U.S. Department
of Transportation
**Federal Highway
Administration**

Publication No. FHWA-NHI-10-087
February 2011

NHI Course No. 130095

Analysis and Design of Skewed and Curved Steel Bridges with LRFD



REFERENCE MANUAL

NATIONAL HIGHWAY INSTITUTE
Training Solutions for Transportation Excellence

AUTHORIZED IACET PROVIDER

Technical Report Documentation Page

1. Report No.	2. Government Accession No.	3. Recipient's Catalog No.
FHWA NHI 10-087		FHWA NHI 10-087

4. Title and Subtitle	5. Report Date
Analysis and Design of Skewed and Curved Steel Bridges with LRFD – Reference Manual	December 2010
	6. Performing Organization Code: FHWA/OPCD/NHI

7. Author (s)	8. Performing Organization Report No.
Michael A. Grubb, P.E. (BSDI, Ltd.), Dann H. Hall (BSDI, Ltd.), John M. Yadlosky, P.E. (HDR), Kenneth E. Wilson, P.E., S.E. (Baker), Laura E. Volle, P.E. (Baker)	RM114904

9. Performing Organization Name and Address	10. Work Unit No. (TRAIS)
Michael Baker Jr., Inc. Airside Business Park, 100 Airside Drive Moon Township, PA 15108	11. Contract or Grant No.: DTFH61-06-D-00009

12. Sponsoring Agency Name and Address	13. Type of Report and Period Covered
Federal Highway Administration National Highway Institute (HNHI-10) 1310 N. Courthouse Road Arlington, VA 22201	Final Submission July 2008 – December 2010
	14. Sponsoring Agency Code: FHWA

15. Supplementary Notes

Baker Principle Investigator: Jeffrey J. Campbell, P.E.
Baker Project Manager: Scott D. Vannoy, P.E.
FHWA Contracting Officer's Technical Representative: Louisa M. Ward
FHWA Contracting Officer's Task Manager: Firas I. Sheikh Ibrahim, Ph.D., P.E.
Review Team Members: Thomas K. Saad, P.E., Dennis R. Mertz, Ph.D., P.E., Silas C. Nichols, P.E., Brian M. Kozy, Ph.D., P.E.

16. Abstract

This document provides instructional material covering the analysis, design, fabrication and construction of skewed and horizontally curved steel bridges using Load and Resistance Factor Design (LRFD). This manual is based on the *AASHTO LRFD Bridge Design Specifications*, Fifth Edition, 2010. It has been developed for highway structural engineers with 0 to approximately 20 years of experience and is presented in US Customary Units.

This manual is comprised of five chapters. The first chapter provides a general overview, it describes the evolution of curved girder bridge design specifications, and it provides a review of LRFD fundamentals. The second chapter describes structural analysis for skewed and curved steel girder bridges, and it includes influence surfaces, bearing constraints, approximate methods, 2D refined methods, 3D refined methods and recommended levels of analysis. The third chapter provides design considerations, and it includes preliminary design decisions, girder design verifications and design of detail items. The fourth chapter describes fabrication and construction considerations unique to skewed or curved steel girder bridges. The fifth chapter provides LRFD step-by-step design examples for a skewed and curved I-girder bridge and for a curved tub girder bridge. AASHTO references are provided throughout this manual.

Key reference documents used in the development of this manual are given immediately following each section in each chapter (as applicable).

17. Key Words	18. Distribution Statement
Curved Bridges, Skewed Bridges, Steel Bridge Design, LRFD, I-Girder, Box Girder, Torsion, System Behavior, Refined Analysis, Lateral Flange Bending, Cross-Frames, Fabrication, Construction, No-Load Fit	This report is available to the public from the NHI Bookstore at http://www.nhi.fhwa.dot.gov/training/nhistore.aspx

19. Security Classif. (of this report)	20. Security Classif. (of this page)	21. No. of Pages	22. Price
Unclassified	Unclassified	1,470	

ACKNOWLEDGEMENTS

We would like to express appreciation to the following individuals who served on the Technical Review Committee:

Dennis R. Mertz, Ph.D., P.E.
Professor of Civil Engineering
University of Delaware
358B DuPont Hall
Newark, DE 19716

We would also like to acknowledge the contributions of the following staff members at Michael Baker Jr., Inc.:

Maureen Kanfoush
Cheryl Epperson
Brittani Renee Russell
Justin W. Bouscher, P.E.
Michael S. Pichura, E.I.T.

In addition, we would like to thank the following individuals who provided technical support throughout the development:

Domenic Coletti, P.E. (HDR Engineering, Inc.)
Brandon W. Chavel, Ph.D., P.E. (HDR Engineering, Inc.)
A. Richard Lawin (Bridge Software Development International, Ltd.)
Scott Krause (High Steel Structures)
Bala Sivakumar, P.E. (HNTB Corporation)
Marcia Baldwin (PerformTech)
Nancy Rosenshine (Perform Tech)

Foreword

This Reference Manual has been written to accompany NHI Course No. 130095 and has been prepared for Design Engineers and Owners of steel bridges with curved girders and/or skewed supports. This work is based on the Fifth Edition of the *AASHTO LRFD Bridge Design Specifications* and the Third Edition of the *AASHTO LRFD Bridge Construction Specifications*. It should be treated as an extension of NHI Course No. 130081 addressing the design of straight steel girder bridges using the same specifications. Steel can be a versatile material that can be designed to meet a wide array of demands of modern highway engineering.

The intent of the publication is to bring more than six decades of aggregate experience with hundreds of these structures to those readers who work in these areas. This Reference Manual addresses the design, fabrication and construction of curved and/or skewed steel girder superstructures. Proper analysis and design of these types of superstructures requires more advanced techniques than commonly used in the design of straight girder bridges without severe skews. Many of the issues that need to be addressed in the Plans and Specifications involve construction, and how they are considered to avoid problems as the project progresses to completion.

These types of girder bridges are, in some ways, similar to straight girder bridges without skew. However, their sometimes subtle behavior introduces issues that must be addressed but can be safely ignored in the design of other girder bridges. The most significant of these issues is non-uniform torque, which involves the interaction between the girders at levels that can be ignored in straight girder bridges without skew. The issue of non-uniform torque appears in handling the curved girders, steel erection, deck placement, barrier placement and application of live load. Phased construction and redecking also introduce special issues that the Design Engineer must consider during the design of these bridges.

The concepts necessary to make these considerations are presented for a structural engineer. Analysis techniques, including approximate methods, 2D grid modeling and 3D modeling, are examined and compared.

It is the earnest hope of the authors that the Design Engineer and Owner will gain a broader comprehension of the entire process, from design through procurement and construction, of these very interesting structures.

NHI Course No. 130095
Analysis and Design of Skewed and Curved Steel Bridges with LRFD
Table of Contents

Chapter 1 Introduction to Skewed and Curved Girder Bridges 1.1.1

Section 1.1 Overview 1.1.1

1.1.1 Introduction 1.1.1
1.1.2 Introduction to Skewed and Curved Bridges 1.1.2
1.1.3 Torsion Theory 1.1.11
1.1.4 Comparison of System Behavior and Individual Girder Behavior 1.1.28
1.1.5 Geometric Terms Commonly Used when Defining Curved Alignments 1.1.45
1.1.6 References 1.1.48

Section 1.2 Evolution of Curved Girder Bridge Design Specifications 1.2.1

1.2.1 Introduction 1.2.1
1.2.2 Research Overview 1.2.2
1.2.3 References 1.2.54

Section 1.3 Review of LRFD Fundamentals 1.3.1

1.3.1 Introduction 1.3.1
1.3.2 Loads 1.3.2
1.3.3 Load Factors and Combinations 1.3.41
1.3.4 Limit States 1.3.49

Chapter 2 Structural Analysis 2.1.1

Section 2.1 General 2.1.1

2.1.1 Introduction 2.1.1
2.1.2 System Modeling 2.1.2
2.1.3 Dead Load 2.1.3
2.1.4 Influence Lines and Influence Surfaces 2.1.3
2.1.5 General LRFD Analysis Requirements 2.1.34
2.1.6 Girder Stiffness 2.1.36
2.1.7 Effective Width of Deck 2.1.38
2.1.8 Uplift 2.1.40
2.1.9 Neglect of Curvature Effects 2.1.43
2.1.10 Uplift Case Study 2.1.47
2.1.11 References 2.1.49

Section 2.2 Bearing Constraints 2.2.1

2.2.1 Introduction 2.2.1
2.2.2 Bearing Loads and Types 2.2.2
2.2.3 Bearing Orientation and Restraint 2.2.3
2.2.4 Effect of Pier Flexibility on Bearing Constraint 2.2.13

Section 2.3 Approximate Methods of Analysis 2.3.1

2.3.1 Introduction 2.3.1
2.3.2 V-Load Method (I-Girders) 2.3.2
2.3.3 M/R Method (Box/Tub Girders) 2.3.24
2.3.4 Levels of Analysis Matrix 2.3.29
2.3.5 References 2.3.33

Section 2.4 2D Methods of Analysis 2.4.1

2.4.1 Introduction 2.4.1
2.4.2 2D Finite Element Modeling 2.4.2
2.4.3 Suggested Methods of Representing Truss-Type Cross-Frames in 2D Models 2.4.8
2.4.4 Advantages, Disadvantages and Limitations of 2D Finite Element Analysis 2.4.19

Section 2.5 3D Methods of Analysis 2.5.1

2.5.1 Introduction 2.5.1
2.5.2 3D Finite Element Analysis 2.5.2
2.5.3 3D Finite Element Modeling 2.5.21
2.5.4 Investigation of a 3D Finite Element Beam Example 2.5.45
2.5.5 Advantages, Disadvantages and Limitations of 3D Finite Element Analysis 2.5.59
2.5.6 Case Study – 3D Investigation of an I-Girder Bridge with a Straddle Beam 2.5.62

Section 2.6 Recommended Level of Analysis 2.6.1

2.6.1 Introduction 2.6.1
2.6.2 Differences in Analysis Results Using Various Levels of Analysis 2.6.2
2.6.3 Completed Levels of Analysis Matrix 2.6.83

Chapter 3 Design Considerations 3.1.1

Section 3.1 Preliminary Design Decisions 3.1.1

3.1.1 Introduction 3.1.1
3.1.2 Primary Layout Considerations for Preliminary Design 3.1.2
3.1.3 Girder Depth and Substructure Considerations 3.1.66
3.1.4 I-Girder Sizing 3.1.89
3.1.5 Box Girder Design 3.1.107
3.1.6 Case Study – 3D Investigation of Framing Plan Layout Issues in a Skewed I-Girder Bridge 3.1.121
3.1.7 References 3.1.127

Section 3.2 Girder Design Verifications 3.2.1

3.2.1 Introduction 3.2.1
3.2.2 LRFD Flexural Design Resistance Equations 3.2.2
3.2.3 LRFD Constructibility Design 3.2.15
3.2.4 LRFD Service Limit State Design 3.2.36
3.2.5 LRFD Fatigue and Fracture Limit State Design 3.2.63
3.2.6 LRFD Strength Limit State Design for Flexure 3.2.111
3.2.7 LRFD Strength Limit State Design for Shear 3.2.175
3.2.8 References 3.2.189

Section 3.3 Design of Detail Items 3.3.1

3.3.1 Introduction 3.3.1
3.3.2 Shear Connectors 3.3.2
3.3.3 Single-Angle Members 3.3.20
3.3.4 Tee and Double-Angle Members 3.3.39
3.3.5 Diaphragms 3.3.56
3.3.6 Bracing Member Connections 3.3.60
3.3.7 Bolted Girder Splices 3.3.135
3.3.8 Web Stiffeners 3.3.168
3.3.9 Bearings 3.3.191
3.3.10 References 3.3.223

Chapter 4 Fabrication and Construction Considerations 4.1.1

Section 4.1 Fabrication 4.1.1

4.1.1 Introduction 4.1.1
4.1.2 Fabrication of Curved Girders 4.1.2
4.1.3 Detailing Cross-Frames and Their Connections 4.1.25
4.1.4 Shop Fit-Up and Assembly Issues 4.1.48
4.1.5 References 4.1.54

Section 4.2 Construction 4.2.1

4.2.1 Introduction 4.2.1
4.2.2 Contractor's Construction Plan 4.2.2
4.2.3 Design Engineer's Construction Plan 4.2.20
4.2.4 Case Study – Phased Construction Issues 4.2.37
4.2.5 References 4.2.40

Chapter 5 LRFD Step-by-Step Design Examples 5.1.1

Section 5.1 Skewed/Curved I-Girder 5.1.1

5.1.1 Introduction 5.1.1
5.1.2 Design Parameters 5.1.2
5.1.3 Steel Framing 5.1.3
5.1.4 Preliminary Member Sizes 5.1.14
5.1.5 Loads 5.1.18
5.1.6 Structural Analysis Results 5.1.21
5.1.7 Limit States 5.1.31
5.1.8 Sample Design Calculations 5.1.32

Section 5.2 Curved Tub Girder 5.2.1

5.2.1 Introduction 5.2.1
5.2.2 Design Parameters 5.2.2
5.2.3 Steel Framing 5.2.3
5.2.4 Bearing Configuration 5.2.9
5.2.5 Preliminary Member Sizes 5.2.9
5.2.6 Loads 5.2.17
5.2.7 Structural Analysis Results 5.2.20
5.2.8 Limit States 5.2.24
5.2.9 Sample Design Calculations 5.2.25

Chapter 1
Introduction to Skewed and Curved Girder Bridges

Section 1.1
Overview



1.1.1 Introduction

This section discusses the applications, advantages and challenges of skewed and curved steel bridges, issues that are unique to these bridges, torsion theory and its application to I- and box sections, and basic concepts of curved girder geometry. This section also describes the behavior of skewed and curved girder bridges, with an emphasis on the importance of considering system behavior in the analysis of these bridges. This section of the Manual serves as a general overview only. Many of the concepts introduced in this section will be expanded upon in greater detail in subsequent sections of this Manual.

1.1.2 Introduction to Skewed and Curved Bridges

1.1.2.1 Curved Bridges

A horizontally curved girder is defined in *AASHTO LRFD* as an I-, closed-box, or tub girder that is curved in a horizontal plane. A horizontally curved bridge can consist of simple-span straight girders kinked at the supports to follow the curve, continuous kinked (chorded) girders or curved girders. In each case, the concrete deck is ordinarily horizontally curved, with the deck overhang being variable in the first two cases and constant in the third.

According to *AASHTO LRFD* Article C6.10.1, bridges containing both straight (tangent) and curved segments are to be treated as horizontally curved bridges since the effects of curvature on the support reactions and girder deflections, as well as the effects of flange lateral bending, usually extend beyond the curved segments. Continuous kinked (chorded) girders are also to be treated as horizontally curved girders.

Curved girders generally are not stable by themselves and need the support of adjacent members to establish equilibrium, particularly during the erection.



Figure 1.1.1 Integral Steel Cap on a Curved I-Girder Bridge Without the Deck

The earliest curved girders were probably made from rolled shapes that were cold bent about their weak axis. As girder welding became more acceptable, curved girders grew in popularity. Horizontally curved girders are used in buildings, such as for balconies. However, the most widespread use of curved girders is in the highway bridge market. They are commonly used in interchanges requiring complex geometries to minimize right-of-way acquisition and where smooth transitions in direction must be accomplished at high speeds.

Curved steel girder bridges have been built in the United States since the 1950s. Some of the earliest horizontally curved girder bridges in the U.S. were box sections made by welding together four plates. Today, curved-girder bridges represent a significant percentage of the total steel-bridge market. Figure 1.1.1 shows a curved I-girder bridge prior to the deck being placed.

Horizontally curved girders offer certain advantages over kinked or chorded girders including:

- Overall simplification of the structure by allowing curved girders to follow the roadway alignment
- Use of longer spans
- Continuity over several spans permitting simplified framing, efficient use of material, increased vertical clearance and fewer joints
- Reduced number of piers
- Simplified forming of the deck with a constant deck overhang
- Simpler reinforcing bar schedule

Aesthetics of highway bridges are being assigned an ever-higher priority. In addition to their structural and economic advantages, curved steel girder bridges provide improved aesthetics at constricted sites. Their graceful appearance is typically well received by the public.

Curved girder bridges, such as the one shown in Figure 1.1.2, demonstrate the aesthetic benefits of matching the structural lines with the traffic flow. The increasing need for horizontally curved bridges is driven by the demand for efficient high-speed highway interchanges and magnificent approaches to major stream crossings. This figure visually shows the versatility welded structural steel can provide when an aesthetic curved bridge is desired.



Figure 1.1.2 Curved I-Girder Bridge

While there is no aesthetic comparison of a curved girder bridge to a segmented curved structure (as shown in Figure 1.1.3) with its seemingly myriad piers and its

interrupted girder lines, the fact is that this inherent aesthetic beauty of curved girders can be obtained for usually less cost than the perfunctory alternative.



Figure 1.1.3 Segmented Curved I-Girder Bridge

However, there are challenges in designing and building horizontally curved girder bridges:

Fabrication requires either additional labor or additional material depending on how the girders are fabricated. Additional labor is used if the girders are fabricated straight and heat curved. Additional material is required of the flanges are cut curved and then the girders are fabricated into a curved shape. Additional labor is also required in the latter case due to handling.

Shipping may add some cost to horizontally curved girders.

Torsion introduces issues when lifting the girders and during erection. Often additional lifting points and temporary supports are needed, increasing costs. Much of these costs would also be encountered if segmented girders were used.

The design of curved girders is slightly more complex than straight girders, but the simpler reinforcing schedule and overhang design of horizontally curved decks on curved girders often balances the increased effort to design the curved girders and cross-frames.

Curved girder bridges are competitive with straight girder bridges on a horizontal curve, but each structure may need to be evaluated as an individual case.

During inspections of curved bridges, greater attention must be paid to cross-frames, diaphragms, cross-girders and lateral bracing since these members are considered to be primary load-carrying members in these bridges. They are also primary members in kinked-girder bridges. Bottom lateral bracing members must also be considered to be primary load-carrying members since they resist significant loads throughout the life of the bridge.

1.1.2.2 Skewed Supports

Skewed supports are employed to match the supports to the underlying alignment of roads, railroads or streams. Skewed supports are often used with either straight or curved alignments.

Skewed supports allow for reduced span lengths and bridge deck area. Reduced spans, in turn, permit reduced girder depths. Skewed supports introduce increased cost with longer abutments and piers compared to right supports. A schematic of a curved bridge with skewed supports is illustrated in Figure 1.1.4.

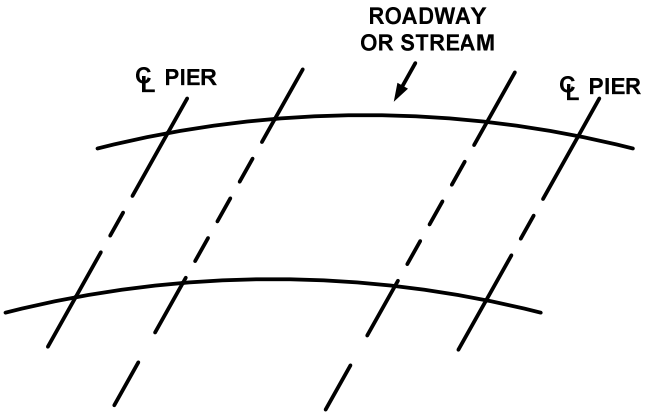


Figure 1.1.4 Curved Bridge with Skewed Supports to Match Roadway/Stream

Skewed supports present additional challenges in the design and construction of straight or curved girders due to the differential deflections of adjacent girders. Interconnection of the girders creates restoring forces in the cross-frames and deck when the structure is loaded. These restoring forces cause torsion in the girders. These load effects lead to girder rotations, larger cross-frame forces and unique thermal movements.

1.1.2.3 Unique Issues with Skewed and Curved Girder Bridges

The objectives of good bridge design include economy, elegance, constructibility and durability. Economy relates to efficient use of the materials and labor while minimizing delays through the reduction of Requests for Information (RFIs). An ill-conceived bridge is never economical or elegant. A well-conceived bridge has an efficient span arrangement with a minimal number of open joints. Unless site constraints make it extremely impractical, spans should be set that permit

reasonable and economical girder depths. This is particularly important for bridges having either curved girders and/or skewed supports since shallower girders tend to accentuate issues associated with these bridges. Selection of an efficient number of girders in the cross-section is particularly important and often overlooked in the early stages of design when this important decision is made. Identification of field-splice and shop-splice locations will be examined in Section 3.1. Utilizing proper types of bearings and joints to permit the bridge to function properly is important. Investigation of construction issues at design will be seen to be very important for both skewed and curved bridges. Such investigations usually will reduce bid costs by providing additional information on design plans and specifications that will lead the contractors to prepare bids based on knowledge rather than uncertainty.

Clearly, to accomplish all these objectives in practical levels of time and cost demands a true professional who is steeped in the technology, construction and enabling technologies that permit him/her to succeed. Success is not measured in the plan set, but only after bidding, construction, acceptance by the public and years of service. Fortunately, the tools and enabling technologies are available to the enterprising engineer. This Manual has been written to prepare the engineer to develop successful designs of steel-girder bridges having horizontally curved girders and/or skewed supports.

First, unique fundamental behavioral issues related to skewed and curved steel bridges must be considered. In addition to vertical bending and shear, torsion in skewed and curved bridge girders results in shear and warping stresses not significant in typical girder bridges, but that must be considered during the design of curved and/or skewed bridges. Warping of I-sections results in transverse shears in the flange and concomitant lateral bending stresses (Figure 1.1.6). In box sections, the torsion results in torsional shear stresses and cross-section distortion stresses. Warping is less severe in closed sections such as box girders.



Figure 1.1.5 Curved Girder Bridge

In skewed and curved bridges, significant load is often transferred between the girders. As mentioned earlier, curved girders depend on their neighbor girders for stability, which is accomplished by shifting load to the next girder away from the center of curvature. This action prevents the girders from twisting further. However, they do twist due to the curvature. Connection to the adjacent girders, usually at cross-frames, interrupts the torsion creating what is referred to as "non-uniform torsion". Of course, this causes increased cross-frame forces and deck stresses. Vertical deflections of adjacent girders differ, resulting in lateral deflection and twist of the girders. Hence, deflection control becomes more critical. Torsion changes the vertical and horizontal reactions, as do thermal loads, wind loads and centrifugal force; all of which have a significant impact on bearing design.

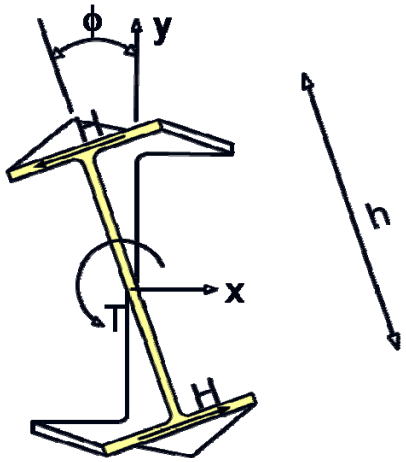


Figure 1.1.6 I-Girder Subjected to Torsion

The integrated behavior of the entire system must be recognized in the analysis of curved-girder bridges due to the significant interaction between components. Bracing members between girders must be included in the analysis and designed as primary load-carrying members. Greater durability and integrity of the bridge can be attained by including all of the structure in the analysis. By computing the force effects on the bearings, bracing and the deck, these components may be designed from rationally computed forces. For example, lateral forces due to vertical as well as lateral loads on laterally restrained bearings can be computed. This information permits rational design of the bearings for lateral forces, particularly those due to vertical loads. This design information leads to much better bearing performance; this is particularly true for bearings in bridges with skewed supports. Rational design of cross-frame members and their connections can be made. The deck reinforcing can be rationally designed for both shear and transverse bending.

A refined analysis model is shown below in Figure 1.1.7. Refined analysis employing such models ensures much more accurate recognition of system behavior.

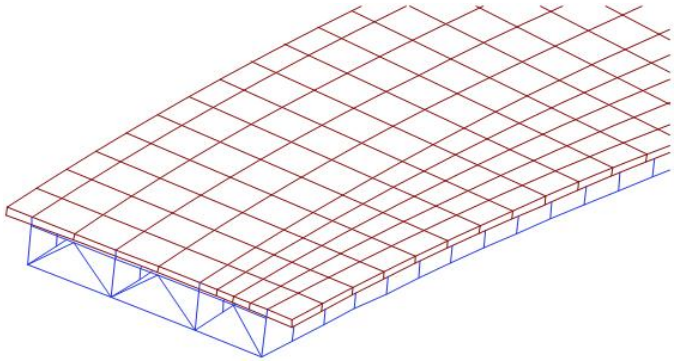


Figure 1.1.7 3D Analysis Model of Curved I-Girder Bridge with Deck

Rational (sanity) checks of statics, strength of materials and deflections are particularly important when refined analyses are employed since the analysis involves calculations performed by a computer and depends on input assumptions made within the computer, and the correctness of the algorithms within the software. There are two methods most commonly employed for checking. First is simply to check global statics; e.g. ensuring that the sum of the vertical reactions equals the vertical applied loads. The second methodology is to use the program to solve classical problems that have been solved by classical methods. These approaches will be examined in more detail later.

In skewed and curved girder bridges, the effects of torsion and amplification of deflections must be considered in the girder design. As mentioned previously, for I-girders, lateral flange bending stresses due to torsion are the primary concern. For box girders, shear stresses and cross-section distortion stresses due to torsion are the primary concern.

For certain bridges with skewed supports and/or curved girders, it may be desirable to provide a Construction Plan in the bid documents indicating what constructibility considerations were made during design. This Construction Plan would be based on the assumptions made at design. For example, it might include components such as an erection plan assumed in developing cambers and stresses, the assumption in design for temporary supports and the deck casting sequence assumed in design. It typically would not include means and methods that have been by rubric, or established custom, determined by the contractor and should remain as such.

Bracing members provide system stability for curved girders and are critical to controlling deflections; thus, they are designed as primary members. This is not directly true for bridges with skewed supports. However, skews may introduce unusually large cross-frame forces, deck stresses and lateral bearing forces compared to “right” bridges. The composite interaction of the cross-frames with the deck through the shear studs is considered in the design of shear connectors in both skewed and curved girder bridges. Transverse deck moments can be significant

enough that additional reinforcing beyond the nominal amount required for the deck may be required.

There are several factors that the fabricator, erector and general contractor should be aware of in order to build bridges with horizontally curved girders and/or skewed supports.

The first decision the fabricator must address when confronted with a curved-girder project is the method of fabrication of the girders. Welded girders may be built by either cut curving the flanges or heat curving flanges of girders built straight. Cut curving is shown in Figure 1.1.8. This method requires additional plate beyond that required for the final girder flanges, which must be ascertained at the time of ordering of the plate from the steel mill. If the decision is made to heat curve the flanges, the plate order will be different. These issues are examined in more detail in Sections 3.1.4.3.4 and 4.1.2.1.

Whichever method the fabricator selects to curve the flanges, handing and shipping of curved girders presents an additional set of challenges that are examined later in Sections 3.1.2.3 and 4.1.2.3.



Figure 1.1.8 Cut Curved I-Girder Flanges in the Shop

Erection of horizontally curved steel girders is more complex than the erection of straight steel girders due to the inherent instability of the girders, as discussed earlier. Frequently the erector is called on to retain an engineer to analyze the system during different stages of the erection to ensure that effects such as girder twist and stability are properly considered during the erection process. Temporary supports are often found to be necessary that might not have been required if the girders were straight. These issues are examined later on in Section 4.2.

Photos of curved I-girder bridges during construction are presented in Figure 1.1.9 and Figure 1.1.10.

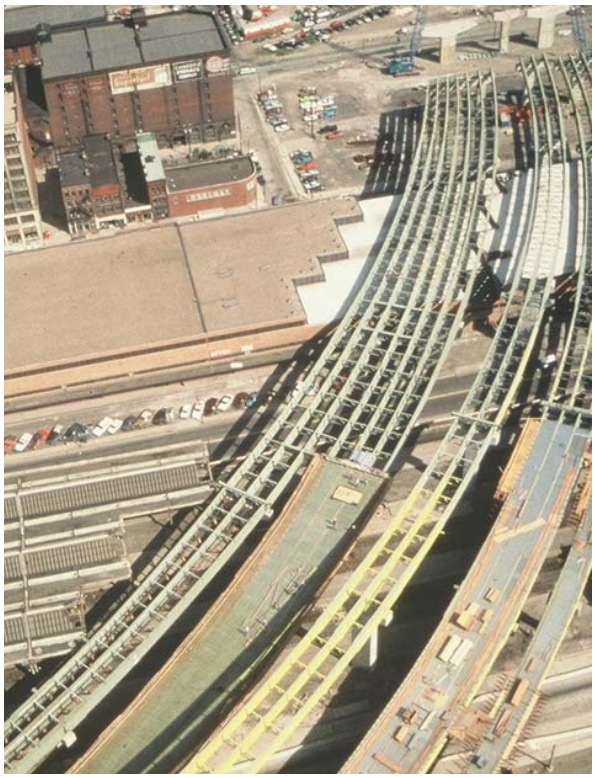


Figure 1.1.9 Curved I-Girder Bridge during Construction

Girders in skewed and curved bridges erected with their webs plumb in the so-called "no-load condition" will be out-of-plumb when the dead load is applied, except at radial supports. Special detailing of the cross-frames in skewed and curved bridges may be required to achieve girder webs in the plumb position after the dead load has been applied.

Skewed supports can complicate the deck-casting. In structures with severe skews, the contractor may choose to skew the screed parallel to the supports in an attempt to equalize the load on the girders. This leads to a longer screed. If the bridge is wide, transverse casts may be required introducing longitudinal construction joints. This also complicates the calculation of deflections, girder moments and cross-frame forces. These issues will be discussed later in Section 3.2.3.

Deck overhang brackets create lateral flange bending moments in the top and bottom flanges of the exterior girders. It is desirable to place the bottom of the bracket at the bottom flange in order to maximize the moment arm and reduce the lateral force on the flanges, which in turn reduces the lateral flange moments. The lateral flange moments may be significant on the top flange of the outside convex curved girder where the brackets caused lateral flange moments that are additive to

those due to curvature in the positive moment regions of the girder. These issues are also discussed further in Section 3.2.3.



Figure 1.1.10 Temporary Supports on Curved I-Girder Bridge

1.1.3 Torsion Theory

1.1.3.1 General

Strength-of-materials teaches that application of a load in a plane other than one through the shear center of the cross-section will cause torsion in the cross-section. The member will twist to the extent that torsional restraints prevent such twisting. The torsional stresses consist of shear and flexural stresses. These stresses must be combined with the stresses due to flexure.

The shear center is defined as the unique point for a cross-section through which any load will create no torsion. The shear center is the point about which a section rotates when subjected to torque. Flexural bending does not create torsion when the applied loads pass through the shear center. This can be tacitly assumed in the analysis with little error in many cases. However, there are many cases where loads do not pass through the shear center, in which case they may create significant torsional stresses. Curved girders and bridges with skewed supports are two cases where torsion should not be ignored without careful consideration.

The shear center of a section must be located in order to evaluate the torsional stress. The shear center does not necessarily coincide with the centroid of the cross-

section. For doubly-symmetric sections, such as the I-sections shown in the left and center sketches of Figure 1.1.11, the shear center coincides with the centroid. For singly-symmetric and unsymmetrical sections, such as channels, tees and single angles, the shear center does not coincide with the centroid. For the channel shown in the right sketch of Figure 1.1.11, the shear center is actually located outside of the section. All of the sections shown in this figure are categorized as open sections. This simply means that the elements of the section do not form a closed or box-type shape. Open sections warp out-of-plane when subjected to torsion.

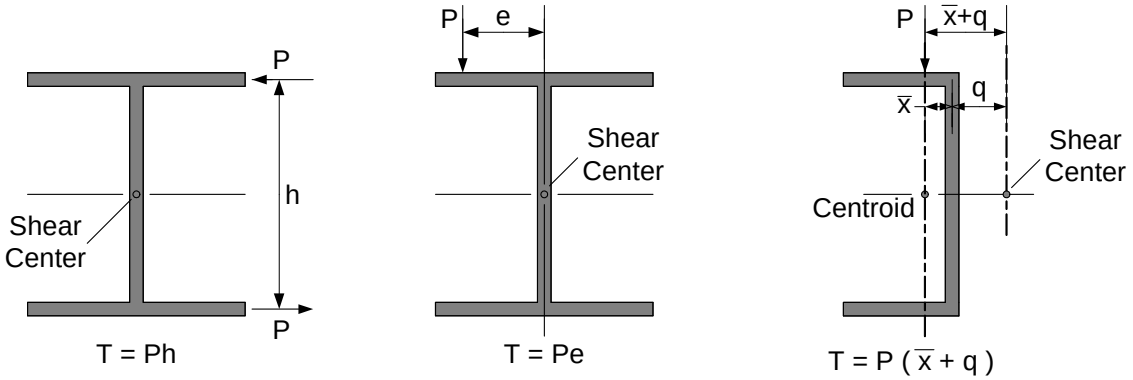


Figure 1.1.11 Torsional Loadings on an I-Section and a Channel

Potential sources of torsion in steel bridges include curvature, support skew, lateral loads (such as wind) and eccentric loads (such as loads induced by deck overhang brackets acting on exterior girders during construction). Due to the torsional effects resulting from curvature, a single curved girder by itself is not stable without some form of torsional restraint. This restraint is typically provided by the cross-frames between the individual girders.

1.1.3.2 I-Sections

1.1.3.2.1 St. Venant Torsion

The simplest form of torsion is referred to as pure torsion or St. Venant torsion. Pure torsion can best be visualized by a prismatic round member free to twist at one end and restrained against twisting at the other end (Figure 1.1.12). If a torque, or torsional moment, is applied to the free end, the torque will travel unreduced to the opposite (torsionally restrained) end where it will be resisted by a torque equal but opposite to the applied torque. The only stresses generated are torsional shear stresses, τ. Hence, the energy induced can be described by a single term. The magnitude of the resulting total angle of twist, ϕ, is computed as:

$$\phi = \frac{TL}{GJ} \qquad \text{Equation 1.1.1}$$

where:

G = shear modulus (ksi)

J = torsion constant or polar moment of inertia; for a solid round = $\pi r^4/2$ ($in.^4$)

L = member length (in.)

T = applied torque (kip-in.)

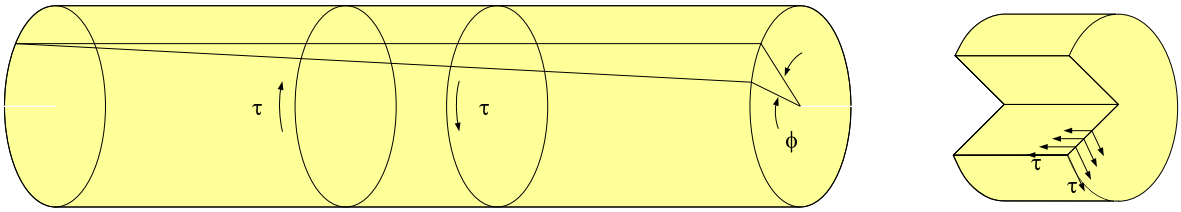


Figure 1.1.12 Solid Round Member Subjected to Torsion

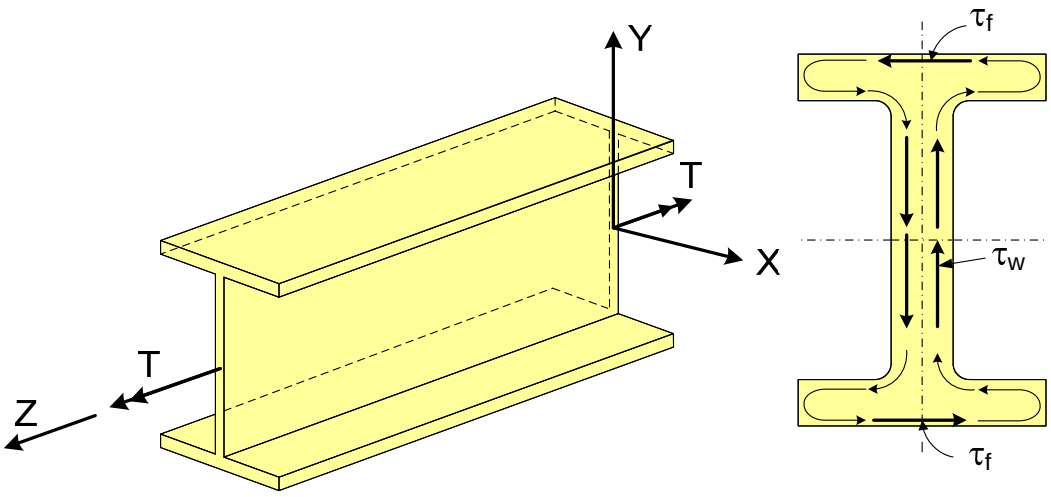


Figure 1.1.13 Torsion and Shear Stress on I-Girder

The rate of twist per unit length, $d\phi/dz$, may be assumed constant for an open cross-section, such as the I-girder section shown in Figure 1.1.13, when the cross-section is assumed not to distort and the torsion is pure and not interrupted by other loads or torsional restraints. The assumption of no distortion allows a torisonal constant to be computed. The section may be thought of as three interconnected rectangular elements (i.e., two flanges and a web) with respect to twist. This assumption is not true for many steel bridge girders where the web is deep and will distort. When the assumption of no distortion is appropriate, the St. Venant torsion shear distribution in

an I-section will be almost identical to that which exists in three separate narrow rectangles.

For a narrow rectangle subject to pure torsion, the relationship between the resisting torque T_s and the twist per unit length can be expressed as shown in Equation 1.1.2 (*1*):

$$T_s = G\left(bt^3/3\right)\frac{d\phi}{dz}$$

Equation 1.1.2

where:

b = width of the rectangle (in.)
t = thickness of the rectangle (in.)

For an I-section, the total St. Venant resisting torque consists of the individual contributions from three narrow rectangles is given as follows:

$$T_s = G\sum\frac{bt^3}{3}\frac{d\phi}{dz} = GJ\frac{d\phi}{dz}$$

Equation 1.1.3

where:

J = St. Venant torsional constant = $\sum bt^3/3$ (in.^{4})

and b and t are the individual width and thickness of each flange and web element. In *AASHTO LRFD* Appendix A6, a more accurate approximation of *J* for an I-section, neglecting the effect of web-to-flange fillets, is given as:

$$J = \frac{Dt_w^3}{3} + \frac{b_{fc}t_{fc}^3}{3}\left(1-0.63\frac{t_{fc}}{b_{fc}}\right) + \frac{b_{ft}t_{ft}^3}{3}\left(1-0.63\frac{t_{ft}}{b_{ft}}\right)$$

Equation 1.1.4
AASHTO LRFD Equation A6.3.3-9

where:

b_{fc} = width of the compression flange (in.)
b_{ft} = width of the tension flange (in.)
D = depth of the web (in.)
t_{fc} = thickness of the compression flange (in.)
t_{ft} = thickness of the tension flange (in.)
t_w = thickness of the web (in.)

For flanges with $b_f/2t_f$ greater than 7.5, the term in parentheses for that flange in the preceding equation may be taken equal to one. More accurate values of *J* for rolled I-shapes, including the effect of the web-to-flange fillets, are tabulated in the AISC *Steel Construction Manual* (*2*).

St. Venant torsional shear stresses in the flanges (τ_f) and web (τ_w) can be approximated from the following formulas:

$$\tau_f = \frac{T_s t_f}{J} \qquad \tau_w = \frac{T_s t_w}{J}$$

Equation 1.1.5

which are for a narrow rectangle, again summing the contributions from the separate rectangular components. As shown in Figure 1.1.13, peaks of shear stress occur on the outer fibers at the center of the flange and on the outer fibers at the mid-height of the web.

1.1.3.2.2 Warping Torsion

If a non-circular cross-section is subjected to a torsional moment, the cross-section will twist. However, it will also deform longitudinally so that plane sections do not remain plane, as shown in Part A of Figure 1.1.14. This cross-sectional deformation is referred to as warping, as shown in Part B of Figure 1.1.14. If warping is restrained, which is typically the case, additional torsion resistance results from transverse shears that develop in the girder flanges due to the flexural resistance of the flanges. This additional component of the torsion resistance resulting from restraint of warping is known as warping torsion.

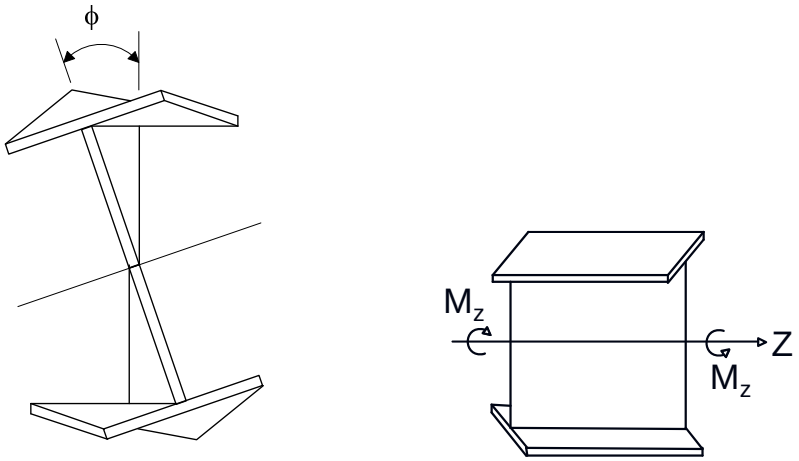
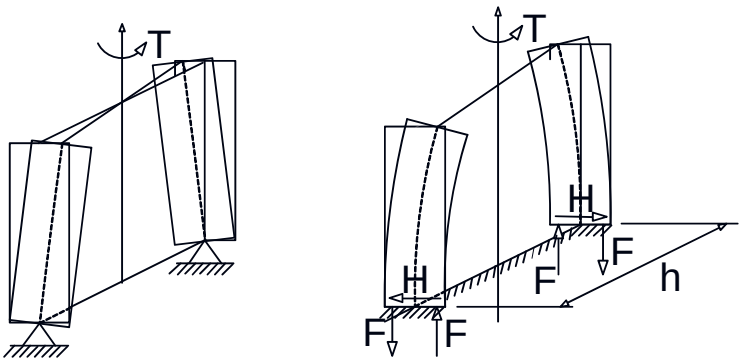


Figure 1.1.14 Twisting and Warping of an I-Section



Warping No Warping

Part A **Part B**

Figure 1.1.15 Warping Torsion Resistance

Part A of Figure 1.1.15 shows a doubly symmetric I-section free at one end and prevented from twisting, but not warping, at the base subjected to a torque, *T*. In Part B of Figure 1.1.15, the same I-section is restrained from warping as well as twisting at its base. As a result, the forces, *F*, are developed and exerted by the support due to restraint of warping. The forces, *F*, acting in the directions shown represent the lateral flange bending moments. These forces cause flange shear stresses, which result in transverse shear forces, *H*, in each flange, as shown in Part B of Figure 1.1.15. These transverse shears bend each flange much like a rectangular beam about its own major axis. Bending in the web is neglected due to its lack of rigidity in the weak direction. In this case, the transverse shear times the distance, *h*, between flange centers results in a couple having the same direction as the resisting torque. Thus, the restraint at the end provides the warping torsion resistance.

Thus, whenever warping restraint is present in an I-section, only part of the applied torque need be resisted in St. Venant torsion. The remainder is carried by so-called warping torsion that is developed due to the transverse shears that result from the flexural resistance of the flanges. The equation for the warping component of the total torque for an I-section is given by the following equation:

$$T_w = -EC_w \frac{d^3\phi}{dz^3}$$

Equation 1.1.6

where:

C_w = warping torsional constant = $I_y h^2/4$ (in.^{6}). Warping torsional constants are available in the literature for other shapes.

h = distance between the centerlines of the flanges (in.)

I_y = moment of inertia of the I-section about a vertical axis in the plane of the web (in.^{4})

Warping torsion is also commonly referred to as “non-uniform torsion” since the shear stress patterns under St. Venant torsion are disturbed because of warping restraint. Thus, non-uniform torsion results from a variation of torque along the span and/or where there are discontinuities in the torque introduced along the span (such as at cross-frames in horizontally curved bridges).

1.1.3.2.3 Torsion Resistance for Design

The total torsion resistance for I-sections is the sum of the St. Venant torsion resistance and the warping torsion resistance, or the resistance that results from the restraint of warping. The differential equation defining the total torsional moment resistance *T* whenever warping restraint is present is given by the following equation:

$$T = T_S + T_W = GJ\frac{d\phi}{dz} - EC_W\frac{d^3\phi}{dz^3}$$

Equation 1.1.7

Knowing the boundary conditions, the differential equation can be solved for the twist angle ϕ and its various derivatives leading to exact theoretical solutions for the various torsional stresses and lateral flange bending moments.

In design, it is often convenient and always conservative to base the design on the dominant type of torsion resistance for the section under consideration and neglect the effects of the other type of torsion resistance. For closed cross-sections, such as box girders, and for certain smaller singly-symmetric and unsymmetrical open cross-sections, such as rolled channels, tees or angles, St. Venant torsion generally predominates. For larger open cross-sections, such as I-sections, warping torsion is generally predominant.

For I-girder design, the St. Venant torsion component is typically ignored for sections with slender webs and all torsion is assumed resisted by warping torsion. Without a significant force couple distance between the shear flows across the thickness of any given element of the I-section, the ability of I-sections to develop St. Venant torsion shear resistance is low. The reason for this is that web distortion causes the section to no longer obey strength-of-materials theory (Figure 1.1.16).

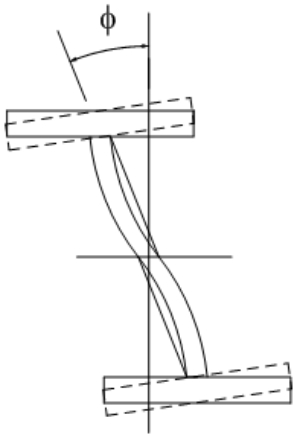


Figure 1.1.16 Web Distortion

The more slender the web, the less significant the St. Venant torsion stiffness becomes. For this reason, St. Venant torsion stiffness is conservatively neglecting in determining the elastic lateral-torsional buckling resistance of slender-web I-sections in the *AASHTO LRFD* Specifications.

For compact web and noncompact web sections, an additional safeguard is specified to allow the use of the full St. Venant torsional stiffness in determining the elastic lateral-torsional buckling resistance in *AASHTO LRFD* Appendix A6 as follows:

$$\frac{I_{yc}}{I_{yt}} \geq 0.3$$

Equation 1.1.8
AASHTO LRFD Equation A6.1-2

where:

I_{yc} = moment of inertia of the compression flange of the steel section about the vertical axis in the plane of the web (in.^{4})
I_{yt} = moment of inertia of the tension flange of the steel section about the vertical axis in the plane of the web (in.^{4})

This limit guards against the use of extremely monosymmetric non-composite I-sections. Cross-section distortion can significantly reduce the influence of the St. Venant torsional stiffness on the lateral-torsional buckling resistance of these sections.

As shown in Figure 1.1.17, warping torsion results in the development of transverse shears in the flanges, along with lateral flange bending moments. The warping torque is typically not used in the design of open sections.

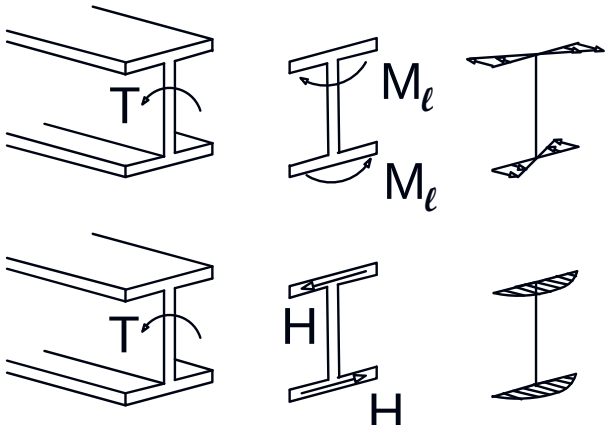


Figure 1.1.17 I-Sections with Effects of Warping Torsion

The lateral flange bending moment times the distance between the flange centers is often referred to as the "bimoment" (in units of kip-in^2), which is most commonly used in the computation of certain fundamental torsional section properties. These properties are not employed in conventional designs.

Individual I-girders with slender webs subject to torsion are typically designed for the force effects shown in Figure 1.1.18.

The girders are designed for the normal stresses, as shown in Part A of Figure 1.1.18, and for shears, as shown in Part B of Figure 1.1.18, resulting from the vertical (major-axis) bending moment.

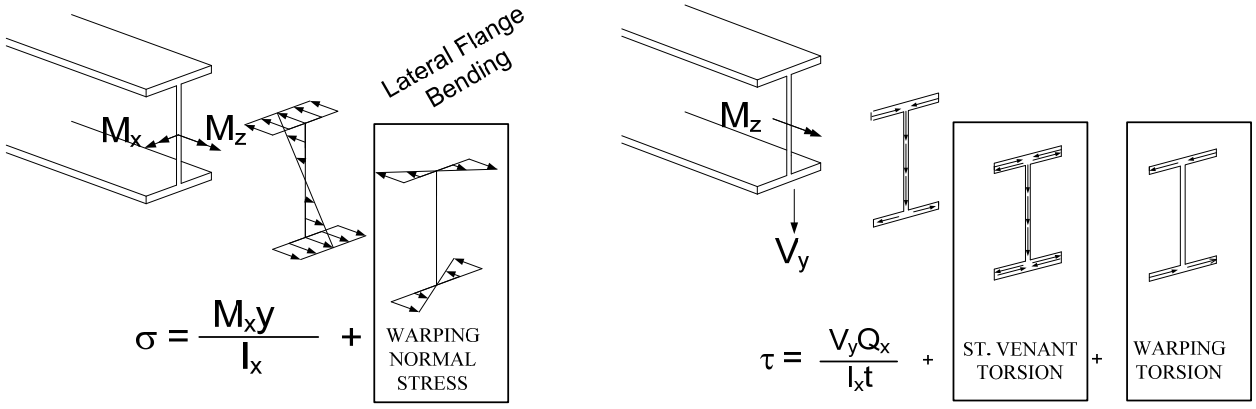


Figure 1.1.18 I-Section Bending Stresses and Shears for Design

The girder flanges are also designed for the lateral flange moments resulting from warping torsion. Shears due to St. Venant torsion and warping torsion in I-sections are generally small and may usually be neglected. Lateral flange bending stresses are the primary action consideration in the design of I-sections for torsion.

Lateral flange bending can be determined by solving a complex differential equation, by reasonable approximations or by direct computation in a 3D finite element model of the section that properly recognizes the lateral bending stiffness. The latter two methods are commonly employed in practical design.

1.1.3.3 Closed (Box) Sections

1.1.3.3.1 General

Closed, or box, sections are many times stiffer in torsion that are open sections. St. Venant torsion is dominant over warping torsion. Additionally, box sections are subject to cross-section distortion that should be considered in design in certain cases.

Figure 1.1.19 shows qualitatively the deformations of a box section due to vertical bending and torsion. Flexure causes vertical deflection; torsion causes twist and cross-section distortion. The final deflected condition is a combination of the three effects.

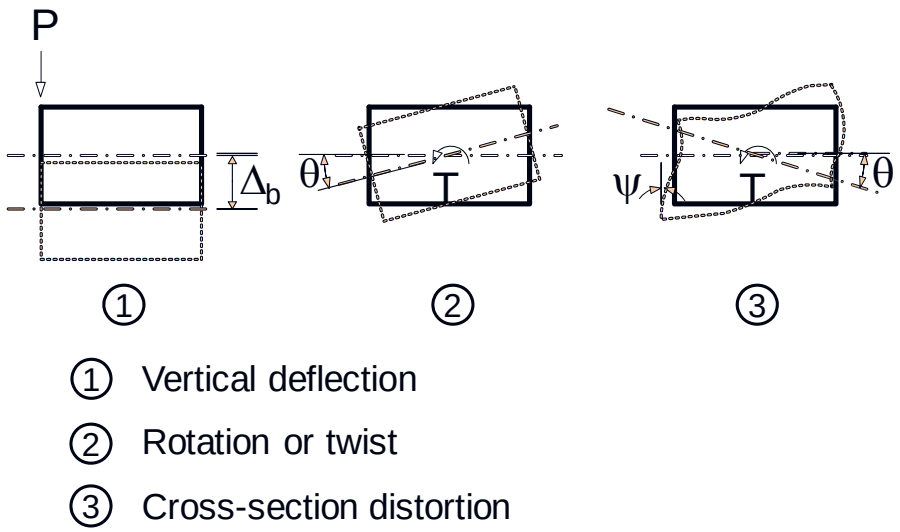


Figure 1.1.19 Deformation of Box Sections

The series of drawings in Figure 1.1.20 illustrates simplistically how a vertical load applied off the shear center can be separated into vertical bending and torsion components using superposition. The load, *P*, is divided equally to the two webs for bending. The torque is represented with a couple of magnitude *Pb*/2.

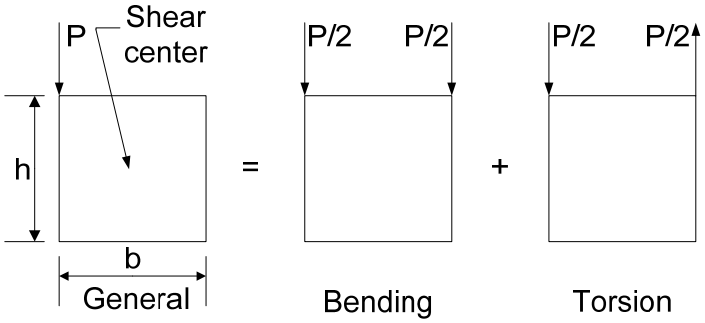


Figure 1.1.20 Vertical Bending and Torsion Components – Box Section

The resulting bending and torsion components to be considered are two normal stresses, three shear stresses and a set of through-thickness bending stresses.

Figure 1.1.21 shows qualitatively the normal and shear stress distributions in the box section due to vertical bending near mid-span (Parts A and B) and at a support (Parts C and D).

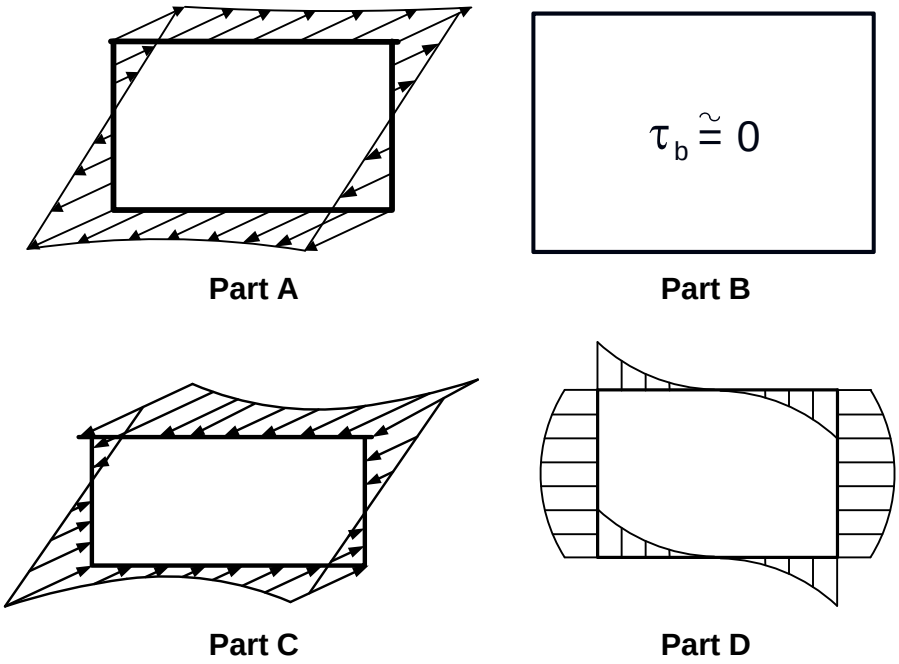


Figure 1.1.21 Normal and Shear Stress Distributions – Box Section

The curvature in the normal and shear stress distributions is due to the effects of shear lag caused by a perturbation in the shear, such as that due to the effect of any concentrated load (such as reactions). The average normal stress across the flange is nearly the same as the integrated normal stress times the area since statics must be satisfied.

This shear lag effect is also present in the deck, but recent research has shown that in most cases its effect may be ignored (this is discussed further in Section 2.1.7).

The series of drawings in Figure 1.1.22 illustrates how the torsion load can be further separated into St. Venant torsion and distortion components. The vertical and horizontal forces shown in the figure are applied directly to the webs and flanges, respectively. The magnitude, *H*, of the horizontal forces applied to the flanges is found from the condition that the total applied torsional moment must be the same as for the box to the left. That is,

$$(P/2)\ b = (P/4)\ b + Hh$$

Equation 1.1.9

$$\therefore\ H = (P/4)\ b/h$$

Equation 1.1.10

In the distortion case of Figure 1.1.22, the applied forces are self-equilibrating and only cause distortion of the cross-section.

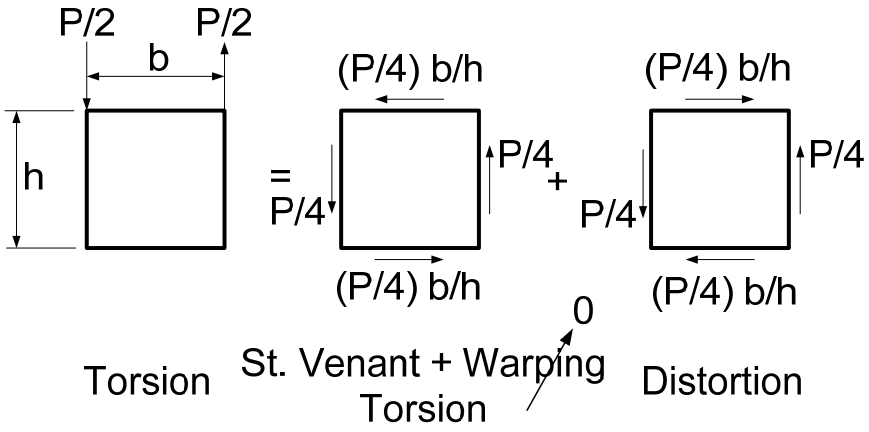


Figure 1.1.22 Torsion Components – Box Section

The warping torsion constant for box sections is usually assumed equal to zero. *This means that shear and normal stresses due to warping torsion are typically quite small and are usually neglected for box sections*. However, as discussed further below, in certain cases including for box sections in skewed and/or curved bridges, normal warping stresses due to cross-section distortion must be considered for fatigue and for checking slip in bolted flange splices. These stresses may be ignored at the strength limit state.

1.1.3.3.2 St. Venant Torsion

Figure 1.1.23 illustrates the St. Venant torsion stress for a box section. As discussed above, in open sections, torsional shear flows around the individual elements. In closed sections, torsional shear flows around the whole section. In a single-cell section, the torsional shear flows around the circumference of the section. For a single cell box section, the uniform St. Venant torsional shear flow, $f = t\tau$ in units of force/length, that develops around the circumference of the box can be determined from the equation shown inside the box

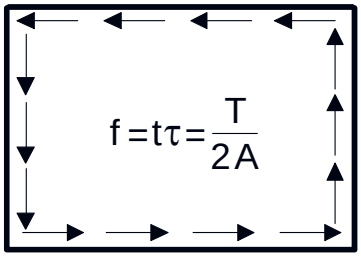


Figure 1.1.23 St. Venant Torsion Shear Flow – Box Section

where *T* is the torque, *A* is the enclosed area of the box and *t* is the thickness of the element under consideration.

To develop this equation, first consider the hollow cylindrical tube shown in Part A of Figure 1.1.24 subject to a torque, *T*.

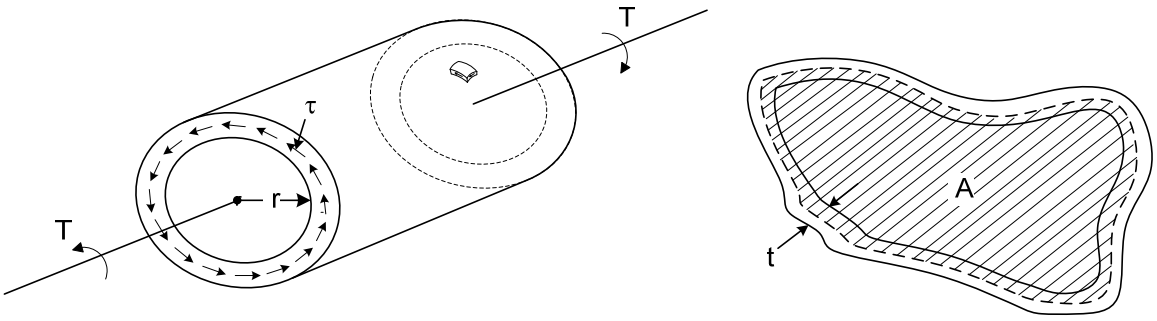


Figure 1.1.24 Cylindrical Tube and Enclosed Area of a Hollow Shaft

The torque is resisted by shear stresses, τ, concentrated within the tubular wall. Assuming the wall is thin with respect to the radius, but thick enough to prevent local buckling, the radial variation of the shear stresses through the thickness may be neglected and the shear flow in the wall may be assumed acting at a distance *r* from the longitudinal axis. *r* is the radius to the middle of the wall from the shear center. For equilibrium in the general case, the shear flow must be taken as the integration

of the torsion over the circumference of the section within the enclosed area. For the cylindrical tube shown in Part A of Figure 1.1.24:

$$T = (\tau t 2\pi r)r$$

Equation 1.1.11

or

$$f = \tau t = \frac{T}{2A}$$

Equation 1.1.12
AASHTO LRFD Equation C6.11.1.1-1

where $A = \pi r^2$ or the enclosed area within the effective radius (Part B of Figure 1.1.24 -- as opposed to the actual cross-sectional area of the material in the tube wall).

Similarly, for the thin-walled rectangular box section shown in Figure 1.1.25 subjected to a torque, *T*:

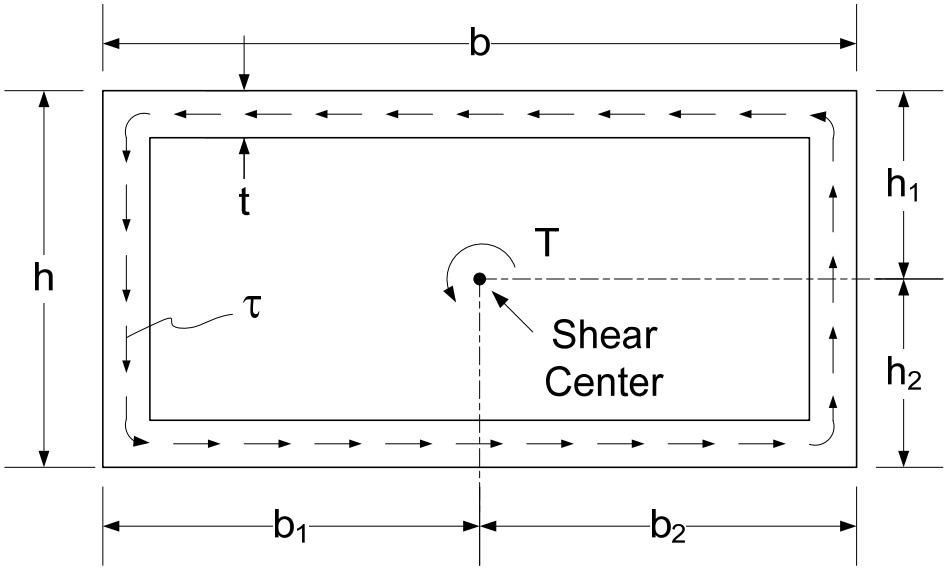


Figure 1.1.25 Shear Flow for a Thin-Walled Rectangular Box Section

$$T = \tau t * [h * (b_1 + b_2) + b * (h_1 + h_2)]$$

Equation 1.1.13

Since:

$$A = bh = (b_1 + b_2)(h_1 + h_2)$$

Equation 1.1.14

$$T = \tau t * [(b * h) + (b * h)]$$

Equation 1.1.15

Therefore:

$$f = \tau t = \frac{T}{2(b * h)} = \frac{T}{2A}$$

Equation 1.1.16

Thus, for any thin-walled single-cell closed shape, the torsional shear stress at any point is equal to the torque divided by the product of the wall thickness at that point and twice the enclosed area. The preceding is true even when the wall thickness varies as long as the change is not abrupt enough to cause a concentration of stress; the shear flow follows the peripheral line and is constant.

The St. Venant torsional constant, *J*, for a rectangular box section with adequate torsional stiffness is determined from Bredt's formula and is given as follows:

$$J = 4\frac{A_o^2}{\sum \frac{b}{t}}$$

Equation 1.1.17
AASHTO LRFD Equation C6.7.4.3-1

where *b* is the width of the plate element under consideration. *AASHTO LRFD* Article C6.7.4.3 permits this equation to be used to compute *J* for tub-girder sections if the distortion of the section is adequately controlled. Cross-section distortion of boxes is usually constrained by internal cross-bracing members. The necessary spacing of internal bracing is difficult to determine, but is a function of the box stiffness and the applied torsion. This issue will be examined in more detail in Sections 3.1.2.8 and 3.2.

In the U.S., most box girders used in bridge superstructures are tub girders having open tops. The open top is braced with a top lateral bracing system that forms a pseudo-box section. The top lateral bracing is designed to resist the shear flow combined with the flexural bending moment in the box. Formulas are available in References 3 and 4 to calculate the thickness of an equivalent plate for different possible configurations of top lateral bracing for use in determining *J*. True (rectangular) box beams in the U.S. are usually limited in application to straddle beams or integral pier caps.

The torsional stiffness of a box section is between 100 and 1,000 times the torsional stiffness of a comparable I-section. This great stiffness is a double-edged sword. When used on horizontally curved alignments, a single box has the ability to resist torsi on alone, unlike open sections that depend on adjacent open sections for stability. Box girders are often used with little or no external cross-

frames/diaphragms, except at supports, even on a significantly curved alignment. This frequently simplifies erection compared to curved I-girders, which may require more lateral bracing and sometimes additional temporary supports. The other edge of the sword limits the twist the box will permit during fit-up. The torsional stiffness in this regard is particularly evident with boxes resting on skewed supports.

Shear flow increases shear in one box web and reduces shear in the other web. In the composite section, the shear flow is resisted, in part, by the deck. The amount of horizontal shear in the concrete deck is determined by the relative shear stiffness of the top flange lateral bracing or top box flange and the deck. In bridges with skewed supports, the horizontal shear in the deck can be substantial and should be considered in the design of the reinforcing steel. The horizontal shear in the bottom box flange is considered by specification in the design of the bottom flange plate. The horizontal shear in the top flanges of tub girders is typically neglected; the top lateral bracing is designed to resist the shear flow induced before the concrete deck hardens.

According to *AASHTO LRFD* Article 6.11.1.1, shear due to St. Venant torsion must be considered at all limit states for all single box or multiple box sections in skewed and/or curved bridges, and/or for sections that do not have fully effective box flanges (discussed further in Section 3.1.5.4.2.1). As specified in *AASHTO LRFD* Articles 6.13.6.1.4b and 6.13.6.1.4c, shear due to St. Venant torsion is also to be considered at all limit states in the design of bolted web splices and bolted box-flange splices for the preceding cases.

1.1.3.3.3 Cross-Section Distortion

Figure 1.1.26 shows the three stress components associated with distortion of a box cross-section; normal warping stress, warping shear and through-thickness bending stress. The through-thickness bending stress distribution shown on the right-hand side of Figure 1.1.26 represents the transverse bending stresses in the outside fiber of the flanges and webs.

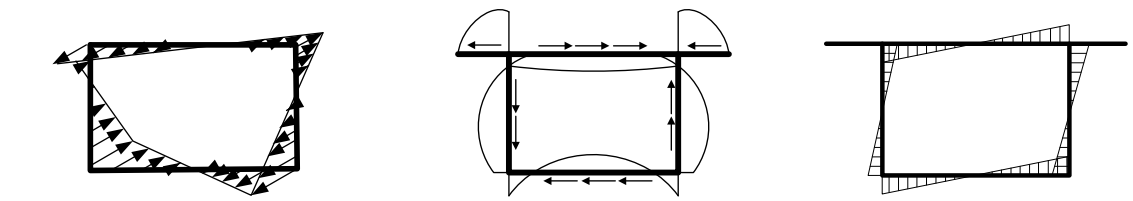


Figure 1.1.26 Distortion Stresses – Box Section

Distortion stresses occur when the section is not round and shear flow changes direction at the box corners, which warps the section. The amount of warping is related primarily to the amount of distortion in the cross-section of the box.

The transverse bending stresses are associated with the shear flow vector changing direction. Since torsion is not mitigated along the section, the section tends to continue to distort and warp until interrupted. In box sections, since the transverse bending stiffness of the flanges and webs alone is not sufficient to retain the box shape, this interruption is accomplished with intermediate internal cross-frames or diaphragms. These members provide quite rigid restraint against movement of the four corners of the box, hence restoring the box to its original shape. Astute location of these braces controls the distortion and associated warping actions.

According to *AASHTO LRFD* Articles 6.11.1.1 and 6.13.6.1.4c, the normal warping stresses due to cross-section distortion must be considered for fatigue and for checking slip in bolted flange splices for all single box or multiple box sections in skewed and/or curved bridges, and/or for sections that do not have fully effective box flanges (discussed further in Section 3.1.5.4.2.1). Normal warping stresses are largest at the corners of the box section where critical welded details are often located. The range of live load longitudinal warping stresses should therefore be added to the range of live load major-axis bending stresses in the bottom flange when checking fatigue. Normal warping stresses due to cross-section distortion may be ignored at the strength limit state. It is apparent that the warping stresses in a flange average out and have been shown to be not deleterious with respect to achieving the capacity of the flange plate. Warping shear stresses due to cross-section distortion are ignored in the specifications.

As discussed previously, when box sections are subject to torsion, the cross-section becomes distorted and is restored at cross-frames/diaphragms, giving rise to secondary transverse bending stresses. Loading the opposite side of the bridge produces reversal of these bending stresses. Thus, according to *AASHTO LRFD* Articles 6.11.1.1 and 6.11.5, transverse bending stresses due to cross-section distortion are to be considered for fatigue for all single box or multiple box sections in skewed and/or curved bridges, and/or for sections that do not have fully effective box flanges. In addition, for these cases, the transverse bending stresses due to the factored loads are to be limited to 20 ksi at the strength limit state. Adequate internal cross bracing usually controls the magnitude of these stresses in boxes of typical proportion such that they are not critical to the ultimate resistance of the box section at the strength limit state.

Transverse bending stresses have caused fatigue cracking in the webs of tub girders where transverse web stiffeners were not attached to the flange. Transverse web stiffeners add significantly to the stiffness of the web so the box distortion is concentrated at their terminus. Attachment of the stiffeners to the flanges, including stiffeners not serving as cross-frame connection plates, prevents this distortion at the stiffener locations. Hence, the welded attachment resists the distortion force. The fatigue resistance of the base metal at the termination of the fillet welds connecting transverse stiffeners to webs and flanges when subject to transverse bending is not

currently quantified in the specifications, but is anticipated to be as low as Category E. Transverse bending stresses are particularly large in boxes subject to large torque, including single box bridges, sharply curved boxes and boxes resting on skewed supports.

The Beam-on-Elastic Foundation (BEF) analogy (*5*) is typically used to calculate the distortion stresses and stress ranges, as illustrated in Section 3.2. Refined analysis methods are generally not used to calculate these stresses due to the refinement of the mesh necessary for their accurate calculation.

1.1.4 Comparison of System Behavior and Individual Girder Behavior

This section addresses the system behavior of skewed girder bridges and curved girder bridges. It emphasizes the knowledge available from a system approach that is not available when studying a single girder.

1.1.4.1 I-Girder Bridges

The model shown in Figure 1.1.27 illustrates the instability of a single simple-span curved I-girder without torsional restraint. The applied vertical load, *P*, creates a torque equal to the load times its eccentricity, *e*, or offset from a chord drawn between the two supports. This torque is unresisted in the illustration. The girder can be made torsionally stable by adding a support or by addition of a torsional restraint at some point on the girder.

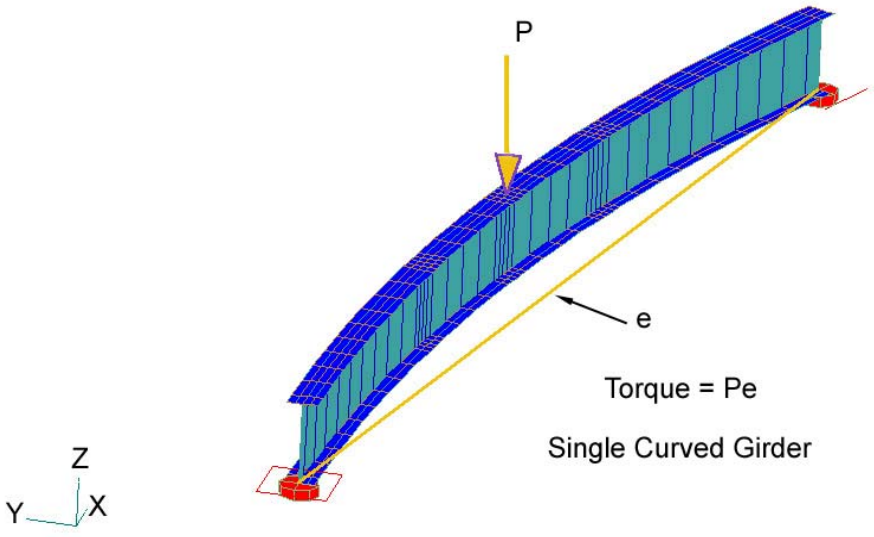


Figure 1.1.27 Model of Single Curved I-Girder with Load and Eccentricity Applied

A curved I-girder bridge would have multiple girders attached together by several cross-frames to provide the necessary stability. This interdependent behavior obviously necessitates an analysis that takes into consideration this interaction. This type of analysis is referred to as a system analysis.

Consider the model of a two-girder simple-span I-girder system with radial supports shown in Figure 1.1.28. The span is 60 feet along the arc. The girders are 4 feet deep; they have a radius of approximately 200 feet and are spaced 10 feet apart. Top and bottom flanges are both 1" x 18". Cross-frames between the girders are located at the supports and at approximately the third points in the span. The cross-frames are all arranged in an X-type configuration. The orientation of the global axes of the model is shown. The origin of the girders is on the left; the girders commence there parallel to the global x-axis.

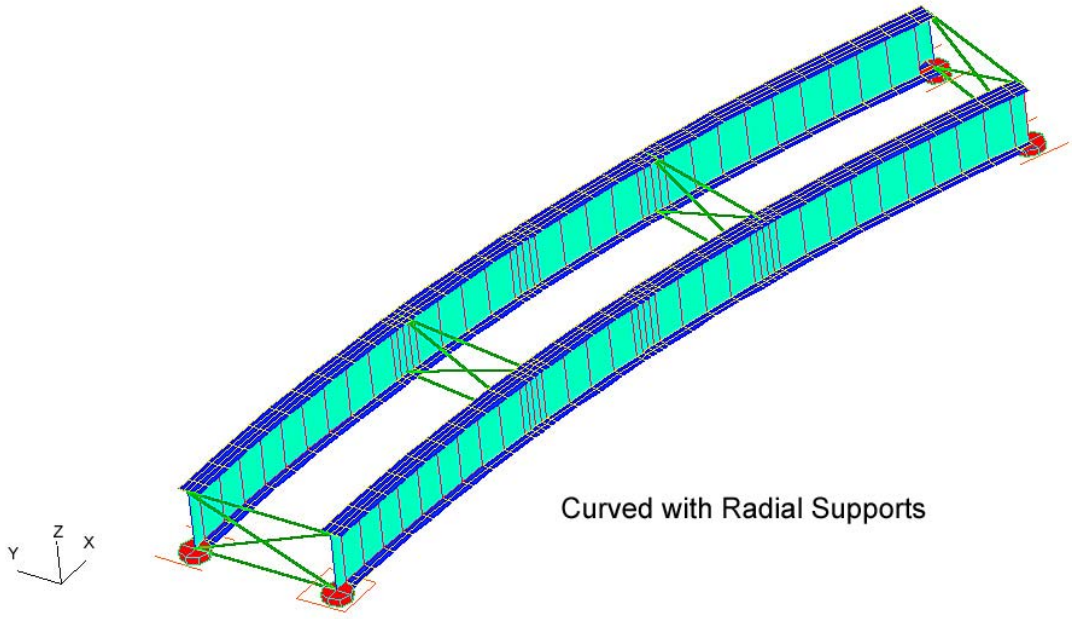


Figure 1.1.28 Model of Two Curved I-Girders with Radial Supports

Stability is achieved by the cross-frames connecting the girders and the four vertical bearings. Note that neither girder alone would be stable. Failure of either girder would cause a significant reduction in the stability of the system and could be expected to lead to collapse.

The four bearings provide the overall system stability, but the cross-frames provide the primary resistance to the torsion caused by the curvature. Unlike their typical characterization as secondary members in straight bridges, cross-frames in a curved bridge must be designed as primary load-carrying members. Hence, unlike straight girder bridges in which individual girders are often isolated from the system and analyzed for design, curved girders must be analyzed as part of a system that includes the cross-frames or diaphragms.

Figure 1.1.29 shows a plan view of the two-girder bridge model from Figure 1.1.28 including the bearing orientation. The behavior of curved and/or skewed girder bridges may be significantly influenced by its bearing restraints. The bearing orientation and restraints are shown. A pair of lines indicates guided bearings; a boxed bearing (see lower left corner of Figure 1.1.29) indicates a fixed bearing.

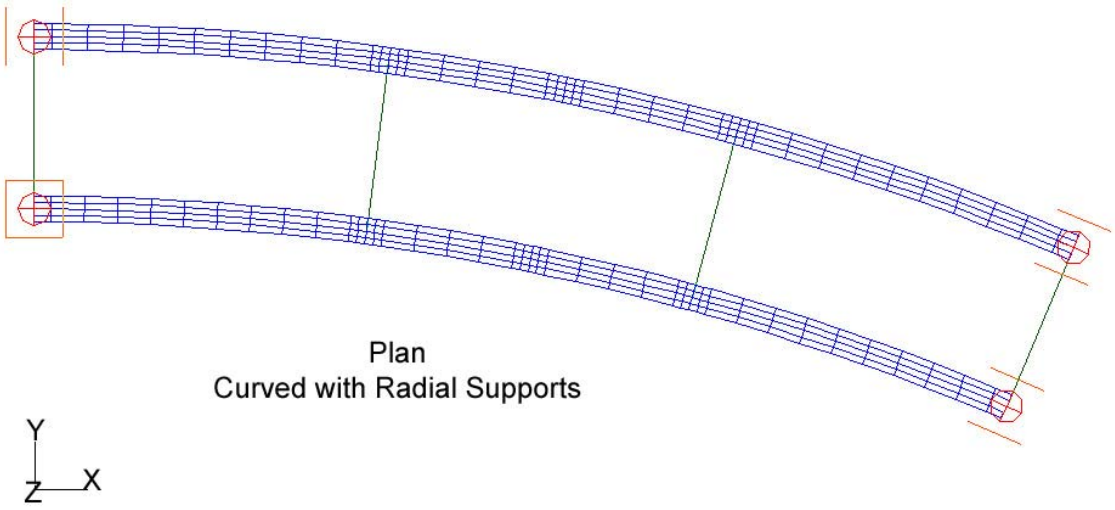


Figure 1.1.29 Plan View of Two-Girder Model

The deformation of the bridge model will next be examined when it is subjected to a uniform vertical load along the full length of both top flanges. Deflections in the subsequent plots are exaggerated to aid in visualization.

Figure 1.1.30 shows a plan view of the deformed shape looking up from the bottom. The top flange is light blue, the bottom flange is brown, and the undeformed model is dark blue.

The effect of the bearing restraints is of interest. At the right end, the bottom flange of both girders got longer due to elastic lengthening of the girders and the freedom of the bearings tangent to the girder lines. The lengthening was greater on the outside girder due to the greater moment (higher tensile stress) in that girder. The bottom flanges of both girders were restrained longitudinally at their left ends. The top flanges of both girders got shorter at both ends due to elastic shortening.

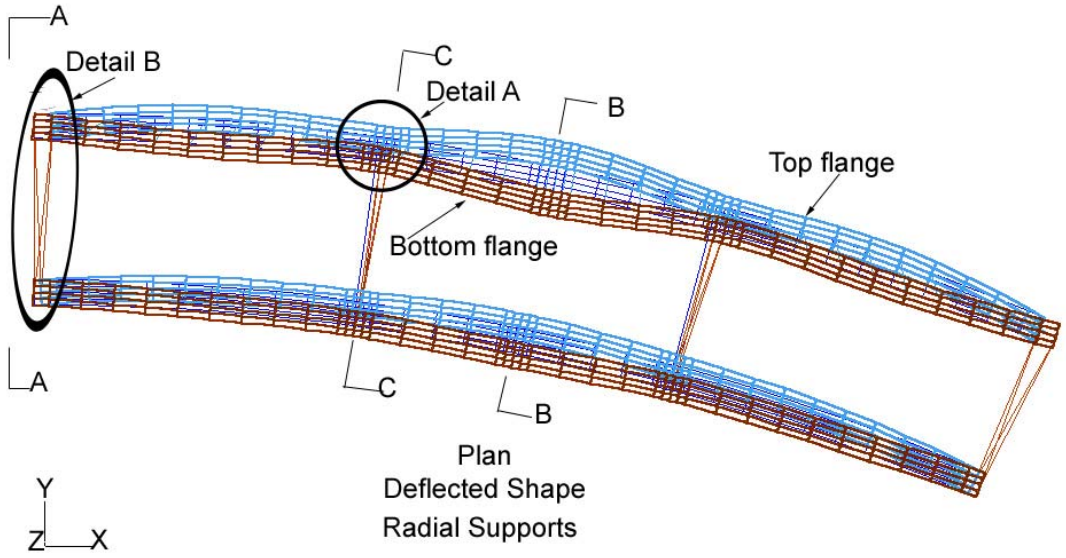


Figure 1.1.30 Plan View of Deflected Shape of Two-Girder Model

The top flanges bowed out, while the bottom flanges tended to straighten. The bowing occurred as a result of radial components of the compressive forces in the flanges due to non-colinearity of the compressive forces. The radial force components in the bottom flanges are due to the tensile forces in those flanges. They act in the opposite direction and tend to straighten or bend the flanges toward the center of curvature. The reversal of curvature near the cross-frames occurs because the moments reverse, much as they do in a continuous beam. In fact, elementary analysis of lateral flange bending can be made by assuming a beam (i.e. the flange) continuous across supports (i.e. the cross-frames).

Part A of Figure 1.1.31 is a free body of a curved compression flange between cross-frames. The flange is assumed subjected to a constant axial force, *P*, induced by a uniform vertical bending moment. The non-collinearity of the flange forces at the cross-frames is accentuated in Part A. The radial components of these forces bow the flange outward. Radial forces, *H*, shown on the free body are restoring forces at the cross-frames.

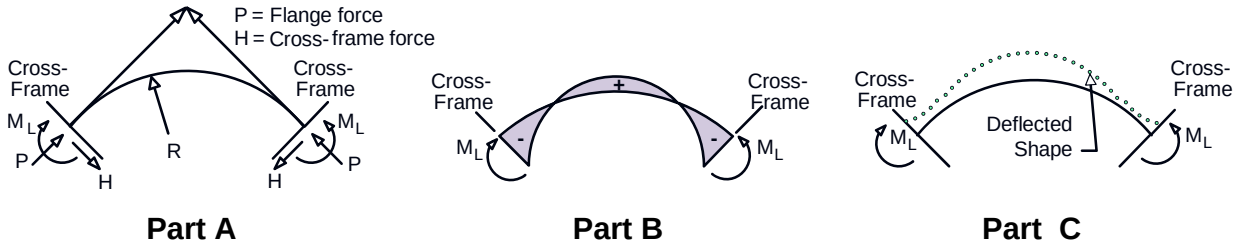


Figure 1.1.31 Curved Compression Flange

In this case, the lateral flange moments at the brace points restrain bowing of the flange. The sense of the lateral moment at cross-frames in compression flanges is usually taken as negative. The sign of the moments reverses over the central region between cross-frames. This phenomenon is exhibited in Part B of Figure 1.1.31. An approximate method for calculating lateral flange moments and stresses at the brace points is presented in Section 2.3.2.

The net effect of the torsion due to curvature in compression flanges is to increase the curvature of the flange, as shown in Part C of Figure 1.1.31. The deflected shape shown in Part C illustrates that the net movement of the flange is outward. Not shown is the inward net movement of the tension flange.

Figure 1.1.32 presents similar diagrams for a curved tension flange between cross-frames. In this case, the radial components of the flange force tend to reduce curvature, while the lateral flange moments at the brace points tend to restore it. The bending sense of the lateral moment at cross-frames in tension flanges is usually taken as positive, with the sign of the moment reversing in between the cross-frames. The net effect on the flange can be to either increase or decrease the curvature of the tension flange, depending on the flange stiffness and curvature. The two tendencies lead to a canting of the girder web from its original orientation.

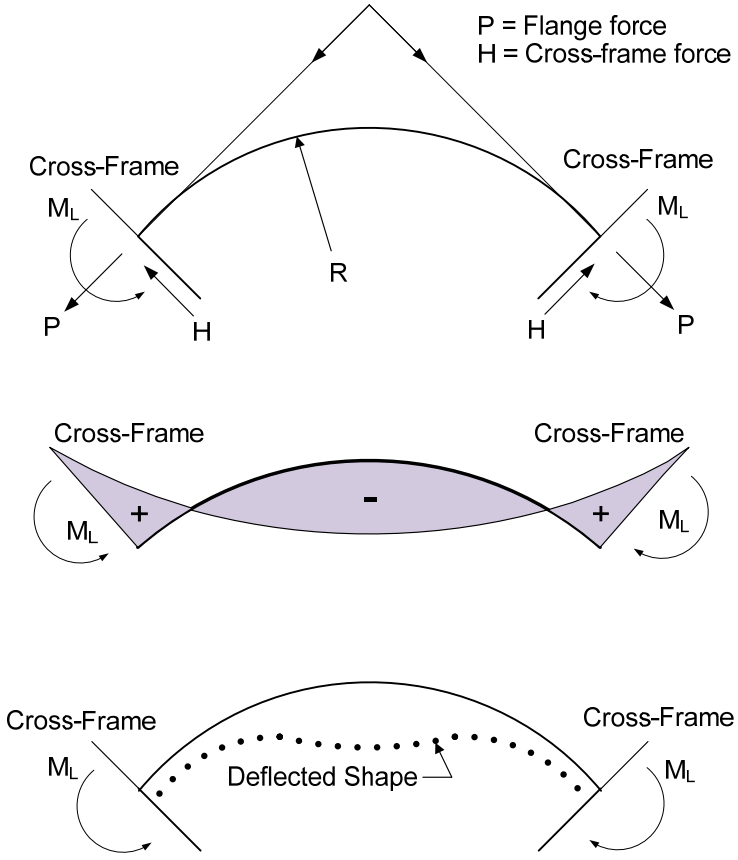


Figure 1.1.32 Curved Tension Flange

Flange lateral bending effects due to curvature and other effects (such as inclined webs, deck overhang bracket forces, top lateral bracing forces and wind) must also be considered in the top flanges of horizontally curved tub girders.

Figure 1.1.33 shows a close-up of the outside girder flanges at the left interior cross-frame of the two-girder model bridge, indicated in Figure 1.1.30 as Detail A.

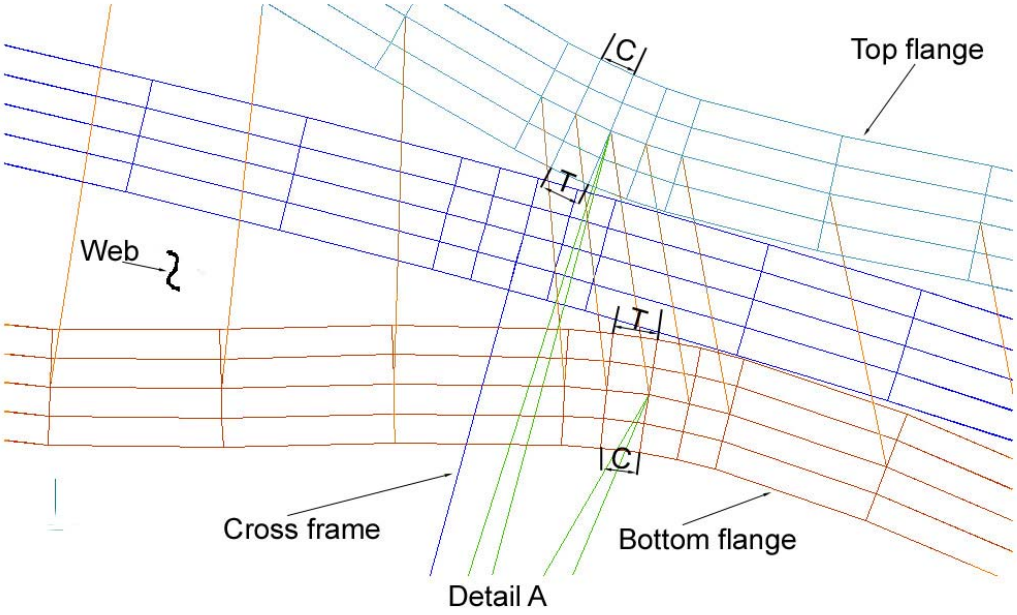


Figure 1.1.33 Detail A of Two-Girder Model in Figure 1.1.30

The set of blue lines in Figure 1.1.33 represent the original, unloaded top flange. Its curvature is uniform. The short elements near the center were introduced to reveal the bending across the flange in the vicinity of the cross-frame. The lines connecting the top and bottom flanges are web element lines. The lines extending to the bottom of the detail are the cross-frame members. In the not-loaded (undeformed) case, the cross-frame members lie in a vertical plane so only one line is visible. The sense of bending can be visualized by the shorter element measured as *C* and the longer element measured as *T* as compared to the element length in the undeformed flange.

The bottom flange exhibits the opposite behavior. The elements on the outside of the bottom flange have lengthened, and the elements on the inside of the flange have shortened.

Figure 1.1.34 shows Detail B, a plan view of the left end of the model at the radial support of Figure 1.1.30. The orientation of the axes in this figure shows that the view has been rotated 90 degrees from the preceding views.

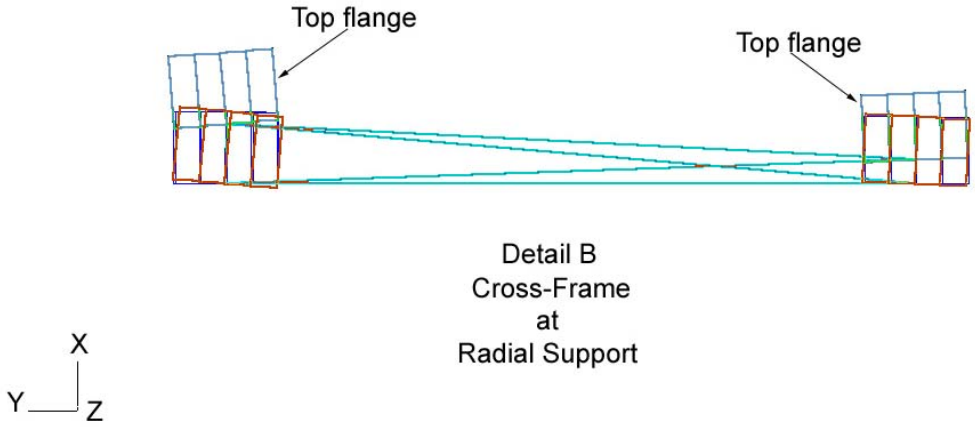


Figure 1.1.34 Detail B of Two-Girder Model in Figure 1.1.30, Cross-Frame at Radial Support

Recall that the bearings at this location prevented longitudinal movement; only the top flanges can move longitudinally. The top flanges of both girders have moved into the span (away from the bearings in the positive X direction). This is simply due to shortening of the compression flange. The outer (left) flange moved further due to the larger stresses in the outside girder. Of course, the cross-frame has rotated with the top flanges.

Both top flanges are bowing outward (away from the center of curvature, i.e., in the positive Y direction). The flanges are not continuous here so there is no reversing moment.

Figure 1.1.35 shows an end view of the deformed model of the same support, which is identified as Section A-A in Figure 1.1.30. The view is looking along the positive X axis. One element along the girder is included in the plot.

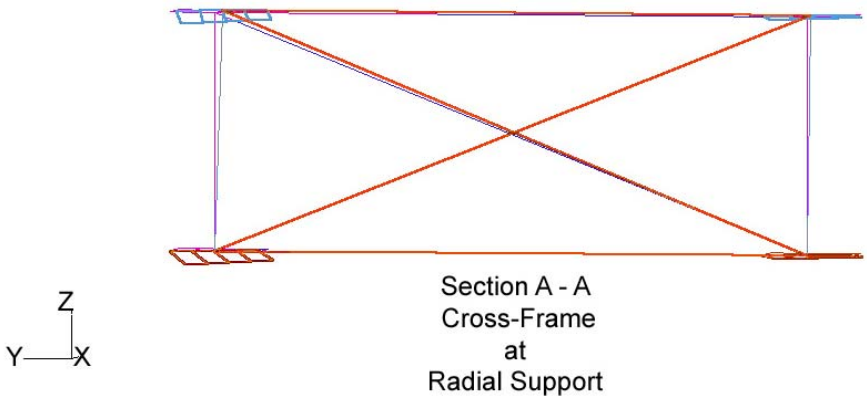


Figure 1.1.35 Section A-A of Two-Girder Model in Figure 1.1.30

The lower element on the left indicates that that girder (on the outside of the curve) has deflected more than the right girder, although equal load intensities were applied to both girders. The girder on the outside of the curve was subject to a larger moment due to its greater length and the load transfer to it via the cross-frames.

The girders did not deflect vertically at the bearings. Nor did they rotate (twist) about their longitudinal axes at the support.

Figure 1.1.36 shows the cross-section at the center of the span, represented by Section B-B of Figure 1.1.30. There is no cross-frame at this section.

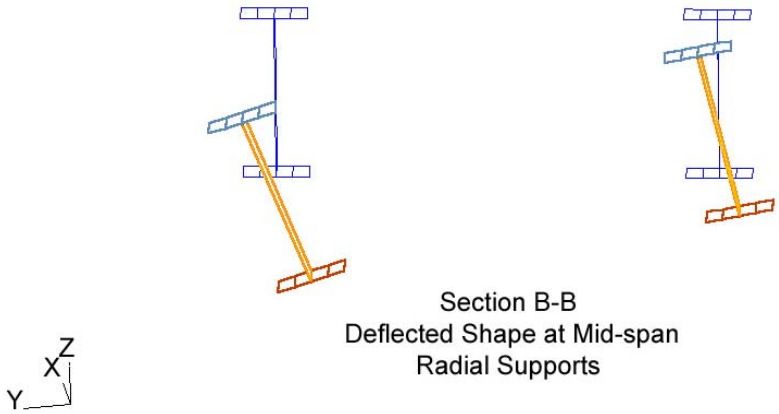


Figure 1.1.36 Section B-B of Two-Girder Model in Figure 1.1.30

The girders did not translate, but deflected downward and rotated about their shear centers. If the top and bottom flanges had been of different sizes, a vertical line through the original undeformed shape would not have passed through the mid-height of the rotated girders, but through the shear center which would not have been located at mid-height.

Figure 1.1.37 shows the cross-section at the left interior cross-frame; Section C-C of Figure 1.1.30.

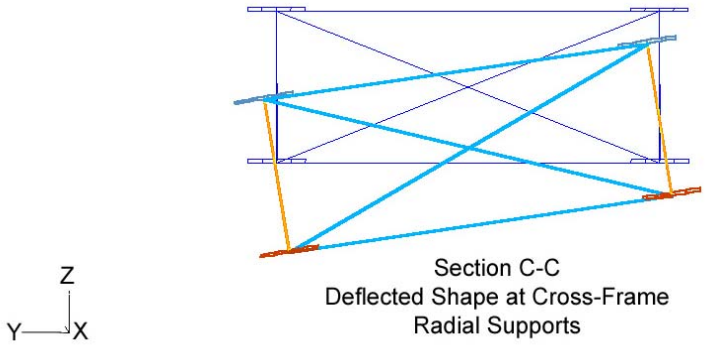


Figure 1.1.37 Section C-C of Two-Girder Model in Figure 1.1.30

Unlike the prior cross-section at mid-span, the girders at this section were forced to rotate together instead of independently by the truss action of the cross-frame, which maintained the rectangular configuration of the girders and cross frame (neglecting the relatively small in-plane elastic axial deformation in the cross-frame members). The distance between the girders and the relative angular orientation remained constant. Thus, the girder flanges remained in common planes while the bridge cross-section rotated. Restoring forces were developed in the cross-frame members.

The relative rotation evident in Figure 1.1.36 demonstrates the effect of the torque in the system rather than in the individual girders.

Skewed supports were introduced to the otherwise same model in Figure 1.1.28. A perspective plot is shown in Figure 1.1.38. The bearing constraints and cross-frames remain the same.

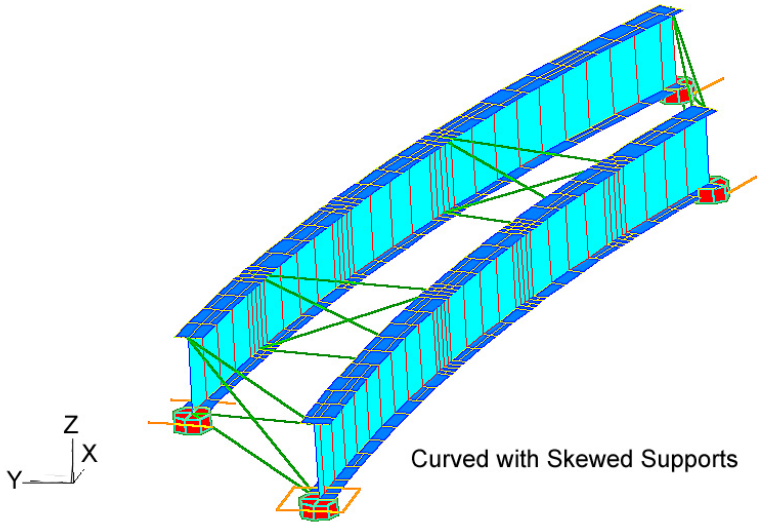


Figure 1.1.38 Skewed Supports Added to Two-Girder Model in Figure 1.1.28

Figure 1.1.39 shows a plan view of the skewed two-girder model.

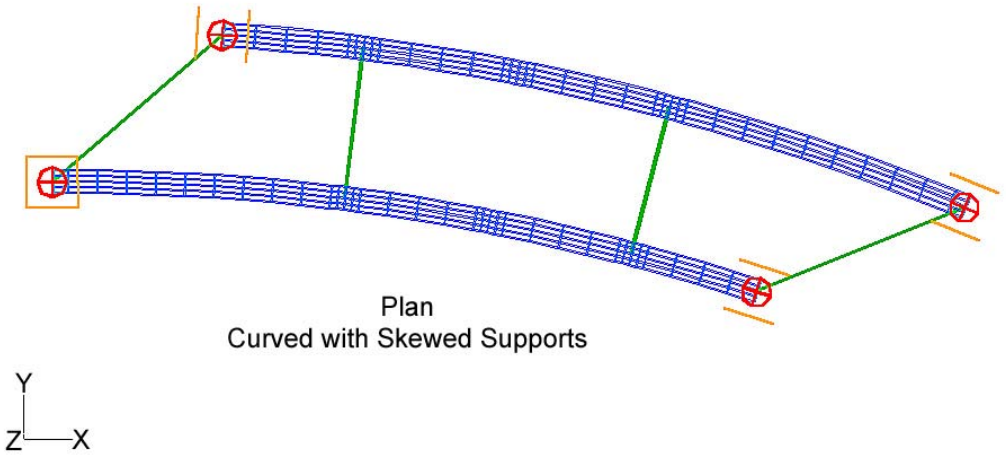


Figure 1.1.39 Plan View of Two-Girder Model in Figure 1.1.38

Figure 1.1.40 shows a plan view of the deformed shape of the skewed model shown in Figure 1.1.38, which is the two-girder model with skewed supports subjected to the same uniform load as applied to the non-skewed model. The top flange is light blue, the bottom flange is brown, and the undeformed model is dark blue.

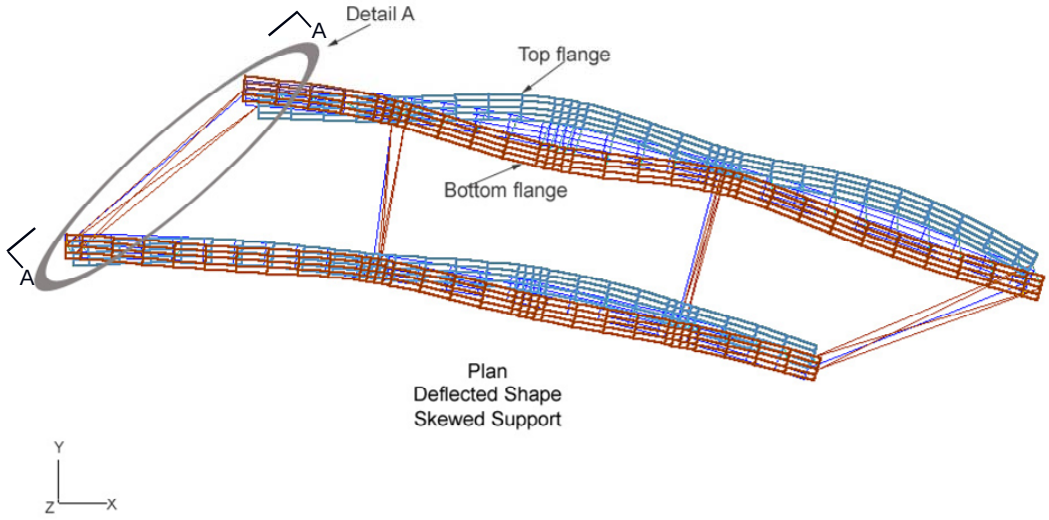


Figure 1.1.40 Plan View of Deflected Shape of Two-Girder Model in Figure 1.1.38

The lengthening of the bottom flanges and shortening of the top flanges is evident. The effect of the bearing constraints is evident. Although the tension flanges lengthened, all of the lengthening occurred at the right end where the bearings

permitted freedom of movement tangent to the girder lines. Since there was no restraint of the top flange, both flanges shortened at both ends. The top and bottom flanges are not aligned at the ends, as was the case with the model on radial supports shown in Figure 1.1.30. Again, the top flanges moved outward, away from the center of curvature, while the bottom flanges tended to straighten and even moved past straight and tended to bow inward. This extreme behavior indicates that the skewed case introduced more torsion than the curved case with no skew.

Figure 1.1.41 shows Detail A indicated in Figure 1.1.40. The global-axis indicator shows that this is a plan view.

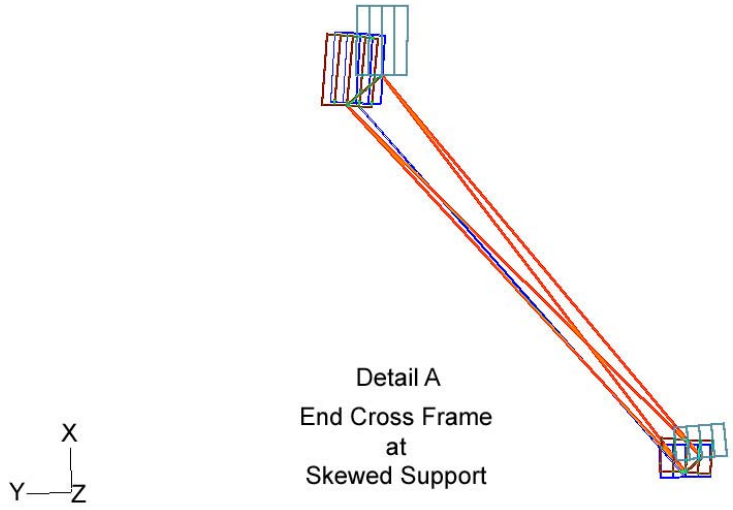


Figure 1.1.41 Detail A of Two-Girder Model in Figure 1.1.40

The top flanges of both girders have shortened (in the positive X direction) and shifted laterally. The top flanges translated in the negative Y direction. Bottom flanges are restrained from moving in the X direction by the bearings. The bearing permitted the bottom flange of the outside girder (upper girder in this plot) to translate slightly in the positive Y direction. The bottom flange of the inside girder is fixed against translation.

The cross-frame must rotate in the positive X direction to remain attached to the top flanges. A view of an interior cross-frame is not shown because is is similar to the case without the skew. The differential deflections at each end of the interior cross-frame in this case occur primarily because the interior cross-frames are connected radially to the adjacent girders at different positions along the length of each girder. Thus, each girder will experience a different vertical deflection and major-axis bending rotation at each end of the cross-frame as the load is applied.

Figure 1.1.42 shows the deformed left support; Section A-A in Figure 1.1.40. The view is looking along the positive X axis.

The rotation (twist) of the girders and the cross-frame is evident. There was essentially no twist in the model with radial supports at the bearings. The twist observed in the skewed case is due to the compatibility of the cross-frame member connectivity. Because the cross-frame member lengths must be maintained, the observed twist is inevitable. It is of interest to note that while one girder rotates away from the bridge, the other rotates toward the bridge. If the skews at both ends are parallel, the girders rotate in opposite directions at their ends.

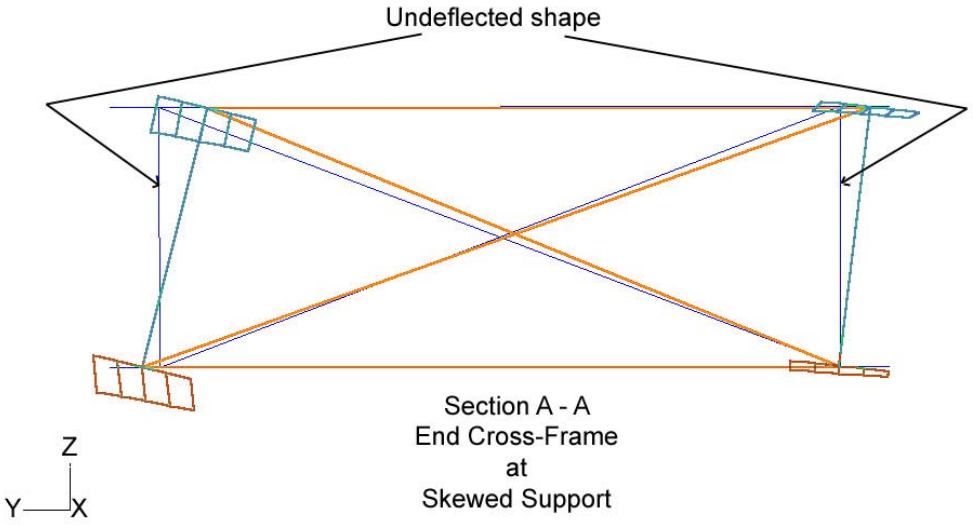


Figure 1.1.42 Section A-A of Two-Girder Model in Figure 1.1.40

The rotation (twist) of the bottom flanges can cause significant issues for bearings and alignment of the entire bridge. These girder rotations about their longitudinal axes will occur at skewed end supports whether the girders are straight or horizontally curved. Larger vertical girder deflections exacerbate the effect. As will be discussed in Sections 4.1 and 4.2, the lateral deflections and girder twist that occur in skewed and curved bridges should be considered during fabrication and construction.

To further describe system behavior as it relates to curved bridges, consider the 3D refined analysis models of the two-girder, 160-ft simple-span, I-girder structure shown in Figure 1.1.43. The girder spacing is 10 feet; the cross-frame spacing is 20 feet; and the girder depth is 6 feet. Both girders are the same size. The girders are singly symmetric with the top flange smaller than the bottom flange.

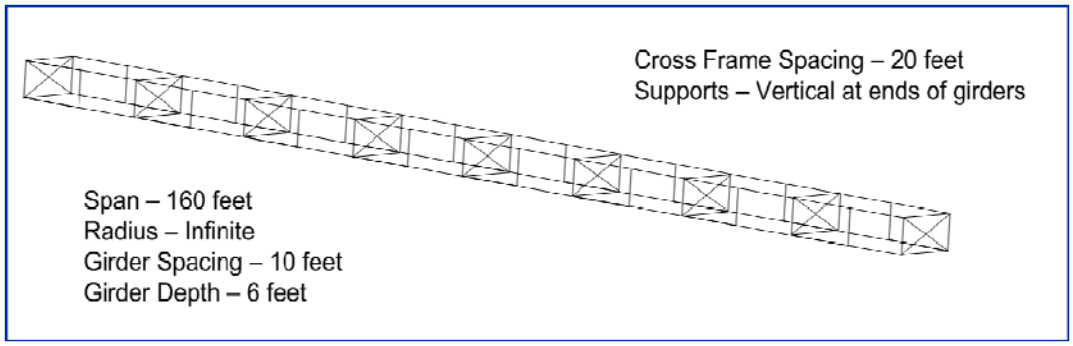


Figure 1.1.43 3D Refined Analysis Model of Straight Girders

For comparison, the two-girder structure shown in Figure 1.1.43 was re-built with a 400-foot radius as shown in Figure 1.1.44.

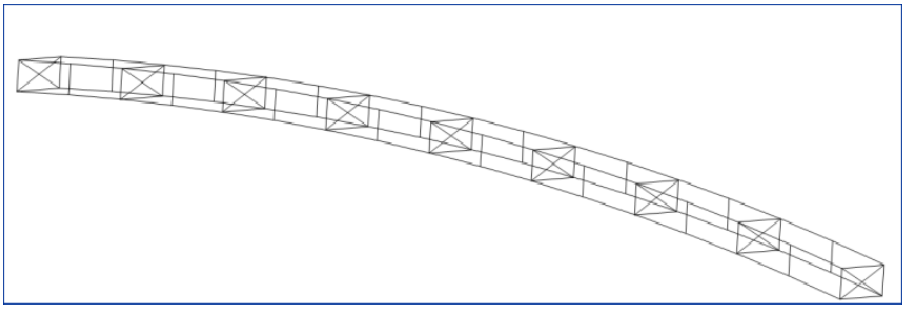


Figure 1.1.44 3D Refined Analysis Model of Curved Girders

An additional comparable model of the two-girder structure was made by kinking the straight girders an amount that gave the same change in alignment as provided by the 400-foot radius model. This model is shown in Figure 1.1.45.

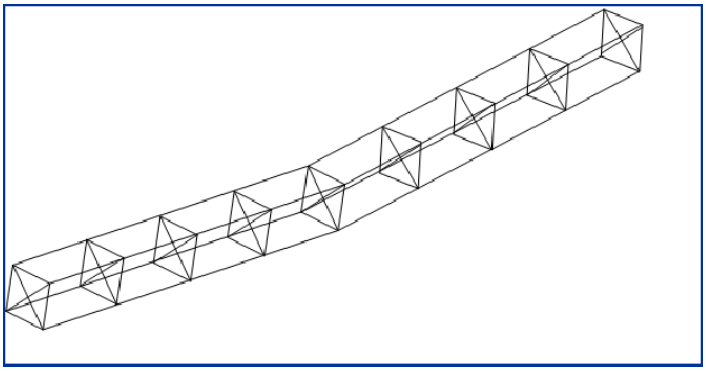


Figure 1.1.45 3D Refined Analysis Model of Kinked Girders

A downward load of 1.0 kip/ft was applied along the length of each girder.

Table 1.1.1 shows reactions and mid-span vertical deflections and mid-span moments for comparison. Note that the total reaction is slightly greater for the

curved and kinked structures than for the straight structure. This is due to the greater length of the curved and kinked structures.

Table 1.1.1 Comparative Reactions, Deflections and Moments of 3D Models

Reactions, midspan deflections and moments

Model girder	Vertical reaction (kips)	Mid-span deflection (in)	Mid-span moment (K ft)
Straight			
Girder 1	80	-3.18	3292
Girder 2	80	-3.18	3292
Total	160		6584
Curved			
Girder 1	-8	-4.17	-547
Girder 2	170	-12.77	7318
Total	162		6771
Kinked			
Girder 1	14	-6.10	-1114
Girder 2	148	-6.63	7862
Total	162		6748

The vertical bending moments in the two straight girders are equal. The sum of the bending moments in the two girders is greater in the curved and kinked cases due to the greater length of the girders. Interestingly, the sum of the moments in the two non-straight cases is nearly equal. In the curved and kinked girders, however, the convex (outside) girder resists more than the total moment although the sum of the moment in the two pairs of girders is nearly equal. The instability of the two girders caused a negative moment in the concave curved girder and uplift at the bearings of that girder. The offset had a similar effect in the kinked-girder case, except that uplift did not occur even though the moment at the kink in the concave girder was negative at mid-span. The reason that there was no uplift in that case is that much of the length of the concave girder was along a straight alignment.

The mid-span deflections in the two kinked girders are nearly equal because the M/EI diagrams along the two girders are nearly equal, except for right at the kink.

In the case of the straight-girder bridge, the cross-frame members act primarily to stabilize the girders and experience little load since the two girders are loaded equally. Whereas in the case of the curved and kinked structures, the cross-frames act as primary load carrying members with the offset being a critical structural effect.

Figure 1.1.46 gives a plot of the bottom flange lateral bending moments in the convex girder from the analysis results. There are no lateral flange moments generated in the straight girder as there is no torque. Lateral moments are shown for the left half of the structure. The cusps in the curved girder are the the cross-frames.

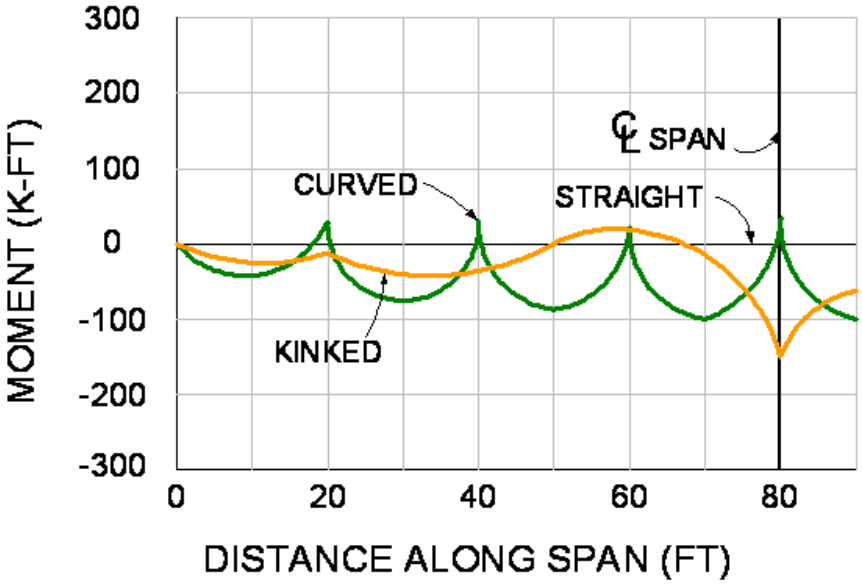


Figure 1.1.46 Bottom Flange Lateral Bending Moments in Convex Girder

Lateral flange bending is distributed along the outside girder in proportion to the vertical bending moment in the structure with uniform curvature. When the offset is created by a kink in the girder, the restoring forces and resulting lateral flange bending are concentrated near the kink.

Figure 1.1.47 shows the computed cross-frame forces for the two offset structures.

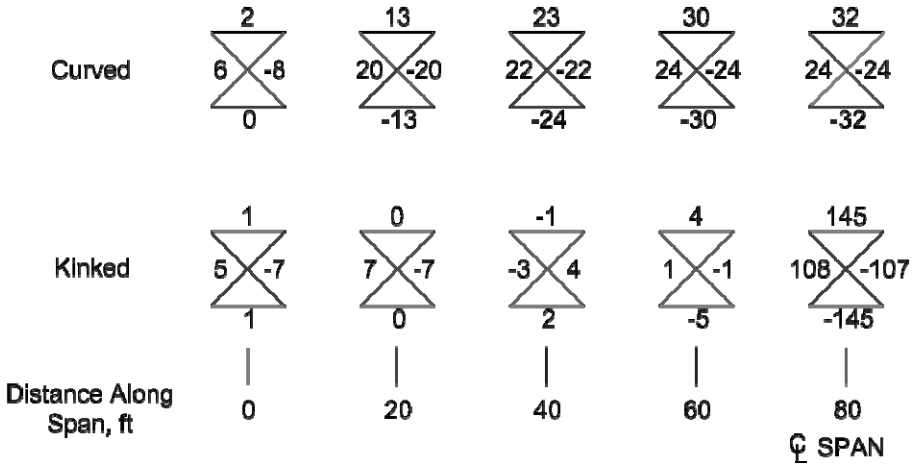


Figure 1.1.47 Computed Cross Frame Forces for Offset Structures

The cross-frame forces at the kink are extremely large. When the girder is kinked, the effect of the non-collinear forces is concentrated at the kink. The cross-frame forces are large because they are required to create equilibrium. If the total non-

colinearity of the girders is accounted for at one point, as in the kinked girder case, the forces in the single cross-frame at that point will be larger than any cross-frame forces in a curved girder with similar offset because the non-colinearity is accounted for over a number of cross frames in a curved girder.

If the cross-frame arrangement were modified in this example such that there was no cross-frame at the kink, the lateral flange bending moment at the kink would be significantly larger than shown because statics would have to be satisfied with lateral moments only. The concomitant cross-frame forces would be mitigated substantially.

This example illustrates the similarities between kinked girders and horizontally curved girders. Because of the similarity of behavior, the *AASHTO LRFD* Specifications require that continuous kinked girders be treated as horizontally curved girders.

Figure 1.1.48 shows the exaggerated deflected shape of the curved model.

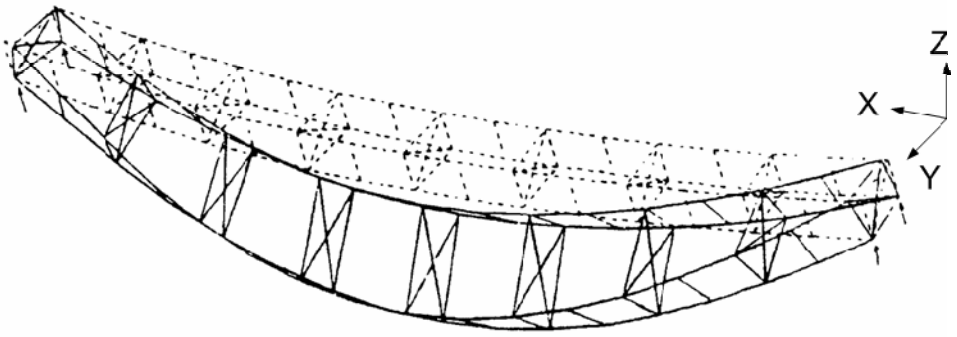


Figure 1.1.48 Exaggerated Deflected Shape of Curved Model

The *AASHTO LRFD* Specifications do not require that second-order deflections be included in the analysis and design of skewed and/or curved bridges. It is left to the Design Engineer to determine if the deflections exceed the point where first-order analyses are appropriate. In this example, the deflections would probably be at a point where first-order assumptions would be of questionable adequacy. Rather than attempt a second-order analysis, the large deflections are probably indicating that the bridge is too flexible and should be modified in some way. For example, in the case here, the two girders are far too unstable and the conception of the bridge should be re-examined. Differential deflections, lateral deflections and twist of all curved girder bridges and bridges with skewed supports should be considered during the fabrication and construction. This will be discussed further in Sections 4.1 and 4.2.

1.1.4.2 Box-Girder Bridges

The major difference between box girders and I-girders subjected to torsion is that the individual box is capable of resisting much larger torques than a typical I-girder of similar vertical bending capacity. The system behavior of curved-box girder bridges

must still be recognized in their analysis, but the treatment of the individual girder element changes and is somewhat more complex in the case of box girders. Since the live load distribution factor for multiple box-girder bridges (*AASHTO LRFD* Article 6.11.2.3) does not address skewed and curved bridges, a refined analysis is inferred at least to determine the live-load effects. Internal and external cross-frames/diaphragms and lateral bracing members are subject to design forces and are to be treated as primary members. A typical two-tub curved box-girder bridge is shown in Figure 1.1.49.

Box-girders on skewed supports are subject to large torques and tend to be particularly problematic to design and to build. Special care should be taken in analyzing and detailing box girders, particularly intermediate cross frames and lateral bracing in order to design a successful bridge.



Figure 1.1.49 Underside of a Two-Tub Curved Box-Girder Bridge

There are three means whereby torsion is generally introduced into box-girder bridges. First is the application of vertical or lateral loads that do not pass through the shear center of the box cross-section. This includes essentially all dead, live, and wind loads. The second means is through horizontal curvature. The third means is through the bearings or supports. A single bearing resists no torsion; stability must be obtained via a set of bearings on a support. A pair of bearings supporting a box girder on a skewed support introduces significant torsion into a box. The reason for this is that the bearing nearest the span receives greater load than does the rear bearing; hence, a torque is introduced by the presence of unbalanced reactions in the two bearings. Since neither of these reactions pass through the shear center of the box, torsion is created. Connections between the boxes tend to restore the

girder to its original position. As a result, the forces in cross frames/diaphragms are often referred to as restoring forces.

The concrete deck of composite box girders is subjected to horizontal shear due to the shear flow in the box in addition to horizontal shears similar to those in an I-girder deck. Hence, it is particularly important to check the deck reinforcement for these additional shear forces.

1.1.4.3 Summary

In summary, the analysis of curved and/or skewed steel-girder bridges (including bridges with continuous kinked girders) should consider the integrated system behavior of all structural components.

As illustrated in this section, recognizing the integrated system behavior properly accounts for the load shifting between girders in such bridges due to the torsional effects resulting from curvature and support skew. Additionally, the Design Engineer must recognize that adjacent girders provide stability in the case of curved I-girder bridges. Because of the necessary load shifting that occurs between girders, cross-frames, diaphragms and lateral bracing members become primary load-carrying members in these structures. Therefore, force effects in these members must be computed in the analysis. This requires consideration of the bridge superstructure as a system rather than analyzing single girders isolated from the system.

Primary torsional effects in the girders include St. Venant torsional shears, and warping torsion. The contribution of each type of torsion depends on the cross-section type and shape of the girder. System analysis of straight non-skewed bridges is also beneficial to more accurately predict stresses and deformations.

1.1.5 Geometric Terms Commonly Used when Defining Curved Alignments

A curved roadway alignment may have a circular curve or a spiral curve. A circular segment has a constant radius, typically defined in degrees of curvature or by its radius and its length. A spiral roadway alignment is defined by its length and minimum, or terminal, radius. A spiral is a curve that commences tangent to a straight segment and transitions to a final radius. The transition in radius is linearly proportional to the length of the spiral.

A circular segment defined in degrees is defined as the number of degrees that the curve encompasses, computed in radians as L/R, where L is the length of the curved arc and R is the radius. Radius is simply the equivalent in degrees. Progressing along the roadway alignment, the curve commences at the point of curvature (P.C.) and terminates at the point of tangency (P.T.) The P.C. and P.T. shown in Figure 1.1.50 assume the curve is measured from left to right. When the curve is measured along a girder, it usually is not designated with the preceeding terms.

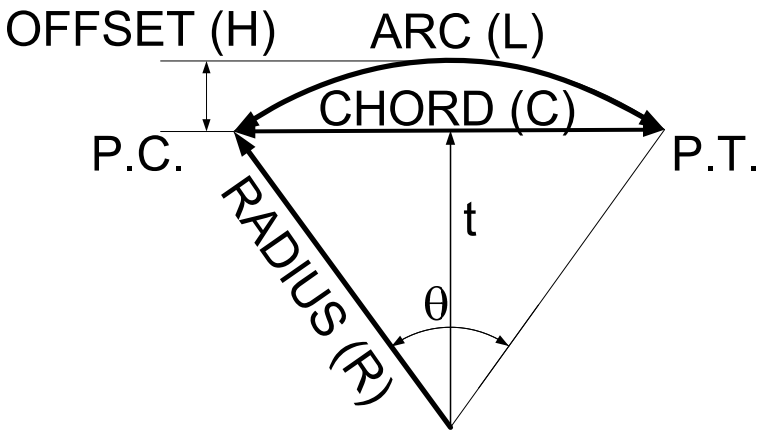


Figure 1.1.50 Geometrics of Circular Curvature

The following equations can be used to compute the various terms presented in Figure 1.1.50:

L = Arc length
R = Radius
Curvature = L/R = θ (degrees or radians)
Chord, C = 2R sin[(L/2)/R]
t = R cos θ/2
Offset, H = R-t

These terms are used by the Design Engineer to compute such quantities as shipping width of a field section or plate width if flanges are to be cut curved.

Varying curvature can be accomplished with compound curves consisting of multiple circular segments, each with a constant radius. A variable curvautre can also be accomplished with a spiral. Bridge fabricators are able to fabricate girders having a spiral alignment.

Typically, the Roadway Engineer lays out the alignment and clearances. The Bridge Engineer is given the alignment and other site constraints within which he/she is to design the structure. In previous times, the bridge alignment often dictated the roadway alignment. This occurs now only with major stream/river crossings. In many ways, this is the result of the Bridge Engineer's ability to adapt modern versatile materials, such as structural steel, to the wide-ranging demands placed on them by the highway and rail industries. It is up to the Bridge Engineer to know when the site constraints will cause a structure to be too expensive, to perform poorly or to be impractical to build. These challenges raise the profession to new levels. Fortunately, the fabricators are capable of fabricating a wide range of structures utilizing modern structural steels supplied by the mills. The highway system permits shipping of very large components. The erectors and general

contractors are capable of building these bridges. But none of these entities are able to execute their skills unless the Bridge Engineer designs a well-conceived and well-detailed bridge. The *AASHTO LRFD Bridge Design Specifications* provide the information necessary to ensure that the latest technology can be applied to design safe, economical structures having uniform live load capacity.

1.1.6 References

1. McGuire, W. 1968. *Steel Structures*. Prentice-Hall, Inc., Englewood Cliffs, NJ.
2. AISC. 2005. *Steel Construction Manual*. 13th Edition, American Institute of Steel Construction, Chicago, IL.
3. Dabrowski, R. 1968. *Curved Thin-Walled Girders*. Translation No. 144, Cement and Concrete Association, London, England.
4. Kolbrunner, C., and K. Basler. 1966. *Torsion in Structures*. Springer-Verlag, New York, NY.
5. Wright, R.N., and Abdel-Samad, S.R. 1968. "BEF Analogy for Analysis of Box Girders." *Journal of the Structural Division*, ASCE, Vol. 94, No. ST7, pp. 1719-1743.

Chapter 1
Introduction to Skewed and Curved Girder Bridges

Section 1.2

Evolution of Curved Girder Bridge Design Specifications



1.2.1 Introduction

Curved girder bridges have grown from relative obscurity to comprise up to a third of the steel bridges built in recent years. The earliest laboratory tests of curved steel girders were performed in the U.S. in the late 1960s and early 1970s. This work resulted in the development of *Tentative Design Specifications for Horizontally Curved Highway Bridges* in an Allowable Stress Design format, which was adopted by AASHTO in 1976. The specifications have since evolved to an LRFD format based on additional analytical and experimental work. This section provides a general overview of the analytical and experimental studies that have led to the current unified *AASHTO LRFD Specification* design provisions for straight and horizontally curved steel bridges.

1.2.2 Research Overview

The earliest analytical studies of curved girders were based on a strength-of-materials approach, with modifications made to account for the effects of cross-section distortion and amplification of lateral deflections. The earliest theoretical work on open and closed curved beams can be traced back to the work of Saint-Venant in 1843 (*1*). In the early 1960s, Vlasov (*2*) and Dabrowski (*3 through 5*) presented rather complete strength-of-materials solutions to the problem of determining stresses and deflections in curved beams. Vlasov first derived the differential equations governing the behavior of horizontally curved thin-walled girders of open cross-section. Dabrowski then refined the equations including several terms neglected by Vlasov.

Although there was a considerable amount of fragmented information available dealing with the structural analysis of horizontally curved members in the U.S., an organized research effort had not been undertaken until the Pennsylvania Department of Transportation initiated an analytical study at Carnegie Mellon University in 1969 (*6*). This study was aimed at collecting and generating a broad spectrum of information on curved-girder highway bridge design and construction. At that time, horizontally curved girder bridges in the U.S., which had been designed and built since the 1950s, were designed without the aid of any specifications related specifically to curved bridge design. Some of the earliest horizontally curved girder bridges in the U.S. were designed by using box sections composed of four plates.

The first extensive study of analysis and design techniques for curved girders was the Consortium of University Research Teams (CURT) Project in the late 1960s and early 1970s conducted under the auspices of the Federal Highway Administration (FHWA) with financial support from 25 participating state highway departments. This project led to the development of the *Tentative Design Specifications for Horizontally Curved Highway Bridges* in an Allowable Stress Design (ASD) format that was adopted by AASHTO in 1976 (*7*). This specification eventually evolved into the *AASHTO Guide Specifications for Horizontally Curved Highway Bridges* (referred to subsequently as *AASHTO Guide Specifications*) in 1980 (*8*). The CURT team included researchers from Syracuse University, the University of Rhode Island, the University of Pennsylvania and Carnegie Mellon University. The project encompassed analytical study and laboratory tests of scaled steel box- and I-girders, which are discussed in greater detail later in this section.

In 1975, the American Iron and Steel Institute (AISI) initiated Project 190 at Washington University to develop Load Factor Design (LFD) criteria for steel curved girder bridges (*9*), which were adopted by AASHTO in 1979 and incorporated in the 1980 *AASHTO Guide Specifications*.

At approximately the same time, experimental work was also being performed at Lehigh University, including the only fatigue tests of curved girders that have been performed in the U.S. The specimens were first tested statically in the elastic range.

One test was performed on a full-scale, two I-girder simple-span unit with no deck (*10 through 12*). The unit was then subjected to cyclic loading until fatigue cracks were observed. The results indicated no significant differences between the fatigue behavior of straight and curved girders. A concrete deck was then added and the unit was tested to failure (*13*). The specimen failed due to crushing of the concrete deck rather than plastification of the steel sections. A similar test of a near full-scale single box girder with top lateral bracing was also performed as part of the same project (*14*). The Lehigh work (*15*), completed in the 1970s, formed the basis of many of the ASD provisions in the *AASHTO Guide Specifications*.

Heins et al. at the University of Maryland and Powell and Mondkar at the University of California at Berkeley also contributed to the body of knowledge on curved I- and box girders (*16 through 19*). Many of these contributions were included as part of the *AASHTO Guide Specifications* and its associated commentary.

Yoo et al. at Auburn University studied the basic buckling and dynamic behavior of curved I-girders, including development of a finite element that has a warping degree of freedom (*20 through 26*).

Several field tests of curved bridges have been conducted. The New York Department of Transportation performed an early test of a simple-span I-girder bridge (*27*). The University of Alabama at Birmingham tested a curved I-girder bridge (*28)*. The University of Maryland tested a curved box-girder bridge during erection and for live load (*29*). The University of Minnesota also tested a curved I-girder bridge during construction (*30*). Several field and laboratory investigations during the construction of curved steel I-girder bridges have also been completed by Linzell et al. at Penn State University (*31 through 35*).

Significant work on curved girders has also taken place in Japan. Fukumoto developed an equation to predict the inelastic strength of I-girders (*36*) and conducted confirming tests on single I-beams (*37*). Nakai et al. also performed numerous component tests of curved beams (*38 through 43*). An empirical equation to predict the strength of curved I-girders was developed from this work (*44*). Inelastic finite element studies were performed by Nakai and Kitada and others (*45*). All of the Japanese research, also discussed in more detail later in this section, eventually culminated in the development of the *Hanshin Guidelines for the Design of Horizontally Curved Girder Bridge*s, published in draft form by the Hanshin Expressway Public Corporation in 1988 (*46*). The Hanshin Guidelines contain design provisions for both box- and I-girders and are ASD-based. Many references are made to the Japanese Bridge Specifications for straight girders (*47*). A text by Nakai and Yoo (*48*) presents additional information on the theoretical background and experimental research leading to the development of the Hanshin provisions.

From the completion of the CURT Project until the late 1990s, additional isolated research on the behavior of horizontally curved girders was conducted in the U.S. (*49 through 51*), but a coordinated and focused effort was lacking. Further experimental studies of curved steel girders were extremely limited. With the acceptance by AASHTO of probabilistic Load and Resistance Factor Design (LRFD)

provisions in 1993 (*52*) as a co-equal alternative design specification to the AASHTO *Standard Specifications for Highway Bridges* for straight bridges (*53*), new experimental data on horizontally curved girders were needed to help generate the necessary statistical data for extension of the LRFD provisions to include horizontally curved girders.

Starting in the late 1990s, the National Highway Cooperative Research Program (NCHRP) initiated Project 12-38 to first develop a revised *AASHTO Guide Specifications* for horizontally curved steel bridges in an LFD format based on state-of-the-art knowledge (*54*). This project led to the development and acceptance by AASHTO of the 2003 *AASHTO Guide Specifications for Horizontally Curved Steel Girder Highway Bridges* (*55*).

At about the same time, the FHWA initiated the Curved Steel Bridge Research Project (CSBRP) to experimentally study the behavior of horizontally curved steel I-girder bridges with the intent of gaining an improved theoretical understanding of their behavior. The CSBRP represented an experimental program of historical significance, with the tests conducted as part of that project representing some of the largest indoor civil-engineering related structural tests ever undertaken. The unique concept of utilizing a full-size three-girder bridge as a test frame to test multiple horizontally curved I-girder components was introduced in the CSBRP (*56*). Most of the previous tests on horizontally curved I-girders employed single girder arrangements, which required artificial torsional restraints at the ends of the torsionally weak I-sections. The tests conducted as part of the CSBRP were the first known tests that tested full-size components to failure as part of a structure that remained elastic and reusable. In fact, parts of the full-size bridge were later re-used for erection studies (*31*) and for testing of the bridge as a full-size composite curved-bridge structure (*56*). By using a full-size curved bridge as a test frame, it ensured for the first time that realistic boundary conditions would be provided for curved-girder component testing. It also ensured that the distortions in the components would be realistic and that material properties would be representative of full-size girders. Compensatory dead load would also not be required for subsequent live load tests.

The results from the CSBRP component tests spurred the introduction into the *AASHTO LRFD Specifications* of the so-called one-third rule equations to predict the resistance of I-girder flanges subject to combined major-axis and lateral bending stresses (*57*). In I-girder bridges, significant lateral flange bending may be caused by the torsion due to curvature, wind, eccentric concrete deck overhang loads acting on cantilever forming brackets placed along exterior girders, and by the use of discontinuous cross-frame lines in conjunction with skew angles exceeding 20° from normal. In order to provide a unified design specification to handle both straight and horizontally curved I-girder bridges with and without skew, a relatively simple approach was needed to predict the resistance of the flanges under the combined flexural and torsional effects. Basically, the one-third rule equations address the combined effects of major-axis bending and lateral bending by handling discretely

braced compression flanges as equivalent beam-columns. The flexural stress (or moment) is considered analogous to the axial loading within the beam-column, and the lateral bending stress is considered analogous to the beam-column bending moment. For discretely braced tension flanges, the one-third rule equations approximate the full plastic strength of a rectangular cross-section subjected to combined major-axis and lateral bending. The resistance equations are written in an interaction format in which the left-hand side of the equations pertains to applied load effects, and the right-hand side of the equations is the appropriate member resistance in major-axis bending. The factor of 1/3 in front of the flange lateral bending stress in the resistance equations provides an accurate linear approximation of the beam-column resistance or the flange plastic strength (as applicable), at least up to the specified limit of $0.6F_{yf}$ on the flange lateral bending stress given in the specifications. The one-third rule equations are discussed in more detail in Section 3.2.2.1.

In addition to the bending component tests, the CSBRP test frame was also used to conduct moment-shear component tests. These tests, along with additional single-girder shear component tests and analytical work conducted at the Georgia Institute of Technology, were all used to confirm the extension of the concept of post-buckling tension-field action to webs of horizontally curved girders (*56*).

With the development of the one-third rule equations to handle the combined effects of major-axis and lateral bending in I-girder flanges, and the extension of post-buckling shear resistance to curved-girder webs, the pieces were in place to perform a complete unification of the design specifications for straight and horizontally curved girders. The extant flexural resistance equations for horizontally curved box girders in the 2003 *AASHTO Guide Specifications* (*55*) already considered the effects of the St. Venant torsional shear stress and converged to the resistance equations for straight box girders in the limit as the radius approached infinity. The final unification of the design provisions for straight and horizontally curved steel I- and box girders in the *AASHTO LRFD Specifications* was completed under NCHRP Project 12-52 (*58*) and first appeared in the 2005 Interim Specifications.

From the preceding chronology of events that led to the evolution of the unified design provisions in the *AASHTO LRFD Specifications* over an approximately 25-year time period, some of the more important and influential work is described in more detail in the following sections, namely the CURT Project and the FHWA CSBRP.

1.2.2.1 CURT Project

The CURT Project (Consortium of University Research Teams) was initiated in October 1969. The charge of the consortium was to:

- Review all published information on the subject of curved bridges
- Conduct analytical and experimental studies to confirm or supplement the published information and assimilate information from related research programs conducted by state highway departments

- Develop simplified analysis and design methods along with supporting computer programs and design aids
- Correlate the developed analysis and design methods with the analytical and experimental data

Culver and his co-workers at Carnegie Mellon University studied the nominal bending strength, lateral stability and local buckling resistance of curved flanges and webs. McManus studied the stability of curved plate girders (*59*). Nasir studied the local buckling resistance of curved plate elements (*60*). Brogan studied the bending behavior of cylindrical web panels (*61*). In addition, the researchers performed experimental scale-model tests on single curved I- and box girders and on a two-girder arrangement of doubly symmetric I-girders, as described in more detail in the following sections.

1.2.2.1.1 Experimental Tests

As part of the CURT Project, Mozer, Culver et al. performed high-bending/low-shear and high-shear experimental tests on horizontally curved I-girders at Carnegie Mellon University (*62 through 64*).

Report P1 (*62*) presents the results of seven tests of curved I-girders that were each tested individually. The compression-flange slenderness ratios of Specimens C7, C8 and C9 were such that local buckling was not expected. Specimens D11, D12, D13 and D14 each had wider flanges and larger flange slenderness ratios than the C-series tests. Radii of curvature varied between 378.0 in. and 1462.0 in. Girder depths varied between approximately 18 in. and 24 in. All specimens had a span of 120 in. The ends of the span were simply supported vertically and pinned torsionally; that is, they were braced at the ends to prevent rotation about the longitudinal axis of the specimens. The load was applied at the center of the span and was eccentric to the girder to create a lateral bending stress at the center of the test panel equal to 0.3 times the vertical bending stress at the same longitudinal position (Figure 1.2.1). Full-depth stiffeners were employed at the supports and at the load points to ensure rigid-body behavior. Intermediate transverse web stiffeners were also provided. Some of the specimens were cut-curved and some were heat-curved (cut- and heat-curving are discussed in more detail in Section 4.1.2.1). Dimensions of the specimens were measured, including web trueness, which was compared to the permissible AWS web trueness (also discussed further in Section 4.1.2.2). Tensile properties and residual stresses were also recorded. Girder rotations were measured and numerous strain gages were employed. The testing arrangement provided for a variable moment throughout and a reasonably uniform shear throughout the 120-in. test length. Failures occurred by either web buckling or flange buckling, and corresponded well with the predicted mode of failure and predicted capacities. The capacities were predicted using equations that were eventually proposed for inclusion in the original *AASHTO Guide Specifications* (*8*); these equations are discussed further later in this section.

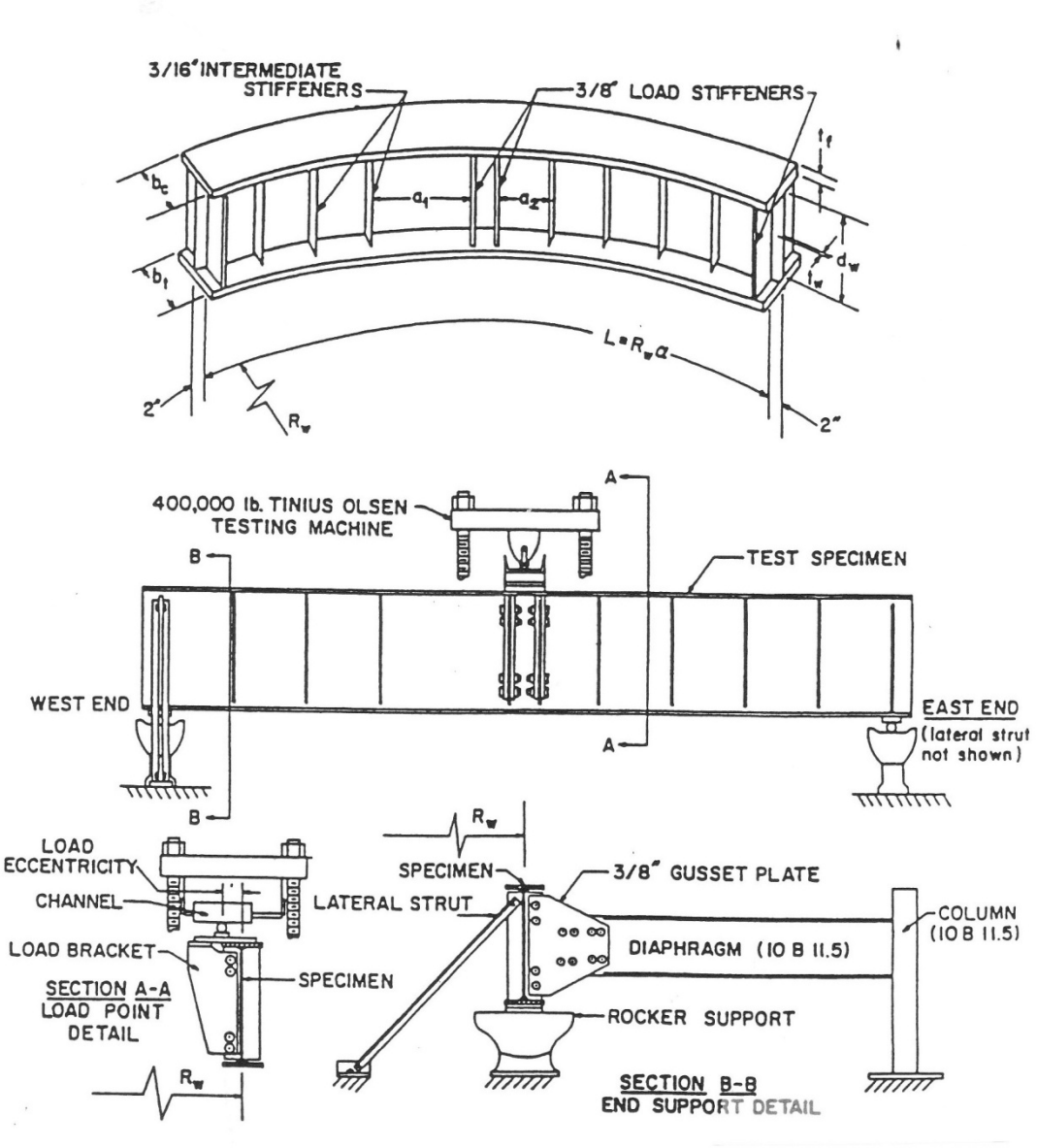


Figure 1.2.1 Mozer-Culver Series C and D Tests

Report P2 (*63*) presents the results of tests for two single curved I-girder specimens; each was tested in three different loading arrangements. Girders were approximately 18 in. deep. The radius of each specimen was approximately 600 in. The length of each specimen was 180 in. The specimens were supported in a similar fashion to the tests described in Report P1. The three different loading arrangements were labeled A, B and C. In Loading Arrangement A, two concentrated loads were employed to test each specimen in nearly pure bending (Figure 1.2.2). The concentrated loads were arranged so that the computed lateral flange bending stress at the center brace points was approximately one-third of the

vertical bending stress. Specimen L1-A had double-sided transverse stiffeners cut short of the tension flange and fitted to the compression flange. Specimen L2-A had full-depth, double-sided transverse stiffeners fitted against both flanges. Loading Arrangements B and C had 120-in. spans for both specimens. For Specimen L1-B, the left support was moved 5 ft into the span and a single load was applied 3.25 ft from the right support. For Specimen L1-C, the right reaction was moved 5 ft into the span and a single load was applied 3.25 ft from the left support. This permitted two panels in Specimen L1 to be tested with similar loading and created a high-shear/high-moment condition in each case. For Specimens L2-B and L2-C, the left support was moved 5 ft into the span and a single load was applied 5 ft from the right support (Figure 1.2.2). In Loading Arrangements B and C, loads were applied eccentrically with respect to the shear center so that the lateral moment could be varied. Specimens L1 were subjected to a larger eccentricity of load and larger lateral flange moments than Specimens L2. Girder deflections, rotations and web distortions in the test panels were carefully measured with dial gages, and numerous strain gages were employed. Failure modes in bending, shear and combined shear and bending were observed and compared to predicted capacities.

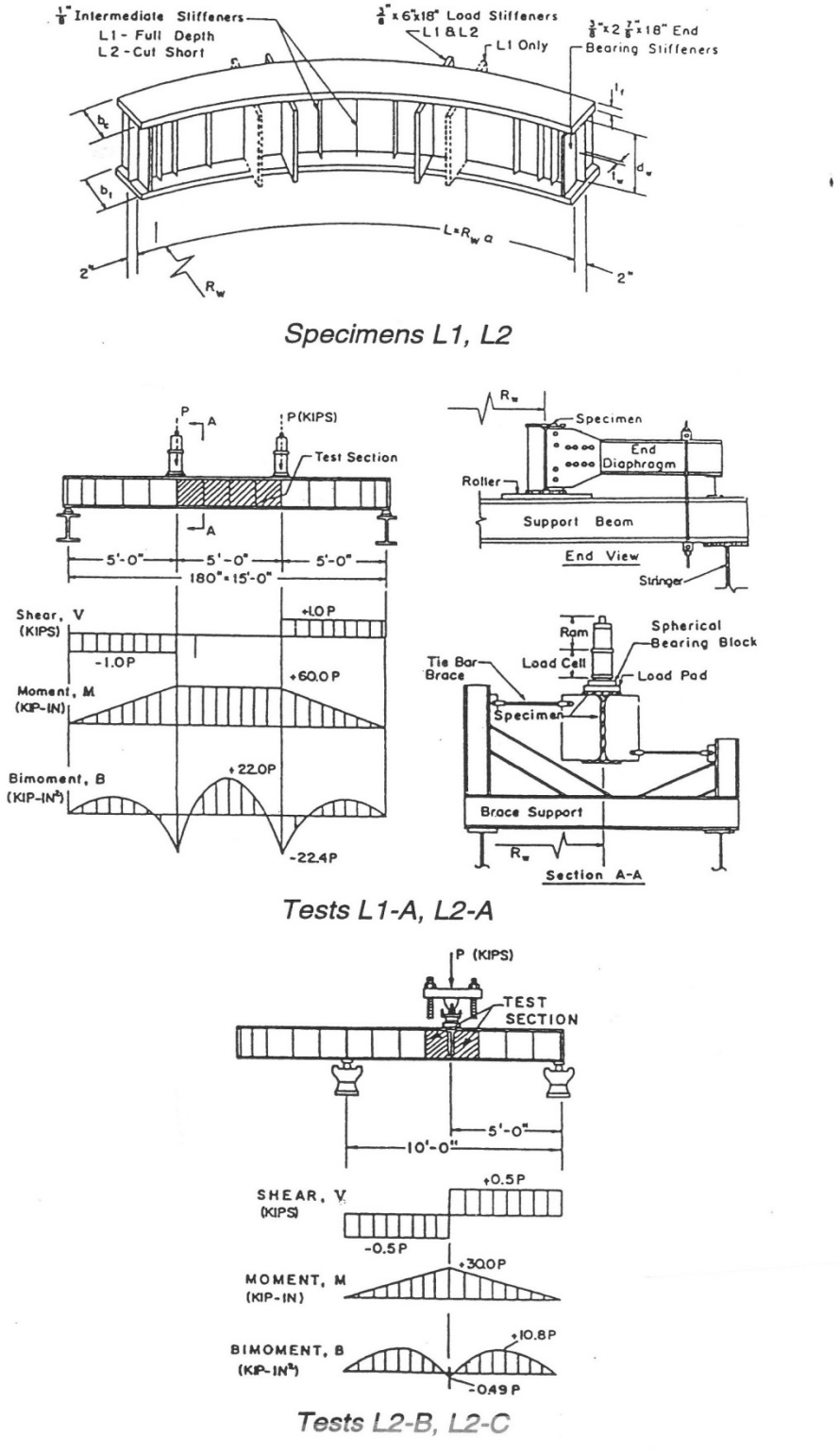


Figure 1.2.2 Mozer-Culver Specimens L1 and L2

Report P3 (*64*) presents the results of tests of a pair of simple-span curved I-girders connected with five intermediate full-depth cross-frames and with near full-depth diaphragms at each support (Figure 1.2.3). The cross-frames could be removed to change the unbraced length for different tests. The girders were spaced 3.0 ft apart. The span was 185 ft and the radius was 51.5 ft, measured along and to the control centerline. A clamping mechanism was employed at the ends of the test structure to provide stability and prevent uplift should it occur. The test girders were not prevented from rotating by these mechanisms, which were described as loose. G-O was the outside girder and G-I was the inside girder. Loads were applied either over Girder G-I or between the girders. Numerous strain gages were employed and measurements included the measurement of cross-frame strains. The tests that were conducted using this configuration are described as follows:

- Tests 1 and 2 were high-shear tests in which a single concentrated vertical load was applied to the top of Girder G-I at the one-sixth point from the support in Test 1 and the five-sixths point in Test 2. Two different stiffener aspect ratios were tested. One web panel failed in shear in each test. The failed web panels were reinforced by welding a ¼-in. thick plate to the web at the completion of each test.
- Tests 3 and 4 were combined shear and bending tests. A single concentrated load was applied to the top of Girder G-I at the one-third point for Test 3 and at the two-thirds point for Test 4. Again, ¼-in. thick plates were added to the failed web panels at the completion of each test.
- Test 5 was a bending test in which loads were applied at the third-points of the span to the top of Girder G-I (Figure 1.2.3). The center cross-frame was removed for this test to provide an unbraced length of approximately 60 in. This provided an L/b ratio of 15, which was greater than the upper limit of 10 proposed for this ratio by the researchers. However, the unbraced length in adjacent panels was half that in the center span. The flange lateral bending stress at the brace points in Girder G-I was approximately 0.75 of the vertical bending stress. Girder G-I was tested to failure in this test.
- Test 6 was similar to Test 4 and thus provided an additional test under combined shear and bending. The load was applied at the one-third point of the span, but 2.25 ft from Girder G-I to prevent uplift of that girder. This test was not brought to failure in order to preserve Girder G-O.
- Test 7 was similar to Test 5, except that the loads were again applied 2.25 ft from Girder G-I to prevent uplift. Also, the cross-frames at the one-sixth point and at the five-sixths point were removed to provide an equal unbraced length for the three panels.
- Test 8 was a bending test with the loads again applied at the third-points of the span, but 2.25 ft from Girder G-I. The cross-frame arrangement was the same as for Test 7. The flange lateral bending stress at the brace points in Girder G-O was approximately 0.57 of the vertical bending stress. Girder G-O was tested to failure in this test.

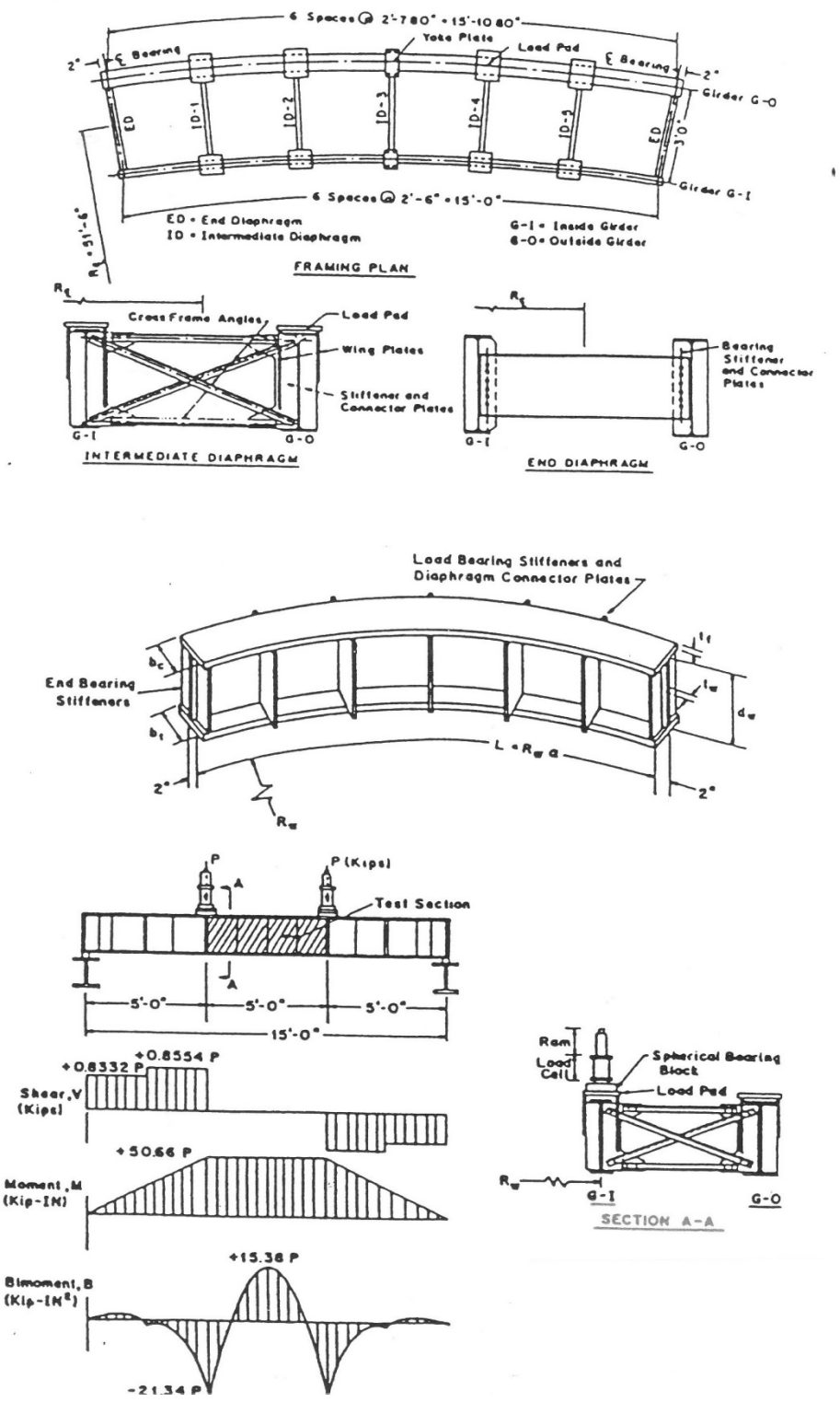


Figure 1.2.3 Mozer-Culver Two-Girder Tests

Forces reported in the cross-frame members in Tests 5 and 8 were not in equilibrium based on first-order analyses; the top-chord force was larger than the bottom-chord force in several locations. The top-chord force was nearly twice the computed value based on small deflection theory in some locations (Figure 1.2.4). Reported compression forces were higher than the predicted values, and the tension forces were lower than the predicted values. The top flange deformed as an arch, thus also creating a larger force in one cross-frame diagonal than in the other in each cross-frame. The vector sum of the horizontal cross-frame forces at a point on a flange must correspond with the lateral bending in the flange. The measured stresses due to flange lateral bending correlated well with the cross-frame forces. That is, where the top chord had a larger force than the bottom chord, there was a similar difference in the flange lateral bending stress at the same point. The difference between the top and bottom flange lateral bending moments and stresses was likely due to second-order amplification and radial effects discussed further in Section 3.2.2.1. Chord forces and end diaphragm stresses in Test 8 were non-linear with increasing load, which indicated load shifting from Girder G-O to Girder G-I as Girder G-O yielded. As the applied load increased, Girder G-O became less stiff due to yielding, resulting in that girder carrying a smaller portion of the additional load. Girder yielding tends to reverse the sense of force in the cross-frames. Due to this shift of load between girders as they yield and change their stiffness, inelastic moment in curved girders cannot be accurately predicted from elastic analyses.

Box girder tests performed during the CURT Project by Mozer and Culver were less extensive than were the I-girder tests. The box girder tests consisted of six small specimens and two larger ones. As of this writing (2010), there have been fewer tests conducted on curved steel box girders than on curved steel I-girders.

Report B1 (*65*) describes the tests on the smaller box specimens. Figure 1.2.5 describes the smaller box specimens B1 and B2, and Figure 1.2.6 describes the smaller box specimens B3 through B6. All six specimens had transverse web stiffeners spaced from 0.3 to 1.0 times the web depth. Intermediate diaphragms were ¼-in. thick plates. A plate was used as a tension flange for each pair of specimens B1-B2, B3-B4 and B5-B6 to represent an uncracked concrete deck. The yield stress of the steel was approximately 40 ksi. The boxes were tested as simple spans. Eight tests were performed on the six specimens. Figure 1.2.7 is a schematic of the test arrangement for specimens B1 through B6. In addition to torque due to curvature, torque was applied at one end through an eccentric ram.

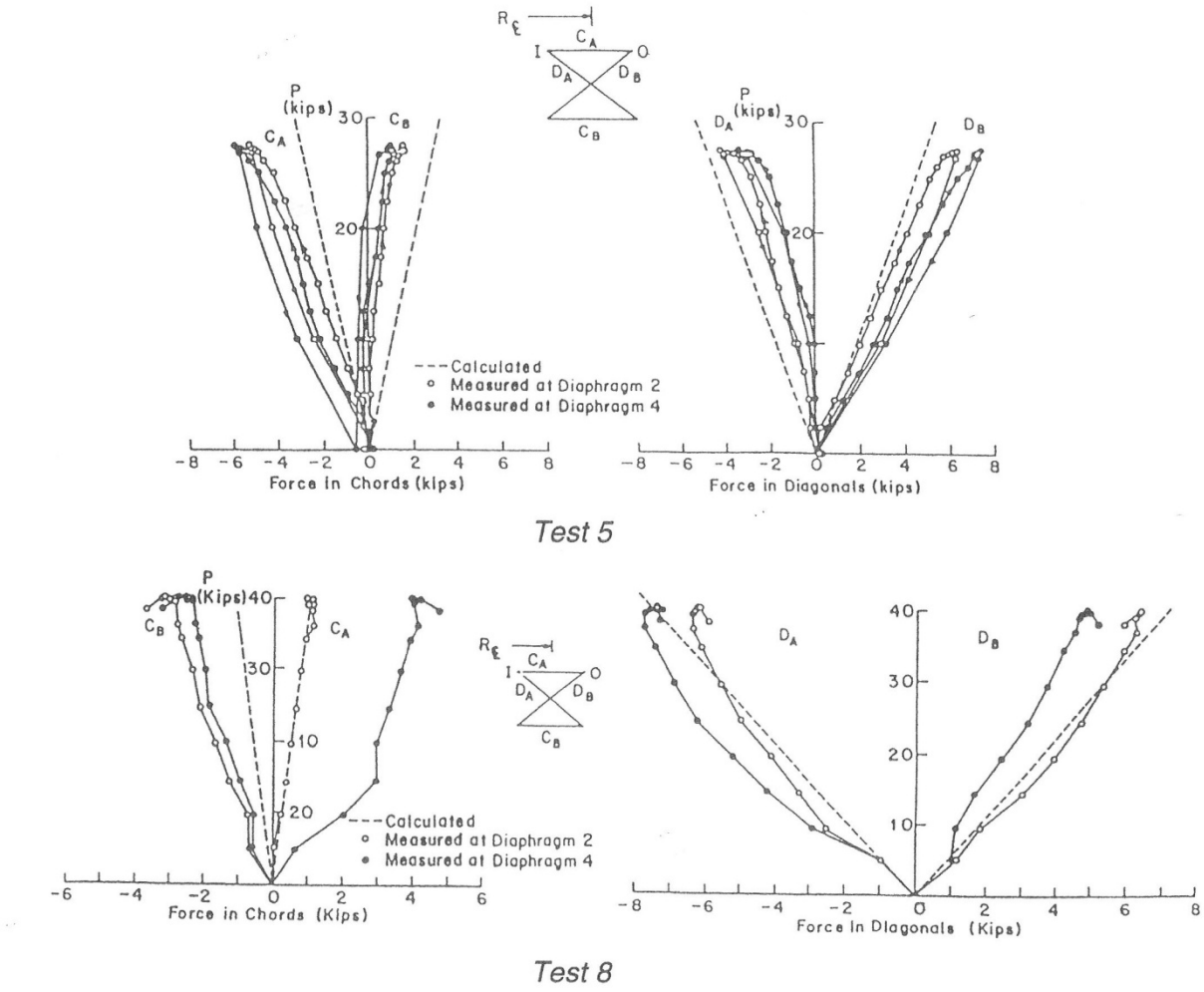
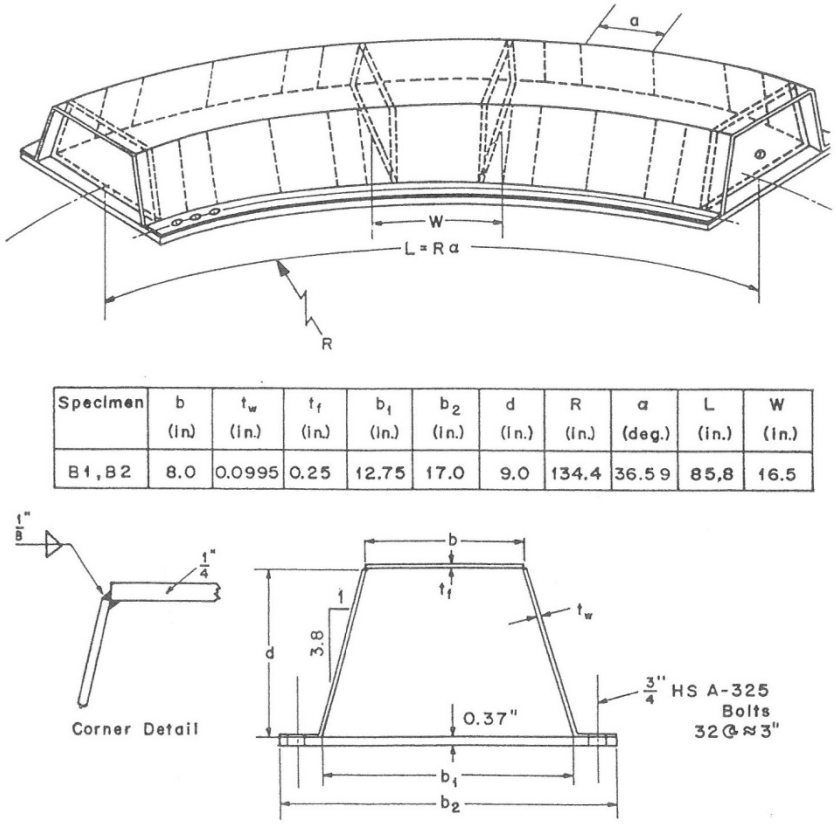


Figure 1.2.4 Mozer-Culver Tests 5 and 8 – Comparison of Cross-Frame Forces

The two concentrated loads provided a center region of low bending shear. The bending loads and end torque were increased monotonically. Because the torque and bending loads were applied separately, different ratios of vertical and torsional loads could be applied. Torque due to the applied eccentric load was constant along the span, whereas torque due to curvature associated with bending changed from negative to positive along the span. Thus, the bending stress was greatest at mid-span, and the sum of the bending and torsional shear stresses was greatest at the supports where the bending stress was small. Maximum applied loads during the tests were compared to calculated critical loads. The ultimate capacity of box-girder sections is dependent on the torsional shear stress, compression-flange buckling resistance and cross-section distortion. The research showed that compression flanges of curved boxes have little post-buckling strength (*65 through 67*). In the tests, longitudinal stiffeners were observed to twist, permitting the compression flange to twist out of plane. The torsional shear and curvature were the contributing factors.



Specimen	b (in)	t_w (in.)	t_f (in.)	b_1 (in.)	b_2 (in.)	d (in.)	R (in.)	α (deg.)	L (in.)	W (in.)
B1, B2	8.0	0.0995	0.25	12.75	17.0	9.0	134.4	36.59	85,8	16.5

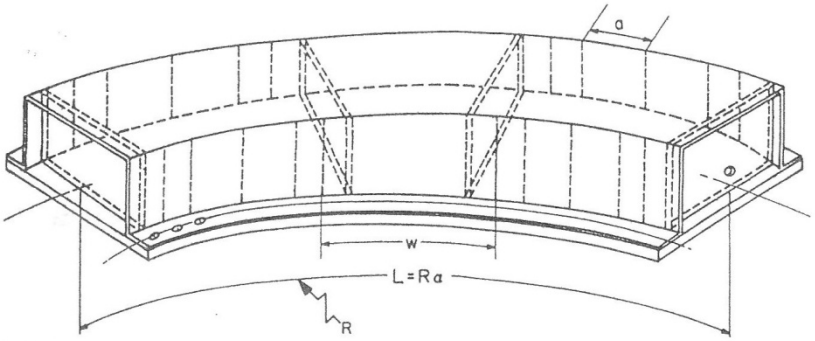
Figure 1.2.5 Mozer-Culver Box-Girder Specimens B1 and B2

The torsional shear stress should be considered in conjunction with the compression flange bending stress in determining the buckling resistance of the flange. Excessive out-of-plane web deformation of the box specimens was also observed under large torque.

Reports B2 and B3 (*66 through 67*) describe the tests on the larger box specimens. Figure 1.2.8 describes the larger box specimen B7, and Figure 1.2.9 describes the larger box specimen B8. The radius of each specimen was 434 ft. The purpose of these tests was to evaluate the deflection and behavior of box sections with practical web and flange slenderness ratios. A schematic of the test arrangement for Specimens B7 and B8 is shown in Figure 1.2.10. Three testing arrangements were used:

- A simple span of 240 in. with concentrated loads at the quarter-points of the span
- A simple span of 240 in. with a concentrated load at mid-span
- Two equal 120-in. spans with equal concentrated loads at the span quarter-points

Thirteen tests in the elastic range were performed on these specimens (*66*). Tests to failure were subsequently performed (*67*). Several tests were performed with different internal cross-frame spacings. It was observed that the cross-frame spacing greatly affected the vertical deflection and rotation of the box specimens. Measured displacements indicated that the internal cross-frames were effective in reducing the box deformations. Measured box rotations were greater than the computed rotations, which assumed no deformation of the box. Internal cross-frame members retain the box shape. Closer-spaced internal bracing reduces cross-section distortion and distortion-related transverse bending stresses in the box elements. As will be discussed further in Section 3.2.5, Wright and Abdel-Samad present a procedure to estimate internal box cross-frame forces and transverse bending stresses due to cross-section distortion using a beam-on-elastic foundation analogy (*68*). Bracing connections in box sections are important. Numerous cracks in the box webs were observed during the inspection of a box bridge on an interchange (*69*). Analytical examinations indicated large internal bracing forces in the box structures and inadequate bracing connections, resulting in fatigue cracks in the web that required expensive retrofitting.



Specimen	b (In.)	t_w (In.)	t_f (in.)	b_1 (In.)	b_2 (in.)	d (In.)	R (In.)	α (deg.)	L (In.)	W (In.)	d_t (in.)
B3	12.75	0.0995	0.0995	12.75	17.0	9.0	646.5	7.92	89.3	25.8	2.08
B4											2.09
B5							134.4	36.59	85.8	26.8	2.04
B6											2.08

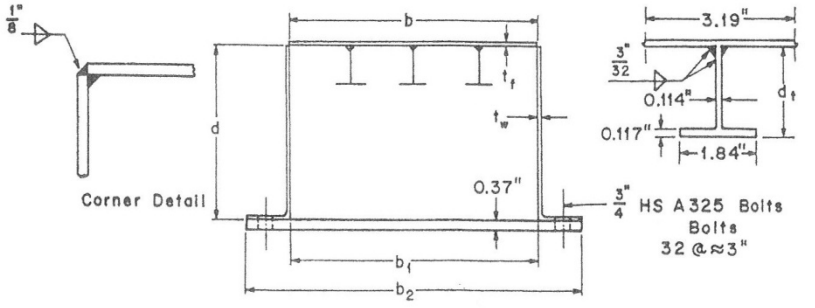


Figure 1.2.6 Mozer-Culver Box-Girder Specimens B3 through B6

1.2.2.1.2 Predictor Equations

The predictor equations for determining the nominal flexural resistance of horizontally curved I-girders in the 1980 (referred to subsequently as the "original *AASHTO Guide Specifications*"), 1993 and 2003 *AASHTO Guide Specifications* were based on the work of McManus as part of the CURT Project (*59*). (It should be noted that subsequent discussion related to the 1980 and 1993 *AASHTO Guide Specifications* is related to the Load Factor Design portion of those specifications only.) McManus examined doubly symmetric curved I-beams in pure bending. The beams had coincident shear center and center of gravity, and were assumed prismatic with equal vertical and lateral moments applied at their ends. Singly symmetric and composite I-sections were discussed but not investigated. Warping due to non-uniform torsion, cross-section deformation and radial effects were all considered. Amplification of deformations due to warping and twist was also addressed.

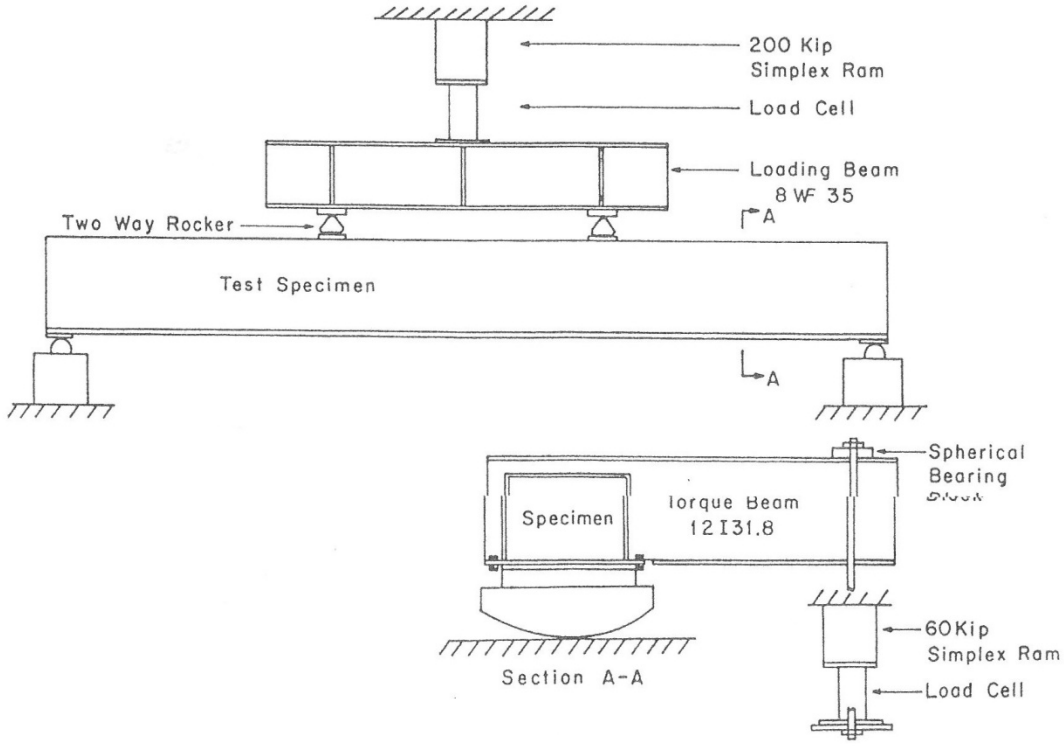


Figure 1.2.7 Test Arrangement for Specimens B1 through B6

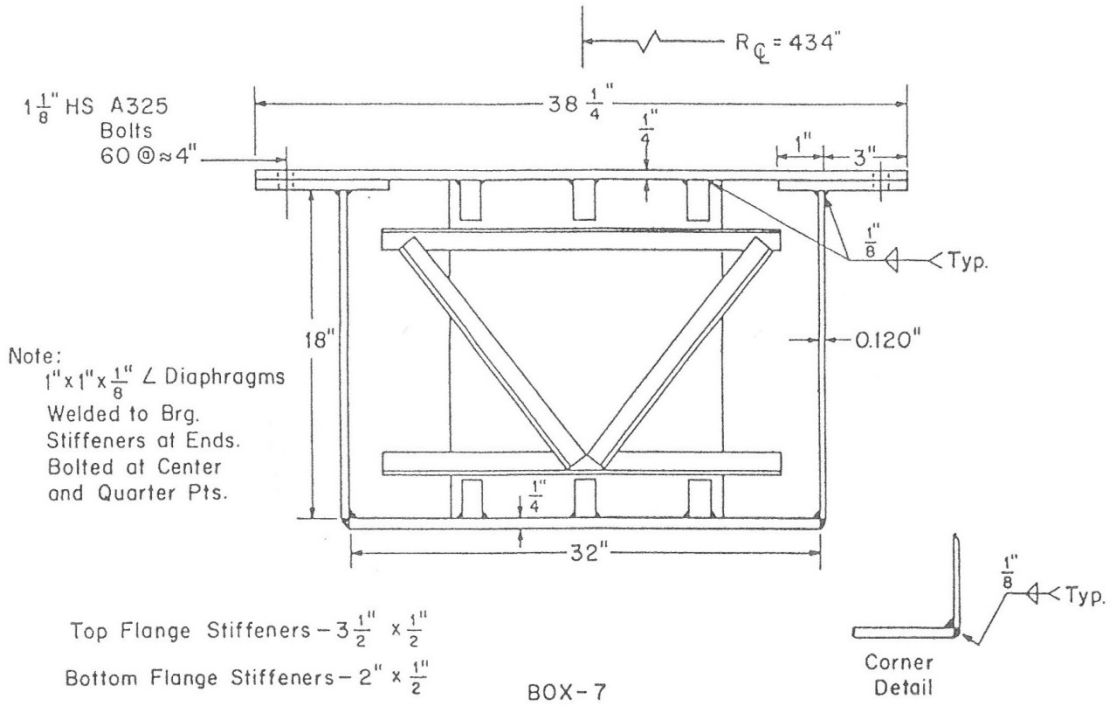


Figure 1.2.8 Mozer-Culver Box-Girder Specimen B7

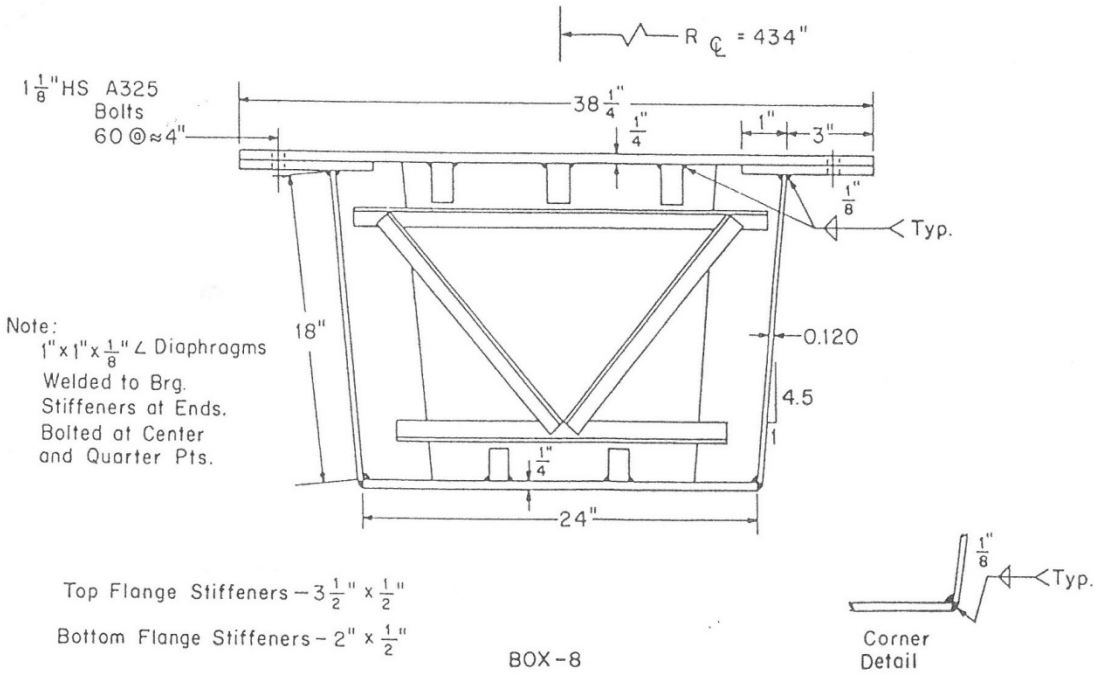


Figure 1.2.9 Mozer-Culver Box Girder Specimen B8

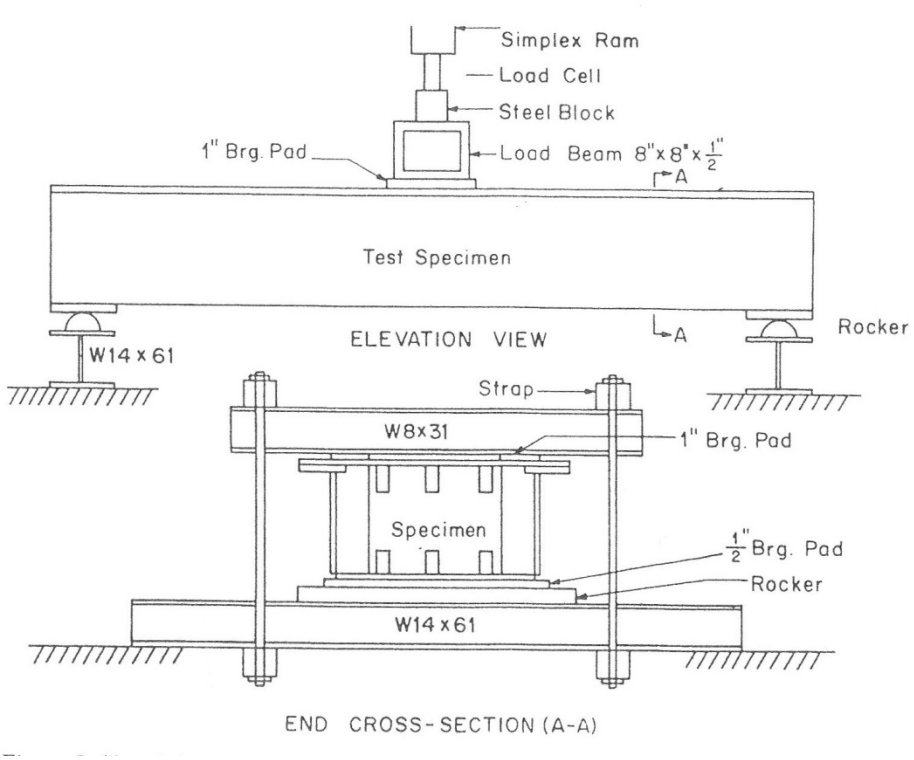


Figure 1.2.10 Test Arrangement for Specimens B7 and B8

Cross-sections with discretely braced compression flanges were defined as either compact sections or non-compact sections. Strictly speaking, failure of a curved compact section would be defined as the load at which plastification of the entire cross-section occurred due to a combination of vertical and lateral bending. However, in fact, these sections typically fail by plastification of the compression flange with little yielding occurring in the web. Thus, the resistance of curved compact sections was conservatively limited to permit plastification of only the compression flange; as a result, the webs were not subject to yielding and therefore not subject to compactness requirements. Compact sections were limited to steels having a specified minimum yield stress not exceeding 50 ksi since the research that led to the development of the empirical resistance equations for flanges of compact sections was limited to those steels. Non-compact sections were defined as sections in which the compression flange was assumed to reach the yield stress at the flange tip prior to local buckling.

McManus defined a compact section as one in which the compression flange had a b/t ratio not exceeding $3{,}200/\sqrt{F_y}$, with F_y taken in units of psi. Sections with a web slenderness ratio only up to 150 were investigated. Nasir found that if the compression-flange slenderness did not exceed the preceding limit, local buckling of the flange did not occur at reasonable radii for steels with a yield stress up to 50 ksi (*60*). In the 2003 *AASHTO Guide Specifications*, the preceding flange slenderness

limit was liberalized to 18 (i.e., independent of the yield stress), which corresponded to the flange slenderness limit for compact sections in straight girders at a yield stress of 50 ksi.

To formulate the predictor equations for flanges of compact and non-compact sections, McManus developed families of strength curves for the plastic and first-yield conditions using approximate solutions to more complex differential equations defining the contribution of the various effects that were considered. For discretely braced compression flanges, these strengths, in terms of moments, were divided by the critical lateral torsional buckling moment for an equivalent straight girder. This moment was determined from the equation for the critical lateral torsional buckling stress that existed in the *AASHO Standard Specifications* provisions at that time:

$$F_{cr} = F_y\left(1 - 3\lambda^2\right)$$

Equation 1.2.1

where:

$$\lambda = \frac{1}{\pi}\left(\frac{\ell}{b}\right)\sqrt{\frac{F_y}{E}}$$

b = compression-flange width
ℓ = length between compression-flange brace points

Equation 1.2.1 tacitly assumes that the girder cross-section is not maintained.

Non-dimensional ratios that resulted from the approximate solutions were defined as the product of two rho (ρ) factors, which were defined in terms of the following non-dimensional parameters: 1) warping stress-to-bending stress ratio (f_w/f_b); 2) ratio of the unbraced length to the girder radius (ℓ/R); and 3) ratio of the unbraced length to compression-flange width (ℓ/b). For both compact and non-compact sections, the ρ factors were only considered applicable within the limits of these parameters that were imposed in the empirical study (i.e., $\ell/b \le 25$, $\ell/R \le 0.1$ and $f_w/f_b \le 0.5$). f_b is defined as the largest vertical bending stress at either brace point, and f_w is the total first-order elastic flange lateral bending stress at the critical brace point. Only stresses at brace points were considered since the stress condition midway between brace points was implicitly considered in the original development of the predictor equations, as discussed later in this section. Changes in flange size between brace points were not considered in the development of the equations. The 2003 *AASHTO Guide Specifications* further clarified that the f_w/f_b ratio need only be checked at locations where f_b exceeded the greater of $0.33F_y$ or 17 ksi (i.e., at sections where strength might be critical).

The development of these equations considered the condition resulting from amplification of the lateral deflection of the compression flange due to arching action. Failure of most curved I-girders occurs at mid-span between brace points. Under

large vertical bending moments, the lateral bending stresses are actually larger at midpoint than at the brace points because of this arching effect, which causes additional lateral bending in the flange.

The predictor equation developed by McManus for the critical vertical bending stress in the discretely braced compression flange of a compact section is given as:

$$F_{cr} = F_{bs}\,\bar{\rho}_b\,\bar{\rho}_w$$

Equation 1.2.2

where:

F_{bs} = F_{cr} from Equation 1.2.1

$$\bar{\rho}_b = \frac{1}{1+\frac{\ell}{b}\left(1+\frac{\ell}{6b}\right)\left(\frac{\ell}{R}-0.01\right)^2}$$

$$\bar{\rho}_w = 0.95 + 18\left[0.1-\frac{\ell}{R}\right]^2 + \frac{\frac{f_w}{f_b}\left[0.3-0.1\frac{\ell}{R}\frac{\ell}{b}\right]}{\bar{\rho}_b\left(F_{bs}/F_y\right)}$$

R = girder radius

(f_w/f_b) = ratio of the first-order elastic flange lateral bending stress to the vertical bending stress (positive when the lateral flange moment is a restoring force)

The critical stress given by Equation 1.2.2 was limited to the yield stress by limiting the product of $\bar{\rho}_b$ and $\bar{\rho}_w$ to 1.0. This limits F_{cr} to F_{bs}, which in turn may not exceed F_y. For short unbraced lengths with small curvature, Equation 1.2.2 can give bending strengths greater than the yield moment. In fact, as the radius increases and the lateral bending stress approaches zero, the product of the ρ factors can be as large as 1.13, which is approximately equal to the shape factor (i.e., the ratio of the plastic moment to the yield moment) for a doubly symmetric I-section. However, for reasons stated previously, the critical stress was limited to the yield stress.

At the time the CURT Project was completed, the AASHTO *Standard Specifications* (Load Factor Design) had a requirement to reduce the width *b* of the compression flange of singly symmetric sections in Equation 1.2.1 by 10 percent. This was done to account in an approximate fashion for the fact that when the neutral axis is near the tension flange, a relatively large portion of the web participates in carrying the compression (*70*). Although the use of 0.9*b* in Equation 1.2.1 was prescribed for singly symmetric sections in the *Standard Specifications*, it was not prescribed in the

original *AASHTO Guide Specifications*. It was, however, prescribed in the 2003 *AASHTO Guide Specifications*.

In the original *AASHTO Guide Specifications*, the compression flange tip stress was not limited for compact sections. Thus, should the compression flange be subject to an average stress equal to the yield stress, there would theoretically be no capacity remaining in the flange to resist the lateral bending. In the 2003 *AASHTO Guide Specifications*, the critical vertical bending stress in the compression flange of a compact section was also limited to F_y minus 1/3 of the flange lateral bending stress. The factor of 1/3 was derived from the plastic capacity of the flange under combined vertical and lateral bending (*54*, *71, 72*). A small portion of the web is permitted to yield in this case. Yielding of the web is theoretically precluded if a factor of 1/2 is used instead of 1/3.

The critical vertical bending stress for a discretely braced tension flange in a compact section was specified to be F_y in the original *AASHTO Guide Specifications*. Again, by limiting the average normal tension stress to F_y, regardless of the magnitude of the lateral bending stress, there would likely be insufficient capacity remaining for the tension flange to resist lateral bending without yielding of the web. Since there were no provisions covering yielding of the web, the section might have been considered overstressed in such cases. It was assumed in the original research that the vertical bending stress in a discretely braced tension flange should be conservatively limited to F_y times the product of the ρ factors since only doubly symmetric sections were studied. Therefore, in the 2003 *AASHTO Guide Specifications*, the ρ factors were reinstated in determining the critical vertical bending stress for discretely braced tension flanges; the $\bar{\rho}$ factors specified for compact sections (see above) were used. The tension flange tip stress was also limited to F_y minus 1/3 times the flange lateral bending stress.

The predictor equation developed by McManus for the critical vertical bending stress in the discretely braced compression flange of a non-compact section is given as:

$$F_{cr} = F_{bs}\rho_b\rho_w$$

Equation 1.2.3

where:

F_{bs} = F_{cr} from Equation 1.2.1

$$\rho_b = \frac{1}{1+\left(\frac{\ell}{R}\right)\left(\frac{\ell}{b}\right)}$$

ρ_w = if (f_w/f_b) is positive, the smaller of:

$$\rho_{w1} = \frac{1}{1-\left(\frac{f_w}{f_b}\right)\left(1-\frac{\frac{\ell}{b}}{75}\right)}$$

or:

$$\rho_{w2} = \frac{0.95+\frac{\frac{\ell}{b}}{\left(30+8000\left(0.1-\frac{\ell}{R}\right)^2\right)}}{1+0.6\left(\frac{f_w}{f_b}\right)}$$

If (f_w/f_b) is negative, use ρ_{w1}.

The ρ_b factor reflected the effects of the vertical bending stress, and the ρ_w factor reflected the effects of the flange lateral bending stress and curvature. The research leading to the development of these ρ factors was also based on the study of sections that were doubly symmetric. The empirical basis of the preceding equations again required that the straight-girder lateral torsional buckling capacity be used with the ρ factors. The use of 0.9*b* for singly symmetric sections in Equation 1.2.1 was again prescribed in the 2003 *AASHTO Guide Specifications*. The compression flange tip stress, $f_b + f_w$, was also limited to F_y in both the original and the 2003 *AASHTO Guide Specifications*.

In the original *AASHTO Guide Specifications*, the compression-flange slenderness, *b*/*t*, for a non-compact section was limited to $4{,}400/\sqrt{F_y}$, with F_y taken in units of psi. In the 2003 *AASHTO Guide Specification*s, *b*/*t* was limited to $1.02\sqrt{E/|(f_b + f_w)|} \le 23$. This equation yielded a permissible *b*/*t* ratio approximately 10 percent less than the maximum permissible value for theoretical prevention of elastic local flange buckling at the yield stress under uniform compression. Research by Davidson et al. (*73*) indicated that local buckling of curved girder flanges may be more critical than for straight flanges. An upper limit of 23 was specified to ensure that potential local buckling failures would be in the inelastic range, and hence, more gradual. Tests of slender curved girders also indicated that local buckling may be critical above this limit (*60*, *62*).

The critical vertical bending stress for a discretely braced tension flange in a non-compact section was specified to be $F_y\rho_b\rho_w$ in the original *AASHTO Guide*

Specifications. The tension flange tip stress, $f_b + f_w$, was also limited to F_y. In a 1993 re-issue of the *AASHTO Guide Specifications*, the ρ factors were removed. The ρ factors were reinstated in the 2003 *AASHTO Guide Specifications*; the $\bar{\rho}$ factors specified for compact sections were again used. The tension flange tip stress was also limited to F_y minus 1/3 times the flange lateral bending stress.

Continuously braced flanges are flanges that are encased in concrete or anchored by shear connectors. Starting with the 1993 re-issue of the original *AASHTO Guide Specifications*, the critical average longitudinal flange stress in a continuously braced flange subject to compression or tension was limited to F_y. Also, flange lateral bending stresses did not need to be considered after the flange was continuously braced. Significant additional flange lateral bending stresses do not develop once the concrete has hardened. Any lateral bending stresses induced in the flange prior to deck hardening remain, but need not be considered. The lateral capacity of the deck is considered more than adequate to compensate for any lateral force that may be shed from a flange tip that yields prematurely.

Although curved hybrid I-girders (but not box girders) were permitted in the original *AASHTO Guide Specifications*, they were not permitted in the 2003 *AASHTO Guide Specifications*. The design of hybrid girders is based on the assumption that a portion of the lower-strength web yields. Since at the time there were only incidental tests and investigations of curved hybrid girders, and little or no study of the test results with regard to hybrid action, it was decided not to permit their use in the 2003 *AASHTO Guide Specifications* until further investigations were completed.

The provisions for the design of horizontally curved box-girder flanges in the original *AASHTO Guide Specifications* were adapted from the strength provisions for straight box-girder flanges given in the AASHTO *Standard Specifications*. The predictor equations for determining the critical stresses for compression and tension flanges in the *Standard Specifications* were essentially modified to reflect the effect of the torsional shear stress. The equations were carried forward to the 2003 *AASHTO Guide Specifications* without modification, and also to the *AASHTO LRFD Specifications* (with some slight modification) in the 2005 Interim Specifications as part of the unification of the design provisions for both straight and horizontally curved girders. These equations are discussed in more detail in Section 3.2.6.

In the original *AASHTO Guide Specifications*, the web slenderness, D/t_w, of horizontally curved I- and box girders with unstiffened webs was limited to 150 (this limit was later removed in the 1993 re-issue of the *AASHTO Guide Specifications*). The slenderness of webs with transverse stiffeners, but no longitudinal web stiffeners, was limited as follows:

$$\frac{D}{t_w} \le \frac{36{,}500}{\sqrt{F_y}}\left[1 - 8.6\left(\frac{d_o}{R}\right) + 34\left(\frac{d_o}{R}\right)^2\right]$$

Equation 1.2.4

where:

d_o = transverse stiffener spacing
F_y = specified minimum yield stress in psi
R = girder radius within the panel

For webs with transverse and longitudinal web stiffeners, the slenderness was limited as follows:

$$\frac{D}{t_w} \le \frac{73{,}000}{\sqrt{F_y}}\left[1 - 2.9\sqrt{\frac{d_o}{R}} + 2.2\left(\frac{d_o}{R}\right)\right]$$

Equation 1.2.5

for the case where one longitudinal stiffener was placed a distance *D*/5 from the compression flange. Should an additional equal sized longitudinal stiffener be placed *D*/5 from the tension flange, the slenderness was instead limited to $73{,}000/\sqrt{F_y}$.

When the clear distance between the neutral axis and the inside face of the compression flange, D_c, exceeded *D*/2, *D* was to be replaced by $2D_c$ when checking the applicable limit.

Due to curvature effects, the web of a curved girder subject to bending tends to deform outward in the compression region and flatten out in the tension region. These deformations result in web bending stresses that vary through the thickness of the plate. Analysis of curved web panels by Brogan (*61*) and Culver et al. (*74*, *75*) using a double-shell technique to account for the shell action of a curved web panel indicated that a reduced slenderness given by Equation 1.2.4 would provide a through-thickness bending stress in the curved web panel roughly equivalent to that in a straight-girder web panel with the maximum permitted AWS out-of-flatness, which was found to be approximately $0.2F_{yw}$. The aspect ratio (i.e., the ratio of transverse stiffener spacing to web depth) in the study was limited to 1.0, and only doubly symmetric girders with a web area equal to the total flange area were investigated. In the limit as the radius approaches infinity, the permissible web slenderness converged to the LFD slenderness limit for straight girders given in the AASHTO *Standard Specifications*, which was determined based on fatigue tests that indicated that the web bending stresses due to initial imperfections in the web panel would not cause fatigue problems up to that limit (*76*).

Based on their test results (*15*), Daniels et al. felt that Equation 1.2.4 was too severe and proposed an alternate reduction factor expressed as a linear function of d_o rather than the quadratic form proposed in the CURT Project. Basically, a smaller initial out-of-flatness was assumed to account for the deflections of the curved web boundary. Interestingly, this limit was eventually adopted in the Allowable Stress

Design (ASD) portion of the *AASHTO Guide Specifications*, but was never carried forward to the Load Factor Design (LFD) portion.

For webs with transverse and longitudinal web stiffeners, a similar analytical model was used, except that the model considered bending in both directions rather than only in a strip of web (*73*). The investigation was again limited to doubly symmetric girders. Since the addition of longitudinal stiffeners significantly reduces out-of-plane bending of the web, it was decided that no reduction in the permitted web slenderness would be necessary when a second longitudinal stiffener was provided in the tension region of the web.

In the 2003 *AASHTO Guide Specifications*, the web slenderness of horizontally curved I- and box girders with unstiffened webs was conservatively limited to 100 for girder radii less than or equal to 700 ft since there were no reported tests of unstiffened curved girders with web slenderness ratios greater than about 70. The specified limit of 100 was approximately equal to the web slenderness limit for compact webs with a yield stress up to 50 ksi specified for straight girders in the *AASHTO LRFD Specifications*. Above a radius of 700 ft, the permitted web slenderness increased linearly with respect to the reduced curvature up to a maximum limit of 150 at a radius of 2,000 ft according to the following equation (in which R is given in units of ft):

$$\frac{D}{t_w} \le 100 + 0.038(R - 700) \le 150$$

Equation 1.2.6

The slenderness of webs with transverse web stiffeners, but no longitudinal web stiffeners, was limited to 150. The slenderness of webs with transverse and longitudinal web stiffeners was limited to 300.

In both the original *AASHTO Guide Specifications* and the 2003 *AASHTO Guide Specifications*, transverse stiffeners were to be spaced such that the maximum design shear due to the factored loads did not exceed the shear yield or shear buckling capacity of the web, with the spacing not to exceed the web depth, *D*. Post-buckling strength due to tension-field action was conservatively not recognized. At the time, only stiffened curved web panels with aspect ratios, d_o/D, up to 1.0 had been tested. The transverse stiffener spacing at simple end supports was conservatively limited to 0.5*D*.

In the 2003 *AASHTO Guide Specifications*, at sections where transverse stiffeners were no longer required for shear, but the web slenderness exceeded the maximum slenderness permitted for an unstiffened web (see above), the transverse stiffener spacing in those regions was limited as follows:

For R ≤ 700 ft:

$$d_o = D$$

Equation 1.2.7

For R > 700 ft:

$$d_o = \left[1.0 + 0.00154\left(R - 700\right)\right] D \le 3D$$

Equation 1.2.8

In Equation 1.2.8, R is given in units of ft. The maximum permitted slenderness for an unstiffened web increased linearly from 100 at a radius of 700 ft up to 150 at a radius of 2,000 ft, according to Equation 1.2.6. According to a handling requirement given in the AASHTO *Standard Specifications*, the maximum permitted transverse stiffener spacing for a straight-girder web at a slenderness of 150 is 3*D*. Thus, for handling and to perhaps help retain the cross-section shape, the maximum permitted spacing of the additional required stiffeners in this region in curved-girder webs was increased linearly from *D* at a radius of 700 ft up to 3*D* at a radius of 2,000 ft and beyond, according to Equation 1.2.8.

In addition, in the 2003 *AASHTO Guide Specifications*, elastic bend-buckling of the web was to be investigated at each limit state, including for constructibility. As in the original *AASHTO Guide Specifications*, post bend-buckling resistance was not recognized in curved web panels (i.e., a web load-shedding factor R_b was not provided). The original *AASHTO Guide Specifications* indirectly controlled the compressive stress (and therefore bend-buckling) in the web by providing the explicit limits on D/t_w, discussed above, expressed as a function of F_y. Limiting the slenderness as a function of F_y assumed that the factored stress at all sections was equal to F_y. At sections where the factored stress is below F_y, a higher slenderness should be permitted. In the 2003 *AASHTO Guide Specifications*, absolute limits on D/t_w that were independent of F_y were provided (see above). The maximum longitudinal compressive stress in the web was then explicitly limited to the web bend-buckling stress, which was logical since bend-buckling is an elastic phenomenon not related to the yield stress of the material. Thus, for webs with or without stiffeners, the compressive flexural stress in the web at each limit state was limited to the web bend-buckling resistance, F_{crw}, given as follows:

$$F_{crw} = \frac{0.9Ek}{\left(\frac{D}{t_w}\right)^2} \le F_y$$

Equation 1.2.9

where:

k	=	bend-buckling coefficient
	=	$7.2(D/D_c)^2$ for unstiffened webs
	=	$9.0(D/D_c)^2$ for webs with transverse stiffeners but no longitudinal stiffeners
	=	for webs with transverse and longitudinal stiffeners:
	=	$5.17(D/d_s)^2 \geq 9.0(D/D_c)^2$ for $d_s/D_c \geq 0.4$
	=	$11.64(D/[D_c-d_s])^2$ for $d_s/D_c < 0.4$
D_c	=	depth of the web in compression
d_s	=	distance along web between longitudinal stiffener and the compression flange

The permissible bend-bucking stress given by Equation 1.2.9 is a function of the depth of the web in compression, D_c, which in turn is related to the factored accumulated stress in the web. The critical compressive stress for the web should not exceed the critical compressive stress for the adjacent flange adjusted for the thickness of the flange.

For curved unstiffened webs, the bend-buckling coefficient, *k*, in the 2003 *AASHTO Guide Specifications* was conservatively limited to $7.2(D/D_c)^2$, which was approximately 20 percent lower than the value of $9.0(D/D_c)^2$ given in the AASHTO *Standard Specifications* for flat webs. For a flat plate subject to a symmetrical bending stress pattern and with clamped edges top and bottom, *k* is equal to 39.6 (*77*). In the AASHTO *Standard Specifications*, it was assumed that the flanges offered only some partial degree of rotational restraint, resulting in a *k* value for a symmetrical section of 36.0. Both of the preceding cases assume pure bending with no shear present. Coincident shear and bending was not considered in either the original *AASHTO Guide Specifications* or the 2003 *AASHTO Guide Specifications*. Shear and bending are simultaneously large near interior supports. Therefore, to provide a level of conservatism for cases where an unstiffened web panel is subject to high bending and shear, based primarily on the paucity of tests of curved unstiffened web panels, a lower value of *k* was specified for unstiffened webs in the 2003 *AASHTO Guide Specifications*. For symmetrical sections, the resulting *k* value is 28.8. Both the original *AASHTO Guide Specifications* (prior to 1990) and the *Standard Specifications* (prior to 1987) followed a different tact by instead lowering the shear buckling strength of unstiffened web panels, presumably to account for possible moment-shear interaction effects. For curved web panels with transverse stiffeners but no longitudinal stiffeners, *k* was increased to the value given in the *Standard Specifications* because transverse stiffeners tend to strengthen curved web panels and because of the unrecognized post-buckling bending and shear resistance of transversely stiffened webs.

Longitudinal web stiffeners help to restrain deeper webs from bend-buckling. The equations for *k* for transversely and longitudinally stiffened webs were developed to permit the bend-bucking stress to be computed for a web with a longitudinal stiffener in any vertical location (*78*). In unshored construction, loads are placed on both the non-composite and composite sections. On long spans where the dead load is

large, the non-composite girder may have more than half of the web in compression in positive moment regions. When the girder becomes composite, the neutral axis shifts upward and another case must be checked. The equations for *k* allow the engineer to investigate various trial positions of the longitudinal stiffener on the web for each stress state in order to determine the most efficient location. Near points of permanent-load contraflexure, it may be possible to locate the stiffener on the web such that the bend-buckling stress is satisfactory with either edge of the web in compression. The *k* value is not permitted to be less than that for a web with only transverse stiffeners.

The specified bend-buckling coefficients are improperly conservative when both edges of the web are in compression such that the neutral axis lies outside the web, which can occur near points of permanent-load contraflexure when stresses due to moments of opposite sign acting on the non-composite and composite sections are accumulated. Thus, the provisions limited *k* to a minimum value of 7.2 in such cases, which is approximately the k value for a flat web under uniform compression (and no shear) with clamped edges (*77*).

Further more detailed information on the CURT Project and on the subsequent development of the original *AASHTO Guide Specifications* and the 2003 *AASHTO Guide Specifications* (and other design provisions in those specifications not discussed herein) may be found in the project reports and in Reference 54.

1.2.2.2 FHWA Curved Steel Bridge Research Project (CSBRP)

As discussed previously, the FHWA Curved Steel Bridge Research Project (CSBRP) was initiated in 1992 to study the fundamental behavior of horizontally curved steel I-girder bridges. The primary focus of the CSBRP was experimental laboratory testing utilizing a re-usable full-size three-girder bridge as a test frame to test multiple horizontally curved I-girder component specimens, followed by testing to failure of the test frame as a full-size composite curved bridge. It was envisioned that parts of the full-size bridge could potentially also be used for separate erection studies. The research team for the project included HDR Engineering, Inc., BSDI, Ltd., Georgia Institute of Technology and Auburn University.

Tests that had been conducted up to that time as part of the CURT Project and elsewhere had generally been conducted on relatively small-scale doubly symmetric specimens composed of very thin plate material. Many of these specimens were subject to unrealistic boundary conditions at their ends and relatively large initial distortions associated with the welding of thinner plate or sheet.

Straight girder bridges generally can be thought of as composed of a series of connected individual elements each possessing their own strength and stability. As a result, individual members can be tested alone as single components. The entire *AASHTO LRFD Specification* is based on designing each individual member to ensure that its component strength is not exceeded, with little attention given to the

system behavior. Unlike straight girders, horizontally curved I-girders depend on adjacent members for their stability and must be braced laterally to adjacent members in order to be stable since applied vertical loads produce torsion as well as bending. Equilibrium is provided by the adjacent girders and bracing members between them, combined with the internal vertical bending and flange lateral bending moments.

Thus, to properly examine the behavior of horizontally curved I-girders, it is desirable to test individual components in-situ, or as part of a complete bridge structure that resists vertical loads and torsion as a system. This provides more realistic boundary conditions for the component specimens. With the exception of the two-girder tests conducted by Mozer, Culver et al. discussed previously (*64*), previous tests on horizontally curved I-girder component specimens did not adequately represent these conditions. This concept also presents fewer safety concerns because the test arrangement composed of multiple girders is more stable than a single curved girder test. Previous tests were also not conducted on full-scale systems. Tests on full-scale systems eliminate the need for compensatory dead loads and more accurately reflect fabrication influences such as initial flange and web distortions and residual stresses. As a result, the tests were true prototypes with results applicable to real bridges.

Since the testing of components to failure within such a realistic full-size structure had never even been contemplated up to this point, there were a number of challenges and obstacles to overcome to ensure success, including budget, schedule and convincing doubters about the viability of this unique concept. Thus, the development of the final experiment design was a slow evolutionary process. The process initiated with the complete development of the preliminary concept for a full-size test frame, with three I-girders in the cross-section, representing a complete simple-span composite bridge structure. Initially, the frame would be used for the testing of several non-composite I-girder component specimens inserted within the outermost girder of the structure. At the completion of the component tests, a concrete deck would be cast onto the steel test frame after it was modified. At that time, testing of the completed bridge with a series of concentrated loads would allow for the development of influence surfaces for the actions in various components of the frame (influence surfaces are discussed in more detail in Section 2.1.4), and for eventual testing of the composite bridge to failure. Upon the completion of this initial investigation of the three-girder test frame, a second rather detailed investigation was initiated looking into the feasibility of single I-girder component tests as a possible alternative. This alternative was eventually abandoned however due to cost concerns related to the support structures that would be required to provide the necessary stability to the specimen, and safety concerns related to the predicted reversal of force that would occur in critical bracing members beyond the peak load. The process then came full circle back to the development of a more refined design of the three-girder frame for I-girder component testing only, accompanied by a more realistic and pared down experimental plan to fit the available time and budget.

One of the numerous complexities introduced by testing components within an entire curved-bridge structure is that it becomes difficult to predict the behavior of an

individual component within the system. As one girder in a curved bridge system yields, typically the outermost girder first, its stiffness is reduced significantly so as to affect the load distribution in the girders. All the cross-frame forces do not necessarily increase in the same sense with increasing load under this condition. Instead of adding load to the outermost girder, the sense of the load in some of the cross-frame members will tend to reverse with increasing load and the other girders in the system that have remained elastic will begin to carry a disproportionate share of the increased load. The load that is transferred to the innermost girder may begin to drop off due to the tendency of this girder to want to uplift as the outermost girder softens. When the outermost girder will no longer accept any load, the system will continue to accept load along a different increasing load-deflection path as long as the structure has not reached its maximum capacity or become unstable. The load-deflection path for the structure will reach a maximum only when the entire structure has reached its maximum capacity or has become unstable. Such behavior is contradictory to the classical load-deflection behavior often observed in individual member tests where the load drops off after the member reaches its ultimate capacity. Thus, the definition of the ultimate load of a component specimen located, for example, within the outermost girder of a curved structure becomes somewhat subjective. The ultimate load might be defined by the point where one or more of the interior girders is resisting nearly all the additional applied load, or else deflection rather than load might be the condition that defines the ultimate load.

The situation is quite complex in an actual curved bridge with moving loads. The position of the live loads producing the maximum load in the outermost girder may not produce the maximum load at the same time in the adjacent girder. The adjacent girder would have additional capacity in this situation. If the adjacent girder is loaded to its maximum load by the live load position that produces the maximum load in the outermost girder, the bridge may not have much additional capacity once the outermost girder reaches its ultimate load. This behavior is quite different from straight-girder bridges that typically have significant reserve capacity when any girder is loaded to ultimate by live load.

The physical loading of a curved-bridge system during testing was also complicated by the fact that each curved girder in the system would begin to twist and deflect immediately upon loading. Measurement of cross-frame forces and end reactions, which was critical to the accurate determination of the actions in the component specimen, also presented some unique challenges. In addition to vertical reactions, the bearings were also subjected to tangential and radial forces. Resistance to these forces introduced forces not only into the bearings, but also into the girders, which affected the girder moments, shears and torques. Minimum lateral restraints were used in the test in order to minimize these horizontal reactions.

As a result of all these complexities, from the beginning, it was evident that this project would need to involve the careful integration of computer analysis, not only to examine and evaluate the test results, but throughout the development of the experiment design, which only added to the complexity of this unique and historical

test. Sophisticated second-order geometric and material non-linear analyses would be required to predict the behavior of the components within the test frame throughout the full range of loading. These analyses would ensure that potential corruptive secondary effects would be minimized during the tests and that the tests could be safely and successfully carried out for the first time. The predicted actions from these analyses would also be used to safely design the various test-frame components and to develop a theoretically sound and efficient set of component specimens. In the previous curved girder tests carried out in the CURT Project in the early 1970s, the technology was not yet available to practically perform the geometric and material non-linear analyses that were required to predict the behavior of component specimens located within a full-size multi-girder test frame up to their ultimate capacities. For this test program, these analysis tools were available, making it possible to better predict the reactions, movements and internal actions in all members and components of the test frame. These analysis results were an integral part of the successful design of the experimental program. The eventual successful completion of the component test program, with no major problems experienced, lent further credence to the level of effort expended in the development of the experiment plan.

1.2.2.2.1 Experimental Design – Bending Component Tests

The test frame was assembled and tested in the Structures Laboratory at the FHWA Turner-Fairbank Highway Research Center in McLean, Virginia. The laboratory test floor is 50 ft by 120 ft in plan, which provided an ideal platform for the design of the planned full-size testing program. The structural floor system is essentially a 14-ft-deep reinforced concrete box girder with four large cells underneath the working floor level. The floor has 573 tie-down holes approximately 3 in. in diameter spaced on a rectangular grid at 3-ft centers through which Dywidag threadbar rods could be passed to apply loads using a number of possible configurations. Loads could either be applied above or underneath the floor and could be transferred to the specimens using an appropriate configuration of Dywidag rods and reaction beams. The constraints of the rectangular grid of tie-down holes presented one of several challenges encountered in the design of a workable and safe loading system for the component testing.

An important initial decision that had to be made in the design of the test frame was the selection of the number of girders in the cross-section. Initial consideration was given to a two-girder system as tested by Mozer, Culver et al. in the CURT Project (*64*). With a two-girder system, stability is achieved from the interaction between the girders through the cross-frames since neither girder alone would be stable. Failure (loss of stiffness) of one of the girders would reduce the system stability and probably lead to collapse of the entire system. Thus, practically speaking, it would have been risky to fail one girder, or a portion of one girder, in a two-girder system containing an individual component specimen, while attempting to keep the other girder and the cross-frames elastic and the entire system stable. A two-girder system would also be much more susceptible to uplift when one of the girders, or a significant portion of one of the girders, failed. Loads would have to be applied at a location between the girders to ensure stability and prevent uplift at the ends of the

inside girder, which would have complicated the required loading mechanism. It was decided that a three-girder system would provide stability and could be less susceptible to uplift. By ensuring greater stability through the entire range of loading, it was found that it would be possible to fail a component specimen located within the outermost girder, while keeping the remaining two girders and the cross-frames elastic. While the possibility of using four girders was considered, it was rejected due to unnecessary complexity, space limitations in the laboratory and the desire to keep the experiment full-size and eliminate scaling.

A simple span was chosen because of space limitations in the laboratory. With proper loading, a simple-span arrangement could provide near pure bending in the test section and high shear at the ends of the girders. The frame was supported on radial concrete abutments at each end approximately 6.5 ft off the laboratory floor for ease of access. The arc span was set to 90.0 ft along the centerline of the center girder (Girder 2 or G2). As a result, the arc span of the outermost G3 was equal to 93.9375 ft, and its centerline radius was equal to 208.75 ft. The arc span of the innermost girder G1 was equal to 86.0625 ft, and its centerline radius was equal to 191.25 ft. G1 and G3 were each extended 1.0 ft beyond the centerline of the bearings. G2 was extended 1.0 ft beyond the centerline of the east bearing and 1.67 ft beyond the centerline of the west bearing to allow G2 to be attached to a tangential support frame (discussed later). The girder spacing was 8.75 ft, and the centerline radius to G2 was 200.0 ft.

The cross-frame spacing was set at 7.5 ft along the centerline of G2. This rather tight spacing reduced the lateral moments in the center and inside girders, thereby increasing the elastic vertical bending moment capacity of those girders. Every other cross-frame between G2 and G3 was removed, providing a spacing (unbraced length L) of 15.656 ft for the component testing in the center of G3. This provided an R/L ratio for each specimen of 13.33. Most practical curved-girder designs have R/L ratios ranging from 13.33 to 20. As a result, the component tests were conducted near the lower practical range. The extra cross-frame lines between G2 and G1 provided additional stability to those girders, reduced the flange lateral bending stresses in those girders, ensured additional load distribution to G3 supporting the component specimen, and helped ensure that G2 and G1 remained elastic throughout the entire range of test loads. Bottom lateral bracing members were placed between the girders at the ends of the test frame to provide overall stability by ensuring that the girders did not move radially with respect to each other during the tests. A plan view of the test frame on the laboratory floor is given in Figure 1.2.11. A larger plan view of the test frame is provided in Figure 1.2.12.

A set of six component specimens was designed for testing in pure flexure. The test frame described above permitted the use of cost-efficient specimens that required no modifications to the test arrangement. After the six tests were successfully completed, two of the specimens were repaired and modified slightly in order to perform two additional bending tests. In both cases, the web distortions experienced while testing were repaired by carefully applying heat. The distorted top

(compression) flanges were replaced. The compression-flange and web slenderness ratios of the eight flexural specimens, B1 through B8, are compared to the corresponding limits given in the original *AASHTO Guide Specifications* and the 2003 *AASHTO Guide Specifications* (labeled as 'NCHRP 12-38') in Figure 1.2.13. Detailed descriptions of each specimen and the intent of each specimen may be found in Reference 56.

These non-composite component specimens, with varying web and compression-flange slenderness ratios and transverse stiffener spacings, were inserted one at a time into the center of G3 with bolted field splices, with the arc length between the centerline of the splices set at 25.4 ft (Figure 1.2.14). The majority of bridge girders are composite in positive bending so that the top flange is not critical and the web is generally less critical than when the girder is non-composite. In negative bending, the bottom (compression) flange is braced intermittently and at least half of the web is in compression, as was the case for the flexural test specimens.

Design of the bolted field splices in G3 to allow the different component specimens to be installed and removed was challenging because of the different proportions of the component specimens. A scheme was developed that allowed a number of splice plates to be re-used during the component testing. To accommodate each specimen using the same set of splice plates, different numbers of bolts were installed in the flange splices plates. The bolted specimen splices were designed to prevent slip at the full plastic moment capacity. All bolts were 7/8-inch diameter ASTM A 325 high-strength bolts placed in standard-size holes. New bolts were used with each test specimen. Bolted flange splices were designed to develop the plastic capacity of the specimen flanges. It was necessary to stagger the flange-splice bolts to accommodate the largest number of bolts while allowing the splice plates to be re-used. It was also decided to taper the flange splice plates at their ends in order to reduce the number of holes in the flange until the flange could be sufficiently unloaded to accommodate four holes across the width. The web splices were conservatively designed for:

- A design shear assumed equal to 100 kips
- A moment due to the eccentricity of the design shear
- The plastic-moment capacity of the web

These assumptions were extremely conservative since the actual shear in the tests was very low and the curved components failed by lateral bending rather than vertical bending. Additional more detailed information on the design of the bolted field splices may be found in Reference 56.

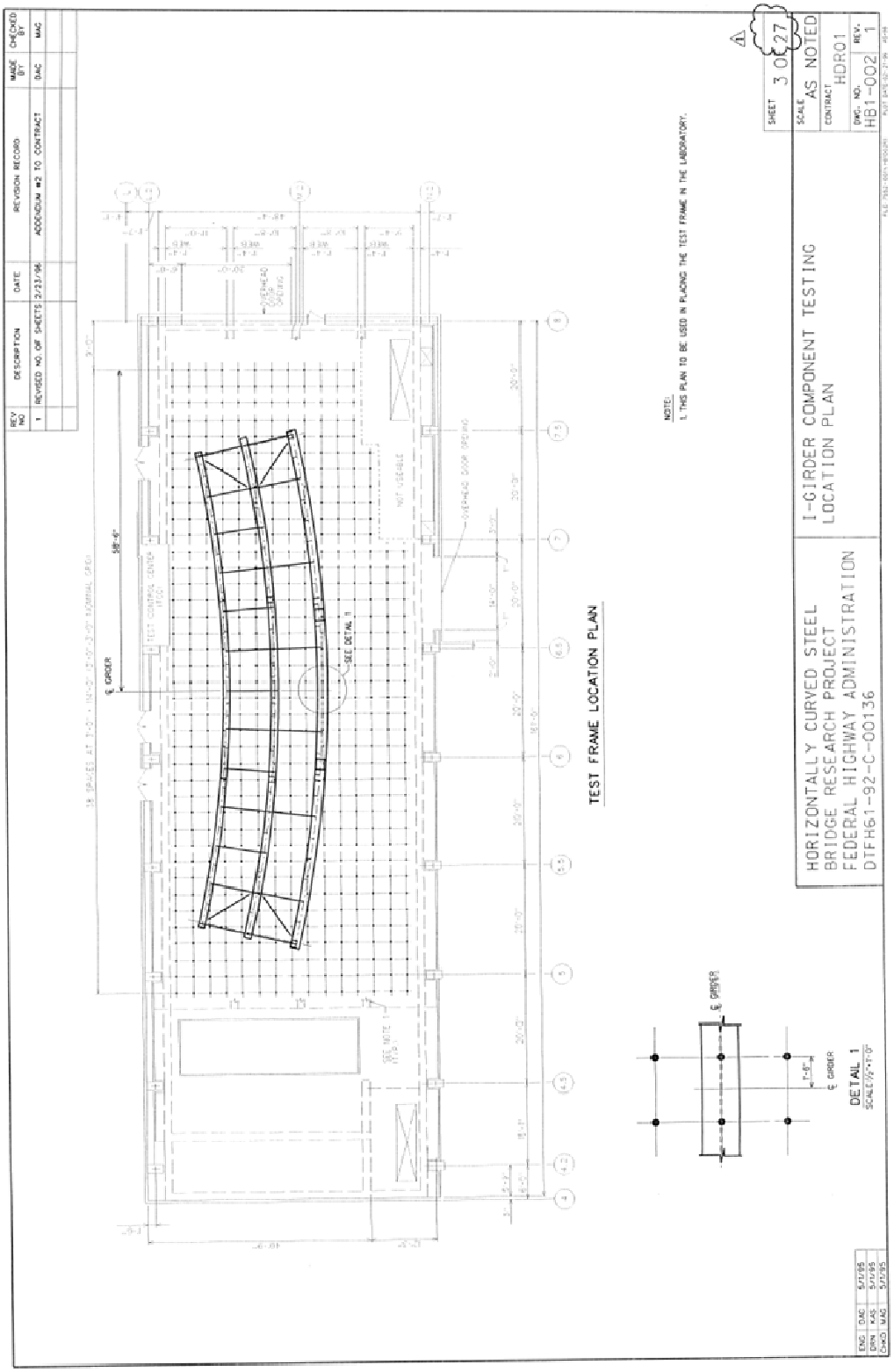


Figure 1.2.11 FHWA CSBRP Test Frame Location Plan

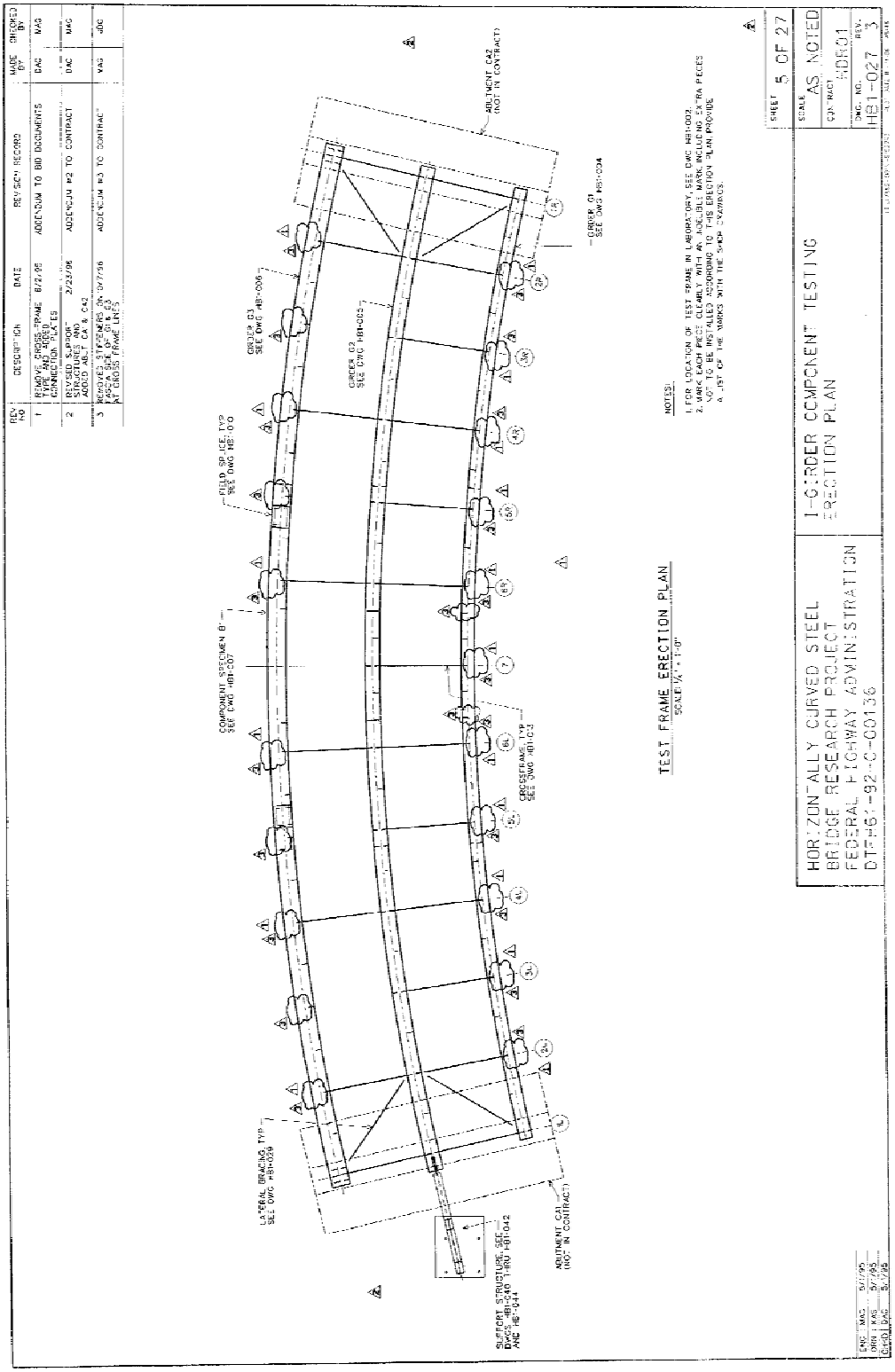


Figure 1.2.12 FHWA CSBRP Test Frame Erection Plan

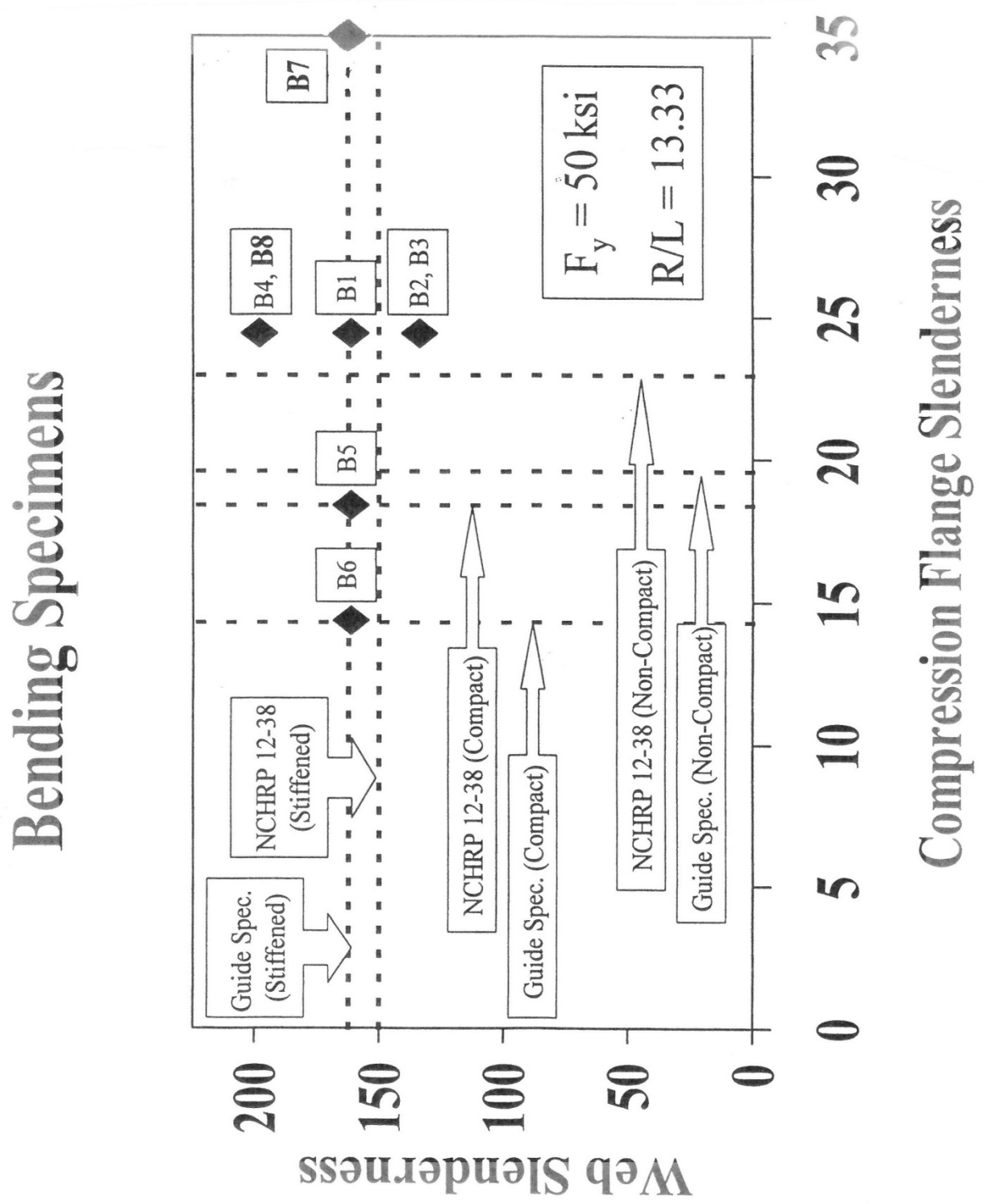


Figure 1.2.13 FHWA CSBRP – Bending Component Specimen Slenderness Ratios

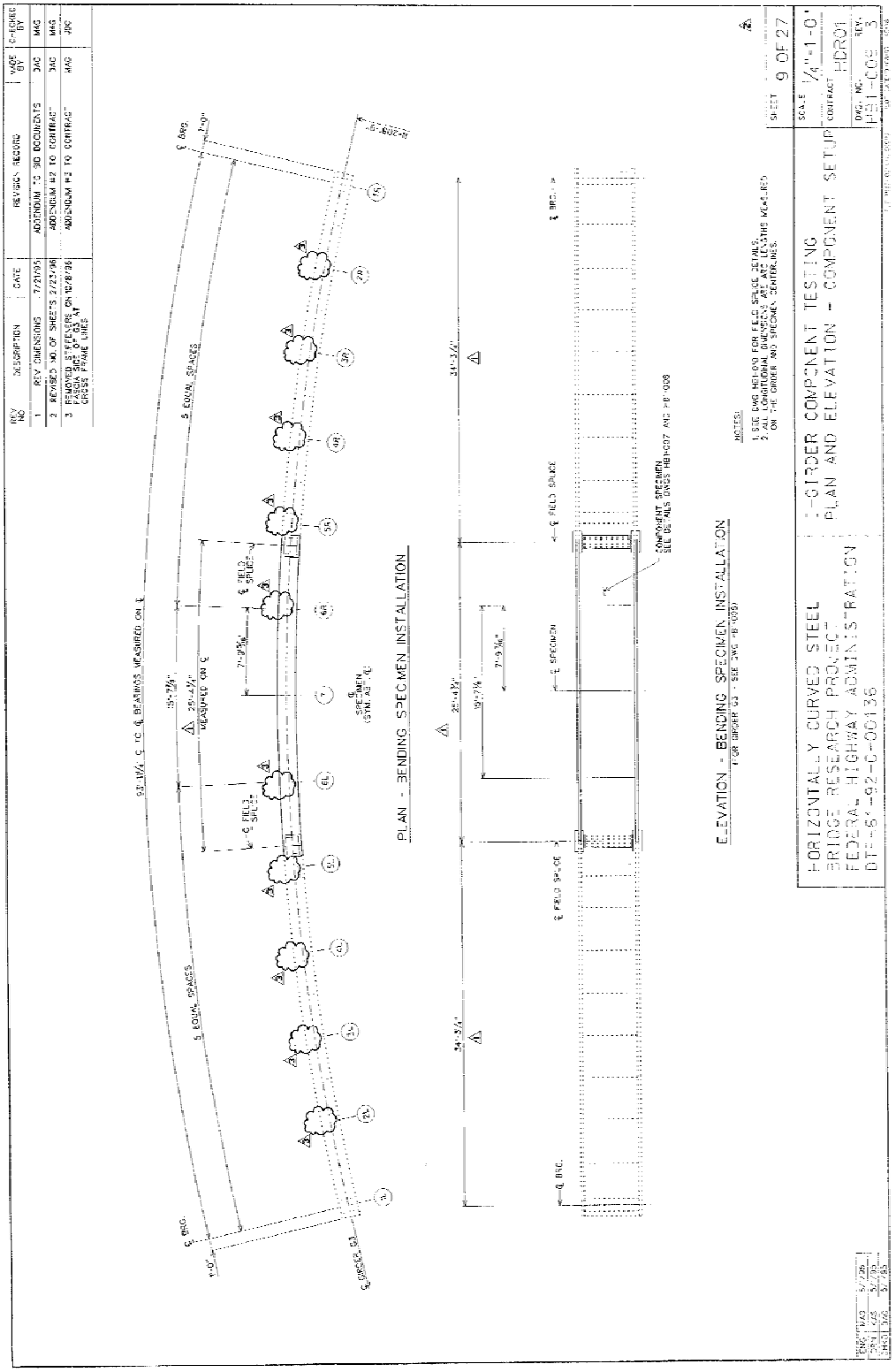


Figure 1.2.14 FHWA CSBRP Component Set-up (Plan and Elevation)

A series of six concentrated loads (two loads on each girder) was applied to the test frame through six load fixtures (discussed later). These loads were centered over each girder such that each girder, including the test specimens, was subjected to nearly pure bending in the central portion of the span. The loads were applied so as to essentially eliminate the potential for uplift and to maximize the moment in each specimen while limiting the stresses in the remaining portions of the frame, including the cross-frames, to the elastic range. By keeping all remaining portions of the test frame elastic throughout the test, it was possible to deduce the moment in the yielded component specimen at the point of failure from statics. However, the shape of the load-deflection curve for the test-frame arrangement was somewhat unusual. The slope of the aggregate load-deflection curve reduced as the test specimen softened, but at the load level at which the test specimen could carry no more load, the aggregate load-deflection curve was still upward sloping since the two girders not containing the test specimen remained elastic. It was not possible to accurately determine the moment in the test specimen from the strain gages mounted on the specimen. Hence, it was necessary to determine the capacity of the specimen indirectly. To accomplish this, a three-pronged strategy utilizing the following three independent, statically-based approaches was developed to deduce the moment in the component specimens from the measurements of stresses in selected locations of the elastic portion of the test frame and the reactions.

- Indirect Statical-Moment Method

  In the indirect statical-moment method, the total vertical bending moment in the three girders at any section, or the statical moment, is determined from the measured applied loads, reactions and the distance of these actions from the point where the statical moment is to be determined. At a given section, the vertical bending moment in one girder (i.e., the girder containing the test specimen) can be determined by subtracting the vertical bending moment in the other two girders from the computed statical moment in the three girders. The vertical bending moments in the two girders are determined from the integration of stresses computed from strain measurements taken on those girders.

- Free-Body Diagram Method

  In the free-body diagram method, a free body is obtained by assuming a cut through the cross-frames between G3 containing the component specimen and G2. The loads applied to the free body are the reactions, applied loads and cross-frame forces. The vertical bending moment in the component can then be determined by applying the vertical components of the external actions to the girder. In addition to the reactions and applied loads, this method requires the determination of the axial forces and moments in the cross-frame members attached to G3.

- G3 Moment Method

  Since the component specimen is assumed to fail at mid-span of G3, the vertical bending moment at other points on G3 is likely to remain elastic at failure and can be determined from the strain gage readings at those points (e.g., at sections near the brace points in the test components where strain gages are located). The vertical bending moment at those sections can be checked by the first method listed above. The vertical bending moment determined from the strain gage readings at those sections should also give a rather close estimate of the vertical bending moment at mid-span since the vertical bending moment is nearly constant within that region.

Because the test frame was non-composite for the component testing, it was decided to make each of the three main girders doubly symmetric. Up to that point, there had been no known tests of full-size singly symmetric horizontally curved I-girders, especially in the inelastic range. The web depth of each girder was 48 in. The web thickness of G1 was 7/16 in. The web thickness of G2 and G3 was ½ in. Top and bottom flange plates on G1 were 1-1/16" x 16". Top and bottom flange plates on G2 were 1-3/16" x 20". Top and bottom flange plates on G3 were 2-1/4" x 24". The decision was made to use AASHTO M 270 Grade 70W steel for the flanges and web of G2 in order to ensure that G2 remained elastic and could sustain the additional load transferred to it as each component specimen shed load. AASHTO M 270 Grade HPS 70W was not readily available at the time the test frame was fabricated. Therefore, the original (non HPS) quenched and tempered M 270 Grade 70W steel was used. Because quenched and tempered Grade 70W steel was only available in plate lengths up to 50 ft, welded shop splices were required in the web and flanges of G2 approximately 25 ft from the end of each girder. The flange and web splices were offset longitudinally by approximately 1.0 ft. The center section of G3 in-between the bolted field splices was set aside during the component testing. This section was fabricated for use during the erection studies and for final testing of the composite bridge. The girder cambers were determined to accommodate the casting of the concrete deck onto the frame at a later stage. Details of the test-frame girders are provided in Reference 56.

As discussed previously in Section 1.1, cross-frames transfer significant loads in horizontally curved bridges and therefore must be treated as primary members. In horizontally curved I-girders subject to a near constant vertical bending moment, the moment creates non-collinear axial forces in the flanges. To satisfy equilibrium, torsion is created along each girder in the system, which in turn creates restoring forces in the cross-frames. The sum of the vertical components of the cross-frame forces represents the load transferred between the girders through the cross-frames necessary to establish system equilibrium. The cross-frames provided stability to the system by transferring load between the girders. As the component specimen softened under load, less load was transferred to G3. In some cases, loads in the cross-frames were reversed and load was actually removed from G3 as the test progressed. As the stiffness of G3 was reduced, the frame tended to become less stable, and reactions at G1 were lessened, tending toward uplift. However, the

applied loads on G1 ensured that uplift could not occur. As explained above, accurate measurement of the actions in all the cross-frame members was essential in order to properly deduce the actions in the yielded component specimens.

Single angles and tee sections are generally used for cross-frame members to allow for the use of simple connection details. However, deducing the axial force in angles or tee sections is very difficult due to the eccentricities of the connections leading to torsional warping and bending stresses in these sections. To avoid these issues, pipes were used for the cross-frame members in the test frame (Figure 1.2.15). Pipes are excellent compression members with doubly symmetric properties. The end connections for the pipes could be designed to introduce less eccentricity. The St. Venant torsional stiffness is also large, and warping torsional stiffness could be ignored. Although the use of pipe sections for the cross-frame members slightly complicated the design of the connection details, the improved confidence in the determination of axial forces and bending moments in the pipes far outweighed the complexities associated with open sections.

The pipe sections selected had axial and flexural stiffnesses approximately equivalent to those of a 5 x 5 x 7/16 single angle member about its geometric axes. The ends of the pipes were closed with plates attached with full penetration welds. A pair of gusset plates was welded to each end plate. The gusset plates were centered on the pipe axis. They were spaced to just fit over the connection plates welded to the girder webs (Figure 1.2.15). The bolted connections were designed as slip-critical gusset-plate connections to ensure that the geometry of the structure did not change during the tests. The number of bolts was minimized by them being in double shear.

An angle capable of carrying the same axial load as the pipe would have been much stiffer than the pipe since it would have had to overcome significant flexural stresses.

Results of a separate non-linear analysis of the frame with the St. Venant torsional stiffness of all the pipes set equal to zero indicated that the additional torsional stiffness offered by the pipes had a negligible effect on the overall behavior of the system. The design of the pipe sections and their connections is discussed in more detail in Reference 56. The process used to determine an appropriate instrumentation scheme and then calibrate the pipe sections to determine the member actions during the component tests is discussed in Reference 79.

The idealized boundary conditions at each of the six bearings at the end supports of the test frame are shown schematically in Figure 1.2.16. Since accurate measurement of horizontal bearing reactions in the laboratory is extremely difficult, these boundary conditions were intended to provide the minimum amount of horizontal restraint to the test frame while still maintaining static equilibrium. Non-guided bearings were used at the ends of G1 and G3 to theoretically allow free translation of the girders (except for friction) in the tangential and radial directions, as well as free rotation of the girders about all three axes. The bearings at both ends of

G2 were guided tangentially; as such, the bearings under G2 provided radial restraint to the girder. Free rotation of G2 about all three axes was permitted. Since the bearings provided no tangential restraint, a tangential support frame was provided at the west end of G2 to supply the necessary tangential restraint to the frame. The frame was oriented to be tangent to the centerline of G2 at the west end. An elevation view of this support frame is shown in Figure 1.2.17. This simple frame consisted of a W12 x 40 column supported by an inclined W12 x 40 strut. To minimize the tangential reaction, the support frame was connected to the neutral axis of the G2 web. The W12 x 40 horizontal arm of the support frame was attached to G2 using a pair of splice plates and a 2-in. diameter pin. The pin was centered within a bean-shaped hole fabricated into the splice plates, with the dimensions of the hole determined to accommodate the predicted maximum end rotation of G2 during the component tests without binding of the pin.

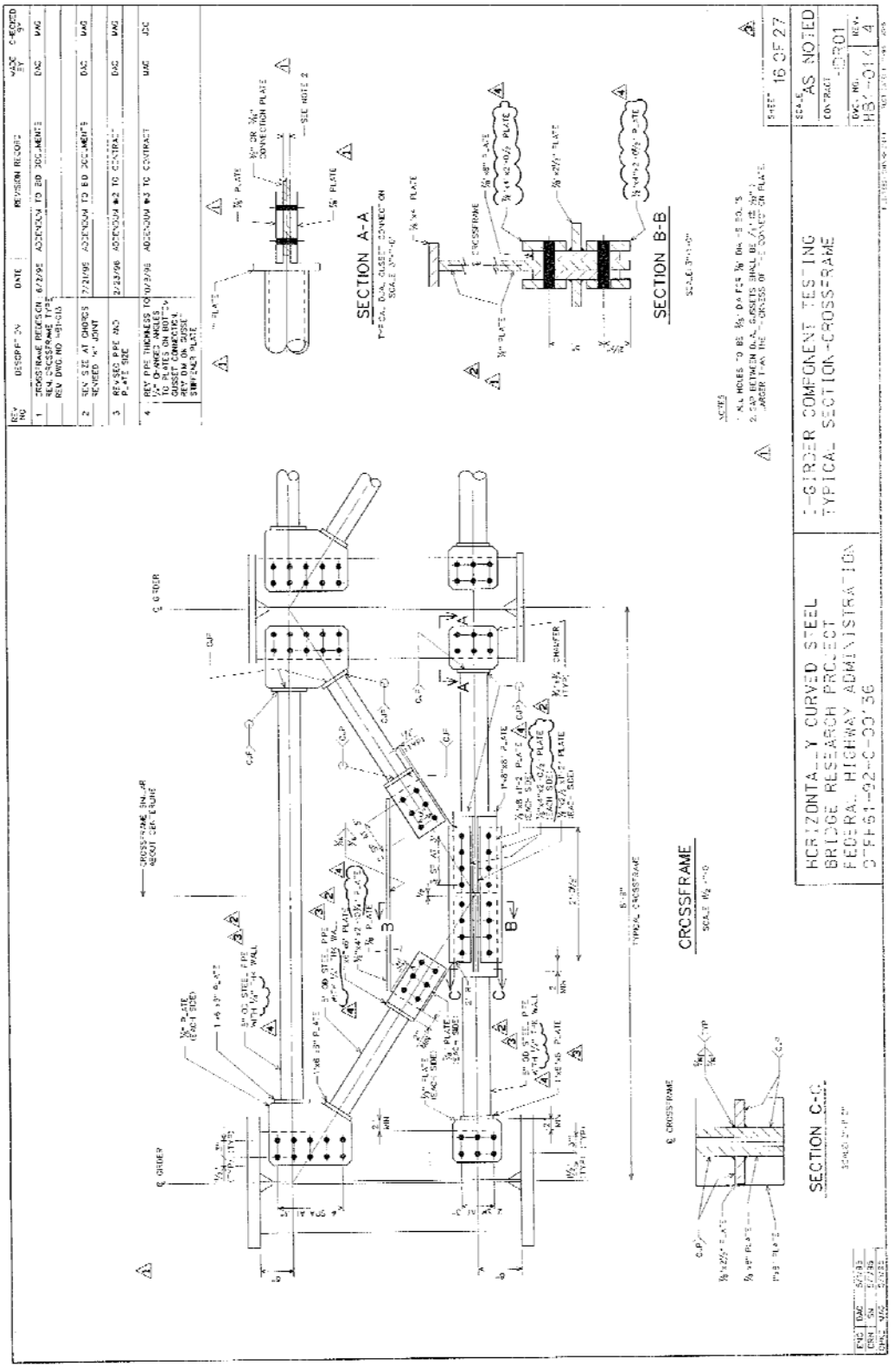


Figure 1.2.15 FHWA CSBRP Typical Section – Cross-Frame

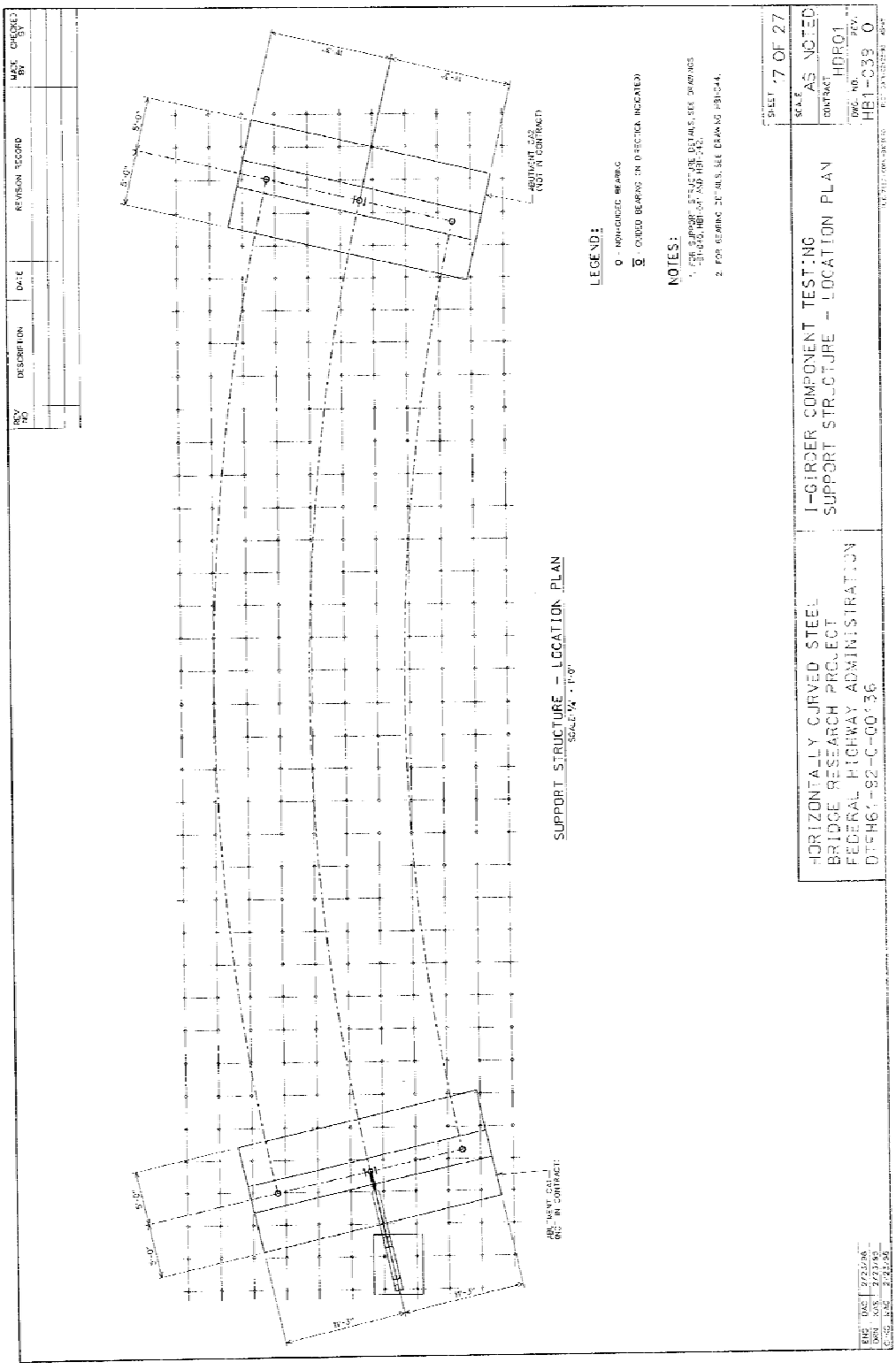


Figure 1.2.16 FHWA CSBRP – Test Frame Boundary Conditions

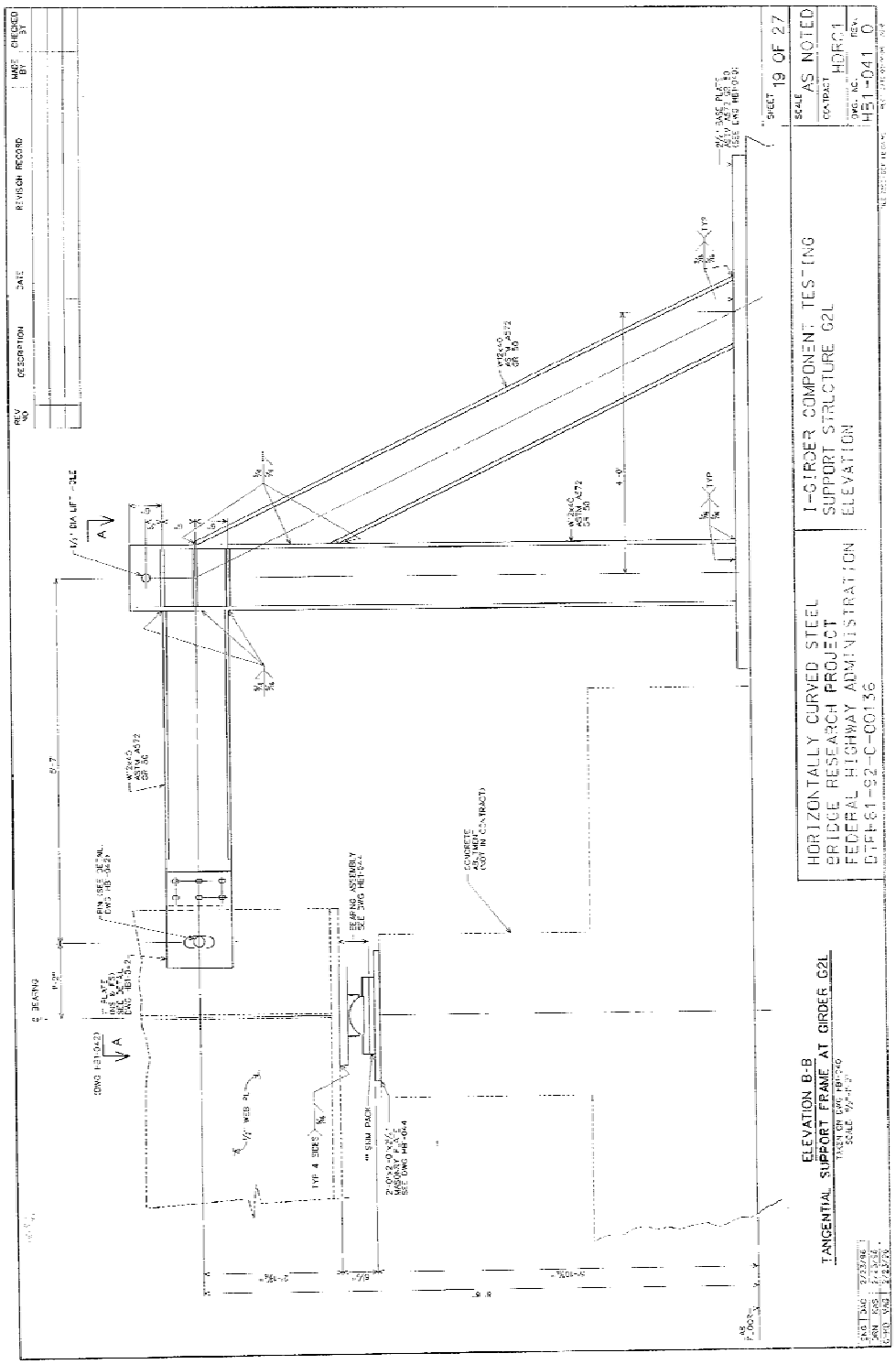


Figure 1.2.17 FHWA CSBRP – Tangential Support Frame (G2)

Because significant rotations were expected in the test program, spherical expansion bearing assemblies were selected for the test-frame girders. Spherical bearings typically consist of woven PTFE either bonded or mechanically fastened to a concave spherical steel plate. That plate then mates with a solid stainless steel plate with a convex spherical surface. The mating spherical surfaces allow for rotation about any axis, and the PTFE provides for a low friction interface. A 16-gage stainless steel sheet is typically seal welded around its entire periphery to the sole plate placed on top of each bearing. This stainless steel sheet mates with PTFE bonded to the flat top of the concave steel plate in order to allow the bearing to translate freely. Guides are usually provided through a recess in the sole plate directly above the bearing that permits translation of the bearing in the desired direction and prevents translation of the bearing in the orthogonal direction.

It was anticipated that horizontal reactions would develop at the test-frame bearings due to artificial or intentional restraints at the bearings, friction and/or corruptive lateral forces resulting from slight unintentional inclinations of the test-frame girders as the test-frame girders twisted and deflected. As mentioned previously, it was desired to minimize these reactions during the component tests due to the difficulty in accurately measuring them, concerns about the potential corruptive effect on the data and concerns about the ability of the load cells (used to measure the vertical reactions at the bearings) to resist significant horizontal forces. Friction was a particular concern because if a sudden movement of the bearings occurred as the frictional resistance in the bearings was overcome, it would contaminate the displacement and strain measurements. To minimize the effects of friction, a maximum coefficient of static friction of 4.5 percent was specified for the bearing design. In addition, the highest unit stress was specified for the design and a rational procedure was developed for minimizing the radius of each bearing. A horizontal design reaction of 10 percent of the maximum anticipated vertical design reaction was assumed at all the bearings, including the non-guided bearings, to conservatively account for the effect of friction and other possible corruptive effects. For the bearings under G2, an additional 10 kips was conservatively added. The final details for the bearings and the bearing design parameters are shown in Figure 1.2.18. Additional more detailed information on the bearing design may be found in Reference 56.

For the bending component tests, it was decided to apply six equal vertical loads at the same time to the flanges of all three girders in the frame at approximately the third points of each girder arc span, which nearly represented the application of a multiple of the deck weight to the non-composite steel girders. As a result, the component specimen in the center of G3 was subjected to a nearly constant vertical bending moment (the vertical bending moment due to the self-weight of the steel was not constant). The loads applied to the outermost G3 were applied just outside the component specimen. As a result of the inherent stability requirements of curved-girder bridges, G3 resisted the largest portion of the total load. Therefore, the component specimen, located within G3, could be loaded to its ultimate load without yielding any remaining portions of the test frame. Equal loading of the test-frame girders also prevented uplift of the innermost G1.

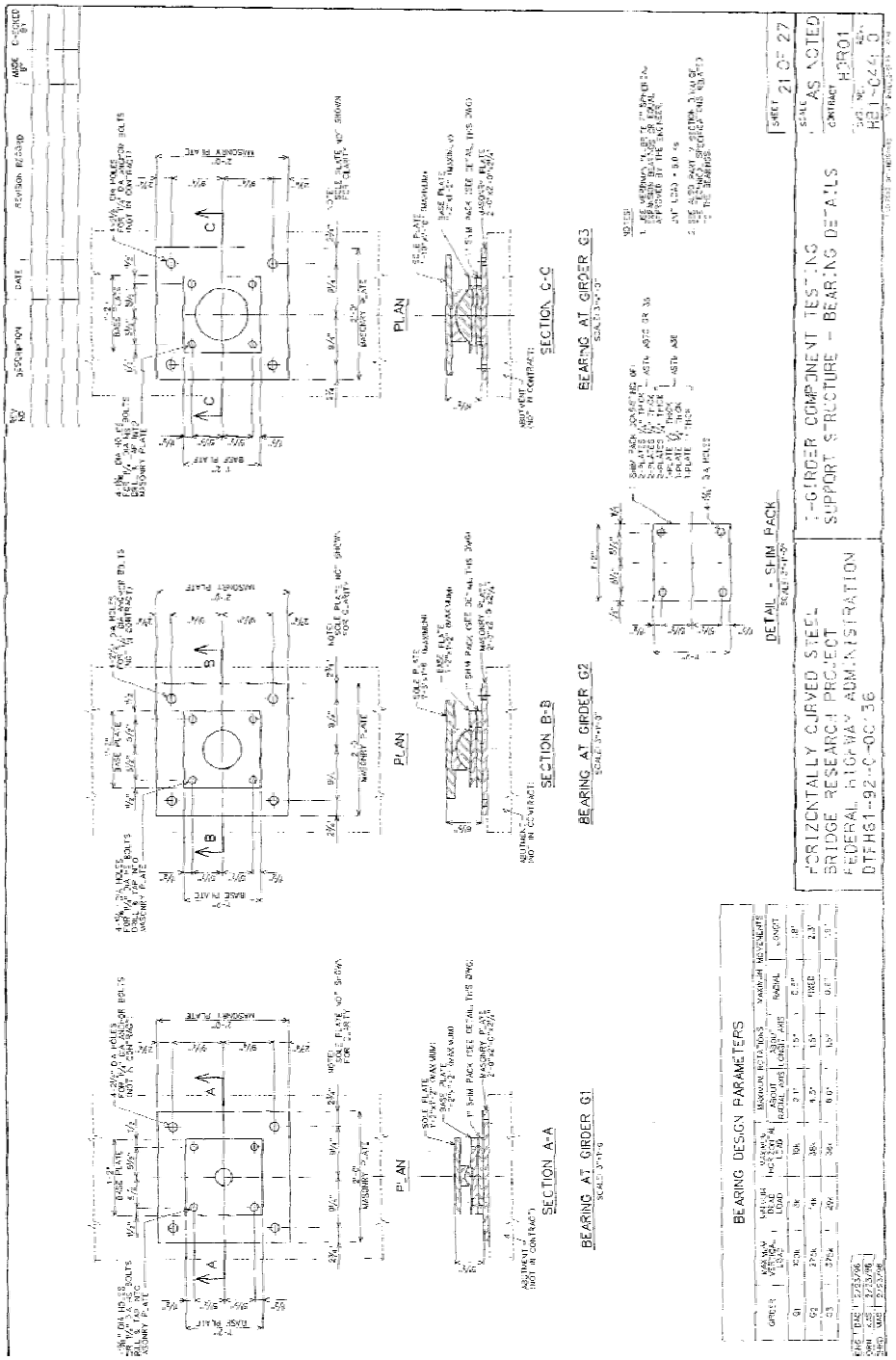


Figure 1.2.18 FHWA CSBRP – Test Frame Bearing Details and Design Parameters

Design of the loading fixtures for the test frame was complicated by the fact that each curved girder would twist and deflect laterally upon loading, which would make it difficult to maintain the applied loads in a vertical position. Any inclination of the applied loads would result in corruptive horizontal forces. Thus, two objectives of the design process for the load fixtures were to: 1) minimize the corruptive effects of any horizontal components of the loads generated by the inclination of the applied loads, and 2) prevent any Dywidag rods that were used as part of the load fixtures from contacting the approximately 3-in. diameter holes in the laboratory floor that they would pass through as the rods would not be designed to resist any bending.

Several different loading schemes were considered involving fairly detailed analytical investigations. Eventually, for the bending tests, it was decided to apply the loads at approximately the third points of each girder using a series of simple orthogonal frames that supported the jacks at each load point in a vertical orientation (Figure 1.2.19). Each orthogonal loading frame was supported near each corner by a Dywidag rod, approximately 14 ft in length, which ran vertically from the frame through a hole in the laboratory floor where it was anchored against the underside of the floor. The four rods for each frame were spaced orthogonally at 6.0 ft to correspond with the holes in the floor. As a result of the location of the holes in the floor with respect to the curved girders, the jacks were not located at the geometric centers of the loading frames. Thus, the tension in the four rods that supported each frame was not exactly equal. However, this did not prove to be significant. Each jack was mounted to a cross beam attached to the orthogonal frame. A greased ball-and-socket type bearing arrangement was used below each jack to maintain the load in a vertical position as the frame moved laterally. The ball was installed at the end of the jack, and the socket was placed on top of a load cell that was used to measure the magnitude of the applied load. The load cell was mounted on a plate attached to the girder top flange. The flexibility of the 14-ft-long Dywidag bars allowed each loading frame to follow the test frame as it moved laterally. The length of the rods reduced the angle caused by the lateral movement, thus making it less likely the rods would contact the edges of the holes in the floor during testing.

This entire undertaking would not have been practical without the advent of modern data-acquisition systems. These systems allowed for the automatic collection and reduction of the enormous amounts of data that were generated in a test of this magnitude in order to properly examine the behavior of the test frame and component specimens. The instrumentation and corresponding data-acquisition systems that were employed during the tests are described in detail in Reference 56.

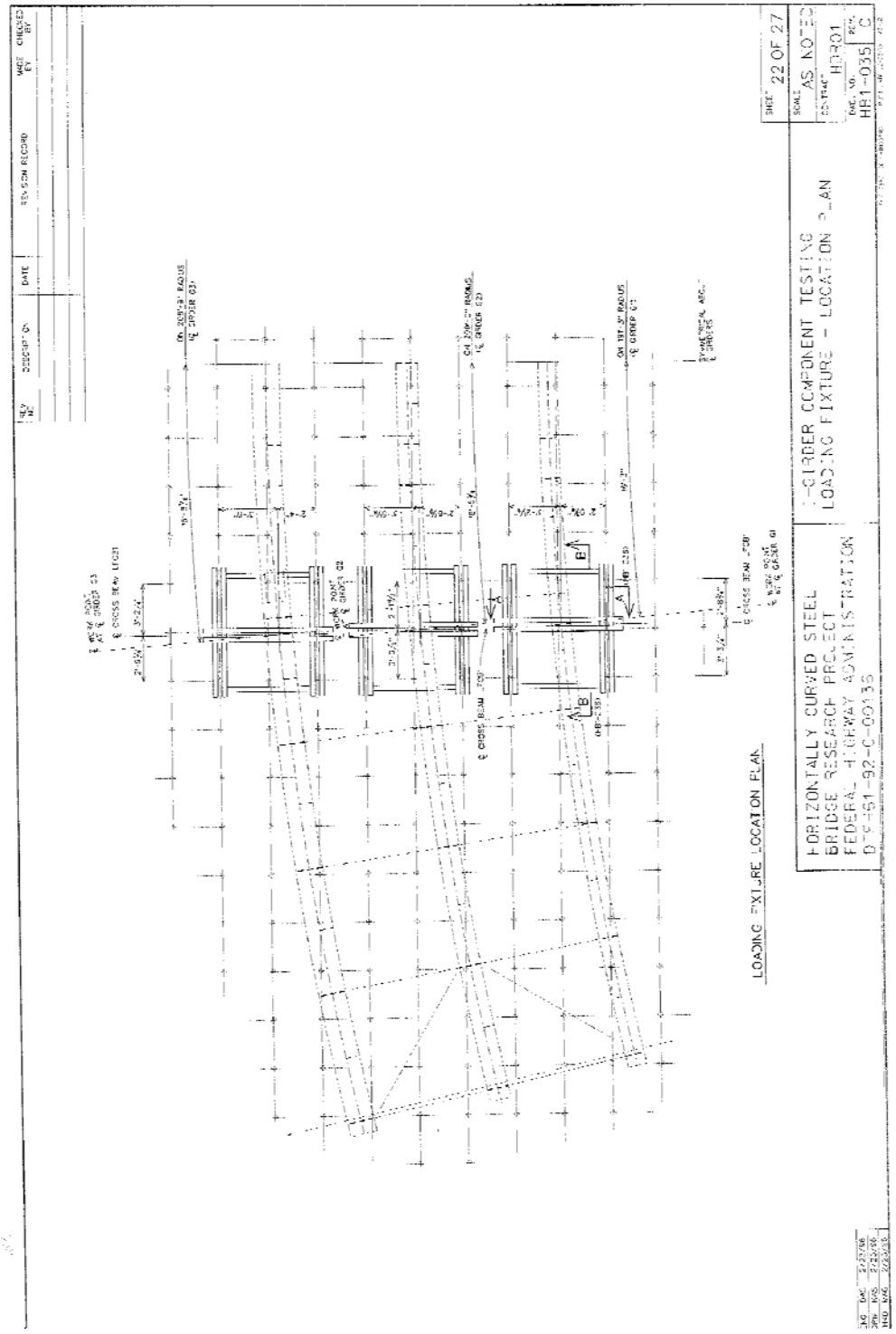


Figure 1.2.19 FHWA CSBRP – Test Frame Loading Fixtures

1.2.2.2.2 Additional Tests

In addition to the eight bending component tests, four full-scale moment-shear component tests (i.e., tests under a moment gradient) were conducted within the test frame. In these tests, the components were again inserted into G3, and only one line of loading fixtures was employed (Figure 1.2.20).

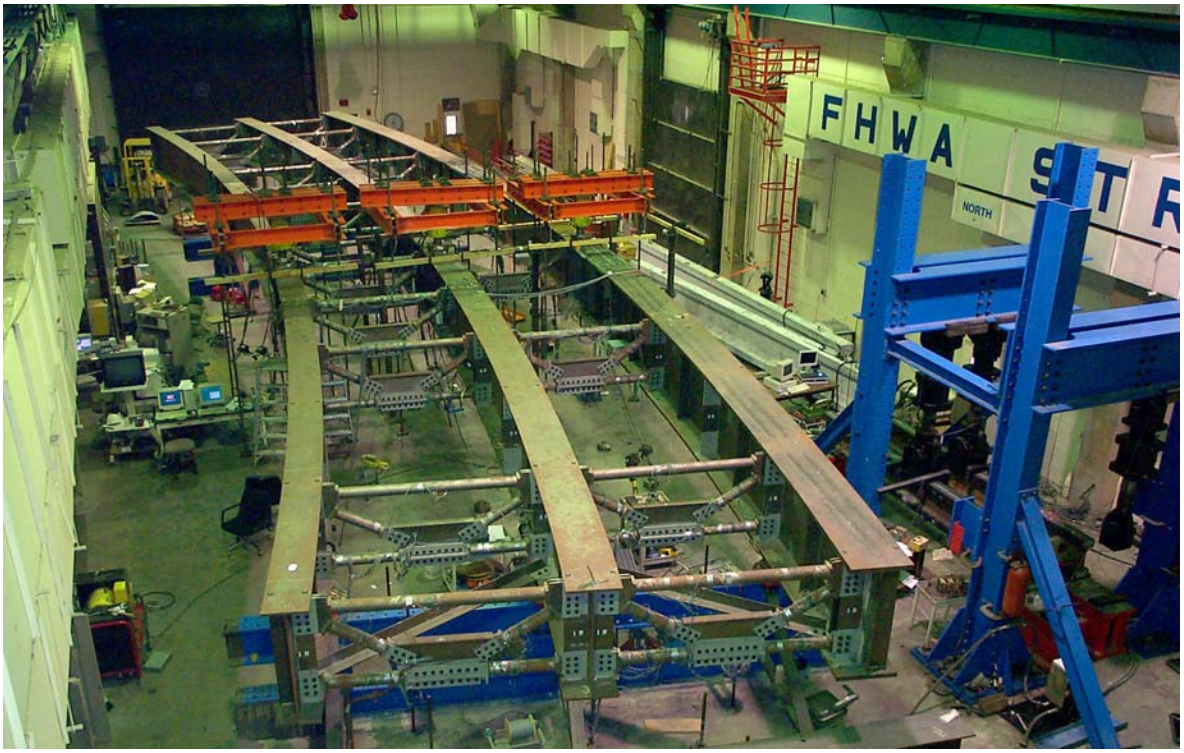


Figure 1.2.20 FHWA CSBRP – Moment-Shear Component Tests

As part of this project, four individual full-scale curved I-girder shear specimens were also tested separately at the Georgia Institute of Technology (*80*). In addition, erection studies were carried out using a new set of girders that were fabricated for the composite bridge tests. For a number of reasons, it was decided to fabricate three new girders for this portion of the test program rather than re-using the original test-frame girders that were employed during the component testing. Instead, the original non-composite test-frame girders G1 and G2 were tested to failure as a pair after the completion of the moment-shear component tests. At mid-span, the outer girder of the pair (G2) was deflected over 30 inches at the final load (Figure 1.2.21).



Figure 1.2.21 FHWA CSBRP – Ultimate Load Test of Original Girder Pair G1-G2

In the erection studies, the new G1 and G2 were first erected as a pair (Figure 1.2.22), and then the new G3 was added to the system. Deflection measurements were made at all steps, and the accumulation of stresses was tracked in the members. A series of point loads was applied, including to the deck overhang brackets, in order to develop an influence surface. The girders were then loaded up to 90 percent of yield in order to measure elastic displacements and distortions.

After the erection studies were completed, a concrete deck was cast onto the three girders (Figure 1.2.23). Measurements in real time were made during the casting of the deck up to mid-span, and over the entire span, to determine the effect of the formwork and the effect of the overhang brackets. The real-time monitoring continued during the curing of the concrete. Loads simulating two HS-20 trucks plus 33 percent dynamic load allowance (impact) were then incrementally applied to the top of the deck. The loads were positioned to maximize the load on G3 (Figure 1.2.24). Holes were cored through the deck to accommodate the Dywidag rods supporting the load fixtures. The composite bridge was able to sustain a significant multiple of the applied truck loads before the test was eventually stopped.



Figure 1.2.22 FHWA CSBRP – Erected G1-G2 Pair Under Gravity (New Girders)

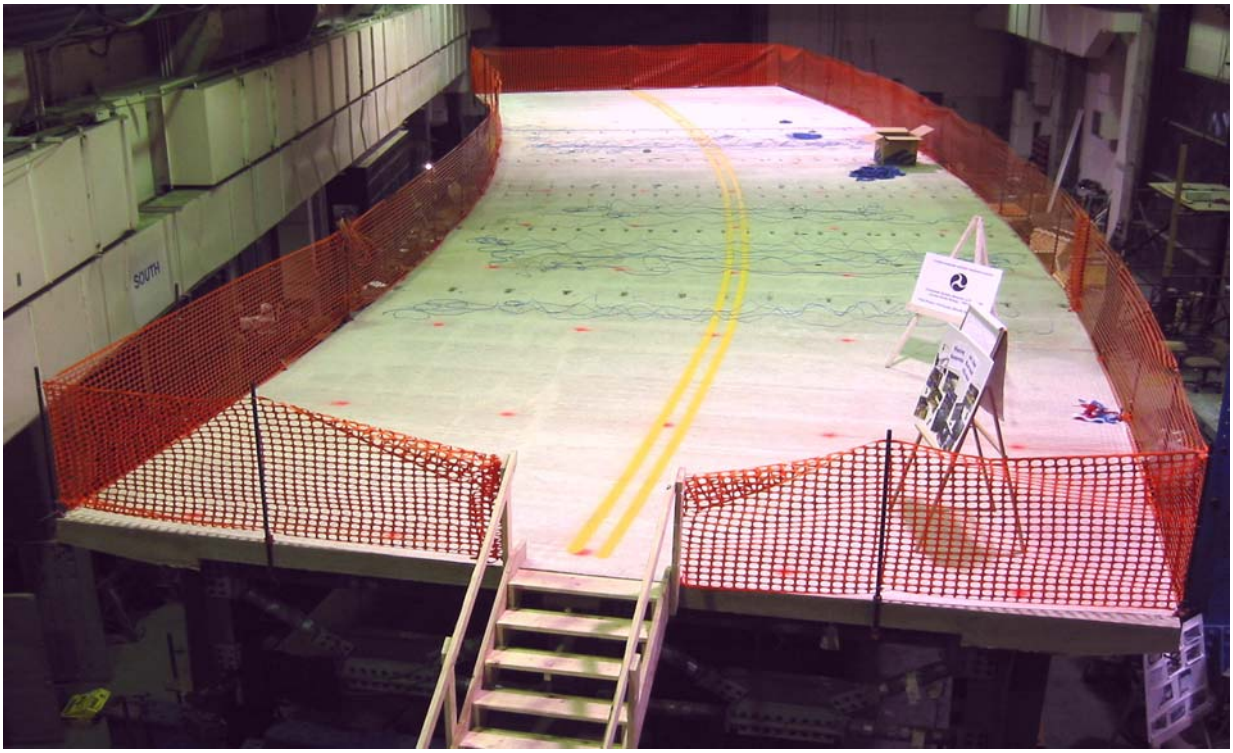


Figure 1.2.23 FHWA CSBRP – Concrete Deck Cast on Three New Girders



Figure 1.2.24 FHWA CSBRP – Loads Simulating Two HS-20 Trucks Plus Dynamic Load Allowance (Impact)

In the interest of brevity, the set-up, conduct and results from these latter phases of the test program (i.e., the shear tests, moment-shear tests, G1-G2 ultimate load test, erection studies and composite bridge test) are not discussed in detail herein. More details on these additional latter phases of the test program are available in Reference 56.

1.2.2.2.3 Summary

After the completion of the component tests, a joint FHWA/AASHTO project was initiated to generate hundreds of additional "virtual" analytical parametric tests using refined non-linear 3D finite element analyses. These "virtual" tests were calibrated utilizing the results from the full-scale laboratory component testing and were used to compile a database for statistical evaluation of the reliability provided by the new proposed equations for predicting the component strength of curved I-girders in bending and shear (*81 through 83*).

In summary, the key advancements resulting from the FHWA CSBRP and related work included: 1) new strength equations (i.e., the one-third rule equations) giving a better statistical prediction of the flexural strength of curved I-girders than the empirical equations from the original and 2003 *AASHTO Guide Specifications*

(developed as part of the CURT Project) (*57*); 2) the extension of post-buckling tension-field action to webs of horizontally curved girders and to the webs of hybrid girders (straight or curved) (*84 through 85*) for determining their shear capacity; 3) the extension of the maximum permitted transverse stiffener spacing from *D* to 3*D* in horizontally curved girders; and 4) the elimination of the moment-shear interaction relationship (*85*).

These advancements, in addition to several enhancements that resulted from the NCHRP 12-38 work to develop the 2003 *AASHTO Guide Specifications*, were combined to allow for the complete unification of the design provisions for straight and horizontally curved steel I- and box girders under NCHRP Project 12-52. Unlike previous specifications, all flexural and shear capacity equations for horizontally curved girders now converged completely to the equations for a straight girder in the limit as the flange lateral bending stresses or St. Venant torsional shear stresses due to curvature effects went to zero. The new flexural resistance equations also allowed for the direct consideration of flange lateral bending effects due to other sources such as wind, skew or deck overhang bracket loads. The new unified provisions were accepted by AASHTO in June 2004 and first appeared in the 2005 Interims to the *AASHTO LRFD Specifications*.

The FHWA CSBRP employed the full capabilities of FHWA Structures Laboratory at the Turner-Fairbank Highway Research Center, modern analytical techniques and instrumentation. The tests conducted as part of this project were historic in that they were the first tests known to the researchers that tested full-size components to failure as part of a structure that remained elastic and was reusable. Using a full-size curved bridge as a test frame also ensured for the first time that realistic boundary conditions would be provided for the component specimen testing. To address the many unknowns in such an ambitious test program, careful integration of analysis was required throughout the entire experimental design process. The extensive analyses that were employed during the design of the test program ensured that such an endeavor could be safely carried out for the first time, while at the same time providing the desired results without any premature failures of any test-frame components. The testing of this full-size simple-span three-girder structure, with its over 4-ft-deep girders and a total weight of nearly 60 tons, represented one of the single largest civil engineering related structural laboratory tests ever undertaken. As such, the design of this historically significant test provided an exceptional challenge and proved to be the final missing step in the approximately 25-year evolutionary development of the current unified *AASHTO LRFD Specifications* design provisions for straight and horizontally curved steel bridges.

1.2.3 References

1. Saint-Venant, B. 1843. “Mémorire sur le calcul de la résistance et de la flexion des pieces solides à simple ou à double courbure, en prenant simultanément en consideration les divers efforts auxquels elles peuvent êntre soumises dans touts les sens.” Compts-Rendus, l’Académic des Paris, Vol. XVII, pp. 942, 1020-1031.
2. Vlasov, V.Z. 1961. *Thin-Walled Elastic Beams*, 2nd Ed., National Science Foundation, Washington, D.C.
3. Dabrowski, R. 1964. “The Analysis of Curved Thin-Walled Girders of Open Section.” Der Stahlbau, 33(12), pp. 364-372.
4. Dabrowski, R. 1965. “Approximate Analysis of Curved Box Girders of Deformable Cross-Section.” 7th IASBE Congress, Preliminary Publication, Zurich, Switzerland, pp. 299-306.
5. Dabrowski, R. 1968. *Curved Thin-Walled Girders, Theory and Analysis*, Cement and Concrete Association, London, England (translated from German).
6. Culver, C.G. 1972. “Instability of Horizontally Curved Members, Design Recommendations for Curved Highway Bridges.” Project 68-32, Final Report to PennDOT, June, pp. 1-101.
7. Consortium of University Research Teams. 1975. “Tentative Design Specifications for Horizontally Curved Highway Bridges.” CURT Report, Part of Final Report, Research Project HPR2-(111), March.
8. AASHTO. 1980 (re-issued in 1993). *Guide Specifications for Horizontally Curved Highway Bridges*, Washington, D.C., pp. 1-111.
9. Galambos, T.V. 1978. “Tentative Load Factor Design Criteria for Curved Steel Bridges, Research Report No. 50.” Department of Civil Engineering, Washington University, St. Louis, MO, May, pp. I-1–C-20.
10. Daniels, J.H., Zettlemoyer, N., Abraham, D., and Batchler, R.P. 1979. “Fatigue of Curved Steel Bridge Elements-Analysis and Design of Plate Girder and Box Girder Test Assemblies.” Lehigh University, Bethlehem, PA, DOT-FH-11-8198.1, pp. 1-109.
11. Daniels, J.H. and Herbein, W.C. 1980. “Fatigue of Curved Steel Bridge Elements – Fatigue Tests of Curved Plate Girder Assemblies.” Lehigh University, Bethlehem, PA, FHWA RD-79-133, pp. 1-150.
12. Zettlemoyer, N., Fisher, J.W., and Daniels, J.H. 1980. “Fatigue of Curved Steel Bridge Elements-Stress Concentration, Stress Range Gradient, and Principal Stress Effects on Fatigue Life.” Lehigh University, Bethlehem, PA, FHWA-RD-79-132, pp. 1-91.
13. Daniels, J.H., Fisher, J.W., Batcheler, R.P., and Maurer, J.K. 1979. “Fatigue of Curved Steel Bridge Elements-Ultimate Strength Tests of Horizontally Curved Plate and Box Girders.” Lehigh University, Bethlehem, PA, DOT-FH-11-8198.7, pp. 1-83.
14. Daniels, J.H., Abraham, D., and Yen, B.T. 1979. “Fatigue of Curved Steel Bridge Elements-Effect of Internal Diaphragms on Fatigue Strength of Curved Box Girders.” Lehigh University, Bethlehem, PA, DOT-FH-8198.6, pp. 1-52.

15. Daniels, J.H., Fisher, J.W., and Yen, B.T. 1980. "Fatigue of Curved Steel Bridge Elements, Design Recommendations For Fatigue of Curved Plate Girder and Box Girder Bridges." Federal Highway Administration, Offices of Research & Development Structures & Applied Mechanics Division, Report No. FHWA-RD-79-138, April, pp. 1-54.
16. Heins, C.P., and Hails, R.L. 1969. "Behavior of Stiffened Curved Plate Model." *Journal of the Structural Division*, ASCE, Vol. 95, No. ST11, Proc. Paper 6876, pp. 2353-2370.
17. Yoo, C., and Heins, C.P. 1972. "Plastic Collapses of Horizontally Curved Bridge Girders." *Journal of the Structural Division*, ASCE, Vol. 98, No. ST4, Proc. Paper 8848, pp. 899-914.
18. Heins, C.P., and Humphreys, R.S. 1979. "Bending and Torsion Interaction of Box Girders." *Journal of the Structural Division*, ASCE, Vol. 105, No. ST5, Proc. Paper 14587, pp. 891-904.
19. Mondkar, D.P., and Powell, G.H. 1974. "CURVBRG – A Computer Program for Analysis of Curved Open Girder Bridges." University of California, College of Engineering, UC-ESEM Report No. 74-17, Berkeley, CA, pp. 1-54.
20. Yoo, C, Buchannan, J., Heins, C.P., and Armstrong, W. 1976. "Analysis of Continuous Curved Box Girder Bridge." TRB Record No. 579, Washington, D.C., October, pp. 61-71.
21. Yoo, C. 1979. "Matrix Formulation of Curved Girders." *Journal of the Engineering Mechanics Division*, ASCE, Vol. 105, No. EM6, December, pp. 971-988.
22. Yoo, C., and Fehrenbach, J.P. 1981. "Natural Frequencies of Curved Girders." Journal of the Engineering Mechanics Division, ASCE, Vol. 107, No. EM2, pp. 339-354.
23. Yoo, C. 1982. "Flexural-Torsional Buckling of Curved Beams." *Journal of the Engineering Mechanics Division*, ASCE, Vol. 108, No. EM6, pp. 1351-1369.
24. Yoo, C., and Pfeiffer, P.A. 1983. "Elastic Stability of Curved Members." *Journal of Structural Engineering*, ASCE, Vol. 109, No. ST12, pp. 2922-2940.
25. Yoo, C., and Littrell, P.C. 1986. "Cross-Bracing Effects in Curved Stringer Bridges." *Journal of Structural Engineering*, ASCE, Vol. 112, No. ST9, pp. 2127-2140.
26. Yoo, C. 1987. "Consistent Discrete Element Technique for Curved Members." *Computers and Structures*, Vol. 25, No. 1, pp. 137-146.
27. Beal, D.B. 1978. "Horizontally Curved Bridges: New York Field Testing and Design Studies, Final Report on Research Project 42-1." Engineering Research and Development Bureau, New York State DOT, Research Report 61.
28. Gambrell, S.C., Jr., and Skelton, T.J. 1986. "Structural Behavior of the Homewood Bridge after Fourteen Years Traffic." The University of Alabama-Birmingham, Department of Engineering Mechanics, August.
29. Buchanan, J.D., Yoo, C.H., and Heins, C.P. 1974. "Field Study of a Curved Box Beam Bridge." University of Maryland, Department of Civil Engineering, September.
30. Galambos, T.V., Hajjar, J.F., Leon, R.T., Huang, W., Pulver, B., and Rudie, B.J. 1996. "Stresses in Steel Curved Girder Bridges." University of Minnesota Center for Transportation Studies, Research Report No.96-28, August.

31. Linzell, D.G., Leon, R.T., and Zureick, A.H. 2004. “Experimental and Analytical Studies of a Horizontally Curved Steel I-Girder Bridge during Erection.” *Journal of Bridge Engineering*, ASCE, Vol. 9, No. ST6, November/December, pp. 521-530.
32. Domalik, D.E., Shura, J.F., and Linzell, D.G. 2005. “Design and Field Monitoring of Horizontally Curved Steel Plate Girder Bridge.” Transportation Research Record No. 1298, Transportation Research Board, Washington, D.C., pp. 83-91.
33. Nevling, D., Linzell, D., and Laman, J. 2006. “Examination of Level of Analysis Accuracy for Curved I-Girder Bridges through Comparisons to Field Data.” *Journal of Bridge Engineering*, ASCE, Vol. 12, No. ST1, March/April, pp. 160-168.
34. Bell, B., and Linzell, D. 2007. “Erection Procedure Effects on Deformations and Stresses in a Large Radius, Horizontally Curved I-Girder Bridge.” *Journal of Bridge Engineering*, ASCE, Vol. 12, No. ST1, July, pp. 467-476.
35. Linzell, D.G., and Shura, J.F. 2010. “Erection Behavior and Grillage Model Accuracy for a Large Radius Curved Bridge.” *Journal of Constructional Steel Research*, Vol. 66, pp. 342-350.
36. Fukumoto, Y., and Nishida, S. 1981. “Ultimate Load Behavior of Curved I-Beams.” *Journal of the Engineering Mechanics Division*, ASCE, Vol. 107, No. EM2, pp. 367-385.
37. Fukumoto, Y., Itoh, Y., and Kubo, M. 1980. “Strength Variation of Laterally Unsupported Beams.” *Journal of the Structural Division*, ASCE, Vol. 106, No. ST1, pp. 165-181.
38. Nakai, H., Kitada, T., Ishizaki, H., and Akehashi, K. 1989. “An Experimental Study on Fatigue Strength of Web Plate in Horizontally Curved Plate Girder.” *Proceedings of Japan Society of Civil Engineers*, 35A, March, pp. 899-909.
39. Nakai, H., Kitada, T., and Ohminami, R. 1985. “Experimental Study on Buckling and Ultimate Strength of Curved Girders Subjected to Combined Loads of Bending and Shear.” *Proceedings of Japan Society of Civil Engineers*, No. 356/I-3, April, pp. 445-454.
40. Nakai, H., Kitada, T., and Ohminami, R. 1983. “Experimental Study on Bending Strength of Web Plate of Horizontally Curved Girder Bridges.” *Proceedings of Japan Society of Civil Engineers*, No. 340, pp. 19-28.
41. Nakai, H., Kitada, T., Ohminami, R., and Fukumoto, K. 1984. “Experimental Study on Shear Strength of Horizontally Curved Plate Girders.” *Proceedings of Japan Society of Civil Engineers*, No. 350/I-2, pp. 281-290.
42. Nakai, H., Nurayama, Y., Kitada, T., and Takada, Y. 1990. “An Experimental Study on Ultimate Strength of Thin-Walled Box Beams Subjected to Bending and Torsion.” *Proceedings of Japan Society of Civil Engineers*, 36A, pp. 63-70.
43. Nakai, H., and Kotoguchi, H. 1983. “A Study on Lateral Buckling Strength and Design Aid for Horizontally Curved I-Girder Bridges.” *Proceedings of Japan Society of Civil Engineers*, No. 339, November, pp. 195-204.
44. Kitada, T., Ohminami, R., and Nakai, H. 1986. “Criteria for Designing Web and Flange Plates of Horizontally Curved Plate Girders.” *Proceedings of the SSRC 1986 Annual Technical Session*, pp. 1-12.

45. Nakai, H., Kitada, T., Ohminami, R., and Kawai, T. 1986. “A Study on Analysis and Design of Web Plates in Curved Girder Bridges Subject to Bending.” Proceedings of Japan Society of Civil Engineers, No. 368/I-5, pp. 235-244.
46. Hanshin Expressway Public Corporation, and Steel Structure Study Committee. 1988. “Guidelines for the Design of Horizontally Curved Girder Bridges (Draft).” Hanshin Expressway Public Corporation, October, pp. 1-178.
47. Japan Road Association. 1990. *Specifications for Highway Bridges, Part I: Common Specifications. Part II: Steel Bridge Specifications*, February, pp. 1-440.
48. Nakai, H., and Yoo, C. 1988. *Analysis and Design of Curved Steel Bridges*. Mc-Graw-Hill Book Company, New York, NY, pp. 1-673.
49. Yang, Y.B., and Kuo, S.R. 1986. “Static Stability of Curved Thin-Walled Beams.” *Journal of Engineering Mechanics*, ASCE, Vol. 112, No. 8, pp. 821-841.
50. Yang, Y.B., and Kuo, S.R. 1987. “Effect of Curvature on Stability of Curved Beams.” *Journal of Structural Engineering*, ASCE, Vol. 113, No. 6, pp. 1185-1201.
51. Yang, Y.B., and Kuo, S.R. 1991. “New Theory on Buckling of Curved Beams.” *Journal of Engineering Mechanics*, ASCE, Vol. 117, No. 8, pp. 1698-1717.
52. AASHTO. 1994. *LRFD Bridge Design Specifications*, First Edition, Washington, D.C.
53. AASHTO. 1992. *Standard Specifications for Highway Bridges*, Fifteenth Edition, Washington, D.C.
54. Hall, D.H., Grubb, M.A., and Yoo, C.H. 1999. “Improved Design Specifications for Horizontally Curved Steel Girder Highway Bridges.” NCHRP Report 424, Transportation Research Board, Washington, D.C., pp. 1-130.
55. AASHTO. 2003. *Guide Specifications for Horizontally Curved Steel Girder Highway Bridges*, Washington, D.C., pp. 1-392.
56. Beshah, F. 2010. “TECH BRIEF”, Curved Steel Bridge Research Project, Federal Highway Administration, Turner-Fairbank Highway Research Center, McLean, VA, November.
57. White, D.W., and Grubb, M.A. 2005. “Unified Resistance Equations for Design of Curved and Tangent Steel Bridge I-Girders.” *Proceedings of the Transportation Research Board Sixth International Bridge Engineering Conference*, Boston, MA, July.
58. Kulicki, J.M., Wassef, W.G., Kleinhans, D.D., Yoo, C.H., Nowak, A.S., and Grubb, M.A. 2006. “Development of LRFD Specifications for Horizontally Curved Steel Highway Bridges.” NCHRP Report 563, Transportation Research Board, Washington, D.C., pp. 1-81.
59. McManus, P.F. 1971. “Lateral Buckling of Curved Plate Girders.” Thesis presented to Carnegie Mellon University in partial fulfillment of the requirements for the degree of Doctor of Philosophy, Pittsburgh, PA, pp. 1-186.
60. Nasir, G.A. 1970. “Buckling of Stiffened and Unstiffened Curved Plate Elements.” Thesis presented to Carnegie Mellon University in partial fulfillment of the requirements for the degree of Doctor of Philosophy, Pittsburgh, PA, pp. 1-243.

61. Brogan, D.K. 1972. “Bending Behavior of Cylindrical Web Panels.” Thesis presented to Carnegie Mellon University in partial fulfillment of the requirements for the degree of Master of Science, Pittsburgh, PA, pp. 1-34.
62. Mozer, J., and Culver, C.G. 1975. “Horizontally Curved Highway Bridges, Stability of Curved Plate Girders.” Report No. P1, U.S. DOT, Federal Highway Administration, Washington, D.C., August.
63. Mozer, J., Ohlson, R., and Culver, C.G. 1975. “Horizontally Curved Highway Bridges, Stability of Curved Plate Girders. “ Report No. P2, U.S. DOT, Federal Highway Administration, Washington, D.C., August.
64. Mozer, J., Cook, J., and Culver, C.G. 1975. “Horizontally Curved Highway Bridges, Stability of Curved Plate Girders.” Report No. P3, U.S. DOT, Federal Highway Administration, Washington, D.C., August.
65. Culver, C.G., and Mozer, J. 1970. “Horizontally Curved Highway Bridges, Stability of Curved Box Girders.” Carnegie Mellon University, Carnegie Institute of Technology, Report No. B1, Pittsburgh, PA, pp. 1-118.
66. Culver, G.G., and Mozer, J. 1971. “Horizontally Curved Highway Bridges, Stability of Curved Box Girders.” Carnegie Mellon University, Carnegie Institute of Technology, Report No. B2, Pittsburgh, PA, pp. 1-91.
67. Culver, C.G., and Mozer, J. 1971. “Horizontally Curved Highway Bridges, Stability of Curved Box Girders.” Carnegie Mellon University, Carnegie Institute of Technology, Report No. B3, Pittsburgh, PA, pp. 1-76.
68. Wright, R.N., and Abdel-Samad, S.R. 1968. “BEF Analogy for Analysis of Box Girders.” Journal of the Structural Division, ASCE, Vol. 94, No. ST7, pp. 1719-1743.
69. Wilson, P.J., Duncan, R.R. III, and Fisher, J.W. 1988. “Repair of Fatigue Cracks in Steel Box Girder Bridges on I-110.” *Proceedings of the 5th Annual International Bridge Conference*, Paper IBC-88-44, Pittsburgh, PA, pp. 234-241.
70. Vincent, G.S. 1969. “Tentative Criteria for Load Factor Design of Steel Highway Bridges.” Bulletin No. 15, American Iron and Steel Institute, March, pp. 1-65.
71. Schilling, C.G. 1996. “Yield-Interaction Relationships for Curved I-Girders.” *Journal of Bridge Engineering*, ASCE, Vol. 1, No. 1, February.
72. Yoo, C.H., and Davidson, J.S. 1997. “Yield Interaction Relationships for Nominal Bending Strength of Curved I-Girders.” *Journal of Bridge Engineering*, ASCE, Vol. 2, No. 2, pp. 37-44.
73. Davidson, J.S., Keller, M.A., and Yoo, C.H. 1996. “Cross-Frame Spacing and Parametric Effects in Horizontally Curved I-Girder Bridges.” *Journal of Structural Engineering*, ASCE, Vol. 122, No. 9, September, pp. 1089-1096.
74. Culver, C.G., Dym, C.L., and Brogan, D.K. 1972. “Bending Behavior of Cylindrical Web Panels.” Journal of the Structural Division, ASCE, Vol. 98, No. ST10, pp. 2291-2308.
75. Culver, C.G., Dym, C.L., and Uddin, T. 1973. “Web Slenderness Requirements for Curved Girders.” Journal of the Structural Division, ASCE, Vol. 99, No. ST3, pp. 417-429.

76. Mueller, J., and Yen, B.T. 1969. “Fatigue Strength of Plate Girders.” Bulletin No. 17, American Iron and Steel Institute, Washington, D.C., April.
77. Timoshenko, S.P., and Gere, J.M. 1961. *The Theory of Elastic Stability*. 2nd Edition, McGraw-Hill Book Company, New York, NY, pp. 1-541.
78. Frank, K.H., and Helwig, T.A. 1995. “Buckling of Webs in Unsymmetric Plate Girders.” *AISC Engineering Journal*, American Institute of Steel Construction, Chicago, IL, Vol. 32, 2nd Qtr., pp. 43-53.
79. Linzell, D.G. 1999. “Studies of a Full-Scale Horizontally Curved Steel I-Girder Bridge System under Self-Weight.” Ph.D. Dissertation, The Georgia Institute of Technology, Atlanta, GA, August.
80. Zureick, A.H., White, D.W., Phoawanich, N.P., and Park J. 2002 “Shear Strength of Horizontally Curved Steel I-Girders – Experimental Tests.” Final Report to Professional Services Industries, Inc. and Federal Highway Administration.
81. Jung, S.K., and White, D.W. 2006. “Shear Strength of Horizontally Curved Steel I-Girders – Finite Element Studies.” *Journal of Constructional Steel Research*, Vol. 62, No. 4, pp. 329-342.
82. White, D.W., Chang, C.-J., and Jung, S.K. 2004. “One-Third Rule for Resistance of I-Section Members Subjected to Combined Major-Axis Bending, Minor-Axis Bending and Torsion – Parametric Studies.” Structural Engineering, Mechanics and Materials Report No. 40, School of Civil and Environmental Engineering, Georgia Institute of Technology, Atlanta, GA.
83. White, D.W., Jung, S.K., and Chang, C.-J. 2004. “One-Third Rule for Resistance of I-Section Members Subjected to Combined Major-Axis Bending, Minor-Axis Bending and Torsion – Supplementary Parametric Studies.” Structural Engineering, Mechanics and Materials Report No. 40, School of Civil and Environmental Engineering, Georgia Institute of Technology, Atlanta, GA.
84. White, D.W., and Barker, M. 2004. “Shear Resistance of Transversely Stiffened Steel I-Girders.” Structural Engineering, Mechanics and Materials Report No. 26, School of Civil and Environmental Engineering, Georgia Institute of Technology, Atlanta, GA.
85. White, D.W., Barker, M., and Azizinamini, A. 2004. “Shear Strength and Moment-Shear Interaction in Transversely Stiffened Steel I-Girders.” Structural Engineering, Mechanics and Materials Report No. 27, School of Civil and Environmental Engineering, Georgia Institute of Technology, Atlanta, GA.

This Page Intentionally Left Blank

Chapter 1
Introduction to Skewed and Curved Girder Bridges

Section 1.3

Review of LRFD Fundamentals



1.3.1 Introduction

In the *AASHTO LRFD Bridge Design Specifications*, bridges are to be designed for specified limit states to achieve the objectives of constructability, safety and serviceability, with due regard given to issues such as economics and aesthetics. At each limit state, the factored resistance of a member or component must not exceed the sum of the factored force effects resulting from a specified combination(s) of design loads. This section presents a general review of the design loads, load factors and load combinations, limit states, and other LRFD fundamentals.

1.3.2 Loads

Loads are classified as permanent loads or transient loads in the *AASHTO LRFD Bridge Design Specifications*.

Permanent loads are loads that are an integral part of the structure and are expected to be constant upon completion of construction. Permanent loads are most frequently dead loads acted upon by gravity. Accumulated locked-in force effects are also classified as permanent loads.

Transient loads are loads that are only present on the structure for a short duration and include vehicular live loads, vehicular centrifugal force, wind loads, force effects due to uniform temperature and temperature gradient, pedestrian live loads and vehicular braking forces.

Each of these loads is described in the following sections. Only the more common loads used in skewed and curved steel bridge superstructure design are discussed. Other loads such as earthquake loads and vehicular collision forces may also need to be considered.

1.3.2.1 Dead Loads

Dead loads in the *AASHTO LRFD* specification are primarily classified as either component dead load (designated as DC), which is assumed to consist of all the structure dead load except for any non-integral wearing surfaces and any specified utility loads, or dead load of any non-integral wearing surfaces and any utilities (designated as DW).

Other dead loads specified by *AASHTO LRFD* include both horizontal and vertical earth pressure, earth pressure surcharge and downdrag on piles and shafts. These loads are not discussed in this section, as they rarely, if ever, influence the design of a bridge superstructure.

1.3.2.1.1 Component Dead Loads

Component dead loads for composite steel-girder design are typically divided into two categories, labeled DC_1 and DC_2. DC_1 loads are considered to be the component dead loads acting on the non-composite section. Typical inclusions in DC_1 are the self-weight of girders, details, deck and deck haunches, stay-in-place forms and cross-frames/diaphragms. DC_2 loads are considered to be the component dead loads acting on the composite section. Raised sidewalks, roadway barriers, railings, lighting structures, sound walls and other attachments to the composite structure are examples of DC_2 loads.

Since DC_1 represents permanent component loads that are applied before the concrete deck has hardened, they are assumed carried by the steel section alone.

Since DC_2 represents permanent component loads that are applied after the concrete deck has hardened, they are assumed carried by the long-term ($3n$) composite section to account for creep effects. Both DC_1 and DC_2 loads are considered as one load type, DC, for purposes of determining the load factor to apply to the force effects in the various load combinations.

Force effects at the service limit state due to DC loads are assigned a load factor of 1.0. DC load factors at the strength and extreme event limit states can vary between 0.90 and 1.50 depending on the effect and load combination being examined. Dead loads are typically not considered in the fatigue limit state evaluation.

Typically, component dead loads are expressed in kips per cubic foot, and the geometric properties of the various bridge components are used to calculate the expected gravitational effects to be used as component dead loads. The Design Engineer is encouraged to investigate local conditions, specific bridge construction specifications or methods, and advances in materials technology to obtain the most appropriate unit weight for determination of permanent component dead loads. *AASHTO LRFD* provides some guidance for typical unit weights in Table 3.5.1-1 in the absence of more precise information. An excerpt of that table for some of the most common structural materials is presented in Table 1.3.1.

Table 1.3.1 Unit Weights of Typical Components

Material		Unit Weight (kcf)
Concrete	Lightweight	0.110
	Sand-lightweight	0.120
	Normal weight with $f'_c \le 5.0$ ksi	0.145
	Normal weight with $5.0 < f'_c \le 15.0$ ksi	$0.140 + 0.001f'_c$
Steel		0.490
Wood	Hard	0.060
	Soft	0.050

(from *AASHTO LRFD* Table 3.5.1-1)

Note that the unit weight of reinforced concrete is generally taken as 0.005 kcf greater than the weight of plain concrete to account for the weight of the reinforcement.

1.3.2.1.2 Wearing Surface and Utility Loads

Non-integral wearing surfaces and utility loads are considered semi-permanent loads and are grouped within the DW load type. Wearing surfaces can be those applied at initial construction or anticipated future wearing surfaces for maintenance of the bridge. Utility loads include the weight of conduits and attachments for not only bridge components but also those using the bridge as a method of crossing. These loads are slightly more variable than those for component dead loads. The wearing

surface that is used in the future may be heavier or lighter than anticipated, depending on advances in technology and common practice by the time a resurfacing is needed. Utilities may also be added or removed, and the weight of conduits and connectors in the future may change. To reflect this variability, at the strength and extreme event limit states, the load factors assigned to the force effects due to non-integral wearing surface and utility loads range from 0.65 for minimum effects to 1.50 for maximum effects. At the service limit states, the force effects due to DW loads are assigned a load factor of 1.0.

1.3.2.2 Construction Loads

Construction loads are permanent loads and other loads that act on the structure only during construction and are removed after the structure opens for service. Construction loads include the weight of equipment such as deck finishing machines, the deck overhang loads or loads applied to the structure through falsework or other temporary supports. Construction dead loads are to be considered as part of the permanent load and construction transient loads are to be considered as part of the live load. Often the construction loads are not accurately known at design time. The Design Engineer should consider talking to local contractors to obtain reasonable estimates of these construction loads, as necessary, and note the magnitude and location of the loads considered in the design on the Plans.

General load factors for these construction loads are described in *AASHTO LRFD* Article 3.4.2. Force effects due to the weight of the structure and appurtenances, or the DC and DW loads as described above, are to be assigned a load factor of 1.25 or greater when investigating the Strength I, III and V load combinations during construction. The load factor applied to the force effects due to the construction loads and any associated dynamic effects is not to be taken less than 1.5 when investigating the Strength I load combination, unless specified otherwise by the Owner.

Wind forces can greatly affect a steel bridge under construction, as the surfaces that wind can affect are greater and more random. However, for the temporary construction condition, the probability of experiencing the full design horizontal wind pressure associated with the maximum base wind velocity is reduced. Hence, when investigating the Strength III load combination (i.e. dead plus wind load with no live load on the structure) during construction, the load factor to be applied to the force effects due to wind on the structure, WS, is to be reduced from 1.4 to not less than 1.25 according to *AASHTO LRFD* Article 3.4.2. .

When the evaluation of construction deflections is required by the contract documents, the Service I load combination is to apply in the absence of any special provisions to the contrary.

Further construction load provisions in *AASHTO LRFD* call for stay-in-place formwork for concrete structure elements to be designed for construction loads.

1.3.2.3 Live Loads

In addition to dead loads, which are continually acting on a bridge, and construction loads, which act on a bridge only during its construction, a bridge must also be designed to resist live loads. The primary difference between dead loads and live loads is that dead loads are permanent but live loads are transient. That is, dead loads act on the bridge at all times, but live loads are not necessarily present at all times. In addition, dead loads are stationary loads, but live loads are moving loads. Two common forms of live loads are vehicular loads and pedestrian loads.

1.3.2.3.1 Design Vehicular Loads

Vehicles crossing a bridge come in various shapes, sizes and weights, such as cars, motorcycles, tractors, buses and trucks. A bridge must be designed to resist all of the live loads that may legally pass across the bridge. However, the vehicles that most significantly affect a bridge are trucks. When compared with the effects of trucks on a bridge, the effects of cars and other vehicles are negligible. Therefore, the vehicular live loads used to design a bridge are based on truck loads.

There are many different types of trucks acting on our bridges today. Trucks come in many different configurations, varying in the following ways:

- Number of axles
- Spacing of axles
- Weight on each axle
- Total truck length
- Total truck weight

Since today's bridges must be able to resist a wide variety of trucks, bridges must be designed to resist all of those trucks. However, for the bridge engineer to consider every possible truck configuration that may act on a bridge would be excessively time consuming and unfeasible. Therefore, the specification writers have developed what is called a notional vehicular load. A notional vehicular load is a theoretical or imaginary load that does not actually exist but is felt to conservatively envelope the load affects of vehicles that may legally act on the bridge. The design vehicular live loads currently specified by *AASHTO* are notional vehicular loads.

Special live loads are specified for checking fatigue, and optionally, live load deflections. Some Owners also require consideration of special design permit loads acting either alone or in combination with the design vehicular live load. These loads are also discussed in more detail below.

The design vehicular load currently used by AASHTO is designated as HL-93, in which "HL" is an abbreviation for highway loading and "93" represents the year of 1993 in which the loading was accepted by AASHTO. The HL-93 live load is based on a 1990 study by the Transportation Research Board (TRB), and it consists of three different load types:

- Design truck (*AASHTO LRFD* Article 3.6.1.2.2)
- Design tandem (*AASHTO LRFD* Article 3.6.1.2.3)
- Design lane (*AASHTO LRFD* Article 3.6.1.2.4)

The following describes how these three different load types are configured in the longitudinal direction, how they are configured in the transverse direction, and how they are combined to form the HL-93 loading.

In the longitudinal direction, the design truck has three axles. The first axle has a specified weight of 8 kips, and the second and third axles have specified weights of 32 kips each. The spacing between the first and second axles is 14 feet, but the spacing between the second and third axles varies between 14 and 30 feet. The axle spacing is selected such that the maximum effect is achieved. The minimum axle spacing of 14 feet usually controls. However, a situation in which an axle spacing greater than 14 feet may control is for a continuous short-span bridge in which the maximum negative moment at the pier is being computed and the second and third axles are positioned in different spans. The design truck is illustrated in Figure 1.3.1.

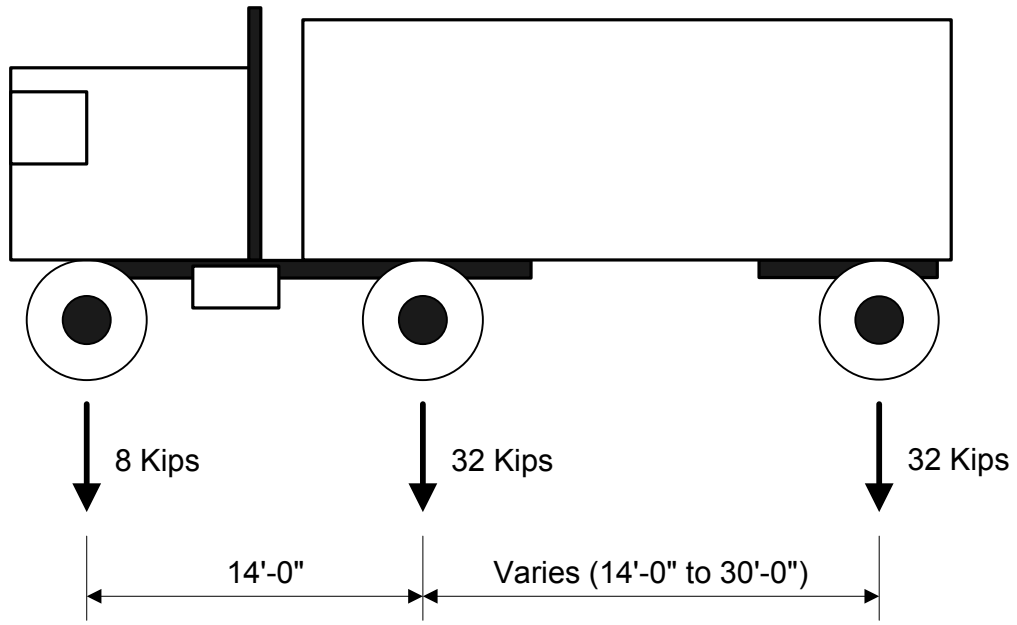


Figure 1.3.1 Design Truck

The design tandem has two axles, each weighing 25 kips. The axle spacing for the design tandem is 4 feet. The design tandem is illustrated in Figure 1.3.2.

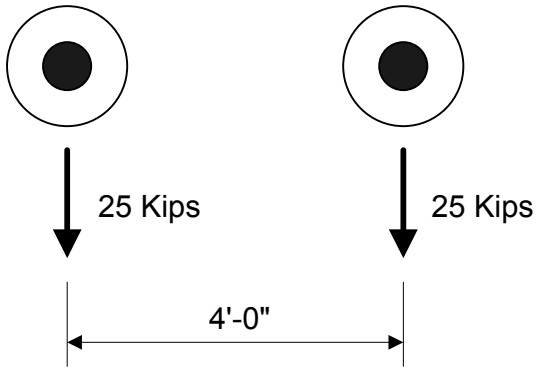


Figure 1.3.2 Design Tandem

The design lane consists of a uniform load of 0.64 kips per linear foot, distributed in the longitudinal direction and is intended to represent a train of trucks. Lengths of design lanes, or parts of design lanes, that contribute to the extreme force effects under consideration are to be loaded with the design lane load. The design lane is illustrated in Figure 1.3.3.

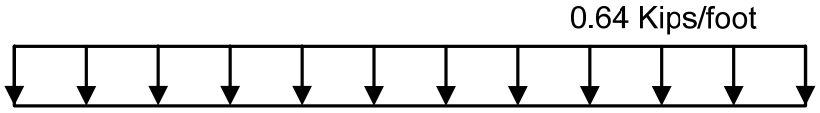
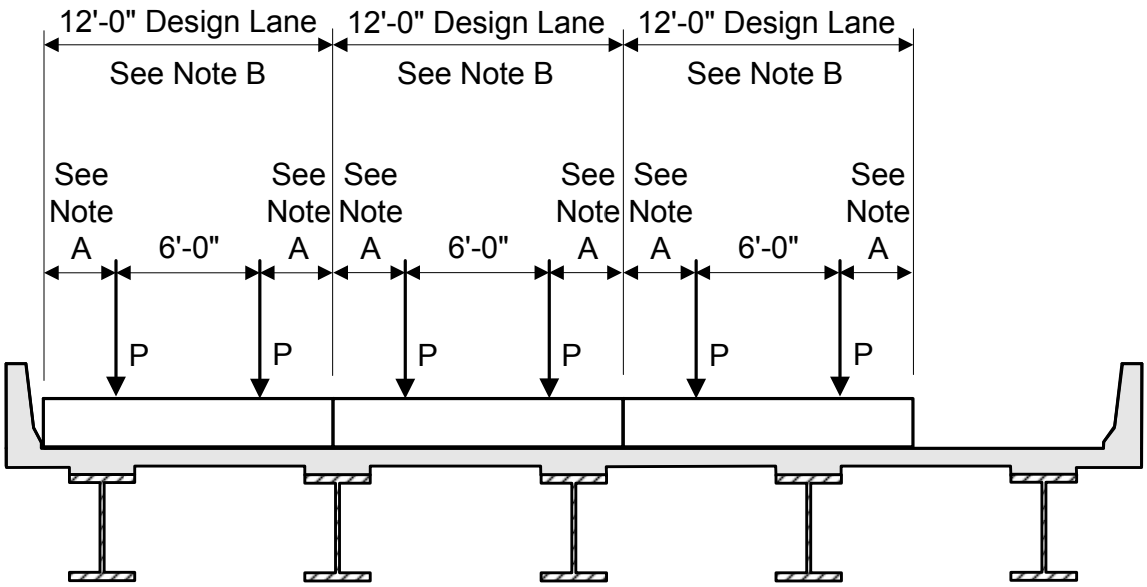


Figure 1.3.3 Design Lane

The design truck and design tandem each have a wheel spacing of 6 feet in the transverse direction and should be located in such a way that the effect being considered is maximized. However, the center of any wheel load must not be closer than 2 feet from the edge of the design lane or from the face of a curb or railing. (The single exception is for the design of the deck overhang in which case the center of the wheel load can be as close as 1 foot from the face of the curb or railing - *AASHTO LRFD* Article 3.6.1.3.1.) The transverse live load configuration for a design truck or design tandem is illustrated in Figure 1.3.4.



P = Wheel Load

Note A: Position wheel loads within the design lane such that the effect being considered is maximized; minimum = 2'-0" (for design of deck overhang, minimum = 1'-0").

Note B: Position design lanes across the roadway such that the effect being considered is maximized.

Figure 1.3.4 Transverse Configuration for a Design Truck or Design Tandem

Similarly, the design lane is distributed uniformly over the 10-foot loaded width, which must be located in its entirety within the 12-foot design lane. Since the design lane is 0.64 kips per linear foot in the longitudinal direction and it acts over a 10-foot width, the design lane load is equivalent to 64 pounds per square foot. Live load placement is discussed further in Section 2.1.4.1.

The HL-93 loading consists of various combinations of the design truck, design tandem and design lane. Specifically, the force effects due to the HL-93 loading are to be taken as the maximum of the force effects resulting from the following two conditions:

- The effect of the design tandem plus the design lane (see Figure 1.3.5)
- The effect of the design truck plus the design lane (see Figure 1.3.6)

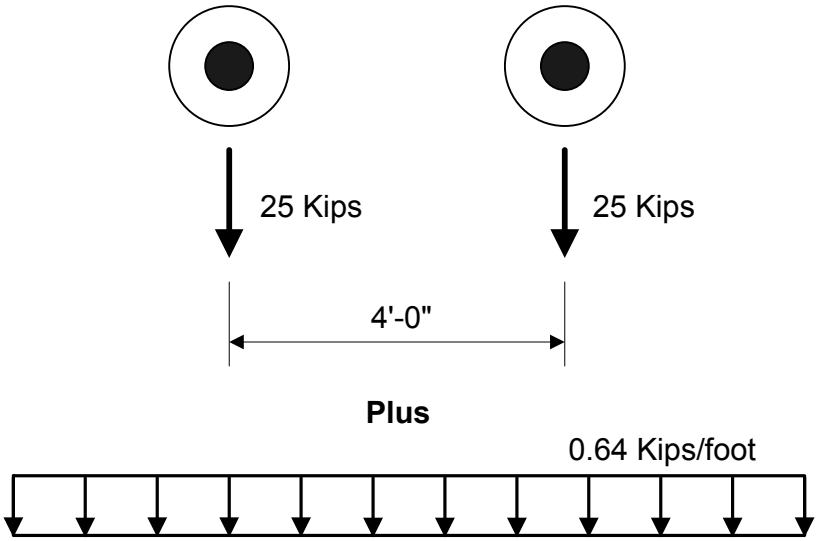


Figure 1.3.5 Design Tandem Plus Design Lane

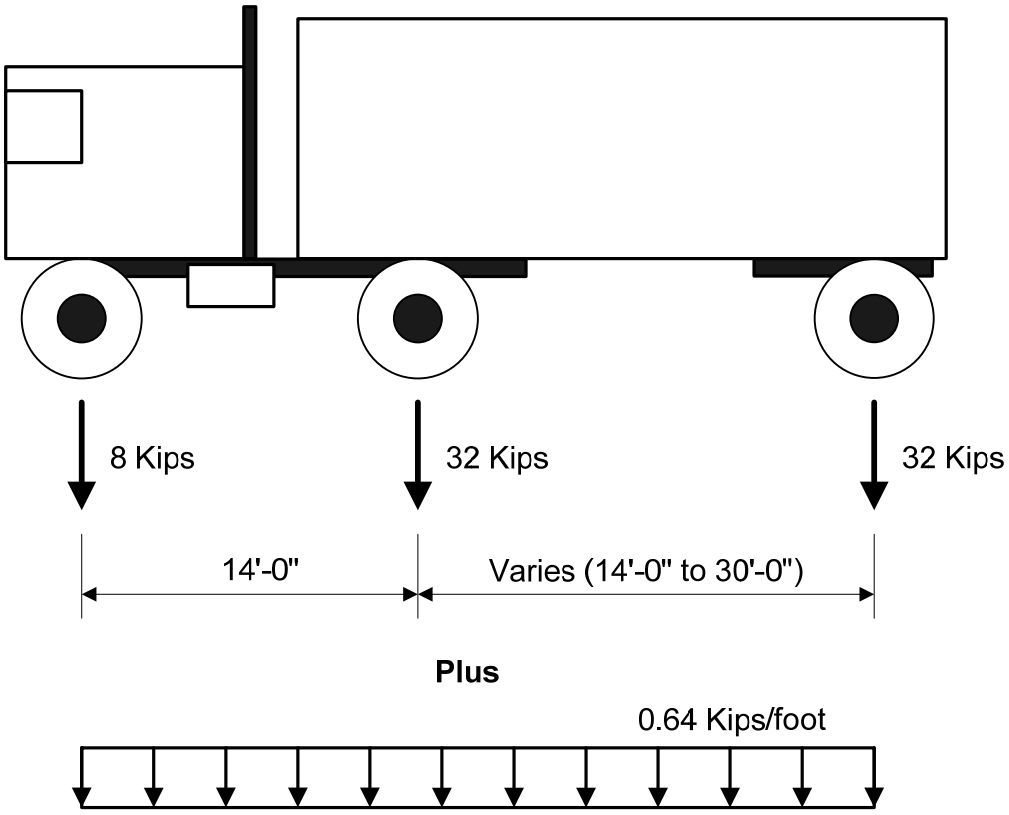


Figure 1.3.6 Design Truck Plus Design Lane

In addition, for negative moment and reaction at interior piers, a third condition is also considered (*AASHTO LRFD* Article 3.6.1.3.1). A second truck is added with a minimum headway between the front and rear axles of the two trucks equal to 50 feet (a larger headway may be used to obtain the maximum effect). The rear axle spacing of the two trucks is set at a constant 14 feet, and all loads are reduced by 10 percent. The two design trucks must be placed in adjacent spans (Figure 1.3.7).
The live load negative moments between points of permanent-load contraflexure are taken as the larger of the moments caused by the HL-93 loading or this special negative-moment loading. The specification is currently silent regarding spans without points of permanent-load contraflexure. Presumably, the special negative-moment loading should be considered over the entire span in such cases.

Live load shear in regions of positive and negative flexure are to be computed using the HL-93 loading only. However, interior-pier reactions are to be calculated based on the larger of the shears caused by the HL-93 loading or the special negative-moment loading.

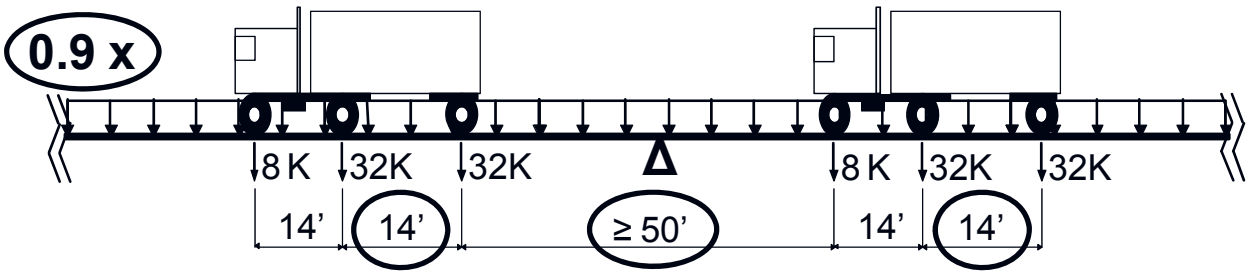


Figure 1.3.7 Special Loading for Negative Moment & Interior-Pier Reactions

In all cases, axles that do not contribute to the extreme force effects under consideration are to be neglected.

For strength and service limit state checks, a 33 percent dynamic load allowance (or impact) factor is applied to the force effects due only to the design truck or design tandem portion of the HL-93 design live load or to the truck portion of the special negative-moment loading (*AASHTO LRFD* Article 3.6.2). The dynamic load allowance is not to be applied to the design lane load in any case. As a result, the dynamic load allowance implicitly remains a function of the span length, although the span length is not explicitly used to compute the allowance (the dynamic load allowance is discussed further in Section 1.3.2.3.8).

The design truck and the design lane are similar to those used in the AASHTO *Standard Specifications for Highway Bridges*, which preceded the *AASHTO LRFD Bridge Design Specifications*. However, in the *AASHTO* Standard Specifications, the design truck and design lane were considered separately and were not combined, whereas they are combined to form the HL-93 live load in the *AASHTO LRFD* Specifications.

The specified load factor applied to the design vehicular live load force effects is 1.75 in the Strength I load combination. This factor is reduced to 1.35 in the Strength V load combination where vehicular live load force effects are considered in combination with those due to wind loads with an assumed velocity of 55 mph. Load factors of 1.0 and 1.3 are applied to the design vehicular live load force effects in the Service I and Service II load combinations, respectively.

1.3.2.3.2 Permit Loads

In addition to design vehicular loads, special design permit loads may also be specified by the Owner for consideration. The configuration, size and weight of design permit vehicles vary from state to state. Likewise, the manner in which permit loads are considered during design also varies from state to state. Therefore, permit loads should be considered during design only as specified by the Owner.

The Owner may specify that the permit load be examined in a single lane or in two adjacent lanes by itself, in all design lanes by itself, and/or in one lane in combination with the design vehicular load in all remaining lanes. Two or more lanes of design permit loads should only be considered on heavy permit routes. The design permit loads should be assumed acting in combination with the HL-93 design lane load discussed previously. For negative moments and interior-pier reactions, a second design permit load should be considered in the same lane, acting in conjunction with 90 percent of the design lane load, with a minimum headway of 50 feet between the front and rear axles of the two permit loads.

Refined analysis approaches are most effectively utilized to investigate the effect of the design permit loads on skewed and curved bridges, particularly for the condition of mixed traffic. *AASHTO LRFD* Article 4.6.2.2.5 provides an approximate approach for such cases that may be used to determine the design force effect per girder from the mixed traffic when distribution factor formulas are used. The use of this approximate approach is not recommended for skewed and curved bridges; refined analysis methods should be employed instead. Recommendations related to the application of multiple presence factors and the dynamic load allowance to the effects of design permit loads determined from refined analysis methods are discussed further in Section 2.1.4.3.

Permit loads are considered in the Strength II Load Combination, with a load factor of 1.35 applied to all live load force effects, including the force effects due to any design vehicular loads that may be applied in combination with the design permit load. This load combination relates to the use of the bridge by Owner-specified special design vehicles, evaluation permit vehicles or both. However, wind is not considered for the Strength II Load Combination. When evaluating the Strength II Load Combination, the permit vehicle should not be assumed to be the only vehicle on the bridge unless such a configuration is assured by traffic control.

.

1.3.2.3.3 Fatigue Load

In addition to the live loadings described above, a fatigue live load must also be considered (*AASHTO LRFD* Article 3.6.1.4.1). Fatigue is defined as the initiation and/or propagation of cracks due to a repeated variation of normal stress with a tensile component. When the load is cyclic, the stress level that leads to initiation and/or propagation of cracks can be significantly less than the material yield stress. The effects of fatigue are based on the following considerations:

- The type and quality of the structural detail
- The magnitude of the stress range
- The number of applications (or cycles) of this stress range

The vehicular live load for checking fatigue in the *AASHTO LRFD* specifications consists of the design truck (without the lane load) with the following adjustments:

- The axle spacing between the two 32-kip axles is a constant 30 feet.
- The fatigue truck is placed in only one lane.

The fatigue load is illustrated in Figure 1.3.8.

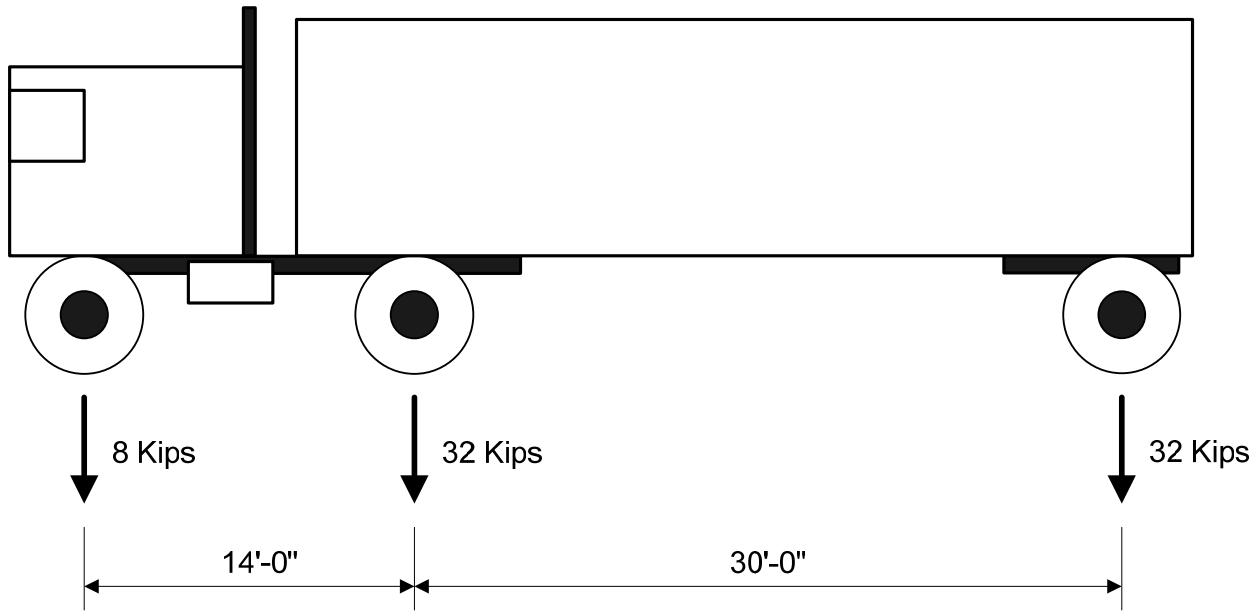


Figure 1.3.8 Fatigue Load

The fatigue load is used to represent the variety of trucks of different types and weights in actual traffic. The constant rear-axle spacing approximates that for the 4- and 5-axle semi-trailers that are the most frequent truck loading and do the most fatigue damage. A reduced dynamic load allowance (discussed further in Section 1.3.2.3.8) of 15 percent is to be applied to the fatigue load (*AASHTO LRFD* Article 3.6.2).

In addition to the actual loading, the number of cycles also influences the fatigue design of a bridge. In the absence of more accurate traffic data, the average daily truck traffic for a single lane averaged over the design life, $(ADTT)_{SL}$, may be computed as follows (*AASHTO LRFD* Article 3.6.1.4.2):

$$ADTT_{SL} = p(ADTT)$$

Equation 1.3.1
AASHTO LRFD Equation 3.6.1.4.2-1

where:

$ADTT_{SL}$ = number of trucks per day in a single lane averaged over the design life
p = fraction of truck traffic in a single lane (Table 1.3.2)
ADTT = number of trucks per day in one direction averaged over the design life

Table 1.3.2 Fraction of Truck Traffic in a Single Lane, *p*
(Based on *AASHTO LRFD* Table 3.6.1.4.2-1)

Number of Lanes Available to Trucks	p
1	1.00
2	0.85
3 or more	0.80

The single-lane *ADTT* is that for the traffic lane in which the majority of the truck traffic crosses the bridge, which is typically the shoulder lane.

ADTT is the number of trucks per day in one direction averaged over the design life. The design life, as presented in *AASHTO LRFD*, is 75 years. In the above equation, the *ADTT* can usually be obtained from the bridge owner. If *ADTT* data is not available, then the *ADTT* can be estimated based on the average daily traffic (*ADT*) and the percentage of truck traffic to total traffic. This percentage can vary widely, depending on the type of roadway crossing the bridge and the location of the bridge, but if more accurate data is not available, the percentages presented in Table 1.3.3 can be used. The *ADTT* can be estimated by multiplying the ADT times the percentage presented in Table 1.3.3.

Table 1.3.3 Percentage of Trucks in Traffic
(Based on *AASHTO LRFD* Table C3.6.1.4.2-1)

Class of Highway	Percentage of Trucks in Traffic
Rural Interstate	20%
Urban Interstate	15%
Other Rural	15%
Other Urban	10%

AASHTO LRFD Article C3.6.1.4.2 suggests taking the *ADTT* as 55 percent of the bi-directional *ADTT* in the absence of data on directionality of truck traffic.

Traffic growth data are usually not predicted for a 75-year design life. Techniques exist to extrapolate available data such as curve fitting growth rate versus time and using extreme value distributions, but some judgment is obviously required in extrapolating the data. *ADTT* values are best determined in consultation with traffic engineers.

The fraction of truck traffic in a single lane, *p*, given in Table 1.3.2 is a function of the number of lanes available to trucks. The probability that all lanes will contain only truck traffic decreases as the number of lanes available to trucks increases. The fraction is assumed to apply to all design lanes on the bridge since future traffic patterns on the bridge are uncertain.

It should be noted that the number of stress cycles does not affect the fatigue load but rather the fatigue resistance.

The *AASHTO* fatigue-design procedures in the Standard Specifications are believed to not accurately reflect actual fatigue loading; these procedures combine an artificially high fatigue stress range with an artificially low number of stress cycles. The specified fatigue load in the *AASHTO LRFD* specifications produces a lower calculated stress range than produced by the loadings in the Standard Specifications. This reduction in calculated stress range is offset by an increase in the number of cycles of loading to be considered. The lower stress range and the increased number of cycles are believed to be more reflective of actual conditions experienced by many bridges.

There are two Fatigue load combinations specified in the *AASHTO LRFD* specifications. The load factor of 1.5 specified for the Fatigue I load combination and applied to the force effects resulting from the single design truck is felt to reflect load levels found to be representative of the maximum stress range of the truck population for infinite fatigue life design. The factor of 1.5 was based on the assumption that the maximum stress range in the random variable spectrum of loading is twice the effective stress range caused by the Fatigue II load combination. The load factor of 0.75 specified for the Fatigue II load combination and applied to the force effects resulting from the single design truck is felt to reflect a load level found to be representative of the effective stress range of the truck population with respect to a small number of stress range cycles and to their cumulative effects for finite fatigue life design. The 75-year $(ADTT)_{SL}$ dictates whether the component or detail under consideration is to be designed for finite life using the Fatigue II load combination or for infinite life using the Fatigue I load combination (*AASHTO LRFD* Table 6.6.1.2.3-2). Fatigue limit state design verifications are discussed in more detail in Section 3.2.5

1.3.2.3.4 Load for Live Load Deflection Evaluation

In *AASHTO LRFD* Article 2.5.2.6.2, optional criteria for live load deflection are provided. These optional criteria permit, but do not require or encourage, the use of past practice for deflection control. The live load deflection criteria are discussed in more detail in Section 3.2.4.2.1.

If the Owner chooses to use the optional criteria for live load deflection, *AASHTO LRFD* Article 3.6.1.3.2 specifies that the deflection should be computed as the larger of the following:

- Live load deflection resulting from the design truck alone.
- Live load deflection resulting from 25 percent of the design truck taken together with the design lane load.

The dynamic load allowance of 33 percent (discussed in Section 1.3.2.3.8) is applied to the design truck only in each case. A load factor of 1.0 is applied to the live load. All design lanes are to be loaded and the multiple presence factor, as defined in *AASHTO LRFD* Article 3.6.1.1.2 and also discussed further in Section 1.3.2.3.7, should be applied.

Live load deflection is a service issue rather than a strength issue. Past experience with bridges designed using the previous AASHTO *Standard Specifications for Highway Bridges* reveals no adverse effects due to excessive live load deflection. Therefore, *AASHTO LRFD* bases the loads for live load deflection on the previous live load rather than on the heavier design live load required for LRFD strength design. The intent of the specified load is to produce live load deflections similar to those produced by the HS20 offloading in the previous *Standard Specifications*. It was decided by the specification writers that it was unnecessary to check live load deflections for the heavier HL-93 design live load used for strength checks. The HL-93 design truck has the same weight as an HS20 truck. The HL-93 design lane load also has the same weight as that specified for HS20. The use of 25 percent of the design truck (0.25 * 72 kips = 18 kips) is similar to the HS20 single concentrated load of 18 kips used in combination with the HS20 lane load for determining bending moments and deflections in longer spans. Of course, the resulting deflections are less than those computed for HS25; hence, the *AASHTO LRFD* live load for deflection is more lenient in this case.

When investigating the deflection for straight-girder systems with little or no skew, all supporting components may be assumed to deflect equally. However, this assumption of equal deflections is not applicable for horizontally curved bridges. For curved-girder systems, the deflection of each girder must be determined individually based on its response as part of a system. Curvature causes each girder to deflect differently than the adjacent girder so that an average deflection has little relevance. For severely skewed bridges, the average deflection also has little meaning due to the differential deflections that occur between girders. Thus, the assumption of equal deflections should also not be considered applicable to severely skewed bridges (i.e. with skew angles greater than 20 degrees from normal).

1.3.2.3.5 Pedestrian Live Load

Pedestrian live load is a uniform load applied to sidewalks and to pedestrian bridges (*AASHTO LRFD* Article 3.6.1.6). Pedestrian live load can be particularly critical for curved bridges when the sidewalk is located on the outside of the curve.

For bridges designed for both vehicular and pedestrian live load and with a sidewalk width exceeding 2 feet, a pedestrian load of 75 pounds per square foot is specified. However, for bridges designed exclusively for pedestrian and/or bicycle traffic, a live load of 85 pounds per square foot is to be applied. Bridges intended for only pedestrian and/or bicycle use should be designed according to the *AASHTO Guide Specifications for the Design of Pedestrian Bridges*.

The actual magnitude of pedestrian load is highly unpredictable, which increases in significance for bridges in which pedestrian load is the only live load. Therefore, for bridges designed exclusively for pedestrian and/or bicycle traffic, AASHTO specifies a greater pedestrian load than for bridges with both vehicular and pedestrian load.

Where vehicles can mount the sidewalk, sidewalk pedestrian load is not to be considered concurrently. If the sidewalk could potentially be removed in the future, the design vehicular live load must be applied 2 feet from the edge of the deck (1 foot from the edge of the deck for the design of the deck overhang).

AASHTO LRFD Article 3.6.1.1.2 specifies that for the purposes of determining the number of loaded lanes, the pedestrian live loads are to be taken as one loaded lane. The multiple presence factor of 1.2 for a single lane (Section 1.3.2.3.7) is not to be applied to pedestrian loads. A multiple presence factor of 1.0 is to be applied to the case of pedestrian live load without vehicular live load. Dynamic load allowance is not to be applied to the force effects due to pedestrian live load. The load factor to be applied to the force effects due to the pedestrian live load in the various strength and service limit state load combinations is the same as for the design vehicular live load.

1.3.2.3.6 Vehicular Centrifugal Force

Vehicular centrifugal force is defined as a lateral force resulting from a change in the direction of a vehicle's movement (*AASHTO LRFD* Article 3.6.3).

Centrifugal forces are to be applied horizontally at a distance 6.0 feet above the roadway surface. A load path to carry the radial forces to the substructure must be provided.

Centrifugal force is applied to the design truck or tandem and to the fatigue live load. However, centrifugal force is not required to be applied to the design lane load, since the spacing of the vehicles in the design lane load at high speed is assumed to be large resulting in a low density of vehicles preceding and/or following the design

truck or tandem. At the strength and service limit states, the design lane load is still considered even though centrifugal force effects are not applied. Permit loads may also not be expected to reach design speeds, so centrifugal force effects may not need to be considered for these loads, at the Owner's discretion.

Force effects from the analysis due to cases with centrifugal force effects included should be compared to effects due to cases with no centrifugal force effects included, and the worst case selected.

Vehicular centrifugal force is computed using the following equation:

$$C = f\frac{v^2}{gR}$$

Equation 1.3.2
AASHTO LRFD Equation 3.6.3-1

where:

f = 4/3 for load combinations other than fatigue, and 1.0 for fatigue
v = highway design speed in ft/sec (1.0 ft/sec = 0.682 mph)
g = gravitational acceleration (= 32.2 ft/sec^2)
R = radius of curvature of traffic lane in feet

The factor, *C*, is multiplied by the total of the axle weights of the design truck or tandem, or the fatigue live load, as applicable.

The HL-93 design vehicular live load specified as a combination of the design truck and lane load represents a group of exclusion vehicles that produce force effects of at least 4/3 of those caused by the design truck alone on short-span or medium-span bridges. Therefore, this ratio is introduced in the *AASHTO LRFD* specifications at the strength and service limit states through the use of the factor, *f*, in the equation for *C*. The factor, *f*, is set to 1.0 at the fatigue limit state, consistent with cumulative damage analysis.

The highway design speed, *v*, is to be taken not less than the value specified in the most current edition of the AASHTO publication, *A Policy of Geometric Design of Highways and Streets*.

Centrifugal force causes an overturning effect on the wheel loads because the radial force is applied 6.0 feet above the top of the deck. Therefore, the centrifugal force tends to increase the vertical wheel loads toward the outside of the bridge and decrease the wheel loads toward the inside of the bridge. The net result is that the outermost girder will receive slightly greater load and the innermost girder will receive slightly less load. This is illustrated in Figure 1.3.9.

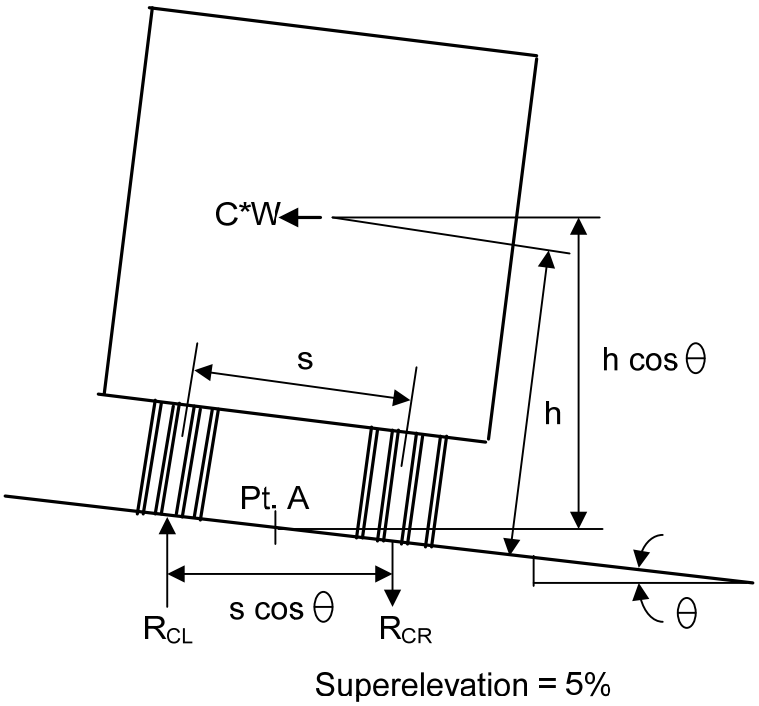


Figure 1.3.9 Vehicular Centrifugal Force Wheel-Load Reactions

The wheel-load reactions, R_{CL} and R_{CR}, due to centrifugal force are computed by summing moments about Point A, as follows:

$$R_{CL} = -R_{CR} = (C * W)\frac{h\cos\theta}{2\left[\frac{s}{2}\cos\theta\right]}$$

Equation 1.3.3

where W is equal to the axle weight. Whenever the wheel spacing, s, is equal to the height at which the radial force is applied above the deck, h (which is typically the case), the equal and opposite wheel-load reactions, R_{CL} and $-R_{CR}$, are simply equal to C multiplied by W. That is, the superelevation has no effect.

However, superelevation helps to balance the effects of the overturning moment due to the centrifugal force. *AASHTO LRFD* Article 3.6.3 permits this beneficial effect to be considered in the computation of the wheel-load reactions due to centrifugal force, as shown in Figure 1.3.10.

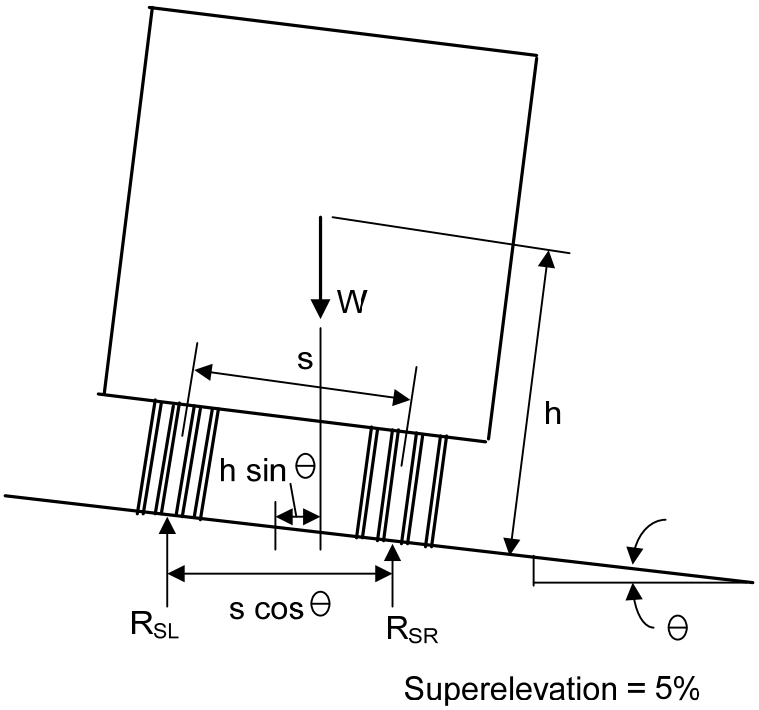


Figure 1.3.10 Effects of Superelevation on Wheel-Load Reactions

The wheel-load reactions, R_{SL} and R_{SR}, due to superelevation are computed by summing moments about the left wheel, as follows:

$$R_{SR} = \frac{\left[\frac{s}{2}\cos\theta + h\sin\theta\right] * W}{s\cos\theta}$$

Equation 1.3.4

$$R_{SL} = 1.0W - R_{SR}$$

Equation 1.3.5

If the superelevation is significant, the Design Engineer may wish to consider its effect for the case with no centrifugal force effects included (that is, a stationary vehicle), since the superelevation will cause an increase in the vertical wheel loads toward the inside of the bridge and an unloading of the vertical wheel loads toward the outside of the bridge, which may potentially be a more critical case for the interior girders. However, since the vehicle is assumed to be stationary, the dynamic load allowance should not be included in this case.

For refined analyses, unit wheel-load factors can be computed based on the sum of the wheel-load reactions due to the centrifugal force and superelevation effects, as shown in Figure 1.3.11.

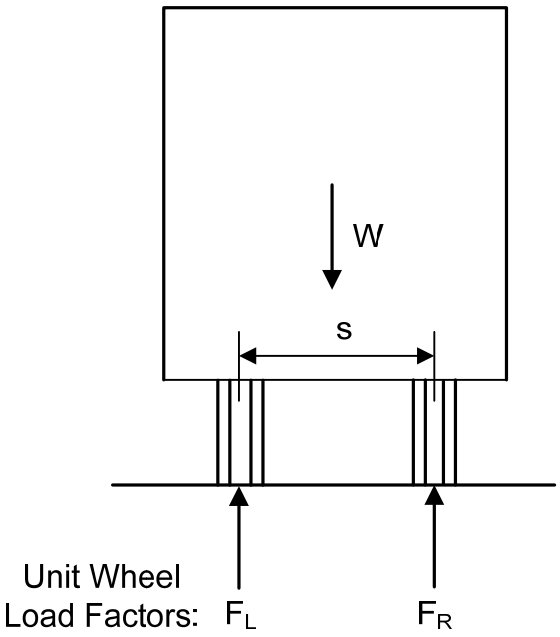


Figure 1.3.11 Unit Wheel Load Factors due to the Combined Effects of Centrifugal Force and Superelevation

The left and right unit wheel-load factors, F_L and F_R, are computed as follows:

$$F_L = 2.0\frac{R_{CL} + R_{SL}}{W}$$

Equation 1.3.6

$$F_R = 2.0\frac{R_{CR} + R_{SR}}{W}$$

Equation 1.3.7

The sum of F_L and F_R must equal 2.0. The factors can be used to increase and decrease accordingly the wheel loads that are applied in the analysis.

For approximate analyses in which a line girder methodology is used (e.g. the approximate V-load analysis method described in Section 2.3.2), it is recommended that a "pile-group analogy" be used to determine the vertical loads acting on each girder resulting from the overturning moment due to centrifugal force effects. The moment that can be balanced by any superelevation may be considered in this approach. This methodology is illustrated after the "Centrifugal Force Design Example," in the "Pile-group Analogy Design Example" given below.

The entire horizontal centrifugal force, *C*W*, is assumed carried to the bridge bearings though transverse bending of the deck slab and transverse shear in the support cross-frames. No particular account need be taken of the horizontal effect of centrifugal force on the bridge superstructure, except that the support cross-frame diagonals should be adequately proportioned to deliver the load to the bearings.

Dynamic load allowance is not to be applied to the force effects due to vehicular centrifugal force. The load factor to be applied to the force effects due to centrifugal force in the various strength, service and fatigue limit state load combinations is the same as for the design vehicular live load.

Centrifugal Force Design Example:

The example skewed and curved I-girder bridge in Section 5.1 has a horizontal curve with a radius of 700 feet along the centerline of the bridge. The highway design speed, *v*, is 35 mph, and the deck cross slope (superelevation) is 5%. Compute the unit wheel-load factors for the combined effects of centrifugal force and superelevation to apply in a refined analysis to determine the vehicular live load force effects at the strength and service limit states.

The first step in this design example is to compute the value of *C*, as follows (Equation 1.3.2):

$$C = f\frac{v^2}{gR} = \left(\frac{4}{3}\right)\frac{(35/0.682)^2}{(32.2)(700)} = 0.156$$

Note that to compute the unit wheel-load factors for determining the live load force effects considering the combined effects of centrifugal force and superelevation at the fatigue limit state, the 4/3 factor would be changed to 1.0 in the preceding equation. This results in a *C* value of 0.117.

The next step is to compute the wheel-load reactions, R_{CL} and R_{CR}, due to centrifugal force effects. Since the wheel spacing, *s*, and the height the radial force is applied above the deck, *h*, are both equal to 6.0 feet, the equal and opposite wheel-load reactions, R_{CL} and $-R_{CR}$, are simply equal to *C* multiplied by *W*, as illustrated below (Equation 1.3.3).

$$R_{CL} = -R_{CR} = (C * W)\frac{h\cos\theta}{2\left[\frac{s}{2}\cos\theta\right]} = C * W = 0.156W$$

This is an upward reaction for the left wheel and an equal and opposite downward reaction for the right wheel.

Next, the effect of superelevation on the individual wheel-load reactions is computed as follows (Equations 1.3.4 and 1.3.5):

$$\theta = \tan^{-1}(0.05) = 2.86^\circ$$

$$R_{SR} = \frac{\left[\frac{s}{2}\cos\theta + h\sin\theta\right] * W}{s\cos\theta} = \frac{\left[\left(\frac{6\text{ ft}}{2}\right)\cos(2.86^\circ) + (6\text{ ft})\sin(2.86^\circ)\right] * W}{(6\text{ ft})\cos(2.86^\circ)} = 0.550\,W$$

$$R_{SL} = 1.0\,W - R_{SR} = 1.0\,W - 0.550\,W = 0.450\,W$$

Unit wheel-load factors due to the combined effects of centrifugal force and superelevation are then computed as follows (Equations 1.3.6 and 1.3.7):

$$F_L = 2.0\frac{R_{CL} + R_{SL}}{W} = 2.0\frac{0.156\,W + 0.450\,W}{W} = 1.212$$

$$F_R = 2.0\frac{R_{CR} + R_{SR}}{W} = 2.0\frac{-0.156\,W + 0.550\,W}{W} = 0.788$$

F_L and F_R represent the factors that must be multiplied by the left wheel load and the right wheel load, respectively, in the analysis to take into account the combined effects of both centrifugal force and superelevation. F_L and F_R are unitless, and their sum is always equal to 2.0.

If no centrifugal force and no superelevation are present, then both F_L and F_R equal 1.0. That is, both the left wheel load and the right wheel load are simply 1.0 times the weight of the wheel. The sum of F_L and F_R is again 2.0.

Force effects from the analysis due to cases with centrifugal force effects included (i.e. utilizing unit wheel-load factors F_L equal to 1.212 and F_R equal to 0.788) are compared to force effects due to cases with no centrifugal force included (i.e. utilizing unit wheel-load factors F_L and F_R equal to 1.0), and the worst case is selected.

From separate computations similar to the above, the unit wheel-load factors, F_L and F_R, for the example bridge at the fatigue limit state (i.e. computed using a factor f equal to 1.0 in Equation 1.3.2) are 1.134 and 0.866, respectively.

Pile-group Analogy Design Example:

For the same example I-girder bridge, compute the vertical loads on the girders due to the overturning moment caused by centrifugal force and superelevation utilizing a pile-group analogy for application in an approximate V-load analysis. The computation will be done for the determination of the live load force effects at the strength and service limit states. The bridge cross-section is shown in Figure 1.3.12.

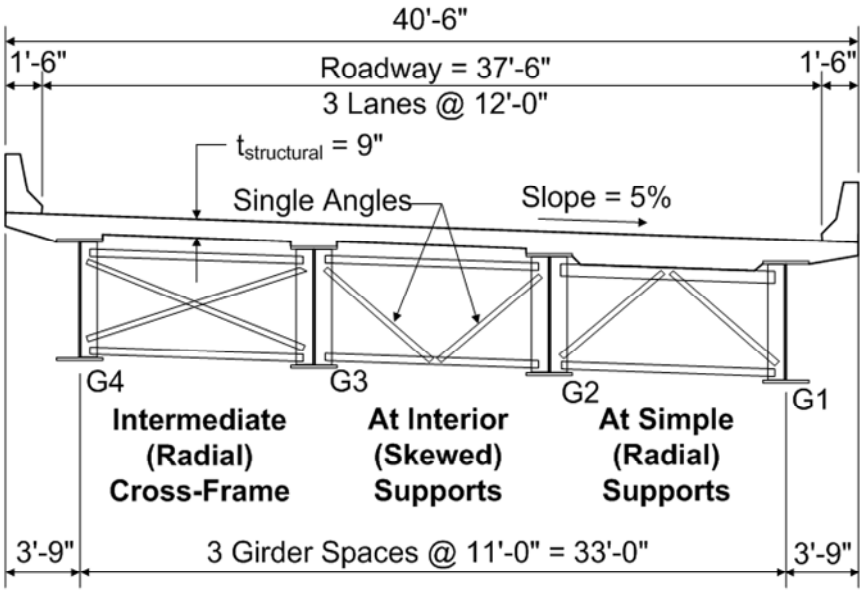


Figure 1.3.12 Example I-Girder Bridge Cross-Section

As previously computed, the value of *C* at the strength and service limit states is 15.6% (0.156*100). However, this value is balanced by the 5% superelevation, as follows:

$$C = C_{centrifugal\ force} - C_{superelevation} = 15.6\% - 5.0\% = 10.6\%$$

Thus, 10.6 percent of the centrifugal force remains to produce an overturning moment about the mid-depth of the slab. With three design lanes of live load permissible on the bridge, the centrifugal force in terms of lanes is computed as:

$$CF = (0.106)(3\ \text{lanes}) = 0.318\ \text{lanes}$$

A "pile-group analogy" can then be used to determine the vertical loads acting on each girder resulting from the overturning moment due to centrifugal force and superelevation effects. The "moment of inertia" of the four girders treated as piles is computed as follows:

$$I_{pile\ group} = 2\left\{[(0.5)(11.0\ \text{feet})]^2 + [(1.5)(11.0\ \text{feet})]^2\right\} = 605\ \text{feet}^2$$

The moment arm for the centrifugal force is computed from the location of the centrifugal force, 6.0 feet above the top of the deck, to the deck mid-depth, as follows:

$$\text{Moment arm} = \frac{6.0 \text{ feet}}{\cos(2.86^\circ)} + \frac{0.75 \text{ feet}}{2} = 6.38 \text{ feet}$$

The vertical load on the left exterior girder, G4, is then computed as follows, similar to the computation of a pile load in a pile group:

$$CF_{\text{Load on G4}} = \frac{(0.318 \text{ lanes})(6.38 \text{ feet})(1.5)(11.0 \text{ feet})}{605 \text{ feet}^2} = 0.055 \text{ lanes}$$

Similarly, the vertical load on the left interior girder, G3, is computed as follows:

$$CF_{\text{Load on G3}} = \frac{(0.318 \text{ lanes})(6.38 \text{ feet})(0.5)(11.0 \text{ feet})}{605 \text{ feet}^2} = 0.018 \text{ lanes}$$

The CF vertical loads on the two right girders, G1 and G2, can conservatively be assumed to be zero since the CF vertical loads would be upward and would be subtracted from all other vertical loads. This is equivalent to the case in which live load is present on the bridge but is not moving.

As discussed further in Section 2.3.2, in the V-load analysis approach, the V-Loads, which account for the effects of curvature, are a function of the summation of primary moments transversely across the structure at each cross-frame line. Since the CF loads act downward on G1 and G2 and upward on G3 and G4, the summation of moments is essentially zero and therefore the V-Loads due to CF are essentially zero. Thus, for the CF loading, only the primary moments need be determined, which can be done on an isolated straight girder basis by applying the above vertical loads to G3 and G4 with each girder isolated and straightened using developed span lengths equal to their respective arc lengths.

1.3.2.3.7 Multiple Presence of Live Load

For a bridge with several design lanes, it is unlikely that each lane will be simultaneously occupied by the full design live load. To account for this improbability, the *AASHTO LRFD* specification specifies multiple presence factors to be applied in certain situations described below (*AASHTO LRFD* Article 3.6.1.1.2). Where applicable, the factors are to be applied to the corresponding live load force effects determined from the analysis. The multiple presence factors are presented in Table 1.3.4.

Table 1.3.4 Multiple Presence Factors
(Based on *AASHTO LRFD* Table 3.6.1.1.2-1)

Number of Loaded Lanes	Multiple Presence Factor
1	1.20
2	1.00
3	0.85
>3	0.65

Since the probability that all lanes will be fully loaded decreases as the number of loaded lanes increases, the multiple presence factor decreases as the number of loaded lanes increases. The statistical calibration of LRFD is based on pairs of vehicles instead of a single vehicle; hence, a multiple presence factor of 1.0 is specified for the case of two lanes loaded. When a single vehicle is on the bridge, it can be heavier than a single pair of vehicles (in two adjacent lanes) and still have the same probability of occurrence. Hence, a multiple presence factor of 1.2 is specified for the case of one lane loaded.

It is important to note the applications for which multiple presence factors should and should not be used. Multiple presence factors should be applied in the following cases:

- For use with refined analysis methods
- For use with the lever rule
- For use whenever a sketch is required to compute the live load distribution
- For use with braking forces

However, multiple presence factors should not be applied in the following cases:

- For use with the approximate live load distribution factors presented in *AASHTO LRFD* Article 4.6.2.2
- For use at the fatigue limit state for which one design truck is used

The multiple presence factors have already been included in the approximate live load distribution factor equations presented in *AASHTO LRFD* Article 4.6.2.2.

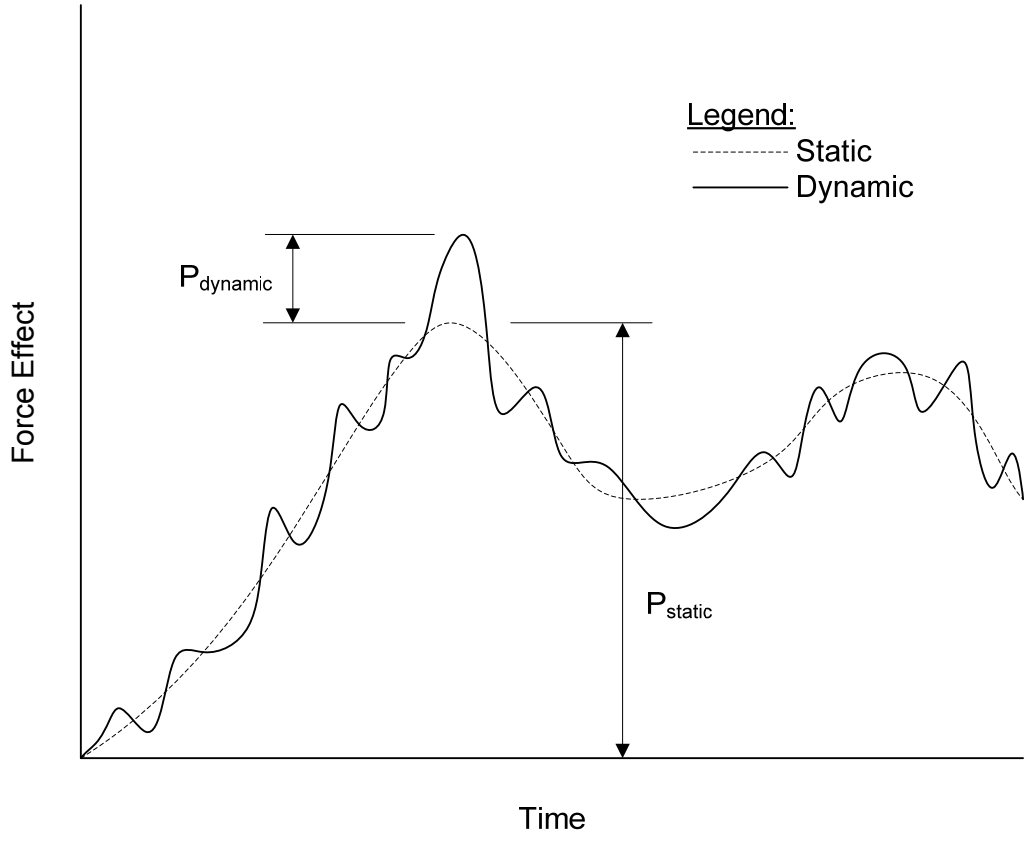
For the fatigue limit state, the factor of 1.2 has already been included in the approximate distribution factor equation for one-lane loaded and must be divided out for fatigue investigations. For other cases (e.g. the lever rule, refined analyses, etc.) involving fatigue investigations, the 1.2 factor should not be applied in determining the distribution factor or should not be applied to the force effects due to the fatigue load determined from the analysis, as applicable.

The application of these multiple presence factors to cases involving design permit loads for refined analyses is discussed further in Section 2.1.4.3.

1.3.2.3.8 Dynamic Load Allowance

The *AASHTO LRFD* vehicular live loads assume a static live load applied to the bridge. However, in reality, the live load is not static but is moving across the bridge. Since the roadway surface on a bridge is usually not perfectly smooth and the suspension systems of most trucks react to roadway roughness with oscillations, a dynamic load is applied to the bridge and must also be considered with the live load. In previous specifications, *AASHTO* referred to this dynamic effect as *impact*. In the *AASHTO LRFD* specification, this effect is referred to as the *dynamic load allowance*.

Dynamic load allowance is defined in *AASHTO LRFD* Article 3.2 as "an increase in the applied static force effects to account for the dynamic interaction between the bridge and moving vehicles." This additional dynamic force effect is illustrated in the generic live load response curve presented in Figure 1.3.13.



P_{static} = Maximum static force effect

$P_{dynamic}$ = Maximum additional dynamic force effect

Figure 1.3.13 Static and Dynamic Live Load Response

Referring to Figure 1.3.13, the dynamic load allowance is equal to:

$$IM = \frac{P_{dynamic}}{P_{static}}$$

Equation 1.3.8

To compute the total live load effect, including both static and dynamic effects, the following equation is used:

$$P_{LL+I} = P_{LL}(1 + IM)$$

Equation 1.3.9

where:

P_{LL+I} = force effect due to both live load and dynamic load allowance
P_{LL} = force effect due to live load only (without dynamic load allowance)
IM = dynamic load allowance (previously referred to as impact)

In previous specifications, *AASHTO* defined impact such that its value increased to a maximum value of 30% as the span length decreased. However, in the *AASHTO LRFD* Specifications, dynamic load allowance is no longer a function of span length, and its value depends only on the component and the limit state. *AASHTO* currently assigns values to dynamic load allowance as presented in Table 1.3.5 (*AASHTO LRFD* Article 3.6.2).

Table 1.3.5 Dynamic Load Allowance, IM
(Based on *AASHTO LRFD* Table 3.6.2.1-1)

Component	Limit State	Dynamic Load Allowance, IM
Deck Joints	All Limit States	75%
All Other Components	Fatigue and Fracture Limit States	15%
	All Other Limit States	33%

Deck joints have a greater dynamic load allowance because the hammering effect of the passing vehicles is more significant for deck joints than for other components, such as girders, beams, bearings and columns.

Dynamic load allowance should not be applied to the following loads:

- Vehicular centrifugal force
- Vehicular braking force
- Pedestrian live load
- Design lane load (dynamic load allowance is applied to the design truck and design tandem but not to the design lane load)

In addition, there are several bridge components for which dynamic load allowance should not be applied, including the following:

- Retaining walls not subject to vertical reactions from the superstructure
- Foundation components that are entirely below ground level
- Wood components
- Any other components identified by the specific agency governing the bridge design

1.3.2.4 Wind Loads

Wind loads represent the typical wind conditions of the local area where the bridge is being constructed. Only exposed surfaces are subject to direct application of wind loads, and different wind load cases exist for wind on structure, wind on live load, wind during construction and wind in the vertical direction. In general, smaller structures are typically not controlled by wind effects, but larger structures with more exposed surfaces can be controlled by wind load.

1.3.2.4.1 Horizontal Wind Pressure

Horizontal wind loads result from the pressure due to wind on both the superstructure and the live load. Wind load on the superstructure, WS, acts at the centroid of the exposed superstructure area, and wind load on the live load, WL, acts at a distance 6 feet above the roadway surface. The exposed superstructure area is the sum of the areas of all components as seen in elevation taken perpendicular to the assumed wind direction.

The base design wind velocity is specified in *AASHTO LRFD* Article 3.8.1.1 as 100 miles per hour. This represents a conservative estimate of the highest wind speeds that a structure will experience over the design life of the structure. The wind pressure from this horizontal wind is applied to all exposed surfaces when the structure is looked at in elevation, perpendicular to the direction of the wind.

For curved structures, the wind force equals the wind intensity times the projected (or planar) area of the bridge. Therefore, the total wind force on a curved bridge is less than that computed if the wind is assumed applied radially along the arc length.

All girders, decks, attachments and other structural components that are exposed in elevation are subject to the same uniform wind pressure. Superelevation and curvature may influence the exposed area and resulting wind pressure on individual curved girders, particularly when the base steel frame is examined for wind during construction. Any analysis of wind loads should include multiple attack angles to determine the wind direction causing the greatest force effect. Note that support cross-frame diagonals should be adequately proportioned to carry WS and WL to the bearings.

For bridges or parts of bridges over 30.0 feet above low ground or water level, the base wind velocity is modified using the following equation from *AASHTO LRFD* Article 3.8.1.1.

$$V_{DZ} = 2.5V_0\left(\frac{V_{30}}{V_B}\right)\ln\left(\frac{Z}{Z_0}\right)$$

Equation 1.3.10
AASHTO LRFD Equation 3.8.1.1-1

where:

V_{DZ}= design wind velocity at a design elevation, Z (mph)
V_0 = friction velocity, see Table 1.3.6
V_{30} = wind velocity at 30.0 feet above low ground or design water level (mph)
V_B = base wind velocity, 100 mph
Z = height of structure at which wind loads are being calculated > 30.0 feet
Z_0 = friction length, see Table 1.3.6

The values of V_0 and Z_0 are terms that are determined from meteorological effects based on the surrounding land conditions of the bridge. The descriptions of these land features are paraphrased from *ASCE 7-93* in *AASHTO LRFD* and are as follows:

- Open country – open terrain with only scattered obstructions with heights generally less than 30.0 feet. This category includes flat, open plains and grasslands.

- Suburban – urban and suburban areas, wooded areas or other terrain with many closely spaced obstructions with the size of a single-family dwelling, or larger. The suburban category shall only be used if the terrain type extends for 1,500 feet or greater in the prevailing upwind direction from the bridge structure.

- City – large city centers with at least half the buildings having a height in excess of 70.0 feet. The city category shall only be used if the terrain type extends for one half mile or greater in the prevailing upwind direction from the bridge structure. In addition to typical wind loads, possible channeling effects and increased wind velocities due to the bridge being located in the wake of larger structures should be considered in the analysis of wind loads.

Once the terrain type is determined, V_0 and Z_0 are selected from *AASHTO LRFD* Table 3.8.1.1-1, shown here as Table 1.3.6.

Table 1.3.6 Values of V_0 and Z_0 for Various Upstream Surface Conditions

Value	Condition		
	Open Country	Suburban	City
V_0 (mph)	8.20	10.90	12.00
Z_0 (feet)	0.23	3.28	8.20

The value of the V_{30} term may be established by the following criteria, as presented in *AASHTO LRFD* Article 3.8.1.1.

- Fastest-mile-of-wind charts available in *ASCE 7-88* for various recurrence intervals
- Site-specific wind surveys
- In the absence of better criterion, the assumption that $V_{30} = V_B = 100$ mph

Calculation of Design Wind Velocity Design Example:

For this example, assume a bridge structure 40.0 feet in height over the design water level. The structure is located in an area where wooded terrain prevails for at least two miles in all directions. From *ASCE 7-88*, the fastest-mile-of-wind is 115 mph for the area in which the bridge is located. Using Equation 1.3.10 as follows:

$$V_{DZ} = 2.5V_0\left(\frac{V_{30}}{V_B}\right)\ln\left(\frac{Z}{Z_0}\right)$$

$$V_{DZ} = 2.5(10.90)\left(\frac{115}{100}\right)\ln\left(\frac{40.0}{3.28}\right) = 78.4$$

Therefore, $V_{DZ} = 78.4$ mph.

1.3.2.4.1.1 Horizontal Wind Pressure on Structures

The load case for horizontal wind on structures, WS, is based on the design wind speed and given base wind pressures in the absence of more precise local information (*AASHTO LRFD* Article 3.8.1.2). The information on base pressures corresponding to the base design wind velocity of 100 mph shown in Table 1.3.7 is taken from *AASHTO LRFD* Table 3.8.1.2.1-1 and is used to determine the design horizontal wind pressure.

Table 1.3.7 Base Pressures, P_B, Corresponding to V_B = 100 mph

Superstructure Component	Windward Load, ksf	Leeward Load, ksf
Trusses, columns, and arches	0.050	0.025
Beams	0.050	N/A
Large flat surfaces	0.040	N/A

The design horizontal wind pressure, P_D, can be calculated using the following equation:

$$P_D = P_B\left(\frac{V_{DZ}}{V_B}\right)^2 = P_B\,\frac{{V_{DZ}}^2}{10{,}000}$$

Equation 1.3.11
AASHTO LRFD Equation 3.8.1.2.1-1

As a limit, the wind load on windward chords of trusses and arches, and beams and girders cannot be less than 0.30 klf. The leeward load on chords of trusses and arches cannot be less than 0.15 klf.

As mentioned previously, various angles of attack for wind direction should be investigated to determine which gives the worst-case response in the bridge structure. The angle of attack is determined as the skew angle from a perpendicular to the longitudinal axis of the member in question. For various standard angles of attack, the value of base pressure, P_B, varies as shown in Table 1.3.8, taken from *AASHTO LRFD* Table 3.8.1.2.2-1. The pressures for lateral loads and longitudinal loads are to be applied simultaneously.

Table 1.3.8 Base Pressures, P_B, for Various Angles of Attack, V_B = 100 mph

Skew Angle of Wind, Degrees	Trusses, Columns and Arches		Girders	
	Lateral Load, ksf	Longitudinal Load, ksf	Lateral Load, ksf	Longitudinal Load, ksf
0	0.075	0.000	0.050	0.000
15	0.070	0.012	0.044	0.006
30	0.065	0.028	0.041	0.012
45	0.047	0.041	0.033	0.016
60	0.024	0.050	0.017	0.019

For girder bridges having an individual span length not exceeding 125 feet and a maximum height above of 30 feet above low ground or water level, base wind pressures of 0.05 ksf and 0.012 ksf may be applied simultaneously in the transverse and longitudinal directions, respectively, in lieu of investigating various angles of attack.

WS is considered in the Strength III, Strength V and Service I load combinations. The Strength III load combination is used to investigate the strength of a member or component assuming the bridge is exposed to a wind velocity exceeding 55 mph. The design vehicular live load is not included in the Strength III load combination. At wind speeds in excess of 55 mph, it is assumed that the higher wind speeds would prevent the presence of maximum live loads on the bridge. In the Strength III Load combination, the load factor applied to the force effects due to WS is 1.4. The Strength V load combination is used to investigate the strength of a member or component assuming the bridge is exposed to a wind velocity of 55 mph under normal use. In the Strength V load combination, the load factor applied to the force effects due to WS corresponding to the load factor specified for WS in the Strength III load combination can be computed as $(1.4)(55/100)^2 = 0.42$, which is rounded to 0.4 in the specification. This corresponds to a load factor on the force effects due to WS of 0.3 under the Service I load combination. The load factor applied to the force effects due to the design vehicular live load plus the associated dynamic effects is reduced from 1.75 to 1.35 when combined with the force effects due to wind load in the Strength V load combination.

As mentioned previously, when investigating the Strength III load combination (i.e. dead plus wind load with no live load on the structure) during construction, the load factor to be applied to the force effects due to wind on the structure, WS, is to be reduced from 1.4 to not less than 1.25 according to *AASHTO LRFD* Article 3.4.2. For investigating wind during the temporary construction condition, consideration might also be given to using a design wind pressure smaller than the design values prescribed above and also to waiving the prescribed minimum value of the distributed wind load (e.g. 0.30 klf for beams and girders) depending on the specific situation and the anticipated maximum wind velocity at the site.

Wind Force on Curved Bridge Design Example:

For the example skewed and curved I-girder bridge in Section 5.1, compute the perpendicular wind force acting on Girder 1 in Span 2 only (shown in plan view in Figure 1.3.14). Assume that the design horizontal wind pressure is P_D = 0.050 ksf for this structure, and assume that the exposed wind height for the superstructure is 10.5 feet.

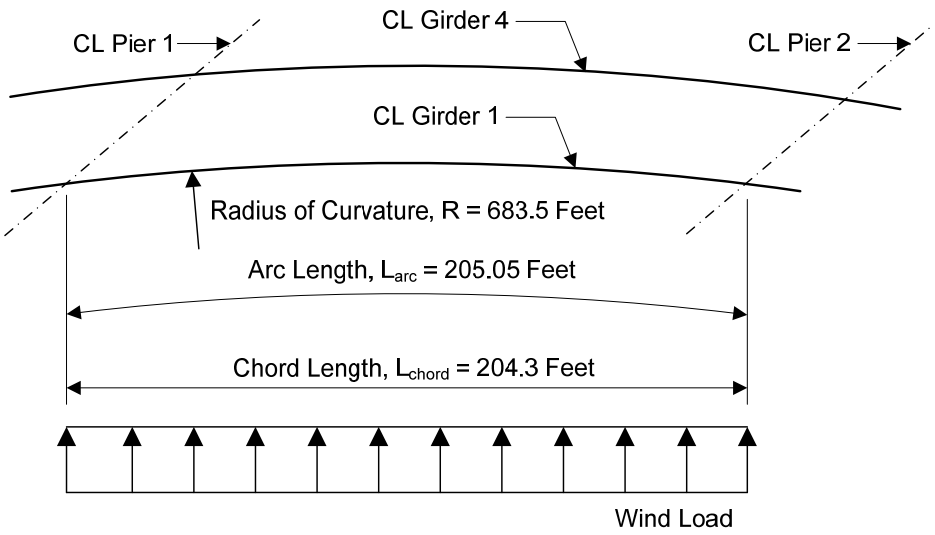


Figure 1.3.14 Plan View of Span 2

Using the equation provided in Section 1.1.3, the chord length is computed as follows:

$$L_{chord} = (2R)\sin\left[\frac{\left(\frac{L_{arc}}{2}\right)}{R}\right] = 2(683.5\,\text{Feet})\sin\left[\frac{\left(\frac{205.05\,\text{Feet}}{2}\right)}{683.5\,\text{Feet}}\right] = 204.3\,\text{Feet}$$

The wind load on the exposed height of the superstructure is computed as follows:

$$\text{Wind load} = (0.050\,\text{ksf})(10.5\,\text{feet}) = 0.525\,\text{Kip/foot}$$

As described previously, wind load on a curved bridge should be computed based on the projected (or planar) area rather than the curved area. Therefore, for the example presented in Figure 1.3.14, the perpendicular wind force acting on Girder 1 in Span 2 only is computed as follows:

$$\text{Wind Force} = (0.525\,\text{Kip/foot})(204.3\,\text{Feet}) = 107.3\,\text{Kips}$$

Notice that the chord length rather than the arc length is used in the above wind load calculation.

When applying the wind force in refined 3D analyses, loads are typically applied as concentrated loads on the exterior windward girder at the top and bottom nodes along the girder. The loads, determined from the wind pressure applied to the appropriate projected tributary area for each node in the analysis model, must be resolved into global x and y components at each node for the analysis (Figure 1.3.15). The wind should also be applied from the opposite side.

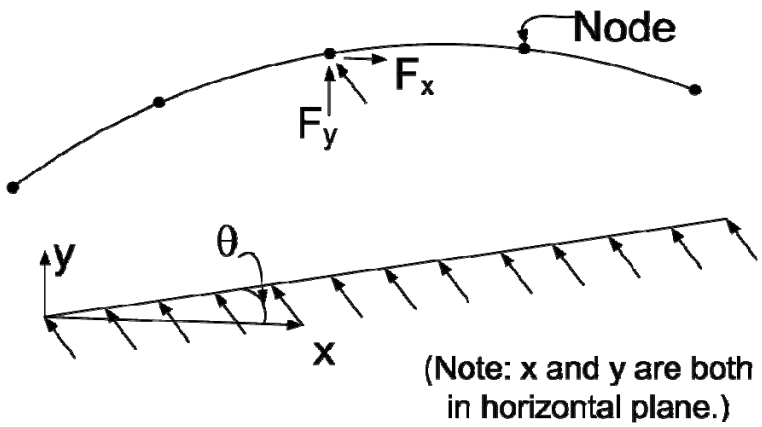


Figure 1.3.15 Resolution of Wind Force for 3D Analysis

1.3.2.4.1.2 Horizontal Wind Pressure on Live Load

In addition to the wind loads that are applied to all exposed surfaces of the bridge superstructure, wind also affects the exposed surfaces of live load traffic passing over the bridge, introducing additional forces that are categorized under load type WL (*AASHTO LRFD* Article 3.8.1.3). At the strength limit state, WL is only considered when investigating the Strength V load combination (discussed previously). The load factor applied to the force effects due to WL in the Strength V load combination is 1.0. WL is also considered in the Service I load combination (load factor equals 1.0).

WL is represented by an interruptible moving force of 0.10 klf acting normal to the roadway and located 6.0 feet above the roadway. Similar to the design lane load, the horizontal line load is to be applied to the same tributary areas producing a force effect of the same kind. For any situation in which an attack angle other than normal to the lane has been found to be the controlling wind direction, the forces for WL will change based on Table 1.3.9, which is transcribed from *AASHTO LRFD* Table 3.8.1.3-1.

Table 1.3.9 Wind Components on Live Load

Skew Angle, Degrees	Normal Component, klf	Parallel Component, klf
0	0.100	0.000
15	0.088	0.012
30	0.082	0.024
45	0.066	0.032
60	0.034	0.038

For girder bridges having an individual span length not exceeding 125 feet and a maximum height above of 30 feet above low ground or water level, wind components on live load of 0.10 klf and 0.04 klf may be applied simultaneously in the transverse and longitudinal directions, respectively, in lieu of investigating various angles of attack.

For vehicles traversing curved bridges, wind on live load results in an overturning force on the vehicle similar to the effect of centrifugal force on vehicles and may be handled in a similar manner.

1.3.2.4.2 Vertical Wind Pressure on Structure

For load combinations in which only wind on the structure is considered (i.e. the Strength III load combination), the wind is applied perpendicular to the longitudinal axis of the bridge, and overturning of the structure is potentially a concern, a vertical upward wind force is to be considered (*AASHTO LRFD* Article 3.8.2). The vertical upward force is to be applied as a longitudinal line load equal to a vertical upward wind pressure of 0.020 ksf times the entire width of the deck, including parapets and sidewalks. The lineal force is to be applied at the windward quarter-point of the deck width in combination with the horizontal wind force on the structure. According to *AASHTO LRFD* Article C3.8.2, the intent of the vertical upward force is to account for the effect of the interruption of the horizontal flow of the air by the superstructure.

1.3.2.5 Thermal Loads

In addition to force effects caused by applied loads, a bridge must also be designed to resist force effects caused by the restraint of deformations resulting from changes in temperature. These force effects can result due to a uniform temperature change or potentially due to a uniform temperature change in combination with a temperature gradient through the depth of the superstructure.

1.3.2.5.1 Uniform Temperature Change

Uniform temperature is characterized by a temperature rise or fall in the entire bridge (*AASHTO LRFD* Article 3.12.2). Although temperature changes in a bridge due not occur uniformly, bridges are generally designed for a uniform temperature change. Uniform temperature change causes the entire superstructure to lengthen due to temperature rise or shorten due to temperature fall. The resulting expansion and contraction directly affects the design of bridge bearings and the required openings in deck joints. In addition, if the supports are constrained, uniform temperature change induces reactions at the bearings and forces in the corresponding substructure units. Thermal effects must be carefully considered when selecting the bearing type, fixity and orientation for curved and/or skewed bridges in order to minimize thermal forces resulting from bearing constraint (see Section 2.2.3).

The thermal movement due to a simple uni-directional uniform temperature change is illustrated in Figure 1.3.16.

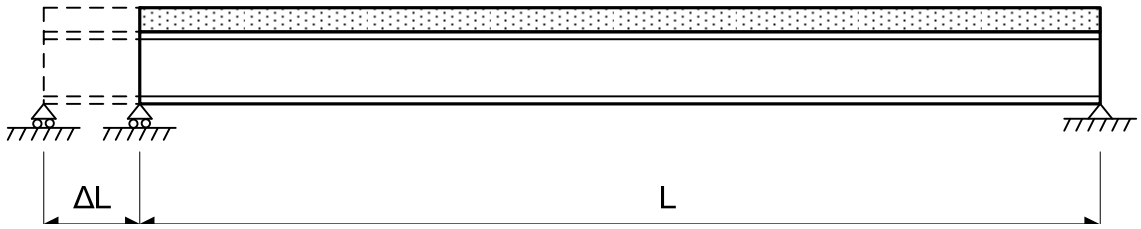


Figure 1.3.16 Uniform Temperature Change

As depicted in Figure 1.3.16, the entire superstructure changes in length when subjected to a uniform temperature change. The magnitude of the change in length, ΔL, is a function of:

- Material properties
- Temperature change
- Expansion length

This relationship is expressed mathematically by the following classical equation:

$$\Delta L = \alpha \, \Delta T \, L$$

Equation 1.3.12

where:

ΔL = total change in length or width due to ΔT
α = coefficient of thermal expansion (see below)
ΔT = design temperature range
L = expansion length

To compute the design movement in an elastomeric bearing, which will not be reset after erection, an additional factor of 1.3 must be included in the above formula. The values for ΔL and L are illustrated in Figure 1.3.16. It is important to note that the expansion length is measured to a point of zero translation. The coefficient of thermal expansion is approximately 0.0000065/˚F for steel, 0.0000060/˚F for normal weight concrete and 0.0000050/˚F for lightweight concrete. The change in temperature is based on the construction temperature assumed at design, the minimum design temperature of the range and the maximum design temperature of the range.

AASHTO provides two methods for determining the minimum and maximum design temperatures. Procedure A, which has traditionally been used by *AASHTO*, is based on the temperature ranges presented in Table 1.3.10.

Table 1.3.10 Temperature Ranges
(Based on *AASHTO LRFD* Table 3.12.2.1.1-1)

Climate	Steel or Aluminum	Concrete	Wood
Moderate	0˚F to 120˚F	10˚F to 80˚F	10˚F to 75˚F
Cold	-30˚F to 120˚F	0˚F to 80˚F	0˚F to 75˚F

As used in Table 1.3.10, moderate climate is defined as climate in which less than 14 days have an average temperature of less than 32˚F, and cold climate is defined as climate in which 14 or more days have an average temperature of less than 32˚F. The temperature range for concrete is less than that for steel or aluminum because concrete generally has more thermal inertia than do steel or aluminum, which makes concrete more resistant to changes in temperature.

Temperature Range Design Example:

To illustrate the application of Table 1.3.10, for a steel girder in cold climate which was assumed constructed at 68˚F, the design temperature rise is 120˚F - 68˚F = 52˚F, and the design temperature fall is 68˚F – (-30˚F) = 98˚F.

Procedure B is based on contour maps, which present contour lines for the maximum and minimum design temperatures for both concrete girder bridges and steel girder bridges. The Design Engineer can locate the bridge site on the contour maps and determine the maximum and minimum design temperatures to within about 10˚F, either by interpolating between contour lines or by using the most conservative adjacent contour line. The use of Procedure B is recommended for steel bridges in order to obtain more realistic temperature ranges.

When two or more adjacent piers have fixed bearings, there is little room to compensate for the ambient temperature during the erection of the girders. To alleviate potential problems, the design engineer can assume a temperature range in the design larger than the temperature range based on the median temperature of the range (which is often assumed as the base construction temperature) in computing the movements and thermal forces on the substructure and superstructure (e.g. ΔT = 100°F). Such an assumption allows for erection of the steel at temperatures other than the assumed construction temperature without requiring flexing of the pier(s) to make-up for the change in the length of the steel. Rocker bearings offer some advantage in that they can be rotated to match the ambient temperature at the time of installation.

Uniform temperature change must be considered in the design of many bridge components, including the following:

- Deck joints
- Bearings
- Piers at which the bearings are constrained against thermal movement

Skewed and curved bridges subject to a uniform temperature change do not expand uni-directionally, but instead expand and contract both radially and tangentially, which complicates the calculation of thermal movements due to the difficulties in determining the proper expansion lengths. Such movements are best predicted by refined analysis (see Section 2.2.3).

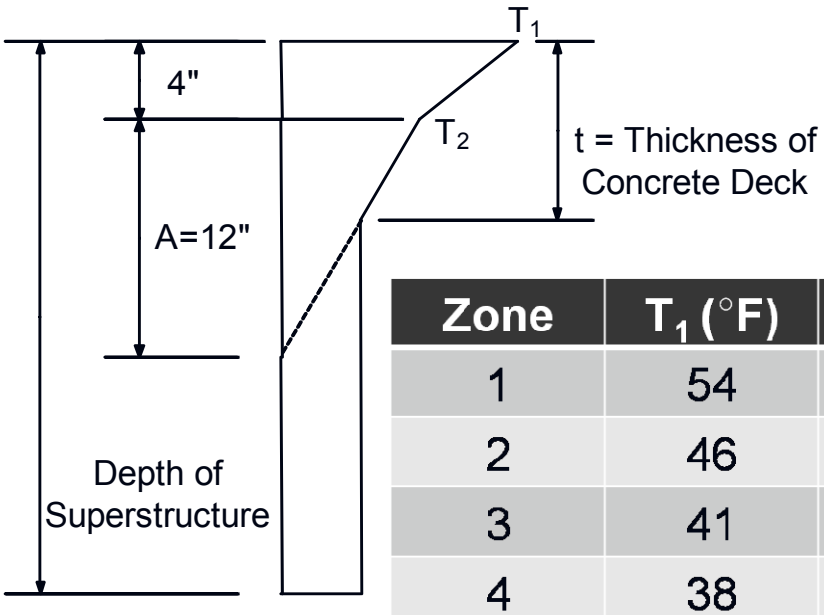
The load factor, γ_{TU}, applied to the force effects due to uniform temperature is specified to be 0.5 for all strength limit state load combinations and 1.0 for all service limit state combinations. For a concrete substructure, the load factor of 0.5 at the strength limit state is to be used in conjunction with the gross moment of inertia. When a refined analysis of a concrete substructure is completed, a load factor of 1.0 is to be used instead at the strength limit state in conjunction with a partially cracked moment of inertia determined by analysis. For a steel substructure, a load factor of 1.0 is to be used. For displacements due to uniform temperature, the load factor is specified to be 1.2 for all strength and service limit state load combinations. According to *AASTHO LRFD* Article C3.4.1-1, a factor greater than 1.0 is used for displacements to avoid undersizing joints, expansion devices and bearings.

1.3.2.5.2 Uniform Temperature Change and Temperature Gradient

A temperature gradient through the depth of the superstructure in combination with a uniform temperature change may lead to uplift in narrow curved and/or skewed structures. When checking uplift in such structures, thermal effects should be considered because they can cause significant vertical reactions. These reactions are properly computed by recognizing the bearing vertical offsets from the neutral axis of the superstructure girders in the analysis. Where uplift is not a consideration, recognition of the offset of the bearings in the analysis may not be necessary. Uplift may simply lead to annoying problems, such as reduced bearing life or unanticipated bending in the deck. However, narrow bridges (such as single tubs) can become unstable under certain conditions due to uplift.

Bridge location plays a more significant role in thermal gradient than in uniform temperature change. Bridges located in western states are generally more sensitive to thermal gradient than bridges located in eastern states. To assist the bridge engineer in computing thermal gradient, *AASHTO* has divided the nation into four solar radiation zones, identified as Zones 1, 2, 3 and 4. Zone 1 has the highest gradient temperatures.

The specified variation in temperature throughout the depth of the superstructure is illustrated in Figure 1.3.17 (*AASHTO LRFD* Article 3.12.3).



Zone	T_1 (°F)	T_2 (°F)
1	54	14
2	46	12
3	41	11
4	38	9

Figure 1.3.17 Positive Temperature Gradient for Steel Girder Superstructures

The figure shows the positive temperature gradient specified for steel superstructures with a concrete deck. This gradient is patterned after a similar gradient given in the Australian bridge specifications. The value for A, as shown in Figure 1.3.17, depends on the superstructure material and depth, and is given as 12 inches for steel. The values for the temperatures (T_1 and T_2) are a function of the solar radiation zone in which the bridge is located. The temperatures form the basis for calculating the change in temperature with depth in the cross-section, not absolute temperatures.

A negative temperature gradient is also specified for consideration in *AASHTO LRFD* Article 3.12.3, which can be obtained by multiplying the temperatures shown in the table in Figure 1.3.20 by –0.30 for plain concrete decks and –0.20 for concrete decks with an asphalt overlay.

When analyzing a bridge for uniform temperature in conjunction with a temperature gradient, the following structure responses should also be considered:

- Axial extension
- Flexural deformation
- Internal stresses

In lieu of project-specific information, the load factor, γ_{TG}, applied to the effects due to temperature gradient is specified to be 0.0 at the strength limit state, 1.0 at the service limit state when live load is not considered, and 0.5 at the service limit state when live load is considered. *AASHTO LRFD* Article C3.4.1 recommends that thermal gradient not be combined with high wind forces.

1.3.2.6 Vehicular Braking Force

When a truck decelerates or stops on a bridge, a longitudinal force is transmitted to the bridge deck, which is also transmitted to the substructure units with fixed bearings. This longitudinal force is known as the braking force.

The braking force is specified in *AASHTO LRFD* Article 3.6.4 as the greater of either:

- 25 percent of the axle weights of the design truck or design tandem
- 5 percent of the design truck plus lane load, or 5 percent of the design tandem plus lane load

The 25% factor is derived using the following kinetic energy formula:

$$F_B = \left(\frac{v^2}{2ga} \right) W = bW$$

Equation 1.3.13

where:

F_B = braking force
v = initial truck velocity (assumed to be 55 mph)
g = gravitational acceleration
a = length of uniform deceleration (assumed to be 400 feet)
W = truck weight
b = braking value

Substituting the assumed values into the above equation leads to a value for *b* of approximately 25%.

AASHTO LRFD Article 3.6.4 specifies that the braking force is to be based on all lanes which are considered to be loaded and which are carrying traffic in the same direction. For bridges that may become one-directional in the future, all design lanes should be simultaneously loaded. In addition, the appropriate multiple presence factor should be applied to the braking force effects.

The braking force is applied 6.0 feet above the roadway surface, and it acts longitudinally in whichever direction causes the maximum force effects.

The load factor to be applied to the braking force effects is the same as for the design vehicular load. Dynamic load allowance is not to be applied to the braking force effects.

1.3.2.7 Accumulated Locked-in Force Effects

Another loading condition that may need to be considered in bridge design is accumulated locked-in force effects. These force effects can result from the

construction process, and they include such effects as secondary forces from post-tensioning. Accumulated locked-in force effects vary both in magnitude and in nature, depending on the bridge type and the erection method.

AASHTO LRFD Table 3.4.1-1 considers accumulated locked-in force effects, EL, as a permanent load, and it is the only permanent load for which *AASHTO* assigns a maximum load factor of 1.00 and a minimum load factor of 1.00 at the strength limit state.

The most common applications of prestressed concrete in steel girder bridges are transverse post-tensioning of the deck and integral pier caps in which the tendons penetrate the girder webs. A composite deck may also be prestressed longitudinally. According to *AASHTO LRFD* Article 3.4.1, the force effects due to the following sources in such applications are to be considered as construction loads, EL: 1) In conjunction with longitudinal prestressing of a precast deck prior to making the deck section composite with the girders, the friction between the precast deck sections and the steel girders; 2) In conjunction with longitudinal post-tensioning performed after the deck becomes composite with the girders, the additional forces induced in the girders and shear connectors; 3) The effects of differential creep and shrinkage of the concrete; and 4) The Poisson effect. The Poisson effect recognizes the bulging of concrete when subject to prestressing. When used in pier caps, post-tensioning causes a transverse Poisson tensile stress resulting in a longitudinal stress in the steel girders.

1.3.3 Load Factors and Combinations

Load and Resistance Factor Design is based on satisfying various limit states. *AASHTO LRFD* defines a limit state as a condition beyond which the bridge or component ceases to satisfy the provisions for which it was designed. For each limit state (discussed later), the following basic equation must be satisfied (*AASHTO LRFD* Article 1.3.2.1):

$$\sum \eta_i \gamma_i Q_i \le \phi R_n = R_r$$

Equation 1.3.14

AASHTO LRFD Equation 1.3.2.1-1

where:

- η_I = load modifier related to ductility, redundancy and operational importance
- γ_i = load factor, a statistically based multiplier applied to force effects
- Q_i = force effect
- ϕ = resistance factor, a statistically based multiplier applied to nominal resistance
- R_n = nominal resistance
- R_r = factored resistance = ϕR_n

In LRFD, the load and resistance factors are statistically calibrated in an attempt to better provide a uniform level of safety for all bridges and components regardless of the bridge type, bridge geometry or material type.

Load modifiers, η, have also been introduced in LRFD. Load modifiers allow the Owner to adjust the margin of safety for a particular bridge to a certain degree based on its operational importance, ductility characteristics and level of redundancy. Ductility and redundancy relate directly to the strength of the bridge. The operational importance relates directly to the consequences of the bridge being out of service. The grouping of these three effects on the load side of the above equation through the use of the load modifier η_i represents an initial attempt at their codification. Improved quantification of these effects may be possible in the future. For loads for which a maximum value of γ_i is appropriate:

$$\eta_i = \eta_D \eta_R \eta_I \geq 0.95$$

Equation 1.3.15
AASHTO LRFD Equation 1.3.2.1-2

where:

η_D = ductility factor specified in *AASHTO LRFD* Article 1.3.3
η_R = redundancy factor specified in *AASHTO LRFD* Article 1.3.4
η_I = operational importance factor specified in *AASHTO LRFD* Article 1.3.5

For loads for which a minimum value of γ_i is appropriate:

$$\eta_i = \frac{1}{\eta_D \eta_R \eta_I} \leq 1.0$$

Equation 1.3.16
AASHTO LRFD Equation 1.3.2.1-3

For typical bridges for which additional ductility-enhancing measures have not been provided beyond those required by the specifications, and/or for which exceptional levels of redundancy are not provided, the three η factors have default values of 1.0 specified at the strength limit state. At all other limit states, all three η factors must be taken equal to 1.0.

In the fundamental equation, products of the load modifiers, the *force effects* due to the loads that apply to the component being designed, and the appropriate load factors for the load combination under consideration are summed. The resulting sum on the left side of the equation is then compared with the factored resistance of the component being designed on the right side of the equation. If the factored resistance exceeds the sum of the factored force effects, then that particular LRFD limit-state design requirement is satisfied.

The factored resistance is equal to a resistance factor times the nominal resistance, as indicated by the dimensions specified in the contract documents and by

permissible stresses, deformations or specified strength of materials. The resistance factor is a statistically based multiplier accounting for variability of material properties and dimensions and uncertainty in the prediction of resistance. For steel structures, the resistance factors are specified in *AASHTO LRFD* Article 6.5.4.2.

The load factors and load combinations are specified in *AASHTO LRFD* Table 3.4.1-1, as presented below in Table 1.3.11. The load factors, γ_p, to be applied to the force effects due to DC and DW loads are given in *AASHTO LRFD* Table 3.4.1-2 (Table 1.3.12)

Table 1.3.11 *AASHTO LRFD* Load Combinations and Load Factors

Load Combination Limit State	*DC DD DW EH EV ES EL PS CR SH*	*LL IM CE BR PL LS*	*WA*	*WS*	*WL*	*FR*	*TU*	*TG*	*SE*	Use One of These at a Time			
										EQ	*IC*	*CT*	*CV*
Strength I (unless noted)	γ_p	1.75	1.00	—	—	1.00	0.50/1.20	γ_{TG}	γ_{SE}	—	—	—	—
Strength II	γ_p	1.35	1.00	—	—	1.00	0.50/1.20	γ_{TG}	γ_{SE}	—	—	—	—
Strength III	γ_p	—	1.00	1.40	—	1.00	0.50/1.20	γ_{TG}	γ_{SE}	—	—	—	—
Strength IV	γ_p	—	1.00	—	—	1.00	0.50/1.20	—	—	—	—	—	—
Strength V	γ_p	1.35	1.00	0.40	1.0	1.00	0.50/1.20	γ_{TG}	γ_{SE}	—	—	—	—
Extreme Event I	γ_p	γEQ	1.00	—	—	1.00	—	—	—	1.00	—	—	—
Extreme Event II	γ_p	0.50	1.00	—	—	1.00	—	—	—	—	1.00	1.00	1.00
Service I	1.00	1.00	1.00	0.30	1.0	1.00	1.00/1.20	γ_{TG}	γ_{SE}	—	—	—	—
Service II	1.00	1.30	1.00	—	—	1.00	1.00/1.20	—	—	—	—	—	—
Service III	1.00	0.80	1.00	—	—	1.00	1.00/1.20	γ_{TG}	γ_{SE}	—	—	—	—
Service IV	1.00	—	1.00	0.70	—	1.00	1.00/1.20	—	1.0	—	—	—	—
Fatigue I—*LL, IM & CE* only	—	1.50	—	—	—	—	—	—	—	—	—	—	—
Fatigue II—*LL, IM & CE* only	—	0.75	—	—	—	—	—	—	—	—	—	—	—

Table 1.3.12 *AASHTO LRFD* Load Factors for Permanent Loads, γ_p

Type of Load, Foundation Type, and Method Used to Calculate Downdrag		Load Factor	
		Maximum	Minimum
DC: Component and Attachments		1.25	0.90
DC: Strength IV only		1.50	0.90
DD: Downdrag	Piles, α Tomlinson Method	1.4	0.25
	Piles, λ Method	1.05	0.30
	Drilled shafts, O'Neill and Reese (1999) Method	1.25	0.35
DW: Wearing Surfaces and Utilities		1.50	0.65
EH: Horizontal Earth Pressure			
• Active		1.50	0.90
• At-Rest		1.35	0.90
• *AEP* for anchored walls		1.35	N/A
EL: Locked-in Construction Stresses		1.00	1.00
EV: Vertical Earth Pressure			
• Overall Stability		1.00	N/A
• Retaining Walls and Abutments		1.35	1.00
• Rigid Buried Structure		1.30	0.90
• Rigid Frames		1.35	0.90
• Flexible Buried Structures other than Metal Box Culverts		1.95	0.90
• Flexible Metal Box Culverts and Structural Plate Culverts with Deep Corrugations		1.50	0.90
ES: Earth Surcharge		1.50	0.75

The four limit states (discussed below) are listed in the left column of Table 1.3.11. Each limit state has several individual load combinations. Each load combination has a unique application along with unique loads and load factors. For example, for the Strength I load combination, dead loads and live loads are included, but wind loads are not included. For the Strength IV load combination, dead loads are included but neither live loads nor wind loads are included.

Table 1.3.11 shows which specific loadings are to be included for each load combination. Also included are the appropriate load factors for each load combination and each loading. Again, the load factors are typically applied to the force effects. The load factors vary for each load combination and each loading. For example, the load factor for live load force effects is 1.75 for the Strength I load combination but is only 1.35 for the Strength V load combination. This accounts for the fact that the Strength V load combination includes several loadings that are not included in the Strength I load combination, and it accounts for the reduced probability that the maximum values of many different loadings will all be applied to the bridge simultaneously.

Each of the load combinations is discussed in more detail in the following:

- Strength I

  Basic load combination used to check the strength of a member or component under normal vehicular use of the bridge in the absence of wind. The basic Strength I load combination is 1.25 times the force effects due to the permanent load of the member components, plus 1.5 times the force effects due to any non-integral wearing surfaces and utilities, plus 1.75 times the design vehicular live load. The load factors for uniform temperature (TU) are reduced at the strength limit state, as some inelastic deformation is expected in the structure that would relieve some of these force effects. For uniform temperature (TU), a reduced load factor of 0.50 is typically used when calculating force effects and an increased load factor of 1.20 is used when calculating displacements. These load factors apply to all strength load combinations.

- Strength II

  Load combination used to check the strength of a member or component when the bridge is loaded with Owner-specified special design permit vehicles, evaluation permit vehicles, or both in the absence of wind. The Strength II load combination is the same as the Strength I load combination with the load factor on live load effects reduced to 1.35.

- Strength III

  Load combination used to check the strength of a member or component assuming the bridge is exposed to a wind velocity exceeding 55 mph in the absence of live load. The basic Strength III load combination is 1.25 times the force effects due to the permanent load of the member components, plus 1.5 times the force effects due to any non-integral wearing surfaces and utilities, plus 1.4 times the force effects due to wind load on the structure.

- Strength IV

  Load combination used to check the strength of a member or component in bridges with very high dead to live load force effect ratios in their final condition. *For steel-girder bridges, this particular load combination can control and should also be considered during the investigation of various construction stages*. In the Strength IV load combination, all permanent-load force effects (for both the construction and final conditions) are factored by 1.5 and live- and wind-load effects are not considered.

- Strength V

  Load combination used to check the strength of a member or component assuming the bridge is exposed to a wind velocity equal to 55 mph under normal use. The basic Strength V load combination is 1.25 times the force effects due to the permanent load of the member components, plus 1.5 times the force effects due to any non-integral wearing surfaces and utilities, plus 1.35 times the design vehicular live load, plus 0.4 times the force effects due to wind load on the structure, plus 1.0 times the force effects due to wind on live load.

.

- Extreme Event I

  Load combination used to check the strength of a member or component assuming the bridge is subject to earthquake loading (EQ). *AASHTO LRFD* Article 3.4.1 directs that the γ_{EQ} load factor applied to live load effects in combination with earthquake load effects should be determined on a project-specific basis. Previous *AASHTO* specifications have set this value to zero, but current research shows that setting γ_{EQ} less than 1.0, or more specifically to 0.50, may be applicable for most average daily truck traffic (*ADTT*) conditions. For more information, refer to *AASHTO LRFD* Articles 3.4.1 and C3.4.1.

- Extreme Event II

  Load combination used to check the strength of a member or component assuming the bridge is subject to ice load (IC), vessel collision (CV), vehicle collision (CT), or check floods or other hydraulic events (WA). The effects of these events are not to be combined at the same time; each is to be checked individually since the joint probability of these events is low. The load factor of 0.5 on live load force effects (other than CT) reflects the fact that if one of these extreme events does occur, the likelihood of the maximum vehicular live load being on the bridge is small.

- Service I

  Load combination relating to the normal operational use of the bridge with a 55 mph wind and all loads taken at their nominal values. This load combination primarily applies to crack control in reinforced concrete structures. However, the live-load portion (only) of the Service I load combination is used for checking live-load deflection in steel bridges (i.e. a load factor of 1.0 is applied to the live load deflections).

- Service II

  Load combination intended to control yielding of steel structures and slip of slip-critical bolted connections. In the Service II load combination, the load factors on the force effects due to DC and DW loads are all reduced to 1.0 and the load factor on force effects due to the design vehicular live load is reduced to 1.3. If the Service II load combination is to be applied to a permit-load situation, it may be desirable to reduce the live load load factor from 1.3 to 1.0. This load combination corresponds to the Overload level in the *AASHTO* Standard Specifications.

- Service III

  Load combination relating to crack control in prestressed concrete superstructures and principal tension in the webs of segmental concrete girders.

- Service IV

  Load combination relating only to crack control in prestressed concrete columns

- Fatigue I

  Load combination relating to infinite load-induced fatigue life. The Fatigue I load combination reflects a load level found to be representative of the maximum stress range of the truck population for infinite fatigue life design. The load factor of 1.5 applied to the fatigue live load effects in the Fatigue I load combination is based on the assumption that the maximum stress range is the random variable spectrum is twice the effective stress range caused by the Fatigue II load combination (see below). No other load effects are considered.

- Fatigue II

  Load combination relating to finite load-induced fatigue life. The Fatigue II load combination reflects a load level found to be representative of the effective stress range of the truck population with respect to a small number of stress range cycles and to their cumulative effects for finite fatigue life design. In the Fatigue II load combination, a load factor of 0.75 is applied to the fatigue live load effects. No other load effects are considered.

Regarding the selection of the appropriate load combinations, all structures utilize the strength and service limit state checks, although not all load combinations within strength and service may apply. For example, the Service I, III and IV load combinations are primarily to control cracking in concrete elements. Therefore,

these load combinations do not apply to skewed and curved steel bridge superstructure elements.

For longer-span bridges in their final condition, the ratio of dead-to-live load force effects is very high and could result in a set of resistance factors different from those determined to be suitable for the sample of smaller-span bridges (with spans not exceeding 200 feet) that were used in the statistical calibration of the specification. Rather than using two sets of resistance factors with the Strength I load combination, it was decided that it would be more practical to include this separate load combination. Although the Strength IV load combination will typically control where the dead-to-live load force effect ratio exceeds about 7.0 for the bridge in its final condition, this load combination may control during the investigation of critical construction stages and should be considered in constructibility design verifications for skewed and curved steel girder bridges (as discussed further in Section 3.2.3.1).

The recurrence interval of extreme events is thought to exceed the design life. The effects of extreme event limit state events may cause some damage to a structure. Stresses and deformations well into the inelastic range are allowed and, in some cases, expected. Prevention of full loss of structural integrity and collapse is the goal of the investigations at the extreme event limit state. Since the structure may undergo significant inelastic deformations at the extreme event limit state, any locked-in force effects due to temperature, creep, shrinkage, support settlement, etc. are expected to be relieved. Extreme event load combinations are applicable for some structures only (not for all) depending on their location. For example, bridges outside of earthquake zones or not crossing rivers do not need to be designed for certain extreme events. *AASHTO* publishes the *Guide Specifications for Bridges Vulnerable to Coastal Storms*. This document provides guidelines for computing wave forces on superstructures based on numerical simulation, actual wave loading data in Gulf Coast states and recent research by the *FHWA*.

Although time-dependent concrete shrinkage effects are included in most of the basic load combinations, the effects of shrinkage on the behavior of composite steel girders are less well understood than creep and are often ignored in U.S. design practice as of this writing. However, some State DOTs require that shrinkage be included as part of the camber considerations. As the concrete deck shrinks, it introduces compression in the flange attached to it while corresponding tensile stresses are introduced in the concrete deck as long as there is no loss of bond between the two materials. The effect of the shortening of both the concrete deck and top flange is to generate a positive moment in the composite girder with its concomitant increase in deflection. The amount of deflection is a function of a number of parameters including the distance of the deck-flange interface from the neutral axis and the stiffness of both the deck and the girder. Shrinkage stresses cannot exceed the modulus of rupture of the deck concrete. Although shrinkage increases the stresses in the girder, it does not appreciably diminish its capacity in the positive moment region because added load will reverse the shrinkage stresses in the deck, which will release its pull on the girder. In the negative moment regions

of a girder, the deck is considered ineffective by the fact that it is usually assumed cracked.

As concrete creeps under a constant sustained loading (e.g. permanent loads applied to the composite section), the strain in the steel girder increases and the steel stresses become larger, while the strains and concomitant stresses in the concrete deck are reduced. The reduction of stress in the concrete is a function of the relative stiffness of the girder and the concrete deck. The actual calculation of creep stresses in composite girders is theoretically complex and not necessary for the design of composite girders. Instead, a simple approach has been adopted for design in which a modular ratio appropriate to the duration of the load is used to compute the corresponding elastic section properties. *AASHTO LRFD* Article 6.10.1.1.1b specifies that for transient loads applied to the composite section, the so-called ″short-term″ modular ratio n is used. For permanent loads applied to the composite section, the so-called ″long-term″ modular ratio of $3n$ is used. The short-term modular ratio is based on the initial tangent modulus, E_c, of the concrete, while the long-term modular ratio is based on an effective apparent modulus, E_c/k, to account for the effects of creep. In U.S. practice, a value of k equal to 3 has been accepted as a reasonable value.

In strength load combinations, where one force effect decreases another force effect, the specified minimum values of the load factors, γ_p, in *AASHTO LRFD* Table 3.4.1-2 (Table 1.3.12) are to be applied instead to the permanent-load force effects. For example, when checking uplift at end supports, the load factor applied to the force effects due to the permanent load of member components would be reduced from 1.25 to 0.9. The load factor applied to the force effects due to non-integral wearing surface loads (if considered in this check) and utility loads would be reduced from 1.5 to 0.65. Special attention should also be given to other situations involving the summing of factored force effects of the opposite sense to ensure that an unconservative result is not obtained. An example would be in the contraflexure regions of continuous spans where dead and live load force effects are often of opposite sign. Consider another example of a cross-frame member carrying a component dead load force of 10 kips tension and live load forces of 15 kips tension and compression. Combining the force effects under the Strength I load combination and applying the maximum load factor of 1.25 to the component dead load tensile force in both live load cases gives 1.25(10) + 1.75(15) = 38.75 kips (tension) and 1.25(10) + 1.75(-15) = -13.75 kips (compression). Applying the minimum load factor of 0.9 to the component dead load tensile force for the live load compression case gives 0.9(10) + 1.75(-15) = -17.25 kips (compression). If compression controls the design of the member, an unconservative result is obtained when the standard maximum load factor is applied to the dead load force.

1.3.4 Limit States

As mentioned Section 1.3.1, in the *AASHTO LRFD* specification, bridges are to be designed for specified limit states to achieve the objectives of constructibility, safety, and serviceability, with due regard to issues of economy and aesthetics. The limit

states specified in the *AASHTO LRFD* specification are intended to provide for a buildable, serviceable bridge capable of carrying the design loads for a specified lifetime. In order to achieve these objectives, the fundamental Equation 1.3.14 must be satisfied at each limit state. The four limit states specified in the *AASHTO LRFD* specification are described in the following. The specific girder design verifications to be satisfied for I- and box girders at each limit state are discussed in greater detail in Section 3.2.

1.3.4.1 Strength Limit State

At the strength limit state (*AASHTO LRFD* Articles 1.3.2.4 and 6.5.4), it must be ensured that adequate strength and stability is provided to resist the statistically significant load combinations the bridge is expected to experience over its design life. Structural damage may occur, but overall structural integrity is maintained. The applicable Strength load combinations, described previously, are used to check the strength limit state. The required Strength limit state verifications for flexure are specified in *AASHTO LRFD* Articles 6.10.6 and 6.11.6 for I- and box girders, respectively. The requirements for shear are specified in *AASHTO LRFD* Articles 6.10.9 and 6.11.9.

Although not specified as a separate limit state, constructibility is one of the basic design objectives of LRFD. The bridge must be safely erected and have adequate strength and stability during all phases of construction. Specific design provisions are given in *AASHTO LRFD* Articles 6.10.3 and 6.11.3 for I- and box-girders, respectively, to help ensure constructibility; in particular, when subject to the specified deck-casting sequence. The constructibility checks are typically made on the steel section only under the factored non-composite dead loads using the appropriate strength load combinations.

1.3.4.2 Service Limit State

To satisfy the service limit state (*AASHTO LRFD* Articles 1.3.2.2 and 6.5.2), restrictions on stress and deformations under regular service conditions are specified to ensure satisfactory performance of the bridge over its service life. As specified in *AASHTO LRFD* Article 6.10.4.1, optional live load deflection criteria and span-to-depth ratios (*AASHTO LRFD* Article 2.5.2.6) may be invoked to control deformations.

Steel structures must also satisfy the requirements of *AASHTO LRFD* Articles 6.10.4.2 and 6.11.4 for I- and box girders, respectively, under the Service II load combination (described previously). The intent of these design checks is to prevent objectionable permanent deformations, caused by localized yielding and potential web bend buckling under expected severe traffic loadings, which might impair rideability.

1.3.4.3 Fatigue and Fracture Limit State

To satisfy the fatigue and fracture limit state (*AASHTO LRFD* Article 1.3.2.3 and 6.5.3), restrictions on stress range under regular service conditions are specified to control crack growth under repetitive loads and to prevent fracture during the design life of the bridge (*AASHTO LRFD* Article 6.6.1). Material toughness requirements are also addressed (*AASHTO LRFD* Article 6.6.2).

For checking fatigue in steel structures, the fatigue live load and Fatigue load combinations, described previously, apply. The nominal fatigue resistance of details is discussed in *AASHTO LRFD* Article 6.6. A special fatigue requirement for webs (*AASHTO LRFD* Article 6.10.5.3) is also specified to control out-of-plane flexing of the web that might potentially lead to fatigue cracking under repeated live loading. Fatigue limit state requirements specific to box girders, primarily addressing the effects of cross-section distortion stresses, are discussed in *AASHTO LRFD* Article 6.11.5.

1.3.4.4 Extreme Event Limit State

At the extreme event limit state (*AASHTO LRFD* Articles 1.3.2.5 and 6.5.5), structural survival of the bridge must be ensured during a major earthquake or flood, or when struck by a vessel, vehicle or ice flow. The applicable Extreme Event load combinations, discussed above, are used to check the extreme event limit state. This limit state will not be covered any further in this Manual.

This Page Intentionally Left Blank

Chapter 2
Structural Analysis

Section 2.1
General



2.1.1 Introduction

The structural theories that have evolved from statics and strength of materials have been used in the analysis of girder bridges and have been taught in structural analysis courses for decades. These concepts, melded with bridge design codes, are used in the design of girder bridges today. Powerful digital computers and modern software have enabled the Design Engineer to better apply these concepts to anticipate the behavior of bridges during design. When properly employed, this technology leads to bolder, better and more efficient bridges that are safe during construction and will dependably serve the public for decades to come.

2.1.2 System Modeling

System modeling implies that the entire structure is modeled and treated structurally as an integrated system. Each element within the system responds to any load introduced into the system. There are different levels of sophistication of system modeling. Grillage models that are two-dimensional models require that certain assumptions be made relating to the depth of the girders, which is not recognized in the model. Three-dimensional models are able to represent the vertical dimension of the bridge without compromising the accuracy. Essentially all girder-bridge-system models are limited to linear-elastic behavior. Non-linear inelastic models are often employed in bridge research work. These models, when properly used, can examine inelastic behavior of girders as they yield or buckle.

2.1.2.1 Skewed Supports

Skewed supports are supports that are other than radial or perpendicular to the girder lines. They are used in situations where a stream, roadway, or railway must be crossed at an angle other than perpendicular. The area of the bridge deck and often the associated cost of the bridge can be minimized by skewing the supports. They also reduce the amount of right-of-way to be required. Skewed supports cause longer more costly abutments and/or piers. They also complicate the design and construction of the bridge. Several structures with skewed supports in the recent past have been razed and rebuilt as a result of issues emanating from their skewed supports. These structures deserve careful design and construction.

2.1.2.2 Curved Girders

Horizontally curved girders have been built in the United States since the late 1950s. The earliest were box girders, which are simpler to analyze because they can be treated quite accurately as closed members in torsion. The solution for tubular members in torsion has been well known for decades. Treating curvature effects on tubular members is rather straightforward. The modern understanding of torsion in open sections was presented by Vlasov in the early 1960s.

These members have become very important in U.S. bridge lore. The Interstate System demanded many “cloverleaf” interchanges to expedite direction changes at high speed. Curved girders were essential in this effort if right-of-way costs were to be held within practical limits.

The *AASHTO LRFD* Specifications have unified the provisions for the analysis and design of curved and straight I- and box-girder bridges for the first time.

2.1.3 Dead Load

The system model contains structural components of the bridge such as the steel framing and the deck. Studies of the erection may be performed by defining only part of the structure. These analyses are useful to check intermediate deflections for fit-up of the steel.

The weight of these components can be represented simply as body forces of the elements. If body forces are used, a density must be defined as well as an acceleration term. If a dynamic analysis is to be made, a mass density should be defined and the acceleration is that of gravity. If a weight density is input, the acceleration factor is 1.0 and dynamic analyses cannot be performed. Body forces are appropriate for members that have stiffness reflected in the analysis. They are not appropriate for dead load components that have no stiffness, such as the concrete deck before it hardens. This load is applied best with concentrated loads at the top girder nodes. Non-structural components such as traffic barriers and sound barriers may be accounted for with concentrated loads. However, if they are to be considered structurally, their stiffness may be included in the model. At any rate, these components, or their weight, should be properly located on the system model.

2.1.4 Influence Lines and Influence Surfaces

Influence Lines

The original concept of influence lines was based on Maxwell's Law of Reciprocal Deflection (1866), which states that for an elastic structure "the deflection at point A in a structure due to a load applied at another point B is exactly the same as the deflection at B if the same load is applied at A" (*1*). The influence line was first used by Professor E. Winkler of Berlin in 1867. The influence line shows graphically how the movement of a unit load across a beam-type structure influences some force effect in the structure.

Application of this principle of influence lines is limited to linear elastic structures and supports with load applied directly to a single line girder. If a support deflects under load, it must deflect elastically in order for the influence line to be considered correct. For example, if a bearing lifts off its support as a unit load transverses the beam, the influence line method is inappropriate because the stiffness of the support is non-linear. Likewise, if permanent set occurs at a support or if the analysis includes non-linear deformation of a member, the influence line method is also not applicable.

The Müller-Breslau Principle is based on the principle of virtual displacements (*1*). It states that *the ordinate values of an influence line for a force effect at a point are proportional to the ordinates of the deflected shape obtained by removing the restraint at that point corresponding to the force effect, and introducing a force effect that causes a unit displacement (or rotation) in the proper sense of the desired action at that point*. That is, the deflected structure draws its own influence line when the proper displacement is applied.

The Müller-Breslau Principle can be used on other than beam structures, such as frames; this review will only address beams. The principle is used to determine qualitative influence lines, which are useful to quickly obtain the correct shape of the influence line and to obtain a better understanding of a particular action. The Müller-Breslau Principle can also be used to obtain the influence line ordinates for statically determinate and indeterminate structures. The principle as stated above is applied in Figure 2.1.1.

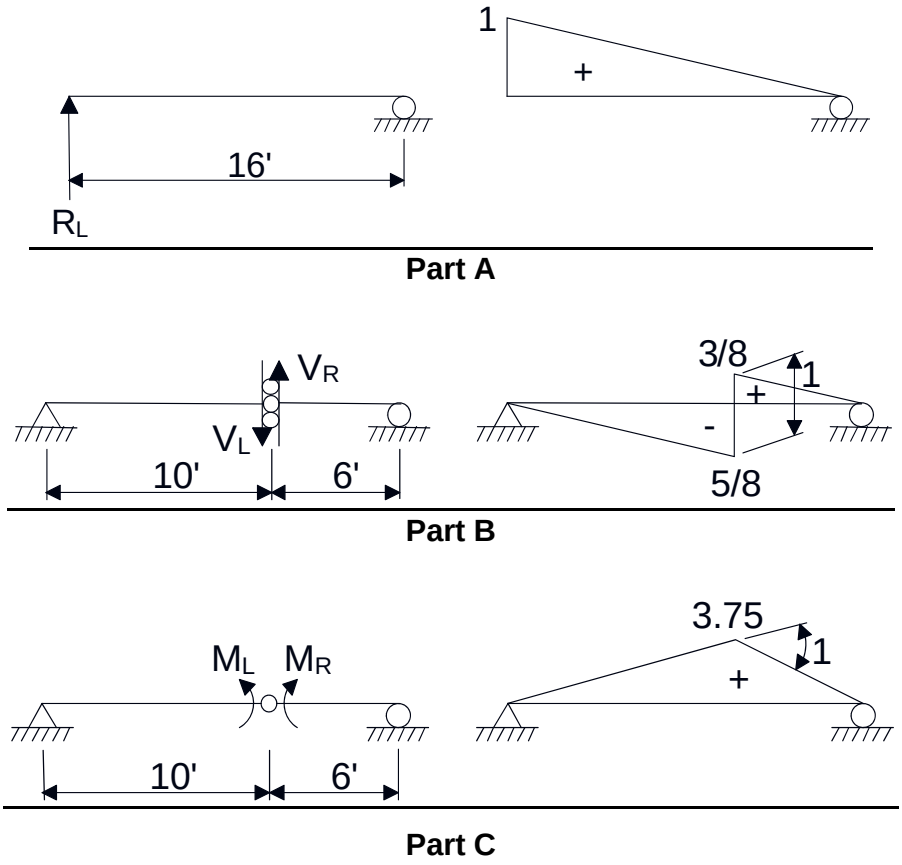


Figure 2.1.1 Application of the Müller-Breslau Principle
A) End Reaction in a Simple-Span Beam; B) Shear at a Section in a Simple-Span Beam; C) Vertical Bending Moment at a Section in a Simple-Span Beam

Determination of the end reaction in a simple-span beam illustrates the application of the Müller-Breslau Principle. Remove the reaction and displace that point by a unit displacement in the direction of the reaction, as shown in Part A of Figure 2.1.1. In this case (as is the case in all determinate structures), the force is zero. The resulting deflected shape is proportional to the true influence line for the end reaction. Since no force was required to cause the deflection, the deflected shape is linear.

The qualitative influence line for shear at a section is found by removing the shear resistance at the section by inserting a roller, as shown in Part B of Figure 2.1.1. Introducing a unit deflection between the free ends at the roller provides the influence line for shear at the point if the deflections properly reflect the sign convention. The magnitude of the displacement of the two ends is proportional to the location of the section in relation to the span. Note that for a statically determinate beam, the resulting influence line is linear because no actual force was required to deflect the structure with the roller installed.

To obtain a qualitative influence line for vertical bending moment at a section (Figure 2.1.1 Part C), remove the moment resistance (i.e. introduce a hinge) at that section while maintaining axial and shear force resistance. Next, apply equal and opposite moments in the proper sense on the left and right sides of the hinge. These moments introduce a unit relative rotation between the two tangents of the deflected shape at the hinge. The corresponding elastic curve is the influence line for bending moment at that section.

For statically determinate structures (e.g. simple-span structures), an influence line is determined by introducing unit deflections; no force is required. *Influence lines are linear for statically determinate structures*.

Influence lines for statically indeterminate structures (e.g. continuous-span structures) are typically determined from an indeterminate analysis. Theoretically, the same result would be obtained using the Müller-Breslau Principle, which introduces a unit deflection or rotation at the point of interest after the proper release is introduced.

The ordinates of influence lines are typically determined by applying a series of vertical unit loads at increments along the girder. Figure 2.1.2 shows a typical influence line for a three-span continuous beam (with equal 100-foot spans) for vertical bending moment at $0.4L_1$ = 40 feet from the abutment in an end span. *Influence lines for bending moment in statically indeterminate structures are curved*.

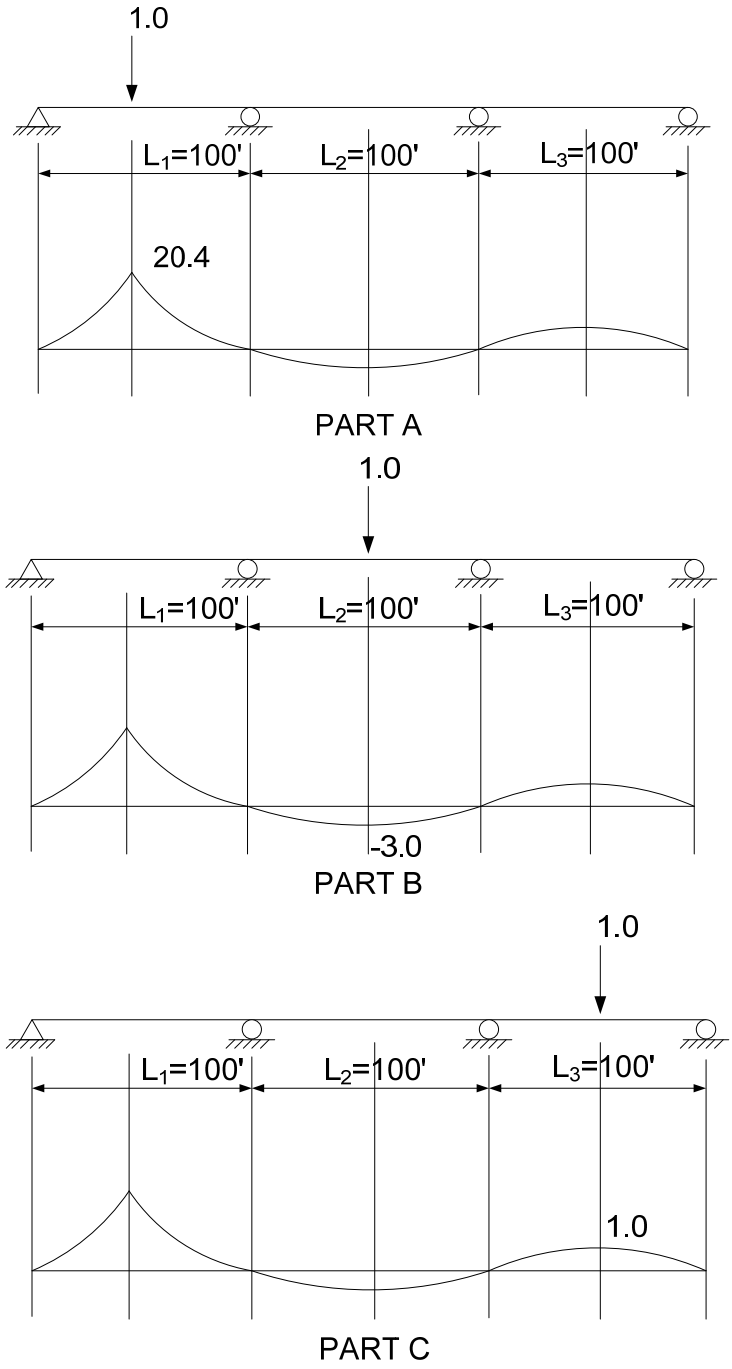


Figure 2.1.2 Development of Influence Line Ordinates for Vertical Bending Moment at 0.4L_1 in a Three-Span Continuous Beam by Application of Unit Loads

A) Unit Load Applied at 0.4L_1 to Obtain Ordinate for Moment at 0.4L_1;
B) Unit Load Applied at 0.5L_2 to Obtain Ordinate for Moment at 0.4L_1;
C) Unit Load Applied at 0.5L_3 to Obtain Ordinate for Moment at 0.4L_1

In Figure 2.1.2 Part A, the influence line ordinate of +20.4 kip-ft/kip at $0.4L_1$ is determined by applying a vertical unit load to the beam at $0.4L_1$. The ordinate represents the vertical bending moment at $0.4L_1$ when a vertical concentrated load is applied at $0.4L_1$. In Figure 2.1.2 Part B, the influence line ordinate of -3.0 kip-ft/kip at $0.5L_2$ is determined by applying a vertical unit load to the beam at $0.5L_2$. This ordinate represents the vertical bending moment at $0.4L_1$ when a vertical concentrated load is applied at $0.5L_2$. Finally, In Figure 2.1.2 Part C, the influence line ordinate of +1.0 kip-ft/kip at $0.5L_3$ is determined by applying a vertical unit load to the beam at $0.5L_3$. This ordinate represents the vertical bending moment at $0.4L_1$ when a vertical concentrated load is applied at $0.5L_3$.

For live load, the objective is to determine maximum and minimum responses of critical actions in the bridge to the specific live load(s) that the bridge is being designed to carry. This is accomplished by systematically applying the live load(s) to the influence line.

The ordinate of the influence line is the response at a specific location to a load of one unit applied at the point of the specific ordinate. Hence, when a concentrated live load (e.g. a wheel load) is applied at that point; the magnitude of the wheel load is multiplied by the ordinate of the influence line to find the response to that wheel load at the specific location of interest.

This is illustrated in Figure 2.1.3 for the *AASHTO LRFD* HL-93 design live load (Section 1.3.2.3.1), which is placed in position for the maximum positive vertical bending moment at $0.4L_1$ in the same three-span continuous beam examined above. The lane load is placed in the first and last spans where the influence line ordinates are positive. The design truck load is placed in the direction shown so that the larger rear-axle load is placed over the larger influence line ordinate adjacent to the critical section at $0.4L_1$.

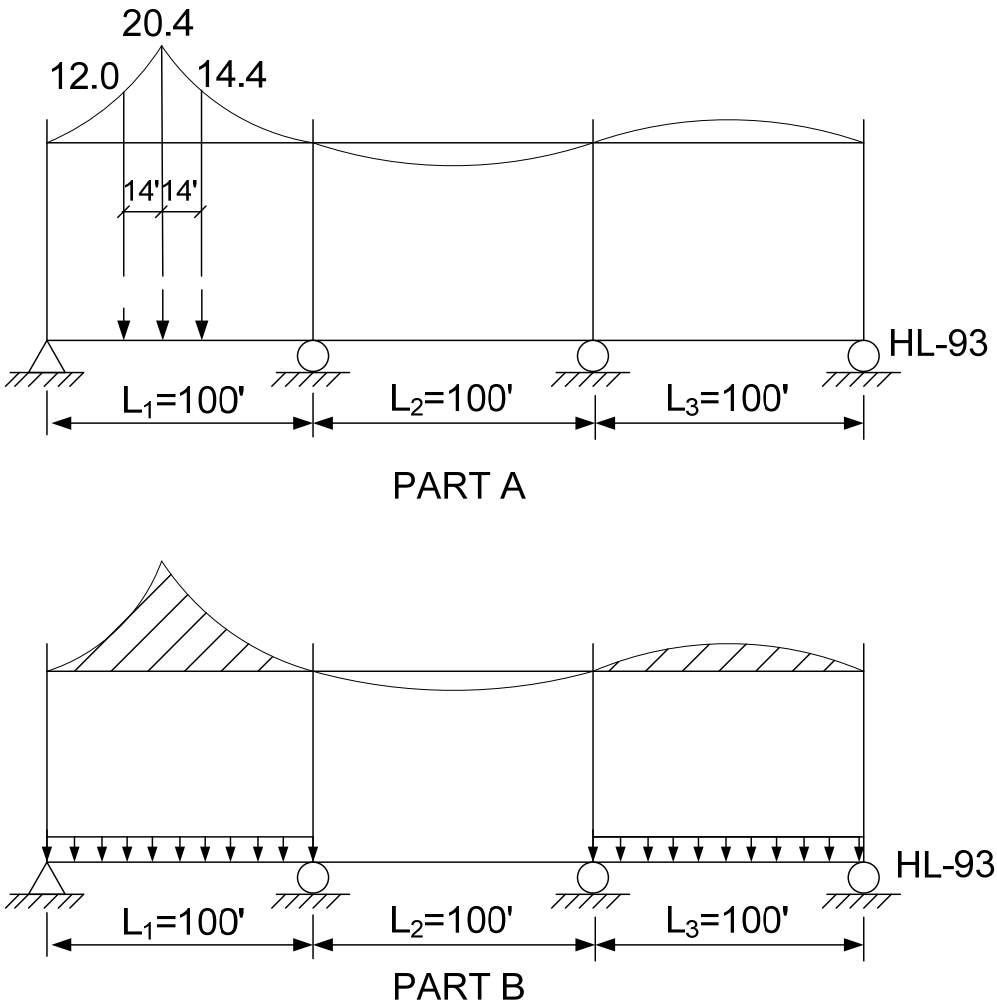


Figure 2.1.3 Application of HL-93 Live Load to an Influence Line for a Three-Span Continuous Beam to Determine the Vertical Bending Moment at $0.4L_1$
A) HL-93 Design Truck Load; B) HL-93 Design Lane Load

For the concentrated load portion of the HL-93 loading, represented by the design truck load, the live load force effect is determined by multiplying the magnitude of each concentrated load by the corresponding influence line ordinate opposite each load (Part A of Figure 2.1.3). The resulting force effect due to the truck load is then multiplied by the dynamic load allowance of 33 percent. For the uniform load portion of the HL-93 loading, represented by the design lane load, the live load force effect is determined by multiplying the magnitude of the uniform load by the area of the influence line opposite the section covered by the load (Figure 2.1.3 Part B). No dynamic load allowance is applied to the resulting force effect from the design lane load.

The total force effect (i.e. the vertical bending moment at $0.4L_1$ in this case) is taken as the sum of the force effects due to the design truck and design lane load. The resulting live load force effect is then multiplied by an appropriate live load distribution factor (LLDF) to account for the transverse load effects. Because influence lines are applied to one-dimensional line-girder configurations, transverse live load effects must be accounted for by applying LLDFs that are applicable to the force effect in the girder under consideration.

AASHTO specifications have favored LLDFs for decades over other methods commonly used in Europe and elsewhere. LLDFs were originally developed assuming non-composite girders with nominal cross-frames. The original factors assumed two lanes loaded. They were developed for straight girders with no skew, which were commonly used in the 1930s and 1940s. Typical in those days were very small overhangs so the exterior girders were less critical than the interior girders. Because the factors were simple, the accuracy varied quite a bit between bridges. Investigations in the 1980s and 1990s resulted in the development of more complex LLDFs found in the *AASHTO LRFD* specifications at present. These factors addressed more parameters than girder spacing in the computation of the LLDFs. Of particular importance in this development was the recognition that the exterior girder in modern bridges is often the critical one. Shear and moment were separated with their own sets of factors. The advent of the single fatigue truck required a set of factors for a single lane loaded. A set of correction factors to be applied to the LLDFs was also created to account in an approximate fashion for the effects of skew.

These advances provided modest improvement in the accuracy of LLDFs. However, they were not able to address curved-girder bridges at all; other methods are required. The digital computer with appropriate software rescued the Design Engineer by providing the ability to analyze the superstructure and, in some cases, the entire bridge as a system.

LLDFs that are computed using the equations presented in the tables given in *AASHTO LRFD* Article 4.6.2.2 are not to be multiplied by multiple presence factors. The effects of multiple presence have already been accounted for in the derivation of the equations. Multiple presence factors are to be applied, however, whenever the lever rule or the special rigid cross-section requirement for exterior beams is applied to compute the distribution factor. Multiple presence factors are discussed in further detail in Section 2.1.4.2.

Since skewed and curved steel bridges are best analyzed as systems, the use of LLDFs is typically not appropriate; thus, influence surfaces rather than influence lines are most often utilized to more accurately determine the necessary live load force effects for these bridge systems. Influence surfaces are examined in more detail below.
Through the application of the Müller-Breslau Principle, influence lines can be instructive. Figure 2.1.4 shows a beam having two equal continuous spans. Part A shows a moment diagram for a uniform dead load applied over the two spans.

Clearly, this loading is not related to live load. No single position of live load will create critical moment and shear in the girder at all locations.

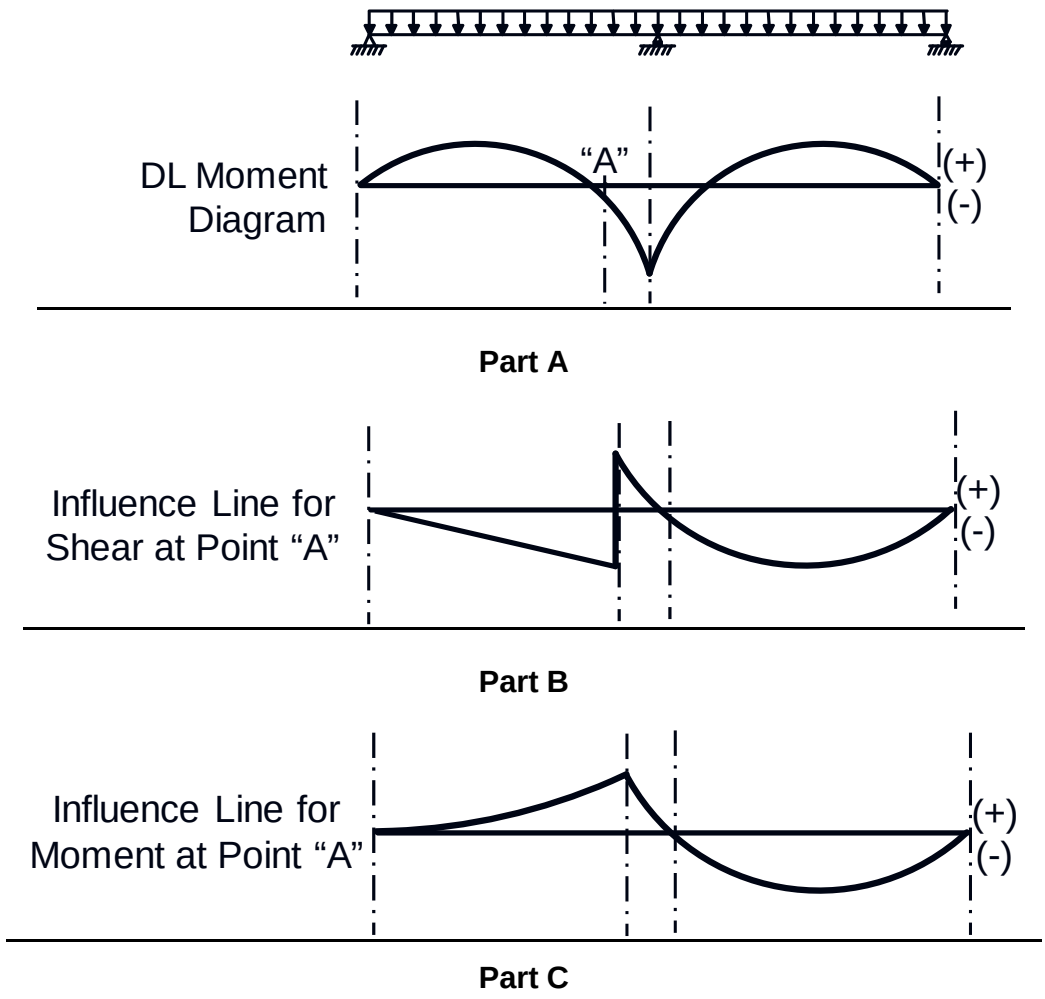


Figure 2.1.4 Positive Live Load Moment Resulting from the Loading Causing the Maximum Shear Range in a Dead Load Negative Moment Region
A) Dead Load Moment Diagram; B) Influence Line for Shear at Point A;
C) Influence Line for Moment at Point A

The live load moment and shear at Point "A" shown in the figure, located in the so-called dead load negative moment region, will be examined. Part B of Figure 2.1.4, shows the influence line for shear at that point. *The influence line for shear is only partially curved in a continuous span*. Similarly, the influence line for moment at Point "A" is shown as Figure 2.1.4 Part C. Clearly, an influence line is not a moment diagram. These influence lines can be determined by employing the Müller-Breslau Principle. A concentrated live load to create maximum shear range at Point "A" must be placed at two closely related positions. The maximum negative shear is found just to the left of Point A; the maximum positive shear is found just to the right of the

point. Interestingly, applying these loads to the moment influence line in Part C indicates that they cause positive moment in the so-called negative moment region of the beam.

Shear connector spacing is usually determined from the fatigue live load shear range; dead load is irrelevant. The live load moment in much of the so-called negative moment region is actually a positive moment for the loading causing the maximum shear range, as demonstrated above. Further, there may be other sources of shear (namely torsion), particularly in skewed and curved bridges. Hence, the argument to not use shear connectors in the dead load negative moment regions is weak indeed. *AASHTO LRFD* Article 6.10.10.1 requires their use throughout the length of curved continuous bridges.

Influence Line Example

A two-span continuous example bridge is shown in Figure 2.1.5.

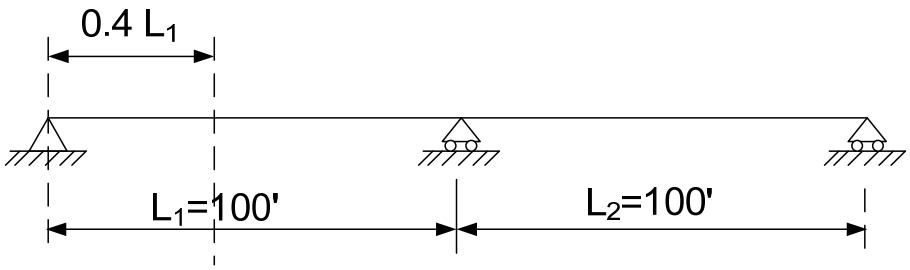
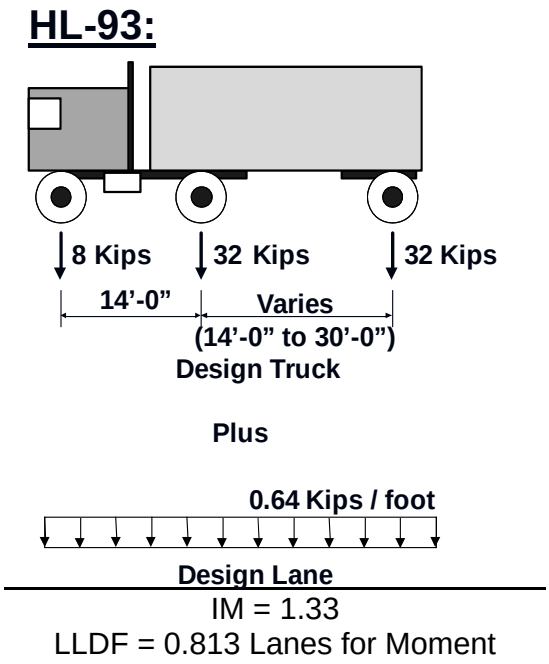


Figure 2.1.5 Example Two-Span Continuous Bridge

Part A: Calculate the approximate critical unfactored positive live load plus impact moment at $0.4L_1$ due to the HL-93 live load. HL-93 includes a truck load and a lane (uniform) load, as illustrated in Figure 2.1.6. The figure also gives the dynamic load allowance (impact) value applied only to the truck load, and the multi-lane live load distribution factor (LLDF) for vertical bending moment in units of lanes.



IM = 1.33

LLDF = 0.813 Lanes for Moment

Figure 2.1.6 HL-93 Live Load plus IM and Multi-Lane Moment LLDF for the Example Two-Span Bridge

This load is applied to the influence line for vertical bending moment at $0.4L_1$ given in Figure 2.1.7. The ordinates of the influence line are given at tenth points of the two spans, or in 10-foot increments in this case. Note that the design lane load is applied only to the positive region of the influence line. The design truck is applied with the center wheel applied at the cusp of the influence line.

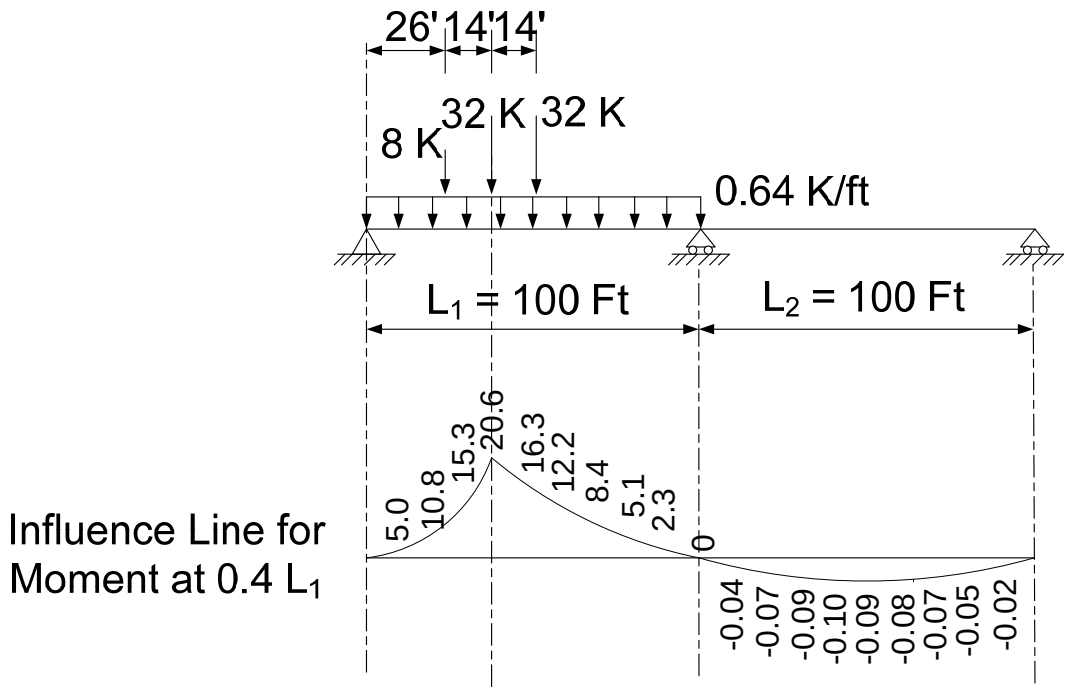


Figure 2.1.7 HL-93 Live Load Applied to Influence Line for Vertical Bending Moment at 0.4L_1 in the Example Two-Span Bridge

The positions of the truck and the lane load are so as to determine the maximum positive HL-93 vertical bending moment at 0.4L_1. Note that the truck could be pointed in either direction, but the right-to-left direction places the heavy rear axle on the larger ordinate in this case.

Interpolation between influence ordinates is necessary. The influence ordinate (Ordinate A) for the leftmost 8-kip axle load is computed as follows:

$$\text{Ordinate A} = 10.8 + \left(\frac{6'}{10'}\right)(15.3 - 10.8) = +13.5 \text{ kip} - \text{ft/kip}$$

The Ordinate B for the middle 32-kip axle load is +20.6 kip-ft/kip. By linear interpolation, the influence ordinate (Ordinate C) for the rear 32-kip axle load is computed as follows:

$$\text{Ordinate C} = 16.3 - \left(\frac{4'}{10'}\right)(16.3 - 12.2) = +14.7 \text{ kip} - \text{ft/kip}$$

The effect of the lane load is found by integrating the area under the positive portion of the plot times the load intensity. Using a linear approximation, the total area under the positive portion of the influence line shown in Figure 2.1.7 is estimated as follows:

$$A = 10\left[\left(\frac{0+5.0}{2}\right)+\left(\frac{5.0+10.8}{2}\right)+\left(\frac{10.8+15.3}{2}\right)+\left(\frac{15.3+20.6}{2}\right)+\left(\frac{20.6+16.3}{2}\right)+\left(\frac{16.3+12.2}{2}\right)+\left(\frac{12.2+8.4}{2}\right)+\left(\frac{8.4+5.1}{2}\right)+\left(\frac{5.1+2.3}{2}\right)+\left(\frac{2.3+0}{2}\right)\right]$$
$$= 960\ \text{ft}^2$$

Accounting for impact (dynamic load allowance) and the live load distribution factor, the approximate critical unfactored positive live load plus impact moment at $0.4L_1$ due to the HL-93 loading is computed as follows:

$$\text{Moment} = (\text{LLDF})(\text{Impact})\left[\sum(\text{Axle Load})(\text{Ordinate})\right] + (\text{LLDF})\left[(\text{Uniform Load})(\text{Area})\right]$$

$$\text{Moment} = (0.813)(1.33)\left[\sum(8\text{K})(13.5)+(32\text{K})(20.6)+(32\text{K})(14.7)\right]+(0.813)\left[(0.64\text{K/ft})(960)\right]$$
$$= 1{,}838\text{K}-\text{ft}$$

Part B: Calculate the approximate critical unfactored range of live load plus impact shear at $0.4L_1$ due to the fatigue live load for the design of the shear connectors for the same bridge analyzed in Part A. The fatigue live load is shown in Figure 2.1.8; the rear-axle spacing is fixed at 30 feet. The figure also gives the dynamic load allowance (impact) value applied only to the fatigue live load, and the single-lane live load distribution factor (LLDF) for shear in units of lanes.

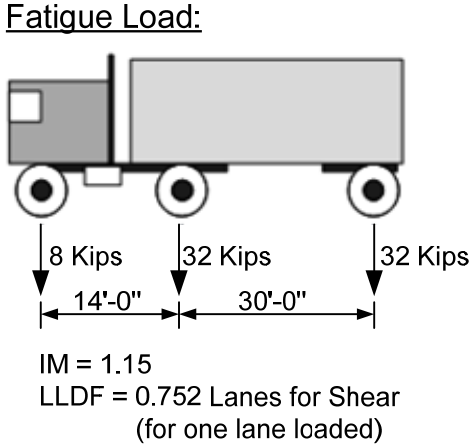


Figure 2.1.8 Fatigue Live Load plus IM and Single-Lane Shear LLDF for the Example Two-Span Bridge

By inspection, the location of the fatigue truck to produce the maximum positive live load plus impact shear due to fatigue is as shown below in Figure 2.1.9. Similarly, the location of the fatigue truck to produce the maximum negative live load plus impact shear due to fatigue is also shown in Figure 2.1.9. These locations give the maximum shear values at $0.4L_1$; they are not loaded simultaneously. In fact, they

are based on the truck headed in opposite directions, which is not realistic for the shear range for the single passage of a truck. However, it is only slightly conservative. The difference between these values is the critical unfactored range for fatigue live load plus impact shear.

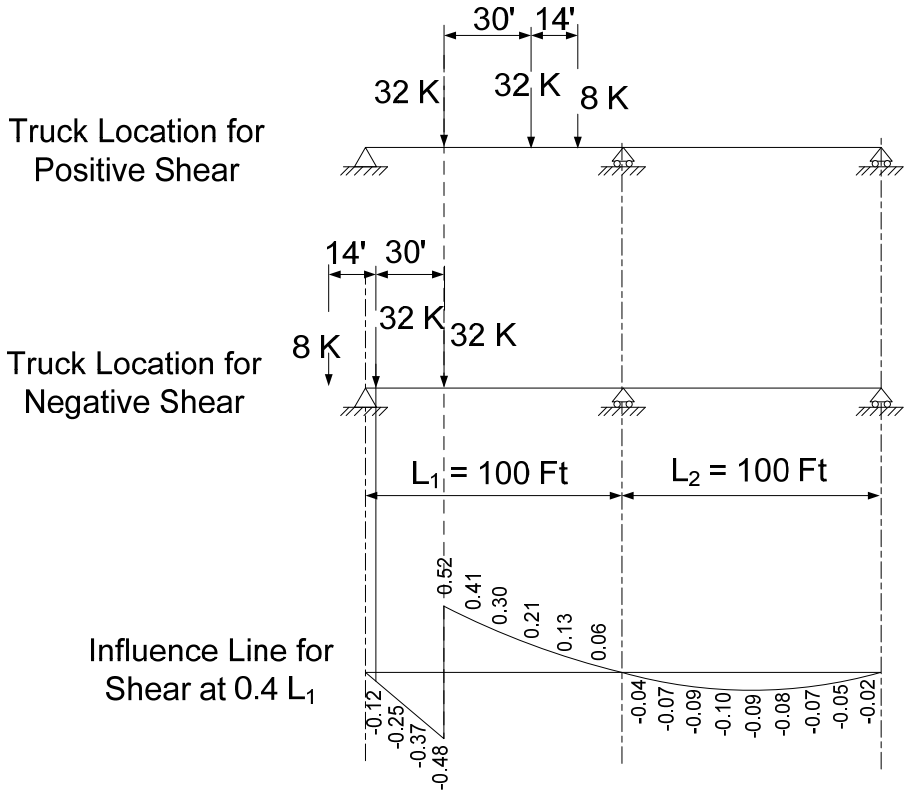


Figure 2.1.9 Fatigue Live Load Applied to Influence Line for Shear at 0.4L_1 in the Example Two-Span Bridge

$$\text{Shear} = (\text{LLDF})(\text{Impact}[\sum(\text{Axle Load})(\text{Ordinate})]$$

The maximum unfactored positive live load plus impact shear at 0.4L_1 due to the fatigue live load is computed as follows:

The Ordinate A for the rear 32-kip axle load is +0.52. The Ordinate B for the middle 32-kip axle load is +0.21. The influence ordinate (Ordinate C) for the rightmost 8-kip axle load is computed as follows:

$$\text{Ordinate C} = 0.13 - \left(\frac{4'}{10'}\right)(0.13 - 0.06) = +0.10$$

$$\text{Shear} = (0.752)(1.15)\left[(32\ \text{K})(0.52) + (32\ \text{K})(0.21) + (8\ \text{K})(0.10)\right] = +24.2\ \text{K}$$

Similarly, the maximum unfactored negative live load plus impact shear at $0.4L_1$ due to the fatigue live load is computed as follows:

The Ordinate A for the rear 32-kip axle load is -0.48. The Ordinate B for the middle 32-kip axle load is =0.12. The leftmost 8-kip axle load is off the bridge.

$$\text{Shear} = (0.752)(1.15)\left[(32\ \text{K})(-0.48) + (32\ \text{K})(-0.12)\right] = -19.2\ \text{K}$$

Therefore, the approximate critical unfactored range of live load plus impact shear at $0.4L_1$ due to the fatigue live load is computed as the difference of these two values, as follows:

$$\text{Shear Range} = +24.2\ \text{K} - (-19.2\ \text{K}) = 43.4\ \text{K}$$

Influence Surfaces

Influence lines are applicable to one-dimensional configurations. Thus, transverse live load effects must be accounted for by applying live load distribution factors to the resulting force effects. Since the use of live load distribution factors is typically not appropriate for skewed and curved steel bridges, which are best analyzed as systems, influence surfaces are most often utilized to more accurately determine the live load force effects in these bridge systems.

The same basic principles discussed previously for influence lines are applicable to influence surfaces. The difference is that influence surfaces consider the transverse position of the live loads as well as the longitudinal position.

There is no need for live load distribution factors to account for transverse effects. Influence surfaces provide influence ordinates over the entire deck. Typically, these ordinates are determined by applying a vertical unit load at selected longitudinal and transverse positions. Live loads are then placed on the surface at critical positions permitted by specification. The load effect that the influence surface was developed for is determined by multiplying the intensity of the load times the corresponding ordinate. Influence surfaces are applicable to all linearly elastic responsive structures.

In skewed and curved bridges, influence surfaces are generally needed for other actions in addition to major-axis bending moment, shear, reactions and deflections. For example, additional surfaces are typically needed for live load cross-frame forces and lateral flange bending moments.

Figure 2.1.10 shows an influence surface for the vertical bending moment in the outside fascia girder G4 in Span 1 of the example I-girder bridge (Section 5.1). The orange represents the deck surface and the zero values of the surface. The framing plan for the bridge is shown in the figure to indicate (with a circle) the location for

which the influence surface is developed. A typical bridge design requires several hundred such influence surfaces that must then be loaded.

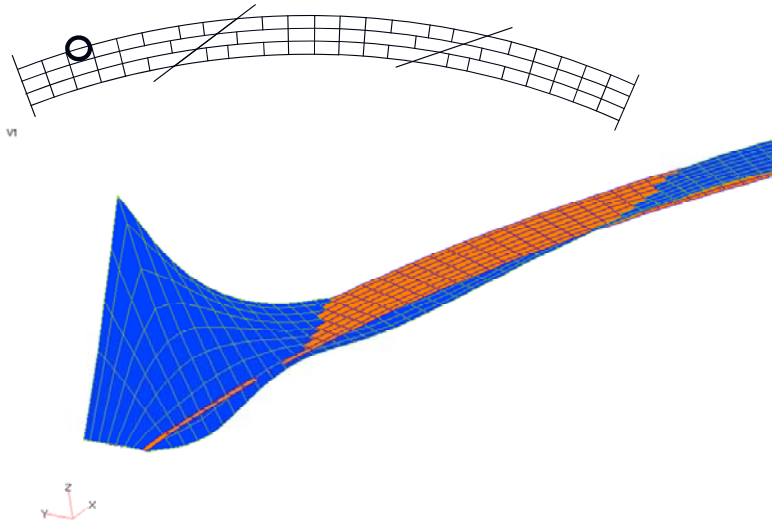


Figure 2.1.10 Influence Surface for Vertical Bending Moment in Span 1 of G4 of the Example I-Girder Bridge

Figure 2.1.11 shows an influence surface for the vertical bending moment in the inside fascia girder G1 at Pier 1 of the same example bridge. The yellow represents the deck surface and the zero values of the surface. Regions of the surface above the yellow represent a positive response. Note that positive moment is introduced at the pier by loading in portions of Span 1. This is due partially to the skew and curvature.

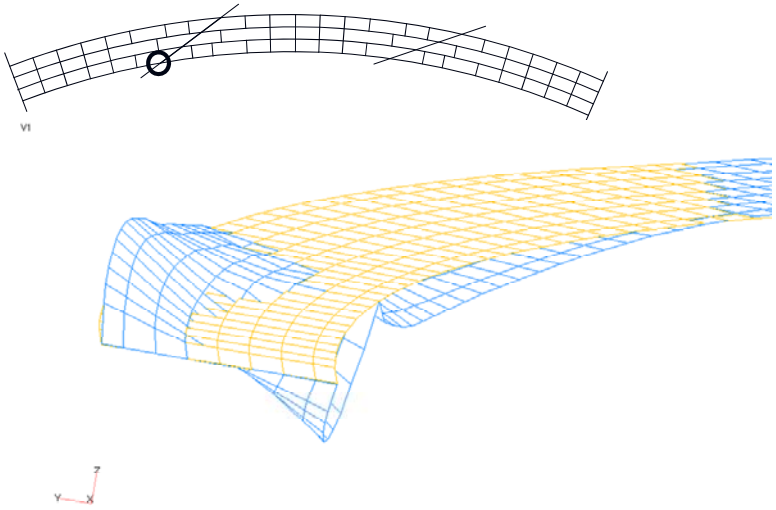


Figure 2.1.11 Influence Surface for Vertical Bending Moment at Pier 1 of G1 in the Example I-Girder Bridge

Figure 2.1.12 shows the influence surface for vertical shear at the location identified (approximately 73.8 feet from the abutment).

.

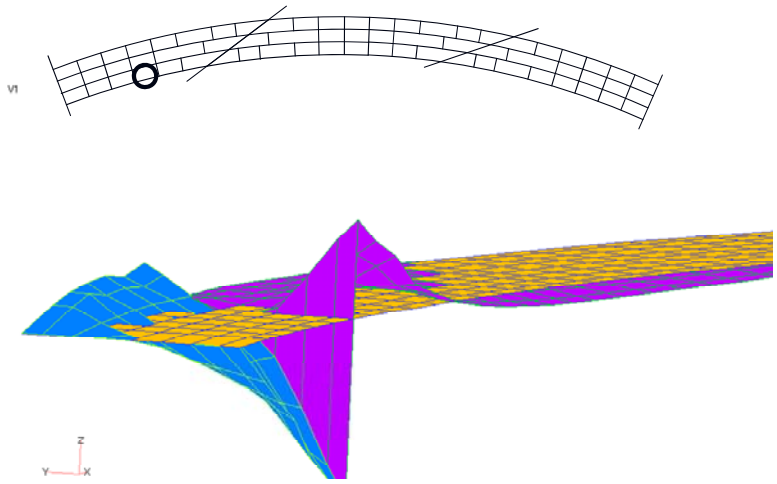


Figure 2.1.12 Influence Surface for Vertical Shear in Span 1 of G1 of the Example I-Girder Bridge

Another category of influence surface is for cross-frame forces, as shown in Figure 2.1.13.

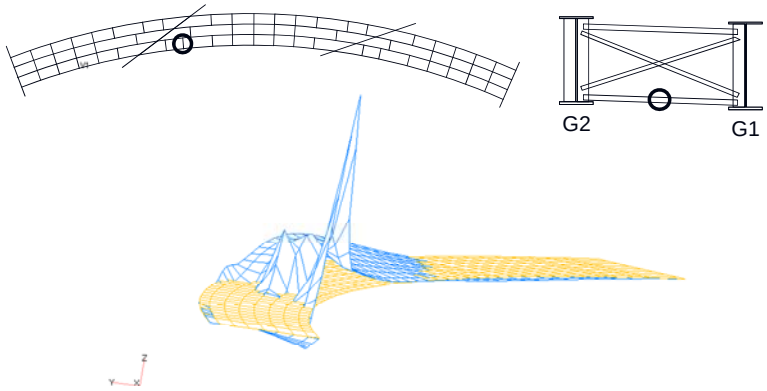


Figure 2.1.13 Influence Surface for Cross-Frame Force in the Bottom Chord of a Cross-Frame in Span 2 of the Example I-Girder Bridge

As discussed in this manual, additional actions must be considered in the design of skewed and curved girder bridges. Cross-frames are treated as primary members in such bridges, so they should be modeled in system analyses. Obviously, it is important to consider the live-load effects for strength and fatigue.

The live load is typically placed in a longitudinal path. The range of force in transverse members (for fatigue design) often occurs when the live load is permitted to roam transversely on the surface. This is evident from viewing the surface shown in Figure 2.1.13. Observe the local peaks in the surface and the non-linear behavior between girders.

Obviously, vehicles rarely if ever, move transversely so the range of force computed by placing the vehicle in two different transverse positions would occur only when two trucks traverse the bridge slightly out-of-phase with each other. *AASHTO LRFD* Article C6.6.1.2.1 suggests that this can be accounted for by using 75 percent of the stress range computed as above for two different transverse load positions.

Figure 2.1.14 shows an influence surface for the bottom flange lateral bending moment in G2 of the example I-girder bridge at a cross-frame located in Span 2. Note that the cross-frames are staggered at this location; this causes larger flange lateral moments.

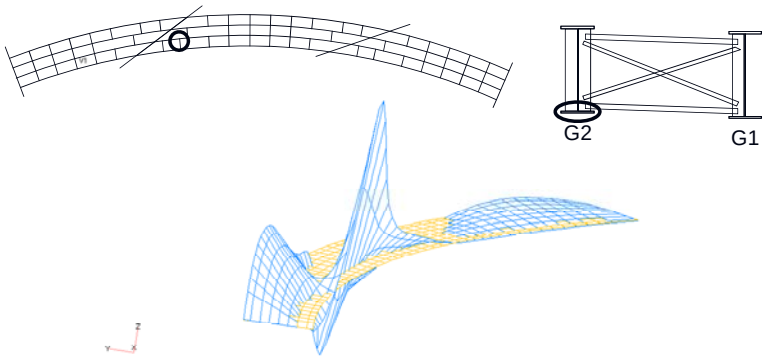


Figure 2.1.14 Influence Surface for Bottom Flange Lateral Bending Moment in G2 of the Example I-Girder Bridge at a Cross-Frame in Span 2

The maximum bottom flange lateral moment at this location is 41 kip-ft for HL-93 loading. The design truck and design lane each produce approximately 20 kip-ft. Design of the flange requires that the stresses due to the lateral moment and the vertical moment be combined. Typically, the two cases are combined although the two actions are not caused by the live load placed in the same position. It is not practical to find the critical combined cases. There are an infinite number of possible live load locations to check. Each case would have to be carried to the final stages and recorded to find where the critical case is located.

The influence surfaces extend to the edges of the deck to ensure that loads beyond the exterior girder will be treated properly. The live load is only permitted to roam on the deck within the realms defined by *AASHTO* (Section 2.1.4.1) and controlled by the Design Engineer.

2.1.4.1 Live Load Placement

The term “design lanes” is generally defined as the number of 12-foot-wide lanes loaded with live load. Design lanes are taken as the integer part of the ratio *w*/12.0, where *w* is the clear roadway width in feet between curbs and/or barriers (*AASHTO LRFD* Article 3.6.1.1.1). Design lanes are defined in the *AASHTO LRFD* Specifications the same as in the *AASHTO* Standard Specifications.

Each design lane is a segment of the deck that may have the specified live load applied within its boundaries. On straight bridges with no skewed supports, design lanes generally may run in a straight line at a specified distance from a curb or barrier. However, when the bridge is curved or has skewed supports, the design lanes may wander in order to produce a critical response. The specifications do not prevent the lanes from wandering. The need to assume this is evident from examination of the influence surfaces.

The design truck is assumed to be six-feet wide and is permitted to be no closer than two feet from the edges of the design lane in which it is placed. The design lane (uniform) load is assumed to be 10-feet wide. The loaded lanes are positioned on the influence surface within the roadway width to produce the extreme force effects in the component under consideration. Live load force effects due to concentrated and uniform loads are determined in the same fashion as discussed previously for influence lines.

An example of lane positioning is shown in Figure 2.1.15. In this case, three design lanes are shown to produce the maximum effect in the left-most girder. Note that this positioning is only certain for the position over the point investigated. At other points on the bridge, the design lanes may have wandered on the deck. Usually, it is assumed that lanes may not cross each other.

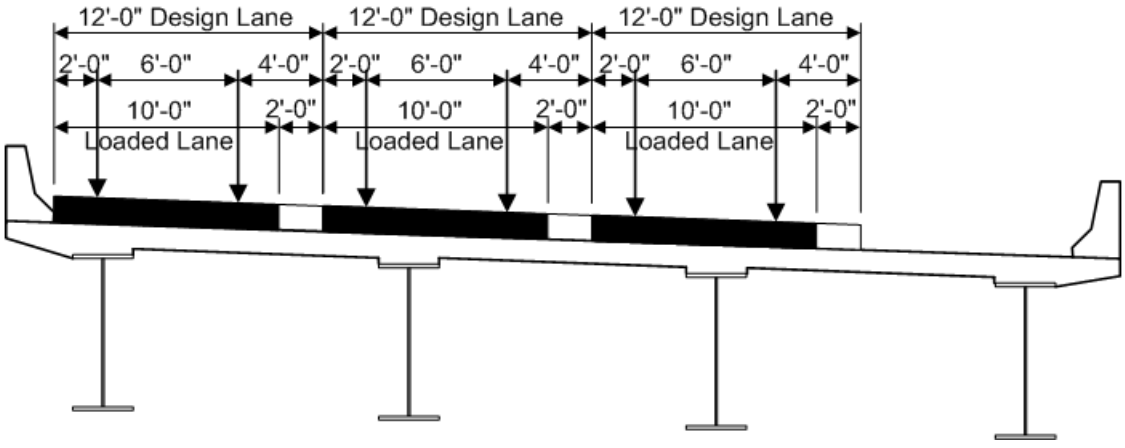


Figure 2.1.15 Positioning of Design Lanes and Loaded Widths within Lanes

Roadway widths from 20.0 to 24.0 feet are to have two design lanes, with each taken equal to one-half the roadway width. In cases where traffic lanes are less than 12.0 feet in width, the number of design lanes is to be taken equal to the number of traffic lanes, with the width of each design lane taken as the width of the traffic lane (*AASHTO LRFD* Article 3.6.1.1.1). Design lanes may be assumed to be 10 feet wide rather than 12. Some Owners prefer this option as a standard.

Design vehicle wheel loads are to be positioned transversely such that the center of a wheel load is not closer than 2.0 feet from the edge of the design lane, as mentioned above. For design of the deck overhangs, wheel loads are to be positioned not closer than 1.0 foot.

Loads need not be positioned side-by-side within their lanes on the surface. Typically, for skewed and curved bridges, the loads will need to be placed in staggered positions (or possibly even in different spans) within adjacent lanes in order to determine the critical responses. Wheel loads may be adjusted by the unit wheel-load factors to account for centrifugal force effects (Section 1.3.2.3.6).

2.1.4.2 Multiple Presence Factors

Multiple presence factors account for the probability of simultaneous lane occupation by the full design live load. The multiple presence factors shown below in Table 2.1.1 are taken from *AASHTO LRFD* Article 3.6.1.1.2.

Table 2.1.1 Multiple Presence Factors, *m*

Number of Loaded Lanes	Multiple Presence Factor, *m*
1	1.20
2	1.00
3	0.85
>3	0.65

These factors are applied whenever refined analyses are employed. For example, they are used when determining force effects from influence surfaces.

Multiple presence factors are not to be used in conjunction with the live load distribution factors given in *AASHTO LRFD* Articles 4.6.2.2 and 4.6.2.3, except where the lever rule or the special analysis for exterior girders in beam-slab bridges specified in *AASHTO LRFD* Article 4.6.2.2.2d is used.

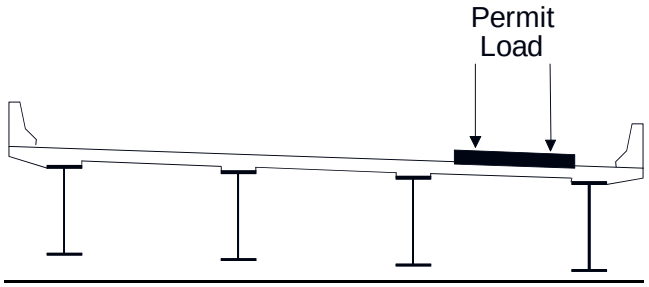
The calibration of the *AASHTO LRFD* Specification is based on pairs of vehicles instead of a single vehicle. The HL-93 is a so-called notional load rather than an actual load. When a single vehicle is on the bridge, its notional load can be heavier than each one of a single pair of notional vehicles and still have the same probability of occurrence. Therefore, a multiple presence factor of 1.2 is used for a single lane loaded.

The multiple presence factor is not applied at the fatigue limit state (*AASHTO LRFD* Article 3.6.1.1.2). The 1.2 factor has been included in the approximate distribution factor equation for one-lane loaded and should be factored out for fatigue. For other cases, such as the lever rule, the special analysis for exterior girders and refined analyses, the 1.2 factor should not be applied to the single fatigue vehicle.

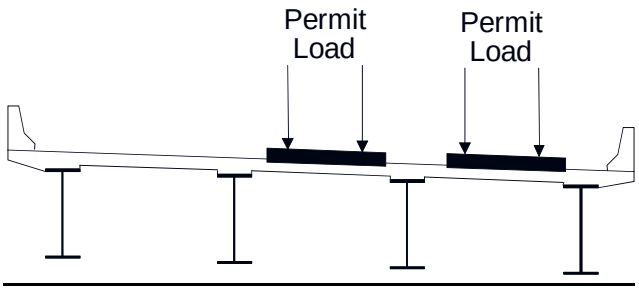
2.1.4.3 Design Permit Loads

Special design permit loads are sometimes specified by the Owner as additional design live loads. The configuration, size and weight of design permit vehicles are specified by the Owner. The manner in which permit loads are considered at design differs from state to state.

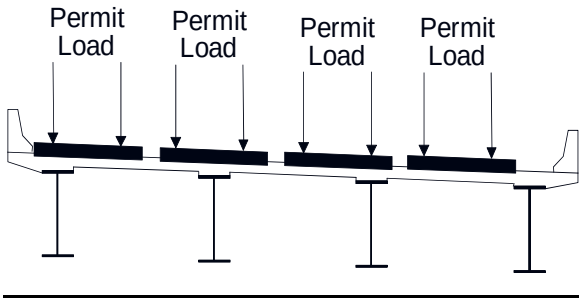
The Owner may require that design permit loads be placed in only one lane (Figure 2.1.16 Part A), in two lanes (Figure 2.1.16 Part B), or in all design lanes (Figure 2.1.16 Part C). The Owner may require that the permit load be placed in one lane with the HL-93 design live load placed in one or more of the remaining design lanes (Figure 2.1.16 Part D). More than one lane of design permit load is usually considered for routes with a large number of permit vehicles. The reason that HL-93 is considered in the other lanes is that permitted loads are often not escorted so traffic is not necessarily forbidden on the structure when a permit vehicle is present. The horizontal dark bars in Figure 2.1.16 represent the HL-93 design lane load, which is recommended to be placed in the same lane(s) in conjunction with the design permit load(s) (discussed further below).



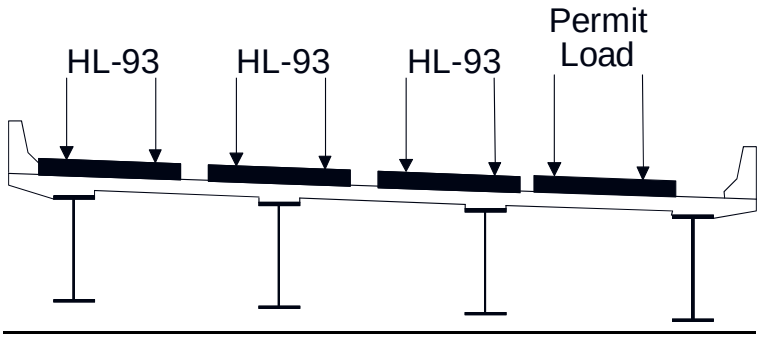
Part A



Part B



Part C



Part D

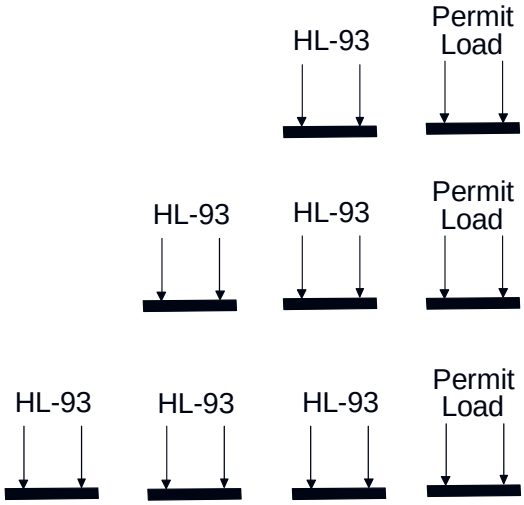
Figure 2.1.16 Design Permit Loads
A) Design Permit Load in One Lane; B) Design Permit Load in Two Lanes; C) Design Permit Load in All Lanes; D) Design Permit Load in One Lane with HL-93 in All Remaining Lanes

AASHTO LRFD Article 4.6.2.2.5 provides an empirical method to obtain a distribution factor for live loads when design permit loads are placed in one lane with HL-93 loading placed in the other lanes. This method basically differentiates between a distribution factor for a group of equal live loads and a distribution factor that acknowledges different loads in the lanes. As an alternative to the method proposed, the Design Engineer may consider the pile analogy method described in *AASHTO LRFD* Article C4.6.2.2.2d. It should also be noted that these methods are applicable only when all of the girders have the same stiffness.

Empirical methods are generally not applicable for skewed and curved bridges which require some type of system approach for analysis. Finite element methods, either 2D grillage or 3D, should be employed in these cases.

It has been observed that there is some inconsistency and incompleteness in the instruction regarding the application of design permit loads in the *AASHTO LRFD* Specification. For this reason, the following recommendations are presented below. Special emphasis is made for structures analyzed using a system approach, such as skewed and curved bridges requiring a system analysis.

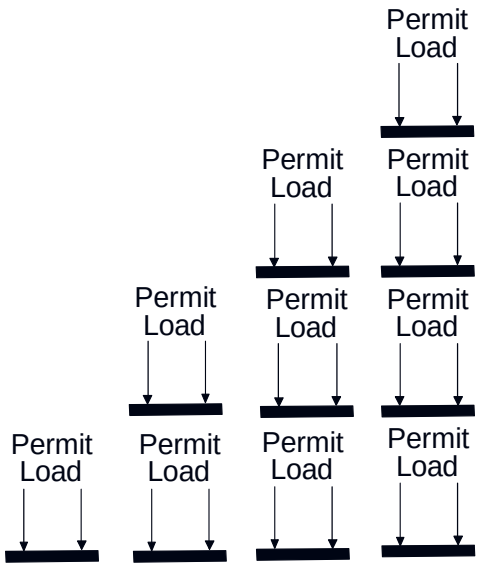
- The Strength II load combination specified in *AASHTO LRFD* Table 3.4.1-1 (Section 1.3.3) should be used for all design permit cases. In all cases, a single design permit vehicle should be considered in conjunction with an HL-93 design lane load placed in the same lane. The lane load is included since normal traffic is often not controlled in the presence of permit loads and the lane load is a major contributor to the live load force effects in longer spans. The Strength II live load factor of 1.35 should be applied to all live load force effects, including the force effects due to the HL-93 loads (or portion of the HL-93 loads) that may be applied in combination with the design permit load(s).
- A second design permit vehicle should be considered in the same lane as the first permit vehicle when computing negative girder moments between points of permanent-load contraflexure and interior-pier reactions. In this case, both permit vehicles should be considered acting in conjunction with 90 percent of the HL-93 design lane load placed in the same lane. A variable headway with a minimum of 50 feet should be assumed between the front and rear axles of the two permit loads.
- A dynamic load allowance (IM) of 33 percent should be applied to the design permit loads (and to the HL-93 design truck load(s) when considered).
- For checks of permanent deformations at the service limit state, a load factor of 1.10 should be applied to all live load force effects, including those due to the HL-93 loads (or portion of the HL-93 loads) applied in combination with the design permit load.
- Figure 2.1.17 gives suggested multiple-presence factors to be used for live load force effects where one design permit load is considered in combination with the full HL-93 design live load in one or more of the remaining design lanes. Only one design permit load should be assumed acting in combination with HL-93 loading in one or more of the remaining design lanes; HL-93 loading should not be considered to act in combination with two or more simultaneous design permit loads. Figure 2.1.18 deals with the case where there are one or more simultaneous design permit loads on the bridge. Note that the multiple presence factors are different for the HL-93 load (or portion of the HL-93 load) and the permit load in each case. The permit load is assumed to be a true load while the HL-93 load is a notional load.



Design Permit Load	HL-93 Design Lane Load & HL-93 Design Truck Load
$m = 0.85$	$m = 1.0$
$m = 0.65$	$m = 0.85$
$m = 0.65$	$m = 0.65$

IM = 33% applied to design permit load & HL-93 design truck load

Figure 2.1.17 Suggested Multiple Presence Factors for Case with One Design Permit Load and HL-93 Load in One or More of the Remaining Lanes



Design Permit Load	HL-93 Design Lane Load
$m = 1.0$	$m = 1.2$
$m = 0.85$	$m = 1.0$
$m = 0.65$	$m = 0.85$
$m = 0.65$	$m = 0.65$

IM = 33% applied to design permit load

Figure 2.1.18 Suggested Multiple Presence Factors for Case with One or More Simultaneous Design Permit Loads

Figures 2.1.17 and 2.1.18 recommend that the multiple presence factor applied to the force effects due to the design permit load be dropped one category from the factor applied to the HL-93 force effects for a given number of lanes loaded (i.e. the factor specified in *AASHTO LRFD* Table 3.6.1.1.2-1 and discussed previously). For the force effects due to: 1) the HL-93 design lane load of 0.64 klf applied in conjunction with the single design permit load as previously recommended; and 2) the HL-93 truck *and* lane load applied in one or more of the remaining design lanes, it is recommended that the appropriate multiple presence factor for HL-93 loading be applied as specified in *AASHTO LRFD* Table 3.6.1.1.2-1. The single design permit load should be treated as one lane in determining the total number of lanes loaded.

For example, for the case of a single design permit load applied in combination with two lanes of HL-93 (i.e. a total of three design lanes loaded), the specified multiple presence factor of 0.65 for four or more lanes loaded would be applied to the design permit load, and the multiple presence factor of 0.85 for three lanes loaded would be applied to the force effects due to the HL-93 design lane load applied in conjunction with the design permit load, and to the force effects due to the HL-93 truck and lane load applied in the two adjacent lanes (Figure 2.1.17). With two simultaneous design permit loads assumed, it is recommended that the specified multiple presence factor of 0.85 for three lanes loaded from *AASHTO LRFD* Table 3.6.1.1.2-1 be applied to the force effects due to the design permit loads, and the multiple presence factor of 1.0 for two lanes loaded from *AASHTO LRFD* Table 3.6.1.1.2-1 be applied to the force effects due to the HL-93 design lane load applied in conjunction with each design permit load (Figure 2.1.18).

Note that when two or more permit vehicles are considered, they are not necessarily side-by-side; they may be offset from each other along the length of the bridge much as the HL-93 vehicle may be.

Influence Surface Example

For the bridge and influence surface shown in this example, the following will be computed by positioning the wheels of the single fatigue truck at least 2.0 feet from the curb line and by including the effects of centrifugal force:

A. The approximate critical unfactored positive live load plus impact vertical bending moment at Node 24 (Figure 2.1.20).

B. The approximate critical unfactored negative live load plus impact vertical bending moment at Node 24 (Figure 2.1.20).

Figure 2.1.19 shows a cross-section of the example I-girder bridge (Section 5.1), which is used in this illustration.

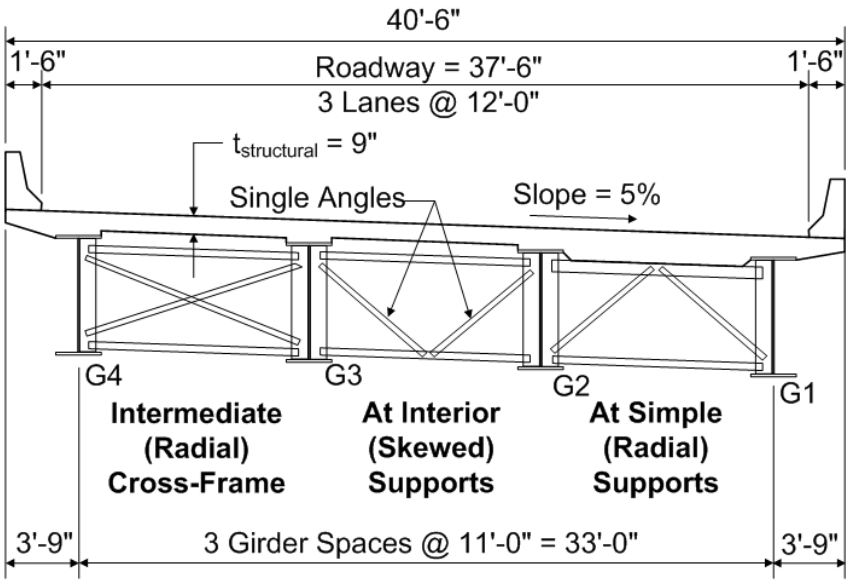


Figure 2.1.19 Example I-Girder Bridge Cross-Section

Figure 2.1.20 is a plan view of the example bridge with a contiguous cross-frame arrangement, which is also assumed in this illustration.

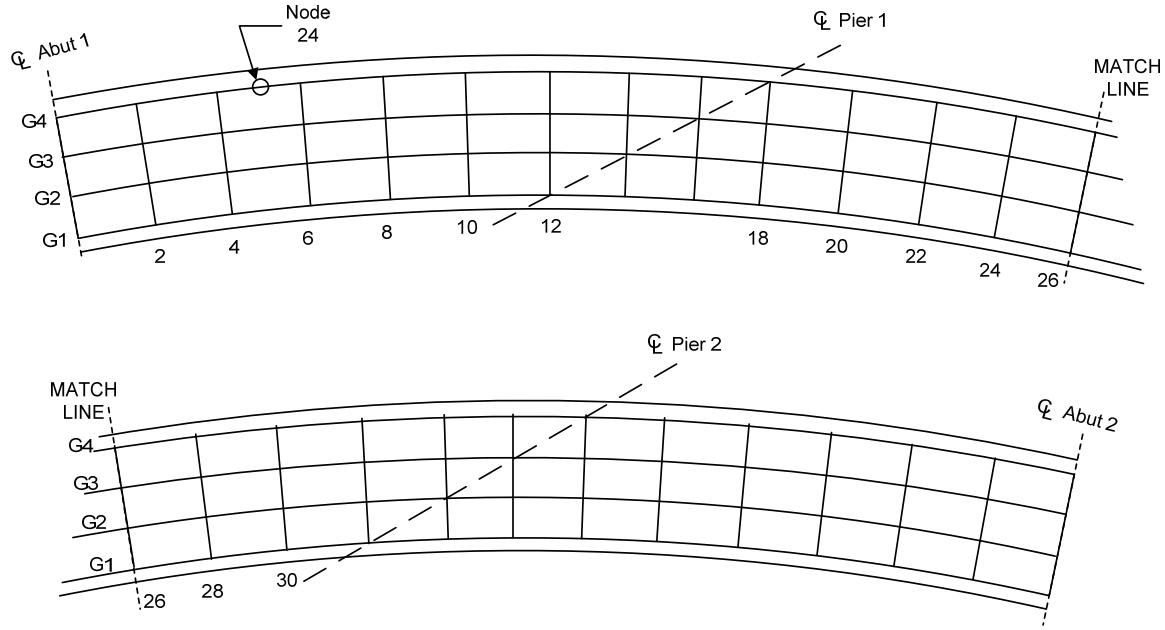


Figure 2.1.20 Plan View of the Example I-Girder Bridge with a Contiguous Cross-Frame Arrangement

Node 24 is shown in Figure 2.1.20. This example is based on the influence surface for vertical bending moment at Node 24. The girder lines and the edge of the deck are included in this plan view as well.

The influence surface shown in Figure 2.1.21 is for the vertical bending moment at Node 24, which is in the outside fascia G4 in Span 1 of the example bridge. The influence surface ordinates are provided in subsequent figures.

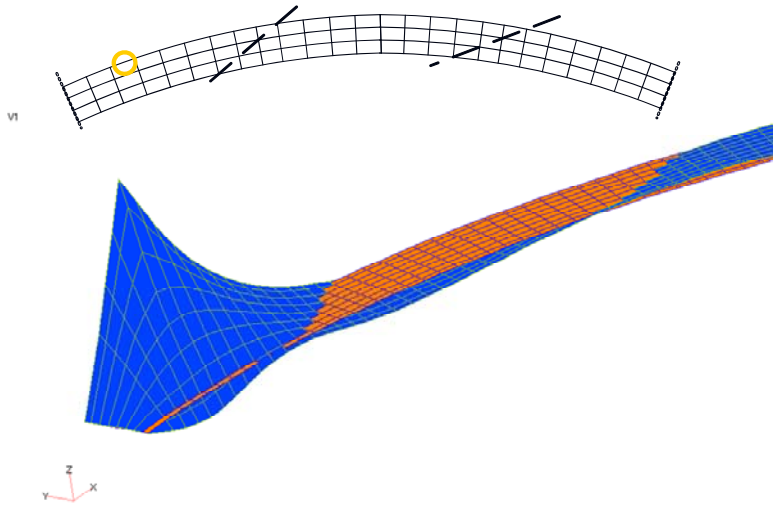
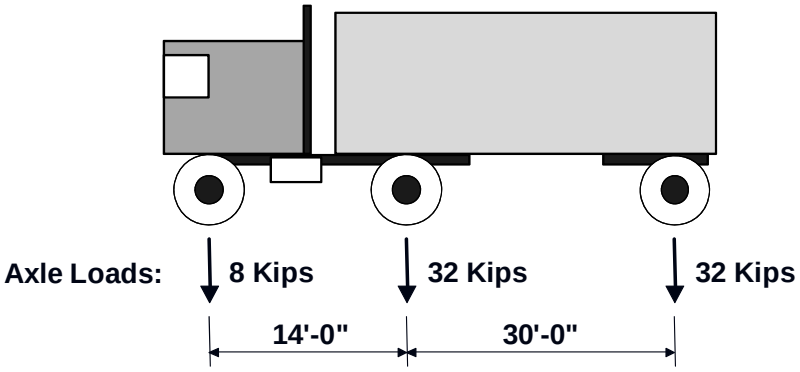


Figure 2.1.21 Influence Surface for Vertical Bending Moment at Node 24 in Span 1 of G4 of the Example I-Girder Bridge

Figure 2.1.22 presents the fatigue live load (Section 1.3.2.3.3) used in this example. The fatigue live load is a single truck, without the lane load, with a dynamic load allowance of 15 percent applied.



IM = 1.15

Figure 2.1.22 Fatigue Live Load

The rear-axle spacing of the fatigue live load is a constant 30’-0". The constant rear-axle spacing approximates that for the 4- and 5-axle semi-trailers that do most of the

fatigue damage to bridges. The fatigue live load occupies a single lane on the bridge; it does not occupy multiple lanes. The multiple presence factor of 1.2 is *not* to be applied for fatigue investigations.

The unit wheel load factors to be applied to the fatigue live load to account for the effects of centrifugal force computed in Section 1.3.2.3.6 are:

- Outside wheels = 1.134
- Inside wheels = 0.866

Figure 2.1.23 illustrates a schematic of the wheels of the fatigue live load (drawn to scale) that will be placed on the influence surface in subsequent figures.



Figure 2.1.23 Schematic of the Wheels of the Fatigue Live Load (drawn to scale)

Part A: The approximate critical unfactored positive live load plus impact vertical bending moment at Node 24 due to the fatigue live load will be calculated in Part A.

Figure 2.1.24 presents the influence surface ordinates in Span 1 for the vertical bending moment at Node 24 that are required to accomplish this computation.

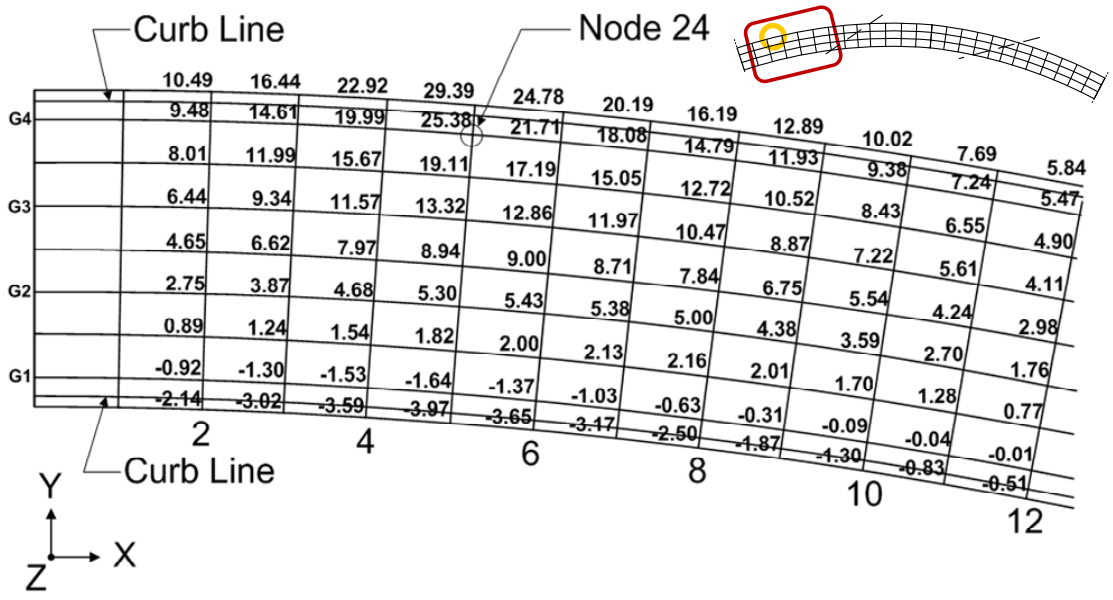


Figure 2.1.24 Influence Surface Ordinates in Span 1 for Vertical Bending Moment at Node 24

The schematic wheel-load model of the fatigue live load (Figure 2.1.23) is positioned on the influence surface in Figure 2.1.25 so as to maximize the positive vertical bending moment at Node 24 based on the influence ordinates shown. The wheel loads must be least two feet from the curb line.

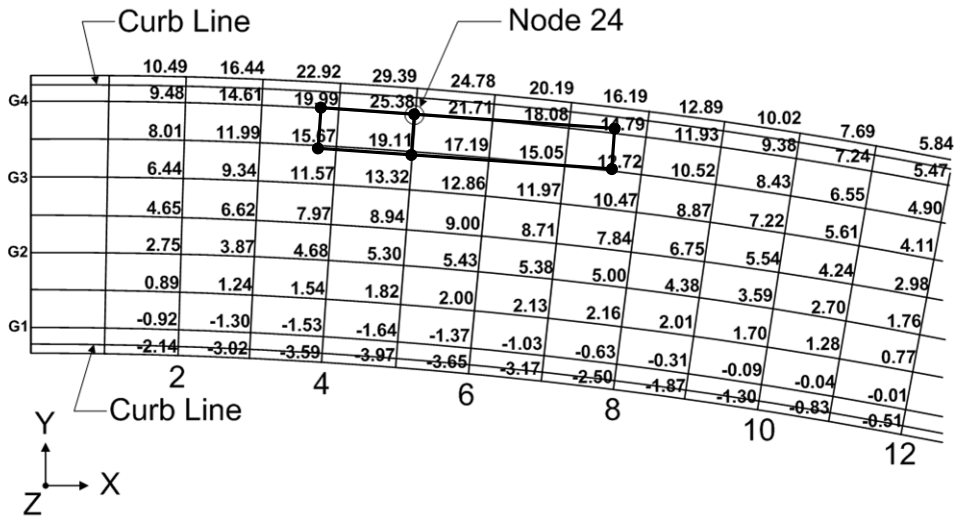


Figure 2.1.25 Wheel-Load Model of the Fatigue Live Load Positioned on Influence Surface to Maximum the Positive Vertical Bending Moment at Node 24

Figure 2.1.26 illustrates in general how the influence surface ordinates shown in Figure 2.1.24 are obtained. An influence surface ordinate corresponds to a specific force effect at a specific location.

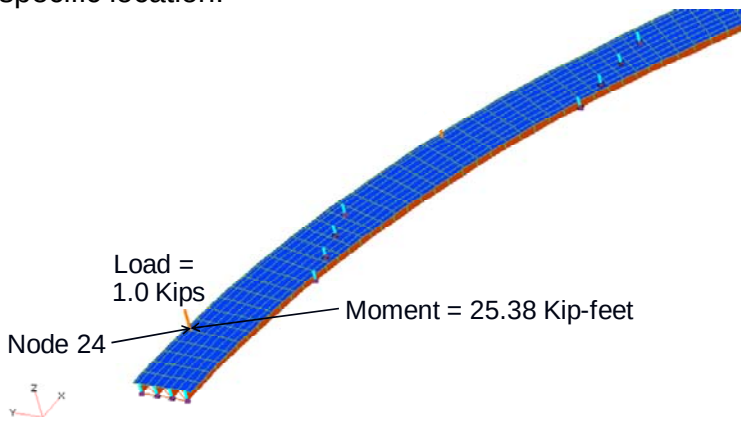


Figure 2.1.26 Determination of the Influence Surface Ordinate for Vertical Bending Moment at Node 24 for a Load Applied at Node 24

For example, to determine the influence surface ordinate for the vertical bending moment at Node 24 caused by a load applied directly to Node 24, the 3D model of

the bridge (in this case) is analyzed for a vertical unit load applied at Node 24 (Figure 2.1.26). The corresponding influence surface ordinate has a value equal to the vertical bending moment at Node 24 caused by that unit load (or 25.38 kip-feet/kip in this case). The ordinates at other nodes in that span shown in Figure 2.1.24 are determined in a similar fashion.

The following equation is used to compute the approximate critical unfactored positive live load plus impact vertical bending moment at Node 24 due to the fatigue live load:

$$\text{Moment} = \sum \left[(\text{WheelLoad})(\text{Impact})(\text{Effect of Centrifugal Force})(\text{Influence Surface Ordinate}) \right]$$

For this illustration, influence surface ordinates not directly under a wheel load are determined using linear interpolation. The solution is the sum of the six components from each of the six individual wheel loads.

The columns in the following computations are as follows:

- First column – wheel load (kips)
- Second column – dynamic load allowance (impact) (unitless)
- Third column – unit wheel-load factor to account for effects of centrifugal force (unitless)
- Fourth column – estimated influence surface ordinate (kip-ft/kip)
- Fifth column – positive live load plus impact moment due to the wheel load under consideration (kip-ft)

In the third column, the larger unit wheel-load factor for centrifugal force is applied to the outside wheels (i.e. the wheel loads closest to the edge of deck), and the smaller unit wheel-load factor is applied to the inside wheels.

$$(4.0)(1.15)(1.134)(18.8) = 98$$

$$(16.0)(1.15)(1.134)(25.4) = 530$$

$$(16.0)(1.15)(1.134)(16.0) = 334$$

$$(4.0)(1.15)(0.866)(14.5) = 58$$

$$(16.0)(1.15)(0.866)(18.8) = 300$$

$$(16.0)(1.15)(0.866)(13.0) = 207$$

$$\sum = 1{,}527$$

Therefore, the approximate critical unfactored positive live load plus impact vertical bending moment at Node 24 due to the fatigue live load is 1,527 kip-feet.

Part B: The critical unfactored negative live load plus impact vertical bending moment at Node 24 due to the fatigue live load is computed in Part B.

Figure 2.1.27 presents the influence surface ordinates in Span 2 for the vertical bending moment at Node 24 in Span 1 that are required to accomplish this computation. Note that the ordinates are all negative in Span 2.

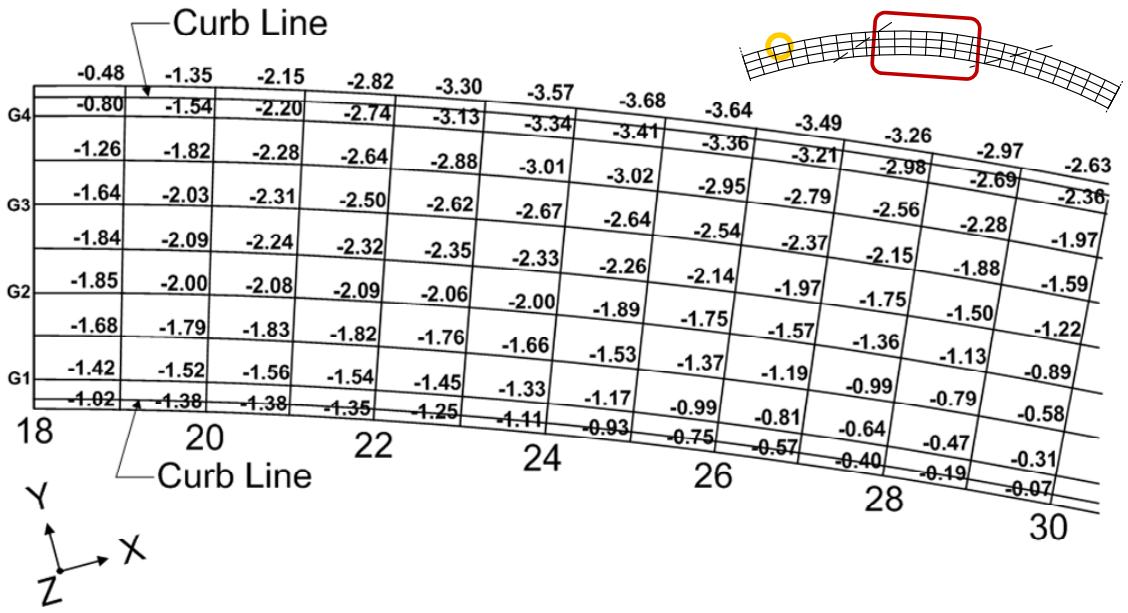


Figure 2.1.27 Influence Surface Ordinates in Span 2 for Vertical Bending Moment at Node 24

In this case, to determine the influence surface ordinate for the vertical bending moment at Node 24 in Span 1 caused by a load applied at a specific location over G4 in Span 2, the 3D model of the bridge (in this case) is analyzed for a vertical unit load applied at that location in Span 2 (Figure 2.1.28). The corresponding influence surface ordinate has a value equal to the vertical bending moment at Node 24 caused by that unit load (or -3.41 kip-feet/kip in this case). Again, the ordinates at the other nodes in that span shown in Figure 2.1.27 are determined in a similar fashion.

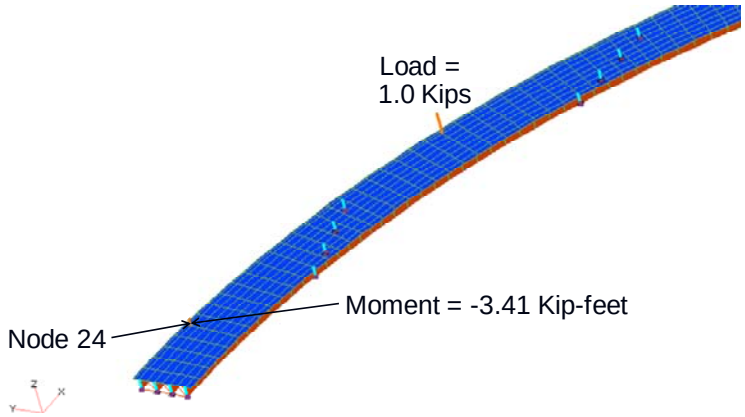


Figure 2.1.28 Determination of the Influence Surface Ordinate for Vertical Bending Moment at Node 24 for a Load Applied Over G4 in Span 2

The schematic wheel-load model of the fatigue live load (Figure 2.1.23) is positioned on the influence surface in Figure 2.1.29 (in Span 2) so as to maximize the negative vertical bending moment at Node 24 in Span 1 based on the influence ordinates shown. Once again the wheel loads must be least two feet from the curb line.

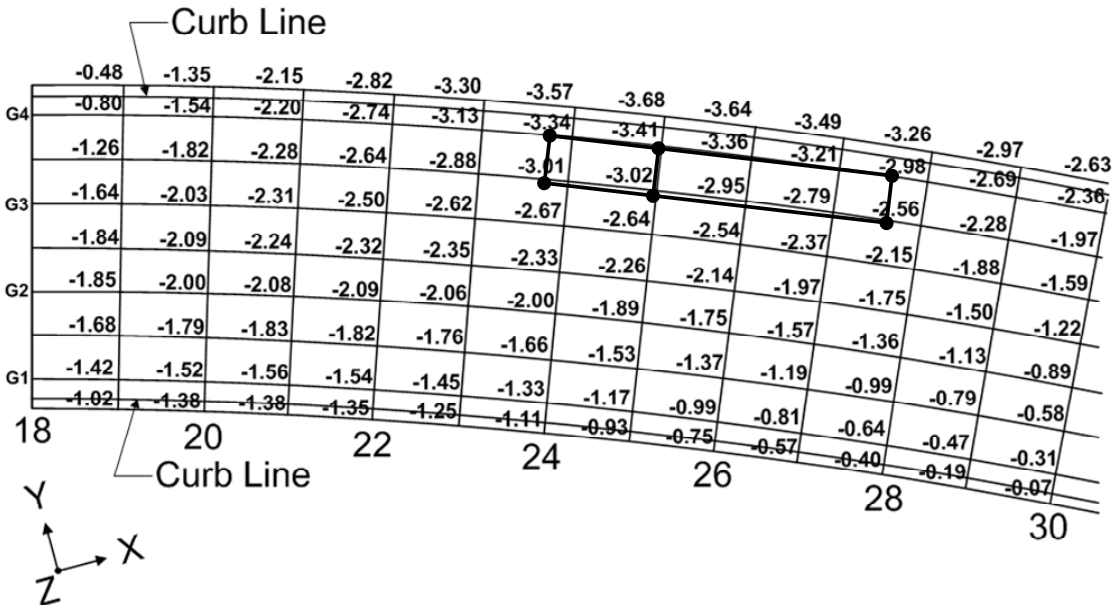


Figure 2.1.29 Wheel-Load Model of the Fatigue Live Load Positioned on Influence Surface to Maximum the Negative Vertical Bending Moment at Node 24

The equation shown previously in Part A is used to compute the approximate critical unfactored negative live load plus impact vertical bending moment at Node 24 due to the fatigue live load. Influence surface ordinates not directly under a wheel load are once again determined using linear interpolation. The solution is the sum of the six

components from each of the six individual wheel loads. The data in the columns below are the same as defined previously in Part A:

$$(4.0)(1.15)(1.134)(-3.3) = -17$$

$$(16.0)(1.15)(1.134)(-3.4) = -71$$

$$(16.0)(1.15)(1.134)(-3.1) = -65$$

$$(4.0)(1.15)(0.866)(-3.0) = -12$$

$$(16.0)(1.15)(0.866)(-3.0) = -48$$

$$(16.0)(1.15)(0.866)(-2.6) = -41$$

$$\sum = -254$$

Therefore, the approximate critical unfactored negative live load plus impact vertical bending moment at Node 24 due to the fatigue live load is -254 kip-feet.

2.1.5 General LRFD Analysis Requirements

This section reviews some of the general *AASHTO LRFD* specification requirements for structural analysis, including requirements for curved girder bridge analysis.

According to *AASHTO LRFD* Article 4.6.1.2.1, for structures curved in plan, the moments, shears and other force effects required to proportion the superstructure components are to be based on a rational analysis of the entire superstructure. As illustrated in this manual, equilibrium of curved girder bridges is developed by transfer of load between the girders (more so in curved I-girder bridges than in curved box-girder bridges). Thus, the analysis must recognize the integrated behavior of all the structural components. Bracing members are considered to be primary members in these bridges since their action is necessary to provide equilibrium. The concrete deck acts in transverse flexure, longitudinal flexure, vertical and horizontal shear. Torsion increases the horizontal deck shear in curved and/or skewed box-girder bridges.

The entire superstructure, including bearings (Figure 2.1.30), is to be considered as integral with the structural unit. An analysis should consider the bearing orientation and the restraint of the bearings afforded by the substructure, including the stiffness of the substructure. The resulting lateral reactions are considered in designing the

bearings, cross-frames/diaphragms, lateral bracing, deck and substructure. The lateral restraint offered by integral abutments or piers can be recognized in a proper analysis.



Figure 2.1.30 Bearings

When girder sections are subjected to significant torsion, as they are in curved bridges and in bridges with skewed supports, the girder sections do not remain plane. Experience has shown that distortion of I-shaped cross-sections need not be considered in the structural analysis of a properly braced bridge. Cross-section distortion can have a significant effect on the torsional behavior of steel box girders and its effect is typically attenuated by the provision of sufficient internal cross bracing. Although the section is allowed to distort, the position of the loads is assumed not to change in linear elastic analyses. Classical methods of analysis are usually based on strength of materials assumptions that do not recognize the effects of cross-section distortion. Refined analyses (e.g. 3D finite element analyses) in which the actual cross-section shape of the I- or box girder is rigorously modeled can recognize cross-section distortion and its effect on structural behavior.

Centrifugal force effects are considered in the analysis of horizontally curved bridges, as discussed further in Section 1.3.2.3.6.

As specified in *AASHTO LRFD* Article 4.5, mathematical models are to include loads, geometry and material behavior of the structure, and where appropriate, the response characteristics of the foundation. The choice of the model is to be based on the limit states investigated, the force effect being quantified, the complexity of the structure and the accuracy required of the analysis.

Linear elastic behavior of materials is assumed so specification of material properties is rather straightforward. An elastic modulus (Young's Modulus) and a Poisson's Ratio is specified for each material. From these properties the shear modulus can be computed. The density of the material is required to address the weight or mass of each element. This property may be specified as the mass density with a gravitational constant or as a gravitational density with a gravitational constant of 1.0 if no dynamic analyses are to be performed. If dynamic analyses are

employed, the mass density is appropriate. In these cases, a gravitational constant other than unity is required. Specification of a weight density is generally preferred since it is more common. In these cases, a gravitational constant of 1.0 is specified. A fourth optional property is the thermal coefficient of expansion, which is necessary if a thermal analysis is required.

A second basic assumption made is that deflections are small. This means that it is assumed that the structure does not deflect enough to cause the point of application of the loads to be displaced enough to affect the analysis results. For example, a catenary cable changes shape under load and generally would not satisfy this assumption.

By assuming first-order small deflection theory and elastic behavior, influence surfaces can be employed for live load analysis.

Another requirement related to linear behavior is that changes in structure stiffness during loading are not permitted. For example, lift-off at a bearing as load is applied would change the structure stiffness and cause the model to behave in a non-linear fashion. Such behavior is not considered in the analyses discussed in this manual.

2.1.6 Girder Stiffness

The stiffness of the steel girders is straightforward. In a 2D grillage analysis, the section properties of the girders must be entered along the spans. In a 3D analysis, the plate sizes are entered and the computer computes the actions without section properties. In both cases, the steel properties must match the actual girders; a uniform beam property over the span length will give erroneous results.

Until recently, it was common to assume that the concrete in the negative moment regions between points of dead load contraflexure was not effective in analyses for loads applied to the composite section. *AASHTO LRFD* Article 6.10.1.5 essentially states that the stiffness properties of the full composite section are to be used for permanent loads and transient loads applied to flexural sections where a concrete deck is attached to the top flange of the steel girder with shear connectors. The effect of concrete creep is accounted for by adjusting Young's Modulus.



Figure 2.1.31 Curved I-Girder Bridge

Field tests of live loads on continuous composite bridges have shown that the portions of the girders in the so-called negative moment regions act compositely under service loads. Moments and deflections computed with a proper finite element model assuming full composite action agree much better with field measurements than those computed with a similar finite element model assuming no composite action in these regions. The composite action in these regions gives greater girder moments at the pier and slightly smaller mid-span moments compared to analyses based on assuming composite action in the so-called positive moment regions only. The increase in negative girder moments occurs over a relatively short length of what is typically a larger cross-section, while the reduction in moment occurs over a much longer positive moment region.

AASHTO LRFD Article 6.10.10.1 requires that curved continuous composite bridges be provided with shear connectors throughout the length of the bridge because significant torsional shear exists that might not be resisted by the bond between the deck and the top flange if shear connectors are omitted. Although the specifications are silent on this issue, it is suggested that shear connectors also be employed throughout the length of the bridge when supports are skewed for similar reasons. They are certainly not forbidden in the so-called negative moment regions on any girder bridge.



Figure 2.1.32 Three-Span Curved Girder Bridge

It is important to recognize the effects of any changes to the relative girder stiffness on the analysis results. Re-analysis should be made whenever revisions are considered to girder and/or cross-frame/diaphragm sizes. It should always be remembered that any increase in stiffness attracts load to the point of increased stiffness and vice versa. For example, should the depth of one girder be larger than the adjacent girders in the cross-section, that girder will tend to attract more load than it would if all the girders were of the same depth. Curved-girder bridges, in particular, are sensitive to changes in relative girder stiffness because the outside girder typically carries a larger than average share of the load. If the outside girder is sized up, its stiffness will increase and it will draw additional load. This situation will also cause an increase in cross-frame forces in the exterior bay as more load is shifted through the cross-frames to the outside girder.

2.1.7 Effective Width of Deck

The concrete deck of composite girders subject to vertical bending is loaded through horizontal shear via the shear connectors. When the shear first is introduced, the effective width of concrete is very small. However, the shear stiffness of the deck soon distributes the force from the shear connectors to the rest of the deck. It takes some length of girder before the force in the concrete reaches equilibrium. At this point, the force in the deck near the shear connectors is somewhat higher than at the extreme edges. This shear-lag phenomenon is evident in Figure Part A. The fact that the stress in the deck is not uniform is addressed by the effective width approach. The thickness of the deck is tacitly assumed constant and equal to the full structural deck thickness. The effective width of the deck used in the computation of the composite section properties accounts for the shear-lag effect.

.

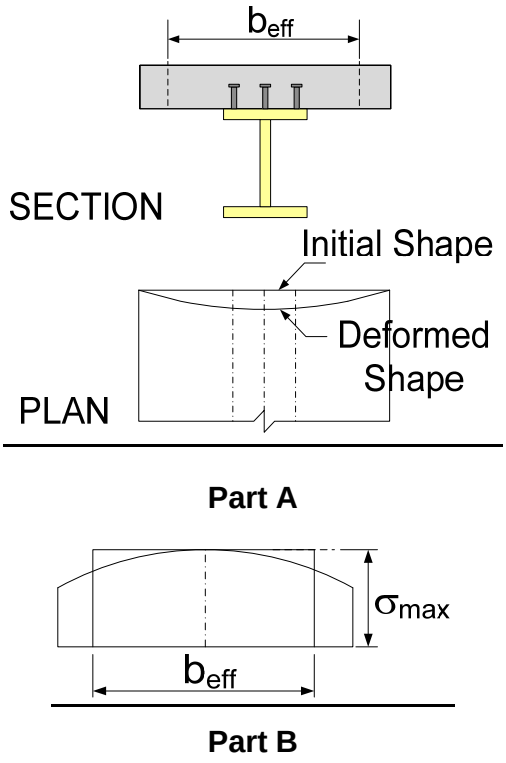


Figure 2.1.33 Effective Width of Deck
A) Shear Deformation of Deck; B) Non-Uniform Stress Distribution over Deck Width Replaced by Assumed Uniform Stress Distribution over b_{eff}

The effective width is the width of deck over which the assumed uniformly distributed longitudinal stresses result in approximately the same deck force and member moments calculated from elementary beam theory (i.e. assuming plane sections remain plane) as would be produced by the actual non-uniform stress distribution (Figure 2.1.33 Part B).

AASHTO LRFD Article 4.6.2.6.1 specifies that for conventional composite girder bridges (i.e. beam-slab bridges) in which the largest skew angle, θ, in the bridge system does not exceed 75° (measured relative to a normal to the centerline of the bridge), the effective width of the deck for determining cross-section stiffnesses for analysis and for determining flexural resistances may be taken as the corresponding tributary width of the deck perpendicular to the axis of the member (Figure 2.1.34). In other situations, the slab effective flange width should be determined by a refined analysis (refer to the *AASHTO LRFD* specification).

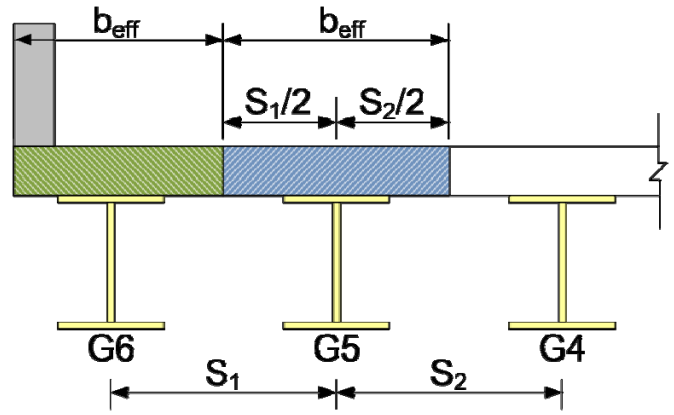


Figure 2.1.34 Effective Deck Width Based on Tributary Width of Deck over Each Girder

2.1.8 Uplift

Uplift is an important consideration in the safe design and proper performance of skewed and curved girder bridges. Uplift is assumed to occur any time the factored reactions causing uplift exceed the factored permanent load reactions available to resist uplift. Uplift can occur due to gravity loads in the completed bridge or at any stage of construction of the bridge. It may also occur due to thermal forces. An example of uplift on a bearing is shown in Figure 2.1.35.



Figure 2.1.35 Uplift on a Bearing

Uplift may simply lead to annoying problems, such as reduced bearing life or additional bending in the deck. However, narrow bridges (e.g. single tubs) can become unstable under certain conditions due to uplift. When uplift occurs in completed bridges under live load, it leads to unloading of supports that in some cases may cause instability leading to structural failure.

Uplift is a non-linear phenomenon that may require changing the boundary conditions and cannot be treated properly with software that uses influence surfaces. Typically, the analysis reflects the assumption that the bearing is tied down, which is incorrect.

Redecking of bridges under traffic can lead to uplift that does not occur under normal operating conditions. In checking for uplift during redecking with part of the deck intact for traffic, relocated barriers and removed deck loads are considered. The presence or absence of any future wearing surface should also be recognized in these investigations.

As previously discussed, thermal effects should be considered when checking uplift, particularly for skewed and curved structures, because these bridges can experience significant vertical reactions due to thermal forces. These reactions are properly computed by recognizing the bearing vertical offsets from the neutral axis of the superstructure girders. Both uniform temperature and thermal gradient conditions need to be considered. It should be noted that a 2D grid analysis will not recognize thermally induced uplift or any other vertical reaction since all forces are in-plane.

Potential uplift at bearings must be investigated at each critical construction stage, in particular during steel erection and deck casting.

Although it is desirable to avoid uplift, there are cases where reverse reactions are identified and countermeasures must be taken. Uplift can sometimes be addressed by modification of the framing, though the provision of tie-down devices or counterweight(s), or by removal of the bearing. Where a decision is made to permit uplift, the analysis should be modified to recognize the absence of vertical restraint at the support experiencing lift-off, which may result in uplift at other locations.

When checking for uplift at the strength limit state, the appropriate minimum load factor, γ_p, specified in *AASHTO LRFD* Table 3.4.1-2 should be applied to any upward permanent load reactions resisting uplift. Potential uplift of the superstructure at any support under the combination of permanent load and other specified load types (including uniform temperature change, thermal gradient and/or wind load) may be investigated according to the following suggested load combinations, as applicable, *subject to the approval of the Owner*.

In many cases, as mentioned previously, uplift may simply lead to annoying problems, such as reduced bearing life or unanticipated bending in the deck. In such cases, potential instability of the bridge due to uplift is typically not a concern and the inequality given by Equation 2.1.3 may be applied. However, narrow bridges can become unstable under certain conditions due to uplift. When uplift

occurs in such bridges, it can lead to unloading of supports that in some cases can cause instability leading to structural failure. Where potential instability due to uplift is deemed to be of concern, the inequalities given by Equations 2.1.1 and 2.1.2 may be employed instead.

On the left-hand side of the inequalities given by Equations 2.1.1 through 2.1.3, the appropriate minimum load factors specified in *AASHTO LRFD* Table 3.4.1-2 are applied to the vertical reactions due to dead loads resisting uplift, including any wearing surface and/or utility loads. Reactions due to a future wearing surface load resisting uplift should conservatively be ignored. On the right-hand side of the inequalities are any uplift reactions that may be caused by various loads; reactions due to loads not causing uplift or not considered are ignored in checking the inequality.

- Where potential uplift may cause instability of the bridge:

$$0.9R_{DC} + 0.65R_{DW} > 1.25R_{(DC)_u} + 1.50R_{(DW)_u} + 1.75R_{LL+IM} + 0.5R_{TG} + 0.5R_{TU} + 0.5R_{WS} + 0.5R_{WL}$$

Equation 2.1.1

and:

$$0.9R_{DC} + 0.65R_{DW} > 1.25R_{(DC)_u} + 1.50R_{(DW)_u} + 1.75R_{LL+IM} + 1.0R_{TG} + 1.0R_{TU}$$

Equation 2.1.2

- Where potential uplift does not cause instability of the bridge:

$$0.9R_{DC} + 0.65R_{DW} > 1.0R_{(DC)_u} + 1.0R_{(DW)_u} + 1.0R_{LL+IM} + 0.5R_{TG} + 1.0R_{TU}$$

Equation 2.1.3

where:

R_{DC} = vertical reaction due to component dead loads resisting uplift (kips)

R_{DW} = vertical reaction due to wearing surface and/or utility loads resisting uplift (kips)

$R_{(DC)_u}$ = uplift reaction due to component dead loads; zero if no uplift or not considered (kips)

$R_{(DW)_u}$ = uplift reaction due to wearing surface and/or utility loads; zero if no uplift or not considered (kips)

R_{LL+IM} = uplift reaction due to the design vehicular live load specified in *AASHTO LRFD* Article 3.6.1.2 (Section 1.3.2.3.1) plus the corresponding dynamic load allowance specified in *AASHTO LRFD*

Article 3.6.2.1 (Section 1.3.2.3.8); zero if no uplift or not considered (kips)

R_{TG} = uplift reaction due to the temperature gradient specified in *AASHTO LRFD* Article 3.12.3 (Section 1.3.2.5.2); zero if no uplift or not considered (kips)

R_{TU} = uplift reaction due to the uniform temperature change specified in *AASHTO LRFD* Article 3.12.2 (Section 1.3.2.5.1); zero if no uplift or not considered (kips)

R_{WS} = uplift reaction due to the wind pressure on the structure specified in *AASHTO LRFD* Article 3.8.1.2 (Section 1.3.2.4.1.1); zero if no uplift or not considered (kips)

R_{WL} = uplift reaction due to the wind pressure on vehicles specified in *AASHTO LRFD* Article 3.8.1.3 (Section 1.3.2.4.1.2); zero if no uplift or not considered (kips)

Where the applicable inequality is not satisfied, uplift is assumed to occur at the support under consideration. Where uplift occurs and is to be countered with a tie-down device or counterweight, the suggested factored design uplift reaction, R_u, for the design of any countermeasure may be computed as follows *subject to the approval of the Owner*:

$$R_u = 0.9R_{DC} + 0.65R_{DW} + 1.25R_{(DC)_u} + 1.50R_{(DW)_u} + 1.75R_{LL+IM} + 0.5R_{TG} + 0.5R_{TU}$$

Equation 2.1.4

The signs of the various reactions must be considered in applying Equation 2.1.4. Reactions due to loads not causing uplift or not considered should be ignored. The effects of thermal movements of the superstructure should be considered when designing tie-down devices or counterweights.

Design checks for potential uplift under any extreme event limit state force effects should be handled separately according to the appropriate design provisions for those situations. Potential uplift due to water loads, WA, acting on the superstructure in an extreme event may also need to be considered at the discretion of the Owner

2.1.9 Neglect of Curvature Effects

This section reviews the *AASHTO LRFD* specification requirements and conditions as to when certain effects of horizontal curvature may be neglected in the analysis of horizontally curved I-girder bridges and horizontally curved closed box or tub girder bridges. For curved I-girder bridges, these conditions are listed in *AASHTO LRFD* Article 4.6.1.2.4b. For curved closed box or tub girder bridges, these conditions are listed in *AASHTO LRFD* Article 4.6.1.2.4c.

The conditions under which the effects of horizontal curvature may be ignored in the analysis for determining the vertical bending moments and bending shears are reviewed. When the bridge under consideration satisfies all the applicable listed

conditions, an individual I-girder or an individual closed box or tub girder in that bridge may be analyzed as an isolated straight girder with a span length(s) equal to the girder arc length(s) for the determination of the vertical bending moments and bending shears.

AASHTO LRFD Article 4.6.1.2.4b specifies that I-girder bridges satisfying the following four conditions may be analyzed neglecting the effects of curvature in determining the vertical bending moments and bending shears:

- All girders must be concentric;
- Bearing lines must not be skewed more than 10° from radial;
- The stiffnesses of the girders must be similar. Similar girder stiffnesses are required to avoid large and irregular changes in stiffness that could alter the transverse distribution of load; under such conditions, a refined analysis is more appropriate;
- For all spans, the arc span, L_{as}, divided by the girder radius, R, in feet must be less than 0.06 radians, where L_{as} is to be taken as follows:

  For simple spans:
  L_{as} = arc length of the girder
  For end spans of continuous members:
  L_{as} = 0.9 times the arc length of the span
  For interior spans of continuous members:
  L_{as} = 0.8 times the arc length of the span



Figure 2.1.36 Curved I-Girder Bridge under Construction

Where the preceding requirements are satisfied, non-composite dead loads (i.e. DC_1 loads) preferably are to be distributed equally to all the girders for the analysis since

the cross-frame/diaphragms provide restoring forces that prevent the girders from deflecting independently in such cases the loads must be nearly equal. Certain dead loads, e.g. wearing surface loads (DW), may be distributed uniformly to the girders as permitted in *AASHTO LRFD* Article 4.6.2.2.1.

Heavier DC_2 line loads such as parapets, barriers, sidewalks or sound walls should not be distributed equally to all the girders. Engineering judgment must be applied in distributing these loads. Usually the largest portion of the DC_2 load on an overhang is assigned to the fascia girder (the outside fascia girder is often critical in curved girder bridges), or to the fascia girder and the first interior girder. In fact, the exterior girder may receive more than the weight of a barrier, etc. on the extreme deck overhang due to the cantilever effect, with resulting uplift of one or more interior girders.

As discussed previously, skew produces torsion in girders, which should be dealt with by other analytical means that generally involve a more refined analysis. Estimating the distribution of DC_2 line loads (e.g. parapets, etc.) to the individual girders for line girder analyses is particularly difficult in skewed bridges because the loads may only be on one side of the bridge over significant portions of the span. Phased construction or deck placement situations that place half the deck weight on one side of a girder may also create significant torsion that should be recognized not only in deflection calculations, but also stress determinations.



Figure 2.1.37 Curved Girder Bridge with Skewed Supports

AASHTO LRFD Article 4.6.1.2.4c specifies that closed box or tub girder bridges (Figure 2.1.38) satisfying the following four conditions may be analyzed neglecting the effects of curvature in determining the vertical bending moments and bending shears:

- All girders must be concentric;
- Bearing lines must not be skewed;
- For all spans, the arc span, L_{as}, divided by the girder radius, R, in feet must be less than 0.3 radians, where L_{as} is to be taken as follows:

  For simple spans:
  L_{as} = arc length of the girder
  For end spans of continuous members:
  L_{as} = 0.9 times the arc length of the span
  For interior spans of continuous members:
  L_{as} = 0.8 times the arc length of the span

- The girder depth must be less than the width of the box at mid-depth of the box. If the box is haunched or tapered, the shallowest girder depth is to be used on conjunction with the narrowest width of the box at mid-depth.



Figure 2.1.38 Curved Tub Girder Bridge

Where the bridge satisfies the preceding conditions and the approximate live load distribution factor for box sections specified in *AASHTO LRFD* Article 4.6.2.2.2b is used to determine the live load vertical bending moments and bending shears, the bridge should also satisfy the special geometric restrictions for the use of the distribution factor given in *AASHTO LRFD* Article 6.11.2.3.

As discussed previously, torsion is often more significant in box sections than in open I-sections. Torsional shears are typically large and the box web shears are particularly affected by the torsional shears. Double bearings also resist significant torque compared to a box-centered single bearing. Thus, the torsional effects should be evaluated by a rational means that recognizes the specific location of loads, as well as the torsional stiffness of the entire cross-section. The approximate M/R Method discussed in Section 2.3.3 addresses the torsional effect of the geometry of the section and the application of loads to a degree.

2.1.10 Uplift Case Study

In this case study, a straight three-span continuous I-girder bridge has four variable-depth steel I-girders. The girder depth is 4.7 feet in the end spans and tapers to 8 feet at the piers and remains at that depth over the center span. All four supports are sharply skewed. Spans are 101-206-101 feet. The intended framing is shown below (Figure 2.1.39).

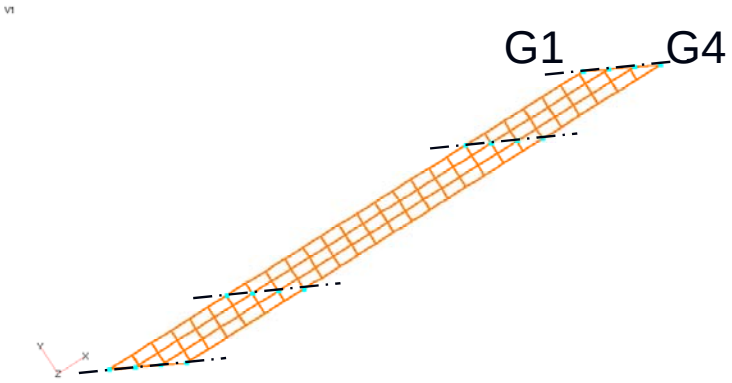


Figure 2.1.39 Framing Plan of Three-Span Continuous I-Girder Bridge for Uplift Case Study

The vertical reactions (kips) of the four girders at the right (far) end of the bridge computed from 3D analyses are given in Table 2.1.2. Girders are numbered from left to right looking at the above plot. The load factor is 1.0 for the dead and live load reactions in the table. These load factors were chosen by the Design Engineer to check for uplift. A negative reaction in the table indicates the maximum upward reaction that resists the maximum downward force at the bearing. A positive reaction in the table indicates the maximum downward reaction that resists the maximum uplift force at the bearing due to the load under consideration.

Table 2.1.2 Original Vertical Girder Reactions (kips) at Right (Far) End

Girder No.	Steel Weight	Deck Weight	Composite Dead Load	Live Load		Total	
				Down	Uplift		
1	0	-2	-2	-93	49	-97	45
2	-11	-25	4	-84	20	-116	-12
3	-9	-22	-7	-78	15	-116	-23
4	-8	-16	-24	-57	1	-105	-47

Girder 1 is experiencing uplift under dead plus live load. A similar situation existed at the left (near) end of the bridge, but the reactions are not shown.

Maximum factored tension and compression forces in the two cross-frames adjacent to the Girder 1 and Girder 2 bearings near the obtuse corner at the right end of the bridge where uplift of Girder 1 occurred were 48, -34 kips and 26, -35 kips. These forces were in the chord members of the K-type cross-frames.

The uplift problem was caused by the poor span ratio, the sharply skewed supports and the shallower end-span girders.

In order to maintain vertical clearances, the girder depths had to be maintained. As shown in the plot in Figure 2.1.40, the two cross-frames adjacent to the Girder 1 and Girder 2 bearings near the obtuse corner were removed. A counterweight was also introduced in-between Girders 1 and 2 near the same corner. In addition, top flange lateral bracing was added in some of the outer bays at the request of the Contractor to stabilize the girders during the erection. The bracing was added at the level of the top flange rather than at the bottom flange to minimize its effect on the live load and composite dead load. By placing the bracing at the level of the top flange, it was located near the neutral axis of the composite section minimizing its effect on loads applied to the composite section.

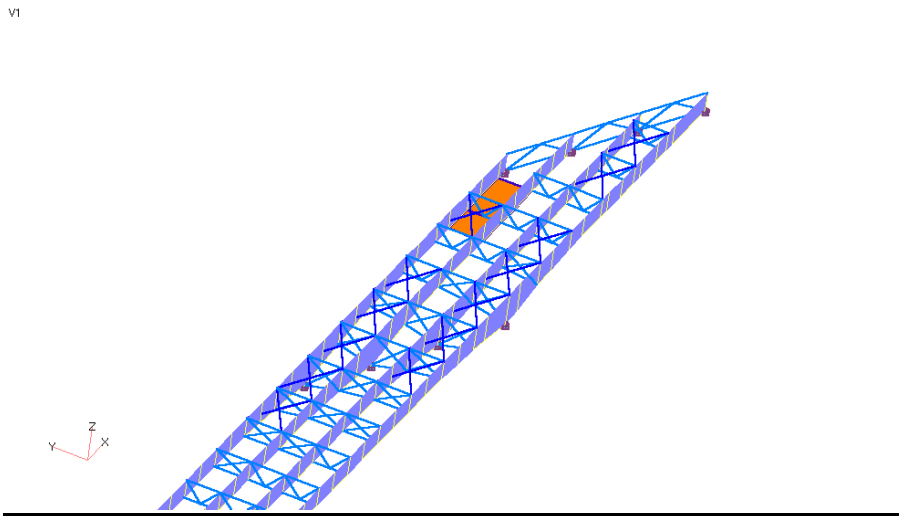


Figure 2.1.40 Design Modifications Introduced to Alleviate Uplift

The resulting reactions from the analysis based on these design changes were as shown in Table 2.1.3 (again, the load factor applied to the dead and live load reactions in the table is 1.0.).

Table 2.1.3 Vertical Girder Reactions (kips) at Right (Far) End after Design Modifications

Girder No.	Steel Weight	Deck Weight	Composite Dead Load	Live Load		Total	
				Down	Uplift		
1	-59	-6	-5	-87	45	-157	-25
2	-29	-19	5	-84	20	127	-23
3	-17	-24	-4	-79	17	-124	-28
4	-11	-21	-25	-57	2	-114	-55

It should be noted that the removal of the two cross-frames had a minimal effect in this particular case.

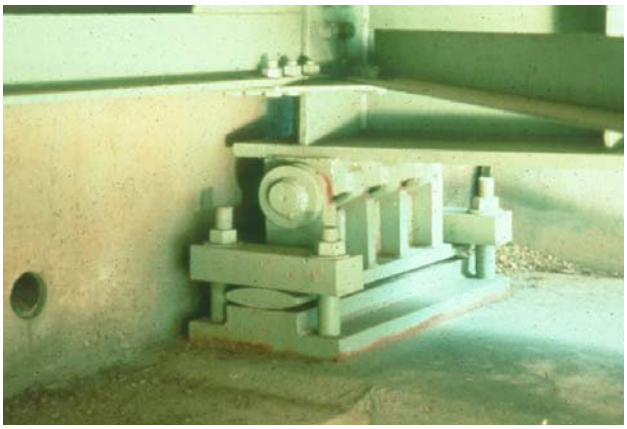
2.1.11 References

1. McCormac, J.C. 1975. *Structural Analysis*. Third Edition, Intext Educational Publishers, New York, NY.

This Page Intentionally Left Blank

Chapter 2
Structural Analysis

Section 2.2
Bearing Constraints



2.2.1 Introduction

Bearings are often thought to act as the boundary conditions for the superstructure. In fact, the true boundary conditions of the superstructure consider the flex in the piers and sometimes even the foundation. The behavior of the superstructure is often very dependent on the effective horizontal restraints on the superstructure. The action at the bearings can have significant effect on the superstructure components due to thermal, vertical and lateral loads. This is particularly true with bridges having skewed supports. The proliferation of bearing types makes the proper selection and orientation of bearings important and somewhat complex.

2.2.2 Bearing Loads and Types

Fifty years ago most bridge bearings were steel rocker type or steel sliding type. Slowly, rubber bearings and Teflon bearings were introduced, followed quickly by spherical bearings. Pot and disc bearings were introduced in the past thirty years.

Lateral loads including those due to vertical dead and live loads can have a significant effect on bearing performance. These loads are often very significant in bridges with skewed supports. They may, in fact, exceed the vertical load in extreme cases. They are the cause of many bearing failures when they are not considered in design. Bearings may be designed to be fixed against lateral moment, guided to move in only one direction or free to move in any direction. Guided bearings are given an orientation that is usually based on thermal effects. However, they must also consider numerous other influences. Restraint of bearings is muted by the flexibility of the substructure in many cases. This added movement should be considered in design of the bearings and the substructure. .

Rocker bearings permit longitudinal movement in one or no direction and rotation about one axis. Rubber bearings permit translation in any direction, but are often longitudinally guided by restraints. They permit rotation about any axis. Pot and spherical bearings permit translation with other sliding components that may or may not be guided by restraints.

Fortunately, the movements and forces on bearings may be calculated by analysis, as are girder moments and shears, so that the bearings may be designed for computed forces and movements. This helps ensure that the bearings will not fail under load or movement. *AASHTO LRFD* Article 14.4 requires that bearings be designed for all forces and movements. Bearing design involves bearing restraints, strength and bearing type. Their design for bridges having skewed supports is usually an iterative process. Lateral constraints have a significant effect on the magnitude of forces in cross-frames or diaphragms at the bearings.

Table 2.2.1 presents some characteristics of each of the seven common bearing types employed in steel-bridge construction. Relative cost and relative degree of required maintenance are presented. Each bearing type has unique properties that make it suitable for some bridge applications and less suitable for others.

Table 2.2.1 Characteristics of Bearing Types used in Steel-Bridge Construction

Type	Plain Elastomeric	Steel Reinforced Elastomeric	Rocker	Cylindrical	Disc	Spherical	Pot
Rotation-Vertical Axis	Limited	Limited	Unsuitable	Unsuitable	Suitable	Suitable	Limited
Lateral Load	Limited	Limited	High	Moderate	Low	Low	High
Relative Cost	Low	Low	Moderate	High	Moderate	High	Moderate
Relative Degree of Maintenance	Low	Low	High	Moderate	Low	Moderate	High

As a general rule, vertical load dictates initial cost. Some bearings accommodate rotation about one axis only, while other bearing types accommodate rotations about two axes or possibly all three axes. Some bearing types also require additional elements (i.e., sliders and guideways) to accommodate horizontal movements.

It is important to know the capabilities of each bearing type so that the most suitable type can be selected for each unique bridge application. This is particularly true when it comes to selecting bearings for curved and/or skewed bridges.

Vertical loads that must be considered in the design of the bearings include dead load, live load (vehicular and pedestrian load), wind load (on the structure, on the live load and during construction) and thermal load (uniform temperature change perhaps in combination with a thermal gradient).

Horizontal loads in the longitudinal and/or transverse direction must be resisted by fixed bearings and guided expansion bearings. Horizontal loads that must be considered in the design of the bearings include dead load, live load, wind load, thermal load, braking force, centrifugal force (for horizontally curved structures) and forces due to extreme events (e.g., seismic, ice, etc.).

Each of these loads is discussed in detail in Section 1.3.2. Further information on bearing types and bearing design is contained in Section 3.3.9.

2.2.3 Bearing Orientation and Restraint

2.2.3.1 General

Bearing orientation is important to control thermal movements and forces and to mitigate thermal forces. Bearings also resist horizontal forces due to dead and live loads, thermal effects, wind, centrifugal force, braking force, extreme events, etc. Restraints and orientation must be chosen with consideration to all of these forces.

Narrow straight bridges with perpendicular supports undergo minimal lateral movement under a uniform temperature change. Hence, lateral thermal movements can be ignored with respect to design of the bearings. However, if the bridge is

wide, has skewed supports, or is curved, lateral expansion and contraction should not be ignored.

Longitudinal restraint at the reactions may introduce moments at the ends. This situation is particularly critical with skewed supports. The bearing restraint acts eccentric with respect to the neutral axis of the girders. Typically, this causes negative moments because the bottom flange is mostly in tension and is attempting to lengthen. The longitudinal reactions can be due to thermal and/or vertical loads. Even dead load effects may not be permanent as bearings or anchorages fail or if the bearings are replaced after the bridge is built. So it is not advisable to take advantage of the negative moments in design. However, it is desirable to check the girder design for the case where the bearings are constrained. The negative moments near piers may be larger and cross-frame/diaphragm actions are usually critical for the constrained bearing case. The girders may be analyzed assuming minimal bearing restraint to obtain the maximum positive moments for the design of the girders.

2.2.3.2 Optimal Bearing Orientation for Thermal Movements

A point of fixity (i.e. zero translation) with respect to thermal movement can be arbitrarily chosen. A uniform temperature increase will cause expansion of the structure radially from that point if there are no horizontal restraints. Obviously, if guided bearings are assumed aligned along these rays, there will be no thermal restraint in the bearings. This simple principle applies to wide, skewed and curved bridges. Figure 2.2.1 shows a schematic of the principle. Excessive reactions and distortions can be created when the bearings are not able to accommodate the deflections and rotations induced in the bridge.

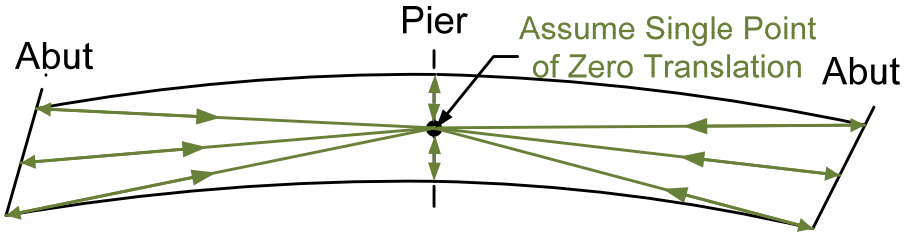


Figure 2.2.1 Thermal Expansion and Contraction Along Rays Emanating from a Single Point of Zero Translation Toward the Bearings

The thermal effects can be minimized in continuous units by making a bearing on an interior pier, rather than a bearing at an abutment, serve as a single point of zero translation.

In many cases, it may be necessary to fix additional bearings transversely on a pier to provide sufficient resistance for other horizontal force effects (e.g., seismic). In such cases, it may be necessary to locate the assumed point of zero translation off a bearing, e.g., at mid-span, and again, guide all the expansion bearings toward that

point (Figure 2.2.2). Several analytical investigations may be necessary to determine the optimum orientation of the bearings to successfully mitigate the resulting horizontal thermal reactions.

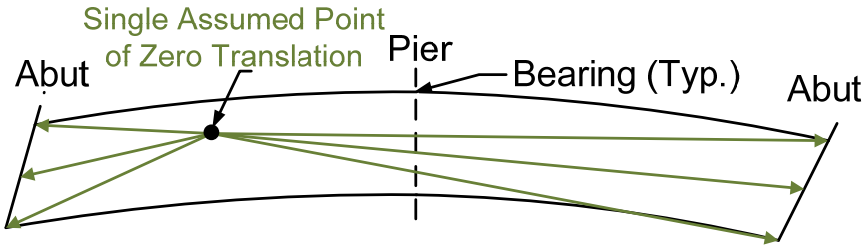


Figure 2.2.2 Locating Assumed Point of Zero Translation Off a Bearing When More than One Bearing is Restrained Transversely on a Pier

2.2.3.3 Bearings at Skewed Supports

The bearings of sharply skewed bridges, curved or straight, are often more problematic than those of straight or curved bridges without skew. Large horizontal reactions can be created in the bearings due to vertical and horizontal loads in skewed bridges (Section 1.3.2) in addition to thermal effects. These reactions increase with increased skew angle and vertical deflection of the girders. The greater the girder rotations at bearings, the greater the lateral reactions tend to be. This situation is particularly critical at end supports.

These large horizontal forces are evidenced by the failure of anchor bolts, concrete, bearings and end cross-frames on skewed bridges when these forces are not adequately taken into account at design (Figure 2.2.3).



Figure 2.2.3 Distressed Bearing on a Skewed Support

It is not uncommon for the lateral forces on pot bearings resting on skewed supports (Figure 2.2.4) to distort the pot, leading to leakage and bearing failure.



Figure 2.2.4 Pot Bearing

2.2.3.4 Mitigation of Horizontal Thermal Reactions

Generally, the more constraint provided in the bearings, the larger the forces involved.

- One approach discussed in Section 2.2.3.2 is to consider establishing one point of thermal fixity (zero translation). Expansion bearings at all other points should then be guided along rays toward that point. Such an arrangement will theoretically result in zero horizontal thermal reactions under a uniform temperature change. This concept can also be combined with freeing the bearings under the extreme outward girders. “Free” in this case means no horizontal constraint. This option is investigated in the bearing orientation example given below.
- Another approach is to consider using all free elastomeric bearings at each support to allow the bridge to essentially “float” on the bearings under nominal horizontal loads, while eliminating the need to utilize more expensive pot bearings. Shear keys can be used to provide the necessary horizontal restraint under extreme events, such as earthquakes, thereby relieving the bearings from the need to resist such large horizontal loads. Independent shear keys also restrain the bridge from “walking” off the bearings. In this case, a nominal representative longitudinal and transverse stiffness is provided by the shear resistance of each bearing. Since the bearings are relatively flexible with respect to the piers, their stiffnesses (Section 2.2.4) might be ignored in this case. Round elastomeric bearings are best for free

bearings. The "floating" option is investigated for the example skewed and curved I-girder bridge in Section 5.1.6.2.

- For severely skewed bridges, calling for jacking of the bridge to lift and reset the girders to relieve any horizontal dead load reactions may be desirable. Lifting girders for bearing replacement has the same effect. Sometimes when a girder is jacked, the latent lateral force due to dead load or thermal load causes the piston to bind on the cylinder requiring a larger pressure than would be expected in order to elevate the girder. The bridge may "jump" when lifted in such cases. This has been observed most often with skewed supports.

Bearing Orientation Example

Consider the plan view of a straight simple-span skewed bridge with eight girders in the cross-section and staggered cross-frames shown in Figure 2.2.5. The model used in the analysis is a 3D finite element type. This model recognizes the eccentricity of the bearings with respect to the neutral axis of the composite girders.

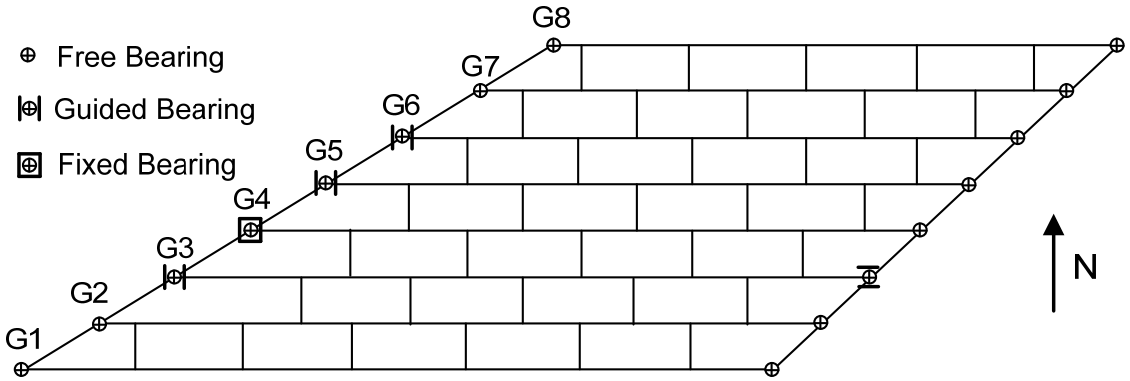


Figure 2.2.5 Plan View of Straight Simple-Span Skewed Bridge w/ Bearing Constraints Shown

The modulus of elasticity of the concrete deck (not shown in Figure 2.2.5) is based on the short-term modular ratio, *n* (no creep effects are assumed for thermal effects, which are assumed to be relatively ephemeral). The other parameters given for the exercise are as follows:

α = 0.0000065 in/in/degree F (steel)
α = 0.0000060 in/in/degree F (concrete)
ΔT = +70° F
Length of G1 = 136 ft
Length of G8 = 102 ft
Depth of steel girders = 66.25 inches
Deck thickness = 7.5 inches
Neutral axis = 47.6 inches from the bottom of steel

For ease of discussion, the girders are assumed to lie west-east. The southernmost girder, G1, is the longest girder at approximately 136 feet, while the northernmost girder, G8, is the shortest girder at approximately 102 feet.

Referring to Figure 2.2.5, the orthogonal constraints of the bearings are oriented along and perpendicular to the girder lines. The middle four bearings constrain their respective girders longitudinally at the west end, while only one girder (G4) is constrained transversely. All girders are free longitudinally, and only one girder (G3) is constrained transversely at the east end. All other bearings are free.

In an actual bridge design, more than one bearing would typically be employed at each end to resist transverse movement and forces. However, only one such constraint is used in this analysis to separate the effect of the overall lateral bridge movement from the lateral constraint forces that would be generated due to expansion of the bridge between adjacent bearings, as discussed further below.

The superstructure, including the concrete deck, is subjected to a uniform 70 degree F temperature increase in the 3D analysis of the bridge.

The difference in the longitudinal expansion of G1 and G8 is significant, as would be expected, due to their different girder lengths. As shown in Figure 2.2.6, G1 expanded the most in the longitudinal direction: [0.57 – (-0.16)] = 0.73 inches. The theoretical expansion of G1 assuming it is isolated from the system is: 0.0000065 x 136 x 12 x 70 = 0.74 inches (Equation 1.3.12). G8 expanded the least: [0.78 – 0.19] = 0.59 inches (not shown in Figure 2.2.6). The theoretical expansion of G8 assuming it is isolated from the system is: 0.0000065 x 102 x 12 x 70 = 0.56 inches (Equation 1.3.12). The expansions from the analysis are reported at the bottom of the steel. They are slightly less than computed because of the smaller coefficient expansion of the concrete, which was ignored in the hand calculations.

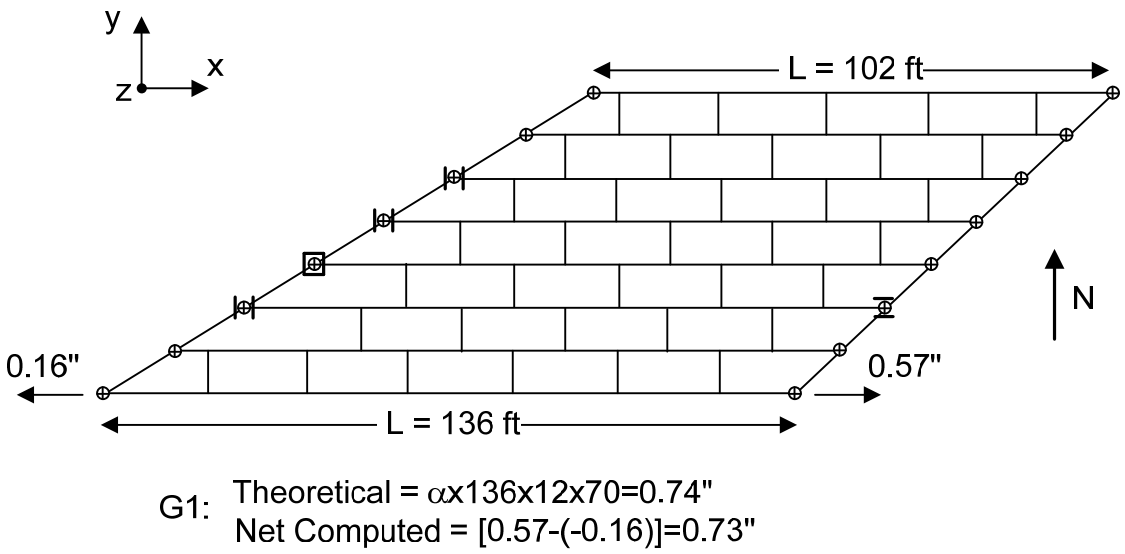


Figure 2.2.6 Longitudinal Thermal Expansion of G1 – Theoretical vs. Net Computed Expansion from the 3D Analysis

Particularly interesting, however, is that the difference in longitudinal expansion between G1 and G8 was arrived at by the expansion of each girder in a completely different fashion. The west end of G1 expanded negatively or to the west, while the west end of G8 expanded positively or to the east. The reason for these movements is the skew and the bearing constraints at the west end. The largest positive expansion was observed at the east end of G8, which represents the most distant corner from the longitudinal constraints at the west end.

The effect of lateral expansion should not be ignored in wide bridges. Assuming more than one bearing must eventually be constrained in the transverse direction, if the lateral thermal movement between adjacent bearings is larger than the freedom provided in the lateral constraints, local lateral forces resulting from the bearings pushing against their neighbors will develop. These forces are separate from the lateral forces that develop due to global rotation of bridges with skewed supports.

In this example, the east bearing of G3 is fixed transversely, while its neighbors are permitted to move transversely. As seen in Figure 2.2.7, the transverse (lateral) movement (y-direction) of the east bearing of G2 was -0.021 inches, and the similar movement at G4 was 0.087 inches. The relative movement of G2 can be ignored. The relative movement of G4 is more than one-sixteenth-inch and, depending on the type of bearing, may be enough to bind the bearing and cause significant lateral forces if the bearing under that girder was transversely constrained. A second analysis with a gap element or a weak lateral constraint introduced may be made to recognize the freedom or play in the bearing in order to determine a more realistic lateral force should it be desired to constrain the bearing at G4 in the transverse direction.

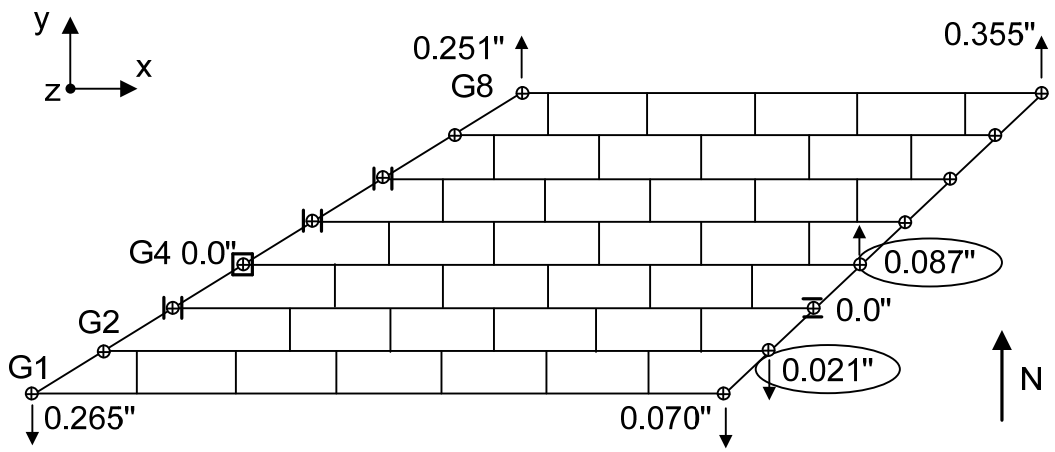


Figure 2.2.7 Transverse (Lateral) Thermal Expansion with a Single Bearing Constrained Transversely at Each End

The magnitudes of the resulting horizontal reactions (i.e., in the x-y plane) are presented in Figure 2.2.8. Recall that the bearing constraints are oriented orthogonal to the girders. The bridge expands in both the longitudinal and transverse directions, because of the skew and the configuration of the bearing constraints and the longer Girder 1. The superstructure twists slightly in the counterclockwise direction in the horizontal plane. Further twist is resisted by the transverse constraints at each end. Note that only the center four girders are constrained in the longitudinal direction at the west end. Constraint of the bearings under the extreme outward girders would result in even larger horizontal forces.

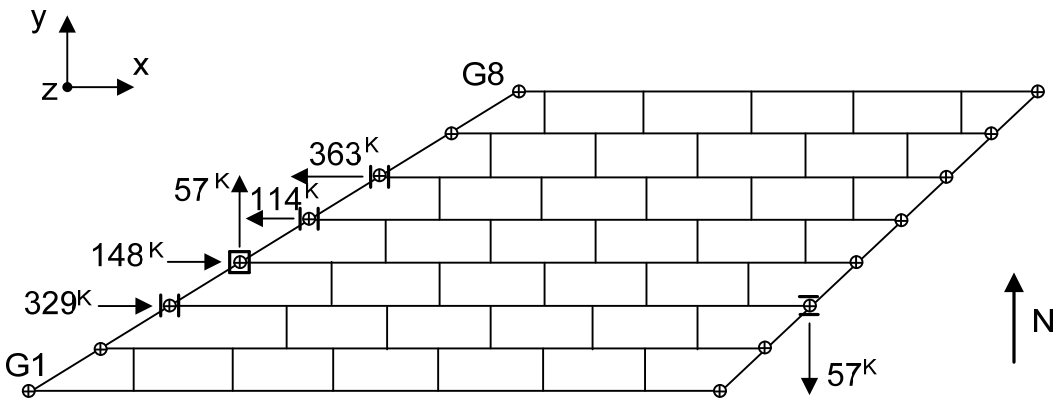


Figure 2.2.8 Horizontal Bearing Reactions (X-Y Plane) due to Thermal Expansion – Bearing Constraints Orthogonal to Girders

The 57-kip force at the east bearing of G3 generates a torque of:

57 kips x 47.6 in./12 = 226 k-ft

It is of interest to note that this torque would not be computed with a grid analysis that applied the bearing restraints at the neutral axes. This torque is resisted by vertical reactions at all bearings and lateral reactions at the west end which generate similar torques. The sums of the forces in the x and y directions are zero. The sum of moments is difficult to compute because of the three-dimensional character of the problem that combines internal torsional moments with external moments.

Consider a different case with the orientation of the bearings revised such that all the guided bearings are guided toward the fixed bearing at the west end of G4, which is the recommended solution in this case. That is, the three guided bearings at the west end under G3, G5 and G6 are all guided along the support line toward the fixed bearing under G4, and the guided bearing at the east end under G3 is guided along the ray emanating from the fixed bearing under the west end of G4 toward the bearing at the east end of G3 (Figure 2.2.9). This means that the west bearing of G4 is the point of thermal fixity (zero translation) discussed above.

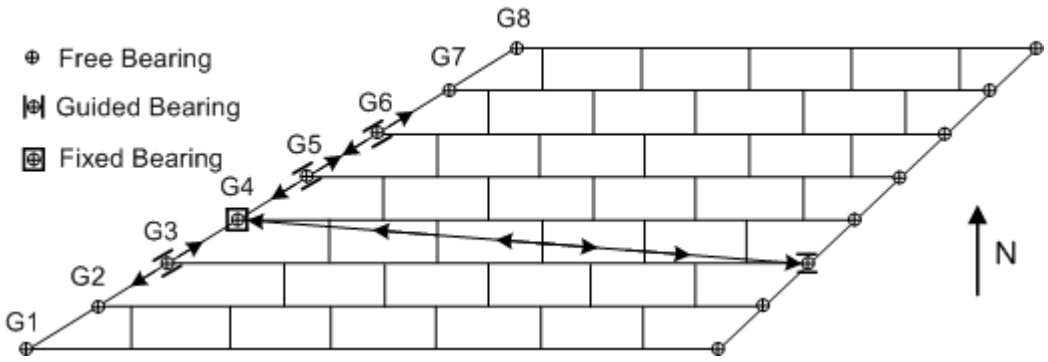


Figure 2.2.9 Guided Bearings All Guided Toward Fixed Bearing at West End of G4

Note the significant reduction in the horizontal reactions (i.e. in the x-y plane) that results (Figure 2.2.10) compared to the case shown previously (Figure 2.2.8). The longitudinal and transverse components of the reactions at all the guided bearings at both the west and east ends are shown in Figure 2.2.10. *The reactions are not zero because of the slightly different coefficients of thermal expansion assigned to the steel girders and concrete deck. In a separate analysis, the coefficients of thermal expansion were made the same and all horizontal reactions went to zero.* A significant reduction in the vertical reactions (not shown in Figure 2.2.8 or Figure 2.2.10) was also noted in this case. It is important to note that this bearing configuration would also need to be checked to ensure that it is satisfactory for dead and live loads and other potential horizontal loads.

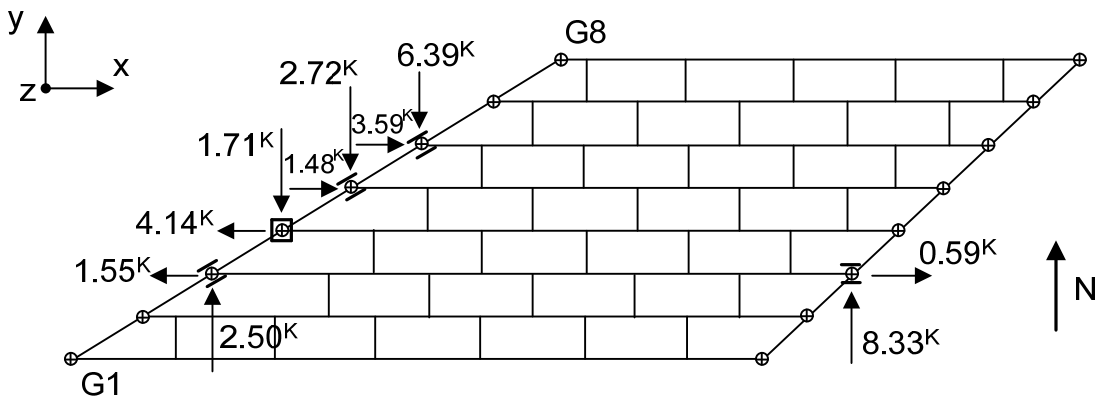


Figure 2.2.10 Horizontal Bearing Reactions (X-Y Plane) due to Thermal Expansion – Guided Bearings All Guided Toward Fixed Bearing at West End of G4

For the guided case, the net longitudinal expansion of G1 was [0.55 – (-0.21)] = 0.76" and the net longitudinal expansion of G8 was [0.84 – 0.27] = 0.57". The lateral expansion of G1 at the west and east corners was -0.145" and -0.148", respectively. The lateral expansion of G8 at the west and east corners was +0.193" and +0.185", respectively.

2.2.3.5 Bearing Arrangement for Box Girders

The arrangement of bearings can have a significant influence on the design of box girders and their cross frames/diaphragms. A single bearing might be centered over the shear center to minimize the torque resisted by the support. However, the torsion in the box must be removed. At such a support, torque is resisted via the cross-frame(s) or diaphragm(s) connecting the box to its neighboring box(es). Of course, a single box is unstable with a single bearing.

AASHTO LRFD Article 6.11.1.2 specifies that if single bearings narrower than the bottom flange are used, they are to be aligned with the center of the box and all other supports must have adequate resistance against overturning under any design load combination. *AASHTO LRFD* Article 6.11.1.2 allows double bearings to be placed between or outboard of the webs. Placing the bearings outboard of the box reduces overturning loads on the bearings and reduces uplift reactions. Wide box spacing, large overhangs, and curvature all can create large uplift forces in addition to the severe uplift issue related to skewed supports. Potential uplift should be investigated with and without a future wearing surface.

A skewed support with two bearings under a box along the skew line will generate a torque because the advance bearing will be more heavily loaded than the rear bearing. The net force in the two bearings will be eccentric with the shear center; hence the torque. If a single bearing is used in these cases, the diaphragm between

boxes will resist the torque. The moment and shear in the connecting diaphragm will be large.

Single-box cross sections are often economical structures, but their design introduces some unique concerns. All torsional loads are resisted by bearing pairs. Skewed single boxes are so problematic that they are best not used. Significant torsional loads may occur during construction as well as in the completed bridge under thermal and live loads. Positions of live load must be investigated for both flexure and torsion.

Orientation of guided bearings can usually be addressed in a manner similar to the orientation of bearings on I-girder bridges.

2.2.4 Effect of Pier Flexibility on Bearing Constraint

2.2.4.1 General

A fixed bearing located on a pier actually moves as a function of the pier stiffness when subjected to load. The displacement of such bearings equals the horizontal bearing force multiplied by the corresponding pier stiffness. The flexibility of the piers must be recognized in the analyses of bridges. Recognition of the inherent flexibility of the piers in the analysis provides relief of the horizontal reactions at constrained bearings and also the cross-frame/diaphragm forces adjacent to laterally constrained bearings.

It is significant to note that a free bearing can create significant force on a pier. If the dead load vertical reaction is 400 kips for example, the lateral force on the substructure is 40 kips for a sliding bearing if the coefficient of friction is 10 percent. This is usually not significant on the superstructure, but it may be significant on the overturning of the pier if the force was assumed to be zero.

2.2.4.2 Determination of Pier Stiffnesses

The pier stiffnesses must be calculated in the direction of the constraint(s). Thus, both longitudinal and transverse pier stiffnesses may be required. Depending on the configuration of the pier, the response of the pier in the longitudinal and transverse directions may be quite different.

The longitudinal pier stiffness (i.e., assuming a right bridge, the stiffness of the pier in the direction parallel to the longitudinal centerline of the bridge) for a typical pier configuration can be represented schematically as a “flagpole” of length, *L* (Part A of Figure 2.2.11). The “flagpole” is fixed at the bottom at an assumed point of fixity, which is dependent on the pier configuration and soil conditions, and free at the top with a longitudinal load, *P*, assumed applied at the top. The deflection, Δ, is in the longitudinal direction, as defined above.

The transverse pier stiffness (i.e., assuming a right bridge, the stiffness in the direction perpendicular to the longitudinal centerline of the bridge) can be represented schematically as a "portal frame", as shown for a two-column bent in Part B of Figure 2.2.11. The "portal frame" is also fixed at an assumed point of fixity, which is again dependent on the pier configuration and soil conditions. The deflection, Δ, is in the transverse direction in this case. Points of contraflexure are assumed to exist in the pier columns and in the cap beam as the "portal frame" deflects in the transverse direction under the load, *P*.

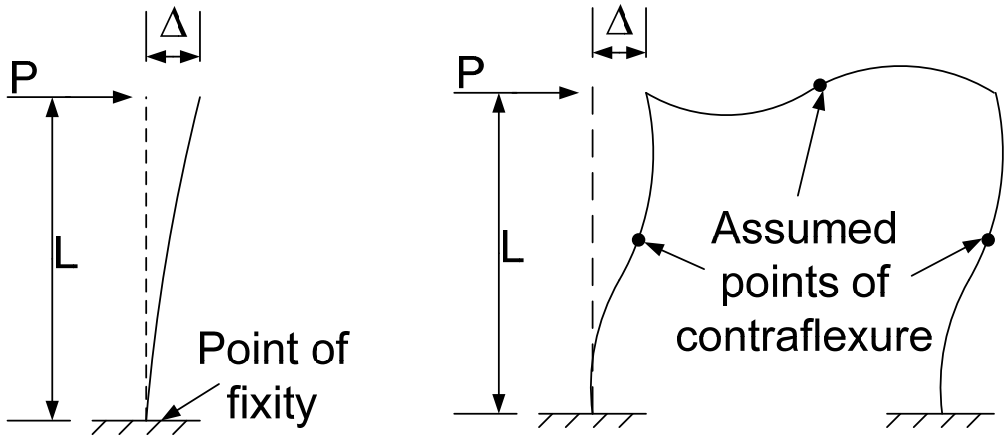


Figure 2.2.11 Schematic Representations of a Typical Pier in the Longitudinal and Transverse Directions
A) "Flagpole" - Longitudinal Pier Stiffness; B) "Portal Frame" - Transverse Pier Stiffness

Of course, refined finite element models of each pier could be built and analyzed in order to determine more accurate values of the pier stiffnesses, or the substructure could be explicitly modeled and combined with the refined model of the superstructure. However, for most typical pier configurations, the horizontal pier stiffnesses may be reasonably estimated in a quicker fashion using the classical conjugate-beam method.

2.2.4.2.1 Conjugate-Beam Method

The conjugate-beam method makes use of an "analogous" or "conjugate" beam that has its supports changed so that correct relationships are obtained. Shear and moment in the conjugate beam, when loaded with the *M*/*EI* diagram, correspond with the rotation and deflection (respectively) of the actual beam. The loads and properties of the actual beam have no effect on the manner in which the conjugate beam is supported. The lengths of the two beams are also equal. The only factor affecting the supports of the conjugate beam is the supports of the actual beam.

Referring to Figure 2.2., a simple support in the actual beam is also a simple support in the conjugate beam. A free end in the actual beam becomes a fixed end in the conjugate beam so that shear and moment are developed at that end when loaded with the *M*/*EI* diagram to reflect the slope and deflection in the actual beam at the free end. Conversely, a fixed end in the actual beam becomes a free end in the conjugate beam since no slope or deflection can occur at a fixed end; thus, no shear or moment can be developed in the conjugate beam at that point. An interior support in a continuous beam with no vertical deflection, but having slope, is a hinge in the conjugate beam. Conjugates for other support conditions may be found in many older textbooks on structural analysis.

Moments, shears and reactions in the conjugate beam are simply computed by statics as the conjugate beam is always statically determinate, even if the actual beam is statically indeterminate. For the simply supported beam loaded by a uniformly distributed load shown on the right-hand side of Figure 2.2.12, the maximum vertical deflection at midspan is computed as the maximum midspan moment in the conjugate beam (which is also a simply supported beam in this case) when loaded with the *M*/*EI* diagram.

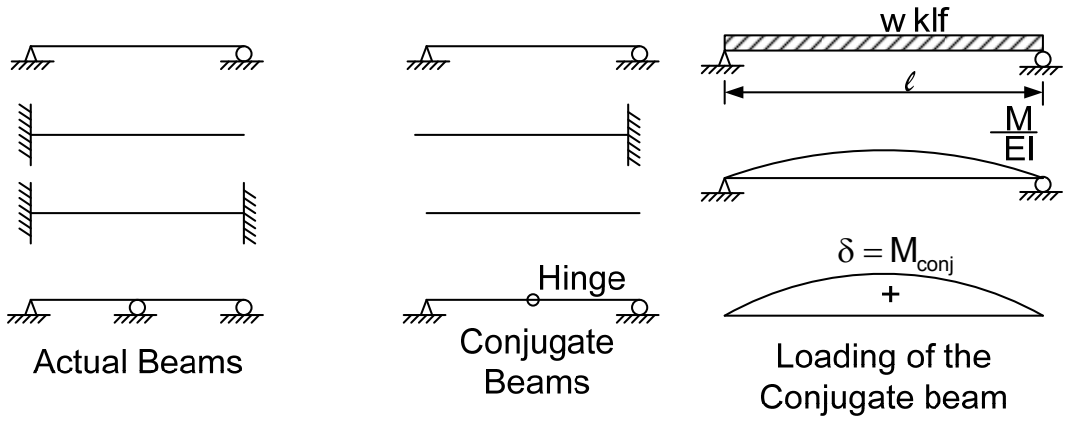


Figure 2.2.12 Conjugate-Beam Method

2.2.4.2.2 Longitudinal Pier Stiffness

The conjugate-beam method will now be applied to the calculation of the longitudinal pier stiffness. Assume that the “flagpole” with a total length of *L* shown on the right-hand side of Figure 2.2.13 represents schematically the behavior of the two-column bent shown on the left-hand side of the figure in the longitudinal direction (i.e. in its weak direction or into the page in this case).

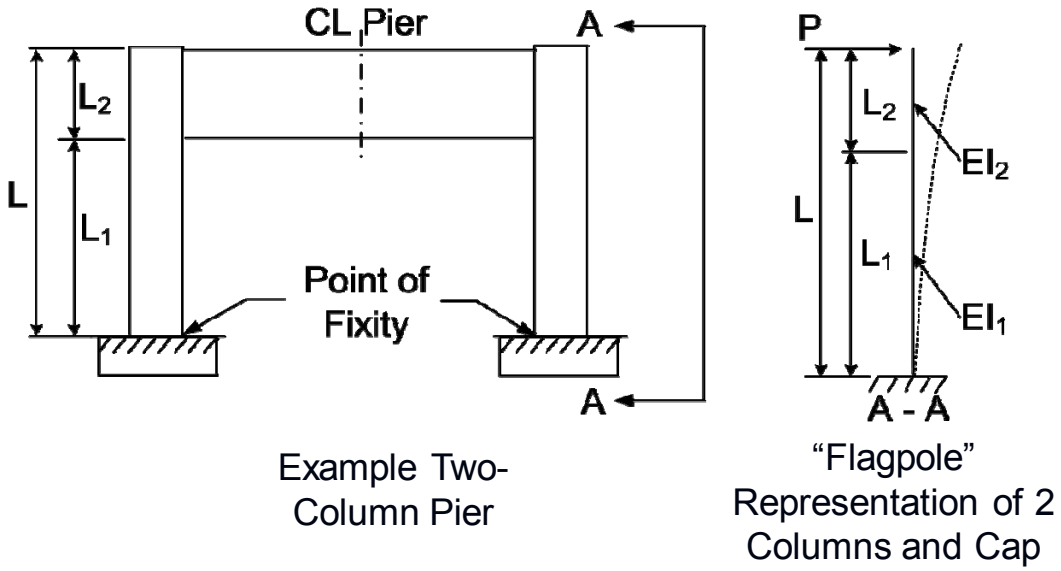


Figure 2.2.13 "Flagpole" Representation of an Example Two-Column Pier for Calculation of the Longitudinal Pier Stiffness

The "flagpole" is fixed at the bottom at an assumed point of fixity, which is assumed to be at the bottom of the columns in this illustration for simplicity, and free at the top with a longitudinal load, P, assumed applied at the top. The deflection, Δ, is again in the longitudinal direction as defined in Section 2.2.4.2 (i.e., into the page in this case).

The "flagpole" represents both pier columns and the pier cap and is assumed to have two stiffnesses, EI_1 and EI_2, along its length. I_1 represents the moment of inertia of two pier columns from the assumed point of fixity up to the bottom of the pier cap (i.e., over the length L_1) about the longitudinal axis of the pier. I_2 represents the moment of inertia of the pier cap along with the portion of the column adjacent to the cap (i.e., over the length L_2) about the longitudinal axis of the pier. The moment, M, at the bottom of the "flagpole" is PL.

The conjugate beam for the "flagpole" loaded by the appropriate M/EI diagram is shown on the right-hand side of Figure 2.2.14. Where there is a significant change in stiffness within the column, this is reflected in the M/EI diagram, as shown in the figure. The free end at the top of the "flagpole" becomes a fixed end in the conjugate beam, while the fixed end at the bottom of the "flagpole" becomes a free end in the conjugate beam.

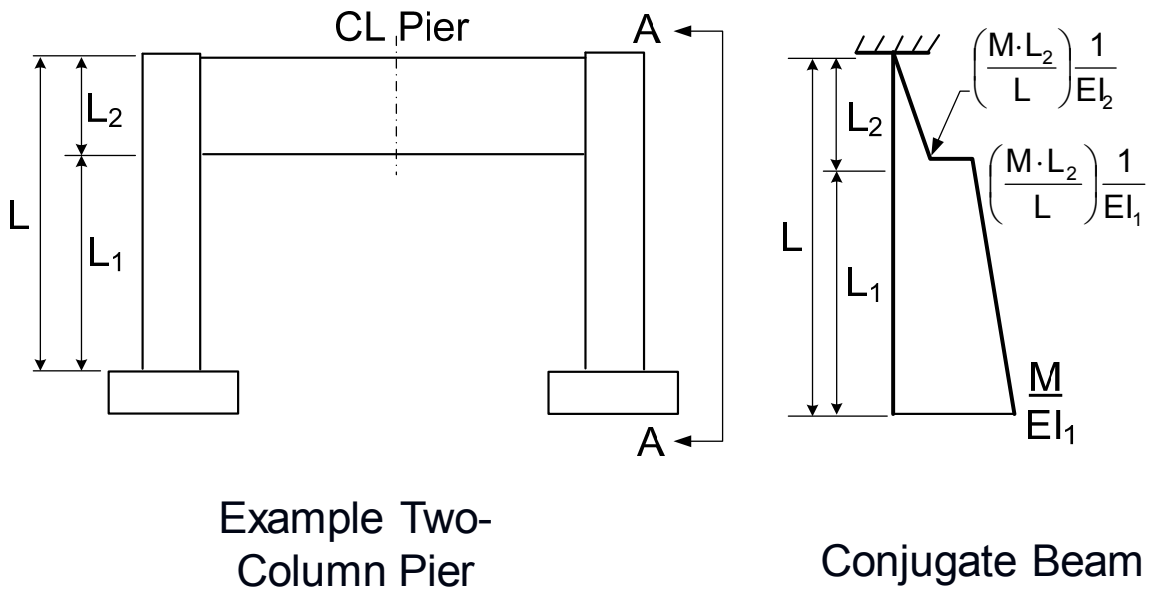


Figure 2.2.14 Conjugate Beam of the "Flagpole" for the Example Two-Column Pier Loaded by the *M*/*EI* Diagram

The longitudinal deflection at the top of the pier, Δ, is computed as the moment at the fixed end of the conjugate beam. Since $\Delta = P/K_L$, the longitudinal pier stiffness, K_L, is then computed from the deflection.

Referring to the conjugate beam of the "flagpole" in Figure 2.2., taking moments about the fixed end of the conjugate beam and substituting $M = PL$ gives:

$$\Delta = \frac{PL_2^3}{3EI_2} + \frac{PL_1L\left(L_2 + \frac{2}{3}L_1\right)}{2EI_1} - \frac{PL_1L_2\left(L_2 + \frac{2}{3}L_1\right)}{2EI_1} + \frac{PL_2L_1\left(L_2 + \frac{L_1}{2}\right)}{EI_1}$$

Equation 2.2.1

Since $\Delta = P/K_L$, where K_L is the longitudinal pier stiffness, then:

$$K_L = \left[\frac{L_2^3}{3EI_2} + \frac{L_1L\left(L_2 + \frac{2}{3}L_1\right)}{2EI_1} - \frac{L_1L_2\left(L_2 + \frac{2}{3}L_1\right)}{2EI_1} + \frac{L_2L_1\left(L_2 + \frac{L_1}{2}\right)}{EI_1}\right]^{-1}$$

Equation 2.2.2

The first term is typically small since I_2 is so large relative to I_1 and will be ignored. Thus:

$$K_L = \left[\frac{L_1 L \left(L_2 + \frac{2}{3} L_1 \right)}{2EI_1} - \frac{L_1 L_2 \left(L_2 + \frac{2}{3} L_1 \right)}{2EI_1} + \frac{L_2 L_1 \left(L_2 + \frac{L_1}{2} \right)}{EI_1} \right]^{-1}$$

Equation 2.2.3

In Equation 2.2.3, I_1 represents the *total* moment of inertia of all the columns in the pier over the length, L_1, about the longitudinal axis of the pier.

An example calculation of K_L for a three-column pier, using Equation 2.2.3, is given in Section 2.2.4.2.5.

2.2.4.2.3 Transverse Pier Stiffness

The conjugate-beam method will now be applied to the calculation of the transverse pier stiffness. Assume that the "portal frame" configuration and deflected shape shown in Figure 2.2.15 represents schematically the behavior of the two-column bent shown on the left-hand side of the figure in the transverse direction (i.e. in its strong direction), with the transverse load, P, applied at the top of one column (at Point B).

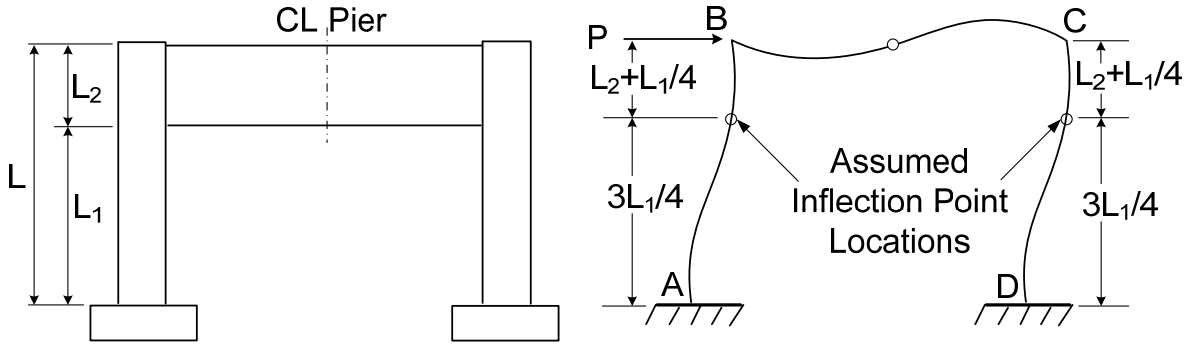


Figure 2.2.15 "Portal Frame" Representation of an Example Two-Column Pier for Calculation of the Transverse Pier Stiffness

Again, both pier columns in the "portal frame" are assumed fixed at the bottom at an assumed point of fixity, which is assumed to be at the base of the columns in this illustration for simplicity. The moments of inertia, I_1 and I_2, in this case over the

lengths L_1 and L_2, respectively, are about an axis transverse to the pier (i.e., out of the page).

Points of contraflexure are assumed at a distance of $3L_1/4$ from the assumed points of fixity in both columns in this example case (the determination of the estimated location of the points of contraflexure for different cases is discussed further in Section 2.2.4.2.3.1).

It can next be assumed that the horizontal shear is divided equally to each pier column at the contraflexure points. If the columns are of different stiffness, it is suggested that the shear be distributed in proportion to the ratio, I_1/L_1^3, of the columns. With two columns of equal stiffness, each column is assigned $P/2$ (Figure 2.2.16). With three columns of equal stiffness, each column would be assigned $P/3$, etc.

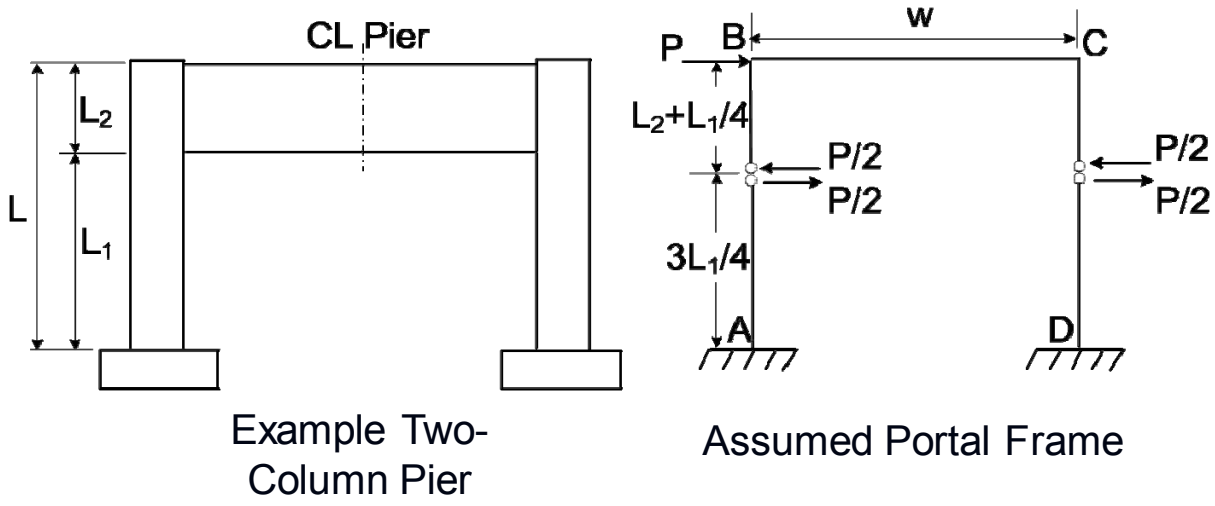
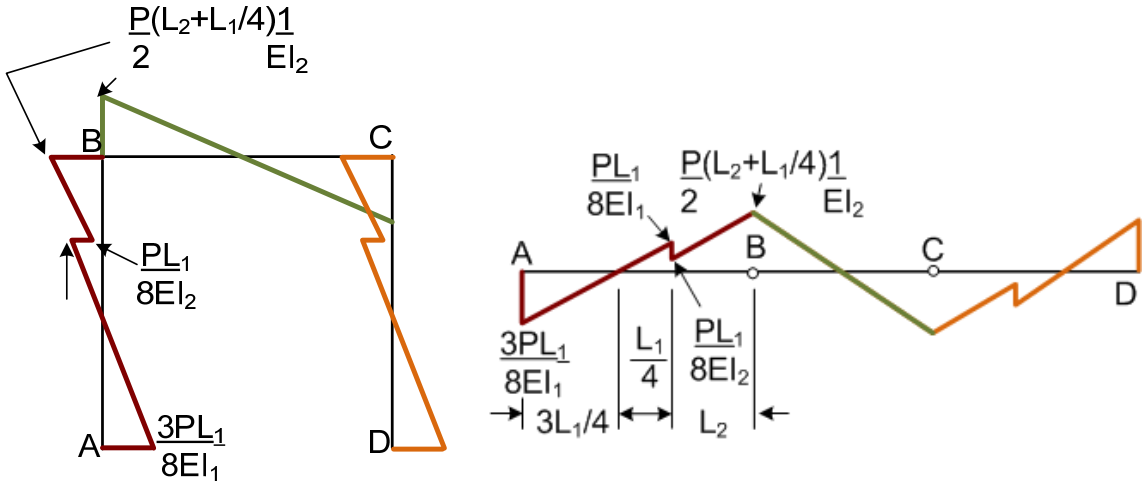


Figure 2.2.16 Distribution of the Horizontal Shear to the Individual Columns in the "Portal Frame"

The resulting M/EI diagram for the "portal frame" is presented in Part A of Figure 2.2.17. Where there is a significant change in stiffness within the columns, this is again reflected in the M/EI diagram, as illustrated in the figure.



Part A **Part B**

Figure 2.2.17 Conjugate Beam of the "Portal Frame" for the Example Two-Column Pier Loaded by the *M*/*EI* Diagram
A) "Portal Frame" *M*/*EI* Diagram; B) Conjugate Beam for the "Portal Frame" Loaded by the *M*/*EI* Diagram

The conjugate beam for the "portal frame" is shown in Part B of Figure 2.2.17. To determine the conjugate beam for this case, joints B and C in the "portal frame" are treated as interior supports in a beam continuous from joints A to D. Neglecting axial deformation of the member joints, joints B and C cannot deflect vertically, although they may be displaced laterally. Rotation is permitted at these joints. Figure 2.2.12 shows that an interior support with no vertical deflection, but having slope, is a hinge in the conjugate beam. Thus, joints B and C in the "portal frame" become hinges in the conjugate beam. The fixed supports at joints A and D in the "portal frame" become free in the conjugate beam. Note that the areas of the *M*/*EI* diagram must be precisely balanced between downward and upward loads since there are no supports in the conjugate beam in this case.

The conjugate beam is then used to compute the transverse deflection, Δ, at joint B in the "portal frame". For simplicity, only the values of the *M*/*EI* diagram between joints A and B are shown on the conjugate beam (Part B of Figure 2.2.17), as these values are the only ones pertinent to computing the transverse deflection at joint B. The transverse deflection at joint B is computed as the moment about the internal hinge at Point B in the conjugate beam when loaded with the *M*/*EI* diagram. Since $\Delta = P/K_T$, the transverse pier stiffness, K_T, is then computed from the deflection.

The solution for the transverse stiffness of the pier is a function of the assumed location of the point of contraflexure in each column, which will result in a unique equation for K_T for each individual case. An approach to make a reasonable estimate of the location of the point of contraflexure is discussed in the next section. An example calculation of K_T for a three-column pier is given in Section 2.2.4.2.5.

2.2.4.2.3.1 Location of Point of Contraflexure in Pier Columns

A reasonable assumption of the location of the point of contraflexure in the pier columns must be made in order to arrive at a solution for the transverse pier stiffness, K_T, using the equivalent "portal frame" approach described above.

Figure 2.2.18 provides a plot for estimating the location of the assumed point of contraflexure as a fraction, x, of the pier-column length, L_1, (measured from the assumed point of fixity) versus the pier-cap to pier-column stiffness ratio, R, which is given as follows:

$$R = \frac{\left(\frac{I_{cap}}{L_c^{\,3}}\right)_{pier\ \ cap}}{\left(\frac{I_{col}}{L_1^{\,3}}\right)_{pier\ \ column}}$$

Equation 2.2.4

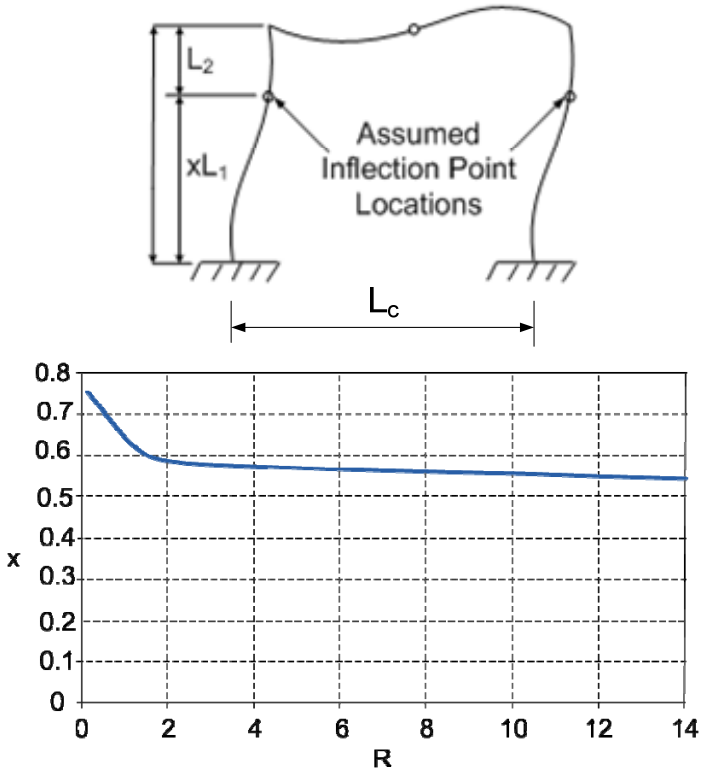


Figure 2.2.18 Plot for Estimation of the Location of the Assumed Point of Contraflexure in Pier Columns for Calculation of the Transverse Pier Stiffness

In the calculation of the pier-cap stiffness, (I_{cap}/L_c^3), in the numerator of Equation 2.2.4, I_{cap} is taken as the bending stiffness of the cap about an axis transverse to the

pier (i.e. out of the page), and L_c is taken as the centerline distance between the pier columns (Figure 2.2.18).

In the calculation of the pier-column stiffness, (I_{col}/L_1^3), in the denominator of Equation 2.2.4, I_{col} is taken as the bending stiffness of an individual column about an axis transverse to the pier, and the distance, L_1, is the length of the individual column from the assumed point of fixity to the base of the cap (Figure 2.2.18)

An examination of the plot in Figure 2.2.18 indicates that the assumed contraflexure point location asymptotically approaches $0.5L_1$ as the stiffness of the individual pier columns decreases with respect to the stiffness of the pier cap (and a condition of full fixity is approached at the point where the cap meets the top of the column); that is, as the value of the ratio R increases. Conversely, as the stiffness of the pier cap decreases significantly with respect to the stiffness of the individual pier columns and R approaches zero, the assumed contraflexure point location approaches a value of $0.75L_1$.

The plot is deemed applicable regardless of the number of pier columns. To ensure a reasonable scale, only data for cases up to and including R = 14 are included in the plot. For values of R greater than 14, the Design Engineer can make use of the fact that at an R value of 96.0, the contraflexure point location is estimated to be at $0.53L_1$.

2.2.4.2.4 Resolution of Pier Stiffnesses

In cases where the piers are skewed, the calculated longitudinal and transverse pier stiffnesses, K_L and K_T, must be resolved in directions parallel to the directions of bearing constraint; that is, the stiffnesses, K_x and K_y, in the directions of bearing constraint must be determined. The orientation of these different stiffness values in the case of a skewed pier is shown in Figure 2.2.19. In this case, the directions of bearing constraint are assumed to be along the global x and y axes.

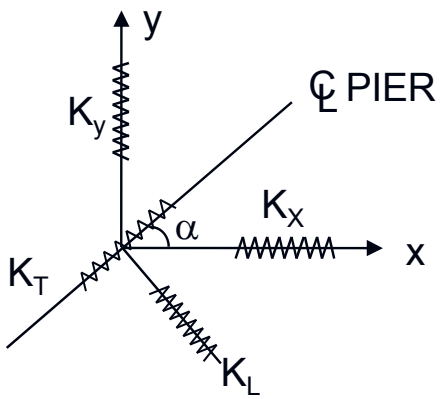


Figure 2.2.19 Resolution of Pier Stiffnesses, K_L and K_T, at a Skewed Pier

Following is the derivation of the stiffness equations necessary to perform this transformation.

First, assume the skewed pier shown in Figure 2.2.19 is translated in the positive global x-direction an amount equal to Δ_x, as illustrated in Figure 2.2.20.

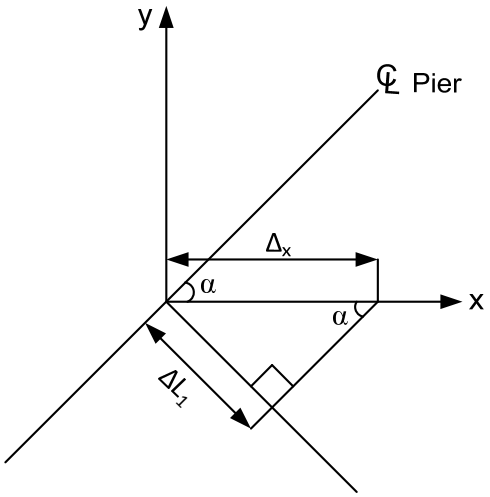


Figure 2.2.20 Imposed Translation, Δ_x, of the Skewed Pier in Figure 2.2.19 for Calculation of the Global Stiffness Coefficients Related to ΔL_1

An element oriented normal to the skewed pier and parallel to the direction of the calculated longitudinal pier stiffness, K_L, shortens by an amount equal to ΔL_1 as a result of the displacement, Δ_x. Referring to Figure 2.2.20, ΔL_1 is equal to the following:

$$\Delta L_1 = \Delta_x \sin\alpha$$

Equation 2.2.5

where α is the skew angle of the pier with respect to the direction of the longitudinal restraint of the bearing (Figure 2.2.19).

The force, F, required to shorten the element an amount equal to ΔL_1 is:

$$F = K_L \sin\alpha\Delta_x$$

Equation 2.2.6

The global x and y components of the force, F, resulting from the displacement, ΔL_1, can then be computed as follows:

$$F_{x1} = K_L \sin^2\alpha\Delta_x$$
$$F_{y1} = -K_L \cos\alpha \sin\alpha\Delta_x$$

Equation 2.2.7

Thus, the stiffness coefficients in the global x and y directions related to the displacement ΔL_1 are as follows:

$$k_{x1} = K_L \sin^2 \alpha$$
$$k_{y1} = -K_L \cos\alpha \sin\alpha$$

Equation 2.2.8

Next, assume the skewed pier is translated in the positive global y-direction an amount equal to Δ_y, as illustrated in Figure 2.2.21.

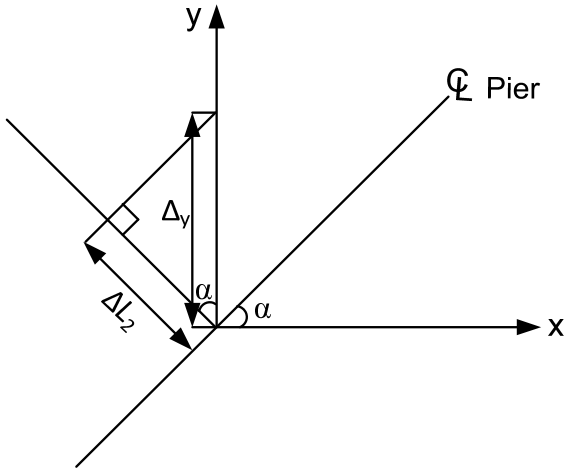


Figure 2.2.21 Imposed Translation, Δ_y, of the Skewed Pier in Figure 2.2.19 for Calculation of the Global Stiffness Coefficients Related to ΔL_2

An element oriented normal to the skewed pier and parallel to the direction of the calculated longitudinal pier stiffness, K_L, shortens by an amount equal to ΔL_2 as a result of the displacement, Δ_y. Referring to Figure 2.2.21, ΔL_2 is equal to the following:

$$\Delta L_2 = \Delta_y \cos\alpha$$

Equation 2.2.9

The force, F, required to shorten the element an amount equal to ΔL_2 is:

$$F = K_L \cos\alpha \Delta_y$$

Equation 2.2.10

The global x and y components of the force, F, resulting from the displacement, ΔL_2, can then be computed as follows:

$$F_{x2} = -K_L \cos\alpha \sin\alpha \Delta_y$$

$$F_{y2} = K_L \cos^2\alpha \Delta_y$$

Equation 2.2.11

Thus, the stiffness coefficients in the global x and y directions related to the displacement ΔL_2 are as follows:

$$k_{x2} = -K_L \cos\alpha \sin\alpha$$

$$k_{y2} = K_L \cos^2\alpha$$

Equation 2.2.12

Next, assume the skewed pier is again translated in the positive global x-direction an amount equal to Δ_x, as illustrated in Figure 2.2.22.

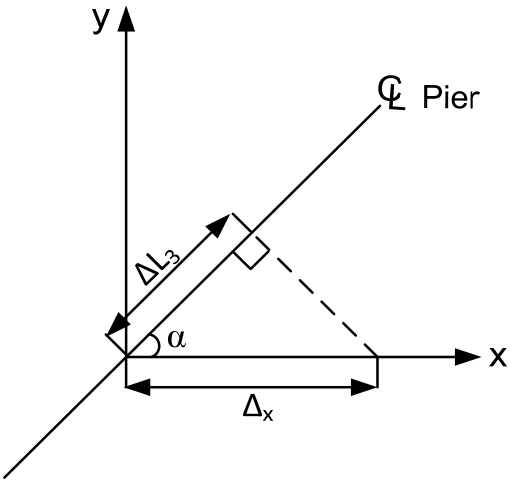


Figure 2.2.22 Imposed Translation, Δ_x, of the Skewed Pier in Figure 2.2.19 for Calculation of the Global Stiffness Coefficients Related to ΔL_3

An element oriented along the skewed pier and parallel to the direction of the calculated transverse pier stiffness, K_T, shortens by an amount equal to ΔL_3 as a result of the displacement, Δ_x. Referring to Figure 2.2.22, ΔL_3 is equal to the following:

$$\Delta L_3 = \Delta_x \cos\alpha$$

Equation 2.2.13

The force, *F*, required to shorten the element an amount equal to ΔL_3 is:

$$F = K_T \cos\alpha \Delta_x$$

Equation 2.2.14

The global x and y components of the force, *F*, resulting from the displacement ΔL_3 can then be computed as follows:

$$F_{x3} = K_T \cos^2\alpha \Delta_x$$
$$F_{y3} = K_T \cos\alpha \sin\alpha \Delta_x$$

Equation 2.2.15

Thus, the stiffness coefficients in the global x and y directions related to the displacement ΔL_3 are as follows:

$$k_{x3} = K_T \cos^2\alpha$$
$$k_{y3} = K_T \cos\alpha \sin\alpha$$

Equation 2.2.16

Finally, assume the skewed pier is again translated in the positive global y-direction an amount equal to Δ_y, as illustrated in Figure 2.2.23.

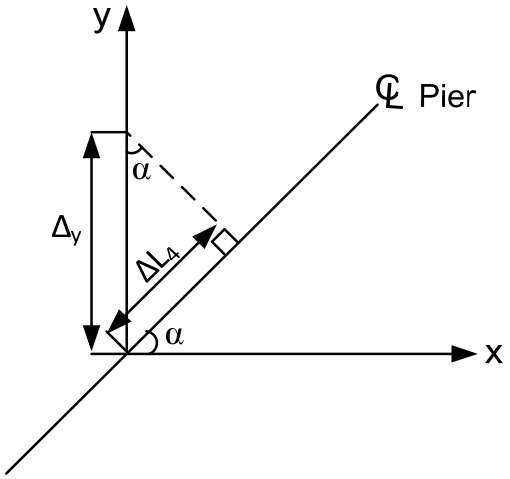


Figure 2.2.23 Imposed Translation, Δ_y, of the Skewed Pier in Figure 2.2.19 for Calculation of the Global Stiffness Coefficients Related to ΔL_4

An element oriented along the skewed pier and parallel to the direction of the calculated transverse pier stiffness, K_T, shortens by an amount equal to ΔL_4 as a result of the displacement, Δ_y. Referring to Figure 2.2.23, ΔL_4 is equal to the following:

$$\Delta L_4 = \Delta_y \sin\alpha$$

Equation 2.2.17

The force, F, required to shorten the element an amount equal to ΔL_4 is:

$$F = K_T \sin\alpha\Delta_y$$

Equation 2.2.18

The global x and y components of the force, F, resulting from the displacement ΔL_4 can then be computed as follows:

$$F_{x4} = K_T \cos\alpha \sin\alpha\Delta_y$$
$$F_{y4} = K_T \sin^2\alpha\Delta_y$$

Equation 2.2.19

Thus, the stiffness coefficients in the global x and y directions related to the displacement Δ_y are as follows:

$$k_{x4} = K_T \cos\alpha \sin\alpha$$
$$k_{y4} = K_T \sin^2\alpha$$

Equation 2.2.20

For assumed values of the bearing reactions, R_x and R_y, the displacements Δ_x and Δ_y can thus be determined by solving the following two equations simultaneously based on the global stiffness coefficients determined above:

$$R_x = k_{x1}\Delta_x + k_{x2}\Delta_y + k_{x3}\Delta_x + k_{x4}\Delta_y$$

Equation 2.2.21

$$R_y = k_{y1}\Delta_x + k_{y2}\Delta_y + k_{y3}\Delta_x + k_{y4}\Delta_y$$

Equation 2.2.22

Substituting and rearranging gives:

$$R_x = \left[K_L \sin^2\alpha + K_T \cos^2\alpha\right]\Delta_x + \left[(-K_L + K_T)\cos\alpha\sin\alpha\right]\Delta_y$$

Equation 2.2.23

$$R_y = \left[(-K_L + K_T)\cos\alpha\sin\alpha\right]\Delta_x + \left[K_L \cos^2\alpha + K_T \sin^2\alpha\right]\Delta_y$$

Equation 2.2.24

The stiffnesses, K_x and K_y, can then be calculated from the corresponding displacements as:

$$K_x = \frac{R_x}{\Delta_x}$$

Equation 2.2.25

$$K_y = \frac{R_y}{\Delta_y}$$

Equation 2.2.26

If there is no restraint at the bearing in the x or y direction, R_x or R_y (as applicable) is set to zero and the resulting displacement and corresponding stiffness in that direction is ignored.

The use of Equations 2.2.23 through 2.2.26 is demonstrated below in Section 2.2.4.2.5.

2.2.4.2.5 Pier Stiffness Example

The calculation of the horizontal pier stiffnesses for the skewed interior piers assumed for the example skewed and curved I-girder bridge (Section 5.1) will be demonstrated using the approximate procedures discussed above. The calculated pier stiffnesses are applied at the fixed and guided bearings on the piers in a 3D thermal analysis of the example bridge (Section 5.1.6.2). The stiffnesses are assigned to foundation elements (Section 2.5.2.3.5) in the 3D model of the example bridge in the appropriate directions of bearing constraint. The effect of including the pier stiffnesses on the thermal analysis results is examined further in Section 5.1.6.2.

A schematic of the assumed pier configuration is shown below in Figure 2.2.24. A 70-foot long three-column concrete bent is assumed for the skewed interior piers. The columns are each assumed to be 37-feet in length measured from assumed points of fixity at the base of each column (i.e., L_1 = 37 feet); the base of each column is used as the assumed point of fixity in this illustration for simplicity. A diameter, d, of 4 feet is assumed for each column. The center-to-center column spacing, L_c, is assumed to be 28 feet and the distance from the centerline of the outer columns to the ends of the pier cap is assumed to be 7 feet. The rectangular pier cap is assumed to be 5 feet in depth (i.e., L_2 = 5 feet) and 4 feet wide. The 28-day compressive strength of the concrete in the columns and pier cap is assumed to be f'_c =5.0 ksi.

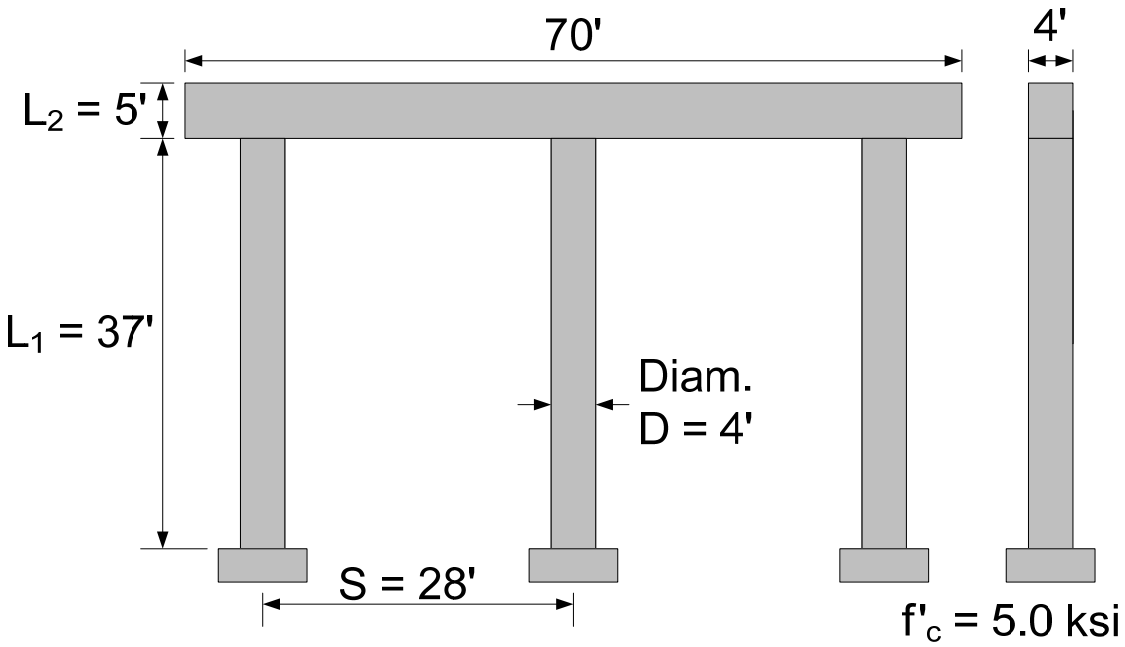


Figure 2.2.24 Assumed Pier Configuration for the Skewed Interior Piers from the Example I-Girder Bridge (Section 5.1)

Modulus of Elasticity of the Pier Columns

First, calculate Young's modulus, *E*, for the concrete columns:

Young's modulus, E_c, of the pier concrete is calculated as follows:

$$E_c = 33{,}000 w_c^{1.5} \sqrt{f_c'}$$

Equation 2.2.27
AASHTO LRFD Eq. 5.4.2.4-1

A unit weight, w_c, of 0.145 kips/ft^3 will be assumed for the concrete in this calculation since 0.005 kips/ft^3 of the specified unit weight of 0.150 kips/ft^3 for normal-weight concrete is typically assumed to account for the reinforcement. Substituting the assumed strength of 5.0 ksi for f'_c gives:

$$E_c = 33{,}000(0.145)^{1.5} \sqrt{5.0} \cong 4{,}000 \text{ ksi} = 576{,}000 \text{ ksf}$$

The full modulus of elasticity of the concrete is assumed for the thermal analysis (i.e. a modular ratio of *n* is assumed).

Longitudinal Pier Stiffness

Calculate the longitudinal pier stiffness (i.e. the stiffness in the weak direction of the pier). First, calculate I_1 for the three circular 4-foot-diameter pier columns (Figure 2.2.25):

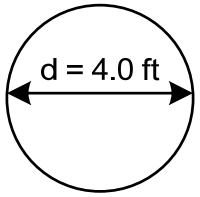


Figure 2.2.25 Cross-Section of Pier Columns

$$I_1 = n * \frac{\pi d^4}{64} = 3 * \frac{\pi (4.0)^4}{64} = 37.7 \text{ ft}^4$$

Substituting into Equation 2.2.3 gives:

$$K_L = \left[\frac{37(42)\left(5 + \frac{2}{3}(37)\right)}{2(576{,}000)(37.7)} - \frac{37(5)\left(5 + \frac{2}{3}(37)\right)}{2(576{,}000)(37.7)} + \frac{5(37)\left(5 + \frac{37}{2}\right)}{576{,}000(37.7)} \right]^{-1} = 881 \text{ kips/ft}$$

For a 100-kip load applied to the top of the pier in the longitudinal direction (i.e. in the weak direction of the pier):

$$\Delta = \frac{P}{K_L} = \frac{100(12)}{881} = 1.36 \text{ inches}$$

From a refined 3D analysis of the pier only, applying a load of 100/3 = 33.33 kips at the top of each column in the longitudinal direction gives:

$$\Delta = 1.37 \text{ inches}.$$

Transverse Pier Stiffness

The transverse pier stiffness (i.e. the stiffness in the strong direction of the pier) will next be calculated. First, calculate the ratio, *R*, from Equation 2.2.4.

For the cap, I_{cap} in Equation 2.2.4 is taken as the bending stiffness of the cap about an axis transverse to the pier, and L_c is taken as the centerline distance between the columns.

$$I_{cap} = \frac{1}{12}(4.0)(5.0)^3 = 41.67 \text{ ft}^4$$

$$L_c = 28.0 \text{ ft}$$

For the columns, I_{col} in Equation 2.2.4 is taken as the bending stiffness of a single column about an axis transverse to the pier and the distance, L_1, is taken as the length of the column from the assumed point of fixity to the base of the pier cap.

$$I_{col} = \frac{\pi d^4}{64} = \frac{\pi(4.0)^4}{64} = 12.57 \text{ ft}^4$$

$$L_1 = 37.0 \text{ ft}$$

Therefore:

$$R = \frac{\left(41.67/28^3\right)}{\left(12.57/37^3\right)} = 7.65$$

From the plot provided in Figure 2.2.18, determine the assumed contraflexure point location in each column based on an R value of 7.65 (Figure 2.2.26):

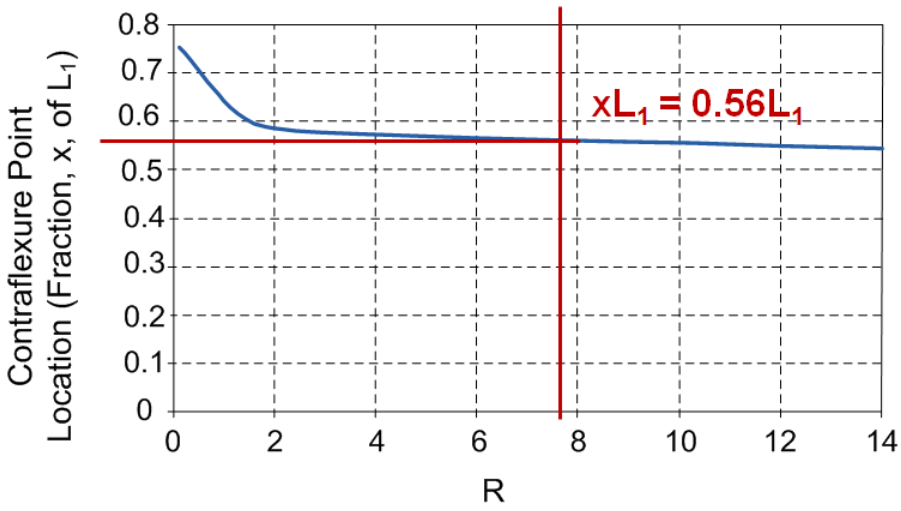
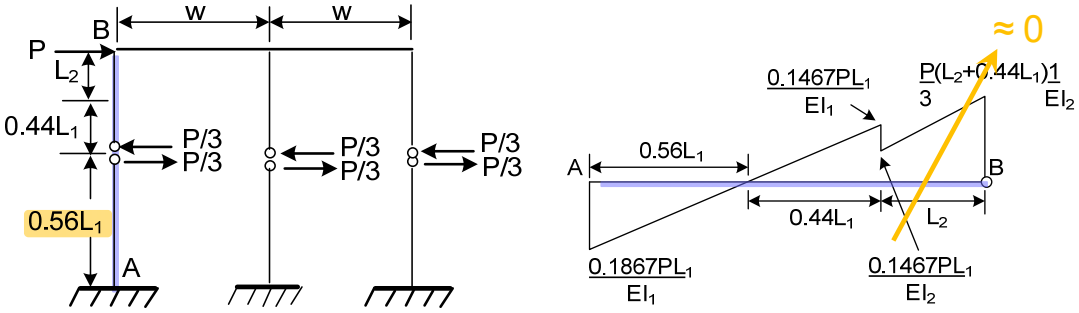


Figure 2.2.26 Determination of the Location of the Assumed Contraflexure Point in Each Pier Column for the Example Pier

The fraction, x, of the column length, L_1, is determined from the plot to be 0.56. Thus, the assumed point of contraflexure is $0.56L_1$ from the assumed point of fixity in each column (Part A of Figure 2.2.27)..

With three columns of equal stiffness, each column is assigned one-third of the horizontal shear, or $P/3$, at the assumed contraflexure points in each column (Part A of Figure 2.2.27).



Part A **Part B**

Figure 2.2.27 "Portal Frame" Representation and Conjugate Beam Between Joints A and B for the Example Pier
A) Distribution of Horizontal Shear, *P*, to Pier Columns at Contraflexure Points
B) Conjugate Beam Between Joints A and B

Only the portion of the resulting conjugate beam between joints A and B in the portal frame is shown in Part B of Figure 2.2.27, as this is the only portion that is pertinent to computing the transverse deflection at joint B. The transverse deflection, Δ, at joint B is computed as the moment about the internal hinge at joint B in the conjugate beam when loaded with the *M*/*EI* diagram.

Note that the portion of the *M*/*EI* diagram extending over the length L_2 may typically be ignored (Part B of Figure 2.2.27) because I_2 of the cap and the portion of the pier column adjacent to the cap is generally so large relative to I_1 that this portion does not materially affect the result.

Referring to Part B of Figure 2.2.27 and taking moments about the internal hinge at joint B in the conjugate beam results in the following expression for the transverse deflection, Δ, at joint B in the "portal frame:

$$\Delta = \frac{1}{2}\left(\frac{0.1867PL_1}{EI_1}\right)(0.56L_1)(L_2 + 0.44L_1 + 0.373L_1)$$
$$-\frac{1}{2}\left(\frac{0.1467PL_1}{EI_1}\right)(0.44L_1)(L_2 + 0.1467L_1)$$

Since $\Delta=P/K_T$, where K_T is the transverse pier stiffness, then:

$$K_T = \left[\frac{0.05228L_1^2}{EI_1}(L_2 + 0.8133L_1) - \frac{0.032274L_1^2}{EI_1}(L_2 + 0.1467L_1) \right]^{-1}$$

Note that in this case, I_1 is taken as the stiffness of an individual column in the transverse direction, or 12.57 ft^4. Substituting:

$$K_T = \left[\frac{0.05228(37)^2}{576{,}000(12.57)}(5.0 + 0.8133(37)) - \frac{0.032274(37)^2}{576{,}000(12.57)}(5.0 + 0.1467(37)) \right]^{-1}$$

$$= 3{,}530 \ \text{kips/ft}$$

For a 100-kip load applied to the top of the pier in the transverse direction (i.e. in the strong direction of the pier):

$$\Delta = \frac{P}{K_T} = \frac{100(12)}{3{,}530} = 0.34 \ \text{inches}$$

From a refined 3D analysis of the pier applying a load of 100 kips at the top of one column in the transverse direction,

$$\Delta = 0.31 \ \text{inches}.$$

Resolution of the Pier Stiffnesses

As discussed in Section 2.2.4.2.4, the calculated longitudinal and transverse pier stiffnesses, K_L and K_T, must be resolved in directions parallel to the directions of bearing constraint in cases where the piers are skewed; that is, the stiffnesses, K_x and K_y, in the directions of bearing constraint must be determined for input into the 3D analysis model. Equations 2.2.23 through 2.2.26 will be used to resolve the stiffnesses.

The angle, α, in this case, or the skew angle of the pier with respect to the direction of the longitudinal restraint of the bearing, is approximately equal to 30° (rounded - refer to the fold-out sheets for the example I-girder bridge given in Section 5.1). The longitudinal pier stiffness, K_L, was determined to be 881 kips/ft and the transverse pier stiffness, K_T, was determined to be 3,530 kips/ft.

Longitudinally Constrained Bearings



The resolved stiffness, K_x, will first be calculated for the longitudinally constrained bearings on the skewed piers of the example I-girder bridge (K_y is equal to zero in this case).

R_x in Equation 2.2.23 is assumed equal to 100 kips (note that any value could be assumed for R_x). R_y in Equation 2.2.24 is taken equal to zero since there is no restraint in the transverse direction in this case. Substituting K_L, K_T and α into Equations 2.2.23 and 2.2.24 results in the two simultaneous equations shown below:

$$2{,}867.75\Delta_x + 1{,}147.02\Delta_y = 100$$
$$1{,}147.02\Delta_x + 1{,}543.25\Delta_y = 0$$

Solving these two simultaneous equations gives Δ_x equal to 0.0496 ft and Δ_y equal to –0.0369 ft. A refined 3D analysis applying a load of 100/3 = 33.33 kips at the top of each column of the *skewed* pier in the positive longitudinal (x) direction yielded Δ_x equal to 0.0465 ft and Δ_y equal to –0.0364 ft.

From Equation 2.2.25:

$$K_x = \frac{100}{0.0495} = 2{,}016 \ \text{k/ft}$$

Since there is no restraint in the transverse direction in this case, Δ_y is ignored and K_y is taken equal to zero.

Transversely Constrained Bearings



The resolved stiffness, K_y, will next be calculated for the transversely constrained bearings on the skewed piers of the example I-girder bridge (K_x is equal to zero in this case).

R_y in Equation 2.2.24 is assumed equal to 100 kips (note that any value could be assumed for R_y). R_x in Equation 2.2.23 is taken equal to zero since there is no restraint in the longitudinal direction in this case. Substituting K_L, K_T and α into Equations 2.2.23 and 2.2.24 results in the two simultaneous equations shown below:

$$2{,}867.75\Delta_x + 1{,}147.02\Delta_y = 0$$
$$1{,}147.02\Delta_x + 1{,}543.25\Delta_y = 100$$

Solving these two simultaneous equations gives Δ_x equal to –0.037 ft and Δ_y equal to –0.0925 ft. A refined 3D analysis applying a load of 100/3 = 33.33 kips at the top of each column of the *skewed* pier in the positive transverse (y) direction yielded Δ_x equal to -0.037 ft and Δ_y equal to 0.0887 ft.

From Equation 2.2.26:

$$K_y = \frac{100}{0.0925} = 1{,}081 \ \text{k/ft}$$

Since there is no restraint in the longitudinal direction in this case, Δ_x is ignored and K_x is taken equal to zero.

Fixed Bearings 

Lastly, the resolved stiffnesses, K_x and K_y, will be calculated for the fixed bearings on the skewed piers of the example I-girder bridge.

R_x and R_y in Equations 2.2.23 and 2.2.24 are both assumed equal to 100 kips (note that any values could be assumed for R_x and R_y). Substituting K_L, K_T and α into Equations 2.2.23 and 2.2.24 results in the two simultaneous equations shown below:

$$2{,}867.75\Delta_x + 1{,}147.02\Delta_y = 100$$
$$1{,}147.02\Delta_x + 1{,}543.25\Delta_y = 100$$

Solving these two simultaneous equations gives Δ_x equal to 0.01274 ft and Δ_y equal to 0.0553 ft. A refined 3D analysis applying a load of 100/3 = 33.33 kips at the top of each column of the *skewed* pier simultaneously in both the positive longitudinal (x) and transverse (y) directions yielded Δ_x equal to 0.010 ft and Δ_y equal to 0.0523 ft.

From Equations 2.2.25 and 2.2.26:

$$K_x = \frac{100}{0.01274} = 7{,}894 \ \text{k/ft}$$
$$K_y = \frac{100}{0.0553} = 1{,}808 \ \text{k/ft}$$

The preceding resolved stiffness values are used in the thermal analysis of the example I-girder bridge described in Section 5.1.6.2.

This Page Intentionally Left Blank

Chapter 2
Structural Analysis

Section 2.3

Approximate Methods of Analysis



2.3.1 Introduction

This section describes two common approximate methods of analysis for curved steel bridges. For I-girder bridges, the V-load approximate method of analysis is described. For box-girder bridges, the M/R approximate method of analysis is described. The theory behind the development of the both methods is instructive in understanding the basic distribution of forces within curved bridge systems. The development and application of both methods is described in this section. Limitations of both methods are also discussed. An approximate calculation of lateral bending stresses in I-girder flanges and top flanges of tub girders due to curvature, based on V-load theory, is presented. A Levels of Analysis

2.3.2 V-Load Method (I-Girders)

2.3.2.1 General

AASHTO LRFD Article 4.6.2.2.4 specifies that approximate methods may be used for the analysis of curved steel bridges. The Design Engineer must ascertain that the approximate analysis method used is appropriate by confirming that it satisfies the requirements for acceptable methods of structural analysis given in *AASHTO LRFD* Article 4.4.

Even with the ever-increasing use of refined analysis techniques as discussed in subsequent sections, treatment of approximate methods of analysis is appropriate for several reasons. First, they provide some historical perspective on the evolution of analysis approaches for curved bridges; second, the techniques are relatively simple to employ and may be useful in the preparation of preliminary designs or perhaps as some measure of validation for more complex analysis techniques; and third, the methods are useful in aiding in the basic understanding of the distribution of forces and the overall behavior of curved bridges.

The application of approximate methods of analysis should be limited to preliminary design and/or to the design of relatively simple structures with basic geometry and framing. The application of these techniques to more complex bridges can result in reduced accuracy; in particular, with regard to the prediction of the structure deformations. Strict rules and limitations on the applicability of these approximate methods do not exist. The Design Engineer must determine when approximate methods of analysis are appropriate.

In this section, an approximate method of analysis for curved steel I-girder bridges known as the V-load method is discussed. A method to approximate the lateral bending stresses in I-girder flanges (and the top flanges of tub girders) due to curvature, based on V-load theory, is also described. An approximatate method of analysis for curved steel box-girder bridges known as the M/R method is discussed in Section 2.3.3.

2.3.2.2 V-load Procedure

The approximate V-load analysis method was originally developed in the early 1960s as a simplified approximate analysis technique for open-framed curved I-girder bridges (*1*). Open framing was defined as non-composite I-girders connected by cross-frames or diaphragms with no lateral bracing placed near, or in, the plane of the flanges. The approximate method as originally presented was too time consuming and cumbersome for actual design practice at the time; in particular, for multi-girder systems. Hence, the method was later modified and greatly simplified for multi-girder systems (*2*). According to a 1969 survey published in 1973 (*3*), the

method was employed for the design of approximately 75 percent of the curved steel I-girder bridges in the U.S. at that time.

The steps for performing a V-load analysis of a curved I-girder bridge system under normal highway loadings are summarized as follows (limitations of the method are discussed further in Section 2.3.2.3):

1. Isolate and straighten the girders to their developed lengths (with span lengths equal to the curved girder arc lengths) and determine the summation of primary moments, M_p, in each girder at each cross-frame. To determine live load primary moments, use the *AASHTO LRFD* straight-girder distribution factors to distribute the lanes to the individual girders. Use an appropriate distribution of dead loads to the individual girders.
2. Compute the V-loads in the outside and inside girders at each cross-frame from the sum of the primary moments using Equation 2.3.15. To determine the V-loads in the interior girders, apply the proper proportionality factor. The V-loads increase the loads on girders outside the longitudinal centerline and decrease the loads on girders inside the longitudinal centerline. To determine the live load V-loads (Equation 2.3.17), first factor the live load primary moments by the ratio of the V-load lateral distribution factor (Equation 2.3.16) to the *AASHTO* distribution factor. Determine the V-load moments by applying the V-loads to the respective developed straight girders at each cross-frame.
3. Sum the primary and V-load moments to determine the final moments in the curved girders.
4. Determine the cross-frame forces from statics.
5. Compute lateral flange bending moments and stresses from the approximate Equations 2.3.16 and 2.3.17.
6. Repeat the procedure to determine shear, deflections and reactions.

Each of these steps is reviewed in more detail below.

2.3.2.2.1 Step 1 – Primary Moments

In Step 1, the curved structure is straightened out so that the applied vertical loads are assumed to introduce only ordinary bending stresses. The individual curved girders are then isolated and analyzed for both dead and live load as straight girders with developed span lengths equal to their respective arc lengths. The resulting bending moments are termed primary moments, M_p.

Consider the curved-bridge system in Figure 2.3.1 consisting of two prismatic I-girders continuous over one interior support with full-depth cross-frames uniformly spaced a distance *d* along the outside Girder 2. The cross-frames provide the primary resistance to the torsional loads caused by the bridge curvature and must, therefore, be designed as primary members. Girder 2 has a radius *R*, and the distance between the two girders is *D*.

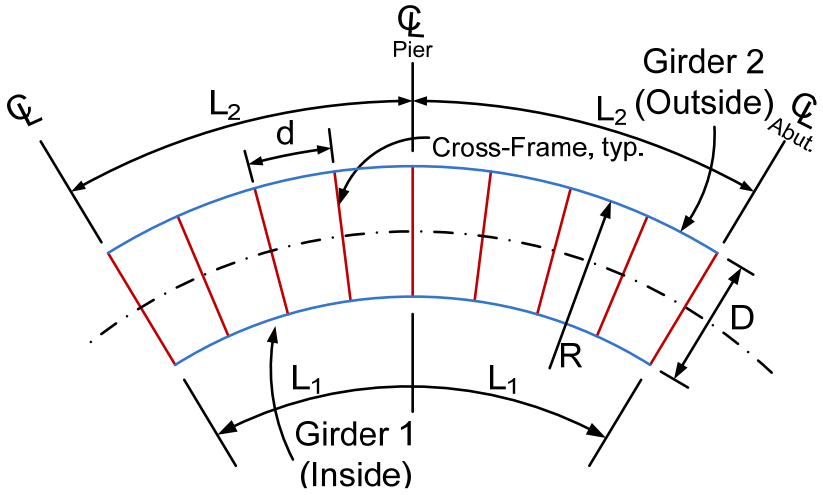


Figure 2.3.1 Sample Two-Span Continuous Curved I-Girder Bridge System

In straight-girder bridge design with limited or no skew, the girders aere typically isolated and individually analyzed and designed. Since an equivalent straight structure is used in the V-load method, the curved girders in this case are also analyzed as isolated straight girders to determine primary moments, using developed span lengths equal to their respective arc lengths, L_1 and L_2 in this case

An appropriate distribution of dead loads to the individual equivalent straight girders must be made to determine the dead load primary moments.

Live-load analysis of a bridge using approximate methods is particularly difficult as it involves moving loads. As discussed in Section 2.1.4, in a live load analysis of an entire bridge, unit loads can be moved across the bridge so that influence surfaces for selected points in the bridge can be developed in order to determine moment and shear envelopes for the individual girders.

For a straight bridge with limited or no skew, a similar approach can be used to develop moment and shear envelopes in a reasonably accurate fashion from influence lines for the isolated girders. Live-load distribution factors, such as those specified by *AASHTO*, must be used in this case to distribute the wheel (or lane) loads laterally to the individual girders. Rather than develop influence surfaces, this latter approach is used for curved bridge analysis with the V-load method because the girders are analyzed as isolated straight girders.

For calculating the primary live load moments in the individual equivalent straight girders, it is recommended that the appropriate live-load distribution factors specified in *AASHTO LRFD* Article 4.6.2.2 be employed. A separate distribution factor is needed, however, to compute the V-load live load moments, as discussed below in Section 2.3.2.2.2.

2.3.2.2.2 Step 2 – V-loads and V-load Moments

In Step 2, fictitious forces known as V-loads are applied to the equivalent straight structure so that the resulting internal forces are the same as in the curved structure when subjected to vertical loads only. The fictitious forces must be self-equilibrating externally applied loads that result in no net vertical, longitudinal or transverse forces on the structure. The moments caused by these externally applied loads are termed the V-load moments.

Figure 2.3.2 presents a partial free-body of a portion of the outside Girder 2 taken from the sample two-span bridge (Figure 2.3.1) in-between two cross-frames. This portion of the girder is taken from the center region of the sample bridge; thus, the girder segment is subjected to near constant vertical bending moment.

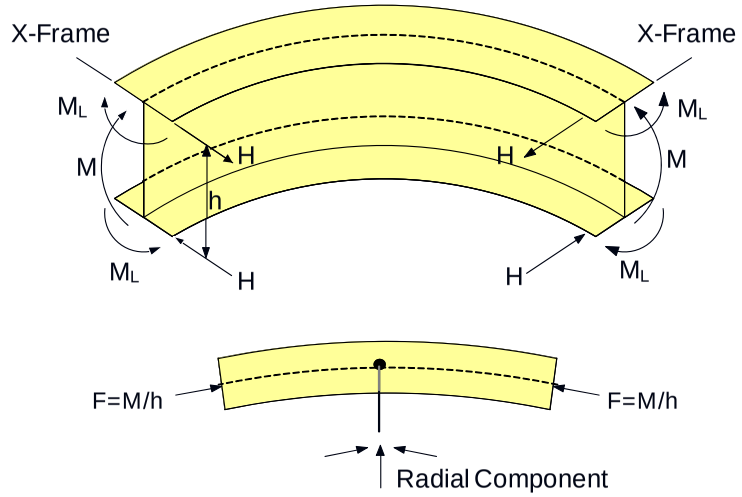


Figure 2.3.2 Partial Free Body of a Segment of Girder 2 from the Sample Bridge in Figure 2.3.1 In-Between Two Cross-Frames

Internally, because of the curvature, the axial forces in the girder flanges created by the vertical bending moment are not collinear along any given segment of the flange. Therefore, to maintain equilibrium, radial flange forces must be created in the girder, as illustrated at the bottom of Figure 2.3.2 for the top flange. In this case, the top flange is in compression so the radial force is directed outward away from the center of curvature.

Ignoring the effect of the web, the axial force in the girder flange may be taken as M/h, where M is the vertical bending moment and h is the depth between flange centerlines.

The radial component of flange force due to curvature may be assumed to act as a radial distributed force, q, over the length of the flange, as illustrated on a plan view

of a segment of the top (compression) flange in-between two cross-frames taken from the sample bridge (Figure 2.3.3).

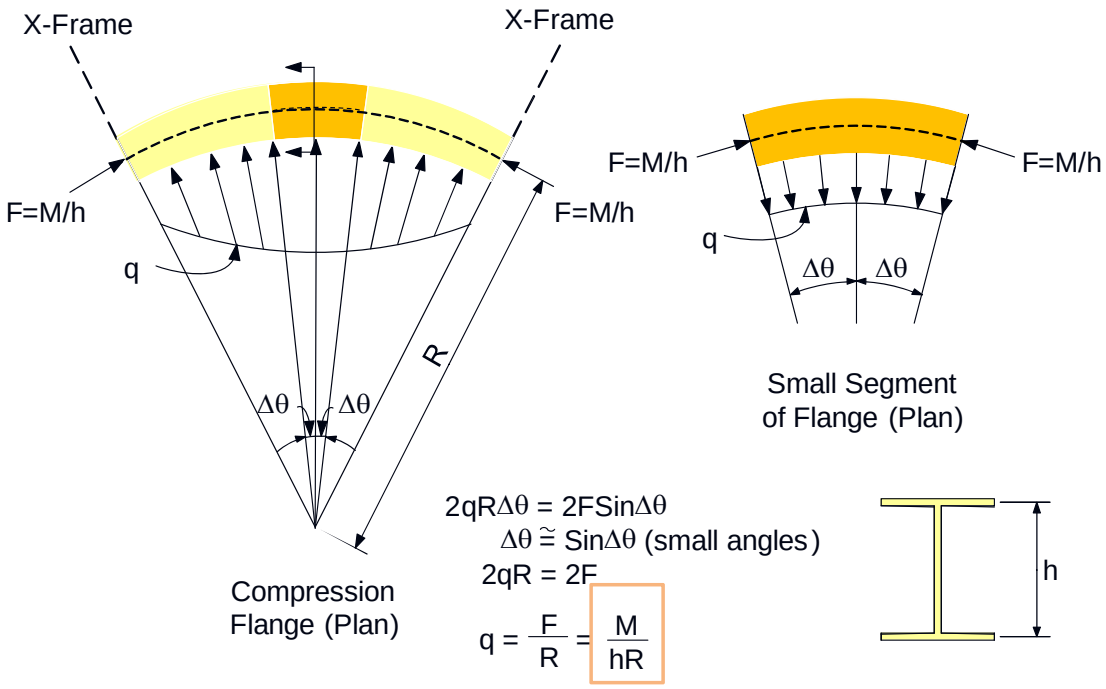


Figure 2.3.3 Determination of the Radial Flange Force, q

The magnitude of *q* can best be derived by the equilibrium condition for a very small segment of the flange, as illustrated in Figure 2.3.3. For the equilibrium condition in this small isolated segment, the direction of *q* must be reversed. Although the radial force, *q*, and axial force, *F*, vary along the flange, for a very small segment of the flange, they may be considered constant. From the equilibrium equation in the radial direction, as shown in the figure, the magnitude of the virtual distributed radial component of flange force on a curved girder flange is determined as $q=M/hR$.

The distribution of the radial forces follows the shape of the vertical bending moment diagram, as shown for each flange in Figure 2.3.4. The radial forces in the flanges are in the opposite direction. The moment of these equal opposing forces causes twisting of the girder about its longitudinal axis.

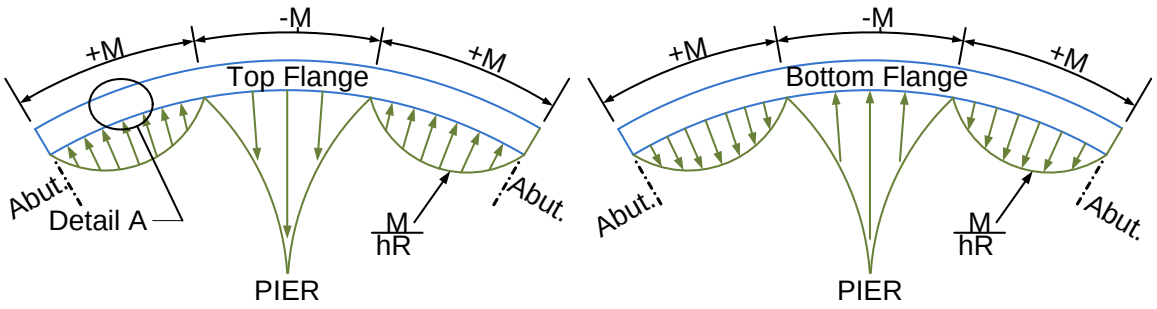


Figure 2.3.4 Distribution of Radial Forces Due to Curvature on the Girder Flanges for the Two-Span Continuous Sample Bridge in Figure 2.3.1

Figure 2.3.5 shows a segment of the curved top flange of the outside girder in a region where the flange is in compression (denoted as Detail A in Figure 2.3.4); the length of the segment is assumed to extend over a distance *d*/2 on either side of a cross-frame (note that lateral flange bending moments are not shown). To determine the torsional load resisted internally at the cross-frame, the assumption is made that the distributed radial flange force has a constant intensity of *M*/*hR* over the length of this segment, where *M* is the vertical bending moment in the curved girder at the cross-frame. The force, *H*, exerted on the flange by the cross-frame is therefore equal to *Md*/*hR*. An equal and opposite reaction force is developed in each flange of each curved girder in the system.

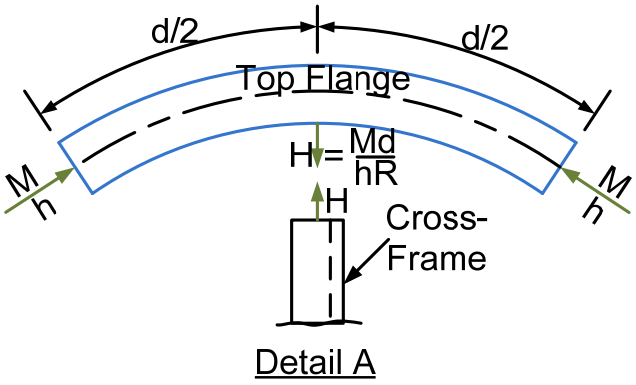


Figure 2.3.5 Segment of the Curved Top Flange in the Compression Region of the Outside Girder of the Sample Bridge Extending d/2 on Each Side of a Cross-Frame (Detail A)

Figure 2.3.6 shows the reaction forces, H_1 and H_2, or restoring forces developed in each flange of each girder in the positive moment region of the sample two-girder bridge (Figure 2.3.1) at a cross-frame. It is assumed that no internal reactions are developed in the web. Equal opposing forces exerted by the cross-frame are shown acting on the girders. The forces at each end of the cross-frame create counterclockwise torsional couples in this case. The corresponding clockwise couples acting on the girders essentially help prevent the girders from tipping over.

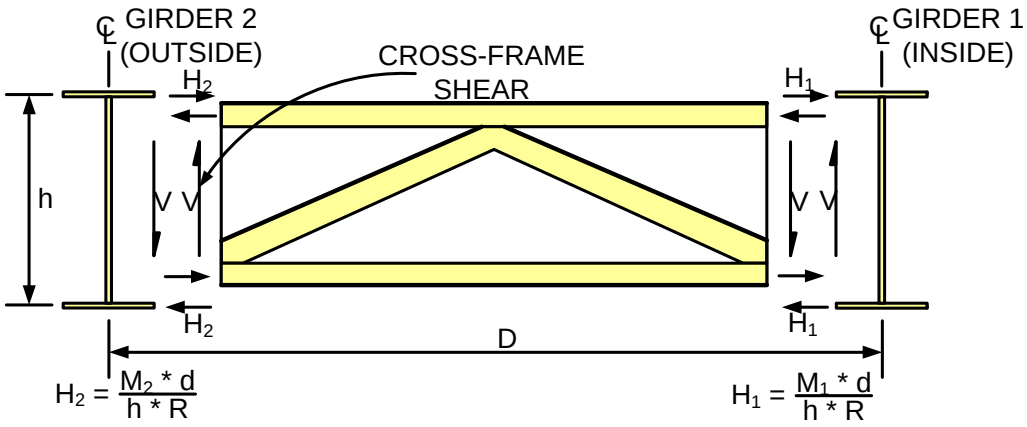


Figure 2.3.6 Cross-Section at a Cross-Frame in the Positive Moment Region of the Sample Two-Span Continuous Bridge in Figure 2.3.1

To maintain equilibrium of the cross-frame, vertical shear forces, *V*, must develop at each end of the cross-frame as a result of cross-frame rigidity and end fixity. These shear forces then react on the girders, resulting in a set of self-equilibrating girder shears.

In the V-load method, these girder shears are applied as external loads to the equivalent straight structure to account for the effects of curvature and are known as the *V-loads*. Applying these external V-loads creates internal forces in the straight structure that will be nearly the same as those that exist in the curved structure under applied vertical loads.

Referring to the free-body diagram of the cross-frame in Figure 2.3.6, moment equilibrium gives:

$$VD = (H_1 + H_2)h$$

Equation 2.3.1

Substituting the values of H_1 and H_2 shown in Figure 2.3.6 gives:

$$V = \frac{M_1 + M_2}{(RD)/d}$$

Equation 2.3.2

or:

$$V = \frac{M_1 + M_2}{K}$$

Equation 2.3.3

where:

$K = (RD)/d$

Note in Equation 2.3.3 that the V-loads are a function of the final moments in the curved girders, M_1 and M_2, which are not yet known.

In a V-load analysis of the sample bridge, the vertical bending moments at the cross-frames in each of the isolated developed straight girders caused by the applied vertical loads are first determined by applying these loads to the equivalent straight girders. These vertical bending moments are again referred to as primary moments and are designated as M_{1p} and M_{2p} in Girders 1 and 2, respectively, in this case.

The corresponding V-load moments caused by the V-loads, M_{1v} and M_{2v}, are then determined by applying the V-loads, *in the proper directions*, to the equivalent straight girders at the cross-frames.

The final moments in the curved girders, M_1 and M_2, are then obtained by summing the respective primary and V-load moments as follows:

$$M_1 = M_{1p} + M_{1v}$$

Equation 2.3.4

$$M_2 = M_{2p} + M_{2v}$$

Equation 2.3.5

The V-load moments may be assumed proportional to their respective girder lengths. Thus:

$$M_{1v} = -M_{2v}\left(\frac{L_1}{L_2}\right)$$

Equation 2.3.6

Substituting Equation 2.3.6 into Equation 2.3.4 and summing M_1 and M_2 gives:

$$M_1 + M_2 = M_{1p} + M_{2p} + \left[M_{2v}\left(1 - \frac{L_1}{L_2}\right)\right]$$

Equation 2.3.7

Since M_{2v} is generally small compared to M_{1p} and M_{2p}, and the term $(1-L_1/L_2)$ is also small, the last term in the brackets in Equation 2.3.7 may be neglected leaving:

$$M_1 + M_2 = M_{1p} + M_{2p}$$

Equation 2.3.8

or:

$$V = \frac{M_{1p} + M_{2p}}{K}$$

Equation 2.3.9

Thus, the V-loads may be obtained with reasonable accuracy in this case by summing the primary moments in the girders at each cross-frame and dividing by *K*. Note that in the computation of *K*, the terms *R*, *D* and *d* are all with respect to the outside girder.

For a three-girder curved system, such as the one shown in Figure 2.3.7, the cross-frame shears between the outside and center girder, and the shears between the center and inside girder are assumed to be equal. Thus, as shown at the bottom of the figure, the V-loads applied to the straight outside and inside girders are equal and opposite, and there are no V-loads applied to the straight center girder since its cross-frame shears cancel.

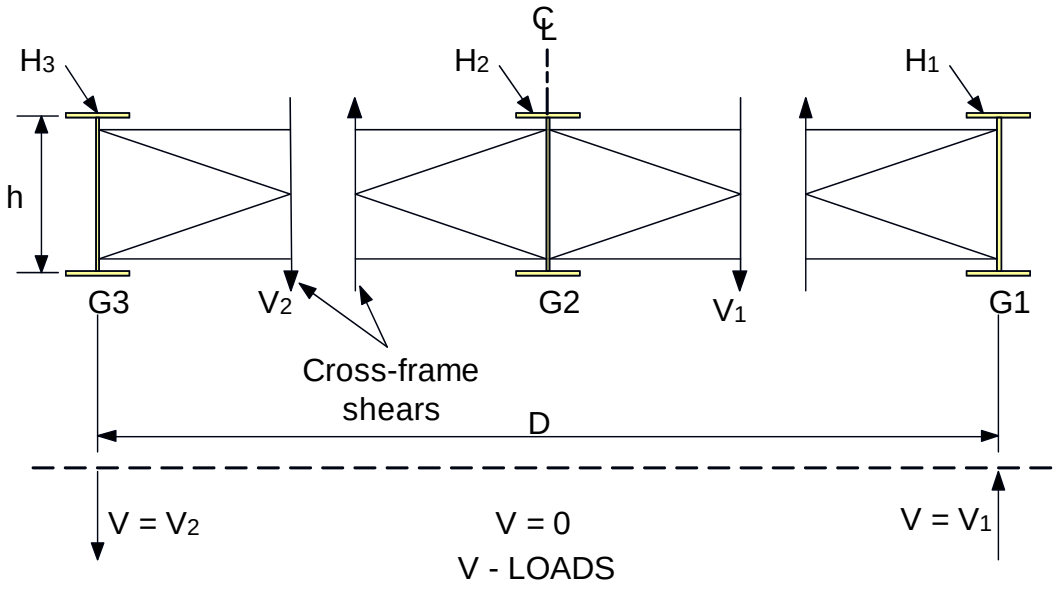


Figure 2.3.7 Cross-Section of a Three-Girder Curved System at a Cross-Frame Line and the V-Loads to be Applied to the Equivalent Straight Structure

It is clear that the shears tend to increase the moments caused by the applied loads on the outside girder. With all signs reversed, vertical shears are also developed to maintain equilibrium in regions of negative flexure in continuous spans. The net effect is that the total load on the curved bridge is generally shifted from the inside

girder to the outside girder as required in order to maintain equilibrium. As a result, the outside girder in a curved bridge is usually heavily loaded and deflected.

For curved systems with more than three girders, the cross-frame shears are not equal. Therefore, the distribution of cross-frame shears across the section becomes important, and the relative stiffness of adjacent girders must be considered.

The V-loads are computed based on the following assumptions:

- All girders in the section have the same vertical stiffness;
- Girder shears across the section are self-equilibrating, and;
- The loading on girders outside the longitudinal centerline of the system is increased, while the loading on girders inside the longitudinal centerline is decreased.

As a result of these assumptions, the shear on a girder may be taken as proportional to the distance of that girder from the longitudinal centerline of the bridge, which implies a linear distribution of shear across the section.

Consider the four-girder system shown in Figure 2.3.8 subject to a net counterclockwise torque due to the effects of curvature. To equilibrate this net torque, internal cross-frame shears, V_1, V_2 and V_3, are developed and are shown acting at inflection points in the cross-frames (arbitrarily shown at distances *a*,*b* and c from the respective girders). Because these shears develop reactions at the adjacent girders, and the shears, V, on the outside and inside girders are assumed to be equal and opposite, $V = V_1 = V_3$.

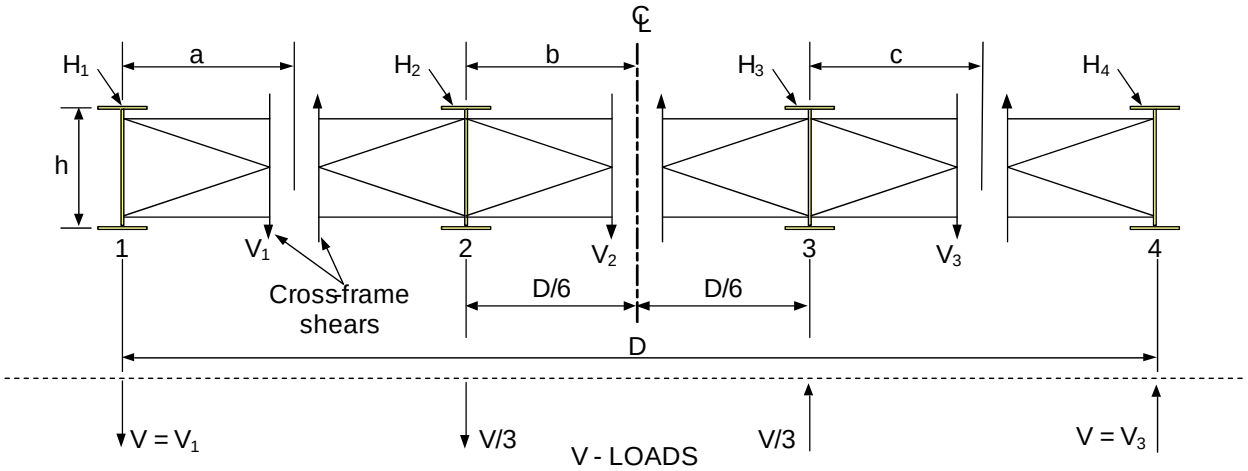


Figure 2.3.8 Cross-Section of a Four-Girder Curved System at a Cross-Frame Line and the V-Loads to be Applied to the Equivalent Straight Structure

Invoking the assumption that the girder shears are proportional to the distance of the girders from the longitudinal centerline of the bridge, the magnitudes of the shears on the two interior girders are equal to (1/3)V in this case. This also means that V_2 =

V_1 + (1/3)V = (4/3)V. The factor, 1/3, is a proportionality factor based on the geometry of the cross-section. Note that the girder shears add up to zero across the section as assumed.

Referring to Figure 2.3.8 and enforcing moment equilibrium between the inflection points at the bottom of each girder results in the following set of four equations:

$$V_1 a = H_1 h = \frac{M_1 d}{R}$$

Equation 2.3.10

$$V_1\left(\frac{D}{3} - a\right) + V_2 b = \frac{M_2 d}{R}$$

Equation 2.3.11

$$V_2\left(\frac{D}{3} - b\right) + V_3 c = \frac{M_3 d}{R}$$

Equation 2.3.12

$$V_3\left(\frac{D}{3} - c\right) = \frac{M_4 d}{R}$$

Equation 2.3.13

Substituting $V_1 = V_3 = V$ and V_2 = (4/3)V, relating the final girder moments to the primary bending moments as discussed above, and solving the four equations simultaneously gives:

$$V = \frac{M_{1p} + M_{2p} + M_{3p} + M_{4p}}{\left(\frac{10RD}{9d}\right)}$$

Equation 2.3.14

or the more general relationship shown below for computing the V-Loads *on the outside and inside girders* of the equivalent straight structure at the cross-frames in a multiple-girder bridge:

$$V = \frac{\sum M_p}{CK}$$

Equation 2.3.15

where:

ΣM_p = summation of primary moments in each girder at a particular cross-frame

C = coefficient which depends on the number of girders in the system (Table 2.3.1)

K = (RD/d) for the outside girder

Table 2.3.1 Coefficient, C, in Equation 2.3.15

No. of Girders in System	Coefficient, C
2	1
3	1
4	10/9
5	5/4
6	7/5
7	14/9
8	12/7
9	15/8
10	165/81

To determine the V-loads on all the other girders in the cross-section, multiply the V-load obtained from Equation 2.3.15 by the appropriate proportionality factor. For example, for a four-girder system with equally spaced girders, the proportionality factor is 1/3. *Special attention must always be paid to the direction of the V-loads*.

V-Load Calculation Example

The calculation of the DC_1 V-loads for the example skewed and curved I-girder bridge (Section 5.1) at the indicated cross-frame line in Span 1 (Figure 2.3.9) is illustrated. This example is for illustrative purposes only as the V-load method is not recommended for use on bridges with severely skewed supports (Section 2.3.2.3). The V-loads in this case are computed at a section in the span removed from the region of the skewed supports.

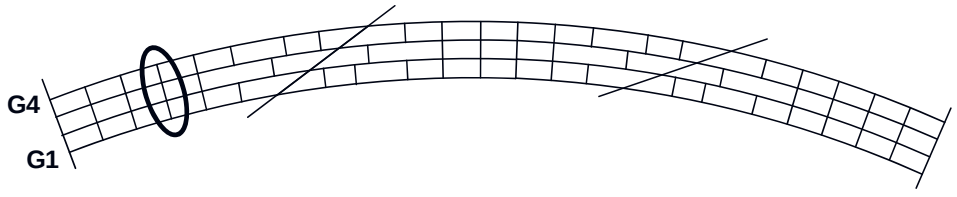


Figure 2.3.9 Example I-Girder Bridge (Section 5.1) – Cross-Frame Line for Sample Calculation of DC_1 V-Loads

The proportionality factor for a four-girder system with equal girder spacing is 1/3. The coefficient, C, in Equation 2.3.15 is 10/9 for a four-girder system (Table 2.3.1). For this bridge, R to the outside girder is 716.5 feet, and the distance, D, between the outside and inside girders, G4 and G1, is 33.0 feet. The cross-frame spacing

along the outside girder at this location is 22.104 feet. These values are used in the calculation of the constant K as follows:

$$K = \frac{RD}{d} = \frac{(716.5)(33.0)}{22.104} = 1{,}070$$

The primary DC_1 moments, M_p, at this cross-frame line were determined by applying the appropriate vertical DC_1 loads to each of the isolated developed straight girders from the bridge, and are given in Table 2.3.2. These moments are substituted into Equation 2.3.15 to determine the V-loads for the outside and inside girders G4 and G1 at this cross-frame line as follows:

$$V = \frac{1{,}303 + 2{,}348 + 3{,}315 + 4{,}011}{\left(10/9\right)(1{,}070)} = \pm 9.2 \text{ kips}$$

The V-loads for girders G2 and G3 are then simply obtained by multiplying this value by the proportionality factor. Thus, the V-loads on G2 and G3 at this cross-frame line are:

$$V = (\pm 9.2)\left(1/3\right) = \pm 3.1 \text{ kips}$$

Figure 2.3.10 shows the DC_1 V-loads applied to the individual straight girders from the example bridge in the proper directions at the indicated cross-frame line in Span 1 (i.e. at Section A-A).

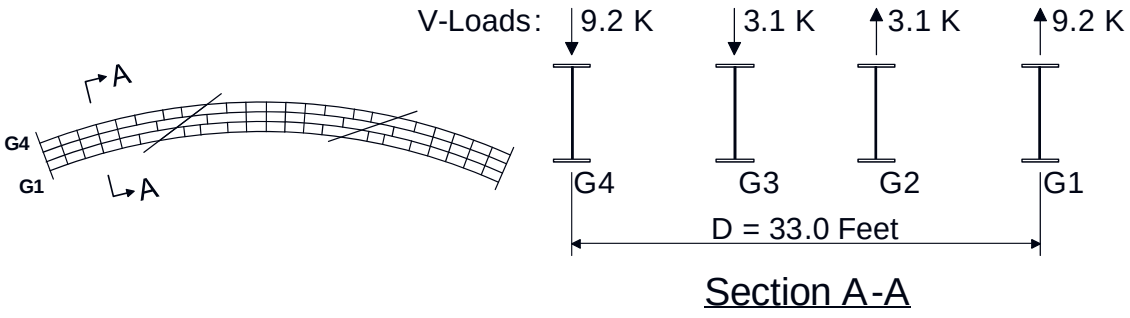


Figure 2.3.10 Example I-Girder Bridge DC_1 V-Loads at a Cross-Frame Line in Span 1 (@ Section A-A)

A similar calculation is repeated at each cross-frame line. The DC_1 V-load moments are then determined by applying the complete set of DC_1 V-loads computed at each cross-frame line to the corresponding isolated developed straight girders (Table 2.3.2). The final DC_1 moments in the curved girders are then computed as the sum of the primary and V-load moments (Table 2.3.2).

Table 2.3.2 DC_1 V-Load Analysis Results at Section A-A

Girder No.	Primary DC_1 Moment, M_p (kip-ft)	V-Load Moment (kip-ft)	Final DC_1 Moment in Curved Girders (kip-ft)
G1	1,303	-423	880
G2	2,348	-166	2,182
G3	3,315	189	3,504
G4	4,011	630	4,641

For live load, the *AASHTO* distribution factors are based upon the live load being positioned to produce the maximum possible moment alternately in each girder. For a given position of the trucks, the V-loads act concurrently on all the girders; thus, using the *AASHTO* distribution factors to compute the V-loads for live load would result in too much total V-load on the structure. Because the V-loads act concurrently, the summation of V-load distribution factors across the section should equal the total number of design lanes on the structure. Since the lateral placement of the lanes has little effect on the sum of the primary moments across a section, the following distribution factor for the V-loads (in lanes) is recommended for use:

$$(\text{D.F.})_{\text{V-Load}} = \frac{N_L}{N_G}$$

Equation 2.3.16

where N_L is the number of design lanes and N_G is the number of girders in the cross-section. There is only one V-load distribution factor for all the girders in a particular bridge.

Hence, to compute the live load V-loads for the live load at a specific location on a particular girder, the original primary live load moments, M_p, in all the girders are first factored by the ratio of the V-load distribution factor to the appropriate *AASHTO* distribution factor as follows:

$$\sum M'_p = \sum M_p \frac{(\text{D.F.})_{\text{V-LOAD}}}{(\text{D.F.})_{\text{Primary}}} \Rightarrow V_{LL} = \frac{\sum M'_p}{C * K}$$

Equation 2.3.17

In determining M_p in all the girders, the live load should be placed at the same relative position in the span of each girder, as the load on the girder under consideration. The summation of the reduced primary moments, M'_p, at each cross-frame is then used in the general equation to compute the set of live load V-loads to

be applied at each cross-frame location for the girder and live load position under consideration (Equation 2.3.17).

2.3.2.2.3 Step 3 – Final Moments in the Curved Girders

Once the dead and live load primary and V-load moments have been determined, Step 3 of the process involves summing the primary and V-load moments to determine the final moments in the curved girders.

2.3.2.2.4 Step 4 – Cross-Frame Forces

In Step 4, cross-frame force effects due to curvature may be calculated in an approximate fashion based on V-load theory. For example, if a cross-frame line is examined in the positive bending region of a four-girder system subject to a net torque due to curvature, the assumed distribution of torque loads and V-loads to the individual girders may be taken as shown at the top of Figure 2.3.11.

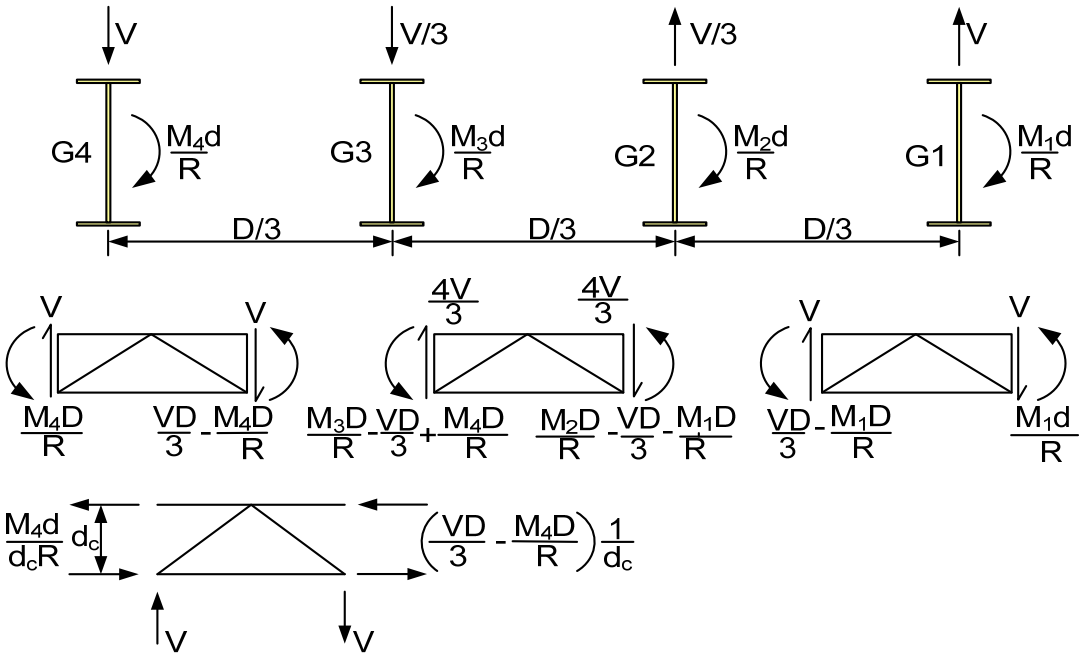


Figure 2.3.11 Estimation of Cross-Frame Forces due to Curvature Effects

From equilibrium considerations, the distribution of end shears and end moments on the cross-frames can then be determined as shown in the center of Figure 2.3.11.

Forces exerted by the top and bottom chords of the cross-frames on the girders can then be determined by dividing the end moments by the vertical distance, d_c, between the working points of the chords, as shown at the bottom of Figure 2.3.11.

With these forces and the cross-frame shears known, the forces can then be resolved accordingly into the individual cross-frame members.

2.3.2.2.5 Step 5 – Lateral Flange Bending Moments & Stresses

In Step 5, an approximate approach is employed to estimate the lateral flange bending moments (and stresses) due to curvature. In the V-load method, each girder is isolated and analyzed as a developed straight girder to determine the vertical bending moments and shears. Similarly, to determine the lateral flange bending moments in the V-load method, each girder flange can be isolated and analyzed as a straight flange rigidly supported at every cross-frame.

Cross-frames in curved bridges help resist lateral flange bending moments and stresses, and thus, act as lateral supports for the flanges. Lateral bending due to curvature is caused by the radial flange forces. Thus, lateral bending moments and stresses can be determined in an approximate fashion in the V-load method by loading each isolated straight flange, assumed supported at each cross-frame, by the appropriate distributed radial flange force, M/hR, as shown for a top flange from a two-span continuous girder in Figure 2.3.12. M is the total vertical bending moment in the girder, equal to the sum of the primary and V-load moments. Note that the cross-frame spacing has been changed from d to ℓ in Figure 2.3.12 to agree with the notation given in the *AASHTO LRFD* Specification.

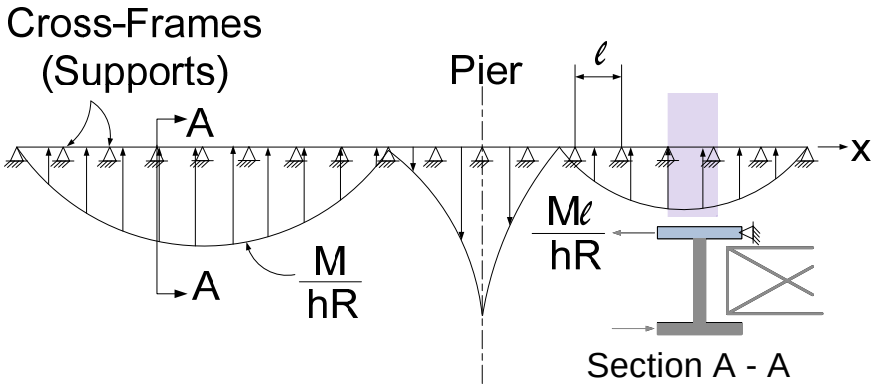


Figure 2.3.12 Schematic of an Isolated Straight Top Flange from a Two-Span Continuous Girder Rigidly Supported at Each Cross-Frame and Loaded by the Distributed Radial Flange Force due to Curvature

A simpler conservative assumption can be made that the lateral distributed force on each flange has a constant value of M/hR, where M is the total vertical bending moment at each cross-frame and h is the vertical depth between the flange centerlines (Figure 2.3.13). For simplicity, the web depth, D, may be conservatively used in place of h, resulting in a lateral distributed force of M/DR.

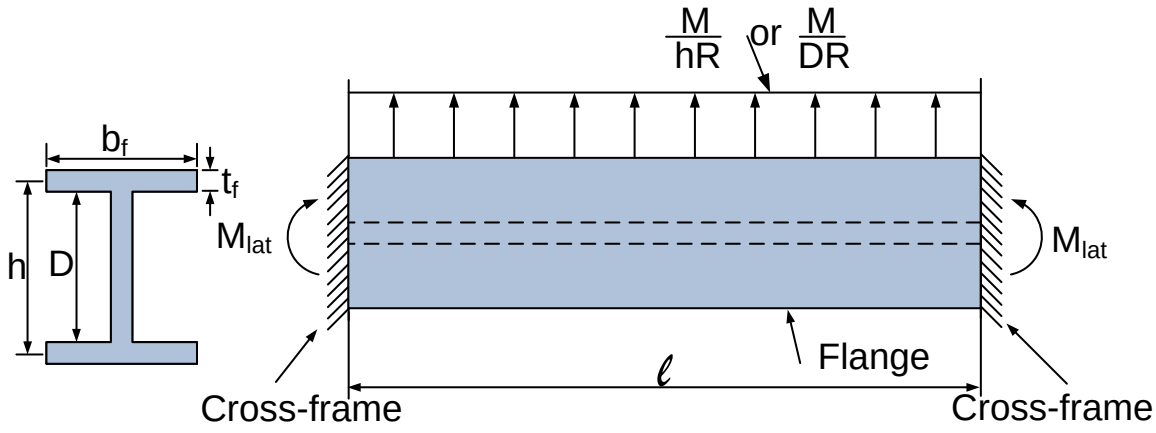


Figure 2.3.13 Plan View of Highlighted Section of Flange in Figure 2.3.12 In-Between Two Cross-Frames Loaded by Assumed Uniformly Distributed Lateral Flange Force due to Curvature

Since the cross-frames are assumed to act as rigid supports for the flanges, the lateral flange moment at each cross-frame, M_{lat}, due to the effects of curvature can then be calculated in an approximate fashion from *AASHTO LRFD* Equation C4.6.1.2.4b-1 as follows:

$$M_{lat} = \frac{M\ell^2}{NRD}$$

Equation 2.3.18
AASHTO LRFD Equation C4.6.1.2.4b-1

where:

M = total vertical bending moment at the cross-frame (kip-ft)
ℓ = unbraced length between cross-frames (ft)
R = girder radius (ft)
D = web depth (ft)
N = a constant taken as 10 or 12 in past practice

Either value of N (i.e., 10 or 12) is acceptable for use, consistent with past practice, depending on the level of conservatism that is desired.

The lateral flange bending stress, f_{lat}, is then determined by dividing the lateral moment by the lateral section modulus of the flange under consideration, $S_{lat} = t_f b_f^2/6$, as follows:

$$f_{lat} = \frac{M_{lat}}{S_{lat}} = \frac{6M_{lat}}{t_f b_f^2}$$

Equation 2.3.19

Equation 2.3.18 for M_{lat} assumes the presence of a cross-frame at the point under investigation. Therefore, at points not actually located at cross-frames, flange lateral moments from the equation may not be strictly correct. The equation also assumes approximately equal adjacent unbraced lengths such that due to approximate symmetry boundary conditions, the ends of the unbraced length are effectively torsionally fixed. Other more appropriate idealizations should be considered when this assumption does not approximate actual conditions; e.g., unbraced lengths adjacent to abutments.

Note that the preceding equations for M_{lat} and f_{lat} may also be used to estimate the lateral flange bending moments and stresses at cross-frames in the top flanges of tub girders prior to hardening of the deck.

Lateral Flange Bending Example

This example illustrates the calculation of the lateral flange bending moments and stresses due to curvature at a selected cross-frame from the example skewed and curved I-girder bridge (Section 5.1) using the approximate procedures discussed above. The results are compared to the results from the refined 3D analysis of the bridge.

The lateral flange bending moments and stresses are calculated at the cross-frame located 66.313 feet from Abutment 1 in Span 1 of G4 (Figure 2.3.14). At this location, the lateral flange bending due to the effects of the discontinuous cross-frames adjacent to the skewed interior support is relatively small; lateral flange bending at this location is primarily due to the effects of curvature. The cross-section of the steel girder at this location is shown in Figure .

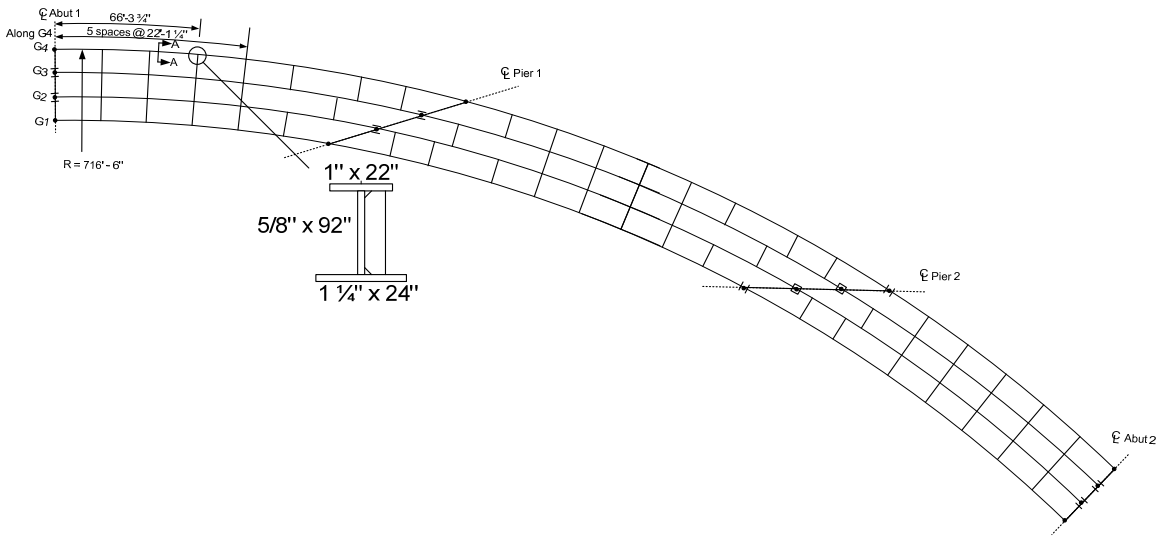


Figure 2.3.14 Example I-Girder Bridge (Section 5.1) – Cross-Section of G4 at Cross-Frame 66.313 Feet from Abutment 1 in Span 1

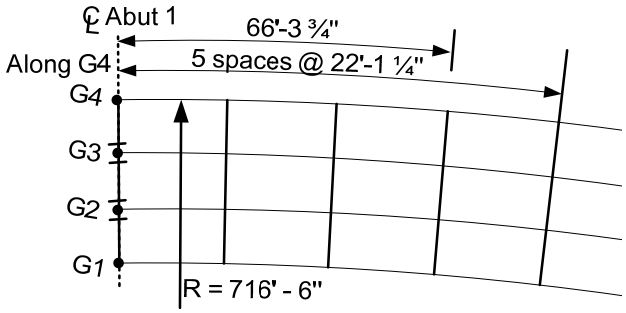


Figure 2.3.15 Detail of Span 1 Region Adjacent to Abutment 1 in Figure 2.3.14

From the 3D analysis of the bridge, the unfactored vertical bending moments at this location are as follows:

M_{DC1} = 4,798 kip-ft
M_{DC2} = 673 kip-ft
M_{DW} = 731 kip-ft
M_{+LL+IM} = 4,990 kip-ft
$M_{deck\ casting}$ = 5,853 kip-ft

Equation 2.3.18 is used to calculate the lateral flange bending moments as follows:

$$M_{lat} = \frac{M\ell^2}{NRD}$$

For this example, *N* is taken equal to 12.

First, the factored lateral flange bending moment in the top flange at this location due to the deck casting sequence is calcuated. Assume the Strength IV load combination controls:

$$M = 1.5(5{,}853) = 8{,}780 \ \text{kip} - \text{ft}$$

$$M_{lat} = \frac{(8{,}780)(22.104)^2}{(12)(716.5)(92/12)} = 65.1 \ \text{kip} - \text{ft}$$

The factored lateral bending moment in the top flange taken directly from the 3D deck-casting analysis at this location is 1.5(27) = 41 kip-ft.

The factored lateral flange bending stress in the top flange at this location due to the deck casting sequence is next calculated from Equation 2.3.19 using the approximate lateral moment as follows:

$$f_{lat} = \frac{6M_{lat}}{t_f b_f^2}$$

$$f_{lat} = \frac{6[(65.1)(12)]}{(1.0)(22.0)^2} = 9.7 \ \text{ksi}$$

Once the deck hardens, lateral flange bending is not a consideration in the top flange because the flange is continuously braced.

Next, the factored lateral flange bending moment and stress in the bottom flange at this location due to the Strength I load combination is calculated. The load modifier, η, is taken equal to 1.0.

$$M = 1.0[1.25(4{,}798 + 673) + 1.5(731) + 1.75(4{,}990)] = 16{,}668 \ \text{kip} - \text{ft}$$

$$M_{lat} = \frac{(16{,}668)(22.104)^2}{(12)(716.5)(92/12)} = 123.5 \ \text{kip} - \text{ft}$$

The factored lateral bending moment in the bottom flange from the 3D analysis at this location, which includes the effects of curvature and any relatively small skew effects in this region, is equal to 66 kip-ft. The approximate equation often gives conservative results for lateral bending due solely to the effects of curvature relative to the 3D analysis results.

The factored lateral flange bending stress in the bottom flange at this location due to the Strength I load combination is calculated from Equation 2.3.19 using the approximate lateral moment as follows:

$$f_{lat} = \frac{6[(123.5)(12)]}{(1.25)(24.0)^2} = 12.4 \text{ ksi}$$

2.3.2.2.6 Step 6 – Shears, Deflections and Reactions

Lastly, Step 6 of the V-load analysis procedure involves repeating the previous steps, and as applicable, to determine the shears, deflections and reactions.

2.3.2.3 Limitations of the V-load Method

In general, the V-load method of analysis is best suited for preliminary design, but may perhaps be suitable for final design of curved structures with radial supports or supports skewed less than approximately 10 degrees from normal.

More specific limitations of this approximate method are summarized below:

- Girders at a given cross-section should have approximately the same vertical stiffness.
- The method is limited primarily to vertical loads only (i.e., not applicable for thermal or wind analyses).
- The method is not directly applicable to continuous structures with reverse curvature.
- The method does not directly account for the horizontal shear stiffness of the concrete deck.
- The method is not directly applicable to closed-framed systems having lateral bracing near, or in, the plane of the bottom flanges (Figure 2.3.16).



Figure 2.3.16 Curved I-Girder Bridge with Bottom Flange Lateral Bracing

- The method does not directly account for girder twist or sources of torque other than curvature; thus, lateral deflections, which become important on bridges with large spans and/or sharp skews, and vertical deflections may be significantly underestimated.
- The method may not detect uplift at end bearings in certain situations.
- The method may significantly underestimate vertical reactions at interior supports on the concave side of continuous-span bridges due to their closer proximity to the center-of-gravity of the bridge system and the concomitant reduction in the eccentric effect at those supports (Figure 2.3.17). Vertical reactions on the concave girder are generally larger than on the convex girder, except possibly for unusual span arrangements. This issue is discussed further in Section 3.1.3.3.1.

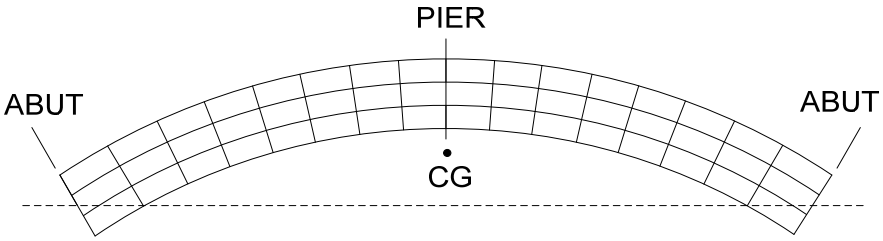


Figure 2.3.17 Plan View of Continuous-Span Curved I-Girder Bridge Illustrating the Proximity of the Concave Interior-Support Reaction to the Center-of-Gravity of the Bridge System

2.3.3 M/R Method (Box/Tub Girders)

2.3.3.1 Description of the Method

This section describes an approximate method of analysis for curved steel box and tub girders known as the M/R method. This approach was developed in the early 1970s by Tung and Fountain (*4*). This method is considered applicable to single-span or continuous-span box or tub girders on radial supports. Curvatures may vary, but may not reverse, within each span. The method also assumes that sufficient internal cross-frames/diaphragms are provided within the box/tub to limit cross-section distortional and longitudinal warping stresses. The method is based on the classical conjugate-beam analysis method (Section 2.2.4.2.1).

The origins of the M/R method relate to the three fundamental equilibrium equations for a curved segment shown below. These three equilibrium equations describe the statics of a curved segment subject to an applied distributed vertical loading, *p*, and an applied distributed torsional loading, *t*, as shown in Figure 2.3.18. In Equation 2.3.21 and Equation 2.3.22, the upper sign applies to a curve with the center of curvature located as shown in Figure 2.3.18, and the lower sign applies to a curve with the center of curvature located on the opposite side of the segment.

$$\frac{dV}{Rd\alpha} = \frac{dV}{dx} = -p$$

Equation 2.3.20

$$\frac{dM}{Rd\alpha} = \frac{dM}{dx} = \mp\frac{T}{R} + V$$

Equation 2.3.21

$$\frac{dT}{Rd\alpha} = \frac{dT}{dx} = \pm\frac{M}{R} - t$$

Equation 2.3.22

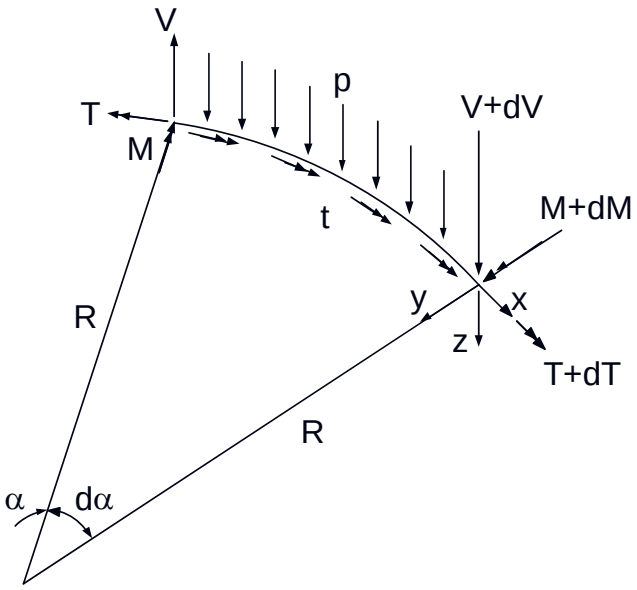


Figure 2.3.18 Curved Segment Subject to a Distributed Vertical Load, *p*, and Distributed Torsional Load, *t*

Integration of Equation 2.3.20 leads to the familiar relationship that the change in shear between any two points on the girder is equal to the area of the distributed vertical load diagram between the two points. In Equation 2.3.21 and Equation 2.3.22, *M* and *T* are coupled together, which complicates the solution. However, when the central angle, α, is small and when the bending-to-torsional stiffness ratio, *EI*/*GJ*, falls below a certain limit for indeterminate structures (Section 2.3.3.3), *M* is not significantly influenced by *T*. Thus, dropping the *T*/*R* term out of Equation 2.3.21 and integrating yields:

$$\frac{dM}{Rd\alpha} = \frac{dM}{dx} = V$$

Equation 2.3.23

This is the familiar relationship that the change in vertical bending moment between any two points is equal to the area under the shear diagram. That is, the vertical bending moment may be evaluated reasonably well by considering the curved girder as a straight girder with a span length equal to its arc length if certain conditions are met (as described in Section 2.3.3.3).

Integration of Equation 2.3.22 yields the relationship that the change in torsional moments between any two points is equal to the area of the ($\pm$ *M*/*R* – *t*) diagram between those two points. The approximate vertical bending moment values obtained based on Equation 2.3.23 may be used in the ($\pm$ *M*/*R* – *t*) diagram, again if certain conditions are met. In addition, the torsional analysis may also be done assuming the girder is straight with a span length equal to the curved girder arc length if similar conditions are met.

Since only the relative change in the torsional moments can be determined from the area under the (± *M*/*R* – *t*) diagram between two points, the torsional moment at a reference section must be known.

For a curved girder span torsionally fixed at each end of a span (but which may otherwise be continuous over several supports) with a constant *EI* and *GJ*, the torque at end A of span AB shown in Figure 2.3.19 is given by:

$$T_A = \frac{1}{L}\int_0^L \left(\pm \frac{M}{R} - t \right)(L - x)dx$$

Equation 2.3.24

In the derivation of Equation 2.3.24, the member is assumed straightened to its developed length and loaded by the torsional load (± *M*/*R* – *t*) computed in an approximate fashion using straight-girder bending moments.

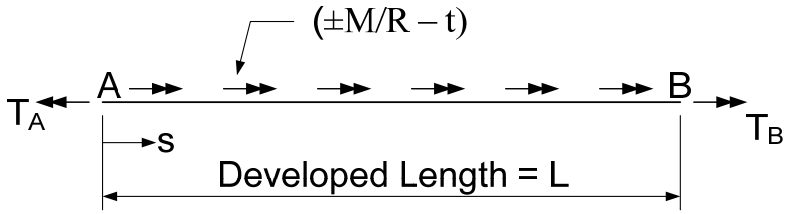


Figure 2.3.19 Torsional Loading on a Developed Girder

The torque at any section located a distance, *s*, from end A is therefore:

$$T = T_A - \int_0^S \left(\pm \frac{M}{R} - t \right)dx$$

Equation 2.3.25

The preceding two equations are analogous to the classical conjugate-beam method for determining deflections of beams.

Thus, for the case of a curved box/tub girder torsionally fixed at the supports, a fictitious simply-supported conjugate beam can be considered loaded with the distributed (± *M*/*R* – *t*) loading for the developed girder, as shown for the interior span of a continuous unit in Figure 2.3.20. The conjugate beam is simply supported because the angle of twist, ϕ, is zero at both torsionally fixed ends in the actual box/tub. To satisfy the original equilibrium equation, a positive (*M*/*R* – *t*) quantity should be applied as an upward load to the conjugate beam. The reaction at end A in the conjugate beam is equal to the end torque in the actual beam, while the shear at any intermediate point in the conjugate beam is equal to the torque at that point in the actual beam.

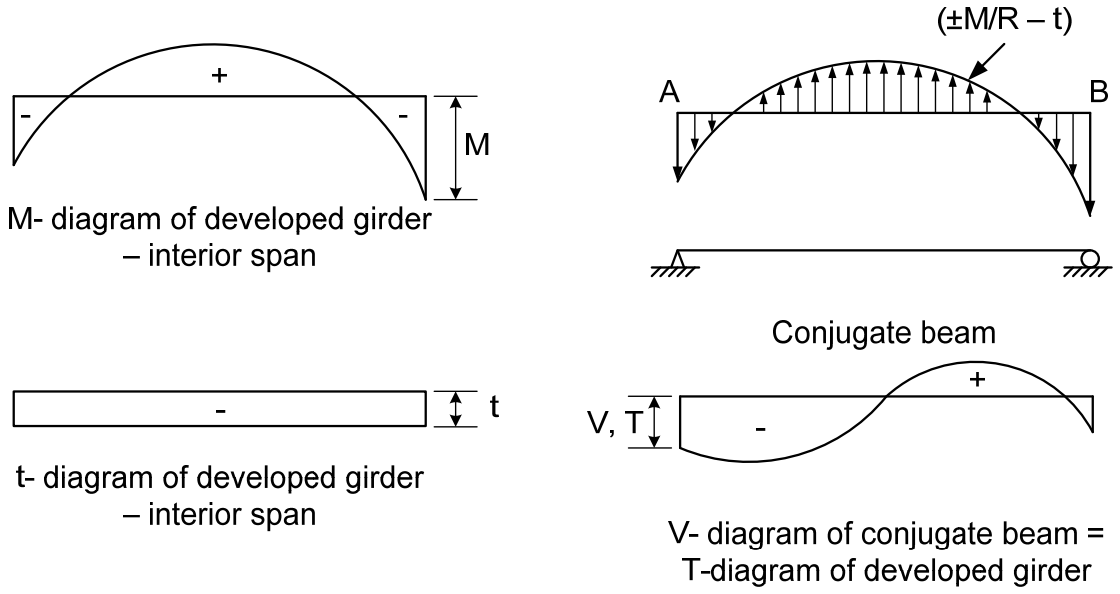


Figure 2.3.20 Conjugate Beam for a Torsionally Fixed Span Loaded with the Distributed (±*M*/*R* – *t*) Loading

Steel box/tub girder bridges supported on two bearings essentially render a torsionally fixed support. The method can be extended to situations in continuous spans in which torsionally free supports are also present (that is, where the box/tub girder is supported on a single bearing).

The angle of twist, ϕ, at any point along the actual girder may be computed using the conjugate-beam analogy. The quantity, $EI\phi$, at any point along the actual girder is equal to the corresponding moment in a simply-supported conjugate beam under the loading $[\pm M/R + (EI/GJ)(\pm M/R - t)]$. When the distributed torque, t, is equal to zero, the numerical value of ϕ can simply be determined as:

$$|\phi| = \frac{1}{R}\left(1 + \frac{EI}{GJ}\right)(|w|)$$

Equation 2.3.26

where w is the corresponding vertical deflection calculated using the approximate bending analysis.

Further information on the *M/R* Method may be found in Reference 4.

2.3.3.2 M/R Procedure

The steps for performing an *M*/*R* analysis of a curved box/tub girder bridge system under normal highway loadings are summarized as follows (limitations of the method are discussed further in Section 2.3.3.3):

1. Isolate and straighten the girder to its developed length (with a span length equal to the curved girder arc length) and provide supports at the actual support locations.
2. Perform a customary line girder analysis to determine the vertical bending moments and shears in the girder. For live load, the *AASHTO LRFD* live load distribution factor for steel box girders (*AASHTO LRFD* Table 4.6.2.2.2b-1) may be used.
3. Considering one span at a time and assuming the supports at each end are torsionally fixed, apply the distributed ($\pm$ *M*/*R* – *t*) loading on the corresponding simply-supported straight conjugate beam to determine the end torisonal moments and the torsional moments within that span. The algebraic difference of the two end torsional moments adjacent to an interior support is the torsional moment reaction at that support. If a support is torsionally free, that support is left out of the conjugate beam so that the beam spans between two adjacent torsionally fixed supports. The vertical bending moments are not significantly affected whether the supports are torsionally fixed or torsionally free. For live load, torque influence lines can be derived by applying the ($\pm$ *M*/*R* – *t*) loading determined for a unit load to the conjugate beam, determining the shears for that loading to obtain the influence ordinates and repeating the procedure along the entire span.
4. Apply the distributed [$\pm$ *M*/*R* + (*EI*/*GJ*)($\pm$ *M*/*R* – *t*)] loading on the simply-supported straight conjugate beams to determine the angles of twist, ϕ.

2.3.3.3 Limitations of the M/R Method

The following are some of the limitations on the applicability of the M/R method:

1. For simple spans, supports must be torsionally fixed with *EI*/*GJ* $\leq$ 4.0 when the central angle $\alpha \leq 25°$, and *EI*/*GJ* $\leq$ 2.5 when $\alpha \leq 30°$.
2. For continuous spans, each span should satisfy the limitations on *EI*/*GJ* specified for simple spans (using a weighted average *EI*/*GJ*). The central angle of the entire unit, or sum of the central angles in the cases of compound curvatures, should not exceed 90°. If one or more supports are not torsionally fixed, there should be at least one torsionally fixed support in the unit, and the central angle (or sum of the central angles) between two adjacent torsionally fixed supports should not exceed 32° when *EI*/*GJ* $\leq$ 4.0 and 40° when *EI*/*GJ* $\leq$ 2.5. In addition, the central angle (or sum of the central angles) between a torsionally free end support and the first torsionally

fixed support should not exceed 20° when $EI/GJ \leq 4.0$ and 25° when $EI/GJ \leq 2.5$.

3. Girders should be on radial supports with single curvature.
4. Sufficient internal cross-frames/diaphragms should be provided according to the provisions of *AASHTO LRFD* Article 6.7.4.3 to limit cross-section distortional and longitudinal warping stresses.

2.3.4 Levels of Analysis Matrix

A Levels of Analysis Matrix is introduced in this section that will be used in subsequent sections of this Manual (i.e. Sections 2.4, 2.5 and 2.6) to evaluate and compare the following analysis methods:

- Approximate methods of analysis; specifically, the V-load method which is only applicable to the analysis of curved I-girder bridges (Section 2.3.2);
- 2D refined methods of analysis (Section 2.4), and;
- 3D refined methods of analysis (Section 2.5).

Two types of 2D analysis models are discussed in Section 2.4. The two types of models are:

- Grid models, and;
- Plate and eccentric beam models.

As each type of model provides somewhat different capabilities, they are listed separately in the matrix. The acronym 'P&EB' is used in the matrix to refer to plate and eccentric beam models.

Strictly speaking, the matrix only pertains to the analysis of skewed and curved *I-girder* bridges. The analysis of box-girder bridges is not explicitly covered.

The blank Levels of Analysis Matrix is presented in Table 2.3.. The top row of the matrix lists the various analysis methods; i.e. the approximate V-load method, refined analysis using 2D grid models, refined analysis using 2D plate and eccentric beam (P&EB) models, and refined analysis using 3D models.

The left-hand column identifies several key issues related to skewed and curved bridge design that are covered at various points throughout the Manual. The matrix is intended to comparatively rank the ability of each analysis method to handle each of these issues and provide meaningful results.

Issues identified in the matrix include the computation of vertical bending moments and shears, the computation of vertical deflections, the computation of lateral bending moments and stresses, and the computation of lateral deflections. Single girder stability, refers to the capability of the method to permit the analysis and investigation of the stability of a single curved steel I-girder during the erection sequence. The matrix also deals with the ability to provide and load influence surfaces for live load analysis, the ability of handle thermal loads, the

Table 2.3.3 Levels of Analysis Matrix

Issue		V-Load	2D Grid	2D P&EB	3D
Vertical Bending	C				
	S				
Vertical Deflection	C				
	S				
Lateral Bending	C				
	S				
Lateral Deflection	C/S				
Single Girder Stability	C/S				
Influence Surface Concept	C				
	S				
Thermal Load	C/S				
Wind Load	C/S				
Horizontal Bearing Constraint	C/S				
Cross-Frame Actions	C				
	S				
Lateral Bracing	C/S				
Substructure Interaction	C/S				
Transverse Deck Stresses	C/S				
Phased Construction	C				
	S				
Vertical Reactions/Uplift	C				
	S				

ability to handle wind loads, the ability to input and consider various types of horizontal bearing constraints, and the ability to determine and provide cross-frame member actions. Finally, the matrix includes the ability to include lateral bracing members in the analysis model, the ability of the method to incorporate substructure conditions such as straddle beams and integral piers in the analysis model (i.e. substructure interaction), the ability to compute and provide transverse deck stresses, the ability to handle the various aspects involved with phased construction, and the ability to provide vertical reactions and detect potential uplift.

The letter ‘C’ in the matrix refers to curved girder bridges with radial supports. The letter ‘S’ in the matrix refers to straight or curved bridges with significant skews. For

certain specific issues, a differentiation on this basis is best made to provide a realistic ranking. Where such a differentiation was not deemed necessary, the symbol 'C/S' is used.

Column(s) dealing with a particular analysis method are filled in at the end of each section dealing with that particular method. The completed matrix is then presented and reviewed in Section 2.6.

The ranking system that is used to fill in the matrix is described as follows:

0 = No capability to handle the issue under consideration or provide the necessary results related to that particular issue
1 = Very limited capability to handle the issue under consideration in some approximate fashion that provides questionable results related to that particular issue
2 = Reasonable capability to handle the issue under consideration in a fashion that provides approximate but acceptable results related to that particular issue
3 = Capable of handling the issue under consideration in a rigorous fashion that provides accurate results related to that particular issue.

2.3.4.1 V-load Method

Table 2.3.4 presents rankings in the Levels of Analysis matrix for the approximate V-load Method of analysis described in Section 2.3.2.

In the V-load method, vertical bending moments and shears, vertical deflections and lateral flange bending moments and stresses are approximated reasonably well in curved bridges with radial supports, or in bridges with small skews ($\leq 10°$). The method begins to break down in these areas as the skew angle increases.

While approximate equations are available to estimate lateral flange moments and stresses due to curvature (Equations 2.3.18 and 2.3.19), similar equations to estimate lateral flange bending moments and stresses due to the effects of skew in conjunction with the use of discontinuous cross-frames are currently not available.

Since the V-load method does not directly account for the girder twist due to torsional effects, the method is not able to provide lateral deflections.

Influence surfaces are obviously not utilized since the V-load method deals with isolated girders straightened to their developed lengths. Influence lines are utilized instead to determine live load vertical bending moments and shears.

The V-load method is not applicable for thermal or wind loads. The effect of horizontal bearing constraints also cannot be considered. Cross-frame forces can be determined, but they must be estimated in an approximate fashion from statics utilizing approximate end moments and shears derived from V-load theory (Section 2.3.2.2.4).

Table 2.3.4 Levels of Analysis Matrix for the V-load Analysis Method

Issue		V-Load	2D Grid	2D P&EB	3D
Vertical Bending	C	2			
	S	1			
Vertical Deflection	C	2			
	S	1			
Lateral Bending	C	2			
	S	0			
Lateral Deflection	C/S	0			
Single Girder Stability	C/S	1			
Influence Surface Concept	C	0			
	S	0			
Thermal Load	C/S	0			
Wind Load	C/S	0			
Horizontal Bearing Constraint	C/S	0			
Cross-Frame Actions	C	1			
	S	1			
Lateral Bracing	C/S	0			
Substructure Interaction	C/S	0			
Transverse Deck Stresses	C/S	0			
Phased Construction	C	1			
	S	1			
Vertical Reactions/Uplift	C	1			
	S	1			

Since the V-load method again deals with isolated girders, the method is unable to incorporate lateral bracing members or the effects of substructure interaction (i.e. straddle beams, integral piers, etc.) directly into the analysis and is also not able to provide transverse deck stresses.

Phased construction could probably be handled in a very approximate fashion utilizing the V-load method. However, the analysis would not be able to directly consider the lateral deflection or rotation of adjacent phases.

Finally, the V-load method may not be able to detect potential uplift at end bearings in certain situations, particularly when there are significant skews.

2.3.5 References

1. Richardson, Gordon and Associates. 1963. “Analysis and Design of Horizontally Curved Steel Bridge Girders.” United States Steel Structural Report, ASUSS 88-6003-01, United States Steel Corporation, Pittsburgh, PA.
2. U.S. Steel. 1965. Highway Structures Design Handbook. Volume 1, Chapter 12, ADUSS 88-1895-01, United States Steel Corporation, Pittsburgh, PA.
3. ASCE. 1973. “Survey of Curved-Girder Bridges.” *Civil Engineering*, Joint AASHTO-ASCE Committee on Flexural Members, American Society of Civil Engineers, New York, NY, February.
4. Tung, D.H.H., and Fountain, R.S. 1970. “Approximate Torsional Analysis of Curved Box Girders by the M/R Method.” *AISC Engineering Journal*, Vol. 7, No. 3, Chicago, IL.

This Page Intentionally Left Blank

Chapter 2
Structural Analysis

Section 2.4
2D Methods of Analysis



2.4.1 Introduction

Two-dimensional finite element analysis models have been used in bridge design for a number of years, and were developed during a time when much less computational capacity was available. The two primary types of 2D analysis models generally available for use in design practice are the traditional grid model and the Plate and Eccentric Beam model. Each type of model is described herein. This section also describes two suggested methods of representing truss-type cross-frames in 2D analysis models. Finally, the advantages, disadvantages and limitations of 2D finite element analysis are discussed, and the Levels of Analysis Matrix introduced in Section 2.3.4 is filled in for the two primary types of 2D models.

2.4.2 2D Finite Element Modeling

2D finite element modeling actually encompasses a broad category of analysis models. There are two main types of grid analysis models generally available in design office practice – traditional 2D "grid" or "grillage" models and Plate and Eccentric Beam models. Note that the terms "grid" and "grillage" are more or less interchangeable.

2D analysis models were originally developed during the time when much slower computers and much less computational capacity were available.

For practical 2D modeling, designers have the choice of using either bridge-specific software packages or building their own 2D model in a structural finite-element software package. There are pros and cons to each approach, which will be discussed in more detail. There are also more sophisticated variations on the 2D modeling theme, but most of them are reserved for academic use at this time.

It is particularly important for the Design Engineer to understand the nature of the design software they are using (i.e., what type of analysis is the software performing and what assumptions are being made), as these aspects can dramatically affect the analysis results.

2.4.2.1 Traditional Grid Versus Plate and Eccentric Beam Models

Traditional 2D "grid" or "grillage" models consist of a purely two-dimensional array of nodes and beam elements.

Girders and cross-frames/diaphragms are modeled using beam elements (Section 2.4.2.2.1). Suggested procedures to determine section properties for truss-type cross-frames modeled using single beam elements are discussed in Section 2.4.3. For composite load cases, the deck is effectively modeled in strips in the longitudinal direction by adjusting the girder element cross-section properties to reflect composite section properties. The distribution of applied live load effects to individual girders is accomplished by means of the *AASHTO* empirical live load distribution factors. An example of a typical traditional grid model is shown in Figure 2.4.1.

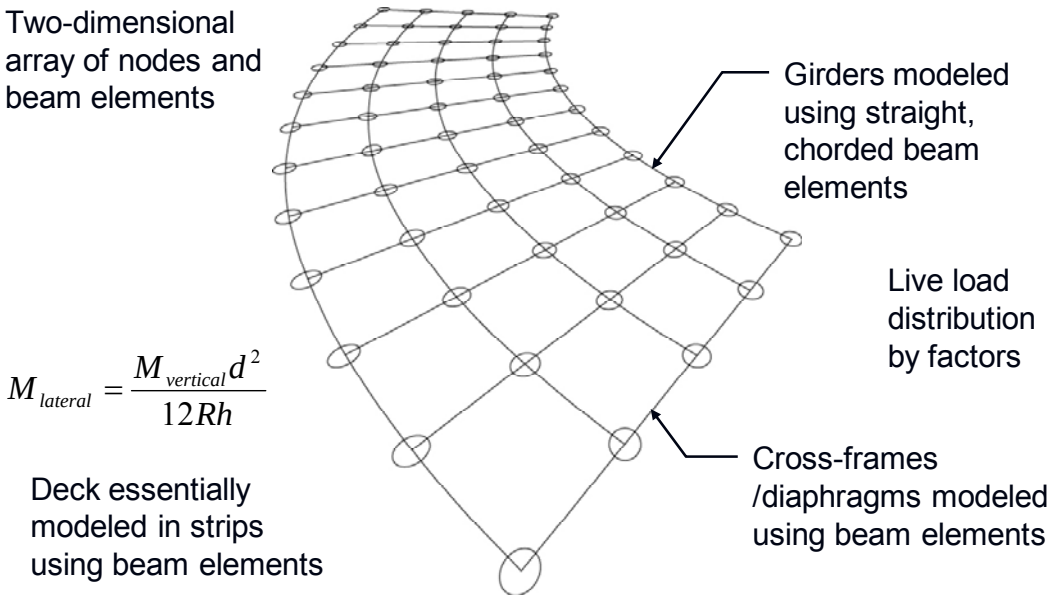


Figure 2.4.1 Traditional 2D "Grid" or "Grillage" Model

The beam elements used to model the girders are straight elements, chorded between nodes in the model. These elements typically do not include a warping stiffness parameter. Lateral flange bending effects may instead be approximated using the V-load formulation discussed in Section 2.3.2.2.5:

$$M_{lateral} = \frac{M_{vertical} d^2}{12Rh}$$

Equation 2.4.1

Design Engineers should take note that some of these approximations may yield erroneous results, particularly in complex bridges.

In Plate and Eccentric Beam models (Figure 2.4.2), the deck is typically modeled using shell elements and is offset from the grid of beam elements used to model the girders and the cross-frames/diaphragms.

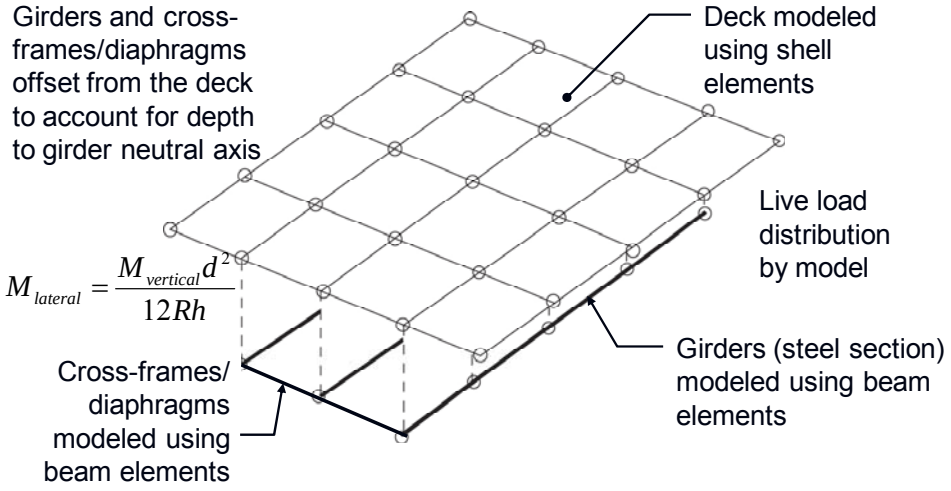


Figure 2.4.2 Contemporary "Plate and Eccentric Beam" Model

This allows for the distribution of live load by means of relative stiffness analysis rather than through the use of empirical live load distribution factors.

However, the girders and cross-frames/diaphragms are still modeled using beam elements, and lateral flange bending effects still must be approximated (e.g. using Equation 2.4.1).

Boundary conditions become a more important consideration for Plate and Eccentric Beam models, as will be discussed in Section 2.4.2.3.

A disadvantage of Plate and Eccentric Beam models is that composite girder moments are not directly available from the analysis results and are more difficult to extract.

The main theme of the differences between using a bridge-specific 2D bridge analysis design package and building a 2D model in a structural finite-element method (FEM) package can be summarized as "control vs. effort" (Table 2.4.1).

Table 2.4.1 2D Modeling: Bridge-Specific vs. Structural FEM Packages

Issue	Bridge Specific	Structural FEM
Automated model generation	Readily available	Becoming more available in some packages
Live load modeling	Generally fully automated	Significant user input
Extracting results	Generally mostly or fully automated	Significant user effort
Design code checks	Generally fully automated for girder design, not so much for cross-frames/diaphragms	Generally must be performed outside of the FEM model, using tools such as spreadsheets
Transparency	Can be somewhat of a "black box"	Generally fairly transparent, since you build it all yourself

With most bridge-specific 2D bridge analysis packages, it is very quick and easy to build a model, run it and get results, including girder code checks. However, these programs can be somewhat of a "black box," and the user is at the mercy of the software vendor with regard to design assumptions and flexibility.

Building the model in a structural FEM analysis package gives the user a great deal of control over modeling assumptions and significant flexibility in modeling any feature of the structure. However, in exchange for this freedom and power, the user typically has to expend a significant amount of effort in building the model (e.g., building the nodal geometry, building the member connectivity and establishing section properties), running live loads on the model (which can be a significant effort), post-processing the results, extracting key design loading information and performing detailed design checks.

2.4.2.2 Elements

2.4.2.2.1 Girders

One of the main elements in a 2D analysis model is the beam element used to model the girders (Figure 2.4.3). In a traditional 2D grid analysis model, this element models both the non-composite steel girder and the composite girder and deck.

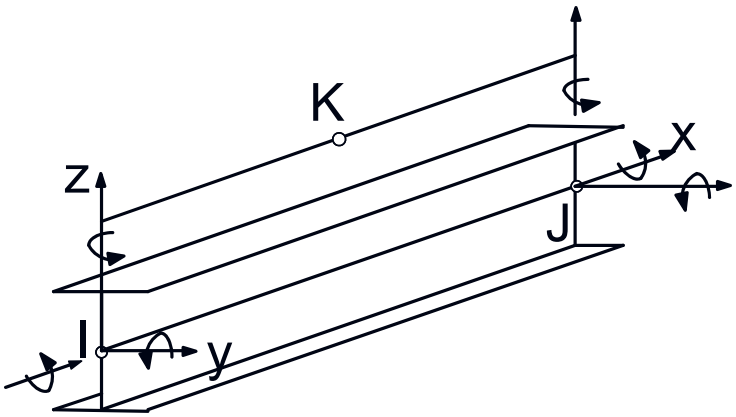


Figure 2.4.3 Beam Element

The elements used are fairly conventional beam-type elements modeling six degrees of freedom (6 DoFs) at each end and representing the flexure, axial and shear stiffness of the girder. A DoF is a direction of movement associated with axial, flexural and shear deformations.

St. Venant torsional stiffness (J) is also typically modeled, but most beam elements do not have the ability to model warping stiffness (C_w). Instead, warping stiffness is neglected, and lateral flange bending stresses are approximated, as discussed above. There has been some debate about the loss of accuracy resulting from not directly modeling the warping stiffness of the girders. To date there is no quantitative guidance in this regard, but many Design Engineers feel that for fairly simple geometries (e.g., gentle curvature, radial supports and constant girder spacing), the loss of accuracy is not significant.

2.4.2.2.2 Deck

In traditional 2D grid modeling (Figure 2.4.1), the deck is not actually fully modeled per se. Instead the effects of the deck are considered in a number of ways. Sometimes this is described as modeling the deck in “strips.”

In the longitudinal direction, the primary effect of the deck on the behavior of the bridge (and on the analysis model of the bridge) is to contribute to the composite section properties of the girders. Thus, girder element section properties are typically adjusted to reflect the effective width of the composite deck.

In the transverse direction, the deck serves primarily to help distribute live loads and composite dead loads to the girders and to tie the girders together (in conjunction with the cross-frames/diaphragms) so they can act together as a system to carry the global overturning moment that occurs in a curved girder bridge. Initial distribution of live load to the nodes of each girder is typically determined by means of empirical live load distribution factors. Assumptions must also be made to distribute the

composite dead loads to the girders (e.g., barriers and wearing surface). The deck stiffness in the transverse direction is either not modeled directly, or else attempts may possibly be made to model the stiffness in strips tributary to the cross-frames/diaphragms.

In Plate and Eccentric Beam models (Figure 2.4.2), the deck is modeled using shell elements. Shell elements are discussed in greater detail in Section 2.5.3.2.2. The deck elements are located at an offset from the grid of girder and cross-frame/diaphragm beam elements so as to account for the depth of the structure from the deck to the neutral axis of the girders.

Among other things, this allows the model to distribute live load and composite dead loads to the girders by means of direct stiffness analysis. This avoids having to use empirical live load distribution factors to determine how much live load is initially applied to each girder line. Similarly this avoids having to use simplified assumptions regarding composite dead load distribution to the girders.

2.4.2.3 Boundary Conditions

For traditional 2D grid models, the boundary conditions are relatively simple; in most cases, pin supports may be assumed at all support locations (Figure 2.4.4). There is no theoretical error introduced in modeling either fixed or expansion bearings as pin supports in a 2D grid model. Longitudinal (tangential) reactions do not develop because the depth of the superstructure is not modeled.

Proper modeling of integral substructures (e.g., integral abutments, integral piers and straddle bents) is difficult with a traditional grid model since there is a strong transverse interaction between the reactions and the superstructure depth is not explicitly modeled.

In a Plate and Eccentric Beam model, the depth of the structure is included in the model. For this reason, greater care must be taken in modeling the boundary conditions. It is important in Plate and Eccentric Beam models to choose boundary conditions that match the actual bearing configurations of the bridge. Otherwise, the model may improperly reflect conditions of moment restraint, which affects the determination of girder moments and deflections.

Care must be taken in these models to release the longitudinal (tangential) translation DoFs at bearings that are free in that direction; otherwise, moment restraint will develop at the bearings from the longitudinal reactions that result. For example, the last case shown on the right in Figure 2.4.4 indicates the moment restraint effect that can occur in a Plate and Eccentric Beam model if pins are provided at both ends of the beam (with the supports located at the bottom flange) such that the longitudinal (tangential) translational DoF is restrained.

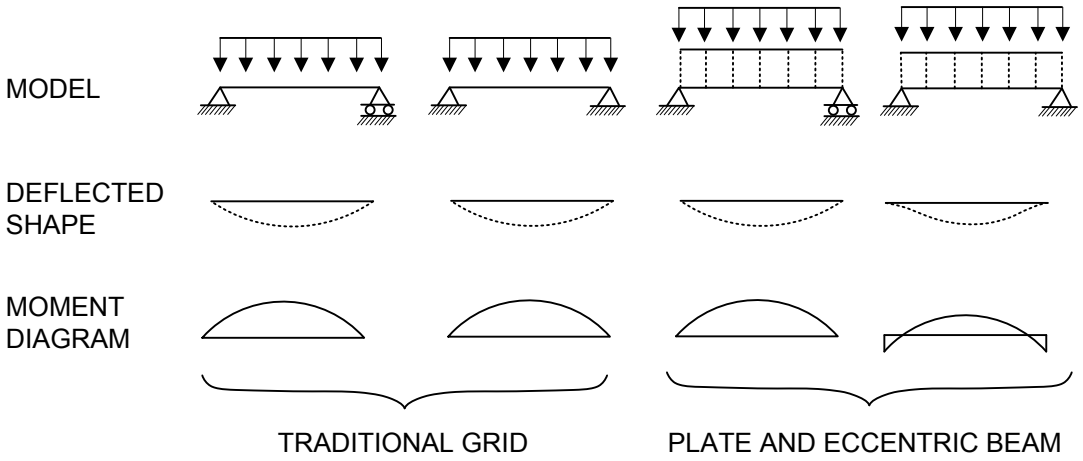


Figure 2.4.4 Effects of Different Boundary Condition Assumptions on Traditional Grid and Plate and Eccentric Beam Models

In a Plate and Eccentric Beam model, if all boundary conditions are modeled as pins, then the model will produce results which show some level of moment restraint. If all bearings on the bridge are fixed, perhaps this would be the correct way to model the bridge. However, the more likely case is that the bridge has some fixed, some guided and some free bearings. Thus, the boundary conditions for a Plate and Eccentric Beam model of that bridge should be chosen to match the actual bearing conditions. Some commercial software may set their default boundary conditions to restrain the longitudinal (tangential) translation DoFs.

Modeling of the boundary conditions for thermal analyses requires special consideration. As discussed in Section 2.2, bearing constraints can cause significant forces even with a uniform temperature change since the supports are not located at the neutral axis of the girders. If thermal effects are to be considered, the boundary conditions must be carefully modeled considering both the bearing fixity and also the specific orientation (direction) of guided bearings.

Care should be exercised when modeling thermal effects in a 2D model. Some commercial 2D modeling packages cannot model a bearing orientation other than locally tangent to the girder at the point of support. Traditional grid models do not permit different temperatures to be introduced through the depth of the structure in order to represent a thermal gradient.

2.4.3 Suggested Methods of Representing Truss-Type Cross-Frames in 2D Models

One major issue in 2D finite element analysis is associated with the modeling of truss-type cross-frames, such as the one shown in Figure 2.4.5. In a 2D model, these cross-frames are modeled using a single beam element. Thus, the stiffness of

a truss-type cross-frame must be represented in terms of the moment of inertia of a single beam element.



Figure 2.4.5 Truss-Type Cross-Frame

There are two suggested approaches that have been mentioned in the literature and are used in some form in commonly available commercial software to calculate an equivalent moment of inertia. These are the "shear stiffness" approach and the "flexure stiffness" approach. The titles are not formal, and there is no single, strong recommendation for the use of one method versus the other. Other methods exist as well. However, these two methods appear to be the most commonly used and are described further in the following.

2.4.3.1 "Shear Stiffness" Approach

In the "shear stiffness" approach, the truss-type cross-frame is modeled separately using the finite element method or similar approach. The most common approach is to model the truss using 3D finite element analysis software. Specific boundary conditions are assumed as shown at the top of Figure 2.4.6, and a unit vertical force is applied to one end of the model. The vertical displacement corresponding to the applied unit force is determined from the analysis model and recorded.

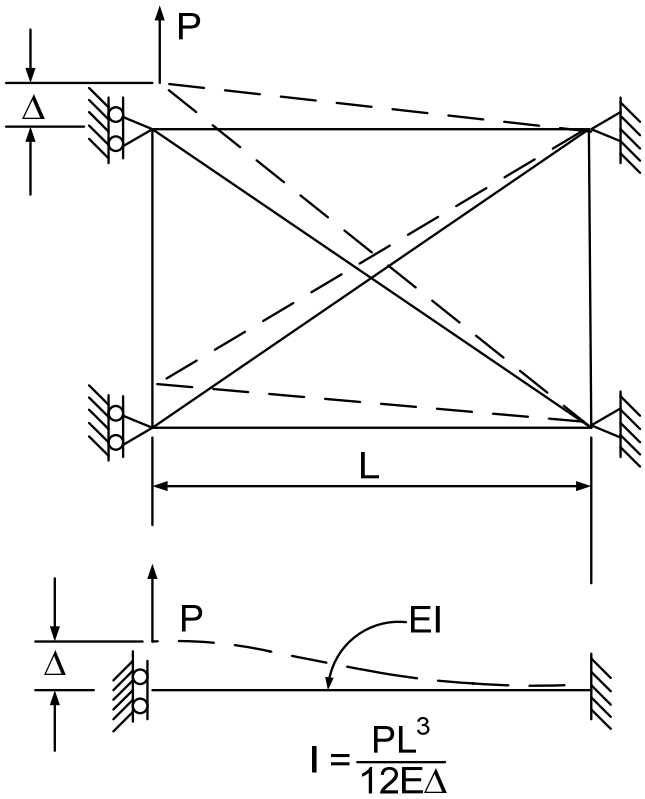


Figure 2.4.6 "Shear Stiffness" Approach Analysis Model of Truss-Type Cross-Frame

Then, the response of this truss model is replicated in an equivalent single beam element model representing essentially a fixed-end beam (see the bottom of Figure 2.4.6 for the associated boundary conditions). The corresponding common beam formula shown in the figure (which can be found in any of a number of textbooks) is then used to back-calculate the equivalent moment of inertia for the beam element corresponding to the applied unit load and resulting displacement.

The equivalent cross-sectional area of the beam element is typically estimated by summing the area of the top and bottom cross-frame chords, although some Design Engineers will also account for the diagonals. The equivalent torsion constant, *J*, is similarly estimated as the sum of the torsion constants of the chords and possibly the diagonals.

The boundary conditions assumed for the truss model in the "shear stiffness" approach are highly idealized and not truly representative of the boundary conditions of the actual cross-frame within the actual bridge system. The boundary conditions essentially assume that the girders on each side of the cross-frame rotate (twist) the same amount so there is no difference in the relative horizontal displacement of the girders.

2.4.3.2 "Flexure Stiffness" Approach

In the "flexure stiffness" approach, the truss-type cross-frame is also modeled separately using the finite element method or similar approach. Most common is to again model the truss using 3D finite-element analysis software. Specific boundary conditions are assumed as shown at the top of Figure 2.4.7, and a unit horizontal force couple is applied to one end of the model. The horizontal displacements at the ends of the top and bottom chord determined from the analysis model are converted to an equivalent end rotation and recorded.

Then, the response of this truss model is replicated in an equivalent single beam element model essentially representing a propped cantilever (see the bottom of Figure 2.4.7 for the associated boundary conditions). The corresponding common beam formula shown in the figure (which can be found in any of a number of textbooks) is then used to back-calculate the equivalent moment of inertia for the beam element corresponding to the applied unit loads and resulting rotation.

The equivalent cross-sectional area and torsion constant are estimated in the same way as described in Section 2.4.3.1 for the "shear stiffness" approach.

The boundary conditions assumed for the truss model in the "flexure stiffness" approach are highly idealized and not truly representative of the boundary conditions of the actual cross-frame within the actual bridge system. The boundary conditions essentially assume that there is no relative vertical deflection between the girders on each side of the cross-frame.

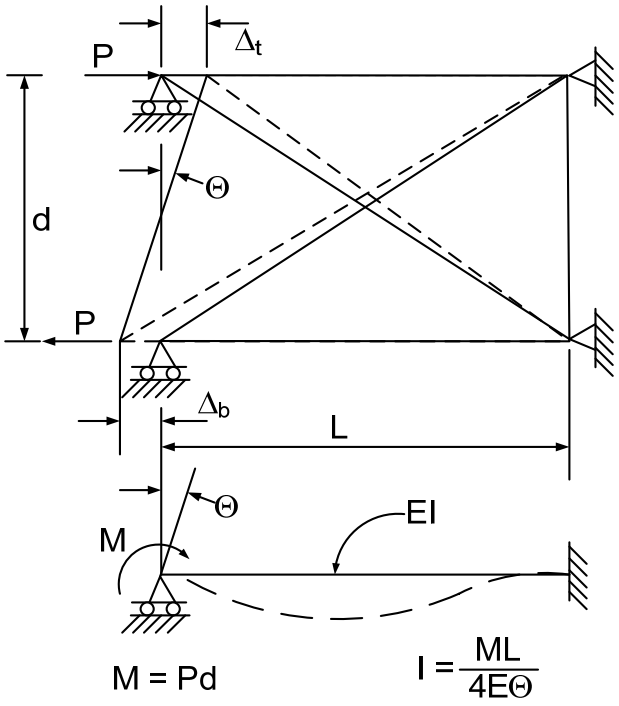


Figure 2.4.7 "Flexure Stiffness" Approach Analysis Model of Truss-Type Cross-Frame

2.4.3.3 Approach Selection & Example Calculation

The decision as to which approach to use depends on the predominant behavior of the system (i.e., shear vs. bending behavior). Neither approach is perfect or "exact." Both approaches are approximations, and each one omits consideration of at least one response parameter. As mentioned, the assumed boundary conditions in each approach are not truly representative of actual behavior. However, for relatively routine bridges (e.g. with radial supports, gentle curvature and reasonable span lengths), these approximations should generally provide reasonable results.

Performing a sensitivity study, where the Design Engineer varies the stiffness of the cross-frame elements in the model to see how the overall results are affected by the cross-frame stiffness assumption, may help provide some level of confidence that the structure will behave relatively consistently regardless of the assumed cross-frame stiffness. Such an approach can also provide the Design Engineer with an envelope of design results (e.g., for girder design, cross-frame design and deflections) that will allow a conservative design to be developed.

In the end, if the Design Engineer is still concerned that the approximations involved in these approaches are not providing a correct enough picture of the response of the structure, it may in fact be a sign that the bridge is not a good candidate for 2D analysis and perhaps a 3D analysis would be more appropriate.

Example: Calculation of the Equivalent Beam Element Moment of Intertia by the "Shear Stiffness" and "Flexure Stiffness" Approaches

A truss-type cross-frame (X-brace) that is 5'-3″ high and 7'-4″ wide (measured from the work points of the truss members) is composed of 5 x 5 x 1/2 angle sections for the truss chords and diagonals. The truss is modeled according to the "shear stiffness" and "flexure stiffness" approaches using a general 3D analysis model in each case, and the results of the unit vertical load and unit horizontal force couple analyses are provided in Figure 2.4.8 and Figure 2.4.9, respectively.

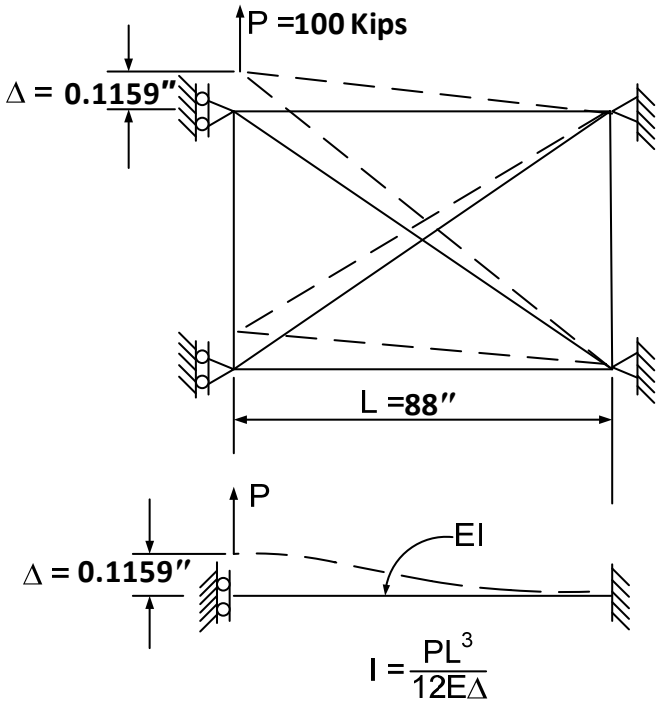


Figure 2.4.8 "Shear Stiffness" Approach – Analysis Results for Example Truss-Type Cross-Frame

Part A: *"Shear Stiffness" Approach*

Use the "shear stiffness" approach to calculate an equivalent moment of inertia for a single beam element to model the cross-frame.

The equivalent moment of inertia is defined as:

$$I = \frac{PL^3}{12E\Delta}$$

Applying the appropriate values from the analysis (Figure 2.4.8) to this equation results in the following:

$$I = \frac{(100\ K)(88")^3}{12(29{,}000\ ksi)(0.1159")} = 1690\ in.^4$$

Part B: *"Flexure Stiffness" Approach*

For the same truss-type cross-frame, use the "flexure stiffness" approach to calculate an equivalent moment of inertia for a single beam element to model the cross-frame.

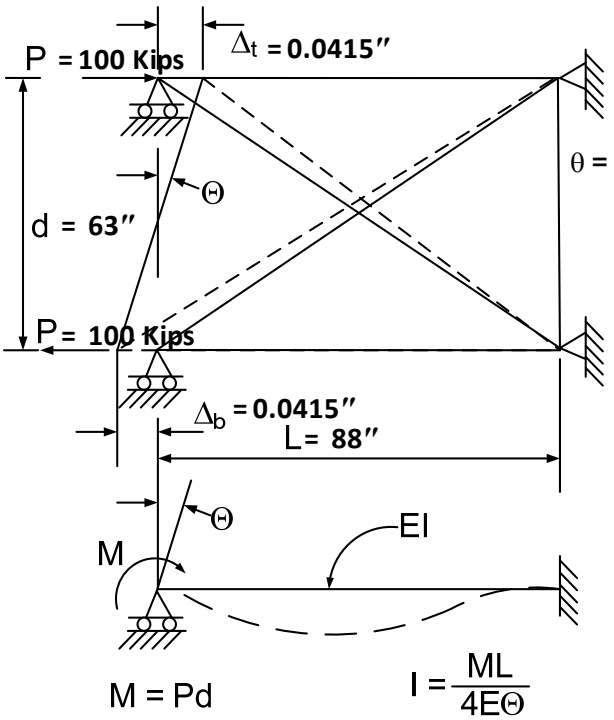


Figure 2.4.9 "Flexure Stiffness" Approach – Analysis Results for Example Truss-Type Cross-Frame

The values needed to compute the equivalent moment of inertia are given in Figure 2.4.9. To compute the equivalent end rotation:

$$\theta = \frac{\Delta_t + \Delta_b}{d} = \frac{(0.0415) + (0.0415)}{63} = 0.001317 \text{ radians}$$

With this equivalent end rotation, the equivalent moment of inertia is computed as follows:

$$I = \frac{ML}{4E\theta} = \frac{(100 \text{ K})(63")(88")}{4(29{,}000 \text{ ksi})(0.001317)} = 3{,}628 \text{ in.}^4$$

It is worth noting that alternative investigations using these same methods yielded dramatically different results. Releasing the horizontal translation restraints at one end of the "shear stiffness" truss model resulted in a moment of inertia, *I*, of 4,396 in^4. Releasing the vertical translation restraints at one end of the "flexure stiffness" truss model resulted in an *I* of 9,424 in^4. Again, sensitivity studies should probably be conducted to determine the effect of all these various solutions on the overall 2D analysis results.

2.4.3.4 Internal Cross-Frame Member Forces

The beam element in the 2D model represents the actual cross-frame in the model. Therefore, the loads calculated from the 2D analysis model for that beam element represent the loads on the actual truss cross-frame.

However, the form of the loads on the beam element is not directly applicable to the truss cross-frame; that is, the 2D model does not directly calculate the forces in the truss cross-frame top chord, bottom chord and diagonals. The forces calculated by the 2D model are the global forces acting on the entire cross-frame. Shears and bending moments are the primary force effects in the beam element representation of the cross-frame, as shown at the top of Figure 2.4.10. One more step must be taken to convert those global forces into the specific internal forces in the cross-frame members.

Another way to think of this is to consider the forces on the beam element as *external forces* acting on the overall cross-frame truss structure, as shown at the bottom of Figure 2.4.10. In order to design the individual truss cross-frame members and connections, the *internal forces,* or the forces in each specific internal member of the truss structure, are needed.

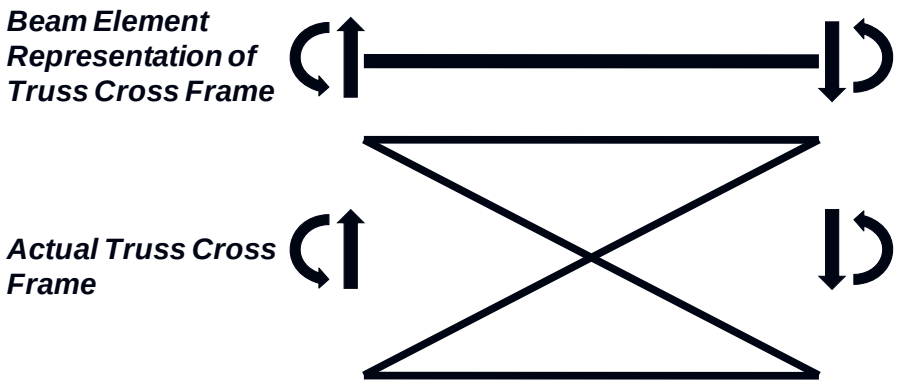


Figure 2.4.10 Global Forces Acting on the Beam Element Representation of the Truss-Type Cross-Frame and the Actual Truss-Type Cross-Frame

Most 2D models consider the self-weight of the structure, and therefore, consider the self-weight of the beam element modeling the cross-frame. For this reason, the shear at the left and right ends of the cross-frame element, as reported in the 2D analysis, may be slightly different. This effect is typically negligible. Design Engineers can simply use the higher of the two shear values.

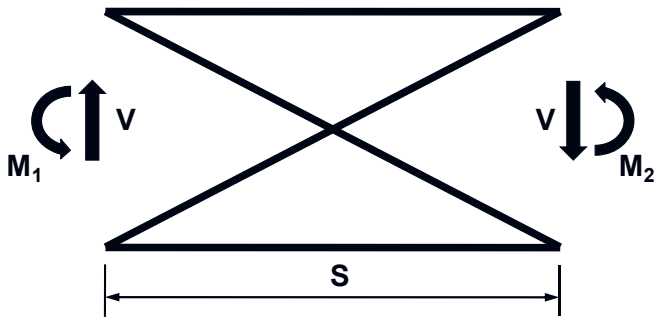


Figure 2.4.11 Global Shear and Moment on the Truss-Type Cross-Frame

The moments, M_1 and M_2, at each end of the beam element modeling the cross-frame, however, are usually significantly different, with the difference representing the fact that shear is being transferred across the length, S, of the cross-frame (Figure 2.4.11). By simple statics (i.e. the sum of the moments about any given point must equal zero), the difference in the moments can be verified. By statics, the moment at one end of the cross-frame must equal the product of the shear times the length of the cross-frame, minus the moment at the other end of the cross-frame. Thus:

$$M_2 = VS - M_1$$

Equation 2.4.2

Keep in mind that consistent sign conventions must be used to perform this calculation.

Depending on the type of cross-frame, different assumptions should be used to proportion the shear to each joint in the cross-frame.

For a K-type cross-frame, all of the shear should be assumed to act at the joint where the diagonal frames into the chord at each end of the cross-frame. The diagonal is the primary load path for the shear force. This can be demonstrated whether the connections in the cross-frame are considered pinned or not. By the principles of relative stiffness, all of the shear will act at the point where there is a very stiff shear load path; i.e., at the joint into which the diagonal frames.

For an X-type cross-frame (Figure 2.4.12), the shear can be assumed proportioned equally to the top and bottom joints at each end of the cross-frame since there is a diagonal framing into each one of those joints.

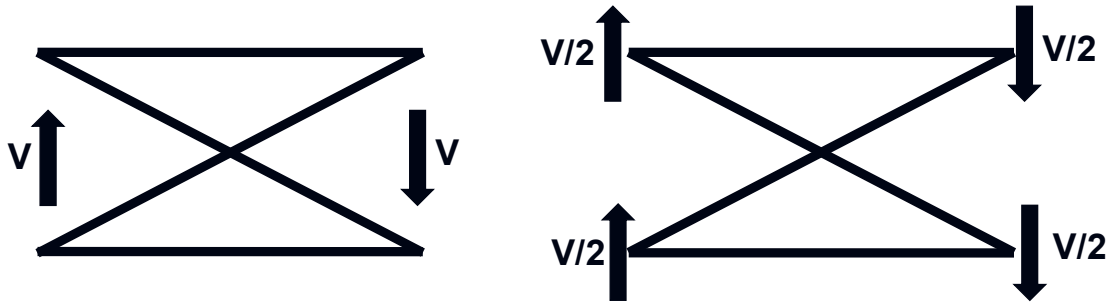


Figure 2.4.12 Assumed Distribution of Shear Forces for an X-Type Cross-Frame

Statics can be used to resolve the moment at each end of the cross-frame into a force couple at each end of the cross-frame by dividing the end moments by the vertical distance, *h*, between the top and bottom chords (Figure 2.4.13).

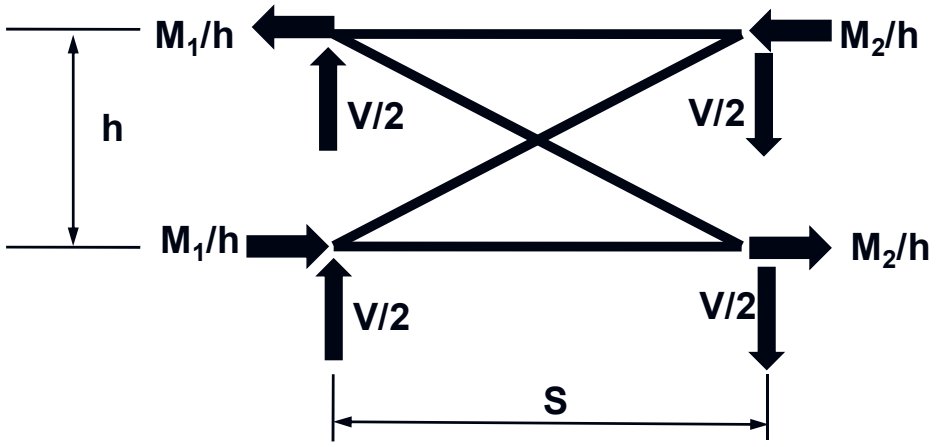


Figure 2.4.13 Resolution of the End Moments into Force Couples (X-Type Cross-Frame)

With the global external forces now resolved into specific external forces at the nodes of the truss, statics (i.e. the method of joints) can further be employed to calculate the specific internal forces in the truss, or the forces in the top chord, bottom chord and diagonals.

Live load moments and shears at each end of the cross-frame are typically not concurrent due to the various positions of the live load required to cause maximum effects in the individual grid elements. Because the live load forces are not concurrent, equilibrium of the cross-frame cannot be attained from the envelope actions typically reported at each end. Thus, for live load, by considering each end of the cross-frame separately and enforcing statics locally at the joints, the critical live load member forces can be deduced.

Example: Calculation of Internal Cross-Frame Member Forces

Given the truss-type cross-frame from the preceding example (Figure 2.4.8) and the global force results in the beam element representing the cross-frame from the 2D analysis model (Figure 2.4.14), calculate the chord and diagonal forces in the cross-frame.

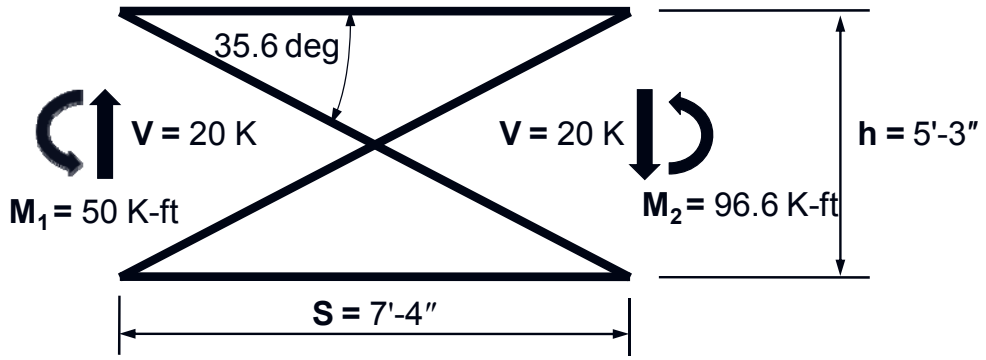


Figure 2.4.14 Global Forces on Example Cross-Frame from 2D Analysis Model

For the case of an X-type cross-frame, the shear is assumed divided equally between the top and bottom node at each end of the cross-frame, as shown in Figure 2.4.15.

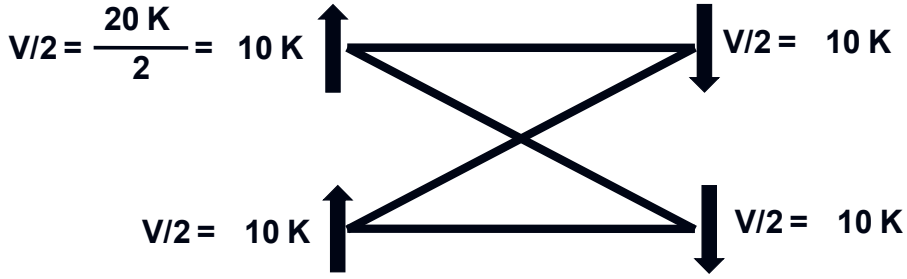


Figure 2.4.15 Assumed Distribution of Shears in the Example Cross-Frame

Statics can be used to resolve the moment at each end of the cross-frame into a force couple at each end of the cross-frame by dividing the end moments by the vertical distance, *h*, between the cross-frame chords (Figure 2.4.16).

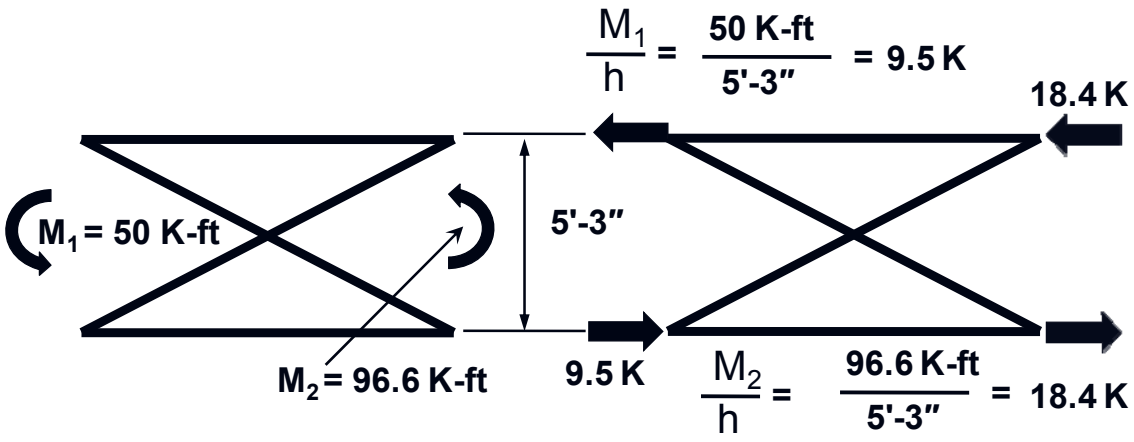


Figure 2.4.16 Resolution of End Moments into Force Couples for the Example Cross-Frame

With the global external forces now resolved into specific external forces at the nodes of the truss, statics (i.e. the method of joints) can be used to calculate the specific internal forces in the truss members. The resulting internal member forces are shown in Figure 2.4.17.

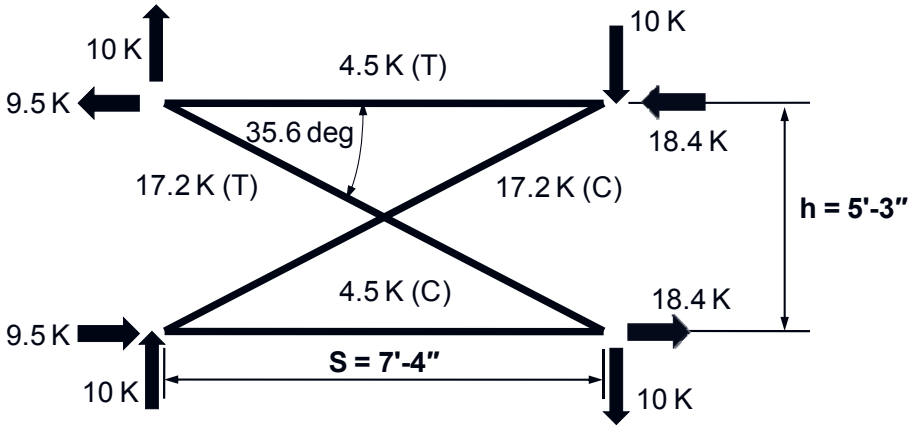


Figure 2.4.17 Example Cross-Frame Internal Member Forces Calculated Using the Method of Joints

2.4.4 Advantages, Disadvantages and Limitations of 2D Finite Element Analysis

The primary advantage of 2D refined methods of analysis is that they are generally less expensive than 3D refined analysis.

Disadvantages of 2D refined methods of analysis include, but are not limited to, the following:

- Warping stiffness for direct modeling of flange lateral bending is typically not included;
- Girders and cross-frames/diaphragms are modeled as single beam elements with no depth;
- Cross-frame/diaphragm actions cannot be obtained directly;
- Horizontal reactions are sometimes not available and/or may not be oriented properly (e.g., for thermal analyses);
- The horizontal shear stiffness of the deck is not properly represented in traditional 2D grid models;
- Questionable accuracy of wind load analysis results, particularly when lateral bracing is present;
- Assumptions usually must be made to distribute dead and live loads to the individual girders in traditional 2D grid models, and;
- Twist and layover of girders during construction cannot be reported directly.

There are exceptions to the above shortcomings that are addressed to a degree through the use of Plate and Eccentric Beam models.

There are currently no specific limitations related to the application of 2D refined analysis methods. However, caution should probably be exercised in situations involving the following:

- Significant curvature and/or skew;
- Longer spans involving the use of deeper girders;
- Irregular span arrangements and/or where uplift might be a concern;
- Variable depth girders;
- The use of lateral bracing;
- Complex framing (i.e., bifurcations or splayed girders, discontinuous girders or staggered cross-frames), and;
- The use of integral abutments, integral piers or straddle bents.

As of this writing (2010), research sponsored by the National Cooperative Highway Research Program (NCHRP Project 12-79) is attempting to identify more specifics related to some of these limitations.

Table 2.4.2 presents rankings in the Levels of Analysis Matrix, introduced in Section 2.3.4, for 2D finite element analysis. To review, '2D Grid' in the matrix represents the traditional grid approach and the acronym 'P&EB' represents the Plate and Eccentric Beam approach. The letter 'C' in the matrix refers to curved girder bridges with radial supports. The letter 'S' refers to straight or curved bridges with significant skews. For certain specific issues, a differentiation on this basis is best made to provide a realistic ranking. Where such a differentiation was not deemed necessary, the symbol 'C/S' is used. The ranking system that is used in the matrix is described further in Section 2.3.4.

Table 2.4.2 Levels of Analysis Matrix for 2D Finite Element Analysis

Issue		V-Load	2D Grid	2D P&EB	3D
Vertical Bending	C		3	3	
	S		2	2	
Vertical Deflection	C		3	3	
	S		1	2	
Lateral Bending	C		2	2	
	S		1	1	
Lateral Deflection	C/S		0	0	
Single Girder Stability	C/S		2	2	
Influence Surface Concept	C		0	3	
	S		0	3	
Thermal Load	C/S		1	1	
Wind Load	C/S		1	2	
Horizontal Bearing Constraint	C/S		0	2	
Cross-Frame Actions	C		2	2	
	S		1	1	
Lateral Bracing	C/S		0	0	
Substructure Interaction	C/S		1	2	
Transverse Deck Stresses	C/S		0	2	
Phased Construction	C		2	2	
	S		1	1	
Vertical Reactions/Uplift	C		3	3	
	S		1	2	

Vertical bending moments, shears and vertical deflections are approximated reasonably well using 2D finite element methods in curved bridges with radial supports and in bridges with smaller skews. The traditional grid approach begins to break down in these areas as the skew angle increases.

With no warping degree of freedom, girder lateral bending moments and stresses must be approximated using the V-load equation in both the traditional grid and Plate and Eccentric Beam approaches. An approximate approach to determine these moments and stresses due to skew effects is not available.

Lateral deflections are not generally available because the superstructure depth is not properly modeled.

Since the traditional grid approach does not typically model the transverse stiffness of the deck, influence surfaces are generally not utilized. Live load distribution factors are usually used instead, and assumptions are usually made to distribute the composite dead loads.

Proper modeling of horizontal bearing constraints and their effects is usually more challenging with 2D analysis methods since the superstructure depth is not recognized.

As illustrated in this section, cross-frame modeling for 2D analysis is approximate at best. Reasonable cross-frame actions can usually be deduced for curved bridges with radial supports or small skews.

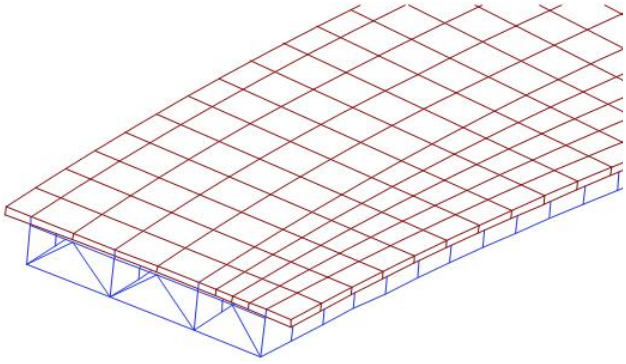
Since 2D analysis models do not model the superstructure depth, the effects of lateral bracing cannot be determined, and the effects of substructure interaction (e.g. when integral piers or straddle bents are employed) are more difficult to properly model.

Since the traditional grid does not typically model the transverse stiffness of the deck, transverse deck stresses are not available.

Proper recognition of uplift in severely skewed bridges is uncertain when 2D analysis methods are used.

Chapter 2
Structural Analysis

Section 2.5
3D Methods of Analysis



2.5.1 Introduction

Three-dimensional structural analysis has come to bridge design in the U. S. slower than in many other areas of structural design, such as buildings, transmission towers and dams. Even today, many bridge superstructure girders are designed as single-dimension lines. Loads are assigned to the line by various assumptions, some rather complex; all have their limitations. The enabling technologies of computers and finite element software permit the confident analysis of complex bridges that permit unique designs constrained only by the laws of physics and the Design Engineer's imagination and skill.

2.5.2 3D Finite Element Analysis

This discussion will cover the basic steps of 3D finite element analysis required to model, analyze and interpret the results necessary to design a steel-girder bridge with horizontally curved alignment and/or skewed supports. Solution of a simple finite element problem will be examined to demonstrate the principle of finite elements. This example will be followed by a discussion of the output information that can be provided. Then, the steps required to build a model of a steel-girder bridge will be examined. Finally, an example of a relatively simple bridge will be studied to demonstrate the advantages of a 3D finite element analysis.

There are four significant output areas of particular interest to the designer of girder-bridge superstructures: reactions, deflections, stresses and cross-frame/diaphragm actions. A proper 3D finite element model is capable of providing more accurate results compared to other methods of analysis and even results that are not available by other means.

2.5.2.1 Finite Element Fundamentals

This section demonstrates the fundamentals on which the finite element method is based. It helps to understand the fundamentals of the linear elastic finite element method. This method, which is based on strength-of-materials and statics, is used to arrange the mathematical model of the bridge in a matrix formulation that is amenable to solution by a digital computer.

First, the structure is divided into a finite set of so-called elements. Second, the spring stiffness of the individual elements is computed. For each direction that each element is capable of resisting translation or rotation, a stiffness resisting each motion must be computed. Assembly of these stiffnesses in matrix form is called the element stiffness. Other properties, including the element's mass and material properties, are also included. The element stiffness matrices are defined by the local axes of the element.

The topology of the model defines the orientation and connection of the elements forming the model. The assembled model is defined in a set of so-called global axes. The element connecting points are referred to as nodes (there are special cases where a node may be separated into one or more parts to recognize actions such as friction; there cases are not discussed herein). Models of bridge and most other structures require a foundation. The points of foundation are called boundaries that support the model as do the bearings of a bridge.

The final step in setting up the problem is to resolve the stiffnesses, using transformations, to get the stiffnesses oriented in the global axes at each node. This information is assembled into the global matrix of the structure. There are potentially three translations and three rotations at each node. Each direction of movement is called a degree of freedom (DoF). The DoFs identified herein are directions of

movement associated with axial, flexural, torsional and shear deformations (the torsional warping degree of freedom, which is typically not available in most finite element software packages, is ignored). All of the DoFs at each node have unknown displacements that must match with all deformations of the neighboring elements connected at that node. In actual solver packages, the node equations are shuffled to minimize the number of active terms, or terms in any equation.

Each step in the preceding process will be examined below. Fortunately, the software develops the information in an optimum matrix and solves the matrix with little assistance from the Design Engineer.

2.5.2.1.1 Global and Local Axes

Generally, nodal locations are specified in the global coordinate system, while element properties are local in nature. Cartesian coordinates are typically used to define global coordinates, although other systems such as cylindrical may be used to simplify the model.

Local axes are local with respect to each element and are used to define the individual elements. The local axes are used to specify the sequence of element node numbering, which in turn is used to define the output such as moments, shears, axial force and stresses. For example, a beam element is a straight element between two nodes, but typically requires a third node to define the orientation of its local axes. The signs of the responses are sometimes related to node sequencing; however, these nuances are too complex and inconsistent between finite element packages to discuss here. Suffice it to say that use of the finite element method requires careful attention to signs and the sequencing of element node numbering.

2.5.2.1.2 Material Properties

This discussion is limited to materials that obey Hooke's Law, which requires that the material behave in a linear elastic manner, or deform and return proportionally to changes in stress. The materials are isotropic, or have uniform properties along three axes. Other properties such as yield stress or tensile stress are not used since the material is elastic. Although finite element analysis applies to non-linear and non-isotropic materials, this discussion does not address those issues.

The following material properties are either input by the user or computed by the software. It is critical that the input properties have units consistent with those used to define the model. For example, if length is input in feet and weight is input in pounds, E, Young's Modulus would have units of pounds/foot^2.

- Young's Modulus (E, force/length^2) - the ratio of the axial stress to the axial strain
- Poisson's Ratio (ν) - the ratio of the transverse strain to the axial strain when a load is applied in the axial direction

- Shear Modulus (G, force/length^2) - the ratio of the shear stress to the shear strain and is usually computed internally in the software. When Hooke's Law applies, $G = E/2(1+\nu)$
- Thermal Coefficient of Expansion (α, length/length/degree temperature change) - the ratio of the change in volume with temperature change. The linear case is usually assumed
- Density (ρ, mass or weight/length^3) - the unit mass or weight of the material in the element. If density is input as mass/length^3, the acceleration in the vertical direction is input as the acceleration due to gravity (g = 32.2 feet/sec^2 if length is input in feet). If density is input as weight/length^3, the acceleration due to gravity is input as 1.0. Note that if a dynamic analysis is required, density must be input in units of mass/length^3

2.5.2.1.3 Degrees of Freedom (DOFs)

In finite element (F.E.) analysis, a degree of freedom (DoF) is defined as the ability of a node to translate in one of three axes (x, y, z), or to rotate about one of the three axes. Thus, each node has six degrees of freedom (Figure 2.5.1). An element can restrain from one to six of these DoFs. The terminology assigns an element a DoF as a restraint of the movement in one of the three local translations or three rotations.

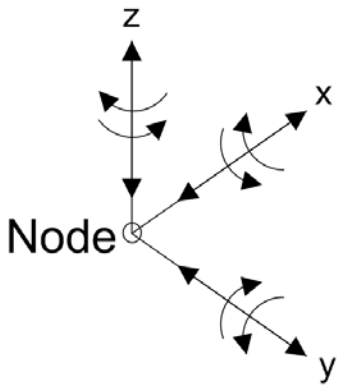


Figure 2.5.1 Degrees of Freedom (DoFs) at a Node

Thus, although the nodes at each end of a truss element have six DoFs, a truss element is said to have one only DoF since it can only restrain movement in its axial direction; i.e., along its own local axis. However, that element may provide up to three translational DoFs at each end of the element in a finite element model depending on its orientation in the global coordinate system. Each node may have two or more elements attached that provide rotational restraints as well as translational restraints. The truss element has no rotational DoFs and therefore does not provide any rotational restraint at either node. If there are no elements at a node that have rotationally restrained DoFs attached to the node, that node will

rotate freely. If there is only one such element, the model will be unstable since it will rotate without restraint.

There are rules about which DoFs must be released or introduced to replicate the proper behavior of the model. This is too complex an issue for discussion here.

2.5.2.1.4 Three-Member Truss

To illustrate the fundamentals of the finite element method, a problem consisting of a three-member truss shown in Figure 2.5.2 will be used. The truss lies in the global x-y plane so the z-axis is ignored. The truss is an equilateral triangle having 10-foot-long sides. Each member is steel with an area, A, of 10 in^2. A vertical 100-kip load is applied at the apex of the truss. The truss is supported at the base nodes by two rigid vertical supports. There is also a rigid horizontal support in the longitudinal (x) direction at the lower left node. The global x and y coordinates of each node are shown. The x-axis of the coordinate system is parallel with the bottom member. The truss is stabilized in the z-direction. The three members are modeled using truss elements each with a single axial DoF.

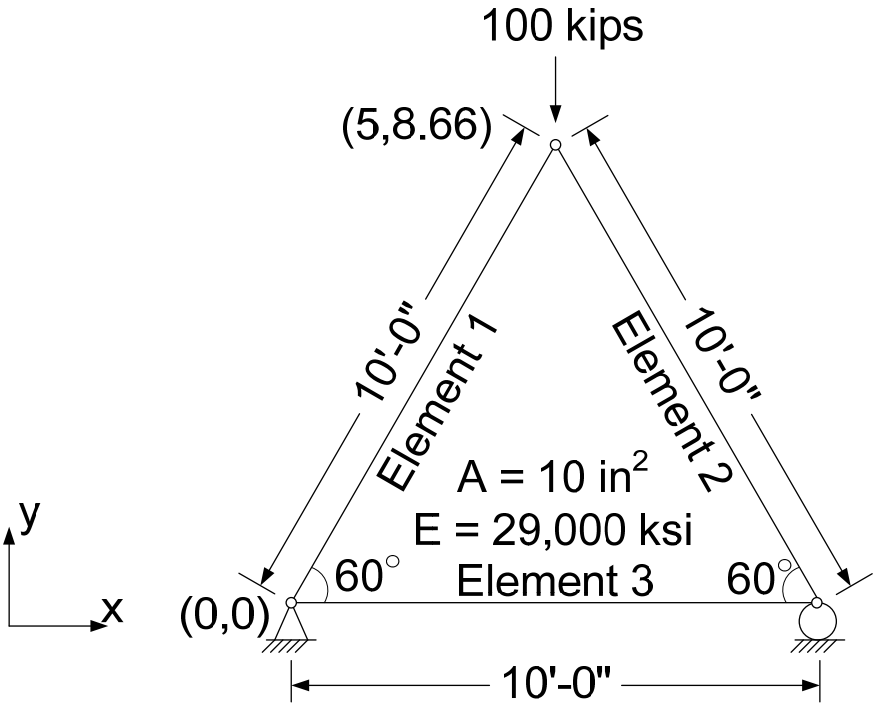


Figure 2.5.2 Example Three-Member Truss

After the model is defined, the first step in a finite element analysis is to compute the element stiffnesses for each applicable DoF. Although the element has only one degree of freedom, solution of the problem using the finite element method requires recognition that each end of each element can translate independently and, in this case, in two directions. Hence, the single element DoF must be changed to four global translational DoFs; two at each end of the element. In order to solve the

problem in Cartesian coordinates, each pair of DoFs is defined for the global x and y axes. Recall that the DoFs in the z-axis are ignored and there are no bending moments in these members.

Figure 2.5.3 shows Element 1 from the truss model isolated, with the four global forces at the ends of the element shown as $F_{1\text{-}4}$.

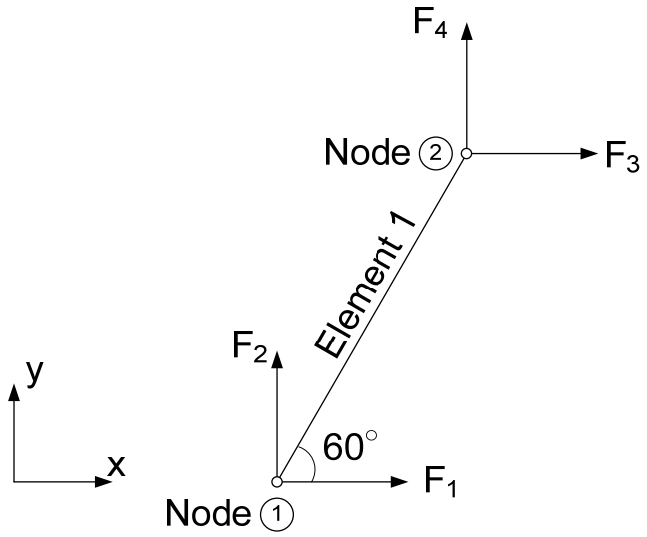


Figure 2.5.3 Element 1 from the Example Three-Member Truss in Figure 2.5.2

To compute the translations in the x- and y-directions at each node (and associated forces) requires element stiffness terms for the x- and y-directions at each node. Once the four global stiffnesses for each element are defined, the nodal stiffnesses can be written in terms of the combined stiffnesses of the elements connected at each node. Assuming all element nodes are attached at a global node such that they move the same, the total force in a global direction at a node equals the sum of the forces for all elements attached to that node, which must balance out any external force (if present) in that direction at that node.

In this model, only forces are considered. If the members were beam elements, additional DoFs for bending and shear would be present at each node. Like actions would be summed at the nodes. The deformations in this case would include rotations as well as translations.

In this case, the element axial stiffness at each node in the element's local coordinate system is $\mathbf{k}_e = AE/L$, where E = Young's Modulus = 29,000 ksi. Thus:

$$\mathbf{k}_e = \frac{AE}{L} = \frac{10 * 29{,}000}{10} = 29{,}000 \text{ kips/ft}$$

Equation 2.5.1

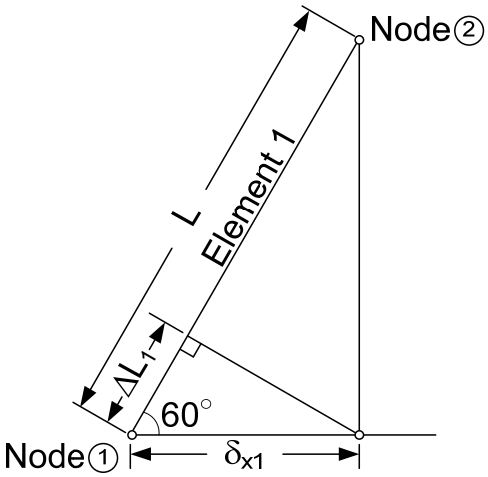


Figure 2.5.4 Element 1 from the Example Three-Member Truss with Node 1 Displaced δ_{x1} in the +x Direction

Looking at the isolated Element 1 once again in Figure 2.5.4, assume Node 1 is displaced in the positive x-direction an amount δ_{x1}, while Node 2 remains stationary. As a result of this displacement, Element 1 shortens by an amount equal to ΔL_1. The force, *F*, required to shorten Element 1 an amount equal to ΔL_1 is equal to:

$$F = \mathbf{k}_e \Delta L_1$$

Equation 2.5.2

$$\Delta L_1 = \delta_{x1} \cos 60°$$

Equation 2.5.3

Therefore, substituting in for ΔL_1, the equation for F becomes:

$$F = \mathbf{k}_e \cos 60° \delta_{x1}$$

Equation 2.5.4

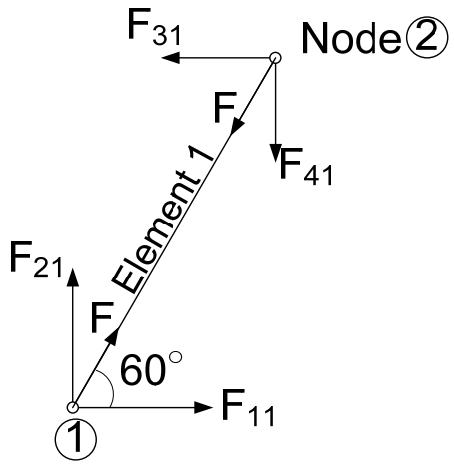


Figure 2.5.5 Force Components in Element 1 from the Example Three-Member Truss due to $+\delta_{x1}$ Displacement

Figure 2.5.5 shows the notation for the components of the force due to the $+\delta_{x1}$ displacement. The component of the force *F* in the x-direction at Node 1 for a displacement $+\delta_{x1}$, F_{11}, is equal to:

$$F_{11} = F\cos 60°$$

Equation 2.5.5

Thus:

$$F_{11} = \mathbf{k}_e \cos^2 60° \delta_{x1}$$

Equation 2.5.6

Since:

$$F_{11} = k_{11}\delta_{x1}$$

Equation 2.5.7

where k_{11} is the stiffness at Node 1 in the x-direction, then:

$$k_{11} = \mathbf{k}_e \cos^2 60°$$

Equation 2.5.8

Statics demands that the reaction force, F_{31}, in the x-direction at Node 2 due to the horizontal displacement at Node 1 be equal and opposite to F_{11}. Thus:

$$F_{31} = -\mathbf{k}_e \cos^2 60° \delta_{x1}$$

Equation 2.5.9

and

$$k_{31} = -\mathbf{k_e} \cos^2 60°$$

Equation 2.5.10

The component of the force *F* in the y-direction at Node 1, F_{21}, is equal to:

$$F_{21} = F \sin 60°$$

Equation 2.5.11

Thus:

$$F_{21} = \mathbf{k_e} \cos 60° \sin 60° \delta_{x1}$$

Equation 2.5.12

and

$$k_{21} = \mathbf{k_e} \cos 60° \sin 60°$$

Equation 2.5.13

Statics again demands that the reaction force, F_{41}, in the y-direction at Node 2 due to the horizontal displacement at Node 1 be equal and opposite to F_{21}. Thus:

$$F_{41} = -\mathbf{k_e} \cos 60° \sin 60° \delta_{x1}$$

Equation 2.5.14

and

$$k_{41} = -\mathbf{k_e} \cos 60° \sin 60°$$

Equation 2.5.15

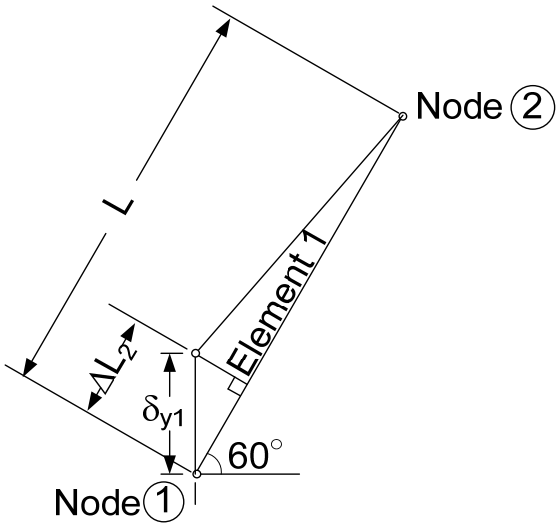


Figure 2.5.6 Element 1 from the Example Three-Member Truss with Node 1 Displaced δ_{y1} in the +y Direction

Next, assume element Node 1 is displaced in the positive y-direction an amount δ_{y1}, as shown in Figure 2.5.6, while element Node 2 remains stationary. As a result of this displacement, Element 1 shortens by an amount equal to ΔL_2. The force, *F*, required to shorten Element 1 an amount equal to ΔL_2 is equal to:

$$F = \mathbf{k_e} \Delta L_2$$

Equation 2.5.16

$$\Delta L_2 = \delta_{y1} \sin 60°$$

Equation 2.5.17

Therefore, substituting in for ΔL_2, the equation for F becomes:

$$F = \mathbf{k_e} \sin 60° \delta_{y1}$$

Equation 2.5.18

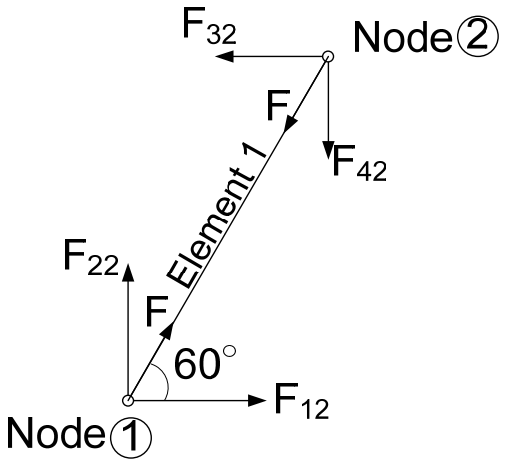


Figure 2.5.7 Force Components in Element 1 from the Example Three-Member Truss due to $+\delta_{y1}$ Displacement

The component of the force *F* in the y-direction at Node 1 for a displacement $+\delta_{y1}$, F_{22}, shown in Figure 2.5.7, is equal to:

$$F_{22} = F \sin 60°$$

Equation 2.5.19

Thus:

$$F_{22} = \mathbf{k_e} \sin^2 60° \delta_{y1}$$

Equation 2.5.20

Since:

$$F_{22} = k_{22} \delta_{y1}$$

Equation 2.5.21

where k_{22} is the stiffness at Node 1 in the y-direction, then:

$$k_{22} = \mathbf{k_e} \sin^2 60°$$

Equation 2.5.22

Statics demands that the reaction force, F_{42}, in the y-direction at Node 2 due to the vertical displacement at Node 1 be equal and opposite to F_{22}. Thus:

$$F_{42} = -\mathbf{k_e} \sin^2 60° \delta_{y1}$$

Equation 2.5.23

and

$$k_{42} = -\mathbf{k_e} \sin^2 60°$$

Equation 2.5.24

The component of the force *F* in the x-direction at Node 1, F_{12}, is equal to:

$$F_{12} = F \cos 60°$$

Equation 2.5.25

Thus:

$$F_{12} = \mathbf{k_e} \sin 60° \cos 60° \delta_{y1}$$

Equation 2.5.26

and

$$k_{12} = \mathbf{k_e} \sin 60° \cos 60°$$

Equation 2.5.27

Statics again demands that the reaction force, F_{32}, in the x-direction at Node 2 due to the vertical displacement at Node 1 be equal and opposite to F_{12}. Thus:

$$F_{32} = -\mathbf{k_e} \sin 60° \cos 60° \delta_{y1}$$

Equation 2.5.28

and

$$k_{32} = -\mathbf{k_e} \sin 60° \cos 60°$$

Equation 2.5.29

Upon repeating the preceding operations at element Node 2, the stiffness matrix, K_1, can be assembled for Element 1 as follows:

$$\begin{bmatrix} k_{11} & k_{12} & k_{13} & k_{14} \\ k_{21} & k_{22} & k_{23} & k_{24} \\ k_{31} & k_{32} & k_{33} & k_{34} \\ k_{41} & k_{42} & k_{43} & k_{44} \end{bmatrix}$$

Equation 2.5.30

Or:

$$K_1 = k_e * \begin{bmatrix} \cos^2 60^\circ & \sin 60^\circ \cos 60^\circ & -\cos^2 60^\circ & -\sin 60^\circ \cos 60^\circ \\ \cos 60^\circ \sin 60^\circ & \sin^2 60^\circ & -\cos 60^\circ \sin 60^\circ & -\sin^2 60^\circ \\ -\cos^2 60^\circ & -\sin 60^\circ \cos 60^\circ & \cos^2 60^\circ & \sin 60^\circ \cos 60^\circ \\ -\cos 60^\circ \sin 60^\circ & -\sin^2 60^\circ & \cos 60^\circ \sin 60^\circ & \sin^2 60^\circ \end{bmatrix}$$

Equation 2.5.31

Or for Element 1:

$$K_1 = k_e * \begin{bmatrix} 0.25 & 0.433 & -0.25 & -0.433 \\ 0.433 & 0.75 & -0.433 & -0.75 \\ -0.25 & -0.433 & 0.25 & 0.433 \\ -0.433 & -0.75 & 0.433 & 0.75 \end{bmatrix}$$

Equation 2.5.32

There are four displacements; two at each node. Thus, there are four responding forces for each displacement so there are 16 directional stiffness values. $\mathbf{k_e}$ is a scalar that is factored outside of the matrix since, in this case, it is the same for all elements.

Using a similar procedure, the stiffness matrix, K_2, for Element 2 is determined to be:

$$K_2 = k_e * \begin{bmatrix} 0.25 & -0.433 & -0.25 & 0.433 \\ -0.433 & 0.75 & 0.433 & -0.75 \\ -0.25 & 0.433 & 0.25 & -0.433 \\ 0.433 & -0.75 & -0.433 & 0.75 \end{bmatrix}$$

Equation 2.5.33

Since Element 3 lies along the x-axis, the trigonometric functions are either ±1.0 or 0.0. Therefore, the stiffness matrix, K_3, for Element 3 is:

$$K_3 = k_e * \begin{bmatrix} 1.0 & 0.0 & -1.0 & 0.0 \\ 0.0 & 0.0 & 0.0 & 0.0 \\ -1.0 & 0.0 & 1.0 & 0.0 \\ 0.0 & 0.0 & 0.0 & 0.0 \end{bmatrix}$$

Equation 2.5.34

After the element stiffnesses are computed, the topology of the model is defined, as shown in Figure 2.5.8. That is, the entire structure is reassembled in terms of the global coordinates. Referring to the figure, the topology of the example truss is included as Table 2.5.1.

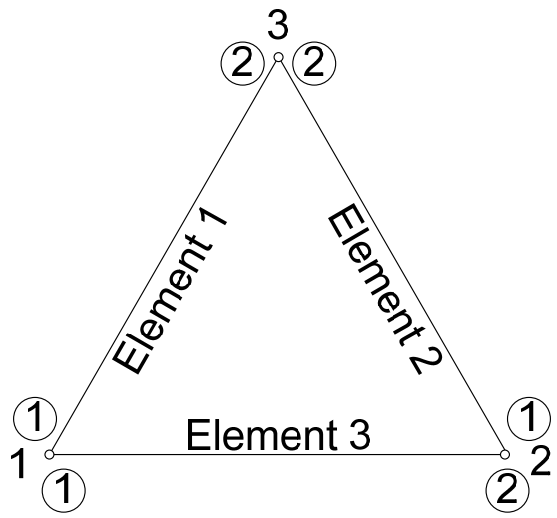


Figure 2.5.8 Local and Global Coordinates for the Example Three-Member Truss

Table 2.5.1 Topology of the Example Three-Member Truss

Element	Local Node	Global Node
1	1	1
	2	3
2	1	2
	2	3
3	1	1
	2	2

The element stiffnesses are then appropriately combined to form a global stiffness matrix, which results in a set of equations for each node. The unknowns of the equations are the x- and y- global deflections, termed u and v, at each global node, as shown in Figure 2.5.9.

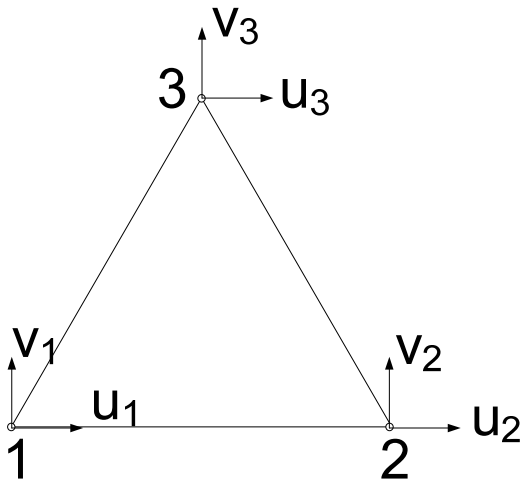


Figure 2.5.9 Global u and v Deflections at Global Nodes of the Example Three-Member Truss

The global stiffness equation written in matrix notation is as follows:

$$[K]\{\xi\} = \{R\}$$

Equation 2.5.35

where:

[K] represents the global stiffness matrix
{ξ} represents the global displacement matrix
{R} represents the force matrix

The global stiffness equation (in matrix form) for the truss problem is given in Figure 2.5.10. The first subscript in each term in the global stiffness matrix identifies the element stiffness associated with the force components at each global node (1,3,5 = force component in the global x-direction at global nodes 1, 3 and 2, respectively; 2,4,6 = force component in the global y-direction at global nodes 1, 3 and 2, respectively). The second subscript in each term identifies for the element stiffness associated with a particular global force component, the displacement at that global node (1, 3, 5 = global x-displacement at global nodes 1, 3 and 2, respectively; 2, 4, 6 = global y-displacement at global nodes 1, 3 and 2, respectively). Note that the 100 kip vertical force at global Node 3 is included in the force matrix on the right-hand side of the global stiffness equation shown in Figure 2.5.10.

$$\begin{matrix}\text{Node 1}\\ \\ \text{Node 2}\\ \\ \text{Node 3}\end{matrix}\begin{bmatrix} k_{11} & k_{12} & k_{13} & k_{14} & k_{15} & k_{16} \\ k_{21} & k_{22} & k_{23} & k_{24} & k_{25} & k_{26} \\ k_{31} & k_{32} & k_{33} & k_{34} & k_{35} & k_{36} \\ k_{41} & k_{42} & k_{43} & k_{44} & k_{45} & k_{46} \\ k_{51} & k_{52} & k_{53} & k_{54} & k_{55} & k_{56} \\ k_{61} & k_{62} & k_{63} & k_{64} & k_{65} & k_{66} \end{bmatrix} \begin{Bmatrix} u_1 \\ v_1 \\ u_2 \\ v_2 \\ u_3 \\ v_3 \end{Bmatrix} = \begin{Bmatrix} H_1 \\ R_1 \\ 0.0 \\ R_2 \\ 0.0 \\ 100.0 \end{Bmatrix}$$

Figure 2.5.10 Global Stiffness Matrix

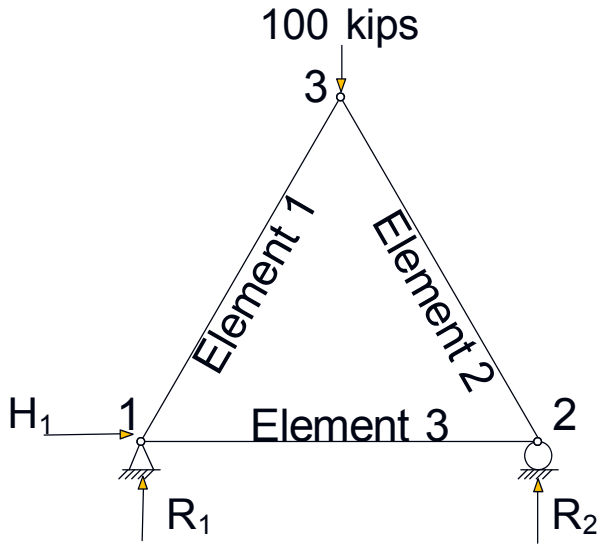


Figure 2.5.11 Global Forces and Reactions for the Example Three-Member Truss

H_1 and R_1 in the force matrix on the right-hand side of the equation are the horizontal and vertical reactions at global Node 1, respectively, and R_2 is the vertical reaction at global Node 2. These are also shown in Figure 2.5.11. In summary, the rows of the stiffness matrix are as follows:

- The first row defines the horizontal force at global Node 1.
- The second row defines the vertical force at global Node 1.
- The third row defines the horizontal force at global Node 2.
- The fourth row defines the vertical force at global Node 2.
- The fifth row defines the horizontal force at global Node 3.
- The sixth row defines the vertical force at global Node 3.

In Figure 2.5.12, element stiffness coefficients in the global stiffness matrix that are nil have been inserted where an element does not affect the solution. For example, Element 2 does not influence the force at global Node 1 because it is not in contact

with that node, so both of the element stiffness coefficients for Element 2 related to global Node 1 (i.e. the horizontal and vertical effects) are zero.

$$\begin{array}{c} \\ \text{Node 1} \\ \\ \text{Node 2} \\ \\ \text{Node 3} \end{array} \begin{array}{c} \begin{array}{cccccc} \text{EL 1} & & \text{EL 2} & & \text{EL 3} & \end{array} \\ \begin{bmatrix} k_{11} & k_{12} & 0.0 & 0.0 & k_{15} & k_{16} \\ k_{21} & k_{22} & 0.0 & 0.0 & k_{25} & k_{26} \\ 0.0 & 0.0 & k_{33} & k_{34} & k_{35} & k_{36} \\ 0.0 & 0.0 & k_{43} & k_{44} & k_{45} & k_{46} \\ k_{51} & k_{52} & k_{53} & k_{54} & 0.0 & 0.0 \\ k_{61} & k_{62} & k_{63} & k_{64} & 0.0 & 0.0 \end{bmatrix} \end{array} \begin{Bmatrix} u_1 \\ v_1 \\ u_2 \\ v_2 \\ u_3 \\ v_3 \end{Bmatrix} = \begin{Bmatrix} H_1 \\ R_1 \\ 0.0 \\ R_2 \\ 0.0 \\ 100.0 \end{Bmatrix}$$

Figure 2.5.12 Updated Global Stiffness Matrix

The equations are then solved simultaneously to yield the global deflections. In this case, six simultaneous equations are required to solve for the six unknowns (i.e. the six translations). Using the element stiffnesses, the global deflections can then be used to solve for the element forces in this case, as will be illustrated below.

For the example truss, the solution of the six simultaneous equations yields the following set of global deflections for the 100 kip load applied at the apex (global Node 3):

- u_1 = 0.0 ft
- u_2 = 0.0009961 ft
- u_3 = 0.0004980 ft
- v_1 = 0.0 ft
- v_2 = 0.0 ft
- v_3 = -0.002588 ft

Using the computed global deflections, the horizontal forces at global Node 1 are summed. Note that actions at both ends of Elements 1 and 3 (framing into Node 1) affect the force in each element, as can be seen in Figure 2.5.13.

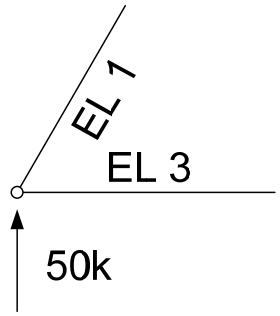


Figure 2.5.13 Detail of Global Node 1 of the Example Three-Member Truss

Since there are no external forces in the x-direction at the Node 1, the sum of the member forces must be zero: Note that in the following, two displacements (i.e. u_1 and v_1) are known to be zero.

|--Element 1--|-----Element 3----|

$$\left[k_{11}u_1 + k_{12}v_1 + k_{15}u_3 + k_{16}v_3\right] = 0.0$$

$$\left[29{,}000\right] * \left[0.25(0.0) + 0.433(0.0) - 0.25(0.0004980) - 0.433(-0.002588)\right] = 0.0$$

Equation 2.5.36

A similar check will be made summing the vertical forces at global Node 1. In this case, due to symmetry, the vertical reaction at Node 1 is 50 kips. This external force must balance the member forces at this node: In the general case, the reaction would not be known. However, some displacements would be zero such that the number of unknowns would remain at six. If a support has a stiffness other than rigid, the reaction can be solved for with the addition of a spring stiffness for the reaction.

|--Element 1---|-----Element 3-----|

$$\left[k_{21}u_1 + k_{22}v_1 + k_{25}u_3 + k_{26}v_3\right] = 50.0$$

$$\left[29{,}000\right] * \left[0.433(0.0) + 0.75(0.0) - 0.433(0.0004980) - 0.75(-0.002588)\right] = 50.0$$

Equation 2.5.37

Separate checks similar to the above are made at global Nodes 2 and 3 and equilibrium is confirmed. The sum of the vertical forces at Node 3 is shown to be equal to the 100 kip vertical load applied at Node 3.

The axial force in Element 1 will next be calculated from the global deflections. Since there is no deflection at global Node 1, only the deflections at global Node 3 are used to calculate the force. The global deflections are transformed to axial deflections along Element 1 as follows:

$$\Delta L = u_3 \sin 60^\circ + v_3 \cos 60^\circ = 0.0004980(12)(0.866) + (-0.002588)(12)(0.5) = -0.0239 \text{ in.}$$

Equation 2.5.38

$$P = \mathbf{k_e} * \Delta L = \left(\frac{29{,}000}{12}\right) * (-0.0239) = -57.9 \text{ kips}$$

Equation 2.5.39

The 3D analysis of the truss resulted in an axial force in Element 1 of –57.7 kips.

Next, the axial force in Element 3 is calculated from the global deflections. The horizontal deflection of global Node 2 is 0.0009961(12) = 0.01195 inches, which is along Element 3. Therefore:

$$P = \mathbf{k}_e * \Delta L = \left(\frac{29{,}000}{12} \right) * 0.1195 = -28.9 \text{ kips}$$

Equation 2.5.40

The 3D analysis of the truss resulted in an axial force in Element 3 of 28.9 kips.

2.5.2.2 Finite Element Output

Translations and rotations of each node in the three global axes are available. From this information, element stresses may be calculated. Specific information for each element depends on the element type and its stress functions. Truss elements, for example, provide only the axial force and/or stress. Beam elements provide the following at each node: axial force, shear in two directions, torque and bending moment about two local element axes. Output available for shell and solid elements depends on the stress functions available in the software. The stress functions of shell and solid elements are more complex than are beam elements. Therefore, the accuracy of the stresses is not reliable for some element proportions outside the range of applicability. It is imperative that the user know these limitations before using results from the analyses.

Mid-length edge stresses of properly proportioned shell elements usually are most reliable. Bending and membrane behavior may be treated separately within shell elements, but the resulting stresses are usually combined. Shear stresses of course are also provided. Principal stresses are also typically available. Proper orientation of the element in the model is important so that the results are properly interpreted.

In the case of composite deck and girder interaction, the effective portion of the deck must be determined. The analysis of the deck recognizes shear lag and automatically apportions the so-adjusted amount of composite behavior if the deck is properly modeled. The neutral axis of the composite section can be backed out of the analysis using the stresses in the top and bottom of the steel section. Determining the ratio of these stresses over the steel depth locates the neutral axis. The amount of effective deck is then computable. A moment of inertia of the effective composite section can then be calculated. From the moment of inertia and the aforementioned stresses, a vertical bending moment in the girder can be determined.

It is somewhat ironic that traditional analyses result in girder moments that are converted to stresses via strength of materials assumptions, while in 3D finite element analysis, stresses must be converted into moments that can then be re-converted back into stresses. There are advantages however to dealing in girder moments. For example, the Design Engineer may resize a flange from the bending moment by re-calculating the section properties of the resized section and applying the new section modulus to the moment from the analyses. Modest changes in the section properties have a minimal effect on the moments. However, in every case a final analysis is required to ascertain deflections for camber setting. This concept is

well known to Design Engineers who have designed girders using traditional techniques.

One of the most significant advantages of using a 3D analysis model is the ability to determine horizontal reactions. These reactions are significant for thermal loads, but are also important for loads due to gravity. These reactions have a major impact on stresses in the superstructure, as well as on the substructure and the bearings. As discussed in Section 2.2.3, horizontal reactions influence the cross-frame forces, vertical deflections, girder and deck stresses. This is particularly true in the case of skewed supports where horizontal reactions are notoriously large. It is not unusual for the horizontal reactions due to dead or live load to be larger than the vertical reactions due to the same load.

Longitudinal reactions usually cause a “hogging” moment, or negative moment that counters the positive moment due to vertical loads. To design girders for these reduced loads may be unsafe since one cannot be certain that the reactions will act throughout the life of the bridge as assumed in the analysis. For example, when bearings are replaced, the bridge is jacked and lateral reactions are released. Also, corrosion or dirt may forbid a bearing from acting as designed. This can result in very large horizontal reactions that change the behavior of the bridge. If the bridge is load tested, these reactions will usually cause measured strains in the positive moment regions to be lower than they would be if the bearings were functioning properly. This may lead to a potentially higher load rating than appropriate. If a large load traverses the bridge, the horizontal reaction may be so large that the bearing is freed and the positive moment could be dramatically increased. A proper rating analysis using a 3D analysis is more accurate than a load test in this instance.

The negative-moment region of continuous spans presents a different issue in that the hogging moment is additive to the gravity-induced moments. The moment and compressive stress is actually increased in these regions. The longer the expansion length, the more critical the issue, since thermal movements are more significant (larger) in longer spans. The effect may be critical when dead load is added to a bridge after the bearings become restrained. This may happen during construction or long after the bridge has been put in service.

Transverse deck stresses may be computed rather simply with a full 3D finite element analysis, as can the horizontal deck shear. Transverse deck stresses, of course, occur after the deck has become composite. The most significant dead load causing transverse bending is loads placed on the cantilevered overhangs. They include the self-weight of the deck when the forms are removed and any traffic barrier or sound wall. Live load stresses on the overhang may occur with unusually large overhangs and due to vehicle impact. These stresses are computable by hand and are generally treated in the design of the overhang. Transverse deck stresses between the girders are often not computed. Generally these stresses are not significant. The empirical method of deck design assumes that load transferred mainly by shear and bending is not very important. There are however occasions

where this assumption does not hold. If the girders are flexible in either bending or torsion, the support points of the deck cannot be assumed rigid, and in fact, they deflect. This causes the effective span of the deck to increase, with a concomitant increase in the transverse deck stresses. When box girders having single bearings are used, the effective deck span may be significantly greater than that between the flanges resulting in larger deck stresses than would be the case when the flanges do not twist due to torsion. Similar increases in the effective transverse span of the deck occur when girders deflect causing a dishing or hogging of the deck that is not evident in an analysis that does not consider the interaction of the deck with the girders.

When the transverse forces in a cross-frame do not sum to zero, as is often the case in a composite section, the remainder of the force is resisted by the deck. The deck stresses can be estimated from this observation. As discussed in Section 3.1.2.8.3, cross-frames are frequently removed on skewed bridges, particularly near the bearings. At other times, they are removed when analysis indicates that the forces in them are exorbitant. When cross-frames are removed, the deck is asked to resist more of the load formerly carried by the removed cross-frame. As discussed throughout this Manual, the load transferred between girders in horizontally curved bridges and skewed bridges is greater than in comparable bridges that are not curved or skewed. Hence, transverse deck stresses are more significant in these bridges.

It is interestingly ironic that two of the stiffest components in a girder bridge are ignored in many, if not most, analyses. They are: lateral restraint of bearings, particularly at abutments, and horizontal shear stiffness of the deck. Horizontal deck shear can be very large in bridges with skewed supports. As the skew and/or the vertical deflection increases, horizontal shear increases in the deck. Although it is difficult to quantify the amount of reinforcing required to respond to this force, it must be agreed that when horizontal shear is very large and is not accounted for, the durability of the deck may be compromised. The authors know of no study of the relationship of horizontal deck shear and deck durability.

As discussed in Section 1.1, in skewed and curved bridges, the girders often rotate about their longitudinal axis, particularly under steel and wet concrete loads. The amount of these movements is reported directly when a 3D model is employed since the top and bottom lateral displacements are available. This information is valuable in determining where the loaded bridge will potentially end up, and whether or not special detailing might be required to accommodate these movements as discussed further in Section 4.1.3.

2.5.3 3D Finite Element Modeling

A 3D finite element model of a composite girder-bridge superstructure is a refined mathematical three-dimensional representation of the superstructure, including girders, deck, cross-frames/diaphragms and supports. Instead of representing each girder as a single element, a 3D model defines the girders with a group of pieces or a finite number of elements. The other components are defined similarly. These

discrete elements or components are assigned properties and given a connectivity to each other and to the supports in a manner that mathematically represents the actual structure.

The finite element method can be used in one, two or three dimensions. The method depends on strength of materials principles. Thus, all solutions will satisfy strength of materials as well as statics. This knowledge is useful when making checks of results. Proper boundary conditions and proper releases of degrees of freedom are absolutely necessary to obtain correct results. These issues are beyond the scope of this discussion, but should be well understood by any user of finite element modeling techniques.

3D modeling permits the most realistic representation of the structure with few simplifying assumptions. The refinement of the mesh or the elements determines the accuracy of the results. This discussion is limited to 3D models that represent the gross structure. It does not address the connections at the level of weld conformation or individual bolts. It does not discuss buckling of members or the eccentricity of cross-frame members, etc. although the method is capable of addressing these items. Instead, it addresses modeling the structure to obtain reasonably correct results at the macro level that can be solved by employing a mathematically rigorous solution algorithm. This provides a tool that enables a knowledgeable Design Engineer to analyze bridge designs so he/she can confidently prepare designs that are unique, efficient, durable and economical.

This discussion will examine the typical components of a finite element model of a steel-girder composite bridge superstructure and discuss the types of structural elements most commonly used for 3D modeling of those components. Construction of a reasonable 3D finite element model of the bridge superstructure from these elements to provide the desired results on a macro level will also be discussed. Discretization of the model and issues related to node layout will be included as part of this discussion. Also to be discussed are the boundary conditions and loads applied to the analysis model.

2.5.3.1 Node Layout

The Design Engineer should keep in mind the objective of the analyses to be performed when determining the degree of discretization required in the model. Laying out the nodes is important because as long as the framing does not change, member properties can be changed and new analyses made rather efficiently. A relatively coarse mesh is generally satisfactory for determining girder moments and stresses, shears, reactions and cross-frame/diaphragm actions at the macro level. The stress state around a diaphragm access hole might require a more refined mesh than would a beam with no large holes in it, or a beam in which stress concentrations around bolt holes or weld discontinuities are of no interest. Such issues may be important, but are beyond the scope of this discussion.

Discretization, or number of elements, is somewhat subjective but there are concepts that are important to keep in mind. For example, looking at the moment diagram of a continuous beam gives some clues as to how to discretize its elements. Each element is actually a sub-domain that can be seen as a small structure connected to other similar small structures. In order to obtain a reasonable continuum of moment, shear, etc. along the span, the beam needs to be discretized such that the curvature of the beam is properly represented. Typically, a beam element has the characteristic of being isoparametric, meaning that it can represent only one curvature. The element is loaded only at its ends. Concentrated loads or moments may be applied. However, the element can only recognize a singular curvature. If the applied loads require that the element have two curvatures to represent the behavior, an error is introduced. If the element is discretized into two elements, each with a single curvature, the two curvatures can be represented and the solution will be more correct. It is the modeler's responsibility to understand these limitations and to compensate for them in laying out the model. The more interrupted the continuum, the greater the number of elements required to properly represent the behavior.

The first step in creating a 3D finite element model is to describe the node layout for the bridge. Each finite-element package has its own preprocessor that assists in the layout. This discussion does not address the specifics of these operations, but only addresses the issues that the Design Engineer should consider in determining the proper nodal grid.

The model must have nodes that match the layout, or alignment, of the deck and the girders. There are four types of horizontal alignments commonly found on bridges:

- Straight (Figure 2.5.14 Part A)
- Constant radius curved upward or curved downward (Figure 2.5.14 Part B)
- Spiral from straight to curved (Figure 2.5.14 Part C)
- Spiral from curved to straight.

A node is required at each change in alignment.

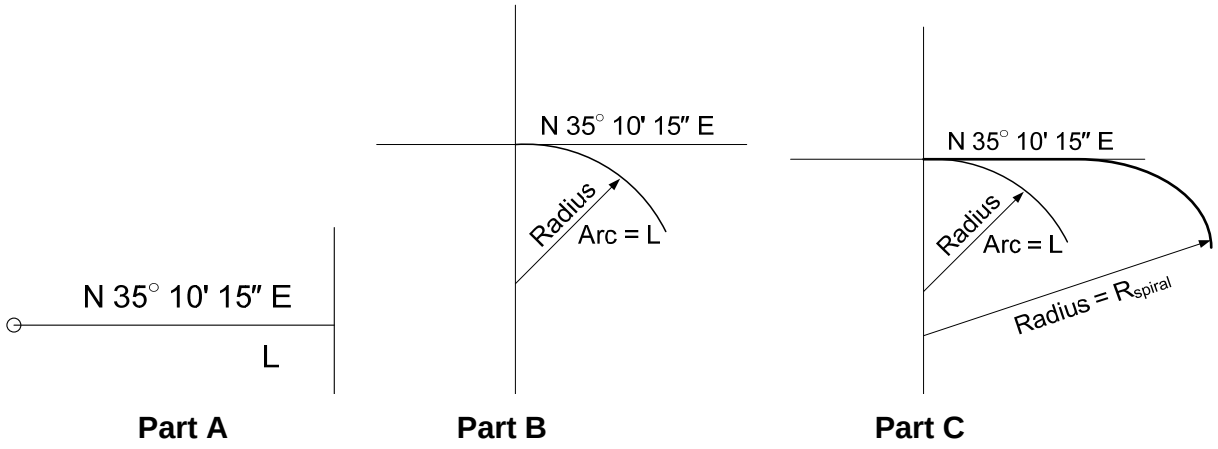


Figure 2.5.14 Horizontal Node Layout for Different Alignments
A) Straight; B) Curved with Constant Radius; C) Spiral from Straight to Curved

Starting with the horizontal roadway alignment is usually the ideal way to commence the layout of the node geometry. The length and shape of each alignment segment must be specified and its location in space defined. This is often done with the control line, or baseline. A straight segment has only one parameter (length) in addition to its bearing and point of initiation. A constant curve segment has an additional parameter; radius. A means of specifying whether the radius curves right or left is also required. A spiral is defined as a line commencing with a straight alignment that increases in curvature linearly over its length to a specified radius at its end. .

Nodes must be also specified at each bearing and cross-frame location. Additional nodes may also be required to accommodate discontinuous girders. Nodes at field-section locations are needed if an erection study is to be undertaken. There are other reasons for placement of nodes that will be examined subsequently.

With skewed supports, it often becomes necessary to compute offset lengths at the supports in order to locate the support nodes along the skew. These lengths are used to determine the proper lengths along the baseline adjacent to the supports that are necessary to project radially from the baseline the correct coordinates for the girder support nodes. Figure 2.5.15 illustrates one possible approach to compute these offset lengths at skewed supports on horizontally curved bridges. Alternatively, node locations may be created from software, such as COGO, that may have been used to layout the bridge for drawing.

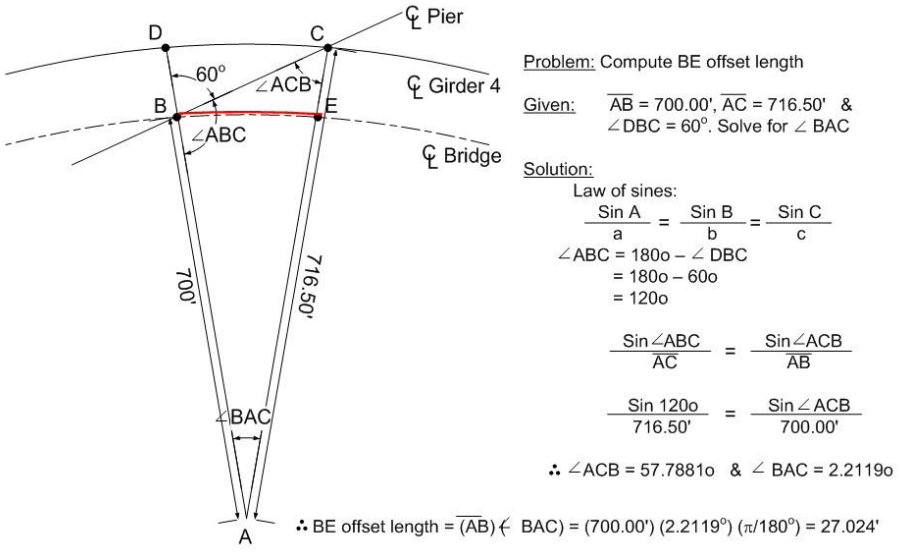


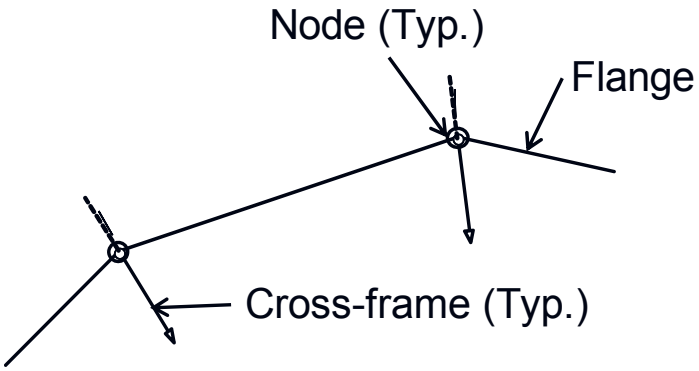
Figure 2.5.15 Offset Length for Skewed Support Nodes

Accurate stresses at nodes of solid and shell element nodes are difficult to obtain and are generally not used. Stresses at mid-element length are used instead. This is an important concept to understand when dealing with a 3D model. The bending moment can be reported directly at a node from the analysis in a grid model or a line model, but this is not true in a 3D model. For example, the cross-section is composed of flange, web and deck elements. A collection of the stresses must be made and the moment calculated from the stresses. However, stresses are determined at mid-element length so the moment is computable only at mid-length of the element; not at a node. Moments at the nodes must be determined by fitting the moment data computed at mid-length of the element. The curvature of the moment curve at interior supports is increasing as the moment approaches the support. Shorter elements near the support provide a better estimate of the maximum moment at the support.

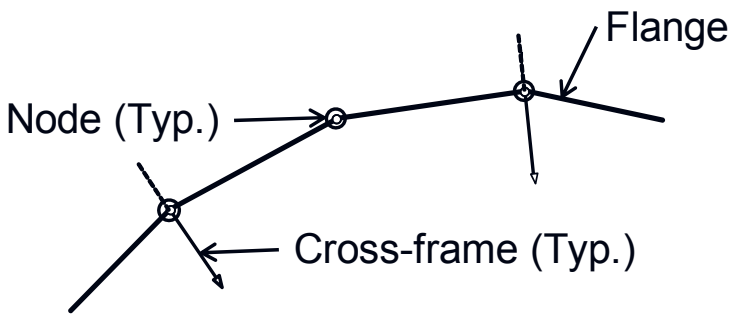
Nodes are required at flange and web size changes in grid analyses if moments are to be used to check sizes. This is not necessary with a 3D analysis since curve fitting is required to get the moment at a node, unless the software can only check stresses at nodes. Flange plate changes located within a few feet of a node do not introduce significant error in the analyses, unless there are too few elements in a span to properly curve fit.

Flange lateral moments are computed at nodes if flanges are modeled using beam elements. In the case of a curved flange, a single straight beam element between cross-frames gives negligible lateral moments because equilibrium at the nodes is established by the restoring forces in the cross-frame members attached at the flange nodes and the lateral moment effect of curvature is negated. Part A of 2.5.16 shows a single flange element between cross-frame nodes. Lateral bending is caused by the non-collinearity of the axial force in the flange. Hence, at least one additional girder node is required along the arc between cross-frames in curved

flanges to activate the non-collinearity effect and generate the flange lateral moments. Figure 2.5.16 Part B shows the two-element flange arrangement needed to create lateral bending.



Part A



Part B

Figure 2.5.16 Cross-Frame Nodes
A) Node at End of Straight Beam Element; B) Additional Node between Cross-Frames Necessary to Create Lateral Bending

Two nodes along the arc between cross-frame nodes have been found to give slightly larger, more realistic lateral flange moments. The lateral moments at interior nodes tend to have the opposite sign of those at the cross-frames.

Additional layers of nodes are required for a 3D model. Other layers of nodes can be built off the basic nodes defining the girders (Figure 2.5.17). The deck may be defined with a single layer of nodes if shell elements are used for the deck. Alternatively, two layers of nodes are required if solid elements are used to model the deck. Vaulted (i.e. variable thickness) decks may be properly modeled by varying the elevation of the bottom layer of deck nodes if solid elements are used. The original girder layout nodes may be used to represent the tops of the girders. A fourth layer of nodes is defined under that layer to represent the bottoms of the girders.

A variable depth girder can be correctly modeled by varying the vertical location of the bottom layer. Superelevation or grade may be modeled by applying a transformation to the model nodes.

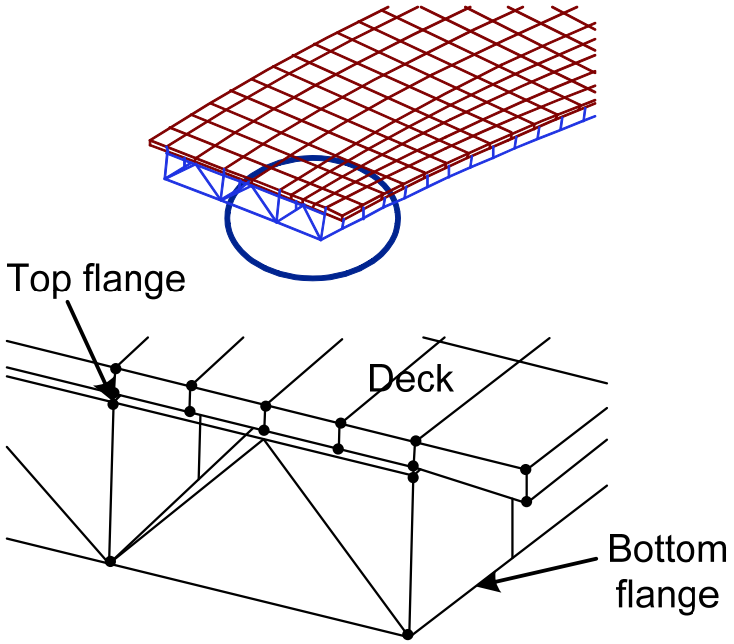


Figure 2.5.17 Node Layers

2.5.3.2 Elements

Several different types of finite elements are used to model the components of a composite girder bridge.

2.5.3.2.1 Beam Elements

The beam element (Figure 2.5.18) typically has six DoFs at each node: bending about two of the local axes; torsion about its third (longitudinal) axis; shears in two planes; and axial force along its longitudinal axis. The typical beam element does not accommodate warping (commonly referred to as the seventh DoF). However, the warping DoF is not needed in a 3D model to model a girder since the girder is modeled with a web (shell element) and individual flanges (beam elements). A third node is assigned to orient the two local axes.

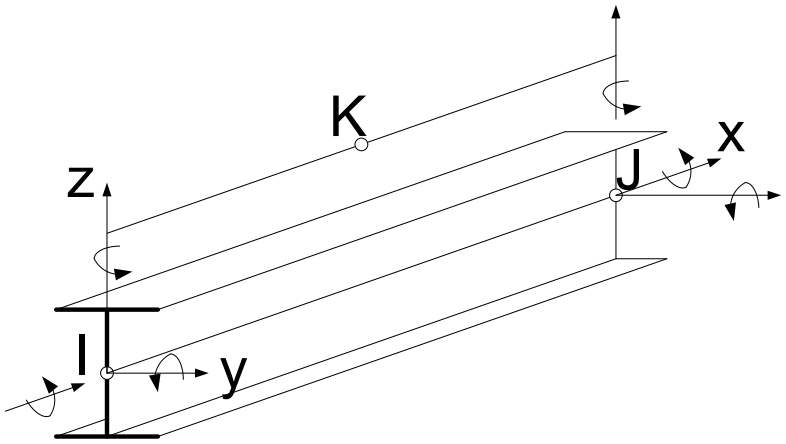


Figure 2.5.18 Beam Element

The properties required for a beam element are: cross-sectional area, bending stiffness about two local axes, torsional stiffness, and two shear areas. The mass or weight of the element is specified and temperatures can be input at each node. Lateral pressures can be applied to a beam element. If a load or pressure is applied to a beam element, the element properties are used to transform loads or pressures to end moments and forces applied at its two nodes.

Typically, a beam element recognizes only single curvature bending. As discussed previously, this type of element is referred to as an isoparametric element. If a beam in the true structure is anticipated to undergo reverse bending (reverse curvature), more than one isoparametric beam element is required to properly recognize its behavior. Of course, there are more elaborate types of beam elements available with more capability.

Girder flanges are typically modeled with beam elements attached to the top and bottom of the web elements (Figure 2.5.19). Deck elements may be connected to the girders with beam elements representing shear connectors. These members also define the location of the deck with respect to the girders (Figure 2.5.19). The element length represents the deck haunch. These elements should be modeled to ensure that the deck does not rotate independently at the nodes in order to ensure that plane sections remain plane. Thus, an additional beam element spanning the nodes defining the top and bottom of the deck elements over each girder (assuming solid elements are used) is usually required.

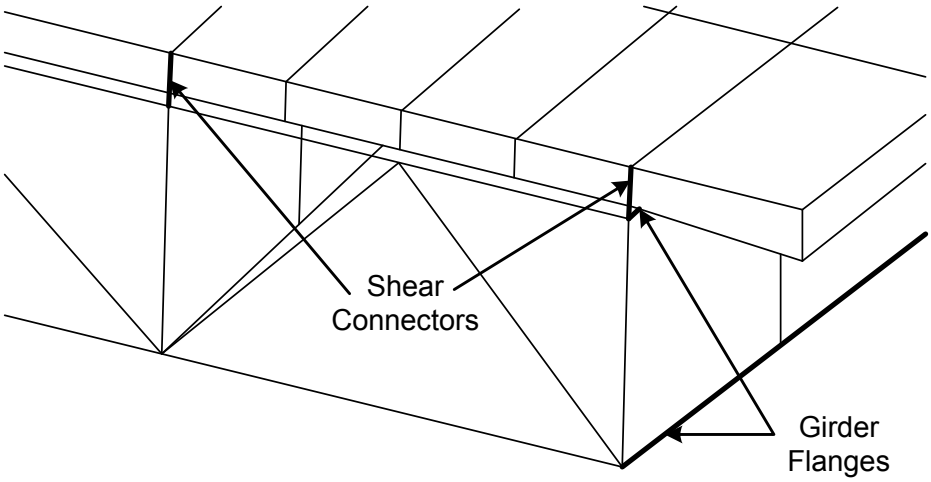


Figure 2.5.19 Beam Elements Used to Model Girder Flanges & Shear Connectors

2.5.3.2.2 Shell Elements

A shell element, typically used to model a girder web, has four nodes (quadrilateral element) with six DoFs at each node -- the three translations and three bending DoFs about the local x, y, and z axes -- for a total of 24 DoFs per element. A shell element is shown in Figure 2.5.20. All six DoFs at each node must be accounted for in the analysis. For example, if only a truss element is connected at a shell element, the three DoFs associated with bending of the shell element at that node cannot be resisted by the truss element and are accounted for by specifying that they are released (or free). If the truss element is oriented such that it cannot resist all three translations, a further modification of DoFs is required. Thicknesses and temperatures may be assigned to each node of a shell element. Pressures may also be applied to the element.

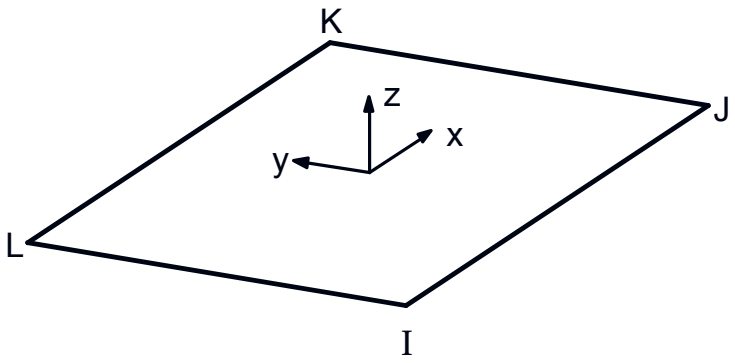


Figure 2.5.20 Shell Element

The nodes of a shell element are typically identified in the counterclockwise direction. The local z-axis is normal to the plane of the element. The reason for a specific pattern is so the output stresses can be identified.

Figure 2.5.21 shows a girder web modeled with a shell element.

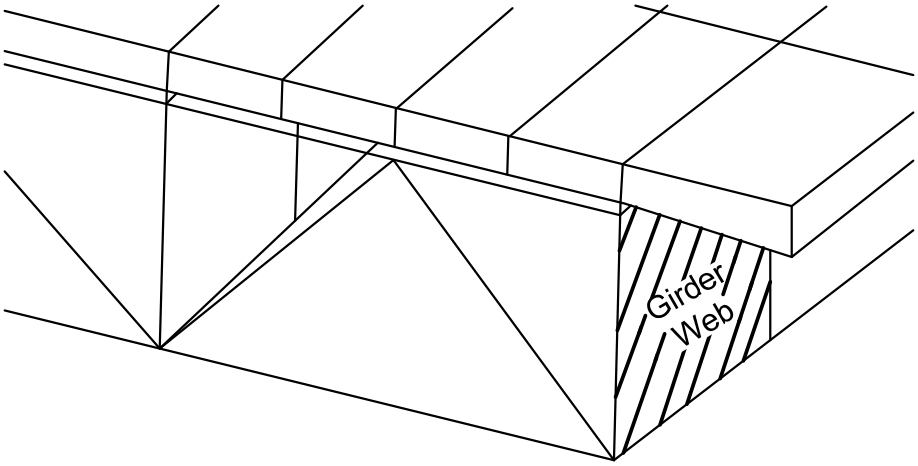


Figure 2.5.21 Shell Element Used to Model a Girder Web

2.5.3.2.3 Solid Elements

Eight-node 3D solid elements are the simplest of all solid elements. This element typically has three translation DoFs at each of the 8 nodes for a total of 24 DoFs. Eight-node solid elements can be collapsed to form triangular solid elements having six nodes. In Figure 2.5.22, the face defined by nodes I, J, K and L in clockwise fashion can be any face. The other face is defined by nodes M, N, O and P, but node M must be behind node I. The order defines the local coordinate system. The thickness of solid elements is not input explicitly, but is instead implicitly defined through the specification of the proper nodal coordinates. Thus, no geometric properties are required; only a material identification is required for these elements.

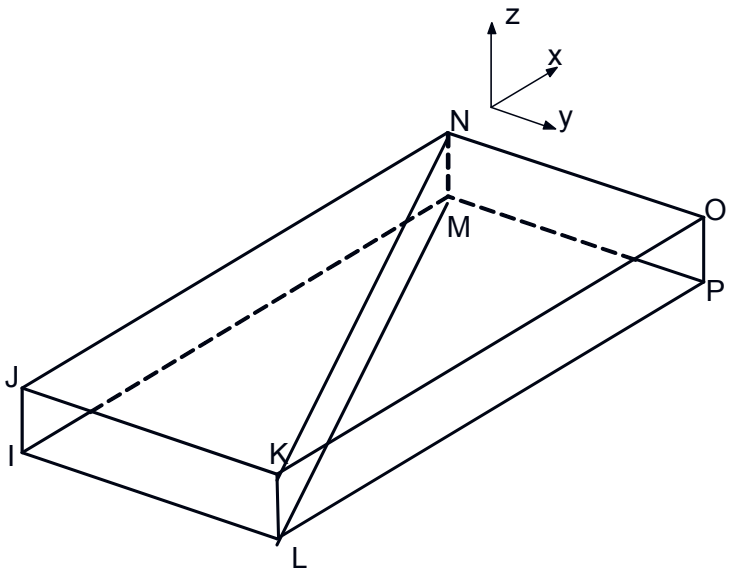


Figure 2.5.22 Solid Element

If a beam element is attached to a solid element and to no other element that takes bending, the two bending and one torsional DoF in the beam element at the connecting node must be specified “free” since the solid element has no ability to react to the bending DoFs of the beam element.

Figure 2.5.23 shows a portion of a composite deck modeled with 8-node solid elements.

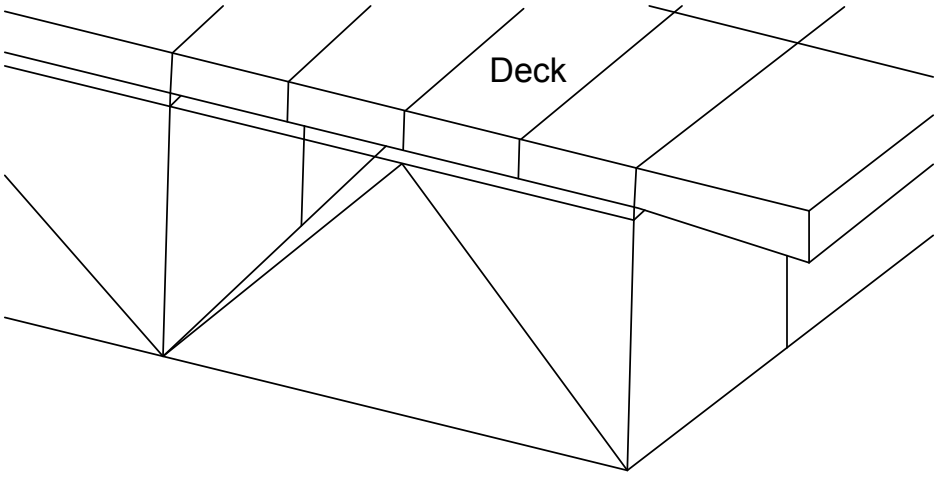


Figure 2.5.23 Solid Elements Used to Model the Concrete Deck

2.5.3.2.4 Truss Elements

The simplest finite element is the truss element shown in Figure 2.5.24. This straight two-node element resists only axial force. The element length is defined by the coordinates of the nodes at its ends. It is assigned a cross-sectional area, and material properties; Young's modulus, density and thermal coefficient of expansion. The truss element reacts to force by changes in its length. The length of the element changes according to force and its stiffness, or an amount equal to PL/AE. Hence, the truss element has one degree of freedom (DoF). Temperatures can be input at each node of a truss element.

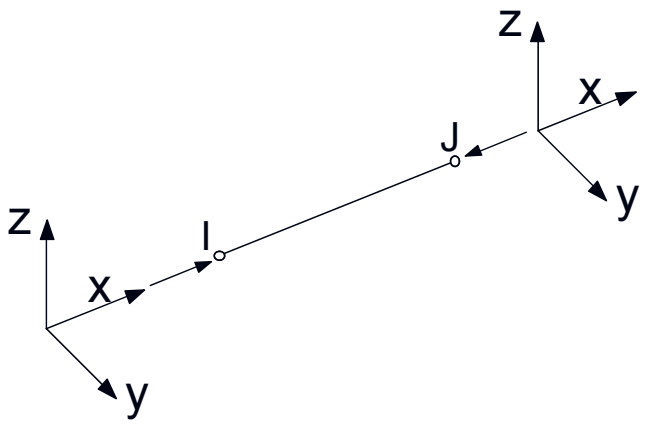


Figure 2.5.24 Truss Element

Cross-frames are typically modeled with truss elements connected to the top and bottom of the web (Figure 2.5.25). Lateral bracing members may also modeled with truss elements. Lateral bracing can also be approximately modeled with an equivalent shell element.

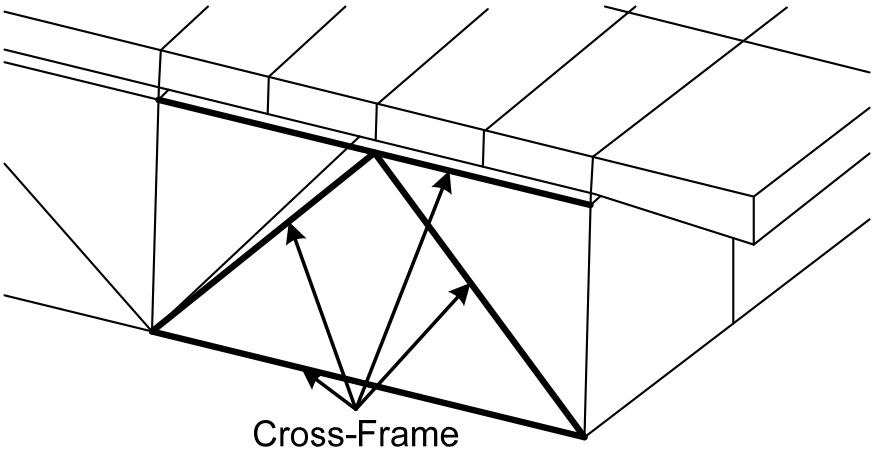


Figure 2.5.25 Truss Elements Used to Model a Cross-Frame

2.5.3.2.5 Foundation Elements

Bridges supported on rigid bearing can be modeled by specifying that the node at the support point be restrained against selected translations and free to rotate (the support would usually be free to rotate). More typically, bearings are modeled with so-called "foundation elements". These dimensionless elements provide for six stiffnesses; three translations and three rotations. The local axes of these elements must be carefully specified.

A foundation element is shown in Figure 2.5.26. The "I" node identifies the element location of action, the "L" node identifies the local y-axis, the "J" node identifies the orientation of the element along the local z-axis, and the "K" node identifies the orientation of the element along the local x-axis. Typically, the z-axis of the foundation element would be the global vertical axis. The x-axis may, for example, be oriented along the girder with the y-axis orthogonal to the girder line. If the bearing is guided, the x-axis of the foundation element may be assigned zero stiffness. The stiffness of the bearing resisting lateral movement would be input as the stiffness along the y-axis. Pier stiffness (Section 2.2.4) may be included in these stiffnesses if the pier is not modeled. If the substructure is explicitly modeled, the foundation element would rest on the pier and would allow the pier stiffness to act on it as well as the superstructure.

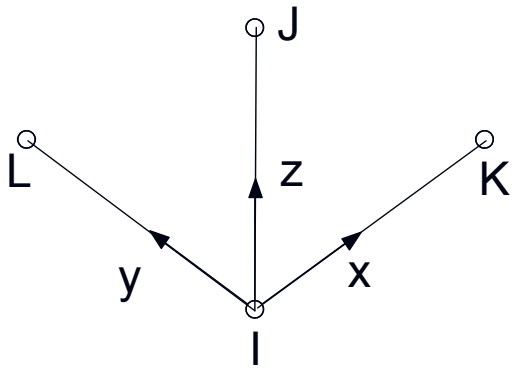


Figure 2.5.26 Foundation Element

2.5.3.2.6 Element Connectivity

The depth of each girder is typically identified by the nodes defining the web elements. A steel girder can be adequately modeled with one or more shell elements representing the depth of the web. The web thickness is input as the thickness of the shell element(s).

The stiffness of very shallow girders may be underestimated if the flange beam elements are common with the top and bottom nodes of the web elements placed at the elevation of the web itself. In girders less than roughly 50 inches deep, it may be desirable to overstate the web depth in order the define the distances between the centers of gravity of the flanges properly (Figure 2.5.27). In the figure, *D* is the assigned web depth.

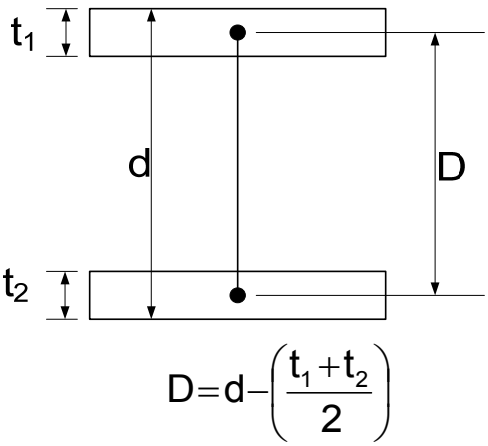


Figure 2.5.27 Overstating of the Web Depth in Shallow Girders

The deck elements are discretized to account for shear lag due to horizontal shear; thus, the deck should be separated into at least two or more isoparametric elements in-between girder lines.

Deck elements must be connected to the girders as discussed in Section 2.5.3.2.1.

Cross-frames are usually used to connect adjacent girders. Since the depth of the webs has been properly represented, the cross-frames can be reasonably represented by attaching them to the top and bottom web nodes. Individual members of the cross-frames may be modeled with either truss or beam elements.

Alternatively, the girders may be connected with diaphragms, which transfer load through bending and shear. Diaphragms may be modeled similar to the girder with a series of shell elements for the web and beam elements for the flanges (Figure 2.5.28). It is important to remember that the diaphragm needs to be divided into enough elements (at least three) along its length to properly represent its deflected shape; often moments in diaphragms reverse sign.

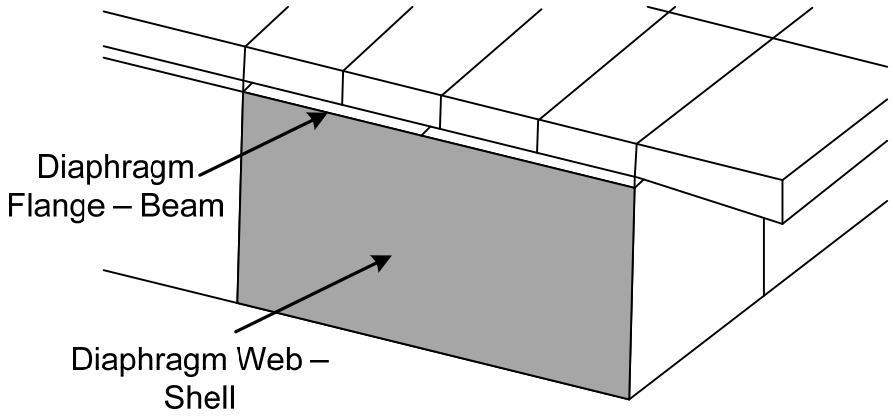


Figure 2.5.28 Shell Elements Used to Model Diaphragm Webs and Beam Elements Used to Model Diaphragm Flanges

2.5.3.3 Boundary Conditions

Bearings can be represented in the 3D model as described in Section 2.5.3.2.5. A bearing with lateral restraint(s) can introduce longitudinal force into the girder and attached diaphragm or cross-frame. Such restraints introduce bending and shear into the girder as well as axial force into the cross-frames. Clearly, it is important that the proper orientation and stiffness of the bearings be modeled.

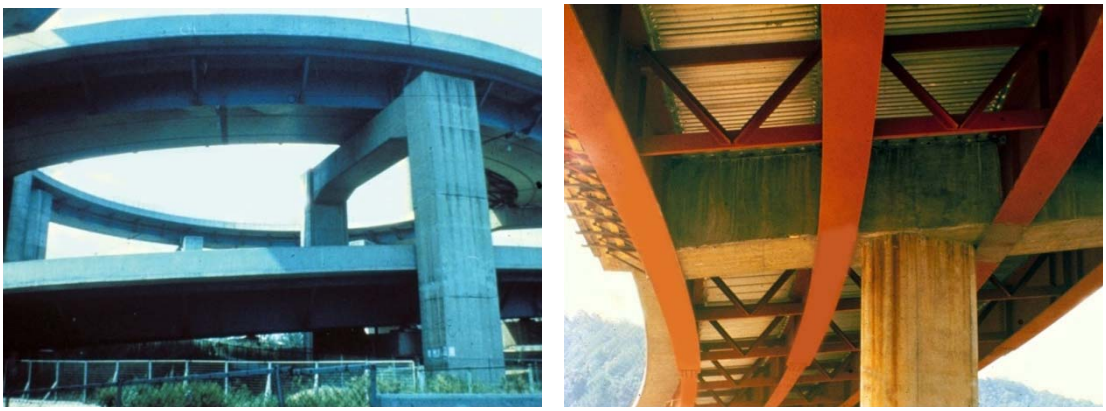
Recognizing the proper bearing arrangement is particularly important for skewed bridges. As discussed in Section 2.2.3, skewed supports can lead to large horizontal forces in the bearings due to gravity as well as thermal loads. These forces can be computed reliably with 3D models. Modeling of a fixed bearing on a pier must recognize the stiffness of the pier (Section 2.2.4).

There is an interaction between restrained bearings on a pier. It is possible the bearings on opposite sides of a skewed pier will have longitudinal thermal forces in opposite directions when the bearings are fixed. In such cases, the longitudinal stiffness of a bearing in the model would be related to the torsional as well as the flexural stiffness of the pier.

Girders may be supported with several types of integral piers. The girders may penetrate an integral pier cap or an articulated pier cap on a pier column. Another type of support is the straddle beam which has two or more supports, with the girders integral with the straddle beam or resting on top of it. The straddle beam may be either simply supported, or if the beam is concrete, it may be integral with the columns forming a bent. However, it is nearly impossible, to properly model these arrangements with bearing stiffnesses alone since there is an interaction between the girder reactions. Stiffnesses of a single bearing cannot properly represent the interactive behavior of the bearings of a multi-girder bridge on a flexible support. The proper way to model these conditions is to explicitly model the straddle beam or entire pier. Modeling the combined girder superstructure and the

substructure is beyond the scope of this discussion, but is an important consideration for this type of bridge.

Figure 2.5.29 Part A shows a concrete straddle beam bent while Figure 2.5.29 Part B shows an integral concrete pier cap. Straddle beams and integral pier caps are discussed further in Section 3.1.3.3. A Case Study involving a 3D investigation of an I-girder bridge with a straddle beam is presented in Section 2.5.6.



Part A **Part B**

Figure 2.5.29 Alternative Supports
A) Concrete Straddle Beam; B) Integral Concrete Pier Cap

2.5.3.4 Loads

2.5.3.4.1 Dead Loads

2.5.3.4.1.1 Structural Steel Weight

Structural steel weight is easily modeled using body-weight of the modeled members. Thus, the steel weight includes the cross-frames as well as the girders. The weight of detail steel such as stiffeners and splices is not included unless specifically included in the model. It can be easily accounted for by changing the density of the steel. If the steel is to be painted, an additional three percent can be added to the steel density to account for the weight of the paint.

It might be noted that the moments, etc. from the analysis of steel weight are based on the assumption that the entire structure is erected in the no-load condition, unless specifically investigated otherwise. Curved bridges and those with skewed supports are often particularly difficult to erect because they deform during the erection process. If the steel is properly detailed to fit in the no-load condition and it is erected without modifications, such as reaming bolt holes or providing oversized or

slotted holes, it can be reasonably assumed that the stresses in the steel frame due to self-weight are roughly correct. This subject is treated in depth in Section 4.1.3.

2.5.3.4.1.2 Concrete Deck Weight

Weight of the wet concrete of the deck may be applied to the non-composite model with concentrated loads at the nodes representing the tops of the girders. The concrete is usually assumed to have no stiffness. Alternatively, deck weight may be specified as a uniform load, but that will be converted to a series of concentrated loads applied at the nodes and perhaps with some nominal end moments. The deck may be modeled using the self-weight of the deck, but that has the disadvantage of dealing with some assigned stiffness. It would be incorrect to use the concrete stiffness, which would distribute the weight differently than if it were wet with no stiffness.

The concentrated load applied to each girder top node is determined by the tributary area of deck associated with the distance between girder nodes and the girder spacings. The action of the cross-frames tends to distribute the load so that the girders deflect nearly equally on a straight bridge with right supports. If all the girders are of equal or nearly equal stiffness in these bridges, the deck weight will be carried nearly equally by all the girders via the restoring forces in the cross-frames. In the case of most skewed or curved girder bridges, the distribution of the deck weight is rather complex and must be ascertained by analysis. However, it is always distributed in a manner consistent with the restoring forces in the cross-frames. This is one of the important functions of the cross-frames.

Where concentrated loads are used to apply the deck weight, the discretization of the model must be sufficient to ensure that the series of concentrated loads applied to the girder nodes will be refined enough to represent the uniform load. This issue can be seen in the following example shown in Figure 2.5.30. The maximum moment due to a uniform load on a simple beam is $1/8w\ell^2$; the maximum shear is $w\ell/2$.

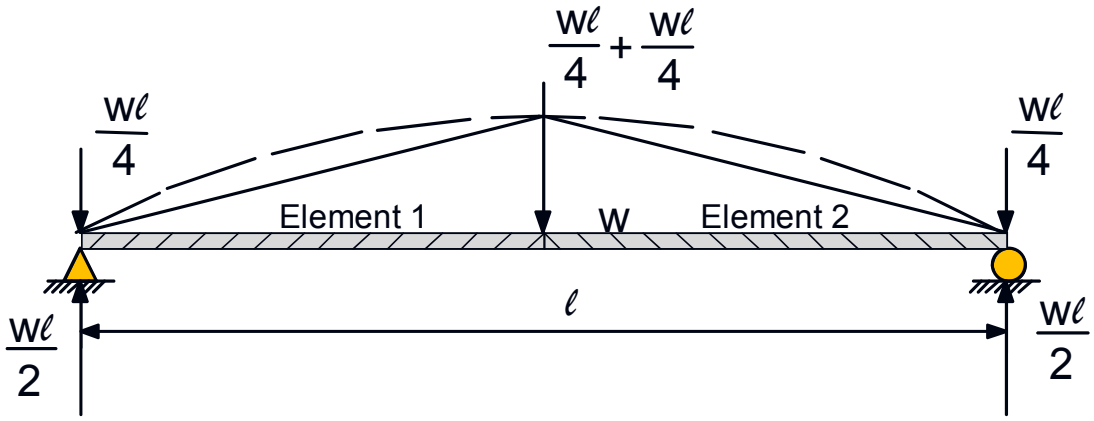


Figure 2.5.30 Discretization of Model for Deck Weight Using Two Elements – Bending Moment

Representing a span with two beam elements with half of the load applied in the center and a quarter of the load applied at each end gives a maximum moment of

$$M_{max} = \left(\frac{w\ell}{2} * \frac{\ell}{2}\right) - \left(\frac{w\ell}{2} * \frac{\ell}{4}\right) = \frac{w\ell^2}{8}$$

Equation 2.5.41

However, the moment diagram is parabolic for the uniform load and triangular for the single concentrated load, as is evident in Figure 2.5.30. The moment along the span at locations other than at the center of the span can be significantly in error depending on the length of the two elements.

As illustrated in Figure 2.5.31, the maximum shear is in error by 50 percent in this case since the loads at the ends of the span are applied to the nodes and not to the beam. Obviously, a more refined model is required.

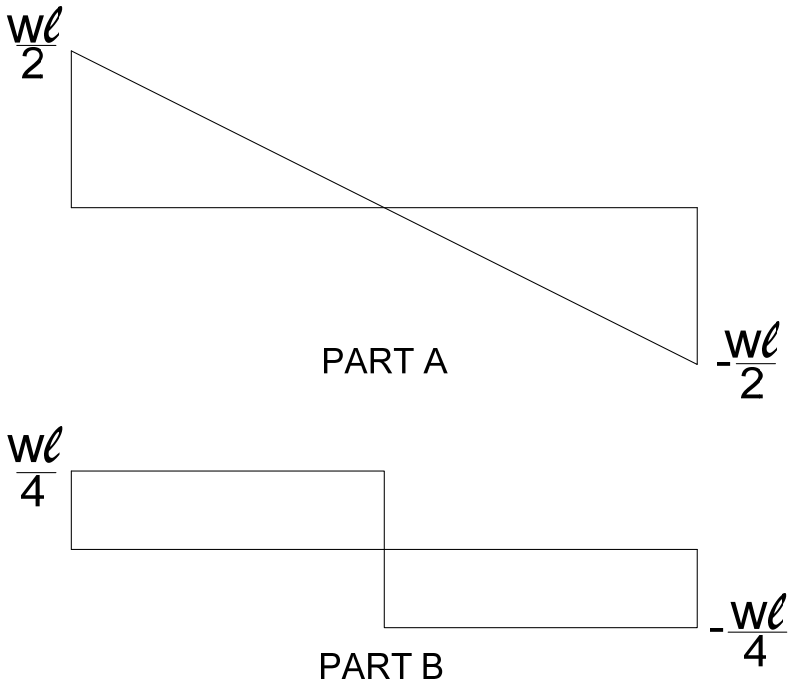


Figure 2.5.31 Shear Diagram for Deck Weight
A) Uniform Load; B) Concentrated Loads Using Two Elements

The weight of deck forms needs to be considered if the forms are to be permanent. This weight can be applied directly to the girders as concentrated loads as done for the deck. This can be accomplished by specifying an increase in the non-structural deck thickness to be used to compute the deck loads applied to the top girder nodes. Recall that these forms exist only between flange edges in the interior bays.

If temporary forms are planned and it is desired to consider their weight in the analysis, their weight can be introduced in a similar manner as for the permanent type. However, in this case, it is necessary to apply a reverse load to the composite section to represent removal of the forms. This consideration is usually not made except in extreme cases.

Deck overhang bracket loads may be addressed more rigorously by the addition of overhang brackets to the 3D model. These additional members receive the weight of the overhang forms, a portion of the deck overhang weight, the weight of the screed rail, the weight of any walkway and railings and perhaps the weight of the deck-finishing machine. As discussed further in Section 3.2.3.3, these loads subject the outside girders to a vertical load and a lateral couple or torque. The cross-frames also act with these loads. The 3D model is able to not only provide the resulting actions in the girder and cross-frames, but is also able to provide vertical and lateral deflections. It is not required to model each overhang bracket; some judgment is required to ensure that adequate nodes are provided to allow for a reasonable number of brackets between cross-frames.

Figure 2.5.32 shows overhang brackets added to a model of a simple span with skewed supports and staggered cross-frames. This extra investigation was undertaken because the Contractor's Engineer was concerned about the effect of the rather large overhang, over four feet, on the fascia girders. The first analysis included a portion of the overhang concrete, the walkway and railing and screed rail. The effect of the finishing machine was also investigated. Small additional diaphragms were added in the exterior bays when the Contractor's Engineer decided that the fascia girders would rotate excessively, and that the lateral flange bending caused by the overhang bracket loads would cause excessive lateral flange bending stresses unless the additional diaphragms were used.

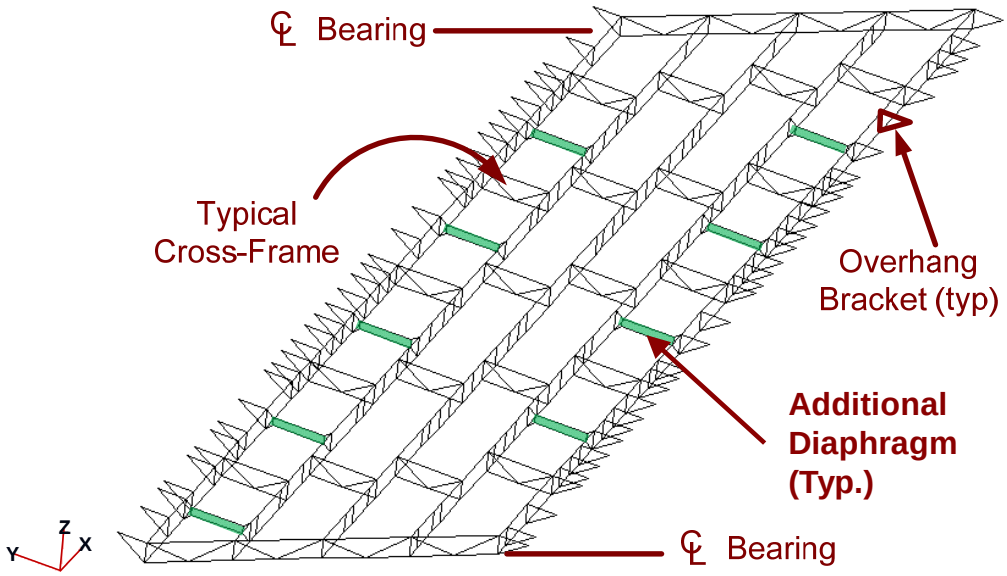


Figure 2.5.32 Overhang Brackets in a 3D Model

Deck staging, as shown in Figure 2.5.33, is investigated by initially assigning the first cast of the deck to the non-composite model. Subsequent casts are assumed to be placed with the concrete in the preceding casts assumed hardened and acting compositely with the girders. These analyses are discussed further in Section 3.2.3.2.

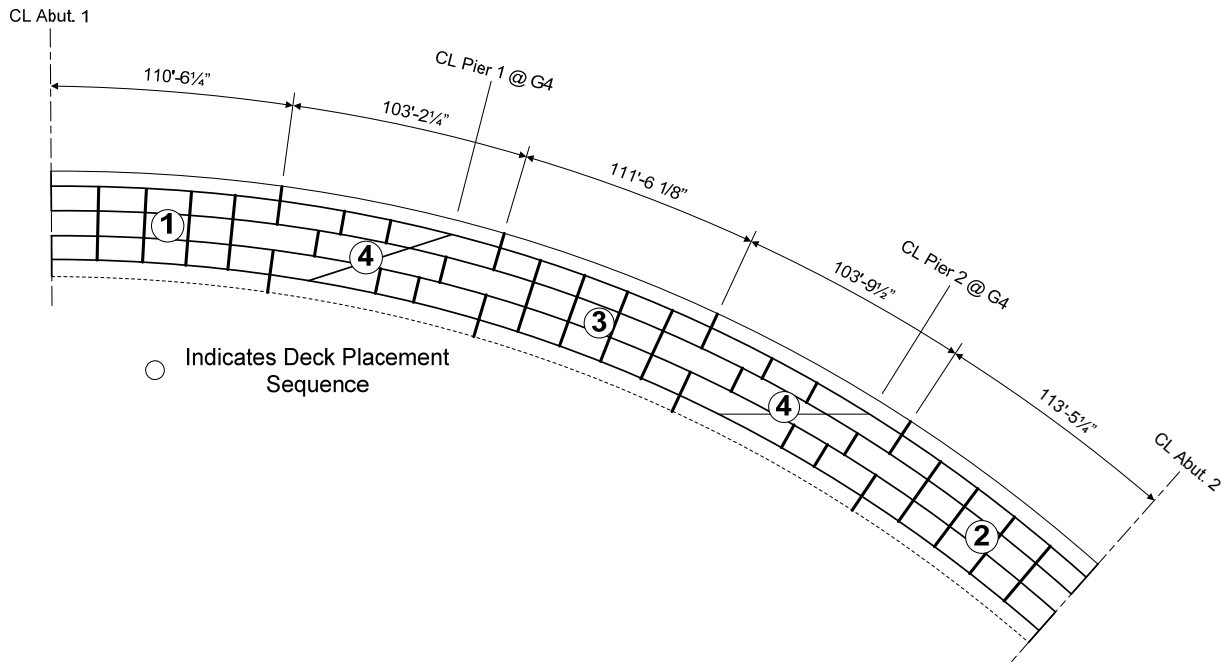


Figure 2.5.33 Deck Staging

The tensile force in the composite deck at the end of an earlier cast due to subsequent deck casts can be determined. This force will be transferred from the deck through the shear connectors to the steel girder. Sufficient shear connectors should be present at this location to handle this force transfer. Otherwise, there is the potential of crushing of the fresh concrete around the studs or damage to the studs themselves.

Some contractors have reported that the deck pans and perhaps the rebar cage act compositely with the girders affecting the behavior. If these effects are of interest, a shell element might be introduced to represent these actions.

2.5.3.4.1.3 Superimposed Dead Loads

Superimposed dead loads applied to the composite section can be properly located on the deck of a 3D model. For example, barrier loads (DC_2 loads) may be placed at the edges of the deck where they are actually located. The traditional approach has been to distribute these loads uniformly to all the girders. Previous specifications never condoned this practice. The provisions called only for curb and railing loads to be uniformly distributed. They did not permit barriers or sound walls, which are much heavier than curbs, to be uniformly distributed. Proper consideration of the location of these loads usually results in the loads causing larger moments in the exterior girders and smaller moments in the interior girders. Barriers or sound walls on large overhangs have even been found to cause reverse loads on the interior girders. The computed reacting forces in the cross-frames are also increased when the barriers are properly located on the edge of the deck. Similarly, utility loads may also be applied at their proper locations.

Future wearing surfaces and deck overlays can be applied to the model as uniform loads acting over the roadway deck area, as a series of concentrated loads, or by inputting an artificial density of the hardened concrete deck.

2.5.3.4.2 Live Loads

Live loads may be applied on the deck of the model or to influence surfaces built from analyses of the model. The influence surface or influence line is a more efficient approach. Special software may be used to accomplish this or loads may be placed by hand—a tedious assignment. The construction of influence surfaces is accomplished by applying a unit load to selected deck nodes. Generally vertical loads are used for gravity loads, although influence surfaces in other than the vertical directions may also be developed. From the individual analysis for each of these loads, responses are found for the actions of interest. Then, the responses are assembled into sets of data; each forming an influence surface.

Loading the influence surface is typically performed with software separate from the finite element solver. Wheel loads are positioned according to the specification rules for live load placement (Section 2.1.4.1) in order to compute the maximum and minimum magnitudes of the desired effect. Lanes of live loads need not necessarily be placed side-by-side within their lanes. This powerful analytical tool can replace wheel-load distribution factors (and associate correction factors). The generation and loading of influence surfaces is discussed in greater detail in Section 2.1.4.

As discussed further in Section 1.3.2.3.6, wheel-load factors can be modified to account for the vertical effects of centrifugal force and superelevation. These modified wheel loads increase or decrease accordingly the wheel loads that are applied to the influence surfaces of curved alignments to account for vertical centrifugal force effects.

2.5.3.4.3 Wind Loads

The application of wind loading to a 3D model of a bridge superstructure is similar in principle to the application of the deck load. Typically, it is assumed that the wind is unidirectional. This means that it is applied at differing angles to horizontally curved bridges as a series of concentrated loads applied in a single uniform direction to the projected area of the bridge. The projected area of the bridge includes the sum of the projected girder areas taken perpendicular to the assumed wind direction. Superelevation and curvature are considered in determining the exposed area and wind load. Areas of the deck and barrier are, of course, included. The overturning wind can be applied in a similar manner.

Wind on the steel frame has been found critical in some recent bridges and increasingly, Owners are requiring designers to check wind on the steel frame after the deck pans are installed and before the deck has hardened. The lateral wind can cause excessive deflections in these cases if there is no lateral bracing. The lateral

strength of the girders alone resists the wind load. Large lateral deflections can occur causing damage to the pans, girders and bearings. The potential of uplift prior to the deck concrete being placed is also a construction check. The critical direction of wind is usually not obvious and several angles of attack are often required to determine the critical condition.

The 3D model recognizes the girder depth, which permits wind loads to be applied to the top and bottom of the girder. These loads are typically applied as concentrated loads to the exterior windward girder at the top and bottom nodes along the girder. Each individual load, computed from the wind pressure and distance between nodes and structure height, is resolved into global x and y components as illustrated in Section 1.3.2.4.

The 3D model provides proper recognition of the horizontal diaphragm shear action of the concrete deck in resisting wind loads applied to the bridge in its final condition. Investigation of the forces due to wind in cross-frames and lateral bracing is also possible.

Wind on live load creates an overturning force on the vehicle similar to the effect of centrifugal force on vehicles and may be handled in a similar to that for centrifugal force, except it is also applied to the lane load instead of only to the truck loading in the case of centrifugal force. Of course, there is also a lateral force that must be considered. The calculation of wind load on the structure (WS) and wind load on the live load (WL) is discussed further in Section 1.3.2.4.

2.5.3.4.4 Thermal Loads

Temperature changes usually cause thermal forces in the superstructure and substructure. Thermal forces are often larger in curved bridges and bridges with skewed supports. These forces are a function of the bearing orientation and the stiffness of the substructure, as well as the magnitude of the temperature change. A uniform temperature change is usually assumed. The different specified coefficients of thermal expansion for concrete and steel can be taken into account. For normal-weight concrete, the coefficient of thermal expansion, α, is 6.0 x 10^{-6}/°F and for steel, α is 6.5 x 10^{-6}/°F. The 3D model permits a different temperature to be applied to the deck. Most 3D packages also allow a thermal gradient to be investigated. Uniform temperature change and thermal gradient are discussed in Section 1.3.2.5.

2.5.3.5 Steps – Analysis and Stress Investigation of Girder Bridges

A summary of the steps required to analyze a skewed and/or curved girder bridge are as follows:

2.5.3.5.1 Build Model

1) Build (input) nodes along the girder lines according to geometry

2) Build girder information and additional nodes to recognize top and bottom of the girders
3) Build the deck information including overhangs and thicknesses
4) Build cross-frames and bearings
5) Define material properties and dead loads
6) Define where influence surfaces are needed

2.5.3.5.2 Analyze Model for Dead Load

1) Analyze non-composite model
2) Analyze composite model
3) Post process raw results to get moments, shears, etc. at girder nodes (special software)

2.5.3.5.3 Analyze Model for Live Load

1) Apply vertical unit loads to deck
2) Solve model for each individual unit load; perhaps several hundred load cases
3) Post process raw results to get moments, shears, etc. at girder nodes (special software)
4) Assemble results into influence surfaces for each response at the loaded nodes
5) Apply the specified live loads to the influence surfaces according to the specification rules for live-load placement to obtain the requested actions (special software)

2.5.3.5.4 Checking

Finally, a stress check of the model sections is made. This may be made with special software or by hand. Alternatively, the check can be made using interactive software with the analysis results concatenated with the model to investigate the design against the analysis results.

This checklist provides some methods to confirm analysis results for a 3D refined analysis.

Some suggested checks of the input are as follows:

- Check geometry nodal coordinates with independently determined coordinates
- Plot model
- Check girder plate sizes and lengths
- Check cross-frame/diaphragm configuration and sizes
- Check lateral bracing configuration and sizes

- Check out-to-out deck width, roadway width, girder spacings, deck overhang lengths, and positions of parapets, sidewalks and utility loads (if present)
- Check bearing constraints

Some suggested checks of the output are as follows:

- Sum vertical dead load reactions for each dead load case and compare to a hand calculation of the expected sums.
- Analyze classical examples with known solutions to confirm that the software is giving proper results and that the user understands the output. This might include a simple beam model built using beam elements for the flanges and shell elements for the web.
- If the software gives moments and shears, the moments in a multiple-girder model at a section in an end span can be checked using statics. That is, the total dead load moment in all of the girders at that section should equal the sum of each dead load reaction times its distance to that section minus the dead load applied to the corresponding girder between that section and the reaction times the distance to the center of gravity of the load from that section.

2.5.4 Investigation of a 3D Finite Element Beam Example

The following 3D finite element beam example will demonstrate some important benefits of 3D modeling through the use of a series of relatively simple illustrations.

Single I-Girder Model

Figure 2.5.34 shows a 3D finite element model of a single straight I-girder, with a simple span of 72 feet. The girder web is 6 feet (72 inches) deep with a web thickness of ½ inch. Top and bottom flanges are each ¾ inches by 16 inches. The moment of inertia of the girder about its major axis is 46,656 in^4. The area of the girder is 60.0 in^2.

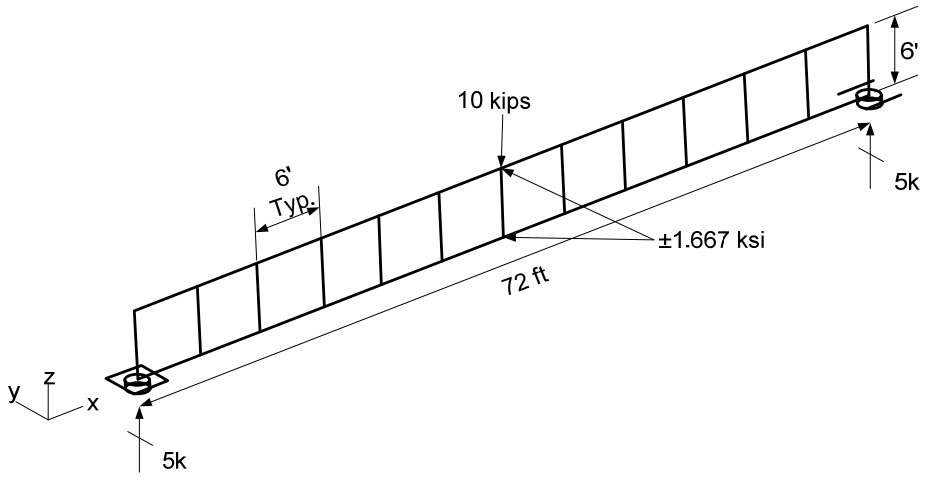


Figure 2.5.34 Single I-Girder Model

The model is made with twelve 6-foot-long shell elements representing the web and twelve 6-foot-long beam elements representing each flange. The beam elements (not shown) are attached to the web nodes. End reactions are each modeled with a foundation element. The girder is longitudinally restrained at one end. Lateral restraining foundation elements (not shown) are added to the top of the girder at its ends to provide stability, but carry no load. These restraining elements are assigned lateral stiffness, but no vertical stiffness or restraint.

A 10-kip concentrated load acting downward (in the minus z direction) is applied to the top of the girder at midspan. The effect of girder self-weight is not considered. The maximum moment at midspan equals an end reaction (5 kips) times half the span length (36 feet), or 180 kip-feet. The maximum flange stress in vertical bending is:

$$f = \pm\frac{180(12)(36.0)}{46{,}656} = \pm 1.667 \text{ ksi}$$

The 3D analysis gives flange stresses (longitudinal) at mid-length of each element. The top and bottom stresses of the symmetrical section are equal but opposite in sign at each longitudinal location. Figure 2.5.35 shows a plot of the bottom flange tensile stresses at the mid-length of each flange element from the analysis. The midspan stress can be computed using the knowledge that the moment (stress) varies as a straight line. The theoretical midspan stress is found by extrapolation. This extrapolation concept can be used to find the stress at point where the moment curve is discontinuous, including at the cusp of influence lines. In this case, extrapolation leads to a midspan stress of 1.667 ksi as computed above. Note that if a simple curve fit were used to obtain the maximum stress, it would be underestimated by approximately 8 percent. Longer elements would cause a greater error.

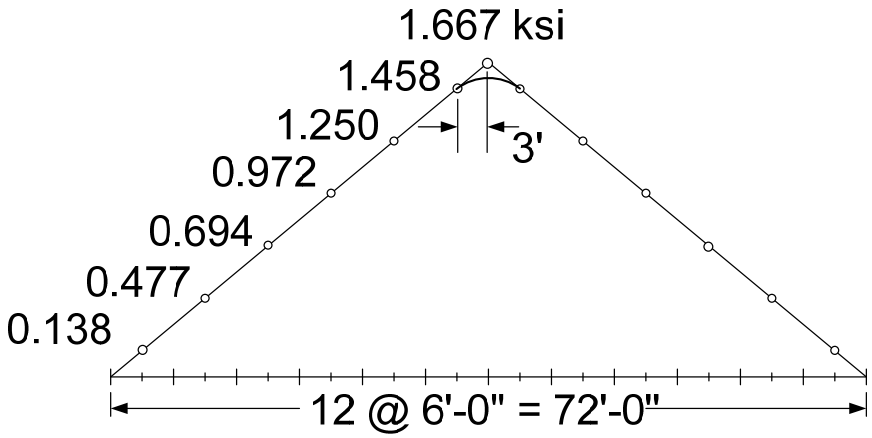


Figure 2.5.35 Stresses at Mid-Length of Each Element of the Single I-Girder Model

Simply stating that a 3D model is used does not necessarily ensure that the "correct" answers are always obtained; significant engineering judgment and knowledge must be employed to ensure proper modeling and correct interpretation of the analysis results.

The example is modified as shown in Figure 2.5.36. The model still has 6-foot long elements, except at the point where the concentrated load is applied where 2-foot long elements are introduced on either side of the load. Analysis of this model yields major-axis bending stresses of ±1.60 ksi at the center of the 2-foot-long flange and web elements, which is much closer to the theoretical maximum stress of 1.667 ksi.

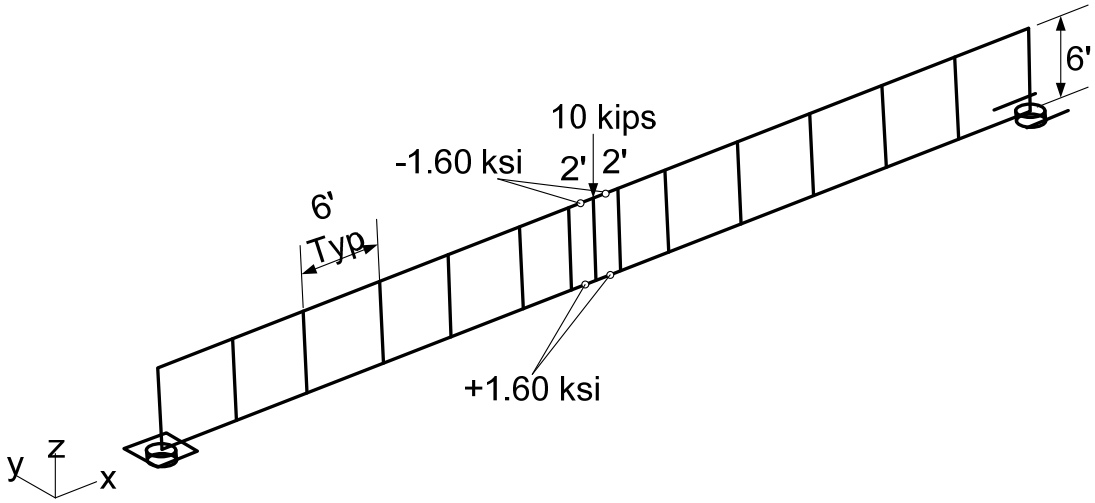


Figure 2.5.36 Addition of Shorter Elements to the Single I-Girder Model Adjacent to the Load

Effect of Bearing Restraint

The effect of bearing restraint will next be examined in the example, which is again modified by restraining both bearings in the longitudinal direction as shown in Figure 2.5.37. A simple-span straight girder has been employed here to demonstrate the effect in a simple fashion. A 2D grid model cannot recognize the longitudinal restraint of the bearings since the bearings in such models are located at the neutral axis of the girder, which would not change length under vertical loading. Longitudinal restraint at the bearings in this case prevents elongation of the bottom flange.

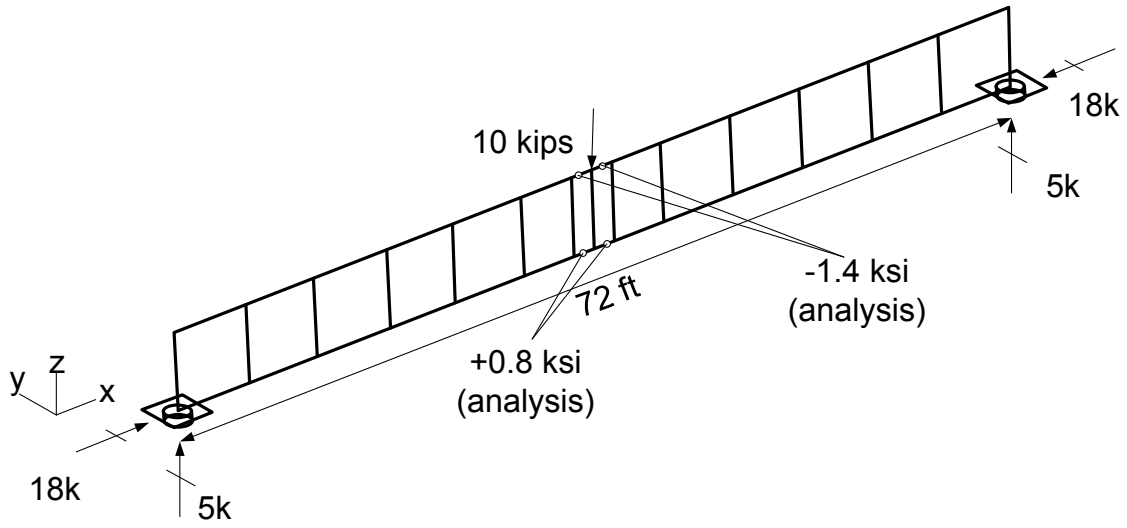


Figure 2.5.37 Single I-Girder Model with Longitudinally Restrained Bearings at Each End

Analysis of the longitudinally restrained 3D model for the 10-kip vertical load at midspan reveals an 18.0 kip longitudinal reaction at each end of the girder (Figure 2.5.37). The longitudinal reaction forces are caused by the restraint of the tension portion of the girder.

The stresses at mid-length of the 2-foot-long elements are –1.4 ksi in the top flange and +0.80 ksi in the bottom flange of the model shown in Figure 2.5.37. The longitudinal reactions cause a "hogging" moment superimposed on the vertical bending moment leading to lower bottom flange stresses. The "hogging" moment induced in the girder due to the longitudinal reactions is:

$$M = 18\left(\frac{6}{2}\right) = -54 \text{ k} - \text{ft}$$

where 6/2 = 3.0 feet is the distance from the longitudinal reaction to the neutral axis of the girder. This "hogging" moment creates bending stresses in the flanges of:

$$f_b = \pm\frac{-54(12)(36.0)}{46{,}656} = \pm 0.5 \text{ ksi}$$

The axial compressive stress in the girder induced by the reactions is:

$$f_{axial} = \frac{-18}{60.0} = -0.3 \text{ ksi}$$

Hence, the total stress in the bottom flange is:

$$f_{bot} = 1.60 - 0.5 - 0.3 = +0.8 \text{ ksi}$$

The top flange stress is:

$$f_{top} = -1.60 + 0.5 - 0.3 = -1.4 \text{ ksi}$$

These stresses are confirmed by the analysis results.

Effect of Composite Deck on "Hogging"

Next, assume for the same girder that the effective top flange area is five times the area of the bottom flange, which is unchanged, to simulate the effect of a composite deck. The neutral axis is raised further from the bearing, increasing the effect of the longitudinal restraints. This case is depicted in Figure 2.5.38. The longitudinal reaction in this case is 16.4 kips. Here the top flange stress is reduced to –0.45 ksi because of the area of the "deck". The bottom flange stress is reduced to +0.67 ksi. For the case of a five-to-one ratio of flange areas and a longitudinal restraint at only one end of the girder, the top flange stress is –0.51 ksi and the bottom flange stress is +1.36 ksi (the longitudinal reaction is zero). The additional longitudinal restraint at the other end of the girder results in a significant stress reduction in the bottom flange of approximately 50 percent. A poorly functioning bearing can create this effect.

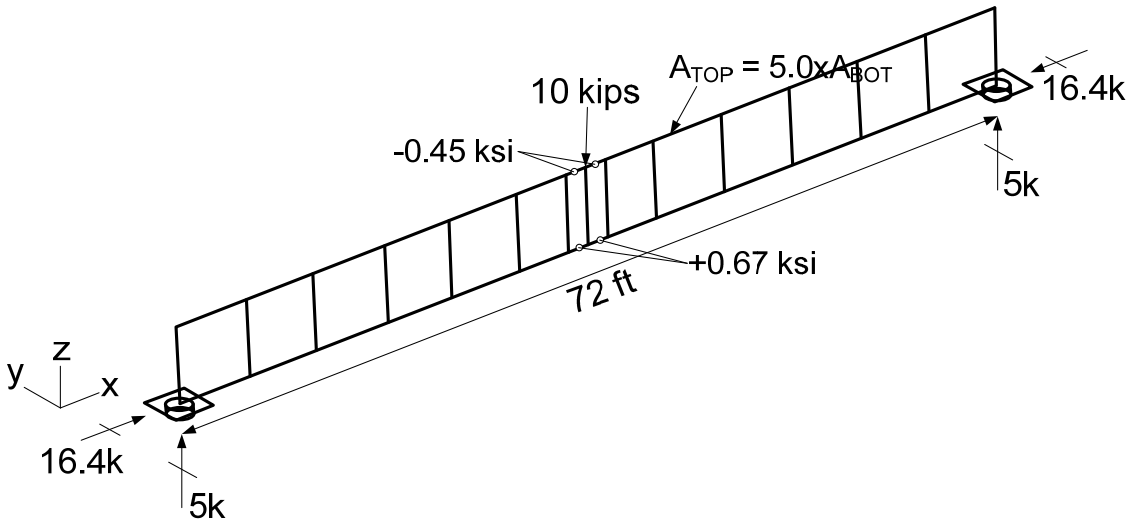


Figure 2.5.38 Single I-Girder Model with a Larger Effective Top Flange Simulating the Concrete Deck

One situation where this condition becomes important is when a bridge is load tested and a stress of 50 percent of the unrestrained stress is measured. If the load rating is performed based on the test stress, an unconservative estimate of the capacity of the bridge would be made. If the bearing restraint is caused by a locked-up bearing, there is no certainty that the constraint will not break free under higher live loads than the test load. Should this happen, an increase of 100 percent in the projected live load stress would occur. In this case, the load testing would have been a disservice to the evaluation of the condition and capacity of the bridge.

The effects of bearing restraint are particularly important in skewed and curved bridges and can be recognized with a 3D analysis. Constraint of the bearings on skewed bridges typically creates longitudinal forces in the girders, as demonstrated in Section 2.2.3.

Two-Girder Model

A second girder is added to the single-girder model with no deck as shown in Figure 2.5.39. Note that only half of the model is shown. Bearing restraints at the end not shown are not restrained longitudinally in this case. The second girder is parallel to and 10 feet away from the first girder. The two girders are connected with three cross-frames; one at each bearing and the third at midspan. Cross-frame members are modeled with truss elements. All cross-frame members are assigned an area of 5.0 in^2. Cross-frame member forces are computed in the model and the behavior is accurately depicted.

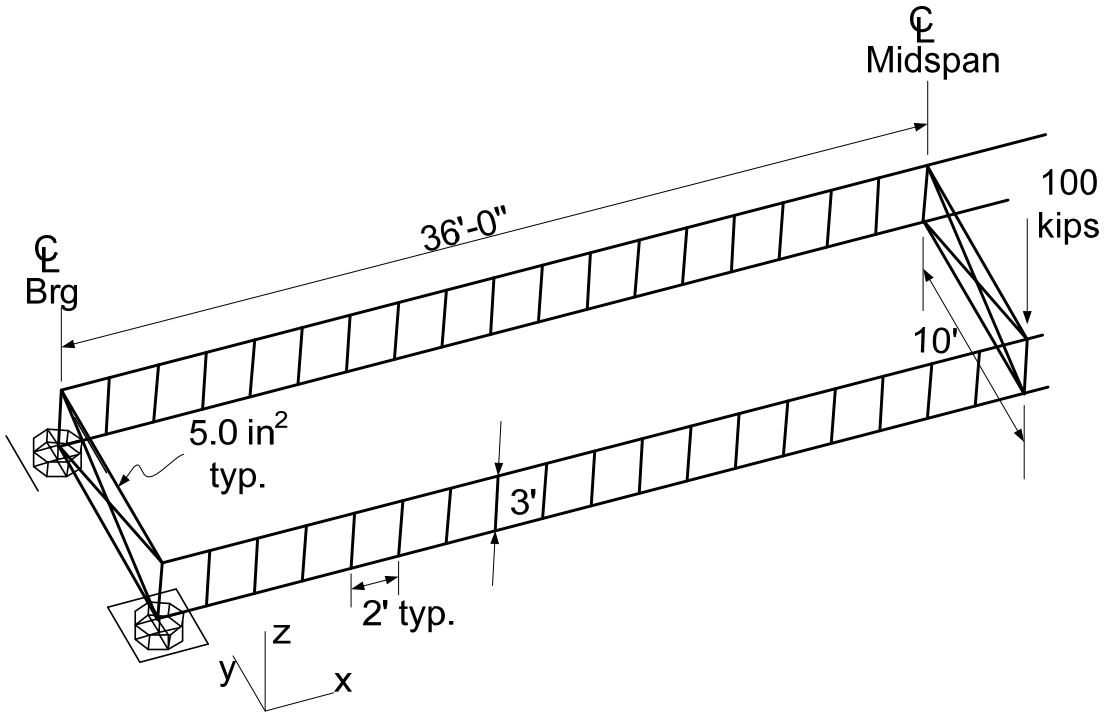


Figure 2.5.39 Two-Girder Model (No Deck)

Note that the depth has been reduced to 3 feet and all girder elements are 2 feet long. A 100-kip vertical load is applied at the top of the right (near) girder at midspan. Boundary conditions are as follows: all supports (bearings) are rigid vertically and are free to rotate about the three global axes. The bearings at the left end of both girders are restrained longitudinally. The near (loaded) girder is restrained transversely at both ends. The bearing constraints at the left end are shown in the figure.

By inspection, external equilibrium requires that the vertical reactions of the far girder be zero. However, the cross-frame at the center of the span transfers some load from the loaded (near) girder to the far girder. However, statics demands that any vertical load so transferred must be transferred back to the near girder through the end cross-frames, since the vertical reactions under the far girder must be zero. In fact, the analysis shows that essentially no vertical load remains in the far girder; the shear in the web elements of the far girder is negligible. These forces on the girders are shown in Figure 2.5.40.

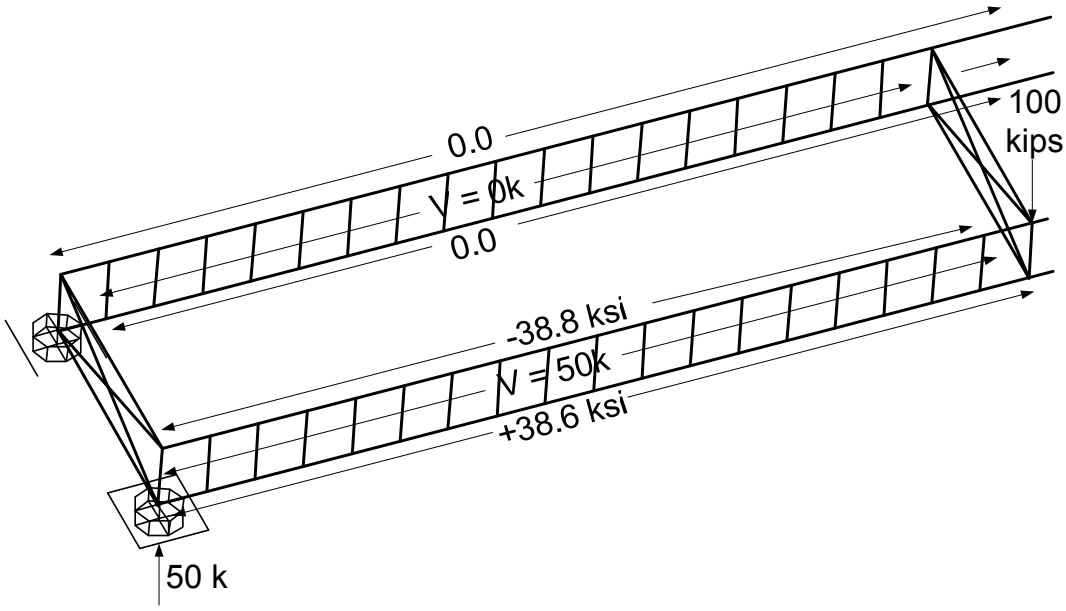


Figure 2.5.40 Two-Girder Model -- Web Shears and Girder Flange Stresses (No Deck)

The maximum vertical deflection of the near girder is 4.6 inches. To accommodate that deflection, both girders deflect laterally at the top and bottom approximately ±1.4 inches (i.e. rotate out-of-plumb) at the point of the load. This rotation is related to the forces reported in the cross-frames. This action also causes lateral flange bending moments of +-8.5 kip-feet in the top and bottom flanges of both girders at midspan. Vertical bending stresses and shear in the far girder are negligible. Computation of the correct girder rotations would be extremely difficult to obtain correctly from a traditional 2D grid model.

It is interesting to note in Figure 2.5.41 that the signs of the forces in the end cross-frame diagonals are reversed from those in the center cross-frames. The net vertical

force in the end cross-frame diagonals is approximately half of the similar total in the center cross-frame diagonals. This is necessary since the vertical reactions in the far girder must be zero.

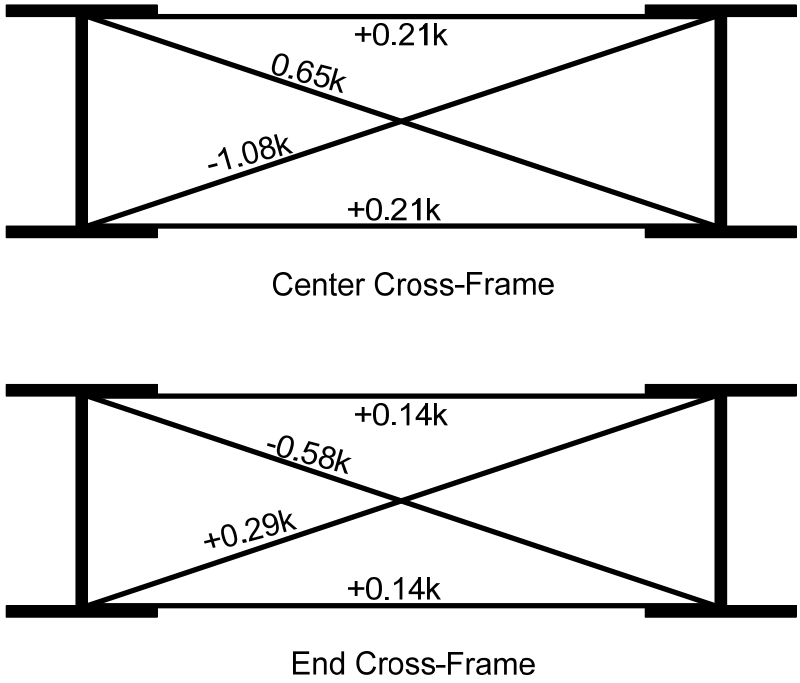


Figure 2.5.41 Two-Girder Model Center and End Cross-Frame Forces (No Deck)

Two-Girder Model with Composite Deck

An 8-inch-thick composite concrete deck is next added to the two-girder model as shown in Figure 2.5.42, with the same 100-kip load applied at midspan of the near girder.

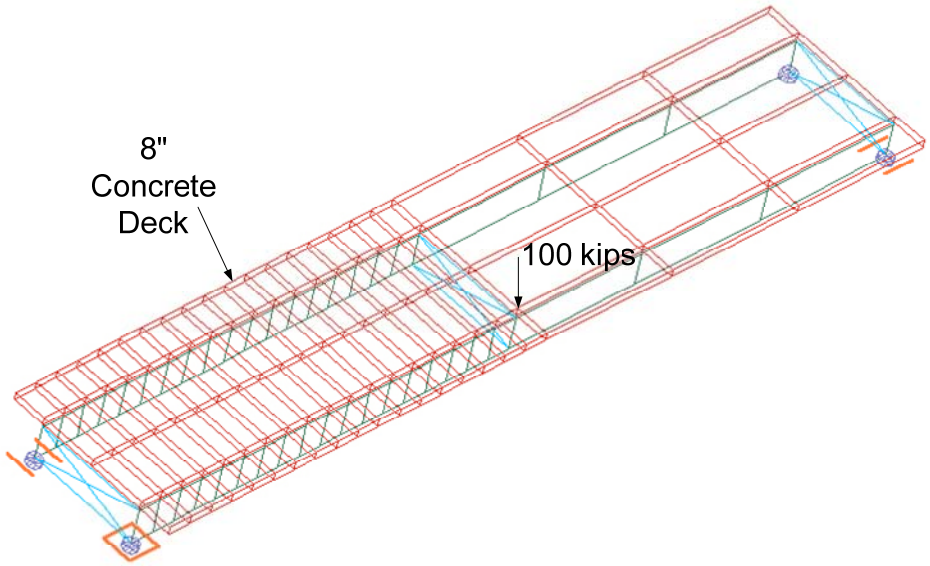


Figure 2.5.42 Two-Girder Model with a Concrete Deck Added

From the analysis, the maximum vertical deflection of the loaded girder is 1.23 inches at midspan. The far girder deflected vertically 0.37 inches at midspan. The bottom of the girders deflected laterally less than 0.23 inches at midspan. Lateral flanges moments in the bottom flange of both girders decreased.

Both girders acted more similarly in this case, which demonstrates the ability of the diaphragm action of the deck to transfer the torsional load by horizontal shear. This behavior is observed because the deck is located away from the neutral axis of the girder. This would not have occurred in a traditional 2D grid model where the deck would be located at the neutral axis of the girders and would not have generated any horizontal shear. The correctness of even offset girders would be questionable in a 2D model that was used to investigate this behavior.

As shown in Figure 2.5.43, in the model with the composite deck (deck not shown), the bottom flange stress in the far girder is approximately 25 percent of that in the near girder. Computed shears in kips for the web elements are given inside each web element.

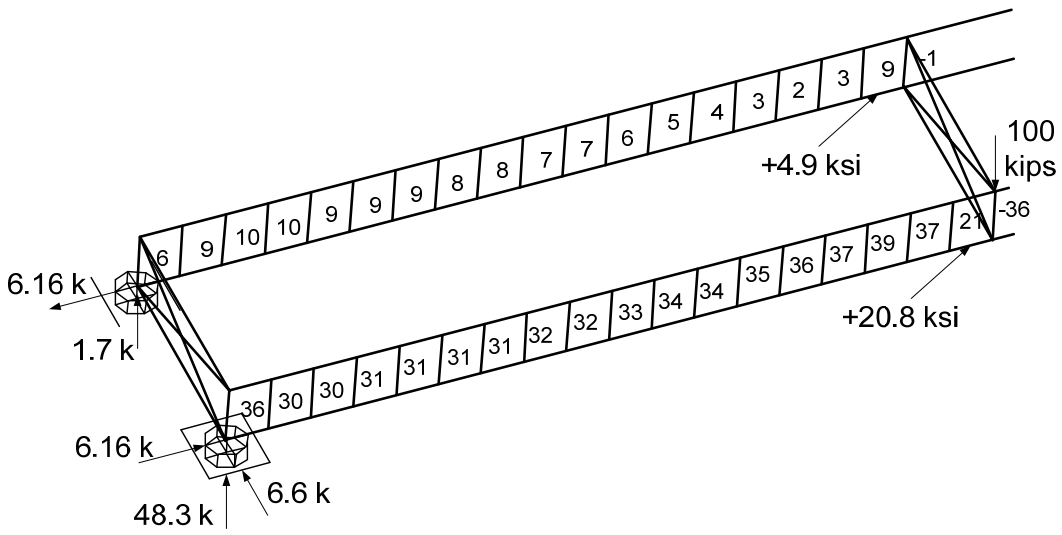


Figure 2.5.43 Two-Girder Model w/ Deck -- Web Shears and Girder Flange Stresses (w/ deck not shown)

The relationship between the shears in the two webs is irregular. Statics indicates that the total shear in the structure is a positive 50 kips in the half-structure shown, and a negative 50 kips in the other half-structure not shown. However, at no point is the sum of the two web shears in any two webs at any section equal to 50 kips. Further, the computed cross-frame forces shown in Figure 2.5.44 are not large enough to transfer the shear in the far web back to the reaction under the near girder, as evidenced by the presence of shear in the far girder. It must be deduced that the deck is carrying the remaining shear. Investigation of the shear in the deck (not shown) confirms this deduction.

The total web shear is only 30 kips just to the left of the load; 20 kips less than the total shear in the left side of the structure. The large applied load creates a local perturbation in the web shears. Deck shear has not distributed the load in the first pair of web elements and is carrying a large portion of the shear. Horizontal shear has distributed 10 kips of the shear to the webs in the next pair of elements. It is of interest to note that simply using the web shear to design the webs would not be correct. The specifications require that girder webs be designed to carry the total shear. Progressing down the bridge to the left, deck shear lag has eventually transferred about 10 kips to the far web, while the shear in the near web has remained about the same. Thus, the total shear in the two webs is 40 kips. The total of 40 kips remains nearly constant over the majority of the span as the deck carries the other 10 kips. At the end of the girder, about 6 kips remains in the far web. While the reaction under the far web is 1.7 kips, the rest of the load was transferred out through the end cross-frame and the deck.

Figure 2.5.44 shows the cross-frame forces for the center and end cross-frames for the case with the composite deck. The forces in the end cross-frame are not nearly large enough to transfer the 4.3 kips from the far web to the near girder reaction.

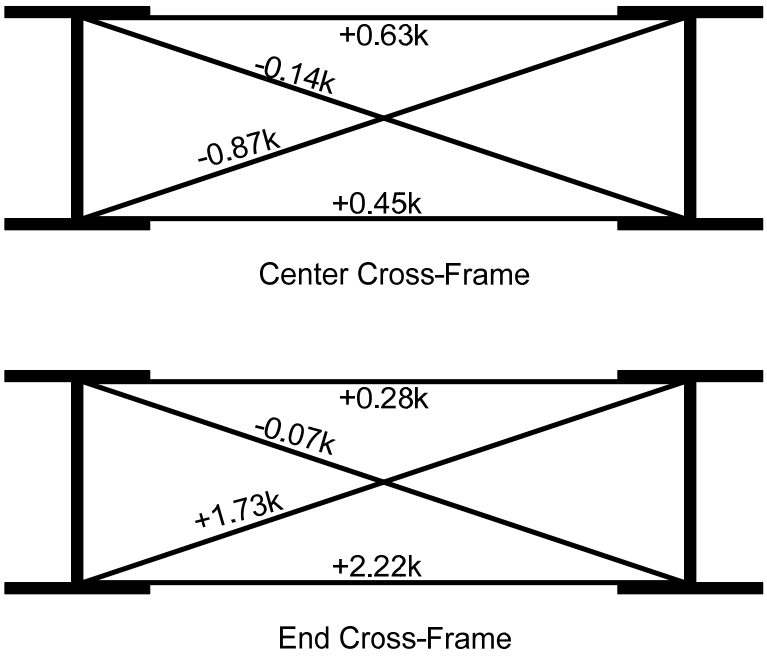


Figure 2.5.44 Two-Girder Model Center and End Cross-Frame Forces (w/ Deck)

It is important to note that the relatively small end cross-frame forces indicate that the transfer of the 6 kips in the far girder web at the end support was largely accomplished through the deck.

The amount of shear in the far web increases from its minimum of 2 kips to a maximum of 10 kips and back to 6 kips at the end. These changes are due to horizontal and vertical deck shear. Vertical deck shear changes over the span due to shear lag, or the shear deformation of the concrete. Even with the far girder resisting up to 20 percent of the vertical load, its vertical reactions were still zero because the end cross-frames and deck shifted most of the load back to the near girder in an attempt to satisfy statics. The reason that “simple” statics does not appear to be satisfied is that the torsional stiffness of the two girders, cross-frames and deck shifted some 3.4 percent of the load to the far reaction.

The longitudinal end reactions of ±6.16 kips further confirm the torsional action of the model. These reactions cause a torque of 6.16 x 10 ft = 61.6.k-ft about the vertical axis that resists the twist of the structure. The longitudinal restraints form a couple. The structure must have transverse restraints at the ends of the girder(s) or else it may have been unstable. This response is important to ascertain when investigating erection of the steel, particularly with horizontally curved and skewed bridges. .The transverse restraints create another torque = 6.6 k x 72 ft = 484 kip-ft that resists rotation of the structure about the vertical axis.

Two-Girder Model with Composite Deck and Bottom Flange Lateral Bracing

Bottom flange lateral bracing is next added to the prior model, as shown in Figure 2.5.45 (deck not shown). The lateral bracing effectively forms the fourth side of a pseudo-box. Prior to this, the two girders and deck formed an "open-section"; the lateral bracing creates a "closed-section" creating significant torsional stiffness. This ensures that the two girders will act more in unison.

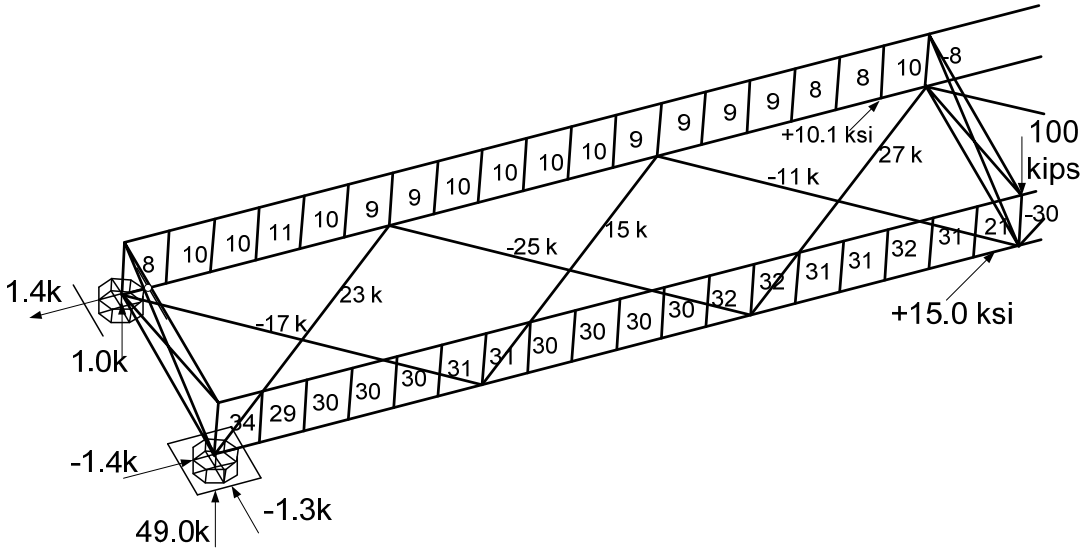


Figure 2.5.45 Two-Girder Model with Deck and Bottom Flange Lateral Bracing

The maximum vertical deflection of the loaded (near) girder is computed to be 0.79 inches. The comparable deflection of the far girder is 0.68 inches. The sum of the midspan deflections is 1.47 inches compared to a total deflection of 1.60 inches for the model with the deck, but without lateral bracing. The model deflected out-of-plumb less than 0.05 inches at midspan. The reason for this reduction in the total deflection is the added stiffness contributed by the longitudinal component of the lateral bracing. Note that the bottom flange stresses in the two girders are less different than in the deck model without lateral bracing.

The cross-frame forces shown in Figure 2.5.46 are from the analysis with lateral bracing. These forces are much larger than in the case with the deck. This is because the pseudo-box is torsionally stiff and the two girders can translate with respect to each other only an amount equal to the elastic lengthening of the lateral bracing. Hence, they must carry nearly the same amount of load. Most of the transfer of load must occur through the central cross-frame. However, statics must still be satisfied; the vertical reactions under the far girder must be near zero.

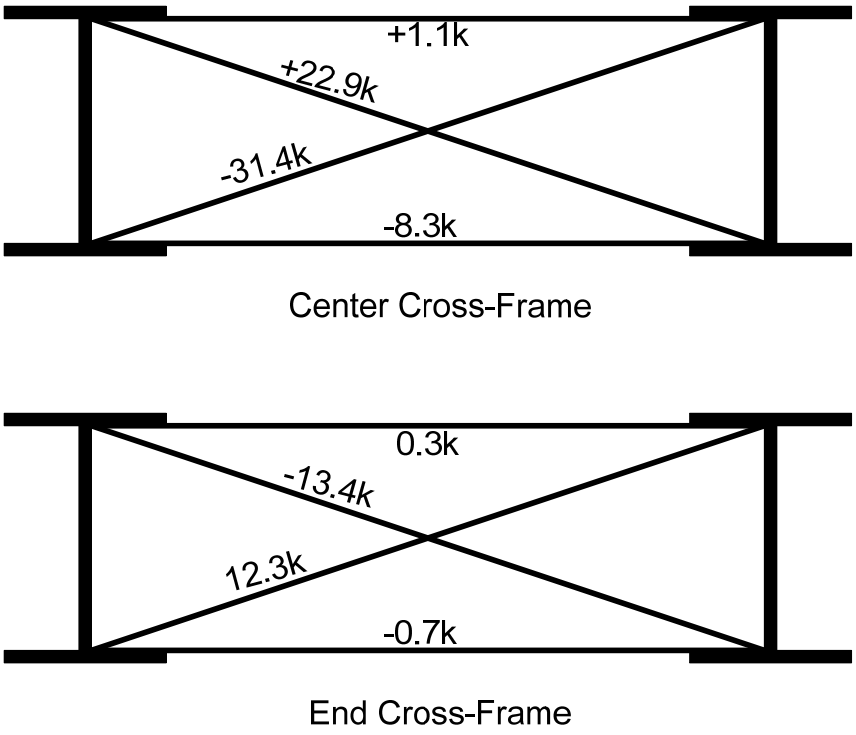


Figure 2.5.46 Two-Girder Model Center and End Cross-Frame Forces (w/ Deck & Bottom Flange Lateral Bracing)

Figure 2.5.47 shows a plot of the longitudinal stress in the bottom of each element from the end bearing up to midspan. The stresses are shown in the near girder only for the case of no deck since the stresses were essentially zero in the far girder for this case. They are shown for both the near and far girders for the other two cases.

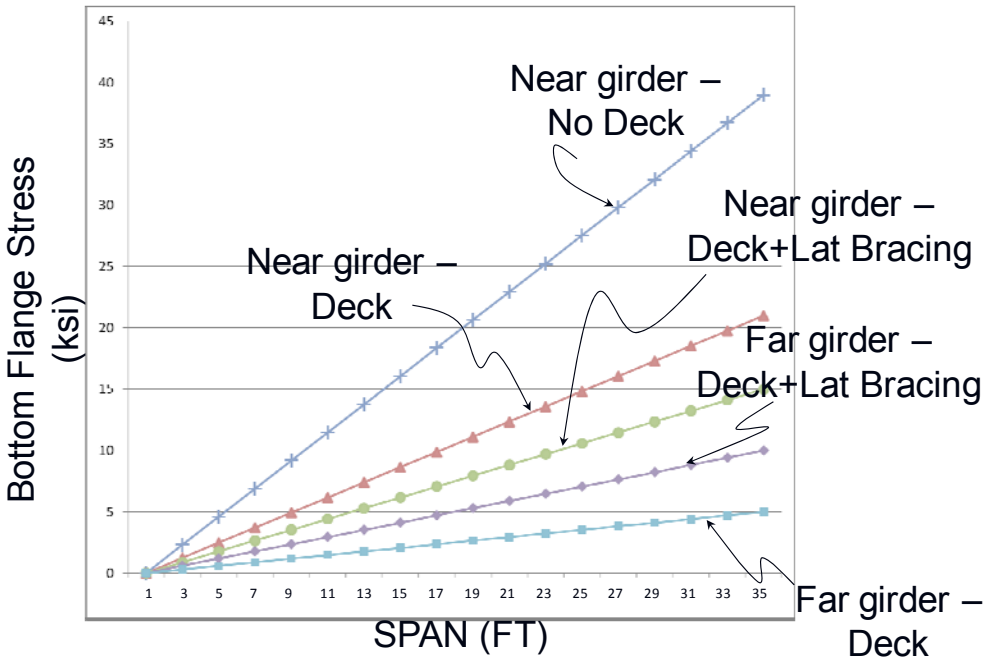


Figure 2.5.47 Two-Girder Model Bottom Flange Stresses

The tendency of the bottom flange stresses to be less different as the torsional stiffness increases is noteworthy. The standard wheel load distribution factors were based on a model that included the deck. In some cases, the cross-frames were included, but in no case was bottom flange lateral bracing included. When lateral bracing is present, girder moments are incorrect; some may be too large, some may be too small. Cross-frame forces computed without considering the presence of lateral bracing are usually vastly underestimated.

Figure 2.5.48 shows a plot of the web shears in each element from the end bearing to midspan. The shears are shown for both girders for the cases of the deck only and of the deck and lateral bracing. The total shear is also shown for both cases.

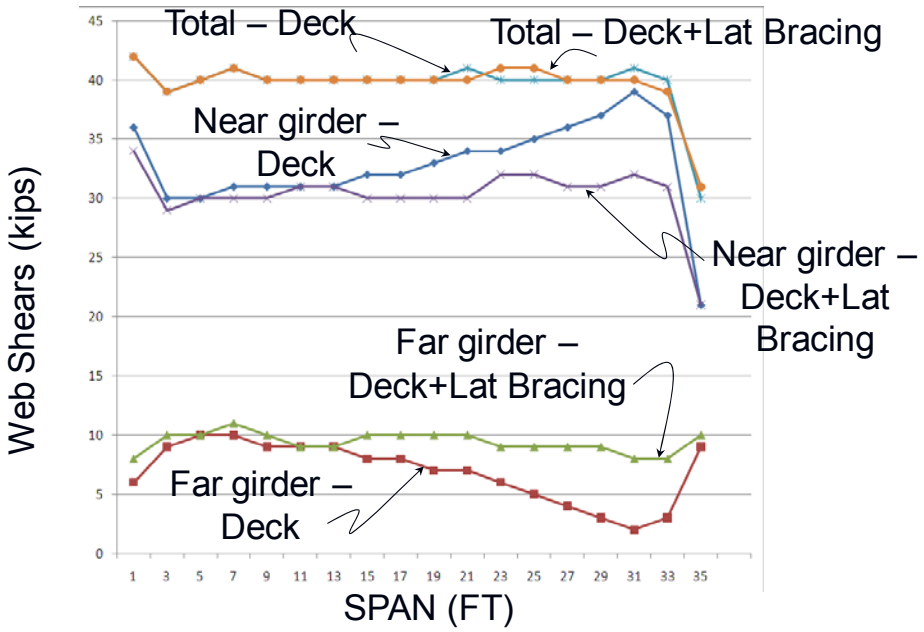


Figure 2.5.48 Two-Girder Model Web Shears

It is noteworthy that in both cases the total shear in both webs is less than the total shear in the structure of 50 kips. In neither case does the far girder web receive as big a portion of the shear as it does of the bending, even though the sum of the shears in the two cases is nearly the same. The reader should also note that the shear is transferred to the far web sooner in the case with lateral bracing. The reason is that the lateral bracing case transfers the majority of the shear via the cross-frame due to the torsional stiffness created by the pseudo-box, while the deck only case transfers the majority of the shear by deck shear, which is mobilized over a greater length of the girder.

2.5.5 Advantages, Disadvantages, and Limitations of 3D Finite Element Analysis

Advantages of 3D finite element methods of analysis include, but are not limited to, the following:

The following is a non-exhausted list of advantages of the 3D finite element method of analysis:

- Permits recognition of the proper location of the deck with respect to the girder neutral axis. This permits consideration of the contribution of the horizontal shear stiffness of the deck, which is the stiffest element in a girder bridge. Deck shear stresses can be determined. This is particularly important in skewed bridges.

- Permits recognition of the proper location of bearings. This permits consideration of lateral and longitudinal bearing constraints. This is critical in computing end cross-frame or diaphragm forces in bridges with skewed supports.
- Permits recognition of lateral bracing. These members greatly affect the distribution of load in structures. The lateral bracing can be very advantageous in curved-girder bridges in many instances when these members are properly modeled.
- Provides the proper modeling of cross-frame members. This assures that the behavior of these members is properly handled in the analysis and that the forces in them can be ascertained directly. It also reduces the effort required to compute and input the troublesome cross-frame equivalents in a 2D model.
- Permits various substructures to be included integrally with the superstructure for analysis. This improves the accuracy of the analysis of both parts of the bridge.
- Permits proper recognition of the torsional stiffness of I-girders, including direct determination of flange lateral moments and girder twist.
- Permits proper loading of tub girders by providing two webs. Hence, torque is properly introduced into the model.
- Transverse deck stresses can be computed that recognize the effect of relative girder deflections. This is important when designing post-tensioned deck slabs.
- Provide proper torsional stiffness of box members by recognizing St. Venant and warping torsional shear simultaneously.
- Variable depth (haunched) girders can be more accurately modeled. The shear component in bottom flanges of haunched girders is recognized.
- Allows for more efficient and detailed modeling of erection sequences.
- This method permits much bolder bridges that are not dependent on rules-of-thumb but on the solid principles of structural analysis.

The following is a non-exhausted list of disadvantages of the 3D finite element method of analysis:

- Requires a greater level of knowledge. Experience with finite element analysis is required to properly construct the models and to compile, interpret and use the results; it should not be used without experienced guidance and assistance.
- Plethora of results to deal with unless a special package is employed.
- Greater modeling effort required unless a pre-processing software for bridges is used.

There are virtually no limitations on the type or complexity of models that can be constructed and analyzed using 3D finite element methods. Limitations that may exist are related to the limitations of the software package, the experience level of the modeler and Design Engineer, and of course, time and cost factors relative to the benefits that would accrue from employing a more sophisticated and complex

analysis for the specific application under consideration. The effort required to build the model and process the results is also very dependent on the pre- and post-processing software available.

Table 2.5.2 contains the filled-in Levels of Analysis Matrix, which was introduced previously in Section 2.3.4, for 3D finite element analysis.

Table 2.5.2 Levels of Analysis Matrix for 3D Finite Element Analysis

Issue		V-Load	2D Grid	2D P&EB	3D
Vertical Bending	C				3
	S				3
Vertical Deflection	C				3
	S				3
Lateral Bending	C				3
	S				3
Lateral Deflection	C/S				3
Single Girder Stability	C/S				3
Influence Surface Concept	C				3
	S				3
Thermal Load	C/S				3
Wind Load	C/S				3
Horizontal Bearing Constraint	C/S				3
Cross-Frame Actions	C				3
	S				3
Lateral Bracing	C/S				3
Substructure Interaction	C/S				3
Transverse Deck Stresses	C/S				3
Phased Construction	C				3
	S				3
Vertical reactions/Uplift	C				3
	S				3

Note that since the 3D finite element method is essentially serving as standard against which the other analysis methods covered in Sections 2.3 and 2.4 are judged, the highest ranking of '3' is provided under all the listed issues in the matrix.

2.5.6 Case Study – 3D Investigation of an I-Girder Bridge with a Straddle Beam

Five continuous horizontally curved steel I-girders are supported by a steel box bent. The girders rest on bearings on top of the bent. The bent is simply supported at its ends. The superstructure unit is composed of several spans. Diaphragms are used between the girders at the bent, while intermediate K-type cross-frames are used elsewhere. A 3D plot of a portion of the girders, cross-frames and box bent is shown in Figure 2.5.49.

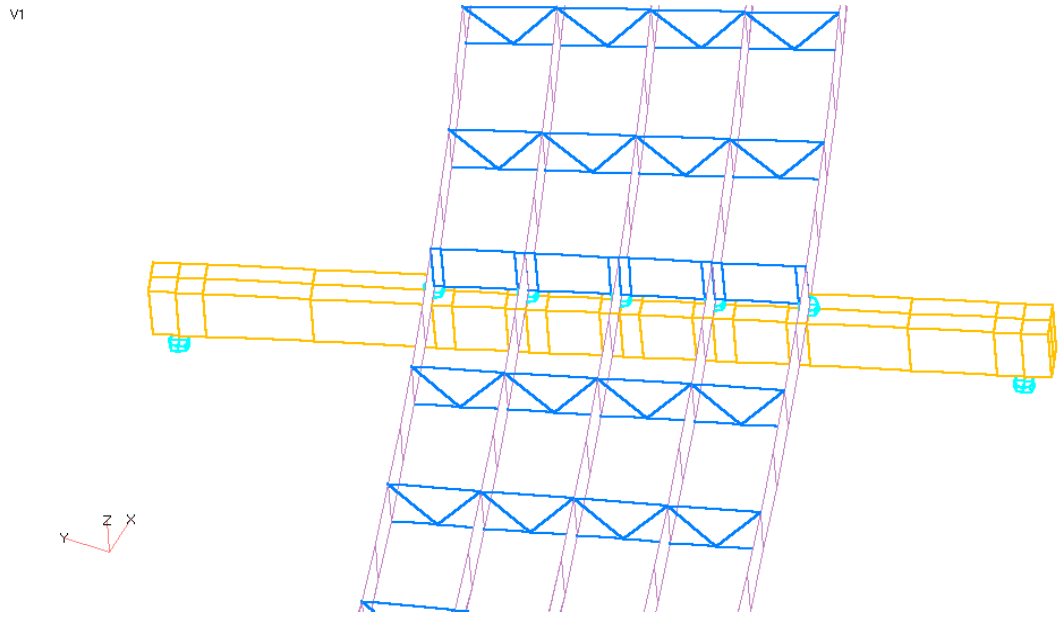


Figure 2.5.49 Case Study Structure

Girders are numbered from left to right looking at the plot. The unfactored vertical dead load reactions on top of the bent are given in Table 2.5.3. The live load plus impact uplift reactions in the table have a load factor of 1.75. The Design Engineer chose these load factors to check uplift. A negative reaction in the table indicates the maximum upward reaction that resists the maximum downward force at the bearing. A positive reaction in the table indicates the maximum downward reaction that resists the maximum uplift force at the bearing due to the load under consideration. The parapets are applied to the composite case. They cause uplift in the center three reactions because their load is applied on the overhang cantilever.

Table 2.5.3 Reactions on the Straddle Beam (kips)

Girder No.	Non-Composite Dead Load	Composite Dead Load	Live Load (Uplift)	Total
1	-491	-115	75	-531
2	-53	14	78	39
3	-64	24	79	39
4	-28	9	70	51
5	-492	-120	88	-524

Clearly, the center three girders are experiencing significant uplift.

The situation arose because the straddle beam tended to deflect out from under the center girders. This caused large loads in the cross-frames at the straddle beam and was the reason that diaphragms were employed there. The revelation of this situation could only be found with an analysis that recognized the interaction between the substructure and the superstructure. Without the interactive analysis, the nominal cross-frames that would have been used would have failed during construction.

The Design Engineer specified that the bolts in the center two diaphragms at the straddle beam be tightened after the non-composite dead load (steel plus deck weight) had been applied. The diaphragms were then made effective to handle the composite dead load and live load. The resulting reactions from the analysis based on this assumption are shown in Table 2.5.4.

Table 2.5.4 Reactions on the Straddle Beam with Revised Construction (kips)

Girder No.	Non-Composite Dead Load	Composite Dead Load	Live Load (Uplift)	Total
1	-324	-115	75	-364
2	-152	14	78	-60
3	-137	24	79	-34
4	-185	9	70	-106
5	-321	-120	88	-353

There was a significant reduction in the diaphragm moments because they were not effective for the non-composite dead load. Forces due to non-composite dead load in adjacent cross-frame members were increased by about 20 percent with this design decision and were sized up slightly.

This Page Intentionally Left Blank

Chapter 2
Structural Analysis

Section 2.6

Recommended Level of Analysis



2.6.1 Introduction

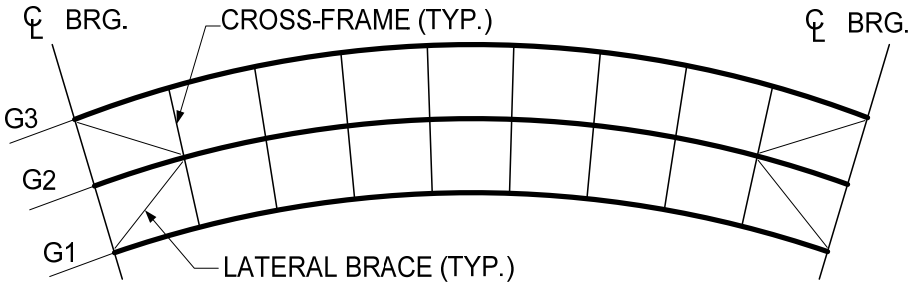
This section presents a comparison of the structural analysis results for a simple-span curved I-girder bridge on radial supports using various methods of analysis. It also presents a comparison of the structural analysis results for the example three-span skewed/curved I-girder bridge presented in Section 5.1. The comparisons are made between analyses conducted using the approximate V-Load method (Section 2.3.2), 2D finite element methods (Section 2.4) and 3D finite element methods (Section 2.5). At the end of this section, the completed Levels of Analysis Matrix introduced in Section 2.3.4 is presented for use in evaluating and comparing the various approximate, 2D and 3D analysis methods described in this Manual.

2.6.2 Differences in Analysis Results Using Various Levels of Analysis

In this section, analysis results are compared for a simple-span curved I-girder bridge on radial supports, and for the skewed and curved example I-girder bridge presented in Section 5.1. Selected analysis results from the approximate V-load method (Section 2.3.2), the 2D finite element method (Section 2.4), and the 3D finite element method (Section 2.5) are compared.

2.6.2.1 Simple-Span Curved I-Girder Bridge

The first bridge to be examined is a simple-span three-girder curved I-girder bridge on radial supports, as seen in Figure 2.6.1. The span length measured along the bridge centerline is 90'-0″, and the centerline radius is 200'-0″. The three girders in the cross-section are spaced at a constant spacing of 8'-9″. The web depth is a constant 48″.



- 90'-0″
- CL Radius = 200'
- Girder Spacing = 8'-9″
- Web Depth = 48″

PLAN

Figure 2.6.1 Plan View of Sample Simple-Span Curved I-Girder Bridge

The bridge is examined using the approximate V-load method, the 2D finite element method and the 3D finite element method. For the 2D finite element analysis, the bridge is examined using only the 2D traditional grid method. Cross-frames in the grid model are represented using the "flexure stiffness" approach discussed in Section 2.4.3.2 (denoted as "Flex" in the plots that follow).

Figure 2.6.2 shows a comparison plot of the total factored Strength I vertical bending moments in the inside fascia G1 of the simple-span bridge.

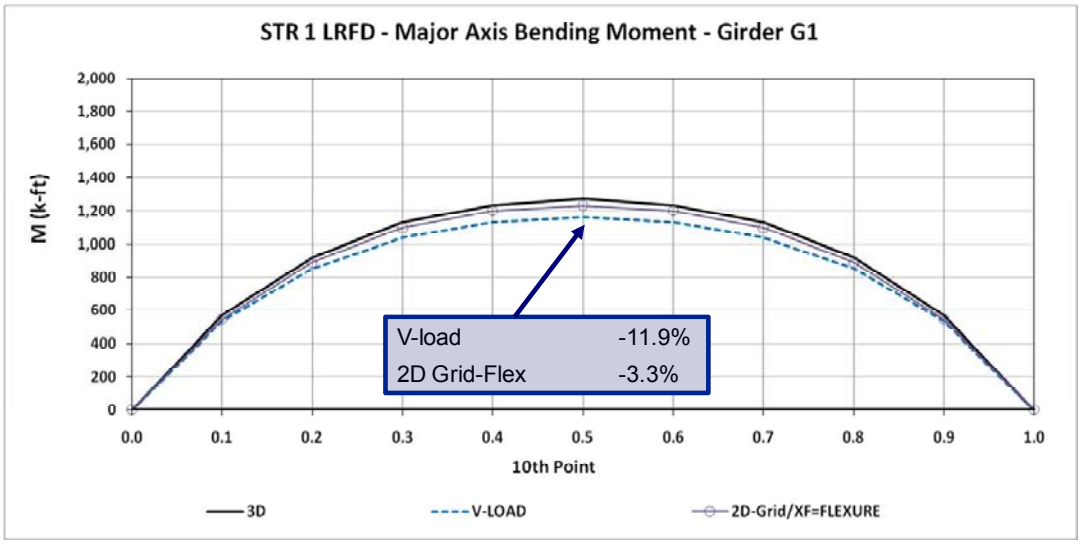


Figure 2.6.2 Strength I Vertical Bending Moment in G1 of the Simple-Span Bridge

The percentages shown for each analysis method in this figure and subsequent figures are with respect to the results determined using the 3D finite element method.

The maximum moment in G1 predicted by the 2D grid method is 3.3 percent lower than the maximum moment predicted by the 3D finite element method. The maximum moment predicted by the V-load method is approximately 12 percent lower.

Figure 2.6.3 shows a comparison of the total factored Strength I vertical bending moments in the outside fascia G3 of the simple-span bridge.

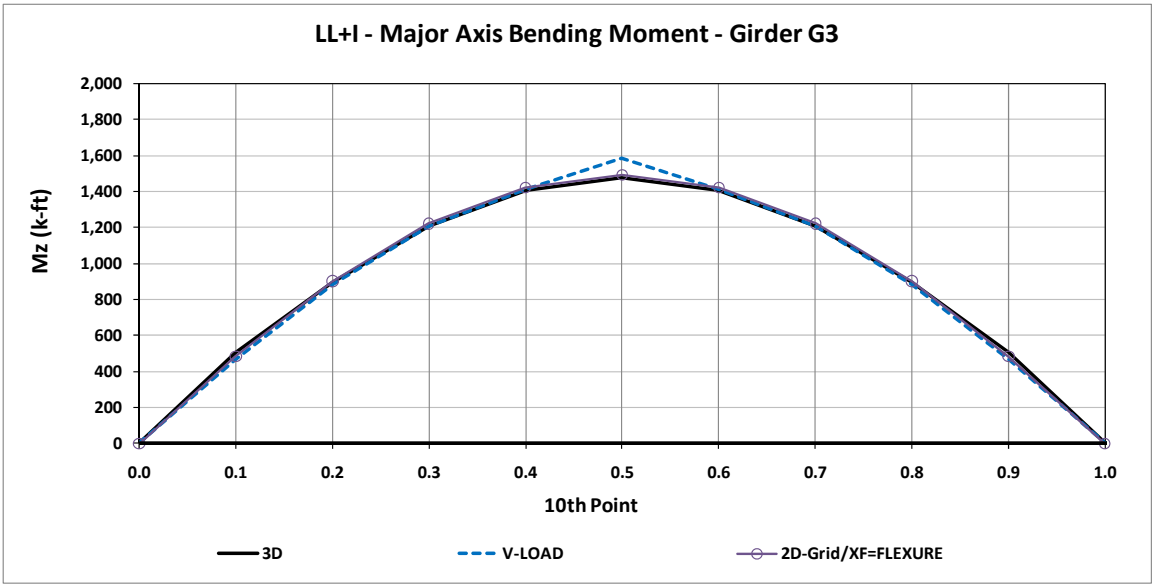


Figure 2.6.3 Strength I Vertical Bending Moment in G3 of the Simple-Span Bridge

Both the V-load method and 2D grid method agree well with the maximum moment predicted by the 3D finite element method in this case.

Figure 2.6.4 shows a comparison plot of the unfactored non-composite dead load (DC_1) vertical displacements of the outside fascia G3; that is, the vertical displacements due to the weight of the steel and concrete deck.

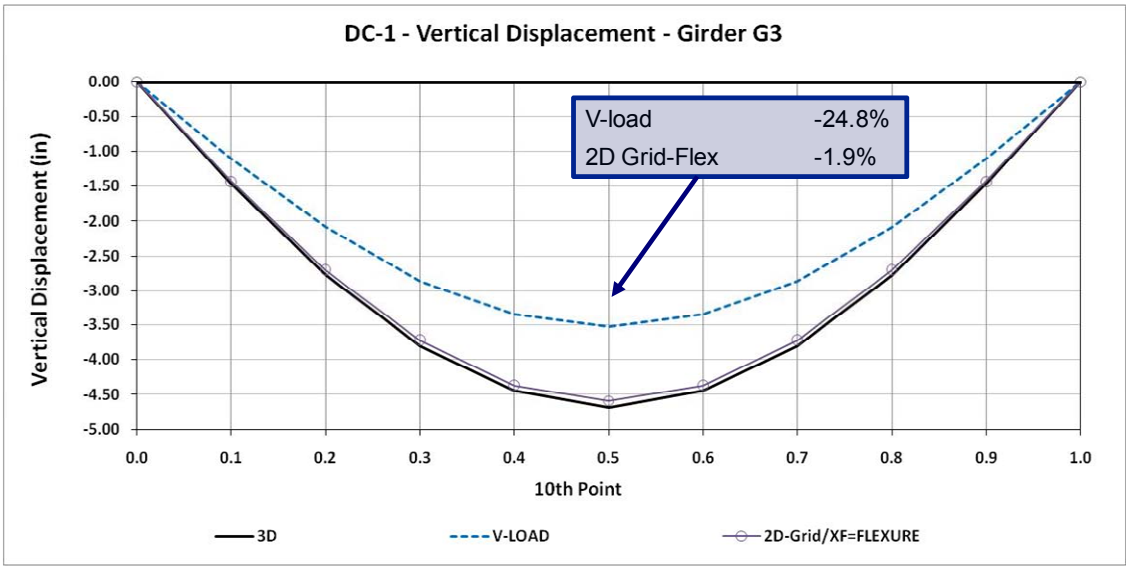


Figure 2.6.4 Unfactored DC_1 Vertical Displacement of G3 of the Simple-Span Bridge

The V-load method significantly underestimates the maximum vertical displacement with respect to the 3D finite element method. The V-load method does not directly take into account the effect of girder twist, which causes additional vertical deflections beyond those produced by bending.

The maximum vertical displacement predicted by the 2D grid method agreed well with that predicted by the 3D finite element method in this case.

Table 2.6.1 shows a comparison of the total factored Strength I cross-frame axial forces in the intermediate K-type cross-frame between G2 and G3 in the simple-span bridge at Line 5L. The configuration and location of the cross-frame in the bridge are shown in Figure 2.6.5, Part A and B, respectively.

Table 2.6.1 Strength I Axial Forces in Cross-Frame Between G2 and G3 at Line 5L of the Simple-Span Bridge

Member	Analysis Method	Strength I – Max. (kips)	Strength I – Min. (kips)
Top Chord	3D	19.8	16.3
	2D Grid – Flex	58.0	30.0
	V-Load	42.0	26.3
Diagonal C	3D	-18.8	-39.8
	2D Grid – Flex	-23.8	-50.0
	V-Load	-25.0	-47.8
Diagonal D	3D	39.8	18.8
	2D Grid – Flex	50.0	23.8
	V-Load	47.8	25.0
Bottom Chord E	3D	-43.8	-71.8
	2D Grid – Flex	-47.8	-94.8
	V-Load	-45.0	-78.3

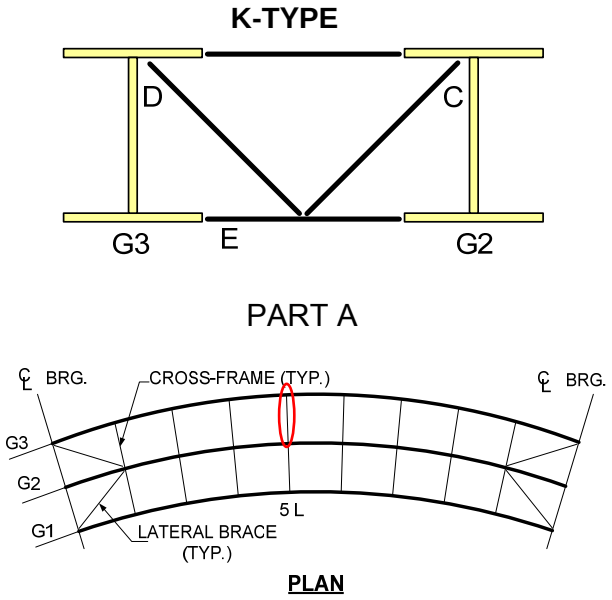


Figure 2.6.5 Cross-Frame at Line 5L in the Simple-Span Bridge: Configuration and Location
A) Configuration; B) Location

The most significant discrepancy in this case is in the prediction of the force in the top chord; unlike the 2D traditional grid method, the 3D finite element method recognizes the horizontal shear stiffness of the deck reducing the composite dead load and live load forces in the top chord.

The force predictions in the other cross-frame members were conservative, but generally not accurate with respect to the predictions from the 3D finite element method.

The bar chart in Figure 2.6.6 shows a comparison of the unfactored DC_1 bottom flange lateral bending moments in the outside G3 at the cross-frame at Line 5L.

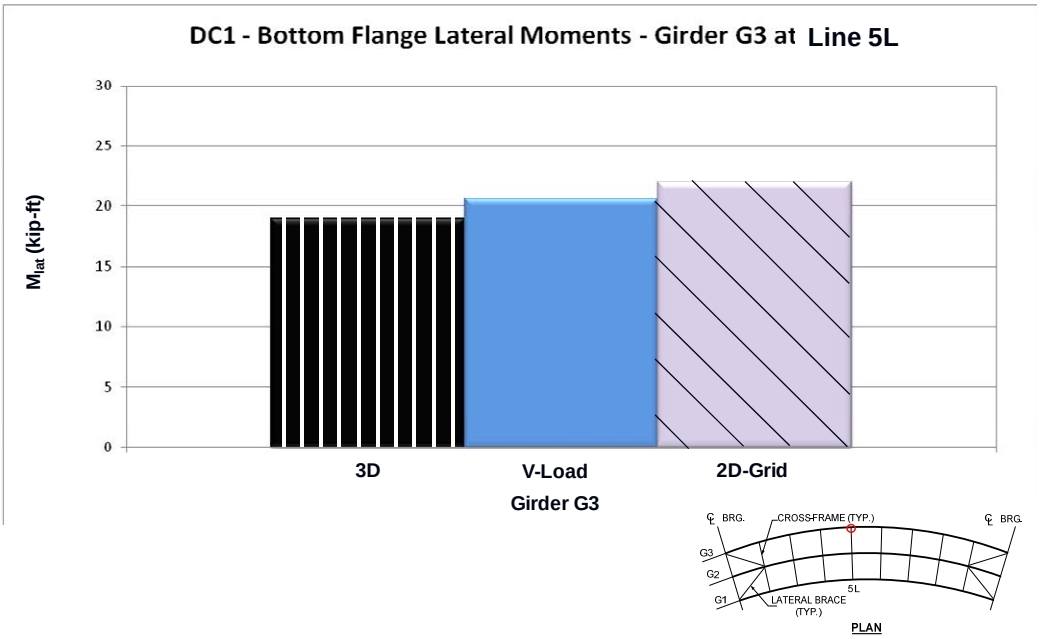


Figure 2.6.6 Unfactored DC_1 Bottom Flange Lateral Bending Moments in G3 of the Simple-Span Bridge at Cross-Frame Line 5L

The approximate V-load equation discussed in Section 2.3.2.2.5 is used to determine the lateral bending moments in the V-load and 2D traditional grid methods.

The bottom flange lateral bracing members are included in the 3D finite element model. Without these members, the lateral bending moment at Line 5L is reduced from 19 kip-ft to 12 kip-ft.

The following is a list some general observations gleaned from the comparative study of the simple-span bridge with radial supports that was investigated using various levels of analysis:

- Reasonable predictions of Strength I vertical bending moments are provided;
- The V-load method is less accurate for the inside fascia G1;
- The V-load method significantly underestimated the DC_1 vertical displacements;
- Lateral bending moments must be determined from an approximate equation,and;
- Cross-frame force predictions are generally conservative, but are not accurate.

The preceding observations are with respect to analysis results determined using the 3D finite element method.
Comparative results for all the girders in the simple-span bridge are provided below.

Comparative Results for the Simple-Span Bridge

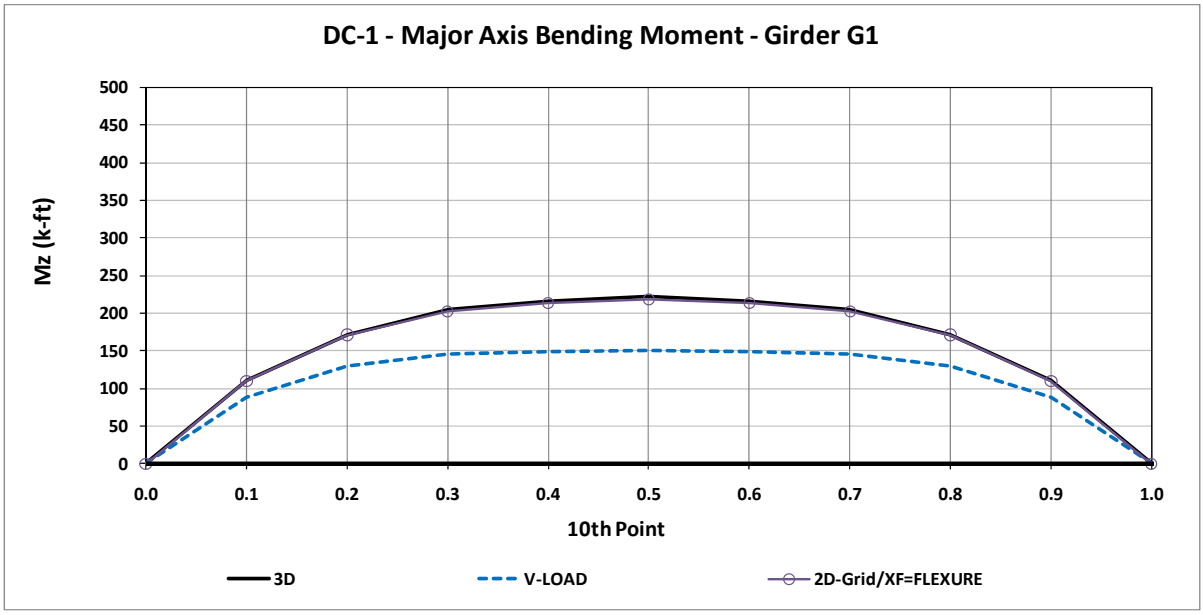


Figure 2.6.7 Unfactored DC_1 Vertical Bending Moment in G1

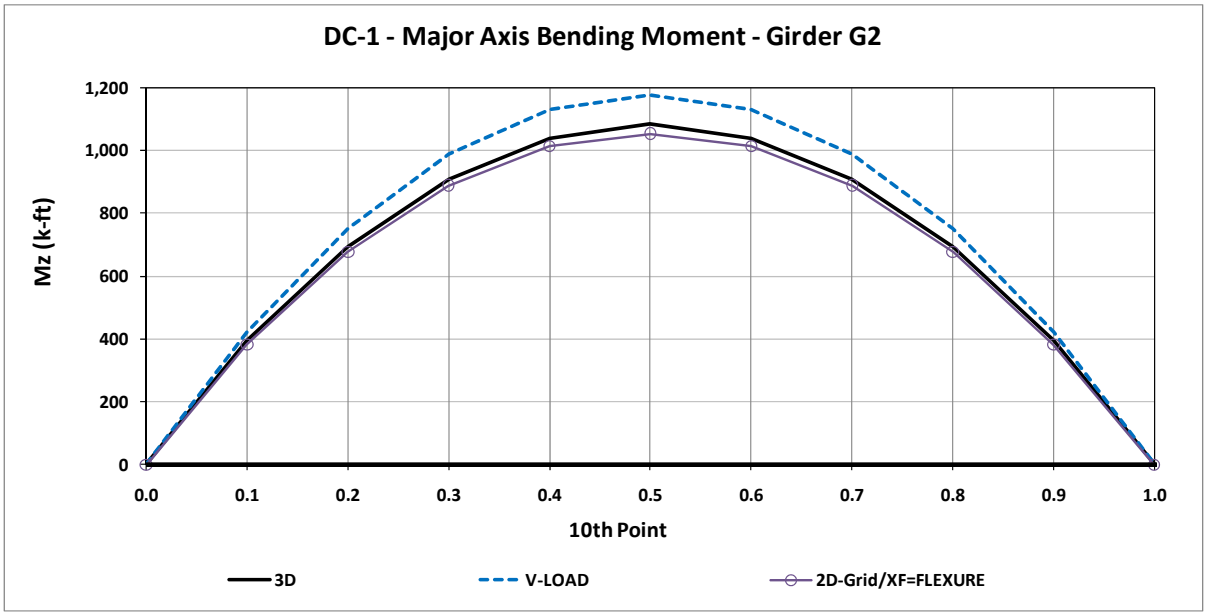


Figure 2.6.8 Unfactored DC_1 Vertical Bending Moment in G2

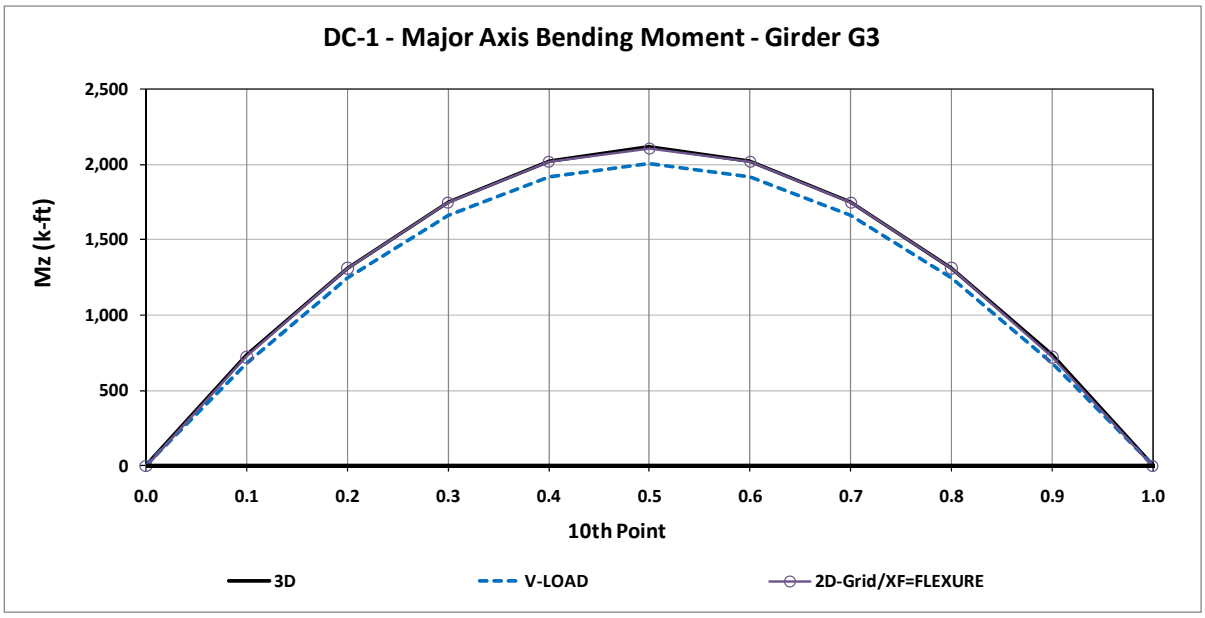


Figure 2.6.9 Unfactored DC_1 Vertical Bending Moment in G3

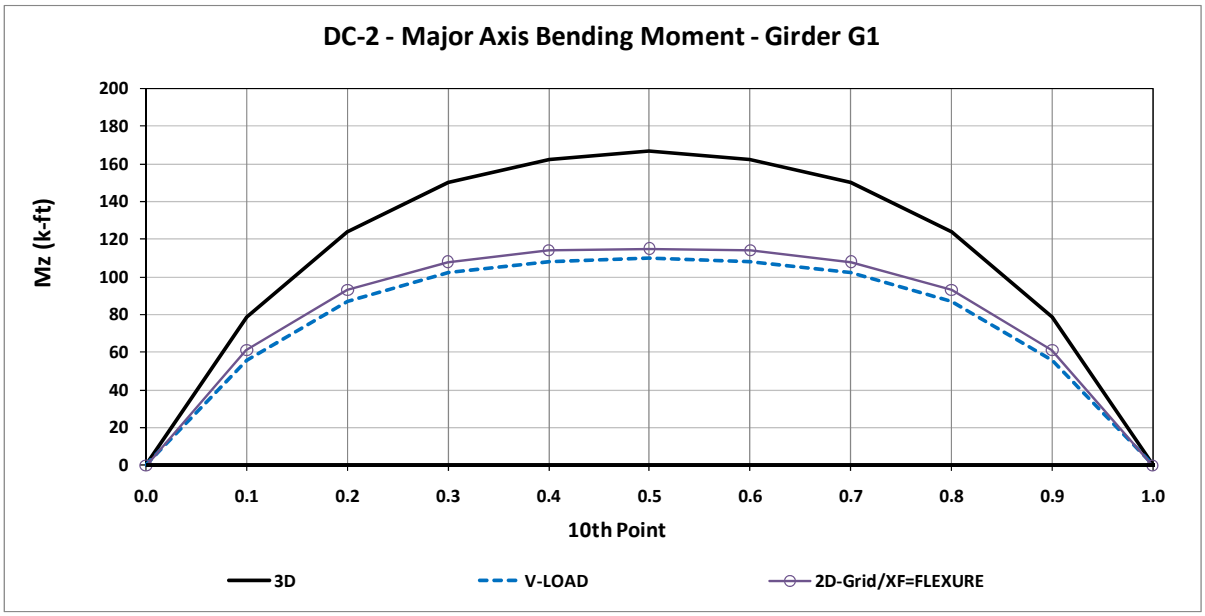


Figure 2.6.10 Unfactored DC_2 Vertical Bending Moment in G1

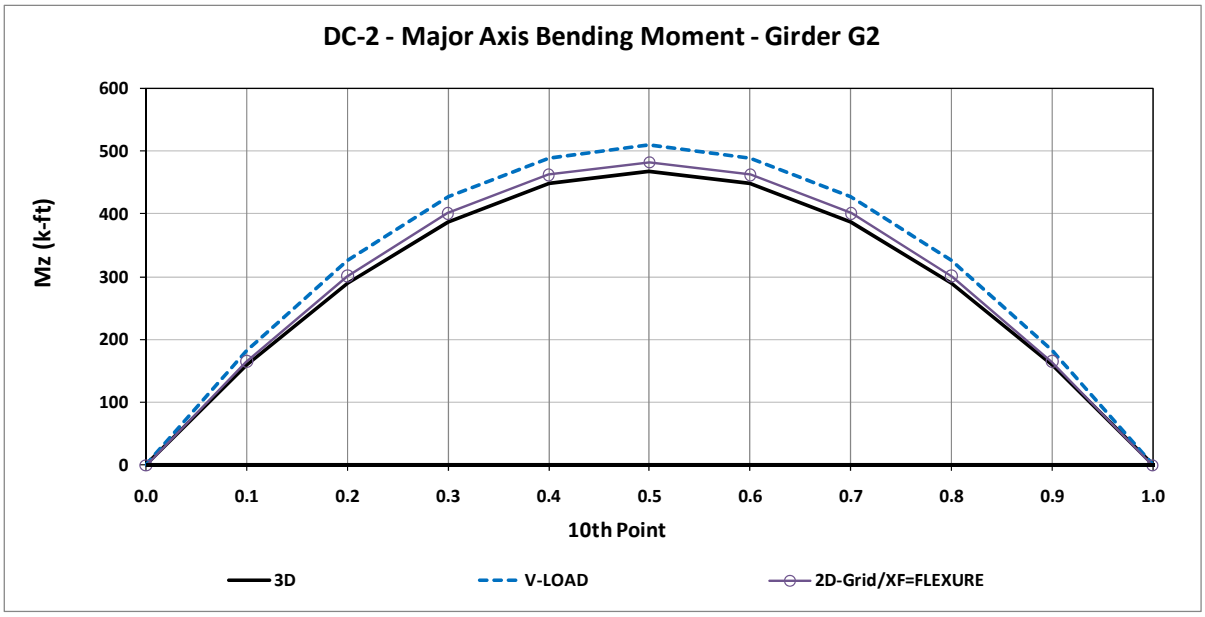


Figure 2.6.11 Unfactored DC_2 Vertical Bending Moment in G2

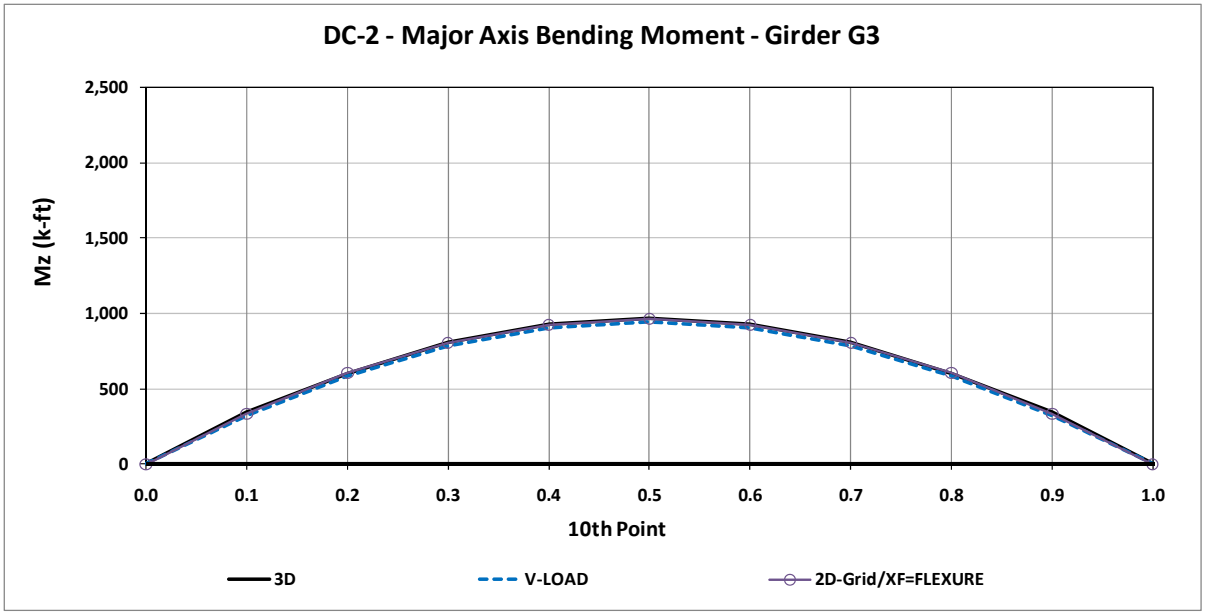


Figure 2.6.12 Unfactored DC_2 Vertical Bending Moment in G3

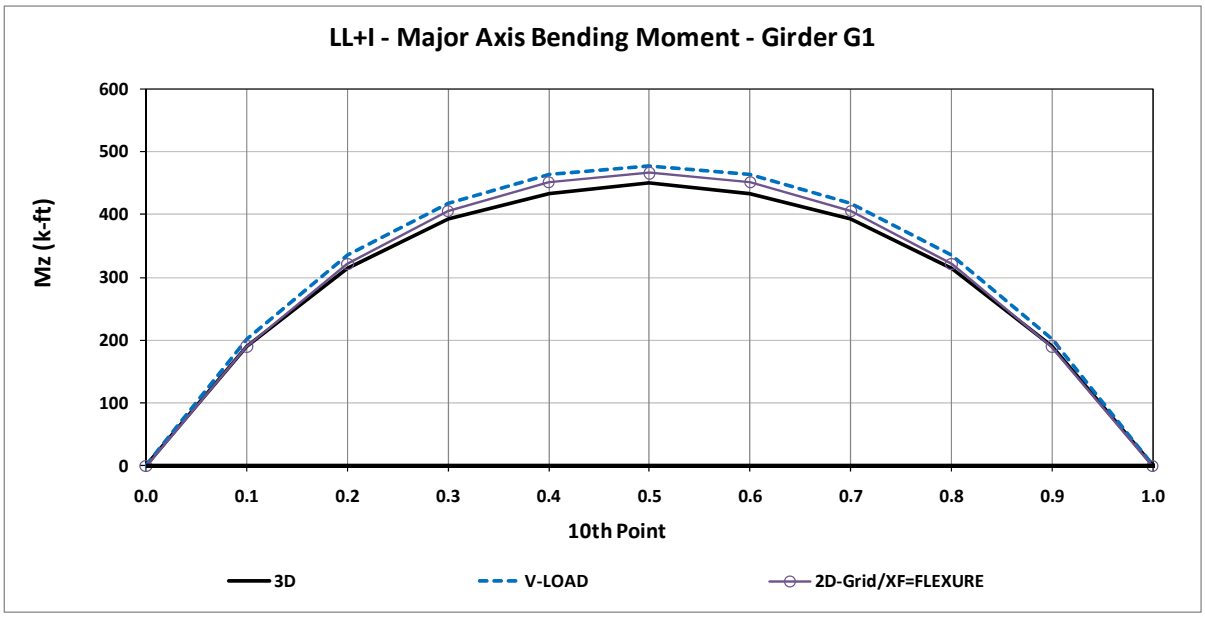


Figure 2.6.13 Unfactored LL+IM Vertical Bending Moment in G1

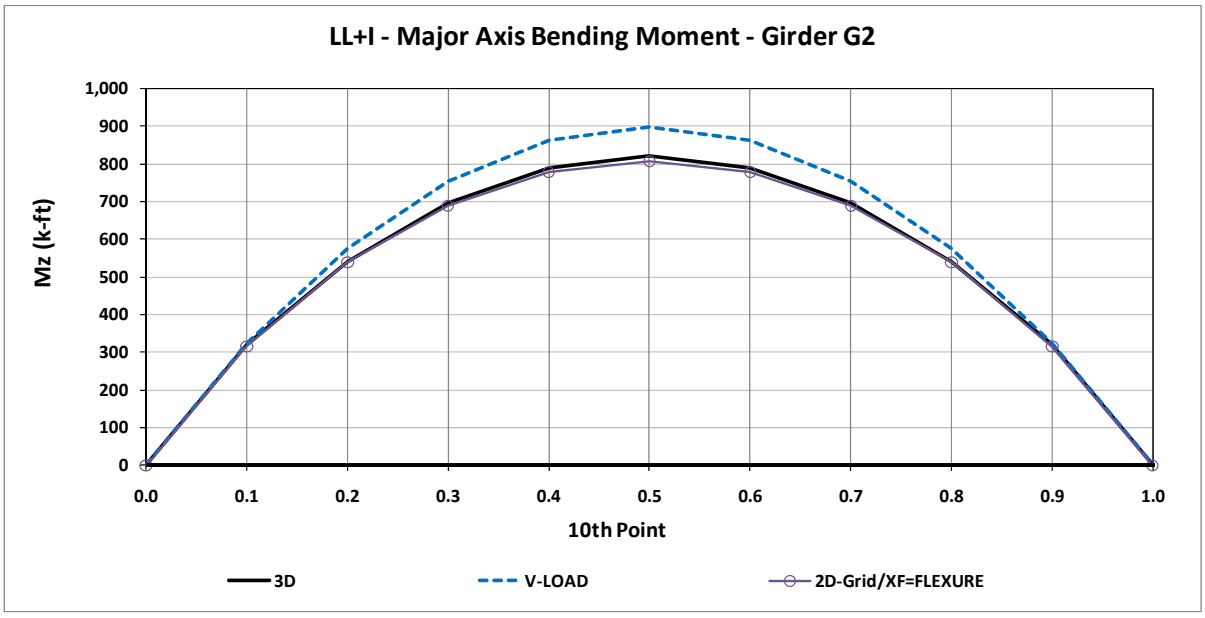


Figure 2.6.14 Unfactored LL+IM Vertical Bending Moment in G2

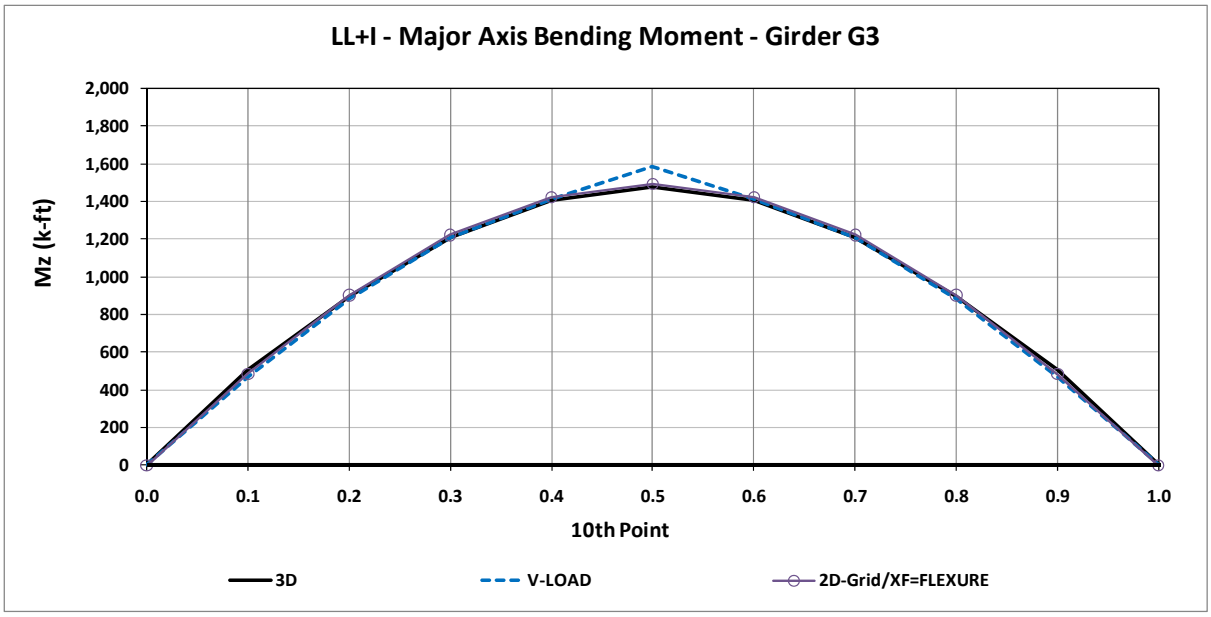


Figure 2.6.15 Unfactored LL+IM Vertical Bending Moment in G3

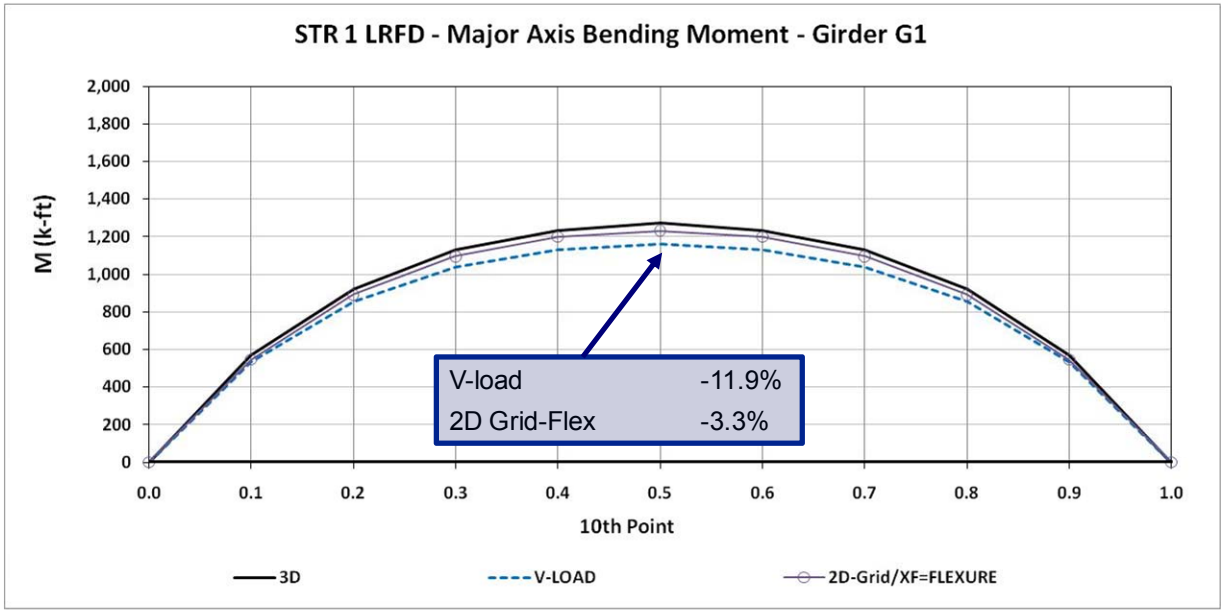


Figure 2.6.16 Strength I Vertical Bending Moment in G1

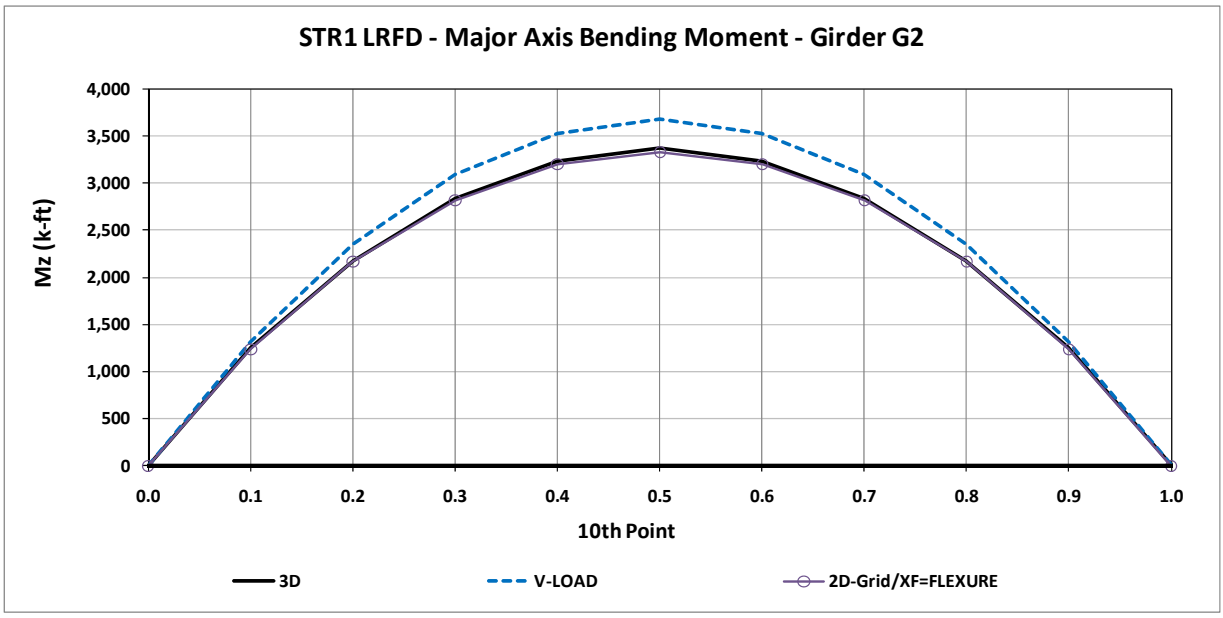


Figure 2.6.17 Strength I Vertical Bending Moment in G2

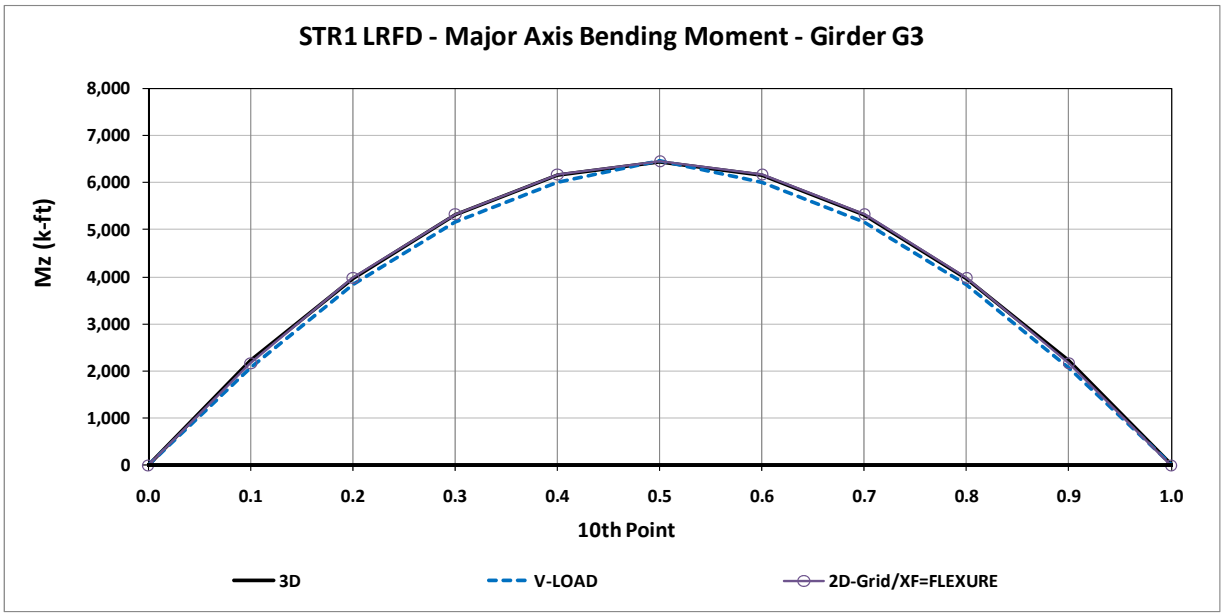


Figure 2.6.18 Strength I Vertical Bending Moment in G3

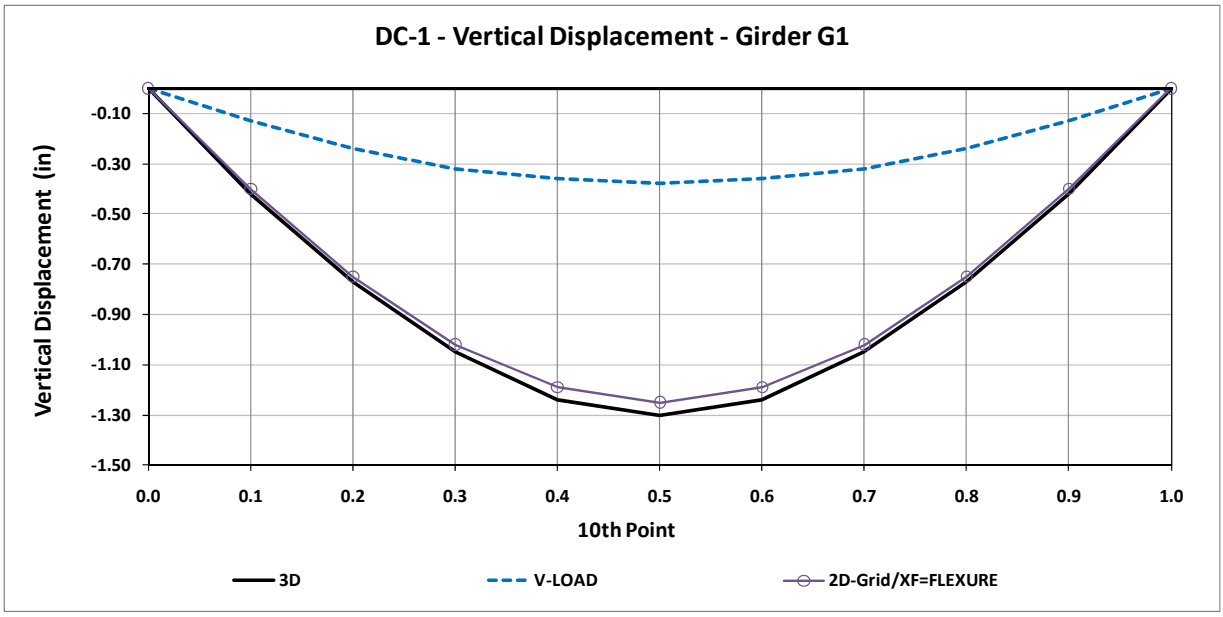


Figure 2.6.19 Unfactored DC_1 Vertical Displacement of G1

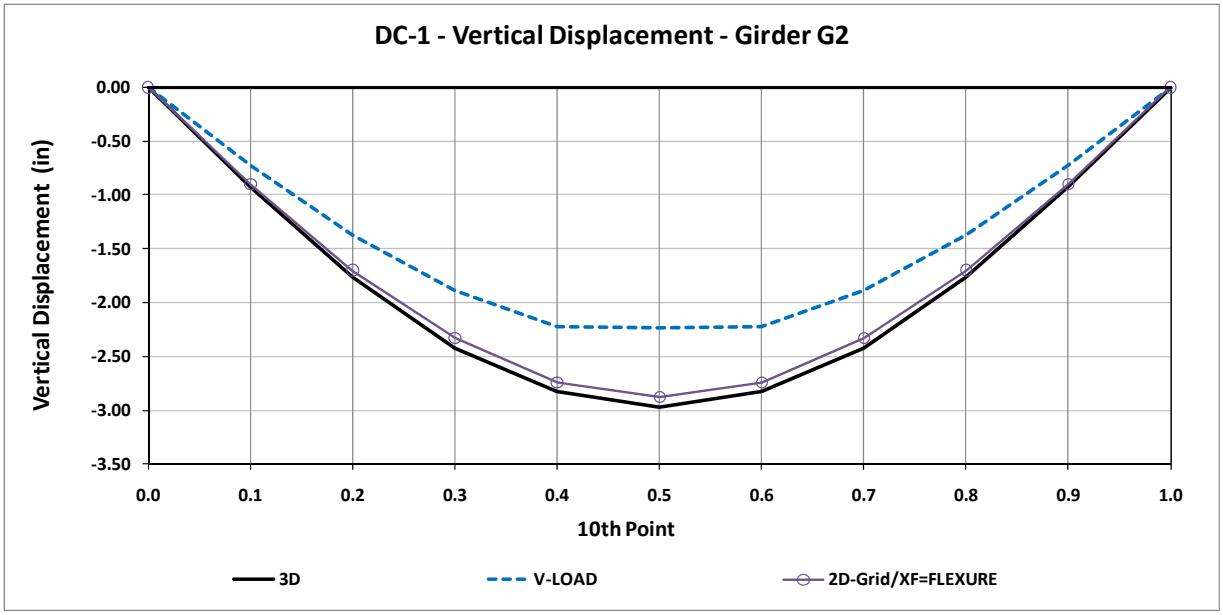


Figure 2.6.20 Unfactored DC_1 Vertical Displacement of G2

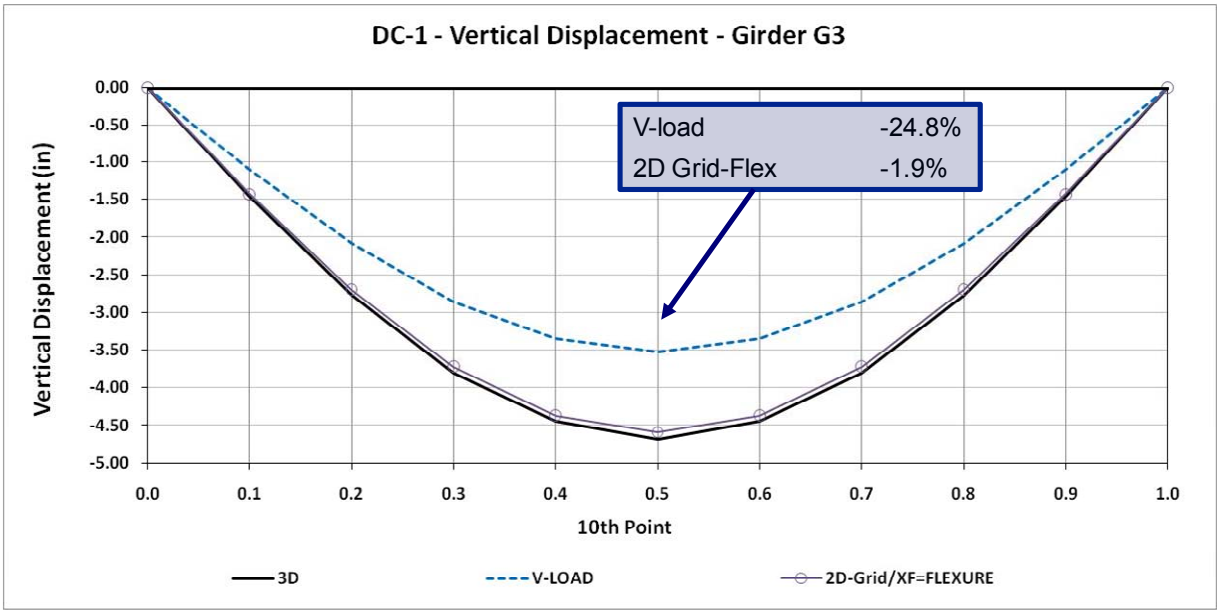


Figure 2.6.21 Unfactored DC_1 Vertical Displacement of G3

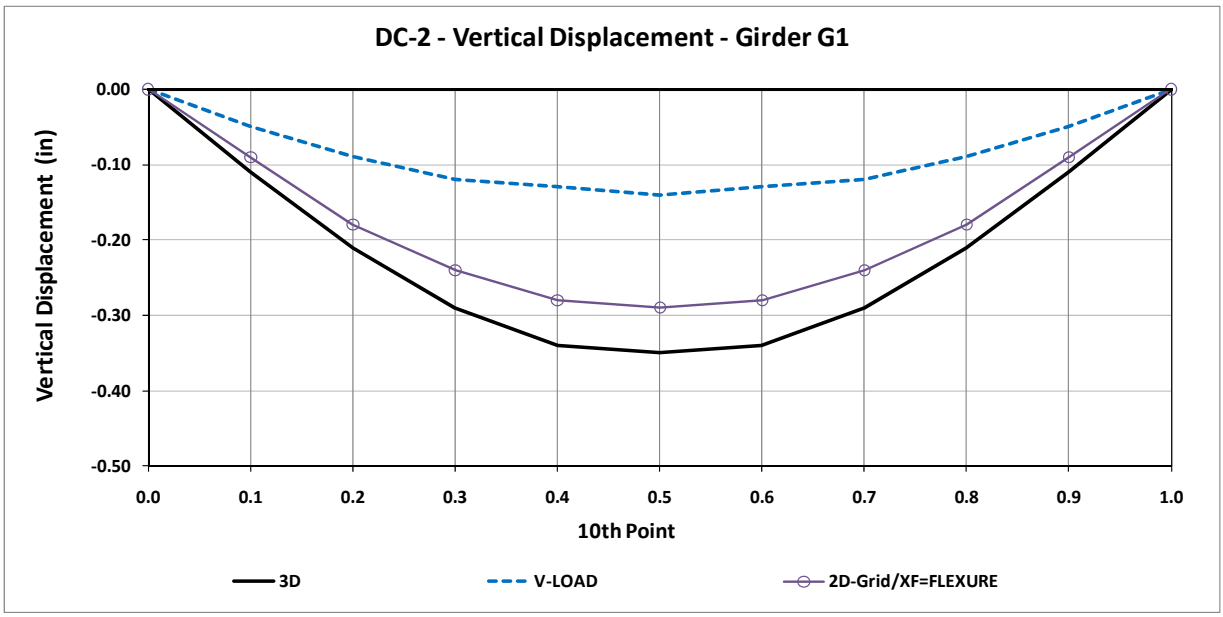


Figure 2.6.22 Unfactored DC_2 Vertical Displacement of G1

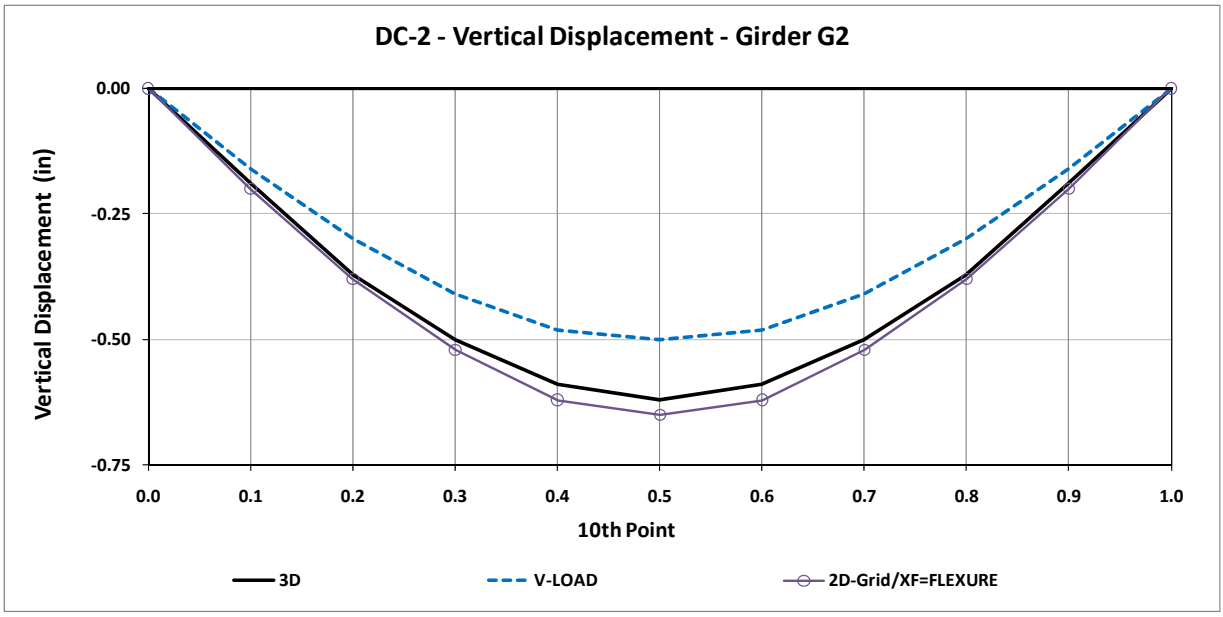


Figure 2.6.23 Unfactored DC_2 Vertical Displacement of G2

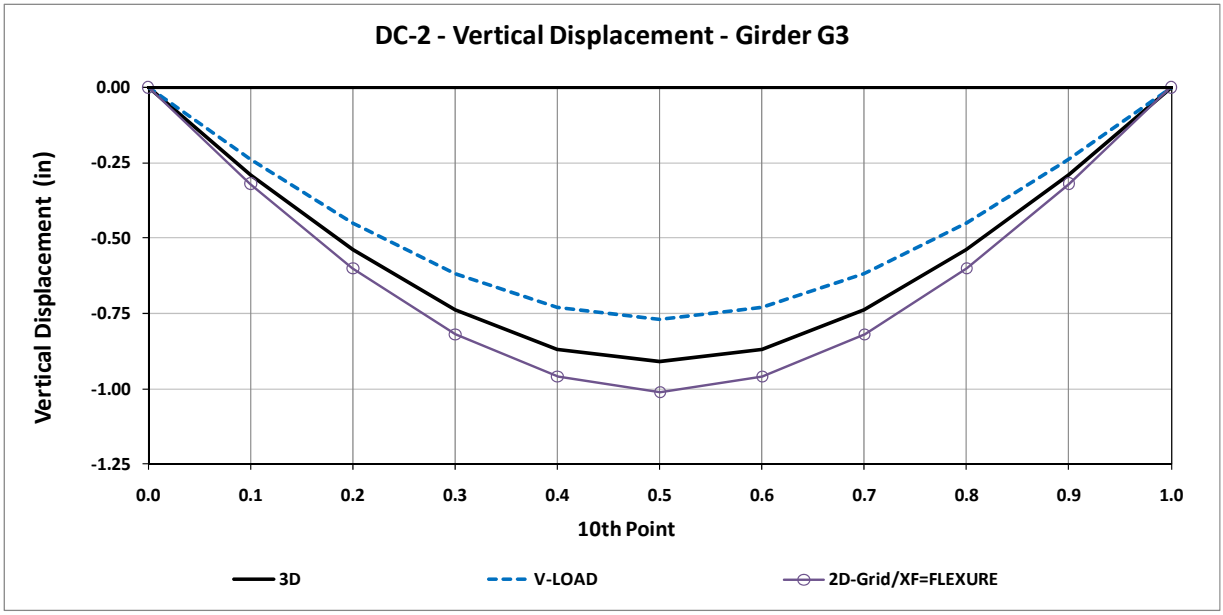


Figure 2.6.24 Unfactored DC_2 Vertical Displacement of G3

2.6.2.2 Example Skewed/Curved I-Girder Bridge

The example skewed/curved I-girder bridge presented in Section 5.1 is a three-span continuous bridge with radial supports at the abutments and two skewed piers, each with a skew angle of approximately 60° measured clockwise from radial (Figure 2.6.22). The span lengths measured along the bridge centerline are 160' – 210' – 160' and the centerline radius is 700 feet. There are four girders in the cross-section spaced at a constant spacing of 11'-0″. The web depth is a constant 92″.

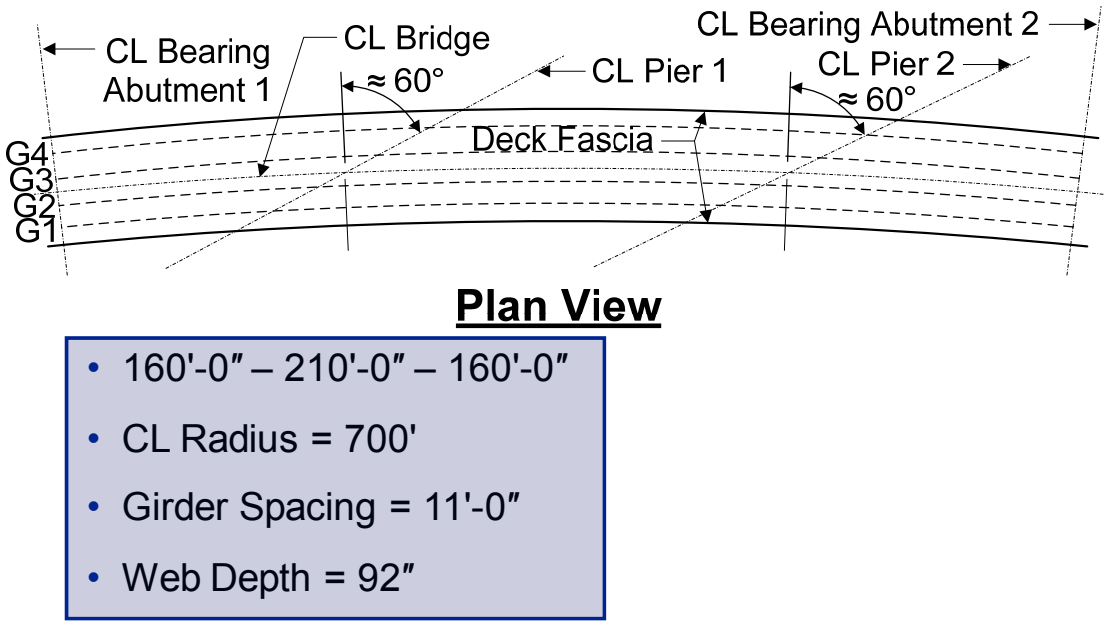
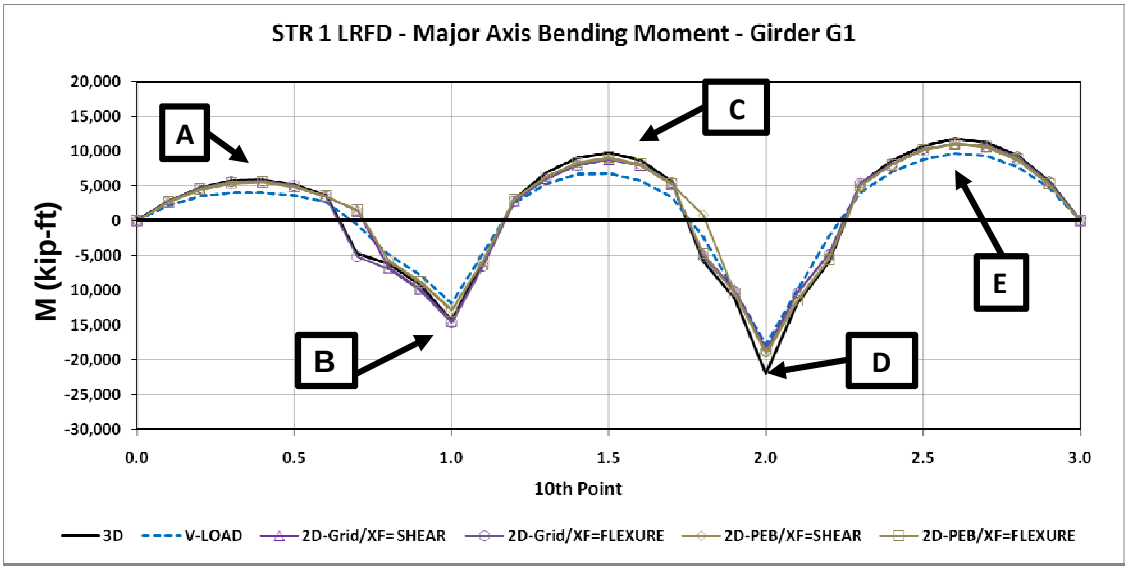


Figure 2.6.25 Plan of Example Skewed/Curved I-Girder Bridge

As discussed in Section 5.1.3.4, discontinuous cross-frame lines were introduced in the design in the region of the skewed piers in order to reduce the transverse stiffness of the superstructure adjacent to the piers, and also the cross-frame forces (refer to Section 5.1.3.4 for the resulting framing plan).

In addition to the V-load and 3D finite element methods, the example bridge is examined using both the 2D grid and 2D Plate and Eccentric Beam (P&EB) methods. For both the 2D grid and 2D P&EB methods, analysis results are presented with the cross-frames in the grid models represented using both the "shear stiffness" and "flexure stiffness: approaches discussed in Section 2.4.3.

Figure 2.6.23 shows a comparison plot of the total factored Strength I vertical bending moments in G1 of the example bridge. Percentages shown for each analysis method with respect to the results determined using the 3D finite element method are shown below the figure.



A

- V-load +1%
- 2D Grid-Shear -4%
- 2D Grid-Flex -5%
- 2D P&EB-Shear -4%
- 2D P&EB-Flex -4%

B

- V-load -19%
- 2D Grid-Shear -17%
- 2D Grid-Flex -16%
- 2D P&EB-Shear -15%
- 2D P&EB-Flex -14%

C

- V-load +20%
- 2D Grid-Shear +9%
- 2D Grid-Flex +6%
- 2D P&EB-Shear +12%
- 2D P&EB-Flex +10%

D

- V-load -14%
- 2D Grid-Shear -7%
- 2D Grid-Flex -7%
- 2D P&EB-Shear -13%
- 2D P&EB-Flex -13%

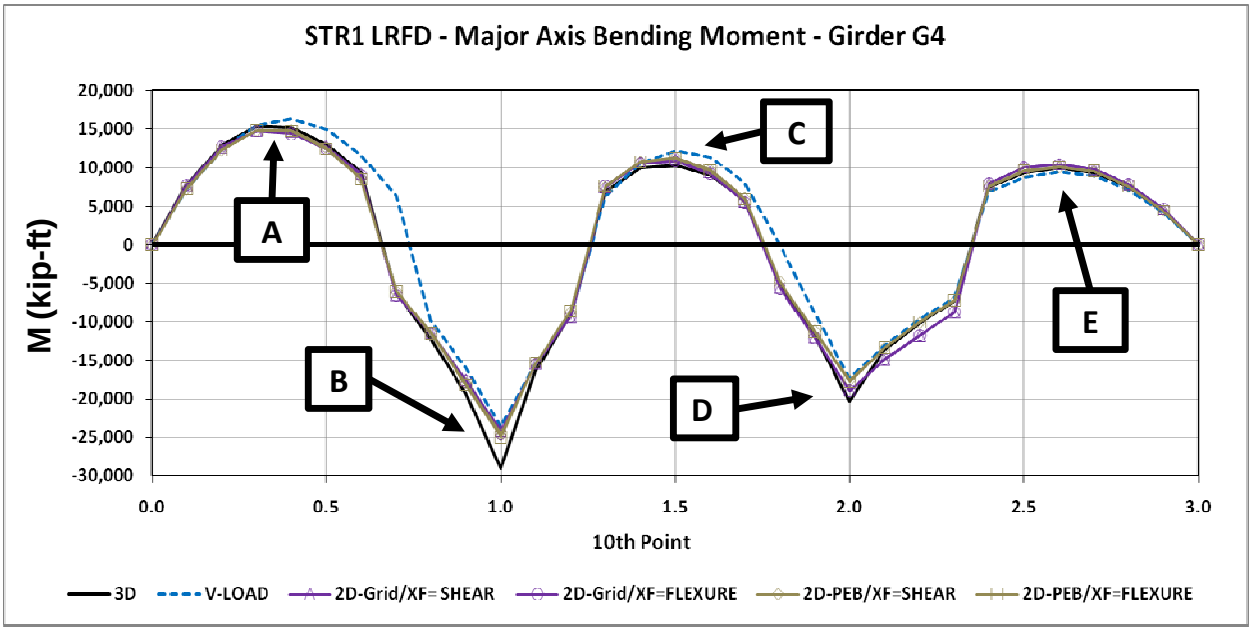
E

- V-load -5%
- 2D Grid-Shear +5%
- 2D Grid-Flex +5%
- 2D P&EB-Shear +1%
- 2D P&EB-Flex +1%

Figure 2.6.26 Strength I Vertical Bending Moment in G1 of the Example I-Girder Bridge

For both the 2D grid and 2D P&EB methods, comparison percentages are listed with the cross-frames represented using either the “shear stiffness” (denoted as “Shear”) or “flexure stiffness” approach (denoted as “Flex”). Except for one case – the 2D grid method at Pier 1 – the analysis methods underestimate the maximum Strength I moments in G1 with respect to the 3D finite element method. Larger discrepancies are generally noted at the skewed piers.

Figure 2.6.27 shows a comparison plot of the total factored Strength I vertical bending moments in G4 of the example bridge. In this case, the largest observed deviations with respect to the 3D finite element method were at the piers and at the maximum moment location in the center span. Interestingly, for both the 2D grid and 2D P&EB methods, the use of the “shear stiffness” or “flexure stiffness” approach to represent the cross-frames did not appear to have a significant effect on the vertical bending moment results in this particular case.



A
- V-load +1%
- 2D Grid-Shear -4%
- 2D Grid-Flex -5%
- 2D P&EB-Shear -4%
- 2D P&EB-Flex -4%

B
- V-load -19%
- 2D Grid-Shear -17%
- 2D Grid-Flex -16%
- 2D P&EB-Shear -15%
- 2D P&EB-Flex -14%

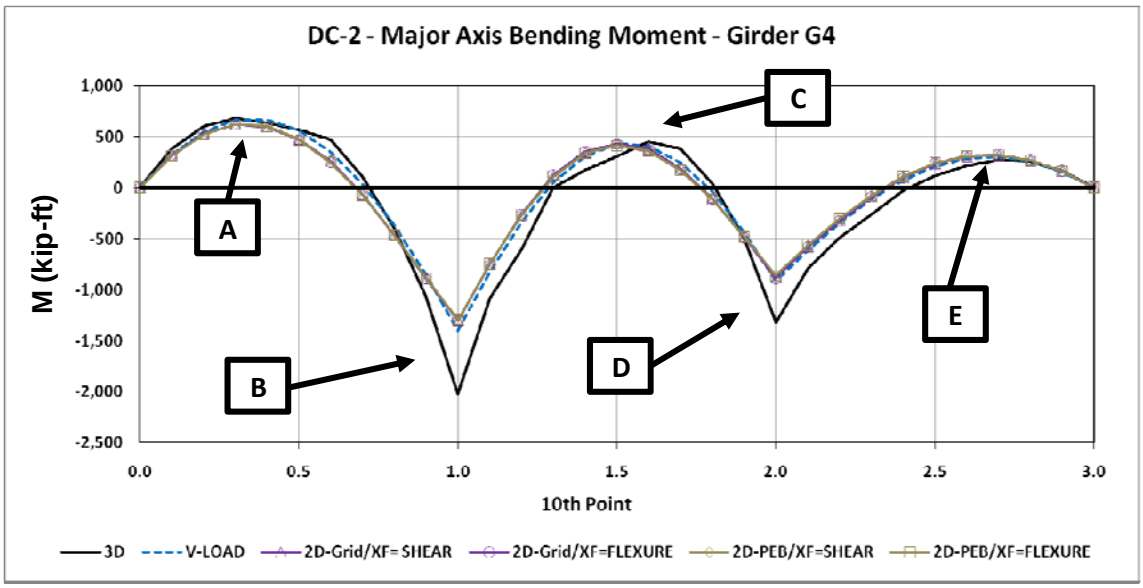
C
- V-load +20%
- 2D Grid-Shear +9%
- 2D Grid-Flex +6%
- 2D P&EB-Shear +12%
- 2D P&EB-Flex +10%

D
- V-load -14%
- 2D Grid-Shear -7%
- 2D Grid-Flex -7%
- 2D P&EB-Shear -13%
- 2D P&EB-Flex -13%

E
- V-load -5%
- 2D Grid-Shear +5%
- 2D Grid-Flex +5%
- 2D P&EB-Shear +1%
- 2D P&EB-Flex +1%

Figure 2.6.27 Strength I Vertical Bending Moment in G4 of the Example I-Girder Bridge

Figure 2.6.28 shows a comparison plot of the unfactored composite dead load (DC_2) vertical bending moments in G4 of the example bridge; that is, the vertical bending moments due to the barrier loads. Again, percentages shown for each analysis method with respect to the results determined using the 3D finite element method are shown below the figure.



A

- V-load -2%
- 2D Grid-Shear -9%
- 2D Grid-Flex -9%
- 2D P&EB-Shear -8%
- 2D P&EB-Flex -9%

B

- V-load -31%
- 2D Grid-Shear -36%
- 2D Grid-Flex -35%
- 2D P&EB-Shear -36%
- 2D P&EB-Flex -36%

C

- V-load +39%
- 2D Grid-Shear +39%
- 2D Grid-Flex +37%
- 2D P&EB-Shear +34%
- 2D P&EB-Flex +32%

D

- V-load -31%
- 2D Grid-Shear -33%
- 2D Grid-Flex -33%
- 2D P&EB-Shear -35%
- 2D P&EB-Flex -35%

E

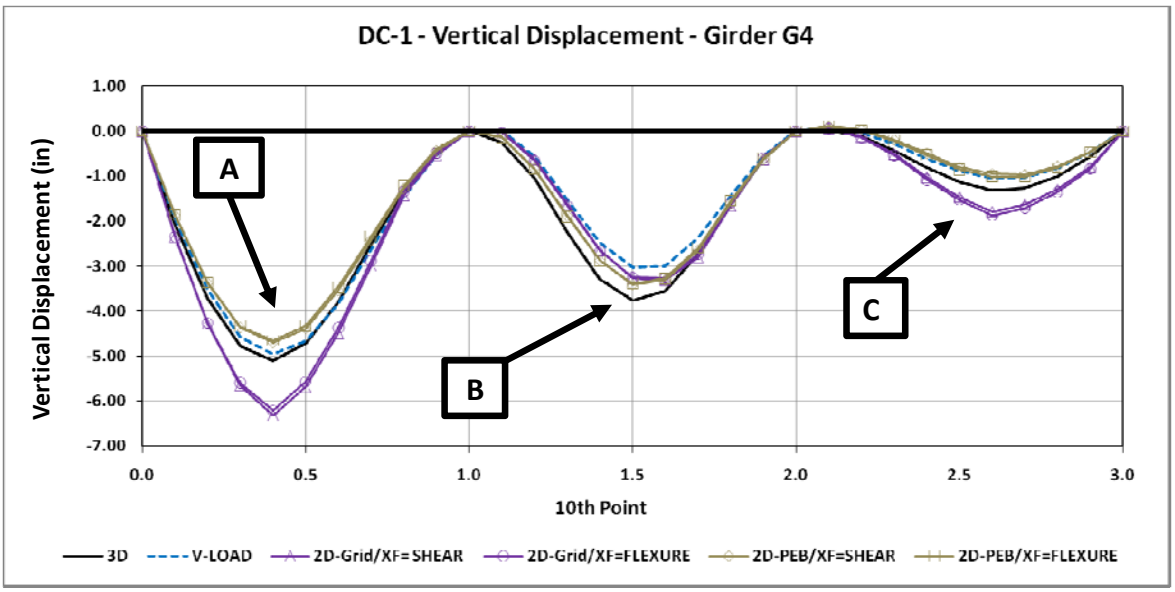
- V-load +9%
- 2D Grid-Shear +15%
- 2D Grid-Flex +17%
- 2D P&EB-Shear +15%
- 2D P&EB-Flex +16%

Figure 2.6.28 Unfactored DC_2 Vertical Bending Moment in G4 of the Example I-Girder Bridge

In the V-load and 2D grid analyses, the barrier loads are assumed equally distributed to all four girders. In the 3D finite element analysis, the barrier loads are placed at their actual locations along the outside edges of the deck.

The pier moments in G2 and G3 due to these loads determined from the V-load and 2D grid analyses (not shown) ranged from approximately 10 to 28 percent *larger* than the pier moments determined from the 3D finite element analysis.

Figure 2.6.9 shows a comparison plot of the unfactored non-composite dead load (DC_1) vertical displacements of G4 of the example bridge; that is, the vertical displacements due to the weight of the steel and concrete deck.



A

- V-load -3%
- 2D Grid-Shear +24%
- 2D Grid-Flex +22%
- 2D P&EB-Shear -8%
- 2D P&EB-Flex -9%

B

- V-load -19%
- 2D Grid-Shear -13%
- 2D Grid-Flex -14%
- 2D P&EB-Shear -9%
- 2D P&EB-Flex -10%

C

- V-load -20%
- 2D Grid-Shear +37%
- 2D Grid-Flex +43%
- 2D P&EB-Shear -27%
- 2D P&EB-Flex -23%

Figure 2.6.29 Unfactored DC_1 Vertical Displacement of G4

The large discrepancies between the 2D grid and 2D P&EB methods in this case are due to the fact that the 2D grid model has an additional girder node in between each cross-frame in this case. When these additional nodes are removed, the 2D grid results are more in-line with the P&EB results. This illustrates the importance of being aware of and understanding the consequences and effects of various modeling assumptions.

Figure 2.6.30 shows a comparison plot of the unfactored bottom flange lateral bending moment due to DC_1 loads in G4 of the example bridge.

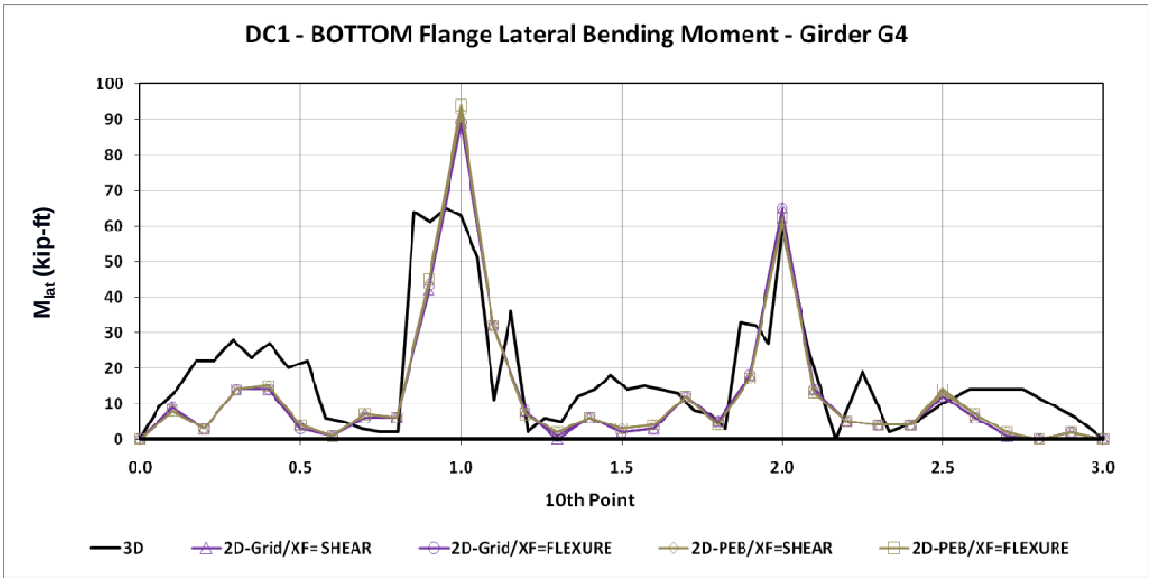


Figure 2.6.30 Unfactored DC_1 Bottom Flange Lateral Bending Moment in G4 of the Example I-Girder Bridge

The lateral flange moments from the V-load method are not included in the comparison.

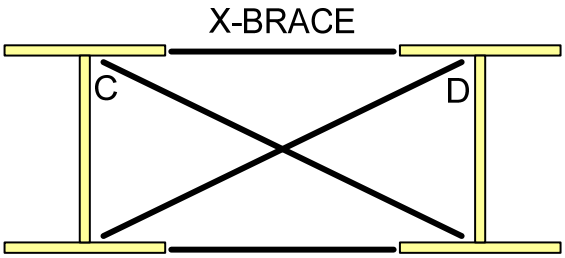
For the 2D grid analyses, lateral flange bending moments must be determined using the approximate V-load equation (Section 2.3.2.2.5), which only accounts for lateral flange bending due to curvature effects.

The lateral flange bending moments determined from the 3D finite element analysis include lateral bending effects due to curvature and due to the effect of the discontinuous cross-frames introduced adjacent to the skewed piers. Lateral bending due to the effect of discontinuous cross-frames is discussed in Section 3.1.2.8.3.2.

Table 2.6.2 shows a comparison of the total factored Strength I cross-frame axial forces in the indicated intermediate X-type cross-frame from the example bridge (Figure 2.6.31).

Table 2.6.2 Strength I Axial Forces in Cross-Frame Between G2 and G3 from the Example I-Girder Bridge (Figure 2.6.27)

Member	Analysis Method	Strength I – Max. (kips)	Strength I – Min. (kips)
Top Chord	3D	43.3	-39.0
	2D Grid – Shear	50.5	10.3
	2D P&EB – Shear	44.5	6.0
Diagonal C	3D	-5.0	-33.0
	2D Grid – Shear	52.5	15.8
	2D P&EB – Shear	44.8	20.3
Diagonal D	3D	29.0	-20.0
	2D Grid – Shear	-15.8	-52.5
	2D P&EB – Shear	-20.3	-44.8
Bottom Chord E	3D	-17.0	-25.8
	2D Grid – Shear	-10.3	-50.5
	2D P&EB – Shear	-6.0	-44.5



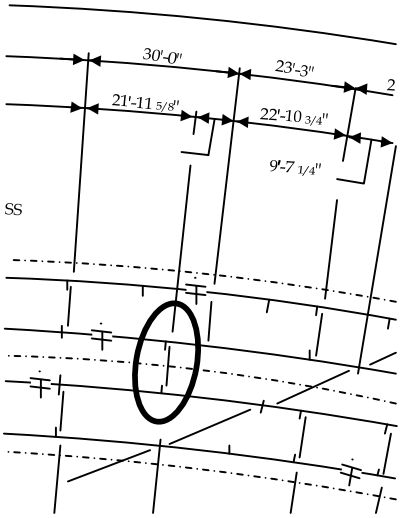


Figure 2.6.31 Cross-frame Detail and Location for Table 2.6.2

Cross-frame forces calculated from the V-load analysis results are not included in the comparison.

The discrepancies are attributed largely to the fact that the dead load forces in the members differed in sign and/or in magnitude between the 3D and 2D methods. Recognition of the horizontal shear stiffness of the deck in the 3D analysis also affects the cross-frame forces.

For both the 2D grid and 2D P&EB methods, the use of the “shear stiffness” or “flexure stiffness” approach to represent the cross-frames did not appear to have a

significant effect on the cross-frame force results in this particular case. Only values calculated based on using the "shear stiffness" approach to represent the cross-frames are shown in Table 2.6.2; values calculated based on the use of the "flexure stiffness" approach are not significantly different.

The list provided below shows some general observations gleaned from the comparative study of the example bridge investigated utilizing various levels of analysis. The observations listed here again are with respect to analysis results determined using the 3D finite element method. These observations may not necessarily apply in total to a different bridge geometry or situation. Judgment is required.

For the most part, the V-load method does not accurately predict the responses. The following observations can be made regarding the 2D grid and 2D P&EB methods:

- Reasonable predictions of Strength I vertical bending moments are made; however, they are less accurate at skewed piers;
- Less accurate predictions of dead load vertical displacements and DC_2 vertical bending moments are made;
- Lateral bending moments must be determined from an approximate equation which only accounts for curvature effects, and;
- Cross-frame force predictions are generally not accurate.

The completed Levels of Analysis matrix in Section 2.6.4 is intended to aid in making the proper judgment regarding the required level of analysis to be applied in a given situation.

Comparative results for all the girders and for some additional cross-frames in the example I-girder bridge are provided below.

Comparative Results for the Example I-Girder Bridge

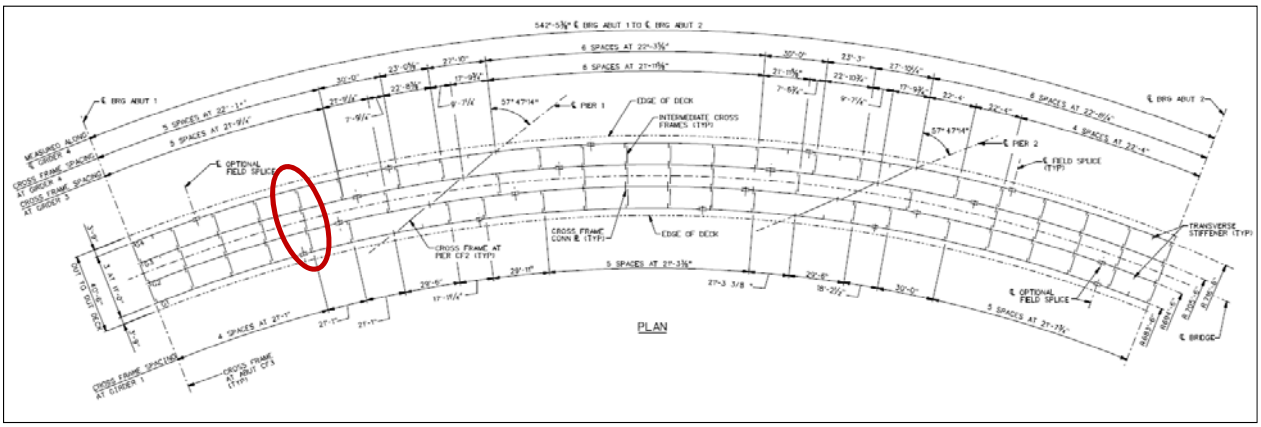


Figure 2.6.32 Cross-Frame Line 5 in the Example I-Girder Bridge

DC1 DEAD LOAD [UNFACTORED]						
XF Bay	Member	3D TOTAL (kip)	2D Grid XF-SHEAR (kip)	2D Grid XF-FLEX (kip)	2D PEB XF-SHEAR (kip)	2D PEB XF-FLEX (kip)
G1-G2	Top Chord	16	14	18	14	18
	Bottom Chord	-18	-14	-19	-14	-19
	Diagonal C	19	-13	-17	-13	-17
	Diagonal D	-18	13	18	13	18
G2-G3	Top Chord	24	20	25	20	25
	Bottom Chord	-25	-20	-27	-20	-27
	Diagonal C	-4	-1	3	-1	3
	Diagonal D	4	1	-1	1	-1
G3-G4	Top Chord	13	14	15	14	15
	Bottom Chord	-15	-14	-16	-14	-16
	Diagonal C	3	-3	0	-3	0
	Diagonal D	-2	3	2	3	2

Figure 2.6.33 Unfactored DC_1 Axial Forces at Cross-Frame Line 5

DC2 DEAD LOAD [UNFACTORED]						
XF Bay	Member	3D STG 7	2D Grid XF-SHEAR	2D Grid XF-FLEX	2D PEB XF-SHEAR	2D PEB XF-FLEX
		(kip)	(kip)	(kip)	(kip)	(kip)
G1-G2	Top Chord	-8	2	2	1	2
	Bottom Chord	-9	-2	-2	-1	-2
	Diagonal C	11	-2	-2	-1	-2
	Diagonal D	-22	2	2	1	2
G2-G3	Top Chord	4	3	4	2	3
	Bottom Chord	-23	-3	-4	-2	-3
	Diagonal C	-5	0	0	-1	0
	Diagonal D	-7	0	0	1	1
G3-G4	Top Chord	-7	2	2	2	2
	Bottom Chord	-10	-2	-2	-2	-2
	Diagonal C	-20	0	0	0	0
	Diagonal D	9	0	0	0	0

Figure 2.6.34 Unfactored DC_2 Axial Forces at Cross-Frame Line 5

+LL+I [UNFACTORED]						
XF Bay	Member	3D	2D Grid XF-SHEAR	2D Grid XF-FLEX	2D PEB XF-SHEAR	2D PEB XF-FLEX
		(kip)	(kip)	(kip)	(kip)	(kip)
G1-G2	Top Chord	4	20	26	10	14
	Bottom Chord	20	18	25	11	16
	Diagonal C	26	16	22	11	16
	Diagonal D	35	16	22	11	16
G2-G3	Top Chord	4	41	51	22	31
	Bottom Chord	35	33	43	18	28
	Diagonal C	25	11	12	4	5
	Diagonal D	14	28	31	18	21
G3-G4	Top Chord	4	6	6	5	5
	Bottom Chord	14	9	12	6	9
	Diagonal C	31	14	16	11	13
	Diagonal D	16	26	28	20	23

Figure 2.6.35 Unfactored +LL+IM Axial Forces at Cross-Frame Line 5

-LL+I [UNFACTORED]						
XF Bay	Member	3D	2D Grid XF-SHEAR	2D Grid XF-FLEX	2D PEB XF-SHEAR	2D PEB XF-FLEX
		(kip)	(kip)	(kip)	(kip)	(kip)
G1-G2	Top Chord	-4	-18	-24	-11	-15
	Bottom Chord	-25	-20	-27	-10	-15
	Diagonal C	-21	-16	-21	-11	-15
	Diagonal D	-45	-16	-21	-11	-16
G2-G3	Top Chord	-2	-33	-41	-18	-26
	Bottom Chord	-65	-41	-54	-22	-33
	Diagonal C	-13	-28	-33	-18	-23
	Diagonal D	-7	-11	-13	-4	-5
G3-G4	Top Chord	-2	-9	-11	-6	-8
	Bottom Chord	-34	-6	-6	-5	-5
	Diagonal C	-24	-26	-29	-20	-24
	Diagonal D	-5	-14	-16	-11	-13

Figure 2.6.36 Unfactored -LL+IM Axial Forces at Cross-Frame Line 5

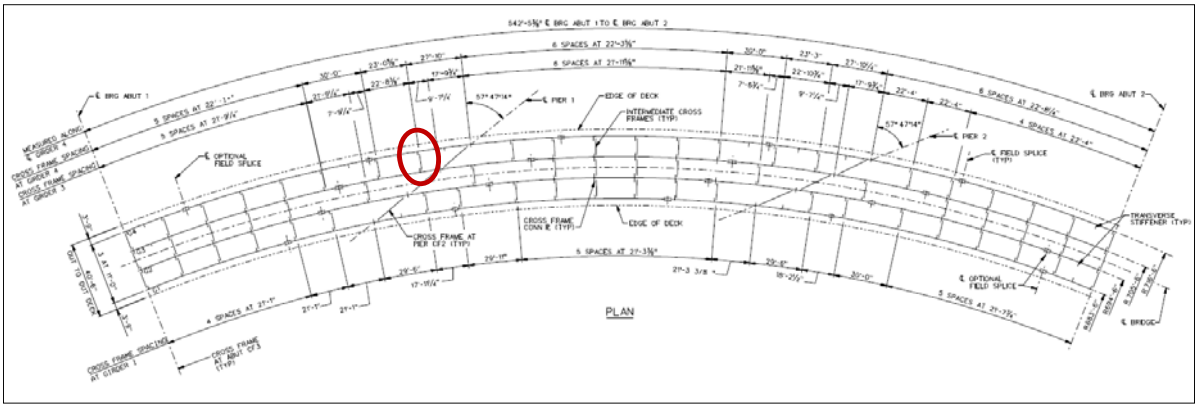


Figure 2.6.37 Cross-Frame Line 9 Between G3 and G4 in the Example I-Girder Bridge

DC1 DEAD LOAD [UNFACTORED]						
XF Bay	Member	3D TOTAL	2D Grid XF-SHEAR	2D Grid XF-FLEX	2D PEB XF-SHEAR	2D PEB XF-FLEX
		(kip)	(kip)	(kip)	(kip)	(kip)
G3-G4	Top Chord	-5	-3	-3	-3	-3
	Bottom Chord	5	3	3	3	3
	Diagonal C	-31	31	31	31	31
	Diagonal D	31	-31	-31	-31	-31

Figure 2.6.38 Unfactored DC_1 Axial Forces at Cross-Frame Line 9 Between G3 and G4

DC2 DEAD LOAD [UNFACTORED]						
XF Bay	Member	3D	2D Grid XF-SHEAR	2D Grid XF-FLEX	2D PEB XF-SHEAR	2D PEB XF-FLEX
		(kip)	(kip)	(kip)	(kip)	(kip)
G3-G4	Top Chord	-11	0	0	0	0
	Bottom Chord	2	0	0	0	0
	Diagonal C	-7	4	4	4	4
	Diagonal D	1	-4	-4	-4	-4

Figure 2.6.39 Unfactored DC_2 Axial Forces at Cross-Frame Line 9 Between G3 and G4

+LL+I [UNFACTORED]						
XF Bay	Member	3D TOTAL	2D Grid XF-SHEAR	2D Grid XF-FLEX	2D PEB XF-SHEAR	2D PEB XF-FLEX
		(kip)	(kip)	(kip)	(kip)	(kip)
G3-G4	Top Chord	12	4	4	6	7
	Bottom Chord	12	9	9	6	9
	Diagonal C	8	15	14	13	15
	Diagonal D	15	14	13	7	7

Figure 2.6.40 Unfactored +LL+IM Axial Forces at Cross-Frame Line 9 Between G3 and G4

-LL+I [UNFACTORED]						
XF Bay	Member	3D TOTAL	2D Grid XF-SHEAR	2D Grid XF-FLEX	2D PEB XF-SHEAR	2D PEB XF-FLEX
		(kip)	(kip)	(kip)	(kip)	(kip)
G3-G4	Top Chord	-16	-9	-9	-6	-9
	Bottom Chord	-7	-4	-4	-6	-8
	Diagonal C	-21	-14	-13	-7	-8
	Diagonal D	-3	-15	-14	-13	-14

Figure 2.6.41 Unfactored -LL+IM Axial Forces at Cross-Frame Line 9 Between G3 and G4

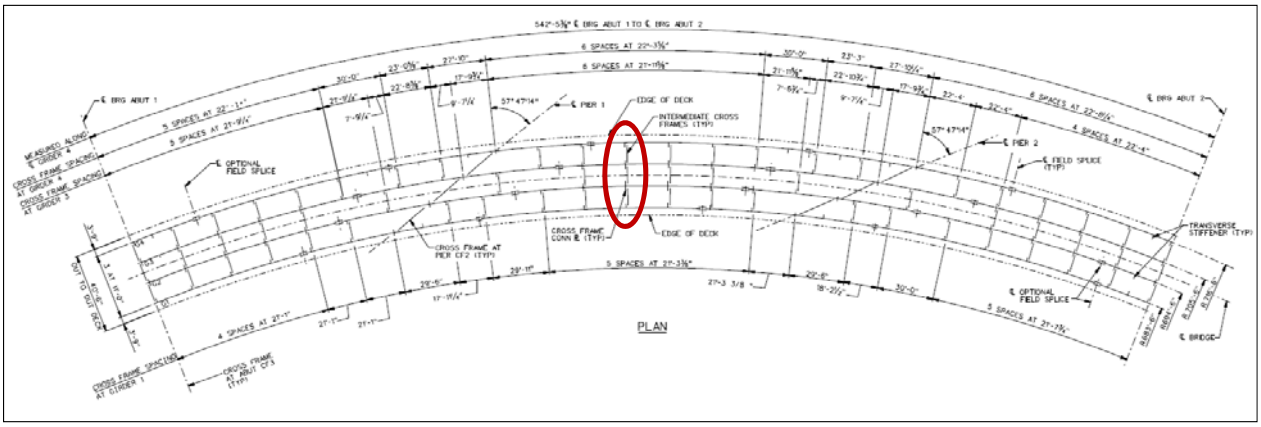


Figure 2.6.42 Cross-Frame Line 14 in the Example I-Girder Bridge

DC1 DEAD LOAD [UNFACTORED]						
XF Bay	Member	3D TOTAL	2D Grid XF-SHEAR	2D Grid XF-FLEX	2D PEB XF-SHEAR	2D PEB XF-FLEX
		(kip)	(kip)	(kip)	(kip)	(kip)
G1-G2	Top Chord	-18	-12	-15	-12	-15
	Bottom Chord	19	12	16	12	16
	Diagonal C	-11	3	5	3	5
	Diagonal D	10	-3	-6	-3	-6
G2-G3	Top Chord	-33	-20	-26	-20	-26
	Bottom Chord	36	20	28	20	28
	Diagonal C	1	-6	-5	-6	-5
	Diagonal D	-4	6	3	6	3
G3-G4	Top Chord	-17	-10	-13	-10	-13
	Bottom Chord	18	10	14	10	14
	Diagonal C	25	-16	-22	-16	-22
	Diagonal D	-27	16	21	16	21

Figure 2.6.43 Unfactored DC_1 Axial Forces at Cross-Frame Line 14

DC2 DEAD LOAD [UNFACTORED]						
XF Bay	Member	3D	2D Grid XF-SHEAR	2D Grid XF-FLEX	2D PEB XF-SHEAR	2D PEB XF-FLEX
		(kip)	(kip)	(kip)	(kip)	(kip)
G1-G2	Top Chord	-7	-1	-1	-1	-1
	Bottom Chord	-2	1	1	1	1
	Diagonal C	3	0	0	-1	0
	Diagonal D	-10	0	0	1	0
G2-G3	Top Chord	4	-2	-2	-1	-2
	Bottom Chord	-8	2	2	1	2
	Diagonal C	-1	-1	-1	-1	-1
	Diagonal D	-2	1	1	1	1
G3-G4	Top Chord	-7	-1	-1	0	-1
	Bottom Chord	-1	1	1	0	1
	Diagonal C	-9	-2	-2	-1	-2
	Diagonal D	2	2	2	1	2

Figure 2.6.44 Unfactored DC_2 Axial Forces at Cross-Frame Line 14

+LL+I [UNFACTORED]						
XF Bay	Member	3D	2D Grid XF-SHEAR	2D Grid XF-FLEX	2D PEB XF-SHEAR	2D PEB XF-FLEX
		(kip)	(kip)	(kip)	(kip)	(kip)
G1-G2	Top Chord	3	3	2	1	2
	Bottom Chord	14	13	15	9	12
	Diagonal C	12	12	13	9	11
	Diagonal D	18	12	13	9	11
G2-G3	Top Chord	4	9	7	4	4
	Bottom Chord	24	22	25	15	21
	Diagonal C	17	14	15	12	14
	Diagonal D	10	23	21	17	19
G3-G4	Top Chord	4	7	7	6	6
	Bottom Chord	11	12	15	9	13
	Diagonal C	25	19	21	17	21
	Diagonal D	4	31	33	25	30

Figure 2.6.45 Unfactored +LL+IM Axial Forces at Cross-Frame Line 14

-LL+I [UNFACTORED]						
XF Bay	Member	3D	2D Grid XF-SHEAR	2D Grid XF-FLEX	2D PEB XF-SHEAR	2D PEB XF-FLEX
		(kip)	(kip)	(kip)	(kip)	(kip)
G1-G2	Top Chord	-1	-13	-14	-9	-12
	Bottom Chord	-5	-3	-3	-1	-2
	Diagonal C	-11	-12	-14	-9	-12
	Diagonal D	-18	-12	-14	-9	-12
G2-G3	Top Chord	0	-22	-24	-15	-20
	Bottom Chord	-12	-9	-7	-4	-5
	Diagonal C	-4	-23	-23	-17	-20
	Diagonal D	-15	-14	-15	-12	-14
G3-G4	Top Chord	-1	-12	-14	-9	-12
	Bottom Chord	-8	-7	-7	-6	-7
	Diagonal C	-10	-31	-34	-25	-31
	Diagonal D	-22	-19	-21	-17	-21

Figure 2.6.46 Unfactored –LL+IM Axial Forces at Cross-Frame Line 14

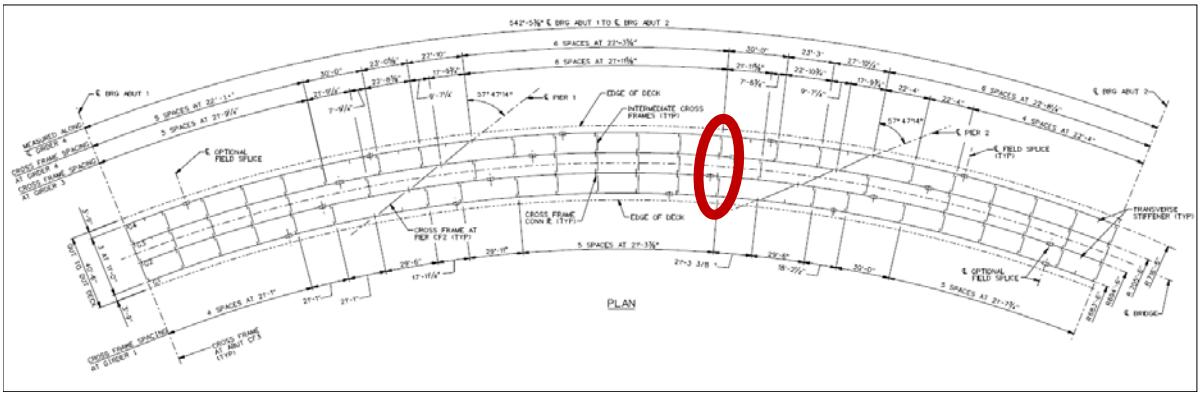


Figure 2.6.47 Cross-Frame Line 17 Between G1 and G2 and Between G3 and G4 in the Example I-Girder Bridge

DC1 DEAD LOAD [UNFACTORED]						
XF Bay	Member	3D TOTAL	2D Grid XF-SHEAR	2D Grid XF-FLEX	2D PEB XF-SHEAR	2D PEB XF-FLEX
		(kip)	(kip)	(kip)	(kip)	(kip)
G1-G2	Top Chord	12	7	7	7	7
	Bottom Chord	-11	-7	-8	-7	-8
	Diagonal C	-14	15	15	15	15
	Diagonal D	14	-15	-15	-15	-15
G3-G4	Top Chord	4	5	5	5	5
	Bottom Chord	-4	-5	-5	-5	-5
	Diagonal C	6	-9	-9	-9	-9
	Diagonal D	-6	9	9	9	9

Figure 2.6.48 Unfactored DC_1 Axial Forces at Cross-Frame Line 17 Between G1 and G2 and Between G3 and G4

DC2 DEAD LOAD [UNFACTORED]						
XF Bay	Member	3D STG 7	2D Grid XF-SHEAR	2D Grid XF-FLEX	2D PEB XF-SHEAR	2D PEB XF-FLEX
		(kip)	(kip)	(kip)	(kip)	(kip)
G1-G2	Top Chord	-11	1	1	1	1
	Bottom Chord	1	-1	-1	-1	-1
	Diagonal C	-6	2	2	1	1
	Diagonal D	-2	-2	-2	-1	-1
G3-G4	Top Chord	-10	1	1	1	1
	Bottom Chord	1	-1	-1	-1	-1
	Diagonal C	-3	-1	-1	-1	-1
	Diagonal D	-4	1	1	1	1

Figure 2.6.49 Unfactored DC_2 Axial Forces at Cross-Frame Line 17 Between G1 and G2 and Between G3 and G4

+LL+I [UNFACTORED]						
XF Bay	Member	3D	2D Grid XF-SHEAR	2D Grid XF-FLEX	2D PEB XF-SHEAR	2D PEB XF-FLEX
		(kip)	(kip)	(kip)	(kip)	(kip)
G1-G2	Top Chord	9	5	6	8	9
	Bottom Chord	1	1	2	3	3
	Diagonal C	4	12	11	8	9
	Diagonal D	6	10	9	8	9
G3-G4	Top Chord	6	5	5	4	5
	Bottom Chord	1	2	2	3	3
	Diagonal C	8	10	10	8	9
	Diagonal D	6	13	13	14	15

Figure 2.6.50 Unfactored +LL+IM Axial Forces at Cross-Frame Line 17 Between G1 and G2 and Between G3 and G4

-LL+I [UNFACTORED]						
XF Bay	Member	3D	2D Grid XF-SHEAR	2D Grid XF-FLEX	2D PEB XF-SHEAR	2D PEB XF-FLEX
		(kip)	(kip)	(kip)	(kip)	(kip)
G1-G2	Top Chord	-14	-1	-2	-3	-3
	Bottom Chord	-4	-5	-6	-8	-9
	Diagonal C	-12	-10	-9	-8	-9
	Diagonal D	-5	-12	-11	-8	-9
G3-G4	Top Chord	-6	-2	-2	-3	-3
	Bottom Chord	-2	-5	-5	-4	-5
	Diagonal C	-4	-13	-13	-14	-15
	Diagonal D	-12	-10	-10	-8	-9

Figure 2.6.51 Unfactored –LL+IM Axial Forces at Cross-Frame Line 17 Between G1 and G2 and Between G3 and G4

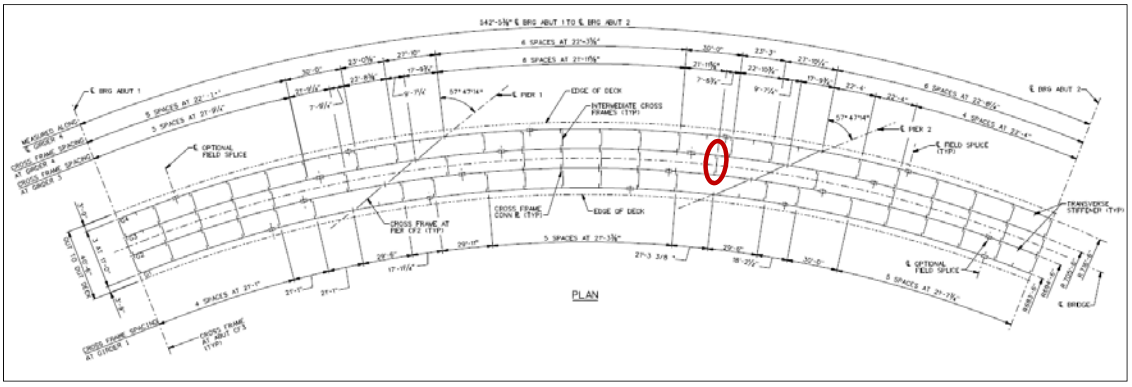


Figure 2.6.52 Cross-Frame Line 18 Between G2 and G3 in the Example I-Girder Bridge

DC1 DEAD LOAD [UNFACTORED]						
XF Bay	Member	3D TOTAL	2D Grid XF-SHEAR	2D Grid XF-FLEX	2D PEB XF-SHEAR	2D PEB XF-FLEX
		(kip)	(kip)	(kip)	(kip)	(kip)
G2-G3	Top Chord	12	7	7	7	7
	Bottom Chord	-12	-7	-7	-7	-7
	Diagonal C	-10	12	12	12	12
	Diagonal D	9	-12	-12	-12	-12

Figure 2.6.53 Unfactored DC_1 Axial Forces at Cross-Frame Line 18 Between G2 and G3

DC2 DEAD LOAD [UNFACTORED]						
XF Bay	Member	3D	2D Grid XF-SHEAR	2D Grid XF-FLEX	2D PEB XF-SHEAR	2D PEB XF-FLEX
		(kip)	(kip)	(kip)	(kip)	(kip)
G2-G3	Top Chord	-4	1	1	9	9
	Bottom Chord	-3	-1	-1	-9	-9
	Diagonal C	-1	2	2	14	14
	Diagonal D	-4	-2	-1	-14	-14

Figure 2.6.54 Unfactored DC_2 Axial Forces at Cross-Frame Line 18 Between G2 and G3

+LL+I [UNFACTORED]						
XF Bay	Member	3D	2D Grid XF-SHEAR	2D Grid XF-FLEX	2D PEB XF-SHEAR	2D PEB XF-FLEX
		(kip)	(kip)	(kip)	(kip)	(kip)
G2-G3	Top Chord	19	16	15	14	16
	Bottom Chord	1	7	7	8	10
	Diagonal C	5	10	10	7	9
	Diagonal D	13	10	10	7	7

Figure 2.6.55 Unfactored +LL+IM Axial Forces at Cross-Frame Line 18 Between G2 and G3

-LL+I [UNFACTORED]						
XF Bay	Member	3D	2D Grid XF-SHEAR	2D Grid XF-FLEX	2D PEB XF-SHEAR	2D PEB XF-FLEX
		(kip)	(kip)	(kip)	(kip)	(kip)
G2-G3	Top Chord	-28	-7	-6	-8	-9
	Bottom Chord	-4	-16	-16	-14	-17
	Diagonal C	-11	-10	-10	-7	-8
	Diagonal D	-15	-10	-10	-7	-8

Figure 2.6.56 Unfactored –LL+IM Axial Forces at Cross-Frame Line 18 Between G2 and G3

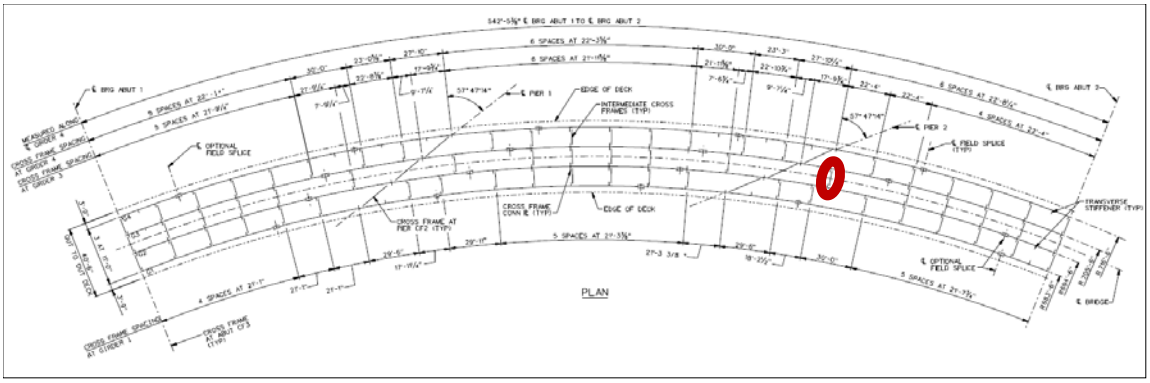


Figure 2.6.57 Cross-Frame Line 22 Between G2 and G3 in the Example I-Girder Bridge

DC1 DEAD LOAD [UNFACTORED]						
XF Bay	Member	3D TOTAL	2D Grid XF-SHEAR	2D Grid XF-FLEX	2D PEB XF-SHEAR	2D PEB XF-FLEX
		(kip)	(kip)	(kip)	(kip)	(kip)
G2-G3	Top Chord	-2	-5	-5	-5	-5
	Bottom Chord	4	5	6	5	6
	Diagonal C	-10	10	10	10	10
	Diagonal D	9	-10	-11	-10	-11

Figure 2.6.58 Unfactored DC_1 Axial Forces at Cross-Frame Line 22 Between G2 and G3

DC2 DEAD LOAD [UNFACTORED]						
XF Bay	Member	3D	2D Grid XF-SHEAR	2D Grid XF-FLEX	2D PEB XF-SHEAR	2D PEB XF-FLEX
		(kip)	(kip)	(kip)	(kip)	(kip)
G2-G3	Top Chord	-3	0	0	9	9
	Bottom Chord	-1	0	0	-9	-9
	Diagonal C	-6	1	1	14	14
	Diagonal D	3	-1	-1	-14	-14

Figure 2.6.59 Unfactored DC_2 Axial Forces at Cross-Frame Line 22 Between G2 and G3

+LL+I [UNFACTORED]						
XF Bay	Member	3D	2D Grid XF-SHEAR	2D Grid XF-FLEX	2D PEB XF-SHEAR	2D PEB XF-FLEX
		(kip)	(kip)	(kip)	(kip)	(kip)
G2-G3	Top Chord	20	4	5	5	7
	Bottom Chord	4	6	7	5	7
	Diagonal C	17	13	13	7	8
	Diagonal D	11	15	14	12	13

Figure 2.6.60 Unfactored +LL+IM Axial Forces at Cross-Frame Line 22 Between G2 and G3

-LL+I [UNFACTORED]						
XF Bay	Member	3D	2D Grid XF-SHEAR	2D Grid XF-FLEX	2D PEB XF-SHEAR	2D PEB XF-FLEX
		(kip)	(kip)	(kip)	(kip)	(kip)
G2-G3	Top Chord	-28	-6	-6	-5	-7
	Bottom Chord	-1	-4	-5	-5	-7
	Diagonal C	-23	-15	-15	-12	-13
	Diagonal D	-10	-13	-13	-7	-8

Figure 2.6.61 Unfactored –LL+IM Axial Forces at Cross-Frame Line 22 Between G2 and G3

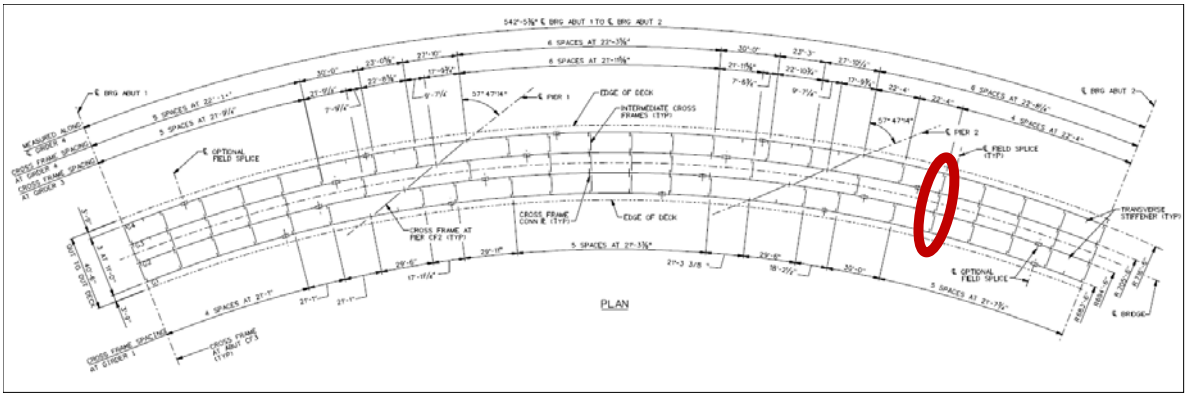


Figure 2.6.62 Cross-Frame Line 24 in the Example I-Girder Bridge

DC1 DEAD LOAD [UNFACTORED]						
XF Bay	Member	3D TOTAL	2D Grid XF-SHEAR	2D Grid XF-FLEX	2D PEB XF-SHEAR	2D PEB XF-FLEX
		(kip)	(kip)	(kip)	(kip)	(kip)
G1-G2	Top Chord	-13	-12	-13	-12	-12
	Bottom Chord	13	12	14	12	12
	Diagonal C	0	-5	-4	-4	-4
	Diagonal D	-1	5	3	4	3
G2-G3	Top Chord	-7	-6	-4	-6	-4
	Bottom Chord	8	6	4	6	4
	Diagonal C	20	-18	-20	-18	-20
	Diagonal D	-20	18	19	18	19
G3-G4	Top Chord	0	0	2	0	2
	Bottom Chord	0	0	-2	0	-2
	Diagonal C	-1	2	3	2	3
	Diagonal D	0	-2	-3	-2	-3

Figure 2.6.63 Unfactored DC_1 Axial Forces at Cross-Frame Line 24

DC2 DEAD LOAD [UNFACTORED]						
XF Bay	Member	3D	2D Grid XF-SHEAR	2D Grid XF-FLEX	2D PEB XF-SHEAR	2D PEB XF-FLEX
		(kip)	(kip)	(kip)	(kip)	(kip)
G1-G2	Top Chord	-7	-1	-1	9	9
	Bottom Chord	-6	1	1	-9	-9
	Diagonal C	9	-1	-1	14	14
	Diagonal D	-18	1	1	-14	-14
G2-G3	Top Chord	4	0	0	9	9
	Bottom Chord	-17	0	0	-9	-9
	Diagonal C	-3	-2	-3	14	14
	Diagonal D	-6	2	3	-14	-14
G3-G4	Top Chord	-8	0	0	9	9
	Bottom Chord	-6	0	0	-9	-9
	Diagonal C	-18	0	1	14	14
	Diagonal D	8	0	0	-14	-14

Figure 2.6.64 Unfactored DC_2 Axial Forces at Cross-Frame Line 24

+LL+I [UNFACTORED]						
XF Bay	Member	3D	2D Grid XF-SHEAR	2D Grid XF-FLEX	2D PEB XF-SHEAR	2D PEB XF-FLEX
		(kip)	(kip)	(kip)	(kip)	(kip)
G1-G2	Top Chord	4	3	3	1	3
	Bottom Chord	19	13	15	9	14
	Diagonal C	18	13	14	10	13
	Diagonal D	27	13	14	11	14
G2-G3	Top Chord	5	4	5	3	4
	Bottom Chord	36	20	27	13	20
	Diagonal C	22	27	31	14	17
	Diagonal D	18	44	48	23	28
G3-G4	Top Chord	5	6	10	3	4
	Bottom Chord	16	14	21	10	16
	Diagonal C	42	24	29	18	23
	Diagonal D	23	34	40	26	32

Figure 2.6.65 Unfactored +LL+IM Axial Forces at Cross-Frame Line 24

-LL+I [UNFACTORED]						
XF Bay	Member	3D	2D Grid XF-SHEAR	2D Grid XF-FLEX	2D PEB XF-SHEAR	2D PEB XF-FLEX
		(kip)	(kip)	(kip)	(kip)	(kip)
G1-G2	Top Chord	-1	-13	-14	-9	-13
	Bottom Chord	-9	-3	-3	-1	-3
	Diagonal C	-15	-13	-14	-11	-14
	Diagonal D	-26	-13	-14	-10	-13
G2-G3	Top Chord	-4	-20	-26	-13	-19
	Bottom Chord	-11	-4	-6	-3	-5
	Diagonal C	-31	-44	-50	-23	-29
	Diagonal D	-32	-27	-31	-14	-17
G3-G4	Top Chord	-1	-14	-19	-10	-15
	Bottom Chord	-8	-6	-11	-3	-5
	Diagonal C	-9	-34	-41	-26	-33
	Diagonal D	-20	-24	-29	-18	-23

Figure 2.6.66 Unfactored –LL+IM Axial Forces at Cross-Frame Line 24

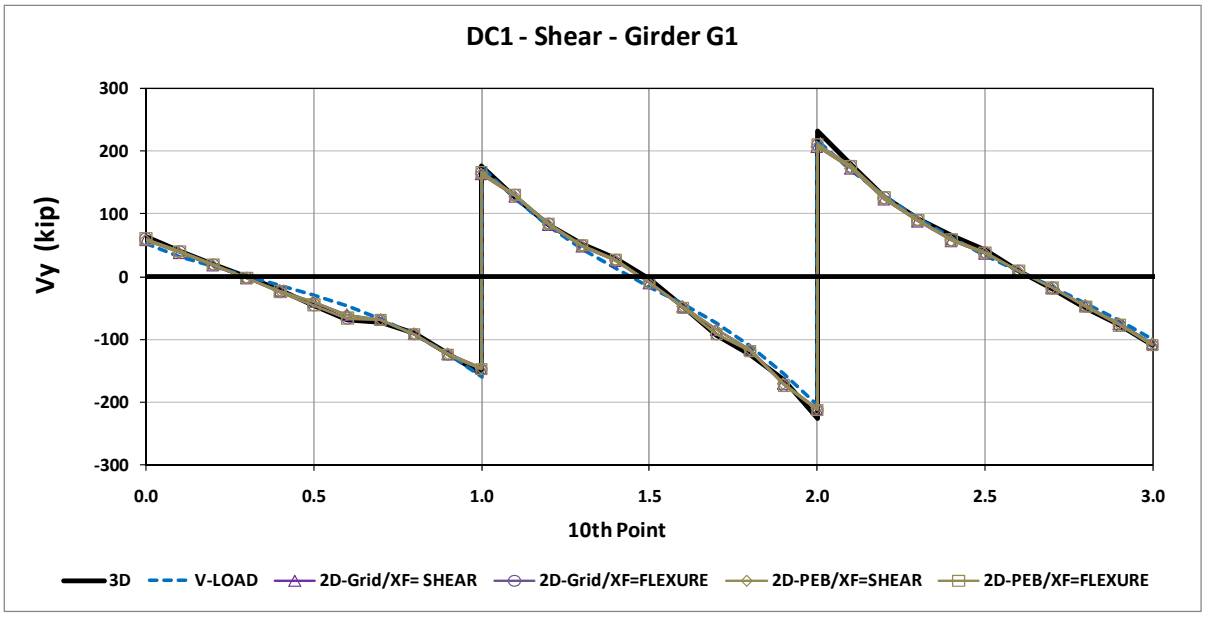


Figure 2.6.67 Unfactored DC_1 Shear in G1

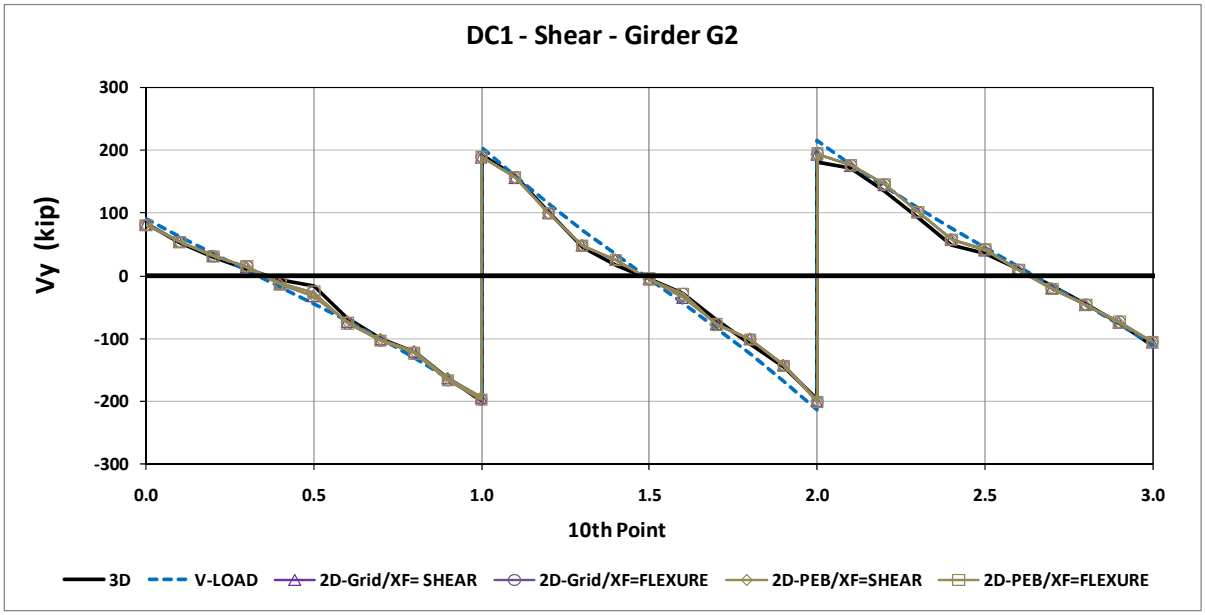


Figure 2.6.68 Unfactored DC_1 Shear in G2

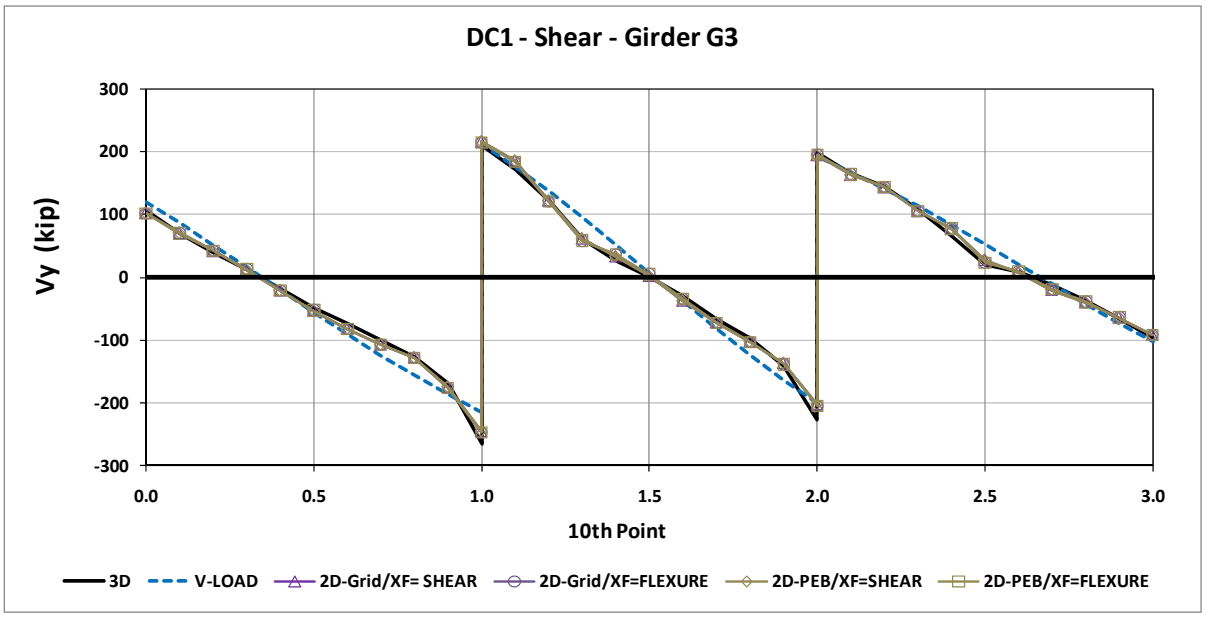


Figure 2.6.69 Unfactored DC_1 Shear in G3

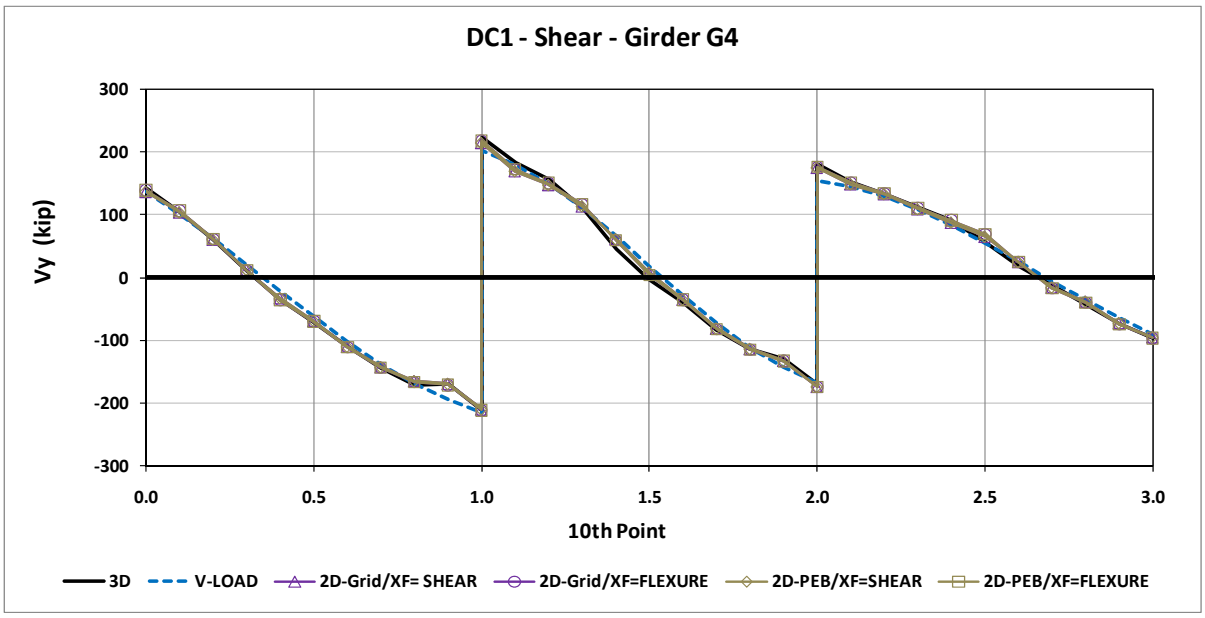


Figure 2.6.70 Unfactored DC_1 Shear in G4

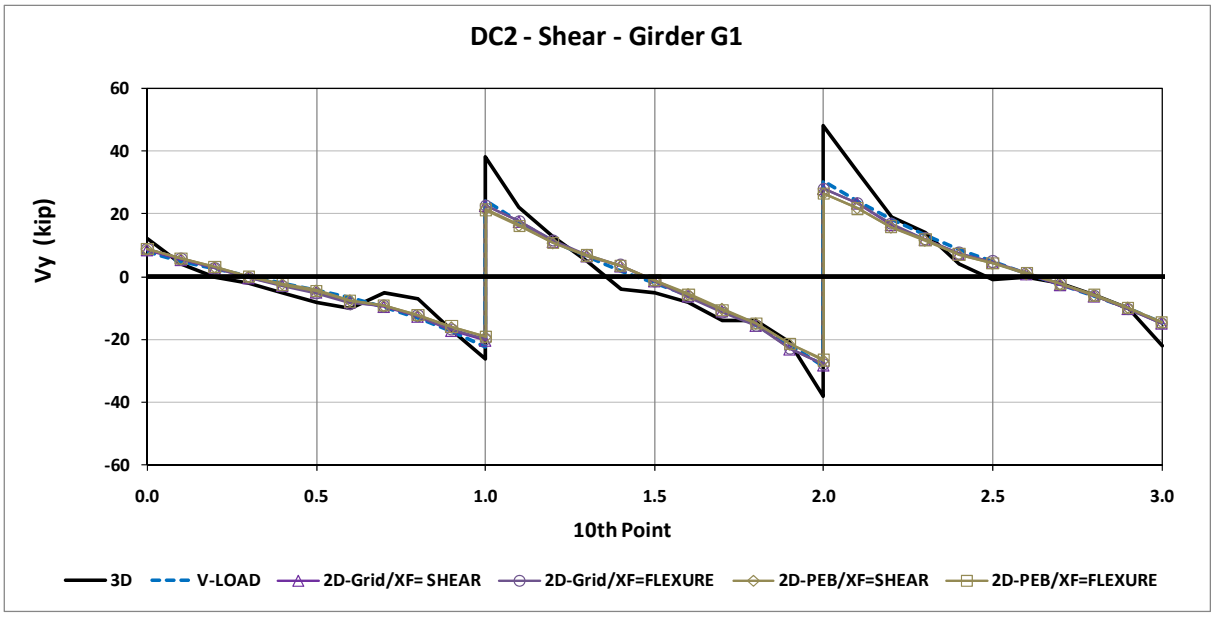


Figure 2.6.71 Unfactored DC_2 Shear in G1

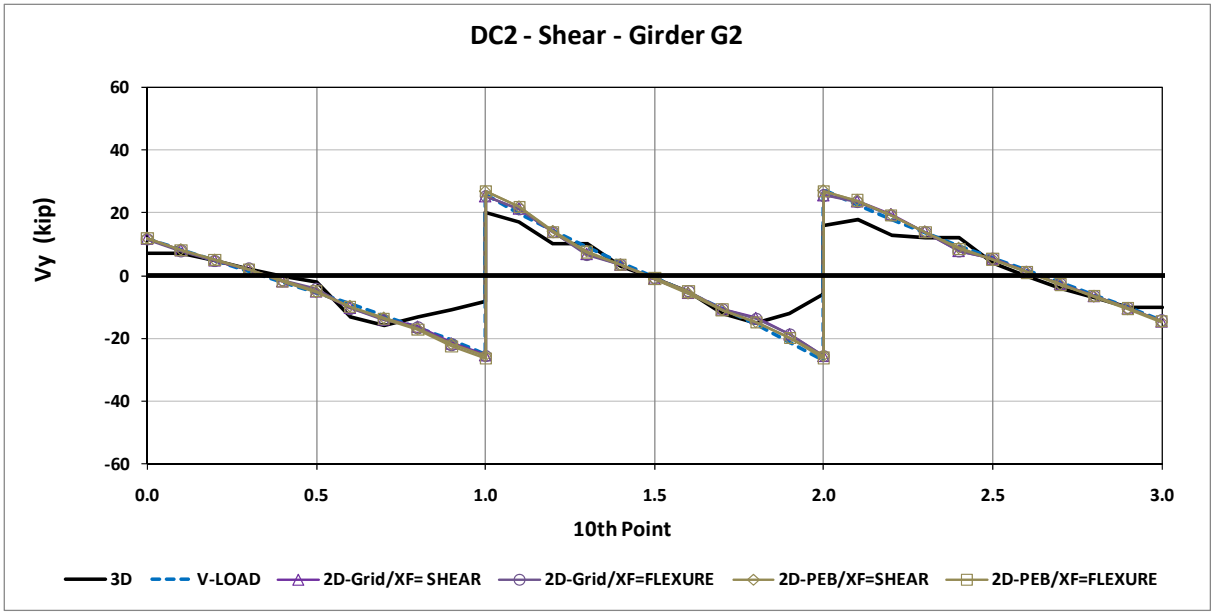


Figure 2.6.72 Unfactored DC_2 Shear in G2

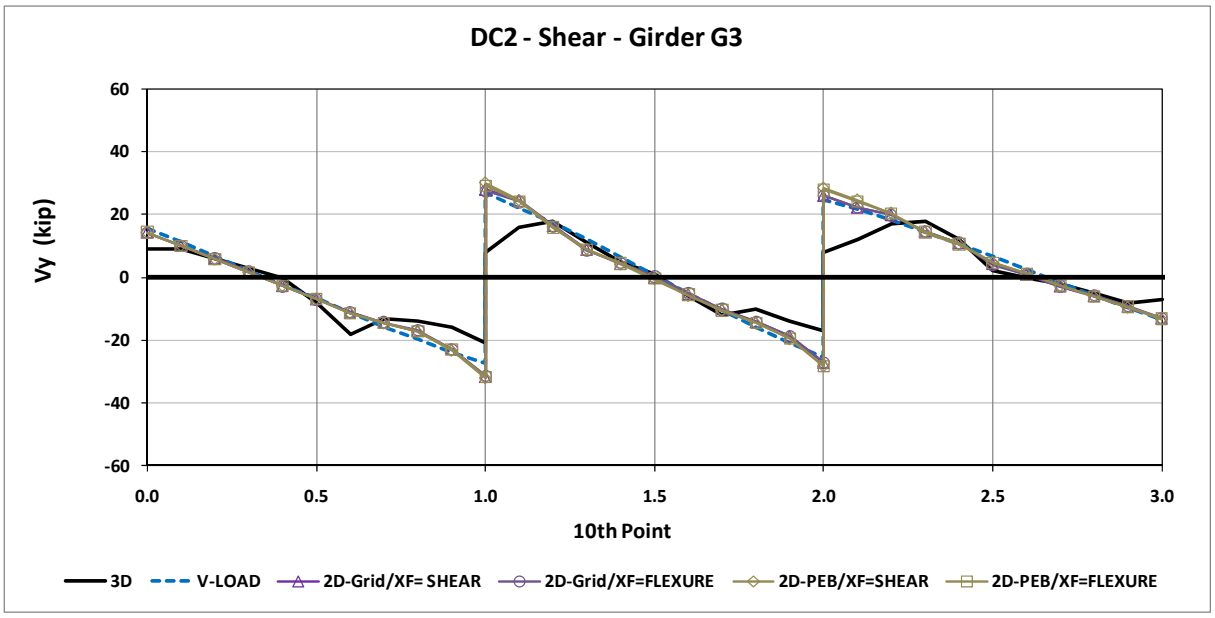


Figure 2.6.73 Unfactored DC_2 Shear in G3

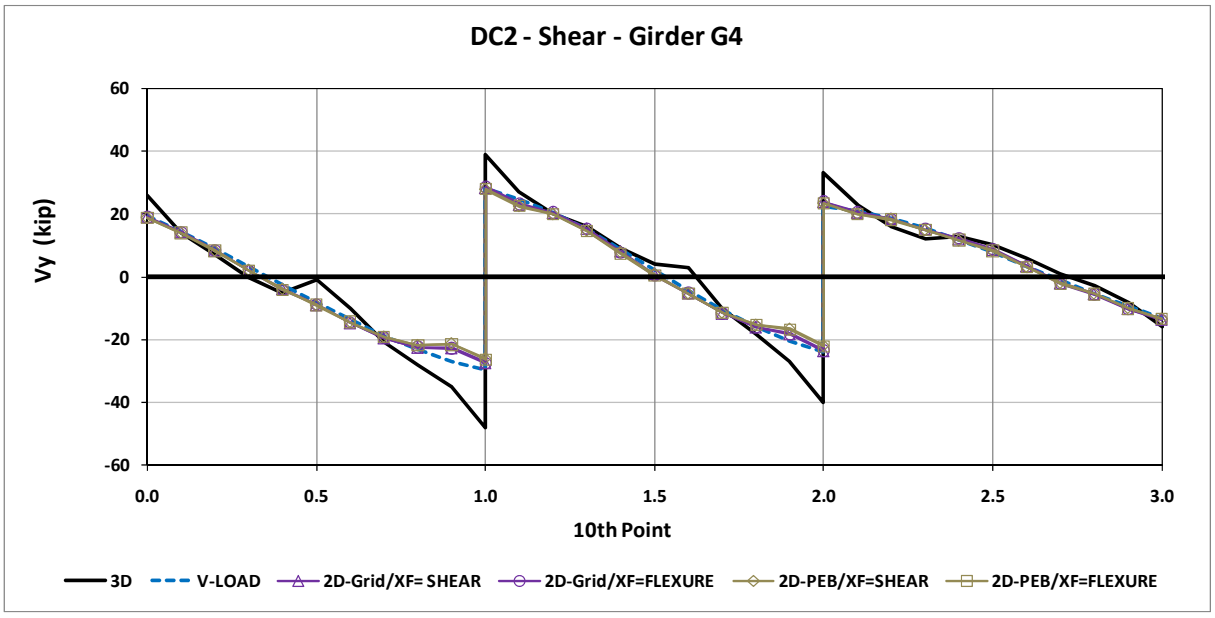


Figure 2.6.74 Unfactored DC_2 Shear in G4

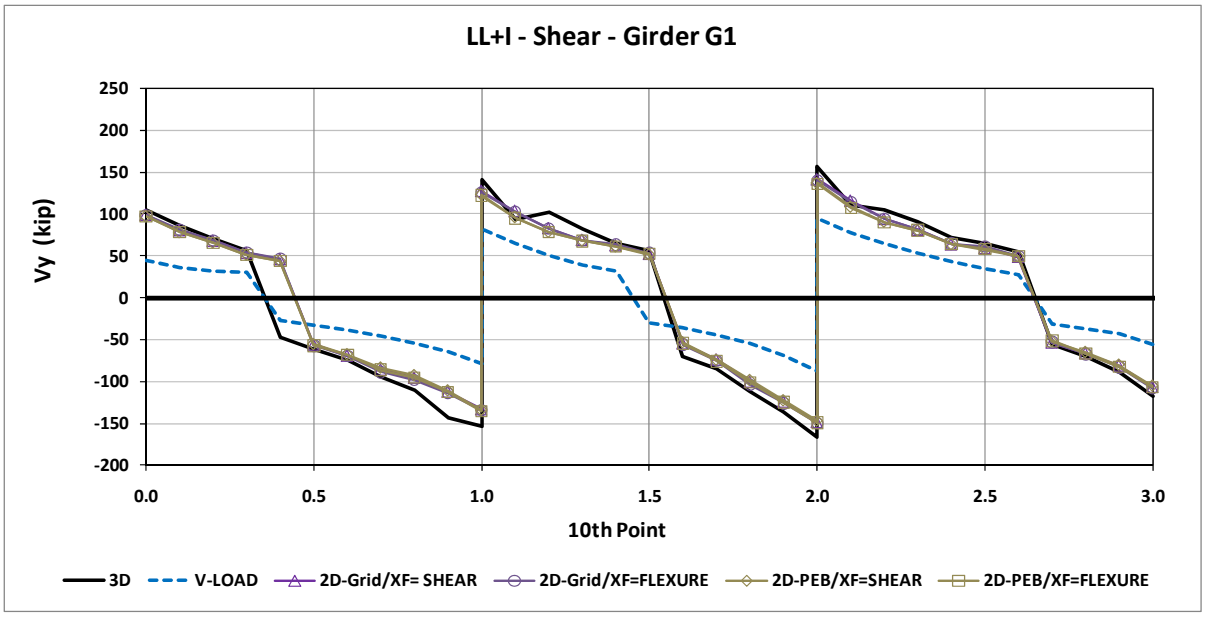


Figure 2.6.75 Unfactored LL+IM Shear in G1

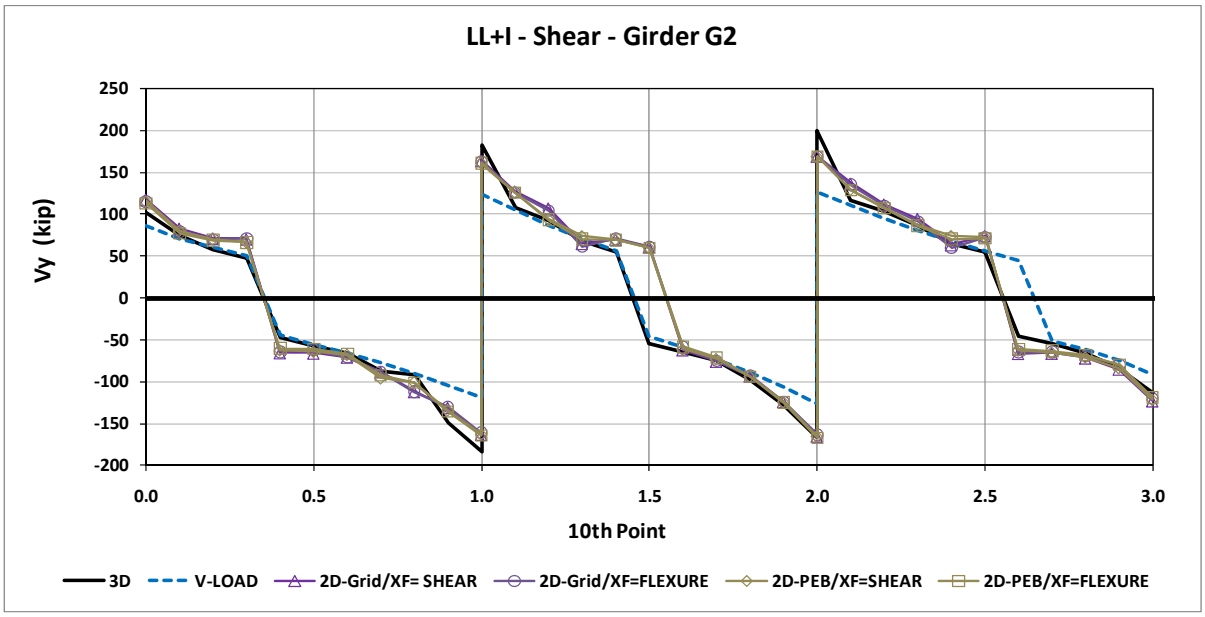


Figure 2.6.76 Unfactored LL+IM Shear in G2

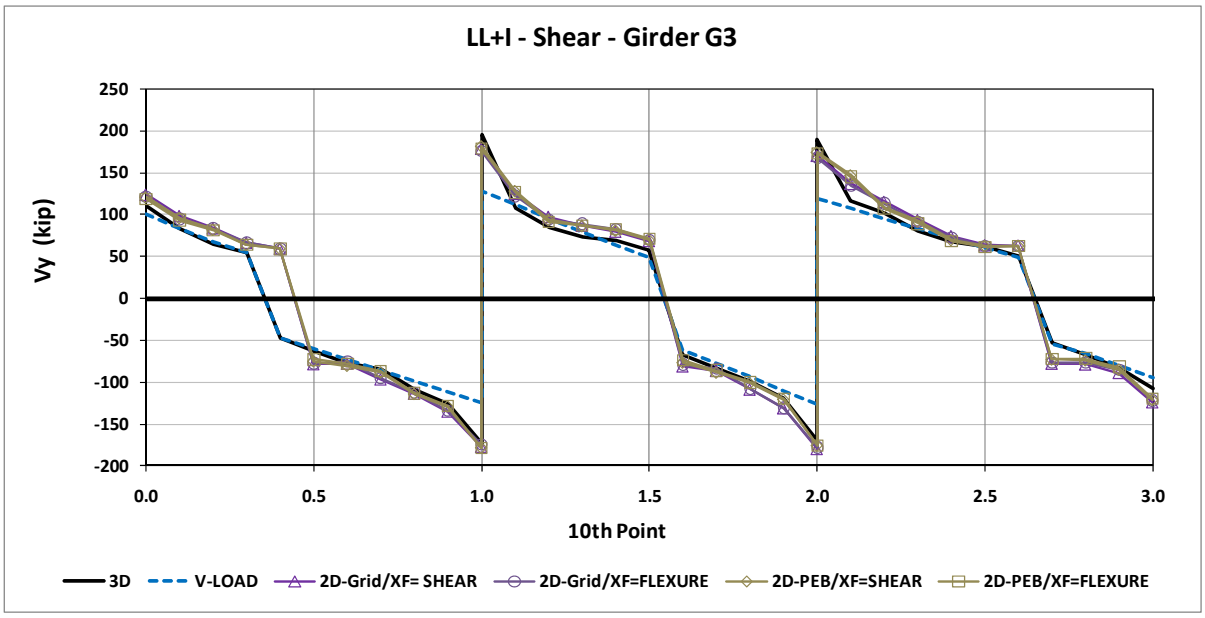


Figure 2.6.77 Unfactored LL+IM Shear in G3

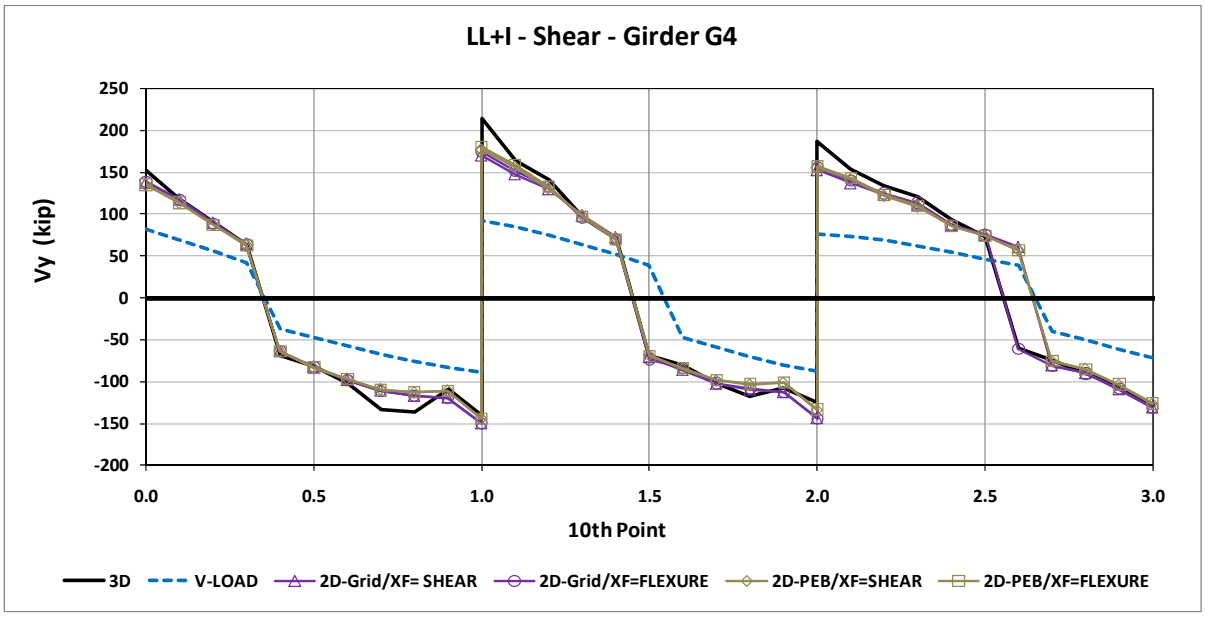


Figure 2.6.78 Unfactored LL+IM Shear in G4

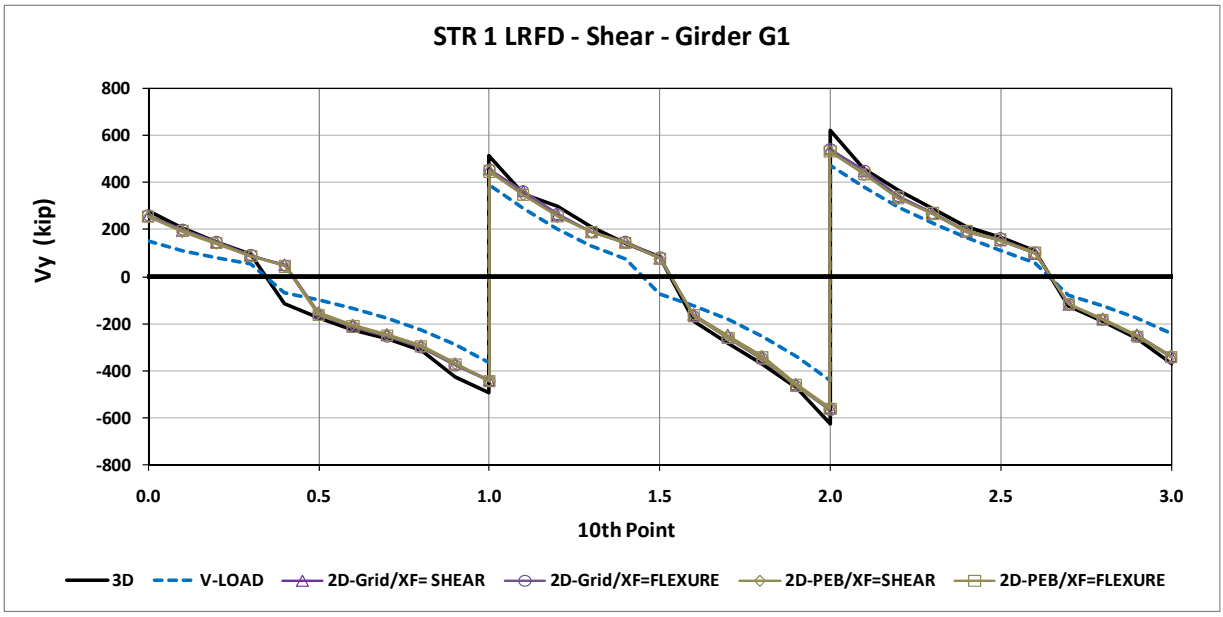


Figure 2.6.79 Strength I Shear in G1

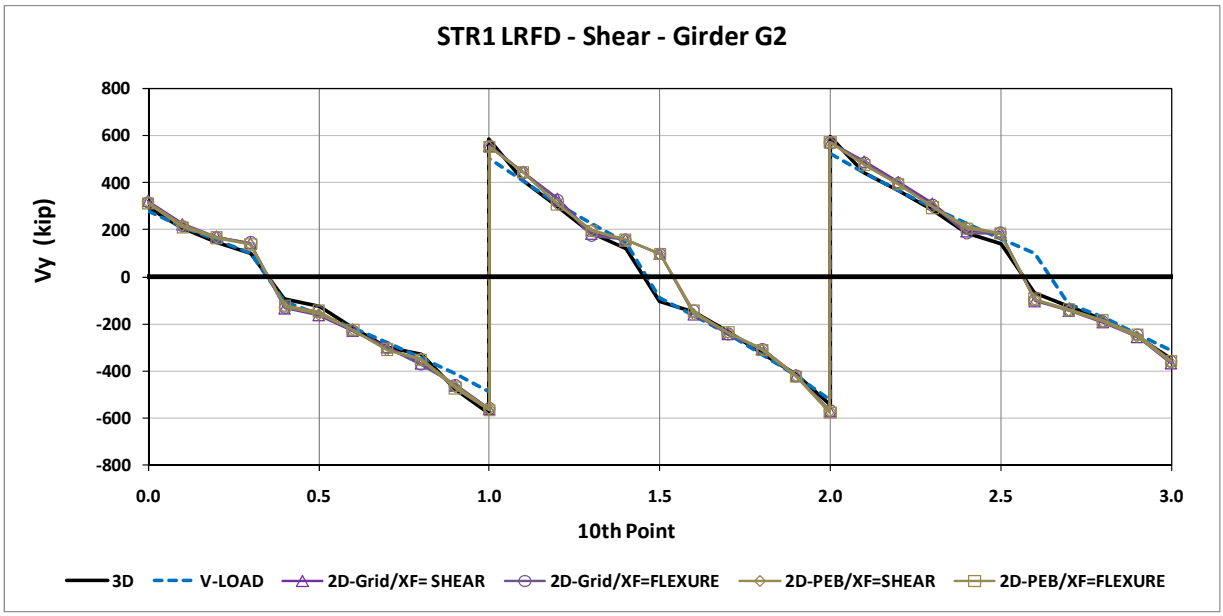


Figure 2.6.80 Strength I Shear in G2

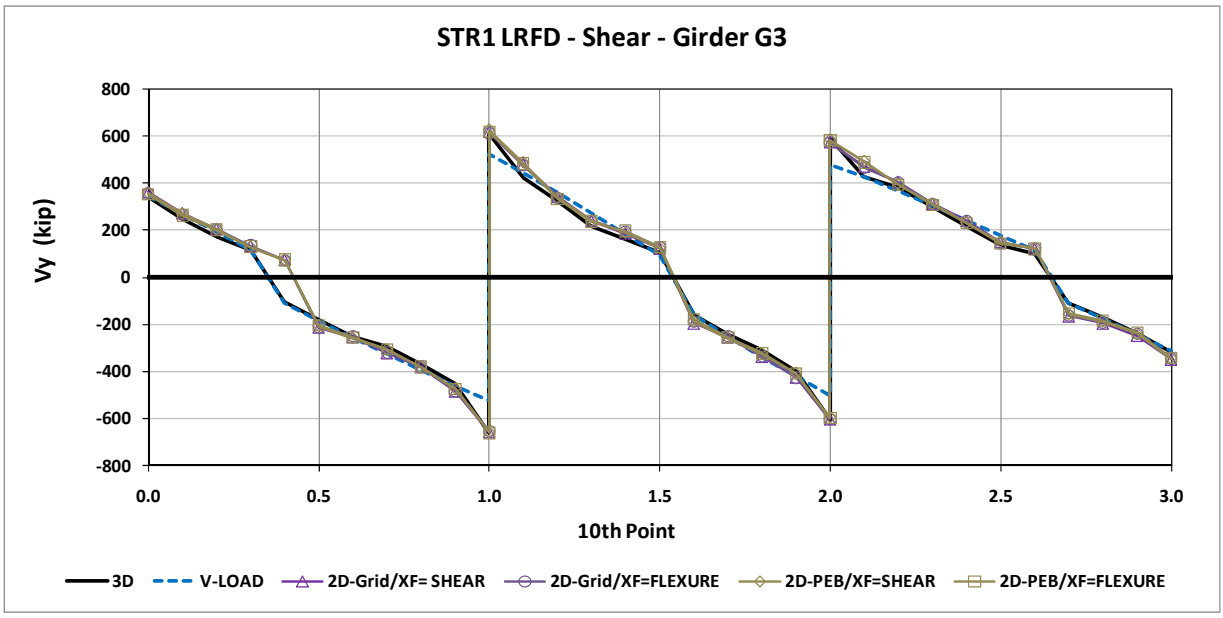


Figure 2.6.81 Strength I Shear in G3

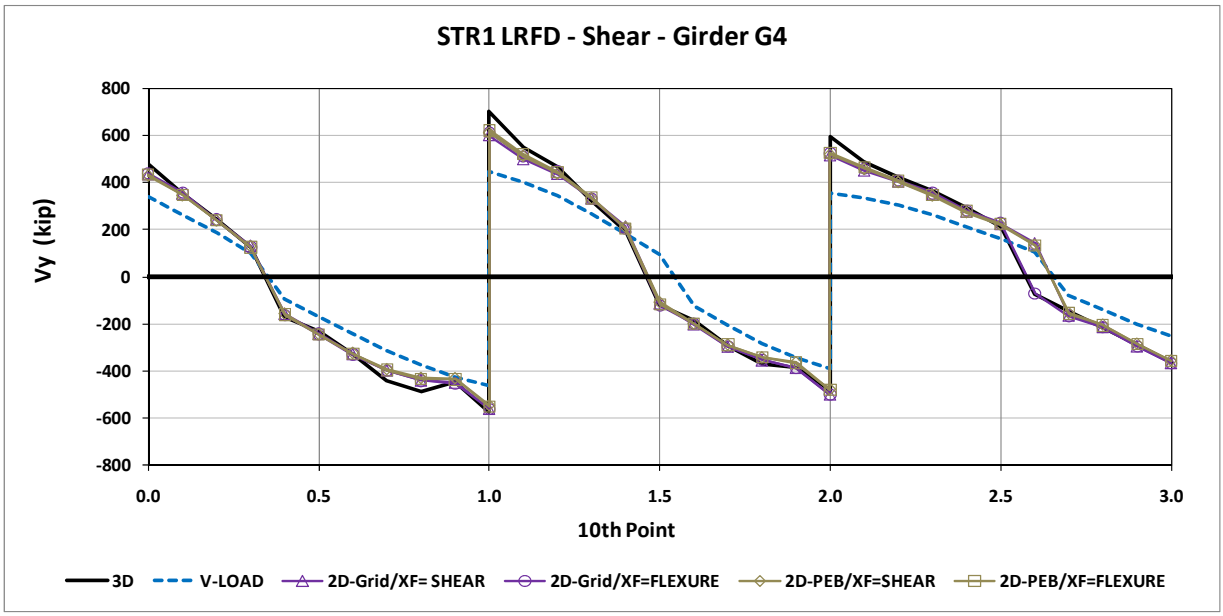


Figure 2.6.82 Strength I Shear in G4

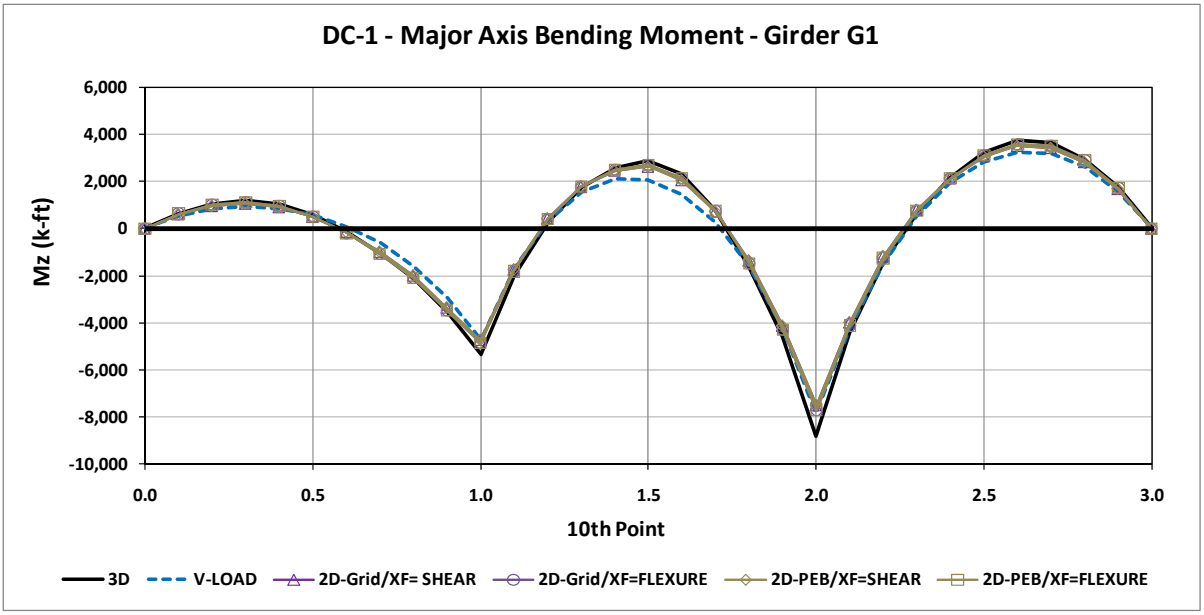


Figure 2.6.83 Unfactored DC_1 Vertical Bending Moment in G1

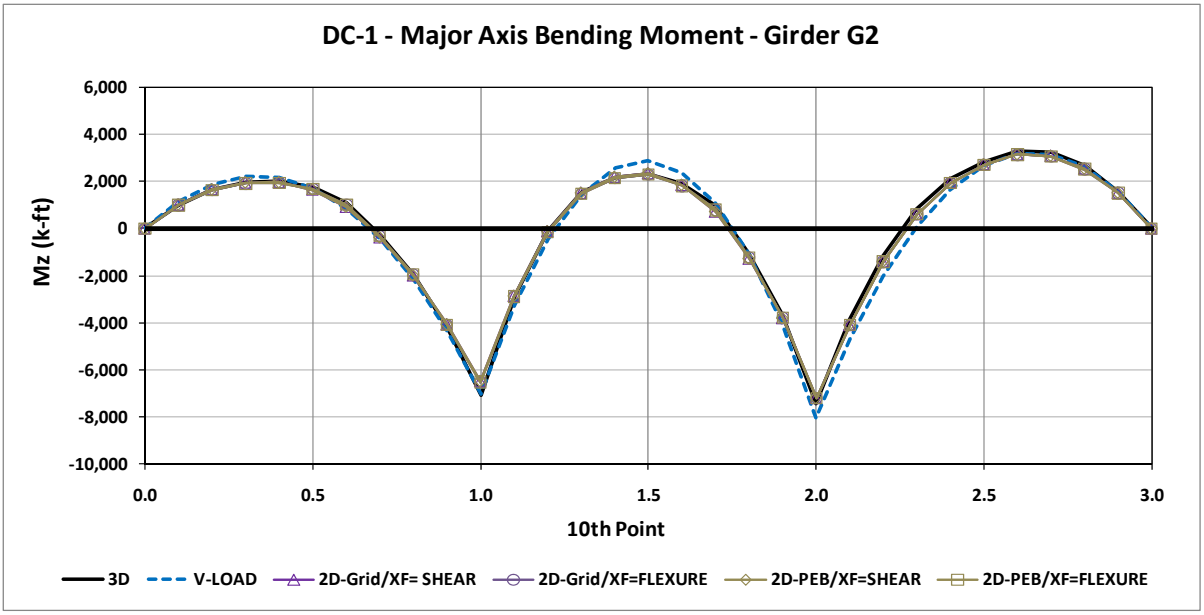


Figure 2.6.84 Unfactored DC_1 Vertical Bending Moment in G2

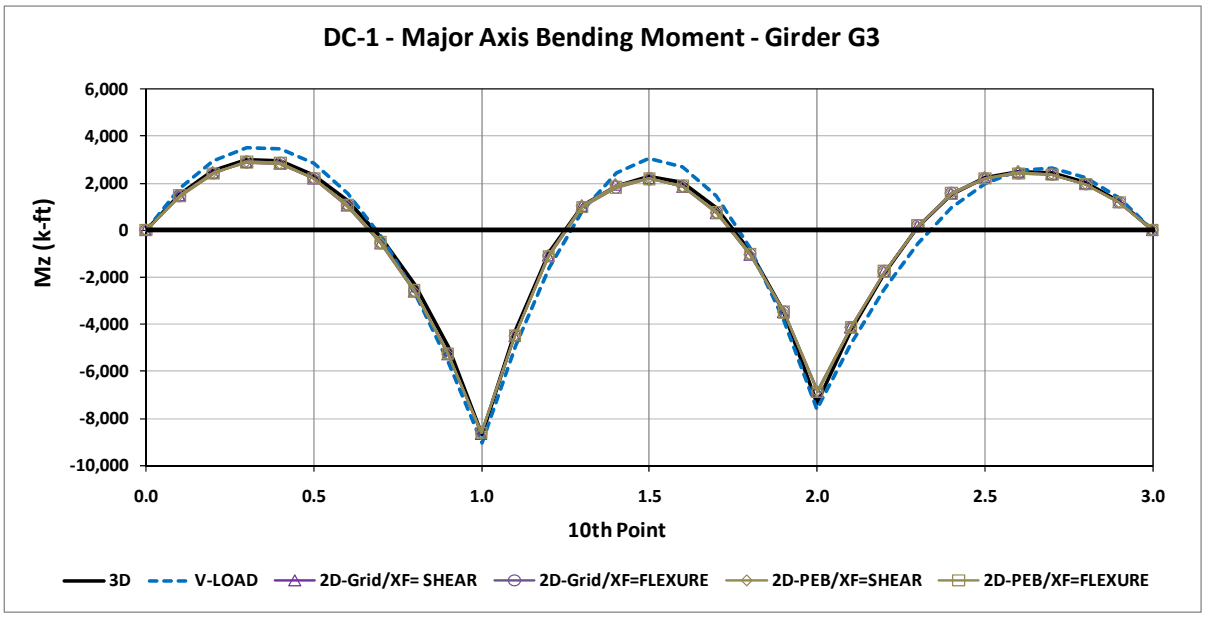


Figure 2.6.85 Unfactored DC_1 Vertical Bending Moment in G3

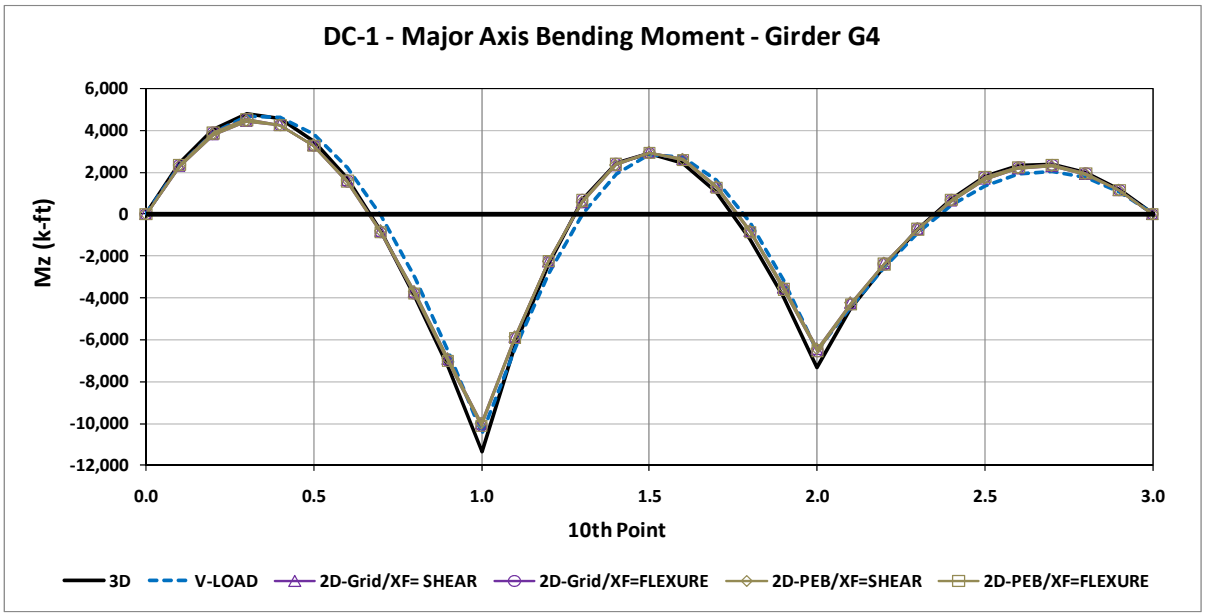


Figure 2.6.86 Unfactored DC_1 Vertical Bending Moment in G4

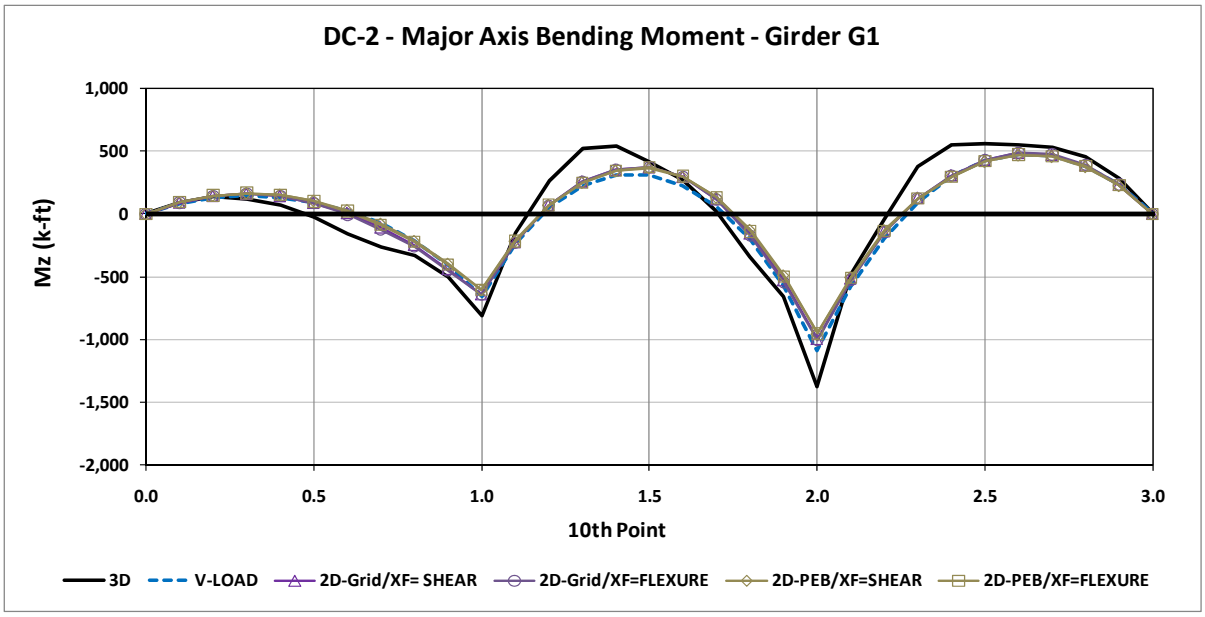


Figure 2.6.87 Unfactored DC_2 Vertical Bending Moment in G1

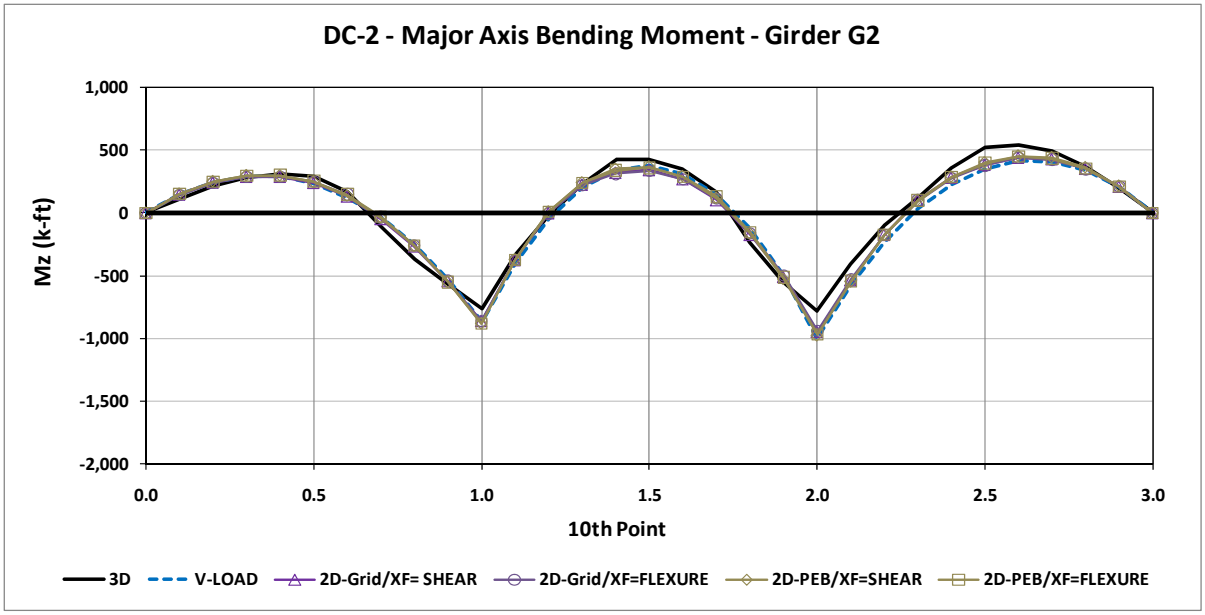


Figure 2.6.88 Unfactored DC_2 Vertical Bending Moment in G2

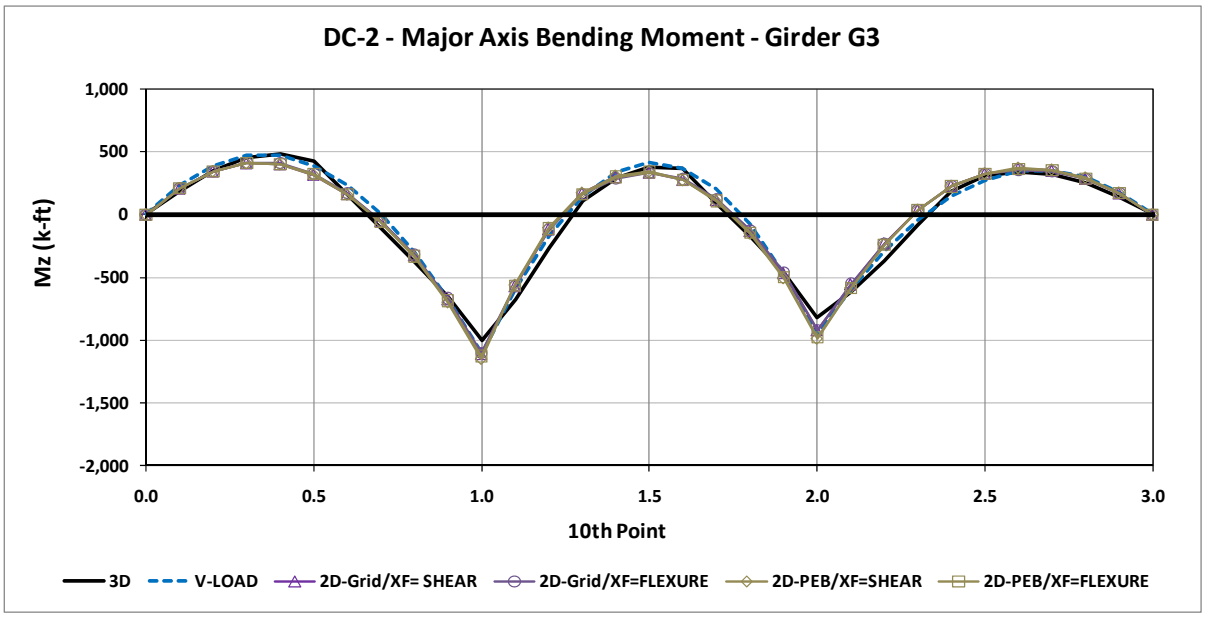


Figure 2.6.89 Unfactored DC_2 Vertical Bending Moment in G3

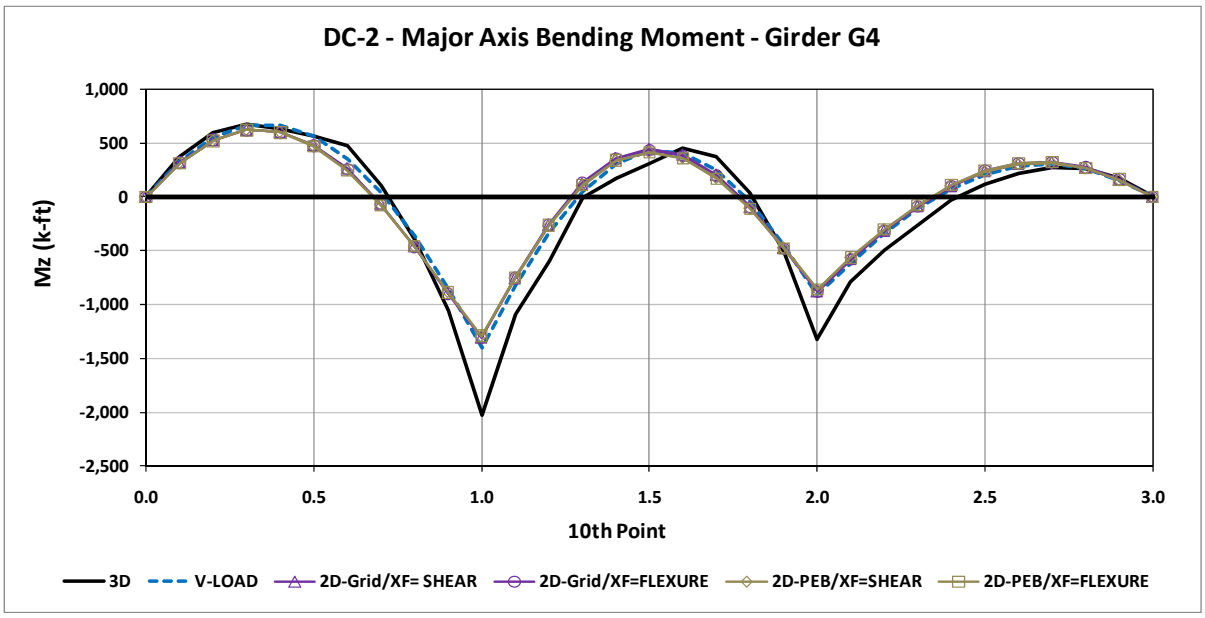


Figure 2.6.90 Unfactored DC_2 Vertical Bending Moment in G4

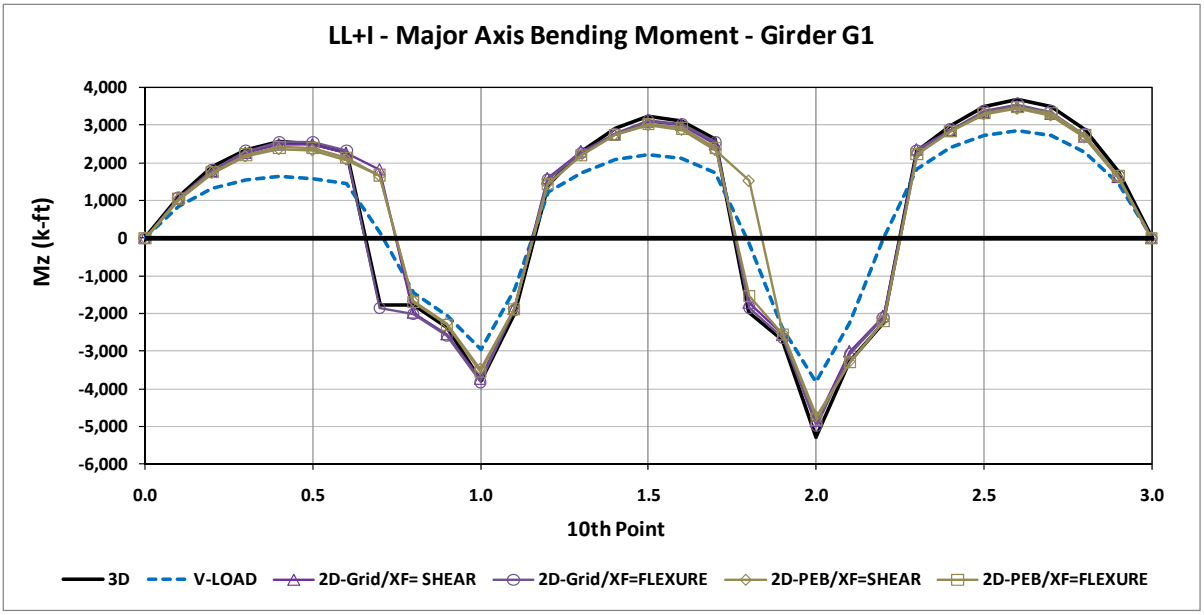


Figure 2.6.91 Unfactored LL+I Vertical Bending Moment in G1

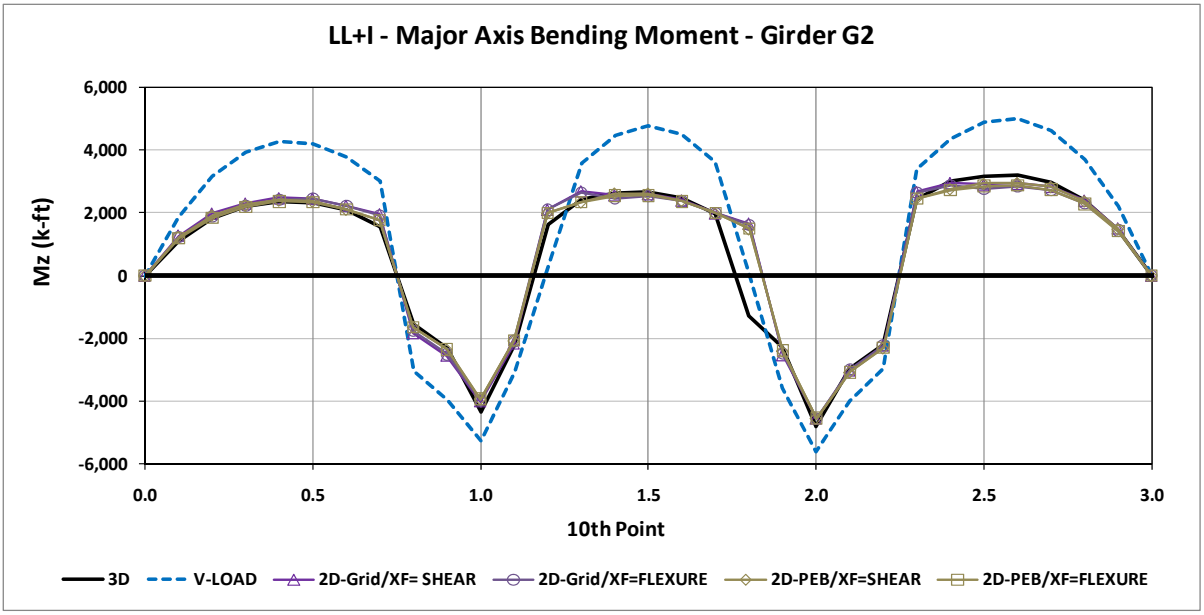


Figure 2.6.92 Unfactored LL+I Vertical Bending Moment in G2

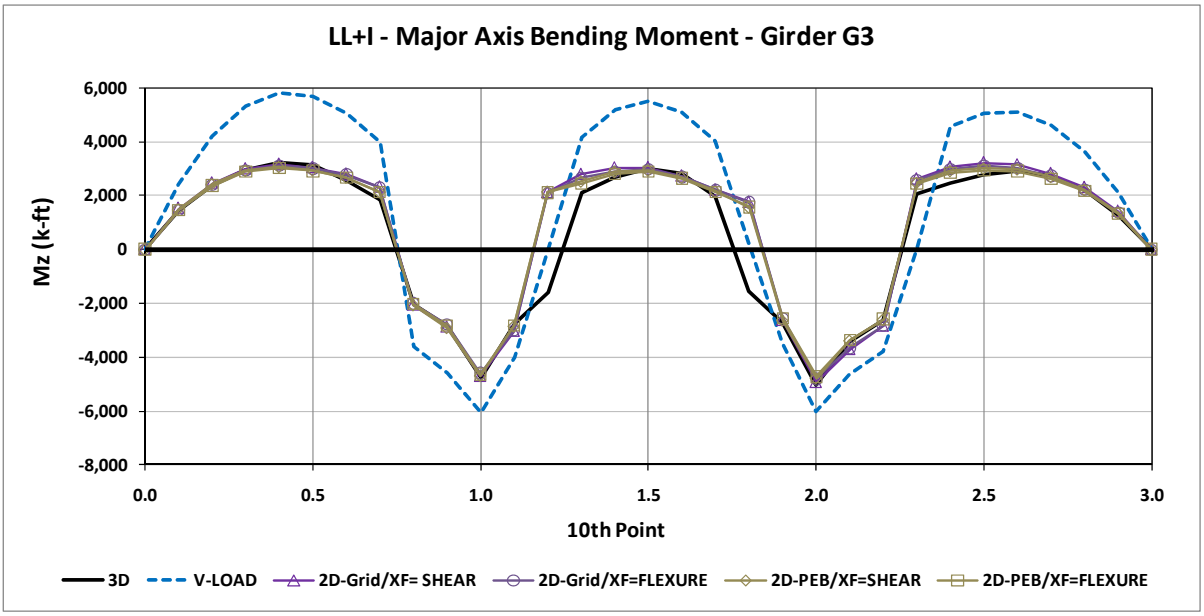


Figure 2.6.93 Unfactored LL+I Vertical Bending Moment in G3

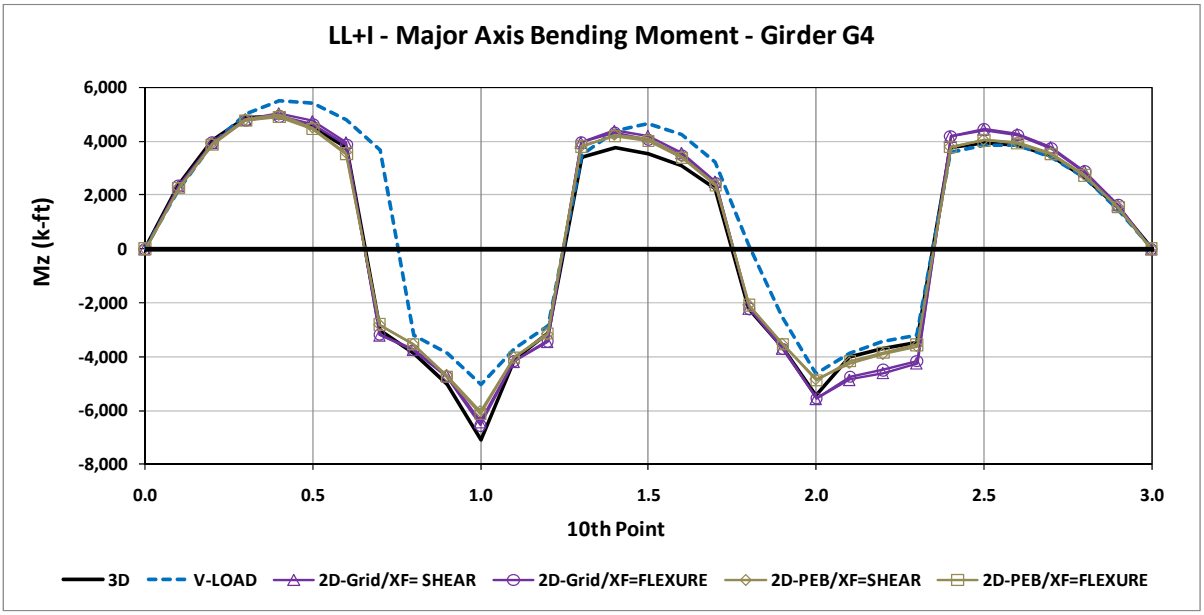


Figure 2.6.94 Unfactored LL+I Vertical Bending Moment in G4

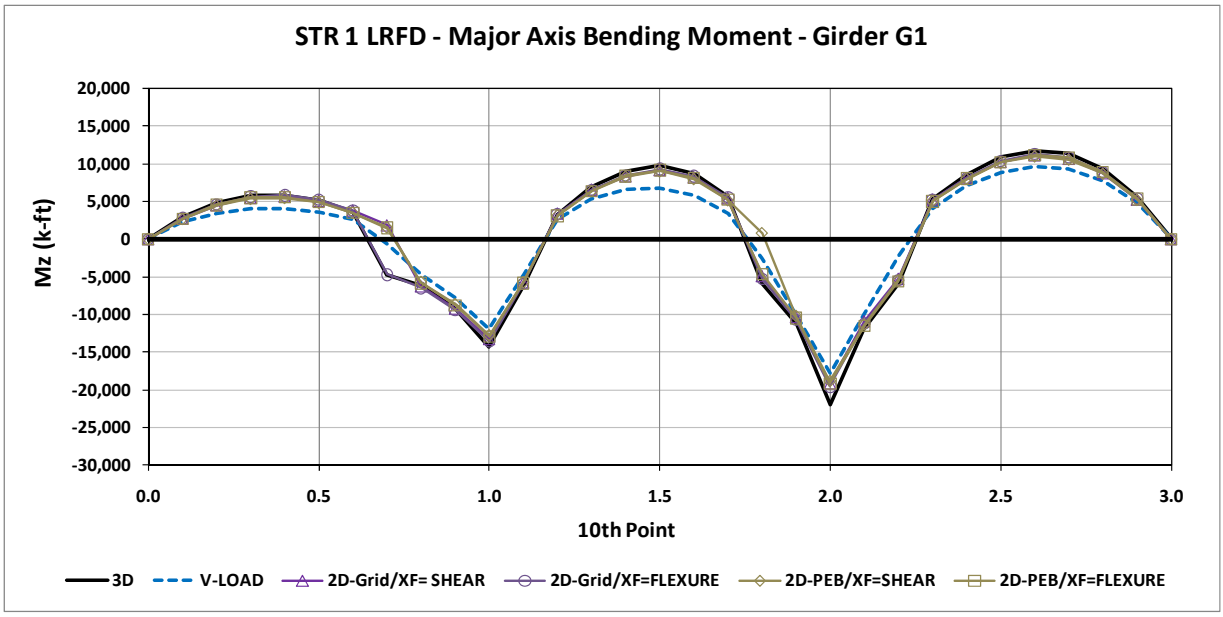


Figure 2.6.95 Strength I Vertical Bending Moment in G1

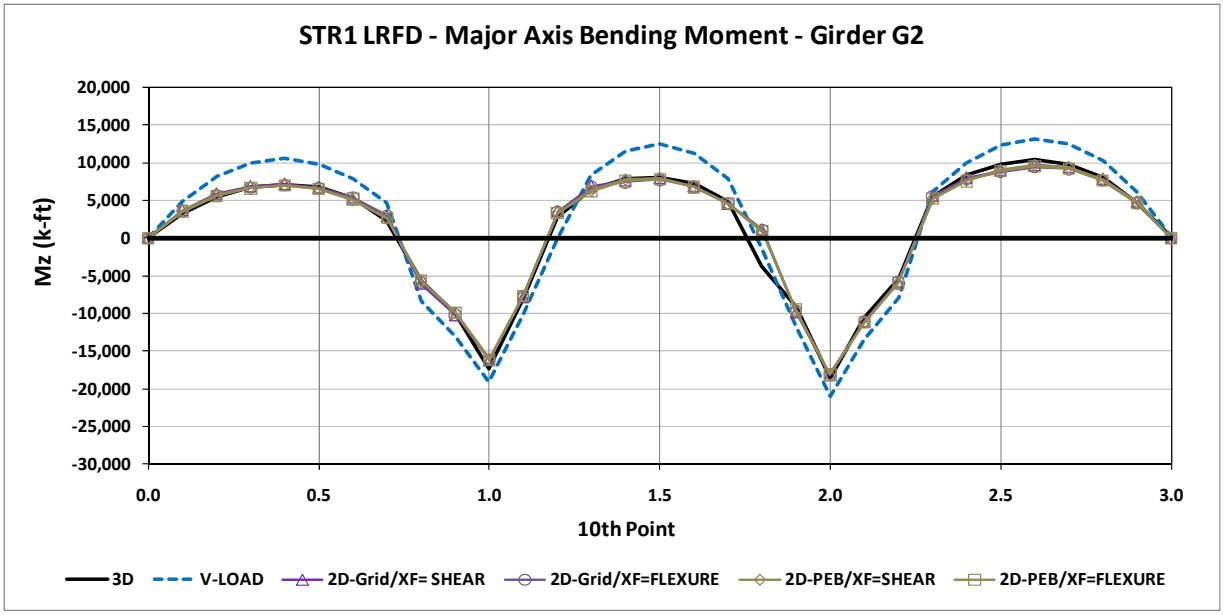


Figure 2.6.96 Strength I Vertical Bending Moment in G2

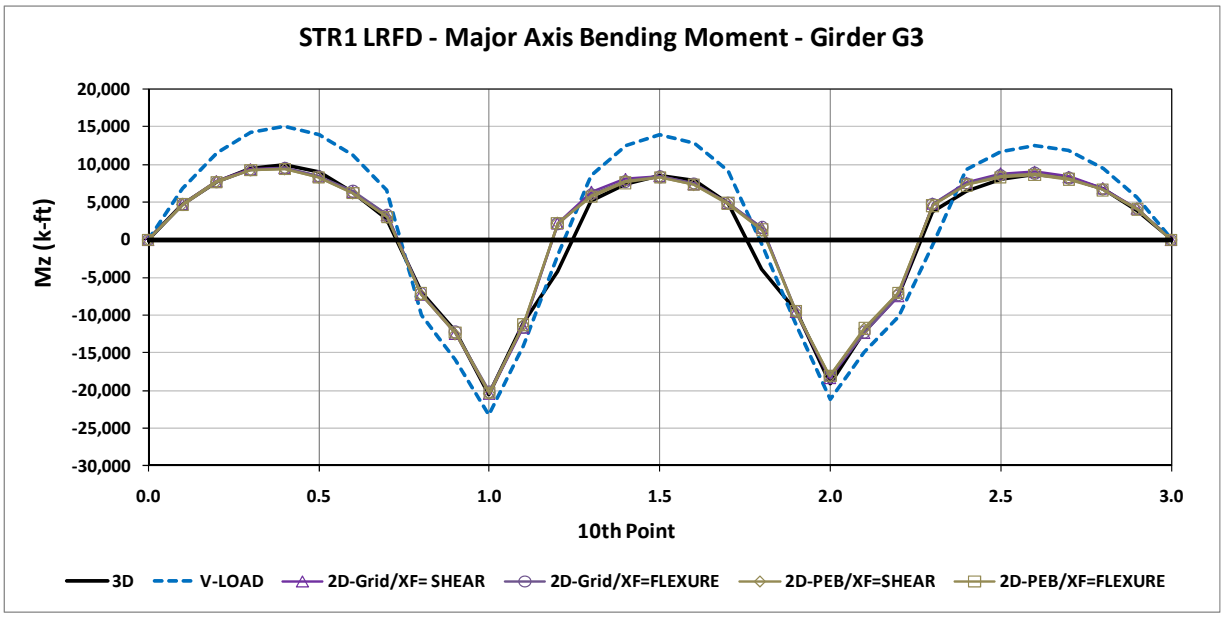


Figure 2.6.97 Strength I Vertical Bending Moment in G3

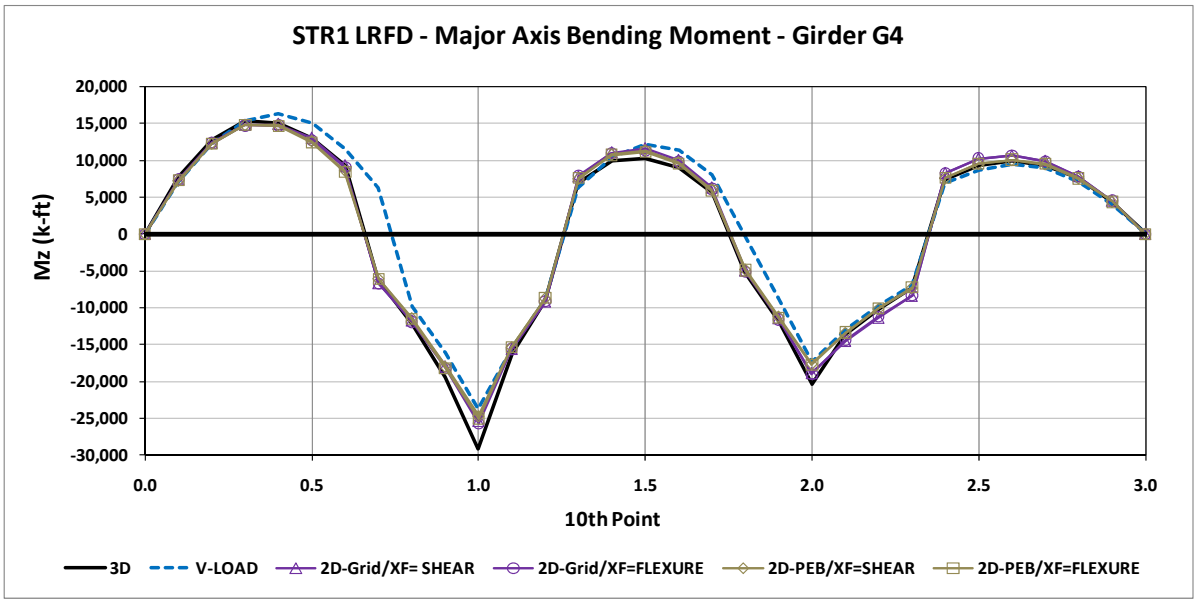


Figure 2.6.98 Strength I Vertical Bending Moment in G4

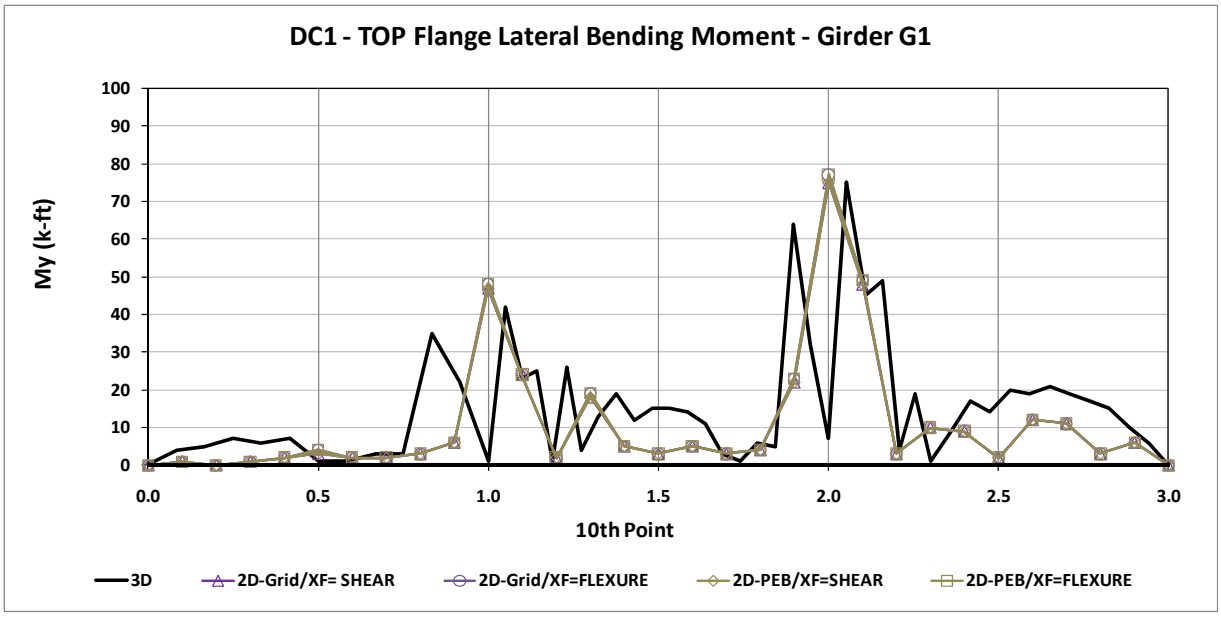


Figure 2.6.99 Unfactored DC_1 Top Flange Lateral Bending Moment in G1

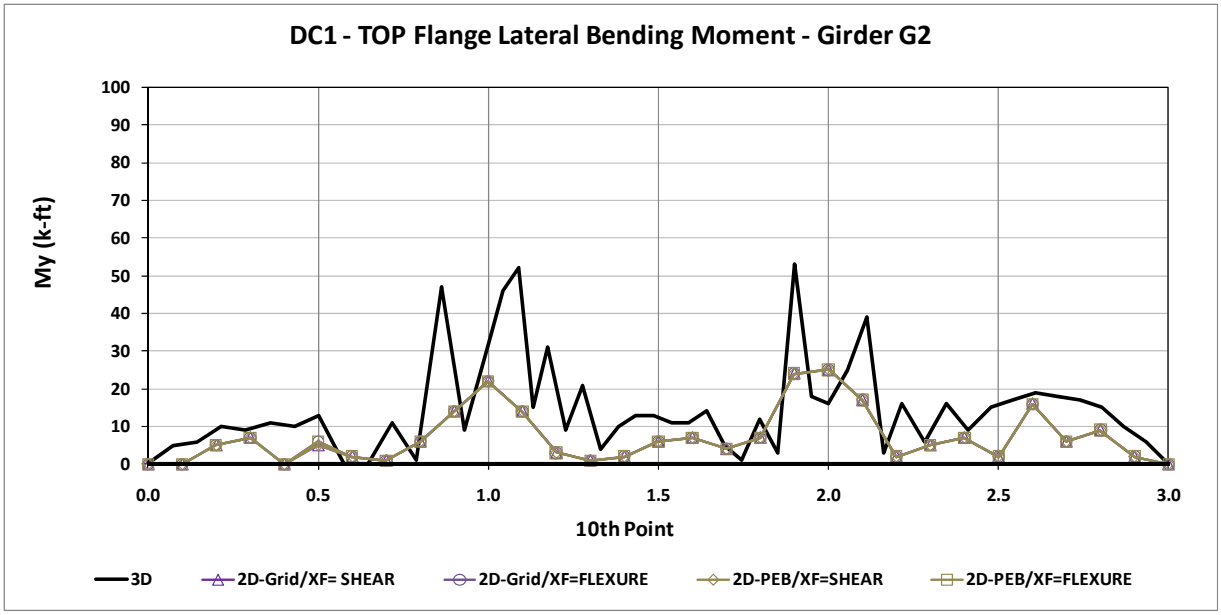


Figure 2.6.100 Unfactored DC_1 Top Flange Lateral Bending Moment in G2

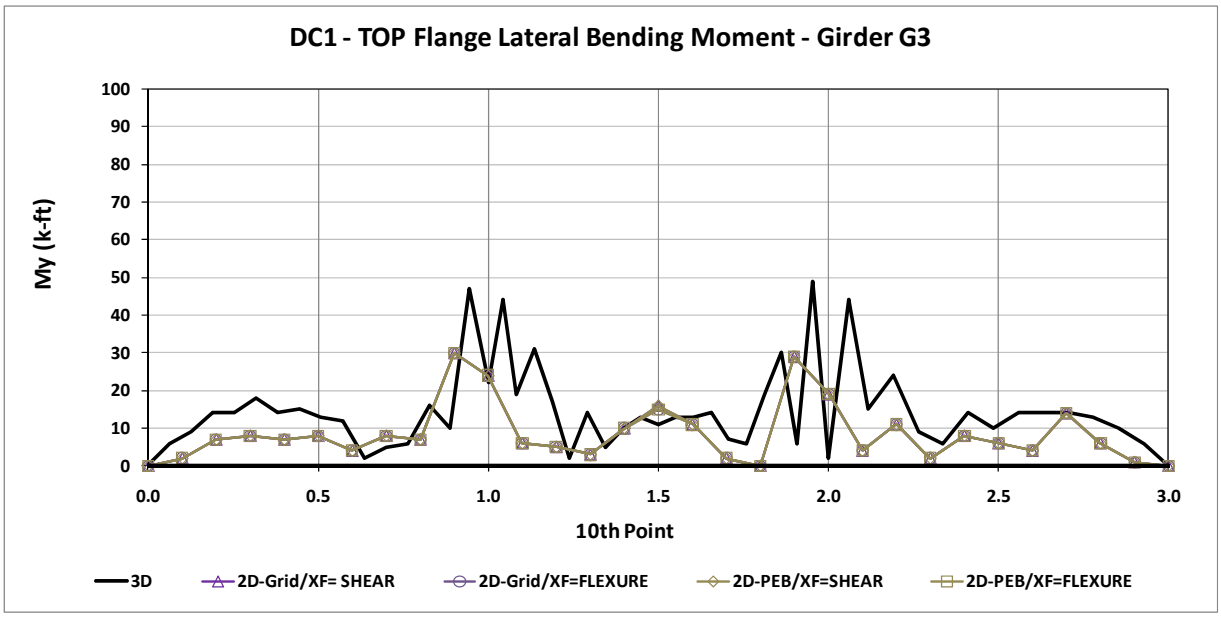


Figure 2.6.101 Unfactored DC_1 Top Flange Lateral Bending Moment in G3

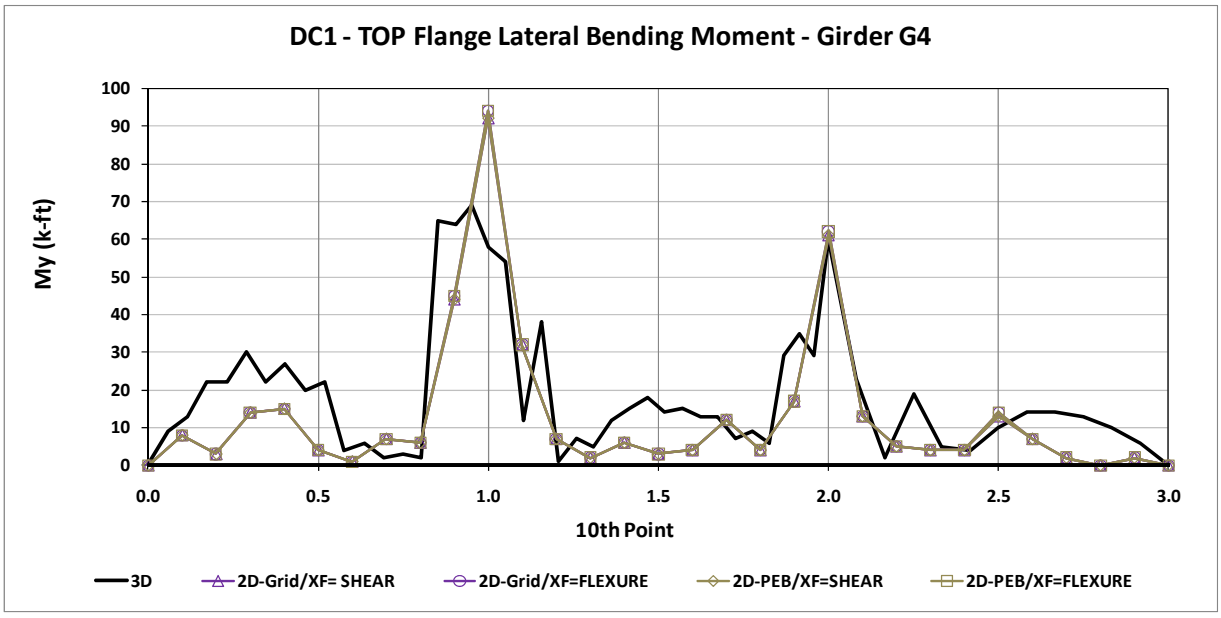


Figure 2.6.102 Unfactored DC_1 Top Flange Lateral Bending Moment in G4

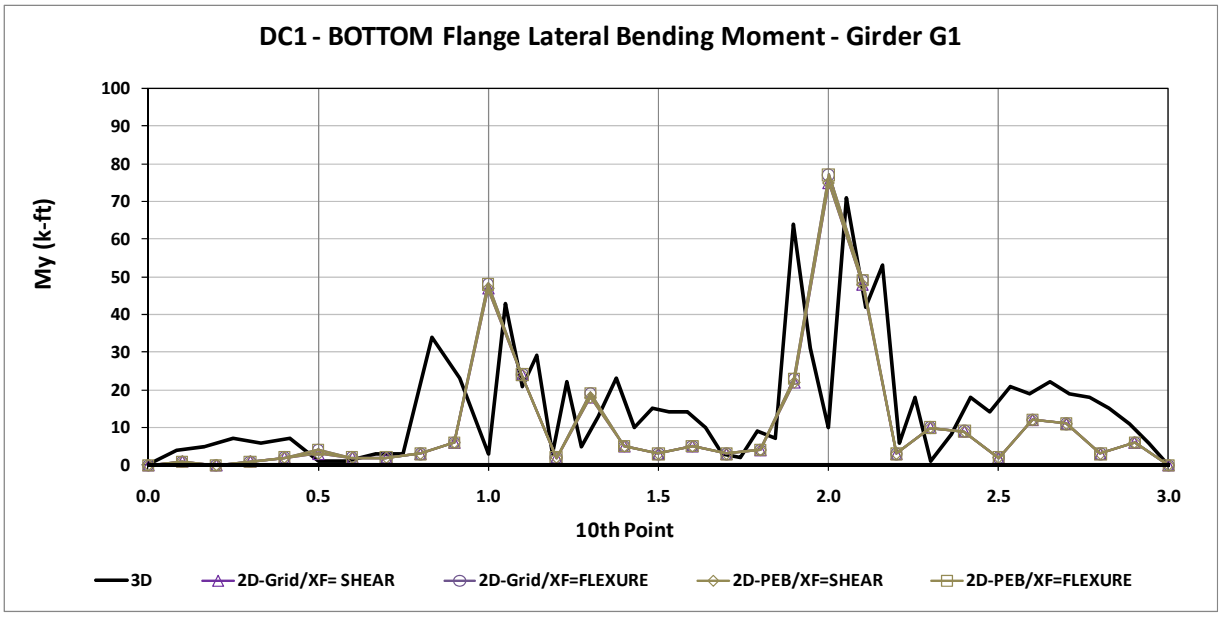


Figure 2.6.103 Unfactored DC_1 Bottom Flange Lateral Bending Moment in G1

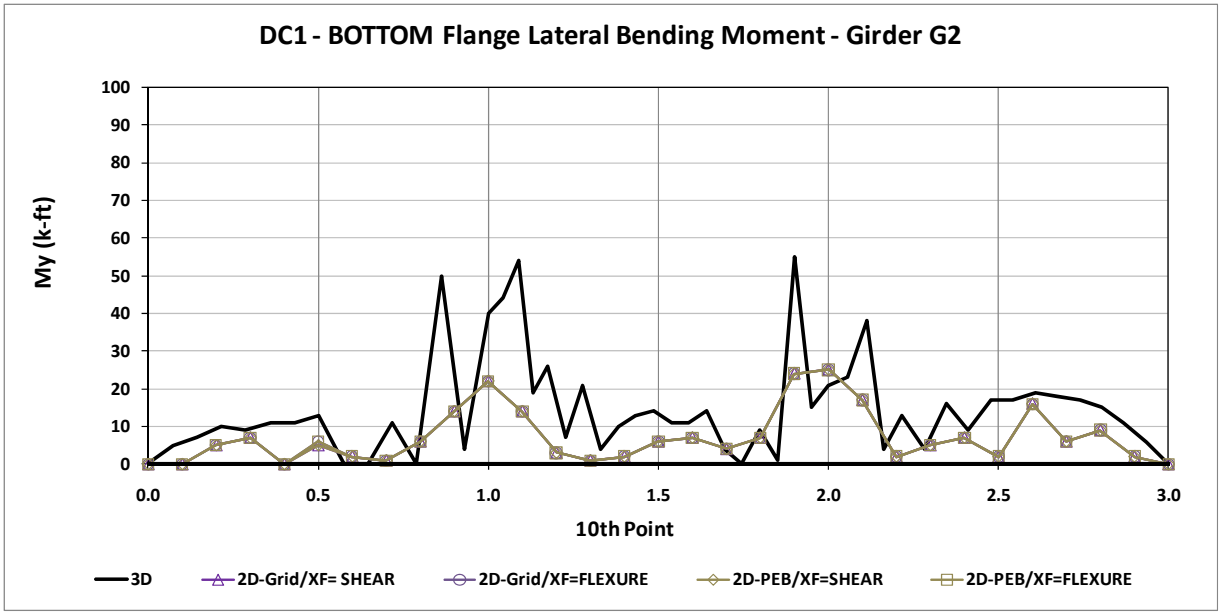


Figure 2.6.104 Unfactored DC_1 Bottom Flange Lateral Bending Moment in G2

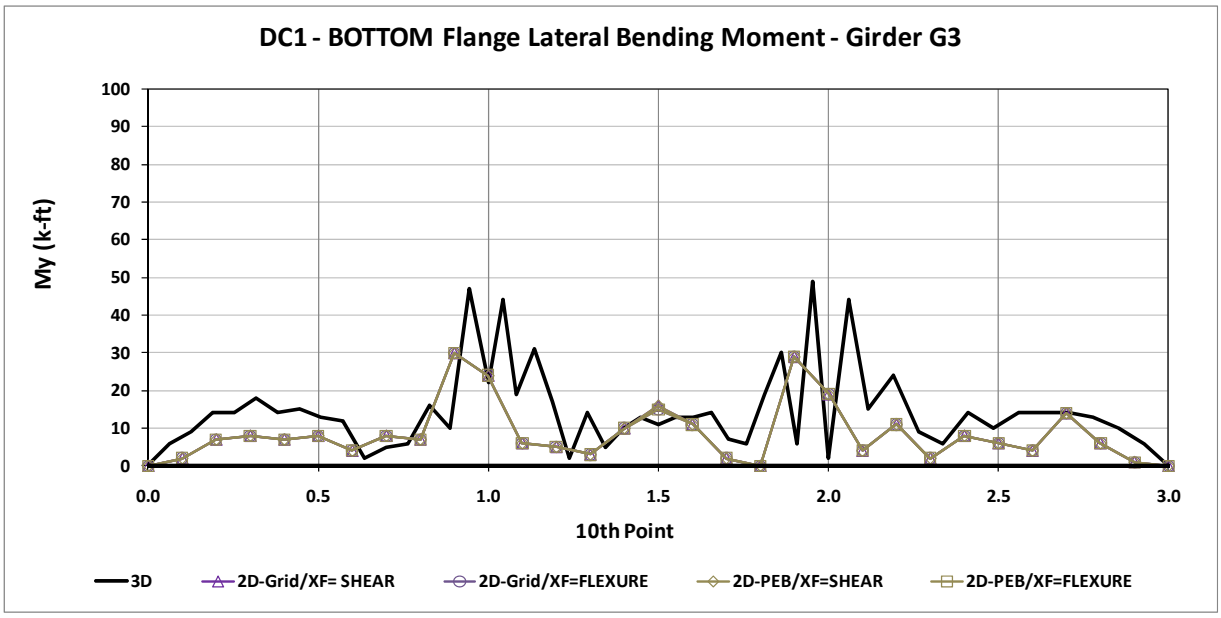


Figure 2.6.105 Unfactored DC_1 Bottom Flange Lateral Bending Moment in G3

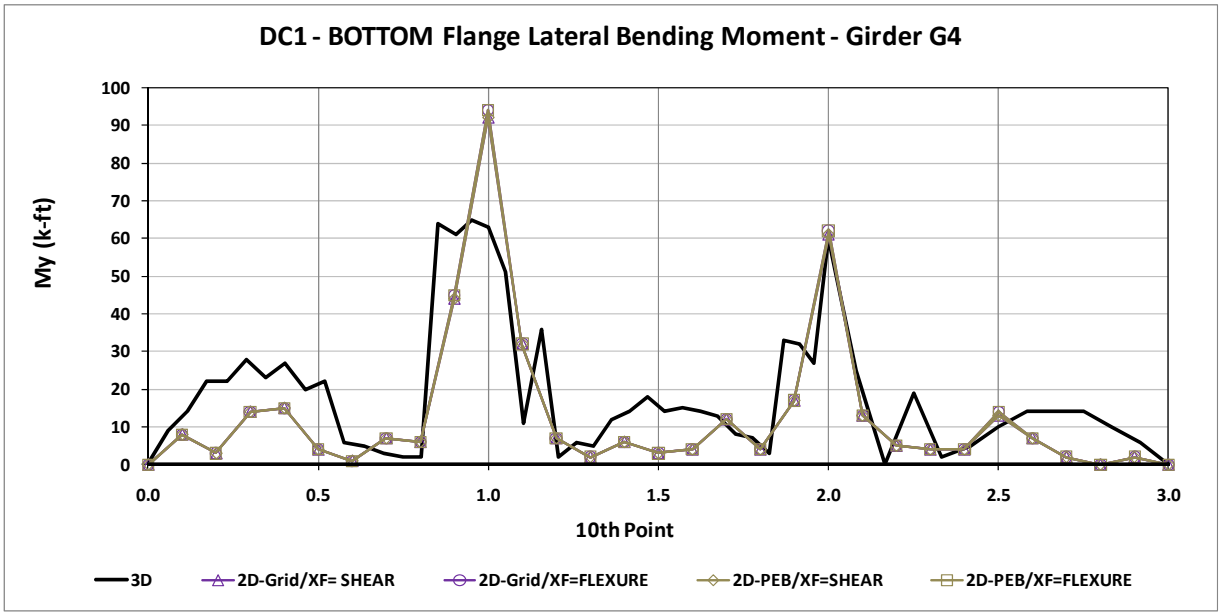


Figure 2.6.106 Unfactored DC_1 Bottom Flange Lateral Bending Moment in G4

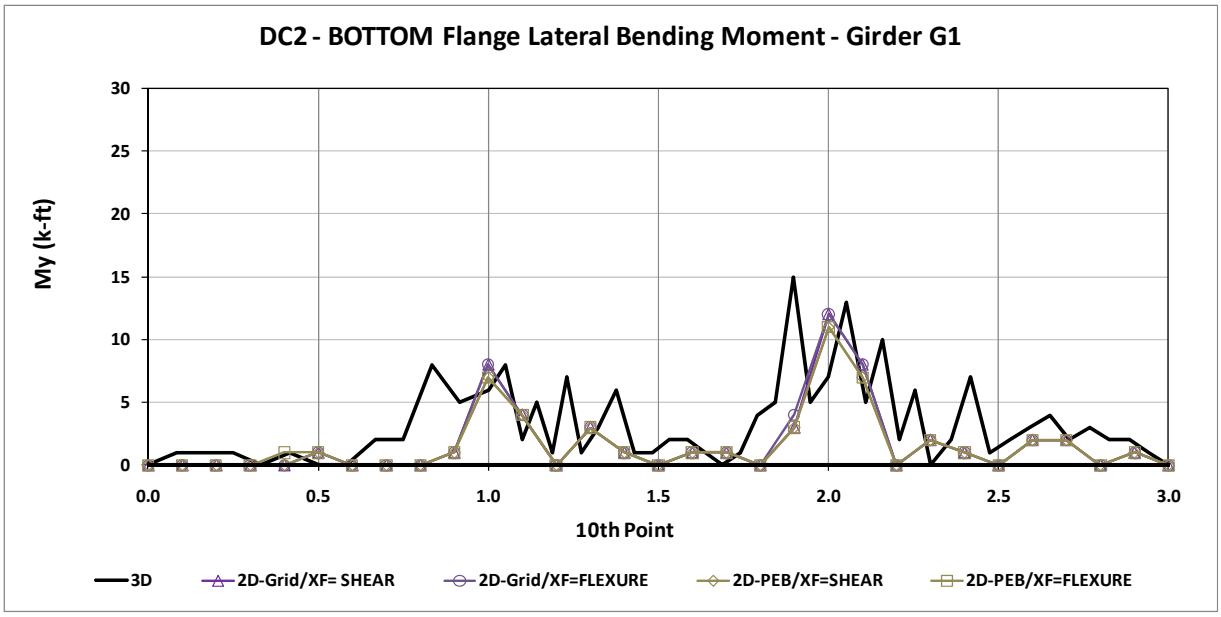


Figure 2.6.107 Unfactored DC_2 Bottom Flange Lateral Bending Moment in G1

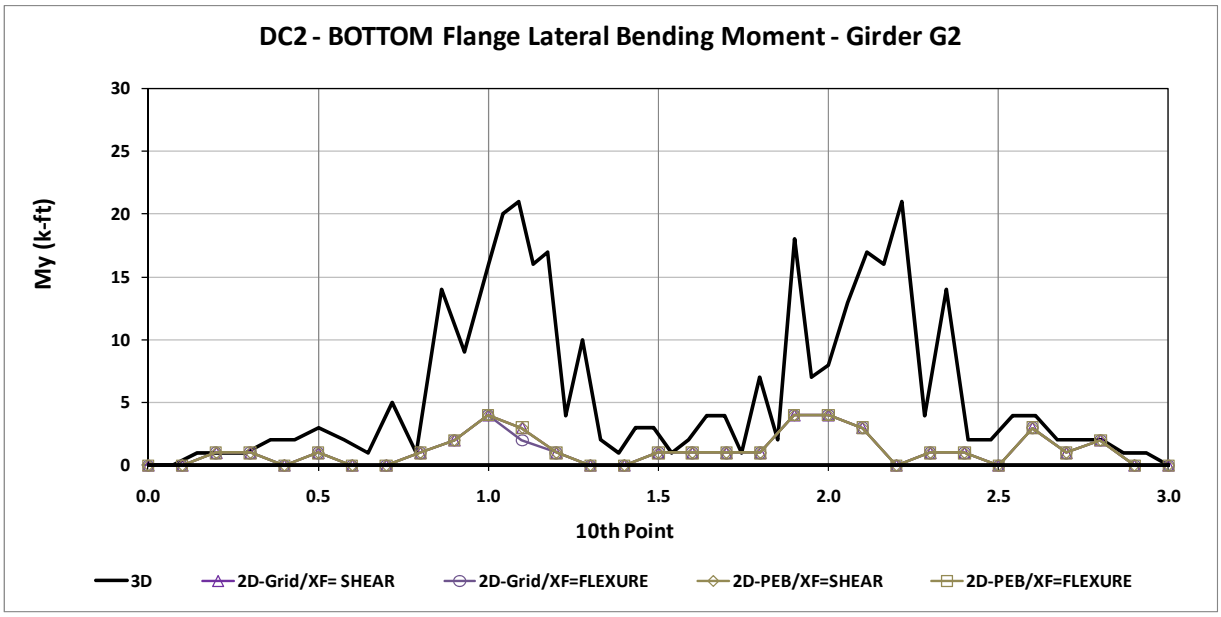


Figure 2.6.108 Unfactored DC_2 Bottom Flange Lateral Bending Moment in G2

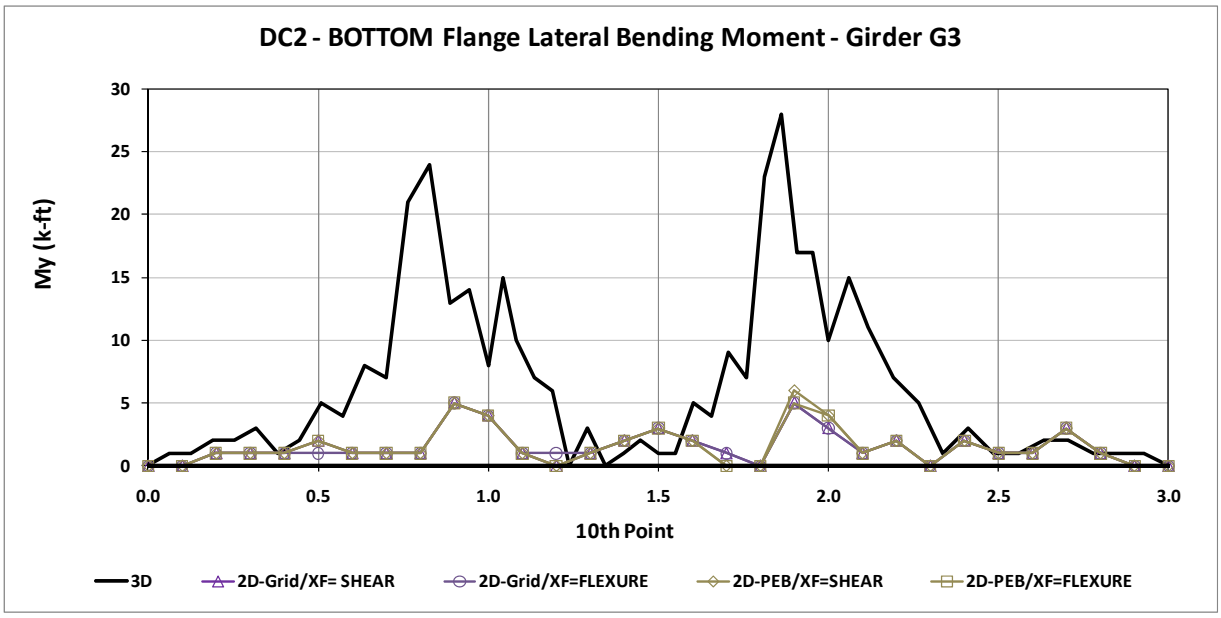


Figure 2.6.109 Unfactored DC_2 Bottom Flange Lateral Bending Moment in G3

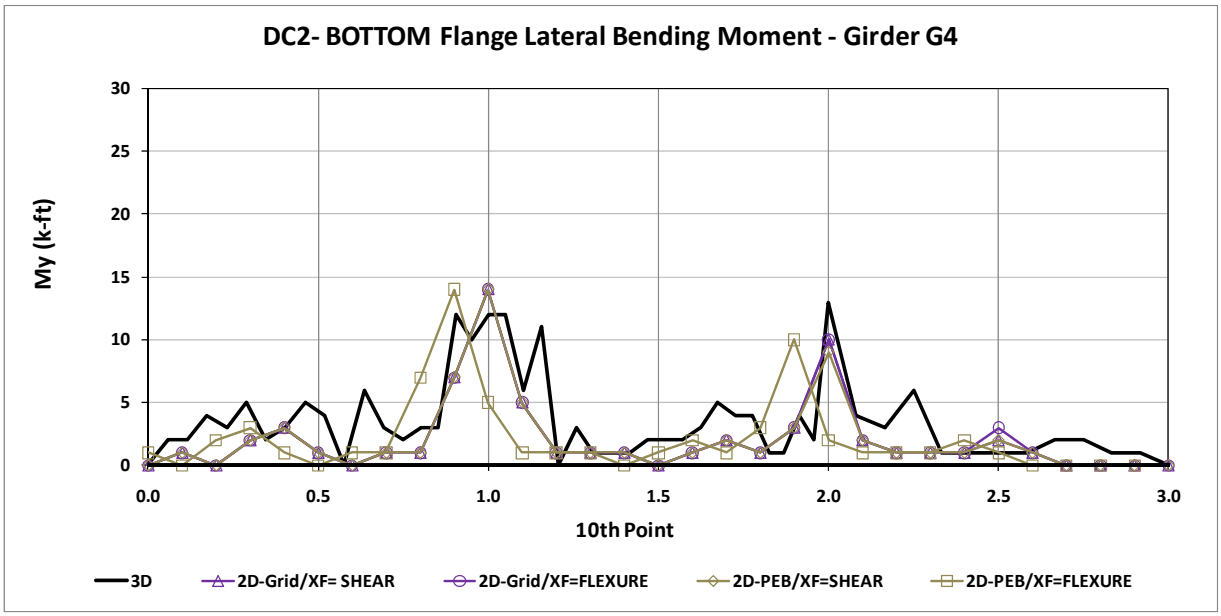


Figure 2.6.110 Unfactored DC_2 Bottom Flange Lateral Bending Moment in G4

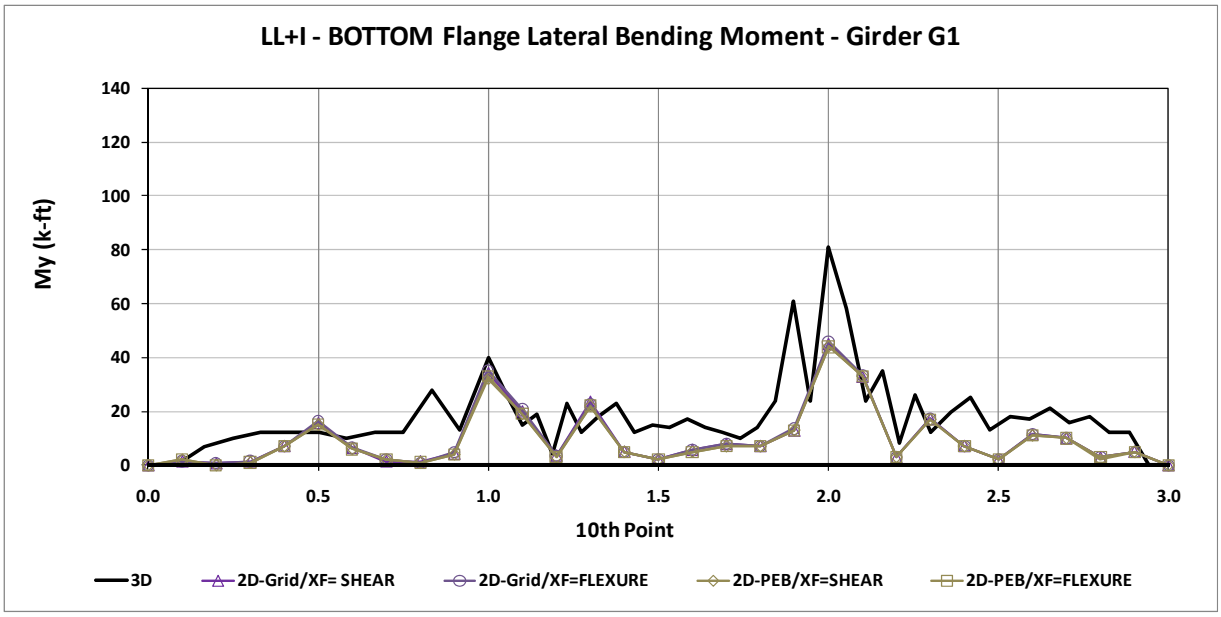


Figure 2.6.111 Unfactored LL+IM Bottom Flange Lateral Bending Moment in G1

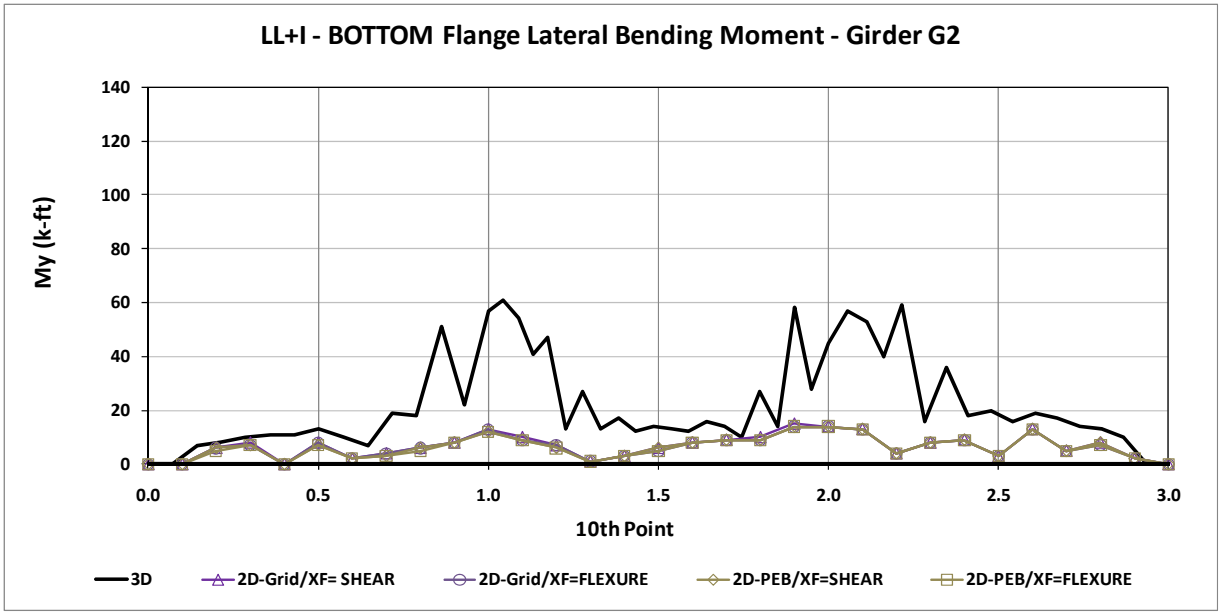


Figure 2.6.112 Unfactored LL+IM Bottom Flange Lateral Bending Moment in G2

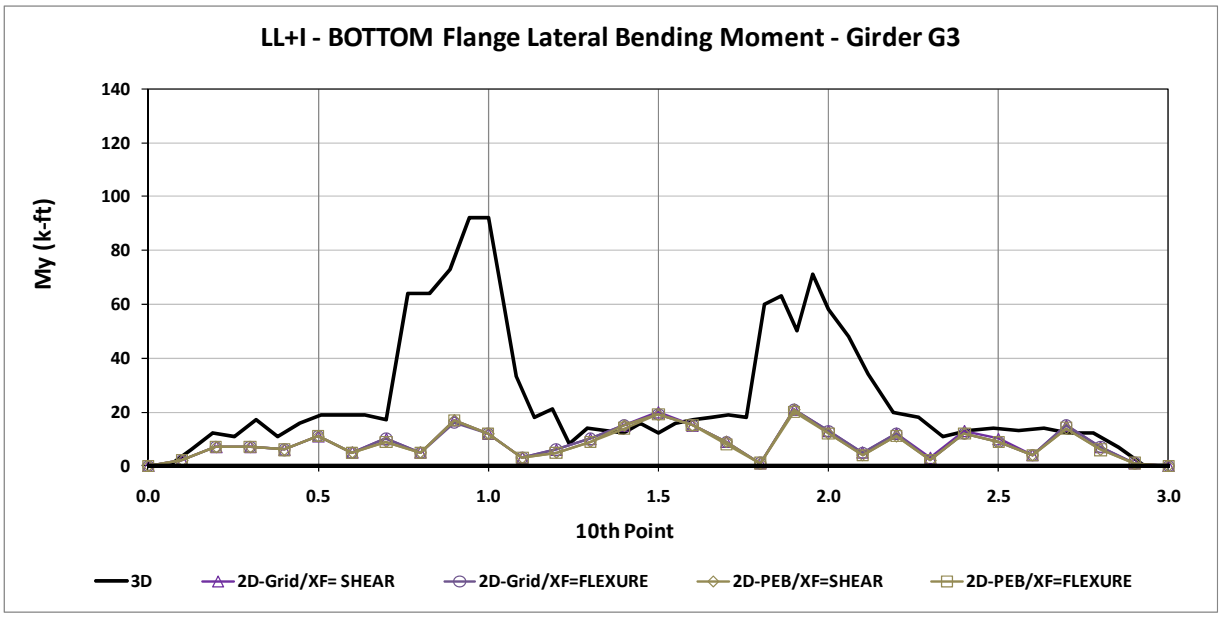


Figure 2.6.113 Unfactored LL+IM Bottom Flange Lateral Bending Moment in G3

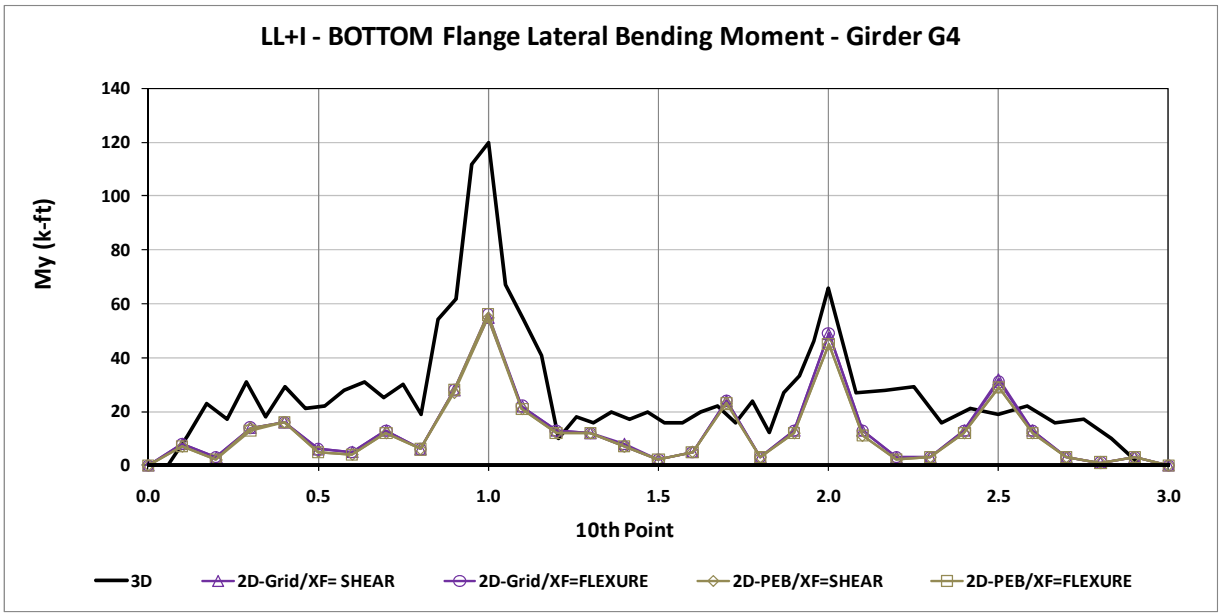


Figure 2.6.114 Unfactored LL+IM Bottom Flange Lateral Bending Moment in G4

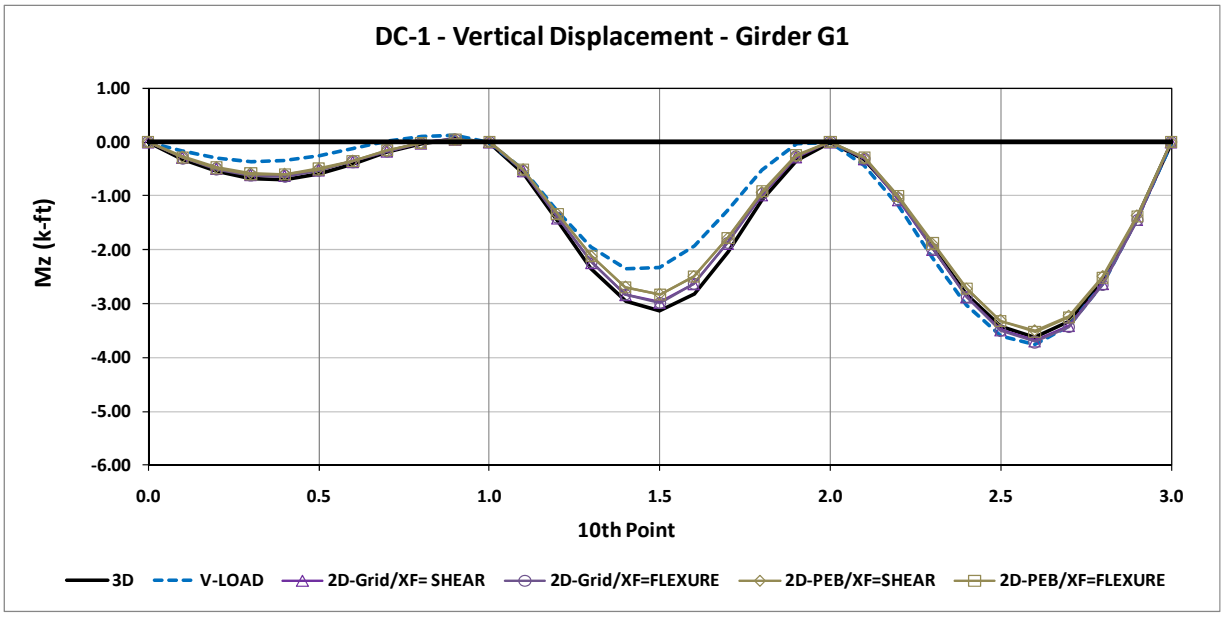


Figure 2.6.115 Unfactored DC_1 Vertical Displacement of G1

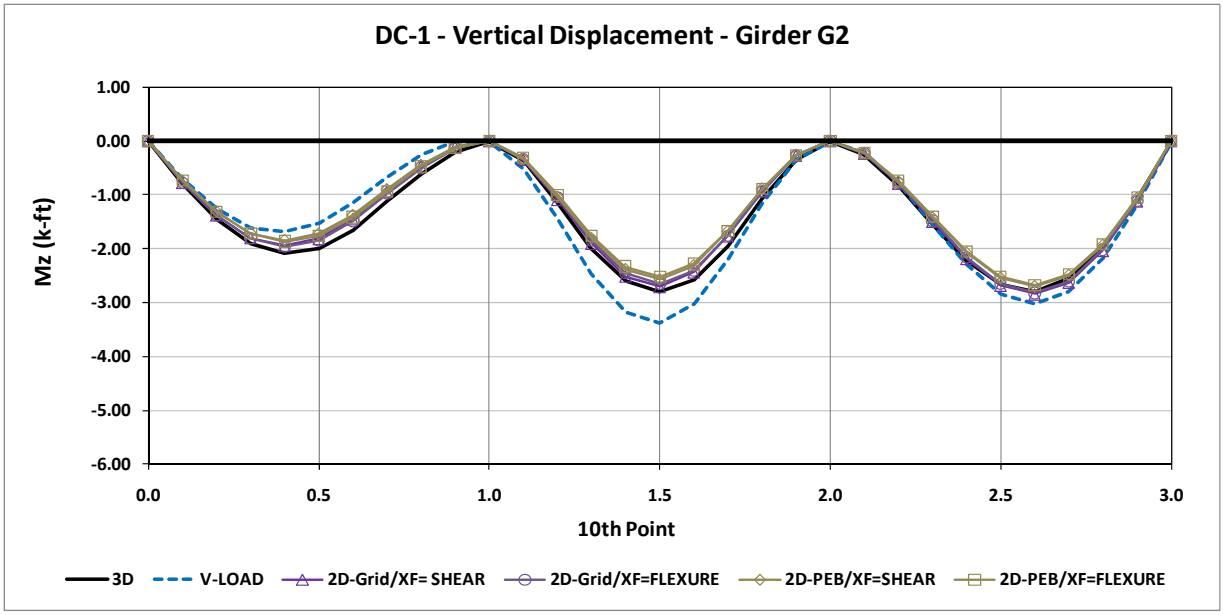


Figure 2.6.116 Unfactored DC_1 Vertical Displacement of G2

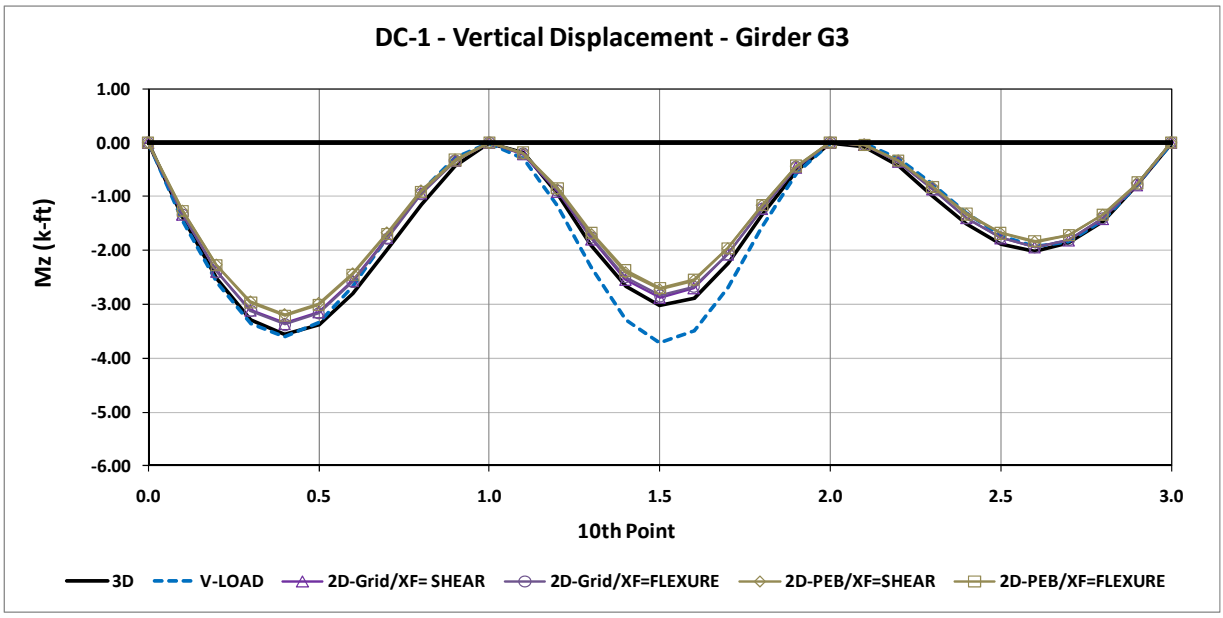


Figure 2.6.117 Unfactored DC_1 Vertical Displacement of G3

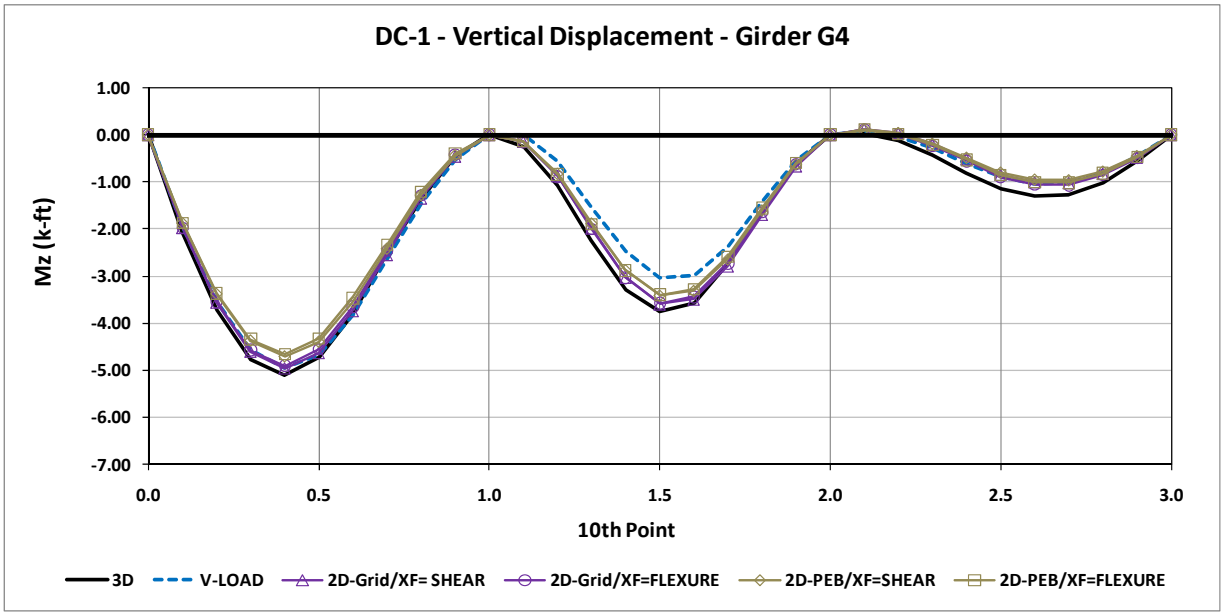


Figure 2.6.118 Unfactored DC_1 Vertical Displacement of G4

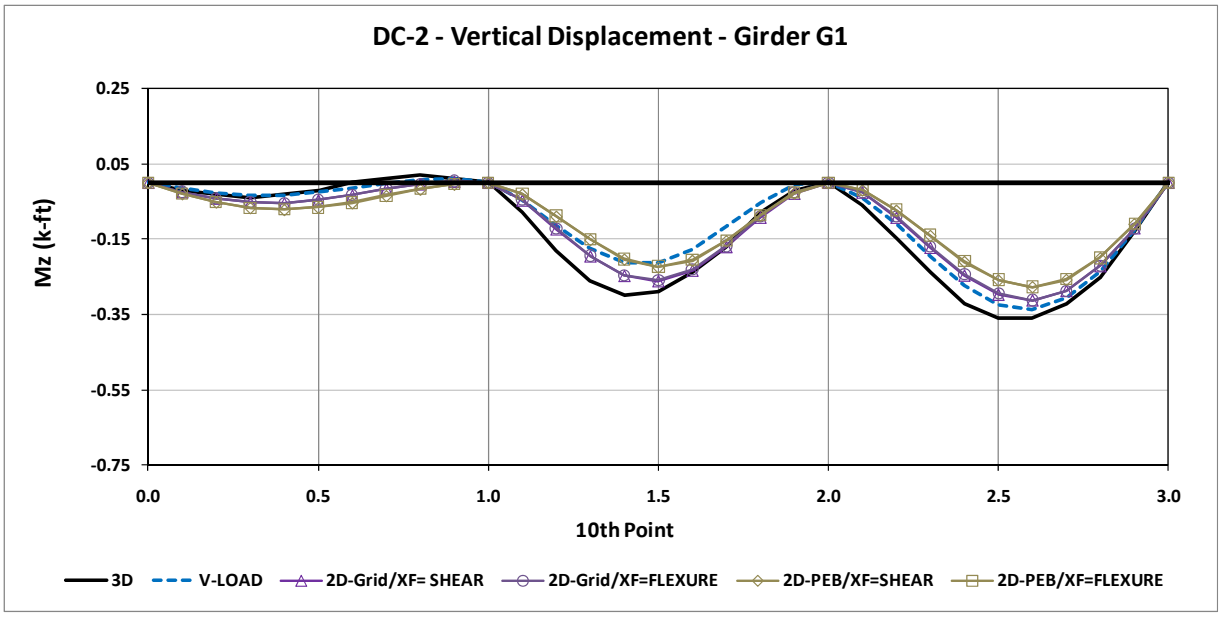


Figure 2.6.119 Unfactored DC_2 Vertical Displacement of G1

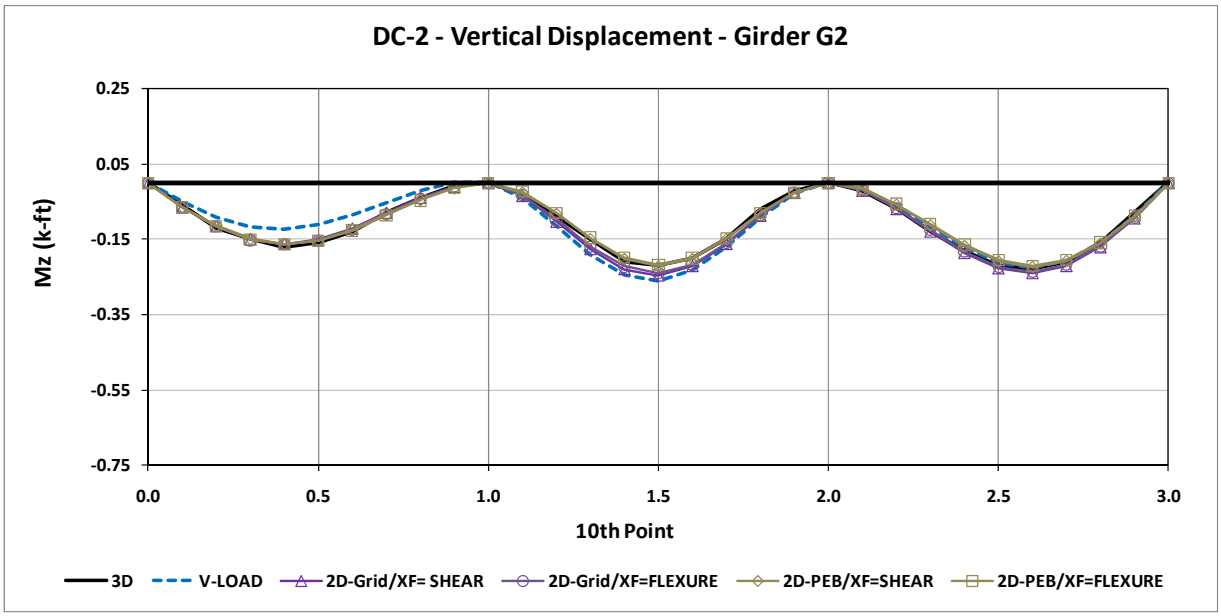


Figure 2.6.120 Unfactored DC_2 Vertical Displacement of G2

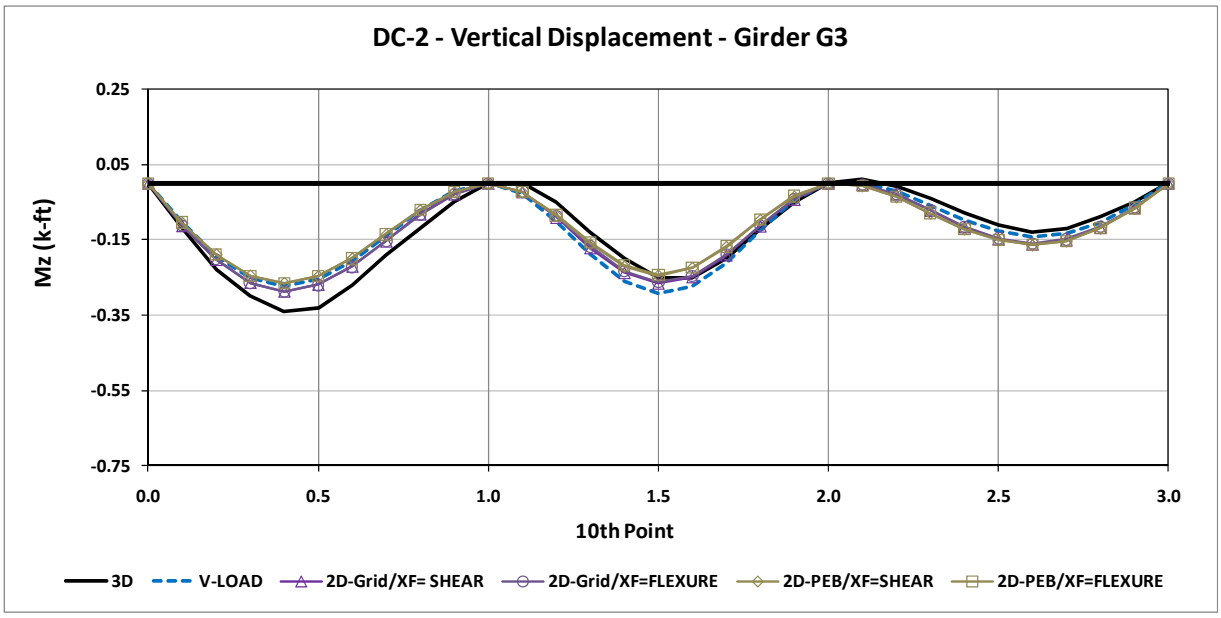


Figure 2.6.121 Unfactored DC_2 Vertical Displacement of G3

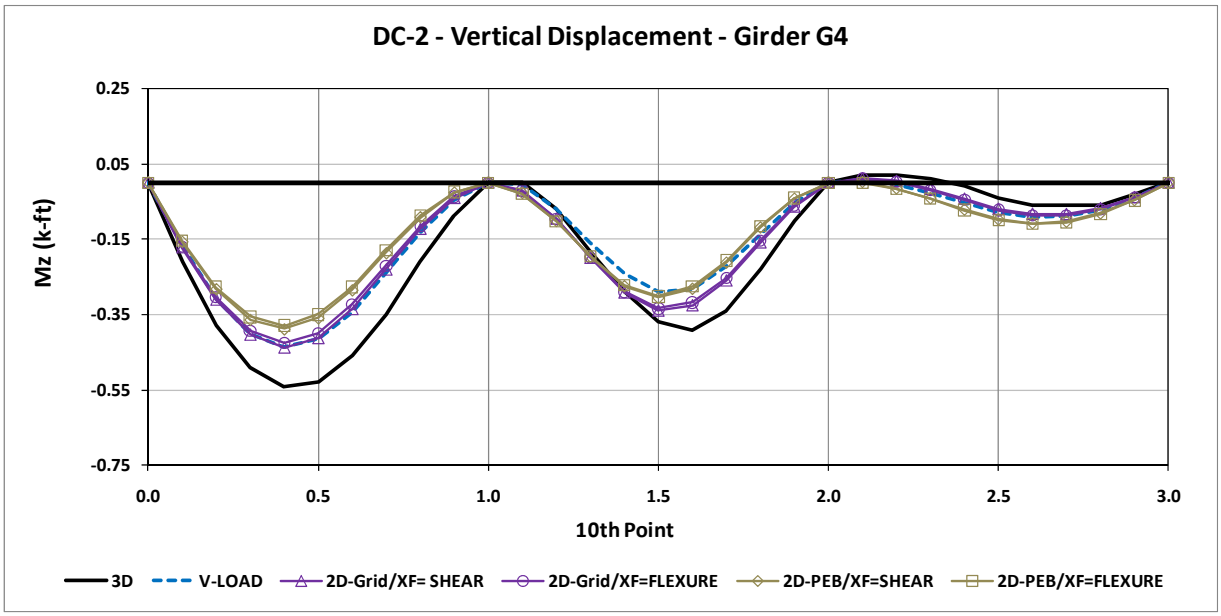


Figure 2.6.122 Unfactored DC_2 Vertical Displacement of G4

LL+I MAXIMUM DISPLACEMENTS							
Girder	Span	V-LOAD	3D	2D Grid XF-SHEAR	2D Grid XF-FLEX	2D PEB XF-SHEAR	2D PEB XF-FLEX
		(in)	(in)	(in)	(in)	(in)	(in)
G1	Span 1	-1.11	-0.49	-0.47	-0.47	-0.45	-0.45
	Span 2	-0.82	-0.97	-1.04	-1.03	-0.91	-0.91
	Span 3	-0.05	-0.94	-1.00	-1.00	-0.90	-0.90
G2	Span 1	n/avail	-0.65	-0.69	-0.67	-0.65	-0.64
	Span 2	n/avail	-0.99	-1.05	-1.03	-0.92	-0.96
	Span 3	n/avail	-0.77	-0.81	-0.79	-0.75	-0.74
G3	Span 1	n/avail	-1.05	-1.07	-1.06	-0.95	-0.94
	Span 2	n/avail	-1.26	-1.34	-1.31	-1.18	-1.17
	Span 3	n/avail	-0.73	-0.77	-0.75	-0.70	-0.69
G4	Span 1	-1.82	-1.58	-1.98	-1.90	-1.61	-1.57
	Span 2	-1.86	-1.69	-2.16	-2.08	-1.72	-1.68
	Span 3	-0.80	-0.88	-0.97	-0.96	-0.81	-0.81

Figure 2.6.123 Unfactored LL+IM Maximum Vertical Displacements

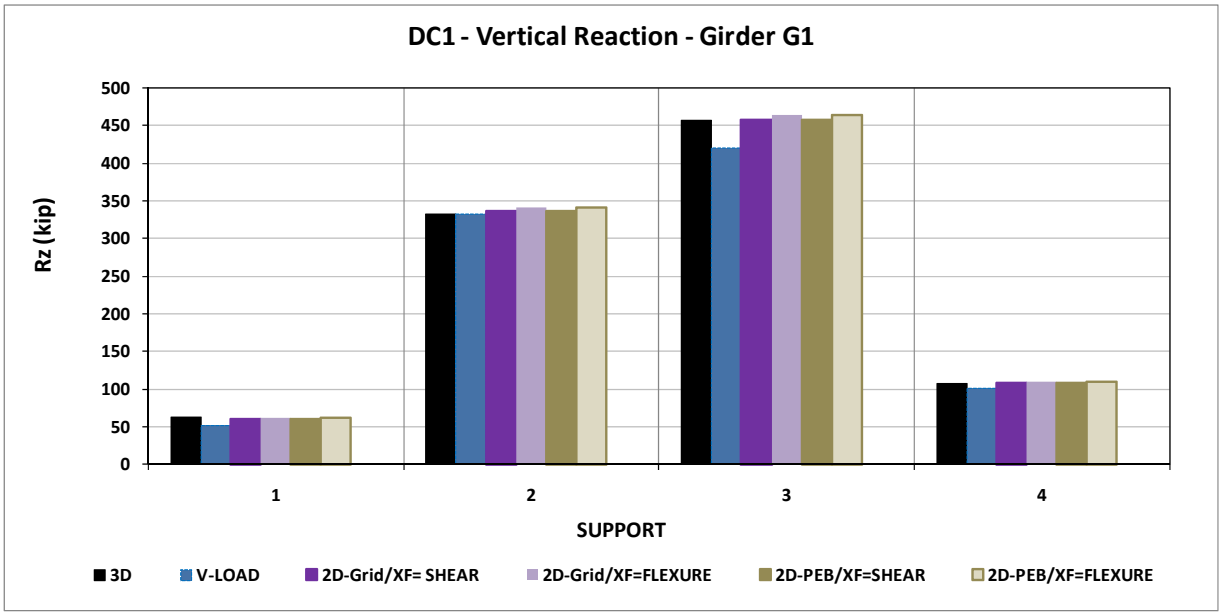


Figure 2.6.124 Unfactored DC_1 Vertical Reactions for G1

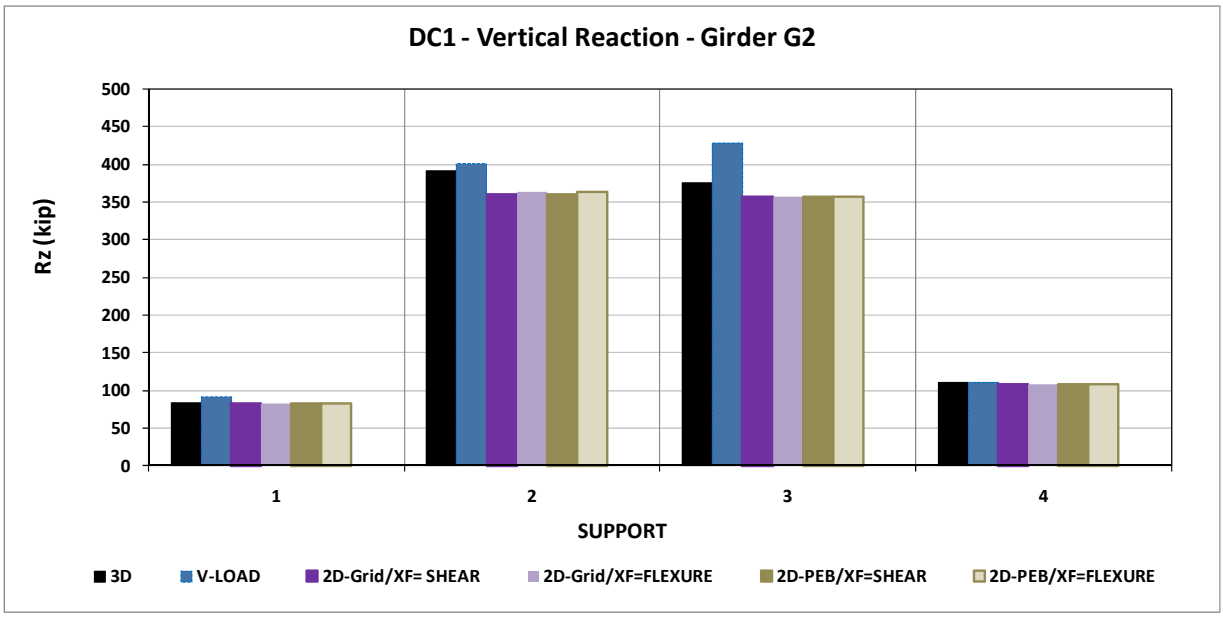


Figure 2.6.125 Unfactored DC_1 Vertical Reactions for G2

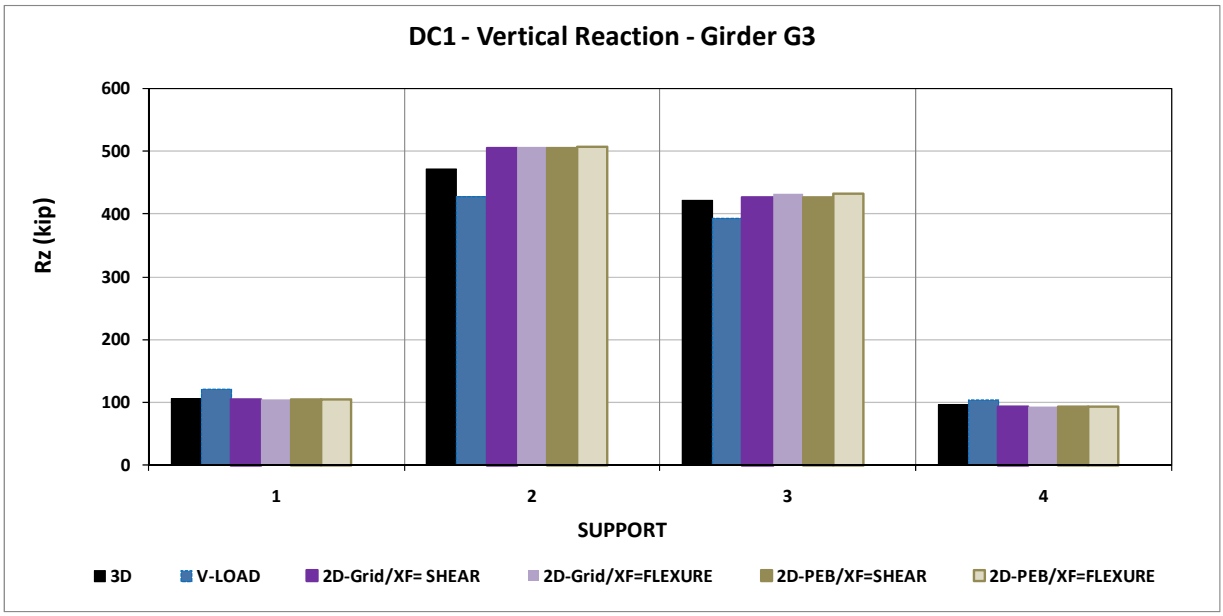


Figure 2.6.126 Unfactored DC_1 Vertical Reactions for G3

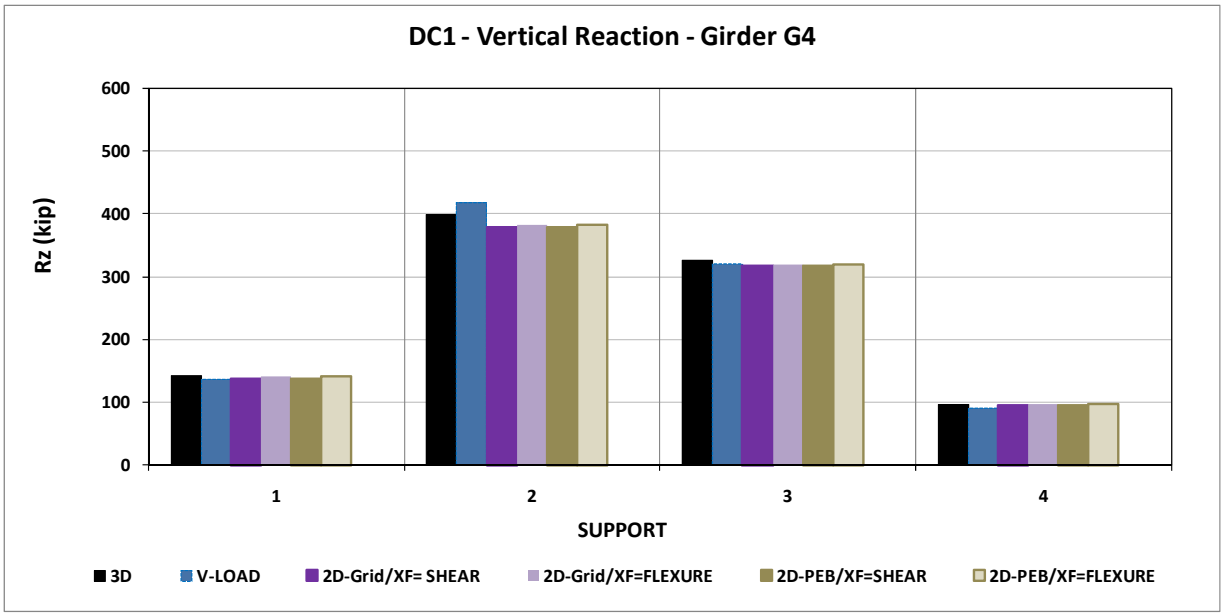


Figure 2.6.127 Unfactored DC_1 Vertical Reactions for G4

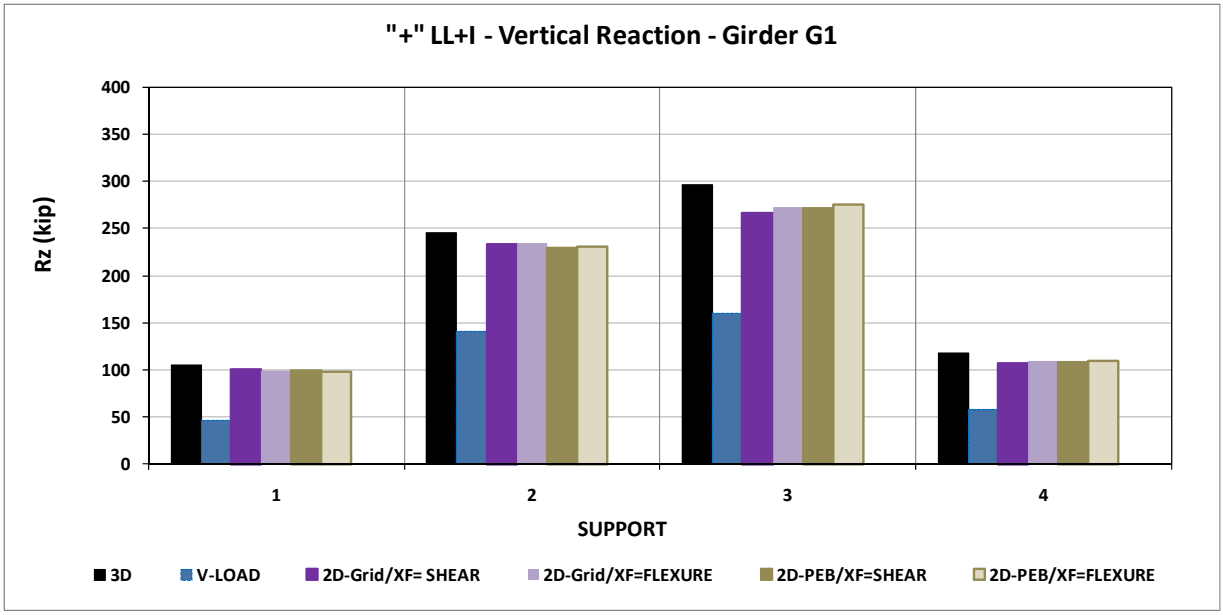


Figure 2.6.128 Unfactored +LL+IM Vertical Reactions for G1

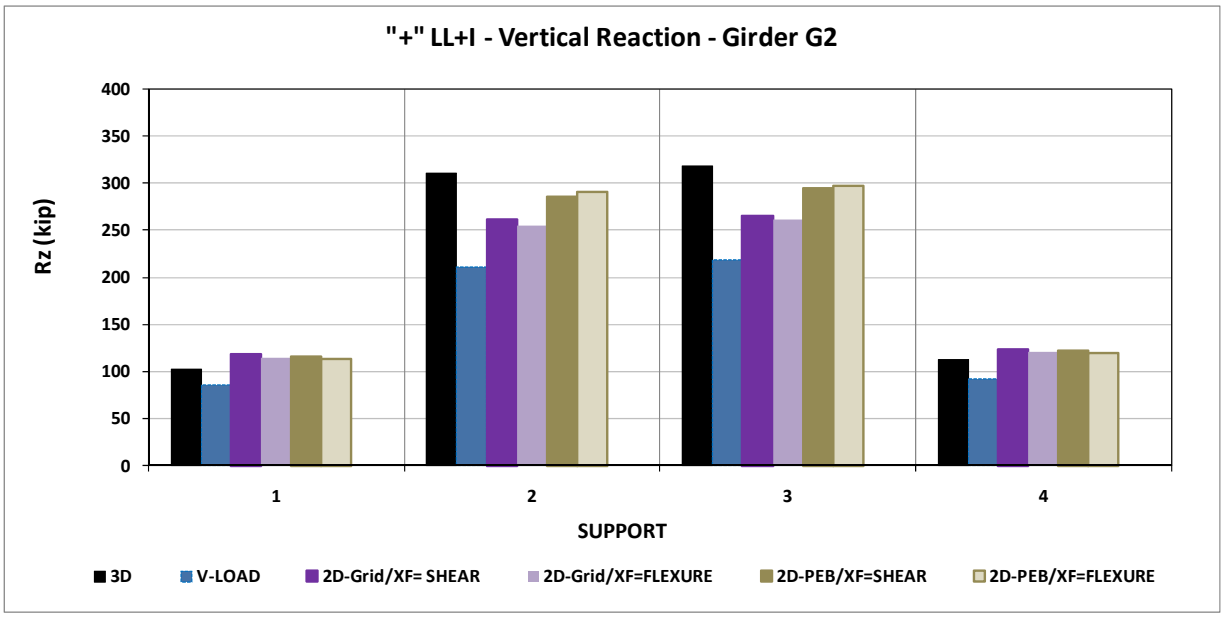


Figure 2.6.129 Unfactored +LL+IM Vertical Reactions for G2

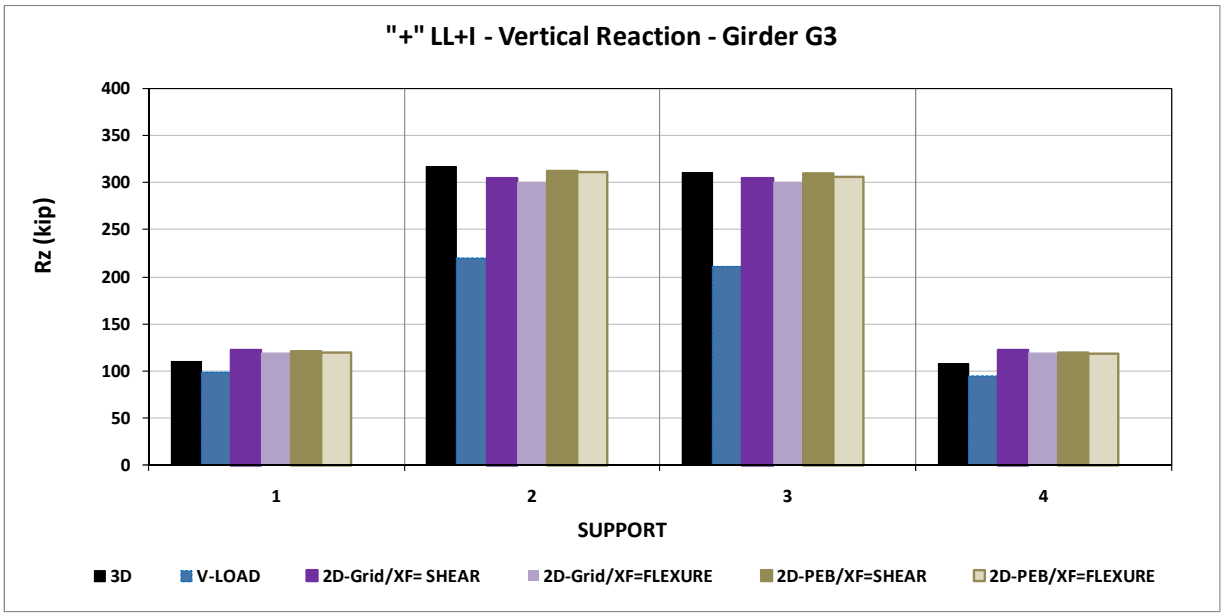


Figure 2.6.130 Unfactored +LL+IM Vertical Reaction for G3

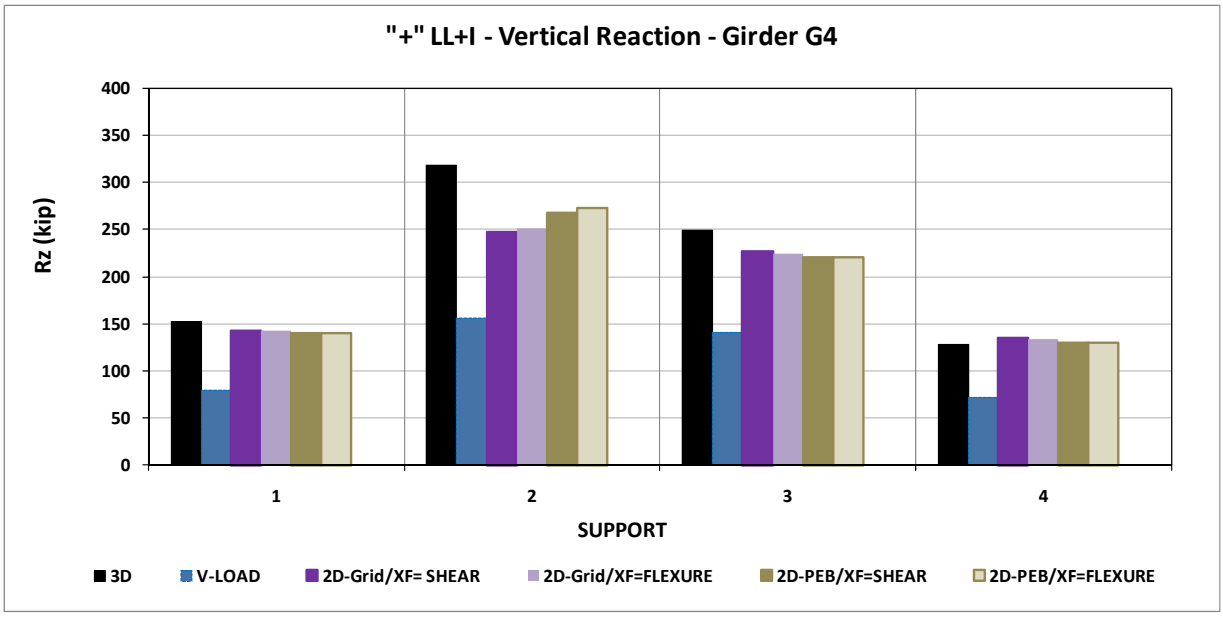


Figure 2.6.131 Unfactored +LL+IM Vertical Reactions for G4

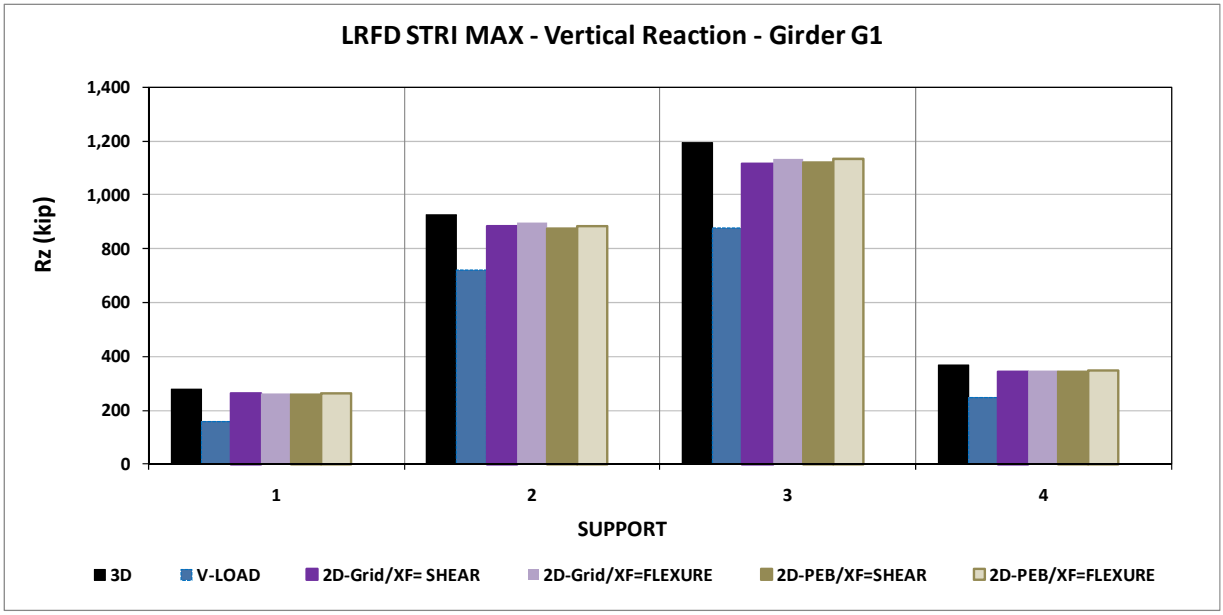


Figure 2.6.132 Strength I Maximum Vertical Reactions for G1

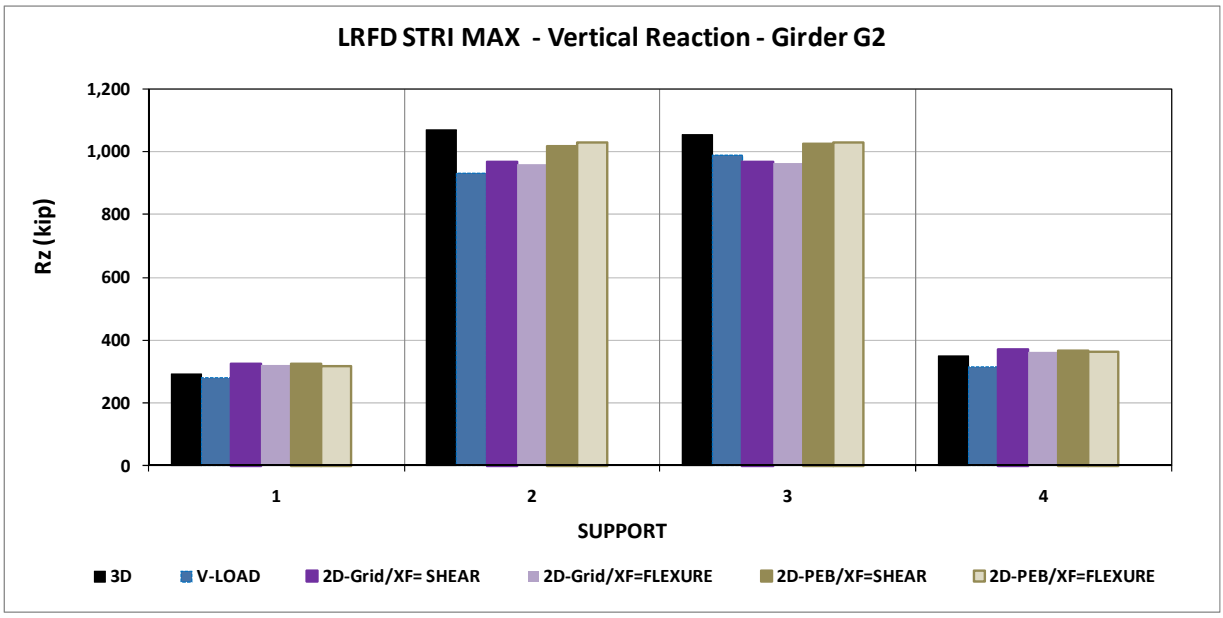


Figure 2.6.133 Strength I Maximum Vertical Reactions for G2

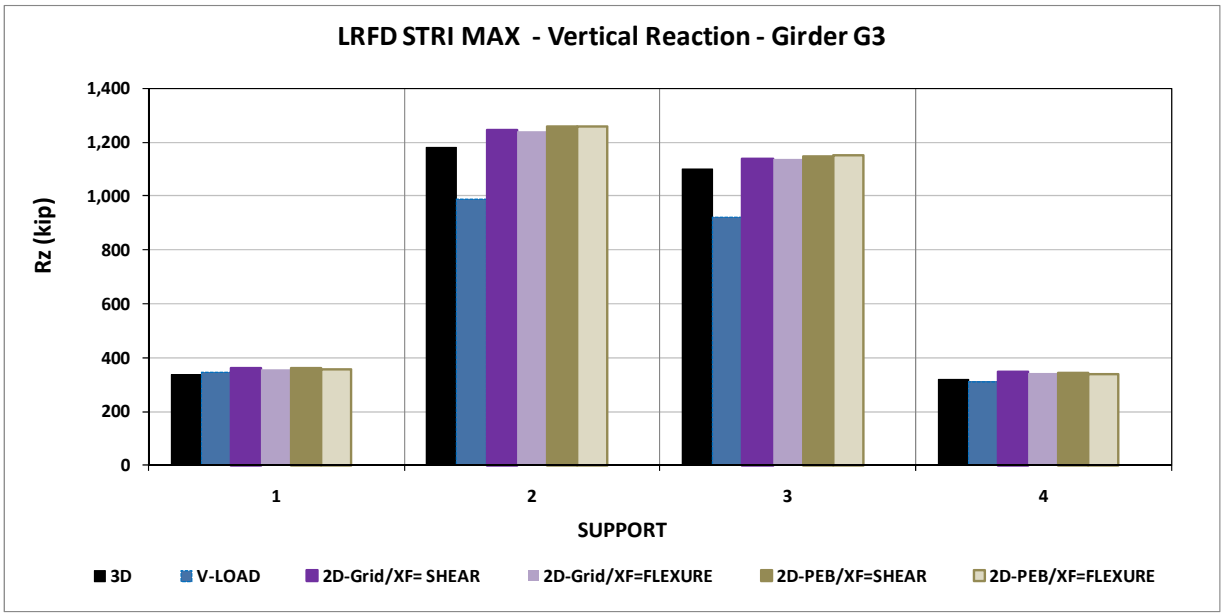


Figure 2.6.134 Strength I Maximum Vertical Reactions for G3

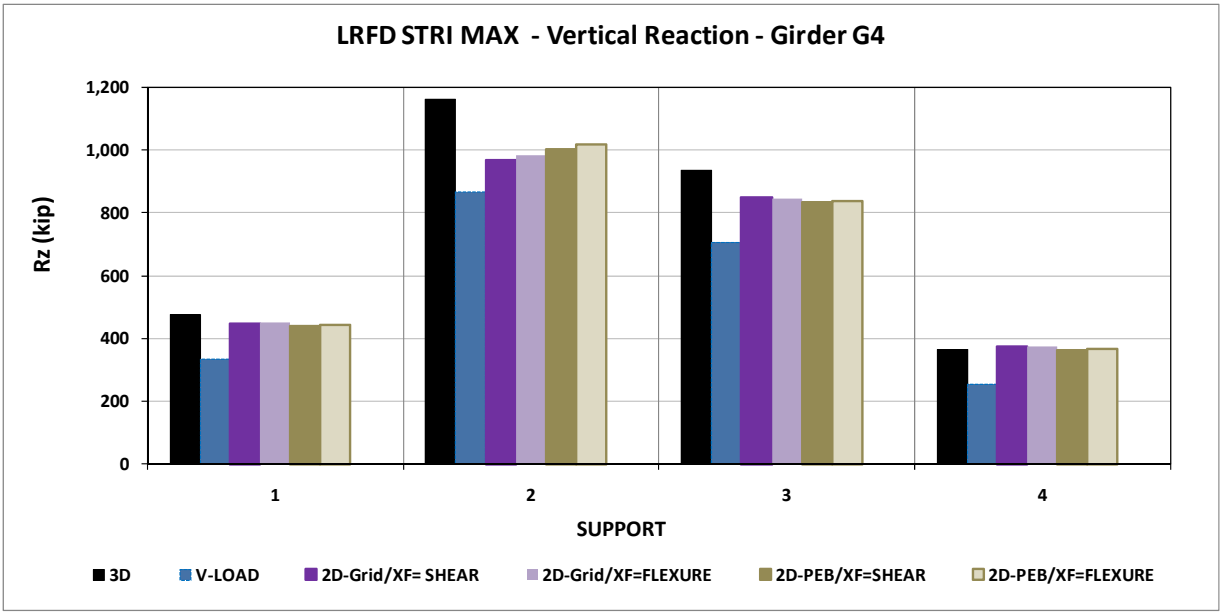


Figure 2.6.135 Strength I Maximum Vertical Reactions for G4

2.6.3 Completed Levels of Analysis Matrix

This section presents the completed Levels of Analysis matrix for all the analysis methods that have been discussed in the preceding sections of Chapter 2 of this manual. The matrix was introduced in Section 2.3.4. To review, '2D Grid' in the matrix represents the traditional grid approach and the acronym 'P&EB' represents the Plate and Eccentric Beam approach. The letter 'C' in the matrix refers to curved girder bridges with radial supports. The letter 'S' refers to straight or curved bridges with significant skews. For certain specific issues, a differentiation on this basis is best made to provide a realistic ranking. Where such a differentiation was not deemed necessary, the symbol 'C/S' is used. The ranking system that is used in the matrix is described further in Section 2.3.4. All rankings are obviously subjective and are open to debate. The rankings are based on the observations made from the analysis results for the two bridges examined previously in this section of the manual, plus the experience of the authors; the matrix is not intended to reflect the findings from a detailed research study. The basic assumptions that were implemented in each analysis approach for this cursory examination are discussed in Sections 2.3, 2.4 and 2.5 of this Manual. The completed matrix is presented in Table 2.6.3.

Table 2.6.3 applies to live load as well as dead load analyses, except where noted. Results are dependent on the ability of the modeling approach to recognize various members and/or conditions. For live load, the actions reported are dependent on the appropriateness and correctness of the post-processing software and not on the structural analysis technique. The matrix presented is useful to make judgments regarding selection of the appropriate methodology for a particular application. Various software packages have features that may make it more or less amenable to a particular issue. In many cases, the pre- and post-processing software is important in selecting a particular package. The above table does not address these issues and should therefore be treated as a guide.

Since the 3D finite element method is serving as the standard against which the other analysis methods are judged in this manual, the highest ranking of '3' is provided under all the listed issues for this method. "3D" in this case is assumed to mean a full 3D model of the superstructure and where required, the substructure. The depth of the structure must be recognized such that the bearings, deck and other features are properly located in the model with respect to the neutral axes of the flexural members.

Both 2D methods are felt to be comparable to the 3D finite element method in terms of the prediction of vertical bending effects in curved bridges without skew or with smaller skews. Both 2D methods begin to break down in this area somewhat as skew effects increase. Some grid or 2D software packages are able to recognize some characteristics that are normally only available in 3D models. Again, it is up to the Design Engineer to determine if the 2D package under consideration is correctly accounting for these characteristics.

The V-load and both grid methods again must rely on an approximate approach to determine lateral bending effects due to curvature. The prediction of lateral bending effects due to skew is less certain with these methods. Lateral deflections cannot be predicted with these methods.

The influence surface concept is not applied in the V-load method and is also typically not applied in the traditional 2D grid method.

The effects of horizontal thermal and wind loads and of horizontal bearing constraints on the analyses for those loads are more difficult to properly address in the two grid methods and cannot be addressed at all in the V-load method.

In both grid methods and in the V-load method, cross-frame actions cannot be obtained directly from the analysis. Internal member forces must be determined through the application of statics.

Note that to compute lateral bracing effects and forces, the use of the 3D finite element method is necessary.

The use of the 3D finite element method is particularly beneficial for examining the interaction of integral piers or straddle beams with the superstructure, for examining transverse deck stresses when necessary and for examining the effects of phased construction.

Table 2.6.3 Completed Levels of Analysis Matrix

Issue		V-Load	2D Grid	2D P&EB	3D
Vertical Bending	C	2	3	3	3
	S	1	2	2	3
Vertical Deflection	C	2	3	3	3
	S	1	1	2	3
Lateral Bending	C	2	2	2	3
	S	0	1	1	3
Lateral Deflection	C/S	0	0	0	3
Single Girder Stability	C/S	1	2	2	3
Influence Surface Concept	C	0	0	3	3
	S	0	0	3	3
Thermal Load	C/S	0	1	1	3
Wind Load	C/S	0	1	2	3

Issue		V-Load	2D Grid	2D P&EB	3D
Horizontal Bearing Constraint	C/S	0	0	2	3
Cross-Frame Actions	C	1	2	2	3
	S	1	1	1	3
Lateral Bracing	C/S	0	0	0	3
Substructure Interaction	C/S	0	1	2	3
Transverse Deck Stresses	C/S	0	0	2	3
Phased Construction	C	1	2	2	3
	S	1	1	1	3
Vertical reactions/Uplift	C	1	3	3	3
	S	1	1	2	3

As discussed in Section 2.3.2, the V-load method may not be able to detect uplift at end bearings in certain situations.

In summary, the approximate V-load method is limited to the analysis of curved I-girder bridges only and is limited to the consideration of vertical loads only. The method is best suited for preliminary design, particularly for structures with radial supports or skews less than approximately 10 degrees. In order to utilize the method, the girders at a given cross-section should have approximately the same vertical stiffness.

In general, 2D grid and 2D P&EB methods should be sufficient for cases involving reasonably regular span or framing arrangements, moderate spans and skews and/or large radii.

The 3D finite element method should be given serious consideration for cases involving irregular span or framing arrangements, long spans, severe skews and/or small radii. The method must be employed to compute lateral bracing effects and forces. The 3D finite element method is beneficial for directly determining cross-frame/diaphragm forces, flange lateral bending and torsion, the effect of constrained bearings and the interaction of integral piers or straddle beams with the superstructure. The 3D finite element method also allows for more efficient and detailed modeling of erection sequences.

The design of the example skewed and curved I-girder bridge (Section 5.1) and the example curved tub-girder bridge (Section 5.2) were both completed using the results from the 3D finite element method.

This Page Intentionally Left Blank

Chapter 3
Design Considerations

Section 3.1

Preliminary Design Decisions



3.1.1 Introduction

When designing skewed and curved steel bridges, several important decisions must be made prior to starting final design. These decisions involve layout considerations, as well as type and size considerations. This section presents guidelines for structural unit lengths, span optimization, field-section sizes, girder spacing, deck overhangs, deck and haunch thicknesses, cross-frames, diaphragms and lateral bracing. It also provides guidance when making decisions about box girders vs. I-girders, span-to-depth ratio, optimum web depth, web proportioning and flange proportioning. This section also includes a case study related to framing plan layout issues.

3.1.2 Primary Layout Considerations for Preliminary Design

The first portion of this section focuses on the primary layout considerations during preliminary design. Careful attention to these issues during preliminary design will provide a cost-effective bridge and will reduce rework during final design.



Figure 3.1.1 Curved Girder Bridge

The typical bridge serves hundreds or even thousands of drivers daily and is often viewed by many more. In fact, bridges are one of the most ubiquitous symbols of the modern infrastructure. More stringent constraints have been placed on bridges as land values have risen and other structures provide obstacles. Fortunately, the options available to the bridge engineer have kept pace. Structural steel is perhaps the most versatile bridge material today. It finds application in sites that have limited clearance due to its potential to be shaped into shallow structures. It can even have its depth smoothly changed with little influence on cost. Steel can be contorted into the tightest alignments. Steel can be combined with concrete in numerous ways resulting in a marvelous melding of the two materials. Steel bridges can be built with minimal interruption to traffic. This is possible because it can be erected quickly and without shoring, although occasional temporary towers permit safe erection.

Because steel can be fabricated and erected in an almost endless number of shapes, it should be always in the mind of the bridge engineer that the structure should be pleasing to the user and to the viewer because it is likely to be viewed for many years.

Other critical factors are initial and maintenance costs. In part, because of steel's versatility there are many ways to cause unnecessary increases in cost as well as

many more ways to design economy into the bridge. The bridge engineer owes the public no less than attractive low-cost structures. This section of the Manual provides recommended means to obtain these objectives within the framework of the *AASHTO LRFD* Specifications.

3.1.2.1 Structural Unit Lengths

One of the first decisions that must be made during preliminary design is the structural unit lengths for the bridge.

Where possible, a single multi-span unit should be employed in lieu of many simple spans or several continuous-span units. Modern design techniques and modern bearings permit the use of much longer multi-span structures than commonly used in the past. Analyses of thermal movements that recognize bearing orientation, bearing restraints and any flex in the substructure are highly desired to evaluate thermal movements and related forces for curved and/or skewed bridges. Elimination of as many end spans and associated joints as possible is desirable for both first-cost and maintenance considerations. Thermal considerations should lead to the use of separate units only after careful consideration of thermal requirements.

The length of bridge without expansion joints is not defined by specification. The elimination of joints – in addition to providing savings in the number of bearings, cross-frames and expansion devices – removes simple supports, which tend to require spans that are shorter than the adjacent spans in order to balance moments and provide economy. Shorter spans within a viaduct-type bridge detract from the aesthetics of equal spans.

Longitudinal forces can be distributed to several piers in proportion to their stiffnesses by the use of fixed pier bearings when designing long continuous units such as the one shown in Figure 3.1.2. Of course the piers must be sufficiently flexible. This option allows less expensive fixed elastomeric bearings to be used. The calculation of the appropriate horizontal pier stiffnesses to use in the analysis for such cases is discussed in Section 2.2.4. Curved alignments may have an advantage over straight alignments if piers are flexible in the transverse direction. This is often accomplished with single column hammerhead-type piers. Continuous curved steel structures over 1,900 feet long have been built and functioned well.



Figure 3.1.2 Curved Girder Bridge with Long Continuous Units

3.1.2.2 Span Arrangement

Steel has the versatility to be built in most any span arrangement. However, steel is most efficient when it is used in properly proportioned span arrangements. As mentioned previously, continuous-span steel bridges are usually more efficient than simple-span steel bridges. Usually the optimum span arrangement for long steel-girder bridges is equal-length interior spans with the length of the end spans approximately 75 percent of the length of the interior spans. Often a span arrangement is provided with all equal spans, which is optimal for prestressed concrete. Such an arrangement, although buildable with steel, is far from optimal. It leads to larger positive moments in the end spans and at times a non-optimal depth of girder. A carefully arranged span arrangement has a positive impact on the economics of the bridge. Selecting a proper span arrangement is particularly important for curved and/or skewed bridges where uplift is a more significant issue.

Span lengths should be proportioned as recommended above to yield approximately equal maximum positive dead load moments in the end and interior spans for straight and horizontally curved continuous spans. Such arrangements are termed “balanced span arrangements”. A balanced span arrangement provides for a single optimum depth. If unbalanced spans are required, it may be desirable to taper the depth of the girder so that different depths are employed more efficiently in different spans. Frequently, a girder depth between two optimal depths is neither optimum for the longer nor the shorter spans because an average girder depth can lead to flanges that are too large for the longer spans and too small for the shorter spans. Also, a shallow depth in the longer spans may cause problematic deflections.

In many cases, unbalanced spans and non-optimal girder depths cannot be avoided. The versatility of steel provides the best and often the only solution. There are choices that can make the situation less dire. Grade separation structures frequently have short end spans. An option in these situations is to examine the use of tall abutments eliminating the short “jump spans”. Lengthening the bridge is an option,

but is often found to be expensive. The traditional option is to use simple end spans, which adds two joints and is not desirable. When underclearance is critical, tie-down end supports with haunched interior span(s) has been employed. Of course, this option demands a foundation that can resist uplift. In the case of curved alignments and/or skewed supports, the uplift issue can often be addressed with judicially located lateral bracing and cross- frames. Varying girder stiffness also has an effect on uplift. Adding concrete integral diaphragms adds significant weight to the end-span reactions and has been found to help resist uplift in many cases.

To illustrate the balanced span concept further, the unfactored moments in a three-span continuous box girder caused by the dead load applied to the noncomposite section (DC_1) are shown in Figure 3.1.3. The span arrangement for this girder (192′-0″ - 236′-0″ - 192′-0″) is reasonably balanced with an end-to-center span ratio of approximately 0.81. The moments assuming the same total length for the box girder, but with a different span arrangement (200′-0″ - 216′-0″ - 200′-0″), are also shown. For this particular unbalanced span arrangement, the end-to-center span ratio is approximately 0.93. Note that the ratio of the maximum positive DC_1 moment in the end span to the maximum positive DC_1 moment in the center span increases from 1.2 to 2.5 when going from the balanced to the unbalanced span arrangement. For a steel-girder design, the larger uneven distribution of the moments from span to span in the unbalanced arrangement will have a significant overall effect on the girder efficiency and economy. Assuming the girder depth is optimized for either the interior or exterior spans, or else averaged, the chosen girder depth will be inefficient for the moments in either some or all spans.

It is prudent to develop a range of steel superstructure and substructure costs for various span lengths. The cost of the deck is ignored in these investigations since its cost is constant with respect to span. The most economical span arrangement is at the minimum point of the total cost curve, or the curve representing the sum of the variable superstructure and fixed substructure cost per pier over the span range under investigation.

For the case illustrated in Figure 3.1.4, the optimum span length is 165 feet for straight girders and 140 feet for curved girders. For multiple continuous-span units, this would be the span length chosen for the interior spans. The length of the end spans would then be chosen to provide a balanced span arrangement.

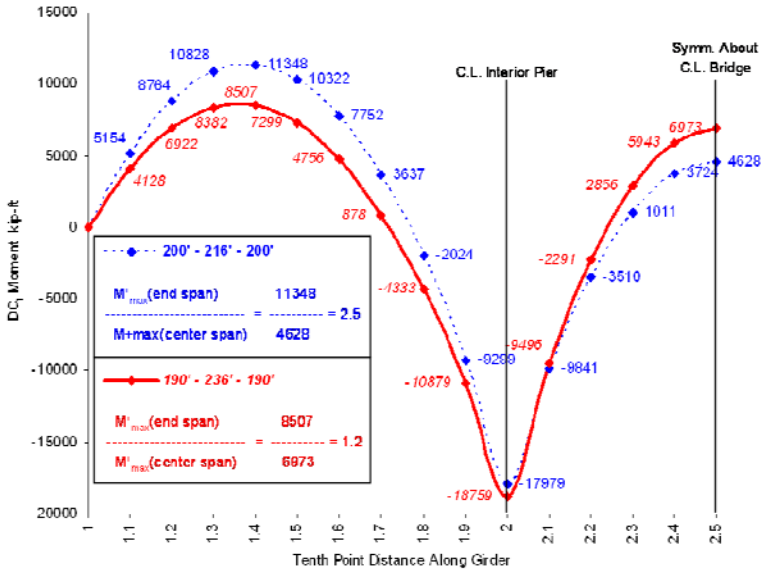


Figure 3.1.3 Component Dead Load (DC_1) Moments for Different Span Arrangements – Box Girder

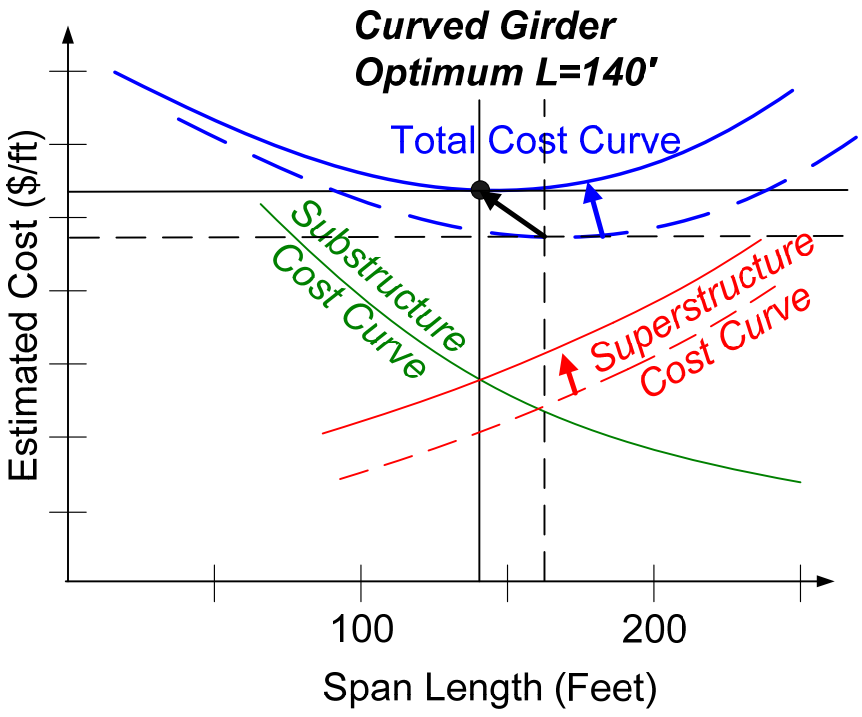


Figure 3.1.4 Cost Curve for Bridge Construction

Figure 3.1.4 demonstrates that the steel cost of curved-girder superstructures typically increases slightly over straight-girder superstructures. This increase results in a decreased optimum span length relative to straight girders for a given set of fixed substructure costs. If individual pier costs vary greatly due to height or subsurface conditions, this approach is of questionable value and a discrete pier investigation is warranted.

3.1.2.2.1 Substructure Costs

Obviously, if the substructure costs are relatively low, the optimum span is shorter than for a case with much larger substructure costs. When other things are not considered, the cost of the substructure should approximately equal the cost of the superstructure steel. An important corollary is that reduction of the pier cost has a double effect in that the savings in the piers justifies less costly (by an equal amount) shorter spans.

Clearly, the shape of the piers and the foundation type and size affect the substructure cost, and thereby, the optimum span length. Estimates of pier cost must include the cost of formwork, reinforcement, concrete and concrete placement. Simplicity and repetition are keys to economy of the piers. Changes to the unit costs that may result from an improved knowledge of specific site conditions should be incorporated in the analysis and the above curves regenerated before selecting the final span arrangement.

Foundation costs are a function of geological conditions and loads. Steel superstructures often provide an advantage over concrete superstructures in that their weight is less. However, this is not always an advantage. In some cases, the lighter gravity load leads to more critical overturning loads. As discussed further in Section 3.1.3.3, an objective for an efficient foundation is one that requires minimal additional material beyond that required for vertical loads. Overturning forces should be handled by a judicious positioning of piles or by the shape and size of a spread footing; preferably, they should not require additional piles or footing size.

To minimize the number of piles, it is necessary to eliminate redundancy in the substructure. For example, a wall pier is typically more expensive than a single column, or hammerhead-type pier. The foundation for a hammerhead pier is usually also more economical .than that for a wall pier. Obviously, when piers are high and/or expensive, there is more incentive to reduce their costs and to introduce some novelty into the design.

Hence, when alternate designs are investigated, the substructure for the steel design must be evaluated and designed concurrently with the superstructure if efficiency is to be obtained. *Since substructure costs have such a substantial impact on the most economical span arrangement, the proper steps must be taken if the Engineer is to ensure that the substructure design is the most efficient possible when combined with the steel superstructure*.

3.1.2.3 Field-Section Size

Field sections or “shipping sections” (sometimes simply called “girders”) are pieces of the bridge girder that are fabricated as a unit and shipped to the bridge site in that manner. A field section is shown in Figure 3.1.5. The limiting length, depth and weight of a field section is a function of the fabricator’s ability to handle the piece in the shop and to ship it. Generally, fabricators are able to fabricate and ship field sections much larger than the optimal size. In rare cases where erection precludes the use of field splices, the larger sections can be made. However, for most structures, the design should be led by optimal-size field sections.



Figure 3.1.5 Girder en Route to Construction Site

The Design Engineer usually does not know which fabricator will actually be doing the fabrication so he/she usually makes decisions on field-section size based on ensuring that at least one fabricator that is likely to bid on the work is capable of handling and shipping the field sections. Often the Design Engineer will provide optional field splices that may be eliminated at the discretion of the fabricator. In design-build situations, the Design Engineer usually works closely with the team in making the decision regarding the size of field sections. This simplifies the decisions but may limit the efficiency of the design compared to that of designs prepared by other teams. An example is girder depth. Another fabricator may be able to ship deeper more efficient girders by barge than the team fabricator may be able to ship.

The number of field sections and the location of splices can have a significant effect on the efficiency of the design. Fewer field splices reduces the cost for splices, other things being equal. For example, a simple span that is too long to fabricate and ship as a single field section may be spliced at the center of the span at the point of maximum moment saving a second splice that would be required if spliced at points of lower moment. Not only is the number of splices reduced, but the splice is made at the point of minimum dead load shear reducing the demand on the web-splice bolts. Further, it may even save a shop splice if the flange plates are too large to

come from the mill. In that case, a uniform-size flange plate would have to be shop-spliced with a hidden cost to the Design Engineer. Not only does the erector have less work, there is one less truck involved in shipping the two field sections than the three field sections to make up one girder line for the span. It should be kept in mind however that the flexural resistance of the tension flange at a bolted splice is limited to the flange yield stress according to the specifications (*AASHTO LRFD* Article 6.10.1.8), which also has to be given some consideration when locating a bolted splice at mid-span, particularly in a straight girder. The choice of field splice locations and the corresponding field section lengths is in many ways project specific.

The weight and length of sections should be determined after consultation with fabricators who are expected to be bidding the work. For example, the crane capacity in the shop legally limits the weight the fabricator can lift with each crane. Sometimes a section can be made slightly lighter to accommodate that capacity relieving the fabricator of calling for an additional crane every time the section is to be moved. Calling for additional cranes to move a section interrupts other production. Sections too long to fit in normal lay-down areas also interrupt normal operations. Flanges too wide to fit in blasting machines or girders too deep to clear overhead cranes are examples of the interrelated factors that affect the cost of fabricating girders.

Material availability from the mills and its cost is significant in some instances, but it is often difficult for the design Engineer to ascertain availability and cost. For example, plates are typically considered standard between 0.375 and 2 inches thick. Above two inches in thickness, there is an extra charged. There may be only one producer that produces bridge quality plates above three inches thick, introducing a substantial extra even though plates up to 4 inches thick are permitted by specification. A deep web plate may be available from one mill but its cost might lead the fabricator to choose to build the girder web up by splicing plates together. Another example is the issue of camber. Camber is typically cut into the web plate. If camber is large, the fabricator may choose to partially shape the web camber by sections of web plate rather than ordering a deep plate to burn out the camber with a large amount of waste. Camber issues are beyond the Engineer to consider at design.

3.1.2.3.1 Shipping

Shipping is very site sensitive. The shipping regulations of the various states differ greatly. It is impractical for the Design Engineer to know the vicissitudes of shipping girder sections. That said, there are specific shipping limits that trip additional costs. For example, it may be that a field section length is slightly over the limit where an escort is not required. If the splice is moved a few feet, a significant savings in shipping cost might be gained. Similar trip points exist for girder weight, depth and width. This information should be ascertained from a fabricator. The width of curved field sections may be a factor. Obviously, the limiting width of a shipping piece might limit the length of a curved girder. Generally, curved girder bridges tend to require shorter field sections, but that is certainly not always true.

The fabricator's contract usually calls for delivery of the fabricated steel to the bridge site. This familiarity with shipping makes the fabricator the source for shipping information. Excessively long, wide or heavy field sections require determination of a specific route, shipping times and frequency of load transporting. Frequently, designs provide for optional field splices to reduce handling and shipping costs. The Design Engineer is encouraged to discuss large bridge design projects in their early stages with the fabricators who are likely to bid on the project. These fabricators will provide parameter information particular to the project. An astutely designed steel girder bridge is one that more than one fabricator must be able to bid competitively. Shipping can be a deal breaker.

Steel I-girders are preferably shipped in the vertical position, although they can be shipped canted or horizontal. Shipping is perhaps the most nebulous of the issues involving steel-girder bridges. The ability to ship a particular girder is dependent on the particular route. This requires that the fabricator study the route in order to give definitive information to the Design Engineer regarding practical girder-size limits.

Examples of special transportation provisions include additional blocking and tie-downs, special multi-axle trailers, escort vehicles, restricted hours for highway use, and special types of railroad cars, etc. Although such special provisions result in additional costs along with added shop handling costs, these costs may be offset by the need to erect fewer sections with fewer field splices, which can result in significant savings.

The curvature affects the feasibility of shipping curved girders and must be taken into account when laying out the splice locations. Often the means of shipping can be predicted. The American highway system has matured to the point that it is the means of choice to ship the majority of steel-bridge components from the fabricator to the bridge site. Essentially all fabricators are capable of shipping by truck. Some fabricators have their own fleet of trucks so they keep trucking costs in-house. Having a personal fleet also permits control over delivery dates, even time of delivery. Since highways are generally publicly owned and used by the public, they are subject to strict regulation to ensure safety and equal use. Load weight, length, and width are controlled, usually by the state, and regulations differ between the states. There are discrete limits on size. Certain sizes may be shipped without an escort; others may require more escorts, and so forth. There may also be limits on the time of day certain loads may be shipped and the number of shipments in a day. For example, it would be nonsensical to design a field section that requires extra shop-crane capacity and an extra escort to ship 250 miles to the bridge site when shortening it by three feet and lightening it by five tons would eliminate both of these extra costs. Therefore, for the Design Engineer to know these limits and take them into account at design is important.

Generally, the curvature limits the length of a shipping field section to a length less than what would be practical for a similar size straight field section. Of course, this

may entail the need for additional field splices in order to reduce the length. For longer field sections, consider showing optional field splice locations on the plans.

The following recommendations related to shipping pieces (for shipment by truck) were provided by a large steel fabricator:

- Whenever the radius of the field section is less than 900 feet, and/or the mid-ordinate is greater than or equal to 18 inches, and/or if the flanges over the majority of the section are light (i.e., less than or equal to 1-inch thick), the Design Engineer should get in touch with a potential fabricator to discuss shipping considerations;
- The total height of the load should be kept below 13′-6″. The height includes the height of the trailer plus the girder depth, including camber and potentially the thickness of the tie-down chains. If the total height limit is exceeded, the use of "drop" trailers (typically 3′-10″ high) can be considered;
- If the planned length of the field section is to exceed 120 feet, the Design Engineer should again communicate with a potential fabricator;
- Field sections weighing more than 35 tons typically require more truck axles than the standard seven axles. A girder weight of 300 to 400 pounds per foot is optimal for shipping. Extreme weight sections are problematic. For long loads that are light (approximately 200 pounds per foot), stability and stresses need to be evaluated. For shorter and heavier loads, it becomes difficult to get the axles under the load. Extra rigging for stability is the fabricator's responsibility, but is reflected in the project cost.

In at least one state, a load for truck shipment is classified as a "super load" if any of the following conditions are met:

- The load length (measured from the front of the tractor to the end of the girder) exceeds 160 feet;
- The total weight of the load, including all equipment, exceeds 100 tons;
- The load width exceeds 16 feet.

In this state, each company is allowed to ship two "super loads" per day. The shipper must pay for any bridge analysis that may be required along the route. State police inspection by each state traversed is usually required. Different travel times may be specified in different areas. Driver regulations may also impact travel times. Different states will likely have different regulations regarding "super loads." Fabricators should always be consulted with regard to trucking of a "super load."

A fabricator might choose rail transportation for particularly deep girders, or girders that are to be shipped a great distance. Since rail access at the bridge site is often not available, such pieces are usually off-loaded and trucked to the site. An interesting aspect of rail transportation is that it can change the competitive situation for a bridge. If the bridge cannot be shipped by truck and must be shipped by rail for whatever reason, the interest is opened for fabricators from greater distances since loading and unloading of the railcars, and demurrage are the largest factors in the cost of rail shipping; rail mileage is a less significant cost than highway mileage.

Again, it should be emphasized that the requirements for a particular project related to rail movement should be investigated with the likely fabricators on an individual project basis.

Presently, there are few steel bridge fabricators located on navigable water in the United States. For certain appropriate structures, water transportation may be practical. Such projects may involve enough sections to fill a barge and be on the water. Otherwise, hybrid shipping may need to be employed entailing trucks as well as a barge. Water shipment may be beneficial when site conditions permit erection directly from the barge. The potential for transporting sub-assemblies or assembling entire bridge spans, floating them into position and erecting them onto their bearings directly from the barge may offer significant economies in certain cases.

3.1.2.4 Girder Spacing

Girder spacing (i.e. the number of girders) is a very important parameter in designing an economical steel-girder bridge. Generally, the fewest girders results in the most economical bridge.

Fewer girders generally provide the following economic benefits:

- Reduced fabrication, inspection, painting, shipping and erection;
- Fewer bearings to purchase, install and maintain;
- Fewer bolts and welded flange splices;
- Reduced fabrication and erection time;
- Reduced structural steel weight;
- Lower total bridge cost.

Like any good idea, there are limits. The associated trade-offs need to be examined in each case. For example, wider girder spacing leads to thicker, heavier concrete decks. Frequently, the girder depth cannot be increased due to the clearance envelope. Flange sizes are limited to practical plate sizes. Live load deflection limits must be met.

In prior editions of the *AASHTO* bridge specifications, the exterior girder was less critical than interior girders. The more recent *AASHTO* Specifications, including the *AASHTO LRFD* Specification, correctly assign more dead and live load to the exterior girders making them, typically, the critical girders in the cross-section. This is particularly true when the overhang is large. As a practical matter, the girders in the cross-section are best made the same size. This means that if the exterior girders control the design, the interior girders are overdesigned if they are made the same size as the exterior girders. If they are sized smaller than the exterior girders, the greater stiffness of the exterior girders will draw load away from the interior ones, leading to the exterior girders being technically underdesigned. Thus, the optimal cross-section is one having a girder spacing and overhang such that the exterior and

interior girders have nearly the same total demand moments. Of course, increasing the girder spacing reduces the overhangs.

There are a number of factors that influence the design of exterior girders differently than interior girders. For the most part, the *AASHTO LRFD* Specification addresses these issues. Curved-girder bridges have a special effect not seen in straight-girder bridges. Exterior girders on the outside of the curve (convex side) receive dead and live load shifted to them, as discussed previously in prior sections of this Manual. It is frequently found that shifting the girders toward the convex side of the deck reduces the demand on the convex girder. This has the effect of resulting in a less stiff convex girder. This in turn draws lesser load, thereby reducing not only flange sizes but also cross-frame forces. The visual effect of different overhang widths is not apparent from normal viewing locations.

Because of steel's greater stiffness than concrete, it is often chosen where depth is limited. Live load deflection often becomes an issue in these circumstances. The tendency often is to add girder lines to reduce deflection. Traditionally, the averaging approach has been used most frequently to determine the appropriate live load assigned to a girder in a straight bridge to compute live load deflection. Unlike the *AASHTO Standard Specifications*, which were ambiguous in this regard, the *AASHTO LRFD* Specification specifies that a multiple presence factor is to be applied. Thus, the more traffic lanes on a bridge, the smaller the live load assigned to a girder. The fewer the girders in the cross-section, the more live load assigned when computing deflection. However, if the wheel load distribution factor for moment or a refined analysis is used to compute live load deflections, the number of girders in the cross-section has a much less significant effect on deflection and fewer girders may in fact be needed than when the averaging approach is used. The most efficient way to increase stiffness of the bridge without increasing girder depth is to increase the size of the bottom flanges.

The maximum flange size is controlled first by the availability of plate and secondly by a number of other matters. As discussed further in Section 3.1.4.3.2, the maximum practical flange thickness is 3 inches. It is suggested not to exceed this limit unless absolutely necessary. When strength and/or stiffness requirements cannot be met with practical size flanges and girder depth cannot be increased, the only alternative is to increase the number of girders.

3.1.2.4.1 Effect on Deck Design

Most states provide standard deck designs. Usually the decks of stringer bridges are designed as transversely reinforced only. Hence, deck thickness increases with increased girder spacing. However, the thickness increases in increments so the spacing can be widened to some degree without attendant increased thickness, which leads to increased concrete and deck reinforcing costs. However, these costs are usually less than the cost of an additional girder line.

When the girder spacing becomes very wide, the cost of forming may increase. When cast-in-place decks are used, the weight of concrete in the flutes of metal

galvanized stay-in-place deck forms must be considered. Much of this weight can be eliminated by placing Styrofoam in the form flutes. Deeper permanent metal deck forms are available that can clear span up to about 13.5 feet between girder top flanges. Precast concrete deck panels are sometimes used as alternative stay-in-place forms, but there forms can only be used for girder spacings up to approximately 10 feet.

Plywood forms are required by some states. Extra wide spacing has been accomplished with wood forms by employing overhang brackets between the girders to reduce the effective span of the wood.

To reduce the weight associated with a thicker deck and wide girder spacing, transversely post tensioned decks have been employed. Post-tensioning in place on steel creates certain issues that need to be addressed. The steel connecting the girders is much stiffer than the deck so it resists shortening, creating hogging in the deck. This is not an insurmountable problem, but it does require a rather refined analysis.

One way that post-tensioned decks have been made more practical is to introduce a vaulted deck. This shape allows the strands to be straight while they produce compression in the top of the deck in the thicker portions in negative moment regions and compression in the bottom of the deck in positive moment regions where the deck is thinner. This approach increases forming costs so it is economical only when spacing is around 30 feet or more. Of course such girder spacing is associated with very large overhangs—perhaps 15 feet. This type of deck has only been designed in conjunction with tub girders.

3.1.2.4.2 Redecking Under Traffic

High usage of the nation's roads has led many states to require that roads remain open to traffic while the deck is being replaced. This is usually accomplished by placing a temporary barrier on the deck, saw cutting the deck over a girder line and removing and replacing that portion of the deck. This process is repeated until the entire deck has been replaced. Various patterns have been employed, but most require that cutting be performed over a girder line and that traffic be maintained without damage to the bridge. Skewed and/or horizontally curved girder bridges can be particularly problematic structures during redecking.

The most critical issue with redecking is the exterior girder on the side with deck and traffic. The removal of weight from the opposite side of the bridge allows the bridge to twist causing an increase in moment in that exterior girder. A second potential issue is uplift at bearings where some of their load has been removed. The uplift issue is more prevalent with skewed supports. Skewed supports can experience uplift that is not found when the total cross-section is effective. Another factor that may exacerbate the uplift issue is the crowding of lanes together during redecking.

Design lanes are usually 12 feet, while during redecking, lane widths of 10 or 11 feet are common.

When a portion of the deck is removed, the load in the girders under the removed portion is relieved. The unloaded girders tend to rise while the cross-frames tend to restrain them. Not infrequently, the cross-frames may be significantly overloaded during this condition. The wet concrete is then placed on the bare girders as a non-composite load. The adjacent composite girders are much stiffer and tend to draw some additional load in excess of the unloading experienced by the earlier deck removal. This additional load must be added to the live load and the load from any temporary barriers. When the entire deck is eventually replaced, it simply returns the bridge to its original stress state and deflected shape. Rarely are cross-frames overloaded as the deck is replaced.

Lane-width requirements and the requirement that cuts must be done over a girder line may control the number of girders in the cross-section. For example, a narrow bridge may require only four girder lines but the girders may not be located such that a lane can remain open when the deck is being replaced. The result is that a fifth girder in the center of the deck is required. Alternatively, if the bridge is wide enough, four girders may be used with wide spacing that permit a single traffic lane with an additional barrier to be supported on two girders. This might cause the exterior girders to be under-designed due to a small overhang, but it almost always more economical than adding an additional girder.

If a four-girder cross section is not wide enough to redeck using two girders, it can be modified by increasing the girder spacing in one bay to accommodate a lane of traffic. The remaining two-bay spacing is reduced. This technique requires a refined analysis because wheel load distribution factors provided in the *AASHTO LRFD* Specification are based on the assumption that the girder spacing is constant in all bays. This technique is particularly useful on curved bridges where the spacing in the bay closest to the center of curvature (i.e. on the concave side of the bridge) is increased while the spacing in the outside bays is decreased. This tends to reduce the moment in the convex critical girder, while perhaps permitting an entire girder line to be eliminated.

3.1.2.4.3 Phased Construction

Phased construction deals with construction of bridges in phases with a longitudinal joint. This method of construction has become increasingly common when replacing existing bridges without detouring traffic. In phased construction, traffic is typically maintained on the existing structure while part of the replacement structure is constructed. Frequently, a portion of the existing bridge is removed so that the existing substructure can be used. Traffic is then shifted to the new phase of the replacement structure, with appropriate temporary barriers added. This phase is followed by demolition of the existing structure. Girders, deck and parapets for the remaining phase of the replacement structure are then constructed and built next to the first phase. Unlike the situation in deck replacement, the first phase has not the benefit of removal of some load. If the second adjacent phase is connected to the

first phase with cross-frames prior to casting the deck, significant load is shifted to the already composite bridge. This increases moments and deflections in the first phase. It is difficult to predict the final position of the bridge due to creep of the deck in the first phase. Extreme forces are often created in the cross-frames connecting the two phases.

The preferred method of construction is to build the second phase independent of the earlier phase. As the final step, the two phases are connected with cross-frames and a closure pour is cast. In some cases, the deck will simply be cast onto the last phase without providing a closure pour. The phased construction is then completed by the removal of any temporary barriers that were placed on the structure during construction. These final steps to join the completed phases and remove any temporary barriers occur on the composite replacement structure.

Interestingly, cross-frame forces in a bridge with skewed supports are relieved somewhat in phased construction because the bridge width is reduced. The transverse stiffness is reduced by the interruption of the cross-frames during placement of the deck.

Phased construction of horizontally curved bridges presents serious issues that must be addressed. If the bridge is built from the concave side, the first phase will cause severe overloading and overdeflection of the convex girder in that phase because it will temporarily be an exterior girder, whereas if the bridge were built in one step, that girder would shift a portion of its load to the adjacent convex girder. The result is that the first phase must be cambered and designed for the controlling first phase.

In cases where a closure pour is provided between the two phases (Figure 3.1.6), the weight of the closure pour, any associated deck forms, and the added cross-frames between the existing and replacement structure should be applied as a composite load to all six girders in the cross-section in the analysis, Removal of any temporary barriers and the addition of any future wearing surface load should also be applied to the completed composite structure.

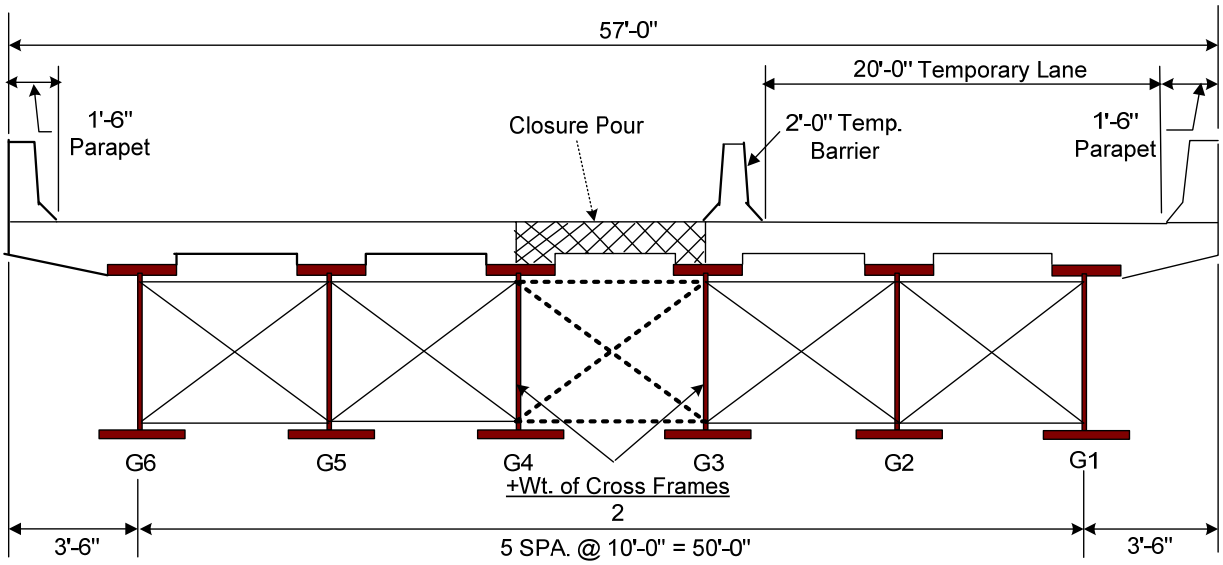


Figure 3.1.6 Phased Construction with a Closure Pour

When the deck is to be cast in phases without providing a closure pour, cross-frame forces in the bay between phases can be mitigated by attaching only the top and bottom chords, as shown in Figure 3.1.7. The diagonals in those cross-frames should not be effective until the deck of both phases has been cast. This procedure still requires that the erector return to the site. To ensure fit-up of the cross-frame diagonals, it may be desirable to use the diagonal holes as a template to field drill the connection-plate bolt holes.

Unlike the scenario with a closure pour, in this case, the adjacent girders in the two phases each have a different stiffness prior to the final deck pour; one girder (G3) is composite and the adjacent girder (G4) is non-composite. Therefore, the stiffer composite girder will tend to draw more load when the final portion of the deck is cast (Figure 3.1.8). Eliminating the cross-frame diagonals for this phase helps reduce some of this load transfer so that the deflections of the adjacent girders will be closer to the case where both girders are assumed to have approximately the same stiffness. The two chords help maintain the alignment and spacing between the girders during the final deck cast. The deck and deck haunch weight (and any associated form weight) from the final portion of the deck cast should be applied as a non-composite load to G4 through G6 and as a composite load to G1 through G3. The weight of the cross-frame chords should also be added as a non-composite load to G4 and as a composite load to G3 in the analysis. Removal of any temporary barriers, addition of any permanent barriers and the addition of any future wearing surface load should be applied to the completed composite structure

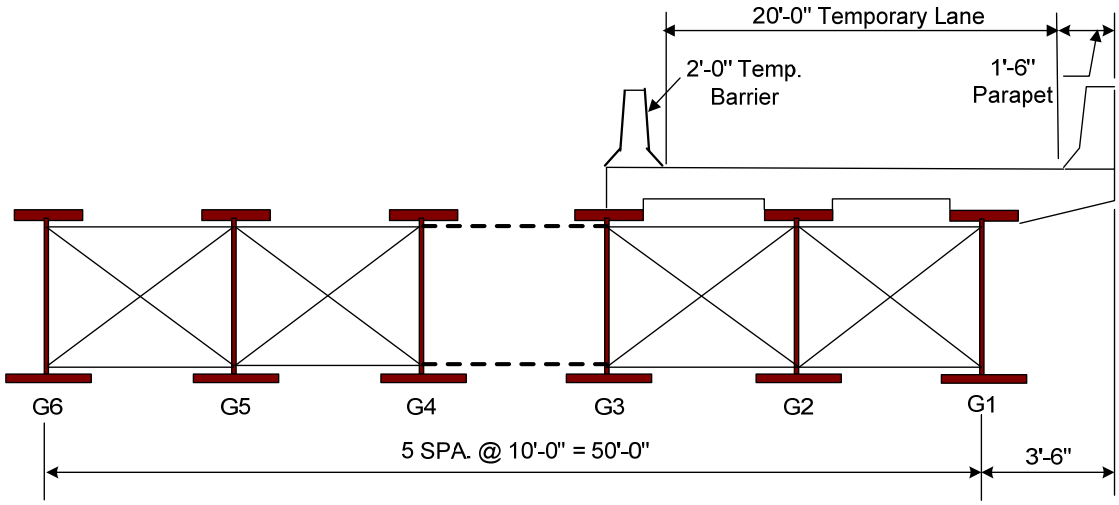


Figure 3.1.7 Phased Construction – No Closure Pour

In both of the above cases for the example bridge shown, the new completed phase of the replacement structure represented by G1 through G3 and the cross-frames in-between those girders must be investigated separately for the dead load acting on that phase only plus the live load placed in the temporary portion of the bridge. The completed bridge must also be evaluated for the combined effects resulting from the addition and removal of the various dead loads during the completion of the phased construction. Usually, the analyses of the phased construction will provide the critical case and is designed first. A check of the completed bridge will usually, but not always, show the girders to be less critically stressed.

Cambering girders for phased construction can be complex. Typically, the closure pour option is employed on longer spans where the dead load is most significant. Deflections are larger and the potential of problematic cross-frame forces in the bay between phases is great. When spans are small to moderate, a closure pour may not be necessary.

The girders may twist under heavy deck loading during phased construction with a closure pour. This is partly due to the uneven deck load on the bridge. The overhang is on one side and the deck is terminated at a girder. This can twist the girders significantly. If the twist occurs only on the second phase, chords as shown in Figure 3.1.8 may restrain the second phase sufficiently. Otherwise, top and bottom lateral bracing in the bays on each side of the closure bay may be required. If the girders are curved, of course the issue is exacerbated.

Specific considerations related to the phased construction of skewed and curved bridges are discussed further in Section 4.2.

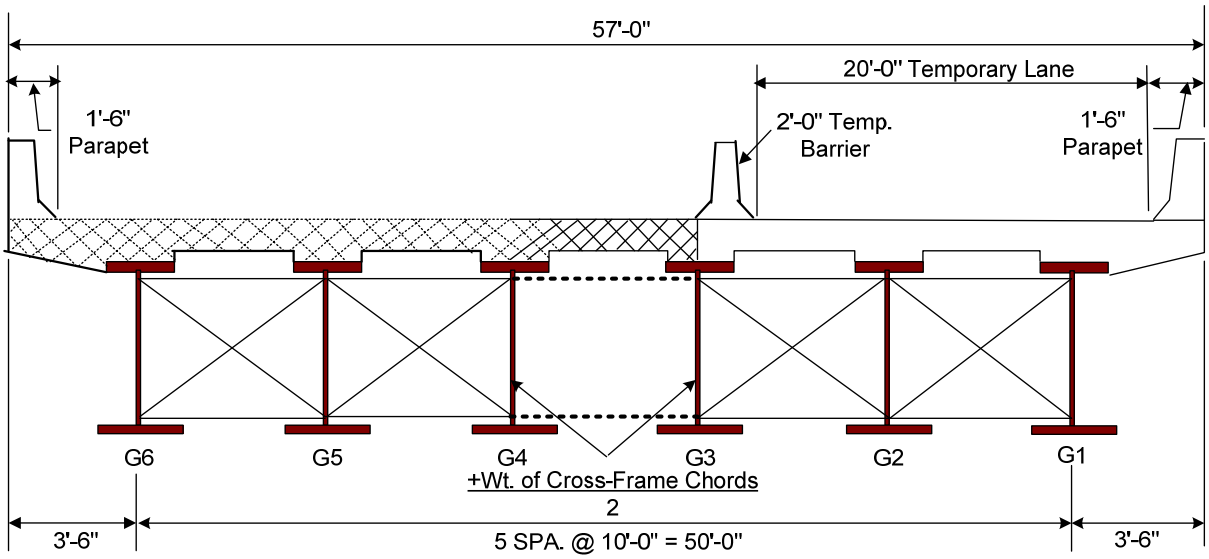


Figure 3.1.8 Phased Construction – No Closure Pour – Deck Cast onto Last Phase

3.1.2.4.4 Varying Roadway Width

Variable deck width introduces challenges to the bridge designer. The versatility of steel is particularly beneficial in these cases. At times the roadway alignment may differ over the supporting girders. For example, a curved deck alignment may be used on straight girders when the curvature is within tolerable limits. In other cases, it may be necessary to splay the girders in plan in order to accommodate the roadway. In extreme cases, the alignment might separate within the same structure. This situation is a so-called bifurcated alignment (Figure 3.1.9).

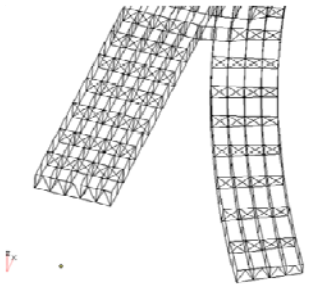


Figure 3.1.9 Splayed-Girder (Bifurcated) Framing Plan

In this case the roadway, before the bifurcation, is narrower than the sum of the two separate roadways. This necessitates the termination of some girders, as shown in Figure 3.1.10. In such cases, the discontinuous girder(s) are usually framed into a bulkhead between girders (Figure 3.1.10). The exterior girders are best not discontinued. First, there is no clean way of attaching the discontinued girder. Second, the exterior girders are frequently the critical girder in the cross-section and adding more load is certainly not desirable. Discontinuing a girder adjacent to an

exterior girder is best avoided since it will likely place additional load on the already critical exterior girder.

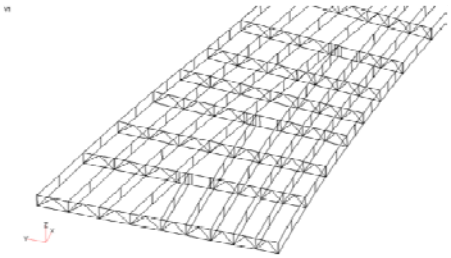


Figure 3.1.10 Discontinuous Girders

To minimize the moment and shear introduced into the bulkhead, it is usually best to discontinue the girders at a point of dead-load contraflexure. This location also reduces the impact on the deck, which is composite with the discontinued girder.

Design of these bulkheads is not treated directly by *AASHTO*. There have been issues raised as to whether or not the bulkheads are fracture critical members. By attaching the bulkhead(s) to the deck with shear connectors, this question is silenced. However, design of the member and its connections deserves careful consideration to avoid fatigue issues. Any moment in the girder at its terminus is transferred into the bulkhead and resisted by twist in the member, which is removed by its end connections and shear connectors. Discontinuous girders are best handled utilizing refined analysis methods.

In situations where the girder spacing varies, it is best to keep the variation within one bay, minimizing the number of different size cross-frames and minimizing changes in formwork and rebar changes.

3.1.2.4.5 Girder-Substringer Bridge Cross-Sections

A girder-substringer framing system, as illustrated in Figure 3.1.11, has been found to be a cost-effective alternative in some cases for continuous-span bridges with spans above 200 to 300 feet, This system consists of widely spaced composite main girders braced laterally by heavy K-shaped cross-frames. Main girder spacings from 16 feet to 28 feet have been used. Halfway in-between the main girders, rolled-beam composite substringers are used to span continuously between the cross-frames and provide support for the deck and live load. The cross-frames are considered primary load-carrying members in this system.

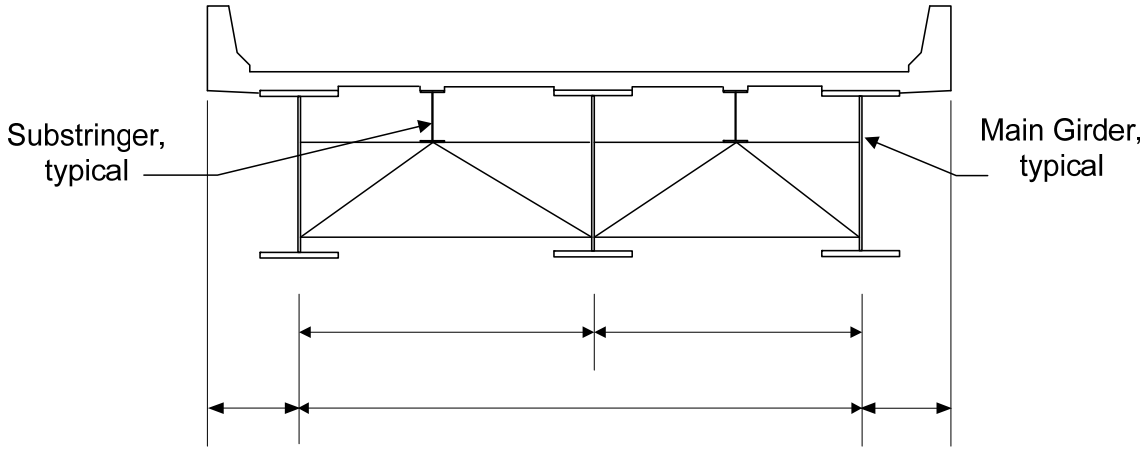


Figure 3.1.11 Girder-Substringer Cross-Section

3.1.2.5 Deck Overhangs

The list below summarizes the typical non-composite and composite loads that may be applied to deck overhangs.

Non-composite loads that are supported by the overhang brackets attached to the exterior girders include:

- Deck forms
- Wet concrete
- Finishing machine
- Screed rail
- Walkway
- Overhang brackets

Composite loads applied to the overhang concrete include:

- Barriers
- Self-weight of concrete
- Barrier impact
- Sidewalk
- Sound walls
- Sign posts
- Live loads (vehicular and potentially pedestrian)

Since the outside girder on a curved bridge must carry a larger share of the total load, the outside girder is particularly affected by larger overhang loads.

Depending on the situation, there are different approaches that can potentially be taken to alleviate any potential issues related to large overhang loads on curved bridges:

- A shifting of all the girders in the cross-section toward the outside of the deck will decrease the overhang on the outside of the curve, reducing the cantilever effect of the overhang loads on the outside girder. The overhang on the inside of the curve will increase, increasing the moment on the inside girder;
- Alternatively, the girder spacing can be increased reducing the overhang on the outside of the curve. The girder spacing between the outside girder and the adjacent interior girder also may be increased to achieve the desired effect;
- Adding bottom flange lateral bracing in the exterior bay will reduce the composite moments in the outside I-girder. Long spans and tight radii typically are cases where this option may be a worthwhile consideration. It works by creating a pseudo-box section after the deck has hardened. This permits the two laterally braced girders to share the load nearly equally. Without the lateral bracing, much of the load is transferred to the outside girder alone. Additional cost for the lateral bracing will be incurred, but the added cost will typically be much less than the costs associated with providing an additional girder to handle the overhang load. Lateral bracing will be discussed further in Section 3.1.2.9;
- Outside girders are particularly affected by sidewalk loads on the outside of a curved bridge. If practical, putting the sidewalk on the inside of the bridge should be considered.
- The non-composite overhang loads are resisted by vertical shear and a couple created by horizontal forces applied to the top flange and to the bottom flange or web. Bearing on the web can lead to web distortion and lowering of the screed rail. This problem has been addressed by adding intermediate web stiffeners. Most contractors either have full-depth brackets or can rent them. The deeper the couple, the less the horizontal force. Hence it is advisable to use girder-depth brackets. Brackets are typically spaced at about three to four feet. Large overhangs can cause significant lateral loads on the exterior girder. The effect of these loads on the girder design is addressed in Section 3.2.3.

3.1.2.6 Deck Thickness

The deck thickness is a function of the girder spacing and the design assumptions. Typically, owner-agencies have tables of deck thickness versus girder spacing. The "empirical deck design method" provided in *AASHTO LRFD* Article 9.7.2 is recommended to be used with caution. The method is based on the assumption that there is a fixed rotation restraint at the edges of the deck span. This is not always true. When the girders twist, the deck moments increase, hence requiring more reinforcement than provided by the method. Differential deflection of the girders creates similar increased moments. In bridges with skewed supports, the horizontal shear force can be significant in the vicinity of the simple supports. The tendency for relative longitudinal movement of the girders is resisted by horizontal shear. Also,

relative vertical deflection of the adjacent girders in skewed bridges increases the vertical shear in the deck. Typically this shear is resisted by the cross-frames, which are significantly stiffer than the deck. Similar issues occur in curved-girder bridges, but typically they are not as severe. A more traditional design approach without such a tacit assumption is presented in the *AASHTO LRFD* Article 9.7.3.

When the deck is properly modeled, shear and flexural stresses can be computed in the deck for superimposed dead load and live load. These analyses must consider the compatible deformation of the steel concurrently with the deck. Usually, a simple rational analysis is sufficient to provide adequate reinforcement. However, in cases where the girders are particularly flexible and/or the skew is particularly sharp, a refined deck analysis may be justified. The deck thickness is typically not changed during the course of the design once it has been set initially, but the amount of reinforcement may change.

3.1.2.7 Haunch Dimensions

Haunch width is usually set to match the top flange width. In some cases, the anticipated deck forming method may affect the choice of the haunch width (e.g., stay-in-place metal deck forms usually include clip angles which are attached to the top flange, dictating that the haunch width match the flange width). Sometimes aesthetic requirements (tapered overhang soffits, desire for constant haunch width even if top flange width varies, etc.) may affect the configuration of the haunch.

Haunch depth is usually set to accommodate all variations in the top flange thickness, along with consideration of the deck cross slope and the anticipated deck forming method (which may involve a minimum haunch thickness requirement). Splice plates and bolt height must be considered. The haunch height is usually increased slightly to ensure clearance for the deck reinforcing. The haunch height is usually included in computing the composite section properties.

3.1.2.8 Cross-Frames and Diaphragms

In the following, the functions of cross-frames/diaphragms, selection of the longitudinal cross-frame/diaphragm spacing, layout or arrangement of the cross-frames/diaphragms in curved and/or skewed I-girder bridges, basic configurations of cross-frames/diaphragms and design considerations for cross-frames/diaphragms will be reviewed.

Although cross-frames and diaphragms account for only a small percentage of the total structure weight, they account for a significant portion of the total erected steel cost of the steel-girder superstructure. Therefore, careful attention should be paid to their design and detailing. The number, arrangement, member size and spacing of cross-frames/diaphragms are important design considerations. These decisions influence not only the design of these members, but the design of the entire superstructure.

Figure 3.1.12 illustrates a cross-frame, a diaphragm and lateral bracing. These are defined in *AASHTO LRFD* Article 6.2 as follows:

- Cross-frame – a transverse truss framework connecting adjacent longitudinal flexural components (or inside a closed box or tub section) used to transfer vertical and lateral loads and to provide stability to the compression flanges;
- Diaphragm – a vertically oriented solid transverse member connecting adjacent longitudinal flexural components (or inside a closed box or tub section) used to transfer vertical and lateral loads and to provide stability to the compression flanges.
- Lateral bracing – a truss placed in horizontal plane between two I-girders (or two flanges of a tub girder) to maintain cross-sectional geometry, and provide additional stiffness and stability to the bridge system;

The functions, configuration and detailing of lateral bracing will be discussed further in Section 3.1.2.9.

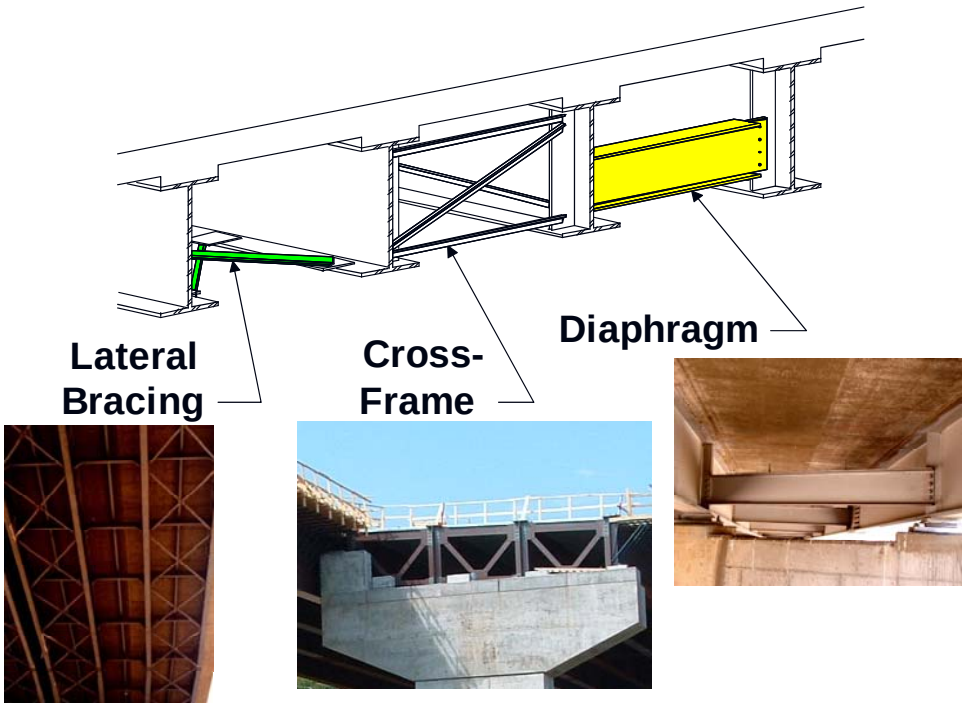


Figure 3.1.12 Definitions of Cross-Frame, Diaphragm and Lateral Bracing

3.1.2.8.1 Cross-Frame/Diaphragm Functions

This section reviews the primary functions of cross-frames/diaphragms in I- and box-girder bridges.

3.1.2.8.1.1 Functions in Right, Straight I-Girder Bridges

Traditionally, cross frames/diaphragms in right, straight bridges provide support to the girders against lateral torsional buckling. They also provide geometric stability to the girders prior to the hardening of the deck. Without them, the girders would deflect independently of each other, making it very difficult to properly cast the deck. Properly erected cross-frames/diaphragms ensure that the girders in these bridges deflect nearly equally as the deck is cast. This ensures that the girders each resist about the same steel and deck non-composite load. The cross-frames/diaphragms transfer load between the girders to ensure that this occurs. *AASHTO LRFD* Article 4.6.2.2.2 indicates that the total deck weight may be distributed equally to the girders when certain specified conditions are satisfied. Cross-frames/diaphragms, along with the deck, also distribute barrier weight, etc. within the superstructure. They also distribute live load within the superstructure.

Cross-frames/diaphragms stabilize the exterior girder when overhang bracket loads are applied. The top flange acts essentially as a continuous beam supported by the cross-frames/diaphragms. The top flange on the exterior girder must resist lateral bending induced by the overhang brackets between each cross-frame/diaphragm. This load may induce significant lateral bending in the top flange. A wider flange is useful to a degree. Intermediate support points have been introduced by various means. However, the spacing of cross-frames/diaphragms may control the girder design if the top flange is slender and/or if the overhangs are large (heavy).

The cross-frames/diaphragms transfer wind load from the superstructure through the bearings to the substructure. They also are effective in earthquakes in that they are the elements attaching the massive deck to the massive substructure.

Although the cross-frames/diaphragms provide lateral stability to the girders, they alone cannot with certainty, provide stability to the steel girders before the deck is placed. If the girders are permitted to move longitudinally with respect to each other, the angle between the cross-frames/diaphragms and the girders is no longer a right angle and the girders may become unstable. Some additional stability is required. Bearings may be locked against longitudinal movement and/or lateral bracing may be added over a portion of the length of a span or spans.

At ends of the bridge, the edges of the deck and the live load must be supported by the top chord of the end cross-frames/diaphragms (refer to *AASHTO LRFD* Article 9.4.4). This member acts in flexure and is often a rolled I-shape or a rolled or bent-plate channel.

Although these are important functions, the cross-frame/diaphragm has not been treated as a primary member deserving design attention in straight bridges with no skew; that is, structural actions are rarely calculated. That does not mean that these members have not been problematic. The most common problem has been fatigue cracks initiating in the area where the web and flange meet. The connection plates were not attached to the flanges for many years. Moment in the connection plates caused high transverse stresses in the web within small web gaps. Cyclic loading

led to fatigue cracks in a number of cases. It should be noted also that cross-frames in the exterior bays transfer parapet (or other) loads on the deck overhangs to the girders. If these loads are large or if the overhang is large, the cross-frame forces in the exterior bay may be significant. Frequently, signs are placed in these locations creating excessive forces in specific cross-frames.

3.1.2.8.1.2 Functions in Horizontally Curved I-Girder Bridges

In curved I-girder bridges, the cross-frames/diaphragms serve all of the above functions, as well as several additional critical functions. As discussed in Section 1.1, the cross-frames/diaphragms provide the primary resistance to torsion. Unlike their typical characterization as secondary members in straight bridges, cross-frames in a horizontally curved bridge with or without skewed supports, must be designed as primary load-carrying members as specified in *AASHTO LRFD* Article 6.7.4.1.

The cross-frames/diaphragms connect adjacent girders so that the concave girder shifts some of its load to its neighboring girder, which must resist that load in order to stabilize the concave girder. The amount of load that is shifted is essentially a function of curvature and length of the span; as the curvature becomes tighter, the cross-frame/diaphragm spacing must be reduced. Regardless of the number of cross-frames/diaphragms in a span, the total load shifted is nearly constant. For example, if there are five cross-frames in a one bay of one span and the total load shift from the inside girder to the outside girder in that bay is 30 kips, the sum of the vertical components in the cross-frame diagonals will equal 30 kips, or 6 kips per cross-frame if they are equally spaced. If there are four equally spaced cross-frames in the same bay of that span, the sum of the vertical components will remain 30 kips, but the vertical force per cross-frame will be 7.5 kips.

If the span is 100 feet and five cross-frames are equally spaced at about 16.7 feet, the lateral flange bending moment is a function of the spacing squared, as demonstrated in Section 2.3.2. If the number of cross-frames is reduced to four so that the cross frame spacing is increased to 20 feet, the lateral flange bending will be increased by the ratio of $(20/16)^2 - 1 = 0.56$ or 56 percent.

3.1.2.8.1.3 Functions in Skewed I-Girder Bridges

In I-girder bridges with skewed supports, the restoring forces in the cross-frames/diaphragms tend to equalize the girder deflections as in right bridges. However, the cross-frames/diaphragms in skewed bridges frequently experience significant forces as they attempt to equalize deflections at the points at which the cross-frames/diaphragms are attached. If the cross-frames/diaphragms are contiguous across the bridge, they act as a transverse truss transferring load across the bridge.

As mentioned previously, although cross-frames/diaphragms in straight I-girder bridges transfer load between the girders, particularly in bridges with sharply skewed supports, their design has traditionally been given insufficient consideration. The specification does not require that the cross-frames/diaphragms in straight bridges with skewed supports be designed as primary members in spite of the fact that the cross-frame/diaphragm forces may be much higher than found in many curved-girder bridges. Cross-frames/diaphragms in these bridges restore the structure by transferring load between girders, brace the girder flanges, resist lateral bending and help resist deck overhang bracket forces.

3.1.2.8.1.4 Functions in Box-Girder Bridges

Cross-frames/diaphragms are employed inside and between boxes. They serve two different sets of functions.

Internal cross-frames maintain the shape of the box. A box section tends to distort when subjected to torsion. This distortion must be limited or the box will lose its capacity in either torsion or in bending and the distortion stresses will become excessive. As discussed previously in Section 1.1.3.3.3, distortion occurs as the shear flow changes direction at the corners of the box. The box distorts between the cross-frames and is returned to its proper shape at the cross-frame minus the elastic shortening of the cross-frame. Unlike bending moment that usually varies along the girder, torque can remain constant over the girder length between the points of application of the torque and points of torsional restraint. The magnitude of distortional warping is related to the magnitude of the torque and the amount of distortion permitted in the box cross-section.

Intermediate internal cross-frames are required in box-section members by specification (*AASHTO LRFD* Article 6.7.4.3). Spacing of the cross-frames may be increased as torsion decreases. Spacing may be more critical in larger and/or torsionally flexible boxes.

Wright et al (*1*) used the analogy of the equations for box distortion and cross-frame forces to those for a beam on an elastic foundation (BEF) to develop charts for the solution of the box distortion problem. Transverse bending in the webs and flanges is analogous to the flex in the BEF beam, while the cross-frame members are analogous to BEF supports. The BEF analogy is discussed further in Section 3.2.5.

Internal cross-frames are attached to transverse stiffeners serving as connection plates. The connection plates are, in turn, welded to the web and to the top and bottom flanges. Hence, the stiffened web is stiffer in transverse bending than the web alone. The bottom flange is not typically stiffened transversely unless a bottom transverse member is provided within the internal cross-frames. When used, these transverse elements typically would be welded to the bottom flange or bolted to the longitudinal flange stiffeners if present. Without transverse stiffening, the bottom flange plate may be susceptible to distortion, which can cause significant through-thickness transverse bending. The transverse bending stresses can be critical at points where the web stiffener is welded to the bottom flange. As mentioned

previously in Section 1.1.3.3.3, the fatigue resistance of the base metal at the termination of these welds with regard to the transverse through-thickness bending stresses in the flange is not currently quantified in the specifications, but is anticipated to be as low as Category E. Through-thickness transverse bending stresses are most severe when the torque in the box is significant; e.g. boxes resting on skewed supports. Steps that can be taken to ameliorate this situation, and the specific cases for which this situation must be considered, are discussed in more detail in Section 3.2.5.

Overhang loads before the deck hardens may cause significant lateral bending in the outer top flange of tub girders, as is the case with I-girders. Overhang brackets are attached to the exterior top flange, applying an outward lateral pull to the flange. The brackets apply a countervailing force on the lower portion of the tub. The same issues apply that were discussed above with regard to I-girders. Internal cross-frames or top struts act as reaction points for the top flange.

Wind loads during construction may also cause significant lateral moments in the top flanges.

As specified in *AASHTO LRFD* Article 6.7.4.3, internal diaphragms are to be provided at each support to resist cross-section distortion; they are to be designed to resist torsion in the box and to transmit vertical and lateral forces from the box to the bearings.

External cross-frames/diaphragms attempt to retain the relative position of adjacent box girders. In addition to vertical load, these members resist and/or introduce torsion in the boxes. To resist the distorting action they tend to cause on the box cross-section, *AASHTO LRFD* Article 6.7.4.3 requires that an interior cross-frame/diaphragm be used in-line with each exterior cross-frame/diaphragm.

According to *AASHTO LRFD* Article 6.7.4.3, for cross sections consisting of two or more boxes, external cross-frames/diaphragms are required at end supports (along with internal diaphragms) to support the deck and the live loads. External cross-frames/diaphragms also act to restrain the rotation of the boxes. External cross-frames/diaphragms must also be provided between girder lines at interior supports, particularly during erection, unless analysis indicates that the boxes are torsionally stable without these members. This is especially true if a box or tub girder has only one bearing per support.

When single bearings are used, the effective distance that the deck spans may be close to the distance between the bearings, which can be twice the distance between adjacent top flanges (assuming equal spacing between box webs). The effective distance depends on the rotation permitted by the external cross-frames/diaphragms and the torsional stiffness of the boxes. Deck stresses and the demand on the external cross-frame/diaphragm increase with increased rotation of the box girders.

Temporary intermediate external cross-frames are sometimes used to control the relative deflection and rotation of adjacent boxes before the deck hardens. These members are removed to maintain the uncluttered appearance of the boxes that is diminished by the presence of too many external cross-frames. Removal of temporary bracing after the deck hardens is usually awkward. If the members are effective (i.e. contain large forces), they can present a danger to workers attempting to remove them when bolts in a partially connected member might fail. Removal of temporary members having large forces introduces restoring forces into the bridge. For example, a member having a force of 100 kips tension introduces a reversed force of 100 kips when it is removed. Removal of temporary cross-frames having large forces may increase deck stresses.

Analysis of the twist in the box due to erection and deck placement can be used to determine if temporary external cross-frames are required. Some suggest that external diaphragms are more attractive on box girder bridges than are cross-frames, which are seen as incongruent with the smooth surfaces of the box girders.

3.1.2.8.2 Cross-Frame/Diaphragm Spacing Requirements

3.1.2.8.2.1 Spacing Requirements for I-Girder Bridges

General

The long-standing requirement limiting the maximum cross-frame/diaphragm spacing in I-girder bridges to 25 feet has been removed. The present provisions (*AASHTO LRFD* Article 6.7.4.1) do not limit cross-frame/diaphragm spacing for straight I-girder bridges. Spacing of cross-frames/diaphragms is to be established by rational investigation of critical construction stages and the final condition to meet the demands of design at each location. The factors determining cross-frame/diaphragm spacing in I-girder bridges are: lateral torsional buckling of the girder compression flange; skew; wind load; lateral loads due to deck overhang brackets; and in the case of curved girders, flange lateral bending due to curvature.

AASHTO LRFD Article C6.7.4.2 recommends that intermediate cross-frames/diaphragms be provided at nearly uniform spacing in I-girder bridges for constructibility, for efficiency of the design, and to allow the more accurate use of approximate methods of analysis for estimating lateral flange bending moments in curved bridges. The approximate V-load equation for estimating the lateral flange bending moments due to curvature, discussed in Section 2.3.2, assumes a uniform spacing of cross-frames/diaphragms. A schematic of uniform, contiguous cross-frame/diaphragm spacing on four curved girders is shown in Figure 3.1.13. A tighter spacing may be desirable adjacent to interior piers to reduce the unbraced length of the compression (bottom) flange. There are other reasons to vary the spacing of cross-frames/diaphragms.

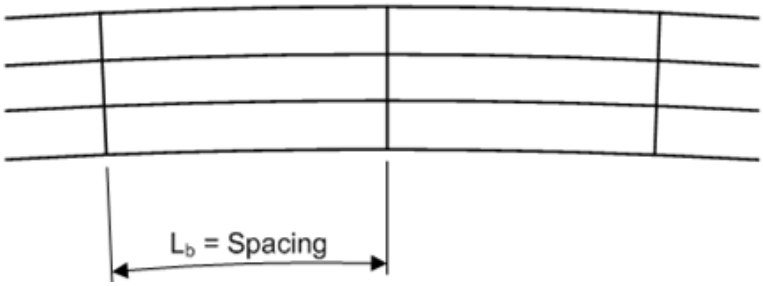


Figure 3.1.13 Uniform Contiguous Cross-Frame/Diaphragm Spacing - Curved I-Girder Bridge

Table 3.1.1 summarizes some of the trade-offs regarding cross-frame/diaphragm spacing. The importance of cross-frame/diaphragm spacing with regard to economy cannot be overemphasized. Although flange overstress can be addressed by the use of a larger flange in many cases, it can also be rectified by judicial arrangement of the cross-frames/diaphragms. Additional cross-frames/diaphragms often are less economical than heaver flanges. However, increasing spacing in some region(s) while reducing the spacing in other region(s) is often economical. For example, assume a uniform spacing of 25 feet on a straight bridge. For this spacing, analysis shows that the compression flange at the pier is overstressed with regard to lateral torsional buckling, but the top flange in the positive moment region has excess capacity. Thus, it may be possible to decrease the spacing adjacent to the pier and increase the spacing slightly beyond 25 feet in the positive moment region and still achieve a satisfactory design.

Table 3.1.1 Cross-Frame/Diaphragm Spacing Trade-Offs

Closer Spacing	Larger Spacing
Lower cross-frame forces	Lower cross-frame cost
Lower lateral flange moments	Larger cross-frame forces
Higher compression-flange moments	Larger lateral flange moments
Higher cross-frame cost	Lower compression-flange capacity

Relatively, the narrower the flanges, the closer the cross-frame/diaphragm spacing must be. However, cross-frames/diaphragms are more costly than flange steel, so wider flanges are usually desirable over additional cross-frames/diaphragms. But, by varying the spacing of a given number of cross-frames/diaphragms, economy in flange material can usually be gained.

Spacing Requirements for Curved I-Girder Bridges

Recall that the lateral force due to curvature is a function of the force in the flange and the curvature. The force in the flange is therefore directly proportional to the vertical moment and inversely proportional to the girder depth. The lateral flange moment is proportional to the lateral force and the square of the distance between

lateral supports; i. e., the cross-frame/diaphragm spacing. The forces in the cross-frames/diaphragms and the magnitude of the lateral flange moment can be modified by changing the cross-frame/diaphragm spacing and/or the girder depth, with no other changes made to the framing.

The total vertical shear within a span is nearly constant within a given span, regardless of the number of cross-frames/diaphragms. Hence, the shear per cross-frame/diaphragm is proportional to the number of cross-frames/diaphragms within a bay within a span. Where the vertical bending moments in a girder are large, a smaller cross-frame/diaphragm spacing reduces the lateral flange bending moment and also improves the lateral torsional buckling resistance of the compression flange. Simply increasing the spacing in regions where the vertical bending moment is smaller and the lateral flange moment is less critical may be satisfactory in lieu of adding a row of cross-frames/diaphragms.

Equation 3.1.1 is given in *AASHTO LRFD* Article C6.7.4.2 and may be used as a guide to determine preliminary cross-frame spacings in horizontally curved I-girder bridges.

$$L_b = \sqrt{\frac{5}{3} r_\sigma R b_f}$$

Equation 3.1.1
AASHTO LRFD Equation C6.7.4.2-1

where:

r_σ = desired bending stress ratio $f_\ell / f_{bu} \le 0.3$
R = girder radius (ft)
b_f = flange width (ft)

The equation is derived from V-load theory (to be discussed in Section 2.3.2) and has been shown to yield good correlation with refined 3D finite element analysis results when the cross-frame spacing is relatively uniform and there is no skew.

In the computation of r_σ, f_ℓ is flange lateral bending stress, and f_{bu} is the largest value of the compressive stress due to vertical bending within the unbraced length under consideration.

As an example, Table 3.1.2 gives results from Equation 3.1.1 for r_σ = 0.15 and b_f = 18 in.

Table 3.1.2 L_b Values from Equation 3.1.1 (for r_σ = 0.15; b_f = 18 in.)

	R = 500 ft	R = 1000 ft	R = 1500 ft
L_b (ft)	14	19	24

However as the user of this equation, one observes that the flange width is considered a given. It might be worthwhile investigating a change in the flange width

to make a given cross-frame/diaphragm spacing work before additional cross-frames/diaphragms are added by rearranging Equation 3.1.1 as follows:

$$b_f = \frac{\lfloor 3/5 L_b^2 \rfloor}{r_\sigma R}$$

Equation 3.1.2

A subsequent check of the flange resistance requirements based on the initial cross-frame/diaphragm spacing determined from Equation 3.1.1 will likely necessitate adjustments to either the flange size or to the cross-frame/diaphragm spacing. Spacing may be varied with flange size and moment. It is desirable to examine the flange width as well as its area. A wider flange reduces the lateral bending stress.

Although the *AASHTO LRFD Specification* does not prescribe a maximum cross-frame/diaphragm spacing for straight I-girder bridges, a maximum spacing requirement is specified for horizontally curved I-girder bridges in the erected condition in *AASHTO LRFD* Article 6.7.4.2. The requirement is given below:

$(L_b)_{max}$ = a minimum of:

- $L_r = \pi r_t \sqrt{(E/F_{yr})}$
- 30.0 feet
- R/10 feet, where R is the minimum girder radius within the panel

The limit of *R*/10 is consistent with past practice. L_r is the limiting unbraced length from *AASHTO LRFD* Eq. 6.10.8.2.3-5 to achieve the onset of nominal yielding in either flange under uniform bending with consideration of compression-flange residual stress effects prior to lateral torsional buckling of the compression flange. The terms r_t and F_{yr} are defined in *AASHTO LRFD* Article 6.10.8.2.3. Limiting the cross-frame/diaphragm spacing to L_r theoretically precludes elastic lateral torsional buckling of the compression flange. At unbraced lengths beyond L_r, significant lateral flange bending is likely to occur, and the amplification factor for flange lateral bending will tend to become large.

The absolute upper limit on the cross-frame/diaphragm spacing in curved I-girder bridges has been established at 30.0 feet.

3.1.2.8.2.2 Spacing Requirements for Box-Girder Bridges

For bridges other than those listed in *AASHTO LRFD* Article 6.11.2.3 (for which the wheel-load distribution factors are applicable), the spacing of internal cross-frames is limited to 40 feet according to *AASHTO LRFD* Article 6.7.4.3. Spacing of the internal cross-frames in box girders is primarily designed to control of distortion of the box. Each internal cross-frame restores the box shape to near its original unstressed

shape. The further apart the cross-frames, the greater the distortion that must be corrected. This induces greater forces in the cross-frame. Of course, the stiffer the box, the greater are the restoring cross-frame forces. Larger restoring forces induce greater box distortion in the vicinity of the cross-frame. Such distortion is associated with potential fatigue and should not be ignored. If the computed cross-frame forces cause problems designing the member connections, the designer might consider reducing the cross-frame spacing. Live load causes much of the cross-frame force (distortion) in straight bridges without skew. Uneven loading of the deck weight on the two webs and parapet weight also may cause large torque. Skew and/or curvature will present significant torque for both dead and live load. The best internal cross-frame spacing is roughly inversely proportional to the torque in the box.

AASHTO LRFD Article 6.11.1.1 limits the through-thickness transverse bending to 20 ksi at the strength limit state and requires that these stresses be considered for fatigue for the appropriate detail. Through-thickness stresses need not be considered for the bridges listed in *AASHTO LRFD* Article 6.11.2.3 for which the wheel-load distribution factors are applicable.

AASHTO LRFD Article C6.7.4.3 recommends limiting the internal cross-frame spacing to control longitudinal warping stresses to approximately 10 percent of the stresses due to major-axis bending. *AASHTO LRFD* Article 6.11.5 requires that longitudinal warping stresses be considered in fatigue. The calculation of transverse bending stresses and longitudinal warping stresses is examined in Section 3.2.5. Where distortion of the section is adequately controlled by the internal cross-frames acting in conjunction with a top lateral bracing system in the case of tub section, the St. Venant torsion constant, *J*, of the box section may be determined from Equation 1.1.17.

For straight boxes without skew satisfying the requirements of *AASHTO LRFD* Article 6.11.2.3 and with fully effective box flanges, and with relatively symmetrical deck weight acting on each box, cross-section distortion stresses have been found to be negligible. A reduction in the number of permanent internal cross-frames and/or top lateral bracing members is therefore permitted in such boxes when checked by proper analysis (see *AASHTO LRFD* Article C6.7.4.3); i.e. the spacing of the internal cross-frames may be permitted to exceed 40.0 ft if confirmed by analysis. However, the cost benefits probably rarely outweigh the risks. Erection conditions are an unknown to the Design Engineer.

Additional struts between the top flanges of tub sections may be necessary to satisfy constructibility provisions (*AASHTO LRFD* Article 6.11.3.2) when internal cross-frames are widely spaced. *AASHTO LRFD* Article C6.11.3.2 suggests that struts that are part of the top lateral bracing may be considered to act as top flange brace points at the discretion of the Design Engineer. The commentary suggests that this assumption may even be appropriate when significant flange lateral bending exists (due to deck overhang loads, curvature, etc.).

Internal cross-frames should be placed at points of maximum moment in each span. They are usually placed near both sides of field splices to aid in fit up in the shop and in the field. Additional internal cross-frames may be used to facilitate transportation and construction.

Additional internal cross-frames, or struts, may be required to reduce the lateral bending in the top flanges of tub sections resulting from transverse loads on these flanges (*AASHTO LRFD* Article C6.11.3.2). According to the commentary, this situation occurs when webs are inclined more than 1-to-4, or where the unbraced length of the top flanges exceeds 30 feet. The lateral load occurs with the inclined web due to web shear creating lateral force on the flanges. In lieu of a refined analysis, the maximum lateral flange bending moments, M_ℓ, due to the transverse load can be estimated as follows:

$$M_\ell = \frac{F_\ell L_b^2}{12}$$

Equation 3.1.3
AASHTO LRFD Equation C6.10.3.4-2

where:

F_ℓ = magnitude of the factored uniformly distributed transverse load (kip/in.)
L_b = unbraced length (in.)

This equation assumes that the flange is continuous at both brace points; the equation is unconservative at simple supports. The entire transverse load at the top is assumed applied to the top flanges (*3*) so the transverse member is assumed to resist the entire transverse load.

Internal cross-frame spacing is influenced by the top lateral bracing arrangement. As the angle between the diagonals and the girder tangents is reduced, the bracing forces due to both torsion and flexure are increased. The brace length is decreased as the angle between the diagonals and the girder flanges increases, increasing the compressive capacity of a given diagonal member. The trade-off is that a flatter angle reduces the number of elements. The configuration of top flange lateral bracing is discussed further in Section 3.1.2.9.2.

3.1.2.8.3 Cross-Frame/Diaphragm Layout in I-Girder Bridges

Judicious layout of the cross-frames/diaphragms can have a significant effect on the economy of I-girder bridges. Although the spacing of the cross-frames/diaphragms is important in controlling the number of cross-frames/diaphragms, their layout can influence the forces in the members and in the girders. The impact of layout is particularly important in I-girder bridges with skewed supports. Large cross-frame/diaphragm forces not only cause large members, they cause extremely expensive, even impractical connections in some cases.

Clearly, cross-frame/diaphragm forces can only be created when there is resistance at the end of the member. In I-girder bridges, this resistance has a few sources. The most critical one is the lateral restraint of a bearing on a rigid abutment. Next, is the resistance of such a bearing on a pier that has lateral flexibility to partially relieve the forces. Third, are opposing cross-frame members in adjacent bays or in the same cross-frame connected at a common node. Finally, the weakest form of resistance is the lateral restraint offered by the flanges.

Changing the number, size and arrangement of the cross-frames/diaphragms often has a significant effect on their forces. ***Hence, it is advisable to check the forces in these members early in the design-prior to resizing girders. If the forces are too large to design practical members or connections, their arrangement should be further investigated before proceeding with the design of the girders***.

A 3D investigation of framing plan layout issues in a skewed I-girder bridge is described in the Case Study given in Section 3.1.6.

3.1.2.8.3.1 Curved I-Girder Bridges Without Skew

AASHTO LRFD Article 6.7.4.2 states that where supports are not skewed, intermediate cross-frames/diaphragms in I-girder bridges should be placed in contiguous lines normal to the girder tangents, as shown in Figure 3.1.14.

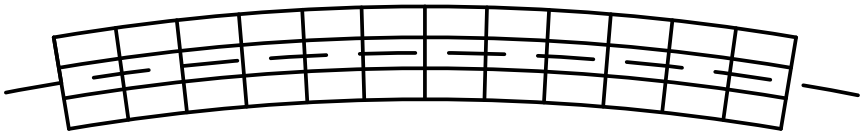


Figure 3.1.14 Contiguous Cross-Frame Arrangement for Non-Skewed Curved Bridge

As discussed above, the spacing may be varied in these cases. Reducing the spacing in the center of this simple span while increasing spacing near the supports may improve the capacity of the flanges in the center of the span while not adding to the number of cross-frames, remembering that cross-frames are expensive compared to flange steel.

3.1.2.8.3.2 Straight or Curved I-Girder Bridges With Skew

AASHTO defines skew as the angle made by the support relative to a line normal to a local tangent to the longitudinal axis of the bridge; thus, a skew angle of 0° denotes a radial support.

AASHTO LRFD Article 6.7.4.2 permits cross-frames/diaphragms to be arranged in contiguous skewed lines parallel to the skewed supports, as shown in Figure 3.1.15 where both supports of a span are parallel and skewed not more than 20 degrees.

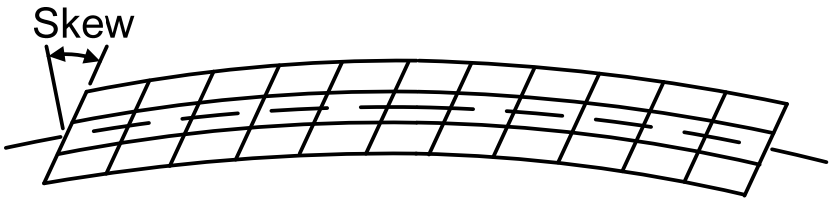


Figure 3.1.15 Contiguous Cross-Frame Arrangement for Skewed Curved Bridge with Parallel Skewed Supports (Skew Angle ≤ 20°)

This requirement is consistent with past practice and is likely based on welding access to the acute corner between the connection plate and web. The forces in the cross-frames/diaphragms also affect the girder forces when the cross-frames/diaphragms are highly skewed because their actions have a longitudinal component. This arrangement permits the cross-frames/diaphragms to be attached to the girders at points of similar length along the girders, i. e., equal stiffness, thus reducing the relative deflection between cross-frame/diaphragm ends and the restoring forces in these members. Cross-frame/diaphragms with greater parallel skew angles have been used with no deleterious effect, but are currently forbidden by the Specifications.

Cross-frames/diaphragms must be placed normal to the girder tangents where both supports within a span are not parallel or are skewed more than 20 degrees. Cross-frames/diaphragms may be placed in a contiguous pattern, as shown in Figure 3.1.16, with the cross-frames/diaphragms opposing each other on both sides of the interior girders. Of course, at the bearings a different arrangement is required. This cross-frame/diaphragm arrangement provides the greatest transverse stiffness; hence, the largest cross-frame/diaphragm forces.

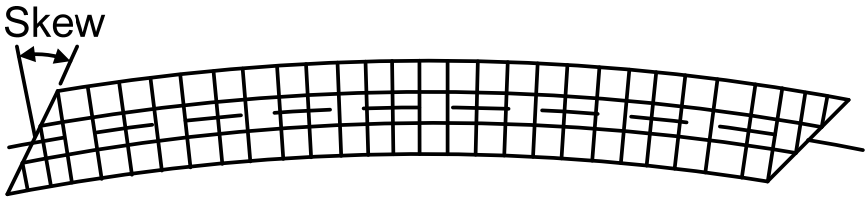


Figure 3.1.16 Contiguous Cross-Frame Arrangement for Skewed Curved Bridge with Skew Angles > 20°

It may be advantageous to use non-contiguous (or discontinuous) cross-frame/diaphragm lines along the entire span as shown in Figure 3.1.17. This pattern effectively reduces the transverse stiffness of the bridge. Alternatively, cross frames may be staggered only near the skewed supports while remaining contiguous in the middle of the span (a pattern not shown).

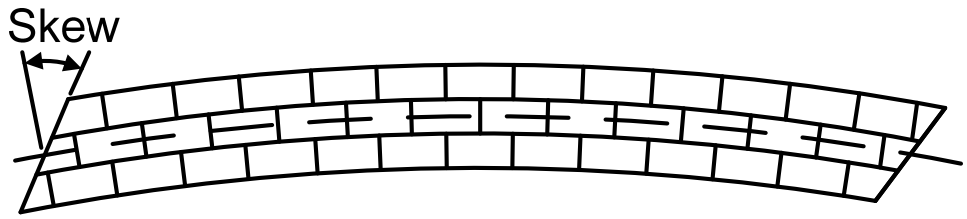


Figure 3.1.17 Discontinuous Cross-Frame Arrangement for Skewed Curved Bridge with Skew Angle > 20°

The reduction of transverse stiffness is accomplished by the transverse flex that occurs in the flanges. The reduction of stiffness is, of course, accompanied with a reduction in the cross-frame/diaphragm forces and associated connection complexity (cost). However, the flex of the flanges must also be accompanied by lateral flange bending. The vertical bending capacity of the flanges is reduced by the lateral bending as evidenced by the one-third rule resistance equation discussed in Section 3.2.2.1.

One of the reasons for very high cross-frame forces near bearings is the restraint that they may provide. This restraint tends to forbid transverse movement; hence, causing very high cross-frame forces. It is imperative to consider bearing restraint when computing cross-frame forces, as discussed further in Section 2.2.3. Changing bearing orientation and restraints often has a significant impact on cross-frame forces near supports. Thus, any investigation of cross-frame arrangement must include simultaneous consideration of bearing restraints. Implicit in this is the use of an analysis that properly recognizes the effect of bearing restraints located off the neutral axis of the girders.

Removal of highly stressed cross-frames/diaphragms, particularly at and near obtuse corners at supports, releases the girders torsionally and is often beneficial in reducing the overall transverse stiffness of the bridge superstructure, as long as the girder twist is not excessive. Highly stressed cross-frame/diaphragm removal also aids in erection by making the installation of the remaining transverse bracing less difficult. Removal of a few highly stressed cross-frames/diaphragms is shown in Figure 3.1.18. One of the disadvantages of this approach is that forces in adjacent cross-frames/diaphragms may increase sharply. Note that this approach also results in discontinuous cross-frame/diaphragm lines, or lines that do not form a continuous line between multiple girders. A preliminary refined analysis of the entire bridge superstructure is useful in indicating which cross-frames/diaphragms are potential candidates for removal.

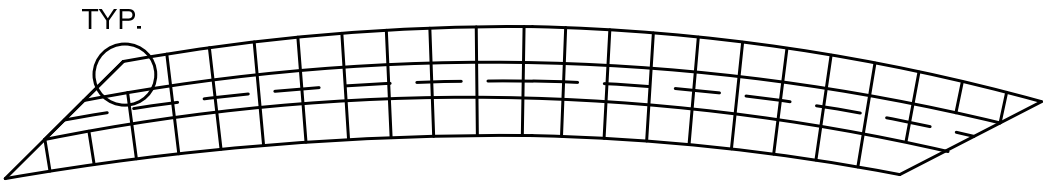


Figure 3.1.18 Removal of Cross-Frame/Diaphragms at Obtuse Corners in Skewed Curved Bridge with Skew Angle > 20°

Discontinuous cross-frame/diaphragm lines can exacerbate the flange lateral bending stresses in the girders, particularly near the locations where the lines are discontinued. However, often the lateral bending is not critical, and the net result is a desirable reduction in the cross-frame/diaphragm forces and resulting costs.

As indicated in *AASHTO LRFD* Article C6.10.1, flange lateral bending effects due to skew should be considered in all regions of the girders where cross-frames/diaphragms are discontinuous. Lateral bending effects due to skew are typically less critical in regions where cross-frames/diaphragms are contiguous.

Exterior girders (i.e., outside and inside girders) always have cross-frames/diaphragms on one side, but since there are no opposing cross-frames/diaphragms on the other side, flange lateral bending due to skew effects is usually smaller in these girders, which is fortuitous since the outside girder in curved bridges often has critical major-axis bending moments compared to the other girders. Interior girders are generally subject to significantly larger lateral flange moments due to skew effects relative to exterior girders, in particular whenever a discontinuous cross-frame/diaphragm arrangement is employed along the entire length of the bridge.

Simple methods to determine flange lateral bending moments and restoring forces in the cross-frame/diaphragms in skewed bridges do not currently exist. These actions are best determined by analysis. In the absence of calculated values, estimates for lateral bending stresses are provided in *AASHTO LRFD* Article C6.10.1. However, their use is not recommended for curved bridges with skewed supports.

Additional options to reduce cross-frame/diaphragm forces in highly skewed bridges include leaving some cross-frames/diaphragms unconnected until after the deck has been cast. This option has the disadvantage of the possibility of poorly braced girders until the deck hardens. Another option is to connect cross-frame chord members, but leave some diagonals free. In this case, the girders tend to deflect independently during deck casting making cambering complicated. Possible variations on these two options are too numerous to examine here. Slotted holes are sometimes used in cross-frame connections of straight skewed bridges to minimize the twist of the girders and reduce the cross-frame forces. Considerations that should be made when this approach is used are discussed further in Section 4.2.3.3. Any of these approaches involve the Erector returning to the bridge after

the deck is cast and working from underneath the deck. Holes usually need to be drilled or at least reamed. The obvious advantage is that cross-frame forces can be greatly reduced. If the parapets are placed before the cross-frames are to be fully installed, it is advisable to consider the investigation of transverse deck stresses.

Another option is to leave restrained bearings free until the deck is cast. Analysis may show that the forces in cross-frames near the bearings may be substantially reduced by this technique.

The "lean-on" bracing option has been promoted by some (*4*). In the "lean-on" bracing system, selected cross-frames are provided with only a top and bottom chord, but no diagonals. In this way, the selected cross-frames continue to function as bracing members for the girder compression flanges, but without the shear stiffness of typical cross-frames. When this system is used, refined analyses should be employed to track deflections, cross-frame forces and transverse deck stresses at various stages.

Skewed Interior Support Lines

AASHTO LRFD Article 6.7.4.2 states that at the discretion of the Owner, cross-frames/diaphragms need not be provided along skewed interior support lines if cross-frames/diaphragms normal to the girders are provided at bearings that resist lateral forces, as shown in Figure 3.1.19. At severely skewed interior supports, e.g., with skews greater than 20°, the detailing of the intersections with the cross-frames/diaphragms oriented normal to the girders is complex. Welding of skewed connection plates to the girder may be problematic where the plate forms an acute angle with the girder. The cross-frames/diaphragms normal to the girders in such cases must be proportioned to transmit all the lateral components of force from the superstructure to the bearings that provide lateral restraint. Otherwise, the lateral bending in the bottom flange near the restrained bearings may be excessive.

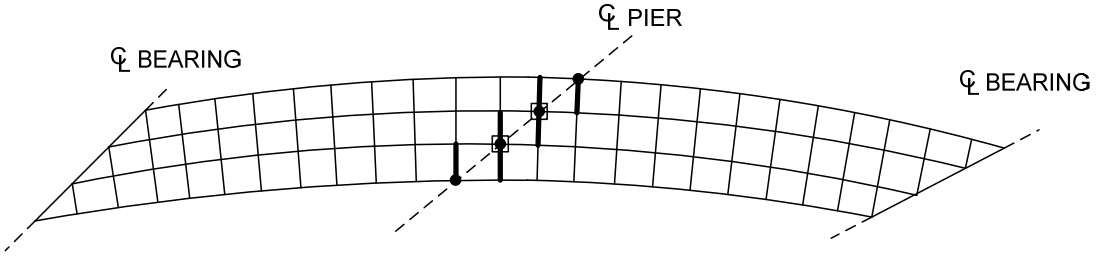


Figure 3.1.19 Skewed and Curved I-Girder Bridge: No Cross-Frame Along the Skewed Interior Support Line

Where discontinuous cross-frames/diaphragms are employed normal to the girders in the vicinity of interior supports, care should be taken to match at least one cross-frame/diaphragm with each bearing that resists lateral force, as shown in Figure 3.1.20. Otherwise, the effect of the lateral moment induced in the bottom flange due to the eccentricity between the intermediate cross-frame/diaphragm and the bearing

should be considered. Also, whenever any bearing along the support line is not matched with a cross-frame/diaphragm, care must be taken to ensure that the bottom flange of the girder is adequately braced. For such cases, the provision of cross-frames/diaphragms along the skewed support line may be necessary. There are no rules for how to arrange bearing restraints and cross-frames/diaphragms at these locations. Ingenuity and trial-and-error are the only tools. In critical cases, often only a least bad arrangement is available.

As illustrated in Figure 3.1.20, the skewed cross-frame/diaphragm in this case braces the bottom flange of the inside and outside girders, and also matches up with the bearings on the two interior girders that resist lateral force. Refined analysis is recommended to allow for a more detailed examination of cross-frame/diaphragm forces, lateral bearing reactions and lateral flange bending whenever removal of cross-frames/diaphragms along, and/or in the vicinity of, severely skewed interior support lines is considered.

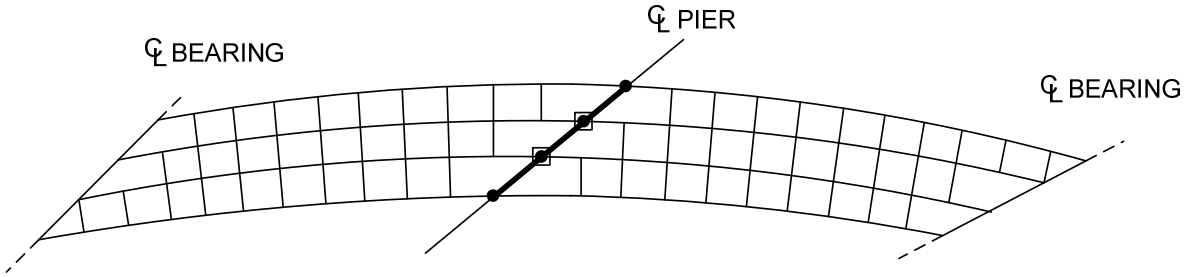


Figure 3.1.20 Skewed and Curved I-Girder Bridge with Discontinuous Cross-Frames: Cross-Frame Along the Skewed Interior Support Line

For skews not exceeding 20°, cross-frames/diaphragms along the skewed support line alone may be sufficient. If cross-frames/diaphragms are also provided normal to the girder tangents, they may be spaced too close together along the girders, introducing significant lateral flange bending stresses into the girders. As discussed in Section 3.1.2.8.5.2, for skewed cross-frames/diaphragms, connection plates should be oriented in the plane of the transverse bracing. The connection plates must be able to transfer the force between the girder and the bracing without undue distortion.

Whatever the case, consideration should always be given to providing a means to allow jacking of the girders at the supports to replace bearings.

Skewed Support Lines at Abutments

At skewed abutments (simple supports), a row of cross-frames/diaphragms is always required along the support line to support the free edge of the deck. Thus, a missing intermediate normal (radial) cross-frame/diaphragm is not a concern.

End rotations of the girders create forces in these cross-frames/diaphragms. At cross-frames/diaphragms along skewed end support lines, tangential components of the skewed end support cross-frame/diaphragm forces act along each girder. In order to maintain static equilibrium, vertical bending moments and shears must develop in the girders at the end supports. Note that the larger the rotation and concomitant deflection of the girders, the larger the end moments. In certain cases, these end moments are important. Since these end moments are usually negative, they can potentially introduce tensile stresses in the deck or subject the bottom flange to compression adjacent to the supports. Generally, these moments can not be avoided altogether. However, by placing the deck at the ends of the bridge last, the tensile stresses in the deck can be minimized. *AASHTO LRFD* Article 6.7.4.2 requires that the effect of the tangential components of force transmitted by the skewed end support members be considered.

The net components of the skewed end support cross-frame/diaphragm forces transverse to the girders introduce a torque at the girder ends. The effect of these transverse forces may need to be considered in the design of the transverse deck reinforcement, particularly when the end cross-frame/diaphragm forces are large.

3.1.2.8.4 Configurations of Cross-Frames/Diaphragms

This section reviews the configuration of cross-frames/diaphragms in I- and box-girder bridges.

3.1.2.8.4.1 Configurations in I-Girder Bridges

Article 6.7.4.2 in *AASHTO LRFD* requires that cross-frames/diaphragms for rolled beams and plate girders should be as deep as practicable, but preferably not less than 0.5 of the beam depth for rolled beams and 0.75 of the girder depth for plate girders (Figure 3.1.21). This requirement is called out to ensure that the cross-frames/diaphragms provide adequate torsional resistance to the beam or girder. The deeper these members are, the lower the forces in them because the moments transferred through them are transferred more efficiently in a deeper section. However, as their sizes are increased, the forces in these members increase. The connection plates also need to be robust enough to transfer the loads to the girders.

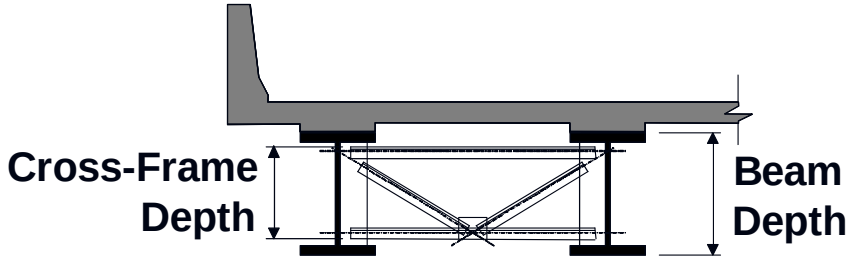


Figure 3.1.21 Cross-Frame and Beam Depth

The X-type configuration, as shown in Figure 3.1.22, is the least expensive configuration of intermediate cross-frames (i.e. cross-frames located at other than end supports). However, if the girder spacing-to-depth is too great, K-type cross frames are preferred in order to steepen the diagonal members. When the angle of the diagonals with respect to the horizontal becomes too shallow for an X-type configuration to be effective (less than about 30 degrees), the unsupported length of the diagonals can become large and the transfer of vertical force between girders imposes a large axial stress in the diagonals. Long members may also be subject to vibration. In such cases, the K-type cross frame is often preferred (*2*). Specific rules in reference to this often are provided by the states.



Figure 3.1.22 X-Type Cross-Frame in an I-Girder Bridge

A typical K-type cross-frame in a curved I-girder bridge is shown in Figure 3.1.23.



Figure 3.1.23 K-Type Cross-Frame in an I-Girder Bridge

The K-node can either be located in the top or bottom chord. The latter configuration is preferred so the diagonals can brace the bottom chord in the vertical direction. However, it is observed that the diagonals have equal and opposite forces hence their horizontal components of force accumulate in one-half of the bottom chord. For this reason, it is often desirable to place the K-node in the top chord to allow these horizontal diagonal forces to accumulate in the lower-stressed top chord. The top chord is more lowly stressed because the deck assists the top chord for superimposed dead load and live load.

At the ends of bridges, the edges of the concrete deck must be supported in order to support the wheel loads coming onto the deck (refer to *AASHTO LRFD* Article 9.4.4). In an I-girder bridge, a rolled I-shape or a rolled or bent plate channel is typically used as the top chord of the end cross-frames in order to provide the necessary support. At end supports, locating the K-node in the center of the upper chord is preferred because it halves the span of the top chord, which must support the deck and the expansion device. The diagonals can also more efficiently carry the wind loads down to the bearings in this configuration; a similar configuration might be considered for the cross-frames at interior-pier supports for this reason.

The cross-frames provide lateral support to the girder compression flanges to resist lateral torsional buckling. They also provide geometric stability to the girders prior to the hardening of the deck. No top chord is used on cross-frames in some cases. If a top chord is not used with K-type cross-frames, the stability of the cross-frame prior to the deck hardening is dependent entirely on the bending stiffness of the bottom chord; this is an unstable condition. If X-type cross-frames are used without a top chord, the upper triangle of the cross-frame truss is eliminated and the stability of the cross-frame may be compromised. *The use of intermediate cross-frames without top chords should be limited to right, straight bridges with regular framing and to spans probably less than 150 feet.*

Diaphragms, such as the one shown in Figure 3.1.24, are used most often in rolled-beam bridges or in plate-girder bridges when the girders are less than about 48 inches deep. Hot-rolled channel sections or rolled I-shapes are most commonly used for diaphragms. Solid-plate diaphragms are rarely used, unless needed as special jacking diaphragms to accommodate bearing replacement.



Figure 3.1.24 Diaphragm in an I-Girder Bridge

Channel sections can either be rolled channels or bent-plate channels (i.e. a plate bent into the shape of a channel by the fabricator) attached directly to the connection plates or attached directly to the stringers using end angles. Bent-plate channels have been used on girders greater than 48 inches deep. The Engineer is encouraged to consult with local fabricators regarding their preference.

Rolled I-shapes can either be attached to connection plates using gusset plates, attached directly to the stringers using end angles, or attached directly to the connection plates. Attaching directly to the connection plates requires coping at the top and bottom. Diaphragms are typically designed for moment and shear. The moments introduce bending into the connection plates.

An advantage of diaphragms for I-girder bridges is that there is typically minimal fabrication involved. Disadvantages are that they often are not full depth, it is difficult to develop the moment in the connections, and they typically require location-specific connection plates with holes located to accommodate any cross-slope or superelevation.

3.1.2.8.4.2 Configuration in Box-Girder Bridges

The use of internal K-type cross-frames with the K-node at the top chord usually provides the best access for internal inspection, while providing the required stiffness. Should it become necessary to reduce the transverse bending stress range in the box flange adjacent to the cross-frame connection plate welds to the flange, the use of transverse cross-frame members attached to the bottom flange as part of the internal cross-frames can reduce the range of transverse bending stress. When bottom transverse cross-frame members are provided, they are to be attached

to the bottom flange, unless a longitudinal flange stiffener(s) is used, in which case the transverse members are bolted to the longitudinal stiffener(s) (*AASHTO LRFD* Article 6.11.5). For closed-box sections, should the top transverse cross-frame members also be called upon to reduce the range of transverse bending stress, they should be similarly attached. In addition, the moment of inertia of the transverse cross-frame member must not be less than the moment of inertia of the largest connection plate for the internal cross-frame under consideration taken about the edge in contact with the web. The moment of inertia of the transverse cross-frame member should be taken about the edge in contact with the flange when it is attached to the flange, or about its neutral axis when bolted to the longitudinal stiffener(s). When transverse bracing members are welded directly to the bottom flange, the transverse bending stress range at the termination of these welds should be checked. When transverse bracing members are connected to longitudinal flange stiffeners, the box flange may be considered stiffened when computing the transverse bending stresses (*AASHTO LRFD* Article C6.11.5).

Internal diaphragms are used at supports. Access holes are provided in the diaphragms at interior supports. *AASHTO LRFD* Article 6.7.4.3 specifies that access holes in internal intermediate diaphragms be at least 18.0 in. wide and 24.0 in. deep; however, a larger hole at least 36.0 in. deep is preferable. In addition to restraining distortion of the box section, the diaphragms at supports also transfer load from the girder webs to the bearing(s). If a single centered bearing is used, the diaphragm must be stout enough to resist the reaction and transfer the load around any access hole. Bearing stiffeners are usually attached to the diaphragms. If a single centered bearing is employed, two stiffeners are generally used. A bearing stiffener on each side of the access hole generally removes the shear from the diaphragm before it is engaged by the hole. Torsion generally causes a different magnitude of shear in the webs of the box on the two sides of the diaphragm. In cases where there is a large torque, the shear may be equal on both sides of the hole. In these cases, some shear must pass over the section containing the hole. If the shear in the diaphragm is high, it may be advisable to investigate the edge stresses around the hole. Reinforcement around the hole may be required, particularly if the access hole requires a large portion of the diaphragm or if a single bearing is located under the diaphragm. Auxiliary stiffeners on the diaphragm or webs may be employed if necessary to spread out the reaction. Refined analysis of internal diaphragms at supports is desirable because they are primary members necessary for the integrity of the bridge.

AASHTO LRFD Article 6.7.4.3 requires that an internal plate diaphragm provided for continuity or to resist torsional forces be connected to the flanges and webs of the box section. It is important to remember that the diaphragm-to-web welds are to be designed for the sum of the web shears on the left and right of the support.

External plate diaphragms with aspect ratios, or ratios of length to depth, less than 4.0 and internal plate diaphragms act as deep beams (*AASHTO LRFD* Article C6.7.4.3) and should be evaluated by considering principal stresses rather than by simple beam theory. Fatigue-sensitive details on these diaphragms and at the

connection of the diaphragms to the flanges should be investigated by considering the principal tensile stresses.

3.1.2.8.5 Design Considerations for Cross-Frames/Diaphragms

3.1.2.8.5.1 General

As a minimum, cross-frames/ diaphragms are to be designed to resist wind loads, to transfer lateral loads between the bearings and the superstructure, and to meet slenderness requirements (*AASHTO LRFD* Articles 6.8.4 or 6.9.3, as applicable) and minimum thickness requirements (*AASHTO LRFD* Article 6.7.3). *AASHTO LRFD* Article 6.7.4.1 also requires that cross-frames/diaphragms that are included in the structural analysis model be designed for the computed force effects. They are to be designed for all applicable limit states.

In a curved-girder bridge, a refined analysis should be used to obtain the actions required to design the bridge (*AASHTO LRFD* Article 4.6.3.3.2). Such analyses typically yield forces in the cross-frame/diaphragm members, which are, as explained above, primary members. The stiffness and size of these members influences the magnitude of the computed actions in them. Disproportionately large cross-frame/diaphragm members will result in large forces that can be reduced by reducing the member sizes. It is best to initially investigate smaller member sizes and increase the sizes as necessary. Significant changes in cross-frame or diaphragm sizes are best investigated with another analysis to assure that the forces have not changed excessively.

Preliminary sizes can be obtained from the permitted slenderness specified in *AASHTO LRFD* Articles 6.8.4 and 6.9.3. Single-element members rather than double angles are preferred for cross-frames. Double angles permit bolts to work in double shear reducing the number. However, they are expensive to fabricate and painting between the angles is difficult. It is preferable for the fabricator to weld the individual members to gusset plates in a jig. The assembled cross-frame can then be shipped for erection. The reader is referred to Sections 3.3.3 and 3.3.4 for further information on the design of single-angle, tee and double-angle members, and to Section 3.3.5 for further information on the design of diaphragms.

Fitting up and welding cross-frames as a unit in the shop is preferred over “knock-down” cross-frames that are shipped in pieces. Cross-frames that can be welded from one side are preferred; that is, no double-angle members. Many fabricators prefer that cross-frames are detailed as parallelograms, rather than as rectangles. Part A of Figure 3.1.25 shows the preferred shape that follows the cross-slope of the bridge. This shape has the advantage of being deeper than possible with the rectangular shape. Note that the cross-frame chords are closer to the flanges. The parallelogram allows holes in the connection plates to be in a single location, increasing fabrication efficiency. A jig can be used to adjust for the cross-slope and accommodate the different required member lengths found with the parallelogram

shape. In cases where there are significant drops between adjacent girders (e.g., a bridge with skewed haunched girders), the cross-frame jig is a necessity.

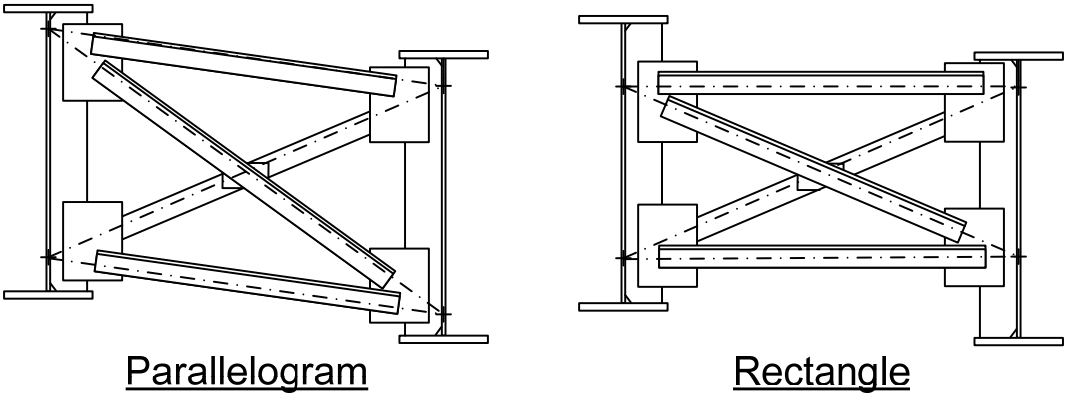


Figure 3.1.25 Cross-Frame Detailing

Figure 3.1.25 Part B shows how the diagonal members in a rectangular cross frame are the same length, but the depth is shallow. As a result, different hole locations are required in most of the connection plates. Locating these holes is obviously expensive.

Rectangular cross-frames with a cross-slope cause opposing horizontal cross-frames that are not in alignment, as shown in Part A of Figure 3.1.18. This subjects the connection plate and web to bending because the chords are not aligned on the two sides of the girders. The lateral forces on exterior girders are less than on interior girders.

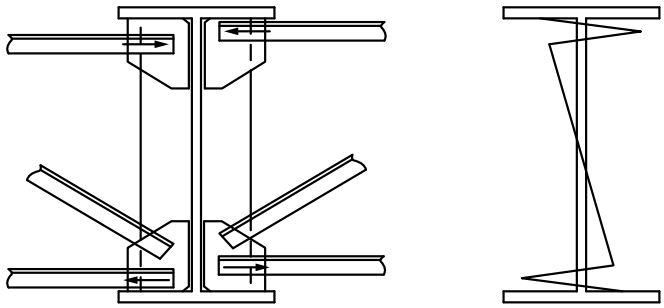


Figure 3.1.26 Connection Plate Bending Resulting from Cross-Frame Alignment

3.1.2.8.5.2 Connection Plate Design

I-Girder Bridges

The complete load path for the cross-frame forces includes a transfer of the net cross-frame force from the connection plates to the girders. Even if the cross-frames are aligned, the net force must be transferred to the flanges. Figure 3.1.26 Part B, shows that when cross-frame members are misaligned on opposite sides of interior girders in I-girder bridges, the moment in the connection plate/web element may be computed by treating the element as a fixed-end beam. The web of the connection plate/web element for an interior girder may be ignored.

The end reactions at the girder flanges represent the net lateral reactions consistent with the lateral flange moment. The welds attaching the connection plates to the flanges must be able to transfer these reactions.

Where end moments are significant, the connection plate fillet welds to the flanges should be checked for combined shear and tension at the strength limit state. Connection plate welds to the web also might also be checked for the net resultant vertical cross-frame force.

All of these forces discussed above must be based on a proper resolution of the dead and live load (plus impact) cross-frame forces. The horizontal forces should be resolved to ensure equilibrium; that is, the proper combination of live loads must be used to obtain equilibrium. Since both maximum and minimum values of the live load forces are obtained, consideration of the proper combinations of these forces is necessary. Although separate influence surfaces are loaded for each member in a refined analysis, equilibrium can still be obtained by combination of the proper live load forces. This issue is examined in more detail in Section 3.3.6.

Local buckling of connection plates for I-girder bridges should be checked when the cross-slope is large and rectangular cross-frames or diaphragms are used. There is usually a significant distance between the cross frame/diaphragm and the flange. The maximum moment in the connection plate may be checked against the resistance factor for flexure, ϕ_f, from *AASHTO LRFD* Article 6.5.4.2 times the nominal local buckling resistance of the connection plate about an axis parallel with the web.

The equations from *AASHTO LRFD* Article 6.12.2.2.1 giving the nominal local buckling resistance of I- and H-shaped members about an axis parallel with the web are appropriate to be applied to rectangular connection plates as follows:

If $\lambda_f \le \lambda_{pf}$, then:

$$M_n = M_p$$

Equation 3.1.4
AASHTO LRFD Equation 6.12.2.2.1-1

If $\lambda_{pf} < \lambda_f \le \lambda_{rf}$, then:

$$M_n = \left[1 - \left(1 - \frac{S_y}{Z_y}\right)\left(\frac{\lambda_f - \lambda_{pf}}{0.45\sqrt{\frac{E}{F_{ys}}}}\right)\right] F_{ys} Z_y$$

Equation 3.1.5
AASHTO LRFD Equation 6.12.2.2.1-2

where:

λ_f = slenderness ratio of the connection plate = b_t/t_t

λ_{pf} = $0.38\sqrt{\frac{E}{F_{ys}}}$

λ_{rf} = $0.83\sqrt{\frac{E}{F_{ys}}}$

F_{ys} = specified minimum yield strength of the connection plate (ksi)

M_p = plastic moment of the effective section (defined below) about the axis parallel with the web (kip-in.)

S_y = elastic section modulus of the effective section (defined below) about the axis parallel with the web (in.^{3})

Z_y = plastic section modulus of the effective section (defined below) about the axis parallel with the web (in.^{3})

For interior girders, S_y, M_p and Z_y may be calculated based on an effective rectangular section consisting of the connection plates on both side of the web. In this case, $M_p = 1.5F_{ys}S_y$ and $Z_y = 1.5S_y$. For exterior girders, S_y, M_p and Z_y may be calculated based on an effective section consisting of the connection plate plus a portion of the web. A portion of the web equal to $18t_w$ is suggested for inclusion with the connection plate in this case. In this case, all properties should be computed about the appropriate neutral axis of the effective tee section. Note that if F_{yw} is smaller than F_{ys}, where F_{yw} is the specified minimum yield strength of the web, the strip of web included in the effective section should be reduced by the ratio of F_{yw}/F_{ys}.

Figure 3.1.27 is a plot of a "Factor" versus b/t assuming that F_{ys} is 50 ksi and that b is the total width (inches) of double-sided connection plates (including the thickness of the web). Multiplying the "Factor" from the plot by the quantity "b^2t" gives the nominal local buckling resistance, M_n (in kip-ft), of the connection plates according to

the above equations. The local buckling resistance of single-sided connection plates cannot be found using this plot.

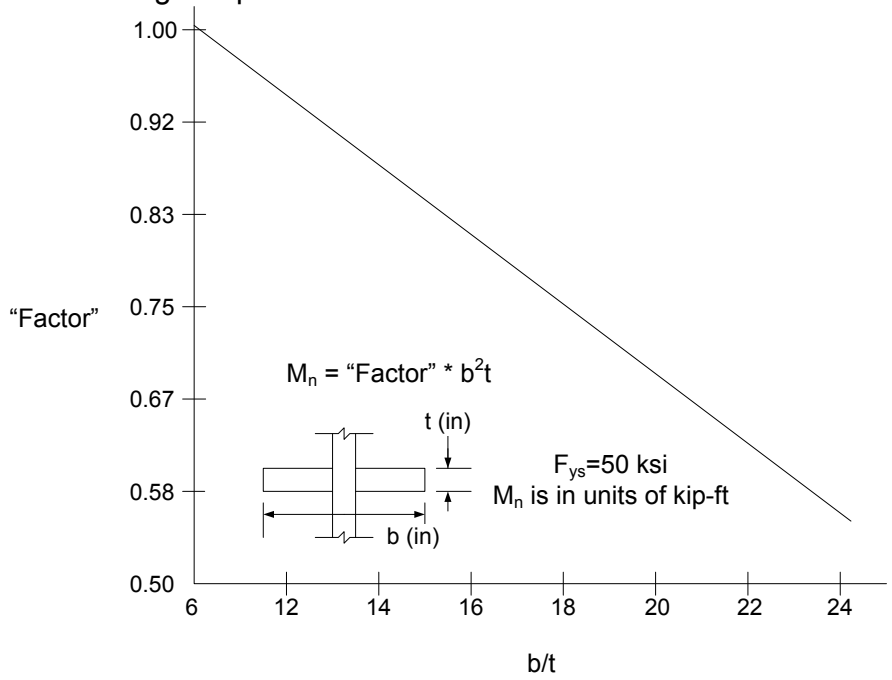


Figure 3.1.27 "Factor" for Computing Nominal Local Buckling Resistance of Double-Sided Connection Plates from Equations 3.1.4 and 3.1.5

Note that connection plates serving as bearing or intermediate transverse shear stiffeners must also satisfy the applicable stiffener design requirements discussed further in Section 3.3.8.

In order for the connection plates for a skewed cross-frame/diaphragm to transfer the forces between the cross-frame/diaphragm members without undue distortion, the connection plates should be oriented in the plane of the cross-frames/diaphragms. Two options for this detail are: a skewed connection plate (Figure 3.1.28); or a bent gusset plate (Figure 3.1.29). The skewed connection plate should be limited to maximum skew angle of 20°. For skew angles not exceeding 20°, it is desirable to give the fabricator the option to use either detail. These details are taken from Reference 2.

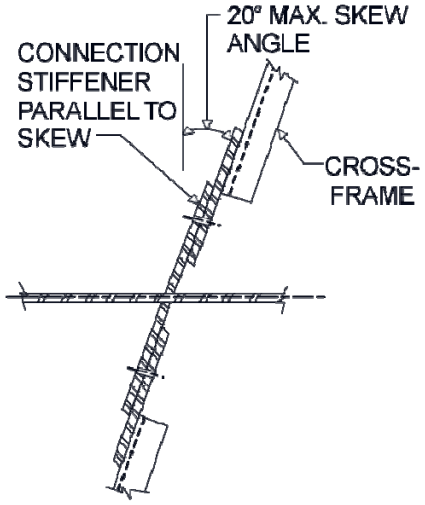


Figure 3.1.28 Skewed Connection Plate

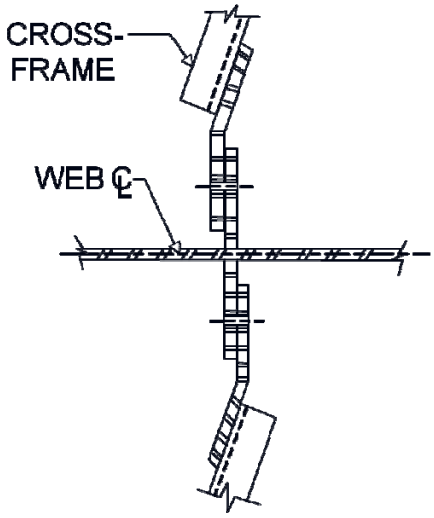


Figure 3.1.29 Bent Gusset Plate

The use of half-rounds (i.e. split pipes) as stiffeners is under investigation for this application. Such stiffeners would also provide improved torsional resistance.

Box-Girder Bridges

The attachment of internal cross-frame connection plates to box flanges is discussed in *AASHTO LRFD* Article C6.6.1.3.1. Fabrication of tub sections is often done by first welding the webs and top flanges. Web stiffeners and connection plates are then welded. The tub shape is then created by bolting in the internal cross frames. The superelevation and twist that might be required in the tub can be introduced in this manner. Finally, the common box flange of the box can be welded to the webs.

Obviously, if the web stiffening extends to the bottom of the webs, automatic continuous welding of the bottom flange would be impossible. If the Design Engineer has permitted, the stiffening and/or connection plates are made short of the bottom of the webs, permitting the web-to-flange welds to be made uninterrupted. Subsequently, the connection plates are extended with lapped tabs that are welded to the bottom flange and the stiffeners. Figures 3.5.A and 3.5.B in Reference 2 show suggested connection details for this particular situation. Figure 3.5.D in Reference 2 shows a suggested connection detail for cases where the box flange is welded to the webs prior to attaching the connection plates and stiffeners. *AASHTO LRFD* Article 6.6.1.3.1 also requires that the connection plates and stiffeners be attached to the flanges to avoid the fatigue issues discussed above.

Details on tub girders have a significant effect on cost. The Design Engineer is encouraged to consult with fabricators likely to build the project regarding the preferred details for fabricating the tub sections. It may be desirable to show alternate details for the connection plates on the design plans.

3.1.2.9 Lateral Bracing

According to *AASHTO LRFD* Article 6.7.5.1, the need for lateral bracing is to be investigated for all stages of construction and the final condition.

3.1.2.9.1 Lateral Bracing Functions

3.1.2.9.1.1 Functions in I-Girder Bridges

Lateral bracing is generally used on the bottom flanges in I-girder bridges (Figure 3.1.30). There are, however, reasons that it might be used on the top flanges. Lateral bracing tends to force the connected girders to act as a pseudo-box if it is used on both top and bottom flanges, or if used only on the bottom flanges after the deck has hardened. Lateral bracing members experience significant load as a result of this box-type action. Lateral bracing is rarely used in all bays of the bridge. Typically, it is used in one or both exterior bays.



Figure 3.1.30 Bottom Lateral Bracing on Curved I-Girder Bridge

Lateral bracing prevents the flanges of the girders to which it is attached from moving longitudinally with respect to each other. Hence, the two flanges have roughly the same stress. Frequently, the cross-frame forces are slightly elevated in the bay with lateral bracing because their diagonals provide the means to transfer the balancing load between the girders.

The outside girder of an I-girder bridge is usually the most highly loaded. This is particularly true with the convex girder of a curved bridge. The outside girder of these bridges often requires heavier flange plates which, in turn, causes increased stiffness drawing even more load, leading to more deflection and increased cross-frame forces. Lateral flange bracing in the outside bay of such bridges reduces the load in the convex girder and its deflection as well because it forces the adjacent girder to share the superimposed dead load and live load. If steel weight and deck weight are causing the convex girder to be highly loaded, top and bottom lateral bracing may be required to create the pseudo box for the non-composite loads.

Lateral bracing can also help control deflections, provide stability and minimize girder out-of-plumbness during construction.

The bare steel girders are subject to lateral wind forces before the deck hardens. The stiffness of an I-girder bridge is equal to the sum of the stiffnesses of the girders. This is often inadequate to prevent damage to the girders and the bearings under the wind forces. Lateral bracing is particularly useful in stiffening the bare steel I-girders against lateral wind loads. Lateral bracing together with the cross-frames provides a rigid truss action to resist the lateral wind force. It is often economical to use lateral bracing over only portions of the spans.

The concept of lateral bracing for wind loads probably arose with truss design where the lateral bracing system is necessary to resist wind. Lateral bracing is not as effective in resisting wind load on a completed multi-girder composite bridge. The lateral wind force on completed girder bridges is resisted primarily by the deck as the

cross-frames/diaphragms transfer the force to the deck, which is must stiffer than any lateral bracing system. The deck resists the wind force as a large diaphragm in shear and bending. The wind force is transferred from the deck to the laterally-restrained bearings through the end cross-frames/diaphragms.

Radial forces in cross-frames of curved-girder bridges cause longitudinal forces in the bridge that may not be balanced out by other cross-frames. Hence, the longitudinal forces may not be in equilibrium, causing potential loss of equilibrium during erection and in any condition before the deck hardens. In smaller bridges, the bending strength of the cross frames may provide the necessary stability. However, in larger spans, the bending strength of the cross-fames may be insufficient. Frequently, the erector will lock down bearings so as to prevent longitudinal movement of the girders, providing another means of obtaining stability. Again, in larger and sharply curved bridges, locking down bearings may not be adequate. A small amount of lateral bracing in several or all bays is effective in these cases. Lateral bracing might only be necessary adjacent to interior supports for continuous-span girders.

AASHTO LRFD Article C6.7.5.2 suggests that lateral bracing be considered to prevent significant relative horizontal movement of I-girders in spans greater than 200 feet. Individual circumstances, such as significant horizontal curvature or skew, or high wind loads acting on the non-composite structure, may warrant inclusion of lateral bracing for smaller spans. Each situation is unique that requires the sound judgment of the Design Engineer. Temporary lateral bracing may be used at the Owner's discretion.

The analysis must be able to recognize the influence of even temporary lateral bracing. If lateral bracing is left on the structure, it will continue to work. This is particularly true for live loads, which usually produce relatively large forces in lateral bracing for reasons discussed above. These forces make the members and their connections to the girders susceptible to fatigue if they have not been designed for fatigue. Lateral bracing might be placed in the plane of the top flange in cases when it is to be employed only for construction. In this location, it senses little effect from live loads so fatigue is unlikely and it most likely need not be considered in the analysis of the final bridge.

Erection of lateral bracing may be problematic because the girders are usually erected and stressed due to self-weight, which may change the bolt-hole positions enough that fit-up is difficult. Some erectors have found that field drilling holes in the gusset plates to match the holes in the flanges works out well. Of course, the holes must be considered in determining the net section of the flanges where flanges are subject to tension (refer to *AASHTO LRFD* Article 6.10.1.8 and Section 3.2.6.1.3). Welding the gusset plates to the flanges presents fatigue issues that are expensive to address. This is another reason that top flange lateral bracing is appealing. Fatigue stresses are far less critical on the top of the girder than at the bottom. Usually, gusset plates can be welded to the top flange with minor changes to handle

fatigue. Further, top flange lateral bracing will have smaller stresses so fewer bolts will be required. Often a single row of bolts is found adequate. Removal of top lateral bracing members may be expensive and problematic if bolted to the top flange.

3.1.2.9.1.2 Functions in Box-Girder Bridges

Lateral bracing of the top flanges of tub girders changes them from an "open section" to a torsionally closed section. They become a closed section for the non-composite loads. Otherwise, tub girders would not become a closed section until the deck hardens. The shear center of an open tub section is located below the bottom flange (*5*). The addition of top lateral bracing shifts the shear center to the inside of the tub resulting in a pseudo-box closed section. When the section becomes closed, the torsional stiffness is significantly increased. Without lateral bracing, a tub section acts as an open section and is torsionally weak. Top-flange bracing retains the shape of the tub.

AASHTO LRFD Article 6.7.5.3 requires lateral bracing over the entire length of the tubs in horizontally curved girders. A full-length lateral bracing system limits distortions that may result from temperature changes occurring prior to deck placement. *AASHTO LRFD* Article C6.7.5.3 recommends full-length lateral bracing be provided with straight tub sections on spans greater than 150 feet.

AASHTO LRFD Article 6.7.5.3 permits the use of partial-length lateral bracing *in straight tub girders* if torsion is known to be small and it can be shown that the section can resist excessive distortion with the partial lateral bracing. Attention should be given to possible loads that might be induced during shipping, erection and placement of the concrete deck. *AASHTO LRFD* Article 6.7.5.3 requires that the local stability of the top flanges and the global stability of the individual tub sections be investigated in tubs with partial length lateral bracing. This requirement applies to the Design Engineer's assumed construction sequence. At least one panel of lateral bracing should be provided on each side of anticipated lifting points. The load effects such as those due to unequal deck weight acting differently on two top flanges or skew acting on the non-composite steel section during shipping or construction should also be considered. Straight tub sections with a partial-length lateral bracing system may be subject to a net torque that must be considered with regard to top-flange lateral bending stresses and cross-section distortion stresses.

Top flange lateral bracing is designed to resist the shear flow in the pseudo-box section resulting from any torsion acting on the steel section due to the design load effects. The bracing also act with the tub in resisting vertical bending. Hence, forces in the bracing due to flexure of the tub during construction must also be considered (based on the assumed construction sequence). Top flange lateral bracing also resists wind loads acting on the non-composite tub section.

When the bridge is analyzed by 3D finite element analysis in which the individual lateral bracing members are included in the model, their forces can be taken from the analysis. When the forces in the bracing members are not computed directly,

the shear flow, *f* (kips/in.), in the top of the pseudo-box section can be computed as follows:

$$f = \frac{T}{2A_o}$$

Equation 3.1.6
AASHTO LRFD Equation C6.11.1.1-1

where:

A_o = enclosed area within the box section (in.^{2})
T = internal torque due to the factored loads (kip-in.)

A_o is to be computed for the non-composite box section. If the top lateral bracing is attached to the webs of the tub, A_o is to be computed using its actual location according to *AASHTO LRFD* Article 6.7.5.3.

The torsional shear (kips) across the top of the tub equals the shear flow times the distance between the tops of the webs. That shear may then be resolved into the vector along the diagonal bracing member. There is also a vector due to flexure that must be included. Bracing member forces due to flexure of the non-composite tub can be estimated by an approach presented in Reference 3. Note that since top lateral bracing contributes to the flexural stiffness of the tub section, the bracing member should be resolved into the section properties when determining stiffness for analysis and for section properties when computing stresses. The lateral system is also subjected to forces after the section becomes composite with the hardened deck. These forces can be significant when the lateral bracing members are large. The distribution of shear flow resisted by the deck and lateral system can be estimated by the ratio of the shear stiffnesses of the two elements.

The equivalent area, $A_{o,}$ of a plate that will represent the shear stiffness of the top lateral bracing may be computed using an equivalent energy method (References 1 and 2 in Section 1.1). The method provides formulas to calculate the equivalent plate thickness for several common configurations of top lateral bracing.

3.1.2.9.2 Configuration of Lateral Bracing

AASHTO LRFD Article 6.7.5.1 states that if permanent lateral bracing members are included in the structural model used to determine live load force effects, they must be designed for all applicable limit states and be considered primary load-carrying members. Since bottom lateral bracing carries significant live load, it must also be detailed very carefully with respect to fatigue if it is left in place.

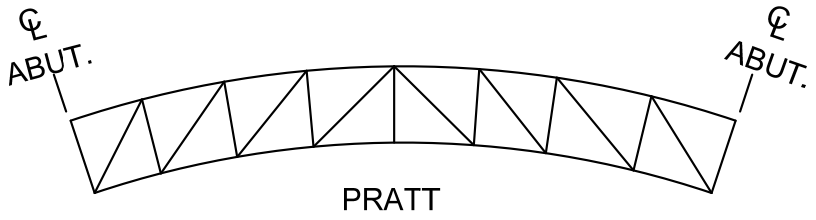
The configuration of lateral bracing may be important economically. This is particularly true in bridges that are subjected to large torsional loads. Lateral bracing configurations with a single diagonal per bay are usually adequate. Other X-type

configurations have twice as many members and connections and are usually avoided.

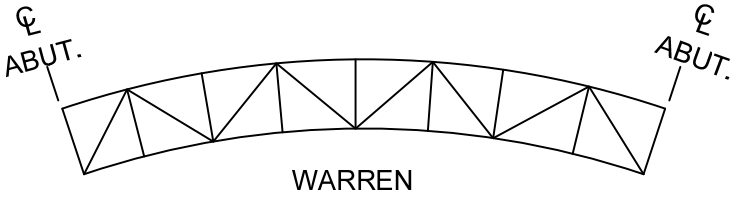
The first decision the Design Engineer needs to make is the bay size for the lateral bracing. The longer the bay, the fewer members required; the longer the members, the greater the unbraced length. However, as mentioned previously, the bracing forces due to both shear flow and flexure are increased with a "flatter" diagonal angle. Generally, the lateral bracing bay length is set equal to half of the cross-frame spacing, so that alternate bays of lateral bracing connect at an internal cross-frame. There is no formula to determine an optimal bay size. However, when members become large and connections become unwieldy, the need for a shorter bay is indicated. Or, if the lateral bracing member can be oriented so that it is in tension for the shear flow in regions where the same member is in compression due to flexure, there is less need to control its length and spanning from cross-frame to cross-frame may be a more economical arrangement. Rarely, is it good design practice to make the angle between the diagonal and the girder tangent greater than 45 degrees.

One commonly asked question is whether lateral bracing members attached to the top flange midway between cross-frames/diaphragms act as a brace point for the top flange in compression when checking for lateral torsional buckling in the presence of flange lateral bending (due to deck overhang loads, curvature, lateral bracing forces, etc.). Usually they are not considered as brace points for the top flanges of the tub. However, there is obviously some argument that the truss action of the lateral system will provide some lateral restraint. *AASHTO LRFD* Article 6.11.3.2 takes the conservative position when it states that the unbraced length of the top flanges of tub sections should be taken as the distance between interior cross-frames/diaphragms. As discussed previously, at locations where only struts exist between the top flanges, top lateral bracing attached to the flanges at these points may be considered to act as brace points at the discretion of the Design Engineer according to *AASHTO LRFD* Article C6.11.3.2.

The Design Engineer has two options regarding the configuration of a single-diagonal lateral bracing system: a Pratt truss pattern, Figure 3.1.31 Part A; or a Warren truss pattern, Figure 3.1.31 Part B. In the Pratt truss configuration, only one member applies force against a flange at a cross-frame/diaphragm. The force is resisted mainly by the strut or top chord of the cross-frame, and to some degree, by lateral bending of the top flange.



Part A



Part B

Figure 3.1.31 Single-Diagonal Lateral Bracing Patterns

The Warren truss pattern applies the force from two lateral bracing members at the intersection, increasing lateral flange moments and strut or cross-frame top chord forces. An approach for estimating the flange lateral bending stresses due to these forces (in lieu of a refined 3D analysis) when a Warren truss pattern is utilized is presented in Reference 3.

When torques are large and a dominate torque direction occurs, it is possible to orient the lateral bracing members such that they are in tension for shear flow, although they may be in compression due to flexure, and vice versa. By configuring the lateral bracing in the Pratt truss pattern with the directions of the diagonals determined from the sign of the torque, significant economy can often be realized with the Pratt truss pattern over the more typical Warren truss pattern that leads to half of the diagonal members in compression. As discussed previously, as the diagonal angle is increased, the bracing force due to both torsion and flexure is reduced, as well as the length of the brace. This becomes important for bracing that must resist compression. A flatter angle, however, reduces the number of elements required in the bracing system. It is for this reason that a Pratt truss pattern that allows tension bracing is economical. It should be noted that usually the direction of the Pratt truss pattern changes over a span. At the central location, it may be desirable to introduce one bay of X-bracing.

AASHTO LRFD Article C6.7.5.3 recommends that the following requirement be satisfied to ensure that a reasonable minimum area is provided for the diagonal members of the top lateral bracing for tub sections:

$$A_d \geq 0.03w \qquad \text{Equation 3.1.7}$$

AASHTO LRFD Equation C6.7.5.3-1

where:

A_d = minimum required cross-sectional area of one diagonal (in.^{2})
w = center-to-center distance between the top flanges (in.)

This requirement was included in the original *AASHTO* Guide Specifications for horizontally curved girders and was intended to ensure that top lateral bracing would be sized to that the tub would act as a pseudo-box section with normal stresses due to warping torsion less than or equal to 10 percent of the major-axis bending stresses and with minimal warping torsional displacements. The criterion was originally developed based on tub sections with vertical webs, with ratios of section width-to-depth between 0.5 and 2.0, and with X-type lateral bracing configurations with the diagonal members at an angle of 45 degrees to the longitudinal centerline of the girder flanges (*7*). Although most tub-girder configurations will likely differ from the configurations for which the above criterion was developed, the criterion at least ensures that some reasonable minimum area will be provided for these members regardless of the configuration. In most cases, larger members will likely be required to resist the applied member forces.

Finally, top lateral bracing should always be continuous across field splice locations. Otherwise, large lateral flange bending stresses might occur in the top flanges of the tub where the bracing is discontinued.

3.1.2.9.3 Detailing of Lateral Bracing

AASHTO LRFD Article 6.6.1.3.2 deals with the detailing of lateral connection plates. Although not required by code, the most desirable connection of lateral bracing members (diagonals and struts) to the girders is to bolt the lateral connection plates (or members) to the flanges rather than to the webs. Welding of the connection plates to the flanges or web typically results in a fatigue Category E detail with a very low fatigue resistance. Bolting improves the fatigue resistance of the connection plate or member (Category B or D) and eliminates the need to provide an expensive radiused transition at the ends of a welded connection plate to improve the fatigue resistance above Category E. *Note however that when the bracing members are bolted to a flange subject to tension, AASHTO LRFD Equation 6.10.1.8-1 must be satisfied at the strength limit state to ensure that fracture on the net section of the flange is prevented – refer to Section 3.2.6.1.3*.

When the connection plate is bolted to the flange, a minimum gap of 4.0 in. should exist between the edge of the flange and first bolt line in the bracing member (Figure 3.1.32) to reduce stresses produced by vibration movement of the lateral bracing (*8*).

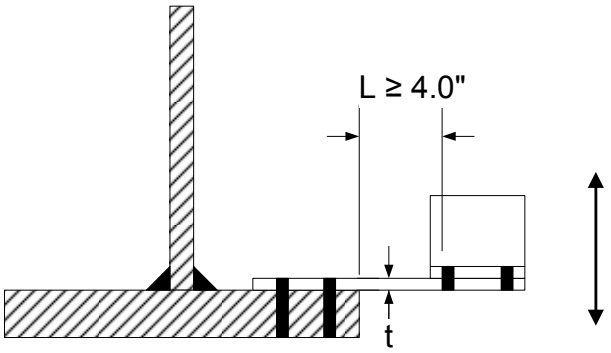


Figure 3.1.32 Lateral Connection Plate Bolted to Flange – Minimum Recommended Gap to Reduce Vibration Stresses

Some Owners specify removable deck forms, even within tub sections. These forms are very difficult to remove when lateral bracing is attached to the flanges, particularly from inside a tub section. To avoid connections of the bracing to the web, it is recommended that the requirement for removable forms be rescinded whenever possible in favor of using permanent metal deck forms, especially within tub sections. One-inch (±) thick fill plates between the lateral connection plate and the underside of the top flange can be used to stay clear of the stay-in-place form installation.

When lateral connection plates are attached to the webs, forces in the lateral bracing members are transferred to the web or connection plates before the forces can be resisted by the flanges. This creates a circuitous load path and potential fatigue prone details; both which must be considered in the design. Also, as specified in *AASHTO LRFD* Article 6.7.5.3, if the bracing is attached to the webs of tub sections, the cross-sectional area of the tub for shear flow A_o must be reduced to reflect the actual location of the bracing, and a means of transferring the forces from the bracing to the top flange must be provided; that is, an adequate load path, with fatigue considered, must be provided between the bracing-to-web connections and the top flanges of the tub.

Where it is not practical to attach lateral connection plates to the flanges, *AASHTO LRFD* Article 6.6.1.3.2 recommends that the connection plates be located a minimum specified distance from the flanges to minimize the effect of out-of-plane distortion stresses on the fatigue resistance of the base metal adjacent to the welds (refer to Section 3.2.5.2.3 for further discussion on distortion-induced fatigue). It is recommended that the connection plate be located a vertical distance not less than one-half the flange width above or below the flange, as applicable, to ensure adequate electrode access and to move the connection plate closer to the neutral axis of the girder to reduce the impact of the weld termination on the fatigue resistance (Figure 3.1.33). The recommended gap also facilitates painting and field inspection. However, even if this is done, a welded Category E detail will not likely suffice at most locations requiring the connection plate to either be cut with a radius or bolted to the web. Should the connection plate be located on the opposite side of

the web from a transverse stiffener, the connection plate must be centered on the stiffener and the stiffener must be rigidly attached to both the compression and tension flanges (Figure 3.1.33).

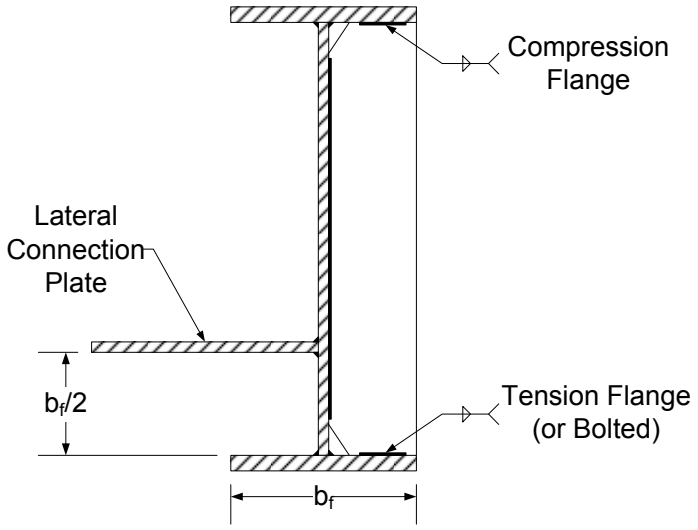


Figure 3.1.33 Recommended Lateral Connection Plate Detail for Plate Attached to the Girder Web – Plate Opposite Transverse Stiffener

The same recommendations apply when the connection plate is located on the same side of the web as a transverse stiffener. The line of action of the laterals should intersect at the transverse stiffener. The stiffener *must* be made discontinuous with the connection plate welded to the discontinuous stiffener, with sufficient copes and a minimum gap of $4t_w$ provided between the stiffener-to-web and lateral connection plate-to-web weld toes, where t_w is the thickness of the web in inches (Figure 3.1.34 – see also *AASHTO LRFD* Figure C6.6.1.3.2-1). As an alternative, the bracing member can be extended and bolted to the stiffener with the connection plate coped around the stiffener (Figure 3.1.35). The ends of the bracing members must be kept a minimum of 4.0 in. from the web and any transverse stiffener to reduce distortion-induced gap stresses resulting from vibrations of the bracing members (Figures 3.1.34 and 3.1.35).

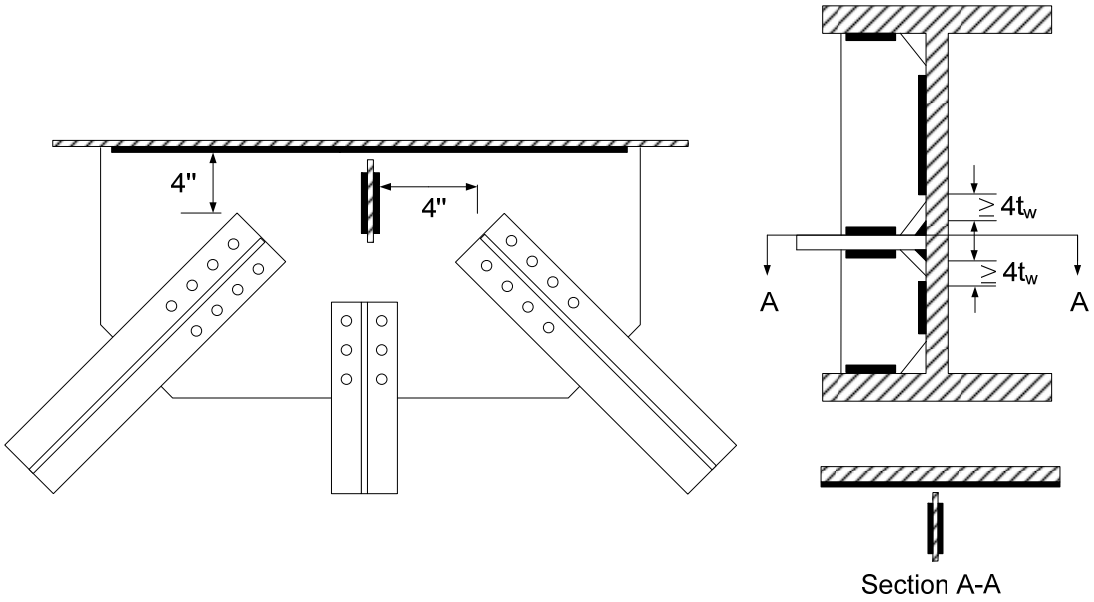


Figure 3.1.34 Recommended Lateral Connection Plate Detail for Plate Attached to Girder Web – Plate on Same Side of Web as Transverse Stiffener

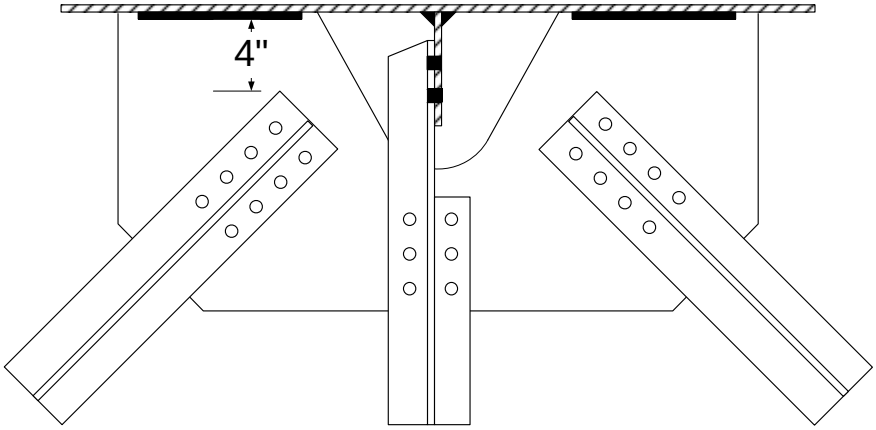


Figure 3.1.35 Alternative Recommended Lateral Connection Plate Detail for Plate Attached to Girder Web – Plate on Same Side of Web as Transverse Stiffener

Should the web be unstiffened opposite the connection plate, the connection plate should be located a minimum of 6.0 inches above or below the flange, as applicable, but not less than one-half the flange width (Figure 3.1.36) in order to prevent large distortion-induced stresses from forming in the web between the connection plate and the flange.

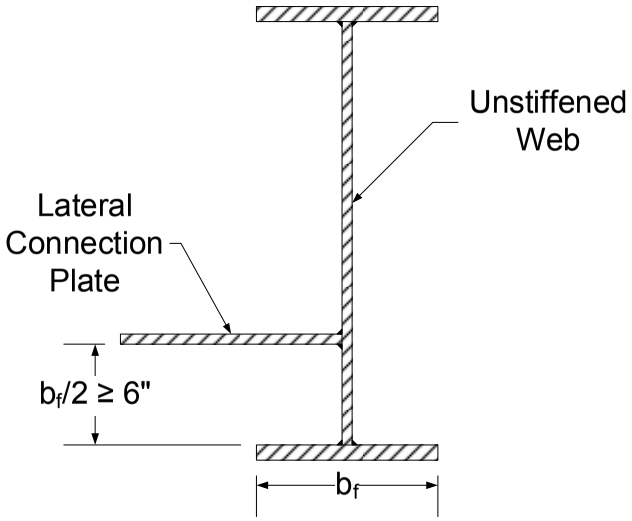


Figure 3.1.36 Recommended Lateral Connection Plate Detail for Plate Attached to Unstiffened Girder Web

The above detailing recommendations for welded lateral connection plates also satisfy the provisions of *AASHTO LRFD* Article 6.6.1.2.4 to avoid so-called "constraint-induced fracture". "Constraint-induced fracture" is a term given to conditions that create highly constrained joints and crack-like discontinuities that can lead to sudden brittle fracture under load with no perceptible fatigue crack growth and no warning, as documented during the Hoan Bridge failure investigation (*9*,*10*). Criteria have been developed in Reference 11 to identify bridges and details susceptible to this failure mode. To avoid details subject to this form of brittle fracture, welds should not be allowed to intersect. Also, attachments that are parallel to the direction of primary stress should be made continuous with any intersecting transverse attachments made discontinuous. The intersecting joint in this case must be detailed to allow a minimum gap of $4t_w$ between weld toes, where t_w is the web thickness in inches, to reduce constraint (see *AASHTO LRFD* Figure C6.6.1.3.2-1).

3.1.2.10 Box Girders Versus I-Girders

Steel box bridge members have been used in large trusses and straddle beams since at least the 1930s. Early box members were built up of four plates riveted to four hot-rolled angles. Access holes were provided for riveting. More recently, however, welded steel box girders, which were not practical until welding became acceptable for connecting major bridge elements, replaced riveted members. The first welded box girder bridges in America were probably constructed in Massachusetts in the 1950s. They were made up of four plates welded into a rectangular box. The two bridges that were constructed had rather severe horizontal curves, which was most likely the reason that the torsionally stiff box sections were used. At that time, behavior of open curved sections was not well understood. Analysis of curved closed-box sections could be done more confidently, although warping behavior was often not explicitly considered; instead, closely spaced internal

cross frames were used in the early box girders to control and minimize warping. Inspection of the Massachusetts box-girder structures in the late 1980s showed the interiors of the boxes to be in pristine condition after more than 30 years of service in the relatively harsh New England environment.

It was likely observed that the amount of steel required for these bridges was excessive. A slightly different box design was introduced by New York State who designed two box-girder bridges in the western tier of the state in the early 1960s. The designs employed lateral bracing between the top flanges of the individual boxes in the positive-moment regions. Hence, the boxes were actually tubs with top flanges. The torsional shear was resisted by a pseudo-box section created by the addition of top-flange lateral bracing members. The lateral bracing was simply designed by resolving the force due to the torsional shear flow into the individual lateral bracing members. Interestingly, the portions of the girders in the dead load negative-moment regions of these continuous-span bridges over the interior supports were closed-box sections built up from four plates. Perhaps the large torsion at the supports was believed better handled with a solid top plate, or perhaps the non-composite behavior in those regions was of concern. One of the bridges was field tested at the time of construction to confirm its behavior. In the 1990s, the bridge was field tested again and a refined analysis was performed; both confirmed that the original design was appropriate.

The early bridges were designed having radial supports. They used either two bearings or a wide rubber bearing at each support so that it could be assumed that most of the torsion would be resisted at supports by the bearings rather than by the diaphragms between the girders. Adequate internal bracing was used to ensure that the boxes did not distort to such a degree that the adequacy of the closed-section analysis could be disputed.

The smooth appearance of tub girders fabricated from welded plates soon became popular with both the public and Design Engineers. As with I-girders and other bridge types, tub girders were found susceptible to fatigue cracking when not properly detailed. For example, some longitudinal tub girders were welded to transverse box members without fully appreciating the implications of fatigue. As with many technological advances, the application preceded full investigation and improper detailing led to premature fatigue cracking in some of these bridges.

Box girders offer some distinct structural advantages over I-girders, particularly when the girders are horizontally curved.

The high torsional resistance of individual box sections permits the box to carry more of the load applied to it rather than shifting much of it to the adjacent girders having greater radius, as is the case with torsionally weaker I-girders. The tendency of box girders to more uniformly share gravity loads reduces the relatively large, and often troubling deflection, of the girder on the outside of the curve. Also, fewer cross-frames/diaphragms are required between the girders; i.e., less material needs to be

added to box girders to resist torsional effects. When a single box girder is used, there is of course no visible bracing.

There are two main advantages of box girders: They can accommodate extremely tight radii of curvature; and they can potentially be more economical than I-girders on longer spans due to their increased torsional stability during erection.

Box girders also offer benefits in durability and maintainability. Fewer elements are available for debris build-up on the outside of the box. Box girders are also easier to inspect since much of the inspection is performed from inside the box.

Because of their smooth uninterrupted profile and the fact that the number of exposed components is minimized, box girders are often chosen based on aesthetic preferences. Their smooth exteriors provide fewer locations for birds to perch.



Figure 3.1.37 Curved Box-Girder Bridge

Box girders are inherently more stable during erection and may often be erected with fewer but larger cranes than required for I-girders. I-girders must be stabilized until they are braced by their neighbors. Overall erection costs for box girders may also be less because there are generally fewer girders and fewer cross-frames/diaphragms than there are for a similar bridge constructed with I-girders. There are also fewer cross-frames/diaphragms to erect than in I-girder alternates. Box girders may also be quicker to construct as there are fewer external bracing members to erect. Box girders are also tend to be more stable under wind loads

before the deck has hardened. The most frequent criticism concerning erection of box girders is that their weight usually requires larger crane capacities.

Some disadvantages of box girders include ineffective bottom-flange material in the contraflexure regions where bending moments are relatively low. Box girders that are too small to navigate through are difficult to inspect.

Boxes can be problematic when resting on skewed supports. Skew introduces torques which can create problems in the field during construction making fit-ups difficult as well as introducing large torsional forces in the lateral bracing. The large torques due to skew also increase the shear stresses in the deck for load applied after the deck has hardened.

Fabrication of box girders is more costly per pound of steel to fabricate than I-girders. The complexity of fabricating trapezoidal box shapes (the most commonly used shape) to accommodate vertical and horizontal curvature, superelevation transitions, and/or skews can contribute to a cost premium versus I-girders. Webs should always be mathematically developable surfaces. This means that a flat plate can be cut to the shape of a web and bent to the proper shape. This is usually accomplished by maintaining a constant slope on the web.

Bridge cross-sections with one or two box girders are frequently defined as fracture critical. Although the jury is out regarding this issue, many Owners have rules defining non-redundant steel structures. Such bridges may therefore contain fracture-critical components, which add additional fabrication and inspection costs.

The detailing of tub or box girders is expensive and has found less standardization of details than for more common I-girder bridges. Hence, it is important that designers spend significant effort detailing tub girders. Usually conversations during design with fabricators who are likely bidders will lead to more fabrication-friendly details.

3.1.3 Girder Depth and Substructure Considerations

3.1.3.1 Span-to-Depth Ratio

To help control elastic deformations at the service limit state, the optional span-to-depth ratios suggested in *AASHTO LRFD* Article 2.5.2.6.3 should be met to establish a reasonable minimum web depth for the design in the absence of specific depth restrictions. However, the Engineer is permitted to use shallower girders where clearance limits girder depth.

The recommended minimum depths in *AASHTO LRFD* Article 2.5.2.6.3 are based on traditional maximum span-to-depth ratios. Span-to-depth ratios for highway bridges date back at least to 1908 when Milo S. Ketchum published "*The Design of Highway Bridges*"; the first such book of its kind (*12*). In this book, Ketchum

presented “General Specifications for Steel Highway Bridges”. Article 54, Depth Limits, from those Specifications indicated that the depth of steel beams preferably should not be less than one-twentieth of the span. This article went on to require that when that limit was not met, the beam must be designed to limit the deflections as if the limiting depth had been met. This stringent depth limit was most likely derived from earlier railroad bridge design provisions. Railroad loads tended to be heavier than highway loads. Further, most railroad bridges had no concrete deck and were not ballasted. The precise reasoning for the requirement is probably lost in antiquity. However, it is believed related to a desire to provide adequate stiffness.

Design stresses for the steel in 1908 were less than 20 ksi. Live loads were roughly equivalent to HS20. The deepest available rolled section at that time was the 21-inch standard beam (wide-flange shapes had not yet been invented). Ketchum gives examples of multi-girder bridges using rolled shapes with spans up to 45 feet. Longer span girder bridges in that era were typically two-girder deck-type or through-type bridges with a floor system spanning between girders. The girders were built-up riveted I-sections. Frequently the girders were not composite with the deck and the two-girder bridges assigned more load to the girders than would occur in a multi-girder bridge.

In 1908, the specified minimum ultimate tensile strength of the steel was about 60 ksi and the minimum specified yield stress was about 30 ksi. Modern bridge steels are designed at twice the design stresses used in 1908. Hence, an efficiently proportioned girder today tends to provide less stiffness and be relatively shallower than would have been the case a century ago. Although design engineers were aware of composite action, they rarely took advantage of it in computation of strength or deflections.

In the First Edition of the AASHO Specifications for Bridges and Structures, 1931, the preferred maximum span-to-depth ratio of steel beams was set at 20. The provisions permitted shallower sections if deflections were limited to those that would have been computed if the girder were designed with a depth of Span/20. This limit was probably taken from Ketchum, although it was the same as the limit given in the AREA Specifications (for railroads) at that time. After about 1910, Universal Mill rolled shapes were available with depths of three feet. The maximum span-to-depth ratio of 20 limited the use of these shapes to spans of about 60 feet in simple-span bridges (most early steel bridges were simple-span bridges). In the Second Edition AASHO Specifications for Bridges and Structures, 1935, the span-to-depth ratio was relaxed from 20 to 25, presumably in recognition of the much deeper wide-flange shapes with much larger and more efficient flanges that had become available after about 1910. The AASHO Specifications required that If the steel beams were shallower than Span/25, they had to be designed such that the deflection would be the same as if they were designed for Span/25. Increasing the ratio to 25 increased the effective span of the available rolled shapes to about 75 feet. The change was not as dramatic as it appeared since the limit was generally applied to many beams rather than only two, and it was also generally applied to bridges with de facto composite decks. In the Third Edition AASHO Specification, dated 1941, a live load deflection limit of Span/800 was also introduced. The span-to-depth and live load

deflection limits were relatively consistent with each other for the typical girder bridges constructed of the traditional steel grades. ASTM A 7 steel, having a specified minimum yield strength of 33.0 ksi, was the most commonly used steel for bridge design at that time, although the use of other grades was not forbidden. The Span/800 deflection limit obviously would have had a greater effect on the designs of that era had the design stresses been higher.

The advent of composite design eventually led to shallower girders being accepted and economical. Recognition of composite action in design implied a stiffer bridge. In earlier times, many bridges were built with decks not integral with the top flange so the depth limits were based on the assumption that no structural interaction existed between the deck and girders; composite design recognized this interaction when it existed. In the early 1950s, it became evident that composite wide flange beams with span-to-depth ratios greater than 25 could be economical. As a result, the preferred maximum span-to-depth ratio was relaxed to Span/30 for the steel beam, and left at Span/25 for the composite beam. As shown below, these preferred ratios remain to the present day.

The enabling use of computers for the analysis and design of bridges in the 1960s led to wider use of more economical continuous span steel-girder bridges. Continuous spans complicated the application of the relatively straightforward span-to-depth ratios. Questions arose with regard to the span length to be used in determining the limiting span-to-depth ratio and live load deflection. Since these were recommended (as opposed to specified) limits, the determination of the appropriate span length in each case was left up to the Owner and the Design Engineer. This resulted in a variety of approaches. A common approach was to liberally define the span length as the distance between points of permanent load contraflexure for determining the maximum span-to-depth ratio, and as the span between supports in determining the Span/800 live load deflection limit.

In the *AASHTO LRFD* Specifications, suggested minimum depths for steel I-girders in simple spans and in continuous spans are given in *AASHTO LRFD* Table 2.5.2.6.3-1 (Table 3.1.3 below). The suggested minimum depths are given as follows:

Table 3.1.3 Suggested Minimum Depths for Steel I-Girders in Simple and Continuous Spans from *AASHTO LRFD* Table 2.5.2.6.3-1

	Simple Spans	Continuous Spans
Overall Depth of Composite I-Beam	0.040L (L/25)	0.032L (L/32)
Depth of I-Beam Portion of Composite I-Beam	0.033L (L/30)	0.027L (L/37)

L in Table 3.1.3 is taken as the span length between bearings. The suggested minimum depths in *AASHTO LRFD* Table 2.5.2.6.3-1 are based on historical values discussed previously. For simple spans, the requirement in the *AASHTO* Standard Specifications is that the span divided by the steel girder depth should not exceed 30. The reciprocal of this value is the constant of 0.033 applied to the span length in Table 3.1.3. For continuous spans, the constant of 0.027 applied to the span length is obtained by reducing the constant 0.033 by 80 percent to account for the effect of end restraint. The suggested minimum overall depth of the composite I-girder for simple spans, i.e. including the deck, is based on applying a constant of 0.040 to the span length. The constant 0.040 is the reciprocal of the traditional maximum span-to-depth ratio of 25 suggested for the overall depth of simple-span composite girders in the Standard Specifications. Similarly, the constant of 0.032 for continuous spans in this case is 80 percent of the simple-span value. Note that an end depth-to-span ratio of 90 percent of the simple-span ratio might be considered in either case to better account for only one end of the span being restrained by continuity. *Although the limits are taken to apply to the overall depth of the girder, it is suggested that they be applied to the web depth for simplicity*.

In the absence of depth restrictions, the above suggested minimum depths for steel I-girders may be used to establish a reasonable minimum vertical web depth for the design of box girders – keeping in mind that the optimum web depth for a box section will typically be slightly less than the optimum web depth of an I-section for the same span because of the inherent torsional stiffness of a box section.

In *AASHTO LRFD* Article 2.5.2.6.3, there is a preferred minimum depth, *D*, recommended for curved steel girder systems of:

$$D \geq \frac{L_{as}}{25} = 0.040 L_{as}$$

Equation 3.1.8

where L_{as} is the arc girder length defined as follows:

- arc span for simple spans
- 0.9 times the arc span for continuous end spans
- 0.8 times the arc span for continuous interior spans

The recommended limit is to be applied to the I-beam portion only of curved steel girders when F_y in regions of positive flexure is less than or equal to 50 ksi, and when:

- F_y in regions of negative flexure is less than or equal to 70 ksi, or;
- A hybrid section is used in regions of negative flexure.

This preferred minimum depth is larger than the traditional values contained in Table 3.1.3. This reflects the fact that the outermost steel girder receives a disproportionate share of the load and should be stiffer. *D is defined in the*

specification as the overall depth of the steel girder, but it is again recommended that D instead be taken as the web depth for simplicity.

As discussed previously, in curved skewed bridges in particular, cross-frame forces are directly related to the relative girder deflections. Therefore, increasing the depth and stiffness of all the girders in a curved skewed bridge leads to smaller relative differences in the deflections and smaller cross-frame forces. Deeper girders also result in reduced out-of plane rotations, which tend to make the bridge easier to erect. Sections deeper than the suggested minimum depth may be desired to provide greater stiffness during erection.

Whenever steels having yield stresses greater than 50 ksi are used for curved girders in regions of positive flexure, an increased minimum girder depth is recommended using Equation 3.1.9 as follows:

$$D \geq \frac{L_{as}}{25}\sqrt{\frac{F_{yt}}{50}} = 0.040\ L_{as}\sqrt{\frac{F_{yt}}{50}}$$

Equation 3.1.9
AASHTO LRFD Equation 2.5.2.6.3-1

where:

F_{yt} = specified minimum yield strength of the bottom (tension) flange

Deeper girders with higher yield steel may be somewhat counterintuitive since stronger steels lead to smaller flanges and stockier webs. The use of higher strength steels tends to shallower girders with larger flanges than those required with a deeper web. The recommended relationship for this case is intended to ensure approximately the same dead and live load deflection as would be obtained at an L_{as}/D ratio of 25 when 50 ksi steel is used. In some cases, a hybrid girder using a 50 ksi top flange and web with a 70 ksi bottom flange is more efficient in positive-flexure. For this reason, the specified minimum yield strength of the bottom (tension) flange, F_{yt}, is used in Equation 3.1.9.

The greatest depth determined from the equation for each span in a continuous girder would be used for the bridge. If the span lengths vary greatly, a tapered girder can be considered. The span-to-depth ratios discussed above are not directly applicable to variable depth girders. Obviously, a conservative approach is to use the recommended minimum depths based on those ratios, as specified, to set the minimum depth. But the depth of the deeper portion of the variable depth girder should be greater than the depth determined from those values for the span between bearings. A suggested more reasonable approach for tapered-depth girders is to apply the recommended values to the depth at a point on the girder approximately 10 percent of the span away from the bearing. In the limit, the deflections of a tapered girder should not be less than the deflections of a constant-depth girder would be if the constant-depth girder met the recommended depth. Such a limit (i.e.

based on deflections) is also suggested for application to girders with parabolic haunches.

Girder depths near those found with the above equations provide the most economical girders so deviating from those values may be uneconomical. The efficiency of the design decreases rapidly as the depth decreases (*13*). When shallower curved girders are used, the Design Engineer needs to carefully evaluate cross-frame forces and girder rotations to ascertain that these matters are within acceptable ranges. Conversely, if a depth far greater than the suggested minimum depth is employed, the flanges designed for flexure are likely to be too small to meet the recommended minimum sizes discussed in later sections of this chapter.

After considering all of the above, many bridges, including curved and skewed bridges, have been successfully built that did not meet these suggested girder depths.

3.1.3.2 Girder Depth

The proper web depth is an important consideration affecting not only the economy, but also the constructibility and performance of steel-girder bridges. This is especially true for skewed and curved steel bridges. The web depth dictates the flange sizes. Since there are minimum flange width-to-web depth and flange width-to-thickness ratios, web depth cannot be selected indiscriminately. As higher strength steels (e.g. ASTM A 709 Grade HPS 70W) are employed, the design flange sizes are smaller than those for a similar web depth with Grade 50 steel. Hence, there is a tendency to reduce the web depth. Such reductions tend to infringe on the recommended span-to-depth ratio.

In the absence of site restrictions on depth, the suggested minimum depths discussed above in Section 3.1.3.1 (based on traditional values of span-to-depth ratios) should be met or exceeded where practical. Deeper girders not only lead to a stiffer bridge, but result in flanges that meet specified depth-to-width limits and girders that are easier to handle. When Grade 70 steels are used, the flange sizes tend to be smaller, potentially infringing on the specified limits.

Girder depths greater than the suggested minimum provide benefits during construction. This is particularly true for curved girders. Shallow skewed bridges may have large cross-frame forces. Increasing the girder depth and reducing the deflections tends to reduce cross-frame forces.

Highway bridge vertical clearance requirements are defined in *AASHTO*, *A Policy on Geometric Design of Highways and Streets*. Typically, the required vertical clearance is 14’-6”. The specified minimum clearance should include 6 inches for future overlays. Clearance requirements for railway bridges are set forth in American Railway Engineering and Maintenance-of-Way Association (AREMA), *Manual for Railway Engineering*. Vertical and lateral clearances for navigable waterways are established with the U.S. Coast Guard. Permits for construction

including temporary supports or causeways for bridges in navigable waterways must be cleared with the Coast Guard

Roadway specifications control roadway profiles to ensure adequate visibility and for other reasons. Hence, it is impractical in many cases to gain vertical clearance by changing profile significantly. It is this exact situation that creates a demand for steel.

The larger Young's Modulus of steel compared to that of concrete allows steel to be the material of choice where structure depth is limited. Frequently, the addition of girders in these situations is considered a necessity. This flawed logic is probably due to the provision in *AASHTO LRFD* Article 2.5.2.6.2 that allows the live load deflection to be computed by using a wheel load factor equal to the number of wheel lines that can be placed on the bridge divided by the number of girders in the cross-section (live load deflection is discussed further in Section 3.2.4.2.1). This method is not applicable to curved-girder bridges and is of questionable use for bridges with skewed supports. The most economical girder bridge, regardless of depth, is one with the fewest girders in the cross-section. There are of course practical limits to the prior statement; for example, if the flanges become too large to be practical, if there are too few girders, and/or if the deck cannot span between the girders.

3.1.3.2.1 Optimum Depth

3.1.3.2.1.1 General

At times, obstacles prevent proper span ratios in continuous-span structures. The temptation is to use an average depth based on the best depth for several spans. This choice rarely gives the best result. Shallow girders, particularly in curved bridges or in bridges with skewed supports, lead to issues during construction and at times in the completed bridge. It is usually desirable to use the near optimal depth for the largest span in the unit if feasible.

The optimum depth is the depth that provides a minimum cost girder for a particular structural unit and is quite elusive. Fortunately, the efficiency of girders does not vary greatly when near the optimum. Composite steel girders are actually designed for two conditions:

- Non-composite condition before the deck hardens
- Composite condition after the deck hardens.

There probably is no algorithm that gives the optimum girder depth.

The optimum depth depends on the span lengths of the unit, target web slenderness, girder spacing, shipping constraints, site constraints, live load deflections, ratio of composite to non-composite load, and many other issues. For example, the optimum depth for the negative moment regions is often not the same as that for the positive moment regions. This is probably where the idea of

haunched girders arose. Usually the optimum depth for the positive moment region is a better choice when combined with heavier flanges in the shorter negative moment regions. Where a deeper web in the positive moment region requires smaller flanges, this may lead to stability issues during shipping and erection. A compromise depth is usually necessary.



Figure 3.1.38 Curved Girder with Large Web Depth

In many cases, the optimum web depth will be greater than the minimum depth based on the traditional span-to-depth ratios.

3.1.3.2.1.2 Optimum Depth for Box Girders

Box webs may either be inclined or vertical. *AASHTO LRFD* Article 6.11.2.1.1 indicates that the inclination of the web plates to a plane normal to the bottom flange should not exceed 1-to-4. Webs attached to top flanges of tub sections must be attached at mid-width of the flanges. Should the flanges be attached to the webs at locations other than mid-width of the flanges, additional lateral bending effects are introduced in the flanges that would require special investigation.

The optimum depth for a box section will typically be slightly less than the optimum depth of an I-section for the same span because of the inherent torsional stiffness of a box section. The web depth obviously dictates the flange sizes for a given design. Therefore, establishing a sound optimum depth for box sections is particularly important because the size of box flanges can typically be varied less over the bridge length. Shallow boxes may be subject to larger torsional shear. Box web depths should not be less than about 5 feet to facilitate fabrication and inspection.

It is interesting to note that the two webs of a box are stressed roughly equally. This means that there will be only one critical location of the live load to produce the maximum moment in the box, whereas there are two critical positions of the live load for two I-girders. The result is that the total live load moment that must be resisted

by two I- girders is greater than the live load moment that must be must be resisted by a box girder supporting the same width of deck. This occurrence is of particular interest when comparing an exterior box girder to an exterior I-girder and the adjacent interior girder. Typically, the exterior I-girder is critical and all girders are often made the same size. The result of comparing a box girder design to an I-girder design is often that the total required moment capacity of the box girder design is less than that required for the I-girder design. This is particularly true when four I-girders are compared to two boxes.

3.1.3.2.2 Constant or Varying Depth

Girder depth is typically varied utilizing either a straight-line taper or a parabolic haunch along the bottom flange. Both I-girder and box-girder members can be designed with a variable depth. Usually box girders are given parabolic haunches rather than tapers. If the webs of a box girder are inclined, the inclination is usually held constant with the bottom flange width varied with the change in depth. Flexural stresses and lateral bending stresses need to be checked at both brace points of I-girder flanges in regions where the girder depth varies.

Variable depth girders may be desirable where clearance issues or awkward span arrangements exist. The most economical means to vary the girder depth is with a straight-line taper (top sketch in Figure 3.1.39). The taper can extend over an entire field section or a portion of a field section. The best detail is to splice the flange over a short distance so that the splice plates are not kinked to the change in slope. The change in depth requires that the cross-frame depth varies. The shorter the length of the taper, the fewer cross-frames will be affected. However, if the change in depth is slight, a long taper can make the change in depth almost invisible to the eye.

Haunched girders have a greater depth at interior supports. Haunching most often is done for aesthetic considerations. A parabolic haunch (middle sketch in Figure 3.1.39) is considered the most aesthetic, although other haunch types are often used. Figure 3.1.40 shows parabolically haunched I-girders with longitudinal web stiffeners.

Haunched girders contribute little to the efficiency of steel girders because the haunch is cut from a wider plate, creating scrap. The distance over which the haunch is effective is relatively short so it does not draw much load away from the adjacent positive moment regions; hence, the positive moment regions receive little reduction in moment. The inclined bottom flange with its vertical component carries some of the shear that normally is resisted by the web. This increased flange force is not evident from a typical beam analysis since the shear component of stress is not a flexural stress. This phenomenon is called the Resal effect after the man who

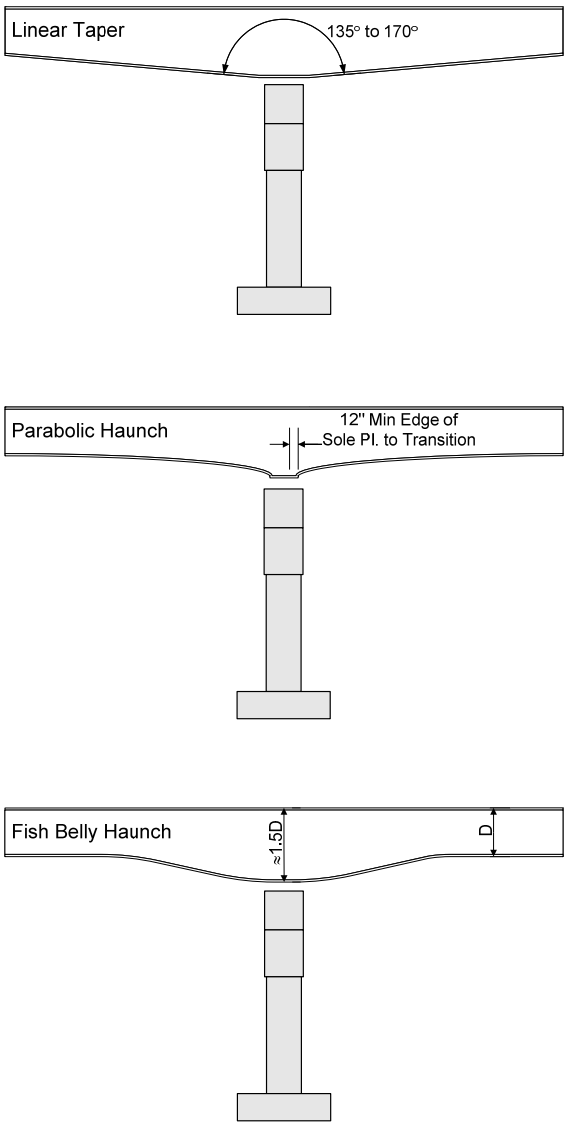


Figure 3.1.39 Variable Web Depth Member Configurations

studied variable depth girders. The effect can be beneficial for concrete girders because it reduces the shear in the web, which is important to the shear-weak concrete. However in steel haunched girder design, the effect may be problematic. In concrete, the haunch usually rests on the foundation so the force can be easily transferred into the foundation without any bearing. In a haunched steel girder, the situation is different. Approaching the bearing, the flange is returned to a horizontal attitude and the Resal force is transferred from the flange into the web. This perturbation in the force field leads to large compression forces in the web in the vicinity of the change in flange attitude. This is addressed either by stiffening the web or by using a smoother transition or “fish belly” to change the slope so that the force can be introduced into the web over a greater distance (bottom sketch in Figure 3.1.39).



Figure 3.1.40 Haunched I-Girders with Longitudinal Web Stiffeners

As discussed previously, application of higher strength (high-performance) steel permits smaller flanges for a given depth girder in a given application. However, the smaller flanges reduce the girder stiffness leading to larger dead and live load deflections for a given depth. Thus, if a 50-ksi design is controlled by deflection, the girder must be deeper if 70-ksi steel is employed. Fortunately, the *AASHTO LRFD* live load specified for computing deflection (*AASHTO LRFD* Article 3.6.1.3.2 – see also Section 1.3.2.3.4) is smaller than HS25 loading (which was used by many State DOTs to compute live load deflection for designs by the *AASHTO* Standard Specifications). Parapet stiffness is also now permitted to be included in computing live load deflections in the *AASHTO LRFD* Specifications (Article 2.5.2.6.2). The result is that many designs meet *AASHTO LRFD* deflection requirements that might not have met the deflection limit when deflection was checked for HS25 loading. Constant web depth members utilizing Grade HPS 70W steel flanges (with Grade 50W steel typically utilized in the web) are sometimes economical for spans up to and even exceeding 500 feet in length when applied in the proper depth. Thus, a parametric study of these applications investigating constant versus variable depth girders is usually justified.

In fabricating a variable web depth member, the desired girder depth is cut into the web plate and then the bottom flange plate is pulled into place and welded to the web plate. In a tapered or haunched girder, a transition is typically made from the sloping part of the taper or haunch to a horizontal bottom flange near the bearing to accommodate the bearing sole plate. The transition is made by using either a welded joint or by bending the flange plate. Bending of the plate depends on the required radius and the length of plate available from the mill. Proportioning of the flange plate at the transition location should allow for the possibility that the

fabricator may bend the plate. As mentioned above, bending of the flange plate into a ″fish belly″ type of transition can help to smooth out the transition, in lieu of a more abrupt transition which can result in an extremely sharp increase in the web stress as the vertical component of the flange force is transferred back into the web. The distance from the edge of the sole plate to the transition should be at least 12 inches in order to clear any distortion that may result from bending or welding of the flange plate and to accommodate any possible future jacking needs for bearing maintenance.

Fabrication costs for variable web depth members are higher than for constant web depth members due to the additional cutting and fitting operations discussed previously. Straight tapers are less costly than parabolic haunches because it is easier to cut the webs, locate and fit web stiffeners, weld flange transitions and fit-up the member at the web-to-flange joint. For bridges with spans exceeding approximately 400 feet, the haunched section may be so deep as to require a longitudinal field splice in the section, which increases fabrication costs significantly. A horizontal field splice may be required because of the maximum plate width availability from the mill and/or because the depth of the haunched section may preclude shipping of the section without a longitudinal field splice (typically when the depth exceeds about 14 feet). Plates are generally available from many plate mills in maximum widths up to 150 inches. Generally, the maximum usable plate width from such a plate is about 144 inches. Larger plate widths may be available from select mills. The Design Engineer is encouraged to contact the fabricator regarding maximum practical plate widths. Longitudinal web splices may either be welded or field bolted. A field bolted splice can either be fabricated using a sub-flange on the bottom of the top section and the top of the bottom section of the web plates (which are then field bolted together), or using side plates similar to a conventional bolted web splice. Note that it may be easier to ship two I-sections than deep tee sections, which may need to be temporarily braced during shipment. Thus, when designing exceptionally deep variable web depth girders, consult with fabricators in the area regarding feasibility of shipping, field-section size/depth and jobsite access.

Variable web depth members are important aesthetically because they visually demonstrate the flow of the forces in the bridge and make the bridge appear thinner. To ensure that the tapers or haunches are long enough in proportion to the span, they preferably should be brought out to the point of dead-load inflection in the span (i.e. where a field splice would typically be located in a continuous span). Parabolic haunches at interior piers typically offer a smoother transition to the rest of the girder and are generally more visually pleasing. Haunches should typically not be deeper than 1.5 times the midspan depth of the girder to prevent the haunch from appearing too heavy in proportion to the midspan section. Conversely, a haunch that is too shallow does not save enough material to justify the added fabrication cost and is not aesthetically pleasing. The total angle at the point of haunch (i.e. between the haunches on either side of the interior pier) preferably should be between approximately 135 and 160 degrees to prevent the appearance of too sharp a haunch at the bearing point (Figure 3.1.39).

When haunched I-girders are employed in conjunction with skewed supports, significant drops are likely to occur between adjacent girders. Thus, the cross-frames would typically be detailed as parallelograms to follow the drops. The effect of these sloping cross-frame members should be considered in the analysis.

In variable web depth tub girders with inclined webs, the inclination of the webs preferably should remain constant to simplify the analysis and fabrication. Assuming a constant distance between the webs at the top of the tub, which is also preferred, along with a varying web depth, the width of the bottom flange must also vary along the length and the web heights at a given cross-section must be kept equal in order to maintain constant web slopes. As described previously, when a vertical curve must also be built into the web because of camber or roadway profile and camber, the establishment of the developed shape of the plate becomes more difficult; that is, the shape of the flat plate pattern from which the web must be cut. Experienced steel detailers and fabricators generally have software available though to establish the necessary pattern. It should be noted that a curved inclined web for a tub section can be cut from a flat plate as part of a cone shape. If, however, the slope varies, the webs are no longer developable and must be heated to conform to the desired shape.

Erection of variable web depth members is affected to some degree by their more complex geometry. However, these complications are generally considered minimal by most erectors. Therefore, erection considerations typically need not enter into the decision process as to whether or not variable web or constant web depth members should be used. An exception might be when the bridge is to be erected by incremental launching, in which case the use of constant web depth members is recommended.

As discussed above, the bottom flange of variable web depth members carries a portion of the vertical shear in the region of the sloping web. Thus, the force in the bottom flange in this region is increased due to the vertical shear component. The major-axis bending moment in this region is developed from the smaller horizontal component of the resultant bottom-flange force. Therefore, if the normal stress in an inclined bottom flange (without considering flange lateral bending) is determined by simply dividing the major-axis bending moment by the elastic section modulus, the bending stress in the flange will generally be underestimated. According to *AASHTO LRFD* Article C6.10.1.4, the horizontal component of the flange force can be determined as:

$$P_h = MA_f / S_x$$

Equation 3.1.10
AASHTO LRFD Equation C6.10.1.4-1

where:

A_f = area of the inclined bottom flange (in.^{2})
M = major-axis bending moment at the section under consideration (kip-in.)
S_x = elastic section modulus to the inclined bottom flange (in.^{3})

According to Reference 14, the normal stress in the inclined flange may then be determined as:

$$f_n = P_h / A_f \cos\theta$$

Equation 3.1.11
AASHTO LRFD Equation C6.10.1.4-2

where θ is the angle of inclination of the bottom flange with respect to the horizontal.

The vertical component of the flange force affects the vertical web shear. According to *AASHTO LRFD* Article C6.10.1.4, the vertical component of the flange force may be determined as:

$$P_v = P_h \tan\theta$$

Equation 3.1.12
AASHTO LRFD Equation C6.10.1.4-3

As pointed out in Reference 14, for fish-belly haunches, P_v is equal to zero near the supports. In regions of positive flexure with tapered or parabolic haunches sloping downward toward the supports, the vertical web shear is *increased* by P_v. For all other cases, the vertical web shear is *reduced* by P_v. The specification allows the Design Engineer to reduce the web dead-load shear by the vertical component of the flange force where desired and permitted by static equilibrium. Reduction of the live-load shear is not recommended in these cases because many combinations of concurrent shear and moment must be evaluated in order to determine the critical (or smallest) shear reduction.

In parabolic haunches, the downward slope of the bottom flange is larger at positions closer to supports. At interior supports, this change in the inclination of the bottom flange along with the compressive stress in the flange introduces a compressive distributed transverse force on the web (*14*). Therefore, *AASHTO LRFD* Article C6.10.1.4 recommends that transverse stiffeners be provided within these types of haunches with a spacing d_o not to exceed approximately 1.5*D*. Otherwise, the Engineer should check the stability of the web under this force.

The bottom flange of a variable web depth member is usually made horizontal in the vicinity of the bearings. Where this transition occurs, the vertical component of the inclined flange force is transferred back into the web as a concentrated load, which causes additional stress in the web and the web-to-bottom flange welds. Thus, additional local stiffening may be required in this area. According to *AASHTO LRFD* Article C6.10.1.4, additional stiffening is not required if the web local yielding provisions of *AASHTO LRFD* Article D6.5.2 (Appendix D6) are satisfied using a length of bearing *N* equal to zero. For compressive concentrated loads, the

provisions of *AASHTO LRFD* Article D6.5.2 generally govern relative to the web crippling provisions of *AASHTO LRFD* Article D6.5.3 when *N* is taken equal to zero. Again, smoothing out the transition with a "fish-belly" flange rather than providing a sharp transition can help to reduce the increase in web stress at these locations.

3.1.3.3 Substructure Considerations with Curved and Skewed Superstructures

3.1.3.3.1 Overturning and Thermal Forces

Curved alignments impact substructure design to a degree. The gravity-load reactions vary much more than in tangent bridges, which have rather uniform reactions on a pier or abutment, due to the effects of curvature. In general, reactions at abutments are largest under the exterior convex girder, while smallest under the concave girders (which are sometimes the exterior girders). The opposite is often found at interior piers; the largest reaction is often under the exterior concave girder. The reason for this is that the center of gravity of the entire bridge is eccentric with respect to a line drawn between the center of the cross-section at the ends, which may be causing an uplift tendency on the convex girder. This is important for pier design since an overturning load is created where on a straight bridge, one would not exist. This eccentricity of load causes a moment in the column of hammerhead piers. In Figure 3.1.41, the reactions at the inside (concave) girders at interior piers B and C are likely larger than at the exterior (convex) girders at those piers. This is due to the "overturning" tendency. The reactions at the outside (convex) girders at the abutments A and D are likely larger than the reactions at the inside (concave) girders. This is due to the curvature.

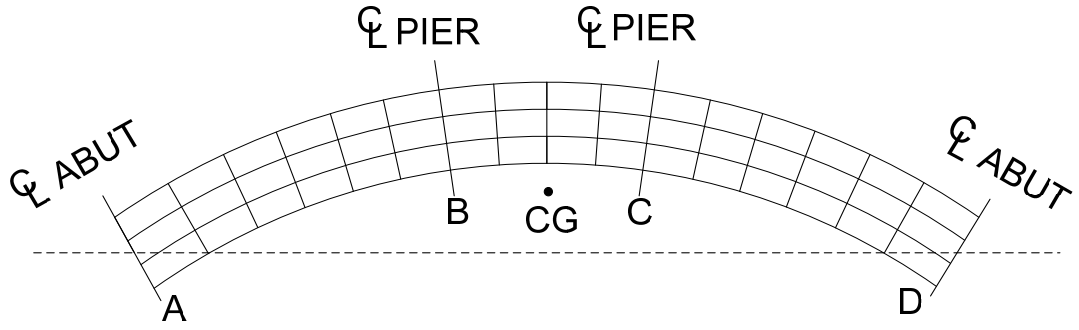
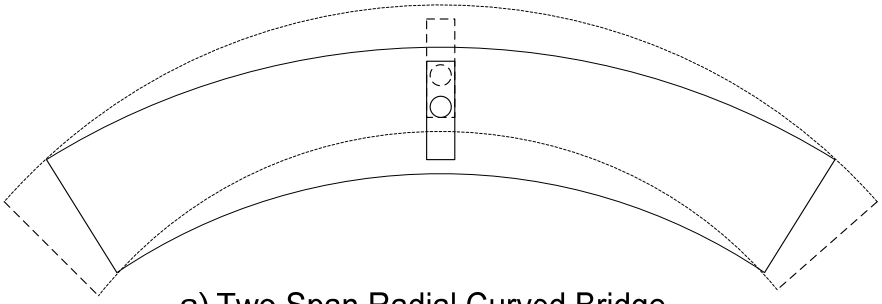


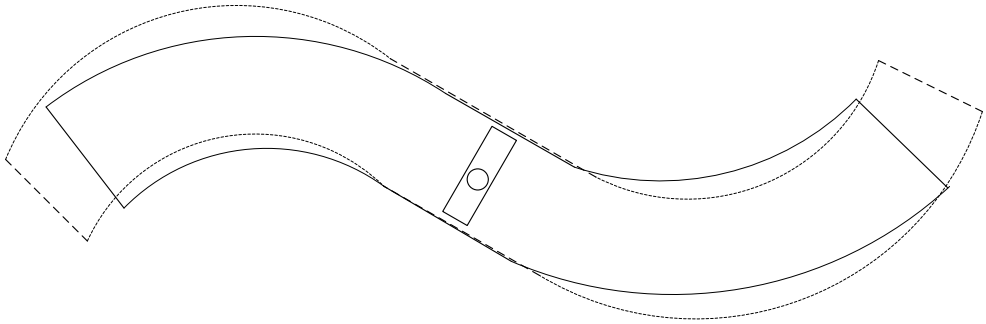
Figure 3.1.41 Curvature and Eccentricity Effects on Girder Support Reactions

Interestingly, this tends to counter the overturning effect caused by centrifugal forces, which produce heavier downward forces on the convex girder.

A second effect of curvature on the substructure design is associated with thermal loads. There is a lateral thermal force exerted on a pier if bearings supporting curved girders are arranged to be guided tangential with the girders or if bearings are fixed at a pier. The reaction on the superstructure is usually not great but it can provide a slight benefit when the lateral pier stiffness is relatively small, allowing the bridge to move laterally relieving the longitudinal movement somewhat. Interestingly, a curved alignment may be able to accommodate a longer expansion length than can a straight alignment. An S-shaped alignment has the unusual character of compensating for the lateral movement due to thermal expansion or contraction as seen in Figure 3.1.42.



a) Two-Span Radial Curved Bridge



b) Two-Span S-Shaped Curved Bridge

Figure 3.1.42 Thermal Expansion of Two-Span Curved Bridges with a Hammerhead Round-Column Pier

The impact of skewed supports on substructure design is usually more severe than is a curved alignment. Thermal forces can play havoc with substructures unless properly managed at design. Fundamentally, the difference between the thermal behavior of a skewed bridge and one with right supports is that the longest expansion length of a skewed bridge is diagonally from acute bearing to acute bearing, while the shortest expansion length is either transversely or diagonally from obtuse angle to obtuse angle. This leads to a twist of the bridge which is usually resisted by laterally restrained bearings. One can imagine a simple-span skewed bridge with two fixed bearings on the extreme girders at one end and a single guided

bearing on the center girder at the other support (Figure 3.1.43 -- perhaps not realistic but demonstrative). As the bridge expands, assuming a uniform temperature increase, the bridge will tend to twist as it expands from the two fixed bearings. The twist is resisted by the lateral restraint at the opposite end of the span as seen in Figure 3.1.43. The lateral reaction creates a couple at the opposite end with very large longitudinal forces. If the bearings at the extreme girders are released and the interior girders are fixed, the distance ΔL is smaller, but so too is the moment arm. The resulting longitudinal forces are reduced somewhat. Again, judicious arrangement of bearings can and does reduce these forces. These forces can be, and often are, large enough to break out anchor bolts and fail the bearings.

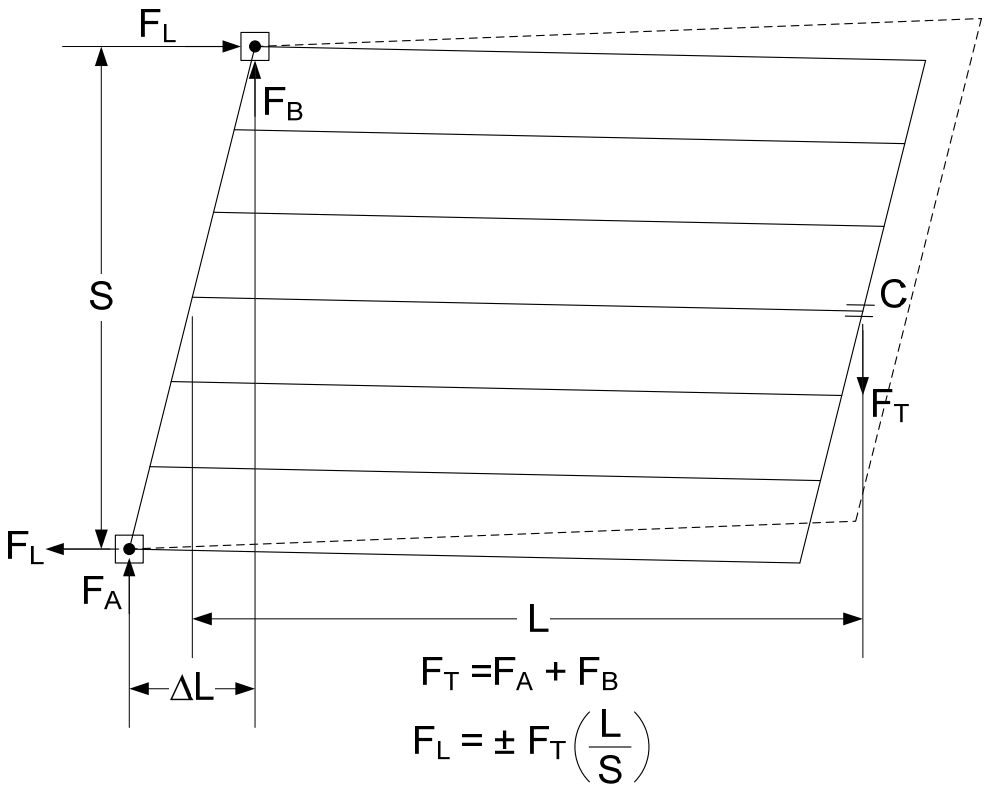


Figure 3.1.43 Twist of a Simple-Span Skewed Bridge Under Uniform Thermal Expansion & Resulting Lateral Reactions

It is important to investigate the bearing arrangement on skewed and/or curved bridges to minimize thermal forces on the piers while controlling the reacting forces on the superstructure. These issues are examined in greater detail in Section 2.2.3.

3.1.3.3.2 Substructure Form

The importance of the foundation and the pier regarding cost and aesthetics cannot be overstated. The first consideration is the geology. If a pile foundation is

anticipated, a small footprint pier is often economical to reduce the number of piles. This can be accomplished by drawing the superstructure loads to a single column (i.e. a hammerhead pier). If a spread footing is anticipated, a larger footprint pier is usually more economical.

A narrow pier tends to drive the superstructure design to also be narrow. A superstructure consisting of a single box girder requiring no pier cap leads to not only an economical pier design, but also to a very economical superstructure. There has been reluctance to use single steel box-girder cross-sections even though there has been a paucity of fractures in the U.S. of newer bridges constructed with modern bridge steels. There are many examples of single-girder bridges built in the U.S. The Storrow Drive Bridge in Boston over the Charles River is perhaps the largest such American structure. There are a number of similar, less noticeable bridges in the Boston Central Artery project, in Ft. Lauderdale, FL and in Seattle, WA.

Each situation presents unique challenges to the Design Engineer. To achieve a truly efficient steel design, the superstructure and substructure type must be viewed in unison with respect to economic, structural and aesthetic demands.

The type of substructure is defined by considering its many functions and the existing soil conditions. The substructure is designed for various specified combinations of the resulting vertical and lateral load effects. Different load factors are applied to each force effect to account for the probability of the combination of individual design loads occurring simultaneously. Further, maximum live loads are reduced from the maximum vertical live load in order to cause the maximum overturning moment; e.g. live load is applied in only one span or on only one half of the cross-section to obtain maximum overturning with concomitant reductions in the maximum vertical load. Vertical loads are primarily dead and live loads plus impact. Lateral loads include wind on the structure and on the live loads; braking; bearing friction; thermal forces; ice; stream flow; earth pressure; ship impact; debris; and seismic forces. Lateral loads are resisted by overturning moments and shear in the piers and abutments.

Overturning moments can cause an increase in the size of the foundation beyond that required for only vertical loads. An objective for an efficient foundation is one that requires minimal additional piles beyond that required for vertical loads alone. Transferring the vertical loads to the ground through a minimum number of pier columns is usually desirable, if not necessary, to accomplish this objective. For example, single-shaft piers carry the entire vertical load as well as resist lateral loads. The critical moment in the shaft is partially due to transversely and longitudinally eccentric vertical loads. Usually the maximum moment and maximum axial load are not coincident. In multiple-column piers, there are multiple or redundant paths for live loads, which in essence provide an uneconomical vertical load capacity in excess of the design vertical load.

Where appropriate, the uneconomical redundant load path dilemma can be avoided by considering the use of single shaft piers that support multiple girders with a pier cap, or optimally a single box girder without a pier cap.

3.1.3.3.3 Clearance Envelopes

Since the purpose of a bridge is to span an obstacle, there is usually some clearance requirement involved. For example, river crossings must account for flood volumes of water; intersections must account for traffic height and safety limits on columns; and navigation channels have specified clearances.

Highway grade separations require that the Engineer thread the structure through a space that provides vertical and lateral clearances without demanding too much grade on the overpassing roadway. These restraints limit the girder depth, which in turn limits span lengths. The lower roads limit placement of piers. The Design Engineer is compelled toward the use of poor span ratios, skewed supports, and often times, to some kind of support structure that straddles the roadway. These straddle-beam structures have been used in some congested metropolitan areas for decades. However, they are becoming more common throughout the nation as right-of-way becomes harder to obtain and the road system becomes more complex.

3.1.3.3.3.1 Straddle Beams

Straddle beams usually straddle a roadway that passes under the planned bridge. They rest on two or more columns. There are several varieties of straddle beams; they may be made of concrete or steel; they may be integral with the columns supporting them; they may support the girders on their top or integrally. Like single box-girder cross-sections, some are concerned about the use of non-redundant steel straddle beams, although the *AASHTO* fracture control plan with its demanding Charpy values for steel used in fracture-critical components and more stringent fabrication and inspection requirements has precluded any recent failures.

The simplest straddle beam is probably the single box beam supporting girders on bearings resting on the top of the box. Stability of the box is one problem. Typically four bearings, two at each support, are used. The stability of the straddle beam depends on its bearings not experiencing uplift. Tie-down bearings are usually not practical, but some have opted to build a bent with steel columns integral with the straddle beam. The options with girders on top of the straddle beam usually provide transversely free bearings to minimize lateral forces on the bent. However, some friction should be considered in designing the bent. One interesting aspect of design is the forces in the cross-frames at the straddle beam. Since the straddle beam deflects unequally under the girders as the bridge is built, significant load is transferred to the girders over the stiffest portions of the straddle beam. This affects the forces in the cross-frames as well as the moments in the girders, and to some degree, the straddle beam. This issue is examined more closely in the Case Study given in Section 2.5.6.

The advantage of these bents is their simplicity and speed of erection. This is particularly important where traffic is extreme.

A more common straddle bent is one with integral girders. This arrangement eliminates the concerns of stability once the bridge is constructed. Again, the straddle beam may be either steel or concrete. Again, the perceived advantage of concrete is that it is not fracture critical. The disadvantage is that the girder sections must be held in place while the concrete is formed, cast and until it has hardened. This time removes much of the advantage of steel construction. Casting off-site has been examined, but the weight of the beam is challenging. More typically, the steel straddle beam is used with the girders either penetrating it or abutted against it. Generally, bolting the intersections is preferred. Earlier, welding was employed, but it was learned that the steel working orthogonally created stress states leading to metal fatigue. Most commonly, the top flange is spliced over the straddle beam with heavy splice plates. Depending on whether the straddle beam bottom flange is below the bottom flange of the girders or intersecting it, the details vary. If a common flange plate is used, the biaxial stress state in the plate should be checked; *AASHTO LRFD* Equation C6.11.8.1.1-1 (Equation 3.2.110) is suggested for possible use in making this check. Web connections to the straddle beam are usually bolted with the bolts designed for shear and flexure.

AASHTO LRFD Article 6.6.2 requires that non-redundant fracture-critical members be identified on the plans and that they are fabricated according to the fracture control plan given in Section 12 of the *AASHTO/AWS D1.5M/D1.5 Bridge Welding Code*. Not infrequently, designers opt to use multiple plates bolted together to circumvent the redundancy issue. For example, two I-girders might be used as the box webs; the two independent girders would then be bolted together with common flange plates to form a box.

Cambering straddle beams and girders requires special attention. The straddle beam is usually erected without the girders and undergoes deflection prior to erection of the girders due to its own self-weight. The weight of the girders increases the straddle beam deflection further. When the straddle beam is long and flexible, addition of the girders may cause enough deflection that fit-up of the girders becomes a challenge. At any rate, camber of the girders must allow for the deflection of the straddle beam as loads are applied. This means that at the connection point, the girders should be cambered for the total deflection that they undergo due to the loads applied after connection of the girders to the straddle beam, minus the deflection of the straddle beam due to its own self-weight (i.e. prior to the erection of the girders) at that point. Within the girder span(s), the girder cambers should be similarly adjusted using a straight-line proration of the straddle-beam deflection (due to its own weight) at the connection point back to the adjacent support(s). If the adjacent support(s) is rigid, the deflection is zero at that point; if the adjacent support(s) is another straddle beam, the self-weight deflection of that straddle beam is used at that point for determining the straight-line proration. Fit-up of the girders to the straddle beam must account for the camber in the straddle beam at the time of fit-up.

Possible alternative fabrication procedures for closed-box straddle beams are discussed in Reference 2. The design of such straddle beams is assumed covered by the *AASHTO LRFD* Specifications.

3.1.3.3.3.2 Steel or Concrete Integral Cap Beams

Integral cap beams are pier caps that are integral with the girders. Usually they rest on a single pier column. They may be either concrete or steel. If they are concrete, they are generally integral with the pier column (Figure 3.1.44). If they are of steel, they are generally not integral with the pier column. As illustrated below, skewed piers often can be avoided with integral pier caps that are radial with the girders. This keeps the dropped cap out of the clearance envelope. The pier may have a variety of configurations. Typically, a steel cap is used to support the exterior girders, while the center girders are erected first and supported directly on the pier column. Unlike the straddle beam, the cap is often composed of separated sections bolted between the girders.

Alternatively, the cap is made of post-tensioned concrete. This requires that the steel be erected before the concrete cap is formed and cast. Usually, the post-tensioning is performed in two stages; first for dead load and second for live load. The two stages permit a higher post-tensioning force without crushing the concrete. An often overlooked issue with these caps is the Poisson effect due to the post-tensioning. The concrete is often highly stressed orthogonally to the stressing due to this effect, which can result in a longitudinal stress in the steel girders (*AASHTO LRFD* Article 3.4.1). Transverse reinforcing should be introduced to prevent cracking.



Figure 3.1.44 Single-Column Integral Concrete Pier Cap

Skewed Support versus an Integral Pier Cap

Figure 3.1.45 highlights three possible pier configurations for a skewed underpassing roadway or stream. Figure 3.1.45 Part A shows a skewed multi-column pier aligned with the roadway below. This configuration results in increased pier length and cost. Figure 3.1.45 Part B shows a multi-column pier aligned normal to the girders. This configuration may result in vertical clearance violations. Figure 3.1.45 Part C shows a single-column integral pier cap aligned normal to the girders. This final configuration eliminates the vertical clearance problems and allows for the elimination of the skewed support.

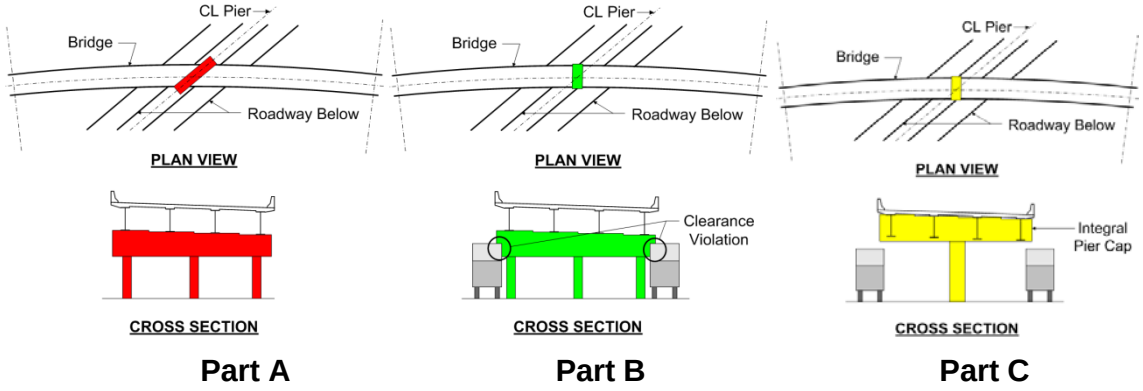


Figure 3.1.45 Possible Pier Configurations for Skewed Alignments

Figure 3.1.44 presents a photograph of the pier configuration depicted in Figure 3.1.45 Part C. This single-column integral pier cap is aligned normal to the girders. It eliminates the vertical clearance problems, and it also allows for the elimination of the skewed support.

3.1.3.3.4 Continuity – Integral Abutments

Most agree that bridge joints are a major factor affecting bridge maintenance. For this reason, many agencies have established policy stating that it is best practice to minimize the number of bridge joints. This policy has been carried to the point of elimination of joints at abutments by attaching the bridge to the approach slab in combination with an integral abutment.

Continuous structural units have become longer over the past two decades. Steel bridge structures up to nearly 2,000 feet long have been built in the U.S. without an intervening joint. Other structures of several hundred feet in length have been built without joints at their ends. Of course the critical issue is thermal movements. All bridges built with few or no joints are not without problems. Earlier, the advantage of long curved structures with relatively low transverse stiffness has been shown to have advantages in allowing greater expansion lengths. Design of the substructure

becomes even more important in these cases where substructure movement is important.

Bridges designed as jointless are popular in some agencies. They have the advantage of preventing water from corroding the ends of the bridge. There are several ways to detail such bridges. Typically, the bridge abutments are made integral with the superstructure. Thermal forces are transferred between the sub and superstructures via connection of the concrete diaphragms at the abutments. There is often reinforcing passing through the girder webs. Sometimes shear studs are added to the girder webs to assist in transferring the load. Design of the studs can be performed by treating the studs as a fastener group designed to develop the end moment in the girders. In the case of a fully integral abutment, piles are generally used. The piles are attached to concrete that acts as the endwall as well as the end diaphragm for the bridge girders. Hence, the ends of the girders act as nearly fixed-end beams resisting the rotation and translation of the girders. Piles are usually oriented in the weak direction parallel to the girders to minimize resistance to expansion and contraction. The piles bear laterally against the soil. The deck is often attached to the approach slabs to further hinder movement, or placed on some interface intended to permit movement when the bridge girders change length due to thermal movements. To properly model this arrangement in an analysis, the friction of the approach slab and the active resistance of the soil acting on the piles should be considered, as well as the flexural stiffness of the piles. The approach slab and the active soil resistance are usually modeled with foundation elements of the proper stiffness to represent the soil behavior. The piles are usually modeled with beam elements.

The effect of fully integral abutments on the girders is often substantial. Negative end moments and thrusts are created in the girders. These end moments and thrusts must be transferred from the girders into the concrete over a relatively short distance. This is done with shear studs. The number of studs can be determined from the force in the girders going into the concrete since it is known that the force at the end of the girder must be zero. Further, the negative moments create tension in the deck, which may cause significant cracking if the deck is not properly detailed. *The effect of thermal forces on a jointless bridge having integral abutments may be significant when the deck is removed on a warm day*.

Skewed abutments provide additional challenges to the Design Engineer when designing integral abutments. Severe bending may be created in the abutment itself due to its longitudinal component of force. This flexure also causes significant additional shear in the abutment that must be reinforced. The piles at the acute angle tend to lift up which increases the force on the piles at the obtuse angle. Hence, an increased number of piles are required. The shear connection also must be beefed up.

Semi-integral abutments are primarily composed of integral concrete end diaphragms, compressible backfill and moveable bearings in a horizontal joint at the

superstructure and a pile-supported abutment interface. A steel cross-frame or diaphragm is often provided to stabilize the girders prior to casting the concrete end diaphragm. Semi-integral abutments are less problematic on skews than are fully integral abutments. Semi-integral abutments do not require modeling of the supporting piles in the analysis. Instead, the superstructure/abutment interfaces are typically modeled with foundation elements. However, end moments are still developed in the girders that need to be removed by shear connectors. Shear forces in the concrete develop when moments in adjacent girders are different. As with fully integral abutments, the concrete forming the abutment must be inserted in the analysis model only for the proper analyses. Often the concrete is placed in the abutments after the steel and deck weights have been recognized by the girders.

3.1.4 I-Girder Sizing

This section will discuss sizing of I-girders, including discussions related to the selection of the steel grade(s), web proportioning and flange proportioning.

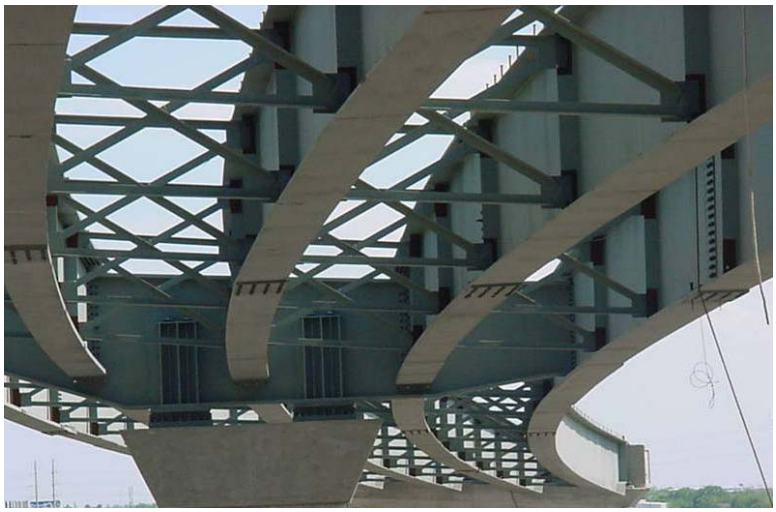


Figure 3.1.46 Curved I-Girder Bridge

3.1.4.1 Steel Grade(s)

The steel industry has developed some new structural steels available to the bridge market. The processes of producing the steels have changed in some instances, resulting in slight differences in availability. The newer higher strength steel, called high-performance steel (or HPS), comes in three strengths -- 50, 70 and 100 ksi yield steels -- with improved toughness and good weathering characteristics. The 50 ksi HPS should only be considered as an option where tough weather-resistant steel is required (e.g. in a fracture-critical application). The most common structural bridge steels in use in the U.S. are the traditional 50 ksi steel and the 50 ksi uncoated weathering steel.

All structural steels have the same Young's Modulus. This means that bridges built from higher strength steel designed to its strength level deflect more unless the structure is made stiffer. In the case of girder bridges, the girders must be made deeper. As discussed above, deeper girders of greater strength tend to have relatively slender flanges.

One way to take advantage of the greater strength is to use hybrid sections with 70 ksi HPS flanges and traditional 50 ksi steel webs. *AASHTO LRFD* Article 6.10.1.3 covers the design of hybrid sections. Designs utilizing 70 ksi compression flanges require closer bracing spacing than those utilizing 50 ksi flanges, potentially requiring more cross-frames/diaphragms. It was suggested earlier that a variable spacing can be applied to the bracing where it is needed without adding cross-frames/diaphragms. A 70 ksi compression flange over an interior pier might demand a closer spacing to take advantage of the strength of the steel. *A bracing spacing that allows only a 50 to 55 ksi factored stress in a 70 ksi flange is an inefficient design*.

It has been found in many instances that the use of 70 ksi HPS for the tension flange in the negative moment region in conjunction with traditional 50 ksi steel in the web and compression flange is the most economical option. Potentially large tensile stresses in the deck caused by the use of 70 ksi in a top tension flange create another issue that is not addressed in the specifications. Experience has shown that the use of one percent longitudinal deck reinforcing has helped to control much of the cracking in the deck when steel strengths of 50 ksi or less are used. If 70 ksi steel is used and a significant portion of the design stress is applied to the composite section, the computed longitudinal tensile deck stress can exceed 1 or even 1.2 ksi. Thermal stresses could raise this level even higher. There are no known investigations of this issue available to the authors at this time.

The use of 70 ksi flanges has particular benefits in curved and skewed bridges. The lateral bending stresses can be resisted by a 70 ksi flange while allowing approximately 50 ksi for the vertical bending stress. Hence, the stiffness of the bridge is not compromised by the use of higher strength steel.

Live load deflection limits are applied differently to curved bridges than to straight bridges. Individual girders should be checked for the allowable deflection based on their response as part of a system, as indicated in *AASHTO LRFD* Article 2.5.2.6.2. Usually the outside girder on the convex side deflects most. The deflection of the convex curved girder is greater than if the span were straight. Deflections of the less stiff 70 ksi girders are more problematic than if designed for 50 ksi. Live load deflection is discussed further in Section 3.2.4.2.1. Although not specified, checks on the individual deflection of individual girders should also be made for straight bridges with skewed supports and skew angles exceeding 20° from normal.

Dead load deflections are similar to live load deflections in that dead load deflections are greater when higher strength steel is used. In curved girders, this leads to more

"girder lean" in the positive moment regions. Lean in curved girders is more difficult to alleviate through special detailing of the cross-frames intended to introduce a reverse twist into the girders during the erection because the radii of the girders must be changed, which introduces stress. This issue is discussed in more detail in Section 4.1.3.1.3.

Fabrication of 70 ksi steel is slightly more expensive than the traditional bridge steels because different consumables are used in welding and the harder steel dulls drills faster. The base price of the steel is also somewhat greater than traditional steel. Hence, it should be used judiciously and where the higher strength can be used to advantage.

Availability of HPS is slightly different from the normal bridge steels. HPS over about two inches thick (check with the producers for the latest information) generally must be quenched and tempered and is available in lengths not greater than 50 feet (note that 100 ksi HPS is only available in lengths not greater than 45 feet). This means that HPS 50 ksi or 70 ksi plates over two inches in thickness should be limited to 50 feet in length without a section change. Typically such plates are employed at piers. Thus, shop splices should be introduced in the flanges within 25 feet of the interior-pier bearing line when HPS greater than two inches in thickness is used. Otherwise, the fabricator will be required to make full-thickness butt welds with no benefit in weight savings.

Although permitted by the specification (*AASHTO LRFD* Article 6.7.7.1), there is not a lot of experience in heat curving HPS as of this writing (2010). The alternative of cut curving HPS also has the disadvantage of scraping plate that is more expensive.

3.1.4.2 I-Girder Web Proportioning

3.1.4.2.1 Web Thickness

As shown in Figure 3.1.47, a limiting D/t_w ratio of 150 is specified for webs without longitudinal stiffeners in *AASHTO LRFD* Article 6.10.2.1. For webs with longitudinal stiffeners, the limiting D/t_w ratio is 300.

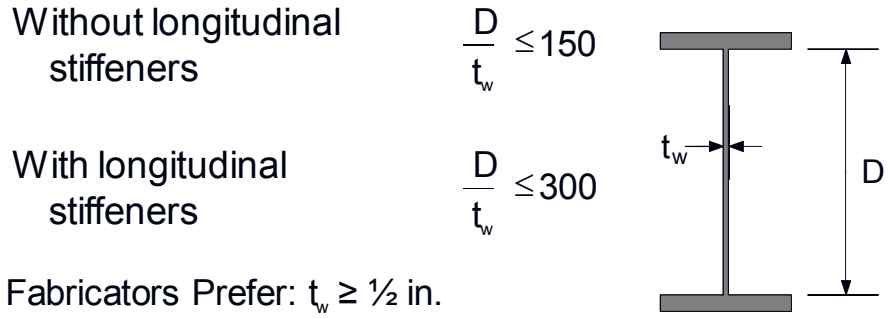


Figure 3.1.47 I-Girder Web Proportioning

where D is the web depth and t_w is the web thickness.

These limits are practical upper limits on the web slenderness expressed as a function of *D*, which served as an upper limit on the slenderness of unstiffened webs in previous versions of the *AASHTO LRFD Specifications* and in the *Standard Specifications*. In these Specifications, the slenderness limit for webs without longitudinal stiffeners was generally expressed as a function of the specified minimum yield strength of the steel and the elastic depth of the web in compression D_c (to accommodate singly symmetric sections). The limit exceeded 150 for girders with a specified minimum yield strength of 50 ksi or below. This limit was established as an upper bound below which fatigue due to excessive transverse web deflections was deemed not to be a consideration (*15, 16*). However, expressing the limit in this fashion makes the initial proportioning of the web more difficult as D_c is not known until the entire cross-section has been defined. Also, the true D_c is a combination of the depth of the web in compression for the non-composite and composite sections prorated based on the portion of load applied in the two conditions. Expressing the limit as a function of *D* allows for straightforward determination of web thickness in preliminary design. To control transverse web displacements in slender-web girders (i.e. girders with larger values of $2D_c/t_w$) at critical limit states, including the fatigue limit state, separate web bend-buckling and shear buckling checks are now specified in the Specifications, as discussed in Section 3.2.

By limiting the slenderness of transversely stiffened webs to 150, transverse stiffeners need only be provided where the web shear requires stiffeners; maximum transverse stiffener spacings up to 3*D* are permitted. By limiting the web slenderness to 150, the need for additional transverse stiffeners for handling (*17*) has been eliminated; stiffeners need only be provided for shear and can potentially be spaced up to the maximum limit of 3*D* for straight and horizontally curved girders. Second, by satisfying the slenderness limit of 150, the web bend-buckling check can be disregarded in the design of composite sections without longitudinal stiffeners in positive flexure after the section is composite. The web bend-buckling resistance F_{crw}, discussed further in Section 3.2.4.3.2.2, for such sections is generally close to or larger than F_{yc} at the strength limit state.

The slenderness limit of 150 is considered valid for sections with specified minimum yield strengths up to and including 100 ksi. Vertical flange buckling limits (*18*) are not considered in the *AASHTO LRFD Specifications*. For girders that satisfy the web slenderness limit of 150, the vertical flange buckling limits do not control unless F_y is greater than 85.0 ksi. Also, tests (*19, 20*) have indicated that the influence of the vertical flange buckling mode, or folding of the compression flange vertically into the web, on the nominal flexural resistance of the girder is small even when the web slenderness significantly violates the vertical flange buckling limits.

For deep girders, longitudinal stiffeners are sometimes employed. Generally they would be much more slender than the 150 limit for transverse stiffened webs. *AASHTO LRFD* Article 6.10.2.1.2 limits these webs such that their slenderness does

not exceed 300. Again, the limit is independent of the yield strength and D_c, which allows for simpler determination of appropriate web thickness. Even for longitudinally stiffened girders with webs that significantly exceed the limit of 300, tests (*19, 21*) have demonstrated that the nominal flexural resistance is not significantly affected by the vertical flange buckling failure mode. Extensive yielding of the compression flange in flexure preceded the vertical flange buckling failure. However, it should be noted that webs that have values of D/t_w larger than 300 are relatively inefficient, are likely to be more susceptible to distortion induced fatigue and are more susceptible to the limit states of web crippling and web local yielding discussed in *AASHTO LRFD* Article D6.5 (Appendix D6).

Fabricators prefer a minimum web thickness of ½" to reduce the deformation of the web and potential weld defects according to the *AASHTO/NSBA Guidelines for Design for Constructibility* (*2*). However, a minimum web thickness of 9/16" has been found to prevent shadowing of the transverse stiffeners on the girder web.

The web thickness over piers may have to be increased over the thickness provided in adjacent regions of positive flexure. This is particularly true if the concrete deck is considered effective in negative flexure at the service limit state, as permitted in *AASHTO LRFD* Article 6.10.4.2.1 when certain specified conditions are satisfied. The web bend-buckling check at the service limit state, specified in *AASHTO LRFD* Article 6.10.4.2.2 (and discussed in Section 3.2.4.3.2.2) will likely control the thickness of the web in these regions.

Depending on the thickness selected, webs may require so-called “partial stiffening” with transverse stiffeners provided in the panels near the abutments and interior piers. Transverse stiffeners are no longer required where the web shear is reduced below the shear-yield or shear-buckling resistance. The Design Engineer should remember that cross-frame/diaphragm connection plates may be considered to act as transverse stiffeners for shear design. Web shear design is discussed further in Section 3.2.7.

A useful guideline for determining the trade-off between adding more transverse stiffeners versus increasing the thickness of the web material is that approximately 10 pounds of web material should be saved for every 1 pound of stiffener material added. Generally, an unstiffened web with no transverse stiffeners (other than the connection plates) is not the most economical alternative. The optimal solution usually includes some stiffeners over the piers and perhaps near the abutments.

3.1.4.3 I-Girder Flange Proportioning

Sizing of flanges is one of the most important issues in obtaining economical curved girder bridges. Basic cross-section proportion limits for flanges of steel I-girders are specified in *AASHTO LRFD* Article 6.10.2.2. The limits apply to both tension and compression flanges.

3.1.4.3.1 Flange Width

The minimum width of flanges is specified as:

$$b_f \geq D/6$$

Equation 3.1.13
AASHTO LRFD Equation 6.10.2.2-2

where:

b_f = width of the flange (in.)
D = web depth (in.)

The cross-section aspect ratio, D/b_f, has a significant effect on the strength and moment-rotation characteristics of I-girders (*39*). Tests on I-sections with very narrow flanges have indicated nominal flexural and shear resistances below those given by the current and previous specifications. Limiting the aspect ratio, D/b_f, to 6 helps to ensure that post-buckling shear resistance due to tension-field action can be developed. *In many cases, a wider flange will be required based on other criteria*.

A minimum width of 12 inches is suggested to prevent flange distortion and cupping due to welding. Typically, somewhat larger minimum flange widths will often be desired for curved girders.

The controlling condition for the top compression flange in regions of positive flexure is usually the non-composite condition. Under this condition, the flange is designed to support its self-weight, the deck and lateral wind on the steel frame. The top flanges of the exterior girders are also designed to resist the lateral force caused by the overhang brackets supporting the wet overhang portion of the deck. The critical non-composite design moment is a function of the deck-casting sequence.

Loads applied to the overhang brackets attached to the flanges cause lateral flange moments. The overhang lateral moment in the convex girder is of the same sense as the lateral flange moments due to curvature. The top flange must have the capacity to resist the vertical and lateral moments.

Equation 3.1.14 is a suggested guideline regarding the minimum width of flanges in compression (Figure 3.1.48). This suggested guideline is based on the experience of erectors (*AASHTO LRFD* Article C6.10.3.4)

$$b_{fc} \geq \frac{L}{85}$$

Equation 3.1.14
AASHTO LRFD Equation C6.10.3.4-1

where:

b_{fc} = width of compression flange (in.)
L = length of girder shipping piece (in.)

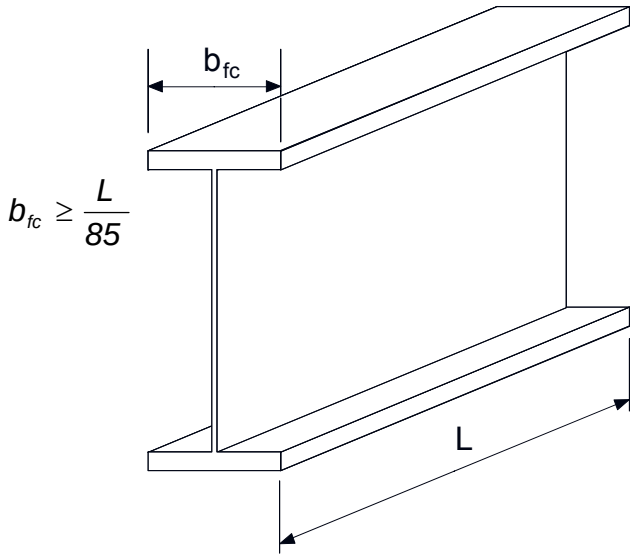


Figure 3.1.48 Field Section L/b Ratio

Satisfaction of this empirical guideline helps ensure that individual field sections are stable during handling in the fabrication shop and for the erector.

Equation 3.1.14 should be used in conjunction with Equation 3.1.13 to establish a *minimum* top-flange width.

Equation 3.1.15 from *AASHTO LRFD* Article 6.10.2.2 limits the width-to-thickness ratio of compression and tension flanges as follows:

$$\frac{b_f}{2t_f} \leq 12.0$$

Equation 3.1.15
AASHTO LRFD Equation 6.10.2.2-1

This requirement is taken from *AASHTO* Allowable Stress Design provisions. It provides a practical upper limit to control flange distortion due to welding.

Equation 3.1.16 from *AASHTO LRFD* Article 6.10.2.2 limits the ratio of the moment of inertia of the compression flange about its strong axis to the moment of inertia of the tension flange about its strong axis as follows:

$$0.1 \leq \frac{I_{yc}}{I_{yt}} \leq 10$$

Equation 3.1.16
AASHTO LRFD Equation 6.10.2.2-4

where:

I_{yc} = moment of inertia of the compression flange of the steel section about the vertical axis in the plane of the web (in.^{4}),

I_{yt} = moment of inertia of the tension flange of the steel section about the vertical axis in the plane of the web (in.^{4}).

This provision prevents the design of unusually unsymmetrical girders where the yield moment, $M_{y,}$ may in fact be larger than the plastic moment, M_p. Sections with an I_{yc}/I_{yt} ratio beyond the specified limits behave more like tee sections with the shear center located at the intersection of the larger flange and the web. Such sections may be particularly difficult to handle. Satisfaction of Equation 3.1.16 also ensures the validity of the lateral-torsional buckling equations (discussed in Section 3.2.6.4.1.2) for cases involving moment gradients.

Additional discussion related to efficient sizing of curved I-girder flange widths for fabrication is provided in Section 3.1.4.3.4.

3.1.4.3.2 Flange Thickness

The minimum thickness of girder flanges is specified in *AASHTO LRFD* Article 6.10.2.2 as follows:

$$t_f \geq 1.1 t_w$$

Equation 3.1.17
AASHTO LRFD Equation 6.10.2.2-3

Equation 3.1.17 ensures that the boundary conditions assumed at the web-flange juncture in the compression-flange local buckling and web bend buckling formulations within the *AASHTO LRFD* Specifications are reasonably accurate. This relationship also ensures that the flanges will provide some level of restraint against web shear buckling. This is only a lower limit, but is often exceeded. *The flange thickness should never be less than ¾ inches* (*2*).

Since the minimum width of plate available from the steel mill is 48 inches, the design is most economical when the entire plate width is utilized. To accomplish this, the Design Engineer should use a minimum number of plate thicknesses and steel grades on a project (Section 3.1.4.3.4). Curved girder bridges often lead to different demands on the girders in a cross-section and hence different flange sizes. Where practical, it is best to vary flange sizes in a cross section by varying the width, keeping the thickness constant.

Flange plate thicknesses are to a large degree dictated by the demanded flange. Although plate pricing from the mills is very complex and should not be a consideration of the Design Engineer, there are several useful limits that the Design Engineer should be aware of in order to keep the mill costs low. Plate thicknesses between 0.375 and 2 inches are considered standard. Thus, it may be good

practice, for example, to change a flange size from 2.25″ x 20″ to 2″ x 22.5″. The practical thickness limit is 3 inches, although the specification provides for thickness up to 4 inches. The 3-inch limit is based on continuous cast steel. Casters produce slabs that are 9-inches thick. Bridge steel toughness requirements necessitate that the plate thickness be reduced by a factor of three, or from 9 inches down to not more than 3 inches. Plate over 3-inches thick must be made by other more expensive processes.

Plate thicknesses should be specified in 1/8-inch increments up to 2½ inches in thickness, and in ¼-inch increments over 2½ inches in thickness (*2*).

The area of the smaller flange plate should not be less than one-half the area of the larger flange plate at welded flange shop splices. A number of states have this as a requirement. It is a reasonable way to control stress concentrations at the splices.

Further discussion related to efficient sizing of curved I-girder flange thicknesses for fabrication is provided in Section 3.1.4.3.4, including discussion related to the efficient location of flange-thickness transitions at shop-welded splices.

3.1.4.3.3 Additional Flange Proportioning Considerations

The first task is to determine where flange splices may be best located. The second task is to estimate the desired number of cross-frames in the span. The first task is performed early so that flange sizing need not be performed at regular increments along the whole span. Although the equations defining the limiting stresses are important, more mundane issues control much of the flange sizing of a well-sized girder. The strength or fatigue limit state usually controls the bottom flange sizes at points of maximum positive moment (for noncompact sections). The strength limit state usually controls the top and bottom flange sizes at interior bearings of continuous spans. Other flange plate sizes are usually best dictated by relative proportioning and fabrication efficiency or other limit-state criteria.

3.1.4.3.3.1 Flange Proportioning Considerations in Negative Moment Regions

A shop splice is almost always used off the pier to reduce the amount of steel. The thickness of the smaller plate is best defined at about one-half the thickness of the pier plate. The width is best held constant assuming that the fabricator will slab weld the flanges (Section 3.1.4.3.4). The smaller plates usually extend to the field splices. The flange plates in the pier field sections are usually controlled by the strength limit state; the service and fatigue limit state checks and constructibility checks usually are not critical.

There are at least three issues involved in determining the sizes of these plates. The first issue is cross-frame spacing. Spacing off the pier must be set to brace the bottom plate such that it can be designed to nearly its yield stress. The cross-frame spacing and the plate width define the lateral torsional buckling capacity. Wider

plates and smaller cross-frame spacings (for a given size flange) provide larger capacity.

The second issue is to find a pier plate that can be spliced down to half of its thickness while maintaining the nominal flexural resistance of the pier plate in the thinner plate. If the thinner plate is too slender, local buckling controls and the nominal flexural resistance will be reduced, making the plate inefficient. The remedy is to use a narrower, thicker pier plate. This may mean that the cross-frame spacing must be reduced to accommodate the narrower plate. It is simplest to locate the cross-frames near splice locations. Of course the smaller plate must have the capacity to handle the moment at the splice. Unfortunately, higher strength steels need stockier plates and hence more bracing to reach the potential capacity of the material. This significantly complicates the design when 70-ksi and higher yield-strength steels are used. The preceding approach is even more important when these more expensive steels are used.

The third issue is to select a plate thickness that will give efficient flanges in at least several of the girders in the cross-section. In straight girders with no skew, the problem is negligible since the girders in a span are most often the same. In curved girder bridges and in some bridges with skewed supports, this issue is more complex. The Design Engineer will find that changing the width of a flange rather than the thickness is likely to provide the most efficient design if it is desirable to change the capacity of the girders within a span (Section 3.1.4.3.4),

Lateral flange bending occurs when either curvature or skewed supports are encountered. Lateral flange bending due to curvature is a function of the square of the cross-frame spacing (Section 2.3.2). Lateral bending increases with the square of the increase in spacing. The one-third rule equations given in the *AASHTO LRFD* Specifications (Section 3.2.2.1) reduce the flange capacity for vertical bending in proportion to one-third of the squared spacing. Cross-frames are often discontinued near skewed supports to avoid complex detailing at the bearings. This discontinuity may cause severe lateral flange bending. There are no known algorithms to solve this issue. Trial and error is needed.

Lateral bending moments should be re-estimated when the cross-frame spacing is changed. This can be accomplished in curved girders by multiplying the original lateral moment by the square of the ratio of the new spacing by the old spacing. A re-analysis is required to obtain lateral flange moments if a staggered cross-frame arrangement is used.

Top-flange sizes in regions of negative flexure are typically controlled by tension-flange yielding at the strength limit state. For girders that are composite throughout their length, the longitudinal deck reinforcement (which must satisfy the minimum one-percent longitudinal reinforcement requirement specified in *AASHTO LRFD* Article 6.10.1.7) within the effective deck width can be included when calculating the composite section properties in these regions. As a result, a top flange with an area

slightly smaller than the area of the bottom flange can be assumed. Also live load stresses and stress ranges for fatigue design can be computed assuming the concrete deck is effective for both positive and negative flexure. This results in a significant reduction in the computed stress range at and near the top flange. The bottom-flange sizes in these regions are typically controlled by either the flange local buckling or lateral-torsional buckling resistance at the strength limit state. Initial trial flange sizes in these regions are primarily educated guesses based on experience. Often, depending on the span arrangement and other factors, the flanges may be somewhat wider than the corresponding flanges in regions of positive flexure. Flange width transitions should be made at the field splices (Section 3.4.1.3.3.3). Changes in the top-flange width can lead to some inconveniences with respect to the deck forming, but these problems are not insurmountable and are relatively minor when compared to the overall economy of the girder design. Other limit state verifications typically do not control in these regions and should be checked last.

3.1.4.3.3.2 Flange Proportioning Considerations in Positive Moment Regions

The flange plates in the positive moment region are easier to design. Design of the top flange (compression) is usually controlled by constructibility; design of the bottom flange (tension) is usually controlled by either strength or fatigue limit state checks (for noncompact sections). The critical parameters in the design of the top flange are flange width and cross-frame spacing. The design stress in the top flange is the sum of the stresses due to the loads applied to the non-composite and composite sections. Lateral flange moments are only considered for the non-composite case since the flange is encased in concrete when the section becomes composite and lateral flange bending cannot be mobilized.

Preliminary analysis gives the moments at the point of maximum positive moment. It is sufficient to design the flanges for maximum moment and check any splice points. Consideration of the moments due to the deck staging is necessary, particularly in the end spans of continuous units, as discussed in Section 3.2.3.2. Lateral flange moments from the overhang brackets acting on the exterior girders also need to be considered as discussed in Section 3.2.3.3.

Preliminary sizing of compression flanges in the positive moment regions of short spans may give small flanges that require close cross-frame spacing to reach an efficient critical stress. Rearranging or addition of a row of cross-frames may be of some benefit, but a larger flange is often most efficient. The flange plates in longer spans are larger so cross-frame spacing is less critical and the present provisions allow the spacing to increase without a numerical limit.

Overhang bracket moments may be problematic leading to reduced cross-frame spacing. Large overhang loads may indicate that the overhangs are too large and increasing the girder spacing may be the best solution (Section 3.1.2.5). This is particularly true if the exterior girder moments are significantly larger than the moments in the interior girders. Properly recognizing the effect of barrier loads leads to larger moments in the exterior girders. Live load action in the exterior girders is

often greater than in the interior girders. Efficient girder spacing was discussed earlier in Section 3.1.2.4.

Modern software makes it easy to modify plate sizes based on an analysis. However, the important part of preliminary sizing is the proportioning of flange sizes along the span to ensure that the moments are approximately correct for resizing. Final size of the top flange and/or the spacing of the cross-frames/diaphragms in these regions will be controlled by either local buckling or lateral torsional buckling.

For exterior girders, which usually control, the critical construction condition will most often be the combined vertical and lateral bending stress in the top flange due to the effect of the deck-casting sequence plus the deck overhang loads. Therefore, it is recommended that the final top-flange size and cross-frame/diaphragm spacing in these regions be determined based on this condition, and then subsequent design verifications be made at the strength, fatigue and service limit states, as applicable. All these design verifications at the various limit states are discussed in greater detail in Section 3.2.

The controlling limit state for the design of bottom flanges in tension in these regions depends on whether the section qualifies as a compact or noncompact section. In horizontally curved bridges, sections in positive flexure must be treated as noncompact sections at the strength limit state. Sections in severely skewed bridges should also be treated as noncompact sections. For a noncompact section, the design of the flange will typically be controlled by tension-flange yielding at the strength limit state. Typically, for composite construction, the bottom flange will be somewhat wider than the top flange. In certain cases, the size of the bottom flange may have to be increased from this level in some areas due to stress-range limitations at the fatigue limit state at certain critical welded details (e.g. cross-frame/diaphragm connection plate welds to the bottom flange near points of permanent load contraflexure). Service limit state verifications will not control for noncompact sections in positive flexure under the load combinations specified in *AASHTO LRFD* Table 3.4.1-1. Constructibility verifications on the bottom flanges will typically not control in these regions.

There are usually a number of additional splice locations in large spans. For example, frequently it is found to be efficient to splice the bottom flange near abutments. The same objectives as described above are used to keep flange width constant within all field sections where slab welding is anticipated.

AASHTO LRFD Article 6.6.2 specifies that all primary longitudinal superstructure components sustaining tensile stress under the Strength I load combination be designated on the plans (to indicate where Charpy V-notch testing of the material is required). The top flange tension region extends into the positive dead load region some distance due to live load which overcomes dead load.

3.1.4.3.3.3 Flange Proportioning Considerations at Field Splices

Field splices are usually bolted although some states permit field welding. The design of bolted field splices for flexural members is discussed in Section 3.3.7. *AASHTO LRFD* Article 6.10.1.8 requires that the ultimate strength of the net section of the bolted joint be checked at the last row of bolts in the splice (refer to Section 3.2.6.1.3 – Equation 3.2.72) in order to prevent the possibility of net section fracture. This provision should never be allowed to control the plate thickness at a splice. When this requirement appears to control, the number of bolt lines can be reduced (note however that *AASHTO LRFD* Article 6.13.6.1.4a requires that there be at least two row of bolts on each side of the web), or the bolts lines may be staggered. This provision seems to be more critical at bottom flange splices of box girders.

There is no structural reason to maintain a constant flange width over an entire span. In areas where there is anticipated significant pedestrian traffic under the bridge, it may be desirable to employ a constant width bottom flange to improve the looks of the bridge. This choice is a relatively expensive choice in some instances because the *b*/*t* requirements may force the designer to use thicker plates than required. The sudden change in flange width can be softened by using a radiused wider plate or by tapering the wider plate to the narrower width. The top and bottom flange widths at a section are often different.

It may be best to change the width of the flanges and keep the thickness constant at the field splice to avoid the need for a filler plate. They add some to the cost and additional bolts are required to develop these plates (Section 3.3.7.4.2). The savings may not justify the effort, except if the splice is repeated a number of times.

3.1.4.3.4 Sizing Flanges for Fabrication

As a practical matter, fabricators order plate for flange material from the mills in widths 48 inches and above; typically, the most economical plate size to buy from a mill is between 72 and 96 inches. Plate with additional width and length is ordered to account for cutting (about 1/8 inch per cut between plates and along sides), plate sweep tolerance, and waste (about ½ inch on each outside edge). For example, a plate 74 inches wide might be ordered to cut five 14-inch-wide flange plates.

It is not economical to design flanges such that something less than 48 inches in width of a given grade and thickness of plate material will be required. Flanges should be designed so that the material can be cut from plate of a single plate of given grade and thickness, preferably between 72 and 96 inches wide, even where girder flanges vary from girder to girder. *In other words, size flanges so that as many pieces as possible can be obtained from a wide plate with minimal waste*. Where cut curving is to be employed, consider the flange offset due to curvature. The cut curving process is discussed further in Section 4.1.2.1.1.

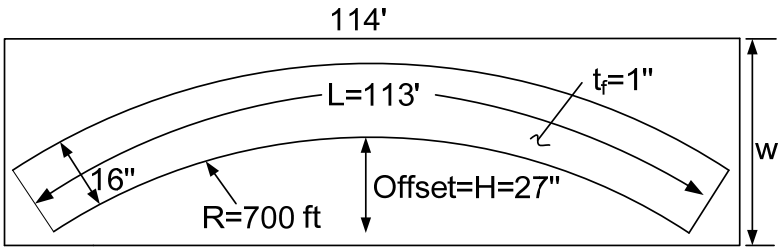
To minimize waste, it is also important to limit the number of different flange plate thicknesses specified for a given project. Larger order quantities of plate cost less, and minimizing the number of different thicknesses simplifies fabrication and

inspection and reduces mill quantity extras. For curved-girder flanges it is especially important to minimize the number of thicknesses of plate that must be ordered to minimize waste, in particular where cut curving is employed. *Thus, re-use flange thicknesses where possible in the design and adjust the flange width accordingly, while preferably maintaining constant top and bottom flange widths within a given field section. Also, as mentioned previously, it is preferred to select flange thicknesses in at least 1/8-inch increments up to 2½ inches and in ¼-inch increments over 2½ inches, and to limit flange thicknesses to 3 inches or below if possible*.

Fabricators will either weld the shop splices in the individual flanges after cutting them to width, or utilize slab welding, which is the process of butt-welding wide plates of different thicknesses together from which individual flanges may be stripped. Stripping the individual plates from a single wide plate allows for fewer weld starts and stops and results in only one set of run-on and run-off tabs. The process of slab welding is discussed in detail in Section 4.1.2.1.3.

The Design Engineer should be aware if the fabricator plans to use slab welding and if so, where, as it can affect the sizing of the flanges. If the use of slab welding is expected, it will be used only within a field section. The process is most often employed for the pier sections. When utilized, the flange widths for an individual girder must be kept constant within the field section. Necessary changes in flange widths can be made at field splices.

Figure 3.1.49 demonstrates the amount of scrap generated when a 1″ x 16″ curved flange 113-ft long with a 700-ft radius is cut from a single plate. The offset, H = 27 inches, is calculated using the equation from Section 1.1.5. The amount of scrap generated is 12,458 lbs of steel, or twice the weight of the flange. If flanges from all four girders in the example bridge are cut from individual plates, the amount of scrap generated is 49,832 lbs of steel.



Allow 3 in. for cutting and plate camber

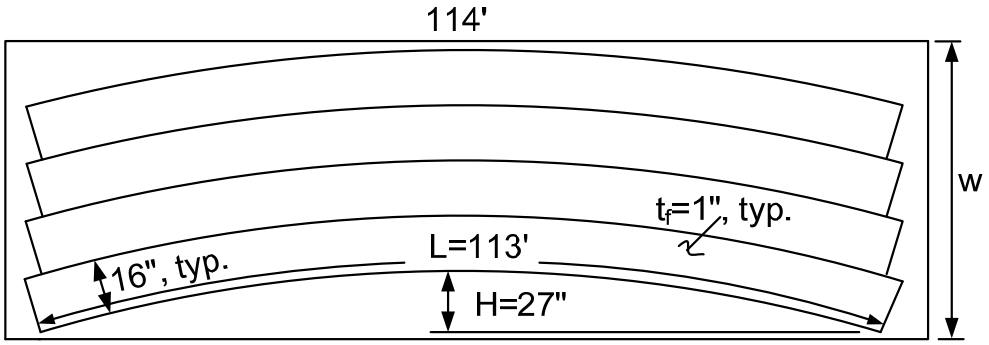
w = 27″+16″+3″ = 46″ (min. plate = 48″)

Plate wt. = (48″)(1″)(114′)(3.4 lbs/in^2/ft) = 18,605 lbs
Flange wt. = (16″)(1″)(113′)(3.4 lbs/in^2/ft) = 6,147 lbs
Scrap = 12,458 lbs

Scrap from 4 flanges = 4 x 12,458 = 49,832 lbs

Figure 3.1.49 Scrap Calculations – Curved Flange Cut from a Single Plate

Figure 3.1.50 reviews the calculation of the amount of scrap generated if four such flanges are nested and cut from a single plate. Nesting is the technique of laying out cutting patterns on a plate to minimize scrap. The individual flanges will be heat curved slightly to different radii.



w = 27″+(16″x4)+3″ = 94″

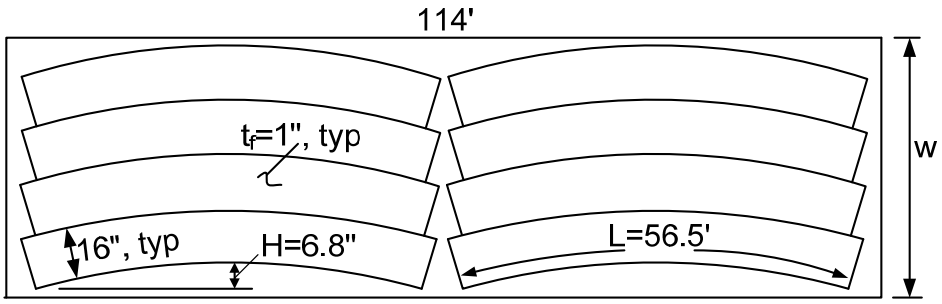
Plate wt. = (94″)(1″)(114′)(3.4 lbs/in^2/ft) = 36,434 lbs
Flange wt. = 6,147 lbs x 4 = 24,588 lbs
Scrap = 11,846 lbs

Figure 3.1.50 Scrap Calculations - Nested Curved Flanges Cut from a Single Wide Plate

The amount of scrap generated is reduced from 49,832 lbs when the flanges are cut from individual plates to 11,846 lbs.

All flanges in the section must have the same thickness.

Figure 3.1.51 shows a pattern that provides eight half-length flanges of the same size. This pattern requires four welded flange splices. Note that the offset is only 6.8 inches. The amount of scrap from this pattern is reduced to only 4,094 lbs, or a savings of 7,752 lbs over the scrap from four full-length flanges nested on a single plate. The savings at 40 cents per pound is $3,100. The fabricator may only choose this option if the design uses equal-thickness flanges.



Assume 8 half-length flanges are taken from a single plate – flanges to be spliced

$$w = 6.8'' + (16'' \times 4) + 3'' \approx 74''$$

Plate wt. = $(74'')(1'')(114')(3.4\ \text{lbs/in}^2\text{/ft}) = 28{,}682$ lbs
Flange wt. = 24,588 lbs
Scrap = 4,094 lbs

Figure 3.1.51 Scrap Calculations – Nested Half-Length Curved Flanges Cut from a Single Wide Plate

Table 3.1.4 provides a summary of the scrap generated by each of the three cut-curving options presented on the preceding three figures.

Table 3.1.4 Summary of Cut-Curving Options

Option	Description	Scrap (lbs)
1 (Figure 3.1.49)	4 individual plates	49,832
2 (Figure 3.1.50)	4 flanges from single plate	11,846
3 (Figure 3.1.51)	8 half-length flanges from single plate (with splice)	4,094

Dividing the scrap savings of 7,752 pounds between Options 2 and 3 by the four welded shop splices that must be introduced in the flange plates in Option 3 yields a scrap savings per splice of 1,938 lbs. This savings may be enough to justify the introduction of the welded splices.

This example demonstrates that cutting four flanges from a single plate significantly reduces scrap. Long constant-size plates, as often found in the positive moment regions, may be spliced by the fabricator to further reduce scrap. The Design Engineer may change plate size in cases where shop splices are anticipated for economy to take advantage of the splices.

Figure 3.1.52 shows how nested curved flange plates can be laid out for slab welding. This layout can only be employed by the fabricator if the Design Engineer has planned ahead. Note that the butt splices are nearly equidistant from the pier, but the length of the pier plates need not be equal on both sides of the bearing.

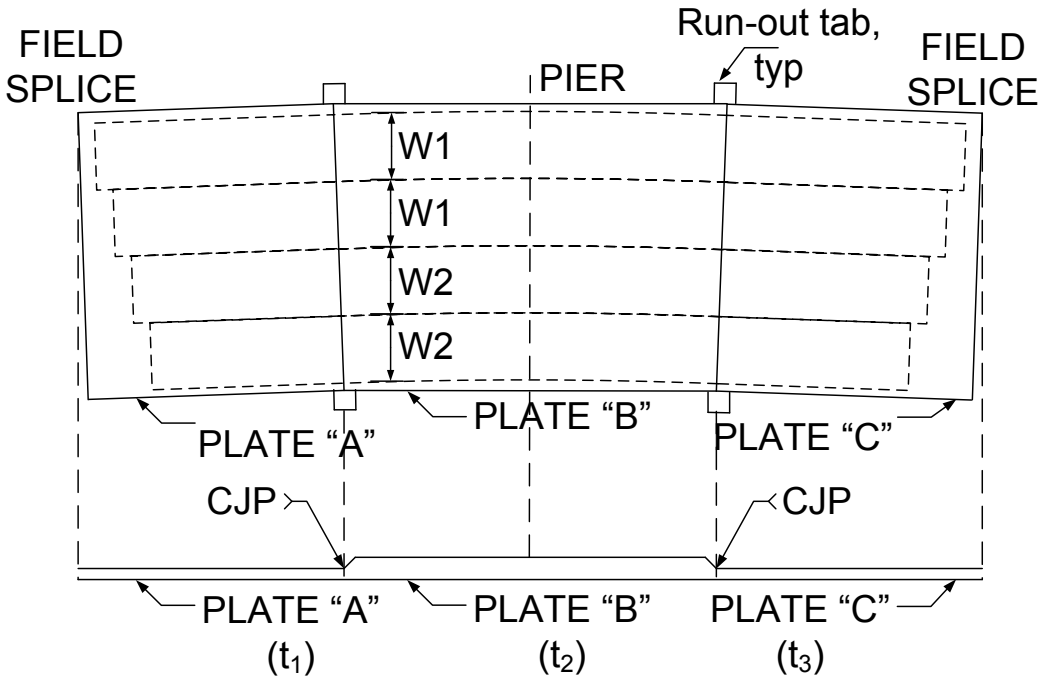


Figure 3.1.52 Nesting for Cut-Curving – Pier Sections

Slab welding can only be used when flange plates have the same thickness, but they may have different widths as long as the spliced plates in each girder have the same width as the pier plate.

Four flanges from either Plate "A" or "C" are best kept to about the same length to minimize scrap. Of course, Plates A and C need not be the same length.

It should be noted that the pier sections of Girders 1 and 2 and of Girders 3 and 4 in the I-girder design example (Section 5.1) were each designed according to the above recommendations to allow for efficient nesting for possible slab welding and cut curving (refer to the girder elevations on the fold-out plan sheets provided in Section 5.1). In this particular case, because of the relatively sharp radius and skew, it was not efficient to nest the flanges for all four girders on one set of plates.

If heat curving is employed to fabricate the girders, the pier-section flanges are likely to be slab welded in the straight condition as shown in Figure 3.1.53. The heat curving process is discussed further in Section 4.1.2.1.2.

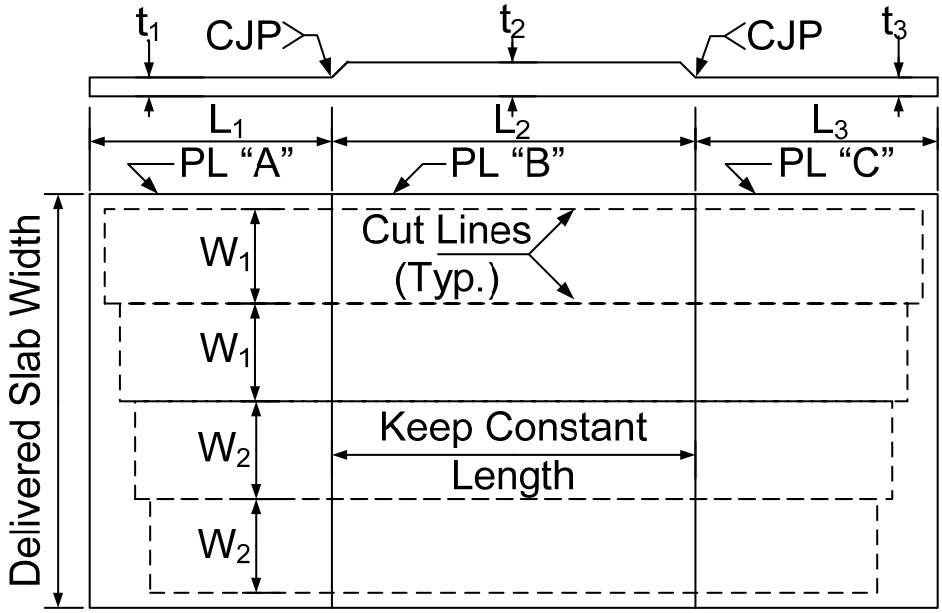


Figure 3.1.53 Nesting for Heat Curving – Pier Sections

The girders will be curved after fabrication. The same recommendations regarding flange-plate length, width and thickness discussed in the preceding paragraphs for cut curving apply.

The Design Engineer might well consult with fabricators that may bid the work regarding their preferences that might affect cost. Most fabricators are helpful in this regard. The information may be contradictory at times and the Design Engineer must be aware of suggestions that make the project unique to one fabricator.

Welded transitions in flange thickness are preferred over transitions in width. The design plans should consider allowing the option to move a shop splice, subject to the approval of the Design Engineer. When evaluating such a request, the Design Engineer must consider the effect of the longer thick plate on deflections. Usually a change in the location of a splice does not change deflections significantly. However, removal of a welded splice may have a pronounced effect on deflections.

Parameters affecting the cost of shop-welded splices vary from shop to shop and for a number of subtle reasons. Reference 2 provides a table of estimated equivalency of weight savings per inch of butt weld to flange material to aid in the evaluation of flange shop splices (Table 1.5.2.A). Roughly, a butt weld costs 1,000 pounds of

material. The Design Engineer is always advised to consult a fabricator whenever practical. The maximum length of flange plate is optimally about 80 feet or less.

Typically, no more than three different flange sizes are necessary in a field section.

3.1.5 Box Girder Design

3.1.5.1 Box and Bridge Cross-Section Configuration

Box and bridge cross-section configuration is the most critical issue in the design of box girder bridges. The shape and number of boxes in the cross-section is central to an efficient and aesthetic bridge. Traditionally, *AASHTO* provisions have limited the box and bridge cross-section configuration because the live load distribution factors for boxes were developed based on a limited range of parameters. The efficient cross-section usually lies outside of these limitations. Fortunately, when a refined analysis is used, the live load distribution is not dependent on wheel load distribution factors; hence the Design Engineer is freed up to select a more economical cross-section. This usually entails fewer box girders. The girders may be wider or narrower than the spacing between them.

Steel box girders are used as stringers, as straddle beams and in various other applications. Boxes may either be closed (steel on four sides), as shown in Figure 3.1.54 Part A, or open top tub sections, as shown Figure 3.1.54 Part B. Closed boxes are generally employed as straddle beams in the U.S. Tub girders are used as stringers with a composite deck attached to the top flanges. The tubs generally have lateral lacing connecting the top flanges to form a pseudo box that is able to resist torsion before the deck hardens.

In many other countries, closed box girders are more common, but OSHA regulations tend to make them expensive in the U.S. Some of the earliest box girders in the U.S. were the closed type. Others had closed sections in the negative moment regions and tub sections in the positive moment regions. Over time, the tub section has become the dominant steel box configuration in the U.S.

Typically, box-stringer webs are inclined so that the bottom flange is as narrow as practical. *AASHTO LRFD* Article 6.11.2.1.1 suggests that the taper on the webs should not exceed 1-to-4.

The composite deck acts as the box top, closing the tub and forming a box. There are certain cases denoted in the specifications that permit lateral bracing to be eliminated. In these cases, the tub acts as an open section until the deck hardens. Other sections, such as boxes formed with truss-type webs, with pipe flanges or multi-cell boxes are not addressed in the *AASHTO LRFD* Specifications. I-girders connected with top and bottom lateral bracing act as a closed-box section and may be treated as such. This situation was discussed in Section 3.1.2.9.1.1. Hence, a composite I-girder cross-section with one or more bay(s) of bottom lateral bracing may be more accurately analyzed by treating each pair of I-girders as a box section.

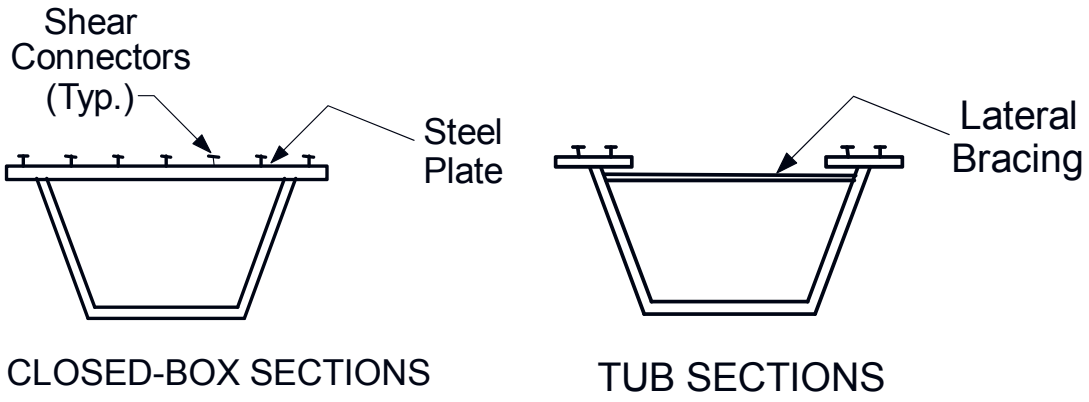


Figure 3.1.54 Box Girder Types

Closed-box sections are defined in the *AASHTO LRFD* Specifications as flexural members having a cross-section composed of two vertical or inclined webs enclosed at the top with a steel plate. The top plate typically acts as deck forms between the webs. A closed steel box may have a cost advantage over a laterally braced tub when torsion is very large.

A closed box girder has the advantage of being hermetically sealed. Experience has demonstrated that corrosion inside of closed steel box sections is insignificant when the box is hermetically sealed. The sections need not be hermetically sealed to prevent corrosion of the interior if provision is made for drainage and air circulation. Tub girders cannot be hermetrically sealed because moisture may enter through the concrete deck. However, corrosion of the interior of tub girders has been shown to be minimal when the tubs are adequately drained and ventilated.

Trapezoidal tub girders, as depicted in Figure 3.1.55, are the most popular steel box girder configuration in the U.S. A full-length top lateral bracing system must be provided for curved tub girders to form a pseudo-box to ensure that the member acts as a torsionally closed member for non-composite and composite loads. Painting the interior of tub sections a light color facilitates inspection to allow for easier detection of any fatigue cracks. Light colored paint also reduces solar-caused temperature gain of the tub before the deck forms are installed. The paint quality need not match that normally used for exterior surfaces, particularly when provisions are made to drain and ventilate the interior of the box.

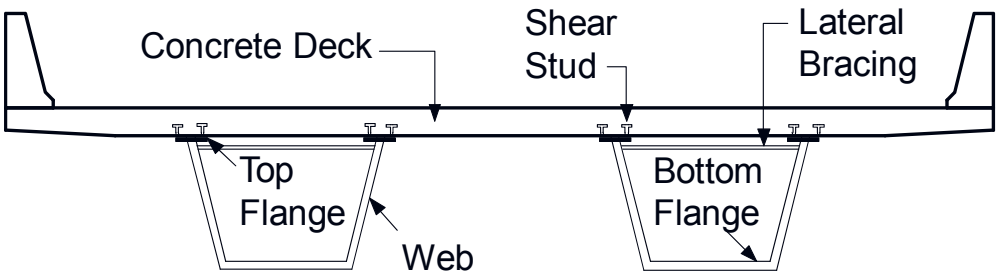


Figure 3.1.55 Trapezoidal Tub Girders

One reason that tub girders are popular is that they permit a wide spacing between webs on top and a relatively narrow steel flange at the bottom.

Box-girder bridges typically employ multiple single-cell steel boxes as shown in Part A of Figure 3.1.56. However, single-box bridges as shown in Part B of Figure 3.1.56 are frequently economical and have found application in numerous ramp bridges. There are very few multi-cell steel box bridges in the U.S. The specifications do not address this configuration. One of the few such structures in the U.S. is the ramp structure on the western side of the Fort Duquesne Bridge in Pittsburgh, Pennsylvania, which was constructed in the late 1960s. Analysis of a multi-cell single box requires consideration of the torques in adjacent cells and the complex addition of torsional and flexural shears. Fabrication, shipping and erection of these structures are also difficult. The use of a nearly full-width bottom flange required by these structures is rarely economical.

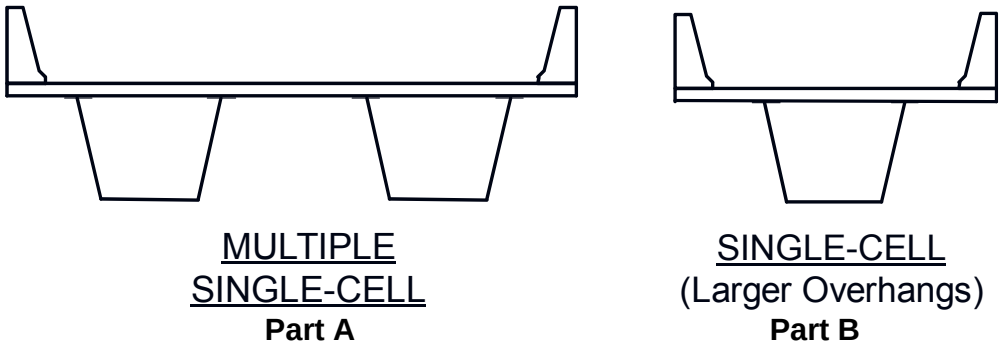


Figure 3.1.56 Box-Girder Cross-Sections

Single (one-cell) box girders are often found economical when they can be used in place of two boxes. The single box has been found to be very competitive with multi-stringer I-girder bridges. The economy of single-box cross-sections results from reduced fabrication, reduced steel and simpler erection. Further, a single box carries all of the live load regardless of the transverse position of the load. The torsional stiffness of the box transfers the load to the box. The torsion is carried predominately by shear, which is capable of transferring the loads from the outside of the bridge to the central box girder. In a multi-girder section, the girders carry

different portions of the live load depending on where the live load is placed. Since the single box carries all of the dead load and live load, the ratio of dead to live is usually greater than if multiple girders are used. This results in a design that is less susceptible to fatigue. Further, the substructure supporting a single box is more economical than a wider redundant substructure likely required when more than one box is used in the cross-section.

The issue of redundancy is always raised with a single box girder cross-section. Depending on circumstances, a single box may be non-redundant. Most of the discussion revolves around the potential of a brittle fracture of the steel. If a fracture should occur in a continuous-span single box bridge, failure could occur if the box is overstressed at the piers. However, modern bridge steels have proven to be quite ductile and no brittle fractures have been reported in steels that are twenty years or less in age. Single box sections are permitted in the *AASHTO LRFD* Specifications without limitation; shear due to St. Venant torsion and cross-section distortion stresses must be considered. However, the Federal Highway Administration may not share fund these bridges. The steel box must be positioned in a central location with respect to the cross-section, and the center of gravity of the dead load should be as close to the shear center of the box as possible. The use of single box cross-section needs two bearings at some supports for stability and equilibrium.

As with prestressed concrete box-girder bridges, a transversely post-tensioned concrete deck may be used when large deck overhangs or girder spacings are employed. This type of construction is used in Europe; it has not been employed in the U.S. at this time.

A bridge width that is too great for a single box may be designed with a minimum number of boxes. The Macmillan Yard Bridge, Toronto, Canada has a cross-section with a 100-foot vaulted deck resting on two steel box girders. The span between the boxes is approximately 30 feet. Overhangs are approximately 15 feet. This vaulted deck was transversely post-tensioned as a prestressed concrete box girder bridge might have been built. Vaulting permits straight (undeviated) transverse strands to be effective in positive and negative bending. This particular bridge was bid successfully against a similar post-tensioned segmental concrete design. The Storrow Drive Bridge across the Charles River in Boston is another example of a single-box steel bridge carrying a wide deck (approximately 80 feet in width). The deck on this bridge is supported on transverse floor beams and is not post-tensioned.

A box cross section is more economical with fewer narrower boxes. A steel box-girder bridge with a cross-section configuration similar to that of a segmental concrete box bridge is often competitive. A steel bridge with two boxes usually cannot be competitive with a single box segmental box girder bridge. The reason is the configuration.

The design of box sections for flexure and torsion (both straight and horizontally curved) is covered in *AASHTO LRFD* Article 6.11. The flexural resistance of non-composite closed-box sections used as compression or tension members is specified in *AASHTO LRFD* Article 6.12.2.2.2. *AASHTO LRFD* Article C6.11.1 indicates that the provisions are applicable when applied to box sections in continuous, simple or tied-down curved or straight spans up to approximately 350 feet long. Further, the provisions may be applied to longer spans if a thorough evaluation, consistent with basic structural engineering fundamentals, is conducted. The article also refers to an alternative straight box-girder specification for further information on the design of long-span straight steel box-girder bridges (*24*). Differences between this specification and the *AASHTO LRFD* Specification primarily relate to the calculation of the effective width for box flanges, the nominal flexural resistance of unstiffened and stiffened box flanges and the web shear capacity.

The *AASHTO LRFD* provisions in Article 6.11 require that composite box sections used as primary longitudinal flexural members have a composite concrete deck throughout their length in the final condition. *AASHTO LRFD* Article 6.10.1.5 specifies the concrete deck be assumed effective in compression and tension over the entire bridge for analysis of the composite case. Torsion exists along the entire bridge in composite box girders. Therefore, shear connectors are required over the entire bridge. As indicated in *AASHTO LRFD* Article C6.11.1, as of this writing (2010), the specifications do not address the use of composite concrete on the bottom flanges of box girders.

In the 10th Edition of the AASHO Bridge Specifications (1969), provisions for computing the wheel load distribution factor for straight box girders were introduced. A similar equation (in units of lanes) was carried forward to *AASHTO LRFD* Article 4.6.2.2.2b (Table 4.6.2.2.2b-1). The equation was derived based on folded-plate theory, which was shown at the time to be valid to analyze the behavior of multiple box-section bridges based on analytical and experimental model studies of simple-span bridges (*25*). To ensure that the equation was applied within the limitations and bridge characteristics of the research study upon which it was based, limits were placed on the cross-section as part of the specifications. Since refined analysis methods were not readily available or widely used at that time, designs outside the specified limits were rarely done. It was further determined from the research that when the cross-section restrictions are satisfied, secondary bending stresses due to cross-section distortion and shear due to St. Venant torsion may be neglected if the box flange is fully effective.

Bridge cross-section limitations were not included in the initial version of the AASHTO *Guide Specifications for Horizontally Curved Bridges* (1980). In lieu of distribution factors, rational analysis was required to distribute the loads in horizontally curved bridges. As discussed previously in Section 1.2, the *AASHTO LRFD* Specifications unified the provisions for the design of straight and horizontally curved bridges into a single specification. In addition, with the more common availability and use of refined methods of analysis, the overall scope of the provisions was broadened to allow the consideration of a wider variety of box-girder

bridge types and cross-sections that were outside of the initial specified limitations. However, since the distribution factor equation was also implemented in the *AASHTO LRFD* Specifications as an acceptable approximate analysis method for determining live load moments in straight bridges, it was necessary to continue the restrictions on the cross-section in order to permit its use. These restrictions are specified in *AASHTO LRFD* Article 6.11.2.3.

Bridges not satisfying one or more of the special restrictions specified in *AASHTO LRFD* Article 6.11.2.3 (and/or that do not have fully effective box flanges) must be investigated using one of the available methods of refined structural analysis, or other acceptable methods of approximate structural analysis specified in *AASHTO LRFD* Articles 4.4 or 4.6.2.2.4. This includes single box cross-sections and multiple box cross-sections in horizontally curved bridges. The additional torsional effects resulting from support skew are not comprehended by the specified live load distribution factor. Hence, a more refined analysis is required whenever one or more supports are skewed, even if the bridge satisfies the preceding cross-sectional limitations. *Skewed supports are particularly problematic for box-girder bridges and special care should be taken in analyzing and detailing box girders with skewed supports in order to provide a successful bridge*. A refined analysis is also recommended in *AASHTO LRFD* Article C6.11.2.3 if the straight portion of a bridge satisfies the preceding requirements, but also contains horizontally curved segments, as the effects of horizontal curvature generally extend beyond the curved segments. Torsion, unlike bending moment, is not mitigated by length Refined analysis methods may be employed, even if the bridge satisfies all the specified restrictions. For bridges not satisfying the specified restrictions and/or without fully effective box flanges, secondary bending stresses due to cross-section distortion and shear due to St. Venant torsion must be considered. The consideration of these actions in the design of the various components of the box section is discussed further in Sections 3.2 and 3.3.

Transverse through-thickness bending stresses are of particular concern for boxes subject to large torques; e.g. single box sections, sharply curved boxes and boxes resting on skewed supports. Longitudinal warping stresses must be considered for fatigue, particularly at the corners of the box section where critical details are often located (*1*). Tests have indicated that longitudinal warping stresses do not adversely affect the strength of boxes of proportions defined in the provisions. The application of the beam-on-elastic-foundation (BEF) analogy to compute cross-section distortional stresses (*1*) is discussed further in Section 3.2.5.2.2.3.

3.1.5.2 Steel Grade(s)

The advantages of using higher-strength high performance steel (HPS) for box flanges in compression are less evident as the local buckling resistance of box flanges (unstiffened or stiffened) is a function of Young's modulus rather than the yield strength of the steel. Since the modulus is not increased with yield strength,

the compressive resistance of a plate of increased yield strength may not significantly improve with an increase in yield strength.

Longitudinal flange stiffeners are primary load carrying members. Therefore their specified minimum yield strength must not be less than the specified minimum yield strength of the box flange to which they are attached as specified in *AASHTO LRFD* Article 6.11.11.2. Rolled structural tees are not available in HPS; therefore, when HPS is used for box flanges, tees must be fabricated from plates or from cut plate.

3.1.5.3 Box Girder Web Proportioning

3.1.5.3.1 Web Thickness

Cross-section proportion limits for webs of box sections are specified in *AASHTO LRFD* Article 6.11.2.1. As specified in *AASHTO LRFD* Article 6.11.2.1.2, for webs without longitudinal stiffeners, the webs must be proportioned such that:

$$\frac{D}{t_w} \le 150$$

Equation 3.1.18
AASHTO LRFD Equation 6.11.2.1.2-1

where D is the web depth and t_w is the web thickness.

Longitudinal web stiffeners are required on webs that do not satisfy Equation 3.1.18. Webs with longitudinal stiffeners must be proportioned to satisfy Equation 3.1.19 as specified in *AASHTO LRFD* Article 6.11.2.1.3.

$$\frac{D}{t_w} \le 300$$

Equation 3.1.19
AASHTO LRFD Equation 6.11.2.1.3-1

Additional discussion regarding web slenderness limits is given in Section 3.1.4.2.1.

Note that for sections with inclined webs, *AASHTO LRFD* Article 6.11.2.1.1 requires that the distance along the web be used for checking all design requirements. Therefore, in checking Equations 3.1.18 and 3.1.19 for the case of an inclined web, the web height, D, must be taken as $D/\cos\theta$, where θ is the angle of inclination of the web plate with respect to the vertical.

As discussed later on in Section 3.2.7, computation of the shear must also take into account the slope of the web; that is, the vertical shear determined from the analysis must be divided by $\cos\theta$. Torsional shear is to be added if it is computed separately from the vertical bending shear. Vertical bending shear in the box is divided evenly between the two webs. St. Venant torsion causes web shears to have opposite

signs in opposing webs. Hence, torsional shear is additive to flexural shear in one web and subtractive in the other. A 3D finite element refined analysis provides both shears since both webs are modeled. Usually, the design is for the critical web and the other web is stiffened the same. Of course, live load causes opposite torques that must be checked. These different shears are also reflected in the reactions when two bearings are used at a support. One bearing will have a larger reaction than its neighbor.

Additional guidelines for I-sections provided in Section 3.1.4.2.1 regarding minimum web thickness, change in web thickness along the girder, and determining the trade-off between adding more stiffeners versus increasing the thickness of web material should be considered applicable to webs of box sections as well.

3.1.5.4 Box Girder Flange Proportioning

3.1.5.4.1 Top Flanges of Tub Sections

AASHTO LRFD Article 6.11.2.2 specifies that top flanges of tub sections subject to tension or compression satisfy the following requirements:

$$\frac{b_f}{2t_f} \le 12.0$$

Equation 3.1.20
AASHTO LRFD Equation 6.11.2.2-1

$$b_f \ge D/6$$

Equation 3.1.21
AASHTO LRFD Equation 6.11.2.2-2

and:

$$t_f \ge 1.1t_w$$

Equation 3.1.22
AASHTO LRFD Equation 6.11.2.2-3

These requirements are the same as those specified for flanges of I-sections in *AASHTO LRFD* Article 6.10.2.2. They are discussed further in Section 3.1.4.3. For sections with inclined webs, *AASHTO LRFD* Article 6.11.2.1.1 requires that the distance along the inclined web be used for checking all design requirements. Therefore, in checking Equation 3.1.21 for an inclined web, *D* is taken as $D/\cos\theta$, where θ is the angle of inclination of the web plate with respect to vertical.

Recommendations regarding minimum flange width and thickness and flange transitions given in Section 3.1.4.3 are applicable to top flanges of tub sections. The two top flanges of a tub section should be the same size. The top flange width should not be less than 16 inches to accommodate the connection of lateral bracing

members. In cases where lateral bracing members are not bolted to the flanges (not recommended), the flanges may be smaller. *For cases where a full-length top lateral bracing system is provided (required for horizontally curved tub sections and strongly recommended for straight tub sections resting on skewed supports), Equation 3.1.14 need not be considered for the top flanges.*

The sizes of top flanges of tub sections in regions of positive flexure are generally governed by constructibility. The establishment of a reasonable preliminary design width and thickness for the flanges in these regions is based on experience, keeping the minimum width and thickness discussed in Section 3.1.4.3. The final size of the top flanges and/or the spacing of the cross-frames/diaphragms in these regions will generally be controlled by either local buckling or lateral-torsional buckling under construction conditions. A critical construction condition is often the combined vertical and lateral bending. The outermost flange of the exterior tub often has the largest vertical bending stress due to deck-casting plus the lateral bending stress due to curvature and deck overhang loads. It is suggested that the top-flange size in positive moment regions be investigated early in the design based on the critical construction condition. Subsequent design verifications can be made for strength, fatigue and service limit states. The specific design verifications at the various limit states are discussed in greater detail in Section 3.2.

The sizes of top flanges of tub sections in negative flexure are typically controlled by tension-flange yielding at the strength limit state. The specification requires that box girders be composite throughout, including in the negative moment regions. Again, preliminary sizes in these regions are based on experience. The top flanges in the negative moment regions near the piers of continuous spans may be wider and thicker than those in regions of positive flexure. Widths should be constant within a field section to permit slab welding of the flanges. Transitions in width should be made at the field splices. Changes in the top-flange width cause some inconvenience in that the length of the forming must be changed. This issue is minor when compared to the improved economy of the structural steel. Other limit states, including the fatigue limit state (discussed in Section 3.2), may be critical in the design of the top flanges in regions of negative flexure in some cases. Web bend-buckling at the service limit state may be critical in the negative moment region if the deck is considered to be effective in tension (refer to Section 3.2.4.3.1). This is caused by the higher neutral axis, which causes more than half of the web to be in compression.

The top flange lateral bracing resists the torsional shear before the top flanges become continuously braced by the hardened concrete deck. Once the concrete hardens, it assists the top lateral bracing in resisting the torsional shear. The torsional shear produces horizontal shear in the deck that should be considered when designing the deck reinforcing steel. Lateral bending stresses occur in the top flanges prior to hardening of the concrete deck and must be considered. Once the deck has hardened, flanges are continuously braced so lateral flange bending, local buckling and lateral-torsional buckling usually need not be considered. If a precast deck is used, the engineer may chose to investigate local buckling if the deck does not adequately brace the flange.

AASHTO LRFD Article 6.10.1.7 requires that the longitudinal deck reinforcement be equal to or greater than one-percent of the total cross-sectional area of the deck. This requirement is provided to control deck cracking. This reinforcement should be included in the composite section properties and often permits a reduction in the size of the top flanges. When the top flange has a yield strength greater than 50 ksi, slightly more longitudinal reinforcing may be desirable to account for the larger strains in the deck, which are compatible with the strains associated with the higher strength steel.

Top flanges should be evaluated for lateral loads from the webs in cases where the webs are sloped more than 1-to-4.for loads applied prior to hardening of the deck.

3.1.5.4.2 Bottom/Top Box Flanges

A box flange is defined in the *AASHTO LRFD* Specifications as a flange that is connected to two webs. The flange may be a flat unstiffened plate, a stiffened plate or a flat plate with reinforced concrete attached to the plate with shear connectors. Thus, unstiffened or stiffened bottom flanges of tub and closed-box sections and top flanges of closed-box sections are classified as box flanges under this definition.

For box sections with inclined webs, the width of bottom box flanges is a function of the web spacing and depth as well as the slope of the webs. Inclined webs are advantageous in reducing the bottom flange width while maintaining the spacing at the top of the box to economically support the deck. *AASHTO LRFD* Article 6.11.2.1.1 specifies that the inclination of the web plates to a plane normal to the bottom flange should not exceed 1-to-4. Where the live load distribution factor equation is used to determine the live load flexural moments, the inclination of the web plates may not exceed 1-to-4. However, this limitation does not apply to curved tub girders and should not be applied to boxes resting on skewed supports. A narrower bottom box flange is desirable. However, caution should be exercised when deviating too much from the constraint applied to the web slope. Lateral bending stresses in the top tub flanges increase as the slope of the web exceeds 1-to-4. This is due to the transverse component of shear force in the web.

Recommendations regarding flange thickness transitions given in Section 3.1.4.3 should also be considered for box flanges. A savings of 800 to 1,200 pounds of flange steel justifies a flange butt splice in top flanges of tub girders (*2*). For wider box flanges, there are additional issues involved. One fabricator has suggested that to warrant the introduction of a shop splice between 48-inch-wide straight box flanges 1½ and 2 inches in thickness composed of ASTM A 572 Grade 50 material, at least 2,250 pounds of material must be saved. This number will vary depending on the width, thickness and grade of the plates being joined, and whether the plates are straight or curved. Box flanges must be cut curved from large plates. Thus, depending on the radius, it may be desirable to introduce additional shop splices in the flange to reduce waste. Therefore, it is recommended that fabricators who are

likely bidders on the job be consulted with regard to the issue of shop splices in box flanges.

Box flanges should extend at least one inch beyond the outside of each web to facilitate welding (*AASHTO LRFD* Article C6.11.2.2) Wider flange lips provide a place for birds to perch, which might otherwise be prevented with a steel tub.

The closed box presents special design considerations. Closed-box sections are often used as straddle beams rather than as girders in the U.S. Top flanges of straddle-beam box sections are designed similarly to bottom flanges of tub girders. However, composite closed-box girders present some different issues. They must be stiff enough to support the weight of the wet concrete. They also must act compositely with the deck. This means that the flange must be thick enough to receive shear studs; a minimum ¾-inch-thick flange is acceptable. In positive flexure, the top flange is generally controlled by constructibility verifications (as discussed in Section 3.2.3) if it is to be composite in the final condition. For closed-box sections in positive flexure (or tub sections in negative flexure), the thickness of the non-composite box flange is usually controlled by its local buckling resistance (see Sections 3.2.2.2 and 3.2.6.4.2.2). It is recommended that the initial flange thickness in these cases be determined based on the local buckling resistance. Subsequent design verifications will then need to be made at the other limit states, as described in more detail in Section 3.2. Deflection of the flange should be checked to ensure that the integrity of the box shape is maintained when concrete is placed on the flange. The shear connection pattern needs to be determined to ensure proper attachment of the deck to the flange (see Section 3.3.2.1.1.2). If the flange is wide enough to experience shear lag, the shear connectors should be distributed across the flange width according to the shear distribution in the flange plate. Shear is highest near the webs at supports. The horizontal shear through the top flange should be checked.

Non-composite box flanges in compression may require longitudinal stiffening to prevent buckling under combined uniform axial compression and St. Venant torsional shear. *Unstiffened box flanges are preferred***.** However, an unstiffened box flange should not be so slender that its buckling resistance becomes impractical. Longitudinal flange stiffeners may be added to increase the compressive resistance of thin flanges. As discussed further in the next paragraph, the cost of these stiffeners is significant and they should be employed only after a thickness increase is evaluated. A minimum thickness of ¾" is recommended for unstiffened box flanges for ease of handling and to minimize distortion and possible cupping of the flange during welding, with the maximum ratio of width to thickness of the flange recommended not to exceed around 120 (*26*). A lesser thickness might be considered for a stiffened box flange; however, it is recommended that fabricators first be consulted before utilizing box flange thicknesses below ¾".

Provisions for longitudinally stiffened box flanges have been part of the *AASHTO* design specifications since box girders were first included. However, they are best avoided where possible. They are costly and can be a time-consuming design matter. Narrower flanges can often be designed efficiently without stiffening in either

tension or compression. Usually box flanges narrower than 60 inches can be designed to be efficient without stiffening and often flanges up to 70 inches do not require stiffening. Box sections do not need to be as deep as do I-sections because the two webs act as an integral unit, sharing the load. This is particularly true for curved alignments. The shallower the box, the stockier the box flange can be (i.e. greater b/t) and the more efficient the flange can be without stiffening. There probably is not a good rule regarding longitudinal flange stiffeners, but a weight savings of flange equal to at least 10 times the stiffener weight would be required to approach parity. High strength steel (above 50 ksi) is usually not economical in box flanges. Flanges that can be designed for 86 to 90 percent of the yield stress at the strength limit state without a longitudinal stiffener usually should not be stiffened. In short, shallower, narrower boxes provide for better economy. If the inside of the box is to be painted, the cost of cleaning and painting the tee section(s) (i.e. stiffeners) offsets some of the advantage of adding the stiffeners (*2*). Another economic advantage of smaller box girders occurs in the contraflexure regions where flange demand is a minimum. A wider box flange requires more steel to simply close the box in these areas than does a narrower one.

Structural tees are recommended for longitudinal flange stiffeners. They provide better lateral torsional buckling resistance than do bars or angles. Tees also provide a high ratio of out-of-plane stiffness to stiffener cross-sectional area. These issues are discussed in *AASHTO LRFD* Article C6.11.11.2. Further discussion of the design of longitudinal flange stiffeners is provided in Section 3.2.6.4.2.2. The tee(s) must be spliced to ensure that the stiffeners are continuous at field section splices, which can complicate both the fabrication and field assembly. The stiffeners should be continuous through internal diaphragms; consideration should be given to attaching the stiffeners to the internal diaphragms as recommended in *AASHTO LRFD* Article C6.11.11.2.

If more than one longitudinal stiffener in a flange section is used, their required moment of inertia is increased substantially. The reason for this is that the webs are assumed to be perfectly rigid and the flange panels with one stiffener are assumed rigidly connected at the webs. When two or longitudinal stiffeners are used to achieve the desired buckling coefficient, their size increases dramatically becoming impractical (as discussed further in Section 3.2.6.4.2.2). Rare is the instance where more than one longitudinal stiffener is economical.

The provisions allow different assumptions regarding the plate-buckling coefficient for uniform normal stress for a longitudinally stiffened flange. A value from 2 to 4 is typically selected by the Design Engineer. The value of 4 assumes that the stiffener is rigid enough that the flange will buckle with no deformation of the stiffener. Lower values assumed the stiffener is permitted to flex before the plate reaches its capacity. This option improves potential economy because a smaller stiffener may be adequate. The Design Engineer is advised to develop or obtain an interactive spreadsheet or program to investigate the design with different coefficients. The

optimum choice provides the flange/stiffener combination that is both adequate and economical for the location.

Termination of the longitudinal flange stiffener is another consideration. The stiffener is not required after the compression stress in the flange drops to a level that the flange is adequate without stiffening. The Design Engineer must check deck staging to be sure that the flange is not subjected to excess compression caused by significant ephemeral negative moments at the terminus during deck placement. Lifting field sections with slender box flanges during shipping or erection can be problematic. The thickness of a stiffened flange may have to be increased at the termination of a longitudinal flange stiffener.

The terminus of a welded longitudinal stiffener with no special transition radius provided creates a fatigue Category E or E′ detail (depending on the detail thickness), which essentially forbids the practice. The fatigue category can be improved by introducing a radius at the terminus and grinding the weld to a smooth radius (see Condition 4.3 in *AASHTO LRFD* Table 6.6.1.2.3-1). It is obviously expensive to terminate the stiffener in regions of net tensile stress. As discussed in Section 3.2.6.4.2.2, it is optimal to terminate a longitudinal stiffener at a bolted splice, which frequently occurs at or near points of dead load contraflexure. The flexural stresses at the joint are zero since the ends of the plates are stress free. However, there are live load stresses in these regions so it cannot be said that the adjacent flange plates are free of flexural stress. It may be that the live load negative moment is large enough to cause the unstiffened flange to be thickened in order to terminate the stiffener. Other potential alternatives for termination of the longitudinal flange stiffener are discussed in Section 3.2.6.4.2.2.

Box flanges in tension are designed against yielding. The flexural stress is combined with the St. Venant torsional shear stress so that a check of the principal stress can be made. Longitudinal stiffeners are not required when the flange is in tension. However, they may assist in maintaining the flatness of a slender flange.

The controlling limit state for the design of bottom box flanges in tension depends on whether the section qualifies as a compact or noncompact section. *Box girders in straight or horizontally curved bridges in positive flexure regions must be treated as noncompact sections at the strength limit state.* This means that tension flanges will be controlled by yielding. Fatigue may be critical in some cases. Constructibility verifications will not typically control the design of box flanges in these regions.

For closed-box sections in regions of negative flexure, the controlling limit state for the design of the top flange in tension will typically be yielding at the strength limit state once the top flange is continuously braced by the hardened deck.

AASHTO LRFD Article 6.11.1.4 specifies that inspection access holes in box sections should be located in areas of low stress in the bottom flange. The access holes should be large enough to provide easy access (at least 18 inches by 36 inches). Access holes should be provided at each end of the bridge. The effect of access holes on stresses in the flange should be investigated to determine if

reinforcement around the hole is required. Rarely should access holes be located in compression flanges. When they must be so located, the flexural resistance of the remaining flange on each side of the hole is to be determined. *AASHTO LRFD* Article 6.10.8.2.2 (discussed further in Section 3.2.6.4.1.2) can be used to determine the local buckling resistance, with the flange slenderness based on the projecting width of flange on either side of the hole.

3.1.5.4.2.1 Effective Width of Box Flanges

Shear lag may be significant in wider box flanges, especially near interior supports. This phenomenon occurs most severely when a concentrated load or reaction is experienced by the girder. Simply, the full flange width does not experience flexural stress suddenly. Instead the portion of the box flange nearest the web sees more stress while the central portion of the flange experiences less of the load. Over some distance, more of the load is distributed to the central portion of the flange, which tends to equalize the stress across the flange. This condition is treated in most specifications by indicating that only a portion of the flange may be used in determining section properties.

If a 3D finite element model is used to model the box, several elements can be used to model the box flange. Edge stresses in the elements provides a pattern of the shear lag at particular points.

In cases where a refined analysis is not available, *AASHTO LRFD* Article 6.11.1.1 specifies that the entire box flange may be considered effective in flexure with a uniform flexural stress when the width of the box flange does not exceed one-fifth of the effective span, which is defined as the span length for simple spans. The effective span in continuous spans is defined as the distance between points of dead load contraflexure or between a simple support and a point of dead load contraflexure.

A flange width of one-fifth of the effective span is to be considered effective in cases where the flange width exceeds one-fifth of the effective span. The effective flange width is used for section properties to calculate factored flexural stresses as suggested in *AASHTO LRFD* Article C6.11.1.1. The entire flange width is used to calculate the flexural stiffness of the box for analysis and for calculating the nominal flexural resistance of the box flange.

The effective width requirement is based on analyses of simple-span box-girder bridges using a series of folded-plate equations (*27*). Span-to-flange width ratios between 5.65 and 35.3 were included in the study. The effective flange width (as compared to the full flange width) ranged from 0.89 for the bridge with the smallest span-to-width ratio to 0.99 for the bridge with the largest span-to-width ratio. It should be noted that continuous spans were not investigated. As discussed above, interior reactions present the most significant situation for shear lag. Based on the parametric results described, the researchers deemed it reasonable to assume that

a flange is fully effective as long as the width of the flange does not exceed one-fifth of the span. The rule was extended to continuous spans by assuming that the effective span be defined as described above. *AASHTO LRFD* Article C6.11.1.1 states that for extremely wide box flanges, a special investigation of shear lag is warranted regardless of the effective span-to-flange width ratio.

3.1.6 Case Study – 3D Investigation of Framing Plan Layout Issues in a Skewed I-Girder Bridge

The structure in this case study is a straight continuous skewed I-girder bridge with two equal spans of 169′-0″. Supports are skewed approximately 45 degrees from normal. The cross-section has seven girders spaced at 9′-0″. The girder depth is constant at approximately 70 inches. Top flanges in the positive moment regions are 1″ x 18″ and bottom flanges are 1-1/4″ x 20″. Top and bottom flanges in the negative moment region are 2-1/4″ x 24″.

Cross-frames are normal to the girder lines, except at the abutments. There are no cross-frames between bearings along the skewed interior support line to simplify the detailing. At the abutments, diaphragms are employed between girders to support the ends of the concrete deck. Interior cross-frames are K-type with the K-node at mid-length of the bottom chord. The area of all typical cross-frame members is 5.0 in^2. Cross-frames are staggered and are spaced longitudinally at approximately 18′-0″. The transverse stiffness of the framing is significantly reduced because of the staggered cross-frames. Less load is transferred across the bridge to the obtuse corners at the bearings than if the cross-frames were contiguous. There are a total of 120 cross-frames and diaphragms including 12 along the skews. This framing arrangement is referred to as Option 1.

Bearing constraints are as shown on the plot of the framing plan shown in Figure 3.1.57. The bearing arrangement was determined based on considerations not discussed. Cross-frames were used on both sides of each of the interior bearings along the pier. These cross-frames transfer lateral loads, such as wind, to the bearings. Bearing stiffnesses at the pier have been adjusted in the analysis to account for the pier flexibility.

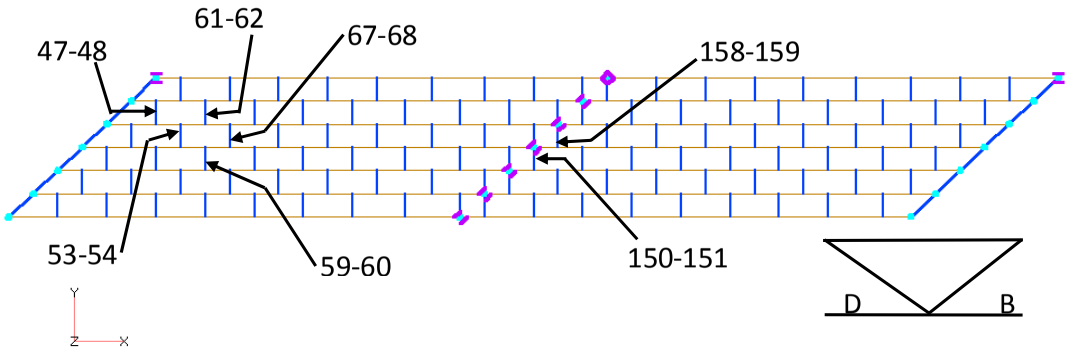


Figure 3.1.57 Framing Plan for Option 1

Critical cross-frame forces from the 3D analysis of the bridge are given in Table 3.1.5 below. The diagonals have equal but opposite forces. When Member B has the critical force, the diagonal over Member B has the same sense and the other diagonal has equal but opposite sense. The locations of these cross-frames are shown in Figure 3.1.57. The smaller node number is the node toward the bottom of the plot. Corresponding lateral flange bending moments at each cross-frame determined from the analysis are also given. Interestingly, none of the cross-frames attached to the exterior girders are identified as having large forces. The reason is that the exterior girders are able to deflect with less restraint than the interior girders experience from having cross-frames on the opposite side of the girder.

Table 3.1.5 Critical Cross-Frame Forces & Lateral Flange Moments (Option 1)

Nodes	Max. Factored Cross-Frame Force (kips)	Lateral Moments (kip-ft)			
		Dead Load		Live Load	
		Top	Bottom	Bottom	
47-48	-50 in B	-14	2	55	-56
53-54	56 in D	-31	6	56	-43
59-60	62 in D	-34	13	46	-29
61-62	58 in B	-28	14	59	-43
67-68	65 in B	-38	18	57	-54
150-151	-90 in B; -184 in D	28	-52	70	-91
158-159	-100 in B; -169 in D	29	-56	77	-100

The node having the largest reported lateral moment is not identified, but it can be deduced from the cross-frame force. For example, Member B is connected to Node 47, so the lateral moment is reported in the girder at Node 47.

Dead load lateral flange bending moments in the bottom flange due to the weight of the concrete parapets are opposite in sense to the lateral flange moments due to the weight of the deck and the self-weight of the girders. Without the properly placed parapet loads, the bottom flange lateral moments would be larger than the reported totals in every case. This observation is lost when parapet loads are distributed across the structure.

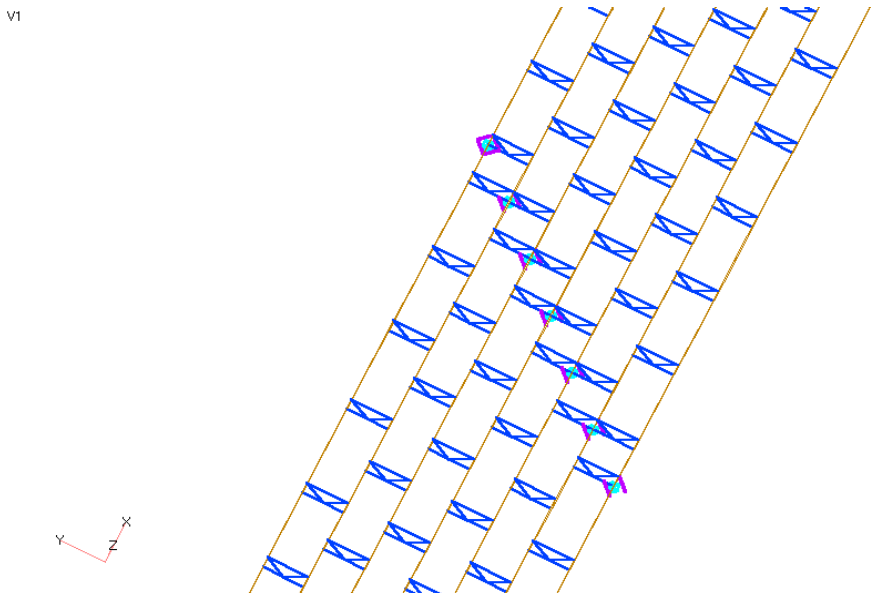


Figure 3.1.58 Rotated Plan View of Option 1

In this study, two additional framing options are examined that might lead to lower cross-frame forces, lateral flange bending moments and cost. Although the bearing arrangement may affect the results, it was not changed in these investigations.

Although the problem is one commonly faced, it probably has no definitive solution and is not amenable to rules. Costs of labor and material vary from time to time and with locale. However, the issues create enough cost that further investigation is warranted. Costs in cases such as these arise from the size of the cross-frame members, the cost of the cross-frame connections (both of the members to gusset plates and the gusset plates to the connection plates), and the cost of the additional shear connectors necessary to resist the net lateral force acting on the shear connectors at the cross-frames. Of course, the total number of cross-frames influences the fabrication, shipping and erection costs. Discontinuous or staggered cross-frames cause an increase in the lateral flange bending moments in the girders, which is addressed through the use of the one-third rule equations; increased lateral flange bending in the girders results in reduced vertical bending capacity.

The second option (Option 2) that was investigated involved maintaining the girder framing arrangement and sizing from Option 1. However, in this option, the cross-frame lines were made contiguous except at the pier. The cross-frame spacing was maintained at 18 feet. This framing is shown in Figure 3.1.59. A line of cross-frames was introduced along the skewed pier to transfer lateral loads to the bearings, since no perpendicular cross-frames were employed at the bearings. There are a total of 114 cross-frames and diaphragms in this option, including 18 along the skews, compared to 120 cross-frames and diaphragms in Option 1.

.

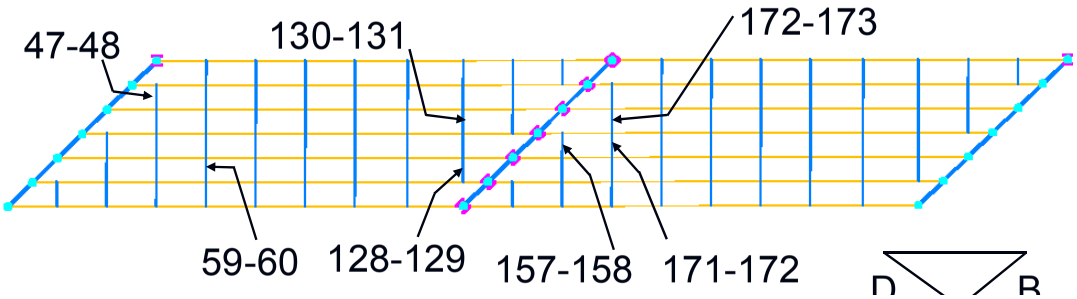


Figure 3.1.59 Framing Plan for Option 2

Critical cross-frame forces from the 3D analysis of the bridge with the revised framing are given in Table 3.1.6, along with the corresponding lateral flange bending moments. The locations of these cross-frames are shown in Figure 3.1.59.

Table 3.1.6 Critical Cross-Frame Forces & Lateral Flange Moments (Option 2)

Nodes	Max. Factored Cross-Frame Force (kips)	Lateral Moments (kip-ft)			
		Dead Load		Live Load	
		Top	Bottom	Bottom	
47-48	-92 in B	-3	4	6	-2
59-60	109 in D	-1	1	2	-1
128-129	-147 in D	27	-47	36	-59
130-131	-143 in B	-2	7	16	-16
157-158	-104 in B	0	-1	6	-8
171-172	-106 in D	-4	2	2	-1
172-173	-177 in B	2	-11	15	-19

Option 2 increased the transverse stiffness of the structure, which led to an increase in cross-frame forces accompanied by a substantial reduction in lateral flange bending. The increased transverse stiffness was evidenced by the 50 percent increase in critical cross-frame forces in the positive moment regions. Lateral flange bending moments in these regions were negligible, which would require only a slight increase, if any, in flange sizes to accommodate them relative to Option 1. Critical cross-frame forces in the negative moment regions were about the same as for Option 1. Lateral flange bending moments in these regions were not negligible because the normal cross-frames were still discontinued to eliminate the connections to the cross-frames along the skewed pier. Although not shown here, the effect on the shear connectors of the lateral force at the cross-frames was also negligible.

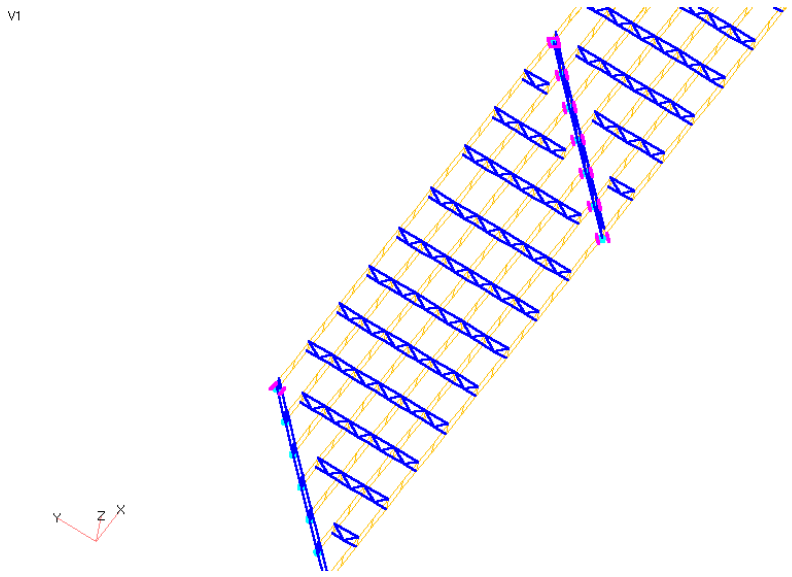


Figure 3.1.60 Rotated Plan View of Option 2

The third option (Option 3) that was examined involved an increase of the cross-frame spacing from 18 feet to 27 feet. The *AASHTO LRFD* Specification permits the cross-frame spacing to exceed 25 feet. In this option, contiguous cross-frame lines were maintained as in Option 2, except at the pier where again, a line of cross-frames was introduced along the pier with no perpendicular cross-frames connected to them. There are only 82 cross-frames and diaphragms in this option, including 18 diaphragms along the supports. A plan view of Option 3 is shown in Figure 3.1.61.

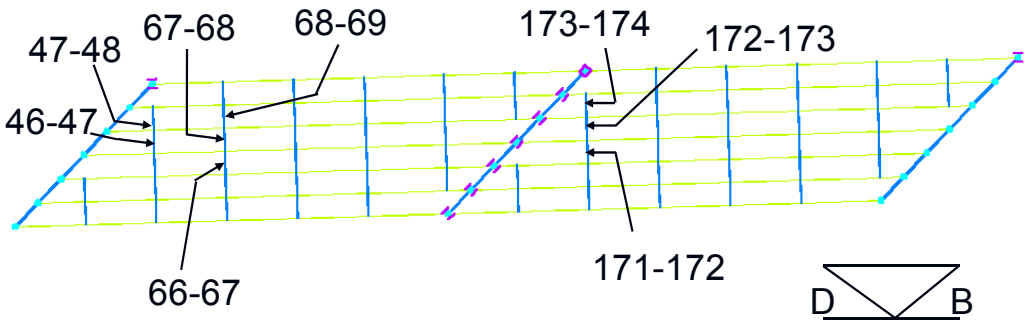


Figure 3.1.61 Framing Plan for Option 3

Critical cross-frame forces from the 3D analysis of the bridge with the revised framing are given in Table 3.1.7, along with the corresponding lateral flange bending moments. The locations of these cross-frames are shown in Figure 3.1.61.

Table 3.1.7 Critical Cross-Frame Forces & Lateral Flange Bending Moments (Option 3)

Nodes	Max. Factored Cross-Frame Force (kips)	Lateral Moments (kip-ft)			
		Dead Load		Live Load	
		Top	Bottom	Bottom	
46-47	120, -103 in B	-3	3	4	-1
47-48	102 in B	-3	13	5	-2
66-67	111 in B; 134 in D	0	1	2	-1
-67-68	134 in B; 134 in D	0	0	1	-1
68-69	134 in B; 97 in D	0	0	1	0
171-172	-148 in B; -186 in D	0	-5	7	-11
172-173	-183 in B; -163 in D	-8	9	6	-2
173-174	-165 in B	-7	10	9	-5

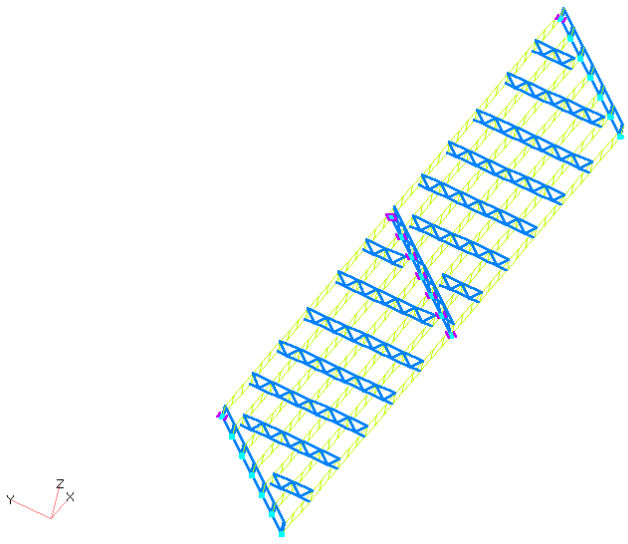


Figure 3.1.62 Rotated Plan View of Option 3

Cross-frame forces in the positive moment regions in this option are at least double those in Option 1. Cross-frame sizes would have to be increased over the original 5.0 in^2. Tee sections may be required. Bolted connections of the gusset plates to the connection plates would likely require a significant increase in the number of bolts. The larger cross-frame forces would also likely have an effect on the number of shear connectors required in these regions. Lateral flange bending moments are not critical in this case.

Conclusions

Option 3 has the least number of cross-frames. However, several of them would have to use larger members. Option 1 has the lowest cross-frame forces, but may impact the girder designs based on the larger lateral flange bending moments.

It is not practical to design cross-frames and connections for all options. However, a summary of all cross-frame forces in each of the three options was not given and might have been instructive as to how many members would have to be increased in size. The actual sizes of the members and connections were not provided. However, based on the information provided, Option 1 looks to be the lowest cost option of the three reported. The cross-frame forces at the interior bearings are extremely large and may be problematic in sizing their connections in all cases. However, a final decision would require additional information.

Results for thermal and wind cases are not reported. They may have a material effect on the final decision. Since the wind can come from either direction, it can introduce critical, additive, forces in any member, as can thermal forces when temperatures increase or decrease. .

Inverting the cross frames (i.e. putting the K-node on the top chord) usually reduces the force in the bottom chord. This happens because the additional horizontal force component from the diagonals is accumulated in the top chord rather than in the bottom chord. The top chord forces are generally lower since the top chord is close to the deck, which shares loads applied to the composite section.

As explained above, different bearing orientations and restraints were not investigated. They can have a very great impact on cross-frame forces as seen at the pier in these cases. If the pier bearings could be released from lateral restraint, the cross-frame forces there would be reduced. In fact, cross-frames would not even necessarily be required at pier bearings that are not laterally restrained. This introduces other issues beyond this example, but the option is available in some cases.

In this case study, the differences are not as great as occur in some projects. This study demonstrates that when a challenging situation arises, there are options to examine other than simply providing heavier members and connections.

3.1.7 References

1. Wright, R.N., and Abdel-Samad, S.R. 1968. “BEF Analogy for Analysis of Box Girders.” *Journal of the Structural Division*, ASCE, Vol. 94, No. ST7, pp. 1719-1743.
2. AASHTO/NSBA Steel Bridge Collaboration. 2003. “Guidelines for Design for Constructibility, G12.1.” American Highway of State Highway and Transportation Officials, Washington, D.C., Publication No. GDC-1.

3. Fan, Z., and Helwig, T.A. 1999. "Behavior of Steel Box Girders with Top Flange Bracing." *Journal of Structural Engineering*, ASCE, Vol. 125, No. ST8, August, pp. 829-837.
4. Herman, R., Helwig, T., Holt, J., Medlock, R., Romage, M., and Zhou, C. 2005. "Lean-On Cross-Frame Bracing for Steel Girders with Skewed Supports." *Proceedings of the 2005 World Steel Bridge Symposium*, Orlando, FL, available from the National Steel Bridge Alliance, Chicago, IL.
5. Heins, C.P. 1975. *Bending and Torsional Design in Structural Members*. Lexington Books, D.C. Heath and Company, Lexington, MA.
6. Timoshenko, S.P., and Gere, J.M. 1961. *Theory of Elastic Stability*. Mc-Graw-Hill, New York, NY, pp. 132, 136-137.
7. Heins, C.P. 1978. "Box Girder Bridge Design – State of the Art." AISC Engineering Journal, American Institute of Steel Construction, Chicago, IL, 4th Qtr.
8. National Highway Institute. 1990. "Economic and Fatigue Resistant Steel Bridge Details – Participant Notebook." National Highway Institute Course No. 13049, Federal Highway Administration, Publication No. FHWA-1-11-90-043, June.
9. Wright, W.J., Fisher, J.W., and Kaufmann, E.J. 2003. "Failure Analysis of the Hoan Bridge Fractures." *Recent Developments in Bridge Engineering*, Mahmoud ed. Swets & Zeitlinger, Lisse.
10. Kaufmann, E.J., R.J. Connor, and J.W. Fisher. 2004. *Failure Investigation of the SR 422 over the Schuylkill River Girder Fracture – Draft Final Report*, ATLSS Engineering Research Center, Lehigh University, Bethlehem, PA.
11. Mahmoud, H.N., R.J. Connor, and J.W. Fisher. 2005. "Finite Element Investigation of the Fracture Potential of Highly Constrained Details." *Journal of Computer-Aided Civil and Infrastructure Engineering*, Blackwell Publishing, Inc., Malden, MA, Vol. 20.
12. Ketchum, M.S. 1908. *The Design of Highway Bridges*. First Edition, McGraw-Hill, New York, NY.
13. Fountain, R.S., and Thunman, Jr., C.E. 1987. "Deflection Criteria for Steel Highway Bridges." Proceedings of the AISC National Engineering Conference, New Orleans, LA, April 29-May 7.
14. Blodgett, O.W. 1982. *Design of Welded Structures*. The James F. Lincoln Arc Welding Foundation, Cleveland, OH.
15. Yen, B.T., and Mueller, J.A. 1966. "Fatigue Tests of Large Size Welded Plate Girders." *WRC Bulletin No. 118*, November.
16. Mueller, J.A., and Yen, B.T. 1968. "Girder Web Boundary Stresses and Fatigue." *WRC Bulletin No. 127*. January.
17. Basler, K. 1961. "Strength of Plate Girders in Shear." *Journal of the Structural Division*, ASCE, Vol. 87. No. ST7, October.
18. AISC. 2005. *Specification for Structural Steel Buildings*. ANSI/AISC 360-05, American Institute of Steel Construction, Chicago, IL, March 9.
19. Cooper, P.B. 1967. "Strength of Longitudinally Stiffened Plate Girders. *Journal of the Structural Division*, ASCE, Vol. 93, No. ST2, April.
20. Lew, H.S., and Toprac, A.A. 1968. "Static Strength of Hybrid Plate Girders." *SFRL Technical Report*, University of Texas, Austin, TX.

21. Owen, D.R.J., Rockey, K.C., and Skaloud, M. 1970. “Ultimate Load Behavior of Longitudinally Reinforced Webplates Subjected to Pure Bending.” IABSE Publications, Vol. 30-1.
22. White, D.W., and Barth, K.E. 1998. “Strength and Ductility of Compact-Flange I Girders in Negative Bending.” *Journal of Constructional Steel Research*, Vol. 45, No. 3.
23. FHWA. 1980. “Proposed Design Specifications for Steel Box Girder Bridges.” *FHWA-TS-80-205*, Federal Highway Administration, Washington, D.C.
24. Johnston, S.B., and Mattock, A.H. 1967. “Lateral Distribution of Load in Composite Box Girder Bridges.” *Highway Research Record, No. 167*, Bridges and Structures, Transportation Research Board, Washington, D.C.
25. Coletti, D., Fan, Z., Gatti, W., Holt, J., and Vogel, J. 2005. “Practical Steel Tub Girder Design.” available from the National Steel Bridge Alliance, Chicago, IL, April.
26. Goldberg, J.E., and Leve, H.L. 1957. “Theory of Prismatic Folded Plate Structures.” *IABSE*, Vol. 16, International Association for Bridge and Structural Engineers, Zurich, Switzerland.

This Page Intentionally Left Blank

Chapter 3
Design Considerations

Section 3.2
Girder Design Verifications



3.2.1 Introduction

This section of the Manual discusses the basis of the LRFD flexural design resistance equations for I-girders and box girders in skewed and curved bridges. The specific LRFD design verifications for I-girders and box girders for constructibility, at the service limit state, at the fatigue limit state and at the strength limit state are then presented. Strength limit state design verifications for flexure are discussed for sections subject to negative flexure, positive flexure and stress reversal. Strength limit state design verifications for shear are also reviewed.

3.2.2 LRFD Flexural Design Resistance Equations

3.2.2.1 I-Girders

3.2.2.1.1 General

The *AASHTO LRFD* flexural resistance equations for the design of steel I-girders are discussed in this section. The same equations are used to check both straight and horizontally curved I-girders with or without skew.

In I-girder bridges, significant flange lateral bending may be caused by wind, by the use of discontinuous cross-frame/diaphragm lines in conjunction with skews exceeding 20° from normal (radial), by torsion due to curvature and by torsion due to eccentric concrete deck overhang loads acting on cantilever forming brackets placed along fascia girders. After the flange lateral bending stresses due to one or more of these effects have been determined, the issue then becomes how to effectively and rationally combine these stresses with the flange major-axis (vertical) bending stresses to check the capacity of the flange (or section). For I-girders, the so-called "one-third rule equations" are used in the *AASHTO LRFD* Specifications to combine the lateral flange bending stresses, f_ℓ, with the vertical bending stresses, f_{bu}, to check the flexural resistance.

The form of the one-third rule equation shown in Equation 3.2.1 is used at sections for which the vertical flexural resistance is expressed in terms of flange stress:

$$f_{bu} + \frac{1}{3} f_\ell \le F_r$$

Equation 3.2.1

where:

- f_{bu} = flange vertical bending stress determined as specified in *AASHTO LRFD* Article 6.10.1.6 (ksi)
- f_ℓ = flange lateral bending stress (ksi)
- F_r = factored flexural resistance in terms of flange vertical bending stress = $\phi_f F_n$ (ksi)
- F_n = nominal flexural resistance in terms of flange vertical bending stress (ksi)
- ϕ_f = resistance factor for flexure = 1.0 (*AASHTO LRFD* Article 6.5.4.2)

The second form of the one-third rule equation shown in Equation 3.2.2 is used at sections for which in the vertical flexural resistance is expressed in terms of moment:

$$M_u + \frac{1}{3} f_\ell S_x \le M_r$$

Equation 3.2.2

where:

M_r = factored flexural resistance in terms of vertical bending moment = $\phi_f M_n$ (kip-in.)
M_n = nominal flexural resistance in terms of vertical bending moment (kip-in.)
M_u = member vertical bending moment determined as specified in *AASHTO LRFD* Article 6.10.1.6 (kip-in.)
S_x = elastic section modulus about the major-axis of the section to the flange under consideration ($in.^3$)

The proper application of each form of the one-third rule equation is discussed below in Section 3.2.2.1.4. *When the effects of flange lateral bending are judged to be insignificant or incidental, the flange lateral bending term, f_ℓ, is simply set to zero in the applicable equation*.

The one-third rule equations address the combined effects of vertical bending and lateral bending by handling discretely braced compression flanges as equivalent beam-columns. A discretely braced flange is defined as a flange supported at discrete intervals by bracing sufficient to restrain lateral deflection of the flange and twisting of the entire cross section. A flange encased in concrete or attached by shear connectors is considered to be a continuously braced flange. The stress f_{bu} and moment M_u are analogous to the axial loading in the beam-column and the stress f_ℓ is analogous to the beam-column bending moment. M_u is considered analogous to axial loading since it produces axial stresses in the flanges.

For discretely braced tension flanges, the one-third rule equations approximate the full plastic strength of a rectangular cross section subjected to combined vertical and lateral bending.

The resistance equations are written in an interaction format in which the left-hand side of the equations pertains to the applied load effects, and the right-hand side of the equations is the appropriate member resistance in vertical bending. The conceptual basis of these equations and development of the 1/3 factor applied to f_ℓ will be explained in further detail in the next section.

In both forms of the equations, all terms are to be taken positive in sign. However, when summing dead and live load stresses to obtain the total vertical and lateral bending stresses, f_{bu} and f_ℓ, to apply in the equations, the signs of the individual dead and live load stresses must be considered.



Figure 3.2.1 Curved I-Girder Bridge Under Construction

3.2.2.1.2 Conceptual Basis

To explain the conceptual basis of the one-third rule equations, consider an isolated flange of an I-girder subjected to combined vertical and lateral bending. If the flange behaves compactly (e.g. a tension flange), it can be assumed to eventually develop the resistances associated with the idealized fully-plastic stress distribution shown on the right-hand side of Figure 3.2.2.

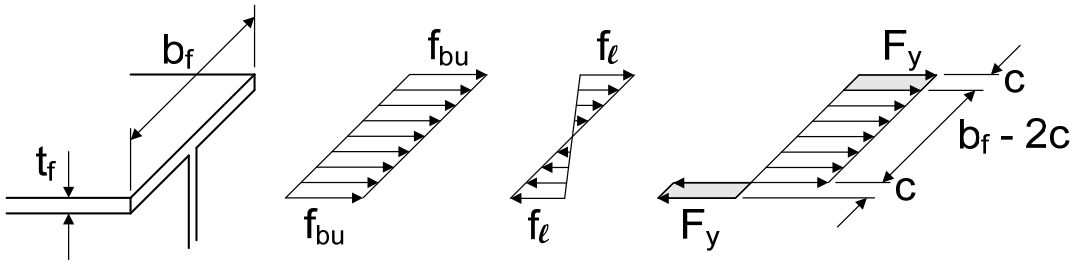


Figure 3.2.2 Fully-Plastic Stress Distribution under Combined Vertical and Lateral Bending (Compact Flange)

Referring to Figure 3.2.2, within this idealized stress distribution, the lateral moment resistance is generated by the strips of width c at the tips of the flange, and the remaining width ($b_f - 2c$) develops the resistance to the flange force associated with vertical bending. By equating the flange lateral bending moment related to the elastically computed lateral bending stress, $f_\ell S_\ell$, where S_ℓ is the lateral section modulus of the flange, to this lateral moment resistance, one obtains:

$$M_\ell = \frac{f_\ell b_f^2 t_f}{6} = F_y c t_f (b_f - c)$$

Equation 3.2.3

where b_f is the flange width and t_f is the flange thickness. This quadratic equation can then be solved for the width *c* to obtain:

$$c = \frac{b_f}{2}\left(1 - \sqrt{1 - \frac{2}{3}\frac{f_\ell}{F_y}}\right)$$

Equation 3.2.4

Similarly, by equating the elastic flange force, *P*, due to vertical bending to the fully-plastic flange force based on the remaining flange width as follows:

$$P = f_{bu} b_f t_f = F_y (b_f - 2c) t_f$$

Equation 3.2.5

and substituting the value of *c* from the Equation 3.2.4, the elastically-computed vertical bending stress associated with the flange fully-plastic resistance may be expressed as:

$$f_{bu} = F_y \frac{b_f - 2c}{b_f} = F_y \sqrt{1 - \frac{2}{3}\frac{f_\ell}{F_y}}$$

Equation 3.2.6

If one considers practical bridge I-girders, where f_ℓ is typically much smaller than F_y (e.g., $f_\ell \le 0.6F_y$), the preceding equation is approximated accurately by the simple linear equation:

$$f_{bu} = F_y - \frac{1}{3} f_\ell$$

Equation 3.2.7

The top curve in Figure 3.2.3 shows a plot of the theoretical fully-plastic strength of a discretely braced tension flange for various combinations of the major-axis bending stress, f_{bu}, and flange lateral bending stress, f_ℓ, as given by the exact Equation 3.2.6. The values of f_{bu} and f_ℓ have both been normalized by the flange yield strength, F_{yf}. Also plotted is the simpler linear Equation 3.2.7 based on the use of $1/3f_\ell$, which is shown to give a reasonable approximation of the more exact solution up to the specified limit on f_ℓ of $0.6F_{yf}$ given in *AASHTO LRFD* Article 6.10.1.6. The total of the lateral bending stresses from all sources, including curvature, wind, skew and/or deck overhang forces, is limited to $0.6F_{yf}$ because beyond that limit, the reduction in

vertical bending resistance due to the flange lateral bending tends to be greater than that comprehended by the one-third rule equation.

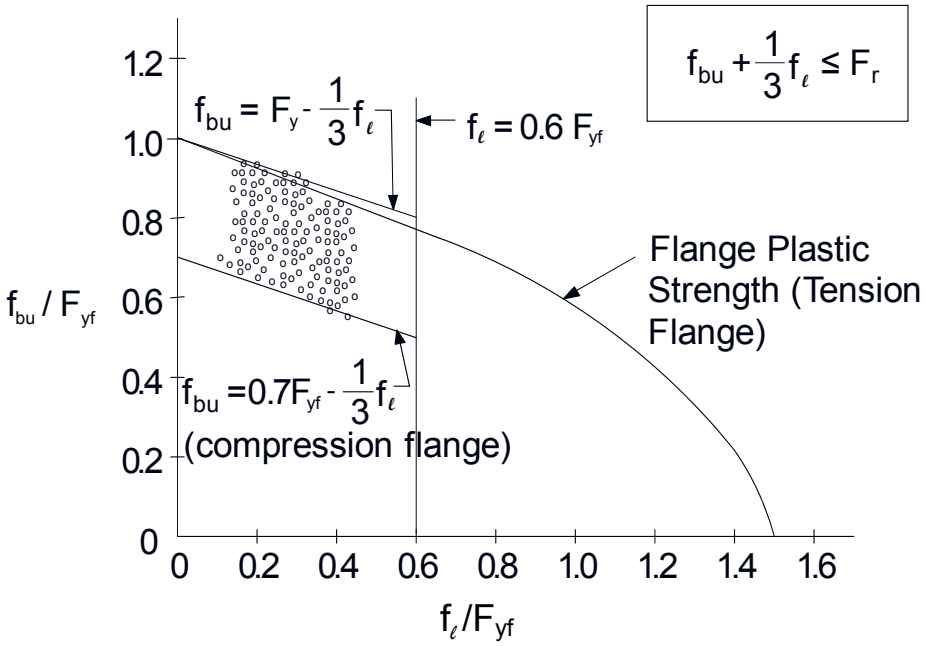


Figure 3.2.3 Normalized Plot of f_{bu} vs. f_ℓ

Research has shown that the 1/3 coefficient on f_ℓ also accurately captures the strength interaction between f_{bu} and f_ℓ for discretely braced compression flanges, including the various yielding and stability effects, again up to the limit of $0.6F_{yf}$ on f_ℓ. In this case, the resistance of the compression flange may be governed by either flange local buckling or flange lateral-torsional bucking and the flange may not be able to reach F_{yf} under the combined effects. In the case shown in Figure 3.2.3, the compression flange is only assumed able to reach $0.7F_{yf}$, for example, due to the effects of local or lateral-torsional buckling. In such cases, the slope of the line relating f_{bu} and f_ℓ, again based on the 1/3 coefficient, was found to be an excellent lower-bound fit to a large series of analytical, numerical and experimental results (represented by the series of dots in the figure). As such, the one-third rule equations may be considered both semi-analytical and semi-empirical.

The final stress form of the one-third rule equation (Equation 3.2.1) was obtained by changing F_{yf} (or $0.7F_{yf}$ for the compression flange in this case) to the factored flexural resistance of the flange, $F_r = \phi_f F_n$, and by bringing the flange lateral bending stress term, $1/3f_\ell$, over to the left-hand side of the equation since it represents a load effect (refer to the box in the upper right-hand corner of Figure 3.2.3). The moment form of the equation (Equation 3.2.2) was obtained by multiplying Equation 3.2.1 through by the elastic section modulus about the major-axis of the section. A more detailed

discussion of the derivation and validation of the one-third rule equations is provided in Reference 1.

3.2.2.1.3 Secondary Flange Lateral Bending Stresses

In addition to flange lateral bending resulting from non-uniform torsion due to curvature and other effects, other secondary effects generate additional flange lateral bending. These effects include the amplification effect and the radial effect.

3.2.2.1.3.1 Amplification Effect

The secondary effect causing the most significant lateral flange bending is the amplification effect as illustrated schematically in Figure 3.2.4, which results due to the lateral deflection of a discretely braced compression flange. As the compression flange curvature increases under load, additional lateral moment occurs due to the axial force in the compression flange acting through the lateral deflection of the flange (similar to the P-delta effect or amplification effect in beam-columns). This effect occurs in both straight and curved flanges. The amplification effect is considered negligible in the tension flange as the lateral deflections of that flange tend to be much smaller. Taking the equivalent beam-column analogy one step further, as applied to girder flanges in the one-third rule equation development, consideration must therefore be given to amplifying the compression-flange lateral bending stresses in certain situations.

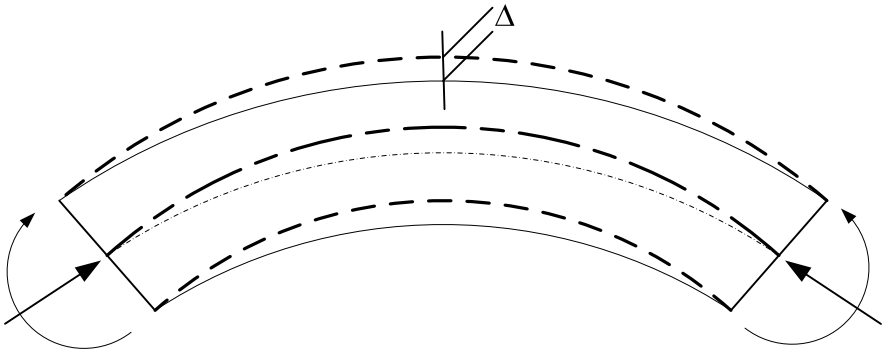


Figure 3.2.4 Amplification Effect in a Discretely Braced Compression Flange

The additional lateral bending in the compression flange due to the amplification effect may be estimated directly from a geometric nonlinear (i.e., elastic large deflection or second-order) analysis of the superstructure, or more simply and conveniently, by amplifying first-order compression-flange lateral bending stresses by the approximate amplification factor shown below in Equation 3.2.9. In bridge members, it is generally impractical to calculate second-order flange lateral bending stresses directly for the case of moving live loads.

In beam-column members subject to axial compression, secondary bending moments arise equal to the compression force times the lateral deflection of the member. Therefore, internal bending moments are amplified. In an analogous

fashion, first-order flange lateral bending stresses in discretely braced compression flanges may need to be amplified to guard against large unbraced lengths in which second-order lateral bending effects may be significant.

AASHTO LRFD Article 6.10.1.6 specifies that for discretely braced compression flanges, if the following equation is not satisfied, then second-order elastic compression-flange lateral bending stresses must be determined:
:

$$L_b \le 1.2L_p\sqrt{\frac{C_bR_b}{f_{bu}/F_{yc}}}$$

Equation 3.2.8
AASHTO LRFD Equation 6.10.1.6-2

where:

C_b = moment-gradient modifier specified in *AASHTO LRFD* Article 6.10.8.2.3
F_{yc} = specified minimum yield stress of the compression flange (ksi)
L_b = unbraced length (in.)
L_p = limiting unbraced length to reach a lateral-torsional buckling resistance equal to F_{max} specified in *AASHTO LRFD* Article 6.10.8.2.3 (in.)
R_b = web load-shedding factor specified in *AASHTO LRFD* Article 6.10.1.10.2

The second-order elastic lateral bending stresses may be determined by conservatively amplifying the first-order values based on the following equation in lieu of a direct geometric non-linear analysis:

$$f_\ell = \left(\frac{0.85}{1-\frac{f_{bu}}{F_{cr}}}\right)f_{\ell 1} \ge f_{\ell 1}$$

Equation 3.2.9
AASHTO LRFD Equation 6.10.1.6-4

where:

f_{bu} = largest value of the factored compressive vertical bending stress throughout the unbraced length in the flange under consideration (ksi)
$f_{\ell 1}$ = factored first-order compression flange lateral bending stress (ksi)
F_{cr} = elastic lateral-torsional buckling stress determined from *AASHTO LRFD* Eq. 6.10.8.2.3-8 (ksi)

Note that the right-hand side of Equation 3.2.8 is the limiting value of the unbraced length, L_b, for which f_ℓ equals $f_{\ell 1}$ in Equation 3.2.9. *It also should be noted that F_{cr} for use in* Equation 3.2.9 *is not limited to $R_bR_hF_{yc}$ as it would be when calculating the elastic lateral-torsional buckling resistance for the design of the compression flange (refer to AASHTO LRFD Article C6.10.1.6 and Section 3.2.6.4.1.2).*

Similar equivalent expressions are specified for use in *AASHTO LRFD* Article 6.10.1.6 (i.e. *AASHTO LRFD* Equations 6.10.1.6-3 and 6.10.1.6-5) whenever the vertical flexural resistance is expressed in terms of moment rather than flange stress.

Equation 3.2.9 represents an established form of the amplification equation used to estimate maximum second-order elastic moments in braced beam-column members whose ends are restrained by other framing (*1*). The purpose of this equation is to guard conservatively against large unbraced lengths in which second-order flange lateral bending effects are significant; for example, in certain construction situations such as when determining the effect of eccentric concrete deck overhang loads acting on exterior-girder flanges. For cases where the amplification of construction dead-load stresses is large, an additional alternative would be to consider conducting a direct geometric nonlinear analysis to more accurately determine the second-order effects. In the final constructed condition, the amplification factor need only be considered for the bottom flange in negative-flexure regions in continuous spans. In these cases, however, F_{cr} is increased significantly due to the moment gradient that exists in these regions, through the moment-gradient modifier C_b.

As shown in Reference 2, these equations give accurate to conservative estimates of flange second-order lateral bending stresses. The equations tend to be significantly conservative for larger unbraced lengths in which f_{bu} also approaches F_{cr}. In cases where the amplification resulting from this equation is large, consideration may be given to using an effective length factor k less than 1.0 in the calculation of the elastic lateral-torsional buckling resistance to appropriately increase F_{cr}. The base lateral-torsional buckling equations in the *AASHTO LRFD* Specifications conservatively assume k = 1.0. *AASHTO LRFD* Article C6.10.8.2.3 makes reference to a procedure (*3*, *4*) that can be used to calculate a reduced effective length factor for lateral-torsional buckling that accounts for the restraint from adjacent unbraced lengths that are less critically loaded than the unbraced length under consideration. The resulting lower value of k can be used to appropriately increase F_{cr} and to modify the unbraced length L_b in special situations. The use of this procedure is demonstrated in Reference 5.

The application of Equations 3.2.8 and 3.2.9 is demonstrated in the skewed/curved I-girder example provided in Section 5.1.

3.2.2.1.3.2 Radial Effect

A secondary effect causing additional flange lateral bending in horizontally curved girders is the so-called radial effect. A curved girder subjected to bending tends to deform radially as soon as loading commences, causing both flanges to undergo increased bowing. This effect can be thought of as resulting from a uniform load applied to both flanges in the radial direction.

The flange lateral moments due to the radial effect vary between brace points as shown in Figures 1.1.31 and 1.1.32 for the compression and tension flanges,

respectively. However, unlike the non-uniform torsion effect, the lateral moments in both flanges due to the radial effect have the same sign. Therefore, as a result of the radial effect, the lateral moments in the compression flange are amplified and the lateral moments in the tension flange are decreased. For a doubly-symmetric girder, the radial effect also causes the cross-frame forces acting on the compression and tension flanges to be different.

Flange lateral bending due to the combination of non-uniform torsion and the radial effect can be estimated reasonably accurately using a 3D refined analysis if the flanges and web are modeled discretely in-between brace points. Approximate analysis approaches to estimate flange lateral bending due to the radial effect are not currently available; however, this is generally compensated for by the conservative approximations often used to estimate lateral bending due to non-uniform torsion (as discussed in Section 2.3.2) and the amplification effect (as discussed in the Section 3.2.2.1.3.1).

3.2.2.1.4 Application of One-Third Rule Equations at Each Limit State

This section discusses the application of the one-third flexural resistance equations for I-girder design at each limit state in the *AASHTO LRFD* Specification. Depending on the limit state and the specific application, one or more different forms of the one-third rule equations may be applied. The different forms of the equations that appear in the specifications are summarized in Table 3.2.1 and discussed in more detail below. The one-third rule equations are intended for application only to I-girders with a concrete deck; through-girders are not comprehended.

Table 3.2.1 Summary of Limit State Application of One-Third Rule Equations

Discretely braced flanges:	**Equation**
Strength limit state (main provisions) and constructibility (strength)	$f_{bu} + \frac{1}{3} f_\ell \le F_r$ Equation 3.2.1
Strength limit state (Appendix A6)	$M_u + \frac{1}{3} f_\ell S_x \le M_r$ Equation 3.2.2
Constructibility (yielding)	$f_{bu} + f_\ell \le \phi_f R_h F_{yf}$ Equation 3.2.10
Service limit state	$f_{bu} + \frac{1}{2} f_\ell \le F_r$ Equation 3.2.11
Continuously braced flanges:	
All limit states	$f_{bu} \le F_r$ Equation 3.2.12

The first equation in Table 3.2.1 is the stress-based form of the one-third rule equation (Equation 3.2.1). *This form of the equation must be used at all sections in kinked (chorded) continuous or horizontally curved-girder bridges, and at all composite sections subject to negative flexure and at all non-composite sections in straight-girder bridges whose supports are skewed more than 20° from normal.* This form of the equation must also be used at sections in straight-girder bridges whose supports are normal or skewed not more than 20° from normal, and with intermediate cross-frames/diaphragms placed in contiguous lines placed parallel to the supports, that do not satisfy certain conditions that are spelled out in the specifications (refer to *AASHTO LRFD* Articles 6.10.2.2.2 and 6.10.2.2.3). Note that Equation 3.2.1 may optionally and conservatively be used at sections in such bridges that do satisfy those conditions. Equation 3.2.1 appears only in the main provisions of Section 6 and is used to check the resistance of discretely braced flanges at the strength limit state (*AASHTO LRFD* Articles 6.10.7.2 and 6.10.8.1). It is also used when checking the strength of discretely braced compression flanges for constructibility (*AASHTO LRFD* Article 6.10.3.2.1).

The second equation in Table 3.2.1 is the moment-based form of the one-third rule equation (Equation 3.2.1). *This form of the equation may not be used at any section in a kinked (chorded) continuous or horizontally curved-girder bridge*. This form of the equation may be used at composite sections subject to negative flexure or at non-composite sections in straight-girder bridges whose supports are normal or skewed not more than 20° from normal, and with intermediate cross-frames/diaphragms placed in contiguous lines placed parallel to the supports. Other conditions, spelled out in *AASHTO LRFD* Articles 6.10.2.2.3 and *AASHTO LRFD* Appendix A6, must also be satisfied in order to utilize Equation 3.2.2 to check discretely braced flanges of such sections at the strength limit state. Equation 3.2.2 appears throughout *AASHTO LRFD* Appendix A6, which accounts for the ability of stockier web I-sections in straight bridges with limited skews to develop flexural resistances significantly greater than M_y. Equation 3.2.2 may also be used at composite sections in positive flexure in straight-girder bridges at the strength limit state when the conditions spelled out in *AASHTO LRFD* Article 6.10.2.2.2 are satisfied.

Research has not yet been conducted to extend the provisions of *AASHTO LRFD* Appendix A6 to sections in kinked (chorded) continuous or horizontally curved-girder bridges, or to composite sections subject to negative flexure or non-composite sections in straight-girder bridges with skew angles exceeding 20 degrees from normal. The effects of the transverse redistribution of loads that occurs as interior-pier sections begin to yield in these bridges have not been examined. Severely skewed bridges with contiguous cross-frames have greater transverse stiffness relative to those with discontinuous cross-frames and thus already have relatively large cross-frame forces in the elastic range. As pier sections yield and begin to lose stiffness and shed their load, the forces in the adjacent cross-frames will increase. There is currently no established procedure to predict the resulting increase in the forces short of doing a refined non-linear 3D analysis. Such analyses cannot be performed with moving live loads since the influence surface method requires an elastic structure. With discontinuous cross-frames, significant lateral

flange bending effects usually occur. The resulting lateral bending moments (and stresses) are amplified in the bottom (compression) flange adjacent to the pier as the flange deflects laterally. There is currently no means to accurately predict these amplification effects as the flange is also yielding. Accurate prediction of even the first-order lateral bending effects requires a refined analysis model that should include the modeling of any actual lateral bearing restraints. Skewed supports also result in twisting of the girders, which is not recognized in plastic-design theory. The relative vertical deflections of the girders create eccentricities that are also not recognized in the theory. Thus, until further research work is done to examine these effects in greater detail, the conservative approach has been taken in the specification.

The moment form of the one-third rule equation will not be discussed further in this Manual. The application of this form of the equation is demonstrated and discussed in greater detail elsewhere (*6-8*).

The third equation of Table 3.2.1, Equation 3.2.10, is used to check for nominal yielding of discretely braced flanges (in compression or tension) of I-sections in flexure during construction. The 1/3 factor applied to the lateral bending stress is changed to 1.0 in this equation to prevent nominal yielding at the flange tips. The hybrid factor, R_h, is also introduced to account for the effect of the limited localized yielding that occurs in webs of hybrid sections on the flange stress. Note that the first and third equations of Table 3.2.1 are also to be used to check the top flanges of tub sections for flexure during construction.

The fourth equation of Table 3.2.1, Equation 3.2.11 is used to check the resistance of discretely braced flanges of I-girder sections at the service limit state. The equation is intended to limit the combined stresses in discretely braced flanges at the service limit state (under the Service II load combination) to prevent objectionable permanent deflections due to expected severe traffic loadings that might impair rideability. The factored resistance of the flange, F_r, on the right side of the equation in this case is taken as $0.95R_hF_{yf}$ for composite sections and $0.80R_hF_{yf}$ for non-composite sections. The 1/3 factor applied to the lateral bending stress is conservatively changed to ½ in this equation. Changing the factor to ½ allows the equation to approximate more rigorous yield-interaction equations corresponding to a load at the onset of yielding at the web-flange juncture under combined major-axis and lateral bending (*9*, *10*). The effect of any minor yielding that occurs at the flange tips prior to this stage is comprehended. By controlling the yielding at the web-flange juncture in this fashion, the resulting permanent deflections under the combined stresses will be small.

Amplification of the first-order lateral bending stresses may be required in discretely braced compression flanges, as discussed in Section 3.2.2.1.3.1, prior to the application of each of the preceding equations. First-order lateral bending stresses in discretely braced tension flanges are not to be amplified (i.e. the amplification factor is to be taken as 1.0).

Finally, the resistance equation for checking continuously braced flanges for flexure at all limit states is presented as the last equation in Table 3.2.1, Equation 3.2.12. When compared with the resistance equations for discretely braced flanges, the f_ℓ term is eliminated altogether for continuously braced flanges. For continuously braced flanges, in which the flange is encased in concrete or attached to the deck by shear connectors, lateral flange bending need not be considered.

Discretely braced compression flanges are subject to flange local buckling and lateral torsional buckling. Discretely braced tension flanges and continuously braced flanges (in tension or compression) are subject only to yielding. The determination of the factored flexural resistance, F_r, of discretely and continuously braced flanges at the strength limit state and for checking strength for constructibility will be discussed later in Sections 3.2.3 and 3.2.6. The application of the one-third rule equation is demonstrated in the skewed/curved I-girder example provided in Section 5.1.

3.2.2.2 Box Girders

Design provisions for straight composite steel tub girders were first introduced in the 10th Edition of the *AASHO* Bridge Specifications dated 1969. These provisions, developed as part of a joint effort between the American Iron and Steel Institute (AISI) and the University of Washington, were based on analytical work as well as some model tests. The provisions applied solely to tangent multi-box cross-sections. By implication, skewed supports were not considered. Torsion was implicitly considered and recognized in the distribution of live loads, but was thought to be insignificant in the design of tub girders based on the parameters covered by the research and limited in the specifications. The capacity of the bottom plate in compression was based on classical plate buckling equations (*11*). Special wheel-load distribution factors were developed to assign live load to the tub girders (*12*). To ensure that the wheel-load distribution factors were applied within the limits of the research study from which they were developed, limits were placed on the cross-section within the provisions.

Design provisions for horizontally curved box girders were included in the First Edition of the *AASHTO Guide Specifications for Horizontally Curved Bridges* dated 1980. These provisions considered more general design parameters. Torsion was explicitly considered. However, skewed supports were not specifically addressed, although clearly skewed supports create more torsion than does curvature in many typical bridges. This does not imply that skewed supports could not be considered within these provisions, but they clearly did not recognize the criticalness of skews. The original allowable stress design provisions were developed under the Consortium of University Research Team (CURT) Project, which was under the direction of the FHWA, a group of state DOTs, and industry representatives (*13*). The CURT Project is discussed further in Section 1.2. The Guide Specifications also included Load Factor Design provisions, which were developed separately under AISI Project 190 (*14*). The bridge cross-section was not limited in the curved-girder

provisions; instead, a rational analysis was required to distribute the loads. Box flange plate capacity was again based on classical plate buckling equations, only including the effect of shear stress (*15*). (*A box flange is explicitly defined in AASHTO LRFD Article 6.2 and herein as a flange that is connected to two webs*). The consideration of torsion implied consideration of forces developed in internal cross-frames and lateral bracing, as well as bracing between adjacent girders. Since consideration of distortional stresses was also required by these provisions, the computation of the distorsional warping stiffness of the box sections became necessary. This could be determined by using the BEF analogy (*16*). Torsional moments resulting from the superstructure analysis could be used in conjunction with the BEF analogy to compute cross-frame forces as well as through-thickness bending stresses due to cross-section distortion.

There were several failures of major steel box bridges around the world, generally during construction, which demonstrated that these bridges were not without their concerns. The British formed a special commission called the Merrison Commission to investigate these failures. From the work of that commission came the Rules by the same name. These new rules were extremely conservative in their attempt to ensure that no additional failures of box- girder bridges would occur. When applied literally, the rules ensured that no such bridges would fail because they would be too expensive to build. This conundrum prompted a major research project in Britain, which included both analytical studies and supportive testing. The research, completed in about 1980, resulted in the development of the modern BS54 box-girder design provisions.

In the late 1970s, the FHWA formed a task force to develop a new American design specification, specifically for steel box-girder bridges. The firm of Wolchuk and Mayrbaurl developed the *Proposed Design Specifications for Steel Box Girder Bridges* in 1980 (*17*). The vast majority of this work was derived from the British research. Although the proposed specifications were mainly directed toward larger box girder bridges than were typically built in the United States, it has been employed in the design of several bridges in the U.S.

The 2003 *AASHTO Guide Specifications for Horizontally Curved Steel Girder Highway Bridges* employed much of the earlier work from the 1980 AASHTO Guide Specifications. These specifications were developed by BSDI, Ltd. and Auburn University under the direction and sponsorship of the National Cooperative Highway Research Program (NCHRP), and included Load Factor Design provisions only (*18*). Several refinements were introduced in these provisions related specifically to tub girders. Shear connectors were required to be designed for torsional shear as well as vertical bending. These provisions also included special considerations for box girders during construction. Single-box and composite closed-box cross-sections were also covered more extensively than in any previous *AASHTO* provisions.

The design provisions from the 2003 *AASHTO* Guide Specifications were later incorporated, with some slight modification, into the *AASHTO LRFD* Specifications

as part of the 2005 Interims to the Third Edition of the specifications. This was done as part of a larger overall effort to unify the design provisions for straight and horizontally curved girder bridges. With the completion of this effort, the *AASHTO LRFD* flexural resistance equations for box girders now provide a unified approach for consideration of the combined effects of normal stress and St. Venant torsional shear stress in box flanges during construction, and in the final constructed condition at the strength limit state. This was done by utilizing the classical plate buckling equations from the earlier Guide Specifications, again with some slight modification. Combined major-axis and flange lateral bending from any source can also now be considered in the top flanges of tub sections during construction by applying the one-third rule equations that were developed for I-sections. Hence, the same equations can now be used to check the flexural resistance of box sections in both straight and horizontally curved girders at the appropriate limit states. These flexural resistance equations will be presented and discussed in greater detail in Sections 3.2.3 and 3.2.6.

3.2.3 LRFD Constructibility Design

3.2.3.1 General

Although not identified as a formal limit state, the *AASHTO LRFD* Specifications provide significant emphasis on constructibility and specify it as a primary objective of bridge design in *AASHTO LRFD* Article 1.3.1. *AASHTO LRFD* Article 2.5.3 states that bridges should be designed such that fabrication and erection can be performed without undue difficulty or distress, and so that locked-in construction force effects are within tolerable limits. If a particular sequence of construction has been assumed by the Design Engineer in order to induce a particular set of dead load stresses (e.g. a particular deck-placement sequence), that sequence must be identified in the contract documents. Also, for bridges considered to be of unusual complexity, at least one means of constructing the bridge must be provided by the Design Engineer in the contract documents to assist the Contractor in preparing a reasonable bid. Responsibility for the actual construction of the bridge (i.e. the “means and methods”) is left to the Contractor, who may still use a more innovative or custom construction sequence in order to gain an advantage over the competitors, if desired. The actual responsibilities of the Design Engineer in this regard are not well defined and are generally left up to the Owner to specify. In addition, according to *AASHTO LRFD* Article 2.5.3, if the design requires temporary bracing, strengthening or support (e.g. falsework) during the erection by the specified sequence, this must be also be identified in the contract documents. These construction issues are discussed in greater detail in Section 4.2.

AASHTO LRFD Article 6.5.1 requires that steel bridges be investigated for each stage that may be critical during construction, handling, transportation and erection. This is particularly important with respect to modern steel-girder designs, which are typically more slender than in the past due to the advent of composite construction, the introduction of higher-strength steels, and the increased use of limit-states design approaches leading to a lower load factor applied to dead-load effects. In

composite construction, the steel girders alone must be strong enough to carry the full non-composite dead loads. Since the composite section assists in resisting the live loads, smaller top flanges can be used in regions of positive flexure. Thus, more than half the depth of the web is in compression in these regions during construction. For tub sections in particular with a wide bottom flange relative to the top flanges, typically more than half of the depth of the web is in compression in regions of positive flexure during construction. Therefore, investigation of critical construction stages when the girders are non-composite is particularly important. Also, the use of higher-strength steels and limit-states design approaches, with their smaller factor of safety on dead load than traditional working stress design, have resulted in much lighter girders overall for the noncomposite condition than were required prior to these advancements.

All design checks for strength during construction are to be made using the appropriate factored loads specified in *AASHTO LRFD* Articles 3.4.1 and 3.4.2. The applicable strength load combinations for these design checks include Strength I, Strength III and Strength IV (see Section 1.3.3 for additional information on these load combinations). Strength III is for dead load in combination with wind load. For Strength IV, a load factor of 1.5 is applied to the dead load with no live load considered. *Note that although the Strength IV load combination will typically only control where the dead-to-live load force effect ratio exceeds about 7.0 for the bridge in its final condition, this load combination can control for critical construction stages and should be considered in all constructibility design checks for strength of steel bridges.* Traditional service-load design approaches have effectively applied a load factor ranging from about 1.67 to 1.82 to the dead load, with the *AASHTO* service-load design method effectively applying the latter. The base strength load combinations in more recent limit-state design approaches have applied a load factor ranging from about 1.25 to 1.3 to the dead load. The load factor of 1.5 specified for the Strength IV load combination is approximately an average of the dead load factors applied in the service-load and limit-states design approaches. With the advent of higher-strength steels and composite construction resulting in lighter non-composite girders, the application of the Strength IV load combination when checking the constructibility of steel bridges helps to ensure a level of strength and stability of the bare non-composite girder during critical construction stages that at least approaches that attained in the past using more traditional design methods.

When considering construction loads, or dead loads and temporary loads that act on the structure only during construction, the provisions of *AASHTO LRFD* Article 3.4.2 apply for determining the appropriate load factor to be applied to these loads in each strength combination. For Strength I, a load factor of 1.5 is to be applied to construction loads. For the calculation of deflections, all load factors are to be taken as 1.0. Slip of bolted connections is to be checked using the appropriate factored loads, with the slip resistance of the connection to be determined as specified in *AASHTO LRFD* Article 6.13.2.8.

Wind-load effects on the non-composite structure prior to casting of the deck are an important consideration. As specified in *AASHTO LRFD* Article 4.6.2.7.3, the need for temporary wind bracing to control lateral bending and lateral deflections during construction must be investigated. Since box girders are torsionally stiff and tub girders must always be provided with at least some degree of top lateral bracing, wind load generally has less effect on box girders than on I-girders during construction.

Potential uplift at bearings is also an important consideration and must be investigated at each critical construction stage according to *AASHTO LRFD* Article 6.10.3.1. Should concentrated loads not be applied to the web through a deck or deck system, and bearing stiffeners also not be provided at such locations, the web must satisfy the provisions of *AASHTO LRFD* Article D6.5 (Appendix D6) to prevent web crippling and web local yielding.

AASHTO LRFD Article 6.10.3.5 refers to the provisions of *AASHTO LRFD* Article 6.7.2, which state that vertical camber must be specified to account for the dead-load deflections. The deflections due to the steel weight, concrete weight, future wearing surface or other loads not applied at the time of construction are reported separately. When phased construction is specified, i.e. when the superstructure is built in separate longitudinal units with a longitudinal joint, the sequence of the load application must be recognized in determining the stresses and the required cambers. This requires analysis of the planned construction stages. Phased construction issues are discussed in greater detail in Sections 3.1.2.4 and 4.2.

3.2.3.2 Deck Placement Analysis

3.2.3.2.1 General

Steel girders in unshored composite construction must support their own weight plus the weight of the wet concrete deck slab, cross-frames, deck forms and construction equipment. The girders become composite once the concrete deck hardens and their behavior changes. The complicating factor is that, depending on the length of the bridge, the construction of the deck may likely require placement in sequential stages, as seen in Figure 3.2.5. Site conditions and access and other factors typically limit how much concrete can be cast in a single day.



Figure 3.2.5 Bridge Deck Under Construction in Sequential Stages

If the deck is placed in sequential stages, then certain sections of the girder will become composite before other sections, which must be considered in the load analysis. Temporary construction moments must be computed for each stage. These temporary construction moments, along with the torsional effects induced in the girders and bracing members during the deck casting, can be significantly greater than if the deck were placed in adjacent spans concurrently and must be considered during design. In addition, construction reactions and deflections must also be considered.

Therefore, as specified in *AASHTO LRFD* Article 6.10.3.4, sections in positive flexure that are composite in the final condition, but non-composite during construction (i.e. unshored construction), must be investigated during the various stages of the deck placement. Changes in load, stiffness and bracing during the various stages of the deck placement are to be considered. Potential uplift at the bearings is also to be investigated according to *AASHTO LRFD* Article 6.10.3.1. Once the critical deck-casting moments are determined from the analysis, the maximum flexural stresses, f_{bu}, in the flanges of the bare steel girders due to the factored moments are to be determined in order to perform the necessary constructibility verifications to ensure adequate strength for flexure, as specified in *AASHTO LRFD* Article 6.10.3.2 for I-sections and *AASHTO LRFD* Article 6.11.3.2 for box sections. Design verifications for shear are also required for shear according to *AASHTO LRFD* Articles 6.10.3.3 and 6.11.3.3 for I-sections and box sections, respectively.

Common practice when casting includes both positive and negative moment regions is to cast the slab in the positive moment regions first, and then cast the slab in the negative moment region over the support in order to minimize cracking at the top of

the slab. This is illustrated for a two-span continuous bridge at the top of Figure 3.2.6. However, when concrete is cast in a span adjacent to a span that already has a hardened deck, induced negative moments in the adjacent spans will cause tensile stresses and torsional shear stresses in the cured concrete that may result in transverse deck cracking. Thus, checks on the concrete deck stresses during the deck placement must also be made as specified in *AASHTO LRFD* Article 6.10.3.2.4. As discussed below in Section 3.2.3.2.5, provision of the minimum required one percent longitudinal reinforcement in the deck at these sections can help control the cracking.

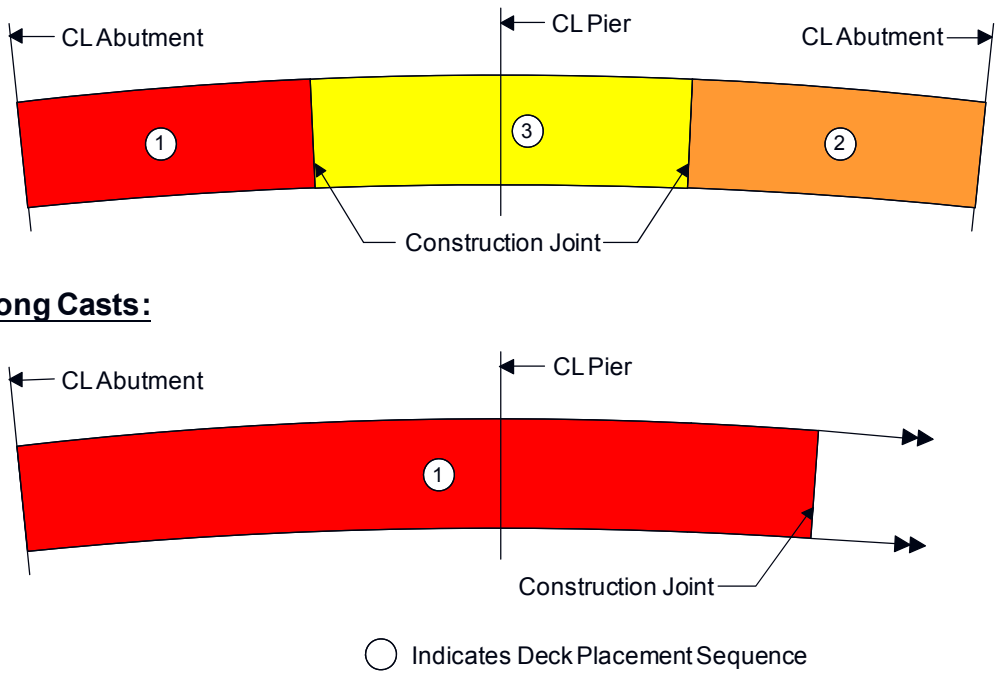


Figure 3.2.6 Casts with Both Positive and Negative Moment Regions

In a long cast, e.g. extending from one end of the bridge over an interior support into an adjacent span (refer to the bottom of Figure 3.2.6), it is possible that the concrete in the negative moment region over the support will harden and be subject to tensile stresses during the remainder of the cast, which may result in early age cracking of the deck. A retarder admixture may be required in the casts over the piers to reduce the potential for early cracking. Also, for such casts, or for casts on bridges that are short and narrow enough that the deck may be cast from one end of the bridge to the other (instead of in stages), the end span must still be checked for the critical instantaneous unbalanced case where wet concrete exists over the entire end span, with no concrete yet on the remaining spans.

3.2.3.2.2 Skewed Supports / Curvature

Skewed supports and/or curvature can complicate the deck-casting sequence. Keeping the deck placement reasonably symmetrical laterally minimizes eccentric or unbalanced loading and helps reduce differential deflections between adjacent

girders. It is preferable on skewed bridges where the differential deflections between girders are reasonably small to keep the finishing machine normal to the girders as it reduces the length of the machine. However, in cases with severe skews leading to large differential deflections, it may be necessary to consider skewing the finishing machine to avoid casting significantly more concrete than needed to meet the specified minimum deck thickness or roadway elevations and achieve the proper bridge geometry. Thus, for these structures, using refined analysis methods to perform the deck-staging analysis is obviously desirable.

Multiple casts may have to be made in the lateral direction also in wide structures that have multiple girders and/or with severe skews. Such casts result in the introduction of longitudinal construction joints.

3.2.3.2.3 Composite Stiffness

During deck placement, the actual composite stiffness depends on the amount of time that the concrete has had to cure before the next portion is cast, but such refinements are usually not considered in the analysis. If a retarder is not used, placed concrete usually obtains composite action in a matter of hours. Thus, the full composite stiffness is often used.

The stiffness of previously cast portions of the concrete deck when computing deflections considering deck staging should be based on a modular ratio closer to the short-term modular ratio since the concrete does not have enough time to creep significantly between casts. At least one State DOT has found the use of a concrete modulus of elasticity equal to 70 percent of the modulus of elasticity at 28 days (which results in a modular ratio of approximately 1.4n) to be appropriate in computing the stiffness.

3.2.3.2.4 Uplift

Uplift can occur at end supports during deck casting if the end spans are lightly loaded and may be particularly critical for curved structures and/or structures with skewed end supports. Thus, the potential for uplift during the deck casting must be investigated.

Options to consider when uplift occurs include:

- Rearranging the concrete placements
- Modifying the framing
- Specifying a temporary load over that support
- Specifying a tie-down bearing
- Removing the bearing
- If the uplift can be tolerated, performing another deck-staging analysis recognizing the absence of vertical restraint at the support experiencing lift-off in order to determine the correct moments and deflections

It is suggested that a load factor of 1.0 be applied to all downward support reactions due to component dead loads causing uplift, and a load factor of 0.9 be applied to all upward support reactions due to component dead loads resisting uplift for the investigation of uplift at critical construction stages.

3.2.3.2.5 Control of Deck Cracking

When the concrete deck is placed in a span adjacent to a span where the concrete has already been placed, as illustrated schematically in Figure 3.2.7, negative moment in the adjacent span causes tensile stresses in the previously placed concrete.

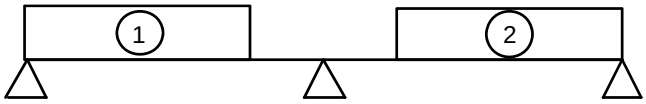


Figure 3.2.7 Sequential Deck Casting

Or in situations where long placements are made such that a negative-flexure region is included in the initial placement, it is possible for the concrete in that region to be subject to tensile stresses during the remainder of the deck placement, which could potentially lead to early cracking of the deck.

AASHTO LRFD Article 6.10.3.2.4 requires that the longitudinal tensile stress in a composite concrete deck due to the factored construction loads satisfy the following equation to control the cracking in the previously placed concrete, unless the total cross-sectional area of the longitudinal reinforcement is at least equal to 1 percent of the total cross-sectional area of the concrete deck (refer also to *AASHTO LRFD* Article 6.10.1.7):

$$f_{deck} \le \phi f_r = 0.9 f_r$$

Equation 3.2.13

where:

- ϕ = resistance factor for concrete in tension = 0.9 for reinforced concrete (*AASHTO LRFD* Article 5.5.4.2.1)
- f_r = deck concrete modulus of rupture specified in *AASHTO LRFD* Article 5.4.2.6 (ksi)

For normal-weight concrete:

$$f_r = 0.24\sqrt{f'_c}$$

Equation 3.2.14

The short-term modular ratio should be used when computing the concrete deck tensile stress; that is, *n* should be used to compute the composite section properties as opposed to 3*n* (refer to *AASHTO LRFD* Article 6.10.1.1.1d). The calculated

stress on the transformed section must be divided by n to obtain the stress in the concrete. f_r is the modulus of rupture, computed using the lower-bound equation for normal-weight concrete shown in Equation 3.2. For lightweight concrete, refer to *AASHTO LRFD* Article 5.4.2.6. A more accurate estimate of the concrete strength at the time the deck casts are made can be used to compute f_r and the modular ratio for this check, if desired.

Sufficient shear connectors should also be present at the end of each cast to transfer the tensile force from the deck to the top flange and prevent potential crushing of the concrete around the studs or fracturing of the studs. To estimate the length over which the tensile force must be transmitted via the factored shear resistance of the connectors, a 45-degree angle might be assumed from the end of the cast to where the concrete deck is assumed effective. If necessary, the tensile force in the deck can be lowered by modifying the placement sequence.

3.2.3.3 Deck Overhang Loads

3.2.3.3.1 General

AASHTO LRFD Article 6.10.3.4 also requires that the effect of forces from deck overhang brackets acting on the fascia girders be considered (Figure 3.2.8). The magnitude and application of the overhang loads assumed in the design should be shown on the contract documents.

The overhang brackets, which are usually spaced at 3 to 4 feet along the exterior girders, are typically attached to the top flanges of the girders. The brackets may either bear directly on the web or be carried to the intersection of the bottom flange and the web, which is preferred. The horizontal components of the bracket reactions transmitted directly onto the exterior girder web may cause the web to exhibit significant plate deformations. Excessive deformations of the web or top flange resulting from the bracket support forces may cause the deck finish to be problematic. Therefore, if the brackets bear on the girder web, particularly in the compression zone of the web, a means should be provided to ensure that the web is not damaged and that the associated deformations permit proper placement of the concrete deck. Also, when the brackets bear on the web, the lateral flange force and the force on the web increase significantly.

The eccentricity of the deck weight and other loads acting on the overhang brackets creates applied torsional moments on the fascia girders. The torsional moments bend the top flanges of exterior I-girders, or the outermost top flanges of tub girders, outward resulting in lateral bending stresses that must be considered in the design of the flanges. The top flange must have sufficient capacity to resist these lateral loads acting in combination with the vertical loads resulting from the deck casting. The effect of the reactions from the brackets on the cross-frame forces should also be considered.

Overhang bracket loads on curved bridges are particularly critical for the girder on the outside of the curve. The top flange is bent outward as the loads are applied to the brackets causing lateral flange moments of the same sense as the lateral flange moments due to curvature in regions of positive flexure. The opposite is true for the girder on the inside of the curve.



Figure 3.2.8 Overhang Brackets on a Curved I-Girder Bridge

3.2.3.3.2 Lateral Flange Forces

The sketch on Figure 3.2.9 shows a deck overhang bracket bearing directly on the bottom flange, which again is the preferred configuration.

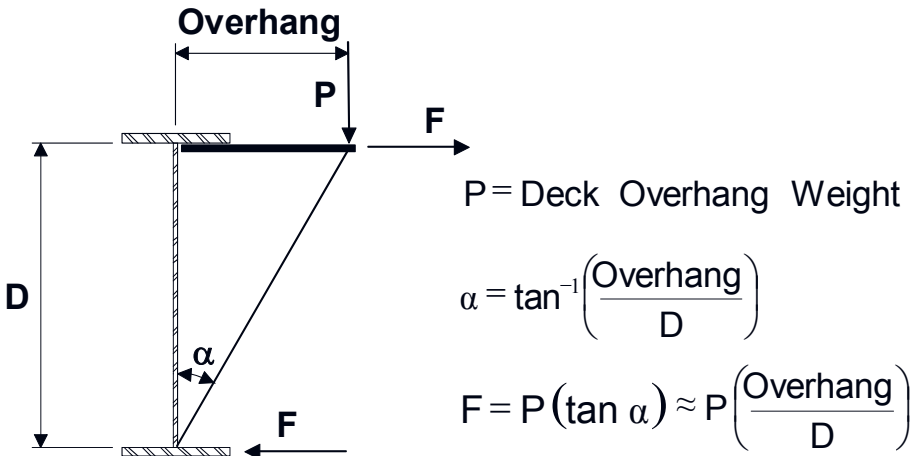


Figure 3.2.9 Lateral Flange Forces from Deck Overhang

The deck overhang weight is resisted by the brackets. If the bracket is assumed to extend near the edge of the deck overhang, it can be assumed that half of the deck overhang weight is placed on the fascia girder and half is placed on the overhang brackets. One-half of the deck haunch weights can also conservatively be included in the total overhang weight.

Besides the weight of the deck, typical loads that act on the overhang only during construction include the overhang deck forms, the screed rail, the railing, the walkway, the overhang brackets and the finishing machine. The Design Engineer should consider talking with local contractors to obtain accurate load values. Refer to *AASHTO LRFD* Article 3.4.2 for the appropriate load factors to be applied to these construction loads.

The lateral force, *F*, on the flanges due to the vertical load, *P*, on the overhang brackets may be computed as shown in Figure 3.2.9. From the equation for *F* shown in the figure, it is evident how *F* increases and the force on the web increases when the bracket bears directly on the web. Since the lateral force is dependent on the assumed angle that the brackets make with the web, the assumed magnitude and application of the overhang loads should be indicated on the contract documents. Should the Contractor deviate significantly from the assumed angle and/or loads, an additional investigation by the Contractor may be necessary.

The deck overhang construction loads are often applied to the non-composite section and removed when the bridge has become composite. Typically, the vertical bending moments due to these loads are small relative to other design loads. However, the Design Engineer may find it desirable in some cases to consider the effect of these moments, particularly in computing deflections for cambers in special situations involving large overhangs. The lateral bending moments due to these loads are often more critical. Where design checks for exterior girder including the

overhang force effects are made under the Strength I load combinations, where a smaller load factor is applied to the component dead load effects than under the Strength IV load combination, consideration might be given to conservatively considering the effect of the additional vertical bending moments resulting from the deck overhang loads.

3.2.3.3.3 Flange Lateral Bending Moments

The approximate equations shown below may be used to estimate the maximum lateral bending moments, M_ℓ, in the flanges (*acting at the cross-frames/diaphragms*) due to the lateral bracket forces in the absence of a more refined analysis. These equations are presented in *AASHTO LRFD* Article C6.10.3.4. The equation to use depends on how the lateral bracket forces are assumed applied to the top flange.

The first equation applies if a statically equivalent uniformly distributed bracket force, F_ℓ (kips/in.), is assumed.

$$M_\ell = \frac{F_\ell L_b^2}{12}$$

Equation 3.2.15

where:

L_b = unbraced length (in.)

The second equation applies if a statically equivalent concentrated lateral bracket force, P_ℓ (kips), is assumed to act at the middle of the unbraced length:

$$M_\ell = \frac{P_\ell L_b}{8}$$

Equation 3.2.16

Bracket dead loads are typically assumed applied uniformly. The finishing machine truss load may be assumed to be applied as a single concentrated load.

The two equations are based on the assumption of interior unbraced lengths in which the flange is continuous with adjacent unbraced lengths. In addition, approximately equal adjacent unbraced lengths are also assumed, such that the ends of the unbraced length under consideration are effectively torsionally fixed. When these assumptions do not approximate actual conditions for the unbraced length under consideration, the Design Engineer should consider other more appropriate idealizations.

Refined 3D analyses of the non-composite bridge for these overhang loads provides more accurate flange lateral bending moments and may identify any rotation of the overhang that could potentially affect the elevation of the screed when finishing the deck (Section 2.5.3.4.1.2).

3.2.3.3.4 Flange Lateral Bending Stresses

Once the lateral bending moments are obtained, the lateral bending stress in the flange under consideration can be computed based on the lateral section modulus of the rectangular flange:

$$f_\ell = \frac{M_\ell}{S_\ell} \le 0.6F_y$$

Equation 3.2.17

where:

f_ℓ = flange lateral bending stress (ksi)
M_ℓ = flange lateral bending moment (kip-in.)
S_ℓ = lateral section modulus of flange = $t_f b_f^2/6$ (in.^{3})

Total lateral bending stresses from all sources (e.g. deck overhang bracket effects, curvature and/or skew as applicable in this case) are limited to a maximum value of $0.6F_{yf}$ according to *AASHTO LRFD* Article 6.10.1.6. Beyond that limit, the reduction in the major-axis bending resistance of the flange due to flange lateral bending tends to be greater than that comprehended by the one-third rule equations used to check the resistance of the flange for the combined vertical and lateral bending effects.

3.2.3.3.4.1 Amplification of Lateral Bending Stresses

As discussed previously in Section 3.2.2.1.3.1, according to *AASHTO LRFD* Article 6.10.1.6, lateral bending stresses determined from a first-order analysis may be used in discretely braced compression flanges for which Equation 3.2.8 is satisfied. In applying this equation for the case of lateral bending stresses due to deck overhang effects (acting in combination with lateral bending stresses due to curvature and/or skew as applicable), f_{bu} is to be taken as the critical factored vertical compressive bending stress determined from the deck-casting analysis.

If the equation is not satisfied (which will often be the case for typical cross-frame/diaphragm spacings used in bridges), then *AASHTO LRFD* Article 6.10.1.6 requires that second-order elastic compression-flange lateral bending stresses be determined. These stresses may be determined by conservatively amplifying the first-order values based on Equation 3.2.9 in lieu of a direct geometric nonlinear analysis.

The amplified or second-order lateral bending stress in the compression flange, including the effects of the deck overhangs, curvature and/or skew as applicable, is then appropriately combined with the flexural stress, f_{bu}, in that flange determined from the deck-casting analysis to perform the necessary constructibility verifications specified in *AASHTO LRFD* Article 6.10.3.2 (for I-girders) or *AASHTO LRFD* Article

6.11.3.2 (for top flanges of tub girders). These verifications are described in more detail below in Section 3.2.3.4.

Tension flange lateral bending stresses are not to be amplified. Therefore, bottom flanges in regions of positive flexure, which are often also wider than top flanges, are typically not critical for the constructibility verifications.

3.2.3.4 LRFD Constructibility Design Verifications

A helpful flowchart detailing the required LRFD constructibility design verifications discussed below is provided in *AASHTO LRFD* Figure C6.4.1-1 (Appendix C6). The application of these design verifications is illustrated in the design examples presented in Sections 5.1 and 5.2.

3.2.3.4.1 I-Sections

3.2.3.4.1.1 General

The provisions for design for constructibility for I-section flexural members are given in *AASHTO LRFD* Article 6.10.3. The provisions are intended to provide adequate strength and stability of the main load-carrying members during construction, to properly account for dead load deflections, and to control the slip in load-resisting bolted connections at each critical construction stage to ensure that the proper geometry of the structure is maintained. *AASHTO LRFD* Article 6.10.3.1 states that nominal yielding or reliance on post-buckling resistance is not to be permitted for main load-carrying members during the critical stages of construction. An exception is permitted for the localized yielding of the web that may occur in hybrid members. To achieve these objectives, the requirements of *AASHTO LRFD* Articles 6.10.3.2 (Flexure) and 6.10.3.3 (Shear) must be satisfied at each critical construction stage, as detailed below. The required check on the concrete deck tensile stress during construction specified in *AASHTO LRFD* Article 6.10.3.2.4 was discussed previously in Section 3.2.3.2.5

3.2.3.4.1.2 Flexure

An important distinction is made between discretely braced and continuously braced flanges in the constructibility design provisions for flexure given in *AASHTO LRFD* Article 6.10.3.2. As discussed previously in Section 3.2.2.1.1, a discretely braced flange is braced at discrete intervals by bracing sufficient to restrain lateral deflection of the flange and twisting of the entire cross-section at the brace points. Both flanges along the entire length of the girder are considered to be discretely braced flanges for the non-composite steel I-girder during construction. A continuously braced flange is encased in hardened concrete or anchored by shear connectors. Lateral flange bending need not be considered for a continuously braced flange. A continuously braced compression flange is also assumed not to be subject to local or lateral-torsional buckling (local buckling and lateral-torsional buckling are discussed further in Section 3.2.6.4.1.2).

There are three equations that must be satisfied for discretely braced flanges in compression, as shown below and as presented in *AASHTO LRFD* Article 6.10.3.2.1. Each of these requirements must be satisfied for critical stages of construction.

The first equation for discretely braced flanges in compression is as follows:

$$f_{bu} + f_{\ell} \le \phi_f R_h F_{yc}$$

Equation 3.2.18
AASHTO LRFD Equation 6.10.3.2.1-1

where:

- ϕ_f = resistance factor for flexure specified in *AASHTO LRFD* Article 6.5.4.2 = 1.0
- f_{bu} = factored compression-flange vertical stress determined as specified in *AASHTO LRFD* Article 6.10.1.6 (ksi). f_{bu} is always taken as positive.
- f_{ℓ} = factored flange lateral bending stress determined as specified in *AASHTO LRFD* Article 6.10.1.6 (ksi). f_{ℓ} is always taken as positive.
- R_h = hybrid factor specified in *AASHTO LRFD* Article 6.10.1.10.1 (Section 3.2.6.3). For hybrid sections in which f_{bu} does not exceed the specified minimum yield strength of the web, R_h is to be taken equal to 1.0.

Equation 3.2.18 ensures that the maximum combined factored vertical and lateral bending stress in the compression flange during construction will not exceed the specified minimum yield strength of the flange times the hybrid factor R_h. As such, this equation is a yielding limit state check. For girders subject to significant lateral bending stresses and for members with compact or noncompact webs, Equation 3.2.18 will often control. However, the equation does not need to be checked for slender-web sections when f_{ℓ} is equal to zero. The definitions of compact, noncompact and slender-web sections are discussed further in Section 3.2.6.4.1.1. In categorizing the web as compact, noncompact or slender for these checks, the properties of the non-composite steel section are used. *Non-composite sections in all kinked (chorded) continuous and horizontally curved-girder bridges and in straight-girder bridges whose supports are skewed more than 20° from normal must always be treated as slender web sections, regardless of their web slenderness, in applying the specifications.*

The hybrid factor, R_h, is discussed further in Section 3.2.6.3. Note that for sections that are composite in the final condition, but non-composite during construction, different values of R_h must be computed for the checks in which the member is non-composite and for the checks in which the member is composite.

The second equation for discretely braced flanges in compression is as follows:

$$f_{bu} + \frac{1}{3} f_\ell \le \phi_f F_{nc}$$

Equation 3.2.19
AASHTO LRFD Equation 6.10.3.2.1-2

where:

F_{nc} = nominal flexural resistance of the compression flange determined as specified in *AASHTO LRFD* Article 6.10.8.2 (ksi)

Equation 3.2.19 ensures that the member has sufficient strength with respect to flange local buckling and lateral-torsional buckling under the maximum combined factored vertical and lateral bending stress in the compression flange during construction. Equation 3.2.19 is based on the stress-based form of the one-third rule equation (i.e. Equation 3.2.1) since the nominal flexural resistance for constructibility is always expressed in terms of the flange stress. The calculation of the flange local buckling (FLB) resistance and lateral-torsional buckling (LTB) resistance, F_{nc}, according to the *AASHTO LRFD* Specification provisions is discussed in detail in Section 3.2.6.4.1.2. Equation 3.2.19 will generally control for members with noncompact flanges having large unsupported lengths during construction in combination with zero or small values of f_ℓ. A noncompact flange is a compression flange with a slenderness ratio between the limiting values of λ_{pf} and λ_{rf} specified in *AASHTO LRFD* Article 6.10.8.2.2 (and discussed further in Section 3.2.6.4.1.2).

Note that for sections in *straight* I-girder bridges with compact or noncompact webs, *AASHTO LRFD* Article 6.10.3.2.1 permits the LTB resistance to be determined from the provisions of *AASHTO LRFD* Article A6.3.3 (Appendix A6), which include the beneficial effect of the St. Venant torsional constant, *J*. For straight members having larger unbraced lengths that utilize such sections, the additional LTB resistance obtained by including the contribution of *J* may be beneficial. The LTB resistance M_{nc} computed from the provisions of Appendix A6 is expressed in terms of moment because, in general, Appendix A6 permits flexural resistances to exceed the yield moment resistance M_{yt} or M_{yc}, as applicable. Therefore, if the LTB resistance is computed from Appendix A6 in such cases, the resulting LTB resistance M_{nc} must be divided by S_{xc} (taken equal to M_{yc}/F_{yc}) to express the resistance in terms of stress for application in Equation 3.2.19. The calculated resistance F_{nc} may exceed F_{yc} in some cases, however Equation 3.2.18 will control ensuring that the combined factored stress in the flange will not exceed F_{yc} during construction.

AASHTO LRFD Article 6.10.1.6 specifies that for design checks involving lateral-torsional buckling, the vertical bending compressive stress, f_{bu}, and flange lateral bending stress, f_ℓ, are to be taken as the largest values throughout the unbraced length in the flange under consideration, which is consistent with established practice in applying beam-column interaction equations involving member stability checks. For design checks involving flange local buckling, f_{bu} and f_ℓ may be taken as the corresponding values at the section under consideration. However, when maximum values of these stresses occur at different locations within the unbraced

length, which is often the case, it is conservative to use the maximum values in the local buckling check. As discussed previously in Section 3.2.2.1.3.1, amplification of the flange lateral bending stresses in discretely braced compression flanges may be required in some cases. *The sign of f_{bu} and f_ℓ is always taken as positive in these equations. However, when summing the lateral flange bending stresses due to curvature, skew and/or deck overhang effects to determine f_ℓ to apply in the equations, the signs of the individual stresses must be considered*. *AASHTO LRFD* Article 6.10.1.6 further specifies that the sum of the factored flange lateral bending stresses due to all sources (after amplification) cannot exceed $0.6F_{yf}$.

The third equation for discretely braced flanges in compression is as follows:

$$f_{bu} \le \phi_f F_{crw}$$

Equation 3.2.20
AASHTO LRFD Equation 6.10.3.2.1-3

where:

F_{crw}= nominal bend-buckling resistance for webs determined as specified in *AASHTO LRFD* Article 6.10.1.9 (ksi)

Equation 3.2.20 ensures that theoretical web bend-buckling will not occur during construction. The calculation of the web bend-buckling resistance, F_{crw}, is discussed in Section 3.2.4.3.2.2. F_{crw} is to be checked against the maximum compression-flange vertical bending stress due to the factored loads, f_{bu}. Utilizing the maximum compression stress in the web rather than the stress in the compression flange in order to obtain greater precision is not warranted for this check. Because the compression-flange stress is limited to F_{crw} during construction according to Equation 3.2.20, the web load-shedding factor, R_b, is always taken equal to 1.0 when computing the nominal flexural resistance of the compression flange for the constructibility checks (the web load-shedding factor, R_b, is discussed further in Section 3.2.6.2). As a result, the R_b factor is not included in Equations 3.2.18 and 3.2.19. Note also that the web slenderness of compact and noncompact web sections is limited such that theoretical web bend-buckling will not occur at elastic stress levels, computed according to beam theory, at or below F_{yc}. Therefore, the specification indicates that Equation 3.2.20 need not be checked for these sections.

Options to consider should Equation 3.2.20 be violated under the construction condition are given at the end of *AASHTO LRFD* Article C6.10.3.2.1 and include:

- Providing a larger compression flange or a smaller tension flange to reduce the elastic depth of the web in compression, D_c;
- Adjusting the deck-placement sequence to reduce the compressive stress in the web;
- Providing a thicker web; or
- As a last resort, should the previous options not prove practical or cost-effective, providing a longitudinal web stiffener.

According to *AASHTO LRFD* Article 6.10.1.6, for design checks involving web bend-buckling or yielding, f_{bu} and f_ℓ may be taken as the corresponding values at the section under consideration. As discussed above, it is conservative to use the maximum values of these stresses within the unbraced length in this check.

AASHTO LRFD Article 6.10.3.2.2 requires that a discretely braced tension flange satisfy the following relationship during critical stages of construction to prevent nominal yielding under the combined factored vertical bending and lateral bending stresses:

$$f_{bu} + f_\ell \le \phi_f R_h F_{yt}$$

Equation 3.2.21
AASHTO LRFD Equation 6.10.3.2.2-1

AASHTO LRFD Article 6.10.3.2.3 requires that the following relationship be satisfied for continuously braced flanges in compression or tension during critical stages of construction to prevent nominal yielding of the flange:

$$f_{bu} \le \phi_f R_h F_{yf}$$

Equation 3.2.22
AASHTO LRFD Equation 6.10.3.2.3-1

As mentioned previously, flange lateral bending need not be considered for a continuously braced flange. The lateral resistance of the concrete deck is generally adequate to compensate for the neglect of any initial lateral bending stresses in the steel prior to placement of the deck and any additional lateral bending stresses induced after the deck has been placed.

The design of discretely braced flanges in tension, continuously braced flanges, and discretely braced flanges in compression in regions of negative flexure is usually not controlled by constructibility verifications.

3.2.3.4.1.3 Shear

AASHTO LRFD Article 6.10.3.3 requires that webs satisfy the following equation during critical stages of construction:

$$V_u \le \phi_v V_{cr}$$

Equation 3.2.23
AASHTO LRFD Equation 6.10.3.3-1

where:

ϕ_v = resistance factor for shear specified in *AASHTO LRFD* Article 6.5.4.2 (= 1.0)

V_u = factored shear in the web at the section under consideration due to the permanent loads and construction loads applied to the non-composite section (kips)

V_{cr} = shear-yielding or shear-buckling resistance determined from *AASHTO LRFD* Equation 6.10.9.3.3-1 (kips)

The nominal shear resistance for this check is limited to the shear-yielding or shear-buckling resistance. The use of tension-field action is not permitted to resist construction loads. Use of tension-field action is permitted at the strength limit state after the deck has hardened or is made composite (if the section along the entire panel is proportioned according to the requirements for tension-field action). The calculation of V_{cr} and the post-buckling shear resistance due to tension-field action is discussed further in Section 3.2.7.

3.2.3.4.2 Box Sections

3.2.3.4.2.1 General

The provisions for design for constructibility for box-section flexural members are given in *AASHTO LRFD* Article 6.11.3. These provisions essentially refer back to the design provisions for constructibility given in *AASHTO LRFD* Article 6.10.3 for I-section flexural members, with a few exceptions as discussed below. The design provisions for constructibility are intended to provide adequate strength and stability of the main load-carrying members during construction, to properly account for dead-load deflections, and to control the slip in load-resisting bolted connections at each critical construction stage to ensure that the proper geometry of the structure is maintained. *AASHTO LRFD* Article 6.10.3.1 states that nominal yielding or reliance on post-buckling resistance is not permitted for main load-carrying members during critical stages of construction. An exception is permitted for the localized yielding of the web that may occur in hybrid members.

The geometry of individual box sections must be maintained throughout all stages of construction as specified in *AASHTO LRFD* Article 6.11.3.1. Eccentric loads that may occur during construction should be considered. The need for temporary or permanent intermediate internal and/or external cross-frames/diaphragms, top lateral bracing, or other means must be investigated to ensure that deformations of the box are controlled. Important considerations in investigating the need for these members are discussed in 3.1.2.8 and 3.1.2.9. As indicated in *AASHTO LRFD* Article C6.11.3.1, temporary cross-frames/diaphragms that are not part of the original design should be removed because the structural behavior of the box section, including the load distribution, may be affected if these members are left in place. As discussed further in Section 3.1.2.8.1.4, released temporary members

may have large built-up forces in them after the deck has hardened, which may introduce restoring forces into the bridge upon removal.

AASHTO LRFD Article C6.11.3.1 suggests that for painted box sections, an allowance be made in the dead load for the weight of the paint. An allowance of three percent of the steel weight has been found to be a reasonable allowance.

To ensure the goal of providing adequate strength and stability of box-section flexural members during construction, without permitting nominal yielding (except for localized web yielding in hybrid sections) or relying on post-buckling resistance, the requirements of *AASHTO LRFD* Articles 6.11.3.2 (Flexure) and 6.10.3.3 (Shear) must be satisfied at each critical construction stage. The required check on the concrete deck tensile stress during construction specified in *AASHTO LRFD* Article 6.10.3.2.4, which is also applicable to box girders, was discussed previously in Section 3.2.3.2.5 and will not be repeated here. Further information regarding the construction of composite steel box-girder bridges may be found in Reference 19.

3.2.3.4.2.2 Flexure

Top Flanges of Tub Sections

AASHTO LRFD Article 6.11.3.2 specifies that for critical stages of construction, the constructibility design provisions of *AASHTO LRFD* Articles 6.10.3.2.1 through 6.10.3.2.3 for flexure of I-sections are to be applied to the top flanges of tub sections. A single exception is that the provisions of *AASHTO LRFD* Article A6.3.3 (Appendix A6) are *not* to be applied in determining the lateral torsional buckling resistance of top flanges of straight tub sections in compression with compact or noncompact webs.

The equations of *AASHTO LRFD* Articles 6.10.3.2.1 through 6.10.3.2.3 are discussed in detail above in Section 3.2.3.4.1.2 and are not repeated here. Essentially, a single top flange of a tub section is considered equivalent to the top flange of an I-section in applying the equations; therefore, it is recommended that the checks using these equations be made for half of the tub section. *AASHTO LRFD* Article 6.11.3.2 conservatively suggests that the unbraced length be taken as the distance between interior cross-frames/diaphragms in calculating the lateral torsional buckling resistance of the flanges. Further discussion on brace points for top flanges of tub sections subject to compression is provided in Sections 3.1.2.8.5.2 and 3.1.2.9.2. The web depth, D, and the depth of the web in compression, D_c, should each be measured along the web slope n computing the web bend-buckling resistance, F_{crw}, for use in Equation 3.2.20 for sections with inclined webs; that is, D_c should be divided by cos θ, where θ is the angle of inclination of the web plate with respect to the vertical. The calculation of the web bend-buckling resistance, F_{crw}, is discussed further in Section 3.2.4.3.2.2. The effects of St. Venant torsional shear stress in the top flanges are neglected in checking all these equations.

The equations of *AASHTO LRFD* Articles 6.10.3.2.1 and 6.10.3.2.2 (i.e. Equations 3.2.18, 3.2.19 and 3.2.21) allow for the direct consideration of flange lateral bending

in discretely braced top flanges of tub sections due to various sources, if deemed significant. Potential sources of lateral flange bending include curvature, wind loads and eccentric concrete deck overhang loads acting on the outermost flanges of fascia girders. Additional potential sources of significant lateral bending in discretely braced top flanges occur in tub girders with inclined webs and with web slopes exceeding 1 to 4, in tub girders where the unbraced length of the top flange exceeds 30 feet, and in tub girders with Warren Truss top lateral bracing configurations, as discussed further in Sections 3.1.2.8.5.2 and 3.1.2.9.2.

Box Flanges

AASHTO LRFD Article 6.11.3.2 specifies that non-composite box flanges in compression satisfy the following requirements for critical stages of construction:

$$f_{bu} \le \phi_f F_{nc}$$

Equation 3.2.24
AASHTO LRFD Equation 6.11.3.2-1

and:

$$f_{bu} \le \phi_f F_{crw}$$

Equation 3.2.25
AASHTO LRFD Equation 6.11.3.2-2

where:

- ϕ_f = resistance factor for flexure specified in *AASHTO LRFD* Article 6.5.4.2 = 1.0
- f_{bu} = factored longitudinal flange stress at the section under consideration calculated without consideration of longitudinal warping (ksi)
- F_{crw}= nominal web bend-buckling resistance determined as specified in *AASHTO LRFD* Article 6.10.1.9 (see Section 3.2.4.3.2.2) (ksi)
- F_{nc} = nominal flexural resistance of box flanges in compression determined as specified in *AASHTO LRFD* Article 6.11.8.2 (see Section 3.2.6.1) (ksi). In computing F_{nc} for constructibility, the web load-shedding factor, R_b (Section 3.2.6.2), is to be taken equal to 1.0.

Equation 3.2.24 is a check for local buckling of the flange during critical stages of construction. *Note that lateral flange bending and lateral-torsional buckling are not a consideration for box flanges*. Equation 3.2.25 ensures that theoretical web bend-buckling will not occur during construction at sections where non-composite box flanges are subject to compression. This check only need be made for sections with slender webs. The calculation of the web bend-buckling resistance, F_{crw}, is discussed further in Section 3.2.4.

Non-composite box flanges in tension and continuously braced box flanges in tension or compression must satisfy the following requirement for each critical stage of construction:

$$f_{bu} \le \phi_f R_h F_{yf} \Delta$$

Equation 3.2.26
AASHTO LRFD Equation 6.11.3.2-3

where:

$$\Delta = \sqrt{1 - 3\left(\frac{f_v}{F_{yf}}\right)^2}$$

Equation 3.2.27
AASHTO LRFD Equation 6.11.3.2-4

f_v = factored St. Venant torsional shear stress in the flange at the section under consideration not to exceed the factored torsional shear resistance of the flange F_{vr} given by *AASHTO LRFD* Equation 6.11.1.1-1 (Equation 3.2.71) (ksi)

$$= \frac{T}{2A_o t_f}$$

Equation 3.2.28
AASHTO LRFD Equation 6.11.3.2-5

A_o = enclosed area within the box section (in.^{2})
R_h = hybrid factor determined as specified in *AASHTO LRFD* Article 6.10.1.10.1
t_f = thickness of the flange under consideration (in.)
T = internal torque due to the factored loads (kip-in.)

Equation 3.2.26 is a yielding check based on the von Mises yield criterion (*20*), which is used to consider the effect of the St. Venant torsional shear in combination with flexure. The enclosed area A_o in Equation 3.2.28 is to be computed for the non-composite box section. If top lateral bracing in a tub section is attached to the webs, A_o is to be reduced to reflect the actual location of the bracing (*AASHTO LRFD* Article 6.7.5.3).

The effects of longitudinal warping stresses in the flanges due to cross-section distortion are not considered in checking Equations 3.2.24 and 3.2.26. However, the effects of these distortion-related stresses must be considered in certain cases when checking bolt slip in flange splices for the construction condition, as discussed further in Section 3.3.7.2.5. Also, in checking these equations, the torque *T* should comprehend the critical torque induced in the girder during the deck-placement sequence.

Non-composite box flanges on top of closed-box sections receive the weight of the wet concrete and other loads during construction before the deck hardens. Therefore, the flange must be designed as a non-composite box flange for those loads. *AASHTO LRFD* Article 6.11.3.2 specifies that the maximum vertical

deflection of the non-composite box flange due to the unfactored permanent loads, including the self-weight of the flange, and any unfactored construction loads must not exceed 1/360 times the transverse span between webs. Through-thickness bending stresses in the flange due to the factored permanent loads and factored construction loads must not exceed 20.0 ksi. The flange may be considered to act as a simple span between webs in making these checks. Transverse and/or longitudinal stiffening of the box flange may be necessary to control the flange stresses and deflections under these loads.

3.2.3.4.2.3 Shear

AASHTO LRFD Article 6.11.3.3 refers back to the shear requirement specified in *AASHTO LRFD* Article 6.10.3.3 (see Section 3.2.3.4.1.3).

The provisions of *AASHTO LRFD* Article 6.11.9, as applicable, are to be applied in checking Equation 3.2.23,. That is, for box sections with inclined webs, the web must be designed for the total vertical shear in the plane of the web, V_{ui}, taken equal to V_u divided by $\cos\theta$, where θ is the angle of inclination of the web plate with respect to the vertical (see Equation 3.2.153). Also, in computing the shear-yielding or shear-buckling resistance, V_{cr}, for the case of inclined webs from *AASHTO LRFD* Equation 6.10.9.3.3-1, the web depth, D, must be taken as the depth of the web measured along the slope or $D/\cos\theta$. The calculation of V_{cr} is discussed further in Section 3.2.7.

V_u is to be taken as the sum of the flexural and St. Venant torsional shears in checking this requirement fr all box sections for which the effects of St. Venant torsion must be considered (including all box sections in curved and/or skewed bridges). In cases where there is significant St. Venant torsional shear, the dead load shear in one web is greater than the flexural dead load shear by the amount of the torsional shear and less than the flexural shear by the same amount in the other web at the same cross-section. For practicality, both webs are generally detailed as if they had the same critical shear. Shears in the web due to warping torsion and due to cross-section distortion may be ignored in making this check for typical box sections, as indicated in *AASHTO LRFD* Article C6.11.9.

3.2.4 LRFD Service Limit State Design

3.2.4.1 General

AASHTO LRFD Article 1.3.2.2 specifies that the service limit state be taken as restrictions on stress, deformations and crack width under regular service conditions. As mentioned in the Commentary to this article, service limit state criteria are more experience-based and somewhat less scientifically oriented.

AASHTO LRFD Article 6.5.2 specifies that for steel structures, the provisions of *AASHTO LRFD* Article 2.5.2.6, dealing primarily with the control of elastic live-load deformations and the consideration of span-to-depth ratios, are to apply as applicable. Permanent deformations must also be controlled for I- and box-section flexural members to prevent objectionable permanent deformations caused by localized yielding and potential web bend-buckling under expected severe traffic loadings, which might impair rideability (*AASHTO LRFD* Articles 6.10.4.2 and 6.11.4). These checks are made under the Service II load combination (refer to Section 1.3.3). A check on the tensile concrete deck stresses under the Service II load combination must also be made as specified in *AASHTO LRFD* Article 6.10.1.7 to ensure that the minimum required one percent longitudinal reinforcement is provided in the deck at the appropriate sections to help control the cracking of the deck.

A helpful flowchart detailing the required LRFD service limit state design verifications discussed below is provided in *AASHTO LRFD* Figure C6.4.2-1 (Appendix C6). The application of these design verifications is illustrated in the design examples presented in Sections 5.1 and 5.2.

3.2.4.2 Elastic Deformations

AASHTO LRFD Article 6.10.4.1 deals with checks related to the control of elastic deformations in steel I-girder bridges under normal service conditions. For box-girder bridges, *AASHTO LRFD* Article 6.11.4 refers back to *AASHTO LRFD* Article 6.10.4.1. Specifically, this article then refers back to the applicable provisions of *AASHTO LRFD* Article 2.5.2.6 dealing with optional live-load deflection criteria and the criteria for span-to-depth ratios. Span-to-depth ratios were discussed previously in Section 3.1.3.1. Live load deflection is discussed below.

3.2.4.2.1 Live Load Deflection

Limitation of live load deflection is a service limit state; such criteria are specified in *AASHTO LRFD* Article 2.5.2.6.2 and limit the computed elastic live-load vertical deflections. Although the criteria are optional, most states require their application. The obvious reason for these provisions is to provide a level of stiffness. However, the reason(s) for a required stiffness is less clear.

Until the 1960s, bridges were designed to a working level; i.e., they were designed for a desired service level. Live load deflection has been a service design consideration from early times in the design of steel highway bridges in the U.S. Limits on live load deflection can be traced back to the railway specifications of the late 1800s, which gave limitations similar to those now given in the *AASHTO LRFD* Specifications (*21*). The requirement to limit deflection of a railroad bridge seems rather self-evident when one considers the rocking forces that could lead to catastrophe on a bridge that was too flexible. Large deflections could also lead to secondary stresses that might cause fatigue cracking that was not well understood in the early days of iron and steel bridges. The first specified live load deflection limit

for steel highway bridges in the U.S. was in the Third Edition *AASHO Specification,* 1941. The suggested limit of Span/800 under vehicular load, which remains in the specification today (*AASHTO LRFD* Article 2.5.2.6.2), is thought to have been recommended by the Bureau of Public Roads after studying several steel-beam bridges that were reportedly subjected to objectionable vibrations (*21*). This limit, in addition to the maximum span-to-depth ratio of 25 that was recommended at that time, were the first attempts to control service load deformations. This was only reasonable since the entire philosophy of working stress design was based on serviceability and not strength.

The advent of higher strength steels and concomitant increases in design stresses led to concern about the effect of live load deflection on economics. As early as the 1950s, *ASCE* began an investigation of the basis for these limits and found numerous shortcomings, including no clear basis for their use, and no evidence of structural damage that could be attributed to excessive deflections (*22*). Competition with prestressed concrete bridges in the 1960s led to further investigations as to the need for this serviceability limit. Field investigations at that time, again, showed no direct correlation.

Not only did the limitation remain, but In the early 1960s an additional limit was introduced; the live load deflection limit on steel bridges with both pedestrian and vehicular loads was set at Span/1000 as a result of isolated concerns related to human response. The criteria remained optional. One legend has it that this limit arose when a mother and wife of a political figure who was pushing her baby in a carriage across a bridge attributed the awakening of her baby to vibration of the bridge (*21*). This complaint prompted the state's governor to chastise the State Bridge Engineer. The issue of human comfort becomes a serviceability issue when people who might use a bridge find its motion objectionable. This is a departure from the other structural criteria provided in the Specification.

The complex issue of the human response of occupants of moving vehicles and of pedestrians to motion has been extensively studied. However, there still are no definitive guidelines on the tolerable limits of dynamic motion or static deflection to ensure creature comfort. Guidelines for limiting the natural frequency of bridges to provide tolerable motion are contained in the *Ontario Highway Bridge Design Code* (*23*), in which the deflection limits are tied to the first fundamental frequency of the superstructure. These limits are provided in the form of graphs and are separated in conjunction with the anticipated pedestrian use. These provisions require that the designer compute the natural frequency of the composite bridge. Wright and Walker found a tenuous theoretical relationship between deflection and natural frequency (*24*). They observed that user comfort was an important factor. They reported that psychologists had found that humans think that vertical deflection they sense is about ten times the actual deflection. Wright and Walker postulated that human discomfort is due to acceleration, not deflection alone. They proposed a parameter, defined as the dynamic component of acceleration in the fundamental mode of vibration, be limited to 100 in^2/sec. The authors suggest that such acceleration is

within the tolerable range experienced in building elevators contemporary with the writing of the paper (1960s). They further suggested that only bridges designed for pedestrian traffic or stationary vehicles be limited in motion by such a serviceability criterion. The issue of bridge vibrations and their relation to human response, along with the development of a reasonable means of controlling bridge vibrations to ensure adequate creature comfort, remains a complex and subjective issue in need of further study.

Other suggested live load deflection limits contained in *AASHTO LRFD* Article 2.5.2.6.2 include a limit of Span/300 for vehicular loads on cantilever arms, and a limit of Span/375 for combined vehicular and pedestrian loads on cantilever arms.

The 'Span' is typically taken as the full span length of the girder (arc span length for curved girders) when checking all the deflection limits. The limit on span-to-depth ratio for continuous spans is usually determined by defining the span as the length between points of permanent load contraflexure. This leads to shallower bridges with an increased flexibility when the limiting live load deflection is defined based on the actual span. Some states conservatively limit deflection by using the distance between points of permanent load contraflexure in computing the permissible deflection. Field tests have confirmed that decks of continuous composite girders in negative moment regions actually behave compositely. Tradition has assumed those regions to be non-composite. Use of the entire deck obviously reduces the computed deflections and brings them closer to actual with regard to the behavior of the deck.

The combination of moving from 33- to 70-ksi yield-stress steel, along with the introduction of composite design, LFD and then LRFD, and the increase of the span-to-depth ratio for steel girders from 25 to 30 had a net effect of roughly increasing the permitted live load deflection by about threefold. Field experience of bridges built has provided scant evidence that the increased flexibility of steel bridges had led to any reduced functionality. It seems that some logical limit exists, but such a limit has proved elusive. It has also been shown that computation of live load deflection as specified in *AASHO* and *AASHTO* is not likely to predict the actual deflection. And so, as the live load deflection limit has become an increasingly critical factor in the design of steel bridges utilizing the higher-strength high performance steels (HPS), an additional investigation has recently been launched into the potential need for improved live load deflection criteria for steel bridges (*25*).

The live load used to compute live load deflection has traditionally been the same as the design live load. This made sense for design based on service loads only. However, for strength-based design, a different and lighter load for service limit state checks is logical since the criteria are based on a different philosophy. In strength design, the capacity of the structure is challenged. Serviceability relates to the structure response to likely loads; these likely loads are reasonably less than the load used to check structural strength. However, even in service load design, live load application has often been different from application for design of the elements. For example, the 1941 *AASHO* Bridge Specifications permitted the Engineer to compute the moment in a stringer for deflection purposes by assuming that all of the

lanes are loaded with the design load and that the resulting load is uniformly distributed equally to all stringers where adequate depth diaphragms or cross-frames exist. This provision has since been interpreted to allow a reduction in load based on the multiple presence factor provision. The practice of loading all lanes appears to be at odds, at least in some cases, with the provision in the 1935 Edition (Art. 3.2.11), which states: "In calculating stresses in structures which support cantilevered sidewalks, the sidewalk shall be considered as fully loaded on only one side of the structure if this condition produces maximum stress." This provision reveals an understanding that loading on the far side of a multi-stringer bridge unloads the near side; this understanding has been borne out in refined analyses. If one visualizes the entire cross-section rotating as a rigid body under each of the above load cases, it is apparent that the opposite side of the bridge rises when one side is loaded. Hence, from the time it was introduced, the assumption of uniform loading of girders for computation of deflection was known to be simply a means to require less stiffness.

The provisions of *AASHTO LRFD* Article 2.5.2.6.2 allow all integer 12-foot wide design lanes to be loaded with all girders assumed to deflect equally. This clause should only be applied for straight-girder bridges when the longitudinal stiffness of the individual girders at all cross-sections is the same. *Cases where the clause should not be applied include cases with skewed supports and skew angles exceeding 20 degrees from normal, different girder depths, or girders with different flange sizes. The assumption of equal live load deflection should not be applied to horizontally curved bridges.* The *AASHTO LRFD* specifications are silent with regard to the application of this assumption to bridges with skewed supports. The live load deflection of individual girders should be computed for curved girders (*AASHTO LRFD* Article 2.5.2.6.2) based on analysis of the superstructure as a structural system with live loads applied according the loading provisions of the Specifications.

There are other bridges where the equal deflection assumption is not rational. As mentioned above, loading of all lanes simultaneously of relatively wide bridges may not give a rational deflection.

An example can best demonstrate the fallacy of assuming equal deflection of girders in a wide bridge. Consider a 518-foot span made continuous by adjoining spans of slightly less length. The straight bridge has seven design lanes and seven girders in the cross-section. All girders have the same longitudinal stiffness and are connected with cross-frames and a composite concrete deck. The design live load is HS20; although not designed for HL-93 loading, the special *AASHTO LRFD* live load for live load deflection (discussed below) is intended to give deflections similar to HS20. The live load deflection limit is Span/800, where Span is the distance between bearings. In this case, the limit is 7.77 inches.

For this case, the live load distribution factor for deflection may be computed as follows by assuming all lanes are loaded and all girders are deflecting equally.

AASHTO LRFD Article 2.5.2.6.3 specifies that the multiple presence factors *m* given in *AASHTO LRFD* Article 3.6.1.1.2 should be applied in calculating live load deflections. These factors are given in *AASHTO LRFD* Table 3.6.1.1.2-1 as follows: for one lane loaded, *m* = 1.2; for two lanes loaded, *m* = 1.0; for three lanes loaded, *m* = 0.85; for more than three lanes loaded, *m* = 0.65 (see Section 1.3.2.3.7 for further discussion on multiple presence factors). Therefore:

$$(DF)_{LLdef} = m\left(\frac{N_L}{N_b}\right)$$

Equation 3.2.29

where:

DF = distribution factor (lanes)
m = multiple presence factor specified in *AASHTO LRFD* Article 3.6.1.1.2
N_L = number of design lanes (roadway width/12 with fractions dismissed)
N_b = number of girders in the cross-section

$$(DF)_{LLdef} = 0.65\left(\frac{7}{7}\right) = 0.65 \text{ lanes}$$

Some states specify that the distribution factor used for moment is to be used to calculate live load deflections. When the distribution factor for moment is used, the lanes are implicitly located in the critical position. The width of the bridge and the number of girders are less significant since the wheel load distribution factors are based on two lanes of traffic regardless of the bridge width. When a refined analysis is used to compute live load deflections, the number of girders in the cross-section also has a much less significant effect on deflection and fewer girders may in fact be needed than when the averaging approach is used. This issue is examined in more detail for a straight simple-span I-girder bridge with right supports in Reference 6. It is incorrect to add girders to reduce the live load deflection of a multi-girder steel bridge. The most efficient way to increase stiffness of the bridge without increasing girder depth is to increase the size of the bottom flanges. When a refined analysis is used or when the exterior girder is investigated, it is also possible to place the live load in the striped lane(s) rather than in the critical transverse position. Such analyses would represent a more realistic service condition than the hypothetical situation that would be employed for a strength check.

Analysis of a single girder from the bridge with the preceding distribution factor gives a live load deflection of 6.8 inches, which is well below the deflection limit.

As shown in Table 3.2.2, a refined 3D analysis of this bridge gives a live load deflection of 8.30 inches in one exterior girder (Girder 1) for four lanes loaded using an impact factor of 10 percent and a multiple presence factor of 0.65.

Table 3.2.2 Refined 3D Analysis Results for Live Load Deflection of a Wide Bridge

No. of Lanes Loaded	m	Live Load Deflection (in.)
1	1.2	-5.70
2	1.0	-8.18
3	0.85	-7.26
4	0.65	-8.30
Opposite Side: 2	1.0	1.30

Evidently, for this particular bridge, four lanes loaded results in the largest deflection (it should be noted that the center lanes were loaded two spans away from the span investigated to compute this deflection). When the multiple presence factors are considered, two lanes loaded gives almost the same live load deflection as does four lanes loaded in this case. Clearly, it does not appear reasonable to assume seven lanes loaded to calculate a live load deflection that meets the deflection limit, while the loading of only two lanes fails the same criteria. An argument can be made that deflection is only a relative issue and no hard rules are available as to the true deflection that should be permitted. However, it appears to be unreasonable to compute a smaller deflection on a bridge because it is wider than another bridge with the same span and girder spacing.

Also, as noted in the last row of Table 3.2.2, when the live load is restrained to the two lanes on the far (opposite) side of the deck in the area of the other exterior girder (i.e. Girder 7), the computed live load deflection in Girder 1 in an upward deflection of 1.3 inches (downward deflections are negative and upward deflections are positive in the table). This deflection was the result of loading in the same span; loading in adjacent spans on the opposite side of the bridge was inconsequential. Thus, the addition of live load on the opposite side of the span of interest would actually unload Girder 1. This phenomenon is the reason that the 1935 AASHO Specification disallowed loading sidewalks on both sides in order to reduce the effect of a single sidewalk, as discussed previously.

With the adoption of Load Factor Design (LFD) in the *AASHTO* Standard Specifications, many states increased live load to HS25 for strength. Some used the HS25 design live load to compute live load deflection; however, others departed from using the same live load for strength and service as discussed above and used the HS20 live load for checking deflection. The use of a 25-percent larger live load eliminated some of the economy possible with the lower factor applied to dead load in LFD. Since the same factors were not used for deflection, it was logical to keep the same traditional live load.

As specified in *AASHTO LRFD* Article 3.6.1.3.2 and discussed further in Section 1.3.2.3.4, the live load deflection check consists of evaluating two separate live load conditions:

- Design truck alone
- Design lane plus 25% of design truck

The dynamic load allowance of 33 percent is applied to the design truck only in each case. A load factor of 1.0 is applied to the live load according to the Service I load combination (refer to Section 1.3.3). As discussed further in Section 1.3.2.3.4, the specified load is intended to produce live load deflections similar to those produced by the HS20 loading in the *Standard Specifications*.

Concrete barriers and sidewalks, and even railings, often contribute to the stiffness of composite superstructures at service load levels. Therefore, *AASHTO LRFD* Article 2.5.2.6.2 permits the entire width of the roadway and the *structurally continuous* portions of railings, sidewalks and barriers (i.e. continuous cast-in-place barriers) to be included in determining the composite stiffness for deflection calculations. The assumption of the full deck width, as provided in *AASHTO LRFD* Article 6.10.1.5 for determining the composite cross-section stiffness for the analysis, gives more functionally correct results. Because the inclusion of the concrete items other than the deck can cause complications in the calculation of the composite stiffness (and in modeling with regard to their inclusion in refined analyses), it is suggested that these items be ignored. If the parapets are on the exterior of the deck, they tend to stiffen the exterior girders drawing load to those girders. Hence, computation of the deflections of the critical exterior based on refined analysis methods show that the computed deflections are not materially reduced by the consideration of the parapets.

The preceding discussion is not intended to insinuate that flexibility should not be controlled. Wherever possible, it is best to meet or preferably exceed the minimum girder depths recommended in the specifications. Of course, there are situations such as curved girder bridges and bridges with differing girder stiffnesses where the uniform deflection assumption is not permitted or recommended. In these cases, specific loading is required for computation of live load deflections. It would likely be more consistent to consider the same assumption for all bridges.

3.2.4.2.2 Dead Load Deflection

All versions of the AASHTO Specifications, including the *AASHTO LRFD* Specification, are essentially silent regarding dead load deflections (as mentioned previously, *AASHTO LRFD* Article 6.7.2 does state that vertical camber be provided to account for the dead load deflections). Prior to composite design, the steel bridge girder was designed to support both dead and live load. With the advent of composite design, much of the dead load is applied on the non-composite structure while the live load is applied to the composite one. This has led to the reduction of the recommended depth of the steel section from $1/25^{th}$ of the span to $1/30^{th}$ of the span. This combined with higher strength steels and a smaller factor applied to

dead load for design has, in many cases, results in very slender steel sections. Although there are no provisions for limiting of dead load deflection, the Engineer is wise to consider vertical deflection of the steel and its potential effects during the various stages of construction of the bridge.

3.2.4.3 Permanent Deformations

3.2.4.3.1 General

Checks are to be made on the flange stresses and for potential web bend-buckling under the Service II load combination to control permanent deformations under repeated severe traffic loadings, which is important to ensure good riding quality.

The standard design Service II loading is defined as 1.0*DC* + 1.0*DW* + 1.3(*LL+IM*), where *DC* represents the component dead loads, *DW* represents the wearing surface and utility loads and (*LL+IM*) represents the design live load plus the dynamic load allowance placed in multiple lanes (see Section 1.3.3). Checks must also be made to prevent slip in slip-critical bolted connections under the Service II loading.

The Service II load combination is intended to be equivalent to the Overload given in the *AASHTO Standard Specifications*. In the *AASHTO Standard Specifications*, the Overload was intended to represent live loads that could be allowed on the structure on infrequent occasions without causing permanent damage. The standard design Overload (i.e. for loadings of H20 or above) was defined as *D* + 5/3(*L+I*), where *D* represents the dead load and (*L+I*) represents the design live load plus impact placed in multiple lanes. Although the live load was to be placed in multiple lanes for design purposes, it can be shown that the live load factor of 5/3 essentially made the loading equivalent to two times the design live load placed in a single lane (*26*).

Under certain conditions, *AASHTO LRFD* Article 6.10.4.2.1 permits flexural stresses caused by Service II loads applied to the composite section to be computed assuming the concrete deck is effective for both positive and negative flexure for the permanent deflection design checks. *AASHTO LRFD* Article 6.10.1.7 lists these conditions as follows:

- Shear connectors must be provided along the entire girder length;
- One-percent longitudinal reinforcement must provided wherever the tensile stress in the concrete deck due to the Service II loads or due to the factored construction loads exceeds ϕf_r (*AASHTO LRFD* Article 6.10.1.7). ϕ is the resistance factor for concrete in tension (= 0.9), and f_r is the modulus of rupture of the concrete taken equal to $0.24\sqrt{f'_c}$ for normal-weight concrete (*AASHTO LRFD* Article 5.4.2.6); and
- The maximum longitudinal tensile stress in the concrete deck at the section under consideration, caused by the Service II loads, must not exceed $2f_r$.

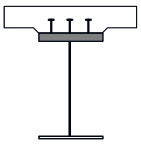
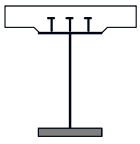
Under these conditions, the crack size is felt to be controlled to a degree such that the concrete deck may be considered effective in tension for computing the flexural stresses acting on the composite section at the service limit state. The limit of $2f_r$ between the use of an uncracked or cracked section for calculation of flexural stresses in the structural steel is similar to the limit suggested in Reference 27 beyond which the effects of concrete cracking should be considered. *When the above conditions are satisfied, the Engineer is strongly encouraged to consider the concrete deck to be fully effective in calculating all Service II flexural stresses, as this assumption better reflects the actual conditions in the bridge*. When one of more of these conditions are not satisfied, the flexural stresses caused by Service II loads applied to the composite section must be computed using the section consisting of the steel section and the longitudinal reinforcement within the effective width of the concrete deck. The properties of the steel section alone are to be used to calculate the flexural stresses in the structural steel for sections that are non-composite for negative flexure. Longitudinal stresses in the concrete deck are to be determined as specified in *AASHTO LRFD* Article 6.10.1.1.1d (refer to Section 3.2.4.4).

3.2.4.3.2 I-Sections

3.2.4.3.2.1 Flange Stresses

AASHTO LRFD Article 6.10.4.2.2 specifies that flange stresses due to the Service II loads in I-sections be limited as shown in Table 3.2. to control permanent deformations in the steel girder at the service limit state.

Table 3.2.3 Flange Stress Checks at the Service Limit State (I-Sections)

Sketch	Description	Equation
	For top steel flange of composite sections	$f_f \le 0.95R_hF_{yf}$ Equation 3.2.30
	For bottom steel flange of composite sections	$f_f + \frac{f_\ell}{2} \le 0.95R_hF_{yf}$ Equation 3.2.31
	For both steel flanges of non-composite sections	$f_f + \frac{f_\ell}{2} \le 0.80R_hF_{yf}$ Equation 3.2.32

f_f is the flange stress due to vertical bending caused by the Service II loads at the section under consideration. f_ℓ is the flange lateral bending stress due to the Service II loads. The other terms are as defined previously. A resistance factor, ϕ, is not shown in these equations because *AASHTO LRFD* Article 1.3.2.1 specifies that the

resistance factor be taken equal to 1.0 at the service limit state. *The sign of f_f and f_ℓ is always taken as positive in these equations. However, when summing dead and live load stresses to obtain the total vertical and lateral bending stresses, f_f and f_ℓ, to apply in the equations, the signs of the individual dead and live load stresses must be considered.* f_ℓ is not included in Equation 3.2.30 because the top flange of composite sections is continuously braced by the concrete deck at the service limit state. Therefore, flange lateral bending stresses are small and may be neglected. For continuous-span members in which non-composite sections are utilized in negative flexure regions only, *AASHTO LRFD* Article C6.10.4.2.2 recommends that Equations 3.2.30 and 3.2.31, as applicable, be applied in those regions. Lateral bending in the bottom flange is only a consideration at the service limit state for all horizontally curved I-girder bridges (with or without skew) and for straight I-girder bridges with discontinuous cross-frame/diaphragm lines in conjunction with skews exceeding 20° from normal. Other significant sources of flange lateral bending, such as concrete deck overhang loads and wind loads, are not a consideration at the service limit state.

A factor of ½ is conservatively included in front of the f_ℓ term in Equations 3.2.31 and 3.2.32. As discussed previously in Section 3.2.2.1.4, when this factor is included, the equations approximate more rigorous yield interaction equations corresponding to a load at the onset of yielding at the web-flange juncture under combined major-axis and lateral bending (*9, 10*). The effect of any minor yielding that occurs at the flange tips prior to this stage is comprehended. By controlling the yielding in this fashion under the combined effects of vertical and lateral bending, with the factored lateral flange bending stresses not exceeding the permissible upper limit of $0.6F_{yf}$ (after any amplification) given in *AASHTO LRFD* Article 6.10.1.6, the resulting permanent deflections will be small. According to *AASHTO LRFD* Article 6.10.1.6, amplification of the first-order flange lateral bending stresses may be required in discretely braced compression flanges. Amplification of tension-flange lateral bending stresses is not required. Amplification of these stresses was discussed previously in Section 3.2.2.1.3.1

The base stress limits of $0.95F_{yf}$ for composite sections and $0.80F_{yf}$ for non-composite sections have been retained from the *AASHTO Standard Specifications*. As discussed in References 26 and 28, these limits arose from bridge experiments conducted as part of the AASHO Road Test at Ottawa, Illinois in the early 1960s (*29*). The six steel bridges in the Road Test were subjected to more than 390,000 vehicle passages, which is roughly equivalent to 20 overload crossings every day for more than 50 years. Two of the bridges were composite and four were non-composite. Each bridge had a span of 50 feet. The total accumulated permanent sets measured at the end of the test traffic are plotted in Figure 3.2.10**.** The differences in the magnitudes of the measured permanent sets in the composite and non-composite bridges are evident in the figure. At stresses approaching 90 percent of F_{yf}, the permanent set was relatively low in composite bridge 2B compared to the permanent set in non-composite bridge 3A. On the basis of this data, the limits were

set as shown in Table 3.2.3. Note that at these two limiting conditions, the measured permanent sets were of comparable magnitude.

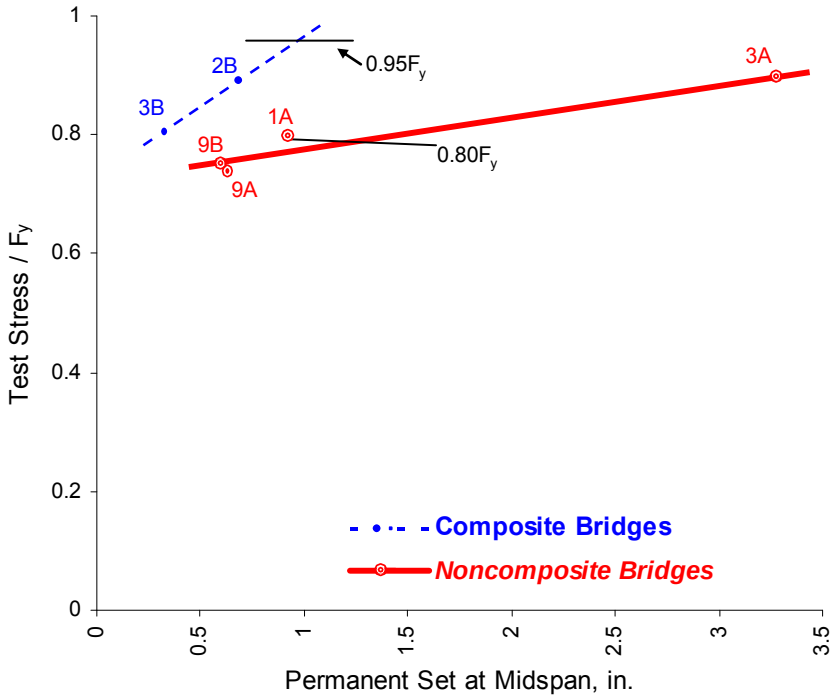


Figure 3.2.10 Measured Permanent Set of AASHO Road Test Bridges

The hybrid factor, R_h, has been conservatively added to the stress limits in the *AASHTO LRFD* Specifications to account for the increase in flange stress caused by early web yielding in hybrid sections. R_h is discussed further in Section 3.2.6.3

AASHTO LRFD Article C6.10.4.2.2 lists sections for which Equations 3.2.30 through 3.2.32 do not control the design under the load combinations specified in *AASHTO LRFD* Table 3.4.1-1 and need not be checked. These sections include:

- composite sections in negative flexure for which the main provisions of *AASHTO LRFD* Article 6.10.8 (assuming slender-web behavior) are applied to determine the nominal flexural resistance at the strength limit state;
- non-composite sections with f_ℓ equal to zero for which the main provisions of *AASHTO LRFD* Article 6.10.8 (assuming slender-web behavior) are applied to determine the nominal flexural resistance at the strength limit state; and
- noncompact composite sections in positive flexure.

As discussed previously, sections in negative flexure in all kinked (chorded) continuous and horizontally curved-girder bridges and in straight-girder bridges whose supports are skewed more than 20° from normal must always be treated as slender-web sections, regardless of their web slenderness. Thus, such sections must always be designed according to the provisions of *AASHTO LRFD* Article

6.10.8 at the strength limit state (i.e. *AASHTO LRFD* Appendix A6 may not be used). Composite sections in positive flexure in all kinked (chorded) continuous and horizontally curved-girder systems must be treated as noncompact sections at the strength limit state according to *AASHTO LRFD* Article 6.10.6.2.2. Although not currently stated in the specifications, consideration should also be given to treating all composite sections in positive flexure in straight-girder bridges whose supports are skewed more than 20° from normal as noncompact sections. Thus, in all these cases, the preceding conditions are met and the nominal flexural resistance of the section at the strength limit state is not permitted to exceed the moment at first yield. *As a result, for these cases under the load combinations specified in AASHTO LRFD Table 3.4.1-1, the flange-stress checks at the service limit state described above do not control and need not be checked*. Web bend buckling, described in the next section, must always be checked however, where applicable.

AASHTO LRFD Article 6.10.4.2.2 optionally permits moment redistribution according to the provisions of *AASHTO LRFD* Appendix B6 prior to making the service limit state design verifications. However, this is only permitted for continuous-span members in straight I-girder bridges with skews not exceeding 10° from normal. Other limitations spelled out in *AASHTO LRFD* Article B6.2 must also be satisfied. Further information on the provisions of *AASHTO LRFD* Appendix B6 may be found in Reference 6.

One final requirement in *AASHTO LRFD* Article 6.10.4.2.2 relates to the rare case of compact composite sections in positive flexure utilized in shored construction. In this case, longitudinal compressive stresses in the concrete deck due to the Service II loads are limited to $0.6f'_c$ to ensure linear behavior of the concrete. As discussed in *AASHTO LRFD* Article C6.10.1.1.1a, the use of shored construction is not recommended. Also, as discussed previously, composite sections in positive flexure in all kinked (chorded) continuous and horizontally curved-girder systems must be treated as noncompact sections. Composite sections in positive flexure in most straight I-girder bridges with skewed supports should also be treated as noncompact sections.

3.2.4.3.2.2 Web Bend Buckling

AASHTO LRFD Article 6.10.4.2.2 specifies that except for composite sections in positive flexure in which the web satisfies the requirement of *AASHTO LRFD* Article 6.10.2.1.1 (i.e. $D/t_w \leq 150$ – no longitudinal web stiffeners), all sections must also satisfy the following check at the service limit state:

$$f_c \leq F_{crw}$$

Equation 3.2.33
AASHTO LRFD Equation 6.10.4.2.2-4

where:

f_c = compression-flange vertical bending stress due to Service II loads (ksi)
F_{crw} = nominal bend-buckling resistance of the web determined as specified in *AASHTO LRFD* Article 6.10.1.9 (ksi)

Again, a resistance factor is not specified (i.e. it is implicitly assumed equal to 1.0) because this is a serviceability check.

A web bend buckling check is specified at the service limit state to control bending deformations and transverse displacements of the web. Regions in negative flexure are particularly susceptible to web bend buckling in composite girders at the service limit state, especially when the concrete deck is considered to be effective in tension as permitted for composite sections in *AASHTO LRFD* Article 6.10.4.2.1 (i.e. when the conditions discussed in Section 3.2.4.3.1 are satisfied). When the concrete deck is considered effective in tension, more than half of the web is likely to be in compression increasing the susceptibility of the web to bend buckling. As a result, the check in this case may often end up governing the web thickness of the girder in these regions when the concrete is assumed effective (as recommended when the appropriate conditions are satisfied). Because an explicit web bend buckling check is specified, the web load-shedding factor R_b is not included in Equations 3.2.30 through 3.2.32. R_b is discussed further in Section 3.2.6.2.

Options to consider should F_{crw} be exceeded are similar to those discussed previously in Section 3.2.3.4.1.2 related to the construction condition, except obviously for the adjustment of the deck-placement sequence.

Web Bend-Buckling Resistance, F_{crw}

The buckling behavior of a slender web plate subject to pure bending is similar to the buckling behavior of a flat plate. A perfectly flat plate with no initial imperfections would not deflect laterally from its initial flat position until its theoretical buckling load is reached. However, in many experimental tests, bending deformations and associated transverse displacements of web plates occur from the onset of load application due to initial web out-of-flatness, and increase progressively throughout the entire range of applied bending moment. As expected, these deformations are largest in the compression zone of the web. Because of the stable postbuckling behavior of the web, however, a significant change in the rate of increase of the transverse displacements of the web as a function of the applied loads is not observed as the theoretical web bend-buckling stress is exceeded (*30*). Therefore, web bend-buckling behavior is essentially a load-deflection rather than a bifurcation phenomenon; that is, a distinct buckling load is not observed.

Since web plates in bending do not collapse when the theoretical buckling load is reached, the available postbuckling strength can be considered in determining the nominal flexural resistance of sections with slender webs at the strength limit state, as discussed further in Section 3.2.6.2. However, in certain situations, it is desirable to limit the bending deformations and transverse displacements of the web. This is particularly true during the construction condition and at the service limit state.

The advent of composite design has led to a significant reduction in the size of compression flanges in regions of positive flexure. As a result, more than half of the web of the non-composite section will be in compression in these regions during the construction condition before the concrete deck has hardened or is made composite. As a result, the web is more susceptible to bend buckling in this condition and is to be explicitly checked in all regions of the non-composite girder during the construction condition (refer to Equation 3.2.20).

A control on the amount of transverse web displacement is also desirable at the service limit state. Regions in negative flexure are most susceptible to web bend buckling in a composite girder at the service limit state, especially when the concrete deck is assumed effective in tension. More than half the web is likely to be in compression in this case.

The *AASHTO LRFD* Specifications use the theoretical web bend-buckling load as a simple index to control the web plate bending strains and transverse displacements during construction and at the service limit state. The web bend-buckling resistance is specified in *AASHTO LRFD* Article 6.10.1.9. The equation for the web bend-buckling resistance, F_{crw}, is provided in *AASHTO LRFD* Article 6.10.1.9.1. This equation is derived from the following equation for the elastic buckling stress of a flat plate subject to pure bending (*11*):

$$F_{cr} = \frac{k\pi^2 E}{12\left(1-\mu^2\right)(b/h)^2}$$

Equation 3.2.34
AASHTO LRFD Article C6.9.4.2

where:

- b = width of the plate along the edge subject to bending (in.)
- E = Young's modulus (29,000 ksi for steel)
- h = thickness of the plate (in.)
- k = bend-buckling coefficient (discussed below)
- μ = Poisson's ratio (0.3 for steel)

Substituting the slenderness ratio D/t_w of the web for b/h, and the values of E, π and μ in Equation 3.2.34 yields Equation 3.2.35 as follows:

$$F_{crw} = \frac{0.9Ek}{\left(\frac{D}{t_w}\right)^2}$$

Equation 3.2.35
AASHTO LRFD Equation 6.10.1.9.1-1

F_{crw} is not to exceed the smaller of R_hF_{yc} and F_{yw}/0.7, where F_{yc} and F_{yw} are the specified minimum yield strengths of the compression flange and web, respectively, and R_h is the hybrid factor. Since the web carries only a relatively small portion of the total bending moment, the transition zone resulting from inelastic buckling is not considered significant and only an elastic buckling equation is provided.

F_{crw} is to be checked against the maximum compression-flange vertical bending stress due to the factored loads. Utilizing the maximum compressive stress in the web rather than the stress in the compression flange in order to obtain greater precision is not warranted for this check. In hybrid sections with a lower yield-strength web, the longitudinal and plate bending strains in the inelastic web at the web-flange juncture are constrained by a stable nominally elastic compression flange (*31*). Since the flange will tend to restrain the longitudinal strains resulting from web bend-buckling at compression-flange stress levels up to R_hF_{yc}, the use of an F_{crw} value that is potentially greater than F_{yw} in hybrid sections is felt to be justified. The upper limit of F_{yw}/0.7 is a conservative limit to cover hybrid sections with F_{yw}/F_{yc} less than 0.7, which are permitted according to *AASHTO LRFD* Article 6.10.1.3, but are not recommended.

Bend-Buckling Coefficient, k

Webs Without Longitudinal Stiffeners

The bend-buckling coefficient, *k*, to be substituted in Equation 3.2.35 for webs without longitudinal stiffeners is given by *AASHTO LRFD* Equation 6.10.1.9.1-2 as follows:

$$k = \frac{9}{(D_c/D)^2}$$

Equation 3.2.36
AASHTO LRFD Equation 6.10.1.9.1-2

where:

D_c = depth of the web in compression in the elastic range (discussed below) (in.)

Equation 3.2.36 yields a *k* value of 36.0 for a doubly symmetric I-girder (i.e. D_c = 0.5*D*). This value is approximately equal to $k_{ss} + 0.8(k_{sf} - k_{ss})$, where k_{ss} = 23.9 and k_{sf} = 39.6 are the bend-buckling coefficients for simply supported and fully restrained longitudinal edge conditions, respectively, along the flanges (*11*). The use of the *k* value from Equation 3.2.36 has been found to provide a reasonable approximation of the theoretical bend-buckling resistance for singly symmetric I-girders.

To ensure that the above boundary conditions at the web-flange juncture are satisfied, *AASHTO LRFD* Article 6.10.2.2 provides minimum flange proportioning requirements that were presented in Section 3.1.4.3. Specifically, the requirement given by *AASHTO LRFD* Equation 6.10.2.2-3 that the thickness of the flanges be greater than or equal to 1.1 times the thickness of the web, and the requirement

given by *AASHTO LRFD* Equation 6.10.2.2-2 that the flange widths equal or exceed 1/6 of the web depth help ensure that the boundary conditions assumed in the web bend-buckling formulation are sufficiently accurate.

Substituting k = 36.0 and the effective web slenderness for a singly symmetric section $2D_c/tw$ for D/t_w in Equation 3.2.35 and rearranging yields the web-slenderness limit, λ_{rw}, for a noncompact-web section given in *AASHTO LRFD* Article 6.10.6.2.3 as follows:

$$\frac{2D_c}{t_w} \le \lambda_{rw} = 5.7\sqrt{\frac{E}{F_{yc}}}$$

Equation 3.2.37
AASHTO LRFD Equation 6.10.6.2.3-1

This limit applies to composite sections in negative flexure and noncomposite sections and distinguishes a non-slender versus a slender-web section. For sections with webs satisfying this limit (i.e. non-slender web sections), theoretical web bend buckling will not occur for elastic stress levels, computed according to beam theory, at or below F_{yc}. Therefore, for these sections, the web load-shedding factor R_b (discussed in Section 3.2.6.2) will always equal 1.0 and the web bend-buckling checks described above need not be made. Both compact-web and noncompact-web sections fall into this category. Sections not satisfying this limit are termed slender-web sections, which rely on significant post bend-buckling resistance at the strength limit state. The slenderness limit λ_{rw} from Equation 3.2.37 is given in Table 3.2.4 for different grades of steel as follows:

Table 3.2.4 Slenderness Limit, λ_{rw}, from Equation 3.2.37 for Different Grades of Steel

F_{yc} (ksi)	λ_{rw}
36.0	162
50.0	137
70.0	116
90.0	102
100.0	97

Although relatively rare, in certain cases, near points of permanent-load contraflexure, both edges of the web (top and bottom) may be in compression when the stresses in the steel and composite sections due to the moments of opposite sign are accumulated. This is particularly true when the concrete is considered to be effective in tension at the service limit state. In such cases, the neutral axis lies above the web and Equation 3.2.36 cannot be used to compute k. Therefore, *AASHTO LRFD* Article 6.10.1.9.1 states that when both edges of the web are in compression, k for use in Equation 3.2.35 is to be taken equal to 7.2. This value is

approximately equal to the theoretical bend-buckling coefficient for a web plate under *uniform* compression assuming fully restrained longitudinal edge conditions along the flanges (*11*). Although such cases are infrequent and the accumulated web compressive stresses are usually small and unlikely to be critical when this occurs, a *k* value is still provided in the specification to allow these cases to be considered in computer software.

Webs With Longitudinal Stiffeners

The bend-buckling coefficient, *k*, for webs with longitudinal stiffeners depends on the distance from the centerline of the closest longitudinal stiffener to the inner surface of compression flange, d_s, with respect to the optimum location of the stiffener, which is at $d_s/D_c = 0.4$. The value of *k* to be substituted in Equation 3.2.35 is therefore given by *AASHTO LRFD* Equation 6.10.1.9.2-1 or *AASHTO LRFD* Equation 6.10.1.9.2-2 as follows:

- If $\frac{d_s}{D_c} \geq 0.4$, then:

$$k = \frac{5.17}{(d_s/D)^2} \geq \frac{9}{(D_c/D)^2}$$

Equation 3.2.38
AASHTO LRFD Equation 6.10.1.9.2-1

- If $\frac{d_s}{D_c} < 0.4$, then:

$$k = \frac{11.64}{\left(\frac{D_c - d_s}{D}\right)^2}$$

Equation 3.2.39
AASHTO LRFD Equation 6.10.1.9.2-2

For existing riveted girders, d_s should be taken between the gage line of the closest angle longitudinal stiffener to the inner leg of the compression-flange element. The development of these equations is discussed in Reference 32. In cases where Equation 3.2.38 controls, the longitudinal stiffener is below its optimum location and web bend-buckling occurs in the panel between the stiffener and the compression flange. In cases where Equation 3.2.39 controls, the stiffener is above its optimum location and web bend-buckling occurs in the panel between the stiffener and the tension flange. In cases where d_s is equal to $0.4D_c$ (i.e. the stiffener is located at its optimum position), web bend-buckling theoretically occurs simultaneously in both panels, in which case, both equations yield a *k* value of 129.3 for the case of a doubly symmetric girder. Note that both equations for *k* assume simply supported longitudinal edge conditions along the flanges.



Figure 3.2.11 I-Girder with Longitudinal Web Stiffeners

Studies on noncomposite girders have indicated that the optimum location of one longitudinal stiffener is $0.4D_c$ for bending and $0.5D$ for shear. The distance $0.4D_c$ is recommended as the optimum location because shear is almost always accompanied by moment and because a properly proportioned longitudinal stiffener can effectively control lateral web deflections under both bending (*33*) and shear.

Changes in flange size can cause D_c to vary along the girder length. Also, as discussed below, D_c in a composite girder is a function of the applied load. Because D_c may vary along the span, it is suggested that the longitudinal stiffener be located based on D_c computed at the section with the largest compressive flexural stress. Since the longitudinal stiffener is normally located a fixed distance from the compression flange, the stiffener cannot be at its optimum location at other sections along the girder length with a lower stress and a different D_c. These sections must also be examined to ensure that they satisfy the specified limit states. *AASHTO LRFD* Article 6.10.11.3.1 requires that longitudinal stiffeners be located at a vertical position on the web such that Equation 3.2.35 is satisfied to prevent web bend-buckling when checking constructibility (refer to Equation 3.2.20), and at the service limit state (refer to Equation 3.2.33). In addition, the stiffener must be located to satisfy all other appropriate design requirements at the strength limit state. Several trial locations of the stiffener may need to be investigated to determine an appropriate location, particularly for composite sections in regions of positive flexure.

The calculated web bend-buckling resistance for composite sections in positive flexure is different before and after placement of the deck and is a function of the applied loading. D_c of the steel section is typically large for non-composite loadings during construction and web bend-buckling must be checked. In a longitudinally stiffened girder, D_c for the composite girder can also be large enough at the service limit state in regions of positive flexure that web bend-buckling may still be of concern. D_c in this case must be calculated based on the accumulated flexural stresses due to the factored loads using Equation 3.2.41.

It is suggested that for composite sections in negative flexure, the longitudinal stiffener initially be located at $0.4D_c$ from the inner surface of the compression flange at the section with the maximum factored compressive vertical bending stress at the strength limit state, with D_c calculated for the section consisting of the steel girder plus the longitudinal reinforcement. For non-composite sections, D_c would be based on the section consisting of the steel girder alone. Based on the required bend-buckling checks and other strength limit state checks, the stiffener may have to be moved up or down from this initial trial position, especially in cases where the concrete deck is assumed effective in tension in regions of negative flexure at the service limit state. D_c in this case must also be calculated based on the accumulated stresses using Equation 3.2.41.

Because simply supported boundary conditions were assumed in the development of Equations 3.2.38 and 3.2.39, it is possible at locations where the longitudinal stiffener is located at an inefficient position for a particular condition, that the web bend-buckling resistance of the longitudinally stiffened web is less than that computed for a web of the same dimensions without longitudinal stiffeners. This anomaly is due to the fact that Equation 3.2.36 for determining k for webs without longitudinal stiffeners was derived assuming partial rotational restraint of the web panel by the flanges. Therefore, the k value from Equation 3.2.36 serves as a lower limit on the k value for a longitudinally stiffened web panel computed from Equation 3.2.38. This lower limit is not applied to Equation 3.2.39 because it would never control in this case. Also, as discussed previously for webs without longitudinal stiffeners, k is to be taken equal to 7.2 for the rare case in which both edges of the longitudinally stiffened web are in compression.

It may be necessary, or desirable, in regions where the web undergoes stress reversal to use two longitudinal stiffeners on the web. Equations 3.2.38 and 3.2.39 conservatively neglect any benefit of placing more than one longitudinal stiffener on the web. However, *AASHTO LRFD* Article 6.10.1.9.2 does permit the Engineer to perform a direct buckling analysis of a web panel with multiple longitudinal stiffeners, if desired, to determine F_{crw} or k for this case. Simply supported boundary conditions should be assumed at the flanges and at the longitudinal stiffener locations in such an analysis. If F_{crw} determined from the bucking analysis is greater than or equal to F_{yc}, then the girder may be proportioned using a web load-shedding factor, R_b, equal to 1.0. The termination of longitudinal stiffeners in these regions is problematic in that a punitive Category E or E' detail exists at the end of the stiffener-to-web welds unless an appropriate transition radius is provided at the termination (refer to *AASHTO LRFD* Table 6.6.1.2.3-1 – Condition 4.3). One way to address this issue is to continue a single longitudinal stiffener from the positive moment region to the negative moment region. A single longitudinal stiffener can be extended over both regions by bending the stiffener from the top portion of the web in the positive moment region to the bottom portion in the negative moment region. Hence, in the contraflexure region, the stiffener will pass through the mid-height of the web. As noted above, the current specification provisions permit the computation of the web bend-buckling resistance with the longitudinal stiffener located at any position on the web.

Rearranging Equation 3.2.35 yields the web slenderness, D/t_w, at or below which theoretical web bend buckling will not occur for elastic stress levels, computed according to beam theory, at or below F_{yc}:

$$\frac{D}{t_w} \le 0.95\sqrt{\frac{Ek}{F_{yc}}}$$

Equation 3.2.40
AASHTO LRFD Equation 6.10.1.10.2-1

The web load-shedding factor, R_b, will always equal 1.0 for sections satisfying this limit,. Based on the k value of 129.3 for the case of a doubly symmetric girder, i.e. $D_c = 0.5D$, with a single longitudinal stiffener located at the optimum position on the web, i.e. $d_s = 0.4D_c$, the slenderness limit from Equation 3.2.40 is given as follows for different grades of steel:

Table 3.2.5 Slenderness Limit from Equation 3.2.40 for Different Grades of Steel

F_{yc} (ksi)	$0.95\sqrt{Ek/F_{yc}}$
36.0	300
50.0	260
70.0	220
90.0	194
100.0	184

The limiting D/t_w will generally be less than the value shown in the preceding table fr singly symmetric girders with $D_c/D > 0.5$ and/or where a single longitudinal stiffener is not located at its optimum position.

The design of longitudinal web stiffeners for both I- and box sections is covered in *AASHTO LRFD* Article 6.10.11.3 and discussed in Section 3.3.8.3.

Depth of the Web in Compression in the Elastic Range, D_c

The depth of the web in compression in the elastic range, D_c, is used primarily in computing the web bend-buckling resistance, F_{crw}, and the web load-shedding factor, R_b. For composite sections in negative flexure and non-composite sections, D_c is also used to determine whether the section qualifies as a slender or a non-slender web section for determining the nominal flexural resistance.

D_c for composite sections is a function of the dead-to-live load stress ratio in the elastic range of stress at the service, fatigue and strength limit states. This is because in a composite girder, the dead and live loads are applied to different

sections. This is an especially important consideration for composite sections in positive flexure as the dead-load stress has a significant effect on the location of the elastic neutral axis. Note that when checking the section for web bend-buckling during construction, however, while the girder is still in the non-composite condition before the concrete deck hardens or is made composite, D_c of the steel section alone (which is a section property independent of the stress) is used in the calculations.

Sections in Positive Flexure

D_c of the composite section (refer to Figure 3.2.12 – the terms shown in the figure are described below) at sections in positive flexure increases with increasing span length because of the increasing dead-to-live load ratio. With increasing spans, the larger non-composite dead load stresses acting on the steel section alone effectively cause the neutral axis to be much lower than it would if all loads were applied to the composite section, which obviously increases the depth of the web in compression. Therefore, in general, it is important in certain cases to recognize the effect of the dead load stress on the location of the neutral axis at these sections.

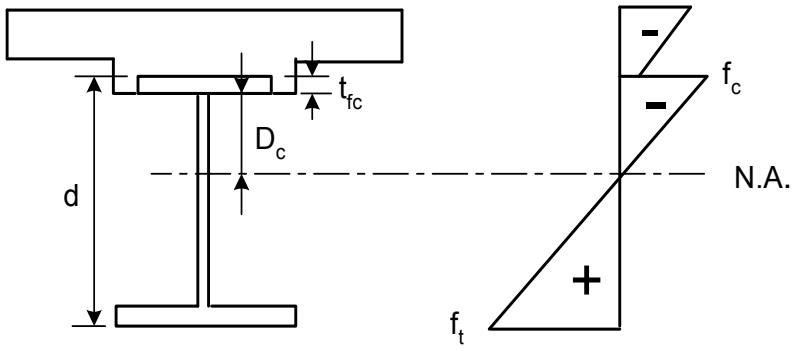


Figure 3.2.12 Dc for a Composite Section in Positive Flexure

AASHTO LRFD Article D6.3.1 in Appendix D6 states that D_c for composite sections in positive flexure is to be taken as the depth over which the algebraic sum of the stresses acting on the steel, long-term composite and short-term composite sections due to the dead and live loads, plus impact, is compressive. The following equation, which can simply be derived from an examination of the stress diagram and cross-section given in Figure 3.2.12, is provided in this article to compute D_c in lieu of calculating D_c utilizing the individual stress diagrams:

$$D_c = \left(\frac{-f_c}{|f_c| + f_t} \right) d - t_{fc} \geq 0$$

Equation 3.2.41
AASHTO LRFD Equation D6.3.1-1

where:

- d = total depth of the steel section (in.)
- f_c = sum of the compression-flange vertical bending stresses caused by the different loads, i.e. DC_1, the permanent load acting on the noncomposite section; DC_2, the permanent load acting on the long-term composite section; DW, the wearing surface load acting on the long-term composite section; and LL+IM, live load plus impact acting on the short-term composite section (ksi). For stresses in compression, f_c is to be taken as negative.
- f_t = sum of the tension-flange vertical bending stresses caused by the different loads (ksi) – see above.
- t_{fc} = thickness of the compression flange (in.)

According to the *AASHTO LRFD* Specifications, for composite sections in positive flexure at the fatigue, service and strength limit states, D_c only needs to be employed in the computation of the nominal flexural resistance for sections in which longitudinal web stiffeners are required based on *AASHTO LRFD* Article 6.10.2.1.1.

For composite sections in positive flexure *without* longitudinal web stiffeners that meet the section proportioning limits of *AASHTO LRFD* Article 6.10.2, and also the ductility requirement of *AASHTO LRFD* Article 6.10.7.3 to prevent premature crushing of the concrete deck, the web bend-buckling resistance, F_{crw}, is generally close to or larger than the yield stress of the compression flange, F_{yc}, at the strength limit state. Also, for loads applied at the service and fatigue limit states after the deck has hardened or is made composite, the increased compressive stresses in the web tend to be compensated for by the increase in F_{crw} resulting from the corresponding decrease in D_c after the section becomes composite. These compensating effects simply continue at the strength limit state. As a result, since theoretical web bend-buckling of these sections is essentially prevented at all elastic stress levels, the web load-shedding factor, R_b, is specified to be 1.0 for composite sections in positive flexure without longitudinal web stiffeners. Since computations of F_{crw} and R_b are not required for these sections, it follows that a computation of D_c is also not required.

The section proportioning requirements of *AASHTO LRFD* Article 6.10.2.1.2 for sections with longitudinal web stiffeners are not generally sufficient to ensure that web bend buckling will not occur. As a result, the specifications require the calculation of F_{crw} and R_b, and consequently D_c, for these sections. The calculation of D_c for composite sections in positive flexure can potentially complicate bridge load rating calculations because of the dependency of the flexural resistance on the applied load. Therefore, avoiding the computation of D_c is desirable where practical.

Sections in Negative Flexure

The concrete deck is typically not considered to be effective in tension for composite sections in negative flexure, except perhaps at the fatigue and service limit states as

permitted by the Specifications when certain conditions are satisfied. The distance between the neutral-axis locations for the steel and composite sections is small when the concrete deck is not considered effective, as the composite section only consists of the steel section plus the longitudinal reinforcement. As a result, the location of the neutral axis for the composite section is essentially unaffected by the dead load stress. In fact, accounting for the effect of the dead load stress actually results in a smaller value of D_c in regions of negative flexure.

Therefore, for the majority of situations involving composite sections in negative flexure, AASHTO LRFD Article D6.3.1 (Appendix D6) of the Specifications conservatively specifies the use of D_c computed for the section consisting of the steel girder plus the longitudinal reinforcement, without considering the algebraic sum of the stresses acting on the non-composite and composite sections. Again, this avoids potential difficulties in bridge load rating calculations since the resulting value of D_c is independent of the applied loading.

A single exception to the preceding requirement is specified in *AASHTO LRFD* Article D6.3.1; that is, if the concrete deck is assumed effective in tension in regions of negative flexure at the service limit state, Equation 3.2.41 *must* be used to compute D_c. When calculating the web bend-buckling resistance F_{crw} at the service limit state, a more precise calculation of D_c, accounting for the *beneficial* effect of the dead load stress in this case, is required when the concrete deck is considered effective in tension. Otherwise, the reduction in F_{crw} will be too large and not reflective of the actual potential web bend-buckling resistance at this limit state.

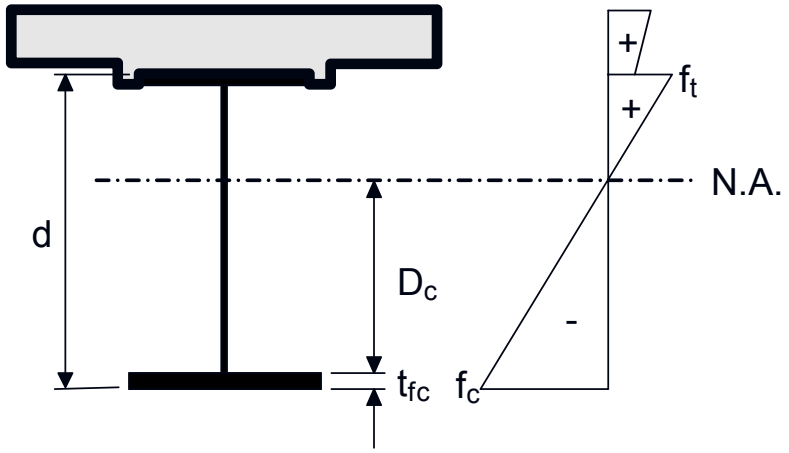


Figure 3.2.13 D_c for a Composite Section in Negative Flexure

D_c of the steel section alone should always be used for non-composite sections.

3.2.4.3.3 Box Sections

3.2.4.3.3.1 Flange Stresses

According to *AASHTO LRFD* Article 6.11.4, flange stresses due to the Service II loads are limited as specified in *AASHTO LRFD* Article 6.10.4.2.2 to control permanent deformations in box sections at the service limit state, with the following exceptions: 1) the f_ℓ term in *AASHTO LRFD* Equation 6.10.4.2.2-2 (Equation 3.2.31) is to be taken as zero, and 2) *AASHTO LRFD* Equation 6.10.4.2.2-3 (Equation 3.2.32) does not apply. Therefore, the specified stress checks reduce to the following:

For the top and bottom steel flange:

$$f_f \leq 0.95 R_h F_{yf}$$

Equation 3.2.42

where:

f_f = flange vertical bending stress at the section under consideration due to the Service II Loads (ksi). f_f is always taken as positive in this equation. However, when summing dead and live load stresses to obtain the total vertical bending stress, f_f, to apply in the equation, the signs of the individual dead and live load stresses must be considered.

R_h = hybrid factor determined as specified in *AASHTO LRFD* Article 6.10.1.10.1

The genesis of the base stress limit given by Equation 3.2.42 is discussed further in Section 3.2.4.3.2.1. The hybrid factor R_h has been conservatively added to the stress limit in Equation 3.2.42 in the *AASHTO LRFD* Specifications to account for the increase in flange stress caused by early web yielding in hybrid sections. A resistance factor, ϕ, is not shown in this equation because *AASHTO LRFD* Article 1.3.2.1 specifies that the resistance factor be taken equal to 1.0 at the service limit state. Note that at sections where access holes are present in the box flange, f_f should be computed using section properties calculated assuming the area of the access hole is subtracted from the box-flange area.

The f_ℓ term is not considered in the stress check for both flanges because flange lateral bending is not a consideration for box flanges and because top flanges are continuously braced at the service limit state. Equation 3.2.32, which applies to both steel flanges of non-composite sections, does not apply because box-section members must be composite along their entire length according to *AASHTO LRFD* Article 6.11.10.

Longitudinal warping stresses due to cross-section distortion and St. Venant torsional shear stresses need not be considered in checking Equation 3.2.42. As

indicated in *AASHTO LRFD* Article C6.11.4, the effect of these stresses on the overall permanent deflections at the service limit state is considered to be insignificant. The effect of longitudinal warping stresses must be considered, however, in certain cases when checking slip of the connections in bolted non-composite box flange splices at the service limit state, as discussed further in Section 3.3.7.2.5.3.

Under the load combinations specified in *AASHTO LRFD* Table 3.4.1-1, Equation 3.2.42 need only be checked for compact sections in positive flexure as indicated in *AASHTO LRFD* Article C6.11.4. Composite sections in positive flexure in all horizontally curved-girder systems must be treated as noncompact sections at the strength limit state according to *AASHTO LRFD* Article 6.11.6.2.2. Although not currently stated in the specifications, consideration should also be given to treating all composite sections in positive flexure in straight-girder bridges whose supports are skewed more than 20° from normal as noncompact sections. *Thus, for all sections in negative flexure and for noncompact sections in positive flexure, Equation 3.2.42 does not control and need not be checked under the load combinations specified in AASHTO LRFD Table 3.4.1-1.* However, web bend buckling must always be considered as discussed in the next section.

AASHTO LRFD Article 6.10.4.2.2 optionally permits moment redistribution for continuous-span members in straight I-girder bridges that satisfy specific limitations spelled out in *AASHTO LRFD* Appendix B6 (Article B6.2) prior to making the service limit state design verifications. However, according to *AASHTO LRFD* Article 6.11.4, the applicability of these moment redistribution procedures to box sections has not yet been demonstrated; therefore, the optional Appendix B6 provisions are not to be applied to box sections at the service limit state.

One final requirement in *AASHTO LRFD* Article 6.10.4.2.2 relates to the rare case of compact composite sections in positive flexure utilized in shored construction. In this case, longitudinal compressive stresses in the concrete deck due to the Service II loads are limited to $0.6f'_c$ to ensure linear behavior of the concrete. As discussed in *AASHTO LRFD* Article C6.10.1.1.1a, the use of shored construction is not recommended. Also, as discussed previously, composite sections in positive flexure in all kinked (chorded) continuous and horizontally curved-girder systems must be treated as noncompact sections. Composite sections in positive flexure in most straight I-girder bridges with skewed supports should also be treated as noncompact sections.

3.2.4.3.3.2 Web Bend Buckling

AASHTO LRFD Article 6.11.4 specifies that except for composite sections in positive flexure in which the web satisfies the requirement of *AASHTO LRFD* Article 6.11.2.1.2 (i.e. $D/t_w \leq 150$ – no longitudinal web stiffeners), all sections must also satisfy Equation 3.2.33 at the service limit state. At sections where access holes are present in the box flange, f_c should be computed using section properties calculated assuming the area of the access hole is subtracted from the box-flange area.

The web depth, D, and the depth of the web in compression, D_c, should each be measured along the web slope in computing the web bend-buckling resistance, F_{crw}, from Equation 3.2.35 for sections with inclined webs; that is, the vertical web depth in each case must be divided by $\cos\theta$, where θ is the angle of inclination of the web plate with respect to the vertical. The reader is referred to Section 3.2.4.3.2.2 for further information on this particular check, the web bend-buckling resistance, F_{crw}, and the depth of the web in compression in the elastic range, D_c.

3.2.4.4 Control of Deck Cracking

AASHTO LRFD Article 6.10.1.7 requires that the longitudinal tensile stress in a composite concrete deck due to the Service II load combination satisfy the following equation to control the cracking in the concrete deck:

$$f_{deck} \le \phi f_r = 0.9 f_r$$

Equation 3.2.43

where:

- ϕ = resistance factor for concrete in tension = 0.9 for reinforced concrete (*AASHTO LRFD* Article 5.5.4.2.1)
- f_r = deck concrete modulus of rupture specified in *AASHTO LRFD* Article 5.4.2.6 (ksi)

For normal-weight concrete:

$$f_r = 0.24\sqrt{f'_c}$$

Equation 3.2.44

The short-term modular ratio should be used when computing the concrete deck tensile stress; that is, n should be used to compute the composite section properties as opposed to $3n$ (refer to *AASHTO LRFD* Article 6.10.1.1.1d). The calculated stress on the transformed section must be divided by n to obtain the stress in the concrete. f_r is the modulus of rupture, computed using the lower-bound equation for normal-weight concrete shown in Equation 3.2. For lightweight concrete, refer to *AASHTO LRFD* Article 5.4.2.6.

A similar requirement is enforced under the factored construction loads (i.e. the deck-placement sequence), as discussed previously in Section 3.2.3.2.5. Basically, the requirement under the service limit state will determine if the cut-off point for the minimum 1 percent longitudinal steel determined for the factored construction loads will need to be extended further into the span.

3.2.5 LRFD Fatigue and Fracture Limit State Design

3.2.5.1 General

AASHTO LRFD Article 1.3.2.3 specifies that the fatigue limit state is to be taken as restrictions on the stress range resulting from a single design truck occurring at an expected number of stress range cycles, which are intended to limit crack growth under repetitive loads to prevent fracture during the design life of the bridge. The fracture limit state is taken as a set of material toughness requirements intended to ensure that the steel has the ability to absorb energy without fracture at minimum specified service temperatures.

AASHTO LRFD Article 6.5.3 states that components and details are to be investigated for fatigue as specified in *AASHTO LRFD* Article 6.6. The investigations are to be made for the applicable Fatigue load combination specified in *AASHTO LRFD* Table 3.4.1-1 using the fatigue live load given in *AASHTO LRFD* Article 3.6.1.4. The fatigue live load is discussed in Section 1.3.2.3.3. The two Fatigue load combinations are discussed in Section 1.3.3. Fracture toughness requirements are to be in conformance with *AASHTO LRFD* Article 6.6.2.

The preceding requirements are reiterated for I-sections, in *AASHTO LRFD* Articles 6.10.5.1 and 6.10.5.2. The design of box sections for the fatigue limit state is covered in *AASHTO LRFD* Article 6.11.5. In addition, a special fatigue requirement for webs is specified in *AASHTO LRFD* Article 6.10.5.3 that is applicable to both I- and box sections. Requirements for fatigue design of shear connectors are covered in Section 3.3.2.2.

A helpful flowchart detailing the required LRFD fatigue and fracture limit state design verifications discussed below is provided in *AASHTO LRFD* Figure C6.4.3-1 (Appendix C6). The application of these design verifications is illustrated in the design examples presented in Sections 5.1 and 5.2.

3.2.5.2 Fatigue Limit State

3.2.5.2.1 General

Fatigue is defined in the *AASHTO LRFD* Specifications as the initiation and/or propagation of cracks due to repeated variation of normal stress with a tensile component. The fatigue life of a detail is defined as the number of repeated stress cycles that result in fatigue failure of a detail, and the fatigue design life is defined as the number of years that a detail is expected to resist the assumed traffic loads without fatigue cracking. In the *AASHTO LRFD* Specifications, the base fatigue design life is taken to be 75 years.

AASHTO LRFD Article 6.6.1.1 specifies that fatigue be categorized as either “load-induced fatigue” (*AASHTO LRFD* Article 6.6.1.2) or “distortion-induced fatigue” (*AASHTO LRFD* Article 6.6.1.3). Load-induced fatigue is defined as fatigue effects

due to in-plane stresses for which components and details are explicitly designed. For load-induced fatigue, specific design verifications are required for both flexure and shear to ensure adequate fatigue resistance for the expected number of stress range cycles, and to control web buckling and the resulting elastic flexing of the web under repeated loading. Distortion-induced fatigue is defined as fatigue effects due to secondary stresses not normally quantified in the typical analysis and design of a bridge. Distortion-induced fatigue is typically controlled by providing rigid load paths to preclude the development of significant secondary stresses that could induce fatigue crack growth.

3.2.5.2.2 Load-Induced Fatigue

3.2.5.2.2.1 Flexure

Stress Range and S-N Curves

Early attempts to quantify the fatigue resistance of a particular structural joint were based on tests on relatively small-scale specimens that simulated a prototype connection (*34*, *35*). The experiments contained a limited number of specimens and many variables were introduced that made it difficult to establish the significance of details, type of steels, stress conditions and the quality of fabrication. Because of the limitations of the test data, only approximate design relationships could be developed. Prior to the Ninth Edition of the *AASHO* Specifications, 1965, welded bridges were checked for fatigue by limiting alternating stresses using American Welding Society (AWS) specifications. The Ninth Edition specifications introduced the concept of cycles of maximum stress combined with the modified Goodman diagram to limit maximum fatigue stresses for nine different conditions. These provisions were based primarily on the tests mentioned above. However, fatigue cracks were still being found in some beams with partial length cover plates after as little as 13 years of service. Fatigue cracks were also found at the ends of web-to-stiffener welds in stiffeners cut short of the beam flange.

Additional experimental data were therefore developed starting in 1968 under National Cooperative Highway Research Program (NCHRP) Project 12-7, which involved the fatigue testing of approximately 500 test beams and girders under constant amplitude loading (*36*, *37*). Large-scale rolled and welded beam specimens were tested both with and without attachments, such as cover plates and transverse stiffeners. The use of large-scale specimens overcame some of the difficulties associated with the previous data, including the effects of residual stresses, defect size and distribution and shear lag. The test data demonstrated that all fatigue cracks commence at an initial discontinuity in the weldment, or at the periphery of the weld, and grow perpendicular to the applied stresses. Such discontinuities are always present regardless of the welding process or techniques used during the fabrication. The data also showed that the termination of groove and fillet welds provides an even more critical crack growth condition than initial discontinuities in the weld due to high stress concentrations resulting from the geometrical conditions.

Analysis of the data from the NCHRP Project showed that the most important factors governing the fatigue resistance are the stress range and type of detail. Other parameters such as the minimum stress, maximum stress, type of steel and stress ratio (i.e. the ratio of minimum stress to maximum stress) do not play an important role. *The stress range is the algebraic difference between the maximum stress and minimum stress at a detail. Stress range means that only the live load plus impact stresses need to be considered; dead load does not contribute to the stress range* (Figure). The fact that stress range is the only significant design parameter is due to the existence of residual stresses in welded steel structures. The welding process results in high tensile residual stresses due to shrinkage of the weld upon cooling, which are at or near the yield point of the weldment and the adjacent base metal. Tensile residual stresses of this magnitude occur regardless of the steel type, which is why the fatigue resistance is independent of the type of steel. Most of the fatigue life occurs in these regions of high tensile residual stress and is exhausted by the time the fatigue crack propagates out of this zone.

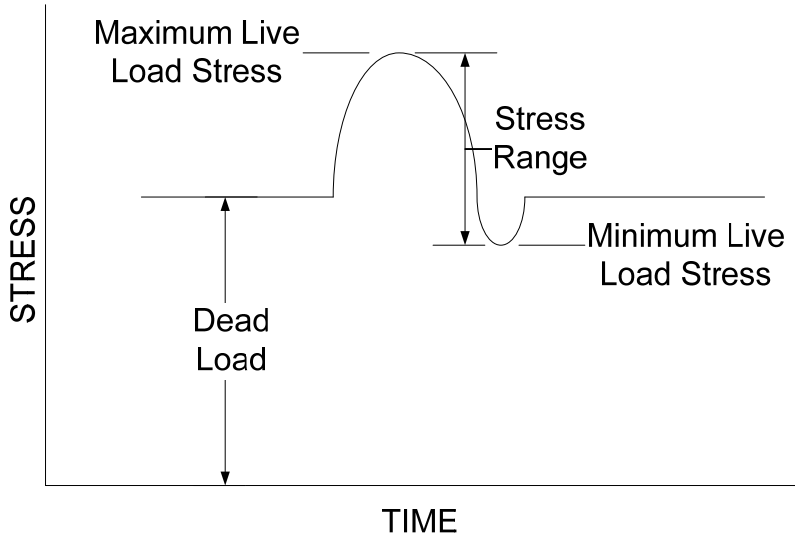


Figure 3.2.14 Components of a Stress Cycle

The tensile portion of a stress cycle propagates a fatigue crack. Therefore, material subjected to a cyclic loading at or near an initial discontinuity will be subject to a fully effective stress cycle in tension, even in cases of stress reversal, because the superposition of the tensile residual stress will elevate the entire cycle into the tensile stress region (Figure 3.2.15). The test data even showed an effective stress cycle in tension in cover-plated beams subjected to cyclic compression alone. Fatigue cracks occurred in the tensile residual stress zone at the cover plate weld terminations, but were arrested as they propagated into the adjacent compressive residual stress regions. No loss in load-carrying capacity was observed. This concept of considering only stress range has also been extended to rolled beam, bolted and riveted details where much different residual stress fields exist; the application of this concept to non-welded details is conservative.

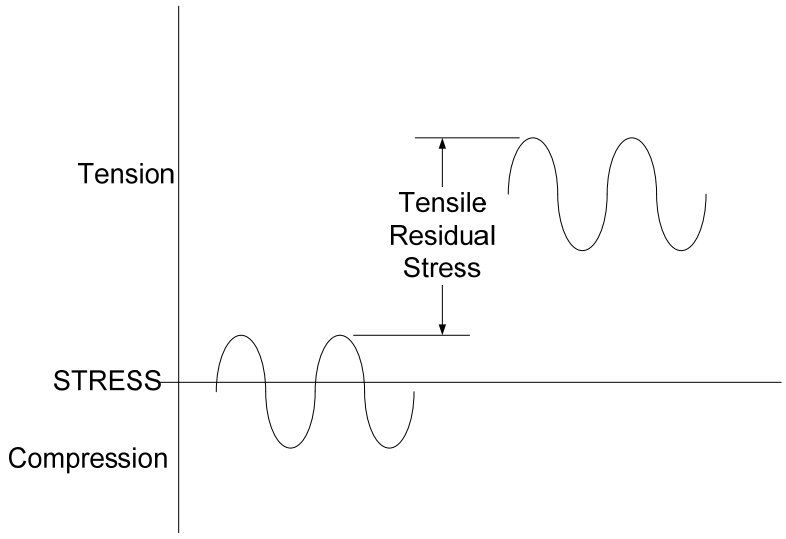


Figure 3.2.15 Effect of Residual Stress on a Stress Cycle

As a result of the observed behavior, fatigue design criteria need only be considered for details subject to effective stress cycles in tension and/or stress reversal. If a detail is subject to stress reversal, fatigue must be considered no matter how small the tension component of the stress cycle since a crack generated in the tensile residual stress zone could still be propagated to failure by the small tensile component of stress. Of course, the detail also must be subject to a net applied tensile stress to begin with when considering the maximum anticipated fatigue live load stress occurring over the fatigue design life acting in conjunction with the stress due to the unfactored permanent loads.

Once it was established that the stress range was the critical parameter defining the fatigue life, a relationship between the nominal fatigue resistance expressed in terms of stress range $(\Delta F)_n$ and the number of stress cycles to failure N, or S-N curve, could be established. Regression analyses showed that such a relationship could be developed with a constant slope in log-log space as follows:

$$\log N = \log A - B \log(\Delta F)_n \qquad \text{or} \qquad N = A(\Delta F)_n^{-B}$$

Equation 3.2.45

where *log A* is the *log N*-axis intercept of the S-N curve and B is the slope constant of the curve. Failure in this case is defined as the growth of a crack large enough in size to result in the inability of a member to carry the load, but does not include brittle fracture where there is limited crack growth.

A least squares linear regression analysis was performed for each type of detail to obtain a curve defining the estimated mean life for that particular detail group; i.e., where half the test data failed prior to reaching the estimated fatigue life and half the data failed after reaching this estimated life. A parallel curve was then drawn two

standard deviations below this mean curve, which represented the 95 percent lower confidence limit. This lower bound curve defined a 97.5 percent probability of survival, or conversely, a 2.5 percent probability of failure. A set of such curves was developed for five different detail categories ranging from A to E, with Category A representing details with the highest fatigue resistance and Category E representing details with the lowest fatigue resistance for the details tested as part of the NCHRP research program. Each curve had a slope constant *B* of approximately 3. These curves first appeared in the 1973 *AASHTO* Interim Specifications. Additional fatigue research conducted in the U.S. and abroad between 1973 and 1986 led to minor adjustments to the fatigue design curves and the inclusion of two additional curves for Categories B′ and E′. The slope constant of each curve was also set equal to 3. The complete set of current AASHTO *S-N* curves given in the *AASHTO LRFD* Specification is shown in Figure 3.2.16.

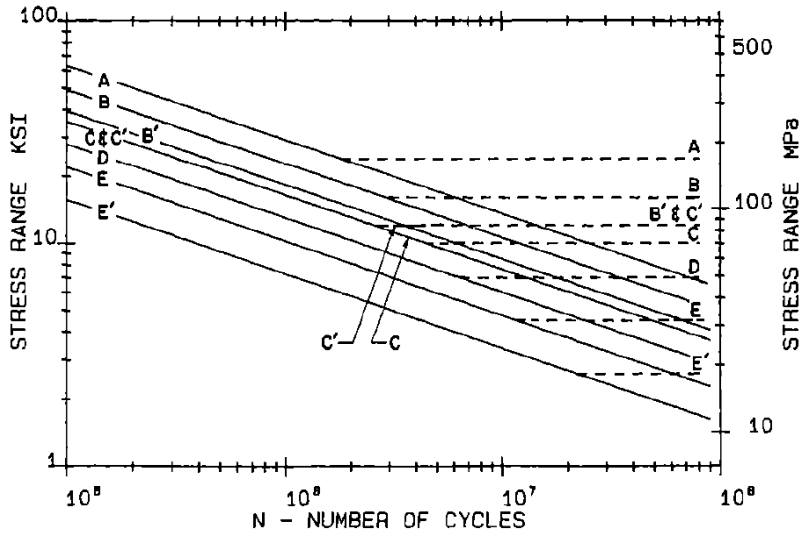


Figure 3.2.16 *AASHTO LRFD* S-N Curves

It was also observed from the test data that as the stress range decreased in magnitude, there was a level at which no fatigue cracking was observed in the test specimens. The maximum stress range at which no fatigue crack growth will occur under constant amplitude loading is termed the constant-amplitude fatigue threshold $(\Delta F)_{TH}$ and is indicated by the dashed horizontal line in Figure 3.2.16 for each detail category. Note that $(\Delta F)_{TH}$ decreases as the severity of the detail category increases. For higher traffic-volume bridges, if the maximum stress range experienced by a detail due to the heaviest truck expected to cross the bridge over the fatigue design life is less than $(\Delta F)_{TH}$, then that detail has a theoretically infinite fatigue life. Therefore, the dashed-line portion of the *S-N* curves will be referred to here as the "infinite-life region". Values for $(\Delta F)_{TH}$ for each detail category are given in *AASHTO LRFD* Table 6.6.1.2.5-3 as follows:

Table 3.2.6 Values for $(\Delta F)_{TH}$ for Each Detail Category

Detail Category	$(\Delta F)_{TH}$ (ksi)
A	24.0
B	16.0
B′	12.0
C	10.0
C′	12.0
D	7.0
E	4.5
E′	2.6

With an identical slope constant of 3 for each curve in Figure 3.2.16, the equation for the sloping portion of the *S-N* curves can be written as follows:

$$(\Delta F)_n = \left(\frac{A}{N}\right)^{\frac{1}{3}}$$

Equation 3.2.46

Values of the *Log N*-axis intercept coefficient *A,* or as referred to in the *AASHTO LRFD* Specification, Detail Category Constant, are given in *AASHTO LRFD* Table 6.6.1.2.5-1 as follows:

Table 3.2.7 Detail Category Constant, A

Detail Category	Constant A times 10^8 (ksi^3)
A	250.0
B	120.0
B′	61.0
C	44.0
C′	44.0
D	22.0
E	11.0
E′	3.9

Equation 3.2.46 controls for lower traffic-volume bridges. The sloping portion of the *S-N* curves will be referred to here as the “finite-life region”.

The above tables reveal that both *A* and $(\Delta F)_{TH}$ are greatest for Detail Category A and are least for Detail Category E′. Therefore, nominal fatigue resistance is also

greatest for Detail Category A and is least for Detail Category E′. The fatigue detail categories are discussed next.

Fatigue Detail Categories

Category A defines the fatigue resistance of the base metal in rolled plates and shapes without welded or bolted details or attachments and provides the maximum possible fatigue resistance of any detail. Category B applies to the base metal at the majority of welded details, including longitudinal fillet (Figure 3.2.17) and full penetration groove welds, transverse groove welds ground flush and transitioned flange splices. Pre-tensioned high-strength bolted connections designed as slip-critical connections installed in holes drilled full size or subpunched and reamed to size are classified as Category B (e.g. bolted flange and web splices, bolted stiffeners and end-bolted cover plates). The fatigue resistance applies to the base metal at the gross section of the connection near the hole(s). Category B also applies to the base metal at the *net* section of high-strength bolted connections designed as bearing-type connections, but fabricated and installed to the requirements for slip-critical connections, with pre-tensioned bolts installed in holes drilled full size or subpunched and reamed to size. The nominal fatigue resistance of uncoated weathering steel base metal designed and detailed in accordance with Reference 38 is also classified as Category B. Category B′, introduced in 1988, applies to longitudinal partial penetration groove welds, full penetration groove welds with backing bars left in place, and straight flange transition splices made with steels with a specified minimum yield strength greater than or equal to 100 ksi. Detail Categories A through B′ rarely control the design.

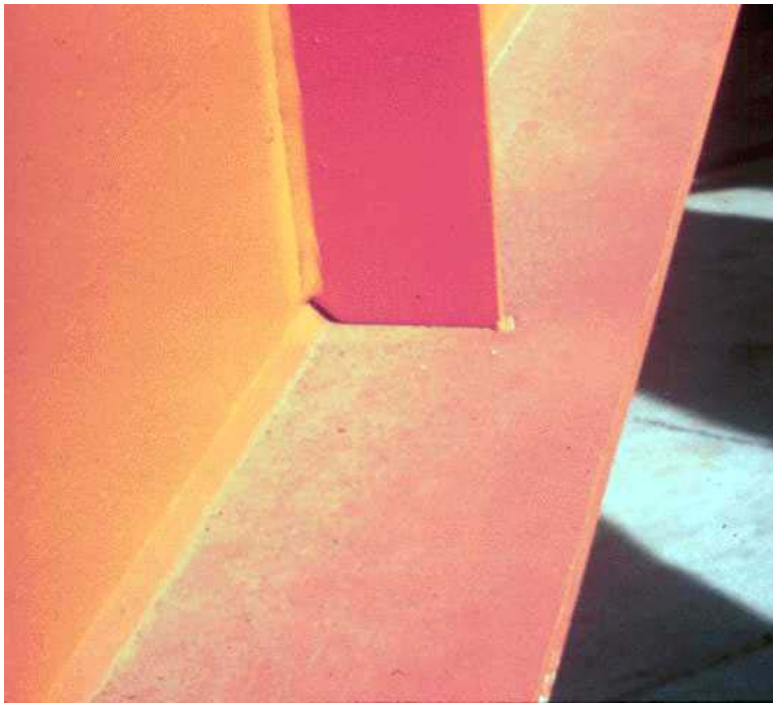


Figure 3.2.17 Longitudinal Flange-to-Web Fillet Weld (Fatigue Category B)

Category C applies to the base metal at short attachments, unimproved transverse groove welds, welded shear studs and certain attachments with specified radius transitions. Category C marks the transition where geometrical stress concentrations begin to influence the fatigue resistance more than initial discontinuities in the weldment (*39*). Category C′ applies specifically to the base metal at the toe of transverse stiffener-to-flange and transverse stiffener-to-web welds. Category D represents a transition between high and low fatigue strength details. The fatigue resistance of Category D details is influenced by any improvements to reduce the geometrical stress concentration and the attachment length. Category D also applies to the base metal at the net section of bolted connections in hot-dipped galvanized members (*40*); the base metal at the gross or net section (as applicable) of pre-tensioned high-strength bolted connections installed in holes punched full size (*41*); the base metal at the net section of joints using A 307 bolts or non-pretensioned high-strength bolts; and the base metal at the net section of open holes in members (*41*).

Category E applies to base metal at the ends of partial length welded cover plates; base metal at the ends of welded longitudinal web or flange stiffeners without specified radius transitions, lateral connection-plate welds, long attachments and small radius transitions; and the base metal at the net section of eyebar heads or pin plates. Base metal in angle or tee section members connected to a gusset or connection plate by longitudinal fillet welds along both sides of the connected element of the member cross-section is also classified as Category E. The fatigue stress range is calculated in this case based on an effective net area of the member as defined in *AASHTO LRFD* Table 6.6.1.2.3-1 and discussed further in Sections 3.3.3.2.5 and 3.3.4.2.3. Category F given in previous specifications for checking shear on the throat of a fillet weld has been eliminated. When fillet welded are properly sized for strength considerations, Category F should not govern. Fatigue will be governed by cracking in the base metal at the weld toe and not by shear on the throat of the weld.

Category E′ details are the lowest fatigue-strength details and are similar to Category E details, but exhibit a reduced fatigue resistance due to a plate-thickness effect, which results in a higher geometrical stress concentration. Category E′ details include the base metal at longitudinal welded attachments with a thickness greater than 1.0 in., at welded cover plate ends on flanges with a thickness greater than 0.8 in. and at the welded ends of cover plates wider than the flange with no transverse end welds.

AASHTO LRFD Table 6.6.1.2.3-1 lists the detail categories for different details. Included in the table is a description of the specific situation, the corresponding detail category and a brief description of potential crack initiation points. For easy reference, the constant-amplitude fatigue threshold, $(\Delta F)_{TH}$, along with the detail category constant, A, have been provided in the table for each detail. The table has been updated to provide more detailed and informative illustrative examples than the table given in previous specifications, and also to combine the detail descriptions

and corresponding illustrative examples within the same table. Additional details have also been added that were not covered in the previous table. Welded stiffeners, which are the most commonly used detail in steel-bridge construction, are now grouped within a separate section of the table. Many of the details are shown in 3D, along with the orientation of the applied stress range. In addition, the potential location of crack initiation is shown in the illustrations.

For example, Figure 3.2.18 shows the illustrative examples given in the table for: 1) base metal at the termination of partial length welded cover plates having square or tapered ends that are narrower than the flange, with or without welds across the ends, or cover plates that are wider than the flange with welds across the ends (Condition 3.5 in the table), and 2) base metal and weld metal in longitudinal web or longitudinal box-flange stiffeners connected by continuous fillet welds parallel to the direction of applied stress (Condition 4.2 in the table). As shown in Figure 3.2.18, the examples confirm for the cases shown in the photograph that the detail category for the ends of a welded partial-length cover plate is Category E′ (since the cover plate is narrower than the flange and the flange thickness is greater than 0.8 inches), and that the detail category for the base metal and weld metal for the continuous fillet weld connecting the longitudinal stiffener to the web is Category B. The illustrative examples are not intended to serve as standard details or necessarily as examples of good detailing practice.

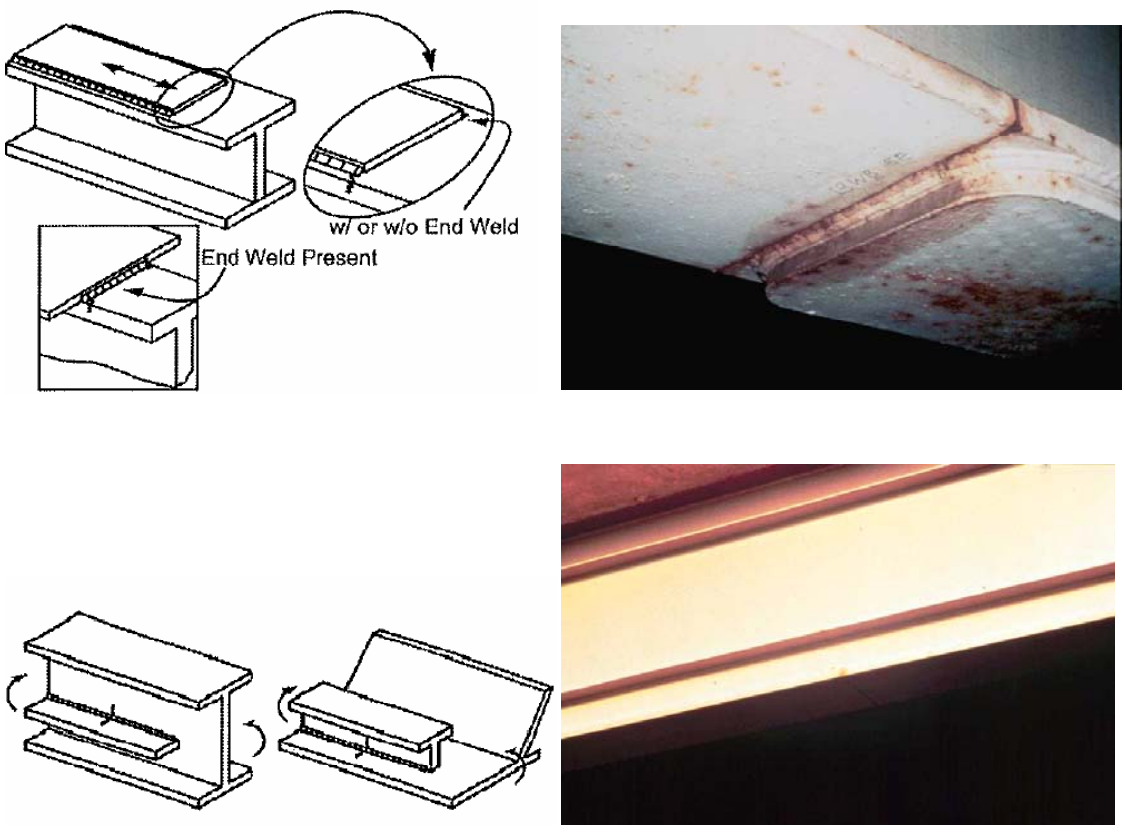


Figure 3.2.18 Sample Illustrative Examples of Fatigue Details

Description	Category	Constant A (ksi3)	Threshold $(\Delta F)_{TH}$ ksi	Potential Crack Initiation Point
3.5 Base metal at the termination of partial length welded cover plates having square or tapered ends that are narrower than the flange, with or without welds across the ends, or cover plates that are wider than the flange with welds across the ends:				In the flange at the toe of the end weld or in the flange at the termination of the longitudinal weld or in the edge of the flange with wide cover plates
Flange thickness ≤ 0.8 in.	E	11×10^8	4.5	
Flange thickness > 0.8 in.	E'	3.9×10^8	2.6	



Description	Category	Constant A (ksi3)	Threshold $(\Delta F)_{TH}$ ksi	Potential Crack Initiation Point
4.2 Base metal and weld metal in longitudinal web or longitudinal box-flange stiffeners connected by continuous fillet welds parallel to the direction of applied stress.	B	120×10^8	16	From the surface or internal discontinuities in the weld away from the end of the weld



Figure 3.2.19 Category B and E' Details

Good Detailing Practices

Examples of design details to optimize the fatigue resistance can be found in References 39, 42 and 43. The following basic general principles of good fatigue design taken from Reference 39 are restated as follows:

- Design the bridge and its assemblage of members as a whole so as to provide easy paths for stress flow. Avoid gross discontinuities by providing gradual changes in cross-section. Put material at the points at which loads are to be resisted and avoid sudden changes in stiffness.
- Select the individual connections on the basis of providing the easiest possible stress path through the connections.
- Although all connections produce stress concentrations, their number and severity should be minimized.
- Position connections near points of low fatigue stress if possible. For example, field splices in continuous girders should preferably be positioned near points of permanent-load contraflexure.
- Avoid the introduction of unnecessary stresses, such as those associated with unnecessary eccentricities.

Details with a fatigue resistance less than Category C should be avoided if possible, but should not necessarily be precluded from use if they can be used in regions of

low stress range. A Category C detail that is overstressed provides less safety than an understressed Category E detail.

Intersecting welds at details should always be avoided. Such details are possible, for example, at the intersection of transverse and longitudinal web stiffeners and at the intersection of lateral connection plates and transverse stiffeners. The restraining effect of the intersecting welds on the plate elements can result in the development of large restraint stresses during cooling, which can potentially result in cracking and low fatigue resistance. In most cases, it is desirable for the longitudinal weld, or the weld parallel to the applied stress, to be continuous to avoid a Category E detail at the weld termination if it is interrupted. End terminations of transverse welds are typically classified as Category C details.

AASHTO LRFD Article 6.6.1.2.4 discusses detailing to reduce constraint-like conditions. This article specified that to the extent practical, welded structures are to be detailed to avoid conditions that create highly constrained joints and crack-like geometric discontinuities susceptible to constraint-induced fracture (i.e. brittle fracture that can occur without any perceptible fatigue crack growth and without any warning). This type of failure was documented during the Hoan Bridge failure investigation (*44*, *45*). Criteria to identify bridges and details susceptible to this failure mode are discussed in Reference 46. Again, intersecting welds are to be avoided. Welds that are parallel to the primary stress, but interrupted by intersecting members, are to be detailed to allow a minimum gap of $4t_w$ between the weld toes, where t_w is the thickness of the web in inches, to reduce constraint. Attached welded elements are less susceptible to fatigue and fracture if the attachment parallel to the primary stress is continuous and the transverse attachment is discontinuous (refer to *AASHTO LRFD* Figures C6.6.1.2.4-1 and C6.6.1.3.2-1 for preferred details at the intersection of a transverse stiffener/connection plate with a longitudinal web stiffener and a lateral connection plate, respectively).

Fillet welds or partial penetration welds providing continuity between intersecting plate members (e.g. at transverse and longitudinal stiffener intersections and at transversely loaded web attachments) are often referred to as cruciform joints (Figure 3.2.20).

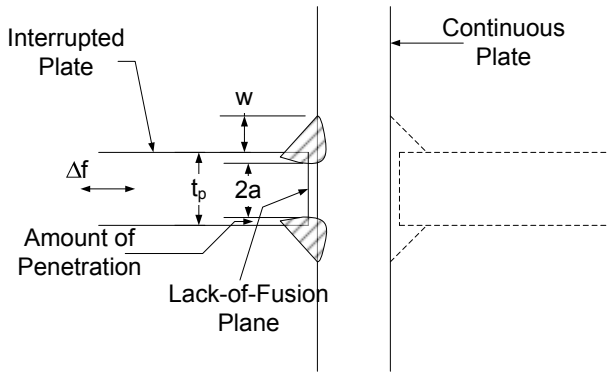


Figure 3.2.20 Cruciform Joint Detail

Such joints are typically fabricated with one plate continuous while the other plate is interrupted, with fillet welds or partial penetration welds provided at the corners. As shown in Figure 3.2.20, a lack-of-fusion plane (or penetration at the weld root) may result depending on the thickness of the interrupted plate, weld size and depth of penetration. When only the continuous plate is loaded, the lack of fusion plane is parallel with the stress field and the fatigue resistance of the base metal at the weld is Category C. If the interrupted plate is loaded, the lack-of-fusion plane is perpendicular to the stress field (i.e. the fillet welds or partial penetration welds are transversely loaded) and the fatigue resistance of the base metal at the weld must be taken from the following equation given in *AASHTO LRFD* Article 6.6.1.2.5:

$$(\Delta F)_n = (\Delta F)_n^C \left(\frac{0.65 - 0.59\left(\frac{2a}{t_p}\right) + 0.72\left(\frac{w}{t_p}\right)}{t_p^{0.167}} \right) \le (\Delta F)_n^C$$

Equation 3.2.47
AASHTO LRFD Equation 6.6.1.2.5-4

where:

$(\Delta F)_n^C$ = nominal fatigue resistance for Detail Category C (ksi)
2a = length of the non-welded root face in the direction of the thickness of the loaded plate (in.). For fillet-welded connections, the quantity ($2a/t_p$) is to be taken equal to 1.0.
t_p = thickness of the loaded plate (in.)
w = leg size of the reinforcement or contour fillet, if any, in the direction of the thickness of the loaded plate (in.)

Equation 3.2.47 accounts for the potential of a crack initiating from the weld root and includes the effects of weld penetration. As a result, the equation is also applicable to partial joint penetration groove welds. The effect of any weld penetration is conservatively ignored by taking the quantity ($2a/t_p$) equal to 1.0. Equation 3.2.47 limits the nominal fatigue resistance based on the crack initiating from the weld root to the nominal fatigue resistance for Category C, which assumes crack initiation from the weld toe. The development of Equation 3.2.47 is discussed in Reference 47.

The severity of the cruciform joint can be reduced by the proper selection of the continuous plate element. For example, as discussed above, at intersections of longitudinal and transverse stiffeners, the longitudinal stiffener (i.e. the loaded element) should be continuous while the transverse stiffener (i.e. the unloaded element) is interrupted. At intersections of transverse stiffeners with lateral connection plates, it is required that the transverse stiffener be interrupted and attached to the lateral connection plate (*AASHTO LRFD* Article 6.6.1.3.2). It should be emphasized that Equation 3.2.47 does *not* apply to the base metal at the toe of

transversely loaded transverse stiffener-to-flange or transverse stiffener-to-web fillet welds, which are classified as Category C′.

Reference 39 discusses the need to provide a sufficient minimum length for the web gap between the end termination of the transverse weld and the weld toe of the longitudinal weld. For example, where transverse stiffeners are welded to the flange, the end of the transverse weld should be terminated at least one inch from the web-to-flange weld toe to prevent intersecting welds and the formation of significant restraint stresses (Figure 3.2.21). The stiffener plate should be coped to avoid interference with the web-to-flange weld. The weld should also be terminated approximately ¼ inch from the plate edges, as wrapping the weld around the plate could result in undercutting of the stiffener plate.

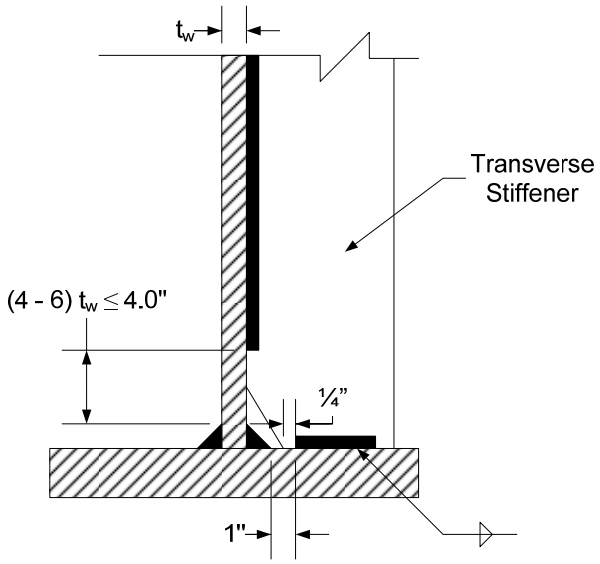


Figure 3.2.21 Transverse Stiffener Detail

As shown in Figure 3.2.21, the minimum distance between the end of the web-to-stiffener weld and the near edge of the web-to-flange fillet weld, or a longitudinal stiffener-to-web weld as applicable, is limited to four times the web thickness, as specified in *AASHTO LRFD* Article 6.10.11.1.1. This limit is specified to eliminate the possibility of a weld intersection and the concomitant high restraint stresses resulting from weld shrinkage. In addition, this limit helps to relieve flexing of the unsupported portion of the web in the gap to avoid fatigue-induced cracking of the stiffener-to-web welds, particularly during handling and shipping of the girders when the stiffeners are cut short from the tension flange (the web gaps should be blocked during shipment in this case). An upper limit on this distance equal to the lesser of six times the web thickness and 4.0 inches is also specified. The $6t_w$ limit is specified to avoid vertical buckling of the unsupported portion of the web. The 4.0-inch limit was arbitrarily selected to avoid large unsupported web segments in cases where the web thickness has been selected for reasons other than stability; an example being the webs of bascule girders at trunions. Additional information

regarding the detailing of stiffeners (transverse, longitudinal and bearing) is provided in Section 3.3.8. Further information regarding the detailing of lateral connection plates for lateral bracing members is provided in Section 3.1.2.9.3.

Nominal Fatigue Resistance

Most of the early laboratory fatigue tests were based on constant-amplitude loading, which consisted of a series of identical load cycles or a constant applied stress range. However, bridges are actually subject to variable-amplitude loading because of the variation of vehicle weights and different possible loading combinations. Variable-amplitude loading consists of a series of cycles of different magnitudes, usually applied in a random sequence. The effects of variable-amplitude loading are typically accounted for using a cumulative damage rule. The most widely used method to account for the effects of cumulative damage is the linear rule proposed by Miner (*48*). According to Miner's rule, fatigue damage occurs when the sum of the cumulative stress cycle ratios for the various stress cycles equals unity, or $\sum n_i / N_i = 1.0$, where n_i is the number of cycles applied at a stress range S_{ri} and N_i is the number of constant amplitude cycles to failure at S_{ri}.

Variable-amplitude fatigue tests were carried out on large-scale beams under NCHRP Project 12-12 (*49*) to evaluate the effectiveness of Miner's linear damage hypothesis in relating variable stress cycles to constant cycle data. The beams were identical to those tested under the original NCHRP Project 12-7. It was determined from the results of this study that an equivalent constant-amplitude stress range, or an *effective stress range*, S_{re}, that causes the same fatigue damage as an equal number of variable-amplitude cycles could be developed by combining Miner's linear damage rule with Equation 3.2.46 as follows:

$$S_{re} = \left(\sum \gamma_i S_{ri}^3\right)^{1/3}$$

Equation 3.2.48

where γ_i is equal to the frequency of occurrence of the stress range S_{ri}. Using an effective stress range allows constant-amplitude fatigue data and resistance curves to be used to define variable-amplitude conditions and also allows the fatigue damage resulting from an arbitrary load spectrum to be related to a single stress range.

Similarly, the gross weight of a fatigue design truck selected so that the fatigue damage caused by a given number of passages of this truck is the same as the damage caused by an equal number of passages of different-sized trucks in actual traffic can be computed as follows:

$$W_F = \left(\sum \alpha_i W_i^3\right)^{1/3}$$

Equation 3.2.49

where α_i is the fraction of trucks with a gross weight of W_i. The stress range caused by the passage of such a truck would be representative of the effective stress range given by Equation 3.2.48. To use Equation 3.2.49, a histogram of truck-weight data for a particular site would be required to arrive at the weight of the fatigue design truck. Since such data are generally not available, a gross weight of 54 kips was originally proposed for the fatigue design truck in Reference 50, which was calculated from Equation 3.2.49 based on weigh-in-motion data and the results of several nationwide traffic surveys (*43*). A constant rear-axle spacing of 30 feet was also proposed for the fatigue design truck in Reference 50 since that spacing was assumed to approximate the spacing for the 4- and 5-axle semitrailers that do most of the fatigue damage to bridges. Further, an impact factor of 1.15 was proposed for fatigue design since the impact factor in this case is for stress range rather than peak stress. Also, it was felt by the Guide Specification writers that an average impact factor rather than a maximum factor would be more appropriate for fatigue design.

These concepts were carried forward to the *AASHTO LRFD* Specifications, with some slight modification. As discussed in Section 1.3.2.3.3, the fatigue design truck is specified to be a single HS20 truck, weighing 72 kips, with a constant rear-axle spacing of 30 feet (*AASHTO LRFD* Article 3.6.1.4.1). A dynamic load allowance (impact factor) of 1.15 is to be applied to the truck (*AASHTO LRFD* Article 3.6.2). *AASHTO LRFD* Article 3.6.1.4.3a specifies that when the bridge is analyzed by a refined analysis method, the truck is to be positioned transversely and longitudinally to maximize the stress range at the detail under consideration regardless of the position of the actual traffic lanes on the deck. *AASHTO LRFD* Article 3.6.1.4.3b specifies that when wheel-load distribution factors are used for the analysis, the appropriate factor specified for one-lane loaded in *AASHTO LRFD* Article 4.6.2.2 is to be used. Further, *AASHTO LRFD* Article 3.6.1.1.2 specifies that the multiple presence factor of 1.2 for one-lane loaded (*AASHTO LRFD* Table 3.6.1.1.2-1) is not to be applied for the fatigue limit state check. Therefore, when using the tabularized equation for the distribution factor for one-lane loaded for the interior girders, the 1.2 multiple presence factor must be divided out of the calculated factor. Or, when using the lever rule or the special analysis equation to compute the factor for one-lane loaded for the exterior girders, or when applying the fatigue design truck to an influence surface in a refined analysis, the 1.2 factor must not be applied.

The fatigue load produces a lower calculated stress range than the design loads that were used to check for fatigue in the *AASHTO* Standard Specifications. Fatigue was checked in the Standard Specifications for multiple lanes of truck loading (using the design truck with variable rear-axle spacing) and multiple lanes of lane loading. In addition, for high-volume roadways, an additional check was made for a single design truck. A reduced impact factor was not applied. The reduction in the calculated stress range in the *AASHTO LRFD* Specifications is offset by an increase in the number of cycles of loading to be considered. In the Standard Specifications, fatigue checks were made for: over 2,000,000 cycles; 2,000,000 cycles; 500,000 cycles and/or 100,000 cycles depending on the case of the roadway (i.e. volume of average daily truck traffic) and the category of loading (truck or lane). Fatigue must be checked in the *AASHTO LRFD* Specifications for a much higher number of

cycles, *N*, in order to achieve a nearly equivalent fatigue design. The lower stress range and increased number of cycles are believed to be more reflective of actual conditions experienced by many bridges. As such, the fatigue provisions given in the *AASHTO LRFD* Specifications can be used more easily for both design and evaluation, whereas the fatigue provisions given in the Standard Specifications, which were based on a much lower number of design cycles than are actually experienced by most bridges, could not easily be used for evaluation.

The preceding discussion on the effective stress range leads to the first principle of fatigue resistance, which applies in the finite-life region, and states that for lower traffic volumes, the fatigue resistance $(\Delta F)_n$ is inversely proportional to the cube of the effective stress range. This principle is reflected by Equation 3.2.46, which represents the equation for the sloping portion of the *S-N* curve. *In the AASHTO LRFD Specifications, the effective stress range is represented by a factored fatigue design truck weighing 54 kips (plus impact), which is specified as the Fatigue II load combination in AASHTO LRFD Table 3.4.1-1. The specified load factor for the Fatigue II load combination is 0.75; 0.75 * 72 kips = 54 kips*.

In the extreme life (or infinite life) region, for which many details on bridges located on high-volume routes are designed, most of the stress cycles in a spectrum will be below the constant-amplitude fatigue threshold $(\Delta F)_{TH}$. These cycles do not cause fatigue damage under constant-amplitude loading. However, under variable-amplitude loading, larger stress cycles that exceed $(\Delta F)_{TH}$ will contribute to fatigue crack growth, which will cause the threshold to decrease in magnitude until all stress cycles will eventually contribute to crack growth. Therefore, in the infinite-life region, fatigue design of welded details subject to variable-amplitude loading requires that the *maximum stress range* be considered in addition to the effective stress range.

As a result, three different cases related to fatigue life are possible depending on the relative values of the effective stress range, maximum stress range and $(\Delta F)_{TH}$: Case 1 -- effective stress range and maximum stress range greater than $(\Delta F)_{TH}$; Case 2 -- effective stress range less than $(\Delta F)_{TH}$ and maximum stress range greater than $(\Delta F)_{TH}$; or Case 3 -- effective and maximum stress ranges both less than $(\Delta F)_{TH}$. These three cases are illustrated in Figure 3.2.22. For the first two cases, the fatigue life is defined by sloping portion of the *S-N* curve and its straight-line extension below $(\Delta F)_{TH}$. Only for the third case will no fatigue crack growth be assured; that is, the detail will have a theoretically infinite fatigue life.

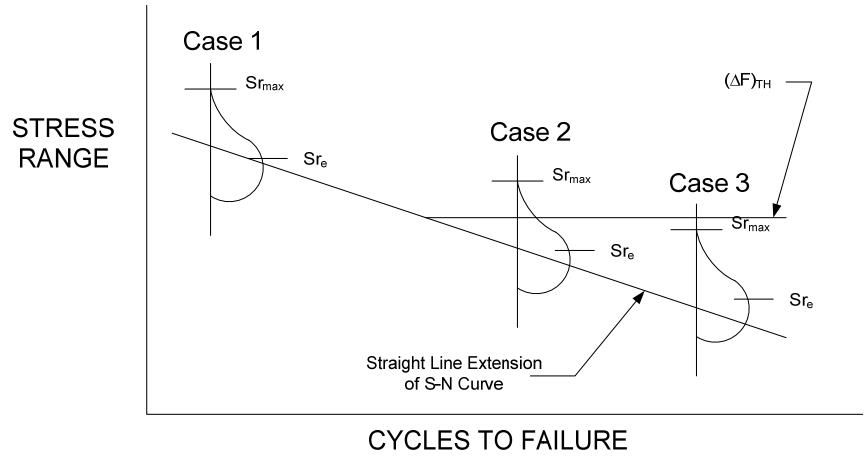


Figure 3.2.22 Three Possible Cases of Variable-Amplitude Loading

The discussion in the preceding paragraph leads to the second principle of fatigue resistance, which applies in the infinite-life region, and states that for higher traffic volumes, the fatigue resistance $(\Delta F)_n$ is infinite if the maximum stress range is less than $(\Delta F)_{TH}$. *In the AASHTO LRFD Specifications, the maximum stress range is assumed to be twice the effective stress range, or twice the live load stress range due to the passage of the effective design truck (plus impact), which is specified as the Fatigue I load combination in AASHTO LRFD Table 3.4.1-1. The specified load factor for the Fatigue I load combination is 1.5; 2 * 0.75 * 72 kips = 1.5 * 72 kips = 108 kips.* That is, the maximum stress range for fatigue design is assumed to be the stress range due to a 108-kip truck (plus impact) with a constant rear-axle spacing of 30 feet. This represents the heaviest truck expected to cross the bridge over its base 75-year fatigue design life.

Therefore, in the *AASHTO LRFD* Specifications, the nominal fatigue resistance, $(\Delta F)_n$, based on the two principles of fatigue resistance is given in *AASHTO LRFD* Article 6.6.1.2.5 as follows:

- For the Fatigue I load combination and infinite life:

$$(\Delta F)_n = (\Delta F)_{TH}$$

Equation 3.2.50
AASHTO LRFD Equation 6.6.1.2.5-1

- For the Fatigue II load combination and finite life:

$$(\Delta F)_n = \left(\frac{A}{N}\right)^{\frac{1}{3}}$$

Equation 3.2.51
AASHTO LRFD Equation 6.6.1.2.5-2

The number of stress cycles, *N*, in Equation 3.2.51 for the required fatigue life as defined in the *AASHTO LRFD* Specifications is to be computed from the following equation:

$$N = (365)(75)n(ADTT)_{SL}$$

Equation 3.2.52
AASHTO LRFD Equation 6.6.1.2.5-3

The number *365* represents the number of days in a year, the number *75* represents the fatigue design life of 75 years (a number other than 75 should be substituted if a fatigue design life other than 75 years is sought), *n* is the number of stress cycles per truck passage taken from *AASHTO LRFD* Table 6.6.1.2.5-2, and $(ADTT)_{SL}$ is the single-lane *ADTT* (Average Daily Truck Traffic) averaged over the design life specified in *AASHTO LRFD* Article 3.6.1.4.2.

The number of stress range cycles per truck passage, *n*, is again specified in *AASHTO LRFD* Table 6.6.1.2.5-2. In many cases, *n* will be taken equal to 1.0. Short-span longitudinal members (with spans less than or equal to 40 feet in length according to *AASHTO LRFD* Table 6.6.1.2.5-2), transverse members loaded directly by a wheel (with a span less than or equal to 20 feet according to *AASHTO LRFD* Table 6.6.1.2.5-2), and areas near interior supports of continuous spans (with 'near' defined in *AASHTO LRFD* Article C6.6.1.2.5 as a distance equal to one-tenth of the span on each side of an interior support) will be subject to more than one stress cycle *n* per truck passage. As span length increases, the effect of the axle loads is attenuated. For cantilever girders, *n* is to be taken equal to 5.0 because these members are susceptible to large vibrations, which cause additional cycles after the truck leaves the bridge.

As specified in *AASHTO LRFD* Article 3.6.1.4.2 and also discussed in Section 1.3.2.3.3, in the absence of better information, $(ADTT)_{SL}$ may be taken as follows:

$$(ADTT)_{SL} = p * ADTT$$

Equation 3.2.53
AASHTO LRFD Equation 3.6.1.4.2-1

where:

$(ADTT)_{SL}$ = the number of trucks per day in a single-lane averaged over the design life
p = fraction of truck traffic in a single lane specified in *AASHTO LRFD* Table 3.6.1.4.2-1 (Table 3.2.8)
ADTT = the number of trucks per day *in one direction* averaged over the design life in the traffic lane carrying the majority of the truck traffic

AASHTO LRFD Article C3.6.1.4.2 contains recommendations on how to compute the *ADTT* based on the average daily traffic (*ADT*) in the absence of site-specific data, and discusses extension of the traffic growth data to the fatigue design life of 75 years (refer also to Section 1.3.2.3.3).

The fraction of truck traffic in a single lane, *p*, is given in Table 3.2.8 and is a function of the number of lanes available to trucks on the bridge travelling in one direction.

Table 3.2.8 Coefficient, p, for Average Daily Truck Traffic

No. of Lanes	p
1	1.00
2	0.85
3 or more	0.80

The probability that all lanes will contain only truck traffic decreases as the number of lanes available to trucks increases. Therefore, it is reasonable that the values for *p* should decrease as the number of lanes available to trucks increases. As discussed in *AASHTO LRFD* Article C3.6.1.4.2, in the absence of truck traffic data in one direction from traffic engineers, designing for 55 percent of the bi-directional *ADTT* is suggested.

The fatigue design for most details (except potentially for Categories E and E′) for higher traffic volumes will be governed by the infinite life check; that is, Equation 3.2.50 utilized in conjunction with the Fatigue I load combination. Table 3.2.9 (*AASHTO LRFD* Table 6.6.1.2.3-2) shows the values of $(ADTT)_{SL}$ for each detail category *above* which the nominal fatigue resistance is governed by $(\Delta F)_{TH}$ (or the infinite-life check):

Table 3.2.9 75-Year $(ADTT)_{SL}$ Equivalent to Infinite Life

Detail Category	75-Year $(ADTT)_{SL}$ Equivalent to Infinite Life (Trucks per Day)
A	530
B	860
B’	1035
C	1290
C’	745
D	1875
E	3530
E’	6485

The values in Table 3.2.9 were computed assuming a 75-year fatigue design life and a number of stress cycles per truck passage, *n*, equal to one, and are rounded up to the nearest five trucks per day. For other values of *n*, the values in the table should be modified by dividing them by *n*. If a fatigue life other than 75 years is sought, the table values must be multiplied by the ratio of 75 divided by the fatigue life sought (in years). The indicated values were determined by equating the infinite life and fatigue life resistances (from Equations 3.2.50 and 3.2.51) taking into account the difference in load factors used with the Fatigue I and Fatigue II load combinations.

AASHTO LRFD Article 6.6.1.2.3 specifies that components and details on fracture-critical members (defined later in Section 3.2.5.3) should be designed for infinite life using the Fatigue I load combination regardless of the $(ADTT)_{SL}$.

Design Verification for Flexure

For load-induced fatigue considerations, each detail must satisfy the following equation specified in *AASHTO LRFD* Article 6.6.1.2.2:

$$\gamma(\Delta f) \le (\Delta F)_n$$

Equation 3.2.54
AASHTO LRFD Equation 6.6.1.2.2-1

where:

γ = load factor for the applicable fatigue load combination (1.5 for Fatigue I or 0.75 for Fatigue II)
(Δf) = live load stress range due to the passage of the fatigue design live load plus impact (ksi)
$(\Delta F)_n$ = nominal fatigue resistance determined as specified in *AASHTO LRFD* Article 6.6.1.2.5 (ksi)

The load modifier, η, and the resistance factor, ϕ, are always taken equal to 1.0 at the fatigue limit state.

The lateral bending stress range in the bottom flange due to the factored fatigue live load plus impact must be included in *(Δf)* for curved bridges, where applicable (*AASHTO LRFD* Article 6.10.5.1). Bottom flange-to-web welds, obviously, need only be checked for the average stress range (due to vertical bending) since the welds are near the mid-width of the flange. However, at points where attachments are welded to the girder bottom flanges, such as at cross-frame connection plates, the flange should be checked for the average stress range plus the lateral flange bending stress range at the critical transverse location on the flange. Bottom flange butt welds should also be checked for the lateral bending stress range in addition to the average stress range. Consideration should also be given to including the bottom-flange lateral bending stress range in straight skewed bridges in regions where cross-frames are discontinuous. The stress range due to flange lateral bending is generally not a consideration for details on the top flange because the flange is continuously braced.

For example, the flange lateral bending stress range, $(\Delta M)_{Lat}$, increases the stress range in the base metal adjacent to the outer termination of the connection plate-to-bottom flange weld as shown in Figure 3.2.23. I_{Lat} is the lateral moment of inertia of the bottom flange = $t_f b_f^3 / 12$.

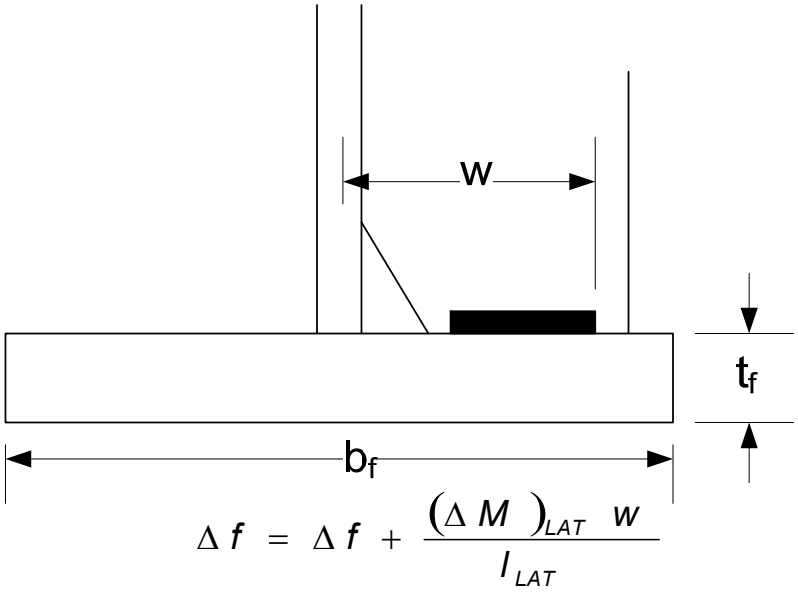


Figure 3.2.23 Effect of Bottom Flange Lateral Bending on the Stress Range

Under certain conditions, *AASHTO LRFD* Article 6.6.1.2.1 permits live load stresses and stress ranges for the fatigue limit state checks to be computed using the short-term composite section assuming the concrete deck is effective for both positive and negative flexure, as discussed previously for the service limit state. *AASHTO LRFD* Article 6.10.1.7 specifies those conditions as the following: 1) shear connectors must be provided along the entire length of the girder; and 2) the minimum 1 percent longitudinal deck reinforcement must be placed wherever the tensile stress in the concrete deck due to either the factored construction loads or load combination Service II exceeds the factored lower-bound modulus of rupture of the concrete. The crack size is felt to be controlled to such a degree under these conditions that full-depth cracks will not occur. Where cracks do occur, the stress in the longitudinal reinforcement will increase until the crack is arrested and the cracked concrete and reinforcement reach equilibrium. With a small number of staggered cracks that do not coalesce at any given section, the concrete can provide significant resistance to tensile stress at service load levels. *Using the short-term composite section to compute the factored fatigue load stresses due to both positive and negative flexure results in a significant reduction in the computed stress range at and near the top flange.* The stress range at or near the bottom flange is largely unaffected because the increase in stiffness for negative flexure is essentially offset by the increase in the distance from the *n*-composite neutral axis to the bottom flange.

The computation of the nominal fatigue resistance, $(\Delta F)_n$, is summarized schematically in Figure 3.2.24. Except as specified for fracture-critical members (as discussed above), where the projected 75-year single lane Average Daily Truck Traffic $(ADTT)_{SL}$ is less than or equal to that specified in Table 3.2.9 for the

component or detail under consideration, the component or detail is to be designed for finite life using the Fatigue II load combination in combination with Equation 3.2.51. The load factor of 0.75 for the Fatigue II load combination, applied to the single design truck, reflects a load level found to be representative of the effective stress range of the truck population with respect to a small number of stress range cycles and to their cumulative effects in steel elements, components and connections for finite fatigue life design. Otherwise, the component or detail is to be designed for infinite life using the Fatigue I load combination in combination with Equation 3.2.50. The load factor of 1.5 for the Fatigue I load combination, applied to the single design truck, reflects load levels found to be representative of the maximum stress range of the truck population for infinite fatigue life design. The factor was chosen on the assumption that the maximum stress range in the random variable spectrum is twice the effective stress range caused by Fatigue II load combination.

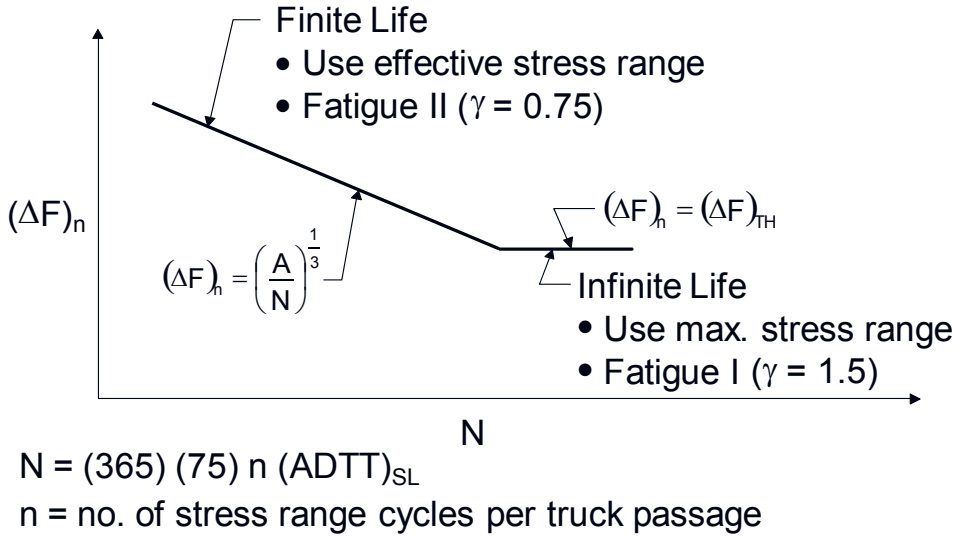


Figure 3.2.24 Nominal Fatigue Resistance, $(\Delta F)_n$

Check for Net Applied Tensile Stress

AASHTO LRFD Article 6.6.1.2.1 specifies that Equation 3.2.54 need only be checked for details subject to a net applied tensile stress. That is, in regions where the unfactored permanent loads produce compression, fatigue need only be considered at a particular detail if the compressive stress at that detail is less than the maximum tensile live load stress caused by the Fatigue I load combination. The Fatigue I load combination again represents the heaviest truck expected to cross the bridge over its 75-year fatigue design life. The effect of any future wearing surface may be conservatively ignored when making this check. If the tensile component of the Fatigue I stress range does not exceed the compressive stress due to the unfactored permanent loads, there is no net tensile stress. As a result, the stress

cycle is compression/compression and a fatigue crack will not propagate beyond a heat-affected zone.

Live load almost always produces negative moments in girders in adjacent spans and often in the same span when supports are sharply skewed. Live load also produces positive moment in girders in regions defined as negative moment regions between points of dead load contraflexure and supports. Thus, it is necessary to test each point in a span to determine if net tension might exist for the fatigue loading.

3.2.5.2.2.2 Shear

AASHTO LRFD Article 6.10.5.3 contains a special fatigue requirement for webs of flexural members. The check is intended to prevent shear buckling of the web under the heaviest truck expected to cross the bridge over its 75-year fatigue design life. In doing so, significant elastic flexing of the web under repeated live loading is not expected to occur. Curved webs are assumed to be initially true. The member is assumed to be able to sustain an infinite number of smaller loadings without fatigue cracking due to this effect.

Interior panels of webs with transverse stiffeners, with or without longitudinal stiffeners, must satisfy the following requirement:

$$V_u \leq V_{cr}$$

Equation 3.2.55
AASHTO LRFD Equation 6.10.5.3-1

where:

V_u = shear in the web at the section under consideration due to the unfactored permanent load plus the Fatigue I load combination – i.e. $V_{DC} + V_{DW} + 1.5\ V_{FAT\ I}$ (kips)

V_{cr} = shear-yield or shear-buckling resistance determined from *AASHTO LRFD* Equation 6.10.9.3.3-1 (kips)

The nominal shear resistance for this check is limited to the shear-yielding or shear-buckling resistance. The use of tension-field action is not permitted. The calculation of V_{cr} is discussed further in Section 3.2.7.2. The live load shear due to the Fatigue I load combination for this check is intended to be that of the heaviest truck expected to cross the bridge in 75 years.

This requirement need not be checked for unstiffened webs or end panels of stiffened webs because the shear in these cases is already limited to V_{cr} at the strength limit state. Thus, Equation 3.2.55 would not control.

The provisions of *AASHTO LRFD* Article 6.11.9, as applicable, are to be applied in checking Equation 3.2.55 for box sections. Inclined webs must be designed for the component of the vertical shear in the plane of the web, V_{ui}, taken equal to V_u

divided by cosθ, where θ is the angle of inclination of the web plate with respect to the vertical (see Equation 3.2.153). Also, in computing the shear-yielding or shear-buckling resistance, V_{cr}, for the case of inclined webs, the web depth, *D,* must be taken as the depth of the web measured along the slope or *D*/cosθ. V_u is to be taken as the sum of the flexural and St. Venant torsional shears in checking this requirement for all box sections for which the effects of St. Venant torsion must be considered (including all box sections in curved and/or skewed bridges). Proper determination of this value considers coincident flexure and torsion. Conservatively, critical torsion and critical flexural shears can be added. In these cases, the dead and live load shears in one web are greater than in the other web at the same cross-section since the torsional shear is of opposite sign in the two webs. For practical reasons, however, both webs are usually detailed for the critical shear. Shears in the web due to warping torsion and cross-section distortion may be ignored in all cases in making this check.

An explicit check on web bend buckling is not specified at the fatigue limit state under this load condition, as the web bend-buckling check at the service limit state (discussed in Sections 3.2.4.3.2.2 and 3.2.4.3.3.2) will always control. This includes composite sections in positive flexure with longitudinal web stiffeners. The smaller value of F_{crw} resulting from the larger value of D_c at the fatigue limit state (i.e. larger than the value at the service limit state) in this case tends to be compensated for by the lower web compressive stress due to the load condition specified for the fatigue limit state shear check.

3.2.5.2.2.3 Cross-Section Distortion Stresses (Box Sections)

As specified in *AASHTO LRFD* Article 6.11.5 and discussed previously in Section 1.1.3.3.3, both longitudinal warping stresses and transverse bending stresses due to cross-section distortion must be considered at the fatigue limit state for all box sections that do not have fully effective box flanges, and/or for all the following sections:

- Single box sections in straight or horizontally curved bridges;
- Multiple box sections in straight bridges not satisfying the restrictions specified in *AASHTO LRFD* Article 6.11.2.3; or
- Multiple box section in horizontally curved bridges;

Skewed box-girder bridges are comprehended in the above list. As discussed in Section 1.1.4.2, skewed supports create significant torque in box sections regardless of whether the bridge is straight or curved.

The cross-section becomes distorted giving rise to secondary bending stresses when box sections are subject to torsion. Horizontal curvature produces torque when the curvature causes load to be applied eccentric to the shear center at the supports. The torque decreases at increasing distances from the supports into simple spans. The phenomenon is less evident in continuous spans where the

interaction between spans is complex. Torque in straight girders is produced by applying load eccentric to the shear center. If loads are applied through the shear center; for example, applied equally to the top and bottom flanges along the entire length of a symmetric straight box, there is no torque created. Skewed supports create such an unsymmetrical loading condition however. If there are two bearings, the reactions in the two bearings are significantly different, creating torque in the box. If there is one bearing, torque is created by diaphragms connecting adjacent boxes. It is easily seen that loading the opposite side of a box produces reversal of these secondary distortional bending stresses. Therefore, in the cases listed above, distortional stresses must be considered when checking fatigue. Although the stresses might be thought of as "distortion-induced", they are calculable and are treated herein as load-induced. Transverse bending stresses are typically most critical for cases where the St. Venant torques are significant, e.g. boxes resting on skewed supports, single box sections and sharply curved boxes.

AASHTO LRFD Article 6.11.5 requires that the stress range due to longitudinal warping be considered in checking the fatigue resistance of the base metal at all details on the box section according to Equation 3.2.54 for the above cases; the longitudinal warping stresses are generally assumed to be additive to the longitudinal vertical bending stresses. This assumption is conservative since the critical longitudinal warping stresses are usually produced by eccentric live loads, whereas the critical vertical bending stresses are produced by more centrally located (i.e. different) live load positions

AASHTO LRFD Article 6.11.5 also requires that the transverse bending stress range be investigated in the base metal adjacent to flange-to-web fillet welds and adjacent to the termination of fillet welds connecting transverse elements to webs and box flanges for the above cases. This investigation is separate from the fatigue check for longitudinal stress ranges in the box.

The condition at welded transverse elements is usually the critical case for transverse bending. A stress concentration occurs at the termination of these welds as a result of the transverse bending. The *AASHTO LRFD* Specification does not specifically address the fatigue resistance of this detail when subject to transverse bending. *AASHTO LRFD* Article C6.11.5 indicates that the fatigue resistance of the base metal adjacent to the welds for this case may be perhaps as low as fatigue Category E. A means of reducing the criticalness of these details is to attach all transverse web stiffeners to the top and bottom flanges. Attachment of the transverse stiffeners to the flanges reduces the sharp through-thickness bending within the unstiffened portions of the web adjacent to the termination of the stiffener-to-web welds, which is typically the most critical region. *AASHTO LRFD* Article 6.6.1.3.1 already requires attachment of cross-frame connection plates to the top and bottom flanges. This provision was found necessary in order to transfer load from the cross-frames directly to the flanges rather than through the web via transverse bending. The same logic applies to all transverse stiffener termini when transverse bending exists in the web. The same check must then be made in the box flange at the terminus of the stiffener-to-flange fillet weld.

AASHTO LRFD Article 6.11.5 further specifies that at the termination of fillet welds connecting cross-frame connection plates to box flanges subjected to calculated torque (i.e. in the above cases only), the need for a transverse member across the bottom of the tub (and/or across the top of a closed box) as part of the internal cross-frames to resist the transverse bending stress range in the box flange must be considered. These members would typically be provided adjacent to the box flanges. When necessary, these members, which are part of the internal cross-bracing, can significantly reduce the transverse bending stress range and help ensure integrity of the cross-section. Closer spacing of the cross-frames also leads to lower transverse bending stresses. To better control the distortion of box flanges in such cases, transverse cross-frame members next to box flanges, that are required to control cross-section distortion stresses, must be attached to the flange. If a longitudinal flange stiffener(s) is present, the transverse members must be bolted to the longitudinal stiffener(s) and not welded to the box flange. This detail avoids the use of more discontinuous fillet welds. Where the transverse bracing members are welded directly to the box flange, the stress range due to transverse bending should also be considered in checking the fatigue resistance of the base metal adjacent to the termination of these welds. Where the transverse bracing members are connected to longitudinal flange stiffeners, the box flange may be considered stiffened (see the section on the BEF Analogy below) when computing the transverse bending stresses (*AASHTO LRFD* Article C6.11.5). The moment of inertia of these transverse bracing members is not to be less than the moment of inertia of the largest transverse connection plate for the internal cross-frame under consideration taken about the edge in contact with the web. The moment of inertia of the transverse cross-frame member should be taken about the edge in contact with the flange when it is attached to the flange, or about its neutral axis when bolted to the longitudinal stiffener(s). The transverse connection plates must still be attached to both flanges as required in *AASHTO LRFD* Article 6.6.1.3.1.

The largest transverse bending stress range is caused by positioning the live load first on one side and then on the opposite side of the box (as in the case for longitudinal warping). This implies that either the vehicle moves sideways on the deck or two trucks traverse the bridge in separate transverse positions, with one vehicle leading the other. *AASHTO LRFD* Article 6.11.5 applies a factor of 0.75 to the computed range of distortionally-induced stresses to account for the unlikely event of this occurring over millions of cycles, but in no case is the stress range to be less than the calculated stress range due to the load positioned in one lane. This factor is in addition to and distinct from the load factor of 0.75 specified for the Fatigue II load combination in *AASHTO LRFD* Table 3.4.1-1. No allowance is made for the fact that two vehicles are required to cause the largest stress cycle. The Design Engineer may consider a reduction in the number of stress cycles (i.e. less than the design number) when computing the fatigue resistance for cases in which the nominal fatigue resistance is calculated based on a finite life, since two cycles are required to cause a single cycle of stress.

AASHTO LRFD Article 6.11.1.3 requires that the total throat thickness of the flange-to-web welds be not less than the smaller of the web or flange thickness when fewer than two intermediate internal cross-frames are provided in a span. The reason for this is to ensure that the smaller section is fully developed for transverse bending. This article permits flange-to-web fillet welds on both sides of the web when two or more intermediate internal cross-frames are provided in each span. The welds must meet the minimum and maximum size requirements specified in *AASHTO LRFD* Article 6.13.3.4.

Consideration might be given to ignoring the distortional stresses in certain cases if it can be demonstrated that the torques are of comparable magnitude to the torques for cases where research has shown that these stresses are small enough to be neglected (*12*); e.g. a straight bridge of similar proportion satisfying the restrictions specified in AASTHO LRFD Article 6.11.2.3; or if the torques are deemed small enough in the judgment of the Owner and the Design Engineer. In such cases, however, it is strongly recommended that all web stiffeners be attached to both flanges in order to enhance fatigue performance.

BEF Analogy

The beam on elastic foundation (BEF) analogy for determining distortional stresses in box girders is based on the work reported in Reference 16 and sponsored by the American Iron and Steel Institute. The approach is described in detail in Reference 51, which forms the basis for the following discussion. The application of the BEF analogy is illustrated in the curved tub girder design example presented in Section 5.2 (specifically Section 5.2.9.3).

Consider the deflection δ_1 due to the uniform torsional load with no cross-frames/diaphragms present, as shown in Figure 3.2.25.

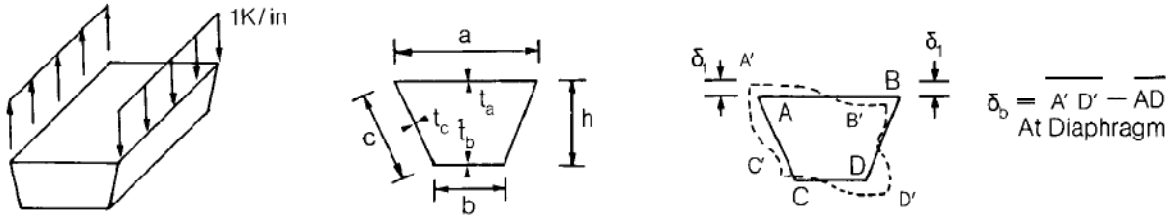


Figure 3.2.25 Box Under Uniform Torsional Loading

δ_1 is the reciprocal of the torsional stiffness of the box and is analogous to the reciprocal of the foundation modulus in the BEF problem. δ_1 (in units of in^2/kip) is computed as follows:

$$\delta_1 = \frac{ab}{24(a+b)}\left\{\frac{c}{D_c}\left[\frac{2ab}{a+b} - v(2a+b)\right] + \frac{a^2}{D_a}\left[\frac{b}{a+b} - v\right]\right\}$$

Equation 3.2.56

where:

a, b, c = dimensions of box section as shown in Figure 3.2.25 (in.).

v = compatibility shear at the center of the bottom flange for unit loads applied at the top corners of a box section of unit length (Figure 3.2.25)

$$= \frac{\frac{1}{D_c}\left[(2a+b)abc\right]+\frac{1}{D_a}\left[ba^3\right]}{(a+b)\left\{\frac{a^3}{D_a}+\frac{2c\left(a^2+ab+b^2\right)}{D_c}+\frac{b^3}{D_b}\right\}}$$

Equation 3.2.57

D_a, D_b, D_c = transverse flexural rigidities of an unstiffened plate (kip-in.^{2}/in.)

$$D_a = \frac{Et_a^3}{12(1-\mu^2)}$$

Equation 3.2.58

$$D_b = \frac{Et_b^3}{12(1-\mu^2)}$$

Equation 3.2.59

$$D_c = \frac{Et_c^3}{12(1-\mu^2)}$$

Equation 3.2.60

t_a, t_b, t_c = thickness of top flange, bottom flange and web, respectively (Figure 3.2.25) (in.)

μ = Poisson's ratio (= 0.2 for concrete – see *AASHTO LRFD* Article 5.4.2.5; 0.3 for steel)

The center of the bottom flange was chosen as the location for computing the compatibility shear because the transverse bending moment and thrust are zero at this point (*16*).

When transverse stiffeners are present on either the flanges or the webs, they should be considered in calculating the transverse flexural rigidities for resisting transverse bending. The rigidity, *D*, of the stiffened plate is computed as:

$$D = \frac{EI_s}{d}$$

Equation 3.2.61

where:

d = stiffener spacing (in.)

I_s = moment of inertia of the stiffened plate for transverse bending (based on the effective width of the plate defined by Equation 3.2.62 below) including the transverse stiffener (in.^{4})

The stiffness of the transverse stiffener is assumed distributed evenly along the stiffened plate.

The effective width of plate, d_o, acting with the stiffener can be determined from the following semi-empirical relationship (*16*) as:

$$d_o = \frac{d\tanh\left(5.6\frac{d}{h}\right)}{\frac{5.6d}{h}\left(1-\mu^2\right)}$$

Equation 3.2.62

where:

h = length of web or box-flange element, as applicable (i.e. dimension "b" or "c" as shown in Figure 3.2.25 (in.)

The BEF stiffness parameter β (in units of $in.^{-1}$) is a measure of the torsional stiffness of the beam and is analogous to the beam-foundation parameter in the BEF problem. β is calculated as follows:

$$\beta \approx \left(\frac{1}{EI\delta_1}\right)^{\frac{1}{4}}$$

Equation 3.2.63

where:

I = moment of inertia of the box section ($in.^4$)

The cross-frames/diaphragms in the box girder restrict the box distortion and are analogous to the supports in the BEF. The cross-frames/diaphragms are incorporated in the solution by the dimensionless ratio, *q*, of the cross-frame/diaphragm stiffness to the box stiffness per unit length, which is defined as follows:

$$q = \left[\frac{E_b A_b}{L_b \ell \delta_1}\right]\delta_b^2$$

Equation 3.2.64

where:

A_b = cross-sectional area of one cross-frame/diaphragm bracing member ($in.^2$)
E_b = Young's modulus of the cross-frame/diaphragm material (ksi)
ℓ = cross-frame/diaphragm spacing (in.)
L_b = length of the cross-frame/diaphragm bracing member (in.)

δ_b = deformation of the bracing member due to the applied torque (Figure) (in.^{2}/kip)

$$= \frac{2(1+a/b)}{\sqrt{1+\left[\frac{a+b}{2h}\right]^2}}\delta_1$$

Equation 3.2.65

h = vertical web depth of the box section (in.)

Equation 3.2.64 assumes that the cross-bracing member is effective in both compression and tension. If the bracing slenderness is large and the member is only considered effective in tension, then A_b in Equation 3.2.64 should be taken as one-half the area of one brace.

The distortional stresses in the box section can be determined analogously by solving the BEF problem. The moment in the BEF is analogous to the distortional longitudinal warping stress, σ_{dw}. The deflection of the BEF is analogous to the distortional transverse bending stress, σ_t. The reactions in the BEF are analogous to the forces in the cross-bracing, F_b. Solutions to the BEF problem for these three components are presented in graphical form in Figure 3.2.26 through Figure 3.2.35 below. These figures each give a BEF factor (or "C" value), which is then used in the appropriate corresponding equation given below (i.e. Equation 3.2.66, 3.2.67 or 3.2.70) to calculate the distortion-related stresses (and stress ranges) or forces (and force ranges). The graphs give relationships for the distortional stresses at either the cross-bracing or at midpanel between the cross-braces, and also for the cross-bracing force, under either a uniform torque per unit length m, or a concentrated torque T (or a range of m or T). Relationships are given for the concentrated torque T (or range of torque T) applied at either midpanel or at the cross-bracing. Given the box geometry, the value of β from Equation 3.2.63, the loading, the cross-bracing stiffness ratio, q, from Equation 3.2.64 and the spacing of the cross-bracing, ℓ, the appropriate value of "C" can be obtained from the graphs for use in the following equations. Since only two loading positions are considered in the graphs for T, it may be necessary in some cases to interpolate between the appropriate graphs for each position. The principle of superposition applies for more than one torque.

The distortional longitudinal warping stress, σ_{dw}, at any point on the cross-section is obtained as follows:

$$\sigma_{dw} = \frac{C_w y}{I\beta a}(m\ell \text{ or } T)$$

Equation 3.2.66

where:

C_w = BEF factor for distortional longitudinal warping stress obtained from Figure 3.2.26, Figure 3.2.27 or Figure 3.2.28, as applicable

y = distance along the transverse vertical axis of the box from the neutral axis to the point under consideration (in.)

All other terms are as defined previously. The range of longitudinal warping stress is obtained by substituting the range of *m* or *T*, as applicable, in Equation 3.2.66.

The distortional transverse bending stresses, σ_t, in the web or box flange at the top or bottom corners of the box section are obtained as follows:

$$\sigma_t = C_t F_d \beta \frac{1}{2a} (m\ell \text{ or } T)$$

Equation 3.2.67

where:

C_t = BEF factor for distortional transverse bending stress obtained from Figure 3.2.29, Figure 3.2.30, Figure or Figure 3.2.32, as applicable

F_d = transverse bending stress in the web or box flange, as applicable, due to the applied torque (in.$^{-1}$)

= $\frac{bv}{2S}$ for the bottom corner of the box

Equation 3.2.68

= $\frac{a}{2S}\left(\frac{b}{a+b} - v\right)$ for the top corner of the box

Equation 3.2.69

S = section modulus per unit length of the web or box flange, as applicable, for transverse bending (in.^{3}/in.). For a stiffened plate, the section modulus per unit length should be based on the effective width of the plate defined by Equation 3.2.62 and include the transverse stiffener.

All other terms are as defined previously. The critical transverse bending stress may be in either the web or the adjacent box flange(s). The range of transverse bending stress is obtained by substituting the range of *m* or *T*, as applicable, in Equation 3.2.67.

The axial force in the cross-bracing due to distortional forces applied to the box, F_b, is obtained as follows:

$$F_b = C_b \left[\frac{\sqrt{1 + \left(\frac{a+b}{2h}\right)^2}}{2\left(1 + \frac{a}{b}\right)} \right] \frac{(m\ell \text{ or } T)}{a}$$

Equation 3.2.70

where:

C_b = BEF factor distortional cross-bracing force determined from Figure 3.2.33 or Figure 3.2.34, as applicable

h = vertical web depth of the box section (in.)

Again, all other terms are as defined previously. The range of axial force is obtained by substituting the range of *m* or *T*, as applicable, in Equation 3.2.70. Note that Figure shows the effect of β on the influence line for cross-bracing forces when the cross-bracing is rigid.

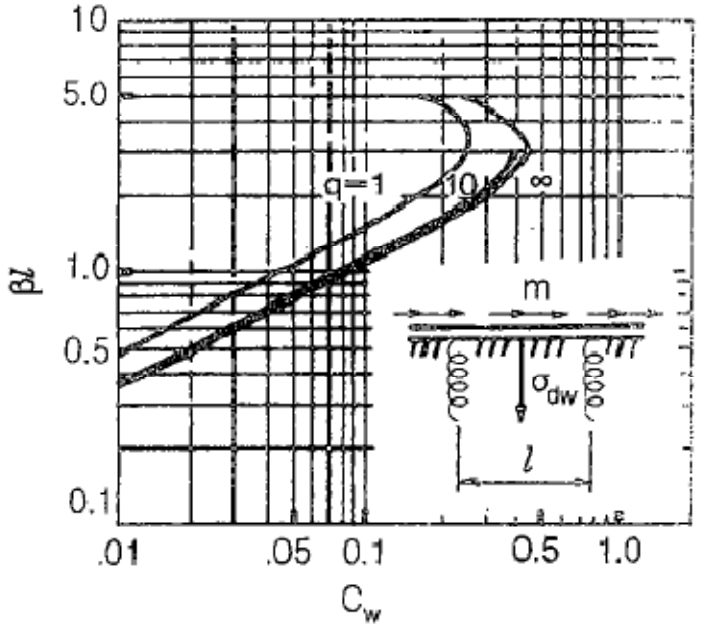


Figure 3.2.26 BEF Factor C_w for Distortional Longitudinal Warping Stress at Midpanel due to a Uniform Torque *m*

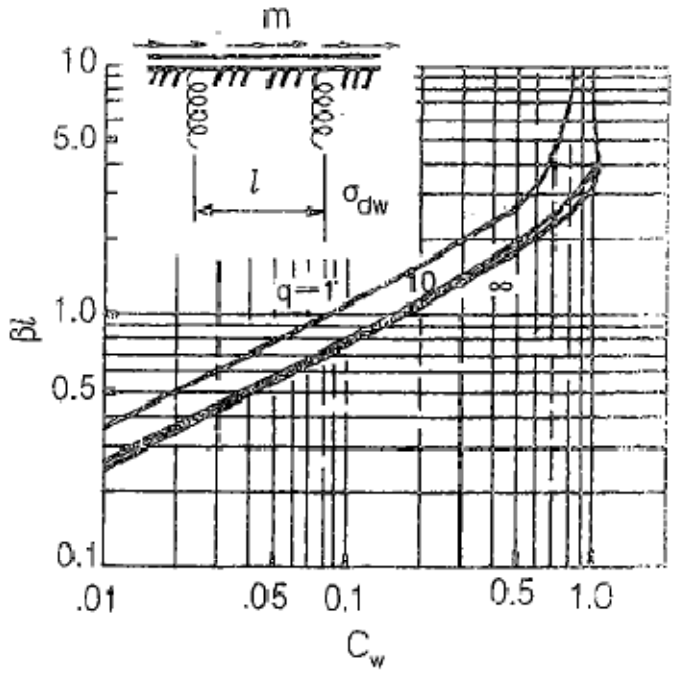


Figure 3.2.27 BEF Factor C_w for Distortional Longitudinal Warping Stress at Cross-Bracing due to a Uniform Torque *m*

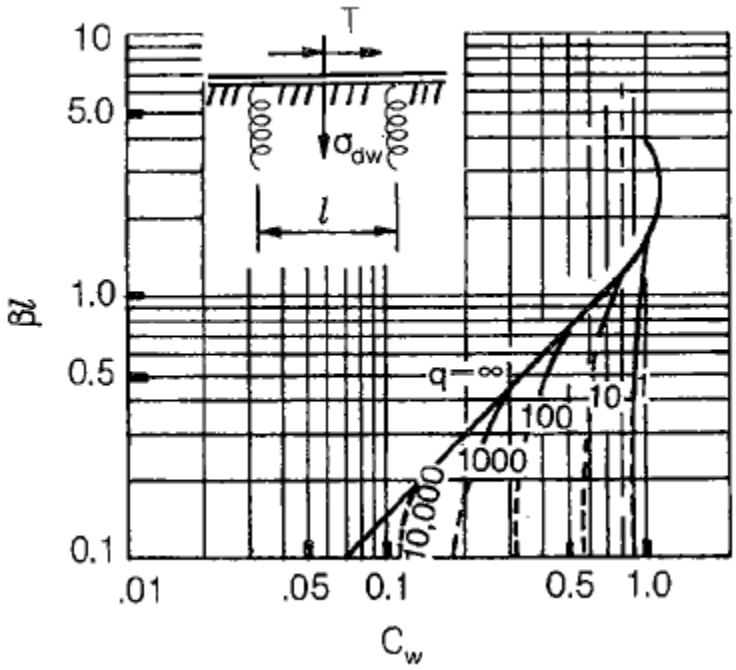


Figure 3.2.28 BEF Factor C_w for Distortional Longitudinal Warping Stress at Midpanel due to a Concentrated Torque *T* at Midpanel

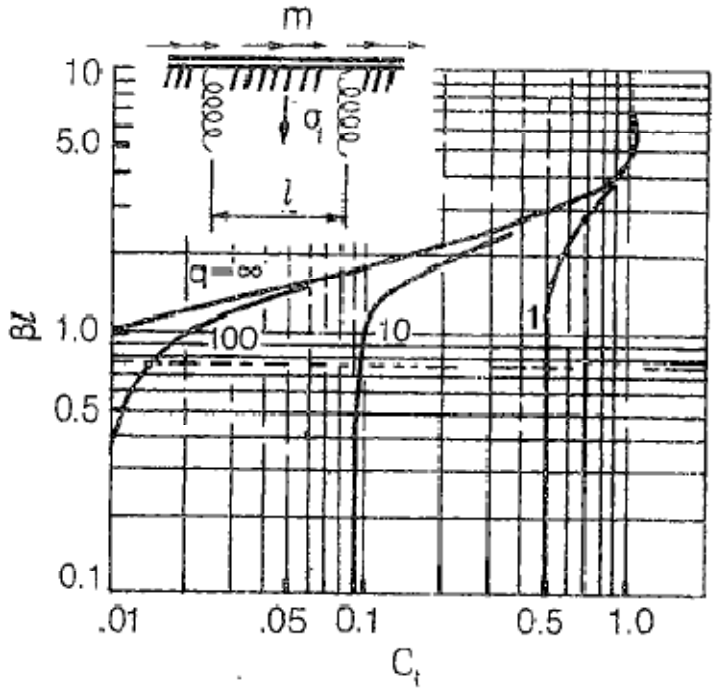


Figure 3.2.29 BEF Factor C_t for Distortional Transverse Bending Stress at Midpanel due to a Uniform Torque *m*

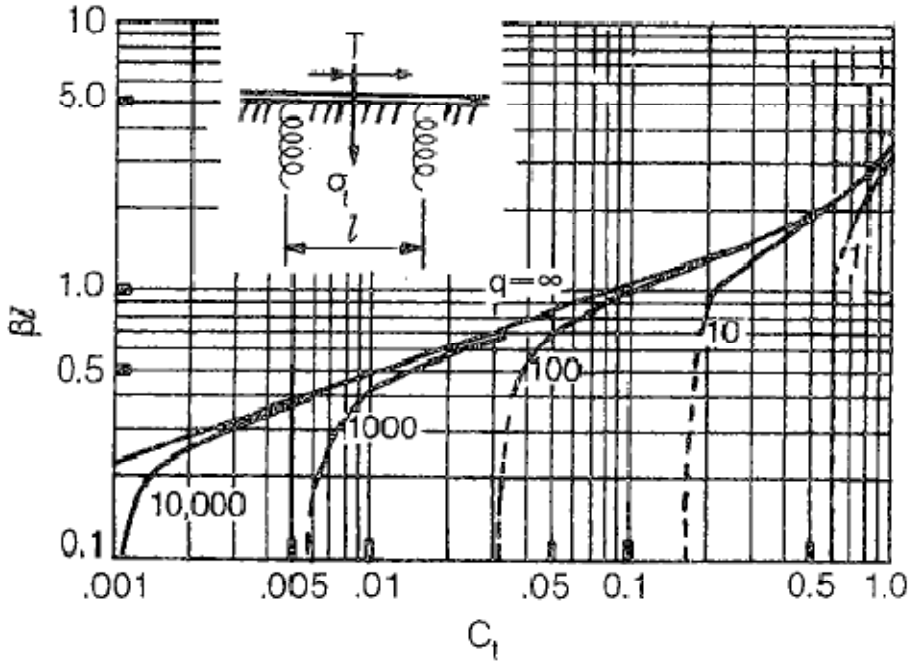


Figure 3.2.30 BEF Factor C_t for Distortional Transverse Bending Stress at Midpanel due to a Concentrated Torque *T* at Midpanel

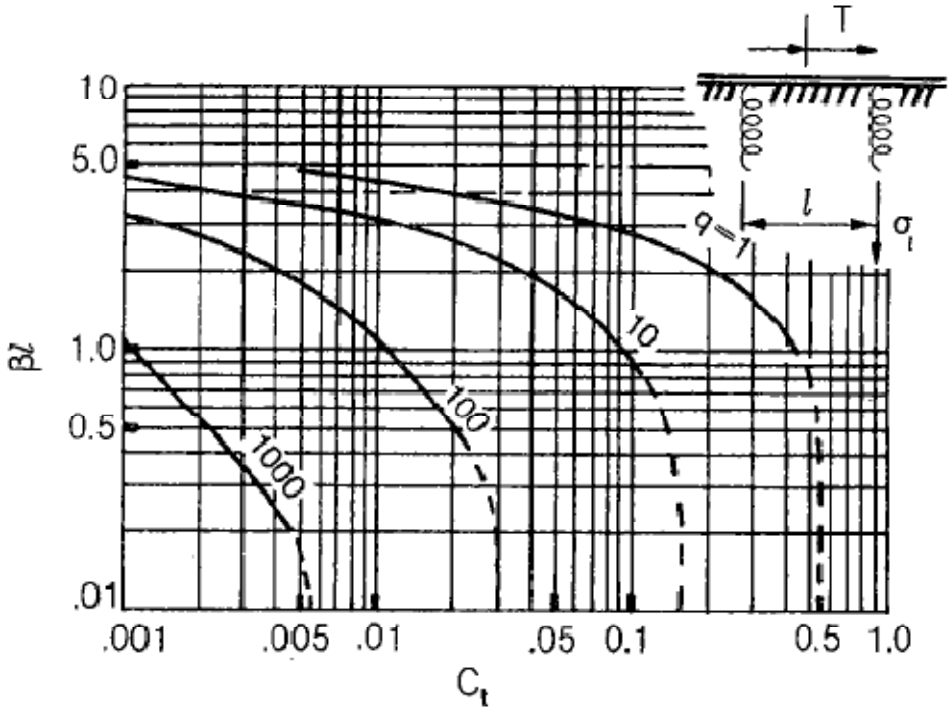


Figure 3.2.31 BEF Factor C_t for Distortional Transverse Bending Stress at Cross-Bracing due to a Concentrated Torque *T* at Midpanel

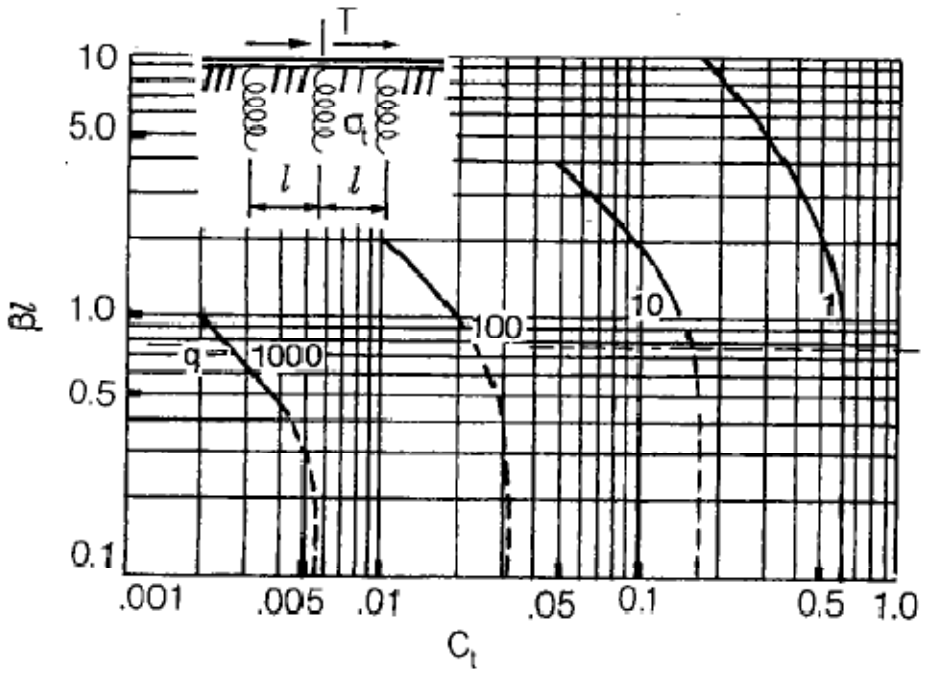


Figure 3.2.32 BEF Factor C_t for Distortional Transverse Bending Stress at Cross-Bracing due to a Concentrated Torque *T* at Cross-Bracing

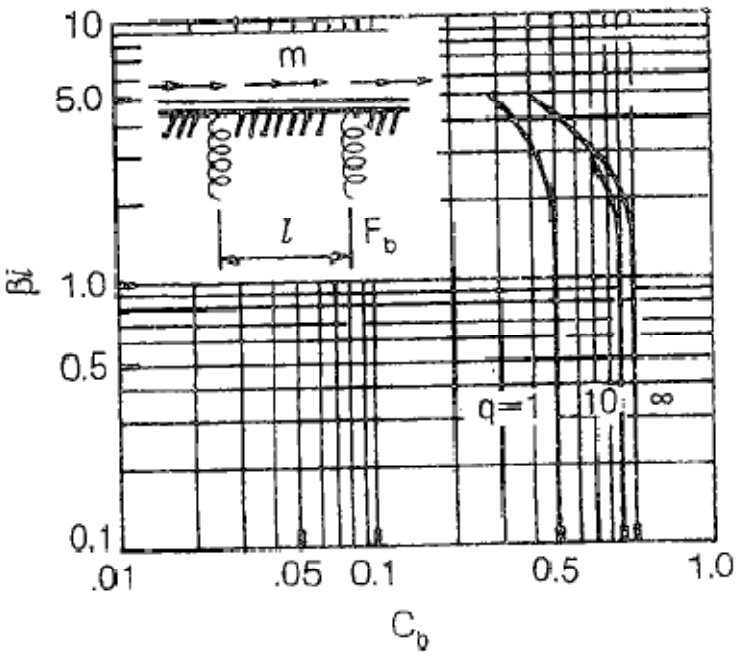


Figure 3.2.33 BEF Factor C_b for Distortional Axial Cross-Bracing Force due to a Uniform Torque *m*

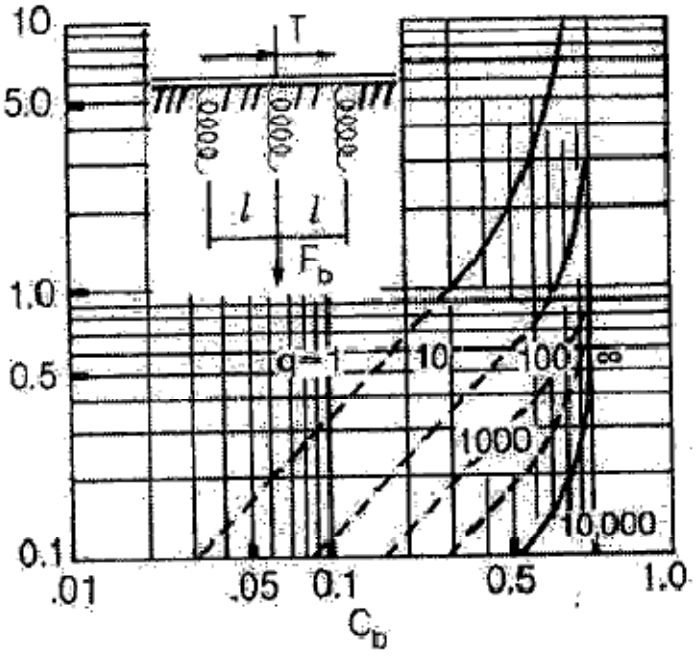


Figure 3.2.34 BEF Factor C_b for Distortional Axial Cross-Bracing Force due to a Concentrated Torque *T* at Cross-Bracing

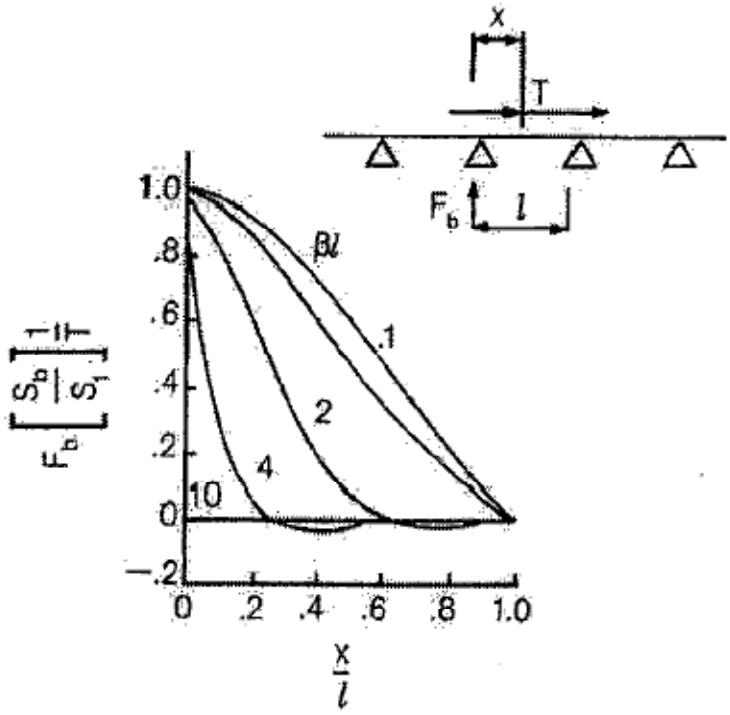


Figure 3.2.35 Influence Line for Distortional Axial Cross-Bracing Force for a Rigid Cross-Brace due to a Concentrated Torque *T*

3.2.5.2.3 Distortion-Induced Fatigue

Distortion-induced fatigue is defined in the *AASHTO LRFD* Specifications as fatigue effects due to secondary stresses not normally quantified in the typical analysis and design of a bridge. These secondary stresses are typically caused by out-of-plane distortions generated by forces resulting from the three-dimensional interaction of bridge members. The resulting localized stresses can be significant in magnitude and generally are not explicitly considered in the design process.

There must be an unstiffened gap, constraints at boundaries of the unstiffened gap and out-of-plane distortion for a bridge detail and/or weldment to be susceptible to distortion-induced fatigue. In the past, short unstiffened gaps were often intentionally designed into bridge structures to avoid a fatigue-sensitive weldment on the tension flange. In fact, transverse welds on tension flanges were prohibited by *AASHTO* up until 1974. As a result, welded cross-frame/diaphragm connection plates and transverse stiffeners often had web gaps introduced above the tension flange. Web gaps were also introduced when lateral connection plates for lateral bracing were coped and not connected to transverse stiffeners. Bolted connections resulted in the introduction of additional web gaps. Intersecting components of a bridge at such details will result in small displacements perpendicular to the web plate that cause bending stresses within the gaps (Figure 3.2.36), which can result in fatigue crack

propagation in the web plate, and in some cases when left unarrested, further propagation into the flange producing failure of the member. For the bending stresses to develop, sufficient constraint must exist at the ends of the web gap.

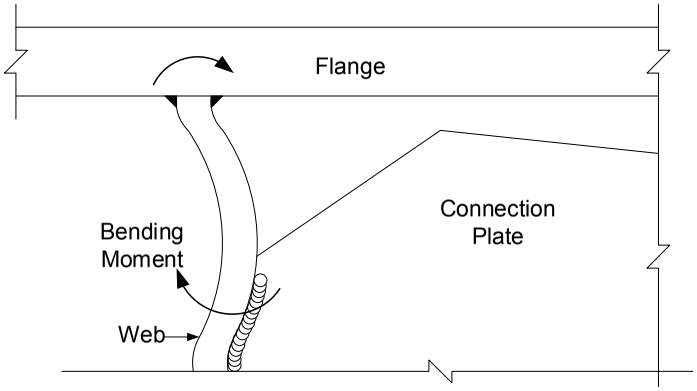


Figure 3.2.36 Web Gap Distortion

Some cases of web gap cracking have been attributed to high frequency vibration of plate elements. For example, vertical vibrations of relatively flexible lateral bracing members have resulted in out-of-plane movements of lateral connection plates attached to either the web or the flange (*39*). Even with small amounts of vibration, a very small gap between the lateral bracing member and the flange connection can lead to large out-of-plane bending stresses. Suggested lateral bracing details to limit the effects of out-of-plane distortion are discussed in Section 3.1.2.9.3, which is an especially important consideration for tub girders. Load-induced fatigue is usually not critical for top lateral bracing in tub girders since the concrete deck is much stiffer than the bracing; thus, the live load forces in the bracing members are usually relatively small. However, since the concrete deck resists the majority of the torsional shear in such cases, it is recommended that the transverse reinforcement in the deck be checked for the torsional shear.

In multiple-girder bridges, out-of-plane distortions of web gaps result from differential displacements between adjacent longitudinal members under eccentric loading causing forces to develop at the intersections between transverse and longitudinal members (Reference 39 details conditions resulting in out-of-plane distortions in other types of bridge structures). The magnitude of the resulting secondary stresses that develop in the web gap is difficult to estimate and the fatigue resistance of the details under these conditions is also difficult to quantify. As a result, the design approach taken is to avoid such details and to provide rigid load paths to preclude the development of significant secondary stresses. *AASHTO LRFD* Article 6.6.1.3 requires that sufficient load paths be provided by connecting all transverse members to the appropriate components comprising the cross-section of the longitudinal member, with the load paths provided by attaching the components through either welding or bolting.

AASHTO LRFD Article 6.6.1.3.1 deals with the detailing of transverse connection plates to prevent distortion-induced fatigue. Transverse connection plates (or

transverse stiffeners serving as connection plates) attached to cross-frames, diaphragms or floorbeams are to be bolted or welded to both the compression and tension flanges of the cross-section in order to eliminate any web gaps. To ensure that the connection is not undersized, particularly at locations where larger out-of-plane forces may develop, it is recommended in *AASHTO LRFD* Article 6.6.1.3.1 that in the absence of better information, the welded or bolted connection in straight, non-skewed bridges be designed for a minimum of a 20.0 kip lateral force (*39*). For straight, skewed bridges and horizontally curved bridges with or without skew, it is recommended in *AASHTO LRFD* Article C6.6.1.3.1 that the force be determined by analysis. The attachment of internal cross-frame connection plates to box flanges is discussed in *AASHTO LRFD* Article C6.6.1.3.1 and Section 3.1.2.8.5.2.

3.2.5.3 Fracture Limit State

3.2.5.3.1 General

Fracture is defined as a tensile mode in which the metal of an element breaks into two parts. By definition, any force in the fractured element is redistributed into the remaining structure. The ability of the structure to absorb this energy without further damage and carry some additional load is called structural redundancy. In a steel bridge member, fracture can either be a ductile fracture, brittle fracture or a combination of the two modes.

Ductile fracture is characterized by plastic deformation prior to separation of the member or component. Ductile fracture is preferable over brittle fracture because there is generally a warning in the form of excessive deformations or deflection prior to failure. The existence of large plastic deformations is indicative that the material has basically followed its stress-strain curve through yielding until the ultimate strength is reached, as shown qualitatively in Figure 3.2.37 for a typical mild steel. Ductile failures generally occur at connections where there is cross-section loss due to plastic deformation in the vicinity of holes and/or concentrations of stress. The design of members or components for ductile fracture is based on the net section.

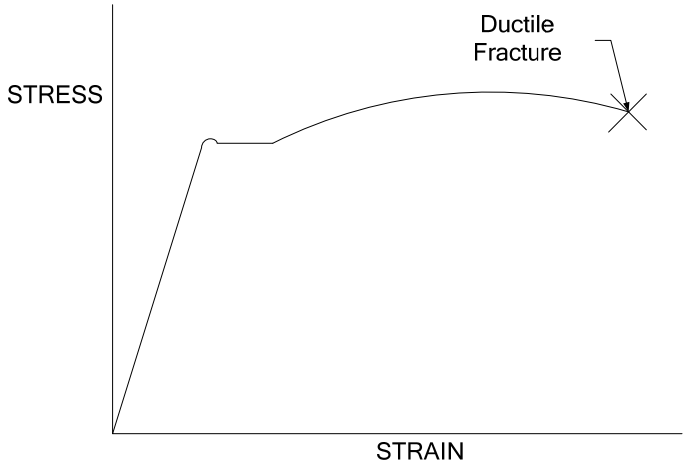


Figure 3.2.37 Typical Stress-Strain Curve for Mild Steel

Brittle fracture is sudden and without warning. With brittle fracture, there is little or no plastic deformation or yielding prior to separation of the member or component. Thus, the ultimate strength of the member is typically not reached (Figure 3.2.38). Since the average stress level at the time of brittle fracture is usually below the yield stress, there is less internal energy and the strength of the member or component is reduced. Brittle fracture typically initiates at an initial flaw or discontinuity in the steel. When a critical stress level is reached at a flaw, crack growth will continue in an unstable fashion at a nearly instantaneous rate until complete separation occurs. Thus, there is an interaction between the crack size and the tensile stress level. As crack size increases, the tensile stress level at which brittle fracture occurs decreases, while smaller cracks can tolerate higher tensile stress levels prior to failure. Hence, it is obviously important to control the size of any discontinuities during the fabrication process.

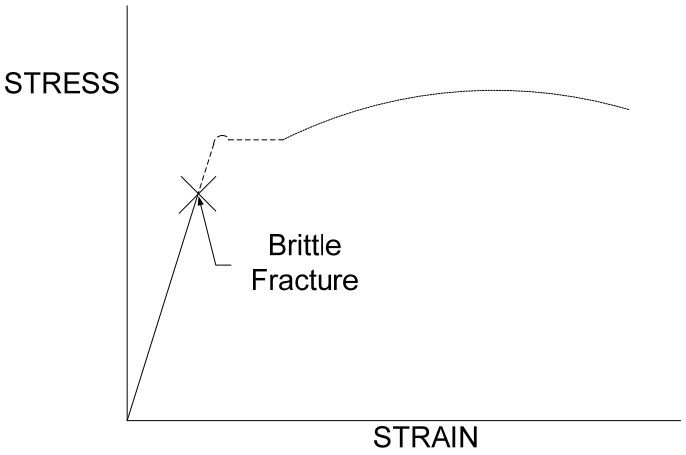


Figure 3.2.38 Stress-Strain Curve Indicative of a Brittle Fracture

Fracture toughness is a material property, much like the properties of yield or ultimate stress, which is defined in the *AASHTO LRFD* Specifications as a measure of the ability of a structural material or element to absorb energy without fracture. As the fracture toughness of steel increases, its ability to tolerate combinations of higher tensile stress and larger cracks prior to unstable crack growth also increases. The fracture toughness of the steel is ideally defined as the area under the stress-strain curve. Thus, a material experiencing a ductile fracture has a much larger area under the stress-strain curve (Figure 3.2.37), and thus, a larger fracture toughness (versus a material experiencing a brittle fracture). Materials such as steel, aluminum and copper have relatively high fracture toughness versus materials such as concrete, cast iron and stone.

The fracture toughness of steel is a function of the material properties, temperature, load rate and degree of constraint. As the yield strength of the steel increases, the ductility of the steel and its ability to plastically deform generally decreases. Alloying and heat treatment of these steels during manufacture is used to increase the fracture toughness. Fracture toughness decreases with temperature. At a certain temperature, called the transition temperature, bridge steels change from ductile to brittle. Slow static load rates result in a higher fracture toughness than rapid dynamic load rates. Truck loading on bridges generally results in an intermediate load rate. Highly constrained details, such as those utilizing thick plates, large welds and/or complex geometries, will also exhibit a lower fracture toughness because of the reduced ability of the steel to deform around a crack. As plate thickness increases, the ability of the plate to plastically deform also decreases.

Pre-existing cracks are introduced during the welding process and cannot be avoided. Quality control procedures during fabrication are intended to minimize the size of the initial flaws to increase both the fatigue and fracture resistance of welded details. The intent of the fatigue-design provisions in *AASHTO* is to prevent or limit stable crack growth, or small incremental crack growth (i.e. fatigue crack propagation) under cyclic loading over the service life of the structure, as continued fatigue crack growth will eventually result in brittle fracture if it not detected and arrested. Using a detail with a higher fatigue resistance or lowering the stress range at the detail can increase the fatigue design life or number of cycles required for failure. The inherent fracture toughness of the steel will limit the fatigue design life due to the maximum crack size that can be tolerated prior to brittle fracture (i.e. unstable crack growth).

Previous *AASHTO* specifications specified separate permissible stress ranges for redundant and non-redundant members, with the limiting values for nonredundant members arbitrarily specified to be 80 percent of the limiting values specified for redundant members. However, as discussed below, larger fracture toughness is demanded in the *AASHTO* Specifications for members used in non-redundant applications. Since the reduction in permissible stress range in combination with the requirements for greater fracture toughness were considered by the specification writers to be an unnecessary double penalty for non-redundant members, only the

permissible stress ranges for redundant members were carried forward to the *AASHTO LRFD* Specifications and are to be applied to both redundant and non-redundant members.

AASHTO has adopted a fracture control plan to ensure that bridge details do not fail due to brittle fracture. The fracture control plan was originally issued as an *AASHTO* Guide Specification in 1978 and is now instead given in Section 12 of the *AASHTO/AWS D1.5M/D1.5 Bridge Welding Code* (*52*). The plan places controls on material properties and initial flaw sizes to provide adequate performance. The fracture control plan specifies: design and review responsibilities; welding inspector, fabricator and NDT personnel qualification and certification; welding requirements; welding procedures; welding repair procedures and required fracture toughness of the steel and weld metal. Stringent preheat and interpass temperature requirements are included to minimize the potential for hydrogen-induced cracking, which results from the presence of hydrogen (moisture) in the molten weld metal. As the weld cools and solidifies, the hydrogen migrates to the grain boundaries of the metal resulting in a weakened plane in the weld, which eventually cracks due to the presence of restraint and tensile residual stresses. The crack reduces the strength of the weld and may potentially lead to fatigue crack growth.

The fracture control plan came into being after there were some fractures of steel bridge members a few decades ago that could be traced to low toughness material. Since the plan has been applied to U.S. bridge construction, there have been no such failures. Recent failures of steel bridges associated with tensile stress, such as the Hoan Bridge in Milwaukee, have been traced to inadequate detailing that did not provide an adequate load path. There have been far more sudden collapses of bridges associated with stability failures, particularly during construction, than due to fracture. Nonetheless, redundant bridges are desirable. However, when a less redundant design is found desirable, it can be built under the current provisions.

The fracture control plan utilizes the Charpy V-Notch impact test to determine the fracture toughness requirements for various bridge steels. Small, notched steel specimens are loaded at very high strain rates as the specimen absorbs the impact from a pendulum (Figure 3.2.39). The maximum height the pendulum rises after impact measures the amount of energy absorbed in foot-pounds. When sets of specimens are tested at different temperatures, there is a shift or transition in energy absorption with temperature, as shown in Figure 3.2.40. It is obviously desirable for bridge steels to be operating in the area to the right of the transition zone.



Figure 3.2.39 Charpy V-Notch Testing Machine

The Charpy V-Notch impact test is a relatively severe test of fracture toughness and does not define the conditions under which bridge steels actually operate. The load rate that a Charpy impact specimen is subject to in the transition zone is approximately five times that expected during bridge loading. The fracture toughness decreases as the load rate increases at a given temperature. The constraint around the fracture zone of the Charpy specimen is typically more severe than found in bridges. Although plates thicker than the thickness of a Charpy specimen are used in bridges, a minimum level of fracture toughness is reached in the Charpy test, as the test represents a plane-strain condition. No further reduction in fracture toughness than the level attained in the Charpy test is realized with increasing plate thickness. The temperatures at which the impact tests are performed are also generally higher than the bridge is subject to.

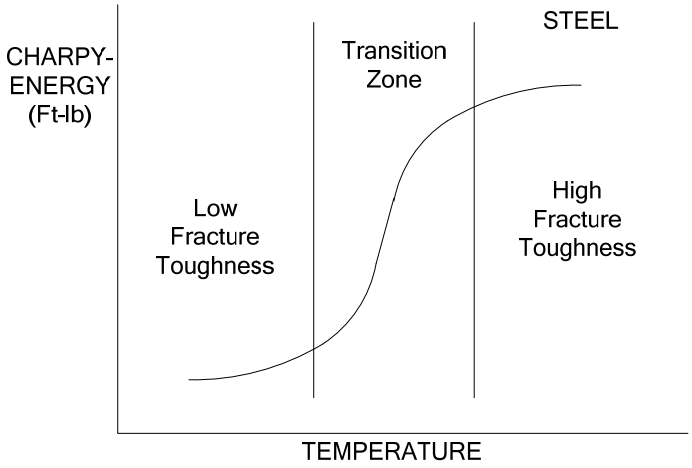


Figure 3.2.40 Typical Plot of Charpy Energy Versus Temperature for a Steel

The *AASHTO* fracture control plan uses three different temperature zones (designated Zones 1, 2 and 3) to qualify the fracture toughness of bridge steels. The three zones are differentiated by their minimum operating (or service) temperatures, which are given in *AASHTO LRFD* Table 6.6.2-1. The required fracture toughness increases as the minimum expected service temperature for the bridge decreases. The fracture toughness requirements (*AASHTO LRFD* Table 6.6.2-2) for various bridge steels are given in terms of the energy (in foot-pounds) absorbed by the Charpy specimens at specified test temperatures for the three different temperature zones. The Charpy test temperatures are on average 70 degrees higher than the minimum service temperature for each zone to compensate for the higher load rates experienced by the test specimens (*53*). For higher strength steels, the requirements are generally more stringent for thicker plates. For the newer high performance steels (HPS), which provide significant improvements in fracture toughness, it was decided that these steels would be required to meet more stringent Zone 3 requirements in all three temperature zones (*54*).

Separate fracture toughness requirements are given in *AASHTO LRFD* Table 6.6.2-2 for nonfracture-critical and fracture-critical members (or components). A fracture-critical member (FCM) is defined as an element that should it fracture, would release energy into the structure that the structure could not safely absorb without further damage. For this reason, further precautions are taken in the fabrication of fracture-critical members (FCMs). FCMs are subject to more stringent Charpy V-Notch fracture toughness requirements than nonfracture-critical members. FCMs must also be fabricated in accordance with the fracture control plan given in Reference 52. According to *AASHTO LRFD* Article 6.6.2, the Engineer has the responsibility to identify all bridge members or components that are fracture critical and clearly delineate their location on the contract plans. Examples of FCMs in bridges include certain truss members in tension, suspension cables, tension components of girders in two-girder systems, pin and link systems in suspended spans, cross-girders and welded tie girders in tied-arches. In addition, any attachment having a length in the direction of the tension stress greater than 4 inches and welded to the tension area of a component of a FCM is also to be considered fracture critical.

AASHTO LRFD Article 6.6.2 requires that all primary *longitudinal* superstructure components and connections, except as noted, sustaining tensile force effects due to the Strength I load combination, along with transverse floorbeams subject to such effects, be subject to mandatory Charpy V-Notch fracture toughness testing. The components and connections requiring such testing (e.g. flange and web material subject to tension) must be so designated on the contract plans. The exceptions are noted as follows (unless designated otherwise on the contract plans): splice plates and filler plates connected in double shear in bolted splices; intermediate transverse web stiffeners not serving as connection plates; bearings, sole plates and masonry plates; expansion dams; and drainage material. The specification of mandatory fracture toughness testing for other primary components and connections sustaining tensile force effects under the specified load combination, e.g. primary connections and components other than floorbeams that are *transverse* to the primary longitudinal components (e.g. cross-frames/diaphragms and lateral bracing in skewed and/or curved bridges) is left to the discretion of the Owner.

3.2.5.3.2 Redundancy Considerations

The term redundancy implies the exceeding of what is considered necessary or normal. Hence, the implication in structural redundancy is the inclusion of something that is not necessary for the normal functioning of the structure. In order to design structures with the least cost, that style of structural redundancy is a type the Engineer tries best to avoid.

Structural redundancy became a matter of some discussion when several structures suffered major fractures. It was observed that a fracture failure in bridges such as the Silver Bridge, which had no redundancy, led to the loss of life. On the other hand, fracture failures experienced by other bridges, such as the I-79 Bridge over Neville Island, which was structurally redundant, only led to minimal inconvenience. Since those days, much effort has been spent defining structural redundancy, when it exists, and how it can best be obtained. This approach falls under the rubric of designing for failure, since if the bridge does not fail, structural redundancy is not called upon. But the importance of bridges and the human lives they carry seems to call out for at least some level of redundancy in every structure.

Wherever possible, bridge details and concepts should be developed to provide some level of redundancy. In the *AASHTO LRFD* Specifications, redundancy is defined as the quality of a bridge that enables it to perform its design function in a damaged state. A redundant member is defined as a member whose failure does not cause failure of the bridge. The implication is that the failure of a single member will be identified before a second member fails. Generally, the *AASHTO LRFD* Specification specifies capacity of individual elements or members. However, *AASHTO LRFD* Article 1.3.4 Redundancy addresses the entire structure. This article recommends either multi-load-path structures or continuous ones in order to provide redundancy. The article goes on to identify bridges that are thought to

collapse if one main element should fail. Such bridges are to be called out on the Plans as “failure-critical”. The member(s) that cause the structure to be failure-critical are to be identified as “fracture-critical”. Another term often used to define such a structure is one susceptible to “progressive collapse”. A load modifier η_R is provided that suggests a factor of 1.05 be applied for members in non-redundant structures. However, there are no instructions as to how to make the proper analysis or the level of live load that the bridge should be able to carry in its damaged condition. Load factors to be applied to the analysis of the damaged structure are also lacking. At least three types of redundancy can be defined: 1) multiple load path redundancy, usually as seen in a cross-section; 2) statical redundancy or continuity of the load path from span to span (i.e. statical indeterminacy); and 3) internal member redundancy (i.e. providing multiple unwelded or mechanically fastened components of a beam, truss or arch member to act as crack arrestors). The type of redundancy that must be demonstrated in identifying FCMs is often dependent on the Owner who can accept an analysis as demonstration of adequate redundancy. Specification of FCMs is often satisfactory. The most conservative and often uneconomical choice is multiple load path redundant structures.

Structural redundancy exists in most highway bridges. However, it is not always simple to determine the presence or absence of adequate redundancy as defined herein. For example, it may not exist in a single box girder cross-section of either steel or post-tensioned concrete; it may or may not exist in a horizontally curved multi-girder bridge. Therefore, it becomes necessary to consider a methodology for the determination of whether redundancy exists. *AASHTO LRFD* Article 6.6.2 does permit the use of refined analyses with assumed hypothetical cracked components to demonstrate redundancy, or to confirm that part of a hypothetically damaged structure is not fracture critical. Owners are becoming more receptive to such analyses. However, as discussed in *AASHTO LRFD* Article C6.6.2, the criteria for these analyses have not yet been codified so that items such as the loading cases to be considered, the location of the potential cracks, the degree of the dynamic effects to be included, the software to be used along with the degree of refinement of the model should all be agreed upon by the Owner and the Design Engineer. Relief from the full factored loads in the applicable strength limit state load combinations should be considered. The number of loaded design lanes versus the number of striped traffic lanes should also be given some consideration in the analysis.

A bridge would be expected to support its design load after a fracture occurs. Assume that it will not be expected to support more than the design live load. The bridge must also support its dead load. A load factor of 1.3 is suggested for both of these loads based approximately on the dead-load factor applied in the LFD and LRFD methodologies. The lower factor applied to the live load is based on expected overloading. The method of loading must be considered in a fracture investigation. Much of the load (i.e. the dead load) is applied to a noncomposite structure, but the fracture effect acts entirely on the composite structure. The live load is applied to the composite structure in both cases.

The dead load is applied as in design. However, the fracture introduces a redistribution of internal actions and external reactions as a result of the fracture. In a steel structure, introduction of the fracture is rather straightforward. The stress at the fracture face must be zero. Thus, forces are applied to the fractured structure at the location of the assumed fracture in a reverse sense to those applied under dead load, forcing the net resultant stresses at the fracture face to be zero. The resulting load case is additive to the dead load cases originally employed during the design.

Ensuring that adequate reinforcing within the deck and adequate shear connection of the deck to the girders are provided to resist the effects of the fracture are important factors in determining the redundancy of composite steel bridges.

The process is similar but more complex in a post-tensioned concrete structure. The typical case would be a segmental box girder with a portion of the bottom flange destroyed. The force in the broken strands would be reversed and applied to the remaining structure. Grouting of the strands must be considered. The multiple strands provide some redundancy against failure of a strand. The same concept can be employed in steel structures by using multiple elements to from a member. Typically, this type of redundancy occurs with riveted members. Modern truss members and arch ties have been made of built-up bolted members to provide redundancy, as have girder bridges that were considered non-redundant. In these structures, the remaining elements in the member need to be examined to ensure that they are adequate. Additional bolt shear forces are encountered should an element fail when the force in the failed element is redistributed through the bolts in the vicinity of the failure to the functioning elements.

Perhaps the best approach is to design and build the structure such that it does not fail; hence avoiding the need for providing structural redundancy as defined herein. This approach also has been investigated intensely since the 1960s—and with great success. It was observed that most all of the steel bridges that failed were either welded using the older technologies that existed at the time, as in the case of Neville Island girder-bridge, or of old material and/or out-of-date design practice, as in the case of the Silver Bridge. Investigations showed that tougher steel, better design of details, and more intense inspection makes steel bridges much tougher and extremely resistant to fracture. This research is borne out as is evidenced in the paucity of fractures of newer bridges in the United States. Generally, the additional costs associated with the work and material specification necessary to satisfy the fracture control plan is not great and can usually be more than offset by the increased efficiency of the structural form. Cross-sections having a single tub or widely-spaced tubs are a good example of such economy. Single tubs save not only on steel and fabrication costs; they permit significantly reduced-cost substructures. A number of these bridges have been built across the nation and are functioning safely.

AASHTO LRFD Article 6.11.5 specifies that box flanges in tension in single-box cross sections are to be considered FCMs, unless by analysis the bridge can be

shown to support the dead load and the live load after sustaining a fracture of the flange and both webs at any point along the girder. If the bridge cannot be shown to be redundant, it does not mean that it cannot be built within the specification. It simply means that the elements leading to the non-redundant condition must be designated FCMs. Another way to address the issue is with multiple load paths. The tension flanges in the negative-moment regions of a single-box bridge may be shown to be redundant via the multiple longitudinal reinforcement provided in the composite deck. There must be adequate shear connection of the deck to permit the section to remain structurally intact. In cross-sections comprised of two box girders, the bottom flanges in positive moment regions are to be considered fracture-critical components according to *AASHTO LRFD* Article 6.11.5 unless adequate strength and stability of the hypothetically damaged structure can be verified by refined analysis. Where cross-sections contain more than two box sections, none of the components of the box sections are to be considered fracture critical according to this article.

3.2.6 LRFD Strength Limit State Design for Flexure

3.2.6.1 General

AASHTO LRFD Article 1.3.2.4 specifies that the strength limit state is to be taken to ensure that strength, as well as both global and local stability, are provided to resist the statistically significant load combinations that a bridge is expected to experience over its design life. As mentioned in the Commentary to this article, structural damage and distress may be expected to occur at the strength limit state, but overall structural integrity should be maintained.

AASHTO LRFD Article 6.5.4 states that the strength load combinations specified in *AASHTO LRFD* Table 3.4.1-1 (discussed in Section 1.3.3) in combination with the resistance factors specified in *AASHTO LRFD* Article 6.5.4.2 are to be used to check the strength limit state. In all the subsequent discussions below, the resistance factor for flexure, ϕ_f, is to be taken as 1.0, as specified in *AASHTO LRFD* Article 6.5.4.2.

As discussed in *AASHTO LRFD* Articles C6.10.6.2.1 and C6.11.6.2.1, the flexural design provisions in the *AASHTO LRFD Specifications* assume low or zero levels of axial force in the member. Should a concentrically applied axial force due to the factored loads, P_u, in excess of ten percent of the factored axial resistance of the member, P_r, be applied at the strength limit state, the section should instead be checked according to the beam-column interaction equations given in *AASHTO LRFD* Article 6.8.2.3 or 6.9.2.2, as applicable. According to the beam-column interaction equations in these articles, when P_u is ten percent of P_r, the flexural resistance of the member is reduced by five percent. The specification writers felt that it would be reasonable to ignore the effect of the axial force in the design below this level. For cases where the axial force is deemed significant, the reader is referred to Reference 55 for a more in-depth discussion regarding the design of composite steel bridge girders subjected to combined axial compression and flexure, such as might

occur in a cable-stayed system with a composite I- or box-girder deck system. A combination of flexural and thermal loads can also produce this situation; this is particularly true when there are stiff restraints against thermal movement.

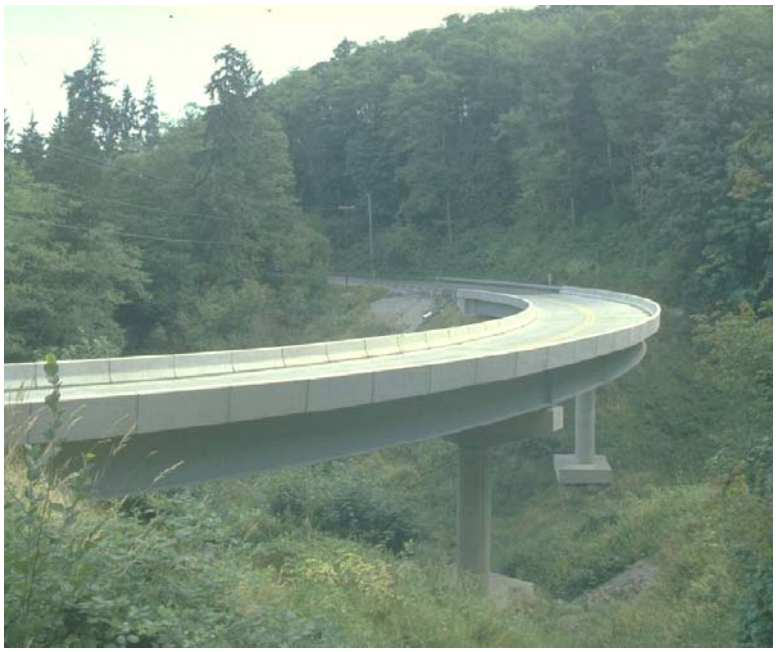


Figure 3.2.41 Curved Girder Bridge

3.2.6.1.1 I-Sections

AASHTO LRFD Article 6.10.6 provides a "roadmap" to direct the Design Engineer to the appropriate articles giving the specific strength limit state checks that are to be made for composite or non-composite I-section flexural members in regions of negative or positive flexure, as discussed in more detail below in Sections 3.2.6.4.1 and 3.2.6.5.1. The application of these design verifications is illustrated in the I-girder design example presented in Section 5.1.

Helpful flowcharts detailing the design checks for flexure to be made at the strength limit state (discussed below) for I-sections are provided in Appendix C6 of the *AASHTO LRFD Specifications*. A flowchart summarizing the basic "roadmap" presented in *AASHTO LRFD* Article 6.10.6 is given in *AASHTO LRFD* Figure C6.4.4-1. The design checks for noncomposite sections and composite sections in negative flexure (according to the slender-web provisions given in *AASHTO LRFD* Article 6.10.8) are summarized in the flowchart given in *AASHTO LRFD* Figure C6.4.6-1. A related flowchart for determining unbraced length requirements to develop the maximum potential lateral-torsional buckling resistance in the presence of a moment gradient (according to the provisions of *AASHTO LRFD* Article D6.4.1 in Appendix D6) is given in *AASHTO LRFD* Figure C6.4.8-1. The design checks for

composite sections in positive flexure are summarized in the flowchart given in *AASHTO LRFD* Figure C6.4.5-1.

3.2.6.1.2 Box Sections

AASHTO LRFD Article 6.11.6 provides a "roadmap" to direct the Design Engineer to the appropriate articles giving the specific strength limit state checks that are to be made for box-section flexural members in regions of positive or negative flexure, as discussed in more detail below in Sections 3.2.6.4.2 and 3.2.6.5.2. The application of these design verifications is illustrated in the tub-girder design example presented in Section 5.2.

The effect of the St. Venant torsional shear stress, f_v, in box flanges must be considered for sections in bridges outside the special restrictions discussed in *AASHTO LRFD* Article 6.11.2.3 (which includes all box sections in skewed and/or curved bridges). f_v may be taken equal to zero for sections in bridges meeting the special restrictions. In cases where f_v is judged to be insignificant or incidental, or is not to be considered, all terms related to f_v are simply set equal to zero in the appropriate equations given in Sections 3.2.6.4.2 and 3.2.6.5.2. The equations then reduce to the equations for determining the nominal flexural resistance of straight box sections in the absence of St. Venant torsion. Again, the Design Engineer should consider torque whenever the supports are skewed.

f_v is determined by dividing the St. Venant torsional shear flow given by *AASHTO LRFD* Equation C6.11.1.1-1 (Equation 1.1.12) by the thickness of the box flange. The nominal flexural resistance of the box flange for such cases is based on the von Mises yield criterion, which is used to consider the effect of the St. Venant torsional shear in combination with flexure. Maximum bending moments and torques are typically not produced by concurrent loads. However, the coincident flexure and torsion due to moving loads to produce the critical von Mises stress is too complex to treat in a practical manner; therefore, maximum envelope values may be used to make all design checks. The Specification is currently silent regarding the inclusion of the elastic shear flow in the box flange due to flexure (i.e. $f = VQ/I$). As pointed out in Reference 55, consideration of the flexural shear stress in the flange may be prudent in cases there the thickness of the box flange is equal to or only slightly larger than the thickness of the web. In such cases, the shear flow in the box flange will be essentially the same as the shear flow in the web at the web-flange junctures.

AASHTO LRFD Article C6.11.1.1 states that for torques applied to the non-composite section, the enclosed area, A_o, used in computing the shear flow is to be computed for the non-composite box section. If top lateral bracing in a tub section is attached to the webs, A_o is to be reduced to reflect the actual location of the bracing (*AASHTO LRFD* Article 6.7.5.3). Because shear connectors are required along the entire length of box sections as specified in *AASHTO LRFD* Article 6.11.10, the concrete deck is considered effective in resisting torsion along the entire span. Thus, for torques applied to the composite section in regions of positive or negative flexure, A_o is to be computed for the composite section using the depth from the bottom flange to the mid-thickness of the concrete deck. The depth may be conservatively determined by neglecting the thickness

of the concrete deck haunch or by using a lower bound estimate of the actual thickness of the haunch, if desired.

The torsion acting on the composite section introduces horizontal shear in the concrete deck that should be considered in the design of the deck transverse reinforcement, particularly for boxes resting on skewed supports. *For tub sections, the deck should be assumed to resist all the torsional shear acting on top of the composite box section*. If top flange lateral bracing is present, it may be modified to an equivalent plate for the analysis. For closed-box sections, the torsional shear in the concrete deck can be determined by multiplying the torsional shear acting on top of the composite box section by the ratio of the thickness of the transformed concrete deck to the total thickness of the top flange plus the transformed deck, as suggested in *AASHTO LRFD* Article C6.11.10. Consideration may be given to adjusting the thickness of the deck for the difference in the Poisson's ratio of the concrete (μ = 0.2) and the steel (μ = 0.3). Adequate shear connection must be provided to ensure that the two materials act in concert.

AASHTO LRFD Article 6.11.1.1 specifies that in cases where the St. Venant torsional shears must be considered, the St. Venant torsional shear stress, f_v, in box flanges due to the factored loads at the strength limit state must not exceed the factored torsional shear resistance of the flange, F_{vr}, given as follows:

$$F_{vr} = 0.75\phi_v \frac{F_{yf}}{\sqrt{3}}$$

Equation 3.2.71
AASHTO LRFD Equation 6.11.1.1-1

where:

ϕ_v = resistance factor for shear specified in *AASHTO LRFD* Article 6.5.4.2 (= 1.0)

It is unlikely, however, that such a level of torsional shear stress will actually be experienced in practical box-girder designs.

3.2.6.1.3 Sections with Holes in the Tension Flange

AASHTO LRFD Article 6.10.6.2.1 specifies that if there are holes in the tension flange of a flexural member at the section under consideration, the tension flange must satisfy the following requirement at the strength limit state (*AASHTO LRFD* Article 6.10.1.8):

$$f_t \le 0.84\left(\frac{A_n}{A_g}\right)F_u \le F_{yt}$$

Equation 3.2.72
AASHTO LRFD Equation 6.10.1.8-1

where:

A_n = net area of the tension flange determined as specified in *AASHTO LRFD* Article 6.8.3 (in.^{2})
A_g = gross area of the tension flange (in.^{2})
f_t = vertical bending stress on the gross area of the tension flange due to the factored loads (ksi)
F_u = specified minimum tensile strength of the tension flange determined as specified in *AASHTO LRFD* Table 6.4.1-1 (ksi)

It is assumed that the holes are the size of those typically used for connectors, such as bolts. For larger holes, the provisions of *AASHTO LRFD* Article 6.8.1 should be applied instead. If Equation 3.2.72 is satisfied, fracture on the net section of the tension flange is theoretically prevented and need not be explicitly checked. The factor of 0.84 in Equation 3.2.72 is approximately equivalent to the ratio of the resistance factor for fracture of tension members, ϕ_u = 0.80, to the resistance factor for yielding of tension members, ϕ_y = 0.95 (*AASHTO LRFD* Article 6.5.4.2).

As will be discussed in Sections 3.2.6.4 and 3.2.6.5, at compact composite sections in positive flexure and at composite I-sections in negative flexure designed according to the optional provisions of *AASHTO LRFD* Appendix A6, with no holes in the tension flange, the nominal flexural resistance is permitted to exceed the moment at first yield at the strength limit state. However, pending further research, the specification currently requires that Equation 3.2.72 still be checked at such sections where there are holes in the tension flange, which will likely prevent holes from being located in these sections at or near points of maximum applied moment where significant yielding of the web (i.e. beyond the localized yielding of the web permitted in hybrid sections) may occur.

Where an access hole is provided in a box flange in tension, the hole should be deducted in determining the *gross area* of the flange for checking this requirement, as specified in *AASHTO LRFD* Article 6.8.1. Thus, yielding is effectively being checked on the net area of the flange at the hole through the use of Equation 3.2.72. Equation 3.2.72 was not specifically developed for the case at hand; i.e. large access holes in the flange. At the edges of a round unreinforced hole, the theoretical stress concentration factor is approximately 3.0. Therefore, the material adjacent to either side of the hole will yield first. At bolt holes, which are relatively small in width in relation to the width of the flange, the section will continue to resist load as the yielding spreads across the plate due to strain hardening at those sections. If Equation 3.2.72 is satisfied, yielding across the gross section will theoretically be achieved prior to fracture on the net section and each fiber of the cross-section can be assumed to be at the yield stress. Access holes are much larger relative to the width of the flange and there has been no research to determine whether sufficient strain hardening exists to permit development of the yield stress across the entire net section. Therefore, it is recommended here that until further research is conducted, the tensile stress f_t on the adjusted gross area of the box flange due to the factored loads at the strength limit state at access holes conservatively be limited to $0.33F_{yt}$ in lieu of using Equation 3.2.72.

3.2.6.2 Web Load-Shedding Factor, R_b

As discussed in Section 3.2.4.3.2.2, once the theoretical web bend-buckling load is reached, a slender-web section does not fail but has significant postbuckling resistance that can be utilized at the strength limit state. As buckling of the compression zone of the web increases, the ability of the web to carry its portion of the load, as computed by ordinary beam theory, decreases. However, this does not mean failure. Instead, a redistribution of stress to the stiffer longitudinal elements (i.e. the compression flange and the immediately adjacent portion of the web) occurs. The tension flange stress is not increased significantly by the shedding of the web compressive stresses. As a result, for a given moment, the stress in the compression portion of the web that is deflecting laterally is less than that calculated for a linear distribution and the stress in the compression flange is greater, as illustrated in Figure 3.2.42. Therefore, yielding may occur in the compression flange before the yield moment calculated from ordinary beam theory is attained.

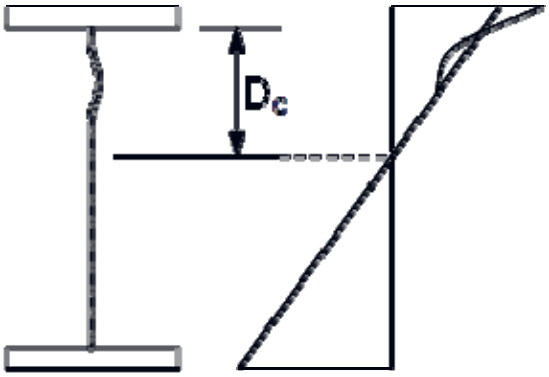


Figure 3.2.42 Load Shedding from the Web to the Compression Flange

To account for this postbuckling resistance in the design of a slender-web section at the strength limit state, or a section with a web slenderness exceeding λ_{rw} as given by Equation 3.2.37, an approximate method was needed to account for the extra load the compression flange must carry after the web becomes partially ineffective. Basler and Thurlimann (*56*) developed such an approach by assuming a linear distribution of stress acting on an effective cross-section, with the nominal flexural resistance, M_n, reached when the extreme fiber of this effective section in compression reached either the yield stress or a critical buckling stress, as applicable. The effective section assumed that a portion of the web in which the buckling (or out-of-plane deformation) occurs becomes ineffective (Figure 3.2.42).

They assumed an effective width, b_e, equal to $30t_w$ for a web with a slenderness D/t_w of about 345. This value was the limiting slenderness to preclude the failure mode of vertical flange buckling, or buckling of the compression flange into the web, for 33,000-psi yield strength steel at an assumed web-to-flange area ratio A_w/A_f of 2 (where A_f is the area of each flange), and an assumed residual tension stress level of 16.5 ksi. The nominal flexural resistance was then assumed to increase linearly

from the resistance of this effective section up to a value of M_y at a web slenderness of λ_{rw}. A more general linear equation containing A_w/A_f as a parameter was then developed as follows:

$$\frac{M_n}{M_y} = 1 - 0.0005\frac{A_w}{A_f}\left(\frac{D}{t_w} - \lambda_{rw}\right)$$

Equation 3.2.73

The expression on the right-hand side of the preceding equation has come to be known as the web load-shedding factor, R_b. The load-shedding factor, which is less than or equal to 1.0, can be used to either reduce the section modulus to the compression flange effectively increasing the compression-flange stress, or to reduce the nominal flexural resistance of the compression flange. Design specifications, including the *AASHTO LRFD* Specifications, have traditionally followed the latter course. In the *AASHTO LRFD* Specifications, the web load-shedding factor to be applied to the nominal flexural resistance of the compression flange at the strength limit state is specified in *AASHTO LRFD* Article 6.10.1.10.2. Note that the effect of load shedding to the compression flange is not considered significant and is ignored whenever the nominal flexural resistance exceeds the yield moment M_y.

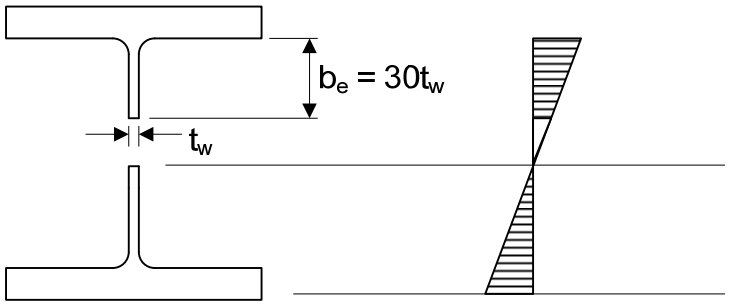


Figure 3.2.43 Effective Cross-Section Assumed in the Derivation of R_b

The preceding equation assumes that the ratio of A_w/A_f does not exceed approximately 3. To accommodate larger ratios up to 10, the *AASHTO LRFD* Specifications utilize a form of the more general equation developed by Basler (*33*) in which the coefficient of 0.0005 in Equation 3.2.73 is replaced by the following coefficient:

$$\frac{a_r}{1200 + 300a_r}$$

Equation 3.2.74

where:

a_r = A_w/A_{fc}

A_{fc} = area of the compression flange (in.^{2})

The ratio of the web area to the compression-flange area will always be less than or equal to 5.45 for sections with flanges satisfying the minimum flange proportioning requirements given by *AASHTO LRFD* Equations 6.10.2.2-2 and 6.10.2.2-3 in the *AASHTO LRFD* Specifications (i.e. $b_f \geq D/6$ and $t_f \geq 1.1t_w$, respectively). Hence, even though the modified coefficient given by Equation 3.2.74 is used, it is not necessary to specify the limiting ratio of 10.

Furthermore, to better accommodate singly symmetric sections, the *AASHTO LRFD* Specifications have replaced a_r in Equation 3.2.74 with a_{wc}, where a_{wc} is typically equal to the ratio of two times the web area in compression to the area of the compression flange. In addition, D/t_w in Equation 3.2.73 is replaced by the effective web slenderness ratio, $2D_c/t_w$, resulting in the following equation for R_b given as Equation 6.10.1.10.2-3 in the *AASHTO LRFD* Specifications:

$$R_b = 1 - \left(\frac{a_{wc}}{1200 + 300a_{wc}} \right) \left(\frac{2D_c}{t_w} - \lambda_{rw} \right) \leq 1.0$$

Equation 3.2.75
AASHTO LRFD Equation 6.10.1.10.2-3

where:

a_{wc} = $2D_c t_w / b_{fc} t_{fc}$

b_{fc} = width of the compression flange (in.)

t_{fc} = thickness of the compression flange (in.)

For compression flanges that have cover plates, the cover-plate area may be added to the compression-flange area in the denominator of the equation for a_{wc}.

The denominator (under the radical) of λ_{rw} in Equation 3.2.75 in previous specifications was the actual compression-flange bending stress due to the factored loads rather than F_{yc}. While this refinement can lead to an increase in the value of R_b in some cases, the increase is not likely to be overly significant. Also, using the actual flange stress to compute the nominal flexural resistance can lead to difficulties in load rating since the flexural resistance is a function of the applied load. Therefore, F_{yc} is now conservatively utilized in the equation for λ_{rw}. *AASHTO LRFD* Article C6.10.1.10.2 suggests a preferred alternative should a larger value of R_b be desired at a section where the nominal flexural resistance of the compression flange is significantly below F_{yc}. The suggested alternative is to substitute the *smaller* of the following values for F_{yc} when determining λ_{rw} for use in Equation 3.2.75, and also in Equations 3.2.40 and 3.2.76, as applicable:

- The nominal flexural resistance of the compression flange F_{nc} calculated assuming R_b and R_h are equal to 1.0 (see Section 3.2.6.3 for a discussion on the hybrid factor R_h);
- The compression-flange bending stress due to the factored loads when the tension-flange bending stress due to the factored loads reaches a value of $R_h F_{yt}$.

The concrete deck acting as a compression-flange element typically contributes a large fraction of the flexural resistance at composite sections subject to positive flexure,. To account for this in an approximate fashion in a longitudinally stiffened composite section in these regions, which may be subject to web bend-buckling at the strength limit state, a fraction of the transformed concrete deck area based conservatively on the long-term 3*n* composite section may be included with the steel compression-flange area in computing the a_{wc} term in Equation 3.2.75 as follows:

$$a_{wc} = \frac{2D_c t_w}{b_{fc} t_{fc} + b_s t_s \left(1 - f_{DC1} / F_{yc}\right) / 3n}$$

Equation 3.2.76
AASHTO LRFD Equation 6.10.1.10.2-6

where:

b_s = effective flange width of the concrete deck (in.)
f_{DC1} = compression flange vertical bending stress caused by the factored permanent load applied before the concrete deck has hardened or is made composite (ksi)
t_s = thickness of the concrete deck (in.)

For these sections, D_c in Equation 3.2.76 is a function of the accumulated stresses and must therefore be calculated using Equation 3.2.41.

As discussed previously in Section 3.2.4.3.2.2, for composite sections in positive flexure *without* longitudinal stiffeners, web bend-buckling is not considered a concern, and therefore, the R_b factor is always taken equal to 1.0 for these sections according to *AASHTO LRFD* Article 6.10.1.10.2. Even if this were not specified to be the case, including the transformed concrete area in the a_{wc} term for these sections as shown in Equation 3.2.76, would likely ensure a value of R_b equal to 1.0 in most every case.

For composite sections in negative flexure, D_c in Equation 3.2.75 should conservatively be computed using the section consisting of the steel girder plus the longitudinal deck reinforcement.

One-half of the effective box flange width should be used in conjunction with one top flange and a single web in calculating R_b for a tub section, as indicated in *AASHTO LRFD* Article C6.11.8.2.2. The effective box flange width is defined in *AASHTO LRFD* Article 6.11.1.1. One-half of the effective top and bottom box flange width should be used in conjunction with a single web for a closed-box section.

AASHTO LRFD Article 6.10.1.10.2 lists the four specific conditions for which the R_b factor may be explicitly taken equal to 1.0 as follows:

- When the section is composite and in a region of positive flexure and the web slenderness D/t_w does not exceed 150 (i.e. longitudinal web stiffeners are not required);
- When checking constructibility according to the provisions of *AASHTO LRFD* Article 6.10.3.2 (since the web bend-buckling resistance F_{crw} must not be exceeded during construction as discussed previously);
- When one or more longitudinal web stiffeners are provided and Equation 3.2.40 is satisfied (i.e. whenever the web slenderness D/t_w does not exceed the slenderness at or below which theoretical web bend buckling will not occur for elastic stress levels at or below F_{yc} at the strength limit state);
- When Equation 3.2.37 is satisfied for webs without longitudinal web stiffeners (i.e. whenever the web slenderness $2D_c/t_w$ does not exceed the noncompact-web slenderness limit λ_{rw} at or below which theoretical web bend buckling will not occur for elastic stress levels at or below F_{yc} at the strength limit state).

Otherwise, R_b must be calculated from Equation 3.2.75.

Bend buckling of longitudinally stiffened webs is prevented during construction and at the service limit state in the *AASHTO LRFD* Specifications, but is permitted at the strength limit state as discussed above. It should be noted, however, that the current longitudinal stiffener proportioning requirements given in *AASHTO LRFD* Article 6.10.11.3 do not ensure that a horizontal line of near zero lateral deflection will be maintained throughout the post-buckling response of the web. As a result, when computing R_b from Equation 3.2.75 at the strength limit state for longitudinally stiffened webs in regions of positive or negative flexure, the presence of the longitudinal stiffeners is conservatively ignored (i.e. the noncompact-web slenderness limit λ_{rw} is used in Equation 3.2.75 rather than the limiting slenderness to prevent theoretical web bend buckling in longitudinally stiffened webs given by Equation 3.2.40).

In the specifications, bend buckling of the web is not considered to have any effect on the shear buckling resistance of the web (and vice versa). The shear resistance of slender-web sections is not reduced as a result of bend buckling (and vice versa) because in such webs, most of the shear resistance results from tension-field action (refer to Section 3.2.7) with only a small contribution from the portion of the web adjacent to the flange.

3.2.6.3 Hybrid Factor, R_h

A hybrid section is defined as a fabricated steel section with a web that has a specified minimum yield strength less than one or both flanges. As a result, yielding

of the lower strength web will occur before the maximum flange strength has been reached. Therefore, the web will participate to a lesser extent than in a homogeneous section when the moment capacity of the hybrid section is attained.

Hybrid sections are covered in general in *AASHTO LRFD* Article 6.10.1.3. Although the specifications can be applied safely to all types of hybrid sections, for greater design efficiency, it is recommended in *AASHTO LRFD* Article 6.10.1.3 that the difference in the specified minimum yield strengths of the web and the higher strength flange be limited to one steel grade. That is, the specified minimum yield strength of the web should not be less than the larger of 70 percent of the specified minimum yield strength of the higher strength flange and 36.0 ksi.

As for a homogeneous section, a hybrid section unloads elastically. If the yield stress in the web is exceeded during the initial loading, a small residual curvature will remain in the girder after unloading. However, under all subsequent loading and unloading cycles, the section will behave elastically if the moment upon reloading does not exceed the previously applied maximum moment. Also, as in a homogeneous section, residual stresses will cause inelastic behavior in a hybrid section during the initial application of the load, but the ultimate resistance of the section will generally not be affected by the presence of residual stresses. Additional more detailed information on the overall behavior of hybrid sections, along with initial design recommendations, may be found in References 31 and in References 57 through 61.

Hybrid sections utilizing HPS 70W steel for both flanges and Grade 50W steel for the web have recently proven to be a popular and economical option, primarily in regions of negative flexure (*62*, *63*). Hybrid sections utilizing a tension flange with a higher yield stress than the web and a compression flange with the same yield stress as the web may also prove economical in regions of positive or negative flexure. Because of stability issues before the concrete deck cures in regions of positive flexure, it is often necessary to use a top flange that is not fully stressed at the strength limit state. Test data for hybrid sections with nominally larger yield strengths in the web than in one or both flanges are limited. Therefore, in such cases, *AASHTO LRFD* Article 6.10.1.3 limits the nominal yield strength that may be used for the web in determining the flexural and shear resistance of the section to 120 percent or less of the specified minimum yield strength of the lower strength flange. This is felt to be a range that is supported by the limited available test data. An exception is permitted for composite sections in positive flexure with a higher strength steel in the web than in the compression flange, in which case the full web strength may be used in determining the flexural and shear resistance. Design issues to consider when hybrid sections are utilized are discussed in Sections 3.1.4.1 and 3.1.5.2.

Section 3.2.6.2 discussed the redistribution of stress that occurs in slender-web sections from the compression zone of the web to the compression flange as a result of localized bend buckling of the web. A similar redistribution of stress from the web to the flanges occurs in hybrid sections as a result of the early localized yielding of the lower strength web; the primary difference being that in the case of the hybrid

section, the redistribution occurs to both the compression and tension flanges (Figure 3.2.44). In the first case, the web load-shedding factor, R_b, is used to account for the reduced contribution of the web to the nominal flexural resistance resulting from web bend buckling. In the case of the hybrid section, the hybrid factor, R_h, is used to account for the effect of earlier yielding of the lower strength steel in the web.

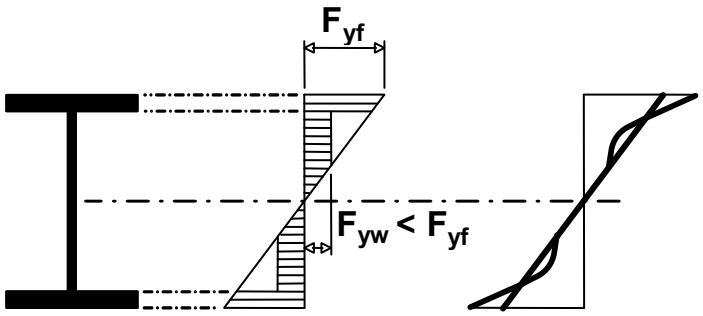


Figure 3.2.44 Load Shedding from the Web to the Flanges Due to Early Web Yielding in a Hybrid Section

As is the case with the load-shedding factor, the hybrid factor, which is less than or equal to 1.0, can be used to either reduce the section modulus to each flange effectively increasing the flange stresses, or to reduce the nominal flexural resistance of each flange. Again, design specifications, including the *AASHTO LRFD* Specifications, have traditionally followed the latter course. In the *AASHTO LRFD* Specifications, the hybrid factor to be applied to the nominal flexural resistance of each flange of a hybrid section is specified in *AASHTO LRFD* Article 6.10.1.10.1. For rolled shapes, which are obviously homogeneous sections based on the nominal yield strength, homogeneous built-up sections and built-up sections with a higher-strength steel in the web than in both flanges, R_h is to be explicitly taken equal to 1.0 according to *AASHTO LRFD* Article 6.10.1.10.1.

The specification allows the Design Engineer to compute R_h for all other cases based on a direct iterative strain compatibility analysis. In lieu of such an analysis, the R_h factor is to be determined as follows:

$$R_h = \frac{12 + \beta\left(3\rho - \rho^3\right)}{12 + 2\beta}$$

Equation 3.2.77
AASHTO LRFD Equation 6.10.1.10.1-1

where:

β = $\dfrac{2D_n t_w}{A_{fn}}$

ρ = the smaller of F_{yw}/f_n and 1.0

A_{fn} = sum of the flange area and the area of any cover plates on the side of the neutral axis corresponding to D_n (in.^{2}). For composite sections in negative flexure, the area of the longitudinal reinforcement may be included in calculating A_{fn} for the top flange.

D_n = larger of the distances from the elastic neutral axis of the cross-section to the inside face of either flange (in.). For sections where the neutral axis is at the mid-depth of the web, the distance from the neutral axis to the inside face of the flange on the side of the neutral axis where yielding occurs first.

f_n = for sections where yielding occurs first in the flange, a cover plate or the longitudinal reinforcement on the side of the neutral axis corresponding to D_n, the largest of the specified minimum yield strengths of each component in the calculation of A_{fn} (ksi). Otherwise, the largest of the elastic stresses in the flange, cover plate or longitudinal reinforcement on the side of the neutral axis corresponding to D_n at first yield on the opposite side of the neutral axis.

Equation 3.2.77 is the basic fundamental equation for R_h originally derived for doubly symmetric I-sections (*57, 59*) (or for sections where the elastic neutral axis is reasonably close to the mid-depth of the web), and included for such sections in previous *AASHTO LRFD Specifications*. Previous specifications also included a separate more complex R_h equation for singly symmetric composite sections subject to positive flexure (*59*). The more complex equation for composite sections has been eliminated in the *AASHTO LRFD* Specifications in lieu of the basic Equation 3.2.77, which has been generalized to consider all possible combinations associated with different positions of the elastic neutral axis and different yield strengths of the top and bottom flange elements in a non-iterative fashion.

A “flange element” is considered to be a flange, a cover plate or plates attached to that flange or the longitudinal reinforcement (associated with the top flange only). Singly symmetric sections (both non-composite and composite) are handled using the base equation by focusing on the side of the neutral axis where nominal yielding occurs first, or the side of the neutral axis subject to the most extensive web yielding prior to first yielding of any flange element. All flange elements on the side of the neutral axis where nominal yielding occurs first are conservatively assumed to be located at the edge of the web in the calculation of R_h. In addition, any shift in the neutral axis caused by the effect of web yielding is considered negligible. These assumptions are similar to the assumptions made originally in the development of the R_h equation for singly symmetric composite sections (*59*), and are not considered overly punitive since computed R_h values are typically close to 1.0.

The first step in computing R_h using Equation 3.2.77 is to determine D_n. According to the definition, D_n is to be taken as the larger of the distances from the elastic neutral axis of the cross-section to the inside face of either flange. The following suggestions are made regarding the calculation of D_n for composite sections:

- For composite sections in positive flexure, D_n may conservatively be taken as the distance from the neutral axis of the short-term *n* composite section to the inside face of the bottom flange.
- Except as noted in the next bullet item, for composite sections in negative flexure, it is recommended that the elastic neutral axis based on the section consisting of the steel girder plus the longitudinal reinforcement be used in determining D_n.
- For composite sections in negative flexure at the service limit state in which the concrete deck is considered to be effective as permitted in *AASHTO LRFD* Article 6.10.4.2.1, D_n may conservatively be taken as the distance from the neutral axis of the short-term *n* composite section to the inside face of the bottom flange. Note that when the concrete deck is *not* considered to be effective in negative flexure, the same value of R_h is used at the strength and service limit states.

In all of the above cases, a more accurate solution can be obtained by calculating the neutral axis location based on the sum of the accumulated factored stresses at the appropriate limit state. However, using the above suggested neutral axes locations for the computation in each case will prevent the flexural resistance from being a function of D_n with D_n being a function of the applied load, which can result in potential complications in load rating. Also, significant differences in the calculated values of R_h, which are generally close to 1.0 in most cases as mentioned above, as a function of the neutral-axis location are not anticipated nor deemed worthy of introducing any additional complexity into the calculation.

In cases where the neutral axis is located at the mid-depth of the web, D_n is to be taken as the distance from the neutral axis to the inside face of the flange on the side of the neutral axis where yielding occurs first. Should yielding occur simultaneously on both sides of the neutral axis, D_n should be taken as the distance to the flange element with the smaller value of A_{fn}.

Once the value of D_n has been established, the next step is to calculate A_{fn}. A_{fn} is defined as the sum of the areas of the flange elements on the side of the neutral axis corresponding to D_n. This would include the flange area, the area of any cover plates, and for composite sections in negative flexure, the area of the longitudinal reinforcement if D_n happens to be measured to the top flange. With D_n and A_{fn} established, the constant β used in Equation 3.2.77 can then be calculated.

In order to calculate the constant ρ used in Equation 3.2.77, the stress f_n must first be calculated. According to the stated definition of f_n, for sections where nominal yielding occurs first in a flange element on the side of the neutral axis corresponding to D_n, which is the case in most instances, f_n is to be taken as the largest of the specified minimum yield strengths of each flange element included in the calculation of A_{fn}. Should yielding occur first on the other side of the neutral axis, f_n is to be taken as the largest of the calculated elastic stresses in the various flange elements

on the side of the neutral axis corresponding to D_n when nominal first yielding occurs on the opposite side. f_n is then divided into the specified minimum yield strength of the web F_{yw} in order to determine ρ, which cannot exceed 1.0.

One-half of the effective box flange width should be used in conjunction with one top flange and a single web in calculating R_h for a tub section, as indicated in *AASHTO LRFD* Article C6.11.8.2.2. The effective box flange width is defined in *AASHTO LRFD* Article 6.11.1.1. One-half of the effective top and bottom box flange width should be used in conjunction with a single web for a closed-box section.

Finally, as discussed in *AASHTO LRFD* Article C6.10.3.2.1, for hybrid sections that are composite in the final condition but non-composite during construction (i.e. sections in bridges built using unshored composite construction), R_h must be calculated separately for the non-composite and composite sections. For the constructibility design checks, R_h for the non-composite section would be applied, and for all subsequent checks in which the member is composite, R_h for the composite section would be applied. For constructibility checks of a hybrid girder where the flange flexural stress, f_{bu}, does not exceed the specified minimum yield strength of the web, R_h is to be taken equal to 1.0.

3.2.6.4 Sections in Negative Flexure

3.2.6.4.1 I-Sections

3.2.6.4.1.1 General

Composite I-sections subject to negative flexure at the strength limit state (and also non-composite I-sections subject to positive or negative flexure during construction) are classified in the *AASHTO LRFD* Specification as follows:

- *Compact Web Sections*: a non-composite section or a composite section in negative flexure that has a web with a slenderness at or below which the section can achieve a maximum flexural resistance M_{max} equal to the plastic moment M_p prior to web bend buckling having a statistically significant influence on the response;
- *Noncompact Web Sections*: a non-composite section or a composite section in negative flexure that has a web satisfying specific steel grade requirements and with a slenderness at or below which theoretical web bend-buckling does not occur at elastic stress levels, computed according to beam theory, smaller than the maximum flexural resistance;
- *Slender Web Sections*: a non-composite section or a composite section in negative flexure that has a web with a slenderness at or above which the theoretical bend-buckling stress is reached in the web prior to reaching M_y.

Figure 3.2.45 illustrates the basic relationship between the maximum potential flexural resistance, M_{max} (or equivalently F_{max}), and the web slenderness, $2D_c/t_w$, for all three types of sections; compact web, noncompact web and slender web

(*assuming yielding with respect to the compression flange controls and that lateral-torsional buckling and local buckling are prevented*). The plot shown in Figure 3.2.45 assumes that compression-flange yielding controls.

Compact web sections are typically shallower sections with thicker webs; that is, rolled beams and welded girder sections with proportions similar to rolled beams that are typically used on bridges with shorter spans. Sections with compact webs are able to develop a maximum potential flexural resistance equal to their full plastic moment capacity, M_p, provided that specific steel grade, ductility, flange and web slenderness and lateral bracing requirements are satisfied. The web slenderness requirement for a compact web section is stated in *AASHTO LRFD* Article A6.2.1 (Appendix A6) as follows:

$$\frac{2D_{cp}}{t_w} \le \lambda_{pw(D_{cp})}$$

Equation 3.2.78
AASHTO LRFD Equation A6.2.1-1

where D_{cp} is the depth of the web in compression at the plastic moment determined as specified in *AASHTO LRFD* Article D6.3.2 (Appendix D6), and $\lambda_{pw(D_{cp})}$ is the limiting slenderness ratio for a compact web section given as follows:

$$\lambda_{pw(D_{cp})} = \frac{\sqrt{\frac{E}{F_{yc}}}}{\left(0.54\frac{M_p}{R_h M_y} - 0.09\right)^2} \le \lambda_{rw}\left(\frac{D_{cp}}{D_c}\right)$$

Equation 3.2.79
AASHTO LRFD Equation A6.2.1-2

Equation 3.2.79 is modified relative to the slenderness limit given in previous specifications for these sections. The modified limit accounts for the higher demands on the web placed on singly symmetric I-sections with larger shape factors M_p/M_y (*64*, *65*).

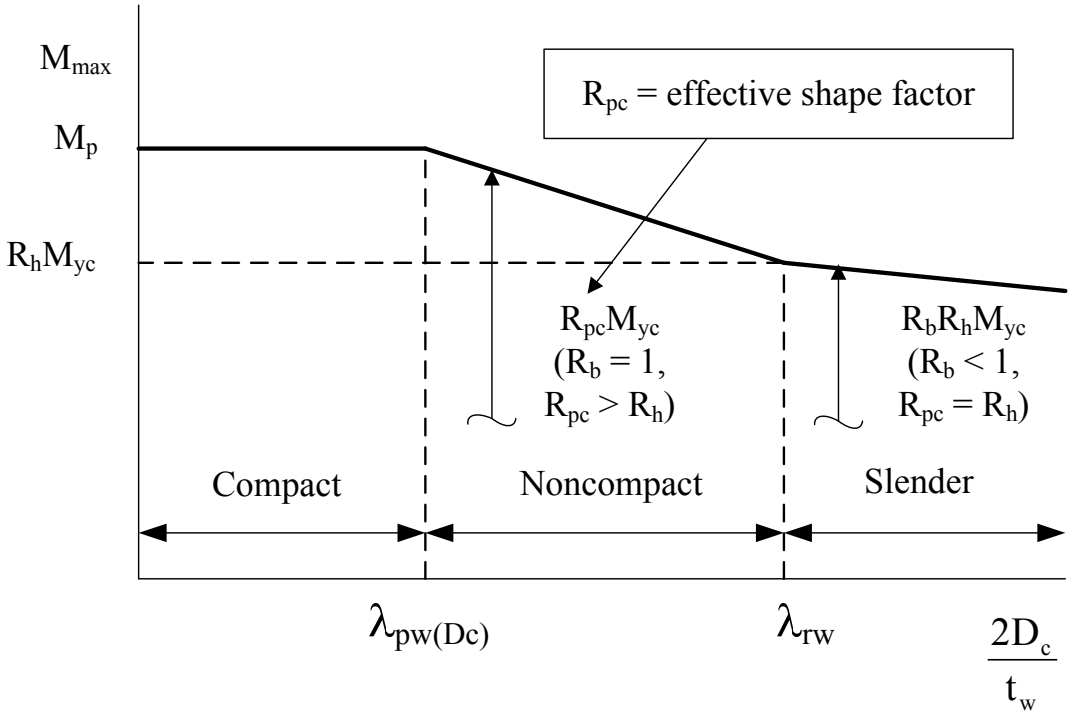


Figure 3.2.45 M_{max} versus Web Slenderness for Composite I-Sections Subject to Negative Flexure and Non-Composite I-Sections

For a shape factor equal to 1.12, which is the typical shape factor for a doubly symmetric non-composite I-section, and a shape factor equal to 1.30, which is representative of the shape factor for a composite I-section subject to negative flexure, the limit from Equation 3.2.79 is as follows (Table 3.2.10):

Table 3.2.10 Web Slenderness Limit for Compact Web Sections, $\lambda_{pw(Dc)}$, from Equation 3.2.79 for Shape Factors M_p/M_y of 1.12 and 1.30

F_{yc} (ksi)	M_p/M_y = 1.12	M_p/M_y = 1.30
36	107	76
50	91	64
70	77	54
90	68	48
100	54	45

In some cases, if certain requirements are met, the available inelastic rotation capacity in these sections can be utilized to allow a redistribution of the bending moments from the interior piers to more lightly loaded sections in positive flexure prior to making the design verifications at the service and strength limit states.

Noncompact web sections are section of intermediate depth with a web slenderness satisfying the following requirement:

$$\frac{2D_c}{t_w} \le \lambda_{rw} = 5.7\sqrt{\frac{E}{F_{yc}}}$$

Equation 3.2.80
AASHTO LRFD Equation A6.2.2-1

The limiting value of λ_{rw} from Equation 3.2.80, which defines the limit below which theoretical web bend buckling does not occur for elastic stress values smaller than F_{yc}, is given as follows for different grades of steel (Table 3.2.11):

Table 3.2.11 Web Slenderness Limit for Compact Web Sections, λ_{rw}, from Equation 3.2.80

F_{yc} (ksi)	λ_{rw}
36	162
50	137
70	116
90	102
100	97

Because web bend buckling is not assumed to occur, R_b is taken equal to 1.0 for these sections. The maximum potential flexural resistance of a noncompact web section is taken as the smaller of $R_{pc}M_{yc}$ and $R_{pt}M_{yt}$ (assuming specific steel grade, compression-flange slenderness and compression-flange bracing requirements are satisfied), and falls between M_{max} for a compact web and a slender web section as a linear function of the web slenderness ratio, $2D_c/t_w$. M_{yc} and M_{yt} are the yield moments with respect to the compression and tension flanges, respectively. R_{pc} and R_{pt} are termed web plastification factors for the compression and tension flange, respectively. The web plastification factors are essentially effective shape factors that define a smooth linear transition in the maximum flexural resistance between M_y and M_p. Referring to Figure 3.2.45 which assumes that compression-flange yielding controls, at the slenderness limit $\lambda_{pw(Dc)}$ delineating a compact web and a noncompact web section, R_{pc} is taken equal to the cross-section shape factor, M_p/M_{yc}, corresponding to the compression flange. At the slenderness limit λ_{rw} delineating a noncompact web and a slender web section, R_{pc} is equal to the hybrid factor R_h.

Sections having a web with a slenderness exceeding λ_{rw} from Equation 3.2.80 are termed slender web sections. Sections with slender webs rely upon significant web post bend buckling resistance at the strength limit state. Because web bend buckling is assumed to occur in such sections, the web load-shedding factor, R_b (discussed previously in Section 3.2.6.2), must be introduced to account for the effect of the post bend- buckling resistance or redistribution of the web compressive stresses to the compression flange resulting from the bend buckling of the web. The

hybrid factor R_h (discussed previously in Section 3.2.6.3) must also be introduced to account for the redistribution of stress to both flanges resulting from local yielding of the web in a hybrid section. Therefore, the maximum potential flexural resistance M_{max} is taken as the smaller of $R_b R_h M_{yc}$ and $R_h M_{yt}$. Unlike a compact web section, a slender web section has little or no available inelastic rotation capacity after reaching M_{max}. Therefore, the flexural resistance drops off quite rapidly after reaching M_{max} and redistribution of moments is obviously not permitted when these sections are used at interior piers.

The design of composite I-sections subject to negative flexure at the strength limit state is covered in either *AASHTO LRFD* Article 6.10.8 or *AASHTO LRFD* Appendix A6. *The provisions of AASHTO LRFD Article 6.10.8 presume slender-web behavior, and therefore, limit the nominal flexural resistance to be less than or equal to the nominal moment at first yield, M_y.* However, it is considered more appropriate to express the maximum resistance in terms of stress for sections in which the maximum resistance is always less than or equal to M_y. In composite construction, the combined effects of the loadings acting on different states of the member cross-section (i.e. non-composite, long-term composite and short-term composite) are better handled by working with flange stresses rather than moments. Bridge engineers are also generally more accustomed to working with stresses and analysis software can typically obtain stresses more directly than moments. Therefore, in the *AASHTO LRFD* Specifications, the flexural resistance for slender web sections is expressed in terms of stress (with the maximum potential flexural resistance given the moniker F_{max}).

For compact web and noncompact web sections in which the maximum potential flexural resistance equals or exceeds M_y, expressing the flexural resistance in terms of stress would generally result in stress limits greater than the yield stress for cases where the resistance exceeds M_y. Therefore, the resistance equations are more conveniently written in terms of bending moment for these sections. For sections in which the flexural resistance is expressed in terms of moment, moments acting on the noncomposite, long-term composite and short-term composite sections may be directly summed for comparison to the nominal resistance. Effects of partial yielding within the cross-section and the sequence of application of loads acting on the different sections need not be considered. Therefore, in *AASHTO LRFD* Appendix A6, which may optionally be applied to compact web and noncompact web sections satisfying specific steel grade and web and flange proportioning requirements in straight I-girder bridges with limited skews, the nominal flexural resistance equations are expressed in terms of bending moment and the nominal flexural resistance is permitted to exceed M_y. The slender web provisions of *AASHTO LRFD* Article 6.10.8 may be applied to sections in these bridges with compact webs or noncompact webs that are nearly compact, but at the expense of some economy with the potential loss in economy increasing with decreasing web slenderness.

As discussed previously in Section 3.2.2.1.4, composite I-sections in negative flexure in all kinked (chorded) continuous and horizontally curved I-girder bridges and in straight I-girder bridges whose supports are skewed more than 20° from normal must always be treated as slender web sections, regardless of

their web slenderness, in applying the specifications. Thus, the nominal flexural resistance of these sections in these bridges is not permitted to exceed M_y. As a result, the optional provisions of *AASHTO LRFD* Appendix A6 may not be applied to compact web or noncompact web sections in these bridges.

AASHTO LRFD Appendix A6 may optionally be applied to composite I-sections subject to negative flexure with compact or noncompact webs in straight-girder bridges whose supports are normal or skewed not more than 20° from normal, and with intermediate cross-frames/diaphragms placed in contiguous lines placed parallel to the supports. Other conditions, spelled out in *AASHTO LRFD* Articles 6.10.2.2.3 and *AASHTO LRFD* Appendix A6, must also be satisfied in order to utilize these provisions to check discretely braced flanges of such sections. The following discussion will focus only on the slender web provisions of *AASHTO LRFD* Article 6.10.8. Further information on the provisions of *AASHTO LRFD* Appendix A6 may be found in References 6 through 8.

AASHTO LRFD Article 6.10.6.2.3 optionally permits moment redistribution according to the provisions of *AASHTO LRFD* Appendix B6 prior to making the strength limit state design verifications. However, this is only permitted for continuous-span members in straight I-girder bridges with skews not exceeding 10° from normal. Other limitations spelled out in *AASHTO LRFD* Article B6.2 must also be satisfied. Further information on the provisions of *AASHTO LRFD* Appendix B6 may be found in Reference 6.

3.2.6.4.1.2 Discretely Braced Compression Flanges

AASHTO LRFD Article 6.10.8.1.1 specifies that at the strength limit state, discretely braced compression flanges must satisfy the one-third rule equation expressed in terms of stress (Section 3.2.2.1.1) as follows:

$$f_{bu} + \frac{1}{3} f_{\ell} \le \phi_f F_{nc}$$

Equation 3.2.81
AASHTO LRFD Equation 6.10.8.1.1-1

where:

f_{bu} = factored compression-flange vertical bending stress determined as specified in *AASHTO LRFD* Article 6.10.1.6 (ksi). f_{bu} is always taken as positive.

f_{ℓ} = factored flange lateral bending stress determined as specified in *AASHTO LRFD* Article 6.10.1.6 (ksi). f_{ℓ} is always taken as positive.

F_{nc} = nominal flexural resistance of the compression flange determined as specified in *AASHTO LRFD* Article 6.10.8.2 (ksi)

A discretely braced flange is once again a flange braced at discrete intervals by bracing sufficient to restrain lateral deflection of the flange and twisting of the entire cross-section at the brace points. *At the strength limit state, discretely braced compression flanges would typically be the bottom flanges in regions of negative flexure in continuous-span members*. Equation 3.2.81 must be satisfied for both local buckling and lateral-torsional buckling using the appropriate value of F_{nc} determined for each case, as specified in *AASHTO LRFD* Articles 6.10.8.2.2 and 6.10.8.2.3, respectively. The computation of F_{nc} for local buckling and lateral-torsional buckling is discussed below.

AASHTO LRFD Article 6.10.1.6 specifies that for design checks involving lateral-torsional buckling, the compressive vertical bending stress, f_{bu}, and flange lateral bending stress, f_ℓ, are to be taken as the largest values throughout the unbraced length in the flange under consideration. This is consistent with established practice in applying beam-column interaction equations involving member stability checks. *For design checks involving flange local buckling, f_{bu} and f_ℓ may be taken as the corresponding values at the section under consideration.* However, when maximum values of these stresses occur at different locations within the unbraced length, which is often the case, it is conservative to use the maximum values in the local buckling check.

The sign of f_{bu} and f_ℓ is always taken as positive in the preceding equation. However, when summing dead and live load stresses to obtain the total factored vertical and lateral bending stresses, f_{bu} and f_ℓ, to apply in the equation, the signs of the individual dead and live load stresses must be considered.

According to *AASHTO LRFD* Article 6.10.1.6, amplification of the first-order flange lateral bending stresses may be required in discretely braced compression flanges. Amplification of these stresses was discussed previously in Section 3.2.2.1.3.1. *AASHTO LRFD* Article 6.10.1.6 further specifies that the sum of the factored flange lateral bending stresses due to all sources (after amplification) cannot exceed $0.6F_{yf}$.

Local Buckling Resistance

Both rolled and built-up steel I-sections are composed of flat plate elements. When these elements are compressed, for example a discretely braced flange, they may buckle locally out of their original planes, as illustrated in Figure 3.2.46.



Figure 3.2.46 Local Buckling of Compression Flange

The width-to-thickness ratio of the compression flange in a flexural member is the controlling parameter for local buckling. The critical elastic buckling stress for a perfectly flat plate with no residual stress subjected to a uniform uniaxial compressive stress is given as follows (*11*):

$$F_{cr} = \frac{k_c \pi^2 E}{12\left(1-\mu^2\right)\left(b_{fc}/t_{fc}\right)^2}$$

Equation 3.2.82

where:

b_{fc} = width of the plate along the edge subject to compression (in.)
E = Young's modulus (29,000 ksi for steel)
t_{fc} = thickness of the plate (in.)
k_c = plate buckling coefficient (discussed below)
μ = Poisson's ratio (0.3 for steel)

The plate buckling coefficient, k_c, depends on the boundary conditions of the plate element. For one-half of a girder compression flange, the longitudinal edge representing the flange-web juncture may be assumed pinned or restrained against rotation. The other longitudinal edge of the flange is free. For idealized pinned conditions at one edge and the other edge free, k_c is equal to 0.425 for a long plate typical of practical structural members; for fully-restrained conditions along one edge, k_c increases to 1.277 (*11*). If an objective is to reach F_{yc} prior to elastic local buckling of the flange, substituting F_{yc} for F_{cr} and $b_{fc}/2$ for b_{fc} in Equation 3.2.81 and rearranging yields:

$$\frac{b_{fc}}{2t_{fc}} \le 0.95\sqrt{\frac{Ek_c}{F_{yc}}}$$

Equation 3.2.83

Research by Johnson (*66*) has resulted in the following general expression for k_c for built-up I-sections:

$$k_c = \frac{4}{\sqrt{\frac{D}{t_w}}}$$

Equation 3.2.84
AASHTO LRFD Equation A6.3.2-6

This expression accounts for the fact that thinner webs in built-up sections tend to offer less rotational restraint to prevent flange local buckling. The calculated value of k_c from Equation 3.2.84 must fall between the range of 0.35 and 0.76.

The lower-bound value of 0.35 (which controls at D/t_w values greater than approximately 130) is back-calculated by equating the local buckling resistances given in the *AASHTO LRFD* Specifications to measured resistances from tests conducted by Johnson and others with D/t_w values ranging from 72 to 245. The fact that the lower-bound value is less than 0.425 (which assumes idealized simply supported boundary conditions along the web-flange juncture) is indicative of the fact that web local buckling in more slender webs tends to destabilize the compression flange. The upper-bound value of 0.76 corresponds to the traditional value that has been assumed for rolled shapes (*67*).

A k_c value of 0.35 is conservatively assumed for all sections in *AASHTO LRFD* Article 6.10.8.2.2, which is assumed to apply only to slender web sections. This results in the following limiting slenderness ratio, λ_{rf}, for a so-called *noncompact flange* (when k_c is taken equal to 0.35 and F_{yr} is substituted for F_{yc} in Equation 3.2.83):

$$\lambda_{rf} = 0.56\sqrt{\frac{E}{F_{yr}}}$$

Equation 3.2.85
AASHTO LRFD Equation 6.10.8.2.2-5

where:

F_{yr} = compression-flange vertical bending stress at the onset of nominal yielding within the cross-section, including residual stress effects, taken as the smaller of $0.7F_{yc}$ and F_{yw}, but not less than $0.5F_{yc}$ (ksi)

F_{yr} is discussed further below under “lateral-torsional buckling”. In the *AASHTO LRFD* Specifications (Article 6.2), a *noncompact flange* is defined as a discretely braced compression flange with a slenderness at or below which localized yielding

within the cross-section associated with a hybrid web, residual stresses and/or cross-section monosymmetry has a statistically significant effect on the nominal flexural resistance.

The local buckling resistance is governed by elastic buckling for a compression-flange slenderness, $b_{fc}/2t_{fc}$, greater than λ_{rf} from Equation 3.2.85, resulting in a so-called *slender flange*. However, elastic local buckling typically does not control for practical bridge-girder sections. The flange-proportioning limit specified in *AASHTO LRFD* Article 6.10.2.2 (discussed in Section 3.1.4.3.3), which limits $b_{fc}/2t_{fc}$ to a practical maximum value of 12.0, precludes elastic flange local buckling for specified minimum yield strengths of the compression flange, F_{yc}, up to and including 90 ksi. In fact, because of this, elastic flange local buckling resistance equations are not provided in the *AASHTO LRFD* Specification. The use of the inelastic flange local buckling resistance equation (discussed below) is permitted for the rare case in which $b_{fc}/2t_{fc}$ may be in the elastic buckling range for F_{yc} greater than 90 ksi.

Flanges may be required to undergo significant plastic compressive strain without having local buckling occur in order to achieve the maximum potential local buckling resistance, F_{max}. For plastic design, a girder will have adequate rotation capacity at a plastic hinge if its flanges are capable of straining to the point of incipient strain hardening prior to buckling, which is typically at a point approximately 15 to 20 times the yield strain. To achieve this condition, the compression-flange slenderness should not exceed the following limit:

$$\frac{b_{fc}}{2t_{fc}} \le 0.30\sqrt{\frac{E}{F_{yc}}}$$

Equation 3.2.86

The development of this limit is beyond the scope of this document, but is described in detail elsewhere (*68, 69*). Because residual stress effects and material imperfections have less effect in the plastic range, and because compressive plastic strains only about one-half the strain necessary to reach strain hardening are required to simply reach maximum flexural resistance equal to the plastic moment, this limit was felt to be too severe to reach F_{max} (*69*). Therefore, the limit was increased to the following slenderness limit, λ_{pf}, for a so-called *compact flange*:

$$\lambda_{pf} = 0.38\sqrt{\frac{E}{F_{yc}}}$$

Equation 3.2.87
AASHTO LRFD Equation 6.10.8.2.2-4

The limiting ratio, λ_{pf}, is given as follows for different grades of steel:

Table 3.2.12 Compression-Flange Slenderness Limit for a Compact Flange, λ_{pf}, from Equation 3.2.87

F_{yc} (ksi)	λ_{pf}
36	10.8
50	9.2
70	7.7
90	6.8
100	6.5

A *compact flange* is defined in the *AASHTO LRFD* Specifications (Article 6.2) as a discretely braced compression flange with a slenderness at or below which the flange can sustain sufficient strains such that the maximum potential flexural resistance is achieved prior to flange local buckling having a statistically significant influence on the response (assuming bracing requirements are also satisfied to develop the maximum potential resistance).

Limits on the width-to-thickness ratio of compression flanges were typically specified in previous specifications as a function of the yield strength of the flange and were taken to be an indirect check on the local buckling resistance of the flange. In the *AASHTO LRFD* Specifications, the compression-flange local buckling resistance is now explicitly calculated as a function of $b_{fc}/2t_{fc}$ and the yield strength of the flange, with $b_{fc}/2t_{fc}$ capped at the specified upper limit of 12.0. For local buckling, the equations defining the nominal flexural resistance of the compression flange, F_{nc}, in *AASHTO LRFD* Article 6.10.8.2.2 are expressed in terms of stress as follows (the equations are shown graphically in Figure 3.2.47):

- If $\lambda_f \le \lambda_{pf}$, then:

$$F_{nc} = F_{max} = R_b R_h F_{yc}$$

Equation 3.2.88
AASHTO LRFD Equation 6.10.8.2.2-1

- Otherwise:

$$F_{nc} = \left[1 - \left(1 - \frac{F_{yr}}{R_h F_{yc}}\right)\left(\frac{\lambda_f - \lambda_{pf}}{\lambda_{rf} - \lambda_{pf}}\right)\right] R_b R_h F_{yc}$$

Equation 3.2.89
AASHTO LRFD Equation 6.10.8.2.2-2

where:

λ_f = slenderness ratio for the compression flange = $b_{fc}/2t_{fc}$
λ_{pf} = limiting slenderness ratio for a compact flange (Equation 3.2.87)
λ_{rf} = limiting slenderness ratio for a noncompact flange (Equation 3.2.85)
R_b = web load-shedding factor determined as specified in *AASHTO LRFD* Article 6.10.1.10.2 (Section 3.2.6.2)
R_h = hybrid factor determined as specified in *AASHTO LRFD* Article 6.10.1.10.1 (Section 3.2.6.3)

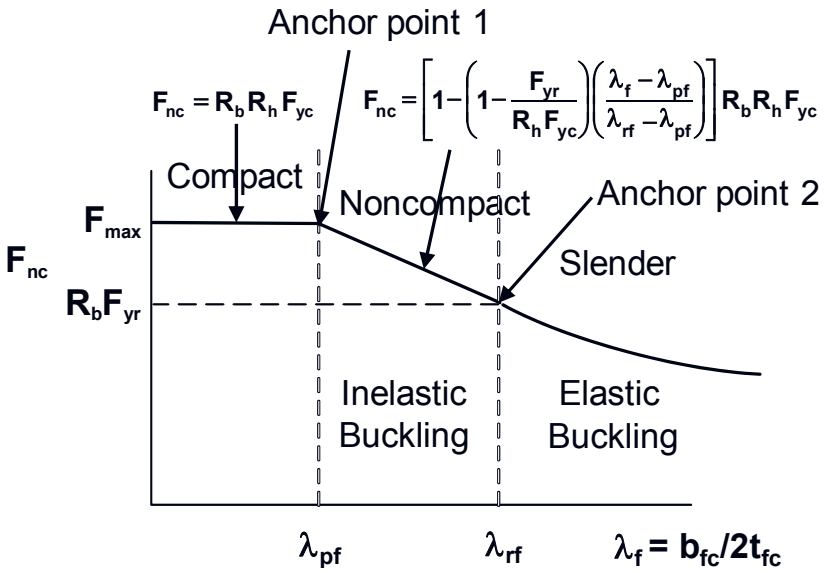


Figure 3.2.47 Local Buckling Resistance, F_{nc}

λ_{pf} and λ_{rf} are Anchor Points 1 and 2, respectively, as shown on Figure 3.2.47. For intermediate values of $b_{fc}/2t_{fc}$ between λ_{pf} and λ_{rf}, residual stresses and initial imperfections give rise to inelastic local buckling, represented in the *AASHTO LRFD* Specifications by a linear transition curve given by Equation 3.2.89. As mentioned previously, an elastic local buckling equation is not provided. The relatively minor influence of moment gradient effects is also neglected for flange local buckling.

Lateral Torsional Buckling Resistance

An I-section member may deflect laterally in a torsional mode before the compressive bending stress reaches the yield stress if the compression flange does not have adequate lateral support. The bracing must be sufficient to restrain lateral deflection of the flange and twisting of the entire cross-section at the brace points for a compression flange to be considered adequately braced.

Figure 3.2.48 shows a doubly symmetric I-section member in pure bending, simply supported and held against twisting at both ends. It is assumed that the compression flange is sturdy enough that it will not buckle locally and that the cross-section will not distort prior to buckling of the entire member between points of lateral support of the compression flange. Under uniform compression, the top flange would buckle downward in its weak direction if this motion were not prevented by the web. Instead, if the force in the compression flange is large enough, the flange will tend to buckle horizontally, or in the only direction that it is free to move. The bottom flange, which is in tension, tends to remain straight. Therefore, the top flange tending to

buckle, bends further than the bottom flange, which tends to remain straight. As a result, the entire cross-section rotates as one rigid unit, as shown in Figure 3.2.48.

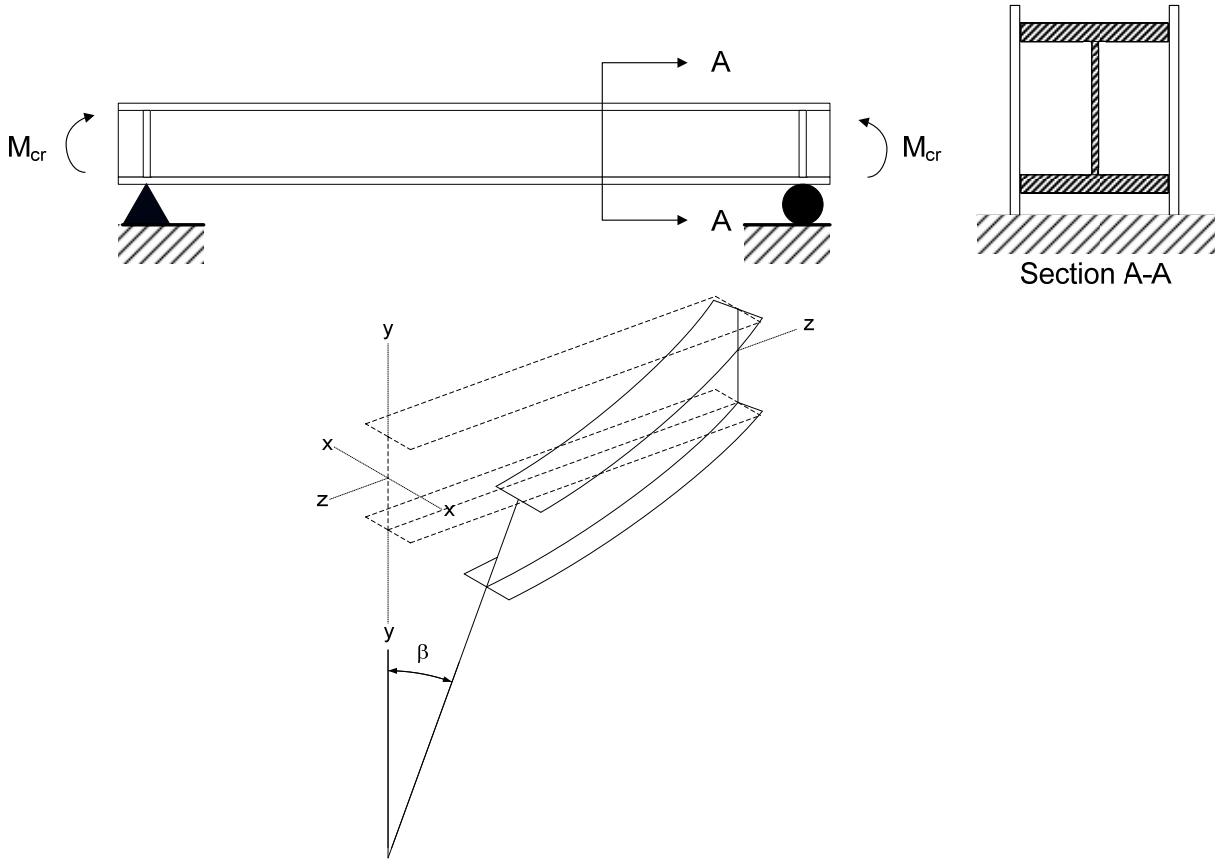


Figure 3.2.48 Lateral-Torsional Buckling of a Doubly Symmetric I-Section Member

The principal variable affecting the lateral-torsional buckling resistance is the distance between the points of lateral support. However, other variables affect the resistance as well including, but not limited to, the end restraints, type and position of the loads, material properties, residual stresses, initial imperfections and cross-section distortion.

For an ideal straight and centered member, there is no tendency for this lateral-torsional motion until the moment reaches a critical magnitude, M_{cr}, at which the member becomes unstable and can undergo lateral deflections and rotations leading to collapse. The tendency for an I-section member to twist is resisted by a combination of St. Venant torsion and warping torsion. The general equation for the *elastic* lateral-torsional buckling resistance, M_{cr}, for a doubly symmetric I-section bent about the strong axis is given as (*70*):

$$M_{cr} = \frac{C_b \pi}{kL_b}\sqrt{EI_y GJ}\sqrt{1+\frac{\pi^2 C_w E}{GJ(kL_b)^2}(C^2+1)} \pm \left(\frac{C\pi}{kL_b}\right)\sqrt{\frac{C_w E}{GJ}}$$

Equation 3.2.90

where:

- C = coefficient to account for load height effect
- C_b = moment-gradient modifier
- C_w = warping constant = $I_y h^2/4$ (in.^{6})
- E = Young's modulus
- G = shear modulus
- h = vertical distance between flanges
- I_y = moment of inertia about the vertical axis in the plane of the web (in.^{4})
- J = St. Venant torsion constant (in.^{4})
- k = effective length factor
- L_b = unbraced length

Other more complex formulations have been developed for singly symmetric sections (*3, 71, 72*). The resistance to the differential bending of the flanges in their own plane increases with the bending rigidity of each flange in its own plane and with the distance between the flanges, as reflected in the warping constant C_w.

It is assumed in the development of Equation 3.2.90 that the end supports for the member are torsionally simple, which means the end sections are prevented from twisting about the z-axis (Figure 3.2.48), but are free to warp out of plane. The effect of any warping restraint can be accounted for with the effective length factor, *k*. For the case of no warping restraint, *k* = 1.0, and for full warping restraint, *k* = 0.5 (*73*). The base lateral-torsional buckling equations in the *AASHTO LRFD* Specifications conservatively assume *k* = 1.0. Warping restraint exists from adjacent unbraced lengths that are less critically loaded than the unbraced length under consideration, which can result in a reduced effective length factor for lateral-torsional buckling. A reduced effective length factor can be used to modify the unbraced length, L_b (i.e. kL_b), and to increase the elastic lateral-torsional buckling stress, F_{cr}, by a factor of ($1/k^2$) (*5*). As mentioned previously in Section 3.2.2.1.3.1, *AASHTO LRFD* Article C6.10.8.2.3 makes reference to a procedure (*3-5*) that can be used to calculate a reduced effective length factor for lateral-torsional buckling in special circumstances (e.g. when it becomes necessary to reduce the amplification of first-order flange lateral bending stresses).

The beneficial effect of a variation in the moment gradient along the length between brace points is accounted for by using the moment gradient modifier C_b, which can take a value between 1.0 and 2.3 depending on the ratio and relative sign of the end moments. The C_b factor is discussed in greater detail below.

The coefficient, *C*, in Equation 3.2.90 accounts for the tipping or stabilizing effect that occurs if transverse loads are applied at the top or bottom flange of the member.

Top flange loading aggravates the tendency toward lateral bucking and therefore the last term in the brackets of Equation 3.2.90 should be subtracted if the load is applied through the top flange. Bottom flange loading has a stabilizing effect and therefore the last term should be added if load is applied through the bottom flange. For a simple span, C = 0.45 for a uniformly distributed load and 0.55 for a concentrated load. If the load is applied through the centroid or if the beam is loaded by end moments, C is taken equal to zero. Most specifications, including the *AASHTO LRFD* Specifications, neglect the effect of load height. The neglect of this effect is believed justified because of the conservative approximations made in simplifying the theoretical formulas for use in design and also by the relative severity of the loading condition on which the provisions are based. Also, when loads are applied to the top flange, the members transmitting the load typically provide restraint to the twisting (e.g. the concrete deck). More recent formulations have accounted for the effect of the load height instead through the C_b factor (*3*). *AASHTO LRFD* Article C6.10.8.2.3, points out that for unusual situations with no intermediate cross-bracing and for unbraced cantilevers with significant loading applied to the top flange, load-height effects should be considered in the calculation of C_b. In such cases, C_b can actually be less than 1.0. Solutions for unbraced cantilevers are given in Reference 74.

Equation 3.2.90 (minus the load height effect) is simplified in the *AASHTO LRFD* Specifications and extended to cover singly symmetric sections by introducing an effective radius of gyration for lateral-torsional buckling r_t, which is essentially the radius of gyration of the compression flange plus 1/3 of the depth of the web in compression. Also, within the provisions of *AASHTO LRFD* Article 6.10.8, the St. Venant torsional constant, J, in Equation 3.2.90 is assumed equal to zero. As discussed previously, the provisions of *AASHTO LRFD* Article 6.10.1.8 are assumed to apply to slender web sections. For very slender web sections, such as deep longitudinally stiffened girders, the contribution of J to the elastic lateral-torsional buckling resistance is generally small. Distortion of the web into an S shape and the corresponding raking of the flanges relative to each other is likely to reduce the buckling resistance further. For composite I-sections subject to negative flexure, the specification equation is generally conservative since it neglects the restraint provided to the bottom (compression) flange by the lateral and torsional stiffness of the concrete deck. However, for very slender web sections, the effect of this restraint is reduced by cross-section distortion and the fact that the deck may not provide an effectively fixed torsional restraint to such relatively large girders. For less slender sections approaching the noncompact web section slenderness limit, λ_{rw} (Equation 3.2.85), ignoring J tends to be conservative, but the resulting simplification of the equation leads to greater overall design convenience. For compact web and noncompact web sections designed according to the optional provisions of *AASHTO LRFD* Appendix A6, J is included in the elastic buckling equation since these stockier sections are not subject to significant web distortion.

Lateral-torsional buckling in the elastic range is of primary importance for relatively slender girders braced at longer than normal intervals. Therefore, the elastic lateral-torsional buckling resistance is most useful when considering the resistance of such girders during the construction phase. In most cases, girders will be braced at

intervals such that the girder will buckle laterally and torsionally only after some portions of the girder have exceeded the yield strain. This phenomenon is referred to as inelastic lateral-torsional buckling.

Inelastic lateral-torsional buckling is complex, as it is influenced by the magnitude and distribution of residual stresses, initial geometric imperfections, and the reduction in various stiffness properties (i.e. Young's modulus, shear modulus, minor-axis bending stiffness, St. Venant torsional stiffness and warping torsional stiffness) as a result of yielding due to in-plane flexure prior to buckling. Many researchers have employed a tangent-modulus approach to investigate the effect of inelastic lateral-torsional buckling. The *AASHTO LRFD* Specifications have adopted a simple linear expression to approximate the lateral-torsional buckling resistance of discretely braced compression flanges in the inelastic range.

The equations defining the nominal flexural resistance of the compression flange, F_{nc}, for lateral-torsional buckling in *AASHTO LRFD* Article 6.10.8.2.3 are expressed in terms of stress as follows (the equations are shown graphically in Figure 3.2.49):

- If $L_b \le L_p$, then:

$$F_{nc} = R_b R_h F_{yc}$$

Equation 3.2.91
AASHTO LRFD Equation 6.10.8.2.3-1

- If $L_p < L_b \le L_r$, then:

$$F_{nc} = C_b \left[1 - \left(1 - \frac{F_{yr}}{R_h F_{yc}} \right) \left(\frac{L_b - L_p}{L_r - L_p} \right) \right] R_b R_h F_{yc} \le R_b R_h F_{yc}$$

Equation 3.2.92
AASHTO LRFD Equation 6.10.8.2.3-2

- If $L_b > L_r$, then:

$$F_{nc} = F_{cr} \le R_b R_h F_{yc}$$

Equation 3.2.93
AASHTO LRFD Equation 6.10.8.2.3-3

where:

L_b = unbraced length (in.)

L_p = limiting unbraced length to achieve the nominal flexural resistance F_{max} equal to $R_b R_h F_{yc}$ under uniform bending (in.)

$$= 1.0 r_t \sqrt{\frac{E}{F_{yc}}}$$

Equation 3.2.94
AASHTO LRFD Equation 6.10.8.2.3-4

L_r = limiting unbraced length to achieve the onset of nominal yielding in either flange under uniform bending with consideration of compression-flange residual stress effects (in.)

$$= \pi r_t \sqrt{\frac{E}{F_{yr}}}$$

Equation 3.2.95
AASHTO LRFD Equation 6.10.8.2.3-5

C_b = moment gradient modifier (discussed below)

F_{cr} = elastic lateral-torsional buckling stress (ksi)

$$= \frac{C_b R_b \pi^2 E}{\left(\frac{L_b}{r_t}\right)^2}$$

Equation 3.2.96
AASHTO LRFD Equation 6.10.8.2.3-8

F_{yr} = compression-flange stress at the onset of nominal yielding within the cross-section, including residual stress effects, but not including compression-flange lateral bending, taken as the smaller of $0.7F_{yc}$ and F_{yw}, but not less than $0.5F_{yc}$ (ksi)

R_b = web load-shedding factor determined as specified in *AASHTO LRFD* Article 6.10.1.10.2 (Section 3.2.6.2)

R_h = hybrid factor determined as specified in *AASHTO LRFD* Article 6.10.1.10.1 (Section 3.2.6.3)

r_t = effective radius of gyration for lateral torsional buckling (in.)

$$= \frac{b_{fc}}{\sqrt{12\left(1 + \frac{1}{3}\frac{D_c t_w}{b_{fc} t_{fc}}\right)}}$$

Equation 3.2.97
AASHTO LRFD Equation 6.10.8.2.3-9

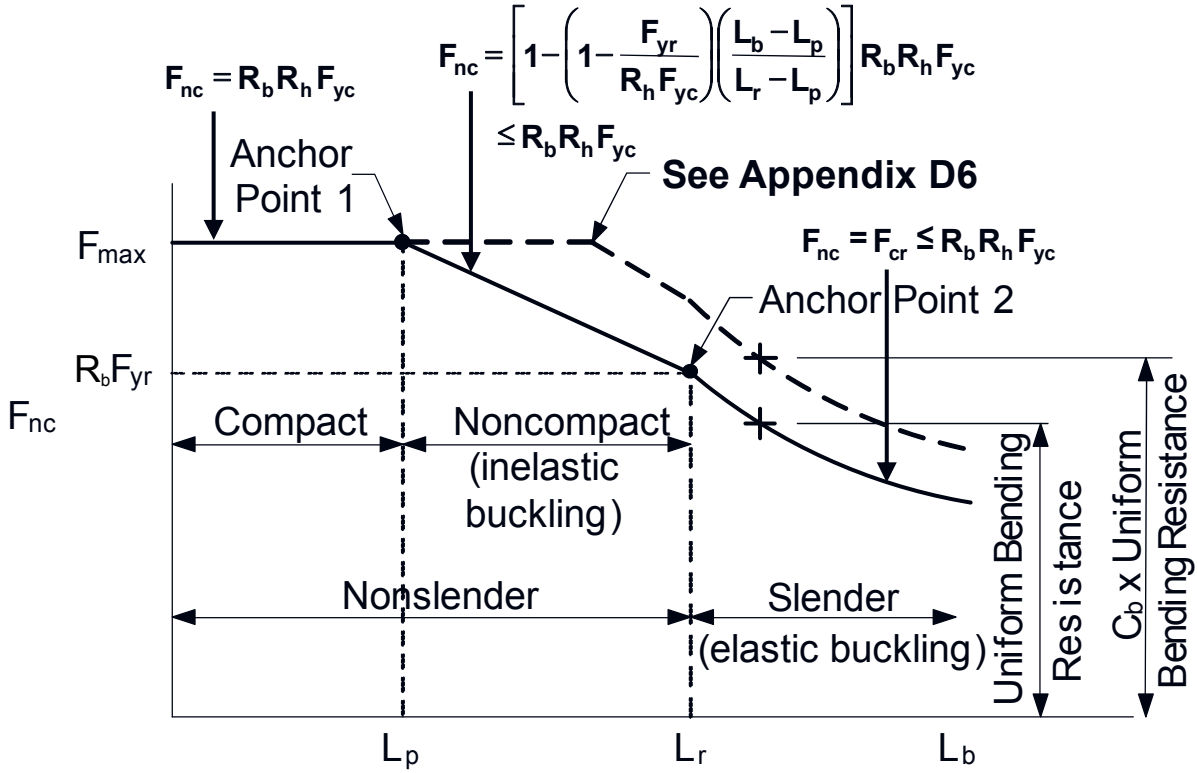


Figure 3.2.49 Lateral Torsional Buckling Resistance, F_{nc}

Brace points defining the unbraced length, L_b, of the compression flange are considered to be points where lateral deflection of the girder flange and twisting of the entire cross-section are restrained. In the past, points of contraflexure have sometimes been considered to act as brace points. Since this practice can lead to significantly unconservative estimates of the lateral-torsional buckling resistance, the *AASHTO LRFD Specifications* do not imply that points of contraflexure should be considered as brace points. Instead, the effects of moment gradient are to be handled directly through the use of the moment gradient modifier C_b (discussed below).

The solid curve in Figure 3.2.49 represents the lateral-torsional buckling resistance for the case of uniform vertical bending. The dashed curve represents the lateral-torsional buckling resistance under moment gradient conditions (Figure 3.2.50). L_p and L_r are Anchor Points 1 and 2, respectively, as shown on Figure 3.2.49. L_p and L_r are given by Equations 3.2.94 and 3.2.95, respectively.

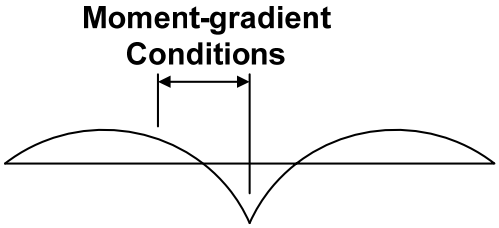


Figure 3.2.50 Moment Gradient Conditions

L_p defines the *compact unbraced length* limit. A member braced at or below the compact unbraced length limit is able to achieve the maximum potential lateral-torsional buckling resistance (F_{max} in Figure 3.2.49) of $R_bR_hF_{yc}$ under uniform vertical bending, which is independent of the unbraced length. The limit is more restrictive than the limit given in previous Specifications. It was developed based on a linear regression analysis for a wide range of data from experimental tests under uniform major-axis bending (with an effective length factor k for lateral-torsional buckling effectively equal to 1.0) that fell within the inelastic lateral-torsional buckling region (*75*). ***Note that in many cases, particularly under uniform vertical bending, it will not be economical to brace the girder at a distance equal to L_p or below in order to reach F_{max}.***

L_r defines the *noncompact unbraced length* limit. The lateral-torsional buckling resistance of a member braced at or below the noncompact unbraced length limit is expressed in Equation 3.2.92 as a linear function of the unbraced length, as illustrated in Figure 3.2.49, which represents the inelastic lateral-torsional buckling resistance. L_r is the unbraced length at which the inelastic and elastic lateral-torsional buckling resistances are the same. The resistance at this point is assumed to be R_bF_{yr}. F_{yr} is taken as the smaller of $0.7F_{yc}$ and F_{yw}, but not less than $0.5F_{yc}$. With the exception of hybrid sections with F_{yw} significantly smaller than F_{yc}, $F_{yr} = 0.7F_{yc}$. This limit corresponds to an assumed nominal compression flange residual stress effect of $0.3F_{yc}$. As pointed out in *AASHTO LRFD* Article C6.10.8.2.3, the $0.5F_{yc}$ limit on F_{yr} avoids anomalous situations for some types of cross-sections in which the inelastic buckling equation gives a larger resistance than the corresponding elastic buckling curve.

Unbraced lengths greater than L_r are termed *slender unbraced lengths* and their resistance is controlled by elastic lateral-torsional buckling. As mentioned previously, lateral-torsional buckling in the elastic range is of primary importance for relatively slender girders braced at longer than normal intervals, which most typically occurs during a temporary construction condition. Equation 3.2.96 for the elastic lateral-torsional buckling stress, F_{cr}, is a conservative approximation of Equation 3.2.90 (assuming load-height effects are not considered). To handle singly symmetric I-sections, an effective radius of gyration, r_t, is introduced as follows:

$$r_t = \frac{b_{fc}}{\sqrt{12\left(\frac{h}{d} + \frac{1}{3}\frac{D_c t_w}{b_{fc} t_{fc}}\frac{D^2}{hd}\right)}}$$

Equation 3.2.98
AASHTO LRFD Equation C6.10.8.2.3-1

where *d* is the overall depth of the steel section and *h* is the depth between the flange centerlines. The expression for r_t given in Equation 3.2.97 is a simplification of Equation 3.2.98 obtained by assuming that $D = h = d$. However, Equation 3.2.98 is still provided in the Commentary to the specification (*AASHTO LRFD* Article C6.10.8.2.3) should the Design Engineer require a more precise calculation of the elastic lateral-torsional buckling stress. The web term $D_c t_w$ in both expressions for r_t accounts for the destabilizing effects of the flexural compression in the web on the lateral-torsional buckling resistance.

Moment Gradient Modifier, C_b

The effect of a variation in the vertical bending moment along the length between brace points, or a moment gradient (Figure 3.2.50), is accounted for by applying the moment gradient modifier, C_b, to the base inelastic and elastic lateral-torsional buckling equations. When the moment and corresponding flange compressive vertical bending stress are constant along the unbraced length, C_b has a base value of 1.0. Under moment gradient conditions, C_b may be taken greater than 1.0, which effectively increases the lateral-torsional buckling resistance with the increase capped at $F_{max} = R_b R_h F_{yc}$ (refer to the dashed curves in Figure 3.2.51). C_b may conservatively be taken equal to 1.0 in all cases, except for some rare cases involving no cross-bracing within the span, as discussed below.

C_b is specified as follows in *AASHTO LRFD* Article 6.10.8.2.3:

- For unbraced cantilevers and for members when $f_{mid}/f_2 > 1$ or $f_2 = 0$:

$$C_b = 1.0$$

Equation 3.2.99
AASHTO LRFD Equation 6.10.8.2.3-6

- For all other cases:

$$C_b = 1.75 - 1.05\left(\frac{f_1}{f_2}\right) + 0.3\left(\frac{f_1}{f_2}\right)^2 \le 2.3$$

Equation 3.2.100
AASHTO LRFD Equation 6.10.8.2.3-7

where:

f_2 = except as noted in the following, largest factored compressive vertical bending stress at either end of the unbraced length of the flange under consideration, calculated from the critical moment envelope value (ksi). f_2 shall be taken as positive. If the stress is zero or tensile in the flange under consideration at both ends of the unbraced length, f_2 shall be taken as zero.

f_0 = factored vertical bending stress at the brace point opposite to the one corresponding to f_2, calculated from the moment envelope value that produces the largest compression at this point in the flange under consideration, or the smallest tension if this point is never in compression (ksi). f_0 shall be taken as positive in compression and negative in tension.

f_1 = factored vertical bending stress at the brace point opposite to the one corresponding to f_2, calculated as the intercept of the most critical assumed linear stress variation passing through f_2 and either f_{mid} or f_0, whichever produces the smaller value of C_b (ksi). f_1 may be determined as follows:

- When the variation in the moment along the entire length between brace points is concave in shape:

$$f_1 = f_0$$

Equation 3.2.101
AASHTO LRFD Equation 6.10.8.2.3-10

- Otherwise:

$$f_1 = 2f_{mid} - f_2 \geq f_0$$

Equation 3.2.102
AASHTO LRFD Equation 6.10.8.2.3-11

where:

f_{mid} = factored vertical bending stress at the middle of the unbraced length under consideration, calculated from the moment envelope value that produces the largest compression at this point, or the smallest tension if the point is never in compression (ksi). f_{mid} shall be taken as positive in compression and negative in tension.

Vertical bending stresses are used in Equation 3.2.100 since dead and live load bending moments are applied to different sections in composite girders, which is significant when the nominal flexural resistance is not permitted to exceed the moment at first yield. However, as pointed out in *AASHTO LRFD* Article C6.10.8.2.3, the ratio of the major-axis bending moments at the brace points may be used in lieu of the bending stresses for convenience, if the Design Engineer feels that the use of the moment ratios does not have a significant effect on the calculated value of C_b.

It is convenient and always conservative to use the critical moment envelope values to compute the above stresses, particularly since concurrent moment values at the brace points are not normally tracked in the analysis. It can be shown that the use of the critical moment envelope values to compute f_2, f_{mid} and f_o is always conservative since a more critical stress distribution along the unbraced length, in terms of computing C_b, cannot exist for all possible concurrent loadings.

The application of the C_b equation to different cases will be illustrated through the examples given in Figure 3.2.51. In examining these cases, recall that according to the definitions given above, in the calculation of C_b, compressive stresses are to be taken as positive and tensile stresses are to be taken as negative.

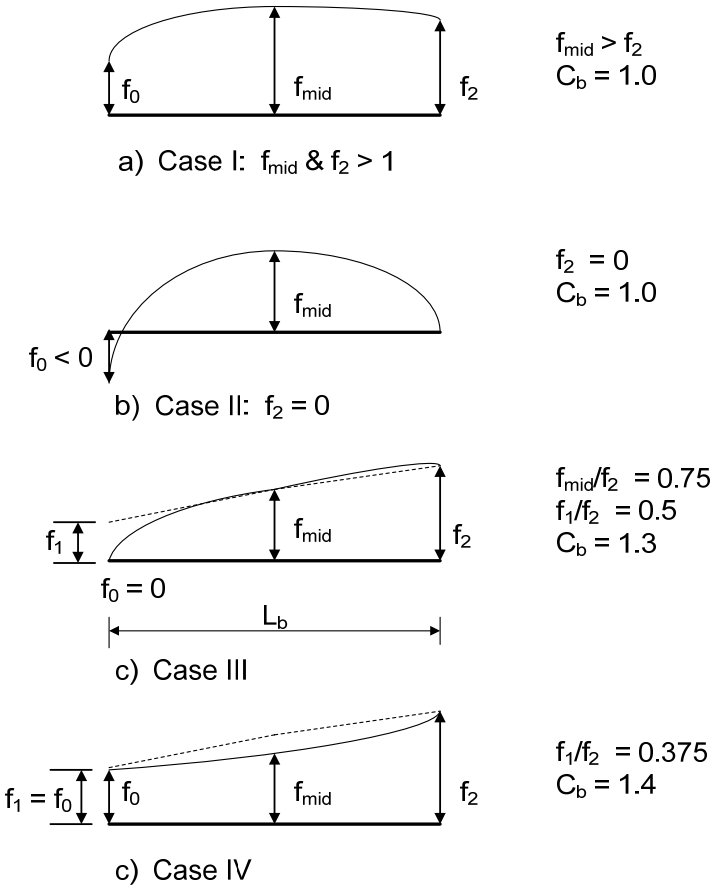


Figure 3.2.51 Moment Gradient Modifier, C_b – Example Cases

The first two cases illustrate when C_b must be taken equal to 1.0. In Case I shown in Figure 3.2.51 Part a, the compressive stress at the middle of the unbraced length, f_{mid}, is greater than the largest compressive stress at either end of the unbraced length, f_2. Therefore, C_b must be taken equal to 1.0. This is a common situation in regions of positive flexure when investigating the lateral-torsional buckling resistance

of the top flange of the non-composite girder in critical unbraced lengths during construction.

In Case II shown in Figure 3.2.51 Part b, the stress in the top flange at one end of the unbraced length is zero and the stress in the top flange at the other end of the unbraced length is tensile. As stated in the above definition of the stress f_2, when this situation occurs, f_2 is to be taken as zero. And further, when f_2 is equal to zero, C_b must be taken equal to 1.0. The situation shown in Figure 3.2.51 Part b represents the rare case of a continuous span with no cross-bracing within the span. A case (not shown) where the stress would be zero at both ends of the unbraced length (and f_2 must then also be taken equal to zero according to the definition) would be a simply supported span with no cross-bracing within the span.

The last case (also not shown) for which C_b must be taken equal to 1.0 is for an unbraced cantilever, which is carried over from previous specifications. As discussed previously, for situations involving no cross-bracing within the span or unbraced cantilevers with significant loading applied to the top flange, consideration should be given to including load-height effects in the calculation of C_b (*3*, *74*). In such situations, the calculated C_b values may actually be less than 1.0. As pointed out in *AASHTO LRFD* Article C6.10.8.2.3, when C_b is less than 1.0, F_{nc} may be smaller than F_{max} even when L_b is less than L_p. Therefore, in these cases, it is recommended that F_{nc} be calculated from Equation 3.2.92 whenever L_b is less than or equal to L_r.

Equation 3.2.100 requires in certain situations the approximation of the stress variation along the unbraced length as the most critical of: 1) a line that passes through f_2 and f_{mid}, or 2) a line that passes between f_2 and f_0, whichever produces the smaller value of C_b. The intercept of the most critical line at the opposite end from f_2 is denoted as f_1. The preceding approximation is represented by Equation 3.2.102. For example, Case III shown in Figure 3.2.51 Part c represents a simply-supported member braced only at its ends and at midspan (only one-half of the member is assumed shown in the figure). In previous specifications, using the compressive stresses at each end of the unbraced length would have given a C_b value of 1.75 according to Equation 3.2.100. However, more accurate equations yield a C_b value of 1.3 for this case (*67*) since the flange compression is significantly larger within the unbraced length than the linear variation implicitly assumed by Equation 3.2.100 due to the parabolic shape of the moment diagram. As shown in Figure 3.2.51 Part c, a line passing through f_2 and f_{mid} will produce a smaller value of C_b for this case than a line passing between f_2 and f_0 since the slope of a line through f_2 and f_{mid} is flatter and closer to that produced by a uniform moment. This fact is reflected when using Equation 3.2.102, which yields $f_1 = 2(0.75f_2) - f_2 = 0.5f_2 > f_0$. Substituting $f_1/f_2 = 0.5$ into Equation 3.2.100 yields $C_b = 1.3$.

It should be noted, however, that in most cases, Equation 3.2.102 will not need to be employed. The most common application of Equation 3.2.100 in design is for unbraced lengths in continuous spans in regions of negative flexure adjacent to interior piers, which are typically subject to significant moment gradients (Figure 3.2.50). ***The Design Engineer is strongly encouraged to calculate C_b for***

unbraced lengths adjacent to interior piers. The unbraced lengths on either side of the pier should be checked to determine which side will yield the lower value of C_b. As shown in Case IV in Figure 3.2.51 Part d, in these cases, where f_{mid} is smaller in magnitude than the average of f_0 and f_2 (or where the moment diagram is concave in shape along the entire length between brace points, which is the case in these regions), f_1 will always equal f_0. Therefore, the specification indicates that for cases where the moment diagram is concave in shape along the entire length between brace points, f_1 in Equation 3.2.100 may simply be taken equal to f_0, or the stress at the brace point opposite to the one corresponding to f_2, and Equation 3.2.102 need not be employed. This of course assumes that the section within the unbraced length is prismatic, or if a flange transition is present that it is located a relatively short distance (i.e. $0.2L_b$) from the brace point with the smaller moment. As discussed further below, when this is not the case, C_b must be taken equal to 1.0. Sample illustrations of the calculation of the C_b factor for other cases, including cases of reverse curvature bending, are provided at the end of *AASHTO LRFD* Appendix C6. Further more detailed discussion on the derivation and calculation of the C_b factor may also be found in Reference 55.

As represented by the dashed curves shown in Figure 3.2.51, under moment gradient conditions (i.e., $C_b > 1.0$), in addition to an increase in the base lateral-torsional buckling resistance, the maximum potential lateral-torsional buckling resistance, $F_{max} = R_b R_h F_{yc}$, can be reached at larger unbraced lengths. The provisions of *AASHTO LRFD* Article D6.4.1 (Appendix D6) can be used to calculate the maximum unbraced lengths to achieve F_{max} under moment gradient conditions, and are recommended for use whenever C_b is greater than 1.0. The modifications to Anchor Points 1 and 2 to account for the effect of the moment gradient are given as follows in *AASHTO LRFD* Article D6.4.1:

- If $L_b \le L_p$, then:

$$F_{nc} = R_b R_h F_{yc}$$

Equation 3.2.103
AASHTO LRFD Equation D6.4.1-1

- If $L_p < L_b \le L_r$, then:

  - If $L_b \le L_p + \dfrac{\left(1 - \dfrac{1}{C_b}\right)}{\left(1 - \dfrac{F_{yr}}{R_h F_{yc}}\right)}\left(L_r - L_p\right)$, then:

$$F_{nc} = R_b R_h F_{yc}$$

Equation 3.2.104
AASHTO LRFD Equation D6.4.1-2

- Otherwise:

$$F_{nc} = C_b\left[1-\left(1-\frac{F_{yr}}{R_h F_{yc}}\right)\left(\frac{L_b - L_p}{L_r - L_p}\right)\right]R_b R_h F_{yc} \le R_b R_h F_{yc}$$

Equation 3.2.105
AASHTO LRFD Equation D6.4.1-3

➢ If $L_b > L_r$, then:

- If $L_b \le \pi r_t\sqrt{\frac{C_b E}{R_h F_{yc}}}$, then:

$$F_{nc} = R_b R_h F_{yc}$$

Equation 3.2.106
AASHTO LRFD Equation D6.4.1-4

- Otherwise:

$$F_{nc} = F_{cr} \le R_b R_h F_{yc}$$

Equation 3.2.107
AASHTO LRFD Equation D6.4.1-5

Effect of Section Transitions within the Unbraced Length

The base lateral-torsional buckling equations in the specifications assume that the member is prismatic within the unbraced length. According to Reference 76, under uniform vertical bending, the reduction in the elastic lateral-torsional buckling resistance due to a transition to a smaller section is approximately 5 percent when the transition is placed at 20 percent of the unbraced length from one of the brace points, and when the lateral moment of inertia of the flange in the smaller section is equal to one-half the corresponding value in the larger section. The reduction is less under moment gradient conditions as long as the larger bending moment occurs within the larger section, the lateral moment of inertia of the flange in the smaller section is greater than one-half the corresponding value in the larger section, and/or the section transition is placed closer to the brace point. Therefore, *AASHTO LRFD* Article 6.10.8.2.3 permits the effect of the section transition on the lateral-torsional buckling resistance to be ignored when the stated conditions above are satisfied. If there is more than one transition within the unbraced length, any transition within 20 percent of the unbraced length from the brace point with the smaller moment may be

ignored and the lateral-torsional buckling resistance based on the remaining sections may then be computed as described in the next paragraph.

For unbraced lengths containing a transition to a smaller section at a distance greater than 20 percent of the unbraced length from the brace point with the smaller moment, the lateral-torsional buckling resistance, F_{nc}, at each section within the unbraced length may be taken as the smallest resistance within the unbraced length according to *AASHTO LRFD* Article 6.10.8.2.3 (note that the transition can either be in the compression or tension flange). The resulting lateral-torsional buckling resistance must then not be exceeded at any section within the unbraced length. In addition, the C_b factor must be taken equal to 1.0 and the unbraced length must not be modified by an effective length factor. Essentially, the nonprismatic member is being replaced with an equivalent prismatic member. The cross-section of the equivalent member that gives the correct lateral-torsional buckling resistance is generally some weighted average of all the cross-sections along the unbraced length. If the cross-section that gives the smallest uniform vertical bending resistance is used (i.e., calculated assuming C_b is equal to 1.0) and the calculated resistance based on that cross-section is not exceeded anywhere along the unbraced length, a conservative solution is obtained. A suggested procedure to obtain a more refined estimate of the lateral-torsional buckling resistance for this case is given in Reference 5.

The preceding requirements are summarized in Figure 3.2.52 for a section change due to a single flange transition. *To avoid a significant reduction in the lateral-torsional buckling resistance in such cases according to the above criteria, consider locating flange transitions within 20 percent of the unbraced length from the brace point with the smaller moment and ensure that the lateral moment of inertia of the flange (or flanges) of the smaller section is equal to or larger than one-half the corresponding value(s) for the flange(s) of the larger section at the transition.*

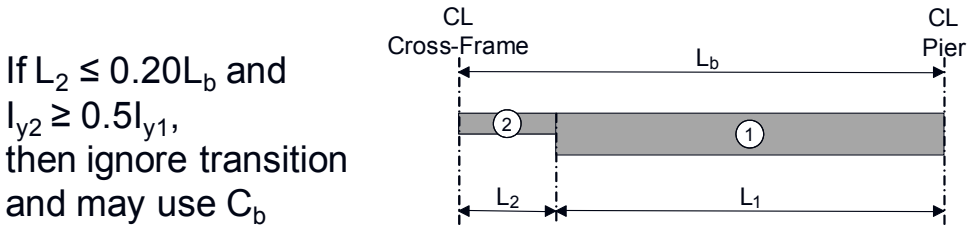


Figure 3.2.52 Unbraced Length with a Single Flange Transition

3.2.6.4.1.3 Continuously Braced Tension Flanges

Tension (top) flanges in regions of negative flexure in continuous-span composite members are typically classified as continuously braced flanges. A continuously braced flange is defined as a flange encased in concrete or anchored by shear connectors. Since in negative flexure regions, the top flange is in tension and the flange is usually continuously braced, only yielding of the flange is a concern and any flange lateral bending stresses need not be considered.

Continuously braced flanges in tension or compression must satisfy the following relationship at the strength limit state (*AASHTO LRFD* Article 6.10.8.1.3):

$$f_{bu} \leq \phi_f R_h F_{yf}$$

Equation 3.2.108
AASHTO LRFD Equation 6.10.8.1.3-1

The specification considers the effects of any potential web bend buckling to be negligible for such cases, and therefore, the web load-shedding factor, R_b, is not included in Equation 3.2.108. Again, lateral bending does not need to be considered in Equation 3.2.108 because the flanges in these cases are continuously supported by the concrete deck.

3.2.6.4.2 Box Sections

3.2.6.4.2.1 General

AASHTO LRFD Article 6.11.6.2.3 specifies that for closed-box and tub sections subject to negative flexure at the strength limit state, the provisions of *AASHTO LRFD* Article 6.11.8 are to be applied. The provisions of *AASHTO LRFD* Article 6.11.8 limit the nominal flexural resistance to always be less than or equal to the moment at first yield *for all types of box girder bridges*. Therefore, the nominal flexural resistance for these sections is always expressed in terms of the elastically computed flange stress.

Further, according to *AASHTO LRFD* Article 6.11.6.2.3, the optional provisions of *AASHTO LRFD* Appendices A6 and B6 are *not* to be applied to box sections. These optional appendices apply only to the design of I-section flexural members. Their applicability to the design of box-section flexural members has not yet been demonstrated.

3.2.6.4.2.2 Box Flanges in Compression

AASHTO LRFD Article 6.11.8.1.1 specifies that for box sections subject to negative flexure, box flanges in compression (i.e. bottom flanges) must satisfy the following requirement at the strength limit state:

$$f_{bu} \le \phi_f F_{nc}$$

Equation 3.2.109
AASHTO LRFD Equation 6.11.8.1.1-1

where:

f_{bu} = factored longitudinal flange stress at the section under consideration calculated without consideration of longitudinal warping (ksi)

F_{nc} = nominal flexural resistance of the box flange in compression determined as specified in *AASHTO LRFD* Article 6.11.8.2 (discussed below) (ksi)

Equation 3.2.109 is intended to ensure that box flanges in compression have sufficient local buckling resistance. Flange lateral bending and lateral-torsional buckling are not a consideration for box flanges. Longitudinal warping stresses are typically ignored at the strength limit state, as permitted in *AASHTO LRFD* Article 6.11.1.1.

In general, bottom box flanges at interior-pier sections are subject to a complex stress state. The flanges are subject to biaxial bending due to vertical bending of the box section and due to vertical bending of the internal diaphragm over the bearing sole plate. Bending of the internal diaphragm over the bearing sole plate may be particularly significant for boxes supported on single bearings. The flange is also subject to shear stresses due to the vertical shear in the internal diaphragm, and in cases where it must be considered, the St. Venant torsional shear. Thus, for cases where the bending of the internal diaphragm and/or the flange shear stresses are deemed significant, *AASHTO LRFD* Article C6.11.8.1.1 suggests that the following equation be used to check the combined stress state in the box flange at interior-pier sections at the strength limit state. The equation represents the general form of the Huber-von Mises-Hencky yield criterion for combined stress (77):

$$\sqrt{f_{bu}^2 - f_{bu}f_{by} + f_{by}^2 + 3(f_d + f_v)^2} \le \phi_f R_b R_h F_{yc}$$

Equation 3.2.110
AASHTO LRFD Equation C6.11.8.1.1-1

where:

f_{by} = factored stress in the box flange caused by the vertical bending of the internal diaphragm over the bearing sole plate (ksi)

f_d = factored shear stress in the box flange caused by the internal diaphragm vertical shear (ksi)

$$= \frac{VQ}{It_{fc}}$$

Equation 3.2.111
AASHTO LRFD Equation C6.11.8.1.1-2

f_v = factored St. Venant torsional shear stress in the box flange (ksi)

I = moment of inertia of the effective internal diaphragm section (discussed below) (in.^{4})
Q = first moment of one-half the effective box-flange area about the neutral axis of the effective internal diaphragm section (discussed below) (in.^{3})
R_b = web load-shedding factor determined as specified in *AASHTO LRFD* Article 6.10.1.10.2 (Section 3.2.6.2)
R_h = hybrid factor determined as specified in *AASHTO LRFD* Article 6.10.1.10.1 (Section 3.2.6.3)
V = factored vertical shear in the internal diaphragm due to flexure plus St. Venant torsion (kips)

f_{bu} and f_{by} are to be taken as signed quantities in Equation 3.2.110. As indicated in *AASHTO LRFD* Article C6.11.8.1.1, for a box supported on two bearings, f_{by} in Equation 3.2.110 is typically relatively small and may be neglected in making this check. f_{by} should be considered for boxes resting on single bearings and may be computed using the effective section discussed in the next paragraph.

In calculating f_d from Equation 3.2.111, and also f_{by}, a portion of the box flange may be considered effective with the internal diaphragm. *AASHTO LRFD* Article C6.11.8.1.1 currently suggests that a flange width equal to six times its thickness may be considered effective with the internal diaphragm. Further, whenever an access hole is provided within the internal diaphragm for inspection purposes, the effect of the hole should be considered in computing the section properties of the effective diaphragm section. The application of Equations 3.2.110 and 3.2.111 is demonstrated in the tub-girder design example given in Section 5.2.

Recall as discussed previously in Sections 3.2.6.2 and 3.2.6.3 that to calculate the web load-shedding factor, R_b, and the hybrid factor, R_h, for a tub section, where applicable, one-half of the effective box flange width should be used in conjunction with one top flange and a single web (refer to *AASHTO LRFD* Article C6.11.8.2.2). One-half of the effective top and bottom box flange width should be used in conjunction with a single web for a closed-box section. The effective box flange width is defined in *AASHTO* LRFD Article 6.11.1.1 and discussed further in Section 3.1.5.4.2.1.

Nominal Flexural Resistance of Box Flanges in Compression, F_{nc}

The nominal flexural resistance of box flanges in compression, F_{nc}, in the *AASHTO LRFD* Specifications is based on local buckling of the flange under combined uniform axial compression and shear (lateral-torsional buckling is not a consideration for box flanges). In general, the resistance is defined for three distinct regions based on the flange slenderness. For unstiffened flanges, the slenderness is based on the full flange width between webs, b_{fc}. For longitudinally stiffened flanges, the slenderness is based on the larger of the width of the flange between longitudinal flange stiffeners or the distance from a web to the nearest longitudinal flange stiffener, w. The local buckling resistance of longitudinally stiffened flanges is dependent on the rigidity of the longitudinal stiffener(s).

As for the compression-flange local buckling and lateral-torsional buckling resistance curves for I-section members, the local buckling resistance curves for box flanges are fitted to two anchor points (Figure 3.2.53).

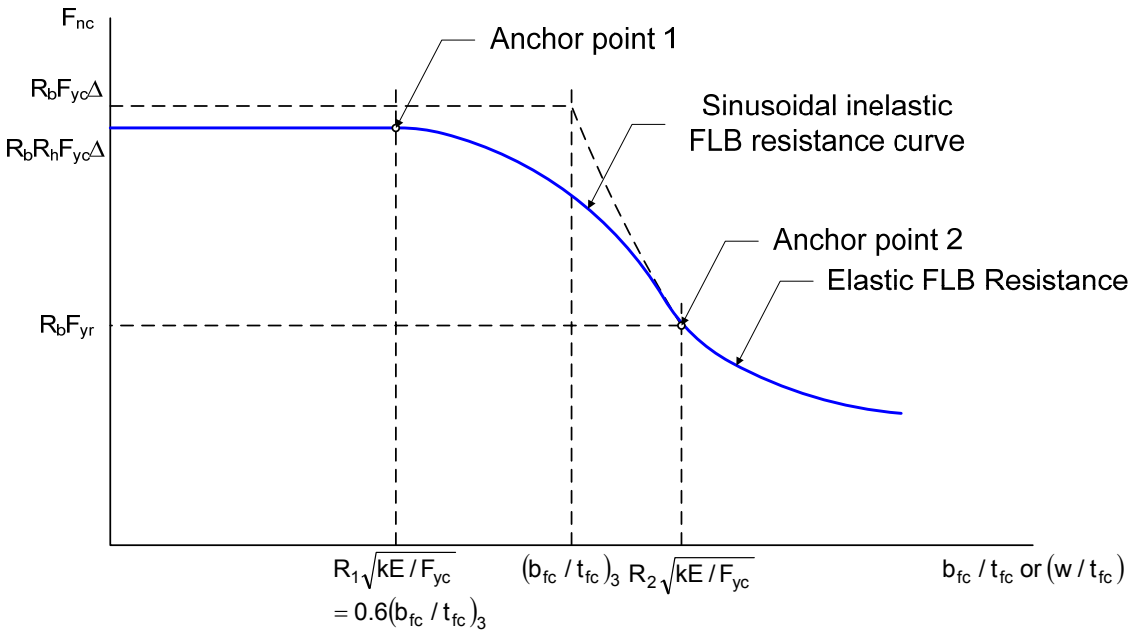


Figure 3.2.53 Local Buckling Resistance Curves for Box Flanges in Compression

These anchor points are discussed in more detail below. Note that the inelastic local buckling resistance of the box flange is represented by a sinusoidal function rather than by a linear interpolation between the two anchor points, as is the case for I-section members. The equations are based on the tacit assumptions that the flange panel is of infinite length and that the panel is subjected to a uniform stress field over its full width and length. Since the moment gradient in negative moment regions increases rather sharply near interior supports, the true stress usually decreases over the panel length from a maximum at one end of the panel. Further the panel is not of infinite length. So the true strength of actual box flanges in negative flexure is greater than implied. Still, it is advisable to use the critical stress in the panel to make the following checks.

At access holes in box flanges subject to compression, it is recommended that the nominal flexural resistance of the remaining flange on each side of the hole be determined according to the provisions of *AASHTO LRFD* Article 6.10.8.2.2, with λ_f taken as the projecting width of the flange on that side of the hole divided by the flange thickness (refer to Section 3.2.6.4.1.2). The equations in *AASHTO LRFD* Article 6.10.8.2.2 are the local buckling resistance equations for I-girder compression flanges, with the flange width based on the projecting width of the flange on the side of the hole under consideration.

Unstiffened Box Flanges

According to *AASHTO LRFD* Article 6.11.8.2.1, the nominal flexural resistance of box flanges in compression without flange longitudinal stiffeners (i.e. unstiffened flanges) is to be determined as specified in *AASHTO LRFD* Article 6.11.8.2.2. *AASHTO LRFD* Article 6.11.8.2.2 defines the nominal local buckling resistance of the flanges as follows:

- If $\lambda_f \le R_1\sqrt{\frac{kE}{F_{yc}}}$, then:

$$F_{nc} = R_b R_h F_{yc} \Delta$$

Equation 3.2.112
AASHTO LRFD Equation 6.11.8.2.2-1

- If $R_1\sqrt{\frac{kE}{F_{yc}}} < \lambda_f \le R_2\sqrt{\frac{kE}{F_{yc}}}$, then:

$$F_{nc} = R_b R_h F_{yc}\left[\Delta - \left(\Delta - \frac{F_{yr}}{R_h F_{yc}}\right)\left\{1 - \sin\left[\frac{\pi}{2}\left(\frac{R_2 - \frac{b_{fc}}{t_{fc}}\sqrt{\frac{F_{yc}}{kE}}}{R_2 - R_1}\right)\right]\right\}\right]$$

Equation 3.2.113
AASHTO LRFD Equation 6.11.8.2.2-2

- If $\lambda_f > R_2\sqrt{\frac{kE}{F_{yc}}}$, then:

$$F_{nc} = \frac{0.9ER_b k}{\left(\frac{b_{fc}}{t_{fc}}\right)^2} - \frac{R_b f_v^2 k}{0.9Ek_s^2}\left(\frac{b_{fc}}{t_{fc}}\right)^2$$

Equation 3.2.114
AASHTO LRFD Equation 6.11.8.2.2-3

where:

λ_f = slenderness ratio for the compression flange

$$= \frac{b_{fc}}{t_{fc}}$$

Equation 3.2.115
AASHTO LRFD Equation 6.11.8.2.2-4

$$\Delta = \sqrt{1-3\left(\frac{f_v}{F_{yc}}\right)^2}$$

Equation 3.2.116
AASHTO LRFD Equation 6.11.8.2.2-5

b_{fc} = compression-flange width between webs (in.)
f_v = factored St. Venant torsional shear stress in the flange at the section under consideration not to exceed the factored torsional shear resistance of the flange, F_{vr}, given by Equation 3.2.71 (ksi)

$$= \frac{T}{2A_o t_{fc}}$$

Equation 3.2.117
AASHTO LRFD Equation 6.11.8.2.2-6

A_o = enclosed area within the box section (in.)
F_{yr} = smaller of the compression-flange yield stress at the onset of nominal yielding, with consideration of residual stress effects, or the specified minimum yield strength of the web (ksi)

$$= (\Delta - 0.4)F_{yc} \le F_{yw}$$

Equation 3.2.118
AASHTO LRFD Equation 6.11.8.2.2-7

k = plate-buckling coefficient for uniform normal stress
= 4.0
k_s = plate-buckling coefficient for shear stress
= 5.34
R_1 = constant which when multiplied by $\sqrt{kE/F_{yc}}$ yields the slenderness ratio equal to 0.6 times the slenderness ratio for which F_{nc} from Equation 3.2.114 is equal to $R_b F_{yc}\Delta$

$$= \frac{0.57}{\sqrt{\frac{1}{2}\left[\Delta + \sqrt{\Delta^2 + 4\left(\frac{f_v}{F_{yc}}\right)^2\left(\frac{k}{k_s}\right)^2}\right]}}$$

Equation 3.2.119
AASHTO LRFD Equation 6.11.8.2.2-8

.

R_2 = constant which when multiplied by $\sqrt{kE/F_{yc}}$ yields the slenderness ratio for which F_{nc} from Equation 3.2.114 is equal to R_bF_{yr}

$$= \frac{1.23}{\sqrt{\frac{1}{1.2}\left[\frac{F_{yr}}{F_{yc}}+\sqrt{\left(\frac{F_{yr}}{F_{yc}}\right)^2+4\left(\frac{f_v}{F_{yc}}\right)^2\left(\frac{k}{k_s}\right)^2}\right]}}$$

Equation 3.2.120
AASHTO LRFD Equation 6.11.8.2.2-9

R_b = web load-shedding factor determined as specified in *AASHTO LRFD* Article 6.10.1.10.2 (Section 3.2.6.2)
R_h = hybrid factor determined as specified in *AASHTO LRFD* Article 6.10.1.10.1 (Section 3.2.6.3)
t_{fc} = thickness of the compression flange (in.)
T = internal torque due to the factored loads (kip-in.)

Referring to Figure 3.2.53, Anchor Point 1 is based on the constant R_1 given by Equation 3.2.119. The anchor point $R_1\sqrt{kE/F_{yc}}$ is equal to 0.6 times the flange slenderness $(b_{fc}/t_{fc})_3$ at which the elastic flange local buckling stress given by Equation 3.2.114 is equal to $R_bF_{yc}\Delta$. For the case of f_v equal to zero and thus Δ equal to 1.0, R_1 is equal to 0.57 and the limiting Anchor Point 1 value of b_{fc}/t_{fc} for F_{yc} = 50 ksi and k = 4.0 is 27.5.

Anchor Point 2 is based on the constant R_2 given by Equation 3.2.120. The anchor point $R_2\sqrt{kE/F_{yc}}$ is equal the flange slenderness at which the elastic flange local buckling stress given by Equation 3.2.114 is equal to R_bF_{yr}, where F_{yr} is given by Equation 3.2.118. For the cases of f_v equal to zero and thus Δ equal to 1.0, R_2 is equal to 1.23 and the limiting Anchor Point 2 value of b_{fc}/t_{fc} for F_{yc} = 50 ksi and k =4.0 is 59.2.

Full yielding of the plate can be achieved as defined by the von Mises yield criterion for combined normal and shear stress (*20*) (Equation 3.2.112) for stocky box flange plates with a flange slenderness less than or equal to $R_1\sqrt{kE/F_{yc}}$. The resistance is governed by elastic buckling for slender plates with a flange slenderness greater than or equal to $R_2\sqrt{kE/F_{yc}}$. In this region, a non-linear interaction curve is used to relate the theoretical elastic Euler buckling equations for an infinitely long plate under a uniform normal stress and under shear stress resulting in Equation 3.2.114 (*3, 11*, *78*). The specified plate-buckling coefficient for uniform normal stress, k = 4.0, and the specified shear-buckling coefficient, k_s = 5.34, both assume simply supported boundary conditions at the edges of the flanges (*11*). For intermediate values of flange slenderness in-between the two limiting anchor points, the resistance is defined by a transition region reflecting the fact that partial yielding due to residual

stresses and initial imperfections do not permit the attainment of the elastic buckling stress. As mentioned previously, the resistance was arbitrarily defined in this region as a sine curve (Equation 2.113) in the original *AASHTO* box-girder design specifications. This assumption has been retained in the *AASHTO LRFD* Specifications. A residual stress level of $0.4F_{yc}$ was assumed in the original derivation of Equation 3.2.113 (*78*).

Longitudinally Stiffened Box Flanges

The nominal flexural resistance of the flange in compression may decrease to an impractical level when an unstiffened box flange becomes too slender. Longitudinal stiffeners can then be added to the flange to increase the nominal flexural resistance.

The design of longitudinal compression-flange stiffeners for box sections is covered in *AASHTO LRFD* Article 6.11.11.2. Longitudinal compression-flange stiffeners on box sections are to be equally spaced across the flange width. Since the stiffeners are primary load carrying members, the specified minimum yield strength of the stiffeners must not be less than the specified minimum yield strength of the box flange to which they are attached. Also, the stiffeners should be included in the section properties of the closed-box or tub section where they are used since they contribute to the flexural stiffness and strength of the section.

Structural tees are preferred for use as longitudinal flange stiffeners because tees increase the lateral torsional buckling resistance of the stiffeners, and also provide a high ratio of out-of-plane stiffness to stiffener cross-sectional area. Using flat bars as stiffeners is an undesirable alternative. Structural tees are not available in grades of steel exceeding 50 ksi. In cases where higher strength tee sections are required (e.g. tees on Grade HPS 70W steel flanges), the tees must be fabricated from plates or bars cut from plate.

As indicated in *AASHTO LRFD* Article C6.11.11.2, longitudinal flange stiffeners should be continuous through internal diaphragms (cut-outs can be provided in the diaphragm to accommodate the stiffeners). Consideration should be given to attaching the longitudinal flange stiffeners to the internal diaphragms; tees can conveniently attached to the diaphragms with a pair of clip angles, as illustrated in Figure 3.2.54.

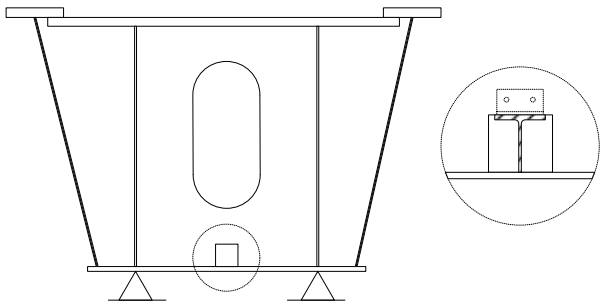


Figure 3.2.54 Suggested Longitudinal Flange Stiffener Detail at an Internal Diaphragm

Longitudinal flange stiffeners are best discontinued at field splice locations at the free edge of the flange where the flange stress is zero, particularly when the span balance is such that the box flange on the other side of the field splice does not require stiffening. In such cases, the compressive resistance of the unstiffened box flange on the other side of the splice must always be checked (see above) to determine if the flange is satisfactory without a stiffener or is a slight increase in the flange thickness will suffice without providing a stiffener. Figure 3.2.55 illustrates a suggested box-flange bolted splice detail to accommodate a termination of the stiffener at the free edge of the flange. When the stiffener is terminated as such, fatigue of the base metal at the stiffener-to-flange weld termination need not be checked in regions subject to a net applied tensile stress (as defined in *AASHTO LRFD* Article 6.6.1.2.1) because the flange stress is zero at the termination.

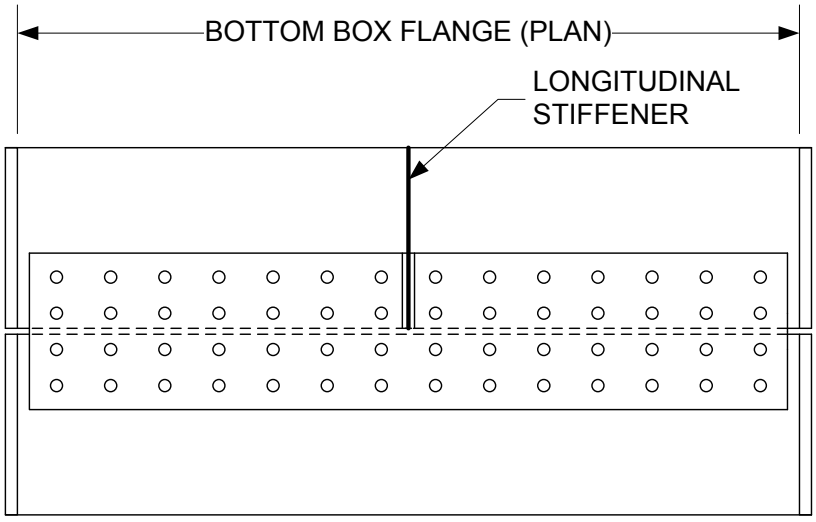


Figure 3.2.55 Suggested Box-Flange Bolted Splice Detail at Flange Stiffener Termination

Should it become necessary to terminate the stiffener beyond the field splice in a region subject to a net applied tensile stress (or should the stiffener be terminated *before* the field splice in such a region), the termination becomes more difficult and

the base metal at the termination of the stiffener-to-flange weld must be checked for fatigue according to the stiffener terminus detail (usually a low Category E or E′ detail unless an appropriate transition radius is provided at the termination – refer to *AASHTO LRFD* Table 6.6.1.2.3-1 – Condition 4.3). Possible options to consider include thickening the flange in the region of the termination to eliminate the need for the stiffener, running the stiffener the full length of the span if the remaining length of unstiffened flange is reasonable (note that this option may help to stiffen a relatively thin tension flange. If a smaller tee section will suffice over the remaining length, it can be spliced onto the existing stiffener), and lastly, including an appropriate transition radius at the end of the stiffener to raise the fatigue detail category accordingly, which is the most costly and least desirable option. The Design Engineer is advised to consult with a fabricator regarding the relative cost of each of these options. Splicing the flange stiffener across the field splice is recommended whenever it becomes necessary to run the stiffener beyond the splice.

AASHTO LRFD Article 6.11.8.2.3 specifies that the nominal flexural resistance of a longitudinally stiffened box flange in compression, F_{nc}, be determined using the same basic equations specified for unstiffened box flanges in compression given in *AASHTO LRFD* Article 6.11.8.2.2 (see above), with the following substitutions:

- The width, w, is to be substituted for b_{fc};
- The plate-buckling coefficient for uniform normal stress, k, is to be taken as:
  - If n = 1, then:

$$k = \left(\frac{8 I_s}{w t_{fc}^3} \right)^{\frac{1}{3}}$$

Equation 3.2.121
AASHTO LRFD Equation 6.11.8.2.3-1

  - If n = 2, then:

$$k = \left(\frac{0.894 I_s}{w t_{fc}^3} \right)^{\frac{1}{3}}$$

Equation 3.2.122
AASHTO LRFD Equation 6.11.8.2.3-2

with $1.0 \leq k \leq 4.0$

- The plate-buckling coefficient for shear stress, k_s, is to be taken as:

$$k_s = \frac{5.34 + 2.84\left(\frac{I_s}{wt_{fc}^3}\right)^{\frac{1}{3}}}{(n+1)^2} \le 5.34$$

Equation 3.2.123
AASHTO LRFD Equation 6.11.8.2.3-3

where:

I_s = moment of inertia of a single longitudinal flange stiffener about an axis parallel to the flange and taken at the base of the stiffener (in.^{4})
n = number of equally spaced longitudinal flange stiffeners
w = larger of the width of the flange between the longitudinal flange stiffeners or the distance from a web to the nearest longitudinal flange stiffener (in.)

The prescribed values of k and k_s for a longitudinally stiffened flange are typically smaller than the prescribed values for an unstiffened flange due to the finite flexibility of the longitudinal stiffeners. The shear-buckling coefficient for the stiffened plate, k_s, given by Equation 3.2.123 is taken from Reference 78. The plate-buckling coefficient for uniform stress, k, is related to the stiffness of the longitudinal flange stiffeners, I_s, and the number of stiffeners, n, according to Equations 3.2.121 and 3.2.122. Equations 3.2.121 and 3.2.122 are derived directly by algebraic manipulation of the following equation for the requirement moment of inertia, I_ℓ, of each longitudinal flange stiffener about an axis parallel to the flange and taken at the base of the stiffener (*AASHTO LRFD* Article 6.11.11.2):

$$I_\ell \ge \psi wt_{fc}^3$$

Equation 3.2.124
AASHTO LRFD Equation 6.11.11.2-2

where:

ψ = $0.125k^3$ for $n = 1$
= $1.120k^3$ for $n = 2$

Equation 3.2.124 is a simplified approximate expression that yields values of the elastic critical stress for a longitudinally stiffened box flange close to those obtained using the exact but more complex equations of elastic stability (*11*). The simplified expression assumes that the box flange and the stiffeners are infinitely long and ignores the effect of any transverse bracing or stiffening. As a result, when n exceeds one, the required moment of inertia from Equation 3.2.124 begins to increase dramatically. When n exceeds 2, for which the value of ψ for application in Equation 3.2.124 is equal to $0.07k^3n^4$, the required moment of inertia becomes nearly impractical. For the rare situation where an exceptionally wide box flange is required and n may need to exceed 2, *AASHTO LRFD* Article C6.11.11.2 suggests

that transverse flange stiffeners be considered to reduce to size of the longitudinal stiffeners to a more practical value. The design of a box flange with longitudinal and transverse flange stiffeners is discussed in more detail below.

Equation 3.2.124 provides the minimum *required* moment of inertia I_ℓ. As discussed previously, when an *actual* assumed longitudinal flange stiffener moment of inertia I_s is used in determining the plate-buckling coefficient k from Equation 3.2.121 or 3.2.122, as applicable, Equation 3.2.124 is automatically satisfied for that value of k since Equations 3.2.121 and 3.2.122 are simply algebraic manipulations of Equation 3.2.124. As an alternative to using Equations 3.2.121 or 3.2.122, however, the Design Engineer can assume a value of k ranging from 1.0 to 4.0 (although a k value ranging from 2.0 to 4.0 typically should be assumed), and then determine the minimum required moment of inertia for each longitudinal stiffener to provide that assumed value of k (as a minimum) from Equation 3.2.124.

AASHTO LRFD Article C6.11.8.2.3 states that k will be at or near a value of 4.0 if the longitudinal flange stiffeners are very rigid and plate buckling will therefore be forced to occur between the stiffeners. For lower values of k, the stiffeners are less rigid and the nominal flexural resistance of the flange will be reduced. ***Therefore, using Equations 3.2.121 and 3.2.122, or alternatively Equation 3.2.124, the Engineer should attempt to efficiently balance the required stiffener size against the required flange resistance in order to provide an economical design. Selecting a k value of 4.0 to provide the largest longitudinal stiffener(s), or selecting a longitudinal stiffener(s) to provide the largest permitted k value of 4.0, may not always provide the most economical solution.*** Also, as discussed above, as the number of longitudinal stiffeners n increases beyond one, the required moment of inertia to achieve a desired k value begins to increase dramatically and eventually becomes impractical. Therefore, equations for k are only provided for values of n up to and including two. ***For boxes of typical proportions, where longitudinal flange stiffeners are required, it is strongly recommended that the number of longitudinal flange stiffeners not exceed one***. In rare cases where an exceptionally wide box flange is required and the number of longitudinal flange stiffeners may need to exceed two, the addition of transverse flange stiffeners should be considered as discussed below. Further discussion on longitudinally stiffened box flanges may be found in Section 3.1.5.4.2.

AASHTO LRFD Article 6.11.11.2 specifies that the projecting width, b_ℓ, of a longitudinal flange stiffener element satisfy the following requirement:

$$b_\ell \le 0.48 t_s \sqrt{\frac{E}{F_{yc}}}$$

Equation 3.2.125
AASHTO LRFD Equation 6.11.11.2-1

where:

t_s = thickness of the projecting longitudinal stiffener element (in.)

For structural tees, b_ℓ is to be taken as one-half the width of the flange. Equation 3.2.125 is intended to prevent local buckling of the projecting elements of the longitudinal stiffener.

Transversely and Longitudinally Stiffened Box Flanges

In rare cases where an exceptionally wide box flange is needed and the number of longitudinal flange stiffeners *n* may need to exceed 2, the use of transverse flange stiffeners should be considered to reduce the required size of the longitudinal flange stiffeners to a more practical value. The required size of the longitudinal stiffeners is based on an infinite length of panel. This assumption becomes significantly conservative when more than two longitudinal stiffeners are used. Also, for cases where *n* is equal to 2 and a plate-buckling coefficient *k* greater than about 2.5 is required, the use of transverse flange stiffeners can help to reduce the size of the longitudinal flange stiffeners over that required by Equation 3.2.124.

The use of transverse stiffeners reduces the length of the panel from infinity to the spacing of the transverse stiffeners. Equations for the design of transversely and longitudinally stiffened box flanges at the strength limit state are provided in *AASHTO LRFD* Article C6.11.11.2 and are reviewed below. These equations are based on classical plate-buckling equations (*11*).

As indicated in *AASHTO LRFD* Article C6.11.11.2, for the exceptional case where transverse flange stiffeners are deemed necessary, the plate-buckling coefficient *k* for uniform normal stress to be used in determining the nominal compressive resistance of the flange (from Equation 3.2.112, 3.2.113 or 3.2.114, as applicable) at the strength limit state may be taken as follows:

$$k = \frac{\left[1+\left(a/b_{fc}\right)^2\right]^2 + 87.3}{(n+1)^2\left(a/b_{fc}\right)^2\left[1+0.1(n+1)\right]} \le 4.0$$

Equation 3.2.126
AASHTO LRFD Equation C6.11.11.2-3

where:

a = longitudinal spacing of the transverse flange stiffeners (in.) $\le 3b_{fc}$

Further, in determining the required moment of inertia of the longitudinal flange stiffeners I_ℓ from Equation 3.2.124 when transverse stiffeners are present, the constant ψ is to be taken as 8.0. The number of longitudinal flange stiffeners *n* preferably should not exceed 5 when transverse flange stiffeners are provided. When *n* does not exceed 5, transverse flange stiffeners spaced at a distance not exceeding 4*w* (see the preceding sections for the definition of *w*) will provide a *k* of approximately 4.0 according to Equation 3.2.126.

When the *k* value from Equation 3.2.126 is used to determine the nominal flexural resistance of the flange, the moment of inertia, I_t, of each transverse flange stiffener *about an axis through its centroid* and parallel to its bottom edge must satisfy the following:

$$I_t \geq 0.05(n+1)^3 w^3 \frac{f_s}{E} \frac{A_f}{a}$$

Equation 3.2.127
AASHTO LRFD Equation C6.11.11.2-4

where:

A_f = area of the box flange including the longitudinal flange stiffeners (in.^{2})
f_s = largest of the longitudinal flange stresses due to the factored loads in the panels on either side of the transverse flange stiffener under consideration (ksi)

In addition, the specified minimum yield strength of the transverse flange stiffeners should not be less than the specified minimum yield strength of the box flange according to *AASHTO LRFD* Article C6.11.11.2.

Transverse flange stiffeners can take one of two forms; either individual tees can serve as transverse flange stiffeners, or a bottom strut provided within the internal cross-bracing of the box satisfying the requirements of *AASHTO LRFD* Article 6.7.4.3 can serve as a transverse flange stiffener if the strut also satisfies the stiffness requirement given by Equation 3.2.127. Regardless of which form is used, the transverse flange stiffeners should be attached to the longitudinal flange stiffeners by bolting, with the connection to each longitudinal flange stiffener designed to resist the following vertical force, F_s, at the strength limit state:

$$F_s = \frac{\phi_f F_{ys} S_s}{n b_{fc}}$$

Equation 3.2.128
AASHTO LRFD Equation C6.11.11.2-1

where:

F_{ys} = specified minimum yield strength of the transverse flange stiffener (ksi)
S_s = section modulus of the transverse flange stiffener (ksi)

Individual tees serving as transverse flange stiffeners should also be attached to the webs of the box section. As indicated in *AASHTO LRFD* Article C6.11.11.2, the connection of the transverse flange stiffeners to each web should be designed to resist the following vertical force, F_w, at the strength limit state:

$$F_w = \frac{\phi_f F_{ys} S_s}{2b_{fc}}$$

Equation 3.2.129
AASHTO LRFD Equation C6.11.11.2-2

Should a bottom strut be provided within the internal cross-bracing of the box to control distortion of the box flange and reduce the transverse bending stress ranges in the flange for fatigue, as discussed previously in Section 3.2.5.2.2.3, the bottom strut and its connections need *not* satisfy the requirements of Equations 3.2.127, 3.2.128 and 3.2.129, *unless* the strut is also intended to serve as a transverse flange stiffener at the strength limit state and the *k* value from Equation 3.2.126 is utilized in the design of the box flange.

3.2.6.4.2.3 Continuously Braced Tension Flanges

AASHTO LRFD Article 6.11.8.1.2 specifies that for box sections subject to negative flexure, continuously braced flanges in tension (i.e. top flanges) must satisfy the following requirement at the strength limit state:

$$f_{bu} \le \phi_f F_{nt}$$

Equation 3.2.130
AASHTO LRFD Equation 6.11.8.1.2-1

where:

F_{nt} = nominal flexural resistance of the flange in tension determined as specified in *AASHTO LRFD* Article 6.11.8.3 (discussed below) (ksi)

A continuously braced flange is defined as a flange encased in concrete or anchored by shear connectors. Lateral flange bending stresses and St. Venant torsional shears need not be considered for continuously braced top flanges of tub sections. The torsional shear must be considered in the continuously braced top flange of a closed-box section however.

Nominal Flexural Resistance of the Tension Flange(s), F_{nt}

For sections in negative flexure, the nominal flexural resistance of the (top) tension flange(s) is controlled by yielding. According to *AASHTO LRFD* Article 6.11.8.3, the nominal flexural resistance of the tension flanges of tub sections, F_{nt}, is to be taken as:

$$F_{nt} = R_h F_{yt}$$

Equation 3.2.131
AASHTO LRFD Equation 6.11.8.3-1

where:

R_h = hybrid factor determined as specified in *AASHTO LRFD* Article 6.10.1.10.1 (Section 3.2.6.3)

The nominal flexural resistance of the (top) tension flange of closed-box sections, F_{nt}, is to be taken as:

$$F_{nt} = R_h F_{yt} \Delta$$

Equation 3.2.132
AASHTO LRFD Equation 6.11.7.2.2-5

where:

$$\Delta = \sqrt{1 - 3\left(\frac{f_v}{F_{yt}}\right)^2}$$

Equation 3.2.133
AASHTO LRFD Equation 6.11.7.2.2-6

f_v = factored St. Venant torsional shear stress in the flange at the section under consideration not to exceed the factored torsional shear resistance of the flange, F_{vr}, given by Equation 3.2.71 (ksi)

$$= \frac{T}{2A_o t_{ft}}$$

` Equation 3.2.134
AASHTO LRFD Equation 6.11.7.2.2-7

A_o = enclosed area within the box section (in.^{2})
t_{ft} = thickness of the tension flange (in.)
T = internal torque due to the factored loads (kip-in.)

3.2.6.5 Sections in Positive Flexure

3.2.6.5.1 General

In the *AASHTO LRFD* Specifications, the nominal flexural resistance of composite sections *in straight girders* subject to positive flexure that satisfy specific steel grade, web slenderness and ductility requirements is permitted to exceed the moment at first yield at the strength limit state. Sections meeting these requirements are termed *compact sections*. The nominal flexural resistance of sections not meeting one or more of these requirements, termed *noncompact sections*, is not permitted to exceed the moment at first yield. For compact sections, the nominal flexural resistance is most appropriately expressed in terms of moment and for noncompact sections, the nominal flexural resistance is most appropriately expressed in terms of the elastically computed flange stress (for reasons discussed previously in Section 3.2.6.4.1.1).

According to AASHTO LRFD Articles 6.10.6.2.2 and 6.11.6.2.2, composite I- and box sections in positive flexure in kinked (chorded) continuous or

horizontally curved steel girder bridges are always to be considered as noncompact sections at the strength limit state. Research has not yet been conducted to support the design of these sections as compact sections with flexural resistances exceeding the moment at first yield. *Although the specification is currently silent on the issue, composite sections in positive flexure in straight-girder bridges whose supports are skewed more than 20° from normal should also be treated as noncompact sections for similar reasons.* For sections that do qualify and/or are considered to be compact sections, consideration could always be given to treating the section as a noncompact section, which simplifies the calculations somewhat and should not result in a significant loss of economy as other limit-state criteria (e.g. service limit state or fatigue limit state criteria) are likely to control the design of the section.

As such, the following discussions will focus on the design provisions for noncompact composite sections in positive flexure. Further discussion on the design provisions for compact composite sections in positive flexure may be found in References 6 and 55.

The nominal flexural resistance of the top (compression) flange is limited to the specified minimum yield strength of the flange times the flange-stress reduction factors R_b and R_h for noncompact composite sections in positive flexure. The nominal flexural resistance of the bottom (tension) flange is limited to the specified minimum yield strength of the flange times R_h.

Noncompact sections must also satisfy a ductility requirement to prevent premature crushing of the concrete deck prior to reaching the specified nominal flexural resistance. The maximum longitudinal compressive stress in the concrete deck at the strength limit state is also limited to $0.6f'_c$ to ensure linear behavior of the concrete, which is assumed in the calculation of the steel flange stresses. These concrete deck requirements are discussed further in Section 3.2.6.5.4.

Top (compression) flanges of composite sections in positive flexure are continuously braced flanges. For a continuously braced compression flange, one side of the flange is effectively prevented from local buckling, or else both sides of the flange must buckle in the direction away from the concrete deck, resulting in highly restrained boundary conditions at the web-flange juncture. The concrete deck also helps restrain lateral deflections of the flange associated with local and lateral-torsional buckling. As a result, continuously braced compression flanges need not be checked for local or lateral-torsional buckling according to the *AASHTO LRFD* Specifications. Lateral flange bending stresses also need not be considered for continuously braced flanges, including any lateral flange bending stresses induced in the non-composite flange before it becomes continuously braced. The lateral resistance of the composite concrete deck is generally sufficient to compensate for the neglect of any initial lateral bending stresses in the flange, as well as any additional lateral bending stresses that may be induced after the deck has been placed.

3.2.6.5.2 I-Sections

The nominal flexural resistance of noncompact composite I-sections in positive flexure is specified in *AASHTO LRFD* Article 6.10.7.2.

3.2.6.5.2.1 Continuously Braced Compression Flanges

AASHTO LRFD Article 6.10.7.2.1 specifies that at the strength limit state, the (top) compression flange of noncompact composite I-sections in positive flexure must satisfy the following:

$$f_{bu} \le \phi_f F_{nc}$$

Equation 3.2.135
AASHTO LRFD Equation 6.10.7.2.1-1

where:

f_{bu} = factored flange vertical bending stress at the section under consideration (ksi).
F_{nc} = nominal flexural resistance of the compression flange determined as specified in *AASHTO LRFD* Article 6.10.7.2.2 (discussed below) (ksi)

Again, flange lateral bending is not considered for the compression flange in Equation 3.2.135 because at the strength limit state, the flange is continuously supported by the concrete deck.

Nominal Flexural Resistance of the Compression Flange, F_{nc}

AASHTO LRFD Article 6.10.7.2.2 specifies that the nominal flexural resistance of the compression flange, F_{nc}, of a noncompact composite I-section in positive flexure is to be taken as:

$$F_{nc} = R_b R_h F_{yc}$$

Equation 3.2.136
AASHTO LRFD Equation 6.10.7.2.2-1

where:

R_b = web load-shedding factor determined as specified in *AASHTO LRFD* Article 6.10.1.10.2 (Section 3.2.6.2)
R_h = hybrid factor determined as specified in *AASHTO LRFD* Article6.10.1.10.1 (Section 3.2.6.3)

Local and lateral buckling of the top flanges is not a concern because the flanges are continuously braced; therefore, the nominal flexural resistance is based on nominal yielding.

Note that for composite sections in positive flexure with $D/t_w \leq 150$ (i.e. no longitudinal web stiffeners), R_b is to be taken equal to 1.0 because web bend buckling and subsequent load shedding are unlikely for these sections at the strength limit state.

3.2.6.5.2.2 Discretely Braced Tension Flanges

The (bottom) tension flange of noncompact composite I-sections in positive flexure must satisfy the one-third rule equation expressed in terms of stress (Section 3.2.2.1.1) as follows:

$$f_{bu} + \frac{1}{3} f_{\ell} \leq \phi_f F_{nt}$$

Equation 3.2.137
AASHTO LRFD Equation 6.10.7.2.1-2

where:

f_{ℓ} = factored flange lateral bending stress at the section under consideration (ksi)
F_{nt} = nominal flexural resistance of the tension flange determined as specified in *AASHTO LRFD* Article 6.10.7.2.2 (discussed below) (ksi)

The stress format is more appropriate in members for which the maximum resistance is always less than or equal to the yield moment in vertical bending.

Since the bottom (tension) flange is not continuously supported, lateral bending must be considered in flexural resistance computations for the tension flange. Possible sources of lateral bending in the bottom flange of these sections at the strength limit state include curvature, wind loading and the effect of staggered cross-frames/diaphragms and/or support skew. *AASHTO LRFD* Article 6.10.1.6 specifies that the sum of the flange lateral bending stresses due to all sources cannot exceed $0.6F_{yf}$. Amplification of the flange lateral bending stresses is not required in this case since the bottom flange is in tension.

Nominal Flexural Resistance of the Tension Flange, F_{nt}

AASHTO LRFD Article 6.10.7.2.2 specifies that the nominal flexural resistance of the tension flange, F_{nt}, is to be taken as:

$$F_{nt} = R_h F_{yt}$$

Equation 3.2.138
AASHTO LRFD Equation 6.10.7.2.2-2

Load shedding of the web compressive stresses to the tension flange as a result of bend buckling of the web is considered insignificant; therefore, the R_b factor is not included in Equation 3.2.138.

3.2.6.5.3 Box Sections

The nominal flexural resistance of noncompact composite box sections in positive flexure is specified in *AASHTO LRFD* Article 6.11.7.2. Longitudinal warping stresses are typically ignored at the strength limit state, as permitted in *AASHTO LRFD* Article 6.11.1.1. St. Venant torsion and cross-section distortion stresses must be considered, however, for noncompact sections.

3.2.6.5.3.1 Continuously Braced Compression Flange(s)

AASHTO LRFD Article 6.11.7.2.1 specifies that at the strength limit state, the (top) compression flange(s) of noncompact composite box sections in positive flexure must satisfy the following:

$$f_{bu} \le \phi_f F_{nc}$$

Equation 3.2.139
AASHTO LRFD Equation 6.10.7.2.1-1

where:

f_{bu} = factored longitudinal flange vertical bending stress at the section under consideration calculated without consideration of longitudinal warping (ksi).

F_{nc} = nominal flexural resistance of the compression flange determined as specified in *AASHTO LRFD* Article 6.11.7.2.2 (discussed below) (ksi)

Again, flange lateral bending is not considered for the compression flange(s) in Equation 3.2.139 because at the strength limit state, the flange is continuously supported by the concrete deck.

Nominal Flexural Resistance of the Compression Flange(s), F_{nc}

AASHTO LRFD Article 6.11.7.2.2 specifies that the nominal flexural resistance of the compression flanges, F_{nc}, of a noncompact composite tub section in positive flexure is to be taken as:

$$F_{nc} = R_b R_h F_{yc}$$

Equation 3.2.140
AASHTO LRFD Equation 6.10.7.2.2-1

where:

R_b = web load-shedding factor determined as specified in *AASHTO LRFD* Article 6.10.1.10.2 (Section 3.2.6.2)

R_h = hybrid factor determined as specified in *AASHTO LRFD* Article6.10.1.10.1 (Section 3.2.6.3)

Local and lateral buckling of the top flanges is not a concern because the flanges are continuously braced; therefore, the nominal flexural resistance is based on nominal yielding. St. Venant torsional shears are also typically neglected in tub girder top flanges.

The nominal flexural resistance of the compression flange of noncompact composite closed-box sections in positive flexure, F_{nc}, is to be taken as:

$$F_{nc} = R_b R_h F_{yc} \Delta$$

Equation 3.2.141
AASHTO LRFD Equation 6.11.7.2.2-2

where:

$$\Delta = \sqrt{1 - 3\left(\frac{f_v}{F_{yc}}\right)^2}$$

Equation 3.2.142
AASHTO LRFD Equation 6.11.7.2.2-3

f_v = factored St. Venant torsional shear stress in the flange at the section under consideration not to exceed the factored torsional shear resistance of the flange, F_{vr}, given by Equation 3.2.71 (ksi)

$$= \frac{T}{2A_o t_{fc}}$$

Equation 3.2.143
AASHTO LRFD Equation 6.11.7.2.2-4

A_o = enclosed area within the box section (in.^{2})
t_{fc} = thickness of the compression flange (in.)
T = internal torque due to the factored loads (kip-in.)

Local buckling of the top box flange is not a concern because the flange is continuously braced at the strength limit state; therefore, the nominal flexural resistance is based on nominal yielding.

Note that in both of the above cases, for composite sections in positive flexure with $D/t_w \le 150$ (i.e. no longitudinal web stiffeners), R_b is to be taken equal to 1.0 because web bend buckling and subsequent load shedding are unlikely for these sections at the strength limit state.

3.2.6.5.3.2 Box Flanges in Tension

AASHTO LRFD Article 6.11.7.2.1 specifies that at the strength limit state, the (bottom) tension flange of noncompact composite box sections in positive flexure must satisfy the following:

$$f_{bu} \le \phi_f F_{nt}$$

Equation 3.2.144
AASHTO LRFD Equation 6.11.7.2.1-2

where:

F_{nt} = nominal flexural resistance of the tension flange determined as specified in *AASHTO LRFD* Article 6.11.7.2.2 (discussed below) (ksi)

The stress format is more appropriate in members for which the maximum resistance is always less than or equal to the yield moment in vertical bending. Lateral bending is not a consideration for the tension flange in Equation 3.2.144 because the tension flange is always a box flange in this case (and lateral bending is not a consideration for box flanges).

Nominal Flexural Resistance of the Tension Flange, F_{nt}

AASHTO LRFD Article 6.11.7.2.2 specifies that the nominal flexural resistance of the tension flange of noncompact composite closed-box and tub sections in positive flexure, F_{nt}, based on nominal yielding is to be taken as:

$$F_{nt} = R_h F_{yt} \Delta$$

Equation 3.2.145
AASHTO LRFD Equation 6.11.7.2.2-5

where:

$$\Delta = \sqrt{1 - 3\left(\frac{f_v}{F_{yt}}\right)^2}$$

Equation 3.2.146
AASHTO LRFD Equation 6.11.7.2.2-6

f_v = factored St. Venant torsional shear stress in the flange at the section under consideration not to exceed the factored torsional shear resistance of the flange, F_{vr}, given by Equation 3.2.71 (ksi)

$$= \frac{T}{2A_o t_{ft}}$$

Equation 3.2.147
AASHTO LRFD Equation 6.11.7.2.2-7

t_{ft} = thickness of the tension flange (in.)

Load shedding of the web compressive stresses to the tension flange as a result of bend buckling of the web is considered insignificant; therefore, the R_b factor is not included in Equation 3.2.145.

3.2.6.5.4 Concrete Deck Requirements

Additional requirements related to the concrete deck to be checked for composite sections in positive flexure at the strength limit state are discussed in the following.

3.2.6.5.4.1 Longitudinal Compressive Deck Stress

According to *AASHTO LRFD* Articles 6.10.7.2.1 (for I-sections) and 6.11.7.2.1 (for box sections), the maximum factored longitudinal compressive stress in the deck at noncompact composite sections in positive flexure at the strength limit state, f_c, is limited as follows:

$$f_c \le 0.6f'_c$$

Equation 3.2.148

This limit is intended to ensure linear behavior of the concrete, which is assumed in the calculation of the steel flange stresses.

As pointed out in *AASHTO LRFD* Articles C6.10.7.2.1 and C6.11.7.2.1, this check is unlikely to control except in cases involving: 1) shored construction, or unshored construction where the non-composite steel dead load stresses are low, combined with 2) geometries causing the neutral axis of the short-term and long-term composite section to be significantly below the bottom of the concrete deck. Equation 3.2.148 ensures that noncompact composite I-sections in positive bending with a relatively large F_{yt}/f'_c or F_{yc}/f'_c and a relatively small concrete deck, resulting in a location of the neutral axis well below the concrete deck, will not be permitted. In such rare cases, Equation 3.2.148 may be satisfied by increasing the concrete f'_c, the slab thickness, the size of the steel top flange, and/or the girder spacing.

3.2.6.5.4.2 Ductility Requirement

According to *AASHTO LRFD* Articles 6.10.6.2.2 (for I-sections) and 6.11.7.2.2 (for box sections), noncompact composite sections in positive flexure must also satisfy the following ductility requirement specified in *AASHTO LRFD* Article 6.10.7.3:

$$D_p \le 0.42D_t$$

Equation 3.2.149
AASHTO LRFD Equation 6.10.7.3-1

where:

D_p = distance from the top of the concrete deck to the neutral axis of the composite section at the plastic moment (in.)
D_t = total depth of the composite section (in.)

This requirement is intended to prevent premature crushing of the concrete deck prior to reaching the specified nominal flexural resistance. Satisfying this requirement also helps permit the web bend buckling check to be neglected for

composite sections in positive flexure without longitudinal stiffeners after the deck hardens.

Although noncompact sections in positive flexure are not permitted to exceed the moment at first yield, the ductility requirement shown in Equation 3.2. must still be satisfied to ensure a ductile failure, and to prevent premature crushing of the deck for sections that may utilize up to 100-ksi steel and/or that are utilized in shored construction. The D_p/D_t ratio is limited to 0.42 to ensure significant yielding of the bottom flange when the crushing strain is reached at the top of the concrete deck. D_t should be computed using a lower-bound estimate of the deck and haunch thickness, or be determined conservatively by neglecting the thickness of the haunch.

3.2.6.6 Regions of Stress Reversal

Girder regions of stress reversal are typically located near points of permanent load contraflexure in continuous spans. These regions can extend over much of the span in some cases depending on the span ratio.

Careful attention must be paid to the design of welded details for load-induced fatigue in these regions since fatigue stress ranges are often significant in these regions. In particular, as discussed previously in Sections 3.2.4.3.2.2 and 3.2.6.4.2.2, special attention must be paid to the termination of welded longitudinal web and flange stiffeners in these regions. Welded cross-frame/diaphragm connection plates (Category C′) located in these regions may also be critical for fatigue. In such cases, the location of the connection plate along the girder may need to be adjusted slightly to satisfy the fatigue limit state requirements.

Shear connectors should not be discontinued in these regions for reasons discussed further in Section 3.3.2.1.1.4.

The girder should be checked in these regions at the strength limit state for the dead load plus positive live load condition and the dead load plus negative live load condition. The signs of the individual dead and live load stresses must be considered when summing to obtain the total factored vertical and lateral bending stresses for each condition,. When the sign of a particular dead load stress is opposite in sign to the live load stress when factoring and combining the stresses, the dead load stress should be unloaded by applying the appropriate *minimum* load factor, γ_p, specified in *AASHTO LRFD* Table 3.4.1-2, in combination with a factor equal to $1/\eta \leq 1.0$ (*AASHTO LRFD* Equation 1.3.2.1-3) applied to that stress.

Different section properties are used for computing composite section stresses at the strength limit state in these regions due to positive and negative moments. *AASHTO LRFD* Article 6.10.1.1.1b specifies that the associated composite section properties may be used to compute the factored vertical bending stresses at the strength limit state due to live and permanent loads if the resulting net unfactored stress in the

concrete deck is compressive. When the net unfactored stress in the concrete deck is tensile, the factored vertical bending stresses must be computed ignoring the concrete deck according to *AASHTO LRFD* Article 6.10.1.1.1c. For example, if the unfactored live load compressive stress in the deck overcomes the unfactored tensile stress in the deck due to the DC_2 and *DW* loads, the factored DC_2 and *DW* stresses in the girder at that location may be computed using the long-term composite (3*n*) section. Conversely, if the unfactored live load tensile stress in the deck overcomes the unfactored compressive stress in the deck due to the DC_2 and *DW* loads, the factored DC_2 and *DW* stresses in the girder at that location are to be computed using only the steel section plus the longitudinal reinforcement within the effective width of the deck.

Bottom flanges slightly beyond the point of dead load contraflexure are subjected to a net factored compressive stress. Flanges in these regions must be checked to ensure they have adequate local and/or lateral torsional buckling resistance; unstiffened box flanges are often found problematic.

Bolted girder splices are often located around points of dead load contraflexure. Flanges subject to a net tensile stress at bolted splices must be checked for net section fracture (refer to Section 3.2.6.1.3). The number of bolt holes in a row can be decreased along with a concomitant lengthening of the splice to gain relief.

3.2.7 LRFD Strength Limit State Design for Shear

3.2.7.1 General

The algebraic sum of the applied loads and reactions on either side of the transverse cross-section of a girder is the shear force, *V*, at that section. Shear can only occur in the presence of bending, but is usually considered independent of bending in design practice (note that this discussion only deals with shear due to bending and not shear caused by torsion, which is discussed in Section 1.1.3). *V* is resisted by internal shear stresses that are maximum on horizontal and vertical planes passing through the neutral axis of the section. The elastic flexural shear stress, f_v, is given by the following fundamental equation:

$$f_v = \frac{VQ}{It}$$

Equation 3.2.150

where:

- I = moment of inertia of the section about the strong axis (in.^{4})
- Q = first statical moment of the cross-sectional area above the point where the shear stress is calculated taken about the neutral axis of the cross-section (in.^{3})
- t = thickness of the girder where the shear stress is calculated (in.)

The distribution of elastic flexural shear stresses through the depth of an I-section is shown in Figure 3.2.56. The distribution of these stresses in a closed box section

was shown previously in Figure 1.1.21 Part D. Note that in both cases the shear stress in the flanges is generally small and is typically ignored (unless perhaps if the thickness of a box flange is equal to or only larger than the thickness of the web, it may be prudent to consider the flexural shear flow in the design of the box flange). The variation in the shear stress in the web is also small so the shear stress in the web may be approximated as an average shear stress equal to the shear force divided by the web area or V/Dt_w. Shear forces resisted in this manner are typically referred to as shears carried by beam action.

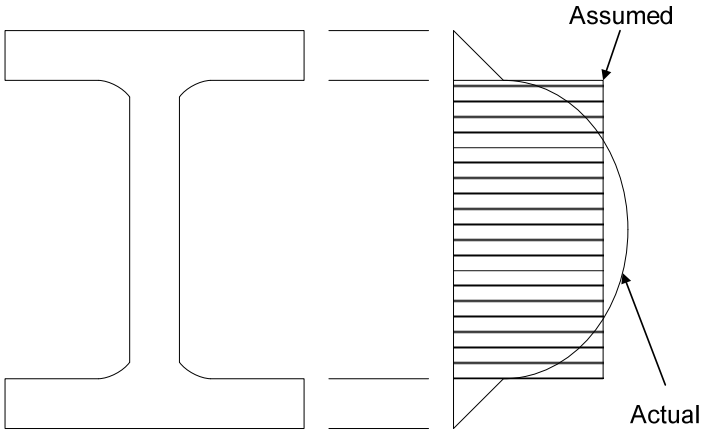


Figure 3.2.56 Distribution of Elastic Flexural Shear Stresses (I-Section)

The shear force causing yielding in shear is known as the plastic shear force, V_p. The shear yield stress, τ_y, is taken equal to $F_{yw}/\sqrt{3}$. Therefore, V_p is calculated as follows:

$$V_p = \frac{F_{yw}}{\sqrt{3}} D t_w = 0.58 F_{yw} D t_w$$

Equation 3.2.151
AASHTO LRFD Equation 6.10.9.2-2

Deflections due to shear are typically much smaller than bending deflections and usually do not need to be considered, except for beams with large depth-to-length ratios.

The vertical shear force in composite girders is assumed resisted by the web of the steel girder. The horizontal shear force per unit length, VQ/I, where I is the moment of inertia of the transformed composite section, that develops during bending of the girder (sometimes referred to as shear flow) must be transferred between the deck and girder by shear connectors to prevent slip along the concrete/steel interface. This facilitates composite action between the girder and the deck. The design of

shear connectors for this horizontal shear flow is discussed in Section 3.3.2. Flange-to-web welds are also typically designed for the horizontal shear flow.

Webs must satisfy the following relationship at the strength limit state:

$$V_u \leq \phi_v V_n$$

Equation 3.2.152
AASHTO LRFD Equation 6.10.9.1-1

where:

V_n = nominal shear resistance (kips)
V_u = factored shear in the web at the section under consideration (kips)

The resistance factor for shear, ϕ_v, is to be taken as 1.0, as specified in *AASHTO LRFD* Article 6.5.4.2.

The nominal shear resistance, V_n, depends on if the web is considered stiffened or unstiffened. The maximum transverse stiffener spacing requirements that determine whether or not a web is considered stiffened or unstiffened are a function of the web depth, *D*. *AASHTO LRFD* Article 6.10.9.1 specifies that interior web panels of non-hybrid (homogeneous) and hybrid members: 1) without a longitudinal stiffener and with a transverse stiffener spacing not exceeding 3*D*, or 2) with one or more longitudinal stiffeners and with a transverse stiffener spacing not exceeding 1.5*D* are considered stiffened (Figure 3.2.57 Part A). Otherwise, the panel is considered unstiffened. Stiffened web panels are able to develop post-buckling shear resistance (Section 3.2.7.3). The shear resistance of unstiffened webs is limited to the shear-yield or shear buckling resistance, V_{cr} (Section 3.2.7.2). The spacing of transverse stiffeners for end panels of stiffened webs, with or without a longitudinal stiffener must not exceed 1.5*D* (Figure 3.2.57 Part B). The shear resistance of end panels is limited to V_{cr}.

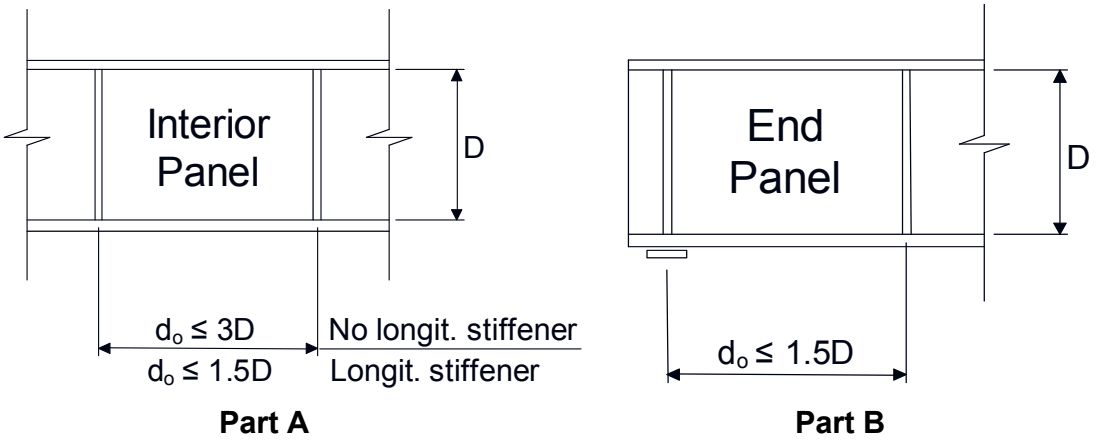


Figure 3.2.57 Maximum Transverse Stiffener Spacing Requirements
A) Interior Panel with or without Longitudinal Web Stiffeners; B) End Panel

Since longitudinal stiffeners divide a web panel into subpanels, the shear resistance of the entire panel could potentially be taken as the sum of the shear resistances of the subpanels. Although a longitudinal stiffener located at its optimum position on the web for flexure also increases the buckling resistance of the web in shear, the increase is relatively small compared to the increase in the bend-buckling resistance resulting from the longitudinal stiffener(s). Therefore, the specifications conservatively neglect the influence of the longitudinal stiffener in computing the nominal shear resistance of the web; that is, the total web depth *D* is used in computing the shear resistance.

A flowchart for shear design is given in *AASHTO LRFD* Figure C6.10.9.1-1. This flowchart applies for both hybrid and non-hybrid I- and box girders, and to both straight and horizontally curved girders. In the *AASHTO LRFD* Specifications, shear design is identical for both straight and horizontally curved girders.

3.2.7.1.1 I-Sections

Shear design provisions for I-section flexural members at the strength limit state are covered in *AASHTO LRFD* Article 6.10.9. The application of these design verifications is illustrated in the I-girder design example presented in Section 5.1.

The design of transverse web stiffeners for I-sections is covered in *AASHTO LRFD* Article 6.10.11.1 and discussed in Section 3.3.8.1.

3.2.7.1.2 Box Sections

Shear design provisions for box-section flexural members at the strength limit state are covered in *AASHTO LRFD* Article 6.11.9. For determining the factored shear resistance of a single web of a box section, *AASHTO LRFD* Article 6.11.9 essentially

refers back to the provisions of *AASHTO LRFD* Article 6.10.9 for I-sections (with a few exceptions as discussed further in the following). The application of these design verifications is illustrated in the tub-girder design example presented in Section 5.2.

For box sections with inclined webs, the web must be designed for the component of the vertical shear in the plane of the web according to *AASHTO LRFD* Article 6.11.9. That is, each web must be designed for a factored shear, V_{ui}, taken as follows:

$$V_{ui} = \frac{V_u}{\cos \theta}$$

Equation 3.2.153
AASHTO LRFD Equation 6.11.9-1

where:

V_u = vertical shear due to the factored loads on one inclined web (kips)
θ = angle of inclination of the web plate to the vertical (degrees)

Box-section webs are usually detailed to be of equal height. However, if the deck is superelevated, the box is typically rotated to match the deck slope, which simplifies fabrication by maintaining symmetry of the box sections. However, rotating the box increases the inclination angle of the web over what it would have been if the box were not rotated. In such cases, consideration should be given to adjusting the vertical shear in that web accordingly.

Also, according to *AASHTO LRFD* Article 6.11.9, for all box sections in bridges outside the special restrictions discussed in *AASHTO LRFD* Article 6.11.2.3 (which includes all box sections in skewed and/or curved bridges), V_u is to be taken as the sum of the flexural and St. Venant torsional shears. Proper determination of this value considers coincident flexure and torsion. Conservatively, critical torsion and critical flexural shears can be added. In these cases, the dead and live load shears in one web are greater than in the other web at the same cross-section since the torsional shear is of opposite sign in the two webs. For practical reasons, however, both webs are usually detailed for the critical shear. Shears in the web due to warping torsion and due to cross-section distortion may be ignored in all cases, as indicated in *AASHTO LRFD* Article C6.11.9.

In computing the nominal shear resistance, V_n, and the maximum transverse stiffener spacing requirements for the case of inclined webs, the web depth, D, must be taken as the depth of the web measured along the slope or $D/\cos\theta$.

AASHTO LRFD Article 6.11.9 specifies that for box flanges, b_{fc} or b_{ft} in Equation 3.2.164 (refer to Section 3.2.7.3), as applicable, is to be taken as one-half the effective flange width between webs, but not to exceed $18t_f$, where t_f is the thickness of the box flange. The effective flange width is determined as specified in *AASHTO LRFD* Article 6.11.1.1 (refer to Section 3.1.5.4.2.1).

The design of transverse web stiffeners for box sections is covered in *AASHTO LRFD* Article 6.10.11.1 and discussed in Section 3.3.8.1.

3.2.7.2 Shear-Buckling (or Shear-Yield) Resistance, V_{cr}

Consider a theoretically flat web panel hypothetically subjected to pure shear, as shown in Figure 3.2.58 Part A. The length of the panel between transverse stiffeners is d_o, and the clear height of the panel between flanges is D. As shown in Figure 3.2.58 Part B and 3.2.58 Part C, an element in pure shear is equivalent to an element rotated 45 degrees and acted upon by a principal tensile stress and an equal principal compressive stress acting in the perpendicular direction.

Assume then that the web will buckle in shear perpendicular to the direction of the principal compressive stress. The panel, if properly supported around the edges, does not fail at this point unless the stress is well above the proportional limit. The buckled plate is able to support the diagonal compression through beam shear since unrestrained out-of-plane deflection of the panel is prevented by the diagonal tension. For web panels with significant post-buckling resistance (discussed in Section 3.2.7.3), it is assumed that the diagonal compression retains the value of beam shear resistance it had when the plate buckled all the way up to complete failure.

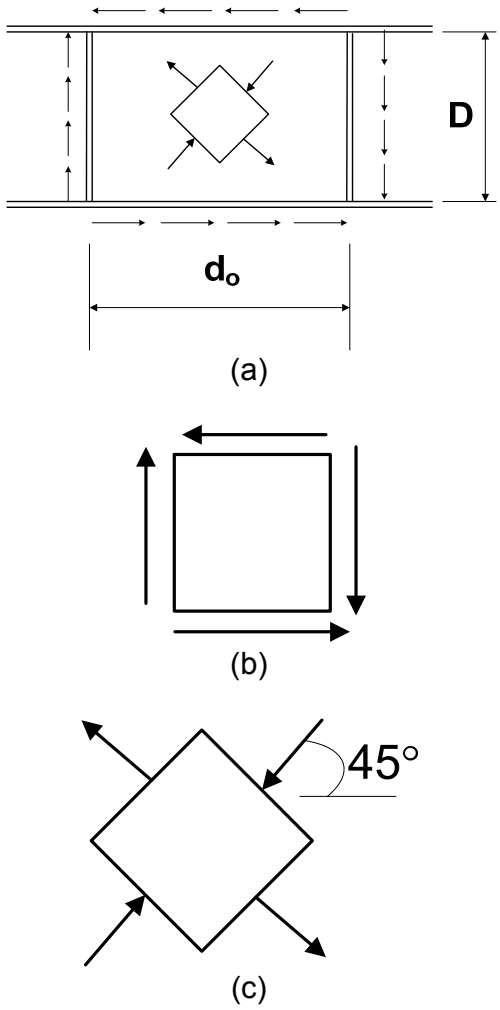


Figure 3.2.58 (a) Web Panel Subjected to Pure Shear, (b) Web Element Subject to Pure Shear, (c) Equivalent Principal Stresses

The elastic buckling stress of a flat plate subject to pure shear is given as follows (*11*):

$$\tau_{cr} = \frac{k\pi^2 E}{12\left(1-\mu^2\right)\left(D/t_w\right)^2}$$

Equation 3.2.154

Assuming simply supported boundary conditions along the edges, which is the typical assumption used in design practice, the shear buckling coefficient *k* is given as (*11*):

$$\text{For } \frac{d_o}{D} \le 1: \qquad k = 4.0 + \frac{5.34}{\left(\frac{d_o}{D}\right)^2}$$

Equation 3.2.155

$$\text{For } \frac{d_o}{D} > 1: \qquad k = \frac{4.0}{\left(\frac{d_o}{D}\right)^2} + 5.34$$

Equation 3.2.156

Equations 3.2.155 and 3.2.156 have been consolidated into a single simplified expression for *k* in the *AASHTO LRFD* Specifications, which is independent of the panel aspect ratio, as follows:

$$k = 5 + \frac{5}{\left(\frac{d_o}{D}\right)^2}$$

Equation 3.2.157
AASHTO LRFD Equation 6.10.9.3.2-7

It can be seen from the preceding equation that decreasing the transverse stiffener spacing increases the value of *k*. This, in turn, also increases V_{cr}. *For an unstiffened web, k is taken equal to 5.0*, which is a conservative approximation of the exact value of *k* = 5.34 for an infinitely long strip with simply supported edges (*11*).

For design, Equation 3.2.154 is expressed in non-dimensional form by introducing the constant *C*, which is defined as the ratio of the shear buckling stress, τ_{cr}, to the shear yield stress, τ_y. Therefore, substituting $\nu = 0.3$ in Equation 3.2.154:

$$C = \frac{\tau_{cr}}{\tau_y} = \frac{k\pi^2 E\sqrt{3}}{F_{yw}(12)(1-0.91)(D/t_w)^2} = \frac{1.57}{\left(\frac{D}{t_w}\right)^2}\left(\frac{Ek}{F_{yw}}\right)$$

Equation 3.2.158
AASHTO LRFD Equation 6.10.9.3.2-6

which is given as *AASHTO LRFD* Equation 6.10.9.3.2-6.

As is the case for lateral-torsional buckling and flange local buckling, residual stresses and geometric imperfections can cause inelastic buckling in shear as the critical stress approaches the yield stress. A transition curve for inelastic buckling

was developed by Basler (*79*) based on the assumption that $\tau_{cr} = \sqrt{0.8\tau_y \tau_{cr}}$. That is, it was assumed that the proportional limit for shear is $0.8\tau_y$, which is higher than for flanges in compression because the effect of residual stresses is less for shear. Therefore, dividing τ_{cr} under the preceding radical by τ_y to obtain *C*, and substituting the value of *C* from Equation 3.2.158 gives:

$$C = \sqrt{0.8C} = \sqrt{0.8\frac{1.57}{\left(\frac{D}{t_w}\right)^2}\left(\frac{Ek}{F_{yw}}\right)} = \frac{1.12}{\frac{D}{t_w}}\sqrt{\frac{Ek}{F_{yw}}}$$

Equation 3.2.159
AASHTO LRFD Equation 6.10.9.3.2-5

which is given as *AASHTO LRFD* Equation 6.10.9.3.2-5. When *C* exceeds 0.8, *C* is taken from Equation 3.2.159. Therefore, substituting a *C* value of 0.8 in Equation 3.2.158 and solving for D/t_w gives $D/t_w = 1.40\sqrt{Ek/F_{yw}}$ above which *C* is calculated from Equation 3.2.159 and at or below which *C* is calculated from Equation 3.2.158.

When *C* is equal to 1.0, the shear resistance is equal to the shear yield stress. Therefore, substituting a *C* value of 1.0 into Equation 3.2.159 and solving for D/t_w gives $D/t_w = 1.12\sqrt{Ek/F_{yw}}$ below which *C* is taken equal to 1.0 and shear yielding controls.

The relationship between the buckling strength in shear and the web slenderness ratio, D/t_w, based on the preceding equations for the constant *C*, is shown graphically in Figure 3.2.59.

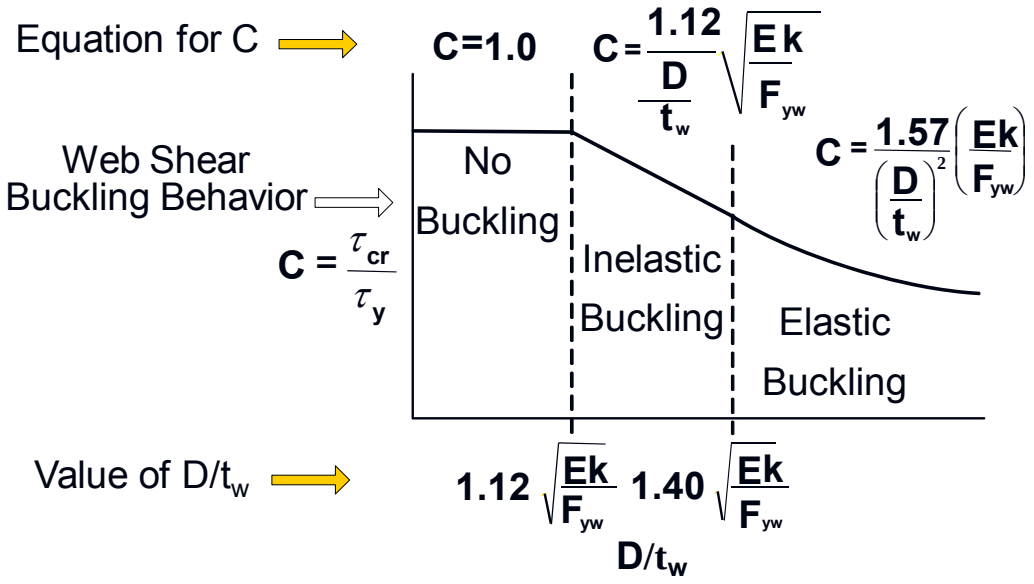


Figure 3.2.59 Web Shear Buckling Resistance – the Constant C

The nominal shear resistance of the girder based on shear buckling (elastic or inelastic) or shear yielding can be computed as:

$$V_n = V_{cr} = \tau_{cr} D t_w$$

Equation 3.2.160

Substituting $C = \tau_{cr}/\tau_y$ gives:

$$V_n = V_{cr} = C\tau_y D t_w = CV_p$$

Equation 3.2.161
AASHTO LRFD Equation 6.10.9.2-1

3.2.7.3 Post-Buckling Shear Resistance (Tension-Field Action)

A web plate stiffened adequately by flanges and transverse stiffeners can carry shear forces considerably greater than its shear buckling resistance; that is, the panel has considerable post-buckling shear resistance. After the web buckles, the girder acts in a manner similar to a Pratt truss with part of each web panel acting as a diagonal tension member carrying the tension forces by membrane action of the web (so-called tension-field action), with the compression forces carried by the transverse stiffeners in conjunction with the adjacent portions of the web (Figure 3.2.60). The ability of a plate girder to carry shear in the post-buckling range by truss action was recognized as early as 1898 (*79*). Early applications of the diagonal

tension-field theory were primarily in the aircraft industry where strength-to-weight ratios are critical factors and thin metal construction is employed.

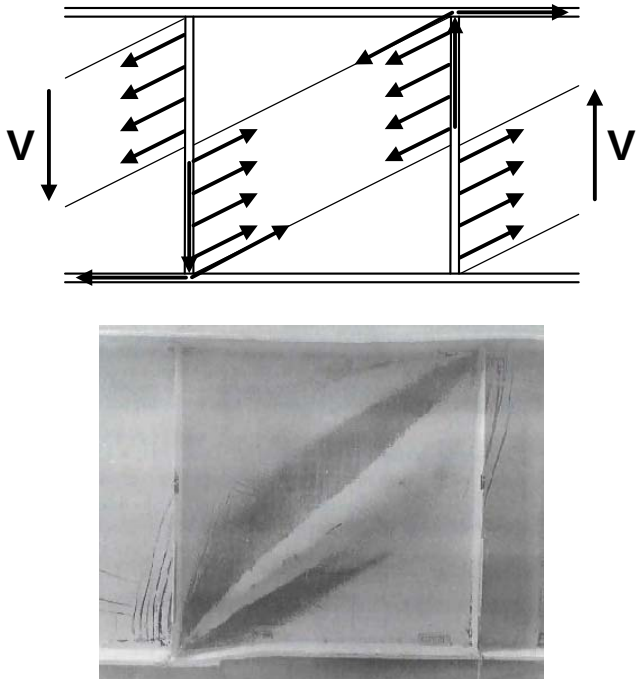


Figure 3.2.60 Web Post-Buckling Shear Resistance – Tension-Field Action

As mentioned in Section 3.2.7.2, it is assumed that the diagonal compression retains the value of beam shear resistance it had when the plate first buckles all the way up to complete failure. Therefore, the nominal shear resistance for post buckling can be computed by summing the contributions of beam action, V_{cr}, and tension-field action, V_{tf}.

The development of V_{tf} has been the subject of numerous research studies worldwide and many different theories have been espoused. An in-depth discussion of all these theories or even the development of the classical value of V_{tf} as developed by Basler (*69*, *73*, *79*), which is still used in many design specifications including the *AASHTO LRFD* Specifications, is beyond the scope of this document. The Basler formulation, which neglects any contribution of the flanges in resisting the diagonal tensile stresses, and conservatively assumes that the angle of the diagonal tension field is at 45 degrees from the horizontal, results in the following expression for V_{tf}:

$$V_{tf} = \frac{0.87V_p(1-C)}{\sqrt{1+\left(\frac{d_o}{D}\right)^2}}$$

Equation 3.2.162

Therefore, the total nominal shear resistance can be written as:

$$V_n = V_p\left[C + \frac{0.87(1-C)}{\sqrt{1+\left(\frac{d_o}{D}\right)^2}}\right]$$

Equation 3.2.163
AASHTO LRFD Equation 6.10.9.3.2-2

Previous specifications included a moment-shear interaction relationship for web panels subject to tension-field action. According to this relationship, the bending and shear resistance of web panels subject simultaneously to both high shear and bending stresses was reduced due to the yielding that could potentially occur under the action of the combined stresses. Relatively recent research (*80*) has led to the removal of this relationship in the *AASHTO LRFD* Specifications. Instead, web panels with the entire section along the panel proportioned to satisfy the following criterion:

$$\frac{2Dt_w}{(b_{fc}t_{fc} + b_{ft}t_{ft})} \le 2.5$$

Equation 3.2.164
AASHTO LRFD Equation 6.10.9.3.2-1

are assumed able to develop the full post-buckling shear resistance due to tension-field action given by Equation 3.2.163. If Equation 3.2.164 is satisfied, along with the requirement on the cross-section aspect ratio given by Equation 3.1.13, and if the maximum moment within the web panel is used to check the flexural resistance, then it is felt that the shear resistance equations given in the specification adequately reflect the majority of the available experimental test results without the need to consider moment-shear interaction effects. The moment-shear interaction relationship was not originally developed to handle the effect of moving loads. Although maximum moment and shear envelope values were typically used to check this relationship, these values generally were not caused by concurrent loadings, which added a level of conservatism. Determining the most critical combination of concurrent moment and shear to check this relationship was not practical. In addition, the anchorage of the tension field and additional shear resistance provided by the composite concrete deck is conservatively neglected in all the shear resistance equations.

If Equation 3.2.164 is not satisfied, the total area of the flanges within the panel is small relative to the area of the web and the full post-buckling resistance generally cannot be developed. Rather than reducing the shear resistance to V_{cr}, it was felt to

be conservative to use a lesser level of the post-buckling shear resistance given by the following equation (*69*):

$$V_n = V_p\left[C + \frac{0.87(1-C)}{\sqrt{1+\left(\frac{d_o}{D}\right)^2}+\frac{d_o}{D}}\right]$$

Equation 3.2.165
AASHTO LRFD Equation 6.10.9.3.2-8

which is given as *AASHTO LRFD* Equation 6.10.9.3.2-8. The extra d_o/D term in the denominator reflects the solution that neglects the shear contribution within the wedges outside of the tension band that was implicitly included by Basler in the development of Equation 3.2.163.

A relatively recent development also incorporated in the *AASHTO LRFD* Specifications is the extension of the post-buckling shear resistance due to tension-field action to webs of hybrid girders (*80-82*). In previous specifications, the shear resistance of hybrid girder webs was conservatively limited to V_{cr} given by Equation 3.2.161.

Equations 3.2.163 and 3.2.165 are applied to stiffened interior web panels. End panels, adjacent to a discontinuous end of a girder, are not permitted to develop any post-buckling resistance. Instead, the shear resistance of these panels is limited to V_{cr} (Equation 3.2.161) in order to provide a sufficient anchor for the development of the tension field in the immediately adjacent interior panels; that is, to absorb any imbalance of the computed horizontal component of the diagonal tension stress in the adjacent panels. In determining V_{cr} for the end panel, the shear buckling coefficient, k, is to be calculated from Equation 3.2.157 based on the spacing from the discontinuous end of the girder to the first transverse stiffener adjacent to that end, which cannot exceed 1.5D.

3.2.7.4 Summary – LRFD Shear Design Requirements

3.2.7.4.1 Unstiffened Webs

The nominal shear resistance, V_n, of nonhybrid and hybrid unstiffened webs is specified in *AASHTO LRFD* Article 6.10.9.2. The nominal shear resistance is limited to the shear-buckling (or shear-yield) resistance, V_{cr}, which was derived in Section 3.2.7.2 and is given by Equation 3.2.161. Consideration of post-buckling shear resistance due to tension-field action is not permitted for unstiffened webs.

The shear buckling coefficient k is to be taken as 5.0 in calculating the appropriate value of the constant C for an unstiffened web (from Equation 3.2.158 or 3.2.159, as applicable). When C is equal to 1.0, the nominal shear resistance is controlled by

shear yielding. The plastic shear force, V_p, for use in Equation 3.2.161 is calculated from Equation 3.2.151. For special considerations related to the determination of the shear resistance of box-section webs, refer to Section 3.2.7.1.2.

In determining whether or not transverse stiffeners are required at a particular section, the Design Engineer will first have to determine the nominal shear resistance of the web, assuming it is unstiffened, to determine if it is less than the shear in the web due to the factored loads at that section. If so, transverse stiffeners are required. *Note that cross-frame/diaphragm connection plates can be considered to act as transverse stiffeners*.

3.2.7.4.2 Stiffened Webs

The nominal shear resistance, V_n, of non-hybrid and hybrid stiffened webs is specified in *AASHTO LRFD* Article 6.10.9.3. Requirements for interior web panels are given in *AASHTO LRFD* Article 6.10.9.3.2 and requirements for end panels are given in *AASHTO LRFD* Article 6.10.9.3.3. The maximum shear in the panel due to the factored loads is to be used to determine the required stiffener spacing, which cannot exceed the maximum values stated in Section 3.2.7.1. The total web depth D is to be used in determining the nominal shear resistance of web panels with longitudinal stiffeners (i.e. the influence of the longitudinal stiffener is conservatively neglected). For special considerations related to the determination of the shear resistance of box-section webs, refer to Section 3.2.7.1.2.

3.2.7.4.2.1 Interior Panels

Stiffened interior web panels of both non-hybrid and hybrid sections are capable of developing post-buckling shear resistance due to tension-field action. As discussed previously in Section 3.2.7.3, in order to develop the full post-buckling resistance, the section along the entire panel must be proportioned to satisfy the relationship given by Equation 3.2.164.

The nominal shear resistance may be taken as the full post-buckling shear resistance given by Equation 3.2.163 if the web-to-flange area ratio given by Equation 3.2.164 is satisfied everywhere within the panel. If Equation 3.2.164 is not satisfied, the total area of the flanges is small relative to the area of the web within the panel such that it is assumed that the full post-buckling resistance cannot be developed. In such cases, V_n is to be based on the available post-buckling resistance given by Equation 3.2.165 in lieu of limiting V_n to V_{cr}. The calculation of the constant C for use in Equation 3.2.163 or 3.2.165, as applicable, is to be based on the shear buckling coefficient k given by Equation 3.2.157, which is a function of the transverse stiffener spacing d_o.

3.2.7.4.2.2 End Panels

End panels of stiffened webs, or the panels immediately adjacent to wherever the girder is discontinuous, are not permitted to develop any post-buckling shear resistance. The shear resistance of these panels is instead limited to V_{cr} (Equation 3.2.161) in order to provide a sufficient anchor for the development of the tension field in the immediately adjacent interior panels. The shear buckling coefficient, k, used to compute the constant C in this case is to be calculated based on the spacing from the discontinuous end of the girder to the first transverse stiffener adjacent to that end.

3.2.8 References

1. White, D.W., and Grubb, M.A. 2005. "Unified Resistance Equations for Design of Curved and Tangent Steel Bridge I-Girders." *Proceedings of the Transportation Research Board Sixth International Bridge Engineering Conference*, Boston, MA, July.
2. White, D.W., Zureick, A.H., Phoawanich, N., and Jung, S.K. 2001. "Development of Unified Equations for Design of Curved and Straight Steel Bridge I-Girders." Final Report to the American Iron and Steel Institute Transportation and Infrastructure Committee, Professional Service Industries, Inc. and the Federal Highway Administration. School of Civil and Environmental Engineering, Georgia Institute of Technology, Atlanta, GA.
3. Galambos, T.V., ed. 1998. *Guide to Stability Design Criteria for Metal Structures*. 5th Edition, Structural Stability Research Council, John Wiley and Sons, Inc., New York, NY.
4. Nethercot, D.A., and Trahair, N.S. 1976. "Lateral Buckling Approximations for Elastic Beams." *The Structural Engineer*. Vol. 54, No. 6.
5. NSBA. 2006. "Design Example 1: Three-Span Continuous Straight Composite I-Girder." *NSBA Steel Bridge Design Handbook*, available from the National Steel Bridge Alliance (www.steelbridges.org), Chicago, IL.
6. HNI. 2007. "Load and Resistance Factor Design (LRFD) for Highway Bridge Superstructures – Design Manual." FHWA Report No. FHWA-NHI 07-035, Federal Highway Administration, National Highway Institute, Washington, D.C.
7. NSBA. 2007. "Design Example 2A: Two-Span Continuous Straight Composite I-Girder." *NSBA Steel Bridge Design Handbook*, available from the National Steel Bridge Alliance (www.steelbridges.org), Chicago, IL.
8. NSBA. 2007. "Design Example 2B: Two-Span Continuous Straight Wide Flange Beam." *NSBA Steel Bridge Design Handbook*, available from the National Steel Bridge Alliance (www.steelbridges.org), Chicago, IL.
9. Schilling, C.G. 1996. "Yield-Interaction Relationships for Curved I-Girders." *Journal of Bridge Engineering*, American Society of Civil Engineers, New York, NY, Vol. 1, No. 1, pp. 26-33.
10. Yoo, C.H., and Davidson, J.S. 1997. "Yield Interaction Equations for Nominal Bending Strength of Curved I-Girders." Journal of Bridge Engineering, American Society of Civil Engineers, New York, NY, Vol. 2, No. 2, pp. 37-44.
11. Timoshenko, S.P., and Gere, J.M. 1961. *Theory of Elastic Stability*. Mc-Graw-Hill, New York, NY.

12. Johnston, S.B., and Mattock, A.H. 1967. “Lateral Distribution of Load in Composite Box Girder Bridges.” *Highway Research Record*, No. 167, Bridges and Structures, Transportation Research Board, Washington, D.C.
13. Consortium of University Research Teams. 1975. “Tentative Design Specifications for Horizontally Curved Highway Bridges.” CURT Project, Part of Final Report, Research Project HPR2-(111), March.
14. Galambos, T.V. 1978. “Tentative Load Factor Design Criteria for Curved Steel Bridges.” Research Report No. 50, Department of Civil Engineering, St. Louis, MO, May.
15. Culver, C.G., and Mozer, J. 1971. “Horizontally Curved Highway Bridges, Stability of Box Girders.” Department of Civil Engineering, Carnegie Mellon University, Pittsburgh, PA, Report No. B2 submitted to the FHWA, Contract No. FH-11-7389, July.
16. Wright, R.N., and Abdel-Samad, S.R. 1968. “BEF Analogy for Analysis of Box Girders.” *Journal of the Structural Division*, ASCE, Vol. 94, No. ST7, pp. 1719-1743.
17. FHWA. 1980. “Proposed Design Specifications for Steel Box Girder Bridges.” *FHWA-TS-80-205*, Federal Highway Administration, Washington, D.C.
18. Hall, D.H., Grubb, M.A., and Yoo, C.H. 1999. “Improved Design Specifications for Horizontally Curved Steel Girder Highway Bridges.” *NCHRP Report 424*, Transportation Research Board, Washington, D.C.
19. United States Steel. 1978. *Steel/Concrete Composite Box-Girder Bridge: A Construction Manual*. available from the National Steel Bridge Alliance, Chicago, IL, December.
20. Boresi, A.P, Sidebottom, M., Seely, F.B., and Smith, J.O. 1978. *Advanced Mechanics of Materials*, 3rd ed. John Wiley and Sons, New York, NY.
21. Fountain, R.S., and Thunman, Jr., C.E. 1987. “Deflection Criteria for Steel Highway Bridges.” Proceedings of the AISC National Engineering Conference, New Orleans, LA, April 29-May 7.
22. ASCE. 1958. “Deflection Limits of Bridges. Progress Report of the Committee on Deflection Limitations of Bridge of the Structural Division.” *Journal of the Structural Division*, ASCE, New York, NY, Vol. 84, No. ST3, May.
23. Ontario Ministry of Transportation. 1991. *Ontario Highway Bridge Design Code*. Quality and Standards Division, Structural Office, Toronto, Canada.
24. Wright, R.N., and Walker, W.H. 1971. “Criteria for Deflection of Steel Bridges.” *AISI Bulletin No. 19*, American Iron and Steel Institute, Washington, D.C., November.
25. Roeder, C.W., Barth, K., and Bergman, A. 2002. “Improved Live Load Deflection Criteria for Steel Bridges.” Final Report for NCHRP Project 20-7[133], National Cooperative Highway Research Program, Transportation Research Board, Washington, D.C., November.
26. Vincent, G.S. 1969. “Tentative Criteria for Load Factor Design of Steel Highway Bridges.” *AISI Bulletin No. 15,* American Iron and Steel Institute, Washington, D.C., March.
27. CEN. 2004. Eurocode 4, EN: 1994-1-1:2004, European Committee for Standardization, Brussels, Belgium.

28. Hansell, W.C., and Viest, I.M. 1971. “Load Factor Design for Steel Highway Bridges.” *AISC Engineering Journal*, American Institute of Steel Construction, Chicago, IL, October.
29. The AASHO Road Test. 1962. “Report No. 4, Bridge Research, Highway Research Board Special Report 61D.” Publication No. 953, National Academy of Sciences, National Research Council, Washington, D.C.
30. Basler, K., Yen, B.T., Mueller, J.A., and Thurlimann, B. 1960. “Web Buckling Tests on Welded Plate Girders.” *WRC Bulletin No. 64*, Welding Research Council, New York, NY.
31. ASCE. 1968. “Design of Hybrid Steel Beams.” Joint ASCE-AASHO Subcommittee on Hybrid Beams and Girders, *Journal of the Structural Division*, American Society of Civil Engineers, Vol. 94, No. ST6, New York, NY.
32. Frank, K.H., and Helwig, T.A. 1995. “Buckling of Webs in Unsymmetric Plate Girders.” *AISC Engineering Journal*, American Institute of Steel Construction, Chicago, IL, Vol. 32, 2nd Qtr.
33. Cooper, P.B. 1967. “Strength of Longitudinally Stiffened Plate Girders.” *Journal of the Structural Division*, American Society of Civil Engineers, New York, NY, Vol. 93, No. ST2, April.
34. Munse, W.H., and Grover, L.H. 1964. “Fatigue of Welded Steel Structures.” Welding Research Council, New York, NY.
35. Gurney, T.R. 1968. “Fatigue of Welded Structures.” Cambridge University Press.
36. Fisher, J.W., Frank, K.H., Hirt, M.A., and McNamee, B.M. 1970. “Effect of Weldments on Fatigue Strength of Steel Beams.” NCHRP Report 102, Highway Research Board, Washington, D.C.
37. Fisher, J.W., Albrecht, P.A., Yen, B.T., Klingerman, D.J., and McNamee, B.M. 1974. “Fatigue Strength of Steel Beams with Transverse Stiffeners and Attachments.” NCHRP Report 147, Highway Research Board, Washington, D.C.
38. FHWA. 1989. *Technical Advisory on Uncoated Weathering Steel in Structures*. Federal Highway Administration, U.S. Department of Transportation, Washington, D.C., October.
39. NHI. 1990. “Economical and Fatigue Resistance Steel Bridge Details – Participant Notebook.” National Highway Institute Course No. 13049, Federal Highway Administration, Publication No. FHWA-1-11-90-043, June.
40. Huhn, H., and Valtinat, G. 2004. “Bolted Connections with Hot Dip Galvanized Steel Members with Punched Holes.” *Proceedings of the ECCS/AISC Workshop, Connections in Steel Structures V: Innovative Steel Connections*, European Convention for Constructional Steelwork/American Institute of Steel Construction, Amsterdam, June 3-5.
41. Brown, J.D., Lubitz, D.J., Cekov, Y.C., and Frank, K.H. 2007. “Evaluation of Influence of Hole Making Upon the Performance of Structural Steel Plates and Connections.” Report No. FHWA/TX-07/0-4624-1, University of Texas at Austin, Austin, TX.
42. Fisher, J.W. 1977. “Bridge Fatigue Guide – Design and Details.” American Institute of Steel Construction, Chicago, IL.
43. Schilling, C.G. 1986. “Fatigue.” Chapter I/6. *Highway Structures Design Handbook*. Available from the National Steel Bridge Alliance, Chicago, IL, February.

44. Wright, W.J., Fisher, J.W., and Kaufmann, E.J. 2003. “Failure Analysis of the Hoan Bridge Fractures.” Recent Developments in Bridge Engineering, Mahmoud ed., Swets & Zeitlinger, Lisse.
45. Kaufmann, E.J., Connor, R.J., and Fisher, J.W. 2004. “Failure Investigation of the SR 422 over the Schuylkill River Girder Fracture – Draft Final Report.” ATLSS Engineering Research Center, Lehigh University, Bethlehem, PA.
46. Mahmoud, H.N., Connor, R.J., and Fisher, J.W. 2005. “Finite Element Investigation of the Fracture Potential of Highly Constrained Details.” *Journal of Computer-Aided Civil and Infrastructure Engineering*, Blackwell Publishing, Inc., Malden, MA, Vol. 20.
47. Frank, K.H., and Fisher, J.W. 1979. “Fatigue Strength of Fillet Welded Cruciform Joints.” Journal of the Structural Division, American Society of Civil Engineers, New York, NY, Vol. 105, No. ST9, September.
48. Miner, M.A. 1945. “Cumulative Damage in Fatigue.” *Journal of Applied Mechanics*. Volume 12, September.
49. Schilling, C.G., Klippstein, K.H., Barsom, J.M., and Blake, G.T. 1975. “Fatigue of Welded Steel Bridge Members Under Variable-Amplitude Loadings.” Final Report – NCHRP Project 12-12, Transportation Research Board, Washington, D.C., August.
50. AASHTO. 1989. *Guide Specifications for Fatigue Design of Steel Bridges*. American Association of State Highway and Transportation Officials, Inc., Washington, D.C.
51. Heins, C.P., and Hall, D.H. 1981. “Designers Guide to Steel Box Girder Bridges.” Booklet No. 3500, Bethlehem Steel Corporation, Bethlehem, PA, February.
52. AASHTO/AWS D1.5M/D1.5. 2008. *Bridge Welding Code*. American National Standard/American Association of State Highway and Transportation Officials/American Welding Society.
53. AISI. 1975. *The Development of AASHTO Fracture-Toughness Requirements for Bridge Steels*. American Iron and Steel Institute, Washington, D.C., February.
54. Wilson, A.D. 2002. “Availability and Future Development of High Performance Steel.” Proceedings of the 2002 NABRO/FHWA HPS Conference, Salt Lake City, UT.
55. NSBA. 2010. “Chapter 6: Structural Behavior of Steel.” *NSBA Steel Bridge Design Handbook*, available from the National Steel Bridge Alliance (www.steelbridges.org), Chicago, IL.
56. Basler, K., and Thurlimann, B. 1961. “Strength of Plate Girders in Bending.” *Journal of the Structural Division*, American Society of Civil Engineers, New York, NY, Vol. 87, No. ST6, August.
57. Frost, R.W., and Schilling, C.G. 1964. “Behavior of Hybrid Beams Subjected to Static Loads.” *Journal of the Structural Division*, American Society of Civil Engineers, New York, NY, Vol. 90, No. ST3, June.
58. Schilling, C.G. 1967. “Web Crippling Tests on Hybrid Girders.” *Journal of the Structural Division*, American Society of Civil Engineers, New York, NY, Vol. 93, No. ST1, February.

59. Schilling, C.G. 1968. "Bending Behavior of Composite Hybrid Beams." *Journal of the Structural Division*, American Society of Civil Engineers, New York, NY, Vol. 94, No. ST8, August.
60. Carskaddan, P.S. 1968. "Shear Buckling of Unstiffened Hybrid Beams." *Journal of the Structural Division*, American Society of Civil Engineers, New York, NY, Vol. 94, No. ST8, August.
61. Toprac, A.A., and Natarajan, M. 1971. "Fatigue Strength of Hybrid Plate Girders." *Journal of the Structural Division*, American Society of Civil Engineers, New York, NY, Vol. 97, No. ST4, April.
62. Lywin, M.M. 2002. *High Performance Steel Designer's Guide*. Federal Highway Administration, Western Resource Center, San Francisco, CA, April.
63. Horton, R., Power, E., Ooyen, K.V., and Azizinamini, A. 2000. "High Performance Steel Cost Comparison Study." Conference Proceedings, Steel Bridge Design and Construction for the New Millennium with Emphasis on High Performance Steel, November 30 – December 1, Federal Highway Administration, Washington, D.C.
64. White, D.W., and Barth, K.E. 1998. "Strength and Ductility of Compact-Flange I-Girders in Negative Bending." *Journal of Constructional Steel Research*, Elsevier, Orlando, FL, Vol. 45, No. 3.
65. Barth, K.E., White, D.W., Righman, J.E., and Yang, L. 2005. "Evaluation of Web Compactness Limits for Singly and Doubly Symmetric Steel I-Girders." Journal of Constructional Steel Research, Elsevier, Orlando, FL, Vol. 61, No. 10.
66. Johnson, D.L. 1985. "An Investigation into the Interaction of Flanges and Webs in Wide Flange Shapes." *Proceedings of the SSRC Annual Technical Session*, Cleveland, OH, Structural Stability Research Council, University of Missouri, Rolla, MO.
67. AISC. 2005. *Specification for Structural Steel Buildings*. ANSI/AISC 360-05, American Institute of Steel Construction, Chicago, IL, March 9.
68. Hall, D.H. 2000. "The Effect of Material Properties on the Stability of Steel Girder Bridges." *Proceedings of the SSRC Annual Technical Session*, Memphis, TN, Structural Stability Research Council, University of Missouri, Rolla, MO.
69. Salmon, C.G., and Johnson, J.E. 1996. *Steel Structures – Design and Behavior*, Fourth Edition, HarperCollins College Publishers, New York, NY.
70. Brockenbrough, R.L., and Johnston, B.G. 1981. *USS Steel Design Manual*. United States Steel Corporation, ADUSS 27-3400-04, Pittsburgh, PA, January.
71. Kitipornchai, S., and Trahair, N.S. 1980. "Buckling Properties of Monosymmetric I-Beams." *Journal of the Structural Division*, American Society of Civil Engineers, New York, NY, Vol. 106, No. ST5, May.
72. Kitipornchai, S., and Trahair, N.S. 1986. "Buckling Properties of Monosymmetric I-Beams Under Moment Gradient." *Journal of the Structural Division*, American Society of Civil Engineers, New York, NY, Vol. 112, No. ST4.
73. McGuire, W. 1968. *Steel Structures*. Prentice-Hall, Inc., Englewood Cliffs, NJ.
74. Doswell, B. 2002. "Lateral-Torsional Buckling of Wide Flange Cantilever Beams." *Proceedings of the 2002 Annual Stability Conference*, Structural Stability Research Council, University of Missouri, Rolla, MO.
75. White, D.W. 2004. "Unified Flexural Resistance Equations for Stability Design of I-Section Members – Overview." Structural Engineering, Mechanics and

Materials Report No. 24a, School of Civil and Environmental Engineering, Georgia Institute of Technology, Atlanta, GA.
76. Carskaddan, P.S., and Schilling, C.G. 1974. “Lateral Buckling of Highway Bridge Girders.” Research Laboratory Report 22-G-001 (019-3), United States Steel Corporation, Monroeville, PA.
77. Ugural, A.C., and Fenster, S.K. 1978. *Advanced Strength and Applied Elasticity*. Elsevier-North Holland Publishing Co., Inc., New York, NY.
78. Culver, C.G. 1972. “Design Recommendations for Curved Highway Bridges.” *Final Report for PennDOT Research Project 68-32*, Civil Engineering Department, Carnegie-Mellon University, Pittsburgh, PA, June.
79. Basler, K. 1961. “Strength of Plate Girders in Shear.” *Journal of the Structural Division*, American Society of Civil Engineers, Vol. 8, No. ST7, October.
80. White, D.W., Barker, M., and Azizinamini, A. 2004. “Shear Strength and Moment Shear Interaction in Transversely-Stiffened Steel I-Girders.” Structural Engineering, Mechanics and Materials Report No. 27, School of Civil and Environmental Engineering, Georgia Institute of Technology, Atlanta, GA.
81. White, D.W., and Barker, M. 2004. “Shear Resistance of Transversely Stiffened Steel I-Girders.” Structural Engineering, Mechanics and Materials Report No. 26, School of Civil and Environmental Engineering, Georgia Institute of Technology, Atlanta, GA.
82. Jung, S.-K., and White, D.W. 2006. “Shear Strength of Horizontally Curved Steel I-Girders – Finite Element Studies.” *Journal of Constructional Steel Research*, 62(4).

Chapter 3
Design Considerations

Section 3.3
Design of Detail Items



3.3.1 Introduction

This section of the Manual discusses LRFD design requirements for detail items such as shear connectors, single-angle members, tee and double-angle members, diaphragms, bracing-member connections, bolted girder splices, stiffeners (i.e., transverse web stiffeners, bearing stiffeners and longitudinal web stiffeners) and bearings. The design of these items is particularly important for skewed and/or curved bridges. The load shifting between girders in such bridges due to the torsional effects resulting from curvature and support skew directly affects the design of many of these items and increases their relative importance. These effects must be considered in the design of these items as discussed herein.

3.3.2 Shear Connectors

3.3.2.1 General

The composite action between the deck and steel girders in composite construction is ensured by the use of welded mechanical shear connectors between the girder and the deck (Figure 3.3.1). The primary function of the shear connectors is to transfer the horizontal shear between the deck and the girder forcing the steel girder and concrete deck to act together as a structural unit by preventing slip along the concrete-steel interface. Shear connectors also help control deck cracking in regions of negative flexure in regions where the deck is subject to tensile stress and also has longitudinal reinforcement present.

The design of shear connectors for I-sections is covered in *AASHTO LRFD* Article 6.10.10. The design of shear connectors for box sections is covered in *AASHTO LRFD* Article 6.11.10. The application of these provisions, as discussed in the following, is illustrated in Section 5.1.8.5 of the I-girder design example and Section 5.2.9.5 of the tub girder design example.

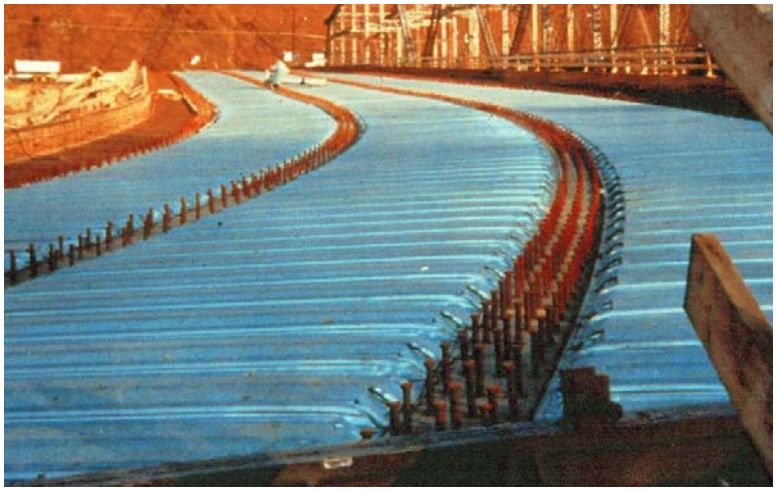


Figure 3.3.1 Stud Shear Connectors on Curved Girders

The shear connectors must be capable of resisting both horizontal and vertical movement between the concrete deck and the steel, and allow compaction of the concrete around them so that their entire surfaces are in contact with the concrete. Typically, stud shear connectors are used, but channel shear connectors are also permitted and may be designed according to the provisions of *AASHTO LRFD* Article 6.10.10. However, channel shear connectors are not commonly used on modern bridges. Common sizes of studs may be found in manufacturer's catalogs.

3.3.2.1.1 Layout Requirements

Requirements for the layout of stud shear connectors are discussed in the following. These requirements include such items as the minimum height-to-diameter ratio, transverse spacing and clear distance, cover and penetration and the maximum and minimum pitch. If any of these requirements are not satisfied, then composite action may not be assumed.

3.3.2.1.1.1 Minimum Height-to-Diameter Ratio

AASHTO LRFD Article 6.10.10.1.1 specifies that the ratio of the height to the diameter of a stud shear connector must be greater than or equal to 4.0 (Figure 3.3.2). The stud height includes the head, but the stud diameter is measured at the shaft rather than the head.

$$\frac{\text{Height}}{\text{Diameter}} \geq 4.0$$

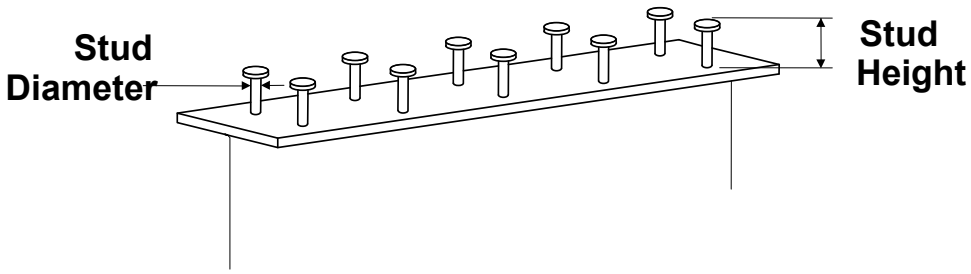


Figure 3.3.2 Minimum Height-to-Diameter Ratio

3.3.2.1.1.2 Transverse Spacing and Clear Distance

AASHTO LRFD Article 6.10.10.1.3 specifies that stud shear connectors are to be spaced no closer than 4.0 stud diameters center-to-center transversely across the top flange(s) of I-sections and tub-girder sections (Figure 3.3.3). As also illustrated in Figure 3.3.3, the clear distance between the edge of the top flange and the edge of the nearest shear connector is not to be less than 1.0 in.

Transverse Spacing ≥ 4.0 x (Stud Diameter)

Clear Distance ≥ 1.0 Inch

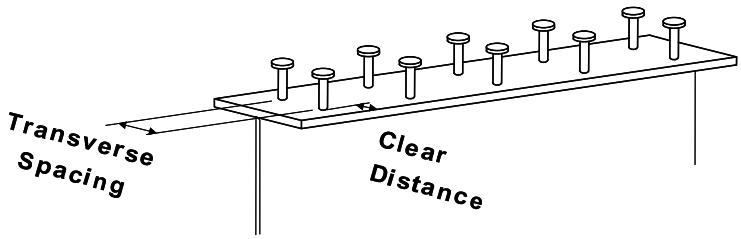


Figure 3.3.3 Transverse Spacing and Clear Distance

Closed-Box Sections

Shear connectors for closed-box sections should be uniformly distributed across the width of the top (box) flange to ensure composite action of the entire flange with the concrete. *AASHTO LRFD* Article 6.11.10 specifies that the maximum transverse spacing, s_t, between shear connectors on composite box flanges of closed-box sections must satisfy the following requirement to help prevent local buckling of the flange plate between connectors when subject to compression:

$$\frac{s_t}{t_f}\sqrt{\frac{F_{yf}}{kE}} \le R_1$$

Equation 3.3.1
AASHTO LRFD Equation 6.11.10-1

where:

k = plate-buckling coefficient for uniform normal stress on box flanges determined as specified in *AASHTO LRFD* Article 6.11.8.2 (Section 3.2.6.4.2.2)

R_1 = limiting slenderness ratio for the box flange determined from *AASHTO LRFD* Equation 6.11.8.2.2-8 (Equation 3.2.119)

3.3.2.1.1.3 Cover and Penetration

AASHTO LRFD Article 6.10.10.1.4 specifies that the clear depth of concrete cover over the tops of shear connectors must not be less than 2.0 in., and the shear connectors should penetrate at least 2.0 in. into the concrete deck (Figure 3.3.4). Otherwise, the deck haunch should be appropriately reinforced to contain the studs and develop their load in the deck.

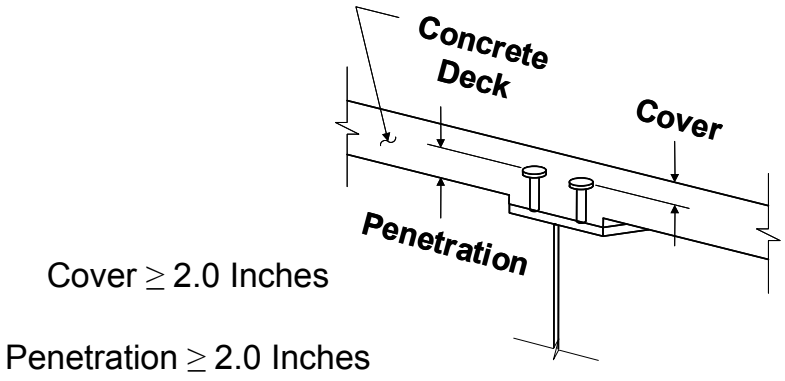


Figure 3.3.4 Cover and Penetration

The Design Engineer should be aware that steep cross-slopes and wide flanges on curved girder bridges may result in little or no haunch above the flange on the low side of the slope if not properly accounted for when setting the initial haunch dimensions.

3.3.2.1.1.4 Minimum and Maximum Pitch

Shear connectors may be spaced at regular or variable intervals longitudinally along the girder. The longitudinal center-to-center spacing of shear connectors is referred to as the pitch. *AASHTO LRFD* Article 6.10.10.1.2 specifies that the pitch must not exceed 24.0 in. and must not be less than six stud diameters (Figure 3.3.5). As described in more detail below, the pitch of the shear connectors is typically determined first to satisfy the fatigue limit state, as specified in *AASHTO LRFD* Article 6.10.10.2 and 6.10.10.3 (as applicable). The resulting number of shear connectors is then checked to ensure that it is not less than the number required to satisfy the strength limit state, as specified in *AASHTO LRFD* Article 6.10.10.4.

Pitch ≤ 24 Inches

Pitch ≥ 6 x (Stud Diameter)

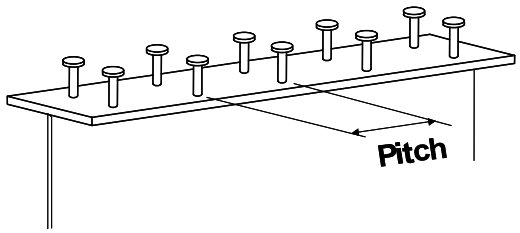


Figure 3.3.5 Minimum and Maximum Pitch

AASHTO LRFD Article 6.10.10.1 specifies that simple-span composite bridges are to have shear connectors provided throughout the length of the span. Straight continuous composite I-girder bridges are to normally be provided with shear connectors throughout the length of the bridge, again to help control cracking in regions of negative flexure, but it is not required. However, if the longitudinal reinforcement in the deck in regions of negative flexure is considered in determining the composite I-section properties in these regions, then shear connectors must also be provided in these regions.

Should shear connectors not be provided in these regions, the longitudinal reinforcement cannot be considered in the computation of the composite I-section properties. .In addition, if shear connectors are omitted in regions of negative flexure in straight I-girder bridges, additional connectors must be placed in the region of the points of permanent load contraflexure according to the provisions of *AASHTO LRFD* Article 6.10.10.3, and the longitudinal deck reinforcement must be extended into the positive flexure region beyond the additional connectors a distance not less than the development length specified in Section 5 of the *AASHTO LRFD* Specifications (*AASHTO LRFD* Article 6.10.1.7). Discontinuing the shear connectors in these regions effectively causes the deck slab to act as a partial-length cover plate, which has two potential problematic effects. First, the slab is likely to crack near the point at which it is no longer acting compositely with the steel girder. Second, the shear connectors and their welds at the discontinuity may be overloaded much as the welds at the termination of a partial length cover plate, particularly if sufficient shear connectors are not provided to transfer the appropriate deck forces back into the girder. In fact, field tests have confirmed that the deck continues to act compositely without shear connection in these regions. When it ceases to act compositely, a tell-tail rust line often develops between the deck and the girder flange that is evident in inspections. This situation may be followed with the deterioration of the deck. Points of permanent load contraflexure should not be related to shear connector design. As demonstrated previously in Section 2.1.4, over most of the region of negative moment due to permanent load, the live load to obtain the maximum shear range produces positive moment, not negative moment.

AASHTO LRFD Article 6.10.10.1 further specifies that curved continuous composite bridges *must* be provided with shear connectors throughout the length of the bridge because torsional shear exists and is developed in the full composite section along the entire bridge (note that the same requirement applies to all types of composite box-girder bridges). For bridges containing one or more curved segments, the effects of curvature usually extend beyond the curved segment. Therefore, it is conservatively specified that shear connectors be provided along the entire length of the bridge in this case as well. As torsional shear also exists along the entire span of straight continuous skewed I-girder bridges and must be developed in the full composite section, consideration should also be given to providing shear connectors along the entire length of these structures.

3.3.2.2 Fatigue Limit State Design

According to the provisions of *AASHTO LRFD* Article 6.10.10.1.2, the pitch of the shear connectors along the longitudinal axis of the girder is to be initially determined to satisfy the fatigue limit state. The resulting number of shear connectors is then to be checked against the number required to satisfy the strength limit state.

The required pitch of the shear connectors at the fatigue limit state is based on the horizontal fatigue live load shear range between the deck and top flange of the girder. In straight girders, if torsion is ignored, the shear range is due only to vertical bending. However, in certain cases, skew can introduce significant torsion. Curvature and other conditions can also introduce torsion. St. Venant torsional shears are significant in certain types of box sections and must be considered in the design of the shear connectors. The shear connector design provisions in the *AASHTO LRFD* Specifications allow for flexural and torsional components of the shear to be considered in these cases and to be added vectorially, as discussed in more detail below.

In addition to determining the required pitch, the base metal at stud welds to flanges subject to net tension must be checked for load-induced fatigue for Detail Category C (*AASHTO LRFD* Table 6.6.1.2.3-1 – Condition 8.1). Refer to *AASHTO LRFD* Article 6.6.1.2 and to Section 3.2.5.2.2.

3.3.2.2.1 Pitch

According to *AASHTO LRFD* Article 6.10.10.1.2, the pitch, *p*, of the shear connectors at the fatigue limit state must satisfy the following:

$$p \le \frac{nZ_r}{V_{sr}}$$

Equation 3.3.2
AASHTO LRFD Equation 6.10.10.1.2-1

where:

- n = number of shear connectors in a cross-section (Figure 3.3.6)
- V_{sr} = horizontal fatigue shear range per unit length (discussed below) (kips/in.)
- Z_r = fatigue shear resistance of an individual shear connector determined as specified in *AASHTO LRFD* Article 6.10.10.2 (Section 3.3.2.2.1.3) (kips)

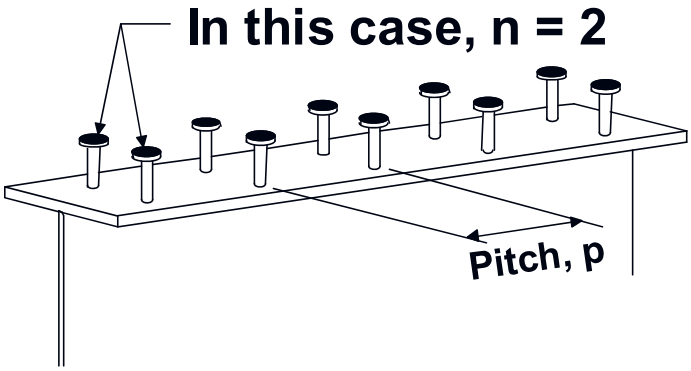


Figure 3.3.6 Number of Shear Connectors in a Cross-Section (n)

The horizontal fatigue shear range per unit length, V_{sr}, is determined as follows:

$$V_{sr} = \sqrt{(V_{fat})^2 + (F_{fat})^2}$$

Equation 3.3.3
AASHTO LRFD Equation 6.10.10.1.2-2

where:

V_{fat} = longitudinal fatigue shear range per unit length (Section 3.3.2.2.1.1) (kips/in.)
F_{fat} = radial fatigue shear range per unit length (Section 3.3.2.2.1.2) (kips/in.)

That is, the horizontal shear range is taken as the vectorial sum of the longitudinal and radial fatigue shear ranges.

For curved and/or skewed bridges, it is recommended that V_{sr} and the resulting pitch, p, for the fatigue limit state be determined at each cross-frame.

Closed-Box Sections

For composite box flanges in closed-box sections, V_{sr} is to be determined as the vector sum of the longitudinal fatigue shear range given by Equation 3.3.4 (see below) and the torsional fatigue shear range in the concrete deck, in lieu of using Equation 3.3.3 (*AASHTO LRFD* Article 6.11.10). According to *AASHTO LRFD* Article C6.11.10, the torsional shear range resisted by the concrete deck can be determined by multiplying the torsional shear range acting on the top of the box section by the ratio of the thickness of the transformed concrete deck to the total thickness of the top flange plus the transformed concrete deck.

3.3.2.2.1.1 Longitudinal Fatigue Shear Range, V_{fat}

The longitudinal fatigue shear range per unit length, V_{fat} (kips/in.), is determined as follows:

$$V_{fat} = \frac{V_f Q}{I}$$

Equation 3.3.4
AASHTO LRFD Equation 6.10.10.1.2-3

where:

- I = moment of inertia of the short-term composite section (in.^{4})
- Q = first moment of the transformed short-term area of the concrete deck about the neutral axis of the short-term composite section (in.^{3})
- V_f = vertical shear force under the applicable Fatigue load combination specified in *AASHTO LRFD* Table 3.4.1-1 (Fatigue I or Fatigue II), with the fatigue live load taken as specified in *AASHTO LRFD* Article 3.6.1.4 (kips)

As discussed in Section 1.3.2.3.3, the fatigue live load is specified to be a single HS20 truck, weighing 72 kips, with a constant rear-axle spacing of 30 feet (*AASHTO LRFD* Article 3.6.1.4.1). For the Fatigue I load combination, which is used for infinite life design, a load factor of 1.5 is applied to the vertical shears resulting from the single design truck. For the Fatigue II load combination, which is used for finite life design, a load factor of 0.75 is applied to the vertical shears resulting from the single design truck. A dynamic load allowance (impact factor) of 1.15 is also to be applied (*AASHTO LRFD* Article 3.6.2). The appropriate Fatigue load combination to use in determining V_f is discussed below in Section 3.3.2.2.1.3.

For girders in curved bridges, the parameters *Q* and *I* in Equation 3.3.4 are always to be determined including the effective width of the concrete deck in all regions of the girder, including in regions of negative flexure (similar values of *Q* and *I* should also be considered for use for girders in straight skewed bridges). V_{fat} is produced by placing the factored fatigue live load immediately to the left and right of the point under consideration. With the load in these positions, positive moments are produced over significant portions of the girder length. As a result, it is reasonable to assume that the concrete deck within the effective width is fully effective along the entire span in determining the stiffness used in the analysis to determine the shear range. In addition, the horizontal shear force in the deck is typically assumed to be effective along the entire span in the analysis. In order to satisfy this assumption, the shear force in the deck should be developed along the entire span.

As mentioned in *AASHTO LRFD* Article C6.10.10.1.2, in negative flexure regions *of straight girders only* (preferably without skew), *Q* and *I* are permitted to be determined using only the longitudinal reinforcement within the effective flange width in line with previous specifications, unless the concrete is considered effective in tension in determining stress ranges for checking fatigue as permitted

in *AASHTO LRFD* Article 6.6.1.2.1 (refer to Section 3.2.5.2.2). When only the longitudinal reinforcement is considered, it must be ensured that the pitch of the shear connectors in these regions does not exceed the permitted maximum pitch of 24.0 in.

The effective width of the concrete deck is likely to be different for the interior and exterior girders in the cross-section, which in conjunction with different fatigue shear ranges in the girders, may result in slightly different pitches for each girder. However, for practical purposes, unless the differences are deemed significant, it is recommended that the same pitches be used on all the girders.

Box Sections

AASHTO LRFD Article 6.11.10 specifies that for all single box sections, horizontally curved box sections, and multiple box sections in bridges not satisfying the limitations of *AASHTO LRFD* Article 6.11.2.3, or with box flanges that are not fully effective according to the provisions of *AASHTO LRFD* Article 6.11.1.1, shear connectors are to be designed for the sum of the flexural and St. Venant torsional shears. In such cases, for which the St. Venant torsional shears are considered to be more significant, V_f in Equation 3.3.4 is to be computed by summing the maximum flexural and torsional shears in the web subject to additive shears. The maximum flexural and torsional shears are used, although they are typically not produced by concurrent loads, because the interaction between flexure and torsion due to moving live loads is too complex to treat in a practical manner. The shear range and resulting pitch should be computed using one-half the moment of inertia I of the box. The top flange over the web opposite to the web subject to additive flexural and torsional shears, or the other half of the flange for a closed-box section, should contain an equal number of shear connectors.

3.3.2.2.1.2 Radial Fatigue Shear Range, F_{fat}

Curvature, skew and other conditions may cause torsion, which introduces a radial component of the horizontal shear. The radial shear range, F_{fat}, so determined is typically computed with the fatigue live load positioned to produce the largest positive and negative major-axis bending moments in the span. The longitudinal shear range, V_{fat}, is produced by placing the fatigue live load immediately to the left and to the right of the point under consideration. Therefore, vectorial addition of the longitudinal and radial components of the shear range is conservative because the longitudinal and radial shears are not produced by concurrent loads.

The radial fatigue shear range per unit length, F_{fat} (kips/in.), is to be taken as the larger of the following:

$$F_{fat1} = \frac{A_{bot}\sigma_{flg}\ell}{wR}$$

Equation 3.3.5
AASHTO LRFD Equation 6.10.10.1.2-4

$$F_{fat2} = \frac{F_{rc}}{w}$$

Equation 3.3.6
AASHTO LRFD Equation 6.10.10.1.2-5

where:

σ_{flg} = range of longitudinal fatigue stress in the bottom flange under the applicable Fatigue load combination without consideration of flange lateral bending (ksi)
A_{bot} = area of the bottom flange (in.^{2})
F_{rc} = net-range of cross-frame/diaphragm force at the top flange (kips)
ℓ = distance between brace points (ft)
R = minimum girder radius within the panel (ft)
w = effective length of concrete deck (in.) taken as 48.0 in., except at end supports where *w* may be taken as 24.0 in.

F_{fat1} is used to determine the radial fatigue shear range due to curvature between brace points and is taken as zero for straight spans or segments. F_{fat2} is the radial fatigue shear range where significant torsion is caused by effects other than curvature, such as skew. F_{fat2} is likely to control when discontinuous cross-frames are used in conjunction with skew angles exceeding 20 degrees in either a straight or a horizontally curved bridge. For all other cases, F_{fat2} may be taken equal to zero.

These two equations are provided to ensure that a load path is provided through the shear connectors to satisfy equilibrium at a section through the girders, deck and cross-frame. The equations yield approximately the same value if the span or segment is curved and there are no other sources of torsion.

Radial Fatigue Shear Range due to Curvature, F_{fat1}

F_{fat1} is the radial fatigue shear range resulting from the effect of any curvature between brace points. The shear range is taken as the radial component of the longitudinal range of force, $A_{bot}\sigma_{flg}$, in the bottom flange under the applicable Fatigue load combination calculated without consideration of flange lateral bending. The range in the bottom flange is used as a measure of the vertical bending moment due to the fatigue load. σ_{flg} is preferably computed at a cross-frame and also at the mid-thickness of the bottom flange since it is being used to compute a flange force *F*.

Referring to the top of Figure 3.3.7, which represents a segment of a curved bottom flange between two cross-frames, the radial component of flange force due to curvature can be assumed to act as a radial distributed force, *q*, over the length

of the flange segment. Although the radial force, *q*, actually varies along the flange as a function of the axial flange force, *F*, due to vertical bending, for a small segment of the flange, both *q* and *F* may be considered constant. Based on this assumption, the magnitude of *q* is derived in Section 2.3.2 as follows:

$$q = \frac{F}{R}$$

Equation 3.3.7

or:

$$q = \frac{A_{bot}\,\sigma_{flg}}{R}$$

Equation 3.3.8

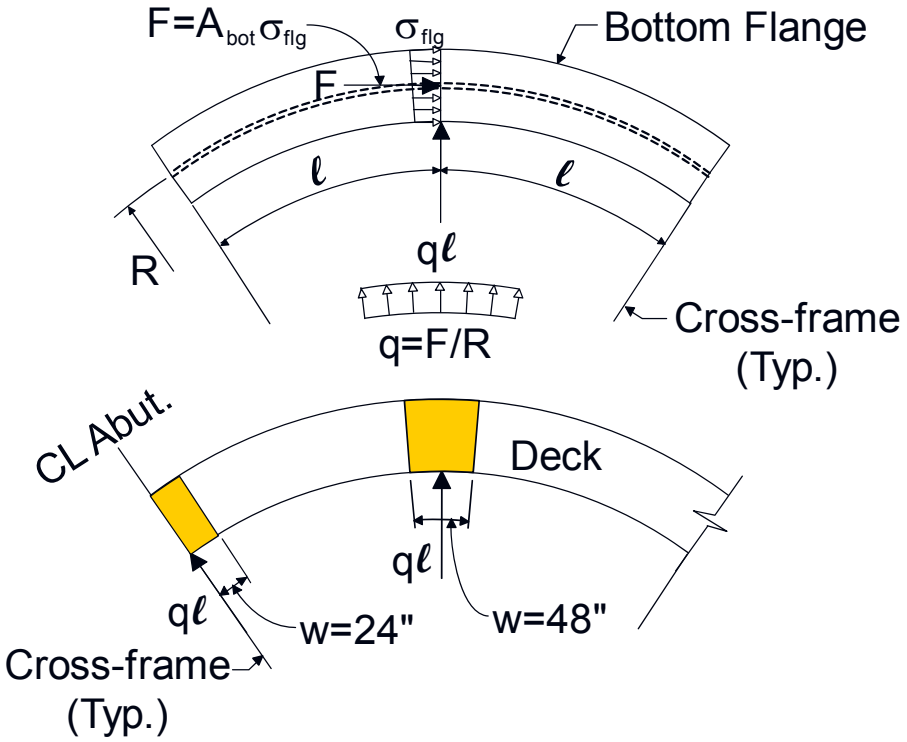


Figure 3.3.7 Derivation of F_{fat1} (Equation 3.3.5)

As shown at the bottom of Figure 3.3.7, multiplying *q* from Equation 3.3.8 by the cross-frame spacing, ℓ, and distributing the resulting radial shear range over an effective length of deck, *w*, gives F_{fat1} in kips/inch as given by Equation 3.3.5. *w* is taken as 48.0 inches, except at end supports where *w* is halved to 24.0 inches. This length is considered representative of the effective length of the deck assumed acting with the flange in the transverse direction.

F_{fat1} may be taken equal to zero for straight spans or segments. *F_{fat1} may be ignored for box sections used in horizontally curved spans or segments, as*

permitted in AASHTO LRFD Article 6.11.10, because of the inherent conservatism in the shear connector design requirements for box sections.

Radial Fatigue Shear Range due to Effects Other than Curvature, F_{fat2}

F_{fat2} is the radial fatigue shear range where significant torsion is caused by effects other than curvature, such as skew. F_{fat2} is computed from the net *range* of cross-frame/diaphragm force at the top flange under the applicable Fatigue load combination, F_{rc}.

As illustrated in Figure 3.3., F_{rc} is to be taken as the resultant range of horizontal force at the level of the top chord from all members and/or cross-frames at the point under consideration that is resisted by the shear connectors. F_{rc} is then distributed over the effective length of deck, w, shown in Figure 3.3. to give F_{fat2} in kips/inch as given by Equation 3.3.6.

As shown at the bottom of Figure 3.3., at skewed cross-frames, the normal (radial) component of the resultant range of force in that cross-frame at the level of the top chord must be computed. Should a normal (radial) cross-frame intersect the skewed cross-frame at the point under consideration, the normal (radial) component of the skewed cross-frame resultant force range should then be appropriately combined with the resultant range of horizontal force at the level of the top chord in the normal (radial) cross-frame to determine F_{rc}.

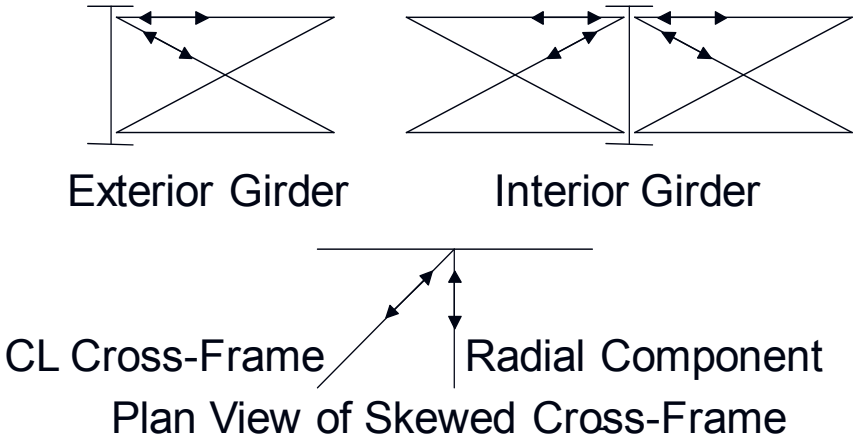


Figure 3.3.8 Resolution of the Horizontal Cross-Frame Force Ranges due to the Factored Fatigue Load at the Level of the Top Chord to Determine F_{rc}

According to *AASHTO LRFD* Article C6.10.10.1.2, in lieu of a refined analysis, F_{rc} may be taken equal to 25.0 kips for an exterior girder, which is typically the critical girder (refer to Figure 3.3.8). *This is typically a conservative value so more accurate determination of this value via refined analysis is suggested*. F_{rc} should not be multiplied by the factor of 0.75 that is recommended for application when determining ranges of force in cross-frames in *AASHTO LRFD* Article C6.6.1.2.1.

F_{fat2} is most likely to control when discontinuous cross-frame lines are used in conjunction with skew angles exceeding 20 degrees. For all other cases, F_{fat2} may be taken equal to zero according to *AASHTO LRFD* Article 6.10.10.1.2.

3.3.2.2.1.3 Stud Fatigue Shear Resistance, Z_r

The fatigue shear resistance of an individual stud shear connector, Z_r, to be used in Equation 3.3.2 for determining the shear connector pitch is to be taken as follows (*1*):

- Where the projected 75-year single-lane Average Daily Truck Traffic $(ADTT)_{SL}$ is greater than or equal to 960 trucks per day, the Fatigue I load combination is to be used and the fatigue shear resistance for infinite life is to be taken as:

$$Z_r = 5.5d^2$$

Equation 3.3.9
AASHTO LRFD Equation 6.10.10.2-1

- Otherwise, the Fatigue II load combination is to be used and the fatigue shear resistance for finite life is to be taken as:

$$Z_r = \alpha d^2$$

Equation 3.3.10
AASHTO LRFD Equation 6.10.10.2-2

where:

α = constant = $34.5 - 4.28 \log N$
d = diameter of the stud (in.)
N = number of stress cycles specified in *AASHTO LRFD* Article 6.6.1.2.5
= $(365)(75)n(ADTT)_{SL}$

Equation 3.3.11
AASHTO LRFD Equation 6.6.1.2.5-3

n = number of stress range cycles per truck passage taken from *AASHTO LRFD* Table 6.6.1.2.5-2

If a fatigue design life other than 75 years is sought, a number other than 75 may be inserted in Equation 3.3.11.

The specified value of the 75-year $(ADTT)_{SL}$ above which the infinite life check governs (i.e. 960 trucks per day) is calculated assuming a 75-year life and one stress range cycle per truck passage (i.e. n = 1.0 in Equation 3.3.11). For other values of the fatigue design life, the specified value of $(ADTT)_{SL}$ = 960 trucks/day should be multiplied by the ratio of 71,768 divided by the fatigue life sought in years. For other values of n, the specified of $(ADTT)_{SL}$ should be divided by the appropriate value of n taken from *AASHTO LRFD* Table 6.6.1.2.5-2.

The reader is referred to *AASHTO LRFD* Article 6.10.10.2 for the appropriate values of Z_r for channel shear connectors.

3.3.2.3 Strength Limit State Design

The resulting number of shear connectors determined to satisfy the fatigue limit state must be checked against the number required to satisfy the strength limit state.

The design requirement at the strength limit state computes the minimum number of shear connectors, *n*, necessary to develop a specified nominal longitudinal force, *P*, within regions on either side of the point of maximum positive design live load plus impact moment. The regions are defined off the point of maximum live load plus impact moment because it applies to the composite section and is easier to locate than a maximum of the sum of all the moments acting on the composite section. The equation for determining *n* in each region is given in *AASHTO LRFD* Article 6.10.10.4.1 as follows:

$$n = \frac{P}{Q_r}$$

Equation 3.3.12
AASHTO LRFD Equation 6.10.10.4.1-2

where:

P = total nominal shear force within the region under consideration determined as specified in *AASHTO LRFD* Article 6.10.10.4.2 (Section 3.3.2.3.1) (kips)

Q_r = factored shear resistance of one shear connector (Section 3.3.2.3.2) (kips)

Similar to V_{sr} for the fatigue limit state, *P* has both a longitudinal and a radial component, as discussed below in Section 3.3.2.3.1.

Since *P* is in terms of total nominal shear force over a specified region and Q_r is in terms of shear resistance per shear connector, it is clear that *n* will result in the required number of shear connectors over the specified region.

3.3.2.3.1 Nominal Shear Force, *P*

According to *AASHTO LRFD* Article 6.10.10.4.2, for simple spans and for continuous spans between points of maximum positive design live load plus impact moment and an adjacent end of the member, the total nominal shear force, *P*, is to be taken as:

$$P = \sqrt{P_p^2 + F_p^2}$$

Equation 3.3.13
AASHTO LRFD Equation 6.10.10.4.2-1

where:

P_p = total longitudinal force in the concrete deck at the point of maximum positive live load plus impact moment (discussed below) (kips)

F_p = total radial force in the concrete deck at the point of maximum positive live load plus impact moment (discussed below) (kips)

P_p is taken as the lesser of the following forces based on either the ultimate-strength properties of the concrete deck (P_{1p}), or the ultimate-strength properties of the steel girder (P_{2p}):

$$P_{1p} = 0.85 f_c' b_s t_s$$

Equation 3.3.14
AASHTO LRFD Equation 6.10.10.4.2-2

or:

$$P_{2p} = F_{yw} D t_w + F_{yt} b_{ft} t_{ft} + F_{yc} b_{fc} t_{fc}$$

Equation 3.3.15
AASHTO LRFD Equation 6.10.10.4.2-3

where:

b_s = effective width of the concrete deck (in.)

t_s = thickness of the concrete deck (in.)

F_p is taken as follows:

$$F_p = P_p \frac{L_p}{R}$$

Equation 3.3.16
AASHTO LRFD Equation 6.10.10.4.2-4

where:

L_p = arc length between an end of the girder and an adjacent point of maximum positive live load plus impact moment (Figure 3.3.9) (ft)

R = minimum girder radius over the length, L_p (ft)

F_p is provided in Equation 3.3.13 to account for the radial effect of curvature, and is required for curved spans or segments to bring the smallest of the longitudinal forces in either the deck or the girder (from Equation 3.3.14 or Equation 3.3.15) into equilibrium. The resulting longitudinal force, P_p, is assumed to be constant over the length, L_p, when computing the radial component, F_p, using Equation 3.3.16. Note that for straight spans or segments, F_p may be taken equal to zero.

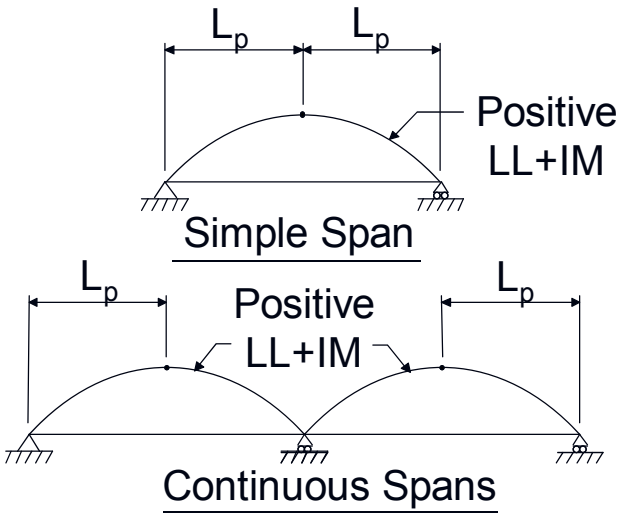


Figure 3.3.9 Definition of Arc Length, L_p

For continuous spans between the point of maximum positive design live load plus impact moment and the centerline of an adjacent interior support, the total nominal shear force, *P*, is to be taken as:

$$P = \sqrt{P_T^2 + F_T^2}$$

Equation 3.3.17
AASHTO LRFD Equation 6.10.10.4.2-5

where:

P_T = total longitudinal force in the concrete deck between the point of maximum positive live load plus impact moment and the centerline of an adjacent interior support (discussed below) (kips)

F_T = total radial force in the concrete deck between the point of maximum positive live load plus impact moment and the centerline of an adjacent interior support (discussed below) (kips)

P_T is taken as follows:

$$P_T = P_p + P_n$$

Equation 3.3.18
AASHTO LRFD Equation 6.10.10.4.2-6

where:

P_n = total longitudinal force in the concrete deck over an interior support (discussed below) (kips)

The number of shear connectors required between points of maximum positive design live load plus impact moment and the centerline of an adjacent interior support is computed from the sum of the critical forces at the maximum positive and negative moment locations according to Equation 3.3.18. The sum of the critical forces at the maximum moment locations is conservatively used in order to

provide adequate shear resistance for any live load position. Many shear connectors in this region resist reversing forces in the concrete deck depending on the live load position since there is no one point where the moment always changes sign.

P_n is taken as the lesser of the following forces based on either the ultimate-strength properties of the steel girder (P_{1n}), or a conservative approximation of the combined contribution of both the longitudinal reinforcement and the concrete that remains effective in tension based on its modulus or rupture (P_{2n}):

$$P_{1n} = F_{yw}Dt_w + F_{yt}b_{ft}t_{ft} + F_{yc}b_{fc}t_{fc}$$

Equation 3.3.19
AASHTO LRFD Equation 6.10.10.4.2-7

or:

$$P_{2n} = 0.45f_c^{'}b_s t_s$$

Equation 3.3.20
AASHTO LRFD Equation 6.10.10.4.2-8

In this region, sufficient shear connectors are necessary to transfer the ultimate tensile force in the longitudinal reinforcement from the concrete deck to the steel section. The tension force given by Equation 3.3.20 is a conservative approximation to account for the combined contribution of the longitudinal reinforcement and the concrete deck that remains effective in tension based on its modulus of rupture. *AASHTO LRFD* Article C6.10.10.4.2 permits a more precise value to be substituted for P_{2n}.

The radial force, F_T, is taken as follows:

$$F_T = P_T \frac{L_n}{R}$$

Equation 3.3.21
AASHTO LRFD Equation 6.10.10.4.2-9

where:

L_n = arc length between the point of maximum positive live load plus impact moment and the centerline of an adjacent interior support (Figure 3.3.10) (ft)
R = minimum girder radius over the length, L_n (ft)

F_T may be taken equal to zero for straight spans or segments.

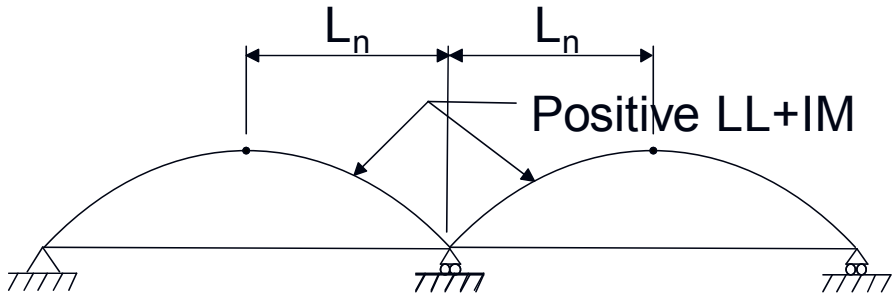


Figure 3.3.10 Definition of Arc Length, L_n

Box Sections

According to *AASHTO LRFD* Article 6.11.10, for box sections, the cross-sectional area of the steel box under consideration and the effective area of the concrete deck associated with that box are to be used to calculate the longitudinal force in Equations 3.3.14, 3.3.15, 3.3.19 and 3.3.20.

Also, for composite box flanges in closed-box sections at the strength limit state, in addition to satisfying the provisions of *AASHTO LRFD* Article 6.10.10.4, the vector sum of the longitudinal and torsional shears due to the factored loads in the concrete deck per connector are not to exceed Q_r from Equation 3.3.22 (see below). The torsional shear in the concrete deck can be determined by multiplying the torsional shear acting on the top of the composite box section by the ratio of the thickness of the transformed concrete deck to the total thickness of the top flange plus the transformed deck. The deck should include adequate transverse reinforcement to resist this torsional shear.

3.3.2.3.2 Factored Shear Resistance of a Stud, Q_r

According to *AASHTO LRFD* Article 6.10.10.4.1, the factored shear resistance, Q_r, of a single shear connector at the strength limit state is to be taken as:

$$Q_r = \phi_{sc} Q_n$$

Equation 3.3.22
AASHTO LRFD Equation 6.10.10.4.1-1

where:

ϕ_{sc} = resistance factor for shear connectors determined as specified in *AASHTO LRFD* Article 6.5.4.2 (= 0.85)

Q_n = nominal shear resistance of a single shear connector determined as specified in *AASHTO LRFD* Article 6.10.10.4.3 (discussed below) (kips)

AASHTO LRFD Article 6.10.10.4.3 specifies that the nominal shear resistance, Q_n, of one stud shear connector embedded in a concrete deck is to be taken as (*2*):

$$Q_n = 0.5A_{sc}\sqrt{f'_c E_c} \le A_{sc}F_u$$

Equation 3.3.23
AASHTO LRFD Equation 6.10.10.4.3-1

where:

A_{sc} = cross-sectional area of a stud shear connector (in.^{2})
E_c = modulus of elasticity of the deck concrete determined as specified in *AASHTO LRFD* Article 5.4.2.4 (ksi)
F_u = specified minimum tensile strength of a stud shear connector determined as specified in *AASHTO LRFD* Article 6.4.4 (ksi)

The specified minimum tensile strength of the connector, F_u, is equal to 60 ksi for a typical stud shear connector (*AASHTO LRFD* Article 6.4.4).

The reader is referred to *AASHTO LRFD* Article 6.10.10.4.3 for the appropriate value of Q_n for channel shear connectors.

3.3.3 Single-Angle Members

3.3.3.1 General

Single angles, as shown in Figure 3.3., are commonly used as cross-frame and lateral bracing members for steel bridges. These members must be designed as primary members in horizontally curved bridges. Similar consideration should be given to the design of these members in straight bridges with significant skews.

Since in most practical applications the angle is connected through one leg only, single-angle bracing members are typically subject to combined axial compression/tension and flexure, or moments about both principal axes due to the eccentricities of the applied axial load. The angle is also usually restrained by differing amounts about its geometric x- and y-axes. As a result, the prediction of the nominal resistance of these members under these conditions is difficult, particularly when the member is subject to compression.

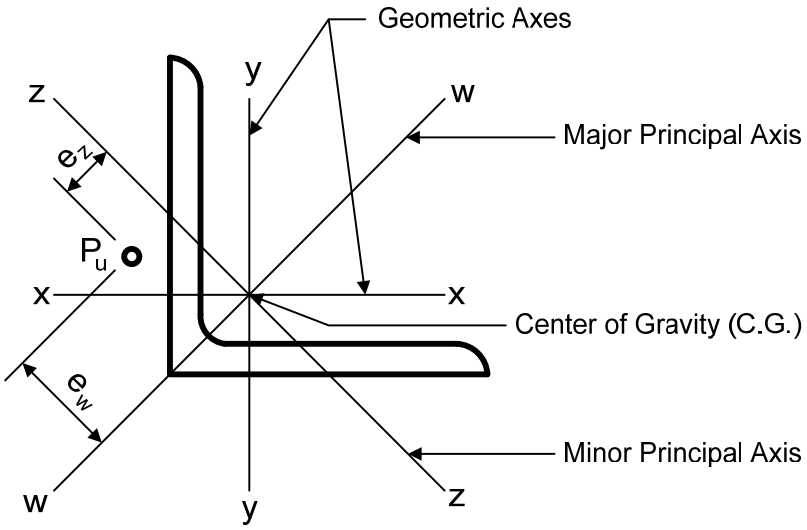


Figure 3.3.11 Single-Angle Member Geometry

As discussed in Section 3.3.3.2, the condition of flexure due to eccentric axial tension is primarily addressed through the use of the shear lag coefficient, *U*, specified in *AASHTO LRFD* Article 6.8.2.2.

As discussed in Section 3.3.3.3, the condition of flexure due to eccentric axial compression may now be efficiently handled through the use of an effective slenderness ratio, $(K\ell/r)_{eff}$, as specified in *AASHTO LRFD* Article 6.9.4.4 (introduced in the Fifth Edition of the *AASHTO LRFD* Specifications). The use of the specified effective slenderness ratio allows single angles satisfying certain conditions that are subject to combined axial compression and flexure to be designed as pin-ended concentrically loaded compression members for flexural buckling only. Furthermore, when the effective slenderness ratio is used, single angles need not be checked for flexural-torsional buckling, and the calculation of the nominal flexural resistance, M_n, of a single-angle member is typically not required. These provisions are based on the provisions for the design of single-angle members used in latticed transmission towers (*3*). Similar provisions are also employed in Section E5 of the 2005 AISC Specification (*4*), the Eurocode 3 standard (*5*) and in British Standard BS5950 (*6*).

The application of these provisions for the design of single-angle members subject to eccentric axial compression, as described in Section 3.3.3.3, is illustrated in Section 5.1.8.7 of the I-girder design example.

3.3.3.1.1 Minimum Thickness

The minimum thickness of the components (i.e. legs, etc.) of single angles that are used as structural members in bridges must exceed the minimum thickness of 5/16″ specified for structural steel in *AASHTO LRFD* Article 6.7.3.

3.3.3.2 Eccentric Axial Tension

3.3.3.2.1 General

The provisions of *AASHTO LRFD* Article 6.8.2 may be applied for single angles subject to eccentric axial tension. *AASHTO LRFD* Article 6.8.2.1 specifies that the factored tensile resistance, P_r, at the strength limit state be taken *as the lesser* of the following:

- The factored tensile resistance for yielding on the gross section taken as:

$$P_r = \phi_y F_y A_g$$

Equation 3.3.24
AASHTO LRFD Equation 6.8.2.1-1

or:

- The factored tensile resistance for fracture on the net section taken as:

$$P_r = \phi_u F_u A_n R_p U$$

Equation 3.3.25
AASHTO LRFD Equation 6.8.2.1-2

where:

ϕ_y = resistance factor for yielding of tension members as specified in *AASHTO LRFD* Article 6.5.4.2 (=0.95)
ϕ_u = resistance factor for fracture of tension members as specified in *AASHTO LRFD* Article 6.5.4.2 (=0.80)
A_g = gross cross-sectional area of the member (in.^{2})
A_n = net area of the member determined as specified in *AASHTO LRFD* Article 6.8.3 (Section 3.3.3.2.2) (in.^{2})
F_y = specified minimum yield strength (ksi)
F_u = tensile strength specified in *AASHTO LRFD* Table 6.4.1-1 (ksi)
R_p = reduction factor for holes taken equal to 0.90 for bolt holes punched full size and 1.0 for bolt holes drilled full size or subpunched and reamed to size
U = reduction factor to account for shear lag; 1.0 for components in which force effects are transmitted to all elements, and as specified in *AASHTO LRFD* Article 6.8.2.2 for other cases (Section 3.3.3.2.3)

The governing value of P_r must not exceed the factored block shear rupture resistance, R_r, of the member determined as specified in *AASHTO LRFD* Article 6.13.4 (and discussed further in Section 3.3.3.2.4).

A ductile steel loaded in axial tension can resist a force greater than the product of its gross area and yield strength prior to fracture due to strain hardening as long as excessive elongation due to uncontrolled yielding does not occur. However,

depending on the ratio of net area to gross area, the geometry of the end connection and the mechanical properties of the steel, the component can fail by fracture of the net area at a load smaller than that required to yield the gross area. Thus, both yielding and fracture must be checked.

Holes in a member cause stress concentrations at service loads, with the tensile stress adjacent to the hole typically about three times the average stress on the net area. As load increases and the deformation continues, all fibers across the section will achieve or eventually exceed the yield strain. Failure occurs when the localized yielding results in a fracture through the net area. Since the width of the member occupied by the net area at bolt holes is generally negligible relative to the overall width of the member, strain hardening is easily achieved in the vicinity of the holes and yielding on the net area at bolt holes is not considered to be significant, except perhaps for built-up members of unusual proportions. A higher margin of safety is typically used when considering the net section fracture resistance versus the yield resistance, as reflected in the specified resistance factors.

The reduction factor, R_p, in Equation 3.3.25 conservatively accounts for the reduced fracture resistance in the vicinity of bolt holes punched full size (*7*). No reduction in the net section fracture resistance is required for holes that are drilled full size or subpunched and reamed to size. In previous specifications, the reduction in the factored resistance for punched holes was accounted for by increasing the hole size for design by 1/16 inches, which penalized drilled and subpunched and reamed holes and did not provide a uniform reduction for punched holes since the reduction varied with the hole size. This reduction has since been removed in favor of the factor, R_p. *AASHTO LRFD Article 6.6.1.2.3 specifies that unless information is available to the contrary, bolt holes in cross-frame and lateral bracing members and their connection plates are to be assumed for design to be punched full size*.

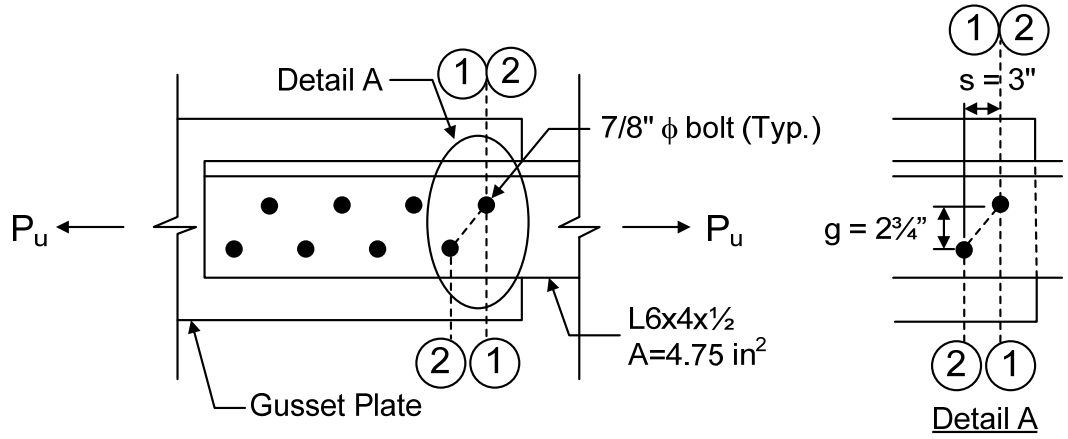
3.3.3.2.1.1 Maximum Slenderness Ratio

Since cross-frames and lateral bracing members in curved bridges are primary members and are subject to stress reversal, the slenderness ratio, ℓ/r, of these members when subject to tension is limited to 140 (*AASHTO LRFD* Article 6.8.4), where *r* is the radius of gyration of the member. A similar limit should be considered for these members in straight bridges with significant skews.

3.3.3.2.2 Net Area, A_n

AASHTO LRFD Article 6.8.3 specifies that the net area, A_n, be taken as the product of the thickness of the angle and its smallest net width. *The width of each standard bolt hole is to be taken as the nominal diameter of the hole*. Maximum holes sizes for different bolt diameters are specified in *AASHTO LRFD* Table 6.13.2.4.2-1. For example, for a 7/8-inch diameter bolt, the maximum hole size of a standard hole is 15/16 inches.

The net width is to be determined for each chain of holes extending across the connected angle leg along any transverse, diagonal or zigzag line. For each chain, the net width is to be determined by subtracting from the total width, the sum of all holes in the chain and adding the quantity $s^2/4g$ for each space between consecutive holes in the chain (i.e. when holes are staggered), where s is equal to the pitch of ay two consecutive holes and g is the gage of the same two holes (Figure 3.3.12). The development of the $s^2/4g$ rule is described in Reference 8. When holes are staggered in both legs of an angle, the gage for holes in opposite adjacent legs is to be taken as the sum of the gages from the back of the angles less the thickness of the angle. For welded single angle connections, A_n is to be taken as the gross area.



$$\text{Chain } 1-1: \quad A_n = 4.75 - [1(0.9375)(0.5)] = 4.28 \text{ in.}^2$$

$$\text{Chain } 2-2: \quad A_n = 4.75 - [2(0.9375)(0.5)] + \left[\frac{(3.0)^2}{4(2.75)}(0.5)\right] = 4.22 \text{ in.}^2 \quad \text{(Governs)}$$

Figure 3.3.12 Net Area Computation – Single Angle with Staggered Bolt Holes

It is conservative to use the least net width in conjunction with the full tensile force to check the connected element. Assuming each bolt transfers an equal share of the load whenever the bolts are arranged symmetrically with respect to the centroidal axis of the connected element, a less conservative alternative is to check each possible chain with a tensile force obtained by subtracting the force removed by each bolt ahead of that chain from the full tensile force.

3.3.3.2.3 Shear Lag Reduction Factor, *U*

As mentioned previously, the eccentricity in these members due to the typical connection through only one leg when subject to tension is addressed through the use of the shear lag reduction factor, *U*, determined as specified in *AASHTO LRFD*

Article 6.8.2.2. As discussed in the Commentary to the *AISC LRFD* Specification (*4*), if the connection is proportioned such that *U* is greater than or equal to 0.6 (which is typically the case), the eccentricity may be ignored in determining the factored resistance of the member.

The *U* factor accounts for shear lag effects associated with end connection geometry. Shear lag is a consideration where the tensile force in the member is applied eccentrically or transmitted by connection to some, but not all of the connection elements; e.g. an angle having a connection to only one leg, or when the connection elements do not lie in a common plane. In such cases, the tensile force is not uniformly distributed over the net area and the critical net section may not be fully effective. Shear lag does not need to be considered when checking yielding on the gross section because the non-uniform tensile stresses over the cross-section tend to be equalized by the yielding. Research on the effects of shear lag in end connections of tension members is described in References 9 and 10.

For single angles, in the absence of more refined analysis or tests, *U* may be determined using the equation given in Case 2 of *AASHTO LRFD* Table 6.8.2.2-1 as shown below:

$$U = 1 - \frac{\bar{x}}{L}$$

Equation 3.3.26

where:

$\bar{x}$ = perpendicular distance from the connection plane or face of the member to the centroid of the member section resisting the connection force (in.)

L = out-to-out distance between the bolts in the connection parallel to the line of force, or maximum length of the longitudinal welds (in.)

Illustrative examples of $\bar{x}$ and *L* for single angles connected with bolts and welds are shown in Figure 3.33. Note that for members connected with combinations of longitudinal and transverse welds, *L* is taken as the maximum length of the longitudinal welds. The transverse weld does little to influence the transfer of the load into the unattached elements of the member cross-section, and thus, does not significantly affect the fracture resistance based on shear lag.

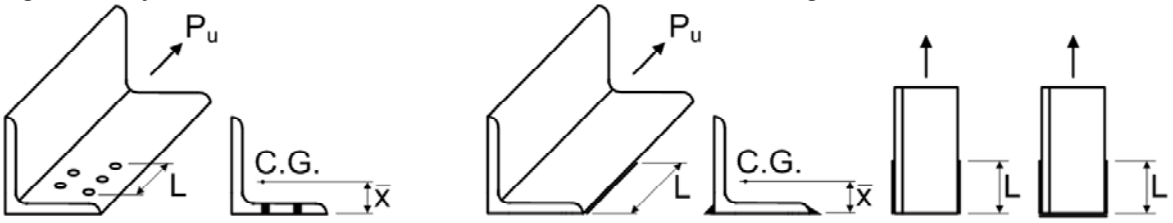


Figure 3.3.13 Determination of $\bar{x}$ and *L* in the Calculation of the Shear Lag Reduction Factor, *U*, from Equation 3.3.26

U for single angles may be determined more simply according to Case 8 in *AASHTO LRFD* Table 6.8.2.2-1; i.e., taken equal to 0.80 with four or more bolts per line in the direction of loading, or as 0.60 with two or three bolts per line in the direction of loading. If Equation 3.3.26 is also used to calculate *U*, then the larger of the applicable constant value or the value from Equation 3.3.26 is permitted for use.

AASHTO LRFD Article 6.8.2.2 further specifies that for members composed or more than one element, the calculated value of U should not be taken to be less than the ration of the gross area of the connected element (or elements) to the member gross area.

3.3.3.2.4 Block Shear Rupture Resistance, R_r

A connected element subject to tension must be checked for a tearing limit state known as block shear rupture. A block shear rupture failure for an angle in tension bolted to a gusset plate is shown in Figure 3.3.14. In Figure 3.3.14, the tearing failure along the bolt holes occurs along section a-b-c. The tearing or shear rupture resistance on section a-b plus the tensile yield resistance on section b-c will result in the total block shear rupture resistance. Note that the failure path is defined by the centerlines of the bolt holes. Tests have shown that it is reasonable to add the resistance in tension yielding on one plane to the shear rupture resistance of the perpendicular plane (*11*, *12*).

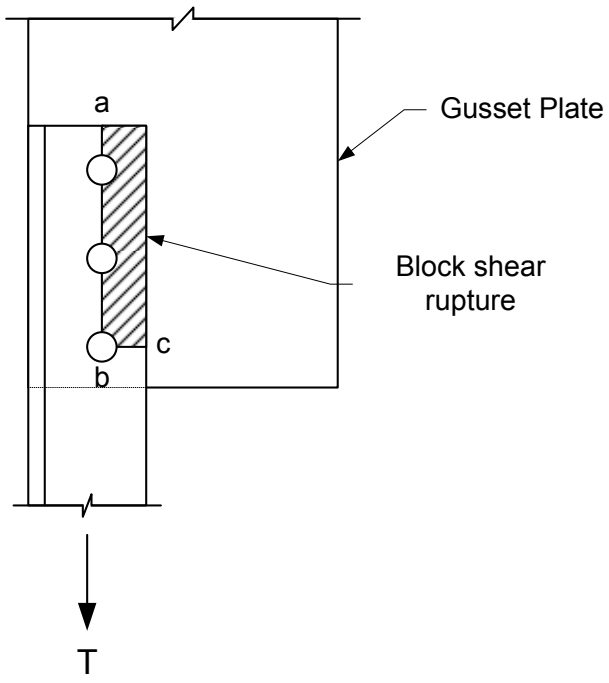


Figure 3.3.14 Tension Failure of a Bolted Single Angle Member by Block Shear Rupture

AASHTO LRFD Article 6.13.4 specifies that block shear rupture is to be checked for the web connection of coped beams and for all tension connections, including connection plates, splice plates and gusset plates. Tests on coped beams have indicated that a block shear failure can occur around the perimeter of the bolt holes (*13*). The block shear rupture mode is not limited to the coped ends of beams, however. Tension member connections are also susceptible, and the block shear rupture mode should also be checked around the periphery of welded connections. The connection is to be investigated by considering all possible failure planes in the connected elements, including those parallel and perpendicular to the applied forces, and determining the most critical set of planes. Planes parallel to the applied force are to be considered to resist only shear stresses and planes perpendicular to the applied force are to be considered to resist only tensile stresses. Block shear rupture is most likely to control in the design of bolted end connections to thin webs of girders (e.g. coped beams) and in the design of short compact bolted connections. It is unlikely to control in the design of bolted flange and web splices of typical proportions.

Therefore, the factored tensile resistance, P_r, computed from Equation 3.3.24 or Equation 3.3.25, whichever controls, must not exceed the factored block shear rupture resistance, R_r, of the member, which must be investigated at the end connections. The factored block shear rupture resistance is determined according to the provisions of *AASHTO LRFD* Article 6.13.4 as follows:

$$R_r = \phi_{bs} R_p \left(0.58 F_u A_{vn} + U_{bs} F_u A_{tn}\right)$$
$$\leq \phi_{bs} R_p \left(0.58 F_y A_{vg} + U_{bs} F_u A_{tn}\right)$$

Equation 3.3.27
AASHTO LRFD Equation 6.13.4-1

where:

ϕ_{bs} = resistance factor for block shear rupture specified in *AASHTO LRFD* Article 6.5.4.2 (=0.80)
A_{vg} = gross area along the plane resisting shear stress (in.^{2})
A_{vn} = net area along the plane resisting shear stress (in.^{2})
A_{tn} = net area along the plane resisting tension stress (in.^{2})
U_{bs} = reduction factor for block shear rupture resistance taken equal to 0.50 when the tension stress is non-uniform and 1.0 when the tension stress is uniform (use 1.0 for angles and tees)

The terms F_y, F_u and R_p are as defined previously.

In determining R_r, the resistance to rupture along the shear plane is added to the resistance to rupture on the tensile plane (Figure 3.3.15). Block shear rupture is a rupture or tearing phenomenon and not a yielding phenomenon. However, gross yielding along the shear place can occur when tearing on the tensile plane commences if $0.58F_uA_{vn}$ exceeds $0.58F_yA_{vg}$. Therefore, the preceding equation limits $0.58F_uA_{vn}$ to not exceed $0.58F_yA_{vg}$.

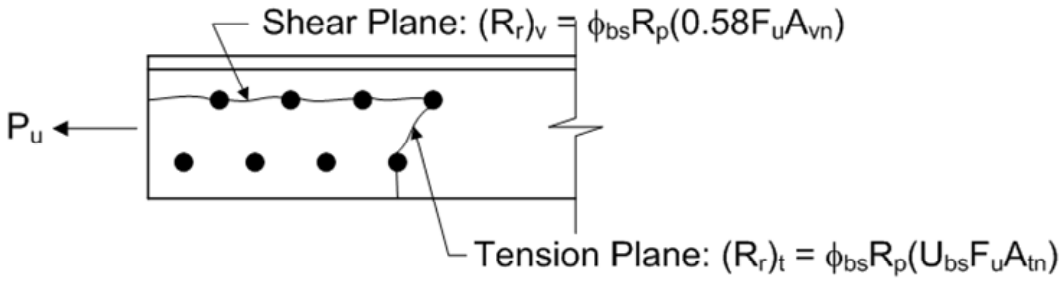


Figure 3.3.15 Factored Resistance of Shear and Tension Planes

The reduction factor, U_{bs}, has been included in Equation 3.3.27 to approximate the effect of a non-uniform stress distribution on the tensile plane in certain cases; e.g., coped beam connections with multiple rows of bolts. In such cases, the tensile stress on the end plane is non-uniform because the rows of bolts nearest the beam end pick up most of the shear (*11*, *14*). For the majority of connections encountered in steel bridges, e.g. angle and tee member connections, U_{bs} will equal 1.0.

In determining the net area of cuts carrying shear stress, the full effective diameter of staggered holes centered within two hole diameters of the cut is to be deducted;

holes further removed are to be disregarded. In determining the net area of cuts carrying tension stress, the effect of staggered holes adjacent to the cuts is to be determined using the $s^2/4g$ correction.

3.3.3.2.5 Fatigue of Single-Angle Member Connections

AASHTO LRFD Table 6.6.1.2.3-1 now provides a simplified procedure for checking fatigue of welded (Condition 7.2) or bolted (Condition 2.5) connections of single-angle members to gusset or connection plates that are subject to a net applied tensile stress (as defined in *AASHTO LRFD* Article 6.6.1.2.1).

When determining ranges of stress in cross-frame members for fatigue design, the low probability of two vehicles being in their critical relative transverse positions over millions of cycles should be considered. *AASHTO LRFD* Article C6.6.1.2.1 recommends that one cycle of stress in a cross-frame member be determined as 75 percent of the stress range in the member determined by the passage of the fatigue load in two different transverse positions, but not less than the stress range caused by the loading of only one lane.

3.3.3.2.5.1 Welded Connections

For single-angle members connected to a gusset or connection plate by longitudinal fillet welds along both sides of the connected element of the member cross-section (Figure 3.3.16), the fatigue stress range, Δf, is to be calculated as follows:

$$\Delta f = \frac{\Delta P}{A_e} = \frac{\Delta P}{UA_g}$$

Equation 3.3.28

where:

A_e = effective net area of the member = UA_g (in.^{2})
A_g = gross cross-sectional area of the member (in.^{2})
ΔP = range of axial force in the member under the applicable Fatigue load combination (kips)
U = shear-lag reduction factor determined from Equation 3.3.26

$\bar{x}$ is to be taken as the distance from the centroid of the member to the surface of the gusset or connection plate, and *L* is to be taken as the maximum length of the longitudinal welds (Figure 3.3.16) in the calculation of the shear-lag reduction factor, *U*.

The effect of the moment due to the eccentricities in the connection may be ignored in computing the stress range when Equation 3.3.28 is used (*15*).

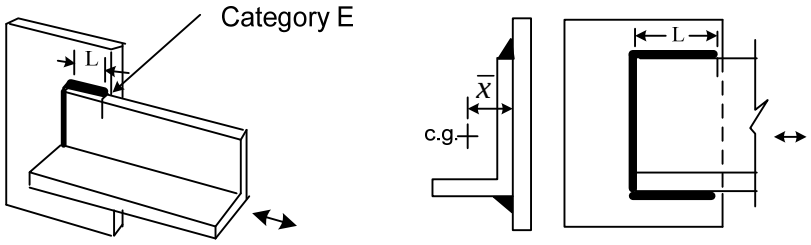


Figure 3.3.16 Welded Connection of a Single-Angle Member to a Gusset Plate

The nominal fatigue resistance of the base metal in single-angle members connected by longitudinal fillet welds along both sides of the connected element of the member cross-section is to be based on detail Category E (Condition 7.2 in *AASHTO LRFD* Table 6.6.1.2.3-1). While the research showed that balancing of the welds offers some increase in the fatigue life (*15*), it is probably not worth the increase in the gusset or connection plate length required to accommodate the longer weld along one leg.

3.3.3.2.5.2 Bolted Connections

For single-angle members connected to a gusset or connection plate with high-strength bolted slip-critical connections (Figure 3.3.17), the fatigue stress range, Δf, is to be calculated from Equation 3.3.28. Slip-critical connections are discussed further in Section 3.3.6.2.1.1.

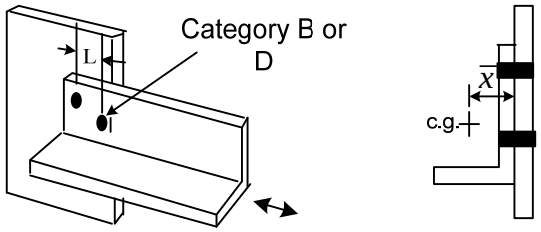


Figure 3.3.17 Bolted Connection of a Single-Angle Member to a Gusset Plate

A_g is to be replaced with the net area of the member, A_n, in Equation 3.3.28 for all other types of bolted connections.

$\bar{x}$ is to be taken as the distance from the centroid of the member to the surface of the gusset or connection plate, and L is to be taken as out-to-out distance between the bolts in the connection parallel to the line of force (Figure 3.3.17) in the calculation of the shear-lag reduction factor, U.

The effect of the moment due to the eccentricities in the connection may be ignored in computing the stress range when Equation 3.3.28 is used.

The nominal fatigue resistance of the base metal in members connected by pre-tensioned high-strength bolts in slip-critical connections is to be determined based on whether the bolt holes are drilled full size or subpunched and reamed to size (Category B), or punched full size (Category D) (Condition 2.1 in *AASHTO LRFD* Table 6.6.1.2.3-1). As mentioned previously, *AASHTO LRFD Article 6.6.1.2.3 specifies that unless information is available to the contrary, bolt holes in cross-frame and lateral bracing members and their connection plates are to be assumed for design to be punched full size*.

Refer to Condition 2.2 or 2.3 in *AASHTO LRFD* Table 6.6.1.2.3-1, as applicable, for all other types of bolted connections. The fatigue resistance of bolted connections is discussed further in Section 3.3.6.2.1.3.

3.3.3.3 Eccentric Axial Compression

3.3.3.3.1 General

For single angles subject to eccentric axial compression, the provisions of *AASHTO LRFD* Articles 6.9.2.1 and 6.9.4 may be applied. *AASHTO LRFD* Article 6.9.2.1 specifies that the factored compressive resistance, P_r, at the strength limit state be taken as:

$$P_r = \phi_c P_n$$

Equation 3.3.29
AASHTO LRFD Equation 6.9.2.1-1

where:

ϕ_c = resistance factor for axial compression specified in *AASHTO LRFD* Article 6.5.4.2 (=0.90)

P_n = nominal compressive resistance (kips) specified in *AASHTO LRFD* Article 6.9.4.1.1 as follows:

- If $\frac{P_e}{P_o} \geq 0.44$, then:

$$P_n = \left[0.658^{\left(\frac{P_o}{P_e}\right)}\right] P_o$$

Equation 3.3.30
AASHTO LRFD Equation 6.9.4.1.1-1

- If $\frac{P_e}{P_o} < 0.44$, then:

$$P_n = 0.877\ P_e$$

Equation 3.3.31
AASHTO LRFD Equation 6.9.4.1.1-2

where:

P_e = elastic critical buckling resistance *for flexural buckling* determined as specified in *AASHTO LRFD* Article 6.9.4.1.2 (Section 3.3.3.3.1.1) (kips)
P_o = equivalent nominal yield resistance = QF_yA_g (Section 3.3.3.3.3) (kips)
A_g = gross cross-sectional area of the member (in.^{2})
F_y = specified minimum yield strength (ksi)
Q = slender element reduction factor (Section 3.3.3.3.3)

Equation 3.3.30 for P_n provides a transition between elastic buckling and yielding, reflecting essentially the effects of residual stress and initial out-of-straightness. Equation 3.3.31 represents an elastic bucking equation for longer columns. The two equations represent a single curve that closely fits SSRC (Structural Stability Research Council) Column Curve 2P (*16*) modified to reflect an initial out-of-straightness criterion of *L*/1500. The development of the mathematical form of the equations representing this curve is discussed in References 17 and 18. Reference 19 shows a reasonable comparison of the results from Equations 3.3.30 and 3.3.31 with physical column test data compiled by Hall (*20*). More detailed discussion on column buckling theory and the genesis of Equations 3.3.30 and 3.3.31 may be found in Reference 21.

Equations 3.3.30 and 3.3.31 are equivalent to the equations given in the 2005 *AISC LRFD* Specification (*4*) for computing the nominal compressive resistance. In the *AASHTO LRFD* Specification, the equations are written in a different format in terms of the critical elastic buckling resistance, P_e, and the equivalent nominal yield resistance, P_o, to allow for more convenient calculation of the nominal resistance for members subject to buckling modes in addition to, or other than, flexural buckling, and to allow for the consideration of compression members with slender elements (Section 3.3.3.3.3).

3.3.3.3.1.1 Elastic Critical Buckling Resistance, P_e (Flexural Buckling)

Flexural buckling of concentrically loaded compression members refers to a buckling mode in which the member deflects laterally without twist or a change in the cross-sectional shape. In general, flexural buckling involves lateral displacements of the member cross-section in the direction of the geometric x- and y-axes that are resisted by the respective flexural rigidities of the member.

The equation used to calculate the elastic flexural buckling resistance, P_e, for single angles subject to eccentric axial compression is specified in *AASHTO LRFD* Article 6.9.4.1.2 as follows:

$$P_e = \frac{\pi^2 E}{\left(\frac{K\ell}{r}\right)^2_{eff}}$$

Equation 3.3.32
AASHTO LRFD Equation 6.9.4.1.2-1

where:

A_g = gross cross-sectional area of the member (in.^{2})

$\left(\frac{K\ell}{r}\right)^2_{eff}$ = effective slenderness ratio (Section 3.3.3.3.2)

3.3.3.3.1.2 Maximum Slenderness Ratio

Since cross-frames and lateral bracing members in curved bridges are primary members, the slenderness ratio, $K\ell/r$, of these members when subject to compression is limited to 120 (*AASHTO LRFD* Article 6.9.3), where K is the effective length factor specified in *AASHTO LRFD* Article 4.6.2.5 and r is the radius of gyration of the member. A similar limit should be considered for these members in straight bridges with significant skews.

AASHTO LRFD Article 6.9.4.4 specifies that the actual maximum slenderness ratio of the angle, as opposed to the effective slenderness ratio,$(K\ell/r)_{eff}$ (Section 3.3.3.3.2), is not to exceed the preceding limit. Thus, if $(K\ell/r)_{eff}$ exceeds the limiting ratio, but the actual maximum slenderness ratio of the angle does not, the design is satisfactory.

3.3.3.3.2 Effective Slenderness Ratio, $(K\ell/r)_{eff}$

According to *AASHTO LRFD* Table 6.9.4.1.1-1, single angles in compression need only be checked for flexural buckling if the provisions of *AASHTO LRFD* Article 6.9.4.4 are employed. These provisions permit the effects of all eccentricities in the member to be neglected when these members are evaluated as axially loaded compression members for flexural buckling only using an appropriate effective slenderness ratio, $(K\ell/r)_{eff}$. The effective slenderness ratio indirectly accounts for the bending in the angles due to the eccentricity of the loading allowing the member to be proportioned as if it were a pinned-end concentrically loaded compression member. *Furthermore, when the effective slenderness ratio is used, single angles need not be checked for flexural-torsional buckling*.

The member must satisfy all of the following conditions specified in *AASHTO LRFD* Article 6.9.4.4, which are typically satisfied by members used in cross-

frames and lateral bracing in steel-bridge applications, in order to use the effective slenderness ratio:

- End connections are to a single leg of the angle, and are welded or use a minimum of two bolts
- The angle is loaded at the ends in compression through the same leg
- The angle is not subjected to any intermediate transverse loads
- If used as web members in trusses, all adjacent web members are attached to the same side of the gusset plate or chord

The equations for the effective slenderness ratio presume significant end rotational restraint about the y-axis, or the axis perpendicular to the connected leg and gusset plate (Figure 3.3.18). As a result, as shown in various tests (*22-24*), the angle tends to buckle primarily about the x-axis due to the eccentricity of the load about the x-axis coupled with the high degree of restraint about the y-axis (References 22 and 24 included tests of unequal-leg angles). Thus, the radius of gyration in the effective slenderness ratio equations is taken as r_x, or the radius of gyration about the geometric axis parallel to the connected leg, as opposed to the minimum radius of gyration about the minor principal axis of the angle, r_z (Figure 3.3.19). When an angle has significant rotational restraint about the y-axis, the stress along the connected leg will be approximately uniform (*25*).

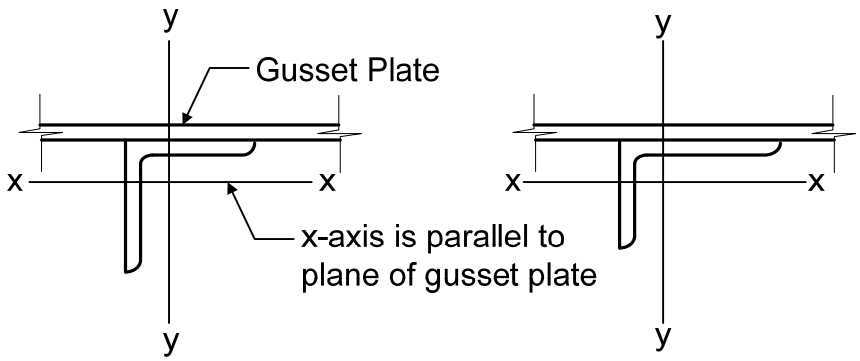


Figure 3.3.18 Single-Angle Geometric Axes Utilized in the Effective Slenderness Ratio Expressions - for Equal-Leg Angle and Unequal-Leg Angle Connected Through the Longer Leg

Lutz (*26*) compared the results from the effective slenderness ratio equations to test results for single-angle members in compression with essentially pinned-end connections reported in References 27 and 28 and found an average value of Pr/Ptest of 0.998 with a coefficient of variation of 0.109. A separate set of equations presented in the 2005 *AISC LRFD* Specification (*4*), which assume a higher degree of x-axis rotational restraint and thus are intended for application only to single angles used as web members in box or space trusses, are not provided in the *AASHTO LRFD* Specifications.

The equations for the effective slenderness ratio, $(K\ell/r)_{eff}$, for the case of equal-leg angles and unequal-leg angles connected through the longer leg (Figure 3.3.18) are as follows.

- If $\ell/r_x \le 80$, then:

$$\left(\frac{K\ell}{r}\right)_{eff} = 72 + 0.75\left(\frac{\ell}{r_x}\right)$$

Equation 3.3.33
AASHTO LRFD Equation 6.9.4.4-1

- If $\ell/r_x > 80$, then:

$$\left(\frac{K\ell}{r}\right)_{eff} = 32 + 1.25\left(\frac{\ell}{r_x}\right)$$

Equation 3.3.34
AASHTO LRFD Equation 6.9.4.4-2

where:

ℓ = distance between the work points of the joints measured along the length of the angle (in.)
r_x = radius of gyration about the geometric axis of the angle parallel to the connected leg (in.)

r_x in the equations should be taken as the smaller value about the angle geometric axes, which is typically listed as r_y for rolled angle shapes, in applying the equations for an unequal-leg angle connected through the longer leg.

The equations for the effective slenderness ratio, $(K\ell/r)_{eff}$, for the case of unequal-leg angles connected through the shorter leg and with ratios of leg lengths, (b_ℓ/b_s), less than 1.7 (Figure 3.3.19) are as follows:

- If $\ell/r_x \le 80$, then:

$$\left(\frac{k\ell}{r}\right)_{eff} = 72 + 0.75\left(\frac{\ell}{r_x}\right) + 4\left[\left(\frac{b_\ell}{b_s}\right)^2 - 1\right] \ge 0.95\left(\frac{\ell}{r_z}\right)$$

Equation 3.3.35
AASHTO LRFD Equation 6.9.4.4-3

- If $\ell/r_x > 80$, then:

$$\left(\frac{k\ell}{r}\right)_{eff} = 32 + 1.25\left(\frac{\ell}{r_x}\right) + 4\left[\left(\frac{b_\ell}{b_s}\right)^2 - 1\right] \geq 0.95\left(\frac{\ell}{r_z}\right)$$

Equation 3.3.36
AASHTO LRFD Equation 6.9.4.4-4

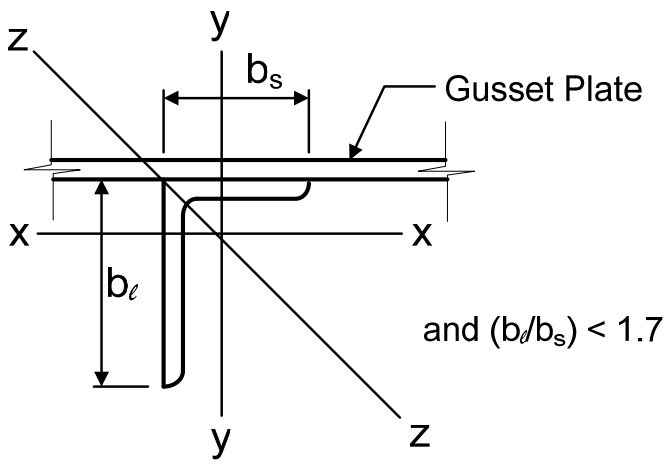


Figure 3.3.19 Unequal-Leg Angles Connected Through the Shorter Leg with Ratio of Leg Lengths < 1.7

The limited available test data for this case (*22*, *24*) give lower capacities for comparable ℓ/r_x values than equal-leg angles (*26*). Stiffening the shorter leg rotationally tends to force the buckling axis of the angle away from the x-axis and closer to the z-axis, or minor principal axis of the angle (*26*) (Figure 3.3.19). Thus, the effective slenderness ratio equations for this case (Equations 3.3.35 and 3.3.36) are modified by adding an additional term based on the ratio of the leg lengths, along with a governing slenderness limit based on ℓ/r_z for slender unequal-leg angles. The upper limit on (b_ℓ/b_s) of 1.7 is based on the limits of the available physical tests.

Single-angle compression members not meeting one or more of the specified conditions, or with (b_ℓ/b_s) greater than or equal to 1.7, should instead be explicitly evaluated for combined axial load and flexure as beam-columns according to Section H2 of the 2005 *AISC LRFD* Specification (*4*). The reader is referred to *AASHTO LRFD* Article C6.9.4.4 for further information on the suggested procedure to follow in the unlikely event that this would be required.

Single-angle members are often employed in X-type configurations in cross-frames. Since the necessary rotational restraint about the y-axis assumed in the effective slenderness ratio equations may not be present at the crossover point of the diagonals (e.g. if the members are only connected with a single bolt at that

point), it is recommended in *AASHTO LRFD* Article C6.9.4.4 that the full length of the diagonal between the connection work points be used for ℓ in applying the effective slenderness ratio equations.

3.3.3.3.3 Equivalent Nominal Yield Resistance, P_o

The last term needed in order to compute the nominal compressive resistance, P_n, is the equivalent nominal yield resistance, P_o, defined in *AASHTO LRFD* Article 6.9.4.1.1 as follows:

$$P_o = QF_yA_g$$

Equation 3.3.37

where:

A_g = gross cross-sectional area of the member (in.^{2})
Q = slender element reduction factor ≤ 1.0

For compression members composed of one or more so-called “slender elements”; that is, elements not meeting the corresponding width-to-thickness ratio limits specified in *AASHTO LRFD* Table 6.9.4.2.1-1, the slender element reduction factor, Q, accounts for the effect of potential local buckling of those elements on the overall buckling resistance of the member and has a value less than 1.0. The value of Q in this instance is determined according to the provisions of *AASHTO LRFD* Article 6.9.4.2.2. The AISC Specification has used this approach, as adopted from Reference 29, since 1969. Prior to 1969, a more conservative approach was used in which any portion of a plate width that exceeded the appropriate width-to-thickness ratio limit was disregarded.

For compression member cross-sections without any slender elements; that is, composed entirely of non-slender elements, Q is taken equal to 1.0 as specified in *AASHTO LRFD* Article 6.9.4.2.1. In such cases, local buckling does not adversely affect the nominal compressive resistance.

For compression member cross-sections composed entirely of unstiffened elements, or plates supported along only one edge parallel to the direction of the compression force, Q is taken equal to the factor for unstiffened elements, Q_s. Unstiffened elements are assumed to reach their limit of resistance when they attain their theoretical local buckling resistance. Q_s is taken as the smallest value for all unstiffened slender elements in the cross-section. Single angles are composed entirely of unstiffened elements (Figure 3.3.20).

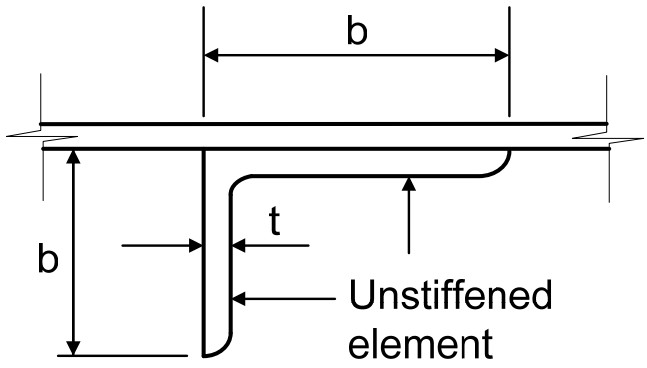


Figure 3.3.20 Unstiffened Elements for a Single-Angle Member

Q_s for slender unstiffened elements is equal to the ratio of the smallest local buckling resistance of all the unstiffened elements in the cross-section divided by F_y. In other words, for a compression member composed entirely of unstiffened elements, the reduced equivalent nominal yield resistance, P_o, of the member is taken as the average axial stress at which the most critical unstiffened element reaches its local buckling resistance (i.e. the elastic or inelastic local buckling resistance depending on the values of b/t and F_y). Additional information on the development of the equations for Q_s may be found in the Commentary to Section E7 of the 2005 *AISC LRFD* Specification (4) and in Reference 30.

b is the full width of the unstiffened element (i.e. outstanding leg) and t is the thickness of that leg (Figure 3.3.20) in the following equations for Q_s for single angles specified in *AASHTO LRFD* Article 6.9.4.2.2:

- If $\frac{b}{t} \le 0.45\sqrt{\frac{E}{F_y}}$, then::

$$Q = Q_s = 1.0$$

Equation 3.3.38

- If $0.45\sqrt{\frac{E}{F_y}} < \frac{b}{t} \le 0.91\sqrt{\frac{E}{F_y}}$, then:

$$Q = Q_s = 1.34 - 0.76\left(\frac{b}{t}\right)\sqrt{\frac{F_y}{E}}$$

Equation 3.3.39
AASHTO LRFD Equation 6.9.4.2.2-5

- If $\frac{b}{t} > 0.91\sqrt{\frac{E}{F_y}}$, then:

$$Q = Q_s = \frac{0.53E}{F_y\left(\frac{b}{t}\right)^2}$$

Equation 3.3.40
AASHTO LRFD Equation 6.9.4.2.2-6

3.3.4 Tee and Double-Angle Members

3.3.4.1 General

Structural tees, as shown in Figure 3.3.21, are sometimes used as cross-frame and lateral bracing members for steel bridges, particularly as the loads in these members become larger. Since in most practical applications, the tee is connected through the flange, tees used as bracing members are also typically subject to combined axial compression/tension and flexure, or a moment about the major-axis of the tee due to the eccentricity of the applied axial load. Double angles can be treated similarly to structural tees. Double angles permit bolts to work in double shear reducing the number. However, as mentioned in Section 3.1.2.8.5.1, they are expensive to fabricate and painting between the angles is difficult.



Figure 3.3.21 Cross-Frame Composed of Structural Tees

The conditions of flexure due to eccentric axial tension and flexure due to eccentric axial compression for tees and double angles are addressed through the use of the beam-column interaction curves specified in *AASHTO LRFD* Article 6.8.2.3 and 6.9.2.2, respectively. Thus, the calculation of the nominal flexural resistance, M_n, of these members is typically required. Also, tees and double angles subject to axial compression can fail either by flexural buckling about their x-axis, or by

torsion combined with flexure about their y-axis (or the axis of symmetry of the section); a condition known as flexural-torsional buckling. An effective slenderness ratio approach, such as the approach discussed in Section 3.3.3.3 for the design of single angles subject to eccentric axial compression, is not available for the design of tees and double angles.

The general geometry of a tee member is shown in Figure 3.3.22. Tees and double angles are singly symmetric members, with the plane of symmetry assumed to be that formed by their weak axis (or y-axis). Legs of double angles in continuous contact or with separators may together be assumed treated as the stem of a tee in applying the specification provisions discussed below.

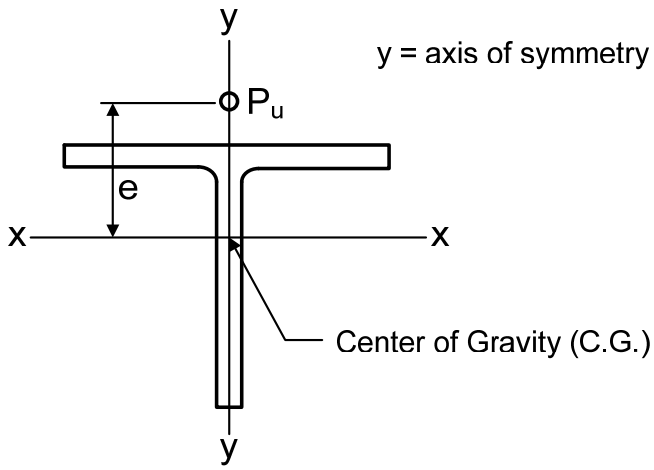


Figure 3.3.22 Tee Member Geometry and Eccentricity of Applied Load, P_u

The application of the provisions for the design of a tee member subject to eccentric axial compression (used as a top lateral bracing member), as described below in Section 3.3.4.3, is illustrated in Section 5.2.9.7 of the tub girder design example.

3.3.4.1.1 Minimum Thickness

The minimum thickness of the components (i.e. flange, stem, etc.) of tees and double angles that are used as structural members in bridges must exceed the minimum thickness of 5/16″ specified for structural steel in *AASHTO LRFD* Article 6.7.3.

3.3.4.1.2 Maximum Slenderness Ratio

The maximum permitted slenderness ratios for tees and double angles subject to tension and tees and double angles subject to compression in curved bridges (and preferably in straight bridges with significant skews) are the same as discussed previously for single angles; i.e. 140 for primary tension members and 120 for primary compression members.

3.3.4.2 Eccentric Axial Tension

3.3.4.2.1 General

The provisions of *AASHTO LRFD* Article 6.8.2.3 dealing with combined axial tension and flexure may be applied for tees and double angles subject to eccentric axial tension. The two interaction equations shown below are provided (bending about the y-axis is not applicable); the equation to use depends on the ratio of the applied factored axial tensile force, P_u, to the factored tensile resistance, P_r, as follows:

- If $\frac{P_u}{P_r} < 0.2$, then:

$$\frac{P_u}{2.0P_r} + \frac{M_{ux}}{M_{rx}} \le 1.0$$

Equation 3.3.41
AASHTO LRFD Equation 6.8.2.3-1

- If $\frac{P_u}{P_r} \ge 0.2$, then:

$$\frac{P_u}{P_r} + \frac{8.0M_{ux}}{9.0M_{rx}} \le 1.0$$

Equation 3.3.42
AASHTO LRFD Equation 6.8.2.3-2

where:

P_u = applied factored axial tensile force (kips)
P_r = factored tensile resistance of the member (Section 3.3.3.2.1) (kips)
M_{ux} = factored moment about the x-axis due to the eccentricity of P_u (kip-in.)
M_{rx} = factored flexural resistance of the member about the x-axis (Section 3.3.4.2.2) (kip-in.)

The factored tensile resistance, P_r, is computed using the exact same procedures discussed in Section 3.3.3.2.1 for the calculation of P_r for single angle members subject to tension. Note that in calculating P_r, the block shear rupture resistance, R_r, must also be considered, as for single angle members (Section 3.3.3.2.4). For tees cut from rolled shapes, the shear lag reduction factor, U, may be determined more simply according to Case 7 in *AASHTO LRFD* Table 6.8.2.2-1. If Equation 3.3.26 is also used to calculate U, then the larger of the applicable constant value or the value from Equation 3.3.26 is permitted for use.

The moment, M_{ux}, is the moment about the x-axis resulting from the eccentricity, e, of the factored axial load, P_u (Figure 3.3.22). M_{rx} is the factored flexural resistance of the member about the x-axis. The calculation of M_{rx} is discussed below in Section 3.3.4.2.2.

3.3.4.2.2 Factored Flexural Resistance, M_{rx}

The factored flexural resistance, M_{rx}, of tees and double angles about the x-axis at the strength limit state is to be taken as follows:

$$M_{rx} = \phi_f M_{nx}$$

Equation 3.3.43
AASHTO LRFD Equation 6.12.1.2.1-1

where:

ϕ_f = resistance factor for flexure specified in *AASHTO LRFD* Article 6.5.4.2 (= 1.0)
M_{nx} = nominal flexural resistance of the member about the x-axis determined as specified in *AASHTO LRFD* Article 6.12.2.2.4 (kip-in.)

AASHTO LRFD Article 6.12.2.2.4 specifies that for tees and double angles loaded in the plane of symmetry, M_{nx} is to be determined as the *smallest* value based on yielding, lateral torsional buckling or flange local buckling, as applicable.

3.3.4.2.2.1 Yielding

For yielding, the nominal flexural resistance is to be taken as:

$$M_{nx} = M_p = F_y Z_x \le 1.6 M_y \quad \text{(for stems in tension)}$$
$$\le M_y \quad \text{(for stems in compression)}$$

Equation 3.3.44
AASHTO LRFD Equation 6.12.2.2.4-1

where:

M_p = plastic moment (kip-in.)
M_y = yield moment based on the distance to the tip of the stem (kip-in.)
Z_x = plastic section modulus about the x-axis (in.^{3})

The limit on M_{nx} of $1.6M_y$ in Equation 3.3.44 for cases where the stem is in tension is intended to indirectly control situations where significant yielding of the stem may occur at service load levels.

3.3.4.2.2.2 Lateral Torsional Buckling

The nominal flexural resistance for lateral torsional buckling is to be taken as:

$$M_{nx} = \frac{\pi\sqrt{EI_y GJ}}{L_b}\left[B + \sqrt{1+B^2}\right] \le M_p$$

Equation 3.3.45
AASHTO LRFD Equation 6.12.2.2.4-2

where:

$$B = \pm 2.3 \frac{d}{L_b} \sqrt{\frac{I_y}{J}}$$

Equation
3.3.46
AASHTO LRFD Equation 6.12.2.2.4-3

d = total depth of the section (in.)
G = shear modulus of elasticity for steel = 0.385*E* (ksi)
I_y = moment of inertia of the cross-section about the y-axis (in.^{4})
J = St. Venant torsional constant (in.^{4})
L_b = unbraced length (in.)

Equation 3.3.45 is a simplified version of the elastic lateral torsional buckling equation developed in Reference 31 and discussed further in Reference 32. The plus sign for the term, *B*, given by Equation 3.3.46 applies when the stem is in tension and the minus sign applies when the stem is in compression. If the tip of the stem is in compression anywhere along the unbraced length, the negative value of *B* is to be used. The lateral torsional buckling resistance for the case where the stem is in compression is substantially smaller than for the case where the stem is in tension.

The St. Venant torsional constant, J, for rolled sections including the effect of the web-to-flange fillets, is tabulated in Reference 33. Equation 1.1.4 may be used for fabricated sections with one of the flange terms removed.

Equation 3.3.45 does not contain the moment gradient modifier, C_b (Section 3.2.6.4.1.2). The C_b factor specified for I-sections is unconservative for tees with the stem in compression. Also, for reverse curvature bending, the portion with the stem in compression may govern the lateral-torsional buckling resistance even though the corresponding moments may be small in relation to the moments in the other portions of the unbraced length. As a result, C_b is conservatively taken equal to 1.0 for all cases. For cases where the stem is in tension, connection details should be designed to minimize end restraint moments that may cause the stem to be in flexural compression at the ends of the member.

3.3.4.2.2.3 Flange Local Buckling

Flange local buckling must be checked for sections where the flange is in compression and the flange slenderness, $\lambda_f = b_f/2t_f$, exceeds the limiting value, λ_{pf}, given below. The nominal flexural resistance for flange local buckling is taken as:

$$M_{nx} = M_p - \left(M_p - 0.7F_yS_{xc}\right)\left(\frac{\lambda_f - \lambda_{pf}}{\lambda_{rf} - \lambda_{pf}}\right) \le 1.6M_y$$

Equation 3.3.47
AASHTO LRFD Equation 6.12.2.2.4-4

where:

λ_f = flange slenderness = $b_f/2t_f$

λ_{pf} = limiting slenderness ratio for a compact flange = $0.38\sqrt{E/F_y}$

λ_{rf} = limiting slenderness ratio for a noncompact flange = $1.0\sqrt{E/F_y}$

b_f = flange width (in.). For double angles, b_f is to be taken as the sum of the widths of the outstanding legs.

S_{xc} = elastic section modulus with respect to the compression flange ($in.^3$)

t_f = flange thickness (in.)

Flange local buckling does not control and need not be checked for cases where the flange is in compression and λ_f does not exceed λ_{pf}.

Equation 3.3.47 corrects an error in 2005 *AISC LRFD* Specification equation for the flange local buckling resistance (*4*), in which a discontinuity in the flexural resistance occurs as the flange slenderness λ_f approaches the compact flange slenderness limit λ_{pf}. The *AISC LRFD* equation approaches M_y instead of the intended value of M_p as the flange slenderness approaches λ_{pf}.

Equation 3.3.47 represents an inelastic flange local buckling equation. An elastic flange local buckling equation for cases with λ_f exceeding λ_{rf} (i.e. with slender flanges) is not provided in the *AASHTO LRFD* Specification (an elastic local buckling equation is provided in Reference 4). None of the tee sections cut from rolled wide-flange sections given in the *AISC Steel Construction Manual* shape property tables (*33*) have slender flange elements, and in general, the limiting slenderness values at which elastic flange local buckling controls are larger than the limiting flange slenderness value of 12.0 for I-sections specified in *AASHTO LRFD* Article 6.10.2.2 (see Equation 3.1.18 – note that this flange slenderness limit is logically assumed to apply also to flanges of tee sections). The limit given by Equation 3.1.18 need only be checked for flanges of fabricated tee sections and for double angles (in tension or compression).

3.3.4.2.2.4 Stem Local Buckling

Local buckling of the stem must be checked for sections where the stem is subject to compression. The nominal flexural resistance for local buckling when stems are loaded in flexural compression is taken as:

$$M_{nx} = 0.424\frac{EJ}{d} \le M_y$$

Equation 3.3.48
AASHTO LRFD Equation 6.12.2.2.4-7

Equation 3.3.48 is indirectly derived from Equation 3.3.45 in the limit of zero unbraced length.

3.3.4.2.3 Fatigue of Tee Member Connections

AASHTO LRFD Table 6.6.1.2.3-1 now provides a simplified procedure for checking fatigue of welded (Condition 7.2) or bolted (Condition 2.5) connections of tee members to gusset or connection plates that are subject to a net applied tensile stress (as defined in *AASHTO LRFD* Article 6.6.1.2.1).. For checking fatigue of welded or bolted connections of double-angle members, refer to Section 3.3.3.2.5 on checking fatigue of single-angle member connections.

When determining ranges of stress in cross-frame members for fatigue design, the low probability of two vehicles being in their critical relative transverse positions over millions of cycles should be considered. *AASHTO LRFD* Article C6.6.1.2.1 recommends that one cycle of stress in a cross-frame member be determined as 75 percent of the stress range in the member determined by the passage of the fatigue load in two different transverse positions, but not less than the stress range caused by the loading of only one lane.

3.3.4.2.3.1 Welded Connections

For tee members connected to a gusset or connection plate by longitudinal fillet welds along both sides of the connected element of the member cross-section (Figure 3.3.23), the fatigue stress range, Δf, is to be calculated as follows:

$$\Delta f = \frac{\Delta P}{A_e} = \frac{\Delta P}{UA_g}$$

Equation 3.3.49

where:

A_e = effective net area of the member = UA_g (in.^{2})
A_g = gross cross-sectional area of the member (in.^{2})
ΔP = range of axial force in the member under the applicable Fatigue load combination (kips)
U = shear-lag reduction factor determined from Equation 3.3.26

$\bar{x}$ is to be taken as the distance from the centroid of the member to the surface of the gusset or connection plate, and *L* is to be taken as the maximum length of the longitudinal welds (Figure 3.3.21) in the calculation of the shear-lag reduction factor, *U*.

The effect of the moment due to the eccentricities in the connection may be ignored in computing the stress range when Equation 3.3.49 is used (*15*).

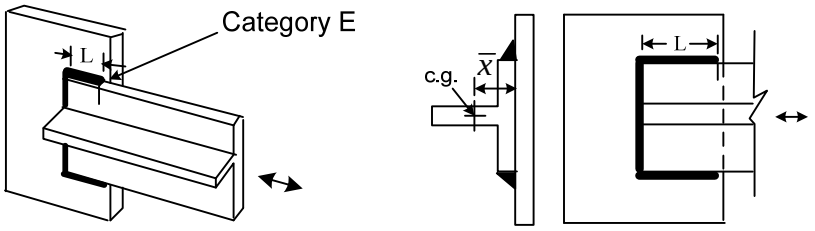


Figure 3.3.23 Welded Connection of a Tee Member to a Gusset Plate

The nominal fatigue resistance of the base metal in tee members connected by longitudinal fillet welds along both sides of the connected element of the member cross-section is to be based on detail Category E (Condition 7.2 in *AASHTO LRFD* Table 6.6.1.2.3-1). While the research showed that balancing of the welds offers some increase in the fatigue life (*15*), it is probably not worth the increase in the gusset or connection plate length required to accommodate the longer weld along one leg.

3.3.4.2.3.2 Bolted Connections

For tee members connected to a gusset or connection plate with high-strength bolted slip-critical connections (Figure 3.3.24), the fatigue stress range, Δf, is to be calculated from Equation 3.3.49. Slip-critical connections are discussed further in Section 3.3.6.2.1.1.

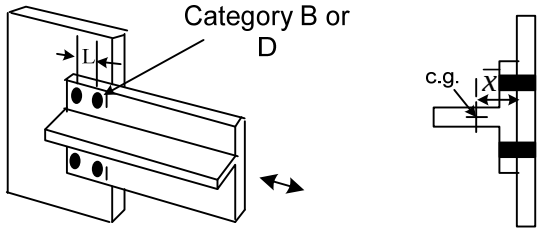


Figure 3.3.24 Bolted Connection of a Tee Member to a Gusset Plate

A_g is to be replaced with the net area of the member, A_n, in Equation 3.3.49 for all other types of bolted connections.

$\bar{x}$ is to be taken as the distance from the centroid of the member to the surface of the gusset or connection plate, and L is to be taken as out-to-out distance between the bolts in the connection parallel to the line of force (Figure 3.3.24) in the calculation of the shear-lag reduction factor, U.

The effect of the moment due to the eccentricities in the connection may be ignored in computing the stress range when Equation 3.3.49 is used.

The nominal fatigue resistance of the base metal in members connected by pre-tensioned high-strength bolts in slip-critical connections is to be determined based on whether the bolt holes are drilled full size or subpunched and reamed to size (Category B), or punched full size (Category D) (Condition 2.1 in *AASHTO LRFD* Table 6.6.1.2.3-1). As mentioned previously, *AASHTO LRFD Article 6.6.1.2.3 specifies that unless information is available to the contrary, bolt holes in cross-frame and lateral bracing members and their connection plates are to be assumed for design to be punched full size*.

Refer to Condition 2.2 or 2.3 in *AASHTO LRFD* Table 6.6.1.2.3-1, as applicable, for all other types of bolted connections. The fatigue resistance of bolted connections is discussed further in Section 3.3.6.2.1.3.

3.3.4.3 Eccentric Axial Compression

3.3.4.3.1 General

The provisions of *AASHTO LRFD* Article 6.9.2.2 dealing with combined axial compression and flexure may be applied for tees and double angles subject to eccentric axial compression. The two interaction equations shown below are provided (bending about the y-axis is not applicable); the equation to use depends on the ratio of the applied factored axial compressive force, P_u, to the factored compressive resistance, P_r, as follows:

- If $P_u/P_r < 0.2$, then:

$$\frac{P_u}{2.0P_r} + \frac{M_{ux}}{M_{rx}} \le 1.0$$

Equation 3.3.50
AASHTO LRFD Equation 6.9.2.2-1

- If $P_u/P_r \ge 0.2$, then:

$$\frac{P_u}{P_r} + \frac{8.0M_{ux}}{9.0M_{rx}} \le 1.0$$

Equation 3.3.51
AASHTO LRFD Equation 6.9.2.2-2

where:

P_u = applied factored axial compressive force (kips)
P_r = factored compressive resistance of the member (Section 3.3.4.3.2) (kips)

M_{ux}= factored moment about the x-axis due to the eccentricity of P_u *with amplification considered* (Section 3.3.4.3.3) (kip-in.)
M_{rx} = factored flexural resistance of the member about the x-axis (Section 3.3.4.2.2) (kip-in.)

The calculation of the factored compressive resistance, P_r, is discussed below in Section 3.3.4.3.2.

The moment, M_{ux}, is the moment about the x-axis resulting from the eccentricity of the factored axial load, P_u. Amplification of M_{ux} must be considered for tees and double angles subject to axial compression, as discussed below in Section 3.3.4.3.3. M_{rx} is the factored flexural resistance of the member about the x-axis and is calculated as discussed previously in Section 3.3.4.2.2.

3.3.4.3.2 Factored Compressive Resistance, P_r

The provisions of *AASHTO LRFD* Articles 6.9.2.1 and 6.9.4 are used to calculate the factored compressive resistance, P_r, for tees and double angles. *AASHTO LRFD* Article 6.9.2.1 specifies that P_r at the strength limit state be taken as:

$$P_r = \phi_c P_n$$

Equation 3.3.52
AASHTO LRFD Equation 6.9.2.1-1

where:
ϕ_c = resistance factor for axial compression specified in *AASHTO LRFD* Article 6.5.4.2 (=0.90)
P_n = nominal compressive resistance (kips) specified in *AASHTO LRFD* Article 6.9.4.1.1 as follows:

- If $\frac{P_e}{P_o} \geq 0.44$, then:

$$P_n = \left[0.658^{\left(\frac{P_o}{P_e}\right)}\right] P_o$$

Equation 3.3.53
AASHTO LRFD Equation 6.9.4.1.1-1

- If $\frac{P_e}{P_o} < 0.44$, then:

$$P_n = 0.877\ P_e$$

Equation 3.3.54
AASHTO LRFD Equation 6.9.4.1.1-2

where:

P_e = elastic critical buckling resistance taken as the *smaller* of the elastic critical buckling resistance for flexural buckling about the x-axis determined as specified in *AASHTO LRFD* Article 6.9.4.1.2, and the elastic critical buckling resistance for flexural-torsional buckling determined as specified in *AASHTO LRFD* Article 6.9.4.1.3 (Section 3.3.4.3.2.1) (kips)

P_o = equivalent nominal yield resistance = QF_yA_g (Section 3.3.4.3.2.2) (kips)

A_g = gross cross-sectional area of the member ($in.^2$)

F_y = specified minimum yield strength (ksi)

Q = slender element reduction factor (Section 3.3.4.3.2.2)

Further information regarding Equations 3.3.53 and 3.3.54 may be found in Section 3.3.3.3.1.

3.3.4.3.2.1 Elastic Critical Buckling Resistance, P_e

The elastic critical buckling resistance, P_e, is used in the computation of the nominal compressive resistance, P_n, from Equation 3.3.53 or 3.3.54, as applicable. According to *AASHTO LRFD* Table 6.9.4.1.1, tees and double angles in compression must be checked for both flexural buckling (about the x-axis only) and flexural-torsional buckling. P_e for use in Equation 3.3.53 or 3.3.54 is taken as the smaller value of these buckling resistances.

Concentrically loaded compression members composed of singly symmetric open cross-sections, where the y-axis is defined as the axis of symmetry of the cross-section (e.g. tees and double angles), can either fail by flexural buckling about the x-axis or by torsion combined with flexure about the y-axis. In such cases, the shear center and centroid of the cross-section do not coincide. As buckling occurs, the axial load has a lateral component resulting from the deflection of the member. The torsional moment caused by this lateral component of axial force acting about the shear center of the section causes twisting of the member. The degree of interaction between the torsional and flexural deformations determines the amount of reduction of the buckling load in comparison to the flexural buckling load (*16*). As the distance between the centroid and shear center increases, the twisting tendency increases and the flexural-torsional buckling load decreases. Because of their relatively low torsional rigidity, flexural-torsional buckling may be a critical mode of failure for thin-walled singly-symmetric open sections. Flexural-torsional buckling is not a consideration for closed sections.

The critical elastic flexural-torsional buckling resistance for open-section singly symmetric members, is always smaller than the critical elastic flexural buckling resistance about the y-axis, P_{ey}. Therefore, for these members, only the elastic flexural buckling resistance about the x-axis, P_{ex}, need be considered along with the elastic flexural-torsional buckling resistance.

Elastic Flexural Buckling Resistance about the x-axis, P_{ex}

The equation used to calculate the elastic flexural buckling resistance about the x-axis, P_{ex}, is specified in *AASHTO LRFD* Article 6.9.4.1.2 as follows:

$$P_{ex} = \frac{\pi^2 E}{\left(\frac{K_x \ell_x}{r_x}\right)^2} A_g$$

Equation 3.3.55
AASHTO LRFD Equation 6.9.4.1.2-1

where:

A_g = gross cross-sectional area of the member (in.^{2})
K_x = effective length factor for flexural buckling about the x-axis determined as specified in *AASHTO LRFD* Article 4.6.2.5
ℓ_x = unbraced length for buckling about the x-axis (in.)
r_x = radius of gyration about the x-axis (in.)

Elastic Flexural-Torsional Buckling Resistance, P_e

The equation used to calculate the elastic flexural-torsional buckling resistance, P_e, for tees and double angles is specified in *AASHTO LRFD* Article 6.9.4.1.3 as follows:

$$P_e = \left(\frac{P_{ey} + P_{ez}}{2H}\right)\left[1 - \sqrt{1 - \frac{4P_{ey}P_{ez}H}{(P_{ey} + P_{ez})^2}}\right]$$

Equation 3.3.56
AASHTO LRFD Equation 6.9.4.1.3-2

where:

$$P_{ey} = \frac{\pi^2 E}{\left(\frac{K_y \ell_y}{r_y}\right)^2} A_g \quad \text{(kips)}$$

Equation 3.3.57
AASHTO LRFD Equation 6.9.4.1.2-1

$$P_{ez} = \frac{GJ}{\bar{r}_o^2} \quad \text{(kips)}$$ (Note: C_w is taken equal to zero for tees and double angles)

Equation 3.3.58
AASHTO LRFD Equation 6.9.4.1.3-5

$$H = 1 - \frac{y_o^2}{\bar{r}_o^2}$$

Equation 3.3.59
AASHTO LRFD Equation 6.9.4.1.3-3

$$\bar{r}_o^2 = y_o^2 + \frac{I_x + I_y}{A_g}$$

Equation 3.3.60
AASHTO LRFD Equation 6.9.4.1.3-6

A_g = gross cross-sectional area of the member (in.^{2})
G = shear modulus of elasticity for the steel = 0.385E (ksi)
I_x = moment of inertia about the x-axis (in.^{4})
I_y = moment of inertia about the y-axis (in.^{4})
J = St. Venant torsional constant (in.^{4})
K_y = effective length factor for flexural buckling about the y-axis determined as specified in *AASHTO LRFD* Article 4.6.2.5
ℓ_y = unbraced length for buckling about the y-axis (in.)
r_y = radius of gyration about the y-axis (in.)
y_o = distance along the y-axis between the shear center and centroid of the cross-section (Figure 3.3.25) (in.)

Values of J, H and $\bar{r}_o^2$ for rolled tee sections are tabulated in the *AISC Steel Construction Manual* (*33*).

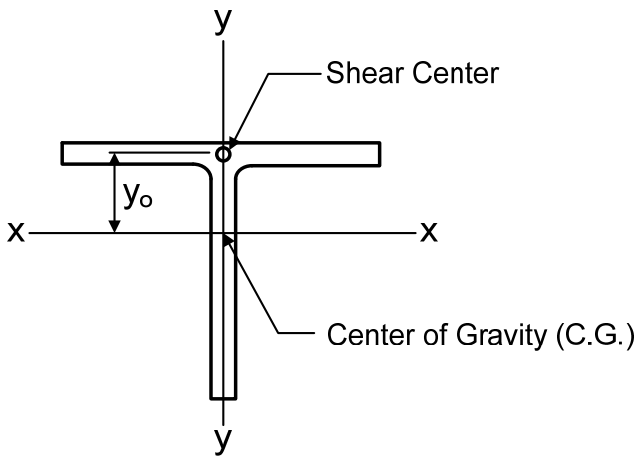


Figure 3.3.25 Calculation of y_o

Should double-angle bracing members subject to compression be interconnected at intervals along their length (i.e. between their ends) in the plane defined by the y-axis of the cross-section, the modified slenderness ratio, $(K\ell/r)_m$, specified for built-up members in *AASHTO LRFD* Article 6.9.4.3.1 should be used in place of $(K_y\ell_y/r_y)$ in Equation 3.3.57 to account for the effect of shear displacements between the two angles. Flexural buckling about the x-axis would be checked in conventional fashion, as shear effects would have no effect on buckling about the x-axis. In addition, *AASHTO LRFD* Article 6.9.4.3.1 specifies that the slenderness ratio of each component shape between connecting bolts or welds not exceed 75 percent of the governing slenderness ratio of the built-up member. When bolts are used, the maximum longitudinal spacing or pitch of the bolts must satisfy the requirements for stitch bolts specified in *AASHTO LRFD* Article 6.13.2.6.3. The reader is referred to Reference 30 for further information.

3.3.4.3.2.2 Equivalent Nominal Yield Resistance, P_o

The last term needed in order to compute the nominal compressive resistance, P_n, is the equivalent nominal yield resistance, P_o, defined in *AASHTO LRFD* Article 6.9.4.1.1 as follows:

$$P_o = QF_yA_g$$

Equation 3.3.61

where:

A_g = gross cross-sectional area of the member (in.^{2})
Q = slender element reduction factor ≤ 1.0

For compression members composed of one or more so-called "slender elements"; that is, elements not meeting the corresponding width-to-thickness ratio limits specified in *AASHTO LRFD* Table 6.9.4.2.1-1, the slender element reduction factor, Q, accounts for the effect of potential local buckling of those elements on the overall buckling resistance of the member and has a value less than 1.0. The value of Q in this instance is determined according to the provisions of *AASHTO LRFD* Article 6.9.4.2.2.

For compression member cross-sections without any slender elements; that is, composed entirely of non-slender elements, Q is taken equal to 1.0 as specified in *AASHTO LRFD* Article 6.9.4.2.1. In such cases, local buckling does not adversely affect the nominal compressive resistance.

For compression member cross-sections composed entirely of unstiffened elements, or plates supported along only one edge parallel to the direction of the compression force, Q is taken equal to the factor for unstiffened elements, Q_s. Unstiffened elements are assumed to reach their limit of resistance when they attain their theoretical local buckling resistance. Q_s is taken as the smallest value for all unstiffened slender elements in the cross-section. Tees (Figure 3.3.26) and double angles are composed entirely of unstiffened elements.

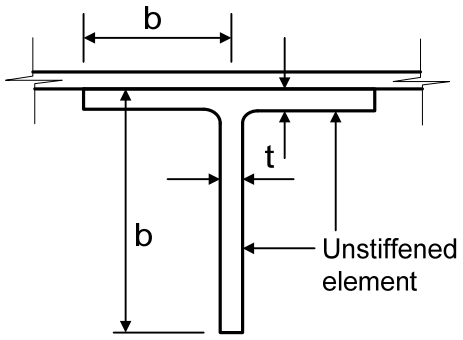


Figure 3.3.26 Unstiffened Elements for a Tee Member

Q_s for slender unstiffened elements is equal to the ratio of the smallest local buckling resistance of all the unstiffened elements in the cross-section divided by F_y. In other words, for a compression member composed entirely of unstiffened elements, the reduced equivalent nominal yield resistance, P_o, of the member is taken as the average axial stress at which the most critical unstiffened element reaches its local buckling resistance (i.e. the elastic or inelastic local buckling resistance depending on the values of b/t and F_y).

b is taken as the full depth of the tee (including the flange) and t is taken as the stem thickness (Figure 3.3.26) in the following equations for Q_s for stems of tees specified in *AASHTO LRFD* Article 6.9.4.2.2. For flanges, b is taken as the half-width of the flange and t is taken as the flange thickness. As mentioned previously, none of the current rolled tee sections have slender flange elements. Should the flange of a fabricated tee section exceed the corresponding width-to-thickness ratio specified for flanges of rolled tee sections in *AASHTO LRFD* Table 6.9.4.2.1-1 and qualify as a slender compression element, the reader is referred to the equations given in *AASHTO LRFD* Article 6.9.4.2.2 for flanges of rolled tee sections in order to obtain Q_s.

The reader is referred to Section 3.3.3.3.3 to utilize the equations given there for single angles in order to obtain Q_s for double angles with separators. The reader is referred to *AASHTO LRFD* Article 6.9.4.2.2 for double angles in continuous contact.

For stems of tees:

- If $\frac{b}{t} \le 0.75\sqrt{\frac{E}{F_y}}$, then:

$$Q = Q_s = 1.0$$

Equation 3.3.62

- If $0.75\sqrt{\frac{E}{F_y}} < \frac{b}{t} \le 1.03\sqrt{\frac{E}{F_y}}$, then:

$$Q = Q_s = 1.908 - 1.22\left(\frac{b}{t}\right)\sqrt{\frac{F_y}{E}}$$

Equation 3.3.63
AASHTO LRFD Equation 6.9.4.2.2-3

- If $\frac{b}{t} > 1.03\sqrt{\frac{E}{F_y}}$, then:

$$Q = Q_s = \frac{0.69E}{F_y\left(\frac{b}{t}\right)^2}$$

Equation 3.3.64
AASHTO LRFD Article 6.9.4.2.2-4

3.3.4.3.3 Amplification of M_{ux}

AASHTO LRFD Article 6.9.2.2 specifies that the moment about the x-axis, M_{ux}, due to the eccentricity of the applied factored axial compressive force, P_u, is to be calculated considering second-order effects arising from the additional secondary moment cause by the axial force acting through the member deflection (Figure 3.3.27).

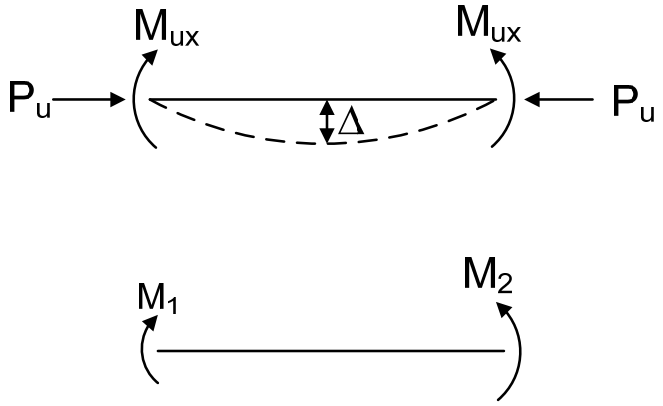


Figure 3.3.27 Amplification of M_{ux} and End Moments M_1 and M_2

The amplification of the first-order moment, $(M_{ux})_1$, can be determined from a second-order elastic analysis, or more simply, from the approximate single-step adjustment specified in *AASHTO LRFD* Article 4.5.3.2.2b as follows (the sidesway term in the equation is not applicable):

$$(M_{ux})_2 = \delta_b (M_{ux})_1$$

Equation 3.3.65
AASHTO LRFD Equation 4.5.3.2.2b-1

where:

$$\delta_b = \frac{C_m}{1-\frac{P_u}{\phi_K P_e}} \geq 1.0$$

Equation 3.3.66
AASHTO LRFD Equation 4.5.3.2.2b-3

C_m = equivalent uniform moment factor. For members braced against sidesway and without transverse loading between supports in the plane of bending:

$$= 0.6 + 0.4(M_1/M_2)$$

Equation 3.3.67
AASHTO LRFD Equation 4.5.3.2.2b-6

P_e = Euler buckling load for buckling about the x-axis (i.e. the axis of bending)

$$= \frac{\pi^2 E I_x}{(K_x \ell_x)^2} \text{ (kips)}$$

Equation 3.3.68
AASHTO LRFD Equation 4.5.3.2.2b-5

ϕ_K = stiffness reduction factor taken equal to 1.0 for steel members
I_x = moment of inertia of the member about the x-axis (in.^{4})
K_x = effective length factor about the x-axis determined as specified in *AASHTO LRFD* Article 4.6.2.5
ℓ_x = unbraced length for buckling about the x-axis (in.)
M_1 = smaller end moment (kip-in.)
M_2 = larger end moment (kip-in.)
P_u = applied factored axial compressive force (kips)

The equivalent uniform moment factor, C_m, given by Equation 3.3.67 depends on the ratio of the moments at the end of the member, with M_1 taken as the smaller end moment and M_2 taken as the larger end moment (Figure 3.3.27). The ratio, (M_1/M_2), is taken as positive when the member is bent in single curvature and negative when the member is bent in reverse curvature. Therefore, for a uniform moment, which is typically the case for an eccentrically loaded tee or double-angle member, C_m is equal to 1.0.

3.3.4.4 Interaction Curves for Tees and Double-Angle Members

For tees and double angles subject to combined axial tension and flexure or combined axial compression and flexure, in which the axial and flexural stresses in the flange of the tee are additive in tension or compression (as applicable), a bulge in the interaction curve occurs as noted qualitatively in Figure 3.3.28 (see upper right and lower left quadrants). Such a condition occurs when a tee is used as a bracing member and the connection of the member is made to the flange. The resulting moment due to the eccentricity of the connection typically places the member design in the upper right or lower left quadrant, and often in the vicinity of

the largest bulge in the resistance envelope. As a result, the *AASHTO LRFD* interaction curves may significantly underestimate the resistance in these cases.

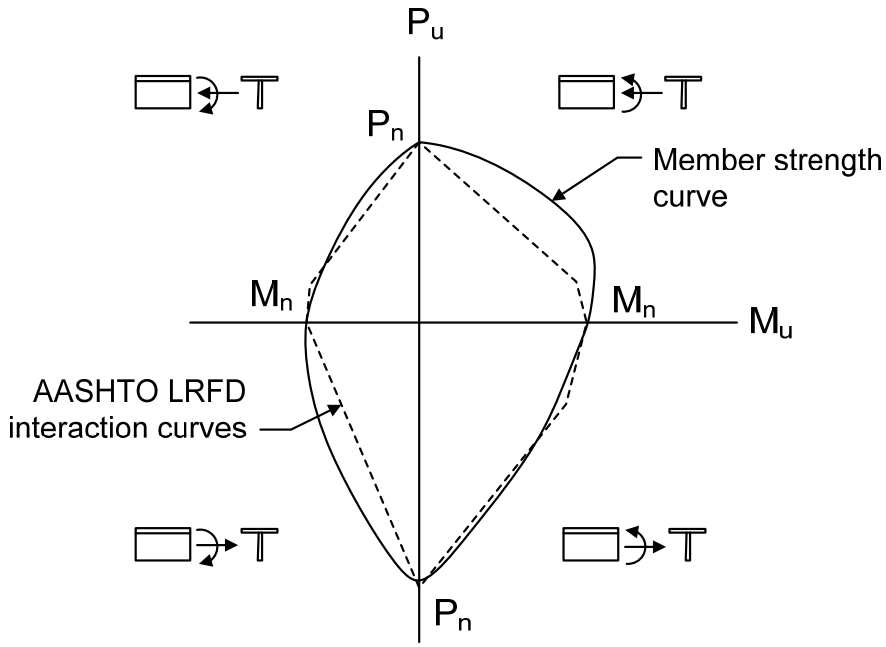


Figure 3.3.28 Interaction Curves for Tees Subjected to Combined Axial Forces and Flexure

The *AASHTO LRFD* interaction curves provide a reasonably accurate estimate of the actual resistance in cases where the stem of the tee is subject to additive axial and flexural tension or compression (see upper left and lower right quadrants of Figure 3.3.28).

As discussed in *AASHTO LRFD* Articles C6.8.2.3 and C6.9.2.2, alternative approaches attempting to capture the bulge in the interaction curve have proven thus far to be generally inconclusive or incomplete. Thus, in the interim, it is recommended that the *AASHTO LRFD* interaction curves be conservatively applied to cases where the axial and flexural stresses in the flange of the tee are additive in tension or compression. Should significant additional resistance be required, the use of one or more of these alternative approaches, as described in greater detail in Reference 30, might be considered.

3.3.5 Diaphragms

3.3.5.1 I-Girder Bridges

Functions and configurations of diaphragms in I-girder bridges were discussed previously in Sections 3.1.2.8.1 and 3.1.2.8.4.1, respectively. Some general design considerations were discussed in Section 3.1.2.8.5.1.

AASHTO LRFD Article 6.7.4.2 specifies that diaphragms for I-girder bridges with span-to-depth ratios greater than or equal to 4.0 may be designed as beams. Diaphragms with span-to-depth ratios less than 4.0 act as deep beams and should be evaluated by considering principal stresses rather than by beam theory (refer to Section 3.3.5.2). The end moments in the diaphragm are also to be considered in the design of the connection between the girders and the diaphragm (*AASHTO LRFD* Article 6.7.4.2).

End diaphragms must be designed for forces and distortion transmitted by the deck and deck joint. They also must be designed to support the deck and the wheel loads coming onto the ends of the deck.

3.3.5.2 Box-Girder Bridges

Functions and configurations of diaphragms in box-girder bridges were discussed previously in Sections 3.1.2.8.1.4 and 3.1.2.8.4.2, respectively. Some general design considerations were discussed in Section 3.1.2.8.5.1.

Solid-plate diaphragms are most commonly used as internal and external diaphragms in box-girder bridges at supports or as internal diaphragms in steel box-section integral bent caps. External diaphragms at end supports act with the internal diaphragm to support the deck and the wheel loads coming onto the ends of the deck. End moments should be considered in the design of the external diaphragms and their end connections to the girders.

Beams deeper than about one-fourth of their span are classified as deep beams in reinforced concrete design. Ordinary beam theory does not apply for deep beams, meaning that shear deformations should be considered and principal stresses should be evaluated. Thus, *AASHTO LRFD* Article C6.7.4.3 indicates that consideration should be given to evaluating the principal stresses in all internal support diaphragms, and in external support diaphragms with aspect ratios (ratios of length to depth) less than 4.0 (external support diaphragms with aspect ratios greater than or equal to 4.0 may be designed as ordinary I-section flexural members). The combined principal stresses in the diaphragm in these cases can be evaluated at the strength limit state using the following general form of the Huber-von Mises-Hencky yield criterion (*34*):

$$\sqrt{\sigma_1^2 - \sigma_1\sigma_2 + \sigma_2^2} \le \phi_f F_y$$

Equation 3.3.69

where:

ϕ = resistance factor for flexure specified in *AASHTO LRFD* Article 6.5.4.2 (= 1.0)

σ_1, σ_2 = critical maximum and minimum principal stresses in the diaphragm (ksi)

$$= \left(\frac{f_{by} + f_{bz}}{2}\right) \pm \sqrt{\left(\frac{f_{by} - f_{bz}}{2}\right)^2 + f_d^2}$$

Equation 3.3.70

f_{by} = for internal diaphragms, factored stress in the diaphragm caused by major-axis bending of the diaphragm over the bearing sole plate (ksi). For external diaphragms, factored stress in the diaphragm caused by major-axis bending of the diaphragm (ksi)

f_{bz} = factored stress in the diaphragm caused by bending of the diaphragm about its longitudinal axis (ksi)

f_d = factored shear stress in the diaphragm caused by the total vertical shear in the diaphragm (ksi)

F_y = specified minimum yield strength of the diaphragm (ksi)

f_{by} and f_{bz} are to be taken as signed quantities in Equations 3.3.69 and 3.3.70. The term f_{bz} is neglected in most all cases. f_{by} may be particularly significant for a box section supported on a single bearing. In calculating f_{by} for internal diaphragms, a width of the bottom box flange equal to six times its thickness may be considered effective with the diaphragm in resisting bending (*AASHTO LRFD* Article C6.7.4.3). More than one loading condition may need to be investigated in order to determine the critical principal stresses in the diaphragm. Should the diaphragm web have a different yield strength than the box flange (for the case of internal diaphragms) or the diaphragm flanges (for the case of external diaphragms), consideration should be given to including the hybrid factor, R_h, (Section 3.2.6.3) on the right-hand side of Equation 3.3.69

Post bend-buckling resistance should not be considered in the design of these critical diaphragm members. Therefore, when considering bending of the diaphragm, *AASTHO LRFD* Article 6.7.4.3 specifies that the diaphragm web satisfy the following requirement:

$$\frac{2D_c}{t_w} \le \lambda_{rw} = 5.7\sqrt{\frac{E}{F_y}}$$

Equation 3.3.71
AASHTO LRFD Equation 6.10.1.10.2-2

where:

D_c = elastic depth of the diaphragm web in compression (in.)

Satisfaction of Equation 3.3.71 ensures that theoretical bend buckling of the diaphragm web will not occur. Thus, the web load-shedding factor, R_b (Section 3.2.6.2), is implicitly taken equal to 1.0 in Equation 3.3.69.

The factored shear resistance of the diaphragm must be checked at the strength limit state as follows:

$$V \le \phi_v V_n$$

Equation 3.3.72

where:

ϕ_v = resistance factor for shear specified in *AASHTO LRFD* Article 6.5.4.2 (= 1.0)
V = total factored vertical shear in the diaphragm (kips)
V_n = nominal shear resistance of the diaphragm (kips)

Post-buckling shear resistance due to tension-field action also should not be considered in the design of these critical diaphragm members. Therefore, *AASTHO LRFD* Article 6.7.4.3 specifies that the nominal shear resistance, V_n, be limited to the shear buckling (or shear yielding) resistance, V_{cr}, given as follows (Section 3.2.7.2):

$$V_n = V_{cr} = CV_p$$

Equation 3.3.73
AASHTO LRFD Equation 6.10.9.3.3-1

where:

V_p = plastic shear force (kips) = $0.58F_yDt_w$
C = ratio of the shear buckling resistance to the shear yield strength determined from *AASHTO LRFD* Equation 6.10.9.3.2-4, 6.10.9.3.2-5 or 6.10.9.3.2-6, as applicable
D = vertical depth of the diaphragm (in.)
t_w = thickness of the diaphragm (in.)

In calculating the constant *C*, the shear buckling coefficient *k* should be taken as 5.0 for unstiffened webs and determined using Equation 3.2.157 for stiffened webs. Bearing stiffeners on internal plate diaphragms may be considered to act as transverse stiffeners.

The section through an access hole in an internal diaphragm at an interior support is especially critical for a section supported on a single bearing, and additional stiffening and/or reinforcement around the hole may be necessary. In such cases, the bearing is typically wider than the access hole so bearing stiffeners provided on each side of the hole can be considered to act as transverse stiffeners to increase the shear resistance of the diaphragm at the hole. If necessary, horizontal stiffeners above and below the hole might be used to increase the flexural resistance of the diaphragm at the hole in lieu of thickening the diaphragm plate.

Because of the presence of access holes and complex details such as stiffening around the holes, and because of the number of load points and more complicated mechanism of load transfer, a more refined analysis of internal plate diaphragms at supports may be desirable to obtain more accurate estimates of the diaphragm flexural and shear stresses. This is particularly true for box sections supported on single bearings. Procedures are available for estimating the moment and shear resistance of steel beams with unreinforced and reinforced web openings (*35*). However, these procedures were primarily developed for rolled I-section flexural

members used in multistory buildings with smaller web openings used to pass utilities through the beams and not for deeper and shorter solid-plate diaphragms used in bridges, with relatively large access holes, that exhibit deep-beam behavior. .

AASHTO LRFD Article 6.11.11.1 specifies that bearing stiffeners for box sections with inclined webs should be attached to either an internal or external diaphragm rather than to the webs so that the bearing stiffeners will be perpendicular to the sole plate. Where a single centered bearing is used and a centered access hole is also provided in an internal diaphragm, the diaphragm must be stout enough to transfer the load around any access hole and to resist the reaction. As mentioned previously, a refined analysis of the diaphragm is desirable is such situations. Stiffening around the hole may be required. Auxiliary bearing stiffeners might be provided to spread out the reaction. Thermal movements of the bridge at expansion bearings may cause the diaphragm to be eccentric with respect to the bearings. *AASHTO LRFD* Article 6.11.11.1 states that the bearing stiffeners and diaphragms should be designed for the resulting eccentricity. The effect of the eccentricity can be recognized by treating the effective bearing stiffener/diaphragm assembly as a beam-column according to the provisions of *AASHTO LRFD* Article 6.9.2.2. The effective bearing assembly consists of the stiffeners plus the portion of the diaphragm web specified in *AASHTO LRFD* Article 6.10.11.2.4b assumed to act with the stiffeners as an effective column section (Section 3.3.8.2.4.1).

Details on diaphragms should be appropriately investigated for the fatigue limit state. On diaphragms for which principal stresses are considered, fatigue-sensitive details should be investigated by considering the principal tensile stress range due to the factored fatigue live load (i.e. factored according to the applicable Fatigue load combination specified in *AASHTO LRFD* Table 3.4.1-1 – refer to Section 1.3.3) that results from the diaphragm acting as a deep beam, which may preclude the use of certain fatigue-sensitive details on the diaphragm. Note that the direction of the principal tensile stress may change for different positions of the live load. Details need only be checked for fatigue if they are subject to a net tensile stress according to the criterion specified in *AASHTO LRFD* Article 6.6.1.2.1.

The application of the preceding provisions to the design of an internal support diaphragm for a tub section is given in Reference 21.

3.3.6 Bracing Member Connections

3.3.6.1 General

Connection design is covered in *AASHTO LRFD* Article 6.13. The design of bolted connections is covered in *AASHTO LRFD* Article 6.13.2. The design of welded connections is covered in *AASHTO LRFD* Article 6.13.3. *AASHTO LRFD* Articles 6.13.4 and 6.13.5 deal with the topics of block shear rupture resistance and the

design of connection elements (e.g. splice plates, gusset plates and lateral connection plates) for tension and shear, respectively.

AASHTO LRFD Article 6.13.1 covers several general considerations related to connection design. Where practical, connections should be made symmetrical about the axis of the members. Members, including bracing, should be connected so that their gravity axes will intersect at a point. Eccentric connections should be avoided, however, where this is not possible, the members and connections must be designed for the combined effects of the shear and moment due to the eccentricity. Bolted connections, except for connections on lacing and handrails, are to contain not less than two bolts.

End connections of stringers, floorbeams and girders should be connected with high-strength bolts. Where bolting is not practical, welded connections may be used, but they must be designed for the vertical loads and any bending moment resulting from restraint against end rotation.

AASHTO LRFD Article 6.13.1 specifies that ***where cross-frames/diaphragms, lateral bracing, stringers or floorbeams for straight or horizontally curved members are included in the structural model used to determine force effects, or are designed for explicitly calculated force effects from the results of a separate investigation (e.g. an approximate wind load analysis), the end connections for those members are to be designed for the calculated factored member force effects. Otherwise, the end connections for these members are to be designed for 75 percent of the factored resistance corresponding to the force effect under consideration.*** The preceding exception results from experience indicating that application of 75 percent and average load provisions to the end connections of these members in which force effects have been determined by analysis, as required in previous specifications, tended to result in large connections with large eccentricities and force concentrations. Therefore, it was felt by the specification writers that the above exception was justified to prevent the complications resulting from such large connections.

3.3.6.2 Bolted Connections

3.3.6.2.1 General

The design of bolted connections is covered in *AASHTO LRFD* Article 6.13.2. As *AASHTO LRFD* Article 6.13.2.1 specifies that bolted steel parts must fit solidly together after the bolts are tightened. The bolted parts may be coated or uncoated. It must be specified in the contract documents that all joint surfaces, including surfaces adjacent to the bolt head and nut, be free of scale (except for tight mill scale), dirt or other foreign material. All material within the grip of the bolt must be steel.

High-strength bolts are to be installed to have a specified initial tension, which results in an initial precompression between the joined parts. At service load levels, the transfer of the loads between the joined parts may then occur entirely via friction with no bearing of the bolt shank against the side of the hole. Until the friction force is overcome, the shear resistance of the bolt and the bearing resistance of the bolt hole will not affect the ability to transfer the load across the shear plane between the joined parts.

In general, high-strength bolted connections designed according to the *AASHTO LRFD* Specification provisions will have a higher reliability than the connected parts because the resistance factors for the design of bolted connections were selected to provide a higher level of reliability than those chosen for member design. Also, the controlling strength limit state in the connected part, e.g. yielding or deflection, is typically reached well before the controlling strength limit state in the connection, e.g. the bolt shear resistance or the bearing resistance of the connected material.

The *AASHTO LRFD* Specifications recognize two types of high-strength bolted connections; slip-critical connections and bearing-type connections. The resistance of all high-strength bolted connections in transmitting shear across a shear plane between bolted steel parts is the same whether the connection is a slip-critical or bearing-type connection. The slip-critical connection has an additional requirement that slip must not occur between the joined parts at service load levels.

3.3.6.2.1.1 Slip-Critical Connections

The load is transferred between the joined parts by friction up to a level of force that is dependent upon the clamping force and the coefficient of friction of the faying surfaces in high-strength bolted slip-critical connections subject to shear. The coefficient of friction depends on the faying surface condition, with mill scale, paint or other surface treatments determining the value of the friction coefficient.

Prior to joint slip, the bolts are not subject to shear nor are the joined parts subject to bearing stress. Once the load exceeds the frictional resistance between the faying surfaces, slip occurs; that is, the friction bond is broken and the two surfaces slip with respect to one another by a relatively large amount. A rupture failure does not occur. Therefore, the connection is able to continue resisting an even greater load through the shear resistance of the bolts and the bearing resistance against the connected material. Final failure of the connection will be by shear failure of the bolts, yielding or tear-out of the connected material or by an unacceptable deformation around the holes; the ultimate resistance of the connection is not related to the slip load.

The slip and bearing resistances are computed separately for application at different load combinations (the calculation of the slip, shear and bearing resistances of bolted connections and the resistance of the connected material is

discussed in more detail below). Because a high tensile force on the bolt is required to develop a significant resisting friction force, only bolts with a high tensile yield strength (i.e. A 325 and A 490 high-strength bolts) can be used in slip-critical connections.

AASHTO LRFD Article 6.13.2.1.1 specifies that slip-critical connections are to be proportioned to prevent slip under Load Combination Service II and to provide bearing, shear and tensile resistance under the applicable strength load combinations. Slip is to be prevented under Load Combination Service II to control permanent deformations caused by slip in bolted joints that could adversely affect the serviceability of the structure. It is further assumed that under the strength load combinations, slip between the bolted parts occurs at the higher loads and that the bolts have gone into bearing against the connected material. Thus, the shear resistance of the bolts and bearing resistance of the bolt holes must be checked under the appropriate strength load combination. In addition, the resistance of the connected material must be checked at the strength limit state.

According to *AASHTO LRFD* Article 6.13.2.1.1, bolted joints subject to stress reversal, heavy impact loads, severe vibration or located where stress or strain due to joint slippage would be detrimental to the serviceability of the structure are to be designated as slip-critical (the reader is referred to this article for the specific list of joints that should be designated as slip-critical). Repeated loading may introduce fatigue concerns if slip occurs in these cases, particularly when oversize or slotted holes are used. ***Bracing member connections should always be designed as slip-critical connections***.

3.3.6.2.1.2 Bearing-Type Connections

In high-strength bolted bearing-type connections, the load is resisted by a combination of the shear resistance of the bolt, the bearing resistance of the connected material and an unknown amount of friction between the faying surfaces. The failure of a bearing-type connection will be by shear failure of the bolts, yielding or tear-out of the connected material or by an unacceptable deformation around the holes, with the final failure load independent of the clamping force provided by the bolts (*36*).

AASHTO LRFD Article 6.13.2.1.2 specifies that bearing-type connections are only to be permitted on bridges for joints subject to axial compression or joints on secondary members. Such connections are to be designed to provide the required factored resistance in shear and bearing at the strength limit state. Connections utilizing A 307 bolts are to be designed as bearing-type connections.

3.3.6.2.1.3 Fatigue Resistance of Bolted Connections

The behavior of a bolted connection under fatigue loading is influenced by the type of load transfer in the connection. In tests of slip-critical lap joints subject to in-plane cyclic loading, crack initiation and growth typically occurred in the gross

section in front of the first bolt hole of the connection (*36*). The cracks initiated on the faying surfaces. Failures that occur at the interface of metallic surfaces that are in contact and that slip a small amount relative to each other under an oscillating load are referred to as fretting failures. The point where fretting is initiated depends on the discontinuities of the mill scale, the clamping zone of the bolt and the frictional resistance of the faying surface.

In bearing-type connections where the load is transmitted primarily by shear and bearing, the crack typically initiates instead at the edge of the bolt hole and grows in the region of the net section, with failure eventually occurring due to fracture of the net section. However, it was observed that slip-critical connections designed based on the gross section (i.e. stress ranges computed on the gross section) and bearing-type connections designed based on the net section (i.e. stress ranges computed on the net section) provide approximately the same nominal fatigue resistance. It was determined that fatigue detail Category B provides a reasonable and conservative lower bound to the test data in both cases (*36*).

Therefore, *AASHTO LRFD* Table 6.6.1.2.3-1 indicates that base metal at the gross section of high-strength bolted slip-critical connections (Condition 2.1) and at the net section of high-strength bolted bearing-type connections (Condition 2.2) subject to a net applied tensile stress (as defined in *AASHTO LRFD* Article 6.6.1.2.1) be designed for fatigue based on Category B. Both of the above conditions assume the connections are made with pre-tensioned high-strength bolts and that the bolts are installed in holes drilled full size or subpunched and reamed to size. Should the bolts be installed in holes punched full size, the connection for each of the above cases is instead to be designed for fatigue based on Category D according to Condition 2.3 in *AASHTO LRFD* Table 6.6.1.2.3-1 (*7*).

Condition 2.3 in *AASHTO LRFD* Table 6.6.1.2.3-1 also covers the fatigue resistance of the base metal at the net section of other mechanically fastened joints, except for eyebars and pin plates; e.g. joints using ASTM A 307 bolts or non pre-tensioned high-strength bolts, and at the net section of all bolted joints in hot dipped galvanized members (*37*). For these cases, the connection is also to be designed for fatigue based on Category D.

The checking of fatigue of bolted bracing member connections for single- and double-angle members, and for tee members, is discussed above in Sections 3.3.3.2.5.2 and 3.3.4.2.3.2, respectively.

Axially loaded joints subject to fatigue loading in direct tension (versus shear), in addition to prying action, are treated differently according to the provisions of *AASHTO LRFD* Article 6.13.2.10.3. The reader is referred to References 21, 33 and 36 for additional information.

3.3.6.2.2 Bolts

3.3.6.2.2.1 Unfinished Bolts

Unfinished bolts, also referred to as common, machine, ordinary or rough bolts, are manufactured from low-carbon steel and are designated as ASTM A 307 bolts. There is no corresponding AASHTO material standard to ASTM A 307. Three grades – Grades A, B, and C – are covered in the ASTM standard. Only Grade A and Grade B bolts are acceptable for use under the *AASHTO LRFD* Specifications. Grade A is the quality that is typically used for general structural applications. Grade A bolt heads and nuts are manufactured with a regular square shape. Grade B bolts are more typically used for flanged joints in piping-systems with cast iron flanges. As indicated in *AASHTO LRFD* Article 6.4.3.1, the specified minimum tensile strength of these bolts (specifically Grades A and B) is 60 ksi. These bolts are typically tightened using long-handled manual wrenches and hardened steel washers are not generally used. Since these bolts do not have a specified proof load, they should only be used for connecting relatively light auxiliary components or members subject to light static loads or for temporary fit-up. These bolts should not be used in connections subject to slip or vibration because of the tendency of the nuts to loosen.

3.3.6.2.2.2 High-Strength Bolts

High-strength bolts are heavy hexagon-head bolts used with heavy semi-finished hexagon nuts. The threaded portion of high-strength bolts is shorter than for bolts used for non-structural applications, which reduces the probability of having the threads present in the shear plane. High-strength bolts produce large and predictable tension when tightened. Initial tensioning of high-strength bolts results in more rigid joints and greater assurance against nut loosening in connections subject to slip or vibration.

High-strength bolts have replaced rivets as the primary means of making non-welded structural connections. Initial experiments on high-strength bolted connections were first reported in Reference 38 in 1934. Follow-up research in 1938 (*39*) indicated that high-strength bolts had fatigue strengths equal to those of well-driven rivets as long as the bolts were sufficiently pretensioned. In 1947, the Research Council on Riveted and Bolted Structural Joints (currently known as the Research Council on Structural Connections or RCSC) was formed to carry out cooperative research into the behavior of various types of connections joined with rivets and bolts. The new Council began by using and extrapolating information from studies of riveted joints in order to evaluate the merits of high-strength bolts used in structural connections. This led to the publication by the Council in 1951 of the first edition of the “Specifications for Structural Joints Using A 325 Bolts”, which permitted the replacement of rivets with bolts on a one-to-one basis. This specification assumed that friction transfer was necessary in all joints at service load conditions. The factor of safety against slip was set at a high enough level to

ensure fatigue resistance that was similar to or better than the fatigue resistance of riveted joints.

Additional research in 1956 (*40*) concluded that for high-strength bolts to be efficient and economical, the minimum initial bolt tension should be as high as practical. Therefore, by 1960, the minimum initial bolt tension was increased. Also, the bearing-type connection was recognized as an acceptable substitute for a riveted connection. It was further recognized that the so-called friction-type connection (now referred to as a slip-critical connection), in which the connection is designed on the basis of slip resistance at service loads, would only be necessary when stress reversals occurred or when direct tension acted on the bolts. In 1960, the turn-of-the-nut installation method was also introduced as an alternative to the torque wrench (or calibrated wrench) method. Furthermore, when the turn-of-the-nut method was used, only one washer located under the head of the element being turned was required, which further improved the economics of high-strength bolting. Previously, two washers were required in the connection. By 1962, the requirement for washers was eliminated, except for special circumstances. In 1964, the higher strength ASTM A 490 bolt was introduced. The philosophy of the design of bearing-type and friction-type connections was revised in later versions of the RCSC Specifications in the mid to late 1980s. The reader is referred to the RCSC Specifications (*41*) and to Reference 36 (both documents are available for download from www.boltcouncil.org) for additional more detailed information on the historical background, research and recommendations that form the basis of the current *AASHTO LRFD* Specification provisions for the design of high-strength bolted connections.

As specified in *AASHTO LRFD* Article 6.4.3.1, ASTM A 325 bolts in diameters of 0.5 inch through 1 inch have a required minimum tensile strength of 120 ksi. ASTM A 325 bolts in diameters of 1.125 inch through 1.5 inch have a required minimum tensile strength of 105 ksi. ASTM A 490 bolts in diameters of 0.5 inch to 1.5 inch have a required minimum tensile strength of 150 ksi. Both A 325 and A 490 bolts are available as Types 1 or 3 (Note: Type 2 bolts are no longer available). The A 325 Type 1 bolt is a medium-carbon steel bolt. The A 490 Type 1 bolt is an alloy steel bolt. Type 1 bolts are to be used with steels other than weathering steel and is the type furnished if not otherwise specified. Type 3 bolts have an atmospheric corrosion resistance and weathering characteristics comparable to weathering steels and are to be used only in weathering steel applications. A 325 and A 490 bolts (and the various bolt types) are distinguished by specific identifying marks described in Reference 41.

Type 1 bolts may be either mechanically or hot-dip galvanized. However, galvanizing of A 490 bolts (by either process) is not permitted due to the potential for hydrogen embrittlement (*41*). When galvanized A 325 bolts are used on weathering steel projects, only hot-dip galvanized bolts should be used as the relatively thin sacrificial coating on mechanically galvanized bolts will corrode too quickly in an uncoated weathering steel application. Galvanized bolts must be

tension tested after galvanizing. The bolts, nuts and washers in any assembly must be galvanized using the same process. Galvanized nuts should be over-tapped to the minimum amount required for the assembly and lubricated with a lubricant containing a visible dye to allow for a visual check of the lubricant at the time of field installation.

Pretensioning of the bolt for high-strength bolts used in slip-critical connections should be as high as possible without causing permanent deformation or failure of the bolt. As shown in Figure 3.3.29, the stress-strain or load-elongation behavior of bolt material in a direct-pull tension test has no well-defined yield point.

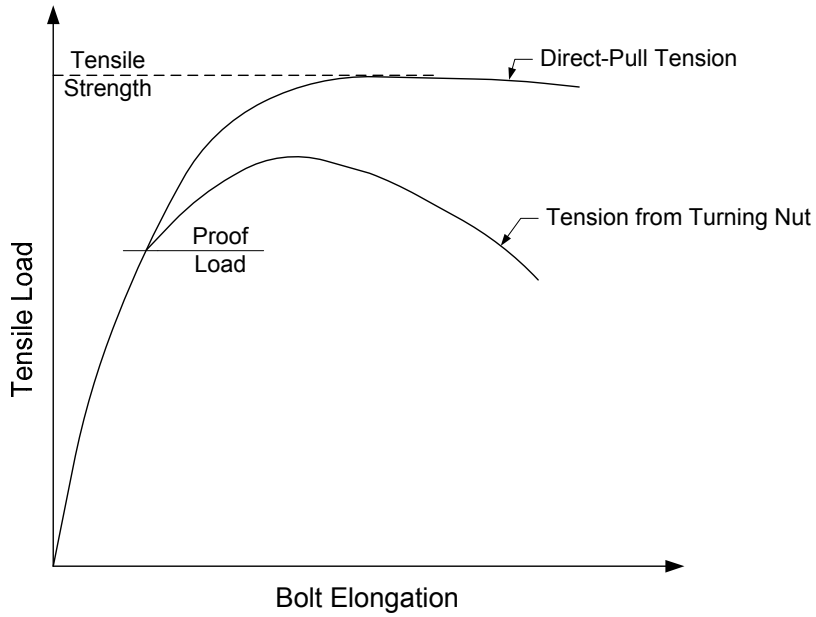


Figure 3.3.29 Typical Tensile Load-Elongation Curve for a High-Strength Bolt

Instead, a so-called proof load is used in lieu of directly specifying a yield stress. The proof load is obtained by multiplying the tensile stress area by a yield stress obtained by using either a 0.2% offset strain or a 0.5% extension under load. The tensile stress area is equal to the following:

$$\text{Tensile stress area} = 0.785 + \left(d - \frac{0.9743}{n} \right)^2$$

Equation 3.3.74

where *d* is the bolt diameter and *n* is the number of threads per inch.

For A 325 and A 490 bolts, the proof load stress is approximately a minimum of 70% and 80%, respectively, of the minimum tensile strength of the bolt, which is also established in a direct-pull tension test (Figure 3.3.29). In actual connections, the pretension in the bolt is established by turning the nut, which results in

elongation of the bolt. Because of the torsional stresses in the bolt caused by tightening in this manner, the tensile strength and total elongation induced in the bolt by turning the nut are somewhat less than in a direct-pull tension test (*42*, *43*). *AASHTO LRFD* Table 6.13.2.8-1 (Table 3.3.1) specifies the minimum required bolt tension for A 325 and A 490 bolts used in slip-critical connections, which is taken equal to 70% of the minimum tensile strength of the respective bolts. The minimum required bolt tension is equal to the proof load for A 325 bolts and about 85 to 90% of the proof load for A 490 bolts.

Table 3.3.1 Minimum Required Bolt Tension for A 325 and A 490 Bolts

Bolt Diameter, in.	Required Tension-P_t (kips)	
	A 325	A 490
5/8	19	24
3/4	28	35
7/8	39	49
1	51	64
1-1/8	56	80
1-1/4	71	102
1-3/8	85	121
1-1/2	103	148

Four general methods of installing the bolts can be used to obtain the minimum required bolt tension: 1) turn-of-the-nut tightening, 2) calibrated wrench tightening, 3) installation of alternative fasteners, or 4) installation of load indicator devices.

The turn-of-the-nut method is the simplest and obtains the pretension by a specified rotation of the nut from the “snug tight” condition, which is defined as the point at which the turned element ceases to rotate freely and the impact wrench begins to impact. If ordinary spud wrenches are used, the “snug tight” position is signaled by the full effort of the worker. A sufficient number of bolts must initially be brought to the “snug tight” position to bring the connection components into full contact. All remaining bolts in the connection are then brought to the “snug tight” position. Once this phase is completed, all nuts in the joint are given an additional rotation depending on the bolt length and the type of connection. The additional rotation causes a specified strain in the bolt controlling the bolt elongation and obtaining bolt tension well beyond the specified proof load. In the plastic range, large changes in bolt strain cause small changes in bolt tension allowing high clamping forces to be consistently obtained under the additional specified rotation regardless of the variation of the initial “snug tightness”.

Calibrated wrench tightening utilizes torque control to obtain the appropriate bolt tensions. Either manual torque wrenches or power wrenches adjusted to stall at a specified torque are used. To prevent large variations in bolt tensions, calibrated wrenches must be set to produce a bolt tension 5% in excess of the values

prescribed in Table 3.3.1. Calibration must be repeated at least daily or whenever the wrench is used to tighten a different size bolt. A hardened washer must be used under the turned element (head or nut).

High-strength bolt installation utilizing alternative fasteners and load indicator devices is discussed in more detail below in Sections 3.3.6.2.2.3 and 3.3.6.2.2.4.

Regardless of the method used, the final tightening sequence should proceed in an orderly fashion from the most rigid part of the connection progressing systematically toward the less rigid areas or free edges. Additional more detailed information on high-strength bolt installation procedures and bolt inspection procedures (including required rotation capacity testing) may be found in References 41 and 44.

3.3.6.2.2.3 Alternative Fasteners

Alternative fasteners or fastener assemblies are permitted if approved by the Engineer and provided they satisfy the general provisions of *AASHTO LRFD* Article 6.4.3.4. Alternative fasteners are generally proprietary fasteners designed to automatically provide the required tension or indirectly indicate the bolt tension. Included in this category are so-called ″twist-off bolts″ (conforming to the requirements of ASTM F 1852).

3.3.6.2.2.4 Load Indicator Devices

Load indicating devices conforming to the requirements of ASTM F 959, or other alternate direct tension indicating devices approved by the Engineer, may be used according to *AASHTO LRFD* Article 6.4.3.5.

Load indicator devices conforming to ASTM F 959 are hardened washers with several formed arches that deform in a controlled manner when subjected to a compressive load. The washer is inserted between the turned element (head or nut) and the gripped material with the protrusions bearing against the underside of the element with a gap maintained by the protrusions. Tightening of the bolt flattens the protrusions and reduces the gap. The bolt tension is then determined by measuring the remaining gap with a feeler gage. For proper tension, the gap should be about 0.015 in. or less (*45*).

Load-indicating devices which are incorporated into assemblies with hardened heavy hex *AASHTO* M 291 (ASTM A 563) Grade DH nuts affixed by the fastener manufacturer are also considered permissible for use, provided both the load-indicating device and heavy hex nut meet the mechanical property requirements of their respective ASTM standards. Such assemblies are referred to as a “captive DTI/nut”.

AASHTO LRFD Article 6.13.2.3.2 specifies that load indicator devices are not to be installed over oversize or slotted holes in an outer ply, unless a hardened washer or a structural plate washer is also provided.

3.3.6.2.2.5 Size of Bolts

AASHTO LRFD Article 6.13.2.5 gives some specific requirements regarding the size of bolts. Bolts are not to be less than 0.625 in. in diameter. Bolts 0.625 in. in diameter are not to be used in primary members, except for 2.5-in. legs of angles and in flanges of sections whose dimensions require 0.625-in. bolts to satisfy other detailing provisions given in the specifications. Structural shapes that do not permit the use of 0.625-in. bolts are to be limited to use in handrails.

The diameter of bolts in angles that serve as primary members is not to exceed one-fourth of the width of the leg in which the bolts are placed. Finally, angles whose size is *not* determined by a calculated demand may use the following bolt sizes: 1) 0.625-in. diameter bolts in 2.0-in. legs; 2) 0.75-in. diameter bolts in 2.5-in. legs; 3) 0.875-in. diameter bolts in 3.0-in. legs; and 4) 1.0-in. diameter bolts in 3.5-in. legs.

3.3.6.2.2.6 Spacing of Bolts

Minimum Spacing and Clear Distance

AASHTO LRFD Article 6.13.2.6.1 specifies that the minimum spacing between centers of bolts in standard holes is not to be less than 3.0*d*, where *d* is the diameter of the bolt (Figure 3.3.30).

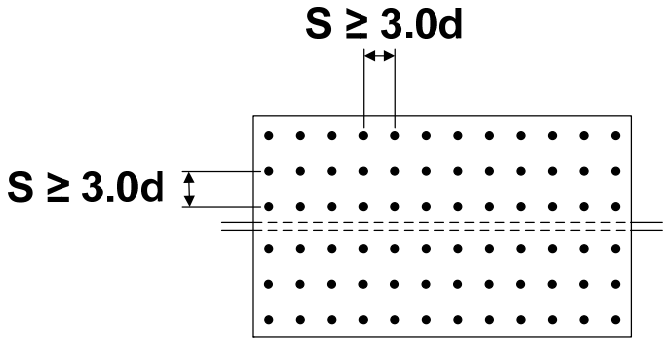


Figure 3.3.30 Minimum Spacing Requirement Between Centers of Bolts

The minimum clear distance, L_c, between the edges of adjacent bolt holes in the direction of the force and transverse to the direction of the force is not to be less than 2.0*d* when oversize or slotted holes are used.

Maximum Spacing for Sealing Bolts

AASHTO LRFD Article 6.13.2.6.2 specifies that to seal against the penetration of moisture in joints, the spacing, *s*, of a single line of bolts adjacent to a free edge of an outside plate or shape must satisfy the following requirement (Figure 3.3.31):

$$s \le (4.0 + 4.0t) \le 7.0 \text{ in.}$$

Equation 3.3.75
AASHTO LRFD Equation
6.13.2.6.2-1

where:
t = thickness of the thinner outside plate or shape (in.)

Where there is a second line of bolts uniformly staggered with the line adjacent to the free edge, at a gage less than 1.5 + 4.0*t*, the staggered spacing, *s*, in the two lines considered together must satisfy the following requirement (Figure 3.3.31):

$$s \le 4.0 + 4.0t - \left(\frac{3.0g}{4.0}\right) \le 7.0 \text{ in.}$$

Equation 3.3.76
AASHTO LRFD Equation
6.13.2.6.2-2

where:
g = gage between bolts (in.)

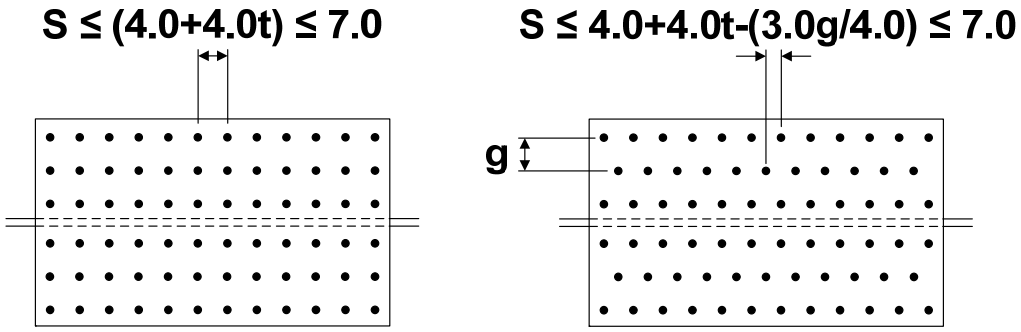


Figure 3.3.31 Maximum Spacing Requirements for Sealing Bolts

In uncoated weathering steel structures, it is critical that the bolt spacing be such that the connection joint is tight and excess moisture cannot enter between the plies of material. If sufficient moisture enters the joint, the resulting corrosion may cause prying, or pack-out, of the joint or bolt failure. Bolt spacing guidelines to insure proper tightness and stiffness of uncoated weathering steel bolted joints to avoid joint prying and corrosion pack-out are provided in Reference 46. The maximum spacing requirements for sealing bolts, given above, automatically satisfy these guidelines.

Maximum pitch requirements for stitch bolts, which fasten together built-up compression or tension members at intervals along their length to ensure that the separate components act as a unit and to prevent buckling of compression members, are specified in *AASHTO LRFD* Article 6.13.2.6.3. The pitch is not to exceed the maximum pitch specified for sealing bolts.

Edge and End Distance Requirements

The edge distance of bolts is defined as the distance perpendicular to the line of force between the center of a hole and the edge of the component (Figure 3.3.32). The minimum edge distance is a function of the diameter of the bolt and the condition of the plate edge (i.e. sheared or rolled or gas cut). *AASHTO LRFD* Article 6.13.2.6.6 specifies that the minimum edge distance is to be taken specified in *AASHTO LRFD* Table 6.13.2.6.6-1 (Table 3.3.2):

Table 3.3.2 Minimum Edge Distances

Bolt Diameter	Sheared Edges	Rolled Edges of Plates or Shapes, or Gas Cut Edges
in.	in.	in.
5/8	1-1/8	7/8
3/4	1-1/4	1
7/8	1-1/2	1-1/8
1	1-3/4	1-1/4
1-1/8	2	1-1/2
1-1/4	2-1/4	1-5/8
1-3/8	2-3/8	1-3/4

The maximum edge distance is not to be more than the lesser of eight times the thickness of the thinnest outside plate and 5.0 in.

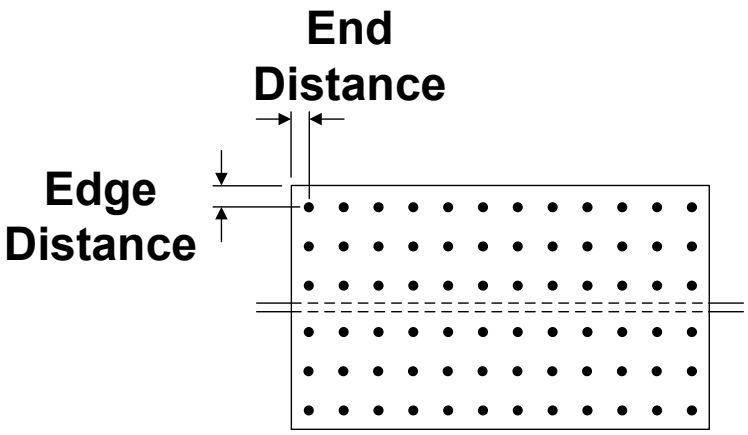


Figure 3.3.32 Edge and End Distance

The end distance of bolts is defined as the distance along the line of force between the center of a hole and the end of the component (Figure 3.3.32). *AASHTO LRFD* Article 6.13.2.6.5 specifies that the end distance for all types of holes is not to less than the appropriate minimum edge distance specified in Table 3.3.2. When oversize or slotted holes are used, the minimum clear end distance, which is defined as the distance between the edge of the bolt hole and the end of the member, must not be less than the bolt diameter.

The maximum end distance is to be taken the same as the maximum edge distance, or the lesser of eight times the thickness of the thinnest outside plate and 5.0 in.

3.3.6.2.3 Nuts

Different grades of high-strength bolts are combined with various heavy hexagon-shaped nuts, which guarantee failure by bolt yielding rather than by stripping of the nut threads.

AASHTO LRFD Article 6.4.3.2 specifies that nuts for use with ASTM A 325 bolts must conform to the requirements of ASTM A 563 Grades DH, DH3, C, C3 and D. Nuts to be used with ASTM A 325 Type 3 bolts must be of Grade C3 or DH3. All plain nuts must have a minimum hardness of 89 HRB.

Nuts to be galvanized must be heat-treated Grade DH nuts and must be lubricated with a lubricant containing a visible dye. To accommodate the relatively thick non-uniform zinc coatings on bolt threads during hot-dip galvanizing, the blank nut is typically hot-dip galvanized and then tapped over-size. This results in a reduction in the thread engagement and the resulting stripping strength. Only the stronger hardened nuts (Grade DH) have adequate strength to meet ASTM thread-strength requirements after over-tapping. Less over-tapping is usually required for mechanically galvanized nuts. Galvanizing increases the friction between the bolt

and nut threads, as well as the variability of the torque-induced pretension (*47*). If the nuts are lubricated, a lower required torque and more consistent results are obtained. Therefore, the supplier must test a galvanized bolt, lubricated galvanized nut and a galvanized washer in an assembled steel joint prior to shipment to show that the galvanized nut with the lubricant provided can be rotated from the snug-tight condition well beyond the rotation required for pretensioned installation without stripping.

Nuts for use with ASTM A 490 bolts must conform to the requirements of ASTM A 563 Grades DH and DH3. Nuts to be used with ASTM A 490 Type 3 bolts must be of Grade DH3.

3.3.6.2.4 Washers

AASHTO LRFD Article 6.4.3.3 specifies that hardened steel washers must satisfy the requirements of ASTM F 436. *AASHTO LRFD* Article 6.13.2.3.2 spells out the conditions under which hardened washers are required in high-strength bolted connections. These conditions include the following:

- When the outer face of the bolted parts has a slope greater than 1:20 with respect to a plane normal to the bolt axis;
- When tightening is performed by the calibrated wrench method. The washer is to be used under the turned element;
- When ASTM A490 bolts are installed in material with a specified minimum yield strength less than 50 ksi regardless of the tightening method. This is to guard against galling and indenting the connected parts since A 490 bolts produce larger clamping forces than A 325 bolts;
- When oversize or short-slotted holes are used in an outer ply. When ASTM A 490 bolts over 1.0 in. in diameter are used in such cases, hardened washers with 0.3125 in. minimum thickness are to be used under both the head and the nut in lieu of standard thickness washers. Multiple hardened washers with a combined thickness greater than or equal to 0.3125 in. are not to be used;
- When long-slotted holes are used. In such cases, structural plate washers or a continuous bar with standard holes not less than 0.3125 in. in thickness are to completely cover long-slotted holes. The hardened washer is then to be placed over the outer surface of the plate washer or bar.

Note that ASTM F 436 weathering steel washers should be used in conjunction with Type 3 high-strength bolts.

3.3.6.2.5 Holes

3.3.6.2.5.1 Size

The maximum permitted size of standard, oversize, short-slotted and long-slotted holes is given in *AASHTO LRFD* Table 6.13.2.4.2-1 (Table 3.3.3). In the table, *d* is the diameter of the bolt:

Table 3.3.3 Maximum Hole Sizes

Bolt Dia.	Standard	Oversize	Short Slot	Long Slot
d	Dia.	Dia.	Width × Length	Width × Length
in.	in.	in.	in.	in.
5/8	11/16	13/16	11/16 × 7/8	11/16 × 1-9/16
3/4	13/16	15/16	13/16 × 1	13/16 × 1-7/8
7/8	15/16	1-1/16	15/16 × 1-1/8	15/16 × 2-3/16
1	1-1/16	1-1/4	1-1/16 × 1-5/16	1-1/16 × 2-1/2
≥ 1-1/8	*d*+1/16	*d*+5/16	*d*+1/16 × *d*+3/8	*d*+1/16 × 2.5*d*

AASHTO LRFD Article 6.8.3 specifies that for design calculations, the width of standard bolt holes is to be taken as the nominal diameter of the hole. The width of oversize and slotted holes is to be taken as the nominal diameter or width of the hole, as applicable, given in Table 3.3.3.

3.3.6.2.5.2 Standard Holes

According to *AASHTO LRFD* Article 6.13.2.4.1a, standard holes (Table 3.3.3) are to be used for high-strength bolted connections, unless specified otherwise.

AASHTO LRFD Article 6.13.1 specifies that unless expressly permitted otherwise by the contract documents, standard holes are to be used in connections in horizontally curved bridges to ensure that the steel fits together in the field during erection. Curved girders depend on their connections to adjacent girders through bracing members for their stability. Therefore, cross-frames/diaphragms on curved girders should be firmly connected to the girders in order for the girders to remain stable during erection. Loosely connected cross-frames/diaphragms and oversize or slotted holes are not recommended for use in horizontally curved bridges as they may compromise the girder alignment and plumbness, as demonstrated in Section 4.1.4.2, making cross-frame/diaphragm fit-up difficult.

3.3.6.2.5.3 Slotted Holes

Section 4.2.3.3 discusses the potential use of vertical slotted holes for cross-frame connections in straight skewed I-girder bridges in an attempt to minimize the twist of the girders and reduce the cross-frame forces. As pointed out in Section 4.2.3.3, such an approach is not recommended as it becomes difficult to control the vertical deflections during the deck placement and care must be taken to ensure the construction plan reflects the analysis assumptions made as to when the bolts are to be tightened.

Short-Slotted Holes

AASHTO LRFD Article 6.13.2.4.1c specifies that short-slotted holes (Table 3.3.3) may be used in any or all plies of either slip-critical or bearing-type connections. In slip-critical connections, the slots may be used without regard to the direction of loading. However, in bearing-type connections, the length of the slot must be normal to the direction of the load.

Long-Slotted Holes

AASHTO LRFD Article 6.13.2.4.1d specifies that long-slotted holes (Table 3.3.3) may be used only one ply of either slip-critical or bearing-type connections. As for short-slotted holes, in slip-critical connections, the slots may be used without regard to the direction of loading. However, in bearing-type connections, the length of the slot must be normal to the direction of the load.

3.3.6.2.6 Factored Resistance of Bolted Connections

3.3.6.2.6.1 Service Limit State

AASHTO LRFD Article 6.13.2.2 specifies that for slip-critical connections at the service limit state, the factored resistance, R_r, of a bolt at the Service II load combination is to be taken as:

$$R_r = R_n$$

Equation 3.3.77
AASHTO LRFD Equation 6.13.2.2-1

where:

R_n = nominal slip resistance of the bolt specified in *AASHTO LRFD* Article 6.13.2.8 (discussed below) (kips)

Slip Resistance of Bolts

The slip resistance of bolts is covered in *AASHTO LRFD* Article 6.13.2.8. The bolt pretension and surface condition of the faying surface (i.e. coefficient of friction) have the greatest effect on the slip-resistance of high-strength bolted connections.

AASHTO LRFD Article 6.13.2.8 specifies that the nominal slip resistance, R_n, of a bolt in a slip-critical connection (subject to shear) is to be taken as:

$$R_n = K_h K_s N_s P_t$$

Equation 3.3.78
AASHTO LRFD Equation 6.13.2.8-1

where:

N_s = number of slip planes per bolt
P_t = minimum required bolt tension specified in *AASHTO LRFD* Table 6.13.2.8-1 (Table 3.3.1) (kips)
K_h = hole size factor specified in *AASHTO LRFD* Table 6.13.2.8-2 (Table 3.3.4)
K_s = surface condition factor specified in *AASHTO LRFD* 6.13.2.8-3 (Table 3.3.5)

In a slip-critical connection subject to combined axial tension and shear, the tensile force reduces the contact pressure between the connected plates thereby reducing the slip resistance to the shear forces. The reduction in slip resistance is approximately proportional to the ratio of the applied tensile force to the bolt installation tension (*41*). Therefore, according to *AASHTO LRFD* Article 6.13.2.11, the nominal slip resistance of a bolt in a slip-critical connection subjected to combined axial tension and shear under service loads (i.e. under Load Combination Service II) must not exceed the nominal slip resistance given by Equation 3.3.78 times the following factor:

$$1 - \frac{T_u}{P_t}$$

Equation 3.3.79
AASHTO LRFD Equation 6.13.2.11-3

where:

T_u = tensile force due to the factored loads under Load Combination Service II (kips)
P_t = minimum required bolt tension specified in *AASHTO LRFD* Table 6.13.2.8-1 (Table 3.3.1) (kips)

The resistance to combined tension and shear once the connection slips and goes into bearing at the strength limit state is discussed in Section 3.3.6.2.6.2.

Since all locations must develop the slip resistance before a total joint slip can occur at that plane, the assumption is made that the slip resistance at each bolt is equal and additive with the slip resistance at the other bolts in the connection. It is

also assumed that the full slip resistances must be mobilized at each slip plane before full joint slip can occur, although the forces at each slip plane do not necessarily develop simultaneously. Equation 3.3.78 is formulated for the case of a single slip plane. Therefore, the total slip resistance of a joint with multiple slip planes can be taken equal to the resistance of a single slip plane multiplied by the number of slip planes N_s.

Hole size factors, K_h, less than 1.0 are provided for bolts in oversize or slotted holes in *AASHTO LRFD* Table 6.13.2.8-2 (Table 3.3.4) because of the greater possibility of significant deformation occurring in joints with oversize or slotted holes. For long-slotted holes, even though the slip load is the same for bolts loaded transverse or parallel to the axis of the slot, the hole size factor for loading parallel to the axis has been reduced, based upon judgment, because of the greater consequences of slip in this case.

Table 3.3.4 Hole Size Factor, K_h

for standard holes	1.00
for oversize and short-slotted holes	0.85
for long-slotted holes with the slot perpendicular to the direction of the force	0.70
for long-slotted holes with the slot parallel to the direction of the force	0.60

The surface condition factor, K_s, is provided in *AASHTO LRFD* Table 6.13.2.8-3 (Table 3.3.5) and is a function of the class of the surface. Three different classes of surfaces are defined based on the mean value of slip coefficients from many tests of clean mill scale, blast-cleaned steel surfaces and galvanized and roughened surfaces. The classes of surfaces are described as follows:

- Class A Surface: unpainted clean mill scale and blast-cleaned surfaces with Class A coatings;
- Class B Surface: unpainted blast-cleaned surfaces and blast-cleaned surfaces with Class B coatings;
- Class C Surface: hot-dip galvanized surfaces roughened by wire brushing after galvanizing.

Table 3.3.5 Surface Condition Factor, K_s

for Class A surface conditions	0.33
for Class B surface conditions	0.50
for Class C surface conditions	0.33

It has been found that if tightly adherent mill scale is on the faying surface of a bolted connection on uncoated weathering steel, the connection slips into bearing at a lower shear stress than on a carbon steel with mill scale (*48*). *However, if the faying surface is blast-cleaned, slip-critical connections on uncoated weathering steel can be designed using a Class B surface condition (49).* Otherwise, a Class A surface condition, which is appropriate for clean mill-scale surfaces, must be used. The slip resistance of bolted joints is not affected by the weathering of uncoated steel surfaces prior to erection, but any loose rust on the connection or faying surfaces must be removed. Pre-construction primers may be used for the cleaned bolted surfaces. Reference 48 indicates that the Class B surface condition can be maintained in such cases for up to one year prior to joint assembly.

Unpainted clean mill-scale faying surfaces and unpainted blast-cleaned faying surfaces must be protected from inadvertent paint overspray. *AASHTO LRFD* Article 6.13.2.8 requires that in uncoated joints, paint (including any inadvertent overspray) be excluded from areas closer than one bolt diameter but not less than 1.0 in. from the edge of any hole and all areas within the bolt pattern. Tests have demonstrated that for material with thickness in the range of 3/8 in. to ¾ in., the transfer of shear by friction between contact surfaces is concentrated in an annular ring around and close to the bolts (*50*). Paint on the contact surfaces away from the edge of the bolt hole by not less than 1.0 in. nor the bolt diameter did not reduce the slip resistance. For joints in thicker material, the minimum bolt pretension may not be adequate to completely flatten and pull the thick material into tight contact around every bolt in the pattern. Therefore, it is specified that all bolt areas within the pattern be kept free of paint, including any overspray.

Joints with painted faying surfaces must be blast-cleaned and coated with a paint that has been qualified by test as a Class A or Class B coating. A Class A coating will not reduce the slip coefficient below that provided by clean mill scale, and a Class B coating will not reduce the slip coefficient below that provided by blast-cleaned steel surfaces. A test method to determine the mean slip coefficient in order to qualify a particular coating for use according to the *AASHTO LRFD* Specifications is provided in Appendix A of Reference 41. The method includes long-term creep test requirements to ensure that the creep deformations caused by the bolt clamping force and joint shear are such that the coating will provide satisfactory long-term performance under sustained loading (*51*). Re-qualification of the coating is required if any essential variable is changed. According to *AASHTO LRFD* Article 6.13.2.8, the contract documents must state that coated

joints not be assembled before the coatings have cured the minimum time used in the qualifying test. Research has indicated that all curing of faying surface coatings ceases at the time the joints are assembled and tightened and that coatings that are not fully cured act as lubricants severely reducing the slip resistance of the joint (*52*). The specification permits the use of faying-surface coatings with a slip resistance less than Class A, (i.e. K_s = 0.33) subject to the approval of the Engineer, provided that the mean slip coefficient is determined by the specified test procedure.

Galvanized faying surfaces must be hot-dip galvanized according to the procedures given in the ASTM A 123 Specification and then must be subsequently roughened by means of hand wire brushing. The mean slip coefficient for clean hot-dip galvanized surfaces is on the order of 0.19 compared to 0.33 for clean mill scale (*41*). Research has indicated that the slip coefficient for galvanized surfaces can be significantly improved by hand wire brushing or light "brush-off" grit blasting (*47*). The treatment must be controlled in order to achieve visible scoring or roughening. Power wire brushing is not satisfactory because it may polish rather than roughen the surface or remove the coating. Tests on surfaces that have been hand wire brushed after coating have indicated a mean slip coefficient of 0.35 (*36*). The surface condition factor, K_s, for treated galvanized surfaces has been conservatively set at 0.33, which is the same as for Class A surfaces. A separate class (Class C) has been provided for galvanized surfaces to avoid potential confusion. Previous Specifications indicated a slip coefficient of 0.40 for galvanized surfaces, which assumed blast-cleaning of the surface after galvanizing; however, this is not the typical practice. Note that field experience and test results have indicated that galvanized surfaces may have a tendency to continue to slip under sustained loading illustrating a creep-type behavior (*36*). Relaxation of bolt tension may also occur where hot-dip galvanized coatings are used, particularly if there are many plies of thickly coated material in the joint. In such cases, this can either be allowed for in the design or else the bolts can be re-tightened after a period of settling-in subsequent to the initial tightening.

Since faying surfaces (that are not galvanized) are typically blast-cleaned as a minimum, a Class A surface condition should only be used to compute the slip resistance when Class A coatings are applied or when unpainted mill scale is left on the faying surface. Most commercially available primers will qualify as Class B coatings.

3.3.6.2.6.2 Strength Limit State

AASHTO LRFD Article 6.13.2.2 specifies that the factored resistance, R_r, of a bolt at the strength limit state (in a slip-critical or bearing-type connection) is to be taken as either:

$$R_r = \phi R_n$$

Equation 3.3.80
AASHTO LRFD Equation 6.13.2.2-2

or:

$$T_r = \phi T_n$$

Equation 3.3.81
AASHTO LRFD Equation 6.13.2.2-3

where:

ϕ = resistance factor for bolts specified in *AASHTO LRFD* Article 6.5.4.2
- = ϕ_s for bolts in shear = 0.80 (for A 325 and A 490 bolts); 0.65 (for A 307 bolts)
- = ϕ_t for bolts in tension = 0.80 (for A 325, A 490 and A 307 bolts)
- = ϕ_{bb} for bolts bearing on connected material = 0.80
- = ϕ_y for yielding in gross section for connected elements in tension = 0.95
- = ϕ_u for fracture in net section for connected elements in tension =0.80
- = ϕ_{vu} for connected elements in shear, rupture in connection element = 0.80

R_n = nominal resistance of the bolt, connected element or connected material (kips)
- = for bolts in shear as specified in *AASHTO LRFD* Article 6.13.2.7 (discussed below)
- = for connected material in bearing joints as specified in *AASHTOLRFD* Article 6.13.2.9 (discussed below)
- = for connected elements in shear or tension as specified in *AASHTO LRFD* Article 6.13.5.2 (discussed below)

T_n = nominal resistance of the bolt (kips)
- = for bolts in axial tension as specified in *AASHTO LRFD* Article 6.13.2.10 (discussed below)
- = for bolts in combined axial tension and shear as specified in *AASHTO LRFD* Article 6.13.2.11 (discussed below)

Shear Resistance of Bolts

The shear resistance of bolts is covered in *AASHTO LRFD* Article 6.13.2.7 (note that the shear resistance of anchor bolts, which are not covered herein, is specified in *AASHTO LRFD* Article 6.13.2.12). The shear failure of a bolt is illustrated in Figure 3.3.33.

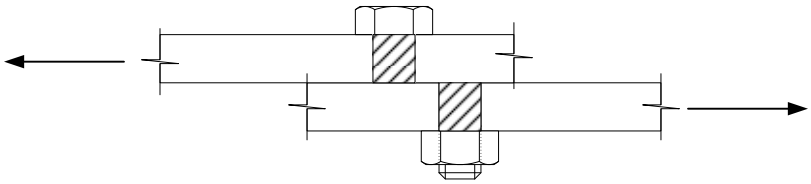


Figure 3.3.33 Shear Failure of a Bolt

AASHTO LRFD Article 6.13.2.7 specifies that the nominal shear resistance of a high-strength bolt (A 325 or A 490 bolt) or an A 307 bolt at the strength limit state in joints whose length between extreme fasteners measured parallel to the line of action of the force is less than 50.0 in. is to be taken as:

- Where threads are excluded from the shear plane:

$$R_n = 0.48 A_b F_{ub} N_s$$

Equation 3.3.82
AASHTO LRFD Equation 6.13.2.7-1

- Where threads are included in the shear plane:

$$R_n = 0.38 A_b F_{ub} N_s$$

Equation 3.3.83
AASHTO LRFD Equation 6.13.2.7-2

where:

A_b = area of the bolt corresponding to the nominal diameter (in.^{2})
F_{ub} = specified minimum tensile strength of the bolt specified in *AASHTO LRFD* Article 6.4.3 (ksi)
N_s = number of shear planes per bolt

For a bolt in a connection greater than 50.0 in. in length, the nominal shear resistance is to be taken as 0.80 times the value given by Equation 3.3.82 or 3.3.83, as applicable. The nominal shear resistance is based on the observation that the shear strength of a single high-strength bolt is about 0.60 times the tensile strength F_{ub} of the bolt (*36*).

The shear resistance is not affected by the pretension in the bolts provided the connected material is in contact at the faying surfaces. In shear connections with more than two bolts in the line of force, the average bolt strength decreases as the joint length increases due to the nonuniform bolt shear force distribution caused by deformation of the connected material. For joints up to 50.0 in. in length, a single reduction factor of 0.80 is implicitly applied to the 0.60 multiplier rather than providing a function that reflects the decrease in average bolt strength with joint length (0.80 * 0.60 equals the 0.48 multiplier given in Equation 3.3.82). This was felt not to adversely affect the economy of very short joints. For bolts in joints

longer than 50.0 in., the nominal shear resistance must be reduced by an additional 20 percent. For bolted flange splices, note that the 50.0 in. length is to be measured between the extreme bolts on only one side of the connection (*AASHTO LRFD* Article C6.13.2.7). The greater than 50.0 in. length reduction does *not* apply when the distribution of shear force is essentially uniform along the joint, such as in a bolted web splice (*41*).

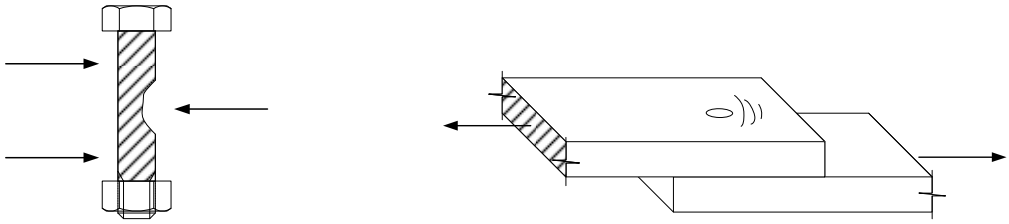
When bolts are positioned so that they cross two planes of contact (i.e. N_S = 2), this is referred to as ′double shear′. Double shear is a symmetrical loading situation with regard to the shear planes and direction of shear transfer. When there is a single plane of contact involved in the load transfer (i.e. N_S = 1), this is referred to as ′single shear′, which is an unsymmetrical loading situation.

The average ratio of the nominal shear resistance for bolts with threads included in the shear plane to the nominal shear resistance for bolts with threads excluded from the shear plane is 0.83 with a standard deviation of 0.03 (*52*). Therefore, a reduction factor of 0.80 is conservatively used to account for the nominal shear resistance when threads are included in the shear plane but calculated with the area corresponding to the nominal bolt diameter (0.48 * 0.80 equals the 0.38 multiplier given in Equation 3.3.83). In determining whether the threads are excluded from the shear planes, the thread length of the bolt is to be determined as two thread pitches greater than the specified thread length. If the threads of a bolt are included in a shear plane of a joint, the nominal shear resistance of the bolts in all shear planes of the joint is to conservatively be taken from Equation 3.3.83. That is, for bolts in double shear with a non-threaded shank in one shear plane and a threaded section in the other shear plane, the sharing of the load between the two dissimilar shear areas is uncertain. Also, knowledge about the specific bolt placement, which might result in both shear planes being in the threaded section, is not ordinarily available to the Design Engineer. *Whenever Equation 3.3.82 is used to compute the nominal shear resistance, the Design Engineer should note on the contract plans that the threads are to be excluded from the shear plane so that the bolt lengths can be detailed accordingly*.

Since the threaded length of an A 307 bolt is not as predictable as that of a high-strength bolt, the nominal shear resistance of an A 307 bolt must always be based on Equation 3.3.83. Also, A 307 bolts with a long grip (i.e. the total thickness of the plies of a joint through which the bolt passes exclusive of any washers or load-indicating devices) tend to bend reducing their shear resistance. Therefore, *AASHTO LRFD* Article 6.13.2.7 requires that when the grip length of an A 307 bolt exceeds 5.0 bolt diameters, the nominal shear resistance must be lowered 1.0 percent for each 1/16 in. of grip in excess of 5.0 bolt diameters.

Bearing Resistance of Connected Material

The bearing resistance of the connected material in a bolted connection is covered in *AASHTO LRFD* Article 6.13.2.9. A bearing failure relates generally to either deformation of the bolt or deformation around a bolt hole, as illustrated in Figure 3.3.34 Part A and Figure 3.3.34 Part B, respectively.



(a) (b)

Figure 3.3.34 Bearing Failure of a) Bolt and b) Connected Material

After a major slip has occurred in a slip-critical connection, one or more bolts are in bearing against the side of the hole. The contact pressure between the bolt and connected material can be expressed as the bearing stress on the bolt or connected material. Tests have always shown that the bearing stress on the bolt is not critical (*36*). For simplicity, the bearing stress is assumed to be a uniform stress distribution equal to the load transmitted by the bolt divided by the bearing area taken as the bolt diameter times the thickness of the connected material. *AASHTO LRFD* Article 6.13.2.9 specifies that the effective thickness of connected material with countersunk holes is to be taken as the thickness of the connected material minus one-half the depth of the countersink.

The actual failure mode depends on the end distance or clear distance between bolts, the bolt diameter and the thickness of the connected material. Either the bolt will split out through the end of the plate because of insufficient end distance, or else excessive deformations are developed in the connected material adjacent to the bolt hole (Figure 3.3.34 Part B) because of insufficient clear distance between the bolts.

The end distance required to prevent the plate from splitting out can be approximated by equating the maximum load, R_n, transmitted by the end bolt to the force corresponding to shear failure of the plate material of thickness, t, along the dotted Lines 1-1 and 2-2 shown in Figure 3.3.35. Although actual splitting would occur along the Lines 1-1 and 2-2 in Figure 3.3.35, the angle α will be assumed equal to zero in order to compute a lower-bound resistance and failure will be assumed to occur along the two solid lines instead.

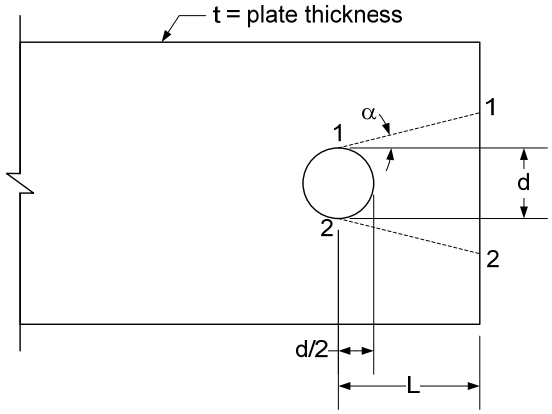


Figure 3.3.35 Bearing Resistance Related to End Distance

Therefore:

$$R_n = 2t(L - \frac{d}{2})\tau_u$$

Equation 3.3.84

where τ_u is the ultimate shear resistance of the plate material. For commonly used steels, τ_u can be assumed approximately equal to $0.75F_u$, where F_u is the ultimate tensile strength of the plate material. Therefore, substituting $0.75F_u$ for τ_u and the clear distance, L_c, from the edge of the hole to the end of the plate in the direction of the force for ($L - d/2$) in Equation 3.3.84 (to simplify the calculations for oversize and slotted holes) gives:

$$R_n = 1.5L_c tF_u$$

Equation 3.3.85

Equation 3.3.85 can be used to determine the bearing resistance between bolt holes by substituting the clear distance between adjacent holes for the clear end distance. The same bearing resistance applies regardless of the bolt shear resistance or the presence or absence of bolt threads in the bearing area. An alternative equivalent relationship relating the bearing stress r_n to F_u as a function of the *L/d* ratio based conservatively on test results of finger-tight bolts (*36*) is given in *AASHTO LRFD* Article C6.13.2.9 as follows:

$$\frac{L}{d} \geq \frac{r_n}{F_u}$$

Equation 3.3.86
AASHTO LRFD Equation
C6.13.2.9-1

Reference 36 further recommends that the ratio of r_n/F_u be limited to 3.0 in order to limit deformations under the factored loads. Substituting $r_n = R_n/dt$ in this ratio and rearranging gives an upper-bound bearing resistance of:

$$R_n = 3.0F_u dt$$

Equation 3.3.87

Equations 3.3.85 and 3.3.87 are given as the bearing resistance equations in Reference 41 for cases where deformation at the bolt holes at service load is *not* a design consideration for standard holes, oversize holes, or short-slotted holes loaded in any direction and long-slotted holes loaded parallel to the applied bearing force.

The more conservative equations from Reference 41 for the preceding cases when deformation at the bolt holes at service load *is* a design consideration are instead specified as follows in *AASHTO LRFD* Article 6.13.2.9 (and are to be applied under the *factored* loads at the strength limit state):

$$R_n = 1.2L_c tF_u \le 2.4dtF_u$$

Equation 3.3.88
AASHTO LRFD Equations 6.13.2.9-1 & 6.13.2.9-2

Equation 3.3.88 is derived based on tests that showed that the total elongation of a standard hole that is loaded to obtain the maximum recommended bearing resistance given by Equation 3.3.87 is on the order of the diameter of the bolt (*36*). Based on these tests, to prevent elongations exceeding 0.25 inches, a reduced limit on the bearing resistance of $2.4dtF_u$ is specified according to Equation 3.3.88.

For long-slotted holes perpendicular to the applied bearing force, the bending component of the deformation in the connected material becomes more critical (*41*). Therefore, for this case, the bearing resistance is further limited as follows:

$$R_n = L_c tF_u \le 2.0dtF_u$$

Equation 3.3.89
AASHTO LRFD Equations 6.13.2.9-3 & 6.13.2.9-4

The design bearing resistance is expressed in terms of a single bolt, although it is truly for the connected material adjacent to the bolt. *Therefore, in calculating the nominal bearing resistance for the connected part, the total bearing resistance may be taken as the sum of the bearing resistances of the individual bolts (holes) parallel to the line of the applied force*.

Shear Resistance of a Connected Element

AASHTO LRFD Article 6.13.5.3 specifies that the *factored* shear resistance, R_r, of a connected element (i.e. a splice plate, gusset plate or lateral connection plate) is to be taken as the smaller value based on shear yielding or shear rupture.

Shear Yielding

For shear yielding, the factored shear resistance of the connected element, R_r, is conservatively based on the shear yield stress (i.e. $F_y/\sqrt{3} = 0.58F_y$) as follows:

$$R_r = \phi_v 0.58 F_y A_{vg}$$

Equation 3.3.90
AASHTO LRFD Equation 6.13.5.3-1

where:

ϕ_v = resistance factor for shear specified in *AASHTO LRFD* Article 6.5.4.2 (= 1.0)
A_{vg} = gross area of the connected element subject to shear (in.^{2})
F_y = specified minimum yield strength of the connected element (ksi)

Shear Rupture

A shear rupture failure of a connected element is illustrated in Figure 3.3.36.

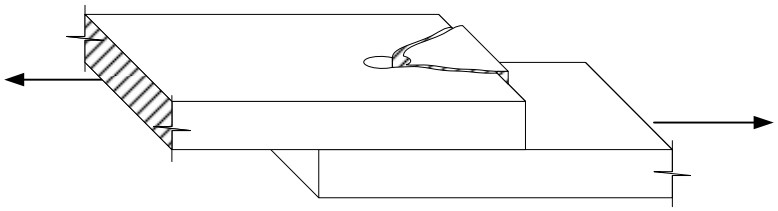


Figure 3.3.36 Shear Rupture Failure of a Connected Element

For shear rupture, the factored shear resistance of the connected element, R_r, is to be taken as follows:

$$R_r = \phi_{vu} 0.58 R_p F_u A_{vn}$$

Equation 3.3.91
AASHTO LRFD Equation 6.13.5.3-2

where:

ϕ_{vu} = resistance factor for shear rupture of connected elements specified in *AASHTO LRFD* Article 6.5.4.2 (= 0.80)
A_{vn} = net area of the connected element subject to shear (in.^{2})
F_u = tensile strength of the connected element specified in *AASHTO LRFD* Table 6.4.1-1 (ksi)
R_p = reduction factor for holes taken equal to 0.90 for bolt holes punched full size and 1.0 for bolt holes drilled full size or subpunched and reamed to size (Section 3.3.3.2.1)

Tensile Resistance of a Connected Element

AASHTO LRFD Article 6.13.5.2 specifies that the *factored* tensile resistance, R_r, of a connected element (i.e. a splice plate, gusset plate or lateral connection plate) is to be taken as the smallest of the resistances based on yielding, net section fracture or block shear rupture.

Yield Resistance

A connected element subject to tension must be checked for yielding on the gross section. Excessive elongation due to uncontrolled yielding of the gross area can limit the structural usefulness of the connected element so that it no longer serves its intended purpose.

According to *AASHTO LRFD* Article 6.13.5.2, the factored yield resistance of a connected element in tension is to be computed from *AASHTO LRFD* Equation 6.8.2.1-1 as follows:

$$R_r = \phi_y F_y A_g$$

Equation 3.3.92
AASHTO LRFD Equation 6.8.2.1-1

where:

ϕ_y = resistance factor for yielding of tension members specified in *AASHTO LRFD* Article 6.5.4.2 (= 0.95)
F_y = specified minimum yield strength of the connected element (ksi)
A_g = gross cross-sectional area of the connected element (in.^{2})

Net Section Fracture Resistance

A connected element subject to tension must be checked for fracture on the net section. The connected element can fracture by failure of the net area (Figure 3.3.37) at a load smaller than that required to yield the gross area depending on the ratio of net to gross area, the properties of the steel (i.e. the ratio of F_u/F_y) and the end connection geometry. Holes in a member cause stress concentrations at service loads, with the tensile stress adjacent to the hole typically about three times the average stress on the net area. As the load increases and the deformation continues, all fibers across the section will achieve or eventually exceed the yield strain. Failure occurs when the localized yielding results in a fracture through the net area.

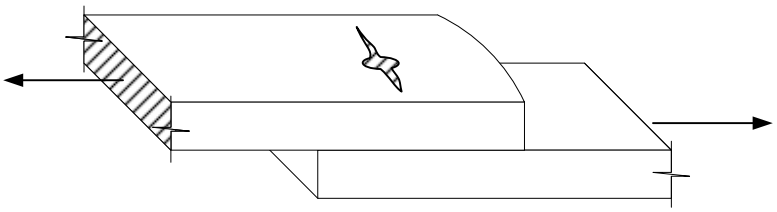


Figure 3.3.37 Tensile Failure of a Connected Element by Net Section Fracture

Typically, a higher margin of safety is used when considering the net section fracture resistance versus the yield resistance. According to *AASHTO LRFD* Article 6.13.5.2, the factored net section fracture resistance of a connected element in tension is to be computed from *AASHTO LRFD* Equation 6.8.2.1-2 as follows:

$$R_r = \phi_u F_u A_n U$$

Equation 3.3.93
AASHTO LRFD Equation 6.8.2.1-2

where:

ϕ_u = resistance factor for fracture of tension members specified in *AASHTO LRFD* Article 6.5.4.2 (= 0.80)
F_u = tensile strength of the connected element specified in *AASHTO LRFD* Table 6.4.1-1 (ksi)
A_n = net cross-sectional area of the connected element determined as specified in *AASHTO LRFD* Article 6.8.3 (in.^{2})
U = reduction factor to account for shear lag (discussed below)

The calculation of the net area, A_n, is discussed above in Section 3.3.3.2.2. *According to AASHTO LRFD Article 6.13.5.2, for lateral connection plates, splice plates and gusset plates, A_n is not to be taken greater than 85 percent of the gross area, A_g, of the plate in checking Equation 3.3.93*. Because the length of these particular elements is small compared to the overall member length, inelastic deformation of the gross area is limited. Tests have shown that when holes are present in such short elements where general yielding on the gross section cannot occur, there will be at least a 15 percent reduction in tensile capacity from that obtained based on yielding of the gross section (*36*).

The reduction factor, *U*, in Equation 3.3.93 accounts for the effect of shear lag in connections, and is discussed further in Section 3.3.3.2.3. Shear lag is a consideration when the connection elements do not lie in a common plane and where the tensile force in the member is applied eccentrically or transmitted by connection to some but not all of the connection elements; e.g. an angle having a connection to only one leg. *As specified in AASHTO LRFD Article 6.13.5.2, for short connection elements such as lateral connection plates, splice plates and gusset plates, where the elements of the cross-section essentially lie in a common plate, U is to be taken equal to 1.0*.

Block Shear Rupture Resistance

The factored block shear rupture resistance, R_r, of the connected element is calculated according to Equation 3.3.27. The reader is referred to Section 3.3.3.2.4 for further discussion regarding block shear rupture.

Compressive Resistance of a Connected Element

The compressive resistance of cross-frame gusset plates and lateral connection plates for lateral bracing members is not currently covered in the *AASHTO LRFD* Specifications. One possible suggestion is to adapt the procedures given in Reference 33 for determining and checking the compressive resistance of these items to fit with the *AASHTO LRFD* Specifications.

Local buckling of cross-frame connection plates serving as transverse stiffeners adjacent to web panels subject to tension-field action is considered in *AASHTO LRFD* Article 6.10.11.1 (Section 3.3.8.1.3). A suggested check for local buckling of cross-frame connection plates in I-girder bridges when the cross-slope is large and rectangular cross-frames or diaphragms are used is discussed in Section 3.1.2.8.5.2.

Tensile Resistance of Bolts

The tensile resistance of bolts is covered in *AASHTO LRFD* Article 6.13.2.10. The tensile failure of a bolt is illustrated in Figure 3.3.38.

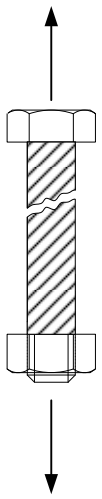


Figure 3.3.38 Tensile Failure of a Bolt

Axial tension occurring without simultaneous shear occurs in bolts for tension members such as hangers or other members whose line of action is perpendicular to the member to which it is fastened. The applied tensile force must be taken as

the force due to externally applied loads plus any tension resulting from prying action produced by deformation of the connected parts. Prying action is not discussed herein; further information on prying action may be found in References 21, 33 and 36. The tensile resistance of bolts (as discussed herein) must typically be considered in combination with simultaneous shear for bolted bracing member connections (as discussed further below under 'Combined Tensile and Shear Resistance of Bolts').

AASHTO LRFD Article 6.13.2.10.1 specifies that high-strength bolts subject to axial tension must be pretensioned to the level given in Table 3.3.1 regardless of whether the design is for a slip-critical or a bearing-type connection. According to *AASHTO LRFD* Article 6.13.2.10.2, the nominal tensile resistance of a bolt, T_n, independent of any initial tightening force is to be taken as:

$$T_n = 0.76 A_b F_{ub}$$

Equation 3.3.94
AASHTO LRFD Equation 6.13.2.10.2-1

where:

A_b = area of the bolt corresponding to the nominal diameter (in.^{2})
F_{ub} = tensile strength of the bolt specified in *AASHTO LRFD* Article 6.4.3 (ksi)

The tensile resistance of a bolt is the product of the tensile strength of the bolt and the tensile stress area through the threaded portion of the bolt given by Equation 3.3.74. The tensile stress area is approximately 76 percent of the nominal cross-sectional area of the bolt for the usual sizes of structural bolt (*41*). Hence, the nominal tensile resistance per unit area (based on the nominal area of the bolt) is taken as 76 percent of the tensile strength of the bolt.

The specified nominal tensile resistance is approximately equal to the initial tightening force specified in Table 3.3.1. Thus, when a tensile force is applied to a high-strength bolt that has been properly pretensioned, the increase in the bolt tension is generally much smaller than the applied load.

Consider a single high-strength bolt and a portion of two connected parts of thickness t subject to an externally applied tensile force, P, as shown in Figure 3.3.39 Part A. Prior to application of the external force, the bolt is installed with a pretension force, T_b. As shown in Figure 3.3.39 Part B, this causes the two parts to be initially compressed by an amount C_i. C_i must equal T_b for equilibrium. The external force P is then applied as shown in Figure 3.3.39 Part C and for equilibrium, P plus C_f must equal T_f, where the subscript f refers to the final condition after the application of the force.

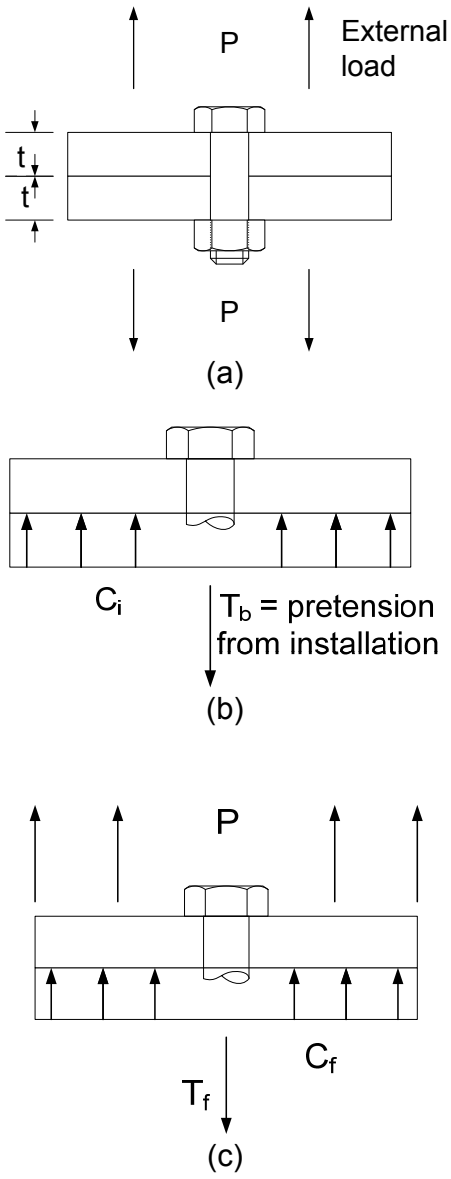


Figure 3.3.39 Pretensioning Effect on a Bolted Joint

The bolt elongates as the tensile force is applied to the joint and the compressed plates simultaneously expand as the initial contact pressure is reduced. The applied force is offset by the increase in the bolt tension and the decrease in contact pressure. As illustrated in Reference 19, the increase in the bolt tension is a function of the relative stiffness of the bolt and connected plates, but it is typically minimal until the parts separate (*36*). There will be little increase in bolt force above the pretension load at service load levels. After the parts separate, the bolt will act as a tension member with the applied force equaling the bolt tension. As a result, bolts in connections subject to axial tension are required to be fully pretensioned.

As mentioned above, pretensioning imposes a small axial elongation of the bolt. A joint subsequently loaded in tension, shear or combined tension and shear imposes significant deformations in the bolt prior to failure that override the small initial elongation and remove the pretensioning. Tests confirm that the initial pretension that would be sustained after the applied load is removed is essentially zero before the bolts fail in shear (*36*). Therefore, the tensile and shear resistances of the bolt are unaffected by the initial pretensioning of the bolt. Any residual torsion induced in the bolt during installation is also small and will be removed when the bolt is loaded to the point of plate separation. Hence, any effect of torsion on the tensile resistance of the bolt need not be considered (*36*).

Combined Tensile and Shear Resistance of Bolts

The resistance of bolts under combined axial tension and shear is covered in *AASHTO LRFD* Article 6.13.2.11. Examples of connections in which the bolts would be subject to combined tension and shear are shown in Figure 3.3.40.

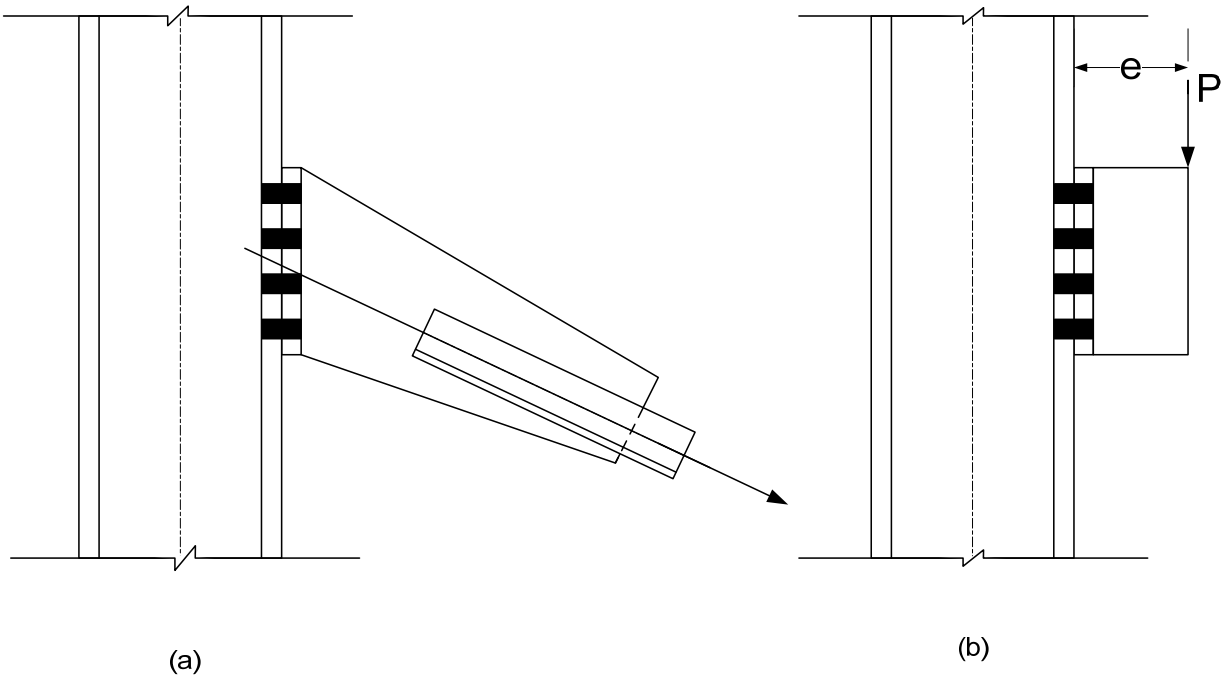


Figure 3.3.40 Bolted Connections Subject to Combined Tension and Shear

Once a bolt slips and goes into bearing, the bolt yields under the effects of combined tension and shear at a lower load than if only shear or tension were present. Tests on single high-strength bolts subject to various combinations of tension and shear in this condition were conducted at the University of Illinois (*53*). From these tests, it was determined that when both shear and tensile forces act on a high-strength bolt at the strength limit state, the interaction can be conveniently expressed by an elliptical interaction relationship as follows (*41*):

$$\left[\frac{T_u}{(R_r)_t}\right]^2 + \left[\frac{P_u}{(R_r)_s}\right]^2$$

Equation 3.3.95

where:

P_u = shear force on the bolt due to the factored loads (kips)
T_u = tensile force on the bolt due to the factored loads (kips)
$(R_r)_s$ = factored resistance of the bolt in shear (kips)
$(R_r)_t$ = factored resistance of the bolt in tension (kips)

Equation 3.3.95 accounts for the connection length effect on bolts loaded in shear, the ratio of the shear resistance to tensile resistance of threaded bolts, the ratio of root area to nominal body area of the bolt and the ratio of the tensile stress area to the nominal body area of the bolt. Equations for various cases based on Equation 3.3.95 can be found in Reference 54.

A conservative simplification of the interaction relationship given by Equation 3.3.95 is used in *AASHTO LRFD* Article 6.13.2.11. The nominal tensile resistance, T_n, of a bolt subjected to combined shear and axial tension is taken as follows:

- If $\frac{P_u}{R_n} \le 0.33$, then:

$$T_n = 0.76 A_b F_{ub}$$

Equation 3.3.96
AASHTO LRFD Equation 6.13.2.11-1

- If $\frac{P_u}{R_n} > 0.33$, then:

$$T_n = 0.76 A_b F_{ub} \sqrt{1 - \left(\frac{P_u}{\phi_s R_n}\right)^2}$$

Equation 3.3.97
AASHTO LRFD Equation 6.13.2.11-2

where:

ϕ_s = resistance factor for bolts in shear specified in *AASHTO LRFD* Article 6.5.4.2 (= 0.80)
A_b = area of the bolt corresponding to the nominal diameter (in.^{2})
F_{ub} = tensile strength of the bolt specified in *AASHTO LRFD* Article 6.4.3 (ksi)
P_u = factored shear force on the bolt (kips)
R_n = nominal shear resistance of the bolt determined as specified in Article 6.13.2.7 (kips)

In other words, no reduction in the nominal tensile resistance of the bolt is required when the factored shear force does not exceed 33 percent of the nominal shear resistance of the bolt.

The nominal resistance of a bolt in a slip-critical connection subject to combined tension and shear under service loads (i.e. under Load Combination Service II) was discussed previously in Section 3.3.6.2.6.1.

In the bracket connection shown in Figure 3.3.40 Part B, the eccentric load, *P*, results in a moment on the connection (Figure 3.3.41 Part A) that produces both shear and tension in the upper bolts. The tension is largest on the top row of bolts. As shown in Figure 3.3.41 Part B, the neutral axis under the bending moment, *M*, due to the factored loads occurs at the centroid of the rectangular contact area (i.e. at *d*/2). The initial pretension in the high-strength bolts introduces a precompression stress, f_{bi}, in the contact area of the joined plates (Figure 3.3.41 Part C). Assuming this initial compression stress is uniform over the contact area, *bd*, this stress can be computed as:

$$f_{bi} = \frac{\Sigma T_i}{bd}$$

Equation 3.3.98

where ΣT_i is the minimum required pretension from Table 3.3.1 times the number of bolts in the connection. The tensile stress at the top of the contact area, f_{tb}, due to the applied moment (Figure 3.3.41 Part D) is computed as:

$$f_{tb} = \frac{Md/2}{I} = \frac{6M}{bd^2}$$

Equation 3.3.99

As shown in Figure 3.3.41 Part E, it should be checked that f_{tb} does not exceed f_{bi} in order to ensure that compression remains between the joined parts at the top of the connection. The tensile load, T_u, on the top bolt due to the factored loads is equal to f_{tb} times the bolt tributary area, or the width *b* times the bolt spacing *p* divided by the number of vertical rows of bolts *n*; i.e. $T_u = f_{tb}bp/n$. Substituting f_{tb} from Equation 3.3.99 gives:

$$T_u = \frac{6Mp}{nd^2}$$

Equation 3.3.100

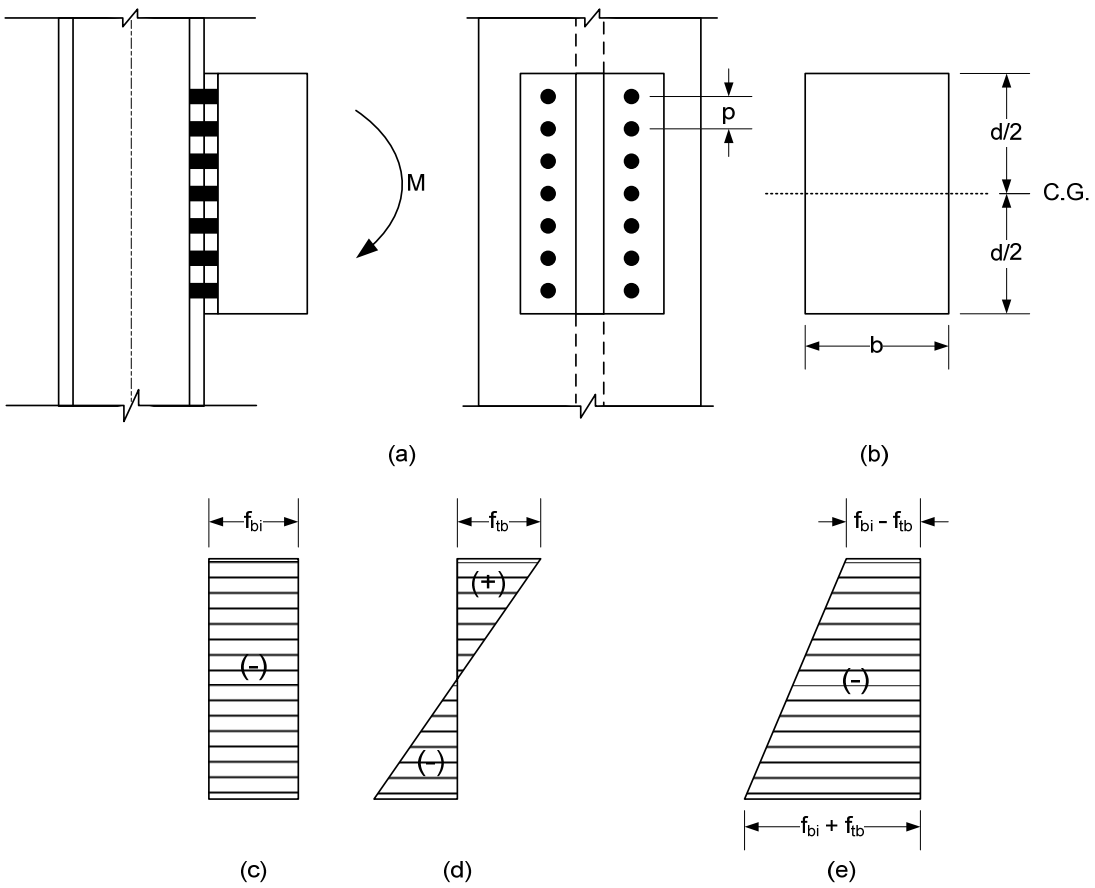


Figure 3.3.41 Tension and Shear from Eccentric Loading – Stresses on Contact Area

Assuming the top bolt is approximately *p*/2 from the top, T_u can be modified as follows (*19*):

$$T_u = \frac{6Mp}{nd^2}\left(\frac{d-p}{d}\right)$$

Equation 3.3.101

For the typical case where all bolts in the connection are the same size, and where f_{bi} is not overcome by f_{tb}, it is shown in Reference 19 that T_u can also be computed from the following simplified formula:

$$T_u = \frac{My_b}{\Sigma y^2}$$

Equation 3.3.102

where y_b is the vertical distance from the centroid of the connection to the extreme row of bolts, and y is the vertical distance from the centroid of the connection to each bolt.

The same equations can be used to calculate T_u for use in Equation 3.3.79 at the service limit state (i.e. under the Service II Load Combination). The shear force, P_u, in each bolt due to the factored loads can be taken simply as the total load, P, divided by the number of bolts in the connection.

3.3.6.2.7 Eccentric Shear

In Figure 3.3.42 Part A, the force, P, is applied on a line of action that does not pass through the center of gravity of the bolt group. The resultant action may be represented as a moment (torque) equal to P times the eccentricity, e, and a concentric force, P, acting on the connection, as shown in Figure 3.3.42 Part B and Figure 3.3.42 Part C.

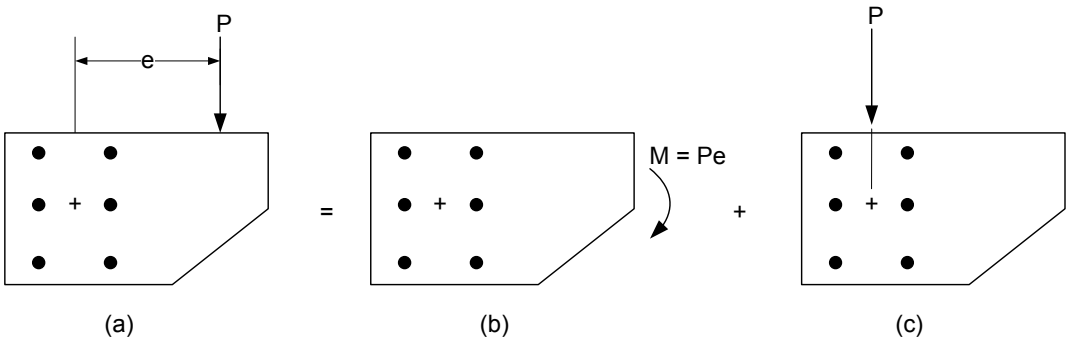


Figure 3.3.42 Bolted Connection Subject to Eccentric Shear

Since both the moment and concentric force cause shears on the bolt group, this particular situation is referred to as eccentric shear. As will be discussed in Section 3.3.7.3, a common example of a connection in a steel bridge subject to eccentric shear is a bolted web splice. Bolted cross-frame member connections are also often subject to eccentric shear.

Bolt groups subject to eccentric shear have typically been analyzed using a traditional elastic vector analysis assuming no friction, that the bolts are elastic and that the plates are rigid ensuring a linear strain variation on the bolts (*36*). The concentric force, P, is assumed to stress the bolts uniformly and the stress due to the torsion is then superimposed vectorially. The torque has traditionally been treated using an adaptation of the theory of twisting of circular steel shafts, as discussed below. Reference 36 discusses an alternative ultimate strength approach in which the translation and rotation of the bolt group is reduced to a pure rotation about a point referred to as the instantaneous center of rotation. An empirical load-deformation relationship is used to relate the shear resistance of each bolt to its deformation (*55, 56*). However, it was felt by the *AASHTO LRFD*

specification writers that the traditional elastic approach provides a more consistent factor of safety and is therefore recommended for use (refer to *AASHTO LRFD* Article C6.13.6.1.4b)

Consider the bolt group acted on by a torque, *M*, as shown in Figure 3.3.43 Part A. Assume the plate, which transmits the torque to the bolts, rotates about an axis through the centroid of the bolt group, and that the bolts all have different areas. It is assumed in this development that constraints on the members or connection do not force rotation about some point other than the centroid of the bolt group, which is typically the case in most practical connections.

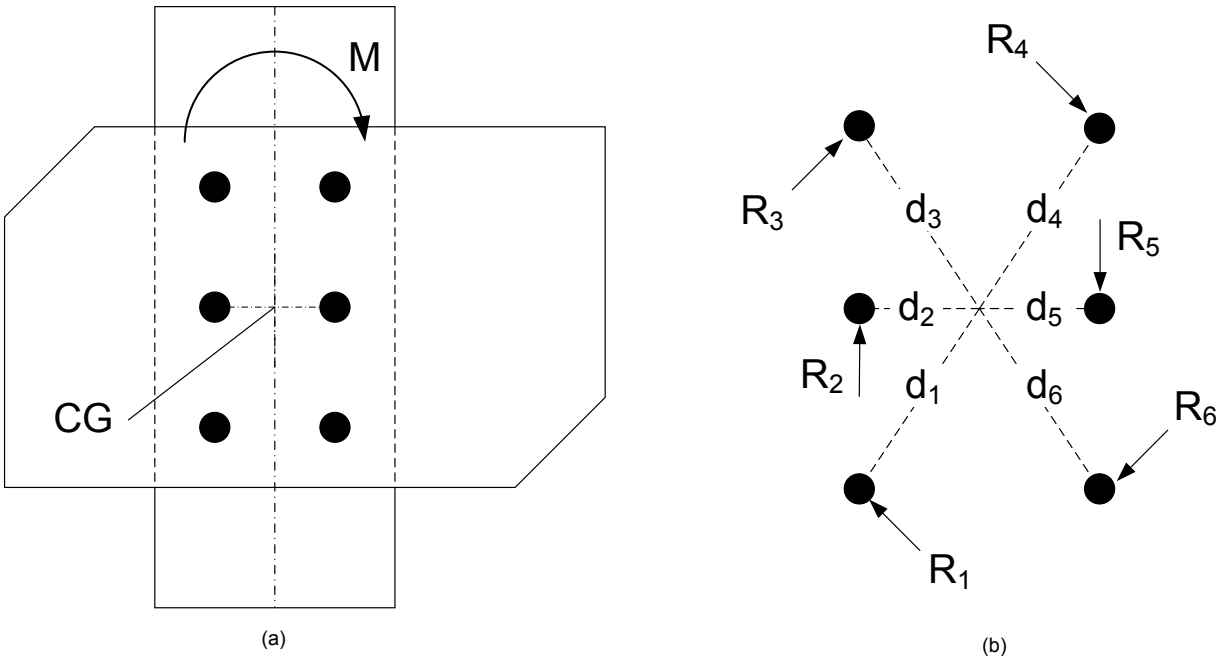


Figure 3.3.43 Analytical Model for Torque on a Bolt Group

Neglecting friction between the plates, the torque on the bolt group is equal to (Figure 3.3.43 Part B):

$$M = R_1 d_1 + R_2 d_2 + R_3 d_3 + ... + R_6 d_6$$

Equation 3.3.103

Assume that the shear stress in each bolt due to the torque acts normal to the radius drawn from the centroid and that the stresses vary linearly with the distance from the centroid. Thus, the bolt furthest removed from the centroid (say Bolt 6 in Figure 3.3.43 Part B for the purposes of this discussion) is the one most heavily stressed. The shear force in Bolt 6 is equal to $R_6 = \tau_6 A_6$. The stresses in the other bolts are then proportional to the stress in Bolt 6. Therefore, the forces acting on the other bolts can be computed as:

$$R_1 = \frac{d_1\tau_6}{d_6}A_1; R_2 = \frac{d_2\tau_6}{d_6}A_2; R_3 = \frac{d_3\tau_6}{d_6}A_3; R_4 = \frac{d_4\tau_6}{d_6}A_4; R_5 = \frac{d_5\tau_6}{d_6}A_5$$

Equation 3.3.104

Substituting the forces into Equation 3.3.103 gives:

$$M = \frac{\tau_6}{d_6}\sum_{i=1}^{n} d_i^2 A_i$$

Equation 3.3.105

where *n* is the total number of bolts in the connection (*n* = 6 in this case).

Rearranging and substituting the polar moment of inertia, I'_p, for the term $\sum_{i=1}^{n} d_i^2 A_i$ gives the following equation for the stress in the most heavily stressed bolt in the group:

$$\tau_6 = \frac{Md_6}{I'_p}$$

Equation 3.3.106

which is analogous to the equation for the shear stress in a circular shaft subject to pure torsion (*8*).

In most cases, the bolts in the connection will be the same size. Therefore, it becomes convenient to factor the bolt cross-sectional area *A* out of I'_p. Therefore, letting $I'_p = A\sum_{i=1}^{n} d_i^2 = AI_p$ results in the following expression for the shear force in the most heavily stressed bolt:

$$R_6 = \frac{Md_6}{I_p}$$

Equation 3.3.107

Referring to Figure 3.3.44, since $d^2 = x^2 + y^2$:

$$I_p = \sum_{i=1}^{n} x_i^2 + \sum_{i=1}^{n} y_i^2$$

Equation 3.3.108

Note that *AASHTO LRFD* Article C6.13.6.1.4b provides the following alternative formula for computing the polar moment of inertia, I_p, about the centroid of the connection assuming a uniform vertical pitch of the bolts (*57*):

$$I_p = \frac{nm}{12}\left[s^2\left(n^2-1\right)+g^2\left(m^2-1\right)\right]$$

Equation 3.3.109
AASHTO LRFD Equation C6.13.6.1.4b-3

where:

m = number of vertical rows of bolts
n = number of bolts in one vertical row
s = vertical pitch of bolts (in.)
g = horizontal pitch of bolts (in.)

To facilitate combination with the direct shear in each bolt due to the concentric force *P*, it becomes convenient to use the *x* and *y* components of the bolt shears due to torsion. Referring again to Figure 3.3.44, $R_6 = R_y\, d_6/x_6$ and $R_6 = R_x\, d_6/y_6$

Substituting into Equation 3.3.107 gives:

$$R_x = \frac{My_6}{I_p}$$

Equation 3.3.110

$$R_y = \frac{Mx_6}{I_p}$$

Equation 3.3.111

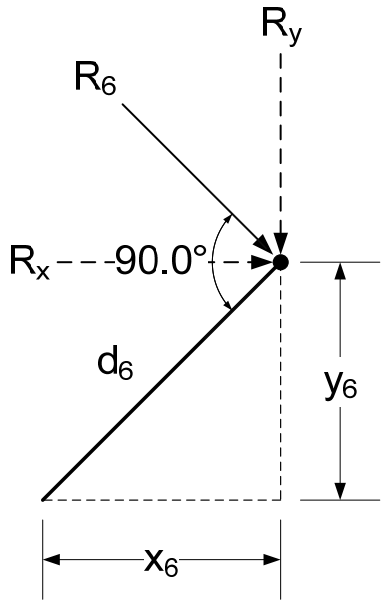


Figure 3.3.44 Horizontal and Vertical Components of Shear Force, *R*

The direct shear force on a bolt in an eccentric shear connection due to the concentric force, P, can be computed as:

$$R_v = \frac{P}{n}$$

Equation 3.3.112

where *n* is again the total number of bolts in the connection.

The total resultant force on the bolt is then computed from the vector sum of the direct shear force and the *x* and *y* components of the shear force due to torsion as follows:

$$R = \sqrt{(R_v + R_y)^2 + R_x^2}$$

Equation 3.3.113

In certain cases, additional horizontal components of shear force may act on a bolt group subject to eccentric shear (e.g. in bolted web splices for sections where the neutral axis is not as the middepth of the web, or in cross-frame connections where the line of action of force in a diagonal member does not pass through the center of gravity of the corresponding bolt group). In such cases, the additional horizontal component would be appropriately combined with R_x in Equation 3.3.113 to determine the resultant bolt force.

As illustrated in the example below, for bolted bracing member connections subjected to eccentric shear, the location of the working point is a critical factor in determining the overall economy of the connection.

Eccentric Shear Design Example (Bolted Bracing Member Connection)

Assume the gusset-plate connection configuration and bolt pattern shown in Figure 3.3.45. All bolts are 7/8-inch diameter A 325 high-strength bolts placed in standard holes. Assume that all bolt spacing and edge and end distance requirements are satisfied, and that the bearing resistance of the bolt holes at the strength limit state has been checked and is satisfactory.

The working point (W.P. in the figure) of the connection has been initially selected as shown. The selection of efficient working points for cross-frame connections can be determined in consultation with a fabricator/detailer. As illustrated later, if there is enough space to place the working point closer to the center of the bolt group, it obviously is desirable. Depending on how the cross-frame is detailed, i.e. if the cross-frame is detailed as a rectangle rather than a parallelogram (which is not preferred), the space available for bolts beyond the working point may vary with the particular bridge cross slope.

From separate calculations (refer to Section 3.3.6.4), the critical resultant strength limit state force combination for the selected gusset-plate connection configuration is a horizontal force of –126.3 kips acting in combination with a vertical force of –46.4 kips.

Check the bolts for shear at the strength limit state assuming the bolts in the connection have slipped and gone into bearing. The bolts are subject to eccentric shear to the in-plane eccentricity and to combined shear and tension due to the out-of-plane eccentricity.

For the eccentric shear (in-plane eccentricity), the traditional elastic vector method is used for calculating the maximum resultant bolt force. The polar moment of inertia, I_p, of the bolts with respect to the centroid of the connection is computed using Equation 3.3.109. For the example connection (referring to Figure 3.3.45), n = 4; m = 4; s = 3.0 in.; and g = 3.0 in. Therefore:

$$I_p = \frac{4(4)}{12}\left[(3.0)^2\left(4^2 - 1\right) + (3.0)^2(4^2 - 1)\right] = 360.0 \text{ in.}^2$$

Determine the vertical bolt force R_v:

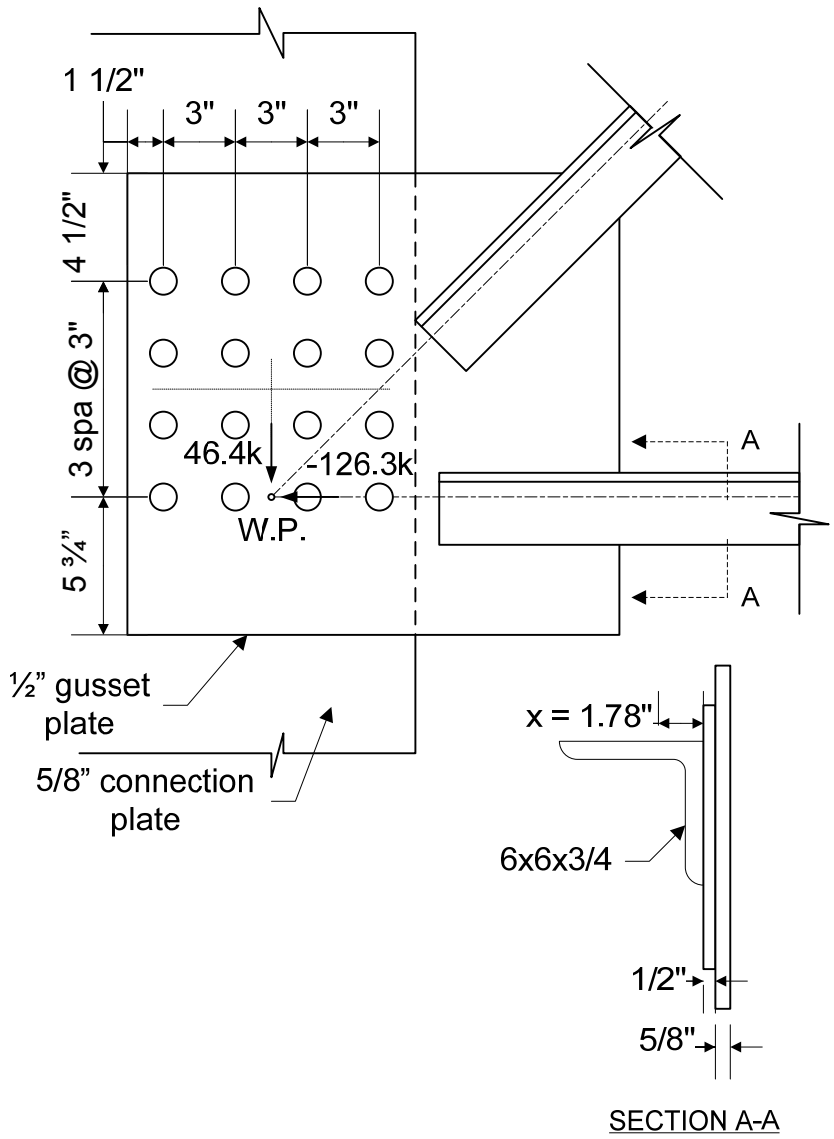


Figure 3.3.45 Example Gusset-Plate Configuration for Bolted Bracing Member Connection – Option 1

$$R_v = \frac{46.4}{16} = 2.90 \text{ kips / bolt}$$

Determine the horizontal bolt force R_h:

$$R_h = \frac{126.3}{16} = 7.89 \text{ kips / bolt}$$

Determine the vertical and horizontal components of the force on the extreme bolt due to the total moment on the connection, M_{tot}:

$$M_{tot} = 126.3(4.5) - 46.4(0.0) = 568.4 \text{ kip} - \text{in.}$$

$$R_{M_v} = \frac{M_{tot}\,x}{I_p} = \frac{568.4(4.5)}{360.0} = 7.11\,\text{kips}$$

$$R_{M_h} = \frac{M_{tot}\,y}{I_p} = \frac{568.4(4.5)}{360.0} = 7.11\,\text{kips}$$

The resultant bolt force on the extreme bolt is:

$$R = \sqrt{\left(R_v + R_{M_v}\right)^2 + \left(R_h + R_{M_h}\right)^2} = \sqrt{(2.90 + 7.11)^2 + (7.89 + 7.11)^2} = 18.03\ \text{kips}$$

The factored shear resistance, R_r, for a 7/8-in. diameter A 325 high-strength bolt in single shear assuming the threads are *excluded* from the shear plane is computed by applying the resistance factor, ϕ_s=0.80, to the nominal shear resistance, R_n, computed from Equation 3.3.82. The result is 27.65 kips/bolt. Therefore:

$$R = 18.03\ \text{kips} < R_r = 27.65\ \text{kips} \quad \text{ok}$$

In addition to shear, the bolts are also subject to tension as a result of the out-of-plane eccentricity. By inspection, the 126.3 kip force controls this computation.

From Table 3.3.1, the minimum required initial pretension, P_t, for 7/8-inch diameter A 325 bolts is 39.0 kips. Therefore, from Equation 3.3.98 and referring to Figure 3.3.45, the initial precompression stress, f_{bi}, on the contact area is equal to (16)(39.0)/(19.25)(12) = 2.70 ksi. Referring to Section A-A in Figure 3.3.45, the eccentricity to the center of the 5/8-inch-thick connection plate is conservatively computed as e = 1.78 + 0.5 + 0.625/2 = 2.59 in. (the eccentricity of the larger bottom chord member is used). From Equation 3.3.99, the tensile stress on the contact area f_{tb} is equal to $6(126.3)(2.59)/(19.25)(12)^2$ = 0.71 ksi, which is less than f_{bi}. Therefore, the pieces remain in compression (contact).

The nominal shear resistance of each bolt, R_n, is taken as the factored shear resistance, R_r = 27.65 kips/bolt, divided by ϕ_s. Therefore, R_n = 27.65/0.8 = 34.56 kips/bolt. The shear due to the factored loads, P_u, in each bolt is taken as the maximum resultant force R computed above. Therefore, P_u = 18.03 kips. Since P_u/R_n = 18.03/34.56 = 0.52 > 0.33, the nominal tensile resistance of each bolt T_n under combined tension and shear is taken from Equation 3.3.97.

For a 7/8" A 325 bolt: $A_b = \dfrac{\pi(0.875)^2}{4} = 0.60\ \text{in.}^2$

F_{ub} = 120 ksi (*AASHTO LRFD* Article 6.4.3.1)

$$T_n = 0.76(0.60)(120)\sqrt{1-\left(\frac{18.03}{(0.80)(34.56)}\right)^2} = 41.5 \text{ kips}$$

Since: $$T_r = \phi_t T_n$$

$$T_r = 0.80(41.5) = 33.2 \text{ kips/bolt}$$

The tensile force in each bolt to the factored loads, T_u, may be computed from Equation 3.3.101 as follows:

$$T_u = \frac{6(126.3)(2.59)(3)}{4(12)^2}\left(\frac{12-3}{12}\right) = 7.7 \text{ kips} < T_r = 33.2 \text{ kips} \quad \text{ok}$$

Alternatively, T_u may be computed from Equation 3.3.102, where y_b = 4.5 in. and $\Sigma y^2 = 8[(1.5)^2 + (4.5)^2] = 180.0$ in.^{2} Therefore:

$$T_u = \frac{126.3(2.59)(4.5)}{180.0} = 8.2 \text{ kips} < T_r = 33.2 \text{ kips} \quad \text{ok}$$

Since the bolted connection is a slip-critical connection, *AASHTO LRFD* Article 6.13.2.1.1 also requires that the connection be proportioned to prevent slip under Load Combination Service II specified in *AASHTO LRFD* Table 3.4.1-1. From separate calculations, the critical resultant Service II force combination for the selected gusset-plate connection configuration is a horizontal force of –97.8 kips acting in combination with a vertical force of –35.9 kips.

Determine the vertical bolt force R_v:

$$R_v = \frac{35.9}{16} = 2.24 \text{ kips / bolt}$$

Determine the horizontal bolt force R_h:

$$R_h = \frac{97.8}{16} = 6.11 \text{ kips / bolt}$$

Determine the vertical and horizontal components of the force on the extreme bolt due to the total moment on the connection, M_{tot}:

$$M_{tot} = 97.8(4.5) - 35.9(0.0) = 440.1 \text{ kip} - \text{in.}$$

$$R_{M_v} = \frac{M_{tot}\, x}{I_p} = \frac{440.1(4.5)}{360.0} = 5.50 \text{ kips}$$

$$R_{Mh} = \frac{M_{tot}\, y}{I_p} = \frac{440.1(4.5)}{360.0} = 5.50 \text{ kips}$$

The resultant bolt force on the extreme bolt is:

$$R = \sqrt{\left(R_v + R_{Mv}\right)^2 + \left(R_h + R_{Mh}\right)^2} = \sqrt{(2.24 + 5.50)^2 + (6.11 + 5.50)^2} = 13.95 \text{ kips}$$

The factored slip resistance, R_r, for a 7/8-in. diameter A 325 high-strength bolt assuming a Class B surface condition for the faying surface, standard holes and a single slip plane per bolt is equal to the nominal slip resistance, R_n, computed from Equation 3.3.78. The result is 19.50 kips/bolt. However, in the presence of tension (due to the out-of-plane eccentricity), the slip resistance must be reduced according to Equation 3.3.79.

P_t in Equation 3.3.79 is equal to the minimum required bolt tension specified in *AASHTO LRFD* Table 6.13.2.8-1 (specified as 39.0 kips for a 7/8-inch diameter A 325 bolt – Table 3.3.1). Under the Service II load combination, the tensile force due to the factored loads, T_u, may be computed from Equation 3.3.102 as follows:

$$T_u = \frac{97.8(2.59)(4.5)}{180} = 6.3 \text{ kips}$$

Therefore, the factored slip resistance, R_r, modified for the effect of the tension is computed from Equation 3.3.79 as:

$$R_r = 19.50\left(1 - \frac{6.3}{39.0}\right) = 16.35 \text{ kips}$$

$$R = 13.95 \text{ kips} < R_r = 16.35 \text{ kips} \quad \text{ok}$$

The slip resistance under the Service II load combination controls the design of the bolted connection in this case. Note that similar computations would need to be done if the cross-frame members had been bolted directly to the connection plate.

If it were possible, the moment on the connection could be reduced significantly in this particular case by moving the working point to the left. For example, if the working point could be moved 3 inches to the left along the bottom row of bolts, the total moment on the connection under the Service II load combination would be reduced from 440 kip-in. to:

$$M_{tot} = 97.8(4.5) - 35.9(3.0) = 332.4 \text{ kip} - \text{in.}$$

which may allow for an overall reduction in the number of bolts.

Assume that enough space is available to move the bottom row of bolts down (or move the bottom cross-frame member up) such that the working point can be located at the center of the bolt group (Figure 3.3.46).

As slip controls, check the slip resistance of the bolts in the resulting reduced bolt pattern shown in Figure 3.3.46 (the critical Service II resultant cross-frame forces are shown in the figure). Note that by going to this pattern, the size of the gusset plate is obviously reduced and the size of the connection plate is also reduced.

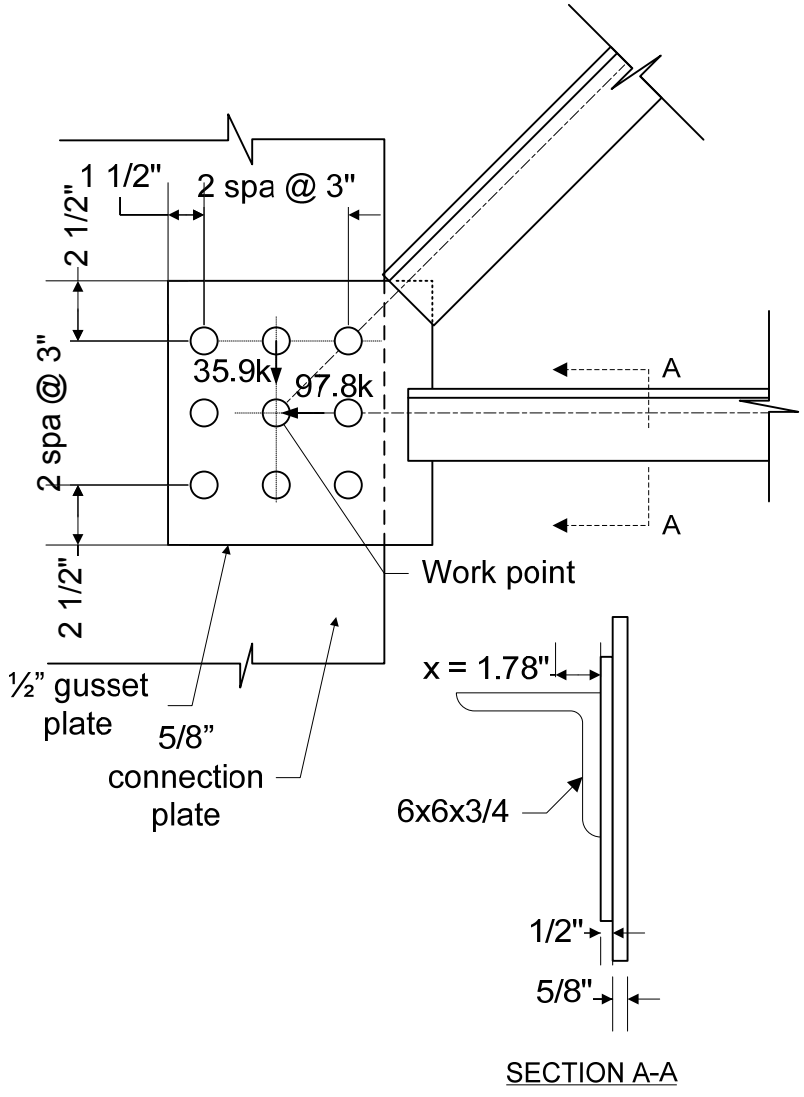


Figure 3.3.46 Example Gusset-Plate Configuration for Bolted Bracing Member Connection – Option 2

Determine the vertical bolt force R_v:

$$R_v = \frac{35.9}{9} = 3.99 \text{ kips / bolt}$$

Determine the horizontal bolt force R_h:

$$R_h = \frac{97.8}{9} = 10.87 \text{ kips / bolt}$$

The total moment on the connection M_{tot} is:

$$M_{tot} = 97.8(0.0) - 35.9(0.0) = 0.0 \text{ kip} - \text{in.}$$

The resultant bolt force on the extreme bolt is:

$$R = \sqrt{R_v^2 + R_h^2} = \sqrt{(3.99)^2 + (10.87)^2} = 11.58 \text{ kips}$$

To account for the tension on the bolts, y_b = 3.0 in. and $\Sigma y^2 = 3[(3.0)^2 + (3.0)^2] = 54.0$ in.^{2} T_u is therefore computed from Equation 3.3.102 as follows:

$$T_u = \frac{97.8(2.59)(3.0)}{54.0} = 14.07 \text{ kips}$$

Therefore, the factored slip resistance, R_r, modified for the effect of the tension is computed from Equation 3.3.79 as:

$$R_r = 19.50\left(1 - \frac{14.07}{39.0}\right) = 12.47 \text{ kips}$$

$R = 11.58$ kips < $R_r = 12.47$ kips ok

3.3.6.3 Welded Connections

3.3.6.3.1 General

Welding is the process of joining two pieces of material, usually metals, by heating the pieces to a suitable temperature such that the materials are soft enough to coalesce or fuse into one material. The pieces are held in position for welding and may or may not be pressed together depending on the process that is used. Also, the pieces may be joined directly to each other or they may be joined using filler material. Although there are some forty different welding processes, arc welding, in which electrical energy in the form of an electric arc is introduced to generate the

heat necessary for welding, is the most commonly used process in the steel-bridge construction industry. The heat of the electric arc as the current passes through the system simultaneously melts a consumable electrode (deposited as filler material) and the parts of the material being joined, with the joint resulting from the cooling and solidification of the fused material. To protect the molten region from impurities, the zone to be welded is typically blanketed in an atmosphere supplied by a flux, which may be a fusible coating on the welding rod, a fusible powder spread over the line of the weld or a gas sprayed over the weld. To produce a weld of the desired quality, the properties of the electrode must be carefully controlled. Proper control of the current and voltage along with a skilled welder are also required in order to produce a quality weld.

Welding in its simplest form has been around for several thousand years, primarily in the form of forge welding in which pieces of metal were heated and hammered into the desired shapes. Brazing of metals was also done for many years. Significant advancements in welding technology did not occur, however, until the late 1800s. Resistance welding, which combines electrical energy with mechanical pressure, originated around 1877 (*58*). Examples of resistance welding include spot and seam welding primarily used for welding of light-gage steel plates and open-web steel joists.

In the late 1880s and early 1890s, the metal arc process made its initial appearance in Russia and in the U.S. at about the same time using uncoated bare electrodes (*59*). Around the same time period, coated metal electrodes were introduced to eliminate many of the problems associated with the use of bare electrodes (*58*). During World War I (1914-1918), welding techniques were primarily applied to repairing damaged ships. Right after the war, experimentation with electrodes and gases to shield the arc and weld area led to the development of gas metal arc welding and gas tungsten arc welding. In 1932, the use of granular flux to protect the weld was introduced, which along with the use of a continuously fed electrode led to the development of the commonly used submerged arc welding process in which the arc is buried under the granular flux (*59*). Research and advancements continue today with the increased usage of automated welding techniques and welding robotics.

The introduction of welding has led to significant advancements in steel-bridge design and fabrication. Welding is now used for the vast majority of shop connections. Welded connections are usually neater in appearance than bolted connections. Welded connections also allow the Design Engineer more freedom to be innovative and build-up cross-sections to transmit the loads in the most efficient manner. Several factors influence the cost of welding, including but not limited to, the amount of weld material required, the costs of preparing the edges to be welded, the ratio of actual arc time to overall welding time and the amount of handling required. Shop welding is almost always less expensive than field welding. Reasons for this include the more ready availability of automatic welding machines and special jigs for holding the pieces in more favorable positions, a less hostile environment, the ability to more easily perform proper preheating of the joint and the ability to schedule a smooth continuous operation versus having to wait for

cranes or special erection equipment to become available. More extensive information and discussion related to the variables influencing welding costs may be found in References 60 through 62.

The weldability of a steel is a measure of the ease of producing a crack-free and sound structural joint. The weldability of structural steel is primarily controlled by its carbon content. While carbon (C) is beneficial to the strength of the steel, it is detrimental to ductility. A high carbon content combined with the heat generated during welding may cause a brittle zone in which weld cracks may develop. A carbon content of about 0.20 percent results in a very weldable steel. Good weldability can be obtained with an upper limit on carbon content of about 0.25 percent. In certain steels, the addition of alloys to enhance the strength and/or corrosion resistance can increase the hardness of the steel. Increased hardness results in an increased likelihood of brittle zones forming. Higher concentrations of carbon and other alloying elements such as manganese (Mn), chromium (Cr), silicon (Si), molybdenum (Mo), vanadium (V), copper (Cu) and nickel (Ni) tend to increase the hardness and decrease the weldability of the steel. Each of these alloying elements tends to influence the hardness and weldability of the steel to different magnitudes. Therefore, an approximate guide to the weldability of alloy steels against that of plain carbon steels is necessary. The most common standard used is the carbon equivalent (%CE) given as follows (*63*):

$$\%CE = \%C + \left(\frac{\%Mn + \%Si}{6}\right) + \left(\frac{\%Cr + \%Mo + \%V}{5}\right) + \left(\frac{\%Cu + \%Ni}{15}\right)$$

Equation 3.3.114

For %CE less than 14 percent, the steel is considered to have excellent weldability. For %CE between 14 and 45 percent, modest preheat and low hydrogen electrodes become necessary. For %CE greater than 45 percent, weld cracking is likely; therefore, larger preheats and low hydrogen electrodes are required.

Weldability should be determined on the basis of actual rather than specified chemical compositions as compositions listed on actual mill certification reports are typically below the maximum alloy contents set by the specifications. Most of the bridge steels specified in the ASTM A 709 Specification can be welded without special precautions or procedures. However, special procedures should be followed to improve weldability and ensure high-quality welds when high-performance steels (HPS) are used (*64*).

The design of welded connections is covered in *AASHTO LRFD* Article 6.13.3. *AASHTO LRFD* Article 6.13.3.1 requires that all base metal, weld metal and weld design details conform to the requirements of Reference 65 (i.e. the *AASHTO/AWS D1.5M/D1.5 Bridge Welding Code*).

3.3.6.3.2 Welding Processes

Welding processes that are used for arc welding carbon and low-alloy steels typically used in bridge construction include: shielded metal arc welding (SMAW), submerged arc welding (SAW), flux cored arc welding (FCAW), gas metal arc welding (GMAW), narrow-gap improved electroslag welding (NGI-ESW), and stud welding (SW). Note that the Design Engineer does not typically specify the welding process to be used or the exact filler metal (electrode/flux material) to be employed. These decisions are usually left with the fabricator. However, a basic understanding of the commonly used welding processes and corresponding AWS filler-metal designations is helpful. More extensive discussion of these processes and the decisions that go into selecting a particular process may be found in References 60 and 62.

More detailed information on filler-metal designations used with each process may be found in References 62 and 65. Information on potential defects in welds and weld inspection and control may be found in References 21, 60, 62 and 65.

3.3.6.3.3 Types of Welds

As shown in Figure 3.3.47, there are four basic types of welds – groove, fillet, slot and plug. Fillet welds represent the largest percentage of welds used in welded construction, and are the most commonly used welds for bracing member connections. Slot and plug welds are primarily used in lap joints in combination with fillet welds to assist in transmitting the shear when the size of the connection limits the length available for fillet or other edge welds. Slot and plug welds can also help prevent the overlapping parts from buckling. However, because of fatigue concerns, slot and plug welds are rarely used in bridge construction, and then, only to resist compression or shear stress; therefore, they are not covered any further here.

Weld symbols are used to allow the Design Engineer to instruct the fabricator and detailer as to the type and size of weld required for a particular connection (and vice versa). A standard system of designating welds by symbols that communicate the desired weld size, location and type has been developed by the AWS (*66*). *AASHTO LRFD* Article 6.13.3.1 specifies that all welding symbols must conform to this system.

If a particular welded connection is used in many different parts of the structure, it may only be necessary to show a typical detail utilizing the welding symbols. For special complex or confusing connections, additional sketches may be necessary to indicate what is required. Welding symbols should be used to communicate and not to confuse. The Design Engineer will typically use welding symbols to convey a minimum amount of information to the fabricator/detailer regarding the welded connection on the design drawings (e.g. type and size of weld, etc.). The fabricator/detailer will then provide welding symbols for the same connection, often conveying more detailed information about the connection, on the shop drawings for review and approval by the Design Engineer. Therefore, the Design Engineer

should have a complete understanding of weld symbols. More detailed information on welding symbols may be found in References 65 and 66 and in most any structural steel textbook.

3.3.6.3.3.1 Groove Welds

Groove welds are most often used to connect structural members that are aligned in the same plane (i.e. butt joints). They can also be used in tee and corner joints. As shown in Figure 3.3.48, there are two basic subcategories of groove welds: complete penetration groove welds (CJP) and partial penetration groove welds (PJP).

CJP groove welds have the same resistance as the pieces joined and are intended to transmit the full load of the members that are joined. PJP groove welds do not extend completely through the thickness of the pieces being joined and are subject to special design requirements. PJP welds are sometimes used when stresses are low and there is no need to develop the complete strength of the base material. Note that both types of welds may be single- or double-sided welds. Double-sided welds, which require access to both sides of the joint, may require less weld metal and result in less distortion and are of particular importance when joining thick members.

Groove welds are classified according to their particular shape. Most groove welds require a specific edge preparation and are named accordingly. The selection of the proper groove weld is dependent on the cost of the edge preparations, the welding process used and the cost of making the weld. The decision as to which groove type to use is usually left to the fabricator/detailer, who will select the type of groove that will generate the required quality at a reasonable cost.

Since groove welds are not typically used for bracing member connections, they will not be discussed any further herein. Further information on groove welds may be found in References 21, 62 and 65.

3.3.6.3.3.2 Fillet Welds

Fillet welds are the most widely used welds due to their ease of fabrication and overall economy, and are certainly the most widely used welds for bracing member connections. Fillet welds generally require less precision during fit-up and the edges of the joined pieces seldom need special preparation such as beveling or squaring. Fillet welds have a triangular cross-section and do not fully fuse the cross-sectional area of the parts they join, although full-strength connections can be developed with fillet welds.

AASHTO LRFD Article 6.13.3.6 specifies that fillet welds deposited on the opposite sides of a common plane of contact between two parts are to be interrupted at a

corner common to both welds (e.g. double-sided fillet welds connecting transverse stiffeners, connection plates or bearing stiffeners to a flange).

Basic fillet weld nomenclature is shown in Figure 3.3.49. The size of a fillet weld is given as the leg size of the fillet. If the two legs are unequal, the nominal size of the weld is given by the shorter of the legs.

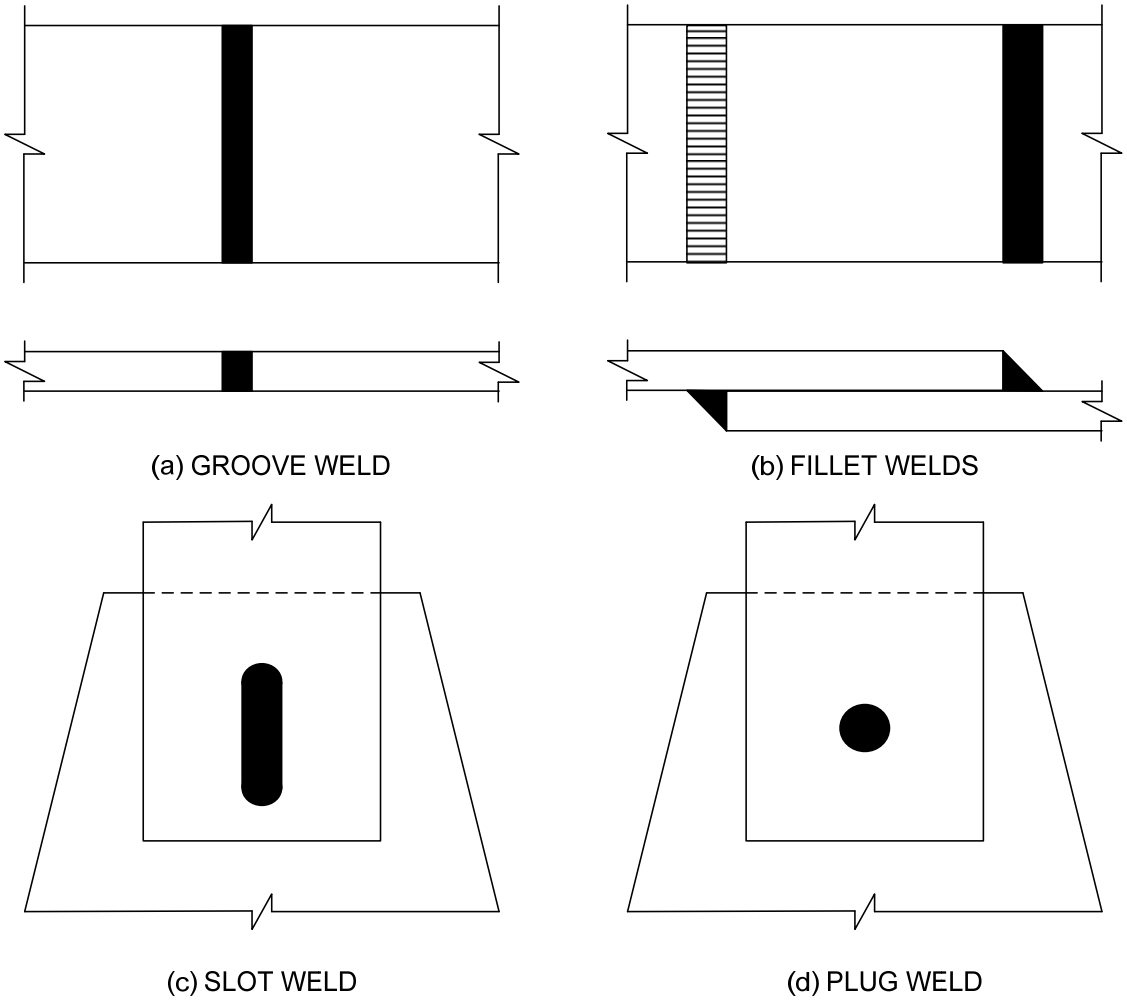
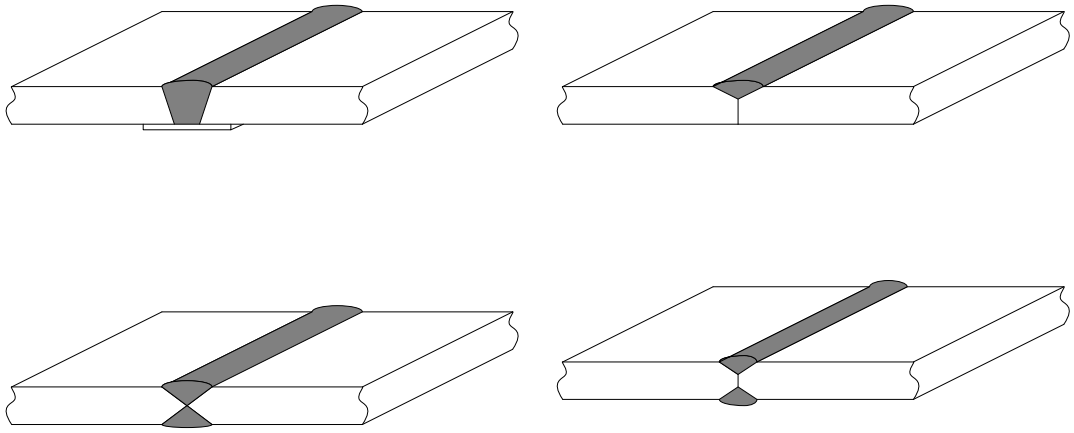


Figure 3.3.47 Types of Welds



Complete Joint Penetration Groove Welds (CJP)

Partial Joint Penetration Groove Welds (PJP)

Figure 3.3.48 Subcategories of Groove Welds

Effective Area of Fillet Welds

The resistance of welds is based on the effective area of the weld, which is taken as the effective length of the weld times the effective throat according to *AASHTO LRFD* Article 6.13.3.3. The effective throat is defined nominally as the shortest distance from the joint root to the face of the weld (neglecting any weld reinforcement), or the minimum width of the expected failure plane.

The effective area of a fillet weld is taken equal to the effective length of the weld times the effective throat (*AASHTO LRFD* Article 6.13.3.3). The effective length is to be taken as the overall length of the full-size fillet. The effective throat is taken as defined below.

Effective Throat

The effective throat dimension of a fillet weld for a typical fillet weld with equal legs of nominal size, *a*, is taken equal to 0.707*a* (Figure 3.3.50 Part A). For the rare case of a fillet weld with unequal leg sizes, the effective throat would be computed as shown in Figure 3.3.50 Part B.

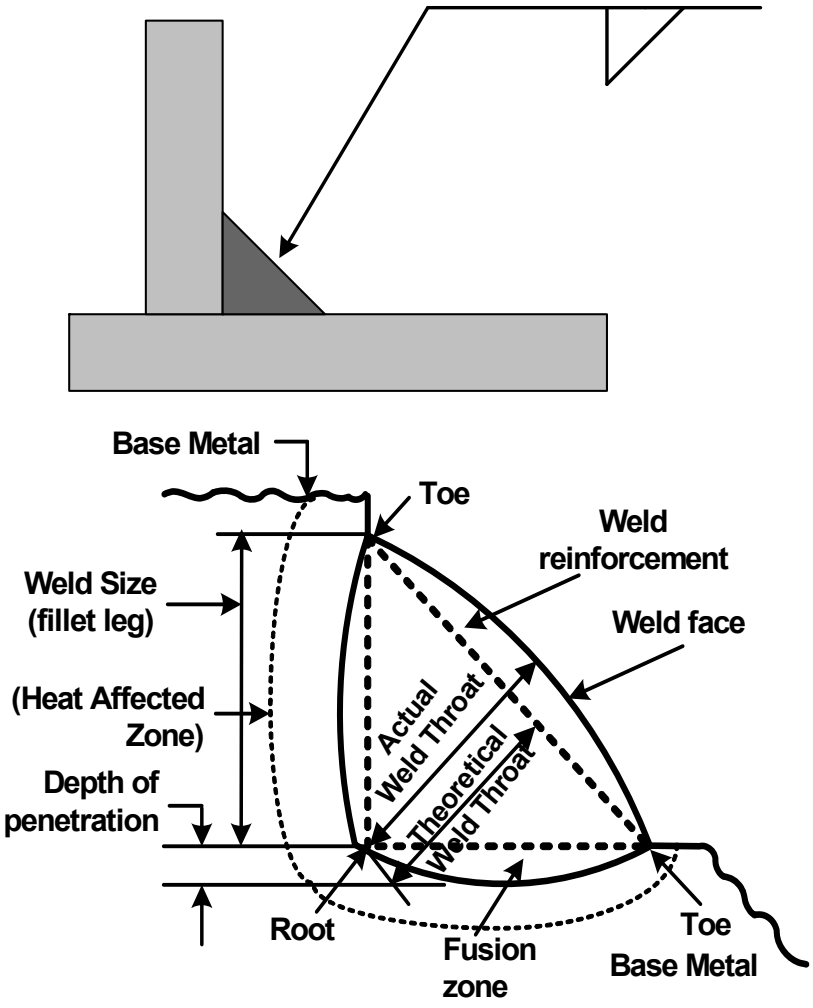


Figure 3.3.49 Fillet Weld Nomenclature

Minimum Effective Length

When placing a fillet weld, the welder builds up the weld to the full dimension as near to the beginning of the weld as possible. However, there is always a slight tapering off of the weld where the weld starts and ends. Therefore, a minimum effective length of the weld is required. As specified in *AASHTO LRFD* Article 6.13.3.5, the minimum effective length of a fillet weld is to be taken as four times its leg size, but not less than 1.5 inches (Figure 3.3.51).

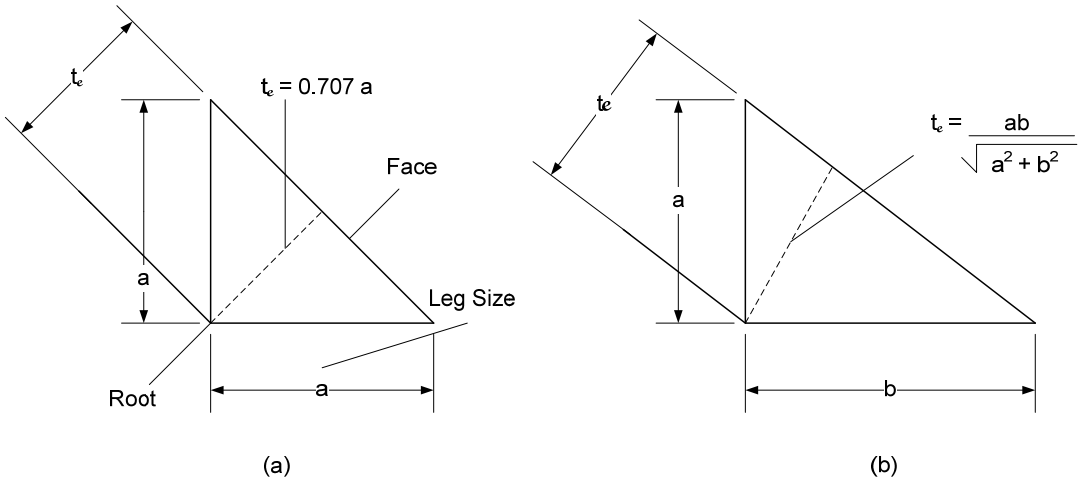


Figure 3.3.50 Effective Throat Dimensions for Fillet Welds
A) Equal Legs; B) Unequal Legs

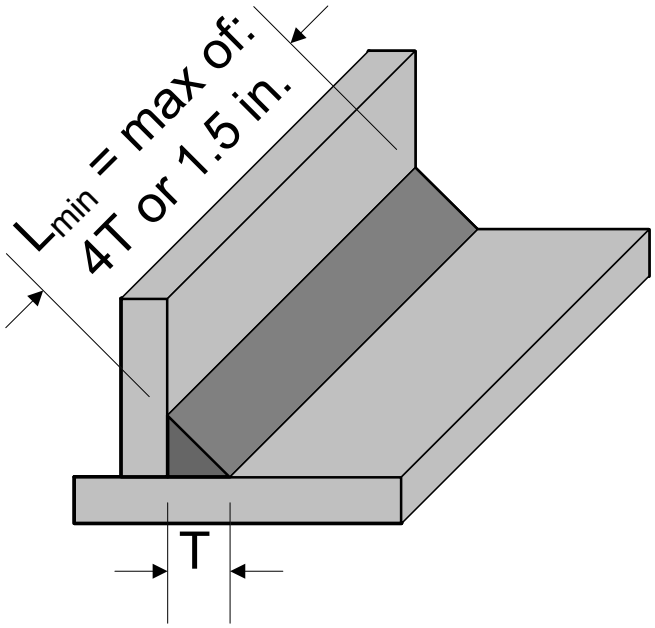


Figure 3.3.51 Minimum Effective Length of Fillet Welds

Maximum Thickness Requirements for Fillet Welds

As specified in *AASHTO LRFD* Article 6.13.3.4 and shown in Figure 3.3.52 Part A and Figure 3.3.52 Part B, maximum thickness (size) requirements for fillet welds *along edges of connected parts* depend on the thickness of the parts being connected (unless the weld is specifically designated on the contract documents to be built out to obtain full throat thickness).

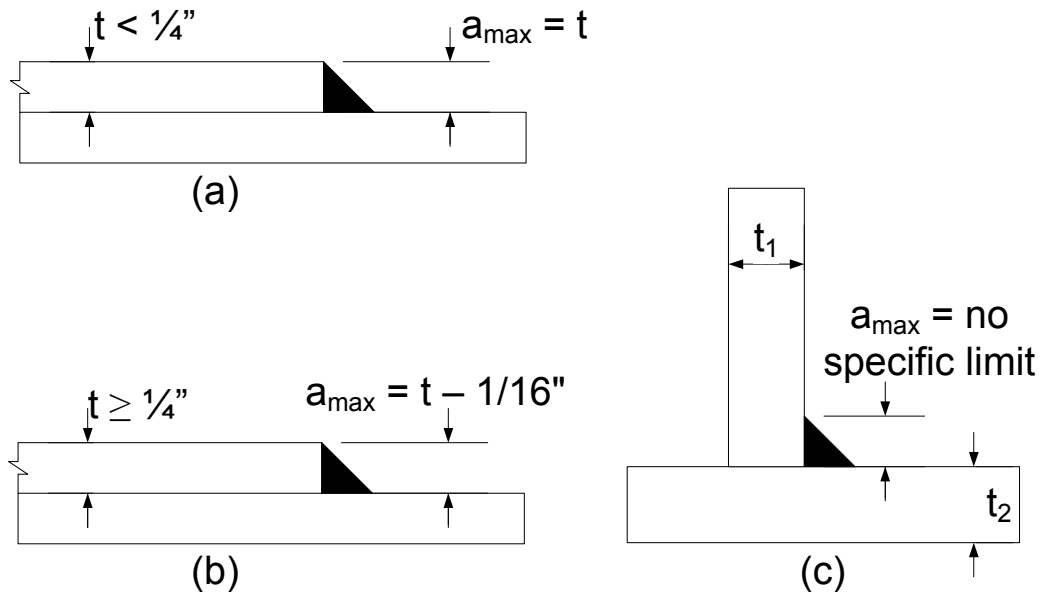


Figure 3.3.52 Maximum Size Requirements for Fillet Welds
A) For $t < ¼''$; B) For $t \geq ¼''$; C) No specific limit

Note that for the case shown in Figure 3.3.52 Part C, no specific limit applies, except as limited by the resistance requirements for the base metal in some instances. The requirements prevent melting of the base metal where the fillet would meet the corner of the plate if the fillet were made the full plate thickness (*19*).

Minimum Thickness Requirements for Fillet Welds

The minimum thickness (size) of a fillet weld is not to be less than that required to transmit the required forces, nor the minimum thickness specified in *AASHTO LRFD* Table 6.13.3.4-1 (Table 3.3.6).

Table 3.3.6 Minimum Thickness Requirements for Fillet Welds

Base Metal Thickness of Thicker Part Joined (*T*)	Minimum Size of Fillet Weld
in.	in.
$T \leq 3/4$	1/4
$3/4 < T$	5/16

The minimum weld size need not exceed the thickness of the *thinner* part joined. Note that the specified minimum weld sizes assume that the required preheats and interpass temperatures are provided (*66*). According to *AASHTO LRFD* Article 6.13.3.4, smaller welds than the minimum size welds may be approved by the

Design Engineer if they are shown to be adequate for the applied stress and if the appropriate additional preheat is applied.

Minimum thickness requirements for fillet welds are based on preventing too rapid a rate of cooling in order to prevent a loss of ductility (i.e. the formation of a brittle microstructure) or a lack of fusion. The thicker the plate joined, the faster the heat is removed from the welding area. As a minimum, a weld of sufficient size is needed to prevent the thicker plate from removing heat at a faster rate than it is being supplied to cause the base metal to become molten. Thus, the minimum weld sizes implicitly imply a specified minimum heat input. In addition, restraint to weld metal shrinkage may result in weld cracking if the welds are too small. Minimum weld sizes are frequently used for the case of longitudinal fillet welds that resist shear (e.g. girder flange-to-web welds). Reducing the amount of weld metal will decrease the amount of distortion in welded assemblies; thus, the smallest acceptable weld size that will provide the required factored resistance should be used.

Since the minimum size requirements for fillet welds imply a minimum level of heat input, the minimum size welds must be made in a single pass, as multiple passes to make the minimum size weld would not provide the assumed minimum level of heat input, essentially defeating the purpose of the requirement. The largest single-pass fillet weld that can be made with the manual SMAW process is typically 5/16 in. (single-pass welds up to about ½ in. can be made with the SAW process).

3.3.6.3.4 Types of Welded Joints

As shown in Figure 3.3.53, there are five basic types of welded joints – butt, lap, tee, corner and edge joints. In practice, different variations and combinations of these joints may be used. Edge joints are more commonly used in sheet metal applications and are not discussed herein.

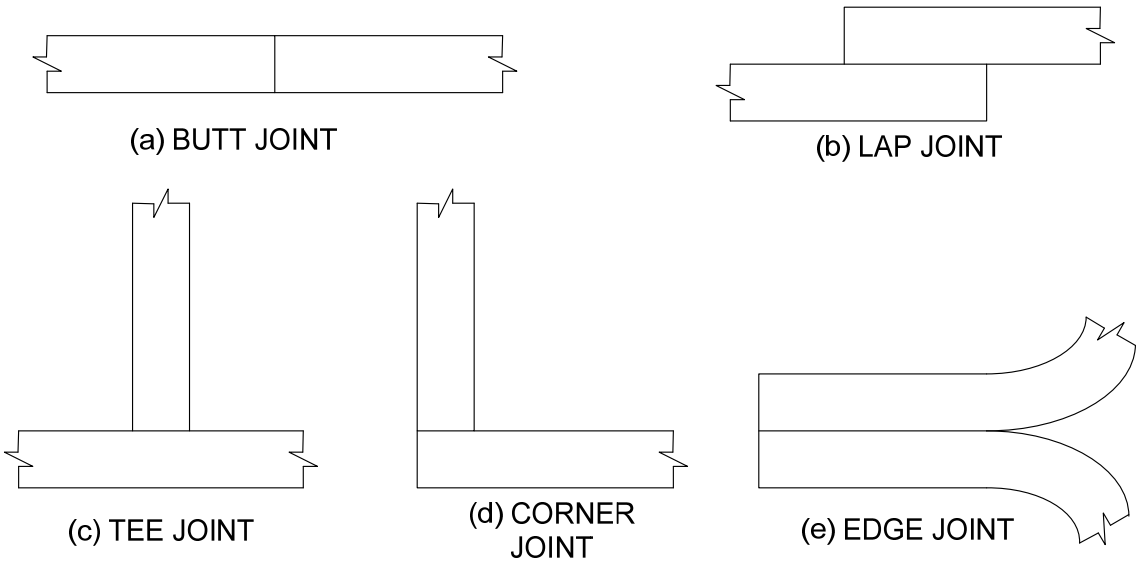


Figure 3.3.53 Types of Welded Joints

The joint type does not necessarily imply a specific type of weld. The selection of the weld type for certain types of joints (e.g. tee and corner joints) is usually dictated by the loading type and magnitude.

Butt joints are used to join the ends of flat plates together (e.g. girder flange and web shop splices). Butt joints in tension subject to fatigue loading are best made with complete penetration groove welds with the weld reinforcement removed. When subject to compression or shear only, partial penetration groove welds may be used providing adequate throats can be developed. The principal disadvantage of butt joints is that the connected edges typically require special preparation (i.e. beveling or grinding) and must be carefully aligned prior to welding.

Lap joints (e.g. cover plates and bracing member-to-gusset plate joints) do not require quite the preciseness in fabrication as other types of joints. The edges of the joined pieces are usually sheared or flame cut and do not require any special edge preparation. Lap joints utilize fillet welds and are the primary joint type for bracing member connections.

Tee joints are used to fabricate built-up sections, or in general, any pieces framing in at right angles (e.g. plate girder web-to-flange connections, stiffener-to-web connections, hangers, brackets). For tee joints subject to longitudinal shear, continuous fillet welds or groove welds can be used to join the pieces; however, fillet welds are usually the most economical option when the fillet weld leg size is less than ¾ in. (*62*). As larger throats are required, partial penetration groove welds (perhaps with external fillet welds) are the most cost-effective option (*62*). Complete penetration groove welds are not recommended for use in tee joints because of the relatively high cost and resulting welding deformations. It should be noted that partial penetration groove welds are assigned a slightly lower fatigue category in this configuration (Category B′ vs. Category B), but this rarely controls.

Corner joints are typically used to form built-up non-composite rectangular closed box sections. For corner joints, internal access to the box section has a major influence on the weld selection. Article 3.1 of Reference 67 discusses suggested details for welding of corner joints in closed box configurations, including large boxes in which a person can safely work and boxes that are too small for a person to work safely inside. The suggested details primarily involve the use of fillet welds alone in all four corners of the box or a combination of fillet welds for one flange and partial penetration groove welds for the second flange. Combinations involving the use of fillet welds and complete penetration groove welds are included, but are generally not recommended due to the expense and the fact that backing bars must generally be left in place. For details where single fillet welds in all four corners, or double fillet welds for one flange in combination with partial penetration groove welds for the second flange, are recommended, the Design Engineer should evaluate the loading conditions (e.g. torsion) and ensure that sufficient internal diaphragms are provided to limit rotations at the corner joints. Corner joints should also be carefully detailed to prevent the possibility of lamellar tearing (*68-71*).

3.3.6.3.5 Factored Resistance of Welded Connections

3.3.6.3.5.1 General

The factored resistance of a welded connection, R_r, at the strength limit state in the *AASHTO LRFD* Specifications is based on either the factored resistance of the base metal or the product of the weld metal strength and the effective area of the weld that resists the load. The weld metal strength is the capacity of the weld metal itself, typically given in units of ksi. As discussed in Section 3.3.6.3.3.2, the effective area of the weld that resists the load is the product of the effective length and the effective throat of the weld.

Weld metal strength may be classified as “matching”, “undermatching” or “overmatching”. Matching weld (filler) metal has the same or slightly higher specified minimum yield and tensile strength as compared to the specified minimum properties of the base metal. For example, matching weld metal for A 709 Grade 50 steel would be E70 filler material where the specified minimum weld/base metal properties for yield strength are 60/50 ksi and for tensile strength are 70/65 ksi. Although the weld metal has slightly higher properties than the base metal in this case, this is considered to be a matching combination. Note that according to Reference 64, matching consumables for A 709 Grade 50W base metal (as specified in Reference 65) are considered to be matching strength for hybrid designs where A 709 Grade HPS 70W base metal is joined to A 709 Grade 50W base metal.

AASHTO LRFD Article 6.13.3.1 specifies that matching weld metal must be used in groove and fillet welds, except that undermatching weld metal is permitted for fillet welds if the welding procedure and weld metal are selected to ensure the

production of sound welds. *According to AASHTO LRFD Article C6.13.3.1*, *the use of undermatched weld metal is strongly encouraged for fillet welds connecting steels with specified minimum yield strength greater than 50 ksi.* Lower strength weld metal will generally be more ductile than higher strength weld metal. Since the residual stresses in a welded connection are assumed to be on the order of the yield point of the weaker material in the connection (*62*), using lower strength weld metal will lower the level of residual stresses in the base metal at the connection reducing the cracking tendencies. Therefore, undermatched welds will be much less sensitive to delayed hydrogen cracking and are more likely to consistently produce sound welds. In such cases, the Design Engineer should indicate where undermatched welds are acceptable on the contract drawings.

Overmatching weld metal offers no significant advantages and increases the level of residual stresses and distortion at the connection. As mentioned above, higher yield strength weld metal is typically less ductile and more crack sensitive. Overmatching weld metal may also force the failure plane into the heat affected zone or fusion boundary, which is an undesirable condition (*62*). Slight overmatching is acceptable in some cases. For example, in the process of adding alloys for improved atmospheric corrosion resistance, most filler metals for welding A 709 Grade 50W weathering steel will deposit weld metal with a specified minimum tensile strength of 80 ksi versus the specified minimum tensile strength of 70 ksi for the base metal. Since this combination performs well and there are limited alternatives, this slight overmatch is acceptable. Since some acceptable weld metals for weathering steel applications are classified as E70, basing the weld design calculations on E70 will give the fabricator the flexibility of using either E70 or E80 weld metal.

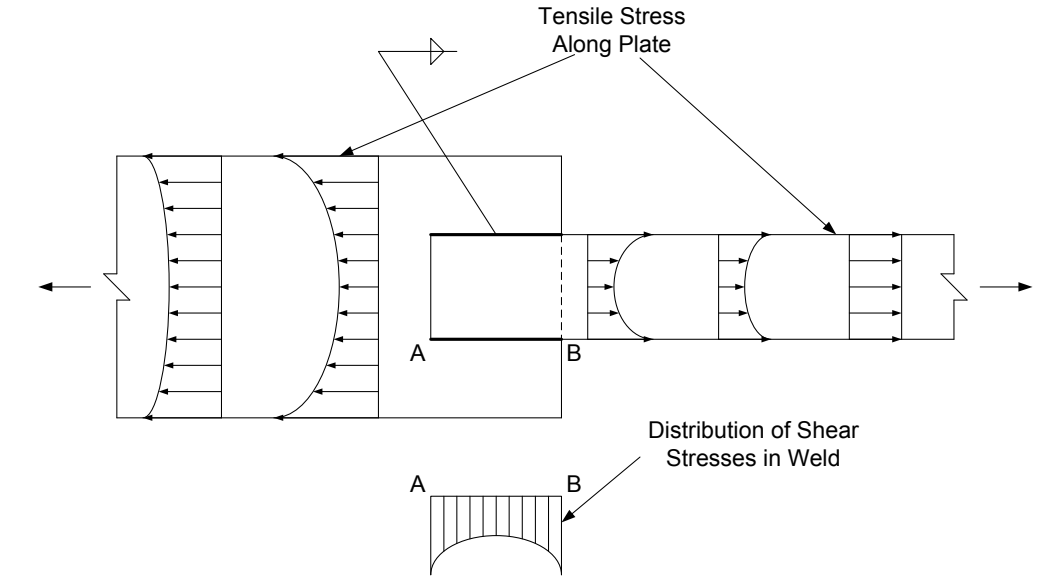
The following section discussed the factored resistance of welded connections made with fillet welds. For determining the factored resistance of welded connections made with CJP or PJP groove welds, the reader is referred to *AASHTO LRFD* Articles 6.13.3.2.2 and 6.13.3.2.3, respectively.

3.3.6.3.5.2 Fillet Welded Connections

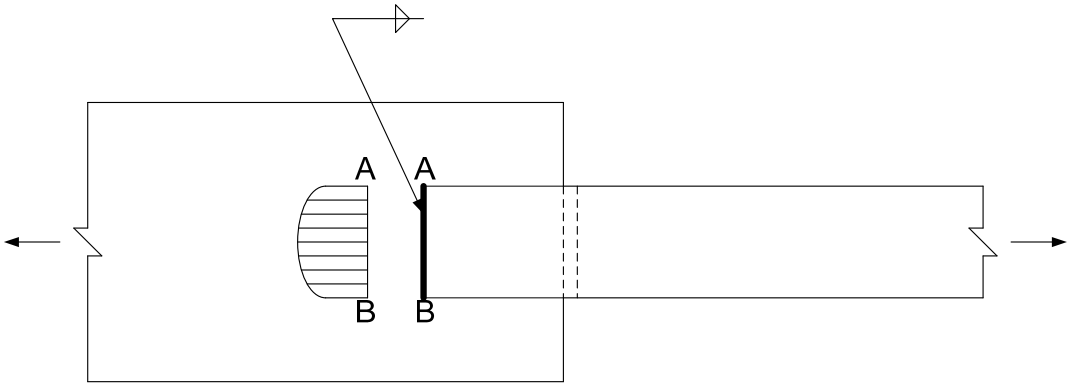
For design purposes, fillet welds are assumed to transfer loads through shear on the effective area of the weld regardless of whether the shear transfer is parallel or perpendicular to the axis of the weld. The factored resistance is actually greater for shear transfer perpendicular to the weld, but there is less deformation capability. In both cases, although the weld fails in shear, the plane of rupture is not the same. However, in the *AASHTO LRFD* Specifications, the additional factored resistance of fillet welds loaded perpendicular to the axis of the weld is ignored and both loading situations are treated the same.

Figure 3.3.54 Part A shows qualitatively a typical elastic shear stress distribution in the longitudinal fillet welds in a lap joint (i.e. for shear transfer parallel to the weld axis). The actual variation of shear stress from Point A to Point B depends on the ratio of the widths of the plates being joined and the length of the weld. Figure

3.3.54 Part B shows a typical elastic shear distribution for fillet welds loaded perpendicular to the weld axis.



(a)



(b)

Figure 3.3.54 Typical Fillet Weld Shear Stress Distributions in a Lap Joint
A) Shear Stress Distribution for Load Parallel to Weld Axis; B) Shear Stress Distribution of Load Perpendicular to Weld Axis

Shear yielding is not critical in the welds because strain hardening occurs without significant overall deformation occurring in either case. Although the elastic shear stress distributions along the length of the weld are not uniform, the available ductility or plastic deformation capability permits lines of fillet weld loaded parallel or perpendicular to the weld to be assumed to resist the load equally along their lengths.

According to *AASHTO LRFD* Article 6.13.3.2.4a, the factored resistance, R_r, of fillet-welded connections at the strength limit state subject to tension or compression parallel to the axis of the weld is to be taken as the corresponding factored resistance of the base metal. Note that fillet welds joining component elements of built-up members (e.g. girder flange-to-web welds) need not be designed for the tensile or compressive stress in those elements parallel to the axis of the welds.

According to *AASHTO LRFD* Article 6.13.3.2.4b, the factored resistance, R_r, of fillet-welded connections at the strength limit state subject to shear on the effective area is to be taken as follows:

$$R_r = 0.6\phi_{e2}F_{exx}$$

Equation 3.3.115
AASHTO LRFD Equation 6.13.3.2.4b-1

where:

ϕ_{e2} = resistance factor for shear on the throat of the weld metal in fillet welds specified in *AASHTO LRFD* Article 6.5.4.2 (= 0.80)

F_{exx} = classification strength of the weld metal (ksi) (e.g. for E70 weld metal, F_{exx} = 70 ksi)

The welds must have typical weld profiles and may be matched or undermatched. The factored shear rupture resistance of the base metal (i.e. $R_r = \phi_u 0.6F_u$) adjacent to the weld leg will seldom control since the effective area of the base metal at the weld leg is typically about 30 percent greater than the weld throat. Therefore, the specification does not require this resistance to be checked. In cases where overmatching weld metal is used, or where the weld throat has excessive convexity such that the resistance is governed by the weld leg, the shear rupture resistance should be checked to avoid overstressing of the base metal.

If a certain size fillet weld must be used in adjacent areas of a particular joint, it is desirable to use the same size weld to allow the same electrodes and welding equipment to be used for that joint and to simplify the inspection.

Fatigue Resistance of Fillet Welded Connections

According to *AASHTO LRFD* Table 6.6.1.2.3-1 (Condition 7.2), the nominal fatigue resistance of the base metal in single- or double-angle members or tee members connected by longitudinal fillet welds along both sides of the connected element of the member cross-section (e.g. a typical lap joint used in a bracing member connection) is to be based on detail Category E. The checking of fatigue of fillet-welded bracing member connections for single- and double-angle members, and for tee members, is discussed above in Sections 3.3.3.2.5.1 and 3.3.4.2.3.1, respectively. As discussed in those sections, while research showed that balancing of the welds offers some increase in the fatigue life of these connections (*15*), it is probably not worth the increase in the gusset or connection plate length required to accommodate the longer weld along one leg.

The reader is referred to *AASHTO LRFD* Table 6.6.1.2.3-1 to determine the fatigue detail category for other types of fillet-welded connections, and for various groove-welded connections (e.g. welded lateral connection plates for lateral bracing members).

Eccentric Shear

As indicated in *AASHTO LRFD* Article 6.13.1, eccentric connections should be avoided, but where they cannot be avoided, members and connections are to be designed for the combined effects of shear and moment due to the eccentricity. *AASHTO LRFD* Article C6.13.3.2.4b indicates that if fillet welds are subject to eccentric loads that produce a combination of shear and bending stresses, they are to be proportioned based on a direct vector addition of the shear forces on the weld. Eccentric shear can result, for example, when the loading of fillet welds is neither parallel to nor transverse to the axis of the welds. Basically, eccentric shear conditions occur when the welds are subject to pure torsion, a combination of shear and torsion or a combination of shear and bending.

As discussed in Section 3.3.6.2.7 for eccentric shear on bolted connections, the resistance of an eccentrically-loaded fillet-weld connection subject to a combination of shear and torsion can be conservatively determined using a traditional elastic vector analysis approach. The following assumptions are made in this approach: 1) assuming each segment of weld is of the same size, it is assumed that concentrically applied load (i.e. direct shear) is resisted equally by each weld segment, 2) any rotation caused by a torsional moment is assumed to occur about the centroid of the weld configuration, 3) load on a weld segment caused by a torsional moment is assumed proportional to the distance of that segment from the centroid of the weld configuration, 4) the direction of the force on a weld segment caused by a torsional moment is assumed perpendicular to the radial distance of the segment from the centroid of the weld configuration, and 5) the resultant force is obtained by combining vectorially the components of the forces caused by direct shear and torsion. Also, for computing forces or stresses on the weld segments, the segment lines are assumed defined by the edges along which the fillets are placed, rather than to the center of the effective throats.

Consider the general case of an eccentrically loaded welded connection subject to combined shear and torsion shown in Figure 3.3.55.

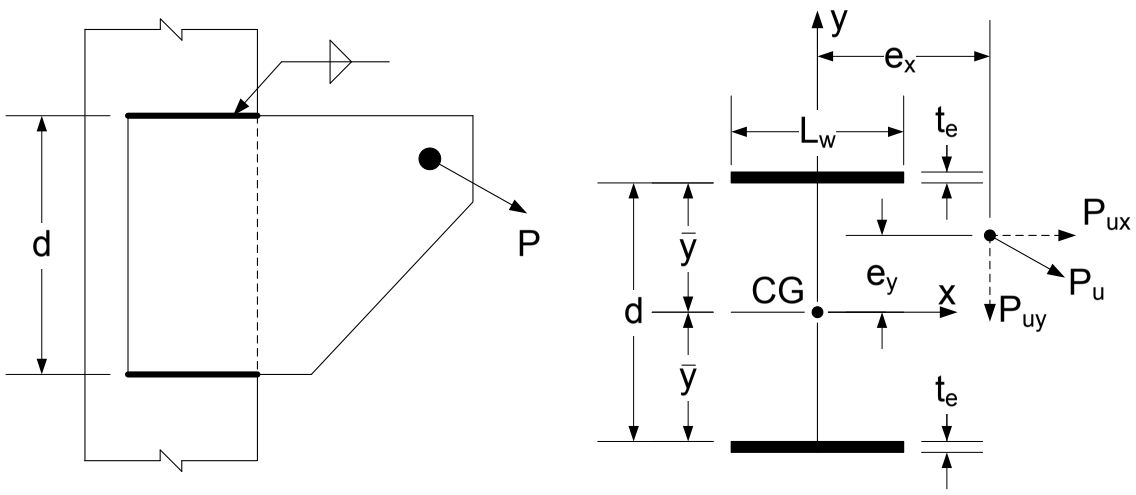


Figure 3.3.55 Eccentrically Loaded Fillet Welded Connection Subject to Combined Shear & Torsion

For this case, the components of stress in the weld segments caused by direct shear are determined as:

$$f_{vx} = \frac{P_{ux}}{A}$$

Equation 3.3.116

$$f_{vy} = \frac{P_{uy}}{A}$$

Equation 3.3.117

where A is the effective weld area taken as the thickness of the effective throat, t_e, times the total length, L_w, of the weld configuration.

The x- and y-components of stress due to the torsional moment can be computed as follows:

$$f_{Tx} = \frac{Ty}{I_p} = \frac{\left(P_{ux}e_y + P_{uy}e_x\right)y}{I_p}$$

Equation 3.3.118

$$f_{Ty} = \frac{Tx}{I_p} = \frac{\left(P_{ux}e_y + P_{uy}e_x\right)x}{I_p}$$

Equation 3.3.119

where I_p is the polar moment of inertia of the weld configuration about the centroid of the weld configuration calculated as follows:

$$I_p = \Sigma(I_x + I_y) + \Sigma A\left(\bar{x}^2 + \bar{y}^2\right)$$

Equation 3.3.120

I_x and I_y are the moments of inertia of each weld segment about their own centroidal axes, A is the area of each weld segment and $\bar{x}$ and $\bar{y}$ are the distances from the centroid of the weld configuration to each individual weld segment. For the case shown in Figure 3.3.55:

$$I_p \cong \frac{t_e}{6}\left[12L_w\bar{y}^2 + L_w^3\right]$$

Equation 3.3.121

When the above stresses are multiplied by effective throat thickness, t_e, the result is a component of force, R, in units of kips/inch.

It becomes convenient in these calculations to treat the welds as lines having length, but with an effective throat thickness (width), t_e, equal to unity (Figure 3.3.56).

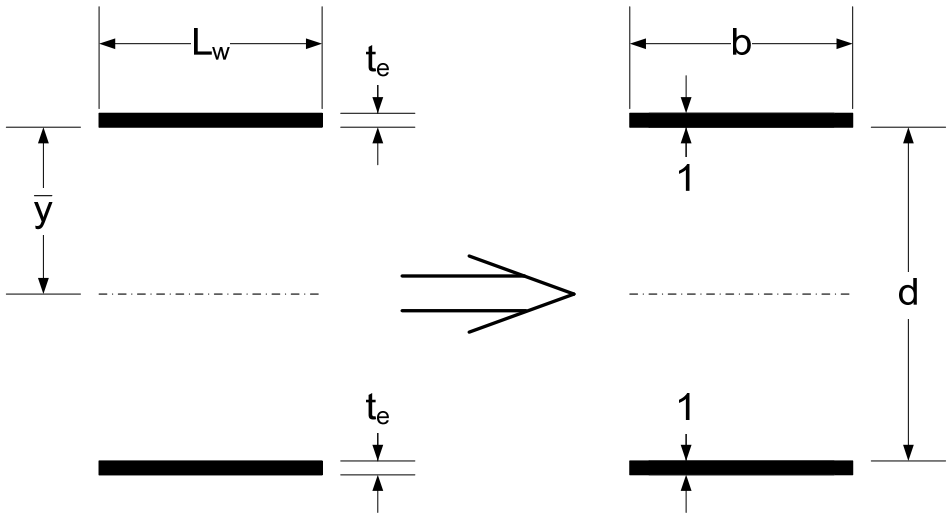


Figure 3.3.56 Weld Configuration Considered as Lines of Unit Thickness

For the above case, setting t_e equal to 1.0 and using the more general terms b and d as shown in Figure 3.3.56, Equation 3.3.121 can be written as follows:

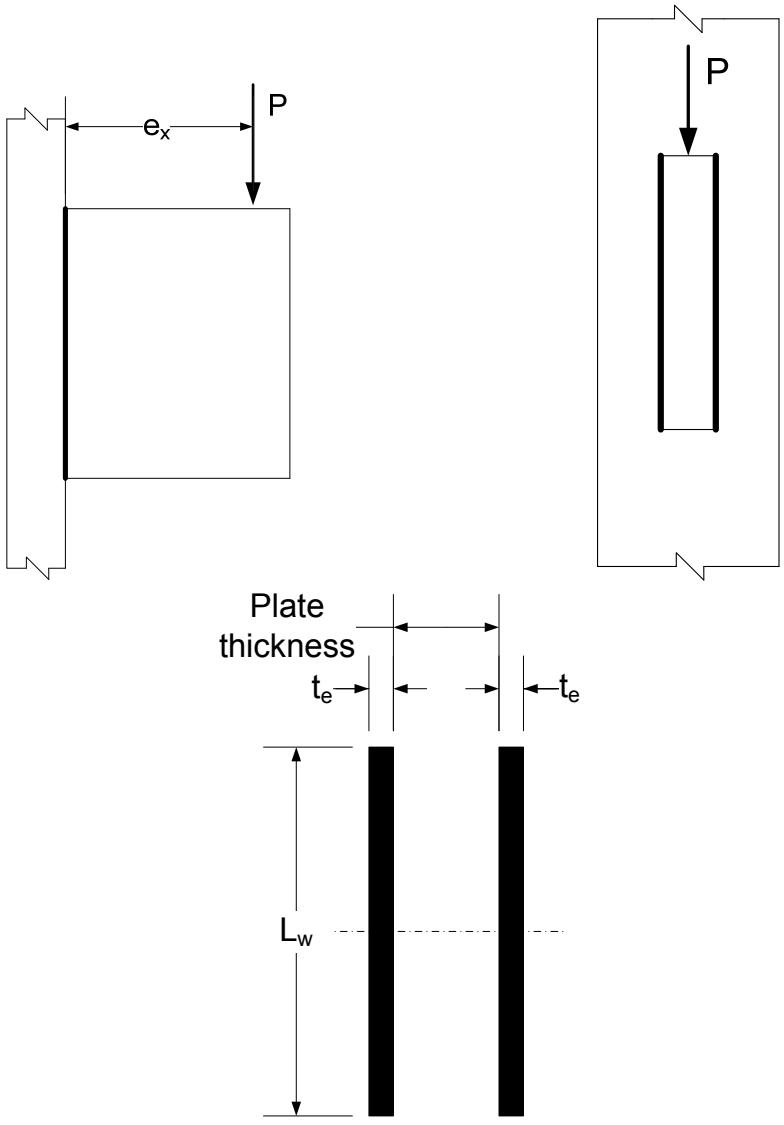


Figure 3.3.57 Eccentrically Loaded Fillet Welded Connection Subject to Combined Shear & Bending

$$I_p \cong \frac{1}{6}\left[12b\left(\frac{d}{2}\right)^2 + b^3\right] = \frac{b}{6}\left[3d^2 + b^2\right]$$

Equation 3.3.122

Properties for other common weld line configurations are tabulated in Reference 19, or can be derived in a similar fashion by the Design Engineer.

A less conservative alternative approach to determine the resistance of a weld configuration subject to eccentric shear is provided in Reference 4. In this approach, an instantaneous center of rotation is located and the load-deformation relationship of a fillet weld is used.

The traditional elastic vector analysis method can also be used for the case where the applied load is eccentric to the plane of the weld configuration subjecting the configuration to combined shear and bending moment (Figure 3.3.57). In essence, the weld configuration is loaded in shear and tension. The compression force from the bending is typically assumed carried by direct compression of the pieces being welded rather than through the welds. The weld segments are again treated as lines with a thickness of unity.

3.3.6.4 Cross-Frame Equilibrium

Individual cross frames are often created in 3D finite element models, permitting them to be individually analyzed. This level of investigation is particularly important in skewed and curved bridges in which these members are often heavily loaded. In addition to dead load analysis, individual influence surfaces may be built for these members (Section 2.1.4). Like other member actions, each maximum and minimum live load response for individual members is for different live load positions. Hence, live load responses, unlike dead load responses, are not in equilibrium for the cross- frame.

Consideration of the proper combination of live load forces is necessary to establish equilibrium. Exact equilibrium cannot be assured in some cases if the loader moves the live loads slightly on the influence surfaces for each individual member. With proper equilibrium established, the appropriate resultant dead and live load factored forces can be combined for the design of the cross-frame connections to the connection plates.

The issue can best be visualized by considering an X-type cross-frame between two I-girders as shown in Figure 3.3.58. Load applied to the left girder causes compression in the diagonal attached to the top flange of the left girder and tension in the other diagonal. A load applied to the right girder causes forces of the opposite sign (Figure 3.3.58). These forces can be thought of as “restoring forces” if the system was in equilibrium before the loads are applied. Restoring forces are forces that attempt to return the system to its original equilibrium condition from its new equilibrium condition. Interestingly, the chord members reach their maximum response when the live load is placed in a different position.

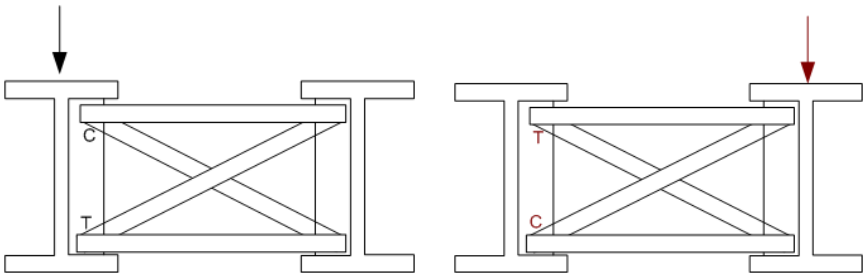


Figure 3.3.58 Cross-Frame Diagonal Forces in an X-Type Cross-Frame due to a Concentrated Load Over Each Girder

Clearly, the maximum force in the diagonals cannot exist at the same time since the live load must be in a different position to attain each maximum. However, the maximum force in one diagonal may well co-exist with the minimum force in the other.

Cross-frame forces alone cannot be in equilibrium for loads applied after the deck hardens because the deck then forms part of the restoring section as discussed in Section 2.5.2.2. Hence, the deck has a horizontal force component in either tension or compression as well as a vertical component in the form of vertical shear. A check of equilibrium is easiest done for the non-composite loads. An equilibrium check for the composite dead loads is usually not possible. The best check for this case is to check for equilibrium in the bottom-flange connections. Cross-frame forces at the bottom of an exterior girder can be checked by combining the horizontal chord force (usually the axial force if the member is horizontal) and the horizontal component of any diagonal member force. The net force must oppose any lateral reaction resulting from lateral bending of the bottom flange at the cross-frame.

Significant lateral bending occurs in interior girder flanges of skewed, straight girders when the cross-frames are staggered. In this case, much of the cross-frame force is due to the effect of the skew. If the girders are horizontally curved, much of the lateral flange bending is due to curvature. If the bridge is both curved and skewed, lateral moments may be large and occur for all of the above reasons.

Figure 3.3.59 shows a sample cross-frame equilibrium calculation for the component cross-frame forces for dead load (DC_1 + DC_2) at the bottom of an exterior girder from a 3D analysis of a straight skewed bridge. The arrows in Figure 3.3.59 indicate the calculated resultant horizontal and vertical forces in the cross-frame diagonal where the diagonal intersects the bottom of the girder. In this case, the net horizontal force is approximately zero, since there is no offsetting horizontal force on the other side of the girder and the lateral flange bending moment (not given) is nearly zero. In this particular case, the bridge is straight and the cross-frames are placed in contiguous lines normal to the girders so that the lateral moments are negligible.

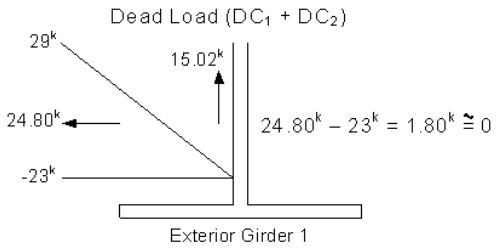


Figure 3.3.59 Equilibrium Check for DC_1 + DC_2 Cross-Frame Horizontal Forces at the Bottom of an Exterior Girder

The connection of the diagonal member to the gusset plate at this point would have to resist a 24.8 kip lateral dead load force and a 15 kip vertical dead load

force (the appropriate load factors would of course have to be applied). The connection of the gusset plate to the girder would only need to be designed for the 15 kip vertical force in this case.

The vertical component of force is not in equilibrium since gravity loads are being transferred between the girders. The difference in the vertical loads from zero at a cross-frame is the net vertical load applied to or removed from the girder at that point.

Figure 3.3.60 shows cross-frame forces due to maximum and minimum live load plus impact (+LL+IM and –LL+IM) for a cross-frame at the bottom of an exterior girder from the same straight skewed bridge. Since the lateral moment is nearly zero, the sum of horizontal forces must be nearly zero. Maximum (positive) force in the diagonal must be combined with the minimum (negative) force in the bottom chord to establish horizontal equilibrium (and vice versa). The values show that this is indeed the case. This means that the same load position produced the minimum force in one member while it produced the maximum force in the other member. This must be the case.

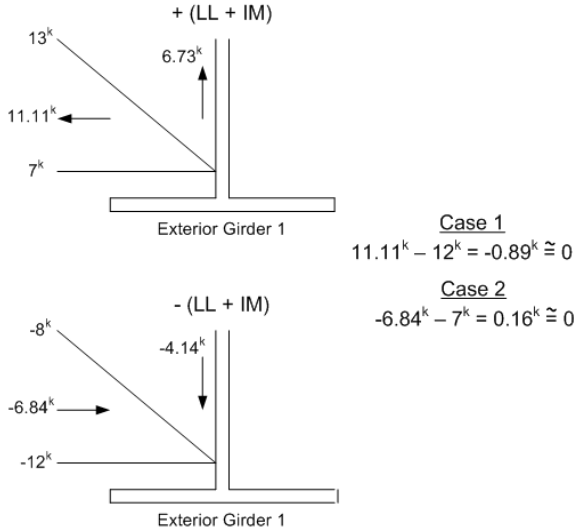


Figure 3.3.60 Equilibrium Check for (+LL+IM) and (-LL+IM) Cross-Frame Horizontal Forces at the Bottom of an Exterior Girder

Once equilibrium is confirmed at the bottom flange, the top-flange connection can be designed using the resultant forces at the top flange without further checking equilibrium. In the case of skewed and/or curved girders, where there is a net lateral force on the top flange, this force may be used to determine the transverse (radial) force to be resisted by the shear connectors (Sections 3.3.2.2.1.2 and 3.3.2.3.1).

Figure 3.3.61 shows cross frames at the bottom flange of the adjacent interior girder. The figure shows the horizontal and vertical forces due to (DC_1 + DC_2),

(+LL+IM) and (-LL+IM) in that order going from top to bottom of the figure. The cross-frame forces at interior girders with contiguous opposing cross frames experience opposing forces, so equilibrium is obtained by considering the forces on both sides of the girder.

Unlike the situation at the exterior girder, the forces for the maximum (positive) live load condition in the diagonal and bottom chord on both sides of the interior girder provide a net horizontal force of approximately zero at the bottom of the girder, and the net minimum (negative) live load condition in the diagonal and bottom chord on both sides of the girder do likewise. Referring to Figure 3.3.58, the reason for this occurrence is that when the adjacent girders each receive live load, they each transfer load to the interior girder through compression. The reverse situation happens when the live load is in place over the interior girder; load is transferred away from the interior girder through tension. Note that the cross-frame force is larger for the case where load is transferred to the girder than when it is transferred away from it. The reason is that two lanes of live load are transferring load to the girder, but only one lane of live load can be placed on the interior girder to transfer load away from it.

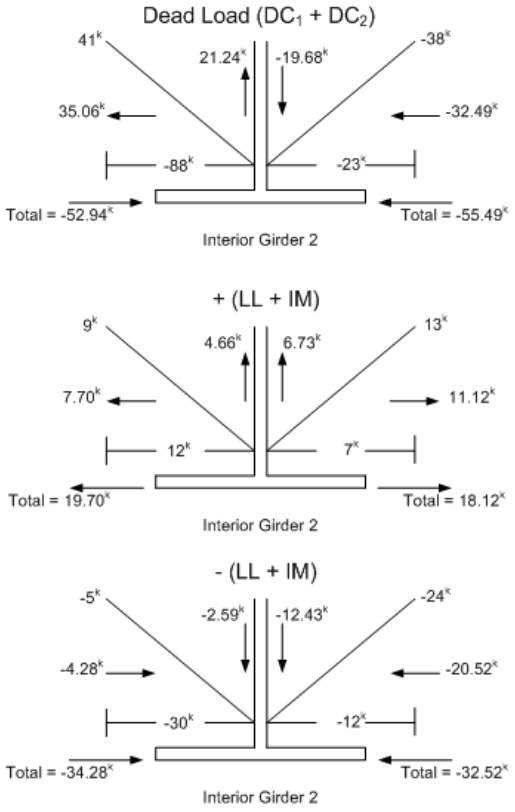


Figure 3.3.61 Equilibrium Check for $DC_1 + DC_2$, (+LL+IM) and (-LL+IM) Cross-Frame Horizontal Forces at the Bottom of an Interior Girder

With equilibrium confirmed, the Design Engineer can then proceed to confidently with design of the cross-frame connections. The resultant horizontal force acting in

combination with the corresponding resultant vertical force is to be used in the design of the connection on each side of the girder. The difference in horizontal force on the two opposing sides of the web in this case must be resisted by attachment of the connection plates to the flanges.

Influence surfaces can be designed for special requirements instead of summing forces as described. For example, an influence surface consisting of the chord force plus the horizontal component of the diagonal force coming into the same joint can be defined. The resulting loading would then be the maximum and minimum horizontal force at the joint. The vertical force is simply the vertical component of the diagonal force. These results can be used to design the bolt group attaching that gusset plate to the connection plate. There still is a need for an influence surface for each individual member however to design the member attachment to the gusset plate. Usually fatigue is the controlling condition.

As mentioned above, the difference in the horizontal force on the two opposing sides of the web equals the force resisted by the web-flange of the girder. Usually, this force is transferred through a load path connecting the connection plate(s) to the flange. These connections are usually welds, although bolts in clip angles are not unheard of. The situation where this force might be significant is with staggered cross-frames on interior girders often found on sharply skewed bridges. The cross-frames on the opposite side of the girder restrain the girder from moving laterally to relieve the cross-frame force, as would be the case for an exterior girder. The net force is resisted by the lateral bending of the flange. The magnitude of the force is dependent on the stiffness of the flange and the spacing of the cross-frames. Staggered cross-frames are a common means of reducing cross-frame forces, as discussed in Section 3.1.2.8.3.2.

The resultant dead and live load forces on the right-hand side of the interior girder (Figure 3.3.61) will now be combined according to the Strength I load combination. The load modifier, η, is taken equal to 1.0. The minimum load factor for component dead load, γ_p = 0.90, from *AASHTO LRFD* Table 3.4.1-2 is considered for application to the (DC_1 + DC_2) resultant force whenever the sign of the force is opposite to the sign of the live load plus impact force to determine if a more critical load combination is produced.

Horizontal resultant force:

(DC_1 + DC_2):	1.0[0.9(-55.49)]	=	-49.9 kips
(+LL+IM):	1.0[1.75(18.12)]	=	31.7 kips
			∑=-18.2 kips

or:

(DC_1 + DC_2):	1.0[1.75(-55.49)]	=	-69.4 kips
(+LL+IM):	1.0[1.75(18.12)]	=	31.7 kips
			∑=-37.7 kips (controls)

(DC_1 + DC_2):	1.0[1.75(-55.49)]	=	-69.4 kips
(-LL+IM):	1.0[1.75(-32.52)]	=	-56.9 kips
			∑=**-126.3 kips**

Vertical resultant force:

(DC_1 + DC_2):	1.0[0.9(-19.68)]	=	-17.7 kips
(+LL+IM):	1.0[1.75(6.73)]	=	11.8 kips
			∑=-5.9 kips

or:

(DC_1 + DC_2):	1.0[1.75(-19.68)]	=	-24.8 kips
(+LL+IM):	1.0[1.75(6.73)]	=	11.8 kips
			∑=-12.8 kips (controls)

(DC_1 + DC_2):	1.0[1.25(-19.68)]	=	-24.8 kips
(-LL+IM):	1.0[1.75(-12.43)]	=	-21.8 kips
			∑=**-46.4 kips**

There are three reasons for the lack of perfect equilibrium in the preceding sample cases: 1) all forces are rounded off to integers, 2) the live load positions may be slightly different for the critical forces in the diagonal and bottom strut, and 3) the effect of small lateral bending moment (in this case) in the bottom flange at the cross-frame is ignored. Again, the bridge was straight and the cross-frames were placed in contiguous lines normal to the girders so that the lateral moments were negligible. Larger lateral moments and resulting deviations from equilibrium of the cross-frame members alone would be expected with cross-frames placed in discontinuous lines (i.e. staggered) and/or with curvature. Although the lateral flange moments would be increased with the cross-frames placed in discontinuous lines, the cross-frame forces would be lessened with the magnitude of the differences being a function of the flange stiffness and relative cross-frame spacings.

In such cases, computation of the net lateral force resisted by the flanges can be estimated by resolving the lateral moment. For the case of staggered cross-frames, the lateral reaction at the cross-frames for establishing equilibrium can be estimated from the equations for the interior reaction and moment in a three-span continuous beam loaded by equal concentrated loads, *P*, at the center of each span as follows:

$$R = 1.14P$$

Equation 3.3.123

where:

$$P = \frac{3.33M_{lat}}{\ell} \text{ (kips)}$$

Equation 3.3.124

ℓ = cross-frame spacing (in.)
M_{lat} = lateral flange moment at the cross-frame (kip-in.)

The lateral reaction would act in the opposite direction at the top-flange connection.

In horizontally curved bridges, there is also a lateral reaction at the cross-frames resulting from the lateral flange moments due to curvature. This lateral reaction can be estimated from the equations for the interior reaction and moment in a three-span continuous beam loaded by a uniform load, *w*, in each span as follows:

$$R = 1.1w\ell$$

Equation 3.3.125

where:

$$w = \frac{M}{RD} \text{ (kips/in.)}$$

Equation 3.3.126

D = web depth (in.)
M = vertical bending moment in the girder at the cross-frame (kip-in.)
R = girder radius (in.)

Statics requires that the lateral reaction at the top-flange connection act in the opposite direction.

The above lateral reactions would only be used as necessary to establish equilibrium (in an approximate fashion) for determining the proper combination of the forces at a particular joint. The lateral reactions do not influence the design of the cross-frame member end connections. However, the reactions so computed should be considered when checking the cross-frame connection plate welds to the flanges, as discussed above. Attachment of connection plates to the flanges avoids transfer of the lateral loads through the web. In older bridges, these connections were not made by code and frequently caused cracks in the web-flange juncture. In recent years, the code has been changed to require these connections.

3.3.7 Bolted Girder Splices

3.3.7.1 General

A splice is defined in *AASHTO LRFD* Article 6.2 as a group of bolted connections, or a welded connection, sufficient to transfer the moment, shear, axial force or torque between two structural elements joined at their ends to form a single, longer element. In steel-bridge design, splices are typically used to connect girder sections together in the field; hence, the term field splices is often used.

The design of splices is covered in *AASHTO LRFD* Article 6.13.6. The design of bolted splices is covered in *AASHTO LRFD* Article 6.13.6.1 and the design of welded splices is covered in *AASHTO LRFD* Article 6.13.6.2. The following discussion concentrates on the specifics related to the design of bolted field splices for girders (i.e. flexural members – Figure 3.3.62), as outlined in *AASHTO LRFD* Article 6.13.6.1.4. Principles of bolted connection design, discussed above in Section 3.3.6.2, are applied in the design of these splices. Section 3.1.2.3 discusses issues related to the selection of field-section size and field-splice locations.



Figure 3.3.62 Bolted Splice on a Curved I-Girder

A schematic of a typical bolted girder splice is shown in Figure 3.3.63 (shown for an I-section). Bolted girder splices generally include top flange splice plates, web splice plates and bottom flange splice plates. In addition, if the plate thicknesses on one side of the joint are different than those on the other side, then filler plates are usually needed. Filler plates are discussed in Section 3.3.7.4. For the flange splice plates, there is typically one plate on the outside of the flange and two smaller plates on the inside, one on each side of the web. For the web splice plates, there are two plates, one on each side of the web. High-strength bolts are used to connect the splice plates to the member in the final condition.

AASHTO LRFD Article 6.13.6.1.1 specifies that at the strength limit state, bolted splices are to be designed to satisfy the general requirements of *AASHTO LRFD* Article 6.13.1; that is, unless specified otherwise, the splices are to be designed for not less than the larger of: 1) the average of the flexural moment-induced stress, shear or axial force due to the factored loads at the point of splice and the factored flexural, shear or axial resistance of the member or element at the same point, or 2) 75 percent of the factored flexural, shear or axial resistance of the member or element. In addition, where a section changes at the splice, the smaller of the two connected sections is to be used in the design. *AASHTO LRFD Article C6.13.6.1.4a suggests that the smaller section at the point of splice in a flexural member be taken as the side of the splice that has the smaller calculated moment of inertia for the non-composite steel section.*

Bolted splices in continuous spans should be made at or near points of permanent load contraflexure if possible, which helps to minimize the flange design forces. *Splices located in areas of stress reversal near points of permanent load contraflexure are to be investigated for both positive and negative flexure in order to determine the governing condition*.

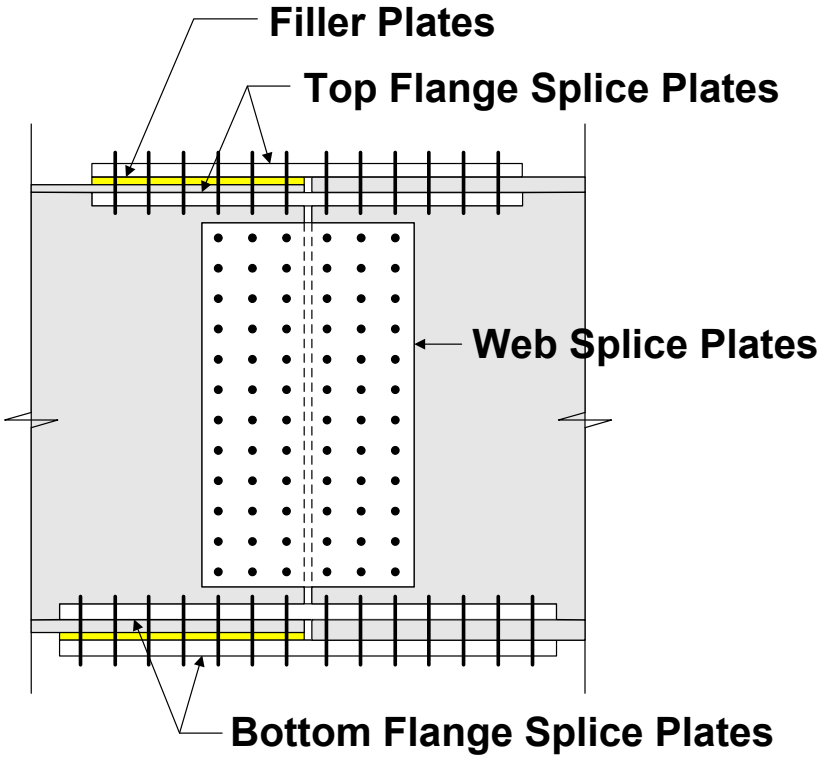


Figure 3.3.63 Typical Bolted Girder Splice

Web and flange splices are not to have less than two rows of bolts on each side of the joint to ensure proper alignment and stability of the girder during construction.

Also, oversize or slotted holes are not to be used in either the member or the splice plates at bolted splices. This is also for improved geometry control during erection, and because a strength reduction (not recognized by the specifications) may occur when oversize or slotted holes are used in eccentrically loaded bolted web connections.

Bolted splice connections for flexural members are to be designed as slip-critical connections. Slip-critical bolted connections were previously discussed in Section 3.3.6.2.1.1. *Slip-critical connections are to be proportioned to prevent slip under Load Combination Service II and to provide bearing, shear and tensile resistance at the strength limit state.* In addition, bolted connections for flange and web splices in flexural members are to be proportioned to prevent slip during the erection of the steel and during the casting of the concrete deck; once again for improved geometry control.

Although there are holes in the tension flange at the point of splice, for simplicity, *AASHTO LRFD* Article 6.13.6.1.4a states that flexural stresses due to the factored loads at the strength limit state and for checking slip of the bolted connections under the Service II load combination at the point of splice are to be determined using the properties of the gross section. However, the factored flexural resistance of the tension flange at the last row of bolt holes for the splice is limited to be less than or equal to the specified minimum yield stress of the tension flange at the strength limit state and when checking constructibility according to the provisions of *AASHTO LRFD* Article 6.10.1.8 (refer to Section 3.2.6.1.3 – Equation 3.2.72) in order to prevent the possibility of net section fracture. As discussed in Section 3.1.4.3.3.3, this provision should never be allowed to control the plate thickness at a splice. When this requirement appears to control, the number of bolt lines can be reduced (note however that *AASHTO LRFD* Article 6.13.6.1.4a requires that there be at least two row of bolts on each side of the web), or the bolts lines may be staggered. This provision appears to be more critical at bottom flange splices of box girders.

As discussed in Section 3.3.6.2.1.3, the nominal fatigue resistance of base metal at the gross section adjacent to slip-critical bolted connections is based on fatigue detail Category B (*AASHTO LRFD* Table 6.6.1.2.3-1 – Condition 2.1) assuming the bolts are installed in holes drilled full size or subpunched and reamed to size (which is typically the case for bolted girder splices). However, as mentioned in *AASHTO LRFD* Article C6.13.6.1.4a, fatigue will generally not control the design of the bolted splice plates for flexural members. The areas of the flange and web splice plates typically equal or exceed the areas of the flanges and web to which they are attached, and the flanges and web are usually checked separately for either equivalent or more critical fatigue category details. Therefore, fatigue of the splice plates will generally not need to be checked unless either of the preceding conditions is not satisfied.

The application of the provisions for the design bolted field splices, as described below, is illustrated in Section 5.1.8.8 of the I-girder design example and in Section 5.2.9.8 of the tub girder design example.

3.3.7.2 Flange Splices

3.3.7.2.1 General

The design of bolted flange splices is covered in *AASHTO LRFD* Article 6.13.6.1.4c. Filler plates for flange splices are discussed in Section 3.3.7.4.2. Lateral bending effects on bolted flange splices are discussed in Section 3.3.7.2.4. Special considerations related to the design of bolted flange splices for box girders are discussed in Section 3.3.7.2.5.

3.3.7.2.2 Strength Limit State

3.3.7.2.2.1 Controlling Flange

The *controlling flange* is defined as the top or bottom flange for the smaller section at the point of splice, whichever flange has the maximum ratio of the elastic flexural stress at its midthickness due to the factored loads to its factored flexural resistance. The opposite flange is termed the *noncontrolling flange*.

The splice must be checked independently for both positive and negative flexure at splices located in regions of stress reversal. For each condition, a different flange may qualify as the controlling flange. For composite sections in positive flexure, the controlling flange is typically the bottom flange. For sections in negative flexure, either flange may qualify as the controlling flange.

Bolted splice plates and their connections on the controlling flange are to be proportioned at the strength limit state to provide a minimum design resistance (force) equal to the design stress, F_{cf}, times the smaller effective flange area, A_e, on either side of the splice. The design stress for the controlling flange, F_{cf}, is to be computed as follows:

$$F_{cf} = \frac{\left(\left|\frac{f_{cf}}{R_h}\right| + \alpha\phi_f F_{yf}\right)}{2} \geq 0.75\alpha\phi_f F_{yf}$$

Equation 3.3.127
AASHTO LRFD Equation 6.13.6.1.4c-1

where:

α = 1.0, except that a lower value equal to F_n/F_{yf} may be used for flanges where F_n is less than F_{yf}
ϕ_f = resistance factor for flexure specified in *AASHTO LRFD* Article 6.5.4.2 (= 1.0)
f_{cf} = maximum factored vertical bending stress at the midthickness of the controlling flange at the point of splice (ksi)
F_n = nominal flexural resistance of the flange (ksi)

F_{yf} = specified minimum yield strength of the flange (ksi)
R_h = hybrid factor determined as specified in *AASHTO LRFD* Article 6.10.1.10.1 (Section 3.2.6.3). For hybrid sections in which F_{cf} does not exceed the specified minimum yield strength of the web, R_h is to be taken as 1.0.

Equation 3.3.127 is based on the general design requirements specified in *AASHTO LRFD* Article 6.13.1 and discussed above in Section 3.3.7.1. The 75 percent rule (i.e. the right-hand side of Equation 3.3.127), which normally governs in regions of lower moment or stress, is interpreted as providing a longitudinal stiffness at the splice that is consistent with the stiffness assumed at that point in the structural analysis. The average rule (i.e. the left-hand side of Equation 3.3.127), which normally governs in regions of higher moment or stress, is interpreted as providing adequate flexural resistance at the splice. The application of Equation 3.3.127 to provide a minimum design resistance for the controlling flange allows for possible unintended shifts in girder moment at the splice and for differences between the actual and predicted moment at the splice, which are certain to be more significant near points of permanent-load contraflexure.

The factor α is included in Equation 3.3.127 to allow for a reduction in the minimum design stress for cases where the nominal flexural resistance of the flange, F_n, is significantly below F_{yf}. An example is a bottom box flange in compression at the point of splice for which the nominal local buckling resistance, F_n, is usually well below F_{yf}. As a result, it would be overly conservative to use F_{yf} in Equation 3.3.127 to determine the minimum design force for designing the splice as the box flange is not permitted to approach a stress level anywhere near F_{yf}. In such cases, α may be taken equal to F_n/F_{yf} (i.e. less than 1.0). For I-section flanges in compression, the reduction in F_n below F_{yf} based on local or lateral torsional buckling is typically not as large as for box flanges. Thus, for simplicity, a conservative value of 1.0 may be used for α in this case even though the specification would permit the use of a lower value. For tension flanges, α should always be taken equal to 1.0.

In Equation 3.3.127, the factored vertical bending stress at the midthickness of the controlling flange, f_{cf}, is divided by the hybrid factor, R_h, instead of reducing F_{yf} by R_h. In actuality, yielding in the web of a hybrid section results in an increase in the flange stress and the flange is permitted to reach F_{yf} (refer to Section 3.2.6.3). When the design stress, F_{cf}, is less than or equal to the specified minimum yield strength of the web, F_{yw}, there is theoretically no yielding in the web and R_h is taken equal to 1.0. The web load-shedding factor R_b (refer to Section 3.2.6.2) is not included in Equation 3.3.127 since the possibility of web bend buckling, and the concomitant shedding of the web compressive stresses to the compression flange, is precluded by the presence of the web splice plates.

To calculate the minimum design force, P_{cf}, for the controlling flange, F_{cf} is multiplied by an effective flange area, A_e. The *smaller* value of A_e on either side of the splice is to be used to compute the minimum flange design force to ensure the design force does not exceed the factored resistance of the smaller flange. For

compression flanges, A_e is to be taken as the gross area of the flange. For tension flanges, A_e is to be calculated as follows:

$$A_e = \left(\frac{\phi_u F_u}{\phi_y F_{yt}} \right) A_n \leq A_g$$

Equation 3.3.128
AASHTO LRFD Equation 6.13.6.1.4c-2

where:

ϕ_u = resistance factor for fracture of tension members specified in *AASHTO LRFD* Article 6.5.4.2 (= 0.80)
ϕ_y = resistance factor for yielding of tension members specified in *AASHTO LRFD* Article 6.5.4.2 (= 0.95)
A_n = net area of the tension flange determined as specified in *AASHTO LRFD* Article 6.8.3 (in.^{2})
A_g = gross area of the tension flange (in.^{2})
F_u = tensile strength of the flange determined as specified in *AASHTO LRFD* Table 6.4.1-1 (ksi)
F_{yt} = specified minimum yield strength of the tension flange (ksi)

The calculation of the net area, A_n, at bolted connections was discussed previously in Section 3.3.3.2.2. For tension flanges, the use of A_e given by Equation 3.3.128 ensures that fracture on the net section of the flange will theoretically be prevented at the splice.

3.3.7.2.2.2 Noncontrolling Flange

Bolted splice plates and their connections on the noncontrolling flange at the strength limit state are to be proportioned to provide a minimum design resistance (force), P_{ncf}, equal to the design stress, F_{ncf}, times the smaller effective flange area, A_e, on either side of the splice. The design stress for the noncontrolling flange, F_{ncf}, is to be computed as follows:

$$F_{ncf} = R_{cf} \left| \frac{f_{ncf}}{R_h} \right| \geq 0.75 \alpha \phi_f F_{yf}$$

Equation 3.3.129
AASHTO LRFD Equation 6.13.6.1.4c-3

where:

f_{ncf} = factored vertical bending stress at the midthickness of the noncontrolling flange at the point of splice concurrent with f_{cf} (ksi)
R_{cf} = the absolute value of the ratio of F_{cf} to f_{cf} for the controlling flange
R_h = hybrid factor determined as specified in *AASHTO LRFD* Article 6.10.1.10.1 (Section 3.2.6.3). For hybrid sections in which F_{cf} does not exceed the specified minimum yield strength of the web, R_h is to be taken as 1.0.

According to Equation 3.3.129, the factored vertical bending stress at the midthickness of the noncontrolling flange, f_{ncf}, concurrent with the stress in the controlling flange is being factored up in the same proportion as the flexural stress in the controlling flange, f_{cf}, (i.e. according to Equation 3.3.127) in order to satisfy the general design requirements of *AASHTO LRFD* Article 6.13.1. To satisfy the requirements of *AASHTO LRFD* Article 6.13.1, the factored-up stress in the noncontrolling flange must be equal to or greater than $0.75\alpha\phi_f F_{yf}$ as a minimum. As was the case for the controlling flange, the factored vertical bending stress, f_{ncf}, is divided by the hybrid factor, R_h.

3.3.7.2.2.3 Flange Splice Plates and Bolts

The calculated minimum design forces in the controlling and noncontrolling flanges, P_{cf} and P_{ncf}, are to be used to check: 1) the resistance of the flange splice plates; 2) the shear resistance of the high-strength bolts (Section 3.3.6.2.6.2); and 3) the bearing resistance at the bolt holes (Section 3.3.6.2.6.2) assuming the bolts have slipped and gone into bearing at the strength limit state.

For a typical flange splice with inner and outer splice plates, an approach is needed to proportion the minimum design force to the inner and outer plates. According to *AASHTO LRFD* Article C6.13.6.1.4c, at the strength limit state, the minimum flange design force may be assumed equally divided to the inner and outer flange splice plates when the areas of the inner and outer plates do not differ by more than 10 percent. In this case, the shear resistance of the bolted connection should be checked for the total minimum flange design force assumed acting in double shear. Should the areas of the inner and outer plates differ by more than 10 percent, the minimum design force in each plate at the strength limit state should be determined by multiplying the total minimum flange design force by the ratio of the area of the splice plate under consideration to the total area of the inner and outer plates. In this case, the shear resistance of the bolted connection should be checked for the larger of the calculated splice-plate minimum design forces assumed acting on a single shear plane.

Flange Splice Plates

Splice Plates in Tension

The minimum design force at the strength limit state in flange splice plates subject to tension is not to exceed the factored resistance of the splice plates in tension specified in *AASHTO LRFD* Article 6.13.5.2; that is, the splice plates are to be checked for yielding on the gross section, fracture on the net section and for block shear rupture (refer to Section 3.3.6.2.6.2). Block shear rupture will not typically control the design of flange splice plates of typical proportion.

Note also that according to *AASHTO LRFD* Article 6.13.5.2, for splice plates subject to tension, A_n must not exceed $0.85A_g$. For narrow splice plates on relatively narrow flanges requiring a relatively large number of bolts, it may be

desirable to taper the splice plates at their ends in order to reduce the number of holes until the plates can be sufficiently unloaded to accommodate more holes across the width. The smallest value of A_e at the end of the taper should probably be used to conservatively compute the flange design forces in this case.

Splice Plates in Compression

AASHTO LRFD Article 6.13.6.1.4c specifies that for flange splice plates subject to compression at the strength limit state, the minimum design force must not exceed the factored resistance in compression given as:

$$R_r = \phi_c F_y A_s$$

Equation 3.3.130
AASHTO LRFD Equation 6.13.6.1.4c-4

where:

ϕ_c = resistance factor for compression specified in *AASHTO LRFD* Article 6.5.4.2 (= 0.90)
A_s = gross area of the splice plate (in.^{2})
F_y = specified minimum yield strength of the splice plate (ksi)

Equation 3.3.130 is a check for yielding on the gross section of the splice plates assuming an unbraced length of zero for the relatively short plates.

Flange Splice Bolts

The shear resistance of the flange splice bolts and the bearing resistance of the flange splice bolt holes is to be calculated according to the procedures discussed in Section 3.3.6.2.6.2. Note that slip of the flange splice bolts is to be checked at the service limit state using a lower minimum design force as discussed below in Section 3.3.7.2.3.

Recall that for a bolt in a connection greater than 50.0 in. in length, the nominal shear resistance is to be taken as 0.80 times the value given by Equation 3.3.82 or 3.3.83, as applicable. For bolted flange splices, the 50.0 in. length is to be measured between the extreme bolts on only one side of the connection (*AASHTO LRFD* Article C6.13.2.7).

The bearing resistance is calculated as the sum of the bearing resistances of the individual bolt holes parallel to the line of the flange design force. When splicing two homogeneous sections of the same specified minimum yield strength, the bearing resistance of the thinner flange splice plate controls if the sum of the inner and outer splice-plate thicknesses is less than the thickness of the thinner flange at the point of splice; otherwise, the thinner flange plate controls. For all other cases, the comparison must be made between the sum of the inner and outer splice-plate

thicknesses times the tensile strength, F_u, of the splice plates to the thickness of each flange times the corresponding F_u of each flange at the point of splice in order to determine which plate controls.

3.3.7.2.3 Service Limit State

The slip resistance of the flange splice bolts (Section 3.3.6.2.6.1) at the service limit state is to be checked under the Service II load combination. The slip resistance of the bolts should also be checked during the deck casting.

For this check, the minimum design force for the flange under consideration is to be taken as the design stress, F_s, times the smaller gross flange area, A_g, on either side of the splice. The design stress, F_s, is to be taken as:

$$F_s = \frac{f_s}{R_h}$$

Equation 3.3.131
AASHTO LRFD Equation 6.13.6.1.4c-5

where:

f_s = maximum vertical bending stress due to Load Combination Service II or the factored vertical bending stress due to the deck-casting sequence (whichever controls) at the midthickness of the flange under consideration for the smaller section at the point of splice (ksi)

R_h = hybrid factor determined as specified in *AASHTO LRFD* Article 6.10.1.10.1 (Section 3.2.6.3). For hybrid sections in which f_s in the flange with the larger stress does not exceed the specified minimum yield strength of the web, R_h is to be taken equal to 1.0.

Since net section fracture is not a concern when checking for slip under this service limit state load combination, the smaller *gross* flange area on either side of the splice is to be used to compute the minimum design force. The smaller gross area on either side of the splice is used to ensure that the design force does not exceed the service limit state resistance of the smaller flange.

As discussed in *AASHTO LRFD* Article C6.13.6.1.4c, when checking the slip resistance of the bolts for a typical flange splice with inner and outer splice plates, the minimum design force at the service limit state should always be assumed divided equally to the two slip planes regardless of the ratio of the splice plate areas. Unless slip occurs on both planes, slip of the connection cannot occur. Therefore, in this case, the slip resistance of the bolted connection should always be checked for the total minimum flange design force assuming two slip planes (i.e. N_s = 2 in Equation 3.3.78).

A check of the flexural stresses in the flange splice plates under the Service II load combination to control permanent deformations in the plates is not currently

required. However, such a check is recommended whenever the combined area of the inner and outer splice plates is less than the area of the smaller flange at the splice. It is recommended that the check be made in this instance by dividing the total minimum design force P_s (calculated from the design stress F_s obtained from Equation 3.3.131) equally to the inner and outer plates, dividing the resulting splice-plate minimum design forces by the gross area of the corresponding plate(s), and then checking that the resulting stresses do not exceed $0.95F_y$, where F_y is the specified minimum yield strength of the splice plate(s).

3.3.7.2.4 Flange Lateral Bending

According to *AASHTO LRFD* Article 6.13.6.1.4c, in cases for straight girders where flange lateral bending is deemed significant (e.g. in straight bridges with significant skew), and for horizontally curved girders (with or without skew), the effects of flange lateral bending must be considered in the design of the bolted splices for discretely braced flanges of I-sections and for discretely braced top flanges of tub sections (a discretely braced flange is defined in *AASHTO LRFD* Section 6.2). Top flanges of I-sections and tub sections are typically discretely braced during the construction condition. Flange lateral bending may be ignored in the design of top-flange splices once the flange is continuously braced. Bottom flanges of I-girders are always discretely braced.

The traditional elastic vector method for eccentric shear (refer to Section 3.3.6.2.7) may be used to account for the effects of flange lateral bending in the design of the flange splice bolts. The direct shear on the flange bolts is caused by either the actual factored flange force, or by the appropriate minimum flange design force, depending on the limit state under investigation (*P* in Figure 3.3.64). The flange force is calculated without consideration of the flange lateral bending. The moment, M_ℓ (Figure 3.3.64), on the bolt group is taken as the calculated factored flange lateral bending moment.

Note in Figure 3.3.64 that the lateral moments in the top and bottom flanges are opposing. The use of the flange lateral moments at the cross-frame closest to the splice is obviously conservative based on the general shape of the lateral moment diagram in-between cross-frames in which the lateral moment actually reverses sign (Figures 1.1.31 and 1.1.32), and the fact that the splice cannot be located right at a cross-frame. If the flange lateral moment is available mid-way between the cross-frames adjacent to the desired splice location (e.g. if a flange node is located halfway between the cross-frames in a refined 3D model – refer to Section 2.5.3.1), a line plotted between the lateral moment at that point and the lateral moment at the cross-frame closest to the splice (with the proper sense of the moments considered) can be used to determine an optimal splice location to minimize the effect of the lateral moment on the design of the splice. *For* curved *bridges with radial supports where the effects of lateral flange bending are due primarily to curvature, the splice is likely to often be at a location where the effects of the flange lateral bending on the splice are minimal and can be ignored*. To

confirm this, the splice location can be checked using the procedure just described, or it can be checked in a more approximate fashion against the location of the point of contraflexure in a fixed-end beam loaded with a uniform load, which is at approximately $0.21L_b$ from the fixed end (i.e from the cross-frame) where L_b is the cross-frame spacing

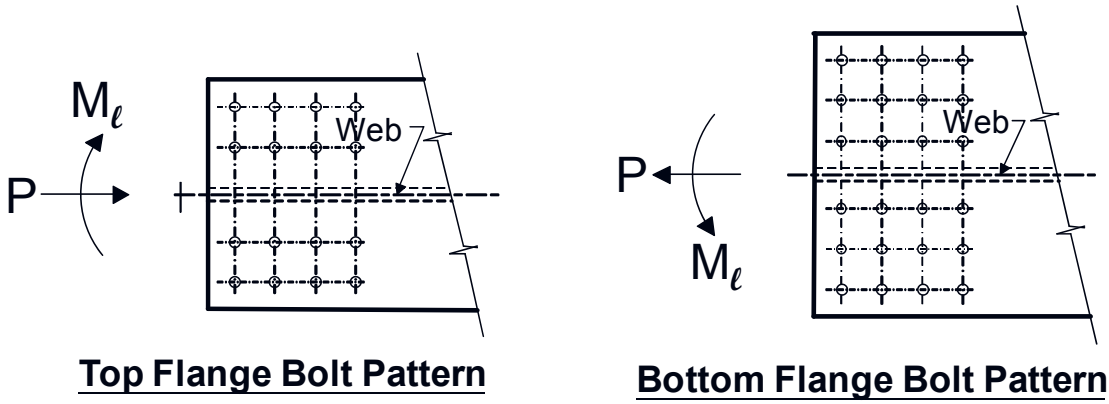


Figure 3.3.64 Top and Bottom Flange Splices Subject to Flange Lateral Bending

Under the combined actions of the flange force, *P*, and the flange lateral bending moment, M_ℓ, top flange splice bolts in I- and tub sections are to be checked for slip for constructibility under the combined actions when the top flange is discretely braced prior to hardening of the deck. *Lateral flange bending effects can be ignored in the design of top flange splices once the deck hardens and the flange is continuously braced*.

Since the bottom flanges of I-girders are always discretely braced, lateral flange bending effects must be considered in the design of bottom flange splices at all limit states. Thus, bottom flange splice bolts are to be checked for slip under the combined actions for the Service II load combination or for constructibility, whichever governs. At the strength limit state, the bolts are to be checked for shear and the bolt holes are to be checked for bearing under the combined actions.

The top and bottom flange splice plates are to be checked at the strength limit state. Since the bottom flange is discretely braced, the splice plates on the bottom flange must be checked for the combined stress due to *P* and M_ℓ. Lateral flange bending can be ignored in the design of the top flange splice plates since the flange is continuously braced at the strength limit state.

The calculation of *P* and M_ℓ for each case is discussed in the following.

For constructibility, *P* is to be taken equal to:

$$P = \frac{f}{R_h} A_g$$

Equation 3.3.132

where:

- f = factored vertical bending stress at the splice at the mid-thickness of the flange under consideration determined from the deck-casting analysis (ksi)
- R_h = hybrid factor for the non-composite section determined as specified in *AASHTO LRFD* Article 6.10.1.10.1 (Section 3.2.6.3)
- A_g = smaller gross flange area on either side of the splice (in.^{2})

and M_ℓ is to be taken equal to the factored flange lateral bending moment at the splice determined from the deck-casting analysis for the same loads. For splices in exterior girders, the factored lateral flange moment due to the deck overhang loads should also be considered.

The stress, *f*, should include the stress due to the steel weight plus stay-in-place form weight plus the weight of the wet concrete.

For Service II, *P* is to be taken equal to:

$$P = \frac{f_s}{R_h} A_g$$

Equation 3.3.133

where

- A_g = smaller gross flange area on either side of the splice (in.^{2})
- f_s = maximum flexural stress due to load combination Service II at the midthickness of the flange under consideration for the smaller section at the point of splice (ksi)
- R_h = hybrid factor specified in *AASHTO LRFD* Article 6.10.1.10.1 (Section 3.2.6.3)

and M_ℓ is to be taken equal to the factored flange lateral bending moment at the splice for the Service II load combination.

For the strength limit state and depending on which flange is under consideration, *P* is to be taken equal to:

$$P = F_{cf} A_e \text{ or } F_{ncf} A_e$$

Equation 3.3.134

where:

- F_{cf} = design stress for the controlling flange given by *AASHTO LRFD* Eq. 6.13.6.1.4c-1 (Equation 3.3.127) (ksi)

F_{ncf}= design stress for the noncontrolling flange given by *AASHTO LRFD* Eq. 6.13.6.1.4c-3 (Equation 3.3.129) (ksi)
A_e = smaller effective area on either side of the splice (in.^{2})

and M_ℓ is to be taken as the factored flange lateral bending moment at the splice for the Strength I load combination. Note that according to *AASHTO LRFD* Article C6.13.6.1.4c, the flange lateral bending moment at the strength limit state need not be multiplied by the factor, R_{cf}, given in Equation 3.3.129 when computing the moment for the design of the splice.

Flange Splice Plates

The equations given below for splice plates subject to tension and for splice plates subject to compression considering the effect of flange lateral bending assume that the areas of the inner and outer flange splice plates do not differ by more than 10 percent. Otherwise, P and M_ℓ should be proportioned to the inner and outer splice plates by the ratio of the area(s) of the inner and outer plate(s) to the total area of the splice plates, with the splice plates than checked individually using their respective actions.

Splice Plates in Tension

Splice plates subject to tension at the strength limit state must be checked for yielding on the gross section (*AASHTO LRFD* Eq. 6.8.2.1-1), fracture on the net section (*AASHTO LRFD* Eq. 6.8.2.1-2) and block shear rupture (refer to *AASHTO LRFD* Article 6.13.4) as follows.

Lateral flange bending is ignored for the top flange splice plates at the strength limit state because the flange is continuously braced. Thus, the following checks are to be made for the top flange splice plates subject to tension:

- For yielding:

$$\frac{P}{(A_g)_{PL}} \le \phi_y F_y$$

Equation 3.3.135

- For net section fracture:

$$\frac{P}{(A_n)_{PL}} \le \phi_u F_u U$$

Equation 3.3.136

- For block shear rupture:

$$P \le R_r$$

Equation 3.3.137

where:

ϕ_y = resistance factor for yielding on the gross section in tension specified in *AASHTO LRFD* Article 6.5.4.2 (= 0.95)
ϕ_u = resistance factor for fracture on the net section in tension specified in *AASHTO LRFD* Article 6.5.4.2 (= 0.80)
$(A_g)_{PL}$ = total gross area of the inner and outer flange splice plates (in.^{2})
$(A_n)_{PL}$ = total net area of the inner and outer flange splice plates (in.^{2})
F_y = specified minimum yield strength of the flange splice plates (ksi)
F_u = tensile strength of the flange splice plates specified in *AASHTO LRFD* Table 6.4.1-1 (ksi)
U = reduction factor to account for shear lag = 1.0 for splice plates (see *AASHTO LRFD* Article 6.13.5.2)
R_r = factored block shear rupture resistance determined as specified in *AASHTO LRFD* Article 6.13.4 (Section 3.3.3.2.4) (kips)

The total net area of the splice plates, $(A_n)_{PL}$, must not be taken as greater than 85 percent of the total gross area of the plates, $(A_g)_{PL}$ when checking net section fracture (*AASHTO LRFD* Article 6.13.5.2).

Since the bottom flange is discretely braced, splice plates in tension on the bottom flange must be checked for the combined stress (i.e. including the flange lateral bending stress). Thus, the following checks are to be made for bottom flange splice plates subject to tension (with flange lateral bending considered):

- For yielding:

$$\frac{P}{(A_g)_{PL}} + \frac{M_\ell}{S_{PL}} \le \phi_y F_y$$

Equation 3.3.138

- For net section fracture:

$$\frac{P}{(A_n)_{PL}} + \frac{M_\ell}{(S_n)_{PL}} \le \phi_u F_u U$$

Equation 3.3.139

- For block shear rupture

$$\frac{P}{(A_g)_{PL}} + \frac{M_\ell}{S_{PL}} \le \frac{R_r}{(A_g)_{PL}}$$

Equation 3.3.140

where:

S_{PL} = total gross lateral section modulus of the inner and outer splice plates (in^3)

$(S_n)_{PL}$ = total net lateral section modulus of the inner and outer flange splice plates ($in.^3$)

$$= \frac{\left[(I_g)_{Outer\ PL} - \sum_{i=1}^{N_b} A_{hole} Y_i^2\right]}{c} + 2\left(\frac{\left[(I_g)_{Inner\ PL} - \sum_{i=1}^{N_b} A_{hole} Y_i^2\right]}{c}\right)$$

Equation 3.3.141

$(I_g)_{Outer\ PL}$ = gross lateral moment of inertia of the outer flange splice plate ($in.^4$)
$(I_g)_{InnerPL}$ = gross lateral moment of inertia of an inner flange splice plate ($in.^4$)
A_{hole} = area of an individual bolt hole ($in.^2$)
c = half the width of the splice plate under consideration (in.)

The distances, Y_i, for each hole in Equation 3.3.141 are shown on the schematic in Figure 3.3.65.

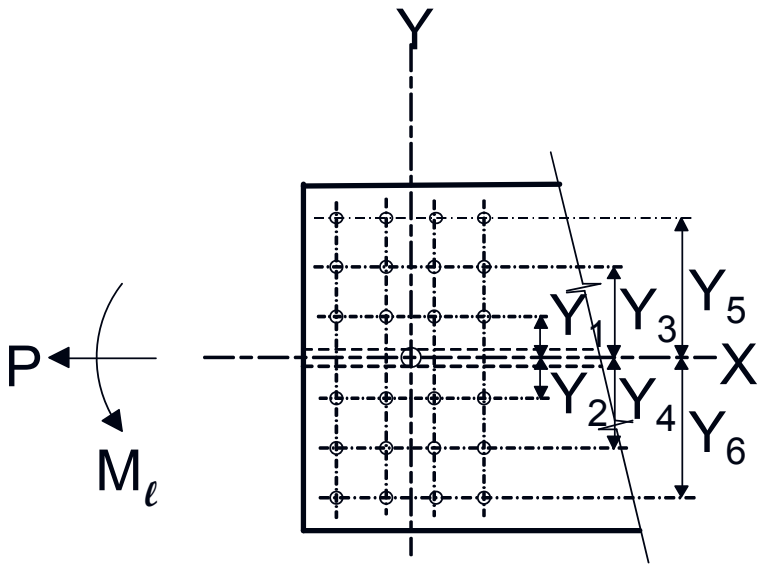


Figure 3.3.65 Distances, Y_i, in Equation 3.3.141

Splice Plates in Compression

Yielding on the gross section of flange splice plates subject to compression may be checked at the strength limit state using the following equations. Again, lateral flange bending is ignored for the top flange splice plates at the strength limit state because the flange is continuously braced. Since the bottom flange is discretely braced, the bottom flange splice plates must be checked for the combined stress. The equations assume an unbraced length of zero for the splice plates.

- For top flange splice plates:

$$\frac{P}{(A_g)_{PL}} \le \phi_c F_y$$

Equation 3.3.142

- For bottom flange splice plates:

$$\frac{P}{(A_g)_{PL}} + \frac{M_\ell}{S_{PL}} \le \phi_c F_y$$

Equation 3.3.143

where:

ϕ_c = resistance factor for compression specified in *AASHTO LRFD* Article 6.5.4.2 (= 0.90)
$(A_g)_{PL}$ = total gross area of the inner and outer flange splice plates (in.^{2})
S_{PL} = total gross lateral section modulus of the inner and outer flange splice plates (in.^{3})
F_y = specified minimum yield strength of the flange splice plates (ksi)

Flange Splice Bolts

To utilize the elastic vector method to determine the maximum resultant force in the extreme bolt under the combined actions, the polar moment of inertia, I_p, of the entire bolt group must first be computed.

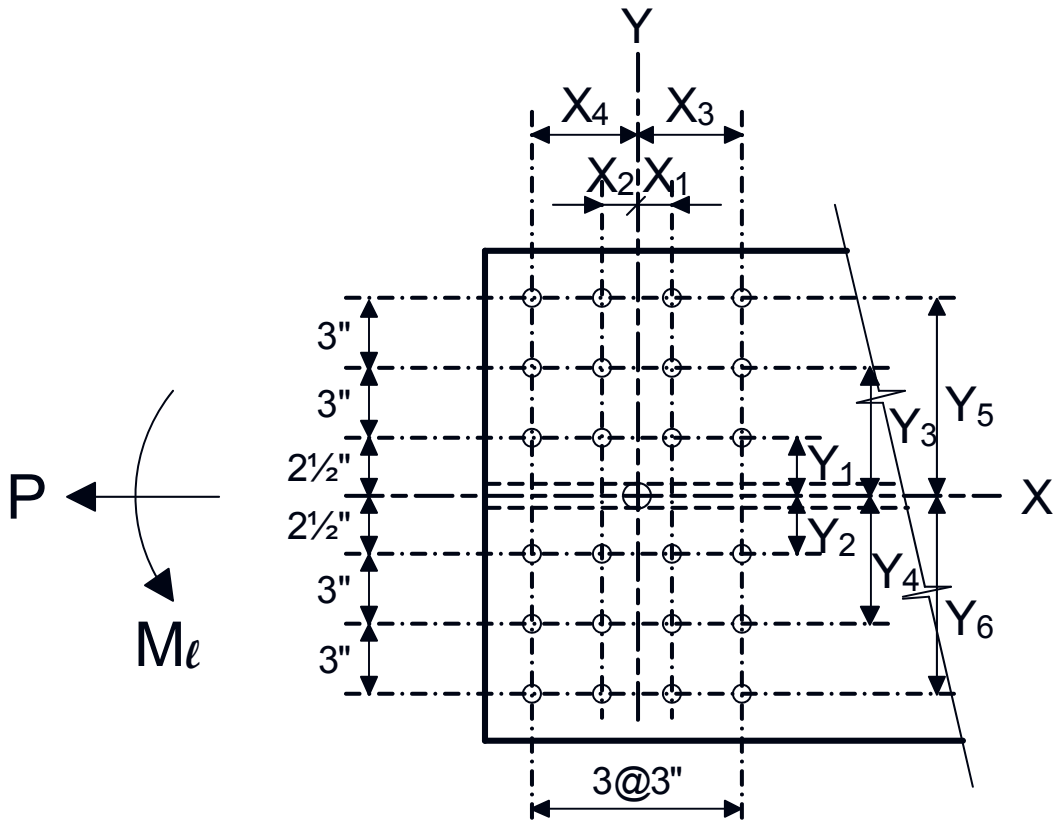


Figure 3.3.66 Sample Bottom Flange Bolt Pattern for Computation of I_p

For example, for the sample bottom-flange bolt pattern shown above in Figure 3.3.66, Ip for the bolt group can be computed using Equation 3.3.108 as follows:

$$I_p = \left[2 * 6 * \left(1.5^2 + 4.5^2\right)\right] + \left[2 * 4 * \left(2.5^2 + 5.5^2 + 8.5^2\right)\right]$$
$$= 1140 \ \text{in}^2$$

After I_p has been computed, the bolt force in the critical extreme bolt in the group due to the flange lateral moment can then be computed. The bolt force due to the moment is computed in two components, as shown below. The longitudinal component, P_{Mx}, is computed as:

$$P_{Mx} = \frac{M_\ell Y}{I_p}$$

Equation 3.3.144

Similarly, the transverse component, P_{My}, is computed as:

$$P_{My} = \frac{M_\ell X}{I_p}$$

Equation 3.3.145

X and *Y* in Equations 3.3.144 and 3.3.145 are defined below in Figure 3.3.67.

The bolt force due to shear, P_v, is taken equal to:

$$P_v = \frac{P}{N_b}$$

Equation 3.3.146

where
- P = applicable flange force (kips)
- N_b = number of bolts in the bolt group

After the bolt forces due to the lateral moment and the shear have been computed, the maximum resultant bolt force in the critical extreme bolt, P_r (Figure 3.3.67), is then computed as:

$$P_r = \sqrt{(P_v + P_{Mx})^2 + P_{My}{}^2}$$

Equation 3.3.147

P_r may then be used to check for slip of the bolts, or to check shear in the bolts and bearing at the bolt holes, as applicable.

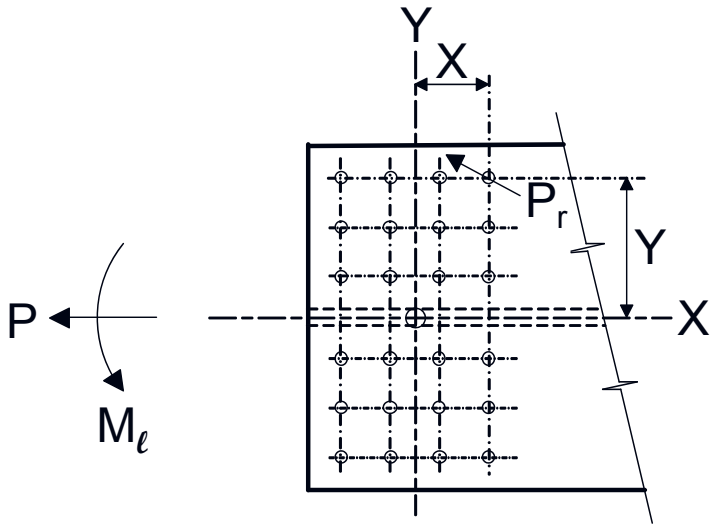


Figure 3.3.67 Resultant Bolt Force, P_r, and Distances *X* and *Y*

When checking the shear resistance of the bolts at the strength limit state, the bolts may be checked using P_r assuming double shear if the areas of the inner and outer flange splice plates do not differ by more than 10 percent. Otherwise, P_r should be proportioned to the inner and outer splice plates by the ratio of the area(s) of the inner and outer plate(s) to the total area of the splice plates. The shear resistance of the bolts would then be checked for the maximum splice plate force assuming single shear. When checking the slip resistance of the bolts at the service limit state, the resultant force, P_r, at the service limit state should always be assumed divided equally to the two slip planes regardless of the ratio of the splice plate areas.

When checking the bearing resistance of the flange at bolt holes, the resistance of the outermost hole, calculated using the clear edge or end distance as applicable, can conservatively be checked against the maximum resultant force, P_r, acting on the extreme bolt at the strength limit state. This assumes the bearing resistance of the flange controls; otherwise, P_r must be appropriately proportioned to the splice plates before making the check as discussed in Section 3.3.7.2.2.3. This check is conservative since the resultant force acts in the direction of an inclined distance that is larger than the clear edge or end distance. If the bearing resistance is exceeded, options include increasing the edge or end distance, calculating the bearing resistance based on the inclined distance, or resolving P_r in the direction parallel to the edge or end distance for making the check.

3.3.7.2.5 Special Considerations for Box-Girder Flange Splices

Special considerations related to flange lateral bending, St. Venant torsional shear and longitudinal warping stress due to cross-section distortion may apply to the design of bolted flange splices for box girders in certain cases as discussed below. Fatigue considerations related to the termination of longitudinal flange stiffeners at bolted flange splices are discussed in Section 3.2.6.4.2.2.

3.3.7.2.5.1 Flange Lateral Bending

AASHTO LRFD Article 6.13.6.1.4c specifies that where applicable, lateral flange bending must be considered in the design of bolted flange splices for discretely braced top flanges of tub sections. Top flanges of tub sections are discretely braced during construction prior to the hardening of the deck. The procedures illustrated in Section 3.3.7.2.4 may be applied in this case.

3.3.7.2.5.2 St. Venant Torsional Shear

AASHTO LRFD Article 6.13.6.1.4c specifies that for all single box sections, and for multiple box sections in bridges not satisfying the requirements of *AASHTO LRFD* Article 6.11.2.3 (including box sections in horizontally curved bridges or on skewed supports), or with box flanges that are not fully effective according to the provisions of *AASHTO LRFD* Article 6.11.1.1, St. Venant torsional shear must also be considered in the design of the bolted splices for box flanges *at all limit states*.

The factored St. Venant torsional shear in the flange can be determined by multiplying the shear flow given by *AASHTO LRFD* Equation C6.11.1.1-1 (Equation 1.1.12) by the width of the box flange. The enclosed area of the box section, A_o, should be computed as discussed in Section 3.2.6.1.2 for torques applied separately to the non-composite and composite sections.

The bolts for box-flange splices can be designed for the effects of the torsional shear using the traditional elastic vector method for eccentric shear (refer to Section 3.3.6.2.7). The direct shear on the flange bolts is caused by either the factored flange force due to the factored loads, or by the appropriate minimum flange design force, depending on the limit state under investigation. The moment on the bolt group is taken as the moment resulting from the eccentricity of the factored St. Venant torsional shear, assumed applied at the centerline of the splice. Note that according to *AASHTO LRFD* Article C6.13.6.1.4c, the flange St. Venant torsional shear at the strength limit state need not be multiplied by the factor, R_{cf}, given in Equation 3.3.129 when computing the moment for the design of the splice.

The box flange splice plates in these cases should also be designed at the strength limit state for the combined effects of the appropriate flange force and the moment resulting from the eccentricity of the factored St. Venant torsional shear.

St. Venant torsional shears are typically ignored in the design of the top flanges of tub sections once the flange is continuously braced and the section is closed, and therefore, need not be considered in the design of the splices for these flanges. The composite deck is assumed to resist the majority of the torsional shear acting on the top of tub sections once the section is closed.

3.3.7.2.5.3 Longitudinal Warping Stress

For the same box sections cited in Section 3.3.7.2.5.2, longitudinal warping stresses due to cross-section distortion (see Section 3.2.5.2.2.3) are to be considered when checking the slip resistance of the bolts for constructibility and at the service limit state, and when checking fatigue of the splices. These stresses can potentially be significant under construction and service conditions in these box sections, and therefore, should be considered in these cases when checking fatigue and when checking for slip of the bolts.

The warping stresses under these conditions can be ignored when checking the top-flange splices after the flange is continuously braced. At the strength limit state, longitudinal warping stresses due to cross-section distortion may be ignored when checking both the top and bottom flange splices, as these stresses are typically limited at the strength limit state through the provision of sufficient internal cross bracing (*AASHTO LRFD* Article C6.7.4.3).

3.3.7.3 Web Splices

3.3.7.3.1 General

The design of bolted web splices for flexural members is covered in *AASHTO LRFD* Article 6.13.6.1.4b. Filler plates for web splices are discussed in Section 3.3.7.4.3. Special considerations related to the design of bolted web splices for box girders are discussed in Section 3.3.7.3.4.

As illustrated in Figure 3.3.68, web splice plates and their connections for flexural members are to be designed in general for a design shear, the moment due to the eccentricity of the design shear at the point of splice, and the portion of the flexural moment assumed resisted by the web at the point of splice.

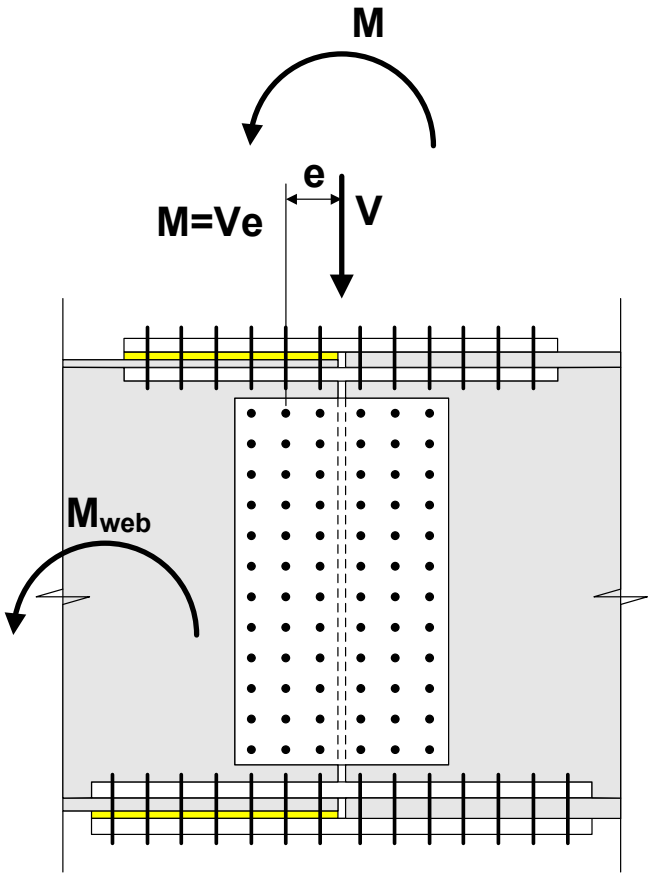


Figure 3.3.68 Design Actions for Bolted Web Splices for Flexural Members

The web moment is assumed applied at mid-depth of the web. Therefore, as discussed further in Section 3.3.7.3.2, at sections where the neutral axis is not at the mid-depth of the web, a horizontal force resultant (not shown in Figure 3.3.68) must also be applied at the mid-depth of the web in order to establish equilibrium.

Webs must be spliced symmetrically by plates on each side of the web. The splice plates must extend as near as practical for the full depth between flanges. Since the web splice is assumed to resist a portion of the flexural moment, maximizing the depth of the web splice plates also maximizes the flexural resistance of the web splice. However, it is important that the splice not impinge on bolt assembly clearances between the top/bottom row of web bolts and the adjacent flange splice bolts. Bolt assembly clearances are given in Tables 7-16 and 7-17 of Reference 33.

Fatigue considerations related to the termination of longitudinal web stiffeners are discussed in Section 3.2.4.3.2.2. If possible, longitudinal web stiffeners are best discontinued at field splice locations at the free edge of the web where the flexural stress in the web is zero, which will require splitting of the web splice plates. The issues related to this are similar to the issues related to the termination of longitudinal stiffeners on box flanges at bolted field splices discussed in Section 3.2.6.4.2.2. As for the box-flange stiffener, splicing the longitudinal web stiffener across the field splice is recommended whenever it becomes necessary to run the stiffener beyond the splice.

3.3.7.3.2 Strength Limit State

3.3.7.3.2.1 Design Shear

Bolted web splice plates and their connections for flexural members are to be proportioned at the strength limit state for a minimum design shear, V_{uw}, taken equal to the following:

- If $V_u < 0.5\phi_v V_n$, then:

$$V_{uw} = 1.5V_u$$

Equation 3.3.148
AASHTO LRFD Equation 6.13.6.1.4b-1

- Otherwise:

$$V_{uw} = \frac{(V_u + \phi_v V_n)}{2}$$

Equation 3.3.149
AASHTO LRFD Equation 6.13.6.1.4b-2

where:

ϕ_v = resistance factor for shear specified in *AASHTO LRFD* Article 6.5.4.2 (= 1.0)
V_u = factored shear at the point of splice (kips)

V_n = nominal shear resistance determined as specified in *AASHTO LRFD* Articles 6.10.9.2 and 6.10.9.3 for unstiffened and stiffened webs, respectively (Section 3.2.7.4) (kips)

Equation 3.3.148 represents an exception to the general design requirements specified in *AASHTO LRFD* Article 6.13.1 and discussed above in Section 3.3.7.1. For cases where the factored shear, V_u, is less than 50 percent of the factored shear resistance, $V_r = \phi_v V_n$, the 75 percent rule is not applied. Instead, the increase in the shear is limited to 50 percent of V_u. This is done for several reasons. First, the opportunities for the shear V_u to change from its calculated value are less than for moment; that is, large unintended shifts in the shear at the splice are unlikely. Second, the maximum shear is usually not concurrent with the maximum moment at the splice, and therefore, the use of lower value of the design shear in these regions was felt by the specification writers to be reasonable. Lastly, a lower value of the design shear is more reasonable for rolled beams. Designing web splices for rolled beams for 75 percent of their factored shear resistance is unreasonable because the factored shear resistance of a rolled beam can be up to 4 to 5 times greater than V_u.

For cases where V_u is greater than or equal to 50 percent of V_r, the average rule is retained for determining the design shear; that is, the minimum design shear is taken as the average of V_u and V_r (Equation 3.3.149).

The web with the smallest nominal shear resistance on either side of the splice should be used to compute the minimum design shear to ensure that the shear resistance of that web is not exceeded.

3.3.7.3.2.2 Moment due to Eccentricity of the Design Shear

Bolted web splices for flexural members are also to be designed at the strength limit state for a design moment, M_{uv}, due to the eccentricity of the design shear at the point of splice as follows:

$$M_{uv} = V_{uw} e$$

Equation 3.3.150

where:

e = eccentricity of the design shear at the point of splice (in.) (refer to Figure 3.3.69)

V_{uw} = design shear for the web splice determined from Equation 3.3.148 or 3.3.149, as applicable (kips)

As specified in *AASHTO LRFD* Article 6.13.6.1.4b and illustrated in Figure 3.3.69, when computing the moment due to the eccentricity of the design shear at the point of splice, the correct eccentricity to use is the horizontal distance from the centerline of the splice to the centroid of the web bolt group on the side of the joint under consideration (*72*).

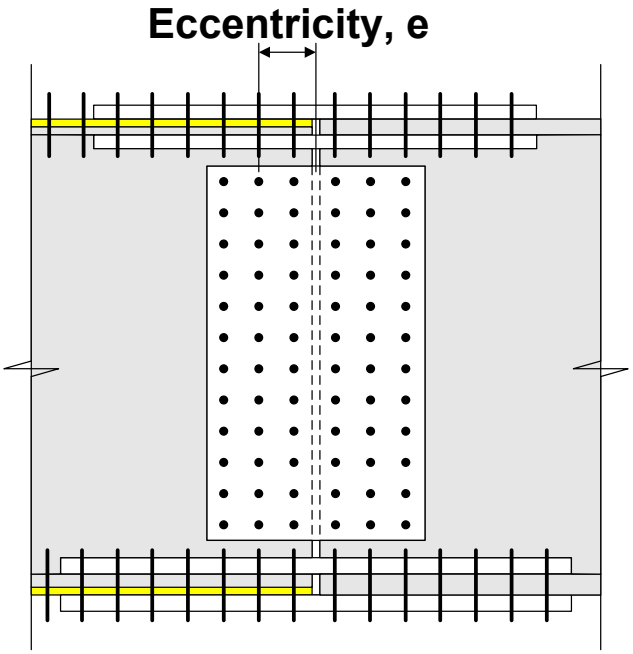


Figure 3.3.69 Eccentricity of the Design Shear for a Web Splice

3.3.7.3.2.3 Design Moment and Design Horizontal Force Resultant

The determination of the proportion of the flexural moment resisted by the web at the point of splice is not necessarily straightforward, particularly for a singly symmetric composite girder. Many different approaches have been used, which have sometimes led to significant variations in the number of web bolts provided in different designs for similar splice geometries.

To simplify the overall computations and eliminate any potential ambiguities, it is suggested in *AASHTO LRFD* Article C6.13.6.1.4b that the calculated portion of the flexural moment resisted by the web be applied at mid-depth of the web. Thus, to establish equilibrium at sections where the neutral axis is not at mid-depth of the web (e.g. in singly symmetric composite sections), a horizontal force resultant must also be applied. In such cases, the horizontal force resultant is also applied at mid-depth of the web and may be assumed applied equally to all the web bolts.

The following equations are provided in *AASHTO LRFD* Article C6.13.6.1.4b to determine a design moment, M_{uw}, and a design horizontal force resultant, H_{uw}, to be applied at mid-depth of the web:

$$M_{uw} = \frac{t_w D^2}{12}\left|R_h F_{cf} - R_{cf} f_{ncf}\right|$$

Equation 3.3.151
AASHTO LRFD Equation C6.13.6.1.4b-1

$$H_{uw} = \frac{t_w D}{2}\left(R_h F_{cf} + R_{cf} f_{ncf}\right)$$

Equation 3.3.152
AASHTO LRFD Equation C6.13.6.1.4b-2

where:

- D = web depth of the smaller section at the point of splice (in.)
- f_{ncf} = factored vertical bending stress at the midthickness of the noncontrolling flange at the point of splice concurrent with f_{cf} (see below); positive for tension, negative for compression (ksi)
- F_{cf} = design stress for the controlling flange at the point of splice determined as specified in *AASHTO LRFD* Article 6.13.6.1.4c (Equation 3.3.127); positive for tension, negative for compression (ksi)
- R_{cf} = the absolute value of the ratio of F_{cf} to the maximum factored vertical bending stress, f_{cf}, at the midthickness of the controlling flange at the point of splice
- R_h = hybrid factor determined as specified in *AASHTO LRFD* Article 6.10.1.10.1 (Section 3.2.6.3). For hybrid sections in which F_{cf} does not exceed the specified minimum yield strength of the web, R_h is taken equal to 1.0.
- t_w = web thickness of the smaller section at the point of splice (in.)

M_{uw} and H_{uw} from the preceding equations, applied together, yield a combined stress distribution equivalent to the unsymmetrical stress distribution in the web. For symmetrical sections with equal compressive and tensile stresses at the top and bottom of the web, H_{uw} will equal zero.

Note that M_{uw} and H_{uw} are conservatively computed using the flexural stresses at the midthickness of the flanges. By utilizing the stresses at the midthickness of the flanges, the same computed stresses are used for the design of the flange and web splices, which simplifies the calculations. The stresses at the inner fibers of the flanges may be used instead, if desired.

In either case, for composite sections, the factored vertical bending stresses are to be computed considering the application of the moments to the respective cross-sections supporting those loads. *Note that all stresses in Equations 3.3.151 and 3.3.152 are to be taken as signed quantities.* Since the sign of M_{uw} corresponds to the sign of the flexural moment for the loading condition under consideration, absolute value signs are applied to the resulting difference of the stresses in Equation 3.3.151 for convenience. H_{uw} from Equation 3.3.152 is taken as a signed quantity; positive for tension, negative for compression.

M_{uw} and H_{uw} are to be computed independently for both positive and negative flexure in areas of stress reversal in order to determine the governing condition. For a composite section subject to positive flexure at the strength limit state, the controlling flange is typically the bottom flange; thus, the top of the web is usually in compression and the neutral axis is usually near the top flange (Figure 3.3.70). To compute minimum design values of M_{uw} and H_{uw} for this case, the stress at the

midthickness of the controlling (bottom) flange is assumed equal to its minimum flange design stress, F_{cf} (from Equation 3.3.127), times the hybrid factor, R_h (Figure 3.3.70). The stress, f_{ncf}, at the midthickness of the noncontrolling flange (the top flange in this case), which is taken as the factored vertical bending stress concurrent with the maximum applied flexural stress, f_{cf}, at the midthickness of the controlling (bottom) flange, is assumed factored up by the ratio, R_{cf}, which is taken as the absolute value of the ratio of F_{cf} to f_{cf}.

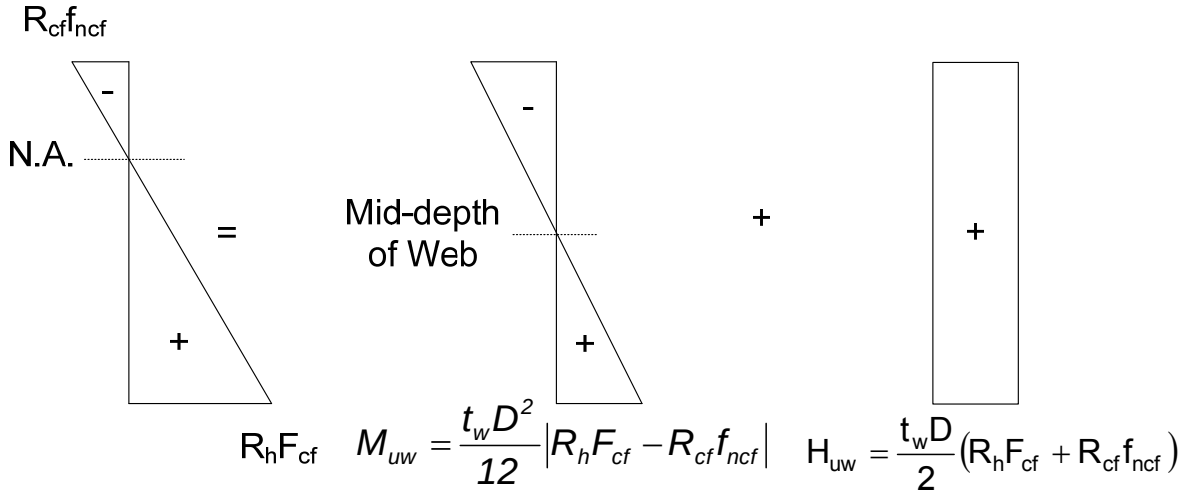
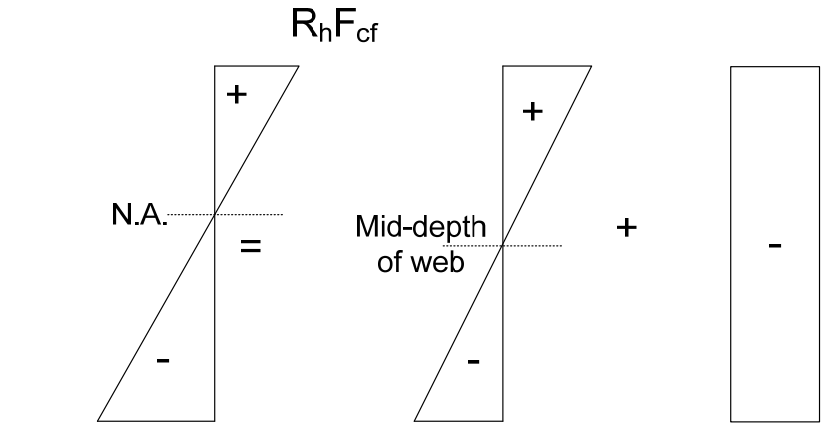


Figure 3.3.70 Assumed Flexural Stress Distribution in the Web for the Design of a Bolted Web Splice in a Composite Section Subject to Positive Flexure

Essentially, by factoring up the stress f_{ncf} by R_{cf}, the stresses in the web are being factored up in the same proportion as the flexural stress in the controlling flange so that the web splice is designed in a consistent fashion; that is, designed to also satisfy the general strength limit state design requirements specified in *AASHTO LRFD* Article 6.13.1. By integrating the resulting stress distribution over the depth of the web, Equation 3.3.151 is derived to determine the value of M_{uw} to be applied at the mid-depth of the web. H_{uw} in Equation 3.3.152 is then simply taken as the average of the factored-up stresses at the midthickness of the top and bottom flange.

For the case of negative flexure at the strength limit state, the controlling flange can either be the top or bottom flange. The top of the web is usually in tension and the neutral axis is usually at or near the mid-depth of the web (Figure 3.3.71). To compute minimum design values of M_{uw} and H_{uw} for this case, the stress at the midthickness of the controlling flange is again assumed equal to its minimum flange design stress, F_{cf} (from Equation 3.3.127), times the hybrid factor, R_h. If the top flange is assumed to be the controlling flange (Figure 3.3.71), the stress, f_{ncf}, at the midthickness of the noncontrolling flange (the bottom flange in this case) is assumed factored up by the ratio, R_{cf}, which would be taken as the absolute value

of the ratio of F_{cf} to f_{cf} for the top flange. M_{uw} and H_{uw} would again then be computed from Equations 3.3.151 and 3.3.152, respectively.



$$M_{uw} = \frac{t_w D^2}{12}\left|R_h F_{cf} - R_{cf} f_{ncf}\right| \qquad H_{uw} = \frac{t_w D}{2}\left(R_h F_{cf} + R_{cf} f_{ncf}\right)$$

Figure 3.3.71 Assumed Flexural Stress Distribution in the Web for the Design of a Bolted Web Splice in a Section Subject to Negative Flexure

For splices not in areas of stress reversal, M_{uw} and H_{uw} need only be computed for the loading condition causing the maximum flexural stress in the controlling flange at the strength limit state; that is, only a single load condition need be checked.

AASHTO LRFD Article 6.13.6.1.4b permits an alternative approach for the design of web splices *for compact web sections at the strength limit state only* (refer to Section 3.2.6.4.1.1 for the definition of a compact web section). In this approach, all the flexural moment is assumed resisted by the flange splices, provided the flanges are capable of resisting the design moment (*72*, *73*). Should the flanges not be capable of resisting the entire design moment, the web splice is assumed to resist any remaining flexural moment in addition to the design shear and the moment due to the eccentricity of the design shear. Note that when this alternate approach is used, the slip resistance of the bolts is still to be checked using conventional assumptions (i.e. that the web resists all its portion of the flexural design moment at the service limit state – see Section 3.3.7.3.3 to follow).

3.3.7.3.2.4 Web Splice Plates and Bolts

The calculated minimum design actions in the web, V_{uw}, M_{uv}, M_{uw} and H_{uw}, are to be used to check: 1) the resistance of the web splice plates; 2) the shear resistance of the high-strength bolts (Section 3.3.6.2.6.2); and 3) the bearing resistance at the bolt holes (Section 3.3.6.2.6.2) assuming the bolts have slipped and gone into bearing at the strength limit state.

Web Splice Plates

AASHTO LRFD Article 6.13.6.1.4b specifies that at the strength limit state, the combined stress in the web splice plates due to M_{uv}, M_{uw} and H_{uw} must not exceed the specified minimum yield strength of the splice plates times the resistance factor, ϕ_f, as follows:

$$f = \frac{M_{uv} + M_{uw}}{S_{PL}} + \frac{H_{uw}}{A_g} \le \phi_f F_y$$

Equation 3.3.153

where:

A_g = gross area of the web splice plates (in.^{2})
F_y = specified minimum yield strength of the web splice plates (ksi)
H_{uw}= design horizontal force resultant (Equation 3.3.152) (kips)
M_{uv}= design moment due to the eccentricity of the design shear at the point of splice (Equation 3.3.150) (kip-in.)
M_{uw}= design moment (Equation 3.3.151) (kip-in.)
S_{PL}= section modulus of the web splice plates based on the gross section (in.^{3})

In addition, the design shear, V_{uw}, must not exceed the lesser of the block shear rupture resistance specified in *AASHTO LRFD* Article 6.13.4 (refer to Section 3.3.3.2.4) or the factored shear resistance of the splice plates specified in *AASHTO LRFD* Article 6.13.5.3 (refer to Section 3.3.6.2.6.2). Note that because of the overall length of the connection, the block shear rupture resistance normally does not control for web splice plates of typical proportion.

Web Splice Bolts

The shear resistance of the web splice bolts and the bearing resistance of the web splice bolt holes is to be calculated according to the procedures discussed in Section 3.3.6.2.6.2. Note that slip of the flange splice bolts is to be checked at the service limit state using lower minimum design actions as discussed below in Section 3.3.7.3.3.

In calculating the shear resistance of the web splice bolts, the greater than 50.0 in. length reduction does *not* apply when the distribution of shear force is essentially uniform along the joint, such as in a bolted web splice (*41*).

The traditional elastic vector method is recommended for calculating the maximum resultant bolt force since the web splice bolts are subject to eccentric shear (refer to Section 3.3.6.2.7). In applying this method to the web bolts, all actions are to be applied at the mid-depth of the web and the polar moment of inertia of the bolt group, I_p, should be computed about the centroid of the connection (Equation 3.3.109 may be used when the vertical pitch of the bolts is uniform). Shifting I_p to

the neutral axis of the composite section (which is typically not at the mid-depth of the web) may cause the bolt forces to be underestimated unless the location of the neutral axis is determined from the summation of the stresses due to the appropriate loadings acting on the respective cross-sections supporting those loadings.

The design horizontal force resultant, H_{uw} (when applicable), may be assumed applied equally as a horizontal shear force to all the web bolts. In determining the maximum resultant bolt force R in the outermost bolt, the horizontal shear force in bolt due to H_{uw} would be appropriately combined with the horizontal component of the bolt shear due to torsion, R_x, in Equation 3.3.113.

The number of bolts in the web splice can potentially be decreased significantly by spacing a group of bolts closer to the mid-depth of the web (where the flexural stress is relatively low) at the maximum spacing specified for sealing (AASHTO LRFD Article 6.13.2.6.2 – Section 3.3.6.2.2.6), and by spacing the remaining two groups of bolts near the top and bottom of the web at a closer spacing.

There are several options for checking the bearing resistance of the web at bolt holes. The resistance of an outermost hole, calculated using the clear edge distance, can conservatively be checked against the maximum resultant bolt force acting on the extreme bolt in the connection (Figure 3.3.72 Part A). Since the resultant force acts in the direction of an inclined distance that is larger than the clear edge distance, the check is conservative.

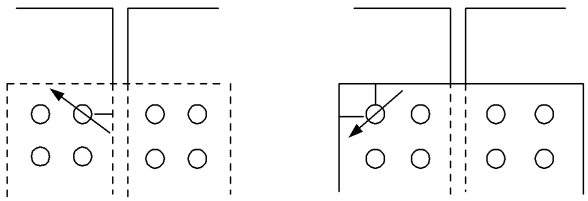


Figure 3.3.72 Critical Locations for Checking Bearing Resistance of Outermost Web Splice Bolt Holes

Alternatively, the bearing resistance can be calculated based on the inclined distance, or else the resultant bolt force can be resolved in the direction parallel to the edge distance. Regardless of which approach is used, should the bearing resistance be exceeded, it is strongly recommended that the edge distance be increased slightly in lieu of increasing the number of bolts or thickening the web, as this is clearly the simplest and most economical solution.

In unusual cases where the bearing resistance of the web splice plate controls (i.e. where the sum of the web splice-plate thicknesses is less than the thickness of the thinner web at the splice), the smaller of the clear edge or end distance on the

splice plates should be used to compute the bearing resistance of the outermost hole (Figure 3.3.72 Part B).

3.3.7.3.3 Service Limit State

The slip resistance of the web splice bolts (Section 3.3.6.2.6.1) at the service limit state is to be checked under the Service II load combination. The slip resistance of the bolts should also be checked during the deck casting.

The design shear for the service limit state, V_s, is to be taken as the shear at the point of splice under Load Combination Service II or the factored shear due to the deck-casting sequence (whichever controls).

The design moment, M_{sv}, at the service limit state due to the eccentricity of the design shear at the point of splice is to be taken as follows:

$$M_{sv} = V_s e$$

Equation 3.3.154

where:

e = eccentricity of the design shear at the point of splice (in.) (refer to Figure 3.3.69)

V_s = design shear for the web splice taken as the shear due to Load Combination Service II or the factored shear due to the deck-casting sequence (whichever controls) at the point of splice (kips)

According to *AASHTO LRFD* Article C6.13.6.1.4b, for checking slip of the web-splice bolts at the service limit state, the portion of the flexural moment resisted by the web (i.e. the design moment M_{sw}) and the design horizontal force resultant, H_{sw}, may be computed as follows:

$$M_{sw} = \frac{t_w D^2}{12}\left|f_s - f_{os}\right|$$

Equation 3.3.155

$$H_{sw} = \frac{t_w D}{12}\left(f_s + f_{os}\right)$$

Equation 3.3.156

where:

D = web depth (in.)

f_s = maximum vertical bending stress due to Load Combination Service II or maximum factored vertical bending stress due to the deck-casting sequence (whichever controls) at the midthickness of the flange under consideration for the smaller section at the point of splice; positive for tension, negative for compression (ksi)

f_{os} = vertical bending stress due to Load Combination Service II or factored vertical bending stress due to the deck-casting sequence (whichever controls) at the midthickness of the other flange at the point of splice concurrent with f_s in the flange under consideration; positive for tension, negative for compression (ksi)

t_w = web thickness (in.)

M_{sw} and H_{sw} are signed quantities in a similar fashion to M_{uw} and H_{uw} at the strength limit state. It is not necessary to determine the controlling and noncontrolling flange when checking for slip; hence the terms F_{cf} and R_{cf} do not appear in Equations 3.3.155 and 3.3.156.

As for the strength limit state, in areas of stress reversal, M_{sw} and H_{sw} must be computed independently for both positive and negative flexure to determine the governing condition. If the splice is not located in an area of stress reversal, M_{sw} and H_{sw} need only be computed for the loading condition causing the maximum vertical bending stress in the flange under consideration.

The maximum resultant bolt force for checking the slip resistance of the web splice bolts should be determined using the traditional elastic vector method for eccentric shear, in a fashion similar to that described above for the strength limit state in Section 3.3.7.3.2.4.

A check of the combined stress due to M_{sv}, M_{sw} and H_{sw} in the web splice plates under the Service II load combination to control permanent deformations in the plates is not currently required. However, such a check is recommended for the unusual case where the combined area of the web splice plates is less than the area of the smaller web at the splice. In this check, the maximum combined stress on the gross section of the web splice plates should not exceed $0.95F_y$, where F_y is the specified minimum yield strength of the splice plates.

3.3.7.3.4 Special Considerations for Box-Girder Web Splices

Special considerations related to St. Venant torsional shear may apply to the design of bolted web splices for box girders in certain cases as discussed below.

AASHTO LRFD Article 6.13.6.1.4b specifies that for all single box sections, and for multiple box sections in bridges not satisfying the requirements of *AASHTO LRFD* Article 6.11.2.3 (including box sections in horizontally curved bridges or on skewed supports), or with box flanges that are not fully effective according to the provisions of *AASHTO LRFD* Article 6.11.1.1, the shear due to the factored loads is to be taken as the sum of the flexural and St. Venant torsional shears *in the web subjected to additive shears* in the design of bolted web splices *at all limit states*.

Also, for boxes with inclined webs, the web splice is to be designed at all limit states for the component of the vertical shear in the plane of the web by dividing the design shear by the cosine of the angle of inclination of the web plate to the vertical.

3.3.7.4 Filler Plates

3.3.7.4.1 General

The design of filler plates is covered in *AASHTO LRFD* Article 6.13.6.1.5. Filler plates are typically used on bolted flange splices of flexural members (and sometimes on web splices) when the thicknesses of the adjoining plates at the point of splice are different (Figure 3.3.73). At bolted flange splices, it is often advantageous to transition one or more of the flange thicknesses down adjacent to the point of splice, if possible, so as to reduce the required size of the filler plate, or possibly change the width of the flanges and keep the thickness constant in order to eliminate the need for a filler plate altogether.

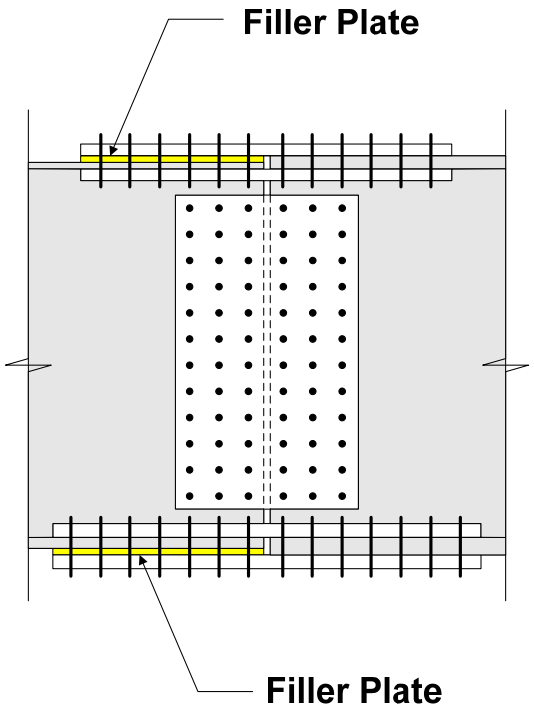


Figure 3.3.73 Filler Plates in Bolted Flange Splices

3.3.7.4.2 Filler Plates for Flange Splices

Fillers in axially loaded connections at the strength limit state must be secured by additional bolts to ensure that the fillers are an integral part of the connection; that is, to ensure that the shear planes are well-defined and that no reduction in the factored shear resistance of the bolts results.

AASHTO LRFD Article 6.13.6.1.5 provides two choices for developing fillers 0.25 in. or more in thickness in axially loaded bolted connections, which include girder

flange splices. The choices are to either: 1) extend the fillers beyond the gusset or splice plate with the filler extension secured by enough additional bolts to distribute the total stress uniformly over the combined section of the member or filler; or 2) in lieu of extending and developing the fillers, reduce the factored shear resistance of the bolts (Section 3.3.6.2.6.2) by the following factor:

$$R = \left[\frac{(1+\gamma)}{(1+2\gamma)} \right]$$

Equation 3.3.157
AASHTO LRFD Equation 6.13.6.1.5-1

where:

γ = A_f/A_p
A_f = sum of the area of the fillers on the top and bottom of the connected plate (in.^{2})
A_p = smaller of either the connected plate area or the sum of the splice plate areas on the top and bottom of the connected plate (in.^{2})

Equation 3.3.157 was developed mathematically (*74*) and compared to the results from an experimental program on axially loaded bolted splice connections with undeveloped fillers (*75*). The reduction factor, *R*, accounts for the reduction in the nominal shear resistance of the bolts due to bending in the bolts and will likely result in having to provide additional bolts in the connection to develop the filler(s). *Note that the reduction factor is only to be applied on the side of the connections with the filler(s)*. For practical reasons, consideration should be given to using the same number of bolts on either side of the splice. Unlike the empirical reduction factor given in Reference 4, Equation 3.3.157 will typically be less than 1.0 for connections utilizing 0.25-in.-thick fillers in order to limit the deformation of the connection. Note that fillers 0.25-in. or more in thickness are not to consist of more than two plates, unless approved by the Design Engineer.

AASHTO LRFD Article 6.13.6.1.5 also requires that the specified minimum yield strength of fillers 0.25 in. or more in thickness not be less than the larger of 70 percent of the specified minimum yield strength of the connected plate and 36.0 ksi. To provide fully developed fillers that act integrally with the connected plate, the specified minimum yield strength of the fillers should theoretically be greater than or equal to the specified minimum yield strength of the connected plates times the factor [1/(1+γ)], where γ is taken as defined above. However, this may not be practical or convenient in some cases due to thinner filler-plate material availability issues. Therefore, in some cases at the strength limit state, premature yielding of the fillers, bolt bending and increased deformation of the connection may occur. To control the potential for excessive deformation of the connection, the lower limit on the specified minimum yield strength of the fillers (given above) is specified. Although in some cases there may be an increased probability of larger deformations in the connection at the strength limit state, the connection bolts will still have adequate reserve shear resistance as long as the fillers are appropriately extended and developed, or in lieu of extending the fillers, additional bolts are added according to Equation 3.3.157. According to *AASHTO LRFD* Article

C6.13.6.1.5, the effects of yielding of the fillers and connection deformation are not considered to be significant for connections with fillers less than 0.25 in. in thickness. Note that for connections involving the use of weathering steels, a weathering grade product should be specified for the filler-plate material.

The resistance to slip between the filler and either connected part at the service limit state is comparable to the slip resistance that would exist between the connected parts if the filler were not present. Therefore, as specified in *AASHTO LRFD* Article 6.13.6.1.5, for slip-critical connections, the factored slip resistance of the bolts (Section 3.3.6.2.6.1) is *not* to be adjusted for the effect of the fillers.

3.3.7.4.3 Filler Plates for Web Splices

AASHTO LRFD Article 6.13.6.1.5 permits the omission of filler plates in bolted web splices where the thicknesses of the adjoining web plates differ by 0.0625 in. (1/16 in.) or less.

3.3.8 Web Stiffeners

Web stiffener design for I-girders is covered in *AASHTO LRFD* Articles 6.10.11 and for box girders in *AASHTO LRFD* Article 6.11.11.1. The design of transverse stiffeners, bearing stiffeners and longitudinal stiffeners will be discussed in each of the following sections.

3.3.8.1 Transverse Web Stiffeners

3.3.8.1.1 General

The design of transverse web stiffeners for I-girders is covered in *AASHTO LRFD* Article 6.10.11.1. For box girders, *AASHTO LRFD* Article 6.11.11.1 refers to the I-girder provisions of *AASHTO LRFD* Article 6.10.11.1 for the design of transverse web stiffeners.

Transverse stiffeners are used to increase the shear resistance of a girder and are aligned vertically on vertical webs or along the slope of inclined webs. Transverse stiffeners consist of plates or angles welded or bolted to either one or both sides of the web (Figure 3.3.74). The term connection plate is given to a transverse stiffener to which a cross-frame or diaphragm is connected. A connection plate can serve as a transverse stiffener for shear design calculations.



Figure 3.3.74 Transverse Web Stiffeners on an I-Girder

AASHTO LRFD Article 6.10.11.1.1 specifies that transverse web stiffeners used as connection plates must be attached to both flanges. According to *AASHTO LRFD* Article 6.6.1.3.1, attachment of the connection plate to the flanges must be made by welding or bolting. The connection to the compression flange is typically welded. The connection to the tension flange is either welded or bolted through a tab plate that has been welded to the connection plate. Design Engineers have specified the use of bolted tab plates to raise the nominal fatigue resistance of the flange base metal at the attachment detail from Category C′ to Category B. This should only be considered at connection plates where fatigue is a significant issue. The bolted tab plate is significantly more expensive to furnish and install than a welded connection. Also, the fatigue category of the base metal at the termination of the weld attaching the connection plate to the web is of the same fatigue category as the base metal at the weld to the tension flange (i.e. Category C′). In most cases, the live load stress range at these two adjacent locations is not significantly different. Therefore, an adjustment of the location of a problem connection plate to eliminate the need for a bolted tab connection should be considered.

Stiffeners in straight girders not used as connection plates are to be tight fit or attached at the compression flange, but need not be in bearing with the tension flange. Generally, attachment of such stiffeners to the compression flange is accomplished by welding. Also, these stiffeners are generally either tight fit or cut short of the tension flange. A tight fit can help straighten the flange tilt without the application of heat (*67*).

According to *AASHTO LRFD* Article 6.10.11.1.1, single-sided stiffeners on horizontally curved girders should be attached to both flanges to help retain the cross-sectional shape of the girder when subjected to torsion and to avoid high localized bending within the web, particularly near the top flange due to the torsional restraint of the concrete deck. For the same reason, it is required that

pairs of transverse stiffeners on horizontally curved girders be tight fit or attached to both flanges. Similar consideration should be given to stiffeners on straight girders resting on skewed supports since they are also subjected to significant torsion.

Special considerations related to the attachment of transverse stiffeners and connection plates to tub-girder flanges are discussed in Section 3.1.2.8.5.2.

As discussed Section 3.2.5.2.2.1 (Figure 3.2.21), the distance between the end of the web-to-stiffener weld and the near edge of the adjacent web-to-flange or longitudinal stiffener-to-web weld is not to be less than $4t_w$ or more than the lesser of $6t_w$ and 4.0 in.

Reference 67 recommends that stiffeners and connection plates be detailed to be normal to the girder flanges unless unusual conditions require them to be detailed otherwise. Also, a minimum spacing of 8 inches or 1-1/2 times the stiffener plate width should be provided between stiffeners or connection plates for welding access.

3.3.8.1.2 Proportioning Requirements for Transverse Web Stiffeners

AASHTO LRFD Article 6.10.11.1.2 specifies that the width, b_t, of each projecting transverse stiffener element (Figure 3.3.75) satisfy the following requirements:

$$b_t \geq 2.0 + \frac{D}{30}$$

Equation 3.3.158
AASHTO LRFD Equation 6.10.11.1.2-1

and:

$$16t_p \geq b_t \geq b_f/4$$

Equation 3.3.159
AASHTO LRFD Equation 6.10.11.1.2-2

where:

b_f = for I-sections, full width of the widest compression flange within the field section under consideration; for tub sections, full width of the widest top flange within the field section under consideration; for closed box sections, the limit of $b_f/4$ does not apply (in.)

t_p = thickness of the projecting stiffener element (in.)

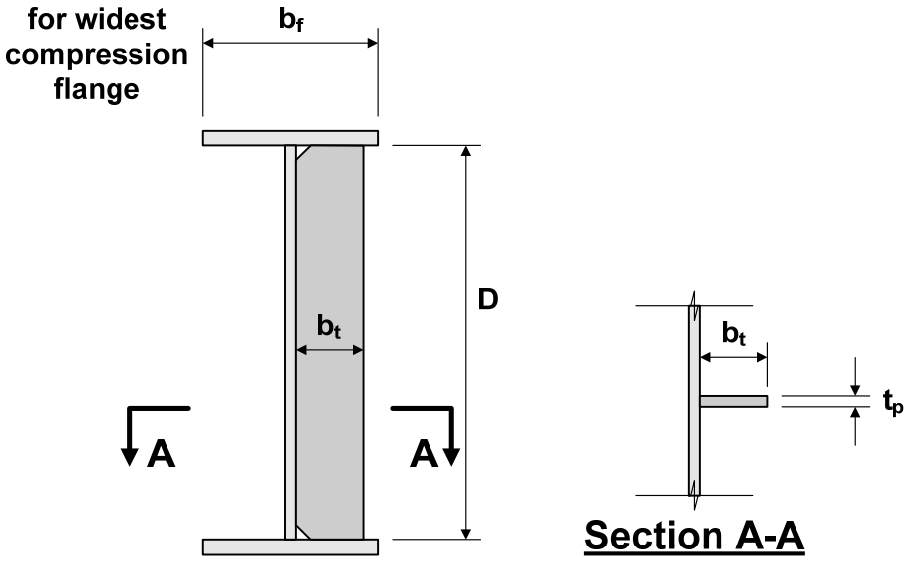


Figure 3.3.75 Projecting Width of Transverse Stiffeners

Equation 3.3.158 (*76*) tends to control relative to Equation 3.3.159 for I-girders with large ratios of D/b_f.

In Equation 3.3.159, the full width of the widest compression flange within the field section under consideration is used for b_f to allow for the use of the same minimum stiffener width throughout the entire field section, if desired, and to help restrain the widest compression flange. Since the bottom flange of tub sections is restrained by a web along both edges, the widest top flange is used for b_f in Equation 3.3.159. Since the web restrains the edges of both flanges of a closed box section, the limit of $b_f/4$ does not apply.

Welded stiffeners and connection plates are commonly made up of less expensive flat bar stock. Flat bars are generally produced in whole-inch width increments and 1/8-in. thickness increments. A ½-inch minimum thickness for stiffeners and connection plates is preferred (*67*).

3.3.8.1.3 Moment of Inertia Requirements for Transverse Web Stiffeners

The transverse stiffener must have sufficient rigidity to maintain a vertical line of near zero lateral deflection of the web along the line of the stiffener in order for the web to adequately develop the shear-buckling resistance, or the combined shear-buckling and postbuckling tension-field resistance. Therefore, the bending rigidity (or moment of inertia) is the dominant parameter governing the performance of transverse stiffeners.

AASHTO LRFD Article 6.10.11.1.3 specifies that for transverse stiffeners adjacent to web panels in which neither panel supports a factored shear force, V_u, larger than the factored shear-buckling resistance (i.e. $V_r = \phi_v V_{cr}$), the moment of inertia of the transverse stiffener, I_t, must satisfy the *smaller* of the following:

$$I_t \geq I_{t1}$$

Equation 3.3.160
AASHTO LRFD Equation 6.10.11.1.3-1

and:

$$I_t \geq I_{t2}$$

Equation 3.3.161
AASHTO LRFD Equation 6.10.11.1.3-2

where:

ϕ_v = resistance factor for shear specified in *AASHTO LRFD* Article 6.5.4.2 (= 1.0)

b = the smaller of d_o and D (in.)

d_o = the smaller of the adjacent panel widths (in.)

I_t = moment of inertia of the transverse stiffener taken about the edge in contact with the web for single stiffeners and about the mid-thickness of the web for stiffener pairs (in.^{4})

I_{t1} = $bt_w^3 J$

Equation 3.3.162
AASHTO LRFD Equation 6.10.11.1.3-3

$$I_{t2} = \frac{D^4 \rho_t^{1.3}}{40}\left(\frac{F_{yw}}{E}\right)^{1.5}$$

Equation 3.3.163
AASHTO LRFD Equation 6.10.11.1.3-4

J = stiffener bending rigidity parameter taken as:

$$= \frac{2.5}{(d_o/D)^2} - 2.0 \geq 0.5$$

Equation 3.3.164
AASHTO LRFD Equation 6.10.11.1.3-5

ρ_t = the larger of F_{yw}/F_{crs} and 1.0

F_{crs} = local buckling stress for the stiffener (ksi) taken as:

$$= \frac{0.31E}{\left(\frac{b_t}{t_p}\right)^2} \leq F_{ys}$$

Equation 3.3.165
AASHTO LRFD Equation 6.10.11.1.3-6

F_{ys} = specified minimum yield strength of the stiffener (ksi)
V_{cr} = smallest nominal shear-buckling resistance of the adjacent web panels (Section 3.2.7.2) (kips)
= CV_p

Equation 3.3.166
AASHTO LRFD Equation 6.10.11.1.3-7

C = ratio of the shear-buckling resistance to the shear yield strength determined from *AASHTO LRFD* Equation 6.10.9.3.2-4, 6.10.9.3.2-5, or 6.10.9.3.2-6 as applicable. For web panels considered unstiffened, the shear buckling coefficient, k, is taken equal to 5.0.
V_p = plastic shear force (kips)
= $0.58F_{yw}Dt_w$

Equation 3.3.167
AASHTO LRFD Equation 6.10.11.1.3-8

V_u = largest of the factored shears in the adjacent web panels (kips)

For transverse stiffeners adjacent to web panels in which the factored shear, V_u, is larger than the factored shear buckling resistance $\phi_v V_{cr}$, and thus the web postbuckling or tension-field resistance is required in one or both panels, the moment of inertia, I_t, of the transverse stiffeners must satisfy the following:

- If $I_{t2} > I_{t1}$, then:

$$I_t \geq I_{t1} + (I_{t2} - I_{t1})\left(\frac{V_u - \phi_v V_{cr}}{\phi_v V_n - \phi_v V_{cr}}\right)$$

Equation 3.3.168
AASHTO LRFD Equation 6.10.11.1.3-9

- Otherwise:

$$I_t \geq I_{t2}$$

Equation 3.3.169
AASHTO LRFD Equation 6.10.11.1.3-10

where:

V_n = smaller of the nominal combined buckling and tension-field shear resistances of the adjacent web panels determined as specified in *AASHTO LRFD* Article 6.10.9.3.2 (Section 3.2.7.3) (kips)

For single-sided stiffeners, a significant portion of the web is implicitly assumed to contribute to the bending rigidity so that the neutral axis of the stiffener is assumed located close to the edge in contact with the web. Therefore, for this case, the moment of inertia is taken about this edge and the contribution of the web to the moment of inertia about the neutral axis is neglected for simplicity.

The smaller moment of inertia from Equation 3.3.160 or 3.3.161 is considered sufficient to develop the shear-buckling resistance of the web, $V_{cr} = CV_p$ *(77)* when a larger shear resistance is not required in either panel adjacent to the stiffener.

For members with $D/t_w = 1.12\sqrt{Ek/F_{yw}}$, which is the D/t_w value at which C is equal to 1.0 and V_{cr} is equal to the plastic shear force, V_p (Equation 3.3.167), Equations 3.3.160 and 3.3.161 give approximately the same value of the I_t required to develop V_{cr}. For members with $D/t_w > 1.12\sqrt{Ek/F_{yw}}$, Equation 3.3.160 gives the smaller value of the I_t to develop the elastic or inelastic value of the shear-buckling resistance V_{cr}, and for members with $D/t_w < 1.12\sqrt{Ek/F_{yw}}$, Equation 3.3.161 gives the smaller value of the I_t required to develop $V_{cr} = V_p$. For the latter case, Equation 3.3.160 requires excessively large stiffener sizes since this equation is based on developing the elastic shear-buckling resistance of the web. Reference 78 gives inelastic buckling solutions, which show that such large stiffeners are not required as D/t_w is reduced below the limit of $1.12\sqrt{Ek/F_{yw}}$. Research based on refined finite-element studies has also confirmed this fact (*77*).

Much larger values of I_t are required to develop the shear-buckling resistance for ratios of (d_o/D) less than or equal to 1.0, (*78*), which is represented by Equation 3.3.160. For ratios of (d_o/D) greater than 1.0, the term, b, in Equation 3.3.160, along with Equation 3.3.164, provide a reasonably constant value of the required I_t to develop the shear-buckling resistance.

The stiffener must generally have a larger I_t than defined by Equation 3.3.160 to develop the web postbuckling or tension-field resistance in one or both panels adjacent to the stiffener (*77*). Equation 3.3.161 provides the larger required I_t necessary in such cases to maintain a line of near zero lateral deflection within the postbuckled web at the stiffener location. Equation 3.3.161 provides an accurate to slightly conservative required stiffener size relative to refined finite-element solutions for straight and horizontally curved I-girders at all values of D/t_w permitted by the *AASHTO LRFD* Specifications (*77*). Although the required stiffener rigidity is insensitive to the parameter (d_o/D) according to Equation 3.3.161, the equation provides an approximate upper bound to the results from a comparable equation proposed in Reference 77 for all values of (d_o/D). The term ρ_t in Equation 3.3.161 accounts for the effect of potential local buckling of stiffeners having a relatively large width-to-thickness ratio, b_t/t_p, and also for the effect of potential early yielding in stiffeners with F_{ys} less than or equal to F_{yw}.

Equation 3.3.161 is intended to provide a required I_t that will allow the development of a factored shear resistance at or near the postbuckling tension-field shear resistance, $\phi_v V_n$, in the adjacent web panel(s). However, in cases where V_u is smaller than $\phi_v V_n$, this value of I_t is not required. Equation 3.3.168 accounts for the fact that the I_t necessary to develop a factored shear resistance greater than or equal to V_u is smaller when V_u is smaller than the full factored combined web shear buckling and postbuckling resistance, $\phi_v V_n$ (*77*). Equation 3.3.168 allows for the calculation of a conservative but more economical stiffener size for large girder depths that is sufficient to develop a girder shear resistance greater than or equal

to V_u. Equation 3.3.169 addresses a small number of cases with stocky webs where V_n is approximately equal to the plastic shear force, V_p.

Previous Specifications included an area requirement for transverse stiffeners adjacent to panels subject to postbuckling tension-field action, which has since been removed. Multiple experimental and refined finite-element based research studies have shown that transverse stiffeners are loaded primarily in lateral bending by the postbuckled web panels, and not by axial forces associated with postbuckling tension-field action, even for web panels with D/t_w up to 300. Therefore, the stiffener moment of inertia has a much stronger correlation with the stiffener performance than the stiffener area. In addition, the research described in Reference 77 indicated that panels designed for shear postbuckling resistance using one-sided stiffeners and two-sided stiffeners based on the traditional area requirement had significantly different values of shear resistance. In fact, in some cases (primarily cases with two-sided stiffeners as D/t_w increased beyond $1.12\sqrt{Ek/F_{yw}}$), the area requirement provided a stiffener size that was insufficient to hold the postbuckled web in position at the stiffener location. Equation 3.3.161 recognizes the fact that one- and two-sided stiffeners, sized such that they have the same value of I_t, provide essentially the same shear resistance for a given stiffener spacing (*77*, *79-82*).

Transverse stiffeners used in panels with longitudinal web stiffeners must also satisfy the following relationship:

$$I_t \geq \left(\frac{b_t}{b_\ell}\right)\left(\frac{D}{3d_o}\right)I_\ell$$

Equation 3.3.170
AASHTO LRFD Equation 6.10.11.1.3-11

where:

b_ℓ = projecting width of the longitudinal stiffener (in.)
b_t = projecting width of the transverse stiffener (in.)
I_ℓ = moment of inertia of the longitudinal stiffener determined as specified in *AASHTO LRFD* Article 6.10.11.3.3 (Section 3.3.8.3) (in.^{4})

Lateral loads along the length of a longitudinal stiffener are transferred to the adjacent transverse stiffeners as concentrated reactions at the stiffener intersections (*83*). Equation 3.3.170 provides a relationship between the moments of inertia of the transverse and longitudinal stiffeners to ensure that the transverse stiffeners do not fail under these concentrated reactions. The relationship applies whether the stiffeners are on the same or opposite side of the web.

3.3.8.2 Bearing Stiffeners

3.3.8.2.1 General

The design of bearing stiffeners for I- and box girders is covered in *AASHTO LRFD* Article 6.10.11.2. *AASHTO LRFD* Article 6.11.1.1 contains a special provision related to bearing stiffeners for box girders (discussed below).

Bearing stiffeners, which are aligned vertically on the web (or preferably on diaphragms in the case of box girders with inclined webs), are designed as columns to resist the reactions at bearing locations and at other locations subjected to concentrated loads where the loads are not transmitted through a deck or deck system (Figure 3.3.76).

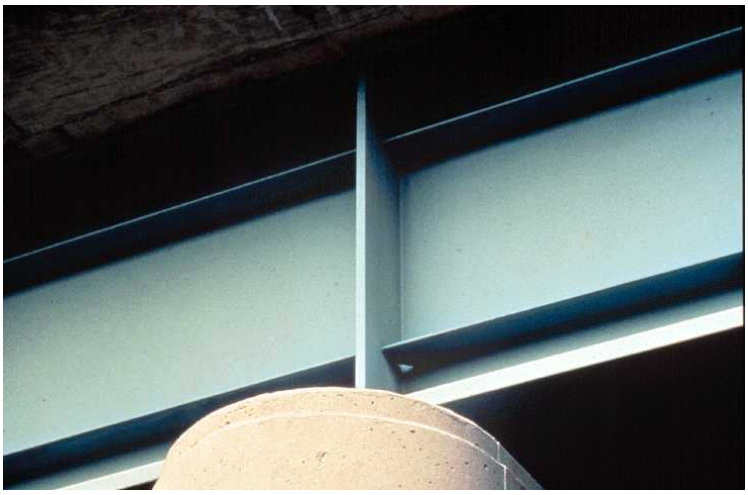


Figure 3.3.76 Bearing Stiffener on I-Girder Web

AASHTO LRFD Article 6.10.11.2.1 specifies that bearing stiffeners be placed on the webs of built-up sections at all bearing locations. At bearing locations on rolled shapes and at other locations on built-up sections or rolled shapes subjected to concentrated loads, where the loads are not transmitted through a deck or deck system, either bearing stiffeners must be provided or else the web must satisfy the provisions of *AASHTO LRFD* Article D6.5 (Appendix D6). Webs without bearing stiffeners at those locations are to be investigated for the limit states of web local yielding and web crippling according to the provisions of *AASHTO LRFD* Article D6.5 (Section 3.3.8.2.5). The section must either be modified to comply with these requirements, or else bearing stiffeners must be placed on the web at the locations under consideration. The Design Engineer should be especially aware of these provisions when concentrated loads (not transmitted through a deck or deck system) are applied during a temporary construction situation; e.g., when girders are incrementally launched over supports.

Bearing stiffeners must consist of one or more plates or angles welded or bolted to both sides of the web, with the connections to the web designed to transmit the full factored bearing force. The stiffeners must extend the full depth of the web and as closely as practical to the outer edges of the flanges.

AASHTO LRFD Article 6.11.11.1 specifies that when inclined webs are used on box sections, the bearing stiffeners should be attached to either an internal or external diaphragm rather than to the webs so that the bearing stiffeners are perpendicular to the sole plate. In such cases, at expansion bearings, thermal movements of the bridge may cause the diaphragm to be eccentric with respect to the bearings. The effect of this eccentricity on the design of the bearing stiffeners and diaphragms should be recognized. Eccentricity effects can be recognized by designing the bearing stiffener assembly as a beam-column according to the provisions of *AASHTO LRFD* Articles 6.10.11.2 and 6.9.2.2. For bearing stiffeners attached to diaphragms, the requirements regarding the effective column section of the bearing stiffeners discussed in Section 3.3.8.2.4.1 are to be applied to the diaphragm rather than to the web (*AASHTO LRFD* Article 6.11.1.1).

Connection of the bearing stiffener to the flange through which it receives its load can either be made by finish-to-bear plus a fillet weld on each side of the stiffener plate (note that fillet welds are not necessary if a cross-frame/diaphragm is not connected to the stiffener plate), or by a full penetration groove weld. Finish-to-bear means allowing the fabricator the option of grinding or milling. *It is recommended that the finish-to-bear option (with or without fillet welds as applicable) always be specified as this approach dramatically reduces the deformations of the flange induced by a full penetration groove weld, and also costs significantly less than a full penetration groove weld.*

Reference 67 recommends that permission be granted for the bearing stiffeners (and bearing diaphragms in box sections) to be detailed either vertical or normal to the girder top flange at the fabricator's option. Reference 67 further indicates that most fabricators prefer the bearing stiffeners to be detailed normal. Also, in cases where multiple bearing stiffeners are used at a given location, a minimum spacing of 8 inches or 1-1/2 times the stiffener plate width should be provided between the stiffener plates for welding access.

3.3.8.2.2 Projecting Width Requirement for Bearing Stiffeners

AASHTO LRFD Article 6.10.11.2.2 specifies that the projecting width, b_t, of each bearing stiffener element (Figure 3.3.77) satisfy the following requirement in order to prevent local buckling of the bearing stiffener plates:

$$b_t \le 0.48 t_p \sqrt{\frac{E}{F_{ys}}}$$

Equation 3.3.171
AASHTO LRFD Equation 6.10.11.2.2-1

where:

F_{ys} = specified minimum yield strength of the stiffener (ksi)

t_p = thickness of the projecting stiffener element (in.)

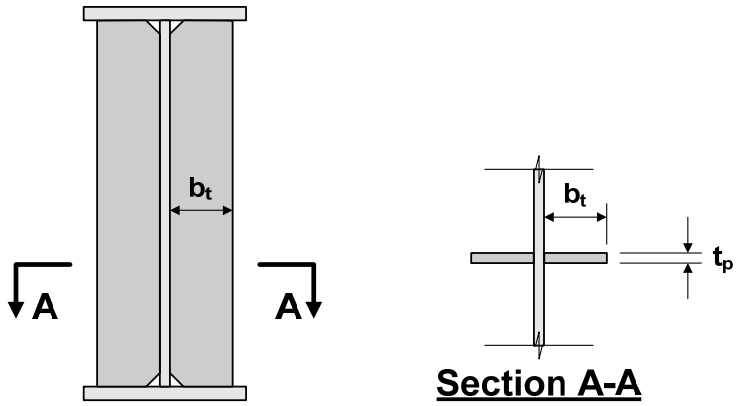


Figure 3.3.77 Projecting Width of Bearing Stiffener

3.3.8.2.3 Bearing Resistance of Stiffeners

Bearing stiffeners must be clipped to clear the web-to-flange fillet welds and to bring the stiffener plates tight against the flange through which they receive their load. As a result, the area of the plates in direct bearing on the flange is less than the gross area of the plates. *AASHTO LRFD* Article 6.10.11.2.3 specifies that the factored bearing resistance of the fitted ends of bearing stiffeners be taken as:

$$(R_{sb})_r = \phi_b (R_{sb})_n$$

Equation 3.3.172
AASHTO LRFD Equation 6.10.11.2.3-1

where:

ϕ_b = resistance factor for bearing on milled surfaces specified in *AASHTO LRFD* Article 6.5.4.2 (= 1.0)

$(R_{sb})_n$ = nominal bearing resistance for the fitted ends of bearing stiffeners (kips) taken as:

= $1.4\ A_{pn} F_{ys}$

Equation 3.3.173
AASHTO LRFD Equation 6.10.11.2.3-2

A_{pn} = area of the projecting elements of the stiffener outside of the web-to-flange fillet welds but not beyond the edge of the flange (in.^{2}). A_{pn} is computed by subtracting the clips from the nominal cross-sectional area of the stiffeners

F_{ys} = specified minimum yield strength of the stiffener (ksi)

The nominal bearing resistance for the fitted ends of bearing stiffeners is given in Reference 4 as $R_n = 1.8F_yA_{pb}$, where A_{pb} is equal to the projected bearing area. The specified nominal bearing resistance is twice the *AISC ASD* (Allowable Stress Design) value of $R_n = 0.9F_yA_{pb}$. Applying the specified *AISC* resistance factor of 0.75 to the nominal *AISC LRFD* nominal bearing resistance gives a factored bearing resistance of $1.35F_yA_{pb}$. Since the *AASHTO LRFD* resistance factors for connection elements are generally 0.05 higher than the *AISC LRFD* resistance factors, the nominal bearing resistance for the fitted ends of bearing stiffeners in the *AASHTO LRFD* Specification was raised to $0.8 * 1.8F_yA_{pb} = 1.4F_yA_{pb}$, which is then used in conjunction with a specified *AASHTO LRFD* resistance factor for bearing on milled surfaces of $\phi_b = 1.0$.

3.3.8.2.4 Axial Resistance of Bearing Stiffeners

Bearing stiffeners are designed as columns. *AASHTO LRFD* Article 6.10.11.2.4a specifies that the factored axial resistance of the stiffeners, P_r, is to be determined as specified in *AASHTO LRFD* Article 6.9.2.1 using the specified minimum yield strength of the stiffener plates, F_{ys}, in order to account for the effect of any early yielding of lower strength stiffener plates. The factored resistance of components in axial compression is given in *AASHTO LRFD* Article 6.9.2.1 as:

$$P_r = \phi_c P_n$$

Equation 3.3.174
AASHTO LRFD Equation 6.9.2.1-1

where:

ϕ_c = resistance factor for axial compression specified in *AASHTO LRFD* Article 6.5.4.2 (= 0.90)
P_n = nominal compressive resistance specified in *AASHTO LRFD* Article 6.9.4.1 (kips)

The nominal compressive resistance, P_n, of bearing stiffeners is to be computed as follows (*AASHTO LRFD* Article 6.9.4.1.1):

- If $\frac{P_e}{P_o} \geq 0.44$, then:

$$P_n = \left[0.658^{\left(\frac{P_o}{P_e}\right)}\right] P_o$$

Equation 3.3.175
AASHTO LRFD Equation 6.9.4.1.1-1

- If $\frac{P_e}{P_o} < 0.44$, then:

$$P_n = 0.877P_e$$

Equation 3.3.176
AASHTO LRFD Equation 6.9.4.1.1-2

where:

P_e = elastic critical buckling resistance for flexural buckling (kips) specified in *AASHTO LRFD* Article 6.9.4.1.2 as:

$$= \frac{\pi^2 E}{\left(\frac{K\ell}{r_s}\right)^2} A_g$$

Equation 3.3.177
AASHTO LRFD Equation 6.9.4.1.2-1

(The flexural buckling resistance is used to compute P_e for bearing stiffeners - see the last entry in *AASHTO LRFD* Table 6.9.4.1.1-1.)

P_o = equivalent nominal yield resistance = $F_y A_g$ (kips). (The slender element reduction factor, Q, is taken equal to 1.0 for bearing stiffeners).

A_g = cross-sectional area of the effective column section of the bearing stiffeners (Section 3.3.8.2.4.1) (in.^{2})

F_y = specified minimum yield strength of the stiffener (ksi)

$K\ell$ = effective length of the effective column section of the bearing stiffeners taken as 0.75*D*, where *D* is the web depth (*AASHTO LRFD* Article 6.10.11.2.4a) (in.)

r_s = radius gyration of the effective column section of the bearing stiffeners about the plane of buckling computed about the mid-thickness of the web (*AASHTO LRFD* Article 6.10.11.2.4a) (in.)

The reduced effective length $K\ell$ = 0.75*D* of the effective column is a result of the end restraint against column buckling provided by the flanges.

Note that the width-to-thickness requirements of *AASHTO LRFD* Article 6.9.4.2.1 are not enforced in bearing stiffener design because the stiffener projecting width requirement specified in *AASHTO LRFD* Article 6.10.11.2.2 (i.e. Equation 3.3.171) is typically more severe. As a result, the slender element reduction factor, *Q*, is taken equal to 1.0 in computing the equivalent nominal yield resistance, P_o, for bearing stiffeners.

3.3.8.2.4.1 Effective Column Section of Bearing Stiffeners

The effective column section of the bearing stiffeners is defined in *AASHTO LRFD* Article 6.10.11.2.4b. For stiffeners bolted to the web (or diaphragm), the effective column section is to consist of only the stiffener elements. For stiffeners welded to the web (or diaphragm), a portion of the web (or diaphragm) is to be included as part of the effective column section, with some exceptions noted below. For stiffeners consisting of two plates welded to the web (or diaphragm), the effective column section is to consist of the two stiffener plates, plus a centrally located strip

of web (or diaphragm) extending not more than $9t_w$ on each side of the stiffeners (Figure 3.3.78).

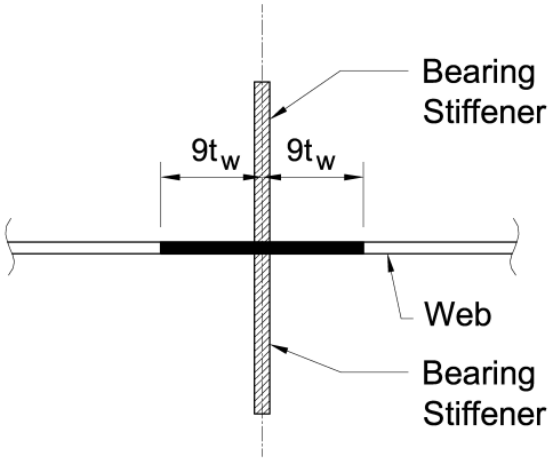


Figure 3.3.78 Effective Column Section for Welded Bearing Stiffener Design (One Pair of Stiffeners Welded to a Web)

If more than one pair of stiffeners is used, the effective column section is to consist of all the stiffener plates, plus a centrally located strip of web (or diaphragm) extending not more than $9t_w$ on each side of the outer projecting elements of the group.

The strip of web is not to be included in the effective section at interior supports of continuous-span hybrid members for which the specified minimum yield strength of the web is less than 70 percent of the specified minimum yield strength of the higher strength flange due to the amount of web yielding that may be expected due to the longitudinal flexural stress. The preceding exception does not apply at the end supports of hybrid members. For unusual cases in which F_{ys} is larger than F_{yw}, the yielding of the lower strength web is to be accounted for by reducing the width of the web strip included in the effective section by the ratio of F_{yw}/F_{ys}.

3.3.8.2.5 Concentrated Loads Applied to Webs Without Bearing Stiffeners

3.3.8.2.5.1 General

At bearing locations on rolled shapes and at other locations on built-up sections or rolled shapes subjected to concentrated loads, where the loads are not transmitted through a deck or deck system, either bearing stiffeners must be provided or else the web must be investigated for the limit states of web local yielding and web crippling as discussed below in Sections 3.3.8.2.5.2 and 3.3.8.2.5.3, respectively (refer to *AASHTO LRFD* Article D6.5 – Appendix D6).

The equations given in *AASHTO LRFD* Article D6.5 are essentially identical to the equations given in Reference 4. *AASHTO LRFD* Article CD6.5.1 notes that the

limit state of sidesway web buckling given in Reference 4 is not included because it governs only for: 1) members subjected to concentrated loads applied directly to the steel section; 2) members for which the compression flange is braced at the load point; 3) members for which the tension flange is unbraced at the load point; and 4) members for which the ratio of D/t_w to L_b/b_{ft} is less than or equal to 1.7. The preceding conditions do not commonly occur in bridge construction.

3.3.8.2.5.2 Web Local Yielding

The limit state of web local yielding is covered in *AASHTO LRFD* Article D6.5.2, and is intended to prevent localized yielding of the web due to a high compressive or tensile stress caused by a concentrated load or bearing reaction. In order to satisfy this limit state without providing bearing stiffeners, webs subject to compressive or tensile concentrated loads must satisfy the following:

$$R_u \le \phi_b R_n$$

Equation 3.3.178
AASHTO LRFD Equation D6.5.2-1

where:

ϕ_b = resistance factor for bearing specified in *AASHTO LRFD* Article 6.5.4.2 (= 1.0)
R_u = factored concentrated load or bearing reaction (kips)
R_n = nominal resistance to the concentrated loading (kips) taken as follows:

- For interior-pier reactions and for concentrated loads applied at a distance from the end of the member that is greater than *d*:

$$R_n = (5k + N)F_{yw}t_w$$

Equation 3.3.179
AASHTO LRFD Equation D6.5.2-2

- Otherwise:

$$R_n = (2.5k + N)F_{yw}t_w$$

Equation 3.3.180
AASHTO LRFD Equation D6.5.2-3

d = depth of the steel section (in.)
k = distance from the outer face of the flange resisting the concentrated load or bearing reaction to the toe of the fillet (in.). For a rolled shape, k is published in the available tables giving dimensions for the shapes. For a built-up section, k may be taken as the distance from the outer face of the flange to the web toe of the web-to-flange fillet weld.
N = length of bearing (in.). N must be greater than or equal to k at end bearing locations.

The preceding equations are largely based on the work described in References 84 and 85. The concentrated load acting on a rolled shape or a built-up section is assumed critical at the toe of the fillet, located a distance *k* from the outer face of the flange resisting the concentrated load or bearing reaction (Figure 3.3.79). For interior concentrated loads or interior-pier reactions, the load is assumed to distribute along the web at a slope of 2.5 to 1 and over a distance of (5*k* + *N*) according to Equation 3.3.179 (see also Figure 3.3.79). An interior concentrated load is assumed to be a load applied at a distance from the end of the member greater than the depth of the steel section *d*. For end concentrated loads or end reactions, the load is assumed to distribute along the web at the same slope over a distance of (2.5*k* + *N*) according to Equation 3.3.180 (Figure 3.3.79).

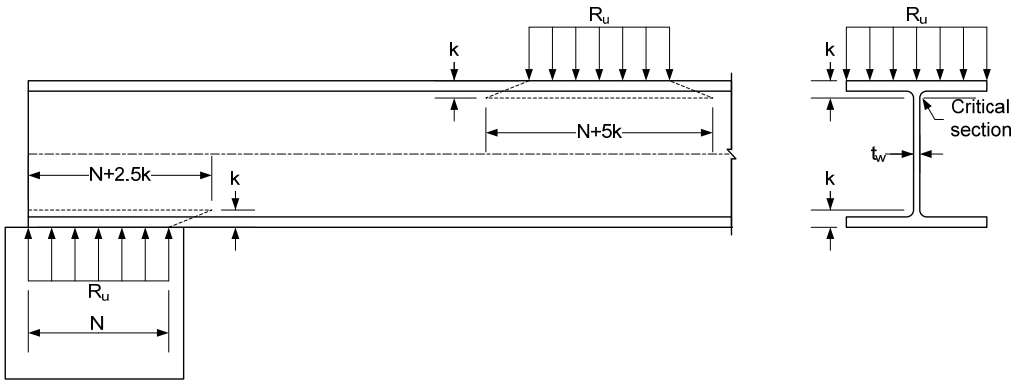


Figure 3.3.79 Local Web Yielding – Bearing Length and k

3.3.8.2.5.3 Web Crippling

The limit state of web crippling is covered in *AASHTO LRFD* Article D6.5.3, and is intended to prevent local instability or crippling of the web due to a high compressive stress caused by a concentrated load or bearing reaction. In order to satisfy this limit state without providing bearing stiffeners, webs subject to compressive concentrated loads must satisfy the following:

$$R_u \le \phi_w R_n$$

Equation 3.3.181
AASHTO LRFD Equation D6.5.3-1

where:

ϕ_w = resistance factor for web crippling specified in *AASHTO LRFD* Article 6.5.4.2 (= 0.80)
R_u = factored concentrated load or bearing reaction (kips)
R_n = nominal resistance to the concentrated loading (kips) taken as follows:

- For interior-pier reactions and for concentrated loads applied at a distance from the end of the member that is greater than or equal to *d*/2:

$$R_n = 0.8t_w^2\left[1+3\left(\frac{N}{d}\right)\left(\frac{t_w}{t_f}\right)^{1.5}\right]\sqrt{\frac{EF_{yw}t_f}{t_w}}$$

Equation 3.3.182
AASHTO LRFD Equation D6.5.3-2

- Otherwise:
  - If $N/d \le 0.2$, then:

$$R_n = 0.4t_w^2\left[1+3\left(\frac{N}{d}\right)\left(\frac{t_w}{t_f}\right)^{1.5}\right]\sqrt{\frac{EF_{yw}t_f}{t_w}}$$

Equation 3.3.183
AASHTO LRFD Equation D6.5.3-3

  - If N/d > 0.2, then:

$$R_n = 0.4t_w^2\left[1+\left(\frac{4N}{d}-0.2\right)\left(\frac{t_w}{t_f}\right)^{1.5}\right]\sqrt{\frac{EF_{yw}t_f}{t_w}}$$

Equation 3.3.184
AASHTO LRFD Equation D6.5.3-4

where:

d = depth of the steel section (in.)
N = length of bearing (in.). N must be greater than or equal to k at end bearing locations.
t_f = thickness of the flange resisting the concentrated load or bearing reaction (in.)

Equations 3.3.182 and 3.3.183 are based on research described in Reference 86. Equation 3.3.184 was developed after additional testing to better represent the effect of longer bearing lengths at the ends of members (*87*).

3.3.8.3 Longitudinal Web Stiffeners

3.3.8.3.1 General

The design of longitudinal web stiffeners is covered in *AASHTO LRFD* Article 6.10.11.3. For box girders, *AASHTO LRFD* Article 6.11.11.1 refers to the I-girder

provisions of *AASHTO LRFD* Article 6.10.11.3 for the design of longitudinal web stiffeners.

Longitudinal stiffeners are aligned horizontally on the web along the length of the girder and divide the web panel into smaller sub-panels (Figure 3.3.80). In the *AASHTO LRFD* Specifications, longitudinal stiffeners are required whenever the web slenderness, D/t_w, exceeds 150, and are used to provide additional bend-buckling resistance to the webs of deeper girders.



Figure 3.3.80 Longitudinal Web Stiffeners on an I-Girder

Longitudinal stiffeners, where required, are to consist of a plate welded to one side of the web or a bolted angle. Welded longitudinal stiffeners are commonly made up of less expensive flat bar stock, which is generally produced in whole-inch width increments and 1/8-in. thickness increments. Longitudinal stiffeners should be used in conjunction with transverse stiffeners to support the longitudinal stiffeners along their length.

AASHTO LRFD Article 6.10.11.3.1 specifies that longitudinal stiffeners are to be located vertically on the web such that adequate web bend-buckling resistance is provided for constructibility and at the service limit state; i.e., the stiffeners must be located such that Equation 3.2.20 is satisfied when checking constructibility and Equation 3.2.33 is satisfied at the service limit state (see Section 3.2.4.3.2.2 regarding the calculation of the web bend-buckling resistance, F_{crw}, for a web with longitudinal stiffeners). It also must be verified that the section has adequate nominal flexural resistance at the strength limit state with the longitudinal stiffener in the selected position (Section 3.2.6).

The depth of the web in compression, D_c, in the elastic range for composite sections in positive flexure changes relative to the vertical position of the longitudinal stiffener after the concrete deck has been placed. D_c for composite sections is a function of the dead-to-live load stress ratio because the dead and live loads are applied to different sections in a composite girder (Section

3.2.4.3.2.2). The dead load stress has a significant effect on the location of the elastic neutral axis for composite sections in positive flexure in particular. The non-composite dead load stresses acting on the steel section alone cause the neutral axis to be lower than it would if all loads were applied to the composite section. This effect increases with increasing span length.

The neutral axis moves higher on the web after the deck has hardened and dead and live loads are applied to the composite section. Thus, D_c changes relative to the vertical position of the longitudinal stiffener, which is usually located a fixed distance from the compression flange in these regions. As a result, the computed web bend-buckling resistance is different before and after placement of the deck and is dependent on the loading. Therefore, several trial locations of the stiffener on the web may be necessary in these regions in order to determine a location of the stiffener to satisfy Equation 3.2.20 when checking constructibility, Equation 3.2.33 at the service limit state, and all applicable strength limit state criteria. *AASHTO LRFD* Article C6.10.11.3.1 provides the following equation for determining an initial trial location of a longitudinal stiffener in regions of positive flexure:

$$\frac{d_s}{D_c} = \frac{1}{1 + 1.5\sqrt{\frac{f_{DC1} + f_{DC2} + f_{DW} + f_{LL+IM}}{f_{DC1}}}}$$

Equation 3.3.185
AASHTO LRFD Equation C6.10.11.3.1-1

where:

d_s = distance from the centerline of a plate longitudinal stiffener, or the gage line of an angle longitudinal stiffener, to the inner surface or leg of a compression-flange element (in.)

D_c = depth of the web of the non-composite steel section in compression in the elastic range (in.)

f_{xx} = factored compression-flange vertical bending stresses at the strength limit state caused by the different loads acting on their respective sections at the section with the maximum compressive vertical bending stress (ksi).

The stiffener will likely need to be moved vertically up or down from this initial trial location in order to satisfy all the specified limit-state criteria.

It is recommended that the longitudinal stiffener initially be located at $0.4D_c$ from the inner surface of the compression flange at composite sections in negative flexure and at non-composite sections. D_c would be conservatively calculated for the section consisting of the steel girder plus the longitudinal reinforcement for composite sections in negative flexure. D_c would be based on the section consisting of the steel girder alone for non-composite sections.

Based on theoretical and experimental studies on non-composite girders, the optimum location of a single longitudinal stiffener is $0.4D_c$ for bending and $0.5D$ for shear. Tests have also shown that longitudinal stiffeners located at $0.4D_c$ on these sections can effectively control lateral web deflections due to bending (*83*). Because shear is always accompanied by moment and because a properly proportioned longitudinal stiffener will also reduce lateral web deflections due to shear, the distance of $0.4D_c$ is recommended. The stiffener may need to be moved vertically up or down from this initial trial location, especially for cases where the concrete deck may be assumed effective in tension in regions of negative flexure at the service limit state as permitted in *AASHTO LRFD* Article 6.10.4.2.1. *AASHTO LRFD* Article D6.3.1 specifies that in this case, D_c at the service limit state must be calculated based on the accumulated stresses using Equation 3.2.41.

Because D_c may vary along the span, it is suggested that the longitudinal stiffener be located based on D_c computed at the section with the largest compressive vertical bending stress. Other sections must also be examined to ensure they satisfy the specified limit states since the stiffener cannot be at its optimum location at other sections along the girder length with a lower stress and a different value of D_c.

In some cases, particularly in regions of stress reversal, it may be necessary or desirable to use two longitudinal stiffeners on the web. The use of two longitudinal stiffeners on the web is discussed in greater detail in Section 3.2.4.3.2.2.

It is preferred that longitudinal stiffeners be placed on the opposite side of the web from transverse stiffeners. At bearing stiffeners and connection plates where the longitudinal stiffener and transverse web element must intersect, a decision must be made as to which element to interrupt. According to *AASHTO LRFD* Article 6.10.11.3.1, wherever practical, longitudinal stiffeners are to extend uninterrupted over their specified length, unless otherwise permitted in the contract documents, since longitudinal stiffeners are designed as continuous members to improve the web bend buckling resistance. In such cases, the interrupted transverse elements must be fitted and attached to both sides of the longitudinal stiffener with connections sufficient to develop the flexural and axial resistance of the transverse element.

If the longitudinal stiffener is interrupted instead, it should be similarly attached to all transverse elements. All interruptions must be carefully designed with respect to fatigue, especially if the longitudinal stiffener is not attached to the transverse web elements, as a punitive Category E or E′ detail may exist at the termination points of each longitudinal stiffener-to-web weld (refer to *AASHTO LRFD* Table 6.6.1.2.3-1 – Condition 4.3). Copes should always be provided to avoid intersecting welds. If an interrupted longitudinal stiffener is attached to a transverse web element, Equation 3.2.47 may apply in checking fatigue (refer to Figure 3.2.20). Should longitudinal stiffeners be discontinued at bolted field splices, consideration should be given to taking the stiffener to the free edge of the web where the normal stress is zero to avoid the fatigue-sensitive details at the

termination of the stiffener-to-web welds. This would require splitting of the web splice plates.

Longitudinal stiffeners are subject to the same flexural strain as the web at their vertical position on the web. As a result, the stiffeners must have sufficient strength and rigidity to resist bend buckling of the web (at the appropriate limit state) and to transmit the stresses in the stiffener and an effective portion of the web as a equivalent column (*83*). Therefore, *AASHTO LRFD* Article 6.10.11.3.1 specifies that the factored vertical bending stress in the longitudinal stiffener, f_s, must satisfy the following requirement at the strength limit state and when checking constructibility:

$$f_s \le \phi_f R_h F_{ys}$$

Equation 3.3.186
AASHTO LRFD Equation 6.10.11.3.1-1

where:

ϕ_f = resistance factor for flexure specified in *AASHTO LRFD* Article 6.5.4.2 (= 1.0)
F_{ys} = specified minimum yield strength of the longitudinal stiffener (ksi)
R_h = hybrid factor determined as specified in *AASHTO LRFD* Article 6.10.1.10.1 (Section 3.2.6.3)

The hybrid factor, R_h, is included in Equation 3.3.186 to account for the influence of local web yielding on the longitudinal stiffener stress in hybrid sections. The appropriate corresponding value of R_h should be applied for the strength limit state and constructibility verifications.

3.3.8.3.2 Projecting Width Requirement for Longitudinal Web Stiffeners

AASHTO LRFD Article 6.10.11.3.2 specifies that the projecting width, b_ℓ, of the longitudinal stiffener satisfy the following requirement in order to prevent local buckling of the stiffener plate:

$$b_\ell \le 0.48 t_s \sqrt{\frac{E}{F_{ys}}}$$

Equation 3.3.187
AASHTO LRFD Equation 6.10.11.3.2-1

where:

F_{ys} = specified minimum yield strength of the stiffener (ksi)
t_s = thickness of the longitudinal stiffener (in.)

3.3.8.3.3 Moment of Inertia Requirement for Longitudinal Web Stiffeners

AASHTO LRFD Article 6.10.11.3.3 specifies that to ensure that a longitudinal stiffener will have adequate rigidity to maintain a horizontal line of near zero lateral deflection in the web to resist bend buckling of the web (at the appropriate limit state), the moment of inertia of the stiffener acting in combination with an adjacent strip of web must satisfy the following requirement (*16*):

$$I_\ell \geq Dt_w^3\left[2.4\left(\frac{d_o}{D}\right)^2 - 0.13\right]\beta$$

Equation 3.3.188
AASHTO LRFD Equation 6.10.11.3.3-1

where:

d_o = transverse stiffener spacing (in.)

I_ℓ = moment of inertia of the longitudinal stiffener including an effective width of the web equal to $18t_w$ taken about the neutral axis of the combined section (in.^{4}). If F_{yw} is smaller than F_{ys}, the strip of web included in the effective section must be reduced by the ratio of F_{yw}/F_{ys}.

β = curvature correction factor for longitudinal stiffener rigidity calculated as follows (equal to 1.0 for longitudinal stiffeners on straight webs):

- For cases where the longitudinal stiffener is on the side of the web away from the center of curvature:

$$\beta = \frac{Z}{6} + 1$$

Equation 3.3.189
AASHTO LRFD Equation 6.10.11.3.3-3

- For cases where the longitudinal stiffener is on the side of the web toward the center of curvature:

$$\beta = \frac{Z}{12} + 1$$

Equation 3.3.190
AASHTO LRFD Equation 6.10.11.3.3-4

Z = curvature parameter taken as:

$$= \frac{0.95d_o^2}{Rt_w} \leq 10$$

Equation 3.3.191
AASHTO LRFD Equation 6.10.11.3.3-5

R = minimum girder radius in the panel (in.)

Reference 83 suggests that the moment of inertia (and radius of gyration – Section 3.3.8.3.4) of the longitudinal stiffener be taken about the neutral axis of an equivalent column cross-section consisting of the stiffener and an adjacent strip of web with a width of $18t_w$. For a web having a lower yield strength than the yield strength of the longitudinal stiffener, the web strip that contributes to the effective column section is reduced by F_{yw}/F_{ys} in computing the moment of inertia of the longitudinal stiffener. Previous specifications required that the moment of inertia (and radius of gyration) of the stiffener be taken about the edge in contact with the web plate.

Longitudinal stiffeners on horizontally curved webs require greater rigidity than on straight webs because of the tendency of curved webs to bow. This is reflected by including the factor, β, in Equation 3.3.188, which is a simplification of a requirement for longitudinal stiffeners on curved webs given in Reference 88. For longitudinal stiffeners on straight webs, β is taken equal to 1.0.

3.3.8.3.4 Radius of Gyration Requirement for Longitudinal Web Stiffeners

AASHTO LRFD Article 6.10.11.3.3 specifies that to ensure the longitudinal stiffener acting in combination with an adjacent strip of web as an effective column section can withstand the axial compressive stress without lateral buckling, the radius of gyration of the effective column section must satisfy the following requirement:

$$r \geq \frac{0.16 d_o \sqrt{\frac{F_{ys}}{E}}}{\sqrt{1 - 0.6 \frac{F_{yc}}{R_h F_{ys}}}}$$

Equation 3.3.192
AASHTO LRFD Equation 6.10.11.3.3-2

where:

d_o = transverse stiffener spacing (in.)
r = radius of gyration of the longitudinal stiffener including an effective width of the web equal to $18t_w$ taken about the neutral axis of the combined section (in.)
F_{ys} = specified minimum yield strength of the longitudinal stiffener (ksi)
R_h = hybrid factor determined as specified in *AASHTO LRFD* Article 6.10.1.10.1 (Section 3.2.6.3)

Equation 3.3.192 is a modification of the original requirement given in Reference 83 that accounts for the possibility of different specified minimum yield strengths for the longitudinal stiffener and compression flange. The hybrid factor, R_h, is also included in the equation to approximate the influence of a lower yield strength web in a hybrid section. For a section with F_{yc}/F_{ys} greater than one, a significantly larger radius of gyration is required than in previous specifications because in this

case, the longitudinal stiffener is subjected to larger stresses compared to its resistance than in an equivalent homogeneous column. Equation 3.3.192 is valid as long as Equation 3.3.186 is satisfied to prevent full nominal yielding of the longitudinal stiffener at the strength limit state.

3.3.9 Bearings

3.3.9.1 General

Bearing selection and design generally involves three basic steps:

1. Obtain the required design input.
2. Select the most feasible bearing type.
3. Design the most feasible bearing type.

The first step is to obtain the required design input. The bearing design input generally depends on whether the bearing is fixed or expansion. The function and capabilities of fixed and expansion bearings are summarized in Table 3.3.7.

Table 3.3.7 Capabilities of Fixed and Expansion Bearings

Capabilities	Fixed Bearing	Expansion Bearing
Resists vertical force	Yes	Yes
Resists horizontal force	Yes	No
Facilitates vertical movement	No	No
Facilitates horizontal movement	No	Yes
Facilitates rotation	Yes	Yes

Bearings can be fixed in both the longitudinal and transverse directions, fixed in one direction and expansion in the other, or expansion in both directions.

When deciding which bearings are fixed and which are expansion on a bridge, several guidelines are commonly considered:

- The bearing layout for a bridge must be developed as a consistent system. Vertical movements are resisted by all bearings, horizontal movements are resisted by fixed bearings and facilitated in expansion bearings, and rotations are generally allowed to occur as freely as possible.
- For maintenance purposes, it is generally desirable to minimize the number of deck joints on a bridge, which can in turn affect the bearing layout.
- The bearing layout must facilitate the anticipated thermal movements, primarily in the longitudinal direction but also in the transverse direction for wide bridges.
- It is generally desirable for the superstructure to expand in the uphill direction wherever possible.

- If more than one substructure unit is fixed within a single superstructure unit, then forces will be induced into the fixed substructure units and must be considered during design.
- For curved bridges, the bearing layout can induce additional stresses into the superstructure, which must be considered during design.
- Forces are distributed to the bearings based on the superstructure analysis.

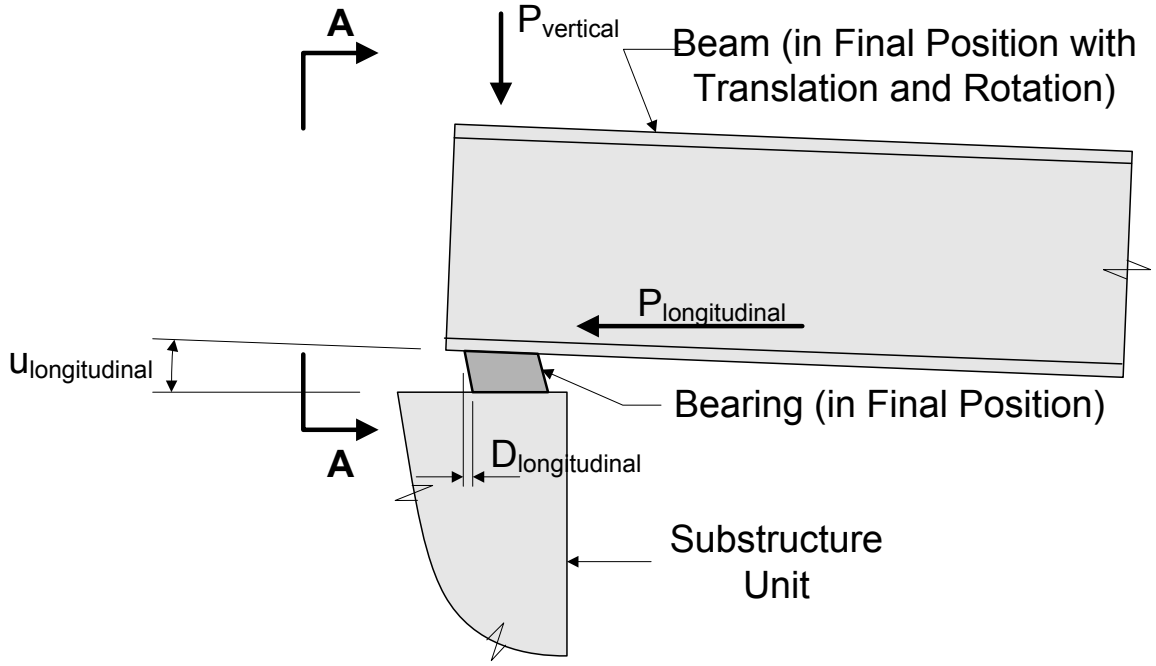
3.3.9.1.1 Loads

Bearings must be designed to resist the loads transferred from the superstructure to the substructure. The primary load is generally the vertical load, which is caused by dead load, vehicular live load, dynamic load allowance, pedestrian live load, and any other vertical loads which may be present. For some bearings, a minimum vertical load is specified in addition to a maximum vertical load.

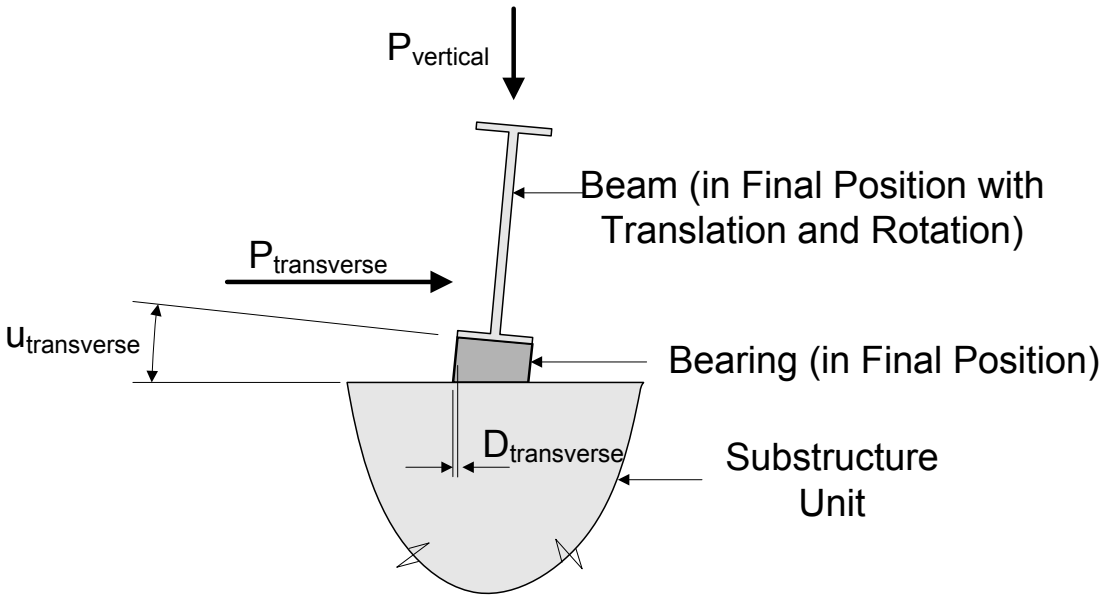
In addition, fixed bearings must also resist horizontal loads in the direction of fixity. Horizontal loads can be caused by wind load on structure, wind on live load, uniform temperature, vehicular braking force, vehicular centrifugal force, earthquake, and any other horizontal loads which may be present.

It is important to note that expansion bearings do not resist horizontal loads in the direction of expansion. For example, if a bearing facilitates expansion in the longitudinal direction, then that bearing will not resist longitudinal loads. Similarly, if a bearing facilitates expansion in the transverse direction, then it will not resist transverse loads. Horizontal loads are generally applied only to fixed bearings.

A schematic showing the various loads acting on a bearing is presented in Figure 3.3.81.



Elevation



View A-A

Figure 3.3.81 Bearings Loads and Moments

3.3.9.1.2 Translation

In addition to resisting loads, a bearing must also facilitate translation in the girders or beams that are being supported. For example, if the superstructure lengthens due to temperature rise or shortens due to temperature fall, then the bearings must be designed to facilitate this longitudinal translation. Although translation is usually greatest in the longitudinal direction, translation in the transverse direction can also be significant, especially on wide, curved, or skewed bridges.

Fixed bearings are designed such that no translation is permitted in the direction of fixity. Expansion bearings are designed to facilitate the anticipated translation in the direction of expansion.

Bearing translation is illustrated in Figure 3.3.81.

3.3.9.1.3 Rotation

A bearing must also facilitate rotation in the girders or beams that are being supported. For example, if a girder deflects due to dead load or live load, then this deflection will cause the end of the girder to rotate in the longitudinal direction (about the transverse axis of the bridge). Similarly, for a curved bridge, the torsional effects in the girders may cause the end of the girder to rotate in the transverse direction (about the longitudinal axis of the bridge). The bearing must be designed to facilitate these anticipated rotations.

Bearing rotation is also illustrated in Figure 3.3.81.

3.3.9.2 Types of Bearings

There are many different types of bearings, and each one has its own unique applications, based on the magnitude of the loads, translations, and rotations about the various axes of the bridge. Some of the most common bearing types are presented in Table 3.3.8, along with a general description of the bearing.

Table 3.3.8 Bearing Type Descriptions

Bearing Type	General Description
Bronze bearing	A bearing in which displacements or rotations take place by the sliding of a bronze surface against a mating surface.
Cotton-duck-reinforced pad (CDP)	A pad made from closely spaced layers of elastomer and cotton-duck, bonded together during vulcanization.
Disc bearing	A bearing that accommodates rotation by deformation of a single elastomeric disc molded from a urethane compound. It may be movable, guided, unguided, or fixed. Movement is accommodated by sliding of polished stainless steel on PTFE.
Double cylindrical bearing	A bearing made from two cylindrical bearings placed on top of each other with their axes at right angles to facilitate rotation about any horizontal axis.
Fiberglass-reinforced pad (FGP)	A pad made from discrete layers of elastomer and woven fiberglass bonded together during vulcanization.
Knuckle bearing	A bearing in which a concave metal surface rocks on a convex metal surface to provide rotation capability about any horizontal axis.
Metal rocker or roller bearing	A bearing that carries vertical load by direct contact between two metal surfaces and that accommodates movement by rocking or rolling of one surface with respect to the other.
Plain elastomeric pad (PEP)	A pad made exclusively of elastomer, which provides limited translation and rotation.
Pot bearing	A bearing that carries vertical load by compression of an elastomeric disc confined in a steel cylinder and that accommodates rotation by deformation of the disc.
PTFE sliding bearing	A bearing that carries vertical load through contact stresses between a PTFE sheet or woven fabric and its mating surface, and that permits movements by sliding of the PTFE over the mating surface.
Steel-reinforced elastomeric bearing	A bearing made from alternate laminates of steel and elastomer bonded together during vulcanization. Vertical loads are carried by compression of the elastomer. Movements parallel to the reinforcing layers and rotations are accommodated by deformation of the elastomer.

Five common bearing types are illustrated in Figure 3.3.82.

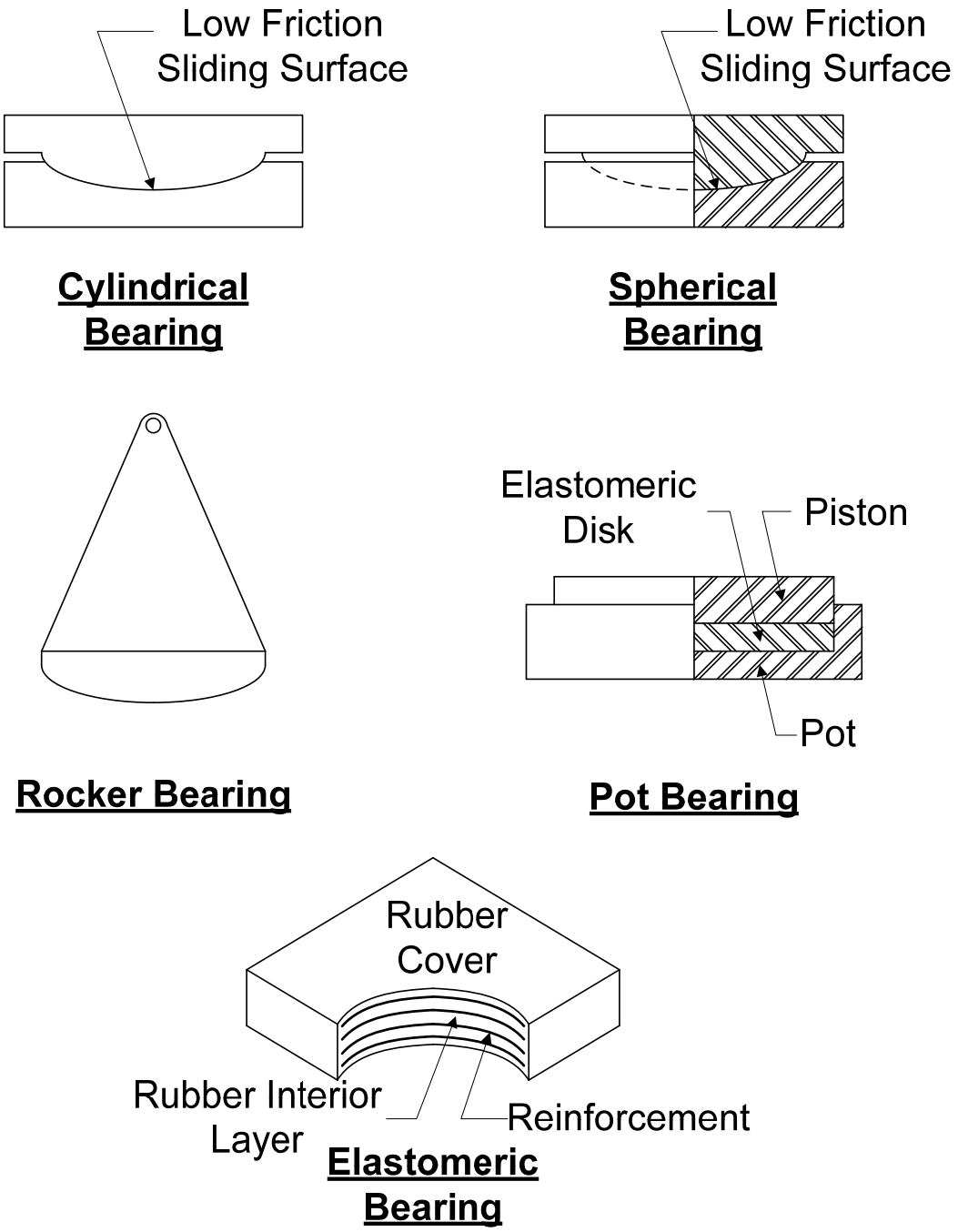


Figure 3.3.82 Common Bearing Types
(Based on *AASHTO LRFD* Figure 14.6.2-1)

After the bearing layout for the entire bridge has been established and the bearing design requirements have been defined, the second step is to select the most feasible bearing type. Several tools are available to the bridge engineer to assist in selecting feasible bearing types.

One such tool is presented in *AASHTO LRFD* Table 14.6.2-1, in which the suitability of various bearing types is presented in terms of movement, rotation, and resistance to loads. This information is presented in Table 3.3.9.

Table 3.3.9 Bearing Suitability
(Based on *AASHTO LRFD* Table 14.6.2-1)

Type of Bearing	Movement		Rotation about Bridge Axis Indicated			Resistance to Loads		
	Long	Trans	Long	Trans	Vert	Long	Trans	Vert
Plain elastomeric pad	S	S	S	S	L	L	L	L
Fiberglass-reinforced pad	S	S	S	S	L	L	L	L
Cotton-duck-reinforced pad	U	U	U	U	U	L	L	S
Steel-reinforced elastomeric bearing	S	S	S	S	L	L	L	S
Plane sliding bearing	S	S	U	U	S	R	R	S
Curved sliding spherical bearing	R	R	S	S	S	R	R	S
Curved sliding cylindrical bearing	R	R	U	S	U	R	R	S
Disc bearing	R	R	S	S	L	S	S	S
Double cylindrical bearing	R	R	S	S	U	R	R	S
Pot bearing	R	R	S	S	L	S	S	S
Rocker bearing	S	U	U	S	U	R	R	S
Knuckle pinned bearing	U	U	U	S	U	S	R	S
Single roller bearing	S	U	U	S	U	U	R	S
Multiple roller bearing	S	U	U	U	U	U	U	S

In the above table:

- S represents suitable
- U represents unsuitable
- L represents suitable for limited applications
- R represents may be suitable but requires special considerations or additional elements such as sliders or guideways

A valuable tool from AISI's *Steel Bridge Bearing Selection and Design Guide* is a set of three preliminary bearing selection diagrams. Separate diagrams are presented for each of the following rotation requirements:

- Minimal design rotation (rotation ≤ 0.005 radians)
- Moderate design rotation (rotation ≤ 0.015 radians)
- Large design rotation (rotation > 0.015 radians)

These three diagrams are presented below in Figure 3.3.83, Figure 3.3.84, and Figure 3.3.85. In each diagram, the limit lines which define the regions are approximate and could be moved approximately 5% in either direction. Therefore, if a specific bearing application falls near a limit line, the engineer should investigate both bearing types.

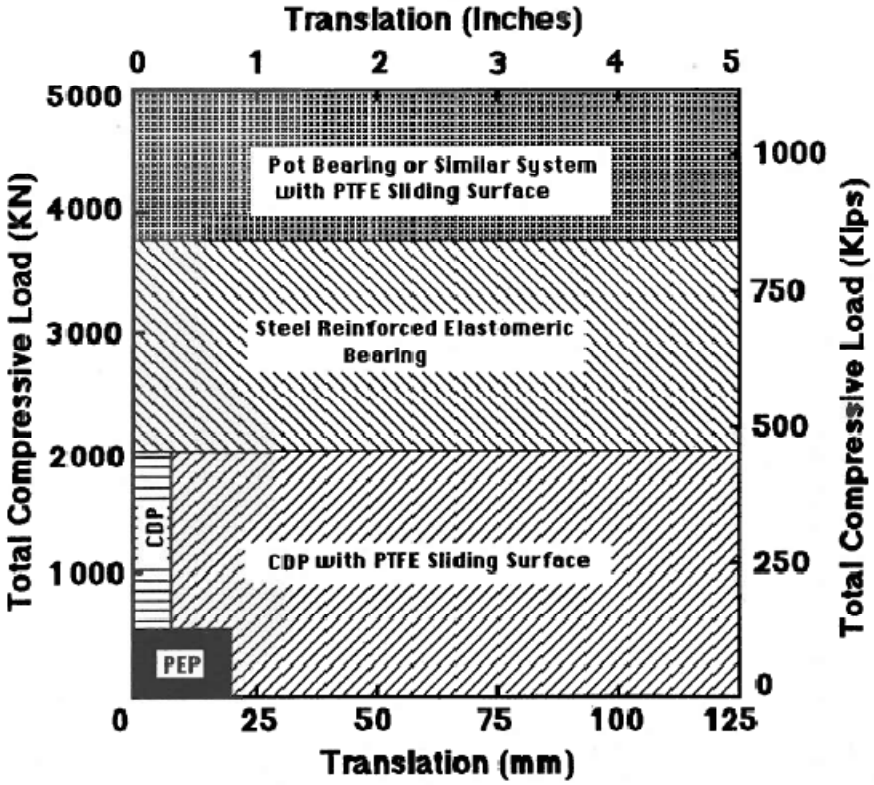


Figure 3.3.83 Preliminary Bearing Selection Diagram for Minimal Design Rotation (Rotation ≤ 0.005 Radians)
(From AISI's *Steel Bridge Bearing Selection and Design Guide*, Figure I-1)

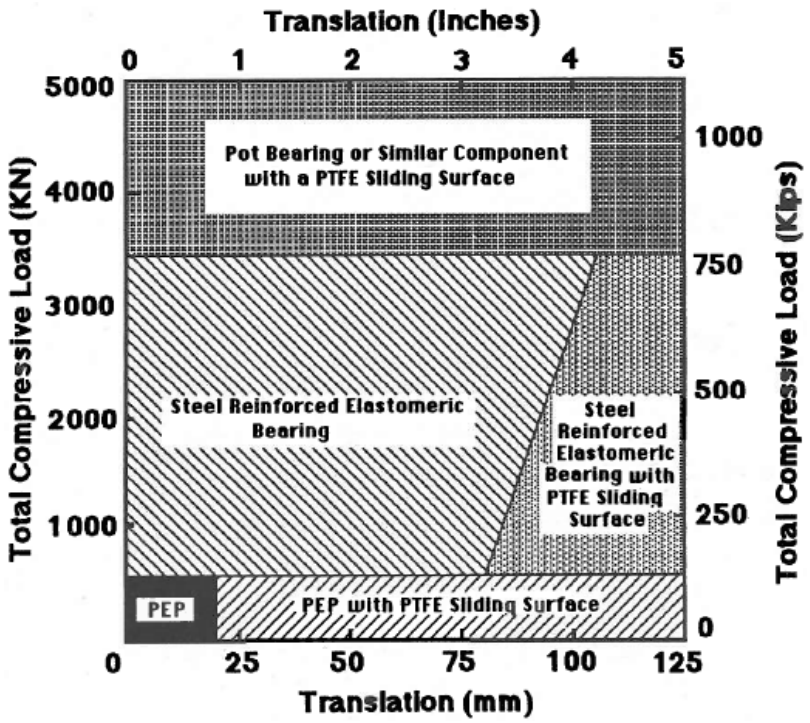


Figure 3.3.84 Preliminary Bearing Selection Diagram for Moderate Design Rotation (Rotation ≤ 0.015 Radians)
(From AISI's *Steel Bridge Bearing Selection and Design Guide*, Figure I-2)

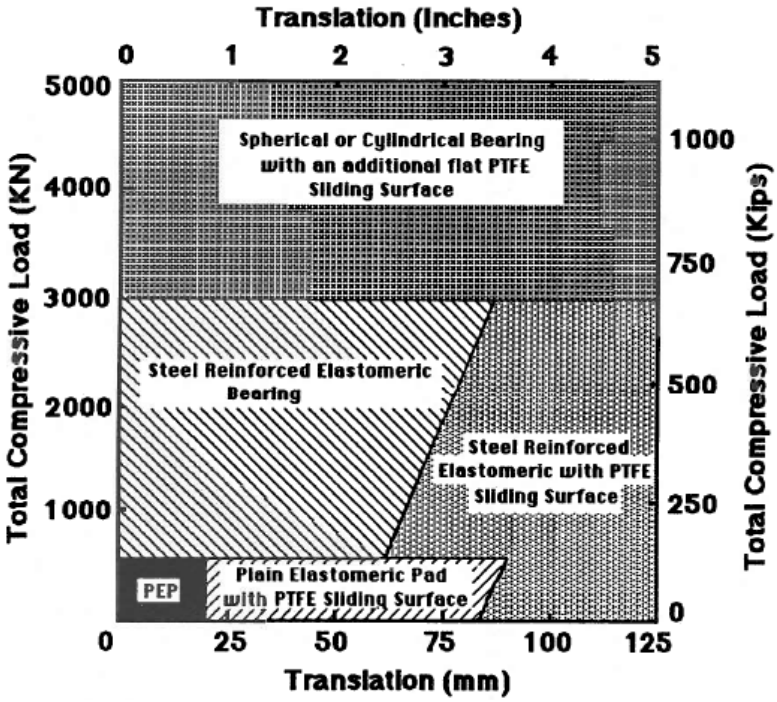


Figure 3.3.85 Preliminary Bearing Selection Diagram for Large Design Rotation (Rotation > 0.015 Radians)
(From AISI's *Steel Bridge Bearing Selection and Design Guide*, Figure I-3)

Some general rules that should be followed during the design of virtually all bearing types are presented in Table 3.3.10.

Table 3.3.10 General Rules for Bearing Design

Observation	General Rule	Consequence of Ignoring Rule
LOAD COMBINATIONS – Some combinations of loads and movements are not possible.	Consider only feasible load and movement combinations, as specified in *AASHTO LRFD* Article 3.4.1.	Using unrealistic load combinations may result in a costly bearing which performs poorly.
LOAD DIRECTIONS – Loads do not necessarily all act in the same direction, and movements do not necessarily take place in the same direction.	Consider the directions of each loading component when computing load and movement combinations.	Adding the absolute values of all loads and movements may result in unrealistic conditions and uneconomical bearings.
INITIAL CONDITIONS – Temporary initial conditions can adversely affect the design of some bearings.	Consider adjusting the position of the bearing during the final stages of construction.	Designing the bearing to resist temporary initial conditions may result in an unnecessarily large and costly bearing.
PROTECTION – Bearings are typically located where dirt, debris, and moisture can collect.	Design and install the bearings to provide protection against the environment and to allow easy access for inspection.	Collection of dirt, debris, and moisture can lead to corrosion and deterioration of the bearing.
SERVICE LIFE – Due to severe demands on a bridge bearing, its service life is often less than that of other bridge components.	Provide allowances for bearing replacement (including space for lifting jacks and employment of appropriate details, such as jacking stiffeners).	Failure to provide jacking details may require expensive retrofits to provide sufficient jacking space and resistance.

The following descriptions and design requirements apply to specific bearing types. For additional details, refer to the appropriate sections of *AASHTO LRFD* Article 14.7.

3.3.9.2.1 Steel Bearings

Steel bearings come in a variety of shapes and sizes. For example sliding bearings consist of two surfaces, frequently one steel and one bronze, with lubrication between them, sliding against each other. Polytetrafluorethylene (PTFE) is often used for lubrication, and it provides favorable chemical resistance and a low coefficient of friction. Steel sliding bearings can be fabricated with flat surfaces to facilitate horizontal movement, or they can be fabricated with curved surfaces to facilitate both horizontal movement and rotation.

Rocker bearings are another type of steel bearings. In rocker bearings, a curved surface is generally placed on top of a flat surface. The two steel parts are constrained by a dowel pin to prevent horizontal movement. Therefore, rocker bearings are generally used at fixed supports.

Another type of steel bearings is roller bearings, in which one or more steel cylinders is placed between two parallel steel plates. Since the rollers facilitate horizontal movement, roller bearings are generally used at expansion supports.

These steel bearing types are described in further detail in various sections of *AASHTO LRFD* Article 14.7.

3.3.9.2.2 Pot Bearings

Pot bearings are commonly used for moderate to large bridges. They carry vertical load by compression of an elastomeric disc contained in a steel cylinder and accommodate rotation by deformation of the disc. Pot bearings are generally used for applications requiring a multidirectional rotational capacity and a medium to large range of load.

The primary components of a pot bearing are illustrated in Figure 3.3.86. The schematic in Figure 3.3.86 shows a sample pot bearing, but it does not necessarily represent the exact configuration of all pot bearings.

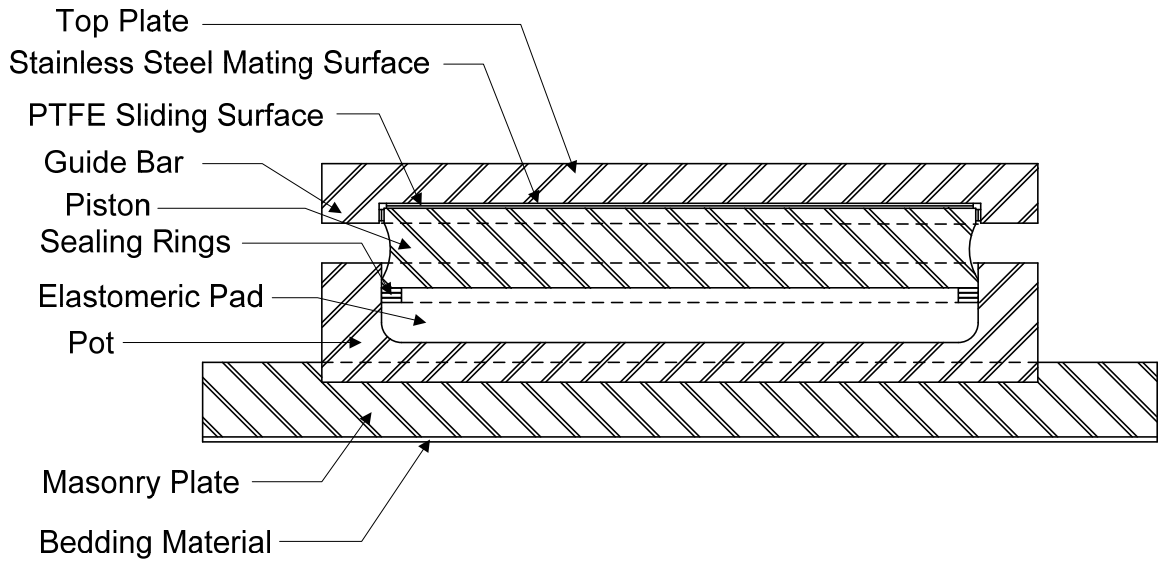


Figure 3.3.86 Components of a Pot Bearing

Pot bearings resist vertical load primarily through compressive stress in the elastomeric pad. The pad can deform and it has some shear stiffness, but it has

very limited compressibility. Pot bearings generally have a large reserve of strength against vertical load.

Pot bearings facilitate rotation through deformation of the elastomeric pad. During rotation, one side of the pad compresses and the other side expands. Pot bearings can sustain many cycles of small rotations with little or no damage. However, pot bearings can experience significant damage when subjected to relatively few cycles of large rotations.

Pot bearings can also resist horizontal loads. Pot bearings can either be fixed, guided, or non-guided. Fixed pot bearings can not translate in any direction, and they resist horizontal load primarily through contact between the rim of the piston and the wall of the pot. Guided pot bearings can translate in only one direction, and they resist horizontal load in the other direction through the use of guide bars. Non-guided bearings can translate in any direction, and they do not resist horizontal loads in any direction.

Although a pot bearing consists of many components (see Figure 3.3.86), only the elastomeric pad, sealing rings, pot, and piston require design computations. Therefore, there are a limited number of design steps:

1. Obtain required design input.
2. Select a feasible bearing type.
3. Select preliminary bearing properties.
4. Design the elastomeric pad.
5. Design the sealing rings.
6. Design the pot.
7. Design the piston.
8. Check the concrete or grout support.

These design steps are presented and illustrated through the following design example.

Pot Bearing Design Example

1. Obtain required design input

The required design input for this bearing design example is as follows:

Service limit state:
Total vertical load = 830 kips

Strength limit state:
Total vertical load = 1250 kips
Design rotation = 0.014 radians

Strength and extreme event limit states:
Total horizontal load = 70 kips

The minimum vertical load on a pot bearing should not be less than 20 percent of the vertical design load.

2. Select a feasible bearing type

To select a feasible bearing type, Figure 3.3.83, Figure 3.3.84, and Figure 3.3.85 may be used. Since the required service rotation is less than 0.014 radians, Figure 3.3.84 is applicable. For a total compressive load of 830 kips and a translation of 0 inches, the preliminary bearing selection diagram in Figure 3.3.84 shows that a pot bearing is a feasible bearing type for this application.

3. Select preliminary bearing properties

The next step is to select the preliminary bearing properties. These are obtained from the *AASHTO LRFD Bridge Design Specifications*, as well as from past experience. For this design, the following preliminary pot bearing properties were selected:

Maximum compressive stress on elastomer at service limit state = 3.5 ksi
Structural weathering steel: AASHTO M270 Grade 50
Pier cap concrete strength, f'_c = 4.0 ksi

4. Design the elastomeric pad

Pot bearings are generally designed for a compressive stress of 3.5 ksi on the elastomeric pad under total service load. The area of the elastomeric pad, as well as the pot, is controlled by this compressive stress requirement.

$$A_{pad} = \frac{830 \text{ kips}}{3.5 \text{ ksi}} = 237 \text{ inches}^2$$

$$D_p = \sqrt{\frac{4\ A_{pad}}{\pi}} = \sqrt{\frac{4(237 \text{ inches}^2)}{\pi}} = 17.4 \text{ inches}$$

Therefore, use an 18-inch diameter elastomeric pad.

$$\sigma_s = \frac{830 \text{ kips}}{\left[\frac{\pi(18 \text{ inches})^2}{4}\right]} = 3.26 \text{ ksi} < 3.5 \text{ ksi} \qquad \therefore \text{OK}$$

Based on *AASHTO LRFD* Article 14.7.4.3, the depth of the elastomeric pad, h_r, must satisfy the following strain requirement:

$$h_r \geq 3.33\, D_p\, \theta_u \qquad \text{Equation 3.3.193}$$

AASHTO LRFD Equation 14.7.4.3-1

where:

D_p = internal diameter of pot
θ_u = design rotation in radians

This equation limits the edge deflections due to rotation in the elastomeric pad to 15 percent of the nominal pad thickness. For this design example:

$$h_r \geq 3.33(18 \text{ inches})(0.014 \text{ radians}) = 0.84 \text{ inches}$$

Therefore, use an elastomeric pad depth, h_r, of 0.875 inches. In addition, the elastomeric pad should have a hardness between 50 and 60 Durometer, it should be lubricated (preferably with silicone grease), and it should provide a snug fit into the pot.

5. Design the sealing rings

Sealing rings provide a seal between the pot and the piston and can be provided in one of two configurations:

- Three rings with rectangular cross-sections
- One ring with circular cross-section

For three rings with rectangular cross-sections, the following geometric constraints are required:

$$\text{Width} \geq 0.02\, D_p \quad \text{and} \quad \text{Width} \geq 0.25 \text{ inches}$$

$$\text{Width} \leq 0.75 \text{ inches}$$

$$\text{Depth} \geq 0.2\ \text{Width}$$

For one ring with a circular cross-section, the cross-sectional diameter must satisfy the following equation:

$$\text{Diameter} \geq 0.0175\, D_p \quad \text{and} \quad \text{Diameter} \geq 0.15625 \text{ inches}$$

For this design example, three rings with rectangular cross-sections are being used. The width and depth of each ring are computed as follows:

$\text{Width} \geq 0.02\ D_p = 0.02(18\text{ inches}) = 0.36\text{ inches}$

and $\text{Width} \geq 0.25\text{ inches}$

$\text{Width} \leq 0.75\text{ inches}$

Therefore, use a ring width of 0.4 inches.

$\text{Depth} \geq 0.2\ \text{Width} = 0.2(0.4\text{ inches}) = 0.08\text{ inches}$

Using a ring width of 0.4 inches and a ring depth of 0.08 inches, the total thickness of the three rings is 0.24 inches. This is less than one-third of the pad thickness (0.875 inches / 3 = 0.292 inches), satisfying a common rule-of-thumb to control the concentration of elastomer strain at the rings.

6. Design the pot

The pot walls must be thick enough to resist both the internal hydrostatic pressure of the elastomeric pad and the pressure from any lateral loads. These two requirements are satisfied using the following two equations:

$$t_w \geq \frac{D_p\ \sigma_s}{1.25\ F_y} \quad \text{and} \quad t_w \geq 0.75\text{ inches} \qquad \text{Equation 3.3.194}$$

AASHTO LRFD Equations 14.7.4.6-5 and 14.7.4.6-6

$$t_w \geq \sqrt{\frac{25\ H_u\ \theta_u}{F_y}} \qquad \text{Equation 3.3.195}$$

AASHTO LRFD Equation 14.7.4.7-1

where:

σ_s = service average compressive stress due to total load
F_y = yield strength of the steel
H_u = lateral load from applicable strength and extreme event load combinations
θ_u = design strength limit state rotation

For this design example,

$$t_w \geq \frac{D_p\ \sigma_s}{1.25\ F_y} = \frac{(18\text{ inches})(3.26\text{ ksi})}{1.25\ (50\text{ ksi})} = 0.94\text{ inches}$$

and $t_w \geq 0.75\text{ inches}$

$$t_w \geq \sqrt{\frac{25\, H_u\, \theta_u}{F_y}} = \sqrt{\frac{25\,(70 \text{ kips})\,(0.014 \text{ radians})}{50 \text{ ksi}}} = 0.70 \text{ inches}$$

Therefore, for this design example, use a pot wall thickness of 1 inch.

Since the pot base must be thick enough to resist the moments from the cantilever bending of the walls, the lateral load equation for the pot wall also applies to the pot base:

$$t_b \geq \sqrt{\frac{25\, H_u\, \theta_u}{F_y}}$$

In addition, for a pot base that bears directly against concrete or grout:

$$t_b \geq 0.06\, D_p \quad \text{and} \quad t_b \geq 0.75 \text{ inches}$$

For a pot base that bears directly on steel girders or load distribution plates:

$$t_b \geq 0.04\, D_p \quad \text{and} \quad t_b \geq 0.50 \text{ inches}$$

For this design example, assuming that the pot base bears directly on load distribution plates:

$$t_b \geq \sqrt{\frac{25\, H_u\, \theta_u}{F_y}} = \sqrt{\frac{25\,(70 \text{ kips})\,(0.014 \text{ radians})}{50 \text{ ksi}}} = 0.70 \text{ inches}$$

$$t_b \geq 0.04\, D_p = 0.04\,(18 \text{ inches}) = 0.72 \text{ inches}$$
and $t_b \geq 0.50$ inches

Therefore, for this design example, the pot wall thickness is 1 inch and the pot base thickness is 0.75 inches.

7. <u>Design the piston</u>

The piston must be thick enough to provide sufficient rigidity and strength. Therefore, the piston thickness must satisfy the following minimum requirement:

$$t_{piston} \geq 0.06\, D_p$$

The height from the top of the rim to the underside of the piston, h_w, must satisfy all three of the following requirements:

$$h_w \geq \frac{1.5\ H_u}{D_p\ F_y} \quad \text{and} \quad h_w \geq 0.125 \text{ inches} \quad \text{and} \quad h_w \geq 0.03\ D_p \qquad \text{Equation 3.3.196}$$

AASHTO LRFD Equations 14.7.4.7-2 and 14.7.4.7-3 and 14.7.4.7-4

Finally, the clearance, c, between the inside diameter of the pot and the diameter of the piston rim must satisfy the following requirements:

$$c \geq \theta_u\left(h_w - \frac{D_p\ \theta_u}{2}\right) \quad \text{and} \quad c \geq 0.02 \text{ inches} \qquad \text{Equation 3.3.197}$$

AASHTO LRFD Equation 14.7.4.7-5

For this design example:

$$t_{piston} \geq 0.06\ D_p = 0.06(18 \text{ inches}) = 1.08 \text{ inches}$$
$$\therefore \text{Use } t_{piston} = 1.25 \text{ inches}$$

$$\frac{1.5\ H_u}{D_p\ F_y} = \frac{1.5(70 \text{ kips})}{(18 \text{ inches})(50 \text{ ksi})} = 0.12 \text{ inches}$$
$$\text{and} \quad 0.03\ D_p = 0.03(18 \text{ inches}) = 0.54 \text{ inches}$$
$$\therefore \text{Use } h_w = 0.54 \text{ inches}$$

$$c \geq \theta_u\left(h_w - \frac{D_p\ \theta_u}{2}\right)$$
$$= (0.014 \text{ radians})\left[0.54 \text{ inches} - \frac{(18 \text{ inches})(0.014 \text{ radians})}{2}\right]$$
$$= 0.0058 \text{ inches} \qquad \therefore \text{Use } c = 0.02 \text{ inches}$$

The PTFE must be designed and recessed based on the PTFE design criteria, and the piston thickness must take into account the PTFE recess requirements.

8. <u>Check the concrete or grout support</u>

The masonry plate of a pot bearing is designed similarly to masonry plates for other applications. Assuming that confinement reinforcement is absent in the concrete, the concrete bearing must satisfy the following requirement:

$$P_r = \phi P_n = \phi[0.85 f'_c\ A_1 m] \qquad \text{Equation 3.3.198}$$

AASHTO LRFD Equations 5.7.5-1 and 5.7.5-2

For this design example, assuming a masonry plate measuring 28 inches by 28 inches and assuming that the modification factor, m, equals 1:

$$P_r = \phi P_n = \phi[0.85f'_c A_1 m] = 0.70[0.85(4.0 \text{ ksi})(28 \text{ inches})^2(1)]$$
$$= 1866 \text{ kips} > 1250 \text{ kips} \qquad \therefore \text{OK}$$

The final pot bearing configuration for this design example is presented in Figure 3.3.87.

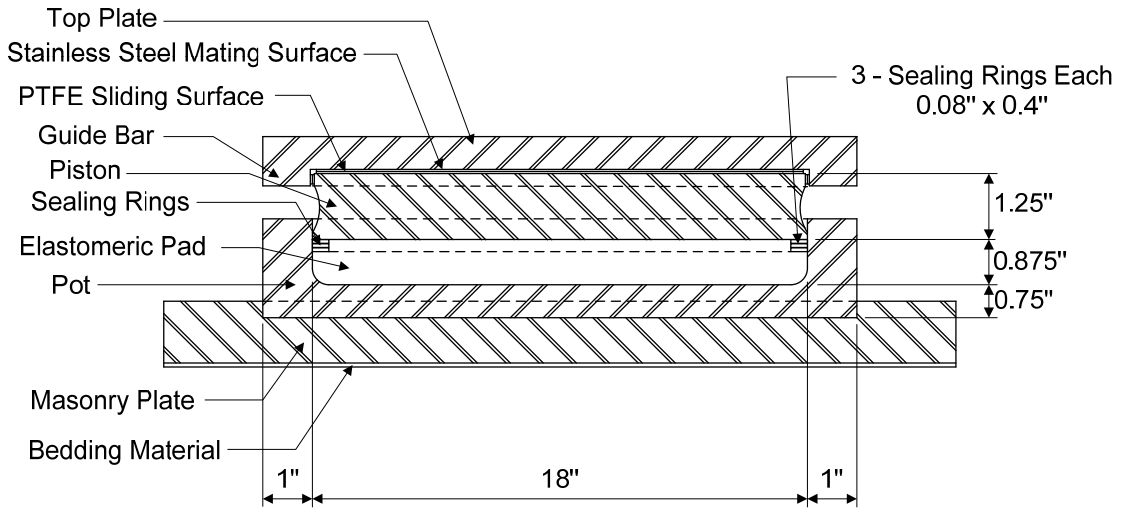
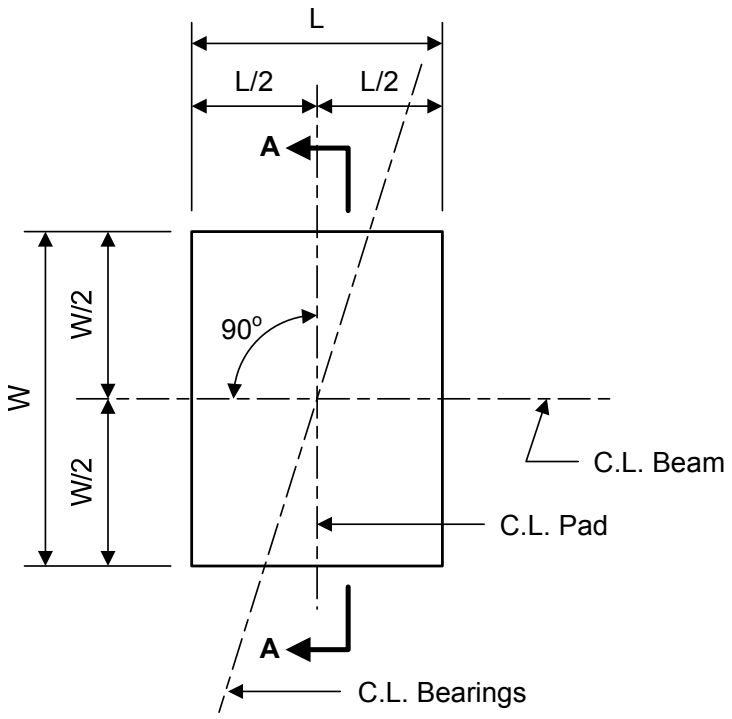


Figure 3.3.87 Final Configuration of Pot Bearing Design Example

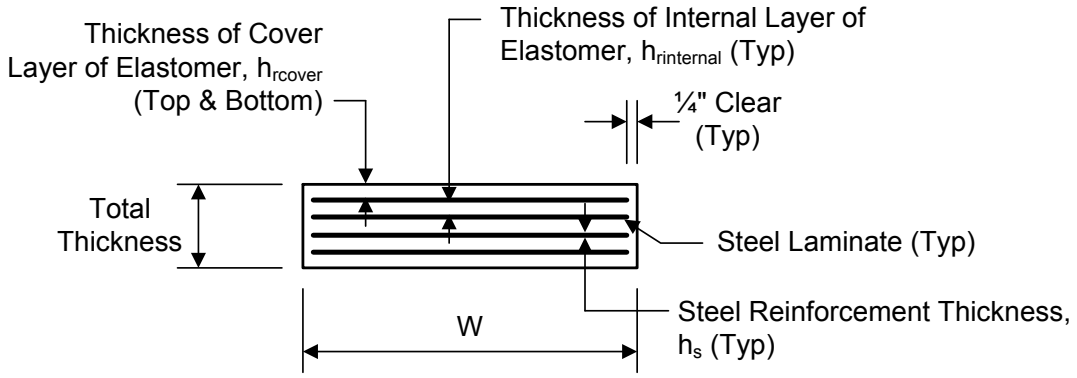
3.3.9.2.3 Elastomeric Bearings

Elastomeric bearings are commonly used on small to moderate sized bridges. There are two general types of elastomeric bearings – plain and reinforced. As the name suggests, plain elastomeric pads consist entirely of elastomer, and they are usually rectangular in shape. Plain elastomeric pads can be used for small bridges, in which the vertical loads, translations, and rotations are relatively small.

Reinforced elastomeric pads are often used for larger bridges with more sizable vertical loads, translations, and rotations. Reinforced elastomeric pads consist of multiple layers of elastomer bonded to layers of reinforcing material, such as steel plate, fiberglass, or cotton-duck. A sample reinforced elastomeric pad is illustrated in Figure 3.3.88.



Plan



Section A-A

Figure 3.3.88 Reinforced Elastomeric Pad

There are two methods available for designing elastomeric bearings – Design Method A and Design Method B. Design Method A usually results in a bearing with a lower capacity than a bearing designed with Method B. However, Method B requires additional testing and quality control.

The design of an elastomeric bearing generally involves the following steps:

1. Obtain required design input.
2. Select a feasible bearing type.
3. Select preliminary bearing properties.
4. Select design method (Design Method A or B).
5. Compute shape factor.
6. Check compressive stress.
7. Check compressive deflection.
8. Check shear deformation.
9. Check rotation (Design Method A) or combined compression and rotation (Design Method B).
10. Check stability.
11. Check reinforcement.
12. Check anchorage (Design Method A) or design for seismic provisions (Design Method B).

Design Method A

For Design Method A, these design steps are presented and illustrated through the following design example for a steel-reinforced elastomeric pad at an abutment. The bearings are expansion only in the longitudinal direction; they are fixed in the transverse direction. The following requirements for Design Method A are further described in *AASHTO LRFD* Article 14.7.6.

1. Obtain required design input

The required design input for this bearing for the service limit state is as follows:

DL = 78.4 kips
LL+I = 110.4 kips
Design rotation = 0.007 radians
Design longitudinal translation = 0.76 inches
Minimum vertical force due to permanent load, P_{sd} = 67.8 kips

Therefore, the total service limit state vertical load is as follows:

DL + LL+I = 78.4 kips + 110.4 kips = 188.8 kips

The design requirements for the strength limit state are as follows:

Factored shear force = 8.6 kips

2. Select a feasible bearing type

To select a feasible bearing type, Figure 3.3.83, Figure 3.3.84, and Figure 3.3.85 may be used. Since the required rotation is 0.007 radians, Figure 3.3.84 is applicable. For a total compressive load of 188.8 kips and a translation of 0.76 inches, the preliminary bearing selection diagram in Figure 3.3.84 shows that steel-reinforced elastomeric bearings are a feasible bearing type.

3. Select preliminary bearing properties

The next step is to select the preliminary bearing properties. These are obtained from the *AASHTO LRFD Bridge Design Specifications*, as well as from past experience. For this design, the following preliminary bearing pad configuration was selected (see Figure 3.3.88 for illustration of terminology):

Pad length, L = 14 inches
Pad width, W = 15 inches
Elastomer cover thickness, h_{rcover} = 0.25 inches
Elastomer internal layer thickness, $h_{rinternal}$ = 0.375 inches
Number of steel reinforcement layers = 9
Steel reinforcement thickness, h_s = 0.1196 inches

In addition, the following material properties were selected:

Elastomer hardness = 50 (*AASHTO LRFD* Article 14.7.6.2)
Elastomer shear modulus, G = 0.095 ksi (*AASHTO LRFD* Table 14.7.5.2-1)
Elastomer creep deflection at 25 years divided by instantaneous deflection = 0.25 (*AASHTO LRFD* Table 14.7.5.2-1)
Steel reinforcement yield strength, F_y = 50 ksi
Steel reinforcement constant-amplitude fatigue threshold for Detail Category A, ΔF_{TH} = 24.0 ksi (*AASHTO LRFD* Table 6.6.1.2.5-3)

4. Select design method (Design Method A or B)

Since additional testing and quality control is not desired for this bridge, Design Method A is selected.

5. Compute shape factor

The next step is to compute the shape factor. The shape factor for individual elastomer layers is the plan area divided by the area of the perimeter free to bulge. For steel-reinforced elastomeric bearings, the following requirements must be satisfied before calculating the shape factor:

1. All internal layers of elastomer must be the same thickness.
2. The thickness of the cover layers cannot exceed 70 percent of the thickness of the internal layers.

For this design example, all internal layers are 0.375 inches thick. The thickness of the cover layers (0.25 inches) is 66.7 percent of the thickness of the internal layers (0.375 inches). Therefore, both of these requirements are satisfied.

For rectangular bearings without holes, the shape factor for the i^{th} layer is:

$$S_i = \frac{L\ W}{2\ h_{ri}\ (L + W)} \qquad \text{Equation 3.3.199}$$

AASHTO LRFD Equation 14.7.5.1-1

For the internal layers of elastomer, the shape factor is computed as follows:

$$S_{internal} = \frac{(14 \text{ inches})\ (15 \text{ inches})}{2\ (0.375 \text{ inches})\ (14 \text{ inches} + 15 \text{ inches})} = 9.66$$

For the cover layers of elastomer, the shape factor is computed as follows:

$$S_{cover} = \frac{(14 \text{ inches})\ (15 \text{ inches})}{2\ (0.25 \text{ inches})\ (14 \text{ inches} + 15 \text{ inches})} = 14.48$$

6. <u>Check compressive stress</u>

For steel-reinforced elastomeric bearings, the compressive stress in the elastomer at the service limit state is limited by each of the following two equations, in which S is based on the thickest layer of the bearing:

$$\sigma_s \le 1.0 \text{ ksi} \quad \text{and} \quad \sigma_s \le 1.0\ G\ S \qquad \text{Equation 3.3.200}$$

AASHTO LRFD Equation 14.7.5.3.2-4

For this bearing design,

$$\sigma_s = \frac{188.8 \text{ kips}}{(14 \text{ inches})(15 \text{ inches})} = 0.899 \text{ ksi} < 1.0 \text{ ksi} \qquad \therefore \text{ OK}$$

$$\sigma_s = 0.899 \text{ ksi} < 0.917 \text{ ksi} = 1.0(0.095 \text{ ksi})(9.66) = 1.0\ G\ S \qquad \therefore \text{ OK}$$

Therefore, the compressive stress requirements are satisfied for this bearing.

7. Check compressive deflection

The instantaneous compressive deflection is obtained from the following equation:

$$\delta = \sum \varepsilon_i \, h_{ri} \qquad \text{Equation 3.3.201}$$

AASHTO LRFD Equation 14.7.5.3.3-1

where:

ε_i = instantaneous compressive strain in the i^{th} elastomer layer
h_{ri} = thickness of the i^{th} elastomeric layer

Since test results are not available for this design example, the instantaneous compressive strain can be approximated from *AASHTO LRFD* Figure C14.7.5.3.3-1. For 50 durometer reinforced bearings with a compressive stress of 0.899 ksi and shape factor of 9.66, the compressive strain is approximately 4.0%. For the cover layers, with a shape factor of 14.48, the compressive strain is approximately 3.3%. Therefore, the instantaneous deflection is computed as follows:

$$\delta = \left[2(0.25 \text{ inches})(0.033)\right] + \left[8(0.375 \text{ inches})(0.040)\right] = 0.137 \text{ inches}$$

In addition, the effects of creep should also be considered. For this design example, material-specific data is not available. As presented in the material properties, the elastomer creep deflection at 25 years divided by the instantaneous deflection equals 0.25 (*AASHTO LRFD* Table 14.7.5.2-1). Therefore, the total deflection value, which includes both the instantaneous deflection and the effects of creep, can be computed as follows:

$$\delta_{total} = \delta_{instantaneous} + \delta_{creep} = (0.137 \text{ inches})(1 + 0.25) = 0.171 \text{ inches}$$

The initial compressive deflection in any layer of a steel-reinforced elastomeric bearing at the service limit state without dynamic load allowance can not exceed $0.07h_{ri}$. For this design example:

$$\delta_{internal} = \varepsilon_{internal} \, h_{rinternal} = (0.040)(0.375 \text{ inches}) = 0.015 \text{ inches}$$

$$0.07 \, h_{rinternal} = (0.07)(0.375 \text{ inches}) = 0.026 \text{ inches} > 0.015 \text{ inches} \qquad \therefore \text{ OK}$$

8. Check shear deformation

The shear deformation is checked to ensure that the bearing can facilitate the anticipated horizontal bridge movement. Also, the shear deformation is limited to avoid rollover at the edges and delamination due to fatigue. The total horizontal movement for this bridge design example is based on thermal effects only and is presented in the design requirements as 0.76 inches. Other criteria that could add to

the shear deformation include construction tolerances, braking force, and longitudinal wind, if applicable. One factor that can reduce the amount of shear deformation is pier flexibility. For a steel-reinforced elastomeric bearing, the smaller of the total elastomer thickness or the bearing thickness must satisfy the following equation:

$$h_{rt} \geq 2\,\Delta_s$$ Equation 3.3.202

AASHTO LRFD Equation 14.7.6.3.4-1

In this example, this requirement is checked as follows:

$$h_{rt} = 2(0.25 \text{ inches}) + 8(0.375 \text{ inches}) = 3.50 \text{ inches}$$

$$2\Delta_s = 2(0.76 \text{ inches}) = 1.52 \text{ inches} < 3.50 \text{ inches} \qquad \therefore \text{ OK}$$

9. <u>Check rotation</u>

Rotation is checked to ensure that no point in the bearing experiences net uplift. The rotation about the transverse axis is checked as follows:

$$\sigma_s \geq 0.5\,G\,S\left(\frac{L}{h_{ri}}\right)^2\left(\frac{\theta_{s,x}}{n}\right)$$ Equation 3.3.203

AASHTO LRFD Equation 14.7.6.3.5d-1

Similarly, the rotation about the longitudinal axis is checked as follows:

$$\sigma_s \geq 0.5\,G\,S\left(\frac{W}{h_{ri}}\right)^2\left(\frac{\theta_{s,z}}{n}\right)$$ Equation 3.3.204

AASHTO LRFD Equation 14.7.6.3.5d-2

where:
n = number of interior layers of elastomer that are bonded on each face

If the thickness of the elastomer cover layers is greater than one-half the thickness of the interior layers, then the value of n may be increased by ½ for each such cover layer. Therefore, for this design example:

$$n = ½ + 8 + ½ = 9$$

For this design example, the service rotation due to total load is about the transverse axis and is presented in the design requirements as 0.007 radians. For elastomeric pads and steel-reinforced elastomeric bearings, an additional rotation of 0.005 radians must be included as an allowance for uncertainties unless an approved quality control plan justifies a smaller value (as specified in *AASHTO LRFD* Article

14.4.2). Since this additional rotation of 0.005 radians must be added to the service rotation of 0.007 radians, the total rotation for this design example is 0.012 radians.

$$0.5\ G\ S\left(\frac{L}{h_{ri}}\right)^2\left(\frac{\theta_{s,x}}{n}\right) = 0.5(0.095\ \text{ksi})(9.66)\left(\frac{14\ \text{inches}}{0.375\ \text{inches}}\right)^2\left(\frac{0.012}{9}\right) = 0.853\ \text{ksi}$$

$$\sigma_s = 0.899\ \text{ksi} > 0.853\ \text{ksi} \qquad \therefore \text{OK}$$

The service rotation due to the total load about the longitudinal axis is negligible compared to the service rotation about the transverse axis. Therefore, the rotation check about the longitudinal axis is not computed in this bearing design example.

10. <u>Check stability</u>

The total thickness of the rectangular pad must not exceed one-third of the pad length or one-third of the pad width, or expressed mathematically:

$$h_{total} \le \frac{L}{3} \quad \text{and} \quad h_{total} \le \frac{W}{3} \qquad \text{Equation 3.3.205}$$

AASHTO LRFD Article 14.7.6.3.6

For this design example:

$$h_{total} = 2(0.25\ \text{inches}) + 8(0.375\ \text{inches}) + 9(0.1196\ \text{inches})$$
$$= 4.5764\ \text{inches}$$

$$\frac{L}{3} = \frac{14\ \text{inches}}{3} = 4.67\ \text{inches} > 4.5764\ \text{inches} \qquad \therefore \text{OK}$$

$$\frac{W}{3} = \frac{15\ \text{inches}}{3} = 5.0\ \text{inches} > 4.5764\ \text{inches} \qquad \therefore \text{OK}$$

Therefore, the bearing pad satisfies the stability requirements.

11. <u>Check reinforcement</u>

The steel reinforcement thickness must be able to sustain the tensile stresses induced by compression in the bearing. The reinforcement thickness must also satisfy the requirements of the *AASHTO LRFD Bridge Construction Specifications*. For this design example, the thickness of the steel reinforcement, h_s, is 0.1196 inches.

For the service limit state:

$$h_s \geq \frac{3\, h_{max}\, \sigma_s}{F_y}$$ Equation 3.3.206

AASHTO LRFD Equation 14.7.5.3.7-1

$$h_s \geq \frac{3\, h_{max}\, \sigma_s}{F_y} = \frac{3(0.375 \text{ inches})(0.899 \text{ ksi})}{50 \text{ ksi}} = 0.0202 \text{ inches} \qquad \therefore \text{OK}$$

For the fatigue limit state:

$$h_s \geq \frac{2.0\, h_{max}\, \sigma_L}{\Delta F_{TH}}$$ Equation 3.3.207

AASHTO LRFD Equation 14.7.5.3.7-2

$$\sigma_L = \frac{110.4 \text{ kips}}{(14 \text{ inches})(15 \text{ inches})} = 0.526 \text{ ksi}$$

As presented in the material properties, the steel reinforcement constant-amplitude fatigue threshold for Detail Category A, ΔF_{TH}, is 24.0 ksi.

$$h_s \geq \frac{2.0\, h_{max}\, \sigma_L}{\Delta F_{TH}} = \frac{2.0(0.375 \text{ inches})(0.526 \text{ ksi})}{24.0 \text{ ksi}} = 0.0164 \text{ inches} \qquad \therefore \text{OK}$$

Therefore, the steel reinforcement thickness satisfies both the service limit state and fatigue limit state requirements.

12. Check anchorage

The bearing pad must be secured against horizontal movement if the factored shear force sustained by the deformed pad at the strength limit state exceeds one-fifth of the minimum vertical force due to permanent load, P_{sd}.

As previously defined, the minimum vertical force due to permanent load, P_{sd}, is 67.8 kips and the factored shear force at the strength limit state is 8.6 kips. The need for anchorage is checked as follows:

$$\frac{P_{sd}}{5} > V_{strength}$$ Equation 3.3.208

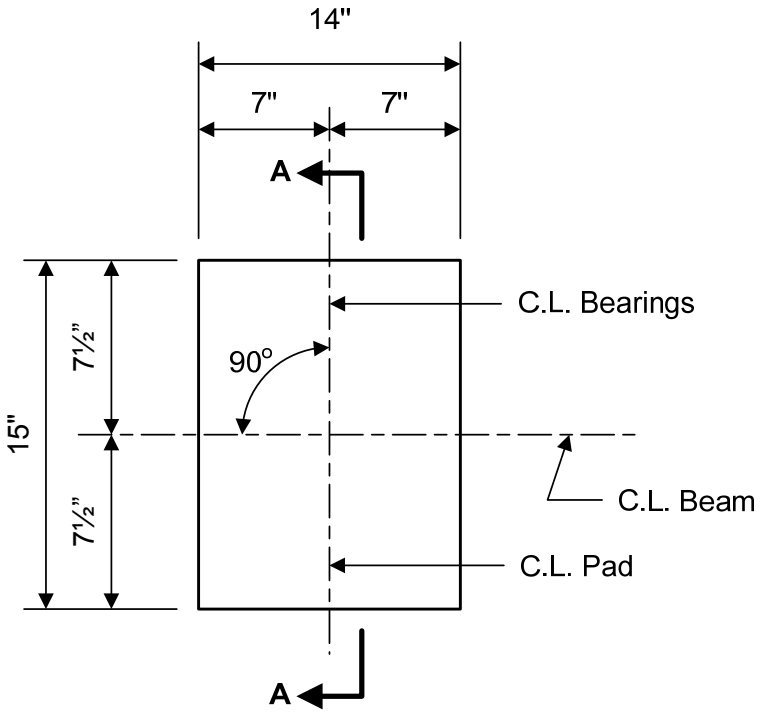
AASHTO LRFD Article 14.7.6.3.7

$$\frac{P_{sd}}{5} = \frac{67.8 \text{ kips}}{5} = 13.6 \text{ kips} > 8.6 \text{ kips} = V_{strength}$$

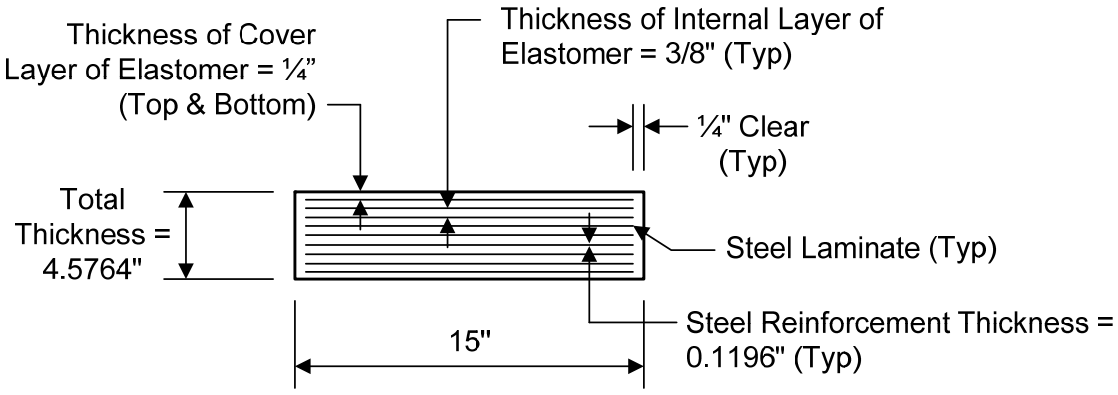
Therefore, for this design example, the bearing pad does not need to be secured against horizontal movement.

The abutment bearings are expansion in the longitudinal direction but fixed in the transverse direction. Therefore, the bearings must be restrained in the transverse direction. Based on the previous computation, the expansion bearing pad does not need to be secured against horizontal movement. However, the horizontal connection must satisfy the seismic requirements of *AASHTO LRFD* Article 3.10.9. This check will be described in a later section of this chapter.

A schematic showing a plan view and sectional view of the final elastomeric bearing configuration is presented in Figure 3.3.89.



Plan



Section A-A

Figure 3.3.89 Final Configuration of Elastomeric Bearing Design Example

Design Method B

Many of the design procedures for Design Method B are similar to those of Design Method A. However, some primary differences between the two methods are summarized in Table 3.3.11.

Table 3.3.11 Elastomeric Bearing Design Methods A and B

Characteristic	Design Method A	Design Method B
Application	Applicable for plain elastomeric pads and steel-reinforced elastomeric bearings	Applicable for steel-reinforced elastomeric bearings only
AASHTO LRFD reference	*AASHTO LRFD* Article 14.7.6	*AASHTO LRFD* Article 14.7.5
Bearing capacity	Stress limits for Design Method A usually result in a bearing with a lower capacity than with Method B	Stress limits for Design Method B usually result in a bearing with a higher capacity than with Method A
Additional testing and quality control	Does not require additional testing and quality control	Requires additional testing and quality control
Design steps unique to that method	• Check rotation • Check anchorage	• Check combined compression and rotation • Design for seismic provisions

3.3.9.2.4 Disc Bearings

Disc bearings consist of an unconfined elastomeric disc. Disc bearings are more economical than many other steel bearing types, and they are frequently used when smaller load capacity is required. Disc bearings may be movable, guided, unguided, or fixed. Movement is accommodated by sliding of polished stainless steel on PTFE.

3.3.9.3 Bearing Anchorage

Bearings which are intended to be fixed in either the longitudinal or transverse direction must be designed for restraint in the direction of fixity. That is, if a bridge is designed such that the bearings at a specific substructure unit are fixed in one or both directions, then those bearings must be designed to provide restraint in those directions.

In addition to the requirements presented in previous sections of this chapter, *AASHTO LRFD* Article 3.10.9 provides additional bearing anchorage requirements. For example, assuming that the bridge in the previous elastomeric bearing design example is located in Seismic Zone 1, *AASHTO LRFD* Article 3.10.9.2 specifies that the horizontal design connection force in the restrained directions must be at least equal to 0.2 times the vertical reaction due to the tributary permanent load and the tributary live loads assumed to exist during an earthquake. This minimum design value is intended to relieve the engineer from a more rigorous analysis for bridges in parts of the country with very low seismicity.

For the previous elastomeric bearing design example, since all abutment bearings are restrained in the transverse direction, the tributary permanent load can be taken as the reaction at the bearing. Assuming that γ_{EQ} equals zero (see *AASHTO LRFD* Article 3.4.1), no tributary live load will be considered.

$$H_{EQ} = 0.2\ DL \qquad \text{Equation 3.3.209}$$

$$H_{EQ} = 0.2\ (78.4\ \text{kips}) = 15.7\ \text{kips}$$

For two 7/8" diameter A 307 bolts with a minimum tensile strength of 60 ksi, the factored shear resistance for threads excluded from the shear plane is computed as follows in accordance with *AASHTO LRFD* Article 6.13.2.7:

$$R_n = 0.48 A_b F_{ub} N_s \qquad \text{Equation 3.3.210}$$

AASHTO LRFD Equation 6.13.2.12

$$R_n = 0.48(2\ \text{bolts})(0.60\ \text{inches}^2/\text{bolt})(60\ \text{ksi})(1\ \text{shear plane/bolt})$$
$$= 34.6\ \text{kips}$$

$$R_r = \phi_s R_n \qquad \text{Equation 3.3.211}$$

AASHTO LRFD Equation 6.13.2.2-2

$$R_r = (0.65)(34.6\ \text{kips}) = 22.5\ \text{kips} > 15.7\ \text{kips} \qquad \therefore \text{OK}$$

After the anchor bolt size and quantity have been determined, the anchor bolt length must also be computed. As an approximation, the bearing stress may be assumed to vary linearly from zero at the end of the embedded length to its maximum value at the top surface of the concrete, in accordance with *AASHTO*

LRFD Article 14.8.3.1. The bearing resistance of the concrete is based on *AASHTO LRFD* Article 5.7.5. Assuming that the modification factor, m, equals 1, the bearing stress is computed as follows:

$$P_r = \phi_b P_n = \phi_b 0.85 f'_c A_1 m \qquad \text{Equation 3.3.212}$$

AASHTO LRFD Equations 5.7.5-1 and 5.7.5-2

$$f_{brg} = \frac{P_r}{A_1} = \frac{\phi_b 0.85 f'_c A_1 m}{A_1} = \phi_b 0.85 f'_c m \qquad \text{Equation 3.3.213}$$

$$f_{brg} = (0.70)(0.85)(4.0 \text{ ksi})(1) = 2.38 \text{ ksi}$$

The total transverse horizontal force acting on each bolt is:

$$H_{EQ} \text{ /bolt} = \frac{15.7 \text{ kips}}{2 \text{ bolts}} = 7.9 \text{ kips/bolt}$$

Using the linear bearing stress approximation from above, the required anchor bolt area resisting the transverse horizontal load can be calculated:

$$A_1 = \frac{H_{EQ}/\text{bolt}}{\frac{0 + f_{brg}}{2}} = \frac{7.9 \text{ kips/bolt}}{\frac{0 + 2.38 \text{ ksi}}{2}} = 6.6 \text{ inches}^2$$

A_1 is the product of the anchor bolt diameter and the anchor bolt length of embedment into the concrete pedestal or beam seat. Since the anchor bolt diameter is known, the required anchor bolt length can be computed as follows:

$$A_1 = (\text{Length}_{bolt})(\text{Diameter}_{bolt}) \qquad \text{Equation 3.3.214}$$

$$\text{Length}_{bolt} = \frac{A_1}{\text{Diameter}_{bolt}} = \frac{6.6 \text{ inches}^2}{0.875 \text{ inches}} = 7.6 \text{ inches} \qquad \text{Use 8 inches}$$

In addition to the above calculations, individual states and agencies may have their own bearing design and anchor bolt requirements.

3.3.10 References

1. Slutter, R.G., and Fisher, J.W. 1966. "Fatigue Strength of Shear Connectors." *Highway Research Record No. 147*, Highway Research Board, Washington, D.C.
2. Ollgard, J.G., Slutter, R.G., and Fisher, J.W. 1971. "Shear Strength of Stud Connectors in Lightweight and Normal Weight Concrete." *AISC Engineering Journal*, American Institute of Steel Construction, Chicago, IL, Vol. 8, No. 2, April.
3. ASCE. 2000. *Design of Latticed Steel Transmission Structures*. ASCE 10-97, American Society of Civil Engineers, Reston, VA.
4. AISC. 2005. *Specification for Structural Steel Buildings*. ANSI/AISC 360-05, American Institute of Steel Construction, Chicago, IL, March 9.
5. CEN. 1993. *Eurocode 3: Design of Steel Structures, Part 1.1 – General Rules and Rules for Buildings*, ENV 1992-1-1, European Committee for Standardization, Brussels, Belgium.
6. BSI. 1990. "BS5950: Part 1: 1990, Structural Use of Steelwork in Buildings, Part 1, Code of Practice for Design in Simple and Continuous Construction: Hot Rolled Sections." British Standards Institution, London.
7. Brown, J.D., Lubitz, D.J., Cekov, Y.C., and Frank, K.H. 2007. *Evaluation of Influence of Hole Making Upon the Performance of Structural Steel Plates and Connections*. Report No. FHWA/TX-07/0-4624-1, University of Texas at Austin, Austin, TX.
8. McGuire, W. 1968. *Steel Structures*. Prentice-Hall, Inc., Englewood Cliffs, NJ.
9. Munse, W.H., Chesson, Jr., E. 1963. "Riveted and Bolted Joints: Net Section Design." *Journal of the Structural Division*, American Society of Civil Engineers, New York, NY, Vol. 83, No. ST2, February.
10. Easterling, W.S., and Giroux, L.G. 1993. "Shear Lag Effects in Steel Tension Members." *AISC Engineering Journal*, American Institute of Steel Construction, Chicago, IL, Vol. 30, No. 3, 3rd Qtr.
11. Ricles, J.M., and Yura, J.A. 1983. "Strength of Double-Row Bolted Web Connections." *Journal of the Structural Division*, American Society of Civil Engineers, New York, NY, Vol. 109, No. ST1, January.
12. Hardash, S., and Bjorhovde, R. 1985. "New Design Criteria for Gusset Plates in Tension." *AISC Engineering Journal*, American Institute of Steel Construction, Chicago, IL, Vol. 22, 2nd Qtr.
13. Birkemoe, P.C., and Gilmour, M.I. 1978. "Behavior of Bearing Critical Double-Angle Beam Connections." *AISC Engineering Journal*, American Institute of Steel Construction, Chicago, IL, Vol. 15, No. 4, 4th Qtr.
14. Kulak, G.L., and Grondin, G.Y. 2001. "AISC LRFD Rules for Block Shear – A Review." *AISC Engineering Journal*, American Institute of Steel Construction, Chicago, IL, Vol. 38, No. 4, 4th Qtr.
15. McDonald, G.S., and Frank, K.H. 2009. "The Fatigue Performance of Angle Cross-Frame Members in Bridges." Ferguson Structural Engineering Laboratory Report FSEL No: 09-1, University of Texas at Austin, Austin, TX, December 2009.

16 Galambos, T.V., ed. 1998. *Guide to Stability Design Criteria for Metal Structures*. 5th Edition, Structural Stability Research Council, John Wiley and Sons, Inc., New York, NY.
17. Tide, R.H.R. 1985. "Reasonable Column Design Equations." Proceedings of the Annual Technical Session and Meeting. Cleveland, OH, April 16-17, Structural Stability Research Council, University of Missouri, Rolla, MO.
18. Tide, R.H.R. 2001. "A Technical Note: Derivation of the LRFD Column Design Equations." *AISC Engineering Journal*, American Institute of Steel Construction, Chicago, IL, Vol. 38, No. 3, 3rd Qtr.
19. Salmon, C.G., and Johnson, J.E. 1996. *Steel Structures – Design and Behavior*, Fourth Edition, HarperCollins College Publishers, New York, NY.
20. Hall, D.H. 1981. "Proposed Steel Column Strength Criteria." *Journal of the Structural Division*, American Society of Civil Engineers, New York, NY, Vol. 107, No. ST4, April.
21. HNI. 2007. "Load and Resistance Factor Design (LRFD) for Highway Bridge Superstructures – Design Manual." FHWA Report No. FHWA-NHI 07-035, Federal Highway Administration, National Highway Institute, Washington, D.C.
22. Usami, T., and Galambos, T.V. 1971. "Eccentrically Loaded Single-Angle Columns." International Association for Bridge and Structural Engineering, Zurich, Switzerland.
23. Woolcock, S.T., and Kitipornchai, S. 1986. "Design of Single-Angle Web Struts in Trusses." *Journal of Structural Engineering*, American Society of Civil Engineers, New York, NY, Vol. 112, No. ST6, June.
24. Mengelkoch, N.S., and Yura, J.A. 2002. "Single-Angle Compression Members Loaded Through One Leg." *Proceedings of the Annual Technical Session and Meeting*, Structural Stability Research Council, University of Missouri, Rolla, MO.
25. Lutz, L.A. 1996. "A Closer Examination of the Axial Capacity of Eccentrically Loaded Single Angle Struts." *AISC Engineering Journal*, American Institute of Steel Construction, Chicago, IL, Vol. 33, No. 2, 2nd Qtr.
26. Lutz, L.A. 2006. "Evaluating Single Angle Compression Struts Using an Effective Slenderness Approach." *AISC Engineering Journal*, American Institute of Steel Construction, Chicago, IL, Vol. 43, No. 4, 4th Qtr.
27. Foehl, P.J. 1948. "Direct Method of Designing Single Angle Struts in Welded Trusses." *Design Book for Welding*, Lincoln Electric Company, Cleveland, OH, November.
28. Trahair, N.S., Usami, T., and Galambos, T.V. 1969. "Eccentrically Loaded Single-Angle Columns." *Research Report No. 11*, Civil and Environmental Engineering Department, Washington University, St. Louis, MO.
29. AISI. 1969. *Specification for the Design of Cold-Formed Steel Structural Members*, American Iron and Steel Institute, Washington, D.C.
30. NSBA. 2010. "Chapter 6: Structural Behavior of Steel." *NSBA Steel Bridge Design Handbook*, available from the National Steel Bridge Alliance (www.steelbridges.org), Chicago, IL.

31. Kitipornchai, S., and Trahair, N.S. 1980. "Buckling Properties of Monosymmetric I-Beams." *Journal of the Structural Division*, American Society of Civil Engineers, New York, NY, Vol. 109, No. ST5.
32. Ellifritt, D.S., Wine, G., Sputo, T., and Samuel, S. 1992. "Flexural Strength of WT Sections." *AISC Engineering Journal*, American Institute of Steel Construction, Chicago, IL, Vol. 29, No. 2, 2nd Qtr.
33. AISC. 2005. *Steel Construction Manual*, 13th ed. American Institute of Steel Construction, Chicago, IL, December.
34. Ugural, A.C., and Fenster, S.K. 1978. *Advanced Strength and Applied Elasticity*. Elsevier-North Holland Publishing Co., Inc., New York, NY.
35. Darwin, D. 1990. *Steel and Composite Beams with Web Openings*. AISC Steel Design Guide Series No. 2, American Institute of Steel Construction, Chicago, IL.
36. Kulak, G.L., Fisher, J.W., and Struik, J.H.A. 1987. *Guide to Design Criteria for Bolted and Riveted Joints*. 2nd Edition, John Wiley & Sons, New York, NY.
37. Huhn, H., and Valtinat, G. 2004. "Bolted Connections with Hot Dip Galvanized Steel Members with Punched Holes." *Proceedings of the ECCS/AISC Workshop, Connections in Steel Structures V: Innovative Steel Connections*, June 3-5, 2004, European Convention for Constructional Steelwork/American Institute of Steel Construction, Amsterdam.
38. Batho, C., and Bateman, E.H. 1934. *Investigations on Bolts and Bolted Joints*. Second Report of the Steel Structures Research Committee, London; His Majesty's Stationary Office.
39. Wilson, W.M., and Thomas, F.P. 1938. "Fatigue Tests on Riveted Joints." Bulletin 302, University of Illinois, Engineering Experiment Station, Urbana, IL.
40. Munse, W.H. 1956. "Research on Bolted Connections." Transactions, American Society of Civil Engineers, New York, NY, No. 121.
41. Research Council on Structural Connections. 2009. *Specification for Structural Joints Using High-Strength Bolts*. c/o American Institute of Steel Construction, Chicago, IL, December 31.
42. Rumpf, J.L., and Fisher, J.W. 1963. "Calibration of A 325 Bolts." *Journal of the Structural Division*, American Society of Civil Engineers, Vol. 89, No. ST6, December.
43. Sterling, G.H., et al. 1965. "Calibration Tests of A 490 High Strength Bolts." *Journal of the Structural Division*, American Society of Civil Engineers, Vol. 91, No. ST5, October.
44. AASHTO. 2010. *LRFD Bridge Construction Specifications*. Third Edition, American Association of State Highway and Transportation Officials, Washington, D.C.
45. Struik, J.H.A., Oyeledun, A.O., and Fisher, J.W. 1973. "Bolt Tension Control with a Direct Tension Indicator." *AISC Engineering Journal*, American Institute of Steel Construction, Chicago, IL, Vol. 10, 1st Qtr.
46. Brockenbrough, R.L. 1983. "Considerations in the Design of Bolted Joints for Weathering Steel." *AISC Engineering Journal*, American Institute of Steel Construction, Chicago, IL, Vol. 20, 1st Qtr.
47. Birkemoe, P.C., and Herrschaft, D.C. 1970. "Bolted Galvanized Bridges: Engineering Acceptance Near." *Civil Engineering*, American Society of Civil Engineers, New York, NY, Vol. 40, No. 4, April.

48. Yura, J.A., Frank, K.H., and Cayes, L. 1981. "Bolted Friction Connections with Weathering Steel." *Journal of the Structural Division*, American Society of Civil Engineers, Vol. 107, No. ST11, November.
49. Mathay, W.L. 1993. *Uncoated Weathering Steel Bridges*. Highway Structures Design Handbook, Volume 1, Chapter 9, available from the National Steel Bridge Alliance, Chicago, IL.
50. Polyzois, D., and Frank, K.H. 1986. "Effect of Overspray and Incomplete Masking of Faying Surfaces on the Slip Resistance of Bolted Connections." *AISC Engineering Journal*, American Institute of Steel Construction, Chicago, IL, Vol. 23, 2nd Qtr.
51. Yura, J.A., and Frank, K.H. 1985. "Testing Method to Determine Slip Coefficient for Coatings Used in Bolted Joints." *AISC Engineering Journal*, American Institute of Steel Construction, Chicago, IL, Vol. 22, No. 3, 3rd Qtr.
52. Frank, K.H., and Yura, J.A. 1981. "An Experimental Study of Bolted Shear Connections." FHWA/RD-81/148, Federal Highway Administration, Washington, D.C., December.
53. Chesson, E., Faustino, N.L., and Munse, W.H. 1965. "High-Strength Bolts Subject to Tension and Shear." *Journal of the Structural Division*, American Society of Civil Engineers, New York, NY, Vol. 91, No. ST5, October.
54. Research Council on Structural Connections. 1988. *Load and Resistance Factor Design Specification for Structural Joints Using ASTM A325 or A490 Bolts*. c/o American Institute of Steel Construction, Chicago, IL, June.
55. Fisher, J.W. 1965. "Behavior of Fasteners and Plates with Holes." *Journal of the Structural Division*, American Society of Civil Engineers, New York, NY, Vol. 91, No. ST6, December.
56. Crawford, S.F., and Kulak, G.L. 1971. "Eccentrically Loaded Bolted Connections." *Journal of the Structural Division*, American Society of Civil Engineers, New York, NY, Vol. 97, No. ST3, March.
57. AISC. 1963. *Manual of Steel Construction*. 6th ed. American Institute of Steel Construction, Chicago, IL.
58. "100 Years of Metalworking – Welding, Brazing and Joining." The Iron Age, June 1955.
59. Miskoe, W.L. 1986. "The Centenary of Modern Welding, 1885-1985 – A Commemoration." *Welding Journal*, Volume 65, April.
60. AWS. 1987, 1991. "Welding Handbook, 8th ed., Vol. 1, Welding Technology, 1987. Vol. 2, Welding Processes, 1991. American Welding Society, Miami, FL.
61. Blodgett, O.W., "How to Determine the Cost of Welding." Bulletin G610, The Lincoln Electric Company, Cleveland, OH.
62. Miller, D.K., and Ogborn, J. 1994. "Welding of Steel Bridges." Highway Structures Design Handbook, available from the National Steel Bridge Alliance, Chicago, IL, Volume 1, Chapter 15.
63. Lincoln Electric Company. 1994. *The Procedure Handbook of Arc Welding*. Lincoln Electric Company, Cleveland, OH.
64. AASHTO. 2003. *Guide Specification for Highway Bridge Fabrication with HPS 70W (485W) Steel*. 2nd ed. American Association of State Highway and Transportation Officials, Washington, D.C., June.

65. AASHTO/AWS D1.5M/D1.5. 2008. *Bridge Welding Code*. American National Standard/American Association of State Highway and Transportation Officials/American Welding Society, available from the American Association of State Highway and Transportation Officials, Washington, D.C.
66. AWS. Standard Symbols for Welding, Brazing and Nondestructive Examination: ANSI/AWS A2.4. American Welding Society, Miami, FL, Latest Version.
67. AASHTO/NSBA Steel Bridge Collaboration. 2003. "Guidelines for Design for Constructibility, G12.1." American Highway of State Highway and Transportation Officials, Washington, D.C., Publication No. GDC-1.
68. Kaufman, E.J., Pense, A.W., and Stout, R.D. 1981. "An Evaluation of Factors Significant to Lamellar Tearing." *Welding Journal*, Research Supplement, Vol. 60, March.
69. AISC. 1973. "Commentary on Highly Restrained Welded Connections." *AISC Engineering Journal*, American Institute of Steel Construction, Chicago, IL, Vol. 10, No. 3, 3rd Qtr.
70. Thornton, C.H. 1973. "Quality Control in Design and Supervision Can Eliminate Lamellar Tearing." *AISC Engineering Journal*, American Institute of Steel Construction, Chicago, IL, Vol. 10, No. 4, 4th Qtr.
71. ASCE. 1982. "Causes and Prevention of Lamellar Tearing." *Civil Engineering*, American Society of Civil Engineers, New York, NY, April.
72. Sheikh-Ibrahim, F.I., and Frank, K.H. 1998. "The Ultimate Strength of Symmetric Beam Bolted Splices." *AISC Engineering Journal*, American Institute of Steel Construction, Chicago, IL, Vol. 35, No. 3, 3rd Qtr.
73. Sheikh-Ibrahim, F.I., and Frank, K.H. 2001. "The Ultimate Strength of Unsymmetric Beam Bolted Splices." *AISC Engineering Journal*, American Institute of Steel Construction, Vol. 38, No. 2, 2nd Qtr.
74. Sheikh-Ibrahim, F.I. 2002. "Design Method for Bolts in Bearing-Type Connections with Fillers." *AISC Engineering Journal*, American Institute of Steel Construction, Chicago, IL, Vol. 39, No. 4, 4th Qtr.
75. Yura, J.A., Hansen, M.A., and Frank, K.H. 1982. "Bolted Splice Connections with Undeveloped Fillers." *Journal of the Structural Division*, American Society of Civil Engineers, New York, NY, Vol. 108, No. ST12, December.
76. Ketchum, M.S. 1920. *The Design of Highway Bridges of Steel, Timber and Concrete*. McGraw-Hill Book Company, New York, NY.
77. Kim, Y.D., Jung, S.K., and White, D.W. 2004. "Transverse Stiffener Requirements in Straight and Horizontally Curved Steel I-Girders." Structural Engineering Report No. 36, School of Civil and Environmental Engineering, Georgia Institute of Technology, Atlanta, GA.
78. Bleich, F. 1952. *Buckling Strength of Metal Structures*. McGraw-Hill, New York, NY.
79. Horne, M.R., and Grayson, W.R. 1983. "Parametric Finite Element Study of Transverse Stiffeners for Webs in Shear." *Instability and Plastic Collapse of Steel Structures, Proceedings of the Michael R. Horne Conference*, L.J. Morris (ed.), Granada Publishing, London, England.
80. Rahal, K.N., and Harding, J.E. 1990. "Transversely Stiffened Girder Webs Subjected to Shear Loading – Part 1: Behaviour." *Proceedings of the Institution of Civil Engineers*, Part 2, 89, March.

81. Stanway, G.S., Chapman, J.C., and Dowling, P.J. 1996. “A Design Method for Intermediate Web Stiffeners.” *Proceedings of the Institution of Civil Engineers, Structures and Buildings*, 116, February.
82. Lee, S.C., Yoo, C.H., and Yoon, D.Y. 2003. “New Design Rule for Intermediate Transverse Stiffeners Attached on Web Panels.” *Journal of Structural Engineering*, American Society of Civil Engineers, Reston, VA, 129(12).
83. Cooper, P.B. 1967. “Strength of Longitudinally Stiffened Plate Girders.” *Journal of the Structural Division*, American Society of Civil Engineers, New York, NY, Vol. 93, No. ST2, April.
84. Johnston, B.G., and Kubo, G.G. 1941. “Web Crippling at Seat Angle Supports.” Fritz Engineering Laboratory, Report No. 192A2, Lehigh University, Bethlehem, PA.
85. Graham, J.D., Sherbourne, A.N., Khabbaz, R.N., and Jensen, C.D. 1959. *Welded Interior Beam-to-Column Connections*. American Institute of Steel Construction, New York, NY.
86. Roberts, T.M. 1981. “Slender Plate Girders Subjected to Edge Loading.” *Proceedings, Institution of Civil Engineers*, Part 2, 71, London.
87. Elgaaly, M., and Salkar, R. 1991. “Web Crippling Under Edge Loading.” *Proceedings of the AISC National Steel Construction Conference*, Washington, D.C.
88. Hanshin Expressway Public Corporation and Steel Structure Study Subcommittee. 1988. “Guidelines for the Design of Horizontally Curved Girder Bridges (Draft).” Hanshin Expressway Public Corporation, October.

Chapter 4
Fabrication and Construction Considerations

Section 4.1
Fabrication



4.1.1 Introduction

The Fabricator adds value to the project by purchasing raw steel from a mill and building it into the girders designed by the Engineer. The Design Engineer, who traditionally, reports to the Owner, is usually quite removed from the Fabricator, although in design-build situations, communications between these two parties may be more frequent. The Design Engineer determines the steel that is ordered and the girder cambers. The Design Engineer's understanding of the Fabricator's work, especially with regard to curved and skewed bridges, can pay handsome dividends in his/her quest for efficient bridges.

4.1.2 Fabrication of Curved Girders

This section discusses the fabrication of horizontally curved steel girders. Provisions specific to curved steel girder fabrication are given in Articles 11.4.12 and 11.8.3 of the *AASHTO LRFD Bridge Construction Specifications* (*1*).

The intent of this discussion is to assist the Design Engineer in understanding the fabrication issues that may be affected by the design. Issues of economy, such as economical splice locations, are addressed in Section 3.1. A significant discussion on heat curving is presented because this information is generally not available to the Design Engineer. Detailing of cross frames for curved girder bridges and bridges with skewed supports is very important to the Fabricator and to the Erector. This single issue generates many requests for information (RFIs) from the Fabricator and the structural detailer. The issue may unexpectedly expose the Design Engineer to liability issues.

The cost of fabricating curved girders is expected to be somewhat greater than the cost of fabricating similar straight girders. The difference lies in the labor cost to heat curve the girders or the material cost related to the fall-off of plate if the flanges are cut-curved. Handling of the girders is also a significant cost factor. Issues related to erection of curved girders are discussed in Sections 4.1.3 and 4.2.

4.1.2.1 Methods of Introducing Curvature in Fabrication

Curvature is usually introduced into horizontally curved welded steel bridge girders by one of two methods:

- Cut curving is a method whereby the flange plates are cut to a curve from plates before they are welded to the web plate. This method often generates significant fall-off (scrap material).
- Heat curving is a method whereby a straight girder is first fabricated and then curved by applying controlled heating to the flanges.

A third method, cold bending, is rarely employed in bridges built in the U.S. Cold bending is accomplished using three-roll benders and is rarely permitted by Owners.

Both of the common methods are addressed in Articles 11.4.12 and 11.8.3.3 of the *AASHTO LRFD Bridge Construction Specifications* (*1*). The method is selected by the Fabricator, but must be spelled out in the Contractor's Construction Plan (Section 4.2.2).

4.1.2.1.1 Cut Curving

Cut curving is preferred my many fabricating shops. Severely curved girders and those with wide and/or thick flanges are usually cut-curved. Scrap is greatly reduced when flanges are nested so they can be cut from a single plate (Section 3.1.4.3.4).

The implementation of numerically controlled burning equipment has made cutting to specific curves very efficient. The efficiency of nested flanges depends on the design of the flanges; it is most efficient when several flanges of the girders in the cross-section are of the same grade and thickness.

4.1.2.1.1.1 Cut Curving I-Girders

Cut curving of I-girders involves the following steps:

- Flanges required to make up the flanges of a girder shipping piece are cut to the proper radius from wider plates. The flanges may be cut individually from individual plates (Figure 4.1.1). Figure 4.1.2 shows the plates slab welded prior to being cut from a single plate. The slab-welding process is discussed in Section 4.1.2.1.3. When flanges are nested, as shown in Figure 4.1.2, they are subsequently heat curved to their final radius after cutting to correct for the effect of girder spacing.

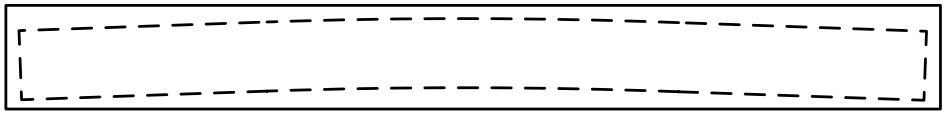


Figure 4.1.1 Single Curved Flange Plate Cut from a Single Ordered Plate

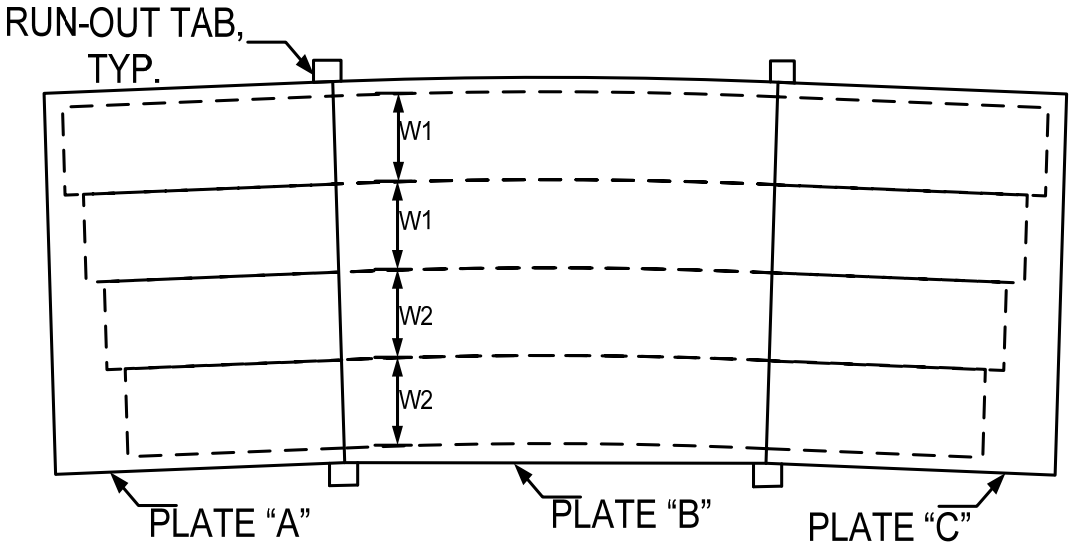


Figure 4.1.2 Slab Welded (Nested) Curved Flanges Prepared to be Cut

- If flange section changes are required in a field section and individual flange plates are cut from a single plate (not shown), they are butt welded together to make up the flanges of each shipping piece if shop splices are required.
- The web position is located on the full-length flanges.
- The web is cut to the proper camber with allowances made for the effect of shrinkage due to flange-to-web welding.

- If the web camber is large (usually in positive moment field sections) the Fabricator may find it economical to partially shape the web camber by sections of web plate rather than ordering a deep plate to burn out the camber with a large amount of waste.

Figure 4.1.3 shows curved flange plates, previously cut and spliced. On the left side of the figure are web plates at various stages of fabrication and assembly.



Figure 4.1.3 Spliced Curved Flange Plates and Web Plates

- Special fixtures or jigs hold the web plates to the stipulated curve for fit-up operations and subsequent welding to the flanges. A typical jig is shown in Figure 4.1.3. Since curved girders with different radii are required for a project, the jig is designed to accommodate different curvatures by altering the elevation of the bearing points.

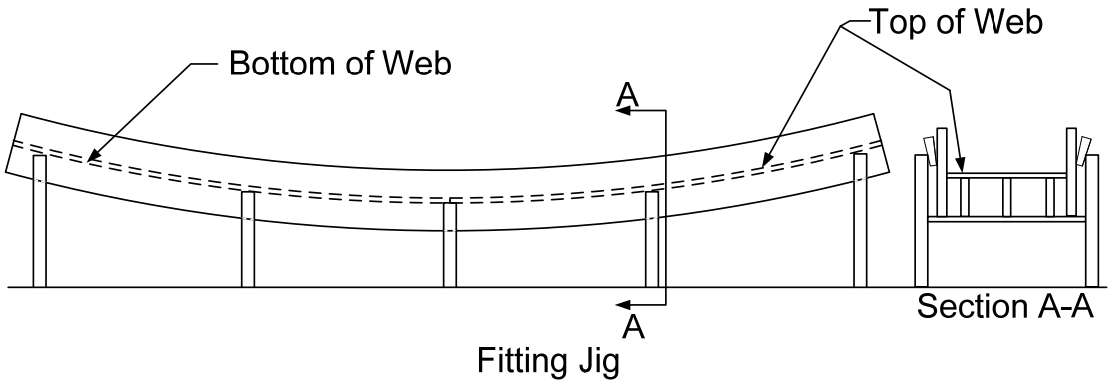


Figure 4.1.4 Special Fixture (Jig) for Web Fit-Up to Cut-Curved Flanges

- Flanges are fitted to the web (or vice versa) on the fitting jig (or the flanges and web may possibly be tack welded in the vertical position prior to laydown in the jig for final welding). Figure 4.1.4 shows the web plate being assembled to the flanges, which have been pre-set in the jig. Chock blocks (or similar) may be used to position the flanges on the web. Clamping fixtures of some type are typically used to apply pressure between the flanges and web during the fitting and tack welding of the flanges to the web in preparation for final welding. Cut-curved flanges of curved girders are sometimes attached to the web in the vertical position. The flanges are brought to the web with “come-a-longs” prior to welding.

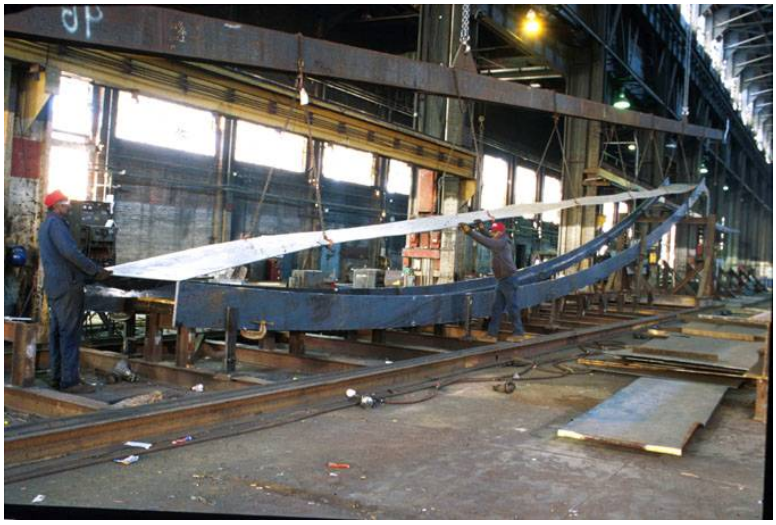


Figure 4.1.5 Fitting of a Web Plate to Cut-Curved Flanges in a Jig

- The last steps include final welding of the flange-to-web welds and the addition of stiffeners and connection plates. Curvature of the girder must be re-checked as the heat from welding can alter the planned curvature. Curvature adjustments are usually made by the controlled application of heat.

4.1.2.1.1.2 Cut Curving Box Girders

Bottom flange plates in horizontally curved tub girders, and top and bottom flange plates in horizontally curved closed-box girders, must always be cut curved. Top flanges of tub girders may either be cut curved or heat curved (discussed below). Heat curving of these flanges may possibly be done after they are welded to the web plates. Inclined webs add a significant complexity to heat curving tub girders.

Typically, the cross-frames are used to position the webs before the bottom flange is attached. This method eliminates the need for complex jigging of the webs. Lateral bracing is also used to hold the webs and top flanges in place. Curved tub or box girders, unlike I-girders, are typically fabricated with a twist to address cross-slope and camber issues. Both webs are usually the same depth but the outside web must be higher than the other. The connection plates must be welded to the webs before the cross-frames can be attached. The connection plates must be cut short of the bottom flange to allow the continuous flange-to-web welds to be laid. The connection plates must later be extended with fillet welded attachments to the bottom flange (Section 3.1.2.8.5.2).

4.1.2.1.1.3 Advantages and Disadvantages of Cut Curving

One advantage of cut curving is that there is no minimum radius that may be obtained. Another advantage is that cut curving takes less time so the fabrication is quicker.

As discussed above, cut curving flanges does not forbid slab welding and stripping. Slab welding allows more economical welding, but requires that the flanges in a girder field section have a common width and that all flanges in the slab have the same grade steel and thickness. Note that any center plates in the field section must be essentially the same length for slab welding. They do not need to be the same length for the flanges to be stripped from the same plate. Note that the flanges in each girder field section may have different (but uniform) widths. The same procedures can be used with heat curved girders, as discussed in the next section.

The largest disadvantage associated with cut curving is that significant amounts of scrap may be generated from the fall-off. The handling during fabrication is made more difficult because the flanges are curved. Lastly, special fixtures may be needed for fit-up.

4.1.2.1.2 Heat Curving

4.1.2.1.2.1 General

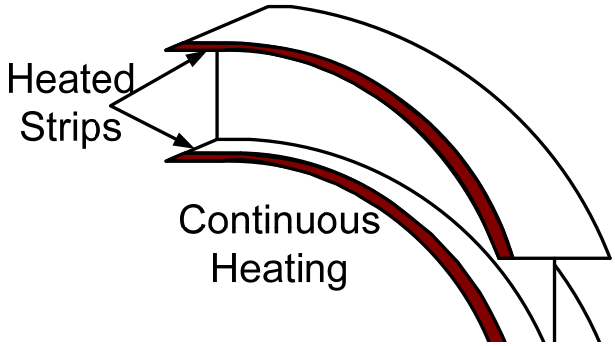
If the radius is large, fabrication of a straight girder followed by heat curving is often preferable. Flanges that are cut curved from a single plate will have nearly the same radius. This radius must always be adjusted slightly to account for the spacing between girders. This adjustment is also performed by heat curving.

The break point between cut curving and heat curving varies between fabricators and with the price of steel. As the curvature and the flange thickness increases, heat curving becomes less desirable.

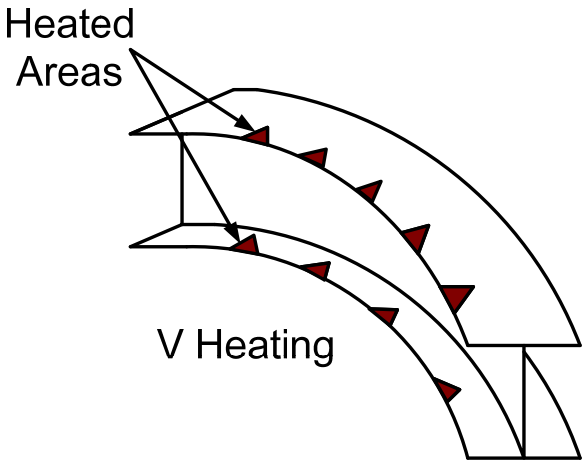
The process of heat curving is quite interesting. A straight girder is fabricated in a conventional manner, complete with all detail material except that all stiffener/connection plates are not welded to the flanges. A thermal gradient is introduced in the top and bottom flanges. The heated side of the flanges expands curving the girder, with the heated side becoming the convex side. The cool side is stressed in compression due to the curving. As the heated side cools, the girder tends to become straight again. However, the yield strength of the heated side has been temporarily reduced so the induced compression stresses on the cool side are able to cause compressive yielding of the heated side. The yielding causes the flange to shorten and thicken. This thickening is called upsetting. The result is that the heated side becomes shorter, so to speak, and becomes the concave side of a curved girder as it reaches ambient temperature.

Slab welding (Section 4.1.2.1.3) can be used with heat curving. The straight girders will be heat curved after they have been fabricated.

Heat curving must be performed in accordance with the provisions of Article 11.4.12.2 of the *AASHTO LRFD Bridge Construction Specifications* (*1*). However, it can be accomplished by either of two means; by continuous heating of the flange tips along their length (Part A of Figure 4.1.6), or by heating the flanges in intermittent triangular (wedge-shaped spots) along their length – a process known as spot or V-heating (Part B of Figure 4.1.6). Usually, V-heating (Figure 4.1.7) is used for larger radius curves because better control can be exercised in the more delicate operation to induce longer curves.



Part A



Part B

Figure 4.1.6 Heat Curving Methods
A) Continuous Heating; B) Spot or V-Heating



Figure 4.1.7 V-Heats

Heat curving can occur either with the web horizontal or vertical. Welding of the stiffeners/connection plates to the flanges is performed after heat curving is complete.

With the web in the horizontal position (Figure 4.1.8) and the girder in positive bending, the self-weight of the girder causes bending about the weak axis that subtracts from the bending due to heating, which is causing negative curvature (negative bending). Gravity adds to the curving as cooling occurs. A check should be made to ensure that the temporarily weakened girder does not yield or buckle locally under self-weight during heating. The provisions of *AASHTO LRFD* Article 6.12.2.2.1 may be used to check for local buckling. The heating and cooling cycle is repeated as necessary to bring the girder to the required curvature. After curving and complete cooling, a final check of the horizontal curvature must be made with the girder positioned vertically in the no-load position.
.

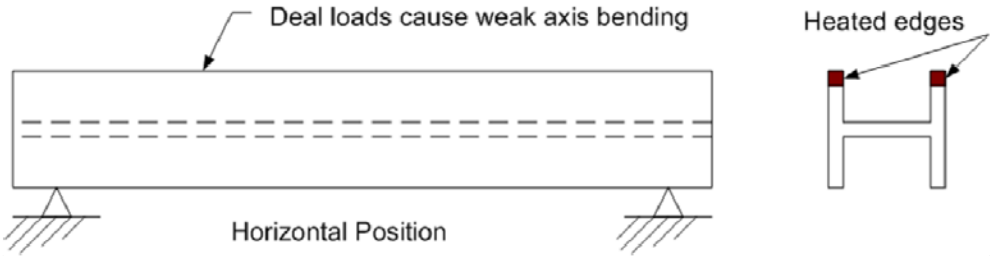


Figure 4.1.8 Heat Curving an I-Girder in a Horizontal Position

With the web in the vertical position (Figure 4.1.9), the self-weight of the girder causes bending about the strong axis of the girder and its effects are less significant with respect to attaining the desired curvature. Remembering that the yield strength of a portion of the flanges is temporarily reduced during heating, the girder should still be checked for the vertical bending due to the self-weight of the girder spanning between support locations. Yielding might impact the vertical camber. Girders are usually not heat-curved in the vertical position by V-heats because the possible curvature is too small.

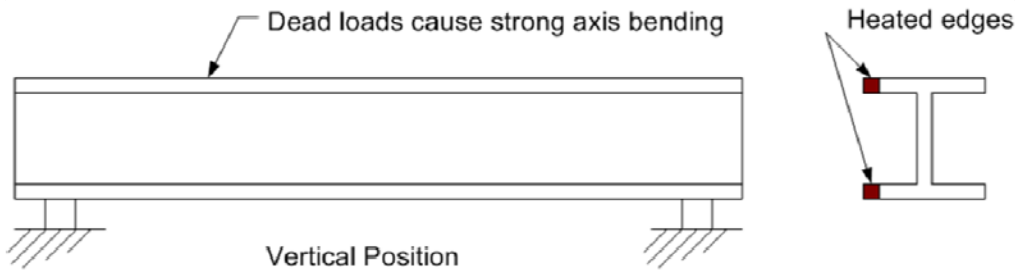


Figure 4.1.9 Heat Curving an I-Girder in a Vertical Position

Article 11.4.12.2.3 of the *AASHTO LRFD Bridge Construction Specifications* specifies that the steel shall not be heated in excess of 1200°F for Grades 36, 50,

50S, 50W, and HPS 50W; the temperature for Grades HPS 70W and HPS 100W is limited to 1100 degrees F. Girders may be artificially cooled after naturally cooling to 600°F. The method of artificial cooling is subject to the approval of the Engineer. The only steels not permitted to be heat curved are the older A852 (Grade 70W) and A514 (Grade 100/100W) steels (i.e. non-HPS grades), which are not recommended for bridge use and are only to be used with the permission of the Owner. They may not be heat curved in any case.

The temperature limitation for heating of higher strength quenched and tempered steel plate is based on the traditional practice of limiting such heating to 50°F below the minimum required tempering temperature so as not to adversely affect the strength of the material. In the absence of other data, the temperature limitation for heat-curving Grade HPS 70W would be specified as 1050°F since the minimum tempering temperature is 1100°F; however, studies have shown that short-time heating to temperatures as high as 1250°F had minimal effect on the strength properties of this grade. Therefore, the limitation of 1100°F was selected for Grade HPS 70W to be consistent with the limit of 1100°F for Grade HPS 100W, which is based on the traditional 50°F limit below its minimum tempering temperature of 1150°F.

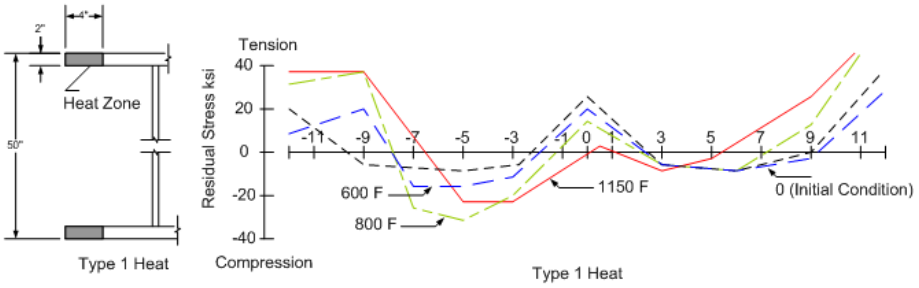
Residual stress is the name given to stresses that reside in a material without any externally applied forces. They are usually a product of the manufacturing process. The plate material supplied from the mill has residual stresses due to differential cooling after rolling of the plate. Additional stresses occur when a flange plate is cut from a wider plate (shear plate) obtained from the mill. Statics requires that the sum of the forces induced in the plate must be zero, which means that there must be tensile and compression stresses. Additional residual stresses are created when the flanges are welded to the web.

These stresses have essentially no effect on the yield capacity of a member because they balance each other out. If a flange is subjected to tension (positive flexure), the tensile stresses will reach the yield point first. This may cause a slight increase in deflection when the applied stresses approach the yield of the material. As load increases, the residual stresses are wiped out and the member fails by yielding (assuming that fracture does not occur) at the exact level that would have occurred if the residual stresses were zero in the beginning.

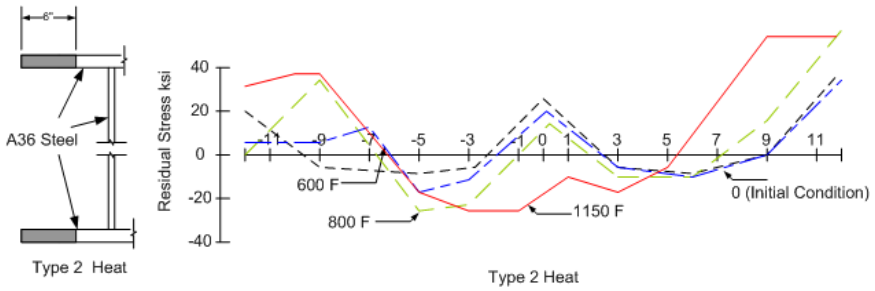
Residual stresses may become problematic with respect to fatigue if they reach levels near the yield stress. Mainly, for this reason, the magnitude of residual stresses due to heat curving has been investigated.

New residual stresses are introduced by the heat-curving process. Figure 4.1.10 shows typical residual stress patterns across a 2″ x 24″ flange plate after heat curving a typical A36-steel 50-inch-deep highway bridge girder. The patterns were determined from an elastic-plastic analysis of the flange plates assuming

temperature-dependent properties for the plates and a typical initial residual stress pattern due to flame cutting and welding the plates (*2*).



PART A



PART B

Figure 1.1.10 Typical Residual Stress Patterns Across a 2″ x 24″ Flange After Heat Curving Determined from an Analytical Study
A) Heated Zone of 4 In. (Type 1); B) Heated Zone of 6 In. (Type 2)

Figure 4.1.10 Part A shows the patterns that were determined in the study assuming a heated zone at each flange edge 4 inches in length (referred to as Type 1 heat), and Figure 4.1.10 Part B shows the patterns that were determined assuming a heated zone at each flange edge 6 inches in length (referred to as Type 2 heat). In each case, the effects of maximum *edge temperatures* ranging from 200°F to 1,150°F, generally in increments of 100°F, were investigated. The assumed temperature distribution along the flange moving away from the edge was calculated from the theoretical solution for a semi-infinite thin plate with a moving-point heat source along its edge.

The x coordinate of “0” in each plot is at the centerline of the web. Each figure shows the initial residual stress pattern assumed in the flange denoted as ″0 (Initial Condition)″, and the pattern that existed after assumed maximum heat-curving temperatures of 600°F, 800°F and 1,150°F were attained and the flanges cooled.

The analyses showed that the pattern (but not magnitude) of residual stresses in the girder after heat curving were generally similar to the pattern that exists before heat curving in girders with initial residual stresses due to gas cutting and welding of the plates; that is, tensile residual stresses existed near the two edges of each flange

and often at the mid-width of the flanges, with compression elsewhere in each flange.

In general, heat curving increases the residual stresses in all parts of the girder except at the mid-width of the flanges, where the initial residual stresses are reduced and may even change from tension to compression in some cases as the heated width and heat-curving temperature are increased. The tensile residual stresses along the heated edges are typically at or near the yield stress (with yielding spreading further into the flange with increasing heated width and heat-curving temperature), while at the opposite flange edges, the tensile residual stresses are somewhat less.

The residual stresses in the web due to heat curving are predominantly compressive and may cause the web to bow slightly during the curving operation. These bows may remain in the web upon cooling if the residual compressive stresses at the flange-to-web weld remain in significant compression.

Figure 4.1.11 shows that at the largest heat-curving temperature assumed in the study (1,150°F), the maximum tensile residual strains at the unheated edges of the flanges were typically approximately half the compressive residual strains that occurred at the heated edges.

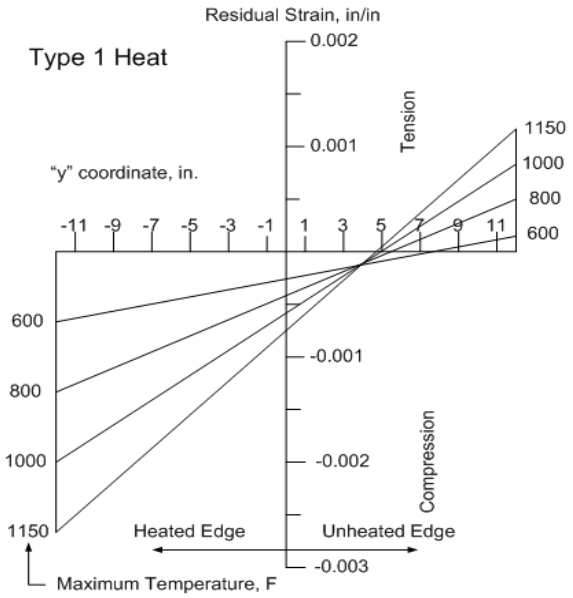


Figure 4.1.11 Tensile Residual Strains at the Flange Edges (Type 1 Heat)

Note that although the residual stresses along the heated edges were tensile, the residual strains along the heated edges were compressive due to the reverse bending that resulted from the shrinkage and yielding that occurred in the heated zones. The maximum residual strain increased in a nearly linear manner as the heat-curving temperature increased for temperatures greater than about 800°F (Figure

4.1.12). The maximum strain also increased as the heated width increased for temperatures greater than about 800°F.

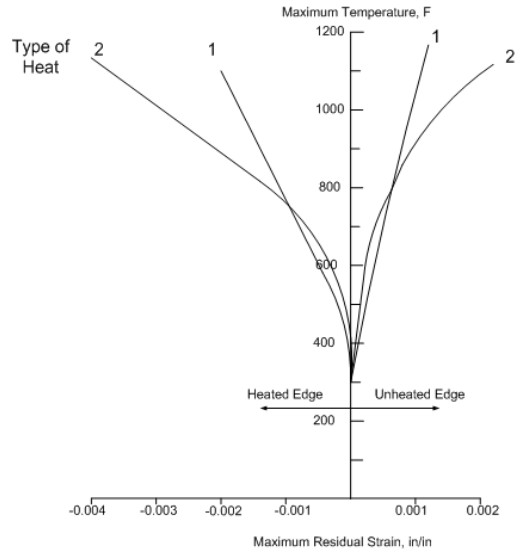


Figure 4.1.12 Maximum Residual Strain at the Flange Edges vs. Heat-Curving Temperature (Type 1 and 2 Heats)

Figure 4.1.13 shows that at heat curving temperatures greater than 800°F, where the curvatures obtained from Type 1 and 2 heats were about the same, the final curvature caused by heat curving generally increased with the maximum heat curving temperature and with the heated width.

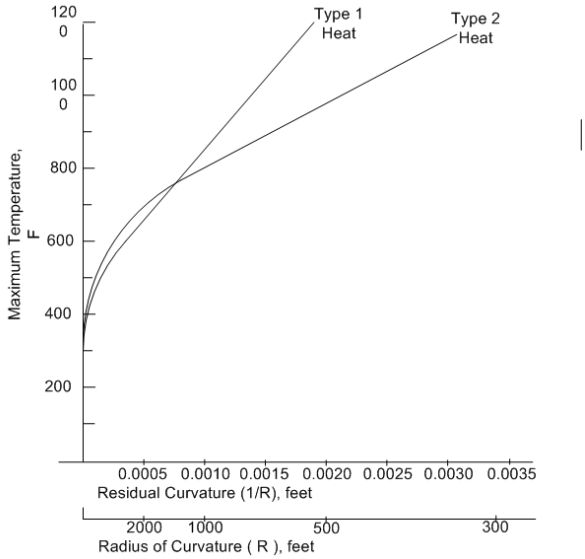


Figure 4.1.13 Final Curvature of Heat-Curved Girder vs. Heat-Curving Temperature (Type 1 and Type 2 Heats)

Since the maximum temperature and heated width are limited by practical considerations, there is a maximum curvature or minimum radius of curvature that can be achieved by heat curving (Section 4.1.2.1.2.3). The minimum calculated radius of curvature at 1,150°F was 540 feet and 298 feet for Type 1 and 2 heats, respectively, in the preceding study.

The behavior of the same girder during an experimental heat-curving operation was in general agreement with the results of the analytical investigation shown herein (*3*).

Although yielding occurs along the heated edges during the heat-curving operation, studies have shown that the changes in the tensile properties of the steel are small and have no significant effect on the overall structural behavior of the girder. Daniels and Batcheler conducted a study that concluded that the residual stresses and strains that are developed due to heat curving also have little or no effect on the fatigue strength of the girders (*4*).

Repeated heating cycles have approximately the same effect on the girder as a single cycle with the same maximum temperature and heated width. Residual stresses and curvature are significantly increased only if a higher maximum temperature or larger heated width is used on a subsequent heating cycle.

4.1.2.1.2.2 Camber Loss due to Heat Curving

Slight inelastic action may occur under initial loading of the girder because of the increased residual stresses due to heat curving and camber loss was theorized to be possible in heat-curved girders with radii less than or equal to 1,000 feet as the residual stresses dissipate. Therefore, the following provided in *AASHTO LRFD* Article 6.7.7.3 may be used to determine additional camber in inches, Δ, that could be specified at any section along the length, *L*, of the girder to compensate for the possible camber loss that might occur in service:

$$\Delta = \frac{\Delta_{DL}}{\Delta_M}\left(\Delta_M + \Delta_R\right)$$

Equation 4.1.1
AASHTO LRFD Equation 6.7.7.3-1

where:

$$\Delta_R = \frac{0.02L^2F_{yf}}{EY_o}\left(\frac{1{,}000 - R}{850}\right)$$

Equation 4.1.2
AASHTO LRFD Equation 6.7.7.3-2

Δ_{DL} = camber at any point along the length, *L* (in.)
Δ_M = maximum value of ΔDL within the length, *L* (in.)
F_{yf} = specified minimum yield strength of a flange (ksi)

L = span length for simple spans or for continuous spans, the distance between a simple end support and the permanent load contraflexure point, or the distance between points of permanent load contraflexure (in.)
R = radius of curvature (ft)
Y_o = distance from the neutral axis to the extreme outer fiber of the cross-section (in.)

Equation 4.1.1 does not apply to girders with radii exceeding 1,000 feet. According to Article 11.8.3.3.1 of the *AASHTO LRFD Bridge Construction Specifications*, the Owner is to determine the necessity of providing this additional camber.

In-service measurements of camber loss have shown that a significant portion of the loss is attributable to construction loads and occurs during construction of the bridge (*5*). New York State has placed thousands of heat-curved girders in service without implementing the requirement for additional camber with no adverse effects reported of camber loss due specifically to heat curving. Their practice has been the typical practice of providing some additional camber in both straight and curved girders to provide for losses due to weld shrinkage. *Therefore, unless deemed necessary by the Owner, it is suggested that the additional camber given by the AASHTO equation not be specified*.

Should the Owner determine the necessity for some camber increase, *AASHTO LRFD* Article C6.7.7.3 suggests that only a portion of the camber increase be considered for inclusion in the bridge profile. It is further suggested that in lieu of other guidelines, the camber might be adjusted using one-half the suggested increase. *AASHTO LRFD* Article 6.7.7.3 also states that camber loss between permanent load contraflexure points adjacent to piers is small and may be neglected.

4.1.2.1.2.3 Minimum Radius of Curvature

There is a minimum radius of curvature that can be achieved by heat curving as mentioned previously. *AASHTO LRFD* Article 6.7.7.2 specifies that for heat-curved girders, the horizontal radius of curvature measured to the centerline of the girder web is not to be less than 150 feet for practical considerations, and is also not to be less than the *larger* of the values calculated from the following two equations:

$$R = \frac{14bD}{\sqrt{F_{yw}}\Psi t_w}$$

Equation 4.1.3
AASHTO LRFD Equation 6.7.7.2-1

$$R = \frac{7{,}500b}{F_{yw}\Psi}$$

Equation 4.1.4
AASHTO LRFD Equation 6.7.7.2-2

where:

Ψ = ratio of the total cross-sectional area to the cross-sectional area of both flanges ($A_{total}/A_{flanges}$)
b = widest flange width (in.)
D = clear distance between flanges (in.)
F_{yw} = specified minimum yield strength of a web (ksi)
R = radius of curvature (in.)

The larger value is conservatively used because the larger radius corresponds to the smaller curvature.

In addition to the preceding requirements, when the flange thickness exceeds 3.0 inches or the flange width exceeds 30.0 inches, the radius is not to be less than 1,000 feet.

The two equations above, which are related to the yield stress and cross-sectional geometry of the girder, were derived to:

- Prevent excessive web bowing due to the combined effects of shear stresses from applied loads and residual compressive stresses in the web (Equation 4.1.3)
- Preclude yielding due to the combined effects of the average compressive residual stresses and shear stresses in the web (Equation 4.1.4)

The web bowing tends to increase as the residual web strain and girder curvature increase. Although the bowing is usually correctible by the usual fabrication methods, it was decided to specify a limiting value of horizontal curvature that would preclude excessive bowing. Equation 4.1.3 controls when D/t_w is greater than or equal to $536/\sqrt{F_y}$ (F_y in ksi). Derivations of these two equations are given in Reference 6.

The equation below shows the calculation of the minimum permissible radius of curvature for heat curving of the positive moment field section in Span 1 of the outermost Girder 4 from the example I-girder bridge (Section 5.1 - refer to the girder elevations on the fold-out plan sheets provided), and the field section over Pier 1 in the same girder, according to the criteria discussed above.

$$R = \frac{14bD}{\sqrt{F_{yw}}\Psi t_w} = \frac{14(24)(92)}{\sqrt{50}(2.106)(0.625)(12)} = 277 \text{ ft}$$

$$R = \frac{7{,}500b}{F_{yw}\Psi} = \frac{7500(24)}{50(2.106)(12)} = 142 \text{ ft}$$

For the field section of Pier 1, the widest flange is b = 33 inches, which is greater than 30 inches. Therefore, the minimum radius of curvature is greater than or equal to 1,000 feet.

For the positive moment field section in Span 1, since the controlling minimum radius is 277 feet and the radius of the girder is 716.5 feet, the field section may be heat curved. For the field section over Pier 1, since the controlling minimum radius is 1,000 ft and the radius of the girder is 716.5 ft, the girder flanges in this field section must be cut curved.

4.1.2.1.2.4 Advantages and Disadvantages of Heat Curving

Advantages of heat curving include the following:

- Fabrication and handling of straight girders is easier than handling curved girders as fabrication equipment is geared more toward straight girders.
- Material savings result from reduced fall-off compared to cut curved flanges.
- Heat curving eliminates the expense of special jigs sometimes required for cut-curving.

Disadvantages of heat curving include the following:

- The radius is limited by the minimum curvature allowed and by the flange width.
- As radius decreases, the time necessary to perform the curving increases causing possible obstruction to production.
- The process may tie up too much shop floor space for an extended period of time.
- There is some potential risk of damaging the girder.
- Although guides for heat curving are available (*7*,*8*), successful heat curving remains more of an art than a science.

4.1.2.1.3 Slab Welding

Slab welding is the process of butt-welding wide plates of different thicknesses together from which individual flanges may be stripped. A sketch of several plates cut from slab weld plates was shown previously in Figure 4.1.2. The decision to utilize slab welding will depend on shop crane capacity, hook height and other individual shop preferences, in addition to the radius, length, width and thickness of the sections and the number of plates having the same dimensions.

Stripping the individual flange plates from a single wide plate allows for fewer weld starts and stops and fewer run-out tabs than when welding shop splices in individual flanges after cutting them to width. Slab welding is used only within a field section and is most often employed for pier sections. *Flange widths must be kept constant within the field section whenever slab welding is employed*.

Slab welding can be used for either cut curving or heat curving. If heat curving is employed to fabricate the girders, the flanges are likely to be nested for slab welding in the straight condition (Figure 4.1.14). The individual straight girders will then be heat curved after completing most of the fabrication.

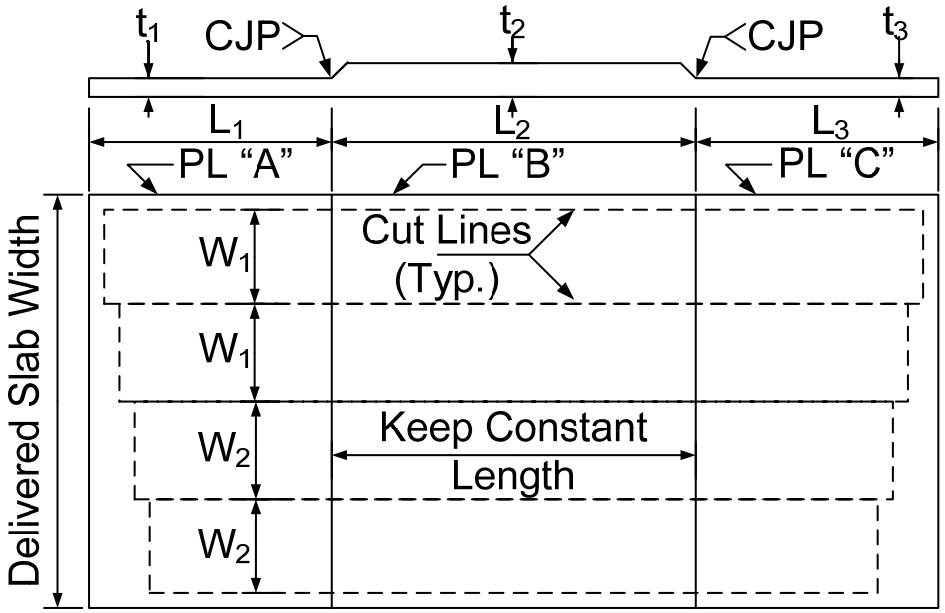


Figure 4.1.14 Nesting for Heat Curving – Slab Welding

In the slab welding process, the individual plates are first blasted, at least in part. The edges of the plates to be butt-welded are prepared and the plates flattened to butt properly. The abutting plates of different thickness are then tack welded and run-out tabs are installed at the ends of the welds. Multi-pass butt welds are then laid. The individual flanges are then cut out with a flame or laser. Flange ends are cut to length. Nested curved flanges have similar radii and have to be heat curved to the final radius, as the final radius varies by the girder spacing in concentric-girder bridges. After cutting, the flanges are flattened if necessary, splice bolt holes are subpunched or drilled, webs are welded to the flanges, stiffeners are attached, and the girder is heat curved to the final radius.

There is an increased premium on the accuracy of the alignment of the slabs and often enough additional material is not available to account for any movement from welding of the slabs together. For girders with larger offsets, the slabs may have to be offset from each other, which can pose a handling problem.

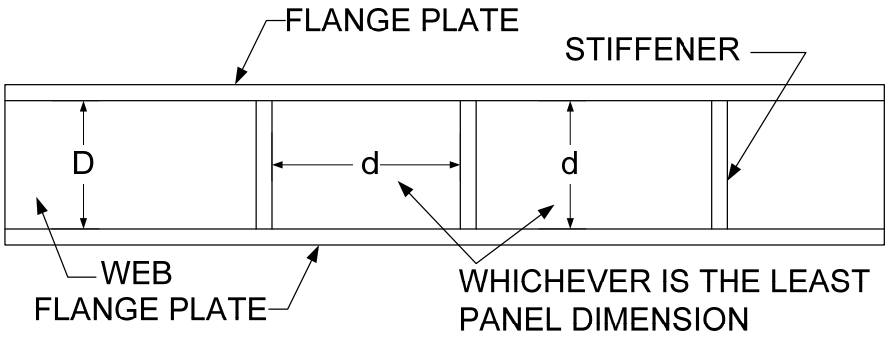
4.1.2.2 Measurements

Measurements that must be made on a fabricated curved I-girder in the shop are discussed in this section; including web trueness, sweep tolerance, camber and girder length.

Dimensional tolerances for horizontally curved girders are covered in Article 11.8.3.6 of the *AASHTO LRFD Bridge Construction Specifications*.

4.1.2.2.1 Web Trueness

Trueness (out-of-flatness) of welded webs must meet the dimensional tolerances specified in Article 3.5 of the *AASHTO/AWS D1.5M/D1.5 Bridge Welding Code* (*9*). Figure 4.1.15 indicates the specified tolerances for cases where intermediate stiffeners are present on either one or both sides of the web. *d* in the figure is the least panel dimension. The maximum permitted variation for unstiffened webs is *D*/150.



	Stiffeners on One Side	Stiffeners on Both Sides
	$D/t_w < 100$	$D/t_w < 150$
Fascia Girders	d/120	d/130
Interior Girders	d/100	d/115
	$D/t_w \geq 100$	$D/t_w \geq 150$
Fascia Girders	d/80	d/105
Interior Girders	d/67	d/92

Figure 4.1.15 Specified Out-of-Flatness Tolerances for Welded Webs

The trueness for curved girders must be determined by measuring offsets from a straightedge oriented vertically between flange-to-web welds at the positions of maximum variation on the web.

Web distortions of twice the permitted amount are satisfactory at an end of a girder that has been drilled, or subpunched and reamed, either during assembly or to a

template for a bolted field splice, provided that when the splice plates are bolted, the web assumes the proper tolerances.

Tolerances on the maximum specified depth, measured at the web centerline, for welded beams and girders are also given in Article 3.5 of the *Bridge Welding Code*, along with tolerances on out-of-straightness and fit of intermediate and bearing stiffeners and tilt (or warpage) of the flanges. The lateral variation between the actual and theoretical web centerline at the flange surface is not to exceed ¼ in.

Revised specifications for web trueness to replace the tolerances shown in Figure 4.1.15 based on the relationship of web distortion to girder moment at first yield are under consideration at this writing (2010).

The maximum permissible web trueness (out-of-flatness) values for the fascia girders and interior girders from the example I-girder bridge (Section 5.1 - refer to the girder elevations on the fold-out plan sheets provided) are as follows:

$$D = 92 \text{ in} = d$$

$$100 < D/t_w = 142.5 < 150$$

The web depth, D, of 92 inches is the least panel dimension, d, over the majority of each girder. The web slenderness, D/t_w, of 147.2 is in-between the limiting values of 100 and 150 given in the table in Figure 4.1.15.

Since stiffeners are only on one side of the web on the fascia girders and D/t_w is greater than 100, the maximum permissible out-of-flatness is:

$$\frac{d}{80} = \frac{92}{80} = 1.15 \text{ in}$$

Since stiffeners are on both sides of the web on the interior girders, and since D/t_w is less than 150, the maximum permissible web out-of-flatness is:

$$\frac{d}{115} = \frac{92}{115} = 0.80 \text{ in}.$$

4.1.2.2.2 Sweep Tolerance

Sweep tolerance for horizontally curved girders is to meet the requirements of Article 3.5.1.4 of the *AASHTO/AWS D1.5M/D1.5 Bridge Welding Code* (*9*). That is, the allowable deviation in the sweep is not to exceed 1/8-inch in 10 feet of length, provided that the member has sufficient lateral flexibility to allow the attachment of

cross-frames/diaphragms, lateral bracing, etc. without damaging the girder or its attachments.

The deviation in the maximum calculated perpendicular offset from the chord relative to the actual measured offset is typically compared to the permissible deviation for curved girders. Measurements are to be made with the girder vertical and in the no-load position.

Referring to Figure 4.1.16, the calculation of the allowable deviation in sweep camber, as defined in the preceding paragraph, for the field section in Span 1 of Girder 4 from the example I-girder bridge (Section 5.2), which has an arc length of 137.4 feet is as follows:

$$\frac{1}{8} * \frac{137.5}{10} = 1.7 \text{ in}$$

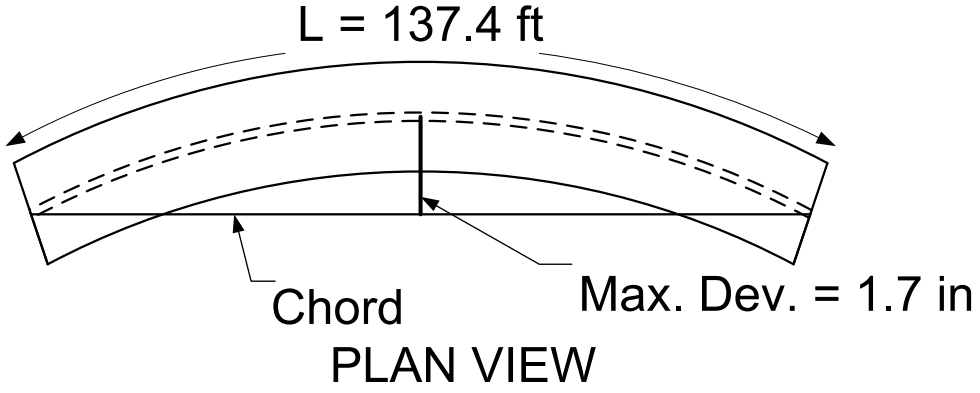


Figure 4.1.16 Calculation of Sweep Tolerance for Field Section in Span 1 of Girder 4 of the Example I-Girder Bridge

4.1.2.2.3 Camber

Vertical camber is provided to compensate for dead load deflections and support rotations about the axis radial to the girder and to provide any vertical curvature required by the profile grade. Horizontal camber may also be provided in some cases to allow for rotation (or twist) of a curved I-girder about the axis tangential to the girder during the erection (Section 4.1.3.1.3.3).

The cambers provided in the contract documents are to be adhered to unless steel erection or deck placement is to be performed in a manner that will lead to deflections different from those used to compute the specified cambers. Different dead load cambers imply that the dead load stresses would also differ from those in the as-designed bridge. The Contractor's approach must be approved by the Owner's Engineer and any documentation required for approval is to be provided. The sequence of load application must be considered at design and included in determining the cambers when phased construction is specified.

Where the Contractor's Construction Plan necessitates that different cambers be provided in the girders from those shown in the contract documents, acceptance by the Owner is to be obtained prior to commencement of the fabrication. Such changes that do not benefit the Owner are usually at no cost to the Owner. In cases where the Owner benefits, such as improved traffic patterns or reduced traffic congestion, the Owner may accept additional cost. The submissions should be approved prior to the submission of the shop drawings for approval.

Camber is difficult to measure on curved girders. Vertical camber is usually checked at intervals along the entire girder length. If horizontal (or twist) camber is not provided, the vertical camber of I-girders should be measured by blocking the girders into their no-load positions with the webs plumb along the girder. If horizontal (or twist) camber should be provided, the vertical camber can best be checked by blocking the girders to the near vertical position while maintaining the no-load out-of-plumb orientation of the webs along the girder length.

Vertical camber can also be checked with the girder web horizontal, as shown in Figure 4.1.17. This alternative is complicated and not necessary.

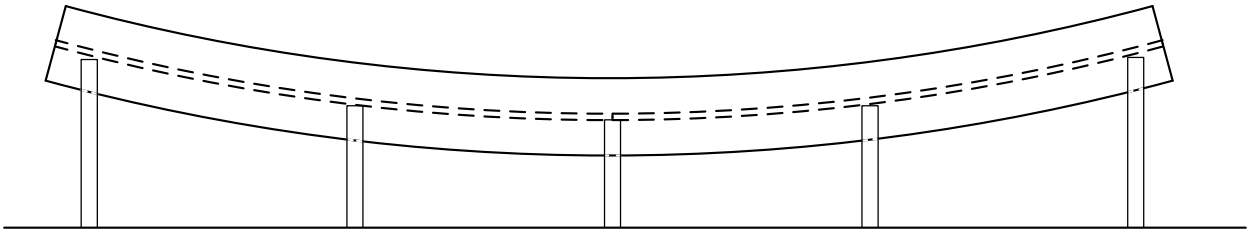


Figure 4.1.17 Vertical Camber Check with Girder Web in the Horizontal Position

4.1.2.2.4 Girder Lengths

Accurate girder lengths are important to ensure that the girders will have the proper length and curvature to match up with the anchor bolts. Pier and bearing locations in the field are not established along a girder arc. Thus, the ends of the girders must be correct.

The use of measuring tapes is usually not practical since curved girder lengths are measured along the arc. Length compensation for temperature is required when length is measured with an optical or laser instrument without temperature compensation. Chord lengths are generally surveyed for curved girders. Offsets and arc length may be checked from that chord.

According to Article 11.8.3.6.4 of the *AASHTO LRFD Bridge Construction Specifications*, girder lengths are to be determined based on a base ambient temperature of 68°F, which corresponds to the temperature used to calibrate Invar

measuring tapes to ensure that they will expand and contract in concert with the steel during fabrication. Some states specify a slightly different base temperature. If the steel temperature during fabrication is greater than 68°F, the steel measured with an Invar tape will be made longer than the length based on 68°F. Conversely, if the steel temperature is colder than 68°F, the girders will be made shorter. This is automatically accomplished when an Invar tape is used to make the measurements. A conscious adjustment in length for temperature may be required when measurements are made by other means.

Expansion bearings are adjusted to accommodate the change in length of the girders should the temperature in the field during erection of the girders differ significantly from 68°F. There is little room to compensate for ambient temperature when two or more adjacent piers have fixed bearings. For such cases, the Design Engineer can assume a temperature range larger than the temperature range based on the median temperature (e.g. 100°F) in computing thermal forces on the substructure and superstructure. Such an assumption allows for erection of the steel at other than the mean temperature without requiring flexing of the pier(s) to make-up for the change in length of the steel. In cases of erection during more extreme temperatures, the piers may need to be jacked into position.

Bearing plates are sometimes clamped to the girder flange or sole plate for shipping so that welding of these plates can be done in the field to allow for any necessary adjustments for the ambient temperature.

4.1.2.3 Shipping Considerations

Article 11.8.2 of the *AASHTO LRFD Bridge Construction Specifications* specifies that the Contractor's Construction Plan must include the shipping weights, lengths, widths and heights, and means of shipping. According to Article 11.8.4 of those same specifications, a Transportation Plan may also be required by the Owner for components that are wider, heavier, deeper or longer than normally permitted for the selected mode of transportation (e.g., truck or rail). The Transportation Plan should include as a minimum:

- The orientation of the girder during shipping;
- The type of girder supports required and their location;
- The type, size and locations of tie-downs, and;
- Any temporary stiffening trusses or beams that are required.

Girder stresses during shipment should be checked for stability, overload and fatigue. Girder cross-section shape must be maintained. Particular attention should be paid to through-thickness stresses such as might occur in the web at the flange if the girder sways during shipment.

Note in Figure 4.1.18 that the girder is tied at its top. This provides not only the necessary stability, but prevents sway that may lead to fatigue of the flange-to-web

weld at the bottom flange. The rig in this picture is separated to accommodate the girder length. At times, the girder is cantilevered significantly beyond the truck



Figure 4.1.18 Trucking a Curved I-Girder

Article C11.8.4 of the *AASHTO LRFD Bridge Construction Specifications* (*1*) provides the following equation, which may be used in lieu of any alternative criteria for the limiting cantilever length, L_c, *in feet* of a single unbraced I-girder to control dynamic lateral bending stresses during shipment:

$$L_c \le 36.0\left(\frac{I}{w}\right)^{0.25}$$

Equation 4.1.5
AASHTO LRFD Bridge Construction Specification Equation C11.8.4-1

where:

I = moment of inertia of the I-girder cross-section about the vertical axis in the plane of the web (in.^{4})
w = I-girder weight per unit length (kip/ft)

The suggested limit is intended to ensure the first mode of vibration of the unbraced cantilever about the weak axis of the I-section is greater than 5 Hz (*10*). Critical lengths for other frequencies may be determined by changing the constant in Equation 4.1.5 from 36.0 to $36.0(5/f)^{1/2}$, where *f* is the desired lower-bound frequency in Hz.

Fatigue stresses in the girders during shipment must not exceed the constant-amplitude fatigue threshold for the appropriate detail categories specified in *AASHTO LRFD* Table 6.6.1.2.5-3. Girder stresses due to self-weight during

shipping are to be computed with a dynamic load allowance of 100 percent and are to satisfy the provisions of *AASHTO LRFD* Articles 6.10.3.2 or 6.11.3.2, as applicable.

The standard truck trailer is 8′-0″ wide. Stability of the girder must be checked; i.e., the load must always be balanced on the trailer. Trailer placement is important to balance the load. Analysis is required by the Fabricator in order to determine the axle loads. Note that the width for shipment is the actual width of the load when balanced on the trailer and not simply the girder mid-ordinate (i.e., the girder offset at mid-length of the shipping piece) plus either one-half or all of the flange width.

Additional discussion on shipping considerations is provided in Section 3.1.2.3.1.

4.1.3 Detailing Cross-Frames and Their Connections

The detailing for camber and the erection of skewed bridges and horizontally curved bridges with or without skewed supports is much more complex than similar tasks for straight girder bridges without skews.

Because of steel's versatility, it is often the material of choice for curved and skewed bridges. Tighter constraints on right-of-way have led to a vastly increased percentage of steel bridges of these two types. Additionally, steel can be used in cases where vertical clearance is limited and concrete girders cannot be used. The trend toward the use of higher strength steels leads to relatively larger deflections associated with the more slender members. These girders present, at times, issues for the Fabricator and Erector. Additional bracing and supports may be needed to control deflections and prevent potential buckling in order to accomplish erection.

Failure of the Design Engineer to properly consider deflections and erection issues may result in difficulties in achieving the intended final position of the girders. Failure to execute adequate analysis, detailing and proper erection may also result in construction delays, claims, and possibly lawsuits. The structural Detailer, Fabricator and Erector are resourceful entities, but the project Owner and Design Engineer can make the builder's job easier and more efficient by considering some of the issues that the building team will face in executing the design provided them.

4.1.3.1 Differential Deflections

4.1.3.1.1 General

Two issues are present in skewed and curved girder bridges that are negligible in traditional straight girder bridges with right supports. The first issue is the unequal deflections of adjacent girders that cause loads to be transferred between girders through the cross-frames and the deck. The second related issue is the non-uniform torsion created in the girders by the connection of points of adjacent girders that have unequal deflections. Curvature also induces non-uniform torsion.

These two phenomena lead to a number of issues that must be addressed if the bridge is to be built without difficulty and function properly over its expected life. Of course, all curved girder bridges and skewed bridges do not exhibit these issues to the same degree. Unfortunately, the extent of the issues for a particular bridge is difficult to quantify. However, common sense indicates that bridges with little relative deflection between adjacent girders at points of cross-frame attachment and those with very large radii would not be as severely affected as those with larger relative deflection in adjacent girders. Simple span skewed and curved girders often are problematic.

As a result, *AASHTO LRFD* Article 6.7.2 on Dead Load Camber now specifies that for straight skewed I-girder bridges and horizontally curved I-girder bridges with or without skewed supports, the contract documents should clearly state an intended erected position of the girders and the condition under which that position is to be theoretically achieved.

Camber addresses the fabricated vertical position of the girders to account for vertical deflection under dead load and geometric requirements. The dead load adjustments are routinely accounted for by reporting the computed vertical deflection due to dead loads. Until recently, girder rotations (i.e. twist or layover) were not accounted for on the Plans. However, as girders have become more flexible and skewed supports have become more common, girder rotations have become addressed more frequently. Analytically, the girders are typically assumed to be vertical at no load. Like vertical deflections, girder rotations may be computed. The ability of various approaches to make these computations is addressed elsewhere in this Manual. When the rotations are properly computed, the Design Engineer and Owner may determine if they are acceptable or not. If they are deemed acceptable, the girders are typically detailed to be vertical in the no-load position (a so-called No-Load Fit). If they are deemed unacceptable, the Plans should indicate the intended erected vertical position (plumbness) under a particular condition (i.e. steel dead load or total dead load) and leave the means and methods required to obtain the desired position up to the Fabricator and the Contractor. The options are discussed in this section. *The computed girder rotations need not be indicated on the Plans.*

If the Plans call for the girders to be plumb under load (either steel or total dead load), the Fabricator can choose the method of detailing the girder and cross- frames to accomplish the required plumbness. There are several means available to the Fabricator to accomplish this and they generally are not amenable to computation. A common method discussed later requires the girders to be twisted out-of-plumb while in the no-load condition to fit the cross-frames, which are detailed to accomplish the correct plumbness. The art of forcing the girders into position to fit-up the cross-frames is not well defined and varies greatly by conditions. Flange stiffness, amount of twist and curvature are some of the variables. The Fabricator should ascertain that the method chosen is viable.

4.1.3.1.2 Intended Final Position of Girders

The intended final positions of I-girders in straight skewed bridges and horizontally curved bridges with or without skewed supports may be defined as either:

- Girder webs theoretically vertical or plumb
- Girder webs out-of-plumb

The three conditions under which these intended final positions can be achieved are:

- No-load
- Steel dead load
- Full dead load

The no-load condition refers to the typical case where the girders are erected under a zero-stress condition; i.e., supported such that the girder self weight stresses are negligible (Figure 4.1.19).



Figure 4.1.19 Curved I-Girders Supported in the No-Load Condition

The steel dead load condition refers to the case after the erection of the steel is complete (i.e., when the steel supports itself). This is shown in Figure 4.1.20.



Figure 4.1.20 Steel Dead Load Condition After Erection of Steel is Completed

The full dead load condition refers to the condition after the full dead load is applied (Figure 4.1.21).



Figure 4.1.21 Full Dead Load Condition After All Dead Load is Applied

4.1.3.1.3 I-Girders

4.1.3.1.3.1 No-Load Fit

A No-Load Fit is defined as when the cross-frames are detailed to fit when the girders are erected in the no-load condition. Usually the girders are plumb in the erected condition without any load. Any cross-slope requirements will be ignored in this discussion for simplicity.

As illustrated in Section 1.1.4.1, when girders in straight skewed I-girder bridges and horizontally curved I-girder bridges with or without skewed supports are erected plumb in the no-load position, with the cross-frames/diaphragms detailed to fit in this position (i.e., when a No-Load Fit is employed), the girder webs will not be plumb under either the steel dead load or full dead load conditions (Table 4.1.1).

Table 4.1.1 Girder Web Plumbness for a No-Load Fit

	PLUMB	OUT-OF-PLUMB
NO-LOAD	●	
STEEL DL		●
FULL DL		●

When a No-Load Fit is employed for bridges with skewed supports, the girders tend to go out-of-plumb along their length including at the supports. This occurs with either straight or horizontally curved girders. The issue is essentially a function of the vertical deflection of the girders. The out-of-plumbness is particularly pronounced at skewed simple supports. This situation can often lead to problems with the bearings, which may not be able to accommodate the rotation imposed on them. A second issue is the lateral movement of the bridge at the elevation of the deck. The lateral forces on the bearings may be extreme if the bearings are laterally restrained, exceeding the vertical reaction in some cases. The Design Engineer should take steps to relieve the lateral restraint on the bearings at design in extreme cases (Section 2.2.3). Of course, the lateral forces are directly related to the forces in the cross-frames or diaphragms at the support. These members must be designed for these forces. The Design Engineer must be very cautious of any changes requested by the Fabricator that may have consequences with regard to this situation.

Out of-plumbness under load of horizontally curved girders occurs in the span, not at the bearings, unless the support is skewed. The out-of-plumbness of curved girders is less severe from an engineering point of view. The girders appear out-of-plumb and may be objectionable from an aesthetic viewpoint. Also, the alignment is slightly in error. The out-of-plumbness should be identified by the Design Engineer and the Owner informed prior to fabrication.

Where a No-Load Fit is employed such that the cross frames are detailed to fit with the girder webs plumb in the no-load position, the required “drop” of the cross-frames (i.e. the distance between the cross-frame and the flange) will be different for different cross-frames by the amount of the cross-slope plus the difference in dead load deflection (Figure 4.1.22).

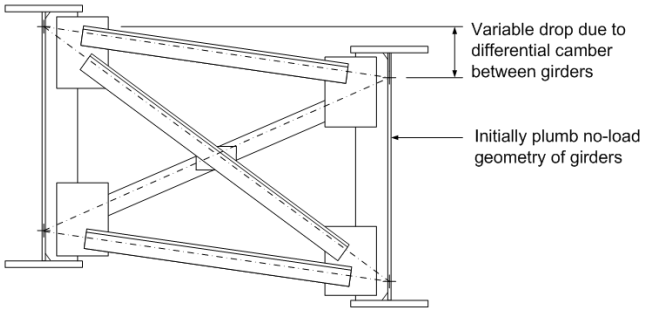


Figure 4.1.22 Variable "Drop" of the Cross-Frames for a No-Load Fit

The resulting out-of-plumbness at the bearings (Figure 4.1.23) and any potential errors in the horizontal roadway alignment under the full dead load condition should be considered at skewed supports whenever a No-Load Fit is employed. At skewed supports, the sole plate may not rest squarely on the bearing unless the sole plate is beveled. This situation is particularly significant with elastomeric bearings and needs to be considered in the design of other types of bearings. The elastomer and the bearing stiffener on one side of the web may be overloaded. Second, the barriers may not line up with the approach slab.

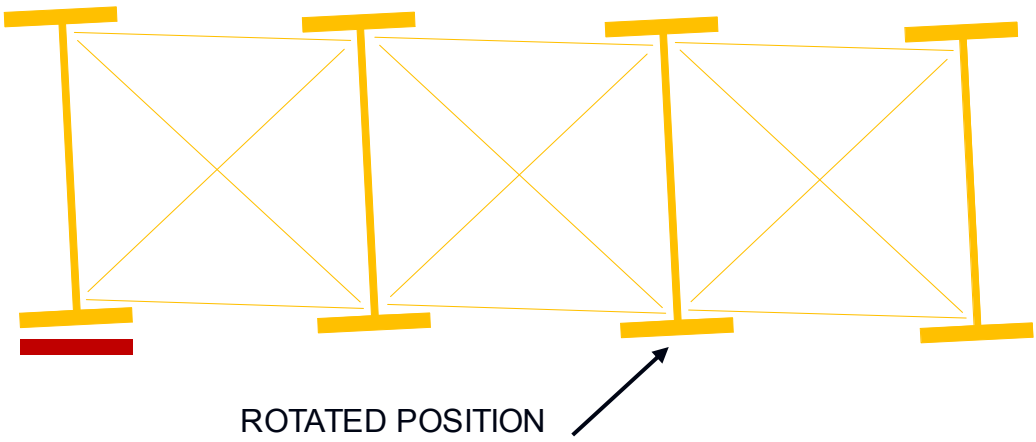


Figure 4.1.23 Out-of-Plumbness at Skewed End Support Resulting from a No-Load Fit

Girder flange rotation about the longitudinal axis of the girder under dead load generally exceeds rotation about that axis due to live load. During construction it may temporarily exceed the full dead load rotation. Excessive rotation can cause permanent damage to bearings. *AASHTO LRFD* Article 2.5.2.6.1 requires that the computed bearing rotations in these bridge types be accumulated over the assumed

construction sequence. The calculated accumulated factored bearing rotations are not to exceed the rotational capacities of the bearings for any construction stage.

The twist angle, ϕ, of the girder about its longitudinal axis at the end supports of skewed bridges, which can be considered in the design of the bearings, can be estimated as follows:

$$\phi = \frac{\theta}{\tan\alpha}$$

Equation 4.1.6

where:

θ = girder end rotation due to the appropriate factored dead load about an axis transverse to the longitudinal axis of the girder (radians)

α = skew angle of the end cross-frame measured with respect to the longitudinal axis of the girder (radians)

In addition, *AASHTO LRFD* Article 2.5.2.6.1 specifies that elastic vertical, lateral and rotational deflections due to the applicable load combinations (including thermal loads) are to be considered to ensure satisfactory performance of the girders, cross-frames, bearings, joints, abutments and piers. The lateral forces at bearings on skewed supports are often quite large (Section 2.2.3). The rotation of the girders at these supports may also be quite large.

The twist and resulting girder layover, LO, is largest at skewed end supports. The layover, LO, is equal to the relative transverse displacement between the top and bottom flanges resulting from the torsional rotation, ϕ_z, of the girder (Figure 4.1.24). In the case shown in the figure, the bottom of the girder did not move because the bearing was fixed transversely.

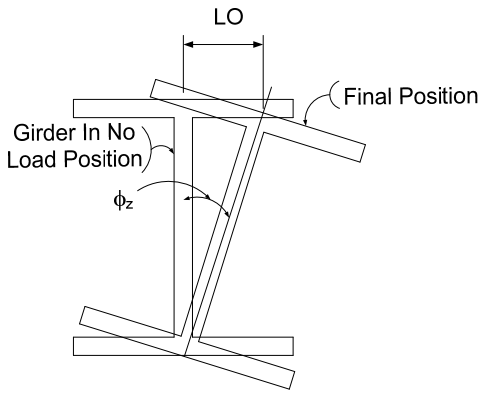


Figure 4.1.24 I-Girder Layover (LO) at a Skewed Support

An equation to estimate LO at skewed cross-frames in lieu of a refined analysis is:

$$LO = \frac{\Delta_x}{Tan\alpha} = \frac{\theta d}{Tan\alpha} \text{ inches}$$

Equation 4.1.7

where:

- θ = girder rotation due to the appropriate dead load about an axis transverse to the longitudinal axis of the girder (radians)
- d = girder depth (in.)
- α = skew angle of the cross-frame measured with respect to the longitudinal axis of the girder (radians)
- Δ_x = longitudinal deflection of the top of the girder at the bearing (in.)

The equation can be derived from geometry of a skewed end support shown in Figure 4.1.25. Note that the top-flange longitudinal deflection, Δ_x, can be estimated as $\theta * d$ (Figure 4.1.26).

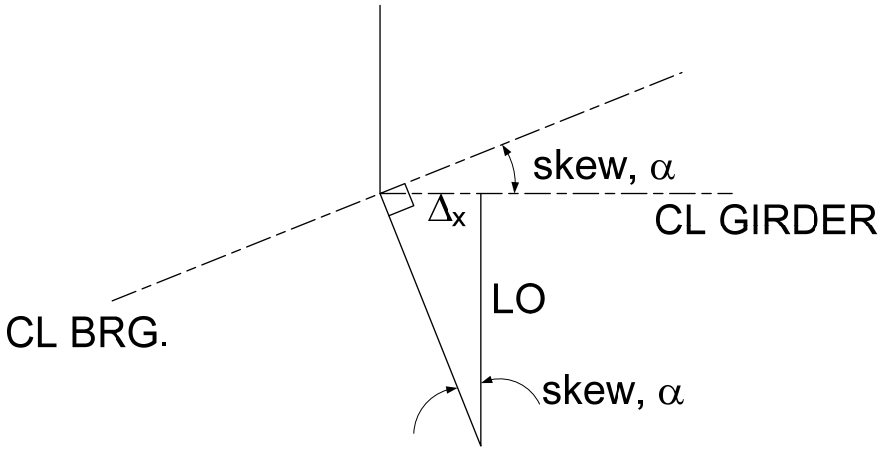


Figure 4.1.25 Derivation of Equation 4.1.7 from the Geometry at a Skewed End Support

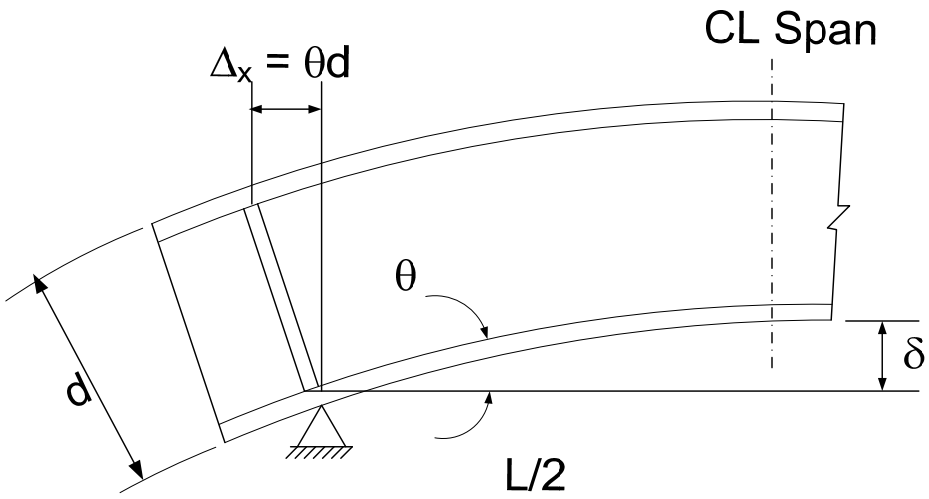


Figure 4.1.26 Girder Rotation, θ, and Top Flange Longitudinal Deflection, Δ_x, at the End Support

Table 4.1.2 shows example web layovers at the end supports computed from Equation 4.1.7 for three different significantly skewed structures (Figure 4.1.27). Numbers shown in the table for the variables that were used in the equation are rounded off. The Design Engineer can evaluate the significance of the amount of layover on a per case basis.

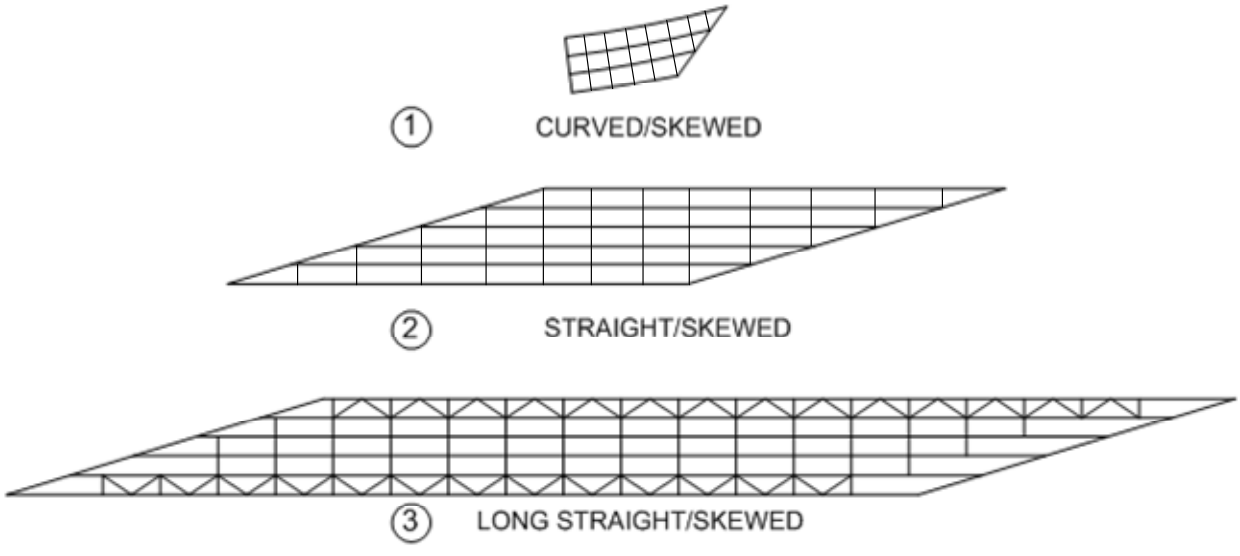


Figure 4.1.27 Skewed Simple-Span Structures 1, 2 and 3 in Table 4.1.2

Table 4.1.2 Computed Web Layover from Equation 4.1.7 for Skewed Structures in Figure 4.1.27

Structure	1	2	3
L, ft	110	160	270
Skew, $\alpha°$	35	20	25
Girder depth, d, ft	5	5.75	10
Rotation, θ, rad	0.007	0.007	0.015
LO, in.	0.623	1.382	3.812

Section 4.2.3.3 discusses the potential use of vertical slotted holes for cross-frame connections in straight skewed I-girder bridges in an attempt to minimize the twist of the girders and reduce the cross-frame forces. As pointed out in Section 4.2.3.3, such an approach is not recommended as it becomes difficult to control the vertical deflections during the deck placement and care must be taken to ensure the construction plan reflects the analysis assumptions made as to when the bolts are loose and load is applied.

Advantages and Disadvantages of a No-Load Fit

The advantages of employing a No-Load Fit are that it is the simplest method of detailing and cross-frame installation is the easiest; that is, a forced fit-up of the cross-frames is not required.

The disadvantages of employing a No-Load Fit are that the girders are out-of-plumb under dead load; it causes the largest cross-frame forces of all the possible options; at skewed supports the deck and barriers may not line up with the approach slab; and at skewed supports, the effect of the out-of-plumbness on the bearing rotations must be considered.

4.1.3.1.3.2 Steel Dead Load or Total Dead Load Fit

Cross-frames are detailed to fit plumb girders after the steel dead load or total (full) dead load is applied when a so-called Steel Dead Load Fit or Total Dead Load Fit is employed. That is, the girders are fabricated plumb and are twisted out-of-plumb in the no-load condition during the erection to fit the cross-frames. Such detailing is consistent with the girders being plumb under either steel dead load only (Table 4.1.3) or total dead load (Table 4.1.4). It must be observed that the cross-frames or diaphragms may not change shape or size as fabrication progresses. This situation is different from the normal assumption that the steel is not stressed when it is fabricated. Self-weight of the steel is applied to the fully erected steel.

Table 4.1.3 Girder Web Plumbness for a Steel Dead Load Fit

	PLUMB	OUT-OF-PLUMB
NO-LOAD		●
STEEL DL	●	
FULL DL		●

Table 4.1.4 Girder Web Plumbness for a Total Dead Load Fit

	PLUMB	OUT-OF-PLUMB
NO-LOAD		●
STEEL DL		●
FULL DL	●	

If the detailing is consistent with the girders being plumb under only steel dead load (i.e., self-weight) the webs will not be plumb under the full dead load (Table 4.1.3) since the webs can be plumb for only one dead load condition at a time.

One might ask why the steel would be plumb under steel dead load only. Additional loads will cause the girders to continue to rotate out-of-plumb. There are a couple of reasons for this assumption. The Erector can check his/her handiwork with a plumb level. The twist introduced during erection will be less than that required to obtain plumb under full dead load. Finally, it has been observed that the girders tend to rotate less than theoretical under deck weight. There are several explanations offered. The deck pans offer shear resistance, the deck reinforcing does the same and the concrete itself introduces some stiffness as it is cast. It has been suggested by some that the girder rotation due to deck placement is roughly half of that computed if the shear stiffness of the deck system is ignored, as is usually done in design.

At this point the discussion must be separated between curved girder bridges with radial supports and straight girder bridges with skewed supports. This discussion

will make several simplifying assumptions. First, all girders are the same size; second, there is no cross-slope considered; third, cross-frames are perpendicular to the girders to which they are attached. Deviations from these assumptions do not negate the remarks to follow, but do complicate the detailing that would be recognized in the sketches.

In curved girder bridges with skewed supports, torque is introduced by both the curvature and the skew magnifying the girder twist that occurs at mid-span and at the end supports. Thus, many of the issues identified for curved bridges with radiual supports and straight bridges with skewed supports are magnified in this case. A Steel Dead Load or Total Dead Load Fit may be employed to counter the effects of the girder twist, but can be more problematic than for bridges that do not have both curvature and skew, or curvature only. In special cases, the option of detailing the girders with a twist camber in the no-load position, as discussed in Section 4.1.3.1.3.3, might be considered for these bridges.

Curved Girder Bridges w/ Radial Supports

Figure 4.1.28 shows an erected curved girder bridge at roughly mid-span before and after dead load has been applied. A Total Dead Load Fit has been employed so that the girders are twisted out-of-plumb in the no-load condition. Note that the length of the cross-frame members did not change (except for elastic shortening). Note that the horizontal distance between the tops of the extreme left and right girders of the bridge in the no-load condition, W', is less than the horizontal distance, W, between the same points after dead load has been applied. The difference equals $W - W'$, where $W' = W\cos\theta$. The change in radius, ΔR, of the leftmost curved girder that must be introduced equals:

$$\Delta R = W(1-\cos\theta)$$

Equation 4.1.8

Thus, the new radius will be $R - \Delta R$. The larger the relative deflection of the girders, the greater the change in radius that must be introduced during the erection. The larger the flange lateral moment of inertia, the greater the force that must be exerted to change the radius.

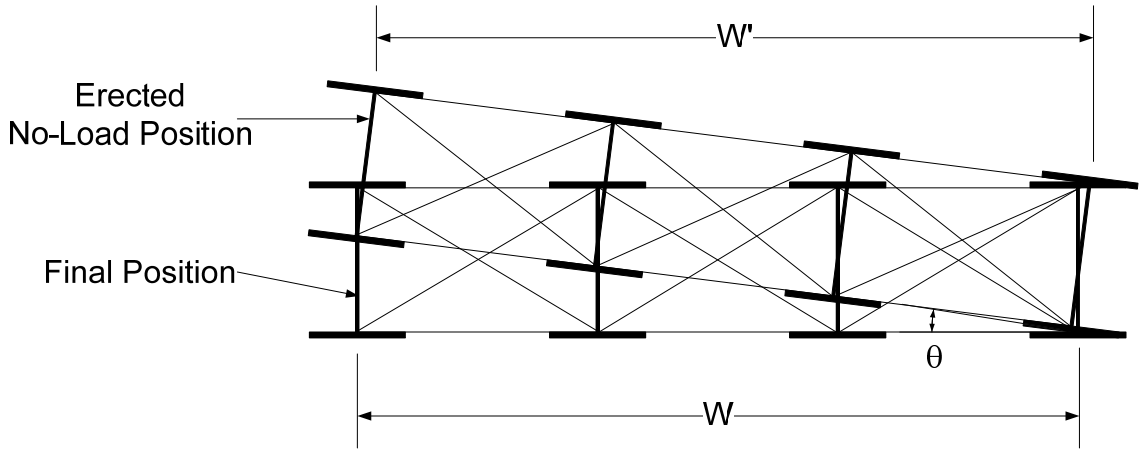


Figure 4.1.28 Erected No-Load Condition and Final Condition of a Curved Bridge at Mid-Span (Total Dead Load Fit)

Note that the flanges lie in single planes, both before and after the dead load is applied. Note that the cross-frames are attached to each of the girders at the same distance from the flanges. This means that the cross-frames must be square and the diagonals must be of equal length.

Note that the relative deflection at the supports is zero and increases to a maximum near the center of the span. Hence, a smaller applied lateral force is expected to be required to make the smaller changes in radii near the supports. It seems that working toward the center cross-frame from the two supports would minimize the lateral force required. A further observation is that the lateral plastic moment of the flange, $(M_p)_\ell$, is computed as follows:

$$\left(M_p\right)_\ell = F_y t_f b_f^2 / 4$$

Equation 4.1.9

If it is assumed that the true yield stress is 60 ksi for nominal 50-ksi material, then Equation 4.1.9 becomes:

$$\left(M_p\right)_\ell = 15 t_f b_f^2$$

Equation 4.1.10

If the spacing of installed cross-frames is *S* and a load, P, is applied at mid-span, the applied moment is $M = P*S/4$. Substituting *M* for $(M_p)_\ell$ in Equation 4.1.10 and rearranging gives:

$$P = 60 t_f b_f^2 / S$$

Equation 4.1.10

For example, a 2″ x 20″ flange composed of nominal 50-ksi material with a cross-frame spacing of 20 feet (240 inches) would require a lateral force, P, of (60 x 2 x 20^2/240) = 200 kips to fully yield the flange. A lateral force of 133 kips would cause yielding in only the extreme fibers. Only 111 kips would cause some yielding in the extreme fibers if the true yield stress of the material was 50 ksi.

The Design Engineer may wish to limit the moment that the Erector can apply to limit yielding of the flanges. Frequently, erectors can apply 100 kips of load with normal equipment in the erection process. Of course, the above example is for only one situation. If the cross-frames near the supports are installed first, a temporary support of some type may be required until the girder is sufficiently braced. The span can be increased and/or other loading patterns might be used by the Erector. Hence, the Design Engineer probably should only control the applied moment. Certainly, the self-weight of the girders impacts the stress state.

These few simple relationships allow the Design Engineer to predict if a Steel Dead Load or Total Dead Load Fit is applicable/feasible. The bridge may be defined as a "complex structure" that must be fit-up in the Fabricator's yard prior to delivery in questionable cases.

If the bridge is determined to not be a candidate for a Steel Dead Load or Total Dead Load Fit, the girders need to be fabricated with different radii (Section 4.1.3.1.3.3), or built with a No-Load Fit and the out-of-plumb webs tolerated.

Straight Girder Bridges w/ Skewed Supports

For straight girder bridges with skewed supports, issues related to twist and web plumbness are most important at supports, particularly at simple supports. A torque is applied to the girders when the two ends of a cross-frame deflect differently. The reason is that the cross-frame experiences restoring forces that attempt to maintain equal deflections of the girders. This force creates a load on the girders that is eccentric with respect to the shear center, which in turn introduces a torque into the girders. The cross-frame forces are larger when the cross-frames are contiguous. Larger differential deflections also cause increased cross-frame forces. Obviously, the forces increase with larger vertical girder deflections and with increased skew.

Fortunately I-girders are weak in torsion, which permits the girders to twist with little resistance except that offered by the opposing cross-frames. Lateral flange bending is increased significantly when the cross-frames are staggered (Section 3.1.2.8.3.2). This occurs because the cross-frames are not aligned so the torque is transmitted along the girder between the points of cross-frame connection. Interestingly, the torque in the exterior girders is less than in the interior girders.

The cross-frames are detailed to be correct under dead load when a Steel Dead Load or Total Dead Load Fit is employed, which means that the girders must be twisted in the direction opposite to that introduced when dead load is applied. Since

I-girders are relatively flexible in torsion, the Erector can usually handle the issue if detailing is done properly.

Skewed Cross-Frames

Simple supports present the critical detailing issue for this category of bridge. The cross-frames at these supports are not perpendicular to the girder lines. As demonstrated previously in Section 1.1.4.1, the girders at each end of a skewed cross-frame rotate about both the transverse (y-axis in Figure 4.1.29) and the longitudinal (x-axis in Figure 4.1.29) axes of the girder. The rotation of the girders about the transverse axis causes the tops of the girders over the bearings to deflect into the span. If the bottoms of the girders are free to move longitudinally, they deflect out of the span. These deflections are due to elastic shortening of the top and bottom of the girder. Rotation of the girders about the transverse axis at supports is usually addressed by detailing the bearing stiffeners to be out-of-plumb in the no-load condition. The stiffeners become plumb as the dead load is applied.

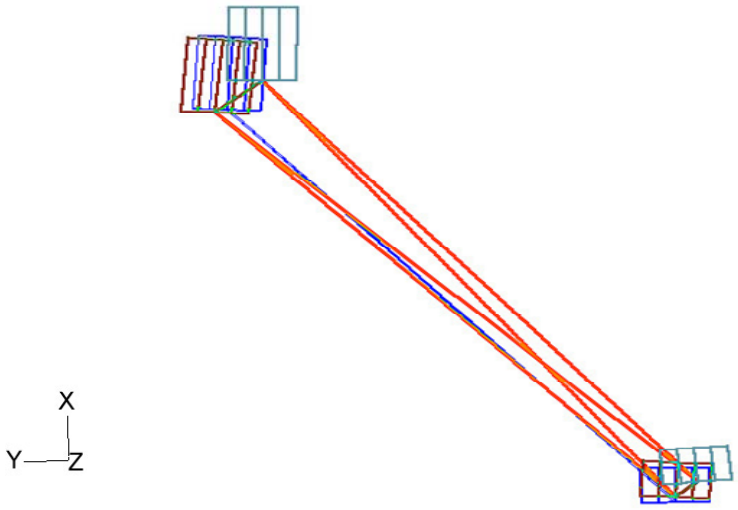


Figure 4.1.29 Plan View of Deflected Shape of an End Cross Frame at a Skewed Support

Since the girder tops move with respect to the bottom of the adjacent girders, the distance between the top of a girder and the bottom of its neighbor changes. However, the cross-frames connecting the girders forbid this change to occur. The only way for the distance to remain constant is for the top of the girder to translate laterally. This is evidenced by an apparent twist in the girders (Figure 4.1.30). Hence, if a No-Load Fit is employed and the girders are plumb in the no-load condition, they will twist out-of-plumb at the supports under dead load. The amount of twist is a function of the dead load deflection and to a small degree, the bearing arrangement.

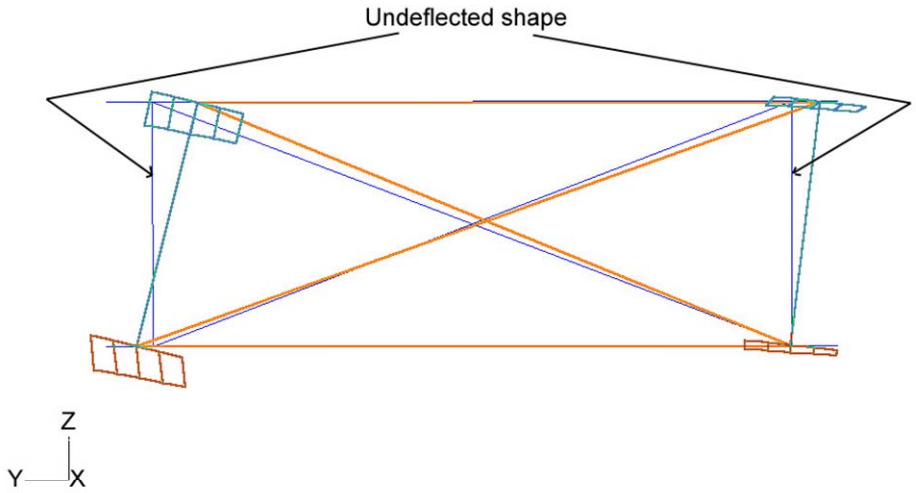


Figure 4.1.30 Cross-Section of End Cross-Frame at a Skewed Support

If the girders are to be plumb under dead load, the cross-frame must have equal length diagonals and be attached to the connection plates at the same height, top and bottom. Further, the cross-frame connection plates must be placed on the girder webs at the locations that will be plumb under dead load. Hence, to fit-up the cross-frames in the no-load condition, the girders must be twisted out-of-plumb during the erection since the tops and bottoms of the girders are not in their final longitudinal positions. As a result, the end cross-frames will not be plumb in the no-load condition. If they were to be erected plumb at no-load, they would be out-of-plumb under dead load.

The use of skewed cross frames parallel to the supports is permitted for skews up to 20 degrees from normal. This means that the cross-frame connections are made at points on the girders that are likely to deflect the same amount. This tends to eliminate the torque introduced with normal cross-frames. The limit on the angle is probably due to the difficulty of welding the skewed connection plates to the girder webs at angles much in excess of 20 degrees. If normal connection plates are used, they need to be bent to receive the skewed cross-frames (Section 3.1.2.8.5.2). This situation introduces an eccentric load on the connection plates. However, the limited experience with significantly skewed cross-frames indicates that they function very well. The advantage of them is that the forces in them are reduced and the twist is reduced, except at simple supports as discussed above. Further, a No-Load Fit can be employed.

Cross-Frames Normal to the Girders

Cross-frames normal to the girders are detailed such that the girder webs will be plumb and the top flanges will lay along a common plane, adjusted for any cross-

slope, after either the steel dead load or full dead load, as applicable, has been applied (Figure 4.1.31).

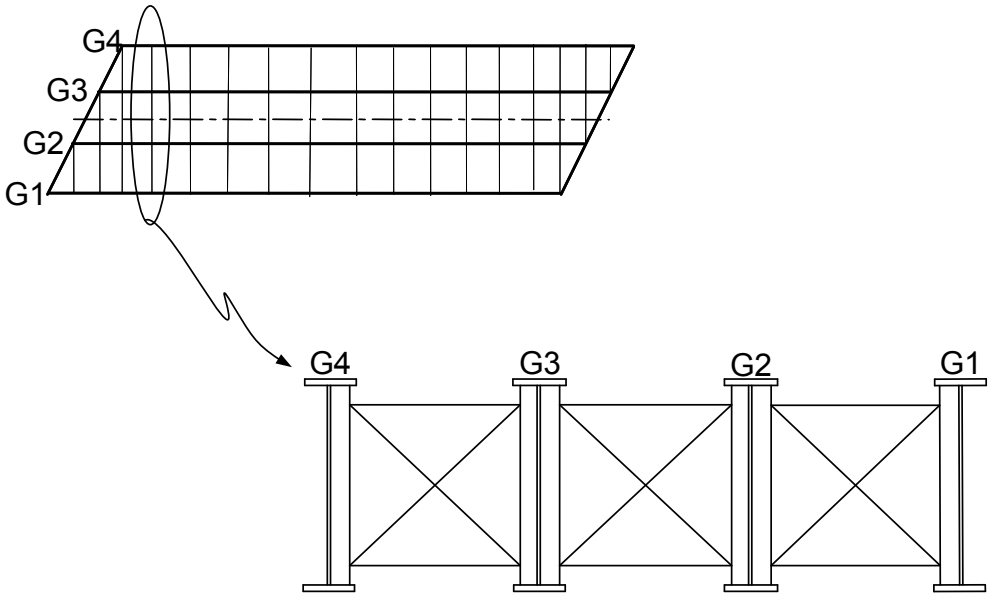


Figure 4.1.31 Steel Dead Load or Total Dead Load Fit Assumption for Cross-Frames Normal to the Girders – Assumes Steel Dead Load or Full Dead Load Applied

A similar approach is used for a Steel Dead Load or Total Dead Load Fit of the intermediate (radial) cross-frames in curved bridges with radial supports.

Consider the four-girders from the sample straight skewed I-girder bridge shown in Figure 4.1.32 initially erected in their no-load position with the girder webs plumb prior to installing the cross-frames (Step 1). The intermediate cross-frames at this section are located perpendicular to the girder lines. For simplicity, it is assumed in the discussion that there is no cross-slope. Each girder has been given a different camber at any given cross-section because of the computed dead load deflections, as shown in Figure 4.1.32.

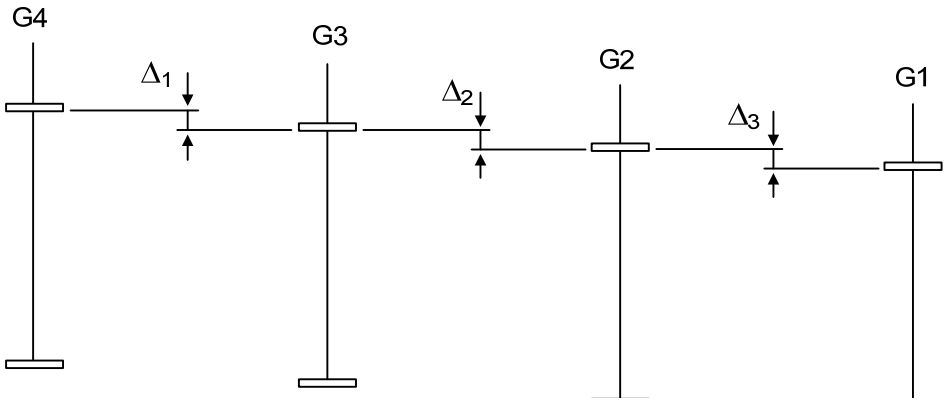


Figure 4.1.32 Step 1 – Girders Erected in their No-Load Position with Webs Plumb Prior to Installing the Cross-Frames

Assume the cross-frames have been detailed such that the girders will be plumb at the full dead load condition (i.e. a total dead load fit). Since the girders at the ends of all intermediate cross-frames will deflect different amounts, the girders must twist when they are loaded after the cross frames are fully installed. Since the cross-frames were detailed to fit plumb girders *after* the dead load has been applied, the girders must be twisted to properly receive the cross-frames.

Thus, a potential erection scheme might be to first erect the cross-frame between G4 and G3 and pin some cross-frame gusset-plate bolt holes to the corresponding connection-plate bolt holes near the top of each girder, with the girders remaining vertical (Step 2 - Figure 4.1.33 Part A). Then, using “come-a-longs” or jacks, the bottom of G3 would be pushed toward G4 so that enough connection-plate bolt holes line up with the cross-frame gusset-plate bolt holes near the bottom of G3 that they can be pinned (Step 3 – Figure 4.1.33 Part B). This operation would then be repeated at the bottom of G4 (Step 4 – Figure 4.1.33 Part C). With the cross-frame now in place, a reverse twist has been introduced into G4 and G3.

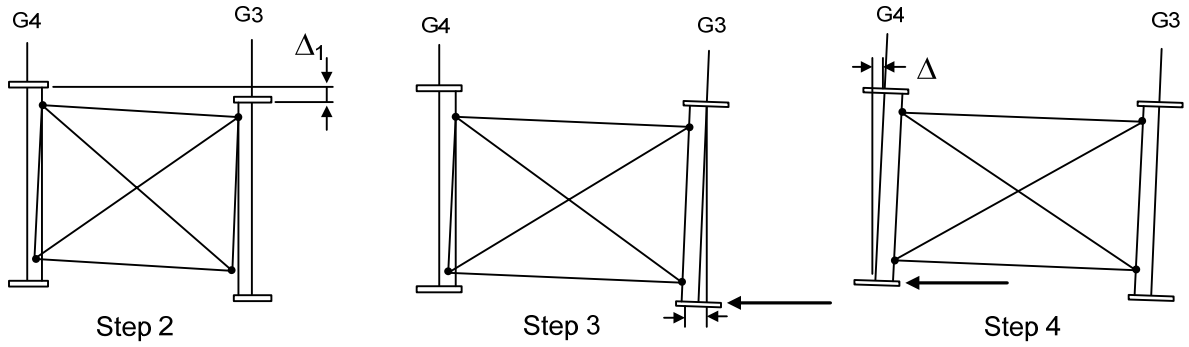


Figure 4.1.33 Installation of Cross-Frame In-Between G4 and G3 - Steps 2, 3, and 4
A) Step 2; B) Step 3; C) Step 4

As a next step, the cross-frame between G3 and G2 would be erected with the top and bottom holes on G3 pinned. The bottom of G2 would then be pushed toward G3 until enough holes lined up near the bottom of G2 for pinning (Step 5 – Figure 4.1.34 Part A). A similar step would be repeated to install the cross-frame between G2 and G1 (Step 6 – Figure 4.1.34 Part B). When this step has been completed, the proper reverse twist has been introduced into the entire cross section.

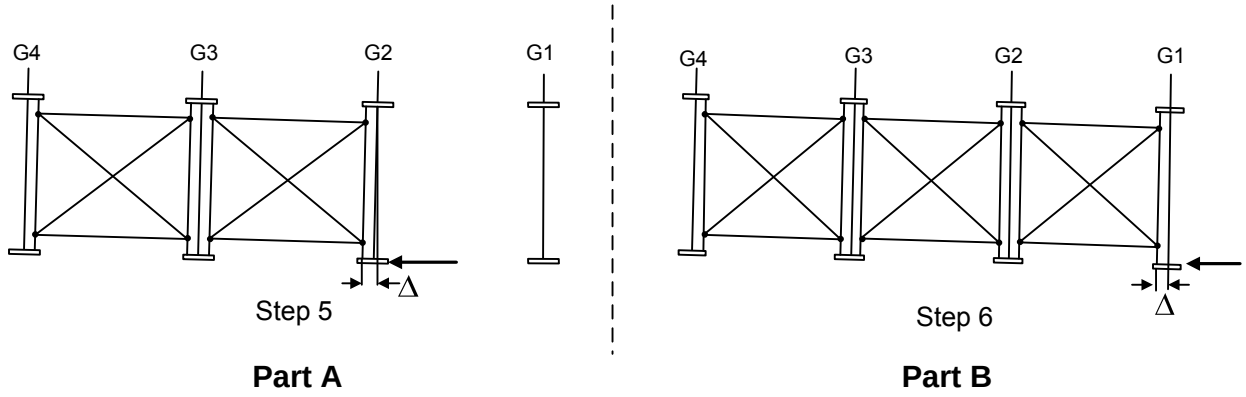


Figure 4.1.34 Installation of Cross-Frames In-Between G3 and G2 and Between G2 and G1 – Steps 5 and 6
A) Step 5; B) Step 6

As a result, the girders will rotate into their final position with all girder webs plumb under dead load (Step 7 – Figure 4.1.35).

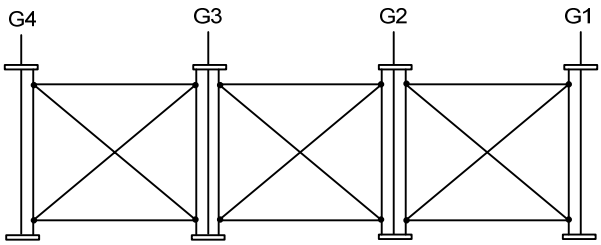


Figure 4.1.35 Cross-Section After Dead Load is Applied – Step 7

Advantages and Disadvantages of a Steel or Total Dead Load Fit

The advantages of employing a Steel or Total Dead Load Fit are that the method provides plumb girders under dead load; the girders will bear more squarely on the bearings; and the lateral position of the deck and barriers with respect to the approaches will be correct (note that the latter two advantages are with regard to a Total Dead Load Fit only).

As with skewed straight girders, when the cross-frames in horizontally curved I-girder bridges are forced into place, the girders are twisted out-of-plumb in the direction contrary to the direction they will twist under load. To accomplish this twist, the radii of the flanges must be slightly changed, resulting in lateral bending, in addition to that due to curvature, introduced into the flanges. The lateral bending stresses due to the change in radius are more significant than the lateral bending stresses introduced in straight girders when they are twisted. The additional lateral stresses in the flanges are a function of the required changes in the flange radii and their lateral stiffness.

These additional lateral bending stresses are of little consequence in the vast majority of cases because the resulting twist of the girders will likely be small enough that the cross-frames will easily pull the girders into their intended position and reverse most of the locked-in lateral bending stresses introduced during installation of the cross-frames.

There is a paucity of research on lateral flange bending stresses that are induced during erection. The subject is not directly addressed in *AASHTO*. Hence, it is currently a matter of engineering judgment. Where a Steel Dead Load or Total Dead Load Fit is used to introduce a twist into curved girders during erection, thin flanges may be subject to local buckling and unusually stocky flanges may be difficult to move into position. Thus, the Design Engineer may be subjected to some risk, when such detailing is called out. There have been cases where the Erector could not distort curved flanges.

An issue when calling for the webs to be theoretically plumb under the full dead load condition is that the Erector will leave the site with the girders out-of-plumb since the full dead load will not have yet been applied. Unless there is a specified amount of out-of-plumb that the girders are to be under self-weight, there is no means to inspect the erection in this regard. Although not typically done in present-day practice, it is suggested that the Plans may specify the expected out-of-plumb of the girders under self-weight.

Another issue when a Total Dead Load Fit is called for under the full dead load condition is the accuracy of the computed rotations. Field observations have indicated that often the girders do not rotate as much as theoretically predicted. There are at least three possible reasons for the differences in the observed and computed rotations:

- The stiffness of the deck forming is typically ignored in the calculations;
- The fresh deck concrete and reinforcing steel exhibit some stiffness;
- If the deck is cast in sections and allowed to harden between casts, the final rotations will be less than if the deck were placed at one time. This should be properly accounted for in the computations.

Some Owners have found success in specifying half of the computed rotation due to the deck weight plus the full rotation due to steel dead load in the detailing for skewed straight-girder bridges. This assumption allows the girders to be reasonably close to plumb if the actual rotation is less than or greater than the computed values.

Bridges with straight or curved girders with normal or radial supports do not exhibit the issues at bearings observed at skewed supports. Of course, skewed supports on horizontally curved girder bridges have the same issues as do straight-girder bridges with skews. Again, the issues are usually most evident at skewed end supports.

4.1.3.1.3.3 No-Load Position with Twist Camber

Issues related to twist are exacerbated, particularly in curved girder bridges with skewed end supports. To circumvent these issues, the girders might be fabricated with a twist about the longitudinal axis of the girder under the no-load position, as depicted in Figure 4.1.36.

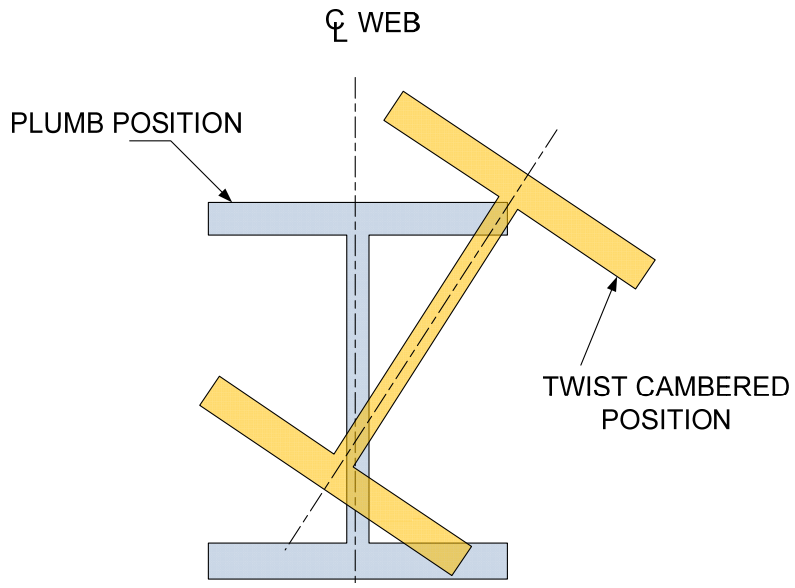


Figure 4.1.36 Twist Cambered No-Load Position

The twist camber is introduced by fabricating the top and bottom flanges with different radii. To facilitate detailing, a horizontal camber for each flange should be calculated and specified on the contract documents. The horizontal cambers might be specified by a given radius or as deviations from a chord between the two ends of the shipping section. The cambers might be specified as the theoretical offsets from the chord, plus or minus (as appropriate) the horizontal deflections resulting from the girder twist determined from a refined analysis, or simply as the horizontal deflections resulting from the twist without the offsets. The method chosen should be noted on the plans. In cases where there is compound curvature or a spiral, it would certainly be desirable to include the offsets to assist detailing.

Flanges should be welded square with respect to the web. The cross-frame drops are for the desired dead load condition, as described previously. Thus, in this case, the cross-frames would be detailed consistently with the girders.

By fabricating the girders in this manner, the webs will end up plumb under dead load *without theoretically inducing any potentially deleterious locked-in stresses in the flanges and cross-frames during the erection.* Again, some fabricators desire the girders to be detailed to have plumb webs under self-weight of the steel only. In this way, the girders are plumb when properly erected. If this approach is chosen, the girders will not be plumb when all of the dead load has been applied (Table 4.1.5).

Table 4.1.5 Girder Web Plumbness for Twist Camber (Steel Dead Load)

	PLUMB	OUT-OF-PLUMB
NO-LOAD		●
STEEL DL	●	
FULL DL		●

Table 4.1.6 Girder Web Plumbness for Twist Camber (Total Dead Load)

	PLUMB	OUT-OF-PLUMB
NO-LOAD		●
STEEL DL		●
FULL DL	●	

Detailing and fabrication costs for twisted curved girders would be expected to be higher than for a traditional curved girder. Since the tools to determine the absolute need for this are not readily available at this time, the Design Engineer is wise to permit the Contractor the option to choose to fabricate the girders in the normal manner with both flanges having the same radii if the Contractor believes that the Erector can erect the girders with the cross-frames and girder detailing inconsistent in order to obtain vertical webs under dead load.

4.1.3.1.4 Tub Girders

Tub girders behave as closed sections with or without the deck. They are torsionally stiff, which means that they must be fabricated with the proper twist in order to be erected. This creates a different issue from I-girders, which can be twisted much easier. Tub girders usually have both webs the same height. This requires that they be fabricated with a built-in twist, as shown in Figure 4.1.37. The induced twist must not only match the cross-slope of the roadway, it must take into account the twist that occurs under dead load. The camber of the two webs is significantly different.

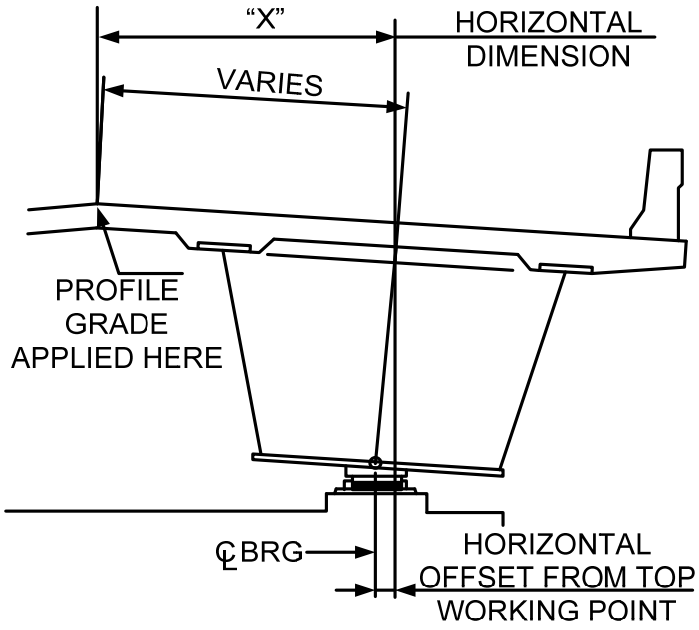


Figure 4.1.37 Cross-Section of Tub Girder with Built-In Twist to Match Roadway Cross-Slope

These girders are fabricated by first welding the top flanges to their respective webs. The webs receive the connection plates. Next, the cross-frames are installed to position the webs and confirm the cambers. Finally, the bottom flange is pulled into place and welded to the webs. As mentioned previously, the connection plates are often clipped short of the bottom flange to permit continuous welds connecting the flange to the webs, and then later extended with fillet welded attachments to the bottom flange (Section 3.1.2.8.5.2).

Tub girders with skewed supports are problematic and often are not amenable to a practical solution. If double bearings are employed on a skewed support, the reaction of the bearing closer into the span is larger than that of the rear bearing, creating what may be a severe torque. This situation often leads to uplift that may be difficult to manage. If a single bearing is used at the support, there is no restraint against twist until installation of the end diaphragms or cross-frames. The girders will twist and make it very difficult to introduce such end-connecting members. It is highly desirable to eliminate skews when tub girders are used.

4.1.4 Shop Fit-Up and Assembly Issues

Shop fit-up and assembly of curved girder sections is covered in Articles 11.8.3.7 and 11.5.3 of the *AASHTO LRFD Bridge Construction Specifications*.

In addition, according to Article 11.8.3.1 of those same specifications, the Fabricator must ensure that the steel can be fit-up in the no-load condition, unless specified

otherwise in the Contractor's Construction Plan. The intent of this provision is to ensure that the steel will be erected in a manner consistent with the analysis for the steel self-weight. The steel may be erected in stages if the analysis reflects the planned erection sequence. Cambers should be adjusted for this process. Attention should be paid to the deck. The stresses and cambers must take into account the distribution of load if the deck is cast on one phase of the bridge and a second phase is cast later.

4.1.4.1 Assembly

According to Articles 11.5.3.1 and 11.8.3.7 of the *AASHTO LRFD Bridge Construction Specifications*, girder field connections are to be preassembled in the shop as necessary prior to shipment to verify the geometry of the completed structure or unit (Figure 4.1.37); that is, to ensure proper fit in the field. Extensive shop fit-up requires that much of the fabrication be completed prior to shipping.

The requirement of Article 11.5.3.1 is typically applied to fit-up and verify the field splices for multi-stringer bridges. If the girder is to be heat-curved, splices may be fit-up prior to heat curving and with the web in either a vertical or horizontal orientation. If the flanges are cut-curved, fit-up of I-girder flange splices is usually performed with the flanges horizontal either before or after welding of the flanges to the web. The design camber must be in the girder when girder field splices are fit-up.

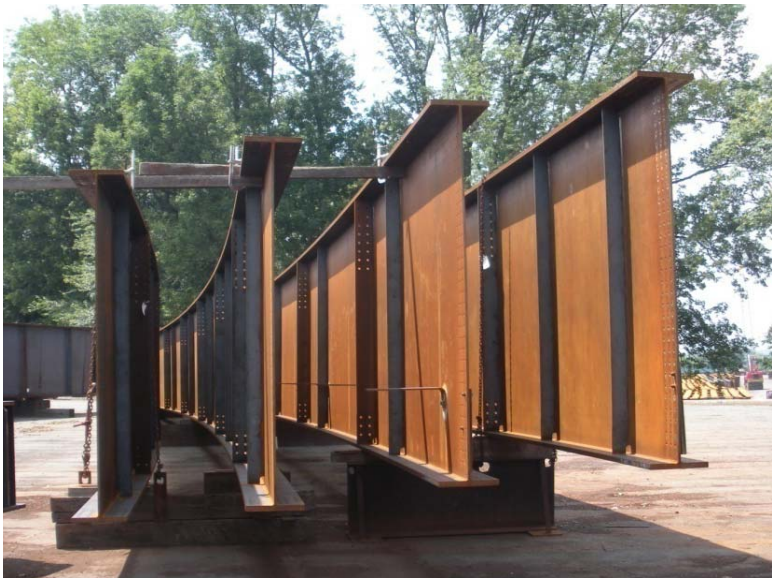


Figure 4.1.38 Preassembled Curved I-Girders

Article 11.8.3.7.1 of the *AASHTO LRFD Bridge Construction Specifications* states "Shop fit-up of bolted connections in load-carrying connections of cross-frames and diaphragms to the girders may be required for structures with complex geometry or stiff elements."

This requirement is rarely invoked because it is usually unnecessary and is relatively expensive. It is most often invoked for tub girders which are very stiff torsionally. Another occasion where it may be desirable is when a Steel Dead Load or Total Dead Load Fit is called for. In such cases when the girders are curved, as discussed above, the fit-up may be difficult and shop assembly to ensure that the girder flanges can be forced may be desirable. It may also be desirable to establish a sequence of installing the cross- frames rather than working it out on the site. Girders with larger radii and/or narrow flanges would likely not be required to be pre-assembled. Straight girders, which are easier to twist for force fitting the cross-frames, are also not likely to require pre-assembly.

A partial fit-up should be sufficient to confirm the practicality of a Steel Dead Load or Total Dead Load Fit. When the cross-frames cannot be force fit by the Fabricator, the girder flanges simply need to be slightly heat curved. Costs are expected to be much lower when this issue is discovered and remedied at the fabricating shop prior to delivery than if an extra or a claim is involved. Performing the remedy in the field is the least desirable. The prior discussion can give the Design Engineer some guidance as to whether a partial assembly by the Fabricator may be needed.

The Design Engineer should note that if the bridge is curved but not skewed, the only issue with a No-Load Fit is rotation (out-of-plumb) of the girders in their final position. If the bridge is curved and skewed and a Steel or Total Dead Load Fit is employed, partial fit-up by the Fabricator may be in order.

In special instances, progressive assembly may be employed in which a minimum of three contiguous sections of the bridge adjusted for line and camber may need to be pre-assembled and fitted one time in a progressive fashion. Full girder assembly, in which the assemblies should not be less than 150 feet long, may be required for structures longer than 150 feet. These methods of assembly are normally employed to structures with particularly rigid or complex framing, or if numerically controlled (NC) drilling is not used. *Full shop assembly of the entire bridge at one time is not required unless specified in the Construction Plan*.

4.1.4.2 Bolt Holes and Bolt Tightening

AASHTO LRFD Article 6.13.1 and Article 11.8.3.5 of the *AASHTO LRFD Bridge Construction Specifications* specify that standard-size bolt holes are to be used in connections of primary load-carrying members in horizontally curved bridges, unless otherwise permitted by the contract documents.

For straight-girder bridges, it is often possible to leave the cross-frame and field splice bolts loose in several spans until the entire bridge is erected to allow fit-up adjustments to be made more easily. The girders can then often be lifted individually to the proper elevation before the bolts are tightened.

As discussed throughout this manual, curved girders depend on their connections to adjacent girders through bracing members for their stability. Thus, cross-frames/diaphragms in curved bridges must be firmly connected to the girders in order for the girders to remain stable during the erection. *Loosely connected cross-frames/diaphragms and oversize or slotted holes are not recommended for use in horizontally curved-girder bridges, as they may compromise the girder alignment and plumbness making cross-frame/diaphragm fit-up more difficult*.

Oversize Bolt Hole Study

A study was conducted on a horizontally curved, simple-span bridge having three I-girders in the cross-section to illustrate the erect of oversize holes on erection. The girders are spaced at 8′-9″ and the girder webs are 48 inches deep. It was assumed that the cross-frames were attached to the girders with loosely connected 7/8-inch-diameter high-strength bolts located in two vertical gage lines of 1-1/16-inch-diameter holes. The oversize holes were assumed to be in both the connection and gusset plates, and it was assumed that the bolts were initially centered within the holes.

The objective of the study was to determine the maximum global displacements of the bridge resulting from the possible displacements of each connection ply; that is, the summation of the local displacements of each ply due to potential slippage in the connection. The displacements were determined based on geometrical considerations.

Three different conditions were examined.

In the first condition shown in Figure 4.1.39, it was assumed that the connection slippage occurred in the horizontal (lateral) direction only with Girder 1 fixed as the reference point. The maximum possible global lateral displacement of the bridge system was computed to be 3/8” at Girder 2 and ¾” at the outside Girder 3.

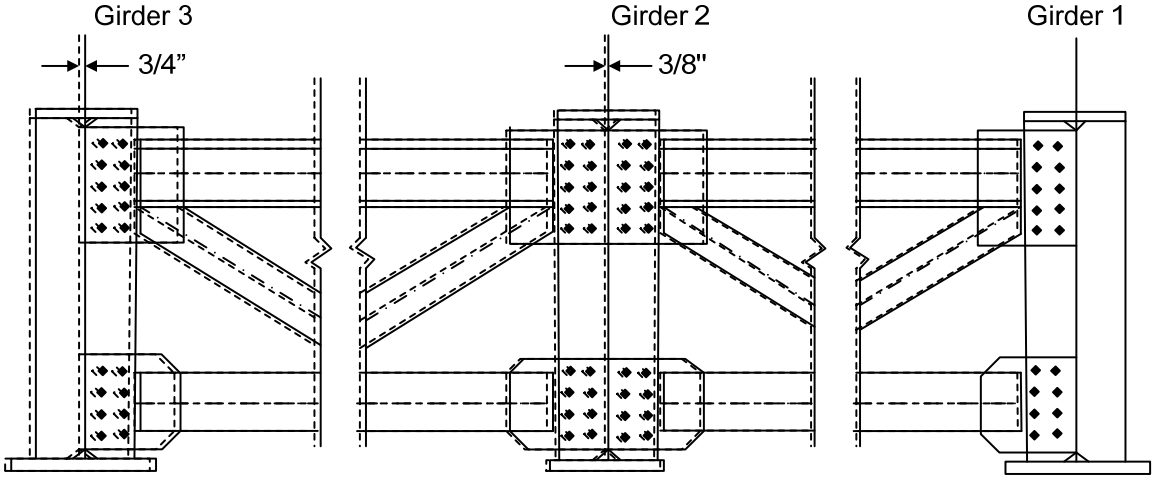


Figure 4.1.39 Horizontal Movement due to Slippage (Girder 1 is Fixed)

In the second condition shown in Figure 4.1.40, it was assumed that the connection slippage occurred in the vertical direction only. The exact same global displacements of the bridge system were computed as in the first condition above.

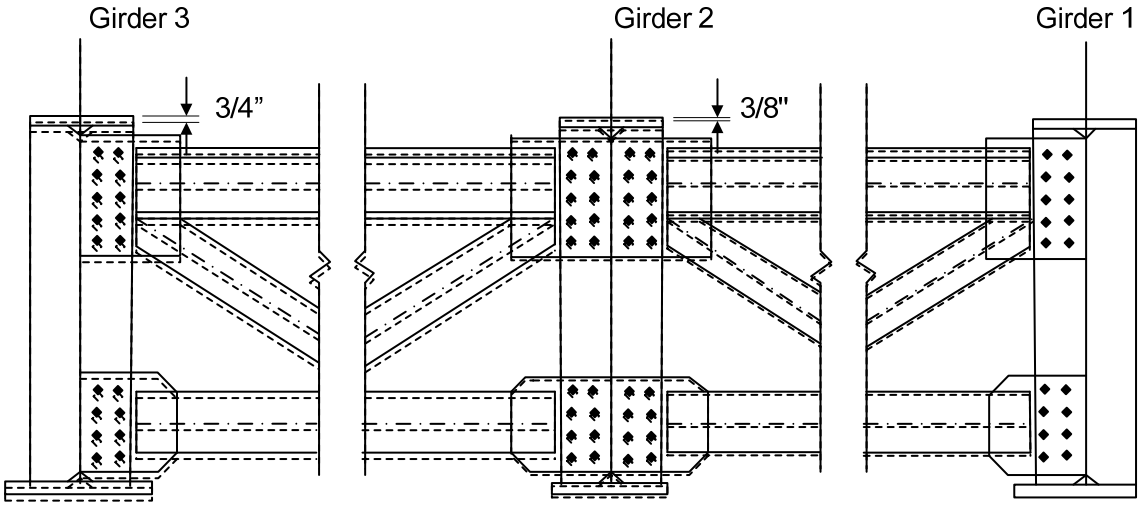


Figure 4.1.40 Vertical Movement due to Slippage (Girder 1 is Fixed)

In the third condition, a rotation of the entire cross-section was assumed due to slippage in the connections, as illustrated in Figure 4.1.41.

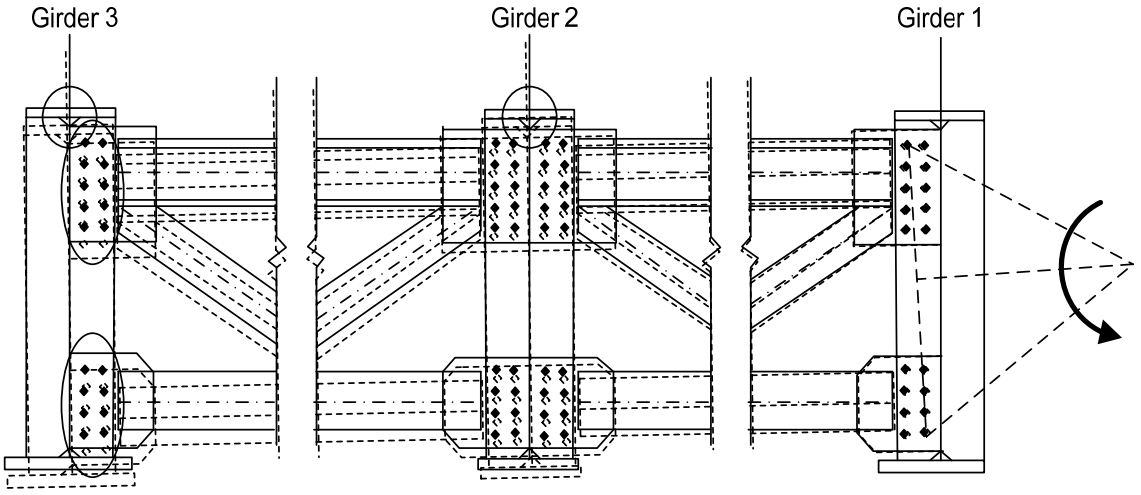


Figure 4.1.41 Assumed Rotation of the Cross-Section after Bolt Slippage

For this cross-section rotation case, from geometry and scaling, the maximum global displacements in the vertical and lateral direction at the outside Girder 3 were computed to be 2.302 inches and 0.371 inches, respectively. As expected, smaller displacements were computed at the interior (center) Girder 2. These movements and dimensions are shown in Figure 4.1.42.

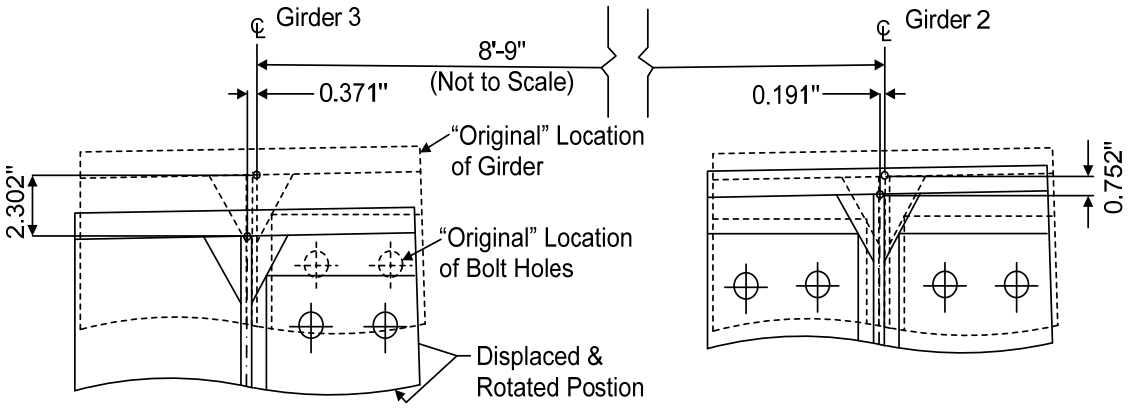


Figure 4.1.42 Vertical and Lateral Displacements of Girders 2 and 3 for the Case Shown in Figure 4.1.41

Movement of a typical initially centered bolt within the oversize hole as a result of the local displacements of each ply resulting from the connection slippage is shown schematically below in Figure 4.1.43. The error would be much greater with more girders in the cross-section.

The displacement occurs by a drop of 3/16 inch and a twist created by the top bolt in the connection plate extending 3/16-inch to the right and by the bottom bolt in the connection plate extending a similar amount to the left of the hole.



Figure 4.1.43 Possible Movement of an Initially Centered Bolt within an Oversize Hole

Larger displacements could have occurred if the bolts had been in less beneficial positions than initially centered in the holes as assumed.

Maneuvering the bridge with cranes to get the girders in the proper alignment elevation is extremely difficult with oversize holes. Fit-up problems generally occur with oversize holes. *The advantage of using oversize or slotted holes to permit error on the part of the Fabricator proves to be a disadvantage to the Erector. This is particularly true for curved girders, which transfer load through the cross-frames. The use of oversize or slotted holes in cross-frame/diaphragm connections is not permitted for curved-girder bridges, unless otherwise permitted in the contract documents*.

4.1.5 References

1. AASHTO. 2010. *LRFD Bridge Construction Specifications*. Third Edition, American Association of State Highway and Transportation Officials, Washington, D.C.
2. Brockenbrough, R.L. 1970. "Theoretical Stresses and Strains from Heat Curving." *Journal of the Structural Division*, American Society of Civil Engineers, New York, Vol. 96, No. ST7.
3. Brockenbrough, R.L., and K.D. Ives. 1970. "Experimental Stresses and Strains from Heat Curving." *Journal of the Structural Division*, American Society of Civil Engineers, New York, Vol. 96, No. ST7.
4. Daniels, J.H., and Bacheler, R.P. 1979. "Fatigue of Curved Steel Bridge Elements: Effect of Heat Curving on the Fatigue Strength of Plate Girders." Report No. FHWA-RD-79136, Federal Highway Administration, Washington, D.C., August.
5. Hilton, M.H. 1984. "Deflections and Camber Loss in Heat-Curved Girders." *Transportation Research Record 950*, Vol. 2, Transportation Research Board, Washington, D.C.
6. Brockenbrough, R.L. 1970. "Criteria for Heat Curved Steel Beams and Girders." *Journal of the Structural Division*, American Society of Civil Engineers, New York, Vol. 96, No. ST10.
7. Brockenbrough, R.L. 1972. *Fabrication Aids for Continuously Heat-Curved Girders*, ADUSS 88-5538-01, United States Steel Corporation, Pittsburgh, PA, April.
8. Brockenbrough, R.L. 1973. *Fabrication Aids for Girders Curved with V-Heats*, ADUSS 88-5539-02, United States Steel Corporation, Pittsburgh, PA, January.
9. AASHTO/AWS D1.5M/D1.5. 2008. *Bridge Welding Code*. American National Standard/American Association of State Highway and Transportation Officials/American Welding Society, available from the American Association of State Highway and Transportation Officials, Washington, D.C.
10. Young, W.C., and Budynas, R.G. 2002. *Roark's Formulas for Stress and Strain*. 7th Edition, McGraw-Hill, New York, NY.

Chapter 4
Fabrication and Construction Considerations

Section 4.2
Construction



4.2.1 Introduction

A hundred years ago most bridges were designed and built by bridge companies. In the 1930s, bridge design firms appeared to design the more complex trusses and suspension bridges. Today most girder bridges are designed and built by different firms, removing the Design Engineer from the construction. As girder bridges have become more complex, this divorce can have bad consequences. Plans are only the first step in the process. They must be based on knowledge of the processes to occur. The *AASHTO LRFD* Specification now requires a Design Engineer's Construction Plan for complex bridges in an attempt to again unify the planning of the designer and the builder.

4.2.2 Contractor's Construction Plan

4.2.2.1 General

The purpose of the Contractor's Construction Plan is to specifically define the means and methods to be utilized in the construction of the bridge. Examples of means and methods include consideration of site conditions, determining the necessary crane locations, reach and capacities, determining the need for any ancillary rigging and the development of an overall erection plan. The Plan also covers a myriad of other issues such as access, grubbing, foundations, substructure construction, deck placement and scheduling. Only the fabrication and erection of the steel is particularly germane to the subject at hand.

When a steel curved girder bridge is built according to the *AASHTO LRFD* Specifications, the Contactor's Construction Plan is to address the special provisions given in Article 11.8 Additional Provisions for Curved Steel Girders in the *AASHTO LRFD Bridge Construction Specifications (1)*. These provisions require that the Contractor's Construction Plan address issues not required in most straight bridges. The Contractor's Construction Plan, including the special provisions of Article 11.8, is to be signed by a Professional Engineer and approved by the Owner. Interestingly, bridges with skewed supports are not addressed in these special provisions. This manual addresses both curved girder bridges and bridges with skewed supports. As has been shown, bridges with skewed supports have certain additional issues that may impact construction. It is suggested that Owners require that bridges with skewed supports be included under these special provisions.

AASHTO Specifications have required a Contractor's Construction Plan for all bridges. It is a legal document provided by the Contractor, whereas the Design Engineer's Construction Plan is advisory. The purposes of the Design Engineer's Construction Plan are three-fold: First is to level the playing field at bidding; second is to reduce some of the Design Engineer's responsibility by showing that the design has considered one method of construction making construction of the bridge feasible; third is to instruct the Contractor of any subtle assumptions in design that may relate to construction.

An example of the first purpose is identification of the anticipated need for temporary towers during the erection of the bridge. This information allows bidding Contractors to prepare fairer bids.

An example of the second purpose of the Design Engineer's Construction Plan relates to wind loads acting on the bare steel to identify the potential need for lateral bracing to prevent excessive deflections and stresses.

An example of the third purpose would be identification of cambers defined for a phased construction process that was assumed at design. A different phasing process may require that the Contractor re-compute the cambers.

Table 4.2.1 Contractor's vs. Design Engineer's Construction Plan

	Contractor	Design Engineer
Purpose:	Identify site constraints.	Level the playing field at bidding.
	Develop means and methods to build bridge including an erection scheme and required equipment.	Reduce some of the Engineer's responsibility by showing that the design is feasible to build.
	Obtain approvals from Owner, associated agencies and any temporary access permits.	Include descriptions of any subtle assumptions of construction sequence assumed at design.

The Contractor's Construction Plan may incorporate the Design Engineer's Construction Plan, or create a completely different scenario for the construction. However, the Contractor would use the Design Engineer's Construction Plan to know what changes, if any, in the design would be required to accommodate a different construction scenario. .

The Contractor remains responsible for the construction even if the Contractor decides to incorporate the Design Engineer's Construction Plan. *At all times, the Contractor remains responsible for the means and methods that are employed in the actual construction*. The Contractor's Construction Plan is considerably more detailed than the construction plan provided in the contract documents. The Design Engineer's Construction Plan is informative, not instructive.

The design-build environment is different and depends on the contractual arrangement. The law relating to these arrangements is not well developed in some situations. These arrangements are not addressed herein.
.



Figure 4.2.1 I-Girder Bridge Erection using Temporary Supports

According to Article 11.8.2 of the *AASHTO LRFD Bridge Construction Specifications*, the Contractor's construction plan is to include:

- Fabrication procedures, including method of curving the girders;
- Shipping weights, lengths, widths and heights and means of shipping;
- Erection plan, including sequence of erection, crane capacities, and the location, capacity and elevations of any temporary supports; and
- Deck placement sequence, including the time between placements, and the magnitude and position of any temporary load required to prevent girder lift-off at bearings.

The Fabricator delivers the girders to the site, but the Contractor is responsible to specify a site to off-load. The erection is often dictated by site-specific conditions such as traffic and right-of-way. Access routes for concrete ready-mix trucks and any required pumping must be identified.

As the Contractor prepares the plan, he/she will often need additional information and submit requests for information (RFIs) to the Owner who may either respond or communicate with the Design Engineer. These RFIs deal with clarifications or permission to change a requirement of the contract. Addition of or elimination of welded splices are examples of changes to the Design Plans that must be approved by the Owner and the Owner's Engineer.

There are numerous requirements the Contractor must follow in preparing the Construction Plan, including the Owner's requirements and the requirements of the *AASHTO LRFD Bridge Construction Specifications*. The *AISC* and *AASHTO/AWS* specifications are liberally referenced in the above documents.

4.2.2.2 Erection Plan

The *AASHTO*/National Steel Bridge Alliance (NSBA) *Steel Bridge Erection Guide Specification* (*2*) (Figure 4.2.2) have been developed through the *AASHTO*/NSBA Steel Bridge Collaboration. This document provides recommendations for the erection procedures, including recommended drawings and calculation procedures.

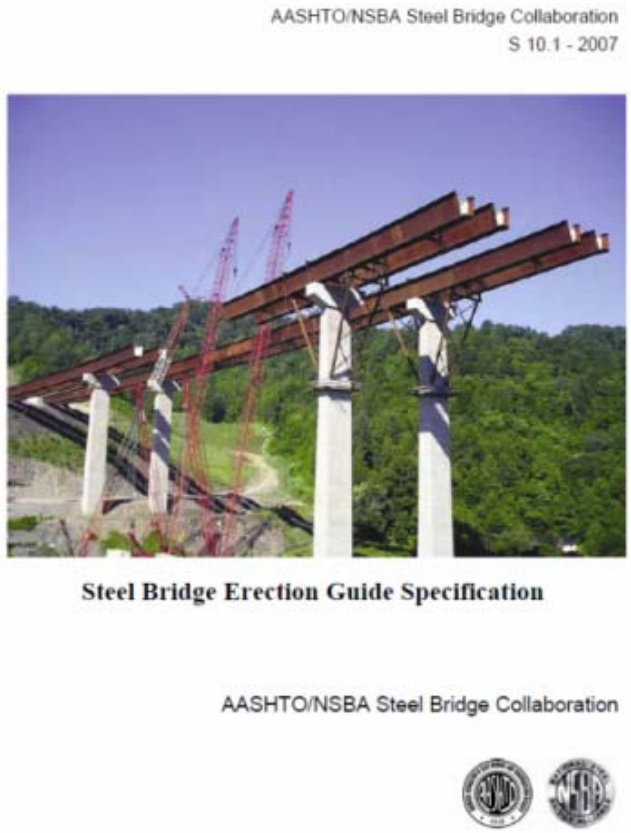


Figure 4.2.2 *AASHTO/NSBA* Steel Bridge Erection Guide Specification

This document requires that the steel erection drawings provide the following:

- Plan of the work area, including permanent and temporary supports, and obstructions such as roads and waterways;
- Erection sequence for all superstructure components, noting the location and use of temporary supports, lifting cranes and holding cranes, temporary bearing restraints and temporary lateral bracing;
- Details of temporary support structures (i.e. elevations, capacities and removal procedures), tie-down devices and blocking for the bearings;
- Details of jacking devices, spreader beams, stiffening trusses and attachments, as well as the lifting weight of girder members (including weights of all rigging and lifting attachments).

The Contractor's Engineer performs a detailed investigation of the anticipated erection sequence. The submitted erection plan provides calculations demonstrating

that the steel is stable and is of adequate structural capacity in each stage of the erection. Reactions, deflections and stresses during the erection are computed. The Contractor's Engineer should ensure there are no girder overstresses, excessive displacements and/or rotations, or instabilities during each stage of construction. Article 11.8.5.1 of the *AASHTO LRFD Bridge Construction Specifications* specifies that factored stresses be checked according to *AASHTO LRFD* Article 6.10.3 or 6.11.3, as applicable, along with Article 11.6.4.2 of the same specifications. A load factor of 1.5 based on the Strength IV load combination (Section 1.3.3) is recommended for these checks. This article further requires that Article 11.6.5 of the same specifications be employed related to field assembly of the bolted girder splices.

The Owner or Owner's Engineer reviews the erection procedure and calculations submitted by the Contractor for completeness and correctness and to ensure the procedure will not be in conflict with the design of the structure. The resulting girder elevations are to be consistent with the design elevations.



Figure 4.2.3 I-Girder Bridge Erection

The Contractor's Engineer should be required to submit the calculations that provide the basis for the details and procedures provided on the erection drawings. As a minimum, the calculations should verify:

- Capacity of cranes and the required reach of lifting and holding cranes;
- Capacity and stability of any temporary support structures;
- Structural adequacy and stability of the girders for each stage of the erection sequence, including considerations of wind loads;
- Capacity of all devices employed in the erection process, such as spreader beams, beam clamps, stiffening trusses and tie-down devices.

The timing of the removal of towers and any temporary bracing must be specified in the Plan. Many failures during erection have occurred when towers or bracing were removed without computations to justify the removal. Any removal of bolts or members to modify the erection should never be done without proper calculations to confirm that the structure will remain safe with the removal. .

4.2.2.3 Temporary Supports

Temporary supports are required more frequently for curved girder bridges than for straight girder bridges of similar spans. Unlike straight girders, a single curved I-girder as seen in Figure 4.2.4 is unstable unless torsionally restrained. There are three types of torsional restraint available:

- One or both ends of the girder may be bolted to another girder that previously has been made stable and is able to provide the required torsional restraint;
- A third support (permanent or temporary support) may be introduced;
- One or preferably more cross-frames may be erected to attach it to another girder.

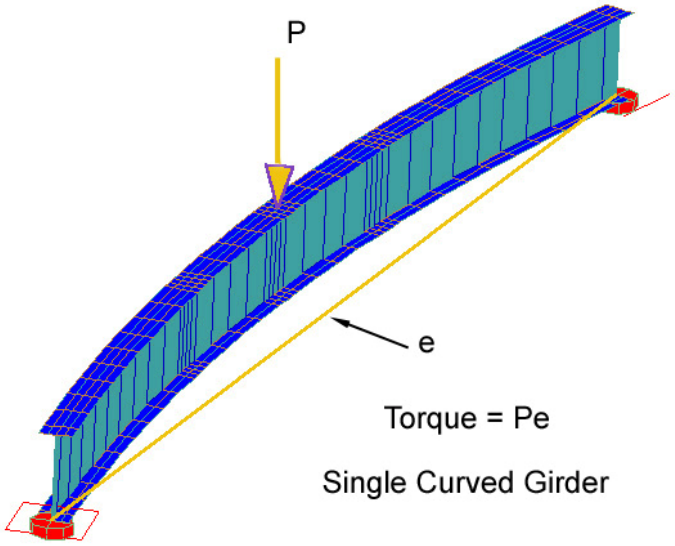


Figure 4.2.4 Single Curved I-Girder

If torsional restraints are applied at the ends of the girder shown, it will twist and deflect laterally as well as vertically. The vertical deflection is much greater than it would be for a straight girder of the same span and flexural stiffness. This extreme position makes it difficult to attach the next steel. Obviously if the girder is torsionally stiff enough, end restraints will permit fit-up of additional steel. When that is not possible, a pair of girders might be assembled and lifted as a unit as shown in Figure 4.2.5. The pair tends to reduce the torsional effects and allow additional steel to be attached. When that is not sufficient, the pair of girders might be lifted with a second holding crane to allow fit-up of additional girders and cross frames. Since the weight

of the girders shifts to the outside girder, the weight of the erected steel becomes extreme.

Erecting the girders from the outside of the curve inward sometimes is effective because the outside girder deflects incrementally as additional girders are added toward the inside of the curve. If the inside girder is erected first, it will deflect in excess of its final position as described above and require lifting.



Figure 4.2.5 Cross-Frames Bracing Two Curved I-Girders During Erection

The above discussion assumes that the bolts in all splices and cross-frame connections are tightened in standard size holes as the erection proceeds. This is a basic requirement when erecting curved girders due to the necessary load transfer between girders.

Many curved girder simple-span bridges can be erected without the aid of a temporary tower if the girders can be erected from the outside of the curve inward and the span is short to medium length. Erection of continuous curved spans is often more complex than simple spans. .When a span of curved girders is erected, the girders will have deflected vertically more than their final deflection. As load is added in adjacent span(s), the girders will eventually be raised to their final self-weight position. The girders in the adjacent span(s) introduce a twist (torque) in the already erected steel. This causes large changes in the elevation and twist in the cantilever girder ends. The addition of each girder field section adds weight and changes the free ends, sometimes significantly, making it very difficult to erect the girders. The Erector has little control of the steel in this situation. Lifting the back span is extremely difficult because all of the girders must be raised at one time.

An analysis of the stresses, deflections, and twists of the girders as the planned erection progresses will indicate if consideration of a temporary tower (as shown in Figure 4.2.6) is in order. Interestingly, the tower in the figure supports only the two convex outside girders of the six-girder cross-section. This saved time in that less ground needed to be moved and the tower could be much smaller than if all six

girders were supported. Jacks are not apparent in this photo. Note the cribbing serving as the tower's foundation.

Another, less desirable approach is to erect two or three girders of the entire unit and return to erect the remainder. This approach may eliminate the need for a temporary tower but necessitates movement of two cranes, the lifting crane and the holding crane, from span to span. Usually this is not a practical option.



Figure 4.2.6 Curved I-Girders on a Temporary Tower

The load capacity and stability of temporary support structures is investigated by the Contractor's Engineer. The vertical and lateral loads that must be resisted by the temporary support are typically due to the self-weight of the structure and wind. Load applied to temporary support structures can change dramatically as steel erection progresses. For curved bridges, it will be different for each girder erected. When temporary supports are utilized, computations are needed to ensure that the girders are not overstressed; to ascertain the temporary support reactions; and to determine the amount of deflection of the erected steel at the temporary supports when they are removed.

Adequate stroke must be provided in the jacks, Figure 4.2.7, for their removal. All jacks at a cross-section should typically be released at once through a manifold arrangement to minimize twisting of the steel and overloading of the cross-frames.



Figure 4.2.7 Jacks on Temporary Supports

The loads that must be resisted by temporary support structures are determined by analysis of each step of the steel erection sequence. Typical components of temporary supports that require design include the tower itself, the upper steel grillage, the lower mat/foundation and any lateral bracing and tie-downs. Accidental longitudinal forces on the tower may occur due to friction in the bearings or thermal or wind movement. Any longitudinal jacking during erection must also be investigated.

4.2.2.4 Girder Splices

Girder splice bolts may be left loose until the camber is to be set in straight girders. As seen earlier, bolts in curved girder splices must be tightened to provide torsional restraint and to control deflections and stresses because these structures act as systems with load being transferred between the girders. The Contractor's Engineer should ensure that the number of bolts that are installed provides enough capacity for the temporary situations that will be encountered prior to completing the bolt patterns.

Since the bolts in curved girder bridges must be tightened when installed and oversize holes are not permitted, the steel needs to be in roughly the no-load position when the bolts are installed. Proper alignment of girder field splices during erection is critical. When a girder cantilevers beyond a pier, the position of the top and bottom flange tips can significantly affect the fit-up of the adjacent girder section. Lifting the cantilever end to adjust the orientation of the web joint becomes more difficult for curved girders, as will be discussed later.



Figure 4.2.8 Cantilevered I-Girder

4.2.2.5 Cranes

Crane access as well as capacity is critical when developing the erection plan. Curved-girder bridges tend to require larger cranes than do straight-girder bridges. As seen earlier, curved girders are often lifted in pairs to improve stability; box girders are usually twice as heavy as single I-girders. Holding cranes are often used if temporary towers are to be avoided, as mentioned earlier. More and larger cranes for these jobs are more expensive. Therefore, it is imperative that erection progress as quickly as possible. This is just another reason for careful planning of the erection of curved-girder jobs. Jobsite access for the large cranes typically required to erect steel I-girders should be verified, and the locations where the various types of cranes (i.e. lifting and/or holding cranes) will be placed are determined in the same manner as for any bridge erection project. The location of the cranes can be affected by the terrain, existing roadways and structures, and by the sequence of erection. Crane locations and reach are shown as part of the erection plan.

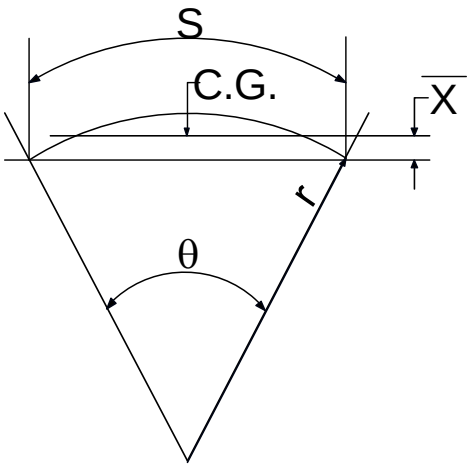
The crane capacity (i.e. type and size), counterweight requirement and boom length are provided in the Contractor's erection plan to allow the assumed crane set-ups for design to be verified in the field. In addition, the required lifting capacity and pick radius for each lifted piece must be shown.



Figure 4.2.9 Cranes Holding I-Girders

4.2.2.6 Lifting of Curved I-Girders

The pick points on curved girders are selected so that the girder section is stable and relatively plumb. They are often found by trial-and-error. Location of the lifting points is complicated by the fact that the center-of-gravity is not located in the plane of the girder web. By treating a curved I-girder as a circular arc, two pick points can be roughly located at the intersections of the arc with a line through the center of gravity of the field section as shown in Figure 4.2.10. However, this computation based simply on geometry is not always valid because of the fact that the actual dimensions of the section often vary from the nominal dimensions and sections are also often non-prismatic, which can shift the center of gravity. Thus, trial lifts are often made, in which a piece is lifted a few inches to test for the most stable lifting locations and adjustments are made as necessary. Lifting points are typically located in the vicinity of the quarter points of the girder.



$$\overline{X} \cong \frac{2r}{\theta}\sin\frac{\theta}{2} - r\cos\frac{\theta}{2}$$

Figure 4.2.10 Locating Pick Points on a Curved I-Girder

Analytical and experimental field studies on lifting of curved I-girders have been conducted (*3*). The studies examined prismatic and non-prismatic field sections and lifting with single and multiple cranes with two or more pick points. The studies indicated that *a*/*L* (refer to Figure 4.2.11) is the critical parameter to control the twist and deformations and to ensure stability; the radius was not a significant parameter.

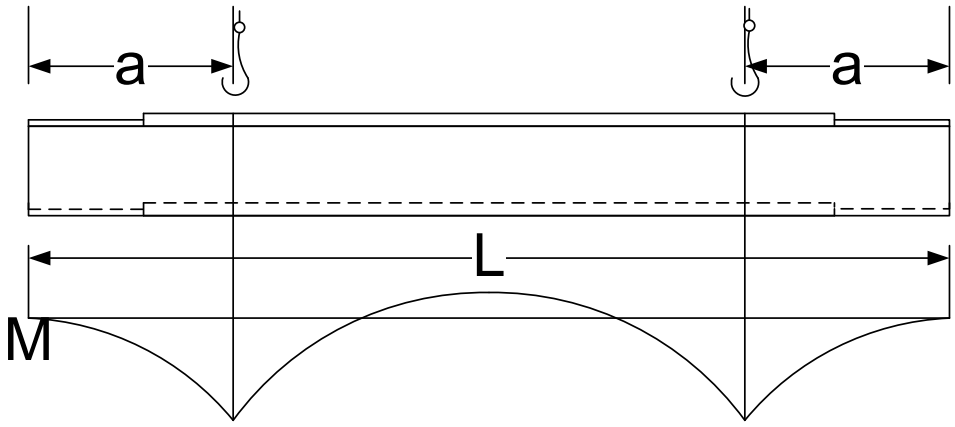


Figure 4.2.11 Moment Diagram Due to Lifting

It was further noted that the critical buckling load rarely controls the design for lifting of curved girders, but is a reasonable estimate for the lifting of straight girders.

A spreadsheet that provides for the analysis of the lifting of a horizontally curved I-girder with one crane and two lift clamps has been developed and is available for free download (*3*).

4.2.2.7 Curved I-Girder Erection Case Study

The bridge in this case study has two spans of approximately 197 and 260 feet. The framing consists of three 8.5-foot deep I-girders spaced 10.33 feet apart. Supports are radial. The horizontal alignment at Pier 1 has a radius of approximately 1,010 feet. At approximately 18 feet from Pier 2, in the second span, the alignment becomes straight. The structural steel has a minimum specified yield stress of 50-ksi. Flange widths vary, but are approximately 30 inches. The composite deck was cast after the steel erection was complete.

Crane and temporary tower locations were limited by site restraints. Erection of each field section was constrained into small increments of time due to trains passing beneath the bridge. Therefore, it was important that the Erector knew exactly what had to be done before issues arose. Hence, there was a need for a careful erection analysis.

4.2.2.7.1 Step 1

Erection commenced at the left support (Pier 1). A temporary tower was placed about 45 feet from Pier 1 to support the three girders during erection. The elevations of the girder supports on the tower were set at the no-load position. Girder 1 is the rightmost girder looking from Pier 1; Girder 2 is in the center; Girder 3 is the leftmost girder (Figure 4.2.12).

The first sections of each of the three girders were 55 feet long. In Step 1, the first section of each girder was erected resting on Pier 1 and the temporary tower; cross-frames were installed. When erected, they extended approximately 10 feet beyond the tower. It is of interest to note that the site conditions (a roadway) constrained the location of the tower, which was placed as far into the span as permitted. The splice locations in this project were selected with input from Contractor and Erector since the bridge was part of a design-build contract. The three bearings at Pier 1 were equipped with temporary longitudinal and transverse restraints in order to provide stability for the girders as erection proceeded. Without longitudinal restraint of the girders, they would be able to move with respect to each other since there were no lateral braces employed in the design. If the girders moved longitudinally with respect to each other, the cross-frames would cease to provide lateral restraint.

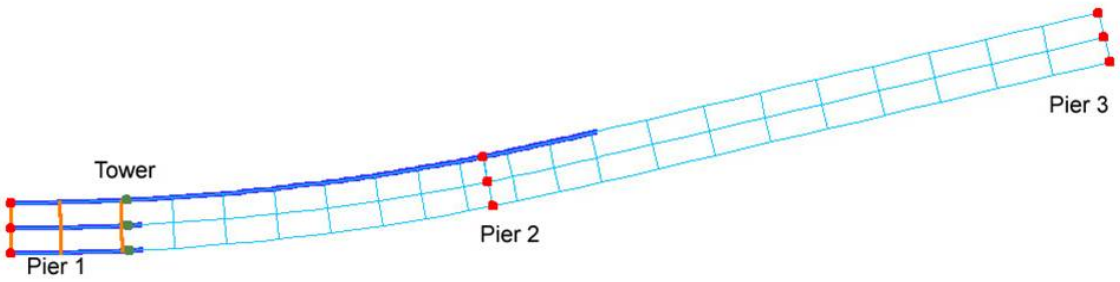


Figure 4.2.12 I-Girder Erection Study – Steps 1 & 2

4.2.2.7.2 Step 2

The next girder piece erected in Step 2 was a single lift composed of two field sections of Girder 3 spliced together prior to their erection. Again, Girder 3 is the girder on the inside (concave side) of the bridge. The Erector would have preferred to erect Girder 1 first, but the site required that the main crane would have had to have been located on the side of Girder 1 and lifting Girders 2 and 3 over previously erected steel was not acceptable. The chosen sequence meant that the girders, when erected, were lower than they would be when erection was completed. This is the case because curved girders shift load to the outside of the curve.

The erected portion extended approximately 60 feet beyond the pier into Span 2 (Figure 4.2.12). A brace was installed at Pier 2. The brace extended from the top of Girder 3 to the bearing location for Girder 2 (Figure 4.2.13). The brace provided the necessary torsional restraint for stability of a single curved-girder section. The force in the brace was an important 4.0 kips. Analysis showed an uplift of approximately 11 kips in Girder 3 at Pier 1. This was remedied by applying a lift of 35 kips at Node 57 on Girder 3 in Span 1 between the tower and Pier 2 (Figure 4.2.13). The advantage of an erection check was that the uplift was discovered analytically and a second helping crane was placed prior to the issue arising in the field, which might have led to a delay or worse. Regardless, the Erector opted to provide tie-downs for the three bearings at Pier 1 for safety.

It is of interest to note that the vertical reaction for Girder 3 at the tower increased to over 50 kips. Without the 35-kip crane lift at Node 57, the maximum vertical deflection in Span 1 of Girder 3 was approximately 0.5 inches and the reaction at Girder 3 on the tower was 110 kips. With the crane lift, the deflections in Span 1 became small and the tower reaction under Girder 3 was halved. The cantilever portion in Span 2 deflected downward, while the maximum deflection in Span 1 was reduced approximately 50 percent to approximately one-quarter inch. The girder twist (out-of-plumb) was reduced from approximately 1.2 inches to about 0.5 inches.

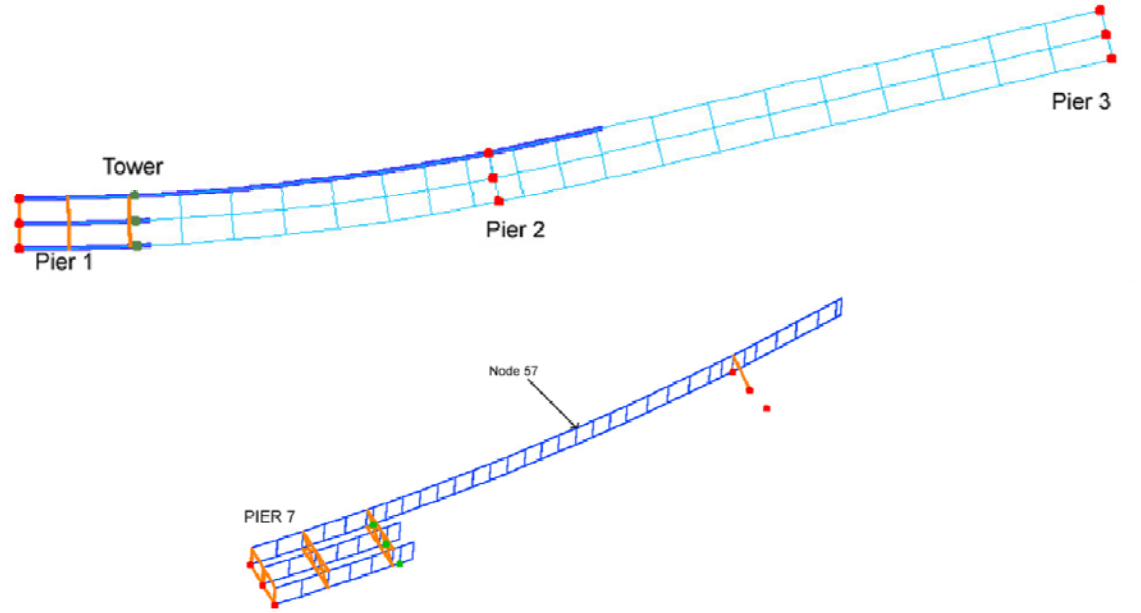


Figure 4.2.13 I-Girder Erection Study – Step 2

4.2.2.7.3 Step 3

In Step 3, the two bolted sections of Girder 2 were then erected, again in a single lift (Figure 4.2.14). An analysis was not developed for the case without cross-frames since the lifting crane held the girder while cross-frames were installed. It should be noted that the 35-kip load was applied to Girder 3 at Node 57 while Girder 2 was erected and the cross-frames were installed. The cross-frames between these girders were attached to Girder 2 prior to erection. Without the helping crane, the first girder would have deflected downward under its own weight approximately 0.6 inches and rotated, thus making it difficult to install the cross-frames connecting Girders 2 and 3. Subsequently, all of the cross-frames in that bay were installed.

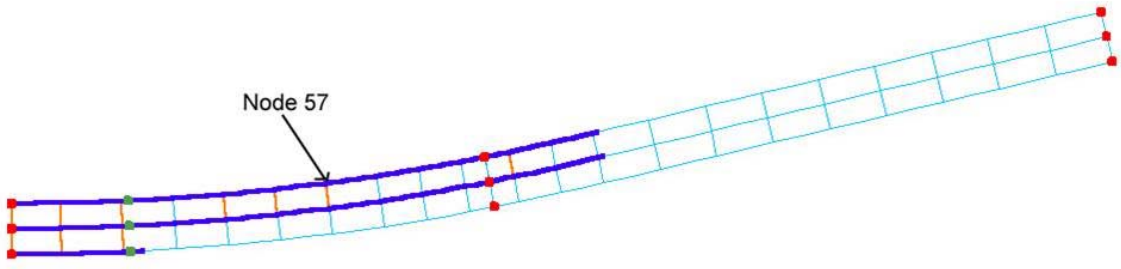


Figure 4.2.14 I-Girder Erection Study – Step 3

4.2.2.7.4 Step 4

In Step 4, the helper crane was moved to Node 56 on Girder 2 where a 40-kip lift was applied (Figure 4.2.15). This lift reduced the vertical deflection of Girder 2 to nearly zero so that Girder 1 could easily be erected in a manner similar to Girder 2. It is of interest to note that the longitudinal reactions at Pier 1 were reduced by the lifting of Girder 2. The parallel two sections of Girder 1 were erected next while the 40-kip lift was applied to Node 56. Three cross-frames were installed in the center of Span 1 in the bay between Girders 1 and 2 to provide stability to Girder 1. A second brace was attached at Pier 2 to the top of Girder 1 and the bearing of Girder 2. Again forces in the braces were nominal. Subsequently, all the cross-frames were installed.

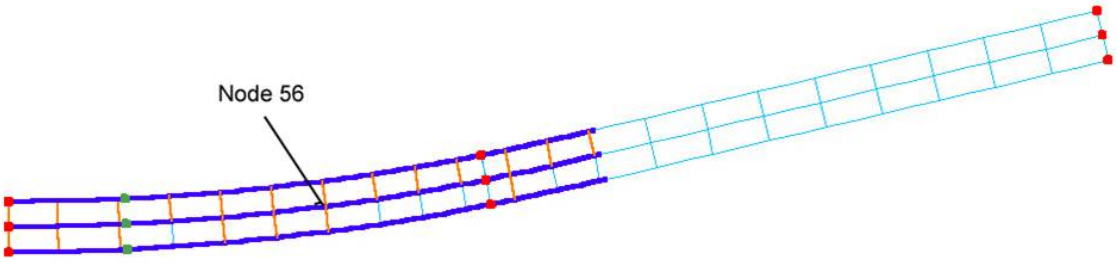


Figure 4.2.15 I-Girder Erection Study – Step 4

4.2.2.7.5 Step 5

In Step 5, two field sections of Girder 3 were spliced prior to lifting and then erected as a single piece (Figure 4.2.16). This piece reached the end of the second span on Pier 3. It should be noted that the second span was essentially straight. If unsupported after this piece was inserted, Girder 3 would have deflected slightly over 3 inches vertically in the second span. With the curve in the second span over a small portion of the girder adjacent to Pier 2, the girder also may have been unstable. Based on the traditional rule of limiting the span of an erected piece to 85 times the compression flange width, 85 x (30/12) ft = 212 feet, which is less than 260 feet. This, the large unsupported length may have led to an unstable condition. A brace was attached at Pier 3 from the top of Girder 1 to the bearing of Girder 2 (Figure 4.2.16). Unlike the brace of the single girder in the curved span, it resisted no significant load because the second span is essentially straight. However, it provided the necessary restraint to the girder. It was also decided to support Girder 3 with a crane load of 86 kips at Node 132 in the second span, as shown in Figure 4.2.16. Computations showed that the cantilever end of the erected portion of Girder 2 would have deflected downward prior to this lift, making it impossible to splice the remainder of Girder 2 to the cantilever end.

The 86-kip lift essentially eliminated deflection of Girder 3 in the second span due to its self-weight; thus, it permitted the cross-frames to be installed more easily. Large deflections of erected girders under their self-weight can be a significant issue even in erecting straight girders that are hung from a crane while the girder is being

erected. Two widely spaced lift points of the girder being erected (i.e. using two cranes) may provide the deflection control needed to match the deflections of adjacent girders. However, in this particular case, the second crane was better employed lifting and stabilizing Girder 3 by itself.

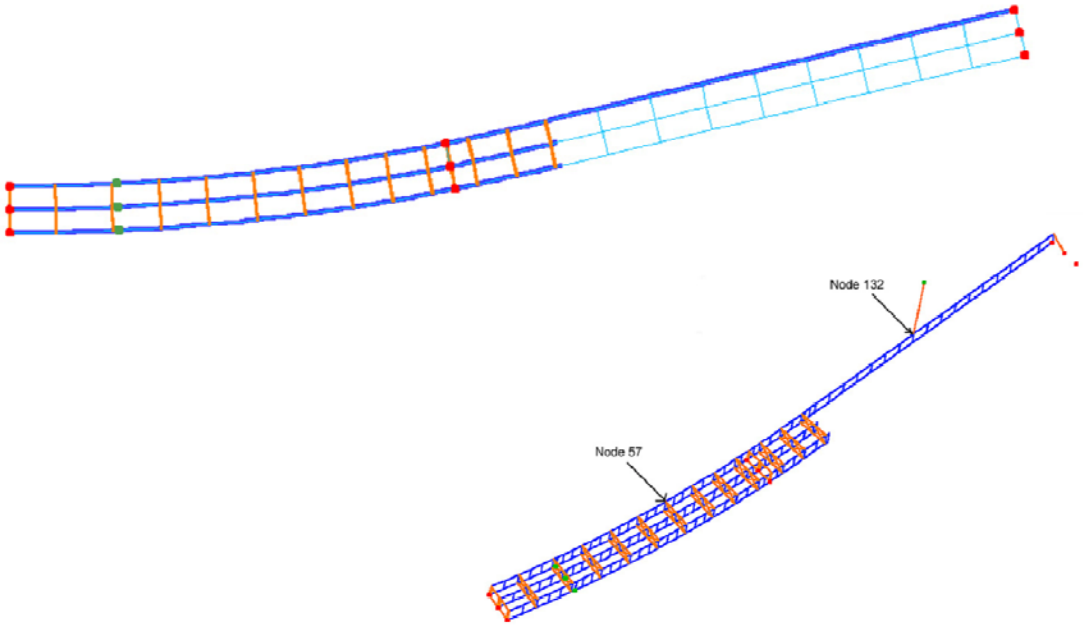


Figure 4.2.16 I-Girder Erection Study – Step 5

4.2.2.7.6 Step 6

In Step 6, the two sections of Girder 2 were erected and three cross-frames were installed in the central region of Span 2 between Girders 2 and 3, while Girder 2 was supported by its lifting crane (Figure 4.2.17). The centrally located cross-frames provided stability to Girder 2 when the crane was released.

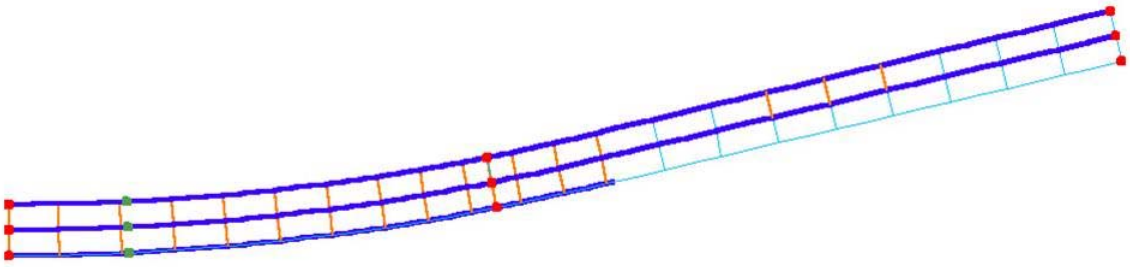


Figure 4.2.17 I-Girder Erection Study – Step 6

4.2.2.7.7 Step 7

In Step 7, the final two sections of Girder 1 were erected and three cross-frames were installed in the central region of Span 2 between Girders 1 and 2 to stabilize Girder 1 (Figure 4.2.18).

The web at the splice must be nearly vertical or tipped slightly upward in order to fit up the adjacent girder section. A downward angled web splice would require that the next section be lowered below its bearing at Pier 3. The girders are fabricated for plumb web splices under dead load. This had not been an issue when fitting up the girders to the first sections near the tower.

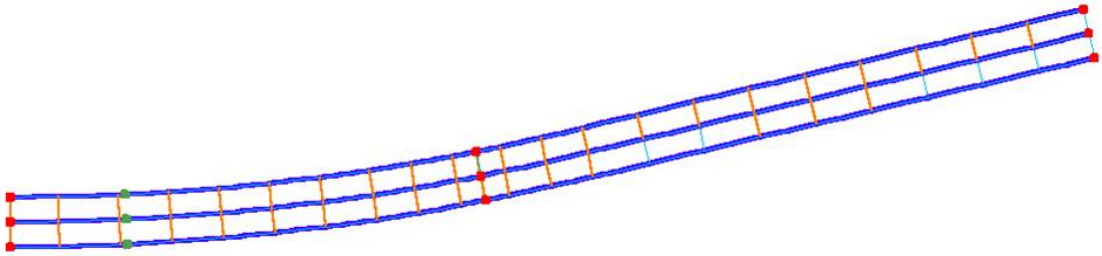


Figure 4.2.18 I-Girder Erection Study – Step 7

4.2.2.7.8 Step 8

In Step 8, remaining cross-frames were installed with all girders under their self-weight (Figure 4.2.19).

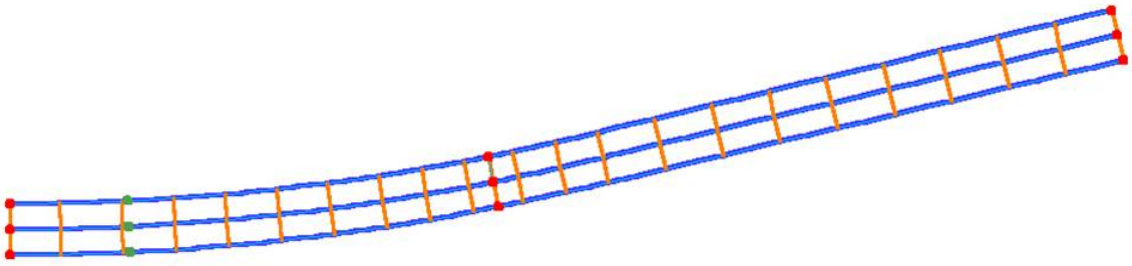


Figure 4.2.19 I-Girder Erection Study – Step 8

4.2.2.7.9 Step 9

Finally, with the steel erected, the tower could be removed in Step 9 (Figure 4.2.20). A final analysis was performed to relieve the 73 kips finally supported by the tower.

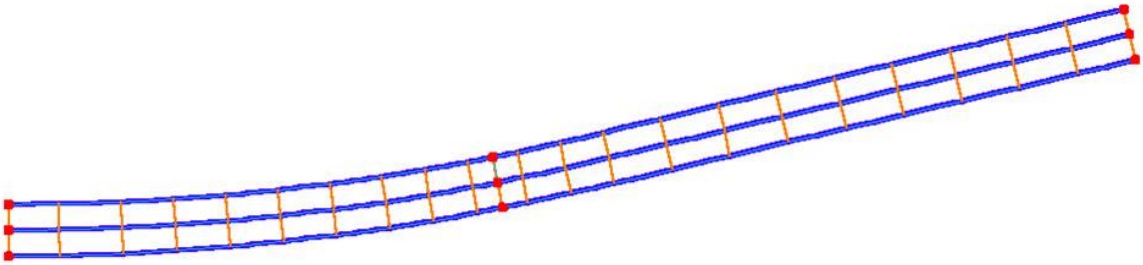


Figure 4.2.20 I-Girder Erection Study – Step 9

4.2.2.7.10 Summary

In summary, the analytical investigation showed a need to design the tower and its foundation to support at least 100 kips for each girder. Thus, more capacity was required than many would have guessed. The need for the tower during the entire erection process was also demonstrated by the significant loads it was required to resist. Its stiffness contributed significant rigidity to the system during the entire process.

Although this bridge had only slight curvature and no skew, the benefits of an analytical investigation of the erection process were evident. A bridge with more significant curvature and/or with skew would benefit even more. The above case was erected quickly. The Erector estimated that at least one day, and perhaps more, was saved by having this advance information available, which was critical in this case because of the small windows of time available to complete the erection over the active railroad tracks.

4.2.3 Design Engineer's Construction Plan

4.2.3.1 General

This section addresses the Design Engineer's Construction Plan. The three-fold purpose of the Design Engineer's Construction Plan was introduced in Table 4.2.1 and the corresponding text.

The Design Engineer's Construction Plan is intended to indicate what constructibility considerations and assumptions were made in the design. The Design Engineer's Construction Plan should instruct Contractors of any subtle assumptions in design that relate to construction sequence or special procedures. The Design Engineer's Construction Plan is not necessarily required in every case, as will be discussed subsequently.

A construction scheme presented as the Design Engineer's Construction Plan is incomplete and merely suggests one viable procedure. The Contractor is not

required to build the bridge according to any scheme presented in the Design Engineer's Construction Plan. Following the Design Engineer's Construction Plan, does not relieve the Contractor or liability or responsibility to develop independently a construction plan that includes the contractor chosen means and methods of building the structure.



Figure 4.2.21 Curved I-Girder Bridge under Construction

AASHTO LRFD Article 2.5.3 states that constructibility issues to be considered at design should include, but not be limited to, consideration of the strength of the steel and stability during critical stages of construction. This article states that "Where the bridge is of unusual complexity, such that it would be unreasonable to expect an experienced contractor to predict and estimate a suitable method of construction while bidding the project, at least one feasible construction method shall be indicated in the contract documents." However, there are no specific rules given to define what is meant by a "complex structure". Thus, it is left up to the judgment of the Design Engineer. Not all curved and skewed steel bridges need be considered "complex".

Conceptually, this is a relatively new requirement for Design Engineers first introduced for curved steel bridges in the 2003 *AASHTO Guide Specifications for Horizontally Curved Steel Girder Highway Bridges*. .

Application of this requirement to a particular curved bridge might involve the Design Engineer performing an analytical investigation of an assumed erection sequence for the bridge. This erection sequence would be based on a limited knowledge of site

conditions, available means and methods of the erection, etc. A design-build arrangement where the Design Engineer is working with/for the contractor is different, in which case the Design Engineer's Construction Plan may well be one in the same as the Contractor's.

Typically, curved girders require more temporary towers than do straight girders of similar length. The Design Engineer investigation may show that a tower or two appears to be required for the erection sequence assumed. The temporary towers may be required to establish the correct elevation of the girders or to provide support so that lateral buckling is prevented. The Plan should not be presented in a way that prevents a cunning Contractor from using a different sequence of erection or an additional crane or two to avoid the tower(s).

The intention is that the Contractor should be made aware that a tower may be required and must be included in his/her bid unless other plans are anticipated. At any rate, no extra would be allowed for a tower not considered originally when preparing the bid.

Frequently, towers cannot be used when they are needed. These cases are the most important cases to identify at design. In these cases, the design must be modified to ensure that the bridge can be constructed. The self-weight of girders often leads to large deflections and twist that makes fit-up of subsequent girders and cross-frames difficult. .

The need for a Design Engineer's Construction Plan and the information to include in that Plan is job-specific.

The sequence of deck placement is considered standard information to be presented in the design plans. However, other information regarding deck placement is not always provided. Overhang bracket loads may be of consequence. The Construction Plan may suggest that brackets should be full-girder depth to prevent web deformations that might occur if partial-depth brackets are employed. This message would inform the Contractor that the webs are not designed to take lateral loads from the brackets. If the deck is exceptionally wide, the Construction Plan may explain whether the deck was assumed to be placed in a single cast or not. Considerations made in the design need to be explained if a longitudinal deck joint is anticipated. Anticipated final deck elevations might be provided to aid the Contractor in planning and the Inspectors in checking.

Steel is typically fabricated to fit in the no-load condition. Exceptions need to be noted in a Construction Plan.

Phased construction of bridges is increasingly common as bridges are replaced with new and often wider ones. Widening of existing bridges is also common. The assumptions of construction sequence need to be delineated to avoid overloading of members and incorrect deck elevations. Temporary loads, both dead and live,

considered in each phase of construction should be stated. Particularly important is when the contractor should bolt up cross-frames between the phases. All closure pours must be specified.

Consideration of wind on the steel frame is another common consideration that may need to be examined. Lateral wind on the steel frame may cause excessive lateral stresses in the girders and excessive deflections. These deflections may even damage bearings and other items. The Construction Plan needs to address the issue if the contractor is responsible to supply temporary lateral bracing. The amount, size and type of bracing need not be defined in the Plan, but if it is required and not called out, the Contractor may be entitled to an extra.

4.2.3.2 Straight Bridges with No Skew

Straight I-girder bridges with no skew will serve as the baseline from which to build the subsequent discussion. Issues identified for these bridges for inclusion in the Design Engineer's Construction Plan should also be considered for all the subsequent bridge types.

Straight I-girder bridges with no skew have been built for decades and most bridge Contractors are familiar with their construction. A typical Design Engineer's Construction Plan for these bridges will likely include considerations related to the deck placement sequence, deck overhangs and perhaps wind loads during construction. Requirements for casting the deck should be called out. For example, if the bridge is so wide that its full width cannot be cast at one time, a longitudinal deck joint may be required. The casting procedure considered in the design should be specified so the Contractor knows what is acceptable from the point of view of capacity and deflections. If the Contactor chooses to cast the deck differently, he/she knows that engineering justification of the change is required. A bay of cross-frames at the longitudinal joint may not be attached until the casting is complete. Slotted holes may be provided at the cross-frame connections to allow for deflection. A closure pour may be specified. The time between casts should be specified as well as the sequence of casting.

Special situations, e.g. situations involving phased construction (Section 4.3.2.2.2), may require the development of a more elaborate Plan.

A single straight I-girder is in static equilibrium. Adjacent straight girders provide an opportunity to brace the compression flanges of the girders with cross-frames. Such bracing is effective if the girders are prevented from moving longitudinally with respect to each other. This can be accomplished either with longitudinal bearing constraints or with lateral bracing between the girders.

Unlike curved girders, straight girders, as seen in Figure 4.2.22, support their own weight without significant torsional restraint. Little of the steel self-weight load is transferred between girders through the cross-frames.



Figure 4.2.22 Erection of Straight I-Girders with No Skew

For straight girders, the Erector can usually leave the bolts in the field splices loose and continue to erect a girder line with little concern for cambers or deflections. Once the girders are erected, a crane can be used to hold a girder at its correct no-load elevation while the bolts in the splices and in the cross-frame connections are tightened. Thus, the erection sequence for these bridges is typically not considered in the Design Engineer's Construction Plan, unless temporary towers are required.

Continuous spans may require temporary support(s). If the girders are heavy, i.e. if the spans are long, it is possible that the first erected girders, usually in an end span, may be of inadequate strength to support themselves until the counterweight of the girders in the adjacent span is present. Temporary towers are usually required in these cases. As important as this case is, usually an experienced Erector does not need to be told this. Another case when temporary towers may be employed is if the cantilever ends of the girders are drooped so that the next field section cannot be spliced to it. The use of "angle wings" may suffice in these cases. These are triangular braces that are supported on the pier foundation with the extended portion supporting the girder some 25 or 30 feet from the pier.

4.2.3.2.1 Wind Loads

It is not the responsibility of the Design Engineer to consider all possible wind load conditions during construction of the bridge. However, it is advisable to consider lateral wind on the erected steel. The only restraint to lateral winds is the sum of the girder flange stiffnesses, unless lateral bracing is provided. Lateral deflections of several feet due to wind are possible in bridges without lateral bracing before the deck is cast. Even if the steel girders can withstand these deflections and stresses, bearings and various connections are likely to be damaged. When the base steel frame is examined for wind load during construction, superelevation and forming increase the exposed area and the resulting wind pressure on the individual girders.

A lesser wind pressure is generally used for the temporary construction condition than the design value. Waiving the minimum wind force of 0.3 klf prescribed for girders (Section 1.3.2.4.1.1) is a consideration for shallow girders.

4.2.3.2.2 Phased Construction

Phased construction is defined as building a bridge in phases. One example of phased construction is shown in Figure 4.2.23. This type of phased construction occurs when traffic is permitted on part of the bridge during construction before the entire bridge can be built. A similar phasing situation occurs when a bridge is being replaced. A portion of the old structure is removed and a part of the new is built. Widening of existing bridges also creates similar issues. Phased construction of modern steel bridges is more critical than perhaps in the past due to higher strength materials with larger deflections and wider girder spacing that leads to a greater difference in deflection between the composite and the non-composite girders than experienced in the past. However, the versatility of steel makes it an ideal material for phased construction.

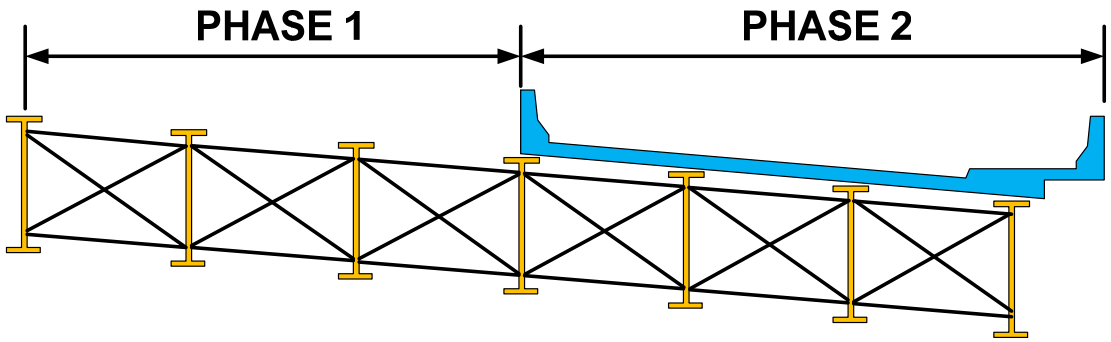


Figure 4.2.23 Phased Construction

There are two basic issues related to phased construction: first, is the large difference in vertical stiffness and deflections between the composite and non-composite girders; second, is the distribution of loads between phases, which is related to the first issue and must be considered in the design and noted in the Plan. These issues were discussed previously in Section 3.1.2.4.3.

It is important that the Contractor construct the bridge in the manner assumed to calculate the cambers and design the girders in order for the deflections and loads to be correct, or else re-engineer the process.

4.2.3.3 Straight Bridges with Skewed Supports

Individual straight I-girders resting on skewed supports are generally as stable as straight I-girders resting on right supports. However, differential girder deflections at perpendicular cross-frames in skewed bridges introduce restoring forces that cause torque to develop in the girders, which causes additional issues that need to be

considered. Issues include end rotations of the girders and the possible provision of vertical slotted holes at the cross-frame connections in an attempt to minimize the twist of the girders and reduce the cross-frame forces.

4.2.3.3.1 Girder End Rotations due to Skew

Girder end rotations (twist) occur about their longitudinal axes at simple supports of skewed I-girder bridges (Section 1.1.4.1). They are problematic in some cases; the larger the vertical deflections, the larger the end rotations. Figure 4.2.24 shows, schematically, twist of an I-girder from plumb to out-of-plumb under load. Twist can be problematical at bearings. Other times it is only an aesthetic issue.

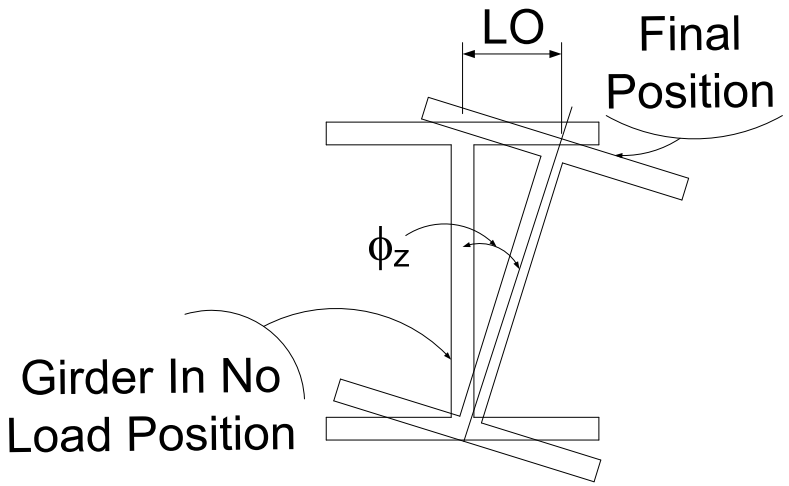


Figure 4.2.24 I-Girder Plumb at No-Load and Out-of-Plumb at Final Dead Load

AASHTO LRFD Article 6.7.2 (Dead Load Camber) states that for skewed I-girder bridges, "…the contract documents should clearly state an intended erected position of the girders and the condition under which that position is to be theoretically achieved" (Section 4.1.3).

Vertical camber is introduced by cutting it into the web or bending the girder. This camber is always introduced into the girder by the Fabricator. The above provision and its accompanying commentary address the possibility of introducing a reverse twist into the girders. Such twist is often introduced into I-girders by the Erector. This is possible when the Fabricator takes it into account when detailing the cross-frames and their attachment to the girders. The objective is to have the girders plumb, or nearly so, in the finished bridge. I–girders are torsionally weak so the Erector can twist and erect straight I-girders contrary to the direction that they will twist under dead load. The torsional stresses introduced during the erection are essentially reversed under dead load and are of little consequence. Figure 4.2.25 shows, schematically, an I-girder with a reverse twist introduced in the no-load position that is made plumb under dead load.

For the purpose of this discussion, vertical cambers for cross-slope or vertical alignment are ignored. Thus, the objective is to have the girder top flanges horizontal and in a horizontal plane. The cross-frames are perpendicular to the girders, however, the points to which they are connected are at different elevations in the no-load condition. Since the girders are to be plumb and at the same elevation under dead load, the cross-frames must be square; i.e. their diagonals must be equal. For this discussion, the cross-frames are all attached at the same distance from the top flange. Since the cross-frames cannot change shape or length, except for nominal elastic shortening or lengthening, they must be square to start if they are to end up square. This means that they can only be attached to the girders if the girders are twisted at the no-load condition.

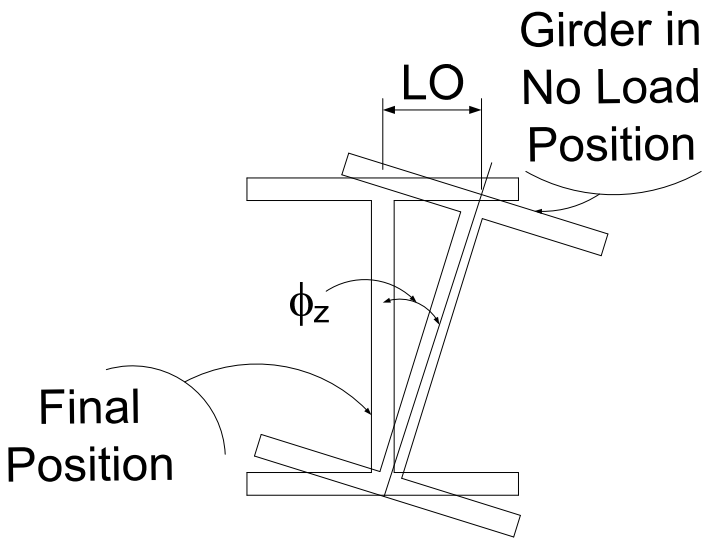


Figure 4.2.25 I-Girder Out-of-Plumb at No-Load and Plumb at Final Dead Load

At simple (skewed) supports, another phenomenon occurs. The top of the girder tends to move into the span due to elastic shortening of the top (compression) flange, while the bottom flange tends to move away from the span due to elastic lengthening of the bottom (tension) flange. The amount that the bottom flange moves is dependent on the bearing constraints. However, neither girder moves appreciably in the vertical direction. The end cross-frames are attached to the ends of the girders and follow the support line. But, the cross-frames still must be square with equal diagonal lengths if the final position of the girders is to be plumb under dead load. If the cross frames are erected plumb under no-load, they will not end up plumb because the top and bottom ends of the connected girders move in opposite directions. Again, the distance between the diagonal corners of the cross-frame must remain equidistant since the cross-frame cannot change size or shape. The only way this happens is for the cross-frame to pull the girder ends, twisting them. If they were plumb at no-load, they become out-of-plumb when dead load is applied. Obviously, the larger the vertical deflection, the larger the longitudinal movement of the girder ends exacerbating the out-of-plumbness, unless accounted for in the detailing.

The detailing can account for the end twist by placing the cross-frame connection plates on the girder webs at the locations that will be plumb under dead load. The cross-frames must be detailed square and attached at the same distance from the top flanges. This will force the girder ends to be twisted out-of-plumb when the cross frames are connected under no-load.

The method of detailing the girders and cross-frames so that the girders are to be plumb at no-load is often referred to as a No-Load Fit, which is described in further detail in Section 4.1.3.1.3.1. The method of detailing the girders and cross-frames so that the girders are plumb at dead load is called a Steel Dead Load or Total Dead Load Fit, which is described further in Section 4.1.3.1.3.2. Another way to express each method is to refer to a No-Load Fit as “detailing for plumb at no-load”, and a Steel Dead Load or Total Dead Load Fit as “detailing for plumb at dead load”. In both cases the girders are detailed to fit-up plumb, but at different loads.

A second effect of this phenomenon is that the cross-frames are stressed as the dead load is applied. Since the end cross-frames have a longitudinal vector component, longitudinal forces are introduced into the girders. Interestingly, these forces generally produce a negative moment in the ends of the girders. Hence, the girders at the simple supports do not have zero stress. This can be of interest to the Design Engineer who might need to account for compression in a flange normally thought of as a tension flange.

The behavior of the girders and cross-frames at the ends of girders with skewed supports is highly dependent on the bearing restraints. Laterally restrained bearings can lead to tremendously large reactions, attendant large cross-frame forces and large longitudinal flange forces.

The Design Engineer’s Construction Plan should identify the anticipated girder twist and layover and the anticipated lateral location of the end of the deck in cases where a No-Load Fit is to be employed. In addition, the Design Engineer should determine if the bearings can accommodate the anticipated girder end rotations.

In cases where a Total Dead Load Fit is to be employed and a reverse twist is to be introduced into the girders such that the web will be plumb at full dead load, the Erector will leave the site with the girder webs still out-of-plumb under their own self-weight. For this condition, the Design Engineer’s Construction Plan should identify the total anticipated girder layover and the expected out-of-plumb of the girder webs under their own self-weight. The *AASHTO/NSBA Steel Bridge Erection Guide Specification* (*3*) provides a suggested tolerance on the deviation from the theoretical erected web position equal to 1/8-inch times the web depth in feet.

Whenever a Steel Dead Load or Total Dead Load Fit is employed, the Design Engineer assumes the responsibility that the girders can be twisted to fit-up the cross-frames.

4.2.3.3.2 Vertically Slotted Gusset-Plate Bolt Holes

Another approach to the twist issue is to employ vertically slotted holes in the gusset plates connecting the cross-frames to the girder connection plates of straight girders. The theory is that the girders are permitted to deflect vertically without interference from their neighboring girders in an attempt to minimize the girder twist and reduce the cross-frame forces. At the same time, the connection plates will provide the necessary lateral restraint of the girders via the sides of the slotted bolt holes. It also allows the girders and cross-frames to be detailed for the webs plumb at no-load.

The use of vertically slotted holes negates any analysis that assumes that the steel frame is effective in resisting its self-weight and the other dead loads applied prior to tightening the cross-frame bolts. *AASHTO LRFD* Article 4.6.2.2.1 suggests that non-composite dead loads, such as the deck, may be assumed uniformly distributed to the girders when certain conditions are met. This assumption would not be applicable with loose bolts in slotted holes, and should generally not be considered applicable in any case to bridges with significant skews. Also, if this approach is assumed to work for differential deflections, the issue of twist at the simple supports is not addressed since the girders do not deflect vertically at the bearings. This method is not applicable to curved girders. Bolt holes in curved girder bridges must be standard size to control the geometry and properly transfer load in these structures (Section 4.2.3.4.2).

In such cases, the Design Engineer's Construction Plan should reflect the analysis assumptions that are made relative to the stage at which the cross-frame connection bolts are to be tightened. If the bolts are to be left loose when the deck is cast, the girders will deflect differently and become difficult to control during the deck casting. The Erector will also have to return to the site to tighten the bolts after the deck is cast. If the bolts are to be tightened prior to the deck casting, the slots must be of the proper size and location to allow the computed deflections to occur freely. The size and location of the slots should be called out in the Plan.

It should be noted that the capacity of the bolts will be less in the slotted holes for all loads that are applied after the bolts are tightened.

4.2.3.4 Curved Bridges with No Skew

The Design Engineer's Construction Plan may need to be more elaborate for curved I-girder bridges without skewed supports (Figure 4.2.26) in order to address more subtle and sometimes complex issues.



Figure 4.2.26 Curved I-Girder Bridge without Skew

4.2.3.4.1 Need for Temporary Supports

Erection of horizontally curved steel I-girders is significantly more complex than the erection of straight steel I-girders. Erection of curved I-girders most always requires more thought and planning.

Curvature causes torsion in the girders due to the offset of the girder weight from a chord through the supports. The torsion must be resisted in order to satisfy the requirements of static equilibrium. Distortions during erection must be controlled so that steel can be connected. Thus, there is a greater potential need for temporary towers during the erection of curved steel I-girders than straight steel I-girders of similar span. Conditions under which a temporary support may be required during an investigation of a potential erection sequence by the Design Engineer were discussed previously in Section 4.2.2.7.

Although temporary towers are often used with straight-girder brides, the need for towers on curved bridges is more subtle and may be ignored at bidding if not specifically identified. Whereas girder splice and cross-frame bolts are often left loose when erecting straight girders, they may not be left loose while erecting curved girders. This essentially requires that the girders be in the proper position (elevation) when the pieces are erected and bolts are installed. Towers are often required to accomplish this.

The inherent character of curved girders to depend on neighboring girders for stability means that their deflections change as girder sections are erected. These issues all lead the potential need for temporary supports. It is not practical for contractors to determine whether or not towers will be required. If the price for one

or more towers is factored into the price of Contractor A and competing Contractor B does not include towers in a bid, Contractor A is at a disadvantage. Then if Contractor B is successful and finds that a tower is required, an extra may be charged. If on the other hand, towers are suggested in the Design Engineer's Construction Plan, both contractors are on equal footing when making their bids. If Contractor B is successful in finding a way to avoid the use of towers through innovative planning and additional engineering, then he/she benefits. If Contractor B bid assuming that towers would not be needed and later finds they are required, Contractor B is responsible for the additional cost over the bid estimate.

A software package has recently been developed that analyzes straight or curved I-girder bridges during girder erection and concrete deck placement. The program uses information readily available to the Design Engineer and develops a model to predict the behavior of these bridges during erection providing the user with displacements, stresses, and rotations (*3*).

4.2.3.4.2 Cross-Frame Connections

Stability of curved steel I-girders depends on their connection to adjacent girders. Therefore, cross-frame connections must be tightened sequentially as erection progresses to control vertical and lateral deflections. The girder alignment and stability must be continuously controlled as erection progresses and the weight shifted between the girders changes as each additional girder is added. If the bolts are permitted to slip during erection, as is permitted with straight girder bridges, the torsional restraint is not available until the bolts engage the holes.

AASHTO LRFD Article 6.13.1 forbids the use of oversize or slotted bolt holes in curved bridges (unless permitted otherwise in the contract documents) for the above reasons. When standard holes are used and field reaming is not permitted, the Erector is assured that the erected steel will have dead load deflections and stresses close to those determined in the analyses.

If phased construction is used, the analysis must be phased consistent with the way structure is to be built. Cambers must be reported for the phased construction and bolt holes must be detailed consistent with the situation of the steel at the time the bolts are to be installed. For example, if lateral bracing is to be installed after the girders are erected, the detailer needs to proceed accordingly. The gusset plates may be used as templates to field-drill the holes in the girder flange or connection plate after the strain due to self-weight of the girders has been introduced. Or the lateral bracing may be installed on a pair of girders prior to their erection. At design the Design Engineer can investigate the elongation of the flanges to determine if erection of the bracing will be problematic.



Figure 4.2.27 Erection of Curved I-Girder Bridge without Skew

If the bridge can be bolted up without reaming bolt holes, the analysis assumptions have been met and stresses can be assumed to be reasonably close to the condition assumed for the detailing.

Unlike straight girders that deflect downward when cantilevered beyond a pier, curved girders in this condition not only deflect downward, but also twist. Their behavior is very difficult to divine without analysis. Since the girders interact, each additional girder section changes the behavior of the erected girders in the cantilevered section, sometimes dramatically. The interaction of the girders means that lifting the girders to adjust the orientation of the field splice usually requires much more lifting capacity and may challenge the cross-frame capacities.

A temporary tower may be required in the back span to alleviate the issues discussed. Adjustments to the elevations of the individual girders at the tower permit fine tuning of the cantilevered girders. This is usually done more easily by analysis than by guessing in the field. Also, jacking individual girders is risky with regard to the cross-frame capacities. Of course, measuring the reactions at the tower jacks confirms the work if analysis data are available to predict the jacking force necessary to achieve a given elevation.

4.2.3.4.3 Girder Rotation

The convex girder (i.e. on the outside of the curve) usually deflects more than the girders on the inside of the curve. The girders will rotate (or twist) out-of-plumb about their tangential axis as the dead loads are applied, as in Figure 4.2.28. The figure shows the original position of the girder vertical. When curved I-girders are erected with plumb webs, it is referred to as a No-Load Fit (Section 4.1.3.1.3.1). This figure is a section of a curved girder between cross-frames near the center of the span.

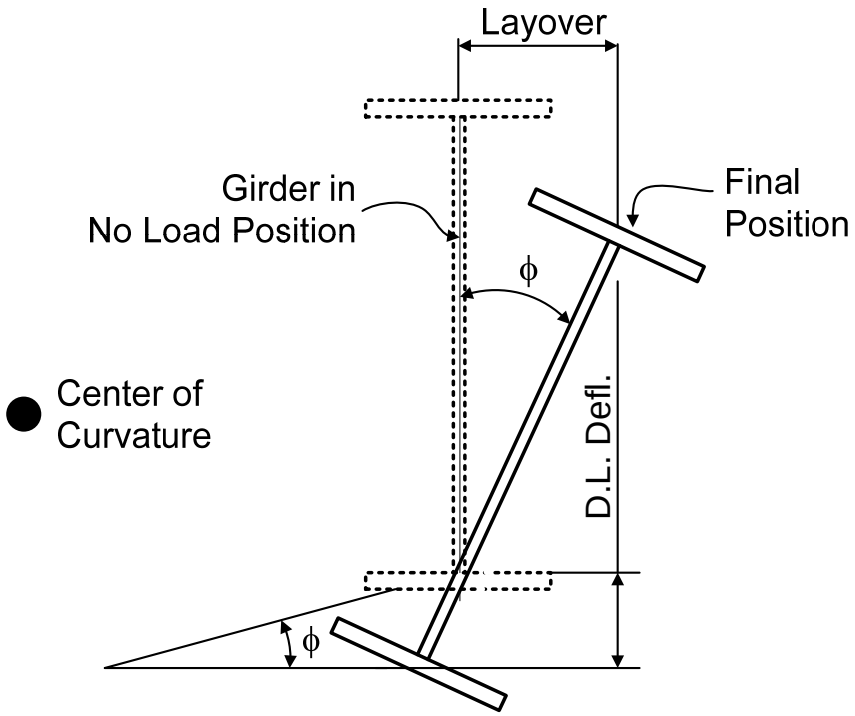


Figure 4.2.28 I-Girder Out-of-Plumb due to Dead Load

Since I-girders are open sections and are relatively weak in torsion, the twisting of straight I-girders to allow fit-up during erection is often accomplished rather easily. Curved girders present different, more complex issues. Curved girders with radial supports do not present issues at simple supports found with skews. They do, however, usually deflect differently at any cross-section in the curved span. Vertical cambering accounts for these differences. This leaves the tops of the girders horizontal but in different planes under no-load. As dead load is applied, the girders deflect vertically, but the cross-frames prevent the girders from moving with respect to each other. Hence, they must twist as they deflect. Normally, the deflection is not severe enough to cause problematic out-of-plumbness of the girders. The main problem is aesthetics. The outside (convex) girder may deflect two or three inches out-of-plumb without concern. But if the out-of-plumbness is much greater, it may become an issue. The girders at the bearings will remain plumb if the supports are radial.

To twist a curved I-girder, the radius of the flanges must be changed. This cannot be done without introducing lateral bending stresses in the flanges in addition to the stresses due to warping torsion. As the curvature becomes greater (i.e. smaller radius) and the flanges become stiffer transversely, the stresses induced by twisting become more severe. At some point, they become so severe that it is not practical to twist the girders in that manner. There have been cases where the Erector was not able to bend the flanges to fit-up the cross-frames where “inconsistent dealing” was called for. This situation may lead to claims.

At the present time, no practical method exists that permits the calculation of these lateral bending stresses. Obviously, smaller flanges allow for easier bending; however, the size and strength of flange that be bent practically is difficult to identify. The parameters affecting the difficulty include: steel strength, flange width and thickness, and the required change in radius. When the Plan calls for a Steel Dead Load or Total Dead Load Fit of curved bridges, the Design Engineer is accepting the responsibility that the flanges can be safely jacked to allow cross-frame fit-up without damage, and that the stresses so-induced are not significant.

4.2.3.4.4 Required Bracing or Restraints

Non-collinear flange forces in curved I-girders are controlled (limited) by cross-frames that attempt to restore the distortion of the flanges (Figure 4.2.29). The girders are globally stable as long as the framing retains its shape and if it is properly restrained at the bearings. If a girder moves radially along the arc with respect to its neighbor, the cross-frame restoring mechanism is upset and the system will probably be unstable. As shown in the plan view in Figure 4.2.29, in the unstable position, the outside girder has moved radially along the arc to the left with respect to the inside girder. The cross-frames are the same length but are no longer radial allowing the outside girder to move closer to the interior girder; a very unstable situation.

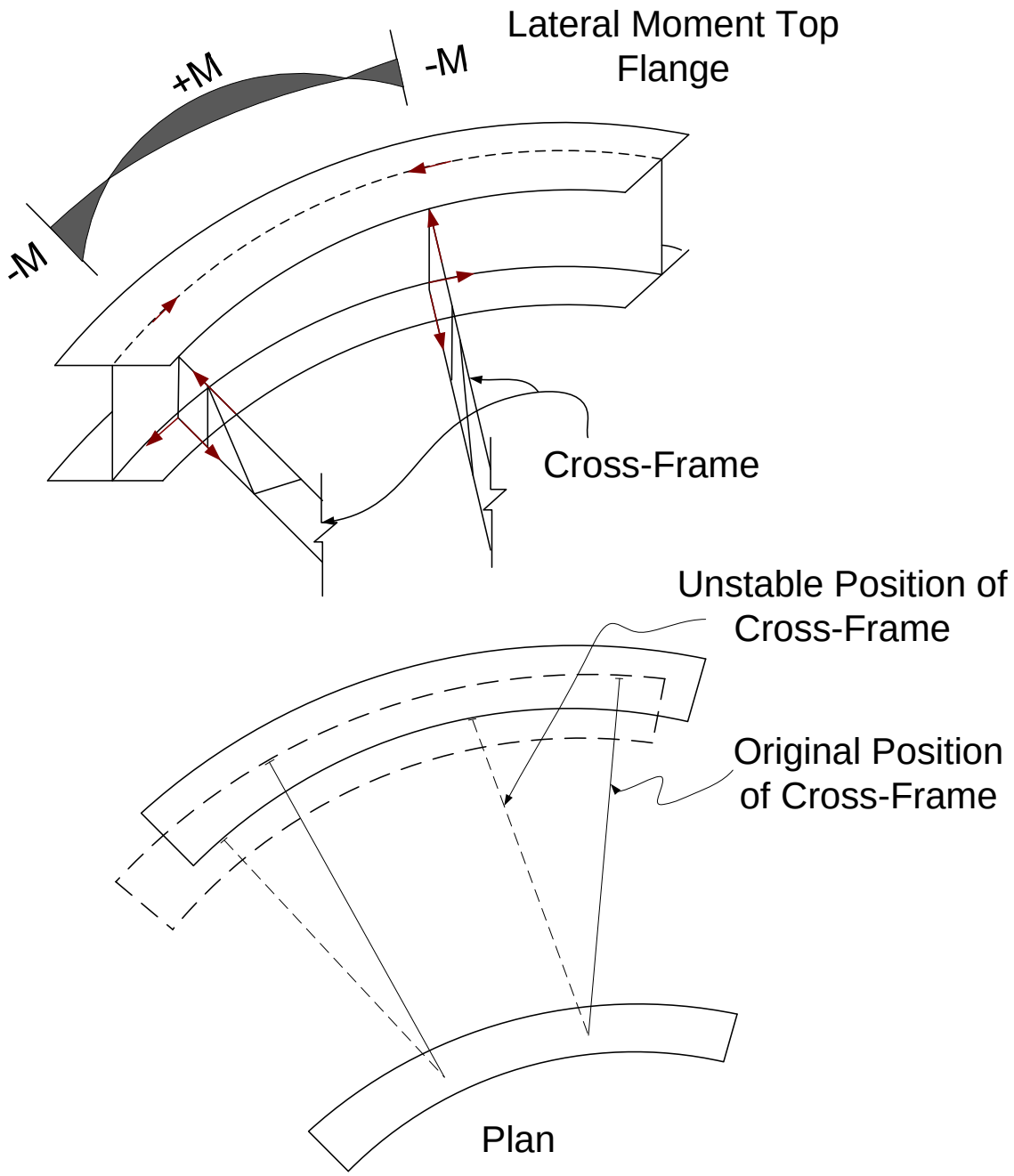


Figure 4.2.29 Relative Tangential Movement in Curved I-Girders

The cross-frames can prevent such movement only through their bending stiffness in the longitudinal (tangential) direction. In larger bridges or in bridges being erected without all of the cross-frames installed and/or that are loaded unsymmetrically (e.g. during the deck casting), i.e. cases in which the cross-frame forces are not balanced, the bending stiffness of the cross-frames alone may be inadequate to provide stability.

If the bearings are adequately restrained longitudinally at all the girders, the global stability is greatly enhanced and is usually adequate. An alternative mechanism to provide global stability is temporary or permanent lateral bracing between the girders. Such bracing may be in only a portion of the span and may be in the top, bottom or in both flange planes. As discussed previously, lateral bracing is also effective in resisting wind loads acting on the undecked structure.

4.2.3.4.5 Phased Construction

Twist of the girders is particularly problematic when curved bridges are to be built in phases. It is necessary for the cross-frames between the flanges to fit-up after the deck has been cast and much of the girder rotation (twist) has occurred. The problem can be manifest even when the deck weight is unevenly applied to the girders.

If the magnitude of the rotation is not excessive, the second phase can be built with only the chords of the cross-frames between the two phases installed until the deck is cast. This will prevent the relative rotation of the two phases while permitting free vertical deflection of the second phase. No closure pour should be necessary unless the Contractor chooses to access the cross-frames between the two phases from above rather than from below the deck.

If global rotations and/or lateral deflections of the girders as determined from a first-order analysis are large, it may be necessary to add top and bottom lateral bracing in one bay of each phase to control rotational deflections. Such bracing also distributes the dead load more evenly between the girders. Large global rotations are signified by large differential deflections between the girders and also large lateral deflections. Such rotations are indicative of a potential second-order global instability. In extreme cases, temporary towers may also be necessary to control the girder rotations.

Excessive rotation can occur with narrow structure widths and/or with longer spans and with even slight curvature and with an unevenly loaded deck weight; for example, a large overhang on one side and no overhang on the other side of a phase of the construction. Such conditions may be particularly critical for simple-span structures utilizing higher strength steels.

Phased construction issues are examined more closely in the Case Study given in Section 4.2.4.

4.2.3.5 Curved Bridges with Skewed Supports

Curved I-girder bridges with skewed supports are a very complex category of I-girder bridge. Many of the construction issues identified previously for straight bridges with skewed supports and for curved bridges with no skew are magnified in this case, increasing the importance of the Design Engineer providing a Construction Plan for this category of bridge.



Figure 4.2.30 Curved Bridge with Skewed Supports

In curved I-girder bridges with skewed supports, torque is introduced by both the curvature and the skew magnifying the girder twist that occurs at mid-span and at the end supports.

A Steel Dead Load or Total Dead Load Fit (Section 4.1.3.1.3.2) may be employed to counter the effects of the girder twist, but can be more problematic than for bridges that do not have both curvature and skew, or curvature only, due to reasons discussed previously (Section 4.2.3.4.3). In special cases, the option of detailing the girders with a twist camber in the no-load position, as discussed in Section 4.1.3.1.3.3, might be considered for these bridges.

4.2.4 Case Study - Phased Construction Issues

The structure in this case study is referred to as a single-point urban interchange (SPUI). The bridge consists of a main structure composed of three spans of 102-150-102 feet with nine straight I-girders in the cross-section spaced at 12′-10″. There are four on-off ramps supported on the exterior girders of the main structure, each with a span of approximately 80 feet. The framing of each of these ramps consists of four straight girders that frame perpendicularly into the exterior girders of the main structure, some additional straight girders framing into the exterior girders of the main structure at an angle, and exterior girders curved to approximately 125-foot radii to accommodate traffic. There is also a raised island on each ramp to direct traffic. Figure 4.2.31 shows only of one-half of the structure.



Figure 4.2.31 Case Study Bridge

The substantial load on the exterior girders of the main structure presented a significant design problem. The girders not only were required to support the additional weight, but the tendency for the ramp girders to rotate also had to be accounted for.

4.2.4.1 Goal

Recommend an approximate cross-frame spacing along the curved exterior girders of the ramp structures considering the fact that they carry very little load due to their proximity to other girders.

Additionally, develop a construction plan (method) that will mitigate the torque on the exterior girders of the main structure and provide a durable structure without joints.

4.2.4.2 Possible Solutions

Investigation of the orthogonal deck stresses and connection moments between the ramps and the main structure utilizing a refined 3D analysis revealed the need to sequence the construction. Additional diaphragms were added between the girders in the exterior bays of the main structure. However, the end rotations of the ramp girders due to dead load were too large for the exterior girders to resist even with the additional heavy diaphragms.

The tight radius of curvature of the curved exterior girders in the ramp structures dictated the required cross-frame spacing. In this case, the rather radical cross-frame spacing shown in Figure 4.2.32 (approximately 6 to 8 feet) was required to control the resulting lateral flange bending moments determined from the analysis.

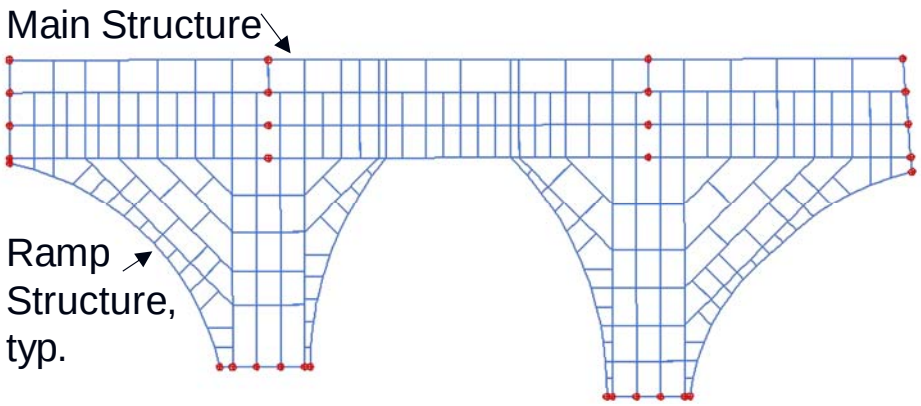


Figure 4.2.32 Case Study Cross-Frame Spacing

Part of the main structure was decked and opened to traffic, but traffic was constricted from the exterior girders, which along with ramp structures, had not yet been decked. It was decided that the ramps would be constructed with simple supports under the ramp girders at the main structure, as shown in Figure 4.2.33. This was accomplished with the use of corbels on the main girders to receive the ramp girders. The corbels permitted rotation of the ends of the ramp girders as the deck was placed on the ramps. After the deck on the ramp girders and over the exterior girders of the main structure was in place, moment connections were then made between the ramp girders and the exterior girders of the main structure. A closure pour was then placed between the ramps and the main structure to complete the deck. The closure pour was heavily reinforced in the direction of the ramp girders to work compositely with the spliced connections to resist the negative moments caused by the superimposed dead load and live load on the ramps.



Figure 4.2.33 Case Study Supports at Intersection of Ramp and Main Girders

It is of interest to note that the Contractor and the Owner desired a construction plan that would allow for a wider deck on the main structure during construction; however, no alternative approach was identified.

4.2.5 References

1. AASHTO. 2010. *LRFD Bridge Construction Specifications*. Third Edition, American Association of State Highway and Transportation Officials, Washington, D.C.
2. AASHTO/NSBA Steel Bridge Collaboration. 2007. “Steel Bridge Erection Guide Specification, S10.1.” American Highway of State Highway and Transportation Officials, Washington, D.C.
3. Stith, J., Schuh, A., Farris, J., Petruzzi, B., Helwig, T., Williamson, E., Frank, K., Englehardt, M., and Kim, H.J. 2010. “Guidance for Erection and Construction of Curved I-Girder Bridges.” Report No. FHWA/TX-10/0-5574-1, Center for Transportation Research, University of Texas at Austin, Austin, TX, May. (software link: http://fsel.engr.utexas.edu/software/index.cfm)

.

Chapter 5
LRFD Step-by-Step Design Examples

Section 5.1
Skewed/Curved I-Girder



5.1.1 Introduction

This example illustrates the design of a three-span continuous horizontally curved steel I-girder bridge with radial abutments and skewed interior piers and spans of 160′ - 210′ - 160′ measured along the arc at the centerline of the bridge. The radius of curvature is 700 feet measured to the centerline of the bridge. This example is intended to illustrate the principles of skewed and curved I-girder design presented in previous sections of this manual. The example illustrates the design of selected critical sections from an exterior girder at the strength, service and fatigue limit states according to the *AASHTO LRFD* Specifications. Constructibility checks and stiffener, shear connector, cross-frame member and bolted field splice designs are also presented.

5.1.2 Design Parameters

An example skewed/curved I-girder bridge is used to illustrate the principles of skewed and curved I-girder design presented in preceding sections of this manual.

The following data apply to this example design:

Specifications: 2010 *AASHTO LRFD* Bridge Design Specifications, Fifth Edition
Structural Steel: AASHTO M 270, Grade 50W (ASTM A 709, Grade 50W) uncoated weathering steel with F_y = 50 ksi
Concrete: f'_c = 4.0 ksi
Slab Reinforcement: AASHTO M 31, Grade 60 (ASTM A 615, Grade 60) with F_y = 60 ksi
Shear Connectors: Three 7/8″-diameter stud connectors per row; F_u = 60 ksi

The girders are composite throughout as required for curved continuous composite bridges in *AASHTO LRFD* Article 6.10.10.1. The steel girders are homogeneous throughout.

Permanent steel deck forms are assumed between the girders; a load of 15 pounds per square foot is assumed for stay-in-place (SIP) forms, which is assumed to include the weight of the concrete in the form flutes. If desired, Styrofoam could be placed in the form flutes to eliminate the concrete add-on in the flutes and reduce the weight of the forms to approximately 4.0 to 5.0 psf. Design Engineers are encouraged to consult with deck-form manufacturers to discuss the various options and obtain more accurate weight information for these forms.

Other permanent (dead) loads applied to the bridge include a load of 495 pounds per linear foot for each concrete deck parapet, and a load of 30 pounds per square foot for a future wearing surface.

The Average Daily Truck Traffic (ADTT) in one direction, considering the expected growth in traffic volume over the 75-year fatigue design life, is assumed to be 2,000 trucks/day for fatigue design.

Steel was selected as the material of choice for this bridge because it is lighter than concrete, which helps to reduce the substructure costs in the poor soil conditions (Section 5.1.3.1). Steel can also better accommodate the curved alignment and skews. Deeper concrete girders would not be able to meet the vertical clearance requirements (Section 5.1.3.1) without span and alignment changes.

Uncoated weathering steel is utilized in the example design. Where site conditions are adequate for successful application, uncoated weathering steel is the most cost-effective material choice for steel bridges in terms of savings in both initial and future

repainting costs. To increase the confidence in the performance of this material, the FHWA issued a Technical Advisory (T5140.22) in 1989 entitled *Uncoated Weathering Steel in Structures.* The guidelines contained in this document, developed in cooperation with the steel industry, suggest good detailing practice to help ensure successful application of the material and are a valuable source of information on the proper environments for the use of weathering steel.

5.1.3 Steel Framing

5.1.3.1 Span Arrangement

Span arrangement considerations are discussed in Section 3.1.2.2. Figure 5.1.1 shows a plan view of the example I-girder bridge.

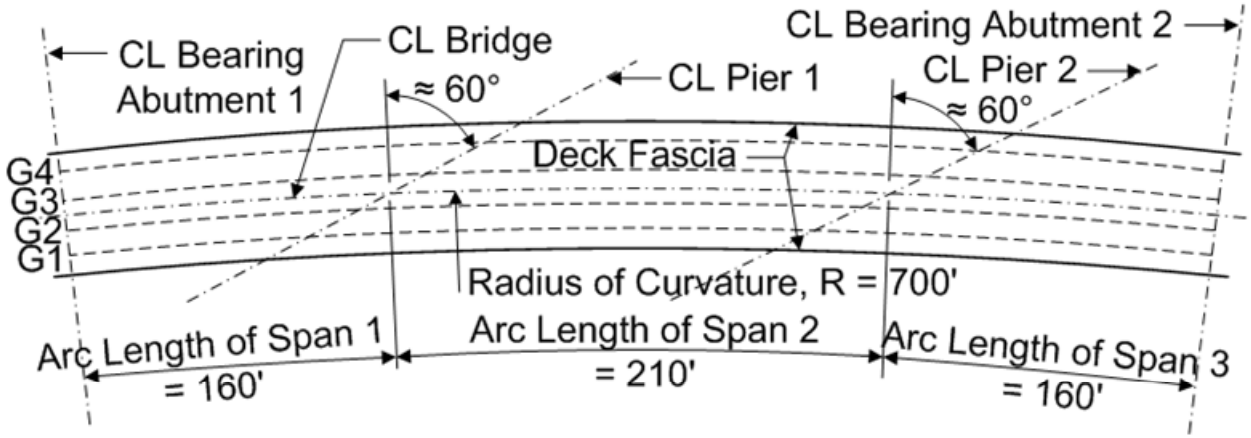


Figure 5.1.1 Plan View of the Example I-Girder Bridge

This example bridge has three spans, with the end spans each 160 feet long and the center span 210 feet long. These span lengths are measured along the arc at the centerline of the bridge. The individual arc span lengths of each girder (in feet) are as follows (Table 5.1.1):

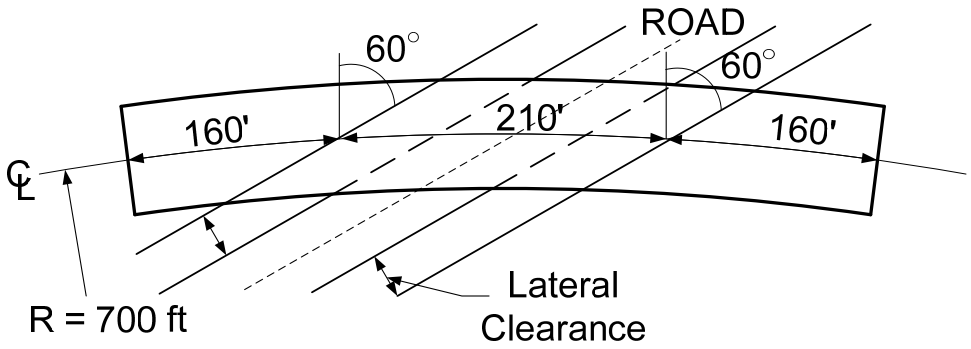
Table 5.1.1 Girder Arc Span Lengths (feet)

	Span 1	Span 2	Span 3
G4	191.41	214.92	136.13
G3	170.70	211.66	151.81
G2	149.08	208.35	168.40
G1	126.50	205.04	185.94

The lateral clearance requirement of 30-ft to accommodate the roadway passing underneath the bridge necessitated the sharply skewed piers and the 210-ft center span (Figure 5.1.2). End spans of 160-ft were then chosen to provide a balanced span arrangement. A three-span continuous unit was chosen to minimize the depth of steel.

The abutments are oriented radially, and both piers have a significant skew. The skew angle of the interior piers is approximately 60 degrees measured clockwise from radial. The abutments were made radial to reduce length and save on the number of deep piles required in the poor soil conditions and to save on square footage of bridge deck.

The radius of curvature is 700 feet measured at the centerline of the bridge. The 700-ft centerline radius was chosen due to right-of-way limitations and to accommodate the design speed of 35 mph.



Clearance requirements: Lateral – 30 ft
Vertical – 16 ft

Poor soil conditions requiring deep piles

Flat terrain

Figure 5.1.2 Alignment, Clearance and Location Considerations for the Example I-Girder Bridge

The height of the approach profile had to be adjusted due to the flat terrain in order to accommodate the necessary girder web depth of 92 inches (Section 5.1.4.1) and still satisfy the vertical clearance requirement. This required the acquisition of additional right-of-way in order to obtain the necessary height at a constant maximum grade.

5.1.3.2 Cross-Section

Figure 5.1.3 shows the cross-section of the example bridge, with the intermediate and support cross-frame configurations noted.

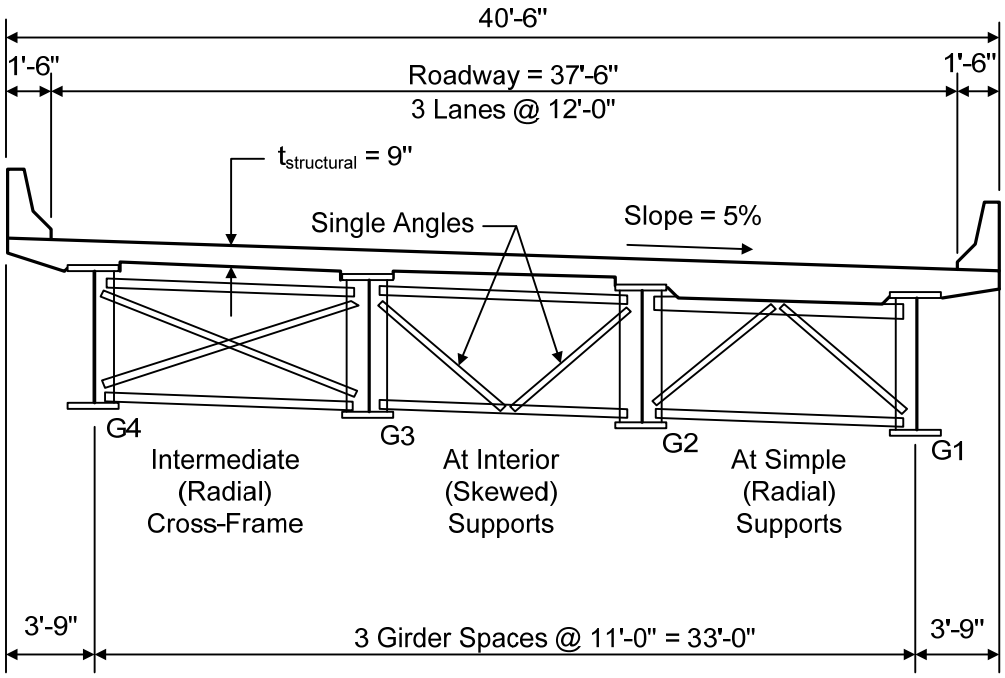


Figure 5.1.3 Cross-Section of the I-Girder Example Bridge

Cross-frame configuration considerations in I-girder bridges are discussed in Section 3.1.2.8.4.1. The cross-frame configuration shown in the left bay is used at all intermediate (radial) cross-frames. The configuration shown in the center bay is used at all interior (skewed) supports. The cross-frame configuration shown in the right bay is used at all simple (radial) supports. The bottom of deck is also different for these locations, as shown in the cross section. At simple supports, the deck rests directly on the top chord of the end cross-frame to support the wheel loads coming onto the bridge.

Girder spacing and deck overhang considerations are discussed in Sections 3.1.2.4 and 3.1.2.5, respectively. Redecking under traffic was assumed not to be an issue for this bridge so a cross-section of four girders at 11'-0″ spacing was selected. The roadway width was dictated by traffic and state standards. As this is a rural bridge, no sidewalks were included. Since overhang loads were not anticipated to be an issue in this case, overhangs were set to be 3'-9″ on both sides of the cross-section. A cross-slope or superelevation of 5 percent was assumed.

The structural thickness of the concrete deck was selected using a standard table to be 9″, with a ½″ structural wearing surface. A 4-inch-thick deck haunch was selected measured from the top of the web to the bottom of the deck. A mildly reinforced

deck with a flat soffitt between the girders is assumed. The deck overhang soffit is tapered from the bottom of the exterior girder haunches to the outside edge of the deck. The thickness of the deck at the edge of the deck is 9½″. Deck and haunch thickness considerations are discussed in Sections 3.1.2.6 and 3.1.2.7, respectively.

5.1.3.3 Field-Section Size

The number of field sections (i.e. girder sections fabricated and shipped to the bridge site) and the location of bolted splices can have a significant effect on the efficiency of the design of steel girders. Fewer field splices reduces shop and field bolting cost. Additionally, the number and location of bolted splices often affects the cost. The choice of field splice locations is in many ways job specific. The weight and length of field sections should be chosen after consulting fabricators expected to bid the work. Additional factors related to the selection of field-section size, including material availability, shipping, handling and erection, are discussed in Section 3.1.2.3.

Field splices are traditionally located in regions of lower moment. Referring to the fold-out sheets are the end of this example, 16 bolted field splices are used in the example; one in each end span and two in the center span resulting in five (5) field sections in each girder line. These splices are located near points of permanent load contraflexure, which tends to reduce the size of these splices. Note that three (3) additional optional field splices are shown in the longer field sections in Span 1 of G4 and in Span 3 of G1 and G2 should the fabricator need to reduce the length of these curved sections for shipment.

The design of one of the bolted field splices is illustrated in Section 5.1.8.8.

5.1.3.4 Cross-Frame Layout

Important functions of cross-frames in skewed and curved I-girder bridges are discussed in Section 3.1.2.8.1.

Cross-frame spacing requirements for I-girder bridges are discussed in Section 3.1.2.8.2.1. Using Equation 3.1.1, calculate a preliminary trial cross-frame spacing, L_b, for the example curved I-girder bridge. Assume an average flange width, b_f = 20 in., and that the desired bending stress ratio, $r_\sigma = f_\ell / f_{bu} = 0.25 < 0.3$. Take R as the centerline radius of 700 ft.

$$L_b = \sqrt{\frac{5}{3} r_\sigma R b_f}$$

$$L_b = \sqrt{\frac{5}{3}(0.25)(700\ \text{ft})\left(\frac{20\ \text{in}}{12\ \text{in/ft}}\right)}$$

$$L_b = 22\ \text{ft}$$

Calculate the maximum permitted cross-frame spacing according to the criteria for curved I-girder bridges discussed in Section 3.1.2.8.2.1. Assume the following values for this check: r_t = 5.8 in; and $F_{yr} = 0.7F_y$ = 35 ksi (girders are homogeneous).

- Check 1: $L_r = \pi\ r_t\sqrt{\frac{E}{F_{yr}}}$

$$= \pi\left(\frac{5.8\ \text{in}}{12\ \text{in/ft}}\right)_t\sqrt{\frac{29000\ \text{ksi}}{35\ \text{ksi}}}$$

$$= 43.7\ \text{ft}$$

- Check 2: $\frac{R}{10} = \frac{700\ \text{ft}}{10} = 70.0\ \text{ft}$

- Check 3: 30.0 ft (governs)

Cross-frame layout considerations in curved I-girder bridges with skew are discussed in Section 3.1.2.8.3.2. Utilizing the preliminary trial cross-frame spacing and maximum permitted cross-frame spacing determined above, assume the trial contiguous cross-frame arrangement for the example bridge shown in Figure 5.1.4.

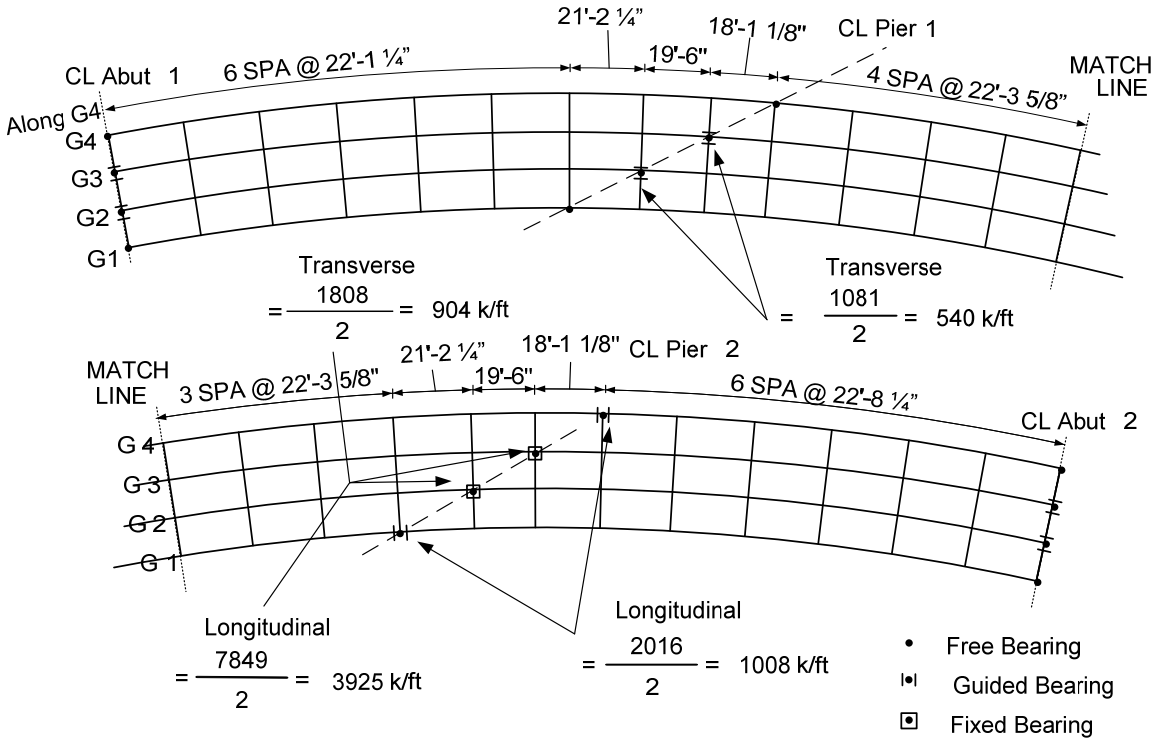


Figure 5.1.4 Trial Contiguous Cross-Frame Arrangement for the Example I-Girder Bridge

As discussed in Section 3.1.2.8.3, it is advisable to check the cross-frame forces early on in the design of the superstructure before advancing the design of the girders too far in order to determine if the forces are too large to design practical members and connections. Therefore, a 3D analysis of the bridge using preliminary girder sizes is conducted in order to evaluate the magnitude of the cross-frame forces to determine if this cross-frame arrangement is indeed satisfactory.

The cross-frame actions are usually critical for the restrained bearing case (Section 2.2.3.1). Thus, it is desirable (although not mandatory) at this stage to anticipate a reasonable bearing configuration that might be used to resist the nominal horizontal loads (e.g. wind loads, temperature change, etc.). The bearing configuration shown in Figure 5.1.4 is assumed. Girders G2 and G3 are assumed restrained transversely (i.e. normal to the girder tangents) at each support. At Pier 2, all four girders are assumed restrained longitudinally (i.e. tangent to the girders). All other bearings on the two fascia girders G1 and G4 are assumed free (i.e. no horizontal restraint). The guided bearings are assumed *not* to be guided toward the two fixed points on Pier 2 in this case (Section 2.2.3.2).

The cross-frames are placed in contiguous lines normal (radial) to the girders. Since cross-frames are provided normal to the girders at all bearings that resist transverse (lateral) forces and are to be proportioned to resist these forces, and the bottom (compression) flanges of the fascia girders G1 and G4 are assumed adequately

braced at the piers, cross-frames are not needed along the skewed support lines in this case and are not provided. This simplifies the detailing.

Fixed points on piers generally flex as a function of the pier stiffness in the direction of the bearing restraint(s). Thus, it is important to recognize the pier stiffness in the analysis where the bearings are constrained (Section 2.2.4). The calculation of the longitudinal and transverse pier stiffness values shown in Figure 5.1.4 (and resolved along the directions of bearing restraint) was illustrated in Section 2.2.4.6. Note that the pier stiffness values are assumed equally divided to the corresponding number of restrained bearings on each pier for the analysis. The stiffnesses are assigned to foundation elements (Section 2.5.2.3.5) in the 3D model in the appropriate directions of bearing constraint. The abutments were assumed to be infinitely rigid.

Figure 5.1.5 shows computed maximum axial forces from the 3D analysis in select cross-frame members. The factored forces are due to combined dead and live load plus impact and include centrifugal force effects. Live load forces are due to the HL-93 design live load. The factored forces are for the Strength I load combination (with η = 1.0). Recall that the configuration of the intermediate (radial) cross-frames is an X-type configuration.

Only the maximum forces in cross-frames that had a total factored member force larger than ± 200 kips are reported in Figure 5.1.5. The critical cross-frames are clustered around the two skewed piers, as expected. In each case, only a single member in each cross-frame had a total factored member force larger than ± 200 kips and that is the force that is indicated. The critical members were not necessarily the same in each cross-frame.

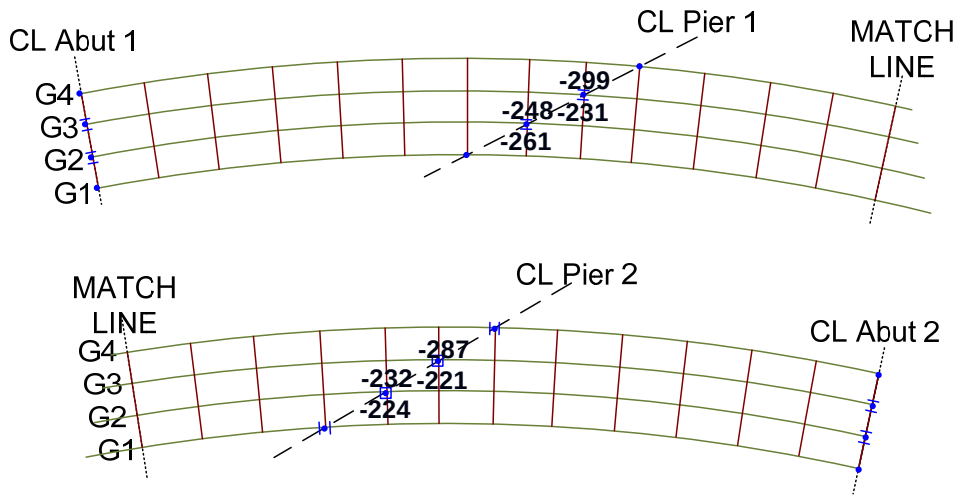


Figure 5.1.5 Maximum Total Factored Axial Forces (>200 kips) in Selected Cross-Frame Members from the 3D Analysis – Contiguous Cross-Frames

An arrangement in which the cross-frames are placed in a contiguous pattern across the bridge provides the greatest transverse stiffness adjacent to skewed supports.

Thus, the largest amount of load possible is transferred across the bridge in these regions and as a result, the cross-frame forces in these regions are relatively large.

An attempt is next made to reduce the transverse stiffness of the superstructure adjacent to the skewed piers by providing discontinuous cross-frames in these regions (Figure 5.1.6). This releases the girders torsionally by allowing the girder flanges to flex laterally and helps to relieve some of the restoring forces in the cross-frame members. Although the forces in the cross-frame members are decreased, discontinuing the cross-frame lines also has the effect of increasing the lateral bending stresses in the girder flanges as illustrated below. These additional lateral flange bending stresses must be considered in the design of the girders. Often, however, the lateral bending is not critical and the net result is a desirable reduction in the cross-frame forces.

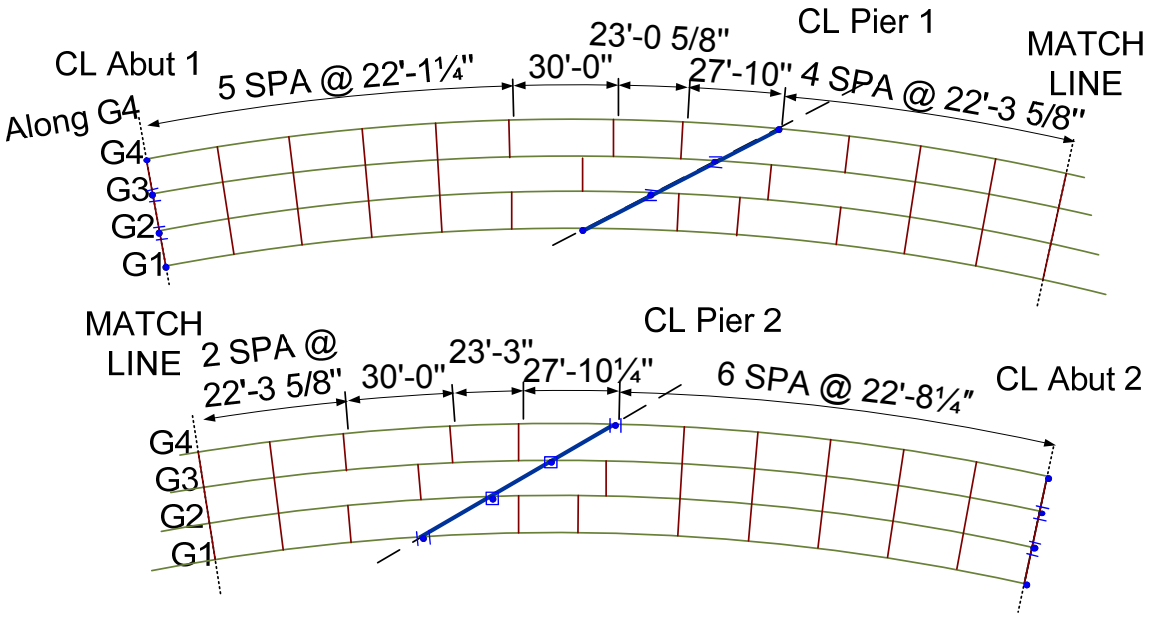


Figure 5.1.6 Trial Discontinuous Cross-Frame Arrangement for the Example I-Girder Bridge

Note the discontinuous (staggered) cross-frame lines adjacent to the skewed piers in Figure 5.1.6. Note also the cross-frames spaced at the maximum permitted spacing of 30 feet along the exterior girder.

The same bearing restraints and longitudinal and transverse stiffness values are assumed as for the previous cross-frame configuration (Figure 5.1.6). In this case, without cross-frame lines provided along the skewed piers, the restrained bearings on the piers supporting girders G2 and G3 would not be matched with a cross-frame to resist the transverse (lateral) forces at those bearings. Also, although the bearings on the piers supporting the fascia girders G1 and G4 are free, relatively large unsupported lengths of the bottom (compression) flange of the those girders

adjacent to the piers would be present without providing cross-frame lines along the skewed piers. Thus, for this particular discontinuous cross-frame arrangement, it becomes necessary to provide cross-frame lines along the skewed piers, as indicated in Figure 5.1.6. Recall that the cross-frame configuration along the skewed piers is a K-type configuration, with the K-node at the middle of the bottom chord.

Figure 5.1.7 computed maximum axial forces from the 3D analysis in select cross-frame members for the assumed discontinuous cross-frame arrangement. .Again, the factored forces are due to the combined dead and live load plus impact and include centrifugal force effects. The factored forces are for the Strength I load combination (with η = 1.0). Live load forces are due to the HL-93 design live load.

Only the maximum forces in cross-frames that had a factored member force larger than $\pm$ 100 kips are indicated in this case. As expected, by providing discontinuous cross-frame lines adjacent to the skewed supports and relieving the transverse stiffness of the superstructure in these regions, a significant reduction in the cross-frame forces is observed with only a few cross-frames now seeing forces larger than $\pm$ 100 kips. *As a result, this discontinuous cross-frame arrangement was selected for further investigation for the example I-girder bridge*.

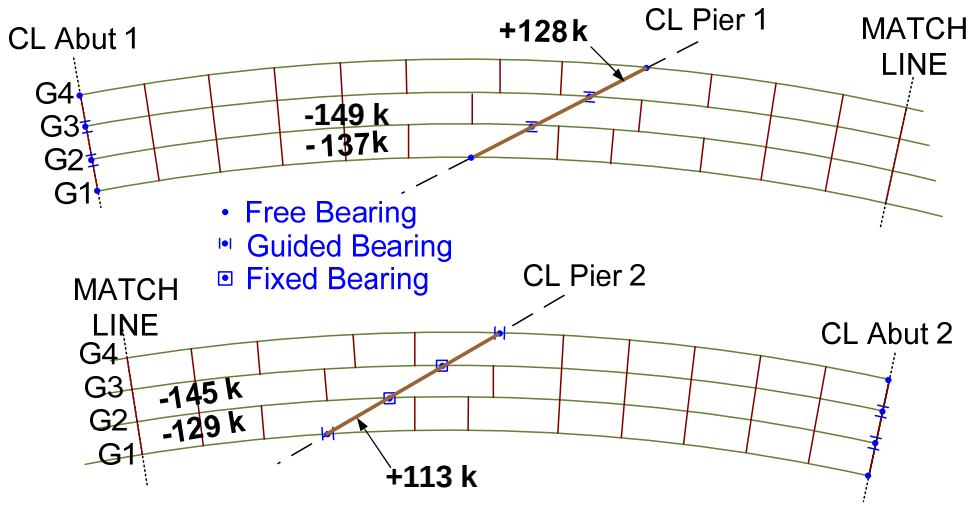


Figure 5.1.7 Maximum Total Factored Axial Forces (>100 kips) in Selected Cross-Frame Members from the 3D Analysis – Discontinuous Cross-Frames

Figure 5.1.8 Part A shows the total factored dead and live load plus impact bottom flange lateral bending stresses at selected cross-frame lines taken directly from the 3D analysis for the first trial case (i.e. contiguous cross-frames). The factored stresses are for the Strength I load combination (with η = 1.0) and include centrifugal force effects. For bottom flanges in compression, the stresses do *not* include the amplification factor. The lateral bending stresses near the abutment are primarily due to the effects of curvature. Near the skewed pier, the bearing restraints acted to reverse the effect of curvature. The stresses are only shown for half of the bridge. Top flange lateral bending stresses are considered negligible because the top flange is continuously braced for the Strength I load combination.

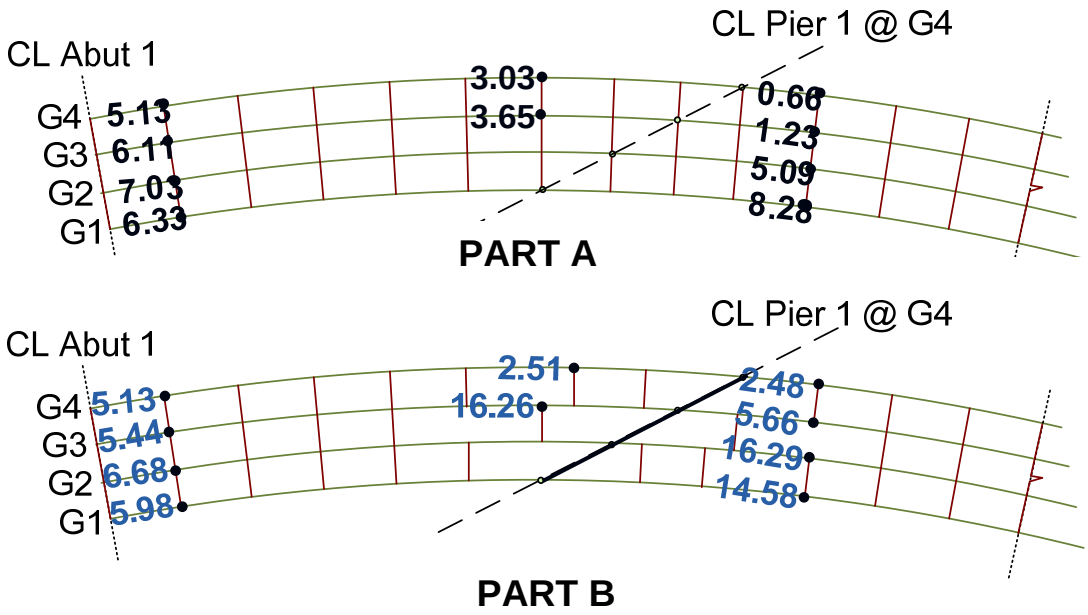


Figure 5.1.8 Total Factored Bottom Flange Lateral Bending Stresses at Selected Cross-Frames from the 3D Analysis
A) Contiguous Cross-Frames; B) Discontinuous Cross-Frames

Figure 5.1.8 Part B shows similar bottom flange lateral bending stresses for the case of discontinuous cross-frames. The lateral bending stresses near the piers are due to the combined effects of curvature and the discontinuous cross-frames that were used in order to counter the effects of the skew. Discontinuous cross-frame lines can exacerbate the flange lateral bending stresses in the girders, particularly near the locations where the lines are discontinued. These flange lateral bending effects due to skew should be considered in the design of the girders whenever discontinuous cross-frame lines are employed.

The lateral bending stresses in Figure 5.1.18 Part B are somewhat larger, in general, in the two interior girders relative to the exterior girders. Since there are no opposing cross-frames on the outside of the fascia girders, flange lateral bending due to skew effects is usually smaller in these girders. Interior girders are generally subject to larger lateral flange moments due to skew effects relative to the fascia girders. Note that the lateral flange bending effects due to the skew are less critical in the regions out in the spans (i.e. away from the skewed piers) where the cross-frames are contiguous. In these regions, the flange lateral bending effects are primarily due to the effects of the curvature in this case.

The possibility of using all free round elastomeric bearings under each girder at each support in order to mitigate the horizontal bearing reactions due to thermal loads is investigated in Section 5.1.6.2. In essence, these bearings allow the bridge to “float”

under nominal horizontal loads (Section 2.2.3.4). Shear keys are assumed provided to handle horizontal restraint under extreme events, such as earthquakes. Such a bearing arrangement would eliminate the need to provide more expensive pot bearings.

A 3D analysis was then conducted for this bearing configuration (in conjunction with the discontinuous cross-frame arrangement) to investigate the total factored cross-frame forces under the combined dead and live loads plus impact to see if any further beneficial reduction in the cross-frame forces could possibly be gleaned from the removal of the horizontal bearing restraints.

In this particular case, very little change in the total factored cross-frame forces occurred due to the removal of the horizontal bearing restraints (Figure 5.1.9). Since there were no depth restrictions in this case, a 92-inch-deep web was employed in the girder design (Section 5.1.4.1). It is anticipated that had it been necessary to employ shallower girders, a more noticeable reduction in cross-frame forces may likely have occurred from the removal of the horizontal bearing restraints. Shallower girders in combination with stiffer piers may likely have resulted in an even further reduction in the forces

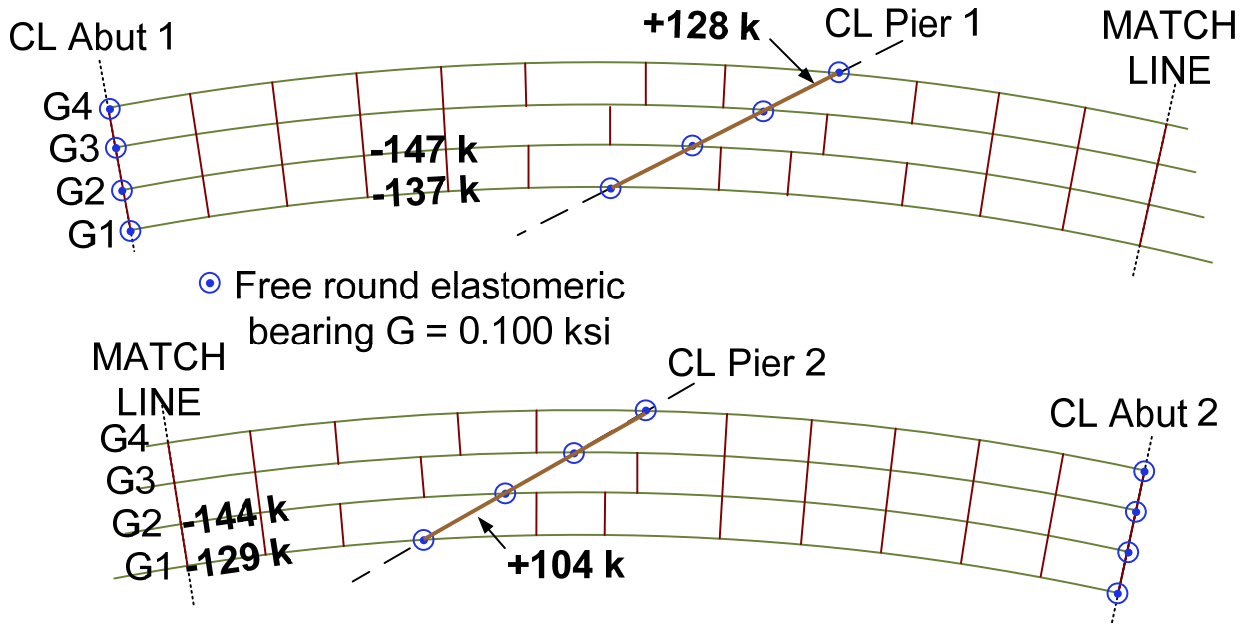


Figure 5.1.9 Maximum Total Factored Axial Forces (>100 kips) in Selected Cross-Frame Members from the 3D Analysis – Discontinuous Cross-Frames w/ Free Elastomeric Bearings

.

5.1.4 Preliminary Member Sizes

5.1.4.1 Web Proportioning

5.1.4.1.1 Web Depth

The first step in sizing the girders for the example bridge is to determine a reasonable web depth. Girder depth considerations are discussed in Section 3.1.3. Figure 5.1.2 shows that the vertical clearance requirement for the example bridge is 16 feet.

Equation 3.1.8 provides a minimum recommended depth for curved steel girder systems for the case where no 70-ksi yield strength steel is used is as follows:

$$D = \frac{L_{as}}{25} = 0.040\ L_{as}$$

The suggested minimum depth for the example bridge is conservatively calculated based on the arc lengths of the longest girder G4. For end spans, L_{as}, for use in the preceding equation is defined as 0.9 times the arc span. For continuous interior spans, L_{as} for use in the equation is defined as 0.8 times the arc span. The arc span length of the end spans of G4 is 191.4 feet. The arc span length of the center span of G4 is 214.9 feet. Therefore:

$$D_{end\ \ span} = 0.040\,(0.9)(191.4) = 6.9\ \ \text{ft} \approx 83\ \ \text{in.}$$

$$D_{center\ \ span} = 0.040\,(0.8)(214.9) = 6.9\ \ \text{ft} \approx 83\ \ \text{in.}$$

The suggested minimum depth conservatively using the full arc span length of the center span is:

$$D = \frac{214.9}{25} = 8.6\ \ \text{ft} \approx 103\ \ \text{in.}$$

Investigations of depths between 83 in. and 103 in. indicated that a constant web depth of 92 in. provides the best overall economy (D in Equation 3.1.8 is defined in the specification as the overall depth of the steel girder, but it is recommended that D instead be taken as the web depth for simplicity). As mentioned in Section 5.1.3.1, although the height of the roadway profile had to be adjusted to accommodate the 92-inch web depth and still meet the vertical clearance requirement, additional right-of-way was able to be acquired relatively easily in this case to obtain the necessary height at a constant maximum grade.

A depth larger than the minimum recommended depth is chosen because of the presence of a significant skew and the desire to lessen the cross-frame forces, the lateral flange bending stresses in the girders, and the girder deflections and rotations. A larger depth will also help provide a greater stiffness to the non-composite girders during construction and better overall economy in this case.

5.1.4.1.2 Web Thickness

Section 3.1.4.2.1 discusses considerations related to the selection of the web thickness. The minimum web thickness for the design is determined from the limiting D/t_w ratio of 150 specified for webs without longitudinal stiffeners in *AASHTO LRFD* Article 6.10.2.1 as follows:

$$\frac{D}{t_w} \le 150$$

$$t_w \ge \frac{D}{150} = \frac{92 \text{ in.}}{150} = 0.613 \text{ in.}$$

A web thickness of 5/8″ is selected. The selected web thickness is greater than the ½" minimum web thickness preferred by fabricators. A constant web thickness is used for each girder.

5.1.4.2 Flange Proportioning

I-girder flange proportioning is discussed in Section 3.1.4.3. The minimum width of flanges is specified as (Equation 3.1.13):

$$b_f \ge D/6$$

Therefore:

$$(b_f)_{min.} = D/6 = 92/6 = 15.3 \text{ in.}$$

Flanges should never be less than 12 inches in width to prevent distortion and cupping due to welding (Section 3.1.4.3.1). A minimum flange width of 16 inches was enforced in the design.

Equation 3.1.14 is a suggested guideline regarding the minimum width of flanges in compression based on the experience of erectors given as follows:

$$b_{fc} \ge \frac{L}{85}$$

where *L* is the length of the girder shipping piece in feet. For example, referring to the fold-out sheets provided at the end of this example, the length of the longest field piece, which is assumed to also equal the length of the longest shipping piece in this

case, is approximately 145 feet (in Span 3 of G1 – assuming the optional field splice is not employed). Therefore, for this particular shipping piece:

$$(b_{fc})_{min} = \frac{L}{85} = \frac{145(12)}{85} = 20.5 \text{ in.}$$

A 1″ x 22″ top flange is used for this shipping piece. Similar checks were made for all the girder field sections.

The minimum thickness of flanges is specified as (Equation 3.1.17):

$$t_f \geq 1.1 t_w$$

or:

$$(t_f)_{min} = 1.1 t_w = 1.1(0.625) = 0.6875 \text{ in.}$$

However, the flange thickness should never be less than ¾ inches (Section 3.1.4.3.2). Therefore, a minimum flange thickness of 0.75 inches was enforced in the design.

Section 3.1.4.3.3.1 discusses considerations related to the proportioning of flanges in negative moment regions. Section 3.1.4.3.3.2 discusses considerations related to the proportioning of flanges in positive moment regions. These guidelines were followed in general in the proportioning of the girder flanges for the example bridge.

Section 3.1.4.3.4 discusses additional important considerations related to the sizing of flanges for efficient fabrication. These considerations are particularly important when sizing flanges for curved girders in order to minimize scrap. In general, the flanges in the example bridge were sized so that as many pieces as possible could be obtained from a wide plate with minimal waste. To minimize waste, it is important to limit the number of different flange plate thicknesses specified for a given project; in this case, only 6 different plate thicknesses were employed for the flanges. Thus, flange thicknesses were re-used in the design with the flange width adjusted accordingly, while maintaining constant top and bottom flange widths within a given field section. Changes in flange width were made at the field splices. The maximum flange thickness used was 2.75 inches (≤ 3.0 inches).

Referring again to the fold-out sheets, the pier sections of G4 and G3 and of G2 and G1 were each designed according to the recommendations in Section 3.1.4.3.4 to allow for efficient nesting of the flanges for possible slab welding (Section 4.1.2.1.3) and cut curving. Note that the flange splices in the adjacent girders were kept equidistant from the pier, but that the lengths of the pier plates were not equal on both sides of the bearing. Similar considerations were made for the flange plates in the positive moment regions to allow for possible nesting of the girder flanges in these regions on a single plate. In this particular case, because of the relatively sharp radius and skew, it was not efficient to nest the flanges for all four girders on one set of plates.

At all welded flange shop splices, it was ensured that the area of the smaller flange plate was not less than one-half the area of the larger flange plate in order to control stress concentrations at the splices (Section 3.1.4.3.2). Good design practice requires that flange transitions and shop-welded splices be located based on demand moments and plate availability, as well as cost comparisons between welding and inspecting of a splice versus extending a thicker plate.

Two additional flange proportion limits are given by Equations 3.1.15 and 3.1.16 as follows:

$$\frac{b_f}{2t_f} \le 12.0$$

$$0.1 \le \frac{I_{yc}}{I_{yt}} \le 10$$

These criteria are each checked for the most critical case (refer to the fold-out sheets):

$$\frac{b_f}{2t_f} = \frac{33}{2(1.375)} = 12.0 \quad \text{ok}$$

All other flanges have a ratio of $b_f/2t_f$ less than 12.0.

$$\frac{I_{yc}}{I_{yt}} = \frac{\frac{1(22)^3}{12}}{\frac{1(22)^3}{12}} = 1.0$$

$$0.1 < 1.0 < 10 \quad \text{ok}$$

At all other sections, the ratio of I_{yc}/I_{yt} is less than 1.0 and greater than 0.1.

5.1.4.3 Cross-Frames

Design considerations for cross-frames are discussed in Section 3.1.2.8.5. Preliminary cross-frame member sizes are required to perform the 3D analysis of the bridge. The 3D finite element method recognizes the individual cross-frame members (Section 2.5.3.2.4). The initial sizes influence the distribution of forces and the magnitude of the computed actions in the members. Disproportionately large cross-frame members will result in large forces that can be reduced by reducing the member sizes. It is best to initially investigate smaller member sizes and increase

the sizes as necessary. Significant changes in cross-frame member sizes are best investigated with another analysis to assure that the forces have not changed excessively.

Single angles are preferred for cross-frame members because they are readily available, inexpensive, easily connected and easily painted. Structural tees are used when forces are large. Double angles are less commonly used because they are expensive to fabricate and painting between the angles is difficult. Sections 3.3.3 and 3.3.4 discuss the design of single-angle, tee and double-angle members.

Preliminary sizes can be obtained from the permitted slenderness specified in *AASHTO LRFD* Articles 6.8.4 and 6.9.3 and/or based on experience. The following preliminary sizes were assumed for the intermediate (radial) cross-frame members and the interior skewed support cross-frame members *for the analysis*:

Top chord: L 5 x 5 x 5/8; A = 5.86 in.^{2}
Bottom chord & diagonals: WT 6 x 22.5; A = 6.61 in.^{2}

End cross-frames require a larger top chord that supports the end dam and deck forms during construction and live loads on the completed bridge. For these cross-frames, an area of 10.0 in.^{2} was assumed for the top chord and an area of 5.86 in.^{2} was assumed for the bottom chord and diagonals *for the analysis*.

The assumed configuration of these cross-frames for the analysis is shown in Figure 5.1.3.

The design of the bottom chord of an intermediate (radial) cross-frame for the actual compressive force obtained from the 3D analysis results is presented in Section 5.1.8.7.

5.1.5 Loads

A refined 3D finite element analysis model of the bridge was constructed and analyzed using many of the concepts discussed in Section 2.5. Loads were applied to the model as described in the following and discussed in greater detail in Section 2.5.3.4.

5.1.5.1 Dead Loads

Dead loads in the *AASHTO LRFD* specification are primarily classified as either component dead load (designated as DC), which is assumed to consist of all the structure dead load except for any non-integral wearing surfaces and any specified utility loads, or dead load of any non-integral wearing surfaces and any utilities (designated as DW). Further discussion on dead loads may be found in Section 1.3.2.1.

5.1.5.1.1 Component Dead Loads

5.1.5.1.1.1 Structural Steel Weight (DC_1)

Structural steel weight was modeled in the analysis using body-weight of the modeled members. The steel weight included the cross-frames as well as the girders. The weight of detail steel such as stiffeners and splices was not included, but was accounted for in the analysis by changing the density of the steel.

5.1.5.1.1.2 Deck/Deck Haunches/SIP Forms (DC_1)

Weight of the wet concrete of the deck was applied to the non-composite 3D model with concentrated loads at the nodes representing the tops of the girders. The concrete was assumed to have no stiffness. The concentrated loads applied to each girder top node were determined by the tributary area of deck associated with the distance between girder nodes and the girder spacings. The thickness of the integral wearing surface was considered. The deck overhang tapers (Figure 5.1.3) were considered in computing the concentrated loads applied to the exterior girders. The weight of the wet concrete in the deck haunches was included in the concentrated loads applied to each girder. An average deck haunch width of 20 inches and deck haunch thickness of 4 inches was assumed (the reduction in weight due to the concrete displaced by the top flanges was ignored). The unit weight of the concrete was taken equal to 0.150 kcf, which includes an additional 0.005 kcf to account for the weight of the rebars.

The weight of the SIP deck forms was applied directly to the girders of the non-composite 3D model as concentrated loads as done for the deck. The forms exist only between flange edges in the interior bays; thus, the weight of the forms and the concrete in the forms was based on the clear span between the top flanges in the interior bays.

5.1.5.1.1.3 Concrete Parapets (DC_2)

The concrete parapet loads were applied as concentrated loads to the nodes at the edges of the deck in the composite 3D model (where the parapets are actually located).

5.1.5.1.2 Future Wearing Surface (DW)

The future wearing surface was applied to the composite 3D model by applying an artificial density of the hardened concrete deck to the deck elements extending over the approximate width of the roadway.

5.1.5.2 Live Loads

Live loads considered in this investigation included the HL-93 design vehicular live load (Section 1.3.2.3.1), the fatigue live load (Section 1.3.2.3.3) and the loading for

live load deflection evaluation (Section 1.3.2.3.4). Design permit loads (Section 1.3.2.3.2) were not considered. As discussed further in Section 1.3.2.3.1, the HL-93 load consists of the combination of a design truck or design tandem, and a design lane load. The special loading for negative moment between points of permanent load contraflexure and for interior-pier reactions (Figure 1.3.7) was also considered in the analysis.

Live loads were applied to influence surfaces (Section 2.1.4) constructed by applying a unit load to selected deck nodes of the composite 3D model. Loading of the influence surfaces was performed with software separate from the finite element solver. Wheel loads were positioned on the surfaces according to the specification rules for live load placement (Section 2.1.4.1) in order to compute the maximum and minimum magnitudes of the desired response. The HL-93 loading was placed in one, two and three design lanes. The fatigue live load was placed in a single lane only. Only lengths of design lanes, or parts of design lanes, that contributed to the extreme force effects under consideration were loaded with the design lane load. Axles that did not contribute to the extreme force effects under consideration were neglected. Multiple presence factors (Section 1.3.2.3.7) and the dynamic load allowance (Section 1.3.2.3.8) were later applied to the live load *responses*, and not to the loads applied to the influence surfaces (see Section 5.1.6.1).

The wheel loads of the design truck(s), design tandem and fatigue live load were modified, however, to account for the vertical effects of centrifugal force and superelevation (Section 1.3.2.3.6). The design lane load was not modified for these effects. Unit wheel-load factors were computed that increased or decreased accordingly the wheel loads that were applied to the influence surfaces to account for vertical centrifugal force effects on this curved bridge. As illustrated in Section 1.3.2.3.6, these unit wheel-load factors were computed to be as follows based on the design speed of 35 mph and the superelevation (deck cross-slope) of 5 percent assumed for the example bridge:

- HL-93 Design Truck(s) & Design Tandem: 1.212 and 0.788
- Fatigue Live Load: 1.134 and 0.866

5.1.5.3 Wind Loads

Wind loads were not considered in this investigation. The reader is referred to Sections 1.3.2.4 and 2.5.3.4.2 for further discussion on wind loads and the application of wind loads to 3D analysis models.

5.1.5.4 Thermal Loads

A uniform temperature change (Section 1.3.2.5.1) was applied to the 3D analysis model of the example bridge. Various bearing configurations were investigated to determine their effect on the thermal analysis results. Section 5.1.6.2 describes this investigation and the results determined for each case.

5.1.6 Structural Analysis Results

5.1.6.1 Dead and Live Load Analysis Results

The unfactored vertical dead and live load bending moments and vertical shears in G4 *at the cross-frames* from the 3D analysis are summarized below in Tables 5.1.2 and 5.1.3.

In the tables, the responses listed under DC_1 represent the sum of the responses due to the steel weight plus the weight of the deck, deck haunches and SIP forms. These loads were applied to the non-composite 3D model in the analysis. Responses listed under DC_2 are the responses due to the weight of the concrete parapets, and responses listed under DW are the responses due to the weight of the future wearing surface. DC_2 and DW loads were applied to the composite 3D model in the analysis.

Reported live load responses represent maximum and minimum envelope values determined from loading of the appropriate influence surfaces. Responses listed under 'HL-93' represent the governing responses due to the HL-93 design vehicular live load (Section 1.3.2.3.1) plus the specified dynamic load allowance (Section 1.3.2.3.8). The listed actions include the appropriate multiple presence factor (Section 1.3.2.3.7) for the governing case (one, two or three lanes loaded). Responses listed under 'Fatigue Load' represent the responses due to the fatigue design live load (Section 1.3.2.3.3) placed in a single lane plus the 15 percent dynamic load allowance; the single-lane multiple presence factor of 1.2 is not applied to the fatigue live load responses.

As discussed in Section 5.1.5.2, centrifugal force effects (Section 1.3.2.3.6) were considered for both the HL-93 and fatigue live load; responses due to cases with centrifugal force effects included were compared to the responses with no centrifugal force considered and the worst case was selected and is reported in the tables.

Table 5.1.2 Unfactored Vertical Bending Moments (kip-ft) in G4 from the 3D Analysis

Cross-Frame Location (ft)	Steel Wt.	Deck + Haunch + SIP Form Wt.	DC_1	DC_2	DW	+(LL+IM) HL-93	-(LL+IM) HL-93	+(LL+IM) Fatigue Load	-(LL+IM) Fatigue Load
Abut. 1	0.	0.	0.	0.	0.	0.	0.	0.	0.
22.104	+615	+2,113	+2,728	+424	+419	+2,689	-498	+912	-113
44.21	+991	+3,403	+4,394	+639	+670	+4,378	-939	+1,420	-213
66.313	+1,083	+3,715	+4,798	+673	+731	+4,990	-1,305	+1,549	-289
88.42	+904	+3,071	+3,975	+584	+607	+4,687	-1,637	+1,427	-365
110.52	+529	+1,642	+2,171	+509	+342	+3,991	-2,114	+1,292	-527
140.52	-434	-1,849	-2,283	-125	-324	+2,059	-3,385	+715	-784
163.57	-1,228	-4,579	-5,807	-755	-851	+1,215	-4,532	+348	-1,008
Pier 1	-2,643	-8,717	-11,360	-2,022	-1,688	+1,349	-7,077	+301	-1,507
22.302	-1,368	-4,655	-6,023	-1,066	-825	+1,122	-4,059	+355	-875
44.604	-507	-1,575	-2,082	-563	-214	+2,521	-3,048	+821	-793
66.906	+161	+841	+1,002	+40	+176	+3,477	-1,964	+1,096	-572
89.208	+518	+2,086	+2,604	+195	+405	+3,764	-1,382	+1,151	-356
111.51	+593	+2,277	+2,870	+333	+433	+3,447	-1,063	+1,049	-173
133.81	+479	+1,724	+2,203	+465	+319	+2,914	-1,130	+991	-265
163.81	-67	-506	-573	+140	-122	+1,660	-1,915	+613	-471
187.06	-590	-2,497	-3,087	-320	-510	+1,146	-3,255	+313	-648
Pier 2	-1,582	-5,752	-7,334	-1,323	-1,137	+1,348	-5,416	+347	-1,008
22.688	-645	-2,474	-3,119	-566	-447	+1,676	-3,773	+441	-916
45.375	-50	-156	-206	-183	-10	+3,369	-3,336	+1,011	-813
68.063	+356	+1,431	+1,787	+114	+290	+3,948	-2,046	+1,203	-588
90.75	+487	+1,925	+2,412	+265	+385	+3,624	-1,309	+1,177	-372
113.438	+354	+1,393	+1,747	+240	+280	+2,335	-646	+805	-180
Abut. 2	0.	0.	0.	0.	0.	0.	0.	0.	0.

Table 5.1.3 Unfactored Vertical Shears (kips) in G4 from the 3D Analysis

Cross-Frame Location (ft)	Steel Wt.	Deck + Haunch + SIP Form Wt.	DC_1	DC_2	DW	+(LL+IM) HL-93	-(LL+IM) HL-93	+(LL+IM) Fatigue Load	-(LL+IM) Fatigue Load
Abut. 1	+33	+109	+142	+26	+22	+152	-36	+55	-8
22.104	+22	+76	+98	+13	+14	+114	-25	+41	-5
44.21	+10	+35	+45	+5	+7	+82	-36	+31	-12
66.313	-2	-8	-10	-2	-1	+51	-57	+21	-23
88.42	-12	-46	-58	-3	-8	+41	-77	+17	-27
110.52	-22	-80	-102	-8	-14	+42	-97	+19	-33
140.52	-34	-122	-156	-25	-22	+23	-142	+7	-49
163.57	-40	-131	-171	-33	-25	+26	-134	+8	-44
Pier 1	-58/+57	-154/+166	-212/+223	-48/+39	-28/+32	+22/+214	-141/-26	+8/+65	-51/-8
22.302	+41	+142	+183	+27	+27	+162	-28	+59	-7
44.604	+33	+121	+154	+21	+21	+139	-25	+47	-7
66.906	+23	+80	+103	+16	+13	+93	-40	+29	-16
89.208	+9	+30	+39	+8	+5	+67	-58	+21	-23
111.51	-1	-8	-9	+5	-2	+52	-70	+20	-24
133.81	-10	-41	-51	0	-8	+52	-87	+20	-29
163.81	-22	-85	-107	-16	-16	+30	-115	+8	-40
187.06	-27	-100	-127	-25	-19	+25	-114	+7	-40
Pier 2	-42/+43	-127/+138	-169/+181	-40/+33	-22/+27	+23/+186	-125/-26	+9/+65	-49/-9
22.688	+30	+111	+141	+20	+21	+137	-16	+52	-7
45.375	+21	+85	+106	+13	+15	+113	-22	+41	-9
68.063	+12	+45	+57	+10	+8	+73	-46	+25	-19
90.75	0	-1	-1	3	0	+48	-69	+15	-27
113.438	-11	-42	-53	-5	-8	+30	-95	+8	-36
Abut. 2	-20	-77	-97	-16	-15	+28	-128	+8	-52

5.1.6.2 Thermal Analysis Results

5.1.6.2.1 General

The bearing configuration options that were investigated for the example bridge and the results of a 3D thermal analysis of the bridge conducted for each of these options is examined herein. This evaluation is intended to demonstrate the effect of various bearing configurations and stiffnesses on the thermal analysis results. Bearing constraints must always be properly recognized in a thermal analysis (Section 2.2).

The bridge is evaluated for the case of selected bearings constrained in the longitudinal (i.e., tangent to the girders) and/or transverse (i.e., normal to the girder tangents) directions. The effects of pier stiffness (Section 2.2.4) are also examined for this case.

The option of using all free round elastomeric bearings under each girder at each support in order to mitigate the horizontal bearing reactions due to thermal loads is also investigated (Section 2.2.3.4). The word "free" in this case is intended to mean no horizontal constraint. In essence, these bearings allow the bridge to "float" under nominal horizontal loads. Shear keys are assumed provided to handle horizontal constraint under extreme events, such as earthquakes.

Various cross-frame arrangements were evaluated for the example bridge in Section 5.1.3.4 to determine the effect of these arrangements on the cross-frame forces and flange lateral bending stresses in the girders. This evaluation indicated that the discontinuous cross-frame arrangement shown in Figure 5.1.10 was optimal in terms of providing a reasonable combination of maximum cross-frame forces and flange lateral bending stresses. It was further determined as part of this investigation that cross-frames were needed along the skewed piers in order to brace the bottom (compression) flange of the fascia girders and to resist the transverse (lateral) forces at the constrained bearings supporting Girders 2 and 3 at the piers (Figure 5.1.10).

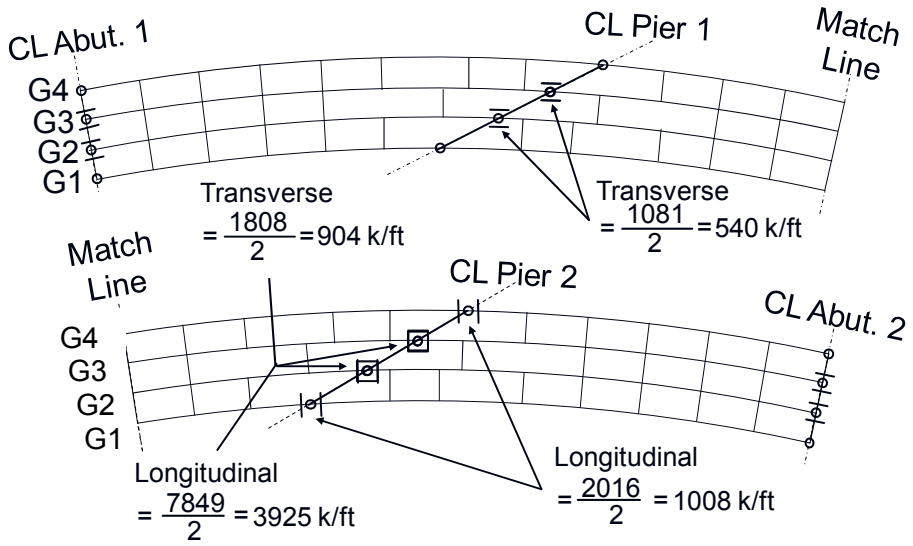


Figure 5.1.10 Selected Cross-Frame Arrangement and Bearing Configuration for the Example I-Girder Bridge

5.1.6.2.2 Constrained Bearings

The bearing configuration shown in Figure 5.1.10 was initially assumed in this investigation. G2 and G3 were assumed constrained transversely (i.e., normal to the girder tangents) at each support. At Pier 2, all four girders were assumed constrained longitudinally (i.e., tangent to the girders). All other bearings on the two fascia girders G1 and G4 were assumed free (i.e., no horizontal constraint). The guided bearings were assumed *not* to be guided toward the two fixed points on Pier 2 in this case.

In addition, longitudinal and transverse pier stiffness values (resolved along the directions of bearing constraint) were calculated in Section 2.2.4.6 and recognized in the analysis where the bearings were constrained. The calculated pier stiffness values were assumed equally divided to the corresponding number of constrained bearings on each pier for the analysis (Figure 5.1.10). The stiffnesses were assigned to foundation elements (Section 2.5.2.3.5) in the 3D model in the appropriate directions of bearing constraint. The abutments were assumed to be infinitely rigid.

The bearings along two girder lines (i.e., G2 and G3) were assumed constrained in the transverse (radial) direction at each support, which may be necessary to help resist additional horizontal loads such as wind and possibly seismic loads. When a thermal analysis is conducted based on such a bearing configuration, large transverse thermal forces are created in the analysis that may not occur in reality depending on the type of bearing that is employed. For example, pot bearings usually have approximately a one-eighth inch gap between the guides and the sole plate. Thus, if the transverse expansion does not exceed this amount, these large transverse forces may not actually materialize.

Additional local transverse forces due to the expansion of the material between adjacent bearings (i.e., the bearings pushing or pulling against their neighbors) may develop during thermal expansion or contraction, which are separate from the transverse forces that develop due to the global thermal movements of the bridge (see the bearing orientation example in Section 2.2.3.4). This transverse expansion can be computed by releasing one of the lines of bearings transversely in the analysis. The transverse movement computed at the released bearings can be compared to the previously mentioned gap to determine if interference might be critical. If so, a second analysis with a gap element or weak lateral restraint introduced might be made to recognize the play in the bearing and determine more realistic transverse thermal forces acting on the actual restrained bearings. In cases where the bearing type selected permits little or no play (e.g. spherical, rocker or others), only the flex of the bearings reduces the expansion forces and the assumption of fully fixed transverse restraints may provide reasonable results.

To illustrate, the transverse bearing constraints at each support along G2 are released for the thermal analysis and the entire transverse pier stiffness of 1081 kips/ft and 1808 kips/ft is applied to the bearings on G3 at Piers 1 and 2, respectively (Figure 5.1.11). Longitudinal pier stiffness values at Pier 2 are also adjusted accordingly.

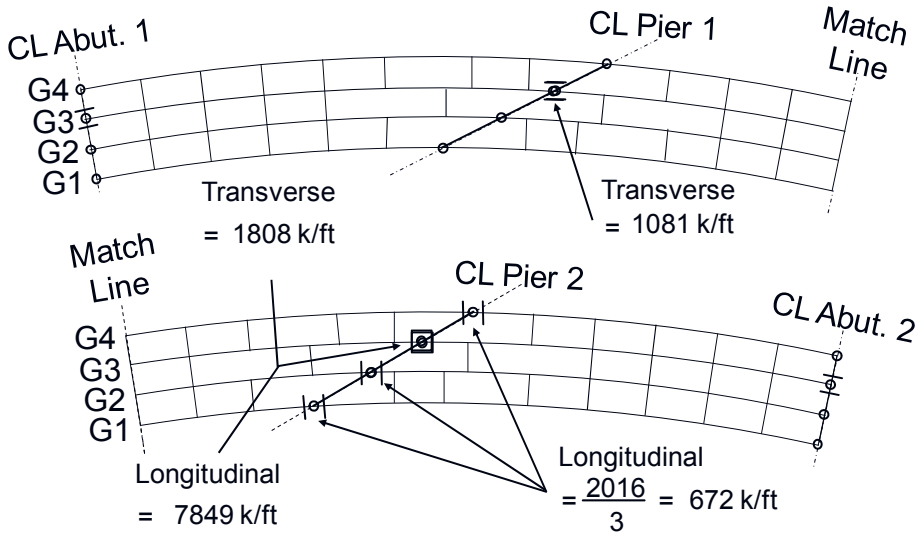


Figure 5.1.11 Updated Bearing Configuration and Pier Stiffness for the Example I-Girder Bridge – w/ Transverse Bearing Constraints Removed at Each Support along G2

The selected design uniform temperature range for the example bridge is -30°F to 120°F (Procedure A – Cold Climate – Section 1.3.2.5.1). The base construction temperature is assumed to be 45°F resulting in a temperature range of ± 75°F for the thermal analysis.

The vertical and horizontal (longitudinal and transverse) bearing reactions for a uniform +75°F temperature increase applied to the example bridge with the assumed bearing configuration shown in Figure 5.1.11 are given in Table 5.1.4. Longitudinal reactions are tangent to the girders and transverse reactions are radial to the girders. All reactions are in kips. The sign convention is according to the axes shown above the table.

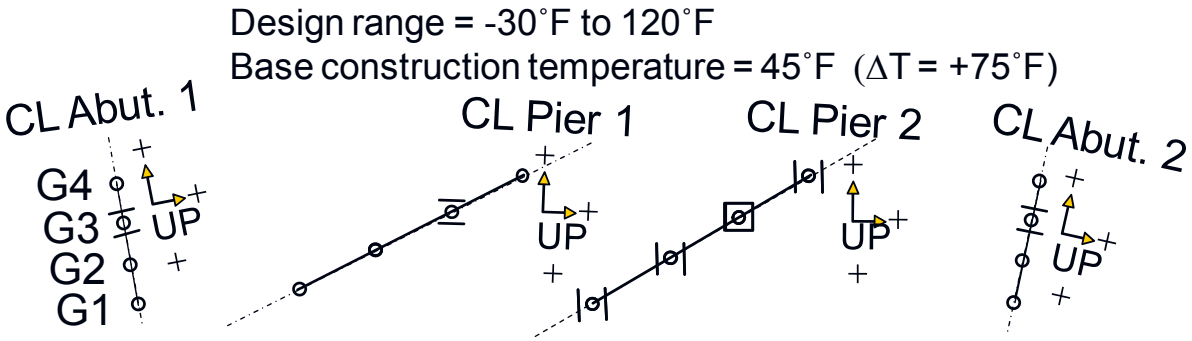


Table 5.1.4 Vertical and Horizontal Bearing Reactions (kips) for a +75°F Uniform Temperature Increase (Bearing Constraints as shown in Figure 5.1.11)

	Abutment 1			Pier 1			Pier 2			Abutment 2		
	Vert.	Long.	Trans.	Vert.	Long.	Trans.	Vert.	Long.	Trans.	Vert.	Long.	Trans.
G4	-0.5	0.0	0.0	-20.4	0.0	0.0	-13.5	-6.6	0.0	-2.0	0.0	0.0
G3	0.3	0.0	-18.9	7.4	0.0	12.2	4.3	-13.0	12.9	1.8	0.0	-9.5
G2	-1.5	0.0	0.0	9.2	0.0	0.0	5.9	4.5	0.0	0.9	0.0	0.0
G1	-9.7	0.0	0.0	10.5	0.0	0.0	14.8	10.7	0.0	-7.4	0.0	0.0

The longitudinal and transverse thermal movements of the girders at each support from the 3D analysis for this case are given in Table 5.1.5. Longitudinal movements are tangent to the girders and transverse movements are radial to the girders. All movements are in inches. Positive directions of movement are indicated by the axes shown above Table 5.1.4.

Table 5.1.5 Longitudinal and Transverse Thermal Movements (in.) at the Bearings for a +75°F Uniform Temperature Increase (Bearing Constraints as shown in Figure 5.1.11)

	Abutment 1		Pier 1		Pier 2		Abutment 2	
	Long	Trans.	Long.	Trans.	Long.	Trans.	Long.	Trans.
G4	-2.210	0.067	-1.101	-0.081	0.035	-0.016	0.913	0.065
G3	-2.194	0.000	-1.195	-0.128	0.057	-0.067	0.918	0.000
G2	-2.174	-0.057	-1.292	**-0.191**	-0.082	**-0.174**	0.921	-0.60
G1	-2.153	-0.119	-1.398	-0.248	-0.194	-0.252	0.922	-0.122

The movements at the constrained bearings on the piers are non-zero because the longitudinal and transverse pier stiffnesses were recognized in the analysis.

The transverse movements of the released bearings on G2 (shown in bold in the table) were –0.191″ and –0.174″ at Piers 1 and 2, respectively. Both movements exceeded 1/8″. Thus, if it were desired to constrain these bearings transversely and pot bearings were utilized, it may be desirable to perform a second analysis with a gap element or weak lateral restraint to recognize the play in the bearings and obtain more reasonable values of the resulting transverse reactions.

The computed reactions and movements are deemed reasonable in this case should only one line of bearings need to be constrained transversely. Note that all actions would be reversed for a uniform -75°F thermal contraction.

The largest cross-frame force from this analysis was –15.04 kips. The cross-frame forces from the analysis due to the uniform temperature change, *TU*, should be appropriately combined with the member dead and live load force effects according to the load combination table (*AASHTO LRFD* Table 3.4.1-1).

5.1.6.2.2.1 Pier Stiffnesses Increased by Factor of 100

Table 5.1.6 shows the vertical and horizontal (longitudinal and transverse) bearing reactions for a uniform +75°F temperature increase for the same bearing configuration as shown in Figure 5.1.11, but *with the longitudinal and transverse pier stiffnesses increased by a factor of 100*. The thermal movements at the supports did not change significantly for this case and are not shown.

Design range = -30˚F to 120˚F
Base construction temperature = 45˚F
Increase longitudinal and transverse pier stiffness by a factor of 100

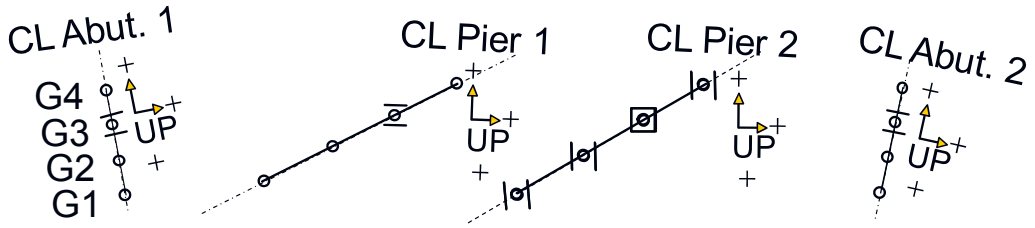


Table 5.1.6 Vertical and Horizontal Bearing Reactions (kips) for a +75°F Uniform Temperature Increase (Bearing Constraints as shown in Figure 5.1.11) – *w/ Longitudinal and Transverse Pier Stiffness Increased by a Factor of 100*

	Abutment 1			Pier 1			Pier 2			Abutment 2		
	Vert.	Long.	Trans.	Vert.	Long.	Trans.	Vert.	Long.	Trans.	Vert.	Long.	Trans.
G4	3.6	0.0	0.0	-58.9	0.0	0.0	16.4	**-364.0**	0.0	29.6	0.0	0.0
G3	-0.6	0.0	-30.8	21.7	0.0	69.9	-20.3	**-338.7**	-13.9	2.8	0.0	-72.6
G2	-4.1	0.0	0.0	26.6	0.0	0.0	-33.6	**193.7**	0.0	-8.2	0.0	0.0
G1	-13.7	0.0	0.0	20.9	0.0	0.0	45.5	**529.3**	0.0	-27.8	0.0	0.0

Note the significant increase in the reactions compared to the reactions in Table 5.1.4; in particular, the longitudinal reactions at Pier 2 (shown in bold in the table). Therefore, with stiffer piers in this particular case, it might be desirable to consider guiding the bearings at each support toward the fixed point(s) on Pier 2 in order to mitigate the horizontal reactions (Section 2.2.3.2). Another option that might be considered to mitigate the horizontal reactions in this case is presented below.

Similar results would have been obtained had the pier stiffness been ignored altogether in the analysis; that is, if the pier stiffness had been assumed to be infinite. This further demonstrates the importance of recognizing the flexibility of the piers in these analyses.

5.1.6.2.3 Free Elastomeric Bearings

The effect of using all free round elastomeric bearings under each girder in the example bridge is investigated next. Again, the term "free" in this case means no horizontal constraint. An advantage of considering the use of such a bearing arrangement in certain instances would be for the mitigation of horizontal bearing reactions due to thermal loads (Section 2.2.3.4). In essence, these bearings allow the bridge to "float" under nominal horizontal loads (e.g. wind and thermal loads). To handle horizontal constraint under extreme events, such as earthquakes, shear keys can be provided. Such a bearing arrangement would eliminate the need to provide more expensive pot bearings. This approach may not be practical if the bridge were on a significant grade.

The design parameters of the elastomeric bearings at the abutments and piers are summarized in Figure 5.1.12. In the design of the pads, the bridge was assumed to move from the center of its length to the pads. The calculated shear stiffness of the pads in the horizontal direction, GA/h_{rt}, is indicated in Figure 5.1.12. These stiffness values were input in the tangential and radial directions at each bearing in the 3D thermal analysis (i.e. assigned to the foundation elements in the 3D model). *The pier stiffnesses input previously were ignored for this case since the bearings are quite flexible relative to the piers*.

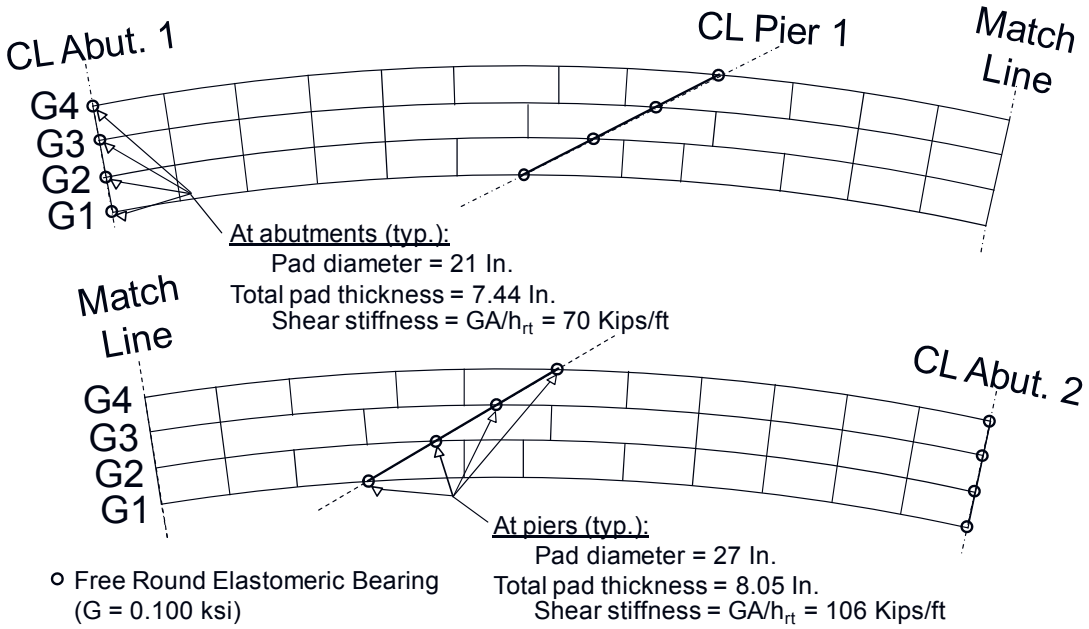


Figure 5.1.12 Free Round Elastomeric Bearings at Each Support in the Example I-Girder Bridge

The vertical and horizontal (longitudinal and transverse) bearing reactions (kips) for a uniform +75°F temperature increase applied to the example bridge for this case are given in Table 5.1.7. The sign convention is again according to the axes shown above the table.

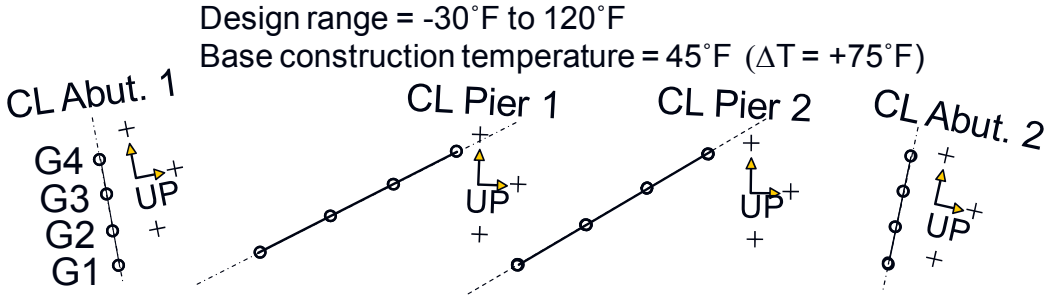


Table 5.1.7 Vertical and Horizontal Bearing Reactions (kips) for a +75°F Uniform Temperature Increase (Free Round Elastomeric Bearings at Each Support – Figure 5.1.12)

	Abutment 1			Pier 1			Pier 2			Abutment 2		
	Vert.	Long.	Trans.	Vert.	Long.	Trans.	Vert.	Long.	Trans.	Vert.	Long.	Trans.
G4	-4.3	8.2	-2.7	-14.7	3.6	-2.3	-8.4	**-6.1**	-3.0	-3.5	-8.2	-2.7
G3	1.3	8.2	-2.4	6.3	4.4	-1.9	2.5	**-5.3**	-2.3	2.0	-8.2	-2.3
G2	1.8	8.2	-2.0	7.4	5.3	-1.4	3.7	**-4.4**	-1.6	2.4	-8.2	-1.9
G1	-7.5	8.1	-1.6	6.4	6.3	-1.0	11.0	**-3.4**	-0.9	-6.4	-8.2	-1.6

The horizontal reactions have been substantially mitigated at Pier 2 (shown in bold in the table); in particular, relative to the preceding case assuming stiff piers (Table 5.1.6). Relatively small horizontal reactions are generated in each direction at each bearing in this case due to the nominal constraint offered by the shear stiffness of the bearings.

The longitudinal and transverse thermal movements of the girders (in.) at each support from the 3D analysis for this case are given in Table 5.1.8. Positive directions of movement are indicated by the axes shown above Table 5.1.7.

Table 5.1.8 Longitudinal and Transverse Thermal Movements (in.) at the Bearings for a +75°F Uniform Temperature Increase (Free Round Elastomeric Bearings at Each Support – Figure 5.1.12)

Movements (Inches)								
	Abutment 1		Pier 1		Pier 2		Abutment 2	
	Long.	Trans.	Long.	Trans.	Long.	Trans.	Long.	Trans.
G4	-1.405	0.470	-0.404	0.268	0.696	0.330	1.406	0.457
G3	-1.403	0.407	-0.500	0.215	0.600	0.253	1.407	0.395
G2	-1.398	0.345	-0.601	0.167	0.497	0.179	1.404	0.332
G1	-1.392	0.282	-0.708	0.114	0.387	0.101	1.400	0.268

Note the overall outward movement of the bridge away from the center of curvature as it “freely” expands in this case. The maximum thermal movements are well within the design horizontal movements of 2.4 inches and 1.7 inches for the bearings at the abutments and piers, respectively.

5.1.7 Limit States

5.1.7.1 Service Limit State

Restrictions on stress and deformation under regular service conditions are specified at the service limit state to ensure satisfactory performance of the bridge over its service life. *AASHTO LRFD* Article 6.10.4.1 specifies that optional live load deflection criteria and span-to-depth ratios (*AASHTO LRFD* Article 2.5.2.6) may be invoked to control deformations.

Steel structures must also satisfy the requirements of *AASHTO LRFD* Article 6.10.4.2 under the Service II load combination (Section 1.3.3). The intent of the design checks specified in *AASHTO LRFD* Article 6.10.4.2 is to prevent objectionable permanent deformations, caused by localized yielding, potential web bend-buckling and connection slip under expected severe traffic loadings, which might impair rideability.

Service limit state verifications are discussed in more detail in Section 3.2.4.

5.1.7.2 Fatigue and Fracture Limit State

Restrictions on stress range under regular service conditions are specified at the fatigue and fracture limit state to control crack growth under repetitive loads and to prevent fracture during the design life of the bridge (*AASHTO LRFD* Article 6.6.1). Material toughness requirements are also addressed (*AASHTO LRFD* Article 6.6.2).

The fatigue load (Section 1.3.2.3.3) and Fatigue load combinations (Section 1.3.3) apply for checking fatigue in steel structures. Fatigue resistance of details is discussed in *AASHTO LRFD* Article 6.6. A special fatigue requirement for webs (*AASHTO LRFD* Article 6.10.5.3) is also specified to control out-of-plane flexing of the web that might potentially lead to fatigue cracking under repeated live loading.

Fatigue and fracture limit state verifications are discussed in more detail in Section 3.2.5.

5.1.7.3 Strength Limit State

At the strength limit state, it must be ensured that adequate strength and stability is provided to resist the load combinations the bridge is expected to experience over its design life. Structural damage may occur, but overall structural integrity is maintained. The applicable Strength load combinations (Section 1.3.3) are used to check the strength limit state.

Although not specified as a separate limit state, constructibility is one of the basic design objectives of LRFD. The bridge must be safely erected and have adequate strength and stability during all phases of construction. Specific design provisions are given in *AASHTO LRFD* Article 6.10.3 to help ensure constructibility of steel

I-girder bridges. The constructibility checks are typically made on the steel section only under the factored non-composite dead loads using the appropriate strength load combinations.

Strength limit state verifications and constructibility verifications are discussed in more detail in Sections 3.2.6 and 3.2.3, respectively.

5.1.7.4 Extreme Event Limit State

At the extreme event limit state, structural survival of the bridge must be ensured during a major earthquake or flood, or when struck by a vessel, vehicle, or ice flow. Extreme event limit states are not covered in this example.

5.1.8 Sample Design Calculations

Sample design calculations at critical sections of G4 from the example I-girder bridge follow. The calculations are intended to illustrate the application of some of the more significant design verifications contained in *AASHTO LRFD* Article 6.10, including design verifications to be made at the service, fatigue and strength limit states. Detailed constructibility verifications are also illustrated. Also included are the shear connector design, transverse web and bearing stiffener designs, a cross-frame member design and a bolted field splice design.

The calculations make use of the unfactored vertical bending moments and vertical shears in G4 from the 3D analysis of the example bridge presented in Section 5.1.6.1. In the calculation of the vertical bending stresses, compressive stresses are shown as negative values and tensile stresses are shown as positive values. The signs of the section moduli are adjusted accordingly to provide the expected sign of the calculation result, in which the sign of the vertical bending moment is maintained.

5.1.8.1 Constructibility Verifications

5.1.8.1.1 Deck Placement Analysis

5.1.8.1.1.1 General

Deck placement analysis is discussed in Section 3.2.3.2. During the deck placement, parts of the girders become composite in sequential stages. Temporary moments induced in the girders during the deck placement can be significantly larger than the final non-composite dead load moments after the sequential placement is complete. A separate 3D analysis was conducted to determine the maximum moments in the girders of the example bridge caused by the assumed deck placement sequence shown in Figure 5.1.13.

Since the differential dead load deflections between the girders are relatively small in this case, the finishing machine is assumed aligned normal (radial) to the girders in order to reduce the length of the machine.

AASHTO LRFD Article 6.10.3.4 requires that changes in the stiffness during the various stages of the deck placement be considered. Therefore, in the analysis, the first cast of the deck is assigned to the non-composite model. Subsequent casts are assumed placed with the concrete in preceding casts assumed hardened and acting compositely with the girders. Should the deck not be cast in separate stages, but instead be cast from one end of the bridge to the other, the end span must still be checked for the critical instantaneous unbalanced case where wet concrete exists over the end span, with no concrete cast yet on the remaining spans.

5.1.8.1.1.2 Deck Placement Analysis Results

Vertical Bending Moments

Unfactored vertical dead load bending moments in each span of the outside G4 from the example bridge (at the cross-frames), including the moments resulting from each individual deck cast, are summarized in Table 5.1.9. The moments due to each

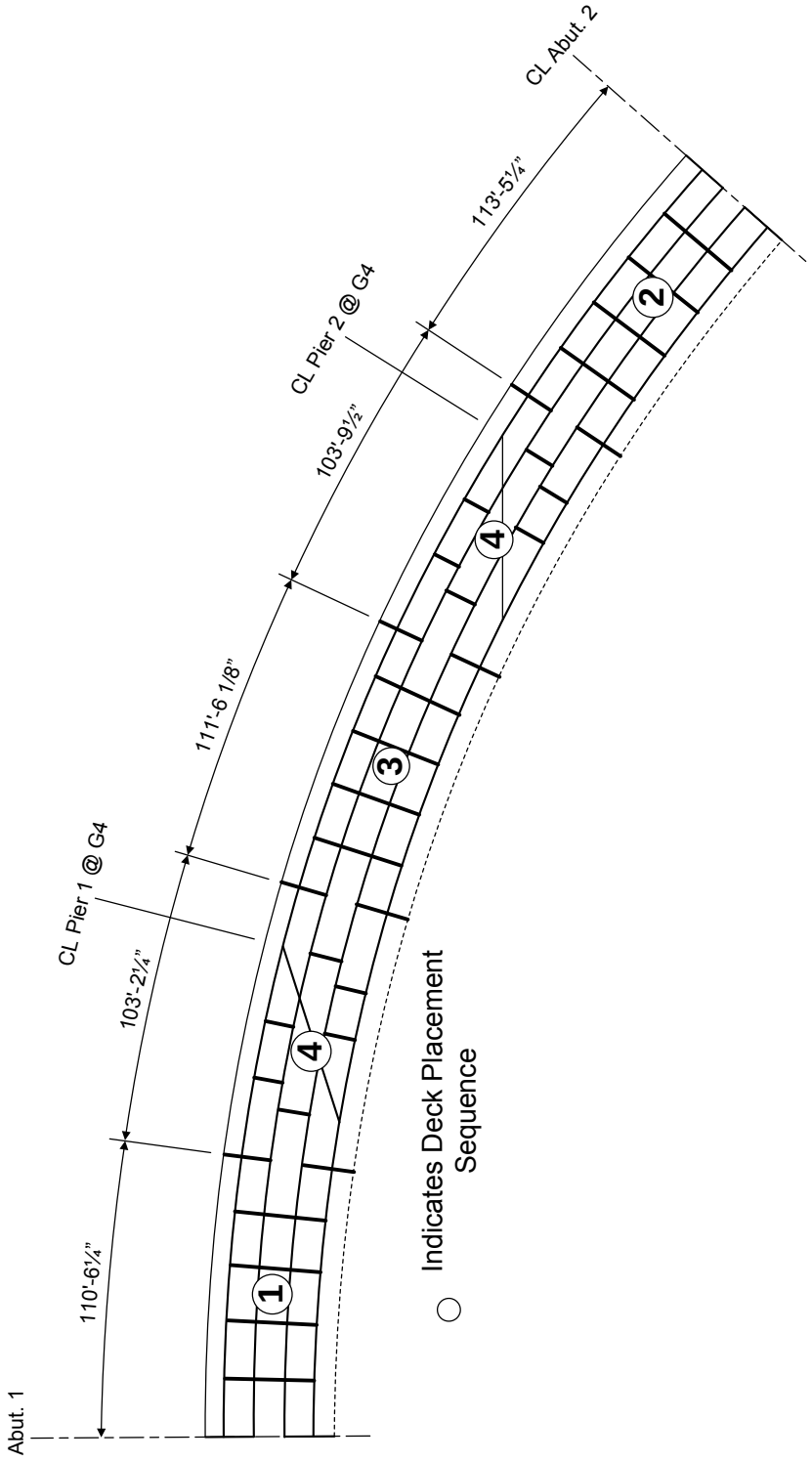


Figure 5.1.13 Assumed Deck Placement Sequence for the Example I-Girder Bridge

deck cast include the moments due to the weight of the stay-in-place (SIP) forms. The assumed weight of the SIP forms includes the weight of the concrete in the form flutes. Although the forms are initially empty, the weight of the deck reinforcement is essentially equivalent to the weight of the concrete in the form flutes.

Table 5.1.9 also gives the moments due to the steel weight, the sum of the moments due to the four casts plus the weight of the SIP forms, the maximum accumulated positive moments during the sequential deck casts (not including the steel weight), and the moments due to the weight of the concrete deck, haunches and SIP forms assuming that the concrete is placed all at once on the non-composite girders.

The slight differences in the moments for each span on the last line of Table 5.1.9 and the accumulated moments due to the four casts plus the weight of the SIP forms are due to the changes in the girder stiffness with each cast. The principle of superposition does not apply directly in the deck-placement analyses since the girder stiffness changes at each step of the analysis. However, note the significant differences between the moments on the last line and the maximum accumulated positive moments during the sequential deck casts. In regions of positive flexure, the non-composite girder should be checked for the effect of this larger maximum accumulated deck-placement moment.

The accumulated positive moment at the critical section in each span is shown in bold in Table 5.1.9, along with the moment due to the steel weight at that section. At the critical section in Span 3 (at the cross-frame located 68.063 ft from Pier 2), the sum of these moments is computed as:

$$M = 356 + 4{,}303 = +4{,}659 \quad \text{kip} - \text{ft}$$

Table 5.1.9 Unfactored Vertical Dead Load Bending Moments (kip-ft) in G4 from the Deck Placement Analysis

Girder 4 Span 1 Unfactored Dead Load Moments at Cross-Frames (kip-feet)									
Length (ft)	0.0	22.104	44.21	66.313	88.42	110.52	140.52	163.57	191.41
Steel Weight	0.	615.	991.	**1083.**	904.	529.	-434.	-1228.	-2643.
Cast									
1	0.	2378.	3904.	4392.	3887.	2746.	278.	-1178.	-2948.
2	0.	153.	285.	378.	458.	640.	887.	1007.	1098.
3	0.	-602.	-1127.	-1511.	-1834.	-2503.	-3373.	-3775.	-4083.
4	0.	198.	374.	517.	662.	928.	525.	-622.	-2635.
Sum of Casts + SIP	0.	2127.	3436.	3776.	3173.	1811.	-1683.	-4568.	-8568.
Max +M	0.	2531.	4189.	**4770.**	4345.	3386.	1165.	0.	0.
Deck, haunches + SIP	0.	2113.	3403.	3715.	3071.	1642.	-1849.	-4579.	-8717.

Girder 4 Span 2 Unfactored Dead Load Moments at Cross-Frames (kip-feet)										
Length (ft)	0.0	22.302	44.604	66.906	89.208	111.51	133.81	163.81	187.06	214.92
Steel Weight	-2643.	-1368.	-507.	161.	518.	**593.**	479.	-67.	-590	-1582.
Cast										
1	-2948.	-2859.	-2745.	-2015.	-1289.	-680.	-225.	424.	757.	1093.
2	1098.	588.	68.	-320.	-614.	-876.	-1223.	-1553.	-1657.	-1643.
3	-4083	-612.	2200.	3486.	3750.	3148.	1819.	-997.	-2517.	-4260.
4	-2635	-1833.	-1207.	-556.	-44.	389.	965.	1048.	226.	-1679.
Sum of Casts + SIP	-8568	-4716.	-1684.	595.	1803.	1981.	1336.	-1078.	-3191.	-6489.
Max +M	0.	0.	0.	1151.	1847.	**1981.**	1336.	424.	757.	1093.
Deck, haunches + SIP	-8717	-4655.	-1575.	841.	2086.	2277.	1724.	-506.	-2497.	-5752.

Girder 4 Span 3 Unfactored Dead Load Moments at Cross-Frames (kip-feet)							
Length (ft)	0.0	22.688	45.375	68.063	90.75	113.438	136.13
Steel Weight	-1582.	-645.	-50.	**356.**	487.	354.	0.
Cast							
1	1093.	1078.	1022.	742.	469.	229.	0.
2	-1643.	913.	2853.	3561.	3264.	2048.	0.
3	-4260.	-4110.	-3621.	-2644.	-1695.	-830.	0.
4	-1679.	-1168.	-856.	-535.	-294.	-131.	0.
Sum of Casts + SIP	-6489.	-3287.	-602.	1124.	1744.	1316.	0.
Max +M	1093.	1991.	3875.	**4303.**	3733.	2277.	0.
Deck, haunches + SIP	-5752.	-2474.	-156.	1431.	1925.	1393.	0.

Vertical Deflections

Unfactored vertical dead load deflections in each span of G4 (at the cross-frames), including the deflections resulting from each individual deck cast, are summarized in similar fashion in Table 5.1.10. Deflections due to DC_2 loads are shown; deflections due to the wearing surface load, DW, are not reported. Negative values are downward deflections and positive values are upward deflections.

Table 5.1.10 Unfactored Vertical Dead Load Deflections (in.) of G4 from the Deck Placement Analysis

Girder 4 Span 1 Unfactored Dead Load Deflections at Cross-Frames (inches)									
Length (ft)	0.0	22.104	44.21	66.313	88.42	110.52	140.52	163.57	191.41
Steel Weight	0.	-0.55	-0.97	-1.18	-1.18	-0.98	-0.50	-0.23	0.
Cast									
1	0.	-2.44	-4.37	-5.52	-5.79	-5.24	-3.35	-1.92	0.
2	0.	-0.24	-0.47	-0.66	-0.80	-0.89	-0.77	-0.51	0.
3	0.	0.94.	1.82	2.56	3.12	3.46	2.98	1.99	0.
4	0.	-0.27	-0.52	-0.71	-0.85	-0.90	-0.65	-0.36	0.
Sum of Casts + SIP	0.	-2.00	-3.54	-4.34	-4.31	-3.56	-1.78	-0.80	0.
DC_2	0.	-0.24	-0.42	-0.52	-0.54	-0.48	-0.28	-0.14	0.
Total	0.	-2.79	-4.92	-6.04	-6.03	-5.03	-2.56	-1.17	0.
Deck, haunches + SIP	0.	-1.80	-3.16	-3.84	-3.76	-3.05	-1.43	-0.58	0.

Girder 4 Span 2 Unfactored Dead Load Deflections at Cross-Frames (inches)										
Length (ft)	0.0	22.302	44.604	66.906	89.208	111.51	133.81	163.81	187.06	214.92
Steel Weight	0.	-0.03	-0.19	-0.45	-0.67	-0.77	-0.71	-0.41	-0.20	0.
Cast										
1	0.	1.37	2.47	3.03	3.06	2.73	2.18	`1.23	0.67	0.
2	0.	0.53	1.12	1.71	2.21	2.55	2.64	2.13	1.40	0.
3	0.	-2.02	-4.11	-5.75	-6.52	-6.34	-5.33	-3.02	-1.60	0.
4	0.	0.08	-0.01	-0.21	-0.47	-0.73	-0.92	-0.82	-0.50	0.
Sum of Casts + SIP	0.	-0.04	-0.54	-1.23	-1.73	-1.80	-1.43	-0.48	-0.03	0.
DC_2	0.	-0.01	-0.08	-0.19	-0.31	-0.38	-0.38	-0.26	-0.14	0.
Total	0.	-0.08	-0.81	-1.87	-2.71	-2.94	-2.53	-1.15	-0.37	0.
Deck, haunches + SIP	0.	-0.24	-0.95	-1.93	-2.73	-3.01	-2.71	-1.49	-0.69	0.

Girder 4 Span 3 Unfactored Dead Load Deflections at Cross-Frames (inches)							
Length (ft)	0.0	22.688	45.375	68.063	90.75	113.438	136.13
Steel Weight	0.	-0.01	-0.10	-0.22	-0.25	-0.17	0.
Cast							
1	0.	-0.44	-0.74	-0.80	-0.64	-0.36	0.
2	0.	-1.39	-2.66	-3.28	-2.96	-1.76	0.
3	0.	0.89	1.30	1.34	1.06	0.58	0.
4	0.	0.25	0.36	0.36	0.28	0.15	0.
Sum of Casts + SIP	0.	-0.70	-1.73	-2.38	-2.26	-1.38	0.
DC_2	0.	0.02	0.00	-0.04	-0.06	-0.05	0.
Total	0.	-0.68	-1.83	-2.64	-2.58	-1.60	0.
Deck, haunches + SIP	0.	-0.05	-0.46	-0.92	-1.05	-0.70	0.

In the analysis, since the concrete does not have enough time to creep significantly between casts, the stiffness of previously cast portions of the deck is based on a modular ratio closer to the short-term modular ratio in computing the moments, deflections and reactions shown for Casts 2, 3 and 4 in Table 5.1.9, Table 5.1.10,

and Table 5.1.11 (note that the effect of this on the moments and reactions is relatively insignificant). A stiffness based on a concrete modulus of elasticity equal to 70 percent of the modulus of elasticity at 28 days (which results in a modular ratio of approximately 1.4*n*) is assumed, which has been found appropriate by at least one State DOT. For the computation of the deflections due to the DC_2 loads, a modular ratio of 3*n* is assumed.

Note the differences in the calculated deflections on the last line for each span (which assume the deck is cast all at once on the non-composite structure) and the sum of the accumulated deflections during the sequential deck casts. As creep of the concrete occurs over time, the accumulated deflections will tend to move toward the values reported on the last line, but they will not likely attain those values. Thus, if the differences in the deflections are deemed significant, e.g. for longer-span bridges, the Design Engineer may need to evaluate which set of deflections should be used, or else perhaps estimate deflections somewhere in-between to compute the girder cambers and avoid potential errors in the final girder elevations.

Vertical Reactions

The unfactored vertical dead load reactions for G4 and for G1 resulting from the deck-placement analysis are given in Table 5.1.11. Negative reactions represent upward reactions that resist the maximum downward force at the support under consideration. Conversely, positive reactions represent downward reactions that resist the maximum uplift force at the support.

For the investigation of uplift at critical construction stages, it is suggested that a load factor of 1.0 be applied to all downward (positive) support reactions due to component dead loads causing uplift, and a load factor of 0.9 be applied to all upward (negative) support reactions due to component dead loads resisting uplift.

Table 5.1.11 Unfactored Vertical Dead Load Reactions (kips) for G4 and G1 from the Deck Placement Analysis

Girder 4 Vertical Reactions (kips)	Abutment 1	Pier 1	Pier 2	Abutment 2
Steel Weight	-33.0	-108.0	-81.0	-20.0
sum	-33.0	-108.0	-81.0	-20.0
Cast 1	-121.0	-39.0	3.0	-10.0
sum	-154.0	-147.0	-78.0	-30.0
Cast 2	-8.0	20.0	-100.0	-105.0
sum	-162.0	-127.0	-178.0	-135.0
Cast 3	32.0	-133.0	-37.0	36.0
sum	-130.0	-260.0	-215.0	-99.0
Cast 4	-10.0	-130.0	-105.0	6.0
sum	-140.0	-390.0	-320.0	-93.0
Sum of Casts + SIP Forms	-107.0	-282.0	-239.0	-73.0
DC_2 + DW	-48.0	-146.0	-122.0	-31.0
Total	-188.0	-536.0	-442.0	-124.0
Deck, haunches + SIP Forms	-109.0	-291.0	-246.0	-77.0
Total	-190.0	-545.0	-444.0	-128.0

Girder 1 Vertical Reactions (kips)	Abutment 1	Pier 1	Pier 2	Abutment 2
Steel Weight	-13.0	-75.0	-112.0	-25.0
sum	-13.0	-75.0	-112.0	-25.0
Cast 1	-62.0	-67.0	1.0	1.0
sum	-75.0	-142.0	-111.0	-24.0
Cast 2	-1.0	26.0	-75.0	-75.0
sum	-76.0	-116.0	-186.0	-99.0
Cast 3	3.0	-110.0	-133.0	1.0
sum	-73.0	-226.0	-319.0	-98.0
Cast 4	8.0	-104.0	-136.0	-10.0
sum	-65.0	-330.0	-455.0	-108.0
Sum of Casts + SIP Forms	-52.0	-255.0	-343.0	-83.0
DC_2 + DW	-22.0	-113.0	-150.0	-39.0
Total	-87.0	-443.0	-605.0	-147.0
Deck, haunches + SIP Forms	-50.0	-257.0	-344.0	-83.0
Total	-85.0	-445.0	-606.0	-147.0

Shown in Table 5.1.11 (under 'sum') are the accumulated vertical reactions for the steel weight plus the individual deck casts, which should be used to check for uplift under the deck placement. A net positive reaction indicates that the girder may lift-off at the support. Due to the reasonably balanced span arrangement along the bridge centerline, lift-off does not occur in any of the girders in this particular example. If the girder is permitted to lift-off its bearing seat, the staging analysis is incorrect unless a hold-down of the girder is provided at the location of a positive reaction.

Options to consider when uplift occurs include: 1) rearranging the concrete casts; 2) modifying the framing; 3) specifying a temporary load over that support; 4) specifying a tie-down bearing; 5) removing the bearing; or 6) if the uplift can be tolerated,

performing another staging analysis with zero bearing stiffness at the support experiencing lift-off to obtain the correct moments and deflections.

Note in this case that the sum of the reactions from the analysis of the staged deck casts differs somewhat from the reactions assuming the deck is cast all at once on the non-composite structure (as given on the next-to-last line of Table 5.1.11); however, it is usually reasonable to ignore these differences and use the reactions as shown on the last line of the table in the design.

Vertical Bending Stress

Calculate the maximum factored dead load vertical bending stress in the top flange of the non-composite steel section at the critical section in Span 3 of Girder 4 (at the cross-frame located 68.063 feet from Pier 2 – Figure 5.1.14) resulting from the deck-placement sequence (refer to the fold-out sheets at the end of this example).

The top flange in regions of positive flexure is most always the critical flange for the constructibility checks. The Strength IV load combination (Section 1.3.3) is considered for the constructibility checks in this example. The load modifier η is taken equal to 1.0. Section properties for the bare steel girder at this section are computed as follows:

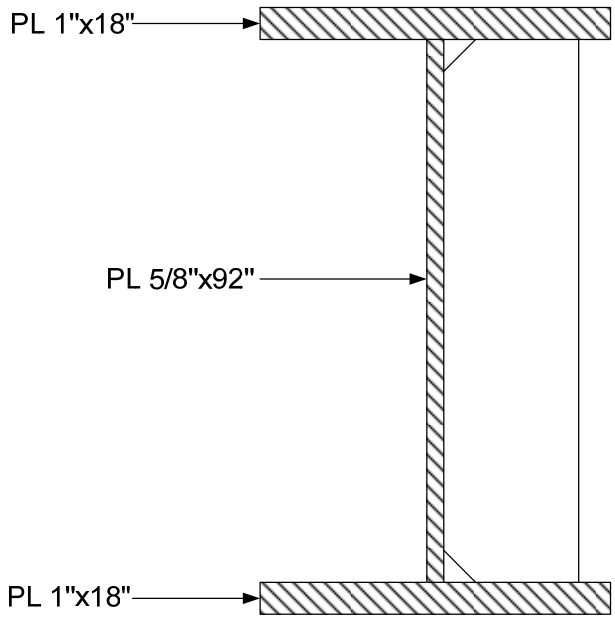


Figure 5.1.14 G4, Span 3, Section at 68.063 Feet from Pier 2

Component	A	d	Ad	Ad^2	I_o	I
Top Flange 1" x 18"	18.00	46.50	837.0	38,921	1.50	38,923
Web 5/8" x 92"	57.50				40,557	40.557
Bottom Flange 1″ x 18"	18.00	–46.50	-837.0	38,921	1.50	38,923
	93.50		0.0		I_{NA} =	118,403 in.^{4}

$d_{TOP\ OF\ STEEL} = 47.00$ in.

$S_{TOP\ OF\ STEEL} = \frac{118{,}403}{-47.00} = -2{,}519$ in.^{3}

$d_{BOT\ OF\ STEEL} = 47.00$ in.

$S_{BOT\ OF\ STEEL} = \frac{118{,}403}{47.00} = 2{,}519$ in.^{3}

For Strength IV:

$$\text{Top flange: } f_{bu} = \frac{1.0(1.5)(4{,}659)(12)}{-2{,}519} = -33.29 \text{ ksi}$$

5.1.8.1.2 Deck Overhang Loads

Deck overhang loads are discussed in Section 3.2.3.3. The deck overhang bracket configuration shown in Figure 5.1.15 is assumed for this example. The brackets extend to the bottom flange, which is preferred. Alternatively, the brackets may bear on the girder web if means are provided to ensure that the web is not damaged and that the associated deformations permit proper placement of the concrete deck.

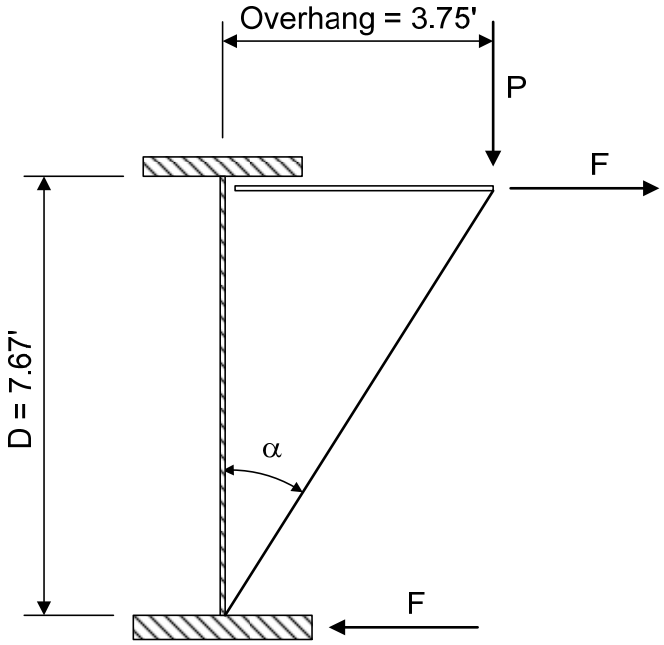


Figure 5.1.15 Assumed Deck Overhang Bracket Configuration for the Example I-Girder Bridge

Although the brackets are typically spaced at 3 to 4 feet along the fascia girder, all bracket loads except for the finishing machine load are assumed applied uniformly.

Calculate the vertical loads acting on the overhang brackets. Because in this case the bracket is assumed to extend near the edge of the deck overhang, assume as an approximation that half the deck overhang weight is placed on the fascia girder and half the weight is placed on the overhang brackets. Conservatively include one-half the deck haunch weight in the total overhang weight. Therefore:

Deck Overhang Weight:

$$P = 0.5 * 150\left[\frac{9.5}{12}(3.75) + \left[\frac{1}{12}\left(\frac{3.5}{2} + 0.5\right)\left(3.75 - \frac{20/2}{12}\right)\right] + \frac{3.00}{12}\left(\frac{20/2}{12}\right)\right] = 279 \text{ lbs / ft}$$

The other half of the overhang weight can be assumed to act at the edge of the top flange (at a distance of 9.0 inches from the shear center of the girder in this case). The effective deck weight acting on the other side of the girder can be assumed applied at the other edge of the top flange. The net torque can be resolved into flange lateral moments that generally act in the opposite direction to the lateral moments caused by the overhang loads. This effect is conservatively neglected in this example.

Construction loads, or dead loads and temporary loads that act on the overhang only during construction, are assumed as follows:

- Overhang deck forms: P = 40 lbs/ft
- Screed rail: P = 85 lbs/ft
- Railing: P = 25 lbs/ft
- Walkway: P = 125 lbs/ft
- Finishing machine P = 3000 lbs

The finishing machine load is estimated as one-half of the total finishing machine truss weight, plus some additional load to account for the weight of the engine, drum and operator assumed to be located on one side of the truss. For checking the Strength IV load combination, however, the finishing machine is considered to be a transient live load and so it is not considered further in this check (since the Strength IV load combination only considers dead loads). Note that the above loads are estimated loads used here for illustration purposes only. It is recommended that the Engineer consider talking to local Contractors to obtain more accurate values for these construction loads.

Referring to Figure 5.1.15, the lateral force on the top flange due to the vertical load on the overhang brackets is computed as:

$$F = P \tan\alpha \cong P\left(\frac{\text{Overhang}}{D}\right)$$

The equations given in *AASHTO LRFD* Article C6.10.3.4 may be used to estimate the maximum flange lateral bending moments in the flanges due to the lateral bracket forces in lieu of a more refined analysis. Assuming the flanges are continuous with the adjacent unbraced lengths and that the adjacent unbraced lengths are approximately equal, the lateral bending moment due to a statically equivalent uniformly distributed lateral bracket force may be estimated as (Equation 3.2.15):

$$M_\ell = \frac{F_\ell L_b^2}{12}$$

Lateral bending stresses determined from a first-order analysis may be used in discretely braced compression flanges for which the unbraced length between cross-frames, L_b, satisfies Equation 3.2.8 as follows:

$$L_b \le 1.2 L_p \sqrt{\frac{C_b R_b}{f_{bu}/F_{yc}}}$$

L_b containing the critical section is equal to 22.6875 feet. L_p is the limiting unbraced length for lateral torsional buckling specified in *AASHTO LRFD* Article 6.10.8.2.3 determined as (Equation 3.2.94):

$$L_p = 1.0 r_t \sqrt{\frac{E}{F_{yc}}}$$

where r_t is the effective radius of gyration for lateral torsional buckling specified in *AASHTO LRFD* Article 6.10.8.2.3 determined as (Equation 3.2.97):

$$r_t = \frac{b_{fc}}{\sqrt{12\left(1 + \frac{1}{3}\frac{D_c t_w}{b_{fc} t_{fc}}\right)}}$$

For the steel section, the depth of the web in compression in the elastic range, D_c, at this section = 92.0/2 = 46.00 inches. Therefore,

$$r_t = \frac{18}{\sqrt{12\left(1 + \frac{1}{3}\frac{46.00(0.625)}{18(1.0)}\right)}} = 4.20 \text{ in.}$$

$$L_p = \frac{1.0(4.20)}{12}\sqrt{\frac{29{,}000}{50}} = 8.43 \text{ ft}$$

C_b is the moment gradient modifier specified in *AASHTO LRFD* Article 6.10.8.2.3 (Section 3.2.6.4.1.2). Since the moment gradient is not significant in this region, C_b will be conservatively taken equal to 1.0. According to *AASHTO LRFD* Article 6.10.1.10.2, the web load-shedding factor, R_b (Section 3.2.6.2), is to be taken equal to 1.0 when checking constructibility since web bend buckling is prevented during construction by a separate limit state check (illustrated below).

AASHTO LRFD Article 6.10.1.6 specifies that f_{bu} in *AASHTO LRFD* Equation 6.10.1.6-2 (Equation 3.2.8) is to be taken as the largest value of the compressive major-axis bending stress throughout the unbraced length under consideration, which in this case is at the location under consideration. Therefore:

$$1.2(8.43)\sqrt{\frac{(1.0)(1.0)}{(-33.29)/(50)}} = 12.40 \text{ ft} < L_b = 22.6875 \text{ ft}$$

Because the preceding equation is not satisfied, *AASHTO LRFD* Article 6.10.1.6 requires that second-order elastic compression-flange lateral bending stresses be determined. The second-order compression-flange lateral bending stresses may be determined by amplifying first-order values (i.e., $f_{\ell 1}$) as follows (Equation 3.2.9):

$$f_\ell = \left(\frac{0.85}{1-\frac{f_{bu}}{F_{cr}}}\right) f_{\ell 1} \geq f_{\ell 1}$$

or:

$$f_\ell = (AF) f_{\ell 1} \geq f_{\ell 1}$$

where *AF* is the amplification factor (note that *AF* is taken equal to 1.0 for tension flanges). F_{cr} is the elastic lateral torsional buckling stress for the flange under consideration specified in *AASHTO LRFD* Article 6.10.8.2.3 determined as (Equation 3.2.96):

$$F_{cr} = \frac{C_b R_b \pi^2 E}{\left(\frac{L_b}{r_t}\right)^2}$$

$$F_{cr} = \frac{1.0(1.0)\pi^2(29{,}000)}{\left(\frac{22.6875(12)}{4.20}\right)^2} = 68.12 \text{ ksi}$$

The calculated value of F_{cr} for use in *AASHTO LRFD* Equation 6.10.1.6-4 (Equation 3.2.9) is not limited to $R_bR_hF_{yc}$ (refer to *AASHTO LRFD* Article C6.10.1.6).

f_{bu} in *AASHTO LRFD* Equation 6.10.1.6-4 (Equation 3.2.9) is again to be taken as the largest value of the compressive major-axis bending stress throughout the unbraced length under consideration. The amplification factor is therefore determined as follows:

$$AF = \frac{0.85}{\left(1 - \frac{|-33.29|}{68.12}\right)} = 1.66 > 1.0 \quad \text{ok}$$

Calculate the factored first-order lateral flange bending stress in the top flange due to the deck overhang loads

- Dead loads:

$$P = 1.0\left[1.5(279 + 40 + 85 + 25 + 125)\right] = 831 \text{ lbs/ft}$$

$$F = F_\ell = P\left(\frac{\text{Overhang}}{D}\right) = 831\left(\frac{3.75}{7.67}\right) = 406 \text{ lbs/ft}$$

$$M_\ell = \frac{F_\ell L_b^2}{12} = \frac{(0.406)(22.6875)^2}{12} = 17.41 \text{ kip-ft}$$

$$f_\ell = \frac{M_\ell}{S_\ell} = \frac{(17.41)(12)}{(1.0)\left(\frac{(18)^2}{6}\right)} = 3.87 \text{ ksi}$$

- Finishing machine: Not considered for Strength IV

AASHTO LRFD Article 6.10.1.6 specifies that for design verifications where the flexural resistance is based on lateral torsional buckling, the vertical bending stress, f_{bu}, and the flange lateral bending stress, f_ℓ, are to be determined as the largest values throughout the unbraced length in the flange under consideration. For design verifications where the flexural resistance is based on yielding or flange local

buckling, f_{bu} and f_ℓ may be determined as the stresses at the section under consideration. For simplicity in this example, the largest values of f_{bu} and f_ℓ within the unbraced length will conservatively be used in all design checks.

The unfactored lateral flange bending moments in the top flange due to DC_1 (i.e. steel weight, total deck plus deck haunch weight and SIP form weight) at selected cross-frames in Span 3 of Girder 4 *resulting from both curvature and skew effects* (taken directly from the 3D analysis results) are as follows:

- 45.375 ft from Pier 2: 2 kip-ft
- 68.063 ft from Pier 2: 10 kip-ft
- 90.75 ft from Pier 2: 14 kip-ft

Strictly speaking, only the top flange lateral moments due to the steel & SIP form weight plus the first two casts would need to be considered; the lateral moments due to Casts 3 and 4 could potentially be ignored since the top flange at the critical section in Span 3 is assumed continuously braced for the succeeding casts. However, this refinement is ignored here for simplicity.

The largest lateral bending moment within the unbraced length adjacent to the section under consideration is 14 kip-ft. The factored lateral bending stress due to curvature and skew effects is therefore computed as:

$$f_\ell = \frac{M_\ell}{S_\ell} = \frac{1.5(14)(12)}{1.0(18)^2/6} = 4.67 \text{ ksi}$$

In the case of G4, in regions of positive flexure, the top-flange lateral bending moments at the cross-frames due to the overhang loads act in the same sense as the lateral bending moments at the cross-frames due to the curvature and skew effects taken directly from the 3D analysis. That is, the lateral moments in each case act to restrain the outward bowing of the top flange caused by these effects. Thus, the lateral bending stresses are additive.

In the case of G1, the top-flange lateral bending moments due to the overhang loads act in the opposite direction to the lateral bending moments due to the curvature and skew effects in regions of positive flexure. This must be considered when summing the lateral bending stresses when checking the top flange of G1 in these regions.

In the following, the factored top flange lateral bending stresses due to the overhang bracket loads and due to curvature and skew effects are summed and the amplification factor is applied:

$$f_\ell \text{ total} = (3.87 + 4.67)\text{AF} = (8.54 \text{ ksi})(1.66) = 14.18 \text{ ksi}$$

First- or second-order flange lateral bending stresses, as applicable, due to all sources are limited to a maximum value of $0.6F_{yf}$ according to *AASHTO LRFD* Equation 6.10.1.6-1:

$$14.18 \text{ ksi} < 0.6F_y = 0.6(50) = 30 \text{ ksi} \quad \text{ok} \qquad (\text{Ratio} = 0.473)$$

5.1.8.1.3 Flexure Verifications

Constructibility design verifications for flexure of I-sections are specified in *AASHTO LRFD* Article 6.10.3.2 and discussed in Section 3.2.3.4.1.2. For critical stages of construction, *AASHTO LRFD* Article 6.10.3.2.1 requires that discretely braced flanges in compression satisfy requirements to prevent nominal yielding at the flange tips, flange local buckling, lateral torsional buckling and web bend buckling.

In the interest of brevity, only the top flange is checked, as the bottom flange is usually not critical for constructibility verifications.

5.1.8.1.3.1 Flange Tip Yielding (Equation 3.2.18)

$$f_{bu} + f_\ell \le \phi_f R_h F_{yc}$$

$$f_{bu} + f_\ell = \left|-33.29\right| \text{ ksi} + 14.18 \text{ ksi} = 47.47 \text{ ksi}$$

$$\phi_f R_h F_{yc} = 1.0(1.0)(50) = 50.0 \text{ ksi}$$

$$47.47 \text{ ksi} < 50.0 \text{ ksi} \quad \text{ok} \qquad (\text{Ratio} = 0.949)$$

5.1.8.1.3.2 Flange Local Buckling (Equation 3.2.19)

$$f_{bu} + \frac{1}{3} f_\ell \le \phi_f (F_{nc})_{FLB}$$

Determine the slenderness ratio of the top flange:

$$\lambda_f = \frac{b_{fc}}{2t_{fc}}$$

$$\lambda_f = \frac{18}{2(1.0)} = 9.0$$

Determine the limiting slenderness ratio for a compact flange from Equation 3.2.87 (alternatively, see *AASHTO LRFD* Table C6.10.8.2.2-1):

$$\lambda_{pf} = 0.38\sqrt{\frac{E}{F_{yc}}}$$

$$\lambda_{pf} = 0.38\sqrt{\frac{29{,}000}{50}} = 9.15$$

Since $\lambda_f < \lambda_{pf}$, the nominal local buckling resistance $(F_{nc})_{FLB}$ is taken as (Equation 3.2.88):

$$(F_{nc})_{FLB} = R_b R_h F_{yc}$$

$$(F_{nc})_{FLB} = 1.0(1.0)(50) = 50.0 \text{ ksi}$$

$$f_{bu} + \frac{1}{3}f_\ell = \left|-33.29\right| \text{ ksi} + \frac{14.18}{3} \text{ ksi} = 38.02 \text{ ksi}$$
$$\phi_f (F_{nc})_{FLB} = 1.0(50.00) = 50.00 \text{ ksi}$$
$$38.02 \text{ ksi} < 50.00 \text{ ksi} \quad \text{ok} \qquad (\text{Ratio} = 0.760)$$

5.1.8.1.3.3 Lateral Torsional Buckling (Equation 3.2.19)

$$f_{bu} + \frac{1}{3}f_\ell \le \phi_f (F_{nc})_{LTB}$$

The limiting unbraced length, L_p, was computed earlier to be 8.43 feet. The effective radius of gyration for lateral torsional buckling r_t for the noncomposite section was also computed earlier to be 4.20 inches.

Determine the limiting unbraced length, L_r, from Equation 3.2.95 as follows:

$$L_r = \pi r_t \sqrt{\frac{E}{F_{yr}}}$$

where:

$$F_{yr} = 0.7F_{yc} \le F_{yw}$$

$$F_{yr} = 0.7(50) = 35.0 \text{ ksi} < 50 \text{ ksi}_{\text{ok}}$$

F_{yr} must also not be less than $0.5F_{yc}$ = 0.5(50) = 25.0 ksi ok.

Therefore:

$$L_r = \frac{\pi(4.20)}{12}\sqrt{\frac{29{,}000}{35.0}} = 31.65 \text{ ft}$$

Since L_p = 8.43 feet < L_b = 22.6875 feet < L_r = 31.65 feet, the nominal lateral torsional buckling resistance is taken as (Equation 3.2.92):

$$(F_{nc})_{LTB} = C_b\left[1-\left(1-\frac{F_{yr}}{R_h F_{yc}}\right)\left(\frac{L_b - L_p}{L_r - L_p}\right)\right]R_b R_h F_{yc} \le R_b R_h F_{yc}$$

Therefore:

$$(F_{nc})_{LTB} = 1.0\left[1-\left(1-\frac{35.0}{1.0(50)}\right)\left(\frac{22.6875-8.43}{31.65-8.43}\right)\right](1.0)(1.0)(50) = 40.79 \text{ ksi} < 1.0(1.0)(50) = 50 \text{ ksi}$$

$$f_{bu} + \frac{1}{3}f_\ell = \left|-33.29\right| \text{ ksi} + \frac{14.18}{3}\text{ksi} = 38.02 \text{ ksi}$$

$$\phi_f (F_{nc})_{LTB} = 1.0(40.79) = 40.79 \text{ ksi}$$

$$38.02 \text{ ksi} < 40.79 \text{ ksi} \quad \text{ok} \qquad (\text{Ratio} = 0.932)$$

5.1.8.1.3.4 Web Bend Buckling (Equation 3.2.20)

$$f_{bu} \le \phi_f F_{crw}$$

Determine the nominal web bend-buckling resistance, F_{crw}, according to the provisions of *AASHTO LRFD* Article 6.10.1.9.1 as follows (Equation 3.2.35):

$$F_{crw} = \frac{0.9Ek}{\left(\frac{D}{t_w}\right)^2}$$

but not to exceed the smaller of $R_h F_{yc}$ and F_{yw}/0.7, where (Equation 3.2.36):

$$k = \frac{9}{(D_c/D)^2}$$

$$k = \frac{9}{(46.00/92.0)^2} = 36.0$$

Therefore,

$$F_{crw} = \frac{0.9(29{,}000)(36.00)}{\left(\frac{92.0}{0.625}\right)^2} = 43.36 \text{ ksi} < \min\left(R_h F_{yc}, F_{yw}/0.7\right) = R_h F_{yc} = 1.0(50) = 50 \text{ ksi}$$

$$\phi_f F_{crw} = 1.0(43.36) = 43.36 \text{ ksi}$$

$$\left|-33.29\right| \text{ ksi} < 43.36 \text{ ksi} \quad \text{ok} \qquad (\text{Ratio} = 0.768)$$

Options to consider should the web bend-buckling resistance be exceeded include:

- Providing a larger compression flange or a smaller tension flange to decrease D_c
- Adjusting the deck-placement sequence to reduce the compressive stress in the web
- Providing a thicker web
- Adding a longitudinal web stiffener should the preceding options not prove to be practical or cost-effective

5.1.8.1.4 Shear Verifications

AASHTO LRFD Article 6.10.3.3 requires that webs satisfy the following requirement during critical stages of construction (Section 3.2.3.4.1.3 - Equation 3.2.23):

$$V_u \le \phi_v V_{cr}$$

For this example, the panel in G4 immediately to the right of Pier 1 (in Span 2) will be checked. The panel is bounded by the bearing stiffeners at Pier 1 and the cross-frame connection plate located 22.302 feet into Span 2 from Pier 1. The bearing stiffeners and connection plate act as transverse stiffeners. The stiffener spacing of 22.302(12) = 267.6 inches is less than the maximum permitted spacing of d_o = 3D = 3(92.0) = 276.0 inches.

Since shear is rarely increased significantly due to deck staging, the DC_1 shear (i.e. shear due to the steel weight, deck plus deck haunch and SIP forms) at Pier 1 equal to 223.0 kips (Table 5.1.3) will be used in this check. Under the Strength IV load combination, at Pier 1:

$$(V_u)_{DC_1} = 1.0(1.5)(223) = 335 \text{ kips}$$

The shear buckling resistance of the 267.6-inch-long panel is determined as (Equation 3.2.161):

$$V_n = V_{cr} = CV_p$$

C is the ratio of the shear buckling resistance to the shear yield strength determined from *AASHTO LRFD* 6.10.9.3.2-4, 6.10.9.3.2-5 or 6.10.9.3.2-6, as applicable. First, compute the shear buckling coefficient *k* from Equation 3.2.157 as follows:

$$k = 5 + \frac{5}{\left(\frac{d_o}{D}\right)^2}$$

$$k = 5 + \frac{5}{\left(\frac{267.6}{92.0}\right)^2} = 5.59$$

Since,

$$1.40\sqrt{\frac{Ek}{F_{yw}}} = 1.40\sqrt{\frac{29{,}000(5.59)}{50}} = 79.7 < \frac{D}{t_w} = \frac{92.0}{0.625} = 147.2$$

Equation 3.2.158 is used to compute *C* as follows:

$$C = \frac{1.57}{\left(\frac{D}{t_w}\right)^2}\left(\frac{Ek}{F_{yw}}\right)$$

$$C = \frac{1.57}{(147.2)^2}\left(\frac{29{,}000(5.59)}{50}\right) = 0.235$$

V_p is the plastic shear force determined as follows (Equation 3.2.151):

$$V_p = 0.58F_{yw}Dt_w$$

$$V_p = 0.58(50)(92.0)(0.625) = 1{,}668 \text{ kips}$$

Therefore,

$$V_{cr} = 0.235(1{,}668) = 392 \text{ kips}$$

$$\phi_v V_{cr} = 1.0(392) = 392 \text{ kips}$$

$$(V_u)_{DC_1} = 335 \text{ kips} < \phi_v V_{cr} = 392 \text{ kips}$$

ok (Ratio = 0.855)

5.1.8.1.5 Concrete Deck

AASHTO LRFD Article 6.10.2.3.4 requires that the factored longitudinal tensile stress in a composite concrete deck not exceed ϕf_r during critical stages of construction, unless the minimum one-percent longitudinal reinforcement is provided according to the provisions of *AASHTO LRFD* Article 6.10.1.7 (Section 3.2.3.2.5).

f_r is the lower-bound modulus of rupture of the concrete determined as follows for normal weight concrete (*AASHTO LRFD* Article 5.4.2.6 – Equation 3.2.14):

$$f_r = 0.24\sqrt{f'_c} = 0.24\sqrt{4.0} = 0.480 \text{ ksi}$$

ϕ is the appropriate resistance factor for concrete in tension specified in *AASHTO LRFD* Article 5.5.4.2.1. For reinforced concrete in tension, ϕ is equal to 0.90.

$$\phi f_r = 0.90(0.480) = 0.432 \text{ ksi}$$

Check the tensile stress in the concrete deck at the end of Cast 2 in Span 3 over G4 (22.688 feet from Pier 2) caused by the negative moments due to Casts 3 and 4.

From Table 5.1.9, the negative moment at the end of Cast 2 due to Casts 3 and 4 is –4,110 + -1,168 = -5,278 kip-feet. The longitudinal concrete deck stress is to be determined as specified in *AASHTO LRFD* Article 6.10.1.1.1d; that is, using the short-term modular ratio n = 8. The calculated stress on the transformed section is to be divided by n to obtain the stress in the concrete. The composite section properties at this section are determined from separate computations similar to the above. Under the Strength IV load combination:

$$f_{deck} = \frac{1.0(1.5)(-5{,}278)(-31.975)(12)}{377{,}558(8)} = +1.006 \text{ ksi} > 0.432 \text{ ksi}$$

Therefore, the minimum one percent longitudinal reinforcement is required at this section. The reinforcement is to be No. 6 bars or smaller spaced at not more than 12 inches. Extend the longitudinal reinforcement to a section approximately 91.0 feet from Pier 2 (into Span 3) where the tensile stress in the deck drops below 0.432 ksi.

Although not done in this example, a more accurate estimate of the concrete strength at the time Casts 3 and 4 are made, and the resulting modular ratio (e.g. using 1.4*n*), could be used in this check if desired.

5.1.8.1.6 Girder Layovers

Girder layovers (in.) from the 3D analysis at the supports and at selected radial cross-sections in each span due to the dead load of the steel, concrete deck and SIP forms are reported in Table 5.1.12. The girder layover is defined as the relative transverse displacement between the top and bottom flanges resulting from the twist or torsional rotation of the girder (Figure 4.1.24).

Table 5.1.12 Girder Layovers (in.) due to the Weight of the Steel, Deck and SIP Forms

Girder Layovers, in. (Steel+Deck+SIP Forms)								
	Abut. 1 (0.0°)	Span 1 (7.95°)	Pier 1	Span 2 (-) (17.99°)	Span 2 (+) (26.91°)	Pier 2	Span 3 (36.13°)	Abut.2 (43.38°)
Girder 4	0.00	+1.169	-0.144	-0.505	+1.021	+0.007	-0.696	0.00
Girder 3	0.00	+1.178	+0.061	-0.400	+0.692	+0.066	-0.697	0.00
Girder 2	0.00	+0.872	-0.087	-0.608	+0.609	-0.078	-0.686	0.00
Girder 1	0.00	+0.965	-0.337	-0.562	+0.113	-0.224	-0.665	0.00

A positive layover is to the left when looking upstation from the left end of the bridge; a negative layover is to the right. The cross-sections listed for each span were selected as the radial cross-section(s) at which the maximum layover of G4 (positive and/or negative, as applicable) occurred within the span under consideration. The location of each cross-section is indicated in terms of degrees measured clockwise from Abutment 1.

In Span 2, two cross-sections are listed in the table; one where the largest negative layover of G4 occurred and one where the largest positive layover of G4 occurred. The girders are obviously twisting within Span 2.

Utilizing a web depth of 92 inches in this case helped to limit the maximum girder layover within the spans to approximately 1.20 inches (or approximately 5/32 inches per foot). The girder layovers are zero at the abutments because the abutments are radial. The maximum girder layover at the two interior piers is less than 3/8". Therefore, it is unlikely that a Steel Dead Load or Total Dead Load Fit (Section 4.1.3.1.3.2) would be required in this particular case to accommodate the girder layovers, which are deemed reasonable.

However, the bearings at the pier need to be checked for the rotation due to the girder layover. If a Steel Dead Load or Total Dead Load Fit were to be employed, site conditions and/or constraints must be such that it would be possible to twist the girder webs out-of-plumb in the no-load condition. Thus, on the Design Plans, it would be indicated that the girder webs are to be theoretically vertical or plumb in the no-load condition. As a result, the girders will be slightly out-of-plumb under the steel and full dead load conditions.

Although the example bridge is skewed, a rough approximation of the expected maximum girder layover within the spans in a horizontally curved bridge can still be obtained from the equation shown in Figure 5.1.16:

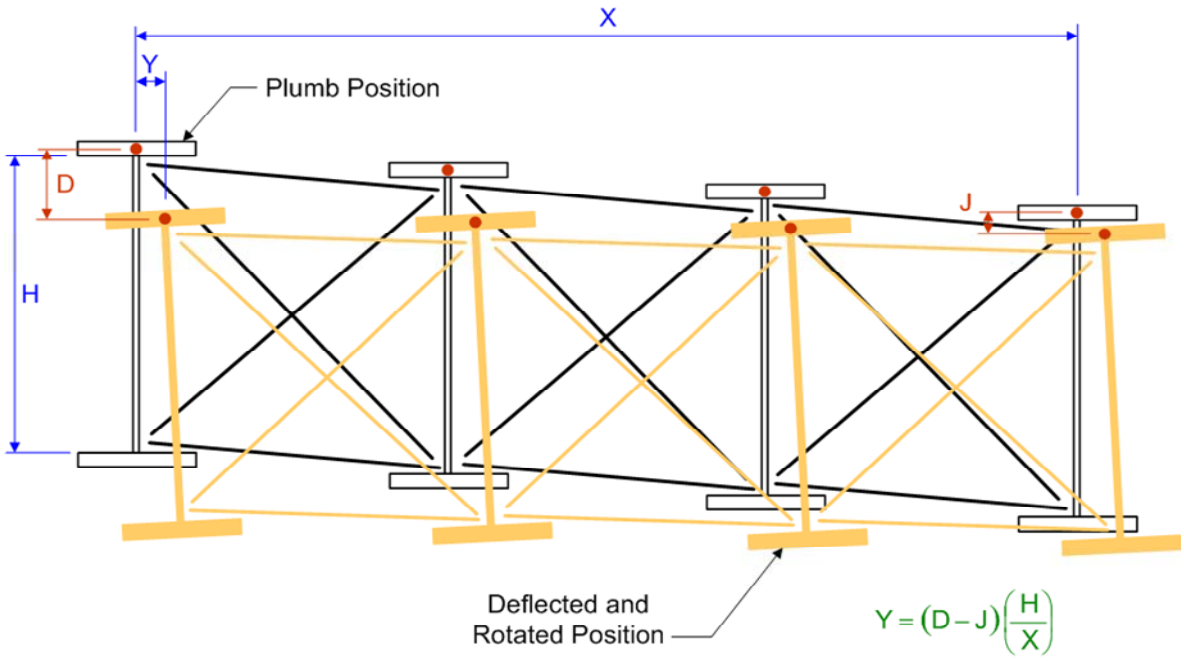


Figure 5.1.16 Approximation of Expected Maximum Girder Layover for a Horizontally Curved Bridge

In this case, *D* is taken as the maximum vertical deflection in Span 1 of G4 due to the dead load of the steel, concrete deck and SIP forms. *J* is taken as the corresponding vertical deflection in Span 1 of G1 at a point projected radially from where *D* is taken. *H* is the web depth and *X* is the spacing between G1 and G4:

D	=	4.57 in.
J	=	0.09 in.
H	=	92 in.
X	=	33 ft. = 396 in.

$$Y = (D - J)\left(\frac{H}{X}\right) = (4.57 - 0.09)\left(\frac{92}{396}\right) = 1.04 \text{ in}$$

5.1.8.2 Service Limit State Verifications

5.1.8.2.1 Live Load Deflections

Live load deflections are discussed in Section 3.2.4.2.1. For control of elastic deformations, *AASHTO LRFD* Article 6.10.4.1 refers back to *AASHTO LRFD* Article 2.5.2.6, which contains optional live load deflection criteria and criteria for span-to-depth ratios. The suggested span-to-depth ratios were utilized earlier in Section 5.1.4.1.1 to establish a reasonable minimum web depth for the example girder design.

The optional live load deflection check consists of evaluating two separate live load conditions (Section 1.3.2.3.4). The two load conditions are (*AASHTO LRFD* Article 3.6.1.3.2):

- The design truck
- The design lane plus 25 percent of the design truck

The dynamic load allowance of 33 percent is applied to the design truck in each case. A load factor of 1.0 is applied to the live load. All design lanes are loaded and the appropriate multiple presence factor is to be applied (i.e. for one lane loaded, m = 1.2; for two lanes loaded; m = 1.0; for three lanes loaded, m = 0.85). For curved-girder bridges, the deflection of each girder must be determined individually based on its response as part of a system.

Span 2 of G4 has an arc span length of 214.92 feet (Table 5.1.1). The maximum live load deflection in Span 2 of G4 will be checked (100.36 ft from Pier 2).

The roadway width can accommodate up to three 12-ft-wide design lanes. From the 3D analysis, the maximum deflections at this point (without impact or multiple presence applied, but with centrifugal force effects considered) due to the design truck and the design lane placed separately in one, two and three design lanes are given in Table 5.1.13 as follows:

Table 5.1.13 Maximum Design Truck and Design Lane Load Deflections (in.) including Centrifugal Force Effects (w/ no impact or multiple presence considered)

Maximum Live Load Deflections (in.) Span 2 – Girder 4 – 100.36 ft from Pier 2		
	Design Truck	Design Lane
One Lane Loaded	0.766	0.832
Two Lanes Loaded	1.211	1.288
Three Lanes Loaded	1.367	1.439

The deflections for the live load conditions to be checked for each case are computed as follows:

- One lane Loaded:

$$1.2\left[1.33\left(0.766\right)\right] = 1.143 \text{ in.}$$
$$1.2\left[0.832 + 0.25\left[1.33\left(0.766\right)\right)\right]\right] = 1.304 \text{ in.} \quad (\text{controls})$$

- Two Lanes Loaded:

$$1.0\left[1.33\left(1.211\right)\right] = 1.611 \text{ in.}$$
$$1.0\left[1.288 + 0.25\left[1.33\left(1.211\right)\right)\right]\right] = 1.691 \text{ in.} \quad (\text{controls})$$

- Three Lanes Loaded:

$$0.85\left[1.33\left(1.367\right)\right] = 1.545 \text{ in.}$$
$$0.85\left[1.439 + 0.25\left[1.33\left(1.367\right)\right)\right]\right] = 1.609 \text{ in.} \quad (\text{controls})$$

The largest live load deflection is for the case of two lanes loaded = 1.691 inches.

The suggested live-load deflection limit for a vehicular load is Span/800 (*AASHTO LRFD* Article 2.5.2.6.2). Therefore,

$$\Delta_{ALLOW} = \frac{214.92(12)}{800} = 3.224 \text{ in.} > 1.691 \text{ in.}$$

ok (Ratio = 0.525)

5.1.8.2.2 Permanent Deformations

AASHTO LRFD Article 6.10.4.2 contains criteria intended to control objectionable permanent deformations due to expected severe traffic loadings that would impair rideability (Section 3.2.4.3). *AASHTO LRFD* Article 6.10.4.2.1 specifies that these checks are to be made under the Service II load combination specified in *AASHTO LRFD* Table 3.4.1-1 (Section 1.3.3).

5.1.8.2.2.1 Flange Stresses

According to *AASHTO LRFD* Article 6.10.4.2.2, flanges must satisfy the following requirements (Section 3.2.4.3.2.1):

Top steel flange of composite sections (Equation 3.2.30):

$$f_f \le 0.95R_hF_{yf}$$

Bottom steel flange of composite sections (Equation 3.2.31):

$$f_f + \frac{f_\ell}{2} \le 0.95 R_h F_{yf}$$

As indicated in *AASHTO LRFD* Article C6.10.4.2.2, under the load combinations specified in *AASHTO LRFD* Table 3.4.1-1, the flange stress checks at the service limit state do not control and need not be checked for composite sections in negative flexure for which the nominal flexural resistance at the strength limit state is determined according to the provisions of *AASHTO LRFD* Article 6.10.8 and for composite sections in positive flexure that are treated as noncompact according to the provisions of *AASHTO LRFD* Article 6.10.7.2.

Sections in curved girders in regions of negative flexure must always be treated as slender-web sections and designed according to the provisions of *AASHTO LRFD* Article 6.10.8. Sections in curved girders in regions of positive flexure must always be treated as noncompact sections and designed according to the provisions of *AASHTO LRFD* Article 6.10.7.2. Therefore, the nominal flexural resistance of these sections at the strength limit state is not permitted to exceed the moment at first yield. As a result, based on the specified load factors and load combinations, the above flange stress checks at the service limit state will not control and need not be checked for sections in curved girders. Thus, they are not demonstrated in this example.

5.1.8.2.2.2 Web Bend Buckling

According to *AASHTO LRFD* Article 6.10.4.2.2, with the exception of composite sections in positive flexure in which the web satisfies the requirement of *AASHTO LRFD* Article 6.10.2.1.1 (i.e. $D/t_w \le 150$) such that longitudinal stiffeners are not required, web bend buckling of all sections under the Service II load combination is to be checked as follows (Section 3.2.4.3.2.2 - Equation 3.2.33):

$$f_c \le F_{crw}$$

Determine the nominal web bend-buckling resistance, F_{crw}, of G4 at Pier 1, and at the flange transition within the unbraced length in Span 1 immediately adjacent to Pier 1 (refer to the fold-out sheets at the end of this example) according to the provisions of *AASHTO LRFD* Article 6.10.1.9.1 as follows (Equation 3.2.35):

$$F_{crw} = \frac{0.9Ek}{\left(\frac{D}{t_w}\right)^2}$$

but not to exceed the smaller of $R_h F_{yc}$ and $F_{yw}/0.7$, where (Equation 3.2.36):

$$k = \frac{9}{(D_c/D)^2}$$

Calculate the compression flange vertical bending stresses at Pier 1 and at the flange transition under the Service II load combination. The load modifier η is always taken as 1.0 at the service limit state. The unfactored vertical bending moments from the 3D analysis (Table 5.1.2 – the moments at the cross-frame adjacent to the transition are used in this illustration), and the section moduli to the bottom flange and to the top of the deck are given as follows (note that live load moments include centrifugal force and dynamic load allowance effects):

- Pier 1:
  - M_{DC1} = -11,360 kip-ft
  - M_{DC2} = -2,022 kip-ft
  - M_{DW} = -1,688 kip-ft
  - M_{-LL+IM} = -7,077 kip-ft
  - S_{steel} = 8,959 in.^{3}
  - $S_{steel+rebar}$ = 9,124 in.^{3} (D_c = 43.55 in.)
  - $S_{n\ top\ of\ deck}$ = -17,201 in.^{3}
- Transition:
  - M_{DC1} = -5,807 kip-ft
  - M_{DC2} = -755 kip-ft
  - M_{DW} = -851 kip-ft
  - M_{-LL+IM} = -4,532 kip-ft
  - S_{steel} = 4,882 in.^{3}
  - $S_{3n\ deck+rebar}$ = 5,653 in.^{3}
  - $S_{n\ deck+rebar}$ = 6,118 in.^{3}
  - $S_{n\ top\ of\ deck}$ = -13,499 in.^{3}

According to *AASHTO LRFD* Article 6.10.4.2.1, for members with shear connectors provided throughout their entire length that also satisfy the provisions of Article 6.10.1.7 (regarding the provision of the minimum one percent longitudinal reinforcement in the deck), the concrete deck may be assumed to be effective for both positive and negative flexure provided that the corresponding longitudinal tensile stresses in the concrete deck at the section under consideration are smaller than $2f_r$, where f_r is the lower-bound modulus of rupture of the concrete specified in *AASHTO LRFD* Article 5.4.2.6.

According to *AASHTO LRFD* Article 6.10.1.1.1d, the longitudinal flexural stresses in the deck due to all permanent and transient loads are to be computed using the short-term modular ratio, n. The calculated stress on the transformed section is to be divided by n to obtain the stress in the concrete. The modulus of rupture of the concrete was computed earlier in Section 5.1.8.1.5 to be f_r = 0.480 ksi. Calculate the longitudinal tensile stress in the deck due to the Service II load combination at Pier 1 and at the flange transition (note the deck is not subject to stress due to DC_1 loads):

- Pier 1:

$$f_{deck} = 1.0\left[\frac{1.0(-2{,}022) + 1.0(-1{,}688) + 1.3(-7{,}077)}{-17{,}201(8)}\right]12 = +1.126 \text{ ksi}$$

$$1.126 \text{ ksi} > 2f_r = 2(0.480) = 0.960 \text{ ksi}$$

- Transition:

$$f_{deck} = 1.0\left[\frac{1.0(-755) + 1.0(-851) + 1.3(-4{,}532)}{-13{,}499(8)}\right]12 = +0.833 \text{ ksi}$$

$$0.833 \text{ ksf} < 2f_r = 2(0.480) = 0.960 \text{ ksi}$$

Therefore, stresses at Pier 1 are computed assuming the concrete deck is not effective in tension (Figure 5.1.17), and stresses at the flange transition are computed assuming the concrete deck is effective in tension (Figure 5.1.18). In both cases, the longitudinal reinforcement is considered to be effective in tension.

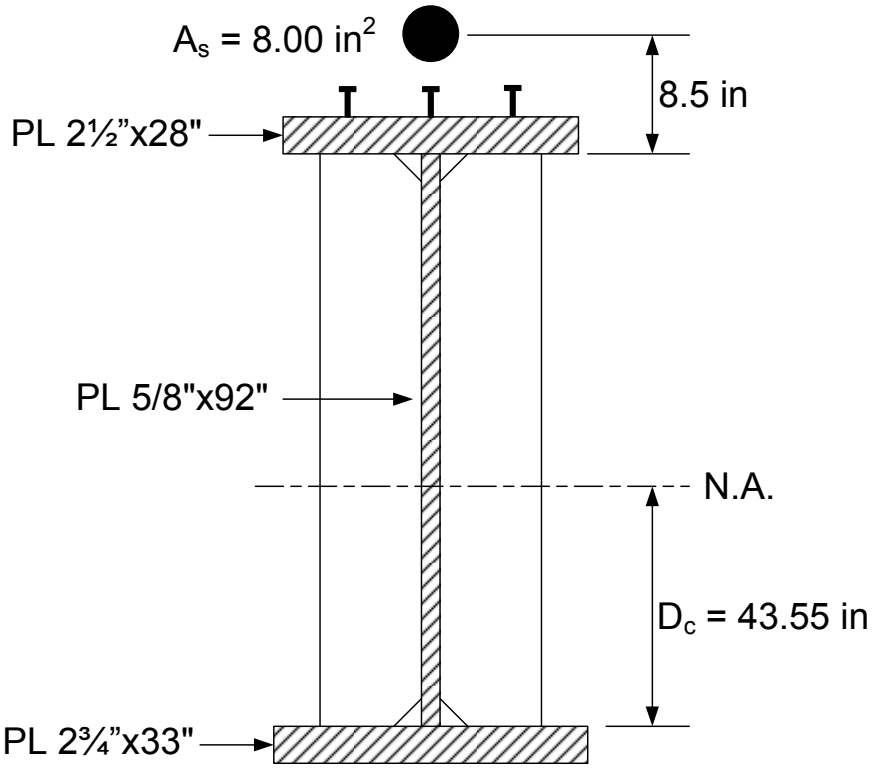


Figure 5.1.17 G4 Section at Pier 1 for Service Limit State Checks

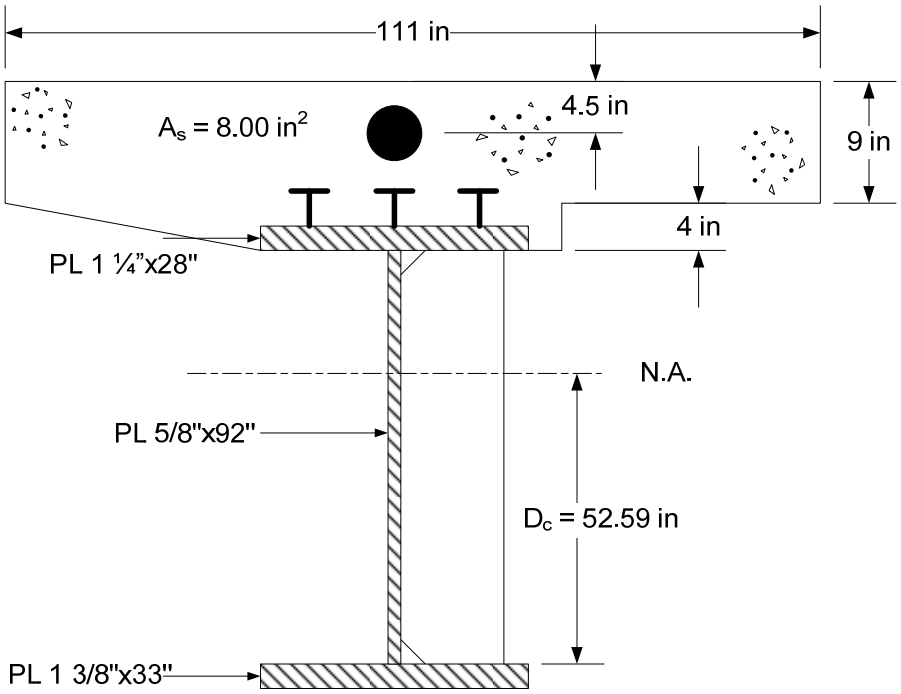


Figure 5.1.18 G4, Span 1, Section at Flange Transition Adjacent to Pier 1 for Service Limit State Checks

The stresses are computed as follows:

- Pier 1:

$$f_c = 1.0\left[\frac{1.0(-11{,}360)}{8{,}959} + \frac{1.0(-2{,}022)}{9{,}124} + \frac{1.0(-1{,}688)}{9{,}124} + \frac{1.3(-7{,}077)}{9{,}124}\right]12 = -32.20 \text{ ksi}$$

- Transition:

$$f_c = 1.0\left[\frac{1.0(-5{,}807)}{4{,}882} + \frac{1.0(-755)}{5{,}653} + \frac{1.0(-851)}{5{,}653} + \frac{1.3(-4{,}532)}{6{,}118}\right]12 = -29.24 \text{ ksi}$$

Calculate F_{crw} at Pier 1. Since the concrete deck is assumed to not be effective in tension at Pier 1, D_c is to be taken as the depth of the web in compression for the steel section plus the longitudinal reinforcement (*AASHTO LRFD* Article D6.3.1 – refer to Figure 5.1.17):

$$k = \frac{9}{\left(\frac{43.55}{92.0}\right)^2} = 40.16$$

$$F_{crw} = \frac{0.9(29{,}000)(40.16)}{\left(\frac{92.0}{0.625}\right)^2} = 48.37 \text{ ksi}$$

$$< \min\left(\frac{R_h F_{yc}, F_{yw}}{0.7}\right) = R_h F_{yc} = 1.0(50) = 50 \text{ ksi}$$

$$\therefore \quad F_{crw} = 48.37 \text{ ksi}$$

$$f_c = |-32.20| \text{ ksi} < 48.37 \text{ ksi}$$

ok $\qquad$ (Ratio = 0.666)

Calculate F_{crw} at the flange transition. According to *AASHTO LRFD* Article D6.3.1 (*AASHTO LRFD* Appendix D6), for composite sections in negative flexure at the service limit state where the concrete deck is considered effective in tension for computing flexural stresses on the composite section, the depth of the web in compression in the elastic range D_c is to be computed from *AASHTO LRFD* Equation D6.3.1-1 as follows (Equation 3.2.41):

$$D_c = \left(\frac{-f_c}{|f_c| + f_t}\right) d - t_{fc} \geq 0$$

This equation recognizes the beneficial effect of the dead-load stress on the location of the neutral axis of the composite section (including the concrete deck) in regions of negative flexure.

From separate calculations similar to the above assuming the deck is effective in tension, f_t at the flange transition under the Service II load combination is equal to +22.03 ksi. Therefore:

$$D_c = \left(\frac{-(-29.24)}{|-29.24| + 22.03}\right) 94.625 - 1.375 = 52.59 \text{ in.} > 0 \quad \text{ok}$$

$$k = \frac{9}{(52.59/92.0)^2} = 27.54$$

$$F_{crw} = \frac{0.9(29{,}000)(27.54)}{\left(\frac{92.0}{0.625}\right)^2} = 33.17 \text{ ksi} < \min\left(R_h F_{yc}, F_{yw}/0.7\right) = R_h F_{yc} = 1.0(50) = 50 \text{ ksi}$$

$$f_c = \left|-29.24\right| \text{ ksi} < 33.17 \text{ ksi}$$

ok (Ratio = 0.882)

5.1.8.2.3 Concrete Deck

AASHTO LRFD Article 6.10.1.7 requires that the minimum one-percent longitudinal reinforcement be present in the concrete deck wherever the longitudinal tensile stress in the deck due to the factored construction loads *and* due to the Service II load combination exceeds ϕf_r (Section 3.2.4.4). Earlier calculations in Section 5.1.8.1.5 showed that the minimum longitudinal reinforcement must extend 91.0 feet from Pier 2 into Span 3 over G4 in order to satisfy this requirement for the construction condition.

Check the tensile stress in the concrete deck due to the Service II load combination at the section 91.0 feet into Span 3 from Pier 2. The unfactored vertical bending moments and section modulus to the top of the deck at this location are given as follows (Table 5.1.2):

M_{DC2} = +265 kip-ft
M_{DW} = +385 kip-ft
M_{-LL+IM} = -1,309 kip-ft
$S_{n \text{ top of deck}}$ = -10,464 in.^{3}

$$f_{deck} = \frac{1.0\left[1.0(+265) + 1.0(+385) + 1.3(-1309)\right](12)}{-10{,}464(8)} = +0.151 \text{ ksi}$$

$$< \phi f_r = 0.90 f_r = 0.432 \text{ ksi} \qquad \text{ok}$$

Therefore, the minimum one-percent longitudinal reinforcement does not need to be extended any further into Span 3.

5.1.8.3 Fatigue Limit State Verifications

5.1.8.3.1 General

Fatigue of the base metal at the connection-plate welds to the flanges of G4 at the cross-frame in Span 3 located approximately 68.0 feet from Pier 2 will be checked (refer to the fold-out sheets at the end of this example). Load-induced fatigue limit state verifications are discussed in Section 3.2.5.2.2.

AASHTO LRFD Article 6.10.5.1 specifies that the stress range due to major-axis bending plus lateral flange bending must be investigated, where applicable, for horizontally curved bridges. For the connection-plate welds to the bottom flange, the stress range due to lateral flange bending is a consideration, as the welds terminate out near the tip of the flange (Figure 3.2.23). For the connection-plate welds to the top flange, the stress range due to lateral flange bending may be ignored as the flange is continuously braced.

The major-axis bending stress range due to the fatigue live load (Section 1.3.2.3.3) modified by the corresponding dynamic load allowance of 15 percent will be used to make these checks. The fatigue-load moments used to compute the stress range are taken from the 3D analysis.

5.1.8.3.2 Single-Lane Average Daily Truck Traffic

From *AASHTO LRFD* Article 3.6.1.4.2, the single-lane average daily truck traffic $(ADTT)_{SL}$ is determined as (Equation 3.2.53):

$$(\text{ADTT})_{\text{SL}} = p * \text{ADTT}$$

For a 3-lane bridge, p is equal to 0.80 (Table 3.2.8). Therefore:

$$(\text{ADTT})_{\text{SL}} = 0.8 * 2{,}000 = 1{,}600 \text{ trucks / day}$$

5.1.8.3.3 Design Verifications for Flexure

According to *AASHTO LRFD* Article 6.6.1.2.1, for flexural members with shear connectors provided throughout their entire length and with concrete deck reinforcement satisfying the provisions of *AASHTO LRFD* Article 6.10.1.7, flexural stresses and stress ranges applied to the composite section at the fatigue limit state may be computed assuming the concrete deck to be effective for both positive and negative flexure.

Shear connectors must be provided along the entire length of the girder in horizontally curved bridges (*AASHTO LRFD* Article 6.10.10.1). Earlier computations made in Sections 5.1.8.1.5 and 5.1.8.2.3 ensure that the longitudinal concrete deck reinforcement satisfies the provisions of *AASHTO LRFD* Article 6.10.1.7. Hence, the concrete deck will be assumed effective in computing all stresses and stress ranges applied to the composite section in the following fatigue calculations.

5.1.8.3.3.1 Top-Flange Connection Plate Weld

Check fatigue of the base metal at the connection-plate weld to the top flange of G4 at the third intermediate cross-frame from Pier 2 in Span 3 (located approximately 68.0 feet from Pier 2 – Figure 5.1.19).

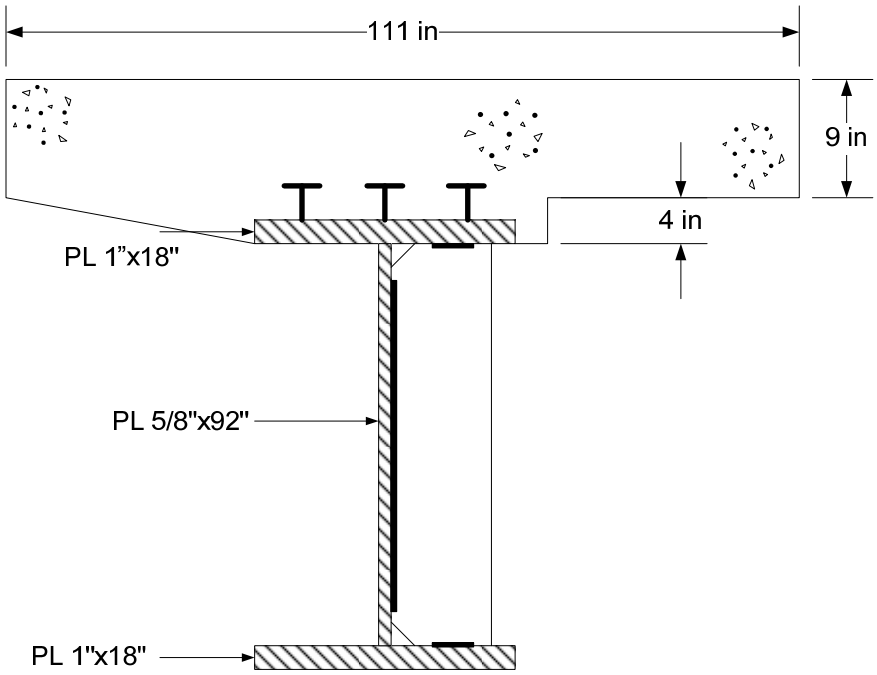


Figure 5.1.19 G4, Span 3, Section at a Cross-Frame 68.063 Feet from Pier 2

The provisions of *AASHTO LRFD* Article 6.6.1.2 apply only to details subject to a net applied tensile stress. According to *AASHTO LRFD* Article 6.6.1.2.1, in regions where the unfactored permanent loads produce compression, fatigue is to be considered only if this compressive stress is less than the maximum tensile stress resulting from the Fatigue I load combination (γ = 1.5). This determination is based on the Fatigue I load combination because this is the largest stress range a detail is expected to experience often enough to propagate a crack. When the tensile component of the stress range cycle resulting from this load combination exceeds the compressive stress due to the unfactored permanent loads, there is a net tensile stress in the component or at the detail under consideration and fatigue must be considered.

Otherwise, the stress cycle is compression-compression and a fatigue crack will not propagate. In this example, the effect of the future wearing surface will be conservatively ignored when determining if a detail is subject to a net applied tensile stress.

The unfactored vertical bending moments due to the DC_1 and DC_2 loads at the cross-frame under consideration (Table 5.1.2), and corresponding moments of inertia and distances from the neutral axis to the top of the web are given as follows:

M_{DC1} = +1,787 kip-ft
M_{DC2} = +114 kip-ft
I_{steel} = 118,397 in.^{4}
$I_{3n\ deck}$ = 208,085 in.^{4}
$y_{top\ of\ web}$ = -46.0 in.
$y_{top\ of\ web}$ = -28.3 in.

The unfactored permanent loads produce compression at the top of the web at this location. The total unfactored permanent-load compressive vertical bending stress at the top-flange weld at this location (neglecting the future wearing surface) is computed as:

$$f_{DC_1} = \frac{1{,}787(12)(-46.0)}{118{,}397} = -8.33 \text{ ksi}$$

$$f_{DC_2} = \frac{114(12)(-28.3)}{208{,}085} = \underline{-0.19 \text{ ksi}}$$

$$-8.52 \text{ ksi}$$

The unfactored negative fatigue load moment (including the 15 percent dynamic load allowance and centrifugal force effects) at the cross-frame under consideration (Table 5.1.2), and the corresponding moment of inertia and distance from the neutral axis to the top of the web are given as follows:

M_{-LL+IM} = -588 kip-ft
$I_{n\ deck}$ = 281,488 in.^{4}
$y_{top\ of\ web}$ = -13.9 in.

The maximum tensile stress at the top-flange weld at this location due to the negative moment caused by the factored fatigue load (factored by the 1.5 load factor specified for the Fatigue I load combination) is:

$$f_{LL+IM} = \frac{1.5(-588)(12)(-13.9)}{281{,}488} = +0.52 \text{ ksi}$$

$$|-8.52| \text{ ksi} > +0.52 \text{ ksi}$$

Therefore, fatigue of the base metal at the connection-plate weld to the top flange at this location need not be checked.

5.1.8.3.3.2 Bottom-Flange Connection Plate Weld

By inspection, the base metal at the connection-plate weld to the bottom flange of G4 at this location is subject to a net applied tensile stress. Therefore, fatigue must be considered.

Determine the fatigue detail category from *AASHTO LRFD* Table 6.6.1.2.3-1. Under the condition of fillet-welded stiffener connections with welds normal to the direction of stress, the fatigue detail category for base metal at transverse stiffener-to-flange fillet welds is Category C′ (Condition 4.1).

AASHTO LRFD Table 6.6.1.2.3-2 (Table 3.2.9) shows the values of $(ADTT)_{SL}$ for each fatigue detail category above which the infinite life check governs. The values in the table assume a 75-year design life and one stress cycle *n* per truck passage.

For continuous spans with span lengths greater than 40.0 feet, the number of stress cycles per truck passage *n* is equal to 1.0 at sections away from the pier (*AASHTO LRFD* Table 6.6.1.2.5-2). Sections ′away from the pier′ are defined as sections greater than a distance of one-tenth the span on each side of the interior support. For other values of *n*, *AASHTO LRFD* Table 6.6.1.2.3-2 should be modified by dividing the values in the table by *n*.

From Table 3.2.9, the 75-year $(ADTT)_{SL}$ equivalent to infinite fatigue life for a Category C′ detail is 745 trucks per day < 1,600 trucks per day. The detail must therefore be checked for infinite life using the Fatigue I load combination (γ = 1.5). In the infinite life region, the nominal fatigue resistance is equal to the constant-amplitude fatigue threshold as follows (Equation 3.2.50):

$$(\Delta F)_n = (\Delta F)_{TH}$$

For a Category C′ detail, $(\Delta F)_{TH}$ = 12.0 ksi (*AASHTO LRFD* Table 6.6.1.2.5-3 – Table 3.2.6). Therefore:

$$(\Delta F)_n = 12.00 \text{ ksi}$$

The unfactored positive fatigue load moment (including the 15 percent dynamic load allowance and centrifugal force effects) at the cross-frame under consideration (Table 5.1.2), and the corresponding moment of inertia and distance from the neutral axis to the bottom of the web are given as follows:

M_{+LL+IM} = +1,203 kip-ft
$I_{n\ deck}$ = 281,488 in.^{4}
$y_{bot\ of\ web}$ = +78.1 in.

The major-axis bending stress range, $\gamma(\Delta f)$, at the connection-plate weld due to the factored fatigue load (factored by the specified 1.5 load factor for the Fatigue I load combination) is computed using the properties of the short-term composite section as:

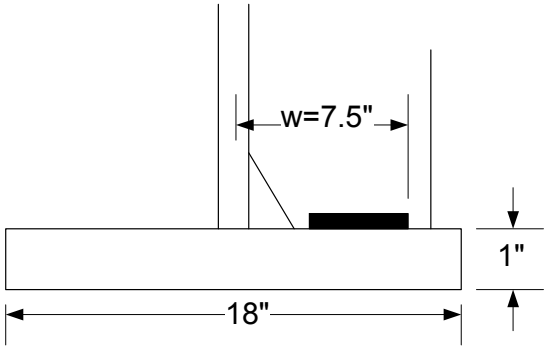
$$\gamma(\Delta f) = \frac{1.5(1{,}203)(12)(78.1)}{281{,}488} + \frac{1.5|-588|(12)(78.1)}{281{,}488}$$
$$= 8.94 \text{ ksi}$$

For this detail, the stress range due to lateral flange bending must also be considered. The unfactored positive and negative fatigue load lateral flange bending moments (including the 15 percent dynamic load allowance and centrifugal force effects) at the cross-frame under consideration from the 3D analysis are given as follows:

$M_{Lat\ (+LL+IM)}$ = +5.33 kip-ft
$M_{Lat\ (-LL+IM)}$ = -2.67 kip-ft

The bottom flange plate is 1″ x 18″. The connection plate-to-flange weld is assumed to terminate on the flange 7.5 inches from the centerline of the web (Figure 5.1.20). The lateral moment of inertia of the bottom flange plate, I_{Lat}, is computed as:

$$I_{Lat} = \frac{1.0(18)^3}{12} = 486 \text{ in.}^4$$



$$(\Delta f)_{tot} = \Delta f + \frac{(\Delta M)_{LAT} w}{I_{LAT}}$$

Figure 5.1.20 Effect of Bottom Flange Lateral Bending on the Stress Range at the End of the Connection Plate to Bottom Flange Weld

Therefore, the lateral bending stress range, $\gamma(\Delta f_{Lat})$, at the connection-plate weld due to the factored fatigue load (factored by the specified 1.5 load factor for the Fatigue I load combination) is computed as:

$$\gamma(\Delta f_{Lat}) = \frac{\Delta M_{Lat} w}{I_{Lat}} = \frac{1.5[5.33(12) + |-2.67|(12)](7.5)}{486} = 2.22 \text{ ksi}$$

The total stress range, $\gamma(\Delta f)_{tot}$, is therefore equal to:

$$\gamma(\Delta f)_{tot} = 8.94 + 2.22 = 11.16 \text{ ksi}$$

According to *AASHTO LRFD* Equation 6.6.1.2.2-1, $\gamma(\Delta f)_{tot}$ must not exceed the nominal fatigue resistance $(\Delta F)_n$ (Equation 3.2.54). Both the resistance factor, ϕ, and load modifier, η, are specified to be 1.0 at the fatigue limit state (*AASHTO LRFD* Article C6.6.1.2.2).

$$\gamma(\Delta f) \le (\Delta F)_n$$

$$11.16 \text{ ksi} < 12.00 \text{ ksi}$$

ok (Ratio = 0.930)

5.1.8.3.4 Design Verifications for Shear

As specified in *AASHTO LRFD* Article 6.10.5.3, interior panels of stiffened webs must satisfy the following requirement (Section 3.2.5.2.2.2 – Equation 3.2.55):

$$V_u \le V_{cr}$$

The factored fatigue load for this check is to be determined using the Fatigue I load combination (*AASHTO LRFD* Table 3.4.1-1), with the fatigue live load taken as specified in *AASHTO LRFD* Article 3.6.1.4. The fatigue live load is modified by the dynamic load allowance of 15 percent (with centrifugal force effects considered).

The live load shear for this check is intended to represent the shear due to the heaviest truck expected to cross the bridge over its 75-year fatigue design life. Satisfaction of the preceding equation is intended to control elastic flexing of the web so that the member is assumed able to sustain an infinite number of smaller loadings without fatigue cracking due to this effect.

Only the interior panels of stiffened webs are checked because the shear resistance of the end panel of stiffened webs and the shear resistance of unstiffened webs are already limited to the shear buckling resistance at the strength limit state.

For this example, the panel in G4 immediately to the right of Pier 1 (in Span 2) will be checked. The panel is bounded by the bearing stiffeners at Pier 1 and the cross-frame connection plate located 22.302 feet into Span 2 from Pier 1. The bearing stiffeners and connection plate act as transverse stiffeners. The stiffener spacing of 22.302(12) = 267.6 inches is less than the maximum permitted spacing of d_o = 3D = 3(92.0) = 276.0 inches.

The unfactored permanent load shears and fatigue live load shear (including the dynamic load allowance and centrifugal force effects) at Pier 1 from the 3D analysis to be used in this check are as follows (Table 5.1.3):

V_{DC1} = +223 kips
V_{DC2} = +39 kips
V_{DW} = +32 kips
V_{+LL+IM} = +65 kips

Therefore:

$$V_u = 223 + 39 + 32 + 1.5(65) = 392 \text{ kips}$$

The shear buckling resistance of the 267.6-inch-long panel is determined as (Equation 3.2.161):

$$V_n = V_{cr} = CV_p$$

C is the ratio of the shear buckling resistance to the shear yield strength determined from *AASHTO LRFD* 6.10.9.3.2-4, 6.10.9.3.2-5 or 6.10.9.3.2-6, as applicable. First, compute the shear buckling coefficient, *k* (Equation 3.2.157):

$$k = 5 + \frac{5}{\left(\frac{d_o}{D}\right)^2}$$

$$k = 5 + \frac{5}{\left(\frac{267.6}{92.0}\right)^2} = 5.59$$

Since,

$$1.40\sqrt{\frac{Ek}{F_{yw}}} = 1.40\sqrt{\frac{29{,}000(5.59)}{50}} = 79.7 < \frac{D}{t_w} = \frac{92.0}{0.625} = 147.2$$

Equation 3.2.158 is used to compute *C* as follows:

$$C = \frac{1.57}{\left(\frac{D}{t_w}\right)^2}\left(\frac{Ek}{F_{yw}}\right)$$

$$C = \frac{1.57}{(147.2)^2}\left(\frac{29{,}000(5.59)}{50}\right) = 0.235$$

V_p is the plastic shear force determined as follows (Equation 3.2.151):

$$V_p = 0.58F_{yw}Dt_w$$

$$V_p = 0.58(50)(92.0)(0.625) = 1{,}668 \text{ kips}$$

Therefore,

$$V_{cr} = 0.235(1{,}668) = 392 \text{ kips}$$

$$V_u = 392 \text{ kips} = V_{cr} = 392 \text{ kips}$$

ok (Ratio = 1.000)

5.1.8.4 Strength Limit State Verifications

5.1.8.4.1 Negative Flexure

Strength limit state verifications for I-sections subject to negative flexure are discussed in Section 3.2.6.4.1. According to *AASHTO LRFD* Article 6.10.6.2.3, sections in negative flexure in kinked (chorded) continuous or horizontally curved steel girder bridges are to be proportioned at the strength limit state according to the provisions specified in *AASHTO LRFD* Article 6.10.8. That is, the sections must always be treated as slender-web sections regardless of the web slenderness meaning that the provisions of *AASHTO LRFD* Appendix A6 may not be used.

According to *AASHTO LRFD* Article 6.10.8.1, for composite sections in negative flexure, the following relationship must be satisfied for a discretely braced compression flange at the strength limit state (Equation 3.2.81):

$$f_{bu} + \frac{1}{3} f_{\ell} \le \phi_f F_{nc}$$

The top (tension) flange in regions of negative flexure is considered continuously braced by the composite concrete deck at the strength limit state. According to *AASHTO LRFD* Article 6.10.8.1.3, continuously braced flanges in tension must satisfy the following relationship at the strength limit state (Equation 3.2.108):

$$f_{bu} \le \phi_f R_h F_{yf}$$

Any flange lateral bending stresses need not be considered once the flange is continuously braced (*AASHTO LRFD* Article C6.10.1.6).

5.1.8.4.1.1 Section at Pier 1 in G4

Assemble the factored stresses for the Strength I load combination needed to check the preceding equations at Pier 1 in G4. The Strength IV load combination does not control by inspection. In this example, the load modifier, η, is taken equal to 1.0 at the strength limit state.

The largest unbraced length, L_b, along G4 adjacent to Pier 1 is equal to 27.833 feet in Span 1 (refer to the fold-out sheets at the end of this example). The section is prismatic within this unbraced length (Figure 5.1.21).

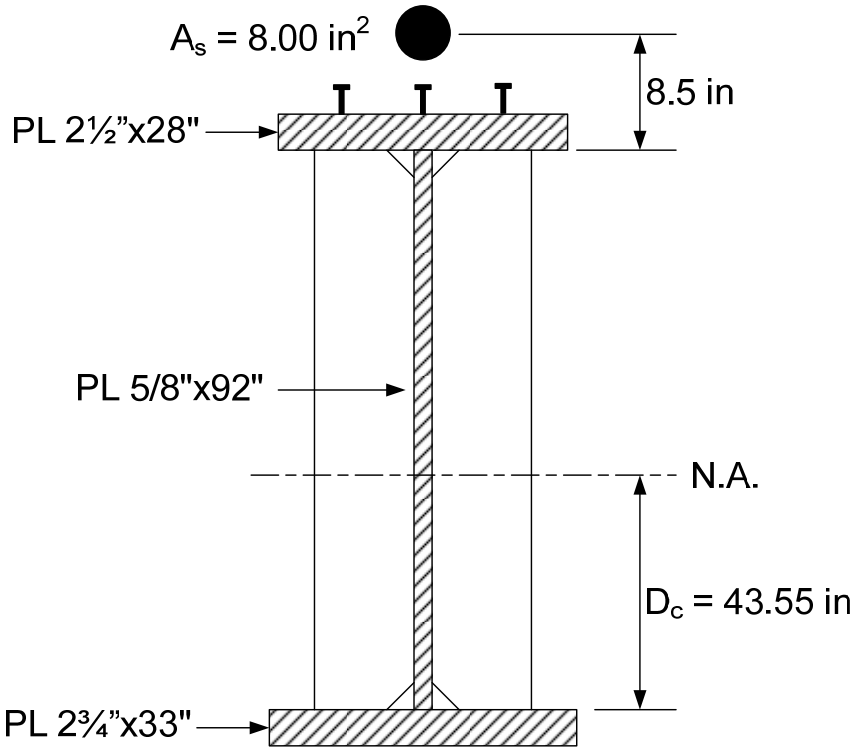


Figure 5.1.21 G4 Section at Pier 1

The unfactored vertical bending moments at Pier 1 in G4 from the 3D analysis (Table 5.1.2), and the section moduli to the top and bottom flanges are given as follows (note that the live load moment includes centrifugal force and dynamic load allowance effects):

M_{DC1} = -11,360 kip-ft
M_{DC2} = -2,022 kip-ft
M_{DW} = -1,688 kip-ft
M_{-LL+IM} = -7,077 kip-ft
$S_{steel\ (top)}$ = -7,465 in.^{3}
$S_{steel\ (bot)}$ = 8,959 in.^{3}
$S_{steel+rebar\ (top)}$ = -8,292 in.^{3}
$S_{steel+rebar\ (bot)}$ = 9,124 in.^{3} (D_c = 43.55 in.)

The factored vertical bending stresses in the top and bottom flanges at Pier 1 in G4 are computed as follows:

- Top flange:

$$f = 1.0\left[\frac{1.25(-11{,}360)}{-7{,}465} + \frac{1.25(-2{,}022)}{-8{,}292} + \frac{1.5(-1{,}688)}{-8{,}292} + \frac{1.75(-7{,}077)}{-8{,}292}\right]12 = 48.07 \text{ ksi}$$

- Bottom flange:

$$f = 1.0\left[\frac{1.25(-11{,}360)}{8{,}959} + \frac{1.25(-2{,}022)}{9{,}124} + \frac{1.5(-1{,}688)}{9{,}124} + \frac{1.75(-7{,}077)}{9{,}124}\right]12 = -41.96 \text{ ksi}$$

The unfactored lateral bending moments in the bottom flange of G4 at Pier 1 and at the other end of the unbraced length (in Span 1 of G4) taken directly from the 3D analysis are given as follows (note that the live load lateral moments include centrifugal force and dynamic load allowance effects):

- Pier 1: M_{DC1} = 58 kip-ft
  M_{DC2} = 12 kip-ft
  M_{DW} = 11 kip-ft
  M_{-LL+IM} = 120 kip-ft

- Span 1: M_{DC1} = 65 kip-ft (at other end of unbraced length)
  M_{DC2} = 3 kip-ft
  M_{DW} = 6 kip-ft
  M_{-LL+IM} = 54 kip-ft

The factored lateral bending stresses in the bottom flange at each location are computed as:

- Pier 1:

$$f_\ell = 1.0\left[\frac{(1.25(58) + 1.25(12) + 1.5(11) + 1.75(120))12}{2.75(33.0)^2/6}\right] = 7.55 \text{ ksi}$$

- Span 1:

$$f_\ell = 1.0\left[\frac{(1.25(65) + 1.25(3) + 1.5(6) + 1.75(54))12}{2.75(33.0)^2/6}\right] = 4.53 \text{ ksi}$$

The largest factored lateral bending stress in this case is at the cross-frame at Pier 1. Lateral bending is not a consideration in the top flange because the top flange is continuously braced at the strength limit state.

Total factored bottom flange lateral bending stresses at each cross-frame in each girder, calculated in a similar fashion, are shown in Figure 5.1.22 for half of the bridge (note: without amplification included). The lateral bending stresses are due to the combined effects of curvature and the discontinuous cross-frames that were utilized to reduce the transverse stiffness of the bridge in order to counter the effects

of the skew. Note in general that the lateral bending stresses are somewhat larger in the two interior girders.

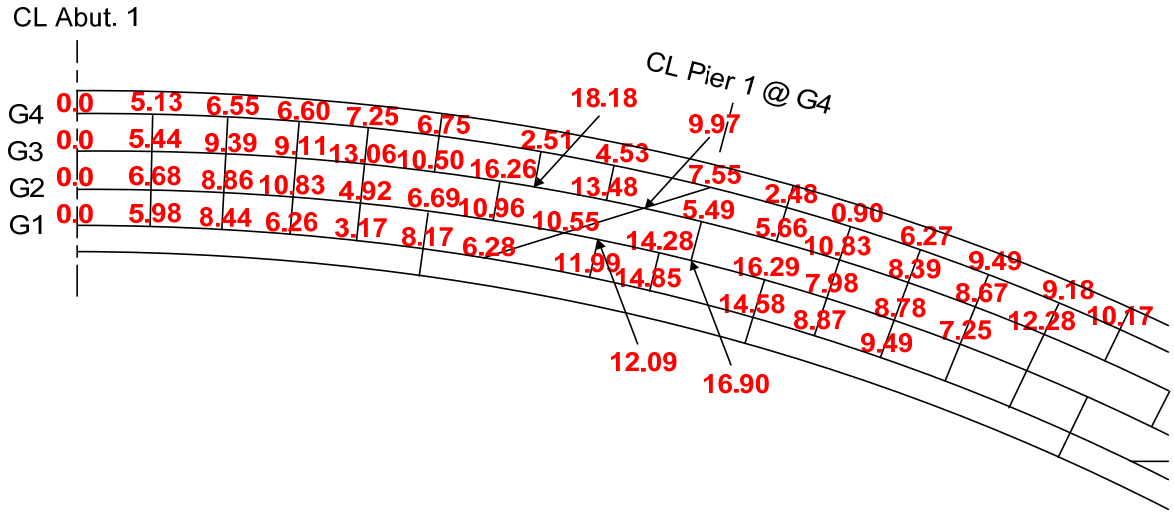


Figure 5.1.22 Total Factored Bottom Flange Lateral Bending Stresses at the Cross-Frames from the 3D Analysis (shown for half of the bridge, no amplification included)

Nominal Flexural Resistance – Bottom Flange

Calculate the nominal flexural resistance, F_{nc}, of the bottom (compression) flange based on local buckling and lateral torsional buckling as follows (Section 3.2.6.4.1.2):

Local Buckling Resistance

Calculate the local buckling resistance of the bottom flange of G4 at Pier 1 according to the provisions of *AASHTO LRFD* Article 6.10.8.2.2. Determine the slenderness ratio of the flange:

$$\lambda_f = \frac{b_{fc}}{2t_{fc}}$$

$$\lambda_f = \frac{33}{2(2.75)} = 6.0$$

Determine the limiting slenderness ratio for a compact flange from Equation 3.2.87 (alternatively, see *AASHTO LRFD* Table C6.10.8.2.2-1):

$$\lambda_{pf} = 0.38\sqrt{\frac{E}{F_{yc}}}$$

$$\lambda_{pf} = 0.38\sqrt{\frac{29{,}000}{50}} = 9.15$$

Since $\lambda_f < \lambda_{pf}$, the nominal local buckling resistance $(F_{nc})_{FLB}$ is taken as (Equation 3.2.88):

$$(F_{nc})_{FLB} = R_b R_h F_{yc}$$

Since the section is a homogeneous built-up section, the hybrid factor R_h is equal to 1.0 (*AASHTO LRFD* Article 6.10.1.10.1 – Section 3.2.6.3).

Calculate the web load-shedding factor, R_b (Section 3.2.6.2), as follows (Equation 3.2.75):

$$R_b = 1 - \left(\frac{a_{wc}}{1200 + 300a_{wc}}\right)\left(\frac{2D_c}{t_w} - \lambda_{rw}\right) \le 1.0$$

From Equation 3.2.37:

$$\lambda_{rw} = 5.7\sqrt{\frac{E}{F_{yc}}}$$

$$\lambda_{rw} = 5.7\sqrt{\frac{29{,}000}{50}} = 137.3$$

$$a_{wc} = \frac{2D_c t_w}{b_{fc} t_{fc}}$$

AASHTO LRFD Article D6.3.1 specifies that for composite sections in negative flexure, D_c is to be computed for the section consisting of the steel girder plus the longitudinal reinforcement at the strength limit state.

$$a_{wc} = \frac{2(43.55)(0.625)}{33(2.75)} = 0.60$$

$$R_b = 1 - \left(\frac{0.60}{1200 + 300(0.60)}\right)\left(\frac{2(43.55)}{0.625} - 137.3\right) = 0.999$$

$$(F_{nc})_{FLB} = (0.999)(1.0)(50) = 49.96 \text{ ksi}$$

Lateral Torsional Buckling Resistance

Calculate the lateral torsional buckling resistance of the bottom flange of G4 within this unbraced length according to the provisions of *AASHTO LRFD* Article 6.10.8.2.3.

Determine the limiting unbraced length, L_p (Equation 3.2.94):

$$L_p = 1.0 r_t \sqrt{\frac{E}{F_{yc}}}$$

where r_t is the effective radius of gyration for lateral torsional buckling specified in *AASHTO LRFD* Article 6.10.8.2.3 determined as (Equation 3.2.97):

$$r_t = \frac{b_{fc}}{\sqrt{12\left(1 + \frac{1}{3}\frac{D_c t_w}{b_{fc} t_{fc}}\right)}}$$

$$r_t = \frac{33}{\sqrt{12\left(1 + \frac{1}{3}\frac{43.55(0.625)}{33(2.75)}\right)}} = 9.08 \text{ in.}$$

$$L_p = \frac{1.0(9.08)}{12}\sqrt{\frac{29{,}000}{50}} = 18.22 \text{ ft}$$

Determine the limiting unbraced length, L_r (Equation 3.2.95):

$$L_r = \pi r_t \sqrt{\frac{E}{F_{yr}}}$$

where:

$$F_{yr} = 0.7F_{yc} \le F_{yw}$$

$$F_{yr} = 0.7(50) = 35.0 \text{ ksi} < 50 \text{ ksi} \quad \text{ok}$$

F_{yr} must also not be less than $0.5F_{yc} = 0.5(50) = 25.0$ ksi ok.

Therefore:

$$L_r = \frac{\pi(9.08)}{12}\sqrt{\frac{29{,}000}{35.0}} = 68.43 \text{ ft}$$

The moment gradient modifier, C_b, will conservatively be assumed to equal 1.0 initially.

Since $L_p = 18.22$ feet < $L_b = 27.83$ feet < $L_r = 68.43$ feet, the nominal lateral torsional buckling resistance $(F_{nc})_{LTB}$ is taken as (Equation 3.2.92):

$$(F_{nc})_{LTB} = C_b\left[1-\left(1-\frac{F_{yr}}{R_hF_{yc}}\right)\left(\frac{L_b-L_p}{L_r-L_p}\right)\right]R_bR_hF_{yc} \le R_bR_hF_{yc}$$

$$(F_{nc})_{LTB} = 1.0\left[1-\left(1-\frac{35.0}{1.0(50.0)}\right)\left(\frac{27.83-18.22}{68.43-18.22}\right)\right](0.999)(1.0)(50)$$

$$= 47.08 \text{ ksi} < 0.999(1.0)(50) = 49.96 \text{ ksi}$$

Therefore:

$$(F_{nc})_{LTB} = 47.08 \text{ ksi}$$

Flange Verifications

With all the required information now assembled, check the flanges of G4 at Pier 1.

According to *AASHTO LRFD* Article 6.10.1.6, lateral bending stresses determined from a first-order analysis may be used in discretely braced compression flanges for which Equation 3.2.8 is satisfied as follows:

$$L_b \le 1.2L_p\sqrt{\frac{C_bR_b}{f_{bu}/F_{yc}}}$$

L_p is the limiting unbraced length for lateral torsional buckling specified in *AASHTO LRFD* Article 6.10.8.2.3 determined above to be 18.22 feet.

f_{bu} in Equation 3.2.8 is to be taken as the largest value of the compressive major-axis bending stress throughout the unbraced length under consideration. Since the member is prismatic within the unbraced length, the largest stress in this case is at Pier 1 and was computed previously to be –41.96 ksi. Therefore:

$$1.2(18.22)\sqrt{\frac{1.0(0.999)}{|-41.96|/50}} = 23.86 \text{ ft} < L_b = 27.83 \text{ ft}$$

Because the preceding equation is not satisfied, *AASHTO LRFD* Article 6.10.1.6 requires that second-order elastic compression-flange lateral bending stresses be determined. The second-order compression-flange lateral bending stresses may be determined by amplifying first-order values (i.e. $f_{\ell 1}$) as follows (Equation 3.2.9):

$$f_\ell = \left(\frac{0.85}{1-\frac{f_{bu}}{F_{cr}}}\right) f_{\ell 1} \geq f_{\ell 1}$$

or:

$$f_\ell = (AF) f_{\ell 1} \geq f_{\ell 1}$$

where *AF* is the amplification factor.

F_{cr} is the elastic lateral torsional buckling stress for the flange under consideration specified in *AASHTO LRFD* Article 6.10.8.2.3 determined as follows (Equation 3.2.96):

$$F_{cr} = \frac{C_b R_b \pi^2 E}{\left(\frac{L_b}{r_t}\right)^2}$$

$$F_{cr} = \frac{1.0(0.999)\pi^2(29{,}000)}{\left(\frac{27.83(12)}{9.08}\right)^2} = 211.4 \text{ ksi}$$

The calculated value of F_{cr} for use in Equation 3.2.9 is not limited to $R_b R_h F_{yc}$ (refer to *AASHTO LRFD* Article C6.10.1.6).

f_{bu} in Equation 3.2.9 is again to be taken as the largest value of the compressive major-axis bending stress throughout the unbraced length under consideration. The amplification factor is therefore determined as follows:

$$AF = \frac{0.85}{\left(1 - \frac{|-41.96|}{211.4}\right)} = 1.06 > 1.0 \quad \text{ok}$$

The second-order elastic compression-flange lateral bending stress to be used in the design verification for the bottom flange is therefore computed as follows. Note that first- or second- order flange lateral bending stresses, as applicable, due to all sources are limited to a maximum value of $0.6F_{yf}$ according to *AASHTO LRFD* Equation 6.10.1.6-1:

Pier 1:

$$f_\ell = (AF)f_{\ell 1} = 1.06(7.55) = 8.00 \text{ ksi} < 0.6F_{yf} = 30.00 \text{ ksi}$$

ok (Ratio = 0.267)

AASHTO LRFD Article 6.10.1.6 specifies that for design checks where the flexural resistance is based on lateral torsional buckling, f_{bu} and f_ℓ are to be taken as the largest values throughout the unbraced length in the flange under consideration. In this case, both stresses are largest at Pier 1. For design checks where the flexural resistance is based on flange local buckling or yielding, f_{bu} and f_ℓ may be determined as the stress at the section under consideration (again Pier 1 in this case).

Check the bottom flange at Pier 1 (Equation 3.2.81):

$$f_{bu} + \frac{1}{3}f_\ell \le \phi_f F_{nc}$$

- Flange local buckling:

$$f_{bu} + \frac{1}{3}f_\ell = |-41.96| \text{ ksi} + \frac{8.00}{3} \text{ ksi} = 44.63 \text{ ksi}$$

$$\phi_f F_{nc} = 1.0(49.96) = 49.96 \text{ ksi}$$

$$44.63 \text{ ksi} < 49.96 \text{ ksi} \quad \text{ok} \quad (\text{Ratio} = 0.893)$$

- Lateral torsional buckling:

$$f_{bu} + \frac{1}{3}f_{\ell} = \left|-41.96\right| \text{ ksi} + \frac{8.00}{3} \text{ ksi} = 44.63 \text{ ksi}$$
$$\phi_f F_{nc} = 1.0(47.08) = 47.08 \text{ ksi}$$
$$44.63 \text{ ksi} < 47.08 \text{ ksi} \qquad \text{ok} \qquad (\text{Ratio} = 0.948)$$

Check the top flange at Pier 1 (Equation 3.2.108):

$$f_{bu} \le \phi_f R_h F_{yf}$$

$$f_{bu} = 48.07 \text{ ksi}$$
$$\phi_f R_h F_{yf} = 1.0(1.0)(50) = 50.00 \text{ ksi}$$
$$48.07 \text{ ksi} < 50.00 \text{ ksi} \qquad \text{ok} \qquad (\text{Ratio} = 0.961)$$

Since a significant moment gradient is present at the pier section, additional economy may be gained in this case, if desired, by calculating and applying the moment gradient modifier C_b. Determine C_b according to the procedure specified in *AASHTO LRFD* Article 6.10.8.2.3 (Section 3.2.6.4.1.2).

In the calculation of C_b, the stress, f_2, is defined as the largest factored vertical bending compressive stress at either end of the unbraced length in the flange under consideration, calculated from the critical moment envelope value, and is to be taken as positive. In this case, f_2 is taken equal to the factored vertical bending compressive stress in the bottom flange of G4 at Pier 1 = 41.96 ksi (calculated previously). C_b at the pier section is to be calculated as follows (Equation 3.2.100):

$$C_b = 1.75 - 1.05\left(\frac{f_1}{f_2}\right) + 0.3\left(\frac{f_1}{f_2}\right)^2 \le 2.3$$

Since the variation in the moment along the entire length between braced points is concave in shape, calculate the stress, f_1, as follows according to *AASHTO LRFD* Article 6.10.8.2.3 (Equation 3.2.101):

$$f_1 = f_o$$

where f_o is the factored vertical bending stress at the brace point opposite to the one corresponding to f_2 (f_o is taken as positive in compression).

From separate calculations, f_o at the brace point in Span 1 of G4 opposite to the brace point at Pier 1 is equal to 23.10 ksi. Therefore:

$$C_b = 1.75 - 1.05\left(\frac{23.10}{41.96}\right) + 0.3\left(\frac{23.10}{41.96}\right)^2 = 1.26 < 2.3$$

ok

f_o at the brace point in Span 2 of G4 opposite to the brace point at Pier 1 is equal to 22.84 ksi, which yields a slightly higher value of C_b equal to 1.27. The lower value of 1.26 will be used.

For values of C_b greater than 1.0, the equations of *AASHTO LRFD* Article D6.4.1 (*AASHTO LRFD* Appendix D6) are to be used to compute the lateral torsional buckling resistance. These equations recognize that the maximum lateral torsional buckling resistance, $(F_{nc})_{LTB} = F_{max} = R_b R_h F_{yc}$, can be reached at larger limiting unbraced lengths under a moment gradient.

According to *AASHTO LRFD* Article D6.4.1, since L_p = 18.22 feet < L_b = 27.83 feet < L_r = 68.43 feet, then (Equation 3.2.104):

$$\text{If } L_b \le L_p + \frac{\left(1 - \frac{1}{C_b}\right)}{\left(1 - \frac{F_{yr}}{R_h F_{yc}}\right)}\left(L_r - L_p\right), \text{ then :}$$

$$\left(F_{nc}\right)_{LTB} = R_b R_h F_{yc}$$

Since:

$$27.83 \text{ ft} < 18.22 + \frac{\left(1 - \frac{1}{1.26}\right)}{\left(1 - \frac{35.0}{50}\right)}(68.43 - 18.22) = 34.54 \text{ ft, then :}$$

$$\left(F_{nc}\right)_{LTB} = 0.999(1.0)(50) = 49.96 \text{ ksi}$$

Separate computations similar to those illustrated previously indicate that the bottom-flange plate of G4 at Pier 1 could safely be reduced from 2-3/4" x 33" to 2-3/4" x 30" when accounting for the effect of the moment gradient by utilizing C_b as demonstrated above.

All of the preceding computations assume an unbraced length in which the member is prismatic. *AASHTO LRFD* Article 6.10.8.2.3 specifies that for unbraced lengths containing a transition to a smaller section at a distance less than or equal to 20 percent of the unbraced length from the brace point with the smaller moment, the lateral torsional buckling resistance may be determined assuming the transition to the smaller section does not exist provided the lateral moment of inertia of the flange or flanges of the smaller section is equal to or larger than one-half the corresponding value in the larger section.

Otherwise, the lateral torsional buckling resistance must be taken as the smallest resistance within the unbraced length under consideration assuming the unbraced length is prismatic. The moment gradient modifier, C_b, must be taken equal to 1.0 in this case. This approximation is based on replacing the nonprismatic member with an equivalent prismatic member. If the cross-section within the unbraced length that gives the smallest uniform bending resistance is used, and the calculated resistance is not exceeded anywhere along the unbraced length, a conservative solution is obtained.

To avoid significant reductions in the lateral torsional buckling resistance in such cases, it is desirable to consider locating flange transitions within 20 percent of the unbraced length from the brace point with the smaller moment (where practical and economical to do so), and ensure that the lateral moment of inertia of the flange (or flanges) of the smaller section is greater than or equal to one-half of the corresponding value(s) for the flange(s) of the larger section at the transition (Figure 3.2.52).

5.1.8.4.2 Positive Flexure

Strength limit state verifications for I-sections subject to positive flexure are discussed in Section 3.2.6.5.2. According to *AASHTO LRFD* Article 6.10.6.2.2, at the strength limit state, composite sections in positive flexure in kinked (chorded) continuous or horizontally curved steel girder bridges are to be considered as noncompact sections designed according to the requirements of *AASHTO LRFD* Article 6.10.7.2. For noncompact sections, the nominal flexural resistance is not permitted to exceed the moment at first yield. The nominal flexural resistance in these cases is therefore more appropriately expressed in terms of the elastically computed flange stress.

According to *AASHTO LRFD* Article 6.10.7.2.1, at the strength limit state, compression flanges of noncompact composite sections in positive flexure must satisfy the following requirement (Equation 3.2.135):

$$f_{bu} \leq \phi_f F_{nc}$$

For composite sections in positive flexure, lateral bending does not need to be considered in the compression flange at the strength limit state because the flange is continuously supported by the concrete deck.

Tension flanges of noncompact composite sections in positive flexure must satisfy the following requirement (Equation 3.2.137):

$$f_{bu} + \frac{1}{3} f_{\ell} \le \phi_f F_{nt}$$

AASHTO LRFD Article 6.10.1.6 specifies that for design checks where the flexural resistance is based on yielding (as is the case here for both flanges), f_{bu} may be taken as the major-axis bending stress due to the factored loads at the section under consideration. f_{ℓ} may also be determined as the stress at the section under consideration.

5.1.8.4.2.1 Section at 66.31 ft from Abutment 1 in Span 1 of G4

Assemble the factored stresses for the Strength I load combination needed to check the preceding equations at the cross-frame located 66.31 feet from Abutment 1 in Span 1 of G4 (Figure 5.1.23 - refer to the fold-out sheets at the end of this example). The Strength IV load combination does not control by inspection. In this example, the load modifier, η, is taken equal to 1.0 at the strength limit state.

The unfactored vertical bending moments at this section from the 3D analysis (Table 5.1.2), and the section moduli to the top and bottom flanges are given as follows (note that the live load moment includes centrifugal force and dynamic load allowance effects):

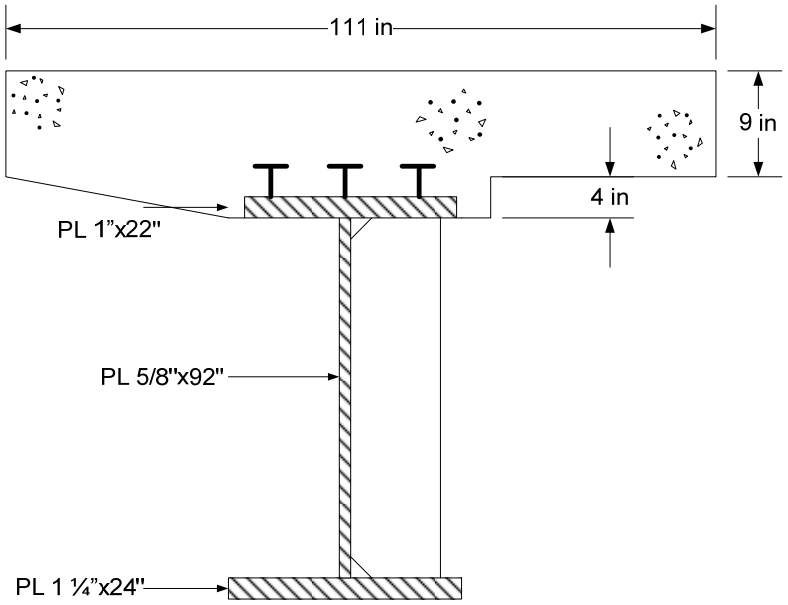


Figure 5.1.23 G4 Section at a Cross-Frame 66.31 Feet from Abutment 1 in Span 1

M_{DC1} = +4,798 kip-ft
M_{DC2} = +673 kip-ft
M_{DW} = +731 kip-ft
M_{-LL+IM} = +4,990 kip-ft
$S_{steel\ (top)}$ = -3,014 $in.^3$
$S_{steel\ (bot)}$ = 3,472 $in.^3$
$S_{3n\ deck\ (top)}$ = -7,706 $in.^3$
$S_{3n\ deck\ (bot)}$ = 4,259 $in.^3$
$S_{n\ deck\ (top)}$ = -19,070 $in.^3$
$S_{n\ deck\ (bot)}$ = 4,673 $in.^3$

The factored vertical bending stresses in the top and bottom flanges at this section are computed as follows:

- Top flange:

$$f_{bu} = 1.0\left[\frac{1.25(4{,}798)}{-3{,}014} + \frac{1.25(673)}{-7{,}706} + \frac{1.5(731)}{-7{,}706} + \frac{1.75(4{,}990)}{-19{,}070}\right]12 = -32{,}39 \text{ ksi}$$

- Bottom flange:

$$f_{bu} = 1.0\left[\frac{1.25(4{,}798)}{3{,}472} + \frac{1.25(673)}{4{,}259} + \frac{1.5(731)}{4{,}259} + \frac{1.75(4{,}990)}{4{,}673}\right]12 = 48.61 \text{ ksi}$$

The total factored lateral bending stress in the bottom flange at this cross-frame determined from the 3D analysis is 6.66 ksi (Figure 5.1.22). Since the cross-frames are contiguous in this region of the bridge, the lateral bending stress at this location is primarily due to the effects of curvature. For flanges in tension, no amplification of the flange lateral bending stress is required (i.e., AF = 1.0). *AASHTO LRFD* Article 6.10.1.6 specifies that the total factored lateral bending stress must not exceed $0.6F_{yf}$.

$$6.60 \text{ ksi} < 0.6F_{yf} = 0.6(50) = 30 \text{ ksi} \quad \text{ok}$$

$$(\text{Ratio} = 0.220)$$

Nominal Flexural Resistance

According to the provisions of *AASHTO LRFD* Article 6.10.7.2.2, the nominal flexural resistance of the compression flange of noncompact composite sections in positive flexure F_{nc} is taken as (Equation 3.2.136):

$$F_{nc} = R_b R_h F_{yc}$$

Since the section is a homogeneous built-up section, the hybrid factor, R_h, is equal to 1.0 (*AASHTO LRFD* Article 6.10.1.10.1 – Section 3.2.6.3).

According to *AASHTO LRFD* Article 6.10.1.10.2, the web load-shedding factor, R_b (Section 3.2.6.2), is to be taken as 1.0 for composite sections in positive flexure in which the web satisfies the requirement of *AASHTO LRFD* Article 6.10.2.1.1 such that longitudinal stiffeners are not required (i.e. $D/t_w \leq 150$). Further explanation as to why such sections are exempt from the calculation of R_b is given in Section 3.2.4.3.2.2.

Therefore:

$$F_{nc} = 1.0(1.0)(50) = 50.00 \text{ ksi}$$

The nominal flexural resistance of the tension flange is (Equation 3.2.138):

$$F_{nt} = R_h F_{yt}$$

Therefore:

$$F_{nt} = 1.0(50) = 50.00 \text{ ksi}$$

Flange Verifications

With all the required information now assembled, check the top flange at this section for the requirements of *AASHTO LRFD* Article 6.10.7.2.1 (Equation 3.2.135).

$$f_{bu} \leq \phi_f F_{nc}$$

$$\phi_f F_{nc} = 1.0(50.00) = 50.00 \text{ ksi}$$

$$\left|-32.39\right| \text{ ksi} < 50.00_0 \text{ ksi} \qquad (\text{Ratio} = 0.648)$$

Check the bottom flange (Equation 3.2.137):

$$f_{bu} + \frac{1}{3} f_\ell \leq \phi_f F_{nt}$$

$$f_{bu} + \frac{1}{3} f_\ell = 48.61 \text{ ksi} + \frac{6.60}{3} \text{ksi} = 50.81 \text{ ksi}$$

$$\phi_f F_{nt} = 1.0(50.00) = 50.00 \text{ ksi}$$

$$50.81 \text{ ksi} > 50.00 \text{ ksi} \quad (\text{Ratio} = 1.016)$$

Concrete Deck Verifications

Concrete deck verifications in regions of positive flexure are discussed in Section 3.2.6.5.4. According to *AASHTO LRFD* Article 6.10.7.2.1, the maximum longitudinal compressive stress in the concrete deck at the strength limit state is not to exceed $0.6f'_c$ to ensure linear behavior of the concrete (Equation 3.2.148).

As specified in *AASHTO LRFD* Article 6.10.1.1.1d, for calculating the longitudinal flexural stresses in the concrete deck due to all permanent and transient loads, the short-term modular ratio, *n*, is to be used. The section modulus to the top of the concrete deck (based on the *n*-composite section) at this section is –11,579 in.^{3}.

Calculate the factored longitudinal compressive stress in the deck at this section; the deck is not subject to DC_1 loads. The deck concrete has a value of 4.0 ksi for f'_c. The stress in the concrete deck is obtained by dividing the stress acting on the transformed section by *n*.

$$f_{deck} = 1.0\left[\frac{1.25(673) + 1.5(731) + 1.75(4{,}990)}{-11{,}579(8)}\right]12 = -1.382 \text{ ksi}$$

$$\left|-1.382 \text{ ksi}\right| < 0.6f'_c = 0.6(4.00) = 2.40 \text{ ksi}$$

$$\text{ok} \qquad (\text{Ratio} = 0.576)$$

Noncompact composite sections in positive flexure must also satisfy the following ductility requirement specified in *AASHTO LRFD* Article 6.10.7.3 to protect the concrete deck from premature crushing (Equation 3.2.149):

$$D_p \le 0.42D_t$$

Calculate the location of the neutral axis at the plastic moment M_p (i.e. the PNA) for the composite section. The equations given in *AASHTO LRFD* Table D6.1-1 will be utilized.

$$P_t = F_{yt}b_t t_t = 50(24.0)(1.25) = 1{,}500 \text{ kips}$$

$$P_w = F_{yw}Dt_w = 50(92.0)(0.625) = 2{,}875 \text{ kips}$$

$$P_c = F_{yc}b_c t_c = 50(22.0)(1.0) = 1{,}100 \text{ kips}$$

$$P_s = 0.85f_c^{'}b_s t_s = 0.85(4.0)(111.0)(9.0) = 3{,}397 \text{ kips}$$

Since $P_t + P_w + P_c = 5{,}475$ kips > $P_s = 3{,}397$ kips, the PNA is in the top flange. Therefore, use Case II in *AASHTO LRFD* Table D6.1-1:

$$\overline{y} = \frac{t_c}{2}\left[\frac{P_w + P_t - P_s}{P_c} + 1\right]$$

$$\overline{y} = \frac{1.0}{2}\left[\frac{2{,}875 + 1{,}500 - 3{,}397}{1{,}100} + 1\right] = 0.945 \text{ in. from the top of the top flange}$$

Check equilibrium by calculating and comparing the total plastic forces acting on the compression and tension sides of the plastic neutral axis:

- Compression side:

$$3{,}397 + 50(22.0)(0.945) = 4{,}437 \text{ kips}$$

- Tension side:

$$50(22.0)(1.0 - 0.945) + 2{,}875 + 1{,}500 = 4{,}436 \text{ kips} \qquad \text{say ok}$$

$$D_p = 9.0 + 4.0 - 1.0 + 0.945 = 12.945 \text{ in.}$$

$$D_t = 1.25 + 92.0 + 4.0 + 9.0 = 106.25 \text{ in.}$$

$$0.42D_t = 0.42(106.25) = 44.625 \text{ in.} > 12.945 \text{ in.}$$

$$\text{ok} \qquad (\text{Ratio} = 0.290)$$

Neither of the preceding concrete deck verifications is likely to control for typical sections utilized in unshored construction. The limit on the longitudinal compressive stress in the deck is unlikely to govern except in cases involving: 1) shored construction, or unshored construction where the noncomposite steel dead load stresses are low, combined with 2) geometries causing the neutral axis of the short-term and long-term composite section to be significantly below the bottom of the concrete deck. The ductility requirement is unlikely to govern for noncompact sections unless sections are utilized in shored construction and/or steels with higher yield strengths (up to 100 ksi) are utilized.

5.1.8.4.3 Shear

5.1.8.4.3.1 General

Strength limit state design for shear covered in Section 3.2.7. *AASHTO LRFD* Article 6.10.6.3 refers to the provisions of *AASHTO LRFD* Article 6.10.9 to determine the nominal shear resistance at the strength limit state. Webs must satisfy the following at the strength limit state (Equation 3.2.152):

$$V_u \le \phi_v V_n$$

Shear design will be demonstrated for an end panel and for two interior panels located in Span 1 of G4 from the example bridge.

The values of the factored shear, V_u, at each cross-frame in Span 1 of G4 under the Strength I load combination are plotted below in Figure 5.1.24 (the Strength IV load combination does not control by inspection). The η factor is taken equal to 1.0. The shears are taken from the 3D analysis. Live-load shears are taken as the shear envelope values.
A sample calculation of V_u at Abutment 1 is given below (the unfactored shears are obtained from Table 5.1.3):

$$V_u = 1.0\left[1.25(142+26)+1.5(22)+1.75(152)\right] = 509 \text{ kips}$$

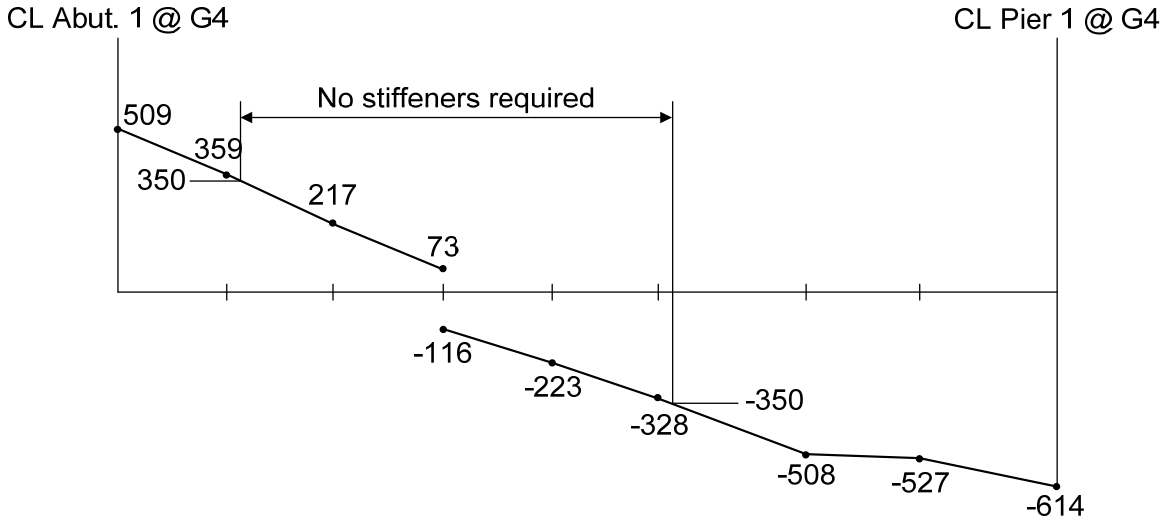


Figure 5.1.24 Factored Design Shears, V_u (kips), at Cross-Frames in Span 1 of G4 (Strength I)

The shears at the cross-frames are plotted because they include the net vertical components of the total factored forces in the cross-frame framing into the girder at each location that result from the effects of curvature and skew.

Note that the shear diagram begins to flatten out as the skewed Pier 1 is approached. In this region, the cross-frame forces are becoming larger due to the effects of the skew.

Figure 5.1.25 shows a plot of the unfactored negative DC_1 shears in Span 1 of G4 at the cross-frames in the region approaching Pier 1 taken from the 3D analysis (Table 5.1.3), which considers the effect of the cross-frames. The dotted line in the figure shows the projected DC_1 girder shears assuming the effect of the cross-frames is neglected. The unfactored DC_1 forces in the diagonals of the two cross-frames adjacent to Pier 1 at Girder 4 taken from the 3D analysis are also shown in the figure. The length of the diagonals is computed as follows:

$$\text{Vertical component} = \frac{92}{160.9} = 0.57$$

$$\ell_{diag} = \sqrt{(92)^2 + (132)^2} = 160.9 \text{ in.}$$

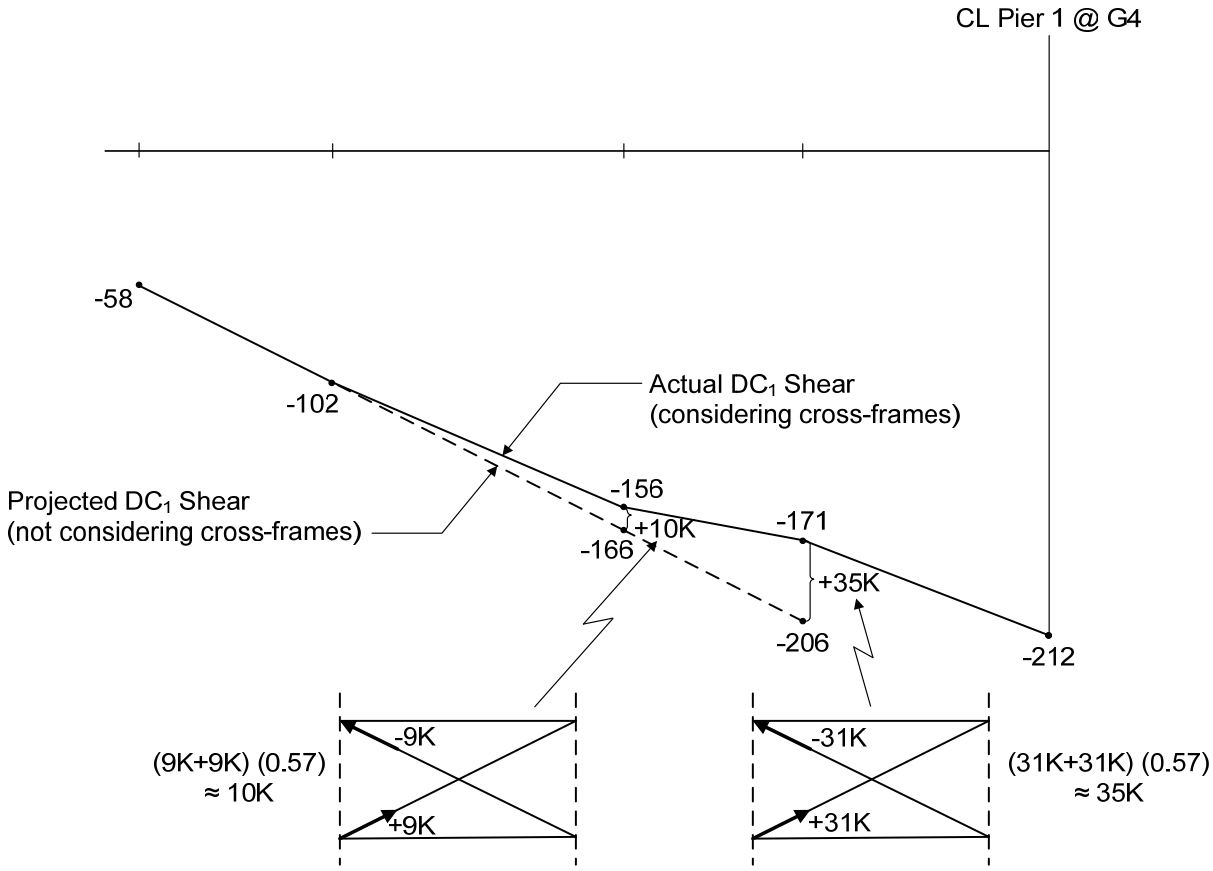


Figure 5.1.25 Unfactored DC_1 Shears (kips) at Cross-Frames in Span 1 of G4 Adjacent to Pier 1

As illustrated in Figure 5.1.25, the difference in the actual and projected DC_1 shears is due to the effect of the net vertical component of the forces in the cross-frames, which must be considered in curved and skewed bridges in order to obtain the proper girder shears.

The kink in the negative shear shown at Pier 1 in Figure 5.1.24 and Figure 5.1.25 reflects an adjustment made in the live load shear in the 3D analysis software so that the total factored interior-pier shears, when properly summed, will match the reported total factored pier reaction, which includes the vertical component of the total factored forces in the cross-frame framing into the pier at G4. In this case, the net vertical component of the cross-frame forces goes directly into the pier reaction and is not seen by the girder.

5.1.8.4.3.2 Unstiffened Web

Determine the nominal shear resistance of an unstiffened web according to the provisions of *AASHTO LRFD* Article 6.10.9.2. The nominal shear resistance of an

unstiffened web is limited to the shear buckling resistance V_{cr} determined as (Equation 3.2.161):

$$V_n = V_{cr} = CV_p$$

C is the ratio of the shear buckling resistance to the shear yield strength determined from *AASHTO LRFD* Equation 6.10.9.3.2-4, 6.10.9.3.2-5 or 6.10.9.3.2-6, as applicable, with the shear buckling coefficient k taken equal to 5.0.

Since:

$$1.40\sqrt{\frac{Ek}{F_{yw}}} = 1.40\sqrt{\frac{29{,}000(5.0)}{50}} = 75.4 < \frac{D}{t_w} = \frac{92.0}{0.625} = 147.2$$

Equation 3.2.158 is used to compute *C* as follows:

$$C = \frac{1.57}{\left(\frac{D}{t_w}\right)^2}\left(\frac{Ek}{F_{yw}}\right)$$

$$C = \frac{1.57}{(147.2)^2}\left(\frac{29{,}000(5.0)}{50}\right) = 0.210$$

V_p is the plastic shear force determined as follows (Equation 3.2.151):

$$V_p = 0.58F_{yw}Dt_w$$

$$V_p = 0.58(50)(92.0)(0.625) = 1{,}668 \text{ kips}$$

Therefore,

$$V_n = V_{cr} = 0.210(1{,}668) = 350 \text{ kips}$$

$$\phi_v V_n = 1.0(350) = 350 \text{ kips}$$

5.1.8.4.3.3 End Panel

V_u is 509 kips at Abutment 1 (Figure 5.1.24), which exceeds $\phi_v V_n$ = 350 kips for an unstiffened web determined above. Therefore, transverse stiffeners are required and the provisions of *AASHTO LRFD* Article 6.10.9.3 apply.

According to *AASHTO LRFD* Article 6.10.9.3.3, the nominal shear resistance of a web end panel is limited to the shear buckling resistance V_{cr} determined as (Equation 3.2.161):

$$V_n = V_{cr} = CV_p$$

First, compute the shear buckling coefficient *k*. According to *AASHTO LRFD* Article 6.10.9.3.3, the transverse stiffener spacing for end panels is not to exceed 1.5*D* = 1.5(92.0) = 138.0 inches. Assume the spacing from Abutment 1 to the first transverse stiffener is one-half of the cross-frame spacing adjacent to Abutment 1; i.e. d_o = 22.104 feet/2 = 11.052 feet = 132.625 inches, which is less than the maximum permitted spacing of 138.0 inches. From Equation 3.2.157:

$$k = 5 + \frac{5}{\left(\frac{132.625}{92.0}\right)^2} = 7.406$$

Since,

$$1.40\sqrt{\frac{Ek}{F_{yw}}} = 1.40\sqrt{\frac{29{,}000(7.406)}{50}} = 91.8 < \frac{D}{t_w} = \frac{92.0}{0.625} = 147.2$$

Equation 3.2.158 is used to compute *C* as follows:

$$C = \frac{1.57}{(147.2)^2}\left(\frac{29{,}000(7.406)}{50}\right) = 0.311$$

Therefore:

$$V_n = V_{cr} = CV_p = 0.311(1{,}668) = 519 \text{ kips}$$

$$\phi_v V_n = 1.0(519) = 519 \text{ kips} > V_u = 509 \text{ kips}$$
$$\text{ok} \qquad (\text{Ratio} = 0.981)$$

5.1.8.4.3.4 Interior Panels

First Interior Panel to the Right of the End Panel Adjacent to Abutment 1 (G4)

According to *AASHTO LRFD* Article 6.10.9.1, the transverse stiffener spacing for interior panels without a longitudinal stiffener is not to exceed 3*D* = 3(92.0) = 276.0 inches. For the first interior panel to the right of the end panel adjacent to Abutment 1 in G4, the transverse stiffener spacing d_o = 11.052 feet = 132.625 inches, which is again equal to one-half the cross-frame spacing adjacent to Abutment 1 (the cross-frame connection plate adjacent to Abutment 1 is assumed to serve as a transverse stiffener). The spacing is less than the maximum permitted spacing of 276.0 inches.

At the first transverse stiffener located d_o = 11.052 feet from Abutment 1, V_u is equal to 431 kips. This value exceeds $\phi_v V_n$ = 350 kips for an unstiffened web so that transverse stiffeners are required. However, V_u in this case is less than the factored shear-buckling resistance of this panel, which was computed above for the adjacent end panel in Section 5.1.8.4.3.3 ($\phi_v V_{cr}$ = 519 kips) that has the same stiffener spacing. Therefore, this panel is satisfactory for shear and development of the post-buckling tension-field shear resistance is not required.

First Interior Panel to the Left of Pier 1 (G4)

At Pier 1, $|V_u|$ is 614 kips, which exceeds $\phi_v V_n$ = 350 kips for an unstiffened web so that transverse stiffeners are required.

For the first interior panel in G4 to the left of Pier 1, assume a transverse stiffener spacing equal to one-half the cross-frame spacing adjacent to Pier 1 in Span 1; that is, d_o = 27.833 feet/2 = 13.917 feet = 167.0 inches, which is less than the maximum permitted spacing of 276.0 inches (note: the bearing stiffeners at Pier 1 and the cross-frame connection plate in Span 1 adjacent to Pier 1 are assumed to act as transverse stiffeners). Separate calculations show that $|V_u|$ exceeds the factored shear buckling resistance, $\phi_v V_{cr}$, of this panel equal to 457 kips. Therefore, this panel must be designed for the additional post-buckling shear resistance due to tension-field action.

For interior panels of both nonhybrid and hybrid members with the section along the entire panel proportioned such that (Equation 3.2.164):

$$\frac{2Dt_w}{\left(b_{fc}t_{fc} + b_{ft}t_{ft}\right)} \le 2.5$$

the nominal shear resistance, V_n, is to be taken as the sum of the shear buckling resistance and the full postbuckling resistance due to tension-field action, or (Equation 3.2.163):

$$V_n = V_p\left[C + \frac{0.87(1-C)}{\sqrt{1+\left(\frac{d_o}{D}\right)^2}}\right]$$

For this panel:

$$\frac{2(92.0)(0.625)}{[33(2.75)+28(2.5)]} = 0.72 < 2.5$$

Therefore, the nominal shear resistance is determined according to Equation 3.2.163. From Equation 3.2.157:

$$k = 5 + \frac{5}{\left(\frac{167.0}{92.0}\right)^2} = 6.517$$

Since:

$$1.40\sqrt{\frac{Ek}{F_{yw}}} = 1.40\sqrt{\frac{29{,}000(6.517)}{50}} = 86.1 < \frac{D}{t_w} = \frac{92.0}{0.625} = 147.2$$

Equation 3.2.158 is used to compute *C* as follows:

$$C = \frac{1.57}{(147.2)^2}\left(\frac{29{,}000(6.517)}{50}\right) = 0.274$$

Therefore:

$$V_n = 1{,}668\left[0.274 + \frac{0.87(1-0.274)}{\sqrt{1+\left(\frac{167.0}{92.0}\right)^2}}\right] = 965 \text{ kips}$$

$$\phi_v V_n = 1.0(965) = 965 \text{ kips} > |V_u| = 614 \text{ kips}$$
$$\text{ok} \qquad (\text{Ratio} = 0.636)$$

5.1.8.5 Shear Connector Design

Shear connector design is covered in Section 3.3.2. Shear connectors are designed according to the provisions of *AASHTO LRFD* Article 6.10.10. The design of shear connectors will be demonstrated for G4 from the example bridge.

Shear connectors are required throughout the entire length of the girders in these structures because of the torsional shear that exists along the entire span of horizontally curved continuous composite bridges. Both stud and channel shear connectors are permitted in *AASHTO LRFD* Article 6.10.10.1.1. Stud shear connectors are much more commonly used and are utilized in this example.

5.1.8.5.1 Stud Proportions

Terminating the studs at approximately the mid-thickness of the concrete deck (i.e. within the core of the deck) will place them well within the limits for cover and penetration specified in *AASHTO LRFD* Article 6.10.10.1.4 (i.e. required cover and penetration both greater than or equal to 2.0 inches), and will also clear the reinforcing steel (Section 3.3.2.1.1.3).

Use the structural thickness of the deck, the deck haunch thickness and the smallest top flange thickness (i.e. 1.0 inch) to estimate a required stud height as follows:

$$\frac{9.0}{2} + (4.0 - 1.0) = 7.5 \text{ in.}$$

Use 7/8″ x 7″ studs. Check that the ratio of the height to the diameter is not less than 4.0, as required in *AASHTO LRFD* Article 6.10.10.1.1 (Section 3.3.2.1.1.1):

$$\frac{h}{d} = \frac{7.0}{0.875} = 8.0 > 4.0 \quad \text{ok}$$

5.1.8.5.2 Pitch

According to the provisions of *AASHTO LRFD* Article 6.10.10.1.2, the pitch of the shear connectors along the longitudinal axis of the girder is to be initially determined to satisfy the fatigue limit state. The resulting number of shear connectors is then to be checked against the number required to satisfy the strength limit state.

5.1.8.5.2.1 Fatigue Limit State

Fatigue limit state requirements for shear connectors are discussed in Section 3.3.2.2. *AASHTO LRFD* Article 6.10.10.1.2 specifies that the pitch, *p*, of the shear

connectors, or center-to-center distance between shear connectors along the longitudinal axis, must satisfy the following requirement (Equation 3.3.2):

$$p \le \frac{nZ_r}{V_{sr}}$$

The horizontal fatigue shear range per unit length, V_{sr}, is to be computed as follows (Equation 3.3.3):

$$V_{sr} = \sqrt{(V_{fat})^2 + (F_{fat})^2}$$

V_{fat} is the longitudinal fatigue shear range per unit length (kips/in.) computed as (Equation 3.3.4):

$$V_{fat} = \frac{V_f Q}{I}$$

For curved girders, the parameters *I* and *Q* are always to be determined using the deck within the effective flange width.

F_{fat} is the radial fatigue shear range per unit length (kips/in.) taken as the larger of either (Equation 3.3.5):

$$F_{fat1} = \frac{A_{bot}\sigma_{flg}\ell}{wR}$$

or (Equation 3.3.6):

$$F_{fat2} = \frac{F_{rc}}{w}$$

Equation 3.3.5 is used to determine the radial fatigue shear range resulting from any curvature between the brace points. The shear range is taken as the radial component of the maximum longitudinal range of force in the bottom flange between brace points, which is used as a measure of the major-axis bending moment. *AASHTO LRFD* Article 6.10.10.1.2 specifies that for straight spans or segments, F_{fat1} may be taken equal to zero.

Equation 3.3.6 provides the radial fatigue shear range in cases where torsion is caused by effects other than curvature, such as skew. This equation will typically control for cases where discontinuous cross-frame lines are used in conjunction with skew angles exceeding 20 degrees (which is the case in this example) in either a straight or a horizontally curved bridge. For all other cases, F_{fat2} may be taken equal to zero according to *AASHTO LRFD* Article 6.10.10.1.2.

F_{rc} in Equation 3.3.6 represents the resultant range of horizontal force from all cross-frames at the point under consideration due to the factored fatigue load plus impact that is resisted by the shear connectors. In this example, F_{rc} is determined from the results of the 3D analysis and both F_{fat1} and F_{fat2} must be considered.

The fatigue resistance, Z_r, of an individual stud shear connector is specified in *AASHTO LRFD* Article 6.10.10.2 (Section 3.3.2.2.1.3). If $(ADTT)_{SL}$ is greater than or equal to 960 trucks per day (assuming a 75-year fatigue design life and one stress range cycle n per truck passage), then the studs must be designed for infinite life using the Fatigue I load combination and the fatigue resistance of an individual stud determined as (Equation 3.3.9):

$$Z_r = 5.5d^2$$

In Section 5.1.8.3.2, the $(ADTT)_{SL}$ for this example was calculated to be 1,600 trucks/day, which exceeds 960 trucks per day.

For continuous spans with span lengths greater than 40.0 feet, the number of stress range cycles per truck passage, n, is equal to 1.5 at sections that are 'near the interior support' (*AASHTO LRFD* Table 6.6.1.2.5-2). Sections ′near the interior support′ are defined as sections less than or equal to a distance of one-tenth the span on each side of the interior support. In these regions, the 75-year $(ADTT)_{SL}$ equivalent to infinite life is equal to 960/1.5 = 640 trucks/day, which is still less than 1,600 trucks/day.

Thus, the studs along the entire span must be designed for infinite life using the Fatigue I load combination, with Z_r taken as follows:

$$Z_r = 5.5d^2 = 5.5(0.875)^2 = 4.21 \text{ kips}$$

The number of shear connectors in a cross-section, n, will be assumed equal to three (3). Requirements for the transverse spacing of shear connectors across the top flange are given in *AASHTO LRFD* Article 6.10.10.1.3 (Section 3.3.2.1.1.2).

A sample calculation of the required shear connector pitch at the fatigue limit state will be made at the cross-frame located 66′-3¾″ from Abutment 1 into Span 1 of G4 (refer to the fold-out sheets at the end of this example and the cross-section in Figure 5.1.23).

First, calculate the longitudinal fatigue shear range per unit length, V_{fat}. From the 3D analysis, the vertical fatigue shear force range per unit length, V_f, at this location is determined for the factored fatigue load (factored by the 1.5 load factor specified for the Fatigue I load combination) including the specified dynamic load allowance of 15 percent as (Table 5.1.3):

$$V_f = 1.5(21 + |-23|) = 1.5(44) = 66 \text{ kips}$$

The first moment, Q_n, of the transformed short-term area of the structural concrete deck about the neutral axis of the short-term composite section at this location is calculated as follows. The transformed area of the concrete deck includes the deck overhang taper (Figure 5.1.3). The thickness at the outside edge of the deck is 9.5 inches. An average 20-inch width is assumed for the deck haunch. The short-term modular ratio n is equal to 8:

$$\text{Effective width of deck} = 3.75(12) + \left(\frac{11.0}{2}\right)(12) = 45 + 66 = 111.0 \text{ in}$$

$$A_{deck} = \left[9.0(66 + 20/2) + \left(\frac{13.0 + 9.5}{2}\right)(45 - 20/2)\right] = 1{,}078 \Big/ 8 = 134.75 \text{ in.}^2$$

$$\bar{y}\, A_{deck} = \left(\frac{9.0}{2}\right)(9.0)(76) + \left(\frac{9.5}{2}\right)(9.5)(35) + \left(9.5 + \frac{3.5}{3}\right)\frac{1}{2}(3.5)(35) = 5{,}311 \text{ in.}^2$$

$$\bar{y} = \frac{\bar{y}\, A_{deck}}{A_{deck}} = \frac{5{,}311}{1{,}078} = 4.93 \text{ in. from the top of the deck}$$

The distance from the neutral axis of the short-term composite section to the neutral axis of the transformed deck = 25.62 in.

$$Q_n = (134.75)(25.62) = 3{,}452 \text{ in.}^3$$

$$I_n = 353{,}749 \text{ in.}^4$$

Therefore, from Equation 3.3.4:

$$V_{fat} = \frac{V_f Q_n}{I_n} = \frac{66(3{,}452)}{353{,}749} = 0.64 \text{ kips / in.}$$

Next, calculate the radial fatigue shear range per unit length, F_{fat}. First, calculate the radial fatigue shear range due to curvature, F_{fat1}, from Equation 3.3.5. From the 3D analysis, the range of moment for the factored fatigue load (factored by the 1.5 load factor specified for the Fatigue I load combination) including the specified dynamic load allowance of 15 percent is (Table 5.1.2):

$$M_{range} = 1.5[1{,}549 + |-289|] = 2{,}757 \text{ kip} - \text{ft}$$

The range of longitudinal stress at the mid-thickness of the 1-1/4" x 24" bottom flange due to the factored fatigue load, calculated without consideration of flange lateral bending, is computed as:

$$\sigma_{f\,lg} = \frac{2{,}757(12)(75.7 - 1.25/2)}{353{,}749} = 7.02 \text{ ksi}$$

A_{bot} = 1.25(24.0) = 30.0 in.^{2}; ℓ = 22.104 ft; R = 716.5 ft; w = 48.0 in.

Therefore, from Equation 3.3.5:

$$F_{fat1} = \frac{A_{bot}\sigma_{f\,lg}\ell}{wR} = \frac{30.0(7.02)(22.104)}{48.0(716.5)} = 0.13 \text{ kips/in.}$$

Next, calculate the radial fatigue shear range due to skew effects, $F_{fat,}$ from Equation 3.3.6. G4 is an exterior girder and the cross-frames radial to G4 are all arranged in an X-type configuration, except at the abutments. In order to compute the resultant range of horizontal cross-frame force at the top flange, F_{rc}, used to compute the radial shear range, F_{fat2}, horizontal components of the range must be computed for the diagonal members in the cross-frame radial to the girder at this location as follows (Figure 3.3.8):

$$\text{Length of diagonal} = \sqrt{(11.0)^2 + \left(\frac{92.0}{12}\right)^2} = 13.4 \text{ feet}$$

$$\text{Horizontal component of diagonal range} = F_{ND}\left(\frac{11.0}{13.4}\right) = 0.82F_{ND}$$

where F_{ND} is the range of factored fatigue load plus impact axial force in the diagonal of the cross-frame radial to the girder. F_{NT} is the range of factored fatigue load plus impact axial force in the top chord of the cross-frame radial to the girder. From the 3D analysis:

Cross-Frame @ 66′-3¾″ from Abutment 1:

F_{NT} = 1.5(1.33) = 2 kips

F_{ND} = 1.5(13.33) = 20 kips

Horizontal component = $0.82F_{ND}$ = 0.82(20) = 16.4 kips

$\therefore$ F_{rc} = 2 kips + 16.4 kips = 18.4 kips

Therefore, from Equation 3.3.6:

$$F_{fat2} = \frac{F_{rc}}{w} = \frac{18.4}{48.0} = 0.38 \text{ kips/in.}$$

F_{fat} is taken as the larger of F_{fat1} and F_{fat2}. Thus:

$$F_{fat} = F_{fat2} = 0.38 \text{ kips/in.}$$

Calculate the horizontal fatigue shear range per unit length, V_{sr} (Equation 3.3.3):

$$V_{sr} = \sqrt{(V_{fat})^2 + (F_{fat})^2} = \sqrt{(0.64)^2 + (0.38)^2} = 0.74 \text{ kips/in.}$$

Calculate the required pitch, p, at this location (Equation 3.3.2):

$$p \le \frac{nZ_r}{V_{sr}} = \frac{3(4.21)}{0.74} = 17.1 \text{ in.}$$

Table 5.1.14 summarizes the required stud pitch along G4 at each cross-frame location to satisfy the fatigue limit state according to *AASHTO LRFD* Equation 6.10.10.1.2-1. *AASHTO LRFD* Article 6.10.10.1.2 specifies that the pitch not be less than six stud diameters = 6(0.875) = 5.25 inches or more than 24.0 inches (Section 3.3.2.1.1.4). Q_n and I_n include the deck plus the longitudinal reinforcement in regions of negative flexure.

A K-type configuration is used at the abutments for the radial cross-frames, with the K-node located at the mid-length of the top strut. Thus, the diagonals have no effect on the computation of F_{rc} in this case and F_{rc} is simply equal to the range of axial force in the top chord of the radial cross-frame at each abutment due to the factored fatigue load plus impact, F_{NT}.

Cross-frames are also present along the skewed support lines at Piers 1 and 2 in this case. These cross-frames are also arranged in a K-type configuration, with the K-node located at the mid-length of the bottom strut. Therefore, in order to compute the resultant range of horizontal cross-frame force at the top flange, F_{rc}, horizontal components of the range must be computed as follows at Piers 1 and 2 (Figure 3.3.8):

Length of skewed top chord =

$$\sqrt{(17.8125)^2 + (11.0)^2} = 20.94 \text{ feet}$$

Length of diagonal in skewed cross-frame =

$$\sqrt{(20.94/2)^2 + (92.0/12)^2} = 12.98 \text{ feet}$$

Horizontal component of diagonal range along skewed top chord =

$$F_{SD}\left(\frac{20.94/2}{12.98}\right) = 0.81F_{SD}$$

Horizontal component of resultant skewed top-chord range =

$$\left(F_{ST} + 0.81F_{SD}\right)\left(\frac{11.0}{20.94}\right) = 0.525F_{ST} + 0.425F_{SD}$$

where F_{ST} is the range of factored axial force in the top chord of the skewed cross-frame and F_{SD} is the range of factored axial force in the diagonal of the skewed cross-frame. All ranges of factored axial force are due to the fatigue load plus impact.

- Pier 1:

  F_{ST} = 1.5(2.67) = 4 kips
  F_{SD} = 1.5(12) = 18 kips

  Horizontal component of resultant
  = $0.525F_{ST} + 0.425F_{SD}$ = 0.525(4) + 0.425(18) = 9.8 kips

  $\therefore F_{rc}$ = 9.8 kips

- Pier 2:

  F_{ST} = 1.5(4) = 6 kips
  F_{SD} = 1.5(5.33) = 8 kips

  Horizontal component of resultant
  = $0.525F_{ST} + 0.425F_{SD}$ = 0.525(6) + 0.425(8) = 6.6 kips

  $\therefore F_{rc}$ = 6.6 kips

Table 5.1.14 G4 Required Stud Shear Connector Pitch – Fatigue Limit State

Location From Support (ft)	V_f (kips)	Q_n (in.^{3})	I_n (in.^{4})	V_{fat} (kips/in.)	F_{fat1} (kips/in.)	F_{rc} (kips)	F_{fat2} (kips/in.)	V_{sr} (kips/in.)	p (in./row)
Abut. 1	94	3,190	318,632	0.94	0.00	4.0	0.17	0.96	13.1
22.104	70	3,190	318,632	0.70	0.07	15.1	0.31	0.76	16.6
44.21	64	3,452	353.749	0.62	0.12	15.8	0.33	0.70	18.0
66.313	66	3,452	353,749	0.64	0.13	18.4	0.38	0.74	17.1
88.42	66	3,452	353,749	0.64	0.13	29.9	0.62	0.89	14.2
110.52	78	3,190	318,632	0.78	0.18	10.9	0.23	0.81	15.6
140.52	84	4,024	447,839	0.75	0.19	16.6	0.35	0.83	15.2
163.57	78	5,042	694,050	0.57	0.17	25.5	0.53	0.78	16.2
Pier 1	110	5,042	694,050	0.80	0.23	9.8	0.20	0.83	15.2
22.302	98	5,042	694,050	0.71	0.13	16.6	0.35	0.79	16.0
44.604	80	4,024	447,839	0.72	0.14	31.9	0.66	0.98	12.9
66.906	68	3,032	294,175	0.70	0.10	16.8	0.35	0.78	16.2
89.208	66	3,032	294,175	0.68	0.09	18.4	0.38	0.78	16.2
111.51	66	3,032	294,175	0.68	0.08	31.5	0.66	0.95	13.3
133.81	74	3,032	294,175	0.76	0.12	12.9	0.27	0.81	15.6
163.81	72	3,733	383,205	0.70	0.13	16.2	0.34	0.78	16.2
187.06	70	4,724	574,647	0.57	0.12	21.8	0.45	0.73	17.3
Pier 2	111	4,724	574,647	0.91	0.16	6.6	0.14	0.92	13.7
22.688	88	4,724	574,647	0.72	0.13	16.6	0.34	0.80	15.8
45.375	76	3,733	383,205	0.74	0.15	30.2	0.63	0.97	13.0
68.063	66	2,958	281,488	0.69	0.11	18.4	0.38	0.79	16.0
90.75	62	2,958	281,488	0.65	0.09	18.4	0.38	0.75	16.8
113.438	66	2,958	281,488	0.69	0.06	16.8	0.35	0.77	16.4
Abut. 2	90	2,958	281,488	0.95	0.00	4.0	0.17	0.96	13.1

5.1.8.5.2.2 Strength Limit State

The resulting number of shear connectors will now be checked against the number required to satisfy the strength limit state. Strength limit state requirements for shear connectors are discussed in Section 3.3.2.3. According to *AASHTO LRFD* Article 6.10.10.4.1, the factored shear resistance of a single shear connector, Q_r, at the strength limit state is to be taken as (Section 3.3.2.3.2 – Equation 3.3.22):

$$Q_r = \phi_{sc} Q_n$$

AASHTO LRFD Article 6.10.10.4.3 specifies that the nominal shear resistance of one stud shear connector embedded in a concrete deck is to be taken as (Equation 3.3.23):

$$Q_n = 0.5 A_{sc} \sqrt{f'_c E_c} \le A_{sc} F_u$$

$$A_{sc} = \frac{\pi}{4}(0.875)^2 = 0.60 \text{ in.}^2$$

$$A_{sc}F_u = (0.60)(60.0) = 36.00 \text{ kips}$$

$$Q_n = 0.5(0.60)\sqrt{4.0(3{,}644)} = 36.22 \text{ kips} > 36.00 \text{ kips}$$

$$\therefore Q_n = 36.00 \text{ kips}$$

$$Q_r = 0.85(36.00) = 30.60 \text{ kips}$$

At the strength limit state, the minimum number of shear connectors, *n*, over the region under consideration is to be taken as (Equation 3.3.12):

$$n = \frac{P}{Q_r}$$

where *P* is the total nominal shear force determined as specified in *AASHTO LRFD* Article 6.10.10.4.2. According to *AASHTO LRFD* Article 6.10.10.4.2, for continuous spans that are composite for negative flexure in the final condition (which is the case in this example), the total nominal shear force, *P*, between the point of maximum positive design live load plus impact moment and an adjacent end of the member is to be determined as (Equation 3.3.13):

$$P = \sqrt{P_P^2 + F_P^2}$$

where P_p is the total longitudinal force in the concrete deck at the point of maximum positive live load plus impact moment taken as the lesser of (Equation 3.3.14):

$$P_{1p} = 0.85f_c'b_s t_s$$

where b_s and t_s are the effective width and thickness of the concrete deck, respectively, or from Equation 3.3.15:

$$P_{2p} = F_{yw}Dt_w + F_{yt}b_{ft}t_{ft} + F_{yc}b_{fc}t_{fc}$$

F_p is the total radial force in the concrete deck at the point of maximum positive live load plus impact moment taken as (Equation 3.3.16):

$$F_p = P_p \frac{L_p}{R}$$

where L_p is the arc length between an end of the girder and an adjacent point of maximum positive live load plus impact moment (Figure 3.3.9), and R is the minimum girder radius over the length, L_p.

F_p is provided to account for the radial effect of curvature and is required for curved spans or segments to bring the smallest longitudinal force from either the deck or girder into equilibrium. F_p may be taken equal to zero for straight spans or segments.

The point of maximum positive live load plus impact moment in Span 1 of G4 is located 66.31 feet from Abutment 1. In Span 3, this point is located 68.06 feet from Abutment 1.

$$P_{1p} = 0.85(4.0)(111.0)(9.0) = 3{,}397 \text{ kips}$$

For the steel section at the point of maximum live load moment in Span 1:

$$P_{2p} = (50.0)(92.0)(0.625) + (50.0)(22.0)(1.0) + (50.0)(24.0)(1.25) = 5{,}475 \text{ kips}$$

For the steel section at the point of maximum live load moment in Span 3:

$$P_{2p} = (50.0)(92.0)(0.625) + (50.0)(18.0)(1.0) + (50.0)(18.0)(1.0) = 4{,}675 \text{ kips}$$

Thus, for both spans:

$$\therefore P_p = P_{1p} = 3{,}397 \text{ kips}$$

In Span 1:

$$F_p = P_p \frac{L_p}{R} = 3{,}397\left(\frac{66.31}{716.5}\right) = 314.4 \text{ kips}$$

$$P = \sqrt{P_p^2 + F_p^2} = \sqrt{(3{,}397)^2 + (314.4)^2} = 3{,}412 \text{ kips}$$

$$n = \frac{P}{Q_r} = \frac{3{,}412}{30.60} = 112 \text{ studs}$$

Compute the required pitch, *p*, in this region at the strength limit state with 3 studs per row:

$$\text{No. of rows} = \frac{112}{3} = 38 \text{ rows}$$

$$p = \frac{66.31(12)}{(38-1)} = 21.5 \text{ in.}$$

In Span 3:

$$F_p = P_p \frac{L_p}{R} = 3{,}397\left(\frac{68.06}{716.5}\right) = 322.7 \text{ kips}$$

$$P = \sqrt{P_p^2 + F_p^2} = \sqrt{(3{,}397)^2 + (322.7)^2} = 3{,}412 \text{ kips}$$

$$n = \frac{P}{Q_r} = \frac{3{,}412}{30.60} = 112 \text{ studs} \quad \text{(38 rows)}$$

$$p = \frac{68.06(12)}{(38-1)} = 22.1 \text{ in.}$$

The total nominal shear force, *P*, between the point of maximum positive design live load plus impact moment and the centerline of an adjacent interior support is to be determined as (Equation 3.3.17):

$$P = \sqrt{P_T^2 + F_T^2}$$

where P_T is the total longitudinal force in the concrete deck between the point of maximum positive live load plus impact moment and the centerline of an adjacent interior support taken as (Equation 3.3.18):

$$P_T = P_p + P_n$$

where P_n is the total longitudinal force in the concrete deck over an interior support taken as the lesser of (Equation 3.3.19):

$$P_{1n} = F_{yw} D t_w + F_{yt} b_{ft} t_{ft} + F_{yc} b_{fc} t_{fc}$$

or from Equation 3.3.20:

$$P_{2n} = 0.45 f_c' b_s t_s$$

Equation 3.3.20 is a conservative approximation of the tension force in the concrete deck to account for the combined contribution of both the longitudinal reinforcement and also the concrete that remains effective in tension based on its modulus of rupture. A more precise value may be substituted, if desired.

F_T is the total radial force in the concrete deck between the point of maximum positive live load plus impact moment and the centerline of an adjacent interior support taken as (Equation 3.3.21):

$$F_T = P_T \frac{L_n}{R}$$

where L_n is the arc length between the point of maximum positive live load plus impact moment and the centerline of an adjacent interior support (Figure 3.3.10). Again, for straight spans or segments, F_T may be taken equal to zero.

The distance between the point of maximum positive live load plus impact moment in Span 1 and the adjacent interior support is (191.406 – 66.31) = 125.1 feet. For Span 3, this distance is (136.13 – 68.06) = 68.1 feet.

For the steel section over Pier 1:

$$P_{1n} = (50.0)(92.0)(0.625) + (50.0)(28.0)(2.5) + (50.0)(33.0)(2.75) = 10{,}913 \text{ kips}$$

For the steel section over Pier 2:

$$P_{1n} = (50.0)(92.0)(0.625) + (50.0)(22.0)(2.0) + (50.0)(25.0)(2.75) = 8{,}513 \text{ kips}$$

For the effective deck in tension and longitudinal reinforcement over both piers:

$$P_{2n} = 0.45(4.0)(111.0)(9.0) = 1{,}798 \text{ kips}$$

Thus, for both spans:

$$\therefore P_n = P_{2n} = 1{,}798 \text{ kips}$$

$$P_t = P_p + P_n = 3{,}397 + 1{,}798 = 5{,}195 \text{ kips}$$

In Span 1:

$$F_T = P_T \frac{L_n}{R} = 5{,}195\left(\frac{125.1}{716.5}\right) = 907.0 \text{ kips}$$

$$P = \sqrt{P_T^2 + F_T^2} = \sqrt{(5{,}195)^2 + (907.0)^2} = 5{,}274 \text{ kips}$$

$$n = \frac{P}{Q_r} = \frac{5{,}274}{30.60} = 173 \text{ studs}$$

Compute the required pitch, *p*, in this region at the strength limit state with 3 studs per row:

$$\text{No. of rows} = \frac{173}{3} = 58 \text{ rows}$$

$$p = \frac{125.1(12)}{(58-1)} = 26.3 \text{ in.}$$

In Span 3:

$$F_T = P_T \frac{L_n}{R} = 5{,}195\left(\frac{68.1}{716.5}\right) = 493.8 \text{ kips}$$

$$P = \sqrt{P_T^2 + F_T^2} = \sqrt{(5{,}195)^2 + (493.8)^2} = 5{,}218 \text{ kips}$$

$$n = \frac{P}{Q_r} = \frac{5{,}218}{30.60} = 171 \text{ studs}$$
(57 rows)

$$p = \frac{68.1(12)}{(57-1)} = 14.6 \text{ in.}$$

The smallest distance between the point of maximum positive live load plus impact moment in Span 2 of G4 and each of the adjacent interior supports is 89.2 feet (to Pier 1). Using calculations similar to the above:

P_p = 3,397 kips
P_n = 1,798 kips

P_T = 5,195 kips
F_T = 647 kips
P = 5,235 kips
n = 172 studs
No. of rows = 58 rows
p = 18.8 in.

Comparing the above values for the strength limit state to the values of the required pitch given for the fatigue limit state in Table 5.1.14, it can be seen that the required pitch is governed by the fatigue limit state at all locations, except for at the cross-frames located 22.688 feet and 68.06 feet into Span 3 from Pier 2. Final recommended pitches for G4 are shown below in Figure 5.1.26.

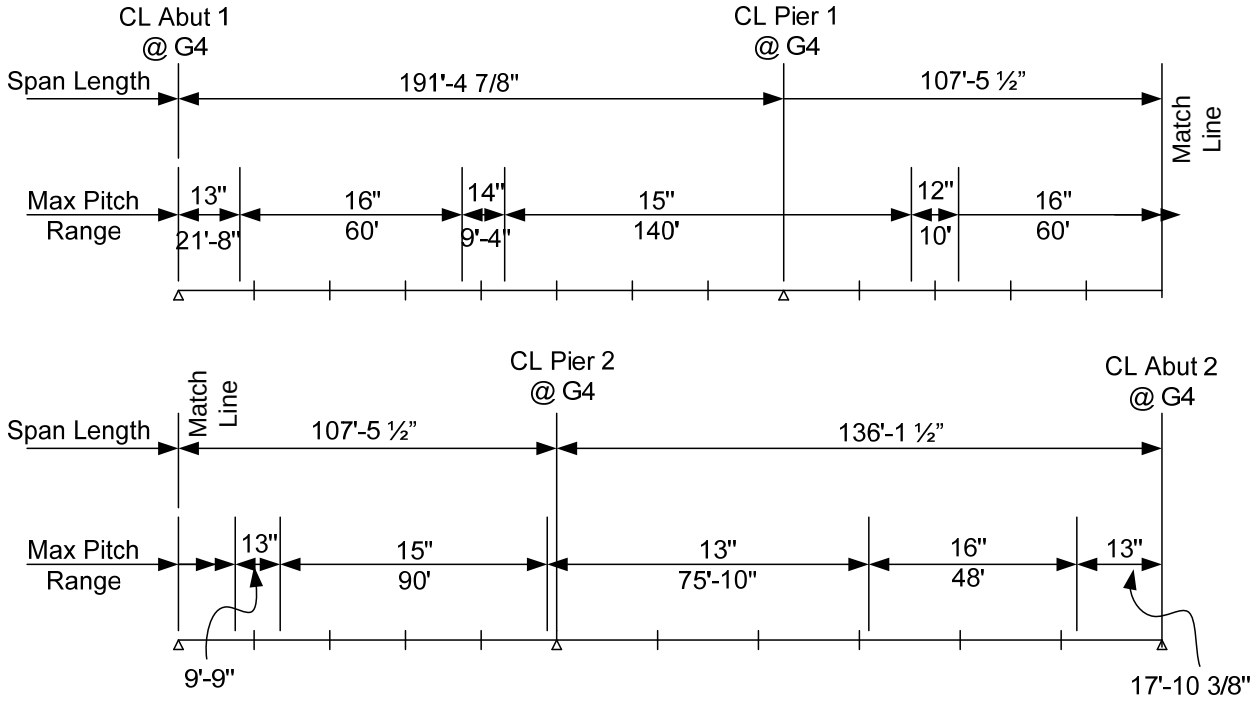


Figure 5.1.26 Recommended Shear Connector Pitch – G4

5.1.8.6 Web Stiffener Design

5.1.8.6.1 Transverse Web Stiffener Design

The design of transverse web stiffeners is covered in Section 3.3.8.1. Transverse stiffeners are designed according to the provisions of *AASHTO LRFD* Article 6.10.11.1. In this example, each intermediate transverse stiffener consists of a plate welded to one side of the web. According to *AASHTO LRFD* Article 6.10.11.1.1, the distance between the end of the web-to-stiffener weld and the near edge of an adjacent web-to-flange or longitudinal stiffener-to-web weld must not be less than $4t_w$, but not to exceed the lesser of $6t_w$ and 4.0 inches.

As specified in *AASHTO LRFD* Article 6.10.11.1.1, single-sided stiffeners on horizontally curved girders should be attached to both flanges to help retain the cross-sectional shape of the girder when subjected to torsion and to avoid high localized bending within the web, particularly near the top flange due to the torsional restraint of the concrete deck. Stiffeners used as connection plates for cross-frames must be attached to both flanges by welding or bolting. Welded connections are generally cheaper. Note that a fatigue Category C' detail still exists at the termination of the connection-plate weld to the web just above (or below) the tension flange even when the stiffeners are bolted to that flange.

The design of the intermediate transverse web stiffener (not serving as a cross-frame connection plate) 11.052 feet = 132.625 inches from Abutment 1 in Span 1 of G4 will be illustrated in this example (refer to the fold-out sheets at the end of this example). Also, the design of the transverse web stiffener 13.917 feet = 167.0 inches to the left of Pier 1 in Span 1 of G4 will be illustrated. Grade 50W steel will be used for the stiffeners (i.e. F_{ys} = 50.0 ksi).

5.1.8.6.1.1 Projecting Width

Transverse web stiffener proportioning requirements are discussed in Section 3.3.8.1.2. Determine the initial trial stiffener proportions using the projecting width requirements of *AASHTO LRFD* Article 6.10.11.1.2. Size the stiffener width, b_t, to be greater than or equal to $b_f/4$, as required in *AASHTO LRFD* Equation 6.10.11.1.2-2 (Equation 3.3.159). b_f is to be taken as the full width of the widest compression flange within the field section under consideration in order to ensure a minimum stiffener width that will help restrain the widest compression flange.

Stiffener Adjacent to Abutment 1 in Span 1 of G4

The top (compression) flange width in this field section is 22 inches.

$$b_t \geq \frac{22.0}{4} = 5.5 \text{ in.}$$

Stiffeners are commonly made up of less expensive flat bar stock. Flat bars are generally produced in whole-inch width increments and 1/8-in. thickness increments.

$$\text{Use } b_t = 6.0 \text{ in.} > 5.5 \text{ in.} \quad \text{ok}$$

Check the proportioning requirement given by Equation 3.3.158:

$$b_t \geq 2.0 + \frac{D}{30}$$

$$2.0 + \frac{92}{30} = 5.1\,\text{in.} < 6.0\,\text{in.} \qquad \text{ok}$$

Try a stiffener thickness, t_p, of 0.5 inches, which is the minimum preferred thickness for stiffeners and connection plates.

Check that (Equation 3.3.159):

$$16\,t_p \geq b_t$$

$$16(0.5) = 8.0\,\text{in.} > 6.0\,\text{in.} \qquad \text{ok}$$

Stiffener Adjacent to Pier 1 in Span 1 of G4

The bottom (compression) flange width in this field section is 33 inches.

$$b_t \geq \frac{33.0}{4} = 8.25\,\text{in.}$$

Use b_t = 8.5 in. > 8.25 in. ok

Check the proportioning requirement given by Equation 3.3.158:

$$b_t \geq 2.0 + \frac{D}{30}$$

$$2.0 + \frac{92}{30} = 5.1\,\text{in.} < 8.5\,\text{in.} \qquad \text{ok}$$

Try a stiffener thickness, t_p, of 0.625 inches.

Check that (Equation 3.3.159):

$$16\,t_p \geq b_t$$

$$16(0.625) = 10.0\,\text{in.} > 8.5\,\text{in.} \qquad \text{ok}$$

5.1.8.6.1.2 Moment of Inertia

The moment of inertia requirements for transverse web stiffeners are specified in *AASHTO LRFD* Article 6.10.11.1.3 (Section 3.3.8.1.3). The moment of inertia requirements ensure that the transverse stiffener has sufficient rigidity to maintain a vertical line of near zero lateral deflection along the line of the stiffener in order for interior web panels to adequately develop the shear buckling resistance, or the combined shear buckling and postbuckling tension-field resistance, as applicable.

For transverse stiffeners adjacent to web panels in which neither panel supports a factored shear force, V_u, larger than the factored shear-buckling resistance (i.e. $V_r = \phi_v V_{cr}$), the moment of inertia of the transverse stiffener, I_t, must satisfy the *smaller* of the following (Equation 3.3.160):

$$I_t \geq I_{t1}$$

and (Equation 3.3.161):

$$I_t \geq I_{t2}$$

I_{t1} is computed from Equation 3.3.162 as follows:

$$I_{t1} = bt_w^3 J$$

where b is taken as the smaller of d_o and D, where d_o is the smaller of the adjacent web panel widths. J is the stiffener bending rigidity parameter taken as (Equation 3.3.164):

$$J = \frac{2.5}{(d_o/D)^2} - 2.0 \geq 0.5$$

I_{t2} is computed from Equation 3.3.163 as follows:

$$I_{t2} = \frac{D^4 \rho_t^{1.3}}{40}\left(\frac{F_{yw}}{E}\right)^{1.5}$$

where ρ_t is taken equal to the larger of F_{yw}/F_{crs} and 1.0, and F_{crs} is equal to the local buckling stress for the stiffener (ksi) taken as (Equation 3.3.165):

$$F_{crs} = \frac{0.31E}{\left(\frac{b_t}{t_p}\right)^2} \leq F_{ys}$$

For transverse stiffeners adjacent to web panels in which the factored shear, V_u, is larger than the factored shear buckling resistance $\phi_v V_{cr}$, and thus the web postbuckling or tension-field resistance is required in one or both panels, the moment of inertia, I_t, of the transverse stiffeners must satisfy the following:

- If $I_{t2} > I_{t1}$, then (Equation 3.3.168):

$$I_t \geq I_{t1} + (I_{t2} - I_{t1})\left(\frac{V_u - \phi_v V_{cr}}{\phi_v V_n - \phi_v V_{cr}}\right)$$

- Otherwise (Equation 3.3.169):

$$I_t \geq I_{t2}$$

Stiffener Adjacent to Abutment 1 in Span 1 of G4

Based on the shear calculations in Sections 5.1.8.4.3.3 and 5.1.8.4.3.4, neither panel adjacent to the stiffener under consideration must support a factored shear, V_u, larger than the factored shear-buckling resistance, $\phi_v V_{cr}$. Thus, in this case, the moment of inertia of the transverse stiffener, I_t, must satisfy the smaller of the limits given by Equations 3.3.160 and 3.3.161.

Compute the stiffener bending rigidity parameter, J, from Equation 3.3.164 as follows. d_o is equal to 132.625 inches and the web depth, D, is equal to 92 inches.

$$J = \frac{2.5}{(132.625/92)^2} - 2.0 = -0.8 < 0.5 \quad \therefore J = 0.5$$

b is taken as the smaller of d_o and D; thus, in this case, $b = D = 92$ inches. Calculate I_{t1} from Equation 3.3.162 as follows:

$$I_{t1} = 92(0.625)^3(0.5) = 11.23 \text{ in.}^4$$

Calculate the local buckling stress of the stiffener, F_{crs}, from Equation 3.3.165 as follows:

$$F_{crs} = \frac{0.31(29{,}000)}{\left(\frac{6.0}{0.5}\right)^2} = 62.4 \text{ ksi} > F_{ys} = 50 \text{ ksi}$$

$$\therefore F_{crs} = 50 \text{ ksi}$$

The term, ρ_t, is equal to the larger of F_{yw}/F_{crs} (i.e. 50 ksi/50 ksi = 1.0) and 1.0. Therefore, in this case, ρ_t is equal to 1.0.

Calculate I_{t2} from Equation 3.3.163 as follows:

$$I_{t2} = \frac{(92)^4 (1.0)^{1.3}}{40}\left(\frac{50}{29{,}000}\right)^{1.5} = 128.2 \text{ in}^4$$

Since I_{t1} is smaller than I_{t2}, Equation 3.3.160 governs the required moment of inertia. Hence, I_t must be greater than or equal to I_{t1} or 11.23 in.^{4}

For single-sided stiffeners, the moment of inertia of the stiffener is to be taken about the edge in contact with the web. Therefore:

$$I_t = \frac{1}{3}(0.5)(6.0)^3 = 36.00 \text{ in.}^4 > 11.23 \text{ in.}^4 \quad \text{ok}$$

Use 1/2″ x 6″ bars for the transverse web stiffener adjacent to Abutment 1 in Span 1 of G4.

Stiffener Adjacent to Pier 1 in Span 1 of G4

Based on the shear calculations in Section 5.1.8.4.3.4, both panels adjacent to the stiffener under consideration must support a factored shear, V_u, larger than the factored postbuckling shear resistance due to tension-field action, $\phi_v V_n$. Thus, in this case, the moment of inertia of the transverse stiffener, I_t, must satisfy either Equation 3.3.168 or 3.3.169, as applicable.

Compute the stiffener bending rigidity parameter, J, from Equation 3.3.164 as follows. d_o is equal to 167 inches and the web depth, D, is equal to 92 inches.

$$J = \frac{2.5}{(167/92)^2} - 2.0 = -1.24 < 0.5 \quad \therefore J = 0.5$$

b is taken as the smaller of d_o and D; thus, in this case, $b = D = 92$ inches. Calculate I_{t1} from Equation 3.3.162 as follows:

$$I_{t1} = 92(0.625)^3(0.5) = 11.23 \text{ in.}^4$$

Calculate the local buckling stress of the stiffener, F_{crs}, from Equation 3.3.165 as follows:

$$F_{crs} = \frac{0.31(29{,}000)}{\left(\frac{8.5}{0.625}\right)^2} = 48.6 \text{ ksi} < F_{ys} = 50 \text{ ksi}$$

$$\therefore F_{crs} = 48.6 \text{ ksi}$$

The term, ρ_t, is equal to the larger of F_{yw}/F_{crs} (i.e. 50 ksi/48.6 ksi = 1.03) and 1.0. Therefore, in this case, ρ_t is equal to 1.03.

Calculate I_{t2} from Equation 3.3.163 as follows:

$$I_{t2} = \frac{(92)^4 (1.03)^{1.3}}{40}\left(\frac{50}{29{,}000}\right)^{1.5} = 133.2 \text{ in}^4$$

Since I_{t2} is greater than I_{t1}, the moment of inertia of the transverse stiffener, I_t, must satisfy Equation 3.3.168 in this particular case. In cases where V_u is smaller than V_n, the value of I_t from Equation 3.3.163 is not required. The required value of I_t from Equation 3.3.163 may be particularly large for deeper girders. Equation 3.3.168 is intended to handle such cases.

V_u in Equation 3.3.168 is the largest of the factored shears in the adjacent web panels. In this case, V_u = 614 kips at Pier 1 (Figure 5.1.24). V_{cr} is the smallest nominal shear-buckling resistance of the adjacent web panels. In this particular case, the shear-buckling resistance of the adjacent web panels is the same (since the panels are the same size) and is computed to be V_{cr} = 457 kips. V_n is the smaller of the nominal combined buckling and tension-field shear resistances of the adjacent web panels. V_n, which was computed in Section 5.1.8.4.3.4 to be 965 kips, is also the same for both panels in this case. ϕ_v is the resistance factor for shear equal to 1.0 (*AASHTO LRFD* Article 6.5.4.2). Therefore, from Equation 3.3.168:

$$I_t \geq 11.23 + (133.2 - 11.23)\left(\frac{614 - 1.0(457)}{1.0(965) - 1.0(457)}\right) = 48.93 \text{ in.}^4$$

For single-sided stiffeners, the moment of inertia of the stiffener is to be taken about the edge in contact with the web. Therefore:

$$I_t = \frac{1}{3}(0.625)(8.5)^3 = 127.9 \text{ in.}^4 > 48.93 \text{ in.}^4 \quad \text{ok}$$

Use 5/8″ x 8-1/2″ bars for the transverse web stiffener adjacent to Pier 1 in Span 1 of G4.

5.1.8.6.2 Bearing Stiffener Design

The design of bearing stiffeners is covered in Section 3.3.8.2. Bearing stiffeners are designed according to the provisions of *AASHTO LRFD* Article 6.10.11.2. Bearing stiffeners are designed as columns to resist the reactions at bearing locations or at other locations subjected to concentrated loads where the loads are not transmitted through a deck or deck system. According to *AASHTO LRFD* Article 6.10.11.2.1,

bearing stiffeners must be placed on the webs of built-up sections at all bearing locations.

Bearing stiffeners are aligned vertically on the web and must extend the full depth of the web and as closely as practical to the outer edges of the flanges. Each stiffener is to either be finished-to-bear (allowing the option of milling or grinding) against the flange through which it receives its load and attached with fillet welds, or else attached to that flange by a full penetration groove weld. The use of finish-to-bear plus fillet welds to connect the bearing stiffeners to the appropriate flange is recommended (note that fillet welds are not necessary if a cross-frame or diaphragm is not connected to the stiffener). Full penetration groove welds are costly and often result in deformations of the flange induced by the full penetration weld.

The design of the bearing stiffeners for G4 at Abutment 1 will be illustrated in this example. Grade 50W steel will be used for the stiffeners (i.e. F_{ys} = 50.0 ksi).

Assemble the bearing reactions due to the factored loads from the 3D analysis at Abutment 1. The unfactored bearing reactions are as follows:

R_{DC1} = 142 kips
R_{DC2} = 26 kips
R_{DW} = 22 kips
R_{LL+IM} = 152 kips

Determine the total factored reaction, R_u, at the strength limit state. The Strength I load combination controls:

$$R_u = 1.0\left[1.25(142+26)+1.5(22)+1.75(152)\right] = 509 \text{ kips}$$

5.1.8.6.2.1 Projecting Width

The projecting width requirement for bearing stiffeners is discussed in Section 3.3.8.2.2. According to *AASHTO LRFD* Article 6.10.11.2.2, the width, b_t, of each projecting stiffener element must satisfy the following requirement (Equation 3.3.171):

$$b_t \le 0.48 t_p \sqrt{\frac{E}{F_{ys}}}$$

Welded bearing stiffeners are also commonly made up of less expensive flat bar stock. Try two 7.0-inch-wide bars welded to each side of the web. Rearranging *AASHTO LRFD* Equation 6.10.11.2.2-1 gives:

$$(t_p)_{min.} = \frac{b_t}{0.48\sqrt{\frac{E}{F_{ys}}}}$$

$$(t_p)_{min.} = \frac{7.0}{0.48\sqrt{\frac{29{,}000}{50.0}}} = 0.61 \text{in.}$$

Try a stiffener thickness t_p of 0.75 inches, which exceeds the 1/2″ minimum preferred thickness for stiffeners and connection plates..

5.1.8.6.2.2 Bearing Resistance

Bearing resistance of the stiffeners is covered in Section 3.3.8.2.3. According to *AASHTO LRFD* Article 6.10.11.2.3, the factored bearing resistance for the fitted ends of bearing stiffeners is to be taken as (Equation 3.3.172):

$$(R_{sb})_r = \phi_b (R_{sb})_n$$

where $(R_{sb})_n$ is equal to the nominal bearing resistance for the fitted end of bearing stiffeners taken as (Equation 3.3.173):

$$(R_{sb})_n = 1.4 A_{pn} F_{ys}$$

A_{pn} is the area of the projecting elements of the stiffener outside of the web-to-flange fillet welds but not beyond the edge of the flange. Assume for this example that the clip provided at the base of the stiffeners to clear the web-to-flange fillet welds is 1.5 inches in length. The resistance factor for bearing on milled surfaces ϕ_b = 1.0 (*AASHTO LRFD* Article 6.5.4.2). Therefore:

$$A_{pn} = 2(7.0 - 1.5)(0.75) = 8.25 \text{ in.}^2$$

$$(R_{sb})_n = 1.4(8.25)(50.0) = 577 \text{ kips}$$

$$(R_{sb})_r = (1.0)(577) = 577 \text{ kips} > R_u = 509 \text{ kips} \quad \text{ok} \quad (\text{Ratio} = 0.882)$$

5.1.8.6.2.3 Axial Resistance

The axial resistance of bearing stiffeners is covered in Section 3.3.8.2.4. For computing the axial resistance of bearing stiffeners that are welded to the web, *AASHTO LRFD* Article 6.10.11.2.4b states that a portion of the web is to be included as part of the effective column section. For stiffeners consisting of two plates welded to the web, the effective column section is to consist of the two stiffener elements,

plus a centrally located strip of web extending not more than $9t_w$ on each side of the stiffeners (Section 3.3.8.2.4.1).

AASHTO LRFD Article 6.10.11.2.4a specifies that the radius of gyration of the effective column section is to be computed about the mid-thickness of the web and the effective length is to be taken as 0.75*D*, where *D* is the web depth. The area of the effective column section is computed as:

$$A_g = 2\left[(7.0)(0.75) + 9(0.625)(0.625)\right] = 17.53 \text{ in.}^2$$

The moment of inertia of the effective column section (conservatively neglecting the web strip) is computed as:

$$I_s = \frac{0.75(7.0 + 0.625 + 7.0)^3}{12} = 195.5 \text{ in.}^4$$

The radius of gyration of the effective column section is therefore computed as:

$$r_s = \sqrt{\frac{I_s}{A_g}} = \sqrt{\frac{195.5}{17.53}} = 3.34 \text{ in.}$$

The effective length of the effective column section is computed as:

$$K\ell = 0.75D = 0.75(92) = 69.0 \text{ in.}$$

Check the limiting slenderness ratio of 120 specified for primary members in compression in *AASHTO LRFD* Article 6.9.3:

$$\frac{K\ell}{r_s} = \frac{69.0}{3.34} = 20.6 < 120 \qquad \text{ok}$$

AASHTO LRFD Article 6.10.11.2.4a specifies that the factored axial resistance, P_r, of the effective column section be calculated according to the provisions of *AASHTO LRFD* Article 6.9.2.1 as follows (Equation 3.3.174):

$$P_r = \phi_c P_n$$

where P_n is equal to the nominal compressive resistance determined as specified in *AASHTO LRFD* Article 6.9.4.1, and ϕ_c is equal to the resistance factor for axial compression = 0.90.

Calculate the elastic critical buckling resistance for flexural buckling, P_e, specified in *AASHTO LRFD* Article 6.9.4.1.2 as follows (Equation 3.3.177):

$$P_e = \frac{\pi^2 E}{\left(\frac{K\ell}{r_s}\right)^2} A_g$$

$$P_e = \frac{\pi^2 (29{,}000)}{(20.6)^2}(17.53) = 11{,}823 \text{ kips}$$

Calculate the equivalent nominal yield resistance, P_o, as follows (*AASHTO LRFD* Article 6.9.4.1.1). The slender element reduction factor, Q, is taken equal to 1.0 for bearing stiffeners:

$$P_o = F_{ys} A_g = 50(17.53) = 876.5 \text{ kips}$$

Since P_e/P_o = 11,823/876.5 = 13.5 is greater than 0.44, the nominal compressive resistance, P_n, of the bearing stiffeners is computed as follows (*AASHTO LRFD* Article 6.9.4.1.1 – Equation 3.3.175):

$$P_n = \left[0.658^{\left(\frac{P_o}{P_e}\right)}\right] P_o$$

$$P_n = \left[0.658^{\left(\frac{876.5}{11{,}823}\right)}\right](876.5) = 850 \text{ kips}$$

The factored compressive resistance, P_r, of the bearing stiffeners is computed as (Equation 3.3.174):

$$P_r = 0.9(850) = 765 \text{ kips} > R_u = 509 \text{ kips} \quad \text{ok} \quad (\text{Ratio} = 0.665)$$

Use 3/4″ x 7″ bars (one pair) for the bearing stiffeners at Abutment 1 on G4.

5.1.8.6.2.4 Bearing Stiffener-to-Web Welds

Design the bearing stiffener-to-web fillet welds. Fillet welds and fillet welded connections are covered in Sections 3.3.6.3.3.2 and 3.3.6.3.5.2, respectively. The girder flanges and web and the stiffeners are ASTM A 709 Grade 50W steel with a specified minimum tensile strength F_u = 70 ksi (*AASHTO LRFD* Table 6.4.1-1).

Assume E70 electrodes (i.e. matching weld metal) with a classification strength, F_{exx}, equal to 70 ksi.

According to *AASHTO LRFD* Table 6.13.3.4-1 (Table 3.3.6), the minimum size fillet weld is ¼ in. when the base metal thickness *T* of the thicker part joined is less than or equal to ¾ in. The girder web is 5/8-in. thick at Abutment 1 and the stiffeners are 3/4-in. thick. Therefore, try the minimum size fillet weld equal to ¼ in. The effective throat of a ¼ in. equal-leg fillet weld is equal to:

$$t_e = 0.707(0.25) = 0.177 \text{ in.}$$

According to *AASHTO LRFD* Article 6.13.3.2.4b, the factored resistance, R_r, of fillet-welded connections at the strength limit state subject to shear on the effective area is to be taken as (Equation 3.3.115):

$$R_r = 0.6\phi_{e2}F_{exx}$$

where ϕ_{e2} is equal to the resistance factor for shear on the throat of the weld metal in fillet welds specified in *AASHTO LRFD* Article 6.5.4.2 = 0.80. Therefore:

$$R_r = 0.6(0.80)(70) = 33.6 \text{ ksi}$$

The factored resistance of a ¼-in. fillet weld in shear in units of kips/inch at the strength limit state is computed as:

$$V_r = R_r t_e = 33.6(0.177) = 5.95 \text{ kips/in.}$$

The governing factored shear rupture resistance of the base metal adjacent to the weld leg at the strength limit state is computed as (Section 3.3.6.2.6.2 – Equation 3.3.91 – substituting the governing plate thickness *t* for A_{vn}):

$$R_r = \phi_{vu}\,0.58R_pF_ut$$

ϕ_{vu} equals the resistance factor for shear rupture of connected elements specified in *AASHTO LRFD* Article 6.5.4.2 (= 0.80). R_p may be taken equal to 1.0 for welded connections. Therefore:

$$R_r = 0.80(0.58)(1.0)(70)(0.625) = 20.3 \text{ kips/in.}$$

which does not control.

The total length of a single bearing stiffener-to-web weld, allowing 2.5 inches for clips at the top and bottom of the bearing stiffeners to clear the flange-to-web welds, is:

$$L_w = 92 - 2(2.5) = 87.0 \text{ in.}$$

The total factored resistance of the four ¼-in. fillet welds connecting the stiffeners to the web (in kips) is therefore:

$$4(5.95)(87.0) = 2{,}071 \text{ kips} > R_u = 509 \text{ kips} \quad \text{ok}$$

Since the stiffeners are located at an abutment, load-induced fatigue of the base metal adjacent to these welds need not be checked.

5.1.8.7 Cross-Frame Member Design

The design of a single angle intermediate (radial) cross-frame member (i.e. a bottom strut) from the example bridge for compression using the effective slenderness ratio procedure discussed in Section 3.3.3.3 is illustrated next.

The largest factored compressive force, P_u, under the Strength I load combination in the cross-frames of the example bridge was determined from the 3D analysis to be –149 kips (Figure 5.1.27). This force was observed in the bottom strut of a single cross-frame between G2 and G3 located approximately 88.4 feet from Abutment 1 in Span 1 (note that all the intermediate cross-frames in the example bridge are arranged in an X-type configuration).

A similar force of –145 kips was observed in the bottom strut of a single cross-frame between G2 and G3 located in Span 2 (Figure 5.1.27). Separate calculations similar to the example calculations below indicate that a relatively large single angle (e.g. 8 x 8 x 5/8) would be required to resist these compressive forces; thus, a structural tee might instead be considered for the bottom chord along these two cross-frame lines. The design of structural tees is covered in Section 3.3.4.

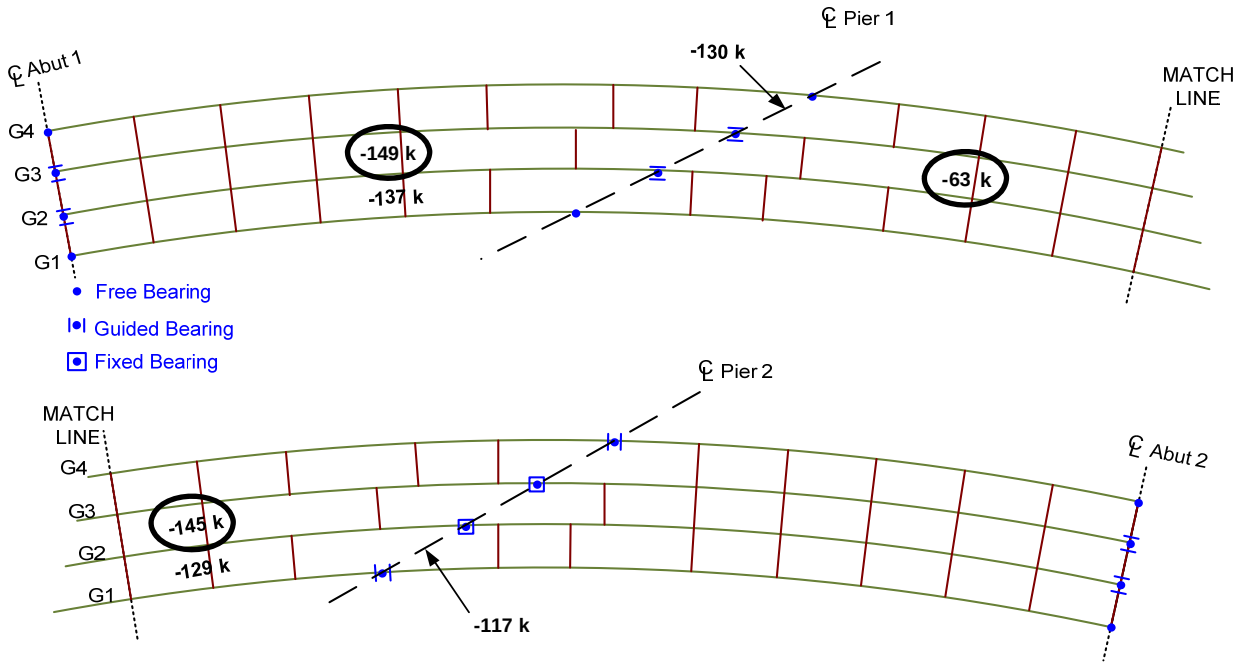


Figure 5.1.27 Critical Total Factored Cross-Frame Forces (Strength I) in the Example I-Girder Bridge from the 3D Analysis – Bottom Strut

The largest compressive force, P_u, in the bottom strut of the intermediate cross-frames located outside of these two cross-frame lines was observed to be –63 kips in a cross-frame located between G2 and G3 in Span 2 (Figure 5.1.27).

Determine if a 6 x 6 x 3/8 single angle would be sufficient in compression to use as the bottom strut for the remaining intermediate cross-frames in the example bridge. Assume the steel for the angle is ASTM A 709 Grade 50W. The thickness of the angle legs exceeds the minimum permissible thickness of 5/16″ specified for structural steel in *AASHTO LRFD* Article 6.7.3.

From the AISC Manual shape property tables, the following section properties are obtained for a 6 x 6 x 3/8 single angle:

$A = 4.36 \text{ in.}^2$
$r_x = 1.88 \text{ in.}$
$r_z = 1.19 \text{ in.}$

First, check the actual maximum slenderness ratio of the angle to ensure it does not exceed the permissible value of 120 for primary members in compression (*AASHTO LRFD* Article 6.9.3). The minimum radius of gyration, r_z, about the minor principal axis is used to calculate the actual maximum slenderness ratio. According to *AASHTO LRFD* Article 4.6.2.5, the effective length factor, K, is to be taken equal to

1.0 for single angles. The unbraced length in the plane of buckling, ℓ, will conservatively be taken as the girder spacing or 11.0 feet. Thus:

$$\frac{K\ell}{r_z} = \frac{1.0(11.0)12}{1.19} = 110.9 < 120 \quad \text{ok}$$

A more refined calculation of ℓ could be considered had the slenderness limit been exceeded.

AASHTO LRFD Article 6.9.2.1 specifies that the factored compressive resistance, P_r, at the strength limit state be taken as (Equation 3.3.29):

$$P_r = \phi_c P_n$$

ϕ_c is the resistance factor for axial compression specified in *AASHTO LRFD* Article 6.5.4.2 = 0.90.

The nominal compressive resistance, P_n, is to be determined as (Equations 3.3.30 and 3.3.31):

- If $\frac{P_e}{P_o} \geq 0.44$, then:

$$P_n = \left[0.658^{\left(\frac{P_o}{P_e}\right)}\right] P_o$$

- If $\frac{P_e}{P_o} < 0.44$, then:

$$P_n = 0.877 P_e$$

P_e is the elastic critical buckling resistance for flexural buckling determined as specified in *AASHTO LRFD* Article 6.9.4.1.2 as follows (Equation 3.3.177):

$$P_e = \frac{\pi^2 E}{\left(\frac{K\ell}{r_s}\right)^2} A_g$$

P_o is the equivalent nominal yield resistance, P_o, determined as specified in *AASHTO LRFD* Article 6.9.4.1.1 (Equation 3.3.37). Q is the slender element reduction factor specified in *AASHTO LRFD* Article 6.9.4.2.2 (Section 3.3.3.3.3):

$$P_o = QF_yA_g$$

According to *AASHTO LRFD* Table 6.9.4.1.1-1, single angles in compression need only be checked for flexural buckling if the provisions of *AASHTO LRFD* Article 6.9.4.4 are employed. These provisions permit the effects of all eccentricities in the member to be neglected when these members are evaluated as axially loaded compression members for flexural buckling only using an appropriate effective slenderness ratio, $(K\ell/r)_{eff}$. The effective slenderness ratio indirectly accounts for the bending in the angles due to the eccentricity of the loading allowing the member to be proportioned as if it were a pinned-end concentrically loaded compression member. Furthermore, when the effective slenderness ratio is used, single angles need not be checked for flexural-torsional buckling.

The member must satisfy all of the following conditions specified in *AASHTO LRFD* Article 6.9.4.4 in order to use the effective slenderness ratio, which are all met in this particular case:

- End connections are to a single leg of the angle, and are welded or use a minimum of two bolts
- The angle is loaded at the ends in compression through the same leg
- The angle is not subjected to any intermediate transverse loads
- If used as web members in trusses, all adjacent web members are attached to the same side of the gusset plate or chord

For an equal-leg angle, the effective slenderness ratio, $(K\ell/r)_{eff}$, is determined as follows (*AASHTO LRFD* Article 6.9.4.4 – Equations 3.3.33 and 3.3.34):

- If $\frac{\ell}{r_x} \le 80$, then:

$$\left(\frac{K\ell}{r}\right)_{eff} = 72 + 0.75\frac{\ell}{r_x}$$

- If $\frac{\ell}{r_x} > 80$, then:

$$\left(\frac{K\ell}{r}\right)_{eff} = 32 + 1.25\frac{\ell}{r_x}$$

where ℓ is the distance between the work points of the joints measured along the angle, and r_x is the radius of gyration about the geometric axis parallel to the connected leg.

Assume the work points of the bottom-strut connection joints at each end of the member are located 6 inches from the centerline of the girder webs. Therefore, ℓ = 11.0 – 2(6.0/12) = 10.0 feet. For equal-leg angles, r_x is taken equal to the actual r_x of the angle about its geometric x-axis. Therefore:

$$\frac{\ell}{r_x} = \frac{10.0(12)}{1.88} = 63.8 < 80$$

Thus:

$$\left(\frac{K\ell}{r}\right)_{eff} = 72 + 0.75\frac{\ell}{r_x} = 72 + 0.75(63.8) = 119.9$$

and:

$$P_e = \frac{\pi^2 E}{\left(\frac{K\ell}{r}\right)^2_{eff}} A_g = \frac{\pi^2 (29{,}000)}{(119.9)^2}(4.36) = 86.8 \text{ kips}$$

Calculate the equivalent nominal yield resistance, P_o. For compression members composed of one or more slender elements; that is, elements not meeting the corresponding width-to-thickness ratio limits specified in *AASHTO LRFD* Table 6.9.4.2.1-1, the slender element reduction factor, Q, accounts for the effect of potential local buckling of those elements on the overall buckling resistance of the member and has a value less than 1.0. The value of Q in this instance is determined according to the provisions of *AASHTO LRFD* Article 6.9.4.2.2.

Q is taken equal to 1.0 as specified in *AASHTO LRFD* Article 6.9.4.2.1 for compression member cross-sections without any slender elements; that is, composed entirely of nonslender elements. In such cases, local buckling does not adversely affect the nominal compressive resistance.

For compression member cross-sections composed entirely of unstiffened elements, or plates supported along only one edge parallel to the direction of the compression force, Q is taken equal to the factor for unstiffened elements, Q_s. Single angles are composed entirely of unstiffened elements (Figure 3.3.20).

When the b/t ratio of the outstanding leg is less than or equal to the following limit (from *AASHTO LRFD* Eq. 6.9.4.2.1-1 with k taken equal to 0.45), the element is nonslender and $Q = Q_s = 1.0$. Check if the legs of the angle under investigation are slender elements:

$$\frac{b}{t} \le 0.45\sqrt{\frac{E}{F_y}}$$

$$0.45\sqrt{\frac{29{,}000}{50}} = 10.8 < \frac{b}{t} = \frac{6}{0.375} = 16.0$$

Therefore, the nominal compressive resistance of the angle must be reduced due to potential local buckling of the slender outstanding leg. Since *b*/*t* is less than $0.91\sqrt{E/F_y} = 21.9$, the slender element reduction factor, $Q = Q_s$, is determined from the following equation (*AASHTO LRFD* Article 6.9.4.2.2 – Equation 3.3.39):

$$Q = Q_s = 1.34 - 0.76\left(\frac{b}{t}\right)\sqrt{\frac{F_y}{E}} = 1.34 - 0.76(16.0)\sqrt{\frac{50}{29{,}000}} = 0.84$$

and:

$$P_o = QF_yA_g = 0.84(50)(4.36) = 183.1 \text{ kips}$$

Since:

$$\frac{P_e}{P_o} = \frac{86.8}{183.1} = 0.47 > 0.44$$

the nominal compressive resistance, P_n, is computed as follows:

$$P_n = \left[0.658^{\left(\frac{183.1}{86.8}\right)}\right](183.1) = 75.7 \text{ kips}$$

The factored compressive resistance, P_r, is taken as:

$$P = \phi_c P_n = 0.90(75.7) = 68.1 \text{ kips} > |P_u| = |-63| \text{ kips}$$

Thus, for compression, use a 6 x 6 x 3/8 single angle as the bottom strut for the remainder of the intermediate cross-frames in the example bridge (i.e. outside the two intermediate cross-frame lines shown in Figure 5.1.27 containing the more heavily loaded bottom struts).

5.1.8.8 Bolted Field Splice Design

5.1.8.8.1 General

The design of bolted girder splices is covered in Section 3.3.7. The following is a complete example design of the bolted field splice in Span 3 of G4 (refer to the fold-out sheets at the end of this example). The splice is located 50 feet from Pier 2. The unbraced length adjacent to either side of the splice is 22.688 feet. The girder plate sizes on the left- and right-hand side of the point of splice are as follows:

Left Side:	Top Flange	1″ x 22″	Right Side:	Top Flange	1″ x 18″
	Web	5/8″ x 92″		Web	5/8″ x 92″
	Bot. Flange	1-3/8″ x 25″		Bot. Flange	1″ x 18″

The sections on both sides of the splice are homogeneous utilizing ASTM A 709 Grade 50W steel for the flanges and web.

AASHTO LRFD Article C6.13.6.1.4a suggests that the smaller section at the point of splice in a flexural member be taken as the side of the splice that has the smaller calculated moment of inertia for the non-composite steel section. The right side of the splice qualifies as the smaller section according to this criterion. Thus, only the calculations for the right side of the splice are shown below.

The elastic section properties of the gross section on the right side of the splice are as follows (Table 5.1.15):

Table 5.1.15 Elastic Section Properties of the Gross Section on the Right Side of the Bolted Splice (in Span 3 of G4)

	I ($in.^4$)	S_{top} ($in.^3$)	S_{bot} ($in.^3$)	Neutral Axis* (in.)
Steel	118,397	2,519	2,519	47.0
Steel + Long. Reinforcement	139,889	3,276	2,727	51.3
3n Composite	208,084	7,102	3,216	64.7
n Composite	281,487	18,892	3,559	79.1

* Neutral axis is measured from the bottom of the steel

The unfactored vertical bending moments and vertical shears at the point of splice from the 3D analysis are as follows:

M_{steel}	=	+50 kip-ft	V_{steel}	=	+20 kips
M_{DC1}	=	+290 kip-ft	V_{DC1}	=	+100 kips
$M_{deck\ casting}$	=	+3,960 kip-ft	$V_{deck\ casting}$	=	+90 kips
M_{DC2}	=	-100 kip-ft	V_{DC2}	=	+13 kips
M_{DW}	=	+66 kip-ft	V_{DW}	=	+14 kips
M_{+LL+IM}	=	+3,613 kip-ft	V_{+LL+IM}	=	+104 kips
M_{-LL+IM}	=	-3,001 kip-ft	V_{-LL+IM}	=	-28 kips

The unfactored lateral flange bending moments at the cross-frame adjacent to the point of splice (45.375 feet from Pier 2 in Span 3) taken from the 3D analysis, which include the combined effects of curvature and skew, are as follows:

Bottom flange:	$(M_\ell)_{steel}$	=	+1 kip-ft
	$(M_\ell)_{deck\ casting}$	=	+23 kip-ft
	$(M_\ell)_{DC1}$	=	+5 kip-ft
	$(M_\ell)_{DC2}$	=	+1 kip-ft
	$(M_\ell)_{DW}$	=	+1 kip-ft
	$(M_\ell)_{+LL+IM}$	=	+16 kip-ft
	$(M_\ell)_{-LL+IM}$	=	-12 kip-ft
Top flange:	$(M_\ell)_{steel}$	=	0 kip-ft
	$(M_\ell)_{deck\ casting}$	=	-5 kip-ft

As discussed in Section 3.3.7.2.4, the use of the flange lateral moments at the cross-frame closest to the splice is obviously conservative based on the general shape of the lateral moment diagram in-between cross-frames in which the lateral moment actually reverses sign, and the fact that the splice cannot be located right at a cross-frame. A line plotted between the lateral moments mid-way between the cross-frames adjacent to the splice (if available) and the lateral moments at the cross-frame closest to the splice (with the proper sense of the moments considered) can be used to determine an optimal splice location to minimize the effect of the lateral moments on the design of the splice.

This example illustrates how to consider the effect of the lateral flange moments in cases where they may be deemed significant at the splice. *For curved bridges with radial supports where the effects of lateral flange bending are due primarily to curvature, the splice is likely to often be at a location where the effects of the flange lateral bending on the splice are relatively minimal and can be ignored*. To confirm this, the splice location can be checked using the procedure described in the preceding paragraph, or it can be checked in a more approximate fashion against the location of the point of contraflexure in a uniformly loaded fixed-end beam, which is at approximately $0.21L_b$ from the fixed end (i.e. from the cross-frame) where L_b is the cross-frame spacing. This assumes reasonably uniform cross-frame spacings adjacent to the splice.

The DC_2 vertical bending moment is negative and the DW vertical bending moment is positive at the point of splice. However, these moments are relatively small since the splice is located near a point of permanent load contraflexure. By inspection, it is apparent that the unfactored tensile/compressive vertical bending stress in the concrete deck due to the DC_2/DW moments is overcome by the unfactored compressive/tensile vertical bending stress in the deck due to the positive/negative live load moment plus impact. Therefore, as specified in *AASHTO LRFD* Article 6.10.1.1.1b, the vertical bending stresses due to the DC_2 and DW moments will be

computed using the 3*n* composite section properties for combination with the positive live load plus impact vertical bending stress. For combination with the negative live load plus impact vertical bending stress, the stresses due to these moments will be computed using the section properties for the steel girder plus the longitudinal reinforcement (Section 3.2.6.6).

Calculate the unfactored vertical bending stresses at the mid-thickness of the bottom flange:

$$f_{DC1} = \frac{290(12)(46.5)}{118{,}397} = +1.37 \text{ ksi}$$

$$f_{DC2} = \frac{-100(12)(64.2)}{208{,}084} = -0.37 \text{ ksi } (3n)$$

$$f_{DC2} = \frac{-100(12)(50.8)}{139{,}889} = -0.44 \text{ ksi } (\text{steel} + \text{reinf.})$$

$$f_{DW} = \frac{66(12)(64.2)}{208{,}084} = +0.24 \text{ ksi } (3n)$$

$$f_{DW} = \frac{66(12)(50.8)}{139{,}889} = +0.29 \text{ ksi } (\text{steel} + \text{reinf.})$$

$$f_{+LL+IM} = \frac{3{,}613(12)(78.6)}{281{,}487} = +12.11 \text{ksi}$$

$$f_{-LL+IM} = \frac{-3{,}001(12)(50.8)}{139{,}889} = -13.08 \text{ ksi}$$

Calculate the unfactored vertical bending stresses at the mid-thickness of the top flange:

$$f_{DC1} = \frac{290(12)(-46.5)}{118{,}397} = -1.37 \text{ ksi}$$

$$f_{DC2} = \frac{-100(12)(-28.8)}{208{,}084} = +0.17 \text{ ksi } (3n)$$

$$f_{DC2} = \frac{-100(12)(-42.2)}{139{,}889} = +0.36 \text{ ksi } (\text{steel} + \text{reinf.})$$

$$f_{DW} = \frac{66(12)(-28.8)}{208{,}084} = -0.11\,\text{ksi}\ \ (3n)$$

$$f_{DW} = \frac{66(12)(-42.2)}{139{,}889} = -0.24\,\text{ksi}\ \ (\text{steel} + \text{reinf.})$$

$$f_{+LL+IM} = \frac{3{,}613(12)(-14.4)}{281{,}487} = -2.22\,\text{ksi}$$

$$f_{-LL+IM} = \frac{-3{,}001(12)(-42.2)}{139{,}889} = +10.86\,\text{ksi}$$

5.1.8.8.2 Flange Splice Design

Bolted flange splice design is covered in Section 3.3.7.2.

5.1.8.8.2.1 Minimum Design Forces

Since the splice is located in an area of stress reversal, checks must be made for both the positive and negative flexure conditions. Compute the combined factored vertical bending stresses at the midthickness of the bottom and top flanges at the strength limit state for each of these conditions using the appropriate load factors given in *AASHTO LRFD* Tables 3.4.1-1 and 3.4.1-2. The Strength I load combination is used (the load modifier, η, is taken equal to 1.0). Note that the minimum load factors, γ_p, from *AASHTO LRFD* Table 3.4.1-2 and a load modifier, $1/\eta$ (≤ 1.0), are applied to the permanent loads when the corresponding stresses are of opposite sign to the live load plus impact stress.

- Bottom Flange

  A. Dead Load + Positive Live Load:

$$f = 1.0(1.25)(+1.37) + (1/1.0)(0.90)(-0.37) + 1.0(1.50)(+0.24) + (1.0)(1.75)(+12.11) = +22.93\,\text{ksi}$$

  B. Dead Load + Negative Live Load:

$$f = (1/1.0)(0.90)(+1.37) + 1.0(1.25)(-0.44) + (1/1.0)(0.65)(+0.29) + 1.0(1.75)(-13.08) = -22.02\,\text{ksi}$$

- Top Flange

  A. Dead Load + Positive Live Load:

$$f = 1.0(1.25)(-1.37) + (1/1.0)(0.90)(+0.17) + 1.0(1.50)(-0.11) + (1.0)(1.75)(-2.22) = -5.61\,\text{ksi}$$

  B. Dead Load + Negative Live Load:

$$f = (1/1.0)(0.90)(-1.37) + 1.0(1.25)(+0.36) + (1/1.0)(0.65)(-0.24) + 1.0(1.75)(+10.86) = +18.07\ \text{ksi}$$

The controlling flange is defined as the top or bottom flange for the smaller section at a point of splice, whichever flange has the maximum ratio of the elastic flexural stress at its midthickness due to the factored loads to its factored flexural resistance (Section 3.3.7.2.2.1). The factored flexural resistance, F_r, of each flange on the right side of the splice is determined from separate calculations similar to those demonstrated previously. The ratios of f/F_r for each condition (positive and negative flexure) are as follows:

- Bottom Flange

  A. Dead Load + Positive Live Load:

     F_r = 50 ksi; $|f/F_r|$ = 0.46

  B. Dead Load + Negative Live Load:

     F_r = 39.1 ksi; $|f/F_r|$ = 0.56

- Top Flange

  A. Dead Load + Positive Live Load:

     F_r = 50 ksi; $|f/F_r|$ = 0.11

  B. Dead Load + Negative Live Load:

     F_r = 50 ksi; $|f/F_r|$ = 0.36

Therefore, the bottom flange is the controlling flange for both the positive and negative flexure conditions. The top flange is the noncontrolling flange (Section 3.3.7.2.2.2) for both the positive and negative flexure conditions in this case.

Positive Flexure

For the case of positive flexure, the minimum design stress for the controlling (bottom) flange at the strength limit state, F_{cf}, is computed as (Equation 3.3.127):

$$F_{cf} = \frac{\left(\left|\frac{f_{cf}}{R_h}\right| + \alpha\phi_f F_{yf}\right)}{2} \geq 0.75\alpha\phi_f F_{yf}$$

The hybrid factor, R_h, is taken as 1.0 for homogeneous sections and α is taken equal to 1.0 for flanges in tension. f_{cf} is the maximum factored vertical bending stress at the midthickness of the controlling flange at the point of splice = +22.93 ksi. Therefore:

$$\frac{\left|\frac{f_{cf}}{R_h}\right| + \alpha F_{yf}}{2} = \frac{\left|\frac{+22.93}{1.0}\right| + 1.0(50)}{2} = 36.47 \text{ ksi}$$

$$0.75\alpha F_{yf} = 0.75(1.0)(50) = 37.50 \text{ ksi} \quad (\text{governs})$$

The minimum design force for the controlling flange, P_{cf}, is taken equal to the design stress, F_{cf}, times the smaller effective flange area, A_e, on either side of the splice. The smaller effective bottom-flange area is on the right side of the splice.

For flanges subject to tension, A_e is computed as (Equation 3.3.128):

$$A_e = \left(\frac{\phi_u F_u}{\phi_y F_{yt}}\right) A_n \leq A_g$$

From *AASHTO LRFD* Table 6.4.1-1, F_u for ASTM A 709 Grade HPS 50W steel is 70 ksi. Assume the bottom flange splice will consist of 4 rows of 7/8-in. diameter A 325 high-strength bolts across the width of the flange (to be confirmed later). *AASHTO LRFD* Article 6.8.3 specifies that the width of standard bolt holes (which must be used for bolted splices in flexural members) for design is to be taken as the nominal diameter of the hole specified in *AASHTO LRFD* Article 6.13.2.4.2. The nominal diameter of a standard hole for a 7/8-in diameter bolt is 15/16 inches (Section 3.3.6.2.5.1). Therefore:

$$A_n = [18.0 - 4(0.9375)](1.0) = 14.25 \text{ in.}^2$$

$$A_g = 18.0(1.0) = 18.00 \text{ in.}^2$$

ϕ_u is the resistance factor for fracture in tension components (=0.80) and ϕ_y is the resistance factor for yielding in tension components (=0.95) (*AASHTO LRFD* Article 6.5.4.2).

$$A_e = \left(\frac{0.80(70)}{0.95(50)}\right)14.25 = 16.80 \text{ in.}^2 < 18.00 \text{ in.}^2$$

$$P_{cf} = F_{cf} A_e = 37.50(16.80) = 630 \text{ kips}$$

For the case of positive flexure, the minimum design stress for the noncontrolling (top) flange at the strength limit state, F_{ncf}, is computed as (Equation 3.3.129):

$$F_{ncf} = R_{cf}\left|\frac{f_{ncf}}{R_h}\right| \geq 0.75\alpha\phi_f F_{yf}$$

f_{ncf} is the factored vertical bending stress at the midthickness of the noncontrolling flange at the point of splice concurrent with f_{cf} and is equal to -5.61 ksi. The top flange is in compression and is continuously braced for this condition. Therefore, since $F_{nc} = F_{yf}$, α must be taken equal to 1.0.

$$R_{cf} = \left|\frac{F_{cf}}{f_{cf}}\right| = \left|\frac{37.50}{+22.93}\right| = 1.64$$

$$R_{cf}\left|\frac{f_{ncf}}{R_h}\right| = 1.64\left|\frac{-5.61}{1.0}\right| = 9.20 \text{ ksi}$$

$$0.75\alpha F_{yf} = 0.75(1.0)(50) = 37.50 \text{ ksi} \quad (\text{governs})$$

The minimum design force for the noncontrolling flange, P_{ncf}, is taken equal to the design stress, F_{ncf}, times the smaller effective flange area, A_e, on either side of the splice. The smaller effective top-flange area is on the right side of the splice. A_e is taken equal to A_g for flanges subject to compression.

$$A_e = A_g = 18(1.0) = 18.00 \text{ in.}^2$$

$$P_{ncf} = F_{ncf} A_e = 37.50(18.00) = 675 \text{ kips}$$

Negative Flexure

For the case of negative flexure, the controlling (bottom) flange is subject to compression. The factored flexural resistance of the bottom flange in compression, F_r, is significantly less than F_{yf} in this particular case; therefore, the factor, α, will be computed. α is taken equal to the nominal compressive resistance of the flange, F_{nc} = 39.1 ksi (lateral torsional buckling controls) divided by F_{yf}, or 39.1/50 = 0.78. The factored vertical bending stress in the controlling flange, f_{cf} = -22.02 ksi. Therefore:

$$\frac{\left|\frac{f_{cf}}{R_h}\right| + \alpha F_{yf}}{2} = \frac{\left|\frac{-22.02}{1.0}\right| + 0.78(50)}{2} = 30.51\,\text{ksi}\ \ (\text{governs})$$

$$0.75\alpha F_{yf} = 0.75(0.78)(50) = 29.25\ \text{ksi}$$

A_e is taken equal to A_g for flanges subject to compression.

$$A_g = 18.0(1.0) = 18.00\ \text{in.}^2$$

$$P_{cf} = F_{cf} A_e = 30.51(18.00) = 549\ \text{kips}$$

For the case of negative flexure, the noncontrolling (top) flange is subject to tension; therefore, α is equal to 1.0. The factored vertical bending stress in the noncontrolling flange, f_{ncf} = +18.07 ksi.

$$R_{cf} = \left|\frac{F_{cf}}{f_{cf}}\right| = \left|\frac{30.51}{-22.02}\right| = 1.39$$

$$R_{cf}\left|\frac{f_{ncf}}{R_h}\right| = 1.39\left|\frac{18.07}{1.0}\right| = 25.12\ \text{ksi}$$

$$0.75\alpha F_{yf} = 0.75(1.0)(50) = 37.50\ \text{ksi}\ \ (\text{governs})$$

Assume the top flange splice will consist of 4 rows of 7/8-in. diameter A 325 high-strength bolts across the width of the flange (to be confirmed later). Therefore:

$$A_n = [18.0 - 4(0.9375)](1.0) = 14.25\ \text{in.}^2$$

$$A_g = 18.0(1.0) = 18.00\ \text{in.}^2$$

$$A_e = \left(\frac{0.80(70)}{0.95(50)}\right)14.25 = 16.80\ \text{in.}^2 < 18.00\ \text{in.}^2$$

$$P_{ncf} = F_{ncf} A_e = 37.50(16.80) = 630\ \text{kips}$$

A summary of the design forces for the bottom and top flange splices at the strength limit state is as follows:

Bottom Flange: P_{cf} = 630 kips (tension)
P_{cf} = 549 kips (compression)

Top Flange: P_{ncf} = 675 kips (compression)
P_{ncf} = 630 kips (tension)

5.1.8.8.2.2 Bottom Flange Splice

The width of the outside splice plate should be at least as wide as the width of the narrowest flange at the splice. Therefore, try a 5/8" x 18" outside splice plate with two 3/4" x 7-1/2" inside splice plates. Include a 3/8" x 18" filler plate on the outside, as shown in Figure 5.1.28. All plates are ASTM A 709 Grade 50W steel.

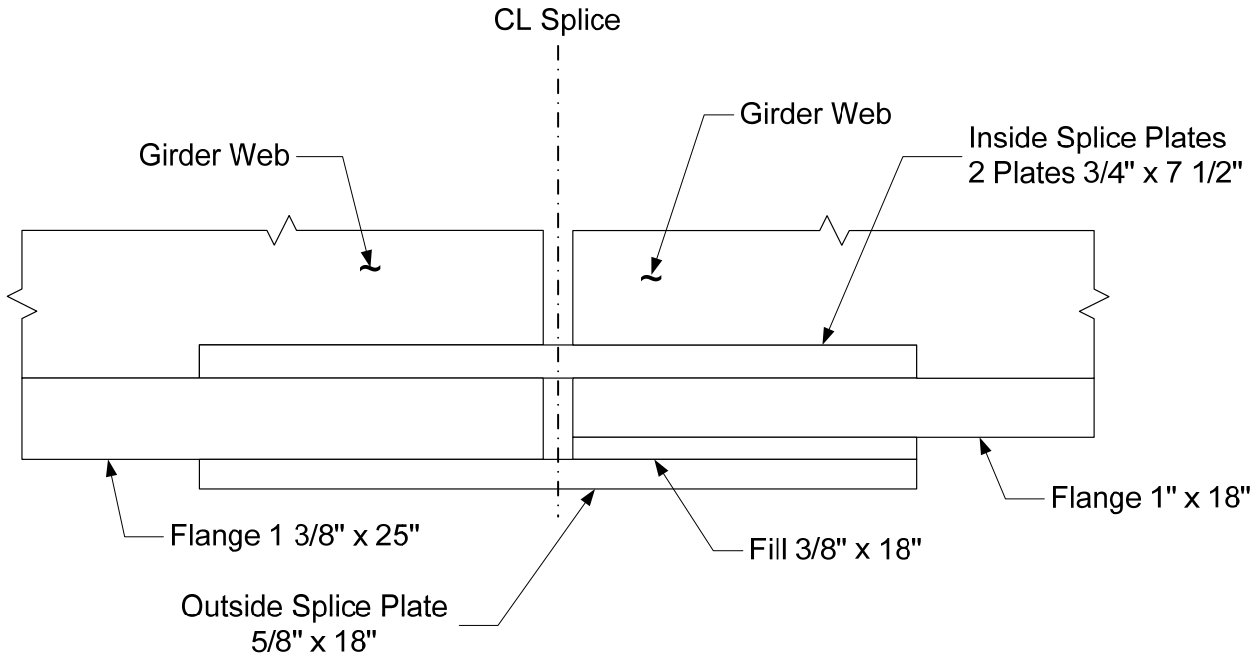


Figure 5.1.28 Elevation View of Bottom Flange Splice in Span 3 of G4 (bolts not shown)

Strength Limit State

Splice Plates

AASHTO LRFD Article 6.13.5.2 specifies that splice plates in tension at the strength limit state be checked for yielding on the gross section, fracture on the net section and block shear rupture. When flange lateral bending is present, splice plates in tension on the bottom flange must be checked for the combined stress (i.e. including the flange lateral bending stress) since the bottom flange is discretely braced (Section 3.3.7.2.4).

For yielding, the splice plates may be checked for the combined stress as follows (Equation 3.3.138):

$$\frac{P}{(A_g)_{PL}} + \frac{M_\ell}{S_{PL}} \le \phi_y F_y$$

M_ℓ is the factored lateral moment in the bottom flange due to the Strength I load combination computed as:

$$M_\ell = 1.0[1.25(5) + 1.25(1) + 1.5(1) + 1.75(16)] = 37 \text{ kip} - \text{ft}$$

Amplification of the lateral moment is not necessary since the flange is subject to tension under vertical bending in this case.

$(A_g)_{PL}$ is the total gross area of the inner and outer splice plates computed as:

$$(A_g)_{PL} = 0.625(18) + 2(0.75)(7.5) = 22.5 \text{ in.}^2$$

S_{PL} is the total gross lateral section modulus of the inner and outer splice plates computed as:

$$S_{PL} = \frac{0.625(18)^2}{6} + \frac{2(0.75)(7.5)^2}{6} = 47.8 \text{ in.}^3$$

Therefore:

$$\frac{630}{22.5} + \frac{37(12)}{47.8} = 37.3 \text{ ksi} < 0.95(50) = 47.5 \text{ ksi} \quad \text{ok}$$

The preceding check and the checks that follow assume that the areas of the inner and outer flange splice plates do not differ by more than 10 percent. In this case, the areas of the inner and outer splice plates are equal. Otherwise, P and M_ℓ should be proportioned to the inner and outer splice plates by the ratio of the area(s) of the inner and outer plate(s) to the total area of the splice plates, with the splice plates than checked individually using their respective actions.

For net section fracture, the splice plates may be checked for the combined stress as follows (Equation 3.3.139):

$$\frac{P}{(A_n)_{PL}} + \frac{M_\ell}{(S_n)_{PL}} \le \phi_u F_u U$$

U is a reduction factor to account for shear lag, which is to be taken as 1.0 for splice plates (*AASHTO LRFD* Article 6.13.5.2).

$(A_n)_{PL}$ is the total net area of the inner and outer splice plates computed as:

$$(A_n)_{PL} = [18 - 4(0.9375)](0.625) + 2[7.5 - 2(0.9375)](0.75) = 17.3 \text{ in.}^2$$

$(S_n)_{PL}$ is the total net lateral section modulus of the inner and outer splice plates computed as (Equation 3.3.141):

$$(S_n)_{PL} = \frac{\left[(I_g)_{\text{Outer PL}} - \sum_{i=1}^{N_b} A_{hole} Y_i^2\right]}{c} + 2\left(\frac{\left[(I_g)_{\text{Inner PL}} - \sum_{i=1}^{N_b} A_{hole} Y_i^2\right]}{c}\right)$$

I_g is the gross lateral moment of inertia of the splice plate(s) under consideration, *c* is the half-width of the splice plate under consideration, and the Y_i distances for each bolt hole are defined in Figure 3.3.63. Therefore, referring to Figure 5.1.30:

$$(S_n)_{PL} = \frac{\left[0.625(18)^3/12 - 2(0.625)(0.9375)\left[(3.0)^2 + (7.0)^2\right]\right]}{(18/2)} + 2\left(\frac{\left[0.75(7.5)^3/12 - 2(0.75)(0.9375)(2.0)^2\right]}{(7.5/2)}\right) = 37.3 \text{ in.}^3$$

Therefore:

$$\frac{630}{17.3} + \frac{37(12)}{37.3} = 48.3 \text{ ksi} < 0.8(70)(1.0) = 56.0 \text{ ksi} \quad \text{ok}$$

Also, according to *AASHTO LRFD* Article 6.13.5.2, for splice plates subject to tension, A_n must not exceed $0.85A_g$.

- Outer plate:

$$0.85(18)(0.625) = 9.56 \text{ in}^2 > A_n = [18 - 4(0.9375)](0.625) = 8.91 \text{ in.}^2 \quad \text{ok}$$

- Inner plates:

$$0.85(2)(7.5)(0.75) = 9.56\ \text{in}^2 > A_n = 2[7.5 - 2(0.9375)](0.75) = 8.44\ \text{in.}^2 \quad \text{ok}$$

The block shear rupture resistance of the splice plates will be checked later.

Flange splice plates subject to compression are checked for yielding on the gross section at the strength limit state. Since the bottom flange is discretely braced, bottom flange splice plates subject to compression must again be checked for the combined stress; the following equation may be used (Equation 3.3.143). The equation assumes an unbraced length of zero for the splice plates.

$$\frac{P}{(A_g)_{PL}} + \frac{M_\ell}{S_{PL}} \le \phi_c F_y$$

ϕ_c is the resistance factor for compression elements (=0.90) (*AASHTO LRFD* Article 6.5.4.2).

M_ℓ is the factored lateral moment in the bottom flange due to the Strength I load combination computed as:

$$M_\ell = (1/1.0)(0.90)(5+1) + (1/1.0)(0.65)(1) + 1.0(1.75)(-12) = -15\ \text{kip} - \text{ft}$$

Since the bottom flange is discretely braced and subject to compression under vertical bending in this case, it is determined using procedures similar to those demonstrated in Section 5.1.8.1.2 that amplification of the lateral moment is required. The amplification factor within this unbraced length is computed to be 1.44. Therefore:

$$\frac{549}{22.5} + \frac{|-15(1.44)|(12)}{47.8} = 29.8\ \text{ksi} < 0.90(50) = 45.0\ \text{ksi} \quad \text{ok}$$

Bolts

Determine the number of bolts for the bottom flange splice plates that are required to develop the governing combined design actions in the flange in shear at the strength limit state assuming the bolts in the connection have slipped and gone into bearing.

A minimum of two rows of bolts must be provided to ensure proper alignment and stability of the girder during construction. The nominal shear resistance, R_n, for a 7/8-in. diameter A325 high-strength bolt in double shear assuming the threads are *excluded* from the shear planes is computed as (Equation 3.3.82):

$$R_n = 0.48 A_b F_{ub} N_s$$

A_b is the area of the bolt corresponding to the nominal diameter equal to $\pi(0.875)^2/4 = 0.60$ in.^{2} F_{ub} is the specified minimum tensile strength of the bolt equal to 120 ksi for bolts less than or equal to 1.0 inch in diameter (*AASHTO LRFD* Article 6.4.3). N_s is the number of shear planes per bolt. Therefore:

$$R_n = 0.48(0.60)(120)(2) = 69.1 \text{ kips/bolt}$$

The factored shear resistance of the bolt, R_r, is equal to R_n times the resistance factor, ϕ_s, for shear on bolts equal to 0.80 (AASHTO LRFD Article 6.5.4.2). Therefore:

$$R_r = 0.80(69.1) = 55.3 \text{ kips/bolt}$$

Since the factored shear resistance of the bolts is based on the assumption that the threads are excluded from the shear planes, an appropriate note should be placed on the contract plans to ensure that the splice is detailed to exclude the bolt threads from the shear planes. It is assumed that the length between the extreme bolts (on one side of the connection) measured parallel to the line of action of the force will be less than 50.0 in. so that no reduction in the factored shear resistance is required (this will be checked later).

The traditional elastic vector method for eccentric shear (Section 3.3.6.2.7) may be used to account for the effects of flange lateral bending in the design of the flange splice bolts. The direct shear on the flange bolts at the strength limit state (*P* in Figure 3.3.62) is caused by the governing minimum flange design force. The moment, M_ℓ (Figure 3.3.62), on the bolt group is taken as the calculated governing factored flange lateral bending moment.

To utilize the elastic vector method to determine the maximum resultant force in the extreme bolt under the combined actions, the polar moment of inertia, I_p, of the entire bolt group must first be computed. Referring to Figure 3.3.64, I_p may be computed as follows (Equation 3.3.108):

$$I_p = \sum_{i=1}^{n} x_i^2 + \sum_{i=1}^{n} y_i^2$$

Assuming the bolt pattern shown below for the bottom flange splice in Figure 5.1.29, I_p is computed as follows:

$$I_p = \left[2 * 4 * \left(3.0^2 + 6.0^2\right)\right] + \left[2 * 5 * \left(3.0^2 + 7.0^2\right)\right] = 940 \text{ in}^2$$

The bolt force due to the moment is computed in two components. *X* and *Y* in the two equations given immediately below are defined in Figure 3.3.65.

The longitudinal component, P_{Mx}, in the extreme bolt is computed as (Equation 3.3.144):

$$P_{Mx} = \frac{M_\ell Y}{I_p}$$

$$P_{Mx} = \frac{37(12)(7.0)}{940} = 3.31 \text{ kips}$$

Similarly, the transverse component, P_{My}, in the extreme bolt is computed as (Equation 3.3.145):

$$P_{My} = \frac{M_\ell X}{I_p}$$

$$P_{My} = \frac{37(12)(6.0)}{940} = 2.83 \text{ kips}$$

The bolt force due to shear, P_v, is taken equal to (Equation 3.3.146):

$$P_v = \frac{P}{N_b}$$

where N_b is the number of bolts in the bolt group.

$$P_v = \frac{630}{20} = 31.5 \text{ kips / bolt}$$

The maximum resultant bolt force in the critical extreme bolt, P_r (Figure 3.3.65), is then computed as (Equation 3.3.147):

$$P_r = \sqrt{(P_v + P_{Mx})^2 + P_{My}{}^2}$$

$$P_r = \sqrt{(31.5 + 3.31)^2 + (2.83)^2} = 34.9 \text{ kips}$$

Filler plates 0.25 in. or greater in thickness in girder flange splices must be secured by additional bolts to ensure that shear planes are well defined and that no reduction in the factored shear resistance of the bolts results (Section 3.3.7.4.2). *AASHTO LRFD* Article 6.13.6.1.5 specifies that this can be accomplished by either: 1) extending the fillers beyond the splice plate with the filler extension secured by

enough additional bolts to distribute the total stress uniformly over the combined section of the member or filler; or 2) in lieu of extending and developing the fillers, reducing the factored shear resistance of the bolts by the following factor (Equation 3.3.157):

$$R = \left[\frac{(1+\gamma)}{(1+2\gamma)} \right]$$

In this example, the factored shear resistance of the bolts on the side of the splice with the filler plate will be reduced by the factor *R* as follows:

$$A_f = 0.375(18.0) = 6.75 \text{ in.}^2$$

$$A_p = \text{flange area} = 1.0(18.0) = 18.0 \text{ in.}^2 \quad \text{(governs)} \quad \text{or}$$

$$A_p = \text{splice plate area} = 2(0.75)(7.5) + 0.625(18.0) = 22.5 \text{ in.}^2$$

$$\gamma = \frac{6.75}{18.0} = 0.375$$

$$R = \frac{1+0.375}{1+2(0.375)} = 0.79$$

$$R * R_r = 0.79 * 55.3 \text{ kips} = 43.7 \text{ kips} > P_r = 34.9 \text{ kips} \quad \text{ok}$$

Therefore, a minimum of 20 bolts is required to provide the necessary factored shear resistance for the bottom flange splice at the strength limit state under the controlling minimum design force. Use twenty (20) 7/8-in. diameter high-strength bolts on each side of the bottom flange splice (4 rows of bolts with 5 bolts per row -- no stagger – Figure 5.1.29). The slip resistance of these bolts at the service limit state and for constructibility is checked later on.

Bolt Spacing

To check the factored bearing resistance of the bolt holes and the block shear rupture resistance of the splice plates and the flange, the bolt spacings and bolt edge and end distances must first be established and checked. Examine the bolt spacings and edge and end distances shown in Figure 5.1.29.

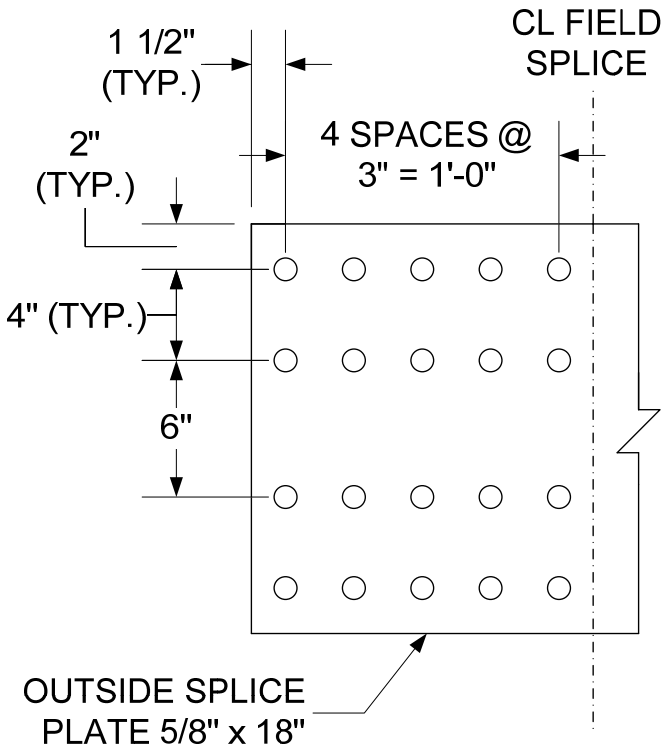


Figure 5.1.29 Bolt Configuration for Bottom Flange Splice in Span 3 of G4

Since the length between the extreme bolts (on one side of the connection) measured parallel to the line of action of the force is less than 50.0 in., no reduction in the factored shear resistance of the bolts is required, as originally assumed.

AASHTO LRFD Article 6.13.2.6.1 specifies that the minimum spacing between centers of bolts in standard holes is not to be less than 3.0*d*, where *d* is the diameter of the bolt (Section 3.3.6.2.2.6). For 7/8-in. diameter bolts:

$$s_{min} = 3d = 3(0.875) = 2.63\,\text{in.} \quad \text{use min. of } 3.0\,\text{in.} \quad \text{ok}$$

AASHTO LRFD Article 6.13.2.6.2 specifies that to seal against the penetration of moisture in joints, the spacing, *s*, of a single line of bolts adjacent to a free edge of an outside plate or shape (when the bolts are not staggered) must satisfy the following requirement (Section 3.3.6.2.2.6 - Equation 3.3.75):

$$s \le (4.0 + 4.0t) \le 7.0\,\text{in.}$$

where *t* is the thickness of the thinner outside plate or shape. First, check for sealing along the edges of the outer splice plate (which is the thinner plate) parallel to the direction of the applied force:

$$s_{max} = 4.0 + 4.0(0.625) = 6.5 \text{ in.} > 3.0 \text{ in.} \quad \text{ok}$$

Check for sealing along the free edge at the end of the splice plate:

$$s_{max} = 4.0 + 4.0(0.625) = 6.5 \text{ in.} > 6.0 \text{ in.} \quad \text{ok}$$

The edge distance of bolts is defined as the distance perpendicular to the line of force between the center of a hole and the edge of the component. In this example, the minimum edge distance of 1.5 inches (on the inside splice plates – Figure 5.1.30) satisfies the minimum edge distance requirement of 1½ inches specified for 7/8-in. diameter bolts and sheared edges in *AASHTO LRFD* Table 6.13.2.6.6-1 (Section 3.3.6.2.2.6 – Table 3.3.2). The maximum edge distance of 2.0 inches also satisfies the maximum edge distance requirement of 8.0*t* (not to exceed 5.0 in.) = 8.0(0.625) = 5.0 in. specified in *AASHTO LRFD* Article 6.13.2.6.6.

The end distance of bolts is defined as the distance along the line of force between the center of a hole and the end of the component. In this example, the end distance of 1½ inches satisfies the minimum end distance requirement of 1½ inches specified for 7/8-in. diameter bolts and sheared edges in Table 3.3.2. The maximum end distance requirement of 8.0*t* (not to exceed 5.0 in.) = 8.0(0.625) = 5.0 in. is also obviously satisfied. Although not specifically required, note that the maximum distance from the corner bolts to the corner of the splice plate, equal to $\sqrt{(1.5)^2 + (2.0)^2} = 2.5 \text{ in.}$, also satisfies the maximum end distance requirement. If desired, the corners of the plate can be clipped to meet this requirement.

Bearing Resistance

The bearing resistance of the connected material at the strength limit state is calculated as the sum of the bearing resistances of the individual bolts (holes) parallel to the line of the applied force (Section 3.3.6.2.6.2).

The splice is subject to lateral bending; thus, the resultant force, P_r, in the extreme outer bolt acts in the direction of an inclined distance that is larger than the clear end distance. In lieu of calculating the bearing resistance based on this inclined distance, the resistance of the outermost hole, calculated using the clear end distance, will conservatively be checked against the maximum resultant bolt force, P_r.

Check the splice plates (the outer plate controls). For standard holes, the nominal bearing resistance, R_n, parallel to the applied bearing force is taken as follows (Equation 3.3.88):

$$R_n = 1.2 L_c t F_u \le 2.4 d t F_u$$

For the outermost bolt adjacent to the end of the splice plate, the end distance is 1.5 in. (Figure 5.1.29). The diameter of the hole is 0.9375 in. Therefore, the clear end distance, L_c, between the edge of the hole and the end of the splice plate is:

$$L_c = 1.5 - \frac{0.9375}{2} = 1.03 \text{ in.}$$

Therefore:

$$R_n = 1.2 L_c t F_u = 1.2(1.03)(0.625)(70) = 54.1 \text{ kips (governs)}$$

or:

$$R_n = 2.4 d t F_u = 2.4(0.875)(0.625)(70) = 91.9 \text{ kips}$$

The factored bearing resistance of the flange, R_r, is computed as (Equation 3.3.80):

$$R_r = \phi_{bb} R_n$$

R_r = 0.80(54.1 kips) = 43.3 kips > $P_r/2$ = 34.9 kips/2 = 17.5 kips ok

Check the thinner bottom flange at the splice. For the outermost bolt adjacent to the end of the flange, the end distance is 2 inches (which also satisfies the minimum end distance requirement discussed above). Therefore, the clear end distance, L_c, between the edge of the hole and the end of the flange is:

$$L_c = 2.0 - \frac{0.9375}{2} = 1.53 \text{ in.}$$

Therefore:

$$R_n = 1.2 L_c t F_u = 1.2(1.53)(1.0)(70) = 128 \text{ kips (governs)}$$

or:

$$R_n = 2.4 d t F_u = 2.4(0.875)(1.0)(70) = 147 \text{ kips}$$

The factored bearing resistance of the flange, R_r, is computed as (Equation 3.3.80):

$$R_r = \phi_{bb} R_n$$

R_r = 0.80(128 kips) = 102 kips > P_r = 34.9 kips ok

Block Shear Rupture Resistance

Check the block shear rupture resistance (Section 3.3.3.2.4) of the bottom flange splice plates and the bottom flange when subject to the minimum design force in tension at the strength limit state.

Assume the potential block shear failure planes on the outside and inside splice plates shown below in Figure 5.1.30.

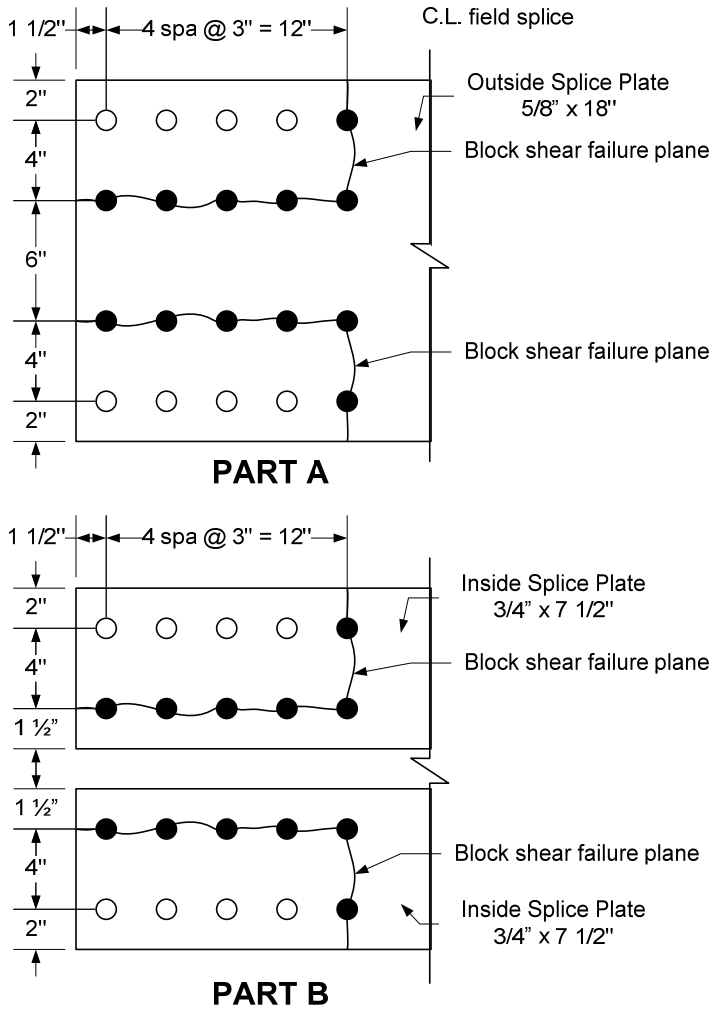


Figure 5.1.30 Assumed Block Shear Failure Planes for Bottom Flange Splice Plates
A) Outside Splice Plate; B) Inside Splice Plates

Determine the block shear rupture resistance for the outside splice plate. A_{tn} is the net area along the place resisting the tensile stress.

$$A_{tn} = 2\left[4.0 + 2.0 - 1.5(0.9375)\right](0.625) = 5.74 \text{ in}^2$$

A_{vn} is the net area along the place resisting the shear stress.

$$A_{vn} = 2[4(3.0) + 1.5 - 4.5(0.9375)](0.625) = 11.60 \text{ in}^2$$

A_{vg} is the gross area along the plane resisting the shear stress.

$$A_{vg} = 2[4(3.0) + 1.5](0.625) = 16.88 \text{ in}^2$$

The factored block shear rupture resistance, R_r, is determined as (Equation 3.3.27):

$$\begin{aligned} R_r &= \phi_{bs} R_p (0.58 F_u A_{vn} + U_{bs} F_u A_{tn}) \\ &\le \phi_{bs} R_p (0.58 F_y A_{vg} + U_{bs} F_u A_{tn}) \end{aligned}$$

ϕ_{bs} is the resistance factor for block shear rupture taken equal to 0.80 (*AASHTO LRFD* Article 6.5.4.2). The reduction factor, R_p, is taken equal to 1.0 for holes drilled full-size (Section 3.3.3.2.1). The reduction factor, U_{bs}, is taken equal to 1.0 since the tension stress is uniform (Section 3.3.3.2.4). Therefore:

$$\begin{aligned} R_r &= 0.80(1.0)[0.58(70)(11.60) + 1.0(70)(5.74)] = 698 \text{ kips} \\ &< 0.80(1.0)[0.58(50)(16.88) + 1.0(70)(5.74)] = 713 \text{ kips} \quad \text{ok} \end{aligned}$$

Determine the block shear rupture resistance for the inside splice plates.

$$A_{tn} = 2[4.0 + 2.0 - 1.5(0.9375)](0.75) = 6.89 \text{ in}^2$$

$$A_{vn} = 2[4(3.0) + 1.5 - 4.5(0.9375)](0.75) = 13.92 \text{ in}^2$$

$$A_{vg} = 2[4(3.0) + 1.5](0.75) = 20.25 \text{ in}^2$$

$$\begin{aligned} R_r &= 0.80(1.0)[0.58(70)(13.92) + 1.0(70)(6.89)] = 838 \text{ kips} \\ &< 0.80(1.0)[0.58(50)(20.25) + 1.0(70)(6.89)] = 856 \text{ kips} \quad \text{ok} \end{aligned}$$

Check the block shear rupture resistance according to Equation 3.3.140 as follows:

$$\frac{P}{(A_g)_{PL}} + \frac{M_\ell}{S_{PL}} \le \frac{R_r}{(A_g)_{PL}}$$

$$\frac{630}{22.5} + \frac{37(12)}{47.8} = 37.3 \text{ ksi} < \frac{(698 + 838)}{22.5} = 68.3 \text{ ksi} \quad \text{ok}$$

Check the critical girder flange at the splice. Two potential failure modes are investigated for the flange as shown below in Figure 5.1.31.

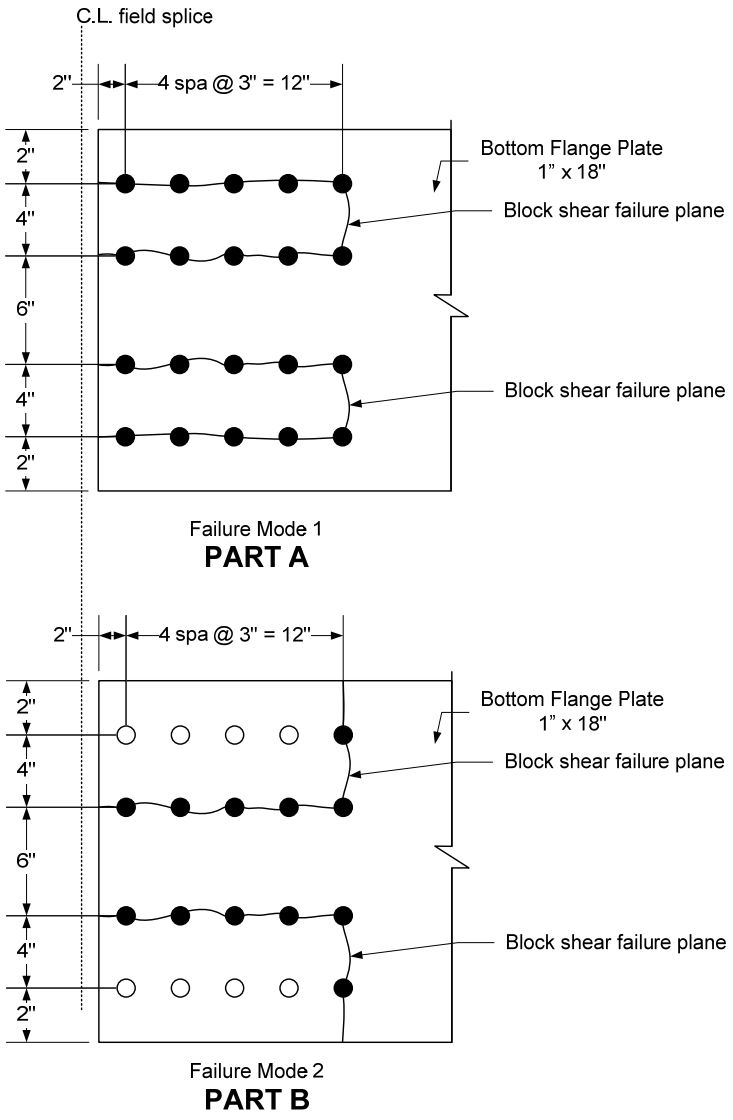


Figure 5.1.31 Assumed Block Shear Failure Planes for Critical Bottom Flange at the Splice
A) Assumed Failure Mode 1; B) Assumed Failure Mode 2

For Failure Mode 1:

$$A_{tn} = 2[4.0 - 0.9375](1.0) = 6.13 \text{ in}^2$$

$$A_{vn} = 4[4(3.0) + 2.0 - 4.5(0.9375)](1.0) = 39.13\ \text{in}^2$$

$$A_{vg} = 4[4(3.0) + 2.0](1.0) = 56.00\ \text{in}^2$$

$$R_r = 0.80(1.0)[0.58(70)(39.13) + 1.0(70)(6.13)] = 1{,}614\ \text{kips}$$
$$< 0.80(1.0)[0.58(50)(56.00) + 1.0(70)(6.13)] = 1{,}642\ \text{kips} \quad \text{ok}$$

$$\frac{630}{1.0(18)} + \frac{37(12)}{1.0(18)^2/6} = 43.2\ \text{ksi} < \frac{1{,}614}{1.0(18)} = 89.7\ \text{ksi} \quad \text{ok}$$

For Failure Mode 2:

$$A_{tn} = 2[4.0 + 2.0 - 1.5(0.9375)](1.0) = 9.19\ \text{in}^2$$

$$A_{vn} = 2[4(3.0) + 2.0 - 4.5(0.9375)](1.0) = 19.56\ \text{in}^2$$

$$A_{vg} = 2[4(3.0) + 2.0](1.0) = 28.00\ \text{in}^2$$

$$R_r = 0.80(1.0)[0.58(70)(19.56) + 1.0(70)(9.19)] = 1{,}150\ \text{kips}$$
$$< 0.80(1.0)[0.58(50)(28.00) + 1.0(70)(9.19)] = 1{,}164\ \text{kips} \quad \text{ok}$$

$$\frac{630}{1.0(18)} + \frac{37(12)}{1.0(18)^2/6} = 43.2\ \text{ksi} < \frac{1{,}150}{1.0(18)} = 63.9\ \text{ksi} \quad \text{ok}$$

Net Section Fracture of Flange

Check for net section fracture of the critical bottom flange at the point of splice when subject to tension at the strength limit state according to the following requirement (Section 3.2.6.1.3 – Equation 3.2.72):

$$f_t \le 0.84\left(\frac{A_n}{A_g}\right)F_u \le F_{yt}$$

The flange on the right side of the splice is the critical flange for this particular check.

A_n is the net area of the flange computed as:

$$A_n = [18 - 4(0.9375)](1.0) = 14.25\ \text{in.}^2$$

$$0.84\left(\frac{A_n}{A_g}\right)F_u = 0.84\left(\frac{14.25}{18.00}\right)70 = 46.6 \text{ ksi} < F_{yt} = 50 \text{ ksi}$$

From separate calculations, f_t in the bottom flange at the strength limit state (Strength I) is equal to +23.06 ksi for the section on the right side of the splice, which is less than 46.6 ksi. Therefore, net section fracture of the bottom flange at the point of splice will not occur.

Service Limit State & Constructibility

Bolts

AASHTO LRFD Article 6.13.6.1.4c requires that high-strength bolted connections for flange splices be designed to prevent slip at the service limit state under a Service II design force. In addition, *AASHTO LRFD* Article 6.13.6.1.4a requires that high-strength bolted splices for flexural members be proportioned to prevent slip during the erection of the steel (assuming an erection analysis is conducted) and during the casting of the concrete deck.

For the service limit state check, the Service II design stress, F_s, is to be taken as (Section 3.3.7.2.3 – Equation 3.3.131):

$$F_s = \frac{f_s}{R_h}$$

where f_s is the maximum vertical bending stress due to Load Combination Service II at the midthickness of the flange under consideration for the smaller section at the point of splice.

For the right side of the splice, which is deemed the smaller section in this case, the Service II stress in the bottom flange is computed as follows. Separate computations indicate that the conditions specified in *AASHTO LRFD* Article 6.10.4.2.1 are met such that flexural stresses caused by Service II loads applied to the composite section can be computed using the short-term or long-term composite section, as appropriate, assuming the concrete deck is effective for both positive and negative flexure (Section 3.2.4.3.1).

A. Dead Load + Positive Live Load:

$$f = \left[1.0(1.37 - 0.37 + 0.24) + 1.3(12.11)\right] = +16.98 \text{ ksi (governs)}$$

B. Dead Load + Negative Live Load:

$$f_{-LL+IM} = \frac{-3{,}001(12)(78.6)}{281{,}487} = -10.06 \text{ ksi}$$

$$f = \left[1.0(1.37 - 0.37 + 0.24) + 1.3(-10.06)\right] = -11.84 \text{ ksi}$$

Therefore, f_s is equal to +16.98 ksi and F_s is equal to f_s/R_h = +16.98/1.0 = +16.98 ksi. The design force, P, for the flange splice is taken as F_s times the smaller gross flange area on either side of the splice (Equation 3.3.133), or:

$$P = F_s A_g = 16.98(1.0)(18) = 306 \text{ kips}$$

M_ℓ is the corresponding factored lateral moment in the bottom flange due to the Service II load combination computed as:

$$M_\ell = 1.0(+5 + 1 + 1) + 1.3(+16) = +28 \text{ kip} - \text{ft}$$

The stress on the non-composite section at the mid-thickness of the bottom flange due to the steel weight plus the deck-casting sequence (the Strength IV load combination controls with η taken equal to 1.0) is:

$$f = \frac{1.0(1.5)(50 + 3{,}960)(12)(46.5)}{118{,}397} = +28.35 \text{ ksi} \qquad \frac{f}{R_h} = \frac{+28.35}{1.0} = +28.35 \text{ ksi}$$

The design force, P, for the flange splice is taken as f times the smaller gross flange area on either side of the splice (Equation 3.3.132), or:

$$P = fA_g = 28.35(1.0)(18) = 510 \text{ kips}$$

Determine the factored lateral moment, M_ℓ, in the bottom flange for constructibility. The factored lateral moment due to the steel weight plus the deck staging is 1.0(1.5)(+1 + 23) = +36 kip-ft. Since the splice is in an exterior girder, include the lateral flange moment due to the deck overhang loads. The factored lateral moment due to the deck overhang loads under the Strength IV load combination at the cross-frame was computed earlier to be +17 kip-ft (Section 5.1.8.1.2). Amplification of the lateral moment is not necessary since the flange is subject to tension under vertical bending in this case. In a curved bridge, the lateral flange moment in the outside girder due to the deck overhang loads has the same sense as the lateral flange moments due to curvature. Therefore:

$$M_\ell = +36 + 17 = +53 \text{ kip} - \text{ft}$$

By inspection, the constructibility case controls.

Determine the number of bolts for the bottom flange splice plates that are required to prevent slip. The factored slip resistance, R_r, for a 7/8-in. diameter A 325 high-strength bolt assuming a Class B surface condition for the faying surface, standard holes and two slip planes per bolt (i.e. N_s = 2) is computed as follows (Section 3.3.6.2.6.1 – Equations 3.3.77 and 3.3.78):

$$R_r = R_n = K_h K_s N_s P_t$$

The hole size factor, K_h, is equal to 1.0 for standard holes (Table 3.3.4). The surface condition factor, K_s, for a Class B faying surface is 0.50 (Table 3.3.5). The minimum required bolt tension, P_t, for a 7/8-inch diameter A 325 high-strength bolt is 39 kips (Table 3.3.1). Therefore:

$$R_r = R_n = 1.0(0.5)(2)(39) = 39.0 \text{ kips/bolt}$$

AASHTO LRFD Article 6.13.6.1.5 specifies that the factored slip resistance need not be adjusted for the effect of filler plates.

Referring to the bolt pattern shown for the bottom flange splice in Figure 5.1.29, calculate the maximum resultant force on the extreme bolt under the combined actions. The longitudinal component, P_{Mx}, in the extreme bolt is computed as (Equation 3.3.144):

$$P_{Mx} = \frac{53(12)(7.0)}{940} = 4.74 \text{ kips}$$

The transverse component, P_{My}, in the extreme bolt is computed as (Equation 3.3.145):

$$P_{My} = \frac{53(12)(6.0)}{940} = 4.06 \text{ kips}$$

The bolt force due to shear, P_v, is taken equal to (Equation 3.3.146):

$$P_v = \frac{510}{20} = 25.5 \text{ kips / bolt}$$

The maximum resultant bolt force in the critical extreme bolt, P_r (Figure 3.3.65), is then computed as (Equation 3.3.147):

$$P_r = \sqrt{(25.5 + 4.74)^2 + (4.06)^2} = 30.5 \text{ kips} < R_r = 39.0 \text{ kips} \quad \text{ok}$$

The slip resistance of the selected bolt pattern is satisfactory for constructibility and at the service limit state.

Splice Plates

The combined stress in the bottom flange splice plates under the Service II load combination will be checked against a limiting stress of $0.95F_y$, where F_y is the specified minimum yield strength of the splice plates.

The minimum Service II design force, P, for the splice was computed earlier to be 306 kips. Since the bottom flange is discretely braced, lateral flange bending is considered. The Service II lateral moment, M_ℓ, was computed above to be 28 kip-ft. Since the design actions at the service limit state are always assumed divided equally to the two slip planes regardless of the ratio of the splice plate areas (*AASHTO LRFD* Article C6.13.6.1.4c), the splice plates may be checked as follows:

$$\frac{P}{(A_g)_{PL}} + \frac{M_\ell}{S_{PL}} \le 0.95F_y$$

$(A_g)_{PL}$ and S_{PL} were computed earlier to be 22.5 in.^{2} and 47.8 in.^{3}, respectively. Therefore:

$$\frac{306}{22.5} + \frac{28(12)}{47.8} = 20.63 \text{ ksi} < 0.95(50) = 47.5 \text{ ksi} \quad \text{ok}$$

Fatigue

Since the combined area of the inside and outside flange splice plates is greater than the area of the smaller flange at the splice, fatigue of the splice plates need not be considered (*AASHTO LRFD* Article C6.13.6.1.4a). However, the check will still be illustrated below to assist with cases in which fatigue may be a concern. The fatigue stresses in the base metal of the bottom flange splice plates adjacent to the slip-critical bolted connections will be checked.

By inspection, the bottom flange is subject to a net tensile stress. The unfactored vertical bending moments at the point of splice due to fatigue live load (Section 1.3.2.3.3) plus the specified 15 percent dynamic load allowance are:

$M_{+\text{Fat LL+IM}}$ = +1,095 kip-ft
$M_{-\text{ Fat LL+IM}}$ = - 773 kip-ft

Since the bottom flange is discretely braced, lateral flange bending is considered. The unfactored lateral flange moments in the bottom flange due to the fatigue live load plus impact at the adjacent cross-frame are:

$(M_\ell)_{+\text{Fat LL+IM}}$ = +4 kip-ft
$(M_\ell)_{-\text{ Fat LL+IM}}$ = -4 kip-ft

The conditions spelled out in *AASHTO LRFD* Article 6.6.1.2.1 are met such that the fatigue live load stresses can be computed using the short-term composite section assuming the concrete deck is effective for both positive and negative flexure (Section 5.1.8.3.3).

For checking the base metal at the gross section of high-strength bolted slip-resistant connections with the bolts installed in holes drilled full-size, the fatigue detail category is Category B (*AASHTO LRFD* Table 6.6.1.2.3-1 – Condition 2.1). From Table 3.2.9, the 75-year $(ADTT)_{SL}$ equivalent to infinite fatigue life for a Category B detail is 860 trucks per day, which is less than the computed $(ADTT)_{SL}$ of 1,600 trucks per day for this case (Section 5.1.8.3.2). The detail must therefore be checked for infinite life using the Fatigue I load combination (γ = 1.5). In the infinite life region, the nominal fatigue resistance is equal to the constant-amplitude fatigue threshold as follows (Equation 3.2.50):

$$(\Delta F)_n = (\Delta F)_{TH}$$

For a Category B detail, $(\Delta F)_{TH}$ = 16.0 ksi (*AASHTO LRFD* Table 6.6.1.2.5-3 – Table 3.2.6).

Using the section properties of the smaller section at the point of splice, the factored live load stress range at the midthickness of the bottom flange is computed as:

$$\gamma(\Delta f) = \frac{1.5[1{,}095 + |-773|](12)(78.6)}{281{,}487} = 9.39 \text{ ksi}$$

The range of flange force in flange is computed from the stress range as follows:

$$\Delta P = 9.39(1.0)(18) = 169.0 \text{ kips}$$

The splice plates may be checked for fatigue as follows:

$$\frac{\Delta P}{(A_g)_{PL}} + \frac{\Delta M_\ell}{S_{PL}} \le (\Delta F)_{TH}$$

$(A_g)_{PL}$ and S_{PL} were computed earlier to be 22.5 in.^{2} and 47.8 in.^{3}, respectively. Therefore:

$$\frac{169.0}{22.5} + \frac{1.5[4 + |-4|](12)}{47.8} = 10.52 \text{ ksi} < 16.0 \text{ ksi} \quad \text{ok}$$

5.1.8.8.2.3 Top Flange Splice

The width of the outside splice plate should be at least as wide as the width of the narrowest flange at the splice. Therefore, try a 1/2" x 18" outside splice plate with

two 5/8" x 7-1/2" inside splice plates (Figure 5.1.32). A filler plate is not required since the flanges are the same thickness on both sides of the splice. All plates are ASTM A 709 Grade 50W steel.

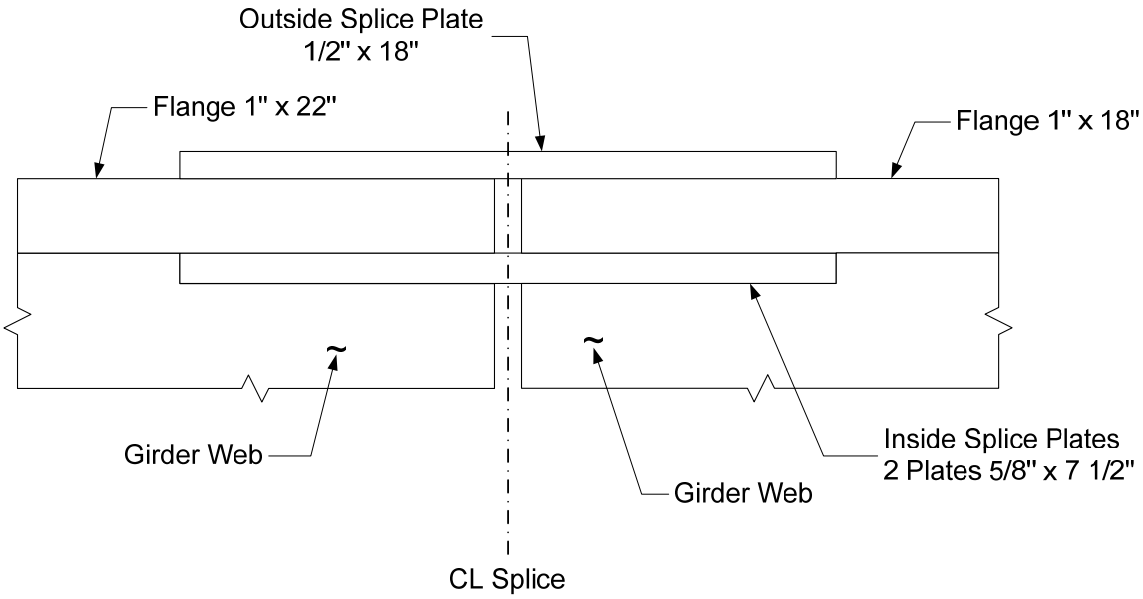


Figure 5.1.32 Elevation View of Top Flange Splice in Span 3 of G4 (bolts not shown)

Strength Limit State

Splice Plates

AASHTO LRFD Article 6.13.5.2 specifies that splice plates in tension at the strength limit state be checked for yielding on the gross section, fracture on the net section and block shear rupture. Lateral flange bending is ignored for the top flange splice plates at the strength limit state because the flange is continuously braced (Section 3.3.7.2.4).

For yielding, the splice plates may be checked as follows (Equation 3.3.135):

$$\frac{P}{(A_g)_{PL}} \le \phi_y F_y$$

$(A_g)_{PL}$ is the total gross area of the inner and outer splice plates computed as:

$$(A_g)_{PL} = 0.5(18) + 2(0.625)(7.5) = 18.4 \text{ in.}^2$$

Therefore:

$$\frac{630}{18.4} = 34.2 \text{ ksi} < 0.95(50) = 47.5 \text{ ksi} \quad \text{ok}$$

The preceding check and the checks that follow assume that the areas of the inner and outer flange splice plates do not differ by more than 10 percent, which is the case here. Otherwise, P and M_ℓ should be proportioned to the inner and outer splice plates by the ratio of the area(s) of the inner and outer plate(s) to the total area of the splice plates, with the splice plates than checked individually using their respective actions.

For net section fracture, the splice plates may be checked as follows (Equation 3.3.136):

$$\frac{P}{(A_n)_{PL}} \le \phi_u F_u U$$

U is a reduction factor to account for shear lag, which is to be taken as 1.0 for splice plates (*AASHTO LRFD* Article 6.13.5.2).

$(A_n)_{PL}$ is the total net area of the inner and outer splice plates computed as:

$$(A_n)_{PL} = [18 - 4(0.9375)](0.5) + 2[7.5 - 2(0.9375)](0.625) = 14.1 \text{ in.}^2$$

Therefore:

$$\frac{630}{14.1} = 44.7 \text{ ksi} < 0.8(70)(1.0) = 56.0 \text{ ksi} \quad \text{ok}$$

Also, according to *AASHTO LRFD* Article 6.13.5.2, for splice plates subject to tension, A_n must not exceed $0.85A_g$.

- Outer plate:

$$0.85(18)(0.5) = 7.65 \text{ in}^2 > A_n = [18 - 4(0.9375)](0.5) = 7.12 \text{ in.}^2 \quad \text{ok}$$

- Inner plates:

$$0.85(2)(7.5)(0.625) = 7.97 \text{ in}^2 > A_n = 2[7.5 - 2(0.9375)](0.625) = 7.03 \text{ in.}^2 \quad \text{ok}$$

The block shear rupture resistance of the splice plates will be checked later.

Flange splice plates subject to compression are checked for yielding on the gross section at the strength limit state as follows (Equation 3.3.142). Again, lateral flange

bending is ignored for the top flange splice plates at the strength limit state because the flange is continuously braced. The equation assumes an unbraced length of zero for the splice plates.

$$\frac{P}{(A_g)_{PL}} \le \phi_c F_y$$

ϕ_c is the resistance factor for compression elements (=0.90) (*AASHTO LRFD* Article 6.5.4.2). Therefore:

$$\frac{675}{18.4} = 36.7 \text{ ksi} < 0.90(50) = 45.0 \text{ ksi} \quad \text{ok}$$

Bolts

Determine the number of bolts for the top flange splice plates that are required to develop the governing minimum design force in the flange in shear at the strength limit state assuming the bolts in the connection have slipped and gone into bearing.

A minimum of two rows of bolts must be provided to ensure proper alignment and stability of the girder during construction. The factored shear resistance, R_r, for a 7/8-in. diameter A325 high-strength bolt in double shear assuming the threads are *excluded* from the shear planes was computed previously to be R_r = 55.3 kips/bolt (Section 5.1.8.8.2.2). It is assumed that the length between the extreme bolts (on one side of the connection) measured parallel to the line of action of the force will be less than 50.0 in. so that no reduction in the factored shear resistance is required (this will be checked later).

Since lateral bending is ignored in the top flange at the strength limit state, the minimum number of bolts required to develop the governing minimum design force in the flange in shear at the strength limit state (in the absence of a filler plate) is:

$$N = \frac{P}{R_r} = \frac{675}{55.3} = 12.2 \text{ bolts} \quad \text{Use N = 16 bolts}$$

Use sixteen (16) 7/8-in. diameter high-strength bolts on each side of the top flange splice (4 rows of bolts with 4 bolts per row -- no stagger – Figure 5.1.33). The slip resistance of these bolts at the service limit state and for constructibility is checked later on.

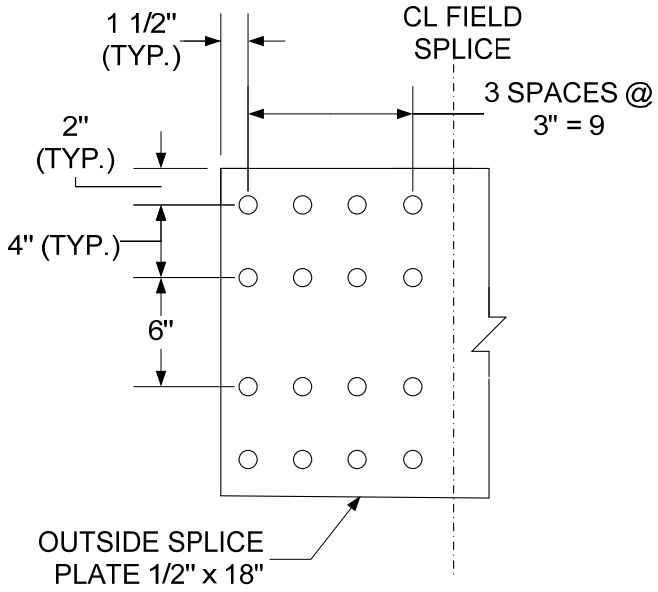


Figure 5.1.33 Bolt Configuration for Top Flange Splice in Span 3 of G4

Bolt Spacing

The bolt spacing and edge and end distances shown in Figure 5.1.33 satisfy the appropriate requirements, as demonstrated previously for the bottom flange splice in Section 5.1.8.8.2.2.

Since the length between the extreme bolts (on one side of the connection) measured parallel to the line of action of the force is less than 50.0 in., no reduction in the factored shear resistance of the bolts is required, as originally assumed.

Bearing Resistance

Check the bearing resistance at the bolt holes at the strength limit state.

Check the splice plates (the outer plate controls). For the four bolts adjacent to the end of the splice plate, the end distance is 1.5 in. Therefore, the clear end distance, L_c, between the edge of the hole and the end of the splice plate is:

$$L_c = 1.5 - \frac{0.9375}{2} = 1.03 \text{ in.}$$

Therefore:

$$R_n = 4(1.2L_c tF_u) = 4\left[1.2(1.03)(0.5)(70)\right] = 173 \text{ kips (governs)}$$

or:

$$R_n = 4(2.4dtF_u) = 4\left[2.4(0.875)(0.5)(70)\right] = 294 \text{ kips}$$

For the other twelve bolts, the center-to-center distance between the bolts in the direction of the applied force is 3.0 in. Therefore, the clear distance, L_c, between the edges of the adjacent holes is:

$$L_c = 3.0 - 0.9375 = 2.06 \text{ in.}$$

Therefore:

$$R_n = 12(1.2L_c tF_u) = 12[1.2(2.06)(0.5)(70)] = 1{,}038 \text{ kips}$$

or:

$$R_n = 12(2.4dtF_u) = 12[2.4(0.875)(0.5)(70)] = 882 \text{ kips (governs)}$$

The total nominal bearing resistance of the splice plate is therefore:

$$R_n = 173 \text{ kips} + 882 \text{ kips} = 1{,}055 \text{ kips}$$

$$R_r = 0.80(1{,}055 \text{ kips}) = 844 \text{ kips} > \frac{675}{2} = 338 \text{ kips} \quad \text{ok}$$

Check the flange at the splice. For the four bolts adjacent to the end of the flange, the end distance is 2 inches (which satisfies the minimum end distance requirement). Therefore, the clear end distance, L_c, between the edge of the hole and the end of the flange is:

$$L_c = 2.0 - \frac{0.9375}{2} = 1.53 \text{ in.}$$

Therefore:

$$R_n = 4(1.2L_c tF_u) = 4[1.2(1.53)(1.0)(70)] = 514 \text{ kips (governs)}$$

or:

$$R_n = 4(2.4dtF_u) = 4[2.4(0.875)(1.0)(70)] = 588 \text{ kips}$$

For the other twelve bolts, the center-to-center distance between the bolts in the direction of the applied force is 3.0 in. Therefore, the clear distance, L_c, between the edges of the adjacent holes is:

$$L_c = 3.0 - 0.9375 = 2.06 \text{ in.}$$

Therefore:

$$R_n = 12(1.2L_c tF_u) = 12[1.2(2.06)(1.0)(70)] = 2{,}076 \text{ kips}$$

or:

$$R_n = 12(2.4dtF_u) = 12[2.4(0.875)(1.0)(70)] = 1{,}764 \text{ kips (governs)}$$

The total nominal bearing resistance of the flange is therefore:

$$R_n = 514 \text{ kips} + 1{,}764 \text{ kips} = 2{,}278 \text{ kips}$$

$$R_r = 0.80(2{,}278 \text{ kips}) = 1{,}822 \text{ kips} > 675 \text{ kips} \quad \text{ok}$$

Block Shear Rupture Resistance

Check the block shear rupture resistance (Section 3.3.3.2.4) of the top flange splice plates and the top flange when subject to the minimum design force in tension at the strength limit state.

Assume the same potential block shear failure planes on the outside and inside splice plates as shown previously for the bottom flange splice plates in Figure 5.1.30.

Check the outside splice plate. A_{tn} is the net area along the place resisting the tensile stress.

$$A_{tn} = 2[4.0 + 2.0 - 1.5(0.9375)](0.5) = 4.59 \text{ in}^2$$

A_{vn} is the net area along the place resisting the shear stress.

$$A_{vn} = 2[3(3.0) + 1.5 - 3.5(0.9375)](0.5) = 7.22 \text{ in}^2$$

A_{vg} is the gross area along the plane resisting the shear stress.

$$A_{vg} = 2[3(3.0) + 1.5](0.5) = 10.50 \text{ in}^2$$

The factored block shear rupture resistance, R_r, is determined as (Equation 3.3.27):

$$R_r = 0.80(1.0)[0.58(70)(7.22) + 1.0(70)(4.59)] = 491 \text{ kips}$$
$$< 0.80(1.0)[0.58(50)(10.50) + 1.0(70)(4.59)] = 501 \text{ kips} \quad \text{ok}$$

Check the block shear rupture resistance according to Equation 3.3.137 as follows:

$$P \le R_r$$

$$R_r = 491 \text{ kips} > \frac{630}{2} = 315 \text{ kips} \quad \text{ok}$$

Determine the block shear rupture resistance for the inside splice plates.

$$A_{tn} = 2[4.0 + 2.0 - 1.5(0.9375)](0.625) = 5.74 \text{ in}^2$$

$$A_{vn} = 2[3(3.0) + 1.5 - 3.5(0.9375)](0.625) = 9.02 \text{ in}^2$$

$$A_{vg} = 2[3(3.0) + 1.5](0.625) = 13.12 \text{ in}^2$$

$$R_r = 0.80(1.0)[0.58(70)(9.02) + 1.0(70)(5.74)] = 614 \text{ kips}$$
$$< 0.80(1.0)[0.58(50)(13.12) + 1.0(70)(5.74)] = 626 \text{ kips} \quad \text{ok}$$

$$R_r = 614 \text{ kips} > \frac{630}{2} = 315 \text{ kips} \quad \text{ok}$$

Check the critical girder flange at the splice. The same two potential failure modes are investigated as for the bottom flange (Figure 5.1.31).

For Failure Mode 1:

$$A_{tn} = 2[4.0 - 0.9375](1.0) = 6.13 \text{ in}^2$$

$$A_{vn} = 4[3(3.0) + 2.0 - 3.5(0.9375)](1.0) = 30.88 \text{ in}^2$$

$$A_{vg} = 4[3(3.0) + 2.0](1.0) = 44.00 \text{ in}^2$$

$$R_r = 0.80(1.0)[0.58(70)(30.88) + 1.0(70)(6.13)] = 1{,}346 \text{ kips}$$
$$< 0.80(1.0)[0.58(50)(44.00) + 1.0(70)(6.13)] = 1{,}364 \text{ kips} \quad \text{ok}$$

$$R_r = 1{,}346 \text{ kips} > 630 \text{ kips} \quad \text{ok}$$

For Failure Mode 2:

$$A_{tn} = 2[4.0 + 2.0 - 1.5(0.9375)](1.0) = 9.19 \text{ in}^2$$

$$A_{vn} = 2[3(3.0) + 2.0 - 3.5(0.9375)](1.0) = 15.44 \text{ in}^2$$

$$A_{vg} = 2[3(3.0) + 2.0](1.0) = 22.00 \text{ in}^2$$

$$R_r = 0.80(1.0)\left[0.58(70)(15.44) + 1.0(70)(9.19)\right] = 1{,}016 \text{ kips}$$
$$< 0.80(1.0)\left[0.58(50)(22.00) + 1.0(70)(9.19)\right] = 1{,}025 \text{ kips} \quad \text{ok}$$

$$R_r = 1{,}016 \text{ kips} > 630 \text{ kips} \quad \text{ok}$$

Net Section Fracture of Flange

Check for net section fracture of the critical top flange at the point of splice when subject to tension at the strength limit state according to *AASHTO LRFD* Equation 6.10.1.8-1 (Section 3.2.6.1.3 – Equation 3.2.72).

The flange on the right side of the splice is the critical flange for this particular check.

A_n is the net area of the flange computed as:

$$A_n = \left[18 - 4(0.9375)\right](1.0) = 14.25 \text{ in.}^2$$

$$0.84\left(\frac{A_n}{A_g}\right)F_u = 0.84\left(\frac{14.25}{18.0}\right)70 = 46.6 \text{ ksi} < F_{yt} = 50 \text{ ksi}$$

From separate calculations, f_t in the top flange at the strength limit state (Strength I) is equal to +24.18 ksi for the section on the right side of the splice, which is less than 46.6 ksi. Therefore, net section fracture of the top flange at the point of splice will not occur.

Service Limit State & Constructibility

Bolts

For the right side of the splice, which is deemed the smaller section, the Service II stress in the top flange is computed as follows. Separate computations indicate that the conditions specified in *AASHTO LRFD* Article 6.10.4.2.1 are met such that flexural stresses caused by Service II loads applied to the composite section can be computed using the short-term or long-term composite section, as appropriate, assuming the concrete deck is effective for both positive and negative flexure. Flange lateral bending is not considered because the flange is continuously braced at the service limit state.

A. Dead Load + Positive Live Load:

$$f = \left[1.0(-1.37 + 0.17 + -0.11) + 1.3(-2.22)\right] = -4.20 \text{ ksi} \quad \text{(controls)}$$

B. Dead Load + Negative Live Load:

$$f_{-LL+IM} = \frac{-3{,}001(12)(-14.4)}{281{,}487} = +1.84 \text{ ksi}$$

$$f = \left[1.0(-1.37 + 0.17 + -0.11) + 1.3(+1.84)\right] = +1.08 \text{ ksi}$$

Therefore, f_s is equal to –4.20 ksi and F_s is equal to f_s/R_h = -4.20/1.0 = -4.20 ksi. The design force, P, for the flange splice is taken as F_s times the smaller gross flange area on either side of the splice (Equation 3.3.133), or:

$$P = F_s A_g = \left|-4.20\right|(1.0)(18) = 75.6 \text{ kips}$$

The stress on the non-composite section at the mid-thickness of the top flange due to the steel weight plus the deck-casting sequence (the Strength IV load combination controls with η taken equal to 1.0) is:

$$f = \frac{1.0(1.5)(50 + 3{,}960)(12)(-46.5)}{118{,}397} = -28.35 \text{ ksi} \qquad \frac{f}{R_h} = \frac{-28.35}{1.0} = -28.35 \text{ ksi}$$

The design force, *P,* for the flange splice is taken as *f* times the smaller gross flange area on either side of the splice (Equation 3.3.132), or:

$$P = fA_g = \left|-28.35\right|(1.0)(18) = 510 \text{ kips}$$

Because the top flange is discretely braced during construction, consider the flange lateral bending. Determine the factored lateral moment, M_ℓ, in the top flange for constructibility. The factored lateral moment due to the steel weight plus the deck staging is 1.0(1.5)(0 + -5) = -7.5 kip-ft. Since the splice is in an exterior girder, include the lateral flange moment due to the deck overhang loads. The factored lateral moment due to the deck overhang loads at the cross-frame under the Strength IV load combination was computed earlier to be -17 kip-ft (Section 5.1.8.1.2). The flange is subject to compression under vertical bending and amplification of the flange lateral moment (stress) is required in this case; the amplification factor, AF, for the top flange within this unbraced length was computed previously to be 1.66 (Section 5.1.8.1.2). In a curved bridge, the lateral flange moment in the outside girder due to the deck overhang loads has the same sense as the lateral flange moments due to curvature. Therefore:

$$M_\ell = -7.5 + -17 = -24.5 \text{ kip} - \text{ft} * AF = -24.5 * 1.66 = -40.7 \text{ kip} - \text{ft}$$

By inspection, the constructibility case controls.

Determine the number of bolts for the top flange splice plates that are required to prevent slip. The factored slip resistance, R_r, for a 7/8-in. diameter A 325 high-strength bolt assuming a Class B surface condition for the faying surface, standard holes and two slip planes per bolt (i.e. N_s = 2) was computed earlier to be R_r = 39.0 kips/bolt (Section 5.1.8.8.2.2).

Referring to the bolt pattern shown for the top flange splice in Figure 5.1.33, calculate the maximum resultant force on the extreme bolt under the combined actions.

The polar moment of inertia of the bolt group, I_p, is computed as follows (Equation 3.3.108):

$$I_p = \left[2*4*\left(1.5^2+4.5^2\right)\right]+\left[2*4*\left(3.0^2+7.0^2\right)\right] = 644\,\text{in}^2$$

The longitudinal component, P_{Mx}, in the extreme bolt is computed as (Equation 3.3.144):

$$P_{Mx} = \frac{|-40.7|(12)(7.0)}{644} = 5.31\,\text{kips}$$

The transverse component, P_{My}, in the extreme bolt is computed as (Equation 3.3.145):

$$P_{My} = \frac{|-40.7|(12)(4.5)}{644} = 3.41\,\text{kips}$$

The bolt force due to shear, P_v, is taken equal to (Equation 3.3.146):

$$P_v = \frac{510}{16} = 31.9\ \text{kips / bolt}$$

The maximum resultant bolt force in the critical extreme bolt, P_r (Figure 3.3.65), is then computed as (Equation 3.3.147):

$$P_r = \sqrt{(31.9+5.31)^2+(3.41)^2} = 37.37\,\text{kips} < R_r = 39.0\,\text{kips} \quad \text{ok}$$

The slip resistance of the selected bolt pattern is satisfactory for constructibility and at the service limit state.

Splice Plates

The combined stress in the top flange splice plates under the Service II load combination will be checked against a limiting stress of $0.95F_y$, where F_y is the specified minimum yield strength of the splice plates.

The minimum Service II design force, *P*, for the splice was computed earlier to be 75.6 kips. Since the top flange is continuously braced at the service limit state, lateral flange bending is ignored. The design actions at the service limit state are always assumed divided equally to the two slip planes regardless of the ratio of the splice plate areas (*AASHTO LRFD* Article C6.13.6.1.4c). Therefore, the force on the outside and inside splice plates will be taken as 75.6/2 = 37.8 kips. The resulting stress on the gross area of the outside splice plate is:

$$f = \frac{37.8}{(0.5)(18)} = 4.2 \text{ ksi} < 0.95(50) = 47.5 \text{ ksi} \quad \text{ok}$$

The stress on the gross area of the inside splice plates is:

$$f = \frac{37.8}{2(0.625)(7.5)} = 4.0 \text{ ksi} < 0.95(50) = 47.5 \text{ ksi} \quad \text{ok}$$

Fatigue

Since the combined area of the inside and outside flange splice plates is less than the area of the smaller flange at the splice, check the fatigue stresses in the base metal of the top flange splice plates adjacent to the slip-critical bolted connections.

The factored fatigue live load plus impact moments at the point of splice were given earlier (Section 5.1.8.8.2.2). The conditions spelled out in *AASHTO LRFD* Article 6.6.1.2.1 are met such that the fatigue live load stresses can be computed using the short-term composite section assuming the concrete deck is effective for both positive and negative flexure (Section 5.1.8.3.3).

First, determine if the top flange splice plates are subject to a net tensile stress under the unfactored permanent loads plus the Fatigue I load combination, as specified in *AASHTO LRFD* Article 6.6.1.2.1. The future wearing surface will be conservatively neglected in this calculation.

$$f_{DC_1} = \frac{290(12)}{-2{,}519} = -1.38 \text{ ksi}$$

$$f_{DC_2} = \frac{-100(12)}{-7{,}102} = +0.17 \text{ ksi}$$

$$f_{-\text{Fat LL+IM}} = \frac{1.5(-773)(12)}{-18{,}892} = +0.74 \text{ ksi}$$

Since |-1.38 + 0.17| = 1.21 ksi > 0.74 ksi, the top flange splice plates are not subject to a net tensile stress under the specified load combination and fatigue need not be checked.

5.1.8.8.3 Web Splice Design

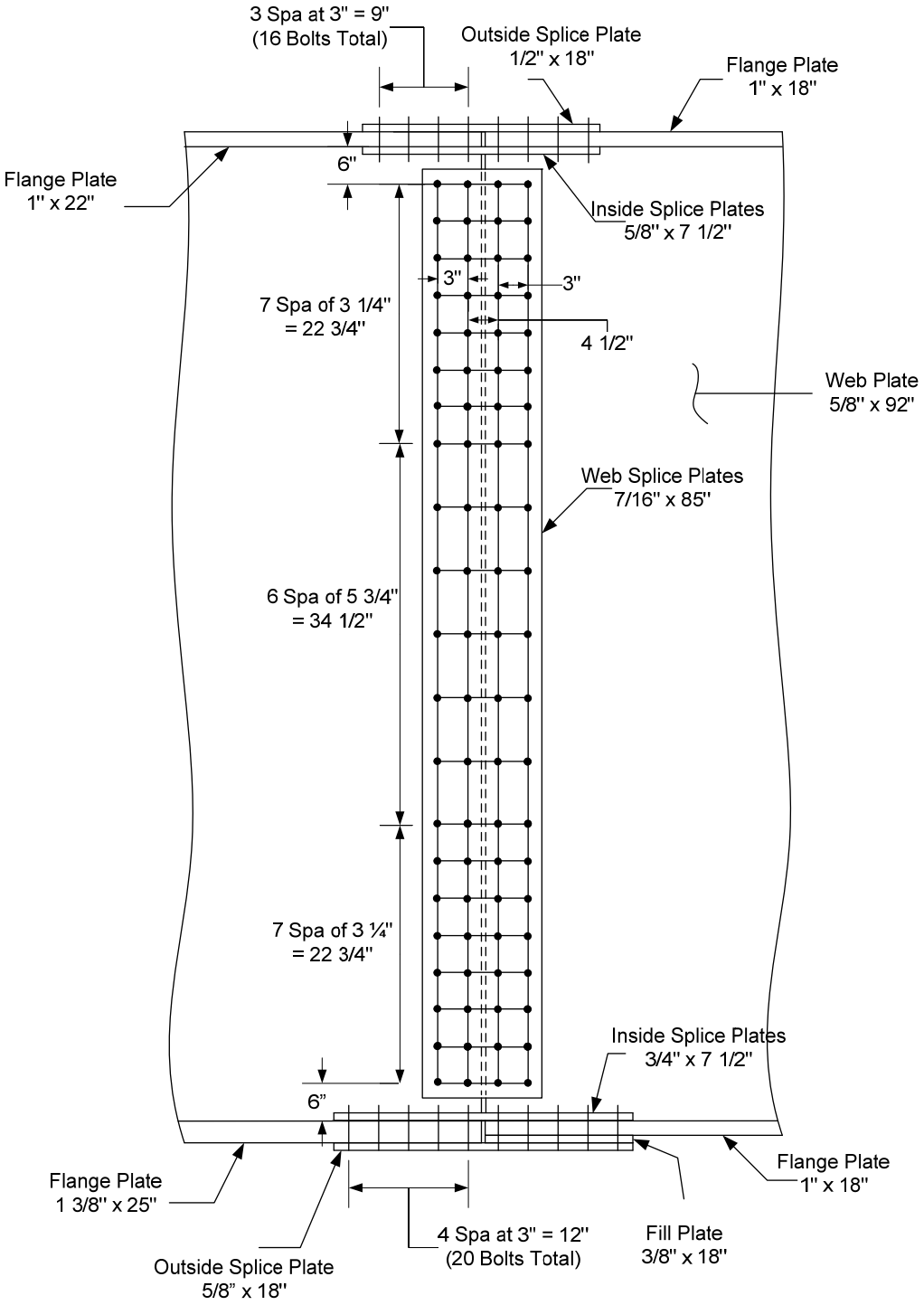
5.1.8.8.3.1 General

Bolted web splice design is covered in Section 3.3.7.3. The web splice will be designed based on the conservative assumption that the maximum moment and shear at the splice will occur under the same loading condition.

Two vertical rows of bolts with 21 bolts per row will be investigated. According to *AASHTO LRFD* Article 6.13.6.1.4a, a minimum of two rows of bolts is required on each side of the joint to ensure proper alignment and stability of the girder during construction. The bolts are spaced horizontally and vertically as shown in Figure 5.1.34.

The outermost bolts are located 6 inches from the flanges to provide ample clearance for assembly (see Table 7-16 of the AISC *Steel Construction Manual* for bolt assembly clearances). The web is spliced symmetrically by plates with a thickness not less than one-half the web thickness. Assume 7/16″ x 85″ splice plates on each side of the web. The splice plates are ASTM A 709 Grade 50W steel (F_u = 70 ksi). A filler plate is not required since the webs are the same thickness on both sides of the splice.

In this illustration, the number of bolts in the web splice is decreased by spacing the group of bolts closest to the mid-depth of the web (where the flexural stress is relatively low) at the maximum spacing specified for sealing (*AASHTO LRFD* Article 6.13.2.6.2), and by spacing the remaining two groups of bolts near the top and bottom of the web at a closer spacing (Figure 5.1.34).



Notes: 1) All bolts are 7/8" dia. (ASTM A325) H.S. Bolts
2) A 0.5 in. gap is assumed between the edges of the field pieces

5.1.34 Elevation View of Bolted Field Splice in Span 3 of G4

5.1.8.8.3.2 Strength Limit State

Design Shear

Determine the design shear in the web, V_{uw}, at the point of splice at the strength limit state (Section 3.3.7.2.2.1).

Compute the maximum factored shear at the splice, V_u, at the strength limit state using the appropriate load factors given in *AASHTO LRFD* Tables 3.4.1-1 and 3.4.1-2. The Strength I load combination is used (the load modifier, η, is taken equal to 1.0). Note that the minimum load factors, γ_p, from *AASHTO LRFD* Table 3.4.1-2 and a load modifier, $1/\eta$ (≤1.0), are applied to the permanent load shears when the corresponding shears are of opposite sign to the live load plus impact shear.

A. Dead Load + Positive Live Load Shear:

$$V_u = 1.0\left[1.25(+100+13)+1.5(+14)+1.75(+104)\right] = +344 \text{ kips (governs)}$$

B. Dead Load + Negative Live Load Shear:

$$V_u = (1/1.0)\left[0.90(+100+13)+0.65(+14)\right]+1.0(1.75)(-28) = +61.8 \text{ kips}$$

Calculate the factored shear resistance, $V_r = \phi_v V_n$, of the web panel containing the splice. The maximum factored shear, V_u, in this panel is +369 kips at the cross-frame adjacent to the splice. The factored shear resistance of the web assuming it is unstiffened was computed previously to be V_r = 350 kips (Section 5.1.8.4.3.2). Thus, transverse stiffeners are required in this panel.

Assuming the cross-frame connection plates act as transverse stiffeners, the transverse stiffener spacing, d_o, in this panel is equal to the cross-frame spacing of 22.688 feet or 272.25 inches. This is less than the maximum permitted spacing for a stiffened interior web panel without longitudinal stiffeners equal to 3*D*, or 3(92.0) = 276 inches (Figure 3.2.57 Part A). In order for a stiffened panel to develop the full post-buckling shear resistance, the section along the panel must satisfy the following relationship (Section 3.2.7.3 – Equation 3.2.164):

$$\frac{2Dt_w}{\left(b_{fc}t_{fc}+b_{ft}t_{ft}\right)} \le 2.5$$

For the smaller section in the web panel:

$$\frac{2(92.0)(0.625)}{\left[18(1.0)+18(1.0)\right]} = 3.2 > 2.5$$

The total area of the flanges within the panel is small relative to the area of the web and the full post-buckling resistance cannot be developed. Therefore, the nominal shear resistance, V_n, must be computed as follows (Equation 3.2.165):

$$V_n = V_p\left[C + \frac{0.87(1-C)}{\sqrt{1+\left(\frac{d_o}{D}\right)^2}+\frac{d_o}{D}}\right]$$

The shear buckling coefficient, k, is computed from Equation 3.2.157 as follows:

$$k = 5 + \frac{5}{\left(\frac{d_o}{D}\right)^2}$$

$$k = 5 + \frac{5}{\left(\frac{272.25}{92.0}\right)^2} = 5.57$$

Since:

$$1.40\sqrt{\frac{Ek}{F_{yw}}} = 1.40\sqrt{\frac{29{,}000(5.57)}{50}} = 79.6 < \frac{D}{t_w} = \frac{92.0}{0.625} = 147.2$$

The constant, *C*, is computed from Equation 3.2.158 as follows:

$$C = \frac{1.57}{\left(\frac{D}{t_w}\right)^2}\left(\frac{Ek}{F_{yw}}\right)$$

$$C = \frac{1.57}{(147.2)^2}\left(\frac{29{,}000(5.57)}{50}\right) = 0.234$$

The plastic shear force, V_p, is computed from Equation 3.2.151 as follows:

$$V_p = 0.58F_{yw}Dt_w$$

$$V_p = 0.58(50)(92.0)(0.625) = 1{,}668 \text{ kips}$$

Therefore:

$$V_n = 1{,}668\left[0.234 + \frac{0.87(1-0.234)}{\sqrt{1+\left(\frac{272.25}{92.0}\right)^2}+\frac{272.25}{92.0}}\right] = 573 \text{ kips}$$

$$V_r = \phi_v V_n = 1.0(573) = 573 \text{ kips} > V_u = 369 \text{ kips} \quad \text{ok}$$

AASHTO LRFD Article 6.13.6.1.4b specifies that the equation to use to compute the design shear, V_{uw}, for the splice depends on the value of V_u at the splice with respect to $V_r = \phi_v V_n$ as follows:

$$0.5\phi_v V_n = 0.5(573) = 286 \text{ kips}$$

$$V_u = 344 \text{ kips} > 286 \text{ kips}$$

Therefore, the design shear, V_{uw}, is to be computed using Equation 3.3.149 as follows:

$$V_{uw} = \frac{(V_u + \phi_v V_n)}{2}$$

$$V_{uw} = \frac{(344 + 573)}{2} = 458 \text{ kips}$$

Moment due to the Eccentricity of the Design Shear

Calculate the design moment, M_{uv}, due to the eccentricity of the design shear at the point of splice at the strength limit state as follows (Section 3.3.7.3.2.2 - Equation 3.3.150):

$$M_{uv} = V_{uw} e$$

Referring to Figure 5.1.34, the correct eccentricity, *e*, to use is the horizontal distance from the centerline of the splice to the centroid of the web bolt group on the side of the joint under consideration as follows (Figure 3.3.67):

$$e = \left(2.25 + \frac{3.0}{2}\right)\frac{1}{12} = 0.3125 \text{ ft}$$

$$M_{uv} = 458(0.3125) = 143\ \text{kip} - \text{ft}$$

Design Moment and Design Horizontal Force Resultant

Determine the portion of the flexural moment to be resisted by the web, M_{uw}, and the horizontal design force resultant, H_{uw}, in the web at the strength limit state. Use the equations provided in *AASHTO LRFD* Article C6.13.6.1.4b (Section 3.3.7.3.2.3 - Equations 3.3.151 and 3.3.152). Again, since the splice is located in an area of stress reversal, checks must be made for both the positive and negative flexure conditions.

- Positive Flexure

The controlling flange for the case of positive flexure was previously determined to be the bottom flange (Section 5.1.8.8.2.1). The maximum factored vertical bending stress at the midthickness of the controlling flange, f_{cf}, and the minimum design stress for the controlling flange, F_{cf}, were previously computed for this loading condition to be:

$$f_{cf} = +22.93\ \text{ksi}$$
$$F_{cf} = +37.50\ \text{ksi}$$

For the same loading condition, the concurrent flexural stress at the mid-thickness of the noncontrolling (top) flange was computed to be:

$$f_{ncf} = -5.61\ \text{ksi}$$

The portion of the flexural moment assumed to be resisted by the web is computed as (Equation 3.3.151):

$$M_{uw} = \frac{t_w D^2}{12}\left|R_h F_{cf} - R_{cf} f_{ncf}\right|$$

where the hybrid factor R_h is taken as 1.0 for a homogeneous section and ratio, R_{cf}, is computed as follows:

$$R_{cf} = \left|\frac{F_{cf}}{f_{cf}}\right| = \left|\frac{+37.50}{+22.93}\right| = 1.63$$

Therefore:

$$M_{uw} = \frac{0.625(92.0)^2}{12}\left|1.0(+37.50) - 1.63(-5.61)\right| = 20{,}562\ \text{kip} - \text{in.} = 1{,}713\ \text{kip} - \text{ft}$$

The design horizontal force resultant for this loading condition is computed as (Equation 3.3.152):

$$H_{uw} = \frac{t_w D}{2}\left(R_h F_{cf} + R_{cf} f_{ncf}\right)$$

$$H_{uw} = \frac{0.625(92.0)}{2}\left[1.0(+37.50) + 1.63(-5.61)\right] = +815 \text{ kips}$$

Note that all stresses in the above equations are to be taken as signed quantities. Since the sign of M_{uw} corresponds to the sign of the flexural moment for the loading condition under consideration, absolute value signs are applied to the resulting difference of the stresses for convenience. H_{uw} is always taken as a signed quantity; positive for tension, negative for compression.

Check the above computed values of M_{uw} and H_{uw}. For the web, the section modulus $S = (0.625)(92.0)^2/6 = 882$ in.^{3} and the area $A = 0.625(92.0) = 57.5$ in.^{2}. Therefore:

$$f_{bot} = \frac{1713(12)}{882} + \frac{815}{57.5} = 37.50 \text{ ksi} = R_h F_{cf} \quad \text{ok}$$

$$f_{top} = \frac{1713(12)}{-882} + \frac{815}{57.5} = -9.13 \text{ ksi} \cong R_{cf} f_{ncf} = 1.63(-5.61) \quad \text{ok}$$

The use of $R_h F_{cf}$ and the application of the factor R_{cf} to f_{ncf} in essence is factoring up the stresses in the web by the same amount as the stresses in the controlling flange so that the web splice is designed in a consistent fashion at the strength limit state.

The total moment on the web splice for this condition is equal to the sum of M_{uv} and M_{uw}:

$$M_{tot} = M_{uv} + M_{uw} = 143 + 1{,}713 = 1{,}856 \text{ kip} - \text{ft}$$

- Negative Flexure

The controlling flange for the case of negative flexure was also previously determined to be the bottom flange (Section 5.1.8.8.2.1). The maximum factored vertical bending stress at the midthickness of the controlling flange, f_{cf}, and the minimum design stress for the controlling flange, F_{cf}, were computed for this loading condition to be:

f_{cf} = -22.02 ksi
F_{cf} = -30.51 ksi

For the same loading condition, the concurrent flexural stress at the mid-thickness of the noncontrolling (top) flange was previously computed to be:

$$f_{ncf} = +18.07 \text{ ksi}$$

The ratio, R_{cf}, is computed as follows:

$$R_{cf} = \left|\frac{F_{cf}}{f_{cf}}\right| = \left|\frac{-30.51}{-22.02}\right| = 1.38$$

Therefore:

$$M_{uw} = \frac{0.625(92.0)^2}{12}\left|1.0(-30.51) - 1.38(+18.07)\right| = 24{,}443 \text{ kip} - \text{in.} = 2{,}037 \text{ kip} - \text{ft}$$

The design horizontal force resultant for this loading condition is computed as:

$$H_{uw} = \frac{0.625(92.0)}{2}\left[1.0(-30.51) + 1.38(+18.07)\right] = -160 \text{ kips}$$

Check the above computed values of M_{uw} and H_{uw}:

$$f_{bot} = \frac{-2{,}037(12)}{882} - \frac{160}{57.5} = -30.51 \text{ ksi} = R_h F_{cf} \quad \text{ok}$$

$$f_{top} = \frac{-2{,}037(12)}{-882} - \frac{160}{57.5} = +24.93 \text{ ksi} = R_{cf} f_{ncf} = 1.38(+18.07) \quad \text{ok}$$

The total moment on the web splice for this condition is equal to the sum of M_{uv} and M_{uw}:

$$M_{tot} = M_{uv} + M_{uw} = 143 + 2{,}037 = 2{,}180 \text{ kip} - \text{ft}$$

Bolts

Check the web-splice bolts for shear at the strength limit state assuming the bolts in the connection have slipped and gone into bearing (Section 3.3.7.3.2.4).

The web-splice bolts are to be designed for the effects of the design shear, the moment due to the eccentric design shear, and the flexural moment and horizontal design force resultant in the web, which are all assumed applied at the mid-depth of the web. The traditional elastic vector method is used for calculating the maximum resultant bolt force (Section 3.3.6.2.7).

The polar moment of inertia, I_p, of the bolts with respect to the centroid of the connection is computed as follows (Equation 3.3.108):

$$I_p = \sum_{i=1}^{n} x_i^2 + \sum_{i=1}^{n} y_i^2$$

Referring to Figure 5.1.34, I_p is computed as:

$$I_p = \left[2 * 21 * \left(1.5^2\right)\right] + \left[2 * 2 * \begin{pmatrix} 5.75^2 + 11.50^2 + 17.25^2 + 20.50^2 + 23.75^2 + 27.00^2 \\ + 30.25^2 + 33.5^2 + 36.75^2 + 40^2 \end{pmatrix}\right]$$

$$= 28{,}751\,\text{in}^2$$

Determine the vertical bolt force, R_v, due to the design shear, V_{uw}, assuming two vertical rows with 21 bolts per row for a total number of bolts, N_b, equal to 42:

$$R_v = \frac{V_{uw}}{N_b} = \frac{458}{42} = 10.90\,\text{kips/bolt}$$

- Positive Flexure

Determine the bolt force due to the horizontal design force resultant, H_{uw}:

$$R_h = \frac{H_{uw}}{N_b} = \frac{815}{42} = 19.40\,\text{kips/bolt}$$

Determine the vertical and horizontal components of the force on the extreme bolt due to the total moment on the web splice, M_{tot}:

$$R_{M_v} = \frac{M_{tot}x}{I_p} = \frac{1{,}856(12)(3.0/2)}{28{,}751} = 1.16\ \text{kips}$$

$$R_{M_h} = \frac{M_{tot}y}{I_p} = \frac{1{,}856(12)(40.0)}{28{,}751} = 30.99\ \text{kips}$$

The resultant bolt force on the extreme bolt is:

$$R = \sqrt{\left(R_v + R_{M_v}\right)^2 + \left(R_h + R_{M_h}\right)^2} = \sqrt{(10.90 + 1.16)^2 + (19.40 + 30.99)^2} = 51.81\text{kips (governs)}$$

- Negative Flexure

Determine the bolt force due to the horizontal design force resultant, H_{uw}:

$$R_h = \frac{H_{uw}}{N_b} = \frac{|-160.0|}{42} = 3.81 \text{ kips / bolt}$$

Determine the vertical and horizontal components of the force on the extreme bolt due to the total moment on the web splice, M_{tot}:

$$R_{M_v} = \frac{M_{tot} x}{I_p} = \frac{2{,}180(12)(3.0/2)}{28{,}751} = 1.36 \text{ kips}$$

$$R_{M_h} = \frac{M_{tot} y}{I_p} = \frac{2{,}180(12)(40.0)}{28{,}751} = 36.40 \text{ kips}$$

The resultant bolt force on the extreme bolt is:

$$R = \sqrt{(R_v + R_{M_v})^2 + (R_h + R_{M_h})^2} = \sqrt{(10.90 + 1.36)^2 + (3.81 + 36.40)^2} = 42.04 \text{ kips}$$

The factored shear resistance, R_r, for a 7/8-in. diameter A 325 high-strength bolt in double shear assuming the threads are *excluded* from the shear planes was computed earlier to be 55.3 kips/bolt (Section 5.1.8.8.2.2). The greater than 50.0 in. length reduction does *not* apply when computing the factored shear resistance of the bolts in a web splice since the distribution of shear force is essentially uniform along the joint. Therefore:

$R = 51.81$ kips $< R_r = 55.3$ kips ok

Bolt Spacing

Check the bolt spacings and bolt edge and end distances for the web splice (Figure 5.1.34).

AASHTO LRFD Article 6.13.2.6.1 specifies that the minimum spacing between centers of bolts in standard holes is not to be less than 3.0*d*, where *d* is the diameter of the bolt (Section 3.3.6.2.2.6). For 7/8-in. diameter bolts:

$$s_{min} = 3d = 3(0.875) = 2.63 \text{ in.} < 3.0 \text{ in.} \quad \text{ok}$$

AASHTO LRFD Article 6.13.2.6.2 specifies that to seal against the penetration of moisture in joints, the spacing *s* of a single line of bolts adjacent to a free edge of an outside plate or shape (when the bolts are not staggered) must satisfy the following requirement (Section 3.3.6.2.2.6 – Equation 3.3.75):

$$s \le (4.0 + 4.0t) \le 7.0 \text{ in.}$$

where *t* is the thickness of the thinner outside plate or shape. Check for sealing along the vertical edges of the web splice plates:

$$s_{max} = 4.0 + 4.0(0.4375) = 5.75 \text{ in. ok}$$

The edge distance of bolts is defined as the distance perpendicular to the line of force between the center of a hole and the edge of the component. In this example, the edge distance from the center of the vertical line of holes to the edge of the splice plate of 2 inches (Figure 5.1.35) satisfies the minimum edge distance requirement of 1½ inches specified for 7/8-in. diameter bolts and sheared edges in *AASHTO LRFD* Table 6.13.2.6.6-1 (Section 3.3.6.2.2.6 – Table 3.3.2). This distance also satisfies the maximum edge distance requirement of 8.0*t* (not to exceed 5.0 in.) = 8.0(0.4375) = 3.5 in. specified in *AASHTO LRFD* Article 6.13.2.6.6.

The end distance of bolts is defined as the distance along the line of force between the center of a hole and the end of the component. In this example, the end distance of 2½ inches at the top and bottom of the web splice plates (Figure 5.1.35) satisfies the minimum end distance requirement of 1½ inches specified for 7/8-in. diameter bolts and sheared edges in *AASHTO LRFD* Table 6.13.2.6.6-1 (Table 3.3.2). The maximum end distance requirement of 8.0*t* (not to exceed 5.0 in.) = 8.0(0.4375) = 3.5 in. specified in *AASHTO LRFD* Article 6.13.2.6.5 is also satisfied. Although not specifically required, note that the distance from the corner bolts to the corner of the web splice plate, equal to $\sqrt{(2.0)^2 + (2.5)^2} = 3.2 \text{ in.}$, also satisfies the maximum end distance requirement.

Bearing Resistance

Check the bearing resistance at the web-splice bolt holes at the strength limit state (Section 3.3.6.2.6.2).

The resistance of an outermost hole, calculated using the clear edge distance (which is smaller than the clear vertical distance between the bolt holes), can conservatively be checked against the maximum resultant bolt force acting on the extreme bolt in the connection (Figure 3.3.70 Part A). Since the resultant force acts in the direction of an inclined distance that is larger than the clear edge distance, the check is conservative. Other options for checking the bearing resistance are discussed in Section 3.3.7.3.2.4.

Check the web. Based on the edge distance from the center of the hole to the edge of the field piece of 2 inches (which also satisfies the minimum edge distance requirement discussed above), the clear edge distance is computed as:

$$L_c = 2.0 - \frac{0.9375}{2} = 1.53 \text{ in.}$$

The nominal bearing resistance, R_n, parallel to the applied bearing force for standard holes is taken as follows (Equation 3.3.88):

$$R_n = 1.2L_c tF_u \le 2.4dtF_u$$

$$R_n = 1.2L_c tF_u = 1.2(1.53)(0.625)(70) = 80.33 \text{ kips (governs)}$$

or:

$$R_n = 2.4dtF_u = 2.4(0.875)(0.625)(70) = 91.88 \text{ kips}$$

The factored bearing resistance of the flange, R_r, is computed as (Equation 3.3.80):

$$R_r = \phi_{bb} R_n$$

R_r = 0.80(80.33) = 64.26 kips > R = 51.81 kips ok

Check the splice plates. Based on the edge distance from the center of the hole to the edge of the splice plate of 2 inches, the clear edge distance is computed as:

$$L_c = 2.0 - \frac{0.9375}{2} = 1.53 \text{ in.}$$

$$R_n = 1.2L_c tF_u = 1.2(1.53)(0.4375)(70) = 56.23 \text{ kips (governs)}$$

or:

$$R_n = 2.4dtF_u = 2.4(0.875)(0.4375)(70) = 64.31 \text{ kips}$$

The factored bearing resistance of the flange, R_r, is computed as (Equation 3.3.80):

$$R_r = \phi_{bb} R_n$$

R_r = 0.80(56.23) = 44.98 kips > R/2 = 51.81 kips/2 = 25.91 kips ok

Had the bearing resistance been exceeded in either case, the preferred option would be to increase the edge distance slightly in lieu of increasing the number of bolts or thickening the web and/or splice plates.

Splice Plates

Block Shear Rupture Resistance of Splice Plates

Check the block shear rupture resistance (Section 3.3.3.2.4) of the web splice plates at the strength limit state. Because of the overall length of the connection, the block shear rupture resistance normally does not control for web splice plates of typical proportion, but the check is illustrated here for completeness. Assume the block shear failure plane on the web splice plates shown below in Figure 5.1.35.

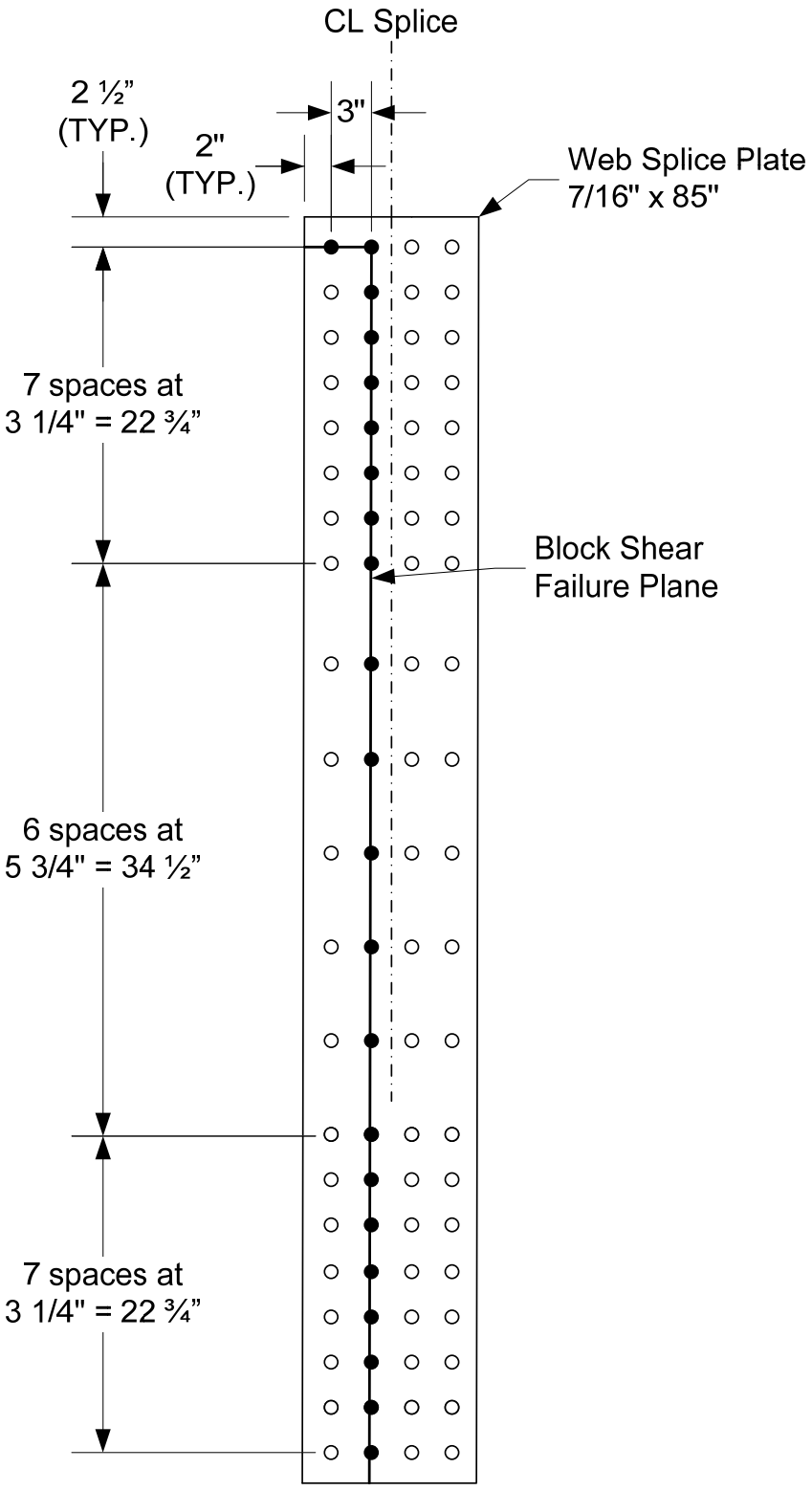


Figure 5.1.35 Assumed Block Shear Failure Plane for the Web Splice Plates

A_{tn} is the net area along the place resisting the tensile stress.

$$A_{tn} = 2[3.0 + 2.0 - 1.5(0.9375)](0.4375) = 3.14 \text{ in}^2$$

A_{vn} is the net area along the place resisting the shear stress.

$$A_{vn} = 2[85.0 - 2.5 - 20.5(0.9375)](0.4375) = 55.37 \text{ in}^2$$

A_{vg} is the gross area along the plane resisting the shear stress.

$$A_{vg} = 2[85.0 - 2.5](0.4375) = 72.19 \text{ in}^2$$

The factored block shear rupture resistance, R_r, is determined as (Equation 3.3.27):

$$\begin{aligned} R_r &= 0.80(1.0)[0.58(70)(55.37) + 1.0(70)(3.14)] = 1{,}974 \text{ kips} \\ &> 0.80(1.0)[0.58(50)(72.19) + 1.0(70)(3.14)] = 1{,}851 \text{ kips} \\ \therefore R_r &= 1{,}851 \text{ kips} \end{aligned}$$

$$R_r = 1{,}851 \text{ kips} > V_{uw} = 458 \text{ kips} \quad \text{ok}$$

Flexural Yielding of Splice Plates

Check for flexural yielding on the gross section of the web splice plates at the strength limit state as follows (Section 3.3.7.3.2.4 – Equation 3.3.153):

$$f = \frac{M_{uv} + M_{uw}}{S_{PL}} + \frac{H_{uw}}{A_g} \le \phi_f F_y$$

$$A_g = 2(0.4375)(85.0) = 74.38 \text{ in.}^2$$

$$S_{PL} = \frac{2(0.4375)(85.0)^2}{6} = 1{,}054 \text{ in.}^3$$

For positive flexure:

$$f = \frac{[143 + 1{,}713](12)}{1{,}054} + \frac{815}{74.38} = 32.09 \text{ ksi} < \phi_f F_y = 1.0(50) = 50 \text{ ksi} \quad \text{ok}$$

For negative flexure:

$$f = \frac{[143 + 2{,}037](12)}{1{,}054} + \frac{|-160|}{74.38} = 26.97 \text{ ksi} < \phi_f F_y = 1.0(50) = 50 \text{ ksi} \quad \text{ok}$$

Shear Yielding and Shear Rupture of Splice Plates

Check for shear yielding on the gross section of the web splice plates under the design shear, V_{uw}, at the strength limit state. *AASHTO LRFD* Article 6.13.5.3 specifies that for shear yielding, the factored shear resistance of a connected element, R_n, is conservatively based on the shear yield stress (i.e. $F_y/\sqrt{3} = 0.58F_y$) as follows (Section 3.3.6.2.6.2 – Equation 3.3.90):

$$R_r = \phi_v 0.58 F_y A_{vg}$$

$$R_r = 1.0(2)0.58(50)(0.4375)(85.0) = 2{,}157 \text{ kips}$$

$$R_r = 2{,}157 \text{ kips} > V_{uw} = 458 \text{ kips} \quad \text{ok}$$

Check for shear rupture on the net section of the web splice plates under the design shear, V_{uw}, at the strength limit state. For shear rupture, the factored shear resistance of the connected element, R_r, is to be taken as follows (Equation 3.3.6.2.6.2 – Equation 3.3.91). The reduction factor, R_p, in the following equation is taken as 1.0 for holes drilled full-size:

$$R_r = \phi_{vu} 0.58 R_p F_u A_{vn}$$

$$R_r = 0.80(2)1.0(70)(0.4375)[85.0 - 2\text{1}(0.9375)] = 3{,}200 \text{ kips}$$

$$R_r = 3{,}200 \text{ kips} > V_{uw} = 458 \text{ kips} \quad \text{ok}$$

5.1.8.8.3.3 Service Limit State and Constructibility

AASHTO LRFD Article 6.13.6.1.4b requires that high-strength bolted connections for web splices be designed to prevent slip at the service limit state under the maximum resultant bolt force due to Load Combination Service II. In addition, *AASHTO LRFD* Article 6.13.6.1.4a requires that high-strength bolted splices for flexural members be proportioned to prevent slip during the erection of the steel (assuming an erection analysis is conducted) and during the casting of the concrete deck (Section 3.3.7.3.3).

Design Shear

The Service II shears at the point of splice for the positive and negative flexure conditions are computed as follows:

A. Dead Load + Positive Live Load Shear:

$$V_s = [1.0(+100 + 13 + 14) + 1.3(+104)] = +262 \text{ kips (governs)}$$

B. Dead Load + Negative Live Load Shear:

$$V_s = [1.0(+100 + 13 + 14) + 1.3(-28)] = +90.6 \text{ kips}$$

Therefore, the design shear, V_s, for the Service II load combination is equal to +262 kips.

The factored shear due to the steel weight plus the deck-casting sequence (the Strength IV load combination controls with the load modifier, η, taken equal to 1.0) is computed as:

$$V_{stl+deck\ casting} = 1.0(1.5)(+20 + 90) = +165 \text{ kips}$$

which is less than the governing value of V_s. Therefore, the design shear for checking slip of the web bolts will be taken as V_s.

Moment due to the Eccentricity of the Design Shear

Calculate the design moment, M_{sv}, due to the eccentricity of the design shear at the point of splice at the service limit state as follows (Equation 3.3.154):

$$M_{sv} = V_s e$$

$$M_{sv} = (262)(0.3125) = 81.9 \text{ kip} - \text{ft}$$

Design Moment and Design Horizontal Force Resultant

Determine the portion of the flexural moment to be resisted by the web, M_{sw}, and the horizontal design force resultant, H_{sw}, in the web at the service limit state (Section 3.3.7.3.3 - Equations 3.3.155 and 3.3.156).

The maximum Service II flexural stress at the midthickness of the bottom flange, f_s, was computed previously (Section 5.1.8.8.2.2) to be +16.98 ksi due to the positive flexure load condition. The flexural stress in the other (top) flange at the point of splice, f_{os}, concurrent with f_s in the bottom flange for this load condition is –4.20 ksi. The portion of the flexural moment assumed to be resisted by the web is computed as (Equation 3.3.155):

$$M_{sw} = \frac{t_w D^2}{12}\left|f_s - f_{os}\right|$$

$$M_{sw} = \frac{0.625(92.0)^2}{12}\left|+16.98-(-4.20)\right| = 9{,}337\,\text{kip}-\text{in.} = 778\,\text{kip}-\text{ft}$$

The design horizontal force resultant for this loading condition is computed as (Equation 3.3.156):

$$H_{sw} = \frac{t_w D}{12}\left(f_s + f_{os}\right)$$

$$H_{uw} = \frac{0.625(92.0)}{2}\left[+16.98+(-4.20)\right] = +367\ \text{kips}$$

Check the above computed values of M_{sw} and H_{sw}:

$$f_{bot} = \frac{778(12)}{882} + \frac{367}{57.5} = 16.97\ \text{ksi} \cong f_s \quad \text{ok}$$

$$f_{top} = \frac{778(12)}{-882} + \frac{367}{57.5} = -4.20\ \text{ksi} = f_{os} \quad \text{ok}$$

The total moment on the web splice for this condition is equal to the sum of M_{sv} and M_{sw}:

$$M_{tot} = M_{sv} + M_{sw} = 81.9 + 778 = 860\ \text{kip}-\text{ft}$$

In this case, the loading condition causing the maximum Service II flexural stress in the top flange is the same loading condition (i.e. the positive flexure condition). Therefore, slip of the web bolts only needs to be checked for the one load condition.

Bolts

The traditional elastic vector method is again used for calculating the maximum resultant bolt force (Section 3.3.6.2.7).

Determine the vertical bolt force, R_v, due to the design shear, V_s, assuming two vertical rows with 21 bolts per row for a total number of bolts N_b equal to 42 (Figure 5.1.34):

$$R_v = \frac{V_s}{N_b} = \frac{262}{42} = 6.24 \text{ kips/bolt}$$

Determine the bolt force due to the horizontal design force resultant H_{sw}:

$$R_h = \frac{H_{sw}}{N_b} = \frac{367}{42} = 8.74 \text{ kips/bolt}$$

Determine the vertical and horizontal components of the force on the extreme bolt due to the total moment on the web splice, M_{tot}:

$$R_{M_v} = \frac{M_{tot} x}{I_p} = \frac{860(12)(3.0/2)}{28{,}751} = 0.54 \text{ kips}$$

$$R_{M_h} = \frac{M_{tot} y}{I_p} = \frac{860(12)(40.0)}{28{,}751} = 14.36 \text{ kips}$$

The resultant bolt force on the extreme bolt is:

$$R = \sqrt{\left(R_v + R_{M_v}\right)^2 + \left(R_h + R_{M_h}\right)^2} = \sqrt{(6.24 + 0.54)^2 + (8.74 + 14.36)^2} = 24.07 \text{ kips}$$

The factored slip resistance, R_r, for a 7/8-in. diameter A 325 high-strength bolt assuming a Class B surface condition for the faying surface, standard holes and two slip planes per bolt (i.e. N_s = 2) was computed to be 39.0 kips/bolt (Section 5.1.8.8.2.2). Therefore:

$$R = 24.07 \text{ kips} < R_r = 39.0 \text{ kips} \quad \text{ok}$$

Splice Plates

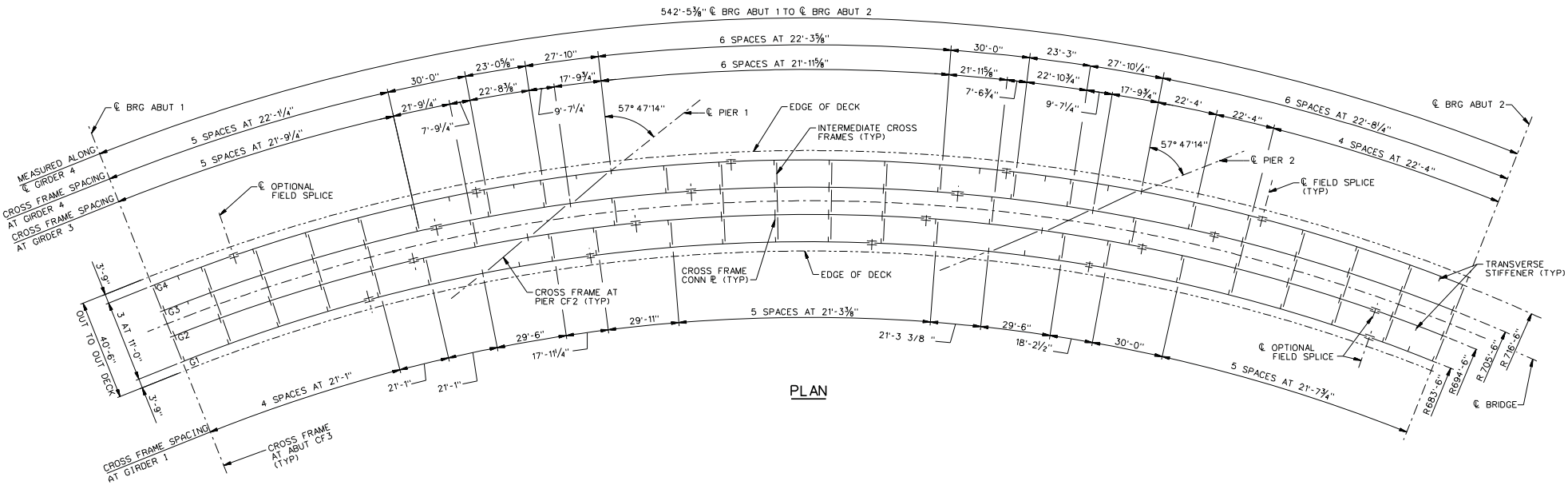
Since the combined area of the web splice plates is greater than the area of the web on both sides of the splice, the flexural stresses in the splice plates at the service limit state under the Service II load combination need not be checked.

5.1.8.8.3.4 Fatigue

Since the combined area of the web splice plates is greater than the area of the web on both sides of the splice, the fatigue stresses in the base metal of the web splice plates adjacent to the slip-critical bolted connections also need not be checked.

5.1.8.9 Fold-Out Drawings of Example I-Girder Bridge

D-9002 CADD (02-98) REVISED (05-97)



PLAN

NOTES:

1. DRAWINGS DEPICTED IN THIS EXAMPLE ARE A PARTIAL REPRESENTATION OF A COMPLETE PLAN SET. FOR GUIDANCE ON THE MINIMUM INFORMATION NECESSARY AND PLAN PRESENTATION, SEE THE AASHTO/NSBA STEEL BRIDGE COLLABORATION, DESIGN DRAWING PRESENTATION GUIDELINES, G1.2.
2. JACKING STIFFENERS, TRANSVERSE STIFFENERS, BEARINGS AND BEARING STIFFENERS, AUXILIARY BEARING STIFFENERS, CONNECTION PLATES, WELDED AND BOLTED CONNECTIONS, ETC. HAVE NOT BEEN DESIGNED. ANY INFORMATION SHOWN FOR THESE ITEMS IS FOR REFERENCE / DISCUSSION PURPOSESS ONLY. SEE THE COURSE NOTES FOR THE DESIGN OF THE SHEAR STUDS FOR G4.
3. CROSS-FRAMES HAVE NOT BEEN DESIGNED. INFORMATION SHOWN REGARDING THE CROSS-FRAMES IN THESE FOUR SHEETS IS FOR REFERENCE / DISCUSSION PURPOSES ONLY. SEE THE COURSE NOTES FOR THE DESIGN OF A SINGLE ANGLE INTERMEDIATE CROSS-FRAME MEMBER.
4. CROSS-FRAMES NOT AT SUPPORTS ARE CF1.

NHI COURSE NO. 130095
ANALYSIS AND DESIGN OF SKEWED AND CURVED STEEL BRIDGES WITH LRFD
I-GIRDER DESIGN EXAMPLE
FRAMING PLAN AND NOTES

RECOMMENDED JANUARY 26, 2010

SHEET 1 OF 4

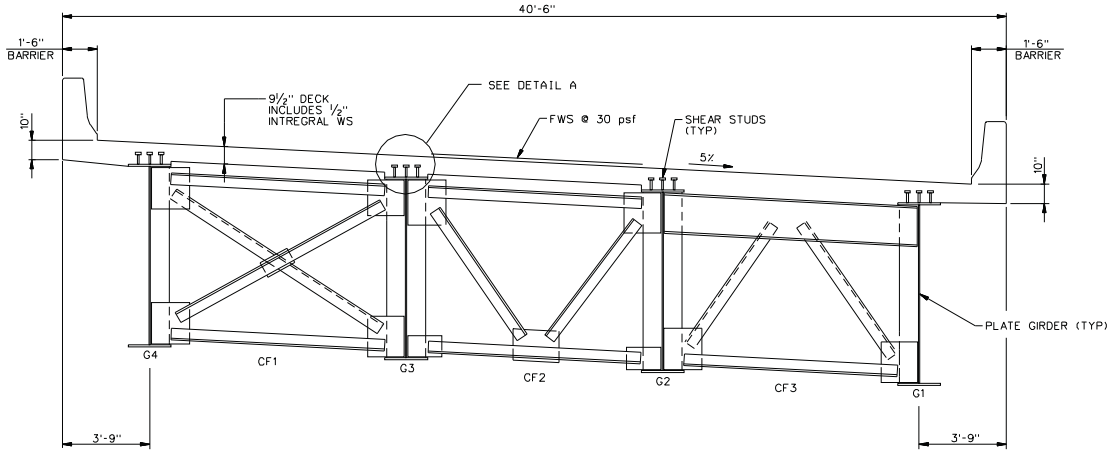
S -

DES: DWG: CKD:

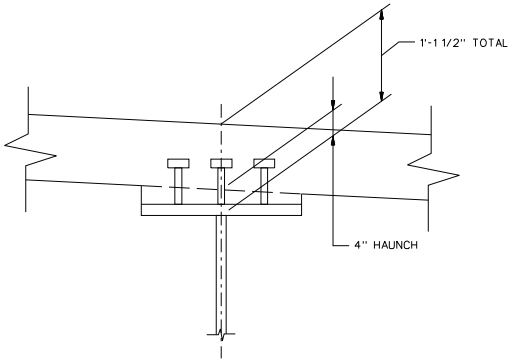
CHECK PRINT
DRAWING ORIGINATOR:
CHECKED BY:
NO.: | DATE: | CORRECTIONS CHECKED BY:
CHANGES MADE BY:
CHANGES VERIFIED BY:

USER: %USER%
PATH: %PWPATHNAME%
FILE: %FILES%
PLOT DATE: %DATE% %TIME%
MODEL: %MODELNAME%

D-9002 CADD (02-90) REVISED (05-97)



TYPICAL CROSS SECTION



DETAIL A
NTS

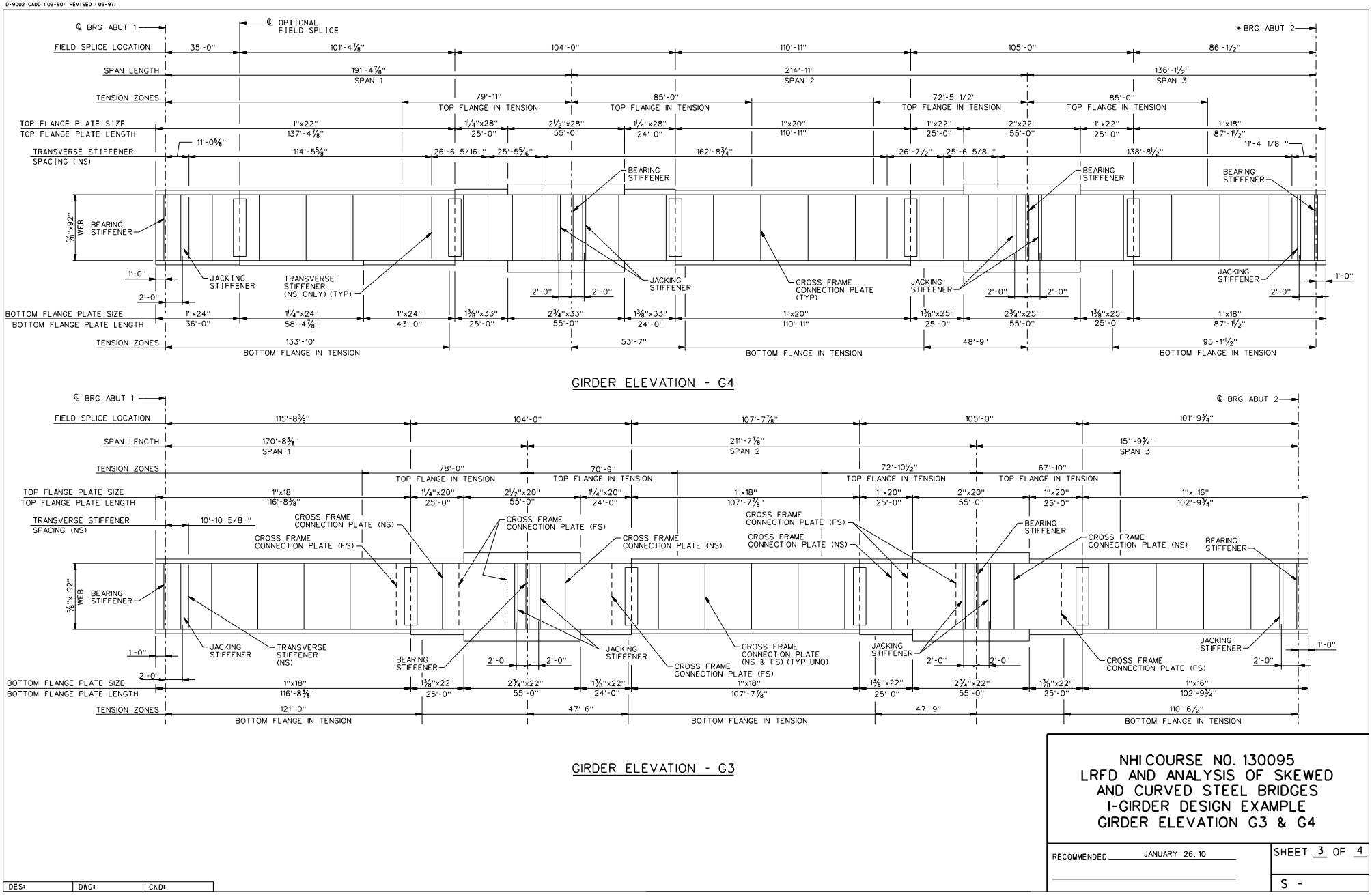
NHI COURSE NO. 130095
ANALYSIS AND DESIGN OF SKEWED
AND CURVED STEEL BRIDGES WITH LRFD
I-GIRDER DESIGN EXAMPLE
TYPICAL SECTION

RECOMMENDED JANUARY 26, 2010

SHEET 2 OF 4

S -

DES. | DWG. | CKD.



GIRDER ELEVATION - G4

GIRDER ELEVATION - G3

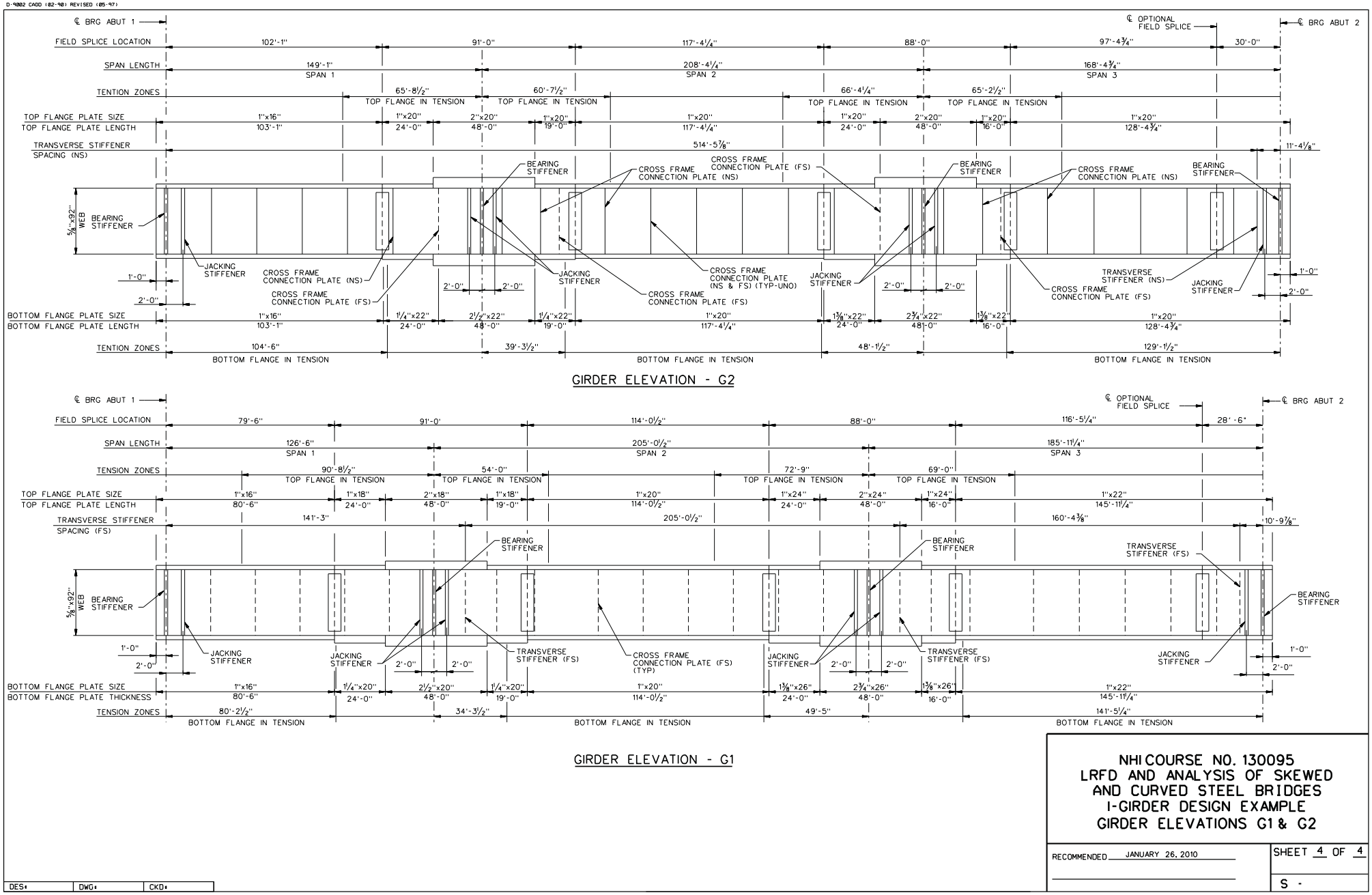
NHI COURSE NO. 130095
LRFD AND ANALYSIS OF SKEWED AND CURVED STEEL BRIDGES
I-GIRDER DESIGN EXAMPLE
GIRDER ELEVATION G3 & G4

RECOMMENDED JANUARY 26, 10

SHEET 3 OF 4

S -

DES: | DWG: | CKD:



GIRDER ELEVATION - G2

GIRDER ELEVATION - G1

NHI COURSE NO. 130095
LRFD AND ANALYSIS OF SKEWED AND CURVED STEEL BRIDGES
I-GIRDER DESIGN EXAMPLE
GIRDER ELEVATIONS G1 & G2

RECOMMENDED JANUARY 26, 2010

SHEET 4 OF 4

S -

Chapter 5
LRFD Step-by-Step Design Examples

Section 5.2
Curved Tub Girder



5.2.1 Introduction

This example illustrates the design of a three-span continuous horizontally curved steel tub girder bridge with radial abutments and spans of 150′ - 200′ - 150′ measured along the arc at the centerline of the bridge. The radius of curvature is 550 feet measured to the centerline of the bridge. This example is intended to illustrate the principles of curved tub-girder design presented in previous sections of this manual. The example illustrates the design of selected critical sections from the tub girder with the largest radius at the strength, service and fatigue limit states according to the *AASHTO LRFD* Specifications. Constructibility checks and stiffener, shear connector, lateral-bracing member and bolted field splice designs are also presented.

5.2.2 Design Parameters

An example curved tub-girder bridge is used to illustrate the principles of curved tub-girder design presented in preceding sections of this manual.

The following data apply to this example design:

Specifications: 2010 *AASHTO LRFD* Bridge Design Specifications, Fifth Edition
Structural Steel: AASHTO M 270, Grade 50W (ASTM A 709, Grade 50W) uncoated weathering steel with F_y = 50 ksi
Concrete: f'_c = 4.5 ksi
Slab Reinforcement: AASHTO M 31, Grade 60 (ASTM A 615, Grade 60) with F_y = 60 ksi
Shear Connectors: Three 7/8″-diameter stud connectors per row; F_u = 60 ksi

The girders are composite throughout as required for curved continuous composite tub girder bridges in *AASHTO LRFD* Articles 6.10.10.1 and 6.11.10. Since torsional shear exists along the entire span in a curved tub girder, shear connectors must be present along the entire span to resist the torsional shear and avoid possible debonding of the deck. The steel girders are homogeneous throughout.

Permanent steel deck forms are assumed between the girders and between the flanges of the individual tub sections; a load of 15 pounds per square foot is assumed for stay-in-place (SIP) forms, which is assumed to include the weight of the concrete in the form flutes.

Other permanent (dead) loads applied to the bridge include a load of 495 pounds per linear foot for each concrete deck parapet, and a load of 30 pounds per square foot for a future wearing surface.

The Average Daily Truck Traffic (ADTT) in one direction, considering the expected growth in traffic volume over the 75-year fatigue design life, is assumed to be 1,250 trucks/day for fatigue design.

Uncoated weathering steel is utilized in the example design. Where site conditions are adequate for successful application, uncoated weathering steel is the most cost-effective material choice for steel bridges in terms of savings in both initial and future repainting costs. To increase the confidence in the performance of this material, the FHWA issued a Technical Advisory (T5140.22) in 1989 entitled *Uncoated Weathering Steel in Structures.* The guidelines contained in this document, developed in cooperation with the steel industry, suggest good detailing practice to help ensure successful application of the material and are a valuable source of information on the proper environments for the use of weathering steel.

5.2.3 Steel Framing

5.2.3.1 Span Arrangement

Span arrangement considerations are discussed in Section 3.1.2.2.

This example bridge has three spans, with the end spans each 150 feet long and the center span 200 feet long, which provides a reasonably balanced span arrangement so that a constant girder depth may be optimally employed. These span lengths are measured along the arc at the centerline of the bridge. The individual arc span lengths of each girder (in feet) measured along the arc at the centerline of each tub are as follows (Table 5.2.1):

Table 5.2.1 Girder Arc Span Lengths (feet)

	Span 1	Span 2	Span 3
G2	153.17	203.23	153.17
G1	146.83	195.77	146.83

The abutments are oriented radially. Box-girders on skewed supports are subject to large torques and tend to be particularly problematic to design and to build. Special care should be taken in analyzing and detailing box girders, particularly intermediate cross-frames and lateral bracing, in order to design a successful bridge.

The radius of curvature is 550 feet measured at the centerline of the bridge. The 550-ft centerline radius was chosen due to right-of-way limitations and to accommodate the design speed of 35 mph.

5.2.3.2 Cross-Section

Figure 5.2.1 shows the cross-section of the example bridge, with the internal intermediate and support cross-frame/diaphragm configurations noted.

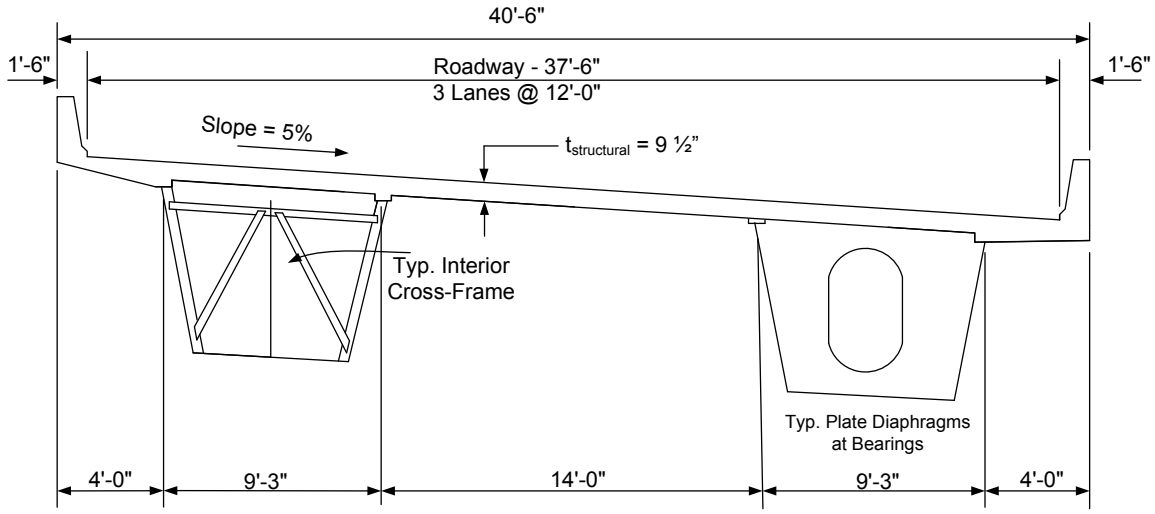


Figure 5.2.1 Cross-Section of the Tub Girder Example Bridge

Trapezoidal tub girders are used, which permit a wide spacing between the webs at the top and a relatively narrow steel flange at the bottom. A box cross-section is more economical with fewer narrower boxes. Box and bridge cross-section configuration issues are discussed in Section 3.1.5.1.

Cross-frame configuration considerations in box-girder bridges are discussed in Section 3.1.2.8.4.2. The cross-frame configuration shown in the left tub in Figure 5.2.1 is used at all intermediate (radial) internal cross-frames. The configuration shown in the right tub is used internally at all supports.

The roadway width is dictated by traffic and state standards. As this is a rural bridge, no sidewalks are included. Overhangs are set to be 4'-0″ on both sides of the cross-section. A cross-slope or superelevation of 5 percent is assumed.

The structural thickness of the concrete deck is selected using a standard table to be 9½″, with a ½″ structural wearing surface. A 5-inch-thick deck haunch is selected measured from the top of the web to the bottom of the deck. The thickness of the deck at the edge of the deck is 9½″. Deck and haunch thickness considerations are discussed in Sections 3.1.2.6 and 3.1.2.7, respectively.

A mildly reinforced deck with a flat soffitt inside and between the girders is assumed. The deck overhang soffit is tapered from the bottom of the haunch to the outside edge of the deck. A vaulted deck with transverse post-tensioning may be the most economical choice for wider spacings and overhangs than were selected for this example (Section 3.1.5.1).

It is assumed that the deck is designed according to the traditional design method. *AASHTO LRFD* Article 9.7.2 permits the use of an “empirical design method”, in which the deck is designed based on the concept of internal arching and is more lightly reinforced. *AASHTO LRFD* Article 9.7.2.4 expresses concerns related to the empirical design method and the effect of relative displacements of torsionally stiff cross-sections (i.e. box sections) without sufficient intermediate cross-frames between the boxes or supplemental transverse deck reinforcement to accommodate the transverse bending of the deck between boxes. In such cases, the girders may not rotate sufficiently to relieve the moment over the webs. As a result, more deck reinforcement may be required than is provided by the “empirical design method”.

5.2.3.3 Field-Section Size

The number of field sections (i.e. girder sections fabricated and shipped to the bridge site) and the location of bolted splices can have a significant effect on the efficiency of the design of steel girders. Fewer field splices reduces shop and field bolting cost. Additionally, the number and location of bolted splices often affects the cost. The choice of field splice locations is in many ways job specific. The weight and length of field sections should be chosen after consulting fabricators expected to bid the work. Additional factors related to the selection of field-section size, including

material availability, shipping, handling and erection, are discussed in Section 3.1.2.3.

Field splices are traditionally located in regions of lower moment. Referring to the girder elevations shown in Figure 5.2.3, eight (8) bolted field splices are used in the example; two in each end span and four in the center span resulting in five (5) field sections in each girder line. These splices are located near points of permanent load contraflexure, which tends to reduce the size of these splices.

In the example design, the field sections in regions of positive flexure each weigh approximately 30 tons and the field sections over each pier weigh approximately 55 tons on average. Each individual box section is 9.25 feet wide at the top and approximately 6.9 feet in height. The longest field sections are the pier sections at approximately 120 feet in length.

The design of one of the bolted field splices is illustrated in Section 5.2.9.8.

5.2.3.4 Cross-Frame Layout

Important functions of cross-frames in box-girder bridges are discussed in Section 3.1.2.8.1.4.

Cross-frame spacing requirements for box-girder bridges are discussed in Section 3.1.2.8.2.2. Spacing of the internal cross-frames in box girders is primarily designed to control of distortion of the box. The spacing of internal cross-frames is limited to 40 feet in curved tub girders according to *AASHTO LRFD* Article 6.7.4.3. Internal cross-frame spacings ranging from 24′-0″ to 28′-10″ (measured along the centerline of the outside tub) are chosen for this example (Figure 5.2.2). Internal cross-frames are placed near both sides of the field splices in each span to aid in fit-up in the shop and in the field. Design checks are made to ensure that the chosen spacings are satisfactory, including checks on the distortional stresses at the strength limit state. The internal K-frames are K-type cross-frames with the K-node at the top chord to provide access for internal inspection along with the required stiffness. A bottom strut to reduce the transverse bending stress range in the box flange adjacent to the cross-frame connection plate welds to the flange is not needed in this case (Section 3.1.2.8.4.2).

AASHTO LRFD Article 6.7.4.3 specifies that internal diaphragms are to be provided at each support to resist cross-section distortion; they are to be designed to resist torsion in the box and to transmit vertical and lateral forces from the box to the bearings. Such diaphragms are provided at each support in this example (Figure 5.2.2). These plate diaphragms must be connected to the flanges and webs of the box section. Access holes are provided in the diaphragms at interior supports.

For cross sections consisting of two or more boxes, external cross-frames/diaphragms are required at end supports (along with internal diaphragms) to support the deck and the live loads (*AASHTO LRFD* Article 6.7.4.3). External cross-frames/diaphragms also act to restrain the rotation of the boxes. External cross-

frames/diaphragms must also be provided between girder lines at interior supports, particularly during erection. In this example, external plate diaphragms are provided at each support (Figure 5.2.2).

Intermediate external cross-frames are also provided between the boxes in this example to retain the relative position of adjacent box girders. *AASHTO LRFD* Article 6.7.4.3 requires that an interior cross-frame be used in-line with each exterior cross-frame to resist the distorting action they tend to cause on the box section. One external cross-frame is placed in each end span and two external cross-frames are placed in the center span (Figure 5.2.2). Each cross-frame has top and bottom chords and is arranged in a K-type configuration with the K-node at the top.

As discussed in Section 3.1.2.8.3, it is advisable to check the cross-frame forces early on in the design of the superstructure before advancing the design of the girders too far in order to determine if the forces are too large to design practical members and connections.

5.2.3.5 Top Lateral Bracing

Important functions of top lateral bracing in tub-girder bridges are discussed in Section 3.1.2.9.1.2.

AASHTO LRFD Article 6.7.5.3 requires lateral bracing over the entire length of the tubs in horizontally curved girders. A full-length lateral bracing system limits distortions that may result from temperature changes occurring prior to deck placement. Top flange lateral bracing is designed to resist the shear flow in the pseudo-box section resulting from any torsion acting on the steel section due to the design load effects. The bracing also act with the tub in resisting vertical bending. Hence, forces in the bracing due to flexure of the tub during construction must also be considered (based on the assumed construction sequence). Since the example bridge is analyzed using a refined 3D analysis in which these members are included in the analysis model, the member forces taken directly from the analysis comprehend these effects. Top flange lateral bracing also resists wind loads acting on the non-composite tub section.

Issues related to the configuration of lateral bracing are discussed in Section 3.1.2.9.2. The Design Engineer has two options regarding the configuration of a single-diagonal lateral bracing system: a Pratt truss pattern (Figure 3.1.41 Part A) or a Warren truss pattern (Figure 3.1.41 Part B). In the Pratt truss configuration, only one member applies force against a flange at a cross-frame/diaphragm. The force is resisted mainly by the strut or top chord of the cross-frame, and to some degree, by lateral bending of the top flange. The Warren truss pattern applies the force from two lateral bracing members at the intersection, increasing lateral flange moments and strut or cross-frame top chord forces. When torques are large and a dominate torque direction occurs, it is possible to orient the lateral bracing members such that they are in tension for shear flow, although they may be in compression due to

flexure, and vice versa. By configuring the lateral bracing in the Pratt truss pattern with the directions of the diagonals determined from the sign of the torque, significant economy can often be realized with the Pratt truss pattern over the more typical Warren truss pattern that leads to half of the diagonal members in compression. In this particular case, the torques are reasonable and the direction of the diagonals was deemed to have a negligible effect on the forces in the bracing members and the top flange lateral bending; thus, the full-length Pratt truss configuration shown in Figure 5.2.2 was chosen for this example.

At all intersections of the lateral bracing diagonals with the flange where a full-depth internal cross-frame does not exist, a strut extending between the two top flanges is assumed. The lateral bracing is continuous across the field splice locations. Otherwise, large lateral flange bending stresses might occur in the top flanges of the tub where the bracing is discontinued.

Important considerations relating to the detailing of lateral bracing connections are discussed in Section 3.1.2.9.3. The most desirable connection of lateral bracing members (diagonals and struts) to the girders is to bolt the lateral connection plates (or members) to the top flanges rather than to the webs. Welding of the connection plates to the flanges or webs typically results in a fatigue Category E detail with a very low fatigue resistance. Bolting improves the fatigue resistance of the connection plate or member (Category B or D) and eliminates the need to provide an expensive radiused transition at the ends of a welded connection plate to improve the fatigue resistance above Category E. Although not checked in this example, wherever the bracing members are bolted to a top flange subject to tension, *AASHTO LRFD* Equation 6.10.1.8-1 must be satisfied at the strength limit state to ensure that fracture on the net section of the flange is prevented (Section 3.2.6.1.3).

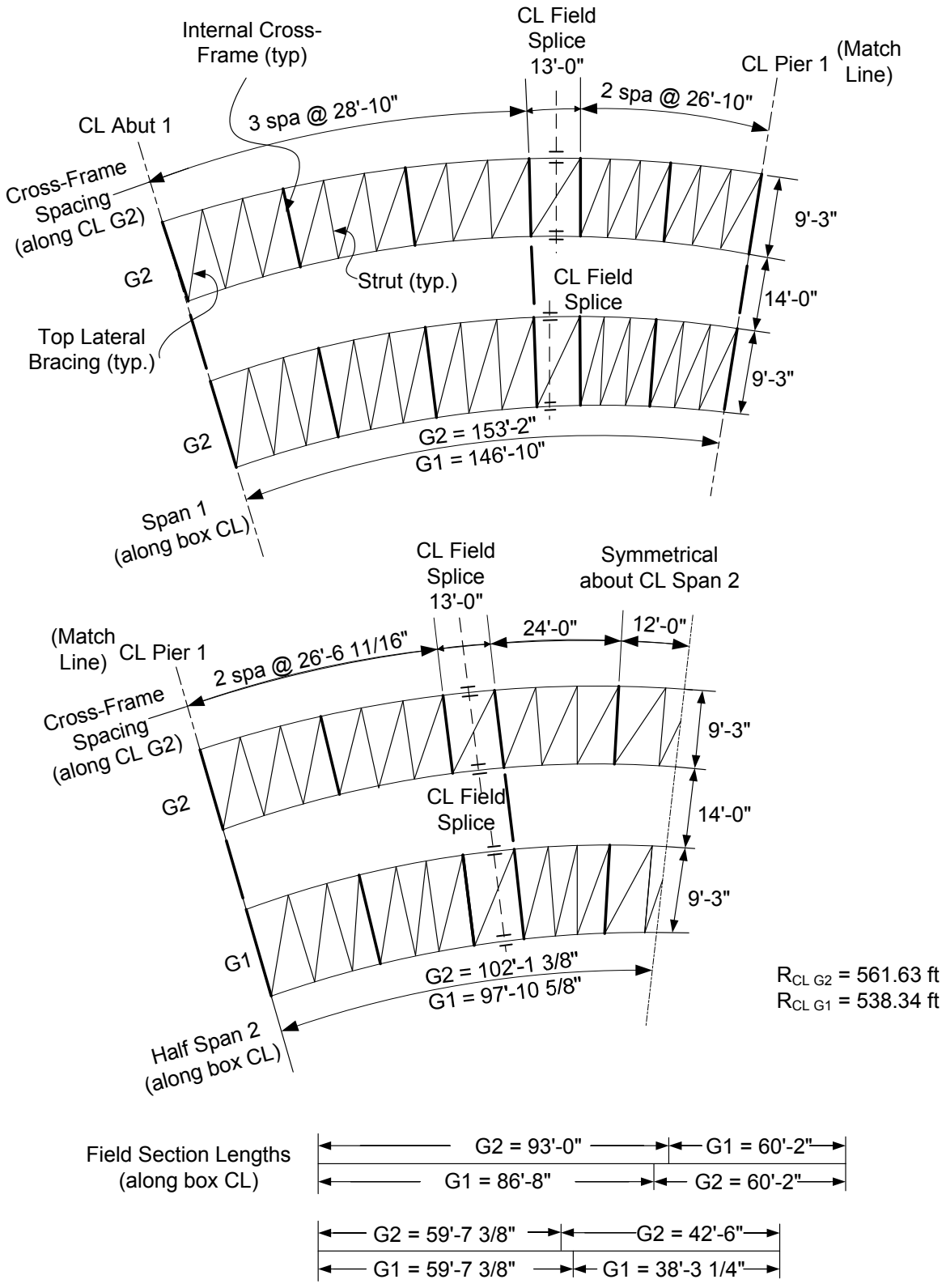


Figure 5.2.2 Framing Plan for the Example Tub Girder Bridge

5.2.4 Bearing Configuration

The bearing configuration can have a significant influence on the design of box girders. If a support has a pair of bearings, the torque resisted by the pair may be rather large. A single bearing centered over the shear center at a support minimizes the torque resisted by that support. The torsion due to vertical load is removed from the box at such a support via the external cross-frame/diaphragm connecting the box to its neighboring box(es).

In this example, single bearings are assumed centered under each box at each support. *AASHTO LRFD* Article 6.11.1.2 specifies that if single bearings narrower than the bottom flange are used, they are to be aligned with the center of the box and all other supports must have adequate resistance against overturning under any design load combination. The position and configuration of the bearings was recognized in the refined analysis of the example bridge to permit direct computation of the reactions. Potential uplift at each bearing was checked and determined not to be a consideration in this case.

Additional considerations related to the bearing arrangement for box girders are discussed in Section 2.2.3.5.

5.2.5 Preliminary Member Sizes

5.2.5.1 Web Proportioning

5.2.5.1.1 Web Depth

The first step in sizing the girders for the example bridge is to determine a reasonable web depth. Girder depth considerations are discussed in Section 3.1.3. There are no depth restrictions assumed in this example.

Equation 3.1.8 provides a minimum recommended depth for curved steel girder systems for the case where no 70-ksi yield strength steel is used is as follows:

$$D = \frac{L_{as}}{25} = 0.040\ L_{as}$$

The suggested minimum depth for the example bridge is conservatively calculated based on the arc lengths of the longest girder G2. For end spans, L_{as} for use in the preceding equation is defined as 0.9 times the arc span. For continuous interior spans, L_{as} for use in the equation is defined as 0.8 times the arc span. The arc span length of the end spans of G2 is 153.2 feet. The arc span length of the center span of G2 is 204.2 feet. Therefore:

$$D_{end\ span} = 0.040(0.9)(153.2) = 5.5\ \text{ft} \approx 66\ \text{in.}$$

$$D_{center\ span} = 0.040(0.8)(204.2) = 6.5\ \text{ft} \approx 78\ \text{in.}$$

The suggested minimum depth conservatively using the full arc span length of the center span is:

$$D = \frac{204.2}{25} = 8.2\ \text{ft} \approx 98\ \text{in.}$$

The optimum depth for a box section will typically be slightly less than the optimum depth of an I-section for the same span because of the inherent torsional stiffness of a box section (Section 3.1.3.2.1.2). The web depth obviously dictates the flange sizes for a given design. Therefore, establishing a sound optimum depth for box sections is particularly important because the size of box flanges can typically be varied less over the bridge length. Shallow boxes may be subject to larger torsional shear. Box web depths should not be less than about 5 feet to facilitate fabrication and inspection.

Investigations of depths between 78 in. and 98 in. indicated that a constant (vertical) web depth of 78 in. provides the best overall economy and establishes a reasonable bottom flange size (*D* in Equation 3.1.8 is defined in the specification as the overall depth of the steel girder, but it is recommended that *D* instead be taken as the web depth for simplicity).

5.2.5.1.2 Web Thickness

Section 3.1.5.3.1 discusses considerations related to the selection of the web thickness for box girders. The minimum web thickness for the design is determined from the limiting D/t_w ratio of 150 specified for webs without longitudinal stiffeners in *AASHTO LRFD* Article 6.11.2.1 as follows (Equation 3.1.18):

$$\frac{D}{t_w} \le 150$$

Inclined webs are used as they are advantageous in reducing the width of bottom box flanges while maintaining the spacing at the top of the box to economically support the deck. *AASHTO LRFD* Article 6.11.2.1.1 specifies that the inclination of the web plates to a plane normal to the bottom flange should not exceed 1-to-4. Although some flexibility is permitted in establishing the web slope when refined analyses are employed, caution should be exercised in deviating too much from the well-established limit on the web slope. Lateral bending stresses in the top tub flanges increase as the slope of the web exceeds 1-to-4. This is due to the transverse component of shear force in the web. A web slope of 1-to-4 is used in this example.

AASHTO LRFD Article 6.11.2.1.1 requires that the distance along the web be used for checking all design requirements for sections with inclined webs. Therefore, in checking Equation 3.1.18 for the case of an inclined web, the web height, *D*, must be taken as *D*/cosθ, where θ is the angle of inclination of the web plate with respect to the vertical. Therefore:

$$t_w \geq \frac{D}{150} = \frac{78/\cos 14^\circ .}{150} = 0.54 \text{ in.}$$

A web thickness of 5/8″ is selected. The selected web thickness is greater than the ½" minimum web thickness preferred by fabricators. A constant web thickness is used for each girder.

5.2.5.2 Flange Proportioning

Box-girder flange proportioning is discussed in Section 3.1.5.4.

The two top flanges of a tub section should be the same size. The minimum width of the top flanges of the tub section is specified as (Equation 3.1.21):

$$b_f \geq D/6$$

Therefore:

$$(b_f)_{\min.} = D/6 = \left(78/\cos 14^\circ\right)/6 = 13.4 \text{ in.}$$

Flanges should never be less than 12 inches in width to prevent distortion and cupping due to welding (Section 3.1.4.3.1). The top flange width should not be less than 16 inches to accommodate the connection of lateral bracing members, particularly when they are bolted to the flanges, which is recommended. A minimum flange width of 18 inches was enforced in the design for the top flanges.

Equation 3.1.14 is a suggested guideline regarding the minimum width of flanges in compression based on the experience of erectors given as follows:

$$b_{fc} \geq \frac{L}{85}$$

where *L* is the length of the girder shipping piece in feet. For cases where a full-length top lateral bracing is provided, which is required for curved tub girders, Equation 3.1.14 need not be considered for the top flanges (Section 3.5.1.4.1).

The minimum thickness of flanges is specified as (Equation 3.1.22):

$$t_f \geq 1.1 t_w$$

or:

$$(t_f)_{min} = 1.1t_w = 1.1(0.625) = 0.6875 \text{ in.}$$

However, the flange thickness should never be less than ¾ inches (Section 3.1.4.3.2). Therefore, a minimum flange thickness of 0.75 inches was enforced in the design.

An additional flange proportion limit for the top flanges is given by Equation 3.1.20 as follows:

$$\frac{b_f}{2t_f} \le 12.0$$

This criterion is checked for the most critical case (refer to the girder elevation below in Figure 5.2.3):

$$\frac{b_f}{2t_f} = \frac{18}{2(1.0)} = 9.0 < 12.0 \text{ ok}$$

All other top flanges have a ratio of $b_f/2t_f$ less than 9.0.

The proportioning of bottom box flanges is discussed in Section 3.1.5.4.2. The width of bottom box flanges is a function of the web spacing and depth as well as the slope of the webs for sections with inclined webs. In this case, the width between the centerlines of the webs is equal to:

Bottom flange width = 9.25(12) – 2(78)(0.25) = 72.0 in.

AASHTO LRFD Article C6.11.2.2 indicates that box flanges should extend at least one inch beyond the outside of each web to allow for welding. Flange lips that are too wide may provide a place for birds to perch, which might otherwise be prevented with a steel tub. Two-inch-wide flange lips are assumed on each side of the web in this example (measured from the centerlines of the web) increasing the total width of the bottom-flange plate to 76.0 in.

Later calculations will show that an unstiffened box flange is satisfactory for this flange width. Unstiffened box flanges are preferred. However, an unstiffened box flange should not become so slender that its buckling resistance becomes impractical. Longitudinal flange stiffeners can be added to increase the compressive resistance to prevent buckling under combined uniform axial compression and St. Venant torsional shear. However, the cost of these stiffeners is significant and they should be employed only after a thickness increase is evaluated. A minimum thickness of ¾" is recommended for unstiffened box flanges (and is enforced in this example) for ease of handling and to minimize distortion and possible cupping of the flange during welding, with the maximum ratio of width to thickness of the flange recommended not to exceed around 120. A lesser thickness might be considered

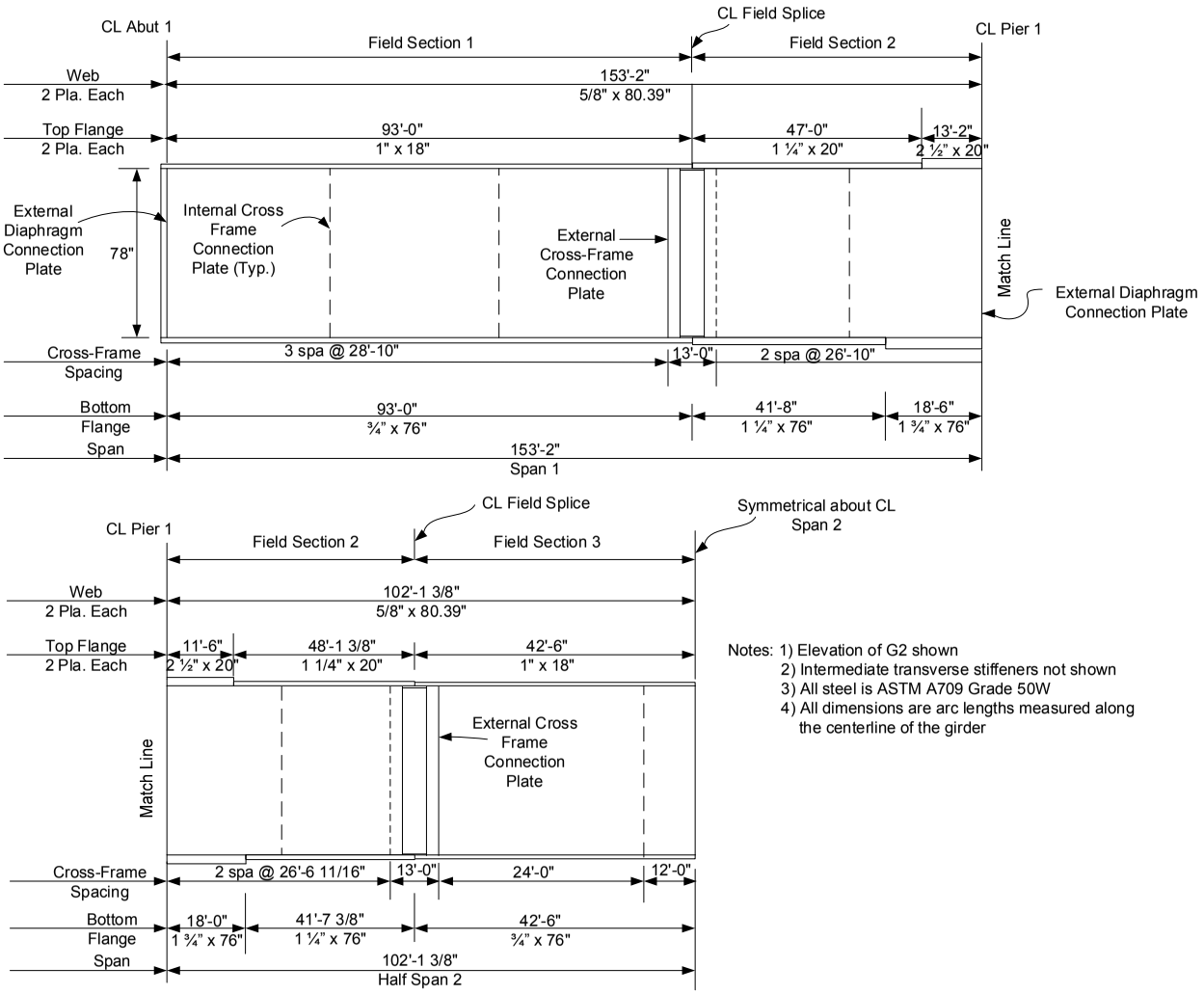
for a stiffened box flange; however, an initial consultation with fabricators is recommended prior to utilizing a box-flange thickness below ¾".

Section 3.1.4.3.4 discusses additional important considerations related to the sizing of flanges for efficient fabrication. These considerations are particularly important when sizing flanges for curved girders in order to minimize scrap. In general, the flanges in the example bridge were sized so that as many pieces as possible could be obtained from a wide plate with minimal waste. To minimize waste, it is important to limit the number of different flange plate thicknesses specified for a given project; in this case, only 5 different plate thicknesses were employed for the flanges. Flange thicknesses were re-used in the design of the top flanges, with the flange width adjusted accordingly, while maintaining constant top-flange widths within a given field section. Changes in top-flange width were made at the field splices. The maximum flange thickness used was 2.5 inches (≤ 3.0 inches).

In this case, the same plate sizes are used for both tub girders in the cross-section. Pier sections were designed according to the recommendations in Section 3.1.4.3.4 to allow for efficient nesting of the flanges for possible slab welding (Section 4.1.2.1.3) and cut curving. Flange splices in the two boxes were kept equidistant from the pier, but the lengths of the pier plates were not equal.on both sides of the bearing. Similar considerations were made for the flange plates in the positive moment regions to allow for possible nesting of the girder flanges in these regions on a single plate. Box flanges must be cut curved from large plates. Thus, depending on the radius, it may be desirable to introduce additional shop splices in the flange to reduce waste. Therefore, it is recommended that fabricators who are likely bidders on the job be consulted with regard to the issue of shop splices in box flanges.

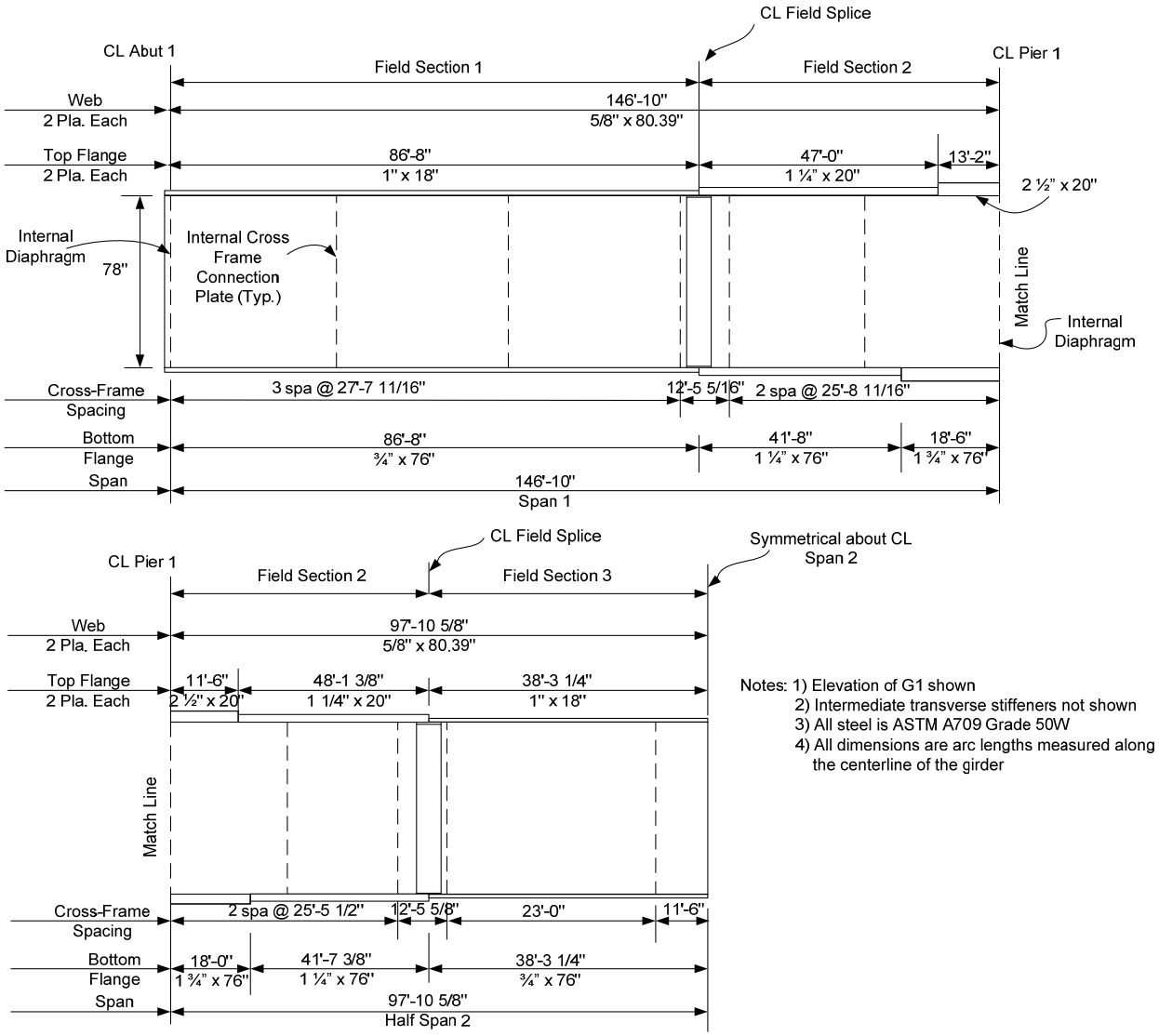
At all welded flange shop splices, it was ensured that the area of the smaller flange plate was not less than one-half the area of the larger flange plate in order to control stress concentrations at the splices (Section 3.1.4.3.2). Good design practice requires that flange transitions and shop-welded splices be located based on demand moments and plate availability, as well as cost comparisons between welding and inspecting of a splice versus extending a thicker plate.

Based on the above minimum proportions and accompanying discussion, the initial trial girder, shown in elevation in Figure 5.2.3, is assumed for each girder in the cross-section.



Notes: 1) Elevation of G2 shown
2) Intermediate transverse stiffeners not shown
3) All steel is ASTM A709 Grade 50W
4) All dimensions are arc lengths measured along the centerline of the girder

PART A



PART B

Figure 5.2.3 Initial Trial Elevation of the Girders for the Example Tub Girder Bridge
A) Outside Girder G2; B) Inside Girder G1

5.2.5.3 Cross-Frames, Top Lateral Bracing and Diaphragms

Preliminary cross-frame and top lateral bracing member sizes are required to perform the 3D analysis of the bridge. The 3D finite element method recognizes the individual cross-frame and top lateral bracing members (Section 2.5.3.2.4). The initial sizes influence the distribution of forces and the magnitude of the computed actions in the members. Disproportionately large members will result in large forces that can be reduced by reducing the member sizes. It is best to initially investigate smaller member sizes and increase the sizes as necessary. Significant changes in

member sizes are best investigated with another analysis to assure that the forces have not changed excessively.

Single angles are preferred for cross-frame and top lateral bracing members because they are readily available, inexpensive, easily connected and easily painted. Structural tees are used when forces are large. Double angles are less commonly used because they are expensive to fabricate and painting between the angles is difficult. Sections 3.3.3 and 3.3.4 discuss the design of single-angle, tee and double-angle members.

Preliminary sizes can be obtained from the permitted slenderness specified in *AASHTO LRFD* Articles 6.8.4 and 6.9.3 and/or based on experience. The following preliminary sizes were assumed for the internal and external cross-frame members *for the analysis*:

Top chord: L 5 x 5 x ¾: $A = 6.94$ in.^{2}
Bottom chord & diagonals: L 5 x 5 x ¾; $A = 6.94$ in.^{2}

The following preliminary sizes were assumed for the top lateral bracing members and struts for the analysis:

Top lateral bracing diagonals: WT 7 x 24: $A = 7.07$ in.^{2}
Struts: WT 7 x 24: $A = 7.07$ in.^{2}

AASHTO LRFD Article C6.7.5.3 recommends that the area of the diagonal members of the top lateral bracing for tub sections not be less than 0.03*w*, where *w* is the center-to-center distance between the top flanges of the tub in inches (Equation 3.1.7). This requirement is easily satisfied in this particular case by the members selected above for the lateral bracing diagonals.

The design of a typical top lateral bracing member for the example tub girder is presented in Section 5.2.9.7.

At the end and interior supports, a thickness of 5/8″ is assumed for the internal plate diaphragms for the analysis. For the external plate diaphragms at both the end and interior supports, a thickness of 5/8″ is assumed for the web and an area of 14.0 square inches is assumed for both the top and bottom flanges for the analysis.

Inspection access through the internal diaphragms at interior supports must be provided with access holes at least 18 inches wide and 24 inches high; however, if feasible, a larger hole at least 36.0 in. deep is preferable. In addition to restraining distortion of the box section, the internal diaphragms at supports also transfer load from the girder webs to the bearing(s). If a single centered bearing is used, the diaphragm must be stout enough to resist the reaction and transfer the load around any access hole. Bearing stiffeners are usually attached to the diaphragms. If a single centered bearing is employed, two stiffeners are generally used. A bearing

stiffener on each side of the access hole generally removes the shear from the diaphragm before it is engaged by the hole. Torsion generally causes a different magnitude of shear in the webs of the box on the two sides of the diaphragm. Reinforcement around the hole may be required, particularly if the access hole requires a large portion of the diaphragm or if a single bearing is located under the diaphragm. Auxiliary stiffeners on the diaphragm or webs may be employed to spread out the reaction. Refined analysis of internal diaphragms at supports is desirable because they are primary members necessary for the integrity of the bridge.

As discussed in *AASHTO LRFD* Article C6.7.4.3, external plate diaphragms with aspect ratios, or ratios of length to depth, less than 4.0 and internal plate diaphragms act as deep beams and should be evaluated by considering principal stresses rather than by simple beam theory. Fatigue-sensitive details on these diaphragms and at the connection of the diaphragms to the flanges should be investigated by considering the principal tensile stresses.

Further information on the design of solid-plate diaphragms for box girders may be found in Section 3.3.5.2.

5.2.6 Loads

A refined 3D finite element analysis model of the bridge was constructed and analyzed using many of the concepts discussed in Section 2.5. Loads were applied to the model as described in the following and discussed in greater detail in Section 2.5.3.4.

5.2.6.1 Dead Loads

Dead loads in the *AASHTO LRFD* specification are primarily classified as either component dead load (designated as DC), which is assumed to consist of all the structure dead load except for any non-integral wearing surfaces and any specified utility loads, or dead load of any non-integral wearing surfaces and any utilities (designated as DW). Further discussion on dead loads may be found in Section 1.3.2.1.

5.2.6.1.1 Component Dead Loads

5.2.6.1.1.1 Structural Steel Weight (DC_1)

Structural steel weight was modeled in the analysis using body-weight of the modeled members. The steel weight included the cross-frames and lateral bracing as well as the girders. The weight of detail steel such as stiffeners and splices was not included, but was accounted for in the analysis by changing the density of the steel.

AASHTO LRFD Article C6.11.3.1 indicates that for painted box sections, the Design Engineer should consider making an allowance for the weight of the paint. An allowance of three percent of the steel weight is considered reasonable. Since unpainted weathering steel is assumed in this example, this allowance is not included.

5.2.6.1.1.2 Deck/Deck Haunches/SIP Forms (DC_1)

Weight of the wet concrete of the deck was applied to the non-composite 3D model with concentrated loads at the nodes representing the tops of the girders. The concrete was assumed to have no stiffness. The concentrated loads applied to each girder top flange node were determined by the tributary area of deck associated with each web based on the the distance between the nodes and the spacings between the webs. The thickness of the integral wearing surface was considered. The deck overhang tapers (Figure 5.2.1) were considered in computing the concentrated loads applied to the exterior girders. The weight of the wet concrete in the deck haunches was included in the concentrated loads applied to each girder. A deck haunch width of 18 inches and deck haunch thickness of 5 inches was assumed (the reduction in weight due to the concrete displaced by the top flanges was ignored). The unit weight of the concrete was taken equal to 0.150 kcf, which includes an additional 0.005 kcf to account for the weight of the rebars.

As mentioned, all the deck weight is applied to the girder top flanges in the analysis. Thus, the DC_1 torques reported below in Table 5.2.4 do not include the torque due to the weight of the deck overhangs acting on the boxes. The reported DC_1 torques result primarily from the application of unequal deck weight loads to the girder top flanges.

The weight of the SIP deck forms was applied directly to the girders of the non-composite 3D model as concentrated loads as done for the deck. The weight of the permanent deck forms is based on the clear span between top flanges. Between the boxes, the maximum clear span is 12′-6″. At least one metal-deck manufacturer is able to span this distance with a 4.5-inch deep bridge deck form constructed of 14-gage material. To prevent over-deflection of the form in this case, Styrofoam must be placed in the form flutes according to the manufacturer to eliminate the concrete add-on in the flutes. The resulting form weight (with the Styrofoam) is assumed to be 7.0 psf. However, a weight of 15.0 psf was conservatively assumed in the analysis. Inside the boxes, a 2.5-inch deep form constructed of 20-gage material is sufficient to span the maximum 7′-9″ clear span. Styrofoam is not required in this case; however, if included the form weight can be reduced from 15.0 psf (with the concrete add-on) to approximately 5.0 psf. Design Engineers are encouraged to consult with deck-form manufacturers to discuss the various options and obtain more accurate weight information for these forms.

5.2.6.1.1.3 Concrete Parapets (DC_2)

The concrete parapet loads were applied as concentrated loads to the nodes at the edges of the deck in the composite 3D model (where the parapets are actually located).

5.2.6.1.2 Future Wearing Surface (DW)

The future wearing surface was applied to the composite 3D model by applying an artificial density of the hardened concrete deck to the deck elements extending over the approximate width of the roadway.

5.2.6.2 Live Loads

Live loads considered in this investigation included the HL-93 design vehicular live load (Section 1.3.2.3.1), the fatigue live load (Section 1.3.2.3.3) and the loading for live load deflection evaluation (Section 1.3.2.3.4). Design permit loads (Section 1.3.2.3.2) were not considered. As discussed further in Section 1.3.2.3.1, the HL-93 load consists of the combination of a design truck or design tandem, and a design lane load. The special loading for negative moment between points of permanent load contraflexure and for interior-pier reactions (Figure 1.3.7) was also considered in the analysis.

Live loads were applied to influence surfaces (Section 2.1.4) constructed by applying a unit load to selected deck nodes of the composite 3D model. Loading of the influence surfaces was performed with software separate from the finite element solver. Wheel loads were positioned on the surfaces according to the specification rules for live load placement (Section 2.1.4.1) in order to compute the maximum and minimum magnitudes of the desired response. The HL-93 loading was placed in one, two and three design lanes. The fatigue live load was placed in a single lane only. Only lengths of design lanes, or parts of design lanes, that contributed to the extreme force effects under consideration were loaded with the design lane load. Axles that did not contribute to the extreme force effects under consideration were neglected. Multiple presence factors (Section 1.3.2.3.7) and the dynamic load allowance (Section 1.3.2.3.8) were later applied to the live load *responses*, and not to the loads applied to the influence surfaces (see Section 5.1.6.1).

The wheel loads of the design truck(s), design tandem and fatigue live load were modified, however, to account for the vertical effects of centrifugal force and superelevation (Section 1.3.2.3.6). The design lane load was not modified for these effects. Unit wheel-load factors were computed that increased or decreased accordingly the wheel loads that were applied to the influence surfaces to account for vertical centrifugal force effects on this curved bridge. Using the procedures illustrated in Section 1.3.2.3.6, these unit wheel-load factors were computed to be as follows based on the design speed of 35 mph and the superelevation (deck cross-slope) of 5 percent assumed for the example bridge:

- HL-93 Design Truck(s) & Design Tandem: 1.296 and 0.704
- Fatigue Live Load: 1.198 and 0.802

5.2.6.3 Wind Loads

Wind loads were not considered in this investigation. The reader is referred to Sections 1.3.2.4 and 2.5.3.4.2 for further discussion on wind loads and the application of wind loads to 3D analysis models.

5.2.6.4 Thermal Loads

Thermal loads were not considered in this investigation. The reader is referred to Sections 1.3.2.5, 2.2 and 5.1.6.2 for further information regarding thermal loads, bearing orientation and constraint and thermal analyses.

5.2.7 Structural Analysis Results

5.2.7.1 Dead and Live Load Analysis Results

5.2.7.1.1 Girders

The unfactored vertical dead and live load bending moments, vertical shears and torques in G2 *at the span tenth-points* from the 3D analysis are summarized below in Tables 5.2.2, 5.2.3 and 5.2.4. The results are not exactly symmetrical about the mid-length of the girder because of the configuration of the top flange lateral bracing. *The shears listed in Table 5.2.3 are the vertical shears in the critical web; that is, the web subject to additive flexural and St. Venant torsional shears*. Looking from the left end of the example bridge, positive St. Venant torques in Table 5.2.4 act in the counterclockwise direction.

In the tables, the responses listed under DC_1 represent the sum of the responses due to the steel weight plus the weight of the deck, deck haunches and SIP forms. These loads were applied to the non-composite 3D model in the analysis. Responses listed under DC_2 are the responses due to the weight of the concrete parapets, and responses listed under DW are the responses due to the weight of the future wearing surface. DC_2 and DW loads were applied to the composite 3D model in the analysis.

Reported live load responses represent maximum and minimum envelope values determined from loading of the appropriate influence surfaces. Responses listed under 'HL-93' represent the governing responses due to the HL-93 design vehicular live load (Section 1.3.2.3.1) plus the specified dynamic load allowance (Section 1.3.2.3.8). The listed actions include the appropriate multiple presence factor (Section 1.3.2.3.7) for the governing case (one, two or three lanes loaded).

Responses listed under 'Fatigue Load' represent the responses due to the fatigue design live load (Section 1.3.2.3.3) placed in a single lane plus the 15 percent dynamic load allowance; the single-lane multiple presence factor of 1.2 is not applied to the fatigue live load responses.

As discussed in Section 5.2.6.2, centrifugal force effects (Section 1.3.2.3.6) were considered for both the HL-93 and fatigue live load; responses due to cases with centrifugal force effects included were compared to the responses with no centrifugal force considered and the worst case was selected and is reported in the tables.

Table 5.2.2 Unfactored Vertical Bending Moments (kip-ft) in G2 from the 3D Analysis

Tenth-Point Location (ft)	Steel Wt.	Deck + Haunch + SIP Form Wt.	DC_1	DC_2	DW	+(LL+IM) HL-93	-(LL+IM) HL-93	+(LL+IM) Fatigue Load	-(LL+IM) Fatigue Load
Abut. 1	0.	0.	0.	0.	0.	0.	0.	0.	0.
15.32	+581	+1,950	+2,531	+341	+394	+2,538	-486	+731	-92
30.63	+955	+3,232	+4,187	+569	+659	+4,224	-971	+1,153	-183
45.95	+1,133	+3,818	+4,951	+676	+789	+5,289	-1,455	+1,372	-275
61.27	+1,132	+3,789	+4,921	+659	+784	+5,752	-1,938	+1,420	-368
76.59	+937	+3,083	+4,020	+542	+641	+5,653	-2,430	+1,308	-467
91.90	+506	+1,615	+2,121	+275	+365	+5,122	-2,892	+1,188	-580
107.22	-161	-577	-738	-91	-47	+4,012	-3,485	+1,019	-712
122.54	-1,029	-3,323	-4,352	-584	-595	+2,559	-4,579	+659	-863
137.85	-2,157	-6,763	-8,920	-1,200	-1,273	+1,271	-5,601	+276	-1,028
Pier 1	-3,538	-10,721	-14,259	-1,985	-2,150	+1,060	-7,758	+231	-1,265
20.42	-1,738	-5,576	-7,314	-972	-1,016	+1,290	-4,409	+316	-788
40.85	-400	-1,443	-1,843	-206	-177	+2,878	-2,619	+792	-604
61.27	+539	+1,648	+2,187	+306	+423	+4,416	-2,071	+1,079	-440
81.69	+1,057	+3,357	+4,414	+644	+784	+5,585	-1,786	+1,281	-319
102.11	+1,255	+4,027	+5,282	+746	+907	+5,947	-1,520	+1,384	-223
122.54	+1,123	+3,566	+4,689	+648	+788	+5,586	-1,786	+1,283	-319
142.96	+596	+1,794	+2,390	+313	+428	+4,417	-2,071	+1,083	-440
163.38	-356	-1,258	-1,614	-202	-171	+2,881	-2,622	+795	-604
183.80	-1,682	-5,356	-7,038	-967	-1,011	+1,295	-4,416	+321	-789
Pier 2	-3,474	-10,521	-13,995	-1,985	-2,148	+1,062	-7,757	+231	-1,264
15.32	-2,134	-6,693	-8,827	-1,204	-1,273	+1,269	-5,605	+269	-1,031
30.63	-1,000	-3,261	-4,261	-590	-597	+2,557	-4,582	+660	-863
45.95	-157	-583	-740	-97	-50	+4,007	-3.484	+1,025	-712
61.27	+475	+1,549	+2,024	+271	+361	+5,117	-2,891	+1,177	-580
76.59	+870	+2,878	+3,748	+539	+638	+5,647	-2,429	+1,303	-465
91.90	+1,065	+3,558	+4,623	+660	+782	+5,754	-1,937	+1,420	-367
107.22	+1,080	+3,642	+4,722	+679	+788	+5,303	-1,453	+1,379	-275
122.54	+902	+3,056	+3,958	+574	+659	+4,268	-971	+1,177	-183
137.85	+535	+1,824	+2,359	+347	+394	+2,477	-485	+699	-91
Abut. 2	0.	0.	0.	0.	0.	0.	0.	0.	0.

Table 5.2.3 Unfactored Vertical Shears (kips) in the Critical Web of G2 from the 3D Analysis

Tenth-Point Location (ft)	Steel Wt.	Deck + Haunch + SIP Form Wt.	DC_1	DC_2	DW	+(LL+IM) HL-93	-(LL+IM) HL-93	+(LL+IM) Fatigue Load	-(LL+IM) Fatigue Load
Abut. 1	+25	+78	+103	+29	+17	+121	-25	+51	-9
15.32	+17	+57	+74	+18	+11	+109	-27	+43	-9
30.63	+9	+31	+40	+11	+6	+92	-34	+36	-11
45.95	+3	+9	+12	+2	+2	+74	-44	+28	-15
61.27	-6	-20	-26	-4	-3	+55	-55	+24	-19
76.59	-13	-44	-57	-8	-8	+36	-73	+15	-25
91.90	-19	-68	-87	-12	-12	+34	-87	+13	-32
107.22	-27	-89	-116	-17	-16	+30	-101	+11	-39
122.54	-34	-106	-140	-24	-19	+18	-115	+5	-44
137.85	-41	-125	-166	-28	-22	+18	-122	+4	-45
Pier 1	-51/+50	-149/+145	-200/+195	-45/+46	-32/+33	+13/+163	-154/-14	+4/+57	-55/-4
20.42	+38	+115	+153	+27	+22	+132	-19	+45	-5
40.85	+30	+98	+128	+18	+18	+119	-31	+41	-8
61.27	+21	+72	+93	+12	+13	+103	-40	+36	-12
81.69	+9	+34	+43	+9	+6	+82	-41	+29	-13
102.11	0	-1	-1	0	0	+60	-60	+21	-21
122.54	-10	-33	-43	-9	-6	+40	-83	+13	-29
142.96	-20	-69	-89	-12	-13	+40	-103	+12	-36
163.38	-30	-97	-127	-19	-18	+31	-120	+8	-41
183.80	-38	-116	-154	-28	-22	+20	-131	+5	-45
Pier 2	-51/+50	-147/+148	-198/+198	-46/+44	-32/+31	+14/+159	-159/-14	+4/+56	-55/-4
15.32	+40	+124	+164	+27	+22	+122	-17	+47	-4
30.63	+33	+103	+136	+23	+19	+115	-18	+43	-5
45.95	+26	+84	+110	+15	+16	+101	-31	+39	-11
61.27	+19	+66	+85	+10	+12	+87	-35	+32	-13
76.59	+11	+42	+53	+9	+7	+73	-35	+25	-15
91.90	+3	+14	+17	+4	+2	+56	-55	+19	-24
107.22	-4	-16	-20	-3	-2	+51	-75	+15	-29
122.54	-11	-37	-48	-12	-7	+38	-94	+11	-37
137.85	-20	-65	-85	-19	-11	+25	-111	+9	-43
Abut. 2	-26	-82	-108	-30	-17	+25	-124	+8	-52

Table 5.2.4 Unfactored Torques (kip-ft) in G2 from the 3D Analysis

Tenth-Point Location (ft)	Steel Wt.	Deck + Haunch + SIP Form Wt.	DC_1	DC_2	DW	+(LL+IM) HL-93	-(LL+IM) HL-93
Abut. 1	+44	+43	+87	+254	+22	+745	-436
15.32	+48	+107	+155	+151	+30	+729	-396
30.63	+15	+14	+29	+103	+13	+644	-376
45.95	+1	+4	+5	+25	+10	+520	-371
61.27	-51	-152	-203	-26	-15	+415	-352
76.59	-44	-147	-191	-36	-26	+338	-457
91.90	-44	-162	-206	-50	-39	+308	-531
107.22	-52	-167	-219	-72	-38	+324	-610
122.54	-43	-101	-144	-133	-26	+434	-696
137.85	+17	+127	+144	-133	+3	+602	-727
Pier 1	+9/+5	+148/-107	+157/-102	-208/+213	+7/+13	+808/+808	-713/-713
20.42	+15	-16	-1	+126	+20	+845	-587
40.85	+72	+213	+285	+77	+50	+806	-409
61.27	+71	+252	+323	+41	+47	+712	-379
81.69	+18	+33	+51	+52	+17	+545	-389
102.11	-20	-62	-82	-12	-3	+481	-499
122.54	-49	-127	-176	-76	-21	+367	-526
142.96	-50	-175	-225	-63	-50	+378	-684
163.38	-66	-197	-263	-97	-50	+421	-783
183.80	-12	+30	+18	-141	-18	+582	-834
Pier 2	-4/-16	+120/-171	+116/-187	-223/+198	-6/-1	+722/+722	-799/-799
15.32	-26	-151	-177	+119	0	+737	-613
30.63	+38	+91	+129	+116	+28	+712	-428
45.95	+49	+154	+203	+52	+37	+628	-308
61.27	+49	+183	+232	+29	+37	+531	-324
76.59	+27	+86	+113	+13	+21	+423	-414
91.90	+9	+12	+21	+2	+9	+334	-419
107.22	-37	-125	-162	-49	-16	+340	-558
122.54	-51	-134	-185	-126	-18	+442	-668
137.85	-88	-245	-342	-172	-33	+458	-710
Abut. 2	-84	-179	-263	-264	-23	+431	-748

5.2.7.1.2 Bracing Members

The maximum total factored tensile force in an internal cross-frame member was 81 kips and the maximum total factored compressive force in an internal cross-frame member was –69 kips. The maximum total factored tensile force in an external cross-frame member was 94 kips and the maximum total factored compressive force in an external cross-frame member was –88 kips. The maximum total factored tensile force in a diagonal member of the top lateral bracing was 56 kips and the maximum total factored compressive force in a diagonal member of the top lateral bracing was –76 kips. The maximum total factored tensile force in a top strut of the lateral bracing system was 50 kips and the maximum total factored compressive force in a top strut of the lateral bracing system was –55 kips. In each case, the maximum tensile and compressive forces were not in the same member. All factored forces were determined accordinng to the Strength I load combination.

5.2.8 Limit States

5.2.8.1 Service Limit State

Restrictions on stress and deformation under regular service conditions are specified at the service limit state to ensure satisfactory performance of the bridge over its service life. *AASHTO LRFD* Article 6.11.4 refers back to the I-girder provisions of *AASHTO LRFD* Article 6.10.4 for the specific service limit state verifications. *AASHTO LRFD* Article 6.10.4.1 specifies that optional live load deflection criteria and span-to-depth ratios (*AASHTO LRFD* Article 2.5.2.6) may be invoked to control deformations.

Steel structures must also satisfy the requirements of *AASHTO LRFD* Article 6.10.4.2 under the Service II load combination (Section 1.3.3). The intent of the design checks specified in *AASHTO LRFD* Article 6.10.4.2 is to prevent objectionable permanent deformations, caused by localized yielding, potential web bend-buckling and connection slip under expected severe traffic loadings, which might impair rideability.

Service limit state verifications are discussed in more detail in Section 3.2.4.

5.2.8.2 Fatigue and Fracture Limit State

Restrictions on stress range under regular service conditions are specified at the fatigue and fracture limit state to control crack growth under repetitive loads and to prevent fracture during the design life of the bridge (*AASHTO LRFD* Article 6.6.1). Material toughness requirements are also addressed (*AASHTO LRFD* Article 6.6.2).

The fatigue load (Section 1.3.2.3.3) and Fatigue load combinations (Section 1.3.3) apply for checking fatigue in steel structures. Fatigue resistance of details is discussed in *AASHTO LRFD* Article 6.6. A special fatigue requirement for webs (*AASHTO LRFD* Article 6.10.5.3) is also specified to control out-of-plane flexing of the web that might potentially lead to fatigue cracking under repeated live loading.

Fatigue and fracture limit state verifications are discussed in more detail in Section 3.2.5.

5.2.8.3 Strength Limit State

At the strength limit state, it must be ensured that adequate strength and stability is provided to resist the load combinations the bridge is expected to experience over its design life. Structural damage may occur, but overall structural integrity is maintained. The applicable Strength load combinations (Section 1.3.3) are used to check the strength limit state.

Although not specified as a separate limit state, constructibility is one of the basic design objectives of LRFD. The bridge must be safely erected and have adequate strength and stability during all phases of construction. Specific design provisions are given in *AASHTO LRFD* Article 6.11.3 to help ensure constructibility of steel I-girder bridges. The constructibility checks are typically made on the steel section only under the factored non-composite dead loads using the appropriate strength load combinations.

Strength limit state verifications and constructibility verifications are discussed in more detail in Sections 3.2.6 and 3.2.3, respectively.

5.2.8.4 Extreme Event Limit State

At the extreme event limit state, structural survival of the bridge must be ensured during a major earthquake or flood, or when struck by a vessel, vehicle, or ice flow. Extreme event limit states are not covered in this example.

5.2.9 Sample Design Calculations

Sample design calculations at critical sections of G2 from the example tub-girder bridge follow. The calculations are intended to illustrate the application of some of the more significant design verifications contained in *AASHTO LRFD* Article 6.11, including design verifications to be made at the service, fatigue and strength limit states. Detailed constructibility verifications are also illustrated. Also included are the shear connector design, transverse web and bearing stiffener designs, a lateral-bracing member design and a bolted field splice design.

The calculations make use of the unfactored vertical bending moments, vertical shears and torques in G2 from the 3D analysis of the example bridge presented in Section 5.2.7.1. In the calculation of the vertical bending stresses, compressive stresses are shown as negative values and tensile stresses are shown as positive values. The signs of the section moduli are adjusted accordingly to provide the expected sign of the calculation result, in which the sign of the vertical bending moment is maintained.

5.2.9.1 Constructibility Verifications

5.2.9.1.1 Deck Placement Analysis

5.2.9.1.1.1 General

Deck placement analysis is discussed in Section 3.2.3.2. During the deck placement, parts of the girders become composite in sequential stages. Temporary moments induced in the girders during the deck placement can be significantly larger than the final non-composite dead load moments after the sequential placement is complete. A separate 3D analysis was conducted to determine the maximum moments in the

girders of the example bridge caused by the assumed deck placement sequence shown in Figure 5.2.4.

AASHTO LRFD Article 6.10.3.4 requires that changes in the stiffness during the various stages of the deck placement be considered. Therefore, in the analysis, the first cast of the deck is assigned to the non-composite model. Subsequent casts are assumed placed with the concrete in preceding casts assumed hardened and acting compositely with the girders. Should the deck not be cast in separate stages, but instead be cast from one end of the bridge to the other, the end span must still be checked for the critical instantaneous unbalanced case where wet concrete exists over the end span, with no concrete cast yet on the remaining spans.

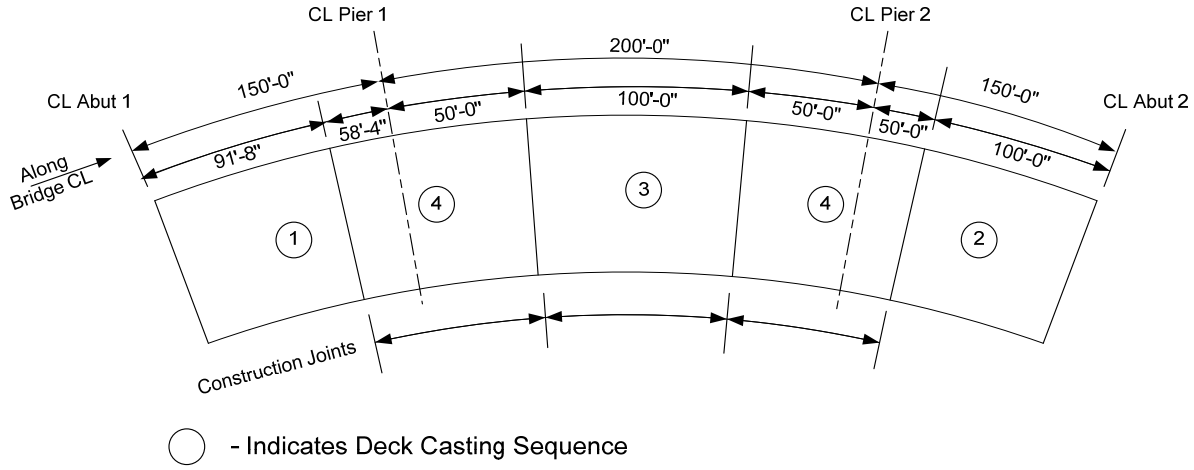


Figure 5.2.4 Assumed Deck Placement Sequence for the Example Tub-Girder Bridge

5.2.9.1.1.2 Deck Placement Analysis Results

Vertical Bending Moments

Unfactored vertical dead load bending moments in each span of G2 from the example bridge (at the span tenth points), including the moments resulting from each individual deck cast, are summarized in Table 5.2.5. The moments due to each deck cast include the moments due to the weight of the stay-in-place (SIP) forms. The assumed weight of the SIP forms includes the weight of the concrete in the form flutes, as discussed previously. Although the forms are initially empty, the weight of the deck reinforcement is essentially equivalent to the weight of the concrete in the form flutes.

Table 5.2.5 also gives the moments due to the steel weight, the sum of the moments due to the four casts plus the weight of the SIP forms, the maximum accumulated positive moments during the sequential deck casts (not including the steel weight),

and the moments due to the weight of the concrete deck, haunches and SIP forms assuming that the concrete is placed all at once on the non-composite girders.

The slight differences in the moments for each span on the last line of Table 5.2.5 and the accumulated moments due to the four casts plus the weight of the SIP forms are due to the changes in the girder stiffness with each cast. The principle of superposition does not apply directly in the deck-placement analyses since the girder stiffness changes at each step of the analysis. However, note the significant differences between the moments on the last line and the maximum accumulated positive moments during the sequential deck casts. In regions of positive flexure, the non-composite girder should be checked for the effect of this larger maximum accumulated deck-placement moment.

The accumulated positive moment at the critical section in each span is shown in bold in Table 5.2.5, along with the moment due to the steel weight at that section. At the critical section in Span 3 (located 91.90 ft from Pier 2 measured along the centerline of the tub), the sum of these moments is computed as:

$$M = 1{,}065 + 5{,}644 = +6{,}709 \ \ \text{kip} - \text{ft}$$

Table 5.2.5 Unfactored Vertical Dead Load Bending Moments (kip-ft) in G2 from the Deck Placement Analysis

Girder 2 Span 1	Unfactored Dead Load Moments (kip-feet)										
Length (ft)	0.0	15.32	30.63	45.95	61.27	76.59	91.90	107.22	122.54	137.85	153.17
Steel Weight	0.	581.	955.	1133.	**1132.**	937.	506.	-161.	-1029.	-2157.	-3538.
Cast											
1	0.	2274.	3845.	4697.	4953.	4536.	3345.	1777.	155.	-1565.	-3065.
2	0.	133.	265.	396.	529.	662.	799.	939.	1075.	1223.	1335.
3	0.	-574.	-1138.	-1703.	-2273.	-2852.	-3442.	-4080.	-4694.	-5355.	-5893.
4	0.	176.	350.	525.	700.	874.	1037.	914.	155.	-1275.	-3362.
Sum of Casts + SIP	0.	2009.	3322.	3915.	3909.	3220.	1739.	-450.	-3309.	-6972.	-10985.
Max +M	0.	2407.	4110.	5093.	**5482.**	5198.	4144.	2716.	1230.	0.	0.
DC_2	0.	341.	569.	676.	659.	542.	275.	-91.	-584.	-1200.	-1985.
Deck, haunches + SIP	0.	1950.	3232.	3818.	3789.	3083.	1615.	-577.	-3323.	-6763.	-10721.

Girder 2 Span 2	Unfactored Dead Load Moments (kip-feet)										
Length (ft)	0.0	20.42	40.85	61.27	81.69	102.11	122.54	142.96	163.38	183.80	204.23
Steel Weight	-3538.	-1738.	-400.	539.	1057.	**1255.**	1123.	596.	-356.	-1682.	-3474.
Cast											
1	-3065.	-2685.	-2260.	-1867.	-1477.	-1045.	-617.	-177.	323.	759.	1186.
2	1335.	889.	412.	-89.	-578.	-1076.	-1582.	-2056.	-2519.	-2990.	-3431.
3	-5893.	-2991.	83.	3008.	4758.	5352.	4853.	2985.	42.	-3058.	-6003.
4	-3362.	-943.	402.	570.	619.	669.	723.	777.	614.	-548.	-2894.
Sum of Casts + SIP	-10985.	-5730.	-1363.	1622.	3322.	3900.	3377.	1529.	-1540.	-5837.	-11142.
Max +M	0.	0.	0.	1622.	3322.	**3900.**	3377.	1529.	323.	759.	1186.
DC_2	-1985.	-972.	-206.	306.	644.	746.	648.	313.	-202.	-967.	-1985.
Deck, haunches + SIP	-10721.	-5576.	-1443.	1648.	3357.	4027.	3566.	1794.	-1258.	-5356.	-10521.

Girder 2 Span 3	Unfactored Dead Load Moments (kip-feet)										
Length (ft)	0.0	15.32	30.63	45.95	61.27	76.59	91.90	107.22	122.54	137.85	153.17
Steel Weight	-3474.	-2134.	-1000.	-157.	475.	870.	**1065.**	1080.	902.	535.	0.
Cast											
1	1186.	1069.	943.	820.	704.	589.	469.	351.	231.	112.	0.
2	-3431.	-1600.	308.	2133.	3782.	4815.	5175.	4863.	3903.	2276.	0.
3	-6003.	-5510.	-4884.	-4261.	-3706.	-3043.	-2424.	-1816.	-1213.	-612.	0.
4	-2894.	-1090.	54.	560.	512.	426.	344.	258.	173.	86.	0.
Sum of Casts + SIP	-11142.	-7131.	-3579.	-748.	1292.	2787.	3564.	3656.	3094.	1862.	0.
Max +M	1186.	1069.	1251.	2953.	4486.	5404.	**5644.**	5214.	4134.	2388.	0.
DC_2	-1985.	-1204.	-590.	-97.	271.	539.	660.	679.	574.	347.	0.
Deck, haunches + SIP	-10521.	-6693.	-3261.	-583.	1549.	2878.	3558.	3642.	3056.	1824.	0.

Vertical Deflections

Unfactored vertical dead load deflections in each span of G2 (at the span tenth points), including the deflections resulting from each individual deck cast, are summarized in similar fashion in Tables 5.2.6 and 5.2.7. Table 5.2.6 reports the deflections under the right web of G2 (when looking down G2 from the left end of the bridge) and Table 5.2.7 reports the deflections under the left web of G2. Deflections due to DC_2 loads are shown; deflections due to the wearing surface load, DW, are not reported. Negative values are downward deflections and positive values are upward deflections.

Table 5.2.6 Unfactored Vertical Dead Load Deflections (in.) of the Right Web of G2 from the Deck Placement Analysis

Girder 2 Span 1 Right Web Unfactored Vertical Dead Load Deflections (in.)											
Length (ft)	0.0	15.32	30.63	45.95	61.27	76.59	91.90	107.22	122.54	137.85	153.17
Steel Weight	0.	-0.22	-0.41	-0.52	-0.56	-0.52	-0.41	-0.26	-0.12	-0.03	0.
Cast											
1	0.	-1.08	-2.00	-2.64	-2.95	-2.91	-2.55	-1.97	-1.31	-0.63	0.
2	0.	-0.08	-0.15	-0.22	-0.27	-0.31	-0.33	-0.32	-0.26	-0.15	0.
3	0.	0.33	0.65	0.93	1.17	1.34	1.43	1.37	1.11	0.64	0.
4	0.	-0.08	-0.15	-0.22	-0.27	-0.30	-0.30	-0.27	-0.18	-0.07	0.
Sum of Casts + SIP	0.	-0.91	-1.66	-2.14	-2.32	-2.18	-1.76	-1.19	-0.63	-0.21	0.
DC_2	0.	-0.07	-0.12	-0.16	-0.17	-0.16	-0.12	-0.08	-0.04	0.	0.
Total	0.	-1.20	-2.19	-2.82	-3.05	-2.86	-2.29	-1.53	-0.79	-0.24	0.
Deck, haunches + SIP	0.	-0.76	-1.37	-1.75	-1.87	-1.71	-1.35	-0.87	-0.42	-0.11	0.

Girder 2 Span 2 Right Web Unfactored Vertical Dead Load Deflections (in.)											
Length (ft)	0.0	20.42	40.85	61.27	81.69	102.11	122.54	142.96	163.38	183.80	204.23
Steel Weight	0.	-0.15	-0.41	-0.68	-0.90	-0.98	-0.91	-0.70	-0.41	-0.16	0.
Cast											
1	0.	0.69	1.20	1.50	1.60	1.50	1.27	0.95	0.61	0.28	0.
2	0.	0.27	0.59	0.94	1.27	1.53	1.65	1.56	1.25	0.72	0.
3	0.	-1.17	-2.49	-3.78	-4.71	-5.05	-4.71	-3.77	-2.46	-1.14	0.
4	0.	-0.09	-0.21	-0.30	-0.37	-0.39	-0.39	-0.35	-0.26	-0.12	0.
Sum of Casts + SIP	0.	-0.30	-0.92	-1.64	-2.21	-2.41	-2.19	-1.60	-0.87	-0.27	0.
DC_2	0.	-0.05	-0.13	-0.23	-0.29	-0.32	-0.29	-0.23	-0.13	-0.05	0.
Total	0.	-0.50	-1.46	-2.55	-3.40	-3.71	-3.39	-2.53	-1.41	-0.48	0.
Deck, haunches + SIP	0.	-0.45	-1.23	-2.11	-2.78	-3.04	-2.81	-2.14	-1.26	-0.47	0.

Girder 2 Span 3 Right Web Unfactored Vertical Dead Load Deflections (in.)											
Length (ft)	0.0	15.32	30.63	45.95	61.27	76.59	91.90	107.22	122.54	137.85	153.17
Steel Weight	0.	-0.02	-0.11	-0.24	-0.38	-0.47	-0.52	-0.48	-0.37	-0.20	0.
Cast											
1	0.	-0.17	-0.30	-0.39	-0.44	-0.44	-0.40	-0.33	-0.23	-0.12	0.
2	0.	-0.69	-1.42	-2.14	-2.73	-3.08	-3.08	-2.73	-2.04	-1.09	0.
3	0.	0.63	1.09	1.32	1.36	1.29	1.14	0.91	0.64	0.33	0.
4	0.	-0.03	-0.08	-0.12	-0.13	-0.13	-0.12	-0.10	-0.07	-0.04	0.
Sum of Casts + SIP	0.	-0.25	-0.72	-1.32	-1.94	-2.36	-2.47	-2.24	-1.70	-0.92	0.
DC_2	0.	0.	-0.04	-0.08	-0.12	-0.16	-0.17	-0.16	-0.12	-0.07	0.
Total	0.	-0.27	-0.87	-1.64	-2.44	-2.99	-3.16	-2.88	-2.19	-1.19	0.
Deck, haunches + SIP	0.	-0.09	-0.38	-0.81	-1.25	-1.58	-1.72	-1.61	-1.26	-0.69	0.

Table 5.2.7 Unfactored Vertical Dead Load Deflections (in.) of the Left Web of G2 from the Deck Placement Analysis

Girder 2 Span 1 Left Web Unfactored Vertical Dead Load Deflections (in.)											
Length (ft)	0.0	15.32	30.63	45.95	61.27	76.59	91.90	107.22	122.54	137.85	153.17
Steel Weight	0.	-0.24	-0.43	-0.56	-0.60	-0.56	-0.44	-0.29	-0.14	-0.04	0.
Cast											
1	0.	-1.12	-2.09	-2.78	-3.12	-3.10	-2.74	-2.14	-1.42	-0.69	0.
2	0.	-0.08	-0.16	-0.22	-0.28	-0.32	-0.34	-0.33	-0.27	-0.16	0.
3	0.	0.35	0.67	0.97	1.21	1.39	1.48	1.43	1.17	0.68	0.
4	0.	-0.08	-0.16	-0.22	-0.28	-0.31	-0.31	-0.27	-0.18	-0.07	0.
Sum of Casts + SIP	0.	-0.94	-1.73	-2.27	-2.47	-2.34	-1,91	-1.31	-0.70	-0.24	0.
DC_2	0.	-0.08	-0.15	-0.19	-0.20	-0.19	-0.15	-0.10	-0.06	-0.02	0.
Total	0.	-1.26	-2.31	-3.02	-3.27	-3.09	-2.50	-1.70	-0.90	-0.30	0.
Deck, haunches + SIP	0.	-0.78	-1.43	-1.84	-1.97	-1.82	-1.44	-0.94	-0.45	-0.11	0.

Girder 2 Span 2 Left Web Unfactored Vertical Dead Load Deflections (in.)											
Length (ft)	0.0	20.42	40.85	61.27	81.69	102.11	122.54	142.96	163.38	183.80	204.23
Steel Weight	0.	-0.14	-0.40	-0.70	-0.93	-1.03	-0.96	-0.74	-0.45	-0.17	0.
Cast											
1	0.	0.74	1.29	1.62	1.73	1.63	1.38	1.04	0.66	0.31	0.
2	0.	0.27	0.61	0.98	1.33	1.60	1.73	1.65	1.33	0.77	0.
3	0.	-1.19	-2.56	-3.92	-4.93	-5.31	-4.98	-4.00	-2.64	-1.23	0.
4	0.	-0.08	-0.22	-0.32	-0.38	-0.41	-0.41	-0.37	-0.27	-0.13	0.
Sum of Casts + SIP	0.	-0.25	-0.88	-1.64	-2.26	-2.50	-2.28	-1.68	-0.92	-0.27	0.
DC_2	0.	-0.06	-0.16	-0.26	-0.33	-0.35	-0.33	-0.26	-0.16	-0.07	0.
Total	0.	-0.45	-1.44	-2.60	-3.52	-3.88	-3.57	-2.68	-1.53	-0.51	0.
Deck, haunches + SIP	0.	-0.41	-1.19	-2.12	-2.86	-3.17	-2.95	-2.26	-1.33	-0.49	0.

Girder 2 Span 3 Left Web Unfactored Vertical Dead Load Deflections (in.)											
Length (ft)	0.0	15.32	30.63	45.95	61.27	76.59	91.90	107.22	122.54	137.85	153.17
Steel Weight	0.	-0.01	-0.10	-0.23	-0.37	-0.48	-0.53	-0.50	-0.39	-0.22	0.
Cast											
1	0.	-0.18	-0.33	-0.42	-0.48	-0.48	-0.44	-0.36	-0.26	-0.13	0.
2	0.	-0.70	-1.46	-2.20	-2.83	-3.21	-3.24	-2.88	-2.17	-1.17	0.
3	0.	0.67	1.16	1.40	1.44	1.36	1.20	0.96	0.67	0.35	0.
4	0.	-0.02	-0.07	-0.11	-0.13	-0.13	-0.12	-0.10	-0.07	-0.04	0.
Sum of Casts + SIP	0.	-0.23	-0.70	-1.34	-2.00	-2.46	-2.59	-2.38	-1.82	-0.99	0.
DC_2	0.	-0.02	-0.05	-0.10	-0.15	-0.19	-0.20	-0.19	-0.15	-0.08	0.
Total	0.	-0.26	-0.85	-1.67	-2.52	-3.13	-3.32	-3.07	-2.36	-1.29	0.
Deck, haunches + SIP	0.	-0.04	-0.30	-0.74	-1.21	-1.58	-1.75	-1.66	-1.31	-0.72	0.

In the analysis, since the concrete does not have enough time to creep significantly between casts, the stiffness of previously cast portions of the deck is based on a modular ratio closer to the short-term modular ratio in computing the moments, deflections and reactions shown for Casts 2, 3 and 4 in Tables 5.2.5 through 5.2.8 (note that the effect of this on the moments and reactions is relatively insignificant).

A stiffness based on a concrete modulus of elasticity equal to 70 percent of the modulus of elasticity at 28 days (which results in a modular ratio of approximately 1.4*n*) is assumed, which has been found appropriate by at least one State DOT. For the computation of the deflections due to the DC_2 loads, a modular ratio of 3*n* is assumed.

Note the differences in the calculated deflections on the last line for each span (which assume the deck is cast all at once on the non-composite structure) and the sum of the accumulated deflections during the sequential deck casts. As creep of the concrete occurs over time, the accumulated deflections will tend to move toward the values reported on the last line, but they will not likely attain those values. Thus, if the differences in the deflections are deemed significant, e.g. for longer-span bridges, the Design Engineer may need to evaluate which set of deflections should be used, or else perhaps estimate deflections somewhere in-between to compute the girder cambers and avoid potential errors in the final girder elevations.

Vertical Reactions

The unfactored vertical dead load reactions for G4 and for G1 resulting from the deck-placement analysis are given in Table 5.2.8. Negative reactions represent upward reactions that resist the maximum downward force at the support under consideration. Conversely, positive reactions represent downward reactions that resist the maximum uplift force at the support.

For the investigation of uplift at critical construction stages, it is suggested that a load factor of 1.0 be applied to all downward (positive) support reactions due to component dead loads causing uplift, and a load factor of 0.9 be applied to all upward (negative) support reactions due to component dead loads resisting uplift.

Table 5.2.8 Unfactored Vertical Dead Load Reactions (kips) for G2 from the Deck Placement Analysis

Girder 2 Vertical Reactions (kips)	Abutment 1	Pier 1	Pier 2	Abutment 2
Steel Weight	-49.0	-194.0	-192.0	-52.0
sum	-49.0	-194.0	-192.0	-52.0
Cast 1	-181.0	-119.0	27.0	-13.0
sum	-230.0	-313.0	-165.0	-65.0
Cast 2	-15.0	23.0	-115.0	-206.0
sum	-245.0	-290.0	-280.0	-271.0
Cast 3	65.0	-149.0	-178.0	84.0
sum	-180.0	-439.0	-458.0	-187.0
Cast 4	-18.0	-288.0	-267.0	-8.0
sum	-198.0	-727.0	-725.0	-195.0
Sum of Casts + SIP Forms	-149.0	-533.0	-533.0	-143.0
DC_2 + DW	-64.0	-211.0	-211.0	-66.0
Total	-262.0	-938.0	-936.0	-261.0
Deck, haunches + SIP Forms	-157.0	-524.0	-517.0	-164.0
Total	-270.0	-929.0	-920.0	-282.0

Shown in Table 5.2.8 (under 'sum') are the accumulated vertical reactions for the steel weight plus the individual deck casts, which should be used to check for uplift under the deck placement. A net positive reaction indicates that the girder may lift-off at the support. Due to the reasonably balanced span arrangement along the bridge centerline, lift-off does not occur in any of the girders in this particular example. If the girder is permitted to lift-off its bearing seat, the staging analysis is incorrect unless a hold-down of the girder is provided at the location of a positive reaction.

Options to consider when uplift occurs include: 1) rearranging the concrete casts; 2) modifying the framing; 3) specifying a temporary load over that support; 4) specifying a tie-down bearing; 5) removing the bearing; or 6) if the uplift can be tolerated, performing another staging analysis with zero bearing stiffness at the support experiencing lift-off to obtain the correct moments and deflections.

Note in this case that the sum of the reactions from the analysis of the staged deck casts differs somewhat from the reactions assuming the deck is cast all at once on the non-composite structure (as given on the next-to-last line of Table 5.2.8); however, it is usually reasonable to ignore these differences and use the reactions as shown on the last line of the table in the design.

Vertical Bending Stress

Calculate the maximum factored dead load vertical bending stress in the top flange of the non-composite steel tub at the critical section in Span 3 of G2 (located 91.90 feet from Pier 2 measured along the centerline of the tub) resulting from the deck-placement sequence.

The top flange in regions of positive flexure is most always the critical flange for the constructibility checks. The Strength IV load combination (Section 1.3.3) is considered for the constructibility checks in this example. The load modifier η is taken equal to 1.0. Section properties for the bare steel girder at this section (Figure 5.2.5) are computed as follows:

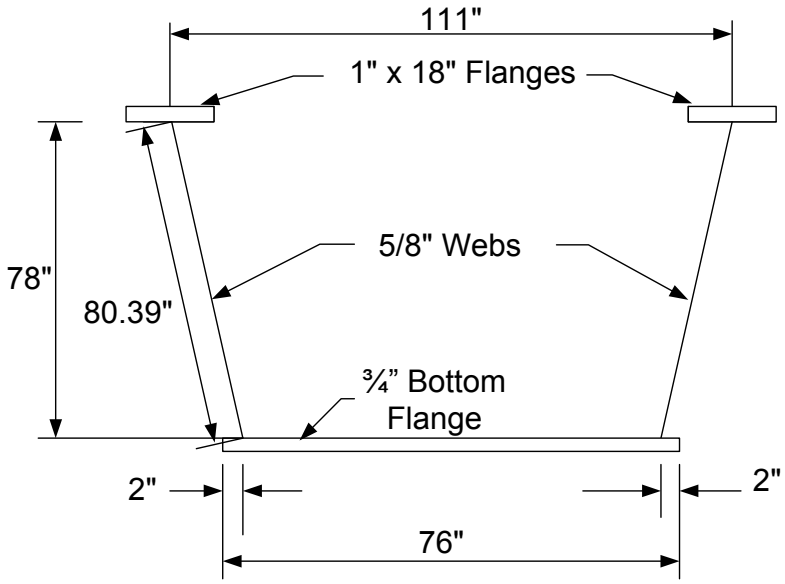


Figure 5.2.5 G2, Span 3, Steel Section at 91.90 Feet from Pier 2

Component	A	d	Ad	Ad^2	I_o	I
2 Top Flanges 1" x 18" + A_d	41.09	39.50	1,623	64,111	3.00	64,114
2 Web Plates 5/8" x 80.39"	100.5				50,934	50,934
Bottom Flange 3/4" x 76"	57.00	−39.38	−2,245	88,395	2.67	88,398
	198.6		−622.0			203,446

$$d_s = \frac{-622.0}{198.6} = -3.13 \text{ in.}$$

$$-3.13(622.0) = -1{,}947$$

$$I_{NA} = 201{,}500 \text{ in.}^4$$

$$d_{TOP\ OF\ STEEL} = 40.00 + 3.13 = 43.13 \text{ in.} \qquad d_{BOT\ OF\ STEEL} = 39.75 - 3.13 = 36.62 \text{ in.}$$

$$S_{TOP\ OF\ STEEL} = \frac{201{,}500}{-43.13} = -4{,}672 \text{ in.}^3 \qquad S_{BOT\ OF\ STEEL} = \frac{201{,}500}{36.62} = 5{,}503 \text{ in.}^3$$

For tub sections with inclined webs, the area of the inclined webs should be used in computing all section properties. In the preceding table, the moment of inertia of *each* inclined web I_{ow} with respect to a horizontal axis at mid-depth of the web is taken as follows:

$$I_{ow} = I_w\left(\frac{S^2}{S^2+1}\right)$$

where:

I_w = moment of inertia of each inclined web with respect to an axis normal to the web (in.^{4})

S = web slope with respect to the horizontal (equal to 4.0 in this case)

The longitudinal component, A_d, of the top flange lateral bracing area (included with the area of the top flanges in the preceding table) is computed as follows:

$$\theta = \tan^{-1}\left(\frac{9.25}{28.833/3}\right) = 43.9^\circ$$

$$A_d = A\cos\theta = 7.07\cos(43.9^\circ) = 5.09 \text{ in.}^2$$

The bottom flange lips are also included in the computation of the section properties.

An effective box-flange width is used in determining the elastic section properties used to calculate the factored vertical bending stresses in the tub section. According to AASHTO LRFD Article 6.11.1.1, box flanges are to be considered fully effective in resisting flexure if the width of the flange does not exceed one-fifth of the effective span. For continuous spans, the effective span is to be taken as the distance between points of permanent load contraflexure, or between a simple support and a point of permanent load contraflexure, as applicable. Should the flange width exceed one-fifth of the effective span, only a width equal to one-fifth of the span is to be considered effective. In calculating the nominal flexural resistance of the box flange, however, the full flange width (neglecting the flange lips) is always to be used regardless of the effective flange width (AASHTO LRFD Article C6.11.1.1). For the section under consideration in Span 3, the effective span is 96 feet based on the location of the point of contraflexure for the steel weight. Therefore:

$$0.2(96)(12) = 230 \text{ in.} > 76.0 \text{ in.}$$

The box flange at this section is fully effective. Further information regarding the effective box-flange width may be found in Section 3.1.5.4.2.1.

For Strength IV:

- Top flange:

$$f_{bu} = \frac{1.0(1.5)(6{,}709)(12)}{-4{,}672} = -25.85 \text{ ksi}$$

5.2.9.1.2 Deck Overhang Loads

Deck overhang loads are discussed in Section 3.2.3.3. The deck overhang bracket configuration shown in Figure 5.2.6 is assumed for this example. The brackets

extend to the bottom flange, which is preferred. Alternatively, the brackets may bear on the girder web if means are provided to ensure that the web is not damaged and that the associated deformations permit proper placement of the concrete deck.

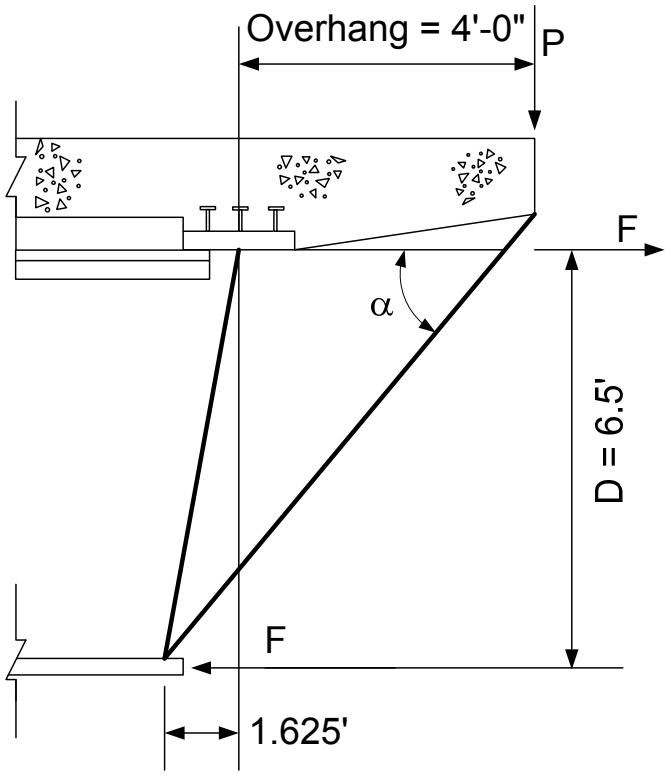


Figure 5.2.6 Assumed Deck Overhang Bracket Configuration for the Example Tub-Girder Bridge

Although the brackets are typically spaced at 3 to 4 feet along the fascia girder, all bracket loads except for the finishing machine load are assumed applied uniformly.

Calculate the vertical loads acting on the overhang brackets. Because in this case the bracket is assumed to extend near the edge of the deck overhang, assume as an approximation that half the deck overhang weight is placed on the outside top flange and web and half the weight is placed on the overhang brackets. Conservatively include one-half the deck haunch weight in the total overhang weight. Therefore:

Deck Overhang Weight:

$$P = 0.5 * 150\left[\frac{10.0}{12}(4.0) + \left[\frac{1}{12}\left(\frac{5.5}{2} + 0.5\right)\left(4.0 - \frac{18/2}{12}\right)\right] + \frac{5.0}{12}\left(\frac{18/2}{12}\right)\right] = 339 \text{ lbs/ft}$$

The other half of the overhang weight can be assumed to act at the edge of the top flange (at a distance of 9.0 inches from the shear center of the girder in this case). The effective deck weight acting on the other side of the web can be assumed applied at the other edge of the top flange. The net torque can be resolved into flange lateral moments that generally act in the opposite direction to the lateral moments caused by the overhang loads. This effect is conservatively neglected in this example.

Construction loads, or dead loads and temporary loads that act on the overhang only during construction, are assumed as follows:

- Overhang deck forms: P = 40 lbs/ft
- Screed rail: P = 85 lbs/ft
- Railing: P = 25 lbs/ft
- Walkway: P = 125 lbs/ft
- Finishing machine P = 3000 lbs

The finishing machine load is estimated as one-half of the total finishing machine truss weight, plus some additional load to account for the weight of the engine, drum and operator assumed to be located on one side of the truss. For checking the Strength IV load combination, however, the finishing machine is considered to be a transient live load and so it is not considered further in this check (since the Strength IV load combination only considers dead loads). Note that the above loads are estimated loads used here for illustration purposes only. It is recommended that the Design Engineer consider talking to local Contractors to obtain more accurate values for these construction loads.

Referring to Figure 5.2.6, the lateral force on the top flange due to the vertical load on the overhang brackets is computed as:

$$F = P/\tan\alpha \cong P\left(\frac{\text{Overhang} + 1.625}{D}\right)$$

The equations given in *AASHTO LRFD* Article C6.10.3.4 may be used to estimate the maximum flange lateral bending moments in the outer top flange due to the lateral bracket forces in lieu of a more refined analysis. Assuming the flange is continuous with the adjacent unbraced lengths and that the adjacent unbraced lengths are approximately equal, the lateral bending moment due to a statically equivalent uniformly distributed lateral bracket force may be estimated as (Equation 3.2.15):

$$M_\ell = \frac{F_\ell L_b^2}{12}$$

Lateral bending stresses determined from a first-order analysis may be used in discretely braced compression flanges for which the unbraced length between cross-frames, L_b, satisfies Equation 3.2.8 as follows:

$$L_b \le 1.2 L_p \sqrt{\frac{C_b R_b}{f_{bu}/F_{yc}}}$$

There is an internal cross-frame adjacent to the section under consideration. The top strut of the lateral bracing framing into the flange on the other side of this section is assumed to act as a brace point, as permitted at the discretion of the Design Engineer in *AASHTO LRFD* Article C6.11.3.2. Although there is not an internal cross-frame at this location, each end of the strut is assumed attached to the flange and is braced at each end by a diagonal member based on the Pratt Truss lateral bracing configuration that is utilized (Figure 5.2.2). In a Warren Truss configuration, the strut would only be braced at one end and two diagonal members would be pushing outward on the flange at the intersection. Therefore, the unbraced length, L_b, of the outer flange containing the section under consideration is taken equal to (28.833/3)(566.25/561.625) = 9.69 feet.

L_p is the limiting unbraced length for lateral torsional buckling specified in *AASHTO LRFD* Article 6.10.8.2.3 determined as (Equation 3.2.94):

$$L_p = 1.0 r_t \sqrt{\frac{E}{F_{yc}}}$$

where r_t is the effective radius of gyration for lateral torsional buckling specified in *AASHTO LRFD* Article 6.10.8.2.3 determined as (Equation 3.2.97):

$$r_t = \frac{b_{fc}}{\sqrt{12\left(1+\frac{1}{3}\frac{D_c t_w}{b_{fc} t_{fc}}\right)}}$$

For the steel section, the depth of the web in compression in the elastic range, D_c, at this section = 43.13 – 1.0 = 42.13/cos14° = 43.42 inches. Therefore,

$$r_t = \frac{18}{\sqrt{12\left(1+\frac{1}{3}\frac{43.42(0.625)}{18(1.0)}\right)}} = 4.24 \text{ in.}$$

$$L_p = \frac{1.0(4.24)}{12}\sqrt{\frac{29{,}000}{50}} = 8.51 \text{ ft}$$

C_b is the moment gradient modifier specified in *AASHTO LRFD* Article 6.10.8.2.3 (Section 3.2.6.4.1.2). Since the moment gradient is not significant in this region, C_b will be conservatively taken equal to 1.0. According to *AASHTO LRFD* Article 6.10.1.10.2, the web load-shedding factor, R_b (Section 3.2.6.2), is to be taken equal to 1.0 when checking constructibility since web bend buckling is prevented during construction by a separate limit state check (illustrated below).

AASHTO LRFD Article 6.10.1.6 specifies that f_{bu} in *AASHTO LRFD* Equation 6.10.1.6-2 (Equation 3.2.8) is to be taken as the largest value of the compressive vertical bending stress throughout the unbraced length under consideration, which in this case is at the location under consideration. Therefore:

$$1.2(8.51)\sqrt{\frac{(1.0)(1.0)}{\left|-25.85\right|/(50)}} = 14.20 \text{ ft} < L_b = 9.69 \text{ ft}$$

Because the preceding equation is satisfied, amplification of the first-order elastic compression-flange lateral bending stresses according to the previsions of AASHTO LRFD Article 6.10.1.6 is not required (i.e. the amplification factor, *AF*, is equal to 1.0).

Calculate the factored first-order lateral flange bending stress in the outer top flange due to the deck overhang loads.

- Dead loads:

$$P = 1.0\left[1.5(339 + 40 + 85 + 25 + 125)\right] = 921 \text{ lbs/ft}$$

$$F = F_\ell = P\left(\frac{\text{Overhang} + 1.625}{D}\right) = 921\left(\frac{4.0 + 1.625}{(78/12)}\right) = 797 \text{ lbs/ft}$$

$$M_\ell = \frac{F_\ell L_b^2}{12} = \frac{(0.797)(9.69)^2}{12} = 6.24 \text{ kip} - \text{ft}$$

$$f_\ell = \frac{M_\ell}{S_\ell} = \frac{(6.24)(12)}{(1.0)\left(\frac{(18)^2}{6}\right)} = 1.39 \text{ ksi}$$

- Finishing machine: Not considered for Strength IV

AASHTO LRFD Article 6.10.1.6 specifies that for design verifications where the flexural resistance is based on lateral torsional buckling, the vertical bending stress, f_{bu}, and the flange lateral bending stress, f_ℓ, are to be determined as the largest values throughout the unbraced length in the flange under consideration. For design

verifications where the flexural resistance is based on yielding or flange local buckling, f_{bu} and f_ℓ may be determined as the stresses at the section under consideration. For simplicity in this example, the largest values of f_{bu} and f_ℓ within the unbraced length will conservatively be used in all design checks.

The largest unfactored lateral flange bending moment in the top flange due to DC_1 (i.e. steel weight, total deck plus deck haunch weight and SIP form weight) within the unbraced length *resulting from curvature and top lateral bracing effects* (taken directly from the 3D analysis results) is 2 kip-ft.

Strictly speaking, only the top flange lateral moments due to the steel & SIP form weight plus the first two casts would need to be considered; the lateral moments due to Casts 3 and 4 could potentially be ignored since the top flange at the critical section in Span 3 is assumed continuously braced for the succeeding casts. However, this refinement is ignored here for simplicity.

The factored lateral bending stress in the outer top flange due to curvature effects is therefore computed as:

$$f_\ell = \frac{M_\ell}{S_\ell} = \frac{1.5(2)(12)}{1.0(18)^2/6} = 0.67 \text{ ksi}$$

In the case of G2, in regions of positive flexure, the lateral bending moments in the outermost top flange at the cross-frames due to the overhang loads act in the same sense as the lateral bending moments at the cross-frames due to the curvature effects taken directly from the 3D analysis. That is, the lateral moments in each case act to restrain the outward bowing of the top flange caused by these effects. Thus, the lateral bending stresses are additive.

In the case of G1, the lateral bending moments in the innermost top flange due to the overhang loads act in the opposite direction to the lateral bending moments due to the curvature effects in regions of positive flexure. This must be considered when summing the lateral bending stresses when checking the top flange of G1 in these regions.

In the following, the factored top flange lateral bending stresses due to the overhang bracket loads and due to curvature skew effects are summed and the amplification factor is applied:

$$f_\ell \text{ total} = (1.39 + 0.67)\text{AF} = (2.06 \text{ ksi})(1.0) = 2.06 \text{ ksi}$$

First- or second-order flange lateral bending stresses, as applicable, due to all sources are limited to a maximum value of $0.6F_{yf}$ according to *AASHTO LRFD* Equation 6.10.1.6-1:

$$2.06 \text{ ksi} < 0.6F_y = 0.6(50) = 30 \text{ ksi} \quad \text{ok} \quad (\text{Ratio} = 0.070)$$

5.2.9.1.3 Flexure Verifications

AASHTO LRFD Article 6.11.3.2 specifies that for critical stages of construction, the constructibility design provisions of *AASHTO LRFD* Articles 6.10.3.2.1 through 6.10.3.2.3 for flexure of I-sections are to be applied to the top flanges of tub sections.

For critical stages of construction, *AASHTO LRFD* Article 6.10.3.2.1 requires that discretely braced flanges in compression satisfy requirements to prevent nominal yielding at the flange tips, flange local buckling, lateral torsional buckling and web bend buckling.

5.2.9.1.3.1 Flange Tip Yielding (Equation 3.2.18)

$$f_{bu} + f_\ell \le \phi_f R_h F_{yc}$$

$$f_{bu} + f_\ell = \left|-25.85\right| \text{ ksi} + 2.06 \text{ ksi} = 27.91 \text{ ksi}$$

$$\phi_f R_h F_{yc} = 1.0(1.0)(50) = 50.0 \text{ ksi}$$

$$27.91 \text{ ksi} < 50.0 \text{ ksi} \quad \text{ok} \quad (\text{Ratio} = 0.560)$$

5.2.9.1.3.2 Flange Local Buckling (Equation 3.2.19)

$$f_{bu} + \frac{1}{3} f_\ell \le \phi_f (F_{nc})_{FLB}$$

Determine the slenderness ratio of the top flange:

$$\lambda_f = \frac{b_{fc}}{2t_{fc}}$$

$$\lambda_f = \frac{18}{2(1.0)} = 9.0$$

Determine the limiting slenderness ratio for a compact flange from Equation 3.2.87 (alternatively, see *AASHTO LRFD* Table C6.10.8.2.2-1):

$$\lambda_{pf} = 0.38\sqrt{\frac{E}{F_{yc}}}$$

$$\lambda_{pf} = 0.38\sqrt{\frac{29{,}000}{50}} = 9.15$$

Since $\lambda_f < \lambda_{pf}$, the nominal local buckling resistance $(F_{nc})_{FLB}$ is taken as (Equation 3.2.88):

$$(F_{nc})_{FLB} = R_b R_h F_{yc}$$

$$(F_{nc})_{FLB} = 1.0(1.0)(50) = 50.0 \text{ ksi}$$

$$f_{bu} + \frac{1}{3}f_\ell = |-25.85| \text{ ksi} + \frac{2.06}{3} \text{ ksi} = 26.54 \text{ ksi}$$

$$\phi_f (F_{nc})_{FLB} = 1.0(50.0) = 50.0 \text{ ksi}$$

$$26.54 \text{ ksi} < 50.0 \text{ ksi} \qquad \text{ok} \qquad (\text{Ratio} = 0.530)$$

5.2.9.1.3.3 Lateral Torsional Buckling (Equation 3.2.19)

$$f_{bu} + \frac{1}{3}f_\ell \le \phi_f (F_{nc})_{LTB}$$

.

The limiting unbraced length, L_p, was computed earlier to be 8.51 feet. The effective radius of gyration for lateral torsional buckling r_t for the non-composite section was also computed earlier to be 4.24 inches.

Determine the limiting unbraced length, L_r, from Equation 3.2.95 as follows:

$$L_r = \pi r_t \sqrt{\frac{E}{F_{yr}}}$$

where:

$$F_{yr} = 0.7F_{yc} \le F_{yw}$$

$$F_{yr} = 0.7(50) = 35.0 \text{ ksi} < 50 \text{ ksi} \qquad \text{ok}$$

F_{yr} must also not be less than $0.5F_{yc}$ = 0.5(50) = 25.0 ksi ok.

Therefore:

$$L_r = \frac{\pi(4.24)}{12}\sqrt{\frac{29{,}000}{35.0}} = 31.95 \text{ ft}$$

Since L_p = 8.51 feet < L_b = 9.69 feet < L_r = 31.95 feet, the nominal lateral torsional buckling resistance is taken as (Equation 3.2.92):

$$(F_{nc})_{LTB} = C_b\left[1-\left(1-\frac{F_{yr}}{R_h F_{yc}}\right)\left(\frac{L_b - L_p}{L_r - L_p}\right)\right]R_b R_h F_{yc} \le R_b R_h F_{yc}$$

Therefore:

$$(F_{nc})_{LTB} = 1.0\left[1-\left(1-\frac{35.0}{1.0(50)}\right)\left(\frac{9.69-8.51}{31.95-8.51}\right)\right](1.0)(1.0)(50) = 49.24 \text{ ksi} < 1.0(1.0)(50) = 50 \text{ ksi} \quad \text{ok}$$

$$f_{bu} + \frac{1}{3}f_{\ell} = \left|-25.85\right| \text{ ksi} + \frac{2.06}{3}\text{ksi} = 26.54 \text{ ksi}$$

$$\phi_f (F_{nc})_{LTB} = 1.0(49.24) = 49.24 \text{ ksi}$$

$$26.54 \text{ ksi} < 49.24 \text{ ksi} \quad \text{ok} \qquad (\text{Ratio} = 0.539)$$

5.2.9.1.3.4 Web Bend Buckling (Equation 3.2.20)

$$f_{bu} \le \phi_f F_{crw}$$

Determine the nominal web bend-buckling resistance, F_{crw}, according to the provisions of *AASHTO LRFD* Article 6.10.1.9.1 as follows (Equation 3.2.35):

$$F_{crw} = \frac{0.9Ek}{\left(\frac{D}{t_w}\right)^2}$$

but not to exceed the smaller of $R_h F_{yc}$ and F_{yw}/0.7, where (Equation 3.2.36):

$$k = \frac{9}{(D_c/D)^2}$$

$$k = \frac{9}{(43.42/80.39)^2} = 30.85$$

Therefore,

$$F_{crw} = \frac{0.9(29{,}000)(30.85)}{\left(\frac{80.39}{0.625}\right)^2} = 48.67 \text{ ksi} < \min\left(R_h F_{yc}, F_{yw}/0.7\right) = R_h F_{yc} = 1.0(50) = 50 \text{ ksi} \quad \text{ok}$$

$$\phi_f F_{crw} = 1.0(48.67) = 48.67 \text{ ksi}$$

$$\left|-25.85\right| \text{ ksi} < 48.67 \text{ ksi} \quad \text{ok} \qquad (\text{Ratio} = 0.531)$$

Options to consider should the web bend-buckling resistance be exceeded include:

- Providing a larger compression flange or a smaller tension flange to decrease D_c
- Adjusting the deck-placement sequence to reduce the compressive stress in the web
- Providing a thicker web
- Adding a longitudinal web stiffener should the preceding options not prove to be practical or cost-effective

5.2.9.1.4 Shear Verifications

AASHTO LRFD Article 6.11.3.3 requires that webs satisfy the following requirement during critical stages of construction (Sections 3.2.3.4.2.3 and 3.2.3.4.1.3 - Equation 3.2.23):

$$V_u \le \phi_v V_{cr}$$

For this example, the panel in G2 immediately to the left of Pier 1 (in Span 1) will be checked. The panel is bounded by the internal diaphragm at Pier 1 and a transverse stiffener located 26.833(566.25/561.625)/2 = 13.527 feet into Span 1 from Pier 1 (measured along the outer web of G2 – Section 5.2.9.4.3.4). The stiffener spacing of 13.527(12) = 162.3 inches is less than the maximum permitted spacing of d_o = 3D = 3(80.39) = 241.2 inches.

Since shear is rarely increased significantly due to deck staging, the DC_1 shear (i.e. shear due to the steel weight, deck plus deck haunch and SIP forms) in the critical web at Pier 1 equal to -200 kips (Table 5.2.3) will be used in this check. The critical web is the web subject to additive flexural and torsional shears. For box sections with inclined webs, the web must be designed for the total vertical shear in the plane of the critical web, V_{ui}, which is taken equal to V_u divided by $\cos\theta$, where θ is the

angle of inclination of the web plate with respect to the vertical (Equation 3.2.153). Under the Strength IV load combination, at Pier 1:

$$(V_u)_{DC1} = 1.0(1.5)|-200| = 300 \text{ kips}/\cos 14^\circ = 309 \text{ kips}$$

The shear buckling resistance of the 162.3-inch-long panel is determined as (Equation 3.2.161):

$$V_n = V_{cr} = CV_p$$

C is the ratio of the shear buckling resistance to the shear yield strength determined from *AASHTO LRFD* 6.10.9.3.2-4, 6.10.9.3.2-5 or 6.10.9.3.2-6, as applicable. In computing the shear-buckling resistance, V_{cr}, for the case of inclined webs, the web depth, *D,* must be taken as the depth of the web measured along the slope or $D/\cos\theta$.

First, compute the shear buckling coefficient *k* from Equation 3.2.157 as follows:

$$k = 5 + \frac{5}{\left(\frac{d_o}{D}\right)^2}$$

$$k = 5 + \frac{5}{\left(\frac{162.3}{80.39}\right)^2} = 6.23$$

Since,

$$1.40\sqrt{\frac{Ek}{F_{yw}}} = 1.40\sqrt{\frac{29{,}000(6.23)}{50}} = 84.2 < \frac{D}{t_w} = \frac{80.39}{0.625} = 128.6$$

Equation 3.2.158 is used to compute *C* as follows:

$$C = \frac{1.57}{\left(\frac{D}{t_w}\right)^2}\left(\frac{Ek}{F_{yw}}\right)$$

$$C = \frac{1.57}{(128.6)^2}\left(\frac{29{,}000(6.23)}{50}\right) = 0.343$$

V_p is the plastic shear force determined as follows (Equation 3.2.151):

$$V_p = 0.58F_{yw}Dt_w$$

$$V_p = 0.58(50)(80.39)(0.625) = 1{,}457 \text{ kips}$$

Therefore,

$$V_{cr} = 0.343(1{,}457) = 500 \text{ kips}$$

$$\phi_v V_{cr} = 1.0(500) = 500 \text{ kips}$$

$$(V_u)_{DC_1} = 309 \text{ kips} < \phi_v V_{cr} = 500 \text{ kips}$$

$$\text{ok} \qquad (\text{Ratio} = 0.618)$$

5.2.9.1.5 Concrete Deck

AASHTO LRFD Article 6.10.2.3.4 requires that the factored longitudinal tensile stress in a composite concrete deck not exceed ϕf_r during critical stages of construction, unless the minimum one-percent longitudinal reinforcement is provided according to the provisions of *AASHTO LRFD* Article 6.10.1.7 (Section 3.2.3.2.5).

f_r is the lower-bound modulus of rupture of the concrete determined as follows for normal weight concrete (*AASHTO LRFD* Article 5.4.2.6 – Equation 3.2.14):

$$f_r = 0.24\sqrt{f'_c} = 0.24\sqrt{4.5} = 0.509 \text{ ksi}$$

ϕ is the appropriate resistance factor for concrete in tension specified in *AASHTO LRFD* Article 5.5.4.2.1. For reinforced concrete in tension, ϕ is equal to 0.90.

$$\phi f_r = 0.9(0.509) = 0.458 \text{ ksi}$$

Check the tensile stress in the concrete deck at the end of Cast 2 in Span 3 over G2 (53.17 feet from Pier 2 measured along the centerline of G2) caused by the negative moment due to Cast 3.

From Table 5.2.5, the negative moment at the end of Cast 2 due to Cast 3 is –3,999 kip-feet (linear interpolation is used). The longitudinal concrete deck stress is to be determined as specified in *AASHTO LRFD* Article 6.10.1.1.1d; that is, using the short-term modular ratio n. Calculate the modular ratio, n (*AASHTO LRFD* Article 6.10.1.1.1b):

$$n = \frac{E}{E_c}$$

where Ec is the modulus of elasticity of the concrete determined as specified in AASHTO LRFD Article 5.4.2.4. A unit weight of 0.145 kcf will be used for the concrete in the calculation of the modular ratio (since 0.005 kcf of the specified unit weight of 0.150 kcf is typically assumed to account for the weight of the reinforcement).

$$E_c = 33{,}000 w_c^{1.5} \sqrt{f_c'}$$

$$E_c = 33{,}000(0.145)^{1.5} \sqrt{4.5} = 3{,}865 \text{ ksi}$$

$$n = \frac{29{,}000}{3{,}865} = 7.5$$

The calculated stress on the transformed section is to be divided by *n* to obtain the stress in the concrete. The composite section properties at this section are determined from separate computations similar to the above. The effective width of the deck is 243 inches (Section 2.1.7). Under the Strength IV load combination:

$$f_{deck} = \frac{1.0(1.5)(-3{,}999)(29.46)(12)}{697{,}719(7.5)} = 0.405 \text{ ksi} < 0.458 \text{ ksi}$$

Therefore, the minimum one percent longitudinal reinforcement is not required at this section. A check is made in Section 5.9.2.2.3 to determine where the longitudinal reinforcement must be terminated in Span 3 to satisfy this condition under the Service II load combination.

Although not done in this example, a more accurate estimate of the concrete strength at the time Cast 3 is made, and the resulting modular ratio (e.g. using 1.4*n*), could be used in this check if desired.

5.2.9.2 Service Limit State Verifications

5.2.9.2.1 Live Load Deflections

Live load deflections are discussed in Section 3.2.4.2.1. For control of elastic deformations, *AASHTO LRFD* Article 6.10.4.1 refers back to *AASHTO LRFD* Article 2.5.2.6, which contains optional live load deflection criteria and criteria for span-to-depth ratios. The suggested span-to-depth ratios were utilized earlier in Section 5.2.5.1.1 to establish a reasonable minimum web depth for the example girder design.

The optional live load deflection check consists of evaluating two separate live load conditions (Section 1.3.2.3.4). The two load conditions are (*AASHTO LRFD* Article 3.6.1.3.2):

- The design truck
- The design lane plus 25 percent of the design truck

The dynamic load allowance of 33 percent is applied to the design truck in each case. A load factor of 1.0 is applied to the live load. All design lanes are loaded and the appropriate multiple presence factor is to be applied (i.e. for one lane loaded, *m* = 1.2; for two lanes loaded; *m* = 1.0; for three lanes loaded, *m* = 0.85). For curved-girder bridges, the deflection of each girder must be determined individually based on its response as part of a system.

Span 2 of G2 has an arc span length of 203.23 feet (Table 5.2.1) measured along the centerline of the tub. The maximum live load deflection in Span 2 of G2 will be checked (102.1 ft from Pier 1).

The roadway width can accommodate up to three 12-ft-wide design lanes. From the 3D analysis, the maximum deflections at this point at the center of the tub (without impact or multiple presence applied, but with centrifugal force effects considered) due to the design truck and the design lane placed separately in one, two and three design lanes are given in Table 5.2.9 as follows:

Table 5.2.9 Maximum Design Truck and Design Lane Load Deflections (in.) including Centrifugal Force Effects (w/ no impact or multiple presence considered)

Maximum Live Load Deflections (in.) Span 2 – G2 – 102.1 ft from Pier 1		
	Design Truck	Design Lane
One Lane Loaded	0.414	0.431
Two Lanes Loaded	0.758	0.782
Three Lanes Loaded	1.018	1.050

The deflections for the live load conditions to be checked for each case are computed as follows:

- One lane Loaded:

$$1.2\left[1.33(0.414)\right] = 0.661\,\text{in.}$$
$$1.2\left[0.431 + 0.25\left[1.33(0.414)\right]\right] = 0.682\,\text{in.} \quad (\text{controls})$$

- Two Lanes Loaded:

$$1.0\left[1.33(0.758)\right] = 1.008 \text{ in.}$$
$$1.0\left[0.782 + 0.25\left[1.33(0.758)\right]\right] = 1.034 \text{ in.} \quad (\text{controls})$$

- Three Lanes Loaded:

$$0.85\left[1.33(1.018)\right] = 1.151 \text{ in.}$$
$$0.85\left[1.050 + 0.25\left[1.33(1.018)\right]\right] = 1.180 \text{ in.} \quad (\text{controls})$$

The largest live load deflection is for the case of two lanes loaded = 1.180 inches.

The suggested live-load deflection limit for a vehicular load is Span/800 (*AASHTO LRFD* Article 2.5.2.6.2). Therefore,

$$\Delta_{ALLOW} = \frac{203.23(12)}{800} = 3.048 \text{ in.} > 1.181 \text{ in.}$$

ok (Ratio = 0.387)

5.9.2.2.2 Permanent Deformations

AASHTO LRFD Article 6.10.4.2 contains criteria intended to control objectionable permanent deformations due to expected severe traffic loadings that would impair rideability (Section 3.2.4.3). *AASHTO LRFD* Article 6.10.4.2.1 specifies that these checks are to be made under the Service II load combination specified in *AASHTO LRFD* Table 3.4.1-1 (Section 1.3.3).

5.9.2.2.2.1 Flange Stresses

According to *AASHTO LRFD* Article 6.11.4, flange stresses due to the Service II loads are limited as specified in *AASHTO LRFD* Article 6.10.4.2.2 to control permanent deformations in box sections at the service limit state, with the following exceptions: 1) the f_ℓ term in *AASHTO LRFD* Equation 6.10.4.2.2-2 (Equation 3.2.31) is to be taken as zero, and 2) *AASHTO LRFD* Equation 6.10.4.2.2-3 (Equation 3.2.32) does not apply. Therefore, the specified stress checks reduce to the following (Section 3.2.4.3.3.1):

For the top and bottom steel flange (Equation 3.2.42):

$$f_f \le 0.95 R_h F_{yf}$$

Under the load combinations specified in *AASHTO LRFD* Table 3.4.1-1, Equation 3.2.42 need only be checked for compact sections in positive flexure as indicated in *AASHTO LRFD* Article C6.11.4. Composite sections in positive flexure in all horizontally curved-girder systems must be treated as noncompact sections at the

strength limit state according to *AASHTO LRFD* Article 6.11.6.2.2. Although not currently stated in the specifications, consideration should also be given to treating all composite sections in positive flexure in straight-girder bridges whose supports are skewed more than 20° from normal as noncompact sections. Thus, for all sections in negative flexure and for noncompact sections in positive flexure, Equation 3.2.42 does not control and need not be checked under the load combinations specified in *AASHTO LRFD* Table 3.4.1-1. Thus, they are not demonstrated in this example.

5.9.2.2.2.2 Web Bend Buckling

AASHTO LRFD Article 6.11.4 specifies that except for composite sections in positive flexure in which the web satisfies the requirement of *AASHTO LRFD* Article 6.11.2.1.2 (i.e. $D/t_w \leq 150$ – no longitudinal web stiffeners), web bend buckling of all sections under the Service II load combination is to be checked as follows (Sections 3.2.4.3.3.2 and 3.2.4.3.2.2 - Equation 3.2.33):

$$f_c \leq F_{crw}$$

The web depth, D, and the depth of the web in compression, D_c, should each be measured along the web slope in computing the web bend-buckling resistance, F_{crw}, from Equation 3.2.35 for sections with inclined webs; that is, the vertical web depth in each case must be divided by $\cos\theta$, where θ is the angle of inclination of the web plate with respect to the vertical. At sections where access holes are present in the box flange, f_c should be computed using section properties calculated assuming the area of the access hole is subtracted from the box-flange area.

Determine the nominal web bend-buckling resistance, F_{crw}, of G2 at Pier 1, and at the bottom-flange transition in Span 1 immediately adjacent to Pier 1 (Figure 5.2.3 – Part A) according to the provisions of *AASHTO LRFD* Article 6.10.1.9.1 as follows (Equation 3.2.35):

$$F_{crw} = \frac{0.9Ek}{\left(\frac{D}{t_w}\right)^2}$$

but not to exceed the smaller of $R_h F_{yc}$ and $F_{yw}/0.7$, where (Equation 3.2.36):

$$k = \frac{9}{(D_c/D)^2}$$

Calculate the compression flange vertical bending stresses in the section at Pier 1 (Figure 5.2.7) under the Service II load combination. The load modifier η is always

taken as 1.0 at the service limit state. The unfactored vertical bending moments from the 3D analysis (Table 5.2.2), and the section moduli to the bottom flange and to the top of the deck are given as follows (note that live load moments include centrifugal force and dynamic load allowance effects):

- Pier 1:

M_{DC1}	=	-14,259 kip-ft
M_{DC2}	=	-1,985 kip-ft
M_{DW}	=	-2,150 kip-ft
M_{-LL+IM}	=	-7,758 kip-ft
S_{steel}	=	11,417 $in.^3$
$S_{3n\ deck+rebar}$	=	12,973 $in.^3$
$S_{n\ deck+rebar}$	=	13,938 $in.^3$
$S_{n\ top\ of\ deck}$	=	-27,924 $in.^3$

According to *AASHTO LRFD* Article 6.10.4.2.1, for members with shear connectors provided throughout their entire length that also satisfy the provisions of Article 6.10.1.7 (regarding the provision of the minimum one percent longitudinal reinforcement in the deck), the concrete deck may be assumed to be effective for both positive and negative flexure provided that the corresponding longitudinal tensile stresses in the concrete deck at the section under consideration are smaller than $2f_r$, where f_r is the lower-bound modulus of rupture of the concrete specified in *AASHTO LRFD* Article 5.4.2.6.

According to *AASHTO LRFD* Article 6.10.1.1.1d, the longitudinal flexural stresses in the deck due to all permanent and transient loads are to be computed using the short-term modular ratio, n. The calculated stress on the transformed section is to be divided by n to obtain the stress in the concrete. The modulus of rupture of the concrete was computed earlier in Section 5.2.9.1.5 to be f_r = 0.509 ksi. Calculate the longitudinal tensile stress in the deck due to the Service II load combination at Pier 1 (note the deck is not subject to stress due to DC_1 loads):

- Pier 1:

$$f_{deck} = 1.0\left[\frac{1.0(-1{,}985) + 1.0(-2{,}150) + 1.3(-7.758)}{-27{,}924(7.5)}\right]12 = +0.815 \text{ ksi}$$

$$0.815 \text{ ksi} < 2f_r = 2(0.509) = 1.02 \text{ ksi}$$

Therefore, stresses at Pier 1 are computed assuming the concrete deck is effective in tension (Figure 5.2.7). The longitudinal reinforcement is considered to be effective in tension.

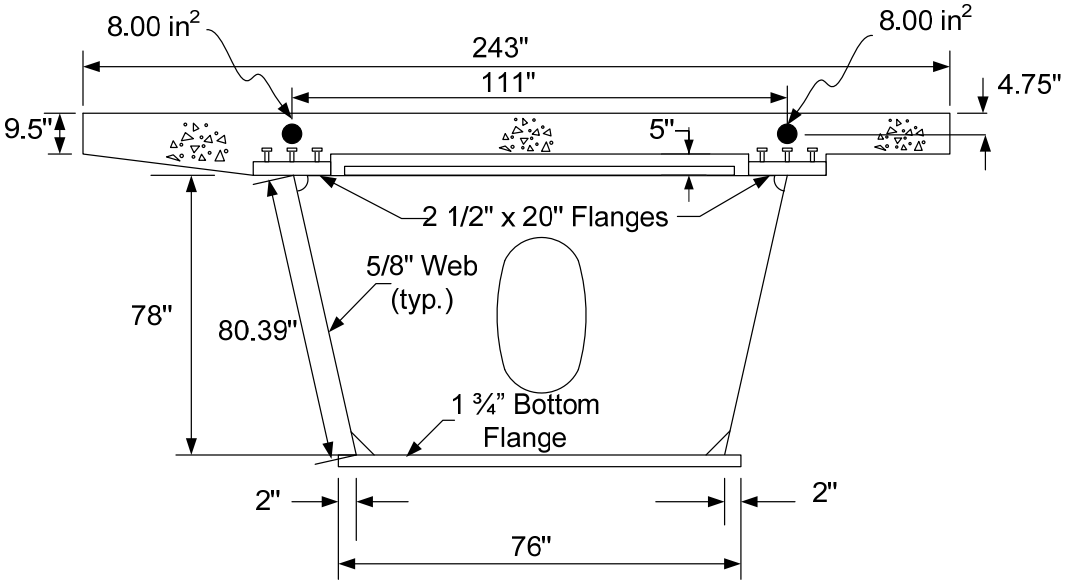


Figure 5.2.7 G2 Section at Pier 1 for Service Limit State Checks

The compressive vertical bending stress in the bottom flange under the Service II load combination is computed as follows:

- Pier 1:

$$f_c = 1.0\left[\frac{1.0(-14{,}259)}{11{,}417} + \frac{1.0(-1{,}985)}{12{,}973} + \frac{1.0(-2{,}150)}{12{,}973} + \frac{1.3(-7{,}758)}{13{,}938}\right]12 = -27.50 \text{ ksi}$$

Calculate F_{crw} at Pier 1. According to *AASHTO LRFD* Article D6.3.1 (*AASHTO LRFD* Appendix D6), for composite sections in negative flexure at the service limit state where the concrete deck is considered effective in tension for computing flexural stresses on the composite section, the depth of the web in compression in the elastic range D_c is to be computed from *AASHTO LRFD* Equation D6.3.1-1 as follows (Equation 3.2.41):

$$D_c = \left(\frac{-f_c}{|f_c| + f_t}\right)d - t_{fc} \geq 0$$

This equation recognizes the beneficial effect of the dead-load stress on the location of the neutral axis of the composite section (including the concrete deck) in regions of negative flexure.

From separate calculations similar to the above assuming the deck is effective in tension, f_t at Pier 1 under the Service II load combination is equal to +22.93 ksi.

Therefore:

$$D_c = \left(\frac{-(-27.50)}{|-27.50| + 22.93} \right) 82.25 - 1.75 = 43.10 / \cos 14^\circ = 44.42 \text{ in.} > 0 \quad \text{ok}$$

$$k = \frac{9}{(44.42/80.39)^2} = 29.48$$

$$F_{crw} = \frac{0.9(29{,}000)(29.48)}{\left(\frac{80.39}{0.625}\right)^2} = 46.51 \text{ ksi} < \min\left(R_h F_{yc}, F_{yw}/0.7\right) = R_h F_{yc} = 1.0(50) = 50 \text{ ksi} \quad \text{ok}$$

$$f_c = |-27.50| \text{ ksi} < 46.51 \text{ ksi}$$

ok (Ratio = 0.591)

5.9.2.2.3 Concrete Deck

AASHTO LRFD Article 6.10.1.7 requires that the minimum one-percent longitudinal reinforcement be present in the concrete deck wherever the longitudinal tensile stress in the deck due to the factored construction loads *and* due to the Service II load combination exceeds ϕf_r (Section 3.2.4.4). Earlier computations in Section 5.9.2.1.5 showed that the factored construction loads did not control this check in Span 3.

Check the tensile stress in the concrete deck due to the Service II load combination at the section 31.0 feet into Span 3 from Pier 2. The unfactored vertical bending moments (Table 5.2.2) and section modulus to the top of the deck at this location are given as follows:

M_{DC2} = -578 kip-ft
M_{DW} = -584 kip-ft
M_{-LL+IM} = -4,550 kip-ft
$S_{n \text{ top of deck}}$ = -24,462 in.^{3}

$$f_{deck} = \frac{1.0[1.0(-578) + 1.0(-584) + 1.3(-4.550)](12)}{-24{,}462(7.5)} = +0.463 \text{ ksi}$$

$$> \phi f_r = 0.90 f_r = 0.458 \text{ ksi}$$

Therefore, terminate the minimum one-percent longitudinal reinforcement approximately 32.0 feet from Pier 2 into Span 3 (measured along the box centerline).

5.2.9.3 Fatigue Limit State Verifications

5.2.9.3.1 General

Fatigue of the base metal at the internal connection-plate welds to the flanges of G2 at the cross-frame in Span 3 located approximately 66.67 feet from Pier 2 (measured along the centerline of the tub) is checked in Section 5.2.9.3.3. Load-induced fatigue limit state verifications are discussed in Section 3.2.5.2.2.

AASHTO LRFD Article 6.10.5.1 specifies that the stress range due to major-axis bending plus lateral flange bending must be investigated, where applicable, for horizontally curved bridges. Lateral bending is not a consideration for box flanges; thus, for the connection-plate welds to the bottom flange, the stress range due to lateral flange bending may be ignored. For the connection-plate welds to the top flange, the stress range due to lateral flange bending also may be ignored as the flange is continuously braced.

AASHTO LRFD Article 6.11.5 specifies that both longitudinal warping stresses and transverse bending stresses due to cross-section distortion be considered at the fatigue limit state for box sections in horizontally curved bridges (Section 3.2.5.2.2.3). Fatigue checks for these distortional stresses are illustrated in Section 5.2.9.3.5.

The vertical bending stress range and torque range due to the fatigue live load (Section 1.3.2.3.3) modified by the corresponding dynamic load allowance of 15 percent will be used to make these checks. The fatigue-load moments and torques used to compute these ranges are taken from the 3D analysis.

5.2.9.3.2 Single-Lane Average Daily Truck Traffic

From *AASHTO LRFD* Article 3.6.1.4.2, the single-lane average daily truck traffic $(ADTT)_{SL}$ is determined as (Equation 3.2.53):

$$(\text{ADTT})_{\text{SL}} = p * \text{ADTT}$$

For a 3-lane bridge, p is equal to 0.80 (Table 3.2.8). Therefore:

$$(\text{ADTT})_{\text{SL}} = 0.80 * 1{,}250 = 1{,}000 \text{ trucks/day}$$

5.2.9.3.3 Design Verifications for Flexure

According to *AASHTO LRFD* Article 6.6.1.2.1, for flexural members with shear connectors provided throughout their entire length and with concrete deck reinforcement satisfying the provisions of *AASHTO LRFD* Article 6.10.1.7, flexural

stresses and stress ranges applied to the composite section at the fatigue limit state may be computed assuming the concrete deck to be effective for both positive and negative flexure.

Shear connectors must be provided along the entire length of the girder in horizontally curved tub-girder bridges (*AASHTO LRFD* Articles 6.10.10.1 and 6.11.10). Earlier computations made in Sections 5.2.9.1.5 and 5.9.2.2.3 ensure that the longitudinal concrete deck reinforcement satisfies the provisions of *AASHTO LRFD* Article 6.10.1.7. Hence, the concrete deck will be assumed effective in computing all stresses and stress ranges applied to the composite section in the following fatigue calculations.

5.2.9.3.3.1 Top-Flange Connection Plate Welds

Check fatigue of the base metal at the connection-plate welds to the top flanges of G2 at the cross-frame in Span 3 located approximately 66.67 feet from Pier 2 (Figure 5.2.8).

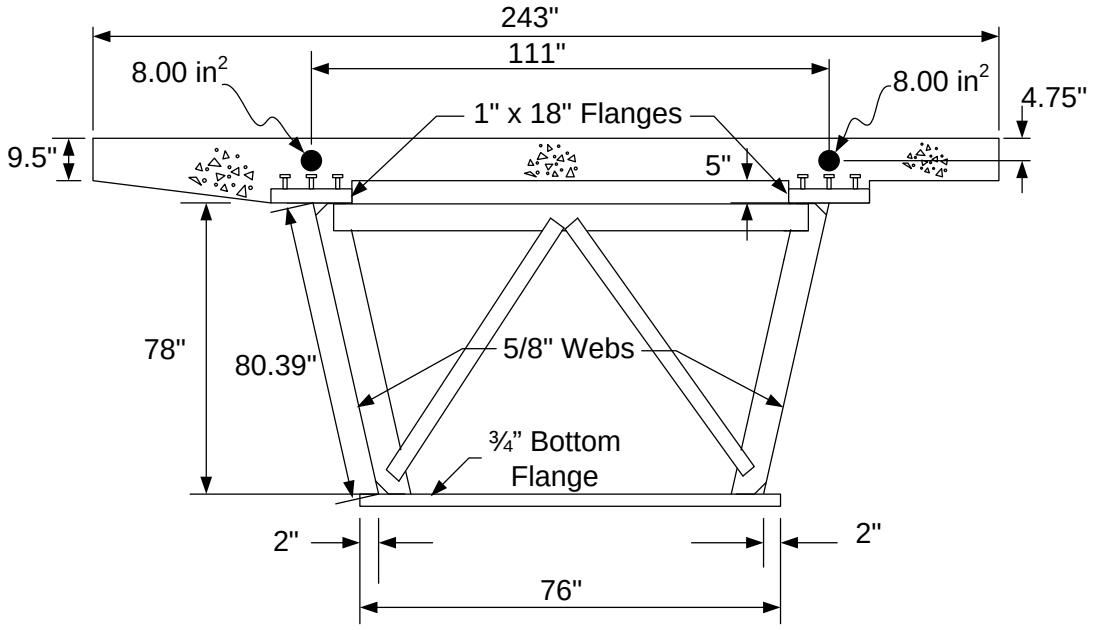


Figure 5.2.8 G2, Span 3, Section at a Cross-Frame 66.67 Feet from Pier 2

The provisions of *AASHTO LRFD* Article 6.6.1.2 apply only to details subject to a net applied tensile stress. According to *AASHTO LRFD* Article 6.6.1.2.1, in regions where the unfactored permanent loads produce compression, fatigue is to be considered only if this compressive stress is less than the maximum tensile stress resulting from the Fatigue I load combination (γ = 1.5). This determination is based on the Fatigue I load combination because this is the largest stress range a detail is expected to experience often enough to propagate a crack. When the tensile component of the stress range cycle resulting from this load combination exceeds the compressive stress due to the unfactored permanent loads, there is a net tensile

stress in the component or at the detail under consideration and fatigue must be considered.

Otherwise, the stress cycle is compression-compression and a fatigue crack will not propagate. In this example, the effect of the future wearing surface will be conservatively ignored when determining if a detail is subject to a net applied tensile stress.

The unfactored vertical bending moments due to the DC_1 and DC_2 loads at the cross-frame under consideration (Table 5.2.2), and corresponding moments of inertia and distances from the neutral axis to the top of the web are given as follows:

M_{DC1} = +365 kip-ft
M_{DC2} = +459 kip-ft
I_{steel} = 201,500 in.^{4}
$y_{top\ of\ web}$ = -42.13 in.
$I_{3n\ deck}$ = 384,332 in.^{4}
$y_{top\ of\ web}$ = -24.46 in.

The unfactored permanent loads produce compression at the top of the web at this location. The total unfactored permanent-load compressive vertical bending stress at the top-flange welds at this location (neglecting the future wearing surface) is computed as:

$$f_{DC_1} = \frac{365(12)(-42.13)}{201{,}500} = -0.92 \text{ ksi}$$

$$f_{DC_2} = \frac{459(12)(-24.46)}{384{,}332} = -0.35 \text{ ksi}$$

$$\Sigma = -1.27 \text{ ksi}$$

The unfactored negative fatigue load moment (including the 15 percent dynamic load allowance and centrifugal force effects) at the cross-frame under consideration (Table 5.2.2), and the corresponding moment of inertia and distance from the neutral axis to the top of the web are given as follows:

M_{-LL+IM} = -537 kip-ft
$I_{n\ deck}$ = 528,681 in.^{4}
$y_{top\ of\ web}$ = -10.60 in.

The maximum tensile stress at the top-flange welds at this location due to the negative moment caused by the factored fatigue load (factored by the 1.5 load factor specified for the Fatigue I load combination) is:

$$f_{LL+IM} = \frac{1.5(-537)(12)(-10.60)}{528{,}681} = +0.19 \text{ ksi}$$

$$\left|-1.27\right| \text{ ksi} > +0.19 \text{ ksi}$$

The distortional longitudinal warping stress is ignored since the top flange is continuously braced. Therefore, fatigue of the base metal at the connection-plate welds to the top flanges at this location need not be checked.

5.2.9.3.3.2 Bottom-Flange Connection Plate Welds

By inspection, the base metal at the connection-plate welds to the bottom flange of G2 at this location is subject to a net applied tensile stress. Therefore, fatigue must be considered.

Determine the fatigue detail category from *AASHTO LRFD* Table 6.6.1.2.3-1. Under the condition of fillet-welded stiffener connections with welds normal to the direction of stress, the fatigue detail category for base metal at transverse stiffener-to-flange fillet welds is Category C′ (Condition 4.1).

AASHTO LRFD Table 6.6.1.2.3-2 (Table 3.2.9) shows the values of $(ADTT)_{SL}$ for each fatigue detail category above which the infinite life check governs. The values in the table assume a 75-year design life and one stress cycle *n* per truck passage.

For continuous spans with span lengths greater than 40.0 feet, the number of stress cycles per truck passage *n* is equal to 1.0 at sections away from the pier (*AASHTO LRFD* Table 6.6.1.2.5-2). Sections ′away from the pier′ are defined as sections greater than a distance of one-tenth the span on each side of the interior support. For other values of *n*, *AASHTO LRFD* Table 6.6.1.2.3-2 should be modified by dividing the values in the table by *n*.

From Table 3.2.9, the 75-year $(ADTT)_{SL}$ equivalent to infinite fatigue life for a Category C′ detail is 745 trucks per day < 1,000 trucks per day. The detail must therefore be checked for infinite life using the Fatigue I load combination (γ = 1.5). In the infinite life region, the nominal fatigue resistance is equal to the constant-amplitude fatigue threshold as follows (Equation 3.2.50):

$$(\Delta F)_n = (\Delta F)_{TH}$$

For a Category C′ detail, $(\Delta F)_{TH}$ = 12.0 ksi (*AASHTO LRFD* Table 6.6.1.2.5-3 – Table 3.2.6). Therefore:

$$(\Delta F)_n = 12.00 \text{ ksi}$$

The unfactored positive fatigue load moment (including the 15 percent dynamic load allowance and centrifugal force effects) at the cross-frame under consideration

(Table 5.2.2), and the corresponding moment of inertia and distance from the neutral axis to the bottom of the web are given as follows:

M_{+LL+IM} = +1,221 kip-ft
$I_{n\ deck}$ = 528,681 in.^{4}
$y_{bot\ of\ web}$ = +67.40 in.

The major-axis bending stress range, $\gamma(\Delta f)$, at the connection-plate weld due to the factored fatigue load (factored by the specified 1.5 load factor for the Fatigue I load combination) is computed using the properties of the short-term composite section as:

$$\gamma(\Delta f) = \frac{1.5(1{,}221)(12)(67.40)}{528{,}681} + \frac{1.5|-537|(12)(67.40)}{528{,}681} = 4.03\ \text{ksi}$$

The distortional longitudinal warping stress range of at the bottom corner of the box, computed below in Section 5.2.9.3.5, is included. The longitudinal warping stresses are assumed additive to the longitudinal vertical bending stresses. The calculated longitudinal warping stress range of 0.78 ksi in the cross-frame panel adjacent to Abutment 1 will be conservatively applied here. Therefore:

$$\gamma(\Delta f)_{tot} = 4.03 + 0.78 = 4.81\ \text{ksi}$$

According to *AASHTO LRFD* Equation 6.6.1.2.2-1, $\gamma(\Delta f)_{tot}$ must not exceed the nominal fatigue resistance $(\Delta F)_n$ (Equation 3.2.54). Both the resistance factor, ϕ, and load modifier, η, are specified to be 1.0 at the fatigue limit state (*AASHTO LRFD* Article C6.6.1.2.2).

$$\gamma(\Delta f) \le (\Delta F)_n$$

$$4.81\ \text{ksi} < 12.0\ \text{ksi}$$

ok (Ratio = 0.401)

5.2.9.3.4 Design Verifications for Shear

As specified in *AASHTO LRFD* Article 6.10.5.3, interior panels of stiffened webs must satisfy the following requirement (Section 3.2.5.2.2.2 – Equation 3.2.55):

$$V_u \le V_{cr}$$

The factored fatigue load for this check is to be determined using the Fatigue I load combination (*AASHTO LRFD* Table 3.4.1-1), with the fatigue live load taken as

specified in *AASHTO LRFD* Article 3.6.1.4. The fatigue live load is modified by the dynamic load allowance of 15 percent (with centrifugal force effects considered).

The live load shear for this check is intended to represent the shear due to the heaviest truck expected to cross the bridge over its 75-year fatigue design life. Satisfaction of the preceding equation is intended to control elastic flexing of the web so that the member is assumed able to sustain an infinite number of smaller loadings without fatigue cracking due to this effect.

Only the interior panels of stiffened webs are checked because the shear resistance of the end panel of stiffened webs and the shear resistance of unstiffened webs are already limited to the shear buckling resistance at the strength limit state.

Inclined webs must again be designed for the component of the vertical shear in the plane of the critical web, V_{ui}, taken equal to V_u divided by $\cos\theta$, where θ is the angle of inclination of the web plate with respect to the vertical (see Equation 3.2.153). Also, in computing the shear-yielding or shear-buckling resistance, V_{cr}, for the case of inclined webs, the web depth, *D,* must be taken as the depth of the web measured along the slope or $D/\cos\theta$.

For this example, the panel in G2 immediately to the left of Pier 1 (in Span 1) will be checked. The shear buckling resistance, V_{cr}, of this 162.3-inch-long panel was computed previously to be 500 kips (Section 5.2.9.1.4).

The unfactored permanent load shears and fatigue live load shear (including the dynamic load allowance and centrifugal force effects) at Pier 1 from the 3D analysis to be used in this check are as follows (Table 5.2.3):

V_{DC1} = -200 kips
V_{DC2} = -45 kips
V_{DW} = -32 kips
V_{-LL+IM} = -55 kips

Therefore:

$$V_u = -200 + (-45) + (-32) + 1.5(-55) = -360 \text{ kips}$$

$$|V_u| = |-360| \text{ kips} < V_{cr} = 500 \text{ kips} \quad \text{ok}$$

$$(\text{Ratio} = 0.720)$$

5.2.9.3.5 Cross-Section Distortion Stresses

When box sections are subject to torsion, the cross-section becomes distorted giving rise to secondary bending stresses. Loading the opposite side of a box produces reversal of these secondary distortional bending stresses. Therefore, in horizontally curved bridges and in straight or curved bridges resting on skewed supports,

distortional stresses must be considered when checking fatigue. Although the stresses might be thought of as “distortion-induced”, they are calculable and are treated herein as load-induced.

AASHTO LRFD Article 6.11.5 requires that the stress range due to longitudinal warping be considered in checking the fatigue resistance of the base metal at all details on the box section; the longitudinal warping stresses are generally assumed to be additive to the longitudinal vertical bending stresses. This assumption is conservative since the critical longitudinal warping stresses are usually produced by eccentric live loads, whereas the critical vertical bending stresses are produced by more centrally located live load positions

AASHTO LRFD Article 6.11.5 also requires for these cases that the transverse bending stress range be investigated in the base metal adjacent to flange-to-web fillet welds and adjacent to the termination of fillet welds connecting transverse elements to webs and box flanges. This investigation is separate from the fatigue check for longitudinal stress ranges in the box. The condition at welded transverse elements is usually the critical case for transverse bending. Transverse bending stresses are typically most critical for cases where the St. Venant torques are significant, e.g. boxes resting on skewed supports, single box sections and sharply curved boxes.

Consideration might be given to ignoring the distortional stresses in certain cases if it can be demonstrated that the torques are of comparable magnitude to the torques for cases where research has shown that these stresses are small enough to be neglected; i.e. if the torques are deemed small enough in the judgment of the Owner and the Design Engineer. In such cases, however, it is strongly recommended that all web stiffeners be attached to both flanges in order to enhance fatigue performance.

AASHTO LRFD Article C6.11.1.1 states that the distortional stresses are best computed using the beam-on-elastic foundation (BEF) analogy, which is utilized in the calculations given below. Further information on cross-section distortional stresses and the BEF Analogy may be found in Section 3.2.5.2.2.3 (the equations utilized below may be found in this section).

It is assumed for this example that all transverse stiffeners are attached to both the top and bottom flanges of the tub. Transverse stiffeners attached to the top and bottom flanges significantly reduce the sharp through-thickness bending that would otherwise occur due to cross-section distortion in the unstiffened portions of the web at the termination of the stiffener-to-web welds. Connection plates are required to be attached to the flanges for this reason.

The critical unfactored torques due to the fatigue load specified in *AASHTO LRFD* Article 3.6.1.4 (i.e. a 72-kip HS20 truck with a constant rear-axle spacing of 30 feet) placed in a single lane, including the 15 percent dynamic load allowance and

centrifugal force effects, at the first transverse stiffener on the outer web of G2 adjacent to Abutment 1 in Span 1 located 120.6 inches from Abutment 1 are as follows:

$+T_{LL+IM}$ = +297 kip-ft
$-T_{LL+IM}$ = -111 kip-ft

Therefore, the total range of torque is $297 + |-111| = 408$ kip – ft.

This range is produced by placing the fatigue truck in two different transverse positions on opposite sides of the tub section (representing two trucks crossing the bridge in separate lanes with one vehicle leading the other), and is larger than the range produced by a single passage of the fatigue load in this case. Therefore, to account for the fact that two separate positions of the truck are required to cause the critical range of torque, a factor of 0.75 is applied to this range, as specified in *AASHTO LRFD* Article 6.11.5.

A stress concentration occurs at the termination of the transverse stiffener welds to the flanges as a result of the transverse bending due to cross-section distortion. The fatigue resistance of this detail when subject to transverse bending is not currently quantified. As recommended in *AASHTO LRFD* Article C6.11.5, fatigue detail Category E should be assumed for computing the nominal fatigue resistance.

Assume the number of stress cycles per truck passage in this region, *n*, is equal to 1.0. The single-lane average daily truck traffic $(ADTT)_{SL}$ is 1,000 trucks/day (Section 5.2.9.3.2). According to *AASHTO LRFD* Table C6.6.1.2.5-1 (Table 3.2.9), since the $(ADTT)_{SL}$ does not exceed the 75-year $(ADTT)_{SL}$ equivalent to infinite life of 3,545 trucks/day for a Category E detail with *n* equal to 1.0, the nominal fatigue resistance, $(\Delta F)_n$, is computed based on finite life as follows (Equation 3.2.51):

$$(\Delta F)_n = \left(\frac{A}{N}\right)^{\frac{1}{3}}$$

The detail category constant *A* for a Category E detail is taken as 11.0 x 10^8 ksi^3 from *AASHTO LRFD* Table 6.6.1.2.5-1 (Table 3.2.7). The number of stress cycles, *N*, is computed as follows (Equation 3.2.52):

$$N = (365)(75)n(ADTT)_{SL}$$

$$N = (365)(75)(1.0)(1{,}000) = 27.4 \times 10^6 \text{ cycles}$$

Therefore:

$$(\Delta F)_n = \left(\frac{11.0 \times 10^8}{27.4 \times 10^6}\right)^{\frac{1}{3}} = 3.42 \text{ ksi}$$

The Fatigue II load combination in *AASHTO LRFD* Table 3.4.1-1 is to be used in the finite life region. The load factor for the Fatigue II load combination is 0.75. Therefore:

$$T_{range} = 408 \text{ kip} - \text{ft} * 0.75 * 0.75 = 230 \text{ kip} - \text{ft} = 2{,}760 \text{ kip} - \text{in.}$$

Calculate the transverse flexural rigidities, D_a and D_b, of the concrete deck and unstiffened bottom box flange, respectively. The modulus of elasticity, E_c, of the concrete is 3,865 ksi (Section 5.2.9.1.5). The Poisson's ratio, μ, is taken as 0.2 for the concrete and 0.3 for the steel. Therefore, from Equations 3.2.58 and 3.2.59:

$$D_a = \frac{Et_a^3}{12(1-\mu^2)} = \frac{3{,}865(9.5)^3}{12\left(1-0.2^2\right)} = 287{,}652 \text{ k} - \text{in.}^2/\text{in.}$$

$$D_b = \frac{Et_b^3}{12(1-\mu^2)} = \frac{29{,}000(0.75)^3}{12\left(1-0.3^2\right)} = 1{,}120 \text{ k} - \text{in.}^2/\text{in.}$$

Calculate the transverse flexural rigidity, D_c, of the stiffened web from Equation 3.2.61. The transverse stiffener will be considered effective in resisting the transverse bending. First, calculate the effective width of the web plate d_o acting with the transverse stiffener (Figure 5.2.9) from Equation 3.2.62. For the web plate, $h = c$ = 78/cos 14° = 80.39 in. The transverse stiffener is assumed to be a 5/8″ x 6″ bar on one side of the web. The larger stiffener spacing in this web panel equal to 28.833(566.25/561.625)(12) – 120.6 = 228.2 inches will be used for d.

$$d_o = \frac{d\tanh\left(5.6\frac{d}{h}\right)}{\frac{5.6d}{h}\left(1-\mu^2\right)} = \frac{228.2\tanh\left[5.6\left(\frac{228.2}{80.39}\right)\right]}{\frac{5.6(228.2)}{80.39}\left(1-0.3^2\right)} = 15.8 \text{ in.}$$

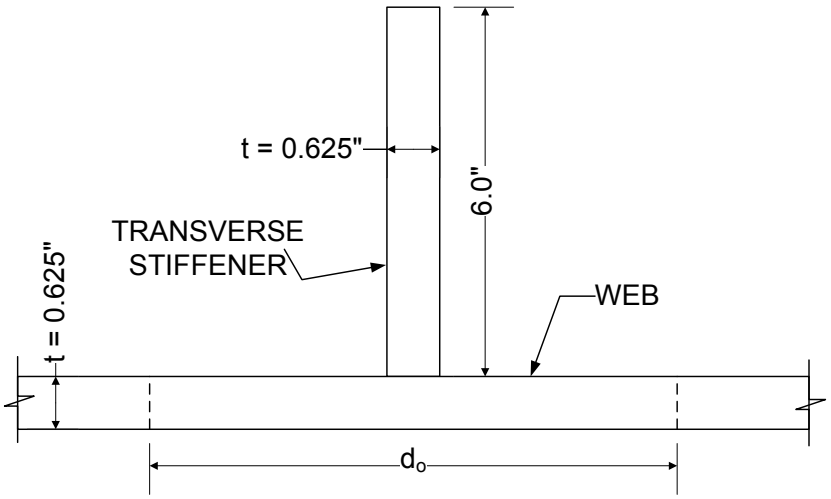


Figure 5.2.9 Effective Width of Web Acting with Transverse Stiffener

Compute the location of the neutral axis of the effective section from the outer web face.

Area of the stiffener =	6.0 * 0.625	=	3.75 in.^{2}
Area of effective web=	15.8 * 0.625	=	9.88 in.^{2}
			13.63 in.^{2}

$$\text{N.A.} = \frac{3.75(0.625 + 6.0/2) + 9.88(0.625/2)}{13.63} = 1.224 \text{ in.}$$

Calculate the moment of inertia I_s of the effective stiffened web plate for transverse bending, including the transverse stiffener:

$$I_s = \frac{1}{12}(0.625)(6.0)^3 + 3.75(6.0/2 + 0.625 - 1.224)^2 + 9.88(0.625/2 - 1.224)^2 + \frac{1}{12}(15.8)(0.625)^3 = 41.40 \text{ in.}^4$$

$$D_c = \frac{EI_s}{d} = \frac{29{,}000(41.40)}{228.2} = 5{,}261 \text{ kip} - \text{in.}^2/\text{in.}$$

Compute the compatibility shear, *v*, at the center of the bottom box flange (Equation 3.2.57):

$$v = \frac{\frac{1}{D_c}\left[(2a+b)abc\right] + \frac{1}{D_a}\left[ba^3\right]}{(a+b)\left\{\frac{a^3}{D_a} + \frac{2c\left(a^2+ab+b^2\right)}{D_c} + \frac{b^3}{D_b}\right\}}$$

$$v = \frac{\frac{1}{5{,}261}\left[(2*111+72)(111*72*80.39)\right] + \frac{1}{287{,}652}\left(72*111^3\right)}{(111+72)\left\{\frac{111^3}{287{,}652} + \frac{2*80.39\left(111^2+111*72+72^2\right)}{5{,}261} + \frac{72^3}{1{,}120}\right\}} = 0.177$$

Calculate the box distortion per kip per inch of load, δ_1, assuming no cross-bracing is present (Equation 3.2.56):

$$\delta_1 = \frac{ab}{24(a+b)}\left\{\frac{c}{D_c}\left[\frac{2ab}{a+b} - v(2a+b)\right] + \frac{a^2}{D_a}\left[\frac{b}{a+b} - v\right]\right\}$$

$$\delta_1 = \frac{111*72}{24(111+72)}\left\{\frac{80.39}{5{,}261}\left[\frac{2*111*72}{111+72} - 0.177(2*111+72)\right] + \frac{111^2}{287{,}652}\left(\frac{72}{111+72} - 0.177\right)\right\}$$

$$= 0.998 \text{ in.}^2/\text{kip}$$

Compute the BEF stiffness parameter, β, from Equation 3.2.63. The *n*-composite moment of inertia, *I,* of the composite box section at this stiffener is 528,681 in.^{4} The cross-frame spacing, ℓ, is 28.833 feet:

$$\beta = \left(\frac{1}{EI\delta_1}\right)^{\frac{1}{4}} = \left(\frac{1}{29{,}000*528{,}681*0.998}\right)^{\frac{1}{4}} = 0.00284 \text{ in.}^{-1}$$

$$\beta\ell = 0.00284(28.833)(12) = 0.983$$

The transverse bending stress range at the top and bottom corners of the tub section may be computed as follows (Equation 3.2.67):

$$\sigma_t = C_t F_d \beta \frac{1}{2a} T_{range}$$

First, compute the section modulus, *S*, per unit length of the stiffened web (including the transverse stiffener). In the following equation, *y* is the distance from the neutral

axis to the extreme fiber of the section consisting of the transverse stiffener and the effective portion of the web plate and *d* is the transverse stiffener spacing.

$$S = \frac{I_s}{yd} = \frac{41.40}{(6.0 + 0.625 - 1.224)(228.2)} = 0.034 \text{ in.}^3/\text{in.}$$

Compute the section modulus, *S*, per unit length of the unstiffened portions of the web, which by inspection is more critical than the unstiffened bottom box flange:

$$S = \frac{1}{6}(1)(0.625)^2 = 0.065 \text{ in.}^3/\text{in.}$$

Because of the relatively large stiffener spacing in this case, *S* of the stiffened web is less than *S* of the unstiffened web, which must be the lower bound. Therefore, the effect of the stiffener will be conservatively ignored in resisting transverse bending in this case and *S* of the unstiffened web will be used in computing the stresses.

For the bottom corner of the box, the transverse bending stress in the web due to the applied torque, F_d, is computed as follows (Equation 3.2.68):

$$F_d = \frac{bv}{2S}$$

$$F_d = \frac{72(0.177)}{2(0.065)} = 98 \text{ in.}^{-1}$$

For the top corner of the box, the transverse bending stress in the web due to the applied torque, F_d, is computed as follows (Equation 3.2.69):

$$F_d = \frac{a}{2S}\left(\frac{b}{a+b} - v\right)$$

$$F_d = \frac{111}{2(0.065)}\left(\frac{72}{111+72} - 0.177\right) = 185 \text{ in.}^{-1}$$

The stress at the top corner of the box controls.

Obtain the BEF factor, C_t, for distortional transverse bending stress. The transverse stiffener will be assumed at mid-panel with the torques conservatively assumed applied at mid-panel. This is the most critical case if one visualizes the analogous deflection of a beam on an elastic foundation. Therefore, C_t will be obtained from the graph given in Figure 3.2.30. If desired, greater precision could be obtained for an actual condition different from that assumed by interpolating between the appropriate graphs.

First, calculate the deformation of the internal bracing member δ_b due to the applied torque (Equation 3.2.65):

$$\delta_b = \frac{2(1+a/b)}{\sqrt{1+\left[\frac{a+b}{2h}\right]^2}}\delta_1$$

$$\delta_b = \frac{2(1+111/72)}{\sqrt{1+\left[\frac{111+72}{2(78.0)}\right]^2}}(0.998) = 3.29 \text{ in.}^2/\text{kip}$$

Calculate the cross-bracing stiffness ratio, q, from Equation 3.2.64. The area of one diagonal, A_b, in the internal K-brace is equal to 6.94 in.^{2} and the length of the diagonal, L_b, is equal to 85.9 in. Assume the bracing member has been designed to be effective in compression; therefore, the full area may be used for A_b.

$$q = \left[\frac{E_b A_b}{L_b \ell \delta_1}\right]\delta_b^2$$

$$q = \left[\frac{29{,}000(6.94)}{85.9(28.833)(12)(0.998)}\right](3.29)^2 = 73.4$$

From the graph in Figure 2.68, for q = 73.4 and $\beta\ell$ = 0.983 (as computed previously), C_t is approximately equal to 0.14. Therefore:

$$\sigma_t = 0.14(185)(0.00284)\left(\frac{1}{2(111)}\right)(2{,}760) = 0.91 \text{ ksi} < (\Delta F)_n = 3.42 \text{ ksi} \quad \text{ok}$$

If necessary, the transverse bending stress could be reduced by decreasing the cross-frame spacing and/or increasing the thickness of the web plate.

The longitudinal warping stress range at the top and bottom corners of the tub section due to cross-section distortion may be computed as follows (Equation 3.2.66):

$$\sigma_{dw} = \frac{C_w y}{I\beta a} T_{range}$$

Obtain the BEF factor, C_w, for distortional longitudinal warping stress. Again, the transverse stiffener will be assumed at mid-panel with the torques conservatively

assumed applied at mid-panel. Therefore, C_w will be obtained from the graph given in Figure 3.2.28. From the graph for q = 73.4 and $\beta\ell$ = 0.983 (as computed previously), C_w is approximately equal to 0.7. Therefore:

$$\sigma_{dw\ top} = \frac{0.7(10.60)}{528{,}681(0.00284)(111)}(2{,}760) = 0.12 \text{ ksi}$$

$$\sigma_{dw\ bot} = \frac{0.7(67.40)}{528{,}861(0.00284)(111)}(2{,}760) = 0.78 \text{ ksi}$$

The longitudinal warping stress range at the bottom of the box is considered in checking the fatigue resistance of the base metal at the connection plate welds to the bottom flange in Section 5.2.9.3.3.2.

5.2.9.4 Strength Limit State Verifications

5.2.9.4.1 Negative Flexure

Strength limit state verifications for box sections subject to negative flexure are discussed in Section 3.2.6.4.2. *AASHTO LRFD* Article 6.11.6.2.3 specifies that for closed-box and tub sections subject to negative flexure at the strength limit state, the provisions of *AASHTO LRFD* Article 6.11.8 are to be applied. The provisions of *AASHTO LRFD* Article 6.11.8 limit the nominal flexural resistance to always be less than or equal to the moment at first yield *for all types of box girder bridges*. Therefore, the nominal flexural resistance for these sections is always expressed in terms of the elastically computed flange stress. Further, according to *AASHTO LRFD* Article 6.11.6.2.3, the optional provisions of *AASHTO LRFD* Appendices A6 and B6 are *not* to be applied to box sections.

AASHTO LRFD Article 6.11.8.1.1 specifies that for box sections subject to negative flexure, box flanges in compression (i.e. bottom flanges) must satisfy the following requirement at the strength limit state (Equation 3.2.109):

$$f_{bu} \le \phi_f F_{nc}$$

Equation 3.2.109 is intended to ensure that box flanges in compression have sufficient local buckling resistance. Flange lateral bending and lateral-torsional buckling are not a consideration for box flanges. Longitudinal warping stresses are typically ignored at the strength limit state, as permitted in *AASHTO LRFD* Article 6.11.1.1.

In general, bottom box flanges at interior-pier sections are subject to biaxial bending due to vertical bending of the box section and due to vertical bending of the internal diaphragm over the bearing sole plate. Bending of the internal diaphragm over the bearing sole plate may be particularly significant for boxes supported on single bearings. The flange is also subject to shear stresses due to the vertical shear in the

internal diaphragm, and in cases where it must be considered, the St. Venant torsional shear. Thus, for cases where the bending of the internal diaphragm and/or the flange shear stresses are deemed significant, *AASHTO LRFD* Article C6.11.8.1.1 suggests that the following equation be used to check the combined stress state in the box flange at interior-pier sections at the strength limit state (Equation 3.2.110):

$$\sqrt{f_{bu}^2 - f_{bu}f_{by} + f_{by}^2 + 3(f_d + f_v)^2} \le \phi_f R_b R_h F_{yc}$$

f_{bu} and f_{by} are to be taken as signed quantities in Equation 3.2.110. In calculating f_d and also f_{by}, a portion of the box flange may be considered effective with the internal diaphragm. *AASHTO LRFD* Article C6.11.8.1.1 currently suggests that a flange width equal to six times its thickness may be considered effective with the internal diaphragm. Further, whenever an access hole is provided within the internal diaphragm for inspection purposes, the effect of the hole should be considered in computing the section properties of the effective diaphragm section.

AASHTO LRFD Article 6.11.8.1.2 specifies that for box sections subject to negative flexure, continuously braced flanges in tension (i.e. top flanges) must satisfy the following requirement at the strength limit state (Equation 3.2.130):

$$f_{bu} \le \phi_f F_{nt}$$

A continuously braced flange is defined as a flange encased in concrete or anchored by shear connectors. Lateral flange bending stresses and St. Venant torsional shears need not be considered for continuously braced top flanges of tub sections. The torsional shear must be considered in the continuously braced top flange of a closed-box section however

5.2.9.4.1.1 Section at Pier 1 in G2

Assemble the factored stresses for the Strength I load combination needed to check the preceding equations for the section at Pier 1 in G2 (Figure 5.2.7). The Strength IV load combination does not control by inspection. In this example, the load modifier, η, is taken equal to 1.0 at the strength limit state.

The unfactored vertical bending moments at Pier 1 in G2 from the 3D analysis (Table 5.2.2), and the section moduli to the top and bottom flanges are given as follows (note that the live load moment includes centrifugal force and dynamic load allowance effects):

M_{DC1} = -14,259 kip-ft
M_{DC2} = -1,985 kip-ft
M_{DW} = -2,150 kip-ft

M_{-LL+IM} = -7,758 kip-ft
$S_{steel\ (top)}$ = -9,614 in.^{3}
$S_{steel\ (bot)}$ = 11,417 in.^{3}
$S_{steel+rebar\ (top)}$ = -11,114 in.^{3}
$S_{steel+rebar\ (bot)}$ = 11,785 in.^{3} (D_c = 38.17 in.)

The factored vertical bending stresses in the top and bottom flanges at Pier 1 in G4 are computed as follows:

- Top flange:

$$f_{bu} = 1.0\left[\frac{1.25(-14{,}259)}{-9{,}614} + \frac{1.25(-1{,}985)}{-11{,}114} + \frac{1.5(-2{,}150)}{-11{,}114} + \frac{1.75(-7{,}758)}{-11{,}114}\right]12 = +43.07 \text{ ksi}$$

- Bottom flange:

$$f_{bu} = 1.0\left[\frac{1.25(-14{,}259)}{11{,}417} + \frac{1.25(-1{,}985)}{11{,}785} + \frac{1.5(-2{,}150)}{11{,}785} + \frac{1.75(-7{,}758)}{11{,}785}\right]12 = -38.37 \text{ ksi}$$

Calculate the factored St. Venant torsional shear stress, f_v, in the bottom flange for the Strength I load combination. f_v is determined by dividing the St. Venant torsional shear flow by the thickness of the box flange (Equation 3.2.117).

As indicated in *AASHTO LRFD* Article C6.11.1.1, for the DC_1 torque, which is applied to the non-composite section, the enclosed area, A_o, is computed for the non-composite box section. The vertical depth between the mid-thickness of the flanges is used. The top lateral bracing is assumed connected to the top flanges so that a reduction in A_o is not required. Therefore:

$$A_o = \frac{(111+72)}{2} * (78.0 + 0.875 + 1.25) * \frac{1\,\text{ft}^2}{144\,\text{in.}^2} = 50.9\,\text{ft}^2$$

Separate calculations indicate that the torques at the left end of Span 2 control at Pier 1. The positive live load plus impact torque also controls. The torques are as follows (Table 5.2.4):

T_{DC1} = -102 kip-ft
T_{DC2} = +213 kip-ft
T_{DW} = +13 kip-ft
T_{-LL+IM} = +808 kip-ft

Note that the minimum load factor, γ_p, from *AASHTO LRFD* Table 3.4.1-2 and a load modifier, $1/\eta$ (≤ 1.0), are applied to the DC_1 torque since it is opposite in sign to the other torques.

$$f_v = \frac{T}{2A_o t_{fc}}$$

$$f_v = \frac{(1/1.0)(0.90)(-102)}{2(50.9)(1.75)} * \frac{1}{12\ \text{in./ft}} = -0.043\ \text{ksi}$$

For the torques applied to the composite section, calculate A_o for the composite section from the mid-thickness of the bottom flange to the mid-thickness of the concrete deck (considering the deck haunch):

$$A_o = \frac{(111+72)}{2} * (78.0 + 0.875 + 5.0 + \frac{9.5}{2}) * \frac{1\,\text{ft}^2}{144\ \text{in.}^2} = 56.3\ \text{ft}^2$$

$$f_v = \frac{1.0\left|1.25(213) + 1.5(13) + 1.75(808)\right|}{2(56.3)(1.75)} * \frac{1}{12\ \text{in./ft}} = 0.719\ \text{ksi}$$

$$f_{v\ \text{total}} = -0.043 + 0.719 = 0.676\ \text{ksi}$$

Check that $f_{v\ total}$ does not exceed the factored torsional shear resistance of the flange, F_{vr} (Equation 3.2.71):

$$F_{vr} = 0.75\phi_v \frac{F_{yf}}{\sqrt{3}}$$

$$F_{vr} = 0.75(1.0)\frac{50}{\sqrt{3}} = 21.65\ \text{ksi} > f_{v\ \text{total}} = 0.676\ \text{ksi} \quad \text{ok}$$

Nominal Flexural Resistance – Bottom Flange

Calculate the nominal flexural resistance, F_{nc}, of the bottom (compression) flange based on local buckling as follows (Section 3.2.6.4.2.2):

Calculate the local buckling resistance of the bottom flange of G2 at Pier 1 according to the provisions of *AASHTO LRFD* Article 6.11.8.2.2.

For an unstiffened flange, the resistance is to be determined based on the flange width b_{fc}, which is taken as the distance between webs.

$$b_{fc} = 72.0 - 0.625 = 71.375\ \text{in.}$$

Determine the slenderness ratio of the flange:

$$\lambda_f = \frac{b_{fc}}{t_{fc}} = \frac{71.375}{1.75} = 40.8$$

From Equation 3.2.116:

$$\Delta = \sqrt{1 - 3\left(\frac{f_v}{F_{yc}}\right)^2}$$

$$\Delta = \sqrt{1 - 3\left(\frac{0.676}{50}\right)^2} \cong 1.0$$

To determine which equation to use, first calculate R_1 (Equation 3.2.119):

$$R_1 = \frac{0.57}{\sqrt{\frac{1}{2}\left[\Delta + \sqrt{\Delta^2 + 4\left(\frac{f_v}{F_{yc}}\right)^2\left(\frac{k}{k_s}\right)^2}\right]}}$$

For unstiffened flanges, k = 4.0 and k_s = 5.34 according to *AASHTO LRFD* Article 6.11.8.2.2. Upon substituting these values and the previously computed values of Δ and f_v into the preceding equation, the denominator of the equation is approximately equal to 1.0. Therefore, R_1 = 0.57.

$$R_1\sqrt{\frac{kE}{F_{yc}}} = 0.57\sqrt{\frac{4.0(29{,}000)}{50}} = 27.5$$

Calculate R_2 (Equation 3.2.120):

$$R_2 = \frac{1.23}{\sqrt{\frac{1}{1.2}\left[\frac{F_{yr}}{F_{yc}} + \sqrt{\left(\frac{F_{yr}}{F_{yc}}\right)^2 + 4\left(\frac{f_v}{F_{yc}}\right)^2\left(\frac{k}{k_s}\right)^2}\right]}}$$

From Equation 3.2.118:

$$F_{yr} = (\Delta - 0.4)F_{yc} \le F_{yw}$$

$$F_{yr} = (1.0 - 0.4)50 = 30.0 \text{ ksi}$$

Upon substituting F_{yr}, k, k_s, Δ and f_v into the preceding equation, the denominator of the equation is again approximately equal to 1.0. Therefore, R_2 = 1.23.

$$R_2\sqrt{\frac{kE}{F_{yc}}} = 1.23\sqrt{\frac{4.0(29{,}000)}{50}} = 59.2$$

Since 27.5 < λ_f = 40.8 < 59.2, then (Equation 3.2.113):

$$F_{nc} = R_b R_h F_{yc}\left[\Delta - \left(\Delta - \frac{F_{yr}}{R_h F_{yc}}\right)\left\{1 - \sin\left[\frac{\pi}{2}\left(\frac{R_2 - \frac{b_{fc}}{t_{fc}}\sqrt{\frac{F_{yc}}{kE}}}{R_2 - R_1}\right)\right]\right\}\right]$$

For a homogeneous girder, the hybrid factor R_h (Section 3.2.6.3) is equal to 1.0. Calculate the web load-shedding factor R_b (Section 3.2.6.2). First, determine if R_b is indeed less than 1.0 by checking *AASHTO LRFD* Equation 6.10.1.10.2-2 as follows. For composite sections in negative flexure, the elastic depth of the web in compression, D_c, at the strength limit state is to conservatively be computed for the section consisting of the steel girder plus the longitudinal reinforcement (*AASHTO LRFD* Article D6.3.1). Also, for box sections with inclined webs, D_c must be measured along the web slope. Therefore:

$$\frac{2D_c}{t_w} = \frac{2(38.17)/\cos 14^\circ}{0.625} = \frac{2(39.34)}{0.625} = 125.9$$

$$\frac{2D_c}{t_w} < \lambda_{rw} = 5.7\sqrt{\frac{E}{F_{yc}}} = 5.7\sqrt{\frac{29{,}000}{50}} = 137.3$$

Therefore, the section is not subject to web bend-buckling at elastic stress levels at the strength limit state and R_b is taken equal to 1.0.

$$F_{nc} = 1.0(1.0)(50)\left[1.0 - \left(1.0 - \frac{30.0}{1.0(50)}\right)\left\{1 - \sin\left[\frac{\pi}{2}\left(\frac{1.23 - (40.8)\sqrt{\frac{50}{4.0(29{,}000)}}}{1.23 - 0.57}\right)\right]\right\}\right] = 45.81\,\text{ksi}$$

Calculate the nominal flexural resistance F_{nt} of the top (tension) flanges. According to *AASHTO LRFD* Article 6.11.8.3, the nominal flexural resistance, F_{nt}, of the tension flanges of tub sections in regions of negative flexure is to be taken as:

$$F_{nt} = R_h F_{yt}$$

Therefore:

$$F_{nt} = 1.0(50) = 50\ \text{ksi}$$

Flange Verifications

With all the required information now assembled, check the flanges of G2 at Pier 1.

Check the bottom flange (Equation 3.2.109):

$$f_{bu} \le \phi_f F_{nc}$$

$$\phi_f F_{nc} = 1.0(45.81) = 45.81\,\text{ksi}$$
$$\left|-38.37\right|\ \text{ksi} < 45.81\,\text{ksi} \qquad \text{ok} \qquad (\text{Ratio} = 0.838)$$

The tub rests on a single bearing. Check the combined stress state in the box flange at Pier 1 in G2 at the strength limit state for the flange acting in combination with the internal diaphragm as follows (Equation 3.2.110):

$$\sqrt{f_{bu}^2 - f_{bu}f_{by} + f_{by}^2 + 3(f_d + f_v)^2} \le \phi_f R_b R_h F_{yc}$$

The internal diaphragm at Pier 1 is assumed for this check to be a 1-1/4-inch-thick A 709 Grade 50W plate with a 1" x 14" top flange. The vertical depth of the plate is 78 inches. An 18-inch wide by 36-inch deep access hole is provided in the diaphragm. The bottom edge of the hole is 16 inches from the bottom of the plate (Figure 5.2.10).

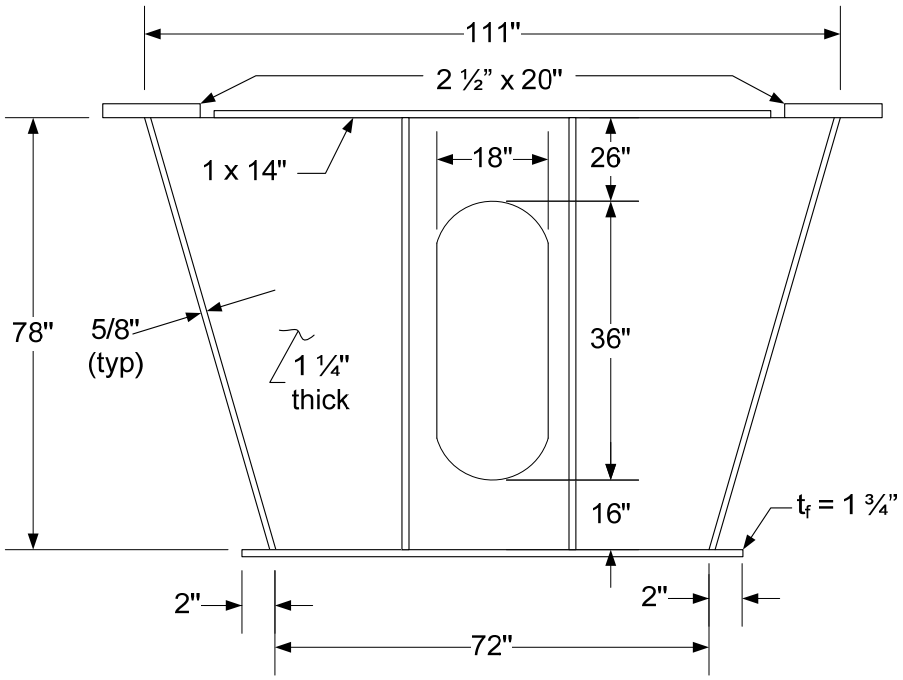


Figure 5.2.10 Internal Diaphragm at Pier 1

Compute the total maximum factored vertical shear in the left and right side of the diaphragm. A 3D analysis of the bridge including a refined model of the internal diaphragm at Pier 1 (including the access hole and bearing stiffeners) was conducted. From this analysis, the following values were determined for the unfactored vertical shear in the left and right side of the diaphragm (on either side of the access hole):

	Left Side	Right Side
Steel:	V = +101 kips	V = -92 kips
Deck(+):	V = +264 kips	V = -264 kips
DC_2:	V = +81 kips	V = -21 kips
DW:	V = +56 kips	V = -55 kips
+LL+IM:	V = +240 kips	V = +19 kips
-LL+IM:	V = -15 kips	V = -233 kips

The negative live load shear is governed by the special negative moment loading case (i.e. 90 percent of two design trucks plus 90 percent of the design lane load plus impact).

The largest total factored vertical shear on the left side of the diaphragm under the Strength I load combination (including the effect of the St. Venant torsional shear) is computed as (the load modifier, η, is taken equal to 1.0):

$$V_{left} = 1.0\left[1.25(101 + 264 + 81) + 1.5(56) + 1.75(240)\right] = +1{,}061 \text{ kips}$$

The largest total factored shear on the right side of the diaphragm is computed as:

$$V_{right} = 1.0\left[1.25(-92 + -264 + -21) + 1.5(-55) + 1.75(-233)\right] = -961 \text{ kips}$$

Although the tub rests on a single bearing, the overall torsional effect on the diaphragm at Pier 1 is relatively small due to the presence of the external diaphragm between the tubs.

Assume a strip of the bottom box flange equal to 6 times its thickness (i.e. 6.0 * 1.75 in. = 10.5 in.) acts with the diaphragm in resisting the diaphragm shear and in resisting major-axis bending of the diaphragm over the bearing sole plate (*AASHTO LRFD* Article C6.11.8.1.1).

Calculate the section properties of the effective section through the center of the access hole for resisting bending. There is significant shear lag around the access hole and plane sections through the hole do not remain plane. Although the material above the hole is effective in bending, it will be conservatively ignored in the calculation of the section properties of the section composed of the bottom flange and the diaphragm below the hole:

Component	A	d	Ad	Ad^2	I_o	I
Web – below hole	20.00	26.00	-520	13,520	427	13,947
Bot. Flange 1-3/4" x 10.5"	18.38	34.88	-641	22,361	4.69	22,366
	38.38		-1,161			36,313
					$-30.25(1{,}161) =$	$-35{,}120$
					$I_{NA} =$	$1{,}193 \text{ in.}^4$

$$d_s = \frac{-1{,}161}{38.38} = -30.25 \text{ in.}$$

$$d_{BOT\ OF\ HOLE} = 17.75 - 5.50 = 12.25 \text{ in.} \qquad d_{BOT\ OF\ FLANGE} = 35.75 - 30.25 = 5.50$$

$$S_{BOT\ OF\ HOLE} = \frac{1{,}193}{12.25} = 97.4 \text{ in.}^3 \qquad S_{BOT\ OF\ FLANGE} = \frac{1{,}193}{5.50} = 217 \text{ in.}^3$$

The first moment, *Q*, of one-half the effective box-flange area about the neutral axis of the effective internal diaphragm section is computed as:

$$Q = \frac{1}{2}(10.5)(1.75)(5.50 - 0.875) = 42.5 \text{ in.}^3$$

The shear stress in the flange is a maximum at the diaphragm and assumed to be zero at each edge of the effective flange (with a linear distribution assumed in-

between); thus, one-half of the flange width must be used to calculate the first moment, *Q*.

The maximum shear stress, f_d, in the box flange caused by the internal diaphragm vertical shear is therefore (Equation 3.2.111):

$$f_d = \frac{VQ}{It_{fc}}$$

$$f_d = \frac{1{,}061(42.5)}{1{,}193(1.75)} = 21.60 \text{ ksi}$$

Calculate the stress in the flange due to major-axis bending of the diaphragm over the bearing sole plate f_{by}. Assume the reaction acts over a one-foot width across the box. The moment due to the factored flexural shear in the section composed of a portion of the flange and diaphragm is taken about a section 6 inches from the centerline of the flange at the assumed bearing. The shear is assumed acting at a point midway between the edge of the access hole and the web, i.e. it is assumed that the shear in the web has been transferred into the diaphragm plate.

$$M = 1{,}061 \text{ kips}[12 \text{ in.} + 27/2 \text{ in.} - 6 \text{ in.}] = -20{,}689 \text{ kip} - \text{in}$$

Although the material above the hole was not included in the section properties above, it forms a couple with the material below the hole to resist the moment. It should be noted that the composite section was ignored for simplicity. In fact, some portion of the deck acts with the diaphragm for the superimposed dead load and live load. This action, in fact, increases the moment resisted in this manner from that computed herein since the tension force in the top includes the deck acting with the diaphragm.

From the refined analysis, the largest average factored bending stress in the material above the hole according to the Strength I load combination is 4.94 ksi. Multiplying this stress by the area of material above the hole = 26(1.25) + 14(1.0) = 46.5 in.^{2} gives a force of 229.7 kips. The distance between the centroids of the top and bottom diaphragm material (including the flanges) is 17.8 + 36.0 + 16.0 + 1.75 – 5.50 = 66.0 inches. Hence, the moment carried by the contribution of this couple is:

$$M = 229.7 \text{ kips} * 66.0 \text{ in.} = 15{,}160 \text{ k} - \text{in.}$$

This moment carried by the couple represents approximately 73 percent of the moment due to the factored shear in this case.

The remaining portion of the moment is assumed resisted by the section below the access hole. Therefore:

$$M = -20{,}689 + 15{,}160 = -5{,}529 \text{ kip} - \text{in.}$$

The transverse bending stress due to the remaining moment in the box flange is computed as:

$$f_b = \frac{-5{,}529 \text{ kip} - \text{in.}}{217 \text{ in.}^3} = -25.48 \text{ ksi}$$

The bending stress at the bottom of the access hole is computed as:

$$f_b = \frac{\left|-5{,}529\right| \text{ kip} - \text{in.}}{97.4 \text{ in.}^3} = 56.76 \text{ ksi}$$

The couple results in an axial compressive stress on the effective section below the access hole. The compressive force, P_c, due to the couple is computed as:

$$P_c = 229.7 / 38.38 = -5.98 \text{ ksi}$$

Therefore, to maintain equilibrium, the stress f_{by} in the box flange caused by vertical bending of the internal diaphragm over the bearing sole plate is computed as:

$$f_{by} = -25.48 \text{ ksi} + 5.98 \text{ ksi} = -19.50 \text{ ksi}$$

The stress at the bottom of the access hole is computed as:

$$f_b = 56.76 \text{ ksi} + 5.98 = 62.74 \text{ ksi}$$

Reinforcement in the form of a horizontal stiffener (flange) at the bottom of the access hole should be considered in this case to reduce the stress, and/or the depth of the material below the hole could be increased.

The total factored St. Venant torsional shear stress, f_v, in the box flange was computed above to be 0.676 ksi. Therefore:

$$\sqrt{(-38.37)^2 - (-38.37)(-19.50) + (-19.50)^2 + 3(21.60 + 0.676)^2} = 50.92 \text{ ksi}$$

$$\phi_f R_b R_h F_{yc} = 1.0(1.0)(1.0)(50) = 50.00 \text{ ksi}$$

50.00 ksi < 50.92 ksi ok (Ratio = 1.018)

Confirm the preceding calculation using the following alternative form of the Huber-von Mises-Hencky yield criterion (Equation 3.3.69):

$$\sqrt{\sigma_1^2 - \sigma_1\sigma_2 + \sigma_2^2} \le \phi_f R_b R_h F_{yc}$$

where:

σ_1, σ_2 = maximum and minimum principal stresses in the bottom flange (ksi)

$$= \left(\frac{f_{bu} + f_{by}}{2}\right) \pm \sqrt{\left(\frac{f_{bu} - f_{by}}{2}\right)^2 + (f_d + f_v)^2}$$

$$\sigma_{1,2} = \left(\frac{-38.37 + -19.50}{2}\right) \pm \sqrt{\left(\frac{-38.37 - (-19.50)}{2}\right)^2 + (21.60 + 0.676)^2} = -53.13, -4.74 \text{ ksi}$$

$$\sqrt{(-53.13)^2 - [(-53.13)(-4.74)] + (-4.74)^2} = 50.92 \text{ ksi} > \phi_f R_b R_h F_{yc} = 50.00 \text{ ksi}$$

There is a slight overstress in this case, but it is acceptable given the numerous conservative assumptions that were made in this calculation.

Check the top flange of G2 at Pier 1 (Equation 3.2.130):

$$f_{bu} \le \phi_f F_{nt}$$

$\phi_f F_{nt} = 1.0(50) = 50.00$ ksi

43.07 ksi $<$ 50.00 ksi ok (Ratio $= 0.861$)

5.2.9.4.1.2 Section Adjacent to the Field Splice in Span 1 of G2

At the section adjacent to the field splice in Span 1 of G2 located 93′-0″ from Abutment 1 (Figure 5.2.8 minus the cross-frame), the section is subject to stress reversal. Thus, the 3/4″ unstiffened box flange on one side of the field splice is subject to compression. A check of the compressive resistance of the box flange at this section is made.

The unfactored vertical bending moments at the field splice in Span 1 of G2 from the 3D analysis (Table 5.2.2), and the section moduli to the top and bottom flanges are given as follows (note that the live load moment includes centrifugal force and dynamic load allowance effects):

M_{DC1} = +1,950 kip-ft
M_{DC2} = +249 kip-ft
M_{DW} = +335 kip-ft
M_{-LL+IM} = -2,926 kip-ft
$S_{steel\ (bot)}$ = 5,503 in.^{3}

$S_{steel+rebar\ (bot)}$ = 5,961 in.^{3} (D_c = 39.74 in.)

The factored vertical bending stress in the bottom flange at this section is computed as follows. By inspection, it is apparent that the compressive vertical bending stress in the concrete deck due to the DC_2/DW moments is overcome by the tensile vertical bending stress in the deck due to the negative live load moment plus impact. Therefore, for combination with the negative live load plus impact vertical bending stress, the stresses due to the positive DC_2/DW moments will be computed using the section properties for the steel girder plus the longitudinal reinforcement (Section 3.2.6.6). Also, in the following, the minimum load factors, γ_p, from *AASHTO LRFD* Table 3.4.1-2 and a load modifier, $1/\eta$ (≤1.0), are applied to the permanent loads since the corresponding stresses are of opposite sign to the live load plus impact stress:

- Bottom flange:

$$f_{bu} = (1/1.0)\left[\frac{0.90(+1{,}950)}{5{,}503} + \frac{0.90(+249)}{5{,}961} + \frac{0.65(+335)}{5{,}961} + \frac{1.75(-2{,}926)}{5{,}961}\right]12 = -5.59 \text{ ksi}$$

Calculate the factored St. Venant torsional shear stress, f_v, in the bottom flange for the Strength I load combination.

For the DC_1 torque, which is applied to the non-composite section, the enclosed area, A_o, is computed for the non-composite box section. The vertical depth between the mid-thickness of the flanges is used. Therefore:

$$A_o = \frac{(111+72)}{2} * (78.0 + 0.375 + 0.5) * \frac{1\,\text{ft}^2}{144\,\text{in.}^2} = 50.1\,\text{ft}^2$$

The torques at this section are as follows:

T_{DC1} = -207 kip-ft
T_{DC2} = -51 kip-ft
T_{DW} = -39 kip-ft
T_{-LL+IM} = -537 kip-ft

$$f_v = \frac{T}{2A_o t_{fc}}$$

$$f_v = \frac{1.0(1.25)(-207)}{2(50.1)(0.75)} * \frac{1}{12\,\text{in./ft}} = -0.29 \text{ ksi}$$

For the torques applied to the composite section, calculate A_o for the composite section from the mid-thickness of the bottom flange to the mid-thickness of the concrete deck (considering the deck haunch):

$$A_o = \frac{(111+72)}{2} * (78.0 + 0.375 + 5.0 + \frac{9.5}{2}) * \frac{1\,ft^2}{144\,in.^2} = 56.0\ ft^2$$

$$f_v = \frac{1.0\left|1.25(-51) + 1.5(-39) + 1.75(-537)\right|}{2(56.0)(0.75)} * \frac{1}{12\,in./ft} = -1.05\ ksi$$

$$f_{v\ total} = -0.29 + -1.05 = -1.34\ ksi$$

Check that $f_{v\ total}$ does not exceed the factored torsional shear resistance of the flange, F_{vr} (Equation 3.2.71):

$$F_{vr} = 0.75\phi_v \frac{F_{yf}}{\sqrt{3}}$$

$$F_{vr} = 0.75(1.0)\frac{50}{\sqrt{3}} = 21.65\ ksi > f_{v\ total} = \left|-1.34\right|\ ksi \quad \text{ok}$$

Nominal Flexural Resistance – Bottom Flange

Calculate the nominal flexural resistance, F_{nc}, of the bottom (compression) flange based on local buckling as follows (Section 3.2.6.4.2.2):

Determine the slenderness ratio of the flange:

$$\lambda_f = \frac{b_{fc}}{t_{fc}} = \frac{71.375}{0.75} = 95.2$$

From Equation 3.2.116:

$$\Delta = \sqrt{1 - 3\left(\frac{\left|-1.34\right|}{50}\right)^2} \cong 1.0$$

Calculate R_2 (Equation 3.2.120):

$$R_2 = \frac{1.23}{\sqrt{\frac{1}{1.2}\left[\frac{F_{yr}}{F_{yc}} + \sqrt{\left(\frac{F_{yr}}{F_{yc}}\right)^2 + 4\left(\frac{f_v}{F_{yc}}\right)^2\left(\frac{k}{k_s}\right)^2}\right]}}$$

From Equation 3.2.118:

$$F_{yr} = (\Delta - 0.4)F_{yc} \le F_{yw}$$

$$F_{yr} = (1.0 - 0.4)50 = 30.0 \text{ ksi}$$

Upon substituting F_{yr}, k, k_s, Δ and f_v into the preceding equation, the denominator of the equation is again approximately equal to 1.0. Therefore, R_2 = 1.23.

$$R_2\sqrt{\frac{kE}{F_{yc}}} = 1.23\sqrt{\frac{4.0(29{,}000)}{50}} = 59.2$$

Since λ_f = 95.2 > 59.2, then (Equation 3.2.114):

$$F_{nc} = \frac{0.9ER_bk}{\left(\frac{b_{fc}}{t_{fc}}\right)^2} - \frac{R_bf_v^2k}{0.9Ek_s^2}\left(\frac{b_{fc}}{t_{fc}}\right)^2$$

Calculate the web load-shedding factor R_b:

$$\frac{2D_c}{t_w} = \frac{2(39.74)/\cos 14^\circ}{0.625} = \frac{2(40.96)}{0.625} = 131.1$$

$$\frac{2D_c}{t_w} < \lambda_{rw} = 5.7\sqrt{\frac{E}{F_{yc}}} = 5.7\sqrt{\frac{29{,}000}{50}} = 137.3$$

Therefore, the section is not subject to web bend-buckling at elastic stress levels at the strength limit state and R_b is taken equal to 1.0.

$$F_{nc} = \frac{0.9(29{,}000)(1.0)(4.0)}{(95.2)^2} - \frac{1.0(-1.34)^2(4.0)}{0.9(29{,}000)(5.34)^2}(95.2)^2 = 11.43 \text{ ksi}$$

Flange Verifications

With all the required information now assembled, check the ¾" unstiffened bottom flange of G2 adjacent to the field splice in Span 1.

Check the bottom flange (Equation 3.2.109):

$$f_{bu} \le \phi_f F_{nc}$$

$$\phi_f F_{nc} = 1.0(11.43) = 11.43 \text{ ksi}$$
$$\left|-5.59\right| \text{ ksi} < 11.43 \text{ ksi} \qquad \text{ok} \qquad (\text{Ratio} = 0.489)$$

5.2.9.4.2 Positive Flexure

Strength limit state verifications for box sections subject to positive flexure are discussed in Section 3.2.6.5.3. According to *AASHTO LRFD* Article 6.11.6.2.2, at the strength limit state, composite sections in positive flexure in horizontally curved steel girder bridges are to be considered as noncompact sections designed according to the requirements of *AASHTO LRFD* Article 6.11.7.2. For noncompact sections, the nominal flexural resistance is not permitted to exceed the moment at first yield. The nominal flexural resistance in these cases is therefore more appropriately expressed in terms of the elastically computed flange stress.

Longitudinal warping stresses are typically ignored at the strength limit state, as permitted in *AASHTO LRFD* Article 6.11.1.1. St. Venant torsion and cross-section distortion stresses must be considered, however, for noncompact sections.

AASHTO LRFD Article 6.11.7.2.1 specifies that at the strength limit state, the (top) compression flange(s) of noncompact composite box sections in positive flexure must satisfy the following (Equation 3.2.139):

$$f_{bu} \le \phi_f F_{nc}$$

Flange lateral bending is not considered for the compression flange(s) in Equation 3.2.139 because at the strength limit state, the flange is continuously supported by the concrete deck.

AASHTO LRFD Article 6.11.7.2.1 specifies that at the strength limit state, the (bottom) tension flange of noncompact composite box sections in positive flexure must satisfy the following (Equation 3.2.144):

$$f_{bu} \le \phi_f F_{nt}$$

Lateral bending is not a consideration for the tension flange in Equation 3.2.144 because the tension flange is always a box flange in this case (and lateral bending is not a consideration for box flanges).

5.2.9.4.2.1 Section at 61.27 ft from Abutment 1 in Span 1 of G2

Assemble the factored stresses for the Strength I load combination needed to check the preceding equations at the section located 61.27 feet from Abutment 1 in Span 1 of G2 (Figure 5.2.8 minus the cross-frame). The longitudinal reinforcement is conservatively ignored in the computation of the composite section properties at this section. The Strength IV load combination does not control by inspection. In this example, the load modifier, η, is taken equal to 1.0 at the strength limit state.

The unfactored vertical bending moments at this section from the 3D analysis (Table 5.2.2), and the section moduli to the top and bottom flanges are given as follows (note that the live load moment includes centrifugal force and dynamic load allowance effects):

M_{DC1} = +4,921 kip-ft
M_{DC2} = +659 kip-ft
M_{DW} = +784 kip-ft
M_{-LL+IM} = +5,752 kip-ft
$S_{steel\ (top)}$ = -4,672 in.^{3}
$S_{steel\ (bot)}$ = 5,503 in.^{3}
$S_{3n\ deck\ (top)}$ = -15,096 in.^{3}
$S_{3n\ deck\ (bot)}$ = 7,079 in.^{3}
$S_{n\ deck\ (top)}$ = -45,576 in.^{3}
$S_{n\ deck\ (bot)}$ = 7,758 in.^{3}

The factored vertical bending stresses in the top and bottom flanges at this section are computed as follows:

- Top flange:

$$f_{bu} = 1.0\left[\frac{1.25(4{,}921)}{-4{,}672} + \frac{1.25(659)}{-15{,}096} + \frac{1.5(784)}{-15{,}096} + \frac{1.75(5{,}752)}{-45{,}576}\right]12 = -20.04 \text{ ksi}$$

- Bottom flange:

$$f_{bu} = 1.0\left[\frac{1.25(4{,}921)}{5{,}503} + \frac{1.25(659)}{7{,}079} + \frac{1.5(784)}{7{,}079} + \frac{1.75(5{,}752)}{7{,}758}\right]12 = +32.37 \text{ ksi}$$

Calculate the factored St. Venant torsional shear stress, f_v, in the bottom flange for the Strength I load combination. f_v is determined by dividing the St. Venant torsional shear flow by the thickness of the box flange (Equation 3.2.147).

As indicated in *AASHTO LRFD* Article C6.11.1.1, for the DC_1 torque, which is applied to the non-composite section, the enclosed area, A_o, is computed for the non-composite box section. The vertical depth between the mid-thickness of the flanges is used. The top lateral bracing is assumed connected to the top flanges so that a reduction in A_o is not required. Therefore:

$$A_o = \frac{(111+72)}{2} * (78.0 + 0.375 + 0.5) * \frac{1\,ft^2}{144\,in.^2} = 50.1\,ft^2$$

The torques are as follows (Table 5.2.4). Separate calculations show that the negative live load plus impact torque controls:

T_{DC1} = -203 kip-ft
T_{DC2} = -26 kip-ft
T_{DW} = -15 kip-ft
T_{-LL+IM} = -352 kip-ft

$$f_v = \frac{T}{2A_o t_{ft}}$$

$$f_v = \frac{(1.0)(1.25)(-203)}{2(50.1)(0.75)} * \frac{1}{12\,in./ft} = -0.281\,ksi$$

For the torques applied to the composite section, calculate A_o for the composite section from the mid-thickness of the bottom flange to the mid-thickness of the concrete deck (considering the deck haunch):

$$A_o = \frac{(111+72)}{2} * (78.0 + 0.375 + 5.0 + \frac{9.5}{2}) * \frac{1\,ft^2}{144\,in.^2} = 56.0\,ft^2$$

$$f_v = \frac{1.0\left|1.25(-26) + 1.5(-15) + 1.75(-352)\right|}{2(56.0)(0.75)} * \frac{1}{12\,in./ft} = -0.666\,ksi$$

$$f_{v\,total} = -0.281 + -0.666 = -0.947\,ksi$$

Check that $f_{v\ total}$ does not exceed the factored torsional shear resistance of the flange, F_{vr} (Equation 3.2.71):

$$F_{vr} = 0.75\phi_v \frac{F_{yf}}{\sqrt{3}}$$

$$F_{vr} = 0.75(1.0)\frac{50}{\sqrt{3}} = 21.65 \text{ ksi} > f_{v\ total} = \left|-0.947\right| \text{ ksi} \quad \text{ok}$$

Nominal Flexural Resistance

AASHTO LRFD Article 6.11.7.2.2 specifies that the nominal flexural resistance of the compression flanges of noncompact composite tub sections in positive flexure, F_{nc}, is to be taken as (Equation 3.2.140):

$$F_{nc} = R_b R_h F_{yc}$$

Local and lateral torsional buckling of the tub top flanges is not a concern because the flanges are continuously braced; therefore, the nominal flexural resistance is based on nominal yielding. St. Venant torsional shears are also typically neglected in tub girder top flanges.

Since the section is a homogeneous built-up section, the hybrid factor, R_h (Section 3.2.6.3), is equal to 1.0. According to *AASHTO LRFD* Article 6.10.1.10.2, the web load-shedding factor, R_b (Section 3.2.6.2), is to be taken as 1.0 for composite box sections in positive flexure in which the web satisfies the requirement of *AASHTO LRFD* Article 6.11.2.1.2 such that longitudinal stiffeners are not required (i.e. $D/t_w \leq 150$). Therefore:

$$F_{nc} = 1.0(1.0)(50) = 50.00 \text{ ksi}$$

The nominal flexural resistance of the tension flange of noncompact composite tub sections in positive flexure, F_{nt}, is based on nominal yielding and is to be taken as (Equation 3.2.145):

$$F_{nt} = R_h F_{yt} \Delta$$

From Equation 3.2.146:

$$\Delta = \sqrt{1 - 3\left(\frac{f_v}{F_{yt}}\right)^2}$$

$$\Delta = \sqrt{1 - 3\left(\frac{\left|-0.947\right|}{50}\right)^2} \cong 1.0$$

Therefore:

$$F_{nt} = 1.0(50)(1.0) = 50.00 \text{ ksi}$$

Flange Verifications

With all the required information now assembled, check the top flanges at this section for the requirements of *AASHTO LRFD* Article 6.11.7.2.1 (Equation 3.2.139):

$$f_{bu} \le \phi_f F_{nc}$$

$$\phi_f F_{nc} = 1.0(50.00) = 50.00 \text{ ksi}$$
$$\left|-20.04\right| \text{ ksi} < 50.00 \text{ ksi} \qquad \text{(Ratio = 0.401)}$$

Check the bottom flange (Equation 3.2.144):

$$f_{bu} \le \phi_f F_{nt}$$

$$\phi_f F_{nt} = 1.0(50.00) = 50.00 \text{ ksi}$$
$$32.37 \text{ ksi} < 50.00 \text{ ksi} \quad \text{ok} \qquad \text{(Ratio = 0.647)}$$

Concrete Deck Verifications

Concrete deck verifications in regions of positive flexure are discussed in Section 3.2.6.5.4. According to *AASHTO LRFD* Article 6.11.7.2.1, the maximum longitudinal compressive stress in the concrete deck at the strength limit state is not to exceed $0.6f'_c$ to ensure linear behavior of the concrete (Equation 3.2.148).

As specified in *AASHTO LRFD* Article 6.10.1.1.1d, for calculating the longitudinal flexural stresses in the concrete deck due to all permanent and transient loads, the short-term modular ratio, *n*, is to be used. The section modulus to the top of the concrete deck (based on the *n*-composite section) at this section is –21,063 in.^{3}.

Calculate the factored longitudinal compressive stress in the deck at this section; the deck is not subject to DC_1 loads. The deck concrete has a value of 4.5 ksi for f'_c. The stress in the concrete deck is obtained by dividing the stress acting on the transformed section by *n*.

$$f_{deck} = 1.0\left[\frac{1.25(659)+1.5(784)+1.75(5{,}752)}{-21{,}063(7.5)}\right]12 = -0.917 \text{ ksi}$$

$$\left|-0.917 \text{ ksi}\right| < 0.6f'_c = 0.6(4.5) = 2.70 \text{ ksi}$$
$$\text{ok (Ratio} = 0.340)$$

Noncompact composite sections in positive flexure must also satisfy the following ductility requirement specified in *AASHTO LRFD* Article 6.10.7.3 to protect the concrete deck from premature crushing (Equation 3.2.149):

$$D_p \le 0.42D_t$$

Calculate the location of the neutral axis at the plastic moment M_p (i.e. the PNA) for the composite section. The equations given in *AASHTO LRFD* Table D6.1-1 for I-sections will be applied to one-half of the composite box section. The longitudinal reinforcement will be conservatively neglected. The longitudinal component of the top-flange lateral bracing area will be included. The web depth, *D*, will be taken as the depth measured along the web slope.

$$P_t = F_{yt}b_t t_t = 50(76.0/2)(0.75) = 1{,}425 \text{ kips}$$

$$P_w = F_{yw}Dt_w = 50(80.39)(0.625) = 2{,}512 \text{ kips}$$

$$P_c = F_{yc}b_c t_c + F_y A_d = 50(18.0)(1.0) + 50(5.09) = 1{,}155 \text{ kips}$$

$$P_s = 0.85f'_c b_s t_s = 0.85(4.5)(234.0/2)(9.5) = 4{,}251 \text{ kips}$$

The conditions in *AASHTO LRFD* Table D6.1-1 are to be checked in the order listed. Since $P_t + P_w + P_c = 5{,}092$ kips $> P_c = 4{,}251$ kips, the PNA is in the top flange. Therefore, use Case II in *AASHTO LRFD* Table D6.1-1:

$$\bar{y} = \frac{t_c}{2}\left[\frac{P_w + P_t - P_s}{P_c} + 1\right]$$

$$\bar{y} = \frac{1.0}{2}\left[\frac{2{,}512 + 1{,}425 - 4{,}251}{1{,}155} + 1\right] = 0.364 \text{ in. from the top of the top flanges}$$

Check equilibrium by calculating and comparing the total plastic forces acting on the compression and tension sides of the plastic neutral axis:

- Compression side:

$$4{,}251 + 1{,}155(0.364) = 4{,}671 \text{ kips}$$

- Tension side:

$$1{,}155(1 - 0.364) + 2{,}512 + 1{,}425 = 4{,}671 \text{ kips} \quad \text{ok}$$

$$D_p = 9.5 + 5.0 + 0.364 = 14.86 \text{ in.}$$

$$D_t = 0.75 + 78.0 + 5.0 + 9.5 = 93.25 \text{ in.}$$

$$0.42D_t = 0.42(93.25) = 39.17 \text{ in.} > 14.86 \text{ in.}$$

ok (Ratio = 0.379)

Neither of the preceding concrete deck verifications is likely to control for typical sections utilized in unshored construction. The limit on the longitudinal compressive stress in the deck is unlikely to govern except in cases involving: 1) shored construction, or unshored construction where the noncomposite steel dead load stresses are low, combined with 2) geometries causing the neutral axis of the short-term and long-term composite section to be significantly below the bottom of the concrete deck. The ductility requirement is unlikely to govern for noncompact sections unless sections are utilized in shored construction and/or steels with higher yield strengths (up to 100 ksi) are utilized.

5.2.9.4.3 Shear

5.2.9.4.3.1 General

Strength limit state design for shear is covered in Section 3.2.7. Shear design provisions for box-section flexural members at the strength limit state are covered in *AASHTO LRFD* Article 6.11.9. Webs must satisfy the following at the strength limit state (Equation 3.2.152):

$$V_u \le \phi_v V_n$$

Shear design will be demonstrated for an end panel and for two interior panels located in Span 1 of G2 from the example bridge.

For box sections with inclined webs, the web must be designed for the component of the vertical shear in the plane of the web according to Equation 3.2.153 (Section 3.2.7.1.2). The factored shear, V_u, is to be taken as the sum of the flexural and St. Venant torsional shears. In computing the nominal shear resistance, V_n, and the maximum transverse stiffener spacing requirements for the case of inclined webs, the web depth, *D,* must be taken as the depth of the web measured along the slope or $D/\cos\theta$.

5.2.9.4.3.2 Unstiffened Web

Determine the nominal shear resistance of an unstiffened web according to the provisions of *AASHTO LRFD* Article 6.10.9.2. The nominal shear resistance of an unstiffened web is limited to the shear buckling resistance, V_{cr}, determined as (Equation 3.2.161):

$$V_n = V_{cr} = CV_p$$

C is the ratio of the shear buckling resistance to the shear yield strength determined from *AASHTO LRFD* Equation 6.10.9.3.2-4, 6.10.9.3.2-5 or 6.10.9.3.2-6, as applicable, with the shear buckling coefficient k taken equal to 5.0.

Since:

$$1.40\sqrt{\frac{Ek}{F_{yw}}} = 1.40\sqrt{\frac{29{,}000(5.0)}{50}} = 75.4 < \frac{D}{t_w} = \frac{80.39}{0.625} = 128.6$$

Equation 3.2.158 is used to compute *C* as follows:

$$C = \frac{1.57}{\left(\frac{D}{t_w}\right)^2}\left(\frac{Ek}{F_{yw}}\right)$$

$$C = \frac{1.57}{(128.6)^2}\left(\frac{29{,}000(5.0)}{50}\right) = 0.275$$

V_p is the plastic shear force determined as follows (Equation 3.2.151):

$$V_p = 0.58F_{yw}Dt_w$$

$$V_p = 0.58(50)(80.39)(0.625) = 1{,}457 \text{ kips}$$

Therefore,

$$V_n = V_{cr} = 0.275(1{,}457) = 401 \text{ kips}$$

$$\phi_v V_n = 1.0(401) = 401 \text{ kips}$$

5.2.9.4.3.3 End Panel

Calculate the factored shear, V_u, at Abutment 1. The load modifier, η, is taken equal to 1.0. The unfactored shears in the critical web are obtained from Table 5.2.3).

$$V_u = 1.0\left[1.25(103+29)+1.5(17)+1.75(121)\right] = 402 \text{ kips} / \cos 14^\circ = 414 \text{ kips}$$

V_u exceeds $\phi_v V_n$ = 401 kips for an unstiffened web determined above. Therefore, transverse stiffeners are required and the provisions of *AASHTO LRFD* Article 6.10.9.3 apply.

According to *AASHTO LRFD* Article 6.10.9.3.3, the nominal shear resistance of a web end panel is limited to the shear buckling resistance, V_{cr}, determined as (Equation 3.2.161):

$$V_n = V_{cr} = CV_p$$

First, compute the shear buckling coefficient, *k*. According to *AASHTO LRFD* Article 6.10.9.3.3, the transverse stiffener spacing for end panels is not to exceed 1.5*D* = 1.5(80.39) = 120.6 inches. Assume the spacing from Abutment 1 to the first transverse stiffener is equal to the maximum permitted spacing of 120.6 inches. From Equation 3.2.157:

$$k = 5 + \frac{5}{\left(\frac{120.6}{80.39}\right)^2} = 7.22$$

Since,

$$1.40\sqrt{\frac{Ek}{F_{yw}}} = 1.40\sqrt{\frac{29{,}000(7.22)}{50}} = 90.6 < \frac{D}{t_w} = \frac{80.39}{0.625} = 128.6$$

Equation 3.2.158 is used to compute *C* as follows:

$$C = \frac{1.57}{(128.6)^2}\left(\frac{29{,}000(7.22)}{50}\right) = 0.397$$

Therefore:

$$V_n = V_{cr} = CV_p = 0.397(1{,}457) = 578 \text{ kips}$$

$$\phi_v V_n = 1.0(578) = 578 \text{ kips} > V_u = 414 \text{ kips}$$

$$\text{ok} \qquad (\text{Ratio} = 0.716)$$

5.2.9.4.3.4 Interior Panels

First Interior Panel to the Right of the End Panel Adjacent to Abutment 1 (G2)

At the first transverse stiffener located d_o = 120.6 inches (10.05 feet) from Abutment 1, V_u is equal to 360 kips. This value is less than $\phi_v V_n$ = 401 kips for an unstiffened web (Section 5.2.9.4.3.2) so that transverse stiffeners are not required.

First Interior Panel to the Left of Pier 1 (G2)

At Pier 1, $|V_u|$ is 643 kips, which exceeds $\phi_v V_n$ = 401 kips for an unstiffened web so that transverse stiffeners are required.

According to *AASHTO LRFD* Article 6.10.9.1, the transverse stiffener spacing for interior panels without a longitudinal stiffener is not to exceed 3*D* = 3(80.39) = 241.2 inches. For the first interior panel in G2 to the left of Pier 1, assume a transverse stiffener spacing equal to one-half the cross-frame spacing adjacent to Pier 1 in Span 1; that is, d_o = 26.833(566.25/561.625)/2 = 13.527 feet = 162.3 inches (measured along the outside web of G2). The cross-frame connection plate is assumed to serve as a transverse stiffener. This spacing is less than the maximum permitted spacing of 241.2 inches. $|V_u|$ exceeds the factored shear buckling resistance, $\phi_v V_{cr}$, of this panel equal to 500 kips (Section 5.2.9.1.4). Therefore, this panel must be designed for the additional post-buckling shear resistance due to tension-field action.

For interior panels of both nonhybrid and hybrid members with the section along the entire panel proportioned such that (Equation 3.2.164):

$$\frac{2Dt_w}{\left(b_{fc}t_{fc} + b_{ft}t_{ft}\right)} \le 2.5$$

the nominal shear resistance, V_n, is to be taken as the sum of the shear buckling resistance and the full postbuckling resistance due to tension-field action, or (Equation 3.2.163):

$$V_n = V_p\left[C + \frac{0.87(1-C)}{\sqrt{1+\left(\frac{d_o}{D}\right)^2}}\right]$$

AASHTO LRFD Article 6.11.9 specifies that for box flanges, b_{fc} or b_{ft} in Equation 3.2.164, as applicable, is to be taken as one-half the effective flange width between webs, but not to exceed $18t_f$, where t_f is the thickness of the box flange.

For the interior web panel under consideration:

$$b_{ft} = 0.5(72.0 - 0.625) = 35.7 \text{ in.} > 18(1.75) = 31.5 \text{ in.}$$

$$\therefore b_{ft} = 31.5 \text{ in.}$$

$$\frac{2(80.39)(0.625)}{[20(1.25)+31.5(1.75)]} = 1.25 < 2.5$$

Therefore, the nominal shear resistance is determined according to Equation 3.2.163. From Equation 3.2.157:

$$k = 5 + \frac{5}{\left(\frac{162.3}{80.39}\right)^2} = 6.23$$

Since,

$$1.40\sqrt{\frac{Ek}{F_{yw}}} = 1.40\sqrt{\frac{29{,}000(6.23)}{50}} = 84.2 < \frac{D}{t_w} = \frac{80.39}{0.625} = 128.6$$

Equation 3.2.158 is used to compute *C* as follows:

$$C = \frac{1.57}{(128.6)^2}\left(\frac{29{,}000(6.23)}{50}\right) = 0.343$$

Therefore:

$$V_n = 1{,}457\left[0.343 + \frac{0.87(1-0.343)}{\sqrt{1+\left(\frac{162.3}{80.39}\right)^2}}\right] = 869 \text{ kips}$$

$$\phi_v V_n = 1.0(869) = 869 \text{ kips} > |V_u| = 643 \text{ kips}$$

ok (Ratio = 0.740)

5.2.9.4.4 Cross-Frame Spacing (Distortional Stresses)

Since the example bridge falls outside the restrictions specified in *AASHTO LRFD* Article 6.11.2.3, transverse bending stresses due to cross-section distortion are limited to 20 ksi at the strength limit state according to *AASHTO LRFD* 6.11.1.1. Adequate internal cross-frames/diaphragms must be introduced to meet this limit, and should also be designed to control the longitudinal warping stresses due to the critical factored torsional loads. *AASHTO LRFD* Article C6.7.4.3 recommends spacing the internal cross-frames/diaphragms to limit such stresses to approximately 10 percent of the stresses due to vertical bending at the strength limit state.

The maximum cross-frame spacing is 28.833 feet in the end spans of G2 (measured along the centerline of the box). Based on this cross-frame spacing, calculate the maximum distortional transverse bending stresses in the end span. The maximum factored torque at the strength limit state (Strength I) in the end spans is at Abutment 2 and is calculated as follows (refer to Table 5.2.4):

$$T = 1.0\left[1.25(-263 + -264) + 1.5(-23) + 1.75(-748)\right] = -2{,}002 \text{ kip} - \text{ft} = -24{,}024 \text{ kip} - \text{in.}$$

Using the BEF Analogy, the transverse bending stress at the top and bottom corners of the tub section may be computed as follows:

$$\sigma_t = C_t F_d \beta \frac{1}{2a} T$$

The other parameters in the preceding equation were determined previously in Section 5.2.9.3.5 for a 28.833-foot cross-frame spacing. Therefore:

$$\sigma_t = 0.14(185)(0.00284)\left(\frac{1}{2(111)}\right)\left|-24{,}024\right| = 8.0 \text{ ksi} < 20.0 \text{ ksi} \quad \text{ok}$$

The longitudinal warping stress at the top and bottom corners of the tub section due to cross-section distortion may be computed as follows (Equation 3.2.66):

$$\sigma_{dw} = \frac{C_w y}{I \beta a} T$$

Again, the other parameters in this equation were determined previously in Section 5.2.9.3.5 (the bottom corner of the box controls). Therefore:

$$\sigma_{dw\ bot} = \frac{0.7(67.40)}{528{,}861(0.00284)(111)}\left|-24{,}024\right| = 6.80 \text{ ksi} > 0.1(32.37) = 3.24 \text{ ksi}$$

The longitudinal warping stress exceeds 10 percent of the maximum factored vertical bending stress in the bottom flange. However, this will be deemed satisfactory because of the conservatism built into the computation of the warping stress in this

case and the fact that the suggested 10 percent limit is only a guideline. The calculated warping stress is reasonably close to the suggested limit.

5.2.9.5 Shear Connector Design

Shear connector design is covered in Section 3.3.2. Shear connectors for box girders are designed according to the provisions of *AASHTO LRFD* Article 6.11.10, which primarily refers back to the provisions of *AASHTO LRFD* Article 6.10.10 for the design of shear connectors for I-girders. The design of shear connectors will be demonstrated for G2 from the example bridge.

According to *AASHTO LRFD* Article 6.11.10, shear connectors are required throughout the entire length of continuous box-girder bridges because of the torisonal shear that exists along the entire span. Shear connectors in horizontally curved box-girder bridges are to be designed for the sum of the flexural and St. Venant torsional shears; that is, V_f in Equation 3.3.4 is to be computed by summing the maximum flexural and torsional shears in the web subject to additive shears. The shear range and resulting pitch should be computed using one-half the moment of inertia, *I*, of the box. The top flange over the web opposite to the web subject to additive flexural and torsional shears should contain an equal number of shear connectors.

Both stud and channel shear connectors are permitted in *AASHTO LRFD* Article 6.10.10.1.1. Stud shear connectors are much more commonly used and are utilized in this example.

5.2.9.5.1 Stud Proportions

Terminating the studs at approximately the mid-thickness of the concrete deck (i.e. within the core of the deck) will place them well within the limits for cover and penetration specified in *AASHTO LRFD* Article 6.10.10.1.4 (i.e. required cover and penetration both greater than or equal to 2.0 inches), and will also clear the reinforcing steel (Section 3.3.2.1.1.3).

Use the structural thickness of the deck, the deck haunch thickness and the smallest top flange thickness (i.e. 1.0 inch) to estimate a required stud height as follows:

$$\frac{9.5}{2} + (5.0 - 1.0) = 8.75 \text{ in.}$$

Use 7/8″ x 8″ studs. Check that the ratio of the height to the diameter is not less than 4.0, as required in *AASHTO LRFD* Article 6.10.10.1.1 (Section 3.3.2.1.1.1):

$$\frac{h}{d} = \frac{8.0}{0.875} = 9.1 > 4.0 \qquad \text{ok}$$

5.2.9.5.2 Pitch

According to the provisions of *AASHTO LRFD* Article 6.10.10.1.2, the pitch of the shear connectors along the longitudinal axis of the girder is to be initially determined to satisfy the fatigue limit state. The resulting number of shear connectors is then to be checked against the number required to satisfy the strength limit state.

5.1.8.5.2.1 Fatigue Limit State

Fatigue limit state requirements for shear connectors are discussed in Section 3.3.2.2. *AASHTO LRFD* Article 6.10.10.1.2 specifies that the pitch, *p*, of the shear connectors, or center-to-center distance between shear connectors along the longitudinal axis, must satisfy the following requirement (Equation 3.3.2):

$$p \le \frac{nZ_r}{V_{sr}}$$

The horizontal fatigue shear range per unit length, V_{sr}, is to be computed as follows (Equation 3.3.3):

$$V_{sr} = \sqrt{(V_{fat})^2 + (F_{fat})^2}$$

V_{fat} is the longitudinal fatigue shear range per unit length (kips/in.) computed as (Equation 3.3.4):

$$V_{fat} = \frac{V_f Q}{I}$$

For curved girders, the parameters *I* and *Q* are always to be determined using the deck within the effective flange width. For tub girders, V_{fat} for one top flange is to be determined for the critical web subject to additive flexural and torsional shears. The resulting pitch is then to be used for the other top flange.

F_{fat} is the radial fatigue shear range per unit length (kips/in.) taken as the larger of either (Equation 3.3.5):

$$F_{fat1} = \frac{A_{bot}\sigma_{flg}\ell}{wR}$$

or (Equation 3.3.6):

$$F_{fat2} = \frac{F_{rc}}{w}$$

Equation 3.3.5 is used to determine the radial fatigue shear range resulting from any curvature between the brace points. The shear range is taken as the radial component of the maximum longitudinal range of force in the bottom flange between brace points, which is used as a measure of the vertical bending moment. *F_{fat1} from Equation 3.3.5 may be ignored for box sections used in horizontally curved spans or segments, as permitted in AASHTO LRFD Article 6.11.10, because of the inherent conservatism in the shear connector design requirements for box sections*.

Equation 3.3.6 provides the radial fatigue shear range in cases where torsion is caused by effects other than curvature, such as skew. Since there is no skew in the example bridge, F_{fat2} is taken equal to zero.

The fatigue resistance, Z_r, of an individual stud shear connector is specified in *AASHTO LRFD* Article 6.10.10.2 (Section 3.3.2.2.1.3). If $(ADTT)_{SL}$ is greater than or equal to 960 trucks per day (assuming a 75-year fatigue design life and one stress range cycle n per truck passage), then the studs must be designed for infinite life using the Fatigue I load combination and the fatigue resistance of an individual stud determined as (Equation 3.3.9):

$$Z_r = 5.5d^2$$

In Section 5.2.9.3.2, the $(ADTT)_{SL}$ for this example was calculated to be 1,000 trucks/day, which exceeds 960 trucks per day.

For continuous spans with span lengths greater than 40.0 feet, the number of stress range cycles per truck passage, n, is equal to 1.5 at sections that are 'near the interior support' (*AASHTO LRFD* Table 6.6.1.2.5-2). Sections ′near the interior support′ are defined as sections less than or equal to a distance of one-tenth the span on each side of the interior support. In these regions, the 75-year $(ADTT)_{SL}$ equivalent to infinite life is equal to 960/1.5 = 640 trucks/day, which is still less than 1,000 trucks/day.

Thus, the studs along the entire span must be designed for infinite life using the Fatigue I load combination, with Z_r taken as follows:

$$Z_r = 5.5d^2 = 5.5(0.875)^2 = 4.21 \text{ kips}$$

The number of shear connectors in a cross-section, n, will be assumed equal to three (3). Requirements for the transverse spacing of shear connectors across the top flange are given in *AASHTO LRFD* Article 6.10.10.1.3 (Section 3.3.2.1.1.2).

A sample calculation of the required shear connector pitch for G2 at the fatigue limit state will be made at Abutment 1.

First, calculate the longitudinal fatigue shear range per unit length, V_{fat}. From the 3D analysis, the vertical fatigue shear force range per unit length, V_f, in the critical web at Abutment 1 is determined for the factored fatigue load (factored by the 1.5 load factor specified for the Fatigue I load combination) including the specified dynamic load allowance of 15 percent as (Table 5.2.3):

$$V_f = 1.5(51 + |-9|) = 1.5(60) = 90 \text{ kips}$$

The first moment, Q_n, of the transformed short-term area of the structural concrete deck about the neutral axis of the short-term composite section at this location is calculated as follows. The transformed area of the concrete deck includes the deck overhang taper (Figure 5.2.1). The thickness at the outside edge of the deck is 9.5 inches. An 18-inch width is assumed for the deck haunch. The short-term modular ratio n is equal to 7.5:

$$\text{Effective width of deck} = (4.0 + 9.25)(12) + \left(\frac{14.0}{2}\right)(12) = 159 + 84 = 243.0 \text{ in}$$

$$A_{deck} = \left[9.5(84 + 111 + 18/2) + \left(\frac{14.5 + 9.5}{2}\right)(48 - 18/2)\right] = 2{,}406/7.5 = 320.8 \text{ in.}^2$$

$$\bar{y}\,A_{deck} = \left(\frac{9.5}{2}\right)(9.5)(243) + \left(9.5 + \frac{5.0}{3}\right)\frac{1}{2}(5.0)(39) = 12{,}054 \text{ in.}^3$$

$$\bar{y} = \frac{\bar{y}\,A_{deck}}{A_{deck}} = \frac{12{,}054}{2{,}406} = 5.01 \text{ in. from the top of the deck}$$

The distance from the neutral axis of the short-term composite section to the neutral axis of the transformed deck = 20.09 in.

$$Q_n = (320.8)(20.09) = 6{,}445 \text{ in.}^3$$

$$I_n = 528{,}681 \text{ in.}^4$$

Q_n and I_n are assumed distributed equally to each web of the tub section. Therefore, from Equation 3.3.4, V_{fat} for the critical web is determined as:

$$V_{fat} = \frac{V_f Q_n}{I_n} = \frac{90(6{,}445/2)}{(528{,}681/2)} = 1.10 \text{ kips/in.}$$

Calculate the horizontal fatigue shear range per unit length, V_{sr} (Equation 3.3.3):

$$V_{sr} = \sqrt{(V_{fat})^2 + (F_{fat})^2} = \sqrt{(1.10)^2 + (0)^2} = 1.10 \text{ kips/in.}$$

Calculate the required pitch, *p*, at this location (Equation 3.3.2):

$$p \le \frac{nZ_r}{V_{sr}} = \frac{3(4.21)}{1.10} = 11.5 \text{ in.}$$

Table 5.2.10 summarizes the required stud pitch along one top flange of G2 at each internal cross-frame location to satisfy the fatigue limit state according to Equation 3.3.2. The same pitch would be used over the other top flange. As specified in *AASHTO LRFD* Article 6.10.10.1.2, the pitch must not be less than six stud diameters = 6(0.875) = 5.25 inches or more than 24.0 inches. In the table, Q_n and I_n are for one-half of the composite box section. Q_n and I_n include the deck plus the longitudinal reinforcement in regions of negative flexure. In the interest of brevity, the pitches for only one-half the girder are shown in Table 5.2.10; the pitches are symmetrical about the longitudinal centerline of the bridge.

Table 5.2.10 G2 Required Stud Shear Connector Pitch – Fatigue Limit State

Location From Support (ft)	V_f (kips)	Q_n (in.^{3})	I_n (in.^{4})	V_{fat} (kips/in.)	F_{fat} (kips/in.)	V_{sr} (kips/in.)	p (in./row)
Abut. 1	90.0	3,223	264,340	1.10	0.0	1.10	11.5
28.83	72.0	3,223	264,340	0.88	0.0	0.88	14.3
57.67	66.0	3,223	264,340	0.80	0.0	0.80	15.8
86.50	66.0	3,223	264,340	0.80	0.0	0.80	15.8
99.50	73.0	4,016	352,990	0.83	0.0	0.83	15.2
126.33	76.0	4,016	352,990	0.86	0.0	0.86	14.7
Pier 1	92.0	4,441	438,130	0.93	0.0	0.95	13.6
26.56	78.0	4,016	352,990	0.89	0.0	0.89	14.2
53.11	76.0	4,016	352,990	0.86	0.0	0.86	14.7
66.11	72.0	3,223	264,340	0.88	0.0	0.88	14.3
90.11	69.0	3,223	264,340	0.84	0.0	0.84	15.0

5.2.9.5.2.2 Strength Limit State

The resulting number of shear connectors will now be checked against the number required to satisfy the strength limit state. Strength limit state requirements for shear connectors are discussed in Section 3.3.2.3. According to *AASHTO LRFD* Article 6.10.10.4.1, the factored shear resistance of a single shear connector, Q_r, at the strength limit state is to be taken as (Section 3.3.2.3.2 – Equation 3.3.22):

$$Q_r = \phi_{sc} Q_n$$

AASHTO LRFD Article 6.10.10.4.3 specifies that the nominal shear resistance of one stud shear connector embedded in a concrete deck is to be taken as (Equation 3.3.23):

$$Q_n = 0.5A_{sc}\sqrt{f_c^{'}E_c} \le A_{sc}F_u$$

$$A_{sc} = \frac{\pi}{4}(0.875)^2 = 0.60 \text{ in.}^2$$

$$A_{sc}F_u = (0.60)(60.0) = 36.00 \text{ kips}$$

$$Q_n = 0.5(0.60)\sqrt{4.5(3{,}865)} = 39.56 \text{ kips} > 36.00 \text{ kips}$$

$$\therefore Q_n = 36.00 \text{ kips}$$

$$Q_r = 0.85(36.00) = 30.60 \text{ kips}$$

At the strength limit state, the minimum number of shear connectors, *n*, over the region under consideration is to be taken as (Equation 3.3.12):

$$n = \frac{P}{Q_r}$$

where *P* is the total nominal shear force determined as specified in *AASHTO LRFD* Article 6.10.10.4.2. According to *AASHTO LRFD* Article 6.10.10.4.2, for continuous spans that are composite for negative flexure in the final condition (which is the case in this example), the total nominal shear force, *P*, between the point of maximum positive design live load plus impact moment and an adjacent end of the member is to be determined as (Equation 3.3.13):

$$P = \sqrt{P_P^2 + F_P^2}$$

where P_p is the total longitudinal force in the concrete deck at the point of maximum positive live load plus impact moment taken as the lesser of (Equation 3.3.14):

$$P_{1p} = 0.85f_c^{'}b_s t_s$$

where b_s and t_s are the effective width and thickness of the concrete deck, respectively, or from Equation 3.3.15:

$$P_{2p} = F_{yw}Dt_w + F_{yt}b_{ft}t_{ft} + F_{yc}b_{fc}t_{fc}$$

F_p is the total radial force in the concrete deck at the point of maximum positive live load plus impact moment taken as (Equation 3.3.16):

$$F_p = P_p \frac{L_p}{R}$$

where L_p is the arc length between an end of the girder and an adjacent point of maximum positive live load plus impact moment (Figure 3.3.9), and R is the minimum girder radius over the length, L_p.

F_p is provided to account for the radial effect of curvature and is required for curved spans or segments to bring the smallest longitudinal force from either the deck or girder into equilibrium. F_p may be taken equal to zero for straight spans or segments.

AASHTO LRFD Article 6.11.10 specifies that for checking the number of shear connectors required to satisfy the strength limit state, the entire cross-sectional area of the steel box section and the effective area of the concrete deck associated with that box is to be used.

The point of maximum positive live load plus impact moment in Span 1 of G2 is located 61.27 feet from Abutment 1 (measured along the centerline of the tub). In Span 3, this point is located 61.27 feet from Abutment 2. Hence, L_p = 61.27 feet in each span.

$$P_{1p} = 0.85(4.5)(243.0)(9.5) = 8{,}830 \text{ kips}$$

For the steel section at these points (note that the longitudinal component of the top-flange bracing area, A_d, is conservatively neglected):

$$P_{2p} = 2(50.0)(80.39)(0.625) + 2(50.0)(18.0)(1.0) + (50.0)(76.0)(0.75) = 9{,}674 \text{ kips}$$

$$\therefore P_p = P_{1p} = 8{,}830 \text{ kips}$$

$$F_p = P_p \frac{L_p}{R} = 8{,}830\left(\frac{61.27}{561.625}\right) = 963 \text{ kips}$$

$$P = \sqrt{P_p^2 + F_p^2} = \sqrt{(8{,}830)^2 + (963)^2} = 8{,}882 \text{ kips}$$

$$n = \frac{P}{Q_r} = \frac{8{,}882}{30.60} = 290 \text{ studs}$$

Compute the required pitch, *p*, in this region at the strength limit state with 6 studs per row (on two flanges):

$$\text{No. of rows} = \frac{290}{6} = 49 \text{ rows}$$

$$\text{Spans 1 \& 3:} \quad p = \frac{61.27(12)}{(49-1)} = 15.3 \text{ in.}$$

The total nominal shear force, *P*, between the point of maximum positive design live load plus impact moment and the centerline of an adjacent interior support is to be determined as (Equation 3.3.17):

$$P = \sqrt{P_T^2 + F_T^2}$$

where P_T is the total longitudinal force in the concrete deck between the point of maximum positive live load plus impact moment and the centerline of an adjacent interior support taken as (Equation 3.3.18):

$$P_T = P_p + P_n$$

where P_n is the total longitudinal force in the concrete deck over an interior support taken as the lesser of (Equation 3.3.19):

$$P_{1n} = F_{yw} D t_w + F_{yt} b_{ft} t_{ft} + F_{yc} b_{fc} t_{fc}$$

or from Equation 3.3.20:

$$P_{2n} = 0.45 f_c' b_s t_s$$

Equation 3.3.20 is a conservative approximation of the tension force in the concrete deck to account for the combined contribution of both the longitudinal reinforcement and also the concrete that remains effective in tension based on its modulus of rupture. A more precise value may be substituted, if desired.

F_T is the total radial force in the concrete deck between the point of maximum positive live load plus impact moment and the centerline of an adjacent interior support taken as (Equation 3.3.21):

$$F_T = P_T \frac{L_n}{R}$$

where L_n is the arc length between the point of maximum positive live load plus impact moment and the centerline of an adjacent interior support (Figure 3.3.10). Again, for straight spans or segments, F_T may be taken equal to zero.

The distance between the point of maximum positive live load plus impact moment in Span 1 and the adjacent interior support is (153.17 – 61.27) = 91.90 feet (measured along the centerline of the tub). For Span 3, this distance is the same. Hence, L_n = 91.90 feet in each span.

For the steel section and effective concrete deck over the interior supports:

$$P_{1n} = 2(50.0)(80.39)(0.625) + 2(50.0)(20.0)(2.5) + (50.0)(76.0)(1.75) = 16{,}674 \text{ kips}$$

$$P_{2n} = 0.45(4.5)(243.0)(9.5) = 4{,}675 \text{ kips}$$

$$\therefore P_n = P_{2n} = 4{,}675 \text{ kips}$$

$$P_T = P_p + P_n = 8{,}830 + 4{,}675 = 13{,}505 \text{ kips}$$

$$F_T = P_T \frac{L_n}{R} = 13{,}505\left(\frac{91.90}{561.625}\right) = 2{,}210 \text{ kips}$$

$$P = \sqrt{P_T^2 + F_T^2} = \sqrt{(13{,}505)^2 + (2{,}210)^2} = 13{,}685 \text{ kips}$$

$$n = \frac{P}{Q_r} = \frac{13{,}685}{30.60} = 448 \text{ studs}$$

Compute the required pitch, p, in this region at the strength limit state with 6 studs per row (on two flanges):

$$\text{No. of rows} = \frac{448}{6} = 75 \text{ rows}$$

$$\text{Spans 1 \& 3:} \quad p = \frac{91.90(12)}{(75-1)} = 14.9 \text{ in.}$$

The distance between the point of maximum positive live load plus impact moment in Span 2 of G2 and each of the adjacent interior supports is 102.1 feet. Using calculations similar to the above:

P_p = 8,830 kips
P_n = 4,675 kips

P_T = 13,505 kips
F_T = 2,455 kips
P = 13,726 kips
n = 449 studs
No. of rows = 75 rows
p = 16.5 in.

Comparing the above values for the strength limit state to the values of the required pitch given for the fatigue limit state in Table 5.2.10, it can be seen that the required pitch is governed by the fatigue limit state at all locations in Span 2 and near the abutments and piers in Spans 1 and 3. The pitch at all other locations in Spans 1 and 3 is governed by the strength limit state. Final recommended pitches for G2 are shown below in Figure 5.2.11.

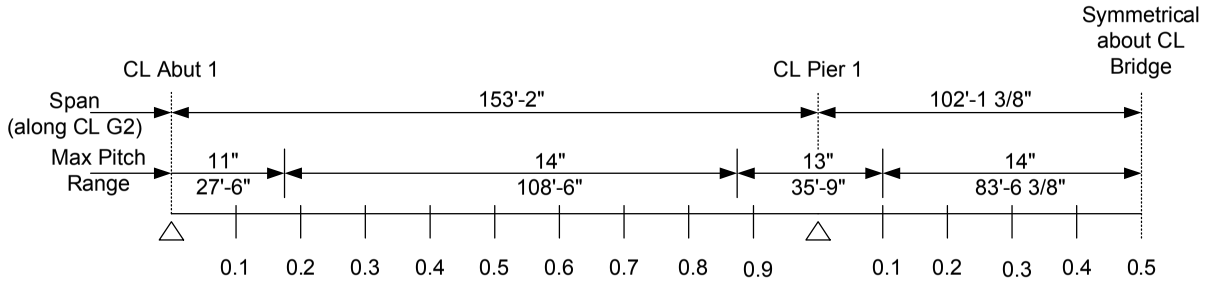


Figure 5.2.11 Recommended Shear Connector Pitch – G2

5.2.9.6 Web Stiffener Design

5.2.9.6.1 Transverse Web Stiffener Design

The design of transverse web stiffeners is covered in Section 3.3.8.1. Transverse stiffeners are designed according to the provisions of *AASHTO LRFD* Article 6.10.11.1. In this example, each intermediate transverse stiffener consists of a plate welded to one side of the web. According to *AASHTO LRFD* Article 6.10.11.1.1, the distance between the end of the web-to-stiffener weld and the near edge of an adjacent web-to-flange or longitudinal stiffener-to-web weld must not be less than $4t_w$, but not to exceed the lesser of $6t_w$ and 4.0 inches.

As specified in *AASHTO LRFD* Article 6.10.11.1.1, single-sided stiffeners on horizontally curved girders should be attached to both flanges to help retain the cross-sectional shape of the girder when subjected to torsion and to avoid high localized bending within the web, particularly near the top flange due to the torsional restraint of the concrete deck. Transverse stiffeners attached to the top and bottom flanges of curved tub girders significantly reduce the sharp through-thickness bending that would otherwise occur due to cross-section distortion in the unstiffened portions of the web at the termination of the stiffener-to-web welds. Stiffeners used as connection plates for cross-frames must be attached to both flanges by welding or bolting. Welded connections are generally cheaper. Note that a fatigue Category C' detail still exists at the termination of the connection-plate weld to the web just

above (or below) the tension flange even when the stiffeners are bolted to that flange.

The design of the intermediate transverse web stiffener (not serving as a cross-frame connection plate) 10.05 feet = 120.6 inches from Abutment 1 in Span 1 of G2 will be illustrated in this example. Also, the design of the transverse web stiffener 13.527 feet = 162.3 inches to the left of Pier 1 in Span 1 of G2 will be illustrated. All distances are measured along the outside web of G2. Grade 50W steel is used for the stiffeners (i.e. F_{ys} = 50.0 ksi).

5.2.9.6.1.1 Projecting Width

Transverse web stiffner proportioning requirements are discussed in Section 3.3.8.1.2. Determine the initial trial stiffener proportions using the projecting width requirements of *AASHTO LRFD* Article 6.10.11.1.2. Size the stiffener width, b_t, to be greater than or equal to $b_f/4$, as required in *AASHTO LRFD* Equation 6.10.11.1.2-2 (Equation 3.3.159). For tub sections, b_f is to be taken as the full width of the widest top flange within the field section under consideration since the bottom flange is restrained by a web along both edges.

Stiffener Adjacent to Abutment 1 in Span 1 of G2

The top flange width in this field section is 18 inches.

$$b_t \geq \frac{18.0}{4} = 4.5 \text{ in.}$$

Stiffeners are commonly made up of less expensive flat bar stock. Flat bars are generally produced in whole-inch width increments and 1/8-in. thickness increments.

$$\text{Use } b_t = 6.0 \text{ in.} > 4.5 \text{ in.} \quad \text{ok}$$

Check the proportioning requirement given by Equation 3.3.158:

$$b_t \geq 2.0 + \frac{D}{30}$$

$$2.0 + \frac{80.39}{30} = 4.7 \text{ in.} < 6.0 \text{ in.} \qquad \text{ok}$$

Try a stiffener thickness, t_p, of 0.625 inches, which exceeds the 1/2″ minimum preferred thickness for stiffeners and connection plates. .

Check that (Equation 3.3.159):

$$16t_p \geq b_t$$

$$16(0.625) = 10.0 \text{ in.} > 6.0 \text{ in.} \quad \text{ok}$$

Stiffener Adjacent to Pier 1 in Span 1 of G2

The top flange width in this field section is 20 inches.

$$b_t \geq \frac{20.0}{4} = 5.0 \text{ in.}$$

Use b_t = 6.0 in. > 5.0 in. ok

Check the proportioning requirement given by Equation 3.3.158:

$$b_t \geq 2.0 + \frac{D}{30}$$

$$2.0 + \frac{80.39}{30} = 4.7 \text{ in.} < 6.0 \text{ in.} \quad \text{ok}$$

Try a stiffener thickness, t_p, of 0.625 inches.

Check that (Equation 3.3.159):

$$16t_p \geq b_t$$

$$16(0.625) = 10.0 \text{ in.} > 6.0 \text{ in.} \quad \text{ok}$$

5.2.9.6.1.2 Moment of Inertia

The moment of inertia requirements for transverse web stiffeners are specified in *AASHTO LRFD* Article 6.10.11.1.3 (Section 3.3.8.1.3). The moment of inertia requirements ensure that the transverse stiffener has sufficient rigidity to maintain a vertical line of near zero lateral deflection along the line of the stiffener in order for interior web panels to adequately develop the shear buckling resistance, or the combined shear buckling and postbuckling tension-field resistance, as applicable.

For transverse stiffeners adjacent to web panels in which neither panel supports a factored shear force, V_u, larger than the factored shear-buckling resistance (i.e. $V_r = \phi_v V_{cr}$), the moment of inertia of the transverse stiffener, I_t, must satisfy the *smaller* of the following (Equation 3.3.160):

$$I_t \geq I_{t1}$$

and (Equation 3.3.161):

$$I_t \geq I_{t2}$$

I_{t1} is computed from Equation 3.3.162 as follows:

$$I_{t1} = bt_w^3 J$$

where b is taken as the smaller of d_o and D, where d_o is the smaller of the adjacent web panel widths. J is the stiffener bending rigidity parameter taken as (Equation 3.3.164):

$$J = \frac{2.5}{(d_o/D)^2} - 2.0 \geq 0.5$$

I_{t2} is computed from Equation 3.3.163 as follows:

$$I_{t2} = \frac{D^4 \rho_t^{1.3}}{40}\left(\frac{F_{yw}}{E}\right)^{1.5}$$

where ρ_t is taken equal to the larger of F_{yw}/F_{crs} and 1.0, and F_{crs} is equal to the local buckling stress for the stiffener (ksi) taken as (Equation 3.3.165):

$$F_{crs} = \frac{0.31E}{\left(\frac{b_t}{t_p}\right)^2} \leq F_{ys}$$

For transverse stiffeners adjacent to web panels in which the factored shear, V_u, is larger than the factored shear buckling resistance $\phi_v V_{cr}$, and thus the web postbuckling or tension-field resistance is required in one or both panels, the moment of inertia, I_t, of the transverse stiffereners must satisfy the following:

- If $I_{t2} > I_{t1}$, then (Equation 3.3.168):

$$I_t \geq I_{t1} + (I_{t2} - I_{t1})\left(\frac{V_u - \phi_v V_{cr}}{\phi_v V_n - \phi_v V_{cr}}\right)$$

- Otherwise (Equation 3.3.169):

$$I_t \geq I_{t2}$$

Stiffener Adjacent to Abutment 1 in Span 1 of G2

Based on the shear calculations in Sections 5.2.9.4.3.3 and 5.2.9.4.3.4, neither panel adjacent to the stiffener under consideration must support a factored shear, V_u, larger than the factored shear-buckling resistance, $\phi_v V_{cr}$. Thus, in this case, the moment of inertia of the transverse stiffener, I_t, must satisfy the smaller of the limits given by Equations 3.3.160 and 3.3.161.

Compute the stiffener bending rigidity parameter, J, from Equation 3.3.164 as follows. d_o is taken as the smaller of the adjacent panel widths equal to 120.6 inches and the web depth, D, is equal to 80.39 inches measured along the web slope.

$$J = \frac{2.5}{(120.6/80.39)^2} - 2.0 = -0.9 < 0.5 \quad \therefore J = 0.5$$

b is taken as the smaller of d_o and D; thus, in this case, $b = D = 80.39$ inches. Calculate I_{t1} from Equation 3.3.162 as follows:

$$I_{t1} = 80.39(0.625)^3(0.5) = 9.81 \text{ in.}^4$$

Calculate the local buckling stress of the stiffener, F_{crs}, from Equation 3.3.165 as follows:

$$F_{crs} = \frac{0.31(29{,}000)}{\left(\frac{6.0}{0.625}\right)^2} = 97.5 \text{ ksi} > F_{ys} = 50 \text{ ksi}$$

$$\therefore F_{crs} = 50 \text{ ksi}$$

The term, ρ_t, is equal to the larger of F_{yw}/F_{crs} (i.e. 50 ksi/50 ksi = 1.0) and 1.0. Therefore, in this case, ρ_t is equal to 1.0.

Calculate I_{t2} from Equation 3.3.163 as follows:

$$I_{t2} = \frac{(80.39)^4(1.0)^{1.3}}{40}\left(\frac{50}{29{,}000}\right)^{1.5} = 74.7 \text{ in}^4$$

Since I_{t1} is smaller than I_{t2}, Equation 3.3.160 governs the required moment of inertia. Hence, I_t must be greater than or equal to I_{t1} or 9.81 in.^{4}

For single-sided stiffeners, the moment of inertia of the stiffener is to be taken about the edge in contact with the web. Therefore:

$$I_t = \frac{1}{3}(0.625)(6.0)^3 = 45.00\ \text{in.}^4 > 9.81\ \text{in.}^4 \quad \text{ok}$$

Use 5/8″ x 6″ bars for the transverse web stiffener adjacent to Abutment 1 in Span 1 of G2.

Stiffener Adjacent to Pier 1 in Span 1 of G2

Based on the shear calculations in Section 5.2.9.4.3.4, both panels adjacent to the stiffener under consideration must support a factored shear, V_u, larger than the factored postbuckling shear resistance due to tension-field action, $\phi_v V_n$. Thus, in this case, the moment of inertia of the transverse stiffener, I_t, must satisfy either Equation 3.3.168 or 3.3.169, as applicable.

Compute the stiffener bending rigidity parameter, J, from Equation 3.3.164 as follows. d_o is equal to 162.3 inches (the stiffener spacings in this panel are equal) and the web depth, D, is equal to 80.39 inches (measured along the web slope).

$$J = \frac{2.5}{(162.3/80.39)^2} - 2.0 = -1.39 < 0.5 \quad \therefore J = 0.5$$

b is taken as the smaller of d_o and D; thus, in this case, $b = D = 80.39$ inches. Calculate I_{t1} from Equation 3.3.162 as follows:

$$I_{t1} = 80.39(0.625)^3(0.5) = 9.81\ \text{in.}^4$$

Calculate the local buckling stress of the stiffener, F_{crs}, from Equation 3.3.165 as follows:

$$F_{crs} = \frac{0.31(29{,}000)}{\left(\frac{6.0}{0.625}\right)^2} = 97.5\ \text{ksi} > F_{ys} = 50\ \text{ksi}$$

$$\therefore F_{crs} = 50\ \text{ksi}$$

The term, ρ_t, is equal to the larger of F_{yw}/F_{crs} (i.e. 50 ksi/50 ksi = 1.0) and 1.0. Therefore, in this case, ρ_t is equal to 1.0.

Calculate I_{t2} from Equation 3.3.163 as follows:

$$I_{t2} = \frac{(80.39)^4 (1.0)^{1.3}}{40}\left(\frac{50}{29{,}000}\right)^{1.5} = 74.7 \text{ in}^4$$

Since I_{t2} is greater than I_{t1}, the moment of inertia of the transverse stiffener, I_t, must satisfy Equation 3.3.168 in this particular case. In cases where V_u is smaller than V_n, the value of I_t from Equation 3.3.163 is not required. The required value of I_t from Equation 3.3.163 may be particularly large for deeper girders. Equation 3.3.168 is intended to handle such cases.

V_u in Equation 3.3.168 is the largest of the factored shears in the adjacent web panels. In this case, $|V_u|$ = 643 kips at Pier 1 (Section 5.2.9.4.3.4). V_{cr} is the smallest nominal shear-buckling resistance of the adjacent web panels. In this particular case, the shear-buckling resistance of the adjacent web panels is the same (since the panels are the same size) and is computed to be V_{cr} = 500 kips (Section 5.2.9.1.4). V_n is the smaller of the nominal combined buckling and tension-field shear resistances of the adjacent web panels. V_n, which was computed in Section 5.2.9.4.3.4 to be 869 kips, is also the same for both panels in this case. ϕ_v is the resistance factor for shear equal to 1.0 (*AASHTO LRFD* Article 6.5.4.2). Therefore, from Equation 3.3.168:

$$I_t \geq 9.81 + (74.7 - 9.81)\left(\frac{643 - 1.0(500)}{1.0(869) - 1.0(500)}\right) = 34.96 \text{ in.}^4$$

For single-sided stiffeners, the moment of inertia of the stiffener is to be taken about the edge in contact with the web. Therefore:

$$I_t = \frac{1}{3}(0.625)(6.0)^3 = 45.00 \text{ in.}^4 > 34.96 \text{ in.}^4 \quad \text{ok}$$

Use 5/8″ x 6″ bars for the transverse web stiffener adjacent to Pier 1 in Span 1 of G2.

5.2.9.6.2 Bearing Stiffener Design

The design of bearing stiffeners is covered in Section 3.3.8.2. *AASHTO LRFD* Article 6.11.11.1 refers to the provisions of *AASHTO LRFD* Article 6.10.11.2 for the design of bearing stiffeners for box sections. Bearing stiffeners are designed as columns to resist the reactions at bearing locations or at other locations subjected to concentrated loads where the loads are not transmitted through a deck or deck system. According to *AASHTO LRFD* Article 6.10.11.2.1, bearing stiffeners must be placed on the webs of built-up sections at all bearing locations. When inclined webs are used on box sections, bearing stiffeners should be attached to either an internal or external diaphragm rather than to the webs so that the bearing stiffeners are perpendicular to the sole plate. Thermal movements of the bridge may cause the

diaphragm to be eccentric with respect to the bearings, which should be recognized in the design of the diaphragm and the bearing stiffeners. Eccentricity effects are not considered in the example (refer to Section 3.3.8.2.1).

Bearing stiffeners are to either be finished-to-bear (allowing the option of milling or grinding) against the flange through which it receives its load and attached with fillet welds, or else attached to that flange by a full penetration groove weld. The use of finish-to-bear plus fillet welds to connect the bearing stiffeners to the appropriate flange is recommended (note that fillet welds are not necessary if a cross-frame or diaphragm is not connected to the stiffener). Full penetration groove welds are costly and often result in deformations of the flange induced by the full penetration weld.

The design of the bearing stiffeners for G2 at Abutment 1 will be illustrated in this example. Grade 50W steel is used for the stiffeners (i.e. F_{ys} = 50.0 ksi).

Assemble the bearing reactions due to the factored loads from the 3D analysis at Abutment 1. The unfactored bearing reactions are as follows:

R_{DC1} = 206 kips
R_{DC2} = 30 kips
R_{DW} = 34 kips
R_{LL+IM} = 244 kips

Determine the total factored reaction, R_u, at the strength limit state. The Strength I load combination controls:

$$R_u = 1.0\left[1.25(206+30)+1.5(34)+1.75(244)\right] = 773 \text{ kips}$$

Assume two bearing stiffeners on the internal diaphragm at the abutment and that the sole plate allows for equal distribution of the total factored reaction to each stiffener. Therefore, design each stiffener for $R_u/2$ = 773/2 = 386.5 kips

5.2.9.6.2.1 Projecting Width

The projecting width requirement for bearing stiffeners is discussed in Section 3.3.8.2.2. According to *AASHTO LRFD* Article 6.10.11.2.2, the width, b_t, of each projecting stiffener element must satisfy the following requirement (Equation 3.3.171):

$$b_t \le 0.48 t_p \sqrt{\frac{E}{F_{ys}}}$$

Welded bearing stiffeners are also commonly made up of less expensive flat bar stock. Try two 6.0-inch-wide bars welded to each side of the diaphragm web. Rearranging *AASHTO LRFD* Equation 6.10.11.2.2-1 gives:

$$(t_p)_{min.} = \frac{b_t}{0.48\sqrt{\frac{E}{F_{ys}}}}$$

$$(t_p)_{min.} = \frac{6.0}{0.48\sqrt{\frac{29{,}000}{50.0}}} = 0.52 \text{ in.}$$

Try a stiffener thickness, t_p, of 0.625 inches, which exceeds the 1/2″ minimum preferred thickness for stiffeners and connection plates.

5.1.8.6.2.2 Bearing Resistance

Bearing resistance of the stiffeners is covered in Section 3.3.8.2.3. According to *AASHTO LRFD* Article 6.10.11.2.3, the factored bearing resistance for the fitted ends of bearing stiffeners is to be taken as (Equation 3.3.172):

$$(R_{sb})_r = \phi_b (R_{sb})_n$$

where $(R_{sb})_n$ is equal to the nominal bearing resistance for the fitted end of bearing stiffeners taken as (Equation 3.3.173):

$$(R_{sb})_n = 1.4 A_{pn} F_{ys}$$

A_{pn} is the area of the projecting elements of the stiffener outside of the diaphragm web-to-bottom flange fillet welds. Assume for this example that the clip provided at the base of the stiffeners to clear the web-to-flange fillet welds is 1.5 inches in length. The resistance factor for bearing on milled surfaces ϕ_b = 1.0 (*AASHTO LRFD* Article 6.5.4.2). Therefore:

$$A_{pn} = 2(6.0 - 1.5)(0.625) = 5.62 \text{ in.}^2$$

$$(R_{sb})_n = 1.4(5.62)(50.0) = 393 \text{ kips}$$

$$(R_{sb})_r = (1.0)(393) = 393 \text{ kips} > R_u/2 = 386.5 \text{ kips} \quad \text{ok} \quad (\text{Ratio} = 0.983)$$

5.2.9.6.2.3 Axial Resistance

The axial resistance of bearing stiffeners is covered in Section 3.3.8.2.4. For computing the axial resistance of bearing stiffeners that are welded to the diaphragm

web, *AASHTO LRFD* Article 6.10.11.2.4b states that a portion of the web is to be included as part of the effective column section. For stiffeners consisting of two plates welded to the web, the effective column section is to consist of the two stiffener elements, plus a centrally located strip of web extending not more than $9t_w$ on each side of the stiffeners (Section 3.3.8.2.4.1).

AASHTO LRFD Article 6.10.11.2.4a specifies that the radius of gyration of the effective column section is to be computed about the mid-thickness of the web and the effective length is to be taken as $0.75D$, where D is the web depth. The thickness of the internal diaphragm web at Abutment 1 is 5/8 inches. The area of the effective column section is computed as:

$$A_g = 2\left[(6.0)(0.625) + 9(0.625)(0.625)\right] = 14.53 \text{ in.}^2$$

The moment of inertia of the effective column section (conservatively neglecting the web strip) is computed as:

$$I_s = \frac{0.625(6.0 + 0.625 + 6.0)^3}{12} = 104.8 \text{ in.}^4$$

The radius of gyration of the effective column section is therefore computed as:

$$r_s = \sqrt{\frac{I_s}{A_g}} = \sqrt{\frac{104.8}{14.53}} = 2.68 \text{ in.}$$

The effective length of the effective column section is computed as:

$$K\ell = 0.75D = 0.75(78) = 58.5 \text{ in.}$$

Check the limiting slenderness ratio of 120 specified for primary members in compression in *AASHTO LRFD* Article 6.9.3:

$$\frac{K\ell}{r_s} = \frac{58.5}{2.68} = 21.8 < 120 \qquad \text{ok}$$

AASHTO LRFD Article 6.10.11.2.4a specifies that the factored axial resistance, P_r, of the effective column section be calculated according to the provisions of *AASHTO LRFD* Article 6.9.2.1 as follows (Equation 3.3.174):

$$P_r = \phi_c P_n$$

where P_n is equal to the nominal compressive resistance determined as specified in *AASHTO LRFD* Article 6.9.4.1, and ϕ_c is equal to the resistance factor for axial compression = 0.90.

Calculate the elastic critical buckling resistance for flexural buckling, P_e, specified in *AASHTO LRFD* Article 6.9.4.1.2 as follows (Equation 3.3.177):

$$P_e = \frac{\pi^2 E}{\left(\frac{K\ell}{r_s}\right)^2} A_g$$

$$P_e = \frac{\pi^2 (29{,}000)}{(21.8)^2}(14.53) = 8{,}751 \text{ kips}$$

Calculate the equivalent nominal yield resistance, P_o, as follows (*AASHTO LRFD* Article 6.9.4.1.1). The slender element reduction factor, Q, is taken equal to 1.0 for bearing stiffeners:

$$P_o = F_{ys} A_g = 50(14.53) = 726 \text{ kips}$$

Since P_e/P_o = 8,751/726 = 12.0 is greater than 0.44, the nominal compressive resistance, P_n, of the bearing stiffeners is computed as follows (*AASHTO LRFD* Article 6.9.4.1.1 – Equation 3.3.175):

$$P_n = \left[0.658^{\left(\frac{P_o}{P_e}\right)}\right] P_o$$

$$P_n = \left[0.658^{\left(\frac{726}{8{,}751}\right)}\right](726) = 701 \text{ kips}$$

The factored compressive resistance, P_r, of the bearing stiffeners is computed as (Equation 3.3.174):

$$P_r = 0.9(701) = 631 \text{ kips} > R_u/2 = 386.5 \text{ kips} \quad \text{ok} \quad (\text{Ratio} = 0.613)$$

Use 5/8″ x 6″ bars (two pair) for the bearing stiffeners on the internal diaphragm plate of G2 at Abutment 1.

5.2.9.6.2.4 Bearing Stiffener-to-Web Welds

Design the bearing stiffener-to-web fillet welds. Fillet welds and fillet welded connections are covered in Sections 3.3.6.3.3.2 and 3.3.6.3.5.2, respectively. The girder flanges, diaphragm web and the stiffeners are ASTM A 709 Grade 50W steel with a specified minimum tensile strength F_u = 70 ksi (*AASHTO LRFD* Table 6.4.1-1). Assume E70 electrodes (i.e. matching weld metal) with a classification strength, F_{exx}, equal to 70 ksi.

According to *AASHTO LRFD* Table 6.13.3.4-1 (Table 3.3.6), the minimum size fillet weld is ¼ in. when the base metal thickness *T* of the thicker part joined is less than or equal to ¾ in. The diaphragm web is 5/8-in. thick at Abutment 1 and the stiffeners are 5/8-in. thick. Therefore, try the minimum size fillet weld equal to ¼ in. The effective throat of a ¼ in. equal-leg fillet weld is equal to:

$$t_e = 0.707(0.25) = 0.177 \text{ in.}$$

According to *AASHTO LRFD* Article 6.13.3.2.4b, the factored resistance, R_r, of fillet-welded connections at the strength limit state subject to shear on the effective area is to be taken as (Equation 3.3.115):

$$R_r = 0.6\phi_{e2}F_{exx}$$

where ϕ_{e2} is equal to the resistance factor for shear on the throat of the weld metal in fillet welds specified in *AASHTO LRFD* Article 6.5.4.2 = 0.80. Therefore:

$$R_r = 0.6(0.80)(70) = 33.6 \text{ ksi}$$

The factored resistance of a ¼-in. fillet weld in shear in units of kips/inch at the strength limit state is computed as:

$$V_r = R_r t_e = 33.6(0.177) = 5.95 \text{ kips/in.}$$

The governing factored shear rupture resistance of the base metal adjacent to the weld leg at the strength limit state is computed as (Section 3.3.6.2.6.2 – Equation 3.3.91 – substituting the governing plate thickness *t* for A_{vn}):

$$R_r = \phi_{vu}\,0.58R_pF_ut$$

ϕ_{vu} equals the resistance factor for shear rupture of connected elements specified in *AASHTO LRFD* Article 6.5.4.2 (= 0.80). R_p may be taken equal to 1.0 for welded connections. Therefore:

$$R_r = 0.80(0.58)(1.0)(70)(0.625) = 20.3 \text{ kips/in.}$$

which does not control.

The total length of a single bearing stiffener-to-web weld, allowing 2.5 inches for clips at the top and bottom of the bearing stiffeners to clear the diaphragm flange-to-web welds, is:

$$L_w = 78 - 2(2.5) = 73.0 \text{ in.}$$

The total factored resistance of the four ¼-in. fillet welds connecting the stiffeners to the web (in kips) is therefore:

$$4(5.95)(73.0) = 1{,}737 \text{ kips} > R_u/2 = 386.5 \text{ kips} \quad \text{ok}$$

Since the stiffeners are located at an abutment, load-induced fatigue of the base metal adjacent to these welds need not be checked.

5.2.9.7 Lateral Bracing Member Design

The design of a top lateral bracing member from the example bridge for compression is illustrated in this section. Top flange lateral bracing is designed to resist the shear flow in the pseudo-box section resulting from any torsion acting on the steel section due to the design load effects, including during the deck-casting sequence (Section 3.1.2.9.1.2). The bracing also acts with the tub in resisting vertical bending. Hence, forces in the bracing due to flexure of the tub must also be considered. Since the bracing is permanent, composite dead load force effects (i.e. due to DC_2 and DW) and live load force effects are considered, although these effects are relatively small in this case since the bracing is located at the top of the tub section.

The largest total compressive force in the top lateral bracing from the example bridge was observed in the diagonal adjacent to Abument 2 in G1. Since the bridge is analyzed by 3D finite element analysis in which the individual lateral bracing members are included in the model, the unfactored compressive forces in this member taken directly from the analysis are as follows (note: the force effects in the member resulting from top-flange lateral bending due to the deck overhang bracket forces were not considered in this particular analysis):

P_{steel} = -10 kips
$P_{deck\ casting(max)}$ = -71 kips
P_{DC1} = -52 kips
P_{DC2} = -1 kip
P_{DW} = -2 kips
P_{LL+IM} = -4 kips

The factored compressive force, P_u, due to the Strength I load combination is computed as (the load modifier, η, is taken equal to 1.0):

$$P_u = 1.0[1.25(-52 + -1) + 1.5(-2) + 1.75(-4)] = -76 \text{ kips}$$

The factored compressive force, P_u, due to the steel weight plus the deck-casting sequence is computed according to the Strength IV load combination as:

$$P_u = 1.0[1.5(-10 + -71)] = -122 \text{ kips (governs)}$$

Determine the suitability of a WT7 x 37 rolled structural tee for use as the top-flange diagonal lateral bracing member. The design of structural tees is covered in Section 3.3.4. Assume the steel for the tee is ASTM A 709 Grade 50W.

From the AISC Manual shape property tables, the following section properties are obtained for a WT7 x 37:

A_g	=	10.90 in.^{2} (> 0.03*w* = 0.03(111) = 3.3 in.^{2} -> Equation 3.1.7)
d	=	7.085 in.
t_w	=	0.450 in.
b_f	=	10.070 in.
t_f	=	0.785 in.
I_x	=	36.0 in.^{4}
S_x	=	6.25 in.^{3}
r_x	=	1.82 in.
y	=	1.32 in.
I_y	=	66.9 in.^{4}
r_y	=	2.48 in.
J	=	1.94 in.^{4}
$\bar{r}_o$	=	3.21 in.
H	=	0.917

The thickness of the tee stem exceeds the minimum permissible thickness of 5/16″ specified for structural steel in *AASHTO LRFD* Article 6.7.3.

First, check the maximum slenderness ratio of the tee to ensure it does not exceed the permissible value of 120 for primary members in compression (*AASHTO LRFD* Article 6.9.3). Since the member is in a horizontally curved bridge and the forces in the tee were determined from an analysis, the member is considered to be a primary member.

Assume the stem of the tee section is pointed down with the flange of the tee bolted to the bottom of the tub top flanges, which is the preferred method of connection. The width, *w*, of the tub section at the top between the centerlines of the flanges is 111 inches and the top flange width is 18 inches. Therefore, the clear distance between the top flanges is 111 in. – 18 in. = 93 inches. The spacing between the strut of the Pratt truss lateral bracing system at this location and the abutment along the outer web of G1 is (27.6406/3)(543.0/538.375)(12) = 111.5 inches (Figure 5.2.2

and Part B of Figure 5.2.3). Thus, the length, ℓ, of the bracing member is computed as:

$$\ell = \sqrt{93^2 + 111.5^2} = 145.2 \text{ in.}$$

AASHTO LRFD Article 4.6.2.5 allows the effective length factor, *K*, to be taken as 0.750 for members with bolted or welded connections at both ends. Assume K_y = 0.750. However, since only the tub flanges are providing restraint for buckling about the x-axis, K_x will conservatively be taken equal to 1.0. The slenderness ratios about each axis in this case are therefore:

$$\frac{K_y \ell_y}{r_y} = \frac{0.750(145.2)}{2.48} = 43.9$$

$$\frac{K_x \ell_x}{r_x} = \frac{1.0(145.2)}{1.82} = 79.8 < 120 \quad \text{ok}$$

A more refined calculation of ℓ could be considered had the slenderness limit been exceeded.

The design of tees for eccentric axial compression is covered in Section 3.3.4.3. *AASHTO LRFD* Article 6.9.2.1 specifies that the factored compressive resistance, P_r, at the strength limit state be taken as (Section 3.3.4.3.2 - Equation 3.3.52):

$$P_r = \phi_c P_n$$

ϕ_c is the resistance factor for axial compression specified in *AASHTO LRFD* Article 6.5.4.2 = 0.90.

The nominal compressive resistance, P_n, is to be determined as (Section 3.3.4.3.2 - Equations 3.3.53 and 3.3.54):

- If $\frac{P_e}{P_o} \geq 0.44$, then:

$$P_n = \left[0.658^{\left(\frac{P_o}{P_e}\right)}\right] P_o$$

- If $\frac{P_e}{P_o} < 0.44$, then:

$$P_n = 0.877 P_e$$

For the design of tees, P_e is taken as the *smaller* of the elastic critical buckling resistance for flexural buckling about the x-axis determined as specified in *AASHTO LRFD* Article 6.9.4.1.2 as follows (Section 3.3.4.3.2.1 - Equation 3.3.55):

$$P_{ex} = \frac{\pi^2 E}{\left(\frac{K_x \ell_x}{r_x}\right)^2} A_g$$

and the elastic critical buckling resistance for flexural-torsional buckling determined as specified in *AASHTO LRFD* Article 6.9.4.1.3 as follows (Section 3.3.4.3.2.1 - Equation 3.3.56):

$$P_e = \left(\frac{P_{ey} + P_{ez}}{2H}\right)\left[1 - \sqrt{1 - \frac{4P_{ey}P_{ez}H}{(P_{ey} + P_{ez})^2}}\right]$$

P_o is the equivalent nominal yield resistance determined as specified in *AASHTO LRFD* Article 6.9.4.1.1 (Section 3.3.4.3.2.2 - Equation 3.3.61). Q is the slender element reduction factor specified in *AASHTO LRFD* Article 6.9.4.2.2 (Section 3.3.4.3.2.2):

$$P_o = QF_yA_g$$

Calculate the equivalent nominal yield resistance, P_o. For compression members composed of one or more slender elements; that is, elements not meeting the corresponding width-to-thickness ratio limits specified in *AASHTO LRFD* Table 6.9.4.2.1-1, the slender element reduction factor, Q, accounts for the effect of potential local buckling of those elements on the overall buckling resistance of the member and has a value less than 1.0. The value of Q in this instance is determined according to the provisions of *AASHTO LRFD* Article 6.9.4.2.2.

Q is taken equal to 1.0 as specified in *AASHTO LRFD* Article 6.9.4.2.1 for compression member cross-sections without any slender elements; that is, composed entirely of nonslender elements. In such cases, local buckling does not adversely affect the nominal compressive resistance.

For compression member cross-sections composed entirely of unstiffened elements, or plates supported along only one edge parallel to the direction of the compression force, Q is taken equal to the factor for unstiffened elements, Q_s. Tees are composed entirely of unstiffened elements (Figure 3.3.20).

None of the rolled tee sections in the AISC Manual shape property tables have slender flanges. When the b/t ratio of the stem of the tee is less than or equal to the

following limit (from *AASHTO LRFD* Eq. 6.9.4.2.1-1 with *k* taken equal to 0.75), the element is nonslender and $Q = Q_s = 1.0$. *b* is taken as the full depth of the tee (including the flange) and *t* is taken as the stem thickness (Figure 3.3.24) in checking this limit. Check if the stem of the tee under investigation is a slender element:

$$\frac{b}{t} \le 0.75\sqrt{\frac{E}{F_y}}$$

$$0.75\sqrt{\frac{29{,}000}{50}} = 18.1 > \frac{b}{t} = \frac{7.085}{0.450} = 15.7$$

Therefore, the nominal compressive resistance of the tee does not have to be reduced due to potential local buckling of the stem. Since the stem is a nonslender element, the slender element reduction factor, $Q = Q_s$, is equal to 1.0.

From Equation 3.3.61:

$$P_o = QF_yA_g = 1.0(50)(10.90) = 545 \text{ kips}$$

Tee sections loaded in axial compression can either fail by flexural buckling about the x-axis or by torsion combined with flexure about the y-axis or flexural-torsional bucking (where the y-axis is defined as the axis of symmetry of the tee section).

The elastic critical buckling resistance for flexural buckling about the x-axis, P_{ex}, is determined as (Equation 3.3.55):

$$P_{ex} = \frac{\pi^2(29{,}000)}{(79.8)^2}(10.90) = 490 \text{ kips}$$

Calculate the elastic critical buckling resistance, P_e, for flexural-torsional buckling. First, calculate P_{ey} as follows (Equation 3.3.57):

$$P_{ey} = \frac{\pi^2E}{\left(\frac{K_y\ell_y}{r_y}\right)^2}A_g$$

$$P_{ey} = \frac{\pi^2(29{,}000)}{(43.9)^2}(10.90) = 1{,}619 \text{ kips}$$

Calculate P_{ez} as follows (Equation 3.3.58). The shear modulus, *G*, is equal to 11,200 ksi for steel:

$$P_{ez} = \frac{GJ}{\bar{r}_o^2}$$

$$P_{ez} = \frac{11{,}200(1.94)}{(3.21)^2} = 2{,}109 \text{ kips}$$

Therefore from Equation 3.3.56:

$$P_e = \left(\frac{1{,}619 + 2{,}109}{2(0.917)}\right)\left[1 - \sqrt{1 - \frac{4(1{,}619)(2{,}109)(0.917)}{(1{,}619 + 2{,}109)^2}}\right] = 1{,}394 \text{ kips}$$

Since P_{ex} is less than P_e for flexural-torsional buckling, flexural buckling about the x-axis controls. Therefore, P_e is equal to P_{ex} = 490 kips.

Since:

$$\frac{P_e}{P_o} = \frac{490}{545} = 0.90 > 0.44$$

the nominal compressive resistance, P_n, is computed as follows (Equation 3.3.53):

$$P_n = \left[0.658^{\left(\frac{545}{490}\right)}\right](545) = 342 \text{ kips}$$

The factored compressive resistance, P_r, is taken as:

$$P_r = \phi_c P_n = 0.90(342) = 308 \text{ kips}$$

Since the tee flange is bolted to the top flanges of the tub, the tee is also subject to a uniform bending moment about the major principal axis (x-axis) due to the eccentricity of the connection at each end of the member. The thickness of the top flanges is 1.0 inch; therefore, the first-order moment, $(M_{ux})_1$, due to the eccentricity is computed as:

$$(M_{ux})_1 = |P_u|(y + \frac{1.0}{2}) = |-122|(1.32 + 0.5) = 222.0 \text{ kip} - \text{in.}$$

Second-order effects arise from the additional secondary moment caused by the axial force acting through the member deflection (Figure 3.3.25). *AASHTO LRFD* Article 4.5.3.2.2b specifies that the single-step adjustment or moment magnification method may be used to determine the second-order elastic moment as follows (Section 3.3.4.3.3 – Equation 3.3.65):

$$(M_{ux})_2 = \delta_b (M_{ux})_1$$

The amplification factor, δ_b, is computed as follows (Equation 3.3.66):

$$\delta_b = \frac{C_m}{1 - \frac{P_u}{\phi_K P_e}} \geq 1.0$$

ϕ_K is a stiffness reduction factor taken equal to 1.0 for steel members. C_m is the equivalent uniform moment factor, which for members braced against sidesway and without transverse loading (other than the self weight of the member) between supports in the plane of bending, is to be taken as (Equation 3.3.67):

$$C_m = 0.6 + 0.4\frac{M_1}{M_2}$$

The tee section is bent in single curvature by equal moments at the end of the member due to the eccentricity. For single curvature, the ratio of the end moments M_1/M_2 = 1.0 is to be taken as positive. Therefore, from the preceding equation, C_m = 1.0.

P_e is the Euler buckling load for buckling about the x-axis (i.e. the plane of bending), which is to be taken as follows (Equation 3.3.68):

$$P_e = \frac{\pi^2 EI}{(K_x \ell_x)^2}$$

K_x is the effective length factor for buckling about the x-axis and ℓ_x is the unbraced length for buckling about the x-axis. For this case, K_x is equal to 1.0 and I is equal to I_x = 24.9 in.^{4}. Therefore:

$$P_e = \frac{\pi^2 (29{,}000)(36.0)}{(1.0 * 145.2)^2} = 489 \text{ kips}$$

$$\delta_b = \frac{1.0}{1 - \frac{|-122|}{1.0(489)}} = 1.33$$

Thus:

$$(M_{ux})_2 = 1.33(222.0) = 295.3 \text{ kip} - \text{in.}$$

Calculate the factored flexural resistance, M_{rx}, of the tee-section member about the strong axis (Section 3.3.4.2.2). The factored flexural resistance, M_{rx}, of tees about the x-axis at the strength limit state is to be taken as follows (Equation 3.3.43):

$$M_{rx} = \phi_f M_{nx}$$

The nominal flexural resistance about the x-axis, M_{nx}, is to be taken as the lowest value based on yielding, lateral torsional buckling or flange local buckling. For yielding, the nominal flexural resistance is given as (Equation 3.3.44):

$$M_{nx} = M_p$$

where $M_p = F_y Z_x$. The plastic section modulus, Z_x, for the tee section neglecting the effect of the web-to-flange fillets is computed by first locating the plastic neutral axis (assumed to be a distance $\bar{y}$ from the top of the flange) as follows:

Depth of stem = (7.085 – 0.785) = 6.30 in.

$$\bar{y}(10.070) = 10.070(0.785 - \bar{y}) + (6.30)(0.450)$$

$$\bar{y} = 0.533 \text{ in.}$$

Taking moments of the cross-sectional areas about the plastic neutral axis yields:

$$Z_x = \frac{10.070(0.533)^2}{2} + \frac{10.070(0.785 - 0.533)^2}{2} + 0.450(6.30)\left[(0.785 - 0.533) + \frac{(6.30)}{2}\right] = 11.39 \text{ in.}^3$$

$$M_p = (50)(11.39) = 569.5 \text{ kip} - \text{in.}$$

M_n for yielding is limited to $1.6M_y$ for stems in tension and to M_y for stems in compression. Determine if the tip of the stem is in compression or tension:

$$f_{tip} = \frac{-122}{10.90} + \frac{222.0}{6.25} = 24.3 \text{ ksi} \quad \text{(tension)}$$

Therefore:

$$1.6M_y = 1.6F_yS_x = 1.6(50)(6.25) = 500.0\ \text{kip}-\text{in.} < M_p$$

$$\therefore M_{nx} = 500.0\ \text{kip}-\text{in.} \quad \text{(for yielding)}$$

For lateral-torsional buckling (Equation 3.3.45):

$$M_{nx} = \frac{\pi\sqrt{EI_yGJ}}{L_b}\left[B + \sqrt{1+B^2}\right] \le M_p$$

From Equation 3.3.46:

$$B = \pm 2.3\frac{d}{L_b}\sqrt{\frac{I_y}{J}}$$

The plus sign on the value of *B* applies when the stem is in tension. Therefore:

$$B = +2.3\frac{7.085}{145.2}\sqrt{\frac{66.9}{1.94}} = +0.659$$

$$M_{nx} = \frac{\pi\sqrt{29{,}000(66.9)(11{,}200)(1.94)}}{145.2}\left[0.659 + \sqrt{1+0.659^2}\right] = 8{,}247\ \text{kip}-\text{in.} > M_p$$

$$\therefore M_{nx} = M_p = 569.5\ \text{kip}-\text{in.} \quad \text{(lateral-torsional buckling)}$$

Since the flange is in compression, the limit state of flange local buckling must also be considered (Section 3.3.4.2.2.3). The flange slenderness, λ_f = $b_f/2t_f$ = 10.070/2(0.785) = 6.4, does not exceed the slenderness limit for a compact flange, $\lambda_{pf} = 0.38\sqrt{E/F_y}$ = 9.2. Therefore, flange local buckling does not control and need not be checked.

Thus, the nominal flexural resistance, M_{nx}, of the tee section is controlled by yielding and is equal to 500.0 kip-in. The factored flexural resistance, M_{rx}, is equal to (Equation 3.3.43):

$$M_{rx} = \phi_f M_{nx} = 1.0(500.0) = 500.0\ \text{kip}-\text{in.}$$

Interaction curves for tee members subject to eccentric axial compression are discussed in Sections 3.3.4.3.1 and 3.3.4.4. The beam-column resistance for the singly symmetric tee-section member will conservatively be checked in this case using Equations 3.3.50 and 3.3.51 (Section 3.3.4.3.1). Since P_u/P_r = $|-122|/308 = 0.40 > 0.2$, Equation 3.3.51 controls as follows:

$$\frac{P_u}{P_r} + \frac{8.0}{9.0}\frac{M_{ux}}{M_{rx}} \le 1.0$$

$$\frac{|-122|}{308} + \frac{8.0}{9.0}\left(\frac{295.3}{500.0}\right) = 0.92 < 1.0 \qquad \text{ok}$$

If a timber were used to brace the member at mid-length in the vertical plane during construction, and upward movement of the tee section was prevented at the brace point, the unbraced length with respect to flexural buckling about the x-axis would be reduced and a smaller tee section could potentially be used.

The above calculations illustrate the design of a lateral bracing member for the largest observed compressive force. Smaller members should be used where feasible at other locations where lower forces are present. Consideration might be given to the development of a practical grouping of different member sizes for the lateral bracing according to the largest demand within various regions of the bridge.

5.2.9.8 Bolted Field Splice Design

5.2.9.8.1 General

The design of bolted girder splices is covered in Section 3.3.7. The following is a complete example design of the bolted field splice in Span 1 of G2 (Figure 5.2.3 Part A). The splice is located 60′-2″ from Pier 1. The girder plate sizes on the left- and right-hand side of the point of splice are as follows:

Left Side:	Top Flanges	1″ x 18″	Right Side:	Top Flanges	1-1/4″ x 20″
	Web	5/8″ x 80.39″		Web	5/8″ x 80.39″
	Bot. Flange	3/4″ x 76″		Bot. Flange	1-1/4″ x 76″

The sections on both sides of the splice are homogeneous utilizing ASTM A 709 Grade 50W steel for the flanges and web.

AASHTO LRFD Article C6.13.6.1.4a suggests that the smaller section at the point of splice in a flexural member be taken as the side of the splice that has the smaller calculated moment of inertia for the non-composite steel section. The left side of the splice qualifies as the smaller section according to this criterion. Thus, only the calculations for the left side of the splice are shown below.

The elastic section properties of the gross section on the left side of the splice are as follows (Table 5.2.11). The section properties include the longitudinal component of the top flange bracing area:

Table 5.2.11 Elastic Section Properties of the Gross Section on the Left Side of the Bolted Splice (in Span 1 of G2)

	I ($in.^4$)	S_{top} ($in.^3$)	S_{bot} ($in.^3$)	Neutral Axis* (in.)
Steel	201,500	4,672	5,503	36.62
Steel + Long. Reinforcement	241,351	6,147	5,961	40.49
3n Composite	384,331	15,095	7,079	54.29
n Composite	528,681	45,576	7,758	68.15

* Neutral axis is measured from the bottom of the steel

The unfactored vertical bending moments and vertical shears in the critical web at the point of splice from the 3D analysis are as follows:

M_{steel} = +467 kip-ft
M_{DC1} = +1,950 kip-ft
$M_{deck\ casting}$ = +4,082 kip-ft
M_{DC2} = +251 kip-ft
M_{DW} = +339 kip-ft
M_{+LL+IM} = +5,066 kip-ft
M_{-LL+IM} = -2,926 kip-ft

V_{steel} = -20 kips
V_{DC1} = -89 kips
$V_{deck\ casting}$ = -89 kips
V_{DC2} = -12 kips
V_{DW} = -12 kips
V_{+LL+IM} = +35 kips
V_{-LL+IM} = -89 kips

The unfactored torques at the point of splice from the 3D analysis are as follows:

T_{steel} = -45 kip-ft
T_{DC1} = -207 kip-ft
$T_{deck\ casting}$ = -217 kip-ft
T_{DC2} = -51 kip-ft
T_{DW} = -39 kip-ft
T_{+LL+IM} = +309 kip-ft
T_{-LL+IM} = -537 kip-ft

The splice is located halfway between the two adjacent cross-frames. The largest unfactored lateral flange bending moments in the top flanges at the point of splice (which are available from the 3D analysis in this case) are as follows:

$(M_\ell)_{steel}$ = +1 kip-ft
$(M_\ell)_{deck\ casting}$ = +4 kip-ft

The DC_2 and DW vertical bending moments are positive at the point of splice. By inspection, it is apparent that the unfactored compressive vertical bending stress in the concrete deck due to the DC_2 and DW moments is overcome by the unfactored tensile vertical bending stress in the deck due to the negative live load moment plus impact. Therefore, as specified in *AASHTO LRFD* Article 6.10.1.1.1b, the vertical bending stresses due to the DC_2 and DW moments will be computed using the 3*n* composite section properties for combination with the positive live load plus impact vertical bending stress. For combination with the negative live load plus impact

vertical bending stress, the stresses due to these moments will be computed using the section properties for the steel girder plus the longitudinal reinforcement (Section 3.2.6.6).

Calculate the unfactored vertical bending stresses at the mid-thickness of the bottom flange:

$$f_{DC1} = \frac{1{,}950(12)(36.245)}{201{,}500} = +4.21\,\text{ksi}$$

$$f_{DC2} = \frac{251(12)(53.915)}{384{,}331} = +0.42 \quad (3n)$$

$$f_{DC2} = \frac{251(12)(40.115)}{241{,}351} = +0.50 \quad (\text{steel} + \text{reinf.})$$

$$f_{DW} = \frac{339(12)(53.915)}{384{,}331} = +0.57\ \text{ksi} \quad (3n)$$

$$f_{DW} = \frac{339(12)(40.115)}{241{,}351} = +0.68\ \text{ksi} \quad (\text{steel} + \text{reinf.})$$

$$f_{+LL+IM} = \frac{5{,}066(12)(67.775)}{528{,}681} = +7.79\ \text{ksi}$$

$$f_{-LL+IM} = \frac{-2{,}926(12)(40.115)}{241{,}351} = -5.84\ \text{ksi}$$

Calculate the unfactored vertical bending stresses at the mid-thickness of the top flange:

$$f_{DC1} = \frac{1{,}950(12)(-42.63)}{201{,}500} = -4.95\ \text{ksi}$$

$$f_{DC2} = \frac{251(12)(-24.96)}{384{,}331} = -0.20\ \text{ksi}\ (3n)$$

$$f_{DC2} = \frac{251(12)(-38.76)}{241{,}351} = -0.48\ \text{ksi} \quad (\text{steel} + \text{reinf.})$$

$$f_{DW} = \frac{339(12)(-24.96)}{384{,}331} = -0.26 \text{ ksi} \quad (3n)$$

$$f_{DW} = \frac{339(12)(-38.76)}{241{,}351} = -0.65 \text{ ksi} \quad (\text{steel} + \text{reinf.})$$

$$f_{+LL+IM} = \frac{5{,}066(12)(-11.10)}{528{,}681} = -1.28 \text{ ksi}$$

$$f_{-LL+IM} = \frac{-2{,}926(12)(-38.76)}{241{,}351} = +5.64 \text{ ksi}$$

5.2.9.8.2 Flange Splice Design

Bolted flange splice design is covered in Section 3.3.7.2.

5.2.9.8.2.1 Minimum Design Forces

Since the splice is located in an area of stress reversal, checks must be made for both the positive and negative flexure conditions. Compute the combined factored vertical bending stresses at the midthickness of the bottom and top flanges at the strength limit state for each of these conditions using the appropriate load factors given in *AASHTO LRFD* Tables 3.4.1-1 and 3.4.1-2. The Strength I load combination is used (the load modifier, η, is taken equal to 1.0). Note that the minimum load factors, γ_p, from *AASHTO LRFD* Table 3.4.1-2 and a load modifier, $1/\eta$ (≤1.0), are applied to the permanent loads when the corresponding stresses are of opposite sign to the live load plus impact stress.

- Bottom Flange

  A. Dead Load + Positive Live Load:

$$f = 1.0(1.25)(+4.21) + (1.0)(1.25)(+0.42) + 1.0(1.50)(+0.57) + (1.0)(1.75)(+7.79) = +20.28 \text{ ksi}$$

  B. Dead Load + Negative Live Load:

$$f = (1/1.0)(0.90)(+4.21) + (1/1.0)(0.90)(+0.50) + (1/1.0)(0.65)(+0.68) + 1.0(1.75)(-5.84) = -5.54 \text{ ksi}$$

- Top Flange

  A. Dead Load + Positive Live Load:

$$f = 1.0(1.25)(-4.95) + (1.0)(1.25)(-0.20) + 1.0(1.50)(-0.26) + (1.0)(1.75)(-1.28) = -9.07 \text{ ksi}$$

B. Dead Load + Negative Live Load:

$$f = (1/1.0)(0.90)(-4.95) + (1/1.0)(0.90)(-0.48) + (1/1.0)(0.65)(-0.65) + 1.0(1.75)(+5.64) = +4.56 \text{ ksi}$$

The controlling flange is defined as the top or bottom flange for the smaller section at a point of splice, whichever flange has the maximum ratio of the elastic flexural stress at its midthickness due to the factored loads to its factored flexural resistance (Section 3.3.7.2.2.1). The factored flexural resistance, F_r, of each flange on the left side of the splice is determined from separate calculations similar to those demonstrated previously. The ratios of f/F_r for each condition (positive and negative flexure) are as follows:

- Bottom Flange

  A. Dead Load + Positive Live Load:

  F_r = 49.95 ksi; $|f/F_r|$ = 0.41

  B. Dead Load + Negative Live Load:

  F_r = -11.4 ksi; $|f/F_r|$ = 0.48

- Top Flange

  A. Dead Load + Positive Live Load:

  F_r = 50 ksi; $|f/F_r|$ = 0.18

  B. Dead Load + Negative Live Load:

  F_r = 50 ksi; $|f/F_r|$ = 0.09

Therefore, the bottom flange is the controlling flange for both the positive and negative flexure conditions. The top flange is the noncontrolling flange (Section 3.3.7.2.2.2) for both the positive and negative flexure conditions in this case.

Positive Flexure

For the case of positive flexure, the minimum design stress for the controlling (bottom) flange at the strength limit state, F_{cf}, is computed as (Equation 3.3.127):

$$F_{cf} = \frac{\left(\left|\frac{f_{cf}}{R_h}\right| + \alpha\phi_f F_{yf}\right)}{2} \geq 0.75\alpha\phi_f F_{yf}$$

The hybrid factor, R_h, is taken as 1.0 for homogeneous sections and α is taken equal to 1.0 for flanges in tension. f_{cf} is the maximum factored vertical bending stress at the midthickness of the controlling flange at the point of splice = +20.28 ksi. Therefore:

$$\frac{\left|\frac{f_{cf}}{R_h}\right| + \alpha F_{yf}}{2} = \frac{\left|\frac{+20.28}{1.0}\right| + 1.0(50)}{2} = 35.14 \text{ ksi}$$

$$0.75\alpha F_{yf} = 0.75(1.0)(50) = 37.50 \text{ ksi} \quad \text{(governs)}$$

The minimum design force for the controlling flange, P_{cf}, is taken equal to the design stress, F_{cf}, times the smaller effective flange area, A_e, on either side of the splice. The smaller effective bottom-flange area is on the left side of the splice.

For flanges subject to tension, A_e is computed as (Equation 3.3.128):

$$A_e = \left(\frac{\phi_u F_u}{\phi_y F_{yt}}\right) A_n \le A_g$$

From *AASHTO LRFD* Table 6.4.1-1, F_u for ASTM A 709 Grade HPS 50W steel is 70 ksi. Assume the bottom flange splice will consist of 18 rows of 7/8-in. diameter A 325 high-strength bolts across the width of the flange (to be confirmed later). *AASHTO LRFD* Article 6.8.3 specifies that the width of standard bolt holes (which must be used for bolted splices in flexural members) for design is to be taken as the nominal diameter of the hole specified in *AASHTO LRFD* Article 6.13.2.4.2. The nominal diameter of a standard hole for a 7/8-in diameter bolt is 15/16 inches (Section 3.3.6.2.5.1). Therefore:

$$A_n = [76.0 - 18(0.9375)](0.75) = 44.34 \text{ in.}^2$$

$$A_g = 76.0(0.75) = 57.00 \text{ in.}^2$$

ϕ_u is the resistance factor for fracture in tension components (=0.80) and ϕ_y is the resistance factor for yielding in tension components (=0.95) (*AASHTO LRFD* Article 6.5.4.2).

$$A_e = \left(\frac{0.80(70)}{0.95(50)}\right) 44.34 = 52.27 \text{ in.}^2 < 57.00 \text{ in.}^2$$

$$P_{cf} = F_{cf} A_e = 37.50(52.27) = 1{,}960 \text{ kips}$$

For the case of positive flexure, the minimum design stress for the noncontrolling (top) flange at the strength limit state, F_{ncf}, is computed as (Equation 3.3.129):

$$F_{ncf} = R_{cf}\left|\frac{f_{ncf}}{R_h}\right| \geq 0.75\alpha\phi_f F_{yf}$$

f_{ncf} is the factored vertical bending stress at the midthickness of the noncontrolling flange at the point of splice concurrent with f_{cf} and is equal to -9.07 ksi. The top flange is in compression and is continuously braced for this condition. Therefore, since $F_{nc} = F_{yf}$, α must be taken equal to 1.0.

$$R_{cf} = \left|\frac{F_{cf}}{f_{cf}}\right| = \left|\frac{37.50}{+20.28}\right| = 1.85$$

$$R_{cf}\left|\frac{f_{ncf}}{R_h}\right| = 1.85\left|\frac{-9.07}{1.0}\right| = 16.78 \text{ ksi}$$

$$0.75\alpha F_{yf} = 0.75(1.0)(50) = 37.50 \text{ ksi} \quad \text{(governs)}$$

The minimum design force for the noncontrolling flange, P_{ncf}, is taken equal to the design stress, F_{ncf}, times the smaller effective flange area, A_e, on either side of the splice. The smaller effective top-flange area is on the left side of the splice. A_e is taken equal to A_g for flanges subject to compression.

$$A_e = A_g = 18(1.0) = 18.00 \text{ in.}^2$$

$$P_{ncf} = F_{ncf}A_e = 37.50(18.00) = 675 \text{ kips/per flange}$$

Negative Flexure

For the case of negative flexure, the controlling (bottom) flange is subject to compression. The factored flexural resistance of the bottom flange in compression, F_r, is significantly less than F_{yf} in this particular case; therefore, the factor, α, will be computed. α is taken equal to the nominal compressive resistance of the flange, F_{nc} = 11.4 ksi divided by F_{yf}, or 11.4/50 = 0.23. The factored vertical bending stress in the controlling flange, f_{cf} = -5.54 ksi. Therefore:

$$\frac{\left|\frac{f_{cf}}{R_h}\right| + \alpha F_{yf}}{2} = \frac{\left|\frac{-5.54}{1.0}\right| + 0.23(50)}{2} = 8.52 \text{ ksi}$$

$$0.75\alpha F_{yf} = 0.75(0.23)(50) = 8.63 \text{ ksi} \quad (\text{governs})$$

A_e is taken equal to A_g for flanges subject to compression.

$$A_g = 76.0(0.75) = 57.00 \text{ in.}^2$$

$$P_{cf} = F_{cf} A_e = 8.63(57.00) = 492 \text{ kips}$$

For the case of negative flexure, the noncontrolling (top) flange is subject to tension; therefore, α is equal to 1.0. The factored vertical bending stress in the noncontrolling flange, f_{ncf} = +4.56 ksi.

$$R_{cf} = \left|\frac{F_{cf}}{f_{cf}}\right| = \left|\frac{8.63}{-5.54}\right| = 1.56$$

$$R_{cf}\left|\frac{f_{ncf}}{R_h}\right| = 1.56\left|\frac{4.56}{1.0}\right| = 7.11 \text{ ksi}$$

$$0.75\alpha F_{yf} = 0.75(1.0)(50) = 37.50 \text{ ksi} \quad \text{(governs)}$$

Assume each top flange splice will consist of 4 rows of 7/8-in. diameter A 325 high-strength bolts across the width of the flange (to be confirmed later). Therefore:

$$A_n = [18.0 - 4(0.9375)](1.0) = 14.25 \text{ in.}^2$$

$$A_g = 18.0(1.0) = 18.00 \text{ in.}^2$$

$$A_e = \left(\frac{0.80(70)}{0.95(50)}\right)14.25 = 16.80 \text{ in.}^2 < 18.00 \text{ in.}^2$$

$$P_{ncf} = F_{ncf} A_e = 37.50(16.80) = 630 \text{ kips / per flange}$$

A summary of the design forces for the bottom and top flange splices at the strength limit state is as follows:

Bottom Flange: P_{cf} = 1,960 kips (tension)
P_{cf} = 492 kips (compression)

Top Flange: P_{ncf} = 675 kips (compression)
P_{ncf} = 630 kips (tension)

5.2.9.8.2.2 Bottom Flange Splice

Try 3/8" x 69-3/8" inside and outside splice plates. Include a 1/2" x 69-3/8" filler plate on the outside, as shown in Figure 5.1.28. All plates are ASTM A 709 Grade 50W steel.

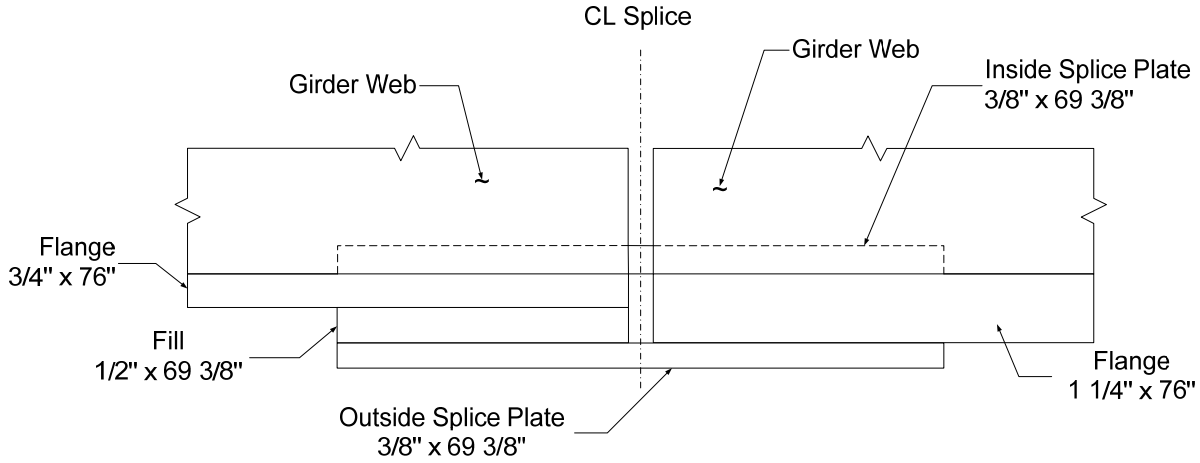


Figure 5.2.12 Elevation View of Bottom Flange Splice in Span 1 of G2 (bolts not shown)

Strength Limit State

Splice Plates

AASHTO LRFD Article 6.13.5.2 specifies that splice plates in tension at the strength limit state be checked for yielding on the gross section, fracture on the net section and block shear rupture.

AASHTO LRFD Article 6.13.6.1.4c specifies that for horizontally curved box-girder bridges, St. Venant torsional shear must be considered in the design of the bolted splices for box flanges at all limit states. The box flange splices in these cases are to be designed at the strength limit state for the combined effects of the appropriate flange force and the moment resulting from the eccentricity of the factored St. Venant torsional shear, M_{SV} (Section 3.3.7.2.5.2).

Longitudinal warping stresses due to cross-section distortion may be ignored when checking both the top and bottom flange splices at the strength limit state, as these stresses are typically limited through the provision of sufficient internal cross bracing (Section 3.3.7.2.5.3).

For yielding, the splice plates may be checked for the combined stress as follows:

$$\frac{P}{(A_g)_{PL}} + \frac{M_{SV}}{S_{PL}} \le \phi_y F_y$$

Calculate the factored St. Venant torsional shear flow, *f*, in the bottom flange at the point of splice for the Strength I load combination. The negative live load plus impact torque controls by inspection.

For the DC_1 torque, which is applied to the non-composite section, the enclosed area, A_o, is computed for the non-composite box section. The vertical depth between the mid-thickness of the flanges is used. Therefore:

$$A_o = \frac{(111+72)}{2} * (78.0 + 0.375 + 0.5) * \frac{1\,ft^2}{144\,in.^2} = 50.1\,ft^2$$

From Equation 1.1.12:

$$f = \frac{T}{2A_o}$$

$$f = \frac{1.0(1.25)(-207)}{2(50.1)} = -2.58\ kips/ft$$

For the torques applied to the composite section, calculate A_o for the composite section from the mid-thickness of the bottom flange to the mid-thickness of the concrete deck (considering the deck haunch):

$$A_o = \frac{(111+72)}{2} * (78.0 + 0.375 + 5.0 + \frac{9.5}{2}) * \frac{1\,ft^2}{144\,in.^2} = 56.0\ ft^2$$

$$f = \frac{1.0\left|1.25(-51) + 1.5(-39) + 1.75(-537)\right|}{2(56.0)} = -9.48\ kips/ft$$

$$f_{total} = -2.58 + -9.48 = -12.06\ kips/ft$$

The factored St. Venant torsional shear at the strength limit state, V_{SV}, at the point of splice is computed as:

$$V_{SV} = f_{total} b_f = \left|-12.06\right| \frac{72.0}{12} = 72.4\ kips$$

Calculate the moment, M_{SV}, in the bottom flange due to the eccentricity of the factored St. Venant torsional shear. Assume the shear is applied at the centerline of the splice (refer to Figure 5.2.13).

$$M_{SV} = 72.4(2.25 + 4.50) = 488.7 \text{ kip} - \text{in.}$$

$(A_g)_{PL}$ is the total gross area of the inner and outer splice plates computed as:

$$(A_g)_{PL} = 2[0.375(69.375)] = 52.0 \text{ in.}^2$$

S_{PL} is the total gross lateral section modulus of the inner and outer splice plates computed as:

$$S_{PL} = 2\left[\frac{0.375(69.375)^2}{6}\right] = 602 \text{ in.}^3$$

Therefore:

$$\frac{1{,}960}{52.0} + \frac{488.7}{602} = 38.5 \text{ ksi} < 0.95(50) = 47.5 \text{ ksi} \quad \text{ok}$$

The preceding check and the checks that follow assume that the areas of the inner and outer flange splice plates do not differ by more than 10 percent. In this case, the areas of the inner and outer splice plates are equal. Otherwise, P and M_{SV} should be proportioned to the inner and outer splice plates by the ratio of the area(s) of the inner and outer plate(s) to the total area of the splice plates, with the splice plates than checked individually using their respective actions.

For net section fracture, the splice plates may be checked for the combined stress as follows:

$$\frac{P}{(A_n)_{PL}} + \frac{M_{SV}}{(S_n)_{PL}} \le \phi_u F_u U$$

U is a reduction factor to account for shear lag, which is to be taken as 1.0 for splice plates (*AASHTO LRFD* Article 6.13.5.2).

$(A_n)_{PL}$ is the total net area of the inner and outer splice plates computed as:

$$(A_n)_{PL} = 2[69.375 - 18(0.9375)](0.375) = 39.4 \text{ in.}^2$$

$(S_n)_{PL}$ is the total net lateral section modulus of the inner and outer splice plates, which may be computed in this case as:

$$(S_n)_{PL} = 2\left(\frac{\left[(I_g)_{PL} - \sum_{i=1}^{N_b} A_{hole} Y_i^2\right]}{c}\right)$$

I_g is the gross lateral moment of inertia of each splice plate, c is the half-width of each splice plate, and the Y_i distances for each bolt hole are defined in Figure 3.3.63. Therefore, referring to Figure 5.2.13:

$$\sum_{i=1}^{N_b} A_{hole} Y_i^2 = 2(0.375)(0.9375)(1.9375^2 + 5.8125^2 + 9.6875^2 + 13.5625^2 + 17.4375^2 + 21.3125^2 + 25.1875^2 + 29.0625^2 + 32.9375^2) = 2{,}558 \text{ in.}^4$$

$$(S_n)_{PL} = 2\left(\frac{\left[0.375(69.375)^3/12 - 2{,}558\right]}{(69.375/2)}\right) = 454 \text{ in.}^3$$

Therefore:

$$\frac{1{,}960}{39.4} + \frac{488.7}{454} = 50.8 \text{ ksi} < 0.8(70)(1.0) = 56.0 \text{ ksi} \quad \text{ok}$$

Also, according to *AASHTO LRFD* Article 6.13.5.2, for splice plates subject to tension, A_n must not exceed $0.85A_g$.

$$0.85(2)(69.375)(0.375) = 44.2 \text{ in}^2 > A_n = 2[69.375 - 18(0.9375)](0.375) = 39.4 \text{ in.}^2 \quad \text{ok}$$

The block shear rupture resistance of the splice plates will be checked later.

Flange splice plates subject to compression are checked for yielding on the gross section at the strength limit state. Since bottom flange splice plates subject to compression must also be checked for the combined stress; the following equation may be used. The equation assumes an unbraced length of zero for the splice plates.

$$\frac{P}{(A_g)_{PL}} + \frac{M_{SV}}{S_{PL}} \le \phi_c F_y$$

ϕ_c is the resistance factor for compression elements (=0.90) (*AASHTO LRFD* Article 6.5.4.2).

Therefore:

$$\frac{492}{52.0}+\frac{488.7}{602}=10.3\text{ ksi}<0.90(50)=45.0\text{ ksi}\quad\text{ ok}$$

Bolts

Determine the number of bolts for the bottom flange splice plates that are required to develop the governing combined design actions in the flange in shear at the strength limit state assuming the bolts in the connection have slipped and gone into bearing.

The nominal shear resistance, R_n, for a 7/8-in. diameter A325 high-strength bolt in double shear assuming the threads are *excluded* from the shear planes is computed as (Equation 3.3.82):

$$R_n=0.48A_bF_{ub}N_s$$

A_b is the area of the bolt corresponding to the nominal diameter equal to $\pi(0.875)^2/4=0.60$ in.^{2} F_{ub} is the specified minimum tensile strength of the bolt equal to 120 ksi for bolts less than or equal to 1.0 inch in diameter (*AASHTO LRFD* Article 6.4.3). N_s is the number of shear planes per bolt. Therefore:

$$R_n=0.48(0.60)(120)(2)=69.1\,\text{kips/bolt}$$

The factored shear resistance of the bolt, R_r, is equal to R_n times the resistance factor, ϕ_s, for shear on bolts equal to 0.80 (AASHTO LRFD Article 6.5.4.2). Therefore:

$$R_r=0.80(69.1)=55.3\text{ kips/bolt}$$

Since the factored shear resistance of the bolts is based on the assumption that the threads are excluded from the shear planes, an appropriate note should be placed on the contract plans to ensure that the splice is detailed to exclude the bolt threads from the shear planes. The length between the extreme bolts (on one side of the connection) measured parallel to the line of action of the force will obviously be less than 50.0 in. in this case so that no reduction in the factored shear resistance is required.

The traditional elastic vector method for eccentric shear (Section 3.3.6.2.7) may be used to account for the effects of the moment due to the eccentricity of the St. Venant torsional shear in the design of the flange splice bolts. The direct shear on the flange bolts at the strength limit state (*P* in Figure 3.3.62) is caused by the governing minimum flange design force. The moment, M_ℓ (Figure 3.3.62), on the bolt

group in this case is taken as the calculated moment due to the eccentricity of the St. Venant torisonal shear, M_{sv}.

To utilize the elastic vector method to determine the maximum resultant force in the extreme bolt under the combined actions, the polar moment of inertia, I_p, of the entire bolt group must first be computed. Referring to Figure 3.3.64, I_p may be computed as follows (Equation 3.3.108). Note in this case the the Y-axis in Figure 3.3.64 is located at the centroid of the bolt group on one side of the splice:

$$I_p = \sum_{i=1}^{n} x_i^2 + \sum_{i=1}^{n} y_i^2$$

Assuming the bolt pattern shown below for the bottom flange splice in Figure 5.2.13, I_p is computed as follows:

$$I_p = \left[2(18)(4.50^2)\right] + \begin{bmatrix} 2(3)(1.9375^2 + 5.8125^2 + 9.6875^2 + 13.5625^2 + 17.4375^2 + 21.3125^2 \\ + 25.1875^2 + 29.0625^2 + 32.9375^2) \end{bmatrix}$$

$$= 22{,}554 \text{ in}^2$$

The bolt force due to the moment is computed in two components. *X* and *Y* in the two equations given immediately below are defined in Figure 3.3.65.

The longitudinal component, P_{Mx}, is computed as:

$$P_{Mx} = \frac{M_{SV} Y}{I_p}$$

$$P_{Mx} = \frac{488.7(32.9375)}{22{,}554} = 0.71 \text{ kips}$$

Similarly, the transverse component, P_{My}, is computed as:

$$P_{My} = \frac{M_{SV} X}{I_p}$$

$$P_{My} = \frac{488.7(4.50)}{22{,}554} = 0.10 \text{ kips}$$

The bolt force due to shear caused by the governing minimum design force, P_v, is taken equal to (Equation 3.3.146):

$$P_v = \frac{P}{N_b}$$

where N_b is the number of bolts in the bolt group.

$$P_v = \frac{1{,}960}{54} = 36.3 \text{ kips}$$

The bolt force due to the factored St. Venant torsional design shear is:

$$P_v = \frac{V_{sv}}{N_b}$$

$$P_{SV} = \frac{72.4}{54} = 1.34 \text{ kips}$$

The maximum resultant bolt force in the critical extreme bolt, P_r (Figure 3.3.65), is then computed as:

$$P_r = \sqrt{(P_v + P_{Mx})^2 + (P_{SV} + P_{My})^2}$$

$$P_r = \sqrt{(36.3 + 0.71)^2 + (1.34 + 0.10)^2} = 37.0 \text{ kips}$$

Filler plates 0.25 in. or greater in thickness in girder flange splices must be secured by additional bolts to ensure that shear planes are well defined and that no reduction in the factored shear resistance of the bolts results (Section 3.3.7.4.2). *AASHTO LRFD* Article 6.13.6.1.5 specifies that this can be accomplished by either: 1) extending the fillers beyond the splice plate with the filler extension secured by enough additional bolts to distribute the total stress uniformly over the combined section of the member or filler; or 2) in lieu of extending and developing the fillers, reducing the factored shear resistance of the bolts by the following factor (Equation 3.3.157):

$$R = \left[\frac{(1+\gamma)}{(1+2\gamma)} \right]$$

In this example, the factored shear resistance of the bolts on the side of the splice with the filler plate will be reduced by the factor *R* as follows:

$$A_f = 0.5(69.375) = 34.7 \text{ in.}^2$$

$$A_p = \text{flange area} = 0.75(76.0) = 57.0 \text{ in.}^2 \quad \text{or}$$

$$A_p = \text{splice plate area} = 2[0.375(69.375)] = 52.0 \text{ in.}^2 \quad \text{(governs)}$$

$$\gamma = \frac{34.7}{52.0} = 0.667$$

$$R = \frac{1 + 0.667}{1 + 2(0.667)} = 0.714$$

$$R * R_r = 0.714 * 55.3 \text{ kips} = 39.5 \text{ kips} > P_r = 37.0 \text{ kips} \quad \text{ok}$$

Therefore, a minimum of 54 bolts is required to provide the necessary factored shear resistance for the bottom flange splice at the strength limit state under the controlling minimum design force. Use fifty-four (54) 7/8-in. diameter high-strength bolts on each side of the bottom flange splice (3 rows of bolts with 18 bolts per row -- no stagger – Figure 5.2.13). The slip resistance of these bolts at the service limit state and for constructibility is checked later on.

Bolt Spacing

To check the factored bearing resistance of the bolt holes and the block shear rupture resistance of the splice plates and the flange, the bolt spacings and bolt edge and end distances must first be established and checked. Examine the bolt spacings and edge and end distances shown in Figure 5.2.13.

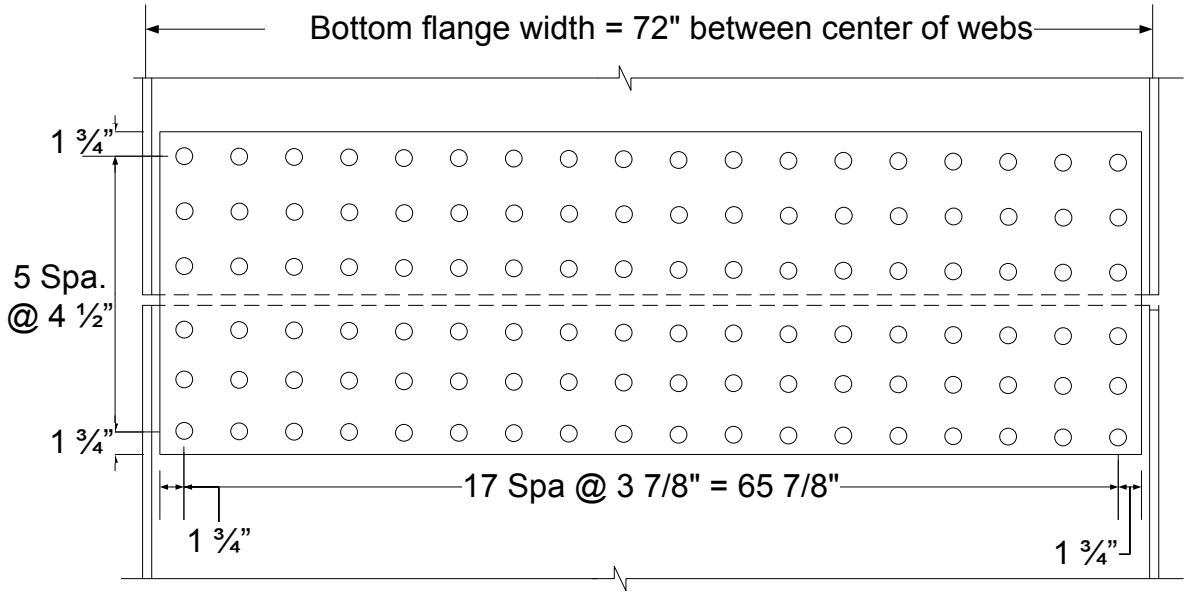


Figure 5.2.13 Bolt Configuration for Bottom Flange Splice in Span 1 of G2

AASHTO LRFD Article 6.13.2.6.1 specifies that the minimum spacing between centers of bolts in standard holes is not to be less than 3.0*d*, where *d* is the diameter of the bolt (Section 3.3.6.2.2.6). For 7/8-in. diameter bolts:

$$s_{min} = 3d = 3(0.875) = 2.63 \text{ in.} \quad \text{use } 3.0 \text{ in. min.} \quad \text{ok}$$

AASHTO LRFD Article 6.13.2.6.2 specifies that to seal against the penetration of moisture in joints, the spacing, *s*, of a single line of bolts adjacent to a free edge of an outside plate or shape (when the bolts are not staggered) must satisfy the following requirement (Section 3.3.6.2.2.6 - Equation 3.3.75):

$$s \le (4.0 + 4.0t) \le 7.0 \text{ in.}$$

where *t* is the thickness of the thinner outside plate or shape. First, check for sealing along the edges of the outer splice plate (which is the thinner plate) parallel to the direction of the applied force:

$$s_{max} = 4.0 + 4.0(0.375) = 5.5 \text{ in.} > 4.5 \text{ in.} \quad \text{ok}$$

Check for sealing along the free edge at the end of the splice plate:

$$s_{max} = 4.0 + 4.0(0.375) = 5.5 \text{ in.} > 3.875 \text{ in.} \quad \text{ok}$$

The edge distance of bolts is defined as the distance perpendicular to the line of force between the center of a hole and the edge of the component. In this example, the edge distance of 1-3/4 inches satisfies the minimum edge distance requirement of 1½ inches specified for 7/8-in. diameter bolts and sheared edges in *AASHTO LRFD* Table 6.13.2.6.6-1 (Section 3.3.6.2.2.6 – Table 3.3.2). The maximum edge distance requirement of 8.0*t* (not to exceed 5.0 in.) = 8.0(0.375) = 3.0 in. specified in *AASHTO LRFD* Article 6.13.2.6.6 is also obviously satisfied.

The end distance of bolts is defined as the distance along the line of force between the center of a hole and the end of the component. In this example, the end distance on the splice plates of 1-3/4 inches satisfies the minimum end distance requirement of 1½ inches specified for 7/8-in. diameter bolts and sheared edges in Table 3.3.2. The maximum end distance requirement of 8.0*t* (not to exceed 5.0 in.) = 8.0(0.375) = 3.0 in. is also obviously satisfied. Although not specifically required, note that the maximum distance from the corner bolts to the corner of the splice plate, equal to $\sqrt{(1.75)^2 + (1.75)^2} = 2.47 \text{ in.}$, also satisfies the maximum end distance requirement. If desired, the corners of the plate can be clipped to meet this requirement.

Bearing Resistance

The bearing resistance of the connected material at the strength limit state is calculated as the sum of the bearing resistances of the individual bolts (holes) parallel to the line of the applied force (Section 3.3.6.2.6.2).

The splice is subject to moment due to the eccentricity of the St. Venant torsional shear; thus, the resultant force, P_r, in the extreme outer bolt acts in the direction of an inclined distance that is larger than the clear end distance. In lieu of calculating the bearing resistance based on this inclined distance, the resistance of the outermost hole, calculated using the clear end distance, will conservatively be checked against the maximum resultant bolt force, P_r.

Check the splice plates. For standard holes, the nominal bearing resistance, R_n, parallel to the applied bearing force is taken as follows (Equation 3.3.88):

$$R_n = 1.2L_c tF_u \le 2.4dtF_u$$

For the outermost bolt adjacent to the end of the splice plate, the end distance is 1.75 in. (Figure 5.2.13). The diameter of the hole is 0.9375 in. Therefore, the clear end distance, L_c, between the edge of the hole and the end of the splice plate is:

$$L_c = 1.75 - \frac{0.9375}{2} = 1.28 \text{ in.}$$

Therefore:

$$R_n = 1.2L_c tF_u = 1.2(1.28)(0.375)(70) = 40.3 \text{ kips (governs)}$$

or:

$$R_n = 2.4dtF_u = 2.4(0.875)(0.375)(70) = 55.1 \text{ kips}$$

The factored bearing resistance of each splice plate, R_r, is computed as (Equation 3.3.80):

$$R_r = \phi_{bb} R_n$$

$$R_r = 0.80(40.3 \text{ kips}) = 32.2 \text{ kips}$$

Since the areas of the inner and outer splice plates are equal, the resultant force, P_r, will be assumed distributed equally to each splice plate. Therefore:

$$P_r / 2 = 37.0/2 = 18.5 \text{ kips} < R_r = 32.2 \text{ kips} \quad \text{ok}$$

Check the thinner bottom flange at the splice. For the outermost bolt adjacent to the end of the flange, the end distance is 2.0 inches (which also satisfies the minimum end distance requirement discussed above). Therefore, the clear end distance, L_c, between the edge of the hole and the end of the flange is:

$$L_c = 2.0 - \frac{0.9375}{2} = 1.53 \text{ in.}$$

Therefore:

$$R_n = 1.2 L_c t F_u = 1.2(1.53)(0.75)(70) = 96.4 \text{ kips (governs)}$$

or:

$$R_n = 2.4 d t F_u = 2.4(0.875)(0.75)(70) = 110 \text{ kips}$$

The factored bearing resistance of the flange, R_r, is computed as (Equation 3.3.80):

$$R_r = \phi_{bb} R_n$$

$$R_r = 0.80(96.4 \text{ kips}) = 77.1 \text{ kips} > P_r = 37.0 \text{ kips} \quad \text{ok}$$

Block Shear Rupture Resistance

Check the block shear rupture resistance (Section 3.3.3.2.4) of the bottom flange splice plates and the bottom flange when subject to the minimum design force in tension at the strength limit state.

Assume the potential block shear failure plane on the outside and inside splice plates shown below in Figure 5.2.14.

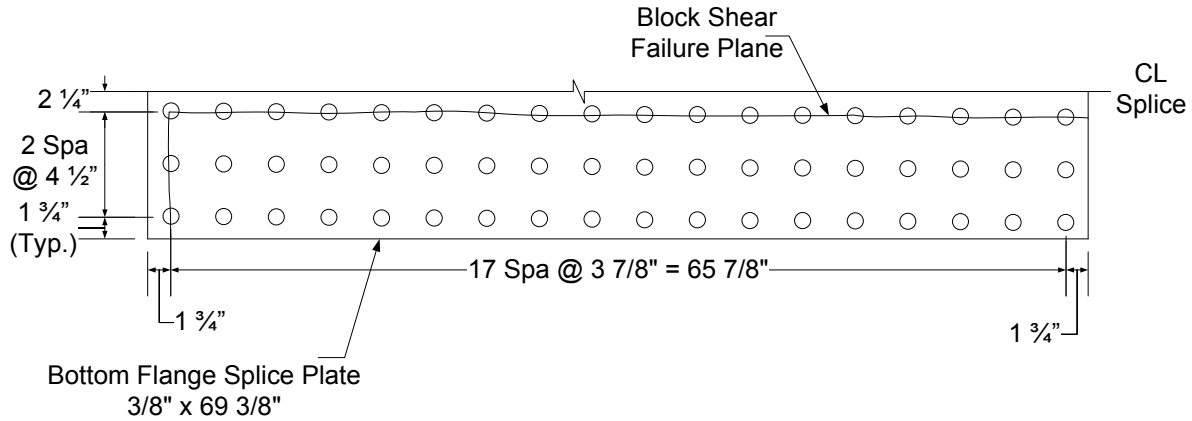


Figure 5.2.14 Assumed Block Shear Failure Planes for Bottom Flange Splice Plates

Determine the block shear rupture resistance for each of the splice plates. A_{tn} is the net area along the place resisting the tensile stress.

$$A_{tn} = 2[69.375 - 1.75 - 17.5(0.9375)](0.375) = 38.4 \text{ in}^2$$

A_{vn} is the net area along the place resisting the shear stress.

$$A_{vn} = 2[2(4.50) + 1.75 - 2.5(0.9375)](0.375) = 6.30 \text{ in}^2$$

A_{vg} is the gross area along the plane resisting the shear stress.

$$A_{vg} = 2[2(4.5) + 1.75](0.375) = 8.06 \text{ in}^2$$

The factored block shear rupture resistance, R_r, is determined as (Equation 3.3.27):

$$\begin{aligned} R_r &= \phi_{bs} R_p (0.58 F_u A_{vn} + U_{bs} F_u A_{tn}) \\ &\le \phi_{bs} R_p (0.58 F_y A_{vg} + U_{bs} F_u A_{tn}) \end{aligned}$$

ϕ_{bs} is the resistance factor for block shear rupture taken equal to 0.80 (*AASHTO LRFD* Article 6.5.4.2). The reduction factor, R_p, is taken equal to 1.0 for holes drilled full-size (Section 3.3.3.2.1). The reduction factor, U_{bs}, is taken equal to 1.0 since the tension stress is uniform (Section 3.3.3.2.4). Therefore:

$$\begin{aligned} R_r &= 0.80(1.0)[0.58(70)(6.30) + 1.0(70)(38.4)] = 2{,}355 \text{ kips} \\ &> 0.80(1.0)[0.58(50)(8.06) + 1.0(70)(38.4)] = 2{,}337 \text{ kips} \\ \therefore R_r &= 2{,}337 \text{ kips} \end{aligned}$$

Check the block shear rupture resistance as follows:

$$\frac{P}{(A_g)_{PL}} + \frac{M_{SV}}{S_{PL}} \le \frac{R_r}{(A_g)_{PL}}$$

$$\frac{1{,}960}{52.0} + \frac{488.7}{602} = 38.5 \text{ ksi} < \frac{2{,}337}{52.0} = 44.9 \text{ ksi} \quad \text{ok}$$

The block shear rupture resistance of the critical bottom flange at the splice is satisfactory by inspection since the end distance for the flange is larger than for the splice plates and a similar block shear failure plane would be assumed. The flange is also not subject to M_{sv}.

Net Section Fracture of Flange

Check for net section fracture of the critical bottom flange at the point of splice when subject to tension at the strength limit state according to the following requirement (Section 3.2.6.1.3 – Equation 3.2.72):

$$f_t \le 0.84\left(\frac{A_n}{A_g}\right)F_u \le F_{yt}$$

The flange on the left side of the splice is the critical flange for this particular check.

A_n is the net area of the flange computed as:

$$A_n = [76.0 - 18(0.9375)](0.75) = 44.34 \text{ in.}^2$$

$$0.84\left(\frac{A_n}{A_g}\right)F_u = 0.84\left(\frac{44.34}{57.00}\right)70 = 45.7 \text{ ksi} < F_{yt} = 50 \text{ ksi}$$

From separate calculations, f_t in the bottom flange at the strength limit state (Strength I) is equal to +20.42 ksi for the section on the left side of the splice, which is less than 45.7 ksi. Therefore, net section fracture of the bottom flange at the point of splice will not occur.

Service Limit State & Constructibility

Bolts

AASHTO LRFD Article 6.13.6.1.4c requires that high-strength bolted connections for flange splices be designed to prevent slip at the service limit state under a Service II design force. In addition, *AASHTO LRFD* Article 6.13.6.1.4a requires that high-strength bolted splices for flexural members be proportioned to prevent slip during the erection of the steel (assuming an erection analysis is conducted) and during the casting of the concrete deck.

Longitudinal warping stresses due to cross-section distortion (see Section 3.2.5.2.2.3) are to be considered when checking the slip resistance of the bolts for constructibility and at the service limit state for flange splices in horizontally curved box-girder bridges (Section 3.3.7.2.5.3). The internal cross-frame spacing adjacent to the splice is 13.0 feet. An examination of the longitudinal warping stresses at the bottom of the box under both conditions for this cross-frame spacing (according to calculations similar to those outlined in Sections 5.2.9.3.5 and 5.2.9.4.4) indicates that they are negligible in this case.

For the service limit state check, the Service II design stress, F_s, is to be taken as (Section 3.3.7.2.3 – Equation 3.3.131):

$$F_s = \frac{f_s}{R_h}$$

where f_s is the maximum vertical bending stress due to Load Combination Service II at the midthickness of the flange under consideration for the smaller section at the point of splice.

For the left side of the splice, which is deemed the smaller section in this case, the Service II stress at the mid-thickness of the bottom flange is computed as follows. Separate computations indicate that the conditions specified in *AASHTO LRFD* Article 6.10.4.2.1 are met such that flexural stresses caused by Service II loads applied to the composite section can be computed using the short-term or long-term composite section, as appropriate, assuming the concrete deck is effective for both positive and negative flexure (Section 3.2.4.3.1).

A. Dead Load + Positive Live Load:

$$f = \left[1.0(4.21 + 0.42 + 0.57) + 1.3(7.79)\right] = +15.33 \text{ ksi} \quad (\text{governs})$$

B. Dead Load + Negative Live Load:

$$f_{-LL+IM} = \frac{-2{,}926(12)(67.775)}{528{,}681} = -4.50 \text{ ksi}$$

$$f = \left[1.0(4.21 + 0.42 + 0.57) + 1.3(-4.50)\right] = -0.65 \text{ ksi}$$

Therefore, f_s is equal to +15,33 ksi and F_s is equal to f_s/R_h = +15.33/1.0 = +15.33 ksi. The design force, P, for the flange splice is taken as F_s times the smaller gross flange area on either side of the splice (Equation 3.3.133), or:

$$P = F_s A_g = 15.33(0.75)(76.0) = 874 \text{ kips}$$

Calculate the factored St. Venant torsional shear flow, f, in the bottom flange at the point of splice for the Service II load combination. The negative live load plus impact torque controls by inspection.

For the DC_1 torque, which is applied to the non-composite section, the enclosed area, A_o, for the non-composite box section is used to calculate the shear flow. A_o for the non-composite section was computed earlier to be 50.1 ft^2. From Equation 1.1.12:

$$f = \frac{T}{2A_o}$$

$$f = \frac{1.0(-207)}{2(50.1)} = -2.07 \text{ kips/ft}$$

The enclosed area, A_o, for the composite box section is used to calculate the shear flow for the torques applied to the composite section. A_o for the composite section was computed earlier to be 56.0 ft^2. Therefore:

$$f = \frac{|1.0(-51) + 1.0(-39) + 1.3(-537)|}{2(56.0)} = -7.04 \text{ kips/ft}$$

$$f_{total} = -2.07 + -7.04 = -9.11 \text{ kips/ft}$$

The factored St. Venant torsional shear at the service limit state, V_{SV}, at the point of splice is computed as:

$$V_{SV} = f_{total} b_f = |-9.11| \frac{72.0}{12} = 54.7 \text{ kips}$$

Calculate the moment, M_{SV}, in the bottom flange due to the eccentricity of the factored St. Venant torsional shear. Assume the shear is applied at the centerline of the splice (refer to Figure 5.2.13).

$$M_{SV} = 54.7(2.25 + 4.50) = 369.2 \text{ kip} - \text{in.}$$

The stress on the non-composite section at the mid-thickness of the bottom flange due to the steel weight plus the deck-casting sequence (the Strength IV load combination controls with η taken equal to 1.0) is:

$$f = \frac{1.0(1.5)(467 + 4{,}082)(12)(36.245)}{201{,}500} = +14.73 \text{ ksi} \qquad \frac{f}{R_h} = \frac{+14.73}{1.0} = +14.73 \text{ ksi}$$

The design force, *P,* for the flange splice is taken as *f* times the smaller gross flange area on either side of the splice (Equation 3.3.132), or:

$$P = fA_g = 14.73(0.75)(76.0) = 840 \text{ kips}$$

Calculate the factored St. Venant torsional shear flow, *f*, in the bottom flange at the point of splice for constructibility (i.e. due to the steel weight plus the deck staging) using A_o of the non-composite section:

$$f = \frac{1.0(1.5)(-45 + -217)}{2(50.1)} = -3.92 \text{ kips / ft}$$

.

The factored St. Venant torsional shear for constructibility, V_{SV}, at the point of splice is computed as:

$$V_{SV} = f * b_f = \left|-3.92\right| \frac{72.0}{12} = 23.5 \text{ kips}$$

Calculate the moment, M_{SV}, in the bottom flange due to the eccentricity of the factored St. Venant torsional shear. Assume the shear is applied at the centerline of the splice (refer to Figure 5.2.13).

$$M_{SV} = 23.5(2.25 + 4.50) = 158.6 \text{ kip} - \text{in.}$$

By inspection, the Service II case controls.

Determine the number of bolts for the bottom flange splice plates that are required to prevent slip. The factored slip resistance, R_r, for a 7/8-in. diameter A 325 high-strength bolt assuming a Class B surface condition for the faying surface, standard holes and two slip planes per bolt (i.e. N_s = 2) is computed as follows (Section 3.3.6.2.6.1 – Equations 3.3.77 and 3.3.78):

$$R_r = R_n = K_h K_s N_s P_t$$

The hole size factor, K_h, is equal to 1.0 for standard holes (Table 3.3.4). The surface condition factor, K_s, for a Class B faying surface is 0.50 (Table 3.3.5). The minimum required bolt tension, P_t, for a 7/8-inch diameter A 325 high-strength bolt is 39 kips (Table 3.3.1). Therefore:

$$R_r = R_n = 1.0(0.5)(2)(39) = 39.0 \text{ kips / bolt}$$

AASHTO LRFD Article 6.13.6.1.5 specifies that the factored slip resistance need not be adjusted for the effect of filler plates.

Referring to the bolt pattern shown for the bottom flange splice in Figure 5.2.13, calculate the maximum resultant force on the extreme bolt under the combined actions. The longitudinal component, P_{Mx}, is computed as:

$$P_{Mx} = \frac{M_{SV} Y}{I_p}$$

$$P_{Mx} = \frac{369.2(32.9375)}{22{,}554} = 0.54 \text{ kips}$$

Similarly, the transverse component, P_{My}, is computed as:

$$P_{My} = \frac{M_{SV} X}{I_p}$$

$$P_{My} = \frac{369.2(4.50)}{22{,}554} = 0.07 \text{ kips}$$

The bolt force due to shear caused by the governing minimum design force, P_v, is taken equal to (Equation 3.3.146):

$$P_v = \frac{P}{N_b}$$

where N_b is the number of bolts in the bolt group.

$$P_v = \frac{874}{54} = 16.2 \text{ kips}$$

The bolt force due to the factored St. Venant torsional design shear is:

$$P_v = \frac{V_{sv}}{N_b}$$

$$P_{SV} = \frac{54.7}{54} = 1.01 \text{ kips}$$

The maximum resultant bolt force in the critical extreme bolt, P_r (Figure 3.3.65), is then computed as:

$$P_r = \sqrt{(P_v + P_{Mx})^2 + (P_{SV} + P_{My})^2}$$

$$P_r = \sqrt{(16.2 + 0.54)^2 + (1.01 + 0.07)^2} = 16.8 \text{ kips} < R_r = 39.0 \text{ kips} \quad \text{ok}$$

The slip resistance of the selected bolt pattern is satisfactory for constructibility and at the service limit state.

Splice Plates

The combined stress in the bottom flange splice plates under the Service II load combination will be checked against a limiting stress of $0.95F_y$, where F_y is the specified minimum yield strength of the splice plates.

The minimum Service II design force, P, for the splice was computed earlier to be 874 kips. The Service II moment due to the eccentricity of the St. Venant torsional shear, M_{SV}, was computed above to be 369.2 kip-in. Since the design actions at the service limit state are always assumed divided equally to the two slip planes regardless of the ratio of the splice plate areas (*AASHTO LRFD* Article C6.13.6.1.4c), the splice plates may be checked as follows:

$$\frac{P}{(A_g)_{PL}} + \frac{M_{SV}}{S_{PL}} \le 0.95F_y$$

$(A_g)_{PL}$ and S_{PL} were computed earlier to be 52.0 in.^{2} and 602 in.^{3}, respectively. Therefore:

$$\frac{874}{52.0} + \frac{369.2}{602} = 17.4 \text{ ksi} < 0.95(50) = 47.5 \text{ ksi} \quad \text{ok}$$

Fatigue

Since the combined area of the inside and outside flange splice plates is slightly less than the area of the smaller flange at the splice, fatigue of the splice plates will be considered (*AASHTO LRFD* Article C6.13.6.1.4a). The fatigue stresses in the base metal of the bottom flange splice plates adjacent to the slip-critical bolted connections will be checked.

By inspection, the bottom flange is subject to a net tensile stress. The unfactored vertical bending moments at the point of splice due to fatigue live load (Section 1.3.2.3.3) plus the specified 15 percent dynamic load allowance from the 3D analysis are:

$M_{+\text{Fat LL+IM}}$ = +1,180 kip-ft
$M_{-\text{ Fat LL+IM}}$ = -589 kip-ft

The unfactored torques in the bottom flange due to the fatigue live load plus impact at the point of splice from the 3D analysis are:

$T_{+\text{Fat LL+IM}}$ = +118 kip-ft
$T_{-\text{ Fat LL+IM}}$ = -218 kip-ft

Longitudinal warping stresses due to cross-section distortion (see Section 3.2.5.2.2.3) are to be considered when checking fatigue of flange splices in horizontally curved box-girder bridges (Section 3.3.7.2.5.3). The internal cross-frame spacing adjacent to the splice is 13.0 feet. An examination of the longitudinal warping stresses at the fatigue limit state for this cross-frame spacing (according to calculations similar to those outlined in Section 5.2.9.3.5) indicate that they are negligible in this case.

The conditions spelled out in *AASHTO LRFD* Article 6.6.1.2.1 are met such that the fatigue live load stresses can be computed using the short-term composite section assuming the concrete deck is effective for both positive and negative flexure (Section 5.2.9.3.3).

For checking the base metal at the gross section of high-strength bolted slip-resistant connections with the bolts installed in holes drilled full-size, the fatigue detail category is Category B (*AASHTO LRFD* Table 6.6.1.2.3-1 – Condition 2.1). From Table 3.2.9, the 75-year $(ADTT)_{SL}$ equivalent to infinite fatigue life for a Category B detail is 860 trucks per day, which is less than the computed $(ADTT)_{SL}$ of 1,000 trucks per day for this case (Section 5.2.9.3.2). The detail must therefore be checked for infinite life using the Fatigue I load combination (γ = 1.5). In the infinite life region, the nominal fatigue resistance is equal to the constant-amplitude fatigue threshold as follows (Equation 3.2.50):

$$(\Delta F)_n = (\Delta F)_{TH}$$

For a Category B detail, $(\Delta F)_{TH}$ = 16.0 ksi (*AASHTO LRFD* Table 6.6.1.2.5-3 – Table 3.2.6).

Using the section properties of the smaller section at the point of splice, the factored live load stress range at the mid-thickness of the bottom flange is computed as:

$$\gamma(\Delta f) = \frac{1.5[1{,}180 + |-589|](12)(67.775)}{528{,}681} = 4.08 \text{ ksi}$$

The range of flange force in flange is computed from the stress range as follows:

$$\Delta P = 4.08(0.75)(76.0) = 233 \text{ kips}$$

The enclosed area, A_o, for the composite box section is used to calculate the range of shear flow, Δf, for the torques applied to the composite section. A_o for the composite section was computed earlier to be 56.0 ft^2. Therefore:

$$\Delta f = \frac{1.5[118 + |-218|]}{2(56.0)} = 4.50 \text{ kips/ft}$$

The factored St. Venant torsional shear range at the service limit state, ΔV_{SV}, at the point of splice is computed as:

$$\Delta V_{SV} = \Delta f * b_f = (4.50)\frac{72.0}{12} = 27.0 \text{ kips}$$

Calculate the range of moment, ΔM_{SV}, in the bottom flange due to the eccentricity of the factored St. Venant torsional shear. Assume the shear is applied at the centerline of the splice (refer to Figure 5.2.13).

$$\Delta M_{SV} = 27.0(2.25 + 4.50) = 182.3 \text{ kip} - \text{in.}$$

The splice plates may be checked for fatigue as follows:

$$\frac{\Delta P}{(A_g)_{PL}} + \frac{\Delta M_{SV}}{S_{PL}} \le (\Delta F)_{TH}$$

$(A_g)_{PL}$ and S_{PL} were computed earlier to be 52.0 in.^{2} and 602 in.^{3}, respectively. Therefore:

$$\frac{233}{52.0} + \frac{182.3}{602} = 4.78 \text{ ksi} < 16.0 \text{ ksi} \quad \text{ok}$$

5.2.9.8.2.3 Top Flange Splices

For the top flange splices, the width of the outside splice plate should be at least as wide as the width of the narrowest flange at the splice. Therefore, try a 1/2" x 18" outside splice plate with two 5/8" x 7-1/2" inside splice plates. Include a 1/4" x 18" filler plate on the outside, as shown in Figure 5.2.15. All plates are ASTM A 709 Grade 50W steel.

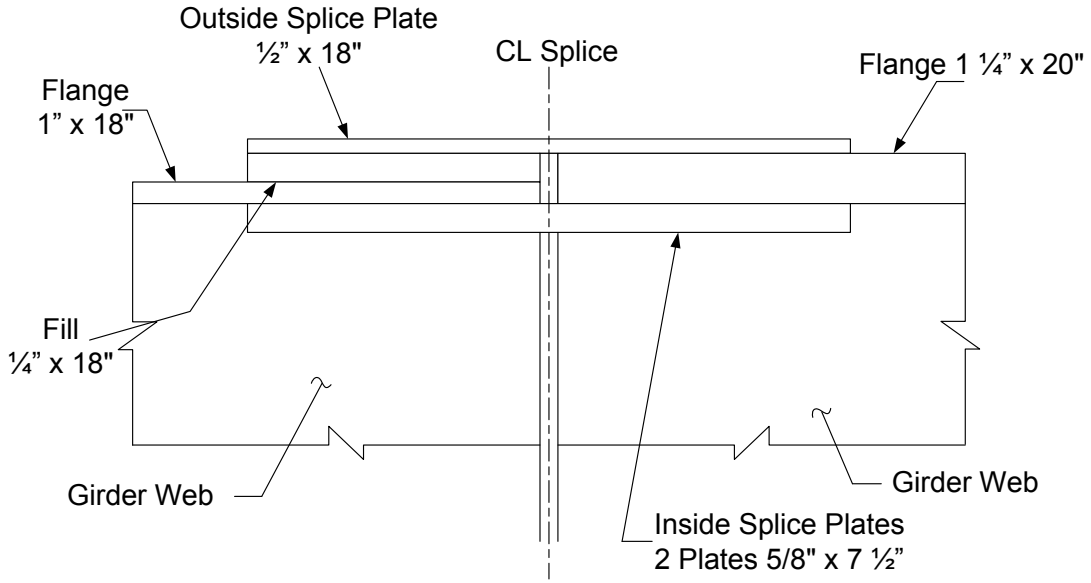


Figure 5.2.15 Elevation View of Top Flange Splice in Span 1 of G2 (bolts not shown)

Strength Limit State

Splice Plates

AASHTO LRFD Article 6.13.5.2 specifies that splice plates in tension at the strength limit state be checked for yielding on the gross section, fracture on the net section and block shear rupture.

Lateral flange bending is ignored for the top flange splice plates at the strength limit state because the flange is continuously braced.

St. Venant torsional shears are also typically ignored in the design of the top flanges of tub sections once the flange is continuously braced and the section is closed, and therefore, need not be considered in the design of the splices for these flanges (Section 3.3.7.2.5.2). The composite deck is assumed to resist the majority of the torsional shear acting on the top of tub sections once the section is closed.

Longitudinal warping stresses due to cross-section distortion may be ignored when checking both the top and bottom flange splices at the strength limit state, as these stresses are typically limited through the provision of sufficient internal cross bracing (Section 3.3.7.2.5.3).

For yielding, the splice plates may be checked as follows (Equation 3.3.135):

$$\frac{P}{(A_g)_{PL}} \le \phi_y F_y$$

$(A_g)_{PL}$ is the total gross area of the inner and outer splice plates computed as:

$$(A_g)_{PL} = 0.5(18) + 2(0.625)(7.5) = 18.4 \text{ in.}^2$$

Therefore:

$$\frac{630}{18.4} = 34.2 \text{ ksi} < 0.95(50) = 47.5 \text{ ksi} \quad \text{ok}$$

The preceding check and the checks that follow assume that the areas of the inner and outer flange splice plates do not differ by more than 10 percent, which is the case here. Otherwise, P and M_ℓ should be proportioned to the inner and outer splice plates by the ratio of the area(s) of the inner and outer plate(s) to the total area of the splice plates, with the splice plates than checked individually using their respective actions.

For net section fracture, the splice plates may be checked as follows (Equation 3.3.136):

$$\frac{P}{(A_n)_{PL}} \le \phi_u F_u U$$

U is a reduction factor to account for shear lag, which is to be taken as 1.0 for splice plates (*AASHTO LRFD* Article 6.13.5.2).

$(A_n)_{PL}$ is the total net area of the inner and outer splice plates computed as:

$$(A_n)_{PL} = [18 - 4(0.9375)](0.5) + 2[7.5 - 2(0.9375)](0.625) = 14.1 \text{ in.}^2$$

Therefore:

$$\frac{630}{14.1} = 44.7 \text{ ksi} < 0.8(70)(1.0) = 56.0 \text{ ksi} \quad \text{ok}$$

Also, according to *AASHTO LRFD* Article 6.13.5.2, for splice plates subject to tension, A_n must not exceed $0.85A_g$.

- Outer plate:

$$0.85(18)(0.5) = 7.65 \text{ in}^2 > A_n = [18 - 4(0.9375)](0.5) = 7.12 \text{ in.}^2 \quad \text{ok}$$

- Inner plates:

$$0.85(2)(7.5)(0.625) = 7.97 \text{ in}^2 > A_n = 2[7.5 - 2(0.9375)](0.625) = 7.03 \text{ in.}^2 \quad \text{ok}$$

The block shear rupture resistance of the splice plates will be checked later.

Flange splice plates subject to compression are checked for yielding on the gross section at the strength limit state as follows (Equation 3.3.142). The equation assumes an unbraced length of zero for the splice plates.

$$\frac{P}{(A_g)_{PL}} \le \phi_c F_y$$

ϕ_c is the resistance factor for compression elements (=0.90) (*AASHTO LRFD* Article 6.5.4.2). Therefore:

$$\frac{675}{18.4} = 36.7 \text{ ksi} < 0.90(50) = 45.0 \text{ ksi} \quad \text{ok}$$

Bolts

Determine the number of bolts for the top flange splice plates that are required to develop the governing minimum design force in the flange in shear at the strength limit state assuming the bolts in the connection have slipped and gone into bearing.

A minimum of two rows of bolts must be provided to ensure proper alignment and stability of the girder during construction. The factored shear resistance, R_r, for a 7/8-in. diameter A325 high-strength bolt in double shear assuming the threads are *excluded* from the shear planes was computed previously to be R_r = 55.3 kips/bolt (Section 5.2.9.8.2.2). It is assumed that the length between the extreme bolts (on one side of the connection) measured parallel to the line of action of the force will be less than 50.0 in. so that no reduction in the factored shear resistance is required (this will be checked later).

In this example, in lieu of extending the filler beyond the splice plate and adding additional bolts, the filler will be developed by reducing the factored shear resistance of the bolts on the side of the splice with the filler plate by the factor *R* as follows:

$$R = \left[\frac{(1+\gamma)}{(1+2\gamma)}\right]$$

$$A_f = 0.25(18.0) = 4.50 \text{ in.}^2$$

$$A_p = \text{flange area} = 1.0(18.0) = 18.0 \text{ in.}^2 \quad \text{(governs)} \quad \text{or}$$

$$A_p = \text{splice plate area} = 0.5(18.0) + 2(0.625)(7.5) = 18.4 \text{ in.}^2$$

$$\gamma = \frac{4.50}{18.0} = 0.25$$

$$R = \frac{1 + 0.25}{1 + 2(0.25)} = 0.833$$

$$R * R_r = 0.833 * 55.3 \text{ kips} = 46.1 \text{ kips}$$

Since lateral bending is ignored in the top flange at the strength limit state, the minimum number of bolts required to develop the governing minimum design force in the flange in shear at the strength limit state is:

$$N = \frac{P}{R * R_r} = \frac{675}{46.1} = 14.6 \text{ bolts} \quad \text{Use N = 16 bolts}$$

Use sixteen (16) 7/8-in. diameter high-strength bolts on each side of the top flange splice (4 rows of bolts with 4 bolts per row -- no stagger – Figure 5.2.16). The slip resistance of these bolts at the service limit state and for constructibility is checked later on.

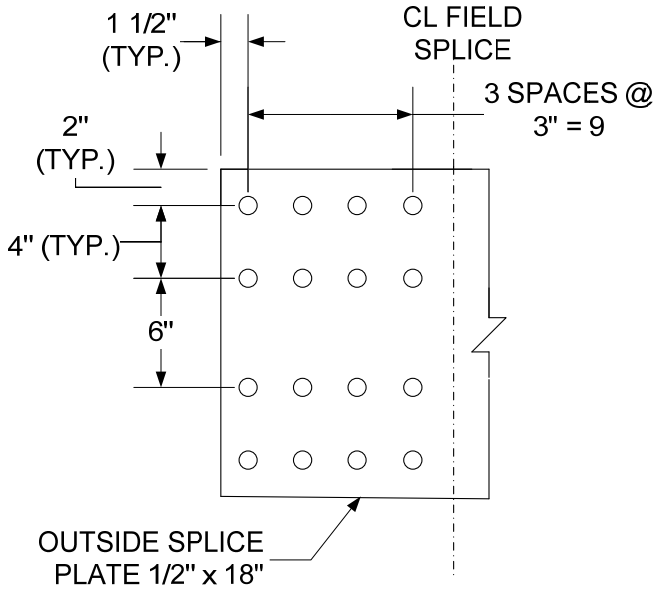


Figure 5.2.16 Bolt Configuration for Top Flange Splice in Span 1 of G2

Bolt Spacing

The bolt spacing and edge and end distances shown in Figure 5.2.16 satisfy the appropriate requirements, as demonstrated previously for the bottom flange splice in Section 5.2.9.8.2.2.

Since the length between the extreme bolts (on one side of the connection) measured parallel to the line of action of the force is less than 50.0 in., no reduction in the factored shear resistance of the bolts is required, as originally assumed.

Bearing Resistance

Check the bearing resistance at the bolt holes at the strength limit state.

Check the splice plates (the outer plate controls). For the four bolts adjacent to the end of the splice plate, the end distance is 1.5 in. Therefore, the clear end distance, L_c, between the edge of the hole and the end of the splice plate is:

$$L_c = 1.5 - \frac{0.9375}{2} = 1.03 \text{ in.}$$

Therefore:

$$R_n = 4(1.2L_c tF_u) = 4\left[1.2(1.03)(0.5)(70)\right] = 173 \text{ kips (governs)}$$

or:

$$R_n = 4(2.4dtF_u) = 4\left[2.4(0.875)(0.5)(70)\right] = 294 \text{ kips}$$

For the other twelve bolts, the center-to-center distance between the bolts in the direction of the applied force is 3.0 in. Therefore, the clear distance, L_c, between the edges of the adjacent holes is:

$$L_c = 3.0 - 0.9375 = 2.06 \text{ in.}$$

Therefore:

$$R_n = 12(1.2L_c tF_u) = 12\left[1.2(2.06)(0.5)(70)\right] = 1{,}038 \text{ kips}$$

or:

$$R_n = 12(2.4dtF_u) = 12\left[2.4(0.875)(0.5)(70)\right] = 882 \text{ kips (governs)}$$

The total nominal bearing resistance of the splice plate is therefore:

$$R_n = 173 \text{ kips} + 882 \text{ kips} = 1{,}055 \text{ kips}$$

$$R_r = 0.80(1{,}055 \text{ kips}) = 844 \text{ kips} > 675 \text{ kips} / 2 = 338 \text{ kips} \quad \text{ok}$$

Check the thinner flange at the splice. For the four bolts adjacent to the end of the flange, the end distance is 2.0 inches (which satisfies the minimum end distance requirement). Therefore, the clear end distance, L_c, between the edge of the hole and the end of the flange is:

$$L_c = 2.0 - \frac{0.9375}{2} = 1.53 \text{ in.}$$

Therefore:

$$R_n = 4(1.2L_c tF_u) = 4\left[1.2(1.53)(1.0)(70)\right] = 514 \text{ kips (governs)}$$

or:

$$R_n = 4(2.4dtF_u) = 4\left[2.4(0.875)(1.0)(70)\right] = 588 \text{ kips}$$

For the other twelve bolts, the center-to-center distance between the bolts in the direction of the applied force is 3.0 in. Therefore, the clear distance, L_c, between the edges of the adjacent holes is:

$$L_c = 3.0 - 0.9375 = 2.06 \text{ in.}$$

Therefore:

$$R_n = 12(1.2L_c tF_u) = 12\left[1.2(2.06)(1.0)(70)\right] = 2{,}076 \text{ kips}$$

or:

$$R_n = 12(2.4dtF_u) = 12\left[2.4(0.875)(1.0)(70)\right] = 1{,}764 \text{ kips (governs)}$$

The total nominal bearing resistance of the flange is therefore:

$$R_n = 514 \text{ kips} + 1{,}764 \text{ kips} = 2{,}278 \text{ kips}$$

$$R_r = 0.80(2{,}278 \text{ kips}) = 1{,}822 \text{ kips} > 675 \text{ kips} \quad \text{ok}$$

Block Shear Rupture Resistance

Check the block shear rupture resistance (Section 3.3.3.2.4) of the top flange splice plates and the top flange when subject to the minimum design force in tension at the strength limit state.

Assume the potential block shear failure planes on the outside and inside splice plates shown below in Figure 5.2.17.

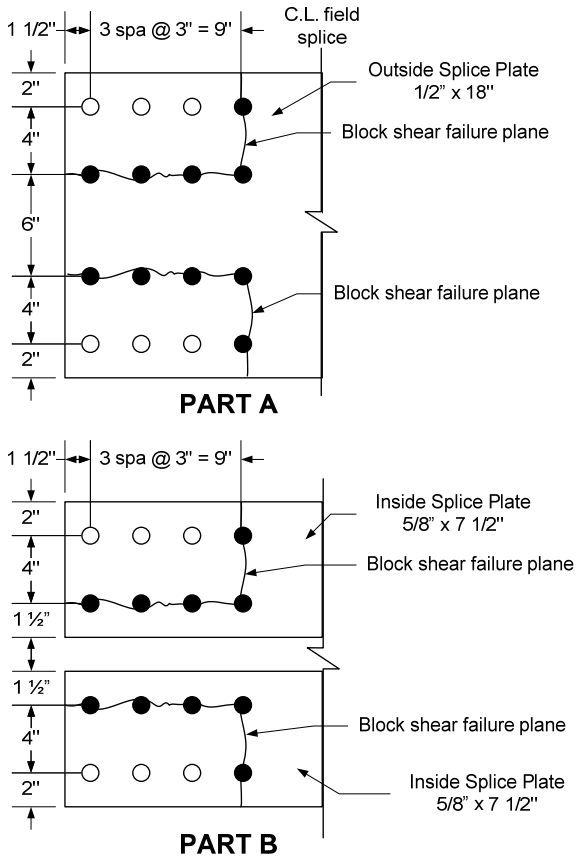


Figure 5.2.17 Assumed Block Shear Failure Planes for Top Flange Splice Plates

A) Outside Splice Plate; B) Inside Splice Plates

Check the outside splice plate. A_{tn} is the net area along the place resisting the tensile stress.

$$A_{tn} = 2[4.0 + 2.0 - 1.5(0.9375)](0.5) = 4.59 \text{ in}^2$$

A_{vn} is the net area along the place resisting the shear stress.

$$A_{vn} = 2[3(3.0) + 1.5 - 3.5(0.9375)](0.5) = 7.22 \text{ in}^2$$

A_{vg} is the gross area along the plane resisting the shear stress.

$$A_{vg} = 2[3(3.0) + 1.5](0.5) = 10.50 \text{ in}^2$$

The factored block shear rupture resistance, R_r, is determined as (Equation 3.3.27):

$$\begin{aligned} R_r &= 0.80(1.0)\left[0.58(70)(7.22)+1.0(70)(4.59)\right] = 491\,\text{kips} \\ &< 0.80(1.0)\left[0.58(50)(10.50)+1.0(70)(4.59)\right] = 501\,\text{kips} \quad \text{ok} \end{aligned}$$

Check the block shear rupture resistance according to Equation 3.3.137 as follows:

$$P \le R_r$$

$$R_r = 491\,\text{kips} > \frac{630}{2} = 315\,\text{kips} \quad \text{ok}$$

Determine the block shear rupture resistance for the inside splice plates.

$$A_{tn} = 2\left[4.0+2.0-1.5(0.9375)\right](0.625) = 5.74\ \text{in}^2$$

$$A_{vn} = 2\left[3(3.0)+1.5-3.5(0.9375)\right](0.625) = 9.02\,\text{in}^2$$

$$A_{vg} = 2\left[3(3.0)+1.5\right](0.625) = 13.12\,\text{in}^2$$

$$\begin{aligned} R_r &= 0.80(1.0)\left[0.58(70)(9.02)+1.0(70)(5.74)\right] = 614\ \text{kips} \\ &< 0.80(1.0)\left[0.58(50)(13.12)+1.0(70)(5.74)\right] = 626\ \text{kips} \quad \text{ok} \end{aligned}$$

$$R_r = 614\ \text{kips} > \frac{630}{2} = 315\ \text{kips} \quad \text{ok}$$

Check the critical girder flange at the splice. Two potential failure modes are investigated for the flange as shown below in Figure 5.2.18.

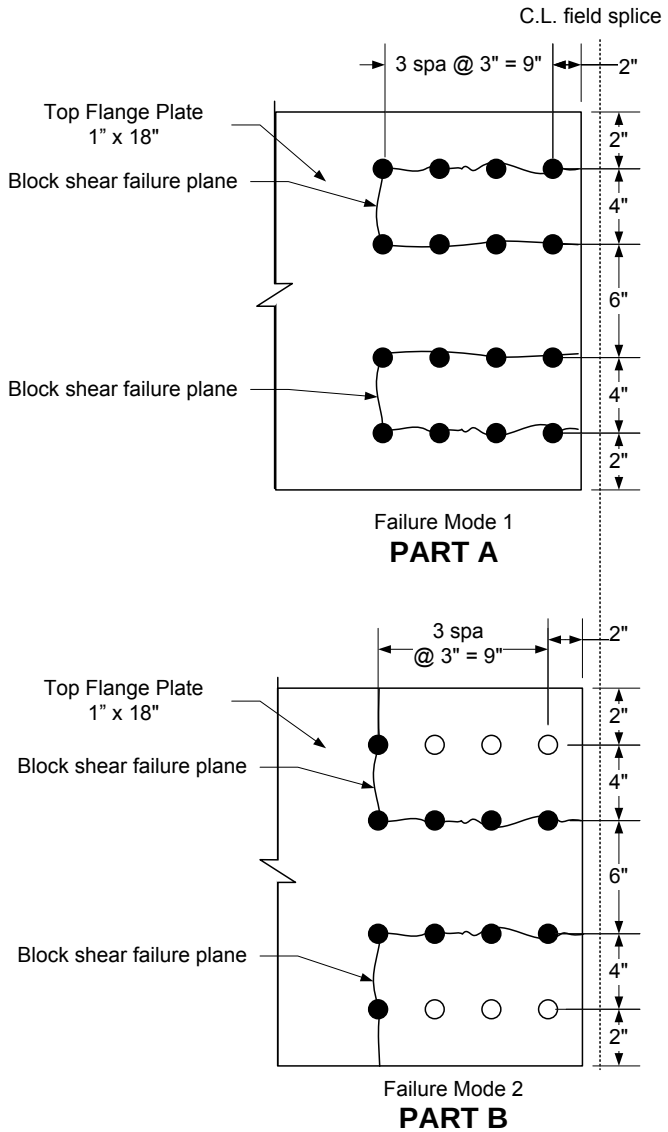


Figure 5.2.18 Assumed Block Shear Failure Planes for Critical Top Flange at the Splice

A) Assumed Failure Mode 1; B) Assumed Failure Mode 2

For Failure Mode 1:

$$A_{tn} = 2[4.0 - 0.9375](1.0) = 6.13 \text{ in}^2$$

$$A_{vn} = 4[3(3.0) + 2.0 - 3.5(0.9375)](1.0) = 30.88 \text{ in}^2$$

$$A_{vg} = 4[3(3.0) + 2.0](1.0) = 44.00 \text{ in}^2$$

$$R_r = 0.80(1.0)\left[0.58(70)(30.88) + 1.0(70)(6.13)\right] = 1{,}346 \text{ kips}$$
$$< 0.80(1.0)\left[0.58(50)(44.00) + 1.0(70)(6.13)\right] = 1{,}364 \text{ kips} \quad \text{ok}$$

$$R_r = 1{,}346 \text{ kips} > 630 \text{ kips} \quad \text{ok}$$

For Failure Mode 2:

$$A_{tn} = 2\left[4.0 + 2.0 - 1.5(0.9375)\right](1.0) = 9.19 \text{ in}^2$$

$$A_{vn} = 2\left[3(3.0) + 2.0 - 3.5(0.9375)\right](1.0) = 15.44 \text{ in}^2$$

$$A_{vg} = 2\left[3(3.0) + 2.0\right](1.0) = 22.00 \text{ in}^2$$

$$R_r = 0.80(1.0)\left[0.58(70)(15.44) + 1.0(70)(9.19)\right] = 1{,}016 \text{ kips}$$
$$< 0.80(1.0)\left[0.58(50)(22.00) + 1.0(70)(9.19)\right] = 1{,}025 \text{ kips} \quad \text{ok}$$

$$R_r = 1{,}016 \text{ kips} > 630 \text{ kips} \quad \text{ok}$$

Net Section Fracture of Flange

Check for net section fracture of the critical top flange at the point of splice when subject to tension at the strength limit state according to *AASHTO LRFD* Equation 6.10.1.8-1 (Section 3.2.6.1.3 – Equation 3.2.72).

The flange on the left side of the splice is the critical flange for this particular check.

A_n is the net area of the flange computed as:

$$A_n = \left[18 - 4(0.9375)\right](1.0) = 14.25 \text{ in.}^2$$

$$0.84\left(\frac{A_n}{A_g}\right)F_u = 0.84\left(\frac{14.25}{18.0}\right)70 = 46.6 \text{ ksi} < F_{yt} = 50 \text{ ksi}$$

From separate calculations, f_t in the top flange at the strength limit state (Strength I) is equal to +4.62 ksi for the section on the left side of the splice, which is less than 46.6 ksi. Therefore, net section fracture of the top flange at the point of splice will not occur.

Service Limit State & Constructibility

Bolts

For the left side of the splice, which is deemed the smaller section, the Service II stress in the top flange is computed as follows. Separate computations indicate that the conditions specified in *AASHTO LRFD* Article 6.10.4.2.1 are met such that flexural stresses caused by Service II loads applied to the composite section can be computed using the short-term or long-term composite section, as appropriate, assuming the concrete deck is effective for both positive and negative flexure. Flange lateral bending is not considered because the flange is continuously braced at the service limit state. St. Venant torsional shears are also not considered in the design of top flange splices.

Longitudinal warping stresses due to cross-section distortion (see Section 3.2.5.2.2.3) are to be considered when checking the slip resistance of the bolts for constructibility and at the service limit state for flange splices in horizontally curved box-girder bridges (Section 3.3.7.2.5.3). The internal cross-frame spacing adjacent to the splice is 13.0 feet. An examination of the longitudinal warping stresses at the top of the box at the service limit state and for constructibility for this cross-frame spacing (according to calculations similar to those outlined in Sections 5.2.9.3.5 and 5.2.9.4.4) indicates that they are negligible in this case.

A. Dead Load + Positive Live Load:

$$f = \left[1.0(-4.95 + -0.20 + -0.26) + 1.3(-1.28)\right] = -7.07 \text{ ksi} \quad \text{(controls)}$$

B. Dead Load + Negative Live Load:

$$f_{-LL+IM} = \frac{-2{,}926(12)(-11.10)}{528{,}681} = +0.74 \text{ ksi}$$

$$f = \left[1.0(-4.95 + -0.20 + -0.26) + 1.3(+0.74)\right] = -4.45 \text{ ksi}$$

Therefore, f_s is equal to –7.07 ksi and F_s is equal to f_s/R_h = -7.07/1.0 = -7.07 ksi. The design force, P, for the flange splice is taken as F_s times the smaller gross flange area on either side of the splice (Equation 3.3.133), or:

$$P = F_s A_g = -7.07(1.0)(18) = 127 \text{ kips}$$

The stress on the non-composite section at the mid-thickness of the top flange due to the steel weight plus the deck-casting sequence (the Strength IV load combination controls with η taken equal to 1.0) is:

$$f = \frac{1.0(1.5)(467 + 4{,}082)(12)(-42.23)}{201{,}500} = -17.16 \text{ ksi} \qquad \frac{f}{R_h} = \frac{-17.16}{1.0} = -17.16 \text{ ksi}$$

The design force, *P,* for the flange splice is taken as *f* times the smaller gross flange area on either side of the splice (Equation 3.3.132), or:

$$P = fA_g = |-17.16|(1.0)(18) = 309 \text{ kips}$$

Because the top flange is discretely braced during construction, consider the flange lateral bending. Determine the factored lateral moment, M_ℓ, in the top flange for constructibility. The factored lateral moment due to the steel weight plus the deck staging at the point of splice is 1.0(1.5)(1 + 4) = +7.5 kip-ft.

The splice on the outside top flange of the tub is subject to lateral flange bending due to the deck overhang loads. Using procedures similar to those demonstrated previously in Section 5.2.9.1.2, the factored lateral moment due to the deck overhang loads at the adjacent cross-frames under the Strength IV load combination for the 13.1-ft cross-frame spacing along the outside top flange at the splice is estimated to be -11.4 kip-ft. Amplification of the lateral moment is not required in this case.

The splice is located halfway between the cross-frames at this location. In a curved bridge, the lateral flange moments in the outside flange of the tub due to the deck overhang loads typically have the same sense as the lateral flange moments due to curvature. However, in this particular case, the cross-frame spacing at the splice is only approximately one-half of the adjacent cross-frame spacings (Figure 5.2.2). Thus, reversal of the lateral flange moment due to the overhang loads does not occur within this shorter unbraced length. A separate line-girder analysis of a three span continuous beam subject to a uniform load with a center span length equal to one-half the length of the adjacent spans indicated that the negative moment at mid-length of the center span is approximately 63 percent of the negative moment at the supports. Therefore, 0.63(-11.4) = -7.2 kip-ft. This moment essentially offsets the top-flange lateral moment of +7.5 kip-ft due to the steel weight plus the deck staging. Hence, flange lateral bending will be ignored in the design of the top-flange splice at this location. Should flange lateral bending be deemed significant, the reader is referred to Section 5.1.8.8.2.3 for an illustration of the suggested procedure for considering flange lateral bending in the design of the splice. :

By inspection, the constructibility case controls.

Determine the number of bolts for the top flange splice plates that are required to prevent slip. The factored slip resistance, R_r, for a 7/8-in. diameter A 325 high-strength bolt assuming a Class B surface condition for the faying surface, standard holes and two slip planes per bolt (i.e. N_s = 2) was computed earlier to be R_r = 39.0 kips/bolt (Section 5.2.9.8.2.2).

Since lateral bending is ignored in this case, the minimum number of bolts required to develop the governing minimum design force is:

$$N = \frac{P}{R_r} = \frac{309}{39.0} = 7.9 \text{ bolts} < 16 \text{ bolts} \quad \text{ok}$$

The slip resistance of the selected bolt pattern is satisfactory for constructibility and at the service limit state.

Splice Plates

The combined stress in the top flange splice plates under the Service II load combination will be checked against a limiting stress of $0.95F_y$, where F_y is the specified minimum yield strength of the splice plates.

The minimum Service II design force, *P*, for the splice was computed earlier to be 127 kips. Since the top flange is continuously braced at the service limit state, lateral flange bending is ignored. The design actions at the service limit state are always assumed divided equally to the two slip planes regardless of the ratio of the splice plate areas (*AASHTO LRFD* Article C6.13.6.1.4c). Therefore, the force on the outside and inside splice plates will be taken as 127/2 = 63.5 kips. The resulting stress on the gross area of the outside splice plate is:

$$f = \frac{63.5}{(0.5)(18)} = 7.1 \text{ ksi} < 0.95(50) = 47.5 \text{ ksi} \quad \text{ok}$$

The stress on the gross area of the inside splice plates is:

$$f = \frac{63.5}{2(0.625)(7.5)} = 6.8 \text{ ksi} < 0.95(50) = 47.5 \text{ ksi} \quad \text{ok}$$

Fatigue

Since the combined area of the inside and outside flange splice plates is greater than the area of the smaller flange at the splice, fatigue of the splice plates need not be considered (*AASHTO LRFD* Article C6.13.6.1.4a). However, the check will still be illustrated below to assist with cases in which fatigue may be a concern.

The factored fatigue live load plus impact moments at the point of splice were given earlier (Section 5.2.9.8.2.2). The conditions spelled out in *AASHTO LRFD* Article 6.6.1.2.1 are met such that the fatigue live load stresses can be computed using the short-term composite section assuming the concrete deck is effective for both positive and negative flexure (Section 5.2.9.3.3).

First, determine if the top flange splice plates are subject to a net tensile stress under the unfactored permanent loads plus the Fatigue I load combination, as specified in *AASHTO LRFD* Article 6.6.1.2.1. The future wearing surface will be conservatively neglected in this calculation.

$$f_{DC1} = \frac{1{,}950(12)}{-4{,}672} = -5.01\,\text{ksi}$$

$$f_{DC2} = \frac{251(12)}{-15{,}095} = -0.20\,\text{ksi}$$

$$f_{-\text{Fat LL+IM}} = \frac{1.5(-589)(12)}{-45{,}576} = +0.23\,\text{ksi}$$

Since |-5.01 + -0.20| = 5.21 ksi > 0.23 ksi, the top flange splice plates are not subject to a net tensile stress under the specified load combination and fatigue need not be checked.

5.2.9.8.3 Web Splice Design

5.2.9.8.3.1 General

Bolted web splice design is covered in Section 3.3.7.3. The web splice will be designed based on the conservative assumption that the maximum moment and shear at the splice will occur under the same loading condition.

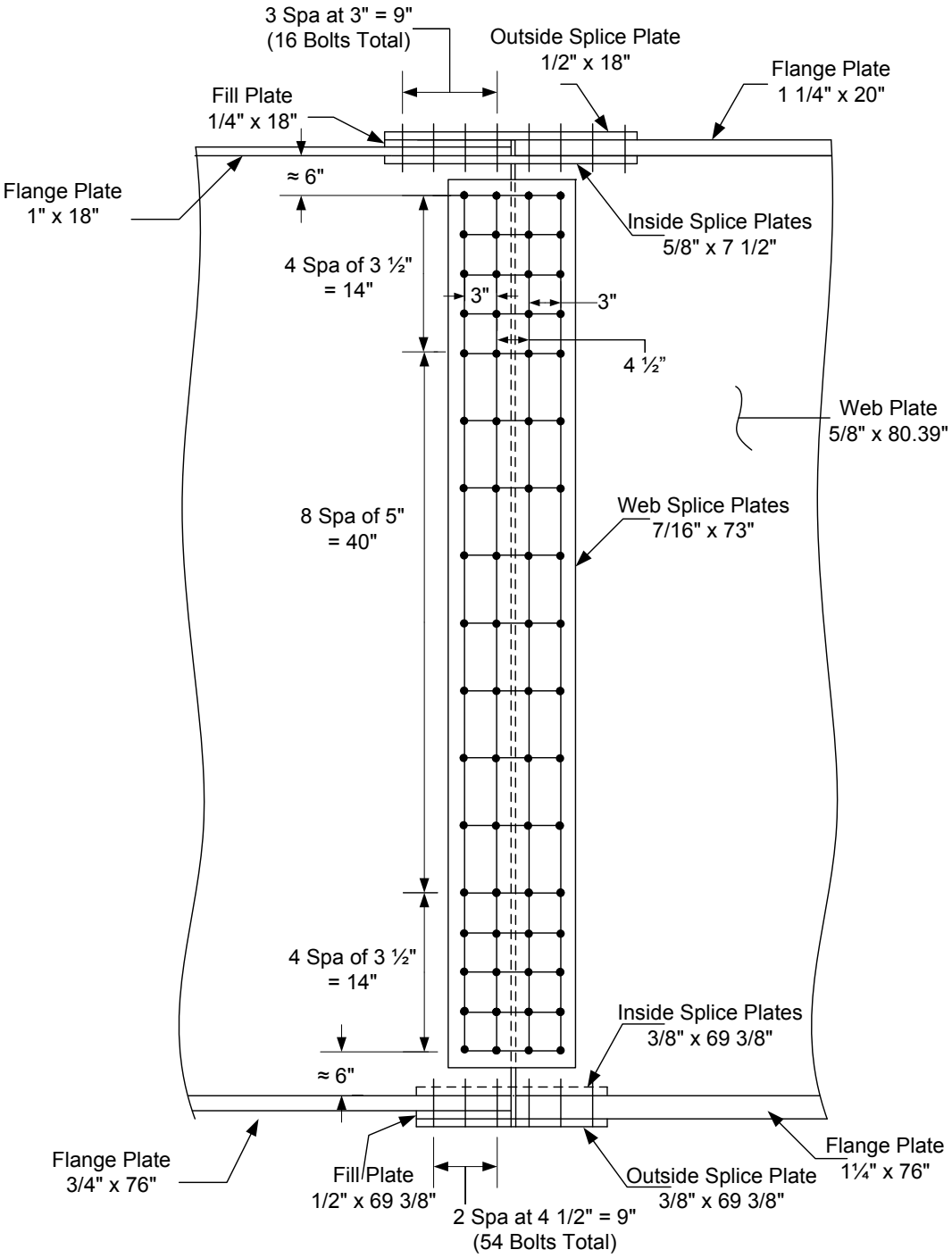
AASHTO LRFD Article 6.13.6.1.4b specifies that for box sections in horizontally curved bridges, the shear due to the factored loads is to be taken as the sum of the flexural and St. Venant torsional shears in the web subjected to additive shears in the design of bolted web splices at all limit states (Section 3.3.7.3.4). Also, for boxes with inclined webs, the web splice is to be designed at all limit states for the component of the vertical shear in the plane of the web by dividing the design shear by the cosine of the angle of inclination of the web plate to the vertical. When designing the web bolts for eccentric shear, this includes the direct shear on the bolts and the vertical component of the bolt shear due to torsion.

Two vertical rows of bolts with 17 bolts per row will be investigated. According to *AASHTO LRFD* Article 6.13.6.1.4a, a minimum of two rows of bolts is required on each side of the joint to ensure proper alignment and stability of the girder during construction. The bolts are spaced horizontally and vertically as shown in Figure 5.2.19.

The outermost bolts are located just over 6 inches from the flanges to provide ample clearance for assembly (see Table 7-16 of the AISC *Steel Construction Manual* for bolt assembly clearances). The web is spliced symmetrically by plates with a thickness not less than one-half the web thickness. Assume 7/16″ x 73″ splice plates on each side of the web. The splice plates are ASTM A 709 Grade 50W steel (F_u =

70 ksi). A filler plate is not required since the webs are the same thickness on both sides of the splice.

In this illustration, the number of bolts in the web splice is decreased by spacing the group of bolts closest to the mid-depth of the web (where the flexural stress is relatively low) near the maximum spacing specified for sealing (*AASHTO LRFD* Article 6.13.2.6.2), and by spacing the remaining two groups of bolts near the top and bottom of the web at a closer spacing (Figure 5.2.19).



Notes: 1) All bolts are 7/8" dia. (ASTM A325) H.S. Bolts
2) A 0.5 in. gap is assumed between the edges of the field pieces
3) The indicated vertical distances are measured along the web slope.

5.2.19 Elevation View of Bolted Field Splice in Span 1 of G2

5.2.9.8.3.2 Strength Limit State

Design Shear

Determine the vertical design shear in the critical web, V_{uw}, at the point of splice at the strength limit state (Section 3.3.7.2.2.1).

Compute the maximum factored vertical shear in the critical web at the splice, V_u, at the strength limit state using the appropriate load factors given in *AASHTO LRFD* Tables 3.4.1-1 and 3.4.1-2. The Strength I load combination is used (the load modifier, η, is taken equal to 1.0). Note that the minimum load factors, γ_p, from *AASHTO LRFD* Table 3.4.1-2 and a load modifier, $1/\eta$ (≤1.0), are applied to the permanent load shears when the corresponding shears are of opposite sign to the live load plus impact shear.

A. Dead Load + Positive Vertical Live Load Shear:

$$V_u = (1/1.0)\left[0.90(-89 + -12) + 0.65(-12)\right] + 1.0(1.75)(+35) = -37.5 \text{ kips}$$

B. Dead Load + Negative Vertical Live Load Shear:

$$V_u = 1.0\left[1.25(-89 + -12) + 1.5(-12) + 1.75(-89)\right] = -300 \text{ kips (governs)}$$

Calculate the factored shear resistance, $V_r = \phi_v V_n$, of the web panel containing the splice. The maximum factored shear, V_u, in this panel is -329 kips/cos14° = -339 kips at the cross-frame adjacent to the splice. The factored shear resistance of the web assuming it is unstiffened was computed previously to be V_r = 401 kips (Section 5.2.9.4.3.2). Thus, transverse stiffeners are not required in this panel. Hence, the factored shear resistance of this panel is taken as the factored shear resistance of the unstiffened web equal to 401 kips.

AASHTO LRFD Article 6.13.6.1.4b specifies that the equation to use to compute the vertical design shear, V_{uw}, for the splice depends on the value of V_u at the splice with respect to $V_r = \phi_v V_n$ as follows:

$$0.5\phi_v V_n = 0.5(401) = 200.5 \text{ kips}$$

$$\left|V_u\right| = \left|-300\right| \text{ kips} > 200.5 \text{ kips}$$

Therefore, the design shear, V_{uw}, is to be computed using Equation 3.3.149 as follows:

$$V_{uw} = \frac{(V_u + \phi_v V_n)}{2}$$

$$V_{uw} = \frac{|-300| + 401}{2} = 350 \text{ kips}$$

Moment due to the Eccentricity of the Design Shear

Calculate the design moment, M_{uv}, due to the eccentricity of the in-plane design shear at the point of splice at the strength limit state as follows (Section 3.3.7.3.2.2 - Equation 3.3.150):

$$M_{uv} = V_{uw} e$$

Referring to Figure 5.2.19, the correct eccentricity, *e*, to use is the horizontal distance from the centerline of the splice to the centroid of the web bolt group on the side of the joint under consideration as follows (Figure 3.3.67):

$$e = \left(2.25 + \frac{3.0}{2}\right)\frac{1}{12} = 0.3125 \text{ ft}$$

$$M_{uv} = \left(350 / \cos 14^\circ\right)(0.3125) = 113 \text{ kip} - \text{ft}$$

Design Moment and Design Horizontal Force Resultant

Determine the portion of the flexural moment to be resisted by the web, M_{uw}, and the horizontal design force resultant, H_{uw}, in the web at the strength limit state. Use the equations provided in *AASHTO LRFD* Article C6.13.6.1.4b (Section 3.3.7.3.2.3 - Equations 3.3.151 and 3.3.152). Again, since the splice is located in an area of stress reversal, checks must be made for both the positive and negative flexure conditions.

- Positive Flexure

The controlling flange for the case of positive flexure was previously determined to be the bottom flange (Section 5.2.9.8.2.1). The maximum factored vertical bending stress at the midthickness of the controlling flange, f_{cf}, and the minimum design stress for the controlling flange, F_{cf}, were previously computed for this loading condition to be:

f_{cf} = +20.28 ksi
F_{cf} = +37.50 ksi

For the same loading condition, the concurrent flexural stress at the mid-thickness of the noncontrolling (top) flange was computed to be:

f_{ncf} = -9.07 ksi

The portion of the flexural moment assumed to be resisted by the web is computed as (Equation 3.3.151):

$$M_{uw} = \frac{t_w D^2}{12}\left|R_h F_{cf} - R_{cf} f_{ncf}\right|$$

where the hybrid factor R_h is taken as 1.0 for a homogeneous section and ratio, R_{cf}, is computed as follows:

$$R_{cf} = \left|\frac{F_{cf}}{f_{cf}}\right| = \left|\frac{+37.50}{+20.28}\right| = 1.85$$

Therefore:

$$M_{uw} = \frac{0.625(78.0)^2}{12}\left|1.0(+37.50) - 1.85(-9.07)\right| = 17{,}200 \text{ kip} - \text{in.} = 1{,}433 \text{ kip} - \text{ft}$$

The design horizontal force resultant for this loading condition is computed as (Equation 3.3.152):

$$H_{uw} = \frac{t_w D}{2}\left(R_h F_{cf} + R_{cf} f_{ncf}\right)$$

$$H_{uw} = \frac{0.625(78.0)}{2}\left[1.0(+37.50) + 1.85(-9.07)\right] = +505 \text{ kips}$$

Note that all stresses in the above equations are to be taken as signed quantities. Since the sign of M_{uw} corresponds to the sign of the flexural moment for the loading condition under consideration, absolute value signs are applied to the resulting difference of the stresses for convenience. H_{uw} is always taken as a signed quantity; positive for tension, negative for compression.

Check the above computed values of M_{uw} and H_{uw}. Assuming the web is vertical, the section modulus S = (0.625)(78.0)^2/6 = 634 in.^{3} and the area A = 0.625(78.0) = 48.75 in.^{2}. Therefore:

$$f_{bot} = \frac{1433(12)}{634} + \frac{505}{48.75} = 37.50 \text{ ksi} = R_h F_{cf} \quad \text{ok}$$

$$f_{top} = \frac{1433(12)}{-634} + \frac{505}{48.75} = -16.76 \text{ ksi} \cong R_{cf} f_{ncf} = 1.85(-9.07) \quad \text{ok}$$

The use of R_hF_{cf} and the application of the factor R_{cf} to f_{ncf} in essence is factoring up the stresses in the web by the same amount as the stresses in the controlling flange so that the web splice is designed in a consistent fashion at the strength limit state.

The total moment on the web splice for this condition is equal to the sum of M_{uv} and M_{uw}:

$$M_{tot} = M_{uv} + M_{uw} = 113 + 1{,}433 = 1{,}546 \text{ kip} - \text{ft}$$

➢ Negative Flexure

The controlling flange for the case of negative flexure was also previously determined to be the bottom flange (Section 5.2.9.8.2.1). The maximum factored vertical bending stress at the midthickness of the controlling flange, f_{cf}, and the minimum design stress for the controlling flange, F_{cf}, were computed for this loading condition to be:

$$f_{cf} = -5.54 \text{ ksi}$$
$$F_{cf} = -8.63 \text{ ksi}$$

For the same loading condition, the concurrent flexural stress at the mid-thickness of the noncontrolling (top) flange was previously computed to be:

$$f_{ncf} = +4.56 \text{ ksi}$$

The ratio, R_{cf}, is computed as follows:

$$R_{cf} = \left|\frac{F_{cf}}{f_{cf}}\right| = \left|\frac{-8.63}{-5.54}\right| = 1.56$$

Therefore:

$$M_{uw} = \frac{0.625(78.0)^2}{12}\left|1.0(-8.63) - 1.56(+4.56)\right| = 4.989 \text{ kip} - \text{in.} = 415.7 \text{ kip} - \text{ft}$$

The design horizontal force resultant for this loading condition is computed as:

$$H_{uw} = \frac{0.625(78.0)}{2}\left[1.0(-8.63) + 1.56(+4.56)\right] = -37 \text{ kips}$$

Check the above computed values of M_{uw} and H_{uw}:

$$f_{bot} = \frac{-415.7(12)}{634} - \frac{37}{48.75} = -8.63 \text{ ksi} = R_hF_{cf} \quad \text{ok}$$

$$f_{top} = \frac{-415.7(12)}{-634} - \frac{37}{48.75} = +7.11\,\text{ksi} = R_{cf} f_{ncf} = 1.56(+4.56) \quad \text{ok}$$

The total moment on the web splice for this condition is equal to the sum of M_{uv} and M_{uw}:

$$M_{tot} = M_{uv} + M_{uw} = 113 + 415.7 = 529\ \text{kip} - \text{ft}$$

Bolts

Check the web-splice bolts for shear at the strength limit state assuming the bolts in the connection have slipped and gone into bearing (Section 3.3.7.3.2.4).

The web-splice bolts are to be designed for the effects of the design shear, the moment due to the eccentric design shear, and the flexural moment and horizontal design force resultant in the web, which are all assumed applied at the mid-depth of the web. The traditional elastic vector method is used for calculating the maximum resultant bolt force (Section 3.3.6.2.7).

The polar moment of inertia, I_p, of the bolts with respect to the centroid of the connection is computed as follows (Equation 3.3.108):

$$I_p = \sum_{i=1}^{n} x_i^2 + \sum_{i=1}^{n} y_i^2$$

Referring to Figure 5.2.19, I_p is computed as:

$$I_p = \left[2 * 17 * \left(1.5^2\right)\right] + \left[2 * 2 * \begin{pmatrix} 5.00^2 + 10.00^2 + 15.00^2 + 20.00^2 + 23.50^2 + 27.00^2 \\ + 30.50^2 + 34.00^2 \end{pmatrix}\right]$$

$$= 16{,}546\ \text{in}^2$$

Determine the in-plane bolt force, R_v, due to the vertical design shear, V_{uw}, assuming two vertical rows with 17 bolts per row for a total number of bolts, N_b, equal to 34:

$$R_v = \frac{V_{uw}}{N_b} = \frac{350}{34} = 10.29\,\text{kips}/\cos 14^\circ = 10.61\,\text{kips/bolt}$$

➢ Positive Flexure

Determine the in-plane bolt force due to the horizontal design force resultant, H_{uw}:

$$R_h = \frac{H_{uw}}{N_b} = \frac{505}{34} = 14.85 \text{ kips/bolt}$$

Determine the in-plane vertical and horizontal components of the force on the extreme bolt due to the total moment on the web splice, M_{tot}:

$$R_{M_v} = \frac{M_{tot}x}{I_p} = \frac{1{,}546(12)(3.0/2)}{16{,}546} = 1.68 \text{ kips}$$

$$R_{M_h} = \frac{M_{tot}y}{I_p} = \frac{1{,}546(12)(34.0)}{16{,}546} = 38.12 \text{ kips}$$

The resultant in-plane bolt force on the extreme bolt is:

$$R = \sqrt{\left(R_v + R_{M_v}\right)^2 + \left(R_h + R_{M_h}\right)^2} = \sqrt{(10.61+1.68)^2 + (14.85+38.12)^2} = 54.38 \text{ kips (governs)}$$

➢ Negative Flexure

Determine the in-plane bolt force due to the horizontal design force resultant, H_{uw}:

$$R_h = \frac{H_{uw}}{N_b} = \frac{|-37|}{34} = 1.09 \text{ kips/bolt}$$

Determine the in-plane vertical and horizontal components of the force on the extreme bolt due to the total moment on the web splice, M_{tot}:

$$R_{M_v} = \frac{M_{tot}x}{I_p} = \frac{529(12)(3.0/2)}{16{,}546} = 0.57 \text{ kips}$$

$$R_{M_h} = \frac{M_{tot}y}{I_p} = \frac{529(12)(34.0)}{16{,}546} = 13.04 \text{ kips}$$

The resultant bolt force on the extreme bolt is:

$$R = \sqrt{\left(R_v + R_{M_v}\right)^2 + \left(R_h + R_{M_h}\right)^2} = \sqrt{(10.61+0.57)^2 + (1.09+13.04)^2} = 18.02 \text{ kips}$$

The factored shear resistance, R_r, for a 7/8-in. diameter A 325 high-strength bolt in double shear assuming the threads are *excluded* from the shear planes was computed earlier to be 55.3 kips/bolt (Section 5.2.9.8.2.2). The greater than 50.0 in. length reduction does *not* apply when computing the factored shear resistance of the

bolts in a web splice since the distribution of shear force is essentially uniform along the joint. Therefore:

$$R = 54.38 \text{ kips} < R_r = 55.3 \text{ kips} \quad \text{ok}$$

Bolt Spacing

Check the bolt spacings and bolt edge and end distances for the web splice (Figure 5.2.19).

AASHTO LRFD Article 6.13.2.6.1 specifies that the minimum spacing between centers of bolts in standard holes is not to be less than 3.0*d*, where *d* is the diameter of the bolt (Section 3.3.6.2.2.6). For 7/8-in. diameter bolts:

$$s_{min} = 3d = 3(0.875) = 2.63 \text{ in.} < 3.0 \text{ in.} \quad \text{ok}$$

AASHTO LRFD Article 6.13.2.6.2 specifies that to seal against the penetration of moisture in joints, the spacing *s* of a single line of bolts adjacent to a free edge of an outside plate or shape (when the bolts are not staggered) must satisfy the following requirement (Section 3.3.6.2.2.6 – Equation 3.3.75):

$$s \le (4.0 + 4.0t) \le 7.0 \text{ in.}$$

where *t* is the thickness of the thinner outside plate or shape. Check for sealing along the vertical edges of the web splice plates:

$$s_{max} = 4.0 + 4.0(0.4375) = 5.75 \text{ in.} > 5.00 \text{ in.} \quad \text{ok}$$

The edge distance of bolts is defined as the distance perpendicular to the line of force between the center of a hole and the edge of the component. In this example, the edge distance from the center of the vertical line of holes to the edge of the splice plate of 2 inches (Figure 5.2.20) satisfies the minimum edge distance requirement of 1½ inches specified for 7/8-in. diameter bolts and sheared edges in *AASHTO LRFD* Table 6.13.2.6.6-1 (Section 3.3.6.2.2.6 – Table 3.3.2). This distance also satisfies the maximum edge distance requirement of 8.0*t* (not to exceed 5.0 in.) = 8.0(0.4375) = 3.5 in. specified in *AASHTO LRFD* Article 6.13.2.6.6.

The end distance of bolts is defined as the distance along the line of force between the center of a hole and the end of the component. In this example, the end distance of 2½ inches at the top and bottom of the web splice plates (Figure 5.2.20) satisfies the minimum end distance requirement of 1½ inches specified for 7/8-in. diameter bolts and sheared edges in *AASHTO LRFD* Table 6.13.2.6.6-1 (Table 3.3.2). The maximum end distance requirement of 8.0*t* (not to exceed 5.0 in.) = 8.0(0.4375) = 3.5 in. specified in *AASHTO LRFD* Article 6.13.2.6.5 is also satisfied. Although not specifically required, note that the distance from the corner bolts to the

corner of the web splice plate, equal to $\sqrt{(2.0)^2 + (2.5)^2} = 3.2$ in., also satisfies the maximum end distance requirement.

Bearing Resistance

Check the bearing resistance at the web-splice bolt holes at the strength limit state (Section 3.3.6.2.6.2).

The resistance of an outermost hole, calculated using the clear edge distance (which is smaller than the clear vertical distance between the bolt holes), can conservatively be checked against the maximum resultant bolt force acting on the extreme bolt in the connection (Figure 3.3.70 Part A). Since the resultant force acts in the direction of an inclined distance that is larger than the clear edge distance, the check is conservative. Other options for checking the bearing resistance are discussed in Section 3.3.7.3.2.4.

Check the web. Based on the edge distance from the center of the hole to the edge of the field piece of 2 inches (which also satisfies the minimum edge distance requirement discussed above), the clear edge distance is computed as:

$$L_c = 2.0 - \frac{0.9375}{2} = 1.53 \text{ in.}$$

The nominal bearing resistance, R_n, parallel to the applied bearing force for standard holes is taken as follows (Equation 3.3.88):

$$R_n = 1.2 L_c t F_u \le 2.4 d t F_u$$

$$R_n = 1.2 L_c t F_u = 1.2(1.53)(0.625)(70) = 80.33 \text{ kips (governs)}$$

or:

$$R_n = 2.4 d t F_u = 2.4(0.875)(0.625)(70) = 91.88 \text{ kips}$$

The factored bearing resistance of the flange, R_r, is computed as (Equation 3.3.80):

$$R_r = \phi_{bb} R_n$$

$R_r = 0.80(80.33) = 64.26$ kips > R = 54.38 kips ok

Check the splice plates. Based on the edge distance from the center of the hole to the edge of the splice plate of 2 inches, the clear edge distance is computed as:

$$L_c = 2.0 - \frac{0.9375}{2} = 1.53 \text{ in.}$$

$$R_n = 1.2L_c tF_u = 1.2(1.53)(0.4375)(70) = 56.23 \text{ kips (governs)}$$

or:

$$R_n = 2.4dtF_u = 2.4(0.875)(0.4375)(70) = 64.31 \text{ kips}$$

The factored bearing resistance of the flange, R_r, is computed as (Equation 3.3.80):

$$R_r = \phi_{bb} R_n$$

R_r = 0.80(56.23) = 44.98 kips > R/2 = 54.38 kips/2 = 27.19 kips ok

Had the bearing resistance been exceeded in either case, the preferred option would be to increase the edge distance slightly in lieu of increasing the number of bolts or thickening the web and/or splice plates.

Splice Plates

Block Shear Rupture Resistance of Splice Plates

Check the block shear rupture resistance (Section 3.3.3.2.4) of the web splice plates at the strength limit state. Because of the overall length of the connection, the block shear rupture resistance normally does not control for web splice plates of typical proportion, but the check is illustrated here for completeness. Assume the block shear failure plane on the web splice plates shown below in Figure 5.2.20.

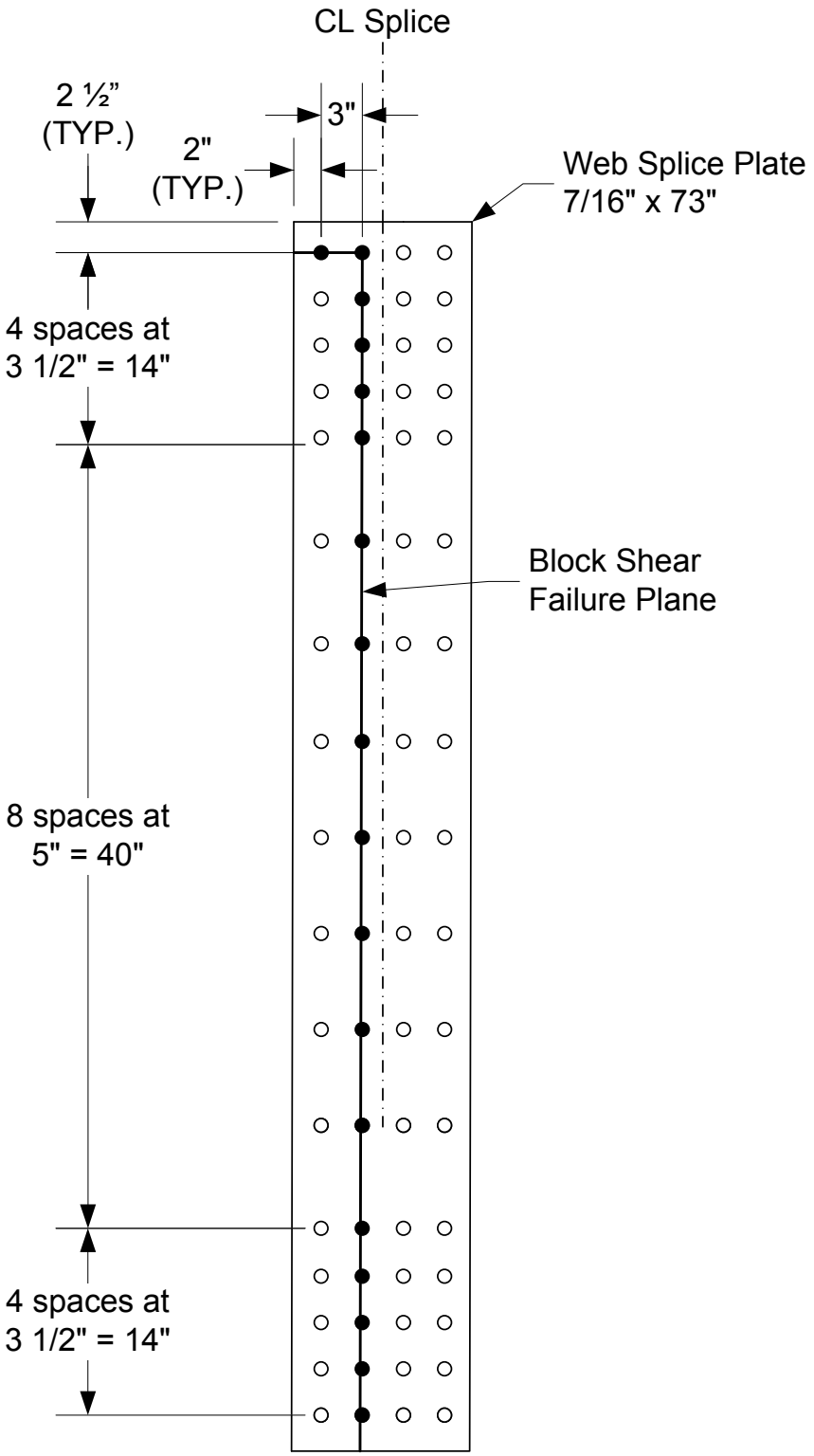


Figure 5.2.20 Assumed Block Shear Failure Plane for the Web Splice Plates

A_{tn} is the net area along the place resisting the tensile stress.

$$A_{tn} = 2[3.0 + 2.0 - 1.5(0.9375)](0.4375) = 3.14 \text{ in}^2$$

A_{vn} is the net area along the place resisting the shear stress.

$$A_{vn} = 2[73.0 - 2.5 - 16.5(0.9375)](0.4375) = 48.15 \text{ in}^2$$

A_{vg} is the gross area along the plane resisting the shear stress.

$$A_{vg} = 2[73.0 - 2.5](0.4375) = 61.69 \text{ in}^2$$

The factored block shear rupture resistance, R_r, is determined as (Equation 3.3.27):

$$\begin{aligned} R_r &= 0.80(1.0)[0.58(70)(48.15) + 1.0(70)(3.14)] = 1{,}740 \text{ kips} \\ &> 0.80(1.0)[0.58(50)(61.69) + 1.0(70)(3.14)] = 1{,}607 \text{ kips} \\ \therefore R_r &= 1{,}607 \text{ kips} \end{aligned}$$

$$R_r = 1{,}607 \text{ kips} > V_{uw} = 350 \text{ kips} / \cos 14^\circ = 361 \text{ kips} \quad \text{ok}$$

Flexural Yielding of Splice Plates

Check for flexural yielding on the gross section of the web splice plates at the strength limit state as follows (Section 3.3.7.3.2.4 – Equation 3.3.153):

$$f = \frac{M_{uv} + M_{uw}}{S_{PL}} + \frac{H_{uw}}{A_g} \le \phi_f F_y$$

$$A_g = 2(0.4375)(73.0) = 63.9 \text{ in.}^2$$

$$S_{PL} = \frac{2(0.4375)(73.0)^2}{6} = 777 \text{ in.}^3$$

For positive flexure:

$$f = \frac{[113 + 1{,}433](12)}{777} + \frac{505}{63.9} = 31.78 \text{ ksi} < \phi_f F_y = 1.0(50) = 50 \text{ ksi} \quad \text{ok}$$

For negative flexure:

$$f = \frac{[113 + 415.7](12)}{777} + \frac{|-37|}{63.9} = 8.74 \text{ ksi} < \phi_f F_y = 1.0(50) = 50 \text{ ksi} \quad \text{ok}$$

Shear Yielding and Shear Rupture of Splice Plates

Check for shear yielding on the gross section of the web splice plates under the in-plane design shear, V_{uw}, at the strength limit state. *AASHTO LRFD* Article 6.13.5.3 specifies that for shear yielding, the factored shear resistance of a connected element, R_n, is conservatively based on the shear yield stress (i.e. $F_y/\sqrt{3} = 0.58F_y$) as follows (Section 3.3.6.2.6.2 – Equation 3.3.90):

$$R_r = \phi_v 0.58 F_y A_{vg}$$

$$R_r = 1.0(2)0.58(50)(0.4375)(73.0) = 1{,}852 \text{ kips}$$

$$R_r = 1{,}852 \text{ kips} > V_{uw} = 350 \text{ kips}/\cos 14^\circ = 361 \text{ kips} \quad \text{ok}$$

Check for shear rupture on the net section of the web splice plates under the design shear, V_{uw}, at the strength limit state. For shear rupture, the factored shear resistance of the connected element, R_r, is to be taken as follows (Equation 3.3.6.2.6.2 – Equation 3.3.91). The reduction factor, R_p, in the following equation is taken as 1.0 for holes drilled full-size:

$$R_r = \phi_{vu} 0.58 R_p F_u A_{vn}$$

$$R_r = 0.80(2)1.0(70)(0.4375)[73.0 - 17(0.9375)] = 2{,}796 \text{ kips}$$

$$R_r = 2{,}796 \text{ kips} > V_{uw} = 350 \text{ kips}/\cos 14^\circ = 361 \text{ kips} \quad \text{ok}$$

5.2.9.8.3.3 Service Limit State and Constructibility

AASHTO LRFD Article 6.13.6.1.4b requires that high-strength bolted connections for web splices be designed to prevent slip at the service limit state under the maximum resultant bolt force due to Load Combination Service II. In addition, *AASHTO LRFD* Article 6.13.6.1.4a requires that high-strength bolted splices for flexural members be proportioned to prevent slip during the erection of the steel (assuming an erection analysis is conducted) and during the casting of the concrete deck (Section 3.3.7.3.3).

Design Shear

The Service II vertical shears in the critical web at the point of splice for the positive and negative flexure conditions are computed as follows:

A. Dead Load + Positive Vertical Live Load Shear:

$$V_S = [1.0(-89 + -12 + -12) + 1.3(+35)] = -67.5 \text{ kips}$$

B. Dead Load + Negative Vertical Live Load Shear:

$$V_S = [1.0(-89 + -12 + -12) + 1.3(-89)] = -229 \text{ kips} \quad (\text{governs})$$

Therefore, the vertical design shear, V_s, for the Service II load combination is equal to $|-229|$ kips.

The factored shear due to the steel weight plus the deck-casting sequence (the Strength IV load combination controls with the load modifier, η, taken equal to 1.0) is computed as:

$$V_{\text{stl+deck casting}} = 1.0(1.5)(-20 + -89) = -164 \text{ kips}$$

which is less than the governing value of V_s. Therefore, the vertical design shear for checking slip of the web bolts will be taken as V_s.

Moment due to the Eccentricity of the Design Shear

Calculate the design moment, M_{sv}, due to the eccentricity of the in-plane design shear at the point of splice at the service limit state as follows (Equation 3.3.154):

$$M_{sv} = V_s e$$

$$M_{sv} = \left(229 / \cos 14^\circ\right)(0.3125) = 73.8 \text{ kip} - \text{ft}$$

Design Moment and Design Horizontal Force Resultant

Determine the portion of the flexural moment to be resisted by the web, M_{sw}, and the horizontal design force resultant, H_{sw}, in the web at the service limit state (Section 3.3.7.3.3 - Equations 3.3.155 and 3.3.156).

The maximum Service II flexural stress at the mid-thickness of the bottom flange, f_s, was computed previously (Section 5.2.9.8.2.2) to be +15.33 ksi due to the positive flexure load condition. The flexural stress in the other (top) flange at the point of

splice, f_{os}, concurrent with f_s in the bottom flange for this load condition is –7.07 ksi. The portion of the flexural moment assumed to be resisted by the web is computed as (Equation 3.3.155):

$$M_{sw} = \frac{t_w D^2}{12}\left|f_s - f_{os}\right|$$

$$M_{sw} = \frac{0.625(78.0)^2}{12}\left|+15.33-(-7.07)\right| = 7{,}098\,\text{kip}-\text{in.} = 592\,\text{kip}-\text{ft}$$

The design horizontal force resultant for this loading condition is computed as (Equation 3.3.156):

$$H_{sw} = \frac{t_w D}{12}\left(f_s + f_{os}\right)$$

$$H_{uw} = \frac{0.625(78.0)}{2}\left[+15.33+(-7.07)\right] = +201\,\text{kips}$$

Check the above computed values of M_{sw} and H_{sw}:

$$f_{bot} = \frac{592(12)}{634} + \frac{201}{48.75} = 15.33\,\text{ksi} = f_s \quad \text{ok}$$

$$f_{top} = \frac{592(12)}{-634} + \frac{201}{48.75} = -7.08\,\text{ksi} \cong f_{os} \quad \text{ok}$$

The total moment on the web splice for this condition is equal to the sum of M_{sv} and M_{sw}:

$$M_{tot} = M_{sv} + M_{sw} = 73.8 + 592 = 666\,\text{kip}-\text{ft}$$

In this case, the loading condition causing the maximum Service II flexural stress in the top flange is the same loading condition (i.e. the positive flexure condition). Therefore, slip of the web bolts only needs to be checked for the one load condition.

Bolts

The traditional elastic vector method is again used for calculating the maximum resultant bolt force (Section 3.3.6.2.7).

Determine the in-plane bolt force, R_v, due to the vertical design shear, V_s, assuming two vertical rows with 17 bolts per row for a total number of bolts N_b equal to 34 (Figure 5.2.19):

$$R_v = \frac{V_s}{N_b} = \frac{229}{34} = 6.74 \text{ kips/cos}14^\circ = 6.95 \text{ kips/bolt}$$

Determine the in-plane bolt force due to the horizontal design force resultant H_{sw}:

$$R_h = \frac{H_{sw}}{N_b} = \frac{201}{34} = 5.91 \text{ kips/bolt}$$

Determine the in-plane vertical and horizontal components of the force on the extreme bolt due to the total moment on the web splice, M_{tot}:

$$R_{M_v} = \frac{M_{tot}x}{I_p} = \frac{592(12)(3.0/2)}{16{,}546} = 0.64 \text{ kips}$$

$$R_{M_h} = \frac{M_{tot}y}{I_p} = \frac{592(12)(34.0)}{16{,}546} = 14.60 \text{ kips}$$

The resultant bolt force on the extreme bolt is:

$$R = \sqrt{\left(R_v + R_{M_v}\right)^2 + \left(R_h + R_{M_h}\right)^2} = \sqrt{\left(6.95 + 0.64\right)^2 + \left(5.91 + 14.60\right)^2} = 21.87 \text{ kips}$$

The factored slip resistance, R_r, for a 7/8-in. diameter A 325 high-strength bolt assuming a Class B surface condition for the faying surface, standard holes and two slip planes per bolt (i.e. N_s = 2) was computed to be 39.0 kips/bolt (Section 5.2.9.8.2.2). Therefore:

$$R = 21.87 \text{ kips} < R_r = 39.0 \text{ kips} \quad \text{ok}$$

Splice Plates

Since the combined area of the web splice plates is greater than the area of the web on both sides of the splice, the flexural stresses in the splice plates at the service limit state under the Service II load combination need not be checked.

5.2.9.8.3.4 Fatigue

Since the combined area of the web splice plates is greater than the area of the web on both sides of the splice, the fatigue stresses in the base metal of the web splice plates adjacent to the slip-critical bolted connections also need not be checked.